American Society of Biomechanics
37th Annual Meeting
Conference Proceedings

Omaha, Nebraska
September 4-7, 2013
CenturyLink Center

Online Program: http://www.openconf.org/asb2013/openconf.php

University of Nebraska Omaha
University of Nebraska Medical Center
University of Nebraska Lincoln
Creighton University

TABLE OF CONTENTS

**Conference program is current as of 08/09/2013. Changes to programming after this date may not be reflected in the following proceedings, however all accepted abstracts are present.*

A SPECIAL THANK YOU TO OUR 2013 SPONSORS

2013 DIAMOND SPONSORS

AMTI FORCE AND MOTION

MotionAnalysis

2013 SILVER SPONSORS

QUALISYS Motion Capture Systems

simpleware

2013 EXHIBITORS

KISTLER measure. analyze. innovate.

Tekscan

novel

VICON

zFlo

GAITRite

DELSYS

NDI

ATI INDUSTRIAL AUTOMATION www.ati-ia.com

The Motion Monitor ...The Total Solution in Motion Capture

xsens

MADONNA Rehabilitation Hospital

MOTION LAB SYSTEMS

BERTEC

POLHEMUS INNOVATION IN MOTION™

COSMED

PROTOKINETICS

C-Motion Research Biomechanics

UNO SCHOOL OF HEALTH, PHYSICAL EDUCATION, AND RECREATION

GREAT LAKES NEUROTECHNOLOGIES

CONTEMPLAS

METRIA INNOVATION INC IMAGE-BASED SPATIAL MEASUREMENT

NORAXON MEASURING FOR EXCELLENCE

ViTRAK Systems Inc

THANK YOU TO OUR 2013 SPONSORS!

ASB 2013 DIAMOND SPONSORS:

AMTI FORCE AND MOTION

MotionAnalysis

ASB 2013 SILVER SPONSORS:

QUALISYS Motion Capture Systems

simpleware

2013 FEDERAL SPONSORS:

NIBIB

NIAMS

2013 FOUNDATION SPONSORS:

THE HAWKS FOUNDATION

University of Nebraska FOUNDATION

University of Nebraska's The Peter Kiewit Institute

ASB SUPPORTING MEMBER:

POLHEMUS INNOVATION IN MOTION™

ASB PARTNER MEMBER:

Tekscan

2013 STATE SPONSORS:

NASA Nebraska Space Grant

Rehabilitation Science Research Laboratory

UNMC Clinical Movement Analysis Laboratory

M2E Mechanical & Materials engineering UNIVERSITY OF NEBRASKA-LINCOLN

IDeA EPSCoR NEBRASKA

UNO SCHOOL OF HEALTH, PHYSICAL EDUCATION, AND RECREATION

MEETING AT A GLANCE

Wednesday September 4	Thursday September 5
12:30-2:00pm Tutorial I (Hilton – St. Nicholas)	7:00-8:00am Breakfast (Grand Ballroom) Past President's Breakfast (Hilton – Herndon)
2:00-5:00pm ASB Executive Board Meeting (Hilton – Blackstone A)	8:00-8:15am Welcoming Comments (CenturyLink – Jr. Ballroom)
2:00-4:00pm Lab Tour – Creighton University	8:15-9:15am Keynote Lecture (CenturyLink – Jr. Ballroom • Nicolaas Bohnen, MD, PhD
2:30-4:30pm Tutorial II (Hilton – Blackstone B)	9:30-11:00am Poster Session I (CenturyLink – Grand Ballroom)
4:00-6:30pm Quick Research studies (CenturyLink – Room 210)	11:30am-12:15pm Podium Sessions (CenturyLink Center)
5:00-6:30pm Student Event (Hilton – Blackstone B)	12:15-1:15pm Lunch (CenturyLink – Grand Ballroom) Diversity Luncheon (CenturyLink – Room 207)
5:00-6:30pm Vendor Reception (Hilton – Liberty Tavern Patio)	1:15-2:15pm Borelli Award Lecture (CenturyLink – Jr. Ballroom) • Kenton R. Kaufman, PhD
6:30-9:00pm Opening Reception (CenturyLink – Aksarben Terrace)	2:30-4:00 Poster Session (CenturyLink – Grand Ballroom)
	4:15-5:15pm Podium Session (CenturyLink Center)
	5:15-6:00 Student Outing (Old Mattress Factory Grill and Bar)

MEETING AT A GLANCE

Friday September 6	Saturday September 7
7:00-8:00am Breakfast (Grand Ballroom) Women in Science Breakfast (Hilton – Blackstone A)	6:30-8:00am 5K Fun Run (Meet in Hilton Lobby)
8:00-9:30am Poster Session (CenturyLink – Grand Ballroom)	7:00-8:00am Breakfast (CenturyLink – Grand Ballroom)
9:45-10:45am Podium Sessions (CenturyLink)	8:00-9:00am Keynote Lecture (CenturyLink – Jr. Ballroom) • Shane Farritor, PhD
11:15am-12:15pm ISB Sponsored Keynote (CenturyLink – Jr. Ballroom) • Taija Finni, PhD	9:30-10:45am Podium Sessions (CenturyLink)
12:15-1:15pm Lunch (CenturyLink – Grand Ballroom) Mentoring Luncheon (CenturyLink – Room 207)	11:00am-12:15pm Podium Sessions (CenturyLink)
1:15-2:15pm Hay Award Lecture (CenturyLink – Jr. Ballroom) • Glenn Fleisig, PhD	12:15-1:15pm Business Meeting and Lunch (CenturyLink – Jr. Ballroom)
2:30-3:45pm Podium Sessions/ASB Fellows Symposium	1:15-2:30pm Podium Sessions/Young Scientist Awards (CenturyLink)
4:00-5:15 Podium Sessions/Symposium	2:45-3:30pm Closing Ceremony and Awards (CenturyLink – Jr. Ballroom)
6:00-9:00 Dinner at the Henry Doorly Zoo	4:00-5:30 Executive Board Meeting (Hilton – Blackstone A)

CENTURYLINK CENTER/HILTON OMAHA FLOOR PLANS

CenturyLink Center Omaha

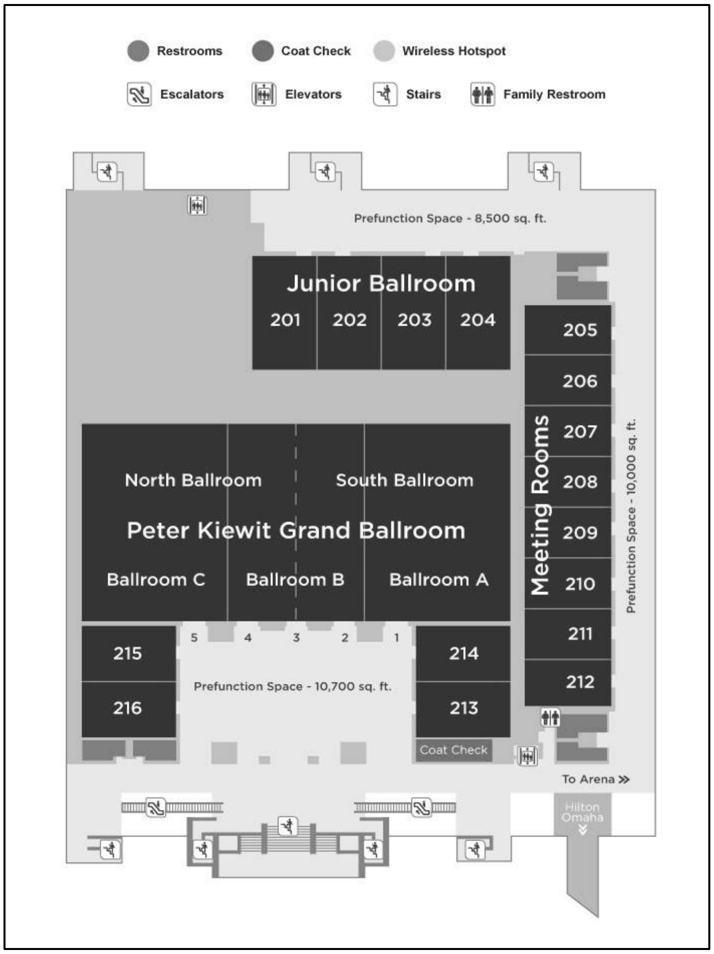

Hilton Omaha

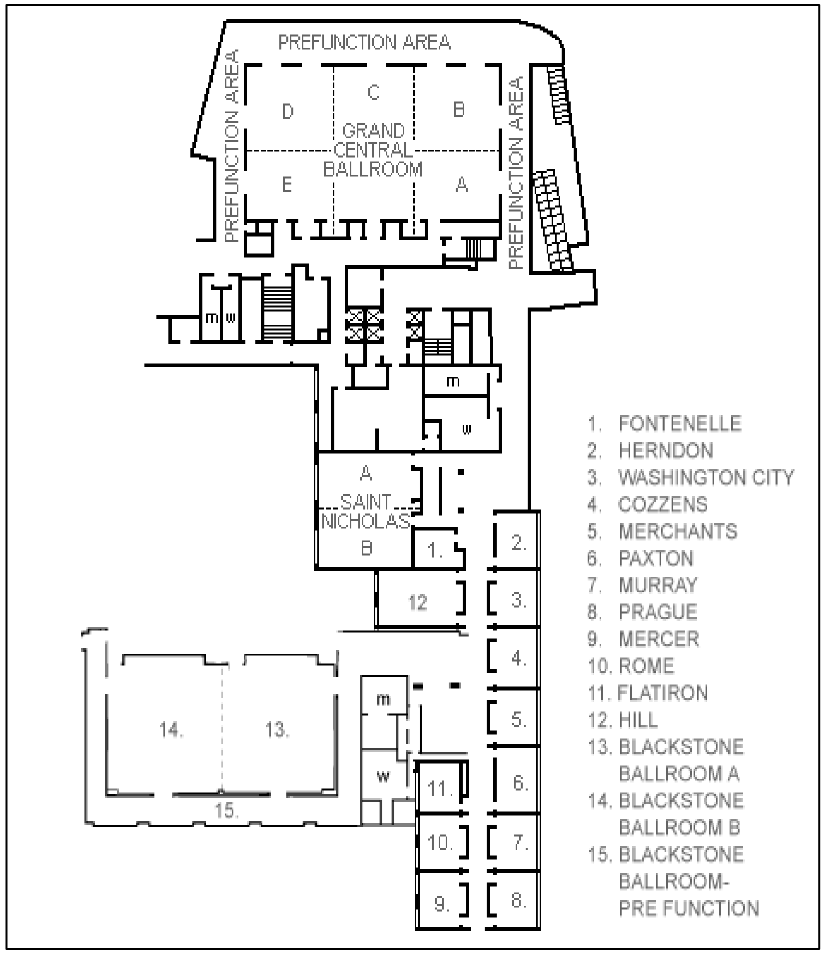

Prepared by MECA
Subject to Change
6/15/13 NB
7/17/13 NB

American Society of Biomechanics
2013 Annual Conference
September 4-7

Peter Kiewit Grand Ballroom

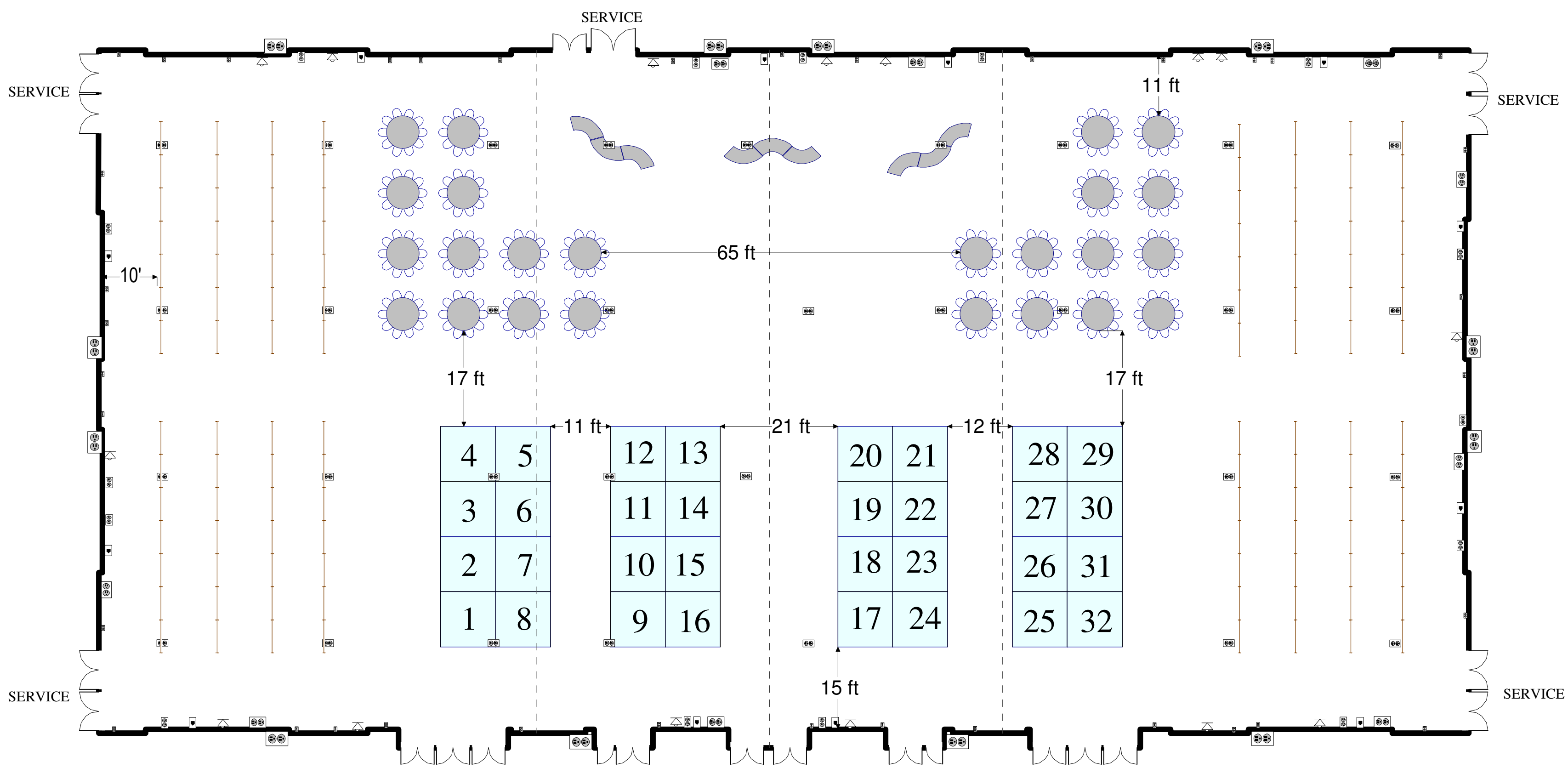

1: Vicon
2: UNO School of Health, Physical Education and Recreation
3: GaitRite/CIR Systems
4: Northern Digital, Inc.
5: Novel
6: Cosmed
7: Metria Innovation
8: ATI Industrial Automation
9: Xsens
10: Motion Lab Systems
11: Empty
12: Polhemus
13: Motion Analysis
14: Delsys
15: Tekscan
16: Tekscan
17: The MotionMonitor
18: Omaha Convention and Visitors Bureau
19: AMTI
20: AMTI
21: Qualisys
22: Empty
23:Madonna Rehab Hospital
24: Madonna Rehab Hospital
25: Bertec
26: zFlo/Contemplas
27: Great Lakes NeuroTechnologies
28:Kistler
29: C-Motion
30: Noraxon
31:ProtoKinetics
32:ProtoKinetics

WELCOME TO ASB 2013!

Thank you all for attending the 37th Annual Meeting of the American Society of Biomechanics. We are excited for the various opportunities and events we have planned for the conference this year. We are pleased with the potential for professional development in the programming, as well as opportunities for networking at our various social events. The opening reception will be held on the terrace of the CenturyLink Center overlooking downtown Omaha, and the banquet dinner for the conference, we are pleased to announce, will be held at the Henry Doorly Zoo (ranked the #1 zoo in the country by TripAdvisor).

This year 480 abstracts were accepted, including 101 abstracts designated for podium presentations that will be presented in over 20 multidisciplinary sessions and 9 invited podium presentations that will be presented in symposium sessions. In addition, we are excited about 24 thematic poster presentations organized in 6 sessions and 346 general posters. Three internationally known keynote speakers are invited. Another highlight of the program are award presentations and many opportunities for networking. The theme of this year's meeting is "thinking beyond biomechanics," bringing together biomechanists and other scientists, who strive to understand how biomechanical principles impact and interact with the broader biological behavior of a system. Thus, we look forward to a multidisciplinary biomechanics program at this year's meeting. Tutorials on Nonlinear Analysis: Theory and Applications and Teaching STEM Concepts with Educational Robots are offered on Wednesday as well as tours of the Rehabilitation Science Research laboratory at Creighton University and the student event.

As the conference has outgrown many university and hotel settings, it has become crucial to expand to a convention center for this year's conference. We are pleased with the outcome and hope that the space is appreciated by all. We would like to give a special thank you to supporters of the conference who have made renting this private facility a possibility. Donors include: The Hawks Foundation, The University of Nebraska Foundation, Peter Kiewit Institute, The University of Nebraska Medical Center College of Public Health, Creighton University Rehabilitation Science Research Laboratory, University of Nebraska at Lincoln Department Mechanical & Materials Engineering, the University of Nebraska at Omaha College of Education, and the School of Health, Physical Education and Recreation. A very special thanks goes out to our Diamond Sponsors, AMTI and Motion Analysis, and our Silver Sponsors, Qualisys and Simpleware. Without generous donations from these sponsors, this meeting would not be possible. In addition to these generous donations to put towards the meeting, we have also received funding from the National Institutes of Health, NASA Nebraska Space Grant, and NSF EPSCoR to assist with student registration fees with the goal of encouraging student attendance and participation at the meeting.

Again, on behalf of the ASB executive board, the local hosting institutions, and all who have been a part of the planning and execution of this conference, welcome you to Omaha and we hope you enjoy your stay.

Sincerely,

Nick Stergiou
Meeting Chair

Rakié Cham
Program Chair

April Chambers
Program Co-Chair

ASB EXECUTIVE BOARD & COMMITTEES

President:
John H. Challis
Pennsylvania State University

Past-President:
Donald D. Anderson
The University of Iowa

President-Elect
Richard Hughes
University of Michigan

Treasurer
Gary Heise
University of Northern Colorado

Treasurer-Elect
Karen Troy
University of Illinois-Chicago

Secretary/Membership Chair
Andy Karduna
University of Oregon

Education Committee Chair:
Gerald Smith
Colorado Mesa University

Communications Committee Chair:
Michelle Sabick
Boise State University

Newsletter Editor
William Ledoux
VA Puget Sound

Program Chair
Rakié Cham
University of Pittsburgh

Program Chair-Elect
Brian Umberger
University of Massachusetts

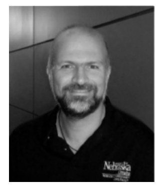

Meeting Chair
Nick Stergiou
University of Nebraska-Omaha

Student Representative
Jennifer Bagwell
University of Southern California

ASB PROGRAM COMMITTEE:

Kai-Nan An, PhD	*(Mayo Clinic)*
Paul DeVita, PhD	*(East Carolina University)*
Clark R. Dickerson, PhD	*(University of Waterloo)*
Jonathan Dingwell, PhD	*(University of Texas at Austin)*
Jinger S. Gottschall, PhD	*(The Pennsylvania State University)*
Chris Hass, PhD	*(University of Florida)*
Thurmon E. Lockhart, PhD	*(Virginia Tech)*
Michael L. Madigan, PhD	*(Virginia Tech)*
Jean L. McCrory, PhD	*(West Virginia University)*
Richard R. Neptune, PhD	*(University of Texas at Austin)*
Maury A. Nussbaum, PhD	*(Virginia Tech)*
Stephen Piazza, PhD	*(The Pennsylvania State University)*
Michelle Sabick, PhD	*(Boise State University)*
Robert A. Siston, PhD	*(The Ohio State University)*
Brian R. Umberger, PhD	*(University of Massachusetts)*

ASB EXECUTIVE COMMITTEE:
Rakié Cham (Program Chair), April Chambers (Program Co-Chair)

LOCAL ORGANIZING COMMITTEE:
Jeff Hawks, Terry Grindstaff, Sara Myers, Ka-Chun (Joseph) Siu.

ASSISTANTS TO THE MEETING & PROGRAM CHAIRS:
Special thanks to Jennifer Yentes, Amanda Fletcher, Jung Chien, and Arash Mahboobin for assistance with conference organization, program development, registration organization, and website construction and maintenance. Also, special thanks to all volunteers who have helped make this conference possible.

ASB REVIEW COMMITTEE

Kai-nan An
Don Anderson
Scott Arnett
Joaquin Barrios
Adam Bartsch
Aditya Belwadi
Kathleen Bieryla
Kimberly Bigelow
Bhushan Borotikar
Brad Bowser
Katherine Boyer
Thomas Buckley
Frank Buczek
Timothy Burkhart
Robert Catena
John H. Challis
April Chambers
Ajit Chaudhari
Li-Shan Chou
Steve Collins
Neil Cronin
Jesse Dean
Geoffrey Desmoulin
Paul DeVita
Clark Disckerson
Angela DiDomenico
Jonathan Dingwell
Janet Dufek
Brent Edwards
Rebecca Fellin
Daniel Ferris
Ken Fischer
Jason Franz
J. Christopher Fritton
Yang-Chieh Fu
Jinger Gottschall
Dave Gutekunst
Gregory Gutierrez
Chris Hass
Kim Hébert-Losier
Bradford Hendershot
Daniel Herman
Brian Higginson
Xiao Hu
Pilwon Hur
Ben Infantolino
Laurel Kuxhaus
Spencer Lake
Patrick Lam
William Ledoux
Sabrina Lee
Thurmon Lockhart
Michael Madigan
Matthew Major
Christopher Massey
Witaya Mathiyakom
Sara Matrangola
Jean McCrory
Jill Meyer
Ross Miller
Chris Mizelle
Melissa Morrow
Sivasankar Murugaiyan
Sara Myers
Rick Neptune
Jennifer Neugebauer
Christopher Neville
Maury Nussbaum
Justus Ortega
Max Paquette
Stephen Piazza
John Popovich
Douglas Powell
Dan Ramsey
Manku Rana
Noah Rosenblatt
Brandi Row
Elizabeth Russell
Michelle Sabick
Kotaro Sasaki
Anne Schmitz
Jason Scibek
Joseph Seay
Matthew Seeley
Na-Jin Seo
Elaine Serina
Anne Silverman
Tarkeshwar Singh
Rob Siston
Ka-Chun Siu
Alexander H. Slocum Jr.
Jeremy Smith
Ewa M. Spiesz
Mark Timmons
Karen Troy
Brian Umberger
Srikant Vallabhajosula
David Wagner
Henry Wang
Ruoli Wang
Feng Wei
Wendi Weimar
Jason Wicke
Erik Wolf
Jianhua Wu
Tong-Ching Tom Wu
Ting Xia
Metin Yavuz
Yener Yeni
Vanessa Yingling
Amir A. Zadpoor

MEETING INFORMATION AT A GLANCE

MEETING LOCATIONS:

All of the academic meeting events will take place at the CenturyLink Center Omaha. All posters will be up in the Grand Ballroom from Thursday morning through Friday afternoon for viewing. Keynote and award lectures will take place in the Junior Ballroom. Podium, Thematic, and Symposium sessions will take place in combined rooms 215-216, 213-214, 211-212, and 208-209. General breakfast, lunch and breaks will be located in the Grand Ballroom with the exhibitors. Events such as Executive Board Meetings, Past President Breakfast, and Women in Science Breakfast will take place at the Hilton Omaha, connected to the CenturyLink Center via skywalk.

REGISTRATION:

Wednesday: The registration desk will be located in the lobby of the Hilton Omaha from 12pm-6:30pm.
Thursday-Saturday: The registration desk will be located at the CenturyLink center in front of the Grand Ballroom from 7am – 5pm on Thursday and Friday, and from 7am – 4pm.

EXHIBITOR BOOTHS:

Exhibitor booths are located in the Grand Ballroom of the CenturyLink Center. Vendor Bingo will be taking place again this year, so visit all of the exhibitors and place your card in the box at the registration desk for your chance to win a prize! Names will be drawn for prizes on Thursday and Friday evenings.

ASB EXECUTIVE BOARD/EXHIBITOR'S RECEPTION:

The ASB Executive board would like to welcome exhibitors to ASB 2013 by hosting a reception on Wednesday, September 4th prior to the opening reception. The reception will take place on the patio of the Hilton. Attendance is limited to the ASB Executive Board, Exhibitor Representatives, and Organizers of the 2013 ASB meeting.

PRESENTER INFORMATION

SPEAKER PRACTICE ROOM:

Due to space constraints, no speaker ready room will be available.

POSTER PRESENTATIONS:

At least one named author is required to be present at each poster during its designated poster session. Posters for the general poster session should be 36” wide x 48” tall (portrait style). Posters shall be posted prior to 8am Thursday morning, and shall be taken down prior to 5:30pm Friday evening. Any posters remaining after 5:30pm on Friday will be discarded.

Poster Session 1: Thursday, September 5th, 9:30-11am
Poster Session 2: Thursday, September 5th, 2:30-4pm
Poster Session 3: Friday, September 6th, 8-9:30am

PODIUM PRESENTATIONS:

Presenters are allotted 10 minutes for the presentation, and 5 minutes for discussion. Speakers will not be allowed to use their own computers for podium presentations. Speakers are strongly encouraged to upload their presentations at the registration desk the day before their assigned time.

THEMATIC POSTER PRESENTATIONS:

Posters will be mounted in the Grand Ballroom prior to 8am Thursday morning. Posters will be moved into the appropriate room for each thematic poster session. Each poster will have a 5 minute formal presentation of approximately 3 PowerPoint slides, followed by approximately 10 minutes of discussion on the theme topic. These sessions are geared towards stimulating scientific discussion among the authors, moderators and audience. Successful discussions should focus on the topic and not on the individual presentation or presenters. Participants should leave having both learned about the work presented, but also know about how the work will be integrated into the field and what some next steps might be. It is strongly encouraged to upload PowerPoint Presentations the day before your assigned session at the registration desk.

INTERNET ACCESS:

Free internet access is available at the CenturyLink center. We strongly encourage conference attendees to limit connections to one device per person.

OPENING RECEPTION:

The opening reception for the conference will take place Wednesday, September 4th on the terrace of the CenturyLink Center (upstairs). Hors D ’Oeuvres will be served during this event.

BANQUET:

The banquet dinner will be an informal gathering at the Henry Doorly Zoo on Friday, September 6th. The Indoor Rainforest, Aquarium and Desert Dome will be open to ASB attendees. A buffet style dinner featuring Omaha Steaks will be served. Busses will be on a loop between the Hilton and the Zoo from 5:30-9pm. The last bus will leave the zoo at 9pm.

BREAKFASTS & LUNCHES:

All meals will be served in the Grand Ballroom of the CenturyLink Center
Breakfast: A variety will be served beginning at 7am daily, Thursday-Saturday.
Lunch: Lunches will be available daily at 12:15, Thursday-Saturday.

Visit the mobile program at
http://www.openconf.org/asb2013/mobile/

SOCIAL PROGRAM

Opening Reception Wednesday, September 4th – 6:30-9pm CenturyLink Center – Aksarben Terrace	The opening reception will be held at the CenturyLink Center Omaha on the Aksarben Terrace (upstairs level), which overlooks downtown Omaha. Hors D' Ouvres and cocktails will be served.
Student Outing Thursday, September 5th – 5:15pm Old Mattress Factory Grill and Bar	The student outing will be held at the Old Mattress Factory Grill an d Bar. This restaurant is a favorite during the College World Series.
Dinner at the Henry Doorly Zoo Friday, September 6th – 6:00-9:00pm Henry Doorly Zoo	The Henry Doorly Zoo has been named the #1 Zoo in America by Trip Advisor. On Friday, the Jungle, Desert Dome, and Aquarium will be open to ASB attendees. For more information, visit http://www.omahazoo.com/.
5K Fun Run Saturday, September 7th – 6:30-7:30am Hilton Omaha Lobby	Meet us in the Hilton lobby for a 5K Fun Run over the Bob Kerry pedestrian bridge!

THURSDAY, SEPTEMBER 5th

KEYNOTE ADDRESS
8:15-9:15 AM
CenturyLink Junior Ballroom

Nicolaas Bohnen, MD, PhD
Professor of Radiology and Neurology, University of Michigan, Ann Arbor, MI

ABOUT THE SPEAKER:
Dr. Bohnen attended medical school in the Netherlands and completed a PhD in neuropsychology. He completed residency training in neurology (Mayo Clinic, Rochester, MN) and nuclear medicine (University of Michigan, Ann Arbor, MI). He was a fellow in movement disorders at the University of Michigan Medical Center. He holds clinical appointments in the Departments of Radiology (Division of Nuclear Medicine), Neurology at the University of Michigan and the Ann Arbor VA where he directs the movement disorders clinic. Dr. Bohnen's research interests include the use of PET and MRI in the study of neurodegenerative disorders and normal aging. He is the Director of the UM Functional Neuroimaging, Cognitive and Mobility Laboratory where his clinical research has a focus on neurobiological correlates of mobility and cognition in normal aging and Parkinson disease and biomarker development for the diagnosis and treatment monitoring in Parkinson disease. His group has helped to identify non-dopaminergic pathologies of mobility impairments and falls in Parkinson disease including cholinergic denervation of the pedunculopontine nucleus, cortical b-amyloid build-up, vascular white matter lesions and more recently brain atrophy changes due to hyperglycemia (diabetes). His research in normal aging aims at the translation of treatment approaches from patients with neurodegenerative disease, such as Parkinson disease, to geriatric mobility problems. His long-term goals are to utilize imaging biomarkers in the effective implementation of targeted and personalized medicine of patients with mobility impairments. His research is funded by grants from the NIH, the Department of Veterans Affairs, and the Michael J. Fox Foundation.

THURSDAY, SEPTEMBER 5th

BORELLI AWARD LECTURE
1:15-2:15 PM
CenturyLink Junior Ballroom

Kenton R. Kaufman, PhD
W. Hall Wendel, Jr. Musculoskeletal Research Professor, Director, Orthopedic Biomechanics/Motion Analysis Laboratory, Mayo Clinic

ABOUT THE SPEAKER:
Dr. Ken Kaufman obtained his PhD from North Dakota State University in 1988. After a time at Children's Hospital in San Diego, he joined the faculty at the Mayo Clinic in 1996. Ken has made outstanding contributions in orthopedics, rehabilitation, prosthetics, orthotics, and quantification of musculoskeletal disease and treatment. He has led studies of microprocessor-controlled knees that have notably improved the functional ability of amputees. Ken's work on orthotics has been sustained since 1992 when he first received NIH funding to work on a Logic Controlled Electromechanical Free Knee Brace -- the original design effort on a class of devices now known as stance-controlled orthoses. Ken's efforts in musculoskeletal medicine have ranged from reducing overuse injuries in military recruits by developing an improved combat boot to pioneering work demonstrating the functional benefit of Botox injections for patients with cerebral palsy. His use of sophisticated motion analysis techniques to document objective outcomes of numerous orthopedic procedures have received the highest research awards in hip surgery, the Stinchfield Award from the Hip Society, as well as in knee surgery, the Insall Award from the Knee Society. More recently, Ken and co-workers have developed a novel fiber-optic sensor that can be inserted using the same clinical techniques used for intramuscular EMG, and he is also actively pursuing strategies for reducing falls in older adults. Ken has made significant and sustained interdisciplinary and translational research contributions, which have advanced, expanded and strengthened the discipline of biomechanics. These contributions include 184 peer-reviewed publications, many of which have appeared in the highest impact biomedical, engineering and clinical journals, 37 book chapters, and over 250 abstracts.
Ken was a founding member of the Commission for Motion Laboratory Accreditation from 1999-2003. He served as President of the Gait and Clinical Movement Analysis Society from 2000-2001, and President of the American Society of Biomechanics from 2006-2007.

FRIDAY, SEPTEMBER 6th

ISB SPONSORED KEYNOTE ADDRESS
11:15 AM-12:15 PM
CenturyLink Center Junior Ballroom

Taija Finni, PhD
Professor of Kinesiologyk, Department of Biology of Physical Activity, University of Jyväskylä, Finland

ABOUT THE SPEAKER:
Taija Finni completed her Ph.D. entitled “Muscle mechanics during human movement revealed by in vivo measurements of tendon force and muscle length” in 2001 at the Department of Biology of Physical Activity, University of Jyväskylä, Finland. She continued to study muscle and tendon function at the University of California, Los Angeles, with J.A. Hodgson, V.R. Edgerton and S. Sinha as a post doc. Currently she is a professor in kinesiology at the Department of Biology of Physical Activity, University of Jyväskylä, Finland. She also holds an adjunct professorship in exercise physiology at the University of Eastern Finland (since 2006). Prof. Finni has published over 50 peer-reviewed articles related to biomechanics and exercise physiology. She also runs translational research related to physical activity and inactivity paradigm. She serves as a biomechanics section editor in Scandinavian Journal of Medicine and Science in Sports and is a member of editorial board in Clinical Biomechanics. She has received recognition in young investigator’s competitions (e.g. 1st prize by ECSS, 1998 and 5th for Promising Young Scientist Award by ISB, 2005).

FRIDAY, SEPTEMBER 6th

HAY AWARD LECTURE
1:15-2:15 PM
CenturyLink Center Junior Ballroom

Glenn S. Fleisig, PhD
Research Director, American Sports Medicine Institute

ABOUT THE SPEAKER:
Glenn Fleisig received his PhD from the University of Alabama at Birmingham in 1994, but by that time he had already established himself as a strong biomechanist in Sports and Exercise Science. Glenn’s background and his entire professional career have been focused on sports biomechanics. After graduating in 1984 with his BS from MIT, interning at the US Olympic Training Center, and completing his MS at Washington University in St. Louis, Glenn was hired in 1987 by James Andrews, MD to develop the research program of the newly created American Sports Medicine Institute, where he has been the principal for the past 25 years.
Glenn is internationally recognized as a leader in throwing biomechanics, particularly with respect to baseball pitching. He has over 75 peer-reviewed publications, mostly in sport biomechanics. He has been invited to write over 30 manuscripts, 12 book chapters, and 50 guest lectures. His conference abstracts total more than 210. Arguably the most important result of his outstanding research in sports biomechanics is the fact that his research on throwing mechanics and injury directly led to widespread implementation of pitch count regulations for youth baseball players.

In addition to his numerous publications on throwing biomechanics related to injury and performance, he has worked to inform the general public through constant interviews and coverage in print, online, television, and radio media. He has analyzed the throwing biomechanics of pitchers for nearly every Major League Baseball team, giving recommendations for reducing injury risk and enhancing performance. He has also been a pitching safety consultant to Little League Baseball and a Medical Safety committee member for USA Baseball. Given that his primary appointment is at a private research institute and not an academic center, it is quite remarkable that Glenn created ASMI’s Student Researcher Program, through which he has supervised 150 students from various universities over the years.

SATURDAY, SEPTEMBER 7th

KEYNOTE ADDRESS
8:00-9:00 AM
CenturyLink Center Junior Ballroom

Shane Farritor, PhD
Professor, Mechanical Engineering, University of Nebraska – Lincoln.

ABOUT THE SPEAKER:
Dr. Farritor's research interests include space robotics, surgical robotics, and biomedical sensors. Shane has founded two startup companies based on his research at UNL. Shane co-founded Virtual Incision Corporation with his surgeon colleague Dr. Dmitry Oleynikov at the University of Nebraska Medical Center. Virtual Incision is developing miniature robotic devices that are placed inside the body during laparoscopic surgery. These new devices could have a significant impact on surgical procedures such as colon resection. Shane's second startup, MRail, is developing a method to improve railroad maintenance by the measurement of vertical rail deflection. Shane is a native growing up in the small central Nebraska town of Ravenna. His wife is a physician at St. Elizabeth's and they have four children. He received the B.S. degree in Mechanical Engineering from the University of Nebraska-Lincoln in 1992, and the M.S. and Ph.D. degrees in Mechanical Engineering from the Massachusetts Institute of Technology, Cambridge, in 1998.

SATURDAY, SEPTEMBER 7th

YOUNG SCIENTIST PRE-DOC AWARD
1:15-1:45 PM
CenturyLink Center Room 215/216

Arin Ellingson, University of Minnesota
Intervertebral Disc Degeneration, Quantified by T2 MRI, Correlated to Biochemistry, Compressive Mechanics, and Global Function Mechanics of the Lubar Spine.*

SATURDAY, SEPTEMBER 7th

YOUNG SCIENTIST POST-DOC AWARD
1:45-2:15 PM
CenturyLink Center Room 215/216

Steven Collins, Carnegie Mellon University
Biomechanics-Centered Design of Robotic Lower-Limb Prostheses

ORAL PRESENATIONS – THURSDAY SEPTEMBER 5th

	Motor Control: Thinking Beyond Biomechanics *Eric Perreault, Jason Kutch*
11:15 AM	Cortical Control Of Pelvic Musculature: Stimulation And Functional Imaging **Rana M, Cosand L, Kirages D, Yani M, Kutch J**
11:30 AM	The Effect Of Optic Flow Speed And Hip Restriction On Cortical Activation During Walking **Yu Y, Mukherjee M**
11:45 AM	Feline Soleus And Lateral Gastrocnemius Self-Reinnervation Results In Increased Ankle Extensor Activity But No Change In Ankle Extensor Moment During Upslope Locomotion **Pantall A, Gregor R, Prilutsky B**
12:00 PM	Want To Test Proprioception? There’s An App For That. **Gillespie E, Hyler J, Lin YL, Karduna A**

CORTICAL CONTROL OF PELVIC MUSCULATURE: STIMULATION AND FUNCTIONAL IMAGING

Manku Rana, Louise Cosand, Daniel Kirages, Moheb S. Yani, Jason J. Kutch

University of Southern California, Los Angeles, CA, USA
email: manku.rana@usc.edu, web: http://ampl.usc.edu

INTRODUCTION

Human pelvic floor musculature is made up of several skeletal muscles with a wide variety of mechanical functions. Pelvic muscles are unique in that they maintain an active contraction, even at rest [1]. This baseline activity is increased in patients with urological chronic pelvic pain disorders (UCPPS) [2,3], and may interfere with function and generate pain. UCPPS patients may have abnormal central nervous system activity [4], but potential impairment sites that might upregulate pelvic muscle activity have not been identified. To better understand the potential cortical contributions to pelvic muscle activity, we present a study to identify the neural substrates that mediate voluntary and involuntary pelvic muscle contraction.

Previous transcranial magnetic stimulation (TMS) studies have shown that the stimulation of medial regions of primary motor cortex (M1) leads to pelvic muscle contraction [5]. However, functional magnetic resonance imaging (fMRI) studies have found the predominant activation of supplementary motor areas (SMA) during voluntary pelvic muscle contractions with only sporadic reports of M1 activation [6,7]. In this study, we use TMS to show that either medial M1 or SMA activation is likely sufficient to cause an involuntary pelvic floor contraction. We additionally use fMRI to show that medial M1 and SMA are likely involved in voluntary pelvic floor contraction.

METHODS

Motor and premotor cortex was stimulated using a Magstim 100 magnetic stimulator (Magstim, Whitland, UK) with a double cone coil. Stimulation was applied at seven different locations (Figure 1) along the midline of the brain. The stimulation locations obtained from Magstim software were registered with T1-weighted structural images of brain, obtained by performing MRI of the head with 3T Siemens Trio (Siemens AG, Munich Germany). The probability of a stimulation location belonging to M1 or SMA region was obtained from the Harvard-Oxford cortical structural atlas in FSL software (FMRIB, Oxford, UK).

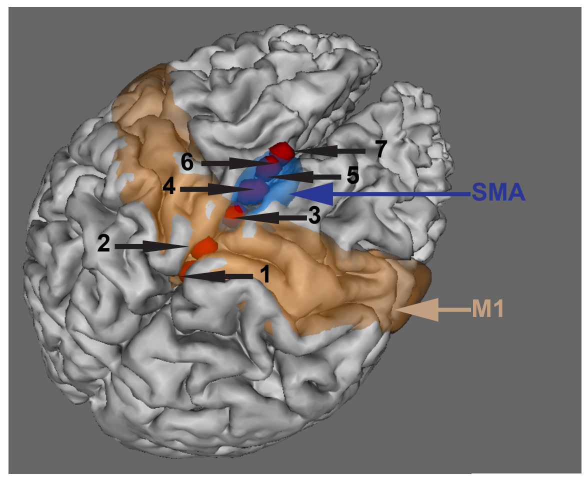

Figure 1: Stimulation sites represented on the T1 images of brain obtained from MRI. The orange and blue regions represent M1 and SMA respectively.

EMG response was obtained from pelvic muscles by using a rectal EMG sensor (The Prometheus Group, Denver, USA). The TMS was applied for ten times per location. An average EMG response was obtained corresponding to each location to obtain the mean motor evoked potential (MEP, Figure 2a) magnitude, as the peak-to-peak voltage, expressed in millivolts.

fMRI data was collected using a 3T Siemens Trio from nine men (mean age of 35 years). To identify brain regions involved in pelvic muscle contraction, participants voluntarily contracted pelvic muscles to the sound of a metronome during a set of fMRI data acquisition runs. Analysis of fMRI data was performed in FSL software, seeking voxels that were significantly correlated to pelvic contraction. Statistical inferences were drawn at the voxel level with $p < 0.05$ corrected for multiple comparisons.

RESULTS AND DISCUSSION

Largest MEP magnitude was obtained at location 2, with a 59% probability of being in M1 and 0% in SMA (Figure 2). Stimulation at location 4, with 84% probability of being in SMA, had the highest MEP magnitude among the locations having 0% probability of being in M1. The results obtained from M1 stimulation are in agreement with the previous TMS studies showing activation of pelvic muscles on stimulation of medial region of primary motor cortex [5].

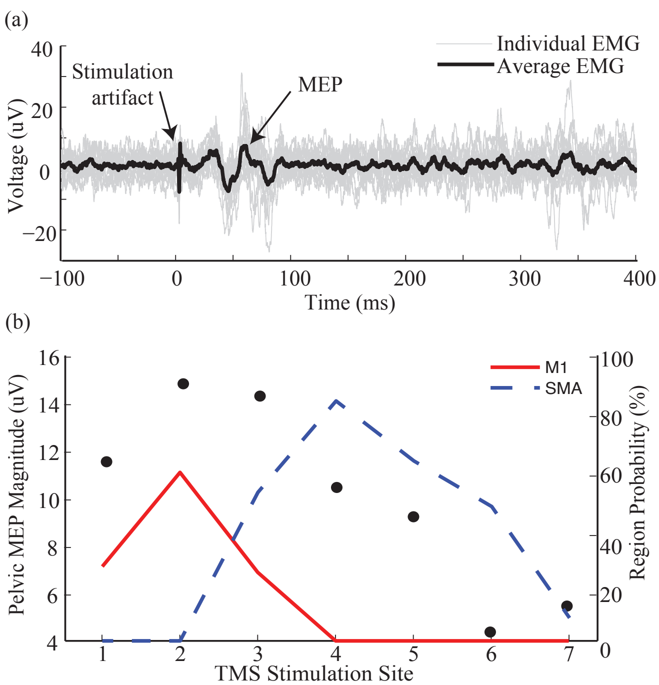

Figure 2: (a) Rectal EMG response obtained at location 2 (b) MEP magnitude obtained at different stimulation sites (black dots) and probability of the location sites to be in M1 (red bold line) or SMA (blue dashed line) regions.

The fMRI results showed activation of both M1 and SMA regions in relation to the voluntary pelvic muscle contractions (Figure 3). The SMA activation is in agreement with the previous fMRI studies [6,7] and M1 has been found active in some fMRI [6] studies on voluntary pelvic muscle contractions.

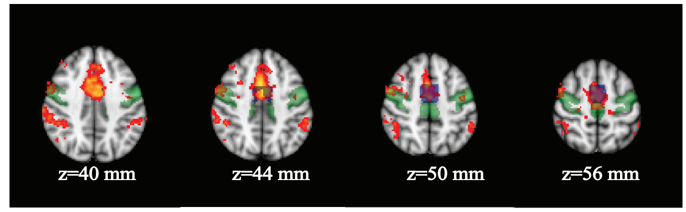

Figure 3: Pelvic contraction z-stat maps, showing the activation intensity in yellow-orange color, superimposed with region probability for M1 (green) and SMA (blue) regions.

None of the previous TMS studies have compared the SMA and M1 stimulation with respect to the pelvic muscles contraction. Our fMRI and preliminary stimulation results indicate a strong representation of pelvic floor muscles in M1 regions, along with SMA.

It has to be noted that the MEP magnitude peaks in the M1 region and then declines gradually (Figure 2b). The non-zero MEP magnitude at farther locations may be the result of the stimulation overflow. Further experiments are needed to study the effects of stimulation overflow, which can be done stimulating at multiple locations in the coronal plane as well as sagittal plane posterior to M1 cortex.

CONCLUSION

These results indicate that both medial M1 and SMA are essential regions to consider in understanding compromised control of the pelvic floor in neuromuscular disorders.

REFERENCES

1. Porter NH, *Ann R Coll Surg Egl*, **31(6)**, 379-404, 1962
2. Cornel EB et al., *Eur Uro* **47(5)**, 607-611, 2011
3. Hetrick DC et al., *Neurourol Urodyn* **25(1)**, 46-49, 2005
4. Anderson RU et al., *J Urol* **179(3)**, 956-960, 2008
5. Lefaucher JP, *Exp Brain Res* **160**, 268-272, 2005
6. Seseke S et al., *NeuroImage* **31**, 1399-1407, 2006
7. Schrum A et al., *J Urol* **186**, 185-190, 2011

ACKNOWLEDGEMENT
We thank Dr. Beth Fisher, Ya-Yun Lee and Allie Southam for helping with the data collection.

THE EFFECT OF OPTIC FLOW SPEED AND HIP RESTRICTION ON CORTICAL ACTIVATION DURING WALKING

[1*]Yawen Yu, and [1]Mukul Mukherjee
[1]University of Nebraska at Omaha, Omaha, NE, USA
Email: yawenyu@unomaha.edu, Web: http://biomech.unomaha.edu/

INTRODUCTION

Human locomotion is tuned to the dynamics of the human-environmental system. Such tuning is evident when the visual information to be perceived is experimentally manipulated using treadmill-based virtual reality (VR) paradigms. When the speed of Optic Flow (OF) in such a paradigm is made to be faster or slower than the individual's Self-Selected Pace (SSP) of walking, changes were observed in locomotion patterns including changes in gait variability [1]. Given the evidence that gait is influenced by higher cortical control mechanisms [2], the brain control mechanisms during walking remain largely unknown due to the technological difficulties encountered in recording brain activity during walking. In contrast to the limitations posed by technologies like fMRI and PET, Functional Near-Infrared Spectroscopy (fNIRS) can be employed to assess the direct linking between cortical activity and locomotor behavior [3]. Such technology can help elicit the brain correlates of locomotion related to the speed of optic flow. In addition, human bipedal locomotion requires greater active control or higher-level control over the medio-lateral (ML) direction than the antero-posterior direction [4]. This assumption is based on increased step width variability in comparison to step length variability that is observable during normal walking. Such variability can be affected by restricting the hip with elastic bands during locomotion [5]. The resulting reduction in step width variability can reduce the metabolic cost of walking [5]. Therefore, the restriction at the hip should intuitively result in changes in the higher/brain control of locomotion. Therefore, in the present study, we sought to examine brain activity during walking as a function of changes in the speed of optic flow and hip restriction.

METHODS

Twelve healthy young adults (age 27.3 ± 5.3) participated in the study. Treadmill-based VR was

Figure 1. Experimental setup.

employed in the current study (Figure 1). Each participant walked on an instrumented treadmill at his or her SSP, with or without hip restriction, while exposed to three different conditions of OF, including self-perceived matched (MOF), Slower (0.5x MOF), and Faster OF (2.0x MOF). Thus, six conditions were formed. Half the participants started with the restriction at hip, while the other half started without hip restriction. Each restriction condition consisted of three blocks, within which the order of conditions of optic flow being presented was randomized with one trial per condition. Each walking trial lasted 70 seconds, during which participants were instructed to walk along with the treadmill-based VR. Between walking trials participants were instructed to stand still with eyes closed, which yielded inter-trial intervals of 50s duration. A continuous wave fNIRS system, the ETG-4000 Optical System (Hitachi Medical Corporation, Tokyo, Japan) utilizing two different wavelengths (~695 and ~830 nm) sampling at 10 Hz was used to measure cortical activity. Task-related cortical activity was computed based on the amount of oxygenated (OxyHb) and deoxygenated (DeoxyHb) hemoglobin during walking (Figure 2). Our paradigm yielded 24 channels on each side of head. A repeated-measure

ANOVA was used to investigate the effects of *OF* (Slower, Matched, Faster) and *Hip Restriction* (with and without) on each channel and separately from the integrated time series data of OxyHb and DeoxyHb. Significance level α was set at 0.05.

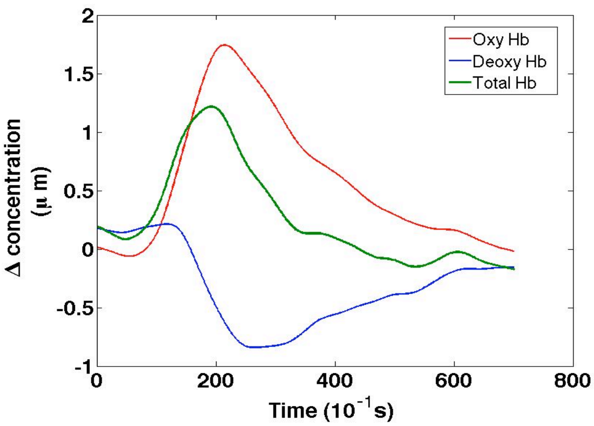

Figure 2: Sketch of the typical cortical activation as revealed by fNIRS.

RESULTS AND DISCUSSION

Effect of Hip Restriction: During walking, borderline effects were determined; specifically, greater amount of OxyHb and less amount of DeoxyHb were found when hip was restricted (*ps* < .080). In addition, such effects were found in areas including pre-central gyrus, post-central gyrus, and angular gyrus. That is, not only the primary motor area but also associated motor areas showed increased activity due to Hip Restriction. *A Significant main effect of Optic Flow was found*. Faster OF was associated with greater amount of OxyHb than matched or slower OF (p = .040); while matched OF was associated with less amount of DeoxyHb than faster/slower OF (p = .018). As this effect was found only in the pre-central gyrus, this demonstrated a more localized effect of the visual sensory feedback. *A borderline interaction effect between Hip Restriction and Optic Flow was found*. Overall, the interaction effect came from the effect of optic flow within the condition of Without Hip Restriction in both OxyHb and DeoxyHb (*ps* < *.080*). This showed an OF effect only when walking normally and a masking of the OF effect in the hip restricted condition. Such effects were observed in the angular gyrus, pre-central gyrus, and post-central gyrus.

Our results, including the interaction effect between Hip Restriction and OF and main effect of Hip Restriction, provide partial support to the assumption that locomotion control in the ML direction requires higher-level neural control [4,5]. When movement in the ML direction was restricted at the hip using elastic bands, the effect of OF on locomotion control was affected. This indicates that when the hip is restricted from free lateral motion (e.g., disease, injury), there may be reduced ability to extract relevant sensory information from the environment. Greater OxyHb that was found in the primary motor area in faster OF condition indicates that more blood flow is needed in this area due to the need for greater neural activity. Several significant effects found in the angular gyrus are consistent with previous results [6]: this area is functionally related to spatial orientation and visual recognition.

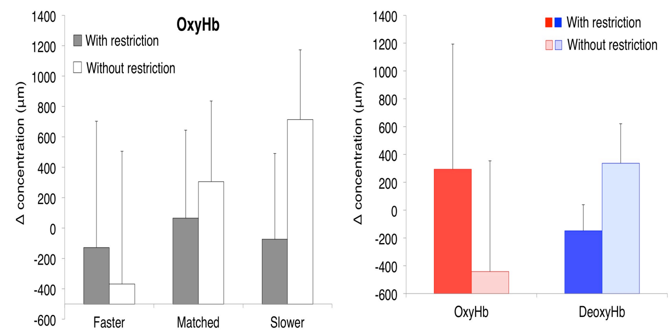

Figure 3. L: OxyHb dynamics as a function of OF and Hip Restriction. **R:** OxyHb and DeoxyHb dynamics as a function of Hip Restriction.

CONCLUSIONS

The present study is the first effort, to our knowledge, that examines how brain activity changes as a result of hip restriction and optic flow speed, which have been known to affect normal gait patterns. Our study demonstrates the feasibility of utilizing fNIRS to explore the brain control aspects of locomotion and locomotor tasks.

REFERENCES

1. Katsavelis D. *NDPLS* **24**, 239-56, 2010.
2. Miyai I, et al. *Neuroimage* **14**, 1186-92 2001.
3. Kurz MJ, et al. *NeuroImage* **59**, 1602-07, 2012.
4. Bauby CE, Kuo AD. *J. Biomech*. **33**, 1433, 2000.
5. Dean JC, et al. *IEEE Trans Biomed Eng* **54**, 1919-26, 2007.

Feline Soleus and Lateral Gastrocnemius self-reinnervation results in increased ankle extensor activity but no change in ankle extensor moment during upslope locomotion

[1]Annette Pantall, [1,2]Robert Gregor and [1]Boris I. Prilutsky

[1]Georgia Institute of Technology, Center for Human Movement Studies, Atlanta, GA, USA
[2]University of Southern California, Los Angeles, CA, USA
email: annette.pantall@ap.gatech.edu web: http://www.ap.gatech.edu/Prilutsky/

INTRODUCTION

Clinically, humans do not fully recover function in many cases following repair of a transected peripheral nerve [1]. This may be the consequence of altered afferent feedback [2], central drive and/or muscle properties resulting in changed motor patterns. Locomotor adaptions during upslope walking immediately following nerve cut and repair of selected ankle extensors in the cat have been reported. Before denervated muscles recover innervation, the mechanical output of the ankle is preserved due to increased activity of intact synergists and functionally appropriate hindlimb kinematic changes (an enhanced ankle yield and reduced knee flexion during stance [3,4]). After reinnervation of injured muscles (between 5-12 weeks; Gregor et al., unpublished data), kinematics of upslope walking recover completely despite the lack of a stretch reflex in the reinnervated muscles [2,7]. These results are puzzling given the important role of length-dependent afferent feedback in muscle recruitment during locomotion [5].

This study aimed to investigate changes in activity of ankle extensors and their mechanics during upslope walking following self-reinnervation of soleus (SO) and lateral gastrocnemius (LG).

METHODS

All experimental and surgical procedures were approved by the Georgia Tech Institutional Animal Care and Use Committee. For the purpose of this study, four female adult cats were investigated. Each cat was trained to walk along an upslope (+27^{o}) walkway with embedded force plates. Under sterile conditions and isoflurane anaesthaesia, medial gastrocnemius (MG), SO, LG (in 4 cats) and plantaris (PL, in 2 cats) were implanted with fine wire EMG electrodes and SO (in 4 cats) and LG (in 1 cat) were implanted with sonomicrometry crystals [4,6]. Prior to recordings, small retroreflective markers were placed on the anatomical landmarks of the right hindlimb. EMG, sonomicrometry, kinematic and ground reaction force data were recorded during locomotion as described previously [3,4,6,7]. After collection of locomotion baseline data, the nerves supplying SO and LG of the right hindlimb were cut and repaired under sterile conditions [3,4,7]. Each cat had multiple walking trials recorded and analyzed before and at least 12 weeks after nerve cut and repair. In the terminal experiments, the absence of stretch reflexes in self-reinnervated muscles was verified [7] and the mass of individual ankle extensors from both hindlimbs was measured.

EMG intensity was normalized to the maximum mean intensity recorded during upslope walking pre-reinnervation. SO and LG fascicle and muscle-tendon unit length (MTL) were normalized to the half of muscle length range in level walking cycle [6]. ANOVA was applied to analyze the effects of self-reinnervation (pre and 12 weeks post) on mean EMG intensity of the ankle extensors, mean and peak of ankle moment and mean length and velocity of fascicles and MTL of SO and LG in stance.

RESULTS AND DISCUSSION

The EMG during upslope walking of a total of 934 stride cycles was analyzed. The mean EMG of SO, MG, LG and PL increased for all cats following self-reinnervation ($p>0.05$; Fig 1). There was no significant change in mean and peak ankle extensor moments across all cats (Fig. 1). An increase in EMG activity generally produces an increase in muscle force and consequently, assuming moment arms are the same, a greater muscle moment.

However, the results indicated that there was no associated increase in the muscle moment. This may have been the result of a decreased moment arm or/and increased co-activation of ankle antagonists. However, as the joint angles [7], MTLs of ankle extensors (Fig. 2) and reciprocal activation of antagonistic muscles (unpublished observations) did not change significantly, it is unlikely the ankle muscle moment arms and coactivation changed [7].

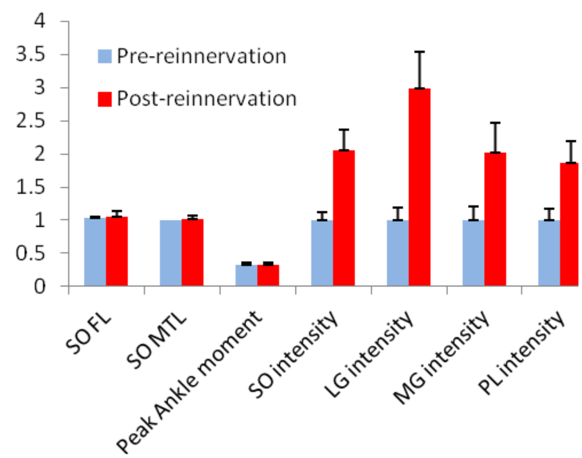

Figure 1: Normalized mean SO fascicle (FL) and MTL lengths, peak ankle moment (in N/kg) and the mean extensor muscle EMG intensity in stance of upslope walking in 4 cats.

The force generated by a muscle is dependent on a number of factors including fascicle length and velocity, muscle physiological cross sectional area (PCSA) and muscle fiber composition. Results showed that overall there was no significant change in fascicle length and peak shortening velocity after reinnervation (Fig 2). There was no difference in mass of ankle extensors between the hindlimbs with intact and self-reinnervated muscles, suggesting that PCSA has not changed after self-reinnervation. We have previously presented findings that following self-reinnervation, the mean EMG frequency decreased suggesting a greater contribution of slow motor units to activity of ankle extensors [8]. This change in motor unit recruitment may result in reduced force production by ankle extensors. Thus, the dissociation between the increased ankle extensor mean EMG and no changes in ankle joint moment after self-reinnervation could result from changes in the fiber type composition and/or recruitment patterns of ankle extensors.

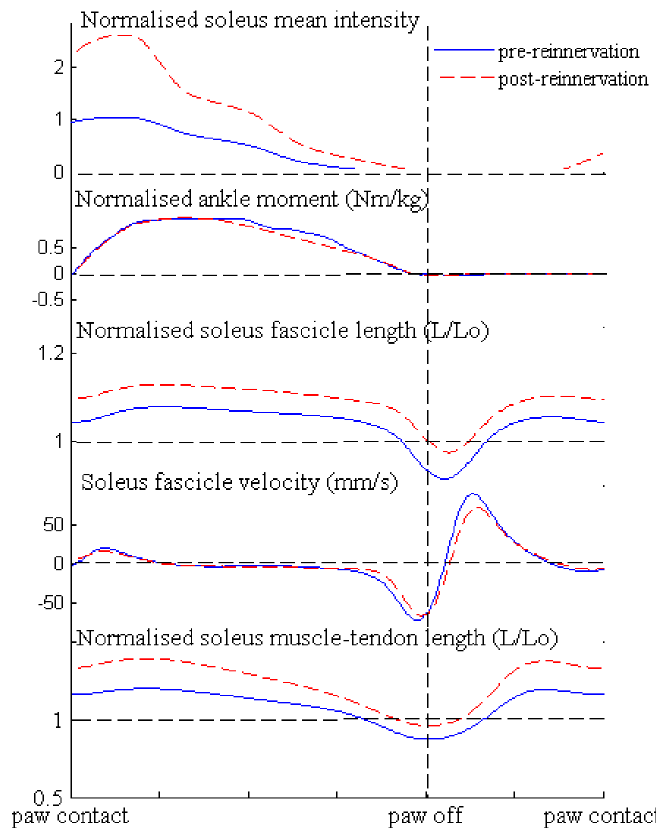

Figure 2: Exemplar plots for Cat 2 showing mean soleus EMG activity, ankle moment, soleus fascicle length and velocity and MTL length in a cycle.

REFERENCES

1.Taylor KS, et al. *Pain* **151**, 582-591, 2010.
2. Cope TC et al. *J Neurophysiol* **71**, 817-820, 1994.
3. Prilutsky BI, et al. *Cells Tissue Organs* **193**, 310-324, 2011.
4. Maas H, et al. *Exp Brain Res* **201**, 681-692, 2010.
5. Pearson KG, Misiaszek JE *Brain Res* **883**, 131-134, 2000.
6. Maas H, et al. *J.Appl Physiol* **106**:1169:1180, 2009.
7. Maas H, et al. *Exp Brain Res* **181**, 377-393, 2007.
8. Pantall A, et al. *Society for Neuroscience*, New Orleans, LO, USA, 2012.

ACKNOWLEDGMENTS

Supported by NIH grant P01 HD32571.
Thanks to Drs. H. Maas, E. Hodson-Tole and M. Bulgakova for help with data collection and analysis.

Want to test proprioception? There's an app for that.

Elizabeth Gillespie, Jacqlyn Hyler, Yin-Liang Lin, Andrew Karduna

Department of Human Physiology, University of Oregon, Eugene, OR, USA
email: karduna@uoregon.edu, web: http://biomechanics.uoregon.edu/obl

INTRODUCTION

Traditionally, proprioception has been assessed with a passive protocol, in which a body segment is moved by an external apparatus. [1,2] Recently, the PI [3] and other investigators [4] have developed protocols based on active movements, which are more representative of function activities. However, even these approaches require expensive testing equipment and the necessity of a visit to a research lab. The gap in the field is that there is no commercially available mobile instrument that will allow for the assessment of proprioception outside of a laboratory setting. The long term goal of this project is to evaluate an inexpensive, portable and quick method for assessing proprioception that would be applicable for both research and clinical purposes. The ability to assess proprioception on a much larger scale than currently possible would allow researchers to answer questions that are currently too difficult or expensive to otherwise address. The objective of this application was to demonstrate the feasibility of this concept by conducting a large scale field based study at the 2012 ASB meeting in Gainesville.

METHODS

<u>Instrumentation</u> We worked with the InfoGraphics Lab at the University of Oregon, to develop a mobile app that runs on Apple's iPod touch (or iPhone). It uses the internal sensors (accelerometers and gyroscopes) to record the orientation of a segment with respect to gravity. Saved files are automatically uploaded to Dropbox.

<u>Logistics</u> Conference attendees were recruited (sometimes aggressively) to participate in this study. With IRB approval, informed consent was obtained with the Canvas mobile app on an iPad (gocanvas.com). Subjects were fitted with Bluetooth noise cancelling headphones, which allowed for us to test three subjects at a time. An iPod Touch (fourth generation) with the app loaded was secured to their humerus. Subjects were instructed about the procedure and allowed sufficient practice trials to familiarize themselves with the protocol.

<u>Protocol</u> Subjects were presented with three target positions: 50, 70 and 90 degrees of shoulder flexion. They were prompted to attain a target position via audio feedback (though the headphones). Once the subjects were within two degrees of the target, the audio signal stopped and subjects held this position for three seconds (they had previously been instructed to use this time to memorize the location of their hand in space). After a verbal cue from the app prompted subjects to relax and return to their arm to the side. After two seconds at this position, subjects were prompted with another verbal cue to return to the target position and hold their arm there for one second. Once testing for a given target was finished, the subject moved on to another target. Each target was presented four times (for a total of 12 targets) in a randomized order. Errors were calculated as the difference between the angle at the repositioned and target positions. Below is a sample of the output from the app where the target angle was 50 degrees (in this case, the subject overshot the presented angle by 7.6 degrees).

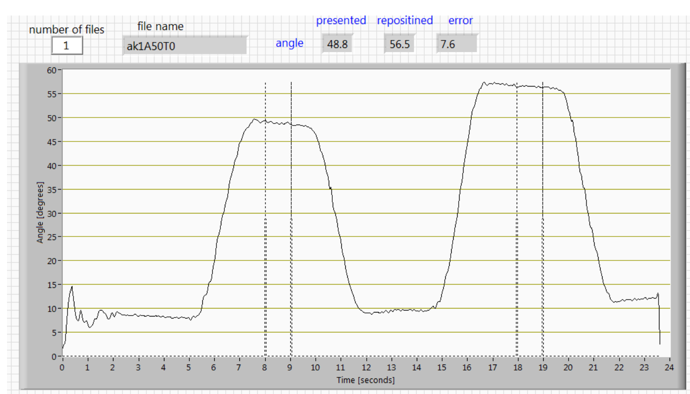

RESULTS AND DISCUSSION

Over the course of the conference, we collected data from a total of 126 willing participants (and 3 alligators). Of these, we focused on the 79 subjects with no shoulder injuries or high level of participation in overhead sports. The results are show in the figure 1. As we have observed in our previous lab based model, [3] errors were found to decrease as the flexion angle increased.

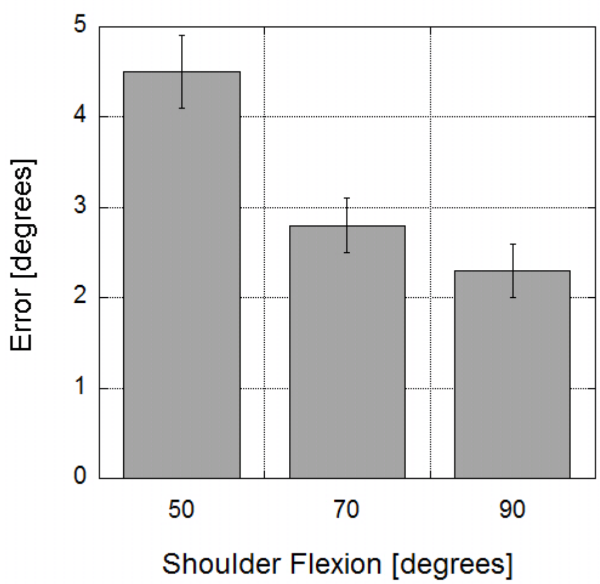

Figure 1. Constant error (+/- sem) as a function of shoulder flexion angle.

There are numerous factors that might explain a decrease in errors as the shoulder approaches 90 degrees of flexion, roughly divided into peripheral and central arguments. On the peripheral side, there is an increase in feedback from the Golgi tendon organs, an alteration in muscle spindle feedback due to alpha-gamma coactivation and a change in the capsuloligamentous and cutaneous feedback. On the central side, there is an increase in the sense of effort, or efference copy, reliance on a gravitational reference frame, and a different cortical representation of hand position and orientation. More physiological based studies need to be performed to determine the mechanisms controlling this response. Additionally, we are currently analyzing the data to examine whether there are any effects of age or sex on end point errors.

CONCLUSIONS

We found this pilot program to be a great way to collect a large amount of data from a very willing population.

REFERENCES

1. Smith JL, et al. *J Appl Physiol*, **106**, 950-958, 2009.
2. Hall LA and McCloskey DI. *J Physiol*, **335**, 519-533, 2009.
3. Suprak DN, et al. *J Orthop Res*, **24**, 559-568, 2006.
4. Tripp BL, et al. *J Athl Train*, **41**, 146-153, 2006.

ACKNOWLEDGEMENTS

Funding provided by a University of Oregon 2012 Summer Research Award.

The mobile app was developed in conjunction with Dana Maher, from the University of Oregon's InfoGraphics Lab (infographics.uoregon.edu).

Thanks to Liz Hsiao-Wecksler for setting up this program, Chris Hass and Mark Tillman for accommodating all of our requests for help at the meeting, and to all the participants who gave their time (mostly willingly) and tired out the students (see figure 2).

Figure 2. Taking a break from data collection.

ORAL PRESENATIONS – THURSDAY SEPTEMBER 5th

	Thematic: Control of Posture in Sports *Michelle Sabick, Scott Breloff*
11:15 AM	Estimating Trunk Muscle Compressive Force In Vertical Dance **Wilson M, Dai B, Zhu QA, Humphrey N**
11:30 AM	Lumbopelvic Control And Injuries In Professional Baseball Pitchers **Chaudhari A, McKenzie C, Pan X, Onate J**
11:45 AM	Relationships Between Trunk Kinematics At The Critical Time Points In Baseball Pitching **Oyama S, Bing Y, Blackburn JT, Padua D, Li L, Myers J**
12:00 PM	A Comparison Of Hip And Trunk Kinematics In Healthy Runners With Strong And Weak Hip Abductors **Hannigan J, Becker J, Chou LS**

ESTIMATING TRUNK MUSCLE FORCE IN VERTICAL DANCE

Margaret Wilson, Boyi Dai, Qin "Arthur" Zhu, and Neil Humphrey

University of Wyoming, Laramie, WY, USA
email: mawilson@uwyo.edu

INTRODUCTION

Vertical dance is a popular form of aerial dance with the dancer suspended by a harness attached to a rope, and the rope is secured on the ceiling or some places overhead. The harness encircles the waist and upper legs and is secured by a buckle, thus the harness supports the mass of the body when the dancer is in the air. The dancer can orient their body (with their feet off the ground) in several different directions relative to gravity: upright, upside down, and perpendicular - where the body is parallel to the floor.

Conducting research with vertical dance poses methodological challenges as the dance form does not take place in a typical environment, the dancer's body is often rotated so that gravity has a different effect, and typical dance positions are performed in a new weight bearing position, with support coming only from the harness and rope, not the feet on the ground. In this orientation, stresses on the spine are experienced in the anterior/posterior axis (rather than the vertical) because of the way the body weight is supported by the harness. These stresses, particularly at the lumbar spine, can be intensified when the dancer's movements are in the horizontal position. Therefore this investigation sought to quantify trunk muscle activity in six positions to better understand optimal training exercises to help the dancer work safely in an airborne dance environment.

METHODS

Four dancers (Table 1) participated in a pilot study, performing 6 typical positions (Figure 1-6) from their vertical dance training. EMG data were collected with a Delsys Myomonitor EMG system (Delsys Inc., MA, USA) at a sampling rate of 1600 Hz. EMG leads were placed on bilateral rectus abdominus, external oblique, erector spinae and latissimus dorsi. Participants completed tests of MVC following the testing.

Table 1. Subject data

	Age	Gender	Height (cm)	Weight (kgs)	Experience
1	23	M	177	77	3 years
2	53	F	149	61	15 years
3	63	M	180	78	15 years
4	20	F	144	56	1 year

The raw EMG data were rectified and filtered at 10 Hz using a Butterworth low-pass filter and then expressed as a percentage of MVC for each position. Using a simplified Granta's model (1) the compressive muscle force was estimated for each position as the product of muscle activation (normalized EMG), muscle cross-sectional area, and muscle gain. Muscle cross-sectional area was estimated using trunk length and trunk breadth [1]. Muscle gain was set at 47.4 N/cm2 [1]. Lumbar compressive force was estimated by summing the vertical component of each muscle force. Rectus abdominus and erector spinae were modeled as parallel to lumbar spine [1]. External oblique and Latissimus dorsi were modeled as 45 degrees from lumbar spine [1]. A one way ANOVA was performed on the estimated compressive muscle forces to examine the position effect. Post-hoc tests were performed using 95% confidence interval for difference. A Type-I error rate was set at 0.05 for significant differences.

RESULTS AND DISCUSSION

See Table 2 for summary of Compressive Forces. ANOVA showed a significant position effect on compressive forces ($p = 0.004$). Post hoc tested demonstrated that the force in inversion was greater than the forces in plank, side lying, spider, and V sit ($p<0.05$). The force in high release was greater than the forces in side lying, spider, and V sit ($p<0.05$).

The force in plank was greater than the forces in V sit (p=0.03).

The greatest means for compressive muscle forces were seen in positions where the dancer is hanging in a vertical axis (both upright and upside down), moving the trunk into a hyper-extended position (Cambre back). The lowest combined means were seen with the dancer is in full hyperextension with the limbs hanging below the pelvis (hanging back bend). This indicates that the dancer is using the skeleton to support the movement more than the trunk muscles.

The trunk muscle force was estimated because EMG data have intrinsic limitations given variability in muscle recruitment patterns. The harness and its potential for movement between positions provided a challenge for data collection. In addition, the muscle force was estimated without considering force-length and force-velocity relationships. Muscle direction was assumed to be constant without including the origin and insertion. The compressive force might be underestimated because only 8 muscles were modeled.

CONCLUSIONS

As vertical dance is gaining popularity, identifying potential stresses on the body in professional and non-professional dance settings is a necessity. Identifying typical muscle recruitment patterns in each movement will help identify key exercises for training. Developing exercises which target awareness and utilization of trunk muscles to support the spine and limbs is being developed, and an intervention protocol is being designed for future research.

REFERENCES

1. Granata KP. *Doctoral Dissertation*, Ohio State University, Columbus, OH, USA, 1993.

Table 2. Compressive forces (N) for each position.

Position	High Release	Inversion	Plank	Side Lying	Spider	V Sit
Mean	1547.1	1903.9	982.9	360.4	490.6	572.6
Standard Deviation	647.2	561.1	383.3	111.1	382. 6	308.9

Figure 1-6. Positions in vertical dance

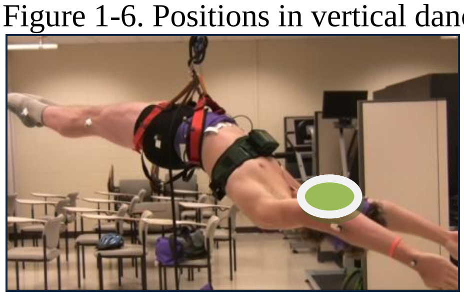

Plank

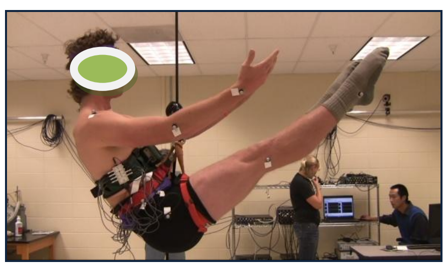

V-Sit

Side-Lying

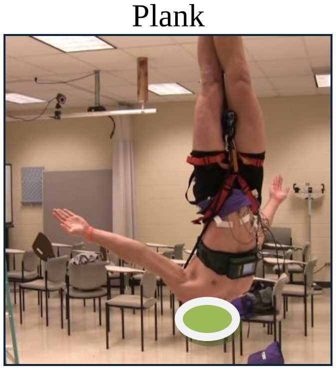

Inversion

High Release

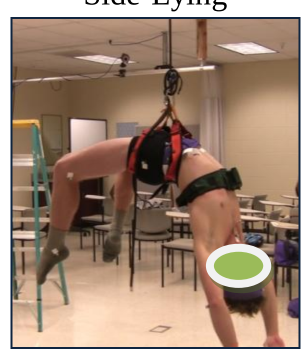

Spider

LUMBOPELVIC CONTROL AND INJURIES IN PROFESSIONAL BASEBALL PITCHERS

[1,2]Ajit M.W. Chaudhari, [1,2]Christopher S. McKenzie, [1]Xueliang Pan and [1]James A. Oñate

[1]The Ohio State University, Columbus, OH, USA
[2]Perfect Practice, Inc., Canal Winchester, OH, USA
email: chaudhari.2@osu.edu

INTRODUCTION

Baseball pitching is a technically and physically demanding activity, requiring coordination of the entire body to deliver the ball with both speed and accuracy. Injuries are very common in baseball pitching at all levels: 26-35% of youth baseball pitchers report elbow or shoulder pain per season [3, 4] and Major League Baseball pitchers lose on average 22 days per season due to injury [2]. Many potential risk factors for pitching injuries have been explored, but the role of motor control of the lumbar spine and pelvis in pitching injury incidence has not been investigated. A recent study demonstrated that pelvic positional control during a standing single-leg-raise test was positively associated with pitching performance [1]. The purpose of this study was to test the hypothesis that pelvic positional control during the single-leg-raise test would be negatively associated with days missed due to injury in professional pitchers.

METHODS

428 professional baseball pitchers (22.4±4.6 years old) from five organizations enrolled in this study during the last 2 weeks of spring training before the 2011 and 2012 baseball seasons after providing IRB-approved informed consent. A previously-described standing single-leg raise test [1] was performed on each participant. In brief, participants stood with weight evenly distributed on both feet, lifted the foot of the kicking leg approximately 10 cm, held that single-leg-stance position for 2 seconds, and then returned to double-leg-stance under control. The anterior-posterior deviation of the pelvis from its starting position relative to the horizon was measured in degrees using an iPod-based tilt sensor (Level Belt Pro, Perfect Practice, Inc.), and the largest peak absolute deviation was recorded for future analysis (APScore).

Through the course of the season, medical staff from each baseball organization recorded days when the participant's activity in practices or games was limited within the organization's own electronic medical record. After completion of the season, these days missed due to injury and all game participation data were compiled for all participants for whom data was available. Participants who retired during the season, who had surgery, or who were traded or released were excluded due to the lack of a complete dataset, leaving 350 pitchers for subsequent analysis.

Pitchers were placed into tertiles based on APScore (LO:<4.0, MD:4.0-7.9, HI:≥8.0; range 1.0-12.5) and into 2 categories based on total number of days missed (<30, ≥30). Pearson Chi-Square and Likelihood Ratio Chi-Square tests were performed to test the hypothesis that those with a greater APScore would be more likely to miss 30+ days due to injury. An *a priori* alpha level of 0.1 was chosen for statistical significance. A secondary examination was also performed of the number of days missed by players who missed one or more days determine whether those with a greater APScore had a tendency to miss more total days when injured.

RESULTS AND DISCUSSION

As shown in Table 1, pitchers with poorer pelvic positional control were significantly more likely to miss 30 or more days due to injury (Pearson Chi-Square, $p=0.045$; Likelihood Ratio Chi-Square, $p=0.067$). The probability of missing 30 or more days in the MD group was 1.44 times that in the LO group, while the probability in the HI group was almost three times that in the LO group.

Single Leg Raise APScore	*Missed < 30 days due to injury*	*Missed 30+ days due to injury*	*Total*
LO: <4.0	124 (89.2%)	15 (10.8%)	139
MD: 4.0-7.9	162 (84.4%)	30 (15.6%)	192
HI: >=8.0	13 (68.4%)	6 (31.6%)	19
All	299 (85.4%)	51 (14.6%)	350

Table 1: Those with poorer pelvic stability (higher APScore in the Single Leg Raise test) were significantly more likely to miss 30 or more days due to injury (Pearson Chi-Square p=0.045).

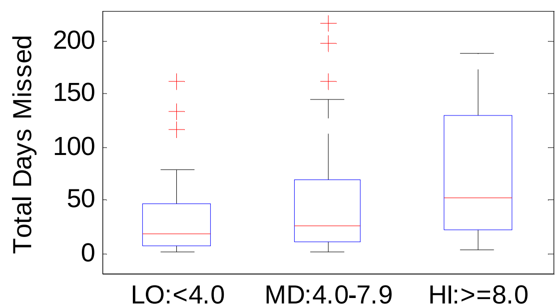

Figure 1: Total days missed due to injury during the course of the season by pitchers in the LO, MD, or HI group who missed at least one day during the season due to injury.

Baseball pitchers with poorer pelvic control also demonstrated a tendency to miss more days due to injury than those with better pelvic control (Figure 1), as shown by the higher median value and higher value for the 75th percentile (top of the box). This result could mean either that the pitchers with poorer control are suffering more injuries, or that each individual injury takes longer to recover from.

To the authors' knowledge, our study is the first to demonstrate that lumbopelvic control is related to injuries in baseball pitchers. Previous studies have shown a relationship between peak ground reaction forces and pitching velocity [5], suggesting that a successful pitch depends on energy generation from the legs and transfer of that energy through the lumbopelvic region to the throwing hand. A lack of lumbopelvic control may lead to an inability of the pitcher to efficiently transfer energy from the legs to the hand, leading to excessive use of the shoulder, arm and wrist muscles to generate ball velocity. It could also lead to early "opening up" of the torso towards the target, forcing the back, shoulder and elbow to the extremes of the range of motion in a whip-like motion, which may cause excessive joint moments that strain the ligaments and other soft tissues leading to back, rotator cuff, medial elbow and other ligament or tendon overuse injuries.

The results of this study should be considered in light of its limitations. A larger sample size would permit a more robust estimate of the difference in injury rates between groups as well as a multi-factorial examination of the relative importance of lumbopelvic control versus other potential injury risk factors. In addition, the players who were released, traded, or retired may have been let go due to poor performance or prior injury history that may or may not have been related to lumbopelvic control deficits to some degree.

CONCLUSIONS

This study observed that poorer lumbopelvic control during a standing single-leg-raise test was a significant predictor of increased risk of missing 30 or more days due to injury in professional baseball pitchers. These results suggest that an increased emphasis on appropriate lumbopelvic control training may reduce the high incidence of injury in baseball pitchers.

REFERENCES

1. Chaudhari AM, et al. *J Strength Cond Res* **25**, 2127-2132, 2011.
2. Conte S, et al. *Am J Sports Med* **29**, 431-436, 2001.
3. Lyman S, et al. *Am J Sports Med* **30**, 463-468, 2002.
4. Lyman S, et al. *Med Sci Sports Exerc* **33**, 1803-1810, 2001.
5. MacWilliams BA, et al. *Am J Sports Med* **26**, 66-71, 1998.

ACKNOWLEDGEMENTS

The authors gratefully acknowledge the Pittsburgh Pirates, Oakland Athletics, Kansas City Royals, Tampa Bay Rays and Cleveland Indians organizations for their participation in this study. Partial funding came from TechColumbus.

RELATIONSHIPS BETWEEN TRUNK KINEMATICS AT THE CRITICAL TIME POINTS IN BASEBALL PITCHING

[1,2]Sakiko Oyama, [2]Yu Bing, [2]J. Troy Blackburn, [2]Darin A. Padua, [3]Li Li, and [2]Joseph B. Myers

[1]University of Texas at San Antonio, San Antonio, TX, USA
[2]University of North Carolina at Chapel Hill, Chapel Hill, NC, USA
[3]Georgia Southern University, Statesboro, GA, USA
email: Sakiko.oyama@utsa.edu

INTRODUCTION

Baseball pitching is one of the most dynamic movements performed in sports. The high complexity of the movement poses a challenge when learning or instructing pitching technique. While there are many technical points to attend to during pitching, it is theorized that there is a limit in the attentional resources that can be used to carry out a task, and thus the number of cues to use when learning or instructing a pitching technique must be limited. [1]

Since pitching is a movement that involves sequential action of body segments, kinematics in the early preparatory phases are likely linked to kinematics in the latter dynamic phases. Understanding the relationship between kinematics at various time points during pitching would help reduce the number of cues to use in coaching, which may lead to effective instruction.

While pitching involves the interaction of multiple segments, trunk kinematics is central to pitching movement, as the trunk is a critical link between the lower and upper extremities. [2,3] Therefore, the purpose of this study was to examine the relationship between trunk forward flexion, lateral flexion, and rotation angles at stride foot contact (SFC), maximal shoulder external rotation (MER), and ball release (REL).

METHODS

A total of 72 high school baseball pitchers (age: 15.5±1.2 years, height: 1.8±0.1 m, mass: 72.7±9.8 kg, dominance: 56 right/16 left) participated. Pitchers were fitted with reflective markers on significant anatomical landmarks. After warm up, participants pitched (fast pitch) from windup until 3 strike pitches were successfully captured.

The pitch trials were performed from an indoor pitching mound to a backstop that was placed 16.4m away. The pitching mound was instrumented with two force plates (sampling frequency: 900Hz), one underneath the pitching rubber and the other on the slope of the mound. The position of the force plate on the slope was adjusted based the pitcher's stride length. A seven-camera motion capture system with automatic marker tracking software was used to capture pitching kinematics (sampling frequency: 300fps).

The trunk segment was defined in accordance to the recommendations from the International Society of Biomechanics. [4] The trunk segment angles relative to the global reference frame (+x: anterior, +y: left, +z: vertical) were calculated using an Euler angle sequence of axial rotation, lateral flexion, and flexion. Positive angles indicated axial rotation to the left, lateral flexion to the left, and forward flexion for the right-handed pitcher. For the left-handed pitcher, positive angles indicated axial rotation to the right, lateral flexion to the right, and forward flexion. The angles were identified at SFC, MER, and REL. The instant of SFC was identified from the force plate data, and MER and REL were identified from the kinematic data. Three-trial averages were used for analyses.

Relationships between the trunk kinematic variables were examined using Pearson product-moment correlation coefficients. Correlation coefficients between .25-.5, .5-.75, and above .75 were considered to indicate fair, moderate to good, and good to excellent relationships, respectively. [5]

RESULTS AND DISCUSSION

At SFC, there were little to no correlations between forward flexion, lateral flexion, and axial rotation angles ($r < .25$). At MER, greater lateral flexion angle was moderately correlated with smaller rotation angle ($r = -.482$, $p < .001$). At REL, greater lateral flexion angle had a good correlation with smaller axial rotation angle ($r = -.784$, $p < .001$) and a moderate correlation with smaller forward flexion angle ($r = -.719$, $p < .001$). The greater forward flexion angle had a fair correlation with greater axial rotation at REL ($r = .469$, $p < .001$).

Moderate correlations were observed between forward flexion angles at SFC and lateral flexion angle at MER ($r = .619$, $p < .001$) and REL ($r = .527$, $p < .001$). The more forward flexed the trunk was at SFC, the less lateral flexion was present at MER and REL (**Figure 2**).

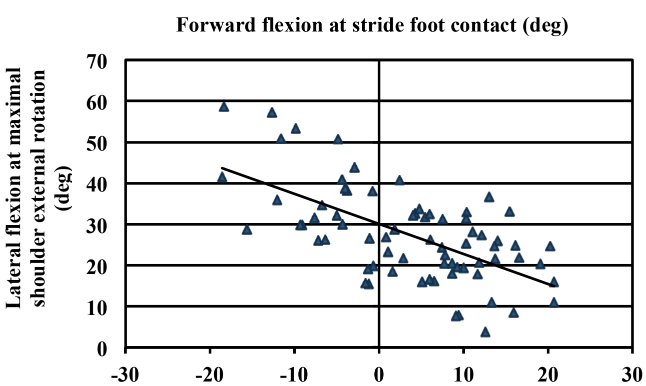

Figure 2. Correlation between forward flexion angles at SFC and lateral flexion angle at MER

There were moderate to high correlations among the segment angles at MER and REL (**Table 1**).

		REL		
		Flexion	Lateral flexion	Rotation
MER	Flexion	.881 (<.001)	-.494 (<.001)	.293 (.013)
	Lateral flexion	.542 (<.001)	.937 (<.001)	.653 (<.001)
	Rotation	.401 (<.001)	-.614 (<.001)	.899 (<.001)

Table 1. Correlation of trunk segment angles between maximal shoulder external rotation and ball release

The correlation between forward flexion angle at SFC and lateral flexion at MER and REL (**Figure 2**) demonstrates that the trunk orientation at SFC is linked to the trunk kinematics in the latter dynamic phases. The relationship indicates that trunk orientation in the sagittal plane translates into trunk orientation in the frontal plane, as the pitcher turns 90° to face the hitter.

At REL and between MER and REL, an axial rotation and forward flexion were positively correlated with each other. On the other hand, greater lateral flexion was negatively correlated with axial rotation and forward flexion angles. These observations suggest that forward trunk flexion and trunk rotation are facilitatory to each other, while lateral flexion is inhibitory to forward flexion and axial rotation. This relationship suggests that some pitchers favor the frontal plane trunk movement, while the others favor the transverse and sagittal plane motion.

Understanding the relationship between the trunk kinematics at various time points is important when instructing or learning a pitching technique. Lateral flexion at MER and REL may be manipulated by changing the forward trunk flexion angle at SFC. Similarly, the balance between frontal vs. transverse and sagittal plane trunk movement may be manipulated by changing one of the three trunk rotations. Baseball coaches may utilize the observations from this study to instruct pitchers on their trunk motion.

REFERENCES

1. Magill RA. *Motor Learning and Control: Concepts and applications,* McGraw-Hill, Inc., 2007.
2. Feltner ME. *Int. J. Sport Biomech* **5**, 403-419, 1989.
3. Hirashima M, et al. *J Biomech* **41**, 2874-83, 2008.
4. Wu G, et al. *J Biomech* **38**, 981-992, 2005.
5. Watkins LP. *Foundations of Clinical Research: Applications to Practice,* Pearson Education, Inc., 2009

A COMPARISON OF HIP AND TRUNK KINEMATICS IN HEALTHY RUNNERS WITH STRONG AND WEAK HIP ABDUCTORS

JJ Hannigan, Jim Becker and Li-Shan Chou

Motion Analysis Laboratory, Department of Human Physiology, University of Oregon, Eugene, OR, USA
email: chou@uoregon.edu, web: http://biomechanics.uoregon.edu/MAL/index.html

INTRODUCTION

Weak hip muscles, particularly the hip abductors, have been suggested as contributing factors for several common running-related injuries [1,3]. It has also been reported that injured runners display abnormal hip kinematics compared to healthy controls [2], and that there are correlations between reduced hip strength and excessive hip internal rotation [3] or hip adduction [1].

Some studies, however, have reported that strengthening these weak muscles did not alter running mechanics [4], which calls into question the relationship between hip strength and running mechanics. Therefore, one purpose of this study was to further investigate this relationship between hip strength and hip kinematics in healthy runners.

In addition, anecdotal evidence from our lab suggests that some runners shift their trunk laterally during stance phase (Figure 1). In theory, this may be an attempt to compensate for weak hip abductors by reducing the load on those muscles. To date, little is known on the relationship between hip strength and trunk kinematics in runners. Therefore, a second purpose of this study was to examine the relationship between hip strength and frontal plane trunk motion.

METHODS

Subjects for this study were part of a larger, ongoing study on running biomechanics and injuries at the University of Oregon Motion Analysis Laboratory. Inclusion criteria for this study were running over 20 miles per week, being injury-free at the time of testing, and completing all components of the protocol required for this study. Based on these criteria, 58 runners were included for analysis (age: 30.20 ± 11.02 years).

Figure 1. Subject displaying excessive lateral trunk lean, pelvic drop, and hip adduction while running

Reflective markers were placed on subjects who ran continuous laps of ~25 meters in the laboratory at their normal training run paces. Whole body kinematic data were collected at 200 Hz using a 10-camera motion capture system (Motion Analysis Corp.) Three AMTI (Advanced Mechanical Technology, Inc.) force plates located in series along the capture region recorded ground reaction forces at 1000 Hz.

After the running protocol, hip abduction strength was measured bilaterally using a Biodex System 3 dynamometer (Biodex Medical Systems, Shirley NY). For this test, subjects pushed against the dynamometer with maximal force three times for five seconds while standing with the hip at 10-degrees of abduction. Mean torque was calculated for each limb and normalized by body mass for analysis.

Limbs with hip abduction strength that is 1.5 standard deviations above the overall mean were considered “strong”, while limbs 1.5 standard deviations below the mean were considered "weak" for this study [5]. For each variable, differences were examined using a 2-tailed t-test. Significance level of $p < .05$ was used for all tests.

RESULTS AND DISCUSSION

Eight runners were identified as having strong hip abductors (age: 22.5 ± 4.9 years; weekly mileage: 44.4 ± 9.4 miles) while four runners were identified as having weak hip abductors (age: 32.8 ± 13.0 years; weekly mileage: 40.0 ± 4.1 miles). There were no significant differences between groups with respect to demographic data ($p > .05$).

Results indicate that individuals with strong hip abductors display significantly less contralateral pelvic drop and hip internal rotation compared to individuals with weak abductors ($p < .05$). No significant differences were found between groups for hip adduction ($p > .05$) (Figure 2; Table 1).

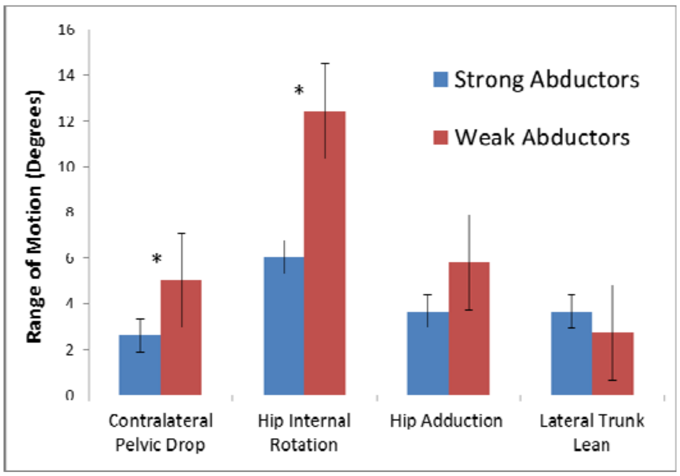

Figure 2. Comparison between strong and weak hip abductor groups for selected kinematic parameters. *indicates a significant difference between groups

These findings support previous research that suggested a relationship between hip abduction strength and hip kinematics [1,3].

In addition, no significant differences were found between groups in regards to frontal plane trunk lean ($p > .05$) (Figure 2; Table 1). This result contradicted our hypothesis that excessive frontal plane trunk motion may be an attempt to compensate for weak hip abductors. More studies are needed to explain this phenomenon.

CONCLUSIONS

Runners with strong hip abductors display significantly less contralateral pelvic drop and hip internal rotation than runners with weak hip abductors. No significant differences were seen between groups for hip adduction or lateral trunk lean. Future studies should examine the effect of hip strengthening on hip kinematics in healthy runners. More research on the relationship between hip strength and trunk kinematics during running also appears warranted.

REFERENCES

1. Dierks TA, et al., *J Orthop Sports Phys Ther*, **38**, 448-56, 2008.
2. Noehren B, et al. *Clin Biomech*, **27**, 366-71, 2012.
3. Souza RB & Powers CM, *Am J Sport Med*, **37**, 579-87, 2009.
4. Willy RW & Davis IS, *J Orthop Sports Phys Ther*, **41**, 625-32, 2011.
5. Butler et al., *Am J Sport Med*, **34**, 1998-2005, 2006.

Table 1: Comparison between strong and weak hip abductor groups for selected kinematic parameters
* indicates a significant difference between groups.

	Range of Motion (degrees)			
	Contralateral Pelvic Drop*	**Hip Internal Rotation***	**Hip Adduction**	**Lateral Trunk Lean**
Strong Hip Abductors	2.6 ± 1.0	6.1 ± 3.5	3.7 ± 2.3	3.7 ± 0.9
Weak Hip Abductors	5.0 ± 0.4	12.4 ± 5.0	5.8 ± 1.5	2.7 ± 0.5

ORAL PRESENATIONS – THURSDAY SEPTEMBER 5th

	Assesssment of Material Properties in Bone by Medical Imaging *Zachary Domire, Ryan Breighner*
11:15 AM	CT Exposure And Energy Effects On Bone Mineral Density Estimation From Calibration Phantoms **Giambini H, Nassr A, Huddleston P, Dragomir-Daescu D, An KN**
11:30 AM	In Vivo Patient-Specific Material Properties Of The Subcalcaneal Fat: An Inverse Finite Element Analysis **Isvilanonda V, Iaquinto J, Williams E, Cavanagh P, Haynor D, Chu B, Ledoux W**
11:45 AM	The Mechanical Consequence Of Actual Bone Loss And Simulated Bone Recovery In Acute Spinal Cord Injury **Edwards WB, Schnitzer T, Troy K**
12:00 PM	Effects Of Charcot Neuropathic Osteoarthropathy On 3-D Foot Bone Orientation Angles Measured Using Quantitative Computed Tomography **Gutekunst D, Liu L, Ju T, Kaufman K, Johnson J, Sinacore D**

CT Exposure and Energy Effects on Bone Mineral Density Estimation from Calibration Phantoms

[1]Hugo Giambini, [1]Ahmad Nassr, [1]Paul M. Huddleston III, [2]Dan Dragomir-Daescu and [1+]Kai-Nan An

[1+] Biomechanics Laboratory, Division of Orthopedic Research, Mayo Clinic,
Rochester, MN USA
[2] Division of Engineering, College of Medicine, Mayo Clinic, Rochester, MN USA

INTRODUCTION

Osteoporosis is characterized by bony material loss and decreased bone strength leading to a significant increase in fracture risk [1]. Areal bone mineral density (aBMD) measured using dual-energy x-ray absorptiometry (DEXA) is considered the gold standard for osteoporosis diagnosis and fracture risk estimation. However, patient-specific QCT (quantitative computed tomography) finite element (FE) models may be used to predict fracture location under physiological loading. Material properties for FE models are obtained by converting grayscale values from the CT into volumetric BMD (vBMD) using a calibration phantom. Any error arising from the CT acquisition protocol will have an effect in the vBMD estimation and material property assignment, thus, resulting in a false fracture risk prediction. The purpose of this study was to investigate the effect of CT exposure and energy on vBMD estimation.

METHODS

A calibration phantom (Mindways, Inc., Austin, TX, USA) containing five rods of reference materials, calibrated against liquid K_2HPO_4/water solutions was scanned 6 times using QCT. The scans were performed using a Somatom Definition Dual-Source Scanner (Siemens, Germany) by varying the exposures and energies according to Table 1. Scans were reconstructed using a high spatial resolution kernel, U70, with a voxel size of 0.4mm isotropic. QCT-DICOM images were uploaded into Mimics (Materialise, Plymouth, MI) and mean CT number values (HU, Hounsfield unit) and standard deviation (noise) were measured for the five calibration rods. A regression curve estimating vBMD from HU values was obtained and extrapolated to cover not only trabecular but cortical bone density as well. Analysis of variance (ANOVA) and Tukey's post hoc were used to compare HU values and noise of each phantom rod and detect differences between energies. Student t-test was used to test for significant differences between exposures.

Table 1.

Exposures (mAs)	**Energy (kVp)**		
110	80	120	140
450	80	120	140

RESULTS AND DISCUSSION

Figure 1 shows the CT image of the calibration phantom in different views. The rods were segmented and measurements of HU and noise obtained for each rod. ANOVA revealed differences (*: $P<0.0001$) for both HU and noise parameters (Figures 2 and 3) when comparing the energy acquisition. The Tukey's post hoc analysis showed differences in all rods (*: $P<0.0001$), except between 120 and 140 kVp (exposure 110 mAs) where the statistical difference for rod 3 was $P=0.024$. When looking at exposure differences (same kVp) in HU values, student t-test showed significant differences to vary among rods with most of them, except one, differing at the lower kVp (80 kVp). At the highest kVp (140 kVp) only rod 5 reached statistical difference (data not shown). On the other hand, noise values differed in all rods (*: $P<0.0001$). Regression curves obtained from the calibration phantom rods are plotted in Figure 3. Regression lines obtained from same energies but different exposures overlap at all HU values. This study shows higher differences in vBMD estimation from calibration phantoms when varying energy as compared to the acquisition exposures. The differences between densities estimated using different energies were smaller within the trabecular bone region compared to the cortical bone density region. However, these trabecular differences were substantial. Comparing an arbitrary HU value of 500 at the two extreme energies (80 and 140 kVp) gave a difference in vBMD estimation of 33% (8% between 120 and 140 kVp). These effects would impact the Young's modulus estimation and a subsequent false estimation of strength and stiffness values in FE models and would also misclassify a number of patients putting them at risk of vertebral fracture. The large standard deviation (noise) values presented in the lower exposure and energy scans could have a negative effect in estimating vBMD, on small sub-regions containing smaller voxel numbers compared to the other acquisitions.

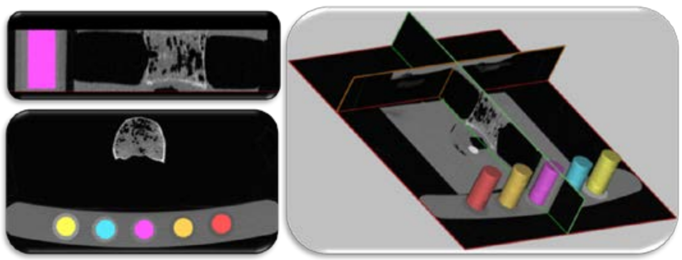

Figure 1: CT scan image showing the 5 calibration rods in different views. Segmented rods (volumetric) are also shown.

2.A

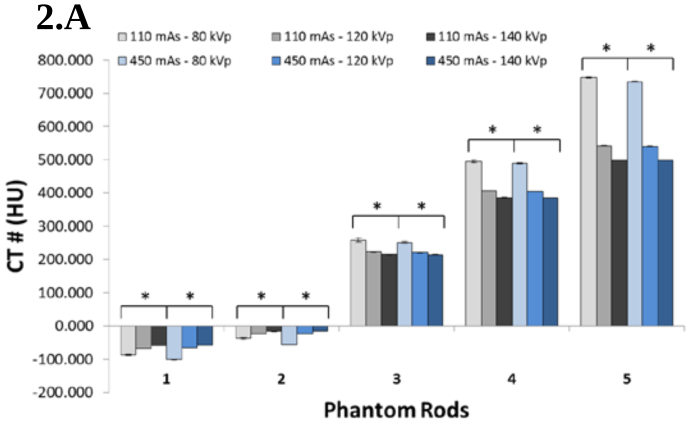

2.B

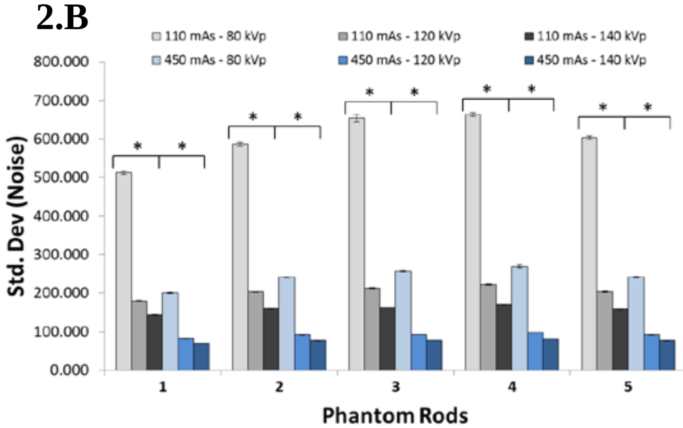

Figure 2: **A**) CT# (HU) and **B**) standard deviation (noise) for the 5 calibration rods at different exposures and acquisition energies (*: P<0.0001).

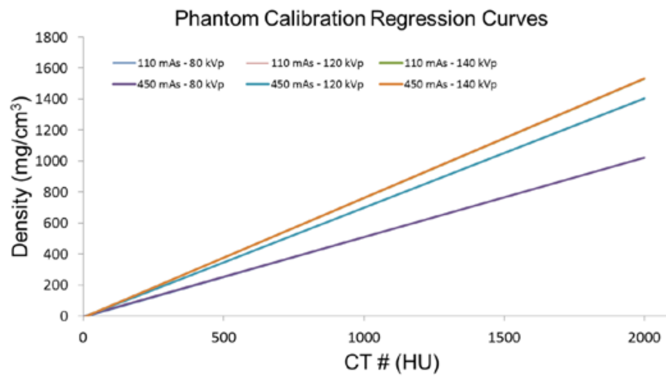

Figure 3: Regression curves used for BMD estimation obtained from the different CT exposure and energy acquisitions.

CONCLUSIONS

The current study demonstrates a significant difference in the estimation of vBMD related to the acquisition energy of the scans. Even though there is a statistical difference between some rods when comparing exposures, these differences have a minor effect on vBMD estimation, as shown by the overlap of the regression curves. Further work is needed to develop a protocol that will combine high spatial resolution and will optimize the exposure and energy to allow for better estimation of fracture risk and vBMD while at the same time reducing the radiation exposure to patients.

REFERENCES

[1] Briggs, A.M., Wrigley, T.V., van Dieen, J.H., Phillips, B., Lo, S.K., Greig, A.M., et al., 2006. The effect of osteoporotic vertebral fracture on predicted spinal loads in vivo. *Eur Spine J* 15, 1785-1795.

ACKNOWLEDGEMENTS

This project was supported by OREF (Orthopedic Research and Education Foundation) and the Mayo Clinic Foundation. The authors would like to thank Beth Cloud for her assistance in the statistical analysis.

IN VIVO PATIENT-SPECIFIC MATERIAL PROPERTIES OF THE SUBCALCANEAL FAT: AN INVERSE FINITE ELEMENT ANALYSIS

[1,2]Vara Isvilanonda, [1,2]Joseph M. Iaquinto, [1,2]Evan D. Williams, [2,3]Peter R. Cavanagh, [4]David R. Haynor, [4]Baocheng Chu and [1,2,3]William R. Ledoux

[1]RR&D Center of Excellence for Limb Loss Prevention and Prosthetic Engineering, Department of Veterans Affairs, Seattle, WA, USA; Departments of [2]Mechanical Engineering, [3]Orthopaedics & Sports Medicine and [4]Radiology, University of Washington, Seattle WA, USA
email: wrledoux@u.washington.edu Web: http://www.amputation.research.va.gov

INTRODUCTION

Subcalcaneal fat serves as shock absorber and provides cushioning to the underlying foot structures and the body as a whole. Changes in mechanical response of the subcalcaneal fat (i.e., stiffening due to age [1] or diabetes [2]) can compromise the ability to dissipate plantar stress and potentially cause tissue injury. Inverse finite element (FE) analysis has been used to quantify mechanical properties of the soft tissue from *in vivo*, *in vitro* or *ex vivo* compression data [3-5]. However, several of these FE models assume simplified anatomy (i.e., 2D, plane strain or axisymmetric), material representation (i.e., lumped skin, fat and muscle) and/or boundary conditions (i.e., neglect bone movement or adjacent structures). In the current study, patient-specific subcalcaneal fat hyperelastic properties were determined from magnetic resonance imaging (MRI) heel compression data using inverse FE analysis. The FE model incorporates 3D anatomically realistic layers of plantar soft tissue (skin, fat and muscle) and physiologic calcaneus movement.

METHODS

A right foot of a 43-year-old male (912 N) subject was scanned using high resolution partial loaded computed tomography (CT) and unloaded MRI. Subsequently, a dynamic hindfoot compression experiment was conducted using an MRI-compatible loading device [6]. The hindfoot was loaded in the antero-posterior direction by a platen up to 11.7mm (55% strain) using a 0.2hz sine wave. The cardiac-gated MR images of the internal tissue were obtained at sixteen phases, each representing a

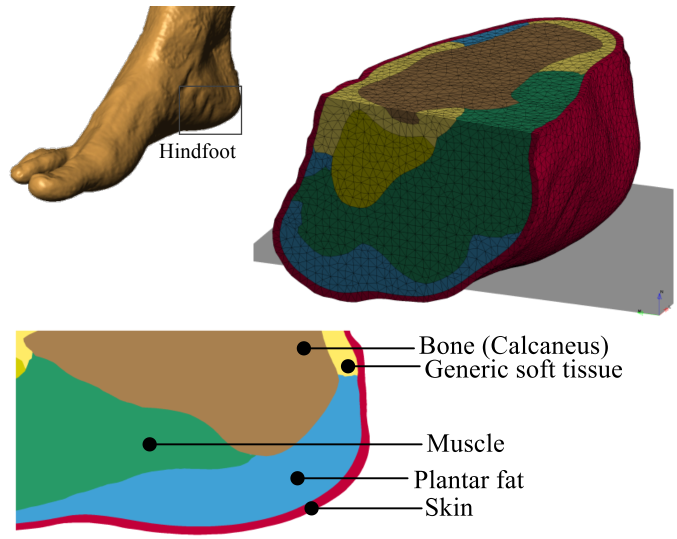

Figure 1: (a) Finite element model of the hindfoot and the loading platen. (b) Sagittal cross section displays different material layers.

point on the loading-unloading curve. Hydraulic pressure in the system was recorded at 2.5khz for force calculation. 3D calcaneus and cuboid surfaces were segmented from the CT data using custom software *Multi-Rigid* [7]. Skin, fat and muscle surfaces were segmented from the unloaded MR data using ScanIP (Simpleware, Exeter, UK) and *Multi-Rigid*. The model including the calcaneus, cuboid, skin, fat, muscle and generic soft tissue (Fig. 1), which were all meshed with 4-noded tetrahedral elements in ANSYS ICEM CFD (ANSYS Inc, Canonsburg, USA). The rigid body transformation of the calcaneus and the loading platen, extracted from the dynamic MR data, were prescribed to the FE model in LS-Prepost (Livermore Software, Livermore, CA). Only the loading cycle was analyzed. The cuboid was rigidly constrained to the calcaneus. Material properties are given in Table 1.

The subcalcaneal fat hyperelastic coefficients (μ_1 and α_1) were identified using inverse FE analysis in LS-OPT (Livermore Software, Livermore, CA). A D-optimal point selection constructed a design of experiment (6 sets of μ_1 and α_1). Subsequently, 6 FE models were generated and solved in LS-DYNA (v971d R5.1.1, explicit analysis). The objective function, defined as the normalized mean squared error (MSE per peak target force squared) between the predicted force and the experimental data, was computed. A successive response surface method (SRSM) was chosen for the quadratic polynomial metamodel-based optimization [8]. The hybrid adaptive simulated annealing optimization algorithm was used [8]. The analysis progressed until the two termination criteria became active:

$$\left|\frac{f^{(k)} - f^{(k-1)}}{f^{(k-1)}}\right| < \varepsilon_f \quad \text{and} \quad \frac{\left\|x^{(k)} - x^{(k-1)}\right\|}{\left\|d\right\|} < \varepsilon_x$$

Where ε_f denotes the objective function accuracy, ε_x refers to the design accuracy, f is the normalized MSE, x refers to the vector of design variables (μ_1 and α_1), d denotes the size of the design space, and *(k)* and *(k-1)* refer to two successive iteration numbers. In this study, $\varepsilon_f = \varepsilon_x = 0.01$ were used.

RESULTS AND DISCUSSION

The model predicted soft tissue thickness (vertical distance from the lowest point on the calcaneus to the platen) and force responses were in good agreement with the test data. Soft tissue thickness has a root-mean-square error (RMSE) of 0.23mm (1.1% of the unloaded thickness). The patient-specific hyperelastic coefficients of the subcalcaneal fat, μ_1 = 0.05476 kPa and α_1 = 26.07, were obtained after 8 iterations. The force-time response has an RMSE of 6.91N (3.2% of the peak target force). The coefficient μ_1 has more influence to the objective function (75.5%) compare to α_1 (24.5%).

The model limitations include using non-patient-specific muscle and skin material properties, lumping generic soft tissue with fat and assuming constant plantar skin thickness. Future analysis will consider a full loading cycle, tighter termination criteria and will identify skin, fat and muscle materials simultaneously by optimizing reaction force and muscle deformation.

REFERENCES

1.Hsu T-C, et al. *Arch. Phys. Med. Rehabil.* **79**, 1998.
2.Pai S, et al. *J. Biomech.* **43**, 1754-1760, 2010.
3.Chokhandre S, et al. **134**, 031002-031009, 2012.
4.Erdemir A, et al. *J. Biomech.* **39**, 1279-1286, 2006.
5.Petre MT. Case Western Reserve University, 2007.
6.Stebbins MJ. University of Washington, 2012.
7.Hu Y, et al. *J. Biomech. Eng.* **133**, 101005, 2011.
8.Stander N, et al. *LS-Opt User's manual*, LSTC, 2010.
9.Muehleman C, et al. *Anat. Rec.* **266**, 81-86, 2002.
10.Zysset PK, et al. *J. Biomech.* **32**, 1005-1012, 1999.
11.Duck FA. *Physical properties of tissue : a comprehensive reference book*, Academic Press, 1990.
12.Then C, et al. *Technol. Health Care* **15**, 385-398, 2007.
13.Gu Y, et al. *Skin Res. Technol.* **16**, 291-296, 2010.
14.Edwards C, et al. *Clin. Dermatol.* **13**, 375-380, 1995.
15.Hibbit D., et al. *ABAQUS/Theory Manual V. 6.7*, Hibbitt, Karlsson & Sorensen Inc., 2007.
16.Hallquist JO. *LS-Dyna Theory manual*, LSTC, 2006.

ACKNOWLEDGEMENTS

This work was supported by the VA Grant A6973R. The authors would like to thank QuocBao Vu for assisting with data analysis.

Table1: Material models and properties.

Material	Model	Properties†	Reference
bone	Rigid	ρ = 0.449e-6 kg/mm^3, E = 20,100 MPa, ν = 0.3	[9],[10]
Plantar fat‡ and **generic soft tissue**	Ogden hyperelastic	ρ = 0.916e-6 kg/mm^3, ν = 0.4998, 1.0e-7<μ_1<5e-4 MPa and 10<α_1<50, initial guess μ_1 = 8.12e-5 MPa and α_1 = 17.97	[11]
muscle††	Ogden hyperelastic	ρ = 1.047e-6 kg/mm^3, μ_1 = 1.558e-3 MPa, α_1 = 1.316, μ_2 = -1.582e-8 MPa, α_2 = 18.36, ν = 0.495	[11], [12]*
skin‡	Ogden hyperelastic	ρ = 1.142e-6 kg/mm^3, μ_1 = 0.0136 MPa, α_1 = 18, ν = 0.48	[11], [13]*

† Density (ρ), modulus of elasticity (E), Poisson's ratio (ν), Ogden hyperelastic coefficients (μ_1 and α_1).
†† Passive mechanical properties for the human gluteus muscle
‡ Poisson's ratio was estimated from the longitudinal ultrasound speed [11], tissue density [11] and elastic modulus [2],[14]
* Conversion from Abaqus Ogden hyperelastic coefficients to LS-DYNA was used due to different definition for μ. Ogden hyperelastic strain energy functions are given in Abaqus and LS-DYNA theory manual [15, 16]

THE MECHANICAL CONSEQUENCE OF ACTUAL BONE LOSS AND SIMULATED BONE RECOVERY IN ACUTE SPINAL CORD INJURY

W. Brent Edwards [1], Thomas J. Schnitzer [2], and Karen L. Troy [1]

[1] University of Illinois at Chicago, Chicago, IL, USA
[2] Northwestern University Feinberg School of Medicine, Chicago, IL, USA
email: edwardsb@uic.edu, web: http://www.uic.edu/ahs/biomechanics

INTRODUCTION

Spinal cord injury (SCI) injury is characterized by a rapid loss of bone mineral at sublesional regions. The clinical consequence of this bone loss is an increased lifetime risk for low-energy fracture that is substantially greater than the general population [1]. These fractures frequently occur around regions of the knee, e.g. the proximal tibia. Fractures after SCI are a source of considerable morbidity, loss of independence, and increased medical costs.

Although the time course and magnitude of bone loss following SCI has been well documented, the biomechanical relevance remains unclear. Bone fractures are ultimately biomechanical events, and small changes in bone mineral may have large mechanical consequences. Though not the standard of care, pharmaceutical treatment represents a potential therapeutic intervention to ameliorate bone loss and reduce fracture occurrence after SCI. However, SCI is also associated with structural changes in geometry and mineral distribution, and therefore pharmaceutical treatments that reverse bone loss alone may not necessarily restore mechanical integrity back to baseline levels.

Our purpose was to quantify changes in torsional stiffness and strength of the proximal tibia due to 1) actual bone loss and 2) simulated bone recovery in acute SCI.

METHODS

Ten adults with acute SCI consented to participate in this institutionally approved study. Subjects received two computed tomography (CT) scans of the knee (120 kV, 200 mAs, pixel resolution 0.352 mm, slice thickness 1 mm). Baseline scans were performed approximately 2 months after SCI and follow-up scans were performed approximately 4 months after baseline. All scans included a calibration phantom to convert CT Hounsfield units to bone apparent density ρ_{app}.

Physical and simulated models:

Proximal tibiae were segmented from the CT scans and four voxel-based geometric models were generated for each subject – two physical (baseline and follow-up) and two simulated (treatment 1 and treatment 2) models. The physical models were generated directly from baseline and follow-up scans. The simulated models represented hypothetical treatments that restored bone mineral back to baseline levels following the acute period of SCI. For treatment 1 models, the ρ_{app} of voxels of follow-up models were uniformly increased so that bone mineral content (BMC) was equal to baseline levels. For treatment 2 models, the ρ_{app} of voxels of follow-up models were also increased so that BMC was equal to baseline, however, the amount of mineral apposition was dependent on the available surface area for remodeling, or surface area density S_v. Martin [2] illustrated that bone S_v (mm^2/mm^3) is related to ρ_{app} (g/cm^3) by a 5th order polynomial: $S_v=0.2+6.8\rho_{app}-2.5\rho_{app}^2-2.3\rho_{app}^3+2.7\rho_{app}^4-0.9\rho_{app}^5$.

Prediction of torsional stiffness and strength:

Torsional stiffness K and strength T_{ult} were predicted for each model using validated subject-specific finite element modeling procedures. Using cadaveric experimentation, these modeling procedures were able to predict *in vitro* torsional stiffness and strength with an r^2 of 0.95 and 0.91, respectively [3]. Briefly, the voxel-based models were converted to 8-node hexahedral elements with 1.5 mm edge lengths. Elements were assigned inhomogeneous nonlinear orthotropic material properties. Pre-yield elastic moduli in the axial direction E_3 (MPa) was defined as: $E_3=6570\rho_{app}^{1.37}$ [4]. Anisotropy was assumed the same throughout with $E_1=0.574E_3$, $E_2=0.577E_3$, $G_{12}=0.195E_3$, $G2_3=0.265E_3$, $G_{31}=0.216E_3$, $\nu_{12}=0.427$, $\nu_{23}=0.234$, and $\nu_{31}=0.405$. The non-linear phase was modeled as bilinear elastic-plastic with a post-yield modulus 5% of the pre-yield modulus. Yield was defined by

Hill's quadratic criterion for orthotropic materials. Yield strains were assumed isotropic in the normal (0.675%) and shear (1.215%) directions [5]. Models were loaded in torsion and K was quantified from the linear portion of the torque-rotation curve. The T_{ult} corresponded to the torque at which 10% of surface elements had failed, defined as a maximum principal strain greater than 1.410% [5].

Data Analysis:
Volumetric bone mineral density (vBMD) and BMC were calculated for each model. Trabecular (Tb) and cortical (Ct) specific BMD and BMC were also determined assuming a threshold of ρ_{app}=1.0 g/cm^3. Paired t-tests were used to examine differences in bone mineral and mechanical behavior between baseline and follow-up models as well as baseline and treatment models (α=0.05).

RESULTS AND DISCUSSION

During the acute period of SCI, subjects lost a mean 8.3% of their vBMD and 8.9% of their BMC (Table 1). Although relative reductions in K were similar in magnitude to relative reductions in bone mineral, relative reductions in T_{ult} were some 1.5 to 2 times greater than the observed reductions in bone mineral (Fig 1). The discrepancy between relative reductions in K and T_{ult} is difficult to interpret, but it does indicate that bone loss had a larger influence on post-yield rather than pre-yield behavior.

Simulations of hypothetical treatments that restored bone mineral back to baseline levels suggested that the declines in proximal tibia mechanical behavior after acute SCI are potentially reversible; for these models K and T_{ult} were not significantly different from baseline. However, substantial scatter in the mechanical behavior after treatment was observed between subjects, and scatter-plots suggested that subjects who lost more than approximately 10% of their bone mineral by follow-up did not restore mechanical behavior back to baseline levels when bone mineral was recovered. Additionally, it should be noted that our modeling procedures cannot account for potential micro-structural changes in trabecular architecture, collagen cross-linking, and remodeling space.

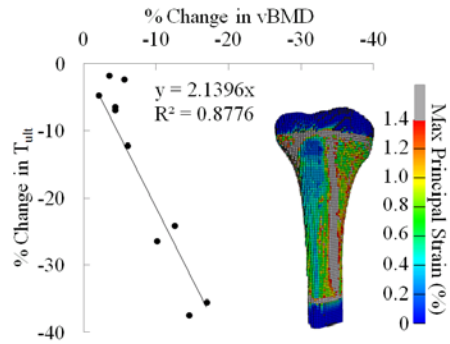

Figure 1. Changes in T_{ult} were 2 fold greater than changes in vBMD. Insert of a finite element model with contour plot of max principal strain at T_{ult}.

The two distinct hypothetical treatments used to restore bone mineral back to baseline levels provides some insight into the mechanisms by which bone mineral is resorbed after SCI. In contrast to treatment 1 simulations, trabecular and cortical BMD and BMC for treatment 2 simulations were not significantly different from baseline. These data, therefore, suggest that the bone remodeling response after SCI is dependent to some degree on the available surface area for remodeling. Indeed, peripheral QCT studies of disuse have observed the greatest declines in bone mineral at regions expressing the largest surface area for remodeling [6].

CONCLUSIONS

Individuals with acute SCI experienced a marked loss of bone mineral at the proximal tibia. Losses in bone mineral were associated with a 1.5 to 2 fold reduction in torsional strength. Reductions in torsional strength may be reversible if pharmaceutical treatment is initiated soon after SCI.

REFERENCES

1. Vestergaard. *Spinal Cord* **36**, 790-796, 1998.
2. Martin. *CRC Critical Reviews in Biomedical Engineering*. CRC Press, **10**, 179-222, 1984.
3. Edwards (2013). *Proceedings of ORS*, San Antonio, TX, USA, 2013.
4. Rho. Med Eng Phys, **17**, 347-355, 1995.
5. Rincón-Kohli (2009). Biomech Model Mechanobiol, 8: 195-208.
6. Rittweger. *Bone* **47**, 511-518, 2010.

ACKNOWLEDGEMENTS

NIH/NIAMS F32 AR061964
Merck & Co, Inc. (investigator-initiated)

Table 1. Percent change in bone mineral and mechanical behavior relative to baseline line (* p<0.05).

	vBMD	BMC	Tb.vBMD	Tb.BMC	Ct.vBMD	Ct.BMC	K	Tult
Follow-up model	-8.3 (4.9)*	-8.9 (5.0)*	-10.3 (9.2)*	-9.7 (9.2)*	-1.1 (2.2)*	-8.0 (5.3)*	-9.9 (6.5)*	-15.8 (13.8)*
Treatment 1 model	0.7 (0.3)*	0.0 (0.0)	-6.0 (7.8)*	-7.2 (8.2)*	5.0 (4.8)*	7.0 (7.3)*	-2.2 (4.7)	-5.0 (10.0)
Treatment 2 model	0.7 (0.3)*	0.0 (0.0)	0.6 (4.8)	-2.9 (8.6)	0.6 (2.5)	0.4 (4.6)	-0.2 (3.4)	-2.4 (4.7)

EFFECTS OF CHARCOT NEUROPATHIC OSTEOARTHROPATHY ON 3-D FOOT BONE ORIENTATION ANGLES MEASURED USING QUANTITATIVE COMPUTED TOMOGRAPHY

[1]David J. Gutekunst, [2]Lu Liu, [2]Tao Ju, [1]Kenton R. Kaufman, [2]Jeffrey E. Johnson and [2]David R. Sinacore

[1]Mayo Clinic, Rochester, MN, USA
[2]Washington University in St. Louis, MO USA
email: gutekunst.david@mayo.edu, web: mayoclinic.org

INTRODUCTION

Individuals with diabetes mellitus (DM) and peripheral neuropathy (PN) are prone to foot deformities that increase plantar pressure and ulcer risk, especially in Charcot neuropathic osteoarthropathy (CN), an inflammatory condition characterized by joint subluxation, dislocation, and fracture. Progressive CN deformity has been shown using sagittal radiographs [1], but many CN foot deformities are multi-planar and difficult to visualize with X-ray. This study's purpose was to use atlas-based, quantitative computed tomography (QCT) methods to measure foot deformities in individuals with acute CN compared to two control groups: a matched group of non-CN individuals with DM and PN, and an unimpaired control (UC) group. We hypothesized that there would be no side-to-side differences in DM+PN or UC group, while the CN group would have significantly different bone orientation angles in the involved foot (Inv) compared to the uninvolved foot (Uninv).

METHODS

Twenty individuals with acute CN, 20 with DM+PN but without CN, and 16 UC individuals provided written informed consent and received bilateral foot and ankle QCT scans. Foot bones were segmented from each other and surrounding soft tissue using semi-automated image analysis. Segmented bone masks and grayscale voxel datasets were imported into custom software [2] which uses locally affine warping to locate anatomical landmarks originally defined on a template bone. Bone surface landmarks were then used to define 3D coordinate axes for tarsal and metatarsal bones. Cardan sequences were used to measure bone-to-bone orientation angles in the sagittal (α), frontal (β), and transverse (γ) planes. The first Cardan rotation (α) from QCT mimics the sagittal X-ray angles (Figure 1):

Calcaneal pitch: sagittal plane angle between calcaneus and the horizontal surface.

Talar declination: sagittal plane angle between a line bisecting talus and the horizontal surface.

Meary's angle: relative angle between the line bisecting talus and the long axis of first metatarsal.

Additionally, *cuboid height* was measured as the vertical distance between the foot's plantar surface and the inferior-posterior aspect of cuboid.

A

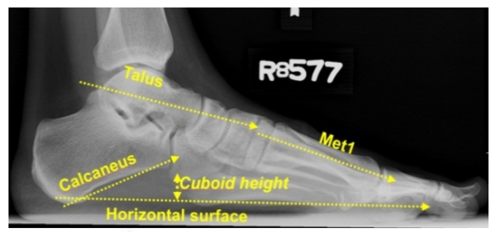

B

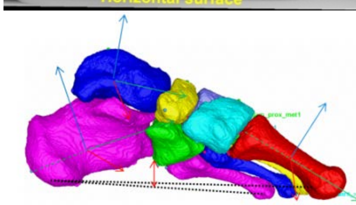

Figure 1: (A) lateral X-ray showing sagittal plane measures; **(B)** 3D Cardan rotation angles, with first rotation (α) mimicking sagittal X-ray measures.

For each bone-to-bone orientation angle, a two-way ANOVA was used to test the effects of Group and Foot. In UC and DM+PN groups, Foot was defined as left or right; in CN, Foot was defined as CN-Inv or CN-Uninv. Significance levels were set at $\alpha \leq 0.05$, with Bonferroni adjustments for post-hoc comparisons. Statistical analyses were completed in SPSS v20.0 (IBM, Chicago, IL).

RESULTS AND DISCUSSION

Exemplar sagittal plane bone meshes of UC and CN-Involved feet are shown in Figure 2. Across all orientation angles, UC and DM+PN groups showed no side-to-side differences, thus left and right side data for UC and DM+PN are combined in Figures 3 and 4. Cuboid height was 6mm lower in CN-Inv feet compared to UC feet, and there was a trend for lower cuboid height in CN-Inv compared to DM+PN and to CN-Uninv feet (both p=0.08).

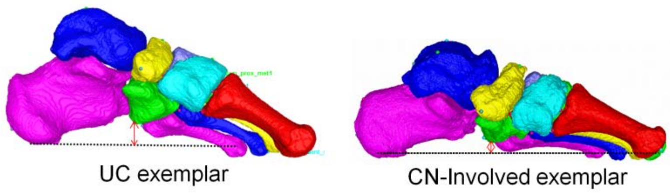

Figure 2: Segmented bone meshes, sagittal view.

Calcaneal pitch was 9° lower in CN-Inv compared to the UC group, 7° lower compared to DM+PN controls, and 4° lower than CN-Uninv feet (Figure 3B). Similarly, talar declination was greater in CN-Inv feet compared to CN-Uninv feet, with a mean side-to-side difference >3° (Figure 3C), while in the DM+PN and UC subjects mean side-to-side differences were 0.5° and 0.8°, respectively. CN-Inv feet had 5° greater talar declination than DM+PN and 4° greater talar declination than the UC group. Meary's angle showed a flattening of the sagittal plane angle of Met1 with respect to Talus in CN-Inv compared to UC and CN-Uninv, due in part to the increased talar declination in CN-Inv feet (Fig 3D).

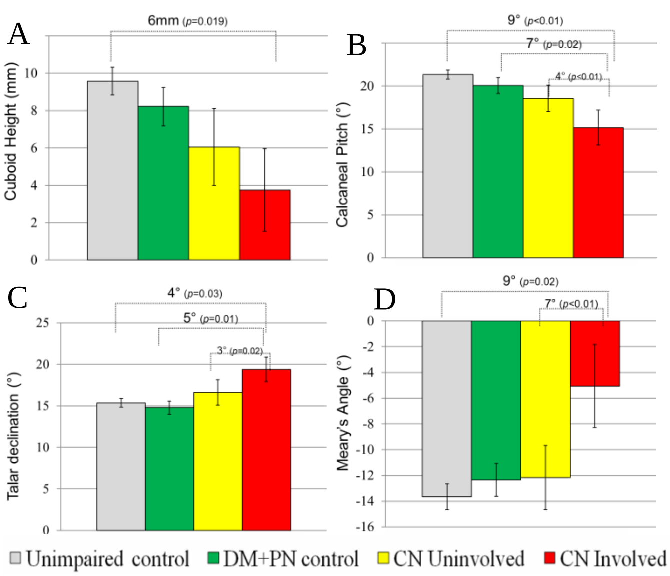

Figure 3: (A) Cuboid height; **(B)** Calcaneal pitch; **(C)** Talar declination; **(D)** Meary's angle.

In the frontal plane, the calcaneus was more everted in the CN-Inv feet compared to the CN-Uninv and DM+PN feet, with a trend toward significantly greater eversion in CN-Inv feet compared to UC.

This calcaneal eversion was also reflected in the frontal plane angle of Met1:Calc, which showed greater relative *inversion* of Met1 in CN-Inv feet compared to CN-Uninv (8°), DM+PN (11°), and UC (10°) (Figure 4A). Similarly, frontal plane angles of Met:Talus showed 8° more Met1 inversion in CN-Inv feet than in UC feet, 6° more than in DM+PN, and 7° more inverted than CN-Uninv feet (Figure 4B).

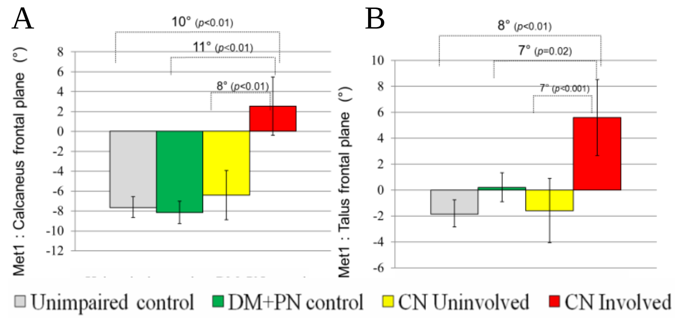

Figure 4: Relative inversion of **(A)** Met1 to calcaneus; **(B)** Met1 to talus.

CONCLUSIONS

Individuals with acute CN have greater 3D foot deformities compared to healthy unimpaired controls and individuals with DM+PN. Results confirm X-ray findings of reduced calcaneal pitch, increased talar declination and Meary's angle, and lower cuboid height [1] and show new deformities in the frontal plane that reflect hindfoot eversion and first metatarsal inversion. This QCT technique expands foot deformity quantification into the frontal and transverse planes, and may improve the ability of surgeons and podiatrists to diagnose and quantify foot mal-alignments in individuals at risk of progressive deformities. Future work will assess morphological changes over time in the neuropathic foot, and seek deformity-based indicators to identify those at risk for ulcers and other sequellae.

REFERENCES

1. Hastings MK, et al. *JBJS Am*, in press.
2. Liu L, et al. *J Digital Imaging*, epub Oct 23 2012.

ACKNOWLEDGEMENTS

Funding support was received from NIH grants: T32 AR056950 (Westendorf), R03 HD068660 (Sinacore), R21 DK079457 (Prior and Sinacore), and T32 HD007434 (Mueller).

ORAL PRESENATIONS – THURSDAY SEPTEMBER 5th

	Thematic: Aging & Falls *Paul DeVita*
11:15 AM	An Eight-Week Balance Exercise Intervention Program In Healthy Older Adults **Hoekstra J, Paquette M, Huang J, Bravo J, Li Y**
11:30 AM	Insights Into The Role Of Lower Extremity Net Joint Moment Contributions To Rapid Voluntary Stepping In The Elderly **Van Ham R, Mahboobin A**
11:45 AM	Knowledge Of The Nature Of The Perturbation Affects Young And Older Adults Differently During Trips In A Mixed Perturbation Paradigm **Coley B, Cham R, Perera S**
12:00 PM	Center Of Pressure Control For Balance Maintenance During Lateral Waist-Pull Perturbations In Older Adults **Fujimoto M, Bair WN, Prettyman M, Beamer B, Rogers M**

AN EIGHT-WEEK BALANCE EXERCISE INTERVENTION PROGRAM IN HEALTHY OLDER ADULTS

Joseph Hoekstra, Max R. Paquette, Jianping Huang, Joshua Bravo and Yuhua Li

University of Memphis, Memphis, TN, USA
email: maxime.paquette@memphis.edu

INTRODUCTION

Previous research has been conducted on strategies for balance improvements and fall prevention through various exercise programs in older adults. The Quick Board (QB; The Quick Board, LLC, Memphis, TN) has been used in athletic settings as a tool for improving lower limb motor functions, such as movement speed, reaction time and agility performance [1]. To date, no studies have investigated the effects of a QB training intervention on movement speed, reaction time and static balance in a healthy elderly population. The purpose of this study was to investigate the effects of an eight-week QFB training intervention on foot movement speed and reaction time, static balance and balance confidence in older healthy adults.

METHODS

Sixteen healthy older adults were randomly assigned to a stationary cycling group (n=8; 70.2 ± 6.0 years) and a QB group (n=8; 71.0 ± 8.6 years). Participants had no previous joint replacement surgeries, no current lower extremity joint injuries and no history of neurological disorders. Participants in each group completed an 8-week intervention with two training sessions per week. The cycling group performed four sets of 5 minute intervals at a self-selected "light" workload with two minute rest breaks on a stationary bike during each session. The QB group performed sets of the QB reaction drill, forward counting drill and backward counting drill with rest breaks during each session. Baseline, 4-week, 8-week and 4-week follow-up measures of static balance, reaction time and movement speed were obtained for all participants. Static balance was measured using average COP sway velocity during double feet quiet standing with eyes open and closed (NeuroCom International, Inc.). Reaction time was measured using the QB reaction drill time (RT) to 10 touches (i.e., respond to visual cues by stepping on correct target) while the movement speed was measured using the QB forward (FC) and backward counting (BC) drills to 10 touches (i.e., left and right rapid stepping on forward and backward targets). In addition, each participant completed the Activity-specific Balance Confidence scale (ABC) at baseline, 8-weeks and 4-week follow-up. A two-way (*Group X Time*) mixed design analysis of variance, with time as the within-subject factor and group as the between-subjects factor, was used to evaluate all variables (SPSS, Chicago, IL, USA). Paired sample t-tests were conducted when interaction effects were observed. Significance was set at an alpha level of 0.05.

RESULTS AND DISCUSSION

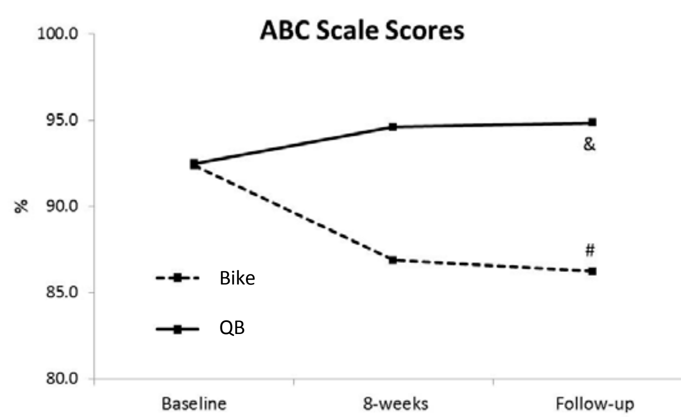

Figure 1: Average ABC scale score for both groups at baseline, 8-weeks and follow-up. #: different from baseline in bike group, &: different from bike group at follow-up.

The ABC scale scores showed a Group x Time interaction effect ($p = 0.04$; Fig. 1). The bike group had lower balance confidence ratings at the follow-up compared to baseline and, the QB group had higher balance confidence ratings compared to the bike group at follow-up (Fig. 1).

Measures of static balance using average COP sway velocity during a 20s double foot quiet standing with eyes-open and closed did not show any significant group or time effects ($p > 0.10$). Fig. 2 shows a *trend* in decreasing COP sway velocity over time in both groups for the eyes-closed quiet standing and, decreasing sway velocity for the QB group only for the eyes-open quiet standing.

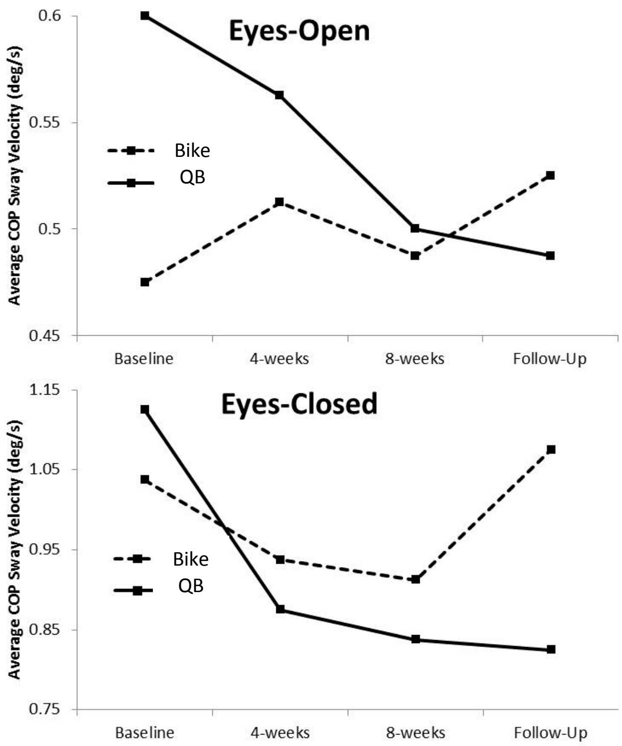

Figure 2: Average COP sway velocity during 20s double foot quiet standing with eyes open (top) and closed (bottom) for both groups at each testing time.

The QB reaction time and forward and backward counting times all showed a significant time effect ($p < 0.05$) where baseline values were significantly different to values at 4-weeks, 8-weeks and follow-up (Table 1). In addition, backward counting showed a significant interaction effect ($p = 0.005$). The post-hoc paired t-test showed that backward counting time was reduced at 4-weeks, 8-weeks and follow-up for the QB group only (Table 1). The finding of increased movement speed for the backward counting task in the QB group compared to the bike group was expected due to weekly practice for the QB group. Thus, it is difficult to associate the QB training with improved movement speed during other tasks as the current study only tested QB movement speed. Pre and post training tests of other reaction time and movement speed tasks would provide insightful information to decipher whether QB drill improvements resulted from a learning effect or a central nervous system training effect. Finally, the small sample size in the current study limits the statistical power.

CONCLUSIONS

Our initial findings show that QB training improves perceived balance confidence compared to a cycling group at 4-weeks following training completion. The QB group tends to improve their QB movement speed performance compared to the cycling group but these findings do not necessarily suggest reaction time and movement speed improvements during other reaction time tasks. Finally, training on the QB or bike does not appear to improve static double foot balance. Future studies should investigate the effects of QB training on ecologically relevant gait tasks such as reacting to an obstacle in the travel path to avoid collisions.

REFERENCES

1. Galpin A, et al. *J Strength Cond Res* 22(6): 1901–1907, 2008.

ACKNOWLEDGEMENTS

The Quick Boards and funding provided in part by The Quick Board, LLC.

Table 1: The Quick Board (QB) reaction time (RT), forward (FC) and backward counting (BC) time for groups and testing times (mean ± SD).

	Baseline		4-weeks		8-week		Follow-up	
Condition	Bike	QB	Bike	QB	Bike	QB	Bike	QB
RT (s) [a, #]	10.2±1.5	10.4±1.8	9.6±1.4	9.0±0.9	9.5±1.1	8.5±1.1	9.7±1.7	8.7±0.9
FC (s) [a, #]	12.6±3.5	12.6±2.2	10.9±2.2	9.7±2.2	10.6±2.8	9.0±1.8	11.1±3.3	9.1±1.5
BC (s) [a, #, c]	12.2±3.2	12.8±2.9	11.0±1.9	9.4±1.5*	10.6±2.9	9.1±1.7*	10.9±3.0	9.2±1.5*

[a]: Time effect; [b]: Group effect; [#]: all testing times are different from baseline; [c]: Interaction effect; [*]: different from baseline in QB group only. ($p < 0.05$)

INSIGHTS INTO THE ROLE OF LOWER EXTREMITY NET JOINT MOMENT CONTRIBUTIONS TO RAPID VOLUNTARY STEPPING IN THE ELDERLY

[1]Raymond Van Ham and [1]Arash Mahboobin

[1]University of Pittsburgh, Pittsburgh, PA, U.S.A.
Email: arm19@pitt.edu

INTRODUCTION

Falls are a serious health hazard to older adults and the costs associated with fall injuries are substantial. For example, among persons aged 65 or older in the United States, approximately 16% reported falling at least once in the past three months; of those, over 30% suffered an injury, resulting in almost $25 billion in annual fall-related costs [1, 2]. Preventing falls would significantly reduce medical costs and enhance quality of life in the aging population.

Experimental studies have provided important descriptions of postural responses under various environmental conditions. However, it is not always straightforward to identify *cause-effect* relationships through experiments alone. Computational modeling and simulation techniques are tremendously useful tools that can complement experimental approaches by identifying causes of failed recovery attempts.

The objective of this study is to determine, through computational modeling and simulation, the impact of aging on lower extremity net joint moment contributions during anticipatory postural adjustments [3] – postural changes associated with voluntary movements that are critical for maintaining balance during locomotor initiation. The knowledge gained can have important implications for understanding neuromuscular impairments leading to appropriate and useful design of rehabilitation strategies.

METHODS

Motion capture data, bilateral ground reaction forces, and EMG data were collected from a healthy young subject (age 23, mass = 79.8 kg, height = 176 cm) and an older subject (age 73, mass = 92.5 kg, height = 174 cm) at the University of Pittsburgh to examine age-related differences during rapid voluntary stepping.

Subjects were asked to complete a simple step reaction time task [4], where they stepped forward with their left foot in response to an auditory cue. There were two stepping locations, short or long, and two response speeds, quick or self-selected.

OpenSim [5] was utilized to develop a 3-D generic musculoskeletal model consisting of 18 degrees of freedom and 60 Hill-type muscles (30 per leg). The generic model was scaled to create *subject-specific* models matching each individual's anthropometry. A weighted least squares problem (inverse kinematics) was solved to obtain a kinematically consistent set of joint angles using the measured motions. The joint angles and the measured ground reaction forces were then used to obtain a dynamically consistent set of joint angles and net joint moments using the residual reduction algorithm [5].

RESULTS AND DISCUSSION

To ensure that the subject-specific models represented the experimental marker set accurately, an iterative marker adjustment algorithm was used that resulted in average root mean square (RMS) marker errors of less than 0.2 cm, indicating a good match between the experimental and model marker locations. Additionally, the RMS errors between the experimental and model markers during inverse kinematics were less than 1.0 cm in all stepping conditions.

Overall, the RMS residual forces and moments obtained during RRA were less than 7 N and 35 Nm, for the young subject, and 13 N and 50 Nm, for the older subject. The RMS errors between the IK-generated and RRA-generated joint angles for the young and older subjects were less than 0.8° and 1.2°, respectively.

Figure 1. Right hip flexion/extension moment. Each graph plots the moment from the stepping (left) leg toe-off (0%) until approximately the stance (right) leg toe-off (100%). Vertical bars indicate heel contact of the stepping leg for the young (black) and older (red) subject. Flexion is positive.

Both subjects exhibited similar kinematic responses; however the young subject showed greater range of hip and knee flexion in all stepping conditions. Ankle flexion/extension moments for the stance (right) and stepping (left) legs, as well as the knee and hip flexion/extension moments for the stepping leg were similar between the two subjects in all stepping conditions. However, notable differences were observed in the stance/support leg hip and knee flexion/extension moments (Fig. 1 and Fig. 2). Compared to the older subject, the young subject exhibited more hip and knee flexion moment in all the stepping trials, particularly prior to the stepping leg's heel contact (i.e., during swing phase). Both subjects exhibited similar moment profiles slightly before and after heel contact of the stepping leg (Fig. 1 and Fig. 2).

The kinematics and dynamics differences observed in this preliminary analysis could be attributed to age-related differences, particularly in the muscles spanning the older subject's hip and knee joints, causing less flexion moment generation capabilities during anticipatory postural adjustments. Future work will focus on estimating individual lower extremity muscle contributions to hip/knee net joint moment generation during voluntary step initiation to determine whether muscle weakness is the contributing factor to these observed age-related differences.

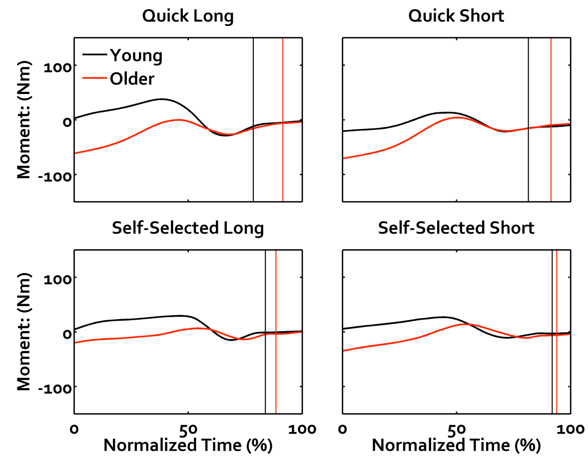

Figure 2. Right knee flexion/extension moment. Each graph plots the moment from the stepping (left) leg toe-off (0%) until approximately the stance (right) leg toe-off (100%). Vertical bars indicate heel contact of the stepping leg for the young (black) and older (red) subject. Flexion is positive.

REFERENCES

1. David JC, et al. *Osteoporosis Int* **21**, 1295-1306, 2010.
2. Stevens JA, et al. *J Saf Res* **39**, 345-349, 2008.
3. Cohen RG, et al. *J Gerontol A Biol Sci Med* **66**, 705-713, 2011.
4. Sparto PJ, et al. *Exp Brain Res* **188**, 633-640, 2008.
5. Delp SL, et al. *IEEE T Bio-Med Eng* **54**, 1940-1950, 2007.

ACKNOWLEDGEMENTS

Funding provided by the Pittsburgh Claude D. Pepper Older Americans Independence Center (P30AG024827).

KNOWLEDGE OF THE NATURE OF THE PERTURBATION AFFECTS YOUNG AND OLDER ADULTS DIFFERENTLY DURING TRIPS IN A MIXED PERTURBATION PARADIGM

Brooke Coley[1], Rakié Cham[1] and Subashan Perera[2]

Human Movement and Balance Laboratory, Department of Bioengineering
Department of Gerontology, University of Pittsburgh, Pittsburgh, PA, USA
Email: bcoley@nsf.gov, web: www.hmbl.bioe.pitt.edu

INTRODUCTION

Trunk kinematics plays a critical role in the recovery outcome of trip perturbations. When equilibrium is unexpectedly challenged, "online" sensory and cortical inputs providing stored information based on previous experiences partially determine reactive motor balance recovery responses [1]. Based on the nature of perturbations, the first encounter with the perturbation is typically the most severe as it generates the most uncertain or naïve response. Experience with and knowledge of a perturbation have been shown to impact perturbation recovery [2-5].

This preliminary study is part of a larger project where both slips and trips are presented in the paradigm. To our knowledge, no study has simultaneously investigated two perturbations occurring during forward locomotion on the same group of subjects inclusive of young and older adults. Focusing on trips, the purpose of this study is to determine whether differences in knowledge and prior exposure conditions impact measures of severity during trips in young and older adults. Frontal plane trunk kinematics will be analyzed to gauge changes in trip severity.

METHODS AND PROCEDURES

Sixteen younger (YA) (ages 21-35) and thirteen older (OA) (ages 65-75) adults, screened for neurological and musculoskeletal abnormalities, were recruited for participations (Table 1). Exclusion criteria included a clinically significant neurological, musculoskeletal, cardiovascular and/or orthopedic disease and the presence of any difficulty that would impede normal walking or an ability to walk and stand independently. Additionally, older adults were screened for osteoporosis (T-score ≤ -2.5) to minimize the risk of bone fracture.

Table 1. Subject characteristics.

Variable	Young (*n*=16; 9M,7F)	Old (*n*=13; 8M,5F)
Age (yrs)	27 ± 5	70 ± 3
Height (cm)	175 ± 8	173 ± 9
Weight (kg)	72 ± 13	77 ± 11
Gait speed (m/s)	1.2 ± 0.2	1.1 ± 0.2
Cadence (steps/minute)	104 ± 11	106 ± 13

Whole-body motion and kinetic data were captured at 120 and 1080 Hz, respectively [6]. Subjects were equipped with a safety harness during all trials to prevent them from hitting the ground in the event of an irrecoverable loss of balance. Subjects were allowed to practice walking prior to data collection and instructed to walk at a comfortable pace while looking straight ahead.

The experimental design consisted of four blocks of trials (Table 2). Block 1 was always presented first with the following two blocks of trials, Blocks 2 and 3, presented randomly. At the beginning of the block before any trials had taken place subjects were told the following script, "In the next set of trials, at some point you will experience a (slip/trip)."

Table 2. Description of the four trial blocks.

Block	Prior Knowledge	Perturbation Type
(1) 5 unperturbed trials - Baseline	Yes, subject will be reassured that no perturbation will occur in the next set of trials	None
(2) 3 slips randomly inserted into a series of 5 unperturbed trials	Yes, subject informed of the type of perturbation at the beginning of the block but not exact timing	Slip, None
(3) 3 trips randomly inserted into a series of 5 unperturbed trials	Yes, subject informed of the type of perturbation at the beginning of the block but not exact timing	Trip, None
(4) 3 trips and 3 slips randomly inserted into a series of 10 unperturbed trials	No, subject will not be informed of the specific type of perturbation (slips/trips are mixed)	Slip, Trip, None

In the perturbation blocks, an unperturbed walking trial was always the first trial in the block and at least one unperturbed walking trial separated perturbations. In Block 4, subjects had no prior knowledge of the nature of the perturbation and/or timing.

Trips were induced with an in-house designed apparatus 90 ms after heel contact. Only blocks 3 and 4 are included in this analysis. For each subject, only the first and last trip perturbations in each block were analyzed. Trip severity was measured by the maximum instantaneous angular deviation in the frontal plane ipsilateral to the perturbed foot. The time window taken was from obstacle impact to landing of the recovery foot. Trunk angle was defined as the angle between the trunk segment (midpoint of the shoulders and the posterior-superior iliac spine) and vertical.

A mixed linear model was fit with angular trunk deviation as the dependent variable and independent variables age group (YA/OA), condition (first trip, last trip, first combo trip, last combo trip), first order effects of these variables as fixed effects and subject as a random effect. Appropriate contrasts were constructed and performed. Statistical significance was set at $\alpha = .05$.

RESULTS

Both young and older adults experienced their greatest deviation in the first trip condition (Figure 1). There was no age group difference

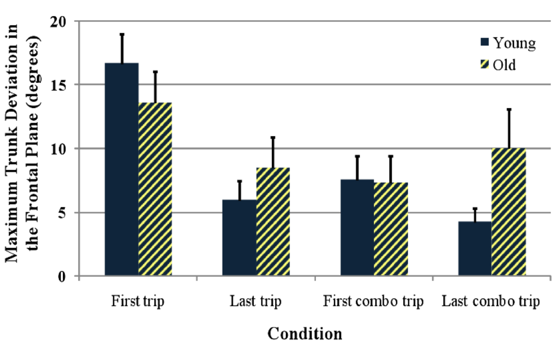

Figure 1. Maximum trunk deviation in the frontal plane. Error bars indicate standard deviation.

in how prior exposure or no knowledge of the nature of the perturbation impacted maximum ipsilateral trunk deviation. However, with increased exposure in the no knowledge condition, there was a significant difference between young and older adults ($p = .007$). Young adults ($p < .0001$) significantly improved trunk deviation compared to older adults that performed similarly to the first trip of the trip block ($p = .149$).

SUMMARY

This study showed the mechanisms by which knowledge and increased exposure affect young and older adults to differ during tripping. The findings of this study showed frontal plane deviation to be comparable amongst adults. However, with greatest experience to trips and lacking knowledge of the nature of the perturbation in the presence of slip perturbations , older adults exhibited trip severity similar to initial trips.

This study underlies the need to further understand older adults' recovery capabilities when knowledge is not provided and more than one specific gait task is explored. With further research, it may be possible to better characterize kinematic and kinetic variables that could identify the existence of overlap in responses to slips and trips. Identification of such overlap could serve as the foundational component of an intervention to train improvement in slip and trip recovery.

REFERENCES

1. Horak FB (1997), *Phys Ther,* 77:517-33.
2. Heiden TL (2006), *Gait & Posture*, 24:237-46.
3. Pijnappels M (2001), *Gait & Posture,* 14:11-8.
4. Pavol M (2001), *J Gerontol Med Sci*, 56:339-53.
5. van Dieen JH (2005), *Safety Science*, 43:1478-91.
6. Moyer B (2006), *Ergonomics*, 49:329-43.
7. Chou LS (2003), *Gait & Posture*, 18: 125-33.
8. Rosenblatt NJ (2010), *Gait & Posture*, 31:380-4.
9. Grabiner MD (2012), *Med Sci Sports Exer*, 44:2410-4

ACKNOWLEDGEMENTS

This study was supported in part by F31 AG025684-03 NIH Ruth L. Kirschstein Award.

CENTER OF PRESSURE CONTROL FOR BALANCE MAINTENANCE DURING LATERAL WAIST-PULL PERTURBATIONS IN OLDER ADULTS

Masahiro Fujimoto, Woei-Nan Bair, Michelle G. Prettyman, Brock A. Beamer and Mark W. Rogers

University of Maryland School of Medicine, Baltimore, MD, USA
email: mfujimoto@som.umaryland.edu, web: http://pt.umaryland.edu/default.asp

INTRODUCTION

An impaired ability to control lateral balance contributes to falls in older adults [1]. When balance is disturbed, the whole-body center of mass (COM) motion needs to be regulated by an active control of the center of pressure (COP) to achieve postural stability. Since the base of support (BOS) provides a possible area for COP movement, the boundaries of the BOS have been considered as stability limits within which balance is maintained by rapidly moving the COP to keep the COM from going beyond the BOS. However, the area in which the COP can functionally move has been reported to decrease with aging [2], thereby constricting the limits of stability. Further, decreases in COP speed during voluntary sway movements have been seen in high fall-risk older adults [3]. Such reduced COP control would affect their ability to recover balance. This study investigated COP control during lateral perturbations in healthy elderly adult non-fallers and fallers. We hypothesized that elderly fallers would demonstrate a slower COP movement with a reduced functional area.

METHODS

Fifty-four community-dwelling older adults (38 Non-Fallers and 16 Fallers) received 60 randomly applied motor-driven lateral waist-pull perturbations with the speed ranging from 7.5 to 37.5 cm/s. Subjects stood in a comfortable position, placing each foot on a separate force platform (AMTI, Newton, MA) that recorded ground reaction forces at 600Hz. Kinematic data were obtained with a 6-camera motion capture system (Vicon 460, Oxford, UK) at 120Hz. Since crossover stepping with passively unloaded leg is a common strategy used by older adults to recover lateral balance [4], responses to the left lateral pull at 30cm/s, where the largest number of subjects (28 Non-Fallers and 7 Fallers) responded with crossover steps using the right leg, were used for all analyses.

The whole-body COM and combined COP positions in the medio-lateral (ML) directions were referenced to the left medial ankle and normalized to the left foot BOS width, while COP velocity prior to step-onset (SO) of the right leg was normalized to the stance width. Left peak hip abductor and ankle invertor moments prior to SO also were calculated. Furthermore, a single-link-plus-foot inverted pendulum model was used to define lateral stability limit at the instant of SO, which was derived using the following equation [5]:

$$\dot{\tilde{X}}_{SO} \leq 1 - \tilde{X}_{SO}$$

where $\tilde{X}_{SO}$ and $\dot{\tilde{X}}_{SO}$ are normalized COM position and velocity at SO in the ML direction, defined as $\tilde{X}_{SO} = (X_{SO} - X_{ma}) / L_f$, $\dot{\tilde{X}}_{SO} = \dot{X}_{SO} / (L_f \omega_0)$ ($\omega_0 = \sqrt{g/l}$, : L_f: BOS width, X_{ma}: medial ankle, l: pendulum length). The lateral stability limit also was adjusted based on COP position at SO, considering it as a functional limit for COP movement. Stability margin was calculated as the shortest distance from the experimental data to the lateral stability limit defined based on both the BOS and functional limit.

An independent t-test was performed to examine group differences. Linear regression analyses were performed to examine the relationship between hip and ankle joint moments and COP measures. Significance level was set at α=.05.

RESULTS AND DISCUSSION

Fallers took more recovery steps than Non-Fallers (mean 2.4±0.4 vs 1.8±0.5). No significant difference was found in normalized peak COP velocity between Fallers and Non-Fallers (Fig.1).

However, normalized COP position at SO for Fallers was located significantly medial to that for Non-Fallers (Fig.1). This suggests that the area functionally used for COP movement to control the COM was significantly reduced in Fallers. In addition, although no significant group differences were detected, peak ankle invertor moment and peak hip abductor moment were significantly correlated with normalized COP position at SO (p=.006) and peak COP velocity (p=.032), respectively, implying different roles of hip and ankle muscles for COP control.

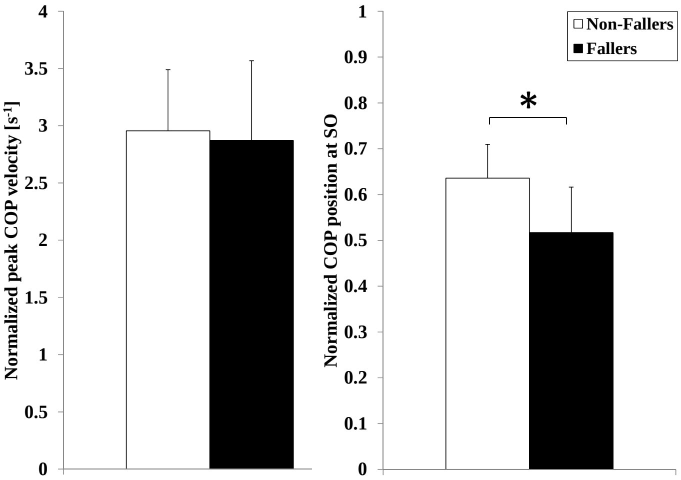

Figure 1: Normalized peak COP velocity and normalized COP position at SO (*p=.001)

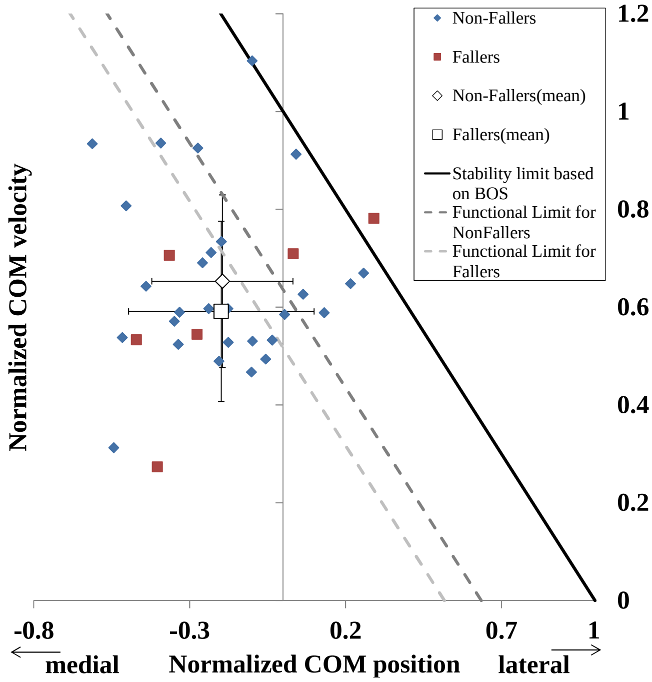

Figure 2: Normalized COM velocity at SO vs. normalized COM position at SO in ML direction.

Although not statistically significant, Fallers demonstrated a smaller normalized COM velocity with a similar COM position at SO compared to Non-Fallers (Fig.2), resulting in a larger stability margin for the stability limit based on the BOS (Fig.3), which is consistent with the previous findings [6]. However, for these crossover steps, the stability margin became smaller than Non-Fallers when the stability limit was adjusted based on the COP position at SO (functional limit) (Fig.3).

These findings suggest that Fallers have reduced functional limits of stability for COM control in the ML direction, possibly due to decreased ankle invertor activity. This could be a cause for lateral instability requiring them to take more steps than Non-Fallers for balance recovery during crossover steps.

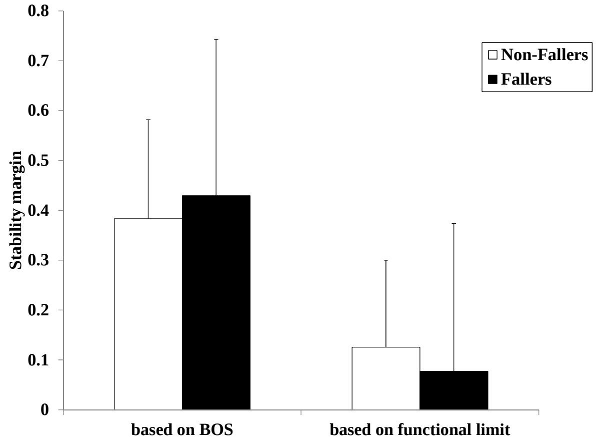

Figure 3: Stability margins based on BOS and functional limit.

REFERENCES

1. Rogers MW and Mille ML. *Exerc. Sport Sci. Rev.* **31**, 182-187, 2003.
2. King JA, et al. *J Gerontol.* **49**(6), M258-263, 1994.
3. Tucker MG, et al. *Clin. Biomech.* **24**, 597-605, 2009.
4. Mille ML, et al. *Clin. Biomech.* **20**, 607-616, 2005.
5. Hof AL, et al. *J Biomech* **38**(1), 1-8, 2005.
6. Patton JL, et al. *Conf. Proc. IEEE Eng. Med. Biol. Soc.* **1**, 3305-3308, 2006.

ACKNOWLEDGEMENTS

This study was supported by NIH grant RO1AG029510 and NIDRR UMANRRT grant H133P100014.

ORAL PRESENATIONS – THURSDAY SEPTEMBER 5th

	Ergonomics: Basic Research *Richard Hughes, Timothy Burkhart*
4:15 PM	Adaptations In Lower Extremity Kinematics Due To Vest-Borne Military Relevant Loads **Fellin R, Frykman P, Sauer S, Seay J**
4:30 PM	Perception Vs. Action: Perceived Obstacle Crossing Ability Of Firefighters In Protective Gear **Petrucci M, Horn G, Rosengren K, Hsiao-Wecksler E**
4:45 PM	Prolonged Sitting Alters Abdominal Muscle Activation And Thoracic Spine Lateral Bending In Transient Pain And Non-pain Developers **Nairn B, Azar N, Drake J**
5:00 PM	Effects Of Localized And Widespread Fatigue On A Repetitive Sawing Task **Cowley J, Dingwell J, Gates D**

ADAPTATIONS IN LOWER EXTREMITY KINEMATICS DUE TO VEST-BORNE MILITARY RELEVANT LOADS

[1]Rebecca E. Fellin, [1]Peter N. Frykman, [1]Shane G. Sauer and [1]Joseph F. Seay

[1]U. S. Army Research Institute of Environmental Medicine, Natick, MA, USA
email: rebecca.e.fellin.ctr@us.army.mil, web: http://www.usariem.army.mil/

INTRODUCTION

Deployed soldiers frequently carry loads up to 121 lb (~55 kg). These large loads likely contribute to the high rate of musculoskeletal overuse injuries in the military. Studies examining pack-borne loads found increased double support and stride width and decreased stride length as load increased [1,2]. Additionally, peak angles of the lower extremity increased with load [2,3]. Hip and ankle range of motion (ROM) across the gait cycle did not change with load although knee ROM decreased with loads 24-kg and up [1]. However, these studies examined peaks loads of 30% BW, 32 kg or 47 kg, which are well below the 55 kg amount deployed soldiers carry. Furthermore, the center of mass (COM) varied across loads due to pack-borne load configurations. Altering the load COM may alter kinematics of the trunk and cause compensations in the pelvis and lower extremities outside of changes due to load magnitude. Therefore, symmetrical torso loads are necessary to elucidate the load magnitude effects separate from alterations to the torso COM caused by pack-borne loads.

The purpose of this study was to examine kinematic changes with symmetrical torso loads. We hypothesized that compared to the bodyweight (BW) condition step rate, stride width, and double support percentage would increase while stride length would decrease. For ROM, we hypothesized that hip, knee and ankle ROM during stance would increase with load compared to BW.

METHODS

Twenty-nine male soldiers (20.6 ± 3.1 yrs; ht: 1.77 ± 0.08 m; wt: 84.9 ± 12.3 kg; mean ± SD) volunteered to participate in this study, which included orientation and data collection sessions. During an orientation session, subjects walked on an instrumented treadmill at the speed and maximum weight they would experience in the data collection. During the data collection session, subjects were instrumented with retro-reflective markers to track pelvis and bilateral lower extremity motion. Subjects then walked in their combat boots at 3 MPH on the treadmill for 5 minutes following which 30 seconds of data were recorded during 4 load conditions: bodyweight only (BW), 15-kg, 35-kg and 55-kg. The BW condition was presented first and the order of the 3 subsequent loads was randomized. The 15-kg load consisted of an armored vest, and subsequent external loads were applied symmetrically via weighted vests. Subjects rested for a minimum of 3 minutes between loads.

Kinematic data were filtered at 6 Hz in Visual3D. 5 strides from the right side were selected for analysis. Spatiotemporal parameters including steps/min, stride length and double support percentage as well as 3D joint angles at the hip, knee and ankle were computed. Sagittal plane ROM was calculated for each joint, and it was defined as the maximum minus minimum value during stance for the hip. Knee ROM was calculated from footstrike to peak knee flexion during midstance. Ankle ROM was calculated from midstance peak plantarflexion to late stance peak dorsiflexion. Variables were averaged across the 5 strides for each condition. Repeated measures ANOVAs were used to compare differences between the load conditions (BW, 15-kg, 35-kg and 55-kg). Post-hoc t-tests were conducted to identify differences between BW and the 3 loads.

RESULTS AND DISCUSSION

Load magnitude influenced all variables except stride width. Spatiotemporal variables, except stride width, were different between BW and 35-kg as well as 55-kg (Table 1). ROM at the hip and ankle was significantly greater in all load conditions compared to BW (Figure 1).

Our results supported most of our spatiotemporal hypotheses. Stride width did not increase, potentially as symmetrical torso loading did not require increased stride width as prior research indicates it did with pack-borne loads [2]. Increased percent double support, from this study and asymmetrical torso loads in the literature, indicated that regardless of COM orientation, soldiers increased double support with added load. It may be a protective mechanism in an attempt to better control loading during weight acceptance. Although only double support percentage changed with the 15-kg load, equivalent to body armor, there were multiple kinematic changes with this load.

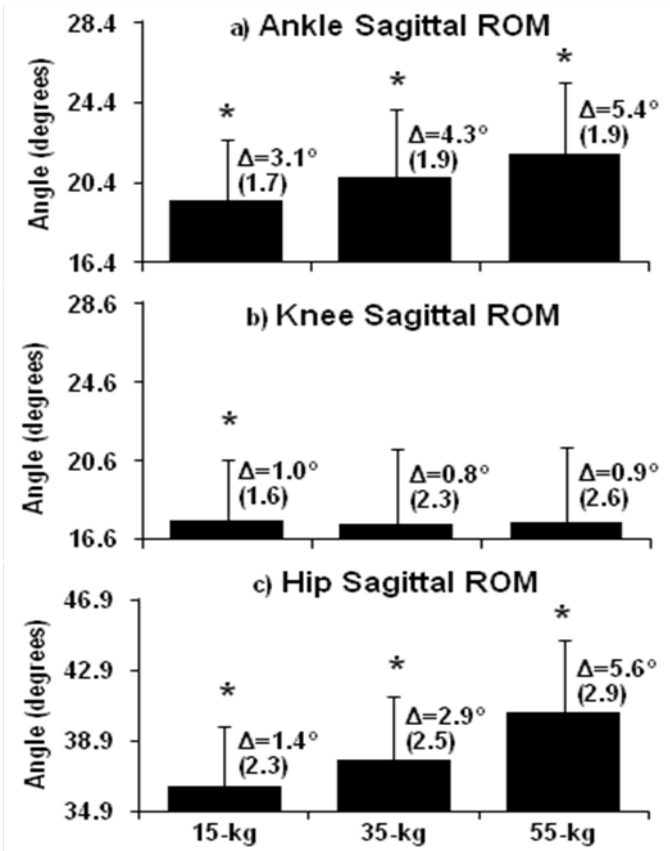

Figure 1: a) ankle b) knee and c) hip ROM. Change values are within subject (mean(SD)) referenced to BW values. Y axis begins at BW value. Error bars=SD. *=Significant change vs BW.

ROM changes were driven by different combinations of changes in peak angles at each joint. Ankle ROM increased due to both peak plantarflexion and peak dorsiflexion increasing in magnitude. Knee ROM did not change as subjects were more flexed both at footstrike and peak knee flexion at midstance. Increased knee flexion at footstrike likely was driven by the slightly shorter stride length. Therefore, the knee musculature must be absorbing the added load as the knee ROM did not change. Hip ROM changes were primarily driven by increased hip extension in terminal stance as hip flexion did not increase until a modest, 1.8 degree, increase with the 55-kg load. No change in hip flexion until 55-kg supported that symmetrical torso loads differ from pack-borne loads as vest-borne loads did not cause increased hip flexion through increased anterior pelvic tilt [1,2].

CONCLUSIONS

Vest-borne loads caused different kinematic responses compared to pack-borne loads. Specifically, symmetrical torso loads do not alter stride width, cause large changes in hip flexion or prevent hip ROM changes. ROM changes during stance indicated that joints in the lower extremity respond differently to added loads. ROM did not change from footstrike to midstance yet increased from midstance to late stance. Late stance hip and ankle changes suggest risk factors for overuse injury may occur during propulsion as well as weight acceptance.

REFERENCES

1. Birrell and Haslam. *Ergonomics* **52**, 1298-1304, 2009.
2. Harman et al. *Army Technical Report*, 2000. http://www.dtic.mil/dtic/tr/fulltext/u2/a377886.pdf
3. Quesada et al. *Ergonomics* **43**, 293-309, 2000.

DISCLAIMER

The views expressed in this abstract are those of the authors and do not reflect the official policy of the Department of Army, Department of Defense, or the U.S. Government. The investigators have adhered to the policies for protection of human subjects as prescribed in Army Regulation 70-25, and the research was conducted in adherence with the provisions of 32 CFR Part 219.

Table 1: Spatiotemporal variables (mean ± SD) across loads. *=Significant change vs BW. DL=double limb.

Variable	BW	15-kg	35-kg	55-kg
Step rate (steps/min)	112.2 ± 5.6	112.5 ± 5.2	114.2 ± 6.2*	115.6 ± 6.5*
Stride length (m)	1.441 ± 0.068	1.433 ± 0.057	1.415 ± 0.071*	1.399 ± 0.072*
Stride width (m)	0.142 ± 0.029	0.137 ± 0.028	0.140 ± 0.035	0.141 ± 0.034
DL Support (%stance)	25.7 ± 1.9	28.0 ± 1.8*	30.1 ± 1.8*	32.7 ± 1.7*

PERCEPTION VS. ACTION: PERCEIVED OBSTACLE CROSSING ABILITY OF FIREFIGHTERS IN PROTECTIVE GEAR

[1]Matthew N. Petrucci, [1]Gavin P. Horn, [2]Karl S. Rosengren, [1]Elizabeth T. Hsiao-Wecksler
[1]University of Illinois, Urbana, IL, USA
[2]Northwestern University, Evanston, IL USA
email: mpetrucc@illinois.edu, web: http://www.mechse.uiuc.edu/research/hsiao-wecksler

INTRODUCTION

An individual's perception of how his or her body fits within the surroundings is a key component for successfully navigating through a cluttered environment that requires moving over, under, or through various obstacles. Possibilities for action, termed "affordances", are based on individual physical attributes and the constraints of a particular obstacle. Affordance judgments are more accurate when we have previous experience with a task [1] or when our physical features (e.g., height) relevant to the passage are easily compared to the size of aperture. Perception remains accurate even when physical features are artificially enlarged [2] or when the body changes over time due to growth or pregnancy [3].

In firefighting, bulky and heavy equipment is necessary for the health and safety of the firefighter. This equipment can affect balance and gait performance and artificially change the size and location of center of mass of the body [4]. It is unclear how wearing firefighting personal protective equipment (PPE) affects firefighter's affordance judgments for navigation. In this study, we examined how well firefighters make perceptual judgments about the ability to navigate over, under or through obstacles while wearing their protective gear.

METHODS

Twenty four subjects (23 male, 1 female, age = 28.6 ± 7.9 yrs, height = 182.1 ± 7.2 cm, weight = 90.7 ± 13.9 kg) were recruited by the University of Illinois Fire Service Institute. IRB approval and informed consent were obtained. All subjects were either career or volunteer firefighters. Testing was done while wearing National Fire Protection Association (NFPA) 1971 compliant PPE including boots, protective clothing, helmet, gloves, and a self-contained breathing apparatus (SCBA) tank.

Three obstacles were tested to simulate difficult situations that would challenge a firefighter's balance or physical ability to pass. Obstacles were always presented in the following order: over, under, through. Participants completed a series of *perception-action* trials to assess affordance judgment error for each obstacle. The participants first completed the perception trials to prevent action trials from informing perception [1].

The 'through' obstacle was a doorway with an adjustable width (height 228 cm), attached perpendicular to a false wall (height 244 cm, width 122 cm). The 'over' and 'under' obstacles consisted of vertical uprights set 122 cm apart to simulate the average width of a hallway. Each upright had a sliding carriage that held cross bars in place. The 'over' obstacle (max height 100 cm) had two PVC cross bars set 10 cm apart, while the 'under' (max height 185 cm) only had a single crossbar. Obstacles could be adjusted to a resolution of 1 cm. Subjects began every trial standing 2.5 m away from the front of each obstacle.

For perception trials, subjects were asked if they thought they could transverse the given obstacle without committing an error. Action trials involved the subjects attempting to actually pass the obstacle without committing an error. Errors were defined as: touching or knocking off the cross bar(s) (over, under), touching hands or knees to the ground (under), or removing the SCBA tank or other shifting of gear (through). Subjects were told to perform the trials at "fireground pace", i.e. acting as quickly as safely possible without running, and to complete trials even if an error was committed. These obstacles and definitions were designed to push the limits of subjects' balance and assess their ability to account for the size of the SCBA tank.

To determine the perceived and actual ability to pass the obstacles, affordance functions were fit to the data based on a normal distribution [1]. The first

4-8 trials began with a binary search method to gain an estimate of the affordance threshold (i.e. the point where they could no longer pass the obstacle). The remaining 6 trials were performed at two points equidistant (0.5 cm) from the estimated affordance threshold. The 50% values of the cumulative distribution functions fit to these data were considered to be the affordance threshold for either perception or action trials.

Statistical differences between perception and action affordance thresholds were assessed using pairwise t-tests (SPSS 20.0; IBM Corp, Armonk, NY). Each threshold value was normalized to relevant body features for each obstacle. These included leg length (over), body height (under), and chest depth (through). Additionally, perceptual judgment error was determined to be the difference between the perceived and action affordance thresholds. Perceptual overestimation of abilities (i.e. saying "yes" to a value that was impassible) was considered to be positive value. Underestimation (i.e. saying "no" to a value that was passable) was considered to be negative.

RESULTS AND DISCUSSION

Significant differences were found between perception and action affordance thresholds for the 'under' ($p < 0.001$) and 'through' ($p = 0.001$) obstacles (**Figure 1**). However, judgment error existed for each obstacle across subjects (**Table 1**). For example, judgment error for the 'under' obstacle was 15 ± 9.5 cm because all but one subject overestimated ability to pass under the obstacle. Typically, subjects failed by having the top of the SCBA tank or the back of the helmet knock off the crossbar. Interestingly, 15 cm equates to the approximate depth of the SCBA tank, suggesting subjects did not accurately consider the depth of the tank while generating their perceptions. In contrast, there was a general underestimation of abilities in the through obstacle (-4.2 ± 5.3 cm) with only 4 subjects overestimating their abilities. This could be due to a lack of understanding of how movable the SCBA pack was on their back while forcing themselves through the doorway.

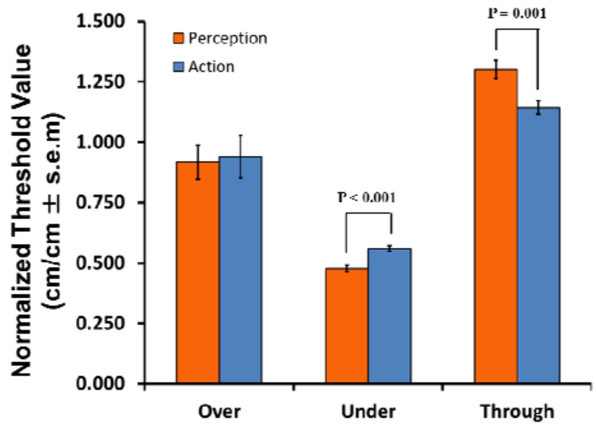

Figure 1: Average (and standard error bars) for normalized perception and action affordance threshold values by obstacle.

A small underestimation of abilities was observed in the 'over' obstacle (-0.5 ± 9.5 cm; **Table 1**). However, the large amount of variability indicates almost the same amount of underestimation and overestimation was present. This was revealed when the absolute value of error was taken, which indicated that nearly 8 cm of judgment error was present.

CONCLUSIONS

These data suggest that firefighters do not have an accurate perception of their abilities while traversing obstacles in their firefighting PPE. Future studies should focus on specific tasks commonly encountered on the fireground.

REFERENCES

1. Franchak, J. *Vision Research* 50(24): 2758-65, 2010
2. Ishak, S. *JEPHPP* 34(6): 1501-14, 2008
3. Franchak, 15th J. *Conf. on Percept & Action*, 2009
4. Park, K. *Ergonomics* 53(7): 882-891, 2010

ACKNOWLEDGEMENTS

This project was funded by the Department of Homeland Security Fire Prevention & Safety Grant #EMW-2010-FP-01606. The authors thank Richard Kesler, David Li, Michael Angelini, Julian Sy, Lela DiMonte, and Dan Warner for their assistance.

Table 1 Judgment errors (relative and absolute) by obstacle type. Positive value corresponds to perceived overestimation actual ability. Notice judgment error becomes apparent in the over obstacle when the absolute value is taken.

	Over	Under	Through
Judgment Error (mean ± SD)	-0.5 ± 9.5 cm	15 ± 9.5 cm	-4.2 ± 5.3 cm
Absolute Judgment Error (mean ± SD)	7.9 ± 5.3 cm	15.2 ± 9.2 cm	5.5 ± 3.9 cm

PROLONGED SITTING ALTERS ABDOMINAL MUSCLE ACTIVATION AND THORACIC SPINE LATERAL BENDING IN TRANSIENT PAIN AND NON-PAIN DEVELOPERS

[1]Brian C. Nairn, [2]Nadia R. Azar and [1]Janessa D.M. Drake*

[1]York University, Toronto, ON, Canada
[2]University of Windsor, Windsor, ON, Canada
*Email: jdrake@yorku.ca

INTRODUCTION

Sitting is a commonly adopted posture during work, and research evidence demonstrates transient back pain can develop over prolonged exposures to sitting [1,2]. Many studies of prolonged sitting have focused strictly on the lumbar spine [1,3] with little attention paid to the thoracic region. Most of the thoracic spine literature has come from short-duration sitting and often included only kinematic data, without regard for the muscle activation patterns associated with the movement patterns [4]. Recently, an on-site case study by Nairn et al. [2] showed notable differences in thoracic spine motion patterns in an individual who developed back pain while seated performing computer-aided drafting (CAD) work for two hours. Examining how different regions of the trunk interact with each other is important to fully understand spine function during prolonged postural exposures. The purpose of this study was to quantify three-dimensional motion from various regions of the spine, and the corresponding muscle activation (EMG) during two hours of uninterrupted simulated seated CAD work. It was expected that participants would split into pain developing (PD) and non-pain developing (NPD) groups and that differences would exist in motion and EMG patterns between these groups.

METHODS

Ten university-aged males were recruited for this study. All were free of neck, back, and shoulder pain for at least one year prior to collection.

Reflective markers were used to track the motion of six regions of the trunk: neck (head-C_7); upper-thoracic (T_1-T_4); mid-thoracic (T_5-T_8); lower-thoracic (T_9-T_{12}), lumbar (L_1-pelvis), and the pelvis. Eight rigid plates (three markers per plate) were attached directly to the skin of the selected vertebrae and individual markers were also adhered to the pelvis and head. Data were analyzed in eight 15-minute time intervals and the kinematic angles were taken as relative angles between adjacent segments. The outcome measures calculated were the average angle and range of motion (ROM) of each time interval.

EMG electrodes were placed over left (L) and right (R) external oblique (EO); internal oblique (IO); rectus abdominis (RA); latissimus dorsi (LD); upper-thoracic erector spinae (UTES); lower-thoracic erector spinae (LTES); lumbar erector spinae (LES); and superficial lumbar multifidus (SLM) muscles. EMG data were normalized to a maximum voluntary contraction (%MVC) from each respective muscle, and the average %MVC from each 15-minute interval was recorded.

Participants sat at a table in an armless and backless office chair for two hours. A laptop was connected to an external monitor, and participants were instructed to read selected passages from the screen and follow along with the mouse and strike the "shift" key on the keyboard after every paragraph. Participant pain/discomfort levels were recorded every 15 minutes using a 100-mm visual analog scale (VAS). Participants who indicated an increase greater than 12 mm were considered PDs (n=4), whereas those who indicated a change of less than 12 mm were considered NPDs (n=6) [5].

RESULTS AND DISCUSSION

The EMG values for IO showed a significant interaction of side and pain group; lumbar ES showed a significant interaction of side and time; and main effects of pain group were found in EO, LIO, RIO, RA, and LD. Figure 1 illustrates the main effects and interactions of pain group on average %MVC. Within the PD group there were higher levels of muscle activation in the abdominal and LD muscles compared to the NPDs.

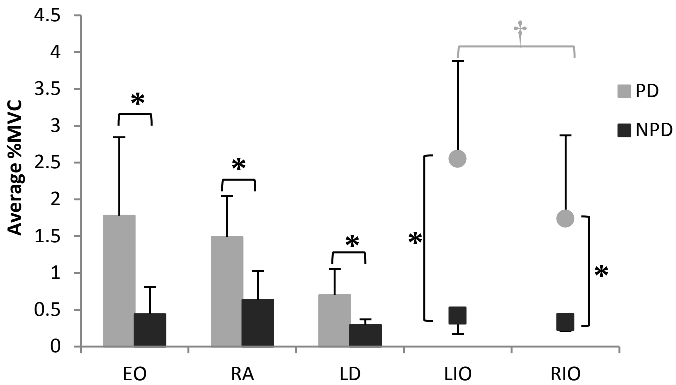

Figure 1: Average %MVC of the abdominals and LD collapsed across time. Significant differences ($p<0.05$) between PD and NPD groups are noted by an asterisk (*) while the dagger (†) denotes a significant difference between left and right IO within the PD group.

There was a significant interaction of pain group and spine region on the lateral bend ROM (Figure 2). Within the NPD group, the mid-thoracic region showed less lateral bend ROM than both the upper- and lower-thoracic regions, but no differences were found within the PD group.

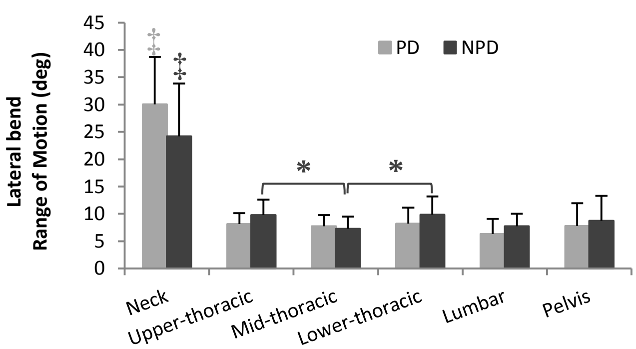

Figure 2: Lateral bend ROM (°) of each region for both PD and NPD groups collapsed over time. The double-dagger (‡) indicates the neck region was significantly greater than all others.

This study showed that some individuals developed transient pain during two hours of undisturbed sitting, while others did not; and differences in both muscle activity and spine kinematics were found between these groups. PDs tended to show higher muscle activations in the abdominals as well as bilateral differences in IO activity compared to the NPDs. It has been suggested that complete relaxation of the muscles (below 1-2% MVC) is necessary to avoid a compromise in muscle performance [6]. Though a link between abdominal muscle activation and reporting of back pain has yet to be established, results of the present study suggest there could be an association between the increased muscle activation and the development of transient pain.

It has also been noted that individuals who were predisposed to sitting-induced back pain showed more instances of shifting compared to non-pain individuals [7]. Results of the present study provide further evidence of NPDs showing overall less movement as indicated by the reduction in lateral bend ROM.

CONCLUSIONS

Forty percent of previously asymptomatic individuals developed back pain over a two-hour period of simulated seated drafting work. Differences in both EMG and spine kinematics were found between pain groups, with the PD group showing higher abdominal muscle activations and the NPD showing less lateral bend ROM. These findings further highlight the importance of analyzing spine motion in different regions and including more than one plane of motion. Additional research to further elucidate the associations between pain development and increased abdominal muscle activation is warranted.

REFERENCES

1. Gregory DE, et al. *Hum Factors* **48**, 142-153, 2006.
2. Nairn BC, et al. *IIE Trans OEHF*, **1**, 76-81, 2013.
3. Callaghan JP, McGill SM. *Ergonomics*, **44**, 280-294, 2001.
4. Claus AP, et al. *Manual Ther* **14**, 404-408, 2009.
5. Kelly AM. *Acad Emerg Med*, **5**, 1086-1090, 1998.
6. McGill SM, et al. *Ergonomics*, **43**, 486-493, 2000.
7. Dunk NM, Callaghan JP. *Work*, **35**, 3-14, 2010.

ACKNOWLEDGEMENTS

Centre of Research Expertise for the Prevention of Musculoskeletal Disorders (CRE-MSD) for funding and Alison Schinkel-Ivy for data collection assistance.

EFFECTS OF LOCALIZED AND WIDESPREAD FATIGUE ON A REPETITIVE SAWING TASK

[1]Jeffrey C. Cowley, [2]Jonathan B. Dingwell and [1]Deanna H. Gates

[1] Dept. of Movement Science, School of Kinesiology, University of Michigan, Ann Arbor, MI, USA
[2] Department of Kinesiology & Health Education, University of Texas, Austin, TX, USA
Email: gatesd@umich.edu Web: http://kines.umich.edu/profile/deanna-gates-phd

INTRODUCTION

Muscle fatigue results in reduced force generating capacity of individual motor units [1] and increased muscle response time [2]. It may also alter muscle coordination [3] and ultimately affect performance. Some have suggested that under muscular fatigue, subjects alter their coordination strategies to achieve the same task goal [1, 4]. However, adaptations in coordination in response to muscle fatigue are not well understood. Studies of the effects of muscular fatigue on performance have utilized different protocols which either localized fatigue to a specific muscle or produced non-specific widespread fatigue across several muscles. It has been proposed that localized fatigue may cause greater changes in muscle activation patterns [3].

Control strategies may be analyzed by assessing how quickly subjects respond to deviations away from a task goal. A goal equivalent manifold (GEM) approach may be used to this end [5]. A GEM analysis allows decomposing movement variability into that which directly affects goal achievement and that which does not. Here, a GEM was defined to analyze changes in control strategies associated with muscular fatigue. We examined changes in performance of a repetitive, timed task under localized and widespread fatigue. We hypothesized that local fatigue would result in greater timing errors and decreased temporal correlations compared to widespread fatigue.

METHODS

20 healthy right-handed subjects (25±2.2 years) performed a bidirectional sawing task (Fig. 1) described previously [6]. Subjects slid a weight along a horizontal track in time with a metronome (~1 Hz). Data collection sessions included a sawing pre-test followed by a fatigue protocol and a sawing post-test. Maximal voluntary contractions (MVC) and rating of perceived exertion (RPE) were obtained at several points during the session to monitor fatigue (Fig. 1). Subjects pushed 10% of push/pull MVC back and forth along the track. A single marker on top of the handle was recorded at 120 Hz using a Vicon motion analysis system. The first fatigue protocol, ‘SAW’ was designed to induce widespread fatigue of the arm and trunk. Subjects performed the same sawing task with 25% of their push/pull MVC for 4 minutes or until RPE ≥ 8[6]. The second fatigue task, LIFT, was designed to localize fatigue to the shoulder flexors. With the elbows extended, subjects lifted a weight (10% of shoulder flexion MVC) to approximately 90° in the sagittal plane at a frequency of ~0.5 Hz [6].

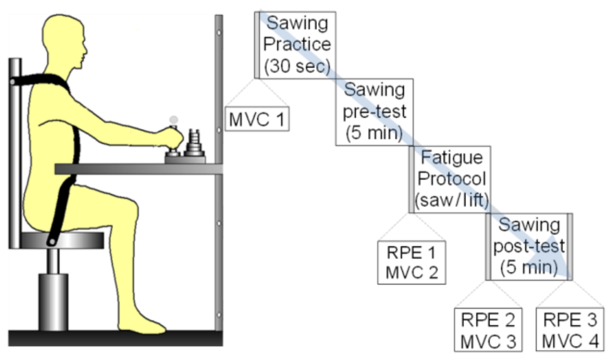

Figure 1: The experimental protocol. Subjects completed two sessions on separate days in random order. The only difference between sessions was the fatigue protocol.

Subjects were instructed to maintain movement time so that the end of each stroke (push or pull) coincided with the metronome beat. A non-dimensional movement distance (D) and speed (S) were obtained by dividing distance by subject height and speed by subject height and metronome frequency. The goal equivalent manifold (GEM) was defined as any combination [D, S] which achieves the correct stroke time. Timing errors, and D, and S were obtained for all push and pull strokes of each trial. Detrended fluctuation analysis was applied to all data series to obtain temporal correlations, α. The value α indicates how quickly deviations are corrected in a data series. Lower values indicate that deviations are corrected more rapidly. EMG instantaneous mean power frequencies (IMNF) were calculated to quantify muscle fatigue [6]. Dependent measures were analyzed using three-factor within subjects ANOVAs to test for differences in fatigue state (Pre/Post), fatigue protocol (SAW/LIFT), and stroke (Push/Pull).

RESULTS AND DISCUSSION

Significant localized muscle fatigue was confirmed by decreased IMNF during both fatigue tasks ($p < 0.05$; Fig. 2). LIFT caused shoulder flexion MVCs to decrease 8% more than SAW ($p = 0.035$).

Timing errors did not change post-fatigue for either fatigue protocol (pre = -0.061, post = -0.051, $p = 0.225$). The standard deviation of timing errors tended to decrease post-fatigue but did not reach significance (pre = 0.087, post = 0.074, $p = 0.052$). The different fatigue protocols affected α differently ($p = 0.025$). Errors were more persistent after LIFT ($p = 0.002$) but not SAW protocol ($p = 0.976$) (Fig. 3B). This suggests that timing errors were corrected less quickly following localized fatigue.

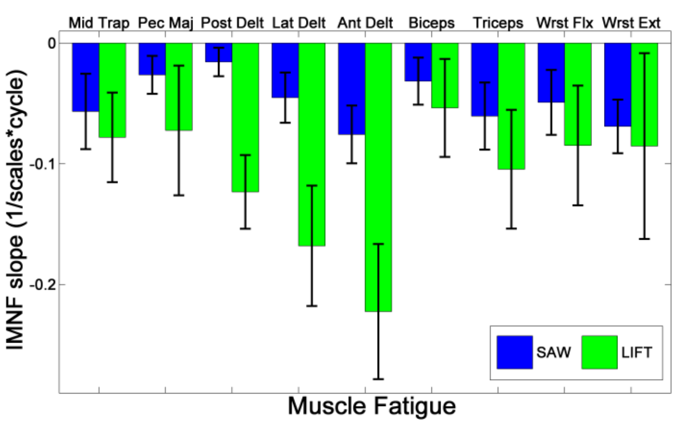

Figure 2. Slope of IMNF for each muscle

Subjects made shorter ($p = 0.002$) and slower ($p = 0.002$) movements after the LIFT task. There were no differences in distance or speed post SAW ($p = 0.158$; $p = 0.328$, respectively). No differences were observed between the push and pull strokes (D: $p = 0.100$, S: $p = 0.744$).

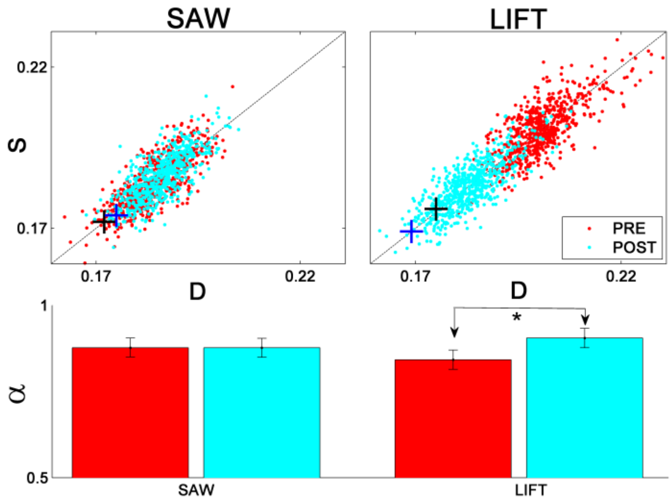

Figure 3: TOP: Movement distance, D, and speed, S, are shown for each stroke ('.') of a representative subject pre and post fatigue. The solid line represents the GEM for the task. Mean pre (black) and post-fatigue (blue) operating points across subjects are highlighted by +. BOTTOM: Mean and 95% CI of α are shown. '*' signifies significant difference ($p < 0.05$).

CONCLUSIONS

Subjects adapted to non-specific widespread fatigue in a way that did not affect movement speed, distance or timing errors. Specific fatigue of the shoulder flexors resulted in shorter, slower movements and greater temporal persistence in timing errors. Localized fatigue may limit options available by limiting the function of a specific muscle group. Neither fatigue protocol prevented subjects from achieving the desired outcome.

REFERENCES

1. Selen L, et al. *Exp Brain Res* **181**, 99-108, 2007.
2. Wilder DG, et al. *Spine* **21**, 2628-39, 1996.
3. Goerlick M, et al. *Appl Ergon* **34**, 317-25, 2003.
4. Cote J. et al. *Exp Brain Res* **147**, 394-8, 2002.
5. Cusumano J. & Cesari P. *Biol Cybern*, **94**, 367-79, 2006.
6. Gates D & Dingwell J *J Biomech*. **43**, 913-19, 2010.

ORAL PRESENATIONS – THURSDAY SEPTEMBER 5th

	Thematic: Biomechanics of Neurodegenerative Diseases (MS/PD) *Chris Hass*
4:15 PM	The Effect Of Moderate Parkinson's Disease On The Preparation For Compensatory Backward Stepping **McVey MA, Barnds A, Lyons KE, Pahwa R, Mahnken JD, Luchies CW**
4:30 PM	Walking Balance Is Improved In Multiple Sclerosis Patients After Elliptical Exercise Training **Cutler E, Wurdeman S, Myers S, Givens D, Stergiou N, Huisinga J**
4:45 PM	Ankle Plantar Flexor Force Control Is Improved After Gait And Balance Rehabilitation In Individuals With Multiple Sclerosis **Davies BL, Arpin DJ, Corr B, Reelfs H, Volkman KG, Harbourne RT, Healey K, Zabad R, Kurz MJ**
5:00 PM	The Effects Of Rest And Fatigue On Balance Performance In Persons With Multiple Sclerosis **Bigelow K, Jackson K**

THE EFFECT OF MODERATE PARKINSON'S DISEASE ON THE PREPARATION FOR COMPENSATORY BACKWARD STEPPING

[1]Molly A. McVey, [1]Annaria Barnds, [2]Kelly E. Lyons, [2]Rajesh Pahwa, and [2]Jonathan D. Mahnken, [1]Carl W. Luchies

[1]University of Kansas, Lawrence, KS, USA
[2]University of Kansas Medical Center, Kansas City, KS, USA
email: luchies@ku.edu

INTRODUCTION

Postural instability leading to falls is one of the most disabling symptoms of Parkinson's disease (PD) with 46% of those with PD falling in a given 3 month period [1]. PD impairs the step response needed to recover from a large balance disturbance and prevent a fall. Investigation of the control of the center of pressure (COP) during the step response has shown impairments in PD, such as the use of multiple anticipatory postural adjustments (APAs) leading to delayed liftoff times and the use of additional and shorter steps to regain balance [2].

Previous studies of postural instability have focused on patients who already exhibit balance deficits, however we have demonstrated impairments in balance recovery in mild PD with no clinical signs of postural instability (H&Y severity level 2) such as a longer weight shift time, altered ankle rotation prior to liftoff, and a more posterior displacement of the COP at landing of the first step in the response [3]. In addition, the COP patterns observed during the step initiation stage of the response were quite different between the two groups. Therefore, the goal of this study was to investigate the COP movement during the preparation stage of the step response in PD patients with moderate PD (clinically diagnosed postural instability- H&Y 3), compared to healthy controls.

METHODS

Ten participants with moderate PD (PD: Age 68 ± 4 years, H&Y 3) and 10 healthy controls (HC: Age 68 ± 5 years) completed the study. All participants gave written informed consent. Participants stood with arms crossed at the chest wearing a rigid waist harness attached via a cable to a weight-drop mechanism (dropped weight = 20% body weight, pull distance = 8.7% waist height), which delivered a posterior pull. The participant was asked to respond naturally. A harness was used for safety.

Data Collection: Motion data were sampled at 100 Hz using an Optotrak (Northern Digital, Inc., Waterloo, Canada) dual bar motion analysis system. Markers were placed bilaterally on the 2nd toe, ankle, heel, calf, and knee. EMG (Delsys, Boston, MA, USA) from the tibialis anterior (TA) and force plate data from three six-component force plates (AMTI, Watertown, MA, USA) were sampled at 1000 Hz. All responses were videotaped.

Data Analysis Data from all trials were processed using MATLAB (Mathworks, Natick, MA, USA). Trials were classified as single or multiple step trials. Only the first step in a multiple step response was compared. A step was defined if the foot lifted off the force plate and repositioned to change the base of support. The foot was required to translate 50 mm or more in order to be considered a step.

The whole body center of pressure (COP) was calculated between disturbance onset to liftoff of the first step, and divided into two stages. Stage 1 was defined as disturbance onset to weight shift onset. Stage 2 was defined as weight shift onset to step foot liftoff. Weight shift onset was defined as the last change in the location of the COP in the medial-lateral (ML) direction prior to liftoff. The anterior-posterior (AP) and ML displacement, path length, average velocity, and the duration of each stage were calculated. APAs were defined based on the movement of the lateral COP signal. The baseline signal was defined by the average of the signal for

500 ms prior to onset of the disturbance. If the COP traveled more than 1cm from the baseline an APA was noted to begin. Trials were classified as having 0, 1, or 2 or more APAs.

Statistical analysis was done with SPSS 20.0 (SPSS Inc., Chicago, IL). The Fisher's Exact Test was used to evaluate group differences in the number of trials where multiple APAs were used and consistency of preparation strategy. Normally distributed COP parameters were analyzed with Student's T-Tests, those that were not were analyzed using the Mann-Whitney U Test. Follow up tests were done to compare stepping strategy (0 or 1 APAs compared to 2 or more APAs) to the COP parameters using linear mixed modeling.

RESULTS AND DISCUSSION

PD, compared to HC, utilized significantly more steps to recover from the balance disturbance (HC: 1.66 ± 0.63, PD: 2.43 ± 0.79, p = .035). PD used multiple APAs in 37% of all trials, compared to HC who never used multiple APAs (p=.0003). There were significant differences in several COP parameters, all in the first stage of the response (table 1). Follow up tests found significant differences in COP parameters based on number of APAs (figure 1). These results suggest that COP measures during the preparation phase of the response may be early indicators of postural instability. This is exciting because the preparation phase of the response cannot be visually observed, so the use of these measures may offer clinical insight that is not otherwise available.

Limitations of this study include the small sample size, the predictable nature of the disturbance, and that PD participants were tested only in the ON medication state. These choices were made to reflect the clinical pull test (UPDRS # 33).

CONCLUSIONS

The preparation phase of the response to an external perturbation is impaired in moderate PD. The use of multiple APAs results in delayed liftoff times and significantly different movement in the COP prior to liftoff. Furthermore, the differences in the response can be attributed to the stage of preparation prior to final weight shift. This portion of the response and these parameters should be further investigated for their value in a more sensitive measure of postural instability.

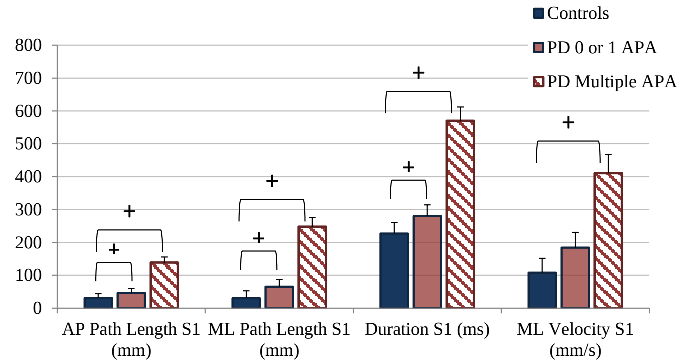

Figure 1. COP Parameters by Step Strategy Type: 0 or 1 APA compared to multiple APAs. + Indicates significant difference in follow up test.

REFERENCES

1. Pickering RM, et al. *Mov Disord* **22,** 1892-1900, 2007.
2. King LA, et al. *Arch Phys Med Rehabil* **91**, 1332-1338, 2010.
3. McVey, MA, et al. *Gait Posture* **30**, 538-542, 2009.

ACKNOWLEDGEMENTS

Assistance from Sommer Amundsen and the Self Graduate Fellowship is acknowledged.

Table 1. COP Parameters for Stage 1 of Response

	HC (N=7)	PD (N=9)	p-value
AP Displ. (mm)	-26 (26)	-66 (47)	0.06
ML Displ. (mm)	26 (29)	53 (72)	0.38
AP Path Length (mm)	34 (22)	85 (49)	0.02*
ML Path Length (mm)	30 (30)	135 (85)	0.01*
Time (ms)	232 (66)	384 (174	0.03*
AP Ave. Vel. (mm/ms)	.13 (.07)	.18 (.09)	0.20
ML Ave. Vel. (mm/ms)	.11 (.10)	.29 (.13)	0.01*

WALKING BALANCE IS IMPROVED IN MULTIPLE SCLEROSIS PATIENTS AFTER ELLIPTICAL EXERCISE TRAINING

[1,2]Eric L. Cutler, [1]Shane R. Wurdeman, [1]Sara A. Myers, [3]Deborah L. Givens, [1,2]Nicholas Stergiou, [4]Jessie M. Huisinga

[1]University of Nebraska at Omaha, Omaha, NE, USA
[2]University of Nebraska Medical Center, Omaha, NE, USA
[3]Creighton University, Omaha, NE, USA
[4]University of Kansas Medical Center, Kansas City, KS, USA
email: ecutler@unomaha.edu, web: nbcf.unomaha.edu

INTRODUCTION

Multiple sclerosis (MS) is a chronic disease of the nervous system. This debilitating disorder often results in a general degradation of motor function. In particular, individuals with MS often exhibit altered balance dynamics while standing [1]. One of the characteristics of this altered balance is a large amount of postural sway [1]. Altered dynamic balance during walking with increased medial-lateral motion of the trunk has also been observed, even in individuals with very mild MS [2]. Static center of pressure measurements have predominantly been used to quantify balance decrements in individuals with MS. However, a recent study utilizing a dynamic measure of balance, margin of stability (MOS), reported individuals with MS exhibit a greater range in MOS than their healthy counterparts [3]. MOS accounts not only for the position of the center of mass but also its velocity [4]. As the MOS decreases, the associated gait is considered to be more mechanically unstable. , Cutler et al.'s [3] findings confirm observations of increased medial-lateral sway in MS patients during gait[2] and are indicative of a decreased ability to control the trajectory of the center of mass.

However, it is unknown if dynamic balance during gait, measured by MOS, can be improved through an intervention for patients with MS. Elliptical exercise has been effective in improving both joint kinetics and quality of life measures in individuals with MS [5,6]. This particular exercise intervention was utilized because it provides a lower limb motion similar to walking and is better able to accommodate individuals with MS than treadmill exercise. Thus, the purpose of this study was to determine if participation in an elliptical exercise program by individuals with MS could improve dynamic balance by improving MOS during gait.

METHODS

Nine subjects (age: 40.3±10.7 yrs, height: 64.8±2.5 cm, mass: 89.9±23.3 kg) diagnosed with MS were consented for and participated in this study. Lower extremity kinematics were recorded by an eight camera system (60 Hz; Motion Analysis Corp., Santa Rosa, CA, USA) while each subject walked over-ground at a self selected pace. Five trials were collected from each subject for each limb. Each subject then participated in 15 exercise training sessions over the course of six weeks. This training was conducted on elliptical machines (Precor, Woodinville, WA, USA) and each session was 30 minutes in duration. Subjects repeated the aforementioned data collection process after completion of the elliptical exercise program.

A custom MATLAB (MathWorks Inc., Natick, MA) code was used to calculate the MOS. Eigenfrequency (ω_0) of the inverted pendulum was calculated, per the equation $\omega_0 = \sqrt{g/l}$, using leg length (l) and the acceleration due to gravity (g). The MOS time series was calculated for each trial, per the equation $MOS = |u_{max} - (x + v/\omega_0)|$, using the position ($x$) and velocity ($v$) of the subject's center of mass and boundary of support of the right foot (u_{max}). The mean, maximum, minimum, and range for the MOS were calculated and used as the outcome variables of this study. A paired t-test was used to test for significant differences with alpha at the 0.05 level.

RESULTS AND DISCUSSION

The elliptical training program had little effect on the mean MOS measurement exhibited by subjects with a decline of less than 0.004 m (Figure 1). The minimum MOS value did increase by 0.008 m post-training. As a result of the exercise training program the maximum MOS value decreased by 0.030 m, which was statistically significant. This post-training increase in minimum MOS and decrease in maximum MOS resulted in a significantly reduced range of MOS after the completion of the exercise training. This reduction was 0.038 m in magnitude.

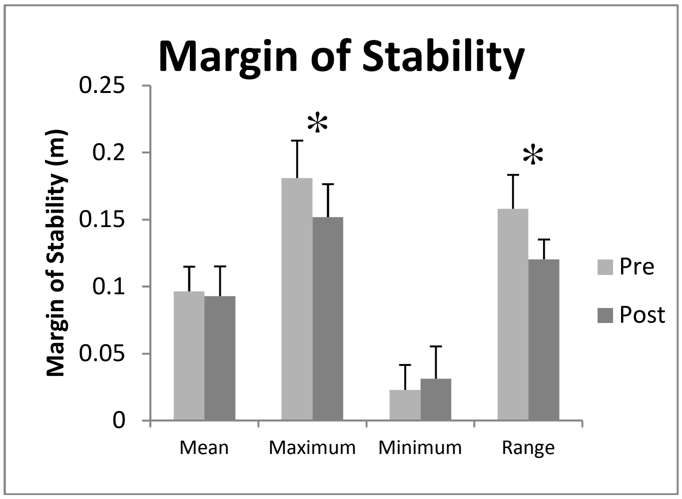

Figure 1: Margin of stability pre vs. post exercise training. *pre vs. post, p<0.05.

As the MOS decreases, the associated gait is considered to be more mechanically unstable. As the extrapolated center of mass nears the border of support a fall becomes more likely to occur [4]. It would appear from our results that neither the mean nor the minimum of the MOS were substantially affected by the elliptical training program. This is indicative of the idea that the training did not cause the medial-lateral path of the extrapolated center of mass to move further away from the boundary of support, a result which would have indicated a reduced risk of falling. However there is a clear decrease in the range of the trajectory of the extrapolated center of mass through the gait cycle after the elliptical training. The decreased range of MOS demonstrates a reduced medial-lateral travel of the extrapolated center of mass. This result is indicative of reduced medial-lateral center of mass sway during gait in subjects with MS who participated in an elliptical exercise training program. Since greater medial-lateral sway is observed in the gait of subjects with MS as compared to healthy controls [2,3], it would appear that elliptical exercise may be able to assist in reducing the effects of MS on dynamic balance during walking.

CONCLUSIONS

Participation in an elliptical exercise training program reduced the medial-lateral center of mass sway in individuals with MS during walking. This represents a change in behavior approaching that of healthy individuals. Elliptical exercise may be able to assist in reducing the effects MS on dynamic balance during walking. Future work will need to determine the best dosing as well as possible other dynamic movement exercise interventions to determine if elliptical is the best method for improving dynamic balance.

REFERENCES

1. Garst GM, et al. *J Neurol Phys Ther* **29,** 170-80, 2005.
2. Spain RI, et al. *Gait Posture* **35**, 573-578, 2012.
3. Cutler E, et al. *Proc Amer Soc Biomech* Gainesville, FL, 2012.
4. Hof AL, Gazendam MGJ, Sinke WE. *J Biomech* **38**, 1-8, 2005.
5. Huisinga, et al. *J Rehab Res Devel* **48**, 881-890, 2011.
6. Huisinga, et al. *J App Biomech* **28**, 249-257, 2012.

ACKNOWLEDGEMENTS

This work was generously supported by grants from the NASA Nebraska Space, the Physical Therapy Department of the Creighton University, and the Nebraska Research Initiative.

ANKLE PLANTAR FLEXOR FORCE CONTROL IS IMPROVED AFTER GAIT AND BALANCE REHABILITATION IN INDIVIDUALS WITH MULTIPLE SCLEROSIS

[1]Brenda L. Davies, [1]David J. Arpin, [1]Bradley Corr, [1]Heidi Reelfs, [2]Kathleen G. Volkman, [1]Regina T. Harbourne, [3]Kathleen Healey, [3]Rana Zabad, [1]Max J. Kurz

[1]Munroe Meyer Institute, University of Nebraska Medical Center, Omaha, NE, USA
[2]School of Allied Health Professionals, University of Nebraska Medical Center, Omaha, NE, USA
[3]College of Medicine, University of Nebraska Medical Center, Omaha, NE, USA
email: mkurz@unmc.edu web: http://www.unmc.edu/mmi/

INTRODUCTION

Multiple sclerosis (MS) is a demyelinating disease that occurs in young adults and often affects the control of the leg musculature. It has been well established that individuals with MS have significantly weaker muscles, and that their musculature fatigues at a faster rate. Recent research has displayed that an intensive gait and posture rehabilitation protocol has the potential to reduce fatigue, and improve the posture and the mobility of individuals with MS [2]. However, it is currently unknown if these improvements may be a result of increased strength or improved control of the leg musculature.

Control of the lower extremity musculature performance is evident by the amount of variability or error in the steady-state isometric muscular force [4]. It has been demonstrated that a greater amount of postural sway is associated with a greater amount of variability in the ankle joint's submaximal steady state force production [4]. This suggests that improvements in postural control should be a result of improved control of the ankle plantar flexor muscles. In spite of these novel insights, it is unknown if the current rehabilitation strategies used with individuals with MS can improve the motor control of the ankle musculature.

The purpose of this study was to determine whether 14-weeks of an intensive gait and balance rehabilitation protocol can improve the muscular control of the ankle plantar flexor muscles of individuals with MS. A secondary purpose of this study was to determine whether the rehabilitation protocol would also improve the postural control and walking speed.

METHODS

Ten adults with relapsing-remitting or secondary progressive MS participated in this investigation (Age: 51.7 ± 8 years). The participants had an average Kurtzke Extended Disability Status Score of 5.3 ± 0.9, which indicated that on average the patients could walk independently for at least 100 meters. Twenty normal, healthy adults acted as a control group (Age: 45.1 ± 14.1 years). The MS group completed testing before and after completing the rehabilitation protocol and the control group completed one testing session.

Muscular control of the ankle plantar flexor muscles was measured using an isokinetic dynamometer (Biodex, Inc., Shirley, NY). The MS group used their most affected leg for the testing, while the control group used their dominant leg. Two maximal isometric voluntary contractions were completed, and the highest maximal voluntary torque (MVT) was used to calculate 20% of the MVT. At least one minute of rest was allowed in between all trials. Two submaximal steady state isometric contractions at 20% MVT were held for 30 seconds each. A custom LabVIEW program was used to display the target and actual force in real-time on a computer screen ~1 m in front of the participants. The middle 15 seconds of each trial was utilized in order to ensure that a steady state contraction had been reached. The coefficient of variation (CV) for each trial was calculated, and the two trials were averaged together for each subject.

Postural control of the MS group was additionally measured based on the composite score from the Sensory Organization Test (SOT) (NeuroCom® International, Clackamas OR), where a higher score indicated a lower amount of postural sway. A fast-as-possible walking velocity was measured using a GAITRite® system (CIR Systems Inc., Sparta, NJ). Two trials were completed and they were averaged together.

The initial two weeks of the rehabilitation program were completed on the UNMC campus under close supervision of a licensed physical therapist. The therapy was conducted twice a day for five days each week. Each session consisted of 20 minutes of static balance training and 20 minutes of dynamic balance training. The sessions focused on learning strategies for static and dynamic postural control. For example, the static balance training included standing on foam or standing with eyes shut, whereas exemplar dynamic balance training included exercises like walking on a treadmill while focusing on foot placement, walking sideways overground or stepping over obstacles. After the initial two weeks, the remaining 12-weeks of training were completed at home twice a day, and were monitored by the physical therapist through weekly phone contact.

RESULTS AND DISCUSSION

The CV of the ankle plantar flexor muscles for the individuals with MS was greater than the controls before the rehabilitation (p=0.03; Figure 1). This suggests that the individuals with MS initially had greater errors in their ability to match and sustain the target value with their ankle joint musculature. However, after rehabilitation, the CV was markedly reduced (p=0.027; Figure 1), and was not significantly different from the CV of the controls (p=0.78). This indicates that the rehabilitation protocol improved and normalized the motor control of the ankle musculature. It has been previously demonstrated that the firing rates of the motor units are diminished and more variable in individuals with MS [1]. Although the specific neural adaptation for improved ankle force control cannot be determined from our data, we suspect that the changes in variability of the motor unit discharge rates and/or changes in the synchrony of common motor units that serve the gastrocnemius and soleus musculature are possible mechanisms [3,5].

Following the rehabilitation protocol, the composite score on the SOT increased (Pre: 51.6 $\pm$ 5, Post: 70.8 $\pm$ 2; p=0.01), indicating that the amount of postural sway was reduced after rehabilitation. Thus, postural control was improved after rehabilitation. Furthermore, our results showed that the fast-as-possible walking velocity improved as well (Pre: 0.97 $\pm$ 0.07 m/s, Post: 1.2 $\pm$ 0.09 m/s; p=0.01). There was a significant negative correlation between CV and SOT scores (r= -0.45; p=0.047) indicating that a better SOT score was associated with less error in the ankle force control. The CV was not correlated with the walking velocity (r= 0.05; p= 0.83). Our results indicate that improved muscular control of the ankle joint has the potential to improve the postural balance of individuals with MS. Based on our results, we suggest that rehabilitation protocols that focus on improving the muscular control of the ankle joint will likely augment clinically relevant improvements in the postural balance of individuals with MS.

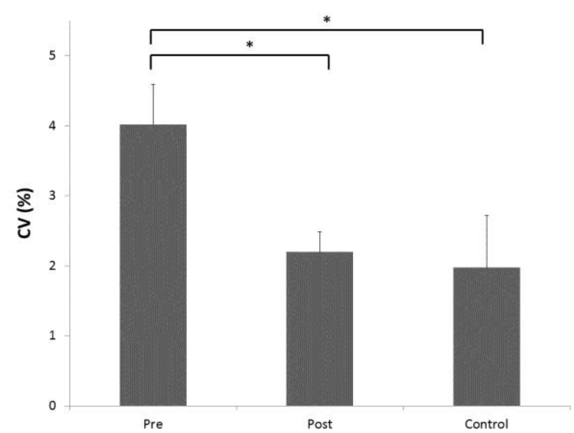

Figure 1: Coefficient of variation ankle plantar flexor muscles (CV) before and after rehabilitation. *p<0.05.

REFERENCES

1. Dorfman LJ, et al. *Electroenceph Clin Neurophys* **73**, 215-224, 1998.
2. Hebert JR, et al. *Phys Ther* **91(8)**, 1166-1183, 2011.
3. Kornatz KW, et al. *J Appl Phys* **98**, 2072-2080, 2005.
4. Kouzaki M & Shinohara M. *Muscle & Nerve* **42**, 78-87, 2010.
5. Semmler JG, et al. *J Neurophys* **92**, 3320-3331, 2004.

The Effects of Rest and Fatigue on Balance Performance in Persons with Multiple Sclerosis

Kimberly Edginton Bigelow and Kurt Jackson

University of Dayton, Dayton, OH, USA
email: Kimberly.Bigelow@udayton.edu web: http://academic.udayton.edu/~ewsl

INTRODUCTION

Multiple Sclerosis (MS) is a chronic, progressive disease of the central nervous system, affecting approximately 400,000 individuals in the United States [1]. Though symptoms are quite varied due to the location of lesions in the central nervous system, two of the most commonly reported disease-related complaints are fatigue and balance deficits [1-3]. As many as 94% of individuals with MS report that they have balance and mobility problems and approximately 90% complain of significant fatigue [2,3]. To date, however, there has been relatively limited work done to examine the relationship between these issues and determine whether they might be confounding factors. A study by Frzovic et al. examined how balance changed throughout the day in individuals with multiple sclerosis, and found that although subjects expressed being more fatigued in the afternoon, their balance performance experienced little change [4]. Frzovic's study supported that requiring consistency in the time of testing may not be necessary when considering how to standardize posturography protocols. The current study tries to advance these findings by examining, instead of solely time of day, the effect of rested versus fatigued conditions. The objective of this study was to determine first, whether individual performance changed on posturography and clinical balance measures in a fatigued condition and second, to determine whether any changes observed were correlated to self-reported fatigue levels.

METHODS

A convenience sample of 15 individuals with MS participated in this study (11 females, 4 males; 54.3 ± 6.9 years; EDSS score: 3.8 ± 1.9). Exclusion criteria included: inability to walk a minimum of 10 meters with or without an assistive device, recent exacerbation of MS symptoms, recent medication changes, and any other condition that would influence walking ability or make participation in moderate physical activity unsafe. This study was approved by the University of Dayton IRB and all subjects gave written informed consent.

Testing occurred over two sessions: a rested condition and a fatigued condition. During the rested condition subjects arrived for testing between 8 am and 9am, having been instructed to refrain from physical activity prior to the test. For the fatigued condition subjects arrived at the lab between 3pm and 4pm. Upon arriving, the six-minute walk test was administered as a means of inducing a controlled moderate fatiguing activity representative of typical community ambulation. The starting condition was counterbalanced for all subjects and the remaining session was completed within 10 days of the first visit.

For each session, subjects first reported their self-perceived fatigue on a visual analog scale (VAS). For the fatigued condition, the 6 minute walk test was then conducted and another VAS measure was immediately taken. Following these VAS scores, the balance testing protocol began. Subjects first participated in a quiet-standing posturography protocol. Center of pressure data was collected under the conditions: eyes open on the flat plate, eyes closed on the flat plate, eyes open on a foam cushion placed on the plate, and eyes closed on the foam cushion. Two trials were taken for each condition, with data collected for 30 seconds at 1000 Hz. Trials where loss of balance occurred were excluded from further analysis. Anterior-posterior (A/P) Sway Range, Medial-lateral (M/L) Sway Range, and Mean Velocity were calculated from the center of pressure data and averaged for each condition. A Limits of Stability (LOS) test was also conducted requiring subjects to utilize an ankle strategy to lean as far forward, backward, left, and right as possible for three trials. From the LOS data, A/P Sway Range and M/L Sway Range were calculated. Following the posturography protocol, the Mini BESTest and Dynamic Gait Index were administered. Upon completion of the tests, subjects reported a final VAS fatigue score. Paired t-tests were used to assess the differences in posturography, clinical, and VAS outcome measures between the rested and fatigued condition. Pearson correlations were calculated to examine the relationship between fatigue and balance. All analyses were performed in SPSS with $p \leq 0.05$.

RESULTS AND DISCUSSION

The results of the clinical balance tests have been presented elsewhere [5], therefore the posturography results are the focus of this abstract. Table 1 shows the data for the quiet-standing posturography results. The eyes closed, foam pad condition proved too challenging for many of the subjects, in both rested and fatigued conditions, and was excluded from analysis.

Table 1. Comparison of Quiet-Standing Postural Sway Measures in Rested vs. Fatigued Condition

Measure	Rested	Fatigued	Sig.
A/P Sway Range (mm)			
EO-Flat Plate	31.0 ± 12.4	35.3 ± 16.9	0.140
EC-Flat Plate	44.0 ± 18.9	50.6 ± 26.0	0.157
EO-Foam	51.5 ± 16.8	60.1 ± 25.0	**0.030***
M/L Sway Range (mm)			
EO-Flat Plate	17.0 ± 7.7	24.4 ± 16.3	0.066
EC-Flat Plate	24.1 ± 12.6	33.3 ± 24.3	**0.044***
EO-Foam	47.7 ± 16.9	50.2 ± 23.0	0.603
Mean Velocity (mm/s)			
EO-Flat Plate	32.6 ± 12.7	36.8 ±16.7	0.189
EC-Flat Plate	48.5 ± 23.9	55.1 ±30.0	0.183
EO-Foam	63.7 ± 21.4	74.1 ± 29.2	**0.038***

Though no differences were observed in the easiest condition (eyes open, flat plate), statistically significant differences were observed in the other two conditions. Interestingly, these changes were not observed for all sway measures. Future studies may wish to examine possible reasons why sway under certain conditions is more affected by fatigue and whether this has clinical implication (i.e. avoid darker areas when experiencing significant fatigue.) The average increase in sway for the significant conditions is approximately 1 cm, which may have implications related to falls. Future research should seek to relate the effect of fatigue and falls due to postural effects. Limits of Stability revealed no statistically significant differences.

Analysis of the VAS fatigue scale showed that subjects felt more fatigued upon arrival for the afternoon sessions than they did in the morning sessions (mean change of 20.9 mm using a 100mm VAS scale). The 6 minute walk test further fatigued subjects (mean change of 8.6 mm). However, despite feeling more fatigued and doing poorer on the Mini BESTest (p=0.002), Dynamic Gait Index (p=0.002), and the selected posturography measures discussed; correlations between fatigue and the dynamic balance measures were low (r_{max}=0.34). These findings suggest that a VAS self-report of fatigue may not relate well with actual performance and ability. However, balance does appear to be affected by fatiguing activities and perhaps time of day. Clinicians working with individuals with MS may wish to take this into account when evaluating patients. It may be useful to purposefully induce fatigue, such as done here using the 6 minute walk test, to evaluate how fatigue affects performance on clinical tests. This study suggests that self-report of fatigue may not be sufficient to be indicative of the effect of performance. Future work is needed to study this further.

CONCLUSIONS

Balance appears to be significantly affected by fatigue in individuals with MS, however these changes are weakly correlated with self-reported fatigue levels. This may have clinical implications for the evaluation and treatment of MS symptoms.

REFERENCES

1. Rumrill PD. *JVR.* 2009;31:75-82.
2. Peterson EW, et al. *Arch Phys Med Rehabil.* 2008;89:1031-1037.
3. Kinkel RP. *Int J MS Care.* Oct 2000. Self-Study Supplement.
4. Frzovic D, et al. *Arch Phys Med Rehabil.* 2000;81:215-221.

ACKNOWLEDGEMENTS

The authors would like to thank Alex Jules for his help with data analysis.

ORAL PRESENATIONS – THURSDAY SEPTEMBER 5th

	Clinical Biomechanics/Journal of Biomechanics Awards *Don Anderson*
4:15 PM	Tibiofemoral Contact Location Changes Associated With Lateral Heel Wedging - A Study Using Weight Bearing MRI **Barrance P, Gade V, Allen J, Cole J**
4:30 PM	A Longitudinal Study Of The Knee Adduction Moment Components Post-Arthroscopic Partial Meniscectomy **Hall M, Wrigley T, Metcalf B, Hinman R, Dempsey A, Mills P, Cicuttini F, Lloyd D, Bennell K**
4:45 PM	Alendronate Treatment Elicits A Reduction In Mechanical Properties And The Density Of Osteocyte Cells In Cortical Tissue **Geissler J, Bajaj D, Allen M, Burr D, Fritton JC**
5:00 PM	Heterogeneous Regional Fascicle Behavior Within The Biceps Femoris Long Head **Bennett H, Rider P, Domire Z, DeVita P, Kulas A**

TIBIOFEMORAL CONTACT LOCATION CHANGES ASSOCIATED WITH LATERAL HEEL WEDGING - A STUDY USING WEIGHT BEARING MRI

[1,2]Peter J. Barrance, [1]Venkata Gade, [1]Jerome Allen, and [3]Jeffrey L. Cole

[1]Kessler Foundation Research Center, West Orange, NJ, USA
[2]University of Medicine and Dentistry of New Jersey, Newark, NJ, USA
[3]Kessler Institute for Rehabilitation, West Orange, NJ, USA
email: pbarrance@kesslerfoundation.org

INTRODUCTION

Lateral and medial shoe wedge orthoses have been proposed as low cost interventions for knee osteoarthritis (OA). These devices can provide relief of knee pain, but there is controversy on the consistency of clinical effectiveness. Some studies and reports have recommended against their use for management of knee OA.

The majority of biomechanical studies into mechanisms of shoe wedging have been conducted using gait analysis methods. Previous studies have reported reduction in external knee adduction moment with lateral shoe wedging [1]. An associated mechanism for pain relief through functional unloading of the medial tibiofemoral compartment in medial knee OA patients has been proposed. Other studies have cited the mixed clinical results as indicative of the need for subject-specific prescription of orthoses. For example, maximal short term pain relief was used to prescribe variable wedging in a previous study [2].

In the current study, we used weight bearing magnetic resonance imaging (MRI) to explore changes in tibiofemoral contact accompanying shoe wedging. The study was conducted in the context of a development effort for the data acquisition and analysis techniques; for this reason, we designed our study to provide more control and experimental reproducibility than would be possible with in-shoe wedging. We used custom shoes with external heel wedging adjustable by the investigator, avoiding the need to remove shoes between trials and perhaps introduce variability in subject positioning. Using biomechanical modeling, we examined the effect of knee flexion and heel wedging on locations of femoral contact on the tibial plateau.

METHODS

Approval for human subject activities was obtained from Kessler Foundation's IRB. 14 subjects (7M,7F,53.6±18.0yrs) with knee OA underwent physical examinations to confirm study eligibility after obtaining informed consent. MRI scanning was performed in a 0.6 T vertically open scanner (Upright MRI, Fonar, NY). Using high-definition reconstruction, images with 0.483 mm pixel spacing and 250 mm field of view were obtained. Two versions of this protocol were used in the study, yielding slices spaced at 0.75 mm or 1.0 mm (scan time 2m16 s or 1m35s respectively).

One of three pairs (small, medium, large sizes) of custom-developed shoes was selected to comfortably fit each subject. Each shoe incorporated an external nylon heel wedge that could be rotated to provide neutral (0°) and 5° lateral wedging conditions. For each wedge condition, the standing subjects used a fiber-optic knee angle visual feedback system [3] to position the knee in neutral flexion (0º) and 20° bilateral knee flexion. One subject did not tolerate 20º standing due to knee pain; 0º trials were analyzed.

Femoral and tibial bone surfaces, along with medial and lateral compartment cartilage surfaces were traced for each image using a digital drawing tablet or a digitizing screen (Wacom, Japan). Custom software was used to project digitized points into 3D coordinates. Coordinates for the bones were placed on the 'neutral wedge / neutral flexion' scan according to anatomical landmarks, and bone surface matching was used to maintain consistent positioning of the tibial plateau coordinate system (C.S.) through the remaining scans. The femoral and tibial cartilage points were projected relative to this tibial plateau C.S., and a cartilage contact

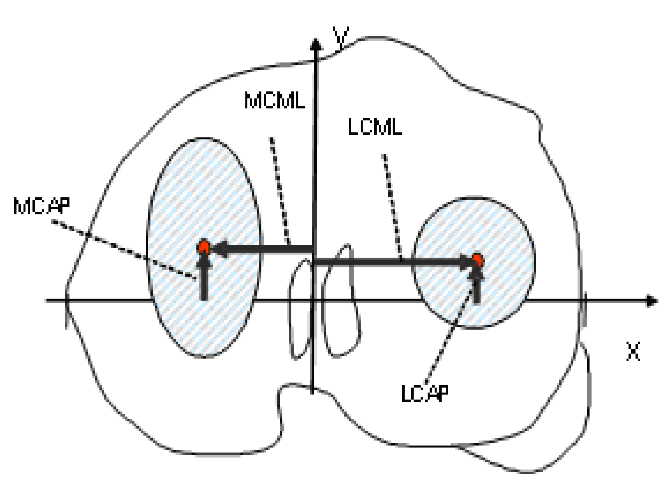

Figure 1: Coordinates of medial and lateral compartment contact centers, as calculated using a cartilage proximity algorithm and referenced to a tibial plateau coordinate system tracked using bone surface matching.

proximity algorithm [4] was used to measure medial/lateral (ML) and anterior/posterior (AP) centers of femoral contact relative to the tibial plateau (Fig 1).

For each outcome variable (MCAP, LCAP, MCML, LCML) a separate ANOVA was performed, with flexion angle (0/20°) and wedge condition (neutral/lateral) as repeated measures. Significance level of α=0.05 was used.

RESULTS AND DISCUSSION

Effect of flexion: ANOVAs yielded significant main effects of flexion on MCAP and LCAP. Pairwise comparisons indicated that both tibiofemoral contact centers moved significantly to the posterior on the tibial plateau (MCAP, LCAP group $\Delta\pm$SE= -1.67±0.5 mm, -8.06±1.0 mm). The findings of posterior contact patch movement with flexion, as well as the greater movement in the lateral compartment, are consistent with previous studies of knee functional anatomy.

Effect of heel wedging: ANOVA analyses did not reveal significant main or interaction effects of wedge condition. We investigated an observed sub-group difference in LCAP between wedge conditions at 20° flexion. At this flexion angle, lateral wedging was associated with an anterior migration of the lateral condyle contact patch (0.64±0.99mm, $p<0.05$, Fig 2). No significant effects of flexion and/or wedge on MCML or LCML coordinates were found.

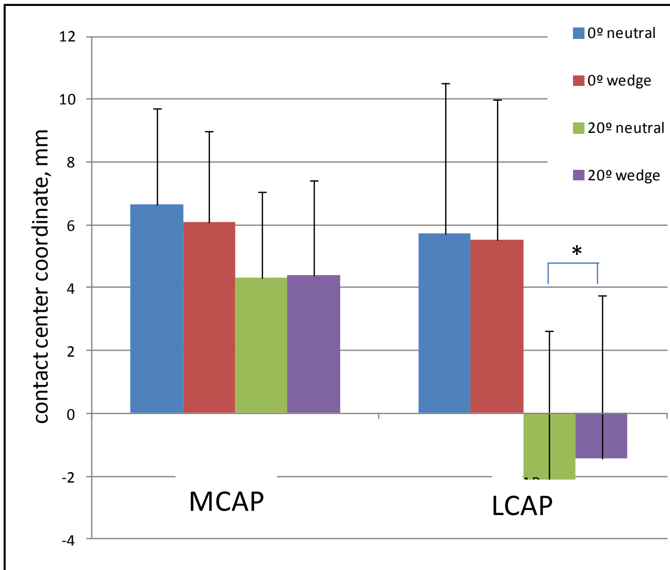

Figure 2: A/P coordinates of contact centers (mean±SD). Lateral wedging was associated with a significant anterior shift in the lateral compartment contact at 20º flexion.

CONCLUSIONS

Grouped responsiveness of contact locations to lateral heel wedging was quite small overall. In the lateral compartment, response appeared to be increased by knee flexion, and wedging was associated with a small but statistically significant shift at 20°. This is consistent with a mechanism wherein increased medial-lateral constraint of the ankle associated with dorsiflexion causes more direct transmission of the wedge effect to the knee. Such an effect underlines the importance of characterizing response at functional joint angles in weight bearing. Review of individual results revealed variability in the directionality of the responses to wedging, which suggests the need for further study into subject-specific evaluation and prescription of wedge orthoses to maximize clinical benefits with these interventions.

REFERENCES

1. Shimada Arch PMR 2006;87:1436-41.
2. Butler J Orthop Res 2007;25:1121-7.
3. Dubowsky SR, Proc. ASB 2009, State College, PA
4. Henderson et al. J Biomech Eng 2011;133:014502.

ACKNOWLEDGEMENTS

This study was supported by Department of Education (NIDRR) grant H133G080136. The authors acknowledge the contribution of Feng Wei PhD, and Carolyn Stolfi, MS in data collection and analysis methods for this project.

A longitudinal study of the knee adduction moment components post-arthroscopic partial meniscectomy

[1]Michelle Hall, [1]Tim V Wrigley, [1]Ben R Metcalf, [1]Rana S Hinman, [2,3]Alasdair R Dempsey, [2]Peter M Mills, [4]Flavia M Cicuttini, [2]David G Lloyd, [1]Kim L Bennell

[1]The University of Melbourne, Melbourne, Victoria, Australia
[2] Griffith Health Institute, Griffith University, Gold Coast, Queensland, Australia
[3]Murdoch University, Perth, Western Australia, Australia
[4]Monash University, Melbourne, Victoria, Australia
email: halm@unimelb.edu.au web: http://www.chesm.unimelb.edu.au/

INTRODUCTION

Following medial arthroscopic partial meniscectomy (APM), patients are at increased risk of developing knee osteoarthritis in the longer-term [1]. Higher medial knee joint loading during gait post-APM is thought to contribute to this increased risk of osteoarthritis. The external knee adduction moment (KAM) is often used as a proxy for dynamic medial knee joint loading and has been found to be higher in patients post-APM surgery as compared to healthy controls [2,3]. Furthermore, we have recently found that over 2 years (from 3-months post-APM surgery), the peak KAM during normal paced walking increased by 9% [2]. The KAM is largely derived as a product of the knee-ground reaction force (GRF) lever arm, and the resultant frontal plane GRF magnitude. For researchers aiming to reduce the KAM post-APM, it is of value to understand which components of the KAM likely contribute to the increase in medial knee joint loads over time in people post-APM.

In individuals measured 3 months post-medial APM (baseline) and 2-years later (follow-up), the purpose of this investigation was to determine: 1) if the knee-GRF lever arm and frontal plane GRF magnitude increased over time; 2) the correlation between the change in peak KAM and a) change in knee-GRF lever arm and b) change in frontal plane GRF magnitude; 3) how much of the variation in change of peak KAM over time is explained by the change in knee-GRF lever arm and the change in frontal plane GRF magnitude.

METHODS

This is a secondary analysis of data collected in a longitudinal study that described and compared the KAM and knee muscle strength in APM participants and healthy controls [2]. Data from 65 individuals with medial APM were collected at baseline 3 months after surgery (86% male; 41 ± 5 yrs; BMI 27.3 ± 4.2 kg/m^2) and 2 years later at follow-up (86% male; age 41 ± 6 yrs; BMI 27.3 ± 4.6 kg/m^2) were analyzed.

Participants walked barefoot at a self-selected normal pace while kinematic data (120Hz) were collected using an eight-camera motion analysis system (Vicon) with kinetic data (1080Hz) recorded using three force plates (AMTI), using the UWA model. The two primary determinants of the KAM; the knee-GRF lever arm and resultant frontal plane GRF were determined at the time of peak KAM by a custom BodyBuilder model (Vicon, Oxford, UK). Specifically, the knee-GRF lever arm was calculated as the perpendicular distance between the frontal plane GRF vector and knee joint center of rotation, and the frontal plane GRF magnitude was defined as the resultant magnitude of GRF vector in laboratory frontal plane [4]. The knee-GRF lever arm and frontal plane GRF magnitude were averaged over five trials. The knee-GRF lever arm was normalized to body height and the frontal plane GRF magnitude was normalized to body weight.

Paired t-tests were used to determine whether the knee-GRF lever arm and the frontal plane GRF changed over time. For variables that significantly changed over time, relationships between their change and change in the peak KAM were determined using Pearson correlation. Forced entry regressions were then used to determine how much variation in the change in peak KAM was explained by change in knee-GRF lever arm, change in frontal plane GRF magnitude and both measures combined. Significance was set at $p<0.05$.

RESULTS AND DISCUSSION

As previously reported, the peak KAM showed a significant 9% increase over the 2 years [2]. Paired t-tests also identified significant increases of 3.4% for the knee-GRF lever arm (p=0.016) and 1.6% for the frontal plane GRF magnitude (p=0.042) in this post-APM cohort. Significant positive correlations were found between the change in peak KAM and each of the change in knee-GRF lever arm (Figure 1), and change in frontal plane GRF magnitude (r = 0.371; p = 0.003). Regression results indicate that change in knee-GRF lever arm was a moderate predictor of the change in peak KAM (R^2 = 0.286, p <0.001). The change in frontal plane GRF magnitude was a weak predictor of the change in peak KAM (R^2 = 0.138, p = 0.003). Together the predictability of the model improved, with change in change in knee-GRF lever arm and frontal plane GRF contributing 36% to the change in peak KAM post-APM (R^2 = 0.357, p < 0.001).

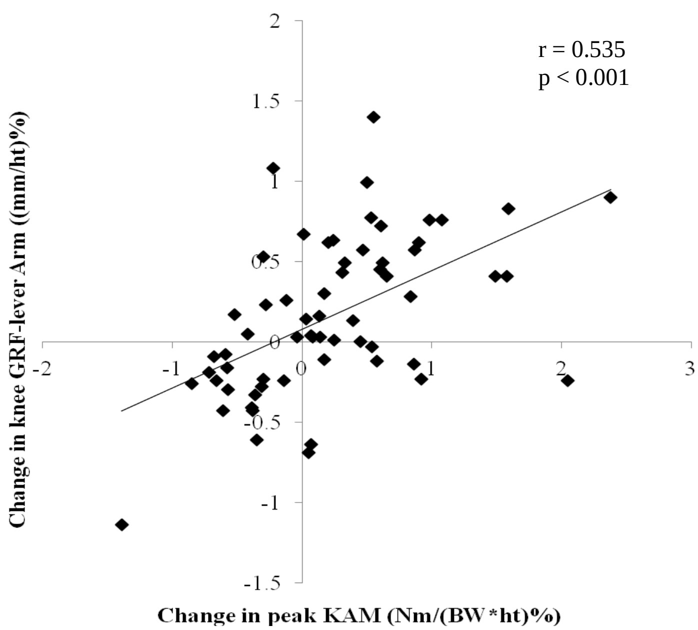

Figure 1. Relationship between change in peak KAM and change in knee-GRF lever arm. KAM: knee adduction moment; GRF: ground reaction force; ht: body height; BW: body weight

Given the association between a higher peak KAM and cartilage degeneration and osteoarthritis progression [5] it is clinically important to investigate the mechanisms underpinning the increases in the peak KAM post-APM surgery. These findings suggest that both the knee-GRF lever arm and frontal plane GRF magnitude could be targeted to potentially reduce peak KAM over time post-APM, although reasons for the increases in knee-GRF lever arm and frontal plane GRF magnitude over time cannot be determined in the current study. Potential factors could include impaired lower limb joint stability and upper body neuromuscular control following APM surgery. The regression analysis results suggest that reducing the knee-GRF lever arm may have greater impact. The knee-GRF lever arm is a function of greater "medial leaning" GRF vector in the frontal plane and/or varus posture of the knee. Three ways to reduce this would be i) more laterally directed acceleration of the upper body centre of mass, ii) greater lateral trunk lean to move the upper body centre of mass relatively closer to the knee, and/or iii) by changing the posture of lower limb so that the knee is located more medially (i.e. greater knee and hip flexion with greater hip internal rotation). A number of conservative interventions such as shoes, braces, gait retraining and/or neuromuscular exercises may potentially help to reduce increases in knee-GRF lever arm post-APM.

CONCLUSIONS

This longitudinal study identified that the increase in peak KAM post-APM is explained by increases in both each of its primary determinants (knee-GRF lever arm and frontal plane GRF magnitude). Further investigation is required identify the mechanisms underlying these changes and to investigate whether postural modifications can help reduce peak KAM in the post-APM population.

REFERENCES

1. Lohmander LS, et al. *Am J Sports Med* **35**, 1756-1769, 2007.
2. Hall M, et al. *Med Sci Sports Exerc* (submitted).
3. Sturnieks DL, et al. *J Orthop Res* **26**, 1075-1080, 2008.
4. Hinman RS, et al. *Clin Biomech* **27,** 27-33, 2012.
5. Miyazaki, T et al. *Ann Rheum Dis* **61**, 617-622, 2002

ALENDRONATE TREATMENT ELICICTS A REDUCTION IN MECHANICAL PROPERTIES AND THE DENSITY OF OSTEOCYTE CELLS IN CORTICAL TISSUE

[1,2]Joseph Geissler, [1]Devendra Bajaj, [3]Matthew Allen, [3]David Burr and [1,2]J. Christopher Fritton

[1]New Jersey Medical School, Department of Orthopaedics, Newark, NJ, USA
[2]New Jersey Institute of Technology, Department of Biomedical Engineering, Newark, NJ, USA
[3]Indiana University of Medicine, Department of Anatomy and Cell Biology, Indianapolis, IN, USA
email: frittojc@umdnj.edu

INTRODUCTION

Bisphosphonates are the most prescribed treatment for osteoporosis [1]. However, side effects are documented; they have been associated with atypical fractures of cortical bone in patients who present with low-energy induced breaks of unclear origin [2]. Possibly because the dosing effects of bisphosphonates are dependent on concentration and the time over which they are taken, longer duration use has been positively associated with greater numbers of atypical fractures [3].

The effects of bisphosphonates on the mechanical properties of cortical bone have been exclusively studied under simple, monotonic, quasi-static loading [4]. However, *in vivo*, bones are naturally loaded cyclically. This repetitive loading results in micro-damage that is normally repaired by targeted remodeling that renews bone tissue [4]. Differences in response to fatigue loading may point to mechanisms behind atypical fracture patterns [2].

We examined the cyclic fatigue properties of bisphosphonate-treated cortical bone at a level in which tissue damage initiates and is accumulated prior to frank fracture in low-energy situations. We also examined mechanisms that can lead to differences in mechanical properties. The hypotheses investigated were long-term bisphosphonate treatment impairs cortical bone: (1) tissue-level mechanical properties under fatigue loading, (2) micro-architecture, and (3) cellularity.

METHODS

In an IACUC approved study, 36 skeletally mature female beagles (1-2 yrs) were divided into 3 equal groups and treated daily for 3 years with vehicle (VEH, 1 ml/kg saline) or one of two alendronate oral doses (ALN, 0.2 or 1.0 mg/kg; Merck) [4].

Following 3 years of treatment, 10th and 11th ribs were excised and evaluated by µCT (SkyScan, 17µm resolution), microscopy and biomechanical tested for density, morphology and resistance to cyclic fatigue loading. Up to 6 cortical bone beams were machined from the medial cortices of each rib with uniform rectangular geometry (0.5x1.5x10mm) using a precision saw (Buehler Isomet 5000). Physiologically relevant (stress amplitudes ranging from 45-85 MPa), 4-point, dynamic bending (Bose Testbench) was applied sinusoidally (2 Hz) to the 72 beams until fracture in a saline bath. The periosteal side was maintained in tension and the endosteal side in compression. Stress and strain were calculated from beam theory. Fatigue life was modeled using a power law. Following mechanical loading, beams were stained with basic fuchsin and plastic embedded for histomorphometric analysis. Cross-sections from each beam were cut, polished to constant thickness, imaged by bright-field microscopy, and analyzed for number and area of pores, osteons, and osteocyte lacuna. Differences between groups were evaluated by ANOVA and Kruskal-Wallis ($p<0.05$). Post-hoc analysis was completed with Bonferroni correction.

RESULTS AND DISCUSSION

Cortical bone beams demonstrated mechanical failure, micro-architectural features and cellularity that were dependent on ALN drug dose. Cyclic fatigue loading of beams resulted in a significant 3-fold reduction in the number of cycles to failure for ALN1.0 treatment compared to VEH (Fig 1).

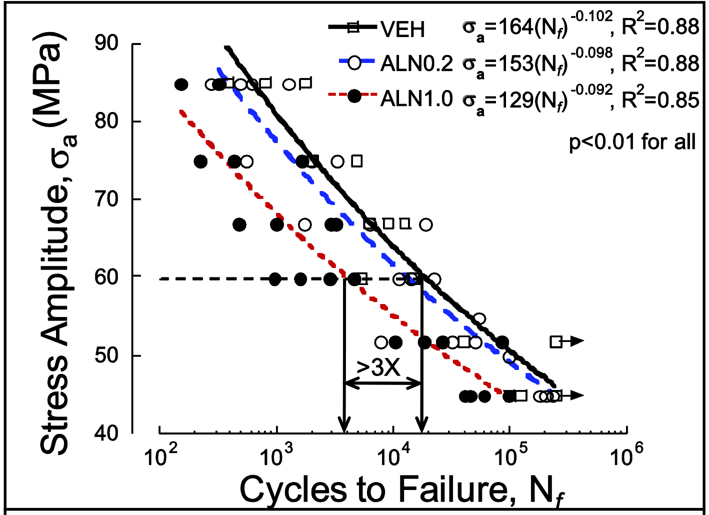

Fig 1: *Fatigue-life diagrams for bone beams cyclically tested under 4-point bending at 6 stress amplitudes.*

Resistance to load (initial stiffness) was also reduced by 21% with ALN1.0. This observation indicates that, prior to exposing the beams to cyclic loading, the drug treatment had already affected the material's mechanical properties.

While not affecting mineral density or the number of osteons, ALN reduced other features associated with bone remodeling. The average size of individual osteons was reduced by 14% in ALN1.0 compared to VEH, as was the density of osteocyte lacunae (-20%) in both ALN1.0 and ALN0.2, compared to VEH. Interestingly, the osteocyte density was directly proportional to the ability of cortical bone tissue to resist loading (R=0.54). This relationship might offer a means of predicting the mechanical properties of osteonal bone.

The observed reduction in osteon size is likely due to decreased individual osteoclast tunneling (Fig 2). The conservation of osteon size not only maintains the amount of interstitial area where damage tends to be found, but also ensures that osteons remain in close proximity to one another, providing structural reinforcement. Reduced osteonal osteocyte lacunar density may be associated with the effects of bisphosphonates on the reduced rate of overall remodeling (Fig 2). These observations have helped us to gain a deeper understanding of the mechanisms behind bone remodeling.

CONCLUSIONS

Combined, these results suggest that tissue-level structural components normally contributing to healthy bone are altered by ALN treatment and contribute to reduced mechanical properties under cyclic loading conditions.

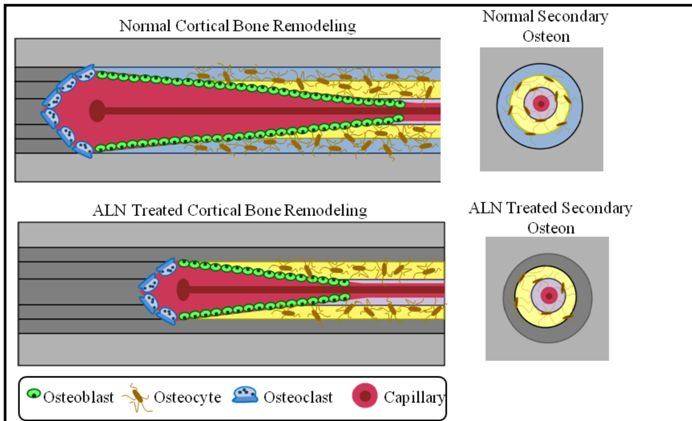

Fig 2: *Model for reduced size of osteons, increased micro-crack length and lower osteocyte density due to ALN treatment.* Reduced osteoclast tunneling leaves behind more, older interstitial tissue where most micro-crack initiate and lengthen. Less interface area between old interstitial and new osteon tissue further reduces the tough, energy-absorbing capacity for slowing crack growth and accumulation and can lead to a significant reduction in tissue stiffness and number of cycles to failure as measured in this study. The formation of a smaller resorption tunnel also requires fewer osteoblasts to refill, resulting in decreased osteocyte formation.

REFERENCES

1. Cummings et al. *JAMA* **280**, 2077-2082, 1998.
2. *FDA Meeting of Advisory Committee for Reproductive Health Drugs and Drug Safety*, September 9, 2011.
3. Dell et al. *J Bone Miner Res* **27**, 2544-2550, 2012.
4. Allen et al. *Calcif Tissue Int* **82**, 354-360, 2008.

ACKNOWLEDGEMENTS

Shahir Monsuruddin, Sadiq Khan, Linda Uko and Edek Williams provided technical assistance. Alendronate was provided at no cost by Merck. Funding was supported by NIH (C06 RR010601, AR062002, AR007581, AR047838, AR063351), NASA (NCC 9-58), Sigma Xi and the NJ Space Grant Consortium.

HETEROGENEOUS REGIONAL FASCICLE BEHAVIOR WITHIN THE BICEPS FEMORIS LONG HEAD

Hunter Bennett, Patrick Rider, Zachary Domire, Paul DeVita, and Anthony S. Kulas

East Carolina University, Greenville, NC, USA
email: bennetth11@students.ecu.edu web: http://www.ecu.edu/cs-hhp/exss/biomechlab.cfm

INTRODUCTION

Biarticular muscles exhibit heterogeneous within muscle behavior at both the muscle fiber and fascicle levels in modeling [1,2] and animal studies [3]. Modeling of regional muscle fibers predicted greater along fiber strain in the region closest to the proximal musculotendinous junction of the biceps femoris long head (BFLH) where, coincidently, the majority of hamstring strains occur [2,4,5]. *In vivo* evidence of heterogeneity in regional fascicle behavior within the BFLH of humans could potentially help explain the disproportionate injury rate in the proximal vs. distal regions, e.g. provide empirical evidence of relatively large proximal fascicle strains. The purpose of this study is to assess the behavior of proximal and distal fascicles in BFLH under selected isometric muscle contraction levels. We hypothesize that the proximal fascicles will be longer [6], and will shorten more than their distal counterparts.

METHODS

Eleven healthy, recreationally active, and resistance trained, subjects (males=5, females=6, age: 21±1yrs, height: 168±10cm, mass: 66±11kg) providing university approved informed consent. Using a GE Logiq E ultrasound unit, panoramic ultrasound images were taken of the BFLH at rest (hip and knee flexed 45°) and during four sustained contractions of 10, 25, 50, and 75% MVIC torque, while prone on a dynamometer. A 13-5 MHz linear array transducer set at a median frequency of 8MHz imaged the muscle along its entire length. Electromyography recorded activation of the BFLH and semitendinosus/semimembranosus (ST/SM) during MVIC and ramp trials of 80% MVIC. Only ST/SM activation was recorded during subsequent study conditions so that panoramic imaging could be performed of the entire BFLH. Activation levels of BFLH and ST/SM during ramp trials were highly non-linear on individual bases (R^2 range = .83-.99, $P<.01$). Regression equations obtained from the power correlation were used to predict BFLH activation from ST/SM activation. Confirming the presence of four distinct activation conditions, a 2 (region) x 5 (contraction) Repeated Measures ANOVA showed significant differences between each of the four isometric conditions for predicted BFLH activation (20.6%±8.7, 29.9%±11.2, 50.4%±14.1, and 66.7%±14.7; $P<.001$) recorded during the four isometric contractions. The midline of each panoramic muscle length was first measured and marked using digital calipers. Fascicles with more than 75% of length in the proximal half were considered proximal fascicles, and those above 75% of length in the distal half were considered distal fascicles. Two fascicle measurements were made in each half of the muscle, and their lengths were averaged to obtain a representation of the fascicle lengths in each region.

The RMANOVA assessed if mean fascicle lengths were different by condition, region, and/or a condition by region interaction. In the presence of a significant condition by region interaction, Tukey's post hoc testing would be performed. To assess whether the changes in fascicles length (cumulative change from passive state) across condition were different in proximal vs. distal regions, paired samples t-tests were performed.

RESULTS AND DISCUSSION

The RMANOVA showed significant main effects for region, with longer proximal fascicles (11.023 cm, 95%CI 10.147, 11.898) than distal counterparts (8.23cm, 95%CI 7.47, 8.99; $P<.001$) across all conditions. A region by condition interaction showed significant incremental shortening in the proximal fascicles from the passive state to 50% BFLH activation while the distal regions showed only significant incremental shortening from passive to 20% BFLH activation (Figure 1, P<.01). In addition, Tukey's post hocs also showed significant cumulative shortening in both the proximal and distal fascicles when each activation level was referenced to the resting state (Figure 1, see brackets **).

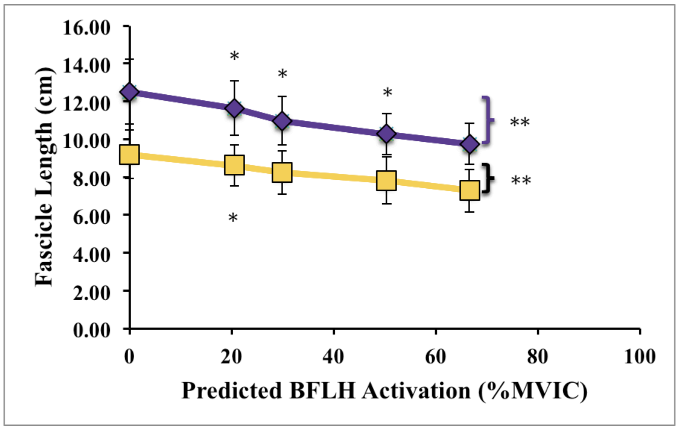

Figure 1: **Regional fascicle lengths according to BFLH activation.** Purple and black brackets refer to total change in proximal and distal fascicle lengths, respectively. * denote significant increment length change, and ** denote lengths had significant cumulative shortening compared to resting states for all conditions and both regions (P<.01).

Paired samples t-tests revealed that the cumulative fascicle shortening, absolute change in length referenced to no contraction, was significantly higher in the proximal vs. distal fascicles at the 29.9%, 50.4%, and 66.7% activation conditions (Figure 2, all P<.001).

Our research study is limited in that it was performed on isometric and not eccentric contractions. While the results show heterogeneity of regional fascicle shortening within the BFLH above ~30% activation, future studies investigating *in vivo* regional fascicle lengthening at different activation levels would further substantiate that heterogeneity is not specific to contraction type.

While this study is to our knowledge the only evidence of *in vivo* non-uniform behavior at the fascicle level of the BFLH, heterogeneity has been found in tissue displacement through imaging of the most proximal tissue during eccentric contractions [6].

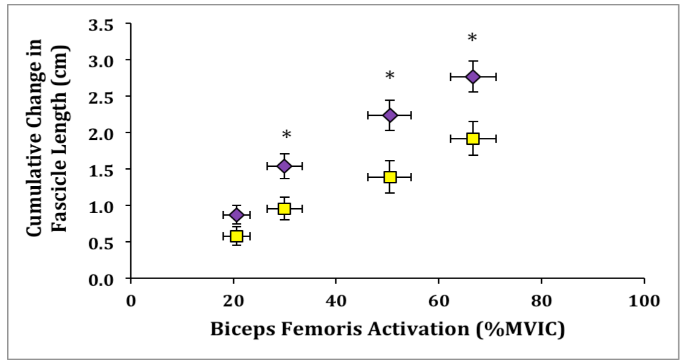

Figure 2. Regional fascicle length changes at each activation level referenced to passive state. Purple denotes proximal and gold denotes distal regions. Asterisks denote significant length change between conditions (p<.01).

CONCLUSIONS

These data confirm our hypothesis that proximal fascicles are longer than their distal counterparts, and that non-uniform shortening exists between the two regions of the BFLH.

This study increases our understanding of within muscle fascicle behavior during isometric contractions. With further research in eccentric contractions we may better understand the mechanisms behind the high injury rate of hamstring strains in the proximal region of the BFLH.

REFERENCES

1. Blemker S, et al. *J Biomech* **38**, 657-665, 2004.
2. Rehorn MR, et al. *J Biomech* **43**(13): 2574-2581, 2010.
3. Ahn AN, et al. *J Physiol* **549**(3): 877-888, 2003.
4. De Smet A & Best T. *AJR* **174**: 393-399, 2000.
5. Askling, et al. *J Sports Med* **35**(2): 197-206, 2007.
6. Silder A, et al. *J Biomech* **43**, 2254-2260, 2010.

ORAL PRESENATIONS – THURSDAY SEPTEMBER 5th

	Thematic: Amputee Gait *Richard Neptune*
4:15 PM	Whole-Body Angular Momentum In Individuals With Unilateral Transtibial Amputation During Stair Walking **Pickle N, Wilken J, Aldridge J, Neptune R, Silverman A**
4:30 PM	Lateral Margins Of Stability In Individuals With Transtibial Amputation Walking In Destabilizing Environments **Beltran E, Beurskens R, Dingwell J, Wilken J**
4:45 PM	Knee Swing-Initiation And Ankle Plantar Flexion Control Using An Active Prosthesis Across Walking Speeds And Users **Fey N, Simon A, Young A, Hargrove L**
5:00 PM	Active Dorsiflexing Prostheses May Reduce Trip-Related Fall-Risk **Rosenblatt N, Bauer A, Rotter D, Hoops M, Grabiner M**

WHOLE-BODY ANGULAR MOMENTUM IN INDIVIDUALS WITH UNILATERAL TRANSTIBIAL AMPUTATION DURING STAIR WALKING

[1]Nathaniel T. Pickle, [2]Jason M. Wilken, [2]Jennifer M. Aldridge, [3]Richard R. Neptune and [1]Anne K. Silverman
[1]Department of Mechanical Engineering, Colorado School of Mines, Golden, CO, USA
[2]Center for the Intrepid, Department of Orthopedics and Rehabilitation, Brooke Army Medical Center, Ft. Sam Houston, TX, USA
[3]Department of Mechanical Engineering, The University of Texas at Austin, Austin, TX, USA
email: npickle@mines.edu website: inside.mines.edu/~asilverm

INTRODUCTION

Whole-body angular momentum (H) must be carefully controlled during walking to maintain dynamic balance and avoid falling. Humans regulate H during walking by altering the net external moment about the body center-of-mass (COM), which equals the time rate of change of H and is a function of ground reaction forces (GRFs) and external moment arms. Muscles are the primary contributors to the net external moment [1], and are therefore the primary regulators of H. Individuals with transtibial amputation (TTA) have altered H compared to able-bodied (AB) individuals during walking on level ground [2], likely due to the functional loss of the ankle plantarflexors. On stairs, TTA also have altered kinematics and kinetics relative to AB [3], but the differences in H between TTA and AB during stair walking remain unclear.

Recently, prostheses with active ankle joints have been developed [4]. These devices generate power at the ankle and reduce the metabolic cost of overground walking in TTA [5]. However, the effects of powered prostheses on H are unknown. Therefore, the goal of this study was to investigate H in TTA using both passive and powered prostheses relative to AB during stair ascent, level walking and stair descent. GRFs, external moment arms and net joint powers were also investigated to help interpret the H results.

METHODS

Nine TTA and nine AB participants completed a biomechanical walking assessment. TTA were assessed while using their clinically prescribed passive energy storing and return (ESR) prosthesis and with the BiOM (iWalk, Bedford, MA) powered prosthesis (PWR). Whole-body kinematics and GRF data were collected at 120 Hz and 1200 Hz, respectively, while participants ascended and descended a 16-step staircase with four instrumented steps using a step-over-step pattern at a fixed cadence of 80 steps/min. The participants also walked on level ground at a fixed walking speed based on leg length.

Kinematic and kinetic data were filtered at 6 Hz and 50 Hz, respectively, using a 4th order low pass Butterworth filter. A 13-segment inverse dynamics model was used to compute net joint powers and H as

$$\vec{H} = \sum_{i=1}^{n} [(\vec{r}_i^{COM} - \vec{r}_{body}^{COM}) \times m_i (\vec{v}_i^{COM} - \vec{v}_{body}^{COM}) + I_i \vec{\omega}_i]$$

where n is the number of segments, $\vec{r}_i^{COM}, \vec{v}_i^{COM}$, and $\vec{\omega}_i$ are, respectively, the position, velocity, and angular velocity of the i^{th} segment, $\vec{r}_{body}^{COM}$ and $\vec{v}_{body}^{COM}$ are, respectively, the position and velocity of the whole-body COM, and m_i and I_i are the mass and inertia matrix of the i^{th} segment. H was normalized by subject height and body weight and expressed from 0 to 100% of the gait cycle. The range of H in all three anatomical planes, peak values of the GRFs, external moment arms, and net joint powers were statistically compared across walking condition (stair ascent, level walking and stair descent) and subject group (ESR, PWR, AB) using a mixed model, repeated measures ANOVA with post hoc pairwise comparisons (α=0.05).

RESULTS AND DISCUSSION

No statistically significant differences in the range of H were observed between groups (ESR, PWR, AB) in the frontal or transverse planes for any walking condition.

During stair ascent, the range of *H* in the sagittal plane during the first half of the gait cycle (during prosthetic limb stance) was greater for both ESR (p=0.008) and PWR (p=0.004) relative to AB (Fig. 1). The range of sagittal *H* during the second half of the gait cycle was similar between AB and both ESR and PWR. The range of *H* was not significantly different between ESR and PWR. Similarly, in level walking, there was no difference in the range of *H* between ESR and PWR. The range of *H* was larger for ESR and PWR relative to AB in the first half of the gait cycle, but not significantly different in the second half, contrary to previous results [2].

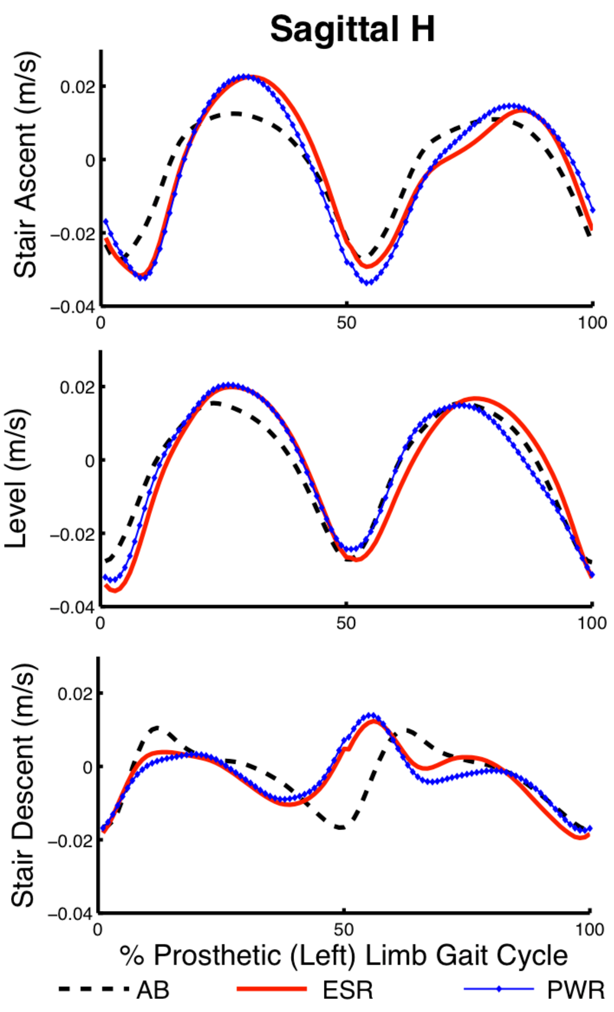

Figure 1: Sagittal plane *H* for AB, ESR, and PWR groups, normalized by subject height and weight.

The peak vertical GRF in the intact (trailing) limb was increased in ESR (p=0.015) and PWR (p=0.001) relative to AB during the push-up phase (0-10% prosthetic limb gait cycle) of stair ascent, contributing to a negative (forward) net external moment and negative slope of the *H* trajectory. In addition, the prosthetic limb anterior external moment arm was increased during pull-up in ESR (p<0.001) and PWR (p=0.017) relative to AB, contributing to a greater positive (backward) external moment from the prosthetic (leading) limb vertical GRF (10-30% of the prosthetic limb gait cycle). Further, peak prosthetic limb hip extension power generation during pull-up was increased in ESR (p<0.001) and PWR (p<0.001) relative to AB during stair ascent, suggesting a greater contribution from the hip extensors to positive *H* [1].

During stair descent, all groups had a significantly reduced range of sagittal *H* relative to level walking, but there were no significant differences between groups. This reduced range of sagittal *H* during stair descent is similar to results for AB during decline slope walking [6], and may be a protective mechanism to reduce fall risk.

CONCLUSIONS

Significant differences in net joint powers between TTA and AB suggest TTA use compensations (e.g., prosthetic limb hip power and intact limb ankle power) during stair walking, regardless of prosthesis type [3]. The lack of significant differences in *H* between the passive and powered prosthesis suggests that, although the powered prosthesis provides increased ankle power generation in the prosthetic limb, it does not provide a distinct advantage over a passive prosthesis in the regulation of *H*.

REFERENCES

1. Neptune RR, et al. *J. Biomech*, **44**, 6-12, 2011.
2. Silverman AK, et al. *J. Biomech,* **44**, 379-385, 2011.
3. Aldridge JM, et al. *Gait & Posture,* **36**, 291-295, 2012.
4. Eilenberg MF, et al. *IEEE Trans. On Neural Systems and Rehab. Eng.,* **18**, 164-173, 2010.
5. Herr HM, et al. *Proc. R. Soc. B.,* **279**, 457-464, 2012.
6. Silverman AK, et al. *J. Biomech,* **45**, 965-971, 2012.

LATERAL MARGINS OF STABILITY IN INDIVIDUALS WITH TRANSTIBIAL AMPUTATION WALKING IN DESTABILIZING ENVIRONMENTS

[1]Eduardo J. Beltran, [1,2]Rainer Beurskens, [2]Jonathan B. Dingwell, and [1]Jason M. Wilken

[1]Department of Orthopedics and Rehabilitation, Center for the Intrepid,
Brooke Army Medical Center, Ft. Sam Houston, TX, USA
[2]Department of Kinesiology, University of Texas at Austin, Austin, TX, USA
email: eduardo.j.beltran.ctr@us.army.mil

INTRODUCTION

The ability to effectively respond to perturbations is required to maintain stability and prevent falls during walking. Individuals with lower-limb amputation face higher risk of falling, possibly due to loss of distal sensation and physical limitations such as lack of ankle control. These patients are therefore commonly assumed to be less stable than able-bodied individuals [1-3]. However, recent findings do not fully support the assumption [2,3].

Assessments of stability commonly focus on the mediolateral (ML) direction because walking is more unstable in that direction [4,5]. Dynamic margins of stability (MOS) [6], a measure that incorporates foot placement and center of mass (COM) velocity, has been used to assess responses to controlled perturbations in healthy adults [4]. Along with the direct measurement of COM motion, it can be used to indentify compensatory strategies adopted by individuals with unilateral transtibial amputation (TTA) [2].

This study quantified MOS and COM motion to assess ML dynamic stability in individuals with unilateral transtibial amputation (TTA) and able-bodied (AB) controls as they responded to continuous ML visual or mechanical perturbations.

METHODS

Thirteen healthy able-bodied individuals (24.8 ± 6.9 yrs) and nine individuals with traumatic unilateral transtibial amputation (30.7 ± 6.8 yrs) participated. Subjects walked in a Computer Assisted Rehabilitation ENvironment (CAREN) system (Motek, Amsterdam, Netherlands). Whole-body kinematics data were collected at 60 Hz using a 24-camera motion-capture system (Vicon, Oxford, UK). Subjects completed five 3-minute walking trials under each of three test conditions. Subjects walked with either no perturbations (NOP) or with pseudo-random mediolateral translations of the platform (PLAT) or visual field (VIS) [4].

MOS [6] were calculated as the ML distance between the lateral edge of base of support (BOS), defined by the 5^{th} metatarsal of the foot in heelstrike, and the extrapolated center of mass (XcoM). XcoM was calculated as

$$XcoM = COM + \dot{COM}/\sqrt{g/l}$$

where g = 9.81 m/s^2 and l was the equivalent pendulum length [7].

The minimum value of MOS during the stance phase of each step was determined for each leg. Also, components of MOS were measured using COM data including the lateral distance between COM and BOS at initial contact ($BOS\text{-}COM_{IC}$), the COM range of motion during stance (ROM), and the COM peak velocity during stance (PV).

All dependent measures were compared using mixed-design ANOVAs (condition × limb × group).

RESULTS AND DISCUSSION

Mean MOS during PLAT and VIS conditions were greater than NOP for both AB and TTA ($p < 0.005$; Fig. 1A). PLAT and VIS also exhibited greater MOS variability than NOP for both groups ($p < 0.001$). For controls, mean MOS were greater on the right side than on the left ($p < 0.05$). No between-group differences were found for either mean MOS or MOS variability.

Mean BOS-COM$_{IC}$ for VIS and PLAT conditions were greater than NOP for both AB and TTA group ($p < 0.001$; Fig. 1B). AB exhibited greater mean BOS-COM$_{IC}$ on the right leg than on the left leg ($p < 0.05$). TTA exhibited greater mean BOS-COM$_{IC}$ on the intact limb than the prosthetic limb ($p < 0.005$). Finally, during the PLAT condition, TTA exhibited greater values than AB for BOS-COM$_{IC}$ variability ($p < 0.005$; not shown), mean and variability of ROM ($p < 0.01$; not shown), and variability of PV ($p < 0.05$; not shown).

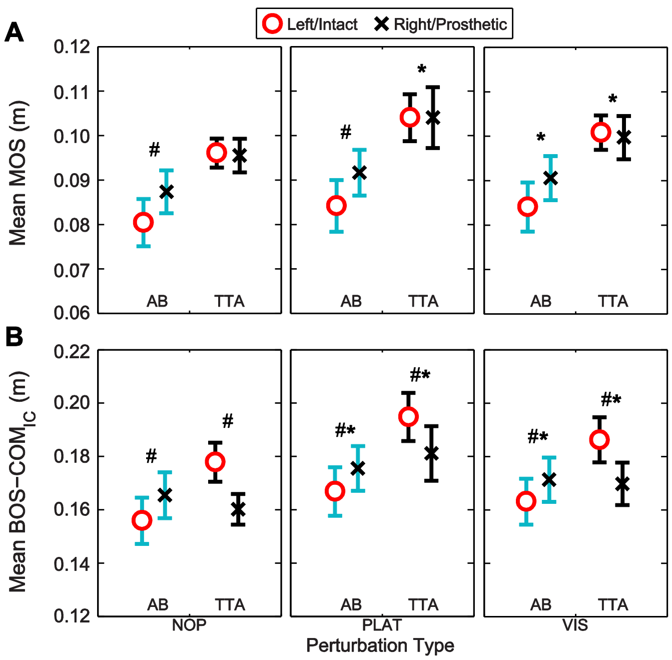

Figure 1. (A) Mean mediolateral MOS and (B) mean distance between COM and BOS at initial contact (BOS-COM$_{IC}$) for controls (AB) and amputees (TTA). '○' indicate left leg for controls and intact limb for amputees. '×'indicate right leg for controls and the prosthetic limb for the amputees. Error bars represent between-subject standard error. '*' indicate significant ($p < 0.05$) differences from NOP. '#' indicate significant differences between limbs.

Individuals with TTA and AB had increased mean MOS and MOS variability in response to the VIS and PLAT perturbations demonstrating a consistent response to the destabilizing effects of the environment. No difference was observed between groups suggesting the individuals with TTA have compensated for impaired limb function. The young age and physical ability of the individuals with TTA may have allowed them to adopt effective strategies for maintaining performance similar to that of age-matched individuals. The significant between-group differences in measures of BOS-COM$_{IC}$ variability, mean and variability of ROM, and variability of PV suggest that individuals with TTA used a wider range of movements to achieve the same mean performance as AB.

CONCLUSIONS

Patients with unilateral TTA who are active and otherwise healthy were not "less stable" (as determined using mean MOS) than able-bodied controls when mechanically or visually perturbed. However, between-limb differences and between-group differences found in COM motion suggest that amputees used different strategies than controls for adjusting stepping movements to respond to the applied perturbations. These different strategies then allowed them to achieve the same mean MOS.

REFERENCES

1. Miller WC, et al., *Arch Phys Med Rehabil* **82**(8): 1031-7, 2001.
2. Gates DH, et al., *Gait Posture* (In press), 2013.
3. Curtze C, et al., *Gait Posture* **33**(2): 292-6, 2011.
4. McAndrew Young PM, et al., *J Biomech* **45**(6): 1053-9, 2012.
5. O'Conner SM, Kuo AD, *J Neurophysiol* **102**(3): 1411-9, 2009.
6. Hof AL, et al., *J Biomech* **38**(1): 1-8, 2005.
7. Massen CH, Kodde L, *Agressologie* **20**: 107-8, 1979.

ACKNOWLEDGEMENTS

Supported by NIH grant 5R01HD059844.

The view(s) expressed herein are those of the author(s) and do not reflect the official policy or position of Brooke Army Medical Center, U.S. Army Medical Department, U.S. Army Office of the Surgeon General, Department of the Army, Department of Defense or the U.S. Government.

KNEE SWING-INITIATION AND ANKLE PLANTAR FLEXION CONTROL USING AN ACTIVE PROSTHESIS ACROSS WALKING SPEEDS AND USERS

Nicholas P. Fey, Ann M. Simon, Aaron J. Young and Levi J. Hargrove

Center for Bionic Medicine, Rehabilitation Institute of Chicago, Chicago, IL, USA
Department of Physical Medicine and Rehabilitation, Northwestern University, Chicago, IL, USA
email: nfey@ricres.org web: http://www.ric.org/research/centers/cbm/

INTRODUCTION

Lower-limb amputees commonly experience abnormal gait characteristics, chronic pain and joint disorders [for review, see 1]. These behaviors are attributed to the absence of muscles and use of prostheses that inadequately restore muscular functions. Moreover, the prevalence and/or intensity of these behaviors generally increase as the level of leg amputation increases [1]. Therefore, advancing prostheses to better emulate the biological system is important, in particular for individuals with a high level of amputation such as above-knee amputees.

The large majority of available prostheses are mechanically-passive devices. Conversely, muscles produce, dissipate or transfer power about the hip, knee and ankle to satisfy energetic requirements of locomotor tasks [e.g., 2]. Recently developed mechanically-active (i.e., powered) prostheses [e.g., 3, 4] have the capacity to more closely approximate the biological system. However, more effective and generalizable control strategies governing the power transfer to each user are needed. Furthermore, strategies that are biomimetic and generalizable across users as well as user-initiated modulations of ambulation speed would be beneficial.

The purpose of this study was to develop a generalizable control strategy of an active knee and ankle prosthesis and demonstrate its performance across various walking speeds and amputee users.

METHODS

An active prosthesis was controlled using a finite state machine and impedance models of the knee and ankle [4]. The models consisted of an angular stiffness, damping and equilibrium position in each state. Within this framework, we implemented four modifications to control stance.

Based on experiments of non-amputee walking [5], we facilitated increasing ankle stiffness during controlled dorsiflexion as a linear function of ankle angle, normalized to user weight. Also based on data from non-amputees [6], we decreased knee stiffness during terminal stance as a linear function of decreasing axial shank force. Similarly, knee swing initiation and powered ankle plantar flexion were controlled by changes of their equilibrium positions as linear functions of shank force.

A rate-based equation, containing straightforward tuning constants, was developed to modify a given impedance parameter, p_i, as a function of decreasing axial shank force, F, (i.e., a load cell measurement).

$$p_i = \boldsymbol{C_i}\ x \left(\frac{F - F_{Initial}}{F_{Initial} - F_{Final}}\right) x\left(p_{i_{Initial}} - \boldsymbol{p_{i_{Final}}}\right) + p_{i_{Initial}}$$

Two tuning constants (in bold) were proportionality constants, $\boldsymbol{C_i}$, which scaled each rate-of-change, and final "desired" impedance values, $\boldsymbol{p_{i_{Final}}}$. Other constants were either detected at state changes or constrained by the state machine.

We tested 4 amputees (3 traumatic, 1 sarcoma; 43±20 years age; 23±21 years post-operation). Amputation level varied from knee disarticulation to the proximal third of the femur. All had Medicare functional classification levels 3 or higher and a minimum of 10 hours experience using the device. For each user, the prosthesis was tuned at their comfortable speed. Subjects walked at 3 self-selected speeds (comfortable, slow and hurried). No additional adjustments were made across speeds. An average of 20 strides was collected per condition. The onboard inertial measurement unit and potentiometers were used to estimate walking speed [7] and joint angles. Knee and ankle power were computed as the product of commanded joint torque and joint velocity.

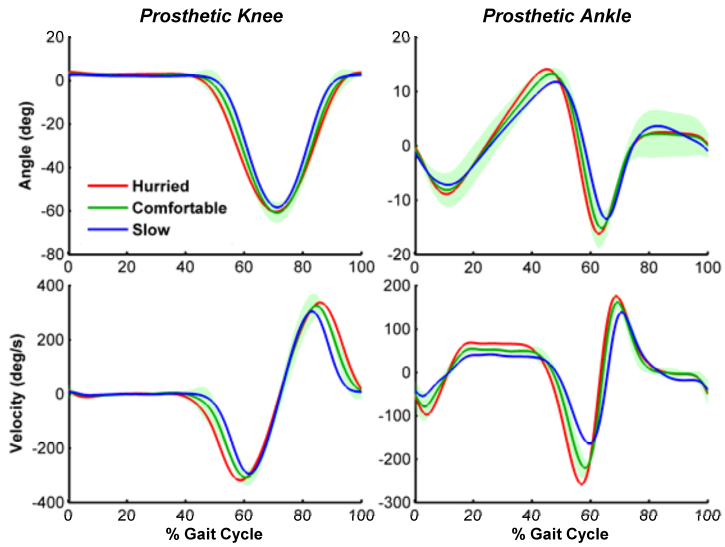

Figure 1: Group averaged prosthetic joint angles and velocities. Comfortable speed standard deviations are shaded.

RESULTS AND DISCUSSION

Seamless modulations of walking speed relative to the comfortable condition were facilitated (i.e., increases *and* decreases of 30±8%). Slow, comfortable and hurried speeds were 0.58, 0.82 and 1.1±0.09 m/s, respectively. As speed increased, increases of peak ankle dorsiflexion and plantar flexion were observed (Fig. 1). Also for increasing speed, negative and positive ankle power increased during stance (Fig. 2). These trends and magnitudes are comparable to non-amputees at these speeds [e.g., 8], especially from mid to late stance. The plantar flexors provide body support and forward propulsion in the second half of stance, and increase their contributions as speed increases [2]. These data suggest the prosthetic ankle behaved similarly.

The stance to swing transition was timed appropriately and performed smoothly since it was a function of a decreasing axial force. This was supported by knee flexion angles initiated earlier as speed increased (Fig. 1). However, *net* knee power over this transition was positive at the two slowest speeds (Fig. 2), contrasting non-amputee data [6, 8]. These differences suggest the prosthetic knee (i.e., with one actuator per degree-of-freedom) may not consistently replace all knee muscle functions (e.g., gastrocnemius and rectus femoris functions, described in [2]). However, these data suggest this control strategy provided appropriate knee flexion kinematics across a range of speeds and users.

These results were produced with little variation of stance phase tuning constants across subjects. Proportionality constants governing decreasing knee stiffness, swing initiation and powered plantar flexion did not vary (1.0, 1.0 and 1.5, respectively). In addition, final plantar flexion equilibrium angles were 10-12º. Final knee flexion equilibrium angles were an exception as they had larger variations (45-70º). These differences were needed to achieve ground clearance for the various amputation levels while the distance between the knee and ankle was fixed (i.e., a current device constraint) [4].

CONCLUSIONS

These rate-based control strategies of an active prosthetic knee and ankle enable amputees to alter their speeds, while displaying kinematic and kinetic profiles supportive of scalable prosthesis function. The generalizability of these strategies was further demonstrated by minimal tuning across users.

REFERENCES

1. Gailey R, et al. *J Rehabil Res Dev* **45** (1), 15-29, 2008.
2. Neptune RR, et al. *Gait & Posture* **28**(1), 135-43, 2008.
3. Au S, et al. *Neural Networks* **21**(4), 654-66, 2008.
4. Sup F, et al. *Int J Rob Res* **27**(2), 263-73, 2008.
5. Rouse RR, et al. *IEEE BioRob*, 2012.
6. Winter DA. *Univ. of Waterloo Press*, 1991.
7. Yang S, et al. *Med Biol Eng Comput* **50**(4), 383-93, 2012.
8. Silverman AK, et al. *Gait & Posture* **28**(4), 602-609, 2008.

ACKNOWLEDGEMENTS

The U.S. Army's TATRC grant 81XWH-09-2-0020 supported this research. We thank Robert Lipschutz, Suzanne Finucane, Elizabeth Halsne and Kim Ingraham for their assistance.

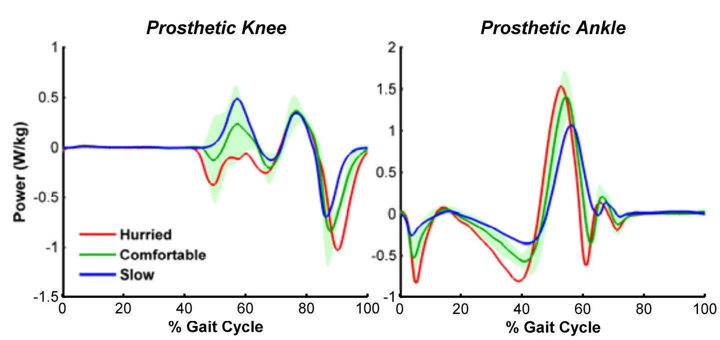

Figure 2: Group averaged prosthetic joint powers. Comfortable speed standard deviations are shaded.

ACTIVE DORSIFLEXING PROSTHESES MAY REDUCE TRIP-RELATED FALL-RISK

[1]Noah J Rosenblatt, [2]Angela Bauer, [2]David Rotter, [1]Mackenzie L. Hoops, [1]Mark D. Grabiner

[1] University of Illinois at Chicago, Department of Kinesiology and Nutrition, Chicago, IL, USA;
[2] Scheck & Siress Prosthetics and Orthotics, Chicago, IL USA,
Website: www.uic.edu/ahs/biomechanics; Email: nrosenbl@uic.edu

INTRODUCTION

A considerable amount of research has focused on reducing falls in older adults, yet little has been directed at reducing falls in amputees, a population known to fall at higher rates than their peers [1] likely due to compromised musculature. During swing, ankle dorsiflexion muscles act to increase toe clearance. For transtibial amputees (TTA), the absence of these muscles may increase fall-risk by decreasing toe clearance and, in turn, increasing the probability that the swing foot will contact an unseen obstacle [2]. The active swing phase dorsiflexion provided by the ProprioFoot is intended to increase toe clearance during level-ground walking. The ProprioFoot also adapts to inclines by increasing stance phase dorsiflexion. Initiating swing with a dosiflexed ankle should also aid toe clearance on inclines. The purpose of this study was to validate these functions. Given that ankle, hip and knee kinematics can all influence toe clearance [3,4] we also sought to characterize the extent to which increased toe clearance reflects active dorsiflexion rather than changes in hip/knee kinematics; if greater toe clearance (and reduced stumbling probability) can be attributed to active dorsiflexion then greater user safety may be attributed to the ProprioFoot. The hypotheses tested were: 1) regardless of incline the ProprioFoot would significantly increase toe clearance and 2) increased toe clearance can be attributed to the active dorsiflexion.

METHODS

Twelve unilateral TTA subjects, all level K3/K4 ambulators, participated (49.0±12.1 yrs; 93.0±23.1 kg; 1.74±0.10 m). Eleven subjects were existing users of conventional prosthetic feet without active dorsiflexion (control subjects) and one used the ProprioFoot. Six control subjects were tested, then fit with the ProprioFoot and allowed four weeks to accommodate to it before retesting. During testing subjects walked at a self-selected speed on a treadmill set to 0% and 5% grade (incline), while wearing a safety harness. For each condition, subjects walked at least two minutes while an 8-camera motion capture system tracked the movements of markers placed on the extremities. Prior to data collection, subjects acclimated to treadmill walking and chose their speed (level: 0.92±0.16 m/s; incline: 0.89±0.17 m/s). For crossover subjects, speeds were matched for each grade.

Toe clearance was quantified as the vertical distance between the marker on the second metatarsal head and the treadmill surface at 50% of swing or when a local minimum occurred, relative to the distance at toe off (TO). For each subject and condition mean values of minimum toe clearance (MTC) were compared using a 2x2 (group x incline) mixed model ANOVA.

For hypothesis two, we used the geometric model described by Moosabhoy and Gard (2006) to express the vertical height of the toe ($T_z(t)$; t is time) as a function of four variables: hip height ($H_z(t)$), and sagittal plane hip, knee and ankle angles ($\alpha(t)$, $\beta(t)$, and $\gamma(t)$, respectively) (Fig 1). The partial derivatives of this function with respect to these four variables represents the sensitivity of $T_z(t)$, to changes in these variables (units: mm/rad). Throughout most of the time period from TO to MTC, the sensitivity of T_z with respect α is negative (increased hip flexion (α) brings the toe closer to the ground). As with healthy able-bodied subjects [4], the sensitivity with respect to α remains negative from TO until just before MTC, whereas the sensitivity with respect to β and γ are positive the

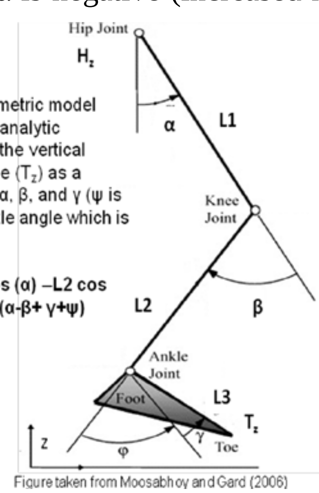

Figure 1. Geometric model used to derive analytic expression for the vertical height of the toe (T_z) as a function of H_z, α, β, and γ (ψ is the neutral ankle angle which is constant):

$T_z = H_z - L1\cos(\alpha) - L2\cos(\alpha-\beta) - L3\cos(\alpha-\beta+\gamma+\psi)$

Figure taken from Moosabhoy and Gard (2006) entire time. Accordingly the motion of the hip from TO until MTC should negatively affect (reduce) MTC and this should be countered by positive contributions of β and γ. To quantify this effect, we used the fact that MTC is the change in T_z between two time points and expressed it as a total differential:

$$MTC = \int_{t=TO}^{t=MTC} \left(\frac{\partial Tz}{\partial \alpha}\frac{d\alpha}{dt} + \frac{\partial Tz}{\partial \beta}\frac{d\beta}{dt} + \frac{\partial Tz}{\partial \gamma}\frac{d\gamma}{dt} + \frac{dHz}{dt} \right) dt$$

(note: $\partial T_z/\partial H_z=1$). This expression accounts for the time course of each variable from TO to MTC, and how, given the values of the other variables, this time course affects toe height. Each term in the parenthesis represents the contribution of a variable to MTC (i.e. α_{con}). For each step MTC ≈ $\alpha_{con} + \beta_{con} + \gamma_{con} + H_{z\_con}$. For analyses, all variables were first normalized (0-100%) to the period of time from TO to MTC then the contributions of each variable were averaged across all steps. A 2x2 mixed model ANOVA was used to test for a main affect of group on γ_{con}. To further explain MTC, the contributions of the other variables were also analyzed.

RESULTS AND DISCUSSION

The results support our hypotheses that regardless of incline the ProprioFoot would significantly increase MTC and increased toe clearance could be attributed to active dorsiflexion. Across grades, the average MTC for the ProprioFoot group was significantly greater than for the control group (Table 1; 30.1±12.3 mm vs. 17.6±6.7 mm, respectively; p=0.04), with values for the latter surprisingly similar to those typically observed by able-bodied individuals [5]. The contribution of the ankle to MTC was positive in the ProprioFoot group, increasing MTC by an average of 6.6 mm, whereas in the control group ankle motion reduced MTC by an average of 2.6 mm (p<0.01). This alone cannot completely explain the nearly 20 mm increase in MTC with the Propriofoot. The ProprioFoot group showed similar positive contributions of the knee (p=0.34) and significantly less negative contribution of α (p=0.02). A significantly less extended hip at TO (p=0.01) explains why the negative effects of the hip were smaller, but why the hip was less extended (even flexed) at TO is unclear. It is possible that by assisting in lowering the foot after heelstrike, the ProprioFoot provides a heel rocker, reducing the need for compensatory strategies during early stance, which could manifest as altered kinematics at TO. Similarly, the adaptations offered during inclined walking, which significantly increase dorsiflexion at TO (p=0.03), may also passively increase hip and knee flexion. A previous study quantifying lower limb kinematics during inclined walking with the ProprioFoot reported similar peak knee flexion angles whether or not the adaptive function was on [6], suggesting the adaptive mode may be insufficient to alter kinematics. The apparent contradiction between the current findings and those of Fradet et al (2010) may reflect different study designs. The latter study used only the ProprioFoot, and thus between-condition comparisons could not include differences in foot design characteristics such as keel length and flexibility. We have done this by comparing the adaptive ProprioFoot to a standard foot.

In conclusion, the active dorsiflexion offered by the ProprioFoot significantly increases MTC, although increased MTC may also reflect altered hip and knee kinematics. The method used here to determine angular contributions to MTC can easily be applied to other variables. By increasing MTC, the ProprioFoot likely increases user safety by reducing the risk of stumbling and the risk of falling.

REFERENCES

1. Miller WC, et al. *Arch Phys Med Rehabil*; 82(8):480-6, 2001.
2. Begg R, et al. *Gait Posture*; 25:191-198, 2007.
3. Winter, DA. *J Biomech*; 21(5):361-7, 1988.
4. Moosabhoy and Gard, *Gait Posture*; 24:493-501, 2006.
5. Khandoker AH, et al. *IEEE Trans Neural Syst Rehabil Eng*; 2008
6. Fradet L, et al. *Gait Posture*; 32:191-8, 2010.

Table 1. Kinematic variables and model output for two groups and grades

grade	group	MTC (mm) #	α_{con} (mm) #	β_{con} (mm) ¶	γ_{con} (mm) #	H_{z_con} (mm)	α at TO (°) #	β at TO (°) #¶	γ at TO (°)
0%	ProprioFoot	31.0 ± 12.5	-31.9 ± 19.3	48.6 ± 15.9	6.6 ± 4.6	25.8 ± 8.7	2.6 ± 4.5	48.2 ± 3.0	-0.1 ± 2.9
	Control	18.4 ± 6.0	-76.3 ± 22.8	60.6 ± 17.9	-2.7 ± 2.7	28.4 ± 13.0	-5.5 ± 4.5	39.5 ± 7.7	-1.1 ± 2.0
5%	ProprioFoot	29.0 ± 14.3	-24.2 ± 19.3	59.5 ± 27.1	6.5 ± 6.1	30.0 ± 8.7	1.5 ± 2.4	45.3 ± 3.7	2.0 ± 3.0&
	Control	16.6 ± 6.9	-73.0 ± 22.8	70.9 ± 20.1	-2.6 ± 2.8	29.2 ± 9.9	-6.3 ± 4.5	35.7 ± 7.7	-1.3 ± 1.8

α>0: hip flexion; β>0: knee flexion; γ>0: dorsiflexion; # significant main effect of group; p<0.5, no significant interaction (grade x group); ¶ significant main effect of grade; p<0.5, no significant interaction (grade x group); & significant between group differences found during post hoc t-test following significant interaction

ORAL PRESENATIONS – FRIDAY SEPTEMBER 6th

	Thematic: Knee Osteoarthritis *Robert Siston*
9:45 AM	Human Knee Joint Muscle Forces And Tissue Stresses-Strains In Gait: Asymptomatic Versus Severe Osteoarthritic Subjects **Adouni M, Shirazi-Adl A**
10:00 AM	Changes In Synovial Fluid Proteins And PRG4 Following Intense Muscular Loading Of The Knee **Abughazaleh N, Abusara Z, Krawetz R, Herzog W**
10:15 AM	Sex Differences In Level Walking Vertical Ground Reaction Force Characteristics In Adults With Medial Knee Osteoarthritis **Morrow M, Evertz L, Kaufman K**
10:30 AM	Knee Flexion Moment During Walking Influences Medial Compartment Cartilage Thickness In Patients With Knee Osteoarthritis **Chehab EF, Favre J, Erhart-Hledik JC, Andriacchi TP**

HUMAN KNEE JOINT MUSCLE FORCES AND TISSUE STRESSES-STRAINS IN GAIT: ASYMPTOMATIC VERSUS SEVERE OSTEOARTHRITIC SUBJECTS

Malek Adouni and Aboulfazl Shirazi-Adl

Department of Mechanical Engineering,
École Polytechnique, Montréal, Québec, Canada
email: aboulfazl.shirazi@polymtl.ca

INTRODUCTION

Human knee is the weight bearing joint most affected by osteoarthritis (OA). Though its multifactorial pathology is not yet well understood, mechanical factors are believed to play an important role in the initiation and progression of the knee OA. Earlier studies on asymptomatic and OA subjects have identified marked differences in gait kinematics-kinetics between these two groups [1]. An accurate knowledge of activation levels in joint musculature as well as resulting contact stresses and stresses/strains within articular cartilage and ligaments of both subject groups is important. Such results help identify the changes in the knee joint mechanical environment with the development of OA and would hence play a crucial role in any successful management of knee OA. In the current work, we use a validated finite element (FE) model [2] to compute lower extremity muscle forces and knee joint stresses/strains in subjects with and without OA during the stance phase of gait. These FE analyses are driven by reported kinematics and kinetics data collected during gait of both asymptomatic subjects and subjects with severe OA [1]. In the model simulating gait of OA subjects, the material properties of the articular cartilage and menisci are either left intact and unchanged as in the model of the asymptomatic group or altered (i.e., with reduced matrix and fibril moduli) to simulate the diseased tissues.

METHODS

An iterative kinematics-driven FE model that accounts for the passive structures of the entire knee joint and active musculature of the lower extremity is employed [2] (Fig. 1). This model incorporates the hip as a 3D and the ankle as a 1D spherical joint whereas the knee is represented realistically as a complex FE model with nonlinear depth-dependent fibril-reinforced cartilage and menisci, ligaments with distinct nonlinear properties and initial strains, patellofemoral and tibiofemoral joints. Based on reported *in vivo* measurements [1,3], hip/knee/ankle joint rotations/moments and ground reaction forces (GRF) at foot during the gait stance phase collected in asymptomatic subjects and subjects with severe knee OA are used to separately drive models of both groups. Analyses are performed at 6 time instances corresponding to beginning 0% (heel strike), 5%, 25%, 50%, 75% and 100% (toe off) of the stance phase. At each stance period, muscle forces at the hip, knee and ankle are predicted using static optimization (sum of cubed muscle stresses) with moment equations (3 at knee, 3 at hip, and 1 at ankle) and upper/lower limits on muscle forces as constraints. The Knee joint response is subsequently analyzed with updated muscle forces as external loads and iterations at deformed configurations continue till convergence is reached. Apart from changes in input kinematics/kinetics, the OA model accounts also for likely alterations in material properties associated with the disease. Additional analyses are thus performed at 5% and 50% stance periods with the cartilage/menisci fibril and matrix moduli reduced both by 25% from their intact values while the Poisson's ratio is either left unchanged or also reduced from 0.49 to 0.45.

RESULTS AND DISCUSSION

In OA subjects compared to normal ones (OA versus N), forces significantly decreased in nearly all muscle groups at most instances of stance (Fig. 2). Mean force over the stance phase in the anterior cruciate ligament (ACL) remained nearly the same. Total contact forces/stresses deceased by an average of 25% with a larger portion of load transmitted via menisci. Alterations in cartilage and menisci material properties simulating OA had negligible effects on muscle forces but further reduced contact pressures (Fig. 3, 50% stance) while increasing cartilage strains and load transmission via menisci.

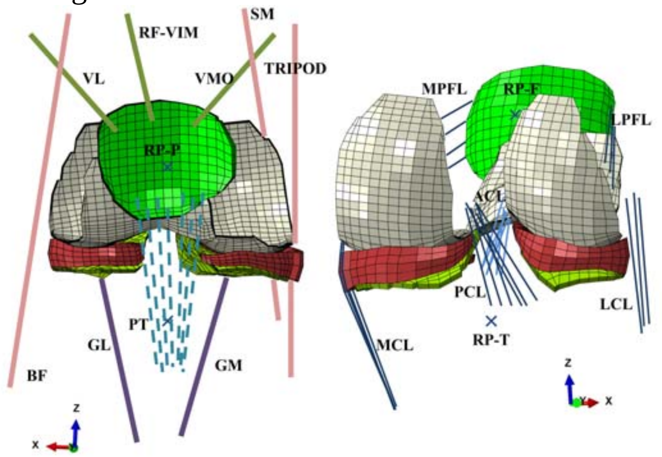

Figure 1: Knee FE model with cartilage layers, menisci, ligaments and muscles. Bony structures are not shown.

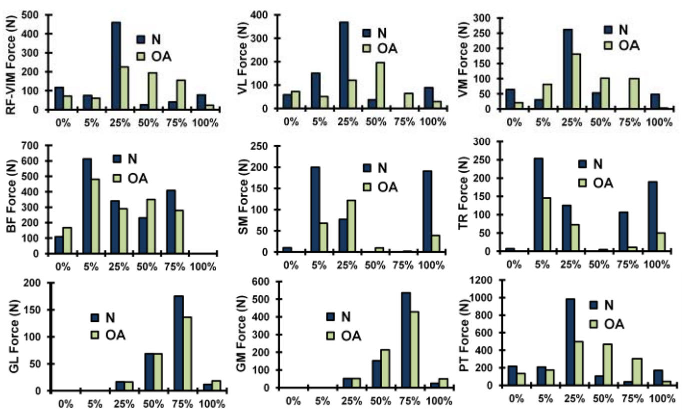

Figure 2: Muscles forces in both N and OA groups during stance phase of gait.

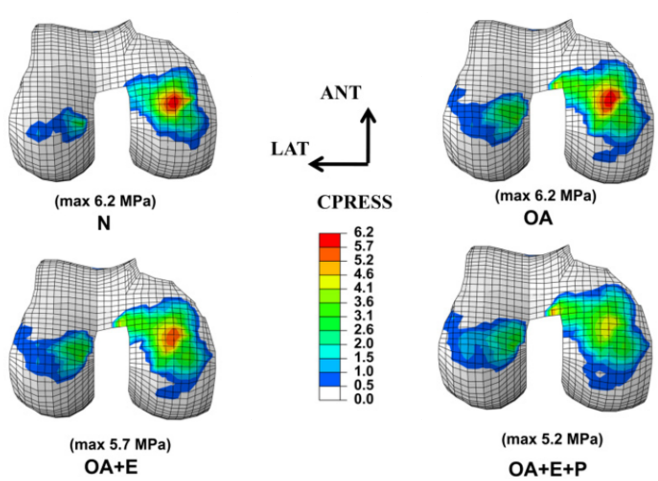

Figure 3: Femoral contact pressures at 50% stance phase in N and OA (with various materials) groups.

In this work, muscle forces and knee joint response were estimated during the stance phase of gait in both asymptomatic and OA subject models while driven by distinct kinematics-kinetics data collected in each group [1]. No co-activity was considered in either normal or OA models. In accordance with the alterations in the joint moments-rotations during gait, muscle forces at the knee joint decreased overall in OA subjects leading to lower contact forces. In contrast to smaller mean/peak contact pressures, the portion of load transmitted via menisci increased in OA group. In addition to altered gait input data, cartilage/menisci fibril and matrix moduli were reduced to represent the expected deteriorations in material properties associated with OA. These changes had smaller effects on muscle, ligament and contact forces but increased contact areas, maximum tensile strains in superficial and deep cartilage layers, and the load transfer via menisci. The peak contact pressures however decreased.

In conclusion, OA-associated alterations in rotations and moments at lower extremity joints recorded during gait of normal and OA subject groups influence activation levels in lower extremity musculature as well as contact forces/stresses and stresses/strains in knee articular cartilage. Reductions in mean and peak contact stresses as well as increases in tissue strains and greater transfer of load via menisci are partly due to reported altered kinetics-kinematics of gait in these groups and partly due to deteriorations in cartilage-menisci material properties.

REFERENCES

1. Astephen et al, *J Orthop Res* 26:332, 2008.
2. Adouni et al, *J Biomech* 45:2149, 2012.
3. Hunt et al, *Clin Biomech* 16:592, 2001.

ACKNOWLEDGEMENTS

Work was supported by the NSERC-Canada and MUTAN-Tunisia.

CHANGES IN SYNOVIAL FLUID PROTEINS AND PRG4 FOLLOWING INTENSE MUSCULAR LOADING OF THE KNEE

Nada Abughazaleh[1], Ziad Abusara[2], Roman Krawetz[3], and Walter Herzog[1,2,3]
Faculties of Engineering[1], Medicine[2] and Kinesiology[3], University of Calgary, Calgary, Canada
email: nabughazaleh@ucalgary.ca

INTRODUCTION

Synovial fluid (SF) lubricates joints and provides nutrition to cartilage. It is composed of soluble molecules, such as morphogens, growth factors, cytokines, and lubricant molecules. There is an extensive body of research of the effects of joint injures and disease on the composition of SF [1, 2]. Excessive joint loading has been associated with the onset and an increased rate of progression of osteoarthritis, but little is known about the effects of exercise loading on synovial fluid composition. The purpose of this study was to load intact knee joints with controlled maximal muscular contractions and identify changes in synovial fluid composition. We hypothesized that protein content, and lubricating protein content, such as PRG4 are upregulated following exercise. Experiments were performed in rabbit knees, loaded by electrical stimulation of the knee extensor group.

METHODS

Twelve knee joints from New Zealand white rabbits were assigned randomly to an experimentally loaded (n=6), and an unloaded control group (n=6). The experimental hind limbs were implemented with a femoral nerve cuff electrode connected to a Grass S8800 stimulator for controlled muscular stimulation. Eccentric knee extensor contractions were used to maximize knee joint loading. Maximal contractions were achieved by stimulating the knee extensors supra-maximally and at a frequency of 100Hz, while the knee was moved from a 150˚ to a 80˚ knee flexion angle at a speed of 70˚/s. Muscle forces were measured using a strain gauged lever that was attached to the distal part of the tibia and the motor driving the leg. Exercise loading consisted of five sets of 10 maximal contractions. Contractions lasted 1.4 seconds at 0.4 Hz. Rest periods between sets were two minutes. The exercise loading resulted in fatigue indicating that the muscles were driven at maximal effort (Figure 1). Following the loading protocol, animals were sacrificed using an overdose of Euthanyl. Following sacrifice, synovial fluid was extracted from the experimentally loaded and the unloaded knees. The synovial fluid was then tested for protein content using Liquid Chromatography–Mass Spectrometry. Paired comparisons of protein content were made between the loaded and unloaded control joints of the same animal.

Following synovial fluid harvesting, the articular surfaces of the knee were preserved and prepared for analysis of cell death using laser scanning confocal microscopy. Specifically, the percentage of dead cells in the femoral groove, lateral and medial femoral condyles, patella and medial and lateral tibial plateaus of control and experimental knee joint surfaces were compared.

RESULTS AND DISCUSSION

Maximal quadriceps forces reached 588±60 N on average in the first and 332±55 N in the last set of loading (Figure 1). Knowing that the average contact area for rabbit patello-femoral and tibio-femoral joints are approximately 21 mm^2, we estimate that peak contact pressures in our experiments reached values of about 28 MPa.

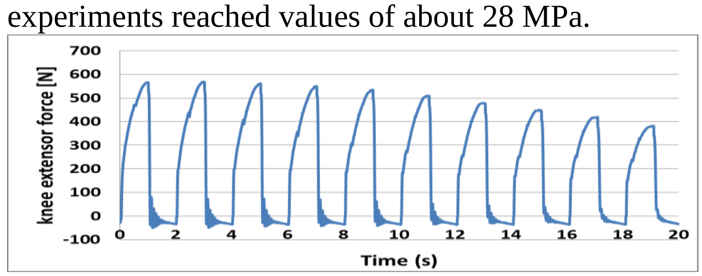

Figure 1: Knee extensor force-time graph of an exemplar set of ten maximal contractions. Note that the maximal force reaches about 600 N and that the force decreases for the ten repeat contractions because of fatigue.

Cell death in the different areas of the knee was the same for loaded and unloaded tissues, indicating that chondrocytes can withstand maximal muscular loading, as applied here. The number of proteins detected in the synovial fluid of experimentally loaded knees was greater than that found in fluid from unloaded control knees (Figure 2). Two proteins that were only found in experimental synovial fluid, and that we would like to emphasize are 14-3-3 protein and creatine kinase.The 14-3-3 protein plays important roles in a range of regulatory processes, including apoptotic cell death and joint inflammation [3].

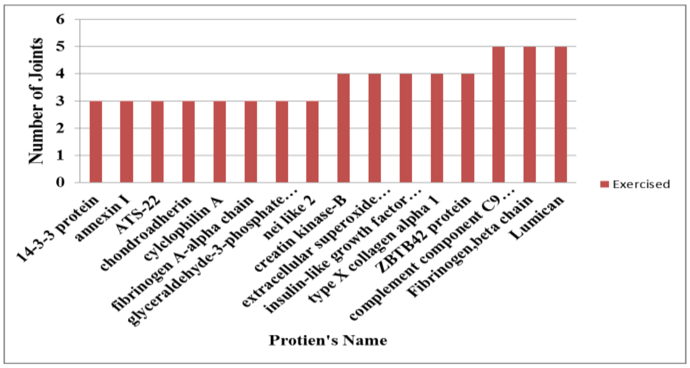

Figure 2: Proteins found only in the synovial fluid of experimentally loaded joints (6 joints).

Creatine kinase catalyzes the conversion of ADP and phosphoryl creatine into ATP and creatine, and restores energy reservoirs. Increasing creatine kinase indicates damage to skeletal muscles [4].

Many proteins were found in the synovial fluids of experimental and control samples. However, many proteins appeared more often in the experimental than the control knees (Figure 2). For example PRG4 was found in the synovial fluid samples of all six exercise-loaded joints, but was only found in three of the unloaded control joint fluids.

Up-regulation of PRG4 may reduce friction in the knee. The increased protein and PRG4 concentration in SF following exercise is consistent with recent results in the mouse knee [5]. In the mouse, we found that small magnitude muscular loading (below about 50% of maximal) did not cause an increase in protein and PRG4 concentrations, while intense exercise (above about 60% of maximal) showed substantial increases in protein and PRG4 concentrations. We also demonstrated that the increase in protein and PRG4 concentrations was eliminated when cell secretion inhibitors were added prior to loading, indicating that the change in synovial fluid content was regulated by an active cellular mechanism. Our results are the first to show that synovial fluid changes dramatically following acute exercise of high intensity. This result has implications for exercise design in rehabilitation, and might be important for elite and recreational athletes as an indicator of overloading of joints.

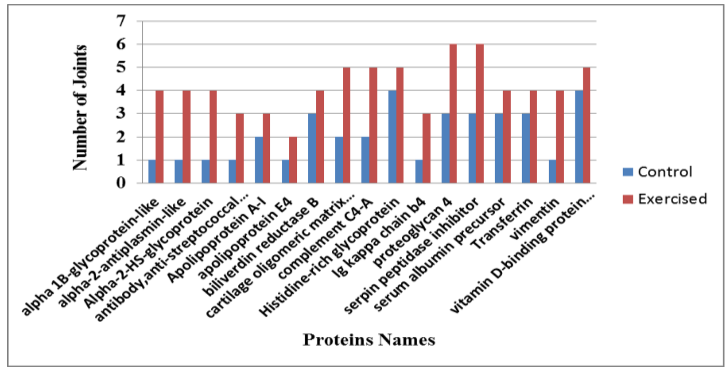

Figure 3: Number of counts (maximum 6) of proteins found in synovial fluid of exercised and control knees, Note that proteins are more often above the detection threshold in exercised compared to control joints.

CONCLUSIONS

Intense muscular exercise causes an acute increase in a number of proteins including PRG4 in synovial fluid of intact knees. These results have implications for the design of rehabilitation strategies and for exercise modulation in recreational and elite athletes.

REFERENCES

[1] Decker B, et al. *Arthritis Rheum* **2**:162–77,1959.

[2] Alexander Y. Hui, et al. *WIREs Syst Biol Med* **157**, DOI: 10.1002. 2011.

[3] Kamran S, et al .*Can J Vet Res*. **75**:271-77, 2011

[4] Baird M, et al. *J Nutr Metab* ***2012***, doi: 10.1155/2012/960363

[5] Abusara Z, et al. *J Biomech.* Doi:10.1016, 2013.

ACKNOWLEDGEMENTS

The AI-HS Team grant on osteoarthritis, the Canada research Chair Programme, CIHR and the Killam foundation.

SEX DIFFERENCES IN LEVEL WALKING VERTICAL GROUND REACTION FORCE CHARACTERISTICS IN ADULTS WITH MEDIAL KNEE OSTEOARTHRITIS

Melissa M. B. Morrow, Loribeth Q. Evertz, and Kenton R. Kaufman

Mayo Clinic, Rochester, MN, USA
email: morrow.melissa@mayo.edu
http://mayoresearch.mayo.edu/mayo/research/biomechanics/

INTRODUCTION

Women are twice as likely as men to suffer from knee osteoarthritis (OA), and they experience greater pain and disability over their lifetime from the chronic disease [1]. The interplay of biomechanics and the pathophysiology of knee OA have been investigated for insight into the progression of the disease and the increased incidence and prevalence in women [2]. The relationship between knee loading during walking and medial knee OA has been previously investigated, but it is unclear if sex differences exist. The purpose of this study was to investigate the effects of sex differences in the vertical ground reaction force characteristics of adults with prevalent knee OA.

METHODS

The study sample consisted of 306 subjects with knee OA who were consented for participation. While 99% of the subjects had bilateral knee OA and 87% of knees had multi-compartment involvement, this analysis excluded those with no medial compartment OA and reduced the sample size to 294 subjects (221 women and 73 men, Table 1).

Table 1. Subject demographics and gait variables

Variables	Women mean (95% CI)	Men mean (95% CI)	*p*
n	221	73	
Age (yrs)	56.5 (55.1-57.9)	59.2 (56.6-61.6)	0.06
BMI (kg/m^2)	32.3 (31.4-33.2)	30.4 (29.0-3l.6)	**0.02***
Velocity (cm/s)	114.6 (112.8-116.5)	118.1 (114.8-121.5)	0.07
Cadence (steps/min)	114.2 (113.0-115.4)	109.3 (107.2-111.4)	**0.00***
Step width (cm)	10.5 (10.2-10.9)	11.1 (10.5-11.8)	0.09

Bilateral weight-bearing radiographic examinations were performed to determine the OA grade according to the Kellgren and Lawrence system. Ground reaction forces were measured with force plates during gait analysis of level walking. The maximum force of the vertical ground reaction force was identified in addition to the timing of the force during the gait cycle (Fig 1). The timing of the maximum force was classified as either during the loading response phase or terminal stance. The heelstrike transient loading rate was calculated as the slope from heelstrike to the heelstrike transient peak (Fig 1). The maximum force and loading rate were normalized to body weight.

T-tests were used to test for sex differences in demographics and gait variables (Table 1). Logistic regression was used to test the effects of sex on the timing of the maximum vertical ground reaction force while controlling for medial knee OA grade. Linear regression was used to adjust the effects of sex on the maximum force and loading rate to the medial knee OA grade.

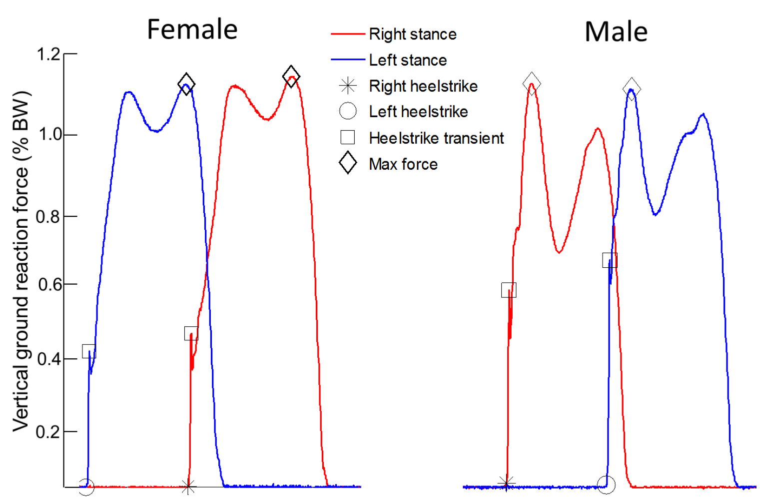

Figure 1. Female and male representative vertical ground reaction force plots over the gait cycle

RESULTS AND DISCUSSION

Women had a significantly higher BMI and cadence than the men (Table 1). The majority of women (73%) experienced a maximum force during terminal stance while the majority of men (60%) applied their maximum force during the initial loading response after heelstrike ($p<0.0001$, Fig 1). There was no effect of OA grade on maximum force timing ($p=0.85$). Similar trends have been shown in men and women without lower extremity joint pathology over the lifespan [3] suggesting that the sexually dimorphic patterns in the vertical ground reaction force may be a risk factor for knee OA development.

There were no effects of sex on the maximum vertical ground reaction force ($p=0.68$, Fig 2) or the heelstrike transient loading rate ($p=0.88$, Fig 3). There was a significant effect of KL OA grade with a reduction in the loading magnitude ($p=0.0004$) and rate ($p=0.02$) as the severity increased (Figs 2 & 3). Previous hypotheses that an increased heelstrike transient loading rate may have detrimental effects on the cartilage in women are not supported by the results of this study.

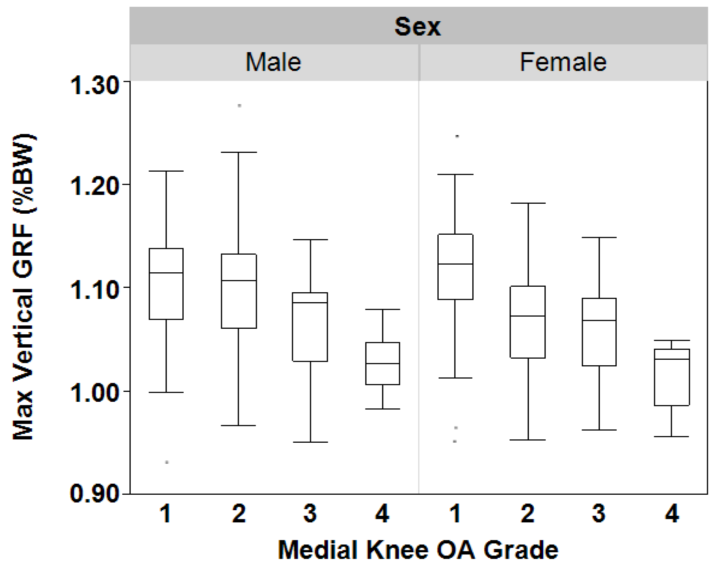

Figure 2. Maximum vertical ground reaction force (GRF) for men and women over the KL OA grades.

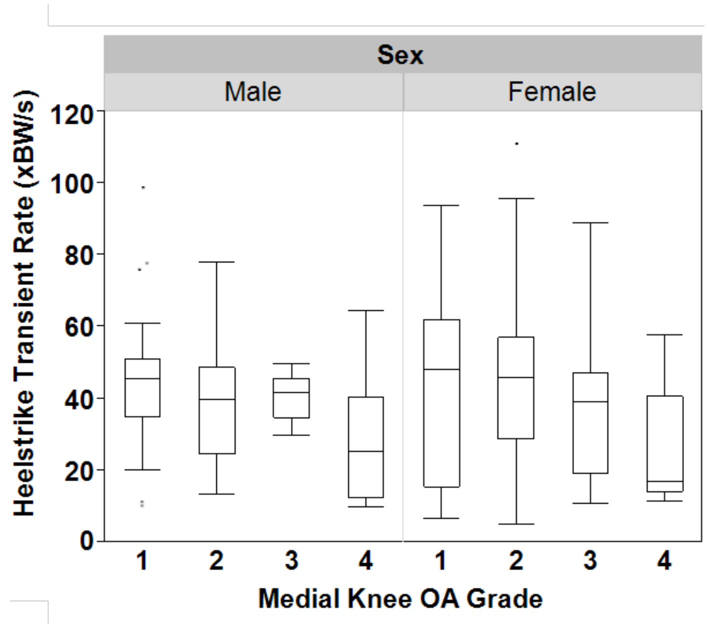

Figure 3. Heelstrike transient loading rate for men and women over the KL OA grades.

CONCLUSIONS

The majority of women walked with a maximum vertical ground reaction force in terminal stance while the majority of men walked with a maximum vertical load during the first peak of the loading response. There were no differences between men and women in the heelstrike transient loading rate and the magnitude of the maximum vertical ground reaction force. Further investigation is warranted in sex differences of loading during walking to identify characteristics that might put women at greater risk of developing medial knee OA.

REFERENCES

1. Srikanth VK et al., *OA and Cart*, 2005. **13**(9):769-81.
2. Sims EL et al. *J Women Aging*, 2009. **21**(3):159-70.
3. Chung MJ and Wang MJ, *Gait & Posture*, 2010. 31(1):131-5.

ACKNOWLEDGEMENTS

This study was funded in part by NIH K12HD065987 and NIH R01AR04876.

KNEE FLEXION MOMENT DURING WALKING INFLUENCES MEDIAL COMPARTMENT CARTILAGE THICKNESS IN PATIENTS WITH KNEE OSTEOARTHRITIS

[1]Eric F. Chehab, [1]Julien Favre, [1,2]Jennifer C. Erhart-Hledik and [1,2]Thomas P. Andriacchi

[1]Stanford University, Stanford, CA, USA
[2]Palo Alto Veterans Affairs, Palo Alto, CA, USA
email: echehab@stanford.edu, web: http://biomotion.stanford.edu

INTRODUCTION

Osteoarthritis (OA) is a disease of the articular cartilage that affects nearly 27 million people in the United States [1]. Knee OA is the most common form of the disease. However, there is limited knowledge regarding the factors affecting the disease progression. Identifying these factors would strengthen our understanding of OA progression and contribute to prevention and treatment programs.

The knee flexion moment has been suggested to be a biomechanical gait measure that is particularly sensitive to OA [2], and could be used to assess the loading environment at the knee [3]. Furthermore, the knee adduction moment has been associated with the radiographic progression of medial compartment knee OA [4]. It remains unclear if these kinetic measures precede the disease or represent a marker of the disease state. Thus, there is a need for a longitudinal study that analyzes the relationship between these two knee moments and change in cartilage thickness in order to identify possible markers for OA progression.

The purpose of this study was to test the relative associations between disease progression, as assessed by changes in cartilage thickness over 5 years, and the magnitude of the adduction and flexion moment at baseline by applying a multiple linear regression model.

METHODS

This IRB-approved study analyzed a group of 18 patients (10 females) with medial compartment knee OA. At baseline, the participants were 60 ± 10 years old (mean ± SD) with a BMI of 27.8 ± 4.5 kg/m^2. Only their index knees, with KL grades of 2.3 ± 0.9, were used for this study. The experimental protocol consisted of a baseline gait test and an MRI scan at baseline after 5 ± 1 years.

A marker-based system (Qualisys, SE) and a force place (Bertec, OH) were used to calculate the knee adduction and knee flexion moments during the baseline gait test following a previously described method [5]. The maximum value of the adduction and flexion moments were extracted during the first half of the stance phase (during foot contact with the force plate) and these maximum values were averaged over three walking trials for every patient.

Each knee was imaged at baseline and follow-up using a 3D-SPGR sequence on 1.5T MRI machine (GE Medical, WI). MR images were segmented and 3D cartilage models were reconstructed using custom software [6]. Mean cartilage thicknesses were calculated over the total medial tibial compartment and total medial femoral load-bearing region. Change in cartilage thickness was defined as the mean cartilage thickness at follow-up minus the mean cartilage thickness at baseline.

Multiple linear regression analyses were used to assess the relationship between baseline knee kinetics (adduction and flexion moments as independent predictors with no interaction term) and changes in femoral and tibial cartilage thicknesses.

RESULTS AND DISCUSSION

The changes in medial tibial cartilage over 5 years were well-modeled by the baseline knee moments (R^2=0.43, p=0.014, Figure 1). Post-hoc analysis showed that the model was indeed largely driven by the flexion moment (p=0.004) and that the contribution of the adduction moment was not significant (p=0.83). On average, a patient with a 1% BW*ht higher baseline knee flexion moment lost 0.15mm more medial tibial cartilage over 5 years. Contrary to the tibia, there was no statistically significant relationship between baseline knee moments and changes in femoral cartilage thickness over 5 years (R^2=0.09, p=0.48).

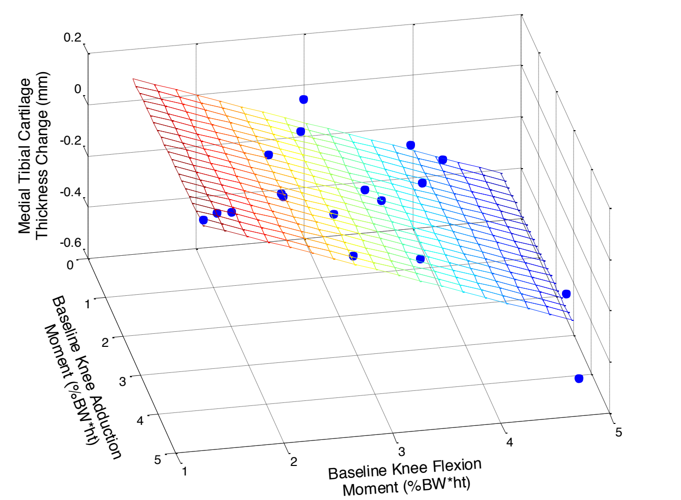

Figure 1: Baseline kinetic measures during walking were associated with medial tibial cartilage changes after 5 years (R^2=0.43, p=0.014).

The finding that baseline knee flexion moment was associated with loss of cartilage over the follow-up period is very important because it provides new evidence for the central role of knee mechanics in disease progression [7] and offers unique insight for prevention programs, such as gait intervention. In this study, a larger flexion moment was associated with greater loss of cartilage thickness. This relationship supports a previously described mechanical pathway to knee OA [7] where diseased cartilage responds negatively to the loading environment and accelerates OA progression in the presence of higher knee loads (flexion moment).

The knee adduction moment is a surrogate measure for the medial-lateral cartilage load distribution [8] and is known to increase with disease severity [9]. In this population of diverse KL-grades, there was no significant relationship between baseline adduction moment and changes in cartilage thickness. This is likely due to the use of absolute thickness change as an indicator of disease progression, as well as the broad range of KL grades; OA-related increases in adduction occur mostly in knees with KL ≥ 3 [9].

The absence of a relationship with femoral cartilage changes is likely due to the large area over which thickness was averaged. An approach that analyzes more specific regions or thickness distribution [10] may be more sensitive to changes in cartilage thickness.

CONCLUSIONS

These results provided insight for the importance of the extrinsic load surrogates during walking in OA progression. The adduction moment has been a useful indicator of the medial-lateral load thickness ratio. Specifically, this study suggests that the magnitude of the flexion moment could possibly be used as a marker for changes in absolute medial compartment thickness in patients with medial compartment OA.

REFERENCES

1. Kotlarz H, et al. *Arthritis and Rheumatism* **60**, 3546-3553, 2009.
2. Boyer KA, et al. *Journal of Orthopaedic Research* **30**, 1118-1124, 2012.
3. Walter JP, et al. *Journal of Orthopaedic Research* **28**, 1348-1354, 2010.
4. Miyazaki T, et al. *Annals of Rheumatic Diseases* **61**, 617-622, 2002.
5. Zabala ME, et al. *Journal of Biomechanics* **46**, 515-520, 2013.
6. Koo S, et al. *Osteoarthritis and Cartilage* **13**, 782-789, 2005.
7. Andriacchi TP, et al. *Annals of Biomedical Engineering* **32**. 447-457, 2004.
8. Schipplein OD, et al. *Journal of Orthopaedic Research* **9** 113-119, 1991.
9. Mündermann A, et al. *Arthritis and Rheumatism* **50**, 1172-1178, 2004.
10. Andriacchi TP. *Arthritis and Rheumatism* **65** 310-313, 2013.

ACKNOWLEDGEMENTS

The authors would like to acknowledge VA Grant #A04-3583R, NIH Grant #R01AR39421, as well as Jessica L. Asay and Anne Mündermann.

ORAL PRESENATIONS – FRIDAY SEPTEMBER 6th

	Ultrasound Assessment of Muscle *Kai-Nan An, Kristin Zhao*
9:45 AM	Automated Measurement Of Muscle Architecture From Ultrasound Images **Infantolino B**
10:00 AM	Measurements Of Shear Elastic Modulus Of The Biceps Brachii Using Shear Wave Elastography **Lee S, Speer S, Rymer W**
10:15 AM	Changes To 3D Muscle Fascicle Geometry During Contraction **Rana M, Hamarneh G, Wakeling J**
10:30 AM	Validation Of Shear Wave Elastography In Skeletal Muscle **Eby S, Song P, Chen S, Chen Q, Greenleaf J, An KN**

AUTOMATED MEASUREMENT OF MUSCLE ARCHITECTURE FROM ULTRASOUND IMAGES

[1]Benjamin W. Infantolino

[1]Penn State - Berks, Reading, PA, USA
email: bwi100@psu.edu

INTRODUCTION

Ultrasound can be used to measure muscle architecture *in vivo* [1]. Unfortunately, this can be time consuming when dealing with dynamic muscle contractions which has led to the development of automated techniques for architecture measurement [2]. Many algorithms track a limited number of points or are difficult to implement for different muscles. Identifying multiple fascicles in ultrasound images allows for assessment of average pennation angle in each frame and does not constrain the algorithm to following one specific object through the entire movement. The purpose of this study is to describe an algorithm that is based on object detection methods to measure average pennation angle and calculate average fascicle length in ultrasound images.

METHODS

The algorithm was implemented in MATLAB (The MathWorks Natick, USA) using the Image Processing Toolbox. A region of interest was defined by the user and for each frame that region of interest was converted from grayscale to black and white. Superficial and deep aponeuroses were located by calculating the sum of each pixel value in each row in an image. The row with the highest sum in the top half and bottom half of the image were identified as the superficial and deep aponeuroses. The distance between aponeuroses was defined as muscle thickness.

After aponeurosis detection, the original grayscale image was further cropped to remove the aponeuroses from the image. The image was converted to black and white but this time the contrast of the image could be manually adjusted to account for varying gain settings on the ultrasound machine. This adjustment allowed the user to produce an ideal image for fascicle detection.

An object detection approach was used to detect fascicles within the ultrasound frames. Fascicles were identified as objects that had fascicle-like attributes (correct orientation, above a minimum size, and line-like quality). The “regionprops” function in MATLAB was used to determine the pennation angle of the fascicle with respect to the horizontal. The average of all the measured pennation angles was assumed to be the pennation angle for the image. Using this average pennation angle and the muscle thickness, average fascicle length was calculated [3].

To validate this algorithm two methods were used, a computer generated video and a physical model. A video was created with “fascicles” that rotated through 20^o. A random amount of rotation ($0 – 0.5^o$) was added to each fascicle for each frame to represent the uneven movement seen in ultrasound. Extraneous objects were added to the video to represent artifacts seen in ultrasound videos. Superficial and deep aponeuroses were also added. Noise was added to the image by blurring the entire image (Figure 1).

In some of the images not all the “fascicles” were detected by the algorithm which is typical for *in vivo* ultrasound. The average angle of the “fascicles” detected by the algorithm was compared to the known average.

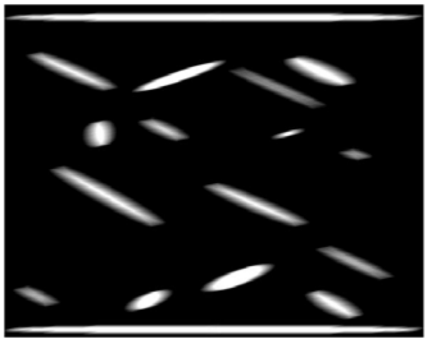

Figure 1. Frame from created video. Objects at the top and bottom represent the aponeuroses while other objects represent fascicles and non-fascicle objects.

In the physical model, rubber bands were placed along a string which moved the bands in the same manner as fascicles. Rubber bands were chosen due to their similar appearance on ultrasound when compared to muscle fascicles (Figure 2).

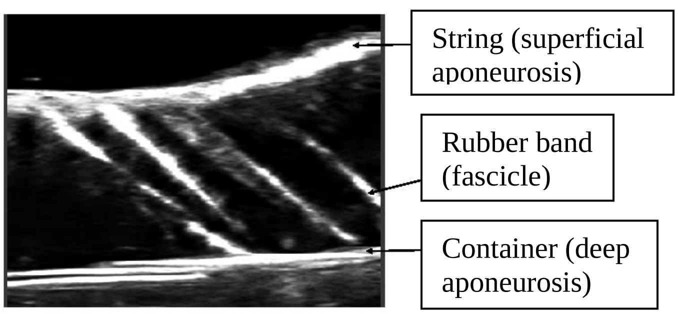

Figure 2. Rubber bands representing fascicles were attached to the bottom of a water bath container and a string was used to move them through a range of motion.

The movement of the bands was captured using a video camera and PC-based ultrasound system (Echoblaster 128, Telemed, Lithuania) simultaneously. Pennation angles were compared between the algorithm and digitization of the video.

RESULTS AND DISCUSSION

The results of the computer generated video tracking indicated no differences between the known and measured angles ($p < 0.05$). Results of the physical tracking model indicated the algorithm produced results that were within the results determined using manual digitization for both length and angle (Figure 3).

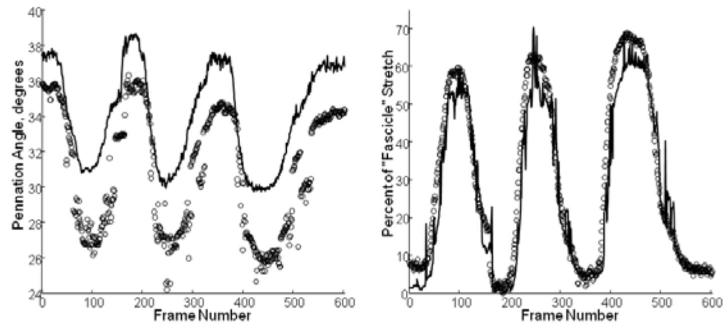

Figure 3. Auotmated and manually measured pennation angles and percent of fascicle length change. The solid black line represents the manually measured values while the open circles represent the algorithm measured values.

CONCLUSIONS

The results indicate that the algorithm is accurate for measuring the orientation and length of fascicle-like structures automatically. The validation methods strived to mimic *in vivo* images by adding noise, random motion, or similar image quality. Automated imaging methods for ultrasound are important for assessing movement of muscles. Many algorithms focus on a single point [4, 5] which can be difficult when points move in and out of the imaging plane.

Limitations did exist in this study. All detected objects have equal weight in the average pennation angle calculation. Non-fascicle objects can be ignored using selection criteria to identify only the most likely objects as fascicles. Another limitation is the ability to generalize these findings to *in vivo* images. The validation methods were selected to mimic *in vivo* images but more research is needed to fully accept this algorithm for automatically measuring fascicles from *in vivo* images.

REFERENCES

1. Narici M. *J Electromyogr Kines* **9**(2), 97-103, 1999.
2. Lee SSM. et al. *J Appl Biomech* **24**(1), 75-82, 2003.
3. Reeves ND. and Narici MV. *J Appl Physiol* **95**(3), 1090-1096, 2003.
4. Loram ID. et al. *J Appl Physiol* **100**(4), 1311-1323, 2006
5. Cronin NJ. et al. *J Appl Physiol* **111**(5), 1491-1496, 2011

MEASUREMENTS OF SHEAR ELASTIC MODULUS OF THE BICEPS BRACHII USING SHEAR WAVE ELASTOGRAPHY

[1,2]Sabrina S.M. Lee, [1]Sam Speer, [1,2]William Z. Rymer

[1]Rehabilitation Institute of Chicago, Chicago, IL, USA
[2]Northwestern University, Chicago, IL, USA
email: s-lee@northwestern.edu

INTRODUCTION

The contractile and elastic components making up muscle have varying mechanical properties that affect both the force generating capacity of muscle and elastic storage. Assessment of these properties is important in understanding changes in muscle function particularly in individuals with impaired muscle function (e.g. reduced force generation and/or range of motion). However, *in vivo* assessment of muscle mechanical properties remains a challenge. Recently, a novel elastographic technique, Supersonic Shear Imaging (SSI) has emerged as a reliable method to estimate *in vivo* shear elastic modulus in soft tissue [1] in real-time. An earlier study of the biceps brachii demonstrated a highly linear relationship between shear elastic modulus and muscle activity during isometric elbow flexion [2]. The shear elastic modulus – length relationship was also investigated in the gastrocnemius muscle [3]. Investigating these two relationships together in the same muscle is important to determine how the mechanical properties are related to muscle function Thus, the purposes of this study were: 1) to compare the shear elastic modulus at different muscle-tendon lengths and 2) to determine the change in shear elastic modulus as load against the muscle increased in the biceps brachii.

METHODS

Eight subjects (4 males, 4 female; age: 29.7 ± 3.6 yrs; height: 1.74 ± 0.11 m, mass: 72.4± 15.8 kg; all right-handed) participated in this study. Subjects were seated with their arms by their side with the humerus aligned with the trunk. For each trial, the subject was instructed to hold a weight (0.9, 1.8, 3.6, 4.5, and 5.4 kg) with the wrist at a neutral angle at the specified elbow flexion position (full extension at 0, 45, 90, and 110 degrees) for five seconds while an ultrasound image was captured. To test the muscle under passive conditions, the subject's forearm was fully supported at each elbow flexion angle. Two trials of each condition (weight and angle) were conducted of the left and right arms.

Ultrasound images were captured using an AixPlorer ultrasonography system (Supersonic Imagine, Aix en Provence, France) with a linear transducer array (4-15 MHz, SuperLiner 15-4, Vermon, Tours, France) in SSI mode [1]. Details of the technology have been described previously [1,4]. In brief, the transducer generates a radiation force through focused ultrasonic beams that induce propagation of transient shear waves. Using high frame rates up to 20 kHz to acquire the raw radiofrequency data, the shear wave velocity is calculated. The transducer was orientated parallel to the muscle fascicles at the mid-belly region of the muscle. The sheer elastic modulus (μ) in the direction of the transducer was calculated as:

$$\mu = \rho c^2$$

where μ is the shear elastic modulus (in kPa), density ρ is assumed to be constant (1000 kgm^{-3}) in human soft tissues (Greenleaf et al., 2003), and c is the shear wave velocity along the principal axis of the transducer. Maps of the shear elastic modulus (15 mm by 15 mm, Fig. 1) were obtained and the spatial average of the shear elastic modulus was determined for a circular region (diameter ranged from 5 to 12 mm).

Analysis of variance was conducted to determine differences in shear modulus between the different elbow flexion angles, loads, and side. Tukey post-hoc analyses identified significant differences between levels. The correlation coefficient of determination, r^2, was calculated between shear modulus and load at each elbow flexion angle to determine the influence of load on shear modulus.

RESULTS AND DISCUSSION

For all elbow flexion angles, the shear elastic modulus increased as the load increased (Figs. 1 and 2) and was significantly different at all loads (Figs. 1 and 2, $p < 0.01$). The shear modulus and load were significantly correlated at each position with r^2 values ranging between 0.77 and 0.90 for left and ride sides (Table 1). The shear modulus values at elbow flexion 45 and 110 degrees were significantly different than at other angles (Figs. 1 and 2, $p < 0.01$) with the greatest shear modulus value occurring at 45 degrees for all the loads. This could be related to the amount of force needed to generate sufficient torque to counteract the load that in turn, is related to the force-length relationship and moment arm of the muscle.

It was interesting that the shear modulus of the left side was significantly higher by 11.7 % across all loads and angles as all subjects were right handed. It is possible that other differences in mechanical properties that affect the force generating capacity exist and are related to handedness.

Table 1: Mean and standard error of the mean values of the coefficient of determination, r^2, between shear modulus and load at various elbow flexion angles of the right and left sides.

Side	Elbow angle (deg)			
	0	**45**	**90**	**110**
Right	0.80 (0.05)	0.85 (0.04)	0.90 (0.02)	0.77 (0.08)
Left	0.80 (0.03)	0.88 (0.01)	0.90 (0.02)	0.84 (0.04)

These results indicate that using SWE can distinguish differences in shear elastic modulus at different muscle-tendon lengths and under different load conditions. This has important implications for individuals with impaired muscle function such as stroke survivors who have substantial decreases in strength and range of motion. It is possible that the mechanical properties in stroke muscle are altered and contribute to decreases in force generation or even force transmission efficiency within the muscle. Thus, we intend to make similar measurements in stroke survivors.

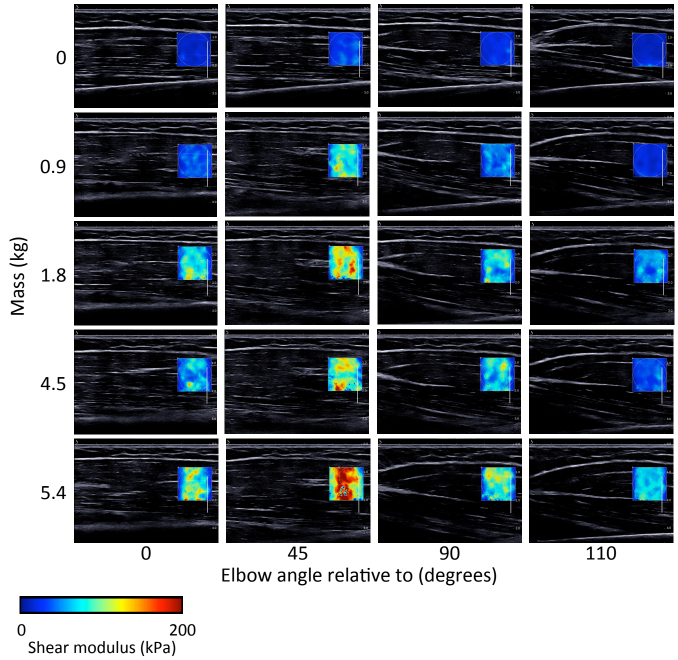

Figure 1: B-mode ultrasound images of the biceps bracchi with shear modulus maps. Images are taken at different loads and elbow flexion angles.

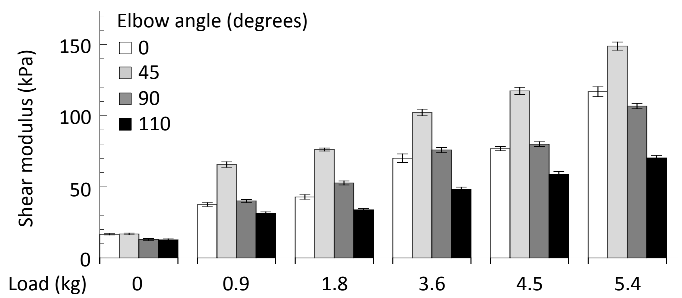

Figure 2: Mean shear modulus values for the different loads and elbow flexion angles. Error bars indicate standard error of the mean.

CONCLUSIONS

These findings indicate that there are strong differences in shear elastic modulus at different muscle-tendon lengths and at different loads.

REFERENCES

1. Bercoff J, et al. *IEEE Trnas Ultrason Ferroelectr Freq Control* **51**, 396-409, 2004.
2. Nordez A, et al. *J Appl Physiol* **108**, 1389-1394, 2010.
3. Maisetti O, et al. *J Biomechanics* **45**, 978-984, 2012.

Changes to 3D muscle fascicle geometry during contraction

[1]Manku Rana, [2]Ghassan Hamarneh and [2]James M. Wakeling

[1]University of Southern California, Los Angeles, CA, USA
[2]Simon Fraser University, Burnaby, BC, Canada
email: manku.rana@usc.edu

INTRODUCTION

Muscle is a three dimensional (3D) entity with varying shape across the length of the muscle and changes shape during contraction. Changes in muscle shape can influence the orientation of the fascicles within the muscle [1]. Dissection studies examining 3D muscle fascicles architecture have reported regional variations in the fascicle architecture [2]. 2D ultrasound studies have shown that the muscle fascicles are curved, and the curvature depends on the contraction state of the muscle [3]. Muscle modeling studies have predicted 3D curving of the fascicles [4], and dissection studies in human first dorsal interosseous muscle (FDI) [5] and animal muscles [6] have shown 3D helical curvature of fascicles.

Previous work on muscle architecture has been mostly in 2D, and a few diffusion tensor MRI and 3D ultrasound studies have quantified the 3D fascicles orientations in passive muscles. 3D fascicle architecture has not been studied during active muscle contractions.

The aim of this study was to obtain the map of muscle fascicle orientations and curvatures in human triceps surae during different muscle lengths and contraction states.

METHODS

Ultrasound images were obtained from six male subjects using a linear ultrasound probe (Echoblaster, Telemed, LT) recording at 20 Hz. Lateral gastrocnemius (LG), medial gastrocnemius (MG) and soleus were imaged for isometric ankle plantarflexions at a fixed knee angle of 135°, a range of ankle angles (-15°, 0, 15 and 30°) and ankle torques (0, 30 and 60 % maximum voluntary contraction (MVC). Images were analyzed to obtain the 2D orientations grids in the image planes. 2D orientation grids from each ultrasound image were reconstructed into 3D grids using 3D position and orientation of the scanning probe using an optical position sensor (Optotrak Certus®, NDI, Ontario). The muscle volume was divided into 5×5×5 mm^3 voxels, which contained a representative value for fascicle orientation represented in polar coordinates as polar angle (considered as pennation angle, β_f) and azimuthal angle (φ_f) [7].

3D curvature maps were obtained from the orientation grids. Fascicle trajectories were tracked locally around each voxel. The local trajectories were used to obtain the curvature magnitude (κ_c) and orientation of normal to curves in polar co-ordinates (β_c and φ_c) using the Frenet-Serret formula.

General linear model ANOVA was used to test the effects of muscle region, ankle angle and ankle torque level on the fascicle orientation, fascicle curvature and orientation of the normal to the curve. Post-hoc Tukey tests were performed to determine the regionalization effects, torque and ankle angles on the dependent variables. The results obtained were considered significant for p-value <0.05.

RESULTS AND DISCUSSION

3D fascicle orientations were regionalized (Figure 1) in all the three muscles (LG, MG and the soleus), and the variations were the maximum along the length of each muscle. In LG, β_f increased from 11.2° to 14.5°, and, φ_f increased from 92.4° to 103.4° from proximal to distal end of the muscle. The regional variations of φ_f indicated helical arrangement of fascicles that was further supported by the regionalization of the fascicle curvature magnitude and direction. Fascicle orientation and curvature changed significantly with contraction level and ankle angle (table 1). There was also a significant interaction between ankle torques and angles on the fascicle architecture. In LG, β_f decreased as the ankle angle increased for 0% MVC but for higher torque levels this trend gradually vanished.

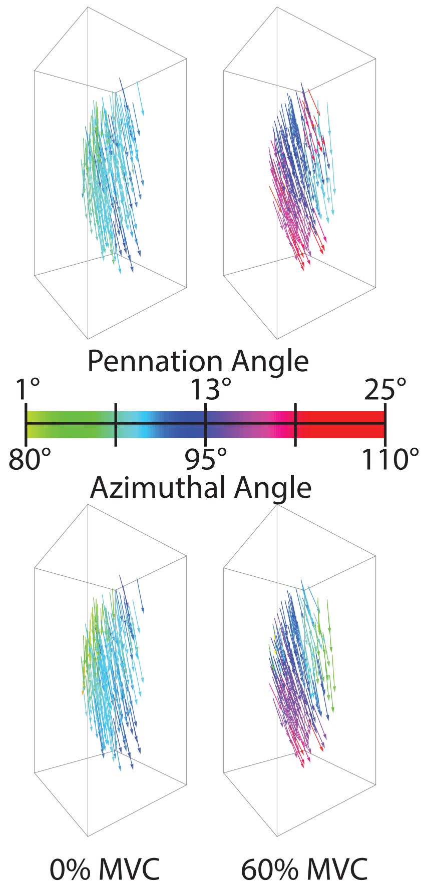

Figure 1: 3D fascicle orientations in the LG for one representative subject at 30° ankle angle. The images show the regionalization of pennation angle and azimuthal angle in the muscle and the change in orientations with torque level.

A curved fascicle generates a pressure difference across the curve with the pressure being greater on the concave side and the magnitude of the pressure differential increasing with the increase in the curvature [4] The curvature maps obtained in this study may be used to predict the intramuscular pressure distributions for different contraction states of muscles.

CONCLUSIONS

This is the first time that 3D fascicle architecture has been quantified in muscles during different contraction states and related to the ankle joint angle and joint torque. The 3D fascicle orientation is regionalized across each muscle in the triceps surae and depends on the muscle length and contraction level. Azimuthal angle (φ_f), a new parameter obtained as a virtue of 3D quantification methods, changed by the same magnitude as the typical 2D orientation measure of pennation angle. The fascicles curve in 3D and curvature magnitude and direction depended on contraction state of the muscle. The 3D curving of the fascicle shows that the 2D planar imaging is not sufficient to capture the complexity of fascicle architectural.

REFERENCES

1. Wakeling JM, et al. *Philos Trans R Soc Lond B Biol Sci* **366**, 1554-1564, 2011
2. Agur AM, et al. *Clin Anat* **16,** 285-293, 2003
3. Muramatsu T, et al. *J Appl Physiol* **92,** 129-134, 2002
4. van Leeuwen JL and Spoor CW**.** *Philos Trans R Soc Lond B Biol Sci* **336**, 275-292, 1992.
5. Infantolino BW, et al. *Anat Rec (Hoboken)* **295**, 1174-1180, 2012
6. Alexander RM. *J Mar Bio Assoc* **49**, 263-290, 1969
7. Rana M, et al. *J Biomech 44*, 2129-2135, 2011

Table 1: Mean (± standard error of mean) fascicle orientations and curvature values for different ankle angles and torque levels in LG.

Ankle Angel	**% MVC**	**β_f (°)**	**φ_f (°)**	**κ_c (m^{-1})**	**β_c (°)**	**φ_c (°)**
-15°	**0%**	13.9 ± 0.05	93.9 ± 0.04	3.7 ± 0.05	92.8 ± 0.16	200.6 ± 1.52
-15°	**60%**	12.7 ± 0.05	98.2 ± 0.05	4.1 ± 0.05	91.1 ± 0.16	182.8 ± 1.45
30°	**0%**	10.5 ± 0.03	93.9 ± 0.04	3.4 ± 0.05	90.8 ± 0.14	190.2 ± 1.5
30°	**60%**	12.9 ± 0.05	97.6 ± 0.06	4.1 ± 0.06	91.7 ± 0.15	195.2 ± 1.3

VALIDATION OF SHEAR WAVE ELASTOGRAPHY IN SKELETAL MUSCLE

[1]Sarah Eby, [2]Pengfei Song, [2]Shigao Chen, [1]Qingshan Chen, [2]James Greenleaf, and [1]Kai-Nan An

[1]Biomechanics Laboratory, Division of Orthopedic Surgery
[2]Physiology and Biomedical Engineering
Mayo Clinic, MN, USA
email: eby.sarah@mayo.edu

INTRODUCTION

Normal skeletal muscle stiffness results from active tension produced by muscle contraction and passive tension produced by the extracellular matrix and connective tissue surrounding individual muscle fibers [1-3]. The extracellular matrix plays a key role not only in force transmission, but also skeletal muscle signaling, growth and metabolism [4]. Therefore, it is imperative to develop noninvasive, reliable measures of muscle stiffness. As skeletal muscle is physically a very dynamic tissue, accurate quantitation of skeletal muscle stiffness throughout its functional range is crucial to improve the physical functioning and independence following pathology. Shear Wave Elastography (SWE) is an ultrasound-based technique that can characterize tissue mechanical properties based on the propagation of remotely induced shear waves [5-8]. Shear modulus, μ, can be calculated from the measured shear wave propagation velocity c_s within a region of interest using Equation (1):

$$\mu = c_s^{\,2}\rho \tag{1}$$

where ρ is density, which can be assumed to be 1000 kg/m^3 for all soft tissues [9]. The objective of this study is to validate shear wave elastography (SWE) throughout the functional range of motion of skeletal muscle.

METHODS

We obtained four right brachialis whole-muscle samples immediately post-mortem from healthy six- to nine-month old female swine. As we completed all testing within five hours of sacrifice, we did not consider rigor mortis a concern [13]. At the time of harvest, we established the initial (L_0) and final lengths (L_1) of the brachialis by flexing the forelimb to 90° and fully extending to 180°, respectively. We harvested the brachialis with intact proximal and distal bony attachments to facilitate mechanical testing. We fixed both bony attachments with bone cement to facilitate attachment to the materials testing system (MTS).

We mounted the specimen on a MTS (model 312, MTS, Minneapolis, MN) for simultaneous tensile testing and SWE evaluation. The MTS stretched the tissue specimen to L_0. Each specimen underwent displacement-controlled tensile testing from L_0 to L_1, at ~1.15% L_0 per second, with simultaneous ultrasound measurements at ten prescribed time points throughout the continuous tensile test. A load cell (model 3397, Lebow Products, Troy, MI) measured force throughout the testing procedure. The specimen was preconditioned for 6 cycles prior to tensile testing using the same loading protocol.

Prior to tensile testing, we fixed a linear-array ultrasound transducer (L7-4, Philips Healthcare, Andover, MA) over the middle third of the muscle specimen. All mechanical testing was well-within the submaximal range, so we tested three transducer-muscle fiber orientations for each muscle specimen: 1) ultrasound transducer aligned parallel with muscle fibers, 2) ultrasound transducer at 45° angle with muscle fibers, and 3) ultrasound transducer aligned perpendicularly with the muscle fibers. Each orientation was repeated five times, for a total of 15 trials with each muscle sample. We calculated shear modulus at each of the ten SWE time points throughout each tensile test using Equation 1.

From the collected MTS data, we calculated strain by dividing the displacement data by initial length, and plotted the stress-strain curve, using CSA calculated from measurements taken at L_0. We defined Young's modulus as the slope between ten consecutive MTS data points from the stress-strain curve. Using this approach, Young's modulus was calculated for each of the ten SWE time points. We used regression to examine the correlation between Young's modulus from MTS and shear modulus from SWE for each of the transducer orientations.

RESULTS AND DISCUSSION

Young's moduli increased with increasing displacement throughout the tensile test for all specimens. Additionally, shear moduli also increased with increasing displacement for trials utilizing parallel ultrasound transducer orientation. Similar increases were not seen with either 45° or perpendicular transducer orientations.

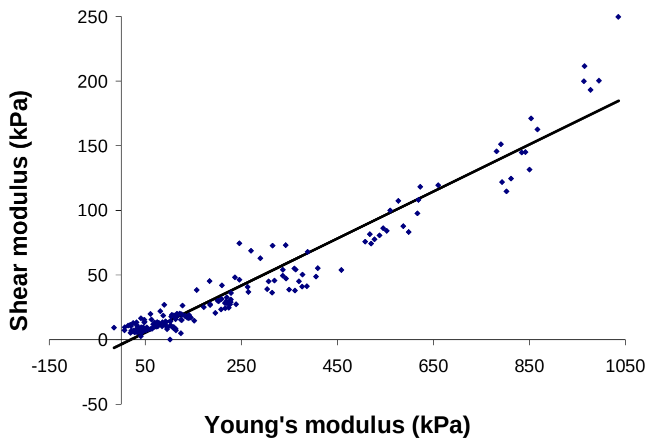

Figure 1: Scatterplot of elastic moduli for parallel ultrasound transducer trials. Generalized linear model regression line from statistics in Table 1.

Generalized estimating equations analyses of all observations from all four specimens are included in Table 1. These results indicate a significant correlation between Young's modulus and shear modulus for parallel transducer orientation (p < 0.0001). The regression coefficient was 0.1818, with a 95% confidence interval of (0.1573 – 0.2064). A scatterplot of all Young's moduli and shear moduli from the parallel transducer trials, with associated generalized linear model regression line, is included in Figure 1. The parameters for 45° and perpendicular transducer orientations were near zero and nonsignificant (0.0061; p = 0.1077, and 0.0043; p = 0.2435, respectively).

CONCLUSIONS

Both parallel SWE and MTS showed increased stiffness measures with increasing tensile load. This study provides the necessary first step for additional studies that can evaluate the distribution of stiffness throughout a muscle.

REFERENCES

1. Hill, AV. *Proc R Soc B* **126**, 136–195 (1938).
2. Huxley, AF. *Prog Biophys Biophys Chem* **7**, 255 (1957).
3. Borg, TK. & Caulfield, JB. *Tissue Cell* **12**, 197–207 (1980).
4. Kjaer, M. *Physiol Rev* **84**, 649–698 (2004).
5. Sarvazyan, AP, et al. *Ultrasound Med Biol* **24**, 1419–35 (1998).
6. Chen, S. et al. *IEEE Trans Ultrason Ferroelectr Freq Control* **56**, 55–62 (2009).
7. Palmeri, ML, et al. *Ultrasound Med Biol* **34**, 546 (2008).
8. Bercoff, J, et al. *IEEE Trans Ultrason Ferroelectr Freq Control* **51**, 396–409 (2004).
9. Yamakoshi, Y, et al. *IEEE Trans Ultrason Ferroelectr Freq Control* **37**, 45–53 (1990).
10. Van Ee, C, et al. *J Biomech Eng* **122**, 9 (2000).

Table 1: Regression coefficients and 95% confidence intervals for shear moduli at three transducer orientations.

Transducer orientation	GEE Parameter	(95% CI)	P-value
Parallel	0.1818	(0.1573 – 0.2064)	<0.0001*
45°	0.0061	(-0.0013 – 0.0135)	0.1077
Perpendicular	0.0043	(-0.0029 – 0.0115)	0.2435

ORAL PRESENATIONS – FRIDAY SEPTEMBER 6th

	Lower Extremity: Gait Analysis *Ajit Chaudhari, Steve Jamison*
9:45 AM	Maximum Ankle Torque Is Positively Correlated With Plantarflexor Moment Arm In Healthy Young Men **Baxter J, Piazza S**
10:00 AM	Partial Rupture Of The Achilles Tendon During Simulated Fire Ground Tasks: Assessment Of Lower-Limb Coordination Using A Dynamical Systems Approach. **Gooyers C, Frost D, McGill S, Callaghan J**
10:15 AM	Knee Muscle Strength And Dynamic Medial Knee Joint Load Post-Arthroscopic Partial Meniscectomy **Hall M, Wrigley T, Metcalf B, Hinman R, Dempsey A, Mills P, Cicuttini F, Lloyd D, Bennell K**
10:30 AM	Limb Asymmetries During Gait In Patients After TKA **Flowers P, Zeni J, Snyder-Mackler L**

MAXIMUM ANKLE TORQUE IS POSITIVELY CORRELATED WITH PLANTARFLEXOR MOMENT ARM IN HEALTHY YOUNG MEN

[1,2]Josh R. Baxter, [1]Stephen J. Piazza

[1]The Pennsylvania State University, University Park, PA, USA
[2]Hospital for Special Surgery, New York, NY, USA
email: *piazza@psu.edu*

INTRODUCTION

The joint moment produced by muscular contraction is the product of the force and the moment arm of the muscle-tendon units crossing the joint. The relative importance of muscle force and muscle moment arm as determinants of strength in humans has not received much attention in previous studies. Maximum plantarflexor torque (pfTOR) has been found to correlate strongly with plantarflexor muscle volume (pfVOL) in young healthy men (1), but no corresponding link has been documented between pfTOR and plantarflexor moment arm (pfMA). Blazevich et al. (2) reported only a weak correlation between maximal knee extensor torque and knee extensor moment arm in young healthy subjects, but reported much stronger correlations between extensor muscle volume and joint strength.

Several recent studies have reported links between locomotor function and pfMA in different populations, including the elderly, distance runners, and sprinters. Walking velocity has been found to correlate positively with pfMA in slower walking elderly adults (3). Distance runners with shorter pfMA demonstrate better running economy (4). Sprinters have been found to have shorter pfMA than height-matched non-sprinters (5,6). It may be that shorter pfMA allows for slower muscle shortening and increased muscle force during rapid joint rotations (7).

The purpose of this study was to measure maximal isometric and isokinetic plantarflexor torque in healthy young men in order to determine if pfTOR is correlated with pfMA. We hypothesized that maximal isometric pfTOR would be positively correlated with pfMA while maximal pfTOR during rapid joint rotations would be negatively correlated with pfMA as longer pfMA would be expected to accentuate force-velocity effects.

METHODS

Subjects. Twenty young, recreationally active, and healthy males (mean age 26.0±3.5y, height 177.7±7.7cm, body mass 76.3±15.6kg, and foot length 268.0±13.0cm) participated in this study.

Dynamometer testing. Subjects were seated in an isokinetic dynamometer (System 3, Biodex Medical Systems) and performed maximal isometric ($0°\cdot s^{-1}$) and isokinetic ($30, 120, 210°\cdot s^{-1}$) contractions. Before each contraction, the foot was placed into 10-15° dorsiflexion and subjects were instructed to press against the plate as hard and as fast as they could while simultaneously releasing the dynamometer brake with a handheld trigger. To acclimate to the isokinetic trials, subjects performed at least three practice contractions at each velocity. Subjects then completed a set of five maximal contractions at each of the four plantarflexion speeds. Rest was provided between contractions and the order of speeds was randomized.

Magnetic resonance (MR) imaging. To quantify pfMA and pfVOL, MR images of the right lower leg and foot of each subject were acquired using a 3.0 T scanner (Siemens Trio) while subjects lay supine with both knees fully extended. The foot was positioned in the scanner with an MR-compatible ankle-positioning device and images were acquired in three ankle postures: 10° dorsiflexion, neutral, and 10° plantarflexion. Previously described techniques were used to calculate pfMA at neutral ankle angle (6) and pfVOL of the posterior compartment (8).

Regression analysis. Linear regressions were performed to determine if pfMA was correlated with pfTOR measured under isometric conditions and at each of the three plantarflexion velocities.

RESULTS AND DISCUSSION

Isometric pfTOR was moderately correlated with both pfVOL (R^2 = 0.322; $p < 0.01$) and pfMA (R^2 = 0.323) (Fig. 1). pfTORs measured during isokinetic tests were weakly correlated with pfVOL at the three speeds tested (R^2 = 0.226 to 0.243) and moderately correlated with pfMA (R^2 = 0.424 to 0.494). There was only a weak correlation between pfMA and pfVOL (R^2 = 0.191; p = 0.054). All of the above correlations were significant ($p < 0.05$) except where indicated.

We found pfTOR to be positively correlated with pfMA across all the plantarflexion speeds we tested. These results support our hypothesis that isometric pfTOR would be positively correlated with pfMA, but reduced ankle leverage did not appear to enhance plantarflexor torque generation in our subjects. In fact, we found a stronger positive correlation between pfTOR and pfMA in our isokinetic tests.

These are the observations of an association between plantarflexor strength and pfMA in humans. Further research is needed to determine whether the correlations reported here would be expected to provide young adults with some functional advantage during locomotion or other activities.

CONCLUSIONS

Plantarflexor torque appears to be positively correlated with pfMA, regardless of the rate of plantarflexion at which this torque is measured. The current findings suggest that joint leverage explained at least as much variance in plantarflexor torque as muscle volume. That pfMA was only weakly correlated with pfVOL suggests moment arm is a less obvious but equally important determinant of ankle strength.

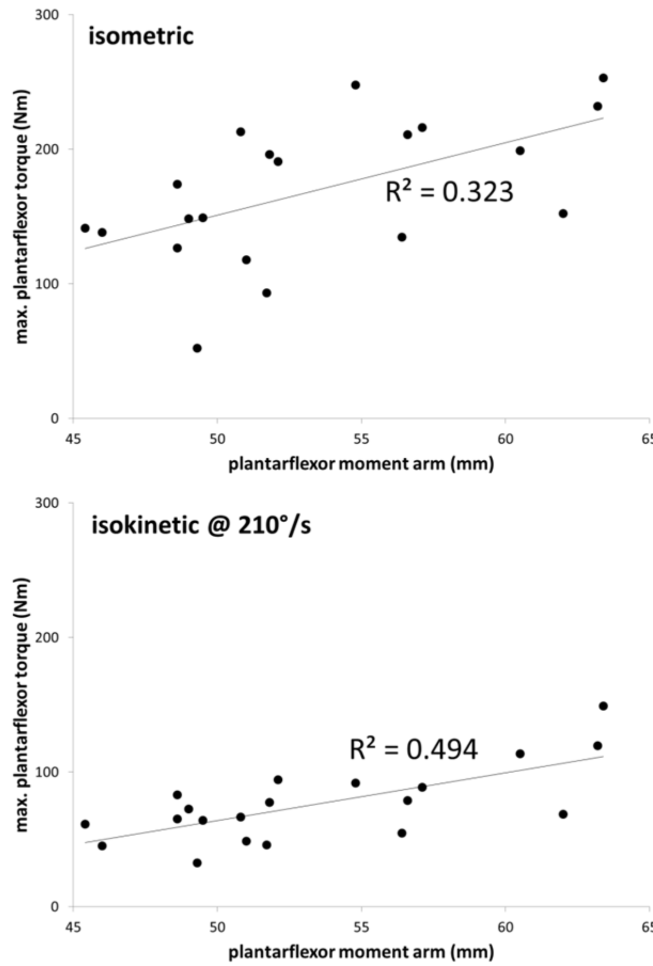

Figure 1: Maximum plantarflexor torque generated under isometric conditions (*top*) and during plantarflexion at 210°/s (*bottom*), plotted versus plantarflexor moment arm in each case. Moderate and significant positive correlations between plantarflexor strength and moment arm were found.

REFERENCES

1. Morse CI et al., *Eur J Appl Physiol*, 2004
2. Blazevich AJ et al., *Eur J Appl Physiol*, 2009
3. Lee SSM et al., *J Biomechanics*, 2012
4. Scholz MN et al., *J Exp Biol*, 2008
5. Lee SSM et al., *J Exp Biol*, 2009
6. Baxter JR et al., *Proc Royal Soc B*, 2012.
7. Lieber RL et al., *Muscle Nerve*, 2000
8. Fukunaga T et al., *J Orthop Res*, 1992

PARTIAL RUPTURE OF THE ACHILLES TENDON DURING SIMULATED FIRE GROUND TASKS: ASSESSMENT OF LOWER-LIMB COORDINATION USING A DYNAMICAL SYSTEMS APPROACH

Chad E. Gooyers, David M. Frost, Stuart M. McGill, Jack P. Callaghan
Department of Kinesiology, University of Waterloo, Waterloo, ON
email: cgooyers@uwaterloo.ca

INTRODUCTION

In a recent study conducted by our group [1], we observed an incumbent firefighter (age = 32 years, height = 172 cm, mass = 80 kg) partially rupture his right Achilles tendon (AT) during an experiment conducted to examine the physical demands of firefighting. The experiment comprised two simulated tasks commonly performed on the fire ground: (i) a hose-advance where participants were instructed to place a 6.4 cm diameter rope (connected to a weighted cable machine at 10 kg resistance) over the right shoulder and initiate forward motion from a left foot forwards stationary stance (Figure 1A); and (ii) a forced entry where participants struck a ceiling-mounted "heavy bag" with a 4.5 kg sledgehammer to simulate forcing entry into a building (Figure 1B). The demands of these tasks were based on the Candidate Physical Ability Test (CPAT), which reflects the critical tasks and essential duties of firefighters.

Although the experiment was designed to evaluate participants' forward motion during the hose advance task, participants also walked backwards (under load) as they returned to the start position to reset for the next trial. By coincidence the data collection system was left running long enough to capture the firefighters' movement patterns during both the advance and the return phase of most trials (30/36). Fortuitously, the participant also contacted the in-ground force platform with his right foot during the majority of these trials (29/30). Though no differences were noted in the peak vertical ground reaction forces recorded during the stance phase of this backwards motion, the participant's right frontal plane ankle moment, a known risk factor for AT rupture [2], was considerably higher during the return phase of the trial performed immediately before the culminating event. However, the participant's lower limb coordination was not examined.

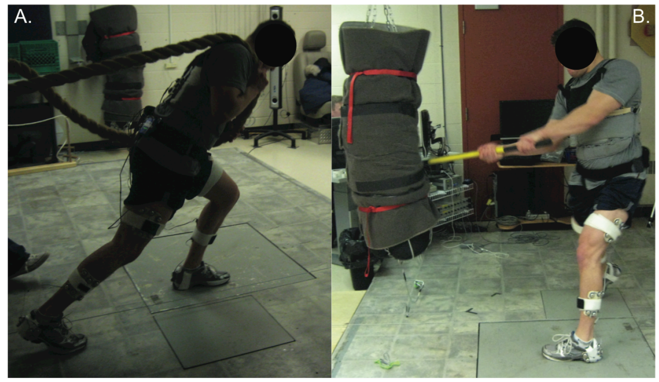

Figure 1: Simulated: (A) hose-advance and (B) forced-entry fire ground tasks.

Therefore, the purpose of this investigation was to assess the bilateral joint coupling between the ankle and knee during the forwards and backwards phases of the hose-advance trials preceding injury using a dynamical systems approach [3].

METHODS

Kinematics of the lower-limbs and trunk were synchronously collected at 32 Hz (Optotrak Certus, Northern Digital Inc., Waterloo, ON, Canada) with ground reaction forces and moments at 2048 Hz from two force platforms (AMTI, Watertown, MA, USA). The firefighter ruptured his right AT during the 37th repetition of the hose-advance task. Forty simulated forced-entry trials were also performed before the injury occurred.

With permission from the participant, all biomechanical data collected were analyzed using an eight-segment rigid link model (bilateral feet, shank, thighs, pelvis and trunk) constructed in Visual3D^{TM} (Version 4.96.6, C-Motion, Inc., Germantown MD, USA). Data from the forward phase of the hose-advance task were truncated to include only the first stride of the movement. Data from the backwards phase were limited to the portion of the movement when the right foot was in contact with the force plate. To facilitate comparisons across trials, kinematic waveforms were time normalized to 101 data points (0 to 100 % of movement) using a shape-preserving, piecewise cubic interpolation method (MATLAB, Version 2012a, The Mathworks, Inc., Natick, MA, USA). Normalized phase plots for the ankle and knee joints (left and right sides) were computed to describe joint coupling via calculation of the continuous relative phase (CRP), defined as the difference between normalized phase angles of the two segments (ankle subtracted from knee). Ensemble averaged curves were calculated for both the forwards and backwards trials preceding the culminating event. The variation of CRP was calculated as the standard deviation of each time-normalized data point.

RESULTS AND DISCUSSION

There was a marked difference in the right lower limb coordination observed in the sagittal plane during the return phase of the 36th trial (~30% movement; Figure 2). The negative sagittal CRP highlights that the ankle had a larger phase angle than the knee. Interestingly, this deviation occurred at the same time that the increased frontal plane moment was observed at the right ankle.

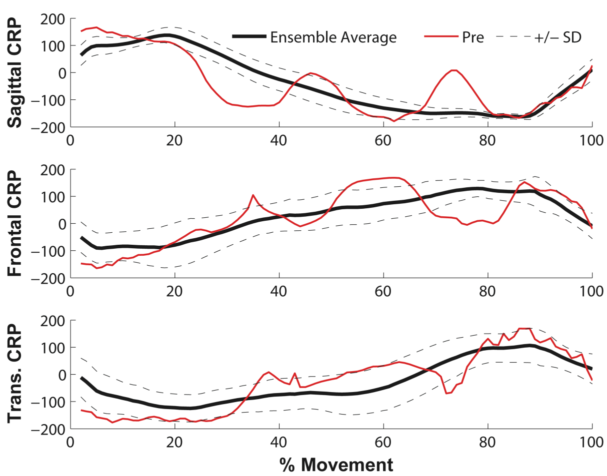

Figure 2: Continuous relative phase (degrees) between the right ankle and knee during stance phase of backwards motion. PRE = backwards phase of the 36th hose advance trial.

A distinct change in joint coupling (> 3 SD) was observed in both the sagittal and frontal planes of movement on the left side immediately before the culminating event during the 37th trial (Figure 3). The positive CRP indicates that the knee had a greater phase angle and approached anti-phase coupling during the initiation of movement.

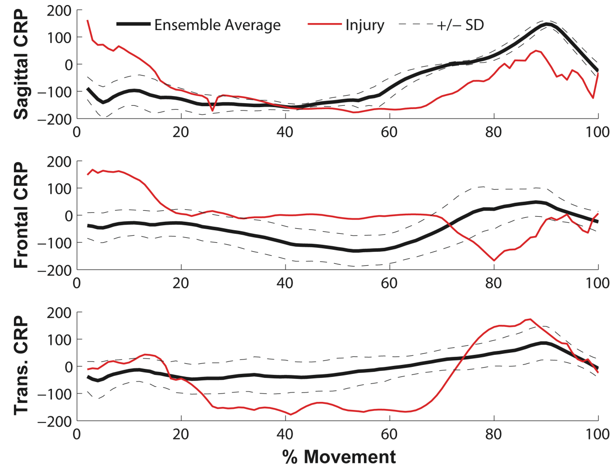

Figure 3: Continuous relative phase (degrees) between the left knee and ankle during the first forward stride during the hose-advance task.

There are two plausible explanations for the increased loading scenario that was observed during the return phase of motion. First, the failure tolerance of the AT was reduced due to repeated loading. When the increased moment was observed, the AT partially ruptured, thus impacting the coordination of movement between the right ankle and knee joint. Second, there was a change in movement behavior, potentially caused by fatigue, which resulted in an acute AT exposure sufficient to cause partial rupture. Although the participant donned his own athletic shoes for the study, this is not the typical footwear worn by firefighters on the fire ground. As such, it is important to acknowledge this potential limitation and the influence that a change from boots to athletic shoes may have on lower-limb joint coordination, and the mechanism of injury.

CONCLUSIONS

The unexpected and rare event that was captured in this work provides insight into the complexity of characterizing overexertion from cumulative injury pathways. Similar analyses of joint coupling between the hip and knee are currently underway.

REFERENCES

1. Gooyers et al. *Clin Biomech*, In Press
2. Hess GW, *Foot & Ankle Specialist* 3, 29-32, 2010.
3. Hamill et al. *Clin Biomech*, 14, 297-308, 1999.

Knee muscle strength and dynamic medial knee joint load post-arthroscopic partial meniscectomy

[1]Michelle Hall, [1]Tim V Wrigley, [1]Ben R Metcalf, [1]Rana S Hinman, [2,3]Alasdair R Dempsey, [2]Peter M Mills, [4]Flavia M Cicuttini, [2]David G Lloyd, [1]Kim L Bennell

[1]The University of Melbourne, Melbourne, Victoria, Australia
[2] Griffith Health Institute, Griffith University, Gold Coast, Queensland, Australia
[3]Murdoch University, Perth, Western Australia, Australia
[4]Monash University, Melbourne, Victoria, Australia
email: halm@unimelb.edu.au web: http://www.chesm.unimelb.edu.au/

INTRODUCTION

Arthroscopic partial meniscectomy (APM) is one of the most commonly performed orthopedic surgeries. Following a meniscal injury individuals are at increased risk of developing knee osteoarthritis with estimates suggesting that 50% of patients have radiographic signs of osteoarthritis within 10-15 years post-surgery [1]. Both knee muscle weakness and a high external knee adduction moment (KAM) during walking are associated with knee osteoarthritis. Also both factors have been observed post-APM [2,3] and may be interrelated [4]. Muscles play a role in controlling joint moments and biomechanical modeling research has found that the quadriceps and hamstrings contribute to support the external knee adduction moment [5,6]. Cross-sectional research also suggests that individuals 3-months post-APM surgery with weak isometric knee extensors have a higher peak KAM during normal paced walking as compared to APM individuals with strength comparable to healthy controls [4]. In an APM population, we have recently found that while knee muscle strength improved over 2 years (from 3 months post-APM surgery), KAM increased over the same time [3]. Considering that muscle weakness can be modified, there is a need to further explore associations between knee muscle strength and dynamic medial knee joint loading post-APM. The purpose of this longitudinal study was to determine whether knee muscle strength three months post-APM surgery was associated with a change in dynamic medial knee joint load over the subsequent 2 years.

METHODS

This is a secondary analysis of longitudinal data collected in a study that described and compared the KAM and knee muscle strength in APM participants and healthy controls [3]. Data from 65 individuals with medial APM were collected at baseline 3 months after surgery (86% male; 41± 5 yrs; BMI 27.3 ± 4.2 kg/m^2) and 2 years later at follow-up (86% male; age 41± 6 yrs; BMI 27.3 ± 4.6 kg/m^2). Maximal isokinetic knee muscle strength was assessed using a KinCom 125-AP dynamometer at baseline and follow-up. During each testing session, participants performed two tests of five maximal concentric-concentric contractions of knee extensors and flexors at 60°/second through a range of 5° to 95° of knee flexion, followed by reciprocal eccentric-eccentric contractions. Peak torque was corrected for gravity and normalized to body mass (Nm/kg). Participants walked barefoot and performed five trials at a self-selected normal and fast walking paces while kinematic data (120Hz) were collected using an eight-camera motion analysis system (Vicon) with kinetic data (1080Hz) recorded using three force plates (AMTI). The first peak KAM and KAM impulse during stance were calculated using inverse dynamics (UWA model), averaged and normalized to the product of body weight and height. For each of the four measures of isokinetic muscle strength participants were categorized into tertiles. Participants in the lowest tertile were categorized as 'weak' while participants in the highest tertile were considered 'strong'. Univariate ANCOVA analyses were used to explore differences in the changes in peak KAM and KAM impulse over 2 years comparing the 'weak' and 'strong' groups. Covariates included change in walking speed (known to affect KAM) and baseline peak KAM and KAM impulse ('scope for change'). Significance was set at $p<0.05$.

RESULTS AND DISCUSSION

There were no significant differences between the strong and weak groups in the change in peak KAM or KAM impulse over the 2-year period (Table 1). However, there was a trend for individuals with weak eccentric quadriceps strength to demonstrate an increase (15%) in KAM impulse during fast pace walking compared to the strong group ($p = 0.057$).

This is the first longitudinal study to evaluate if people with knee muscle weakness at baseline have greater increases in KAM over 2 years post-APM. Overall our data did not find this to be the case. This is despite previous modeling research implicating the role of the quadriceps and hamstrings in supporting the externally applied knee adduction moment [5, 6] and cross-sectional evidence observing that individuals 3-months post-APM surgery with weak isometric knee extensor strength have a higher peak KAM during normal paced walking than APM participants with strength comparable to healthy controls [4]. Possible explanations for our non-significant findings include that the KAM is a net calculation controlled by submaximal activations of multiple lower extremity and upper body muscles. Therefore the premise that increases in KAM would be associated with weak maximal isokinetic knee muscle strength is perhaps too simplistic [4]. These findings suggest that factors other than isokinetic strength may be more important in determining increases in peak KAM following APM. For example, dynamic alignment of the lower extremity or control of upper body posture and movement may influence increases in peak KAM, which are perhaps more reliant on neuromuscular control rather than maximal isokinetic knee muscle strength.

CONCLUSIONS

This exploratory study suggests no association between knee muscle weakness and increase in KAM during walking post-APM. Nonetheless, the trend observed between eccentric knee extensor weakness and increases in KAM impulse during fast pace walking warrants further research.

REFERENCES

1. Lohmander LS, et al. *Am J Sports Med* **35**, 1756-1769, 2007.
2. Sturnieks DL, et al. *J Orthop Res* **26**, 1075-1080, 2008.
3. Bennell KL, et al. *Osteoarthritis Cartilage* **20,** S26-S26, 2012.
4. Sturnieks DL, et al. *Med Sci Sports Exerc* **40**, 991-997, 2008.
5. Lloyd DG, et al. *J Biomech* **34**, 1257-1267, 2001.
6. Winby et al *J Biomech* **42,** 2294–2300, 2009.

Table 1: Normalised change in knee adduction moment and impulse (mean ± SD) over 2 years according to isokinetic knee muscle strength in APM participants

	Normal Pace Walking				**Fast Pace Walking**			
Isokinetic strength (Nm/kg)	Δ Peak KAM (Nm/(BW*ht)%)		Δ KAM Impulse (Nm.s/(BW*ht)%)		Δ Peak KAM (Nm/(BW*ht)%)		Δ KAM Impulse (Nm.s/(BW*ht)%)	
	APM Weak	APM Strong	APM Weak	APM Strong	APM Weak	APM Strong	APM Weak	APM Strong
Concentric quad	0.24 ± 0.87	0.29 ± 0.65	0.03 ± 0.24	0.03 ± 0.22	0.56 ± 1.13	0.17 ± 0.84	0.09 ± 0.23	-0.01 ± 17
Eccentric quad	0.26 ± 0.89	0.13 ± 0.62	0.06 ± 0.23	0.01 ± 0.20	0.56 ± 1.16	0.11 ± 0.84	0.11 ± 0.22	-0.02 ± 0.15
Concentric hams	0.19 ± 0.71	0.43 ± 0.82	0.02 ± 0.22	0.05 ± 0.23	0.38 ± 0.87	0.45 ± 1.11	0.06 ± 0.18	0.04 ± 0.20
Eccentric hams	0.25 ± 0.76	-0.02 ± 0.56	0.01 ± 0.23	-0.03 ± 0.20	0.36 ± 0.91	-0.03 ± 0.66	0.05 ± 0.19	-0.04 ± 0.14

KAM; knee adduction moment: Quad; quadriceps Hams; hamstrings. All values adjusted for baseline scores (peak KAM and KAM impulse) and change in walking speed

LIMB ASYMMETRIES DURING GAIT IN PATIENTS AFTER TKA

[1]Portia Flowers, [1]Joeseph Zeni and [1]Lynn Snyder-Mackler

[1]University of Delaware, Newark, DE, USA
email: pflowers@udel.edu

INTRODUCTION
Total knee arthroplasty (TKA) reduces pain and improves function in patients with knee osteoarthritis (OA). However, movement asymmetries and muscle weakness persist after surgery. These movement asymmetries overload the contralateral joints, which may explain the high prevalence of contralateral knee OA following initial TKA surgery [1]. The purpose of this study was to quantify short and long-term kinetic and kinematic movement asymmetries during gait in patients after unilateral TKA. We hypothesized that 2 years after TKA, patients will have more symmetrical flexion angles at initial contact, excursions and moments, but demonstrate more asymmetrical adduction moments.

METHODS
Thirty subjects who underwent unilateral TKA for osteoarthritis were evaluated. Fifteen subjects were evaluated 6 months after surgery (6M, 9F, age=67.4yrs, BMI=33.61) and fifteen age- and sex-matched subjects were evaluated 2 years after surgery (6M, 9F, age=67.1 yrs, BMI = 31.85). Three dimensional gait analysis was performed using an 8 camera infrared motion system (Vicon) synchronized with two forceplates (Bertec). Knee flexion at initial contact, knee flexion excursion, peak knee flexion moment (PKFM), peak knee extension moment (PKEM), 1st and 2nd peak knee adduction moments (PKAM1, PKAM2), and average adduction moment (KAM_{ave}) were analyzed. Differences between limbs over time were assessed using 2x2 (limb by time) 2-way repeated measures ANOVA.

RESULTS AND DISCUSSION
There were no significant limb by time interactions for any of the kinetic and kinematic variables, indicating a lack of change in asymmetries over time. The main effect between limbs was significant for PKAM1 ($p<0.01$) and PKAM2 ($p<0.01$). The main effect of time was significant for PKAM2 ($p=0.037$) and approached significance for PKAM1 ($p=0.077$). PKAM1 was 0.139 N·m/kg·m greater and PKAM2 was 0.080 N·m/kg·m greater in the non-operated limb compared to the operated limb (Fig. 1), indicating greater medial compartment loading in the non-operated limb. The main effects of limb and time were also significant for KAM_{ave} ($p<0.01$; $p=0.037$). Individuals 2 yrs after TKA had 0.035 N·m/kg·m greater adduction moment than those 6mo after surgery. This increased loading 2 years after TKA may increase the risk of developing OA in the contralateral joint [2] or be representative of disease progression in this group [3].

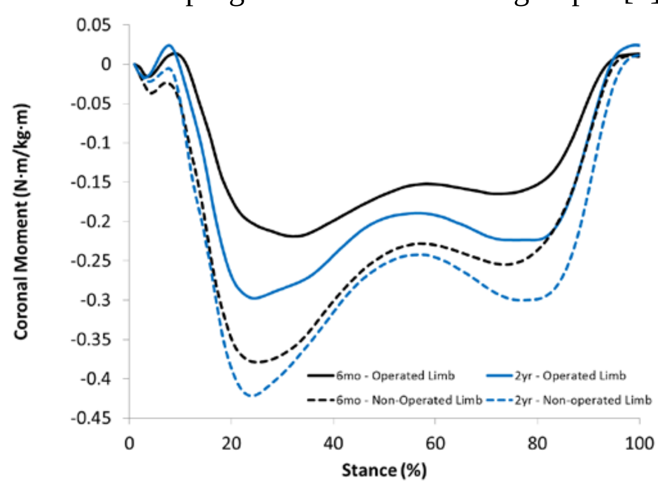

Figure 1: Knee Adduction Moment during stance

For knee flexion angle at initial contact, the main effect of limb was significant ($p=0.008$) and approached significance for the main effect of time ($p=0.067$). The operated limb had 3.4° more flexion at initial contact compared to the non-operated limb. Such asymmetries may be indicative of residual adaptations to reduce joint loading and pain prior to TKA.

The main effect of time was significant for the PKEM ($p=0.034$). Individuals 2 years after TKA surgery had 0.069 N·m/kg·m more external extension moment than those at 6 months and demonstrated a more biphasic sagittal moment pattern. This lack of a knee extension moment may be a result of excessive knee flexion through midstance, which may increase the demand on the quadriceps (Fig. 2).

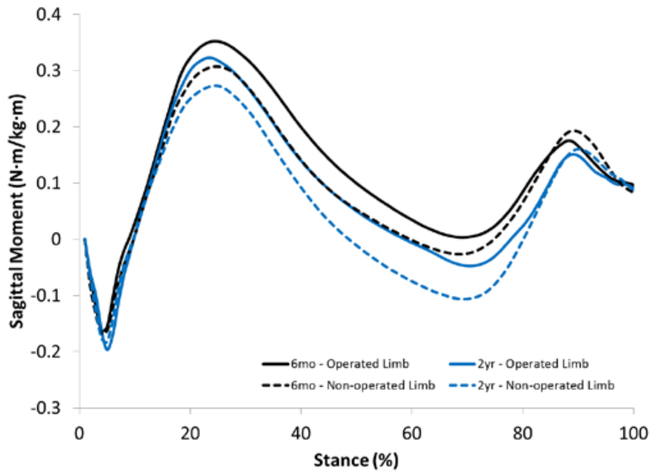

Figure 2: Sagittal Knee Moment during stance

CONCLUSIONS

We did not find any time by limb interactions in our sample, but there were main effects for limb. This suggests that subjects 6 months after TKA ambulate with significant kinematic and kinetic movement asymmetries and these asymmetries persist 2 years after TKA.

There were main effects for knee extension moments over time. This may reflect improved knee extension excursion in both limbs 2 years after TKA. The main effect of limb for flexion at initial contact indicates that the operated limb remains more flexed at initial contact at both timepoints. This may be reflective of reduced range of motion and may place the individual at risk for functional limitations and abnormal loading patterns. Larger adduction moments were also present in the non-operated limb at both time points. Although we hypothesized that adduction moment would become more asymmetrical over time (with an increase in the non-operated limb), this hypothesis was not supported by our data. However, the significant between limb difference is concerning as excessive adduction moment on the non-operated limb may lead to long-term functional decline in these patients. Previous studies have shown that the risk of knee OA progression increases 6.46 times with a 1% increase in knee adduction moment [3]. Although we noticed a slight increase in peak knee adduction moment over time, this trend was not significant.

A longer-term follow up or a larger sample size may be required to demonstrate the expected changes in between-limb symmetry over time. Future work should assess quadriceps strength, pain, and knee range of motion to determine the underlying cause of these movement asymmetries.

REFERENCES

1. Shakoor N. *Arthritis Rheum*, **46**, 3185-89, 2002.
2. Alnahdi, A. *J Orthop Res*, **29**, 647-652, 2011.
3. Miyazaki, T. *Ann Rheum Dis*, **61**, 617-622, 2002.

ACKNOWLEDGEMENTS

This study was supported by NIH grants (P20RR016458, S10RR022396) and a scholarship from the University of Delaware.

Table 1: Gait parameters (mean±SD), *Significant difference between limbs, ¶Significant difference between time points

	6mo		2yr	
	Operated	Non-Operated	Operated	Non-Operated
Knee flexion angle at Initial Contact (°)	-9.26±4.42*	-4.81±4.95	-5.07±5.61*	-2.66±5.34
Knee flexion excursion (°)	10.56±4.11	12.40±4.63	12.02±2.39	11.78±5.61
PKFM (N·m/kg·m)	0.36±0.12	0.31±0.16	0.32±0.15	0.28±0.20
PKEM (N·m/kg·m)	0.00±0.12¶	-0.03±0.09¶	-0.06±0.15	-0.11±0.08
PKAM1 (N·m/kg·m)	-0.24±0.11*	-0.40±0.10	-0.32±0.12*	-0.43±0.13
PKAM2 (N·m/kg·m)	-0.18±0.09*¶	-0.27±0.07¶	-0.24±0.09*	-0.31±0.11
KAMave (N·m/kg·m)	-0.12±0.07*¶	-0.21±0.06¶	-0.17±0.07*	-0.24±0.08

ORAL PRESENATIONS – FRIDAY SEPTEMBER 6th

	Thematic: Variability in Standing, Walking and Running *Jonathan Dingwell*
9:45 AM	Gait Variability Of Individuals With Transtibial Amputations Walking In Destabilizing Environments. **Beurskens R, Beltran EJ, Wilken JM, Dingwell JB**
10:00 AM	Medio-Lateral Restriction And The Speed Of Optic Flow Affect The Temporal Structure Of Gait Variability **Qiao M, Stergiou N, Mukherjee M**
10:15 AM	Day-To-Day Variability Of Home-Based Measures Of Postural Sway In Older Adults **McGrath D, Greene B, Sheehan K, Kenny R, Caulfield B**
10:30 AM	Effect Of Treadmill Versus Overground Running On The Structure Of Variability Of Stride Timing **Lindsay T, Noakes T, McGregor S**

GAIT VARIABILITY OF INDIVIDUALS WITH TRANSTIBIAL AMPUTATIONS WALKING IN DESTABILIZING ENVIRONMENTS

[1]Rainer Beurskens, [2]Eduardo J. Beltran, [2]Jason M. Wilken and [1]Jonathan B. Dingwell

[1]Department of Kinesiology & Health Education, University of Texas at Austin, TX, USA
[2]Department of Orthopedics and Rehabilitation, Center for the Intrepid, Brooke Army Medical Center, Ft. Sam Houston, TX, USA
email: rbeurskens@austin.utexas.edu

INTRODUCTION

During walking people are exposed to many challenges to stability, including slippery surfaces and uneven terrain. These may lead to changes in walking behavior or cause falls and injuries. Walking on uneven surfaces or while exposed to perturbations increases gait variability in both, models and humans [1]. Increased gait variability may predict increased risk of falling [2]. Alternatively, increased gait variability may also result directly from the perturbations themselves and/or reflect subjects' responses to perturbations. An improved understanding of how different types of perturbations affect gait variability, especially in patient groups that are known to be at an increased risk of falling, is needed. The purpose of this study was to determine the effect of unilateral transtibial amputation on gait variability during exposure to continuous medio-lateral perturbations of the walking surface or the visual field.

METHODS

Nine individuals with a unilateral trans-tibial amputation (TTA, 30.7±6.8yrs) and thirteen age matched able-bodied individuals (AB, 24.8±6.9yrs) walked on a 2m×3m treadmill embedded in a 4m diameter moveable platform in a Computer Assisted Rehabilitation Environment (CAREN) virtual reality system (Motek, Amsterdam, Netherlands). Participant movements were recorded using 24 motion analysis cameras (Vicon, Oxford, UK). Subjects completed five 3-min trials under each of the following conditions: no perturbation (NOP), platform (PLAT) perturbations, or visual field (VIS) perturbations. Subjects walked at the same, controlled walking speeds in all three conditions. All perturbations were applied as pseudo-random translations in the medio-lateral direction [3,4]. We calculated means and standard deviations of the following stepping parameters and trunk motions:

- *Step length:* distance between right and left heel strikes in anterior-posterior direction
- *Step width:* distance between right and left heel strikes in medial-lateral direction
- *C7 position:* mean standard deviation of the C7 vertebra position
- *C7 velocity:* mean standard deviation of the C7 vertebra velocity

For each dependent measure, 2-way mixed repeated measures ANOVAs were used to determine between-group differences across conditions. Data were compared separately for platform and visual perturbation trials because of the different nature of each type of perturbation [3,4].

RESULTS AND DISCUSSION

In the PLAT condition, subjects' mean step width ($F(1,20) = 32.3$; $p < 0.001$), step width variability ($F(1,20) = 173.1$), step length variability ($F(1,20) = 34.4$; $p < 0.001$), C7 position ($F(1,20) = 265.7$) and C7 velocity ($F(1,20) = 236.1$; both $p < 0.001$) increased and mean step length ($F(1,20) = 40.9$; both $p < 0.001$) decreased compared to NOP for both groups (AB and TTA). Also, step width and C7 position were slightly more variable for TTA, but only C7 position reached significance ($F(1,20) = 7.25$; $p < 0.05$). Increases in mean step width and step length indicate both groups increased their base of support when walking in mechanically destabilizing environments.

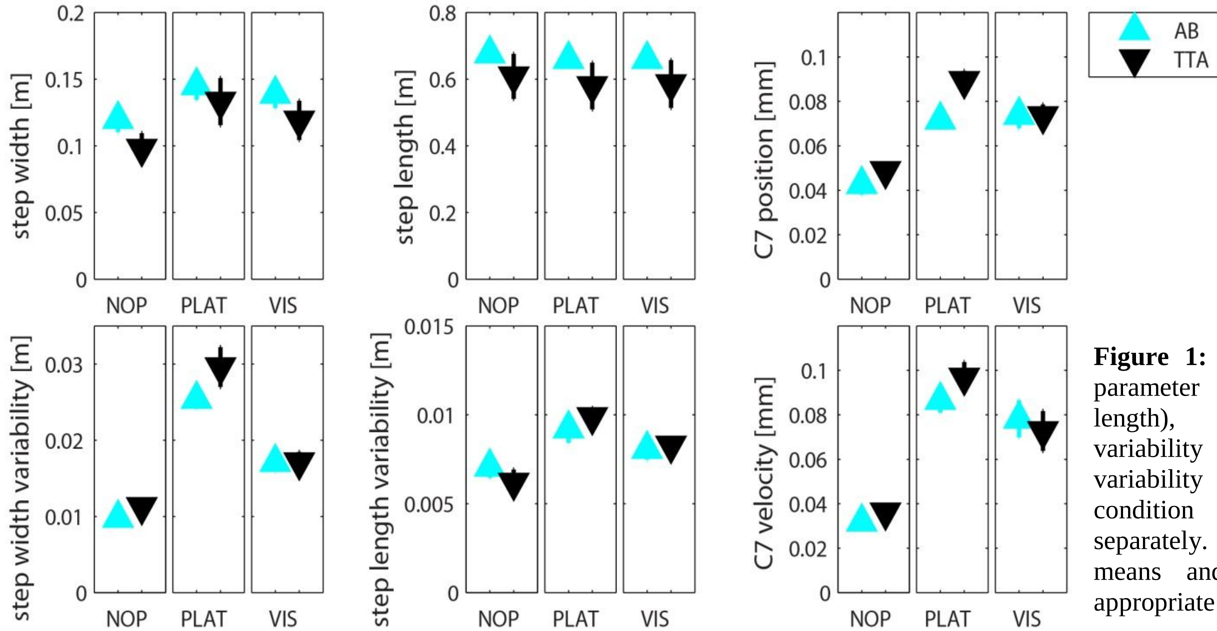

Figure 1: Subjects' stepping parameter (step width, step length), the appropriate variability and C7 vertebra variability for each walking condition and each group separately. Triangles represent means and error bars the appropriate standard error.

Similarly, in the VIS condition, step width (F(1,20) = 27.1), step width variability (F(1,20) = 50.4), step length variability (F(1,20) = 13.2), C7 position (F(1,20) = 39.4) and C7 velocity (F(1,20) = 49.2; all $p < 0.001$) increased and step length (F(1,20) = 31.3) decreased relative to NOP in both groups. Compared to PLAT, the changes in VIS were less pronounced, indicating both groups were more affected by mechanical perturbations than by visual perturbations. This is potentially crucial for TTA patients. Despite their significantly deteriorated somatosensory input, transtibial amputees did not appear to be more sensitive to visual perturbations than healthy controls.

Although TTA patients showed slightly greater trunk movement and step width variability, only trunk movement was significantly different between our two groups. This outcome may be the result of a young, highly active and otherwise healthy patient population.

CONCLUSIONS

Both healthy AB and TTA patients took wider steps to increase their base of support when perturbed. Despite this accommodation, both groups still exhibited increased stepping and trunk (C7) movement variability when perturbed. Interestingly, young active patients with unilateral trans-tibial amputation did *not* demonstrate increased gait variability compared to healthy controls when walking in these mechanically or visually disturbing environments.

REFERENCES

1. Dingwell, JB & Cusumano, JP *Chaos* **10(4)**: 848-863, 2000
2. Maki, BE, *J Am Geriatr Soc* **45(3)**: 313-320, 1997
3. McAndrew, PM, et al. *J Biomech* **44(4)**: 644-649, 2011
4. McAndrew PM, et al., *J Biomech* **43(8)**:1470-75, 2010
5. Wilken, JM et al., *J Am Acad Orthop Surg* **20(1)**: 42-47, 2012

ACKNOWLEDGEMENTS

Supported by NIH grant# R01-HD059844.

The view(s) expressed herein are those of the author(s) and do not reflect the official policy or position of Brooke Army Medical Center, U.S. Army Medical Department, U.S. Army Office of the Surgeon General, Department of the Army, Department of Defense or the U.S. Government

MEDIO-LATERAL RESTRICTION AND THE SPEED OF OPTIC FLOW AFFECT THE TEMPORAL STRUCTURE OF GAIT VARIABILITY

Mu Qiao, Nicholas Stergiou, and Mukul Mukherjee

Nebraska Biomechanics Core Facility, School of Health, Physical Education & Recreation
University of Nebraska at Omaha, Omaha, NE, 68182-0214, USA
email: mqiao@unomaha.edu, web: http://biomech.unomaha.edu/

INTRODUCTION

Gait variability is associated with stability because changes in gait variability are associated with falls. For human walking, the movement in the sagittal plane is more stable than in the frontal plane. As a result, there is more variability in the Medio-Lateral (ML) direction requiring greater active control than in the Antero-Posterior (AP) direction (*1*). Sinusoidal optic flow affected the variability of gait in the ML direction more than the AP direction (*2*). On the other hand, restriction of the ML sway can reduce step width variability and decrease the metabolic cost (*3, 4*). However, it is not clear whether the speed of optic flow can affect walking stability in terms of gait variability. Although ML restriction can affect ML stability, how it impacts the effect of optic flow speed on gait variability is not known. Hence, the aim of this study is to determine the effects of the speed of optic flow and ML restrictions on gait variability. We found that ML restriction reduced both the mean and the variability of step width. The speed of optic flow affected step width, and increasing the speed resulted in decreasing the step width variability. These findings indicate that 1) stabilization in the ML direction can affect gait stability by decreasing both the mean and variability of step width and 2) the speed of optic flow can also affect gait variability in the ML direction.

METHODS

We collected kinematics by using the 3D investigator motion tracking system (60Hz, Northern Digital, Inc., Waterloo, Canada) to track smart marker clusters placed on the foot, shank, thigh, and sacrum. An instrumented split-belt treadmill (300Hz, Bertec Corp., Columbus, OH) was used to record the ground reaction forces (GRFs). Two elastic rubber bands (stiffness = 282 N/m, resting length = 1.07 m) were attached to the waist of the participants. When acting together, the two bands applied forces pulling the participant towards the sagittal plane dividing the two belts (Fig. 1). Ten participants (8 males, age = 28.0 ± 5.6 years; body mass = 72.1 ± 14.1kg; height = 169.7 ± 10.5 cm, preferred walking speed = 1.05 ± 0.22 m/s, mean ± std) performed 3 trials in each condition (each 1 minute long). The Center of Mass (COM) was determined by the sacral markers. Step length and width were calculated using the marker clusters on the feet (Fig. 2). Several variability measures of step length and step width were calculated. These were Root Mean Square (RMS), standard deviation (std), and coefficient of variation (COV, std/mean). A repeated measure factorial ANOVA with participants as the repeated factor was used to determine the effect of main factors (Factor A, restriction, 2 levels, with/without rubber band; Factor B, the gain of optical flow speed to walking speed, 3 levels, 50%, 100% and 200% of the preferred walking speed).

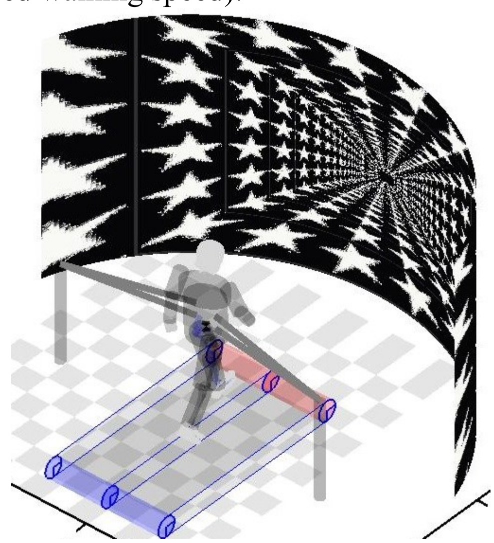

Figure 1: The schematic of the experimental setup with a participant walking in front of the simulated environment and having elastic hip-stabilizers in the ML direction.

RESULTS AND DISCUSSION

The ML restriction reduced the amplitude of COM sway in both AP and ML directions by 36% and 22%, respectively (Fig. 3). However, the effect of optic flow speed on COM excursion was not significant.

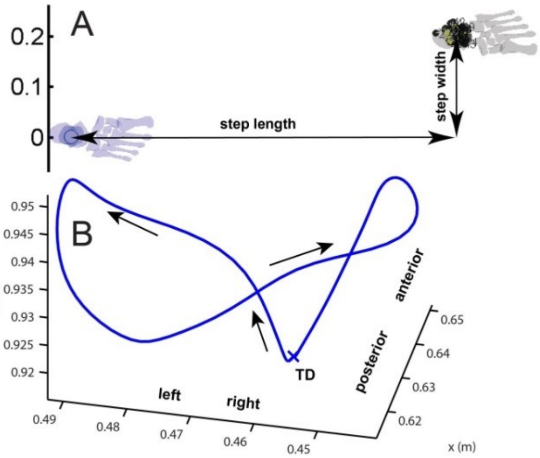

Figure 2: definition of (A) step length and width and (B) ensemble COM trajectory from a complete gait cycle from treadmill walking.

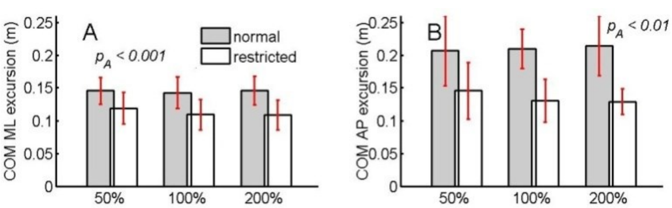

Figure 3: The effect of optic flow (Factor B) and ML restriction (Factor A) on the COM excursion in (A) ML and (B) AP directions (mean ± std).

A significant interaction for step width occurred because the ML restriction reduced the mean step width in the 100% ($p < 0.05$) and 200% ($p < 0.01$) optic flow speed conditions (Fig. 4A). Neither ML restriction nor optic flow speed had any effect on the mean step length (Fig. 4B).

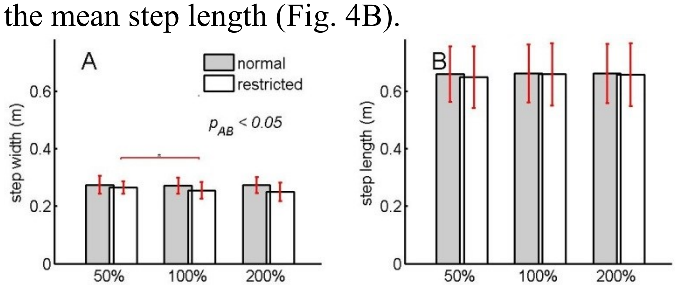

Figure 4: The effect of ML restriction and optic flow on (A) step width and (B) step length.

ML restriction reduced the variability of step width (RMS) by 6% (Fig. 5A, $p_A < 0.05$). When the speed of optic flow increased, the variability of step width decreased (Fig. 5A, $p_B < 0.05$) indicating that the speed of optic flow can also modify the ML stability during human walking. On the other hand, there was no effect of ML restriction or optic flow speed on the step length variability (Fig. 5B). Moreover, there was no effect of ML restriction or optic flow speed on the magnitude of gait variability calculated using std or COV.

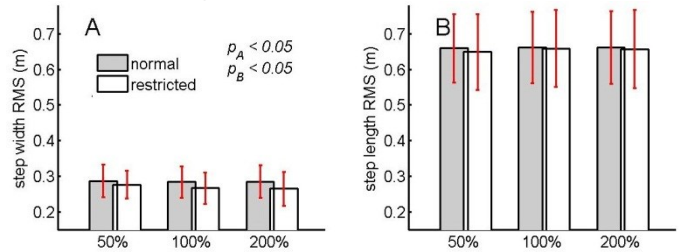

Figure 5: The effect of ML restriction and optic flow on the variability of (A) step width and (B) step length.

CONCLUSIONS

The restriction of ML sway reduced the ML excursion of COM and step width during walking, and therefore has potential to improve gait stability in special populations (*4*). Higher variability in the ML direction is also associated with greater active control to maintain balance resulting in greater metabolic cost (*3*). The speed of optic flow affected gait variability in the ML direction but not in the AP direction. This could be due the virtual environment which did not project visual oscillations in the AP direction as in a previous study (2). However, a lack of differences in the magnitude of gait variability does not predicate the same for the temporal structure of variability. Further, in order to optimize the effect of optic flow on gait variability, the usage of optic flow with a temporally variable structure may have larger and potentially more useful effects.

REFERENCES

1. C. E. Bauby, A. D. Kuo, Active control of lateral balance in human walking. *J. Biomech.* **33**, 1433 (Nov, 2000).
2. S. M. O'Connor, A. D. Kuo, Direction-Dependent Control of Balance During Walking and Standing. *J. Neurophysiol.* **102**, 1411 (Sep, 2009).
3. J. M. Donelan, D. W. Shipman, R. Kram, A. D. Kuo, Mechanical and metabolic requirements for active lateral stabilization in human walking. *J. Biomech.* **37**, 827 (Jun, 2004).
4. J. C. Dean, N. B. Alexander, A. D. Kuo, The effect of lateral stabilization on walking in young and old adults. *IEEE Trans. Biomed. Eng.* **54**, 1919 (Nov, 2007).

DAY-TO-DAY VARIABILITY OF HOME-BASED MEASURES OF POSTURAL SWAY IN OLDER ADULTS

[1,2]Denise McGrath, [2,3]Barry R. Greene, [2]Katie J. Sheehan, [2]Rose A. Kenny, [2]Brian Caulfield,

[1]University of Ulster, Co. Antrim, Northern Ireland
[2]The TRIL Center, University College Dublin, Ireland
[3]Intel labs, Intel Ireland, Leixlip, Co. Kildare, Ireland
email: d.mcgrath@ulster.ac.uk,

INTRODUCTION

Declining postural control is a well documented characteristic of the ageing process. With the current demographic shift towards an ageing population, this is a growing public health concern due to the associated risk of falls and subsequent loss of independence. Over the past two decades, the biomechanics community has championed the use of posturography for the objective measurement of postural control. Measures of postural sway are generally based on center of pressure (COP) deviations beneath the foot when standing on a force platform and have been shown to differentiate between young and older adults [1].

Force plates are very specialized and costly equipment however, and are not readily accessible to the wider community. The Nintendo Wii balance board has recently been shown to be a reliable and valid (compared to a laboratory grade force plate) alternative technology [2], sensitive enough to detect age-related differences in standing balance [3]. This new, low cost solution for reliable measurement of COP deviations yields myriad possibilities for monitoring balance capabilities in older adults. Such a tool could potentially be incorporated into a standard ‘weighing scales’, deployed into a home setting, enabling remote, longitudinal monitoring of postural control. This type of remote monitoring could have far-reaching applications e.g. early detection of declining postural control that could lead to falls prevention, monitoring progress after hospital discharge, examining the effects of changes in medication on the sensory-motor system and evaluation of exercise programs. However, in order to capture a true change in postural control over time, a fundamental precursor to implementing these monitoring paradigms is required: the natural biological variability of the postural sway measures themselves needs to be established.

Like most biological signals, COP exhibits an intrinsic variability that needs to be taken into account, distinct from the measurement error associated with the instrument or conditions. This study sought to remotely measure postural sway parameters in a number of healthy older adults on a daily basis over an 8-week period, using a Nintendo Wii balance board set up in their homes. The aim of the study was to establish the natural variability of postural sway for each individual person, and to investigate if the postural sway parameters were related to age and gait velocity.

METHODS

Eighteen community dwelling older adults (3 male, 15 female; aged ≥65 yrs (Table 1) height: 165cm±8; weight: 79kg±14; Mini Mental State exam: 29±0.8) provided informed consent to participate in a home-based balance trial that required them part-take in a geriatric assessment and to execute a two-footed standing balance trial every day for 8 weeks. Comfortable stance was selected for greatest stability and safety given that the test was unsupervised. A Wii balance board (Nintendo, Japan) was used to record a 60s static balance trial. The sensor data from each daily assessment were sent automatically via a 3G mote to a remote server. Data were monitored to ensure the test was being carried out each day. Each Wii balance board contains four strain gauge pressure sensors, placed at each corner. COP was calculated similar to previously reported methods [2]. The COP time series were sampled at 40Hz and low pass filtered with a 8^{th} order, zero-phase Butterworth filter with a 5Hz corner frequency. Postural sway parameters were calculated according to [1]. Sway length was defined as the total length of the COP path. The mean distance (MDIST) represents the average distance from the mean COP. Mean, standard deviation (SD) and coefficient of variation (CV) were calculated for each parameter across all testing days. Pearson's correlation coefficient was used to investigate relationships between these variables and age and gait velocity.

RESULTS AND DISCUSSION

The mean postural sway values generated by our protocol (Table 1) are similar to those reported in Prieto *et al.* [1] for older adults in a similar stance, using a force plate. This suggests that the Wii balance board is a robust tool for the assessment of postural control. Our data indicate that intra-subject variability was often as large inter-subject variability (Table 1). It must be acknowledged that our protocol was unsupervised, therefore increasing the potential for extraneous movements during the test, despite the fact that each subject was given specific instructions on how to stand and asked to report any disturbances after each test. We believe however, that the weight of the measurement error component was decreased compared with the true score, given the number of trials involved. The postural sway variables had weak to moderate relationships with age and gait velocity (Pearson's correlation coefficient values ranged from 0.35 (Age v MDist) to -0.5 (Gait Velocity v MDist) for mean values and 0.0 (Age v CV Sway Length) to -0.41 (Age v MDist) for variability parameters). This would suggest that the variability reported here is primarily related to the natural biological variability of postural sway in healthy older adults. To the authors' knowledge, this is the first study to quantify this over such a long period of time, in a real-world environment. Future work will seek to incorporate these findings into meaningful, long-term remote monitoring paradigms.

REFERENCES

1. Prieto TE, et al. *IEEE* **43**, 956-966, 1994.
2. Clarke RA, et al. *Gait Posture* **31**,307-310, 2010
3. Kalisch T, et al. *J Aging Res*, **2011**, 2011

Table 1: Descriptive statistics for total sway length and mean distance from the mean COP for each subject

Subject	Age	Gait Velocity (cm/s)	Mean Sway Length (cm)	SD Sway Length (cm)	CV Sway Length	MDist (mm)	SD MDist (mm)	CV MDist
1	81	82.7	75.5	9.7	13.1	7.7	1.4	17.9
2	72	119.2	31.2	7.9	25.3	4.6	1.6	33.8
3	67	136.0	38.7	8.3	22.6	5.6	1.9	30.7
4	67	97.7	38.7	5.9	15.2	5.5	1.3	21.6
5	66	121.7	34.3	5.8	16.8	4.2	1.4	31.5
6	72	89.1	50	11	22.2	8.1	3.1	38.5
7	79	97.7	30.4	4.9	16.3	4.5	1.2	24.9
8	68	116.3	31.8	4.5	14.2	5.6	1.4	24.3
9	78	77.2	37.5	8.2	22.1	6.8	2	30.2
10	66	97.3	23.1	4.7	21.6	4.1	1.9	46.2
11	71	108.6	28.2	4.5	16.5	4.6	1.1	27.4
12	75	93.4	41.2	7.7	19.9	5.7	1.2	20.1
13	73	117.4	43.9	8.4	19.4	7.7	3.3	41.9
14	66	98.5	39.7	9	23.6	7.9	4.4	55.1
15	80	93.0	44.0	7.6	17.3	7.8	2	24.2
16	80	98.1	32.0	9.7	30.2	5.3	2.1	38.7
17	68	115.1	32.0	7.8	24.9	5.8	1.9	32.4
18	67	142.6	28.4	5.2	18.5	4	1.3	33.7
Mean	72.0	105.6	37.8	7.3	20.0	5.9	1.9	31.8
SD	5.5	17.7	11.6	2	4.5	1.4	0.9	9.6
CV	7.7	16.7	30.6	27.7	22.3	24.7	45.4	30.2

EFFECT OF TREADMILL VERSUS OVERGROUND RUNNING ON THE STRUCTURE OF VARIABILITY OF STRIDE TIMING

[1,2]Timothy R. Lindsay, [2]Timothy D. Noakes, and [1]Stephen J. McGregor

[1]Eastern Michigan University, Ypsilanti, MI, USA
[2]University of Cape Town, Cape Town, South Africa
email: tlindsa2@emich.edu

INTRODUCTION

The presence of persistent correlations in human gait has been shown in both treadmill and overground running [1,2]. There are reasons why treadmill and overground gait might elicit different movement patterns, but in the case of walking, reported differences in stride timing persistence are equivocal [3,4]. Further, even if results of walking studies were not equivocal, differences between walking and running gait make extrapolation of such results difficult. Not only is running more physiologically strenuous than walking, but there also may be task execution challenges that are only manifest when higher intensities are performed on the treadmill. Therefore, because there has not yet been a direct comparison of running modes, the purpose of this study was to compare nonlinear gait timing dynamics of paced treadmill and overground running at different speeds.

METHODS

10 trained runners ran for 8 min on an indoor running track at preferred pace (PP). They then completed paced treadmill and track trials at 80%, 100%, and 120% PP for 8 min each. Pacing for track running was accomplished using lights around the track that were lit in sequence to 0.1 $km \cdot h^{-1}$ precision. The treadmill and track sessions were done on separate days and in random order. The order of speeds was also random.

Foot contact was identified using telemetric 3-D accelerometers mounted on the top of the running shoe (316-10G, Noraxon, Phoenix, AZ; mass ~ 20 g each). Stride time series were generated from the peak vertical accelerations in each stride cycle.

We applied detrended fluctuation analysis (DFA), power spectral density analysis (PSD), and multiscale entropy (MSE) analysis [5]. DFA and PSD have a close theoretical relationship and quantify the strength of serial correlations in a data set. MSE quantifies system entropy and complexity. We tested for significant differences due to condition and speed using ANOVA. All analyses were performed in Matlab (R2009a, Mathworks, Natick, MA), except MSE, which was performed in a Cygwin environment.

RESULTS AND DISCUSSION

Treadmill exhibited a higher DFA and lower PSD scaling exponent (Table 1). Treadmill also demonstrated lower sample entropy (S_E) across all scaling factors, with a significant difference between running at 100% and 120% PP (Fig. 1).

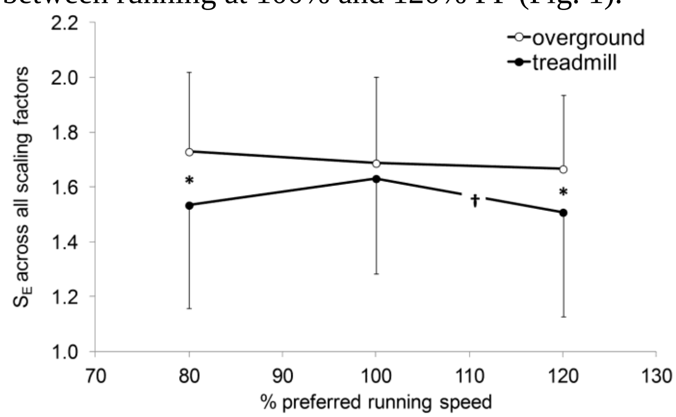

Figure 1: MSE for treadmill and overground running. *significant difference at this particular speed and condition ($p<0.05$), †significantly different between adjacent speeds for that condition ($p<0.05$).

The effect of condition and speed on the full MSE output is displayed in Fig. 2, showing significant differences between treadmill and overground for 80% and 120% PP, but not 100% PP.

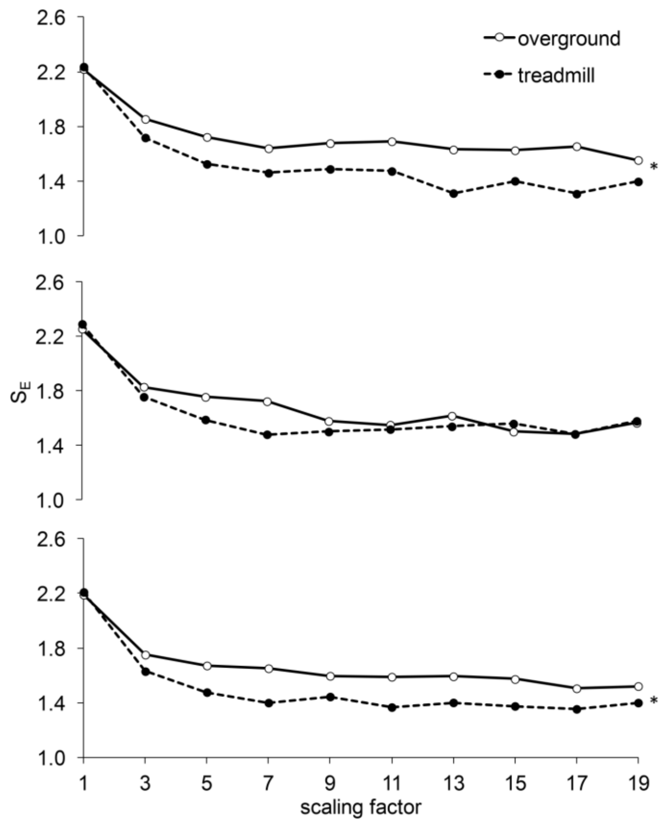

Figure 2: Effect of condition and scaling factor on the MSE output at 80% (top), 100% (middle), and 120% PP (bottom). *significant difference between treadmill and overground, across all scaling factors ($p<0.05$).

While DFA α was higher for treadmill (closer to pink noise), PSD β was lower (closer to white noise) and this agreement was less frequent at 120% PP, due to the decrease in β for that condition. We interpret this loss of correspondence as a reduction in the strength of correlations, which is consistent with the MSE findings. S_E across all scaling factors was lower for treadmill running. Decreased long-term correlations and decreased entropy are both consistent with the notion of increased constraint.

This suggests that factors other than mere running speed may contribute to constraint. Alton et al. suggested that on the treadmill, individuals may feel a greater sense of urgency to move their swing limb forward as the supporting limb is carried backward on the belt, perhaps leading to altered afferent feedback [6]. The agreement between afferent feedback and visual input may also influence operant constraints. This relationship is "normal" in overground conditions, but with treadmill, there may be a conflict between the forward speed seen by the eye and the speed sensed by the legs and feet [7]. The above mechanisms may modify the underlying persistent gait rhythm.

CONCLUSIONS

Treadmill running leads to reduced serial correlations and more regular timing compared to overground running. These dynamics are indicative of higher constraint and therefore a tighter control of stride timing. The underlying rhythm is likely influenced by task and environmental constraints, which may arise from interactions between mechanical, afferent, and visual phenomena. That these changes may be more pronounced during faster running suggests that factors from the task and environment combine to elicit especially constrained behavior.

REFERENCES

1. Jordan, K, et al. *Hum Mov Sci* **26**, 87–102.
2. Meardon, SA, et al. *Gait Posture* **33**, 36–40.
3. Bollens, B, et al. *Gait Posture* **32**, 369–373.
4. Terrier, P. et al. *J Neuroeng Rehab* **8**, 12.
5. Crevecoeur, F. et al. *J Neurosci Methods* **192**, 163–172.
6. Alton, F. et al. *Clin Biomech* **13**, 434–440.
7. Srinivasan, M. *Chaos* **19**, 026112.

Table 1: Effect of condition and speed on DFA and PSD scaling exponents. Values are mean ± SD.

	Treadmill			**Track**		
	80% PP	**PP**	**120% PP**	**80% PP**	**PP**	**120% PP**
DFA α*	0.96 ± 0.08	0.93 ± 0.07	0.94 ± 0.11	0.87 ± 0.12	0.86 ± 0.08	0.87 ± 0.10
PSD β*	0.69 ± 0.17	0.63 ± 0.15	0.54 ± 0.15	0.73 ± 0.16	0.73 ± 0.17	0.78 ± 0.24

*significant difference between conditions ($p<0.05$)

ORAL PRESENATIONS – FRIDAY SEPTEMBER 6th

	Footstrike Patterns in Running *Clare Milner, Eric Foch*
2:30 PM	A Modified Strike Index For Detection Of Foot Strike Pattern In Barefoot Running **Graf E, Rainbow M, Samaan C, Davis I**
2:45 PM	Effect Of Running Velocity On Footstrike Angle In Recreational Athletes **Forrester S, Townend J**
3:00 PM	Energy Expenditure Of The Triceps Surae During Rearfoot And Forefoot Running **Gruber A, Umberger B, Hamill J**
3:15 PM	Impact Characteristics In Novice And Trainied Runners In Traditional And Minimal Footwear **Frank N, Prentice S, Callaghan J**
3:30 PM	Joint Moments And Contact Forces At The L5-s1 Joint During Forefoot And Rearfoot Running **McClellan J, Derrick T, Rooney B**

A MODIFIED STRIKE INDEX FOR DETECTION OF FOOT STRIKE PATTERN IN BAREFOOT RUNNING

Eveline S. Graf, Michael J. Rainbow, Cynthia D. Samaan, Irene S. Davis

Spaulding National Running Center, Department of Physical Medicine and Rehabilitation,
Harvard Medical School, Cambridge, MA, USA
email: egraf@partners.org, web: http://www.runsnrc.org

INTRODUCTION

The strike index (SI) is used to identify the foot strike pattern in runners. It describes the location of the center of pressure (CoP) at initial foot-ground contact with respect to the long axis of the foot. SI is traditionally expressed as the percentage of the total foot length [1]. Based on the SI, runners can be classified as rearfoot (with a SI between 0 and 33%), midfoot (34 to 67%), or forefoot strikers (68 to 100%). This concept was developed for shod running [1] but has also been applied to barefoot running [2].

When forefoot striking, barefoot runners typically contact the ground with the distal area of the metatarsals, not the toes; therefore, the underutilized portion of the forefoot region (from the toes to the distal metatarsals), may reduce the ability of the SI to properly categorize forefoot strikes (Figure 1). Therefore, the purpose of this study was to define a modified strike index (SImod) that neglects the toes, and to compare the sensitivity and specificity of SI and SImod for each strike pattern. It was hypothesized that SImod would identify a larger proportion of forefoot strikes than SI.

METHODS

Eight recreational runners (27.8±7.0 years, 1.7±0.1 m, 74.6±10.6 kg) participated in the study and signed informed consent. Five retro-reflective markers were attached to the left foot: three on the heel (used to track the foot position in dynamic trials), one on the first metatarsal head, and one on the distal end of the second toe. Each subject performed seven barefoot running trials at their self-selected pace. The marker trajectories were collected with a ten-camera Vicon system (250 Hz) while ground reaction forces were simultaneously collected using two AMTI force platforms (1000 Hz) embedded in the floor. Additionally, a high speed video camera (Basler GigE) recorded the steps on the force plates from lateral at 125 Hz.

The strike pattern of each trial was determined as forefoot (FFS), midfoot (MFS), or rearfoot (RFS) based on visual inspection of the high-speed video recordings. Custom code (Matlab, MathWorks) was used to calculate the center of pressure location relative to the foot at touchdown (vertical ground reaction force > 20 N), which was then used to determine the SI and SImod. For the SI, the foot length was defined by the distal marker on the heel and the marker on the second toe. The foot length used to determine SImod was defined as the distance between the distal marker on the heel and the marker on the first metatarsal head. The strike index regions for SI and SImod were defined by dividing the foot length into equal thirds (Figure 1).

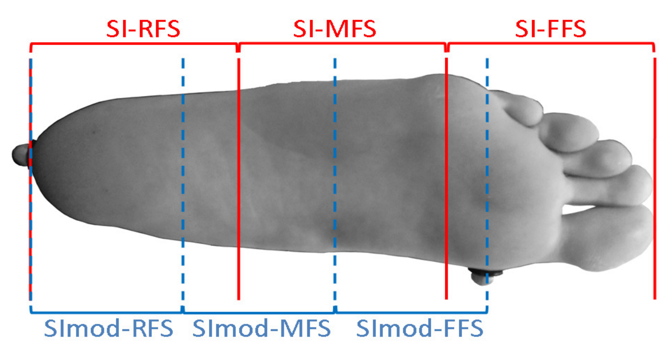

Figure 1: strike index regions for SI (solid) and SImod (dashed)

The validity of SI and SImod to determine the strike pattern was determined by calculating the sensitivity and specificity of both methods for each of the landing patterns.

RESULTS AND DISCUSSION

Out of 56 steps that were analyzed with visual classification there were 37 forefoot, 7 midfoot, and 12 rearfoot strikes. The SI correctly identified 6 forefoot, 5 midfoot, and 12 rearfoot strikes. This resulted in a high sensitivity for rearfoot and midfoot strikes but low sensitivity for the forefoot strikes (Table 1). Therefore, the traditional SI fails at detecting forefoot landings in the barefoot condition. The SI specificity was high for forefoot and rearfoot strikes but low for midfoot which is a result of a large number of false positive ratings for the MFS (Table 1). This can be directly related to the way midfoot strikes are defined by the SI. The SI midfoot contains most of the distal area of the metatarsals which is the region where ground contact during forefoot landing occurs.

Using the SImod, 37 forefoot, 1 midfoot, and 12 rearfoot strikes were correctly classified. This resulted in high sensitivity values for forefoot and rearfoot strikes but a low value for midfoot landings (Table 1). The specificity was high for MFS and RFS and slightly reduced for FFS. Only one step with an index of over 100% (indicating a toe landing) was found (101.4%).

SImod had a higher validity for forefoot strikes, which verified the hypothesis, but a lower validity for midfoot strikes than SI. A large portion of the forefoot area of the SI is made up of the toe region, which is typically not used during forefoot landing. Therefore, forefoot landings where the distal area of the metatarsals touches the ground first are often incorrectly classified as midfoot strikes. This issue is resolved by using the SImod.

SImod is less sensitive at detecting midfoot strikes compared to SI. Midfoot landings are defined as landings where the foot lands flat on the ground. There can be large variability in the CoP location depending on the pressure distribution at touchdown. A midfoot landing where more pressure is exerted on the forefoot compared to the rearfoot causes the CoP to shift distally and into the FFS region of the SImod. This leads to a reduced sensitivity for MFS and a decreased specificity value for FFS and RFS.

Another cause for the decreased specificity of FFS for SImod could be limitations in the strike pattern detection using visual inspection. MFS were more difficult to determine. It is possible that during landings which were classified as midfoot strikes, the forefoot touched the ground just before the rearfoot but that this instance was missed due to the camera angle and the limited frame rates.

CONCLUSIONS

The modified strike index described in this study is more valid for detection of forefoot landing patterns during barefoot running compared to the traditional strike index. Additional research is needed to examine the validity of the SImod during shod running. In order to define the strike index areas, the foot length is divided into equal thirds. Using a different definition of the strike index regions (e.g. MFS area larger than FFS and RFS) may increase the sensitivity of the SImod for MFS. Therefore, further research with an increased sample size is currently being conducted to test this hypothesis.

REFERENCES

1. Cavanagh PR, Lafortune MA. *J Biomech* **13**, 397-406, 1980.
2. Altman AR, Davis IS. *Gait Posture* **35**, 298-300, 2012.

Table 1: Outcomes of diagnostic test (true positive (tp), false positive (fp), false negative (fn), true negative (tn)), sensitivity and specificity of SI and SImod to determine FFS, MFS, RFS

	SI			SImod		
	tp, fp, fn, tn	Sensitivity	Specificity	tp, fp, fn, tn	Sensitivity	Specificity
FFS	6, 0, 31, 19	0.16	1.00	37, 5, 0, 14	1.00	0.74
MFS	6, 31, 1, 18	0.86	0.37	1, 0, 6, 49	0.14	1.00
RFS	12, 1, 0, 43	1.00	0.98	12, 1, 0, 43	1.00	0.98

EFFECT OF RUNNING VELOCITY ON FOOTSTRIKE ANGLE IN RECREATIONAL ATHLETES

Steph Forrester and Jayne Townend
Sports Technology Institute, Loughborough University, Loughborough, UK
email: s.forrester@lboro.ac.uk, web: http://sti.lboro.ac.uk

INTRODUCTION

Footstrike pattern (FSP) during running has recently received increased attention, partly due to its suggested link to injury [1]. FSP can be determined using either a force platform via the Strike Index method [2], or high speed video from either measuring the foot angle at touchdown [3] or from visual classification [4]. The first two methods provide a continuum measure of FSP, whilst the third simply classifies runners based on three categories: rearfoot (RFS) where the heel hits the ground first; midfoot (MFS) where both the heel and ball of the foot lands on the ground approximately together; and forefoot (FFS) where the ball of the foot first strikes the ground.

Using the visual classification method on data from a half-marathon, it was concluded that about 75% of all shod endurance runners are RFS, 24% are MFS, and the remaining 1% are FFS [4]. This study also found evidence for a trend towards a reduced RFS and increased MFS in the faster runners. Taking this to the extreme, endurance running is typically thought to be synonymous with a RFS and sprinting with a FFS FSP. However, it is unclear to what extent these observations are runner specific, due to the increased running velocity, or both, *i.e.* does a typical runner transition from RFS → MFS → FFS as their velocity increases from jogging to sprinting, or is it that individuals work over a narrower band of FSP regardless of running velocity? To help answer this question, the purpose of this study was to determine how FSP, defined by foot angle at touchdown, changed with running velocity in a group of recreational athletes.

METHODS

Eighty five recreational athletes (55M–30F; age 22.4±3.7 yrs; height 1.76±0.09 m; body mass 71.9±12.1 kg) provided informed consent. All were recreational athletes that trained or competed at least three times a week in a sport that involved running, *e.g.* soccer, rugby union, field hockey, and had experienced no lower limb injuries in the six months prior to testing.

Following a short warm up, participants were asked to run on a treadmill at incrementally increasing velocities from 2.2 to 6.1 $m\cdot s^{-1}$. The increments were 0.44 $m\cdot s^{-1}$ until the final increment which was 0.33 $m\cdot s^{-1}$, resulting in ten discrete velocities. All participants progressed from the slowest to fastest velocity and were required to run for 60 seconds at each. Participants were allowed to stop as soon as they felt they could no longer achieve the desired velocity.

Sagittal plane high speed video (Casio Exilim EX-FH100) was captured for each running velocity at 240 Hz (shutter speed: 1/250th second; resolution: 448 × 336 pixels). The capture was for five seconds starting 40 seconds into each running velocity. The high speed video footage was analysed to determine the following variables: foot angle at touchdown (θ_{TD}); stride frequency; stride length; and ground contact time. Foot angle at touchdown was determined with the aid of markers placed on the rear and forefoot of the participant's shoe [3]. Three footstrikes for each velocity were analysed and the mean used in further analysis. Participants were divided into three groups depending on their foot angle at touchdown at the lowest running velocities; these groups corresponded to RFS, MFS and FFS [3]. Significant differences in θ_{TD} with running velocity were examined for each group using a one-way ANOVA with Bonferroni post-hoc (significance $p \le 0.05$).

RESULTS AND DISCUSSION

Of the 85 participants, 83 reached 4 $m\cdot s^{-1}$, thereafter there was a rapid drop off with only 48 participants reaching 5.3 m·s^{-1} and 39 completing all ten velocities (Table 1). For running velocities < 5 m·s^{-1} the %RFS–%MFS–%FFS were consistently around 68%–25%–7%. Thereafter, there was substantial shift from RFS to MFS (44%–51%–5% at the highest velocity) indicating an overall trend in RFS runners towards MFS at running velocities > 5 m·s^{-1}. However, ~65% of the RFS remained RFS throughout and none converted to FFS even at the highest running velocity. These results are in general agreement with the half-marathon data presented in [4].

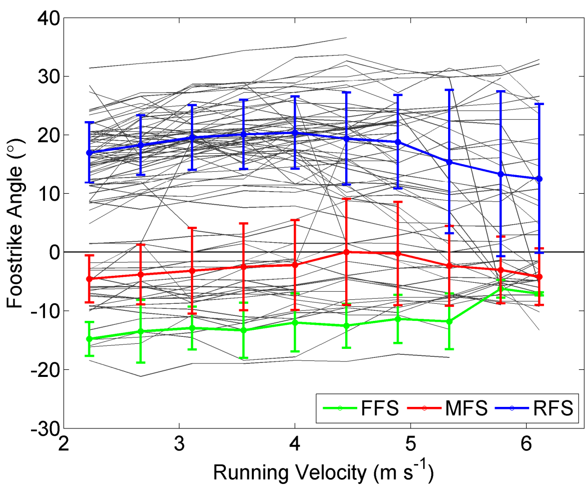

Figure 1. Running velocity versus foot angle at touchdown. The thin lines are for the individual participants and the thick lines the mean (± SD) for each category (RFS, MFS, FFS).

Only the FFS and RFS categories demonstrated a significant change in θ_{TD} with running velocity (Fig. 1). For FFS the angle remained consistent up to 4.0 m·s^{-1} then increased rapidly between 4.0 and 5.3 m·s^{-1} to a second plateau corresponding to a flatter foot at impact. Indeed, of the six FFS runners at the lower velocities, four converted to a MFS at the higher velocities.

For RFS the angle increased (not significant) over the lower velocities (2.2–4.0 m·s^{-1}) and then decreased significantly with further increases in velocity (Fig. 1); the latter in agreement with the earlier discussion. The trend towards a more extreme RFS over the lower velocities was unexpected and possibly worthy of further investigation. It could be hypothesized it was due to participants increasing stride length through increasing hip range of motion without altering knee and ankle kinematics, which may have implications for overstriding. An initial theoretical consideration of this hypothesis using simple trigonometry suggests an increase in θ_{TD} of 6°, comparable to the 4° observed here (Fig. 1); however, confirmation would require further study.

CONCLUSIONS

FSP was affected by running velocity with an overall trend towards a shallower angle (flatter foot) with increasing running velocity above 4.0 m·s^{-1} regardless of whether the runner had a FFS or RFS at lower velocities. These changes were typically gradual with the majority of RFS (almost two-thirds) maintaining a RFS across the full range of velocities range.

REFERENCES

1. Pohl MB, et al. *Clin J Sport Med* **19**, 372–376, 2009.
2. Cavanagh PR, Lafortune MA. *J Biomech* **13**, 397–406, 1980.
3. Altman AR, Davis IS. *Gait and Posture* **35**, 298–300, 2012.
4. Hasegawa H, et al. *J Strength Cond Res* **21**, 888–893, 2007.

Table 1. Overall group results including mean (±SD) of the basic stride parameters (SF = stride frequency, SL = stride length, t_{GC} = ground contact time).

Vel. (m·s^{-1})	2.2	2.7	3.1	3.6	4.0	4.4	4.9	5.3	5.8	6.1
n	85	85	85	84	83	74	63	48	42	39
%R–M–FFS	68–25–7	69–24–7	69–24–7	69–23–8	69–24–7	70–24–5	68–27–5	50–44–6	48–50–2	44–51–5
SF (spm)	78 ± 4	80 ± 4	81 ± 4	83 ± 4	85 ± 4	87 ± 5	90 ± 6	92 ± 6	95 ± 6	97 ± 6
SL (m)	1.7 ± 0.1	2.0 ± 0.1	2.3 ± 0.1	2.6 ± 0.1	2.8 ± 0.1	3.1 ± 0.2	3.3 ± 0.2	3.5 ± 0.2	3.6 ± 0.2	3.8 ± 0.2
t_{GC} (s)	0.35 ± 0.04	0.31 ± 0.03	0.28 ± 0.03	0.26 ± 0.03	0.24 ± 0.02	0.22 ± 0.02	0.21 ± 0.02	0.20 ± 0.02	0.19 ± 0.01	0.18 ± 0.02

ENERGY EXPENDITURE OF THE TRICEPS SURAE DURING REARFOOT AND FOREFOOT RUNNING

Allison H. Gruber, Brian R. Umberger and Joseph Hamill

University of Massachusetts, Amherst, MA, USA
email: agruber@kin.umass.edu, web: http://www.umass.edu/biomechanics/

INTRODUCTION

Effective storage and release of elastic strain energy will reduce muscle fiber mechanical work if the muscle fibers are able to operate at low contraction velocities, and thereby produce force at a lower rate of ATP consumption [1]. The forefoot (FF) running footfall pattern has been claimed to result in greater Achilles tendon elastic energy utilization [e.g., 2], resulting in a lower metabolic cost [3] compared with the rearfoot (RF) footfall pattern. Not only is there direct evidence to the contrary [2], but we have also found greater contractile element (CE) mechanical work in the gastrocnemius (GA) and soleus (SOL) in FF running than in RF running [4], despite greater series elastic element (SEE) work in FF running. These findings imply that FF running may not result in lower muscle metabolic energy expenditure compared to RF, but it is difficult to infer metabolic cost from force and work. Therefore, the purpose of this study was to expand on our earlier work and use a musculoskeletal model to predict metabolic energy expenditure of the GA and SOL in RF and FF running. It was hypothesized that FF running would result in greater muscle energy expenditure than RF running.

METHODS

Ten natural RF runners (7 males, 3 females, age = 28±5 yrs, mass = 70.6±9.8 kg, height = 1.8±0.1 m) and ten natural FF runners (9 males, 1 female, age = 26±8 yrs, mass = 70.5±7.1 kg, height = 1.8±0.1 m) participated after providing informed consent. Each participant performed ten trials of over-ground running with each footfall pattern ($3.5\ m \cdot s^{-1} \pm 5\%$). Inputs to a musculoskeletal model included sagittal plane knee and ankle joint angles and moments averaged over the 10 trials of each participant. Musculoskeletal geometry parameters were scaled to each participant. A two-component Hill model of the GA and SOL was used to calculate MT, CE, and SEE forces, powers, and work. CE metabolic power (CE_{MP}) was predicted as a function of CE velocity and activation [5]. CE metabolic energy expenditure (CE_{ME}) during the entire stance phase and the push-off phase was calculated by integrating CE_{MP} with respect to time. The push-off phase was defined as the time between the first instant the MT produced positive power in the second half of stance through toe-off. A mixed-factor ANOVA was used to detect differences in CE_{ME} between footfall patterns and groups during stance and push-off phases ($\alpha = 0.05$).

RESULTS AND DISCUSSION

No significant group by pattern interactions or group main effects were observed for GA or SOL CE_{EE} during stance or push-off ($P>0.05$). Thus, all results were collapsed across groups. There was no significant difference in GA CE_{EE} between footfall patterns during stance or push-off ($P>0.05$: Figure 1D). However, FF running resulted in 28% greater SOL CE_{EE} than RF running during the stance phase and 33% greater SOL CE_{EE} than RF running during push-off ($P<0.01$; Figure 1D).

Although the elastic energy mechanism does augment the mechanical output of the GA and SOL in FF running compared to RF [4], FF running resulted in greater SOL CE_{ME} but similar GA CE_{ME} than RF running (Figure 1D and E). Therefore, the hypothesis that FF running would result in greater CE_{ME} than RF running was supported for the SOL but not the GA.

GA CE work and CE_{ME} (Figure 1C and E) were similar between patterns because of the offsetting mechanical and metabolic effects of CE shortening

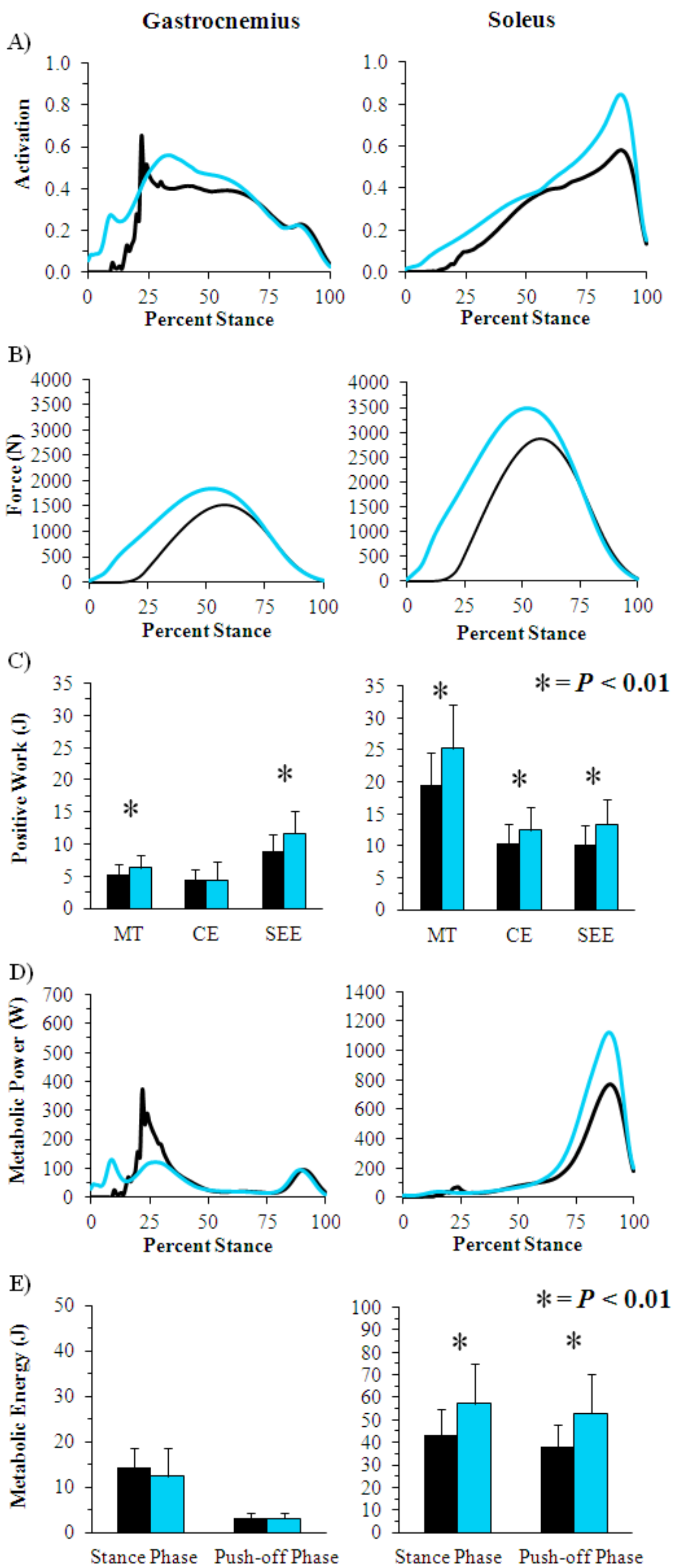

Figure 1: A) Muscle activation, B) muscle force, C) mechanical work of the muscle-tendon complex (MT), contractile element (CE), and series elastic element (SEE) [4], D) CE_{MP}, and E) CE_{ME} during RF (black) and FF (blue) running collapsed across groups.

velocity and force generation: FF running required greater activation in order to generate greater GA force (Figure 1A and B) but it was produced more economically as a result of slower contraction velocities compared to RF running [4].

In the first ~65% of stance, SOL CE_{ME} was similar between patterns (Figure 1D) as a result of offsetting metabolic effects of contraction velocity and force production. Similarly to the GA, RF running resulted in higher SOL CE shortening velocities [4], but lower activation and force production than FF running during this period (Figure 1A and B). During push-off, however, FF running resulted in greater SOL CE work and CE_{ME} (Figure 1C and E) as a result of greater activation (Figure 1A) and shortening velocities [4] compared to RF running, despite similar SOL force production between patterns during this period (Figure 1B).

CONCLUSIONS

Although we found that FF running does result in greater elastic energy utilization of the GA and SOL [4], consistent with previous suggestions [2,3], metabolic energy expenditure of the triceps surae was greater in FF running compared with RF running. These findings can be understood largely in terms of the CE force-velocity relation: a higher force or higher shortening velocity will favor more mechanical work, but will also cost more due to the necessity of higher muscle activation. In the GA, force and velocity offset each other in FF versus RF running, but in the SOL during late stance they do not, resulting in greater SOL energy expenditure in FF running.

REFERENCES

1. Biewener AA & Roberts TJ. *Exerc Sport Sci Rev* **28**, 99-107, 2000.
2. Perl DP, et al. *Med Sci Sports Exerc* **44**, 1335-1343, 2012.
3. Hasegawa H, et al. *J Strength Cond Res* **21**, 888-893, 2007.
4. Gruber AH, et al. *Proceedings of ISB '13*, Natal, Brazil, In Review.
5. Minetti AE & Alexander RM. *J Theor Biol* **186**, 467-476, 1997.

IMPACT CHARACTERISTICS IN NOVICE AND TRAINED RUNNERS IN TRADITIONAL AND MINIMAL FOOTWEAR

Nicholas S. Frank, Stephen D. Prentice and Jack P. Callaghan
University of Waterloo, Waterloo, ON, Canada
email: nfrank@uwaterloo.ca

INTRODUCTION

Midfoot (MFS) and forefoot (FFS) strike patterns during running have been linked to decreased vertical loading rates, regardless of being shod or barefoot [1]. Using a rearfoot strike pattern (RFS) while barefoot or in minimal shoes results in higher vertical loading rates compared to running in traditional shoes due to midsole deformation [1,2].

Of runners who self identified as midfoot strikers in minimal shoes, only 65% truly used a MFS pattern [2]. Those runners who misclassified themselves as MFS actually ran with a RFS and showed higher vertical loading rates (107.8 BW/s) compared to RFS in traditional footwear (68.6 BW/s) [2]. These results show that not all runners are fully aware of how they strike the ground and highlight the consequences of using a RFS in minimal footwear.

When novice runners run on a treadmill in traditional shoes, a RFS is used 98% of the time [3]. Minimal footwear sales have increased in recent years, with all abilities of runners using this type of product; yet the majority of research on minimal shoes has only included trained runners and overlooked novice runners.

The increased likelihood of novice runners using a RFS pattern, combined with less cushioning, and reduced awareness while running with a MFS/FFS pattern served as motivation for this study. The aim of this research was to compare strike patterns in trained and novice runners while wearing traditional and minimal footwear. It was hypothesized that higher average vertical loading rates (AVLR), higher instantaneous vertical loading rates (IVLR) and higher impact peak magnitudes (IP) would be measured in minimal shoes and novice runners compared to traditional shoes and trained runners.

METHODS

Novice (4) and trained (5) runners were included in this study. Novice runners were defined as running less than a total of 10 km in the past 12 months [3]. The trained runner group required participants to be running a minimum of 30 km per week and injury free within the past 3 months.

Four different shoes were tested during overground running on a 36 m runway. The shoes consisted of hard and soft midsoles, in both a minimal and traditional midsole design (Figure 1). Midsoles were made from EVA slabs and cut to specification. Lower limb kinematics were collected at 100 Hz using an OPTOTRAK motion capture system (NDI, Waterloo, ON). The right foot, shank, thigh and pelvis were tracked with rigid bodies consisting of five or more markers. Four AMTI force platforms (Watertown, MA) were embedded in the runway and sampled at 1000 Hz. Photoelectric timing gates were set up around the capture volume and running speed was controlled to 3.84 m/s ± 5%.

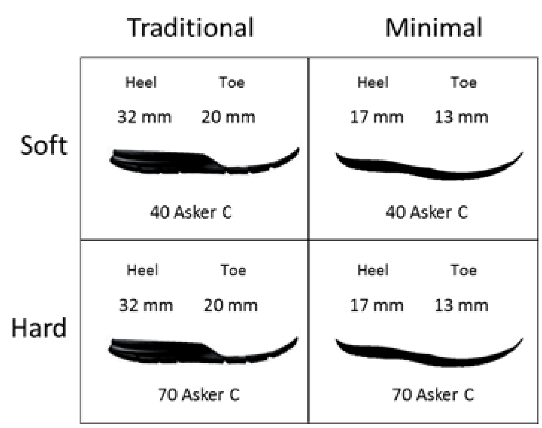

Figure 1: Four shoe conditions were included. Stack height and midsole stiffness are reported.

Ground reaction forces (GRF) were filtered using a 4th order Butterworth filter with a cutoff frequency of 100 Hz. All GRF data were normalized to body weight. AVLR was the average rate between 20% and 80% from footstrike to the impact peak [4]. IVLR was the maximum rate between footstrike and IP. IP magnitude was the first peak in the vertical GRF. If no IP was present, no value was given to that trial. A two-way mixed ANOVA (repeated measure of shoe and between factor of experience) was applied with an alpha-criterion set at $p = 0.05$.

RESULTS

In one of the five trained runners the IP was absent for all shoe conditions. In one of the four novice runners the IP was present only in the traditional shoes. IVLR did not differ across all four shoe conditions (Figure 2, $p = 0.06$) and there was no interaction between shoe and running group observed ($p = 0.10$). IP magnitude was smallest for the traditional hard shoe (1.9 BW) but was not statistically different from any of the other shoe conditions. AVLR did not differ across shoe conditions ($p = 0.07$) and there was no interaction between shoe and running group ($p = 0.95$). IP was also not different across any of the shoe conditions ($p = 0.15$) and there was no main effect of running group between trained and novice runners ($p = 0.93$).

DISCUSSION

The trained runner group showed trends towards lower loading rates in soft midsoles compared to hard midsoles. Loading rates were lower in thicker shoes compared to thin shoes. The novice group did not show this same trend as loading rates were similar across all shoe conditions. Kinematic analysis may reveal group differences which may explain the lack of change in loading rates for novice runners across all shoes tested.

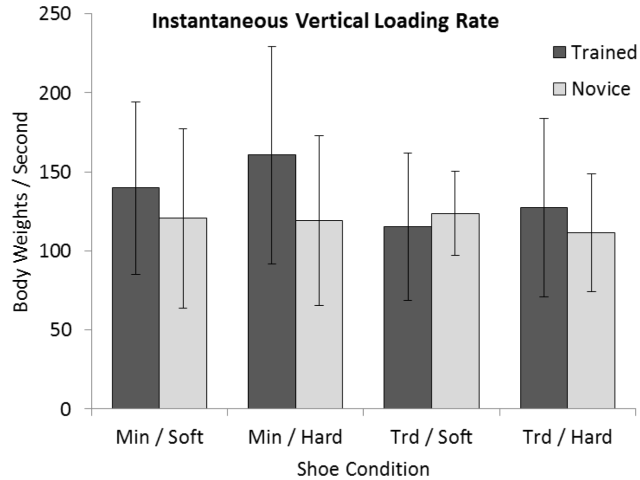

Figure 2: IVLR is displayed for both running groups and all shoes. Error bars represent 1 S.D.

The impact peak in the traditional hard shoe was lower in both running groups. Observed power for IVLR was only 0.58 which provides motivation to collect more participants in each running group as based on the initial trends there are potential differences between novice and trained runners especially for the minimal shoe condition.

REFERENCES

1. Lieberman, et al. *Nature* **463**, 531-536, 2010.
2. Goss, et al. *Proceedings of ASB '12*, Gainesville, FL, USA, 2012.
3. Bertelsen, et al. *Gait Posture*, 2012.
4. Williams, et al. *J Appl* Biomech, **16**, 210-218, 2000.
5. Hamill, et al. *Ftwr Sci*, **3**, 33-40, 2011.

ACKNOWLEDGEMENTS

The authors would like to thank NSERC and Nike Inc. for supplying footwear. Footwear included in this research does not resemble any Nike product.

Table 1: Mean (SD) values for all running shoes and groups.

	AVLR (BW/s)				IVLR (BW/s)				IP (BW)			
	Trained		Novice		Trained		Novice		Trained		Novice	
Minimal/Soft	71.8	(15.7)	71.7	(19.9)	139.9	(56.7)	122	(53.6)	2.22	(0.46)	2.14	(0.41)
Minimal / Hard	79.1	(19.7)	78.7	(27.4)	161.7	(70.6)	122.4	(57.2)	2.19	(0.37)	2.26	(0.54)
Traditional / Soft	63.7	(15.6)	73	(16.4)	113.5	(49.3)	123.2	(17.4)	2.26	(0.33)	2.18	(0.23)
Traditional / Hard	71.9	(16.0)	76.7	(17.3)	127.4	(60.4)	112	(28.5)	1.88	(0.35)	1.92	(0.34)

JOINT MOMENTS AND CONTACT FORCES AT THE L5-S1 JOINT DURING FOREFOOT AND REARFOOT RUNNING

[1]Jeffrey R. McClellan, [1]Timothy R. Derrick and [2]Brandon D. Rooney

[1]Iowa State University, Ames, IA, USA
[2] Brooks Sports Inc, Bothell, WA, USA

INTRODUCTION

Between 9 and 19 million individuals in the United States frequently participate in running [1]. Injuries are common among runners, with injury to the low back comprising between 5 and 15 percent of all injuries [2,3]. Despite this small but important segment of running injuries, little research exists which examines low back mechanics among runners. Additionally, the recent popularization of barefoot/minimalist running has led to the alteration of foot-strike patterns, with the hope that injury reduction may be achieved through gait retraining. Thus, the purpose of this pilot study was to gain a better understanding of low back mechanics at the L5-S1 joint among runners with different foot-strike patterns.

METHODS

Thirty runners (24 male, 6 female)(21.3±2.1 y, 64.7±8.1 kg, 1.78±0.08 m, 99.5±34.1 km/wk) were recruited to participate in this study, with 15 whom habitually ran with a forefoot (FF) strike pattern, and 15 whom habitually ran with a rearfoot (RF) strike pattern. Informed consent was obtained from all participants, after which they were instrumented with 21 retro-reflective markers on the right shoe, leg, pelvis and trunk. Participants ran 10 times at a self-selected speed (FF: 4.39±0.24, RF: 4.26±0.27 m/s) over a force platform (2000 Hz, AMTI, Watertown, MA) while wearing lab provided test shoes. Kinematic and force data were collected concurrently using a three dimensional motion analysis system (200 Hz, Vicon MX, Vicon, Centennial, CO, USA).

All analyses were performed using custom Matlab programs. Joint moment data were low-pass filtered according to Edwards, et al. [4]. A rigid body model was used with inverse dynamics to estimate 3D joint moments, and reaction forces at the L5-S1 joint, using approximations for pelvic mass and moment of inertia [5]. An individually scaled musculo-skeletal model was used to estimate muscle insertion, origin, and moment arm of the erector spinae muscle group, while an approximation of the L5-S1 joint center was derived from this same model [6]. The erector moment arm was assumed to be constant during the stance phase and it was assumed that flexor activity was negligible. Pelvic center of mass was estimated to lie at a point halfway between the L5-S1 joint center and the midpoint between the greater trochanters.

Muscle force was estimated using the moment arm for the erector spinae muscle group and the sagittal joint moments at the L5/S1 joint. Muscle forces and reaction forces were rotated 30 degrees in the sagittal plane to simulate the orientation of the sacrum at the L5/S1 joint, and joint contact forces were calculated by combining the rotated values for muscle force and reaction force. All forces were normalized by bodyweight. T-tests (α=0.05) were performed comparing the peak compressive contact forces (CF), peak shear contact forces (SF), peak extensor muscle forces (MF), and peak negative frontal moment (FM) during stance between FF and RF.

RESULTS AND DISCUSSION

At the beginning of stance, visual inspection of joint moments (Fig. 1) revealed some differences between FF and RF runners. FF runners began stance with a greater extensor moment in the sagittal plane than RF runners, which was followed by a mild flexor moment which did not exist for RF runners. In the Frontal plane, the general patterns appear to be the same, although the pattern for FF runners appears to be offset from that of RF. Calculated muscle forces (Fig. 2) displayed the same patterns seen in the sagittal moments, while the resultant normal joint contact force (Fig. 3) for FF exhibited a mild tensile force near the beginning of stance.

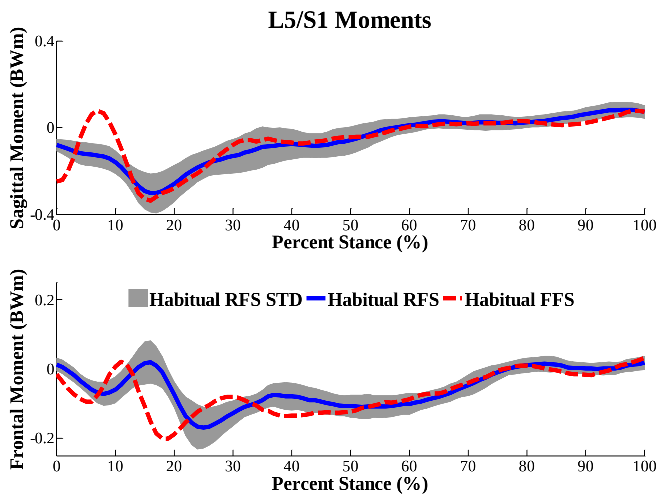

Figure 1: Moments in the sagittal and frontal planes at the L5/S1 joint.

Values for CF of -5.08±1.17 BW (RF) and -6.24±2.55 BW (FF) were recorded, although t-tests did not reach statistical significance (p=0.063). Similar results were recorded for MF with recorded values of -3.99±0.92 BW (RF) and -4.82±1.77 BW (FF) and a p-value of 0.061. Likewise, results for SF showed no statistical significance (p=0.18) with recorded values of 2.83±0.65 BW (RF) and 3.08±0.81 BW (FF). Significant results were recorded for FM (p=0.006) with values of -0.20 ±0.05 BWm for RF and -0.26±0.07 BWm for FF.

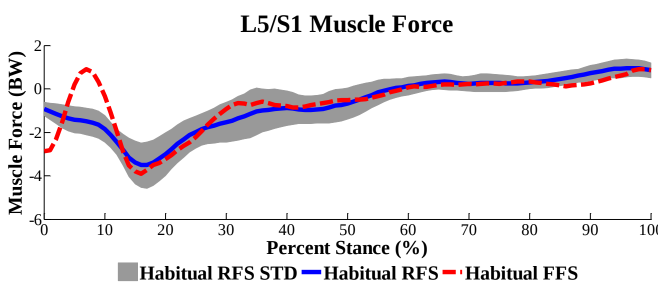

Figure 2: Erector Spinae muscle force.

While visual inspection of the data showed clear differences between the conditions it was unclear if the limitations of the model used may have distorted results. Only one extensor muscle was inserted into the model, however the calculated muscle force shows a flexor force being applied by the forefoot runners at the beginning of stance. It is unclear if using a more robust model would eliminate or reduce these differences. The effect of only calculating muscle forces from the sagittal moments is also unknown as frontal and transverse applications of the force are lost. Even with these limitations the difference in FM during FF indicates that the two running styles do elicit changes at the L5/S1 joint during the early portions of stance.

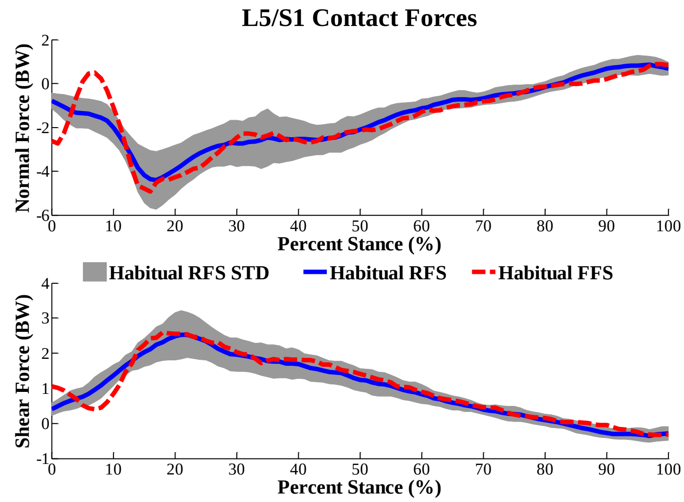

Figure 3: Normal and shear contact forces at the L5/S1 joint.

CONCLUSIONS

An alteration of foot-strike pattern does cause changes at the L5S1 joint during the stance phase of running, while the magnitude and significance of these changes are unknown. Additional models need to be developed which can more accurately predict the effect that running with different foot-strike patterns can have on the low back.

REFERENCES

1. Running USA. http://www.runningusa.org/2012-state-of-sport-part-2, 2012.
2. Jacobs SJ, Berson BL. *Am J Sports Med* **14**, 151-155, 1986.
3. Taunton JE, et al. *Br J Sports Med* **37**, 239-244, 2003.
4. Edwards BW, et al. *Gait & Posture* **34**, 435-438, 2011.
5. Zatsiorsky VM. *Kinetics of human motion*, Human Kinetics Publishers, 2006.
6. Delp SL, et al. *IEEE Trans Biomed Eng* **54**, 1940-1950, 2007.

ORAL PRESENATIONS – FRIDAY SEPTEMBER 6th

	Amputee Mobility *Kenton Kaufman, Jason Wilken*
2:30 PM	Use Of An Amputee Gait Score To Assess Rehabilitation Progress **Kingsbury T, Marks M, Thesing N, Myers G, Isken M, Wyatt M**
2:45 PM	Direct Measures Of Prosthesis Inertia Influence Joint Kinetics During Swing **Smith J, Ferris A, Heise G, Hinrichs R, Martin P**
3:00 PM	Lateral Shear Forces At The Low Back In Persons With Unilateral Transfemoral Amputation During Overground Walking **Hendershot B, Wolf E**
3:15 PM	Interlimb Asymmetries During Stand To Sit And Sit To Stand Tasks In Transtibial Amputees **Ferris A, Smith J, Christiansen C**
3:30 PM	Muscle Contributions Of Amputees And Non-amputees To Circular Turning **Ventura J, Klute G, Neptune R**

Use of an Amputee Gait Score to Assess Rehabilitation Progress

[1]Trevor Kingsbury, [2]Michael Marks, [1]Nancy Thesing, [1]Grant Myers, [3]Mark Isken, [1]Marilynn Wyatt
[1]Naval Medical Center San Diego, San Diego, CA, USA
[2]Improvement Path Systems, Inc. Bingham Farms, MI, USA
[3]Oakland University, MI, USA
email: trevor.kingsbury@med.navy.mil

INTRODUCTION

The use of gait analysis for patients with amputations is a useful tool to evaluate progress made during rehabilitation. While gait data can provide valuable metrics to guide patient care, the ease of acquiring large sets of data for many variables can make interpretation convoluted for a provider without extensive gait training. Originally developed for children with cerebral palsy, the Gillette Gait Index (GGI) utilizes kinematic and temporal spatial data to describe the quality of a subject's gait[1]. Other measures such as the Gait Deviation Index (GDI) and the Gait Profile Score (GPS) have used only kinematic variables to define gait pathology[2,3] . These measures have been tested with amputee gait data with some success, finding that the GGI, GDI, and GPS could differentiate patients with different levels of amputation to some degree[4]. However, when focusing on the rehabilitation of a patient with an amputation, loading of both the amputated and the sound limb are important. Previous research has linked degenerative conditions such as osteoarthritis to loading asymmetries in amputees[5]. Thus, kinetic ground reaction force data is an important variable when evaluating the gait of a patient with an amputation. The goal of this study is do develop an amputee gait score that can assess gait quality through rehabilitation. We hypothesize that a patient's gait score should be at a minimum around 6 months from their baseline study, when they are near the end of physical therapy before discharge.

METHODS

Gait data was collected on 20 normal male subjects and 40 patients with unilateral transtibial amputations. Those forty patients had a total of 173 studies. Baseline studies were collected as soon as the patient could walk without an assistive device and were then followed up over the next year at four time points: 6 weeks, 3 months, 6 months, and 1 year. Due to problems such as socket fit issues, pain, and other activities, not all patients were collected at every time point.

Clinically relevant minimums and maximums were chosen from vectors of gait cycle data. Thirty-six total variables for each study were collected (8 Temporal Spatial, 20 Kinematic, and 8 Kinetic) (Table 1). The data from the 20 normal subjects were normalized to a mean of zero with a unit standard deviation. The 173 studies for patients with unilateral transtibial amputations were normalized to the mean and standard deviation of the 20 normal studies. Absolute step asymmetry, velocity, cadence, and step width were adjusted to account for patients being better than the normal mean. For any patient who had values better than the normal mean value for these variables, the values were set to zero. Additionally, velocity, cadence, step length, and stride length were normalized for patient height. A weighting scheme was then applied to the variables to emphasize key indicators of quality gait in patients with amputations (Table 1). A principal component analysis was run on the normal population and applied to the study population. This was done as a variable reduction technique and to remove the inherent correlation that occurs in gait data. Means were calculated for the normal principal components. A Euclidean distance was taken from the means of the normal principal components to the values of the principal components for each study. This resulted in a single score, for each study, that explained the amount of deviation from normal gait, with a score closer to zero indicating less deviation.

Patient study data was binned by time (in days from baseline) into categories representing baseline, 6 week, 3 month, 6 month, and one year data. An ANOVA model with LSD post hoc tests were used to determine interaction effects if a main overall effect was found.

Table 1: Variables used with their corresponding weights. Variables in italics were evaluated for both left and right sides.

Variable:	% Weight:
Absolute Step Asymmetry	4
Step Length	8
Stride Length	4
Step Width	4
Velocity	10
Cadence	6
% Support Time	2.4
% Swing Time	1.6
Pelvic Obliquity Min	0.4
Pelvic Obliquity Max	1.2
Hip Abduction Max	1.6
Hip Adduction Max	0.4
Lateral Trunk Tilt Max	2
Pelvic Tilt Min	0.4
Pelvic Tilt Max	1.6
Pelvic Tilt Avg	0.4
Trunk Flexion Min	0.4
Trunk Flexion Max	0.8
Trunk Flexion Avg	1.2
Hip Extension Max	2
Hip Flexion Max	1.2
Hip Flexion Max Swing	0.8
Knee Flexion Max at Initial Contact	0.4
Knee Flexion Max in Early Stance	2
Knee Extension Max	0.8
Knee Flexion Max Swing	1.2
Ankle Plantarflexion Max	0.4
Ankle Dorsiflexion Max	0.8
Vertical GRF F1	12
Vertical GRF F2	3.2
Vertical GRF F3	12
Peak Braking Force	4.8
Peak Propulsion Force	4.8
Medial GRF Max	1.6
Lateral GRF Max	1.6

RESULTS AND DISCUSSION

Amputee gait scores at the five timepoints are summarized in Table 2. A significant main effect was found for the time bins ($F = 19.27$, $p < .001$). Post hoc analysis revealed significant interaction effects between baseline and all other times as well as between the 6 week and 6 month time point ($p<.05$) (Figure 1). Thus, patients rapidly improve their gait scores throughout the early part of rehabilitation and appear to stabilize around the six month mark.

Table 2: Descriptive Statistics for the Amputee Gait Scores

	N	Mean	SD	95% Confidence Interval		Minimum	Maximum
				Lower Bound	Upper Bound		
Baseline	39	65.30	13.59	60.90	69.70	34.19	87.58
6 Week	30	49.01	12.38	44.38	53.63	26.69	75.21
3 Month	38	46.59	13.04	42.31	50.88	29.31	78.65
6 Month	45	43.00	10.29	39.91	46.09	22.55	68.75
1 Year	21	45.02	14.92	38.23	51.82	25.96	83.22

Figure 1: Line graph of Amputee Gait Scores

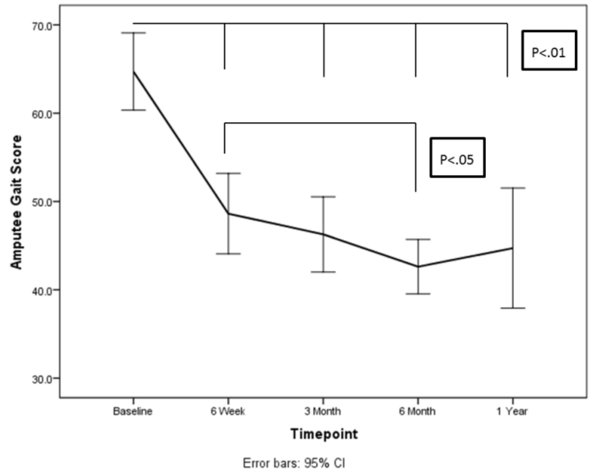

These results coincide with clinical observations of the patients with amputations undergoing rehabilitation. At our center, as a patient progresses between the three and six month mark in their care, they typically scale back on their physical therapy appointments as they move into higher functional activities and return to their jobs. One of the main obstacles they will face is maintaining quality gait throughout their lives without the assistance of intense physical therapy.

Future aims of this project will be to look at patients with other levels of amputations to create a gait scoring guideline for any patient with amputation starting a rehabilitation program. This will hopefully aid the patients and providers in keeping them on track in therapy to provide the best long term outcomes.

REFERENCES

1. Schutte LM, et al. An index for quantifying deviations from normal gait. *Gait and Posture*, 11. 25-31. 2000.
2. Schwartz MH and Rozumalski A. The gait deviation index: A new comprehensive index of gait pathology. *Gait and Posture*, 28. 351-357. 2008
3. Baker R, et al. The Gait Profile Score and Movement Analysis Profile. *Gait and Posture*, 30. 265-269. 2009.
4. Kark L, et al. Use of gait summary measures with lower limb amputees. *Gait and Posture*, 35. 238-243. 2012
5. Snyder RD. The effect of five prosthetic feet on the gait and loading of the sound limb in dysvascular below-knee amputees. *Journal of Rehabilitation Research and Development*, 32. 309-315. 1995.

DIRECT MEASURES OF PROSTHESIS INERTIA INFLUENCE JOINT KINETICS DURING SWING

[1]Jeremy D. Smith, [1]Abbie E. Ferris, [1]Gary D. Heise, [2]Richard N. Hinrichs, and [3]Philip E. Martin

[1]School of Sport & Exercise Science, University of Northern Colorado, Greeley, CO
[2]Kinesiology Program, Arizona State University, Phoenix, AZ
[3]Department of Kinesiology, Iowa State University, Ames, IA
Email: jeremy.smith@unco.edu; website: http://www.unco.edu/nhs/ses/

INTRODUCTION

Modern lower limb prostheses are fabricated using lightweight materials resulting in prosthetic limbs that are often much lighter than the limbs they replace. One consequence of this fabrication practice is that an inertial asymmetry between the prosthetic limb and intact limb is created. Compared with a typical intact shank and foot, the mass of a below-knee prosthesis and residual limb is approximately 35% less and has a center of mass located approximately 35% closer to the knee joint [1]. The lower and more proximally distributed mass produce a much lower (~60%) moment of inertia relative to the knee joint compared to the intact shank and foot. Although Miller [2] previously suggested that using intact inertia estimates for the prosthetic limb have little effect on joint kinetic estimates, her comparisons were limited to resultant joint moments during stance, where the ground reaction force strongly influences lower extremity moments. During swing, it is unclear whether lower inertial properties of the prosthesis influence resultant joint moments. Thus, the purpose of this study was to contrast the effects of using direct measures of the prosthesis inertia versus using estimates of intact limb inertial properties on ankle, knee, and hip resultant joint moments during walking in unilateral, transtibial amputees.

METHODS

Six amputees (5 males; 1 female; age = 46±16 yrs, mass = 104.7±9.7, height = 1.8±0.1) participated in this study. Five of six amputees had amputations due to traumatic injuries with the other due to congenital bone disease. All amputees used a lock and pin type suspension system and a dynamic elastic response prosthetic foot. Participant recruitment focused on amputees who were fully ambulatory, had used a prosthesis for at least one year, and maintained some degree of physical activity. The protocol was reviewed and approved by the University's Institutional Review Board. Informed consent was obtained from each participant.

Participants completed five overground walking trials at preferred speed (1.2±0.1 $m \cdot s^{-1}$) while ground reaction forces (480 Hz) from two force plates and motion data (60 Hz) from a six camera motion analysis system were collected. Retro-reflective markers were placed bilaterally on the greater trochanter, lateral femoral condyle, lateral malleolus, lateral aspect of the heel, and the head of the fifth metatarsal prior to data collection. A three-segment sagittal plane inverse dynamics model was used to compute resultant joint forces and moments. Segment inertial properties for intact body segments were predicted using regression equations from de Leva [3]. Inertial properties of the prosthesis and residual limb were measured directly using oscillation and reaction board techniques [1]. To determine the effect that inertia values (direct measures vs. estimates based on intact segment inertia properties) had on joint moments, a single factor, repeated measures MANOVA was used with a Bonferroni adjustment. Peak resultant joint moments at the ankle, knee, and hip during stance and swing served as primary dependent variables. Significance differences were considered at $p < .05$.

RESULTS

Averaged across participants, prosthetic side mass was 39% less, moment of inertia about a transverse axis through the knee was 52% less, and the center of mass location was 24% closer to the knee compared with values for the intact leg. Peak resultant knee and hip joint moments (Figure 1) during swing were lower when direct measures of prosthesis inertial were used in inverse dynamics assessments compared with use of predicted inertial properties for intact anatomy. Effect sizes suggest these differences were large (Table 1). During stance, several significant differences in moment magnitudes were observed at the ankle and knee (Table 1), but effect sizes for all differences during stance were less than or equal to 0.1.

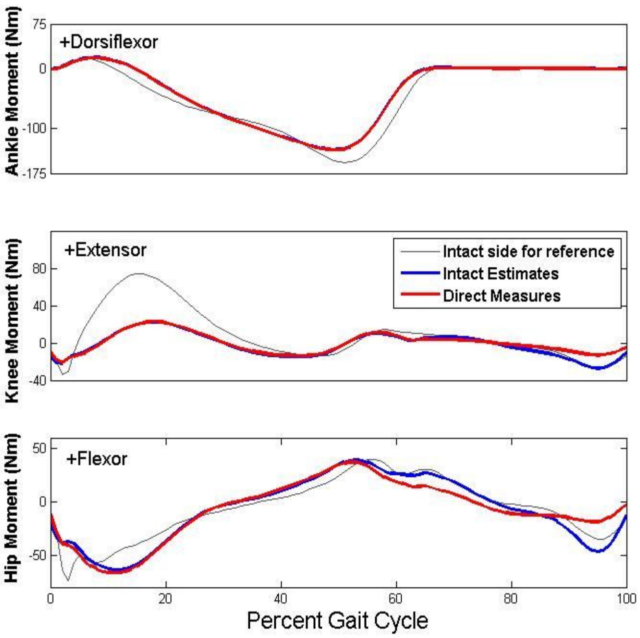

Figure 1: Resultant joint moments about a transverse axis through the ankle, knee, and hip. Foot contacts occur at 0 and 100%, whereas toe-off occurs at ~60% of the gait cycle.

Table 1: Peak resultant joint moments averaged across subjects and statistical comparisons between the two inertial models.

Variable	Inertial Model: Direct Measures	Inertial Model: Intact Estimates	*p* value	Cohen's d (Effect Size)
Ankle				
Early Stance	20.0(5.6)	20.5(5.6)	0.001	0.10
Terminal Stance	-141.5(37.4)	-140.9(37.3)	<0.001	0.01
Knee				
Mid-Stance	27.0(31.8)	26.1(31.4)	0.053	0.03
Terminal Stance	-21.4(21.9)	-22.3(21.2)	0.033	0.04
Initial Swing	4.4(3.3)	8.7(3.4)	0.015	1.26
Terminal Swing	-13.7(3.)	-28.4(4.9)	0.001	3.64
Hip				
Initial Swing	20.6(13.0)	32.7(11.4)	0.002	1.00
Terminal Swing	-19.8(5.2)	-48.4(9.4)	<0.001	3.78

Notes. Mean data are presented as mean(SD).

DISCUSSION

In absolute terms, the largest magnitude difference during stance was less than 1 N·m, which is slightly less than the average moment magnitude difference of 3 N·m Miller [2] reported for the stance phase of running. Moment magnitudes during running are generally larger than during walking, which likely contributed to larger differences reported by Miller. However, Miller concluded that even the 3 N·m difference was unlikely to influence overall conclusions of the study. Thus, although we observed significant differences during stance, it is unlikely these differences have physiological relevance.

In the absence of ground reaction force influences during swing, the motion of the limb is more dependent on system inertia and segment interactions. When using intact segment inertial properties in the model, resultant joint moment magnitudes at the hip and knee were artificially high. This illustrates a limitation of interpreting resultant joint moments as an indicator of muscular demand during swing. Using intact segment inertial properties to model the prosthetic side during swing would suggest a higher muscular demand to control the limb that was actually more comparable to the control utilized in the intact limb. Thus, one might be lead to interpret that prosthetic side joint function during swing as similar to that of an intact leg.

In conclusion, when focusing on swing phase mechanics, researchers should use direct measures of prosthesis inertia in inverse dynamics models, but during stance the inertia parameters seem to have little impact on study outcomes.

REFERENCES

1. Smith, JD & Martin, PE *J Prosthet Orthot* **23**, 114-123, 2011.
2. Miller, DI *J Biomech* **20**, 529-541, 1987.
3. de Leva, P *J Biomech* **29**, 1223-1230, 1996.

ACKNOWLEDGEMENTS

The American and International Societies of Biomechanics provided funding for this study.

LATERAL SHEAR FORCES AT THE LOW BACK IN PERSONS WITH UNILATERAL TRANSFEMORAL AMPUTATION DURING OVERGROUND WALKING

[1,2]Brad D. Hendershot and [1]Erik J. Wolf

[1]Walter Reed National Military Medical Center, Bethesda, MD, USA
[2]Henry M. Jackson Foundation for the Advancement of Military Medicine, Rockville, MD, USA
Email: bradford.d.hendershot.ctr@health.mil

INTRODUCTION

The prevalence of low back pain (LBP) is considerably higher in persons with lower-extremity amputation (52-71%) compared to the general population (6-33%) [1]. Alterations in gait and movement among persons with lower-extremity amputation have been associated with overall increases in trunk and pelvic motion [2]. Persons with unilateral transfemoral amputation (TFA), specifically, tend to walk with larger lateral bending of the trunk toward the prosthetic side in single-limb stance [3]. Due to its relatively large mass compared to the whole body, increases in lateral trunk movement can substantially alter ground reaction force generation, thereby altering joint loads throughout the body [4]. As such, altered gait with increased trunk (and pelvic) motion among persons with TFA likely results in spinal loading patterns distinct from able-bodied individuals. Increased or asymmetric spinal loads are an important proximate cause of LBP [5]; repeated exposure to increased and altered spinal loads may therefore contribute, in part, to LBP onset and recurrence in this population. The goal of the present study was to quantify and compare lumbosacral (L5/S1) lateral shear forces in persons with and without unilateral TFA during overground walking.

METHODS

Data was collected retrospectively from twenty males with unilateral TFA and twenty male non-amputation controls that had completed previous gait evaluations (Table 1); these retrospective analyses were approved by the local IRB. All amputations were traumatic, and the mean (SD) time since amputation was 3.2 (1.7) years.

Participants walked at their self-selected walking velocity across a 10m walkway. Kinematics were recorded (120Hz) using a full-body marker set and a 23-camera motion capture system (Vicon, Oxford, UK). Ground reaction forces were sampled (1200Hz) from four force platforms (AMTI, Watertown, MA, USA) embedded in the walkway. Since the calculation of joint forces at the low back requires responses from both lower extremities, multiple walking trials were collected to obtain 5 "clean" gait cycles; clean gait cycles were identified by clean right and left foot strikes on consecutive force platforms.

Table 1: Mean (SD) participant demographics.

	Control	TFA
Age (yr)	28.1 (4.7)	29.5 (6.7)
Height (cm)	181.7 (6.4)	176.2 (6.7)
Body mass (kg)	85.0 (9.4)	80.6 (12.0)

Lumbosacral joint forces were calculated using a bottom-up inverse dynamics analysis, with a three-dimensional full-body link-segment model developed in Visual3D (C-Motion Inc., Germantown, MD, USA). The trunk was modeled as a single rigid segment, defined proximally by the acromia, C7, and sternal notch, and attached distally to the pelvis at the L5/S1 joint. The location of the L5/S1 joint was estimated using boney pelvis landmarks (ASIS and PSIS) and scaled by pelvis width [6]. L5/S1 lateral shear forces were normalized to participants' body mass. Peak lateral trunk flexion angles in the global coordinate system (relative to vertical) were also calculated. Peak lumbosacral lateral shear forces and trunk lateral flexion angles were obtained during single-limb stance (per side), and averaged across the 5 clean trials for each participant.

Mixed-factor analyses of variance (ANOVA) were used to compare peak L5/S1 lateral shear forces and peak lateral trunk flexion angles between and within (bilaterally) groups. All statistical analyses were performed using JMP (Version 10, SAS Institute Inc., Cary, NC, USA), with statistical significance determined when $p < 0.05$. Summary values are reported as means (SD).

RESULTS AND DISCUSSION

Self-selected walking velocities were similar (p = 0.45) for participants with TFA and controls at 1.34 (0.06) and 1.36 (0.07) m/s, respectively. Overall, peak lumbosacral lateral shear forces were larger (p < 0.001) in participants with TFA compared to controls, with respective values of 1.03 (0.37) and 0.73 (0.20) N/kg. These were larger (p = 0.026) during prosthetic vs. intact single-limb stance among participants with TFA, but bilaterally similar (p = 0.094; i.e., minimal asymmetries) among controls (Fig. 1A). Of note, the lateral shear forces estimated here were directed towards the support leg during single-limb stance (i.e., right shear of trunk on pelvis during right-leg single support). Peak trunk lateral flexion was similarly larger (p < 0.001) overall in persons with TFA compared to controls [4.8 (2.8) vs. 2.0 (1.1) °]. Peak trunk lateral flexion was larger (p < 0.001) toward the prosthetic vs. intact limb in stance among participants with TFA, but bilaterally similar (p = 0.75) among controls (Fig. 1B).

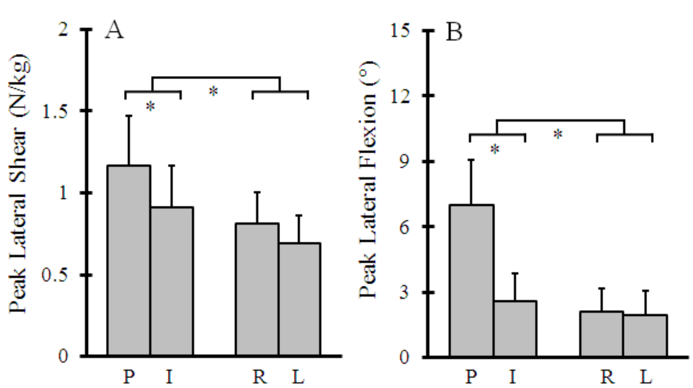

Figure 1: Peak lumbosacral lateral shear force (A) and peak trunk lateral flexion (B) among participants with unilateral TFA and controls. P/I = prosthetic/intact; R/L = right/left. Results from post-hoc contrasts are indicated by brackets (* = significant difference).

Walking is generally less stable in the mediolateral than the anteroposterior direction, requiring active muscle control to maintain balance [8]. Specifically, balance of the trunk and pelvis about the supporting hip in single-limb stance requires a hip abduction moment to counteract the destabilizing laterally-directed gravitational forces and reduce pelvic drop [9]. Increased trunk lateral flexion toward the prosthetic side among persons with unilateral TFA has been suggested to help stabilize the body [10], perhaps as a compensation for weak (or missing) hip-stabilizing musculature in the residual limb. Such a strategy, however, appears to increase lumbosacral lateral shear forces during prosthetic single-limb stance. In conclusion, increased and asymmetric lateral shear forces at the low back combined with altered trunk (and pelvic) motion among persons with unilateral TFA may support a theory suggesting an association between repeated exposure to altered spinal loading and LBP onset and recurrence in this population.

REFERENCES

1. Ehde DM, et al. *Arch Phys Med Rehabil* **82**, 731-34, 2001.
2. Goujon-Pillet H, et al. *Arch Phys Med Rehabil* **89**, 87-94, 2008
3. Jaegers SHMJ, et al. *Arch Phys Med Rehabil* **76**, 736-743, 1995.
4. Gillet C, et al. *Am J Phys Med Rehabil* **82**, 101-109, 2003.
5. McGill SM. *J Biomech* **30**, 465-475, 1997.
6. Reed MP, et al. *SAE Technical Paper*, 1999-01-0959
7. Winter, DA. *Biomechanics and Motor Control of Human Movement*, John Wiley & Sons, 2005.
8. Kuo AD, et al. *Int J Robotics Res* **18**, 917-930, 1999.
9. MacKinnon CD, et al. *J Biomech* **26**, 633-644, 1993.
10. Michaud SB, et al. *JRRD* **37**, 1-10.

INTERLIMB ASYMMETRIES DURING STAND TO SIT AND SIT TO STAND TASKS IN TRANSTIBIAL AMPUTEES

[1]Abbie E. Ferris, [1]Jeremy D. Smith, [2]Cory L. Christiansen and [1]Gary D. Heise
[1]School of Sport & Exercise Science, University of Northern Colorado, Greeley, CO
[2]Interdisciplinary Movement Science Lab, University of Colorado, Anschutz Medical Campus, Denver, CO
Email: abbie.ferris@unco.edu; website: http://www.unco.edu/nhs/ses/

INTRODUCTION

Patients with unilateral, transtibial amputation (TTA) often exhibit functional asymmetries that clinicians, researchers, and patients often attempt to minimize. Compared to traditional surgical techniques transtibial osteomyoplastic amputation (Ertl) has been suggested to lead to improved functional outcomes following amputation [1]. Using a "bone bridge", the Ertl technique connects the tibia and fibula and seals the medullary canal. In addition the anterior and posterior musculatures are sutured together. This technique commonly results in a healthier residual limb through reduced bone spurs, increased venous return, and reduced incidence of ulcers [1, 2]. It has also been suggested that those who undergo an Ertl compared to a traditional amputation have enhanced "end-bearing" capability of the residual limb [3].

Important to activities of daily living, are sitting and standing tasks. It has been estimated that people with TTA sit-to-stand (STAND) roughly 50 times per day [4, 5]. To date, there has only been one biomechanical study of STAND following TTA [6]. Agrawal et al. found patients with TTA produced 27% more vertical ground reaction force (VGRF) with the intact limb during a STAND movement compared with the prosthetic side. Non-amputee controls, however, exhibited less than 10% asymmetry in vertical ground reaction force during the same movement.

While inter-limb asymmetries have been shown to exist during the STAND task, it is unclear if these asymmetries persist in people who underwent an Ertl amputation. Additionally, to our knowledge no study has evaluated the stand-to-sit (SIT) task in a TTA population regardless of surgical technique. The purpose of this study was to evaluate inter-limb asymmetry in persons who have undergone an Ertl amputation during SIT and STAND tasks.

METHODS

Six persons with unilateral Ertl TTA volunteered (78.9±18.9 kg, 1.75±0.08 m). All participants wore an elastic response prosthetic, had been wearing the same prosthesis for at least 6 months, and were considered K3 or above in functional classification.

Participants performed a five times STAND task as fast as possible. Participants were not allowed to push off with their hands during the task. Seat height was adjusted to the height of each individual's intact fibular head height from the ground during standing. The seat was placed in front of two force plates (2000 Hz) embedded into the ground and each foot was placed on a force plate. Of the five cycles, only the middle three were analyzed to avoid any issues with starting and ending the task. SIT and STAND phases were analyzed separately.

VGRFs were low-pass filtered using a recursive, 4th order Butterworth filter (50 Hz cut-off frequency). Peak VGRF, impulse (Imp), symmetry indices (SI), percent net impulse contribution (PC), and task time were calculated for each task/limb. SI was calculated using the methods of Agrawal et al. [6]:

$$SI = 100 - 100 * \frac{I - P}{(I + P)}$$

The SI indicates the distribution of forces between the limbs, it does not indicate the contribution of each limb to the overall movement. PC was computed using:

$$PC = \frac{Imp_{limb}}{Imp_{int} + Imp_{pros}} * 100$$

where Imp_{limb} is the impulse of the limb being compared; Imp_{int} and Imp_{pros} are the impulses of the intact and prosthetic limbs, respectively.

Between limb differences were evaluated using a MANOVA (SPSS 19.0). A paired t-test was used to evaluate differences in time during the STAND and SIT tasks. Statistical significance was set at $p<.05$.

RESULTS

Amputees took longer to stand up than to sit down (1.05 s vs. 0.87 s, $p=.006$). VGRFs during quiet standing were not significantly different between limbs; however, significant asymmetries were found during SIT and STAND (see Table 1, Figure 1). Impulse SI for both SIT (76%±7%) and STAND tasks (82%±5%) indicated an asymmetry towards increased loading of the intact limb. The PC of the intact limb to the total impulse was significantly greater than the prosthetic limb for sitting (16.4% $p=.008$) and standing (17.5%, $p<.001$) (Figure 2).

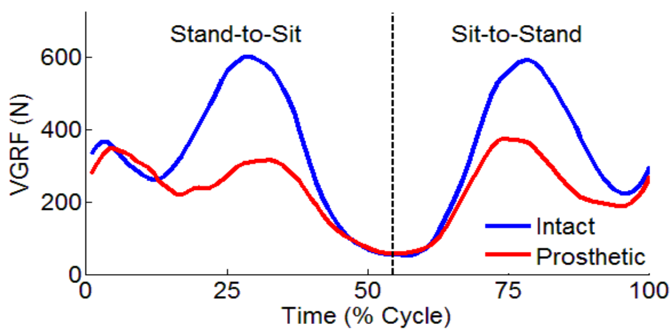

Figure 1. Mean VGRF for the complete trial.

DISCUSSION

During periods of non-movement (Figure 1: 0%, 55%, 100%), loading asymmetry was minimal between limbs. As movement progressed, loading asymmetries increased with more reliance on the intact limb for total force production. The current finding of 76% SI during the STAND task was similar to the results reported by Agrawal et al. [6] (~72-76% during STAND phase). From a force perspective, 62% of the total VGRF was produced by the intact limb in our study. These force discrepancies lead to a functional asymmetry in impulse with the intact limb contributing ~18% more of the total impulse during STAND.

This was the first study to evaluate inter-limb asymmetries during the sitting task in patients with TTA. VGRF asymmetries were similar between STAND and SIT tasks. Even though no significant asymmetries were observed during quiet standing, once movement began, subjects relied on the intact limb for a greater portion of the force production.

Results of our study indicated a significant functional asymmetry during SIT and STAND tasks in persons who received an Ertl amputation. In regards to the number of times this task is completed on a daily basis further understanding of the functional consequences of this loading asymmetry is needed.

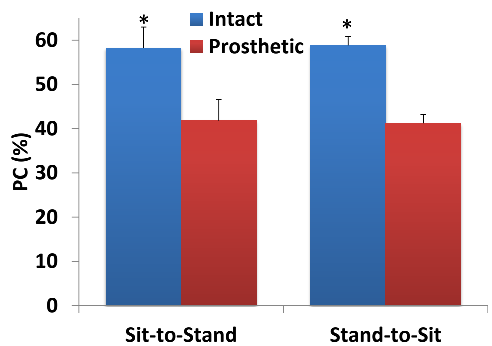

Figure 2. Percent contribution to the task. *Significantly different from prosthetic $p>.05$

ACKNOWLEDGEMENTS

David Hahn, M.D. for assistance with recruitment and his medical expertise with this project.

REFERENCES

1.Ertl JW, et al. February 15, 2013]; Available from: http://ertlreconstruction.com/documents/108.html.
2.Dederich, R. *Journal of Bone & Joint Surgery, British Volume*. **45**(1) 60-66, 1963
3.Dionne, C.P., et al. *J. Prosthet. Orthotics*. **21**(1) 64, 2009
4.Bussmann, J.B., et al. *Arch. Phys. Med. Rehabil.* **85**(2) 240-4, 2004
5.Bussmann, J.B., et al. *Arch. Phys. Med. Rehabil.* **89**(3) 430-4, 2008
6.Agrawal, V., et al. *Ergonomics*. **54**(7) 656-64, 2011

Table 1. Peak VGRFs and Impulse

	Peak Vertical Ground Reaction Force (N)			VGRF Impulse (Ns)	
Limb	STAND	SIT	Quiet Standing	STAND	SIT
Intact	667.5±198.6*	663.0±179.9*	403.9±107.9	341.9±113.5*	290.7±77.9*
Prosthetic	398.1±82.8	458.1±104.9	360.5±85.3	241.6±72.9	201.6±45.9

Note. *Significantly different from prosthetic $p<.05$

MUSCLE CONTRIBUTIONS OF AMPUTEES AND NON-AMPUTEES TO CIRCULAR TURNING

[1]Jessica D. Ventura, [2]Glenn K. Klute and [3]Richard R. Neptune

[1]Department of Kinesiology, Gordon College, Wenham, MA, USA
[2]Department of Veterans Affairs, Puget Sound Health Care System, Seattle, WA, USA
[3] Department of Mechanical Engineering, The University of Texas at Austin, Austin, TX, USA
email: jessica.ventura@gordon.edu, web: http://gordon.academia.edu/JessicaVentura

INTRODUCTION

Walking requires the generation of biomechanical subtasks such as body support, forward propulsion and navigation by turning. Turning involves both the acceleration of the body center-of-mass (COM) and the rotation of the pelvis towards the new heading. To accelerate the COM in the direction of the turn, the medial ground reaction force (GRF) of the outer leg increases relative to straight-line walking and the GRF of the inner leg changes from a medial to lateral directed force [1]. During straight-line walking, computational models suggest the gluteus medius (GMED) is the primary contributor to the medial GRF, while the gastrocnemius (GAS) and soleus (SOL), vasti (VAS), and adductor (ADD) muscles are the primary contributors to lateral GRF [2].

Pelvis rotation into a turn is primarily accomplished by internal rotation of the hip joint during inner leg stance and external rotation of the hip joint during outer leg stance. During straight-line walking, the anterior GMED and iliopsoas (IL) contribute to internal hip rotation and posterior GMED, GMAX, and SOL to external hip rotation [2]. The swing leg also plays an important role in the body's trajectory during walking [3]. Muscles that significantly contribute to motion of the leg during swing, namely the hip flexors and abductors, will also influence pelvis rotation.

To perform a turning task, changes in muscle contributions appear needed to redirect the COM and rotate the pelvis. The goal of this study was to use musculoskeletal modeling and simulation to understand how individual muscles contribute to the turning task in non-amputees and how amputees compensate.

METHODS

Three unilateral transtibial amputees and three speed-matched non-amputees from a larger set of participants [4] were analyzed. Kinematic and GRF data were collected at 120 Hz at 600 Hz, respectively. Participants walked around a 1m radius circular path at their self-selected walking speed (three trials in each direction, Fig. 1).

Musculoskeletal models and forward dynamic simulations of the turning task for each subject were generated using OpenSim [5]. A computed muscle control algorithm solved for the muscle excitations to drive the model to track the experimental kinematics and GRFs. An induced acceleration analysis [6] determined the individual muscle contributions to accelerating the COM and pelvis rotation.

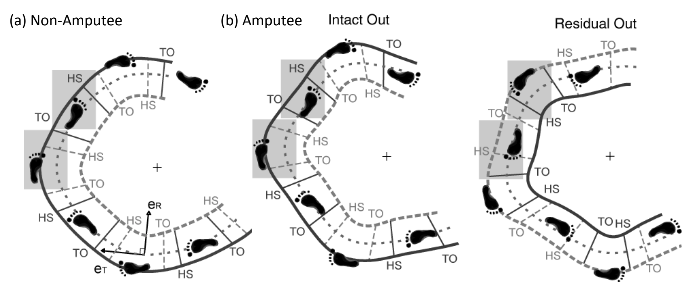

Figure 1: Walking paths of (a) a non-amputee and (b) an amputee, with force plates, COM path, shoulder paths and foot positions. Gait events are shown by lines joining shoulder paths.

Individual muscle contributions to accelerate the COM into the turn were defined in the pelvic reference frame as positive medial accelerations. Muscle contributions were analyzed during single-leg support, where the majority of medial COM acceleration occurs (Fig. 1). Contributions from the three walking trials were averaged for each condition and then across subjects.

RESULTS AND DISCUSSION

The largest contributor to COM medial acceleration during outer leg stance in the non-amputees was the stance leg GMED (Fig. 2). The greatest contributors during inner leg stance were the stance leg iliopsoas (IL) and plantarflexors (SOL and GAS). The greatest contributors to pelvis angular acceleration in the turn direction during outer leg stance were the stance leg IL and swing leg GMED (Fig. 3). During inner leg stance, the greatest contributors were the swing leg IL and ADD.

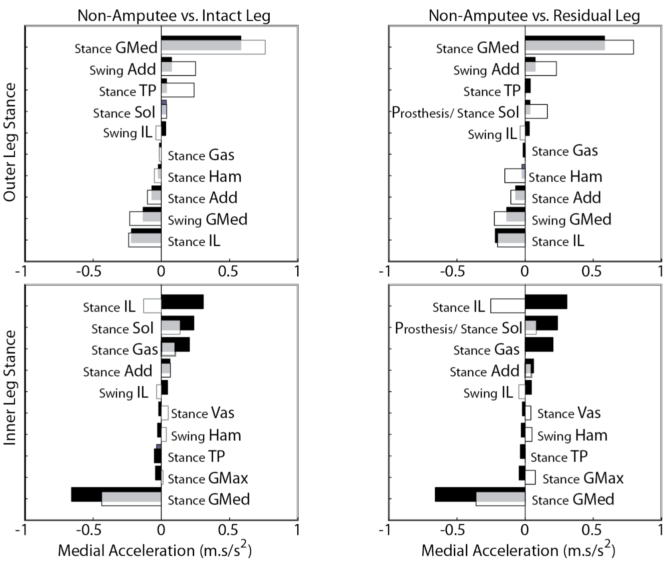

Figure 2: The primary contributors to COM medial acceleration for non-amputees (black) and amputees (white).

The amputees had similar muscle contributions as the non-amputees except for the stance leg IL during inner leg stance, which contributed negatively to medial acceleration, and the stance leg TP during outer leg stance, which contributed largely to the medial acceleration. This suggests that the amputees maintained a different inner leg angle and different outer leg center of pressure than the non-amputees, possibly to increase stability. The prosthesis contributed to the medial acceleration during outer leg stance. The primary differences between amputees and non-amputees were the muscle contributions to the COM medial and pelvis angular acceleration, which were greater during outer leg stance and lower during inner leg stance for the amputees relative to the non-amputees.

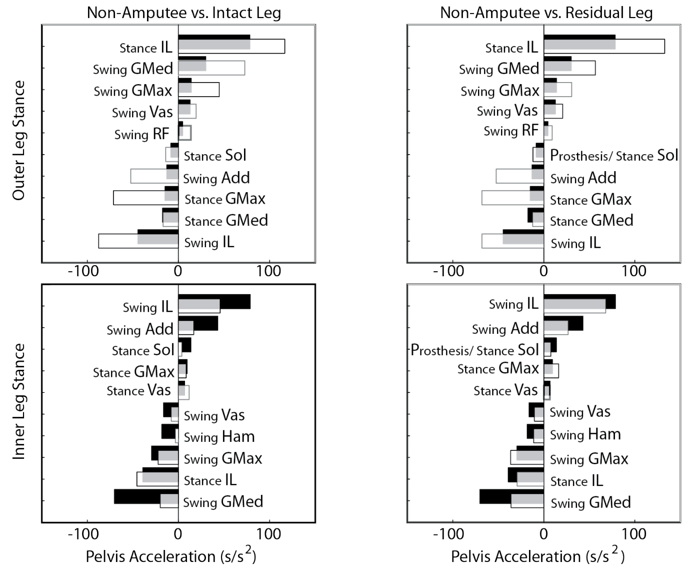

Figure 3: The primary contributors to pelvis angular acceleration for non-amputees (black) and amputees (white).

CONCLUSIONS

Stance leg IL, GMED and plantarflexors and swing leg hip muscles are important contributors to COM medial acceleration and pelvis rotation during turning. To perform the same turning task, amputee muscle contributions in the turn direction decrease during inner leg stance requiring an increase in muscle output during outer leg stance. These differences may be to provide greater stability.

REFERENCES

1. Orendurff MS, et al. *Gait Posture* 23, 106-11, 2006.
2. Pandy MG, et al. *J Biomech* 43, 2055-64, 2010.
3. Winter DA. *Gait Posture* 3, 193-214, 1995.
4. Segal AD, et al. *J Rehabil Res Dev* 46, 375-83, 2009.
5. Delp SL, et al. *IEEE Trans Biomed Eng* 54, 1940-50, 2007.
6. Lin, YC, et al. *Intl J Num Methods BE* 27, 436-49, 2011.

ACKNOWLEDGEMENTS

This research was supported by the Department of Veterans Affairs (A9243C and A7128R) and the National Science Foundation (0346514).

ORAL PRESENATIONS – FRIDAY SEPTEMBER 6th

	Upper Extremity: Clinical Mechanics & Wheelchair Use *Andrew Karduna, K Zhao*
2:30 PM	Kinematic And Functional Evaluation Of Daily Living Tasks In Older Adults With And Without A Rotator Cuff Tear **Vidt ME, Santago AC, Tuohy CJ, Freehill MT, Poehling GG, Miller ME, Saul KR**
2:45 PM	The Influence Of Wheelchair Seat Position On Upper Extremity Demand **Slowik J, Neptune R**
3:00 PM	Risk Of Reduced Subacromial Space In Manual Wheelchair Users Using A Model-based Approach **Zhao K, Van Straaten M, Morrow M, Cloud B, An KN, Ludewig P**
3:15 PM	Subacromial Injection Results In Further Scapular Dyskinesis **Ettinger L, Shapiro M, Karduna A**
3:30 PM	Consideration Of PCSA In Humeral Rotation Co-Activation Calculations **Brookham R, Dickerson C**

KINEMATIC AND FUNCTIONAL EVALUATION OF DAILY LIVING TASKS IN OLDER ADULTS WITH AND WITHOUT A ROTATOR CUFF TEAR

[1,2]Meghan E. Vidt, [1,2]Anthony C. Santago, [3]Christopher J. Tuohy, [3]Michael T. Freehill, [3]Gary G. Poehling, [4]Michael E. Miller, and [1,2,3]Katherine R. Saul

[1]VT-WFU School of Biomedical Engineering and Sciences, Winston-Salem, NC, USA
[2]Wake Forest School of Medicine, Department of Biomedical Engineering, Winston-Salem, NC, USA
[3]Wake Forest School of Medicine, Department of Orthopaedic Surgery, Winston-Salem, NC, USA
[4]Wake Forest School of Medicine, Department of Public Health Sciences, Winston-Salem, NC, USA
email: mvidt@wakehealth.edu, web: www.sbes.vt.edu/kholzbau/MoBL/

INTRODUCTION

Successful completion of daily functional tasks is critical for older adults (age$\geq$60yrs) to maintain their independence. It is estimated that 20-50% of older adults have a rotator cuff tear [1], which is associated with muscle atrophy, decreased strength, and reduced range of motion (ROM). These changes may further exacerbate the functional declines associated with healthy aging. Studies exploring functional performance in older adults are sparse [2], and it is unknown whether rotator cuff injured older adults perform functional tasks differently than their healthy counterparts. In the clinical setting, it is difficult to quantitatively evaluate functional performance, so functional outcome scores are often used. These scores rely on subjective patient self-assessments, and it is unclear whether these scores can successfully classify older adults with a rotator cuff tear. While functional outcome scores are used as a surrogate to evaluate function, it is unknown whether these scores relate to measured kinematics during task performance. Our objective is to obtain functional outcome scores and task kinematics, and assess their relationships for older adults with and without a rotator cuff tear.

METHODS

Six older adults (4M, 2F, mean age 64±2.3yrs) participated; 3 with a degenerative, full-thickness tear of the supraspinatus and 3 age- and gender-matched controls. Subjects performed 7 functional tasks that span the upper limb workspace from a seated position (chair height=0.53m). Tasks included axilla wash, forward reach, functional pull, hair comb, perineal care, upward reach to shoulder height, and upward reach to 115°. Forward and upward reaches were performed with a 2lb dumbbell weight to a distance measuring 80% of the subject's forearm length; functional pull was against 6lb resistance, from an unloaded weight machine. Three trials of each task were recorded; the second trial was used for analysis. Seven Hawk motion capture cameras (Motion Analysis Corp.) recorded locations of 12 retroreflective markers on anatomical landmarks during tasks. Data was post-processed with Cortex (Motion Analysis Corp.), OpenSim (v.3.0, Stanford Univ.), and Matlab (The Mathworks, Inc.). Maximum and minimum joint angles were calculated for 3 shoulder degrees of freedom (shoulder elevation, elevation plane, shoulder rotation); minimum angle was subtracted from maximum angle to calculate ROM.

Participants completed 4 functional outcome scores: Western Ontario Rotator Cuff Index (WORC), American Shoulder and Elbow Surgeons Shoulder Outcome Score (ASES), Simple Shoulder Test (SST), and the Rand 36-Item Short Form Health Survey (SF-36). Repeated measures ANOVA were used to compare participants with a rotator cuff tear to controls for each functional outcome score and task ROM. Regression analyses were used to assess relationships between ROM and outcome scores for outcomes that were different between groups. Since these are preliminary analyses, we did not correct for type I error and assessed differences at $p \leq 0.1$.

RESULTS AND DISCUSSION

All tasks were successfully completed by all subjects, except the hair comb for a single rotator cuff tear participant; this trial was not included in the analyses. Participants in the rotator cuff tear group had reduced shoulder elevation ROM compared to healthy controls for the hair comb (p=0.0125) and perineal care (p=0.0347) tasks (Fig. 1A). Similarly, elevation plane ROM was reduced for participants with a rotator cuff tear for the axilla wash (p=0.0212) and functional pull (p=0.0707) (Fig. 1B).

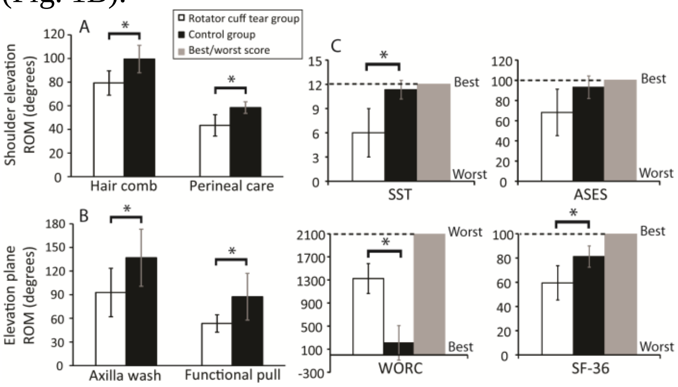

Figure 1: Mean±SD for rotator cuff tear and control groups for (A) shoulder elevation ROM; (B) elevation plane ROM; and (C) functional outcome scores. * indicates p≤0.1.

Subjects with a rotator cuff tear had worse scores than controls on the functional outcome scores (Fig. 1C). These differences were significant for SST (p=0.045), WORC (p=0.007), and SF-36 (p=0.086), with a trend toward significance for ASES (p=0.167). Using regression analyses, we identified relationships between the functional outcome scores and ROM. For the SF-36, 71% and 88% of the variation in elevation angle ROM was accounted for by changes in SF-36 score for the functional pull (p=0.0341) and axilla wash (p=0.0055), respectively (Fig. 2). Similarly, 64% of the variation in shoulder elevation ROM was accounted for by changes in SF-36 score for perineal care (p=0.0561) (Fig. 2). Sixty eight % of the variation in elevation angle ROM was accounted for by changes in ASES score for the functional pull (p=0.0422), while 57% of the variation in shoulder elevation ROM was accounted for by changes in SST score for the perineal care task (p=0.0848). Our findings indicate that even in this preliminary sample, we are able to identify important relationships between subjective, self-assessments of function and quantitative descriptions of function during specific tasks. This work indicates that the SF-36 and SST scores are able to differentiate between patients with and without a rotator cuff tear and are associated with differences in performance during the axilla wash, functional pull, and perineal care tasks.

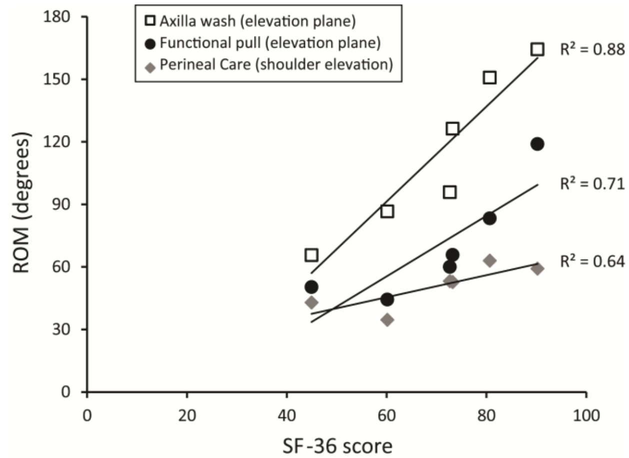

Figure 2: Regression analyses for elevation angle ROM versus SF-36 score for axilla wash and functional pull, and shoulder elevation ROM versus SF-36 score for perineal care.

CONCLUSIONS

We have measured functional kinematics for a group of older adults with and without a rotator cuff tear and identified differences between these groups for functional outcome scores and ROM. Clinical implications of our findings suggest that a few of the many available functional outcome scores should have a priority when evaluating patients with a suspected rotator cuff tear in the clinic. This work is part of an ongoing study which will further evaluate these relationships in a larger cohort. Identification of tasks that require compensation after injury will allow researchers to focus on the muscles that play a role during those specific tasks.

REFERENCES

1. Lin JC, et al. *J Am Med Dir Assoc* **9**, 626-632, 2008.
2. Hall LC, et al. *Clin Biomech* **26**, 579-584, 2011.

ACKNOWLEDGEMENTS

NIH Award #1F31AG040921; WFU Pepper Center, NIA P30 AG021332.

THE INFLUENCE OF WHEELCHAIR SEAT POSITION ON UPPER EXTREMITY DEMAND

Jonathan S. Slowik and Richard R. Neptune

The University of Texas at Austin, Austin, TX, USA
email: jsslowik@utexas.edu, web: http://www.me.utexas.edu/~neptune

INTRODUCTION

The physical demands placed on the upper extremity during manual wheelchair propulsion result in a high prevalence of pain and injury [1]. Seat position is an adjustable parameter that directly influences propulsion mechanics and upper extremity demand, so identifying a position that minimizes demand holds great promise for reducing the risk of pain and injury.

Current clinical guidelines [2] recommend that the seat be positioned as far posterior as possible without compromising user stability and at a height such that the angle between the upper arm and forearm is between 100° and 120° when the hand is placed on the handrim at top dead-center (TDC). These guidelines were primarily based on experimentally identified trends in indirect measures of upper extremity demand such as cadence, push angle, handrim forces and EMG across a relatively small number of seat positions.

Forward dynamics simulations provide an alternative approach to systematically examine the influence of wheelchair seat position on direct measures of upper extremity demand. When integrated with a musculoskeletal model, they can be used to systematically examine quantities that contribute to upper extremity demand across a wide range of seat positions. The purpose of this study was to use forward dynamics simulations of wheelchair propulsion to investigate how seat position influences muscle stresses, muscle-produced joint moments and metabolic cost.

METHODS

The 3D musculoskeletal model used in this study was developed using SIMM/Dynamics Pipeline (Musculographics, Inc.) and based on the work of Rankin et al. [3]. The model had five rotational degrees-of-freedom (DOFs), representing the articulations of the shoulder, elbow and forearm. Twenty-six Hill-type musculoskeletal actuators represented the major upper extremity muscles crossing these joints.

The motion of the hand was prescribed to follow a path on a standard circular handrim during the push phase. The contact angle, release angle and push frequency were dependent on seat position and were calculated using a set of equations developed by Richter [4], assuming an initial position push frequency of 1Hz. Push time was set to 40% of the cycle time. For all seat positions, the average power output to the handrim was set at 10W.

From the initial position (hub-shoulder angle: 0°, TDC elbow angle: 110°), the seat position was systematically varied independently in the superior/inferior and the anterior/posterior directions throughout the range of achievable seat positions, which resulted in 53 investigated positions.

A forward dynamics simulation was generated for each seat position using a simulated annealing optimization algorithm to identify the muscle excitation patterns that minimized the time rate of change in handrim force and muscle-produced joint moments while producing realistic wheelchair propulsion mechanics.

The level of antagonistic muscle-produced joint moments was quantified by the co-contraction moment (τ_{cc}), defined as the difference between the average total magnitude of moments (τ_{total}) and the average net moment (τ_{net}):

$$\tau_{total} = \frac{1}{n_{dof} * t_c} \int_0^{t_c} \left(\sum_{j=1}^{n_{dof}} \sum_{i=1}^{n_{mus}} \left| \tau_{i,j}(t) \right| \right) dt \qquad (1)$$

$$\tau_{net} = \frac{1}{n_{dof} * t_c} \int_0^{t_c} \left(\left| \sum_{j=1}^{n_{dof}} \sum_{i=1}^{n_{mus}} \tau_{i,j}(t) \right| \right) dt \qquad (2)$$

$$\tau_{cc} = \tau_{total} - \tau_{net} \quad (3)$$

where $\tau_{i,j}$ is the moment that the i^{th} muscle applies about the j^{th} DOF and t_c is the cycle time.

Co-contraction moment, muscle stress and metabolic cost (normalized by the total work done on the handrim throughout the cycle) were calculated and compared across seat positions. Metabolic cost was calculated using a previously described model [5].

RESULTS AND DISCUSSION

The average co-contraction moment across all DOFs (Fig. 1) was minimized (4.6 Nm) at a seat position with hub-shoulder angle of -6.4° and TDC elbow angle of 122.2°. Seat positions with hub-shoulder angles between -10° and -2.5° and TDC elbow angles between 110° and 130° had an average co-contraction moment of less than 5 Nm.

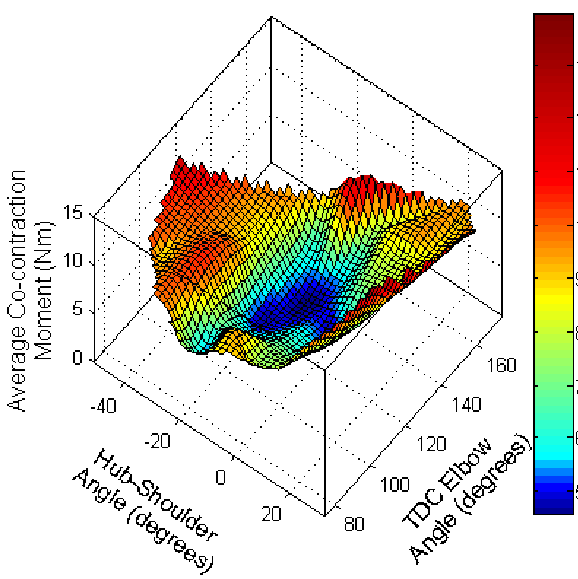

Figure 1: Average co-contraction moment versus seat position.

The overall muscle stress was minimized (72.2 kPa) at a seat position with hub-shoulder angle of -11.5° and TDC elbow angle of 116.9°. Seat positions with hub-shoulder angles between -15° and 0° and TDC elbow angles between 105° and 120° had an associated overall muscle stress level less than 85 kPa.

The normalized metabolic cost was minimized (8.5) at a seat position with hub-shoulder angle of -11.6° and TDC elbow angle of 106.6°. Seat positions with hub-shoulder angles between -15° and 10° and TDC elbow angle between 100° and 120° had an associated normalized metabolic cost less than 10.

Additional analysis found that further posterior seat positions placed some of the major power-producing muscles during the push phase (e.g., anterior deltoid and pectoralis major) under non-optimal operating conditions (i.e. less favorable regions of the intrinsic muscle force-length relationship). Also, a decomposition of the co-contraction moment into individual DOF components found that the muscles crossing the glenohumeral joint predominantly influenced the amount of co-contraction.

All examined upper extremity demand measures were near minimum values at positions with hub-shoulder angles between -10° and -2.5° and TDC elbow angles between 110° and 120°. These results agree with current clinical guidelines given that further posterior positions would likely compromise user stability in a standard manual wheelchair. However, even if a novel wheelchair design could achieve further posterior seat positions while maintaining user stability, our results suggest that there is a limit to how far posterior to position the seat before upper extremity demand begins to increase.

REFERENCES

1. Requejo PS, et al., *Top Spinal Cord Inj Rehabil* **13**, 86-119, 2008.
2. Consortium for Spinal Cord Medicine. *J Spinal Cord Med* **28**, 434-470, 2005.
3. Rankin JW, et al. *J Biomech* **44**, 1246-1252, 2011.
4. Richter WM. *Med Eng Phys* **23**, 707-712, 2001.
5. Umberger BR. *J R Soc Interface* **7**, 1329-1340, 2010.

ACKNOWLEDGEMENTS

The authors thank Dr. Jeff Rankin for help with the initial model development.

Risk of Reduced Subacromial Space in Manual Wheelchair Users Using a Model-Based Approach

[1]Kristin Zhao, [1]Meegan Van Straaten, [1]Melissa Morrow, [1]Beth Cloud, [1]Kai-Nan An, and [2]Paula Ludewig
[1]Mayo Clinic, Rochester, MN USA
[2]University of Minnesota, Minneapolis, MN, USA
email: zhao.kristin@mayo.edu

INTRODUCTION

Spinal cord injured (SCI) individuals rely on manual wheelchairs for mobility as well as for recreation and exercise. Therefore, they are dependent on their shoulders for weight bearing during all of their daily activities. Due to this reliance on their shoulders, as well as the lack of geometrical stability in the joint, shoulder-related pain is reported to be as high as 70% [1].

Imaging, as well as cadaveric and animal studies, implicate subacromial space narrowing (that results in mechanical impingement of the interposed rotator cuff tendons) as a primary mechanism for the shoulder pain in this population. Previous reports have used assumed at-risk scapular and glenohumeral angular kinematics (scapular anterior tilt and internal rotation, glenohumeral internal rotation) to assess risk of subacromial space narrowing. A model-based approach was used in this study to predict the proximity of the rotator cuff insertions on the humerus to the underside of the coracoacromial arch. The goal of this project was to compare the risk between three tasks (wheelchair propulsion, weight relief raises, and scapular plane abduction) using both the modeling approach, as well as assumed at-risk angular kinematics, in a population of wheelchair users with reported shoulder pain.

METHODS

Subjects

Fifteen subjects who use manual wheelchairs as their primary means of mobility (gender: 13M, 2F; age: 39 ± 12 yrs; years post-SCI: 14 ± 9 yrs) were recruited according to Institutional Review Board guidelines. The individuals reported shoulder joint pain caused by mechanical impingement (as determined by a licensed physical therapist). Subjects' injury levels ranged from C6-7 to L2, with one subject who was post-polio.

Kinematic data collection

The subjects' wheelchairs were placed atop a set of custom aluminum rollers for the kinematic data acquisition. Electromagnetic sensors were attached via double-sided adhesive tape to the sternum, the skin overlying the flat superior surface of the scapular acromion process, and to a thermoplastic cuff secured to the distal humerus on the subject's painful arm (Fig. 1). Anatomical coordinate systems were defined on each body segment (scapula, humerus, and thorax), and the global coordinate system was defined, according to ISB standards [2]. The three-dimensional position and orientation of the subject's thorax, scapula, and humerus were collected throughout the dynamic movements at 240Hz using a Liberty (Polhemus, Inc., Colchester, VT) electromagnetic tracking system and accompanying data collection/analysis software, MotionMonitor (Innovative Sports Training, Chicago, IL).

Subjects performed two repetitions of weight relief raises, scapular plane abduction (up to 60 degrees of elevation), and propulsion at a comfortable speed on the aluminum rollers; the final trial was used for analysis. Glenohumeral rotations were expressed using an XZ'Y" Euler sequence [3] and scapulothoracic rotations were expressed using an YX'Z" Euler sequence.

Modeling

A CT scan from a single subject of similar height and weight to our median subject was used to generate reconstructed humerus and scapula bone surface models as well as tendon insertion areas on the humerus for the supraspinatus, infraspinatus, and subscapularis (Figure 1). After defining the ISB coordinate systems on the bone model surfaces, each subject's respective glenohumeral rotation values were used to simulate the motion for all three tasks using a custom Matlab program (Mathworks). The humeral head was centered on the glenoid. At 5% increments across the movement cycles, a proximity (distance) map was defined from each of the tendon insertion areas on the humerus to the acromion and coracoacromial (CA) ligament. Maps were determined by calculating the Euclidean distance from all vertices in the tendon insertion areas to all vertices on the underside of the acromion and CA ligament. The shortest distance across the proximity maps were saved at each increment of the movements.

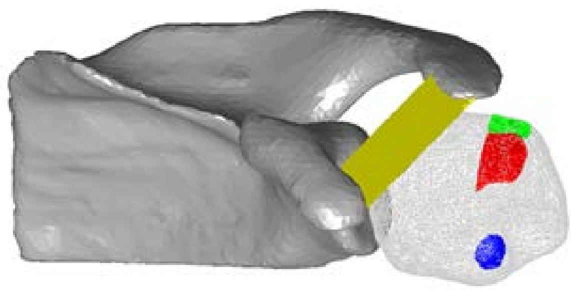

Figure 1: Surface models of the scapula (solid gray) and humeral head (meshed gray) with the CA ligament (yellow), subscapularis tendon footprint (blue), supraspinatus tendon footprint (red), and infraspinatus tendon footprint (green).

RESULTS AND DISCUSSION

The kinematics assumed to reduce the subacromial space were selected from the time series curves at four events across the cycles for each movement. Repeated measures ANOVA ($p<0.05$) were used to assess changes across the three tasks. For both mean and peak rotations, weight relief was found to be consistently at greatest risk (i.e. greater angular values) and scapular plane abduction at least risk (Table 1). However, when using the modeling approach to assess risk (Table 2), propulsion and scapular plane abduction were found to be at greater risk (smaller distances) and weight relief at least risk.

As subacromial impingement risk is directly defined based on glenohumeral motion changes (not indirect shoulder kinematic descriptors including scapulothoracic rotations), it is imperative that future research focus on the glenohumeral articulation rather than on the scapula and humerus motions independently to attempt to define risk. Further, many of the studies which attempt to identify changes in kinematics associated with subacromial risk focus on the scapular plane abduction movement. These data clearly demonstrate that there are differences between tasks, and risk needs to be quantified for the tasks in question rather than translating findings from assessments of other movements.

REFERENCES

1. Anderson, K.D. *J Neurotrauma* **21**:1371-83, 2004.
2. Wu, G., et al., *J Biomech* **35**:543-548, 2002.
3. Phadke, V., et al., *J Biomech* **44**:700-705, 2011.

ACKNOWLEDGEMENTS

Funding for this study was provided by the Paralyzed Veterans of America Foundation.

Table 1: Statistically significant ($p<0.05$) differences in assumed at-risk kinematics across tasks (SCAP=scapular plane abduction, WR= weight relief, PROP=propulsion). Higher risk (red); lower risk (green).

Kinematics	Mean rotations	Peak rotations
Scapula internal rotation	SCAP > WR, PROP	WR, PROP > SCAP
Scapula anterior tilt	WR, PROP > SCAP	WR, PROP > SCAP
Glenohumeral internal rotation	WR > PROP > SCAP	WR > PROP > SCAP

Table 2: Statistically significant ($p< 0.05$) differences in risk (minimum distances) across tasks for each tendon (SCAP=scapular plane abduction, WR= weight relief, PROP=propulsion). Higher risk (red); lower risk (green).

Minimum distances	Acromion
Infraspinatus	PROP < WR, SCAP
Supraspinatus	PROP, SCAP < WR
Subscapularis	SCAP < PROP < WR

SUBACROMIAL INJECTION RESULTS IN FURTHER SCAPULAR DYSKINESIS

[1] Luke R. Ettinger M.S, [2] Matthew M. Shapiro M.D, [1] Andrew R. Karduna Ph.D
[1] University of Oregon, Eugene, OR, USA
[2] Slocum Center for Orthopedics and Sports Medicine, Eugene, OR, USA
email: lettinge@gmail.com

INTRODUCTION

Treatment of subacromial impingement often targets strengthening rotator cuff musculature and reducing pain. However, little is known about the rotator cuff activity in the presence of pain. Work from our laboratory suggests that disabling the rotator cuff (nerve block) results in increased deltoid muscle activity during arm elevation in healthy subjects [1]. Myers et al., suggested that patients with impingement have greater reliance on deltoid activity than healthy controls [2]. Together, these findings suggest that rotator cuff activation may be attenuated by pain inhibition in patients with subacromial impingement.

Patients with impingement have been reported to have greater scapular anterior tilting, which is believed to reduce clearance in the subacromial space [3]. The influence of subacromial pain on scapular tilting is currently unknown.

The goal of this study is to examine the influence of pain on deltoid activity. Additionally, we sought to investigate the influence of pain on scapular tilting during arm elevation. We hypothesize that following an anesthetic injection, patients will have a reduction in deltoid activity due to pain dis-inhibition of the rotator cuff. Further we hypothesize that following a subacromial injection, patients will demonstrate scapular kinematics that more closely resemble healthy control participants' kinematics.

METHODS

Twenty patients with a mean age of 57.5 (± 8.1) years diagnosed with stage 2 subacromial impingement syndrome were included in this study. Additionally, to date, 5 healthy age and arm dominance matched control participants, with a mean age of 60 (± 11.2) years have been included. Patients suspected of having rotator cuff tears were excluded. Surface EMG activity was measured from three shoulder muscles (anterior, middle and posterior deltoid) on the affected arm during three arm elevation trials in the scapular plane. Each arm elevation trial was performed at approximately 30 degrees per second. Three dimensional scapular kinematic data were measured using an electromagnetic tracking device (Polhemus Fastrak). Digitization of anatomic landmarks followed the proposed ISB standards [4]. Subjects completed a visual analog scale (VAS) questionnaire depicting their pain immediately following the arm elevation task. All data were collected before and after a subacromial injection of anesthetic (6 cc 0.5% bupivacaine with epinephrine and 3 cc lidocaine with epinephrine) and corticosteroid (1 cc 40mg methylprednisolone acetate) as part of their normal treatment. The procedure was completed by one of our co-authors (M.S) who is an orthopedic surgeon. Normalization of EMG was calculated as percent maximal voluntary isometric contraction (MVIC) of each muscle during a 5 second contraction, where the amplitude of the contraction was determined by the root mean squared (rms) over the middle two seconds of the muscle contraction. Each muscle's MVIC was determined in a unique testing position, with approximately 20 seconds of rest between testing different muscles. No sensors were removed between the pre and post injection tests. EMG data were sampled at 1200 Hz and kinematic motion data were sampled at 40 Hz. All MVIC data (for normalization) were collected post injection.

RESULTS AND DISCUSSION

Following an anesthetic subacromial injection, there was a reduction in pain of approximately 62%; pre injection VAS 6.3/10 ± 2.4, post injection VAS 2.8/10 ± 1.4. Patients tended toward an anteriorly tilted scapula at all levels of humeral elevation and this trend was increased following a subacromial injection. In contrast, our control participants demonstrated posterior tilt at all levels of humeral elevation (Figure 1). Patients had greater deltoid (anterior, middle and posterior) activity at all levels of humeral elevation compared to healthy controls; additionally deltoid activity was augmented following the subacromial injection for our patient population (Figure 2,3,4).

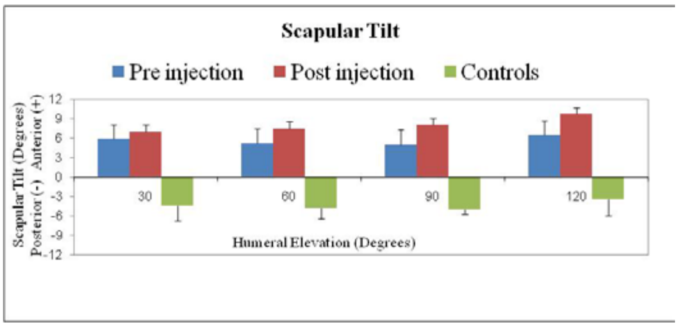

Figure 1: Scapular tilt pre (blue) and post (red) injection in patients with subacromial impingement versus healthy controls (green).

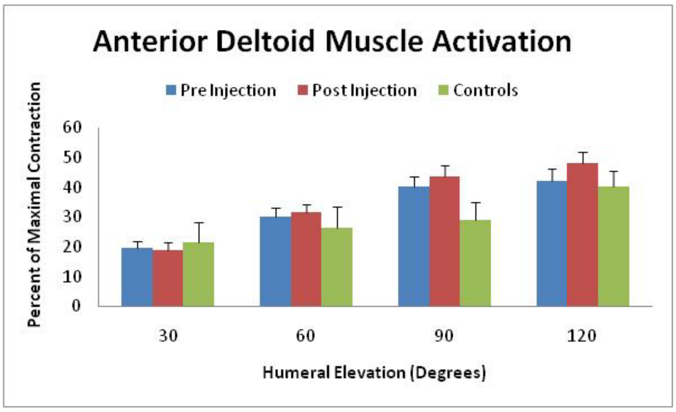

Figure 2: Anterior deltoid activity pre (blue) and post (red) injection in patients with subacromial impingement versus healthy controls (green).

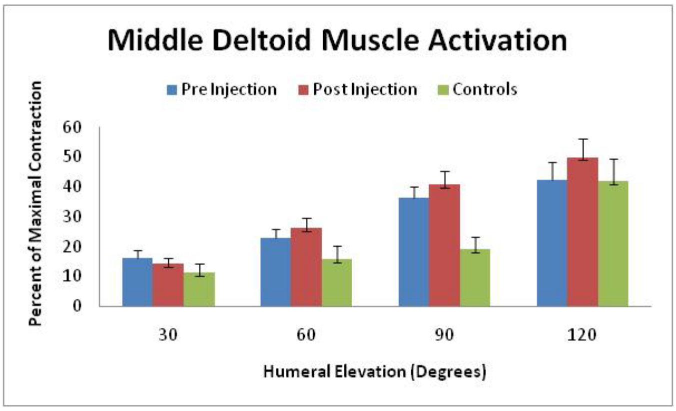

Figure 3: Middle deltoid activity pre (blue) and post (red) injection in patients with subacromial impingement versus healthy controls (green).

The subacromial distance can be influenced by scapular anteior tilting and superior humeral migration. Our results indicate that patients with impingement have greater scapular anteior tilting than control subjects. Further scapular tilting increased following the subacromial injection. Thus our hypothesis was not supported. This finding suggests that pain may be inhibiting scapular tilt to some degree. However, it is likely that the changes measured are transitory and represent the immediate adaptation in scapular neuro-mechanics adopted by this population.

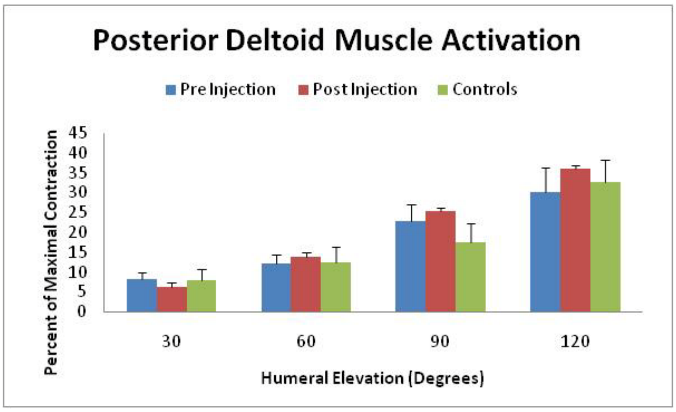

Figure 4: Posterior deltoid activity pre (blue) and post (red) injection in patients with subacromial impingement versus healthy controls (green).

Also contrary to our hypothesis, patients with impingement had greater deltoid activity after injection. However, our hypothesis was supported when comparing the patients with impingement with healthy controls. This finding suggests that patients with impingement may have greater superior humeral head migration than healthy controls, but humeral migration may be exacerbated by a subacromial injection. The greater activation of deltoid muscles in the impinged group may be due to reduced rotator cuff activity [1]. These findings suggest that a reduction of pain may further reduce rotator cuff activity and result in greater superior humeral displacement during arm elevation. However, these results may be due to a transitory or “foreign sensation” adaptation due to the short lived anesthetics.

REFERENCES

1. McCully S, et al., *Journal of Biomechanics*, **40**:1839-1864, 2007.
2. Myers et al., *Sci Med Sport* **12**:603-608, 2009.
3. Ludewig P et al., *Phys Ther* **80**: 276-291, 2000.
4. Wu G, et al., *Journal of Biomechanics* 38: 981-992, 2005.

CONSIDERATION OF PCSA IN HUMERAL ROTATION CO-ACTIVATION CALCULATIONS

[1]Rebecca L. Brookham and [1]Clark R. Dickerson

[1]University of Waterloo, Waterloo, ON, CAN
email: clark.dickerson@uwaterloo.ca

INTRODUCTION

The exemption of co-activation in computational biomechanical models precedes underestimations of muscle force and joint loading. Shoulder co-activation must be quantified as its inclusion in biomechanical models will improve physiological realism, thereby enhancing prediction accuracy. Previously [1, 2], electromyography (EMG) of knee and elbow muscles has been used to define co-activation as a non-weighted ratio of normalized agonist to total (agonist plus antagonist) activation. However, shoulder muscles vary considerably in size and thus have variable potential contributions to force generation. Physiological cross-sectional area (PCSA) should be considered in the examination of shoulder co-activation to assess the importance of these size differences. The purposes of this study were to quantify the co-activation relationships of humeral internal and external rotators in young healthy adults during a subset of exertion intensities and postures using traditional non-weighted and PCSA-weighted calculations. We hypothesized that predictions from PCSA-weighted co-activation models would more closely represent (higher r^2) empirically measured co-activation than non-weighted predictions.

METHODS

Surface EMG electrodes were placed over the right supraspinatus, infraspinatus, pectoralis major (clavicular and sternal insertions), posterior deltoid and latissimus dorsi of 10 males and 10 females (mean [range]: age (years) 22 [18-32], stature (m) 1.7 [1.6-1.8]; weight (kg) 66.6 [48.5-85.0]). Fine wire EMG electrodes were inserted into the right supraspinatus, infraspinatus and subscapularis. Participants performed humeral internal rotation (IR) and external rotation (ER) maximal voluntary force exertions (3 sets each), and the maximum IR and ER strength was determined. Two sets each of muscle-specific maximal voluntary contractions were performed. Participants performed 54 trials of 6s duration isometric humeral IR and ER at varying intensities (20%, 40%, 60% of individual capacity), humeral rotation angles (0°, -45°, 45°) and abduction angles (0°, 45°, 90°) with the elbow flexed to 90°. Raw EMG was high pass filtered (Fc 30Hz), linear enveloped (low pass filtered, Fc 2.5Hz) and normalized. Non- and PCSA-weighted co-activation indexes ($CI_{non\text{-}wght}$ and CI_{PCSA}) were calculated (Eq.1-2). PCSA data were extracted from previous works [3, 4].

$$\boldsymbol{CI_{non-wght}} = \frac{\int_{t1}^{t3}\left[\frac{\sum_{i=1}^{4} E_{R_i}}{4}\right](t)\,dt}{\int_{t1}^{t3}\left[\left[\frac{\sum_{i=1}^{4} E_{R_i}}{4}\right]+\left[\frac{\sum_{i=5}^{7} E_{R_i}}{3}\right]\right](t)\,dt} \qquad \text{Eq.1}$$

$$\boldsymbol{CI_{PCSA}} = \frac{\int_{t1}^{t3}\left[\frac{\sum_{i=1}^{4} E_{R_i}\cdot PCSA_i}{\sum_{i=1}^{4} PCSA_i}\right](t)\,dt}{\int_{t1}^{t3}\left[\left[\frac{\sum_{i=1}^{4} E_{R_i}\cdot PCSA_i}{\sum_{i=1}^{4} PCSA_i}\right]+\left[\frac{\sum_{i=5}^{7} E_{R_i}\cdot PCSA_i}{\sum_{i=5}^{7} PCSA_i}\right]\right](t)\,dt} \qquad \text{Eq.2}$$

Where: E = linear enveloped and normalized EMG; $R_{1\text{-}4}$ = Internal rotators: subscapularis, pectoralis major clavicular / sternal heads and latissimus dorsi, respectively; $R_{5\text{-}7}$ = External rotators: infraspinatus, posterior deltoid and supraspinatus, respectively.

The CIs provide a relative measure of IR activation to total (IR plus ER) activation. A CI of 0 indicates no co-activation (IRs not activated); a CI of 0.5 indicates full co-activation (both IRs and ERs equal) and a CI of 1.0 indicates no co-activation (ERs not activated). EMG signals determined to have artifact were removed from CI ratios and denominators were scaled to reflect this removal (Table 1). Fine wire supraspinatus and infraspinatus channels with artifact were removed and substituted with their respective surface EMG channels. Predictor variables were identified using stepwise multiple linear regression analysis (mixed, 0.25/0.25 enter/exit p-values). Prediction models were developed for non- and PCSA-weighted CIs, separately for both IR and ER type exertions using a repeated measures analysis of variance. The inclusion of interaction effects provided no or little improvement in explained variance, and thus only main effects were considered.

RESULTS AND DISCUSSION

The most parsimonious models for non- and PCSA weighted co-activation during humeral IR and ER exertions ($CI_{non\text{-}wght,IR}$, $CI_{PCSA,IR}$, $CI_{non\text{-}wght,ER}$ and $CI_{PCSA,ER}$: Eq.3-6, resp.) were:
[where A_{abd} = humeral abduction angle is in degrees, and I = intensity, percent maximal voluntary force]

$$\boldsymbol{CI_{non-wght,IR} = 0.70 - [0.0036 \cdot A_{abd}] + [0.0034 \cdot I]}$$

[Eq. 3: whole model p value <0.0001; $\mathbf{r^2 = 0.70}$; independent variable p values = <0.0001, <0.0001, resp. and F ratios = 757.99, 131.34, resp.]

$$\boldsymbol{CI_{PCSA,IR} = 0.72 - [0.0032 \cdot A_{abd}] + [0.0034 \cdot I]}$$

[Eq. 4: whole model p value <0.0001; $\mathbf{r^2 = 0.62}$; independent variable p values = <0.0001, <0.0001, resp. and F ratios = 467.49, 106.11, resp.]

$$\boldsymbol{CI_{non-wght,ER} = 0.22 - [0.00047 \cdot A_{abd}]}$$

[Eq. 5: whole model p value <0.0001; $\mathbf{r^2 = 0.35}$; independent variable p value = <0.0001 and F ratio = 22.09]

$$\boldsymbol{CI_{PSCA,ER} = 0.29 - [0.00060 \cdot A_{abd}] - [0.00064 \cdot I]}$$

[Eq. 6: whole model p value <0.0001; $\mathbf{r^2 = 0.42}$; independent variable p values = <0.0001, 0.0205, resp. and F ratios = 23.61, 5.40, resp.]

Contradicting our main hypothesis, PCSA-weighted predictions were modestly more representative of empirically measured co-activation only during ER exertions. As the summation of IR and ER muscle PCSAs used in this study were approximately equal (34.38 cm^2 vs. 31.15 cm^2) their effects were nearly balanced in the CI equations, deemphasizing any individual PCSA-dependent differences. The observed differences in variance explanation may be indicative of the non-generalizability of the PCSA values taken from cadavers for this healthy young adult population.

The magnitudes of the prediction intercepts are intuitive in that they indicate an increase in activation of IR musculature during IR exertions (intercepts 0.70-0.72), and an increase in activation of the ER muscles during ER exertions (0.22-0.29). Co-activation during humeral rotation is foremost affected by humeral abduction posture, followed by task intensity. As humeral abduction angle increases, there is an increase in activation of ERs relative to total muscle activation (lower CIs). In general, as task intensity increases, activation of humeral IRs increases (higher CIs), which may suggest a protective response of dynamic stabilizers, as the IRs (primarily subscapularis) attempt to protect against large forces which may compromise joint stability.

Co-activation was less predictable (lower r^2) during ER exertions, perhaps due to increased variability of muscle activation strategies attempting to preserve glenohumeral joint stability (anterior dislocations occur during abduction and ER). Shoulder muscle strategies may change with postural adjustments [5]. Further efforts should continue to examine the feasibility of extrapolating these co-activation relationships to other postures and intensities.

CONCLUSIONS

Humeral axial rotational co-activation was more sensitive to abduction angle and task intensity than PCSA. The consideration of PCSA had no or limited improvement in explanation of variance of co-activation relationships, suggesting low utility for such specific exertions.

REFERENCES

1. Kellis E, et al. *J Electrom Kines* **13**, 220-38, 2003.
2. Brookham RL, et al. *J Biomech* **44**, 1582-7, 2011.
3. Veeger H et al, *J Biomech* **7**, 615-29, 1991.
4. van der Helm F et al, *J Biomech* **27**, 551-69, 1994.
5. Lee S-B et al, *J Bone Joint Surg* **82**, 849-57, 2000.

ACKNOWLEDGEMENTS

Support was received from the Natural Science and Engineering Research Council, Canada Foundation for Innovation and the University of Waterloo.

Table 1: Data removed due to motion artifact

	Supraspinatus (fine wire)	Infraspinatus (fine wire)	Subscapularis (fine wire)	Pectoralis Major – Sternal (surface)
% of trials removed	5%	4%	11%	0.09%

ORAL PRESENATIONS – FRIDAY SEPTEMBER 6th

	Gait and Falls *Michael Madigan, Kathleen Bieryla*
4:00 PM	The Point Of Minimum Toe Clearance On The Shoe Is Closer To The Toe Tip At Faster Gait Speeds And More Lateral On Surfaces With Obstacles **Schulz B, Jongprasithporn M, Hart-Hughes S, Bulat T**
4:15 PM	Fall Risks Assessment For The Community Dwelling Obese Elderly Using Wearable Sensors **Wu X, Lockhart T**
4:30 PM	Spatiotemporal Gait Analysis Of Trans-Tibial And Trans-Femoral Amputees At Varying Gait Speeds **Boes M, Tangtragulcharoen T, Kesler R, Nolan L, Hsiao-Wecksler E**
4:45 PM	Effect Of Shoe Tread Depth On Hydrodynamic Pressures In The Shoe-Floor Interface During Slipping **Beschorner K, Chambers A, Redfern M**
5:00 PM	Biomechanics Of Slips And Falls Or Recovery In The Elderly And Young Using Lower And Upper Body Center Of Mass Dynamics **Jayadas A, Boros R**

THE POINT OF MINIMUM TOE CLEARANCE ON THE SHOE IS CLOSER TO THE TOE TIP AT FASTER GAIT SPEEDS AND MORE LATERAL ON SURFACES WITH OBSTACLES

[1]Brian Schulz, [1]Manutchanok Jongprasithporn, [1]Stephanie Hart-Hughes, and [1]Tatjana Bulat

[1]VA HSR&D/RR&D Center of Excellence in Maximizing Rehabilitation Outcomes,
James A. Haley VA Hospital, Tampa, Florida, USA
email: Brian.Schulz@va.gov

INTRODUCTION

Toe speed during gait generally nears its maximum while its height reaches a local minima halfway through swing phase. Trips are thought to frequently occur at these local minima (minimum toe clearance or MTC events) and trip risk has been quantified using the minimum distance between the toe and ground here (MTC) [1]. The location of the point of MTC on the shoe varies with flooring and other factors [2]. We have demonstrated that MTC value and frequency varies with flooring surface and gait speed [3], but the effects of flooring surface and gait speed on the location of the point of MTC on the shoe has never before been evaluated.

METHODS

Fourteen unimpaired younger (age=26±5) and older (age=73±7) subjects, as well as 11 older adults who had fallen in the past 6 months each traversed a 4.88m walkway 4 times at slow, preferred, and fast speeds across surfaces with no obstacles, visible obstacles, and hidden obstacles. Both surfaces with obstacles had the same random obstacle configuration. Shoe and body segment motions were tracked using passive markers and MTC and kinematics calculated using previously-described methods [2]. Also as per these methods [2], MTC events were defined to occur at a point in the swing phase where the following criteria were met: 1) The minimum toe clearance was at a local minima (value is less than that for preceding or following two frames), 2) Toe segment centroid speed (mean speed of the four toe markers) was within the upper quartile for that step, and 3) The minimum toe clearance was lower than the minimum heel clearance. If these criteria were met by more than one point per gait cycle then the smaller MTC value was used. Actual gait speed differed between subjects and groups, so gait speed normalized to leg length was tested as a continuous independent variable (IV). Floor surface and subject group were the other IVs tested. The five dependent variables tested were MTC, the posterior distance of the point of MTC from the toe tip, the mediolateral position of the point of MTC from the toe, and the distance from the whole-body center of mass (COM) from the swing and stance toes. SAS was used for all statistical analyses and effects were considered significant at $p<0.0028$ after corrections for multiple statistical tests.

RESULTS AND DISCUSSION

The preferred and fast gait speeds of the fallers were similar to the slow and preferred gait speed of the younger and older unimpaired subjects. All subjects had similar MTC values on all surfaces and speeds (Figure 1). The point of MTC on the shoe was closer to the toe tip for faster gait speeds and more lateral on surfaces with obstacles (Figures 2 & 3, $p<0.0001$). A more anterior point of swing toe contact during a trip may result in greater plantarflexion moment and more severe disturbance of the swing ankle, making recovery more difficult.
At the instant of MTC, the COM was less anterior to the swing toe and more anterior to the stance toe on surfaces with obstacles (Figure 4, $p<0.0001$). The COM was also less anterior to the both toes at faster gait speeds, but this was only significant for the stance toe ($p<0.0001$). These adaptations to obstacles would likely result in less available time for recovery from a trip (COM more anterior to stance toe), but the swing foot would be in a better position for the recovery step. The reductions in COM-toe distances with increasing speed would increase recovery time and improve foot position.

DISCLAIMER: The contents of this manuscript are those of the authors alone and do not represent the views of the Department of Veterans Affairs or the United States Government.

CONCLUSIONS

All subjects tested thus far similarly adapt MTC to gait speed and changes in flooring surface. The changes in COM position relative to the swing and stance foot at the instant of MTC appear to be generally beneficial, but the more anterior location of the point of MTC on the toe at faster speeds may increase trip severity if the toe contacts the ground.

REFERENCES

1.Winter DA. *Physical Therapy*, 72(1), 45-6, 1992.
2.Thies SB, et al. *J Biomech*, 44(15), 2679-84, 2011
3.Schulz BW, et al. *J Biomech*,44(7),1277-84, 2011.

ACKNOWLEDGEMENTS

VA RR&D Career Development Award (E4941W). We thank Wendy Kimmel, Pradeep Ambati, & Scott Barnett for their assistance.

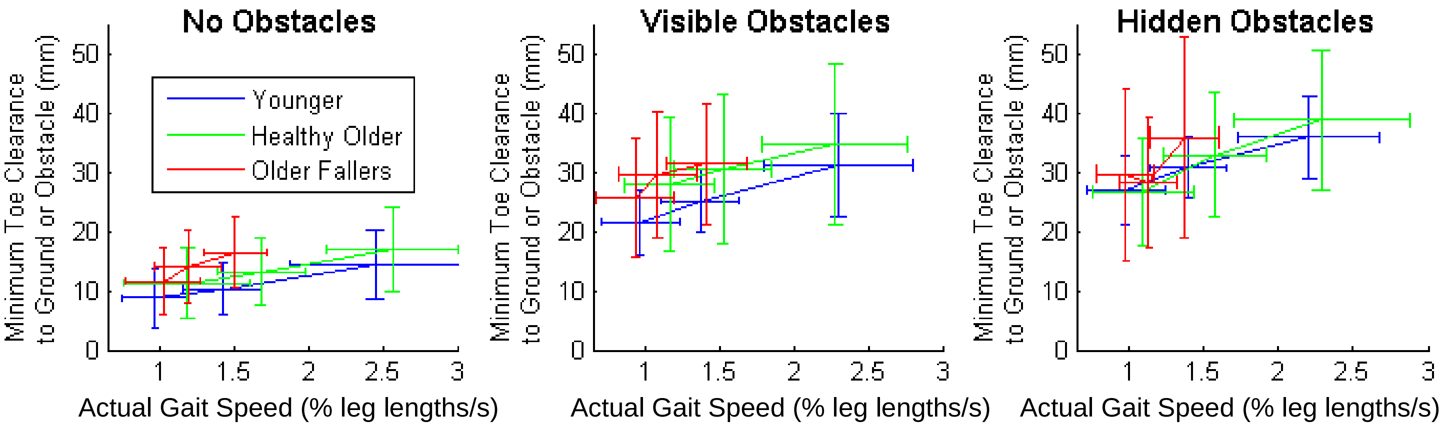

Figure 1: Minimum toe clearance (MTC) by subject group, floor surface, and actual gait speed clustered by instructed gait speed (slow, preferred, and fast).

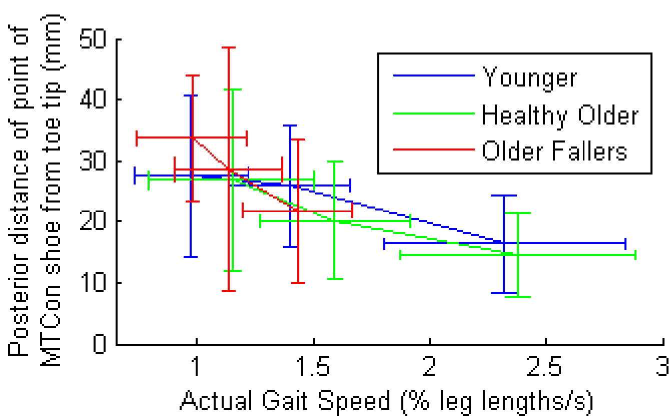

Figure 2: Posterior distance of point of MTC on the shoe from the toe tip. Actual gait speeds clustered by instructed gait speeds.

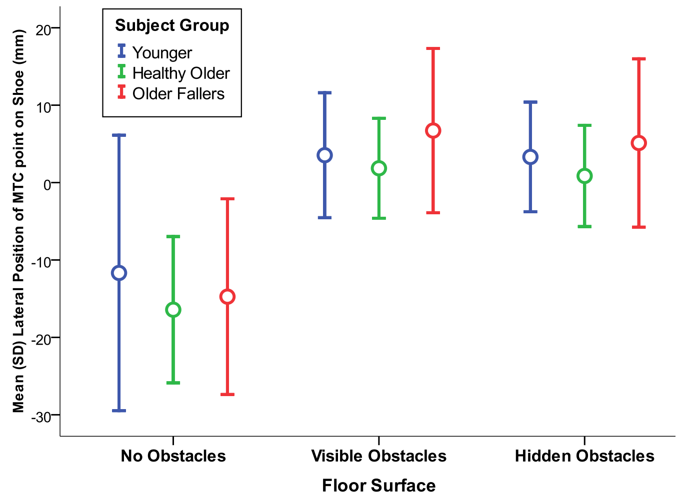

Figure 3: Lateral distance of point of MTC on the shoe from the midpoint of the toe.

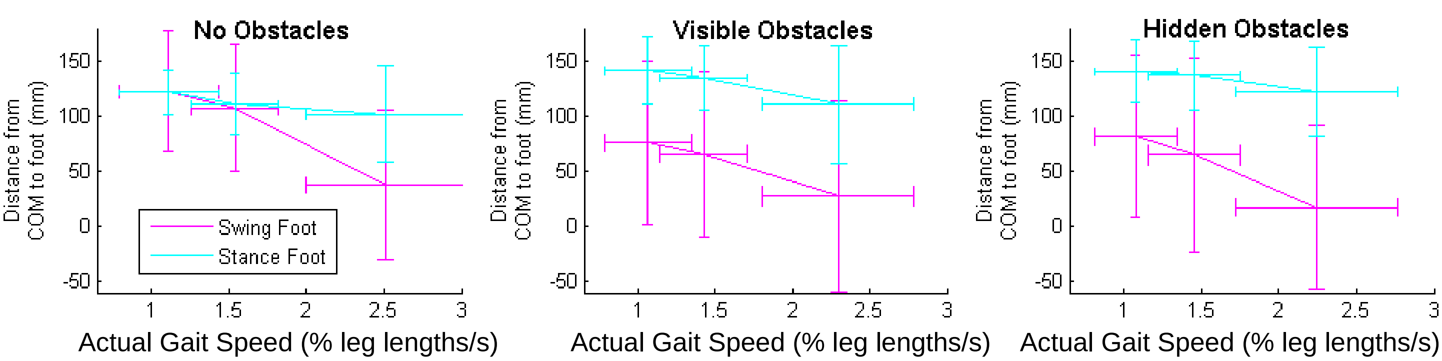

Figure 4: Distance from swing or stance toe to COM at MTC by subject group, floor surface, and actual gait speed clustered by instructed gait speed (healthy slow/faller preferred, healthy preferred/faller fast, and healthy fast).

FALL RISKS ASSESSMENT FOR THE COMMUNITY DWELLING OBESE ELDERLY USING WEARABLE SENSORS

[1]Xuefang Wu and [1,2]Thurmon E. Lockhart

[1]Industrial and System Engineering
[2]Biomedical Engineering and Science
Virginia Tech, Blacksburg, VA, 24061
E-mail: xfwu@vt.edu

INTRODUCTION

In the US, 35.7% of the adults, or over 72 million people are obese. Obesity is not only a contributing cause of many physical health conditions, but also associated with structural and functional limitations [1]. One of the concerns is its association with an increased fall risks and subsequent injuries. Falls have been identified as the most common (36%) cause of injuries in the obese. Middle-aged and older obese adults fell almost twice as frequently (27%) as their lean counterparts (15%) per year [2]. Although epidemiological studies clearly indicated increased risks of falls in the older obese population, it is not clear why they fall more. One way to evaluate their increased fall risks among the obese is to study the difference between obese fallers and non-fallers, if there is any.

Clinical tools such as the Activities-specific and Balance Confidence (ABC) Scale, Timed Up and Go test (TUG), Sit to Stand test (STS) and 10 meter walking test have been demonstrated to predict elderly fallers. Older adults who score low on those scales or requiring longer time to complete the TUG/STS tasks have been identified to have higher fall risks. As such, we will evaluate the fall risks of the obese community-dwelling elderly using these clinical tools.

METHODS

Twenty community-dwelling older adults were enrolled in the study after giving informed consent, which was pre-approved by the Internal Review Borad of Virginia Polytechnic Institute and State University. The inclusion criteria were: (1) age 65years or older, (2) ability to understand the nature of the study and provide informed consent, and (4) ability to walk 10 m without gait aids. Individuals with any medical condition or disability that could prevent them from participating in routine clinical balance tests (e.g., TUG) were excluded. After informed consent was obtained, subjects completed questionnaires containing information on age, residential status, medical history, and fall history during the past twelve months. Participants' height, weight and responses to the Activities-specific Balance Confidence (ABC) scale were also obtained. Among all the participants, there are four obese (BMI>30) non-fallers, four non-obese (18<BMI<25) non-fallers and six obese fallers and six non-obese fallers.

Three custom-made wireless inertial measurement units (TEMPO: IMUs), consisting of one triaxial accelerometer and two gyroscopes were attached on participants' sternum and both ankles (lateral sides) to obtain the temporal and kinematic data. Stopwatch was also used. A standard armchair (seat height of 43cm, arm height of 65 cm) was used for participants to perform the "timed up & go" and sit to stand tasks.

Wearing their own footwear, participants were asked to complete the TUG, STS and 10 meter walking tasks. The participants had a chance to walk through the test once before being timed in order to become familiar with the test. The two consequent trials were timed and recorded for the experiment. Two trials were recorded and timed. The sequence of the trials for each participant was randomized.

The mean of the two timed trials for each mobility task (STS, TUG, 10-meter walking) were used to represent the temporal and kinematic characteristics each participant during the task. Transitional phase time and peak velocity and acceleration during the transitional phase were calculated using MATLAB from the IMU data. Ensemble Empirical Mode Decomposition (EEMD)-Golay was first used to denoise the IMU data. For the 10-meter walking trials, walking velocity (WV), gait cycle time (GCT), double support time (DST), stance time (ST), swing time (SwT), swing angle (SA), step length (SL) and cadence were calculated from the IMUs.

Two-way between-subject ANOVA was performed to determine the interaction effect of obesity×fall, the main effect of obesity and the main effect of fall using JMP 9, with significance level of <0.05.

RESULTS AND DISCUSSION

Our results indicated that fallers have lower ABC scores ($F(1,16)=5.6130$, $p=0.03$), slower walking velocity ($F(1,16)=4.3696$, $p=0.05$) and longer TUG time ($F(1,16)=7.4606$, $p=0.01$) compared with their non-faller counterparts. Obese participants had longer sit to stand time ($F(1,16)=4.1357$, $p=0.05$) than their lean counterparts. No interaction effect was found between the obesity and falls. The mean and standard deviation of all parameters for all four groups of participants can be found in Table 1.

Our study indicated that fallers had a significantly lower ABC score when compared to their non-faller counterparts (Table 1). ABC scores were linked with the psychological factor, referring to the "fear of falling", which has significant implications on an elderly's independence level and results in loss of confidence in performing activities of daily living [3]. Individuals with a fall history are more influenced by the fear of falling complex and seem to be more restricted in their daily activities. Additionally, WV was identified as one of the variables to predict falls. The slowed walking velocity among fallers may reflect degradations in musculoskeletal and sensory systems and lack of confidence in walk safely. Furthermore, our results indicated that fallers took significantly longer time to complete the TUG task than non-fallers. Timed up and go test is designed to assess the four main risk factors associated with the risk of falling among the elderly: 1) strength in lower extremities, 2) coordination, 3) balance, 4) gait. The significant longer completion time among fallers was in agreement with other studies, which indicated that fallers are associated with decreased functional mobility. Decreased functional mobility may be linked to poor muscle strength, poor balance, slow gait speed, fear of falling, physical inactivity, and impairments relating to basic and instrumental activities of daily living. The significant longer STS time among the obese may indicate that obese alterations in dynamic postural control. Our results indicated that obesity does not appear to increase overall fall risk, although some postural control adaptations exist. Larger scale study is warranted to provide more insights in the fall risks of obese.

REFERENCES

1. Hills AP et al. *Obesity Reviews* 3(1), 35-43, 2002.
2. Fjeldstad C et al. *Dynamic Medicine* 7 (4), 27, 2008
3. Lajoie Y and Gallagher SP. *Archives of Gerontology and Geriatrics*, 38: 11-26, 2000.

Table 1: Results for obese and non-obese fallers and non-fallers

	Non-Obese		**Obese**	
Parameter	**Non-Fallers**	**Fallers**	**Non-fallers**	**Fallers**
ABC score	87.68±16.72	64.93±10.89	73.25±19.52	67.4±13.60
Walking Velocity ($m*s^{-1}$)	1.02±0.17	0.92±0.10	1.12±0.25	0.81±0.17
Sit to Stand Time (s)	2.80±1.29	3.70±1.71	4.96±2.05	5.84+1.85
Timed up and go completion time (s)	7.68±1.16	9.32±1.57	7.78±0.77	11.30±1.27
Gait Cycle Time (s)	0.92±0.27	1.16±0.14	0.91±0.23	0.95±0.24
Double Support Time (s)	0.23±0.11	0.28±0.12	0.18±0.12	0.28±0.18
Stance Time (s)	0.54±0.18	0.70±0.13	0.50±0.11	0.54±0.21
Swing Time (s)	0.41±0.07	0.43±0.09	0.43±0.06	0.41±0.10
Swing Angle (°)	32.64±5.33	33.94±5.02	31.29±6.63	28.85±6.60
Step Length (m)	0.41±0.07	0.44±0.07	0.39±0.09	0.38±0.08
Cadence ($step*min^{-1}$)	118.26±17.46	111.62±12.26	129.14±22.55	119.51±19.64

SPATIOTEMPORAL GAIT ANALYSIS OF TRANS-TIBIAL AND TRANS-FEMORAL AMPUTEES AT VARYING GAIT SPEEDS

[1]Morgan K. Boes, [1]Tut Tangtragulcharoen, [1]Richard M. Kesler, [2]Lee Nolan, and [1]Elizabeth T. Hsiao-Wecksler

[1]University of Illinois at Urbana-Champaign, Urbana, IL, USA
[2] Karolinska Institutet, Stockholm, Sweden; Jönköping University, Jönköping, Sweden
email: mboes2@illinois.edu

INTRODUCTION

It is widely known that amputees experience asymmetric gait patterns, i.e., increased swing time, decreased stance time, decreased swing velocity, and increased double support time of the prosthetic limb compared to the intact limb [1-7]. Symmetry of gait kinematics has been investigated in both trans-tibial [1, 2] and trans-femoral [3-5] amputees. Although the metrics used to evaluate symmetry vary across studies, there is general agreement that asymmetry exists in most aspects of amputee gait [2, 3, 6]. However, it is not well known how the amount of gait asymmetry varies as a consequence of amputation level and gait speed.

Few studies have compared asymmetry in trans-tibial and trans-femoral amputees [6, 7]. One used clinically based gait summary measures, finding that each summary measure varied significantly between levels of amputation [6].

A few studies have evaluated the effect of gait speed on amputation with mixed conclusions on the impact of an increased gait speed on gait asymmetries [2-4, 7]. Jaegers, *et al.* suggests that at a rapid walking speed there was less gait asymmetry than at a comfortable walking speed for trans-femoral amputees [4]. Yet, Isakov, *et al.* concludes that at a faster gait speed, temporal and distance parameters were significantly different than at a comfortable walking speed, but the inter-leg differences were not affected for trans-tibial amputees [2]. Nolan *et al.* found that asymmetry in temporal gait metrics decreased and ground reaction force increased with increasing gait speed [7].

This study aimed to determine the effect of level of amputation and gait speed on asymmetry of gait. We hypothesized that in order to walk as fast as possible the level of asymmetry in spatiotemporal gait characteristics (e.g. step width, step length, etc.) would decrease, and that the ability to adapt for faster walking by decreasing asymmetry will be greater in trans-tibial amputees (TT) than trans-femoral amputees (TF).

METHODS

Subjects
The subjects included eight unilateral trans-tibial amputees (4 females; age 38.9 ± 8.6 years (mean ± s.d.), time as amputee of 11.5 ± 12.6 years); seven unilateral trans-femoral amputees (2 female; 35.0±7.5 years of age with time as amputees of 7.9±7.2 years); and nine able-bodied persons (2 female; 32.2±4.0 years of age). All amputations were due to trauma or tumor. Ethical approval for the study was granted by the University Ethics Committee and subjects gave their informed consent.

Protocol
A ProReflex (Qualysis, Sweden) optoelectronic system was used with a 23 marker set for subject tracking. The subjects were asked to walk at three different speeds: comfortable, specified at 1.2m/s, and as fast as possible (AFAP). The speeds were measured by three photocell timing lights. The marker data were processed with a 4th order Butterworth filter in MATLAB (Mathworks, Waltham, MA) to calculate the spatiotemporal gait parameters.

Statistical Data Analysis
The able-bodied (AB) subjects were not used in the statistical analysis as their AFAP speed (2.1±0.6 m/s) was significantly greater than TF (1.4±0.2m/s, $p<0.001$) and TT (1.6±0.2m/s, $p<0.001$).

Four spatiotemporal gait metrics were examined: stance time, swing time, step length, and step width per limb. Comparison of gait metrics were analyzed with a MANOVA with two within-subject factors (3 speeds × 2 limbs) and one between-subject factor (2 amputation levels) (SPSS 20, IBM, New York). Significance level for the MANOA was set at $\alpha = 0.05$, with an adjusted value of $\alpha = 0.008$ for the univariate tests to account for the 6 within-subject factors. Borderline significance was defined as $0.008 \leq p < 0.05$ for the univariate tests. Gait asymmetry was assessed as a significant difference in standard gait parameters assigned to each limb (prosthetic or intact).

RESULTS AND DISCUSSION

As expected, asymmetries in kinematic gait behavior were observed between prosthetic and intact limbs, and changes in gait metrics were noted due to increasing gait speed (Table 1). Differences due to limb were decreased stance time (prosthetic: 0.66 ± 0.02s vs. intact: 0.74 ± 0.02s, $p < 0.001$) and increased swing time (prosthetic: 0.50 ± 0.01s vs. intact: 0.41 ± 0.01s, $p < 0.001$) of the prosthetic limb.

Contrary to our hypothesis, limited changes in asymmetries due to amputation level and gait speed were found. There was no group × limb × speed significance in any of the gait metrics, such that the level of asymmetry of amputee gait was not affected by gait speed and level of amputation. There were no significant differences between groups within a gait speed. The only differences seen based on group (TT vs. TF) were borderline significant in stance time and swing time ($p = 0.04$ and 0.04, respectively), suggesting that TF amputees spend more time in stance and less time in swing than TT amputees. There was a significant difference due to the interaction of group and speed in combined limb

TABLE 1: Average gait metrics as function of gait speed. P-value for main effect of speed.

	Comf. (m/s) TF: 0.8±0.0 TT: 0.9±0.0	Specified (m/s) TF: 1.1±0.0 TT: 1.2±0.0	AFAP (m/s) TF: 1.4±0.1 TT: 1.6±0.1	p-value
Stance Time (s)	TF: 0.87±0.11 TT: 0.80±0.10	TF: 0.72±0.03 TT: 0.66±0.5	TF: 0.62±0.06 TT: 0.55±0.05	< 0.001
Swing Time (s)	TF: 0.50±0.04 TT: 0.49±0.05	TF: 0.48±0.03 TT: 0.44±0.04	TF: 0.44±0.03 TT: 0.39±0.04	< 0.001
Step Length (m)	TF: 0.58±0.04 TT: 0.60±0.05	TF: 0.67±0.03 TT: 0.68±0.04	TF: 0.75±0.08 TT: 0.77±0.09	< 0.001
Step Width (m)	TF: 0.12±0.04 TT: 0.10±0.02	TF: 0.14±0.04 TT: 0.10±0.02	TF: 0.15±0.04 TT: 0.11±0.02	= 0.001

*All values are mean ± standard error

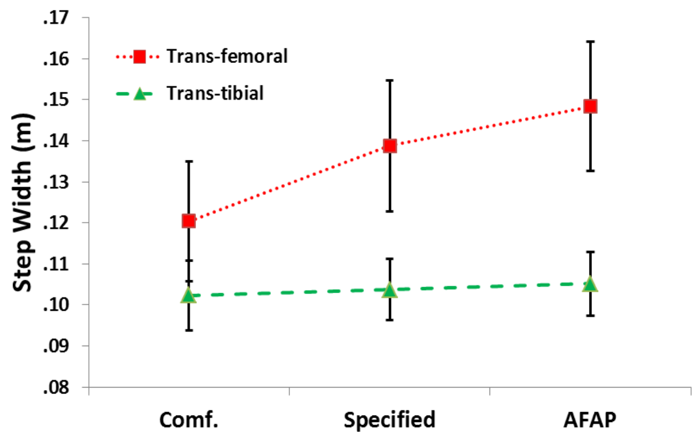

FIG. 1: Average (with standard error bars) step width differences in TF and TT groups for increasing gait speeds.

step width ($p = 0.008$). The TF amputees increased their step width significantly more than TT amputees as gait speed increased (Fig. 1).

CONCLUSIONS

There was no combined group × speed × limb effect in any standard gait metrics, which did not support our hypothesis such that neither amputee group adapted their gait for a faster pace by decreasing the asymmetry. Since the AFAP speed was self-selected, it could be that the subjects were uncomfortable walking at a speed fast enough to elucidate the reduction in asymmetry changes that were expected.

REFERENCES

1. Kovac, I., V. Medved, and L. Ostojic, Coll Antropol, 2010. **34 Suppl 1**: p. 205-13.
2. Isakov, E., et al., Prosthet Orthot Int, 1996. **20**(3): p. 153-8.
3. Roerdink, M., et al., Gait Posture, 2012. **35**(3): p. 446-51.
4. Jaegers, S.M., J.H. Arendzen, and H.J. de Jongh, Arch Phys Med Rehabil, 1995. **76**(8): p. 736-43.
5. Kaufman, K.R., S. Frittoli, and C.A. Frigo, Clin Biomech (Bristol, Avon), 2012. **27**(5): p. 460-5.
6. Kark, L., et al., Gait Posture, 2012. **35**(2): p. 238-43.
7. Nolan, L., et al., Gait Posture, 2003. **17**(2): p. 142-51.

ACKNOWLEDGMENTS

This work was made possible by the hard work of many people including Emily Morris and Shawna Culp.

EFFECT OF SHOE TREAD DEPTH ON HYDRODYNAMIC PRESSURES IN THE SHOE-FLOOR INTERFACE DURING SLIPPING

[1]Kurt Beschorner, [2]April J. Chambers, [2]Mark S. Redfern

[1]University of Wisconsin, Milwaukee, Milwaukee, WI, USA web: http://www.uwm.edu/gabl/
[2]University of Pittsburgh, Pittsburgh, PA, USA
email: beschorn@uwm.edu

INTRODUCTION

Fall accidents accounted for 15% of nonfatal occupational accidents in 2010 [1]. Shoe tread has been found to affect coefficient of friction [2]. Shoe tread is thought to provide drainage channels that prevent pressurized fluid from building up between the shoe and floor [3]. In addition, inadequate tread has been linked with slipping accidents in mail delivery industry [4]. While tread has been linked with higher friction, a gap currently exists regarding whether shoe tread can prevent pressurized fluid buildup during walking and slipping events. Several studies have theorized that hydrodynamic pressures are the critical mechanism causing a slip but no study to date has confirmed their existence during human slipping events [3]. The purpose of this study is to measure hydrodynamic pressures during human slipping events using fluid pressure sensors embedded in the floor. Hydrodynamic pressures and slip outcomes will be compared between treaded and untreaded shoes.

METHODS

Seventeen participants (10 female, mean ± standard deviation: age 23.5 ± 4.0 years, height 1.71 ± 0.072m, weight 70.0 ± 11.8 kg) were unexpectedly slipped while wearing either treaded or untreaded shoes. Subjects experienced one slip while wearing a treaded and an untreaded shoe. The shoes were advertised as slip-resistant footwear. Treaded shoes had the full tread intact (tread depth = 3 mm), while non-treaded shoes had the tread completely abraded from the shoe. Shoe order was randomized.

Slips were induced using a 90:10 glycerol: water solution that was applied to a 24” x 24” vinyl floor tile. At least five dry trials were collected before participants were unexpectedly slipped wearing the first type of shoes. After the first unexpected slip, at least fifteen dry trials with the second pair of shoes were collected to ensure participants returned to a normal gait. Participants listened to music between trails to prevent them from noticing the fluid contaminant being applied to the floor. Motion data were collected at 120 Hz using a 14 camera Vicon motion capture system. Hydrodynamic pressures were measured by fluid pressure sensors that were embedded just beneath the surface of the floor (Setra). The sensors were set up in a 3x3 grid and sensors were spaced 30 mm apart from each other. The starting point for the subject was aligned so that their foot would hit just behind the first row of sensors and slip or step across the sensors. Subjects wore a safety harness to prevent injury.

The primary variables of interest were the hydrodynamic pressures and the peak slip-velocity. Specifically, the maximum hydrodynamic pressure from each sensor was calculated. To more completely describe the hydrodynamic pressure profile, onset durations of hydrodynamic pressures were calculated. Onset was the first moment that the hydrodynamic pressure signal exceeded 5 standard deviations of baseline and offset was when it first dropped below 5 standard deviations of baseline. Peak slip velocity (PSV) was calculated as the maximum resultant velocity of the heel between the beginning and end of the slip. The beginning of the slip was defined as the first local minimum of the heel velocity after heel strike. Slip stop was defined as the first local minimum of the heel velocity after the slip. An ANOVA was performed to determine the effect of tread (independent variable) on the hydrodynamic pressures (dependent variable) and slip-severity (dependent variable). To determine whether hydrodynamic pressures varied medio-laterally across the shoe or during the progression of the slip, another ANOVA was performed with peak pressure as the dependent variable and sensor location as the independent variable.

RESULTS AND DISCUSSION

Untreaded shoes had higher hydrodynamic pressures and led to more severe slips. The average (standard deviation) peak hydrodynamic pressure was 124 kPa (75 kPa) for the untreaded shoes and 1.1 kPa (.29 kPa) for treaded shoes. The average PSV was 1.57 ± 0.80 m/s for untreaded shoes and 0.063 ± 0.017 m/s for treaded shoes. Hydrodynamic pressures were characterized by a single peak and durations were 86 ms (65 ms) in the untreaded conditions (Figure 1). In treaded conditions, hydrodynamic pressures were only observed in one slip for one sensor with duration of 36 ms. Assuming a sliding velocity of 1-1.5 m/s, this duration would correspond with a hydrodynamic pressures occurring over ~10 cm of the shoe surface.

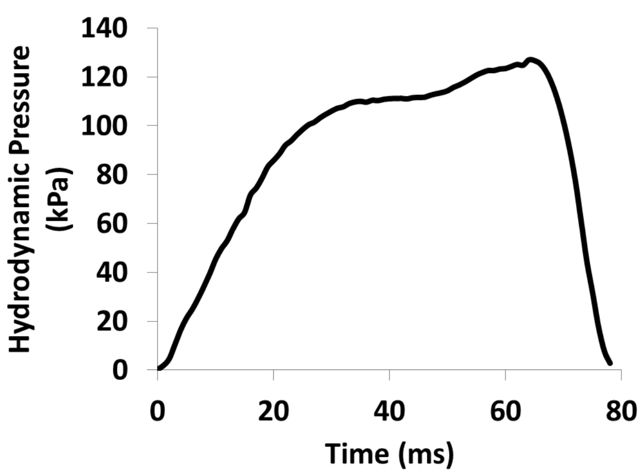

Figure 1: Representative time-series plot of hydrodynamic pressures as foot passes over the pressure sensor. Time=0 represents onset of the hydrodynamic pressures.

These results confirm the existence of hydrodynamic pressures in the shoe-floor interface during actual slipping events. Furthermore, shoe tread has a demonstrated effectiveness in reducing hydrodynamic pressures. Based on the duration of hydrodynamic pressures, tread over the posterior 10 cm of the heel appears to be critical to preventing slipping accidents. Previous researchers have suggested that slip-testing devices should be tribologically fidelic as part of being "biofidelic" (i.e., relevant to human slips). Comparing hydrodynamic pressures of slip-testing devices to human slips may be an approach for testing the devices' tribological fidelity.

Neither the sensor position nor the PSV were significantly correlated with peak hydrodynamic pressures. One explanation for a lack of correlation between sensor position and the hydrodynamic pressures is that the sensors were mapped to the flooring location as opposed to the shoe. Previous research by our group has shown that the highest hydrodynamic pressures occur centrally near the back of the foot [5]. Future analyses may benefit by correlating the position of the sensors to the foot during slipping to the hydrodynamic pressures. In addition, using the instantaneous velocity of the foot when over the sensor as well as other factors (vertical force, for example) may yield better correlation than peak slip velocity.

REFERENCES

1. U.S. Department of Labor- Bureau of Labor Statistics (2011). Nonfatal Occupational Injuries: Table 5.
2. Li KW, et al. *Applied Ergonomics* **37**, 743-748, 2006.
3. Chang et al. *Ergonomics* **44,** 1217-1232.
4. Bentley, T. and Haslam, R., 2001, *Applied Ergonomics* **32**, 127-134.
5. Singh, G. and Beschorner, K.E., 2013, *Ergonomics*, submitted.

ACKNOWLEDGEMENTS

The authors would like to thank Aaron Ledgerwood and Devon Albert for their assistance in data collection, processing and calculations of peak slip velocity. We would like to thank our funding source: NIOSH R01 OH008986.

BIOMECHANICS OF SLIPS AND FALLS OR RECOVERY IN THE ELDERLY AND YOUNG USING LOWER AND UPPER BODY CENTER OF MASS DYNAMICS

Aditya Jayadas and Rhonda L. Boros

Texas Tech University, Lubbock, TX, USA
e-mail: RL.BOROS@TTU.EDU

INTRODUCTION

During gait, the human body is in an inherent state of instability. The gait cycle begins with the initiation of gait, which is an unstable event since the whole body center of mass (WBCOM) is made to fall forward and outside the stance foot [1]. As the swing limb makes contact with the ground to initiate the role of weight acceptance, a high heel contact velocity could lead to a slip-induced fall [2]. When the heel begins to slide after making contact with a slippery surface, a slip-induced fall occurs when the WBCOM of an individual is thrown out of balance with respect to the BOS [3]. In terms of the WBCOM velocity, it has been reported that the WBCOM velocity of older individuals is slower when compared to younger individuals during a slip perturbation, suggesting that the elderly individuals use a slower and less effective reactive response [1]. The purpose of the current study was to explore a novel approach for studying the biomechanics of slips and falls using the dynamics of the lower body center of mass (LBCOM) and the upper body center of mass (UBCOM), and also determine if this approach is better at differentiating fallers and non-fallers as a result of a slippery perturbation.

METHODS

This study was conducted at the Ergonomics Laboratory in the Industrial Engineering Department at Texas Tech University. Twenty-eight healthy subjects (14 young, 14 elderly with equal numbers of males and females) participated in the study. The 14 elderly subjects ranged as follows in age (65-80y), height (1.56-1.93m) and mass (56.4-113.2kg). The 14 younger subjects ranged as follows in age (20-33y), height (1.63-1.88m) and mass (44.7-101.6kg).

Gait trials were performed on a circular track equipped with a fall arrest rig system. Subjects walked at their preferred walking pace over three different weeks and each individual was exposed to three unknown slips for a total of 84 trials. Motion data was captured at 120Hz using an 8-camera motion capture system from Motion Analysis Corporation (Santa Rosa, California, USA). Nineteen (19) reflective markers were used to create a whole body, upper body and lower body biomechanical model in order to summarize the motion of the whole body, the upper body and the lower body as individuals walked over unknown slippery surfaces. All the kinematics data were smoothed using a 4^{th} order zero lag Butterworth filter with a cut off frequency of 6hz. Resultant velocity differences (in the anterior-posterior and medio-lateral directions) for the WBCOM and heel, and the LBCOM and UBCOM were calculated for the duration of slip for all the slip trials, and grouped under "fallers" and "non-fallers" based on if a fall or recovery resulted from the slip event.

RESULTS AND DISCUSSION

14 trials were classified as 'falls' out of the 84 unknown slippery trials. The maximum velocity differences between the sliding heel and the WBCOM, and the LBCOM and UBCOM for the fallers and non-fallers are shown in *Figure 1* and *Figure 2* respectively.

The maximum velocity difference for the sliding heel and WBCOM between the fallers and non-

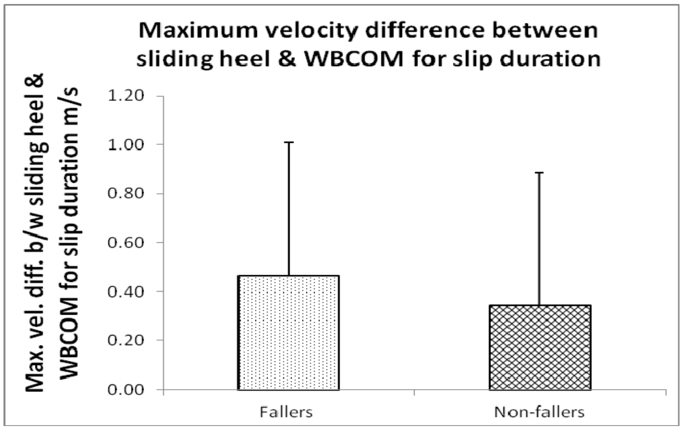

Figure 1: Max. diff. in vel. between the sliding heel and the WBCOM for slip duration.

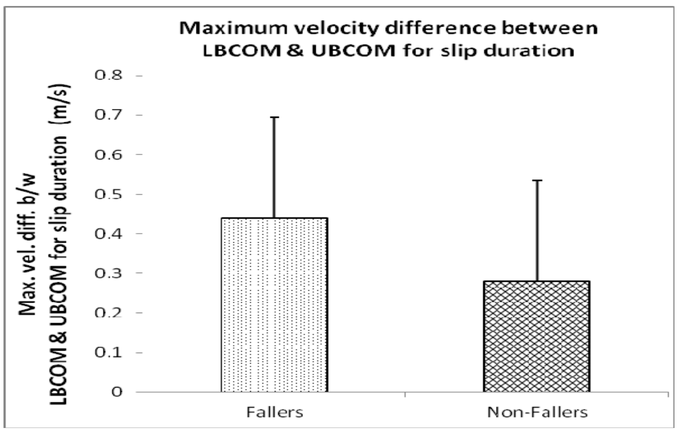

Figure 2: Max. diff. in vel. between the LBCOM and the UBCOM for slip duration.

fallers was found to be statistically insignificant (P=0.24). However, the maximum differences in velocity for the LBCOM and UBCOM between the fallers and non-fallers was found to be statistically significant (P=0.02). This suggests that the maximum difference in velocities between the LBCOM and UBCOM was able to better distinguish fallers and non-fallers, when compared to the maximum difference in velocities between the sliding heel and the WBCOM.

In addition, this new LBCOM-UBCOM velocity difference approach was able to also distinguish between older and younger fallers (P=0.03) and non-fallers (P=0.04) as shown in *Figure 3*. Older fallers experienced higher differences in velocity compared, and younger non-fallers demonstrated greater LBCOM-UBCOM velocity differences compared with older and were still able to recover.

This approach takes into consideration that the majority of the body's mass is in the trunk and upper body, and if individuals can quickly make their upper body “catch up” with their lower body when the feet are sliding under them, they may be able to recover. Also, using the LBCOM, simplifies the process in that the sliding and trailing leg dynamics are both taken into account using one variable rather than leading and trailing legs. In addition, no force plate is required.

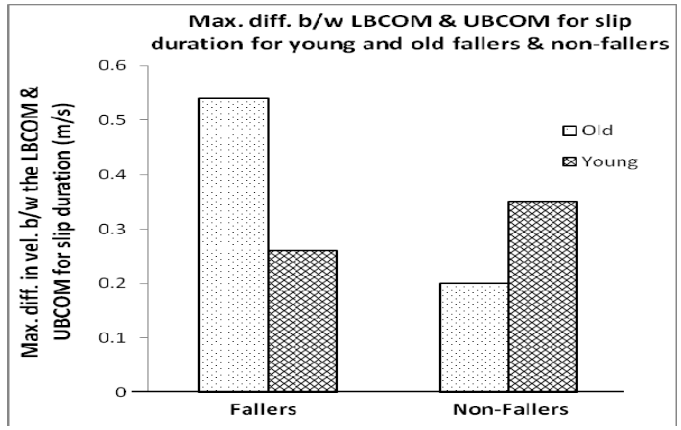

Figure 3: Max. diff. in vel. between the LBCOM and the UBCOM for slip duration for old and young fallers and non-fallers.

CONCLUSIONS

This study demonstrates that a simple variable such as the velocity difference between the LBCOM and UBCOM could be used as an alternative to the WBCOM-heel approach in better understanding the biomechanics of slips and falls in young and elderly individuals. The results from this study suggest that older individuals could benefit from exercise programs like Tai chi which use coordinated upper and lower body movement in order to move their upper body more quickly with respect to their lower body when they encounter a slippery surface.

REFERENCES

1. Lockhart, T. E., et al. *Ergonomics*, **46**, 1136-1160, 2003.
2. Winter, D. A. *Biomechanics and Motor Control of Human Gait*, University of Waterloo Press, 1991.
3. You, J., et al., *Clinical Biomechanics*, **16**, 167-173, 2001.

ORAL PRESENATIONS – FRIDAY SEPTEMBER 6th

	Upper Extremity: Orthopedic Mechanics & Modeling *Clark Dickerson, Katherine Saul*
4:00 PM	Optimizing Physiological Parameters For Modeled Upper Shoulder Muscles **Garner B, White J**
4:15 PM	The Effect Of Biceps Tension On The Glenoid Labrum In Shoulders Having Rotator Cuff Tears **Hwang E, Carpenter J, Hughes R, Palmer M**
4:30 PM	Development And Validation Of A Computational Multibody Model Of The Elbow Joint **Rahman M, Guess T, Johnson M, Cil A**
4:45 PM	Effect Of Forearm Posture On The Elbow Varus Torque Generated By The Flexor Pronator Muscles: Implications For The Ulnar Collateral Ligament **Buffi J, Murray W**
5:00 PM	The Effect Of Material Model, Element Formulation And Bone Marrow Inclusion On The Accuracy Of An Explicit Finite Element Model Of The Distal Radius **Burkhart T, Dunning C**

OPTIMIZING PHYSIOLOGICAL PARAMETERS FOR MODELED UPPER SHOULDER MUSCLES

Brian Garner and Joel White

Baylor University, Waco, TX, USA
email: brian_garner@baylor.edu

INTRODUCTION

In the development of a previous musculoskeletal model of the human upper extremity[1], physiological parameters of muscles actuating the wrist, elbow, and shoulder were optimized to match known muscle volumes and experimentally-measured joint moments over a wide range of motion for every joint[2]. At the time, experimental measurements of strength in the upper shoulder girdle were not available, and so the physiological parameters of upper shoulder muscles could not be effectively optimized or verified. The aim of the present study was to remedy this weakness in the previous model by optimizing the modeled upper shoulder muscles based on experimental data of shoulder shrugging strength reported in a more recent publication[3].

METHODS

The previous upper extremity model was cropped to include nine degrees-of-freedom for the clavicle, scapula, and humerus, actuated by 21 muscle bundles representing upper shoulder muscle groups including serratus anterior, trapezius, rhomboids, pectoralis major, and latissimus dorsi. Contact between the scapula and thorax was enforced with a kinematic constraint. Muscle paths were modeled using obstacle sets, and muscle physiology was modeled using Zajac's four parameters: peak isometric force, optimal fiber length, tendon slack length, and pennation angle. Pennation angles were taken from the literature, while values for the other three parameters were optimized in this study.

The model was used to simulate twelve maximal isometric shoulder shrugging exercises performed in the experimental study[3]. These exercises consisted of four directions of shrugging motion: elevation, depression, protraction, and retraction, with three positions for each (e.g., elevation exercise at depressed, middle, and elevated positions). The model was tasked to activate all muscles contributing to each exercise, and to compute the resulting isometric output force applied at the end of the humerus against a resistance load (Figure 1).

Optimization of muscle physiological parameters was performed using steepest-descent algorithms set to minimize summed-squared error between the simulated and measured output forces over all twelve exercises. As in the previous model, muscle parameters were limited to match known muscle volumes. For simulated elevation and depression exercises the modeled elevation position was prescribed to match the experimental positions, while the protraction position was adjusted by the optimizer. For simulated protraction and retraction exercises the protraction position was prescribed while the elevation position was adjusted.

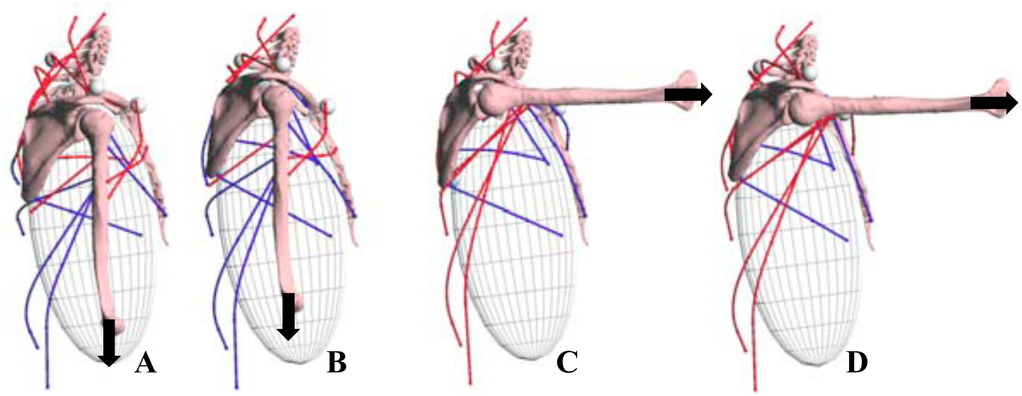

Figure 1: Model simulations of elevation exercises in depressed (A) and elevated (B) positions, and retraction exercises in retracted (C) and protracted (D) positions. Black arrows represent the isometric resistance load. Modeled muscle bundles are shown as red (activated) and blue (relaxed) lines. White balls represent markers used to measure and prescribe positions.

RESULTS AND DISCUSSION

The model was able to position itself to match the experimental positions within about 1 mm of lateral acromion displacement for all exercises. The model also exhibited the monotonically varying strength patterns over the three positions of each exercise direction (Figure 2) that was observed in the experimental data. For example, both measured and simulated elevation strengths tended to decrease in magnitude as shoulder girdle position was moved from a more depressed position to a more elevated position (Figure 2, left plots).

Optimization of the physiological parameters improved the model's ability to reproduce the experimental shoulder shrugging strengths. When the physiological parameters of the initial model were used, the simulated shoulder shrugging strengths varied on average from the experimental strengths by about 28%, 37%, 59%, and 12% for elevation, depression, protraction, and retraction exercises, respectively (Figure 2, blue triangles). After optimization, these errors were reduced to about 3%, 3%, 18%, and 7%, respectively (red x's).

The model had particular difficulty reproducing the magnitudes of output forces measured for the protraction exercises. The experimental magnitudes were on average about 1,330 N, but the optimized model was only able to achieve on average about 1,080 N. Modeled muscle moment arms of the serratus anterior and pectoralis muscles are suspected as contributing to the lack of strength in the protraction direction.

An analysis was performed to investigate whether the difficulty in matching protraction strengths may have affected the computation of muscle parameters for the other exercises. In this analysis the modeled muscle parameters were optimized to match only the experimental strengths of elevation and depression. As shown in Figure 2, this approach resulted in no appreciable change in the simulated shrugging strengths (compare green boxes and red x's).

CONCLUSIONS

Optimization of muscle physiological parameters to match experimental data improved the strength performance of an upper shoulder model, but the model remains weak in the direction of protraction.

REFERENCES

1. Garner, BA, Pandy, MG. *Comp Meth Biomech Biomed Engineering* **4**, 93-126, 2001.
2. Garner BA, Pandy MG. *Annals of Biomedical Engineering*, **31**, 207-229, 2003.
3. Garner, BA, Shim, J. *Clinical Biomechanics* **23**, 30-37, 2008.

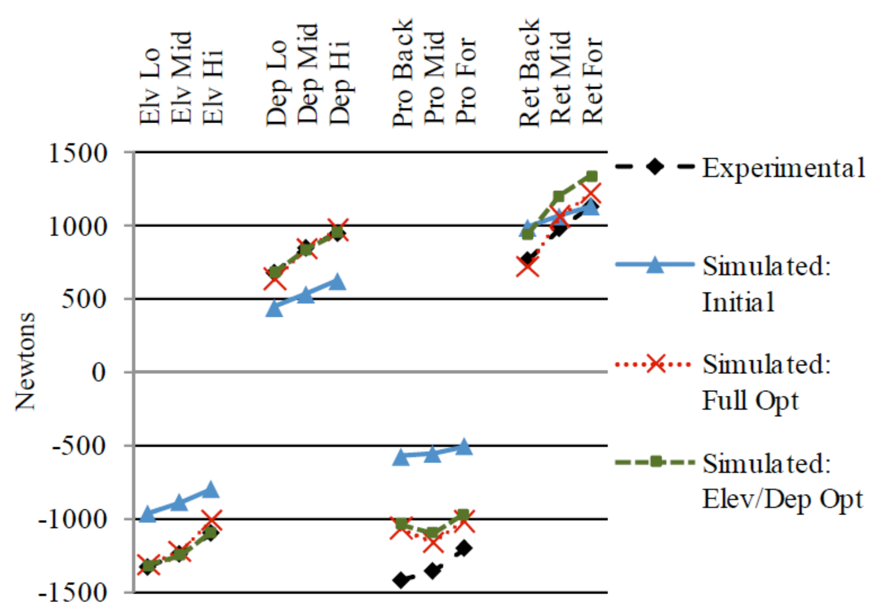

Figure 2: Experimental and simulated isometric shoulder shrugging forces for twelve exercises including elevation and depression at high, middle, and low positions, and protraction and retraction at forward, middle, and back positions. Simulations were performed using the muscle physiological parameter values of the original upper shoulder model (Initial), parameters optimized to minimize error between measured and modeled shrugging forces over all twelve exercises (Full Opt), and parameters optimized to minimize error for only the elevation and depression exercises (Elev/Dep Opt).

THE EFFECT OF BICEPS TENSION ON THE GLENOID LABRUM IN SHOULDERS HAVING ROTATOR CUFF TEARS

Eunjoo Hwang, James E. Carpenter, Richard E. Hughes, and Mark L. Palmer

University of Michigan, Ann Arbor, MI, USA
email: mlpalmer@umich.edu

INTRODUCTION

Rotator cuff tears, the most common injury in shoulder joints, are often accompanied by secondary tears in the superior glenoid labrum [1]. While this high incidence of superior labral pathology has been described in association with rotator cuff pathology, the significance and mechanism of this finding is unclear.

Because the long head of the biceps tendon (LHB) forms a continuous structure with the superior labrum, the LHB has been implicated in the pathogenesis of superior labral injuries [2]. Therefore, we hypothesize that superior humeral head translation, as can be seen in rotator cuff disease, combined with loading on the LHB tendon leads to increased displacement and strain of the superior labrum.

METHODS

Mechanical tests were performed using six shoulders obtained from fresh-frozen cadavers (avg. age=51.7 years, range=47-55) having no evidence of shoulder pathology. Specimens were dissected free of all soft tissue, except for the labrum-LHB complex and articular cartilages. The humerus was positioned in 30˚ of abduction in the scapular plane with 0˚ humeral rotation. A compressive force of 50N in the medial direction was applied to seat the humeral head in the glenoid cavity [3]. Next, a tension load of either 0N or 22N was applied to the LHB tendon. A 22N load was chosen because this magnitude was shown to affect glenohumeral range of motion and kinematics [4]. Finally, the humerus was translated relative to the glenoid by 5mm in the superior direction at a rate of 1mm/sec. This amount of displacement encompasses the range of humeral head translations encountered in patients with rotator cuff disease (excluding massive tears) [5]. Paired beads were affixed to the superior labrum and the glenoid surface, according to the six angular positions (Fig. 1, inset), but the beads on both AB and PB had the same reference bead. Serial radiographs captured the position of the beads to determine the displacement of the superior labrum.

A subject-specific, dynamic finite element (FE) model was developed using a shoulder from a fresh frozen cadaver (84-years-old) prepared similarly to the mechanical testing specimens. The specimen was then scanned using a micro-CT system at a voxel size of 93 microns, segmented using Amira®, and converted to a hexahedral mesh using Hypermesh®. Material properties were assigned based on previous studies [6,7]. To simulate the appropriate vector of the LHB tension, hexahedral elements were added to the distal end of the labrum-LHB complex by following a path through the biceps groove. Boundary conditions matched those of the experiment. However, two additional cases of 55N and 88N were chosen for the LHB tendon to represent the force of maximum isometric contraction calculated from the physiologic cross-sectional area of muscle [8] and the peak force during stretch of an activated muscle [5], respectively. The FE analyses were performed using LS-DYNA®. Both mesh convergence and parameter sensitivity analyses were performed on the model. The outputs from the model were the displacements and the tissue strains in the superior labrum at the locations corresponding to the beads in the mechanical tests.

RESULTS AND DISCUSSION

The tension on the LHB significantly affected the magnitude of the labral displacement (P=0.0002) and the location of the peak displacement. The predicted FE data fell within 1 standard deviation of experimental data. Both the mechanical test and the model showed when the LHB load increased from 0N to 22N, there was a posterior shift in the location of the greatest displacement from the AB to the PB location (Fig. 1). Similarly, the 55N and 88N LHB loading conditions caused both an increase and a posterior shift in the predicted displacements.

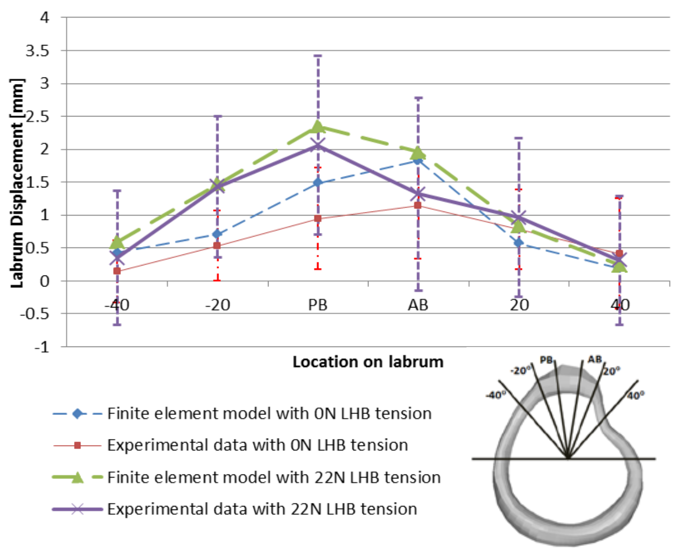

Figure 1: The displacement profile of the superior labrum determined from the FE model and experiments (average ± 1 standard deviation) for 5mm of superior humeral head displacement with 0N and 22N LHB tension.

Increasing LHB tension also increased the strain in the superior labrum by a factor of 43% (Fig 2). The region of the labrum with the highest strain occurred in the origin of LHB (0°, Fig. 2, inset) in the superior labrum and it was independent of the magnitude of the LHB. The high strain around the 20° location is explained by the small cross-sectional area in that portion of the labrum.

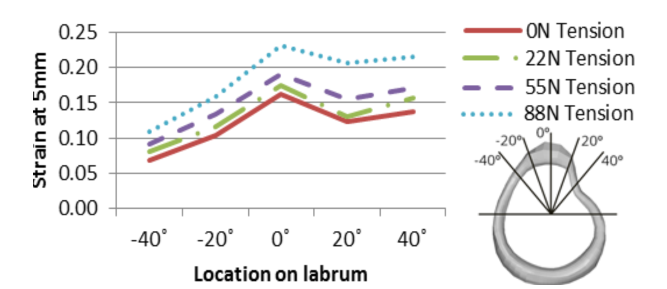

Figure 2: The average strain through the cross section of the labrum on the labral location.

The strain in the PB and AB locations were relatively low in the 0N case compared to the 88N case (Fig. 3). The high strain pathway from the origin of the LHB to the interface between the glenoid bone and cartilage was demonstrated in the labrum with 88N of LHB tension. The strain distributions in the 22N and 55N tension conditions were similar to that in the 88N case.

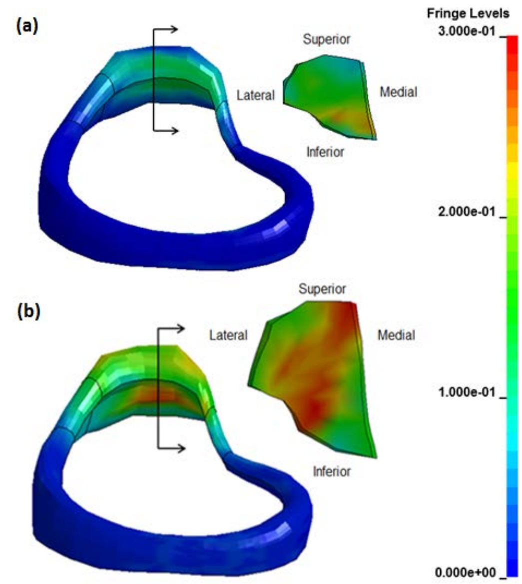

Figure 3: The strain plots for 5mm of superior humeral head displacement with (a) 0N and (b) 88N of LHB tension.

CONCLUSIONS

This study supports the hypothesis that tension on the LHB increases displacement and strain of the glenoid labrum in shoulders with rotator cuff disease. Increasing the LHB tension caused a posterior shift in the location of peak displacement and strain. Additionally, the area of the highest predicted strain in the labrum with LHB tension correlated well with the clinical presentation of the most common superior labral pathology. Therefore, high LHB tension may contribute to injuries of the superior labrum in patients with rotator cuff disease.

REFERENCES

1. Kim TK, et al. *JBJS [Am]* **85A**, 66-71, 2003.
2. Bey MJ, et al. *JSES* **7**, 397-401, 1998.
3. Gatti CJ et al. *ABE* **38,** 3766-3776, 2010.
4. Youm T, et al. *JSES* **18**, 122-129, 2009.
5. Keener JD, et al. *JBJS [Am]* **91**, 1405-1413, 2009.
6. Henak CR, et al. *J Biomech* **44**, 2201-2206, 2011.
7. Smith CD, et al. *J Anat* **21**, 49-54, 2008.
8. Su WR, et al. *Arthroscopy* **26,** 578-586, 2010

DEVELOPMENT AND VALIDATION OF A COMPUTATIONAL MULTIBODY MODEL OF THE ELBOW JOINT

Munsur Rahman, Trent M. Guess, Ph.D., Michael Johnson, M.D., Akin Cil, M.D.

University of Missouri-Kansas City, MO, USA
e-mail: guesstr@umkc.edu, web: http://sce.umkc.edu/~guesstr/

INTRODUCTION

The human elbow joint is a unique joint that produces complex motion of the forearm needed for positioning of the hand. This joint is the second most commonly dislocated joint in adults [1], but compared to the lower limb, elbow injuries and disorders have relatively little evidence related to treatment. Computational multibody modeling can be used as a versatile tool to study the elbow joint. The purpose of this study was to develop and validate an anatomically correct computational elbow joint model that includes representation of articular cartilage, multiple ligament bundles having non-linear toe region, as well as wrapping around bone of the lateral ulnar collateral and annular ligaments. Biomechanical computational models of the elbow exist in the literature, but these models are typically limited in their applicability by assuming joint structure having particular degrees of freedom, prescribing specific kinematics, simplifying ligament characteristics or ignoring cartilage [2, 3].

METHODS AND MATERIALS

Three fresh frozen cadaver elbows were used for this study. The humerus head was cemented inside a cylinder that was attached by a hinge joint to the top ram of a bi-axial mechanical tester (Bose ElectroForce3510-AT) constrained in the vertical direction. The ulna was also fixed to a cup that was connected to the rotating arm of torsion motor via a universal joint. The wrist and hand was disarticulated and the remaining forearm with intact distal radioulnar joint was free from any external mechanical constraint. The triceps tendon was exposed and a suture was used to connect the tendons to 100N load cell attached to the humerus cylinder. Four infrared rigid body markers of an Optotrak Certus system (Northern Digital, Inc., Waterloo, ON, Canada) were firmly attached to the humerus, radius, ulna, and humerous cylinder. The initial position and orientation of cadaveric bone geometries relative to the dynamic simulator were recorded using an Optotrak system. The elbow joint was positioned at a flexion angle of 103^0 before starting the experimental tests (Fig **1**a). A motion profile of 50mm vertical displacement was provided by the machine producing a flexion angle between 97^0 to 112^0. Bone motion as well as triceps tendon forces were recorded during the test. After test completion, the elbow was dis-articulated and points around the origin and insertion sites for the medial collateral ligament (MCL), lateral collateral ligament (LCL), annular ligament, and triceps tendon were collected with an Optotrak digitizing probe.

Three dimensional geometries of the bone were created from medical images. The bone geometries and ligament insertion/origin points were then aligned in the multi-body modeling software ADAMS (MSC Software Corporation, Santa Ana, CA) by using the initial position and point clouds of each bone obtained during experiment (Fig 1**b**). The ligaments and tendons were modeled as non-linear springs using a piecewise function describing the force–length relationship [4]. A subroutine was written in ADAMS to describe this relationship that was derived from the ligament force as a function of strain, the measured zero-load length (the lengths at which ligament bundles first become taut) and the ligament stiffness. The zero-load length of each bundle was determined by calculating the maximum straight-line distance between insertion and origin sites throughout the experimentally measured full range of motion and then applying a correction percentage (80% for each ligament bundle). The cartilages geometries were modeled as rigid bodies of 0.5 mm uniform thickness from the bone surface. Contacts were applied between cartilage geometries using a contact function in Adams that allows for interpenetration of the geometries to simulate deformable contact [5]

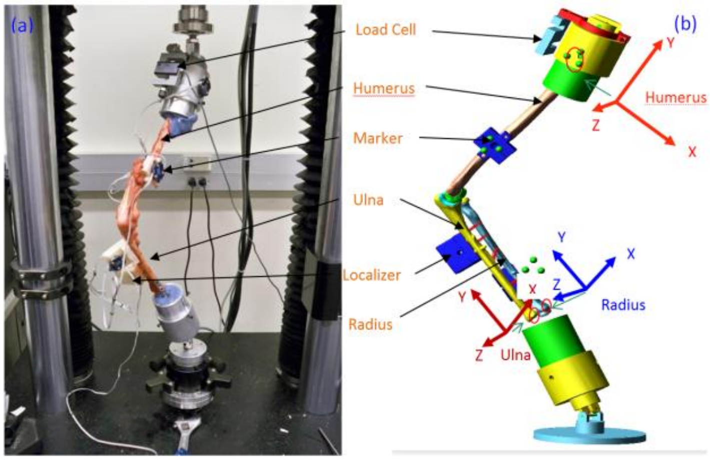

Fig. 1: (**a**) Cadaver elbow in the mechanical tester (**b**) Multi-body model of the elbow. Also shown are the humerus, ulna, and radius coordinate system.

RESULT

Model predicted kinematics of the ulna and radius relative to humerus were compared to experimental motion. Triceps tendon forces were also compared (Fig. **2**). Local coordinate systems for each segment were created as described by Wu *et al.* in International Society of Biomechanics (ISB) recommendation [6].

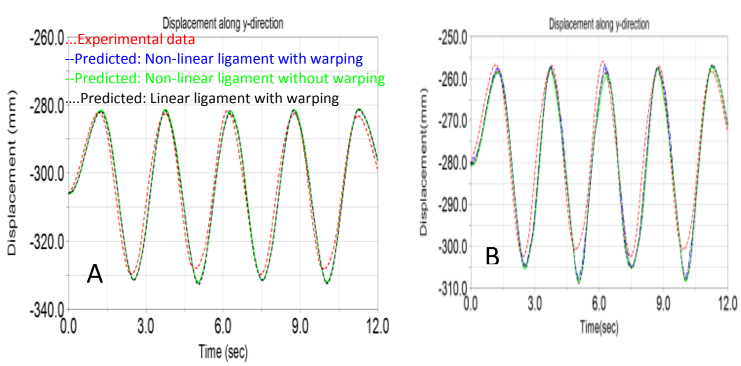

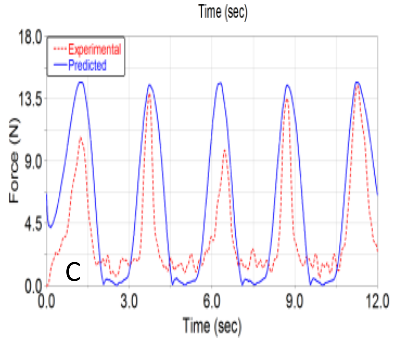

Fig.2: Comparison between predicted and measured kinematics of the ulna coordinate system (A) and radius coordinate system(B) relative to the humerus coordinate system in y-direction for Elbow#1.Also shown is the comparison of triceps tendon forces(C).

Table 1: RMS error between predicted and measured value obtained from Fig.2

	Ulna Coordinate	Radius Coordinate
Warping with Non-linear	3.3	4.0
Warping with Linear	3.4	4.4
No warping with Non-linear	3.4	4.7
Triceps tendon	3.9	

DISCUSSION

The main aim of this study was to create and validate an anatomically correct subject specific computational multibody model of the elbow joint. The key advantages of this model are the ability to predict parameters that are difficult to capture experimentally such as forces within ligaments and contact forces between cartilages covered bones. A small improvement in kinematics, compared to experimental measurements, was seen when the ligaments were taken as multiple bundles versus single elements. Some reductions of RMS error were also observed when non-linear with toe region ligament assumption was compared with previously studied linear without toe region ligaments [2, 3]. Future work includes modeling the cartilage as discrete elements so that contact pressure can be predicted, modeling more ligament wrapping around the joint, and adding muscle forces. The model is the first step in developing a musculoskeletal model of the elbow joint. The developed model will then be used for subject specific full musculoskeletal movement simulations of the upper-extremity.

REFERENCES

[1] J. de Haan, et al. *Open Orthop J*, **5**, pp. 168-76, 2011 **[2]** J. P. Fisk,et al.*Ann Biomed Eng*, **37**, pp. 803-12, 2009. **[3]** R. V. Gonzalez,et al.*J Biomech Eng*,**118**, pp. 32-40,1996. **[4]** J. Wismans,et al, **13**, pp.677-85, 1980. **[5]** A. P. Stylianou,et al.*Comput Methods Biomech Biomed Engin*, 2012. **[6]** G. Wu, et al. *J Biomech*, **38**, pp. 981-992, 2005.

ACKNOWLEDGEMENTS

This research is funded by the School of Medicine, University of Missouri-Kansas City.

EFFECT OF FOREARM POSTURE ON THE ELBOW VARUS TORQUE GENERATED BY THE FLEXOR PRONATOR MUSCLES: IMPLICATIONS FOR THE ULNAR COLLATERAL LIGAMENT

[1,3]James Buffi and [1,2,3,4]Wendy M. Murray

Departments of [1]Biomedical Engineering and [2]PM&R, Northwestern University, Chicago, IL
[3]SMPP, Rehabilitation Institute of Chicago, Chicago, IL; [4]VA Hines, Hines, IL
email: jamesbuffi2013@u.northwestern.edu
web: http://www.smpp.northwestern.edu/research/arms/index.html

INTRODUCTION

Overhead throwing is the primary task for athletes who play the position of pitcher in the sport of baseball. While pitching, extreme levels of valgus torque are generated at the elbow and this creates stress on the elbow structures opposing valgus loads, including the ulnar collateral ligament (UCL) [1]. Accordingly, extreme valgus torque has been highly correlated with serious elbow injury [2].

Previous work has demonstrated that the flexor pronator muscles of the arm (Flexor Digitorum Superficialis, Flexor Carpi Radialis, Flexor Carpi Ulnaris, and Pronator Teres) are primary contributors to varus torques that counter applied valgus torques [3, 5]. These muscles originate on the ulnar side of the distal humerus and have been shown to be highly active during pitching [4]. Additionally, experimental work in cadavers has revealed that tension in these muscles relieves stress on the UCL and can protect it from failure [5].

While research studies have effectively established that the flexor pronator muscles are capable of adding stability to the elbow joint, these analyses have focused on a single, neutral, forearm posture [e.g., 3]. This is problematic for understanding the potential for these muscles to reduce injury risk in pitching because baseball players modify forearm posture to throw different pitches [6]. Moreover, pitches that require a supinated forearm, such as the slider, have been associated with a large increase in elbow injury risk [7].

The purpose of this study was to use a biomechanical model to quantify the effect of forearm posture on the capacity of the flexor pronator muscles to generate varus elbow torque. We hypothesized that specific forearm postures would reduce the varus torque capacity, thereby increasing the risk of UCL failure in those postures.

METHODS

To evaluate the effect of forearm posture on the elbow varus torque generated by the flexor pronator muscles, we modified an existing biomechanical model [8] to include a varus axis of rotation at the elbow. Using this model, we calculated the isometric elbow varus torque produced by each muscle as a function of forearm pronation-supination angle. Analyses were completed using the Software for Interactive Musculoskeletal Modeling (SIMM; Musculographics, Inc.; Santa Rosa, CA). We then used a varus-valgus torque balance to examine how different levels of muscle torque would impact the load on the UCL and the risk of ligament failure.

We implemented the axis of rotation for varus-valgus used in the elbow model described by Buchanan et al. (1998) and calculated the isometric elbow varus torques generated by each of the four forearm flexor pronator muscles at (i) its activation level observed during pitching [4], and (ii) maximum activation. Muscle torques were calculated at one degree increments across the full range of motion for pronation-supination while the elbow was positioned at 90˚ of flexion, the approximate elbow posture adopted while pitching [6]. An individual muscle torque (T_i) was calculated as the product of muscle force (F_i) at the appropriate activation level (α), and moment arm (L_i). That is,

$$(1) \quad T_i(F_i, L_i) = \alpha F_i(l_m(\theta)) * L_i(\theta) ,$$

where the modeled muscle force varies with fiber length (l_m), which varies with forearm rotation angle (θ) [8]. The total, isometric, varus torque produced by the flexor pronator muscles (T_{mus}) was computed as the sum of the individual torques.

We used a torque balance about the varus axis to estimate the torque load imposed on the UCL for both muscle activation patterns evaluated. A preliminary cadaveric study (in which muscles were removed via dissection) reported that external valgus loads (T_{val}) were opposed by the UCL (T_{UCL}), the joint capsule (T_{cap}), and the osseous structures of the joint (T_{oss}) [9]. Thus,

$$(2) \quad T_{UCL} = T_{val} - T_{mus} - T_{cap} - T_{oss} \;,$$

given the capacity of the flexor pronator muscles to generate a stabilizing varus torque (T_{mus}). The cadaveric study reported that the joint capsule and the osseous structures generated a torque equal to 43% of the applied load [9]. Assuming loading of these structures maintains this proportion across valgus loads, an external valgus load of 100 Nm, and the isometric torque-angle profiles calculated using the biomechanical model, we solved for the resulting T_{UCL}. Valgus loads during pitching have been reported to range from 64 to 120 Nm [1].

To quantify the risk of UCL failure, we calculated a safety factor for the UCL as the ratio of the torque associated with UCL failure (34 Nm) [10] to T_{UCL}. Thus, at a safety factor of 1, the UCL experiences its failure torque.

RESULTS AND DISCUSSION

During pitching, it has been shown that the forearm angle is often between 13˚ and 25˚ supination [6], which corresponds to between 23 Nm and 24 Nm of varus muscle torque, assuming the muscle activation levels used during pitching (Fig. 1). For varus muscle torques in this range, the UCL safety factor ranged between 1 and 1.03. Supination beyond 25˚ further decreased the muscle varus torque, suggesting the UCL would experience loads greater than the reported failure limit. To achieve a UCL safety factor of 8, which is considered typical of ligaments [11], the muscles must exert 53 Nm of torque in a supinated posture. Even at maximum activation, the muscles exerted at most 32 Nm in a pronated position, which would correspond to a UCL safety factor of only 1.4 and a forearm position not typically used during pitching (Fig. 1).

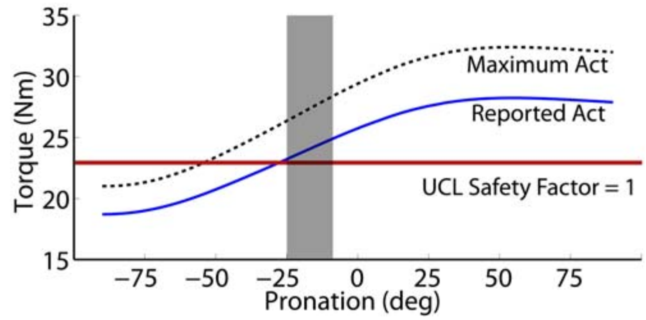

Figure 1. Total isometric varus muscle torque vs. forearm angle at muscle activations reported for pitching (blue curve) and at maximum activations (black dotted curve). Negative angles indicate supination. The shaded gray area represents the range of postures often used when pitching. The red line represents the muscle torque level that results in a UCL safety factor of 1.

A limitation of our study is that pitching is a dynamic task, while our study was a quasi-static analysis. However, changes in the kinematics of the arm would result in changes to the torque capacity regardless of the dynamics of the system.

CONCLUSIONS

Regardless of forearm posture, our biomechanical analysis suggests a 100 Nm valgus load at the elbow is associated with dangerous levels of loading for the UCL. Our results are consistent with a study that reported serious elbow injuries occur to pitchers who experience this loading level [2].

REFERENCES

1. Fleisig GS, et al. *Am J Sports Med*, **23**, 233-239, 1995
2. Anz AW, et al. *Am J Sports Med*, **38**, 1368-1374, 2010.
3. Buchanan TS, et al. *J Biomech Eng*, **120**, 634-639, 1998.
4. Hamilton CD, et al. *J Shoulder Elbow Surg*, **5**, 347-354, 1996.
5. Lin F, et al. *J Shoulder Elbow Surg*, **16**, 795-802, 2007.
6. Fleisig GS, et al. *Am J Sports Med*, **34**, 423-430, 2006.
7. Lyman S, et al. *Am J Sports Med*, **30**, 463-468, 2002.
8. Holzbaur KRS, et al. *An Biomed Eng*, **33**, 829-849, 2005.
9. Morrey BF and KN An. *Am J Sports Med*, **11**, 315-319, 1983.
10. Ahmad CS, et al. *Am J Sports Med*, **31**, 332-337, 2003.
11. Butler DL, et al. *J Biomech Eng*, **122**, 570-575.

ACKNOWLEDGEMENTS

This work was funded by NIH R01 HD046774.

THE EFFECT OF MATERIAL MODEL, ELEMENT FORMULATION AND BONE MARROW INCLUSION ON THE ACCURACY OF AN EXPLICIT FINITE ELEMENT MODEL OF THE DISTAL RADIUS

[1]Timothy A. Burkhart, [1]Cynthia E. Dunning

[1]Western University, London, Ontario, Canada
email: tburkhar@uwo.ca

INTRODUCTION

Explicit finite element modeling (FEM) of human bone tissue has a wide of range of applications in the field of orthopaedics. One example is the analysis of forward fall (impact) initiated distal radius fractures. Finite element modeling is a relatively feasible alternative to expensive and destructive cadaveric testing and by-passes the many safety issues associated with *in vivo* testing of forward falls [1].

Although the prevalence of finite element modeling applications in biomechanics, bioengineering and orthopaedics has grown exponentially (by more than 6000%) over the last 20 years [1] the attention to model validation and verification however, has not kept pace. This is particularly worrisome given the consequences of utilizing inaccurate data in these fields.

It is generally accepted that certain element formulations provide more accurate data than others (single integration point vs. full integration). However, despite work [1] that has eloquently stressed the importance of performing validation and verification studies the interaction of element formulation with different material models and the inclusion/exclusion of bone marrow is less well understood. Therefore, the purpose of this work was to determine the optimal combination of element formulation material model, and bone marrow inclusion on the accuracy of explicit FEM predictions at the distal radius.

METHODS

A previously developed and validated finite element model of the distal radius (Figure 1a) was used for the simulations presented here [2]. Briefly, this model consisted of 1.4 million 8-node hexahedral elements. All three bone components (cortical, cancellous and marrow) were considered and meshed separately (Figure 1b). Cortical bone material properties were calculated from a three point bending test (specimen specific), while those of cancellous and cortical bone were adopted from the literature. The material models of the bone marrow and foam were kept constant as linear elastic and all components of the impactor were modeled as rigid stainless steel.

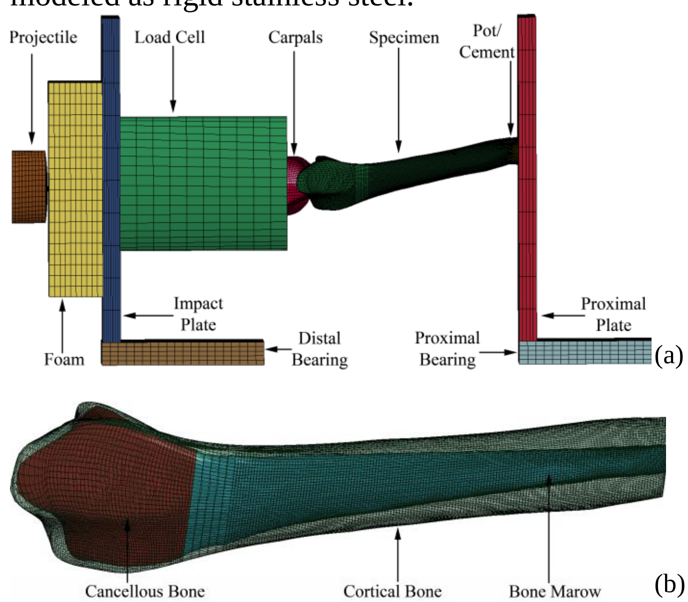

Figure 1: (a) Modeled components of the experimental set-up and (b) a detailed view of the three bone components.

Two different bone material models were assessed - elastic-plastic (EP) and elastic-plastic with failure (EPF). The difference between these two models is that EPF incorporates material softening and deletes an element when the ultimate failure strain is exceeded. Two element formulations were used (constant stress single integration and fully integrated selectively reduced) and all simulations accounted for strain rate effects through a Cowper-Symonds scaling factor [2]. Finally, to determine the role of bone marrow, simulations were conducted with and without the marrow present. Simulations were performed in LS-DYNA® using all combinations of the above parameters

To determine the accuracy of each parameter combination, a validation metric (VM) (Eq.1) [3] and percent differences were calculated for the axial force component (Fz) measured at the load cell and the minimum and maximum principal strains measured proximal to the radial styloid. Modeling results were compared to previously collected specimen specific outputs [4].

$$VM = 1 - \frac{1}{N}\sum_{n=0}^{N} \tanh\left|\frac{y(t_n) - Y(t_n)}{Y(t_n)}\right| \qquad \text{(Eq.1)}$$

RESULTS AND DISCUSSION

Overall, 4 of the 16 simulations were excluded (all were full integration models) as a result of unrealistic computation time (> 200hrs) or negative volume errors. On average examination of the Fz forces shows that EP, single integration point, and marrow-included models all resulted in the highest average validation metrics and lowest % errors (Table 1). However when the parameters were assessed in combination, the EP/no-marrow/single integration model showed the best agreement with experimental data (VM=0.43) and a relatively low % difference (6.6%).

When concerned with the maximum principle strains, the mean EPF, no marrow and full integration conditions had the highest and lowest VM and % differences respectively (Table 1). The combination of parameters with the highest VM (0.53) was the EPF/no-marrow/single integration model. Finally, the mean VMs were the greatest across the EP, no marrow and fully integrated parameters with respect to the minimum principle strains (Table 1) with the best combination of parameters found to be EP/no-marrow/full integration (VM=0.67, difference = 24%).

Validation metrics were similar for all tests performed and there was no correlation to the % differences. This highlights the importance of performing multiple validation measurements that are consistent with the desired application of the model. When considering the computational time, it does not appear that fully integrated elements provide an advantage, contrary to popular belief.

CONCLUSIONS

When taken together, the results suggest that an explicit model of the distal radius can be modeled as elastic plastic without bone marrow and adopting single integration. In any case, it is important that careful consideration is given to these parameters as well as the final application of the modeling results.

REFERENCES

1. Cristofolini L, et al. *Philos Trans A* **368**, 2725-2763, 2010.
2.Burkhart TA, et al. *Proceedings of CSB* Vancouver, BC, Canada, 2012.
3.Oberkapf WL, et al. *Prog Aerosp Sci* **38**, 209-272, 2002.
4.Burkhart TA, et al. *J Orthop Res* **30**, 885-892, 2012.

Table 1: Mean validation metrics (VM) and % differences across each parameter

Parameter	Computational Time (hrs)	Fz VM	Fz % Diff. (N)	Radius Max. VM	Radius Max. % Diff. (με)	Radius Min.VM	Rad Min. % Diff.(με)
EP	9	0.33	13.77	0.36	-70.66	0.46	-32.22
EPF	12	0.30	-25.42	0.40	-79.08	0.40	-45.33
Marrow	10	0.34	-0.21	0.32	-82.85	0.42	-43.53
No Marrow	10	0.30	-8.64	0.41	-70.88	0.44	-36.39
Single	7	0.33	-0.39	0.38	-81.23	0.42	-42.25
Full	18	0.28	-16.69	0.39	-62.16	0.46	-31.82

ORAL PRESENATIONS – FRIDAY SEPTEMBER 6th

	Lower Extremity: ACL *James Ashton-Miller, David Lipps*
4:00 PM	Gastrocnemius Activation Level Markedly Influences ACL Force **Adouni M, Shirazi-Adl A, Marouane H**
4:15 PM	Limited Femoral Internal Axial Rotation Increases ACL Strain During A Cadaver-simulated Pivot Landing **Beaulieu M, Oh Y, Bedi A, Wojtys E, Ashton-Miller J**
4:30 PM	Novel Framework To Personalize Validated Generalized Finite Element Model: Implication For Individual-based ACL Injury Risk Assessment **Kiapour A, Kiapour A, Demetropoulos C, Quatman C, Wordeman S, Hewett T, Goel V**
4:45 PM	Flexion Moment Differences Persist More Than One Year Post-ACL Reconstruction In Paediatric Subjects **Hassan EA, Deluzio K, Borschneck D**
5:00 PM	Is The Strain Concentration At The Femoral Enthesis A Risk Factor For Anterior Cruciate Ligament Injury? **Oh Y, Beaulieu M, Lipps D, Wojtys E, Ashton-Miller J**

GASTROCNEMIUS ACTIVATION LEVEL MARKEDLY INFLUENCES ACL FORCE

Malek Adouni, Aboulfazl Shirazi-Adl and Hafedh Marouane

Department of Mechanical Engineering,
École Polytechnique, Montréal, Québec, Canada
email: aboulfazl.shirazi@polymtl.ca

INTRODUCTION

Medial (MG) and lateral (LG) fascicles of the gastrocnemius are the primary muscles of the leg with major contributions at both ankle and knee joints. Along with quadriceps and hamstrings, they resist external moments, control motions and stabilize the knee joint. The influence of individual and combined activities in quadriceps and hamstrings on ACL loading at various flexion angles has been documented [1]. The antagonistic role of gastrocnemius on ACL loading on the other hand needs further studies [2]. Such knowledge would benefit effective preventive and treatment procedures in both normal and ACL-deficient subjects. In the current work, we use a validated finite element (FE) model [3] to compute the effect of changes in gastrocnemius activation level on lower extremity muscle forces and knee joint response at 75% instance of gait stance phase when gastrocnemius is highly active. These FE analyses are driven by kinematics-kinetics data collected during gait of asymptomatic subjects [4]. Changes in gastrocnemius force are caused here by alterations in properties (i.e., PCSA and level arm) of soles muscle within reported data in the literature. In additional analyses similar to earlier studies [1], the response of the unconstrained knee is investigated in flexion (0-90°) under 3 constant gastrocnemius forces (S-G=400N, G=700N, L-G=900N) selected based on results of gait analyses.

METHODS

The FE model considers bony structures (tibia, patella, femur), TF and PF joints, major TF (ACL, PCL, LCL, MCL) and PF (MPFL, LPFL) ligaments, patellar tendon, as well as active musculature of the lower extremity [3] (Fig. 1). Nonlinear depth-dependent fibril-reinforced cartilage and menisci as well as ligaments with distinct nonlinear properties/initial strains are considered. The hip/knee/ankle joint rotations-moments and ground reaction forces at foot are based on reported *in vivo* gait measurements [4]. Analyses are performed at 75% period of stance corresponding to high activation of gastrocnemius muscles. Muscle forces at the hip, knee and ankle are estimated using optimization. The Knee joint response is subsequently analyzed with updated muscle forces as external loads and iterations at deformed configurations continue till convergence is reached. To assess the sensitivity of response on gastrocnemius activation, analysis is repeated with altered level arm and PCSA of the soles muscle [5] in order to increase (case L-G) or decrease (case S-G) gastrocnemius activation level compared to the reference case (G). To gain more insights, additional analyses are carried out with the unconstrained knee joint model [6] in flexion (0-90°) under gastrocnemius forces (S-G = 400N, G = 700N and L-G = 900N) chosen based on results of gait analyses described above.

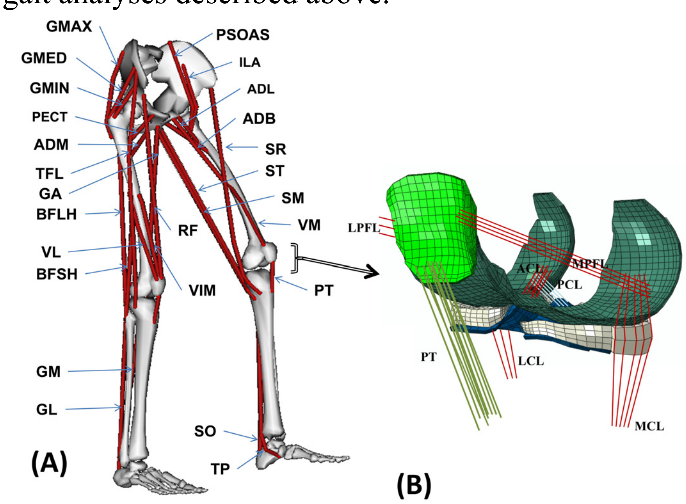

Figure 1: Lower extremity musculature (A), Knee joint FE model (B).

RESULTS AND DISCUSSION

At 75% instance of stance phase, the computed gastrocnemius muscle forces (Lat/Med) varied from minimum of 119N/320 N in S-G case to 180N/508 N in reference G case and to maximum of 235/627 N in L-G case. Forces in medial and lateral hamstrings muscles substantially diminished along with a slight reduction in quadriceps as forces in gastrocnemius fascicles increased (Fig. 2). These changes in muscle activation only slightly altered contact forces/pressures. ACL force however markedly increased with increases in gastrocnemius force (Fig. 3, inlay). The antagonist effect of gastrocnemius activation on ACL force at all flexion angles was further confirmed in subsequent analyses on the knee model studied alone (Fig. 3).

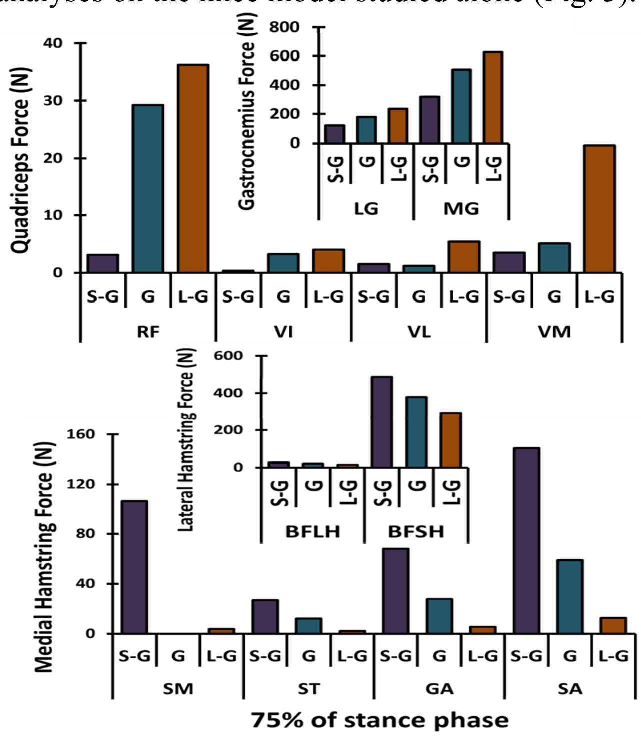

Figure 2: Estimated muscle Forces at 75% instance of stance phase for 3 gastrocnemius force levels (S-G, G, L-G) when altering soleus properties.

The first part of this study on the analysis of an instance of stance phase demonstrated that gastrocnemius muscles at higher activation diminish forces in hamstrings and act as an antagonist of ACL at their peak activation periods of gait. Subsequent simulations under constant isolated contraction of gastrocnemius at three different load levels confirmed these findings at all joint flexion angles. With flexion, the force in the anteromedial (am) bundle increased while that in the posterolateral (pl) bundle diminished. Increases in gastrocnemius force level increased tibial anterior translation and internal rotation in both models. These predictions are corroborated by reported model studies [7] and in vivo measurements of strain at ACL-am [2].

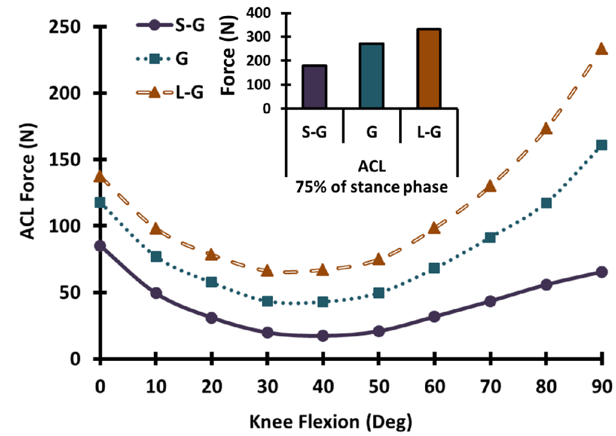

Figure 3: ACL force during gait (inlay) and in the knee model at different flexion angles for 3 activity levels in the gastrocnemius muscles.

In conclusion, while hamstrings and gastrocnemius are both knee joint flexors, they play opposite roles in respectively either protecting or loading ACL. The fact that gastrocnemius is an antagonist of ACL may help both preventing of ACL injury and designing safer rehabilitation programs following ACL reconstruction. It is also noted that the joint flexion initially diminish ACL force under quadriceps [1] and gastrocnemius (Fig. 3) activations. This trend, however, alters at larger flexion angles under gastrocnemius activation yielding large ACL (am bundle) forces at 90^{o} flexion.

REFERENCES

1. Mesfar and Shirazi-Adl, *CB* 21:841, 2006.
2. Fleming et al, *J Orthop Res* 19:1178, 2001.
3. Adouni et al, *J Biomech* 45:2149, 2012.
4. Astephen et al, *J Orthop Res* 26:332, 2008.
5. Delp et al, *IEEE BE* 54:1940, 2007.
6. Adouni/Shirazi-Adl, *CMBBE* 12:661, 2009.
7. O'Connor, *JBJS* 75:41, 1993.

ACKNOWLEDGEMENTS

Work has been supported by the NSERC-Canada.

LIMITED FEMORAL INTERNAL AXIAL ROTATION INCREASES ACL STRAIN DURING A CADAVER-SIMULATED PIVOT LANDING

Mélanie L. Beaulieu, Youkeun K. Oh, Asheesh Bedi, Edward M. Wojtys and James A. Ashton-Miller

University of Michigan, Ann Arbor, MI, USA
email: mbeaulie@umich.edu

INTRODUCTION

A better understanding of the mechanism of anterior cruciate ligament (ACL) injuries is needed to improve prevention strategies and reduce the enormous health and financial burden of these injuries [1,2]. While many factors contributing to injury risk have been investigated, attention has mostly focused on the knee. However, the mechanics of the hip may also contribute to injury risk. For example, restricted passive range of internal rotation at the hip (e.g., femoroacetabular impingement) has been correlated with ACL ruptures in soccer players [3]. It is unknown, however, how limited hip internal rotation increases ACL injury risk. So, we hypothesized that during 'risky' athletic maneuvers, ACL strain increases with the amount of femoral internal axial rotation restriction. We tested this hypothesis in a cadaver model simulating a single-leg pivot landing.

METHODS

Six human knee specimens were harvested from one female and two male donors (age: 55.7 ± 1.4 years; height: 1.70 ± 0.14 m; mass: 73.5 ± 13.0 kg). Each specimen was dissected, leaving the joint capsule, including the ligamentous structures, intact, as well as the tendons of the quadriceps, medial and lateral hamstrings, and medial and lateral gastrocnemii.

Each knee specimen was mounted in a modified version of the Withrow-Oh testing apparatus [4] in 15° of flexion (Fig. 1). As previously described [4], this custom-built apparatus simulates a single-leg pivot landing task by impacting the distal end of the tibia of the inverted knee specimen. An impulsive force induces a compression force, knee flexion moment, and internal tibial torque. A novel addition to the apparatus was a femoral rotation device ('R', Fig. 1) able to limit the range of femoral axial rotation. This device comprised a circular plate able to rotate in the transverse plane on a tapered-roller bearing and two pre-tensioned springs attached tangentially to the perimeter of the plate via aircraft cables. Muscles were simulated by pretensioned elastic structures connected to the tendons. Strain of the anteromedial bundle of the ACL (AM-ACL) was recorded with a DVRT (MicroStrain, Burlington, VT) at 2 kHz. An opto-electric imaging system (Optotrak Certus, NDI, Waterloo, ON) recorded tibiofemoral kinematics at 400 Hz via diode triads secured to the femur and the tibia.

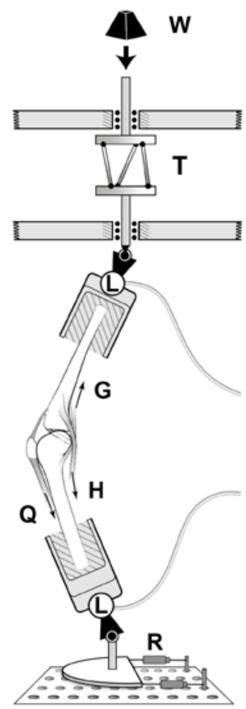

Figure 1: Schematic of *in vitro* apparatus.

In each trial, an impulsive force of two-bodyweights was applied. Each testing session began with five preconditioning trials, followed by five blocks of six trials in an 'A-B-C-D-A' design (Table 1).

Table 1: Testing protocol, including loading condition and range of femoral internal axial rotation for each block of trials.

Protocol		Loading Condition	Femoral Rotation
	A	comp + flex m	≈ 0°
R	B	comp + flex m + int tib trq	≈ 5°
R	C	comp + flex m + int tib trq	≈ 10°
R	D	comp + flex m + int tib trq	≈ 15°
	A	comp + flex m	≈ 0°

comp: compression force; *flex m*: flexion moment; *int tib trq*: internal tibial torque; *R*: randomized sequence.

To limit femoral internal axial rotation, the femoral rotation device was either locked (block 'D') or resisted by high stiffness (block 'C') or low stiffness (block 'B') springs.

Peak AM-ACL relative strain and *peak relative anterior tibial translation* were compared between femoral rotation conditions via two linear mixed models, with *femoral internal axial rotation magnitude* treated as a fixed effect and *knee specimen* and *donor* as random effects. An $\alpha < 0.05$ was taken to indicate statistical significance.

RESULTS AND DISCUSSION

As the available range of femoral internal axial rotation was decreased, both peak AM-ACL relative strain and peak relative anterior tibial translation increased significantly during the simulated pivot landings (Fig. 2). On average, AM-ACL relative strain increased 36% when the range of femoral internal axial rotation was decreased 10° (from large to small femoral rotation); whereas anterior tibial translation increased 22%. Smaller but significant increases in these variables also occurred with 5° of decreased femoral internal axial rotation.

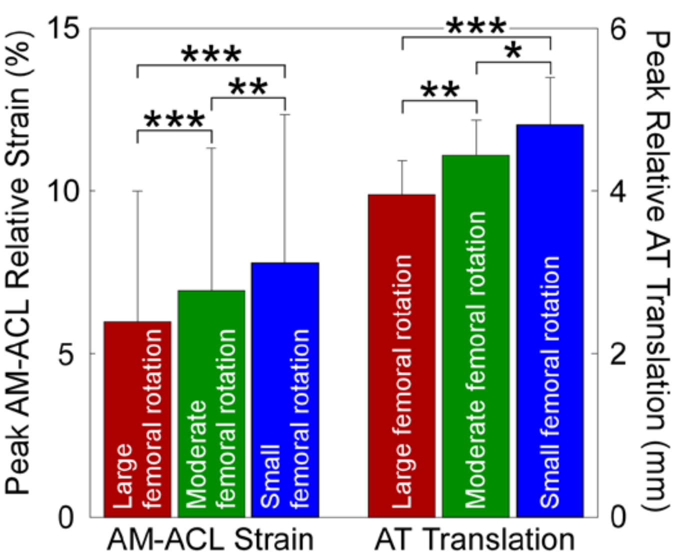

Figure 2: Peak ACL relative strain (left) and relative anterior tibial (AT) translation (right) for each femoral rotation condition during the pivot landings. *p<0.05; **p<0.01; ***p<0.001.

Differences in peak AM-ACL relative strain between femoral rotation conditions can be explained by the compensatory differences in tibial internal axial rotation. As the range of femoral internal axial rotation was progressively limited, the range of tibial internal axial rotation increased (Fig. 3). Given that tibial internal axial rotation is known to strain the ACL during pivot landings [4], it is likely that this increase in axial rotation at the knee joint caused the increase in ligament strain. These results present a plausible explanation as to why athletes with limited range of hip internal rotation are at greater risk of ACL injuries [3].

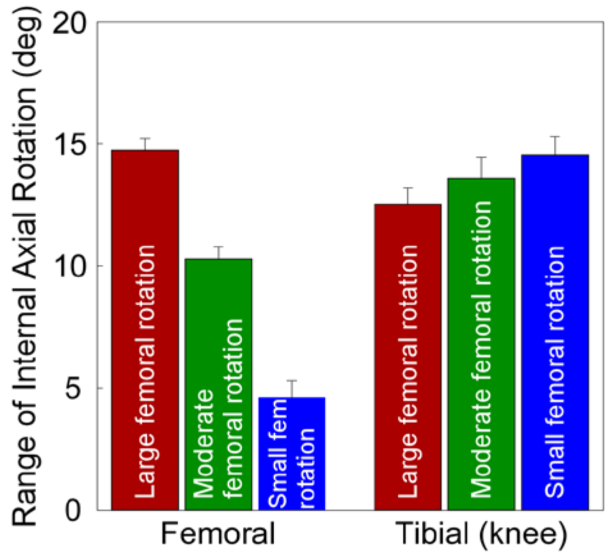

Figure 3: Range of femoral (left) and tibial (right) internal axial rotation for each femoral rotation condition during the pivot landings.

CONCLUSIONS

A restriction of femoral internal axial rotation increases peak AM-ACL relative strain and relative anterior tibial translation during simulated pivot landings.

REFERENCES

1. Brophy RH et al. *Am J Sports Med* **37**, 683-687, 2009.
2. Lohmander LS et al. *Am J Sports Med* **35**, 1756-1769, 2007.
3. Gomes JL et al. *Arthroscopy*, **24**, 1034-1037, 2008.
4. Oh YK et al. *J Orthop Res*, **30**, 528-534, 2012.

ACKNOWLEDGEMENTS

Funding: NIH R01 AR054821 and University of Michigan Rackham Predoctoral Fellowship.
Assistance: Sasha Kapshai and Rebecca Thoppil.

NOVEL FRAMEWORK TO PERSONALIZE VALIDATED GENERALIZED FINITE ELEMENT MODEL: IMPLICATION FOR INDIVIDUAL-BASED ACL INJURY RISK ASSESSMENT

[1]Ata M. Kiapour, [1]Ali Kiapour, [1]Constantine K. Demetropoulos, [2]Carmen E. Quatman, [2]Samuel C. Wordeman [2]Timothy E. Hewett, [1]Vijay K. Goel

[1]Engineering Center for Orthopaedic Research Excellence (ECORE), University of Toledo, Toledo, OH
[2]OSU Sports Medicine, Sports Health and Performance Institute, The Ohio State University, Columbus, OH
email: ata.kiapour@utoledo.edu, web: http://www.eng.utoledo.edu/ecore

INTRODUCTION

The anterior cruciate ligament (ACL) is one of the most frequently injured ligaments of the knee, with a prevalence estimated to be 1 in 3000 in the U.S. population. Current approaches to biomechanical finite element (FE) modeling of the knee are at a crossroads. While the ideal scenario for clinically applicable FE modeling would be a subject-specific approach with detailed, image-based anatomic reconstruction of the joint, the computational intensity of such an approach would almost certainly preclude its clinical applicability. The assumption that an accurate assessment of an individual's ACL injury risk profile can be attained through generalized FE models also has yet to be tested. The current study aims to test a novel framework in which the developed, validated generalized FE model can be customized to each specimen based on ACL structural properties (mechanical and anatomical), posterior slope of the lateral tibial plateau and femoral intercondylar notch width as the most critical anatomic risk factors for ACL injury [1]. We hypothesized that personalized FE models using the proposed framework would result in more accurate predictions of ACL strain (as an established measure of injury risk) compared to the generalized FE model. Thus, these models may serve as individual-based injury risk assessment tools.

METHODS

I) Model Customization Approach: An anatomical non-linear knee FE model, developed from a healthy, young female athlete (25 yrs, 170 cm, 64.4 Kg) was used (Figure 1). The model has been extensively validated against direct cadaveric measurements of joint kinematics, ligament strains and cartilage pressure distribution under quasi-static and dynamic loading conditions [2].

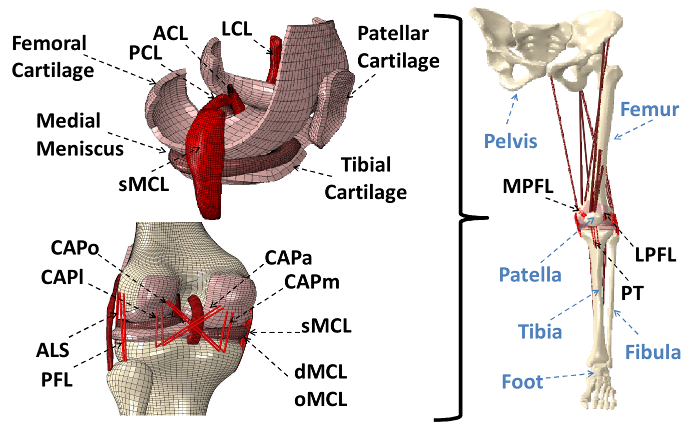

Figure 1: Validated generalized FE model of the knee [4].

Five normal cadaveric legs (41±5 yrs) were acquired, imaged and instrumented with a DVRT displacement transducer across the ACL AM-bundle. A-P knee joint laxity of each specimen was determined using a CompuKT Knee Arthrometer. The 3D ACL geometry of each specimen was generated and meshed following the same technique used in development of the validated generalized FE model. Five personalized FE models were developed by changing the native ACL geometry/mesh to the subject-specific ones. Further, tibial slope and intercondylar notch width of each specimen were measured. In order to modify the lateral tibial slope of each personalized model, tibial plateau was rotated about an axis located above the tibial tuberosity, 2 cm distal to the tibial plateau and normal to the long axis of the tibia to match the measured lateral tibial slope [3]. Finally, the regional nodes/elements across the intercondylar notch of each model were manually manipulated to match the measured intercondylar width of the specimen. Subsequently, personalized FE models were used to simulate instrumented knee laxity tests. Finally, ACL material model coefficients of each personalized model were optimized to reproduce the subject-specific force-displacement curve obtained from knee arthrometry.

II) Approach Validation and Accuracy Evaluation: Model predictions of ACL strain during simulated A-P laxity tests for each personalized FE model were compared to experimentally measured data. Further, cadaveric experiments of bi-pedal landing from a 30 cm height [4], conducted on the specimens, were simulated in the personalized FE models. Finally, FE predictions of peak ACL strain were compared to experimentally measured values to test the reliability/validity of this novel approach for prediction of individual-based ACL injury risk. Additional simulations were conducted using the generalized FE model to further verify the accuracy of the personalized models. Pearson's correlation coefficient (r), root-mean-square errors (RMSE) and ANOVA with a post-hoc Bonferroni for multiple comparisons were used for statistical analyses.

RESULTS AND DISCUSSION

Applied anterior drawer load resulted in elevated ACL strain levels as shown by 4.4±1.4%, 3.2% and 4.2±1.3% in cadaveric experiments, generalized and personalized FE models, respectively. Simulated landings resulted in peak ACL strain of 6.8±1.6%, 5.7±0.9% and 6.5±1.3% in cadaveric experiments, generalized and personalized FE models, respectively. Although both generalized and personalized FE models resulted in similar trends as cadaveric experiments, personalized FE models resulted in more accurate predictions compared to the generalized model.

Strong correlations (Laxity Test: r=0.97, p=0.006; Landing: r=0.94, p=0.01) with low deviation (Laxity Test: RMSE=0.4%; Landing: RMSE=0.7%) were observed between personalized FE models predictions and experimental measurements of ACL strain. However, a lower correlation (r=0.42 p=0.48) with greater deviation (RMSE=1.9%) was observed between generalized FE model predictions and experimental measurements under the similar landing condition (Figure 2). No significant differences were observed between average peak ACL strain reported by cadaveric experiments, generalized FE and personalized FE models (p>0.55). The absence of significance differences between generalized FE model predictions and experimental data highlights the potential application of this modeling approach in overall risk assessment (identification of risk factors and mechanisms) and parametric/sensitivity analyses. However, low correlation and large RMS error, are indicatives of the relatively low accuracy of this approach in individual-based risk assessment. Whereas, personalized FE models resulted in more accurate predictions of ACL strain supported by strong correlations with the RMS error minimized.

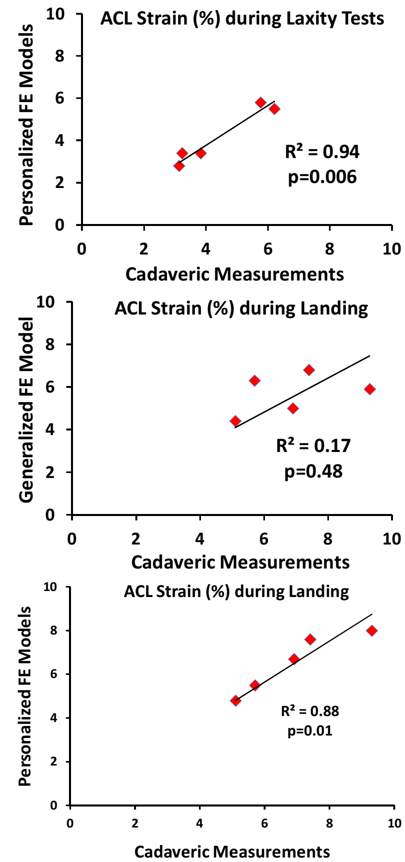

Figure 2: Personalized and Generalized FE models predictions of ACL strain Vs. cadaveric measurements.

CONCLUSIONS

The current findings demonstrate the validity of the proposed novel, computationally efficient approach to generate personalized models and thus supported our hypothesis. This highlights the clinical utility of such personalized models for prediction of an individual's risk of ACL injury (as reported by ACL strain) especially in large-scale clinical studies where subject-specific modeling is not practical.

REFERENCES

1. Simon RA, et al. *J Biomech* **43**, 1702-1707, 2004.
2. Kiapour A. *Proceeding of ORS'12*, CA, USA, 2012.
3. Shelburne KB, et al. *JOR* **29**, 223-231, 2011.
4. Levine JW, et al. *AJSM* **41**, 385-395, 2013.

ACKNOWLEDGEMENTS
Funded by NIH/NIAMS (R01 AR056259 & R01 AR049375).

FLEXION MOMENT DIFFERENCES PERSIST MORE THAN ONE YEAR POST-ACL RECONSTRUCTION IN PAEDIATRIC SUBJECTS

[1]EA Hassan, [1]KJ Deluzio and [2]DP Borschneck

[1]Department of Mechanical and Materials Engineering, Queen's University, Kingston, ON, Canada
[2]Department of Surgery, Queen's University, Kingston, ON, Canada
Elizabeth.Hassan@me.queensu.ca

INTRODUCTION

Although many patients are able to successfully return to sport and leisure activities after replacement of the anterior cruciate ligament (ACL), non-normal kinematics may be observed over a year after surgery. Although gait nominally returns to normal 6 to 12 months post-surgery, multiple studies have noted that a reduced knee flexion moment is present during stance phase of gait, with larger differences observed during demanding activities [1–4].

Surgical techniques that harvest a tendon autograft from either the patellar tendon (extensor) or hamstring tendons (flexors) have been specifically investigated [5-6] with the hypothesis that morphological changes due to the harvest procedure affect the function of the knee extensors and flexors. Therefore, examining the knee flexion moment is a logical starting point for quantifying non-normal knee biomechanics post-ACL reconstruction. Techniques harvesting a hamstring tendon are particularly popular with pediatric surgeons because a soft tissue at the physes is thought to interfere less with normal growth [7].

This was a pilot study, aimed at developing a protocol and metrics that could be used to objectively quantify surgical recovery from ACL reconstruction. Our ultimate goal is to develop a protocol and metrics capable of detecting subtle functional differences due to surgical approach.

METHODS

Subjects: 8 participants were recruited from the practice of a local paediatric orthopaedic surgeon. All were teenage athletes who underwent an ACL reconstruction with hamstring autograft between 6 months and 2 years prior to participation in the study and had returned to unrestricted sporting activities.

Data Collection: Kinematic data was collected with a full body skin-fixed marker set of passive, retro-reflective markers were tracked with a 12 Qualisys Oqus cameras (Qualisys AB, Gothenburg, Sweden). Ground reaction forces were collected with four AMTI force plates (AMTI, Watertown, MA).

Protocol Activities: After a static trial, subjects were instructed to climb stairs, walk, walk backwards, hop off a step and perform unanticipated straight jogs, side and cross cuts. Only the straight jog and cross cut activities will be discussed in this abstract.

Subjects approached the designated force plate at a self-selected jog pace. Upon breaking a laser beam, a randomly selected arrow appeared before the subject after a fixed time delay, indicating the direction (left, straight or right) that the subjects should follow after planting either the specified limb on a marked target. The subjects were instructed to proceed along taped lines at 35 to 60 degrees from their initial heading. A cross-cut activity was one in which the subject headed in the same direction as the planted foot. Three repetitions of each combination of limb (affected and unaffected) and direction were performed, for a total of 18 trials per subject.

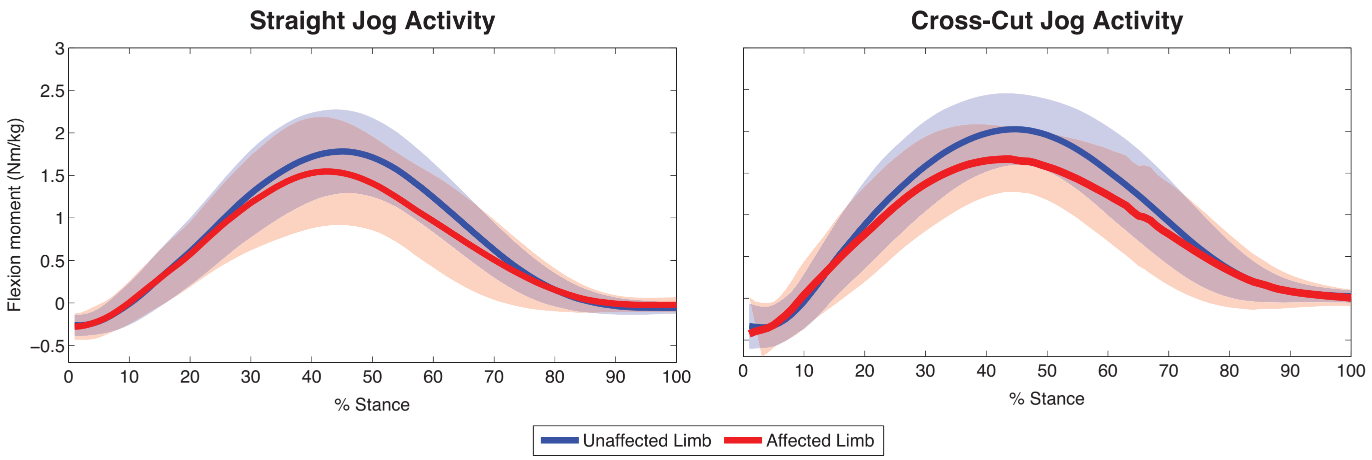

Figure 1: Average waveforms (solid line) and standard deviation (shaded areas) for knee flexion moment during stance phase of straight jog and cross cut jog activity

Data Processing and Analysis: Data was collected and tracked in the Qualisys software package, QTM. Functional hip joint centres, knee joint angles, forces and moments were calculated with Visual3D (C-Motion, Germantown, MD). Principal Component Analysis (PCA) of the knee angle, force and moment waveforms was performed with a custom written algorithm in MATLAB.

RESULTS

The participants were heterogeneous with respect to gender (1 male, 7 female), age (mean 17.1 years, range 15-19), IKDC knee score (mean 87.7, range 64.4-98.9), height (mean 172 cm, range 167-183) and weight (mean 70.4 kg, range 58.5-99.7) and affected limb (4 right, 4 left). The mean self-selected speed was 2.47 m/s (SD 0.17).

Principal component analysis was performed on flexion-extension, abduction-adduction and internal-external rotation angle, force and moment waveforms, normalized over the stance phase. Each set of waveforms was tested with a t-test for significant differences ($p<0.05$) in the Principal Component (PC) scores between affected and unaffected limbs, with all subjects and trials pooled.

Only the flexion moment yielded significant differences between the affected and unaffected limbs, and only for the cross cut activity. Average waveforms for both activities are shown in Figure 1.

PC1 and PC2 were related to the magnitude and location of the peak flexion moment, a high PC1 score corresponds to higher magnitude and earlier peak and a high PC2 scores corresponds to higher magnitude and later peak. PC 3 was related to the rate of loading; a high PC3 score corresponds to a higher loading rate. These interpretations were consistent for both the straight jog and cross-cut activities. PC1 was not significantly different ($p=0.52$), but PC2 ($p=0.031$) and PC3 ($p=0.045$) were different for affected and unaffected limbs for the cross-cut task. No principal components were significantly different for the straight jog task ($p=0.16$, 0.24 and 0.18 respectively).

DISCUSSION AND CONCLUSIONS

Statistically significant differences in the flexion moment were observed during a demanding task, even though the sample was small, relatively heterogeneous and all subjects had returned to unrestricted sporting activities. This supports previous work that showed persistent kinematic and kinetic differences post-ACL reconstruction, particularly during high demand activities. The lack of differences observed during the less demanding straight jog, and the lack of differences in joint angles suggests that protocols that are comprehensive and multimodal are more likely to elicit clinically meaningful differences than those that collect gait kinematics only.

REFERENCES

1. Bush-Joseph CA, et al. *Am J Sp Med* **29, 1**, 36-41, 2001.
2. Hooper, DM et al. *Clin Orthop* **403,** 168-178, 2002.
3. Timoney, JM et al. *Am J Sports Med* **21, 6**, 887-889, 1993.
4. Webster, KE et al. *Am J Sports Med* **33, 2**, 247-254, 1993.
5. Barenius, B et al. *Intl Orthop* **37, 2**, 207-212, 2013.
6. Makihara, Y et al. *Knee Surg Sport Traum Arth* **14, 4**, 310-317, 2006.
7. Utukuri, MM et al. *The Knee* **13, 5**, 345-352. 2006.

IS THE STRAIN CONCENTRATION AT THE FEMORAL ENTHESIS A RISK FACTOR FOR ANTERIOR CRUCIATE LIGAMENT INJURY?

Youkeun K. Oh, Mélanie L. Beaulieu, David B. Lipps, Edward M. Wojtys and James A. Ashton-Miller

University of Michigan, Ann Arbor, MI, USA
email: youkeun@umich.edu

INTRODUCTION

The fibers of the anterior cruciate ligament (ACL) located near the femoral attachment ('femoral enthesis'), especially of the posterolateral (PL) bundle, appear to be particularly prone to failure [1, 2]. The structural vulnerabilities of an enthesis with an acute "take-off" angle have been demonstrated as partial thickness rotator cuff tears, called 'rim-rent' tears [3], as well as the pubovisceral muscle enthesis [4], the reasons for the ACL's susceptibility to injury near its femoral enthesis have not been investigated. Previously, we found that the majority of the knee specimens, which developed partial or complete visible ACL tears, exhibited macroscopic damages near the PL bundle of the femoral enthesis during an *in vitro* knee experiment [1]. Our goal here was to perform a secondary analysis on this data set to determine if the femoral enthesis angle of the ACL can explain the macroscopic damages near the PL bundle of the femoral enthesis. In addition we used a 3-D simulation of the knee and further investigated where the strain concentration occurs during a simulated pivot landing [5].

METHODS

Data from 10 pairs of knee specimens (sex: 5/5 males/females; age: 53 ± 7 years; height: 174 ± 9 cm; mass: 69 ± 9 kg) presented in Lipps et al. [1] were used for this study. As previously described [1], each knee specimen was subjected to repetitive loading that simulated a single-leg pivot landing (impulsive compression, knee flexion moment, internal tibial torque, and physiological muscle forces). From each pair, one knee was subjected to a three-time body weight loading, with the other knee subjected to a four-time body weight loading. The cyclic loading protocol ended when the ACL failed (macroscopic rupture or 3-mm increase in cumulative anterior tibial translation) or a minimum of 50 trials was collected.

Magnetic resonance (MR) images were also collected from which the ACL's angle of origin from the distal femur ('femoral enthesis angle') was measured. Using an oblique-coronal view (along the longitudinal axis of the ACL) of the mid-portion of the ACL (Fig 1.a), the angle between (1) a line drawn along the edge of the lateral femoral condyle where the ACL inserts and (2) an average line of the outer edges of the proximal 25% of the ACL was calculated with custom Matlab code (Fig 1.b).

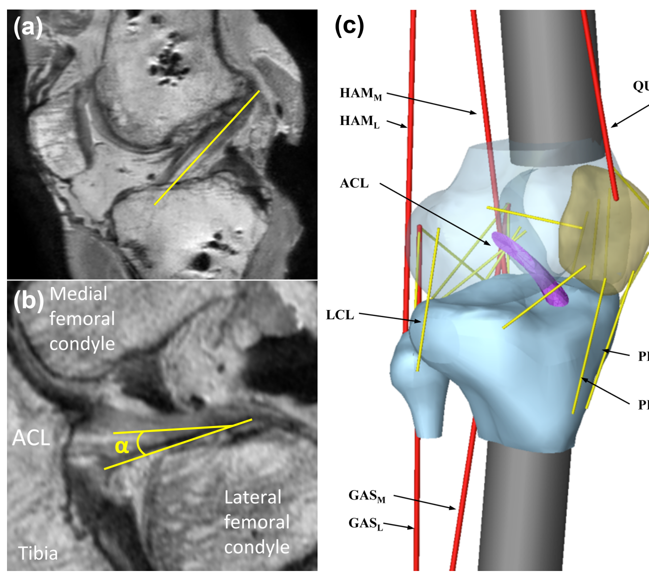

Figure 1: (a) Example of the oblique coronal plane of the mid-portion of the ACL, (b) definition of the femoral enthesis angle (α) and (c) schematic diagram of the knee model.

As previously described [5], a 3-D knee model (Fig 1.c) was constructed to replicate the *in vitro* experimental set-up using T2-weighted MR images (TR/TE: 1000/35 ms, slice thickness: 0.35 mm, FOV: 160 mm) of a male cadaveric knee. The segmented bones and ACL were treated as a rigid body and deformable body, respectively (MD

ADAMS R3, MSC. Software, Inc., Santa Ana, CA). To drive the knee model simulation, the impulsive compressive force, internal tibial torque, and knee abduction moment, measured from the *in vitro* experiment, were applied. The boundary loading condition for the ACL attachment sites was calculated using ADAMS, and then was transferred to finite element software in order to calculate the distribution of the strain throughout the model ACL (ANSYS 14, ANSYS, Inc., Canonsburg, PA).

RESULTS AND DISCUSSION

The femoral enthesis angles for the knee groups that exhibited either a partial tear of PL bundle near femoral enthesis or a permanent elongation were significantly smaller than for the group where the ACL did not fail ($p < 0.05$, Fig 2).

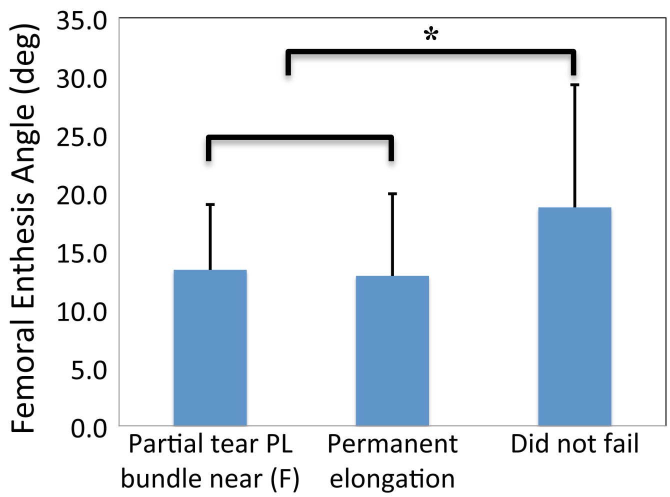

Figure 2: Mean (SD) femoral enthesis angles for each group that showed (left) a partial tear of PL bundle near femoral enthesis, (middle) a 3-mm permanent elongation, and (right) no failure [3]. Error bars represent +1 standard deviation. The asterisk indicates a significant difference.

The knee model simulation confirmed that the highest von Mises elastic strain occurs at the anterior margin of the origin of the PL bundle of the ACL femoral enthesis. Contours of von Mises elastic strain are shown when the AM-ACL relative strain reaches its peak value at ~65 msec during a simulated pivot landing (Fig 3).

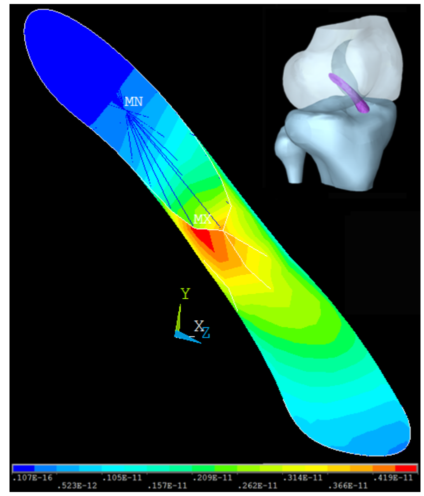

Figure 3: Antero-posterior three-quarter latero-medial view of the left knee and FE model of the ACL. The upper left oval area represents the femoral attachment site of the ACL. The red region shows the highest strain concentration corresponding to the anterior margin of the PL bundle of the ACL femoral enthesis. Note. Because of the oblique viewing angle, the red region appears to be in the middle of the ACL in this view even though it actually is at the femoral origin.

CONCLUSIONS

1. A smaller femoral enthesis angle is a significant predictor of *in vitro* ACL injuries.
2. The anterior margin of the origin of the PL bundle of the ACL femoral enthesis appears to be prone to injury because it exhibits the highest ACL strain concentration during a simulated pivot landing.

REFERENCES

1. Lipps DB et al. *Am J Sports Med* (published online).
2. Myers EG et al. *Am J Sports Med 41*, 3377-3383, 2008.
3. Codman EA. *The Shoulder*, Thomas Todd, 1934
4. Kim J et al. *Neurourol Urodyn* 30, 1366-1370, 2011.
5. Oh Y et al. *Am J Sports Med* 40, 574-583, 2012.

ACKNOWLEDGEMENTS
Funding from PHS R01 AR 054821, a Rackham Predoctoral Fellowship (MLB), and an NDSEG Fellowship (DBL).

ORAL PRESENATIONS – FRIDAY SEPTEMBER 6th

Symposium: A Continuum of Pediatric Biomechanics: From Clinical to Technical *Frank Buczek*
Upper Extremity Biomechanics Of Assisted Mobility Device Usage In Pediatric Orthopaedic Disabilities **Slavens B, Paul A, Graf A, Krzak J, Vogel L, Harris G**
Development And Validation Of A Three-dimensional Model For Kinematic Analysis Of The Thumb **Curran P, Bagley A, Sison-Williamson M, James M**
Design Of A Bilateral Adl Task-oriented, Robot Therapy Environment For Children With Cerebral Palsy **Johnson M, Hughes D, Holley D, Theriault A, Krzak J, Graf A, Gilliam J**

UPPER EXTREMITY BIOMECHANICS OF ASSISTED MOBILITY DEVICE USAGE IN PEDIATRIC ORTHOPAEDIC DISABILITIES

[1]Brooke A. Slavens, [1]Alyssa J. Paul, [2]Adam Graf, [2]Joseph Krzak, [2]Lawrence Vogel and [2]Gerald F. Harris
[1]University of Wisconsin Milwaukee, Milwaukee, WI, USA
[2]Shriners Hospitals for Children - Chicago, Chicago, IL, USA
email: slavens@uwm.edu

INTRODUCTION

According to the latest NIDRR Mobility device report there are an estimated 1.7 million wheelchair or scooter users and 6.1 million users of walkers, crutches, canes, or other devices [1]. Walker use has been reported by 1.8 million persons, while 1.5 million persons use manual wheelchairs and 566,000 persons use crutches [1]. A growing population of pediatric individuals is included within this population. Severe cerebral palsy (CP), spinal cord injury (SCI), myelomeningocele (MM), and osteogenesis imperfecta (OI) are associated with these leading causes of assistive mobility device usage in children and adolescents.

While the number of pediatric individuals using assistive devices is significant, there is limited information on joint dynamics. The relationship between joint forces, assistive devices and the transition effects to adulthood has not been studied. We propose methods for characterizing three-dimensional (3-D) upper extremity (UE) joint forces and moments during assisted mobility (wheelchair mobility, crutch and walker assisted-gait).

High joint forces during assistive device usage have been shown to lead to joint pain and approach levels of injury [2-4]. Quadrapedal gait, as occurs with crutch and walker usage requires high, unnatural demands on the upper extremity. Literature has shown that peak joint forces at the shoulder are directly correlated to device usage. These forces are also anticipated to be of concern at the wrist and elbow. Quantification of 3-D inverse dynamics and correlation among assistive device usage and pathology is essential for improved care of children with severe orthopedic disabilities. The investigation of the joint demands placed on the UE may have significant impact on rehabilitation protocols and transitional care.

METHODS

Advanced mobility modeling techniques using 3-D inverse dynamics methods are proposed. The UE inverse dynamics model computes wrist, elbow and shoulder complex kinematics and kinetics [5].

The model includes the kinetically instrumented assistive device segment(s) of interest (i.e., wheelchair, crutches, or walker) and defines the thorax, shoulder complex, upper arm, forearm and hand. Computed joint motions include the thorax, shoulder complex, elbow and wrist. The model follows ISB recommendations [6].

Wheelchair mobility is one of the three activities of interest. Three subjects with SCI (17 year-old) propelled their manual wheelchair along a 15-meter path at a self-selected propulsion pattern and speed (Figure 1). Kinematic data was collected using a 14 camera Vicon MX motion capture system (120 Hz). 3-D forces and moments were acquired simultaneously (240 Hz) from a SmartWheel (Out-Front, Mesa, AZ) on the subjects' dominant side.

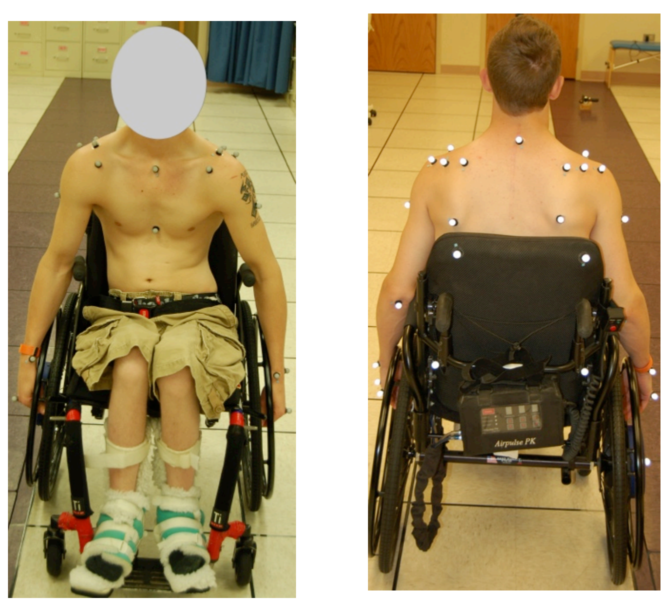

Figure 1: Manual wheelchair user (MWU) with UE model marker set.

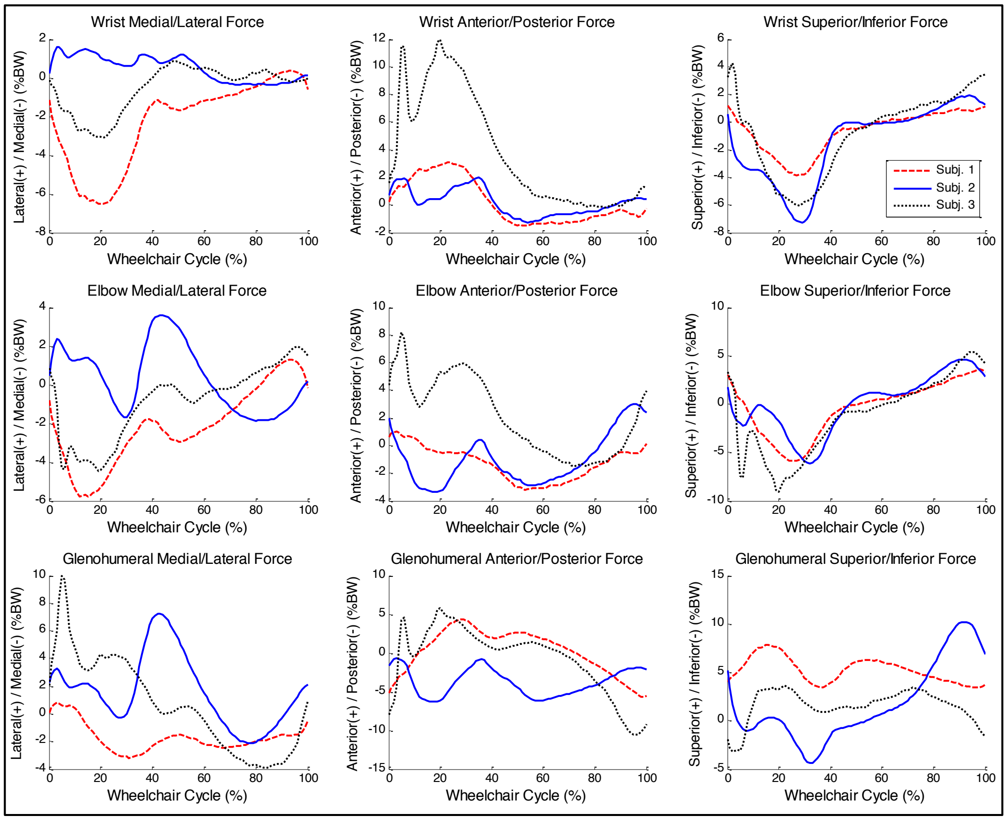

Figure 2: Mean upper extremity joint kinetics during wheelchair mobility for three subjects with SCI.

RESULTS

Ten stroke cycles of each subject were analyzed using our custom pediatric inverse dynamics model. Average joint forces for three subjects' dominant side are presented in Figure 2. Mean shoulder, elbow, and wrist joint forces were computed triaxially.

DISCUSSION

The custom pediatric UE biomechanical model successfully characterized joint dynamics in MWUs with SCI. Subjects displayed similar, yet different morphologies, suggesting the need for subject specific analysis and further characterization of orthopaedic pathologies. Joint forces during crutch and walker assisted gait are proving to be substantially higher than wheelchair mobility, causing even greater concern. The implications for pain and overuse pathology are significant.

CONCLUSIONS

Improved biomechanical understanding of assistive device usage will provide insight for children as they mature. Transition to adulthood will bring about new challenges to be addressed biomechanically. This work provides quantitative framework to support training paradigms, alternative mobility patterns or redesigned assistive devices to reduce joint loading. Future work involves determining correlations among joint dynamics, pain and functional outcomes, as well as to determine the underlying tissue level effects through musculoskeletal modeling of pathology.

REFERENCES

1. Kaye, H.S., et al. (2000) US Dept of Ed, Disability Statistics Report, 14.
2. Kulig, K. et al. (2001) Clin Biomech, 16: 744-51.
3. Boninger, M. L. et al. (2005) JRRD., 42:9-19.
4. Corfman, T.A. et al. (2003) J Spinal Cord Med, 26 (2):135-140.
5. Paul, A. et al. (2012) IEEE EMBC, 4788-4791.
6. Wu, G. et al. (2005) J. Biomech, 38:981-992.

ACKNOWLEDGEMENTS

The contents of this work were developed under a grant from the Department of Education, NIDRR grant number H133E100007. However, the contents of this work do not necessarily represent the policy of the Department of Education, and you should not assume endorsement by the Federal Government.

DEVELOPMENT AND VALIDATION OF A THREE-DIMENSIONAL MODEL FOR KINEMATIC ANALYSIS OF THE THUMB

Patrick Curran, MS[1,2], Anita Bagley, PhD, MPH[2], Mitell Sison-Williamson, MS[2], and Michelle James, MD[2,3]

[1] School of Medicine, University of California, Davis, CA, USA
[2] Shriners Hospitals for Children, Sacramento, CA, USA
[3]Department of Orthopaedics, University of California, Davis, CA, USA
E-mail: patrick.curran@ucdmc.ucdavis.edu

INTRODUCTION

Congenital thumb hypoplasia is a spectrum of clinical abnormalities ranging from a small digit to absence of the thumb. Children with thumb deficiency are unable to achieve normal opposition, impairing prehension and the ability to accomplish fine motor activities [1]. Clinical assessment relies on static uniaxial goniometric measurements and qualitative evaluation of prehension. The purpose of this study is develop and validate a kinematic model of the hand to measure thumb joint range of motion (ROM) and functional workspace for assessment of children with congenital thumb hypoplasia.

METHODS

A biomechanical model of the hand was developed that included twelve retroreflective markers positioned on landmarks of the thumb, hand and fingertips (Figure 1), and eight local joint coordinate systems derived by transposing markers to joint centers. Custom MATLAB software (Mathworks Inc, Natick, MA) calculated joint ROM and functional thumb workspace. Markers were placed on a rigid segment, articulated model of the hand and joint angle calculations were validated by articulating the digits through known angles. For the functional workspace, a 3D triangular mesh shell was generated overlying marker data. Data points within the shell were interpolated and common data points between the thumb-tip and fingertips were determined. The functional workspace calculation was validated by measurement of the intersection of two known volumes.

Twenty healthy subjects (18 right-hand dominant; age = 13.0 ± 3.7 years) performed three trials of the ROM tasks: thumb flexion (F), extension (E), opposition, radial abduction-adduction (AA), palmar AA; finger F, E; total thumb ROM, and Jebsen Taylor tasks [2]: pick up paperclip, penny, bottle cap, can; turn card; stack checkers; simulate feeding. The functional workspace of the thumb was calculated by measuring the volume of intersection between total thumb-tip ROM and finger F/E data (Figure 2). One subject post-opponensplasty was also tested.

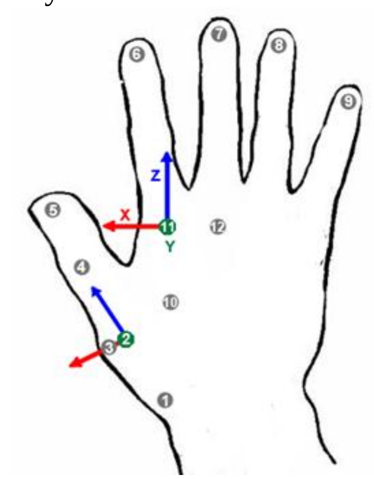

Figure 1: Location of 12 markers and two local joint coordinate systems

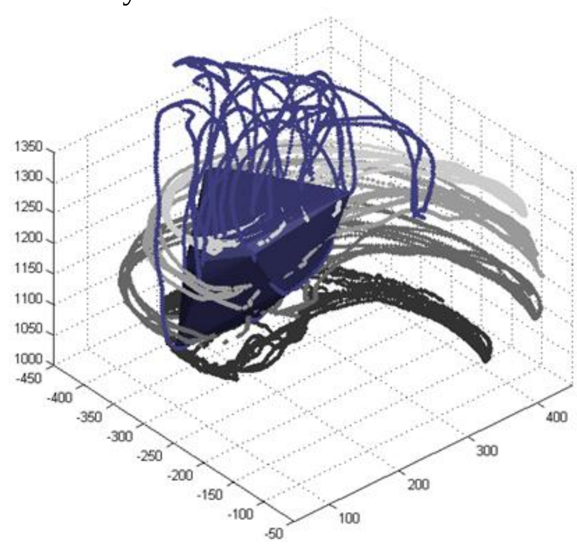

Figure 2: Blue volume shows functional workspace

RESULTS AND DISCUSSION

For the rigid hand model, there were no significant differences between goniometric and calculated joint angles. The mean error for the functional workspace calculation was 3.1% and was not affected by volume size.

For the subjects, there were no significant differences between goniometric and 3D ROM measures (Table 1). The selected functional tasks required significantly less interphalangeal (IP) and metacarpophalangeal (MCP) flexion compared to total ROM.

		Gonio-metric	3D ROM	Task
IP	Flexion	83 (21)	89 (18)	25 (4)*
	Extension	26 (14)	10 (13)	9 (4)
MCP	Flexion	58 (10)	68 (8)	24 (3)*
	Extension	2 (9)	8 (9)	7 (6)
CMC	Flexion	-	35 (13)	37 (5)
	Extension	-	12 (6)	9 (10)
	Abduction	-	23 (11)	21 (4)
	Adduction	-	11 (10)	7 (1)
	Pronation	-	11 (13)	3 (4)
	Supination	-	17 (16)	13 (1)

Table 1: Mean (standard deviation) of maximum joint angles (degrees) in three thumb joints for goniometric, 3D ROM, and functional tasks.
 * $p<0.05$ for 3D ROM and Task

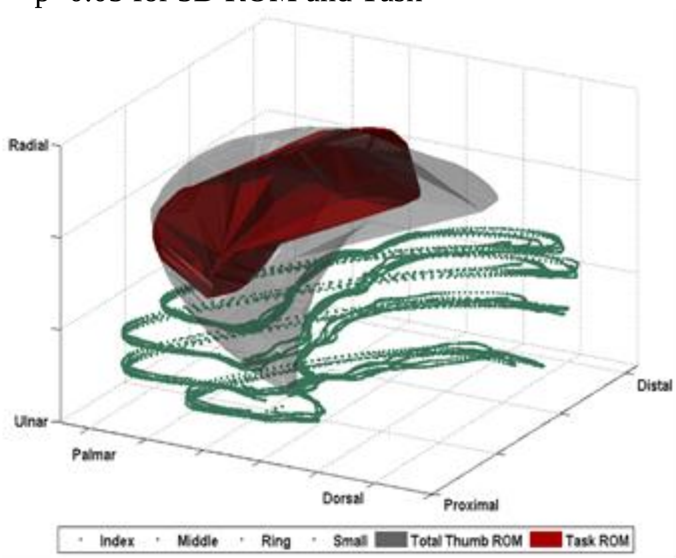

Figure 3a: Total thumb ROM and task ROM for a control subject

Figure 3 demonstrates differences between workspace and functional task volumes for a control subject (Fig 3a) and a post-opponensplasty subject (Fig 3b) and indicates the potential sensitivity of this technique.

CONCLUSIONS

This study presents an accurate kinematic model for measurement of the ROM and functional workspace of the thumb. Current clinical measurements may not adequately assess thumb motion required for prehensile activities. Future investigations will compare the functional ROM and workspace of children with congenital thumb hypoplasia to age-matched control subjects.

REFERENCES

1. Bunnell, S (1938) J Bone Joint Surg Am, 20(2):269-284.
2. Jebsen, RH, et al (1969) Arch Phys Med Rehabil, 50(6):311-319.

ACKNOWLEDGEMENTS

Funding for the work was provided by an OREF/POSNA Research Grant in Pediatric Orthopaedics.

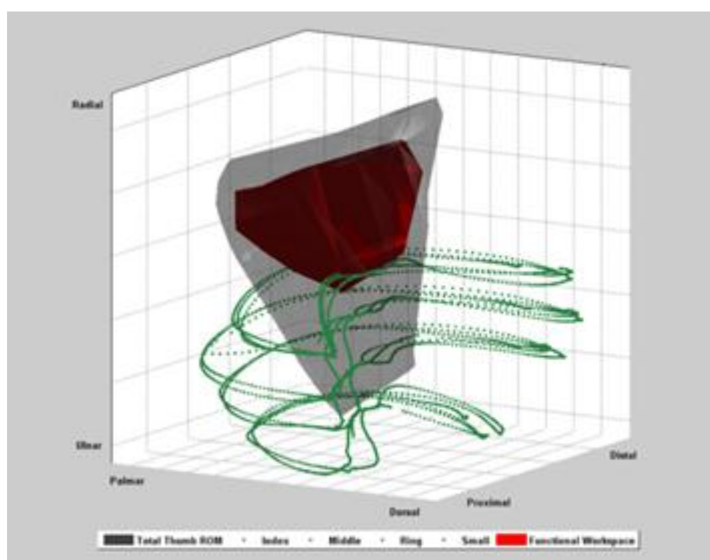

Figure 3b: Total ROM and task ROM for a post-opponensplasty subject

Design of a Bilateral ADL Task-Oriented, Robot Therapy Environment for Children with Cerebral Palsy

[1,2]Michelle J. Johnson [1]Daren Hughes, [2]Devon Holley, [2]Andrew Theriault, [3]Joseph Krzak, [3]Adam Graf and [3]Jasmine Gilliam

[1]Medical College of Wisconsin, Milwaukee, WI, USA
[2]Marquette University, Milwaukee, WI, USA
Shriners Hospitals for Children, Chicago, IL, USA
email: mjjohnso@mcw.edu

INTRODUCTION

Children with cerebral palsy (CP) often present with a variety of impairments affecting the upper limbs (UL); these impairments affect reaching and grasping ability which lead to further difficulties with activities of daily living (ADLs) including selfcare and play [1]. Wrist tendon surgery improves manipulation skills in children with cerebral palsy (CP) [2]. The rate of skill recovery after surgery is about 6 months. We desire to augment surgery with robots to increase the rate and extent of ADL recovery. Robot therapy environments can automate standard therapy to reduce mild to severe limitations in the hemiplegic UL of adults with stroke and children with CP [3, 4]. Previous studies show that goal-directed robot-assisted therapy using the MIT-MANUS robot, which is used extensively with stroke patients, can help improve UL motor control in children with CP [4]. ADLER is an ADL task-oriented robot therapy environment that assists stroke patients to relearn how to perform reach, grasp, and manipulation tasks with their affected UL [5]. Task-oriented therapy with and without robot assistance has been shown to improve motor control and ADL function in stroke patients [6].

Our long term research goal is twofold: 1) to design a bilateral version of ADLER (Bi-ADLER) that is suitable for children with hemiparetic CP to improve their ability to complete unilateral or bilateral coordinated reaching and grasping tasks; and 2) to determine if robot intervention combined with surgery and standard of care therapy (RT+S/OT) increases the rate and extent of ADL functional recovery more so than S/OT alone. In this abstract, we discuss the first aspect of our goal; the Bi-ADLER design process and the clinical needs that motivated them.

METHODS

A needs assessment conducted with pediatric rehabilitation specialists helped determine the requirements for the Bi-ADLER system. A bilateral system was desired to allow for unilateral or bilateral ADL task practice by children with right or left hemiparetic CP ranging in age from 7 to 14 years old. Keeping the child engaged and challenged throughout the therapy while he/she solve reach to grasp tasks is a key aim and is thought to drive motor relearning neural plasticity [6]. After wrist tendon surgery, a common difficulty is to coordinate hand orientation, especially hand flexion and extension (f/e) as well as pronation and supination (p/s), to enable stable manipulation. To train a child to overcome these difficulties, the robot should provide assist-as-needed control for position and orientation of the child’s hand for use in grasp/release exercises. The robot should support a variety of seated tasks in either the horizontal or vertical plane. The tasks should engage the patients and enable therapy sessions from 30 to 60 minutes in duration. The system should be safe with redundant stopping methods. The system should also minimize the child’s ability to use compensatory behaviors such as excessive trunk and shoulder movements; in doing so behaviors that limit ADL function are discouraged [7].

RESULTS AND DISCUSSION

The Bi-ADLER system will have three main components: the task environment, the position and orientation robots, and the control system (Fig. 1).

The *therapy task environment* consists of the restraint chair, a bi-directional table top to provide a workspace for children with either right or left hemiparesis, and a display monitor. The tasks supported are a subset of tasks that are currently being used after S/OT at Shriners Hospital such as string large and/or small beads and sorting cards. Engagement will be maintained by providing the child with real-time feedback on his/her movements and overall performance. Task difficulty level will be tuned to the child's level of motor function.

Two *robots* are used, each with positioning and orienting capability to support arm movements (Table 1). The active robot has 7 degrees of freedom (DOF) RRPRRRR; 5 of these DOFs will be controlled. The positioning part of the robot is an all-aluminum chassis with 3DOF, RRP. Two revolute joints drive the base and shoulder rotations and a prismatic joint drives a telescopic scissor assembly. The orientation part of the active robot will support the impaired wrist; the orthosis has 4 DOF (RRRR), two of which are active and assists in wrist f/e and p/s. This robot can be used with and without the passive one. The passive robot will support the non-impaired arm and will mimick the active robot; it will have 7 non-controlled DOFs and will be mostly SLS Rapid Prototyped construction with a lightweight aluminum prismatic joint assembly. The passive robot will passively measure the non-impaired arm movements. The *control system* uses custom programs built on Mathworks real time data hardware and software to operate the robots, collect data, and coordinate the therapy protocols and safety flags. Three emergency stops are built in: one is user activated to pause the robot and two are therapist activated to pause or shutdown motors.

The Bi-ADLER incorporates features to drive motor learning. The next phase is testing and evaluations with CP children to determine impact.

REFERENCES

1. Koman et al. , The Lancet, 363, 1619-1631, 2004
2. de Roode, CP et al. *Techniques in Hand and Upper Extremity Surgery*. 14:2, 129-134, 2010
3. Loureiro RCV et al. Med Biol Eng Comput. 49(10): 1103–1118, 2011
4. Fasoli, SE, et al. *Am J Phys Med and Rehabil,* 87, 929-936, 2008.
5. Johnson MJ et al. *Med Biol Eng Comput*. 49: 1157–1171, 2011.
6. Schaechter JD. *Prog Neurobiol.* 73:61-72, 2004
7. Mackey, AH et al. *A Phys Med and Rehabil*. 87 207-214, 2006

ACKNOWLEDGEMENTS

Research supported by RERC Technologies for Children with Orthopedic Disabilities (TECP4POD): US Department of Education, NIDRR H133E100007, Department of Physical Medicine and Rehabilitation, Medical College of Wisconsin and NIH NINDS Career Award K25NS058577-1A04.

Table 1: Range of Motions for BiAdler

	Mass	ROM for joints
POSITION		
Link 1	5.6 kg	θ1= ±90 deg
Link 2	8.79 kg	θ2= +45/-90
Link 3	5.52 kg	d3 = 0 to 0.56m
ORIENTATION [7]		
Pitch-like	Joint 4	θ4= ±90 deg
Pro/Sup	Joint 5 (ACTIVE)	θ5= ±80 deg
Yaw-like	Joint 6	θ6= ±45 deg
Wrist flex/ext	Joint 7 (ACTIVE)	θ7= -45/70 deg

Figure 1: Bi-ADLER: Active Prototyped System Configuration.

ORAL PRESENATIONS – FRIDAY SEPTEMBER 6th

	Energetics *Brian Umberger, Gregory Sawicki*
9:30 AM	Adaptation Of Step-To-Step Mechanical Work On Center Of Mass During Split-Belt Treadmill Walking **Cho G, Thajchayapong M, Toney M, Chang YH**
9:45 AM	Reduced Vertical Displacement Reverses Effect Of Speed On Energy **Korgan W, Wurdeman S**
10:00 AM	Effect Of Grade And Velocity On Metabolic Cost And Transition Work During Walking **Auyang A, Grabowski A**
10:15 AM	Redistribution Of Joint Work Within The Stance Phase Of Gait **Diffendaffer A, Yentes J, Wurdeman S, Myers S**
10:30 AM	Revisiting The Prediction Of Walking Mechanics And Energetics In Three Dimensions By Minimum Metabolic Cost **Miller R, Ackermann M, van den Bogert A**

ADAPTATION OF STEP-TO-STEP MECHANICAL WORK ON CENTER OF MASS DURING SPLIT-BELT TREADMILL WALKING

[1,2]Gloria Cho, [2]Montakan 'Ploy' Thajchayapong, [2]Megan E. Toney and [1,2]Young-Hui Chang

[1] Georgia Tech MSPO Program, School of Applied Physiology, Atlanta, GA, USA
[2]Comparative Neuromechanics Lab, School of Applied Physiology, Georgia Tech, Atlanta, GA, USA
email: ploy@ap.gatech.edu , web: http://www.ap.gatech.edu/Chang/Lab/CNL/home.html

INTRODUCTION

The purpose of this work is to try to understand how the body adjusts mechanical work on the center of mass (COM) due to external perturbation. Much of COM work is performed to redirect the center of mass from a downward to an upward velocity during transitions from one step to another, termed step-to-step transitions. In this study, step-to-step transition starts from the minimum center of mass velocity and ends at its maximum.

Split-belt treadmill has been previously used for study walking adaptation. Here we termed adaptation as the ability to adjust the body function from changes in environment.

We hypothesize that external mechanical work on COM would demonstrate adaptation to eventually match with the baseline condition.

METHODS

Subjects were asked to walk on a treadmill consisting of 2 separate belts and each belt can be controlled independently. During different testing periods, subjects walked on the treadmill with the 2 belts either moving at the same speed ("tied" condition) or at different speed ("split-belt" condition). During baseline period, subjects walked on the treadmill with belt tied at 0.5, 1.0 and 1.5 m/s. During adaptation period (10 minutes), treadmill belt speeds were set at 0.5 and 1.5 m/s. The leg was assigned randomly on each belt. At the end of testing session, the treadmill belt was tied and the speed was set at 0.5 m/s.

We used a six camera motion analysis system (120 Hz, Vicon motion system) to determine the sagittal plane positions of the body segments. Mechanical work was calculated from

$$P = \vec{F} \cdot \vec{v}_{COM} \qquad (1)$$

$$W = \int P \, dt \qquad (2)$$

RESULTS AND DISCUSSION

When walking in the split belt treadmill condition, there were two types of transitions recorded and analyzed. When transitioning from the fast belt to the slow belt, the fast leg trails, providing propulsion and the slow leg leads, providing breaking forces to slow the COM velocity.

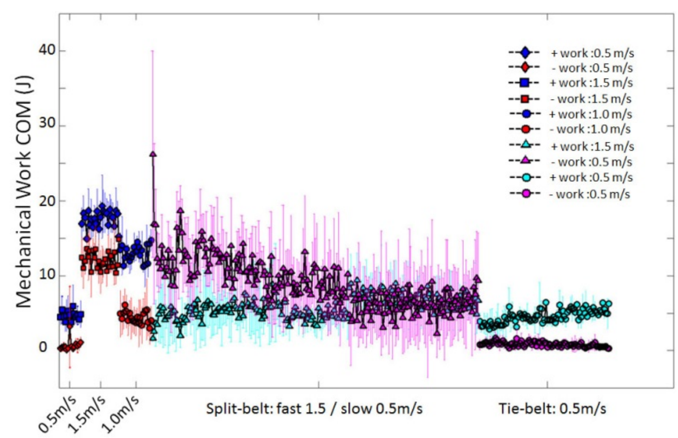

Figure 1. Transitioning from fast to slow belt, the leading leg (red/magenta) requires more steps to reach a steady state compared to the trailing leg (blue/cyan).

During this transition, the leading leg requires more steps to reach a steady state than the trailing leg, demonstrating a typical adaptation. In 2010, Reisman et al. suggested that variables with this typical exponential decay curve (Lam et al, 2006) are generally controlled via feedforward, predictive mechanisms. Because leading leg collision kinetics are dominated by the initial conditions prior to contact, it follows that leading leg control would be governed by feed-forward mechanisms. During transitions in which the body steps from the fast to the slow belt, stance kinetics of the fast leg inform the body that it is walking at 1.5 m/s. When the slow leg then encounters the belt moving at 0.5m/s, in early adaptation the walker has not yet established appropriate feedforward expectations for controlling leading leg collisions. As a result, leading leg collisions of the slow leg (pink triangles, Fig 1) are much larger than what would be expected from slow tied belt, baseline walking (red diamonds, Fig 1).

The leading leg also provides afferent sensory feedback about the encountered conditions, which may inform behavior for the trailing leg. As a result, the trailing leg can make online adjustments to account for unexpected perturbations. When transitioning from fast to slow conditions, the trailing leg positive work undershoots what would be expected from the 1.5m/s baseline (blue squares, Fig 1). The trailing leg also reaches a steady state condition for positive work in fewer steps than the leading leg, indicating that trailing leg propulsive work is likely governed by feedback control mechanisms.

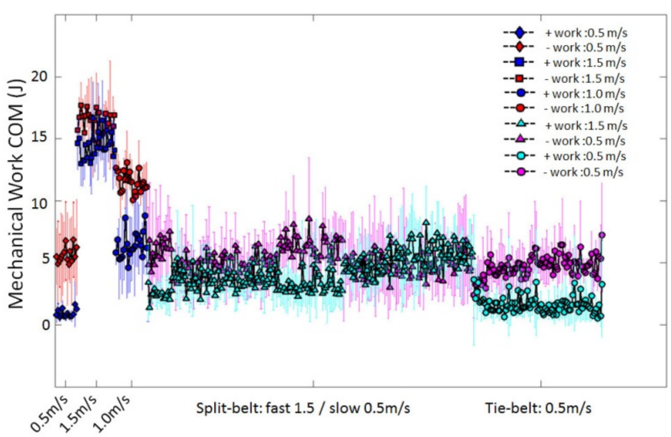

Figure 2. When transitioning from the fast to slow belt, the leading (red) and trailing (blue) legs reach steady state almost immediately after initial exposure to the split belt environment.

When transitioning from the slow to fast belt, the fast leg leads and produces less negative work than would be expected from the baseline trials. The reduced negative work appears close to the work necessary to achieve smooth transitions, and little adaptation is observed. The trailing leg correspondingly produces smaller positive, propulsive work, reaching a steady state in fewer steps similarly to what was previously observed in the fast to slow transitions.

The final steady state value does not consistently match external mechanical work calculated for the respective baseline trials. It appears that the body attempts to match positive and negative braking forces within a transition rather than matching baseline values. This final steady state value may indicate that human walkers attempt to stabilize (make consistent) some larger goal over successive steps over the course of adaptation.

CONCLUSIONS

The results presented here demonstrate that human walkers adapt kinetic parameters when walking in a split belt environment. It appears that leading leg collision kinetics are mediated by feedforward mechanisms, demonstrating a typical adaptation curve. Trailing leg propulsive forces then make online adjustments informed by afferent feedback from the leading leg dynamics. Contrary to our hypothesis, external mechanical work did not return to a recorded baseline value, but instead appeared to match braking and propulsive work within a single step. This trend provides some evidence that human walkers attempt to stabilize some greater whole-body goal when walking in an unusual environment.

REFERENCES

1. Reisman DS, Bastian AJ, Morton SM. Neurophysiologic and rehabilitation insights from the split-belt and other locomotor adaptation paradigms. Phys Ther. 2010;90(2):187-195.
2. Donelan JM, Kram R, Kuo AD. Simultaneous positive and negative external mechanical work in human walking. Journal of Biomechanics. 2002;35:17–124.
3. Adamczyk PG, Kuo AD. Redirection of center-of-mass velocity during the step-to-step transition of human walking. Journal of Experimental Biology. 2009;212:2668–2678.
4. Lam T, Anderschitz M, Dietz V. Contribution of feedback and feedforward strategies to locomotor adaptation. J. Neurophysiol 95:776-773.

REDUCED VERTICAL DISPLACEMENT REVERSES EFFECT OF SPEED ON ENERGY EXPENDITURE

[1]Whitney Korgan, [1,2]Shane R. Wurdeman, [1,2]Jennifer M. Yentes, [1]Troy Rand, [1]Sara A. Myers, [1,2]Nicholas Stergiou

[1]University of Nebraska at Omaha, NE, USA
[2]University of Nebraska Medical Center, Omaha, NE, USA
e-mail: swurdeman@unomaha.edu, web: http://nbcf.unomaha.edu

INTRODUCTION

Previous work utilizing a curved treadmill demonstrated that minimized vertical displacement of the body's center of mass (COM) did not coincide with reduced energy expenditure [1]. The curved treadmill translated the arc motion of the path of the COM bed of the treadmill to below the feet, thereby reducing vertical displacement of the COM in a more natural manner rather than having subjects adjust their gait to minimize movement. However, a limitation of this previous work was the fact that the curved treadmill was not motorized and the flat treadmill used for comparison was motorized. Thus, the purpose of this study was to address this limitation. It was hypothesized that reduced vertical displacement of the COM would still not coincide with reduced energy expenditure in a motorized curved treadmill. This hypothesis would be consistent with the original contention that reducing vertical displacement of the COM, beyond a yet to be determined "optimal" amount, results in reduced gait efficiency.

METHODS

Five subjects (age: 23.8 ± 5.6 years, ht: 170.5 ± 5.9 cm, mass: 67.9 ± 12.9 kg) walked on both a standard motorized flat treadmill and a curved treadmill (Woodway®, Waukesha, WI, USA) with three different speeds; 1.12, 1.56, and 2.01 m/s. The order of the conditions was randomized. The curved treadmill was motorized with the motor from a separate treadmill (Trackmaster® Jas Fitness System, Newton, KS, USA) by replacing the timing belt with a longer belt that was attached externally to an axle that drove the curved treadmill (Figure 1). Three different speeds were initially chosen [3]. Gear ratio limitations, however, prevented the utilization of a speed of 0.67 m/s for the curved treadmill, therefore a speed of 2.01 m/s was added on our conditions. Subjects walked at each speed for three minutes on both treadmills with breaks as needed in between each trial to reduce fatigue. Steady state oxygen consumption relative to body mass (VO2) (K4b2, Cosmed, Chicago, IL) was measured.

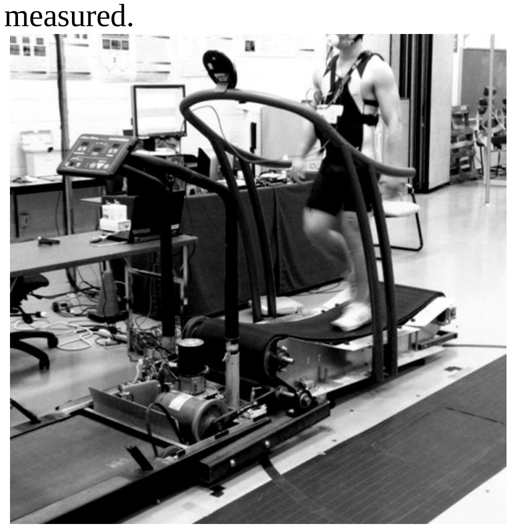

Figure 1: Setup for a flat treadmill motor powering the curved treadmill.

Vertical displacement of COM was recorded through sacral marker movement (60Hz; Motion Analysis Corp., Santa Rosa, CA, USA). Vertical displacement of the sacral marker was quantified as the dispersion about the individual's mean COM height (i.e. standard deviation) as well as maximum range of displacement through all steps within each trial. Significant differences for dispersion and range of sacral marker displacement and VO2 were tested through separate 2x3 fully repeated measures ANOVAs (treadmill x speed). When main effect or interaction was significant, Tukey tests were used for post-hoc analysis (PASW 18.0, IBM Corp., Armonk, NY).

RESULTS AND DISCUSSION

Consistent with previous findings, energy expenditure increased on the curved treadmill (p=0.002, Figure 2). There was a significant interaction, for which post-hoc analysis revealed that VO2 was significantly higher at 1.12 m/s (p<0.05) and 1.56 m/s (p<0.05) on the curved treadmill but not for the 2.01 m/s (p>0.05).

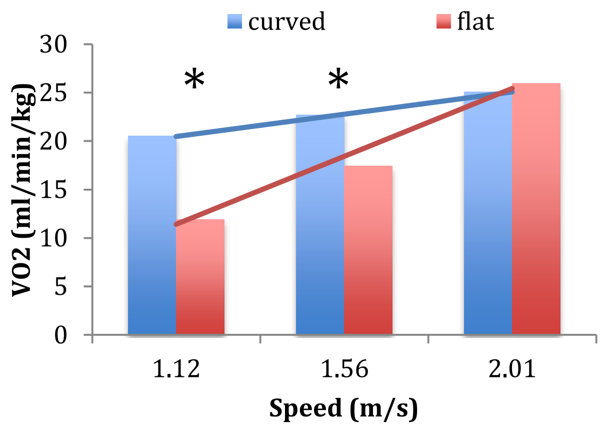

Figure 2: Energy expenditure displayed an interaction between speed and treadmill type.

Results for normalized COM displacement (Figure 3) showed a similar pattern as our previous work with increased discrepancy in COM displacement as speed increased [1]. However, the speeds utilized in this study were increased due to limitations of the adjusted treadmill. Specifically, we previously found increased COM displacement for the flat treadmill at 1.12 m/s but in the current study there was no difference (p<0.05). There is an overall significantly higher COM on the flat than the curved treadmill (p=0.05) Post hoc revealed no significance between individual speeds and treadmills. Thus, we see from the 1.12 m/s and 1.56 m/s conditions that reduced (or equal) vertical COM displacement did not coincide with reduced VO2. However, the interaction that we now see for VO2, not previously seen in the non-motorized testing, may offer additional insight. It appears that as speeds increase, the excessive motion of the COM on the flat treadmill rapidly increases VO2.

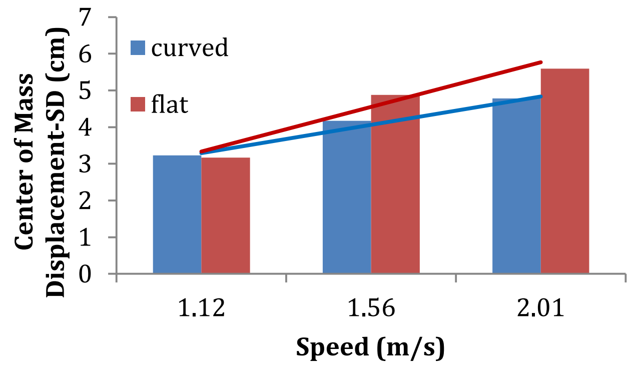

Figure 3: Center of mass displacement in terms of standard deviation increased as speed increased normalized by leg length.

CONCLUSIONS

Walking on a motorized, curved treadmill reduces vertical displacement of the COM but results in increased VO2 compared to a standard, flat treadmill. However, at higher speeds, motion of the COM on the flat treadmill grows considerably greater than on the curved treadmill at which point VO2 on the motorized curved treadmill is no longer different from the standard flat treadmill. This seems to coincide with the notion of an 'optimal' amount of vertical displacement with regards to energy expenditure during locomotion.

REFERENCES

1. Korgan et al. *Proceedings of GCMAS'12*, Grand Rapids, MI, USA, 2012.
2. Korgan et al. *Proceedings of ASB.* Gainesville, FL, USA, 2012
3. Gordon et al. *Arch Phys Med Rehabil* **90**, 136-144, 2009.
4. Snyder et al. *J Strength Cond Res* **25**: S109, 2011.

ACKNOWLEDGEMENTS

Support was provided through a Fund for Undergraduate Scholarly Experience (FUSE) grant, a UNMC Widaman Fellowship, and a NASA EPSCOR grant.

Effect of grade and velocity on metabolic cost and transition work during walking

Arick Auyang[1], Alena M. Grabowski[1,2]
[1]Locomotion Lab, Dept. of Integrative Physiology, University of Colorado Boulder, CO, USA
[2]Eastern Colorado Healthcare System, Department of Veterans Affairs, Denver, CO USA
Email: arick.auyang@gmail.com

Introduction

During level-ground walking, mechanical work from each leg is required to change the direction of the center of mass (COM) during step to step transitions [1]. Previous studies show a correlation between step to step transition (S2ST) work and metabolic cost of transport (COT) during level-ground walking [2], which suggests a relationship when walking at different slopes and velocities. Yet, to our knowledge, no one has established this correlation. This information would be useful in the design and development of assistive devices such as leg prostheses. Walking up steeper slopes requires more metabolic energy [3]. Similarly, more metabolic energy is required at faster velocities [4]. Walking uphill requires more positive trailing leg work (W_{trail}) and walking downhill requires more negative leading leg work (W_{lead}) during S2STs [5].

We sought to determine the relationship between S2ST work and COT during walking across a range of slopes and velocities. We hypothesized that changes in COT would correlate with S2ST work changes in both the leading and trailing legs.

Methods

7 healthy subjects (4 M, 3 F) walked on a dual-belt force-measuring treadmill (Bertec Corp., Columbus, OH) at three velocities (1.0, 1.25, & 1.5m/s) and 7 slopes (0°, +/-3°, +/-6°, & +/-9°). Each trial was six minutes and trial order was randomized.

We measured rates of oxygen consumption and carbon dioxide production using indirect calorimetry (Parvo Medics TrueOne 2400). We calculated metabolic power using a standard equation (Brockway 1987) and COT as the quotient of metabolic power and velocity.

We measured ground reaction forces at 1500 Hz from each leg and normalized all data to each subject's body mass. We then filtered and processed forces using a custom program (Matlab, Natick, MA).

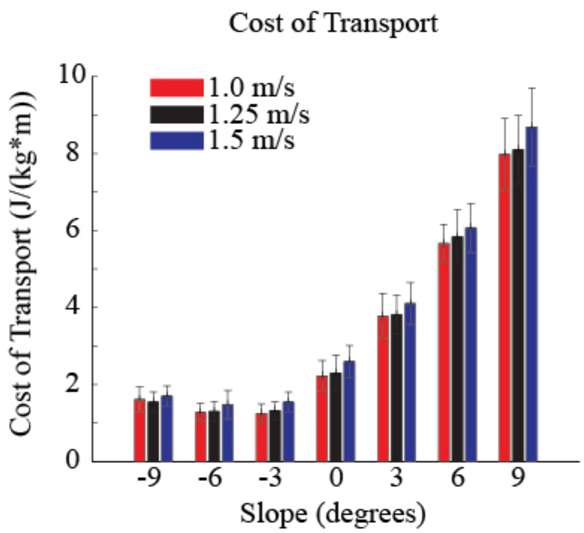

Fig. 1. Average COT (J/kg*m) across slopes at 1m/s (red), 1.25m/s (black), & 1.5m/s (blue). COT increased from -6° to 9° and from 1.25m/s to 1.5m/s.

We calculated individual leg power during S2STs as the dot product of the force and COM velocity vectors. We calculated positive and negative W_{trail} and W_{lead} by integrating S2ST powers with respect to time. Finally, we calculated each leg's net work during S2STs as the sum of the positive and negative work. We correlated COT as a function of S2ST work of each leg at each velocity using 2nd degree polynomial functions.

Results

COT increased from -6° to 9° (**Fig. 1**). COT was minimized at -6° at all velocities. There was a trend for COT to increase with velocity within each grade. W_{trail} increased with slope during S2STs (**Fig. 2a**) and with velocity from -6 to 9°. We found that W_{lead} decreased with slope from 3° to -9° and produced net positive work at 6° and 9° (**Fig. 2b**). W_{lead} decreased with faster velocities from -9° to 0°.

We correlated COT and S2ST work for each leg across all slopes at each velocity using a 2nd degree polynomial fit. R^2 values for W_{trail} were 0.76, 0.76, and 0.72 for 1.0, 1.25, and 1.5 m/s respectively. R^2 values for W_{lead} were 0.84, 0.86, and 0.84, respectively for 1.0, 1.25, and 1.5 m/s (**Fig 3**).

Discussion

Consistent with previous literature, we found that COT increased with velocity and positive slopes. We found that the minimum COT occurs at approximately -6° for all velocities tested. We found that S2ST work changes were consistent with previous studies. At steeper slopes and faster velocities, W_{trail} was greater during the transition period while W_{lead} was more negative work with negative slopes and faster velocities.

We hypothesized that changes in COT at different slopes and velocities could be explained by changes in the S2ST work required for each condition. We found that ~75% of the COT can be accounted for by W_{trail} for all velocities while ~85% can be accounted for by W_{lead}. Our findings suggest that the work performed by each leg during the S2ST phase at different slopes accounts for a large portion of the COT during walking.

Future work should examine ankle dynamics at similar slopes and velocities since ankle work greatly contributes to S2ST work over level-ground. Our results provide insight for assistive device design. Specifically, leg prostheses have been designed to optimize level-ground walking. Our results provide a starting point to evaluate the effectiveness and efficiency of leg prostheses for different slopes and velocities during walking.

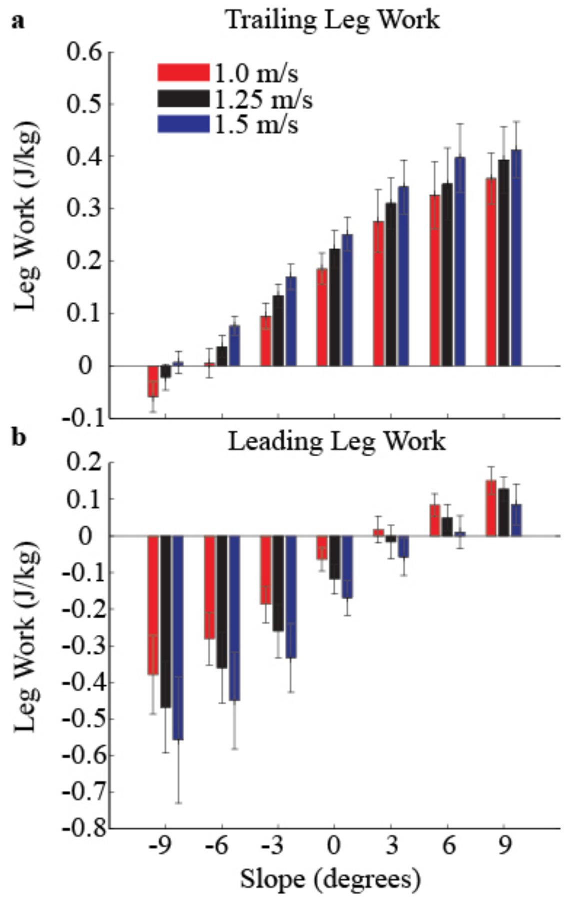

Fig. 2. S2ST mechanical leg work. (**a**) W_{trail} increased with slope. From 0° to 9°, W_{trail} was greater at faster velocities. (**b**) W_{lead} was lower as slope decreased. W_{lead} during downhill slopes was more negative work at faster velocities.

References

1. Cavagna, G.A., N.C. Heglund, and C.R. Taylor. (1977). Am J Physiol, **233**(5).
2. Donelan, J.M., R. Kram, and A.D. Kuo. (2002). J Exp Biol, **205**(Pt 23).
3. Kang, J., et al. (2002). Eur J Appl Physiol, **86**(6).
4. Taylor, C.R., N.C. Heglund, and G.M. Maloiy. (1982). Journal of Experimental Biology, **97**.
5. Franz, J.R., N.E. Lyddon, and R. Kram. (2012). J Biomech, **45**(2).

Acknowledgements

This work is supported by a VA Career Development Award (VA RR&D A7972-W) to A.M.G.

REDISTRIBUTION OF JOINT WORK WITHIN THE STANCE PHASE OF GAIT

[1]Alek Diffendaffer, [1,2]Jennifer M. Yentes, [1,2]Shane R. Wurdeman and [1]Sara A. Myers

[1]University of Nebraska at Omaha, Omaha, NE, USA
[2]University of Nebraska Medical Center, Omaha, NE, USA
email: adiffendaffer@unomaha.edu, web: http://nbcf.unomaha.edu

INTRODUCTION

More positive work than negative work over the stance phase of gait has been reported in both young and older adults [1]. However, the total positive work "reserve" in older adults is less than in young, with total net work values near zero [1]. Joint work is the integration of the joint power versus time curve allowing for the calculation of the rate of energy transfer across each joint center [2] and the total sum can be regarded as a global parameter of the body's behavior [3]. Moreover, it has been reported that older adults redistribute peak joint power throughout the three lower extremity joints at fast and self-selected speeds [4], yet older adults may also redistribute joint work within a specific joint over the stance phase of gait maintaining the same amount of work. Upon visual inspection of the power curves, noticeable differences exist during initial double support, single support and terminal double support between young and older adults. Therefore, the purpose of this study was to investigate both positive and negative work at the ankle, knee, and hip joints during the three different support phases of the gait cycle. It was hypothesized that changes in joint work were due to aging and/or speed.

METHODS

We enrolled 20 young and 20 older adults into this study. After providing informed consent, the subjects were instructed to walk along a 10-meter walkway at their self-selected speed while kinematics (60 Hz; Cortex, Motion Analysis Corp., Santa Rosa, CA, USA) and kinetics were collected simultaneously (600 Hz; Kistler Instruments, Inc., Amherst, NY). A total of five successful trials were collected for all older adults and ten trials for young adults. Gait velocities were calculated from a sacral marker. Subjects were subsequently matched one-to-one based on a criterion of ±10% mean gait velocity. This resulted in eight matched pairs. Joint power at the right ankle, knee and hip was calculated (C-Motion Inc., Germantown, MD) and custom scripts (The Mathworks, Inc., Natick, MA) were used to identify the three support phases of stance [5] and joint work calculation. In addition to work within each support phase, total joint work was computed. Independent t-tests were used to compare young vs. older adults. We further divided each group into slow vs. fast velocity based on their self-selected speed. Separate independent t-tests were used to evaluate joint work of slow vs. fast within each group. The alpha value was set at 0.05.

RESULTS AND DISCUSSION

Gait velocity for the young subjects (25.13±5.72 yrs) was 1.34±0.11 m/s and for the older adults (66.50± 5.73 yrs) was 1.33±0.15 m/s ($p=0.9$). All significant differences in joint work between young and older adults were measured at the knee and hip (Figure 1). Total positive work for young adults was 2.46±0.65 J/kg and for older adults was 1.70±0.38 J/kg ($p=0.01$). Total negative work was -1.12±0.20 J/kg and -1.46±0.31 J/kg for the young and older, respectively ($p=0.02$). These changes led to young adults having a significantly greater ($p=0.001$) total positive net work "reserve" (1.34±0.63 J/kg) compared to the older adults (0.25±0.47 J/kg) across the entire stance phase.

After separating the young adults into slow and fast velocities, their gait speeds were 1.26±0.09 m/s (n=4) and 1.42±0.07 m/s, respectively ($p=0.03$). In addition, the older adults walked at 1.20±0.04 m/s (n=4) and 1.47±0.05 m/s ($p=0.0001$). For young adults, no significant differences were found between the two speeds for any of the dependent variables. However for the older adults, the positive ankle joint work at terminal double support was significantly greater in the fast velocity group (slow: 0.75±0.13 J/kg, fast: 1.23±0.21 J/kg, p=0.008) leading to a significantly greater ankle positive total work (slow: 0.76±0.14 J/kg, fast: 1.24±0.21 J/kg, p=0.009). The fast velocity older adults also had more negative ankle work during initial double support (slow: -0.15± 0.07 J/kg, fast: -0.26±0.02 J/kg, p=0.02). In addition, the fast velocity group demonstrated reduced positive knee joint work during single support (slow: 0.008±0.005 J/kg, fast: 0.001±0.001 J/kg, p=0.04).

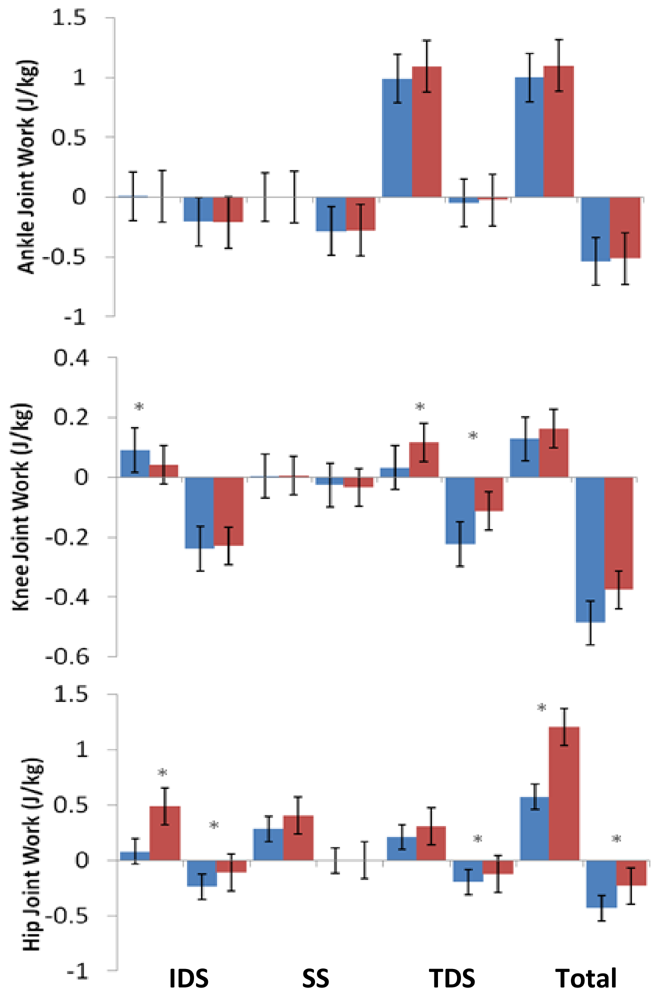

Figure 1: Results of joint work for young (red) and older (blue) during three support phases of stance (IDS: initial double support, SS: single support, TDS: terminal double support, Total: total work across the joint). Magnitudes that were significantly different are indicated by *(p<.05).

Older adults demonstrated the ability to redistribute the amount of work done within the knee and hip joints throughout the stance phase of gait. Older adults redistributed joint work at the knee by generating more work at initial double support and less at terminal double support. Further, they dissipated almost two times the energy at the knee during terminal double support as compared to the young adults. Older adults also demonstrated redistribution of joint work at the hip joint. The hip generated 1/16 of the energy generated by young adults during initial double support yet the older group dissipated more energy during initial and terminal double support at the hip. However, this redistribution was not enough to provide a reserve of positive work that was similar to the young adults. The increased total negative work overall may demonstrate reliance on more energy dissipation by the muscles through the eccentric phases of stance. This may be consistent with more of a "controlled fall" gait as opposed to actively powering forward.

Moreover, when groups were divided into slow vs. fast velocities based upon their own chosen pace, young adults were able to maintain similar joint work profiles regardless of speed. However, older adults demonstrated altered changes mainly at the ankle when divided by speed. It could be that the plantarflexors are most important for speed compensation, yet the hip and knee are affected by aging.

CONCLUSIONS

Older adults redistribute their joint work across the three support phases of gait, however, they are unable to compensate for the deficit in overall power generation. In addition, slower walking older adults demonstrate significant decrements in ankle power generation.

REFERENCES

1. Christiansen C & Heise G. *Proceedings of NACOB '08*, Ann Arbor, MI, USA, 2008.
2. Winter DA. *Biomechanics and Motor Control of Human Movement*, John Wiley & Sons, Ltd., 2005.
3. Hamill J. & Knutzen KM. *Biomechanical Basis of Human Movement.* Williams & Wilkins, 1995.
4. DeVita P & Hortobagyi T. *J Appl Physiol* **88**, 1804-1811, 2000.
5. O'Connor et al. *Gait & Posture* **25**, 469-474, 2007.

ACKNOWLEDGEMENTS

This work was supported by the University of Nebraska Omaha FIRE Grant program. We would like to thank Daniel Leib for assisting with coding.

REVISITING THE PREDICTION OF WALKING MECHANICS AND ENERGETICS IN THREE DIMENSIONS BY MINIMUM METABOLIC COST

[1]Ross H. Miller, [2]Marko Ackermann, and [3]Antonie J. van den Bogert

[1]University of Maryland, College Park, MD, USA
[2]Centro Universitário da FEI, São Bernando do Campo, SP, Brazil
[3]Cleveland State University, Cleveland, OH, USA
email: rosshm@umd.edu, web: http://sph.umd.edu/KNES/faculty/rosshm/

INTRODUCTION

A relatively low rate of energy expenditure is a signature of normal, healthy walking. However, most simulation studies of walking have focused on musculoskeletal mechanics, with metabolic energy receiving comparatively little attention. Anderson and Pandy [1,2] considered both mechanics and energetics in their simulation, and forwarded two important conclusions: first, that minimization of the metabolic cost of transport (CoT) is a valid criterion for predicting walking mechanics without tracking experimental data [1], and second, that muscle forces predicted by forward and inverse dynamics methods are practically identical [2].

Both conclusions have major implications in the study of human walking by simulation methods, and are thus in need of further evaluation. A limitation of the simulation in Ref. [1] that has not been given much attention is that its CoT (4.9 J/m/kg) was well outside a plausible statistical range for real human walking. It therefore seems that both conclusions are potentially invalid; the first because the simulation predicted an unrealistic CoT, and the second because the inverse dynamics muscle forces were compared to forward dynamics forces that incurred an unrealistic CoT.

A possible explanation for why the CoT in Ref. [1] was so high is that the initial kinematic state was prescribed from human experimental data at a point in the gait cycle when the stance leg was near its maximum knee flexion. Other walking simulations have suggested that minimizing energy expenditure leads to a straight knee in stance [3]. It is therefore not clear from Ref. [1] if the CoT was truly minimized, or if minimizing the CoT predicts realistic knee flexion in stance.

In this study, we performed a predictive (minimum CoT) simulation of walking in three dimensions with no explicit dependency on human experimental data. We expected that the resulting gait would have a more realistic CoT than Ref. [1], but an unrealistic pattern of knee motion in stance.

METHODS

A previous 2D musculoskeletal model and random-search optimization framework [4] was modified to simulate the forward dynamics of gait in three dimensions. The model had 18 degrees of freedom and consisted of a pelvis and two legs, with each leg actuated by 12 Hill-based muscle models. The model's height, weight, and muscle mass were representative of an active young adult female. Muscle excitations had a feedback component that maintained an upright pelvic posture, and a feedforward component that was a piecewise linear function of 21 nodal values spaced evenly over the stride duration. The nodal excitations, feedback gains, step duration, and initial kinematic state at heel-strike were optimized to minimize the CoT. Penalty terms rewarded solutions with periodic musculoskeletal states.

Data for a full stride of walking were reconstructed from simulation of one step by assuming bilateral symmetry [1]. For validation, experimental were collected from 14 adults while they walked in a "normal and comfortable" fashion.

RESULTS

The model's average walking speed was 1.38 m/s, near the middle of the range of speeds chosen by the subjects (1.17-1.65 m/s). The CoT was 4.1 J/m/kg, which is 25% above the expected mean CoT for human walking, but only 8% above the expected CoT for walking with suppressed arm swing and trunk motion [5,6], and 16% smaller than the CoT in Ref. [1].

The model walked with a relatively straight knee in the first half of stance before beginning to flex the knee in the second half of stance (Fig. 1). In contrast, the human subjects showed the stereotypical cycle of knee flexion/extension motion during stance (Fig. 2).

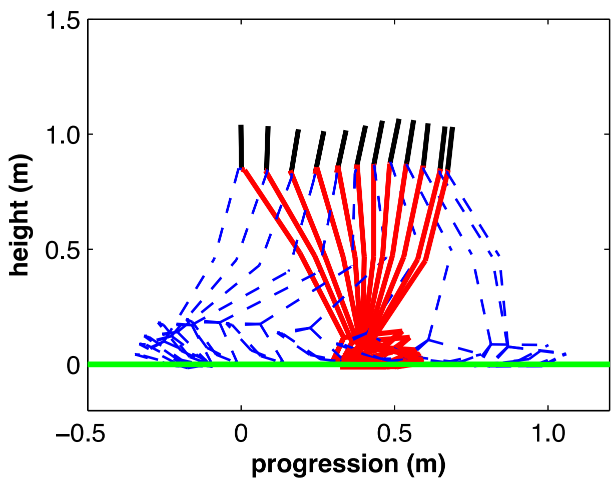

Figure 1. Sagittal plane stick figure tracing of the lower limb motion for the simulated step. Solid line = right leg, dashed line = left leg.

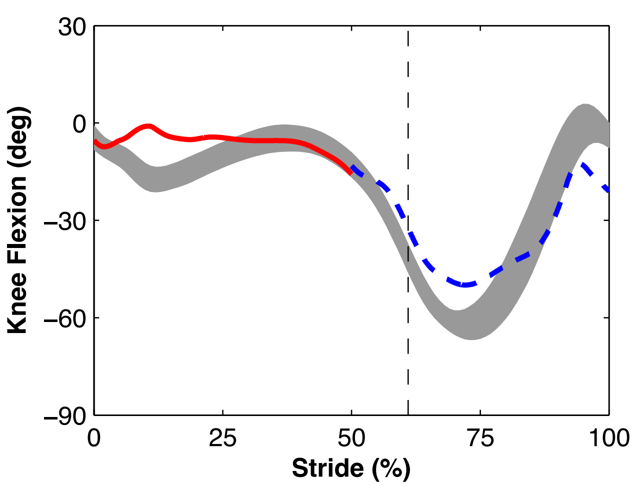

Figure 2. Knee joint angles during the simulated stride assuming bilateral symmetry. Solid line = right leg, dashed line = left leg. The shaded gray area is the mean experimental data +/- one between-subjects standard deviation.

DISCUSSION

As expected, we found that minimizing the CoT predicted an unrealistic (straight-kneed) pattern of knee joint motion during stance in simulated human walking. This finding corroborates previous results from 2D simulations that used a simpler muscle energetics model [3] and suggests that factors other than or in addition to the CoT should be considered when simulating human walking mechanics in a predictive fashion.

Simulations with different cost functions could predict more realistic walking mechanic, but they would not be expected to predict a more realistic CoT since the CoT was explicitly targeted for minimization here. Despite this targeting, we still overestimated the CoT for real human walking by 8-25%. It therefore seems that something essential for predicting simultaneously realistic mechanics and energetics of gait is missing from simulations of this variety, either in the muscle energetics model, or in the musculoskeletal or control models.

The prediction of a straight-kneed gait to minimize the CoT is at odds with experiments on human walking where suppressing knee flexion increased the metabolic cost [7], but that study suppressed knee flexion in both stance and swing, forcing considerable hip circumduction in swing. Volitional suppression of knee flexion in stance could reduce the energy requirements of walking by taking greater advantage of pendular dynamics [8], but this theory remains to be tested in experiments.

REFERENCES

1. Anderson FC & Pandy MG. *J Biomech Engr* **123**, 381-390, 2001.
2. Anderson FC & Pandy MG. *J Biomech* **34**, 153-161, 2001.
3. Ackermann M & van den Bogert AJ. *J Biomech* **43**, 1055-1060, 2010.
4. Miller RH et al. *Proc R Soc B* **279**, 1498-1505, 2012.
5. Umberger BR. *J Biomech* **41**, 2575-2580, 2008.
6. Srinivasan M. *Chaos* **19**, 026112, 2009.
7. Lewek MD et al. *Arch Phys Med Rehab* **93**, 123-128, 2012.
8. Cavagna GA et al. *J Appl Physiol* **18**, 1-9, 1963.

ORAL PRESENATIONS – SATURDAY SEPTEMBER 7th

	Ergonomics: Applied Research *Jack Callaghan, Joan Stevenson*
9:30 AM	Research And Design Of A Mover's Assistive Device For Professional Movers **Stevenson J, Whitfield B, Smallman C, Kudryk I, Reid S, Costigan P**
9:45 AM	Does Promoting Changes In Posture Using A Sit-Stand Workstation Mitagate Low Back Pain During Prolonged Standing? **Gallagher K, Campbell T, Callaghan J**
10:00 AM	Effects Of Using An Assistive Device For Overhead Work **Rashedi E, Kim S, Nussbaum M, Agnew M**
10:15 AM	Evaluation Of A Novel Thoracic Support For Mobile Police Officers During Prolonged Driving Exposures **Gruevski K, Holmes M, Gooyers C, Dickerson C, Callaghan J**
10:30 AM	Nonlinear Model-based Estimation Of Hand-arm Reaction Force In Powered Torque Tool Use **Ay H, Luscher A, Sommerich C, Berme N**

RESEARCH AND DESIGN OF A MOVER'S ASSISTIVE DEVICE FOR PROFESSIONAL MOVERS

[1]Joan Stevenson, [1]Brett Whitfield, [1]Catherine Smallman, [1]Ian Kudryk, [1]Susan Reid, [1]Pat Costigan

[1]Queen's University, Kingston, ON, Canada
email: joan.stevenson@queensu.ca, web: http://www.skhs.queensu.ca/ergbio/

INTRODUCTION

Although assistive devices have advanced over time, professional movers still prefer to move boxes by hand because they find that ergonomic aids are not sufficiently mobile for many situations (i.e., stairs, tight spaces) and are not quick enough to meet their expectations. Yet, movers encounter one of the highest risks of injury [1] and were ranked as the 6th high-risk occupation for the development of musculoskeletal injuries in Washington State [2]. Kudryk [3] identified that 93% of all summer and full-time movers developed musculoskeletal pain that occurred most commonly in the shoulders (63.3%), back (60.0%) and hands (56.7%). He also found that workers believed that carrying loads behind their bodies was easier on their backs and improved their vision. However, some employers do not allow this approach because of concerns for the safety of the goods as well as workers' safety.

The purpose of this presentation is to explain four studies that comprise the development of an ergonomic aid specific to movers' needs. The purposes of these four studies were: 1) to compare box front carries and back carries in terms of muscle electromyography and L4/L5 forces; 2) to describe the design and development of a Mover's Assistive Device (MAD); 3) to examine whether the MAD affected the coordination of movers during front and back box carries; and, 4) to examine the impact of the MAD on front and back box carries.

METHODS

Effect of front carries (FC) and back carries (BC). For Study 1, EMG was monitored from the right side of L3 (LES) and T7 (TES) erector spinae, upper trapezius (TRAP), anterior deltoid (AD), posterior deltoid (PD), rectus abdominalis (RA), external oblique (EO) and flexor digitorum (FD) muscles using a Bortec amplifier. Inexperienced male participants (n=10) carried 20% of his own body weight in a typical moving box during front carries (FC) and back carries (BC) while walking on a treadmill at 2m/s (Figure 1). EMG data were captured for 10 strides and processed using APDF.

Figure1. Back carry (BC) and front carry (FC).

L4/L5 moments and forces were calculated for 9 professional movers for FC (n=47) and BC (n=39) in Study 4. Movers stopped on an AMTI AccuGait force plate with an attached inclining and declining ramp while holding boxes during truck loading or unloading. A Cannon Vixia HFM40 video camera placed perpendicular to the force plate was used to capture 2D body posture. At a point where the force platform record was stable, a single frame was digitized using a custom feet up linked segment model. Trunk posture was also recorded.

Design of a Mover's Assistive Device (MAD). Based on the previous objective and subjective findings, a Mover's Assistive Device (MAD) was created. Several iterations were investigated before developing a version for testing in the laboratory and field. The MAD was designed to allow workers to be equally as fast, fit all sizes and used for both FC and BC of boxes (Figure 2).

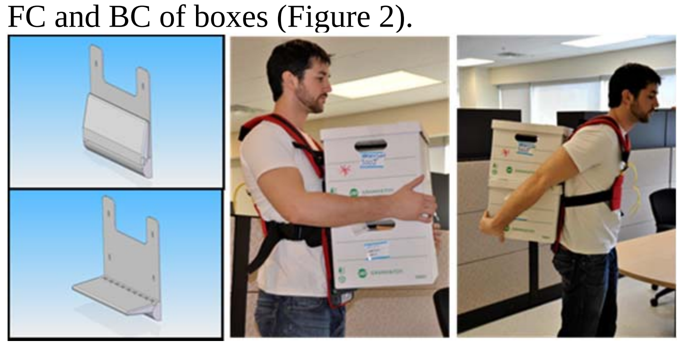

Figure 2: Ledge drawing and straps for FC and BC.

Intersegment coordination for MAD safety. One concern was whether the movers would feel less coordinated in BC versus FC conditions with and without the MAD. Coordination was defined as the 3D continuous relative phase (CRP) angles between the trunk-hip, hip-knee and knee-ankle as well as between the trunk-pelvis and box-trunk. Single and triads of retro-reflective markers were used with 6 Vicon 512 cameras to capture motions of 10 participants who walked at their preferred rates [4] on a treadmill while carrying 5 kg under the four conditions. Euler rotation sequence (flexion-extension, abduction-adduction, internal-external rotation, trunk-pelvis, box-trunk) and joint angular velocities were calculated. Then, all joint angles and velocities were divided into 30 individual gait cycles based on heel strike and normalized to 100% before calculating velocity. These data were normalized again to -1 (minimum) to 1 (maximum) at each time frame to account for amplitude and frequency differences between joints. Phase angles were calculated for each time frame of the gait cycle before calculating the continuous relative phase angles (CRP) and the SD variability of CRP angles.

Effect of MAD for FC and BC. EMG (Study 1) and L4/L5 moments/forces and trunk posture (Study 4) were repeated using the same protocols with 9 inexperienced and 9 experienced male movers respectively. Opinions of MAD were also collected.

RESULTS AND DISCUSSION

Effect of front (FC) and back (BC) carries. Figure 3 shows that the EMG of the TES, LES and Trapezius muscles were much lower for the BC than the FC. In both cases, however, the hand grip muscles were working over 50% of their MVC; these data were borne out by subjective opinions.

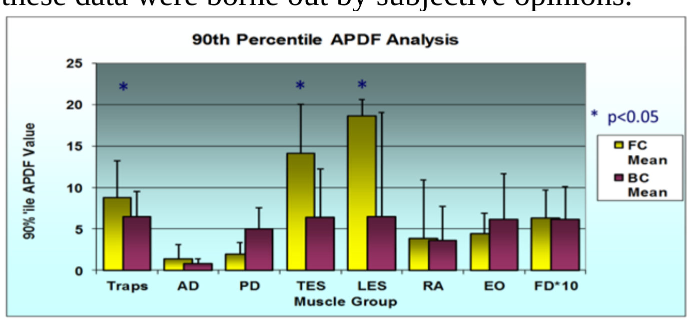

Figure 3. APDF shows BC reduces EMG activity.

Intersegment coordination. Stable coordination patterns are thought to be associated with decreased variability of the continuous relative phase angles [5]. Irrespective of the MAD, the FC technique exhibited lower CRP variability of the lower extremities than the BC technique, thus creating a more stable support for the limbs. Furthermore, MAD use resulted in decreased CRP variability of the lower extremities, which further promoted a stable support for movers. In terms of trunk coordination, no differences were observed across carrying FC and BC techniques. Although all conditions exhibited relatively in-phase coordination patterns, MAD use resulted in decreased perceived discomfort and more in-phase coordination between the trunk-pelvis. This result suggests that there is improved coordination when wearing the MAD.

Effect of MAD on FC and BC. Similar EMG patterns existed for FC and BC for back muscles as shown in Figure 3. The MAD significantly reduced the anterior and posterior deltoid activity for FC and BC respectively as well as hand grip requirements. As with the EMG, the L4/L5 moments/forces were greatly reduced in the BC condition. However, the MAD did not alter spinal loading for either FC or BC (Figure 4a). This was primarily due to forward trunk lean across both conditions (Figure 4b). Movers did like the MAD because it helped reduced their hand grips and did not slow them down.

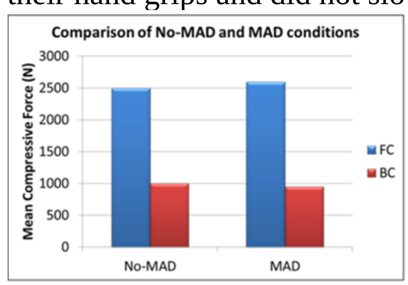

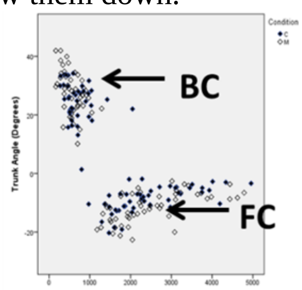

Figure 4. L4/L5 compressive force as a function of a) MAD and b) trunk posture.

ACKNOWLEDGEMENT: Ontario WSIB.

REFERENCES

1. Silverstein B et al. *Amer J. Ind Med* **41**,149-169,2002.
2. Xu Y, et al. *Occ & Env Med* **54 (10)**, 741-745,1997.
3. Kudryk I. *MSc Thesis.* Queen's University, 2008.
4. Dingwell JB, et al. *J Biomech.* **39,** 444-452. 2006
5. Scholz JP. *Phys Ther.* **70,** 827-843,1990.

DOES PROMOTING CHANGES IN POSTURE USING A SIT-STAND WORKSTATION MITAGATE LOW BACK PAIN DURING PROLONGED STANDING?

Kaitlin M. Gallagher, Troy Campbell, Jack P. Callaghan
University of Waterloo, Waterloo, ON, CA
email: kgallagh@uwaterloo.ca

INTRODUCTION

The term "sitting disease" describes the negative health effects of prolonged sitting and has led many to recommended standing or sit-stand workstations in the office place[1]; however, field studies show a relationship between occupational prolonged constrained standing and low back pain (LBP)[2]. Upwards of 40% of asymptomatic individuals demonstrate subjective reports of LBP development during a 2 hour prolonged standing simulation[3]. We investigated the use of a sitting break between bouts of prolonged standing as a way to relieve LBP development. We also investigated posture and movement differences between pain (PD) and non-pain (NPD) developers during sitting and standing.

METHODS

Ten male and ten females (ages 18-35) were recruited for this study. The exclusion criteria were no low back injuries that required a visit to a medical doctor or to miss more than three days of work, the inability to stand for two hours, previous lumbar or hip surgery, or work in an occupation that requires prolonged static standing within the last 12 months.

Participants were outfitted with tri-axial accelerometers in four locations: head, and T1, L1, and S2 vertebrae. Subjective pain ratings were recorded using a 100 mm visual analogue scale (VAS). Participants were asked "indicate the CURRENT level pain in your low back". The scale's endpoints were anchored with "No Pain" and "Worst Pain Imaginable".

Upon entering the lab, participants completed informed consent and a baseline VAS. After participants were outfitted with accelerometers and took a post-instrumentation VAS, they entered the experimental protocol. Participants worked at a computer in a 3:1 stand:sit ratio where they worked for 45 minutes in standing, then transitioned to 15 minutes of sitting. This protocol was then repeated a second time. The computer tasks were randomized within a participant between keyboarding, mousing, and combination tasks. Participants took VAS scores every 5 minutes in standing, 2.5 minutes in sitting, and immediately after they transitioned from standing to sitting (or vice versa).

Participants were categorized as PD if their VAS score reached 10 mm in the standing trial. Neck, thoracic, and lumbar spine angles were calculated form the accelerometers using a custom written MATLAB (v7.11.0, R2010b, The Mathworks, Natick, MA) program. Lumbar spine angle was expressed with respect to maximum lumbar extension. An APDF was calculated to determine the median (50^{th}%ile) and the range (difference between the 10^{th} and 90^{th}%ile) for each angle. A three way general linear model with between factors of gender and pain stature and within factor of time was used to analyze the variables. If there were no main effects or interactions containing gender and time, the variables were collapsed and the model was re-run. Significance was set at p<0.05.

RESULTS AND DISCUSSION

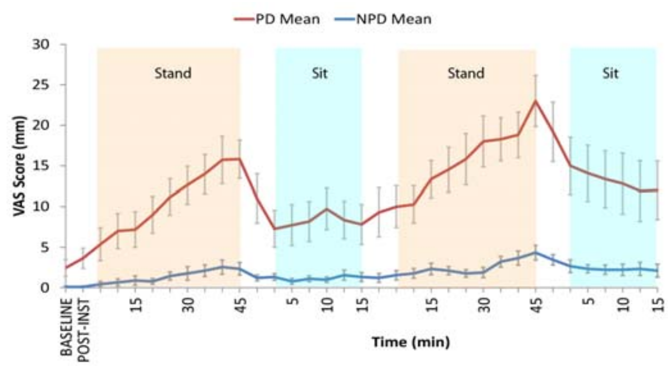

Figure 1. VAS scores over the two-hour experiment protocol.

55% of participants (six males, five females) were classified as PD based on their VAS scores. The PD group demonstrated an increase in VAS scores during the first 45 minute standing period (Figure 1), followed by a decrease when they sat; however, there was a residual pain that persisted during the sitting period. A second increase was noted within the second standing block, which was higher than that seen in the first block of standing, and sitting again reduced this subjective rating.

It was hypothesized that differences in lumbar angles between PD and NPD would exist in standing; however, groups demonstrated similar lumbar angles (approximately 15 degrees from max extension) (Figure 2). A main effect of time (p<0.0001) was found, driven by a significant difference in lumbar angle between sitting and standing.

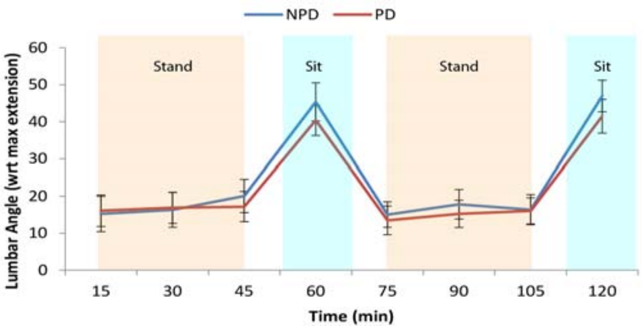

Figure 2. Normalized lumbar spine angle.

Main effects of pain group (p=0.0091) and time (p=0.0405) were found for lumbar spine angle range (Figure 3). Overall, NPD had a greater range of lumbar spine angle compared to PD. Both groups moved significantly less in the first 45 minutes compared to the first bout of sitting. Their range decreased but remained consistent in the second standing block and increased again slightly in sitting.

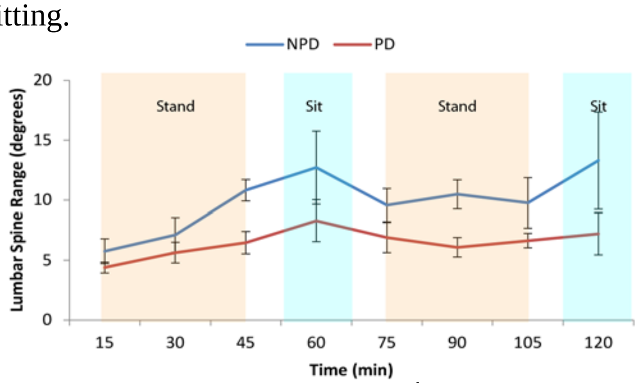

Figure 3. Lumbar spine angle range (90^{th}-10%ile)

The flattened lumbar spine in sitting, compared to the lordotic posture in standing, seems advantageous for the PD because it relieved their pain. Mild flexion is associated with reduced stress on the facet joints, reduced compressive stress on the posterior annulus, and improved transport of disc metabolites[4]. Recommended standing postures, such as one foot elevated or a sloped surface, also provide flattened lordosis. As a result, it was thought that PD would stand in a more extended posture. The key may not be the posture a person is in, but how much they move around this posture that matters. While their median postures are similar, increased movement seen in NPD around this posture may decrease the negative effects of a more lordotic spine. People who stay in this posture will bear the negative effects of a more lordotic posture.

A 15 minute break from standing was not long enough to relieve LBP for the PD. In static flexion, a work/rest ratio of 1:1 (i.e. 30 minutes flexion, 30 minutes rest) is optimal for preventing a prolonged neuromuscular disorder[5], but only up to a point. In this study, the stand:sit ratio was 3:1. As a result, a prolonged effect likely occurred and the 15 minutes of sitting did not relieve this, thus making the baseline for the next 45 minutes even higher and the pain worse in PD.

CONCLUSIONS

Pain developers utilize a smaller range of their lumbar spine angle compared to NPD, which may result in a static lordotic posture that results in a prolonged aggravation of tissue that has not resolve itself after 15 minutes of sitting and worsens when a person stands again. A stand:sit ratio of 3:1 does not allow for proper recovery of low back pain as a result of prolonged standing. The evidence indicates that implementing long exposures at standing workstations introduces the potential for LBP in workers. As a result, future research should investigate a ratio for LBP developers during prolonged standing that still allows for movement in the workplace.

REFERENCES

1. Plotnikoff et al. *Arch Environ Occ Hlth* **67**, 125-7, 2012
2. Tissot et al. *Ergonomics*, **52**, 1402-18, 2009
3. Nelson-Wong et al. *J Electyromyog Kinesiol* **20**, 256-63, 2010
4. Adams et al. *J Bone Jt Surg(Br)*, **67**, 625-9, 1985
5. Sbroccli et al. *Spine*, **29**, 2643-53, 2004.

EFFECTS OF USING AN ASSISTIVE DEVICE FOR OVERHEAD WORK

Ehsan Rashedi, Sunwook Kim, Maury A. Nussbaum and Michael J. Agnew

Virginia Tech, Blacksburg, VA, USA
email: nussbaum@vt.edu

INTRODUCTION

Work-related musculoskeletal disorders (WMSDs) in the upper extremity (UE) are an important issue in the modern U.S. workplace. Shoulder WMSDs in particular accounted for ~13% of all cases in 2011, with greater severity than other body regions [1]. Overhead work – working with the arms at or above the shoulder – is an important risk factor for shoulder injuries [2], since overhead work, by its nature, places concurrent demands (e.g., non-neutral postures and increased muscular activity) on the UE musculature and connective tissues.

Unless overhead work can be eliminated, the effects of overhead work can potentially be reduced by implementing engineering controls. As one example, the use of an inverted drill press in construction reduced extreme UE working postures and shoulder loading [3]. More generally, though, there is a lack of readily-available control measures for overhead work. Here, we explored a new approach – developed from a combination of a commercially-available mechanical arm (zeroG^2; Equipois Inc., Los Angeles, CA) and an exoskeletal vest (Fawcett Exovest^{TM}; The Tiffen Company, Hauppauge, NY) – as a potential assistive device for overhead work and that could be used in manufacturing environments (Figure 1).

METHODS

Twelve male participants, with no self-reported musculoskeletal disorders, completed the experiment after giving informed consent (procedures were approved by the Virginia Tech Institutional Review Board). Participant mean (SD) age, stature, and body mass were 27 (2.6) yrs, 178 (4.6) cm, and 76 (4.6) kg, respectively. A repeated-measures design was used, in which each participant performed a 10-min simulated overhead work task in six trials involving all combinations of two *Intervention* and three *Payload* conditions. Trials involved a 50% duty cycle and 30 sec cycle time. The task involved maintaining a hex socket engaged with a fixed bolt oriented downward, such that the hands were slightly above individual head height (Figure 1). The two *Intervention* conditions were with vs. without use of the assistive device (arm + vest). The three *Payload* conditions involved light (1.1 kg), medium (3.4 kg), and heavy (8.1 kg) masses, selected to represent a range of powered or pneumatic hand tools likely used in auto and aircraft manufacturing environments.

Ratings of perceived discomfort (RPDs) and electromyography (EMG) were obtained from the upper arm, shoulder, and low back. RPDs were collected every four cycles (i.e., every 2 min) using a 10-point scale [4]. EMG was monitored bilaterally from: triceps brachii (TB), anterior and middle deltoid (AD and TB), and iliocostalis lumborum pars lumborum (ILL). Pairs of bipolar Ag/AgCl electrodes (AccuSensor, Lynn Medical, MI) were placed on the skin surface with a 2.5 cm inter-electrode distance. Raw EMG signals were sampled at 960 Hz using a telemetered system (TeleMyo 900, Noraxon, AZ) and bandpass filtered (20 - 400 Hz). In each work period, EMG root mean square (RMS) values were obtained with a time constant of 250 ms, and were averaged over the sampling duration. Mean RMS values were then normalized (nRMS) to corresponding reference RMS values; these were obtained initially, while participants maintained the same working postures without any payload.

For each trial, final values of RPD and the mean values of nRMS in the last cycle (after 20 cycles, or 10 min) were statistically analyzed. Separate repeated-measures analyses of variance (RANOVAs) were performed to assess the effects of *Intervention* and *Payload*. Post hoc comparisons were performed using Tukey's HSD where relevant.

All statistical analyses were conducted using JMP Pro 10 (SAS Institute Inc., Cary, NC), and statistical significance was determined when $p < 0.05$.

RESULTS AND DISCUSSION

RPDs for the upper arm and shoulder significantly decreased with the use of the assistive device (all p values ≤ 0.019). This decrease was most pronounced when handling the medium and heavy payloads, with respective reductions of 47% and 54% (Figure 2). In contrast, low back RPD values increased with the use of assistive device across all conditions ($p = 0.007$). This divergence in effects was likely caused by the fact that the vertical rigid frame of the exoskeletal vest enabled a redistribution of external loads from the shoulder to the torso and pelvis (see Figure 1).

Use of the assistive device had a significant effect on bilateral AD nRMS ($p < 0.0002$), with respective decreases of 41% and 54% on the right and left sides. Although MD was not significantly affected by *Intervention*, the left TB was significantly affected across all levels of *Intervention* and *Payload* (p values ≤ 0.0034). TB nRMS values substantially decreased with the use of the assistive device when handling the medium (45%) and heavy (37%) payloads. On the other hand, increasing payload resulted in greater ILL nRMS bilaterally. Use of the assistive device also caused a substantial increase in right ILL nRMS (> 40%, $p < 0.0001$). This latter effect could be due to the connection of the zeroG^2 arm to the exoskeletal vest being on the left side. As such, it is likely that the right ILL activity increased to equilibrate the resulting asymmetric external torso moment. In addition to observed increased demands on the low back with the assistive device, the rigidity of the vest likely constrained trunk movement, and which may have further increased back muscle activity and contributed to increased levels of perceived discomfort reported for the low back.

Overall, the assistive device seems to effectively reduce demands on the UE, particularly when handling heavier payloads (> 3.1 kg), though also imposing increased demands on the low back. The latter effect, however, was of smaller relative magnitude than the former, and suggests potential utility of this approach as a practical intervention. However, the duration of simulated work was relatively short (10 min) here, and generalization to more realistic (prolonged) working conditions is unclear. Future study is thus warranted to understand the longer-term effects of the assistive device and its acceptance to workers in the field.

Figure 1: The exoskeletal vest (Left) and working posture using the assistive device (Right).

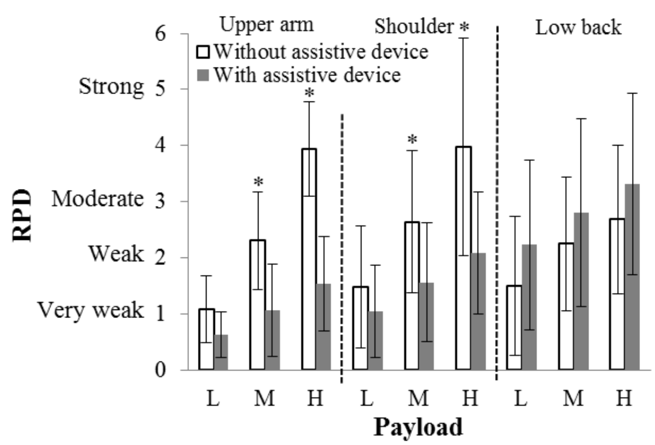

Figure 2: *Intervention* × *Payload* interaction effects on ratings of perceived discomfort (RPDs). The symbol * indicates a significant pairwise difference between *Intervention* conditions.

REFERENCES

1. Bureau of Labor Statistics. *US Department of Labor*, Washington, DC, 2012.
2. McGlothlin JD, et al. *Ergonomics* **36**, 697-717, 1993.
3. Rempel DM, et al. *Professional Safety* **52**, 30-35, 2007.
4. Borg G. *Scand J Work Environ Health* **16**, 55-58, 1990.

EVALUATION OF A NOVEL THORACIC SUPPORT FOR MOBILE POLICE OFFICERS DURING PROLONGED DRIVING EXPOSURES

[1]Kristina M. Gruevski, [2]Michael W.R. Holmes, [1]Chad E. Gooyers, [1]Clark R. Dickerson, [1]Jack P. Callaghan

[1]Department of Kinesiology, University of Waterloo, Waterloo, ON, Canada
[2]Faculty of Health Sciences, University of Ontario Institute of Technology, Oshawa, ON, Canada
email: kmgruevs@uwaterloo.ca

INTRODUCTION

Previous research has noted an increased prevalence of back pain among professional drivers, including mobile police officers [1]. The equipment (duty belt and Kevlar vest) worn by officers creates a unique interface between the occupant and the seat. Low back discomfort was 35% lower in a prototype automobile seat with an active lumbar support system (ALS) and foam structural modifications compared to a standard Crown Victoria Interceptor (CV) seat [2]. Therefore, the aim of this investigation was twofold: (i) to develop a retrofit thoracic support (TS) that when applied to a CV seat mimicked the ALS seat and (ii) to evaluate changes in spine posture and discomfort induced by the TS during prolonged simulated driving.

METHODS

The TS was developed by digitizing the 3D surface profile seat using an active motion capture system (Optotrak Certus, Northern Digital, Inc., Waterloo, ON) and identifying the mapped difference between the surface scans for the ALS and CV seats (Figure 1). The force/deflection properties of the ALS seat in its fully inflated state was measured to select a foam to mimic the seat's stiffness properties. The foam sample (Evazote EV50 foam, Zotefoams, Croydon, Surrey, UK) was tapered at its edges to minimize impedance to axial trunk rotation and the final prototype was covered with a light textile fabric.

Fourteen participants: 7 male (21.3±1.9 years, 1.71±0.06 m, 75.1±9.3 kg) and 7 female (23.3±4.4 years, 1.69±0.06 m, 68.2±7.7 kg) attended two 120 minute driving simulations on separate days, using: (i) a standard CV seat (control) and (ii) the same seat equipped with the TS. Lumbar spine postures were expressed as percentages of a functional range

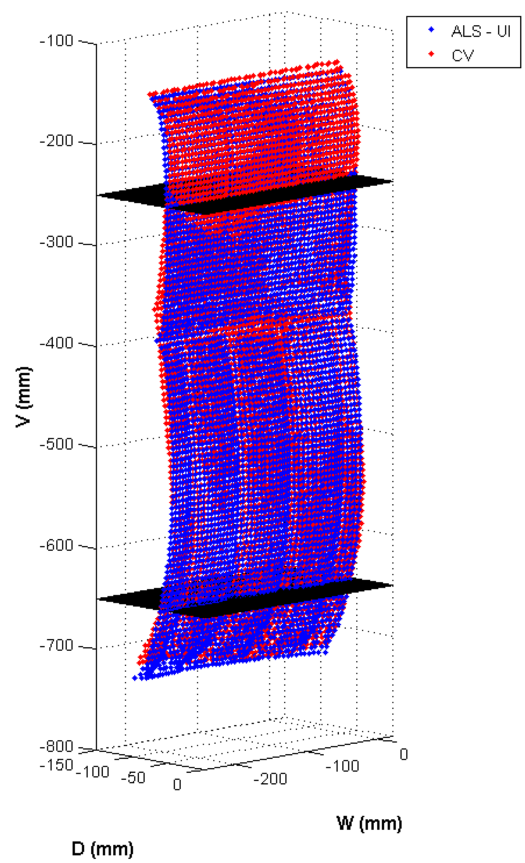

Figure 1: Mapped differences between the highest inflated ALS mechanism position compared to the CV seat. The height (V), depth (D) and width (W) are graphed in mm.

of motion with 0 percent representing standing postures and 100 percent representing maximum flexion. Seat interface pressure was measured on the seat back and seat pan. Discomfort was recorded on a 100mm visual analogue scale (VAS). A three-way mixed general linear model with repeated measures on time and seat was completed.

RESULTS AND DISCUSSION

The TS did not reduce discomfort; however, scores were low in both conditions and comparable to previous work [3]. Over the two hour driving period, discomfort values were below 9mm in both conditions, a threshold that has been used to indicate a meaningful change in the level of discomfort [4]. The seatback pressure profiles were separated into upper and lower sections to identify the contact of the TS with the subject (upper) and isolate the area where the duty belt contacts the seat (lower). Total pressure (p=0.0324; Figure 2) and pressure contact area (p=0.0008) were significantly reduced in the lower half of the backrest for the TS condition. Pressure contact area increased with the TS in the upper half of the seatback, suggesting increased support in the upper half of the seatback and reduced pressure on the lower half of the seatback. The mean of normalized lumbar flexion for the TS seat was 54.2 ± 29.3 % compared to 27.3 ± 34.9 % in the CV condition (Figure 3).

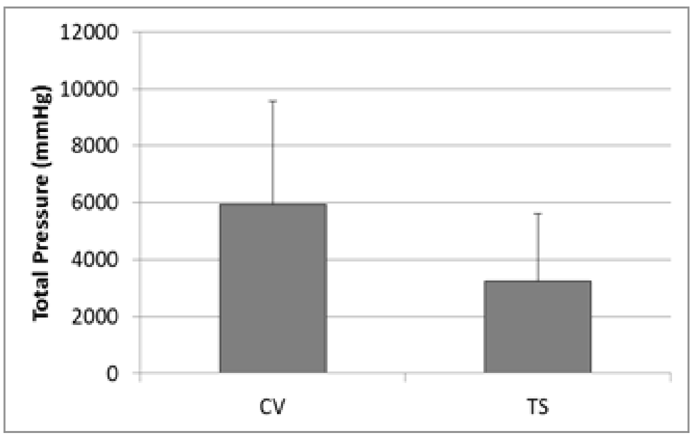

Figure 2: Total Pressure on the lower half of the seat back is reduced in the thoracic condition, α=.05

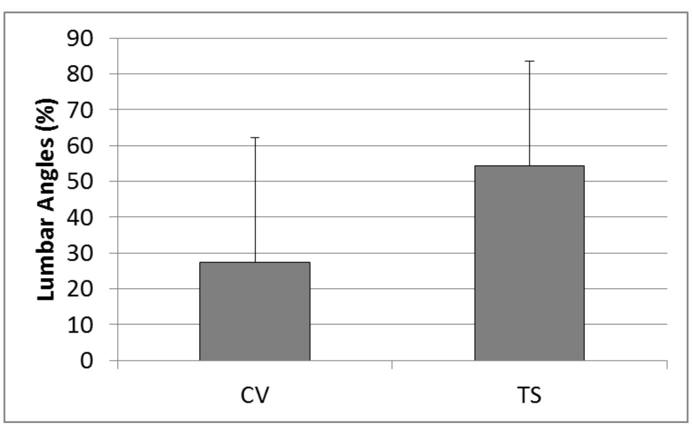

Figure 3: Increased normalized lumbar flexion angles in the TS condition compared to the control seat, α=.05

The lumbar flexion angles in the TS condition were similar in magnitude to previous research involving prolonged non-occupational driving [5]. A recent investigation compared lumbar spine postures between a standard duty belt configuration and a modified configuration removing items on the belt from the low back area [3]. Normalized lumbar postures were found (on average) to have greater flexion in the reduced belt compared to the standard belt with 34.5 ± 29.9 % and 27.5 ± 27.8 % respectively [3], which is similar to the trend observed in the present study. While lumbar spine postures in the CV condition were found to be closer to upright standing values, this may not be representative of postures that reduce discomfort reporting [6]. Previous work has demonstrated that while an in-vehicle lumbar support increased lordosis compared to no support, there was no change in pelvic posture between the two driving conditions [7]. Increased lordosis with a fixed pelvis has been shown to increase discomfort reporting [6] and may increase tension at the lumbosacral junction [7].

CONCLUSIONS

The reduction in interface pressure at the base of the seat back and the promotion of lumbar flexion angles that mimic non-occupational driving postures support the TS as an ergonomic intervention for both male and female mobile police officers.

REFERENCES

1. Gyi & Porter. *Appl Ergon* **30**, 99-107, 1998.
2. Donnelly et al. *JOSE*, **15(3)**, 295–307, 2009.
3. Holmes et al. *Ergonomics*, **56(1)**, 126-136, 2013.
4. Kelly, A. M. *AEM*, **(5)11**, 1086-90, 1998
5. De Carvalho et al. *IJIE*, **41(6)**, 617-624, 2011.
6. De Carvalho & Callaghan. A.C.E. Abstract, 2011
7. De Carvalho & Callaghan. *Appl Ergon* **43(5),** 876-882, 2012

ACKNOWLEDGEMENTS

The authors greatly acknowledge financial support from the Natural Sciences & Engineering Research Council of Canada and the Workplace Safety & Insurance Board of Ontario.

NONLINEAR MODEL-BASED ESTIMATION OF HAND-ARM REACTION FORCE IN POWERED TORQUE TOOL USE

Haluk Ay[1], Anthony F. Luscher[2], Carolyn M. Sommerich[3], Necip Berme[1, 2]
[1] Bertec Corporation, Columbus, OH, USA
[2] Department of Mechanical and Aerospace Engineering, The Ohio State University, Columbus, OH, USA
[3] Department of Integrated Systems Engineering, The Ohio State University, Columbus, OH, USA

INTRODUCTION

Powered torque tools are commonly used in manufacturing industry to tighten fasteners with increased productivity and tightening torque accuracy. However, prolonged exposure to the impulsive forces in torque tool use is associated with muscle fatigue and stress, which may lead to upper extremity injuries and musculoskeletal disorders [1, 2]. This study employed a previously developed and validated nonlinear hand-arm model to estimate hand-arm reaction force during right angle direct current (DC) torque tool use [3, 4]. Experiments were conducted with human subjects and force estimation results were compared to the experimental measurements in terms of peak values and coefficient of determination (R^2).

METHODS

The experiment procedures and the testing apparatus were described in Ay et al. [3]. The subjects (12 male, 10 female) were instructed to resist a precisely controlled half-sine torque pulse while grasping the handle of an instrumented tester bar assembly. The apparatus served as a physical simulation of a right angle torque tool. Two pulse amplitude (20, 30 Nm) and four pulse duration (200, 360, 520, 680 ms) levels were tested with each subject. Hand-arm angular velocity ($\dot{\theta}$) and reaction force (F_h) were measured simultaneously.

The nonlinearity characteristics of the hand-arm model in Ay et al. [3] represented delayed muscle force generation and stiffness modulation in eccentric and concentric exertions. The hand-arm dynamics were quantified with constant mass (m) and damping (c) elements as well as a nonlinear stiffness (k) parameter. The elements of the time series estimated hand-arm reaction force vector ($F_{h,i}$) were calculated using the effective handle length ($L_{h,i}$) and the model parameters (Eqn. 1). In Eqn. 1, $L_{h,i}$ was determined based on the simultaneous bending moment and shear force measurements from the custom load cell in the tester bar assembly. Angular acceleration ($\ddot{\theta}$) and displacement (θ) were calculated using numerical differentiation and integration of $\dot{\theta}$, respectively.

Eqn. 1 $$F_{h,i} = L_{h,i}\left(k_i\theta_i + c\dot{\theta}_i + m\ddot{\theta}_i\right)$$

The peak error and R^2 of estimated force with respect to the experimental measurements were calculated. We conducted two-way ANOVAs to investigate the differences in peak force error and force R^2 due to the main effects as well as the interaction of torque amplitude and duration. Post-hoc comparisons using the Tukey's test were carried out on the statistically significant results.

RESULTS AND DISCUSSION

Sample results of estimated versus experimental hand-arm reaction force profiles at each pulse duration level are shown in Figure 1. Tables 1 and 2 show the mean and standard deviation (SD) values of error in peak force and force R^2 estimation with respect to the experimental measurements.

Table 1: Mean and SD values of peak force error and force R^2 at the tested torque pulse duration levels.

Torque Pulse Duration (ms)	Mean (SD) Error in Peak Force (%)	Mean (SD) Force R^2
200	-1.04 (5.19)	0.87 (0.09)
360	0.94(3.66)	0.90 (0.09)
520	-0.29 (4.44)	0.93 (0.06)
680	-0.46 (5.68)	0.93 (0.08)

Table 2: Mean and SD values of peak force error and force R^2 at the tested torque pulse amplitude levels.

Torque Pulse Amplitude (Nm)	Mean (SD) Error in Peak Force (%)	Mean (SD) Force R^2
20	-0.07 (5.36)	0.89 (0.10)
30	-0.36 (4.24)	0.92 (0.06)

The two-way ANOVA results are shown in Tables 3 and 4. There were no significant interactions between torque amplitude and duration that affected error in peak force (*p = 0.374*) or force R^2 (*p = 0.924*). We found that the error in peak force was not affected by either the torque pulse amplitude (*p = 0.695*) or duration (*p = 0.269*). On the other hand, the differences in force R^2 due to torque amplitude (*p = 0.006*) and duration (*p = 0.001*) were statistically significant. Post-hoc comparisons with Tukey's test showed that mean force R^2 for the 20 Nm condition was significantly different from the 30 Nm condition. Also, the mean force R^2 for the 200 ms condition was significantly different from the 520 ms and 680 ms conditions.

Ay et al. [3] showed that the nonlinear hand-arm model provided accurate *displacement* estimation for various pulse amplitude and duration conditions of powered torque tool use. The results in this study demonstrated that the nonlinear model also provided accurate *reaction force* estimation for the same torque amplitude and duration conditions. Together, these findings suggested that nonlinear characteristics of hand-arm dynamics, which negatively affected the accuracy of linear modeling in torque tool use with respect to torque pulse amplitude and duration, were successfully represented with the developed nonlinear model.

Table 3: The ANOVA table for error in peak force with respect to torque amplitude and duration.

Source	DF	SS	MS	F	P
Torque Amplitude	1	3.6	3.57	0.15	0.695
Torque Duration	3	91.8	30.61	1.32	0.269
Interaction	3	72.7	24.22	1.04	0.374
Error	168	3894.6	23.18		
Total	175	4062.7			

Table 4: The ANOVA table for force R^2 with respect to torque amplitude and duration.

Source	DF	SS	MS	F	P
Torque Amplitude	1	0.053	0.053	7.85	0.006
Torque Duration	3	0.124	0.041	6.13	0.001
Interaction	3	0.003	0.001	0.16	0.924
Error	168	1.132	0.007		
Total	175	1.313			

REFERENCES

1. Chourasia, A. O., *et al.* (2009). Prolonged mechanical and physiological changes in the upper extremity following short-term simulated power hand tool use. *Ergonomics, 52*(1), 15-24.
2. Ku, C. H., *et al.* (2007). Power hand tool kinetics associated with upper limb injuries in an automobile assembly plant. *Journal of Occupational and Environmental Hygiene*, *4*(6), 391-399.
3. Ay, H. *et al.* (2012). A nonlinear hand-arm model for interaction with impulsive forces. *36th Annual Meeting of the ASB*, Gainesville.
4. Ay, H. (2011). Linear and nonlinear models of human hand-arm dynamics and torque tool interaction. *Unpublished doctoral dissertation*. The Ohio State University, Columbus.

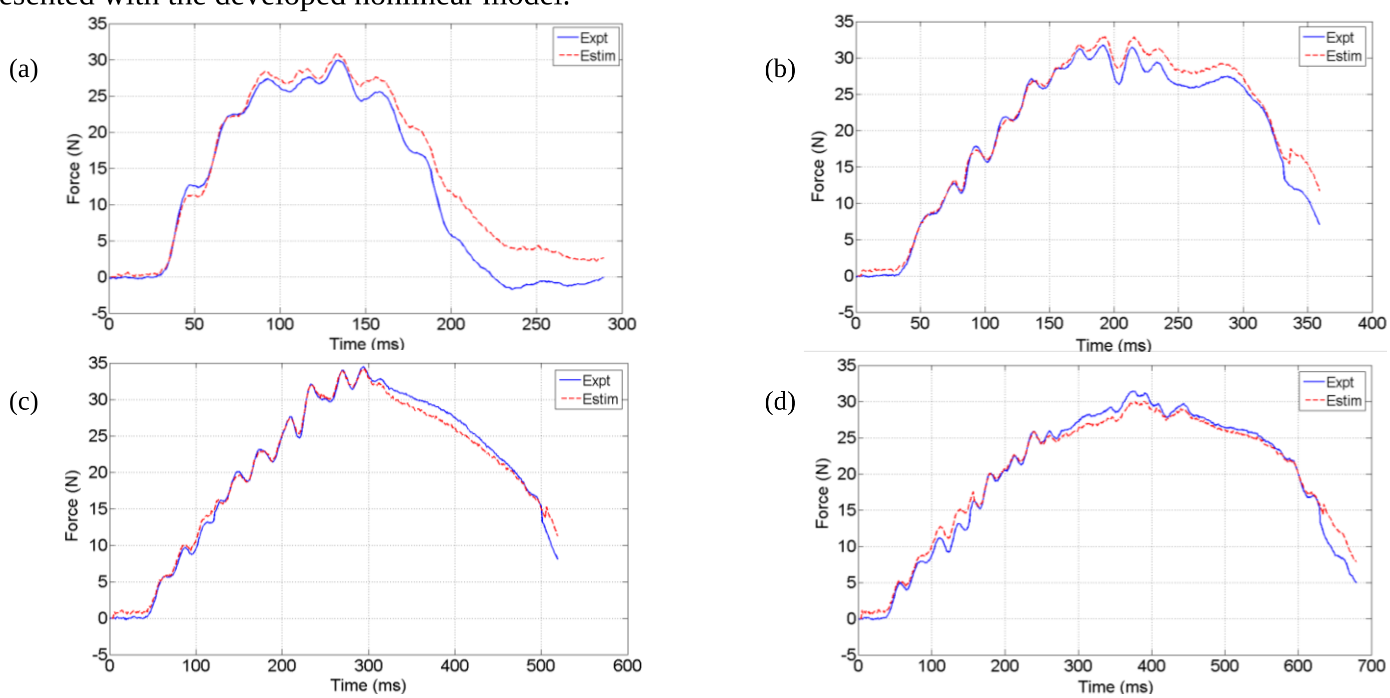

Figure 1: Sample results of estimated versus experimental hand-arm reaction force profiles at 20 Nm amplitude and (a) 200, (b) 360, (c) 520, (d) 680 ms duration levels.

ORAL PRESENATIONS – SATURDAY SEPTEMBER 7th

	Locomotion Following Cerebral Vascular Accident (Stroke/CP) *Chris Hass, Ryan Roemmich*
9:30 AM	Gait Parameter Changes During Sustained Walking In Individuals With Chronic Stroke **Dierks T, Altenburger P, Miller K, Phipps R, Schmid A**
9:45 AM	Walking Dysfunction Is Not Associated With Metabolic Cost In People Post Stroke **Wutzke C, Lewek M**
10:00 AM	A User-Controlled Powered Ankle Exoskeleton To Assist Gait Propulsion Post-stroke **Takahashi K, Sawicki G**
10:15 AM	Assessing Performance Of Three Types Of Biomechanical Models Applied To Pediatric Cerebral Palsy Gait **Buczek F, Rainbow M, Cooney K, Bruening D, Schmitz A, Thelen D**
10:30 AM	Locomotor Adaptation To Resistance During Treadmill Walking In Children With Cerebral Palsy **Wei F, Kim J, Gaebler-Spira D, Schmit B, Wu M**

GAIT PARAMETER CHANGES DURING SUSTAINED WALKING IN INDIVIDUALS WITH CHRONIC STROKE

Tracy A. Dierks[1], Peter A. Altenburger[1,2], Kristine K. Miller[1,3], Rebecca L. Phipps[2], and Arlene A. Schmid[1,3]

[1]Indiana University, Indianapolis, IN, USA; [2]Indiana University Health, Indianapolis, IN, USA; [3]Roudebush VA Medical Center, Indianapolis, IN, USA; email: tdierks@iupui.edu, URL: http://shrs.iupui.edu/physical_therapy/

INTRODUCTION

Gait recovery is a focal point of rehabilitation following stroke. Yet despite improvements in gait speed, it is common for many with chronic stroke to still experience gait deficits and subsequent declines in community ambulation (CA) and participation. CA potential is routinely predicted based on gait speed. Perry et al. (1995) identified 3 levels based on gait speed over 10 m of walking: Unlimited CA (>0.80 m/s), Limited CA (0.40-0.80 m/s), and Household Ambulators (<0.40 m/s). However, functional distances in the community far exceed this length and time. Since fatigue is commonly reported as one of the worst symptoms after stroke (Colle et al, 2006), gait related parameters during extended walking are likely influenced by fatigue, reducing gait speed and further compounding functional recovery. Yet, it is largely unknown how gait parameters are affected during extended functional walking. It is these parameters that might be contributing factors to persistent gait deficits in the chronic stroke stage. PURPOSE: to determine if gait parameters are influenced by sustained walking in persons with chronic stroke, as well as across the 3 levels of CA. We hypothesized a reduced gait speed, with shorter step/stride lengths and more time in stance/double support; most notable in the Household Ambulator group.

METHODS

Subjects were a subset of a study on the impact of mobility on activity and participation in people with chronic stroke (Schmid et al, 2012). Forty-eight subjects performed the 10 m walk test (10MWT) and the 6 minute walk test (6MWT) in random order interspersed with questionnaires and physical outcome measures. For the 10MWT, subjects walked as fast as possible over 10 m with a gait mat (GAITRite, CIR Systems Inc, Sparta, NJ, USA) positioned in the middle. For the 6MWT, subjects walked at a self-selected comfortable pace for 6 minutes while traversing a 30 m walkway with the gait mat in the middle, allowing for multiple gait mat passes. Rating of perceived exertion (RPE) was measured just prior to and immediately after the 6MWT to assess relative task intensity.

Spatiotemporal gait parameters were measured via the gait mat and assessed for the fastest of 2 10MWT trials, and for the 6MWT on the first gait mat pass, the pass with peak gait speed, and on the last pass. Gait parameters were compared as the peak pass minus that on the last pass during the 6MWT, and the 10MWT minus the 6MWT peak pass to determine if subjects could differentiate a fast versus sustainable speed. Repeated measures t-tests were used to assess within-subject differences. Each subject's 6MWT peak speed was used to stratify the sample into the 3 CA levels, and the same comparisons were made (Wilcoxon signed-rank test used due to small sample sizes). Statistical significance indicated at $p \leq 0.05$.

RESULTS AND DISCUSSION

As expected, the group as a whole was unable to sustain gait speed during the 6MWT (Table 1), with a significant reduction of 0.07 m/s, which is consistent with Sibley et al. (2009). The RPE was significantly greater at the end (7.7 vs. 11.8), moving from a "somewhat light" intensity to "somewhat hard", indicating that the task became more difficult at the end. The reduced gait speed and increased RPE were associated with decreased step and stride lengths, more time spent in stance and double support, and more time to complete a step and stride. This indicates that as the task became more difficult, subjects were slowing down by taking shorter steps/strides, and spending more time in stance/double support. Over 80% of subjects were experiencing a declining speed with these altered gait parameters. Thus, even these small reductions in gait parameters might be a limiting factor on confidence and CA.

Using the same subject population, we previously reported that the majority of our subjects indicated that walking farther was more important than walking faster (Combs et al, 2012). Thus, it is not surprising that the group self-selected a 6MWT peak speed that was 0.17 m/s slower than their 10MWT fast pace (Table 1). This faster gait speed was associated with longer steps/strides, and less time in stance/double support, and faster steps/strides/swing phases. These findings indicate an ability to differentiate and modulate a fast speed versus a slower sustainable one. With an emphasis on walking farther, subjects likely selected a slower pace and adjusted gait parameters accordingly for the 6MWT. However, they were not able to sustain this speed and maintain gait parameters. It is possible that subjects were inherently aware of their physical inability to maintain gait parameters and resulting loss in distance walked. This awareness may directly influence subject confidence, as well as CA and participation.

While extended walking resulted in gait parameter changes for the group as a whole, it was not consistent across CA levels. Surprisingly, the majority of changes were due to the Unlimited CA group (n=28), the highest functioning group. In this group, 6MWT peak gait speed significantly dropped from 1.15 m/s (0.24) to 1.07 m/s (0.22) at the end, while the 10MWT was significantly faster at 1.38 m/s (0.38). All other gait parameters (except for base of support) also significantly changed consistent with the group findings. The Limited CA group (n=14) was similar to the Unlimited CA group in that 6MWT peak gait speed dropped from 0.61 m/s (0.11) to 0.55 m/s (0.13) at the end, with a faster 10MWT of 0.71 m/s (0.18). However, changes in the other gait parameters were not consistent. No changes were observed in any gait parameters for the Household Ambulator group (n=6), the lowest functioning level (6MWT peak speed=0.30 m/s (0.07), end=0.28 m/s (0.05); 10MWT speed=0.34 m/s (0.16)). Overall, these CA subgroup findings indicate that gait parameters responded differently across subgroups, suggesting a need for ongoing assessment during rehabilitation.

CONCLUSIONS

Our cohort of chronic stroke survivors displayed an inability to maintain gait speed and adjusted gait parameters as extended walking became more difficult. Subjects were, however, able to differentiate between a fast speed (10MWT) and a slower speed for extended walking (6MWT). The observed differences were primarily due to the Unlimited CA group, which could potentially impact interpretation of 6MWT scores in clinical practice for individuals with chronic stroke.

REFERENCES

Colle F, et al. *Annals Phys Rehabil Med*, 2006;49: 361-364.
Combs SA, et al. *Disability & Rehabil*, 2012;1-8.
Perry J, et al. *Stroke*, 1995;26:982-989.
Schmid A, et al. *Arch Phys Med Rehabil*, 2012;93: 1101-1107.
Sibley KM, et al. *J Neuroeng Rehabil*, 2009;6:27.

Table 1. Spatiotemporal gait variables for the group as a whole during the 10 m walk test (10MWT) and the 6-minute walk test (6MWT) on the first pass (Begin), the peak gait speed pass, and the last pass (End).

		Spatial Gait Variables (m)			Temporal Gait Variables (s)				
	Gait Speed (m/s)	Stride Length	Step Length	Base of Support	Step	Stride	Swing/ Single Support	Stance	Double Support
10MWT	1.06** (0.51)	1.16** (0.39)	0.58** (0.20)	0.14 (0.09)	0.61** (0.14)	1.21** (0.27)	0.40** (0.05)	0.81** (0.24)	0.42** (0.22)
6MWT Begin	0.81^ (0.34)	1.02^ (0.30)	0.51^ (0.15)	0.15 (0.07)	0.68^ (0.15)	1.37^ (0.30)	0.44 (0.07)	0.93^ (0.26)	0.51^ (0.22)
6MWT Peak	0.89*,**,^ (0.38)	1.07*,**,^ (0.33)	0.54*,**,^ (0.16)	0.14 (0.07)	0.66*,**,^ (0.14)	1.32*,**,^ (0.29)	0.44** (0.06)	0.88*,**,^ (0.24)	0.46*,**,^ (0.19)
6MWT End	0.82* (0.36)	1.03* (0.32)	0.51* (0.16)	0.15 (0.09)	0.69* (0.17)	1.39* (0.34)	0.45 (0.07)	0.94* (0.29)	0.50* (0.24)

*Significant difference between 6MWT Peak and 6MWT End. **Significant difference between 6MWT Peak and 10MWT. ^Significant difference between 6MWT Peak and 6MWT Begin.

WALKING DYSFUNCTION IS NOT ASSOCIATED WITH METABOLIC COST IN PEOPLE POST STROKE

Clinton J. Wutzke, Michael D. Lewek

The University of North Carolina at Chapel Hill
email: cwutzke@med.unc.edu

INTRODUCTION

Following stroke, people commonly have reduced walking speed [1] and fatigue quickly [2]. The cause of walking dysfunction is likely multi-factorial as impairments in strength [3], coordination [4], or sensation [5] influence walking in people post stroke. The metabolic cost of walking in people post stroke is greater than unimpaired controls walking at comparable walking speeds [6]. Reduced walking endurance may also be due, in part, to an inefficient walking style. Compensations that occur within limbs and between limbs during gait result in greater metabolic cost of walking [7].

Identification of a relationship between metabolic power and walking endurance in people post stroke may be of importance for clinicians to reduce fatigue and improve quality of life.

The purpose of this study was to determine if functional walking ability was associated with greater metabolic efficiency in individuals with chronic hemiparesis. We hypothesized that individuals with greater metabolic efficiency would be capable of walking a longer distance such that the distance walked during a Six Minute Walk test would be correlated with metabolic cost in people post stroke.

METHODS

Twenty people post stroke ($\bar{x}$ age: 61.4±10.7 years; $\bar{x}$ height: 173.36±8.29 cm, $\bar{x}$ weight: 83.05±13.14 kg, 14M/6F) participated in this study. Ten subjects wore an AFO or bracing on the paretic limb and 12 used an assistive device (10 Single point canes, 2 Quad point canes).

Subjects completed three walking passes on a 14 foot GAITRITE® mat at their comfortable gait speed (CGS). Subjects also completed a 6 Minute Walk Test on a 33.5 meter walkway wearing a K4B2 portable metabolic cart (CosMed, Chicago, IL). Indirect calorimetry was used to determine the average mass specific net metabolic power (W/kg) from the last 30 seconds of the sixth minute during the 6 Minute Walk test.

Pearson product correlation coefficients were calculated to determine the presence of a relationship between metabolic cost of walking (i.e., final 30 sec of 6 min walk test) and 1) walk distance and 2) comfortable walking speed. Significance was determined a priori at α=0.05.

RESULTS AND DISCUSSION

The average comfortable overground gait speed for all subjects was 0.47±0.22 m/s. The average distance during the 6 Minute Walk test was 197.87±96.17 meters. During the sixth minute of the walk test, subjects had an average net metabolic power of 2.75±0.95 W/kg.

The distance walked during the 6 Minute walk test was not correlated with the mass specific net metabolic power during the final 30 sec of the test (r=-0.003, p=0.990, Figure 1).

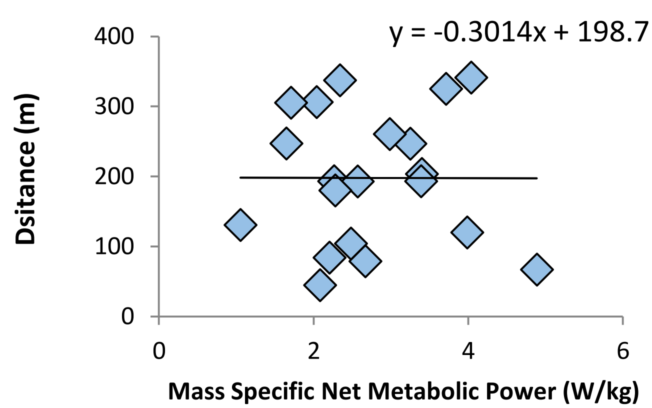

Figure 1: Correlation between Metabolic Power and Six Minute Walk Distance.

Additionally, comfortable gait speed was not associated with net metabolic power of the final 30 seconds of the Six Minute Walk test ($r=0.166$, $p=0.484$, Figure 2).

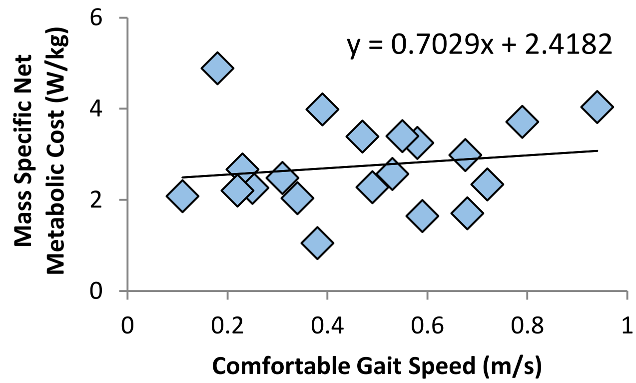

Figure 2: Correlation between comfortable gait speed and Metabolic Cost during Minute Six of Walk test.

Comfortable gait speed was, however, significantly correlated with distance walked during the Six Minute Walk test ($r=0.867$, $p<0.001$, Figure 3).

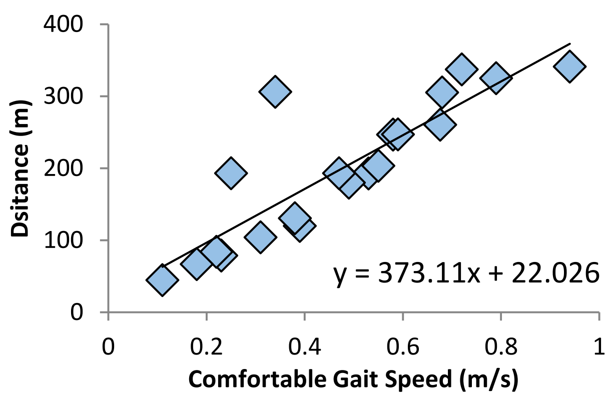

Figure 3: Correlation between comfortable gait speed and Six Minute Walk Distance.

Our hypotheses that metabolic power would be associated with distance walked during the Six Minute Walk Test and comfortable overground gait speed were not supported.

CONCLUSIONS

The results of this study suggest that metabolic power is not associated with distance walked during the Six Minute Walk Test in people post stroke. Reduced walking speed in people post stroke may therefore not be due to avoiding feelings of fatigue or metabolic inefficiency. Although we tested metabolic power, we did not account for local muscle fatigue, which may also play a role in limiting walking ability. Although people post stroke exhibit abnormal and inefficient walking patterns, our data would suggest that the inefficiency of these patterns is not associated with the common reports of reduced walking speed and endurance. Additional factors will need to be evaluated to fully understand the underlying source of reduced walking speed and fatigue in people with chronic hemiparesis.

REFERENCES

1. Hill, K., et al, *Aust J Physiother*; **43**(3): p. 173-180, 1997.
2. Lord S.E., et al, *Arch Phys Med Rehabil*, **85**(2): p. 234-239, 2004.
3. Kim, C.M. & Eng, J.J., PT, **83**: p. 49-57, 2003.
4. Daly, J.J., et al, Rehab Res Prac, pg , 1-8, 2011.
5. Hsu, A., et al, Arch Phys Med Rehabil, **84**: p. 1185-1193, 2003.
6. Platts et al, Med Sci Sports Exerc, **38**(6): p. 1041-1046, 2006.
7. Wutzke, C.J., et al, *J of Biomech*, **45**(14): p. 2405-2410, 2012.

A USER-CONTROLLED POWERED ANKLE EXOSKELETON TO ASSIST GAIT PROPULSION POST-STROKE

[1]Kota Z. Takahashi and [1]Gregory S. Sawicki
[1]Joint Department of Biomedical Engineering, North Carolina State University and University of North Carolina at Chapel Hill, Raleigh, NC, USA
email: ktakaha@ncsu.edu

INTRODUCTION

The gait pattern of individuals with hemiplegia post- stroke is commonly associated with decreased ankle joint power generation in the affected limb [1] - likely contributing to an elevated metabolic cost [2] and a slower self-selected walking speed [1,2]. In healthy individuals, the ankle joint generates more mechanical energy than any other lower extremity joint [3] and plays a critical role in accelerating the body forward [4]. We anticipate, then, that restoring normal ankle mechanics in persons with stroke could greatly improve gait outcomes.

One potential solution may be to assist ankle plantarflexion via an externally powered exoskeleton. These devices have been shown to effectively reduce the metabolic cost of walking in healthy individuals by *replacing* a portion of the biological muscular work [3,4]. Yet, it is unknown whether these devices can *augment* ankle joint function in people with plantarflexion weakness due to stroke.

Here, we introduce a novel user-controlled ankle exoskeleton in which the *magnitude* and *timing* of mechanical actuation of an artificial muscle is dictated by both the user's own central nervous system (soleus electromyography [EMG]) and gait mechanics (anterior-posterior ground reaction force [AP-GRF]). We tested the feasibility of this powered exoskeleton to provide assistance to the paretic limb of a person with hemi-paretic stroke during treadmill walking.

METHODS

We recruited a stroke survivor (age 52, 1.72 m, 79.3 kg) with mild hemiparesis and medium gait impairment (preferred overgound walking speed = 0.72 m/s). The lightweight exoskeleton consisted of

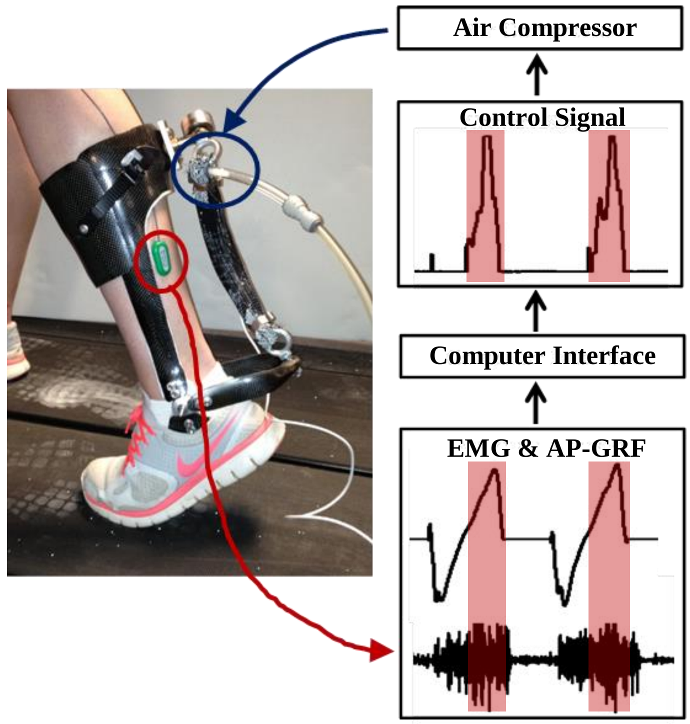

Figure 1: The soleus EMG and AP-GRF (from an instrumented treadmill) were collected in real-time to control the magnitude and timing of exoskeleton actuation. The *proportional myoelectric propulsion* (PMP) controller requires soleus EMG amplitude above a set threshold during the propulsive phase of stance, encouraging the user to activate the muscle to receive mechanical assistance.

custom-fitted carbon fiber shank and foot components hinged at an ankle joint (mass=454 g). An artificial pneumatic muscle (length=16.5 cm) was attached along the posterior shank (moment arm=12 cm) to provide an assistive plantarflexion torque about the ankle.

To control the magnitude and timing of exoskeleton assistance, we collected and processed information from the subject's soleus EMG and the AP-GRF in real-time. We implemented *a proportional myoelectric propulsion* (PMP) control algorithm, in which the exoskeleton supplied assistance torque proportional to the soleus EMG signal *only* during the phase of stance when the AP-GRF was greater than 0 (Figure 1). In essence, the PMP controller strategically aims to augment the propulsive role of the ankle joint muscles under the user's volitional action.

The subject walked on an instrumented treadmill (Bertec, OH, USA) at 70% of the preferred overground walking speed (0.50 m/s), with and without exoskeleton power assistance (i.e., EXO and NoEXO conditions). Within a single data collection session, the subject completed a 5 minute trial of the NoEXO condition, and three repetitions of 5 minute trials of the EXO condition. We obtained measurements of lower extremity mechanics (using inverse dynamics), exoskeleton mechanics (using a compression load cell), and metabolic energy estimates (using indirect calorimetry). We compared the data from the NoEXO condition to the last repetition of the EXO condition.

RESULTS AND DISCUSSION

The magnitude of positive mechanical work done by the paretic ankle joint during the EXO condition was 118% greater than the NoEXO condition (0.074 J/kg versus 0.034 J/kg) (Figure 2). The exoskeleton accounted for 28% of the total ankle positive work during the EXO condition (0.021 J/kg). The average metabolic energy expenditure during the NoEXO and EXO conditions were 3.55 W/kg and 3.52 W/kg, respectively.

CONCLUSIONS

Over three 5 minute bouts of walking, a person with post-stroke hemiparesis demonstrated the ability to use the exoskeleton to increase ankle joint power generation during the propulsion phase of gait. With repeated training sessions, we expect to see further increases in ankle joint power output, an improvement in lower limb mechanical symmetry, and larger reductions in the metabolic cost of walking. We have on-going efforts to improve the PMP control algorithm, including optimizing the timing and magnitude of the exoskeleton actuation that is unique to a given individual's impairment.

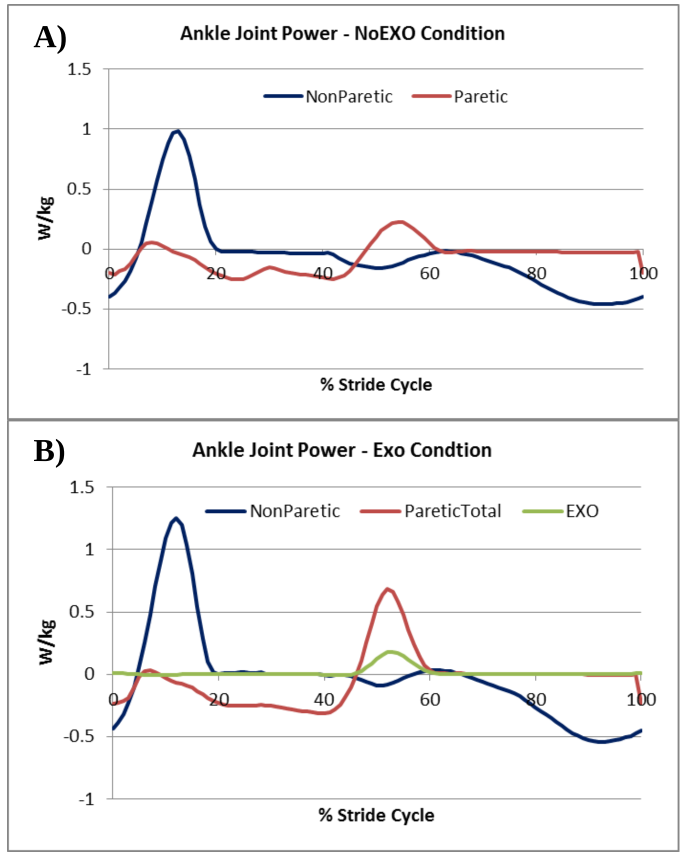

Figure 2: The total ankle joint power profiles during the NoEXO condition (A) and the last repetition of the EXO condition (B). The data were averaged from 10 consecutive steps obtained during the last minute of each condition. In the EXO condition, the total paretic ankle joint power (red) contains contributions from both the exoskeleton (green) and the biological muscles (not shown).

REFERENCES

1. Jonkers I et al. *Gait & Posture* 29, 129-137, 2009
2. Stoquart G et al. *Gait & Posture* 36, 409-413, 2012
3. Farris DJ and Sawicki GS. *J R Soc Interface* 9, 110-118.
4. Neptune RR et al. *J Biomech* 34, 1387-1398, 2001
5. Sawicki GS and Ferris DP. *J Exp Biol* 211, 1402-1413
6. Malcom P et al., *PLoS One* 8, e53137, 2013

ACKNOWLEDGEMENTS

This work was funded by NIH 5R24-HD050821-08 Pilot Grant to GSS

ASSESSING PERFORMANCE OF THREE TYPES OF BIOMECHANICAL MODELS APPLIED TO PEDIATRIC CEREBRAL PALSY GAIT

[1,2] Frank L. Buczek, [3] Michael J. Rainbow, [2] Kevin M. Cooney, [4] Dustin A. Bruening, [5] Anne Schmitz, [6] Darryl G. Thelen
[1] National Institute for Occupational Safety & Health (NIOSH), Morgantown WV, USA
[2] Shriners Hospitals for Children, Erie PA, USA, [3] Harvard Medical School, Cambridge MA, USA
[4,2] Air Force Research Laboratories, Dayton OH, USA, [5] University of Kentucky, Lexington KY, USA
[6] University of Wisconsin-Madison, Madison WI, USA
email: fbuczek@cdc.gov

INTRODUCTION

Gait analyses provide clinical decision-makers with physical examination findings, muscle recruitment patterns, and biomechanical data, all of which augment the basis for orthopedic treatment recommendations. Previous studies have shown that models with six degree-of-freedom (6DOF) joints may better capture non-sagittal joint kinematics and kinetics than the conventional gait model, in both experimental [1] and simulated normal gait [2]. As many biomechanical models and simulations are based upon normal skeletal anatomy and neuro-muscular function, inaccuracies may arise in key gait analysis variables calculated for pathological gait. Still, forward dynamic gait simulations, with a generic musculoskeletal model, can be viewed as a first approximation of abnormal neuromusculo-skeletal function [3]. The purpose of this study is to assess the performance of three types of biomech-anical models using muscle-actuated, forward dynamic simulations [4,5], customized to individual pediatric cerebral palsy gait patterns, as an estimate of true motion. In particular: **CGM** = conventional gait model; **OPT1** = CGM local reference frames [6] with 6DOF tracking; **OPT2** = local reference frames based upon *in vivo* and *in vitro* studies [7], with 6DOF tracking. We hypothesize that OPT2 will match simulations better than OPT1 and CGM.

METHODS

Full-body data collection, using a ten-camera Vicon 612 system and three AMTI force plates, was performed during over-ground gait [1]. Following informed consent approved by the local human subjects committee, five pediatric cerebral palsy patients were fitted with a hybrid marker configuration, allowing the identical stride to be analyzed in Visual3D (C-Motion, Inc.) using CGM, OPT1, and OPT2. Patient-specific gait simulations were generated for strides where bilateral force plate data were available during double support. A generic whole body model was first scaled to match the measured lengths of each patient (Figure). We used a least squares forward dynamics algorithm to compute pelvic motion and joint kinematics that were consistent with experimentally acquired marker kinematics and ground reactions, while satisfying overall equations of motion. Simulated marker kinematics were generated assuming rigid fixation to each segment, and processed in Visual3D using the OPT2 biomechanical model; associated gait data (twenty functionally relevant maxima and minima in joint angles, moments, and powers, see Table) were used as our best estimate of truth (**CLN**).

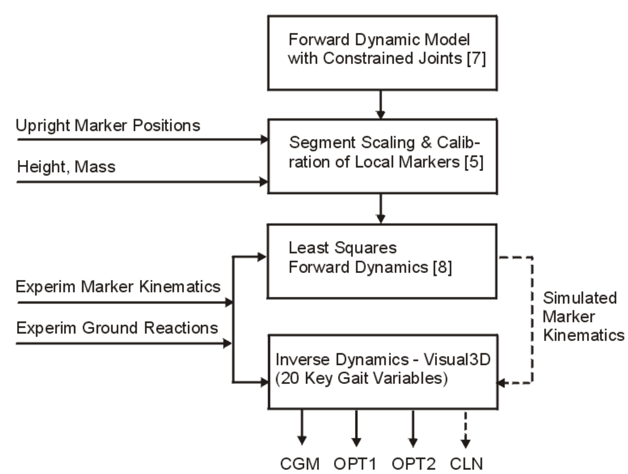

Figure. Forward and inverse dynamics processing [2].

Experimental marker kinematics, affected by soft tissue errors, were processed in Visual3D according to CGM, OPT1, and OPT2 model criteria. Repeated measures ANOVAs, with Tukey HSD *post hoc* comparisons (Statistica 5.1, StatSoft), were used to identify significant differences ($p<0.05$) between all pairs of models.

RESULTS AND DISCUSSION

Our primary hypothesis was supported, with no significant differences found between gait variables calculated using CLN and OPT2 models (Table). Four of twenty variables were significantly different between CLN and OPT1 models; six of twenty variables were significantly different between CLN and CGM models. These differences were not as numerous as those found between models in a previous study of normal children [2]. This is likely due to the much greater variability across the five patients in this study, who presented with either hemiplegic or diplegic cerebral palsy, and who had a variety of surgeries or BOTOX injections prior to their gait evaluation. Statistically under powered, we interpret these findings only as a guide to further analyses. Also important, OPT2 used joint centers different from those used identically in OPT1 and CGM. OPT2 and OPT1 both used 6DOF tracking, unlike the hierarchical tracking used in CGM. Given the pattern of significant differences across these models, it appears as though local reference frames (especially joint center locations) may play a greater role in performance than 6DOF tracking.

CONCLUSIONS

Due to the wide variability across these patients, we conclude only that: (1) differences in joint center locations may play a greater role in the performance of biomechanical models applied to pediatric cerebral palsy gait, than 6DOF tracking, and (2) 6DOF tracking may provide more accurate results for non-sagittal kinematics and kinetics.

REFERENCES

1. Buczek FL, et al. *Gait Posture* **31**, 57-63, 2010.
2. Buczek FL, et al. *Proc.* Amer Soc Biom, 2010.
3. Steele KM, et al. *J.Biomech* **43**, 2099-2105, 2010.
4. Thelen DG, et al. *J. Biomech* **36,** 321-328, 2003.
5. Delp SL, et al. *IEEE Trans Biom Eng* **54**, 1940-1950, 2007.
6. Davis RB, et al. *Hum Mov Sci* **10**, 575-587, 1991.
7. Delp SL, et al. *IEEE Trans Biom Eng* **37**, 757-767, 1990.
8. Remy CD & Thelen DG. *J Biomech Eng* **131**, 031005, 2009.

ACKNOWLEDGEMENTS & DISCLAIMER

Gratefully funded by Shriners Hospitals for Children, grant #8510. Findings are those of the authors and may not represent views of NIOSH.

Table: Statistical comparison of key gait analysis variables across models (**bold** indicates significant at $p<0.05$).

		P-Values (Tukey HSD Post Hoc Comparisons)					
	Key Gait Variable	CLN OPT2	CLN OPT1	CLN CGM	OPT2 OPT1	OPT2 CGM	OPT1 CGM
1	maximum hip extension in late stance (deg)	1.0000	**0.0141**	**0.0073**	**0.0141**	**0.0073**	0.9802
2	maximum hip flexion moment in late stance (Nm/kg)	1.0000	0.2855	0.6402	0.2858	0.6407	0.9007
3	maximum hip flexion power absorption in late stance (W/kg)	1.0000	**0.0216**	0.0808	**0.0216**	0.0808	0.8693
4	maximum knee extension in late swing (deg)	1.0000	**0.0194**	**0.0220**	**0.0194**	**0.0220**	0.9999
5	maximum knee flexion moment in late swing (Nm/kg)	1.0000	0.9595	0.8824	0.9596	0.8826	0.9949
6	maximum knee flexion power absorption in late swing (W/kg)	1.0000	0.9905	**0.0003**	0.9906	**0.0003**	**0.0004**
7	maximum ankle plantarflexion at push-off (deg)	1.0000	0.3257	0.9952	0.3357	0.9952	0.4402
8	maximum ankle plantarflexion moment at push-off (Nm/kg)	1.0000	0.6132	0.1536	0.6132	0.1536	0.7230
9	maximum ankle plantarflexion power generation push-off (W/kg)	1.0000	0.7173	0.0800	0.7172	0.0799	0.3987
10	maximum hip adduction in early stance (deg)	1.0000	**0.0441**	**0.0015**	**0.0441**	**0.0015**	0.2359
11	maximum hip abduction moment in early stance (Nm/kg)	1.0000	0.1356	**0.0240**	0.1356	**0.0240**	0.7424
12	maximum hip abduction power absorption early stance (W/kg)	1.0000	0.7398	0.1633	0.7398	0.1633	0.6184
13	maximum knee adduction moment at initial contact (Nm/kg)	1.0000	0.9326	0.8724	0.9325	0.8723	0.9984
14	maximum knee abduction moment in early stance (Nm/kg)	1.0000	0.9988	0.2031	0.9988	0.2031	0.1609
15	mean hip int/ext rotation across gait cycle (deg)	1.0000	0.9988	**0.0120**	0.9988	**0.0120**	**0.0154**
16	mean knee int/ext rotation across gait cycle (deg)	1.0000	0.9922	0.9584	0.9922	0.9584	0.9961
17	mean ankle int/ext rotation across gait cycle (deg)	1.0000	0.9124	0.4607	0.9124	0.4607	0.8256
18	maximum hip external rotation moment early stance (Nm/kg)	1.0000	0.3471	0.1087	0.3472	0.1088	0.8660
19	maximum knee external rotation moment late stance (Nm/kg)	0.9828	0.2887	0.1224	0.4616	0.2164	0.9412
20	maximum knee internal rotation moment early stance (Nm/kg)	1.0000	0.9961	0.3107	0.9961	0.3106	0.2270

LOCOMOTOR ADAPTATION TO RESISTANCE DURING TREADMILL WALKING IN CHILDREN WITH CEREBRAL PALSY

[1,2]Feng Wei, [1]Janis Kim, [1,2]Deborah J. Gaebler-Spira, [1,2,3]Brian D. Schmit, and [1,2]Ming Wu*

[1]Rehabilitation Institute of Chicago, Chicago, IL, USA
[2]Northwestern University Feinberg School of Medicine, Chicago, IL, USA
[3]Marquette University, Milwaukee, WI, USA
Email: feng.wei@northwestern.edu, *w-ming@northwestern.edu

INTRODUCTION

Cerebral palsy (CP) is the most prevalent physical disability originating in childhood with an incidence of 2.7 per 1000 live births [1]. The development of efficient and independent walking is an important therapeutic goal for many children with CP [2]. Theories of motor learning suggest that task-specific, repetitive practice can improve walking in children with neurological disorders such as CP [3]. As a consequence, there has been a growing interest of using treadmill training, particularly with body weight support, to improve locomotor function in children with CP [2]. However, while significant improvements in walking capacity with treadmill training have been shown, the functional gains are relatively small [2], suggesting a need to improve techniques in order to produce greater functional improvements in children with CP.

Data from hemiparetic subjects practicing upper limb movements with forces that provide passive guidance versus error enhancement indicate that greater improvements in performance are achieved when errors are magnified [4]. These results suggest that causing adaptation by using error-augmentation training might be an effective way to promote functional motor improvement for children with CP. In addition, previous studies have shown that, with repeated exposure to forces that resist hip flexion during swing phase of gait, healthy subjects form anticipatory motor commands in response to the resistance [5]. The development of these anticipatory motor commands is revealed by the presence of aftereffects (i.e., greater stride length and higher stepping) once the disturbance is removed. These aftereffects following a period of training under resistance imply the formation of motor output for a given task. Yet, to date, locomotor adaptation to resistance added during the swing phase of gait has not been investigated in children with CP. We postulate that applying a controlled, resistance load to produce kinematic deviations of the leg during treadmill training will accelerate the motor learning in children with CP.

METHODS

Five children (3 girls and 2 boys, 11.2 ± 2.4 years) with diagnosed CP (spastic diplegia, GMFCS level II) participated in the study after obtaining informed consent. A custom designed, cable-driven robot was utilized to provide controlled, resistance loads to the leg at the ankle (Fig 1) during treadmill walking. A 3D position sensor consisting of a detector rod and three potentiometers was used to measure the ankle position during treadmill walking [6]. The cable-driven robot was highly back-drivable and therefore, had minimal constraints to subject voluntary movements.

A controlled, resistance load approximately equivalent to 15-18% of the maximum voluntary contraction of hip flexion during standing was applied to the right leg of each subject from the late stance to mid-swing phase of gait. The treadmill speed was pre-determined in an earlier overground test using an instrumented walkway (GaitMat II, EQ Inc., Chalfont, PA). The average treadmill speed was set at 0.39 ± 0.20 m/s. A body weight support was provided as necessary to assure stable stepping. Subjects were allowed to hold onto a handrail during walking. Subjects first walked on the treadmill without loads for 2 minutes (baseline), followed by a 10-minute walking with a resistance load applied to the right ankle (adaptation). The load was then removed while subjects continued to walk on the treadmill for another 3 minutes (post-adaptation). The ankle position data obtained from the 3D sensors were recorded on a personal computer with a sampling rate of 500 Hz.

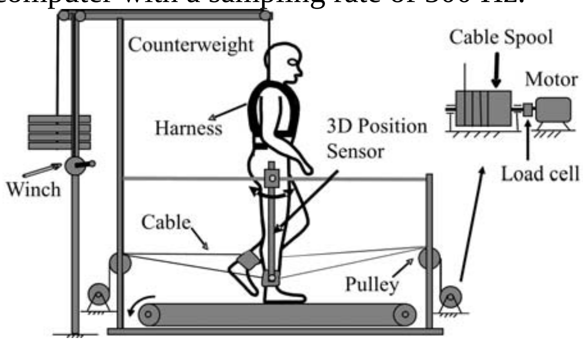

Figure 1: Schematic diagram of the cable-driven robotic treadmill system.

Data processing was performed using custom written routines in MATLAB (MathWorks, Natick, MA). Ankle kinematic data were low-pass filtered at 5 Hz cutoff frequency using a zero-lag, fourth-order Butterworth filter. Stride length, defined as the distance that the treadmill belt moved between two consecutive heel contacts of the right foot [7], was calculated for each subject. In addition, gait patterns in terms of the foot trajectory in the sagittal plane immediately before loading and after load removal were determined and compared.

RESULTS AND DISCUSSION

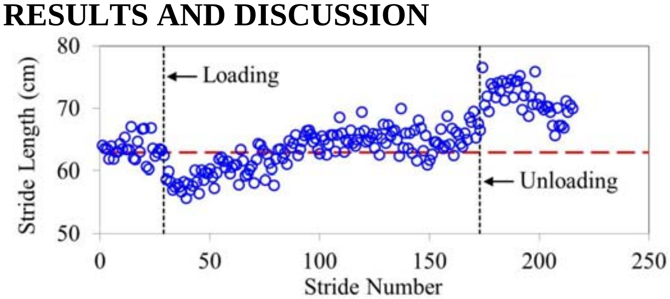

Figure 2: Stride by stride plot of stride length of the right leg for one child with CP (subject 1). Each point shown was an average of 3 stride lengths. The red line was the averaged stride length across the last 5 strides in baseline.

An immediate decrease in stride length was observed in early adaptation period when a resistance load was applied (Fig 2). Then, the stride length gradually returned to a level close to the baseline during the late adaptation period. An aftereffect consisting of an increase in stride length was observed following load removal after 10 minutes of resistance training. Group data indicated that the stride length was significantly greater during post-adaptation period than baseline (ANOVA, p=0.002) (Fig 3). The gait pattern of each subject showed an increase in the horizontal foot trajectory during post-adaptation period versus baseline (Fig 4). In addition, subjects 1 and 3 generated a higher step height (vertical foot trajectory) during the post-adaptation period compared to baseline.

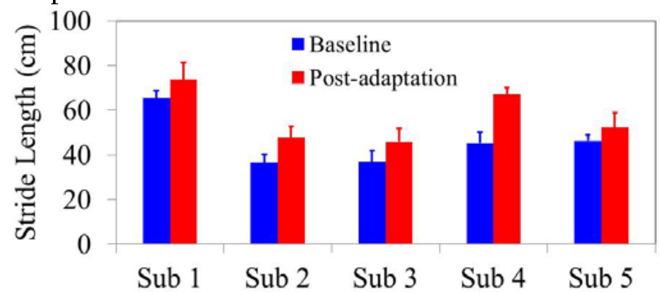

Figure 3: Average stride length of five successive strides in baseline (last five strides before loading) and post-adaptation (first five strides after load removal).

CONCLUSIONS

The kinematic results showed that the added resistance alters gait patterns and motor outputs formed to compensate for leg resistance in children with CP. An aftereffect consisting of an increase in stride length was observed after resistance training, implying the development of anticipatory motor commands during locomotor adaptation in children with CP. While motor adaptation to resistance and associated aftereffects are generally short-lived, the phenomenon may have the potential for clinical significance following repeated exposures. Results from this study may be used in the development of a novel, targeted therapeutic training strategy to improve locomotor function in children with CP through robotic resistance treadmill training.

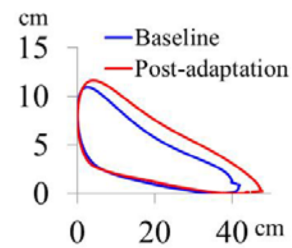

Figure 4: Sagittal view of foot trajectory from subject 1.

REFERENCES

[1] Rosen et al. *J Obstet Gynecol* 167:417-423, 1992.
[2] Dodd et al. *Dev Med Child Neurol* 49:101-105, 2007.
[3] Barbeau, *Neurorehabil Neural Repair* 17:3-11, 2003.
[4] Patton et al. *Exp Brain Res* 168:368-383, 2006.
[5] Lam et al. *J Neurophysiol* 95:766-773, 2006.
[6] Wu et al. *Gait Posture* 33:256-260, 2011.
[7] Yen et al. *Exp Brain Res* 216:473-482, 2012.

ACKNOWLEDGEMENTS

This study is supported by a grant from the NIH/NICHD R21HD066261 (Wu, M).

ORAL PRESENATIONS – SATURDAY SEPTEMBER 7th

Symposium: Biomechanics in Disability Research *Alicia Koontz*
Speed And Force Relations During Prolonged High-Intensity Figure-Of-Eight Wheelchair Propulsion **Hwang S, Lin YS, Wang LH, Koontz AM**
Addressing Shoulder Pain In Manual Wheelchair Users: Characterization Of Field-Based Kinematics & Kinetics And A Tele-Rehab Therapeutic Exercise Program **Morrow M, Van Straaten M, Ludewig P, Cloud B, An KN, Kaufman K, Zhao K**
Biomechanics Of Independent Car Transfer And Wheelchair Loading In Manual Wheelchair Users With SCI **Requejo P**

Speed and Force Relations during Prolonged High-Intensity Figure-of-Eight Wheelchair Propulsion

[1,2]Seonhong Hwang, [1,2]Yen-Sheng Lin, [3]Lin-Hwa Wang, and [1,2]Alicia M Koontz

[1]Human Engineering Research Laboratories, VA Pittsburgh Healthcare System, Pittsburgh, PA
[2]Department of Rehabilitation Science and Technology, University of Pittsburgh, Pittsburgh, PA
[3]Institute of Physical Education, Health & Leisure Studies, National Cheng Kung University, Tainan, Taiwan
email: seh113@pitt.edu

INTRODUCTION

Manual wheelchair (WC) propulsion is essential activity for many individuals with spinal cord injury (SCI), and is believed to a major cause of upper-limb pain and injuries [1]. Propulsion biomechanics has been extensively investigated on unnatural surfaces (e.g. ergometers, treadmills, etc.) at submaximal speeds [2,3]. Few studies have investigated wheelchair propulsion on natural ground surfaces. These studies focused on start-up and steady-state straightaway propulsion and ignored other common mobility tasks such as steering, turning, or braking maneuvers [4]. We developed a figure-of-eight course to study the effects of intensive propulsion an acute changes at the shoulders and wrists using quantitative ultrasound [5,6]. Manual WC users who pushed with higher shoulder forces and moments during the startup straightaway portions of the course showed greater narrowing of the subacromial space post-propulsion – a precursor to shoulder impingement [7]. Turning biomechanics has not been investigated in detail and may provide insight into performance on the court (e.g. WC basketball, rugby etc.) and injury mechanisms. The purpose of this study was to investigate the force and velocity relationships during the turning portions of the course. We hypothesized that individuals with better speed control during the turn would have lower pushrim peak forces before, during and after the turn.

METHODS

Subjects: Ten participants with spinal cord injury (7 males, 3 females; mean age 37 ± 10 years; mean weight 82 ± 22 kg; level of injury C5-L3; mean duration of injury 15 ± 9 years) provided written informed consent prior to the start of this study, which was approved by our local institutional review board. Experimental Protocol: Subjects were asked to propel their wheelchair on concrete floor along a figure-of-eight shaped course with 20 m span, outlined by cones (Fig. 1(A)). Before starting the test, participants were instructed to propel their wheelchair at a self-selected maximum speed through the entire course, and to rapidly come to a complete stop upon completion of each loop before pushing around the subsequent loop. They were asked to propel their wheelchair for four minutes, and then rested for 90 seconds. This sequence was repeated two more times to obtain a total propulsion time of 12 minutes. During the propulsion test, each subject's non-dominant side of the wheelchair was fitted with an instrumented wheel (SmartWheel, Three Rivers Holdings, Inc., Mesa, AZ) to record three-dimensional forces and moments at 240-Hz. Data were collected during the first ('early') and last minute ('late').

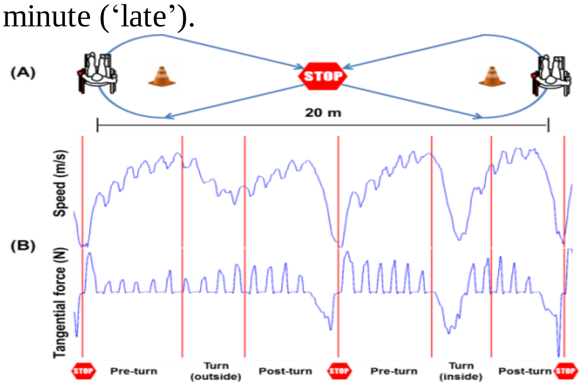

Figure 1: (A) A Schematic of the figure-of-eight shaped propulsion course and (B) wheelchair speed and tangential push force during one cycle of the course.

Data Analysis: The course was divided into three different phases: pre-turning (Pr), turning (T), and post-turning (Po) based on the wheel trajectory. A Vicon motion capture system was used for studying the kinematics of the wheel and the upper extremity; however, only the wheel position was used in this study. The peak speeds and tangential push forces (F_t) for all turns completed in the first and the last minute were computed using a customized Matlab program (The Mathworks, Natick, MA).

The difference between the minimum speed during T and the maximum speed during Pr was divided by the maximum speeds during Pr to account for variation in the subjects' self-selected speeds. The last two positive peaks of F_t during Pr were averaged and defined as the peak Pr F_t. The peak Po F_t was calculated by averaging all positive peaks during Po. During T, the average of the positive peaks of F_t on the outside wheel and the negative peak of F_t on the inside wheel were defined as the outside peak T F_t (push force) and the inside peak T F_t (braking force), respectively. All force values were normalized by dividing by the user-wheelchair weights. The relationship between the peak F_ts during Pr, Po, and T on the outside wheel to the speed changes on the outside wheel was evaluated using a Spearman correlation test. The same test was also performed for the inside wheel. A Wilcoxon signed rank test was used to compare the changes in speed and the peak F_t between the early and the late times of the propulsion task.

Table 1: Velocity and force variables during early and late propulsion

Mean (sd)		Early	Late	z	*p*
Inside	Changes in speed	0.952 (0.084)	0.973 (0.053)	-0.923	0.356
	Pr Ft	**0.638 (0.280)**	**0.479 (0.121)**	**-2.059**	**0.039***
	T Ft	-1.045 (0.261)	-1.016 (0.246)	-0.260	0.795
	Po Ft	0.684 (0.275)	0.568 (0.187)	-1.349	0.177
Outside	Changes in speed	0.456 (0.048)	0.458 (0.069)	-0.071	0.943
	Pr Ft	0.693 (0.239)	0.582 (0.192)	-1.870	0.062
	T Ft	0.823 (0.339)	0.757 (0.205)	-0.923	0.356
	Po Ft	**0.739 (0.295)**	**0.592 (0.163)**	**-2.44**	**0.015***

*Significance level $p < .05$. Wilcoxon signed rank test

RESULTS AND DISCUSSION

In general, peak F_t during T was higher than the peak F_t prior to and after T (Table 1). Peak F_t for the inside arm (braking force) was higher than F_t for the outside arm (propulsive force) during T (Fig 1b). Larger changes in velocity were observed for the inside arm versus the outside arm during T. At the early time, less braking force on the inside arm and more propulsive force on the outside arm was associated with better speed control through the turn (e.g. defined by less change in velocity) (Table 2). Higher propulsive forces on the outside arm also correlated with better speed control at the later time. Peak F_t prior to and after the turn decreased significantly overtime (Table 2) while no change was observed in velocity or peak F_t during T.

CONCLUSIONS

Subjects with better speed control during turns used less braking force and more propulsive force to successfully maneuver themselves around the cones. There was no relationship found between the pre and post turning forces and speed control during turning. The reduction in pre and post turning forces overtime suggests that fatigue may have impaired performance however no changes were found overtime in speed control or the forces used during the turns. The results provide insight into mobility skills training for wheelchair users who participate in court sports. Future studies are needed to determine the relationship between turning mechanics and markers of pathology.

REFERENCES

1. Nyland J, et al. *Spinal Cord* **38**, 649-57, 2000.
2. Rodgers MM, et al. *Arch Phys Med Rehabil* **75**, 85-93, 1994.
3. Rice I, et al. *Spinal Cord* **47**, 413-17, 2009.
4. Gagnon D, et al. *Proceedings of RESNA 2008 Ann Conf*, AL, VA, USA, 2008.
5. Collinger JL, et al. *Phys Med & Rehabil* **2**, 920-5, 2010.
6. Impink BG, et al. *Phys Med & Rehabil* **3**, 803-10, 2011.
7. Lin YS, et al. *Proceedings of RESNA 2008 Ann Conf*, Bellevue, WA, USA, 2013.

ACKNOWLEDGEMENTS

This material is based upon work supported by the Department of Veterans Affairs Rehabilitation Research and Development Service (Project Number: B6252R). This material is the result of work supported with resources and the use of facilities at the Human Engineering Research Laboratories, VA Pittsburgh Healthcare System. The contents of this abstract do not represent the views of the Department of Veterans Affairs or the United States Government.

Table 2: Correlation coefficients between changes in peak speed and forces.

Rho (p-value)	Tangential force (F_t) in the early time						Tangential force (F_t) in the late time					
	Inside			Outside			Inside			Outside		
	Pr	T	Po	Pr	T	Po	Pr	T	Po	Pr	T	Po
Changes in speed	0.17 (0.50)	**-0.60 (0.01)**	0.08 (0.77)	-0.02 (0.93)	**-0.42 (0.09)***	0.03 (0.93)	0.19 (0.51)	0.26 (0.37)	0.38 (0.19)	-0.11 (0.71)	**-0.46 (0.10)***	-0.17 (0.56)

Abbreviation: Pr, pre-turn; T, turn; Po, post-turn; F_t, tangential push force. *: denotes a trend $p \leq 0.1$

ADDRESSING SHOULDER PAIN IN MANUAL WHEELCHAIR USERS: CHARACTERIZATION OF FIELD-BASED KINEMATICS & KINETICS AND A TELE-REHAB THERAPEUTIC EXERCISE PROGRAM

[1]Melissa M. B. Morrow,[1]Meegan G. Van Straaten, [2]Paula M. Ludewig, [1]Beth A. Cloud,
[1]Kai-Nan An, [1]Kenton R. Kaufman, and [1]Kristin D. Zhao

[1]Mayo Clinic, Rochester, MN, USA, [2]University of Minnesota, Minneapolis, MN, USA
email: morrow.melissa@mayo.edu, web: http://mayoresearch.mayo.edu/mayo/research/biomechanics/

INTRODUCTION

Individuals with spinal cord injury often use manual wheelchairs as their primary mode of mobility. However, the joint geometry of the shoulder is not well designed for weight bearing [1], and its musculature is smaller and less efficient for ambulating as compared to the large musculature of the lower extremity. This places manual wheelchair users at a high risk of shoulder pain and injury [2]. Strategies to thwart further disability from shoulder pain include primary prevention and rehabilitation. Two recent projects of the manual wheelchair research program at Mayo Clinic have included efforts to address both strategies: (a) to characterize kinematics and kinetics of manual wheelchair users in their natural environment to understand the mechanisms of pain and injury development; and (b) to test the efficacy of a graded 12-week therapeutic exercise program, utilizing tele-rehabilitation, targeted at shoulder musculature to decrease pain caused by reduction of the subacromial space. Both projects are presented and discussed in this report.

METHODS

Field-Based Kinematics and Kinetics

Twenty adult manual wheelchair users (18-65 years of age) were recruited and consented for participation in the IRB approved study. They had full active upper extremity (UE) range of motion and strength of 4/5 as measured with manual muscle testing throughout the upper extremity. Complaints of pain were documented and disease was confirmed with shoulder MRI.

Prior to participant testing, a custom-built prototype force glove (Fig 1) was developed and validated in the laboratory. The validation procedure used a table-embedded forceplate (AMTI) for sit-and-pivot transfers, and a Smartwheel instrumented wheelchair handrim (Three Rivers) for propulsion. APDM inertial measurement units (IMUs) were used for kinematic collection and were validated against a surface marker motion analysis system.

Figure 1: (A) Participant with IMUs on trunk, upperarm, and wrist. (B) Forceglove on the hand

The field collection included kinematic and kinetic data collection for one typical day in the user's natural environment. The participant donned the force glove and IMUs on one limb. IMUs were worn on the trunk, upper arm and forearm. At the start of the field collection, the participant completed a Wheelchair User's Pain Index (WUSPI) questionnaire [3]. The collections were scheduled to last for 8 hours. The primary variables of interest were kinematics of the elbow, shoulder and trunk and hand forces measured at the base of the palmar surface. The force magnitudes throughout the day were classified as no force, low, medium and high force quantiles.

Therapeutic Exercise Program

Fifteen adult subjects were recruited and consented for participation in the IRB approved study. Inclusion criteria included: 18-65 years of age, manual wheelchair user for at least 1 year, shoulder pain attributed to impingement, and internet access. Complaints of pain were documented and disease was confirmed with shoulder MRI.

Subjects visited the Motion Analysis Laboratory for a baseline and post exercise follow-up data collection after completion of the 12-week exercise program. During the visits, the subjects completed WUSPI, DASH and Shoulder Rating Questionnaire (SRQ) self-report measures. Subsequently, the shoulder range of motion was measured with goniometry, and isometric strength of shoulder musculature was measured with the Quantitative Muscle Assessment system (Aeverl Medical).

During the initial visit, subjects received individualized training with a licensed physical therapist regarding the appropriate way to perform the prescribed exercises targeting the lower trapezius, serratus anterior, and glenohumeral external rotators (Fig 2). Stretches were also prescribed to target the anterior chest and internal rotators, and the posterior capsule. Tele-rehabilitation visits were conducted weekly with the physical therapist for the majority of the subjects using Skype internet videoconferencing software (www.skype.com) to ensure that subjects were completing their exercises with proper technique. Exercises were advanced as the subject demonstrated mastery of earlier phases of exercise. At follow-up, subjects repeated the questionnaires. The study's primary outcome measures were the pain and functional survey scores. Isometric muscle strength was also compared before and after the intervention.

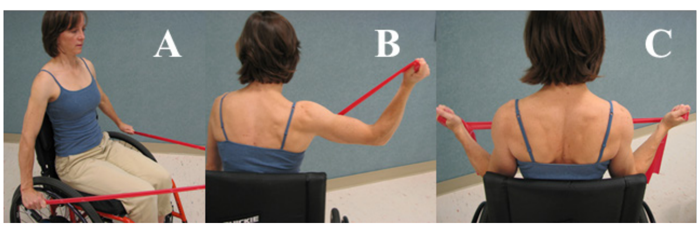

Figure 2. Example exercises for (A) lower trapezius, (B & C) glenohumeral external rotators.

RESULTS AND DISCUSSION

Preliminary analysis of the field-based collection data suggest that lower levels of pain correlated with longer periods of high loading (Table 1) and larger ranges of motion including overhead motion. These results would tend to suggest that the subjects with higher pain levels were compensating for the pain by avoiding high loading tasks and overhead motion.

Table 1. WUSPI scores and distribution of forces into 3 quantiles represented as a percentage of the day

Subject	WUSPI score	No Force (%)	Low Force (%)	Medium Force (%)	High Force (%)
1	16.0	89.20	10.60	0.1	0.09
2	22.3	99.40	0.50	0.03	0.06
3	0.0	87.20	12.69	0.08	0.04
4	6.4	91.99	7.93	0.07	0.01
5	69.4	99.70	0.26	0.01	0.03
6	8.4	98.59	1.38	0.02	0.01
7	1.4	96.03	3.73	0.22	0.02

Table 2. WUSPI scores for baseline, 12 week and 24+ week follow-up

N=11	Mean	SD	Median	Range
Baseline	28.3	24.2	18.7	1.2-76.3
12 week	12.5	12.6	10.4	0-33.4
24+ week	11.6	11.1	7.0	0-27.6

Preliminary analysis of the therapeutic exercise program showed improvement between the baseline and 12 week WUSPI scores (Table 2). The middle trapezius muscle strength improved, on average, by 36%. The strength improvement results suggest a positive benefit to scapular stabilization from the exercise program from increased strength and targeted activation of the middle trapezius. Subjects reported benefit from the education about proper ergonomics to protect their shoulders. Additionally, the tele-rehabilitation component was successfully implemented and provides a format for feasibly implementing home exercise programs in disabled populations.

CONCLUSIONS

Data from these projects will further our understanding of the loading and motion patterns that result in shoulder dysfunction and how best to prevent and rehabilitate shoulder pain and injury.

REFERENCES

1. Requejo, P.S. and S.J. Mulrouy, *Topics in Spinal Cord Inj Rehab*, 2008. **13**(4): p. 86-119.
2. Bayley, J.C., et al, *J of Bone & Joiny Surg*., 1987. **69**(5): p. 676-8.
3. Curtis, K.A., et al., *Paraplegia*, 1995. **33**(5): p. 290-3.

ACKNOWLEDGEMENTS

Funding for both projects was provided by the Paralyzed Veterans of America Foundation.

BIOMECHANICS OF INDEPENDENT CAR TRANSFER AND WHEELCHAIR LOADING IN MANUAL WHEELCHAIR USERS WITH SCI

[1,2]Philip Requejo, [1]Sara Mulroy, [1]Lisa Lighthall Haubert, [1]Somboon Maneekobkonwong, [1]Puja Ruparel, [3]Carmen Muller-Karger, [2]Jill McNitt-Gray

[1]Rancho Los Amigos National Rehabilitation Center, Downey, CA, USA
[2]University of Southern California, Los Angeles, CA, USA
[3]Simon Bolivar University, Caracas, Venezuela
email: requejo@usc.edu web: http://www.usc.edu/agingrerc

INTRODUCTION

The ability to transfer safely to a variety of surfaces is a fundamental requirement of independent mobility for individuals who use a manual wheelchair (WC). Transportation and ability to drive independently are important determinants of employment status and quality of life for individuals with SCI[1]. However, independent driving also requires transferring oneself and lifting a WC in and out of the car. Curtis et al. (1999) reported that for long-term WC users, the greatest amount of shoulder pain was experienced when the functional activity required extremes of shoulder range of motion, overhead positioning, or a high level of upper extremity strength[2]. Since transferring into a car and loading a WC encompass all three of these, it is crucial to identify the specific biomechanical demands at the shoulder in order to develop strategies for prospectively preventing shoulder pathology and loss of functional independence.

The purpose of this study was to examine the biomechanical demands of independent WC-to-car transfer and lifting of the WC frame into and out of a car. We evaluated the shoulder joint kinematics, kinetics and muscle activities of these tasks in order to examine the shoulder joint and muscular demands experienced by individuals who transfer independently with various techniques from their personal manual WCs to vehicles of different heights.

METHODS

Participants: A total of 11 participants with paraplegia from SCI (SCI level thoracic or lower and American Spinal Injury Association Impairment Scale (AIS A, B, or C – either no motor function below the level of SCI or motor function that is less than 3/5 in key muscles) who use a manual wheelchair for community mobility and routinely transfer and drive independently were asked to participate. Prior to data collection, we provided each participant with a copy of the Bill of Rights of Human Subjects and they read and signed an informed consent form that had been approved by the Institutional Review Board. Instrumentation: We instrumented a Toyota Camry (Toyota Motors, Torrance CA) to measure 6-degree-of- freedom reaction forces exerted on the steering column, driver seat, and driver's side overhead grab bar; further described in Requejo et al. 2013[3]. We used a sixteen-camera Optitrack® (Natural Points) motion capture system to track the positions (AMASS, C-Motion, Inc.) of the trunk and the bilateral upper limbs, wheelchair frame, and car positions. We recorded the electromyography (EMG) of key shoulder muscles (2000Hz) using indwelling fine-wire electrodes. Data Collection: Laboratory testing began with the subjects sitting in their personal WC, ready to lift their body into the car. Subjects were then instructed to place their right hand either on the instrumented seat, grab bar, or steering wheel, to assist in pulling or pushing themselves into the car. After subjects had transferred into the car, they were instructed to lift the WC frame from the ground to the passenger seat or rear seat. The order of hand placement and WC frame placement testing was randomized prior to data collection. The car transfer task was conducted twice; once with the instrumented vehicle set up to simulate the height from ground to the seat of an average sedan (~22") and again at a height simulating an SUV (~28"). Three wheelchair frames of varying configurations and weights were evaluated; 1) ultra-lightweight L-shaped Ti-lite Ti (3.8kg.), lightweight box frame Quickie GPV (5.9kg.), and lightweight L-shaped Colours Razorblade (4.5kg.). Data Processing and Analysis: Force, EMG, and motion data were combined using custom software (C3D Server, MLS, Inc.) and Visual3D (C-Motion Inc., Rockville, MD) was used to implement the three-dimensional model of the upper body and calculate the upper extremity kinematics and kinetics during the transfer and loading tasks. Motion and load-cell trajectory data were smoothed with a 6-Hz and 14-Hz zero-phase fourth-order digital Butterworth low-pass filter, respectively. Upper limb segments were defined following the description of Rao et al.[4] Joint kinematics was calculated using Euler/Cardan rotation sequence with the proximal segment defined as the reference frame (i.e. upper arm relative to torso, etc.). The shoulder net joint forces and moments during each phase of the transfer and lifting task were determined using inverse dynamics. The EMG activity recorded during transfer and loading tasks was processed using the International Society of Electrophysiology and Kinesiology (ISEK) recommendations. The duration and median intensity of each muscle were determined for each phase of each trial.

RESULTS AND DISCUSSION

Results: We examined the influences of varying car height, WC frame (weight and dimensions) and right hand placement during car transfer on the shoulder joint kinetics an muscle activities during independent transfers and WC frame loading. Kinematic and kinetic data from an individual with T12 paraplegia (ASIA A) transferring (Figure 1) into the sedan height vehicle and EMG when lifting (Figure 2) an L-Shaped ultra-lightweight WC frame shown as exemplary data. During the loading task, he lifted the frame from the ground with the left arm in a slight external rotation, while holding onto the steering wheel with the right arm. During placement of the frame onto the rear seat, both hands were used but the right shoulder was in maximum external rotation and abduction; an external rotation moment was observed during this time. Muscle activities were highest in right Infraspinatus (INFRA), Subscapularis (SUBSCAP), right Supraspinatus (SUPRA) during this time. The shoulder joint kinematics, kinetics, and muscle activities showed variations between test conditions.

Discussion: The current investigation documented the large forces and extreme position of the shoulder during the body lift of the transfer and release of the WC frame into the rear seat; which may predispose the shoulder joint to high stresses that lead to injury. Information from this research is critical to the development of a comprehensive shoulder pain prevention program that is crucial for preserving independence and community participation for individuals with SCI.

CONCLUSIONS

Quantitative biomechanical analysis of the car transfer and WC loading allowed the identification of the demands associated with high-stress activity that can contribute to the development of shoulder pain in manual WC users.

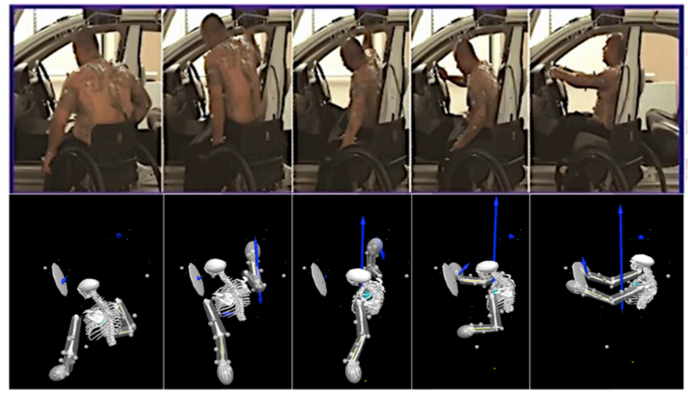

Figure 1: Video and Visual3D movement of the participant transferring into the car.

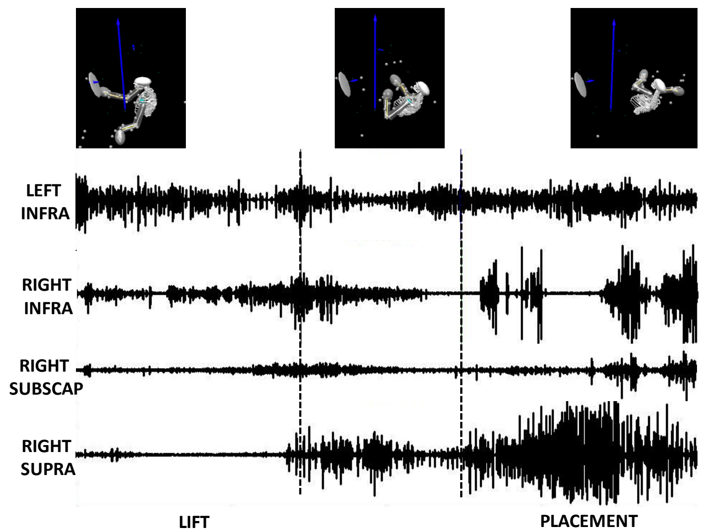

Figure 2: EMG of a participant loading the wheelchair frame into the back seat of the car.

REFERENCES

Fliess-Douer, et al. (2012). *Arch Phys Med Rehab.* 93, 629-635.

Curtis, K.A., et al. (1999). *Arch Phys Med Rehab.* 80**,** 453-457.

Rao, S.S.et al. (1996). *IEEE Trans Rehab. Eng.* 4, 152-160.

Requejo, P., et al. (2012). *RESNA*.

ACKNOWLEDGEMENTS

The contents of this report were developed under a grant from the Department of Education, NIDRR grant number H133E080024. However, those contents do not necessarily represent the policy of the Department of Education, and you should not assume endorsement by the Federal Government.

ORAL PRESENATIONS – SATURDAY SEPTEMBER 7th

	Balance & Falls *April Chambers, Brooke Coley*
11:00 AM	Impact Of Central And Peripheral Vision Loss On Standing Balance **Cham R, Mahboobin A, Redfern M, Nau A**
11:15 AM	On The Proximal Propagation Of An Impulsive Force Along The Adult Human Upper Extremity: Age And Gender Effects **Lee Y, Ashton-Miller J**
11:30 AM	Effects Of Foot Placement On Ladder Slip Outcomes **Pliner E, Beschorner K, Campbell-Kyureghyan N**
11:45 AM	Vestibular Contributions To Blindfolded Path Navigation **Davidson A, Vallabhajosula S, Mukherjee M, Stergiou N**
12:00 PM	Recovery Response To A Destabilizing Perturbation: Preliminary Comparison Between Healthy Controls And Persons With Transtibial Amputation **Sturdy J, Collins JD, Wyatt M, Grabiner M, Kaufman K, Sessoms P**

IMPACT OF CENTRAL AND PERIPHERAL VISION LOSS ON STANDING BALANCE

[1]Rakié Cham, [1]Arash Mahboobin, [1]Mark S. Redfern, and [1]Amy C. Nau

[1]University of Pittsburgh, Pittsburgh, PA, U.S.A.
Email: arm19@pitt.edu

INTRODUCTION

Vision impairments are among the leading risk factors for falls and falls-related injuries. While epidemiological studies have linked visual dysfunction with poor balance and falls, to date, the effect of visual field loss alone has not been investigated. Studies describing the effects of visual field loss in actual patients can be confounded by the presence of systemic or ocular co-morbidities, which can make it impossible to tease out the effects of visual field loss alone. This is particularly true in the case of balance or gait studies in which conditions such as arthritis or knee replacement surgery, common in the older adults, can confuse results. In order to eliminate the potential confounders of non-ocular and ocular co-morbid conditions, we developed a method of inducing visual field loss by using painted contact lenses in otherwise completely normal subjects to isolate the effect of visual field loss alone. This method provides a tool to selectively mimic visual field impairments in the absence of co-existent ocular or systemic co-morbidities that could confound balance testing. A full description of this lens model is described elsewhere [1]. Briefly, a central visual field occlusion is created by application of a soft contact lens that has been painted with an 8mm central opacity. Similarly, circumferential peripheral occlusion is elicited by application of a soft contact lens that is painted black with a clear, 1mm central aperture.

Prior studies have largely failed to elucidate underlying mechanisms explaining how specific visual impairments result in postural instability. The goal of this preliminary study was to determine the impact of restricted central or peripheral visual field losses alone on one specific mechanism for postural instability, namely the ability to integrate sensory information important for balance.

METHODS

Six healthy young adults (mean 23, std. 3) with no balance/mobility impairments were recruited for participation in this study. Subjects were given a comprehensive ocular examination and baseline visual field test prior to the balance testing, which occurred at a subsequent visit. Both the central and peripheral occlusion lenses were worn bilaterally and a control condition without lenses was administered. All subjects wore their habitual spectacle correction over their contact lenses while performing the balance protocols.

The balance protocol consisted of the standard Sensory Organization Test (SOT) [2] conditions 1-6: Condition 1: Eyes open and fixed visual scene (Fixed-Vis)/fixed floor (Fixed); Condition 2: Eyes closed/Fixed; Condition 3: Sway referenced visual scene (SR-Vis)/Fixed; Condition 4: Fixed-Vis/sway referenced floor (SR-F); Condition 5: Eyes closed/SR-F; and Condition 6: SR-Vis/SR-F. The lens conditions were: (1) none, (2) peripheral vision occluded, and (3) central vision occluded. Each SOT condition (60s in duration) was repeated three times, once for each lens condition.

Sway amplitude and velocity were quantified using two variables: root mean square (RMS) of the anterior-posterior COP time series, and mean velocity (MV) [3]. Data from SOT conditions 2 and 5 were not included in the analysis as the eyes are closed in these conditions. A repeated measures ANOVA model was used for the analysis of the data.

RESULTS AND DISCUSSION

The lens conditions were found to have a significant effect on the velocity of sway (MV), but not on the magnitude of sway (RMS). The analysis revealed a statistically significant main effect of lens condition (*F=4.15; p=0.049*), floor condition (*F=92.4; p<0.0001*), and visual scene condition (*F=11.1; p=0.02*) on MV. In addition, there were significant interaction effects on MV, including a floor condition x visual scene condition (*F=9.03; p=0.03*) and lens condition x floor condition x visual scene condition (*F=6.19; p=0.02*). Thus, the impact of the lens condition was influenced by the postural conditions (Fig. 1). More specifically, when correct proprioceptive information was available (fixed floor condition) there was no impact of lens condition on MV. However, when proprioceptive information was incorrect (sway referenced floor) MV was increased with peripheral visual field occlusion compared to central visual field occlusion and to the baseline of no lens condition (Fig. 1a). During the sway referenced visual scene conditions, occluding central vision reduced MV sway and there was no effect of occluding peripheral vision compared to baseline (Fig. 1b).

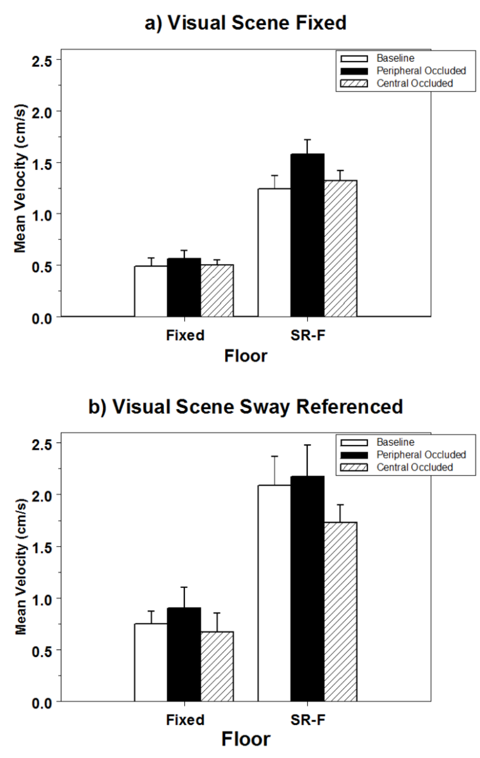

Figure 1. Impact of lens condition on mean velocity (MV) in two somatosensory conditions: Fixed (fixed floor) and SR-F (sway referenced floor).

Our results suggest that peripheral visual inputs influence postural control to a greater extent than central vision in healthy subjects. More specifically, occluding the peripheral visual field increased sway velocity, particularly when the somatosensory information was unreliable. Occluding central vision did not impact standing balance, compared to having a full visual field available. These findings occurred when visual inputs were available/reliable (fixed visual scene). However, when visual information was unreliable (sway-referenced visual scene), occluding peripheral vision did not impact sway velocity, but occluding central vision reduced velocity. Only sway velocity (and not the RMS of sway) was affected by the visual field inputs, suggesting that in healthy adults peripheral vision does not impact the magnitude of sway; however, absence of peripheral vision poses a greater challenge for the postural control system, requiring more effort to maintain balance.

Caution should be exercised if comparing the results obtained in our healthy young subjects wearing contact lenses to an aged cohort. Aging effects such as cognitive decline or motor deficiencies cannot be controlled unless the subjects are age-matched. In addition, it is known that sensory integration for postural control changes as a function of age, with vision and proprioception becoming more important as vestibular function declines. Thus, one would anticipate that the effects in older adults would be even greater as sensory integration processes change. Future studies are planned to compare young and older subjects wearing the contact lenses to investigate the influence of age on the visual field loss and balance.

REFERENCES

1. Nau A. *Optometry* **83**, 76-81, 2012.
2. Nashner LM and Peters JF. *Neurol Clin* **8**, 331-349, 1990.
3. Maurer C and Peterka RJ. *J Neurophysiol* **93**, 189-200, 2005.

ACKNOWLEDGEMENTS

Funding provided by the National Institute of Health CORE Grant (P30 EY008098) and the University of Pittsburgh Central Research Development Fund (CRDF) Grant Program.

ON THE PROXIMAL PROPAGATION OF AN IMPULSIVE FORCE ALONG THE ADULT HUMAN UPPER EXTREMITY: AGE AND GENDER EFFECTS

[1]Yunju Lee and [1]James A. Ashton-Miller

[1]University of Michigan, Ann Arbor, MI, USA
email: yunjulee@umich.edu, web: http://me.engin.umich.edu/brl/

INTRODUCTION

In a fall to the ground, the impact force on the hand reaches 2-3 times body weight [1], enough to cause wrist fracture on a hard surface. The arm muscles precontract to generate enough stiffness to prevent the arm from buckling, thereby protecting the head from impact. The ground reaction force peaks within a few tens of milliseconds on the hand, and within one hundred milliseconds at the proximal extremities [1, 2]. This raises the question as to whether there is sufficient time for any short- or long-loop muscle reflexes to increase the muscular resistance to arm buckling during the fall arrest. So, the goal of this paper was to study the factors that determine arm kinematics under an impulsive end load. We tested the null hypotheses that neither gender, age, nor pre-contraction level affects the time it takes for an impulsive force to propagate proximally along the upper extremity in healthy adults; furthermore, this propagation time is always shorter than the latency of the major triceps EMG response to the impact.

METHODS

Ten healthy young males of mean (SD) age of 25.5 (2.7) years, eight healthy young females of 24.5 (3.1) years, 9 healthy old males of 69.4 (3.4) years and 11 healthy old females of 67.7 (2.4) years participated in the study. Each volunteer lay on an apparatus in the prone position with shoulders and arms slightly flexed. The non-dominant hand was positioned on a 6-axis force transducer mounted at one end of a thin-walled rectangular aluminum beam. With the beam pivoted about a central fulcrum, a weight of 23 Kgf was released from a fixed height to land on the other, raised, damped end of the beam, thereby applying a known impulsive force to the hand when the desired level of triceps muscle precontraction level had reached either 25, 50 or 75% of maximum voluntary contraction levels. Limb kinematic data were acquired at 280 Hz using optoelectronic markers, and the lateral triceps electromyographic (EMG) activity was acquired at 4 kHz.

Descriptive statistics were calculated for peak force, joint marker and EMG onset times. A repeated measures analysis of variance (rm-ANOVA) was used to test the null hypothesis for age, gender, and three different muscle co-contraction levels using SAS 9.3 software. A p-value of less than 0.05 was considered statistically significant.

RESULTS AND DISCUSSION

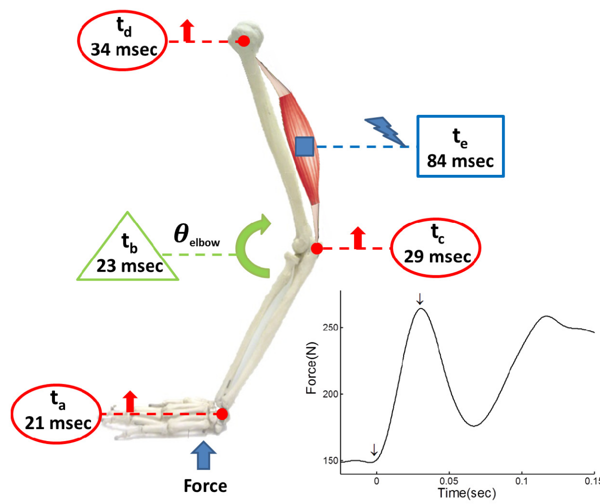

Figure 1: Illustration of onset times (outlined) of landmark movement and EMG onset time. The red circles (t_a, t_c, t_d) denote the onset times of linear displacements at the wrist, elbow and shoulder joints; the green triangle (t_b): the onset of rotation at the elbow joint; the blue rectangle (t_e): the onset of lateral triceps brachii EMG signal. Temporal plot of measured impulsive force shows two arrows indicating the onset of change from the preload force (F_0) and the peak force (F_1) [see text].

Across all subjects, the peak applied force (F_1) occurred (mean ± SD) 27 ± 2 msec after the onset (F_0) of the applied impulse. The onset times for displacements of the wrist, elbow and shoulder markers were 21 ± 3 msec, 29 ± 5 msec and 34 ± 7 msec, respectively. The corresponding onset times for elbow flexion and lateral triceps brachii EMG activity were 23 ± 5 msec and 84 ± 8 msec, respectively (Fig. 1).

The hypothesis was supported in that even the longest latency to onset of the shoulder marker linear displacement was approximately 40 msec, with the displacement onsets at the wrist and elbow being shorter, and all these latencies being substantially shorter than the EMG onset time of the lateral triceps brachii (measured at 84 msec) as well as the time required to alter striated muscle force by 50% of maximum values (90 msec from [3]). So, neither the short- nor long-loop reflexes can alter the state of triceps muscle contraction before the elbow joint is forcibly flexed.

The ANOVA demonstrated significant gender, age, and pre-contraction level effects on onset times (Table 1). Age significantly affected EMG onset time, gender affected wrist and shoulder displacement onset times, and co-contraction level significantly affected all joint onset times, as well as the time to peak force (F_1). While the higher pre-contraction level accompanied a more rapid onset time for each joint marker, the lower pre-contraction level was associated with a more rapid time to the peak force (F_1). In addition, the initial force (F_0) correlated with pre-contraction level as well as peak force, F_1 ($p<0.001$). Although the onset of wrist marker motion was earlier in males, the latency of the impulse propagation to the shoulder marker was slower than in the females.

The results suggest that the elbow started to flex 6 msec before the origin of the triceps started to displace, so the triceps EMG response at 84 msec was most likely triggered by arm flexion rather than by any axial displacement of the femoral origin of triceps in the direction of the impulsive force. These results suggest that there is insufficient time for any neural reflexes to modulate arm buckling resistance before the 84 msec onset of triceps EMG, whether triggered by muscle spindle stretch due to the onset of induced elbow flexion (at 23 msec), or the onset of the proximal displacement of the origin of the triceps muscle near the acromion marker (at 34 msec). Given the 90 msec Thelen et al. [3] found that it takes to volitionally increase tension, and therefore tensile stiffness, of striated muscle to half-maximal values, it is unlikely that any muscle reflex can significantly increase the tensile stiffness of the triceps before it is forcibly stretched at 23 msec, even if the onset of the impulsive force was so rapid that it triggered a flexural stress wave (velocity of 300 m/s [4]) to propagate proximally along the ulna and humerus so as to initiate (after ~2 msec) longitudinal vibrations in triceps muscle spindles.

CONCLUSIONS

There is insufficient time for any muscle reflexes to significantly increase the resistance of the arm muscles to elbow buckling while landing a fall. The arm muscles must be adequately precontracted *prior to* impact in order to prevent arm buckling.

REFERENCES

1. DeGoede KM, et al. *J Biomech* **35**, 843-848, 2002.
2. DeGoede KM, et al. *J Biomech* **36**, 413-420, 2003.
3. Thelen DG, et al. *J Gerontol (Biol Sci Med Sci)* **51A**, M226-M232, 1996.
4. Flynn TW, et al. *Work* **18**, 151-160, 2002.

ACKNOWLDEGEMENTS: NIH P30 AG024824

Table 1: ANOVA p values showing outcomes as a function of the three main effects.

Main Effect	Wrist Onset Time	Elbow Flexion Onset Time	F_1 Latency	Olecranon Latency	Acromion Latency	Triceps EMG Latency
Age	0.8185	0.1736	0.8727	0.1264	0.0614	0.0032*
Gender	0.0105*	0.6652	0.0125*	0.7828	0.0177*	0.92
Co-contraction	<.0001*	0.0001*	0.0005*	<.0001*	0.0009*	0.1504

Effects of Foot Placement on Ladder Slip Outcomes

Erika Pliner, Kurt Beschorner, Ph.D., and Naira Campbell-Kyureghyan, Ph.D.

University of Wisconsin-Milwaukee, WI, USA
email: empliner@uwm.edu

INTRODUCTION

Ladder-related falls are the leading cause of disabling falls to lower levels [1]. Employees injured from ladder-related falls miss an average of 15 work days [1]. Rung shape, orientation, and friction are important factors in generating hand forces and have been deemed important for a safe ladder design [2]. However ladder climbing is a full body activity and few studies have considered the role of the lower-body during slipping. Understanding the effects of climbing technique on ladder slip and fall risk is critical to training safe ladder climbing. Since the foot is the primary load-supporting interface between the ladder and the body [3], foot placement may be a critical variable for estimating slip and fall risk. This study investigates the effects of foot placement on frequency of ladder slips and falls and the kinematic variables involved with slip outcome.

METHODS

The study included 32 participants aged 18-65 with 10 females. IRB approval and written informed consent were obtained prior to testing. Exclusion criteria included musculoskeletal and neurological disorders, pregnancy, and balance disorders. All participants were equipped with standardized attire, footwear and a safety harness. Forty-six reflective markers were placed on anatomical landmarks of the participant and were tracked during each trial (100 Hz). Participants climbed a vertical 12-foot ladder equipped with five reflective markers. Lockable bearings were applied to the fourth rung so that it locked during non-slip trials and spun during slip trials. The safety harness was equipped with a load cell to determine the participant's weight supported by the harness (1000 Hz).

Each participant was randomly assigned to two of four climbing strategy groups. Climbing strategies included two hand positions (rungs or rails) and two foot placements (mid-foot or forefoot). A board was placed a distance of 25% of the subject's foot length anterior to the ladder during the forefoot climbing conditions to ensure forefoot placement. Participants were allowed to acclimate to the ladder prior to data collection. Participants were instructed to climb the ladder at a comfortable but urgent pace. For both of the climbing strategies, participants climbed the ladder 5-8 times with the rung locked in place and then once when the rung could freely spin. Between each trial the participants performed a walking task outside the lab so that they were not aware of the rung's locked/unlocked configuration. The climber's safety was ensured throughout the testing session with a belayer, spotter, and an impact mat.

A trial was classified as a slip if the participant's foot completely slipped off the perturbed rung. For each slip event, the ascent and descent were considered as separate samples. A trial was considered to be a slip if the foot completely slipped off of the rung, which was determined by examining the vertical position of the foot relative to the rung. A slip trial was classified as a fall if the load in the harness supported more than 10% of the participant's body weight. The foot-floor angle was calculated using markers placed on the toe and heel. An ANOVA analysis was performed with age, climb direction, foot placement and hand position as independent variables and with slip outcome as the dependent variable. Because of the low number of fall outcomes, a separate ANOVA analysis was performed with just foot placement as the independent variable and fall outcome as the dependent variable. ANOVA analyses were performed with foot kinematic variables as the dependent variables and foot placement climbing strategy and slip outcome as the independent variables. Foot kinematic variables include foot positioning and foot angles at foot contact time and contralateral foot-off time. The change in foot positioning and foot angle between foot contact and contralateral foot-off times were also analyzed.

RESULTS AND DISCUSSION

Participants slipped off of the rung 16 times and fell five times during the 64 slip trials. Seven slips occurred during ascent and nine slips occurred during descent with two and three falls, respectively. Ten slips were with rail hand positioning and six slips were with rung hand positioning. Out of the five falls, four were under the rail hand placement condition. Slipping was seven times more likely with forefoot than mid-foot placement ($p<0.01$) and falls occurred exclusively with the forefoot placement ($p<0.01$). Therefore it may be determined that forefoot placement puts a climber at greater risk of slipping and falling.

Age group was a significant factor for slipping ($p<0.05$) with the most occurring in the youngest age group (ages 18-29) (7.8% slips), followed by the eldest group (ages 50-65) (3.1% slips) and then the middle group (30-49) (1.6% slips). This suggests that the younger and older age groups are more susceptible to slipping. One possible explanation for this V-shaped relationship may be that experience and age-related changes in strength, coordination and climbing style affect slip risk.

The rung position relative to the toe and normalized to foot length was 0.27 at foot contact and 0.21 at contralateral foot-off for the forefoot condition while it was 0.45 at foot contact and 0.49 at contralateral foot-off for the mid-foot condition. Thus the foot moved posteriorly from foot contact to contralateral foot-off during the forefoot and anteriorly for the mid-foot condition ($p<0.01$). The forefoot also moved more posterior during slipping trials compared with non-slipping trials ($p<0.001$). Thus, the perturbed foot started to slip off the rung prior to contralateral foot-off. Climbing on the forefoot led to smaller foot angles at foot contact ($p<0.05$) and at contralateral foot-off ($p<0.001$). A larger increase in foot angle between foot contact and contralateral foot-off was observed among participants who slipped compared with participants who did not slip ($p<0.05$) (Figure 1). The kinematics of the foot may be an important mechanism for understanding the occurrence of ladder slipping. Specifically, participants who slipped had a greater difference between foot contact angle and contralateral foot-off angle, which suggests that stabilizing the foot as it accepts the weight of the body is critical to preventing slips. Foot stabilization may be accomplished through the production of ankle plantar flexor moments or with use of upper body strategies. Confirming these strategies that maintain stability of the foot angle during climbing may assist in preventing ladder slips.

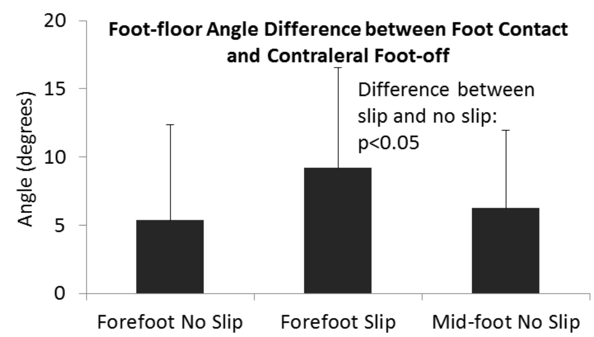

Figure 1: Foot-floor angle difference between foot contact and contralateral foot-off across foot placement and slip outcome groups. Mid-foot slips were omitted due to a small sample size (n=2).

CONCLUSIONS

The findings of this study provide insight into how ladder slips and falls occur. A slip or fall is more likely to occur with a forefoot placement. Stabilizing the foot during weight acceptance either through upper or lower-body strategies may improve slip and fall outcomes.

REFERENCES

1. U.S DoL- BLS, *New Data Highlight Gravity of Construction Falls*, 1996: Washington, D.C.
2. Young et al, 2009, *Human Factors*. 51: p. 705-17.
3. Bloswick and Chaffin, 1990, *International Journal of Industrial Ergonomics*. 6(1): p. 17-27.

ACKNOWLEDGEMENTS

This work was funded by University of Illinois-Chicago/NIOSH/CDC (5T42OH008672-08).

VESTIBULAR CONTRIBUTIONS TO BLINDFOLDED PATH NAVIGATION

[1]Austin Davidson, [2]Srikant Vallabhajosula, [1]Mukul Mukherjee and [1,3]Nicholas Stergiou

[1]Nebraska Biomechanics Core Facility. University of Nebraska at Omaha. Omaha, NE, USA
[2]Department of Physical Therapy Education, Elon University, Elon, NC, USA
[3]College of Public Health, University of Nebraska Medical Center, Omaha, NE, USA
email: ajdavidson@unomaha.edu, web: nbcf.unomaha.edu

INTRODUCTION

During blindfolded path navigation, the ability to orient oneself in space based on perceived motion plays a critical role in successful navigation. The vestibular system is believed to play a key role in providing feedback important for orientation during path navigation through a perception of the body's perception of linear and angular velocity and acceleration [1]. In order to test the effects of the vestibular afference on path navigation, a circular path was chosen because it would have a continuous change in angular displacement. The vestibular system was manipulated with tactors that produced vibratory stimuli on the mastoid process. The goal of this study was to determine the role of the vestibular system during blindfolded circular path navigation. We hypothesized that perturbations to the vestibular system would show a greater positive correlation with effects to the angular components of the circular path compared to linear components. In addition, we compared the results to our previously work on the effects of tactile stimulation on blindfolded path navigation [3].

METHODS

Vestibular perturbation was conducted using four C2 tactors (vibrators; Engineering Acoustics, Inc., Casselberry, FL) attached posterior to mastoid process on either side of subject's head. Ten healthy subjects aged between 19 and 29 years walked on a 7.2m circular path [2]. Subjects walked on a circular path under four conditions: 1) with eyes open and tactors off, 2) with eyes closed and tactors off, 3) with eyes closed and tactors on (left side) and 4) with eyes closed and tactors on (right side). In addition to being blind-folded, subjects wore disposable ear plugs to lessen their ability to orient themselves based on auditory cues. Condition 1 was always performed first to allow subjects to form a cognitive map and conditions 2, 3, and 4 were randomized for each subject. Kinematic data was collected using 12 infrared cameras (Motion Analysis Corp., Santa Rosa, CA). Dependent variables calculated included path length, median radius, walking velocity, linear distance between start and end points (linear error), and angular distance traversed between start and end points (angular error). All variables were determined using the sacral marker data. Post-processing was performed using Matlab (Mathworks, Natick, MA).

RESULTS AND DISCUSSION

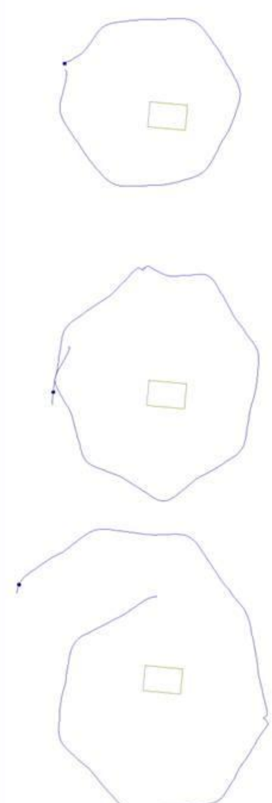

Figure 1a: Example of subject's path with eyes open, tactors off (condition 1)

Figure 1b: Example of subject's path with eyes closed, tactors off (condition 2)

Figure 1c: Example of subject's path with eyes closed, tactors on (condition 3)

Figure 1: Example of path traveled by one subject under three conditions

Figure 1a-c shows a representation of one subject's paths under different conditions.

Table 1: Mean (SE) of dependent variables for the experimental conditions with vestibular perturbation and control (n = 10). The following comparisons were signifcant at p<0.05: # eyes open tactors off Vs eyes closed tactors off, * eyes open tactors off Vs eyes closed tactors on Left, ^ eyes open tactors off Vs eyes closed tactors on Right.

Dependent Variable	***Eyes Open – Tactors Off***	***Eyes Closed – Tactors Off***	***Eyes Closed – Tactors On (Left)***	***Eyes Closed – Tactors On (Right)***
Path Length (m)	7.56 (0.17)	8.55 (0.41)	7.69 (0.27)	7. 92 (0.35)
Median Radius (m)	1.42 (0.02) ^	1.62 (0.10)	1.58 (0.07)	1.72 (0.06)
Walking Velocity (m/s)	0.83 (0.01) #	0.76 (0.02)	0.73 (0.04)	0.74 (0.03)
Linear Error (m)	0.17 (0.08) #*^	1.10 (0.22)	1.43 (0.36)	1.57 (0.32)
Angular Distance (°)	358.44 (0.41) #*^	324.11 (7.68)	312.11 (12.97)	309.78 (12.10)

CONCLUSIONS

Figure 1 shows a clear sequential decrement in path navigation ability with first, removal of vision and second, with removal of vision and vestibular stimulation. The ability to accurately navigate a circular path while blindfolded was reduced when the vestibular system was perturbed in addition to the removal of vision. Figure 2 demonstrates a comparison of vestibular perturbations from this study to our previous study involving tactile perturbations [2]. It is apparent that linear error was more sensitive to tactile perturbations while the greatest impact of vestibular perturbations was on the angular parameters during circular path navigation. However, such an effect can be proven through multiple sensory manipulations on the same group of participants. This is our future direction.

REFERENCES

1. Berthoz A, et al. *Science*, **269(5220)**, 95-98, 1995.
2. Koutakis P, et al. *Gait & Posture*, **37 (2)**, 154-158, 2013.
3. Vallabhajosula S, et al. Proceedings of ASB, 2012 [http://www.asbweb.org/conferences/2012/abstracts/194.pdf]

ACKNOWLEDGEMENTS

Funding provided by the National Institute of Health (Grant No. 1R011AG034995-01A1), and the National Aeronautics and Space Administration (Grant No. NNX11AM06A).

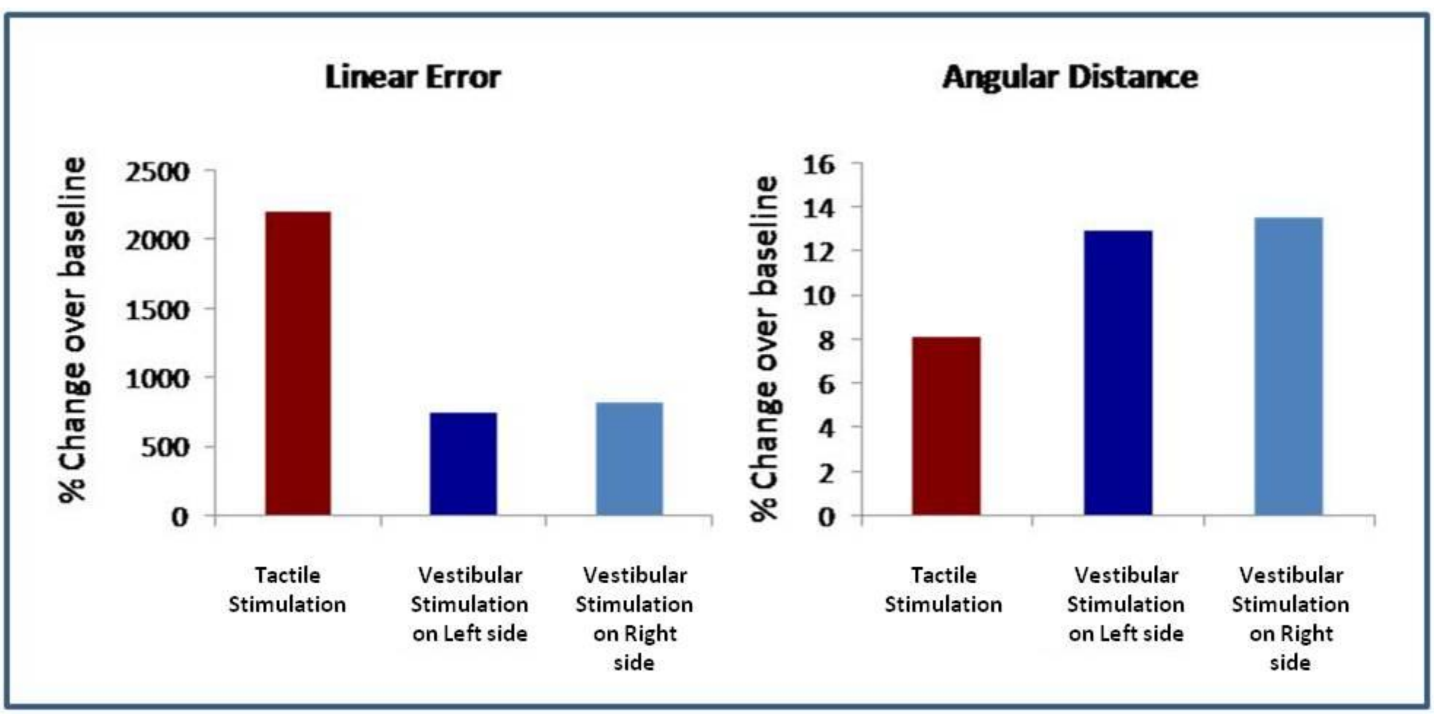

Figure 2: Comparison of vestibular perturbations on path integration to tactile perturbations from previous study.

RECOVERY RESPONSE TO A DESTABILIZING PERTURBATION: PRELIMINARY COMPARISON BETWEEN HEALTHY CONTROLS AND PERSONS WITH TRANSTIBIAL AMPUTATION

[1]Jordan Sturdy, [2]John-David Collins, [1]Marilynn Wyatt, [3]Mark Grabiner, [4]Kenton Kaufman, and [2]Pinata Sessoms
[1]Naval Medical Center San Diego, San Diego, CA, USA
[2]Naval Health Research Center, San Diego, CA, USA
[3]University of Illinois, Chicago, IL, USA
[4]Mayo Clinic, Rochester, MN, USA
email: jordan.sturdy@med.navy.mil

INTRODUCTION

The most common cause of a nonfatal injury in all age groups is falls. A technique for assessing the ability to avoid falling from a destabilizing perturbation has been developed and is being tested with an injured population and healthy controls. Here, we report initial comparisons between a healthy control group and persons with transtibial amputation (TTA).

METHODS

Functional performance of the subject's ability to avoid a potential fall was assessed using a Computer Assisted Rehabilitation Environment (CAREN, Motek Medical BV, Amsterdam, NL), an immersive virtual environment with an instrumented dual-belt treadmill. Data were collected during two visits on able-bodied controls (N=5, mean height= 173.7±5.1 cm and weight= 76.3±9.4 kg), and persons with TTA (N=6, mean height= 176.7±6.1 cm and weight= 76.3±5.1 kg). The TTA group underwent a fall prevention training program in the two weeks between the first and second visits (pre and post tests). Perturbations to able-bodied self specified dominant and non-dominant limbs were contrasted with sound limb (NPL) and prosthetic limb (PL) perturbations in the TTA group. Walking speed was normalized based on each subject's leg length. During each visit, subjects walked on the treadmill for a 10-minute warm-up period. This was then followed by a five minute period during which six destabilizing perturbations, three each for the left and right leg, were randomly delivered. This was implemented by a treadmill deceleration that was followed by an acceleration that increased treadmill velocity to over 4.0 m/s before returning back to the normal walking speed. Subjects were instructed to recover as best they could and continue walking if possible. Each subject wore a safety harness for the entire visit. Full body marker coordinate data were acquired using a 12 camera motion capture system (Motion Analysis Corp., Santa Rosa, CA).

Trunk motion variables previously shown to determine likelihood of a fall[1] were analyzed. Independent samples t-tests were run to compare differences in peak trunk flexion angle and velocity between the control group and the TTA group, both for pre- and post-tests. T-test comparisons between the two TTA visits were also performed.

RESULTS

It has been previously determined that responses to trips after the first perturbation are similar[2]. The final perturbation during each visit for each subject was thus selected for our analyses. No differences were observed between visits for the able-bodied group, and only the second visit was used as the representative control data set for comparison to persons with TTA.

When compared to the controls, persons with TTA exhibited significantly higher peak trunk angle and velocity during the pre-test (Figure 1a) when the NPL was perturbed ($p < 0.014$ and $p < 0.001$ respectively). During the post-test (Figure 1b), only peak trunk velocity was significantly higher ($p < 0.032$) in the TTA group compared to the healthy controls. Notably, persons with TTA exhibited significantly lower post-test values for peak trunk angle and velocity following NPL perturbations compared to pre test ($p < 0.035$ and $p < 0.013$, respectively). For PL perturbations, only peak trunk angle decreased significantly from pre to post test ($p < 0.045$).

(a)

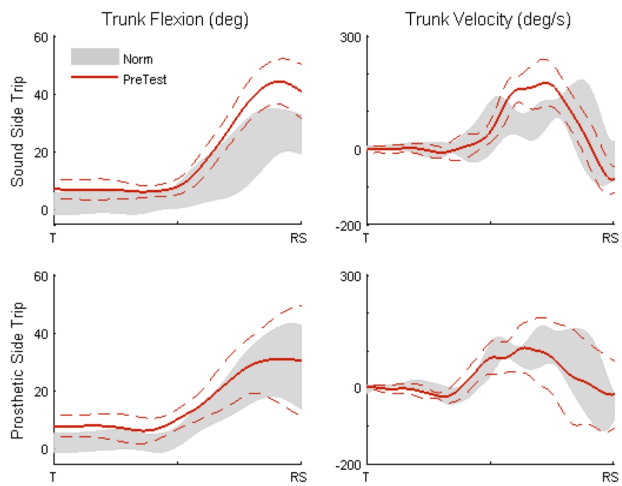

(b)

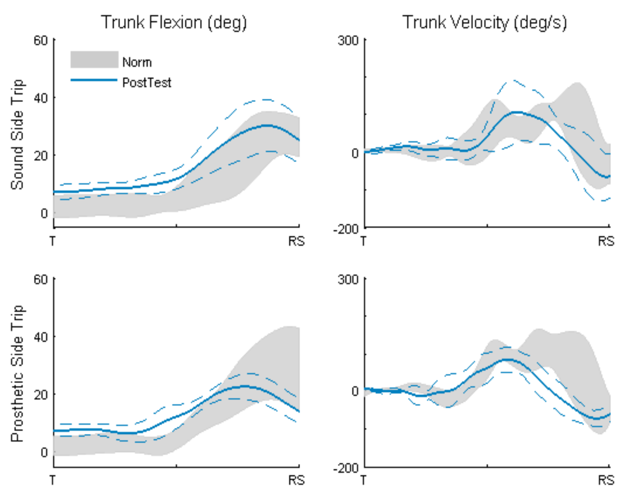

Figure 1: Pre (a) and post (b) test perturbation data values from time of perturbation (T) to recovery step (RS). Solid lines represent means; dotted lines represent one standard deviation for persons with TTA. Shaded region represents the mean ± one standard deviation of the control group.

CONCLUSIONS

Large peak trunk flexion angle and velocity values may be indicators of a higher risk of falling[1]. For persons with TTA these data are significantly higher during pre-test than controls when the NPL is the perturbed limb and the subject must rely on the PL for their initial stabilization.

While both pre- and post-test trunk flexion velocities were significantly higher in persons with TTA than controls during NPL perturbations, the post-test values were significantly lower that the pre-test values. Remaining post-test data seem to approximate control values in recovering from a perturbation. This indicates that training produced an improvement in the ability to control trunk motion following an unexpected perturbation. Anecdotal feedback from TTA subjects state that they are less concerned when they stumble or trip while participating in activities of daily living.

REFERENCES

1. Owings TM, et al. *Clinical Biomechanics* **16**, 813-819, 2001
2. Sessoms, PH, et al. *J. Biomech*, In Review

ACKNOWLEDGEMENTS

This work was supported by DoD Grant DM090896 and the Bureau of Medicine and Surgery Wounded, Ill and Injured grant R116 under work unit no. 60818. The views expressed are those of the authors and do not reflect the official policy or position of the DoN, DoD, or the U.S. Government. Approved for public release; distribution is unlimited. This research was conducted in compliance with all applicable federal regulations governing the protection of human subjects (Protocols NHRC.2013.0001 and NHRC.2011.003)

Table 1: Mean peak values and standard deviations for trunk angle and velocity for both sound limb (NPL) and prosthetic limb (PL) perturbations. * denotes Significance vs. Controls; ^ denotes Significance between TTA-Pre and TTA-Post tests.

Sound Limb (NPL)	Control Dominant	TTA-Pre	TTA-Post	Prosthetic Limb (PL)	Control non-Dominant	TTA-Pre	TTA-Post
Trunk Angle (deg)	24.8 ± 10.5	40.1 ± 6.0 *^	29.3 ± 10.9 ^	**Trunk Angle (deg)**	30.1 ± 8.5	31.4 ± 10.4 ^	22.2 ± 4.2 ^
Trunk Velocity (deg/s)	98.9 ± 20.9	177.7 ± 36.2 *^	129.0 ± 26.3 *^	**Trunk Velocity (deg/s)**	119.6 ± 42.0	134.9 ± 48.5	97.8 ± 35.7

ORAL PRESENATIONS – SATURDAY SEPTEMBER 7th

	Musculoskeletal Modeling *Stephen Piazza, Jeffrey Reinbolt*
11:00 AM	Statistical Functional Mapping From Body Parameters To Gait Kinematics **Yun Y, Deshpande A**
11:15 AM	Consistency Among Musculoskeletal Model Moment Arms **Wagner D, Stepanyan V, Shippen J, DeMers M, Gibbons R, Andrews B, Creasey G, Beaupre G**
11:30 AM	Hill-Type Muscle Model With Slow And Fast Fiber Contractile Elements **Lee SSM, Arnold AS, de Boef Miara M, Biewener AA Wakeling JM**
11:45 AM	Windng Filament Muscle Model For Musculo-Skeltal Simulations **Petak J, Heckathorne N, LeMoyne R, Dyer J, Yeo SH, Dinesh P, Tester J, Nishikawa K**
12:00 PM	Matching Human Walking Using A Six-Link Planar Model **Martin A, Schmiedeler J**

STATISTICAL FUNCTIONAL MAPPING

FROM BODY PARAMETERS TO GAIT KINEMATICS

Youngmok Yun and Ashish D. Deshpande
The University of Texas at Austin, Austin, TX, USA
email: yunyoungmok@utexas.edu, web: http://www.me.utexas.edu/~reneu/

INTRODUCTION

Investigation of the relationships between body parameters and human gait kinematics is challenging because numerous factors affect gait kinematics and their effects are highly nonlinear. One possible approach is to use a biomechanical model [1]. The gait motion generated by optimizing the model with a cost function (metabolic energy) can show the effects of biomechanical elements. However, effectiveness of this method is limited by the simplification in the models, need for a cost function, difficulty in measuring biomechanical parameters and ignorance of variance. Another approach is to use a statistical method based on data. Previous researchers revealed correlations (typically linear) between one or two body parameters (height, age, etc) and gait parameters (step length, gait period, etc) [2]. This approach does not require development of a biomechanical model or choosing of a cost function; however, effects of only one or two body parameters have been analyzed, and also the output is a gait parameter (scalar value) not a gait pattern (time-series).

We have developed a novel statistical method to generate a functional mapping from body parameters to gait kinematics pattern. The mapping is a numerical model, sometimes referred to as a *black-box* model, and Gaussian Process Regression (GPR) algorithm [3] was employed for its generation. From an arbitrary person's body parameters, the function can not only produce time-series of the joint motions representing gait kinematics but also estimate the associated uncertainties. This enables a comprehensive understanding of the correlation and uncertainty between body parameters and gait kinematics, and furthermore provides a low-cost gait kinematics prediction method because the only necessary inputs are the subject's body parameters which are easy to measure.

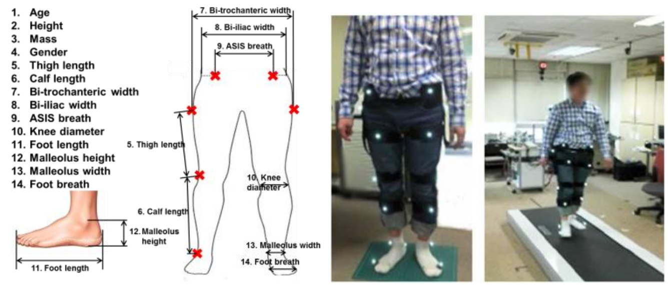

Figure 1: Collection of database. Left: 14 body parameters. Right: recording of gait kinematics with a motion capture device

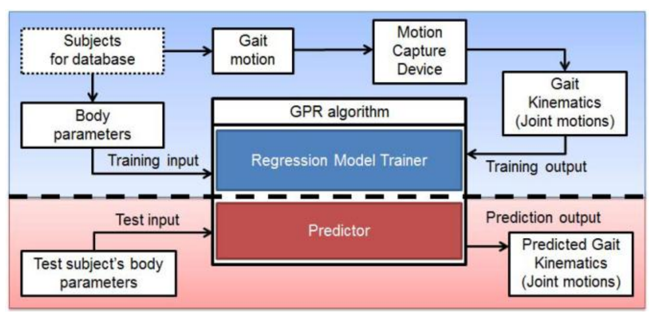

Figure 2: Creation of functional mapping from body parameters to gait kinematics.

METHODS

A total of 113 healthy subjects participated in the experiments for the generation of a large database. Their 14 body parameters (height, etc.) that significantly affect gait patterns were selected as function inputs, and 14 joint motions (knee flexion, etc.) were selected as function outputs representing gait kinematics. Body parameters were measured by the researchers for each individual and the joint motions were recorded by a motion capture device (Figure 1).

The creation of functional mapping from a large database requires the implementation of a nonlinear regression method. We devised a GPR model for this work and trained the model with the database (Figure 2). The GPR model is defined by the mean function of (1) and the covariance function of (2).

$$m(x) = \nu_m \quad (1)$$

$$k(x, x') = \nu_0 \exp\left(-\frac{(\Delta \mathrm{b})^{\mathrm{T}} \Lambda_b (\Delta \mathrm{b}) + \lambda_{\mathrm{t}} \Delta t^2}{2}\right) + \nu_1 \delta(i, j) \quad (2)$$

where b is a vector indicating a subject's body parameters, and t is a normalized time index. Δb is defined as $\mathrm{b} - \mathrm{b}'$ and Δt is defined as $t - t'$. $\delta(i, j)$ is Kronecker delta function. Λ_b is a diagonal matrix. Hyperparameter set is defined as a set of $\nu_m, \nu_0, \nu_1, \Lambda_b, \lambda_{\mathrm{t}}$ and determines the characteristics of GPR model. By selecting the hyperparameter set to maximize likelihood function (in other words to accord with all database), we can find the optimal GPR model.

RESULTS AND DISCUSSION

We built a functional mapping from body parameters to gait kinematics by training GPR model with the database. The input of the function is an arbitrary person's body parameters and the output is probabilistic distribution of the predicted joint motion including the mean trajectory and the standard deviation associated with the uncertainty of the trajectory (Figure 3). Cross-validation (leave-one-out) with all the subjects confirms that the prediction algorithm is effective.

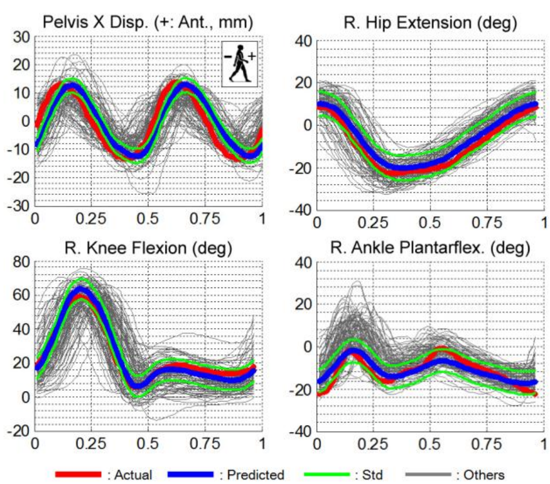

Figure 3: Sample prediction results. x-axes indicate normalized time index. GPR prediction algorithm provides not only time-series of joint motions but also its uncertainty values via standard deviation values.

Selection of the body parameters for the input of the functional mapping is challenging because countless factors influence the human gait pattern and many of the factors are hard to measure, time-variant or even random. Against this situation, we selected 14 body parameters that are proven to have significant effects on the gait pattern and are easy to measure. Then we let the stochastic model handle influence of the other factors. GPR is fully based on Bayesian model, and thus its output is a probabilistic distribution. As a result, the effect of the other factors can be expressed by the uncertainty via standard deviation values of predicted gait pattern.

Our functional mapping gives a novel statistical method to investigate the relationships between body parameters to gait pattern. Previous researches revealed one-to-one or two-to-one mappings between body parameters and gait parameters (e.g., height to step length). Our method enables broader analysis by providing a functional mapping whose input is multi-dimensional and output is multi-dimensional time-series (not scalar). While the previous statistical methods only revealed a slice of the human gait kinematics, our comprehensive input and output functional mapping may lead to a deeper understanding of factors affecting gait kinematics and contribution in rehabilitation, prosthetics and controls of humanoid walking.

The presented method suffers from the disadvantage inevitable in statistical regression method. A drawback is that it is hard to get insight into the physics and biomechanics. We plan to address this weakness by introducing physical models as constraints in the GPR algorithm.

REFERENCES

1. Frank CA, et al. *J. Biomech. Eng.* 2001.
2. Jennifer LL, et al. *Gait & Posture* 2003.
3. Carl ER, et al. *Gaussian process for machine learning*, MIT press, 2006

ACKNOWLEDGEMENTS

The data for this study was collected at the Korean Institute of Science and Technology. A part of this work has been submitted in the form of a journal article which is under review.

CONSISTENCY AMONG MUSCULOSKELETAL MODEL MOMENT ARMS

[1]David W. Wagner, [2]Vahagn Stepanyan, [3]James M. Shippen, [2]Matthew S. DeMers, [4]Robin S. Gibbons, [5]Brian J. Andrews, [1,2]Graham H. Creasey, and [1,2]Gary S. Beaupre

[1]VA Palo Alto Health Care System, Palo Alto, CA, USA
[2]Stanford University, Stanford, CA, USA
[3]Coventry University, Worcestershire, UK
[4]Brunel University, Hertshire, UK
[5]Oxford University, Oxford, UK
email: dwwagner@gmail.com

INTRODUCTION

Musculoskeletal simulation software packages and model repositories have broadened the user base able to perform musculoskeletal analysis and have facilitated in the sharing and distribution of musculoskeletal models. As musculoskeletal modeling continues to become more utilized as an engineering tool, the consistency in results derived from different models and simulation software is becoming more critical. Understanding the absolute and potential trend differences that may result as a function of model selection is essential, especially considering users rarely have the opportunity to duplicate a particular analysis with different generic models or software. The purpose of this study was to compare eight musculoskeletal models, from three modeling packages, and evaluate differences in muscle moment arm lengths.

METHODS

Eight musculoskeletal models (Table 1) were scaled to the same joint-to-joint lengths, consistent with a 50th percentile male by stature, with off-axis dimensions scaled isometrically. Model-predicted moment arm data were obtained using the same method for all models using a direct load measurement method, previously summarized by An et al. [1]. Sub-models of each musculoskeletal model were constructed with only the single muscle (or group of muscle fascicles representing a single muscle) to be evaluated. An external unit torque was applied about the rotational axis of the knee. Knee flexion was varied between -125 degrees and +10 degrees (knee extension) over a time of 1000 seconds. The force of gravity was reduced to zero for each model. Muscle and tendon force for each model were computed using a static optimization procedure. Although an optimization procedure was used, the results are deterministic as only one muscle was included in each model. The muscle moment arm at each knee angle was computed as the applied torque divided by the computed tendon force. The computed moment arms for the models in OpenSim were essentially equivalent to the outputted moment arms from that software's available muscle moment arm calculation function.

RESULTS AND DISCUSSION

The difference between the moment arms for the individual quadriceps muscles within a single model was relatively small (results not shown). For knee flexion angles greater than 20 degrees, the maximum moment arm difference for any given model was 0.68 cm. All the scaled models have both different absolute moment arm lengths and trends over the evaluated knee range of motion (see Fig. 1 for vastus lateralis). Similar results were observed for the other quadriceps muscles (not shown). No single model bounded the upper or lower moment arm limits over the knee angles evaluated.

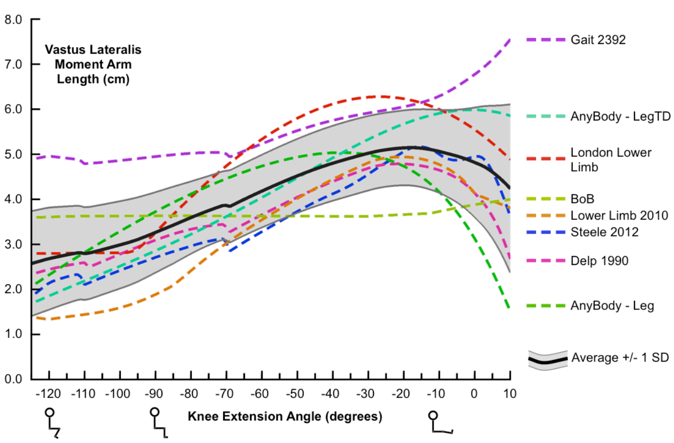

Fig. 1: Muscle moment arms for the vastus lateralis.

The coefficient of variation (COV) was used to evaluate the variance among the musculoskeletal models and with previous studies (Fig. 2). The greatest inter-model agreement, was observed between knee flexion angles of -10 and -60 degrees, angles nearly spanning those observed in normal gait [2]. For knee flexion angles approaching either end of the range of motion limits, the coefficient of variation exceeded 2.5 times the minimum value observed at 23 degrees knee flexion. Excluding the BoB and Gait 2392 models, which have different qualitative trends for the moment arm length versus knee extension angle as the other models and previously reported data [3], the minimum coefficient of variation value decreased from 0.16 to 0.11, the maximum coefficient of variation for deep knee flexion decreased from 0.46 to 0.25, and the inter-model agreement remained relatively unchanged for extended knee postures.

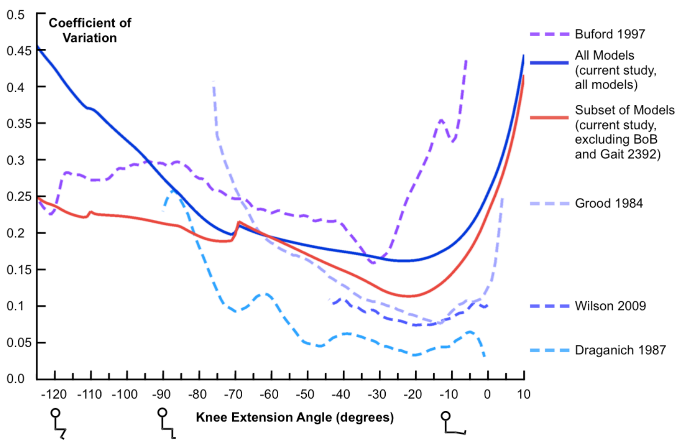

Fig. 2: Comparison of vastus lateralis moment arm variation among musculoskeletal models and previous studies.

Lund et al. [4] defined the examination of the "correctness of variable interaction" as trend validation, a concept that has been previously used to evaluate musculoskeletal model performance [5] and which has also been identified as a prerequisite for using musculoskeletal simulations to address "what-if" or "if-then" scenarios [4], a growing area for future applications of musculoskeletal modeling. Comparing the models tested in this study in the context of variable interaction, the majority of models (7 of 8) exhibited smaller muscle moment arms at large angles of knee flexion compared to moderate or low knee flexion angles, a result consistent with several previous studies [3,6,7]. Six of the eight models exhibited maximum vastus lateralis moment arm lengths at slightly flexed knee postures, an observation also consistent with previous studies [6,7]. The general consistency of these variables among musculoskeletal models is encouraging and suggests similar interpretations from a trend type analysis may be achieved when using the majority of the available models. Additional research is necessary to further identify how differences in moment arms propagate to simulated muscle and joint contact forces.

REFERENCES

1. An KN, et al. *J Biomech Eng* **106**, 280-2, 1984.
2. Perry J. *Gait Analysis: Normal And Pathological Function*, SLACK inc., 1992.
3. Buford WL, et al. *IEEE Trans Rehabil Eng*. **5,** 367-79, 1997.
4. Lund ME, et al. *Proc Inst Mech Eng H.* **226,** 82-94, 2012.
5. Pontonnier C, et al. *ISB Technical Group on Computer Simulation Symposium,* Leuven, Belgium, 2011.
6. Grood ES, et al. *J Bone Joint Surg Am.* **66**, 725-34, 1984.
7. Wilson NA, et al. *J Biomech* **42**,1891-7, 2009.
8. Draganich LF, et al. *J Orthop Res.* **5**, 539-47, 1987.

Table 1. Musculoskeletal models used to compute model-predicted moment arms.

Model Name	Software Package	Availability
AnyBody - Leg	AnyBody (v 4.1.0)	http://forge.anyscript.org/gf/project/ammr/
AnyBody - LegTD	AnyBody (v 4.1.0)	http://forge.anyscript.org/gf/project/ammr/
Biomechanics of Bodies (BoB)	Matlab (v 7.12)	http://www.marlbrook.com/download
Delp 1990	Opensim (v 2.4.0)	https://simtk.org/home/low-ext-model
Steele 2012	Opensim (v 2.4.0)	https://simtk.org/home/mattdemersstuff
Gait 2392	Opensim (v 2.4.0)	https://simtk.org/home/torso_legs
London Lower Limb	Opensim (v 2.4.0)	https://simtk.org/home/low_limb_london
Lower Limb 2010	Opensim (v 2.4.0)	https://simtk.org/home/lowlimbmodel09

HILL-TYPE MUSCLE MODEL WITH SLOW AND FAST FIBER CONTRACTILE ELEMENTS

[1,2,3]Sabrina S.M. Lee, [4]Allison S. Arnold, [4]Maria de Boef Miara, [4]Andrew A. Biewener, [3]James M. Wakeling

[1]Rehabilitation Institute of Chicago, Chicago, IL, USA, [2]Northwestern University, Chicago, IL, USA,
[3]Simon Fraser University, Vancouver, BC, Canada, [4]Harvard University, Cambridge, MA, USA
email: s-lee@northwestern.edu

INTRODUCTION

Hill-type muscle models, which estimate muscle force based on scaled length-tension and force velocity properties [e.g. 1], are arguably one of the most widely-used tools in biomechanics. However, many tests of these models have been limited to *in situ* experiments that do not represent the neural excitation and fascicle strains that occur during *in vivo* dynamic behavior. Rigorous validation of these models requires a comprehensive set of experimental measures, including fascicle length, muscle excitation, and muscle or tendon force. In this study, we investigated the ability of several different Hill-type models to reproduce *in vivo* gastrocnemius forces measured in goats during locomotion. Another important limitation of existing models is the assumption of homogenous fiber type distribution. We have recently developed a modified Hill-based model that incorporates slow and fast contractile elements that are activated independently. Under *in situ* conditions, this novel two-element model predicted forces better than other commonly used one-element models [2]. A second aim of this study was to determine if our novel two-element muscle model predicted force more accurately than one-element models under *in vivo* conditions.

METHODS

Six African pygmy goats (*Capra hircus* L; 3 males, 3 females, mean ± standard deviation; age 21.0 ± 15.5 months, mass 25.85 ± 6.20 kg) were tested at Harvard University's Concord Field Station. All surgical and testing procedures followed IACUC approval. While the goats walked, trotted, and galloped on the treadmill, *in vivo* recordings of muscle excitations (electromyography) and fascicle lengths (sonomicrometry) of the lateral and medial gastrocnemius were made, and Achilles tendon force (tendon buckle transducer) were measured. Additional *in situ* experiments were conducted to characterize the passive and active force-length relationships of the muscles.

Three one-element muscle models and a novel two-element model [2] were tested. The total muscle force F_m was given by:

$$F_m = c\left[\hat{F}_f + \hat{F}_p(l)\right]\cos\beta$$

where β was the pennation angle, $F_p(l)$ was the passive component of the force-length relationship, F_f was the active force from the fibers, and *c* scaled the fiber force to the whole muscle. The maximum shortening velocity, v_o, and the curvature of the force-velocity relation, *k*, were different for each model. The **homogenous** model was comprised of fibers with homogenous properties; v_o, was based on the maximum intrinsic speeds of the different fiber-types weighted by their fractional cross-sectional areas, and *k*, was assigned an intermediate value between the slow and fast fiber limits that depended on the fractional area of the fast fibers. The **hybrid** model was similar to the homogenous model except that v_o represented the fastest fibers and *k* was calculated from the composite force-velocity relation taken from a combination of fast and slow fibers with force proportional to the fractional fiber areas following Hill [5]. The **orderly** recruitment model assumed that as the level of activation increased, the active muscle took the characteristics of progressively faster fiber types [5]; v_o represented the slowest fibers at the lowest activation levels. For these three one-element models, the activation state was determined from the total EMG intensity [2]. The two-element **differential** recruitment model, by contrast, incorporated independently activated slow and fast contractile elements [2]. Wavelet analysis was used to calculate EMG intensity at specific frequency bands, corresponding to faster and slower motor units, from raw EMG [3]. The activation levels for the slow and fast contractile elements in the model were estimated from EMG intensity using transfer functions [3].

Analysis of variance was conducted to determine if differences in the coefficient of determination, r^2, and root mean square error, RMSE, (between the measured and predicted forces) existed between the different models, goats, muscles, fiber-type proportions, and gait conditions. Tukey post-hoc analyses were performed to identify significant differences between levels within a factor.

RESULTS AND DISCUSSION

Overall, the two-element model predicted *in vivo* gastrocnemius forces during locomotion more accurately than the one-element models. In particular, r^2 was up to 8.2% higher and RMSE was up to 21% lower for the two-element model than for the one-element models (Fig. 1).

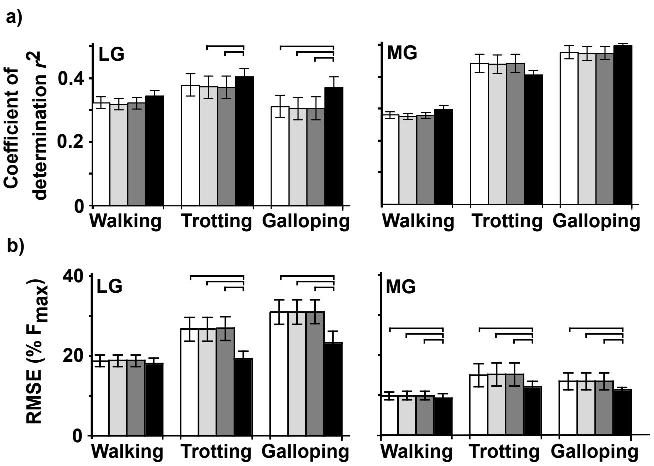

Figure 1: a) Coefficient of determination, r^2, and b) root mean square error, RMSE, for the measured and predicted forces across the gait conditions. Bars show the mean ± SEM pooled from all the goats for the homogeneous (white), hybrid (light grey), orderly (dark grey), and differential models (black). Significant differences between the models are denoted by horizontal bars.

By driving the slow and fast contractile elements independently by the active states of the slow and fast fibers, the differential model accounted for the recruitment patterns of the different motor units across different gait conditions. Data from this and other studies have shown that recruitment of different motor unit types may change in a task-specific fashion, for example, with changes in fascicle strain rates that accompany changes in locomotor speed [4]. Thus, a two-element model that accounts for the recruitment of different fibers enables more accurate prediction of force development during different dynamic tasks (Fig.2).

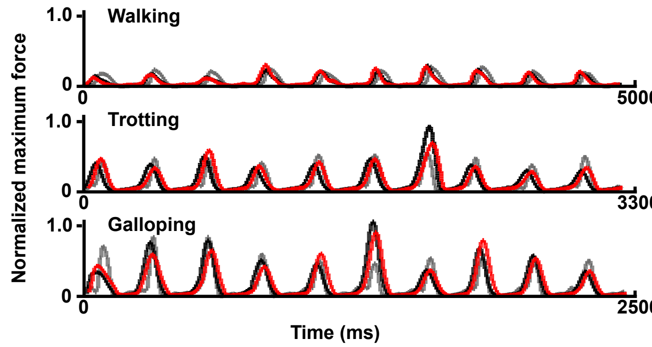

Figure 2: Force profiles of the lateral gastrocnemius muscle during walking, trotting, and galloping. Measured forces (grey) and predicted forces from the one-element homogenous model (black) and two-element differential model (red) are shown. Predicted forces for the other one-element models were very similar to the forces predicted by the homogeneous model.

CONCLUSIONS

An extensive set of experimental measurements in goats has allowed validation of Hill-type models under *in vivo* dynamic conditions. A novel, two-element differential recruitment model predicted *in vivo* gastrocnemius forces more accurately (r^2 up to 8.2% higher and RMSE up to 21% lower) than conventional one-element models during different locomotor tasks.

REFERENCES

1. Zajac FE. *Critical Rev Biomed Eng* **17**, 359-411, 1989.
2. Wakeling JM, et al. *Annal Biomed Eng* **40**, 1708-1720, 2012
3. Lee SSM, et al. *J Electro Kines* **21**, 557-565, 2011.
4. Lee SSM, et al. *J Exp Biol* **216**, 198-207, 2013
5. Hill AV. *First and last experiments in muscle mechanics*, Cambridge University Press, 1970.

ACKNOWLEDGEMENTS

This work was supported by the NIH (R01AR055648).

WINDNG FILAMENT MUSCLE MODEL FOR MUSCULO-SKELTAL SIMULATIONS

[1]Jeremy Petak, [1]Nathan Heckathorn, [2]Robert LeMoyne, [3]John Dyer, [4]Sang Hoon Yeo, [4]Dinesh Pai, [1]John Tester, & [2]Kiisa Nishikawa

[1]Department of Mechanical Engineering, Northern Arizona University;
[2]Department of Biological Sciences, Northern Arizona University;
[3]Electric Torque Machines, Inc., Flagstaff, AZ;
[4]Department of Computer Science, University of British Columbia
email: John.Tester@nau.edu

INTRODUCTION

Understanding how the brain controls muscle force is important for treating neuromuscular disease, injury, and constructing devices that emulate human musculoskeletal systems. Yet, our understanding of this process is remarkably incomplete [1]. One explanation for this problem is that there is more to muscle function than currently understood.

Basic experiments involve the isolation of a single muscle or fiber and the measuring of force generation during isovelocity experiments [1]. A muscle sarcomere-based model (known as the Hill-type model) was created to explain and predict the forces generated during various experiments; it is a three element model consisting of two spring elements and a contractile element. The contractile element provides both force generation and damping to the system [6].

Zajac [2] provided a muscle model based on the sliding filament theory [3], expanding on the Hill-type model. Yet, nearly 25 years of attempts to use Hill-Zajac models have not completely captured true muscle behavior [4]. We suggest that an incomplete understanding of muscle contraction has prevented an understanding of neural control of muscle force. Based on new understanding of how muscles work at the protein level [5], a new model is being proposed, the "Winding Filament Model" (WFM). The goal of this paper is to display preliminary results towards the development of the WFM, as compared to the Hill-type model. The goal of this research is to design a muscle model that more fully describes the features of muscle force generation seen during isovelocity experiments.

METHODS

We developed a "winding filament" hypothesis for muscle contraction [5] in which the N2A region (red dot, Fig. 1) of titin (a giant elastic protein) binds to actin (blue) upon Ca^2+ influx. Titin then winds on the thin filaments during force development because the cross-bridges not only translate, but also rotate the thin filaments.

A mechanical model (Fig. 2) simulates the winding filament hypothesis: a contractile element (CE) turns a pulley (thin filament), which stretches a spring (titin). A ratchet controls unwinding. We used the mechanical model to develop a mathematical model to predict force output during isovelocity eccentric contraction in soleus muscles of cat and mouse. Using MatLab, the Hill-Type model and the WFM were simulated and an iterative process was performed to find optimum values for the spring and damping constants in eccentric contraction and concentric contraction for digitized data from cat soleus muscle [1].

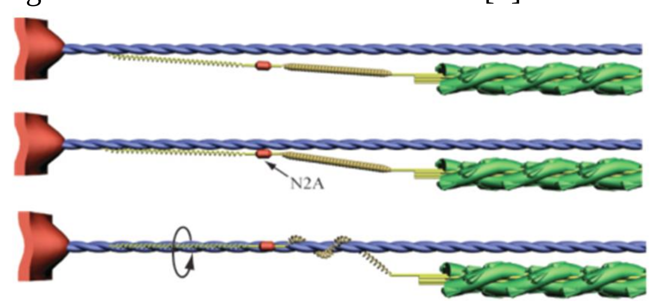

Figure 1: Schematic of N2A binding (above) and filament winding (below), from [5].

RESULTS AND DISCUSSION

The model displays force enhancement and depression in isovelocity experiments, and accounts for 97% of the variance in force during isovelocity

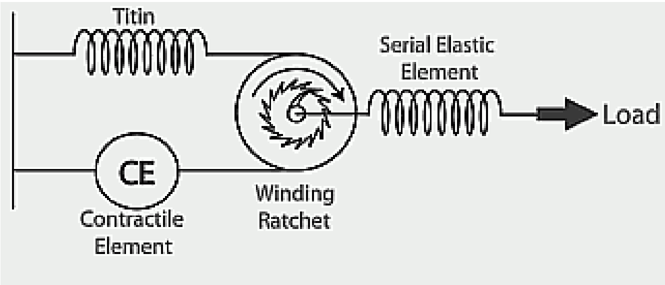

Figure 2: Schematic of Winding Filament Model.

stretch (Fig. 4). In contrast, Hill-type models ***entirely lack*** this history dependence (Fig.3). Hill-type models fail to account for force enhancement because springs are in parallel or series with the CE. The winding filament model however, can account for history dependence because titin is oriented ***simultaneously in parallel and in series*** with the CE. Internal work done by the CE and external work done by applied forces are stored as elastic energy in titin and total force is the sum of the titin force plus CE force.

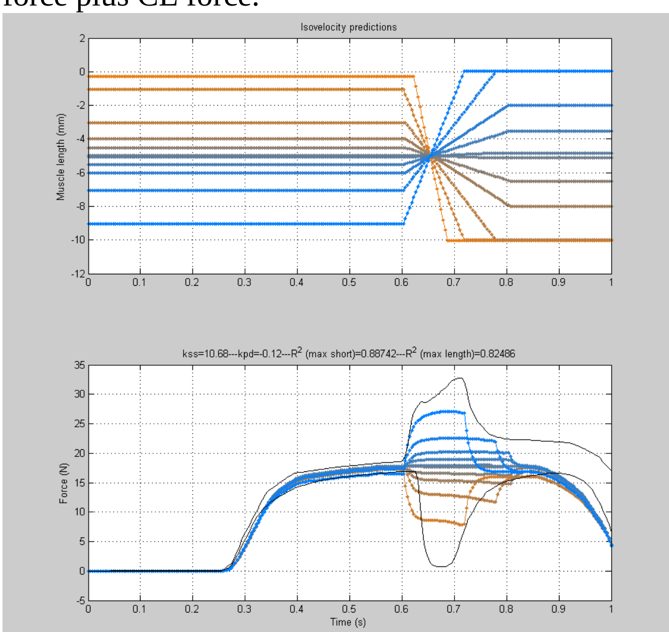

Figure 3: Hill-Type Model Simulation

CONCLUSIONS

The early results of the WFM simulation show muscle characteristics that the Hill-type model does not. For the highest velocity experiments, the Hill-Type model has R-squared values of 0.82 for eccentric contraction and 0.88 for concentric contraction. For the WFM's highest velocity experiments however, the R-squared value is 0.97

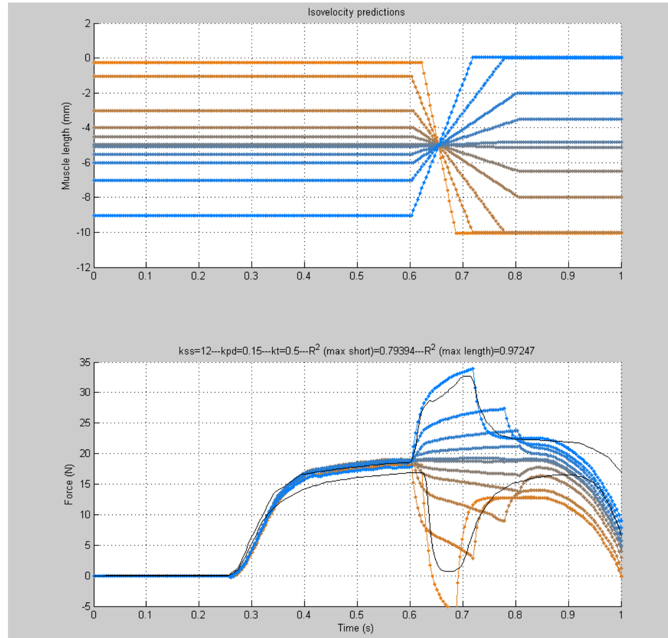

Figure 4: WFM Model Simulation

for eccentric contraction, but the R-squared value of 0.79 for concentric contraction is lower than the Hill-type model. Thus, the WFM needs further development to properly simulate muscle fibers in concentric contraction.

If the model is successful at predicting non-linear changes in muscle force, then it will transform our understanding of the mechanism of muscle contraction. These studies have the potential to improve models of muscle contraction and motor control. Future research will take a fully optimized WFM for human muscle and develop it into control algorithms for a powered prosthetic ankle.

REFERENCES

1. Sandercock & Heckman (1997) J Neurophysiol
2. Zajac (1989) Crit Rev Biomed Engr
3. Huxley (1974) J Physiol
4. Brown et al. (1999) J Mus Res Cell Motil
5. Nishikawa et al. (2012) Proc Roy Soc B
6. McMahon TA (1984) Muscles, reflexes, and locomotion. Princeton University Press: Princeton, N.J.

ACKNOWLEDGEMENTS

Our research results are based upon work supported by the National Science Foundation Partnerships for Innovation award (IIP-1237878). Also supported by NSF IOS-1025896.

MATCHING HUMAN WALKING USING A SIX-LINK PLANAR MODEL

Anne E. Martin and James P. Schmiedeler
Aerospace and Mechanical Engineering, University of Notre Dame
Email: amarti29@nd.edu

INTRODUCTION

Although many amputees prefer energy storage and return (ESAR) prosthetic feet, very few statistically significant results quantify how ESAR feet are superior to conventional prosthetic feet [1]. As a result, prosthetic foot design is largely based on intuition and subjective preference. A model of amputee walking that is complex enough to accurately capture gait dynamics, yet simple enough to allow iterative design, could provide needed justification and enable improved design. Unfortunately, current models are either overly simplistic [2] or too complex [3] to accomplish these goals. Planar models controlled based on hybrid zero dynamics (HZD), a technique from the robotics community, offer a promising compromise [4]. Prior work showed that an HZD-based model can accurately match human hip and knee kinematics at a single walking speed [5]. However, that model is still too complex to be easily used for design. This work simplifies the model and verifies that the new model can mimic human walking at speeds ranging from very slow to very fast.

Due to the deformation of the stance foot, a simple model of the form of the foot is unlikely to yield accurate results. Instead, the function of the foot-ankle complex can be modeled by recognizing that it helps to control both the position of the center of pressure (CoP) under the foot [6] and the whole body center of mass (CoM) acceleration [7]. Prior work showed that the foot-ankle roll-over shape, which is the shape the CoP traces when plotted in a shank-fixed coordinate frame, is a circular arc [8]. By simply modeling the feet as rigid circular arcs, this aspect of ankle function can be replaced. However, the ankle also plays an important role in redirecting the CoM velocity in an energetically optimal manner during the step-to-step transition [9]. Prior work has shown that the ankle generates a large moment [3] and most of the CoM acceleration during late stance [7], indicating the need for ankle joints in a model.

METHODS

Two planar models were created – a six-link model with ankles (Fig. 1) and a four-link model without ankles. The six-link model consists of two circular, massive feet, two massive shanks, two massive thighs, and a point mass at the hip (mass of the HAT). The four-link model is similar, except that the feet are rigidly attached to the shanks. A step consists of a single support phase controlled using an HZD-based approach and an instantaneous double support phase during which the stance leg switches. While humans have a finite time double support phase, condensing it to an instant simplifies the control problem significantly. Model gaits were created to match experimental human walking at a variety of speeds by minimizing the error in model step length, average speed, and joint kinematics.

RESULTS AND DISCUSSION

The six-link model accurately matches human experimental data very well for all speeds. The model step length and speed match the experimental step length and speed exactly (Fig. 2). The average joint error at the hips and knees is 5°, which corresponds to about one standard deviation of the experimental joint angle measurements. The joint error at the ankle is irrelevant because the ankle displacement is largely captured by the model's curved foot shape rather than actual movement of the joint. In contrast, the four-link model only performs well at slow speeds. At faster speeds, the model almost matches the experimental speed but takes much shorter steps than observed in the human data (Fig. 2). Regardless of speed, the four-link model has an average joint error of 11°. Without ankles to inject energy during stance,

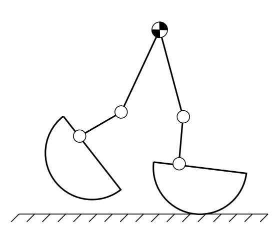

Figure 1: Schematic of the six-link model. For the four-link model, the feet are rigidly attached perpendicular to the shanks.

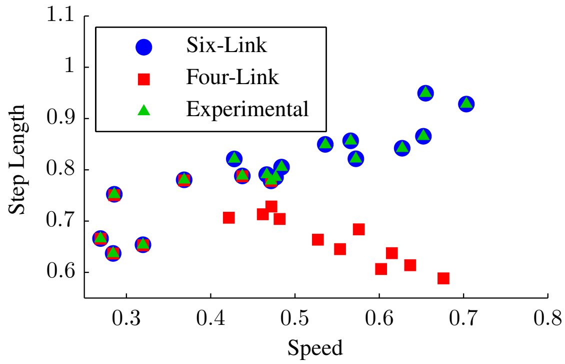

Figure 2: Normalized step length vs. normalized average speed for the four- and six-link models and the human experimental data.

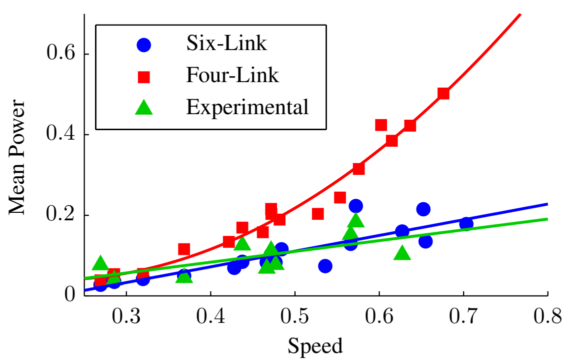

Figure 3: Normalized mean absolute power vs. normalized speed for both models and the human experimental data with reported joint moments. Least squares fits for each data set are shown.

the four-link model must compensate by using a combination of shorter steps to reduce impact losses and jerkier motion to inject additional energy into the gait with the hips and knees. These effects are more significant at higher speeds when more energy is required, which explains the increasing error in matching human gait.

To ensure that the six-link model captures the kinetics of human walking as well as the kinematics, the mean absolute power over a step was computed.

$$\bar{P} = \sum_{i=1}^{N} \frac{\int_0^T |P_i(t)|dt}{T}, \tag{1}$$

where P is power, T is step duration, t is time, and N is the number of joints. The mean absolute power increases linearly with walking speed at approximately the same rate for both humans ($R^2 = 0.48$) and the six-link model ($R^2 = 0.77$) and at a higher quadratic rate for the four-link model ($R^2 = 0.97$, Fig. 3). The experimental trend agrees with prior experimental work [10], and the fit is reasonable due to differing experimental protocols for the available data. Although the four-link model consumes less energy per step, in part because the steps are shorter, it requires a larger mean absolute power because of the forced non-human-like oscillations. Thus, the four-link model overestimates some and underestimates other kinetic measures of human walking, while the six-link model captures the overall human kinetic response even without explicitly attempting to match human energetic data.

CONCLUSIONS

A six-link, planar model with HZD-based control and an instantaneous double support phase captures both the key kinematic and kinetic aspects of human walking with surprising accuracy over a wide range of speeds. Still, it is simple enough to enable iterative prosthetic foot design. The walking gaits presented here will be used to identify an optimization function with which the model can predict human gait over a range of speeds. Those results can then be used to help design prostheses that better mimic human motion and to quantify the effect of increasing levels of ankle actuation in prosthetic devices.

REFERENCES

[1] Hafner, B, et al. *Clin Biomech* **17**, 325–44, 2002.
[2] Kuo, A. *Hum Movement Sci* **26**, 617–56, 2007.
[3] Liu, M, et al. *J Biomech* **41**, 3243–52, 2008.
[4] Westervelt, E, et al. *Feedback Control of Dynamic Bipedal Robot Locomotion*, CRC, 2007.
[5] Srinivasan, S, et al. *J Biomech Eng-T ASME* **130**, 051017, 2008.
[6] Wang, C & Hansen, A. *J Biomech* **43**, 2288–93, 2010.
[7] Anderson, F & Pandy, M. *Gait Posture* **17**, 159–69, 2003.
[8] Hansen, A, et al. *Clin Biomech* **19**, 407–14, 2004.
[9] Donelan, J, et al. *J Biomech* **35**, 117–24, 2002.
[10] Burdett, R, et al. *J Orthop Res* **1**, 63–72, 1983.

ORAL PRESENATIONS – SATURDAY SEPTEMBER 7th

	Instrumentation *Sara Myers, Jason Franz*
11:00 AM	Estimating Soldier Ground Reaction Forces Using An Activity Monitor **Neugebauer J**
11:15 AM	Do We Really Need A Force Platform?: Accelerometry To Measure Postural Sway In Healthy And Pathological Populations **Huisinga J, Mancini M, Horak F**
11:30 AM	Non-Stepping Balance Recovery Capability Differs Between Young And Older Adults **Koushyar H, Bieryla K, Madigan M**
11:45 AM	Feasibility Of A Single Camera Markerless Motion Capture System To Accurately Measure Flexion-Extension **Schmitz A, Ye M, Shapiro R, Yang R, Noehren B**
12:00 PM	A Standing Alignment System Improves Between-Session Repeatability In Gait Kinematics: A Preliminary Study **Samaan C, Schwartz J, Graf E, Davis I, Rainbow M**

ESTIMATING SOLDIER GROUND REACTION FORCES USING AN ACTIVITY MONITOR

Jennifer Neugebauer, Ph.D.
US Army Research Laboratory
Dismounted Warrior Branch, Human Research and Engineering Directorate
Aberdeen Proving Ground, MD 21005
email: jennifer.neugebauer.ctr@mail.mil, web: http://www.arl.army.mil/www/default.cfm?page=31

INTRODUCTION

Methods are needed to quantify ground reaction forces (GRFs) of Soldiers during real-world, operationally-relevant tasks, such as prolonged load carriage, over ground walking, or move-to-shoot tasks. Commonly, this type of analysis is limited to a laboratory setting equipped with sophisticated equipment, such as force plates. Peak vertical GRF (pVGRF) is the GRF with the largest magnitude during gait. Assessment of pVGRF along with the frequency of its occurrence provides a 'snapshot' of a Soldier's loading profile during a task. Methods have been developed in youth and college-age adults to estimate pVGRF using a hip-mounted activity monitor (AM) [1, 2]. AMs provide a lightweight, small, portable means to measure tri-axial accelerations outside of a laboratory and then estimate pVGRF. Soldier specific adaptations to current equations to estimate pVGRF using AMs may need to account for differences due to wearing combat boots and/or carrying load. The purpose of this study was to develop a repeated measures regression model to predict pVGRF from AM acceleration for Soldiers carrying loads up to 45 kg, wearing either athletic shoes or combat boots while walking.

METHODS

Fifteen active-duty Soldiers (age 25.4 ± 5.3 years; mass 85.8 ± 9.5 kg; height 178.6 ± 9.7 cm) walked on an integrated force plate-treadmill (AMTI Corporation, Watertown, MA, USA) at randomly ordered speeds of 0.67-1.61 m/s (0.13 m/s increments) for 45 seconds at each speed (Figure 1). Subjects completed a total of eight conditions which were a combination of two footwear (athletic shoes or combat boots) and four load conditions. The load conditions included (1) no load, (2) 14 kg load (body armor only), (3) 27 kg load (body armor + 13 kg rucksack), and (4) 46 kg (body armor + 32 kg rucksack). Subjects wore a randomly assigned ActiGraph GT3X+ AM (ActiGraph, Pensacola, FL, USA) over the right hip and over the right tibial plateau (used to determine foot strike).

Figure 1. Subject walking with load.

pVGRF and peak vertical hip acceleration (acc_{vert}) were calculated for each speed, footwear, and load condition. R (R Foundation for Statistical Computing, Vienna, Austria) was used to develop a repeated measures fixed effects regression model to predict peak pVGRF. The regression model initially included acc_{vert} (g), subject mass (kg), subject height (cm), load mass (kg), footwear (where athletic shoe = 0, boot = 1), specific AM worn, and acc_{vert}-load mass interaction. A cutoff of $p < 0.05$ was used to determine if effects were included in the model. The final regression model was used to determine the average absolute and average absolute percent difference between measured and predicted peak pVGRF for all trials.

RESULTS AND DISCUSSION

Generally, as peak acc_{vert} increased, pVGRF increased as well. Additionally, as load mass increased, both acc_{vert} and pVGRF increased. The final regression model included the fixed effects of acc_{vert}, subject mass, load mass, footwear, and the interaction between acc_{vert} and load mass (Equation

1). Subject height and the specific AM worn were not significant factors ($p > 0.70$).

$$Y_{ij} = 5.67 + 0.25X_{ij1} + 0.01X_{i2} + 0.01X_{i3} + 0.02X_{i4} + 0.003X_{i5} + e_{ij} \quad (1)$$

where:

Y_{ij} = log transformed pVGRF (ln(N)) for subject i, trial j

X_{ij1} = acc_{vert} (g)

X_{i2} = subject mass (cm)

X_{ij3} = load mass (kg)

X_{ij4} = footwear (athletic shoe = 0, combat boot = 1)

X_{ij5} = interaction of acc_{vert} and load mass

e_{ij} = error in trial j for subject i

The natural log of pVGRF was predicted using Equation 1 for all trials, converted to pVGRF, and compared with the actual pVGRF for all trials (Figure 2 and Figure 3, respectively; two graphs are shown for ease of viewing only).

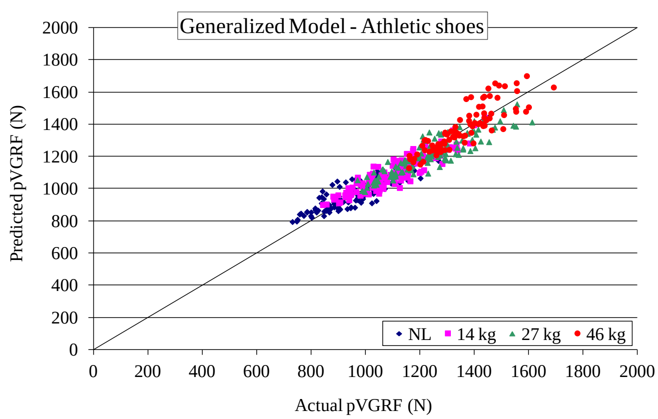

Figure 2. Predicted versus actual pVGRF for all loads tested while wearing athletic shoes ($r^2 = 0.89$ and $p < 0.001$; NL = no load).

The average absolute difference and absolute percent difference between actual and predicted pVGRF was determined for each condition (Table 1) and the average across all conditions was 51.7 N (± 6.9 N) and 4.4% (± 0.5%). The differences between actual and predicted pVGRF are similar those previously reported [1, 2]. Future studies are needed to validate and refine the model for use in field-based studies. Such refinements could account for terrain or the duration of load carriage.

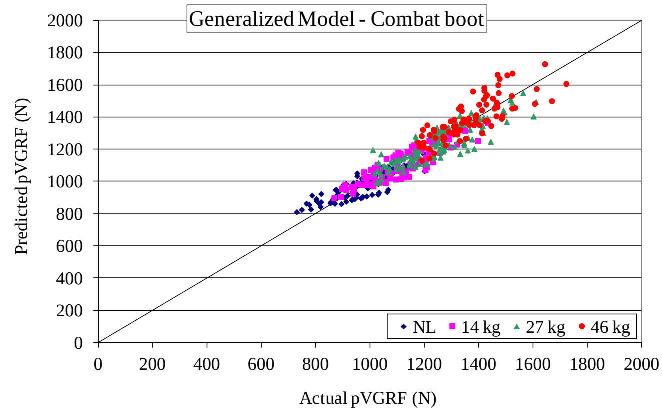

Figure 3. Predicted versus actual pVGRF for all loads tested while wearing combat boots ($r^2 = 0.85$ and $p < 0.001$; NL = no load).

Table 1. The average (avg) absolute (abs) difference (diff) and avg abs % diff between actual and predicted pVGRF for both footwear conditions.

	Athletic Shoes		Combat Boots	
Load	**Avg Abs Diff (N)**	**Avg Abs % Diff (%)**	**Avg Abs Diff (N)**	**Avg Abs % Diff (%)**
No load	48.1	5.1	46.3	4.9
14 kg	43.1	3.9	49.5	4.4
27 kg	54.2	4.2	52.4	4.1
46 kg	54.7	3.9	65.6	4.7

CONCLUSIONS

A generalized regression equation to estimate pVGRF was developed for Soldiers carrying load and wearing either athletic shoes or combat boots. Average absolute percent difference between actual and predicted pVGRF was less than 5% for all trials. The small absolute difference and absolute percent difference suggest that AM data can be used to estimate pVGRF for Soldiers walking with loads wearing either athletic shoes or combat boots.

REFERENCES

1. Collins, et al. (2011) ASB Annual Meeting, Long Beach, CA.
2. Neugebauer, et al. (2012) PLoS ONE 7(10): e48182.

DO WE REALLY NEED A FORCE PLATFORM?: ACCELEROMETRY TO MEASURE POSTURAL SWAY IN HEALTHY AND PATHOLOGICAL POPULATIONS

[1]Jessie M. Huisinga, [2]Martina Mancini, and [2]Fay B. Horak
[1]University of Kansas Medical Center, Kansas City, KS, USA
[2]Oregon Health and Science University, Portland, OR, USA
email: jhuisinga@kumc.edu

INTRODUCTION

To quantify postural control, measures of sway during quiet standing are frequently used. Stabilometry, the measurement of forces exerted against the ground from a force platform during quiet stance, is commonly used to quantify postural steadiness [1]. From stabilometry, a center of pressure (COP) time series is calculated which provides a single global measure of postural control. In order to measure postural control outside of a laboratory environment, accelerometers represent a cheaper, smaller, and more portable solution. In previous studies, COP and acceleration (ACC) time series were moderately correlated in healthy young people standing on one leg [2] which suggests ACC is a valid quantitative measure of postural sway and when the accelerometer is placed on the waist, it's suggested that ACC can better approximate center of mass motion [3]. A recent study also showed ACC sway measures are as sensitive as COP sway measures in differentiating between Parkinson's disease patients and healthy controls [4]. To utilize ACC sway measures in other pathological populations, it is first necessary to validate the sway measures. In persons with multiple sclerosis (PwMS), problems with balance are reported by up to 85% of those diagnosed, but there are few quantitative clinical balance assessment tools available. To date, ACC sway measures have not been validated in PwMS. The purpose of this study was to investigate the relationship between postural sway variables calculated from COP and from ACC time series in PwMS and in healthy controls. Correlation analysis was used to examine the relationship between COP and ACC variables while receiver operator characteristic (ROC) curves were used to examine the ability of COP and ACC sway variables to discriminate between PwMS and healthy controls. We hypothesized that sway variables would show strong correlations in both PwMS and in healthy controls. We also hypothesized that COP and ACC calculated variables would show similar discriminative ability based on the ROC curves.

METHODS

Forty PwMS (age 45.6 ± 11.7 yrs, self-reported EDSS 4.3 ± 1.2) and 20 healthy, age-matched healthy controls (age 41.8 ± 10.7 yrs) participated. Subjects were outfitted with 4 MTX Xsens sensors (49A33G15, Xsens, Enschede, NL, USA) sampling at 50 Hz. The sensors contained 3D accelerometers (±1.7 g) and 3D gyroscopes (±300º/s range) mounted on: (i) sternum, (ii) sacrum (L5 lumbar level), (iii) right and left lower leg. Only the acceleration time series at the lumbar level was used in this analysis. Concurrently, subjects stood on two side-by-side force platforms (one under each foot) with arms crossed and heel-to-heel distance fixed at 10 cm. Pre-processing of COP and ACC signals has been previously described [4]. Subjects stood quietly for 30 seconds with eyes open. Variables of interest, calculated both from the accelerometers (ACC) and from the force platforms (COP), include root mean square (RMS), range, velocity, area, and 95% frequency (F95). The average values across three trials were used for analysis. Data was not normally distributed based on the Shapiro Wilks test, so Spearman correlations were performed between variables calculated from COP and from ACC within the MS group and within the healthy controls. Mann-Whitney U-tests were performed between PwMS and healthy controls. Sensitivity-specificity analyses to determine discriminative ability (ROC curves) between the MS group and healthy controls were also performed for each variable.

RESULTS

Within PwMS, correlation coefficients between COP and ACC variables were RMS (rho = 0.804, $p < 0.001$), range (rho = 0.749, $p < 0.001$), velocity (rho = 0.458, $p = 0.004$), area (rho = 0.815, $p <$

0.001), and F95 (rho = 0.378, p = 0.019). Within healthy controls, correlation coefficients between COP and ACC variables were RMS (rho = 0.577, p = 0.008), range (rho = 0.642, p = 0.002), velocity (rho = 0.195, p = 0.410), area (rho = 0.514, p = 0.020), and F95 (rho = 0.343, p = 0.139). Between groups, RMS, range, velocity, and area were significantly greater in the MS group except for ACC velocity. F95 was not significantly different between groups (Table 1). The area under the curve for ROC analysis between PwMS and healthy controls are presented in Table 2.

Table 2: *Area under the curve values* for ROC curves separating subjects with MS from healthy controls based on variables calculated from COP and ACC time series. Values greater than 0.70 indicate high sensitivity-specificity of the variable to discriminate between groups.

	RMS	Range	Velocity	Area	F95
COP	0.764	0.778	0.754	0.779	0.449
ACC	0.741	0.787	0.596	0.811	0.514

DISCUSSION

Correlation analysis found that sway variables calculated from COP and ACC time series are related in both healthy controls and in subjects with MS. These sway variables also identified significant differences between subjects with MS and healthy controls and were able discriminate between the two groups.

Interestingly, the correlations between COP and ACC variables were stronger in the MS group (rho=0.804 – 0.378) than in healthy controls (rho= 0.642 – 0.343). PwMS have a wider range of both COP and ACC values such that the data are more spread, resulting in stronger correlations. Because two different time series representing different signals are being utilized, a perfect correlation (rho = 1.0) is unlikely. COP is the position of the center of pressure on the ground while the ACC is the acceleration at the lower back which is meant to approximate acceleration of the center of mass. The difference in location of signal (under foot v. lower back) may also help explain the difference in correlation values between groups. Previous work has shown that PwMS have different segment (ankle v. hip) motion during standing compared to controls [5]. Thus, the measurement of COP under the feet and ACC at the lower back could result in different correlations between groups. The difference in group size (MS group n = 40; healthy control n = 20) could also affect the correlation values.

Paired tests and ROC analysis indicate that while the different sway variables may not be strongly correlated, corresponding variables were able to identify significant differences between groups (Table 1). In addition, the discriminative ability of the corresponding variables (COP range v. ACC range) in separating PwMS from healthy controls is also similar (Table 2). These results indicates that either COP or ACC sway variables could be used to measure sway in healthy controls and in subjects with MS in order to identify differences based on the pathology.

REFERENCES

1. Rocchi et al. *Med. Biol. Engin. Comput*, **42**, 71-79, 2004.
2. Adlerton et al. *Physiother Res Int*, **8**, 187-199, 2003.
3. Kamen et al. *Gerontology*, **44**, 40-45, 2000.
4. Mancini, et al. *J Neuroengin Rehab*, **9**, 2012.
5. Huisinga et al., *Proceed Amer Soc Biomech* Gainesville, FL, 2012.

ACKNOWLEDGEMENTS

This work was supported by the National Multiple Sclerosis Society, the Medical Research Foundation of Oregon, and the NIA.

Table 1: Mean values for sway variables based on center of pressure (COP) and accelerometer (ACC) time series.

	COP			ACC		
	MS	Control	p-value	MS	Control	p-value
RMS	8.59 ± 6.34	4.99 ± 1.88	0.002	0.101 ± 0.071	0.061 ± 0.018	0.002
Range	41.72 ± 28.4	24.77 ± 9.21	0.001	0.527 ± 0.331	0.315 ± 0.094	<0.001
Velocity	11.47 ± 6.94	6.98 ± 2.33	0.003	0.188 ± 0.117	0.150 ± 0.073	0.194
Area	24.55 ± 22.76	8.56 ± 4.78	0.001	0.007 ± 0.13	0.002 ± 0.001	<0.001
F95	1.32 ± 0.76	1.56 ± 1.12	0.603	1.71 ± 0.51	1.69 ± 0.35	0.887

NON-STEPPING BALANCE RECOVERY CAPABILITY DIFFERS BETWEEN YOUNG AND OLDER ADULTS

[1]Hoda Koushyar, [2]Kathleen Bieryla and [1]Michael L. Madigan

[1] Virginia Polytechnic Institute and State University, Blacksburg, VA, USA
[2] Bucknell University, Lewisburg, PA, USA
email: koushyar@vt.edu

INTRODUCTION

It is well-documented that older adults have a higher risk for falling than young adults. One contributing factor to this higher risk of falling is thought to be an impaired ability to recover balance after a postural perturbation. Older adults have consistently exhibited an impaired ability to recover balance after a wide range of postural perturbations.

Mackey and Robinovitch [1] determined the largest static angle from which young and older women over 65 could recover balance upon release when using the so-called ankle strategy. Older women exhibited a 19.6% smaller maximum lean (13.1 degrees) compared to young women (16.3 degrees). Constraining balance recovery to the ankle strategy is a fairly significant constraint on body kinematics, particularly when older adults are known to exhibit greater hip motion during non-stepping balance recovery [2]. The purpose of this study was to investigate age differences in non-stepping balance recovery capability without constraining movements to the ankle strategy. As such, participants could bend at the hips, knees, ankles, or raise portions of feet off the floor to maintain balance.

METHODS

Three groups of adults completed the study including five young adults (age = mean 22.8 ± SD 2.6 years), six community-dwelling older adults (age = 73.2 ± 2.2 years), and five assisted-living older adults (age = 85 ± 6.5 years) from a local nursing home. All participants were able to stand unassisted. The study was approved by the local Institutional Review Board, and written consent was obtained from all participants prior to participation.

Participants stood on a pneumatic, instrumented, moving platform (PIMP) that translated 0-0.15 m forward or 0-0.25 m backward in ~350 ms (Figure 1). Forward displacements elicited a backward loss of balance by participants, and backward displacement elicited a forward loss of balance by participants. The time over which the PIMP translated was fairly constant (350 ms), and the translation distance was modulated by increasing the peak translation speed (e.g. 0.4 m/s for a translation distance of 0.08 m, or 1.1 m/s for a translation distance of 0.19 m). A potentiometer was used to measure displacement of the PIMP during each trial.

Figure 1: Photograph of PIMP.

Balance recovery capability was quantified by determining the maximum forward and backward PIMP displacement the participants could withstand without stepping. Participants stood barefoot on the PIMP with their feet approximately shoulder-width apart, eyes open, and while looking straight ahead. They were instructed to remain relaxed, try their best not to step, and remain standing still after the perturbation. The first trial began with the PIMP moving approximately 0.02 m backward. After a successful (i.e. non-stepping) trial, another trial was performed with the displacement increased approximately 0.01 m. After an unsuccessful trial (i.e. the participant stepped or required assistance by a spotter), another trial was performed at the same displacement. This process was repeated until three unsuccessful trials occurred at the same platform displacement. Both forward and backward platform translations were presented in a random order to prevent anticipation of translation direction, and to simultaneously determine the maximum displacement that the participants could withstand without stepping in both directions.

The maximum forward and maximum backward perturbation distance from which balance could be maintained without stepping (i.e. maximum forward distance and maximum backward distance, respectively) were compared between groups using a Kruskal-Wallis one-way analysis of variance by ranks, and a significant effect of group was followed by multiple comparisons between each pair of groups using a Wilcoxon signed-ranks test. A significance level of $p<0.05$ was used, and analysis was performed using JMP v10 (SAS Institute, Inc., Cary, NC).

RESULTS AND DISCUSSION

The maximum forward distance, which elicited a backward loss of balance, was 60% and 54% smaller in the assisted-living older adults compared to young adults ($p=0.011$) and community-dwelling older adults ($p=0.007$), respectively, but did not differ between the young adults and community-dwelling older adults ($p=0.302$). The maximum backward distance, which elicited a forward loss of balance, was 61% and 47% smaller in the assisted-living older adults compared to young adults ($p=0.012$) and community-dwelling older adults ($p=0.008$), respectively, and was 27% smaller among the community-dwelling older adults compared to the young adults ($p=0.027$: Figure 2).

Our results are consistent with prior studies on non-stepping balance recovery in that older adults exhibited compromised balance recovery capability compared to young adults [1]. Our results also showed greater impairment in older adults from an assisted-living center compared to those who were community-dwelling.

One limitation of this study is that, as in earlier work, constraining balance recovery to a non-

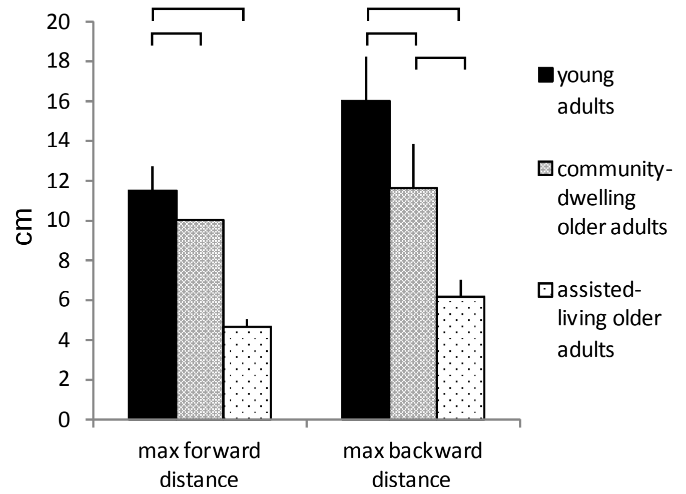

Figure 2: Median values of maximum forward and backward distance across all three groups. Error bars represent interquartile range. Bars at top indicate statistical difference between groups.

stepping strategy when such a constraint is possible, but not typical, reduces the external validity of the study. However, it is possible that the same neuromuscular factors that contribute to the age differences in non-stepping balance recovery also contribute to age differences in balance recovery without any constraints. Moreover, this constraint provides experimental control that improves internal validity, and can facilitate planned future modeling efforts.

CONCLUSIONS

In conclusion, the ability to maintain balance without stepping after a brief support surface perturbation was impaired up to 61% among older adults living in an assisted-living center and up to 27% among community-dwelling older adults compared to young adults. Impaired balance recovery likely contributes to higher fall rates among these individuals.

REFERENCES

1. Mackey DC et al. *Gait Posture* **23**, 59-68, 2006.
2. Woollacott. *J Geron* **48**, 56-60, 1993.

ACKNOWLEDGEMENTS
Support was provided by 5R01OH00988

Feasibility of a single camera markerless motion capture system to accurately measure flexion-extension

[1]Anne Schmitz, [1]Mao Ye, [1]Robert Shapiro, [1]Ruigang Yang and [1]Brian Noehren

[1]University of Kentucky, Lexington, KY, USA
email: anne.schmitz@uky.edu

INTRODUCTION

Traditional motion capture techniques use markers to measure movement. However, markers are prone to soft tissue artifact and experimental error [1] as well as possible impedance to natural motion. Another significant challenge is the ability to use optical motion capture systems in a variety of natural setting such as a patient's home, on the sports field, or in public. This has led to the development of markerless motion capture [2]. The accuracy of marker-based systems has been analyzed using custom built devices [3], *in vivo* imaging [4], external fixators [5], and electrogoniometers [6]. By comparison, the accuracy of markerless motion capture techniques in calculating joint angles has not been studied as extensively. Joint kinematics calculated from marker-based and markerless motion capture have been compared [7], but this only provides a measure of relative accuracy. The absolute accuracy of markerless motion capture has been analyzed using a virtual walking model, but this excludes errors due to camera calibration and foreground/background separation [8]. Also these systems used an array of cameras and were not systems such as the Microsoft Kinect which relies on just two cameras: a depth map and a color camera. Therefore, the goal of this study was to quantify the accuracy of marker-based and markerless motion capture systems in the calculation of joint angles during a static posture and to compare the differences in joint angles during motion using a simulated leg in an experimental setting.

METHODS

Seven retroreflective markers were placed on a testing jig built to simulate a leg (Figure 1). For both a flexed static posture and flexion-extension motion, the positions of these markers were recorded using a 10 camera motion analysis system (Motion Analysis Corp, Santa Rosa, USA) and sampled at 200 Hz [9].

One Kinect camera [10] was used to collect multiple views of the jig in a static posture with the markers attached. Relative transformations among views were calculated based on the markers. All views were then aligned accordingly to build a template where marker positions were included. For the motion of interest, data were collected at 30 Hz using the Kinect. An articulated iterative closest point algorithm [11] was used to align these captured data with the template. Virtual marker trajectories were then exported for the motion of interest.

For both systems, Visual3D (C-motion, Germantown, MD, USA) was used to lowpass filter marker trajectories at 8 Hz and to compute the flexion-extension angle of the distal segment relative to the proximal segment.

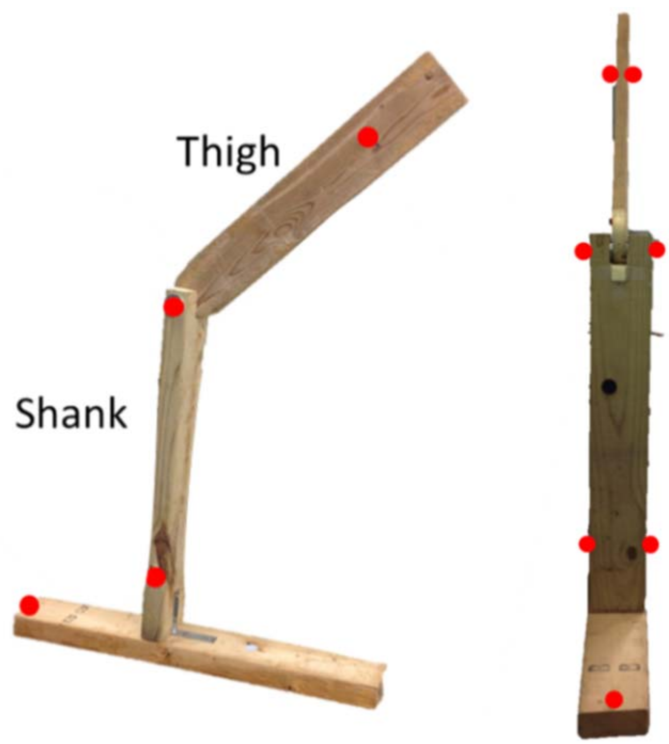

Figure 1: (left) sagittal (right) frontal views of the testing jig

To provide a ground truth measure for the static configuration, the relative position of the thigh with respect to the tibia was measured using a digital protractor (Craftsman, Model 320.48295, accuracy of 0.1 degrees).

RESULTS AND DISCUSSION

Both motion capture techniques produced similar results for calculations of sagittal plane motion (Table 1). In the static posture, both motion capture techniques were able to capture the joint angle within 0.9 degrees. These results provide initial evidence that a precise and accurate algorithm can be developed for measuring kinematic data using the Microsoft Kinetic camera in the sagittal plane. Ongoing studies are determining its accuracy in the frontal and transverse plane as well. These data allow us to know beyond what range differences in dynamic motion are truly indicative of error between systems.

When comparing the two systems during a flexion-extension motion, we found a similar pattern of motion with an average difference of 0.9 ± 1.0 degrees between the two systems (Figure 2). These early results are a promising demonstration of the ability to develop markerless motion capture systems using technology such as the Microsoft Kinect to track motion. Several potential challenges remain to be addressed, such as determining the best orientation of the jig/person to obtain an accurate Kinect template for aligning the motion frames, determining the effect of the low frame rate of the Kinect, and handling marker occlusions in the creation of the Kinect template.

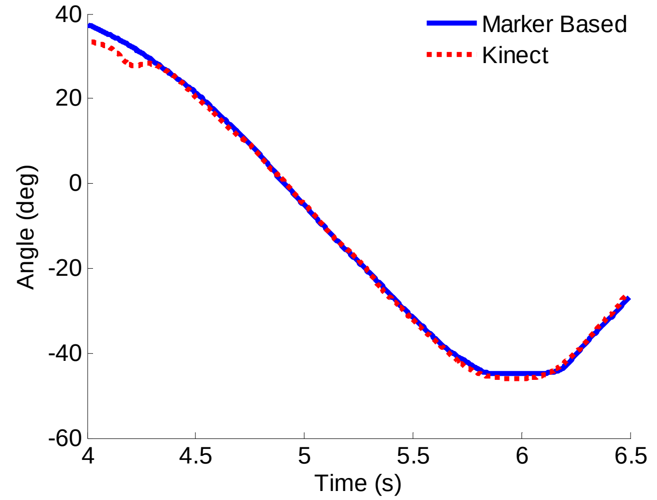

Figure 2: The flexion-extension angle measured by the marker-based and Kinect. Positive angle denotes extension.

CONCLUSIONS

This study shows the feasibility of using a Kinect camera to accurately measure the sagittal angle between two rigid bodies in a static configuration and during motion. Future plans include jig revision and investigation of non-sagittal rotation angles.

ACKNOWLEDGEMENTS

funded by NSF IIS 1231545

REFERENCES

1.Leardini, A., et al. *Gait & Posture* **21**, 212, 2005.
2.Mundermann, L., et al. *J Neuroengr and Rehab* **3**, 2006.
3.Richards, J. G. *Human Move Sci* **18**, 589-602, 1999.
4.Miranda, D. L., et al. *J Biomech* **46**, 567-573, 2013.
5.Holden, J. P., et al. *Gait & Posture* **5**, 217-227, 1997.
6.Kiran, D., et al. *Phys Ther Sport* **11**, 81-5, 2010.
7.Mündermann, L., et al. *Proc of ASB*, Cleveland, OH, 2005.
8.Corazza, S., et al. *Proc of 9th international symposium on the 3D analysis of human movement*, 2006.
9.Noehren, B., et al. *Gait & Posture* **36**, 596-599, 2012.
10.Microsoft. http://www.microsoft.com/en-us/kinectforwindows/
11.Pellegrini, S., et al. *Proc of British Machine Vision Conference*, 2008.

Table 1: Comparison of flexion-extension angle measurement for a jig configuration of -45.6 ± 0.1º

Marker-based	Error in marker-based	Kinect	Error in Kinect	Difference between marker-based and Kinect
-45.0º	0.6º	-44.7º	0.9º	0.3º

A STANDING ALIGNMENT SYSTEM IMPROVES BETWEEN-SESSION REPEATIBILITY IN GAIT KINEMATICS: A PRELIMINARY STUDY

[1]Cynthia Samaan, [2]Joel Schwartz, [1]Eveline Graf, [1]Irene Davis and [1]Michael J Rainbow

[1]Spaulding National Running Centre, Harvard Medical School, Cambridge, MA, USA
[2]Warren Alpert Medical School of Brown University, Providence, RI, USA
email: csamaan@partners.org, web: http://runsnrc.org

INTRODUCTION

Longitudinal biomechanical studies of human gait typically utilize three-dimensional (3-D) optical motion capture (OMC) to track kinematic and kinetic changes. Unfortunately, the subjective placement of anatomical markers has been shown to result in anatomical coordinate systems (ACS) that are inconsistent between sessions. This inconsistency introduces bias, which can corrupt between-session analyses, and greatly reduce the efficacy of 3-D motion analysis to quantify between-session changes [1,2].

Noehren et al. [3] developed a marker placement device that reduced between-session bias. The device was used to manually record the position of anatomical markers to facilitate placement in later sessions. However, use of the device was time intensive, required manual positioning of multiple measurement fixtures, and required careful replacement of anatomical markers during follow-up sessions.

The purpose of this study was to introduce a new alignment system that improves between-session reliability of OMC outcome measures. The system consists of new methodology and an alignment device (AD) that minimizes manual positioning of measurement fixtures and eliminates the need to place physical anatomical markers in follow-up sessions. Here, we describe the alignment system and present preliminary results of a repeatability study on knee and hip joint angles during walking and running.

METHODS

Alignment System: The AD was designed for use during the standing calibration of a motion capture session. It allows the subject to stand consistently between sessions. This is facilitated by two adjustable footplates and an adjustable posterior support. (Fig. 1). During an initial visit, anatomical and tracking markers are manually placed on the subject's lower body. The subject stands in a self-selected posture in the AD, and the footplates and posterior support are positioned against their feet and buttocks. The position of the footplates and posterior support are manually recorded and a standing trial is collected with the OMC system. The locations of the physical anatomical markers are determined with respect to a 5-marker cluster attached to a rigid baseplate. During subsequent sessions, the footplates and resting pad are repositioned according to measurements taken in the initial session. With the aid of the device, the subject replicates their standing posture and a standing calibration trial is recorded. The location of the physical anatomical markers from the initial session are then virtually computed from the 5-marker cluster. Pelvis, thigh, shank, and foot ACS are then created from these virtual markers.

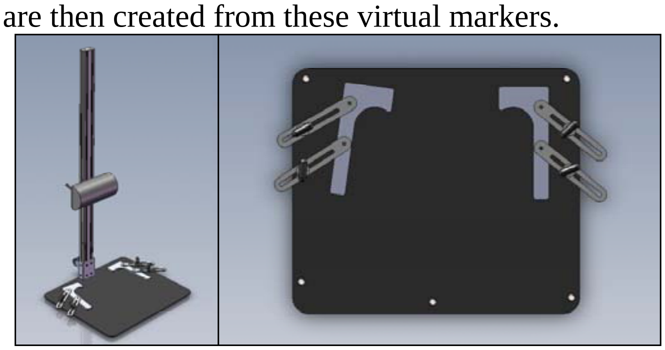

Figure 1: AD with adjustable footplates and posterior support.

Reliability Assessment: A preliminary assessment of the reliability of this system was performed on a single subject over two days. A single investigator performed both data collections. Two analyses were performed; A within day analysis (day 1), and a between-day analysis (day 1 vs. day 2). The within day analysis evaluated the repeatability of the subject's standing posture in the AD. The between-day analysis compared the repeatability of the alignment system with the repeatability of performing two independent gait analyses.

Data Collection: The subject stood within the AD and the footplates and posterior support were adjusted to accommodate their preferred posture. Footplate and anterior support measurements were recorded and a standing calibration was collected with the OMC system. Without removing any physical anatomical or tracking markers, 5 walking and 5 running trials were recorded. To simulate device repeatability, the footplates and posterior support were then set to an arbitrary position and repositioned for the subject using the recorded measurements. The subject then stood in the AD, using the supports to guide their posture, and a second standing trial was recorded. On day 2, this protocol was repeated.

Within-Day Analysis (day 1): Using the 5-marker cluster, the physical markers from the first calibration trial were virtually created in the second calibration trial. Two ACS sets were computed; one set from the physical anatomical markers in the first trial (ACS_{1P}), and the second set from the virtual markers in the second trial (ACS_{1V}). Both sets of coordinate systems were then tracked through the running and walking trials. Hip and knee joint angles were computed. Repeatability was defined as the RMS differences ($RMS_{1P\text{-}1V}$) between joint angles derived from ACS_{1P} and ACS_{1V}.

Between-Day Analysis: Using the 5-marker cluster, the physical markers from the first calibration trial on day 1 were virtually created in the day 2 calibration trial (ACS_{2V}). RMS differences between ACS_{2V} and ACS_{1P} were computed ($RMS_{1P\text{-}2V}$). A second set of RMS differences were computed using physical anatomical markers and kinematics that were captured independently on day 1 and day 2 ($RMS_{1P\text{-}2P}$). We then compared $RMS_{1P\text{-}2P}$ to $RMS_{1P\text{-}2V}$.

Table 1: Within-Day: Standing posture repeatability $RMS_{1P\text{-}1V}$ Error (º)

Activity	Joint	Flex/Ext	Ab/Add	Int/Ext
Walking	Left Knee	1.2	0.5	0.1
	Left Hip	0.7	0.3	0.6
	Right Knee	1.1	1.0	0.3
	Right Hip	0.7	0.2	0.9
Running	Left Knee	1.2	0.5	0.2
	Left Hip	0.7	0.3	0.6
	Right Knee	1.1	1.1	0.5
	Right Hip	0.7	0.2	0.9

RESULTS AND DISCUSSION

Within-Day: We observed small RMS errors between ACS_{1P} and ACS_{1V}, indicating that the AD successfully allowed the subject to reproduce his initial standing posture and the anatomical markers were accurately reproduced (Table 1). The largest $RMS_{1P\text{-}1V}$ difference of 1.2º was in the flexion/extension angle at the left knee.

Between-Day: Compared to the physical markers ($RMS_{1P\text{-}2P}$), the alignment system ($RMS_{1P\text{-}2V}$), resulted in a smaller between-day difference for most ab/adduction and int/external rotation angles at the hip and knee (Table 2). Flexion/extension angles showed greater differences between days (performed worse) for the alignment system compared to the marker condition (negative angles in Table 2). These tended to be small differences (-0.1 to -1.3º) especially when considering the magnitude of flexion excursion during walking and running (hip: 48º and 53º, knee: 63º and 81º). This is contrasted by coronal plane angular excursions of 15º and 17º at the knee, where $RMS_{1P\text{-}2V}$ was lower by up to 6.4º using the alignment system as compared to standard manual marker placement.

CONCLUSIONS

The new alignment system shows promising preliminary results in reducing between-session variability of frontal and coronal plane rotations. Improving on Noehren's [3] concept, the system eliminates the subjective application of anatomical markers after the initial session. Future research will evaluate between-day reliability in a larger subject group and explore refinements to the AD.

REFERENCES

1. della Croce U, et al. *Gait Post* **21**, 226-237, 2005.
2. Gorton GE, et al. *Gait Post* **29**, 398-402, 2009.
3. Noehren B, et al. *J Orthop Res* **28**, 1405-10, 2010.

Table 2: Between-Day: With vs. without the alignment system ($RMS_{1P\text{-}2V}$ vs. $RMS_{1P\text{-}2P}$, +ve: lower $RMS_{1P\text{-}2V}$) (º)

Activity	Joint	Flex/Ext	Ab/Add	Int/Ext
Walking	Left Knee	-0.4	0.3	6.4
	Left Hip	0.6	-0.7	4.0
	Right Knee	-1.3	0.0	0.4
	Right Hip	0.1	1.9	-1.2
Running	Left Knee	-0.8	0.2	6.1
	Left Hip	-0.1	0.0	4.1
	Right Knee	-1.3	2.1	0.4
	Right Hip	-0.1	2.1	-1.4

ORAL PRESENATIONS – SATURDAY SEPTEMBER 7th

Symposium: Teaching Biomechanics *John Challis, Matthew Pain*
Undergraduate Course Case Study: Motion Capture And Animation For Biomechanics **Melissa Gross**
Guided Inquiry In Biomechanics Or: How I Learned To Stop Worrying And Leave The Lectern **Andrew Karduna**
Teaching Biomechanical Analysis Using Matlab/Simulink **James Shippen; Barbara May**

UNDERGRADUATE COURSE CASE STUDY: MOTION CAPTURE AND ANIMATION FOR BIOMECHANICS

Melissa Gross

University of Michigan, Ann Arbor, MI, USA
email: mgross@umich.edu

OVERVIEW

Motion capture technology is widely used in biomechanics research to analyze the kinematics of human movement and in the entertainment industry to animate the movement of digital human characters. At the intersection of science and art, motion capture technology represents a unique opportunity for undergraduate students to apply their conceptual understanding of biomechanical principles in a context that also encourages development of their creativity and communication skills. Despite the ubiquity of motion capture technology in science and industry, and the educational value of deploying it in the classroom, few undergraduate programs offer courses using motion capture technology because of the high cost of motion capture equipment. At the University of Michigan, a fully equipped motion capture facility is available for use by the university community, enabling development of a motion capture and animation course for undergraduate students. The course "Motion Capture and Animation for Biomechanics" is now offered in the School of Kinesiology for advanced undergraduates.

Movement Science 437 is designed as a studio course that gives students hands-on experience with motion capture technology and animation. In the first part of the course, students use animation software to create keyframe and mocap-based animations, completing a series of individual assignments that gradually builds their animation skills. In the second part of the course, students work in teams to complete a small-scale project that addresses a biomechanical question of their own choice. The final product for each project team is a short video that includes live-action video clips, mocap-based animation, kinematic analyses, and voice-over narration.

After completing the course, students are able to:

- create realistic animations of human gait
- use mocap data to animate human characters
- design a biomechanical study with appropriate independent and dependent variables
- plan and conduct a mocap session
- evaluate and correct errors in mocap data
- interpret kinematic data correctly
- use animations to visualize study outcomes
- make an effective scientific video presentation
- work effectively as a member of a project team

By participating in the course, students gain a new appreciation of the digital representation of human movement from both scientific and artistic perspectives, deepen their knowledge of gait biomechanics by "hand" animating the gait cycle, learn to evaluate the biomechanical fidelity of human movement animations, and develop new tools with which to express their own understanding of human movement and to communicate biomechanical principles to others.

COURSE LOGISTICS

The learning environment for the course includes several different spaces housed in the Digital Media Commons, a component of the UM Library. The main instructional classroom is configured with 20 high-end graphics workstations that set the upper limit for enrollment (one student per workstation). Each workstation runs animation software (Autodesk MotionBuilder), motion capture software (Vicon Blade), as well as standard office productivity software. Motion capture data are collected in a nearby video studio configured with an eight-camera VICON motion capture system and professional HD video cameras. Students learn to edit videos with Apple iMovie software in another computer training classroom. A third facility that supports the production, conversion, and editing of digital media, equipped with video and audio equipment and a sound booth, is available to students on a walk-in, self-serve basis (24/7) for recording their narrations and off-hours assistance. Staff members associated with the Digital Media Commons are also available to assist faculty and students during motion capture sessions and to help resolve technical issues.

Collaboration is an important element of the course. Students produce large files that they need to share with their project teams, and the instructor needs access to both animation and project files to provide frequent feedback. Google collaboration tools and Box cloud file storage enable the file sharing that facilitates collaboration in the course.

COURSE DESIGN

The class meets twice per week for two hours. In the first part of the term, students work in a "flipped classroom" setting, that is, they watch tutorials and complete short assignments related to the upcoming class session, and then apply the newly learned material in class. The animation assignments begin with learning the MotionBuilder user interface, and then move on to animating primitive objects (e.g., cubes, spheres, cylinders), adding backgrounds, and rendering the animations from different camera views. The next step is to add realism to their animations by incorporating physics into their digital scenes; for example, students create realistic ball bouncing animations by ensuring that their animated motions are consistent with what they know about projectile motion and collision mechanics. In the next step, students learn to animate human motion by setting their character's body position in each frame ("keyframing") at 24 fps. After reviewing gait biomechanics, they use keyframing to generate realistic gait animations. Finally, students learn to use motion capture data to animate their human characters. Students wrap up this component of the course by learning iMovie and then creating compilations of their animations.

In the second part of the course, students work in teams of three to five members to complete projects. Class sessions are designed to lead them through the sequential steps needed to develop their ideas, design their experiment, acquire their data, analyze and interpret their data, and then communicate their findings. The first step is for each group to decide on the biomechanical question they want to explore. Students use their own interests and a review of the relevant literature to formulate their questions. Next, students design a simple experiment to test their question, and establish an experimental protocol. They state independent and dependent variables, and predict their study outcomes. Each team works with the instructor to conduct their motion capture session. Next, students learn to clean their mocap data, and use the coordinate data to generate linear kinematics. They import their mocap data into OpenSim and generate angular kinematic data. Finally, they create storyboards to organize their video presentations and write scripts for their narrations. Their final project videos include text, images, graphs, videos, animations, and linear and angular kinematic data, assembled with iMovie and overlaid with a voice narration.

STUDENT EXPERIENCE

To date, nearly 100 students have completed the course. Students report that they especially value the hands-on experiences and have gained confidence by learning new and challenging skills. They have learned to depend on other students in their groups and have increased their collaboration skills. They have enjoyed the opportunity to incorporate creativity into their scientific work, while simultaneously developing their research and analytical skills.

ACKNOWLEDGEMENTS

Course development was supported by grants from the UM Center for Research on Teaching and Learning. We are indebted to staff in the UM3D Lab and the Digital Media Commons, especially Steffen Heise.

TEACHING BIOMECHANICAL ANALYSIS USING THE BoB MATLAB/SIMULINK MODEL

James Shippen, Barbara May
Coventry University, UK
email: j.shippen@coventry.ac.uk, web: http://www.coventry.ac.uk

INTRODUCTION

This paper describes a biomechanical modeling package which resides totally within the MATLAB environment – the model is called BoB (Biomechanics of Bodies). It has been developed by the authors to provide a robust platform for research and teaching of biomechanics within a variety of disciplines, for example, rehabilitation therapies, sports science, ergonomics and engineering. It has a short learning curve for basic functionality which makes it an ideal research and teaching tool for academia, health, life sciences and within commercial environment. For many research institutions and commercial organizations MATLAB is the preferred mathematical modeling and simulation environment offering a comprehensive analysis suite, robustness of architecture, stability and a large availability of many existing models.

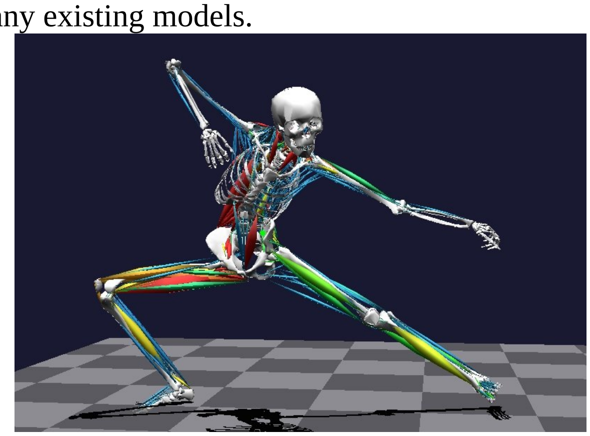

Figure 1: The BoB musculoskeletal model

METHODS

BoB is a MATLAB S-function of the human musculo-skeletal model which runs within the Simulink environment. The model calculates joint torques, muscle load distribution, joint contact forces and graphical output. The skeletal model is composed of 36 rigid segments representing the major bones of the body, eg the femurs, the skull, the radii, etc. These segments are connected by joints representing their anatomical counterparts, for example a hinge joint for the elbow, a spherical joint for the hip joint and a combination of joints to represent the shoulder girdle. A default mass distribution is based on [1] although the user can override the default distribution with an explicit segmental inertia tensor. External loads and torques can be applied to the segments defined in either the local segmental co-ordinate system or in the global co-ordinate system. Inputs to the S-function are the body mass, joint articulation time histories, the external loads and torques acting on the segments and the non-default segmental inertia tensors.

The muscle model consists of 666 locomotor muscle units and are characterized by their maximal isometric load [2]. The torques at the joints are calculated by inverse dynamics; these torques are generated by the muscles which cross these joints. However there were many more muscles than degrees of freedom at the joints (37 degrees of freedom) and therefore there is not a unique solution for the muscle load distribution. Hence an optimization approach using sequential quadratic programming [3] is used to minimize the sum of the 2^{nd} to 4^{th} power of the muscle activations.

Figure 2 shows a typical implementation of the BoB S-function within the Simulink environment – BoB is the large grey rectangle. To the left of BoB are the blocks from the Simulink library which define the joint articulations, external loads and torques as constants, simple functions or from a motion capture system. This model can be quickly and intuitively configured by inexperienced MATLAB users in order to perform a biomechanical analysis. This biomechanical model can also be integrated into existing MATLAB models of engineering systems to incorporate a human model.

RESULTS AND DISCUSSION

Figure 3 shows an example of a validation test of BoB versus other biomechanical modeling systems in terms of joint moment arms. A random muscle biceps femoris breve, is used to compare the joint moment arms for BoB and other modeling packages.

BoB has been used by students to analyse a wide range of biomechanical scenarios from Irish dance [4] to cricket - figure 4 shows an example of muscle loading distribution and trajectory tracks which occurred during cricket fast bowling using motion captured data. The “body-in-a-box” approach used in BoB was found to be intuitive to use and could be implemented with minimal instruction following a very short learning curve.

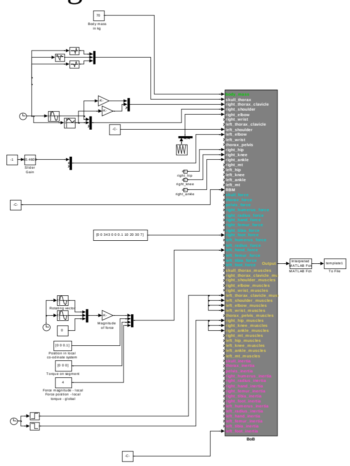

Figure 2: Typical implementation of the BoB S-function

CONCLUSIONS

BoB is a musculoskeletal modeling package within the MATLAB modeling environment which has been found to be fast and intuitive to learn making it very well suited to teaching biomechanics in a variety of disciplines. It enables students to quickly obtain reliable answers to their biomechanical questions. Additionally BoB provides a method for incorporating a bio-mechanical component into the models of any engineering systems. BoB can be downloaded from www.marlbrook.com/download

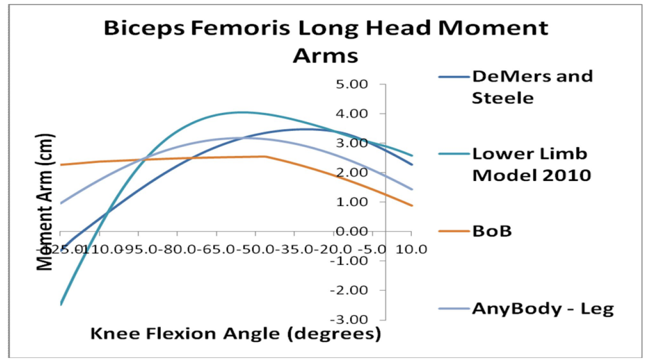

Figure 3: Comparison of biceps femoris breve moment arm for BoB and other modelling systems

REFERENCES

1. Winter D. Biomechanics and Motor Control of Human Movement (2nd ed.). New York: John Wiley & Sons, 1990
2. Shippen J, May B. The calculation of ground reaction forces during dance in the absence of forceplates. Journal of Dance Science and Medicine , Vol 16 Number 1, 2012
3. Powell, M.J.D., "The Convergence of Variable Metric Methods For Nonlinearly Constrained Optimization Calculations," Nonlinear Programming 3 (O.L. Mangasarian, R.R. Meyer, and S.M. Robinson, eds.), Academic Press, 1978.
4. Shippen J, May B. Calculation of Muscle Loading and Joint Contact Forces in Irish Dance. Journal of Dance Science and Medicine, Volume 14 1 pp11-18 2010

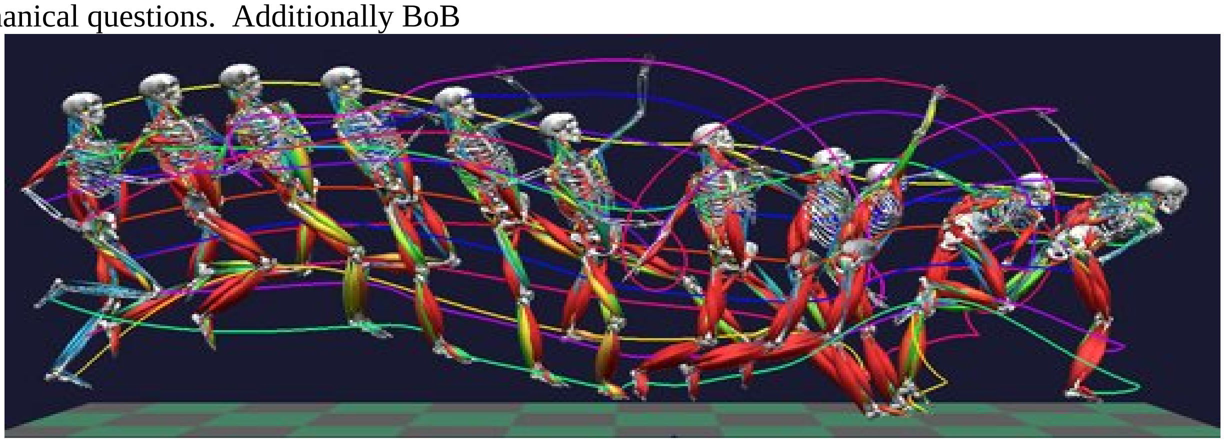

Figure 4: Example of muscle loading distribution and trajectories during cricket bowling

ORAL PRESENATIONS – SATURDAY SEPTEMBER 7th

	ACL-Related Biomechanics in Sports *Timothy Hewett, Stephanie Di Stasi*
1:15 PM	Changes In Biomechanical Hip & Trunk Control, Knee Load & Potential Predictors Of Increased ACL Injury Risk: Randomized Controlled Trial **Hewett T, Myer G, Khoury J, Xu Y, Ford K**
1:30 PM	Pre-operative Self-reported Function Predicts Knee Excursion Asymmetries In ACL-injured Athletes **Di Stasi S, Roewer B, Stammen K, Hewett T**
1:45 PM	Jump Landing Biomechanics Differ In Female Athletes With High Vs Low Baseline Neurocognitive Performance: Implications For Anterior Cruciate Ligament Injury Risk **Herman D, Barth J**
2:00 PM	Gender Differences In Unilateral Landing Mechanics From Absolute And Relative Drop Heights **Sievert Z, Irmischer B, Robinson Y, Seligman J, Weinhandl J**
2:15 PM	Effects Of Two Football Studs On Ground Reaction Force Of Single-Leg Landing And Cutting Movements On Infilled Synthetic Turf **Zhang S, Brock E, Milner C, Brosnan J, Sorochan J**

CHANGES IN BIOMECHANICAL HIP & TRUNK CONTROL, KNEE LOAD & POTENTIAL PREDICTORS OF INCREASED ACL INJURY RISK: RANDOMIZED CONTROLLED TRIAL

[1, 2] Hewett, T E; [2] Xu, YY; [2] Ford, KR; [2]Khoury J; [1, 2] Myer, GD
[1]The Ohio State University, Sports Health & Performance Institute, Columbus, OH,
[2] Cincinnati Children's Hospital Research Foundation, Cincinnati, OH,
Email: tim.hewett@osumc.edu or tim.hewett@cchmc.org.

INTRODUCTION

Over 125,000 anterior cruciate ligament (ACL) injuries occur each year in the United States. External loads on the knee in frontal plane, specifically knee abduction moment (KAM) predict ACL injury risk with high sensitivity and specificity. Neuromuscular deficits associated with increased trunk motion and decreased neuromuscular control associated with increased KAM were examined to determine the effects of multiple biomechanical and neuromuscular risk factors associated with ACL injury risk during knee, hip & trunk challenging tasks including the Drop Vertical Jump (DVJ), Single Leg Drop (SLD) and Single Leg Cross-Over Drop (SCD), respectively.

The purpose of this work was to understand the effects of hip and trunk focused intervention on the potential coupling between biomechanical and neuromuscular risk factors and their effects on neuromuscular control of the trunk, hip and knee. We hypothesized that trunk and hip focused neuromuscular training (Core NMT) would increase neuromuscular control of the trunk and hip and decrease knee load inputs, while Sham sprint training would not influence similar adaptations.

METHODS

A total of 370 athletes from 48 basketball, soccer and volleyball teams were screened prior to their competitive season. A total of 48 teams were randomized into the study, 28 in the Core NMT group and 19 into the Sham group, this resulted in 222 and 148 team members respectively. There are no statistically significant differences between the randomized groups for age, height, weight and BMI. During the screening, the athletes were asked to perform three different types of tasks for which biomechanical measures were taken: DVJ, SLD and SCD. For each task, 3 trials were performed. The athletes were tested again about one year later. We have previously reported (Hewett et al. 2011) using Latent profile analysis (LPA) to create 3 susceptibility groups for risk of ACL injury. We examined pre-post change of the pre-specified bio-mechanical motion variables between the Core NMT and Sham groups using Analysis of Variance (ANOVA). Differences were considered statistically significant at $p<0.05$. We further explored the group by risk profile interaction and conducted stratified analyses if necessary. Statistical analyses were conducted using SAS 9.3. We also examined post treatment effects according to these risk profiles.

RESULTS AND DISCUSSION

Intervention: During the SCD task, Core NMT increased maximum trunk flexion angles (2.8°), while Sham training decreased maximum trunk flexion angles on average by 4.8° ($p<0.001$). In addition, Core NMT decreased maximum trunk extension angles (3.3°), while Sham increased by 6.2° ($p<0.001$). During the SLD task, Core NMT group demonstrated increased hip external rotation moment (2.5 Nm) while Sham demonstrated less hip external rotation impulse (1.5 Nm) during the stabilization phase of landing ($p=0.03$). Also during the SLD task, Core NMT increased hip external rotation moment by 0.03 Nm, while Sham decreased by 0.1 Nm ($p=0.02$). When analyzed by LPA profile, the higher risk profile (profile 3), showed trends toward greater beneficial changes than lower risk profiles. Among the high-risk subjects, there were significant treatment effect in maximum trunk flexion angle during SCD (Core NMT increased by 4.7° the Sham decreased by 8.2°, $p=0.01$), maximum trunk extension angles during SCD (Core NMT decreased by 4.1° the Sham increased by 9.1°, $p=0.03$). In contrast, the treatment effects were not significant among the moderate-risk subjects. There was a significant interaction between intervention group by risk profile for change in knee abduction moment (KAM) during the landing phase of the SCD task, (P=0.003). Among the high-risk subjects, in the Core NMT group KAM was decreased by 4.5 Nm, while in the Sham group KAM was increased by 6.4 Nm (however due to small sample size group difference wasn't statistically significant). While among the moderate risk subjects (Profile 2), Core NMT decreased KAM by 0.74 N-m, while Sham increased KAM by 1.47 N-m during landing phase of the SCD.

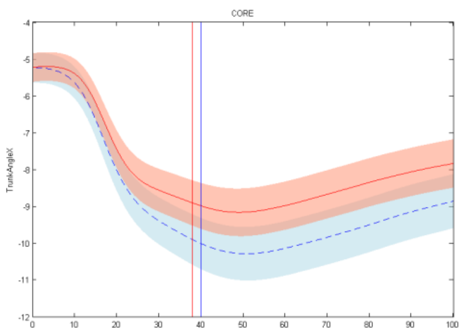

Figure1 Mean and SE of Trunk angle in sagittal plane. **(Red is pre-test; Blue is post-test).**

This is the first study to use biomechanical landing data in an RCT to examine trunk, hip and knee kinematics and kinetics that relate to potential changes in ACL injury risk profiles.

High KAM was observed in those subjects that went on to ACL injury (Hewett 2005).These findings begin to explain the biomechanical underpinnings of increased injury risk; yet, further study is needed to investigate this phenomenon. We continue to examine models and will validate them post intervention to determine potential emergent profiles that result from neuromuscular training. Large cohort Multi-Center studies of prediction of Trunk, Hip and Knee control and ACL injury risk with measured and demonstrably high validity and reliability will be the focus of future analyses.

CONCLUSIONS

Biomechanical and neuromuscular risk factors change with Core NMT may explain underlying mechanics to ACL injury risk reductions evidence with neuromuscular training programs.

REFERENCES:

Hewett TE et al. *J. Bone Joint Surg*, 2004 Aug; 86-A(8): 1601-8. *2004*

Hewett TE, et al. *Am J Sport Med*. **33**, 492-501. 2005.

ACKNOWLEDGEMENTS

This study was funded by National Institutes of Health/NIAMS Grants R01 AR055569, R01 AR055569 and R01 AR056259.

Table 1. Changes in values of variables of interest pre to post intervention (all athletes and by risk profile group (**significant change**).

variable	task	Core NMT		Sham			risk profile
		Mean	StdErr	Mean	StdErr	p-value	
hip external rotation moment impulse	SLD	-0.03	0.02	0.10	0.04	0.02	all
during first 10% of landing phase		-0.01	0.02	0.08	0.03		1*
		-0.01	0.04	0.04	0.06	0.59	2
		-0.06	0.07	0.21	0.09	0.08	3
hip external rotation moment	SLD	-2.52	0.78	1.54	1.19	0.03	all
		-1.05	0.71	-1.96	0.99		1*
		-3.82	1.39	3.13	2.05	0.04	2
		-0.49	2.03	-1.21	2.80	0.87	3
maximum trunk extension angles	SCD	-3.29	1.23	6.18	1.90	<0.01	all
		-2.11	2.10	5.36	2.02		1*
		-1.59	1.92	3.69	2.84	0.26	2
		-4.10	2.61	9.09	3.53	0.03	3
maximum trunk flexion angles	SCD	-2.80	1.08	4.84	1.67	<0.01	all
		-2.11	1.91	3.71	1.68		1*
		-1.20	1.64	2.72	2.43	0.33	2
		-4.66	1.99	8.23	2.70	0.01	3

Data are least squares means & standard errors or *raw means and standard errors due to sample size.

PRE-OPERATIVE SELF-REPORTED FUNCTION PREDICTS KNEE EXCURSION ASYMMETRIES IN ACL-INJURED ATHLETES

[1,2]Stephanie L Di Stasi, [1]Benjamin D. Roewer, [1]Kari L. Stammen, and [1,2,3]Timothy E. Hewett

[1]The Ohio State University, Sports Health and Performance Institute, Columbus, OH, USA
[2]The Ohio State University, Division of Sports Medicine, Columbus, OH, USA
[3]Cincinnati Children's Hospital Medical Center, Cincinnati, OH, USA

email: stephanie.distasi@osumc.edu

INTRODUCTION

Restricted knee motion during activities of daily living is a common impairment following acute rupture of the anterior cruciate ligament (ACL) and may represent impaired joint mobility or an abnormal neuromuscular control strategy [1]. Importantly, the pre-operative condition of the injured knee is known to affect both mid-term and long-term functional outcomes in ACL-injured athletes [2,3]. Specifically, post-injury stiffness is significantly associated with stiffness six months after ACL reconstruction [3]. A knee stiffening strategy during dynamic tasks may be indiscernible without the use of highly sensitive motion analysis systems. Therefore, determinants of neuromuscular dysfunction, which can be easily captured in the clinical environment, may facilitate the development of targeted and effective pre-operative rehabilitation strategies.

Self-report outcome measures provide important data on a patient's perceived level of function in the wake of ACL injury. The Knee Injury and Osteoarthritis Outcome Score (KOOS) is a reliable, valid and responsive outcome measure in individuals with ACL injury, where lower scores represent greater disability [4]. Its relationship to dynamic measures of neuromuscular dysfunction early after ACL injury, however, is unknown. The purpose of this study is to determine whether poorer functional outcome scores of acutely ACL-injured athletes are predictive of pre-operative knee excursion asymmetries during gait.

METHODS

Fifteen athletes who sustained an acute ACL rupture (age: 24.5 ± 11.5 years, mass: 78.4 ± 13.9 kg) underwent three-dimensional motion analysis of walking gait. The Institutional Review Board approved all study methods, and all subjects provided informed consent prior to participation.

Kinematic data during three gait trials were sampled at 240Hz and then low-pass filtered at 6Hz using a bi-directional Butterworth filter. Joint motion was calculated using rigid body analysis and Euler angles with custom Visual 3D (C-motion Inc., Germantown MD) and Matlab (Mathworks Inc. Natick, MA) coding. Ensemble averages were generated for the involved and uninvolved limbs of each athlete. Sagittal plane knee joint excursions were calculated during the stance phase of gait and normalized to 100% for comparison between athletes.

Linear regression analyses were used to examine whether subscales of the KOOS (Symptoms/Stiffness; Pain; Function, Daily Living; and Quality of Life) could independently predict sagittal plane knee excursion asymmetries acutely after ACL injury. *A priori* statistical significance was set at $P < 0.05$, and adjusted R square values are reported.

RESULTS AND DISCUSSION

Pre-operative knee excursion asymmetry during the stance phase of gait significantly predicted self-reported outcomes on two of the four KOOS subscales. Lower scores on the Symptoms/Stiffness and Pain subscales of the KOOS were significant predictors of larger knee excursion asymmetries (Symptoms/Stiffness: $P = 0.048$, adjusted $R^2 = 0.211$; Pain, $P = 0.001$, adjusted $R^2 = 0.531$) early after ACL rupture. Scores on the Function, Daily Living (ADL) and Quality of Life (QOL) subscales were not significantly predictive of knee excursion asymmetries (ADL: P = 0.08, adjusted R^2 = 0.157; QOL: P = 0.057, adjusted R^2 = 0.193)

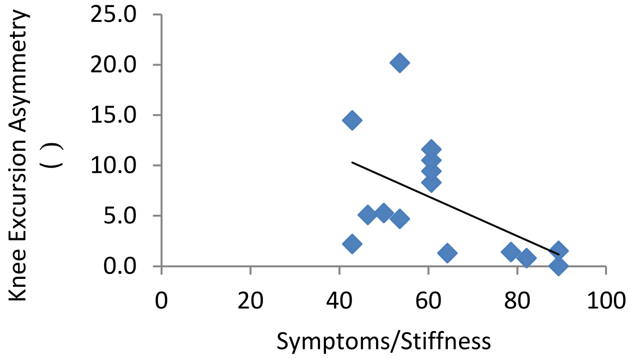

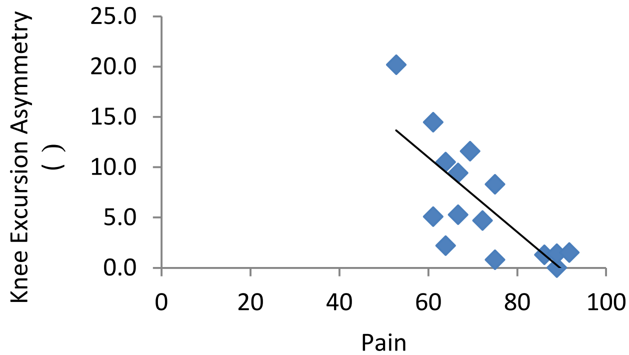

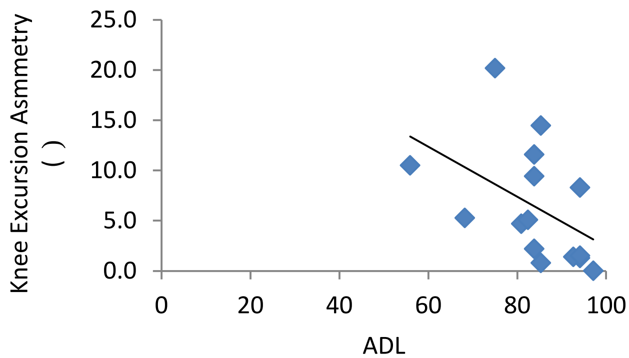

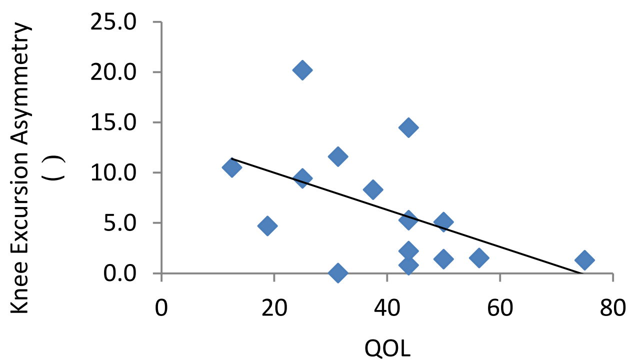

Our data support the findings of previous studies which highlight aberrant gait mechanics as a characteristic of the most poorly performing athletes following ACL injury [1]. Self-report measures, as part of a battery of clinical tests, have successfully identified ACL-deficient athletes capable of returning to sport in the short-term following a bout of neuromuscular training [5]. While these tests are easy to implement, they are time-intensive and require expensive equipment; thus, a single self-report outcome measure that can effectively predict ACL-deficient athletes who may and may not benefit from pre-operative care is of significant value to sports medicine clinicians. Based on these preliminary data, use of the KOOS may help identify those athletes in particular need of targeted rehabilitation prior to ACL reconstruction.

CONCLUSIONS

Delaying ACL reconstruction in order to restore normal joint motion has been advocated as a means to reduce the development of post-operative knee stiffness. Subscales of the KOOS appear to capture important functional and neuromuscular asymmetries in athletes prior to ACL reconstruction; its utility as a clinical surrogate for determining the need for pre-operative rehabilitation is unknown. Whether these early measures of abnormal function predict post-operative outcome is currently under investigation.

REFERENCES

1. Rudolph KS, et al. *J Electro Kines* **8**, 349-362, 1998.
2. Eitzen I, et al. *Br J Sports Med* **43**, 371-376, 2009.
3. Robertson GAJ, et al. *Knee* **16**, 245-247, 2009.
4. Roos E, et al. *J Orthop Sports Phys Ther* **28**, 88-96, 1998.
5. Fitzgerald, et al. *Knee Surg, Sports Traumatol, Arthrosc* **8**, 76-82.

ACKNOWLEDGEMENTS

This study was funded by DJO Global (Vista, CA). Special thanks to Sam Wordeman, Chris Nagelli and the staff of the Biodynamics Laboratory at The Ohio State University.

JUMP LANDING BIOMECHANICS DIFFER IN FEMALE ATHLETES WITH HIGH VS LOW BASELINE NEUROCOGNITIVE PERFORMANCE: IMPLICATIONS FOR ANTERIOR CRUCIATE LIGAMENT INJURY RISK

[1]Daniel Herman, [2]Jeffrey Barth

[1]University of Florida, Gainesville, FL, USA
[2]University of Virginia, Charlottesville, VA, USA
email: dcherman@ufl.edu

INTRODUCTION

Altered neuromuscular characteristics during athletic tasks such as jump landing have previously been demonstrated as compelling risk factors for anterior cruciate ligament injury and injury prevention. Groups at high risk for ACL injury have kinetic and kinematic characteristics such as high ground reaction forces, high frontal and sagittal plane moment at the knee, high frontal plane motion at the knee and trunk, and low sagittal plane motion at the knee and trunk [1]; furthermore, neuromuscular characteristics have the capacity for prediction of injury [2].

Recent studies indicate that poor neurocognitive performance is associated with a high risk of musculoskeletal injury [3]. The mechanisms by which neurocognition affects injury risk are not known, but may exert an affect on neuromuscular performance. Athletes who have temporary alteration of normal neurocognitive performance such as with a concussion demonstrate altered neuromuscular measures of gait during a dual-attention task [4], but we do not how neurocognitive performance at baseline may impact neuromuscular performance during a more rigorous athletic task.

The purpose of this study was to determine if differences in neuromuscular performance during an unanticipated jump landing task exist between female athletes with high and low baseline neurocognitive performance. We hypothesized that female athletes with low baseline neurocognitive performance would demonstrate neuromuscular performance characteristics associated with high ACL injury risk, including increased peak vertical ground reaction force (GRF), peak anterior proximal tibial shear force (TSF), knee abduction moment at GRF (KABM), knee abduction angle at GRF (KABA), and trunk lateral flexion angle at GRF (TLFA), as well as decreased knee flexion angle at GRF (KFA) and trunk flexion angle at GRF (TFA).

METHODS

Subjects included recreational college-aged (18-30yrs) athletes, defined as one who participates in jumping/cutting sports (e.g. basketball, soccer, volleyball, lacrosse) at least three times a week; or 2) participates in these sports at least once a month and previously participated at the high school varsity or collegiate club levels. 58 potential subjects were screened using the computer-based Concussion Resolution Index (CRI). The CRI neurocognitive testing subtest domains include simple reaction time, complex reaction time, and processing speed. Subjects above the 80th percentile in one score and with two scores no lower than 60th percentile were included in the higher performers (HP) group (N=10). Subjects with one subtest score below the 40th percentile and with two scores no higher than the 70th percentile, or with at least two scores below the 30th percentile were included in the low performers (LP) group (N=10).

Whole-body kinematics and kinetics were evaluated by using a high-speed 12-camera optical motion analysis system (200Hz, Vicon, Los Angeles, CA) and two in-ground force platforms (1200Hz, Bertec Inc, Columbus, OH) using a modified Helen Hays marker system and standard calibration, data collection, and data reduction techniques. The subjects completed a jump landing task using a variable landing target. The subject stood on a 30cm box, jumped forward off the box over a distance of ½ the subject's height to land on a set of force plates. During the flight phase before landing, a monitor positioned in front of the subject displayed an arrow pointing right, left, or up at 250msec prior to landing. The subject then jumped off the plates at maximum effort to either landing targets positioned 1m forward and to the right or left of the plates, or vertically to land again on the force plates as indicated by the monitor.

Three trials for each landing condition were recorded, and data from the three vertical landing conditions were averaged for each subject and used for comparison. Forces were normalized to body weight and moments to the produce of body weight and height. Statistical analysis used independent-samples t-tests with alpha set at $p=0.05$.

RESULTS AND DISCUSSION

There were no significant difference between groups in age, height, or weight ($p>0.05$). The LP group demonstrated significantly lower CRI scores in all domains compared to the HP group ($p<0.01$, see Figure 1). Regarding jump landing performance, the LP demonstrated altered jump landing measures (Mean±SD of LP vs HP) including significantly increased GRF (1.94±0.61BW vs 1.41±0.16BW, $p=0.03$) and TSF (0.98±0.17BW vs 0.80±0.15BW, $p=0.04$); increased KABA (6.1 ± 4.7^o vs 1.3 ± 5.6^o $p=0.03$) and TLFA (4.1 ± 4.7^o vs 0.3 ± 1.2^o, $p=0.01$) as well as decreased TFA (5.4 ± 4.5^o vs 11.5 ± 6.1^o, $p=0.03$) (See Figure 3). Differences in KABM and KFA were not statistically significant ($p > 0.8$).

These results are among the first to explore the relationship between neurocognitive performance and neuromuscular performance. The neuromuscular performance differences observed in LP athletes are consistent with elevated ACL injury risk as demonstrated in previous studies. The implications of these findings for ACL injury risk evaluation and injury prevention have the potential to be profound. Improving our understanding of the relationship between these domains may result in an enhanced capability to engage in pre-activity injury risk stratification via use of standard neurocognitive screening tools that are gaining widespread popularity among competitive sports from high school to the professional levels. Return to play criteria following transient alterations in neurocognition such as with a concussion may also be enhanced to incorporate post-concussion musculoskeletal injury risk considerations. Furthermore, both pre-season and post-concussion injury prevention strategies may also be expanded to include neurocognitive rehabilitation and training techniques. Additionally, game/practice factors such as limited minutes to reduce likely additive risk factors such as fatigue may be considered during the immediate return to play period following a concussion. Finally, the knowledge gained as a result of this study and future investigations could also be applied to other populations at high risk for musculoskeletal injury, such as the military, which may help inform assessments of injury risk, duty readiness, and weapon-use performance after traumatic brain injury.

CONCLUSIONS

Neuromuscular performance measures during the jump landing are altered in female recreational athletes who demonstrate relatively low baseline neurocognitive performance in a manner consistent with increase risk for ACL injury.

REFERENCES

1. Chappell JD, et. al. *AJSM* **30**(2): 261-7
2. Hewett TE, et. al. *AJSM* **33**(4): 492-501
3. Swanik CB, et. al. *AJSM* **35**(6): 943-8
4. Catena RD, et. al. *Gait Posture* **25**(3): 406-11

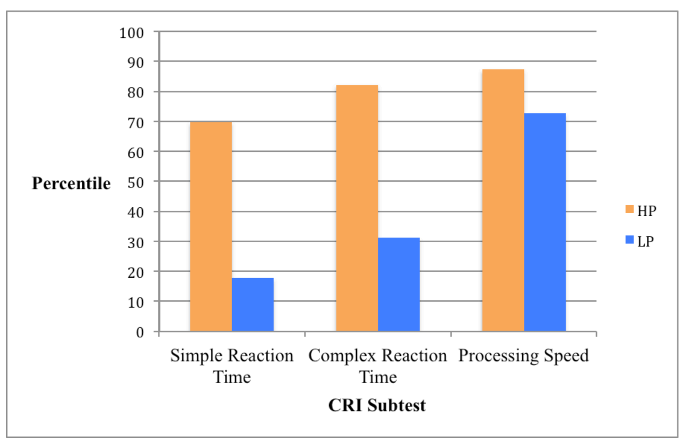

Figure 1: Concussion Resolution Index Scores

GENDER DIFFERENCES IN UNILATERAL LANDING MECHANICS FROM ABSOLUTE AND RELATIVE DROP HEIGHTS

Zach A. Sievert, Bobbie Irmischer, Yashona Robinson, Justin Seligman, Joshua T. Weinhandl

Old Dominion University, Norfolk, VA, USA
email: zsiev001@odu.edu

INTRODUCTION

The growth of female participation in sport has led to an increase in ACL injuries in female athletes. Gender differences in landing mechanics may be due in part to decreased muscle strength, increased flexibility, and delayed hamstring activation relative to the quadriceps often observed in women [1]. These differences may place the knee in a dangerous position, reducing the stabilization and increasing forces transmitted through the joint.

Landing mechanics have been reported using absolute and relative drop. Females exhibited increased knee abduction and vertical ground reaction forces compared to males in unilateral and bilateral landings from absolute heights [2]. Further, gender differences in frontal plane knee have been reported in absolute height unilateral landings [3]. However, when relative drop heights were employed, a gender effect was only reported for hip and knee sagittal plane kinematics [4]. It appears that absolute jump heights may inflate gender differences in landing mechanics. Increased landing height has been associated with increased vertical GRF in unilateral landings [5]. As height increases, the amount of force that must be dissipated increases as well. Thus, landing from a height greater than the participant's jumping ability, may not capture natural landing mechanics. The purpose of this study was to compare ground reaction forces, as well as lower extremity kinematics and kinetics of males and females when landing from absolute heights and a height equal to their maximum jumping ability.

METHODS

Five healthy, recreationally active men (81.2 ± 10.4 kg, 1.78 ± 0.03 m) and five healthy, recreationally active women (59.6 ± 7.4 kg, 1.62 ± 0.11 m) aged 18 to 30 years volunteered to perform unilateral landings onto a force plate. Prior to data collection, participants were informed of study procedures and provided written informed consent in accordance with institutional guidelines. Single reflective markers were placed on specific anatomical landmarks [4] and a static standing calibration trial (neutral position) was collected. Participants were asked to complete five right side unilateral drop landings from 30, 40 and 50 cm, as well as a box set to their vertical jumping ability. Three dimensional marker coordinate data were collected at 200 Hz using an eight-camera Vicon motion analysis system. Synchronously, three-dimensional force data was collected at 1000Hz using a Bertec force plate.

Raw three-dimensional marker coordinate and GRF data were low-pass filtered using a fourth-order, zero lag, recursive Butterworth filter with cutoff frequency of 15 Hz. A kinematic model comprised of eight skeletal segments (trunk, pelvis, and bilateral thighs, shanks, and feet) was created from the standing calibration trial [4]. Three-dimensional ankle, knee, and hip angles were calculated using a joint coordinate system approach [6].

To compare lower extremity joint dynamics between the landing heights peak posterior and vertical GRF, and initial contact (IC) knee joint angles were identified. A 2×4 repeated measures ANOVA (gender×landing height) was performed for each dependent variable (p<0.05).

RESULTS AND DISCUSSION

Gender differences were observed as men landed with 0.68 $N\cdot kg^{-1}$ significantly more peak posterior GRF compared to women (p=0.004) (Table 1), and women landed with 4.1^{o} significantly less IC knee adduction then men (p<0.001) (Figure 1).

When comparing the absolute landing heights to the relative landing height differences were only observed between the peak vertical GRF and IC knee adduction angle. Compared to the 50 cm landing height, landings from a relative height were performed with 6.16 $N \cdot kg^{-1}$ significantly less peak vertical GRF (p=0.005) and 1.4° significantly more knee adduction at IC (p=0.018).

Changes were also observed as absolute height increased. These included decreased knee flexion and external rotation at IC, as well as increased peak posterior and vertical GRF.

The results of the current study support the findings of Yeow et al. [5] who reported an increase in resultant GRF as landing height was increased from 30 cm to 60 cm. These authors also reported a decrease in knee flexion angle as landing height increased which is consisted with the current findings. The observed increases in peak posterior and vertical GRF may be a result of the decreased knee flexion at IC [4]. This stiffer landing style is likely to result in increased loading of the ACL [7].

The decreased knee adduction at IC demonstrated by women in the current study is consistent with findings of Russell et al. [3]. Furthermore, as landing height increased women exhibited a shift towards knee abduction at IC, a position that has been associated with increased ACL injury risk [1]. However, since the average jump height of women in the current study was 27 cm these higher landing heights may have represented a task that is unlikely to occur in a natural environment.

CONCLUSIONS

The observed differences in peak vertical GRF and knee adduction angle at IC suggest between the highest landing height (50 cm) and a height specific to each individuals jumping ability suggest that extreme heights create a task that is unrealistic for many individuals. Future studies investigating landing mechanics should consider implementing drop heights that are scaled based on participants' jumping abilities. Such comparisons are likely to provide a better representation of landing mechanics during game situations when injuries most commonly occur and may help elucidate gender differences responsible for gender disparities in ACL injury rates.

Table 1. Effects of gender and landing height on mean ± stdv peak posterior and vertical GRF ($N \cdot kg^{-1}$).

		Men	Women
GRF_Y*[bc]	Rel	-6.10 ± 0.79	-5.05 ± 0.39
	D30	-5.50 ± 1.02	-5.03 ± 0.68
	D40	-5.80 ± 1.01	-5.06 ± 0.29
	D50	-6.08 ± 0.77	-5.59 ± 0.54
GRF_Z[abcd]	Rel	42.94 ± 9.64	34.74 ± 6.4
	D30	38.10 ± 5.86	35.48 ± 4.91
	D40	42.41 ± 5.65	39.26 ± 5.42
	D50	46.21 ± 4.48	43.80 ± 7.45

* significant gender difference
[a] D30 significantly different from D40
[b] D30 significantly different from D50
[c] D40 significantly different from D50
[d] Rel significantly different from D50

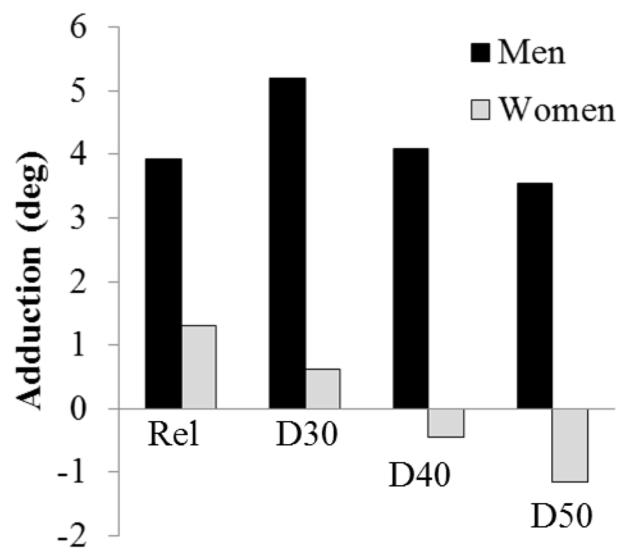

Figure 1. Mean knee adduction angle at IC.

REFERENCES

1. Hewett et al. *Am J Sports Med*. **34**:299-311, 2006.
2. Pappas et al. *CJSM*, **17**:263-8, 2007.
3. Russell et al. *J Ath Train*, **41**:166-71, 2006.
4. Weinhandl et al. *J Appl Biomech*. **26**:444-53, 2010.
5. Yeow et al. *The Knee*, **17**:127-31, 2010.
6. Grood & Suntay, *J Biomech Eng*, **105**:136-44, 1983.
7. Laughlin, et al. *J Biomech*, **44**:1845-51, 2011.

EFFECTS OF TWO FOOTBALL STUDS ON GROUND REACTION FRORCE OF SINGLE-LEG LANDING AND CUTTING MOVEMENTS ON INFILLED SYNTHETIC TURF

[1]Songning Zhang, [2] Elizabeth Brock, and [1]Clare Milner, [3]James T. Brosnan, [3]John C. Sorochan
[1]Biomechanics/Sports Medicine Lab, The University of Tennessee, Knoxville, TN, USA
[2]University of Oregon, Eugene, OR
[3]Department of Plant Sciences, The University of Tennessee, Knoxville, TN, USA
email: szhang@utk.edu, web: web.utk.edu/~sals/resources/biomechanics_laboratory.html

INTRODUCTION

Injuries in American football occur more frequently than any other NCAA sports [5]. Non-contact ACL injuries often occur during fast-paced plant-and-cut movements that involve rapid deceleration, jumping and landing [1, 4]. The introduction of synthetic turf has influenced both the frequency and type of injuries in American football. It has been reported that artificial surfaces contribute to 1.73 ACL injuries per 10,000 exposures compared to 1.24 ACL injuries per 10,000 exposures on natural turfgrass [2].

Muller et al. [6] studied three different movements on sand/rubber infilled synthetic turf with four different studded conditions. Peak vertical ground reaction force (GRF) and its loading rate were not affected by different stud conditions in a 45° cut. Peak vertical and shear GRFs for the soft (longer) ground studs were decreased compared to hard (shorter) ground studs in a 180° cut [6].

Single-leg land-cut and 180° cut movements are common in American football and are associated with rapid deceleration and changes of direction. Thus, the potential for injury during these movements is significant. Furthermore, data examining the biomechanical behaviors of human participants during a single-leg land-cut movement on infilled synthetic turf are limited. Therefore, the purpose of this investigation was to examine effects of natural and synthetic turf studs and a running shoe on GRF variables during single-leg land-cut and 180° cut movements on an infilled synthetic turf.

METHODS

Fourteen active and healthy male recreational football players (age: 20.1 ± 1.4 years, height: 1.80 ± 0.0 m, mass: 85.6 ± 9.7 kg) with a minimum of three years of football experience and exercised at least three times a week participated in this study. Five successful trials were performed in each of six testing conditions: neutral running shoe, natural turf studs (1.27 cm in length, 0.9 cm diameter) and synthetic turf studs (0.95 cm in length, 1.5 cm diameter) for both a 180° cut and single-leg land-cut. Studs were fastened on a pair of football shoe (Scorch X Low D, adidas). The movements were performed on a 51 mm monofilament synthetic turf surface (Astroturf Gameday 3D, AstroTurf, Dalton, GA) on top of and around a force platform in the lab, forming three separate runways. The turf was topdressed with silica sand and rubber at a ratio of 4.89 kg sand: 12.21 kg rubber. Silica sand was distributed first and followed by SBR rubber.

A 9-camera motion analysis system (240 Hz, Vicon Motion Analysis) and a force platform (1200 Hz, AMTI) were used to obtain 3D kinematic and ground reaction force data during the movement trials. Anatomical and tracking reflective markers were placed on the pelvis, and the right thigh, leg, and foot (via cutouts in shoe). The shoe and movement conditions were randomized. Visual3D (C-Motion, Inc.) was used to compute 3D kinematic and kinetic variables. A right-hand rule was used to establish the 3D kinematics/kinetics conventions. Marker trajectories and force platform data were filtered with a zero-lag fourth order low-pass Butterworth filter at 12 and 50 Hz, respectively. A 3 x 2 (stud x movement) repeated measures analysis of variance (ANOVA) was used to examine effects of the three shoe and two movement conditions on selected variables (19.0, SPSS). Post hoc comparisons were performed using a pairwise comparison. The significance level was set at 0.05.

RESULTS AND DISCUSSION

Peak vertical GRFs and vertical GRF loading rate were greater for land-cut movement compared to 180° cut (Table 1). A stud × movement interaction was also detected in time-to-peak vertical GRF (p=0.048). Post hoc comparisons showed that peak vertical GRF was reached later in the natural turf compared to synthetic turf stud during the 180° cut movement (p=0.019). Finally, peak medial GRF showed a significant stud x movement interaction (p=0.002, Table 1). The peak medial GRF was greater in the running shoe compared to natural turf studs (p<0.001) and synthetic studs (p=0.004), and smaller in natural turf studs compared to synthetic turf studs (p<0.001) during the 180° cut. A stud × movement interaction was also detected in peak medial GRF data (p=0.002, Table 1). The peak medial GRF was greater in the non-studded running shoe compared to either the natural turf (p<0.001) or synthetic studs (p=0.004) during the 180° cut movement. Additionally, peak medial GRF with the natural turf stud was significantly lower than both the synthetic turf stud and the non-studded running shoe during the 180° cut movement (Table 1).

The lack of differences in peak vertical GRFs between shoe conditions are supported by the results of Griffin et al. [4] who found that neither sole materials nor shoe conditions significantly changed peak vertical GRF. Gehring et al. [3] found no significant differences in peak vertical GRF during a 180° cut performed by soccer players wearing traditional and bladed studs. Our results show that the single-leg land-cut is associated with elevated peak vertical and medial GRF as well as greater loading rates compared to the 180° cut. Few significant differences were detected in peak vertical GRF between the shoe conditions for either movement. However, during the 180° cut the time-to-peak vertical GRF was longest with the natural turf stud compared to the other shoe conditions. The additional length of the natural turf studs may aid in decreasing vertical GRF and prolonging the time-to-peak vertical GRF compared to synthetic turf studs and non-studded shoe conditions, which may have implications in injury reduction by decreasing the vertical GRF loading rate.

CONCLUSION

In general, few differences in GRF variables were observed between the shoe conditions. However, during the 180° cut movement, natural turf studs produced the lowest peak medial GRF compared to synthetic turf studs and the running shoe. Overall, increased GRFs, especially in combination with rapid change of direction and deceleration may increase the chance of ACL injury.

REFERENCES

1. Boden, B. P., et al. (2000). *Orthopedics* **23**, 573-578.
2. Dragoo, J. L., et al. (2012). *Am J Sports Med*, **40**, 990-995.
3. Gehring, D., et al. (2007). *Int J Sports Med*, **28**, 1030-1034.
4. Griffin, L. Y., et al. (2000). *J Am Acad Orthop Surg*, **8**, 131-150.
5. Hootman, J. M., et al. (2007). *J Athl Train*, **42**, 311-319.
6. Muller, C., et al. (2010). *Sports Biomech*, **9**, 193-205.

Table 1. Mean ground reaction force variables: mean ± SD.

	Land-Cut			180° Cut		
	Running shoe	**Natural turf stud**	**Synthetic turf stud**	**Running shoe**	**Natural turf stud**	**Synthetic turf stud**
Peak vertical GRF (BW) ^{M}	4.8±0.9	5.0±0.7	5.0±0.7	1.9±0.2	1.6±0.2	1.8±0.3
Time-To-Peak vertical GRF(s) $^{M, \&}$	0.048±0.009 $^{\$}$	0.047±0.013 $^{\$}$	0.050±0.013 $^{\$}$	0.066±0.020	0.081±0.032 $^{\%}$	0.063±0.028
Loading rate (BW/s) ^{M}	103.1±38.4	108.7±38.4	103.0±44.2	30.5±13.0	25.3±12.6	27.8±13.2
Peak Medial GRF (BW) $^{C, \&}$	1.3±0.2	1.3±0.3	1.4±0.3	1.4±0.2 $^{*\#}$	1.1±0.1 $^{\%}$	-1.3±0.1

^{C}: Significant Shoe main effect, ^{M}: Significant Movement main effect, $^{\&}$: Significant Shoe condition x Movement Interaction, *: Significant difference between Shoe and Natural turf stud in the same movement, $^{\#}$: Significant difference between Shoe and Synthetic turf stud in the same movement, $^{\%}$: Significant difference between Natural turf stud and Synthetic turf stud in the same movement, $^{\$}$: Significant difference between movement of same stud condition.

ORAL PRESENATIONS – SATURDAY SEPTEMBER 7th

	Motor Control: Standing & Locomotion *Elizabeth Hsiao-Wecksler, Alena Grabowski*
1:15 PM	Biomechanical Analysis Of Gait Termination In Children At Preferred And Fast Walking Speeds **Ridge S, Manal K, Henley J, Miller F, Richards J**
1:30 PM	Heel Rise Occurs Earlier In Stance With Increased Walking Speed **Schrank E, Guinn L, Stanhope S**
1:45 PM	Ankle Dynamics of Walking At Varying Velocities And Inclines **Auyang A, Grabowski A**
2:00 PM	The Cost Of Being Stable: A Quantitative Approach To Examine Trade-Off Between Effort And Stability **Sohn MH, Ting L**
2:15 PM	The Temporal Structure Of Center Of Pressure During Standing Is Affected By Proprioceptive Input **Rand T, Kyvelidou A, Mukherjee M, Myers S**

BIOMECHANICAL ANALYSIS OF GAIT TERMINATION IN CHILDREN AT PREFERRED AND FAST WALKING SPEEDS

Sarah Ridge[1], Kurt Manal[2], John Henley[3], Freeman Miller[3], James Richards[2]

[1]Brigham Young University, Provo, UT; [2]University of Delaware, Newark, DE;
[3]A.I. DuPont Hospital for Children, Wilmington, DE
E-mail: sarah_ridge@byu.edu

INTRODUCTION

Gait termination can be challenging for populations that may already have difficulty with walking, such as children with cerebral palsy. Even in healthy populations, additional challenges may be present when walking at fast speeds. Previous research has shown that as walking velocity increases, so do ground reaction forces and the number of steps required to stop.[1,2] When individuals with some pathologies perform gait termination at preferred walking speeds, they also change their ground reaction forces and take more than one step to stop.[1,2] Although children's steady-state gait patterns mature by the age of 7, mechanics of gait initiation and termination may take longer. Therefore, the purpose of this study was to gain a greater understanding of how healthy children perform planned and unplanned stopping tasks at 2 different speeds.

METHODS

Fifteen healthy, typically developing children between the ages of 11-17 years (mean 14 ± 2.1) participated. Reflective markers were applied to anatomical landmarks to create a 12 segment model. Motion capture data was collected at 60 Hz using 10 Eagle Digital Motion Analysis Cameras (Motion Analysis, Santa Rosa, CA). Four AMTI force plates were used to measure ground reaction force data at 960 Hz.

Subjects performed five sets of trials: 1) walking trials to establish preferred walking speed, 2) unplanned stop at preferred speed (UP), 3) planned stop at preferred speed (PP), 4) unplanned stop at fast speed (UF), and 5) planned stop at fast speed (PF). Fast speed was 150% of the preferred walking speed. During all trials, subjects monitored their speed by watching a screen positioned at the end of the walkway. During unplanned stopping trials, a large STOP sign appeared on the screen signaling that the subject should stop and "freeze". The stop sign was triggered to appear at foot contact of the dominant leg. During planned stopping trials, subjects were directed to stop with their feet together on the furthest of force plates. Data were collected from the time the subject entered the volume until approximately 2 seconds after he/she stopped.

Lower body joint angles, moments, and total body center of mass (COM) were calculated using Visual 3D (C-Motion, Inc., Germantown, MD). Repeated measures ANOVAs were used to compare peaks across speeds (UP to UF and PP to PF). Alpha level was set a $p<.01$. When statistical differences were found, a Tukey's post hoc test was run to determine where the differences occurred.

RESULTS AND DISCUSSION

Data from three subjects were removed from analysis of the unplanned fast and/or planned fast conditions due to lack of ability to either walk fast enough or stop within 1 stop of receiving the stop signal. An additional 3 subjects were not able to stop cleanly on a force plate during the unplanned fast condition, so their data were excluded from kinetic analyses.

Joint angle and moment data for UP, PP, UF, and PF trials are presented in Table 1.

Speed Comparisons within Conditions

Peak ankle angles were not significantly different between fast and preferred speed conditions. However, by looking at the angle as the stop stance phase progressed, it appears that subjects stayed in a more dorsiflexed position during the PF stopping task than they did during PP stopping. This requires the ability to stretch the gastrocnemius and Achilles tendon, which could be difficult for people with spastic muscles.

Peak knee flexion angles were greater during fast speeds than during the respective slow speed trials. During the PF stops, subjects stabilized in similar positions regardless of speed, with the knee in full extension, or static standing, by the time the COM stopped moving forward. During unplanned stops, most subjects stabilized with a more flexed knee, suggesting the need for adequate quadriceps and hamstring strength. Peak knee extension moments were significantly greater during the fast stops compared to the preferred speed stops. This too has implications for people with weak quadriceps that may have difficulty controlling the motion of the knee against larger ground reaction forces. Also of note, most subjects continued to have a greater knee extension moment throughout the stance phase during the UF stops than during the UP stops, suggesting that stabilization requires more knee extensor activity throughout the stop stance phase when the subject entered the stop step at a higher velocity.

Peak hip flexion angles were also greater during fast stopping. Most subjects stabilized by extending the hip slightly; though the degree to which that occurred varied. As with the knee extension moment, the peak hip extension moment was significantly greater during the PF trials than during the PP trials.

Speed Comparisons across Conditions

Some interesting trends were noted when comparing variables across speed and planning conditions. There were many similarities between UP and PF conditions, including peak knee and hip flexion angles. Most subjects used different strategies to stop based on whether the stop was planned or unplanned. However, the mechanics of PF stopping were more similar to those of the UP condition than the PP condition. This data suggests that it may be possible to utilize a PF stopping task as a protocol that stresses the individual and gives clinicians an indication of how children would respond to an unexpected stimulus which required them to stop quickly. Planned stopping, even at a fast speed, is a substantially easier protocol to test and may still provide useful information about mechanical difficulties children may have with gait termination.

REFERENCES

1. Bishop, M, et al. *Neuroscience Letters*, **397**(3), 240-244, 2006.
2. Tirosh & Sparrow. *Gait & Posture*, **19**(3), 243-251, 2004.

Table 1. Peak joint angle (n=12) and moment (n=9) data for the leading leg (non-dominant) from the stop step during planned preferred and planned fast trials. [a] denotes a significant difference from unplanned slower speed condition, while [b] denotes a significant difference from planned slower speed condition.

	Unplanned Preferred	Unplanned Fast	Planned Preferred	Planned Fast
Peak Knee Flexion Angle (degrees)	34.5 ± 10.0	50.9 ± 8.20[a]	22.7 ± 8.78	38.5 ± 9.87[b]
Peak Hip Flexion Angle (degrees)	30.4 ± 7.03	46.0 ± 9.28[a]	22.8 ± 6.13	30.5 ± 7.96[b]
Peak Plantarflexion Moment (Nm/kg*m)	.614 ± .116	.632 ± .100	.432 ± .137	.570 ± .119
Peak Knee Extension Moment (Nm/kg*m)	.261 ± .282	.934 ± .306[a]	.240 ± .177	.810 ± .403[b]
Peak Hip Extension Moment (Nm/kg*m)	.432 ± .112	.560 ± .110	.236 ± .076	.528 ± .146[b]

Heel rise occurs earlier in stance with increased walking speed

[1]Elisa S. Schrank, [1]Lakisha Guinn and [1]Steven J. Stanhope

[1]University of Delaware, Delaware, DE, USA
email: schranke@udel.edu, web: http://www.udel.edu

INTRODUCTION

During typical walking, heel rise (HR) from foot flat has been suggested as a powerful contributor to minimizing the vertical displacement of the center of mass when it is at its lowest, possibly improving energy efficiency [1]. HR has also been associated with increasing energy efficiency by decreasing the ground reaction force moment arm during push off. The extension of the metatarsophalangeal joints and pronation of the subtalar joint in late stance decreases the GRF moment arm around the talocrural joint, thereby increasing the moment arm of the ankle plantar flexor muscles and reducing the load on the musculoskeletal system [2]. These studies demonstrate the importance of HR but to do not provide an understanding of the mechanisms for generating HR. Understanding the mechanisms of HR and the changes with walking speed could be helpful in prescribing prosthetics and orthotics to improve walking speed in impaired populations. Therefore, the purpose of this study was to investigate changes in the timing of HR and the concomitant magnitudes of foot center of pressure, ankle angle, and ankle moment.

METHODS

Eleven unimpaired subjects (height: 1.72 ± 0.08 m, weight: 75.34 ± 21.76 kg, age: 24.2 ± 2.9 years, 6 females) walked at four scaled (by body height, BH) speeds, selected in a random order. A six camera motion capture system (Motion Analysis Corp, Santa Rosa, CA) and four imbedded force plates (AMTI, Inc, Watertown, MA) were used to collect kinematic and kinetic data at 120 Hz and 360 Hz, respectively. A 6 degree of freedom marker set was used to track motion of the lower limbs. For all subjects, at least three trials with good force plate contact (only one entire foot on a force plate at a time) and within ± 0.02 BH/s of each target walking speed (0.4, 0.6, 0.8, and 1.0 BH/s) were analyzed for each limb. Inverse dynamics analyses were performed using Visual3D software (C-motion, Inc, Germantown, MD). HR was defined as when the foot-to-floor angle increased by 0.5° from its orientation at foot-flat. The center of pressure (COP) in the modified foot coordinate system was normalized by foot length and the ankle moments by body weight and height. One way ANOVAs, with Bonferroni corrections for pairwise comparisons were used to evaluate significance ($p \leq 0.05$).

RESULTS AND DISCUSSION

HR occurred at an earlier percent of the stance phase of the gait with increased walking speed for all comparisons between 0.4 BH/s, 0.6 BH/s and 0.8 BH/s ($p<0.005$), but the change in percent stance was not significant between the two fastest speeds. The location of the COP at HR remained constant across all speeds; there were no significant differences between COP locations at HR across all speed except between the slowest and fastest speeds ($p<0.002$) (**Figure 1**). Though there was a significant difference in COP between the slowest and fastest speeds, the magnitude of the average change in COP from the slowest to fastest speed was small, less than 7mm. These results indicate that the COP moved out faster along the longitudinal foot axis with increased walking speed and HR appeared to occur at a threshold COP position.

The ankle angle at HR decreased with increasing walking speed (**Figure 2**). The second rocker of gait is often defined as beginning at foot-flat and ending with HR. This data suggests that with increasing walking speed, the length of the second rocker phase decreased. The ankle moments at HR also decreased with increasing walking speed for all comparisons between 0.4 BH/s, 0.6 BH/s, and 0.8

BH/s ($p<0.005$), but the difference was not significant between the two fastest speeds.

Chen et al. (2012) used finite element analysis to investigate movements of the ankle and foot with variations of force generated by the gastrocnemius-soleus muscle complex [3]. Chen and colleagues reported that changing the load on the Achilles changed the foot geometry and with decreased muscle force, ankle dorsiflexion increased and the metatarsophalangeal joint extension decreased. Those findings are consistent with the decrease in peak ankle dorsiflexion and increase in the angle of peak plantar flexion at toe off with increased speed in this study.

CONCLUSIONS

While HR occurs earlier as a percent of stance with increased walking speed, there appears to be a positional threshold of the COP location along the longitudinal axis of the foot at which HR occurs during gait across various walking velocities. In this study, the ankle angles and moments at HR decreased with increased walking speed. Future studies are needed to determine if these changes are beneficial to increasing walking speed or are a result of gait being more dynamic with increased speed.

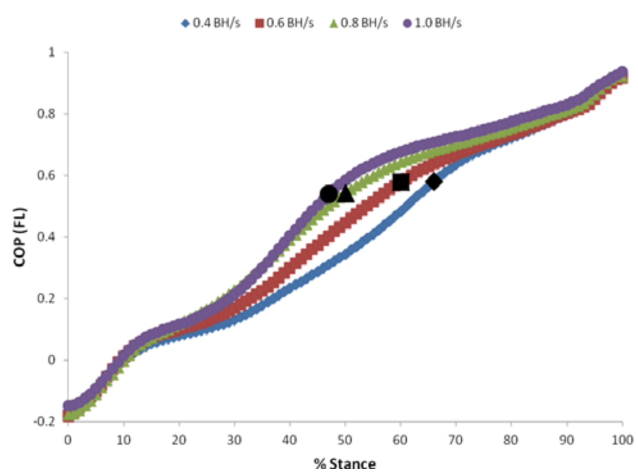

Figure 1: Center of pressure (normalized by foot length) along the longitudinal axis of the foot during stance at four walking speeds. Each shape in black indicates heel rise.

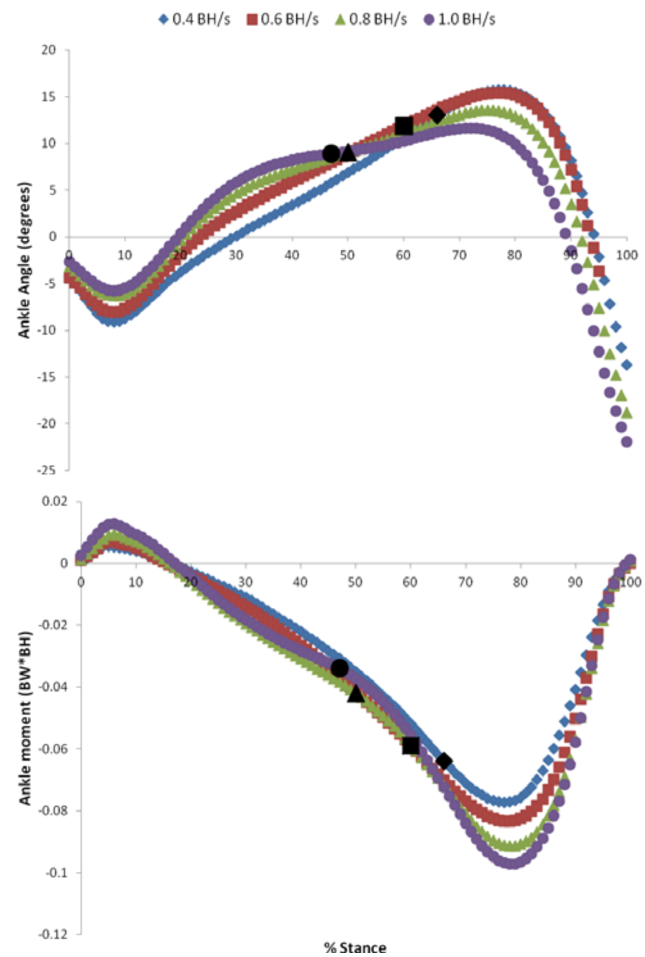

Figure 2: Ankle angle (Top) and moment (Bottom) during stance at four walking speeds. Each shape in black indicates heel rise.

REFERENCES

1. Kerrigan DC, et al. *Arch Phys Med Rehabil* **81**, 1077-1080, 2000.
2. Boonpratatong A and Ren L. *J Bionic Engineer* **7**, 211-218, 2010.
3. Chen WM, et al. *J Biomechanics* **45**, 1783-1789, 2012.

Ankle dynamics of walking at varying velocities and inclines

Arick Auyang[1], Alena M. Grabowski[1,2]
[1]Locomotion Lab, Dept. of Integrative Physiology, University of Colorado Boulder, CO, USA
[2]Eastern Colorado Healthcare System, Department of Veterans Affairs, Denver, CO USA
Email: arick.auyang@gmail.com

INTRODUCTION

Advances in prosthetic materials, design, and technology have enabled persons with lower-extremity amputations to return to a more functional lifestyle [1]; today's prostheses more closely resemble normative biomechanical function during locomotion. Much of the previous research on human locomotion and on new powered ankle-foot prosthetic design has been focused on traversing level surfaces [1]. While this may account for the majority of terrain encountered daily, the ability to vary velocity and traverse terrain is equally important to return people with lower-extremity amputations to full function.

Walking up or down slopes requires significant changes in the mechanical work absorbed and produced by the leading and trailing legs, respectively, during step to step transitions. The leading leg increases absorption of net negative work during downhill walking, while the trailing leg increases production of net positive mechanical work during uphill walking [2]. The ankle produces approximately 80% of the mechanical power required for walking on level ground [3]. Thus, during walking on sloped terrain, the changes observed in the mechanical work of each leg during step to step transitions are likely dependent on the ability of the ankle to absorb or produce work.

Current advanced powered ankle-foot prostheses are based on biological ankle work, specifically the relationship between ankle angle and moment during level-ground walking [1, 4, 5]. The aim of this study was to quantify the biological ankle work in non-amputee subjects across a range of velocities and slopes. We hypothesized that the ankle would produce more net positive work as subjects walked at faster velocities and up steeper slopes.

METHODS

Fifteen healthy subjects (9 M, 6 F) walked on a dual-belt force-measuring treadmill (Bertec Corp., Columbus, OH) at three velocities (1.0, 1.25, and 1.5 m/s) and 7 slopes (0^o, +/-3^o, +/-6^o, and +/-9^o), a total of 21 conditions.

Each trial was thirty seconds long and trial order was randomized. We simultaneously collected ground reaction forces at 1500Hz from each leg and lower limb kinematics using a modified Cleveland Clinic cluster marker set and a high speed motion capture system at 100Hz (Vicon Motion Systems, Centennial, CO).

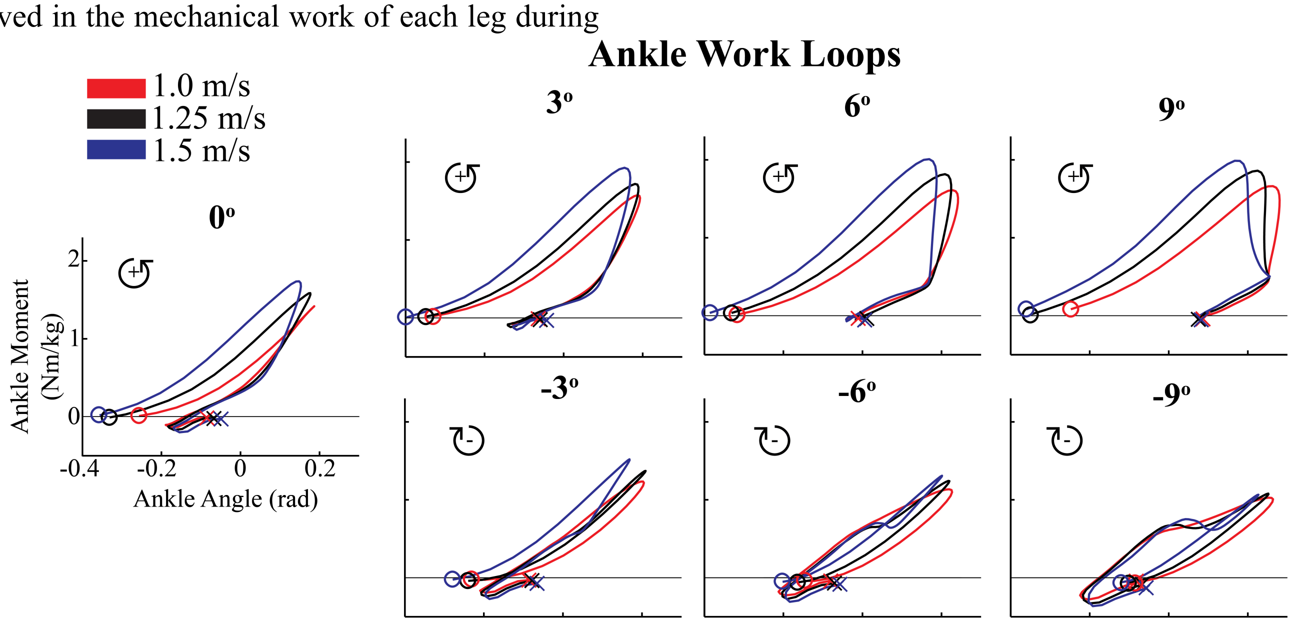

Fig. 1. Ankle work loops defined as ankle moment as a function of ankle angle for -9^o to 9^o for 1.0 m/s (red), 1.25 m/s (black), and 1.5 m/s (blue) from foot strike (X) to toe off (O). Net positive work is represented by the area within the curve when the work loop is in

the counter-clockwise direction while net negative work is represented by the area within the curve when the work loop is in the clockwise direction.

We used inverse dynamics to calculate ankle moments and powers (Visual3D, Germantown, MD). We filtered the data using a low-pass fourth order Butterworth filter with a 20Hz cutoff for force data and 10Hz cutoff for marker data. We calculated ankle work using a custom code (Matlab, Natick, MA). Net ankle work was defined as the integral of ankle power with respect to time over the stance phase. We normalized forces, joint moments, and work to each subject's body mass.

RESULTS

We found that from 0^o to 9^o, net positive ankle work increased with velocity and slope. From -3^o to -9^o, we found that net negative ankle work increased with slower velocities and decreasing slopes (**Fig. 1, Table 1**). Net ankle work at all slopes and speeds were statistically different from each other except for -6^o and -9^o at 1m/s and -6^o and -3^o 1.25m/s ($p<0.05$).

We found that ankle range of motion increased with velocity and slope between -3^o to 9^o and decreased with faster velocities at -6^o and -9^o (**Table 1**). Peak ankle plantarflexion moment increased with both velocity and slope from -9^o to 9^o (**Table 1**).

DISCUSSION

In this study, we provide data for ankle work loops during walking at different velocities and slopes. As hypothesized, we found that net positive ankle work increased with velocity and slope from 0^o to 9^o. We also found that there was greater net negative ankle work at slower velocities and decreasing slopes from -3^o to -9^o. Both ankle range of motion and peak plantarflexion moment changed significantly with velocity and slope.

Data from level-ground walking is important, but not sufficient for the design of fully functional biomimetic lower-extremity prostheses. Consideration of the biological ankle range of motion, torque, and net work during walking at different velocities and slopes is paramount for designing effective, versatile lowered-extremity powered prostheses.

REFERENCES

1. Herr, H.M. and A.M. Grabowski. (2012). Proc Biol Sci, **279**(1728).
2. Franz, J.R., N.E. Lyddon, and R. Kram. (2012). J Biomech, **45**(2).
3. Winter, D.A. (1983). Clin Orthop Relat Res, (175).
4. Au, S.K. and H.M. Herr. (2008). Ieee Robotics & Automation Magazine, **15**(3).
5. Au, S.K., J. Weber, and H. Herr. (2009). Ieee Transactions on Robotics, **25**(1).

Acknowledgements

This work is supported by a VA Career Development Award (VA RR&D A7972-W) to A.M.G.

Net Work (J/kg)	-9^o	-6^o	-3^o	0^o	3^o	6^o	9^o
1.00 m/s	-0.195 (0.081)	-0.160 (0.052)	-0.097 (0.048)	0.028 (0.059)	0.196 (0.061)	0.273 (0.079)	0.363 (0.066)
1.25 m/s	-0.158 (0.080)	-0.107 (0.069)	-0.049 (0.063)	0.124 (0.046)	0.249 (0.040)	0.378 (0.055)	0.468 (0.077)
1.50 m/s	-0.111 (0.063)	-0.046 (0.069)	-0.052 (0.049)	0.226 (0.045)	0.368 (0.053)	0.462 (0.110)	0.543 (0.083)
Range of Motion (rad)	-9^o	-6^o	-3^o	0^o	3^o	6^o	9^o
1.00 m/s	0.500 (0.007)	0.466 (0.013)	0.482 (0.032)	0.519 (0.051)	0.567 (0.050)	0.597 (0.052)	0.634 (0.041)
1.25 m/s	0.486 (0.004)	0.461 (0.008)	0.507 (0.051)	0.557 (0.042)	0.597 (0.037)	0.626 (0.036)	0.672 (0.026)
1.50 m/s	0.443 (0.006)	0.454 (0.014)	0.511 (0.039)	0.565 (0.039)	0.607 (0.035)	0.649 (0.034)	0.702 (0.037)
Peak Moment (Nm/kg)	-9^o	-6^o	-3^o	0^o	3^o	6^o	9^o
1.00 m/s	1.04 (0.218)	1.15 (0.229)	1.25 (0.178)	1.43 (0.149)	1.59 (0.223)	1.63 (0.261)	1.69 (0.310)
1.25 m/s	1.11 (0.237)	1.27 (0.238)	1.39 (0.213)	1.60 (0.174)	1.73 (0.230)	1.83 (0.294)	1.89 (0.347)
1.50 m/s	1.11 (0.237)	1.33 (0.235)	1.53 (0.236)	1.76 (0.200)	1.94 (0.268)	2.02 (0.333)	2.02 (0.392)

Table 1. Mean (±S.D.) net ankle work, ankle range of motion, and peak ankle plantarflexion moment over the stance phase for 1.0 m/s, 1.25 m/s, and 1.5 m/s from -9 ^{o} to 9^{o}.

THE COST OF BEING STABLE: A QUANTITATIVE APPROACH TO EXAMINE TRADE-OFF BETWEEN EFFORT AND STABILITY

[1]M. Hongchul Sohn and [1,2]Lena H. Ting

[1]Georgia Institute of Technology, Atlanta, GA, USA
[2]Emory University, Atlanta, GA, USA
email: lting@emory.edu

INTRODUCTION

It is likely that viable motor solution for unstable tasks reflects a trade-off between *efficiency* and *stability*. Minimizing muscular effort (e.g. sum-squared activation) has been widely accepted as an optimizing criterion for predicting muscle patterns in musculoskeletal models and simulations [1], but may conflict with maintaining stability. For example, subjects increase muscle co-activation, when reaching in a dynamically unstable environment, increasing arm stiffness at the cost of muscular effort [2]. However, little is known about whether effort and stability reflect a true trade-off.

One reason may be that we lack neuromechanical principles to guide selection of muscle activation patterns based on stability. Through the selection of muscle activation patterns producing equivalent motor output, local stability of a musculoskeletal system can be tuned [3]. The linearized dynamics conferred by the active stiffness and viscosity of muscles and the rigid-body mechanics can be quantified by the eigenvalues of the system. For example, during perturbed balance control in cats, the limb is relatively stable (joint angle deviations <5°) during the initial ~100 ms following perturbation, where the dynamics is due only to the relatively low, tonic background muscle activity [4]. However, the minimum-effort solution for a generating a stance-like force vector in a cat hindlimb model yielded unstable limb dynamics [5].

Here, we developed a search algorithm to explore the relationship between effort and stability in the musculoskeletal system. As a proof of concept, we performed the search in muscle activation space using a cat hindlimb model producing an extensor force, in three different cases: **i)** starting with the minimum-effort solution and searching for muscle activation patterns to improve the local stability of the limb, and starting with the maximum-effort solution and searching for muscle activation pattern to **ii)** improve or **iii)** reduce the stability of the limb.

METHODS

We used a highly redundant cat hindlimb model [3] with 7 degrees of freedom and 31 muscles. The model defines a linear mapping between a muscle activation vector ($\vec{e}$) and an endpoint force vector: $\mathbf{RF}_{AFL}\vec{e} = \mathbf{J}^{\mathrm{T}}\vec{\boldsymbol{F}}_{End}$ (**R**: moment arm matrix, $\mathbf{F}_{AFL}$: muscle scaling factors for active force generation, **J**: geometric Jacobian). The model posture was matched to an experimentally-measured posture, and measured extensor force [6] was used as the target endpoint force vector ($\vec{\boldsymbol{F}}_{End}$).

We defined the metric for effort ($\boldsymbol{E}$) to be the sum of squared activations: $\boldsymbol{E} = \sum e_m^2$, m=1~31. We identified the minimum-effort solution ($\vec{e}^{MIN}$) and maximum-effort solution ($\vec{e}^{MAX}$) where the cost $\boldsymbol{E}$ was either minimized or maximized. All costs examined in this study were normalized to that of the maximum, i.e., $\boldsymbol{E}$ of $\vec{e}^{MAX}$ is 100%.

We defined the metric for stability ($\boldsymbol{S}$) as the maximum real part of the eigenvalues (λ) obtained from the linearized system of the full nonlinear equations of motion. The system was linearized about an equilibrium point of constant extensor force generation, using Neuromechanic software [7]. A muscle activation pattern was determined unstable if $\boldsymbol{S}$>0 (Fig.1A, shaded).

We formulated a simple heuristic search to drive $\vec{e}^{MIN}$ and $\vec{e}^{MAX}$ towards specified direction in terms of $\boldsymbol{E}$ and $\boldsymbol{S}$: **i)** $\Delta\boldsymbol{E}$>0 & $\Delta\boldsymbol{S}$<0 (cost↑, stability↑) for $\vec{e}^{MIN}$; **ii)** $\Delta\boldsymbol{E}$<0 & $\Delta\boldsymbol{S}$<0 (cost↓, stability↑) and **iii)** $\Delta\boldsymbol{E}$<0 & $\Delta\boldsymbol{S}$>0 (cost↓, stability↓) for $\vec{e}^{MAX}$. The search algorithm progressed as below:

① Perturb activation of each muscle (m=1~31) individually by Δe_m=1% of its feasible range [8]
② Project each perturbed muscle activation patterns to the solution manifold for the extensor force
③ Evaluate $\Delta\boldsymbol{E}$ and $\Delta\boldsymbol{S}$ of the projected solutions individually
④ For muscles satisfying changes of $\boldsymbol{E}$ and $\boldsymbol{S}$ for **i)**, **ii)** or **iii)**, change e_m by 2% feasible range
⑤ Project combined changes to the solution manifold, and iterate from beginning (100 times)

RESULTS AND DISCUSSION

All three cases converged to a local minimum, and revealed a reciprocal but non-monotonic relationship between $\boldsymbol{E}$ and $\boldsymbol{S}$ (Fig.1).

i) $\vec{e}^{MIN}$ was unstable ($\boldsymbol{E}$=0.77%, $\boldsymbol{S}$=18.8; Fig.1, blue circle) and converged to a stable solution ($\boldsymbol{E}$=25.1%, $\boldsymbol{S}$=-3.26; Fig.1, blue ×). When the solution first became stable, only a 1.2% increase in effort was required (Fig.1, blue dotted circle: $\boldsymbol{E}$=1.93%, $\boldsymbol{S}$=-0.14) with only small changes in muscle activity (Fig 2A).

ii) $\vec{e}^{MAX}$ was stable but costly ($\boldsymbol{E}$=100%, $\boldsymbol{S}$=-2.25; Fig.1, black circle) and could become more efficient and more stable ($\boldsymbol{E}$=32.5%, $\boldsymbol{S}$=-3.45; Fig.1, black ×), ending with similar level of effort and stability as in **i)**, but with a different muscle activation pattern (Fig.2B).

iii) $\vec{e}^{MAX}$ could be driven to be unstable, but converged on a solution ($\boldsymbol{E}$=21.6%, $\boldsymbol{S}$=14.2; Fig.1, red ×) much more costly than $\vec{e}^{MIN}$.

Our result shows that a stable solution can be very close to the unstable minimum-effort solution. Moreover, existence of many local minima suggest that there could be multiple stable solutions that are near-minimum. Considering the stability conferred by active muscle properties may explain the deviations of optimal predictions from experimental data, and may also improve the stability of musculoskeletal simulations [9].

Further exploration of the solution space illustrated (not shown) a bumpy landscape; one implication is that pathological motor patterns with increased stability may be difficult to reduce effort through adaptation because of many local minima.

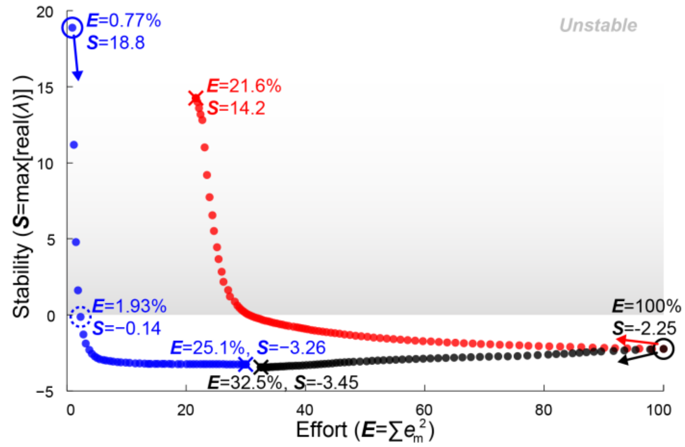

Figure 1: Heuristic search starting from **i)** $\vec{e}^{MIN}$ for more effort and more stability (blue); from $\vec{e}^{MAX}$ for **ii)** less effort and more stability (black), or **iii)** less effort and less stability (red).

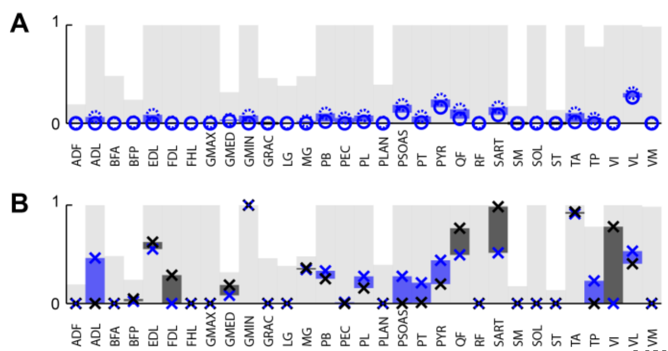

Figure 2: (**A**) Muscle activation patterns for $\vec{e}^{MIN}$ (circle) and the first stable solution (dotted circle); (**B**) converged solutions for case **i)** (blue ×) and **ii)** (black ×). Differences between the two solutions are filled with colors. Gray shaded area represents the total feasible range of activation in each muscle.

REFERENCES

[1] Erdemir A, et al. *Clin Biomech* **22**, 131-154, 2007.
[2] Franklin DW, et al. *J Neurophysiol* **90**, 3270-3282, 2003.
[3] Bunderson NE, et al. *J Biomech* **41**, 1537-1544, 2008.
[4] Jacobs R, Macpherson JM. *J Neurophysiol* **76**, 2402-2411 1996.
[5] Bunderson NE, et al. *J Exp Biol* **213**, 2131-2141, 2010.
[6] Torres-Oviedo G, et al. *J Neurophysiol* **96**, 1530-1546, 2006.
[7] Bunderson NE, et al. *Int J Numer Method Biomed Eng* **28**, 1015-1027, 2012.
[8] Sohn MH, et al. *J Biomech*, 2013 (accepted).
[9] Ting LH, et al. *Int J Numer Method Biomed Eng* **28**, 1003-1014, 2012.

ACKNOWLEDGEMENTS

NIH HD 46922

THE TEMPORAL STRUCTURE OF CENTER OF PRESSURE DURING STANDING IS AFFECTED BY PROPRIOCEPTIVE INPUT

[1]Troy Rand, [1]Anastasia Kyvelidou, [1]Sara Myers

[1]Nebraska Biomechanics Core Facility, University of Nebraska at Omaha, Omaha, NE, USA
email: troyrand@gmail.com, web: nbcf.unomaha.edu

INTRODUCTION

A healthy biological system is characterized by a temporal structure that exhibits fractal properties and is highly complex [1, 2]. The model of optimal variability (Figure 1) describes the temporal structure of variability. Unhealthy systems demonstrate low complexity and can have either low predictability or high predictability. A system with low predictability is noisy and unstable, while a system with high predictability is too stiff and rigid. A healthy system is moderately predictable, demonstrates high complexity and contains a rich structure that can be described with mathematical chaos [1]. Aging and disease are associated with a change in the temporal structure of signals associated with various physiological processes [3], including gait alterations. Recent research in our laboratory has utilized auditory inputs to attempt to restore a healthy level of variability in individuals with compromised gait patterns. Our research has found that temporal structure of gait patterns can be driven through auditory inputs containing signals of varying complexity [4]. These gait patterns change in order to reflect the temporal structure of the music; when music was played with a random temporal sequencing, gait patterns became more random and less predictable, when music was played with a metronomic temporal sequencing then the gait patterns became very ordered and predictable. Currently there is no research that has investigated whether standing posture can be driven using proprioceptive signals with varying temporal structure in an attempt to restore a healthy variability.

The purpose of this research was to determine if applying proprioceptive input of varying temporal structures to a force platform would affect the temporal structure of the COP signal. It was hypothesized that the temporal structure of participants COP would be altered according to the structure of input that is applied. Furthermore, it is hypothesized that by organizing the conditions by predictability the results will exhibit an inverted-u relationship similar to what is seen in the model of optimal variability.

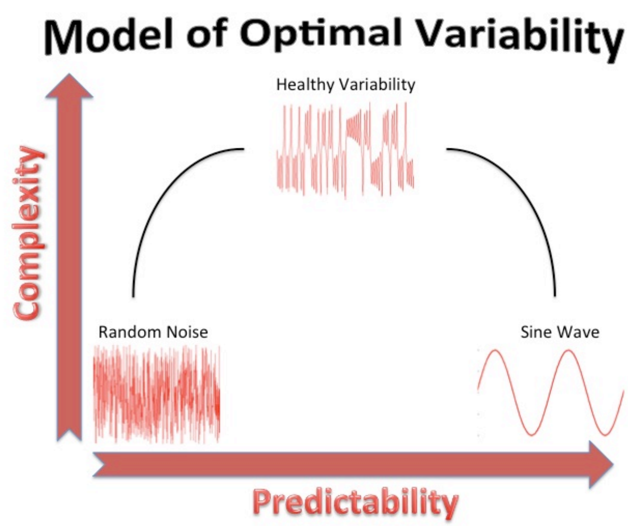

Figure 1: The model of optimal variability shows the temporal structure of variability. Healthy variability exhibits a rich structure and is moderately predictable.

METHODS

Eight healthy participants were screened and participated in this study. The Neurocom® Balance Manager™ System (Neurocom International Inc., Clackamas, OR; 100 Hz) was used to provide the proprioceptive input and record the COP data. The Neurocom force platform can be translated according to any input waveform. For this study there were five conditions; normal standing and four conditions with input waveforms of varying temporal structure (white noise, pink noise, brown noise, and sine wave). Each condition was recorded at 100Hz for one three-minute trial and down sampled to 10Hz for analysis. Detrended Fluctuation Analysis (DFA) was used to analyze the temporal structure of the COP signal. All analysis was performed using custom MATLAB software implementing the methods of Peng, et al. [5]. DFA analysis results in a scaling exponent α that quantifies the long-range correlations. A sine wave produces an alpha value of 0, uncorrelated white noise will produce an α-value of 0.5, pink noise produces an α-value of 1.0 and brown noise an α-value of 1.5. The output from the motor that was driving the platform was analyzed for all conditions and produced α-values of 0.003, 0.49, 1.1, and 1.6 respectively. A 1x5 ANOVA was used to compare the alpha values between the conditions and significance was set to $\alpha = 0.05$.

RESULTS AND DISCUSSION

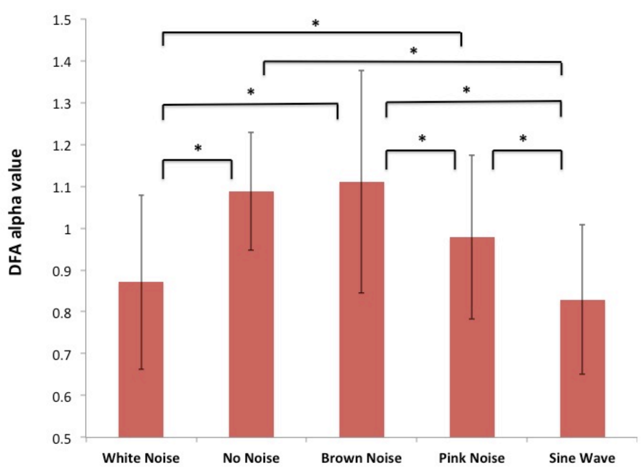

Figure 2: Mean and Standard Deviation of scaling exponent α. The white noise and sine wave conditions showed a significant difference when compared to the brown noise, pink noise and no noise conditions. There was also a significant difference between the pink noise and brown noise conditions.

By organizing the conditions with low predictability (white noise) on the left and high predictability (sine wave) on the right the results exhibit an inverted-u relationship similar to the model of optimal variability (Figures 1 and 2). Significant differences were found in the α-values when comparing both the sine wave and white noise conditions with the no noise, brown noise and pink noise conditions as well as when comparing the pink noise and brown noise conditions (Table 1). Despite large standard deviations for α-values across subjects, each subject exhibited an inverted-u pattern.

The current research is the first time proprioceptive inputs were applied through a force platform in a variety of temporal structures. Our findings suggest that individuals entrain to this input and alter their COP to match the input. This could lead to novel methods of training balance where the goal would be to restore the rich temporal structure of variability instead of trying to stand rigid or by applying a random white noise stimulus.

Conditions	p-value
White Noise vs. No Noise	0.002
White Noise vs. Brown Noise	0.001
White Noise vs. Pink Noise	0.024
Sine Wave vs. No Noise	< 0.000
Sine Wave vs. Brown Noise	0.001
Sine Wave vs. Pink Noise	0.021
Brown Noise vs. Pink Noise	0.024

Table 1: Significant findings showing the sine wave and white noise conditions significantly altered the temporal structure compared to the no noise, brown noise and white noise conditions. The brown noise and pink noise were also significantly different, however neither one was significantly different from the no noise condition.

CONCLUSIONS

Exploring the temporal structure of biological processes has provided many new insights into movement control. Because aging and disease are characterized by a degradation of this temporal structure it is important to investigate new ways to restore this highly complex structure. This study shows that complexity of standing posture can be improved using input with specific temporal structure. Further work will investigate if balance training using these proprioceptive inputs can restore lost complexity of standing posture.

REFERENCES

1. Stergiou, N., et al. *J Neurol Phys Ther,* **30**(3), 120-129, 2006.
2. Goldberger, A., et al. *Yale J Bio Med* **60**, 421-435, 1987.
3. Lipsitz, L., et al. *JAMA*, **267**(13), 1806-1809, 1992.
4. Kaipust, J., et al. *Ann Bio Med Eng,* **38**, 2012.
5. Peng, C., et al. *Chaos*, **5**(1), 82-87, 1995.

ORAL PRESENATIONS – SATURDAY SEPTEMBER 7th

	Low Back Pain *Erika Nelson-Wong, Nadia Azar*
1:15 PM	Modulation Of Trunk Kinematics In Response To Changing Task Constraints In Young Adults With A History Of Low Back Pain And Healthy Controls **Armour Smith J, Kulig K**
1:30 PM	Is Trunk Muscle Co-contraction Associated With Low Back Pain Development During Prolonged Sitting? **Schinkel-Ivy A, Nairn BC, Drake JDM**
1:45 PM	Female Lumbar Spine Kinematics During Coitus: Initial Recommendations For The Low Back Pain Patient **Sidorkewicz N, Cambridge E, McGill S**
2:00 PM	Lumbopelvic Control During Frontal Plane Motion And Hip Muscle Activation In Low Back Pain Cases Versus Controls **Nelson-Wong E, Bourgeois G, DeGrandis C, Hamilton N, Kirven I, Pieratt K, Thornton W**
2:15 PM	Variability Of Vertical Ground Reaction Forces In Adults With Chronic Low Back Pain, Before And After A Limited Protocol Of Chiropractic Care **Russell B, Geil M, Wu J, Hoiriis K**

MODULATION OF TRUNK KINEMATICS IN RESPONSE TO CHANGING TASK CONSTRAINTS IN YOUNG ADULTS WITH A HISTORY OF LOW BACK PAIN AND HEALTHY CONTROLS

[1]Jo Armour Smith, [1]Kornelia Kulig
[1]University of Southern California, Los Angeles, USA
email: joannesm@usc.edu, web: http://pt.usc.edu/joannesm/

INTRODUCTION

Skilled motor performance is associated with the ability to repeatedly achieve a task goal under varying task constraints. This is facilitated by an optimal level of variability in the coordination of degrees of freedom utilized by an individual. Inter-segmental trunk coordination variability during locomotion may be modulated by both mechanical and cognitive task constraints. Limited evidence suggests that these modulations may be different in response to altered cognitive but not mechanical demands in persons with a history of low back pain [1,2]. Overground locomotor perturbations such as ipsilateral walking turns (spin turns) have greater mechanical demand than steady-state locomotion and therefore may highlight subtle modulation in variability in young adults. The aims of this study were to investigate the effect of increased locomotor speed and divided attention on the amplitude of inter-segmental trunk coordination variability during spin turns in young adults, and to compare these adaptations between persons with a history of recurrent low back pain (RLBP) and healthy controls (CTRL).

METHODS

RLBP participants were required to have a greater than one-year history of episodic LBP and to be symptom free at the time of data collection.

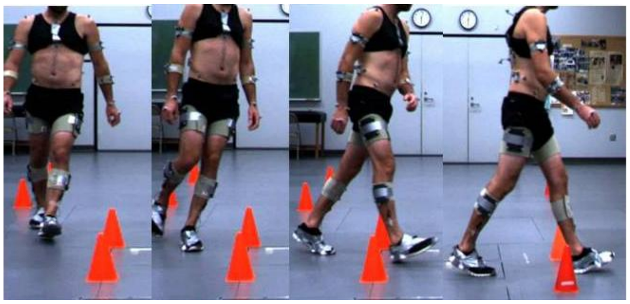

Figure 1: Stride cycle of spin turn to left

Motion capture markers on the greater trochanters, L5/S1 inter-spinous space, iliac crests and anterior superior iliac spines, and a rigid triad of makers on T3, were used to define a kinematic model for the pelvis and trunk respectively (200 Hz, Qualisys AB, Gothenburg, Sweden). Participants walked around a circuit that required them to make a 90-degree spin turn in a defined turning area on each lap of the circuit (Figure 1).

The verbal 2-back task was utilized for the divided attention condition. This task requires participants to listen to a string of digits and respond when they hear a digit that is the same as one presented 2 digits earlier. Participants performed multiple laps of the walking circuit under 3 conditions: self-selected speed (SELF); controlled speed (CONTR, 1.5m/s); and divided attention (ATT, 2-back task + controlled speed). Average locomotor speed was calculated using photo-electric triggers. During the ATT condition, subjects were instructed to prioritize the 2-back task. However, only ATT trials where average speed was maintained at 1.5m/s (± 5%) were retained for analysis. Number of errors on the 2-back task was quantified at baseline in relaxed standing and under the ATT condition.

The stride cycle and stance/swing phases of the turn were defined by footswitches and confirmed by the vertical and horizontal trajectory of heel markers. A minimum of 15 trials were analyzed for each condition and each stride cycle was time-normalized to 201 points. Trunk and pelvis angular displacement were calculated (Visual3D software, C-Motion Inc, MD, USA) and then the coordination between the trunk and the pelvis was quantified as the coupling angle using the vector coding approach. Coordination variability was defined as the angular deviation of the coupling angle for each time point across the repeated trials in each condition, and mean coordination variability was calculated across the time series [3].

RESULTS AND DISCUSSION

Eleven participants were recruited (RLBP n=6, CTRL n=5, mean age 26.3 (2.5) years). Participants with a history of RLBP reported an average of 4.9 (3.5) years of episodic pain. Self-selected locomotor speed was slower than the controlled locomotor speed in all subjects (SELF speed; RLBP 1.21(0.15) m/s; CTRL 1.23(0.08) m/s). Duration of the turn stride cycle in the CONTR condition compared with the SELF condition decreased by an average of 13.6% in the RLBP group and 17% in the CTRL group, confirming that participants modulated their turn speed during the CONTR trials (CONTR stride duration: RLBP 1.05(0.06) s, CTRL 1.00 (0.04) s). Average difference in stride cycle duration between the CONTR and ATT trials was below 5% for both groups. This indicates that the same mechanical conditions were maintained during the divided attention task. Average number of errors on the 2-back task was similar between groups and between the baseline and ATT conditions (baseline; RLBP 0.4 (0.2), CTRL 0.5 (0.2); ATT; RLBP 0.4 (0.3), CTRL 0.3 (0.2) errors per trial). This suggests that all subjects effectively prioritized the 2-back task during the ATT condition.

Average inter-segmental coordination variability increased 23.78% with increased turn speed during the stance phase of the CONTR turns compared with the SELF turns (Effect size (ES) 0.83). RLBP subjects had a slightly larger increase in variability than CTRLs (Figure 2). Variability also increased with increased speed in both groups during swing phase (31.4% increase, ES 0.64), although there was substantial inter-subject variation in the amplitude of the increase (RLBP 7.44 (13.12)º CTRL 6.78 (9.97)º). This increased coordination variability may enhance the ability to correct minor motor errors during the more rapid turn.

Under the divided attention condition, there was small decrease in inter-segmental coordination variability during stance phase in a majority of subjects. However, this difference was within the standard error of the measurement. During swing phase, all but one subject demonstrated decreased coordination variability (mean difference 23.81%, ES 1.43). There was a trend for the decrease in variability to be greater in RLBP participants than controls (RLBP –5.63(2.99)° CTRL – 4.18 (3.98)°, ES 0.42, Figure 3). The consistent modulation in response to the divided attention condition is suggestive of a more constrained locomotor strategy when cognitive load is increased.

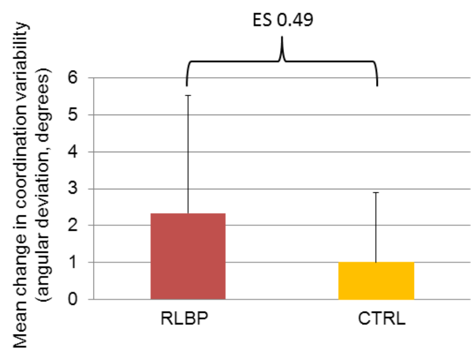

Figure 2: Increase in mean coordination variability with increased locomotor speed during stance phase (RLBP n=6, CTRL n=5)

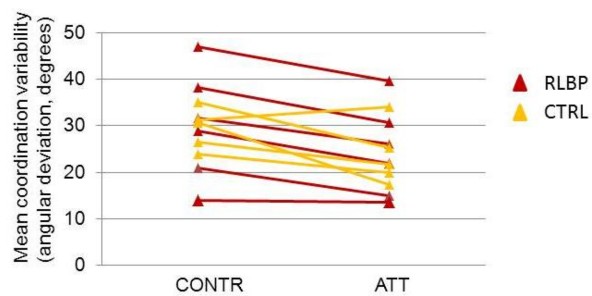

Figure 3: Change in mean coordination variability from CONTR to ATT condition (n=11)

CONCLUSIONS

The amplitude of trunk inter-segmental coordination variability in young adults is a function of both mechanical demand and cognitive control. In this small sample, there was a trend towards increased modulation in response to both constraints in the subjects with a history of RLBP, indicating adaptations in locomotor control in young subjects even when they are asymptomatic.

REFERENCES

1. Seay JF, et al. *Clin Biomech* **26**, 572-8, 2011.
2. Lamoth CJ, et al. *J NeuroEngineering Rehabil* **5,** 13, 2008.
3. Miller RH, et al. *J Biomech* **43**, 2254-2560, 2010.

IS TRUNK MUSCLE CO-CONTRACTION ASSOCIATED WITH LOW BACK PAIN DEVELOPMENT DURING PROLONGED SITTING?

Alison Schinkel-Ivy, Brian C. Nairn, & Janessa D.M. Drake*

York University, Toronto, ON, Canada
*email: jdrake@yorku.ca

INTRODUCTION

Various studies have demonstrated an association between low back pain (LBP) and prolonged sitting. Evidence has shown that altered muscle activation patterns are often observed in chronic-LBP patients, relative to healthy controls. For example, when trunk muscle activation levels are compared between chronic-LBP patients and healthy controls, patients tend to exhibit higher activation levels during slumped sitting [1]. In addition, differences in activation patterns can be found in asymptomatic individuals who develop transient LBP during prolonged static postures, compared to individuals who do not develop pain. During a two hour standing protocol, 'pain developers' (PD) have been characterized by higher flexor-extensor co-contraction levels, as well as higher co-contraction in the bilateral gluteus medius muscles [2]. However, no such analysis of localized co-contraction has yet been conducted for a prolonged sitting protocol. Therefore, the purpose of this study was to investigate whether co-contraction levels between various muscles in the trunk: a) differed between participants who did and did not develop back pain or b) changed over time during the course of a two hour prolonged sitting protocol.

METHODS

Ten university-aged males were recruited to participate in the present study. All participants were asymptomatic for back pain, and had not sought treatment or taken days off school or work due to LBP in the preceding year.

Electrodes were applied bilaterally over the rectus abdominis (RA), external oblique (EO), internal oblique (IO), upper- (UTES) and lower- (LTES) thoracic erector spinae, lumbar erector spinae (LES), latissimus dorsi (LD), and superficial lumbar multifidus (SLM). Three resisted back extension trials were performed to determine the maximum voluntary contraction (MVC); all subsequent EMG signals were normalized to this MVC value. Participants then underwent a two hour prolonged sitting protocol, during which time they read selected passages on a computer screen while seated a standard office workstation. Prior to beginning the protocol, and every 15 minutes throughout, each participant completed a 100-mm Visual Analog Scale (VAS) to document pain in the back. Participants who experienced an increase in VAS of greater than and less than 12 mm were considered pain developers (PD; *n*=4) and non-pain developers (NPD; *n*=6), respectively [3].

Co-contraction indices (CCI) were calculated for all possible pairings of muscles (120 in total) for each minute of data, using a custom program written in Matlab v.R2012a. For each pairing, the CCI values for each 15-minute interval were averaged, yielding eight CCI values for each pairing [2]. CCI values were compared between pain groups and over time, and were correlated to the VAS scores.

RESULTS AND DISCUSSION

Of the 120 muscle pairings, 43 displayed a main effect of pain group, in that pain developers experienced higher co-contraction levels than the non-pain developers (Figure 1). Two pairings (LIO-LLD, REO-RSLM) displayed a main effect of time, in that CCI values were greater in the later time intervals. Finally, interaction effects between pain group and time were observed for six pairings (LLD-RRA, LLD-RUTES, LSLM-REO, LSLM-RLES, RLD-RLES, RLES-RSLM), in that co-contraction was higher in the PD group, and tended to increase over time for that group; whereas the

NPD CCIs tended to remain consistent. The CCI values for 35 of the muscle pairings were significantly correlated to the VAS scores, with the strongest correlations observed for 11 muscle pairings containing either LLES or LSLM (*r* values ranging from 0.410 – 0.605) (Table 1).

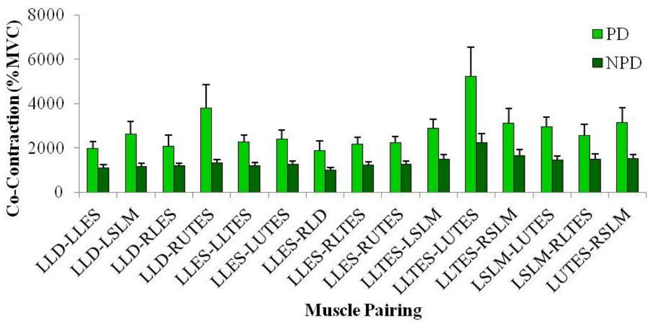

Figure 1: Main effect of pain group on mean (SEM) co-contraction (%MVC), for the back-back muscle pairings. All between-group comparisons were significant ($p<0.05$).

Overall, the results of the present study indicated that PDs exhibited greater co-contraction than NPDs, and that co-contraction increased over time during a prolonged sitting protocol. Higher activation in PD participants agreed well with past literature [2,4]. Activation levels tend to remain higher in LBP patients relative to asymptomatic individuals during slumped sitting [1]. It is thought that this impaired neuromuscular control may be a mechanism employed in an attempt to protect the passive elements of the spine [5]; this may have also been employed by the PD participants in the present study, thereby contributing to their higher co-contraction levels.

Table 1: Muscle pairings that were significantly, moderately correlated with the VAS scores ($p<0.05$).

CCI Pairing	Correlation Coefficient
LEO-LLES	0.523
LEO-LSLM	0.411
LIO-LLES	0.543
LIO-LSLM	0.438
LLES-LRA	0.415
LLES-REO	0.605
LLES-LSLM	0.529
LLES-RLES	0.446
LLES-RSLM	0.489
LSLM-RLES	0.414
LSLM-RSLM	0.410

Moderate correlations were observed between the VAS scores and CCI muscle pairings involving LLES or LSLM. This may indicate that during prolonged sitting, the activation patterns of the lower musculature play a more substantial role in transient LBP than the upper musculature. As the demands of this task are predominantly postural, the greater co-contraction levels of the abdominal and low back musculature may exacerbate the influence of those muscles in transient LBP development.

While past literature has suggested that co-contraction predisposes to LBP development [2], the present data are more indicative of a circular relationship between co-contraction and pain development. High co-contraction may contribute to LBP development, following which co-contraction is increased in an attempt to alleviate pain and reduce tissue stresses, and the cycle is repeated. Over time, this cycle may result in progression to chronic-LBP or mechanical injury.

CONCLUSIONS

In conclusion, differences in co-contraction were observed between pain groups and over time during prolonged sitting; PD participants demonstrated greater co-contraction levels, and co-contraction tended to increase over time. These data indicated that the relationship between co-contraction and pain development may in fact be circular; further work will be required to confirm these trends. Determining the direction of this relationship will facilitate the development of interventions to prevent or minimize the progression of pain over a prolonged static office-type sitting exposure.

REFERENCES

1. Dankaerts W, et al. *Spine* **31**, 2017-23, 2006.
2. Nelson-Wong E, Callaghan JP. *J Electromyogr Kinesiol* **20**, 256-63, 2010.
3. Kelly AM. *Acad Emerg Med* **5**, 1086-90, 1998.
4. Van Dieen JH, et al. *J Electromyogr Kinesiol* **13**, 333-51, 2003.
5. Colloca CJ, Hinrichs RN. *J Manipulative Physiol Ther* **28**, 623-31, 2005.

ACKNOWLEDGEMENTS

Natural Science and Engineering Council of Canada (NSERC) for funding; Dr. Diana DeCarvalho for assistance with MatLab programming.

FEMALE LUMBAR SPINE KINEMATICS DURING COITUS: INITIAL RECOMMENDATIONS FOR THE LOW BACK PAIN PATIENT

[1]Natalie Sidorkewicz, [1]Edward D J Cambridge, [1]Stuart M McGill

[1]University of Waterloo, Waterloo, ON, CAN
email: nsidorke@uwaterloo.ca, web: Spine Biomechanics Laboratory

INTRODUCTION

Qualitative studies investigating the sexual activity of people with low back pain (LBP) found a substantial reduction in the frequency of coitus [1]. Pain during coitus has been linked to mechanical factors, such as movements and postures, which are reported as the primary reason for this decreased frequency [2]. Despite these implications, a biomechanical analysis of coitus, to date, has not been conducted [3]. The main objective of this study was to describe female lumbar spine motion during coitus and compare this motion across five common coital positions.

METHODS

Ten healthy females (29.8 ± 8.0 years, 164.9 ± 3.0 centimeters, 64.2 ± 7.2 kilograms) and ten healthy males participated in this study. These couples had approximately 4.7 ± 3.9 years of sexual experience with each other. Each couple engaged in coitus in five pre-selected positions (presented in random order) for 20 seconds per position. Three-dimensional (3D) lumbar spine kinematic data was continuously collected for the duration of each trial by an electromagnetic motion capture system. The five coital positions chosen were as follows: fQUAD1 – female quadruped with elbow support, male kneeling behind; fQUAD2 – female quadruped with hand support, male kneeling behind; fMISS1 – female supine with minimal hip or knee flexion, male prone on top; fMISS2 – female supine with hip and knee flexion, male prone on top; and fSIDE – female side-lying, male side-lying behind.

The spine kinematic profile across all coital positions was found to be primarily sagittal plane movement (i.e., flexion/extension), cyclic in nature, but variable over time, so the amplitude probability distribution function (APDF) of female lumbar spine kinematics in the sagittal plane, expressed as percentages of lumbar spine active range of flexion and extension motion (% aROM), was deemed the most appropriate analysis tool to compare coital motion across all positions. To determine if each coital position had distinct spine kinematic profiles, separate univariate general linear models (GLM) (factor: coital position = five levels, α=0.05) followed by Tukey's Honestly Significant Difference (HSD) post hoc analysis were used on amplitude probabilities of 0.0, 0.5, and 1.0.

RESULTS AND DISCUSSION

In comparison to all other coital positions, fMISS2 values at amplitude probabilities of 0.0, 0.5, and 1.0 were lowest, followed by fMISS1, fQUAD1, fSIDE, and fQUAD2 (Table 1 and Fig. 1).

Table 1: Female lumbar spine angular displacements (% aROM) at amplitude probabilities of 0.0, 0.5, and 1.0 for all coital positions.

Amplitude Probability	*Lumbar Spine Angular Displacement (% aROM) by Position*				
	fQUAD1	fQUAD2	fMISS1	fMISS2	fSIDE
0.0	-21.97 ± 34.51	9.00 ± 41.62	-49.81 ± 19.90	-65.55 ± 17.75	-4.43 ± 34.83
0.5	14.35 ± 40.76	52.40 ± 44.45	-28.16 ± 13.04	-50.70 ± 16.13	26.65 ± 35.97
1.0	49.00 ± 41.95	77.00 ± 45.17	-2.50 ± 25.45	-28.89 ± 14.53	48.00 ± 34.50

Note: A negative value represents spine flexion and a position value represents spine extension.

Significant differences were found at amplitude probabilities of 0.0 ($F(4,31)=12.602$, $p<.001$), 0.5 ($F(4,31)=19.805$, $p<.001$), and 1.0 ($F(4,31)=22.261$, $p<.001$). At all three amplitude probabilities, fMISS2 was significantly different from fQUAD1 ($p=.006$, $p<.001$, and $p<.001$, respectively), fQUAD2 (p<.001, p<.001, and p<.001, respectively), and fSIDE (p<.001, p<.001, and p<.001, respectively) and fMISS1 was significantly different from fQUAD2 (p=.001, p<.001, and p<.001, respectively) and fSIDE (p=.012, p=.004, and p=.008, respectively). fMISS1 was also significantly different from fQUAD1 at amplitude probabilities of 0.5 (p=.039) and 1.0 (p=.006). fQUAD1 was significantly different from fQUAD2 at an amplitude probability of 0.5 (p=.031).

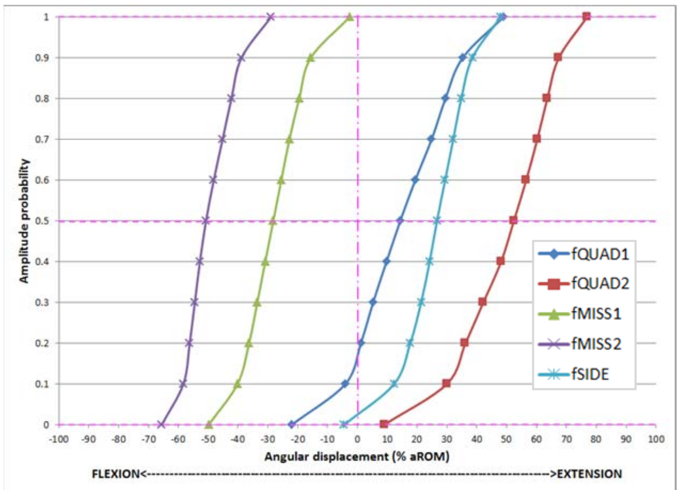

Figure 1: APDF results for female spine kinematics across all coital positions.

Note: The purple dashed horizontal lines indicate the amplitude probabilities at which statistical tests were performed (i.e., 0.0, 0.5, and 1.0). The purple dashed vertical line indicates zero lumbar spine angular displacement (i.e., a neutral spine position) – to the left of this line is lumbar spine flexion and to the right of this line is lumbar spine extension.

The results found in this biomechanical analysis of common coital positions may be useful in a clinical context. In particular, for the flexion-, extension-, and motion-intolerant patient [4], certain common coital positions should be avoided. For the flexion-intolerant female patient, both variations of fMISS should be avoided, especially fMISS2, as they were shown to elicit the most spine flexion. fQUAD2 and fSIDE are the more spine-sparing coital positions for the flexion-intolerant patient, followed by fQUAD1 (Fig. 2).

It should be noted that the coital positions were performed by participants that did not have a pre-existing disabling back or hip condition, so patients with a low back disorder may have different movement patterns during coitus. This study was intended to provide initial recommendations based on a biomechanical analysis in an area that has not previously been explored – this is a starting point for recommendations to evolve from further research on a back-pained population.

CONCLUSIONS

Thus, spine-sparing coitus appears to be possible for the flexion-, extension-, and motion-intolerant patient. Health care practitioners may recommend appropriate coital positions and coach coital movement patterns, such as hip-hinging, to spare the spine.

REFERENCES

1. Akbas NB, et al. *J Neurosurg Spine* **13**, 581-586, 2010.
2. Maigne J & Chatellier G. *Clin Orthop Relat Res* **385**, 82-87, 2001.
3. White AA & Panjabi MM. *Clinical biomechanics of the spine (2nd ed.)*, J.B. Lippincott Company, 1990.
4. McGill SM. *Low Back Disorders (2nd ed.)*, Human Kinetics, 2007.

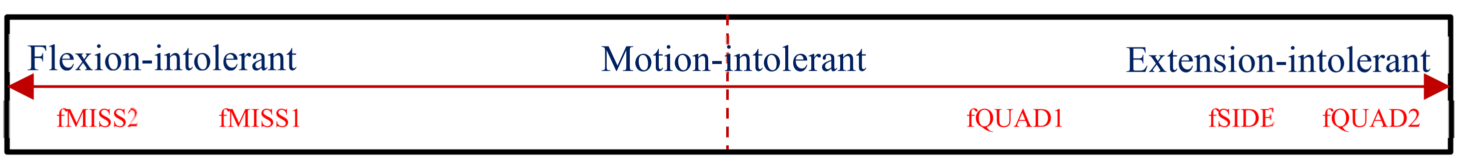

Figure 2: Initial recommendations for female coital positions to avoid (red text) for specific LBP-provoking movements (blue text).

Note: Motions, postures, and loads may exacerbate LBP. Only specific motions were analyzed in this study; therefore, recommendations can only be made for these specific motion intolerances (i.e., flexion-, extension-, and motion-intolerance [in the sagittal plane]) without consideration of spine loads.

LUMBOPELVIC CONTROL DURING FRONTAL PLANE MOTION AND HIP MUSCLE ACTIVATION IN LOW BACK PAIN CASES VERSUS CONTROLS

Erika Nelson-Wong, Greg Bourgeois, Chris DeGrandis, Nathan Hamilton, Ian Kirven, Kassidy Pieratt, and Wesley Thornton
Regis University, School of Physical Therapy, Denver, CO, USA
email: enelsonw@regis.edu

INTRODUCTION

Low back pain (LBP) is a widespread musculoskeletal problem. Diminished lumbopelvic control during frontal plane movement, clinically assessed through the Active Hip Abduction (AHAbd) test, has been proposed as a factor for examination of individuals with LBP [1]. Case-control studies have shown muscle activation timing differences between individuals with and without LBP during AHAbd, with cases having a predominant distal to proximal activation pattern [2]. The test has been shown to have a fairly high rate of false (+) scores, and a low rate of false (-) scores [2]. However AHAbd has also been shown to predict LBP development in asymptomatic individuals [3], therefore a (+) score may be indicative of increased LBP risk in control subjects. Excess hip flexion is one common compensatory motion for individuals with (+) scores on the AHAbd test. This study aimed to determine if hip abductor/hip flexor activation ratios differ between individuals with and without LBP, who have similar AHAbd test scores. It was also of interest to investigate muscle activation sequencing patterns among those with (+) and (-) test scores. It was hypothesized that individuals with (+) test scores would have lower hip muscle activation ratios, and a distal to proximal muscle activation sequencing pattern regardless of LBP status.

METHODS

43 participants (25 LBP cases, 19 male, 28.8 ± 10.5 yrs) volunteered for this study. Electromyography (EMG) was collected from 6 bilateral muscle groups (Internal/External Oblique, Lumbar Erector Spinae, Gluteus Medius, Gluteus Maximus and Rectus Femoris) during performance of the AHAbd Test. Test performance was simultaneously scored by 2 trained examiners. The test was conducted in sidelying and scored based on the ability of the participant to maintain frontal plane lumbopelvic control. Kinematic data were collected concurrently to create a 4-segment model (thorax, pelvis, bilateral thighs) using Visual3D software (C-Motion, Inc, Germantown, MD). Reference contractions were obtained for each muscle group and used to normalize EMG for the motion trials to %RVC. The mean muscle activation was calculated for the gluteus medius (GMed) and rectus femoris (RF) muscles during the active phase of movement (determined from kinematic data). A GMed to RF activation index (GRA) was calculated using Eq.1 [4].

Eq. 1: $$GRA = \left[\frac{meanGMed}{meanRF} * meanGMed\right]$$

Cross-correlation analyses were performed on the linear enveloped data to determine phase relationships (phase lag at peak correlation) between muscles. Data were entered into the cross-correlation equation such that a +ve phase lag indicated the first-listed muscle was activated first and a -ve phase lag indicated the first-listed muscle was activated second.

GRA and phase lag data were entered into *t*-tests for pairwise comparisons by (+) and (-) test score for each LBP group, with a significance criterion of $p < .05$. Accuracy diagnostic statistics for discrimination between case/control were also calculated from contingency tables.

RESULTS AND DISCUSSION

85% of LBP cases and 47% of controls scored (+) on the AHAbd Test, while 15% of cases and 53% of controls scored (-) on the test. Accuracy statistics (95% CI) were: Sn = .85 (.67-.94), Sp = .53 (.31-.74), OR = 6.2 (1.5-25.8).

Cases demonstrated a distal to proximal activation pattern during right AHAbd, activating right gluteus medius 0.024 ± 0.05 s prior to right internal oblique compared with controls who activated right internal oblique 0.037 ± 0.08 s prior to gluteus medius (*p* = .05). Interestingly, cases with (+) test scores showed a proximal-distal pattern while cases with (-) scores activated distal to proximally (*p* =.03). Controls demonstrated a proximal to distal sequence, regardless of AHAbd test score (Fig. 1).

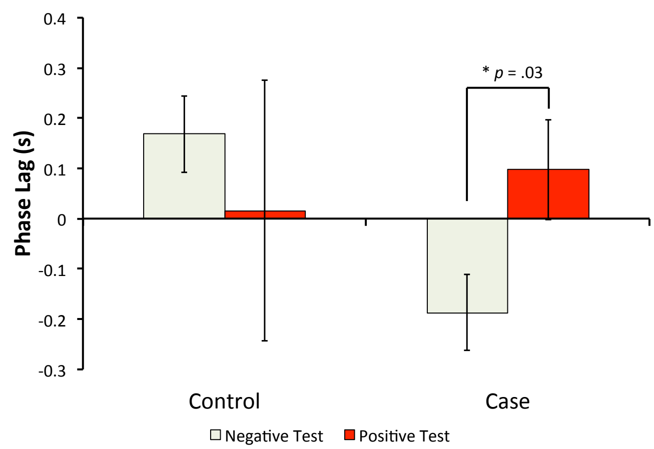

Fig. 1: Cases with (+) AHAbd tests demonstrated a reversal of the distal to proximal muscle sequencing usually seen on AHAbd in people with LBP for gluteus medius and internal oblique.

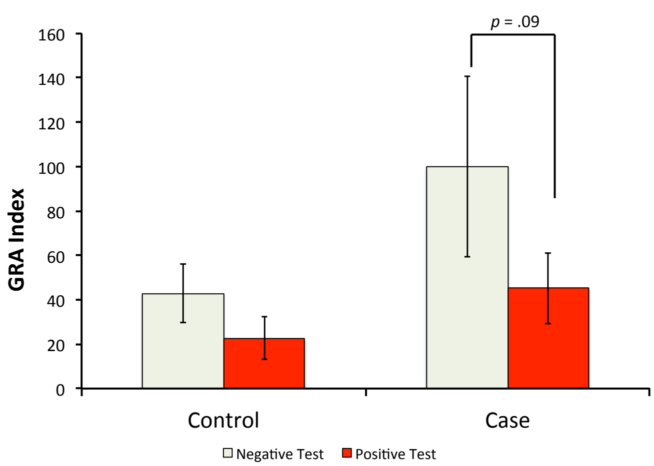

Fig 2: There was a non-significant trend for cases with (-) scores to activate GMed more than RF during the AHAbd test

There was a non-significant trend (p = .09) towards cases with (-) test scores to utilize a higher GMed to RF ratio during AHAbd compared to cases with (+) test scores (Fig. 2).

CONCLUSIONS

The AHAbd test performed well in discriminating between cases and controls in this sample with a relatively high diagnostic odds ratio. Sensitivity was moderately high, while specificity was only fair, indicating that the test does have a tendency towards false positives.

It was interesting that while cases typically exhibit a distal-proximal muscle activation sequence [2], those with positive tests demonstrated the opposite. It is possible that these individuals attempted to maintain lumbopelvic control, although unsuccessfully, by pre-emptively bracing with their abdominal musculature.

There was a trend towards higher GRAs in cases with (-) compared to (+) test scores. Due to common compensatory movement strategies observed in (+) tests, we expected individuals with (+) tests to have lower GRAs, as this would indicate lower GMed and higher RF activation. Data collection is ongoing as larger sample sizes are necessary for adequate statistical power, however these preliminary findings are promising. These findings could help guide specific interventions towards the hip musculature when the goal is to improve lumbopelvic control during frontal plane motions in patients with LBP.

REFERENCES

1. Delitto A, et al. J Orthop Sports Phys Ther 42, A1-A57, 2012.
2. Poupore K, et al. Combined Sections Meeting of the APTA, San Diego, CA, 2013
3. Nelson-Wong E, et al. J Electromyograph & Kinesiol 20, 256-263, 2010.
4. Selkowitz DM, et al. J Orthop Sports Phys Ther 43, 54-64, 2013.

ACKNOWLEDGEMENTS

Regis University Research and Scholarship Council

Variability of vertical ground reaction forces in adults with chronic low back pain, before and after a limited protocol of chiropractic care

[1]Brent da Silva Russell, [2]Mark D. Geil, [2]Jianhua Wu, [1]Kathryn T. Hoiriis
[1]Life University, Marietta, GA, USA
[2]Georgia State University, Atlanta, GA USA
email: brussell@life.edu, web: http://www.life.edu/academics/academics-engagelearn/engaged-osr

INTRODUCTION

Doctors of chiropractic (DCs) have an interest in gait and seem to generally believe that their care has a beneficial effect on gait. However, there has been little research as to whether the primary tool of the DC, "adjustment", or spinal manipulation (SM), has a beneficial effect on gait. This pilot study evaluated the effects of SM, hip joint manipulation and light mobilization and stretching on variability of selected aspects of gait in patients with chronic low back pain (LPB), a population that has previously been shown to have some altered aspects of gait as compared to asymptomatic individuals. It was expected that the chronic LBP participants would have greater pre-care variability than a group of controls, and would have decreased variability post-care. This report is concerned with information immediately pre- and post- for a single visit of care.

METHODS

Nine adult CLBP participants, with pain of at least 7 weeks, and 6 asymptomatic controls were recruited through e-mails to colleagues, and flyers posted at Georgia State University (GSU). Participants completed Quadruple Visual Analog Scale (QVAS) and Quebec Back Pain Disability Scale (QBPDS) questionnaires; CLBP participants were examined in a manner usual to a new chiropractic patient at the private office of the 4th investigator. Four CLBP participants lacking previous diagnostic imaging received x-ray evaluations at no cost to them.

Gait evaluation was done using a Zebris FDM-T treadmill system. Participants received 2 pre-care evaluations, averaged for a baseline measure, and performed at preferred walking speed for 30 seconds; CLBP participants also received a post-treatment evaluation.

The PI provided SM "high velocity low amplitude" (HVLA) procedures directed only toward lumbar spine, hip, and sacroiliac joints perceived through manual examination to have excessive stiffness or abnormal intersegmental motion patterns. HVLA procedures were performed using a treatment table providing drop-section mechanical assistance, and were in some cases supplemented by the use of pelvic wedges, flexion-distraction, mobilization, and light myofascial release (sustained stretches.)

Vertical ground reaction force data was exported to a customized MATLAB program, the stance phase of gait was normalized into 100 equal intervals, and the mean force and standard deviation (SD) were calculated for each interval. The primary outcome measures were the stance phase mean coefficient of variation (MCV) and the Mean Standard Deviation (MSD) over all of stance phase. The MCV was calculated as the root mean square of the standard deviation at each time interval divided by the grand mean of all intervals. MSD is simply the mean of the SDs for all intervals. MCV is the more common outcome, having been used in a number of previous investigations, (e.g., 1, 2) and MSD is a novel outcome measure of vertical GRFs, modeled after its use in a recent kinematic study by Kang and Dingwell. (3)

Also, CVs of several discrete events of stance phase were analyzed, including magnitudes (in Newtons) and timing (in the percentage of stance phase) for the 1st and 2nd peak forces and the mid-stance "valley" between peak forces; the loading rate (in Newtons/sec) from heel strike to the 1st peak force, and the unloading rate (in Newtons/sec) from the 2nd peak force to toe-off (Table 2.)

RESULTS AND DISCUSSION

CLBP participants had higher baseline variability than controls but the differences were statistically not significantly different.

CLBP participants showed a slight decrease in variability from pre- to post-care; the differences were statistically not significantly different but did show small-to-moderate effect sizes (Table 1).

Table 1	MSD Lf (N)	MSD Rt (N)	MCV Lf (%)	MCV Rt (%)
pre	28.9 (8.3)	27.7 (7.0)	6.1 (1.7)	5.8 (1.3)
post	26.0 (7.0)	25.8 (6.4)	5.4 (1.1)	5.3 (.96)
Signif.	p= .056	p= .11	p= .11	p= .09
Effect size	d = 0.37	d = 0.29	d = 0.47	d = 0.45

Variability of LBP participants was not significantly different from the controls in any discrete events of stance phase (Table 2); post-care, they showed significantly lower amounts of variability only in the magnitudes of the first peak forces on both the left and right sides, and for the midstance force on the left side. Other measures showed non-significant decreases or even increases.

Limitations: this was a small pilot study done as a master's thesis project; some CLBP participants had low levels of pain and disability, no walking impairment at baseline, and had little room for improvement. Others may have had additional joint or muscle dysfunctions, not addressed because the care was limited to lumbar, sacroiliac, and hip regions. However, some individual cases suggest an association of decreased variability with treatment improvements. In general, those with higher levels of pre-care variability showed post-care decreases.

CONCLUSIONS

Participants with CLBP had slightly more variability in vertical GRF than controls but most differences were not statistically significant. For the primary outcome measures, decreases in post-care variability had small-to-medium effect sizes but were not statistically significant. This pilot study will guide more research in this area with larger groups and improved participant selection.

REFERENCES

1. Winter DA, 1983, J Mot Behavior.
2. O'Dwyer N, Smith R, Halaki M, Rattanaorasert U, 2009, Gait Posture.
3. Kang HG, Dingwell JB, 2008, Gait Posture.

ACKNOWLEDGMENTS

Edward F. Owens also provided valuable assistance.

Table 2: CVs (%) of events of stance phase: magnitudes of the 1st peak, mid-stance "valley", and 2nd peak forces (PkF1, Mid F, PkF2); timing (% of stance phase, of the 1st peak, mid-stance, and 2nd peak forces (PkF1 %, Mid F %, PkF2 %); and the loading rate from heel strike to PkF1 (Pk1 rate), and the unloading rate from the 2nd peak force to toe-off (Pk2 rate).

Means for the control group (CON, n=6) were compared to the pre-care means of the participants with chronic low back pain (LBP-pre, n=9) with independent t-tests. LBP post-care group means were compared to pre-care means with dependent t-tests. Significant differences are marked with asterisks (*).

Left	PkF1	PkF1 %	Pk1 rate	Mid F	Mid %	PkF2	PkF2 %	Pk2 rate
CON mns	2.58	9.69	11.46	2.67	6.18	2.65	2.53	7.78
LBP-pre mns	3.37	7.22	8.32	4.72	5.68	3.06	3.00	9.21
p-values, CON-LBP	0.09	0.26	0.19	0.07	0.69	0.45	0.58	0.33
LBP-post mns	2.79	8.08	13.51	3.56	5.61	2.80	3.24	8.59
p-values, pre-post	*** 0.04**	0.55	0.38	*** 0.04**	0.90	0.24	0.71	0.51
Right	PkF1	PkF1 %	Pk1 rate	Mid F	Mid %	PkF2	PkF2 %	Pk2 rate
CON mns	2.69	7.41	8.63	2.98	5.67	2.67	2.29	7.67
LBP pre mns	3.15	8.26	9.16	4.56	5.52	3.19	3.24	9.24
p-values, CON-LBP	0.34	0.60	0.69	0.08	0.88	0.25	0.38	0.36
LBP post mns	2.58	9.92	12.14	3.99	6.07	2.84	3.04	8.89
p-values, pre-post	*** 0.01**	0.45	0.48	0.18	0.57	0.11	0.52	0.48

ORAL PRESENATIONS – SATURDAY SEPTEMBER 7th

Young Scientist Awards *Donald Anderson*
Intervertebral Disc Degeneration, Quantified By T2* MRI, Correlated To Biochemistry, Compressive Mechanics, And Global Functional Mechanics Of The Lumbar Spine **Arin M Ellingson; David J Nuckley**
Biomechanics-centered Design Of Robotic Lower-Limb Prostheses **Steven H Collins; Joshua M. Caputo**

Intervertebral Disc Degeneration, Quantified by T2* MRI, Correlated to Biochemistry, Compressive Mechanics, and Global Functional Mechanics of the Lumbar Spine

[1]Arin M. Ellingson and [1]David J. Nuckley

[1]University of Minnesota, Minneapolis, MN, USA
email: ellin224@umn.edu

INTRODUCTION

The causes of low back pain are poorly defined and indistinct; most often implicated as the origin of pain is the intervertebral disc (IVD). Traditionally, a clinical exam assessing functional range-of-motion coupled with T2-weighted MRI (Fig 1B) revealing disc morphology are used to evaluate spinal health, but they fail to correlate well with pain or provide useful patient stratification [1,2].

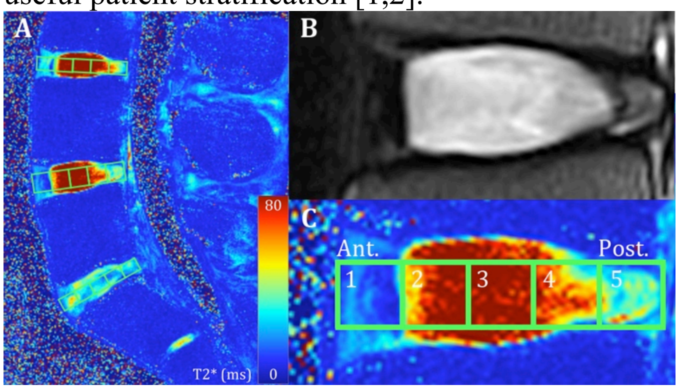

Figure 1- MRI of Lumbar Spine and IVD. A: T2* Map of L-Spine. **B:** Clinical T2-Weighted MRI of Healthy L4-5 IVD. **C:** T2* Map of Same IVD.

Improved imaging techniques, such as quantitative T2* MRI, probe the biochemical properties of tissues, specifically interrogating the water mobility in the macro-molecular network (Fig 1A&C) [3,4]. This is particularly beneficial in detecting the early stages of IVD degeneration, where a decrease in proteoglycans in the nucleus pulposus leads to dehydration and diminished pressurization. Ultimately, these changes to the IVD alter kinematics and stability of the spinal segment.

This study aimed to define the relationship between disc degeneration, quantitatively assessed using magnetic resonance imaging and i. local disc biochemistry, ii. local compressive mechanics, and iii. global functional lumbar spine mechanics.

METHODS

Eighteen cadaveric lumbar spines (L3-S1), acquired from the UofM Bequest Program (53.2±15.5 yrs; range: 21-71 yrs), were imaged using a Siemens 3T MRI scanner (Magnetom Trio; Siemens Healthcare, Erlangen, Germany). Quantitative T2* relaxation maps (MapIt, Siemens Healthcare, Erlangen, Germany) were obtained using the following imaging parameters [TR(ms): 500; TE(ms): 4.18, 11.32, 18.46, 25.60, 32.74, 39.88; Voxel Size(mm): 0.5x0.5x3.0, Slices: 33]. Utilizing MATLAB (Mathworks Inc. Natick, MA), the central ROI mean relaxation value was evaluated in the coronal plane as the intensity changed from lateral to medial to lateral (Fig 2). Based upon Pfirrmann grading criteria, this method quantified the transition zone by computing the slope and intensity by integrating under the curve, altogether defining IVD health.

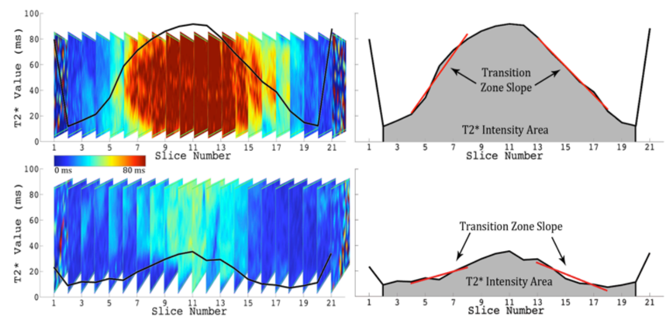

Figure 2- Quantification of Imaging Parameters. Top Left: Coronal Profile of Healthy Disc with Plot of Average T2* Relaxation Time (ms) Overlaid. **Top Right**: Quantification of Transition Zone Slope and T2* Intensity Area of the Healthy Disc. **Bottom Left:** Coronal Profile of Degenerated Disc with Average T2* Relaxation Time (ms) Overlaid. **Bottom Right:** Quantification of Transition Zone Slope and T2* Intensity Area of Degenerated Disc.

In a six-axis Spine Kinetic Simulator (8821 Biopuls, Instron, Norwood, MA), specimens underwent flexion-extension and lateral bending in a pure moment fashion up to 7Nm. Range of motion (ROM), neutral zone ratio (NZR), and bending stiffness were measured. Helical axes (HA) of the L4-L5 spinal segment were computed every 0.05° and averaged over a 1Nm window from -6.5Nm to 6.5Nm [5]. The orientation and location of the HA vector were used for comparison with disc health.

Subsequent experiments probing the local biochemistry and compressive mechanics of the L4-L5 discs were performed at five ROIs (Fig 3). Stress relaxation tests were performed using the hybrid confined/*in situ* indentation test, which utilizes the cartilaginous endplate as the porous indenter. The residual stress and strain were recorded [6].

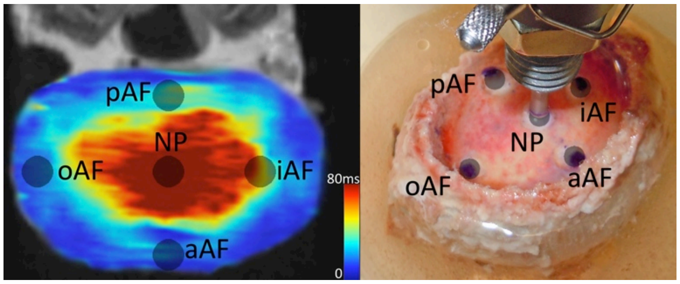

Figure 3- IVD Test Sites (NP: Nucleus Pulposus, AF: Annulus Fibrosus, o: Outer, i: Inner, a: Anterior, p: Posterior). Left. Site Locations on a Transverse Slice of a T2* Map. The Average T2* Relaxation Time was Measured at Each Site. **Right.** Same Test Locations on a Specimen Undergoing Hybrid Confined/In Situ Indentation Tests; Each Site was Assayed for s-GAG Content.

Each test site was then excised and sulfated-glycosaminoglycan (s-GAG) was measured using a 1,9-dimethylmethylene blue assay. Pearson's correlation tests were performed between each measurement and disc health (T2* values).

RESULTS AND DISCUSSION

T2* relaxation time was significantly correlated with the s-GAG content ($p<0.047$) in a site-specific fashion. T2* relaxation times of the NP, iAF, and oAF were significantly correlated with both excised strain and residual stress. The pAF T2* time was also correlated with residual stress. These relationships were particularly strong in the NP and iAF (Fig 5).

There was also a measured change in global spine kinematics as a result of disc degeneration. The T2* Intensity Area and the Transition Zone Slope were both significantly correlated with flexion and lateral bending ROM, NZR, and bending stiffness ($p< 0.044$), but not extension.

The lateral bending HA patterns of the L4-L5 functional spinal unit were also affected by the quality of the IVD (Fig 4). There was a significant correlation between the orientation and location of the HA vector and T2* parameters of disc health, particularly at the end ranges of motion. The HA patterns indicate the more degenerative IVDs have more out-of-plane rotation.

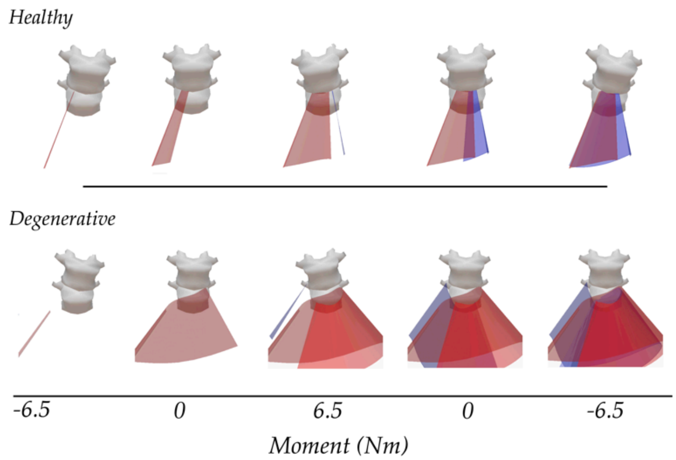

Figure 4- Representative Helical Axis Patterns of a Healthy (top) and Degenerative (bottom) Disc.

CONCLUSIONS

Quantitative T2* MRI is a clinically available imaging sequence capable of detecting proteoglycan content changes, local compression mechanics, and is correlated to global functional motion. The interaction of these changes throughout the degenerative process need further study; however together these data and analyses may prove to be diagnostically powerful for disc health assessment.

REFERENCES

1. Boden SD, et al. *JBJS.* 1990. **2.** Savage RA, et al. *Eur. Spine J.* 1997. **3.** Bittersohl B, et al. *Eur. Radiol.* 2012. **4.** Welsch GH, et al. *Skeletal Radiol.* 2011. **5.** Woltring HJ, et al. *J Biomech.* 1985. **6.** Ellingson AM and Nuckley DJ. *J Biomech.* 2012.

ACKNOWLEDGEMENTS

Funding from NIH/NIAMS T32 AR050938 'Musculoskeletal Training Grant'

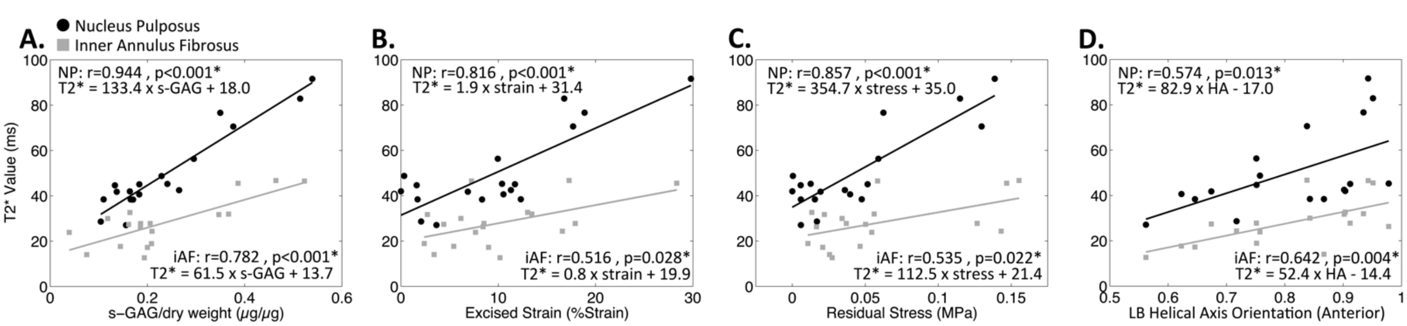

Figure 5. T2* Relaxation Time Correlational Plots of the Nucleus Pulposus and. Annulus Fibrosus. A- T2* vs. s-GAG Content (%dry weight). **B-** T2* vs. Excised Strain (%strain). **C-** T2* vs. Residual Stress (MPa). **D.** Primary Helical Axis Unit Vector Orientation for Lateral Bending. An Orientation of 1.0 Indicates Perfectly Aligned Vectors. Note that the smaller T2* Values Represent More Degenerated Samples Such that Healthy Sample Data are in the Upper Right of Each Plot.

BIOMECHANICS-CENTERED DESIGN OF ROBOTIC LOWER-LIMB PROSTHESES

Steven H. Collins and Joshua M. Caputo

Carnegie Mellon University, Pittsburgh, PA, USA
email: stevecollins@cmu.edu, web: http://biomechatronics.cit.cmu.edu

INTRODUCTION

Robotic ankle-foot prostheses can improve mobility for individuals with amputation, yet we do not know by how much, nor what designs are optimal in general or for a given individual. Improvements in metabolic energy consumption and preferred speed have been demonstrated [1], often using specialized mechanisms to conserve electrical energy [2]. Development has been centered on robotic designs themselves, however, with years of refinement required before the more interesting questions of human biomechanical response can be answered.

Systematic explorations of prosthesis design space, with a focus on human response, would generate a more rational framework for design. Ankle push-off seems a promising place to begin; increased work may improve human economy, but implies heavier motors and batteries. A quantitative characterization of this trade-off could reveal optimal characteristics.

METHODS

We used a versatile ankle-foot prosthesis testbed to explore human responses to changes in push-off work. This testbed, described in detail in [3], was actuated by a powerful motor, connected through a Bowden-cable tether to an instrumented prosthesis end-effector worn by the subject (Fig. 1).

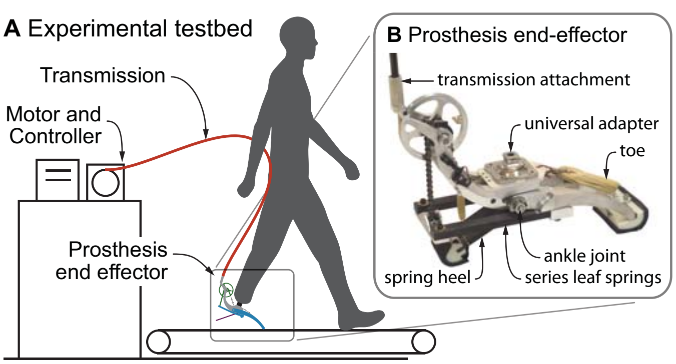

Figure 1: Testbed decouples function from embodiment.

We performed tests on a single healthy subject (N=1, 70 kg, 0.94 m leg length, 22 yrs.) walking on a treadmill at 1.25 m·s^{-1} wearing the prosthesis on one leg using a simulator boot [2]. The prosthesis behaved like a stiffening spring with separate constants during dorsiflexion and plantarflexion [3], resulting in an ankle-joint work loop. Plantarflexion settings were varied across conditions to generate different amounts of net mechanical work per step. We selected values that roughly corresponded to -0.5, 0, 1, 2, 3, and 4 times the net work performed by the biological ankle during walking, and called this scaling term C_w. The subject trained on all conditions one day prior to collection, all conditions lasted 10 minutes, and all were presented in random order. Procedures were approved by CMU IRB.

We measured average metabolic rate during the final 3 minutes of each condition using indirect respirometry, with quiet standing as a baseline. We measured prosthetic ankle torque and position using onboard sensors and used these to calculate prosthetic ankle power. We also calculated average net prosthesis power, defined as positive minus negative work per stride divided by average stride time. We then performed linear regression to obtain a relationship between average net prosthesis power and human metabolic rate across conditions.

RESULTS AND DISCUSSION

Increasing C_w led to increased prosthetic ankle power and work per stride (Fig. 2) as intended. This led to a decrease in metabolic energy expenditure (Fig. 3) with linear coefficient of -1.78 (R^2 = 0.97) and coefficient of performance [4] of 0.45.

This relationship may have interesting implications for the design of robotic ankle-foot prostheses. Parallel and series elasticity and escapements could minimize motor requirements, allowing ideal power and energy densities of about 0.075 W per gram and

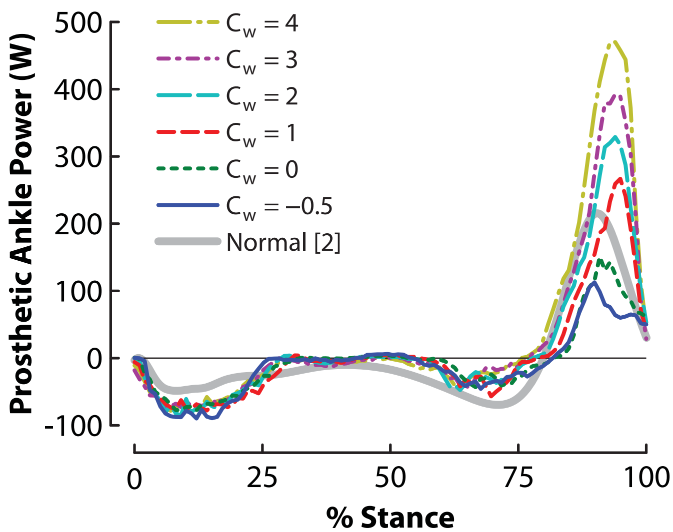

Figure 2: Robotic ankle prosthesis power during the stance period for each condition. Ankle power during normal gait from [2] provided for reference.

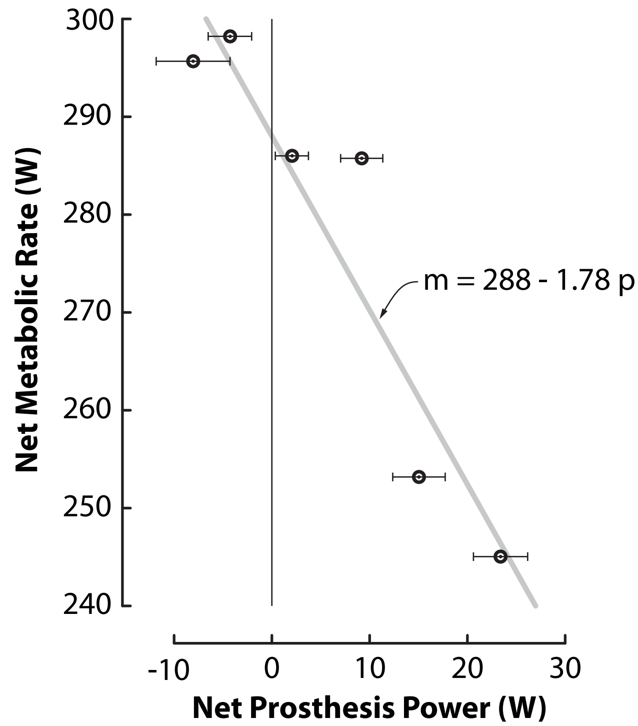

Figure 3: Net human metabolic rate vs. average net prosthesis power. Axis scales are equal. Average net prosthesis power presented with ± st. dev. Net metabolic rate during Normal walking was 223 W.

250 J per gram, respectively, including transmission efficiency [5]. An individual who takes 3000 steps per day would then need 13 + 11 = 24 grams of motor and battery per 1 W push-off assistance. For each gram added at the ankle, we expect a 0.015 W increase in metabolic rate [6], leading to an expected 0.34 W increase per 1 W assistance. Each 1 W of assistance would thus reduce metabolic rate by 0.34 – 1.78 = -1.54 W. In other words, for this individual, a bigger robotic prosthesis is always better. For extreme values this fit will likely break down, but apparently not for the wide range tested here, which far exceeds values for normal walking and commercial robotic prostheses. Benefits would be even greater for batteries stored at the hip or with high nominal prosthesis mass. For lower power or energy density, or more steps per day, a tipping point would be reached at which a passive device would instead be preferable. Similar implications might also be derived for robotic orthoses [7].

Our results must be taken as preliminary, however, due to the small sample size, lack of human kinetics and kinematics measurements, short training period, and use of a simulator boot. We are currently collecting a more complete data set on individuals with amputation. The low coefficient of performance may indicate the possibility of improved delivery of prosthesis work, and a more detailed study of control parameter space is warranted.

CONCLUSIONS

These results illustrate the potential for thorough exploration of biomechatronic design spaces using experimental testbeds and the types of quantitative design frameworks that can be derived with this approach. In particular, our findings suggest that ankle-foot prostheses could provide even more benefit with increased push-off work production. We think this approach could facilitate systematic, rational design of improved robotic prostheses.

REFERENCES

1. Herr HM, Grabowski AM. *Proc. Royal Soc. London B* **279**, 457-464, 2012.
2. Collins SH, Kuo AD. *PLoS ONE* **5**, e9307, 2010.
3. Caputo JM, Collins SH. *J Biomec Eng* **submitted**.
4. Sawicki GS, Ferris DP. *J Exp Biol* **211**, 1402-13.
5. Madden JD. *Science* **318**, 1094-1097, 2007.
6. Browning RC, Modica JR, Kram R, Goswami A. *Med Sci Sport Exer* **39**, 515-525.
7. Collins SH, Jackson RM. *Proceedings of ICORR'13*, Seattle WA, USA, submitted.

GENERAL POSTER SESSION I – Thursday, 9:30-11:00
Grand Ballroom

ERGONOMICS			
1	Development of Biomechanical Index Finger Model to Predict Multi-Segmental Grip Forces for Varying Finger Postures **Hur P, Salehi SH, Seo NJ**	4	Impact Of Wheel Control Methods On Driving Safety And Efficiency **Crocher V, Seo NJ**
7	Frequency Content Of Isokinetic Moment Curves For Differentiating Between Maximal And Non-maximal Shoulder Efforts **Almosnino S, Dvir Z, Stevenson J, Bardana D**	10	Predictive Three Dimensional Surfaces For Localized Joint Level Muscle Fatigue During Intermittent Tasks **Looft J, Frey Law L**
13	Handle Design Based On Pressure Distribution Patterns: Effect Of Handle Shape And Task Direction **Slota G, Seo NJ**	16	A Data-driven Optimization Method To Determine Muscle- Tendon Paths Of The Index Finger **Lee JH, Asakawa DS, Lozano CA, Dennerlein JT, Jindrich DL**
19	Joint Angles Of The Fingers And Thumb During 8 Different Gestures On A Touchscreen Computing Device **Asakawa D, Lozano C, Lee JH, Dennerlein J, Jindrich D**	22	A Biomechanical Assessment Of Breast Kinematics During Different Exercise Modalities **Risius D, Milligan A, Mills C, Scurr J**
25	Scapulothoracic Muscle Activation And Shoulder Kinematics Following A Simulated Work Task With Low Level Forces **Szucs K, Beckas N, Molnar M**		

GAIT			
28	Advanced Age And The Mechanics Of Uphill Walking: A Joint-level, Inverse Dynamic Analysis **Franz J, Kehler A, MacDonald L, Kram R**	31	Region-specific Strain Energy In The Proximal Femur During Load-based Activities In Elderly Women **Kersh M, Martelli S, Zebaze R, Seeman E, Pandy M**
34	Comparison Of Knee Kinematics In Older Adults With Unilateral Transfemoral Amputations During Baseline Walking And Ramp Descent **O'Connell C, Cham R, Chambers A**	37	Real-time Feedback Encourages Old Adults To Increase Their Propulsion During Walking **Franz J, Maletis M, Kram R**
40	Brittle Bone Fracture Risk With Transverse Isotropy **Fritz J, Grosland N, Smith P, Harris G**	43	Multiple Shooting Optimal Control For Aperiodic Multistep Gait Simulation **Celik H, Piazza S**
46	Ankle Fatigue Classification Using Support Vector Machines **Zhang J, Lockhart T, Soangra R**	49	A Comparison Between Angular Momentum And Margin Of Stability In Healthy Younger And Older Adults **Vistamehr A, Neptune R**

52	Effects Of Visual Perception Of Self-motion On Gait In People With Diabetes **Huang CK, Thaisetthawatkul P, Shivaswamy V, Siu KC**	55	Optimal Monitor Location For Posture And Movement Detection **Fortune E, Lugade V, Kaufman K**
58	Fixed Cadence Effect On Shod & Barefoot Gait Kinematics **Romer B, Fox J, Patel J, Rehm J, Weimar W**	61	The Effect Of Load On Sagittal Plane Kinematics During Unanticipated Cutting Maneuvers **Brown T, O’Donovan M, Hasselquist L, Corner B, Schiffman J**
64	Relationship Between Functional Performance, Cognition, Gait And Balance Measures In Older Adults After Resistance Training **Vallabhajosula S, Worley F, Hensley R, Bailey S**	67	Generating Kinematically Consistent Data For Musculoskeletal Inverse Dynamic Analyses Using Finite Element Tools **Chinnakonda MK, Saraswat P, Yao J, Oancea V, Hurtado J, Sett S**
70	Effect Of Shoe Tread Depth On Foot Slipping Kinematics **Albert D, Ledgerwood A, Chambers A, Redfern M, Beschorner K**	73	Assistive Forces Affect The Temporal Structure Of Gait Variability **Cutler E, Wurdeman S, Givens D, Stergiou N**
76	The Effects Of Plantar Fasciitis On Multi-segment Foot Running Gait Kinematics **Bauer R, Mitchell C, Joshi M, Cobb S**	79	Associations Between Cognitive Performance And Gait Variability In Parkinson's Disease **Stegemöller E, Wilson J, Hazamy A, Okun M, Altmann L, Hass C**
82	Variations In Leg Stiffness And Lower Extremity Range Of Motion Variability From Stride Length Perturbations During Gait **Nordin AD, Bailey JP, Dufek JS**	85	Individuals With Anterior Cruciate Ligament Reconstruction Display Altered Mechanics During Split-belt Walking **Roper JA, Roemmich RT, Hass CJ, Tillman MD**
88	What Predicts The First Peak Of The Knee Adduction Moment? Implications For The Treatment Of Knee Osteoarthritis **Schmitz A, Noehren B**	91	Effects Of Load Carriage And Fatigue On Gait Coordination And Variation In Healthy Males **Masterson C, Leib D, Wang H, Dugan E**
94	Biomechanical Value Of Temperature In Assessing Plantar Loading **Yavuz M, Delvadia N, Atves J, Goldfarb J, Stuto J, Franklin A, McGaha R, Rispoli J, Torrence G, Rao N**	97	Assessment Of Body Posture Using Inertial Measurement Units: A Validation Study **Kang GE, Gross M**
100	Comparison Of Functional Outcome Measures Between Patients With Knee Disarticulation And Trans-femoral Amputations Due To Trauma **Thesing N, Kingsbury T, Myers G, Wyatt M**	103	Relationship Between Muscle Force And Size Of Human Intrinsic Foot Muscles **Kurihara T, Otsuka M, Tottori N, Hashimoto T, Isaka T, Yamauchi J**
106	Directional Differences In The Biaxial Material Properties Of Goat Fascia Lata **Eng C, Pancheri F, Lieberman D, Biewener A, Dorfmann AL**	109	Energy Differences Between A Rigid And Deformable Representation Of The Shank During Drop Landings **Pain M**

112	Gait Initiation Variability Following A Concussion **Buckley T, Tapia-Lovler T, Brewer H, Munkasy B**	115	Differences In Passive Contributions In Walking Among Healthy Young And Older Adults And Persons With PAD **Leib D, Wurdeman S, Goodman D, Pipinos I, Johanning J, Myers S**
118	Gender Differences In Response To Load Carriage **Krupenevich R, Mahar T, Ridings J, Tatarski R, Rider P, Domire Z, DeVita P**	121	Persistance Of Asymmetrical Lower-extremity Joint Work Following ACL Reconstruction **Roewer B, Di Stasi S, Hewett T**
124	Contribution Of Thigh And Tibial Motion To Knee Transverse Plane Motion In Runners With Anterior Knee Pain **Rodrigues P, Noehren B, Hamill J**	127	Visual Feedback Improved Movement Symmetry During Sit-to-stand **Abujaber S, Marmon A, Zeni J.**
130	Static And Dynamic Medial Longitudinal Arch Angle In Patellofemoral Pain Syndrome Individuals **Aliberti S, Mezencio B, Amadio A, Serrão J, Hamill J, Mochizuki L**		

MOTOR CONTROL			
133	Altered Power Grip Force Distribution And Phalanx Force Trajectory For Older Individuals **Lambert L, Slota G, Enders L, Seo NJ**	136	Finger Enslaving In The Dominant And Non-dominant Hand **Wilhelm L, Martin J, Latash M, Zatsiorsky V**
139	Neuromuscular Control Of Shot Distance Using The Driver **Peterson T, Requejo P, Flashner H, McNitt-Gray J**	142	A Pilot Study Investigating The Difference In Sense Of Effort Between Chronic Stroke Survivors And Healthy Adults **Jain T, Wauneka C, Ratzki S, Hozie B, VanTowle T, Perry B, Swanson G, Liu W**
145	Muscular Contributions To Knee Accelerations During Single-leg Jump Landing In Australian Football Players **Morgan K, Donnelly C, Reinbolt J**	148	Arm Reaching With Vibrating Manipulandum Within A Dynamic Environment **Wauneka C, Jain T, Liu W**

ORTHOPEDIC MECHANICS			
150	Decreased Bone Material Strength In Severe Osteogenesis Imperfecta (OI) **Albert C, Smith P, Harris G**	153	Development Of Age And Gender-specific Thorax Finite Element Models **Schoell S, Weaver A, Stitzel J**
156	In Vitro Fixation Tests Utilizing An Adjustable Bone Plate **Cervantes TM, SlocumAH, Gupta R, Seldin EB**	159	A Novel Augmented Reality Simulator For Teaching Wire Navigation Skills In Treating Intertrochanteric Hip Fractures **Johns B, Thomas G, Kho J, Karam M, Marsh JL, Anderson D**

162	Isokinetic Knee Torque In Early And Advanced Parkinson's Disease: Relation To Physical Function **Singh G, Lyons K, Liu W, Pahwa R, Sharma N**	165	Subject Specific Multi-body Modles Of The Human Knee; Design Techniques And Experimental Verification **deBock M, Hale R, Gonzalez R**
168	Repeatability Of A Modified Finite Heliax Axis Method: Within And Between Sessions **Graf E, Stefanyshyn D**	171	Anatomical Associations With Knee Kinematics In Maturing Females **Pomeroy S, Goulet G, McLean S**
174	Jumping Performance May Reflect Level Of Competition In Orienteering **Hébert-Losier K**	177	Kinematic Markers Of Prolonged Pronation In Runners **Becker J, Osternig L, James S, Wayner R, Chou LS**
180	Quantification Of The Mechanical And Neural Components Of Finger Enslaving By Using The Blind Source Separation (BSS) Of EMG Data **Paclet F, Léouffre M, Solnik S, Wilhem L, Latash M, Zatsiorsky V**	183	The Functional Role Of The Medial Gastrocnemius During Cycling: A Workloop Approach **Dick T, Wakeling J**
186	The Influence Of Compressive Load Magnitude On The Centre Of Rotation Of Functional Spinal Units During In Vitro Biomechanics Testing **Noguchi M, Gooyers C, Callaghan J**	189	Influence Of Ligaments On Rotation Response Of Cervical Spine: Finite Element Study **Zafarparandeh I, Erbulut D, Lazoglu I, Ozer F**
192	Increase In Broadband Excitation Identifies Vertebral Endplate Fractures **Coombs M, Davis K, Kotowski S, Parkinson R, Callaghan J**	195	Cancellous Bone Fracture Visualization Method **Corbiere N, Kafka O, Issen K, Kuxhaus L**
198	Shoulder Joint Force Sensitivity To Muscle Changes Following Brachial Plexus Birth Palsy **Crouch D, Plate J, Li Z, Saul K**	201	A Finite Element Modeling Approach To Understanding Critical Mechanical Trade-offs In Reverse Shoulder Arthroplasty **Permeswaran V, Goetz J, Hettrich C, Anderson D**
204	The Role Of Pelvic Girdle Position In Force Development And Electromyography Of The Latissimus Dorsi **Patel J, Jagodinsky A, Oliver G, Weimar W**	207	Evaluation Of Midcarpal Capitate Contact Mechanics In Normal, Injured And Post-operative Wrist **Modaresi S, Kallem M, Lee P, McIff T, Toby EB, Fischer K**

OTHER			
210	Kinematic Calibration Of A Thin-film Pressure Grid Using Circular Disk Markers **Sinsel E, Buczek F**	213	Noncontact Photoacoustic And Laser-ultrasound Imaging Of Optical Absorbers And Acoustic Scatterers In Tissue Phantoms **Johnson J, Sabick M, Van Wijk K**
216	Modulation Of Titin Elasticity In Working Muscle To Minimize Energy Loss In Passive Stretch-shortening Cycles **Herzog J, Leonard T, Jinha A, Herzog W**	219	A Practical Approach To Determine Appropriate Cutoff Frequencies For Motion Analysis Data **Carbonneau E, Fontaine R, Smeesters C**

POSTURE & BALANCE			
221	Pilot Study Of The Effect Of An Acute Vestibular Therapy On Postural Stability Of Children With Autism Spectrum Disorder And Typically Developing Children **Smoot S, Kinor D, Bigelow KE**	224	Quantification Of Musculoskeletal Loading Profile Of The Thumb During Pipetting **Wu J, Sinsel E, Shroyer J, Welcome D, Zhao K, An KN, Buczek F**
227	Comparison Of The Kinematics Of The Threshold Of Balance Recovery Of Two Postural Perturbations: Lean Release And Surface Translation **Thiaux V, Robinovitch SN, Smeesters C**	230	Biomechanical Response To Ladder Slipping Events: Effects Of Hand Placement On Response And Recovery **Paul A, Lovell M, Campbell-Kyureghyan N, Beschorner K**
233	Effect Of Compliant Flooring On Postural Stability In An Older Adult Population **Beach R, Jackson K, Bigelow K**	236	Determining Vestibular Contributions To Postural Control During Standing Using Suprathreshold Mechanical Stimulation **Chien J, Mukherjee M**
239	Single-leg Static Stability In Fit, Young Adults: Lower Extremity Strength And Core Strength As Predictors **Silvernale C, Heise G, Esselman E, Smith J**	242	Whole Body Posture For Running Change Of Direction Tasks **Havens K, Sigward S**
245	The Effect Of Recruitment Process On Postural Sway: A Preliminary Comparison Across Three Clinical Studies On Patients With Low Back Pain **Xia T, Long C, Gudavalli R, Owens E, DeVocht J, Wilder D, Meeker W, Goertz C**	248	Characterizing Lumbar Joint Torques During Sitting Following Multidirectional Perturbations: A Case Study **Vette A, Yoshida T, Masani K, Popovic M**
251	Loading Asymmetry During A Stand To Sit Task For People With Multiple Sclerosis **Bowser B, Brown C, White L, Simpson K**	254	Dynamic Postural Stability Deficits Exist In Mechanically Lax Individuals But Not Those With Perceived Functional Ankle Instability **Rosen A, Ko J, Crowell C**
257	Impact Of Obesity On Antropometric Predictors Of Body Fat In Older Adults **Kolling A, Montgomery J, McCrory J, Cham R, Chambers A**		

REHABILITATION			
258	Quantifying Head Injury Severity Following Pediatric Patient Falls **Dufek J, Ryan-Wenger N, Mefferd K**	261	Individual Muscle Contributions To Handcycling Propulsion **Sasaki K**
264	Evaluation Of Novel Biofeedback In Changes Of Activation Of The Trapezius **Gaffney B, Maluf K, Davidson B**	267	Normative 3D Strength Surfaces In Healthy Subjects For The Hip And Trunk Joint Complexes **Looft J, Stockdale A, Avin K, Frey Law L**

270	Comparison Of Supraspinatus And Infraspinatus Surface And Fine Wire Electromyography During Isometric Humeral Rotation **Brookham R, Allen T, Cudlip A, Dickerson C**	273	Neuromagnetic Activity Of The Sensorimotor Cortices During The Motor Planning And Execution Stages In Children With Cerebral Palsy **Arpin D, Becker K, Heinrichs-Graham E, Wilson T, Kurz M**
276	Effects Of A Newly Designed Cervicle Collar On Neck Joint Kinematics **Gardner J, Liu X, Wen C, Zhang S**	279	The Effects Of A Varus Unloader Brace For Lateral Tibiofemoral Osteoarthritis And Valgus Malalignment After Anterior Cruicate Ligament Reconstruction: A Proof Of Concept **Hart H, Ackland D, Schache A, Pandy M, Collins N, Crossley K**
282	The Relationships Of Force Generation Between Biodensity Training And Similar Athletic Tasks **Dai B, Heinbaugh E, Moynes R, Rockey S, Smith D**	285	Effect Of Glenohumeral Abduction On Supraspinatus Repair Tension **Hawthorne J, Carpenter E, Lam P, Murrell G**
288	Data-driven Biomechanical Analysis Of The Upper Trapezius Muscles And Neck Movement: A Pilot Study **Wei Q, Gerber N, Duric Z, Otto P, Vishnoi N, Sikdar S**	291	Time-dependent Changes In Velocity-dependent Stiffness Of The Elbow Joint During Stroke Recovery **Kindig M, Krishnan V, Mirbagheri M**
294	Thermal Conductivity Of Prosthetic Elastomers, Fabrics, Liners, And Socket Materials **Klittich M, Davis B, Webber C, Dhinojwala A**	297	Integration Of Musculoskeletal Analysis With Engineering Design For Virtual Prototyping Of Exoskeletons **Agarwal P, Kuo PH, Neptune R, Deshpande A**
300	A Biomechanical Model For Glenohumeral Joint Evaluation During Pediatric Manual Wheelchair Mobility **Slavens B, Paul A, Graf A, Krzak J, Vogel L**	303	Variability Of Upper Extremity Kinematics And Shoulder Pain During Wheelchair Propulsion: A Vector Coding Analysis **Hsu I, Moon Y, Jayaraman C, Rice I, Sosnoff J, Hsiao-Wecksler E**
306	Enhancing Friction Between Gloves And Pushrims For Wheelchair Racing **Marcou F, Masson G, Martel F, Rancourt D, Smeesters C, Berrigan F, Laroche J, Langelier E**		

SPORTS			
307	A Novel Method To Model A Cyclist In Situ **Meyers AC, Eltoukhy M, Signorile J**	310	Muscular Activation Of Lower Limb Muscles Due To In-flight Posterior Perturbation During Drop Landing **Kakar RS, Arnett SW, Fu YC, Simpson KJ**
313	A Compact Stereo-based Motion Capture Solution For Exercise Monitoring **Lee MW, Jung S, Judkins T, Handelman D, Bachrach B**	316	Kinematic Comparison Of Successful And Unsuccessful Landings During Unanticipated Movement Tasks **Kipp K, Geiser C, Wood C, Meinerz C, Watson K**

319	Differences In The Mechanics Between The Dominant And Non-dominant Plant Limb During Instep Soccer Kicking **Berlin C, Dugan E**	322	Characteristics Of Tibial Strains During Different Type Of Physical Activities **Kia M, Dickin DC, Wang H**
325	Kinematic Analysis Of Soccer Heading; Comparison Of Training Methods **Suzuki S, Nakamura Y, Inoue N**	328	Ground Reaction Forces And Impulse During Landing Is Not Correlated With Ball Speed In High School Baseball Pitchers **Soujoudi M, Oyama S, Myers J**
331	The Relationships Of Bat Quickness And Bat Velocity With Batting Outcomes For Division I Softball Players **Ficklin T, Reilly-Boccia C, Lund R, Beatty K, Hervas J**	334	Relationship Of Rate Of Torque Development And Contractile Impulse During Time Critical Periods **Johnson S, Norcross M, Pollard C, Hoffman M**
337	Biomechanical Variables During Swing Correlated With Impact Peak In Running **Schmitz A, Pohl M, Woods K, Noehren B**	340	Can Increased Running Cadence Simulate The Effects Of Going Barefoot? **Hafer J, Bido J, Plack LA, Metzl J**
343	The Effects Of Fatigue On Vertical Loading During Running **Maas D, Mattison L, Michelson M, Bowser B**	346	Lateral Momentum Generation In An Unexpected Quick First Step **Ramos C, McNitt-Gray J**

DEVELOPMENT OF BIOMECHANICAL INDEX FINGER MODEL TO PREDICT MULTI-SEGMENTAL GRIP FORCES FOR VARYING FINGER POSTURES

Pilwon Hur, Seyed Hadi Salehi and Na Jin Seo
University of Wisconsin-Milwaukee, Milwaukee, WI, USA
email: hur@uwm.edu, web: http:// pantherfile.uwm.edu/seon/www/

INTRODUCTION

Hand and fingers injuries account for 1/3 of all injuries at work, 1/3 of chronic injuries, 1/4 of lost working time, and 1/5 of permanent disability [1]. Many hand injuries occur when a task requires hand strength exceeding one's capability. To reduce these hand injuries, ergonomists have tried to optimize the design of work objects to maximize the hand's physical capacity via biomechanical analyses.

However, these efforts are primarily empirical, limited to specific shapes and sizes of handles examined. These empirical data are not sufficient to extrapolate and predict grip strengths for a new set of handle shapes and sizes. Currently available hand/finger models are also limited, because they are insensitive to changes in finger posture and predict force only at the fingertip.

Therefore, the objective of this study was to develop a novel biomechanical index finger model which can predict the maximal grip force across all phalanges during grip of objects in varying shapes and sizes.

METHODS

A new index finger model was developed by incorporating the tendon pulley mechanism [2], passive properties of soft tissues [3], and extensor mechanism [4] for the seven muscles controlling the index finger. The novelty of this model is that all above three aspects were taken into account concurrently to predict the maximum grip forces across all phalanges for varying postures.

The distal interphalangeal (DIP), proximal interphalangeal (PIP) and metacarpophalangeal (MCP) joints were frictionless hinges with one degree of freedom in flexion/extension. The seven muscles for the index finger were: first dorsal interosseous (FDI), first lumbrical (LUM), first palmar interosseous (FPI), flexor digitorum profundus (FDP), flexor digitorum superficialis (FDS), extensor digitorum communis (EDC) and extensor indicis proprius (EIP). Four more tendons were included for the extensor mechanism: terminal extensor (TE), extensor slip (ES), radial band (RB) and ulnar band (UB). Finally, 5 annular pulleys (A1 through A5) were included (Fig. 1).

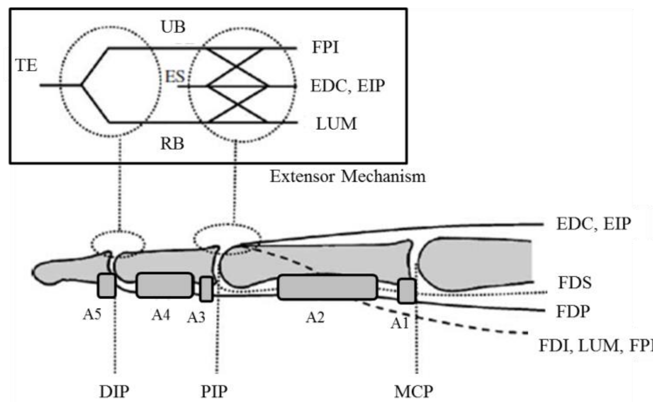

Figure 1: The index finger model with pulleys and the extensor mechanism

The pulley mechanisms defined how muscles' moment arm lengths changed as a function of joint angle. In addition, due to pulleys, tendon tension produced forces not only at the insertion sites, but also at the interaction points with pulleys. For example, FDP inserts at and flexes the distal phalanx (DP). At the same time, FDP influences the middle (MP) and proximal (PP) phalanges due to the interactions with pulleys. The interaction force was computed as a vector sum of the two tendon tensions at each pulley according to their geometric configurations (Fig. 2). All parameter information for pulleys was adopted from [2].

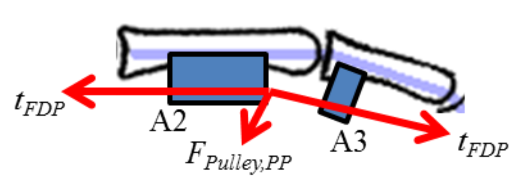

Figure 2: Tendon-pulley interaction force

Passive joint torque at each joint due to the contribution of soft tissues such as ligaments, skin, and joint capsules also changed as a function of joint angle [3] in the model.

The extensor mechanism by Brook [4] was used to model tendon tension distribution in the complicated extensor tendon network depending on the geometric configuration as follows.

$$t_{TE} = 0.992 t_{RB} + 0.995 t_{UB}$$
$$t_{RB} = \alpha_{EDC+EIP} t_{EDC+EIP} + \alpha_{LUM} t_{LUM}$$
$$t_{UB} = \alpha_{EDC+EIP} t_{EDC+EIP} + \alpha_{FPI} t_{FPI}$$
$$t_{ES} = (1-\alpha_{FPI})\, t_{FPI} + (1-\alpha_{LUM})\, t_{LUM} + (1-2\alpha_{EDC+EIP})\, t_{EDC+EIP}$$

where $\alpha_{EDC+EIP}$, α_{FPI}, and α_{LUM} are the contribution of the corresponding muscle(s) to the four tendon tensions in the extensor mechanism. All tendon tensions except the four (t_{TE}, t_{RB}, t_{UB}, t_{ES}) were limited by the physiological cross-sectional area (PCSA) [5] times the maximum muscle stress (s=35 N/cm^2) [6]. The MP length was assumed 24.5 mm and defined other phalanx lengths proportionally [2].

Maximizing external contact forces across all phalanges was the goal of optimization. External contact forces were assumed to be perpendicular to and at the center point of the contacting phalanx. The model and optimization were implemented in MATLAB (v8.0; The MathWorks, Natick, MA).

Find t_i (i=FDP, FDS, LUM, FDI, FPI, EDC+EIP)
$\alpha_{EDC+EIP}$, α_{FPI}, α_{LUM}

Maximize $F_{External,DP} + F_{External,MP} + F_{External,PP}$

Subject to $0 \le t_i \le PCSA \times s$

$$0 \le \alpha_{EDC+EIP} \le 0.5,\ 0 \le \alpha_{FPI},\ \alpha_{LUM} \le 1$$
$$F_{External,j} \ge 0$$
$$F_{Tendon,j} + F_{Pulley,j} + F_{External,j} + F_{Joint,j} = 0$$
$$M_{Tendon,j} + M_{Pulley,j} + M_{External,j} + M_{Joint,j} + M_{Passive,j} = 0$$
$$(j = \text{DP, MP, PP})$$

RESULTS AND DISCUSSION

The predicted grip strength changed with finger posture as shown in the 3 examples in Table 1. Grip strength increased as the finger closed. Grip strength for DP was the greatest followed by PP and MP. These trends agreed with literature [7].

Table 1. Predicted grip strength for 3 finger postures

Segment \ Posture	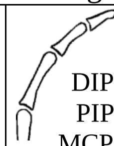 DIP=10 ° PIP=25 ° MCP=30 °	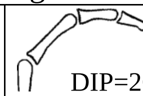 DIP=20 ° PIP=45 ° MCP=45 °	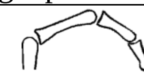 DIP=20 ° PIP=50 ° MCP=70 °
DP	56.8 N	61.3 N	61.3 N
MP	5.3 N	20.3 N	24.7 N
PP	5.5 N	34.4 N	46.7 N

For future work, the model will be scalable according to user-specific PCSA and hand length. The model validation will be performed by comparing the predictions to measured data. In addition, a user interface will be developed so that ergonomists and industrial designers can apply this new index finger model to improve ergonomics of work objects and consumer products, thereby reducing hand injuries.

CONCLUSIONS

A novel index finger model was developed to predict the maximum grip forces across all phalanges for varying finger postures. This model integrated the 5 pulleys, extensor mechanism, and passive properties. Upon addition of scalability and validation, the model will be made accessible to ergonomists and industrial designers via graphical user interface to enhance ergonomic designs of work objects and reduce hand injuries due to overexertion.

REFERENCES

1. Marty J et al. *Ann Chir Main*, pp.1-2, 1983.
2. An KN et al. *J Biomech* **12**, 775–788, 1979.
3. Kamper DG et al. *J Biomech*, **35**, 1581-1589, 2002.
4. Brook N et al. *Med Eng Phys*, **17**, 54-63, 1995.
5. An KN et al. J Orthop Res, **3**, 202-211, 1985.
6. Zajac FE *Crit Rev Biomed Eng*, **17**, 359-411, 1989.
7. Amis A, *J Biomed Eng*, 9, 313-320, 1987.

ACKNOWLEDGEMENTS

We appreciate funding from the National Institute of Occupational Safety and Health, University of Michigan ERC PPRT.

Impact of Wheel Control Methods on Driving Safety and Efficiency

Vincent Crocher and Na Jin Seo

Hand Rehabilitation Lab, University of Wisconsin-Milwaukee, Milwaukee, WI, USA
E-mail: seon@uwm.edu, Web: pantherfile.uwm.edu/seon/www/

INTRODUCTION

People with arm or hand impairment have to drive with only one hand. Driving with one hand while the other hand is in an arm cast significantly hampers driving safety and efficiency [1, 2, 3]. Some spinner knobs are commercially available to supposedly assist with driving. However, the efficacy of these assistive knobs on driving safety and efficiency is currently unknown.

The objective of this study was thus to determine the effect of different wheel control methods on driving safety and efficiency. Especially, use of a spinner knob shown in Fig. 1 was evaluated for driving safety and efficiency, in comparison to the preferred way (habitual driving method), two-hand driving (the method recommended by driving instructors), and one-hand driving (due to casts or hemiparesis).

Figure 1: A spinner knob.

METHODS

Ten healthy subjects with a current driving license drove in the BRDrivingSimEX driving simulator (Beta Research Inc., Los Gatos, CA, USA) using six different wheel control methods: 1-preferred way, 2-two hands, 3-dominant hand only, 4-dominant hand with the spinner knob (illustrated in Fig. 2), 5-non-dominant hand only, and 6-non-dominant hand with the spinner knob. All subjects had no previous experience using any kind of spinner knob.

Figure 2: A subject driving with the spinner knob.

The sequence of testing the 6 wheel control methods was randomized across subjects. For each wheel control method, subjects drove in five driving scenarios: making a left turn, passing large trucks in traffic, entering a freeway in traffic, parallel parking, and forward parking. Presentation of the driving scenarios was also randomized within a wheel control method. The subjects got accustomed to the driving simulator, driving scenarios, and each wheel control method through practice sessions prior to testing.

The driving safety and efficiency for each wheel control method for each subject were assessed with a score, S (Eq. 1), based on five criteria: the number of collisions, the number of seconds over the speed limit, the number of seconds of following another vehicle too closely, the number of lane deviations (unintended line crossings), and the time to complete parking tasks. The number of collisions applied for all scenarios, whereas the speeding, following too close and lane deviations applied for only on-road scenarios.

The coefficients used in Eq. 1 for each criterion were based on the Wisconsin Department of Motor Vehicle point system probationary license drivers [4]. The *MinimumTime* for each of the two parking tasks was the minimum time realized by any subject using any wheel control method. A lower score indicates a safer and more efficient driving.

$$S = \sum_{AllScenarios} (\#Collisions) + \sum_{OnRoadScenarios} \begin{bmatrix} 3\times(\#SecOfSpeeding) \\ +3\times(\#SecOfFollowTooClose) \\ +4\times(\#Deviations) \end{bmatrix} + \sum_{ParkingTasks} \left[8\times\left(\frac{TimeToComplete}{MinimumTime} - 1\right)\right] \quad (1)$$

The score for each wheel control method was normalized by the sum of the scores for all the methods for a given subject. The normalized scores were compared among the wheel control methods. One-way ANOVA did not yield any significant effect ($p>.05$). Thus, only trends are discussed. Additional testing is planned for the future.

RESULTS AND DISCUSSION

Normalized scores for each wheel control method are presented in Fig. 3. The preferred way resulted in the best driving score followed by the dominant hand and two-hand control methods. Driving with one hand was, on average, 8.8% less safe than the preferred way, consistent with the previous study [2]. The present study also showed that driving with the spinner knob was 5.9% less safe for the dominant hand, whereas for the non-dominant hand, use of the spinner knob did not affect the score much (1.1%). Driving with the non-dominant hand, with or without the spinner knob, was found to be the least safe and efficient among all methods.

CONCLUSION

In conclusion, the experiment results suggest that use of the spinner knob only deteriorates driving safety and efficiency when a person drives with the dominant hand. For the non-dominant hand driving, the spinner knob appears to have little impact on driving safety and efficiency. Overall, driving with only one hand, with or without the spinner knob, worsens driving safety and efficiency, compared to the preferred way.

Although some people might think it would be helpful to use a spinner knob when having to drive with only one hand, the present study demonstrates that the spinner knob does not help driving safety and efficiency and rather demotes them for the dominant hand. Since only the sphere knob was evaluated in the present study, other types of assistive knobs such as tri-pin, palm-grip or V-grip (from Howell Ventures Ltd., Upper Kingsclear, Canada) should be evaluated for driving safety and efficiency for people with physical impairments who have to drive with only one hand.

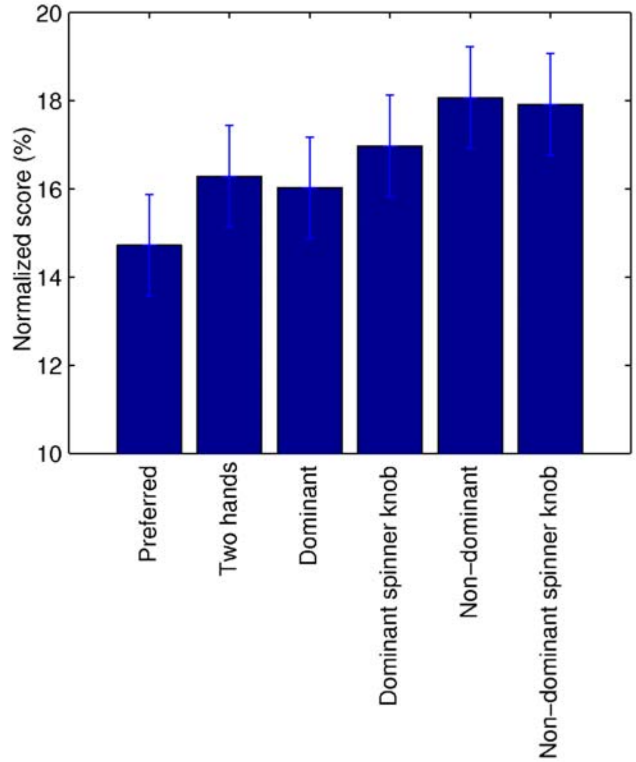

Figure 3: Normalized score for each wheel control method (subjects pooled).

REFERENCES

1. Blair, S. et al. *Injury* **33.1**, 55-56, 2002.
2. Gregory, J.J. et al. *Injury* **40.3**, 253-256, 2009.
3. Kalamaras, M.A. et al. *ANZ Journal of Surgery* 76.6, 439-441, 2006.
4. Wisconsin Administrative Code of Department Transportation, Chapt. 101, 2013.

ACKNOWLEDGMENTS

We thank Aimee Johnson for assisting with the experiments and data analysis and Howell Ventures Ltd. for generous donation of spinner knobs.

FREQUENCY CONTENT OF ISOKINETIC MOMENT CURVES FOR DIFFERENTIATING BETWEEN MAXIMAL AND NON-MAXIMAL SHOULDER EFFORTS

[1]Sivan Almosnino, [1,2]Zeevi Dvir, [1]Joan Stevenson, and [1]Davide Bardana

[1]Queen's University, Kingston, ON, Canada, [2]Tel Aviv University, Ramat Aviv, Israel
email: sivanalm@hotmail.com, web: http://www.skhs.queensu.ca/ergbio/

INTRODUCTION

Work-related injuries of the shoulder complex are common in Canada and impose a significant burden in terms of time off work and related restitutions [1]. The evaluation of shoulder muscular strength may assist clinicians in assessing an injured worker's progression through rehabilitation, and may also contribute to decision-making processes related to disability ratings, and readiness to return to work. However, a fundamental assumption with using strength scores in such settings is that maximal voluntary efforts were exerted by the participant during testing.

One method proposed for differentiating between maximal and non-maximal isokinetic efforts relies on presumed differences in neuromuscular strategies between the two efforts types, which are manifested in the degree of strength curve smoothness. [2]. In particular, it has been suggested that whilst maximal efforts are characterized by relatively smooth strength curves throughout the tested range of motion; those curves obtained during non-maximal effort exertions exhibit high frequency oscillatory irregularities [3]. In these regards, it should be first noted that the aforementioned observations have mostly been made with reference to curves attained from testing of the knee. Thus, it is unclear whether such differences are also apparent for curves attained from testing of shoulder strength. Second, second, attempts to quantify the above-mentioned differences in strength curve morphologies have yielded mixed results [3], which may be partially a consequence of the insensitivity of the outcome measures used for differentiation purposes. As such, exploring the use of other measures is warranted. This investigation assessed the capabilities of the isokinetic-based moment signal's frequency content in discriminating between performance of maximal and non-maximal isokinetic shoulder flexion and extension efforts.

METHODS

The concentric dominant shoulder strength of 27 healthy, university-aged participants (15 men) was measured using a Biodex System 3 isokinetic dynamometer (Biodex Medical Systems Inc., Shirley, NY, USA). Study procedures were approved by the University's General Research Ethics Board, and written informed consent was obtained from all participants.

The experimental protocol entailed performance of 3 sets of 5 shoulder flexion/extension repetitions at preset angular velocities of 30°/sec and 120°/sec. Testing was done in a seated position, and through a 60° range of motion. In the first set, participants were asked to exert their maximal voluntary effort, whilst in the 2nd set the participants were asked to convince the examiner they are exerting their best effort whilst simulating shoulder muscular dysfunction for the explicit purpose of monetary gain. The third set was composed of sub-maximal efforts at a self-chosen, comfortable level. During all conditions, visual via the concurrent moment-time display and audible feedback on performance were provided.

DC bias was removed from all individual moment time series prior to transformation into the frequency domain via Fast Fourier Transform. The frequency content within 95% and 99% of total signal power was then calculated. Cut-off scores for differentiating between maximal and non-maximal efforts were obtained by calculations of one-sided tolerance intervals covering 95% of the population with a confidence level of 95%. The performance of these cut-off scores is reported in terms of the number of misclassification per effort type, and the accompanying specificity and sensitivity percentages.

RESULTS AND DISCUSSION

During performance of feigned and sub-maximal shoulder flexion efforts at both testing velocities the participants performed, on average, at 65% -70% of their maximal capabilities. During performance of shoulder extension repetitions, feigned and submaximal efforts were performed, on average, at 46%-53% of maximal efforts.

Irrespective of signal power percentage or testing velocity, the isokinetic moment curve's frequency content for maximal efforts was, on average, lower than that obtained for both non-maximal effort conditions (Table 1). Furthermore, self-selected submaximal efforts exhibited lower frequency content than that obtained for feigned effort attempts.

The cut-off scores for differentiating between maximal and non-maximal efforts are presented in Table 1. The specificity values across both total signal percentage levels and testing velocities ranged between 88.9% and 100%, whilst sensitivity values ranged between 42.6% and 72.2%. Of note is that the majority of misclassified non-maximal efforts were those performed at the self-selected submaximal level.

CONCLUSIONS

The results of this investigation suggest that the isokinetic moment signal's frequency content possesses some ability to discriminate between maximal and non-maximal shoulder isokinetic efforts, and may be of value in the development of multivariate decision rules in future investigations. The results also indicate a possible avenue of research pertaining to the ability to differentiate between sincere submaximal efforts and purposeful feigned attempts.

REFERENCES

1. Workplace Safety and Insurance Board. Statistical supplement, 2009.
2. Ayalon A., et al. *Isok & Ex Sci* **9**, 45-50.
3. Dvir Z. *Isokinetics*, Churchill-Livingston, 2004.

ACKNOWLEDGEMENTS

Sivan Almosnino is supported by a NSERC-CREATE doctoral stipend and a Canadian Society of Biomechanics travel award.

Table 1: Group mean ± SD frequency content scores for maximal and non-maximal efforts, and performance of the cut-off score (**CS**) in terms misclassifications per effort type, (feign-submaximal), and corresponding specificity (**Sp**) and sensitivity (**Sn**) percentages.

% Signal Power	Velocity	Maximal Efforts (Hz)	Feigned Efforts (Hz)	Submaximal Efforts (Hz)	CS (Hz)	# of Maximal Efforts Misclassified	# of Non-Max Efforts Misclassified	Sp (%)	Sn (%)
95%	30°/sec	0.68±0.16	7.05±8.92	1.18±0.80	1.03	2/27	16/54 (4-12)	92.6	70.4
	120°/sec	3.91±1.39	11.63±5.23	8.65±4.37	7.04	0/27	15/54 (4-11)	100	72.2
99%	30°/sec	3.27±1.67	18.64±14.45	7.56±4.48	5.77	3/27	16/54 (5-11)	88.9	70.4
	120°/sec	16.45±4.72	28.51±7.94	24.37±7.38	27.05	0/27	31/54 (9-22)	100	42.6

PREDICTIVE THREE DIMENSIONAL SURFACES FOR LOCALIZED JOINT LEVEL MUSCLE FATIGUE DURING INTERMITTENT TASKS

[1]John M. Looft, [1]Laura Frey Law

[1]University of Iowa, Iowa City, IA, USA
email: laura-freylaw@uiowa.edu

INTRODUCTION

Muscle fatigue has been defined as "any reduction in the ability to exert force in response to voluntary effort"[1]. The reduction in force due to static muscle contractions was first quantified by Walter Rohmert [2]. The relationship between intensity and endurance time (ET) have been coined "Rohmert Curves", and have been studied by many other researchers [2-8].

Recently, we compiled a large meta-analysis to "update" the "Rohmert curves" for each joint region (ankle, knee, trunk, shoulder, elbow, and hand/grip) [9]. The updated "Rohmert curves" provide more up to date and accurate versions of the static isometric intensity-ET curves for each joint region, however these curves only represent static muscle contractions. Unfortunately, there are few muscle fatigue models that represent the development of fatigue for more complex contractions (i.e. intermittent work rest cycles) that are observed in the work force. Although ET has historically been the main outcome variable for empirical muscle fatigue models [2, 6], it could be problematic for intermittent tasks due to the long ETs that are associated with low intensity and low duty cycle (DC) tasks. Whereas, the decline in peak torque over time provides a metric of fatigue that can be assessed at multiple time points.

Thus the goal of this study was to create localized muscle fatigue models, akin to "Rohmert curves" for intermittent tasks, considering task intensity and DC. This was accomplished by 1) conducting a comprehensive review of literature to extract relevant fatigue data 2) developing a statistical model of percent torque decline as a function of task intensity and DC for individual joint regions (ankle, knee, trunk, shoulder, elbow, and hand/grip).

METHODS

Systematic Review of Literature

A systematic review of localized muscle fatigue was performed using the following databases: PubMed, Cumulative Index to Nursing and Allied Health Literature (CINAHL), Web of Knowledge, and Google Scholar. The search criteria used strategies previously described [9], using search term combinations that would elicit relevant articles reporting torque decline during intermittent tasks.

Inclusion and Exclusion Criteria

The inclusion criteria included: studies with healthy human subjects, ages between 18-55 years old, intermittent/static tasks with force/torque data, a task time of at least 30 seconds, and published in English. Exclusion criteria included: dynamic contractions, simultaneous multi-joint testing (e.g. squat lifts), functional tasks, body/limb weight as primary resistance, and electrically stimulated contractions. Data that involved patient populations or interventions (i.e. creatine supplementation) were not used for the analysis, but any control subjects' data were included [9].

Data Analysis

The authors, number of subjects, sex, and task intensity (% effort) were compiled in the Excel database as previously described [9]; additionally the duty cycle and percent decline at discrete time points (30, 60, 90, and 120 seconds) of the MVC (mean and SD) were recorded. The four discrete time points were chosen based on the available data. When appropriate, graphical data was obtained using pixel analysis (Adobe Photoshop, San Jose, CA) [9]. Only joints with a minimum of 3 (i.e. three points are needed to define a plane) data points at different combination of MVCs and DCs were further analyzed at each time point.

Based on the power relationship observed in the intensity-ET curves for sustained contractions (i.e., 100% DC) [9], a log transform was performed across each data set. The log transformed data set was then plotted in TableCurve3D (SYSTAT

Software Inc, Richmond, CA) and fit to a plane in the form of Equation 1. An exponential transform was then applied to the plane equation in order to transform the plane to a power relationship as previously described [9], where a, b, and c are the model coefficients (Equation 2).

1) $\ln(\%TD) = \ln(a)+b*\ln(DC)+c*\ln(MVC)$
2) $\%TD = a * (DC)^b (MVC)^c$

RESULTS AND DISCUSSION

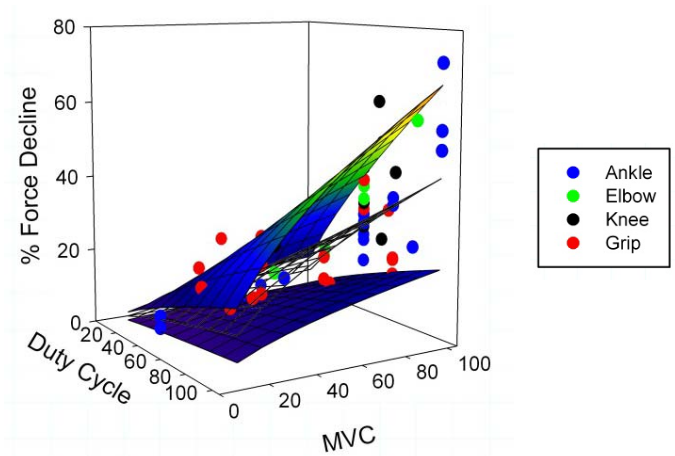

Figure 1: Example of the general empirical torque decline model at 120s. The 95% CI is shown by the colored planes.

69 publications (194 data points) were found, enabling surfaces to be created for 4 joint regions (ankle, knee, elbow, and hand/grip) and a general surface for each of the 4 time points (Figure 1). Based on the power relationship observed in the intensity-ET curves for sustained contractions (i.e. 100% DC) [9], the data points were fit to nonlinear, 3-parameter, power equation (Equation 1). The 3D surface fits varied across joints and times, with median R^2 = 0.500 (range 0.036 to 0.990) (see Table 1). Overall, the joint-specific fits were superior to the general model, indicating heterogeneity between joints.

CONCLUSIONS

This research focused on developing models of muscle fatigue involving intermittent tasks. Overall, model fits were reasonable, suggesting this 3D empirical approach has merit, but the lack of available data and the non-uniformity of the data make deriving firm conclusions challenging. While additional studies are needed to validate and advance the current models, these results suggest 3D fatigue models have merit. These novel approaches could have significant impacts in the ergonomics field to maximize worker effectiveness while minimizing the risks for musculoskeletal disorders.

REFERENCES

1. Chaffin, D.B., G.B.J. Andersson, and B.J. Martin, *Occupational Biomechanics*. 2006, Hoboken: John Wiley & Sons, Inc.
2. Rohmert, W., *Determination of the recovery pause for static work of man.* Internationale Zeitschrift Fur Angewandte Physiologie, Einschliesslich Arbeitsphysiologie, 1960. **18**: p. 123-164.
3. Garg, A., et al., *The effects of maximum voluntary contraction on endurance times for the shoulder girdle.* International Journal of Industrial Ergonomics, 2002. **30**(2): p. 103-113.
4. Hagberg, M., *Work load and fatigue in repetitive arm elevations.* Ergonomics, 1981. **24**(7): p. 543-555.
5. Huijgens, J.M.M., *A model for quantifying static load, incorporating muscle fatigue*, in *Biomechanics Symposium*, W.C. Buskirk, Editor. 1981, American Society of Mechanical Engineers: Boulder, CO. p. 97-99.
6. Iridiastadi, H. and M.A. Nussbaum, *Muscle fatigue and endurance during repetitive intermittent static efforts: development of prediction models.* Ergonomics, 2006. **49**(4): p. 344-360.
7. Monod, H. and J. Scherrer, *The work capacity of a synergic muscluar group.* Ergonomics, 1965. **8**(1-4): p. 329-338.
8. Rose, L., M. Ericson, and R. Ortengren, *Endurance time, pain and resumption in passive loading of the elbow joint.* Ergonomics, 2000. **43**(3): p. 405-420.
9. Frey Law, L.A. and K.G. Avin, *Endurance time is joint specific: A modelling and meta-analysis investigation.* Ergonomics, 2010. **53**(1): p. 109-129.

ACKNOWLEDGMENTS

The authors were funded in part by National Institutes for Health, K01AR056134 and the University of Iowa Heartland Center Graduate Student Fellowship

Table 1: R^2 (n data points) values for 3D torque decline-intensity-DC models

Joint	30 seconds	60 seconds	90 seconds	120 seconds	Median
Ankle	0.597 (7)	0.673 (20)	0.535 (7)	0.832 (24)	0.635
Knee	0.465 (19)	0.258 (23)	0.462 (16)	0.416 (15)	0.439
Elbow	0.794 (7)	0.941 (11)	0.990 (6)	0.990 (7)	0.966
Hand/Grip	0.628 (11)	0.036 (21)	0.968 (8)	0.182 (22)	0.405
General	0.222 (44)	0.216 (75)	0.207 (37)	0.410 (68)	0.219
Median	0.597	0.258	0.535	0.416	0.500

HANDLE DESIGN BASED ON PRESSURE DISTRIBUTION PATTERNS: EFFECT OF HANDLE SHAPE AND TASK DIRECTION

Gregory P. Slota & Na Jin Seo

University of Wisconsin-Milwaukee, Milwaukee, WI, USA
E-mail: gslota@uwm.edu, Web: https://pantherfile.uwm.edu/seon/www/

INTRODUCTION

Everyday kitchen tasks such as chopping with a knife or lifting a pan or pot require gripping long handles while generating a force-moment couple using the hand. In a study of activities of daily living, gripping produced the highest frequency of pain and was related to these kitchen activities [1].

How pain during kitchen tasks could be reduced by better handle design has not been studied despite the high frequency and prevalence of kitchen activities and associated pain. Among the objective measures, contact area and average pressure on the hand have been shown to be an appropriate measurement of hand discomfort and pain, more so than gripping muscle activity [2]. In addition, peak pressure can specify how the hand discomfort compares to pressure pain thresholds [3].

The purpose of this study was to quantify the effect of the handle shape on grip pressure measures during pressing and lifting of simulated long handled kitchen objects. The results of this study can be used to improve handle design to minimize grip discomfort and pain.

METHODS

Subjects (4 males and 5 females, 19-28 year old, healthy, right handed) simulated knife use by pressing the handle down on a load cell and also simulated pot lifting by lifting up the handle against a load cell (Fig 1) using one of the six common handle shapes (Fig 2). Each task was performed for 10 seconds at 20 N (approx. 2L pot of water) with visual feedback of the task force measured using a load cell (AMTI, Watertown, MA, USA). During the task, grip pressures (Fig 3) were measured with a Pliance pressure mat (Novel Electronics Inc., St. Paul, MN, USA) wrapped around each handle and secured in place with tape. The handle was not attached to the load cell requiring the subjects to maintain static equilibrium.

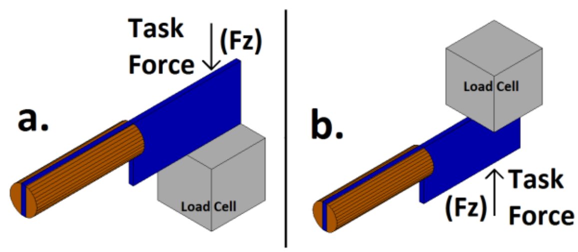

Figure 1: Test set-up with a load cell and handle: a-knife pressing task; b-pot lifting task.

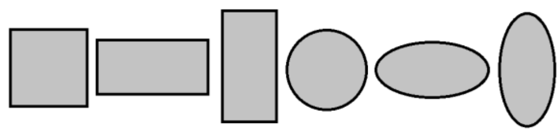

Figure 2: The six handle shapes: square, wide rectangle, tall rectangle, circle, wide oval, and tall oval cross-sections.

The pressure mat was 125x125 mm with 256 sensors calibrated to 600 kPa. All handles had a circumference of 125 mm as smaller handles could result in finger/thumb overlap and larger handles could not be entirely covered by the pressure sensor. Analyses of variance were used to test each measure (contact area, peak pressure, and mean pressure) for the effects of handle shape, task direction, and their interaction.

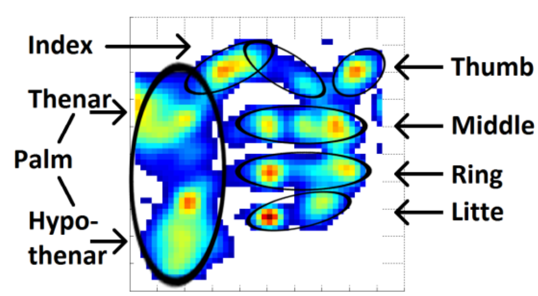

Figure 3: A sample pressure distribution for a max grasp of the circular handle with regions labeled.

RESULTS AND DISCUSSION

Handle shape was found to be a significant main effect for all measured parameters ($p<0.01$). Post-hoc analysis (Table 1) showed that the circular handle had the largest contact area ($p<0.01$ vs. all other shapes) and the lowest peak and mean pressures ($p<0.01$ vs. all other shapes but the tall oval). Pressure concentration patterns were visibly different between the rounded and rectangular handles: Pressure was well distributed for the rounded handles, especially for the circular handle, whereas the rectangular handles tended to have pressure concentrations along the corners (Fig 4a,b). These results suggest that use of a circular handle could distribute pressure over a larger hand area, reducing stress concentrations (lower peak pressure) compared to oval and rectangular handles.

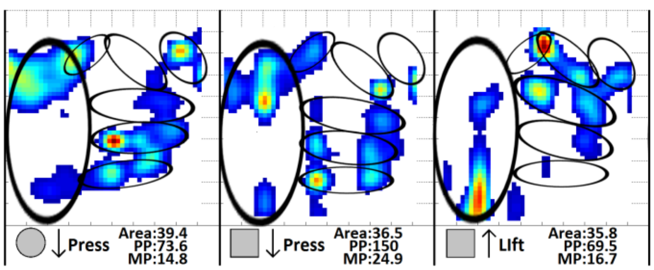

Figure 4: Grip pressure distribution examples: Circular vs. square for pressing (a vs. b), pressing vs. lifting with the square handle (b vs. c).

Peak and mean pressures were higher for the pressing tasks compared to the lifting tasks ($p<0.01$). Pressure was concentrated in the thenar eminence and the ring and little fingers for the pressing tasks, whereas for the lifting tasks, pressure was at the hypothenar area and the index and middle fingers (Fig 4b,c). The interaction post-hoc showed that task direction was significant for the square, wide rectangle, and wide oval handles (Table 1) for both peak and mean pressure. For pressing tasks, these same three handles also resulted in peak pressure exceeding a potential pressure pain threshold of 300 kPa [3] in 15% of trials. These results show that for the same task force magnitude, the handle design consideration is more important for tasks involving pressing down than lifting up.

SUMMARY/CONCLUSIONS

By modifying the handle shape, the peak pressure could be reduced as much as 27.6% (circle vs. wide rectangle), substantially lowering the likelihood of pain during kitchen activities. Specifically, the circular handle resulted in the lowest peak and mean pressures due to a more distributed pressure over a larger contact area than other handle shapes. Peak pressure at the hand was higher during pressing down than lifting up for the square, wide rectangle, and wide oval handles. Especially, peak pressure exceeded a potential pressure pain threshold 15% of the time, indicating hand pain when people press down with a knife at 20 N using those three handles. These results are expected to be useful in redesigning handle shapes of long handled kitchen tools to minimize pressure concentrations and discomfort/pain in the hand.

REFERENCES

1. Kamat, S.R. et al. *Proceedings of KEER-2010*, Paris, France, 2010.
2. Kuijt-Evers, L.F.M. et al. *Applied Ergonomics*, **38**, 643-654, 2007.
3. Cathcart, S., Pritchard S. *J. Headache Pain*, **7**, 21-26, 2006.

Table 1: Mean area and pressures with significant post-hoc results for handle shape and direction

Handle Shape		**Contact Area *‡**		**Peak Pressure *†‡**		**Mean Pressure *†‡**	
		cm^2	post-hoc	kPa	post-hoc	kPa	post-hoc
1	**Square**	32.4		214.6	Press > Lift	43.0	Press > Lift
2	**Tall Rectangle**	31.6		210.4		46.8	Press < Lift
3	**Wide Rectangle**	33.9	Press < Lift	223.6	Press > Lift	43.6	Press > Lift
4	**Circle**	46.1	> 1,2,3,5,6	161.9	< 1,2,3,6	37.1	< 1,2,3,6
5	**Tall Oval**	39.6	> 1,2,3	189.0		40.1	< 2
6	**Wide Oval**	36.3		224.3	Press > Lift	45.1	Press > Lift

(Significant: *****handle shape, †direction, ‡direction×handle shape)

A DATA-DRIVEN OPTIMIZATION METHOD TO DETERMINE MUSCLE- TENDON PATHS OF THE INDEX FINGER

[1]Jong Hwa Lee, [2]Deanna S. Asakawa, [1]Cecil A. Lozano, [3]Jack T. Dennerlein and [2]Devin L. Jindrich

[1]Arizona State University, Tempe, AZ, USA
[2]California State University, San Marcos, CA, USA
[3]Northeastern University, Boston, MA, USA
email: djindrich@csusm.edu web: www.limblab.org

INTRODUCTION

A musculoskeletal model of the human index finger can provide a better understanding of hand dynamics and control during multi-touch gestures used on hand-held touchscreen computing devices. As a first step toward a musculoskeletal model capable of describing the complex, multi-finger gestures used for touchscreen devices, we seek to incorporate intrinsic hand muscles into an existing musculoskeletal model of the human arm [5]. Although several studies have measured hand muscle moment arms in vivo and in situ [1-3], measurements of moment arms alone are insufficient for homeomorphic models like OpenSim [4]. Moment arms are indeterminate: many combinations of muscle- tendon paths could result in the same moment arm. We therefore developed techniques for data-driven optimization to determine attachments that reproduce measured moment arms for intrinsic and extrinsic muscles and tendons of the index finger.

METHODS

We added the following muscles to an upper-extremity model implemented in OpenSim [5]: terminal extensor (TE), extensor slip (ES), radial band (RB), ulnar band (UB), first dorsal interosseous or radial interosseous (RI), lumbricals (LU), and first palmar interosseous or ulnar interosseous (UI). Extensor indicis (EI) was omitted because the moment arms of EI and EDC (extensor digitorum communis) muscles were identical. Experimentally-measured values [1-3] were used as target moment arm relationships for all seven muscles at metacarpophalangeal (MCP), proximal interphalangeal (PIP), and distal interphalangeal (DIP) joints. We normalized moment arms by the length of middle phalanx for DIP and PIP joints, and by the MCP joint's thickness and width for the MCP joint. We employed a simulated annealing [6] algorithm to optimize muscle attachment points. The objective function, $f(\vec{x})$ was defined as the root mean square (RMS) error between the experimentally-derived moment arms, $r_j(\vec{q_i})$ and the modeled-estimate moment arms, $\hat{r}_j(\vec{q_i},\vec{x})$ as follows:

$$\text{Minimize} \qquad f(\vec{x}) = \sqrt{\sum_{i=1}^{m} \frac{\left[r_j(\vec{q_i}) - \hat{r}_j(\vec{q_i},\vec{x})\right]^2}{m}}$$

$$\text{Subject to} \qquad lb_j \le x_j \le ub_j$$

$$g_j(\vec{x}) - \varepsilon_j \le 0$$

Where, $\vec{x}$ was 6×1 vector (described as x,y,z origin and x,y,z insertion points) to be optimized, $\vec{q_i}$ was the joint angle with respect to finger motions (i), and j was each individual muscle. Boundary conditions constrained the path of muscle from violating a feasible region, expanded from bony segment (as a lower bound: lb_j) to external hand dimensions (as an upper bound: ub_j). ε_j was the maximum variations of experimental moment arms, and $g_j(\vec{x})$ was RMS error of ab/adduction moment arms during flexion/extension movements. The inequality constraint imposed the optimal pathway on producing realistic ab/adduction moment arms during flexion/extension simulation. This inequality constraint $\left(g_j(x), \varepsilon_j\right)$ acted as a weight function; ε_j for the extrinsic tendons was a large number so the attachment points were less influenced by ab/adduction motions, while ε_j for the intrinsic muscles was a small number so these muscles were more influenced by ab/adduction movements.

RESULTS AND DISCUSSION

The data-driven optimization approach was able to determine the attachment points of extrinsic and intrinsic muscles, resulting in moment arms that matched experimentally-measured relationships. At the MCP joint, the calculated moment arms of both extrinsic tendons and intrinsic muscles were similar to those measured by An [2] as shown in Fig. 1. The RMS error between modeled and actual moment arms were less than 1.7mm for flexion/extension motions and 2.1mm for ab/adduction movements. At the PIP and DIP joints, the calculated moment arms were compared with the experimentally measured values [1] (Fig. 2). During flexion or extension, the calculated moment arms of intrinsic muscles (UR and RB) matched the slope of experimental values ($R^2 = 0.96$); those of extrinsic tendons (FDP, FDS, ES and TE) showed poorer fits (Fig. 2).

At the PIP joint, the experimental moment arms of extrinsic tendons were constant across varying joint angles (FDP: r_{fdp} =10.8, FDS: r_{fds} =8.9 and ES: r_{es} =-3.6mm), while the calculated moment arms were non-linear functions dependent on joint angle ($0 \leq q \leq 2.09$ rad.) as follows: $r_{fdp} = -3.47q^2 + 9.09q + 4.43$, $r_{fds} = -2.46q^2 + 6.72q + 3.79$ and $r_{es} = 0.37q^2 + 2.73q - 5.69$. At the DIP joint, experimental moment arms were constants ($r_{fdp} = 6.8$ and r_{te} = -3.4 mm), but optimized moment arms were non-linear functions with respect to change in joint angle ($0 \leq q \leq 1.57$ rad.): $r_{fdp} = -3.27q^2 + 5.50q - 4.88$ and $r_{te} = 0.05q^2 + 2.34q - 2.28$. However, for all muscles except for TE, peak moment arms matched the constant measured moment arms at a point within the mid-range of movement.

REFERENCES

1. An KN, et al. *J Biomech* **12**, 775-788, 1979.
2. An KN, et al. *J Biomech* **16**, 419-425, 1983.
3. Armstrong TJ and Chaffin DB. *J Biomech* **11**, 119-128, 1978.
4. Delp SL, et al. *IEEE Trans on BME* **54**, 1940-1950, 2007.
5. Holzbaur K, et al. *Biomed Eng* **33**, 829-840, 2005.
6. Kirkpatrick S, et al. *Science* **220**, 671-680, 1983.

ACKNOWLEDGEMENTS

This study was funded by NSF (IIS/HCC) 0964220.

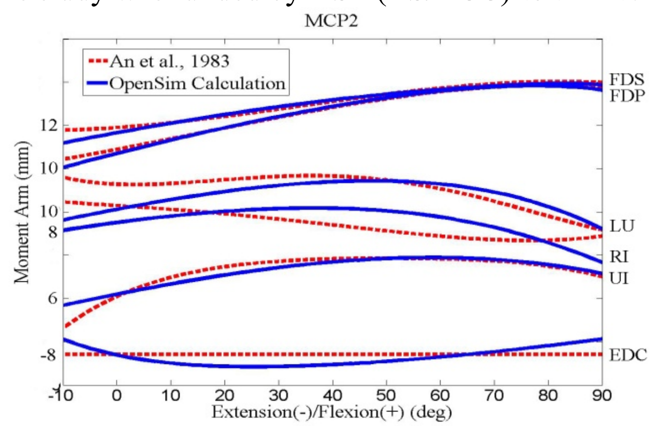

Figure 1: Estimated moment arms at the MCP joint (solid lines) compared with the corresponding experimental values (dashed lines). Positive angles are flexion while negative angles are extension.

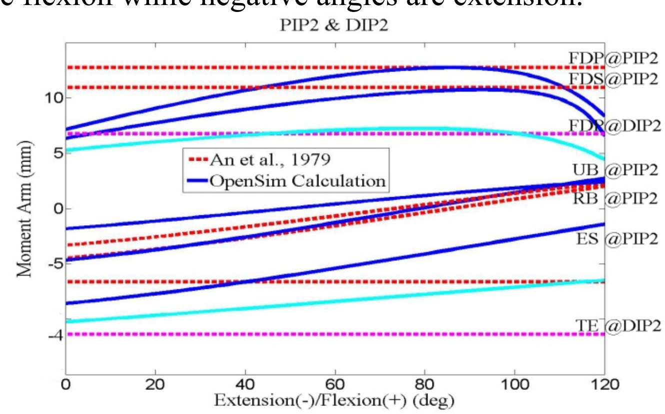

Figure 2: Moment arms at the PIP and DIP joints.

Table 1: Tendon excursion and moment arm root mean square errors between modeled and experimental values at DIP, PIP and MCP joints

		FDP	FDS	EC(ES)	RI	LU(RB)	UI(UB)	TE
DIP	**Moment Arm**	0.73						3.18
	Excursion	0.30						0.83
PIP	**Moment Arm**	2.54	2.19	2.54		0.39	1.08	
	Excursion	0.98	0.94	0.99		0.22	1.43	
MCP	**Moment Arm**	0.28	0.40	1.74	1.70	0.69	1.01	
		(0.44)	(0.92)	(1.33)	(1.86)	(1.87)	(2.09)	
	Excursion	2.49	2.05	1.85	2.14	0.70	0.60	
		(0.47)	(0.10)	(1.25)	(1.71)	(0.62)	(1.40)	

JOINT ANGLES OF THE FINGERS AND THUMB DURING 8 DIFFERENT GESTURES ON A TOUCHSCREEN COMPUTING DEVICE

[1]Deanna S. Asakawa, [2]Cecil Lozano, [2]Jong Hwa Lee, [3]Jack T. Dennerlein and [1]Devin L. Jindrich

[1]California State University San Marcos, San Marcos, CA, USA
[2]Arizona State University, Tempe, AZ, USA
[3]Northeastern University, Boston, MA, USA
email: dasakawa@csusm.edu

INTRODUCTION

Mobile touchscreen computing devices, including tablets and smartphones, are commonly used for both personal and work purposes. Recent statistics show that 45% of Americans own a smartphone[1]. These rapidly spreading hand-held devices increase the possibility of repetitive strain injuries or other musculoskeletal disorders related to the overuse of the fingers and thumb. Previous studies have investigated factors such as thumb posture and motor performance during hand-held smartphone use[2]. The purpose of this study was to quantitatively compare finger joint biomechanics during common one- and two-finger gestures used on a touchscreen hand-held computing device. We hypothesized that two-finger gestures would involve larger changes in joint angles of the digits and greater muscular activity than one-finger gestures.

METHODS

Twelve healthy right-handed subjects (6 male, 6 female, age 20-30 yrs) completed a 3-4 hour experimental session for this study. All subjects reported to be free of any upper extremity musculoskeletal disorders, were frequent touchscreen device users, and were familiar with the finger gestures and computer tablet interactions used in this study. Consent forms and procedures were approved by the Institutional Review Board of Arizona State University and were in accordance with the declaration of Helsinki.

We measured finger joint flexion/extension angles and muscle activations as subjects completed multiple repetitions of 8 different stroke-like gestures on an iPad computer tablet (Apple Inc., Cupertino, CA). We studied 4 gestures that used only the index finger. These one-finger gestures included: panning to the right, left, up and down by sliding the index finger in the respective direction. We also studied 4 gestures that required simultaneous use of the index finger and thumb: rotating to the right (index finger and thumb rotate in a clockwise direction), rotating to the left (index finger and thumb rotate counter in a counter clockwise direction), zooming in (spreading the index finger and thumb farther apart) and zooming out (bringing the thumb and index finger together). Subjects performed gestures on the touchscreen in two conditions: interacting with a software application (contextual), and performing gestures when the computer tablet device was off (non-contextual). For the contextual condition, subjects interacted with the software Google Earth Globe (Google Inc., Mountain View, CA). Each condition was completed 3 times for a total of 48 trials (8 gestures x 2 contexts x 3 replicates). Order of the gestures was randomized and order of device condition among participants was presented in a complete counterbalance. Subjects repeated each gesture for 20 second trials followed by 5 seconds of rest. Device condition was changed every 5 minutes. Continuous data recordings of finger joint angles and electromyographic (EMG) muscular activity were recorded for all gesture repetitions. Joint angles (kinematic data) of all fingers on the dominant were recorded through a wireless CyberGlove II sensor system (CyberGlove Systems, San Jose, CA). Muscular activity in the extensor digitorum and deltoid muscles of the dominant arm were recorded using bi-polar surface EMG (Bortec AMT-8).

RESULTS AND DISCUSSION

Gestures on a touchscreen computer involving both the thumb and index finger produced larger changes in joint angle for all fingers than gestures involving the index finger alone (Fig. 1). The two more proximal joints of each digit showed the greatest movement compared to the distal joints for both the one and two-finger gestures (Fig. 1). The metacarpophalangeal (MCP) and proximal interphalangeal (PIP) joints of the index finger moved more during the two-finger gestures as compared to gestures using the index finger alone.

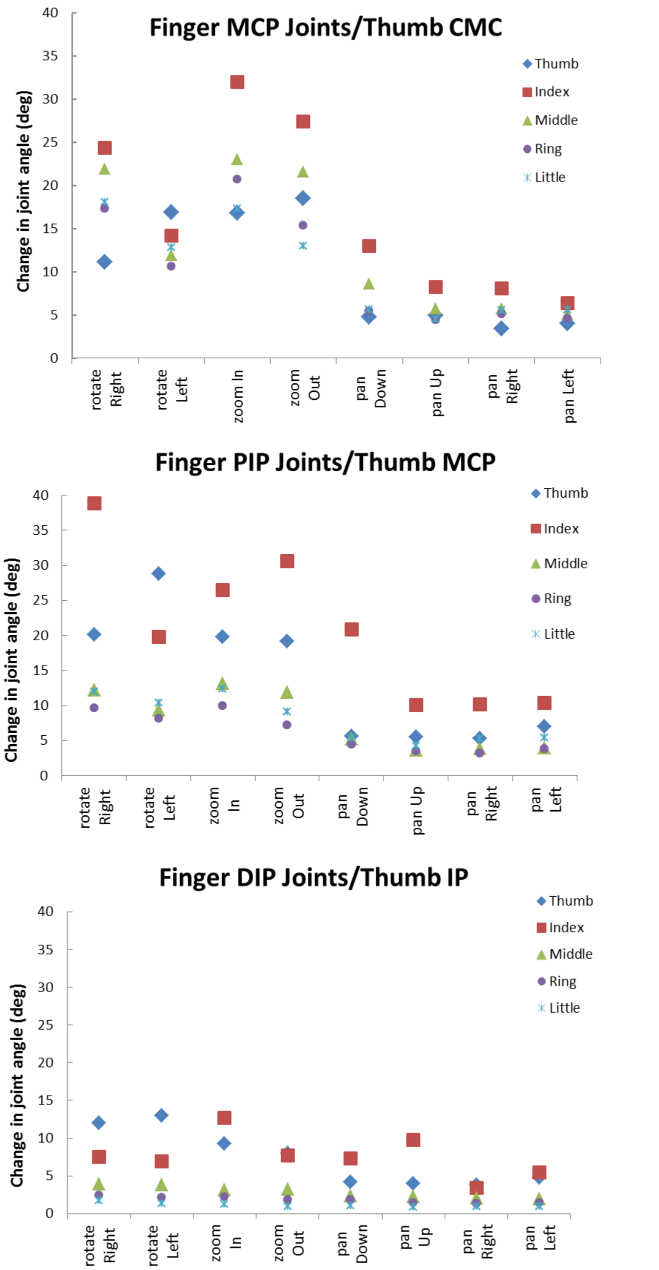

Figure 1: Average change in joint angle for the thumb (diamond), index (square), middle (triangle), ring (circle) and little finger (x) at each joint location for each of 8 touchscreen gestures.

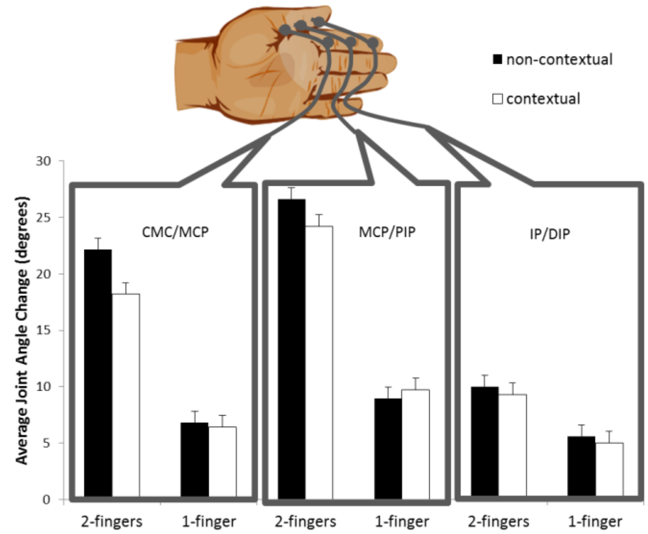

Figure 2. Average change in joint angle for thumb CMC/index finger MCP, thumb MCP/index finger PIP, and thumb IP/index finger DIP for gestures using 2 fingers and 1 finger (index finger alone). For the 2-finger condition, the change in joint angle was averaged for the thumb and index finger.

Similar to the index finger, the joints of the middle, ring and little fingers showed greater change in joint angle during the two-finger gestures as compared to one-finger gestures even though these fingers were not touching the screen (Fig. 1).

In general, the visual display of software reacting to the performed gestures (contextual condition) resulted in smaller finger and thumb joint movements compared to gestures performed with the device turned off (Fig. 2). Also, our results showed muscle activity in the extensor digitorum was greater during the gestures involving 2 fingers. These results support the hypothesis that 2-finger gestures involve larger changes in joint angles of the digits than 1-finger gestures on a touchscreen.

REFERENCES

1. Duggan M. and Rainie L. *Pew Research Center's Internet & American Life Project*, 2012.
2. Trudeau MB. et al. *J. Biomech*,**45**(14)2349-54 2012.

ACKNOWLEDGEMENTS

This study was funded by NSF(IIS/HCC) 096422.

A BIOMECHANICAL ASSESSMENT OF BREAST KINEMATICS DURING DIFFERENT EXERCISE MODALITIES

[1]Debbie Risius, [1]Alexandra Milligan, [1]Chris Mills, and [1]Joanna Scurr

[1]University of Portsmouth, Portsmouth, Hants, UK
email: Debbie.Risius@port.ac.uk, web: http://www.port.ac.uk/breastresearch

INTRODUCTION

Effective sports bras that minimise breast displacement are crucial to reduce breast discomfort during exercise [1]. The majority of breast biomechanics literature centers on treadmill activity. However, until the movement of the breast is understood during different actions, optimum breast support parameters for sport specific activities are unknown. This study aimed to determine the kinematics of female breast movement during; running, jumping and an agility task, in order to inform breast support design during different multiplanar activities.

METHODS

Ten 34D cup participants had passive markers attached to their right nipple and trunk, to calculate relative 3D breast displacement [2]. Supported and unsupported anterioposterior, mediolateral and vertical breast displacement was calculated during treadmill running (10kph), maximum counter movement jumps and an agility T-test.

RESULTS AND DISCUSSION

Exercise modality influenced the magnitude of breast displacement when bare breasted ($p<.006$) and when wearing a sports bra ($p<.013$). The greatest anterioposterior (57 mm) and mediolateral (67 mm) breast movement was found during the agility task, and the greatest vertical breast movement (86 mm) found during jumping (Fig. 1). Agility and running had equal distributions of movement in each direction (30% AP, 36% ML, 33% V), whereas jumping activities produced a larger distribution in the vertical direction (26% AP, 27% ML, 47% V). The sports bra was more effective at reducing anterioposterior breast displacement during running (51%) than either jumping (35%) or the agility task (41%), more effect at reducing mediolateral displacement during jumping (64%) than either running (47%) or the agility task (49%), and more effective at reducing vertical breast displacement during running (66%) than jumping (50%) (Fig. 2).

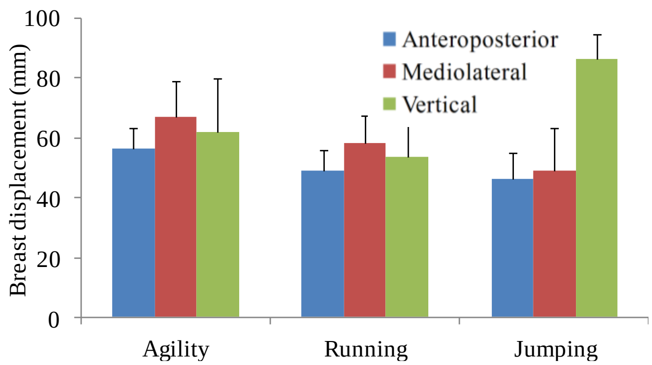

Figure 1: Multiplanar breast displacement during different exercise modalities in a bare breasted condition.

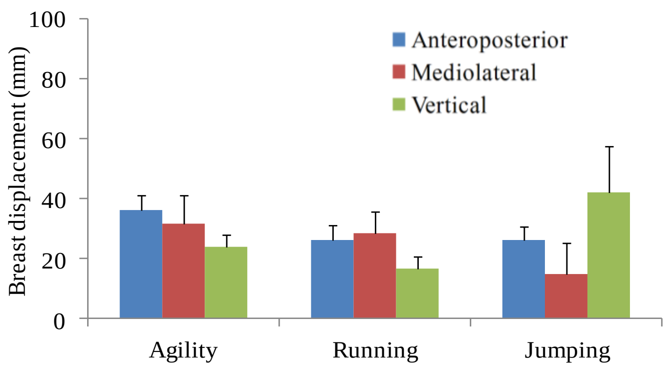

Figure 2: Multiplanar breast displacement during different exercise modalities in a sports bra condition.

Exercise modality has an impact upon the magnitude and distribution of multiplanar breast displacement, and also upon a sports bra's effectiveness at reducing this breast movement. Future studies on sports bra functionality should ensure that the exercise modality is carefully selected, as the results may differ. Sports bra manufacturers may wish to design sport specific products, as a sports bra effectiveness is influenced by the type of exercise [1].

REFERENCES

1. Scurr J, et al. *J Sports Sci* **29**, 55-61, 2011.
2. Scurr J, et al. *J Appl Biomech* **25**, 322-329, 2009.

SCAPULOTHORACIC MUSCLE ACTIVATION AND SHOULDER KINEMATICS FOLLOWING A SIMULATED WORK TASK WITH LOW LEVEL FORCES

[1] Kimberly A. Szucs PhD OTR/L, [2]Nicolas Beckas MS OT, [1]Megan Molnar OTS
[1]Department of Occupational Therapy, Duquesne University, Pittsburgh, PA; szucsk@duq.edu
[2]University of Pittsburgh Medical Center for Rehabilitation Services, Pittsburgh, PA

INTRODUCTION

Chronic shoulder pain is common in persons who frequently engage in repetitive manual work. Biomechanical stress caused by heavy lifting has been well examined and efforts have been taken to minimize these stresses in work environments. However, less is known about the effect of low-intensity, repetitive forces on muscle activation and shoulder biomechanics. Low-intensity forces can cause muscle fatigue, including fatigue of the trapezius muscle [1]; however, it is currently unknown if muscle fatigue resulting from low-intensity forces will lead to biomechanical changes at the shoulder complex, such as altered scapular kinematics. Additionally, most fatigue studies include only the standard 3 anatomical divisions of the trapezius muscle: the upper, middle and lower trapezius. The upper trapezius is not uniformly activated and can be subdivided into 2 functional portions: clavicular trapezius and upper trapezius, which are each preferentially activated [2].

This study aims to determine whether acute muscle fatigue resulting from low-intensity repetitive forces alters shoulder joint kinematics—specifically scapula rotations. Also being explored is whether muscle fatigue caused from low-intensity forces manifests differently between the 4 parts of the trapezius, including the two subdivisions of upper trapezius.

METHODS

A Noraxon Telemyo 900 EMG system (Noraxon U.S.A. Inc., Scottsdale, AZ) was used to record raw surface EMG signals from 4 parts of trapezius (clavicular, upper, middle, and lower subdivisions). This system is differentially amplified and has an input impedance of $>10^{15}\ \Omega$//0.2pF. Data were pre-amplified x10. Bipolar Ag-AgCl electrodes were taped to the skin overlying the muscle belly on the dominant side, parallel to the muscle fiber. Sensors were applied at the following locations:

1. Clavicular fibers of Trapezius: 20% lateral to the midpoint between the origin and insertion of the fibers [2].
2. Upper Trapezius: Halfway along a line between the AC joint and7th cervical spinous process [3]
3. Middle Trapezius: Midway on a horizontal line between the root of the spine of scapula and the 3rd thoracic spinous process [3]
4. Lower Trapezius: Medial and superior to an oblique line between the root of the spine of scapula and the 8th thoracic spinous process [3]

A trakSTAR electromagnetic motion capture system (Ascension Technology Corp., Burlington, VT) was used to capture 3D kinematic data of each subject's thorax, dominant side humerus and scapula. 8 mm surface sensors were taped to the skin over these bony segments using double-sided tape.

Maximum voluntary contractions were collected for each muscle following standard protocols [4]. The same method was used to test the clavicular and upper trapezius. 3D kinematic and EMG data were collected as subjects elevated their arm in the scapular plane for 5 repetitions (Pre-fatigue condition). Subjects then began the 60 minute Fatigue task. This task was designed to simulate a lift-and-place work activity. Subjects repeatedly lifted light-weight foam rings between 45° and 100° of arm elevation in the scapular plane (Fig. 1). The task was completed in sitting to focus on fatiguing the trapezius versus other core or lower extremity musculature. Subjective fatigue during the task was assessed with the Borg CR10 scale at 15 minute intervals. Subjects were encouraged to complete the task for the entire 60 minute protocol but were able to stop if the fatigue in their shoulder reached a 10 on the Borg CR10 scale.

EMG and kinematic data were collected immediately following completion of the Fatigue task (Post-fatigue condition) and following a 15 minute rest period (Rest condition). EMG and kinematic data were synchronized during data collection and captured at 1200 Hz using MotionMonitor software (InnSport, Chicago, Ill).

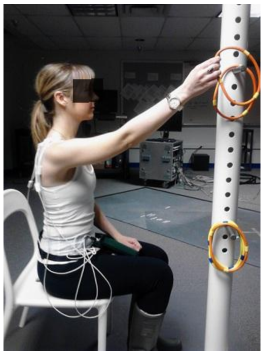

Figure 1: Fatigue task set-up

Data collection and processing is currently ongoing. To date 15 healthy subjects have completed data collection and processing is complete on 7 subjects. Kinematics and EMG data were reduced to every 15° of arm elevation. Raw EMG data were full wave rectified and filtered with a 100Hz low pass fourth-order zero lag Butterworth filter. Separate MVCs for each muscle were calculated using Excel.

RESULTS AND DISCUSSION

Due to the limited data currently available for analysis, descriptive statistics have been calculated and reported here with the available data from 7 subjects. The average Borg rating at completion of the Fatigue Task was 6.5 (±2.3). The average time completed for the Fatigue Task was 30 minutes, with 2 of the 7 subjects completing all 60 minutes. Descriptive statistics of trapezius activation show a trend towards increased percent activation in all four divisions post-fatigue, suggesting the muscles were fatigued by the task (Table 1). In the Rest condition, activation of the clavicular trapezius had returned to pre-fatigue values, while activation of the upper and middle divisions was similar to post-fatigue values. Percent activation of lower trapezius was higher at rest than both pre- and post-fatigue.

A trend towards increased scapular upward rotation, internal rotation and posterior tilt was also observed post-fatigue, suggesting acute fatigue from low-level forces can alter shoulder biomechanics (Fig 2). A similar pattern of increased upward rotation and internal rotation has been observed in persons with subacromial impingement syndrome [5].

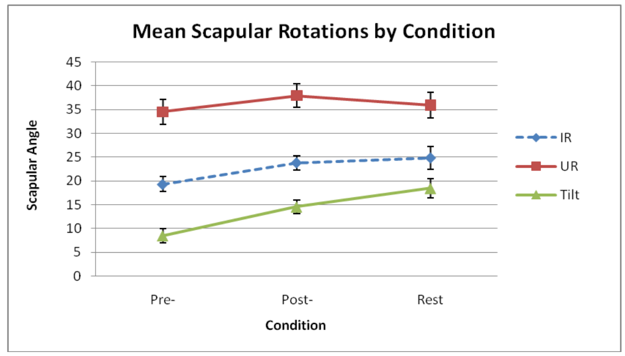

Figure 2: Mean scapular rotations by condition (±SE)

CONCLUSIONS

These preliminary findings support the hypothesis that low-level, repetitive forces contribute to muscle fatigue and altered shoulder biomechanics. Preliminary results from this study justify the need for preventative measures in the workplace such as activity pacing and reasonable task demands.

REFERENCES

1. de Looze M, et al. *Ergonomics* **52**, 428-437, 2009
2. Holtermann A, et al. *JEMK* **19**, 896-902, 2008
3. Soderberg G (editor), NIOSH. 1992
4. Kendall FP, *Muscles: Testing and Function, with Posture and Pain* (5th ed), Lippincott Williams & Wilkins, 2005
5. Ludewig PM & Reynolds JR, *JOSPT* **39**, 90-104, 2009

Table 1: Mean % Activation of Trapezius by Condition

Portion of Trapezius	Pre-Fatigue	Post-Fatigue	Rest
Clavicular	Pre: 64.04% (±4.41)	Post: 71.48% (±5.04)	Rest: 63.88% (±6.99)
Upper	Pre: 49.02% (±4.82)	Post: 59.22% (±6.15)	Rest: 58.11% (±8.30)
Middle	Pre: 47.15% (±5.82)	Post: 52.10% (±6.98)	Rest:51.26% (±8.57)
Lower	Pre: 64.89% (±6.55)	Post: 75.08% (±6.41)	Rest: 78.89% (±9.71)

ADVANCED AGE AND THE MECHANICS OF UPHILL WALKING: A JOINT-LEVEL, INVERSE DYNAMIC ANALYSIS

Jason R. Franz, Alyse Kehler, Lauren E. MacDonald, and Rodger Kram

Locomotion Laboratory, Dept. of Integrative Physiology, University of Colorado, Boulder, CO, USA
Email: jrfranz2@wisc.edu web: https://sites.google.com/site/jasonrfranz

INTRODUCTION

The biomechanical demands of uphill walking can be challenging for community-dwelling old adults. We recently quantified how advanced age (65+ yrs) brings diminished ground reaction forces (GRFs), mechanical work, and leg muscle recruitment during both level and uphill walking [e.g., 1-3]. While these measures have been valuable and informative, they offer only indirect insight into the muscular limitations of old adults walking uphill. In this study we compared the kinetics (moments and powers) of old and young adults at each leg joint to more precisely identify biomechanical factors that may lead to impaired uphill walking ability with age.

One of the most pervasive biomechanical consequences of advanced age is a reduction in ankle joint kinetics. During level walking, for example, even healthy and active old adults generate 17 to 29% less ankle power compared to young adults [1-3]. Reduced ankle joint kinetics in old adults are compensated for by an increase in hip extensor moments and power generation during early stance [e.g., 1] and/or an increase in hip flexor moments and power generation during push-off [e.g., 2]. Uphill walking places increased demands on the leg muscles of old adults that could exacerbate age-related changes in leg joint kinetics.

In this study, we quantified sagittal plane ankle, knee, and hip joint moments and powers in healthy old and young adults during level and uphill walking. We hypothesized that: 1) old adults would exhibit smaller peak ankle joint kinetics and larger peak hip joint kinetics than young adults during both level and uphill walking and 2) these age-related differences in ankle and hip joint kinetics would be greatest during uphill vs. level walking.

METHODS

We analyzed the walking patterns of 10 old adults (mean ± SD, age: 72 ± 5 yrs) and 8 young adults (age: 27 ± 5 yrs) walking at 1.25 m/s on a dual-belt, force-measuring treadmill at four grades (0°, +3°, +6°, +9°). We placed 15 retro-reflective markers on each subject's skin/shoes corresponding to the following anatomical landmarks: anterior superior iliac spines, sacrum, greater trochanters, lateral femoral condyles, tibial tuberosities, lateral malleoli, posterior calcanei, and lateral fifth metatarsal heads. An 8-camera motion analysis system (Motion Analysis Corp, Santa Rosa, CA) captured the three-dimensional marker positions at 100 Hz in synchrony with the GRF data.

We used the analysis methods described by Vaughan et al. [4] to calculate the sagittal plane ankle, knee, and hip joint kinematics and kinetics for each subject over 15 consecutive strides. In a secondary analysis, we integrated the joint power curves with respect to time to calculate the net positive work performed by muscles crossing the ankle, knee, and hip joints. An analysis of variance (ANOVA) for repeated measures tested for significant main effects of and interactions between age and grade with a $p<0.05$ criterion.

RESULTS AND DISCUSSION

As hypothesized, old adults walked with smaller peak ankle joint kinetics (e.g., power generation: -18% at +9°) and larger peak hip joint kinetics (e.g., power generation: +119% at +9°) than young adults, most evident during the late stance phase of both level and uphill conditions (Fig. 1). In partial support of our second hypothesis, the age-related reduction in peak ankle joint moments was greater during uphill (-0.41 Nm/kg) vs. level (-0.30 Nm/kg) walking. Indeed, a significant interaction revealed that only young adults increased their peak ankle extensor moments during uphill vs. level walking (p=0.003).

Old adults performed 317% (level) and 119% (uphill) more trailing leg positive double support work than young adults using muscles crossing the hip (p=0.012). However, this was not enough to compensate for the reduced contribution from muscles crossing the trailing leg knee and ankle joints. Thus, old adults tended to perform 20% (level) and 16% (uphill) less total double support trailing leg positive joint work than young adults (p=0.051).

In addition to their more vigorous hip joint kinetics during push-off, old adults further compensated for reduced propulsive ankle function by performing two to three times more positive work per step than young adults during single support via muscles crossing the stance leg knee joint (Fig. 2). In contrast, old adults performed 75% (level) and 71% (uphill) less single support positive work per step using muscles crossing the hip (p<0.001).

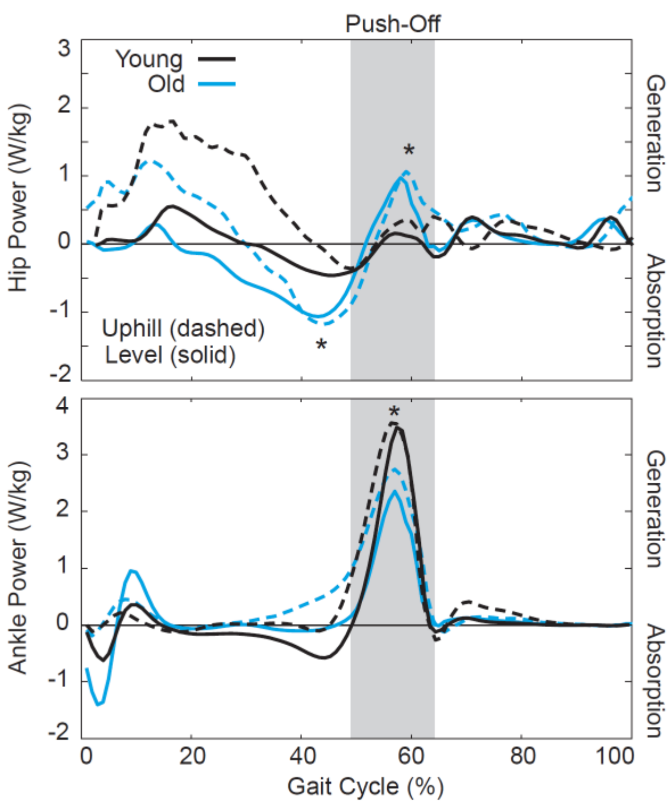

Figure 1. Sagittal plane ankle and hip joint powers of old and young adults during level and uphill (+9°) walking plotted over an averaged gait cycle. Asterisks (*) indicate a significant difference between old and young adults (p<0.05).

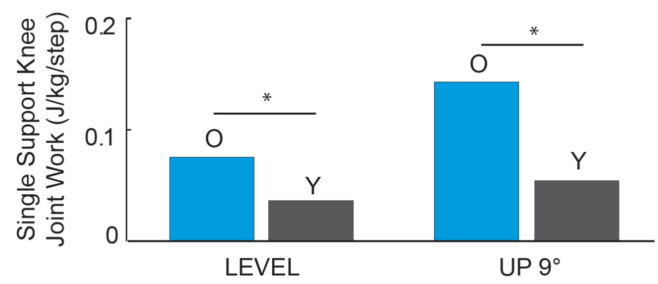

Figure 2. Average knee joint mechanical work per step performed during single support in old (O) and young (Y) adults. Total joint work performed during single support was not significantly different between old and young adults (p=0.593). However, old adults performed more single support positive work than young adults via muscles acting across the knee (p=0.027).

CONCLUSIONS

Old adults exhibit reduced trailing leg propulsive function during uphill walking largely because they generate significantly less ankle power than young adults during push-off. Old adults compensate for reduced ankle power by: 1) generating greater hip power than young adults during push-off to initiate leg swing and 2) performing greater positive work during single support via muscles acting across the knee (i.e., quadriceps). In our opinion, interventions to preserve the uphill walking ability of old adults should focus on the source of their walking impairments rather than observed compensations. Thus, our findings indicate that maintaining ankle power generation and trailing leg propulsive function with age should be the primary focus of "prehabilitation" strategies for old adults.

REFERENCES

1. DeVita P and Hortobagyi T. *J Appl Phys* 2000.
2. Cofre LE et al. *Gait Posture* ***33***, 2011.
3. Franz JR, Kram R. *J Biomech* **46**, 2013
4. Vaughan et al. Dynamics of Human Gait 1999.

ACKNOWLEDGEMENTS

We thank Dr. Alaa Ahmed for her help in developing the inverse dynamics script and the use of the motion capture system. Supported by a grant from NIH (5T32AG000279).

REGION-SPECIFIC STRAIN ENERGY IN THE PROXIMAL FEMUR DURING LOAD-BASED ACTIVITIES IN ELDERLY WOMEN

[1]Mariana E. Kersh, [1]Saulo Martelli, [2]Roger M.D. Zebaze, [2]Ego Seeman, and [1]Marcus Pandy

[1]University of Melbourne, Melbourne, VIC, Australia
[2]University of Melbourne – Austin Health, Melbourne, VIC, Australia
email: mkersh@unimelb.edu.au

INTRODUCTION

Exercise may slow bone loss and maintain bone's structural integrity [1-2]. However, the stresses and strains responsible for focal adaptive changes in bone structure in response to joint and muscle forces during exercise are not quantified. To achieve this, and so design programs to maintain bone health, we compared the strain energy density in four regions of the proximal femur during jumping, stair ascent, and stair descent.

METHODS

Pilot data from five postmenopausal women (age range = 60-74) with no history of fractures or drug therapy influencing the skeleton was obtained. The ethics committees of The University of Melbourne and the Austin Health approved the study.

Subjects were asked to jump in place, and ascend and descend a series of stairs without the use of handrails. Three dimensional joint motion, ground reaction forces and muscle EMG activity were recorded simultaneously for five trails of each task. Computed tomography (CT) data of the femur of the dominant leg for each subject were also acquired (Aquilon CT, Toshiba) (Fig. 1). Scans were taken using 120kV, 200mA, and 0.5mm sized voxels.

A generic musculoskeletal model was scaled to each subject's anthropometry using OpenSim [3]. The joint angles and torques were calculated using inverse kinematic and dynamic analyses, respectively. Muscle forces were calculated using a static optimization algorithm in which the sum of the squares of the muscle activation was minimized. The hip joint reaction force was found by solving a static equilibrium problem for the femur.

Finite element models of the femur of the dominant leg of each subject were created (Fig. 1). Each femur was segmented from the CT scans (Amira v5.3, VSG, USA) and converted into solid models (Geomagic v10, Geomagic, USA). A finite element package (Abaqus v6.11, Simulia, France) was used to discretize the bone into quadratic tetrahedral elements and each element was assigned an isotropic Young's modulus based on the relationships between Hounsfield units and Young's modulus (Bonemat, Supercomputing Solutions, Italy) [4]. The muscle forces and hip joint reaction force from the musculoskeletal model were applied

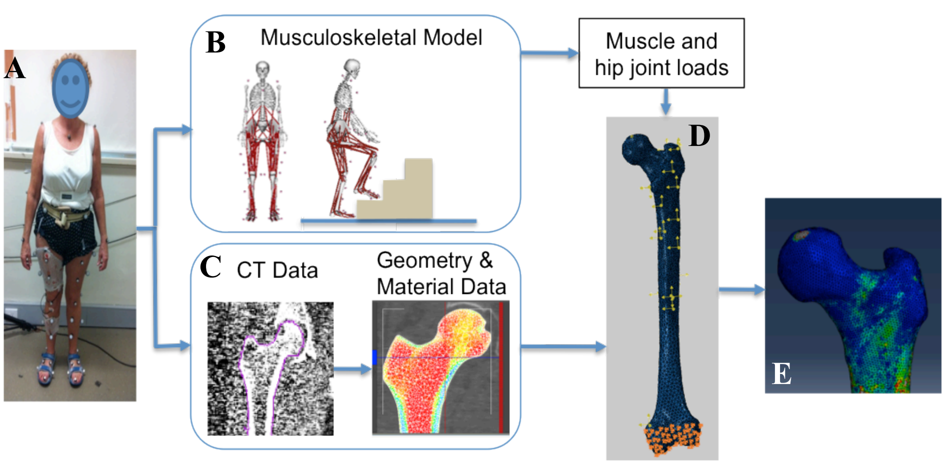

Figure 1: Women over 60 years of age (A) were asked to jump in place, ascend stairs, and descend stairs. Musculoskeletal models (B) were used to calculate muscle and hip joint loads at the femur. CT data from each subject (C) was used to create models of the femur with a heterogeneous distribution of bone strength values. A finite-element model (D) of the femur was used to calculate the stain energy (E) in the proximal femur.

as nodal boundary conditions for each time increment of the activity, and the distal end of the femur was kinematically constrained. A linear implicit analysis was used to calculate the strain energy (a specific indicator of bone remodeling) in the proximal femur.

Strain energy density comparisons: Four regions of the proximal femur were compared: (1) proximal neck, (2) distal neck, (3) greater trochanter, and (4) lesser trochanter (Fig. 2, inset images). The strain energy density within each region (strain energy/volume) was calculated for all activities. A paired t-test ($\alpha = 0.05$) was used to compare the total strain energy density (the area under each curve in Fig. 2) during jumping, stair ascent, and stair descent.

RESULTS AND DISCUSSION

During jumping, there was no difference in the total strain energy density by region (Fig 2). For stair ascent, the total strain energy density within the proximal femoral neck was higher than that in the distal femoral neck ($p = 0.03$) (Fig. 2, compare gray lines in A and B). The strain energy density during stair descent was also higher proximally than distally ($p = 0.03$). Within each region, the total strain energy density was not different regardless of activity.

Two peaks in strain energy were observed during jumping: one for the crouch phase during which the subject prepares to jump and the second for the impact phase of jumping. Interestingly, our results suggest that the act of crouching, which requires hip and knee flexion, generates as much strain energy as impact loading. Understanding the specific contribution of the hip and knee flexors to the strain energy response during jumping may help in the development of non-impact based exercise protocols that are safer for the older populations to which they are targeted.

A limitation of this study is the qualitative verification of muscle force calculations by comparison of their magnitudes with EMG data. Also, the material properties of the finite-element model have been validated against cortical surface strain alone. Finally, the statistical power of this study is limited by the sample size. However, a differentiation of the regional response of bone to loads was possible.

CONCLUSIONS

The effect of stair climbing and descending was higher in the proximal than distal femoral neck. Femoral fractures are more common in the proximal region, and so safely targeting this region with exercises may be a feasible approach to preserving bone structure and reducing age related increases in bone fragility.

REFERENCES

1. Korpelainen R, et al. *Arch Intern Med* **170(17)**, 1548-56,2010.
2. Nikander R, et al. *BMC Medicine* **8(47)**, 1-16, 2010.
3. Delp S, et al. *IEEE Trans Biomed Eng* **54(11)**, 1940-50, 2007
4. Morgan-St.James and Carroll, *Bone* **43(3)**, 521-531, 2003

ACKNOWLEDGEMENTS

We thank Kylie King, Mercy Asideu, and Melissa Munanto for their assistance with this study.

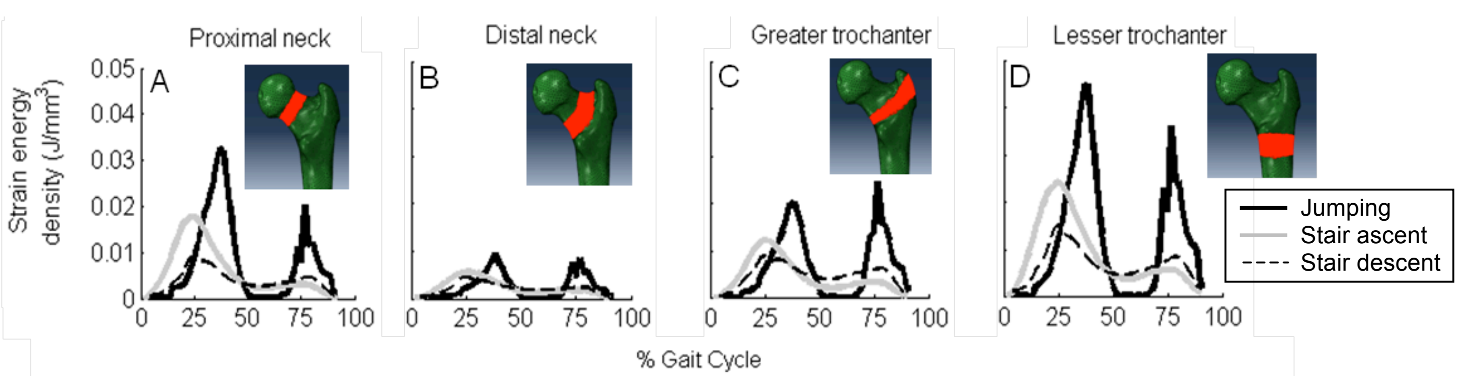

Figure 2. Strain energy density calculated in four regions of the proximal femur for the activities investigated.

COMPARISON OF KNEE KINEMATICS IN OLDER ADULTS WITH UNILATERAL TRANSFEMORAL AMPUTATIONS DURING BASELINE WALKING AND RAMP DESCENT

[1]Caitlin O'Connell, [1]Rakie Cham, [1]April J. Chambers
[1]University of Pittsburgh, Pittsburgh, PA, USA
Email: Caitlino@pitt.edu

INTRODUCTION

Factors associated with both old age and lower extremity amputations have been shown to predispose individuals to falls [1,2]. The loss of muscles, sensory nerves and joints associated with amputation as well as the inherent differences between prosthetic and sound limbs can affect gait [1]. An intra-subject comparison between the prosthetic and sound limb of older adults with a unilateral transfemoral amputation during gait can give insight into the kinematic differences that contribute to an increased risk of falling. This study will include baseline walking and ramp descent, as inclines are environmental obstacles that are difficult to navigate with a prosthetic leg and have not been studied extensively in this population [1,3].

METHODS

Five subjects (age 67.2 ± 2.7 years, 2 female) with a unilateral transfemoral amputation were recruited for the study with additional inclusion criteria of being 2 years post-amputation with an activity level of K2 or K3 according to the Medicare Functional Classification Level Scale. Individuals with comorbidities that could affect gait or balance were not eligible. All subjects wore microprocessor controlled prosthetic knees.

The protocol was approved by the Institutional Review Board and subjects signed a consent form prior to testing. Data was collected in the Human Movement and Balance Laboratory, a gait analysis laboratory equipped with a 14-camera motion capture system (Vicon, Oxford, UK) at a sampling frequency of 120 Hz. An initial static trial was recorded with subjects standing in a modified anatomical position from which joint angles could be normalized. At least three trials were collected for both baseline walking and ramp descent conditions. For the baseline condition, subjects walked on a level ground for approximately 5 m. The ramp descent took place on a 2-m long ramp with an inclination of -4.7° designed to meet building guidelines set by the Americans with Disability Act [4]. For both conditions, subjects were instructed to walk at a self-selected pace and were permitted to use assistive devices necessary to complete each condition. Two subjects required no assistive devices for baseline walking and ramp descent, while two used standard walkers and one subject used a cane for both conditions.

Data was processed using a Woltring filtering routine. Sagittal knee angles were computed using the Euler method with primary rotation taken in the sagittal plane. Static angles were subtracted from dynamic angles for each trial to normalize for differences between the prosthetic and sound limbs. Additionally, gait speed was measured for each trial.

RESULTS AND DISCUSSION

Sagittal knee angles at heel strike (HS) and midswing (MSw) during baseline walking and ramp descent for each subject are reported in Table 1. Based on intra-subject analysis, the angles of the prosthetic limb at HS and MSw were statistically different ($p<0.01$) from the angles of the sound limb for baseline walking and ramp descent. Further, the maximum flexion angle during swing phase is significantly lower in the sound limb during ramp descent when compared to the baseline while the angle of the prosthetic limb at MSw is statistically different ($p<0.01$) but whether the angle increases or decreases compared to baseline prosthetic limb varies between subject. The use of an assistive device may play a role in the knee kinematics during ramp descent, but this interaction could not be quantified due to small sample size. This suggests that microprocessor knees allow for some control of knee flexion during swing phase but the gait adjustments to an inclined surface is dependent on the individual. Gait speed during ramp descent decreased from that of baseline walking for all subjects and is a modification strategy previously identified in the literature [1,3].

Examining the knee flexion angle over an entire gait cycle, the swing phase generally occurs sooner for the prosthetic limb than the sound limb and the prosthetic knee is fully extended for ~10% of the gait cycle before HS to ensure that the prosthetic knee will not buckle when loaded (Figure 1). Differences between sound and prosthetic limbs were largely consistent between baseline and ramp descent for all subjects.

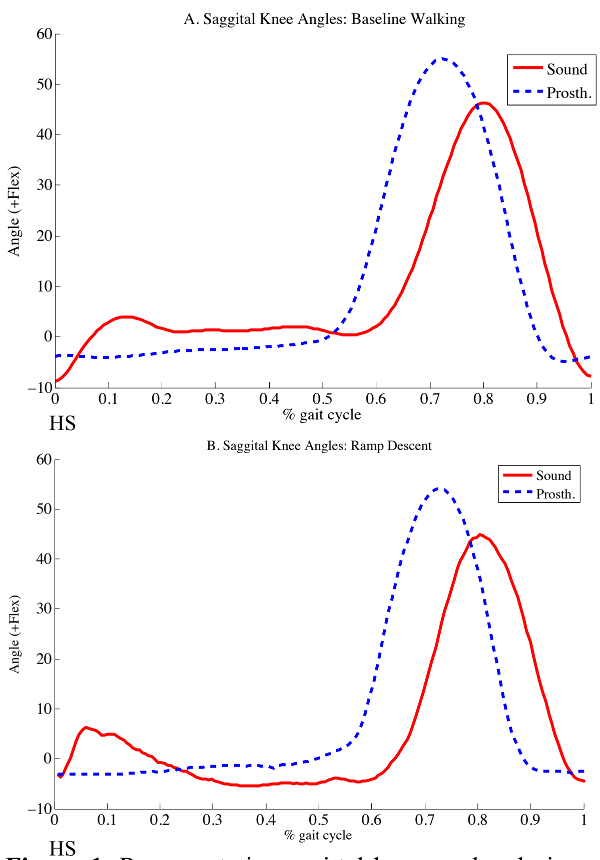

Figure 1. Representative sagittal knee angles during one gait cycle for Subject 1.

CONCLUSION

The differences in knee kinematics between sound and prosthetic limbs of older adults with unilateral transfemoral amputation suggest that different gait modifications are employed when navigating an incline as opposed to a level surface. Further study with a larger sample size is required to identify the specific gait adjustments employed during ramp descent as well as the interaction between knee kinematics and the assistive devices used during gait.

REFERENCES

1. Vrieling et al. *Gait Posture.* **28**, 235-242, 2008.
2. Shumway-Cook et al. *Physical Therapy*. **77**, 812-819, 1997.
3. Fradet, L et al. *Gait Posture.* **32**,191-198, 2010.
4. Appendix A, *Americans with Disabilities Act*, 31-33, 2002.

ACKNOWLEDGEMENTS

Funding provided by the American Orthotic and Prosthetic Association.

Table 1. Sagittal knee angles (+ Flexion) at MSw and HS of sound and prosthetic limbs during baseline walking and ramp descent conditions.

		Baseline Walking					Ramp Descent				
		Sound Limb		Prosthetic Limb		Speed	Sound Limb		Prosthetic Limb		Speed
Subject	Assistive Device	MSw Angle	HS Angle	MSw Angle	HS Angle	(m/s)	MSw Angle	HS Angle	MSw Angle	HS Angle	(m/s)
1	Cane	45.41	-11.05	55.50[a]	-3.93[a]	0.75	33.83[b]	-14.28	53.16[ab]	-3.41[a]	0.51
2	Walker	30.63	-10.82	46.74[a]	1.25[a]	0.29	25.63[b]	-4.98	22.37[b]	2.18[a]	0.10
3	None	50.59	-14.42	68.71[a]	-1.20[a]	1.12	49.53	-16.25	64.69[ab]	-1.57[ab]	1.01
4	None	53.47	1.83	47.90[a]	-5.05[a]	0.94	52.11	-1.39	33.00[a]	-6.33[a]	0.77
5	Walker	52.59	-2.73	39.91[a]	-4.64	0.89	45.37[b]	-1.53	34.56[ab]	-4.77[a]	0.68
Average		46.54	-7.44	51.75	-2.71	0.80	41.29	-7.69	41.56	-2.78	0.61
Standard Deviation		9.43	6.73	10.97	2.68	0.32	11.21	7.10	17.03	3.28	0.34

a- mean angles of prosthetic limb is significantly different ($p<0.01$) from mean angle of sound limb
b- mean angle for ramp descent is significantly different ($p<0.01$) than mean angle during baseline walking

REAL-TIME FEEDBACK ENCOURAGES OLD ADULTS TO INCREASE THEIR PROPULSION DURING WALKING

Jason R. Franz, Michela Maletis, and Rodger Kram

Locomotion Laboratory, Dept. of Integrative Physiology, University of Colorado, Boulder, CO, USA
Email: jrfranz2@wisc.edu web: https://sites.google.com/site/jasonrfranz

INTRODUCTION

Even healthy and physically active old adults exhibit diminished trailing leg propulsive function during walking. For example, old adults exert smaller peak propulsive ground reaction forces (GRFs) and perform significantly less trailing leg positive mechanical work than young adults walking at the same speed [e.g., 1-3]. Eventually, the propulsive deficits of old adults may restrict their walking ability and thus their independence in the community.

Old adults exhibit reduced trailing leg propulsive function during walking largely because they generate significantly less ankle power than young adults during push-off [e.g., 1-3]. However, compared to level walking, old adults have the capacity to significantly increase their push-off muscle activities and propulsive mechanics to walk uphill [3,4]. Based on their ability to successfully walk uphill in previous studies, we propose that old adults have a considerable and underutilized propulsive reserve during level walking.

In this study, we used real-time visual feedback and auditory cues to test the hypothesis that old adults can voluntarily increase their propulsive function during level walking.

METHODS

8 old adults (5F/3M, mean age ± s.d.:72.1 ± 3.9 yrs) walked at 1.25 m/s on a dual-belt, force-measuring treadmill while we recorded right leg GRFs and bilateral electromyographic (EMG) recordings (MG, medial gastrocnemius and SOL, soleus). In different trials, subjects walked: 1) normally, 2) with visual feedback of their peak propulsive GRF, 3) with visual feedback of their mean push-off MG activity, and 4) with an audio metronome set to slower than normal stride frequencies.

Figure 1 summarizes our experimental setup. Briefly, a custom script written in LabView extracted the GRF and EMG signals from each stance phase in real-time, based on a 20 N vertical GRF threshold. This script identified the propulsive peak of the low-pass filtered (20 Hz) anterior-posterior GRF and calculated the mean band-pass filtered (20-450 Hz) and rectified MG activity during the second half of each stance phase. A computer monitor positioned in front of the treadmill displayed points each corresponding to a 2-stride average of those measurements (i.e., one dot appeared every two strides, scrolling from right to left).

For visual feedback trials, we asked subjects to match a target line set to 20% and 40% greater than

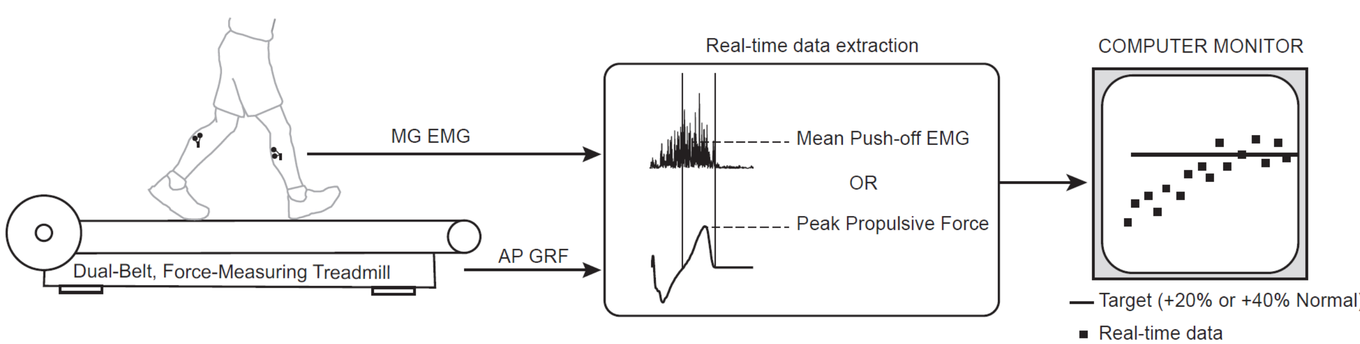

Figure 1. Experimental setup and real-time analysis for visual feedback trials. MG: medial gastrocnemius. AP GRF: anterior-posterior ground reaction force.

normal walking for 2 min (F20/F40 and EMG20/ EMG40). We then turned the monitor off and asked subjects to maintain the same push-off for 1 min. For auditory cueing trials, we asked the subjects to match a metronome set to step frequencies 10% and 20% slower than normal walking (SF10, SF20), corresponding to 10% and 20% longer steps. For comparison, we collected GRF data from 11 young adults (6F/5M, age: 21.0 ± 1.5 yrs) walking normally. A repeated measures ANOVA tested for significant main effects of feedback on GRF and EMG measures ($p<0.05$). Independent samples t-tests compared old and young adult GRF measures.

RESULTS AND DISCUSSION

Walking normally, old adults exerted 12.5% smaller peak propulsive GRFs than young adults ($p<0.05$) (Fig. 2A). However, as hypothesized, old adults were able to significantly and dramatically increase their propulsive GRFs and push-off muscle activities when we provided visual feedback. In fact, visual force feedback elicited propulsive GRFs that were either indistinguishable from (F20) or significantly greater than (F40) those of young adults (Fig. 2A). Those conditions also elicited significant increases in push-off muscle activities (Fig. 2B). With visual EMG feedback, old adults significantly increased their push-off muscle activities but without increasing their propulsive GRFs. Force feedback targets (20% and 40%) required a considerably more vigorous push-off than the same percent increase for EMG feedback targets. Subjects could maintain this more vigorous push-off for at least 40 strides after we removed visual feedback or auditory cueing.

Visual force and EMG feedback elicited ancillary gait pattern changes that require further investigation. These included: a greater first peak vertical GRF, greater center of mass velocity fluctuations, and a greater performance of positive mechanical work, particularly during the single support phase. Auditory stride frequency cueing elicited smaller increases in propulsive GRFs and push-off muscle activities in old adults than using visual feedback of those measures directly (not shown).

CONCLUSIONS

Our findings reveal that old adults do have a considerable and underutilized propulsive reserve during level walking. Moreover, real-time feedback can be used to encourage old adults to voluntarily increase aspects of their propulsion to equal that of young adults. Future studies are needed to explore if longer term feedback studies have beneficial results.

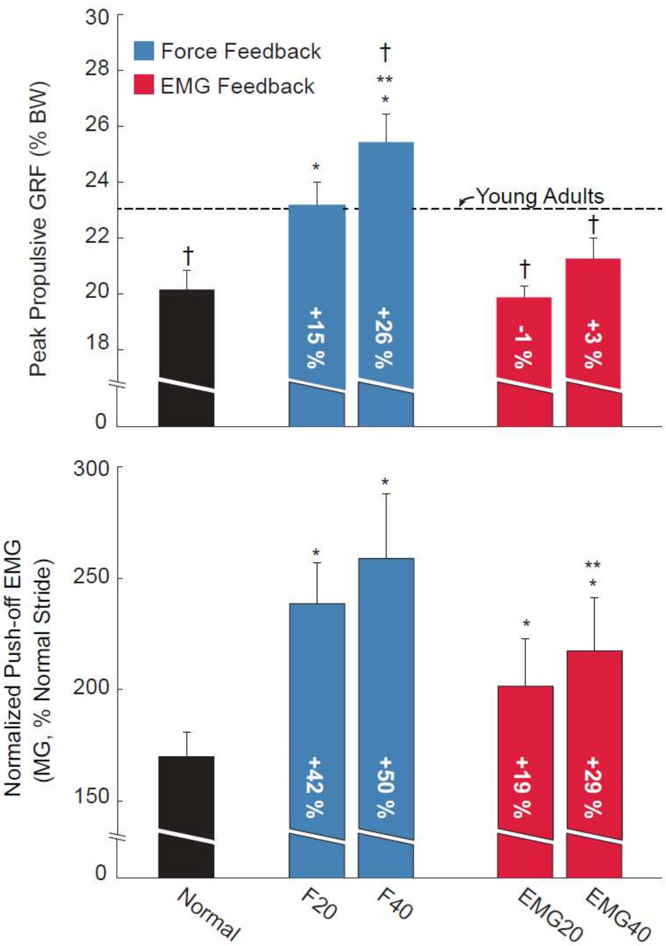

Figure 2. Mean (SE) results for old adults walking with visual force and EMG feedback showing percent change from normal. Single asterisks (*) indicate significantly different from normal walking, double asterisks (**) indicate 40% target significantly different from 20% target, and crosses (†) indicate significantly different from young adults ($p<0.05$ significant).

REFERENCES

1. Ortega JD, Farley CT. *J Appl Physiol* **102**, 2007.
2. Hernandez et al. *Gait Posture* **30**, 2009.
3. Franz JR, Kram R. *J Biomech*, **46**, 2013.
4. Franz JR, Kram R. *Gait Posture*, in press.

ACKNOWLEDGEMENTS

We thank Dr. Alena Grabowski for use of the EMG equipment.

BRITTLE BONE FRACTURE RISK WITH TRANSVERSE ISOTROPY

[1,2]Jessica M. Fritz, [4]Nicole M. Grosland, [3]Peter A. Smith, and [1-3]Gerald F. Harris

[1]Marquette University, Milwaukee, WI, USA
[2]Medical College of Wisconsin, Milwaukee, WI, USA
[3]Shriners Hospitals for Children – Chicago, Chicago, IL, USA
[4]University of Iowa, Iowa, City, IA, USA
email: jessica.fritz@mu.edu

INTRODUCTION

Osteogenesis imperfecta (OI) is a heritable bone fragility disorder characterized by skeletal deformity and "brittle" bones. This fragility is believed to stem from a combination of bone mass deficiency and compromised bone material properties [1-3]. Poor bone quality poses major orthopaedic and rehabilitation challenges. Risk of fracture is a major consideration when prescribing activity restrictions and physical therapy. Quantifying bone fracture risk would be an invaluable clinical treatment tool. Finite element (FE) models have the potential to provide patient-specific feedback on the effects of fracture risk factors in long bones. As more information on OI becomes available, the model is evolving to include the latest data. The latest modification is focused on material properties. It is clear that OI bone does not behave like normal pediatric bone [1-5]. However, quantification of these differences has only recently been explored. Accurate material properties are essential for a computational fracture risk assessment (FE) model. The previous femoral fracture risk assessment model for an OI patient implemented material properties obtained during nanoindentation testing of OI bone specimens [5]. At the time, this was the only data available on OI bone properties. Based on these results, the femur was modeled as an isotropic material. Recent mechanical testing by our group has shed new light on the flexural properties of OI bone. These tests have shown that OI bone is, in fact, not isotropic and has a much lower Young's modulus (E) than what was calculated via nanoindentation testing. Transverse isotropic properties have been implemented into the OI femur model to examine effects on the maximum principal stress experienced during mid-stance of the gait cycle (highest load phase). The goal of study is to compare the isotropic and transverse isotropic models.

METHODS

A previously developed hexahedral FE model of an OI femur was used for this study [4]. The loading and boundary conditions assumed the mid-stance phase of gait; the condylar contact surfaces were fixed in all directions, while the femoral loads and muscle forces were derived from the kinetics of gait of a 12-year-old OI type I subject who underwent gait analysis at Shriners Hospital for Children – Chicago (Fig. 1).

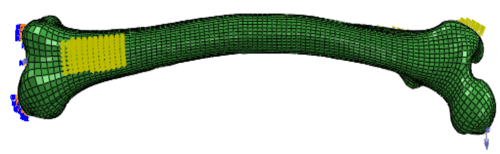

Figure 1: FE model of OI type I femur.

The material properties were assigned to reflect the new OI bone property data. The current FE femur is modeled with transversely isotropic material properties as shown in Table 1.

Table 1: Young's modulus (E, GPa), Poisson's ratio (υ) and shear modulus (G, GPa) for FE model of OI type I femur.

	$E_{11/22}$	E_{33}	$\upsilon_{11/22}$	υ_{33}	$G_{11/22}$	G_{33}
Cortical	4.0	7.0	0.3	0.3	1.5	2.7
Cancellous	3.0	6.0	0.3	0.3	1.2	2.3

The model was analyzed for three different levels of bowing: 5 mm, 15 mm and 25 mm. Maximum and minimum principal stresses were assessed and compared to previous isotropic results.

RESULTS AND DISCUSSION

The results of the maximum and minimum principal stresses and the percent difference between the isotropic and transverse isotropic models are shown in Table 2. As expected, the maximum and minimum principal stresses increased with the new model material properties. Interestingly, the percent difference of maximum principal stress was consistent for all levels of bowing around 10%; however, the minimum principal stress showed greater variation in percent difference as bowing increased. Percent difference of minimum principal stress ranged from 11.5% to nearly 24%.

Table 2: Results of principal stress comparison. An * depicts the transverse isotropic model.

	Maximum Principal Stress (MPa)	Minimum Principal Stress (MPa)
5mm	46.10	-43.50
5mm*	50.75	-48.50
% Diff	10.09	11.49
15mm	46.80	-45.00
15mm*	51.25	-50.60
% Diff	9.51	12.44
25mm	47.50	-47.10
25mm*	52.00	-58.40
% Diff	9.47	23.99

The principal stress results also show distinct differences between the two models. This can be seen in their stress contour plots (Fig. 2). The general location of the extreme stress values remains relatively unchanged between the isotropic and transversely isotropic models. However, the current model shows a very slight distal and anterior shift in the extreme stress areas as well as smaller areas of higher stress. The comparison is between a previous model with higher cortical and cancellous Young's modulus values of 19 GPa and 17 GPa, respectively. The effect of isotropy was examined in the 15 mm bowing model by comparison to the transversely isotropic model. The percent difference in maximum and minimum principal stresses showed a 5% and 7% increase, respectively, between the isotropic and transversely isotropic models.

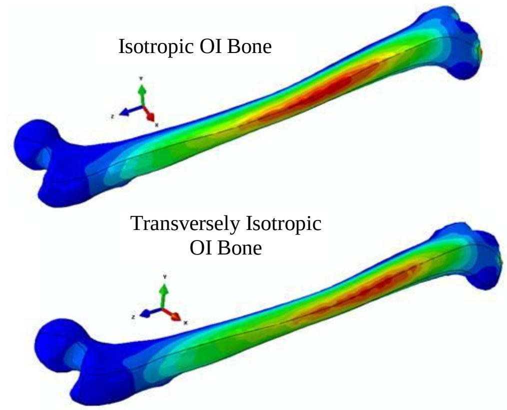

Figure 2: Contour plots of maximum principal stress on 15 mm bowed femur for previous (top) and current (bottom) FE models. Stress levels: red>blue.

CONCLUSIONS

Having a reliable fracture assessment model requires the most accurate input data available. Until recently, OI bone testing had been reported to be closer to an isotropic material than the anisotropic properties of normal bone. With new information indicating that this is not the case, the femur model was reconfigured and assessed to determine the effects of the newly acquired OI bone properties. As expected, the lower E values increased stress values. The femur being modeled as transversely isotropic rather than isotropic also affects the principal stresses due to loading during gait. Increased stresses lead to greater deviation towards fracture risk. This work updates the OI femur model to include recent biomaterial findings.

REFERENCES

1. Rauch F & F Glorieux. *Lancet* 363:1377-85, 2004.
2. Weber M, et al. *Bone* **39**(*3*), 616-22, 2006.
3. Roschger P, et al. *Calcif Tissue Int*, **82**, 263-70, 2008.
4. Fritz JM, et al. *Proceedings of ASB 2011*, Long Beach, CA, USA, 2011.
5. Fan Z, et al. *J Biomed Mater Res A*, **79**, 71-7, 2006.

ACKNOWLEDGEMENTS

Department of Education, NIDRR grant no. H133E100007. Contents do not necessarily represent the policy of the Department of Education.

MULTIPLE SHOOTING OPTIMAL CONTROL FOR APERIODIC MULTISTEP GAIT SIMULATION

Huseyin Celik and Stephen J. Piazza

The Pennsylvania State University, University Park, PA, USA
email: *piazza@psu.edu*

INTRODUCTION

Model-based optimal control is a tool commonly used to create dynamic simulations of locomotion through minimization of some objective function. Such optimization problems usually have components such as time-continuous state equations, boundary conditions, and controllers. Optimal control methods generally require converting these components into linear and nonlinear constraints which make up a nonlinear programming problem (NLP). There are three main methods used for this conversion, each of which produces a different variety of NLP: (1) single shooting; (2) direct collocation; and (3) multiple shooting. Single shooting (e.g., [1]) is the most widely used method and searches for controls that minimize an objective function evaluated during a single forward integration. This problem is usually subject to initial, terminal, and periodicity constraints. Direct collocation is a method borrowed from physics-based computer graphics that has recently been applied to musculoskeletal simulation of human movement (e.g., [2]) in which optimal controls and state trajectories are searched simultaneously to minimize an objective function subject to constraints that represent the dynamic equations of motion, in addition to any initial and terminal constraints. In direct collocation there is no forward integration of the state equations; instead, an Euler discretization scheme is used to transform differential equations into algebraic counterparts.

METHODS

Multiple shooting is a method that combines features of single shooting and direct collocation. In this method, the total simulation time is divided into many short integration intervals (Figure 1), each of which has a set of initial states and constant or linearly varying controls. An objective function is minimized subject to constraints requiring that the terminal values for the states at the end of each integration interval (x_i^-) are equal to the initial values for the next interval (x_i^+). Multiple shooting is a robust option that avoids some of drawbacks of other methods, such as the accumulation of nonlinearity on the boundary conditions and numerical instability (in single shooting) and problems with error-controlled discretization that requires re-gridding (in direct collocation). The method has been used recently to simulate a periodic sprinting gait cycle [3].

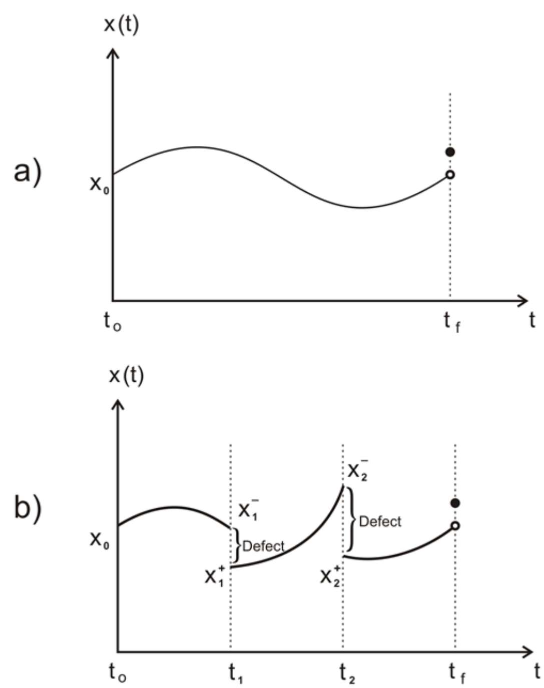

Figure 1: (a) In *single shooting*, the state equations are integrated once from initial to final time. (b) In *multiple shooting*, the state equations are integrated segment by segment. Defects are minimized to ensure continuity of the states.

RESULTS AND DISCUSSION

In our laboratory we have used multiple shooting to simulate an aperiodic sprint race for a simple spring-loaded inverted pendulum (SLIP) model that begins from rest, accelerates, and finishes 20 m from the start. A feedback controller is used to generate an initial guess, but following optimization via multiple shooting the solution exhibits many features recognizable from human sprinting (Figure 2), including starting with the trunk bent forward followed by gradual straightening, and a forward dive at the end.

We tried, but failed, to simulate aperiodic sprinting using both single shooting and direct collocation. In single shooting, singularity in the motion early in the simulation prevented the model from completing the 20 m sprint, and this resulted in numerical problems in the optimization process. In a periodic walking or running step, when states and forces are changing relatively slowly, it is unlikely that time integration of state equations would be as much of a problem. In a much longer and faster motion with many footfalls, however, a more robust integration scheme such as the one we employed in the multiple shooting method is critical for convergence on an optimal solution.

The direct collocation method does not include time integration of state equations, but for our problem often produced infeasible or sub-optimal solutions. We attribute this to migration of the solution manifold as we moved to progressively finer grids throughout the solution process.

We are currently working to extend the methods described to produce an improved simulation of aperiodic sprinting that features additional joints (ankle and knee) and muscle-tendon actuators. This effort will make use of zero-state models of muscle force generation in order to keep the problem dimension small. We plan to use these simulations to enhance our understanding of the musculoskeletal characteristics that determine gait speed in pathological populations as well as in athletes.

REFERENCES

1. Anderson FC and Pandy MG. *J of Biomech* **123**, 381-390, 2001.
2. Van den Bogert AJ, et al. *Proceedings of XII Congress of ISB*, Cape Town, South Africa, 2009.
3. Schultz G and Mombaur K. *IEEE/ASME Trans Mechatronics* **15**, 783-792, 2010.

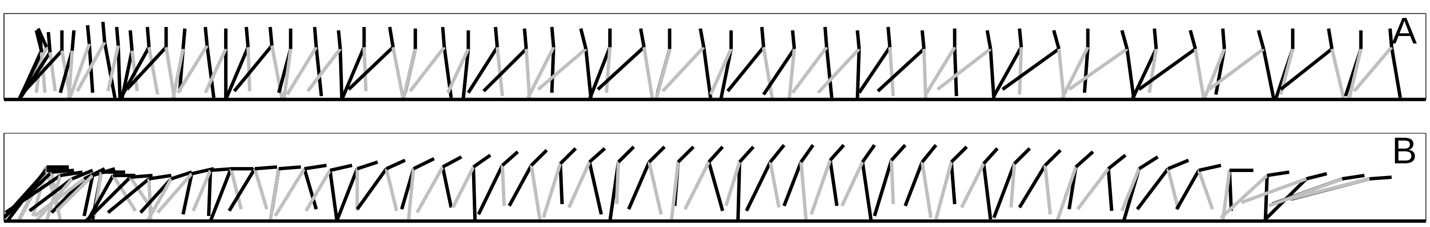

Figure 2: Stick-figure trajectories for the model (A) completing a 20 m initial guess “jog” guided by feedback controller in 6.64 s; and (B) sprinting from rest following optimization, covering 20 m in 2.79 s. The optimized simulation begins with the trunk flexed forward, straightens as the race progresses, and dives forward at the finish. The time between frames in these figures is (A) 125 ms and (B) 53 ms.

Ankle Fatigue Classification Using Support Vector Machines

[1]Jian Zhang, [1&2]Thurmon E. Lockhart, and [2]Rahul Soangra

[1] Industrial & Systems Engineering, Blacksburg, VA, USA
[2] School of Biomedical Engineering & Sciences, Virginia Tech-Wake Forest, VA, USA
email: zhangj@vt.edu, web: http://ise.locomotion.vt.edu

INTRODUCTION

Fall accidents are a significant problem for the elderly, in terms of both human suffering and economic losses. Localized muscle fatigue is a potential risk factor for slip-induced falls as muscle fatigue adversely affects proprioception, movement coordination and muscle reaction times leading to postural instability and gait changes. Specifically, fatigue in ankle is associated with decline in postural stability, motor performance and fall accidents in human subjects. Automated recognition of ankle fatigue condition may be advantageous in early detection of fall and injury risks. In this study, we explore the classification potential of support vector machines (SVM) in recognizing gait patterns associated with ankle fatigue utilizing an inertial measurement unit (IMU) as the wearable technology has the potential to investigate continuous kinematic changes evoked by fatigue.

The SVM is considered a powerful technique for general data classification and has been widely used to classify human motion patterns with good results. The advantage of SVM algorithm [1] is that it can generate a classification result with limited data sets by minimizing both structural and empirical risks. Although numerous studies have been devoted to improving the SVM algorithms, little work has been performed to assess the robustness of SVM algorithms associated with movement variations and fatigue states.

In the current study, we aim to monitor kinematics of walking in unconstrained environments using an IMU situated around the trunk Center-of-Mass (COM) during ankle fatigue and no-fatigue walking conditions. We hypothesize that ankle fatigue will influence walking behavior and this subtle changes in gait can be classified by supervised machine learning techniques such as support vector machines.

METHODS

Seventeen healthy young adults (9 males and 8 females) participated in the study. The participants mean age was 29±11 years, height 174±10 cm, and weight 73±12 kg. The experiment was composed of inducement of fatigue in ankle joints with squatting exercises [2]. Walking trials were conducted both prior and after the fatiguing condition. The IMU node consisted of MMA7261QT tri-axial accelerometers and IDG-300 (*x* and *y* plane gyroscope) and ADXRS300, *z*-plane uniaxial gyroscope aggregated in the Technology-Enabled Medical Precision Observation (TEMPO) platform which was manufactured in collaboration with the research team of the University of Virginia [3].

For the classification, both training and testing data sets consisted of ankle fatigue/no-fatigue walking data. Kinematic data used for SVM input was Representative Gait Cycle (RGC) data. RGC begins when one foot contacts the ground and ends when that foot contacts the ground again using the shank IMU. A perfect representative gait cycle signal between two easily identifiable events of the same foot was chosen for the analysis (Figure 1). This representative gait cycle started at peak right shank angular velocity (left foot mid-stance) and terminated at consecutive peak right shank angular velocity (left foot mid-stance). All IMU signals were truncated to RGC and normalized to 0% to 100%. A repeated-measure design was used to test changes intra-subject in gait parameters from normal walking and post fatigue walking trials.

The SVM classifier has not been applied previously to ankle fatigue and no-fatigue gait patterns. An important characteristic of using SVM classifier in this study was to obtain high ankle fatigue/no-fatigue classification accuracy with three different types of feature input (Table 1): (1) selected "ad hoc" features based on domain knowledge; (2) general features; and (3) concatenated complete gait pattern signals. After extracting features, all features or input variables were normalized by computing their z-scores. Input data was kept in range between 0 and 1. Then Principle Component Analysis (PCA) was employed to decrease the dimensions. The objective of PCA is to perform dimensionality reduction while preserving as much of the randomness in the high-dimensional space as possible. Subsequently, a five-fold cross-validation scheme was adopted to evaluate the generalizability of the SVM classifier. Finally, SVM models were trained over the range $C=2^{-10}$ to 2^{10} using linear, polynomial and radial basis function kernel.

RESULTS AND DISCUSSION

The machine learning classification results demonstrated high intra-individual classification rates across all three-kernel types (i.e., linear, polynomial and radial basis function kernel). We found that linear (accuracy ~97-99%) and RBF (accuracy ~96-98%) kernels perform equally well in intra-individual ankle fatigue/no-fatigue classifications (Table 2). The polynomial kernel had the lowest classification accuracy amongst all three different types of kernels. Our results also indicate that ankle fatigue effects are evident in individuals' gait patterns and extracted features and, SVM accurately classified ankle fatigue/no-fatigue conditions. We found that SVM classifier incorporating trunk kinematic signals during gait has an excellent potential to predict fatigue status intra-individually (~98% accurate predictions).

Previous researchers have adopted various gait feature extraction methods for SVM classification. Results of our investigation indicate that features extraction methods influenced classification accuracy. In ankle fatigue classification, concatenated waveform input resulted in the highest classification accuracies; however, selected feature input had better classification accuracies than general feature input. This may be attributed to intra-individual variability. In essence, concatenated waveform input exhibited superior classification accuracy and had important gait information to classify fatigue; on the contrary, the other two feature extraction methods lacked peculiar information relevant to achieving higher classification results.

Three different types of kernels were employed in SVM: linear, polynomial, and radial basis function. Both linear and RBF kernels performed well in ankle fatigue/no-fatigue classifications. Considering the computational cost, RBF and polynomial kernels need less time compared to linear kernels in the same conditions. As such, RBF kernel is the most promising kernel function in the ankle fatigue classification schemes, and it may also provide better applicability to real time system implementation.

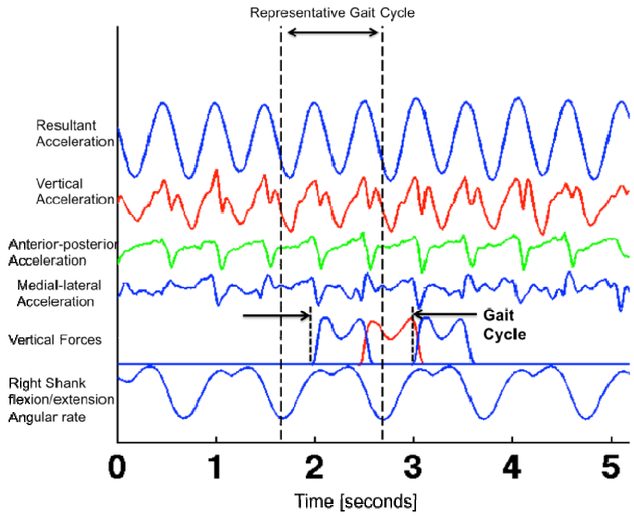

Figure 1: Two consecutive time epochs when right shank attains peak angular velocities were chosen during walking as input gait pattern data mimicking gait cycle and was defined as Representative Gait Cycle. The R-GC data from IMU situated at trunk was truncated for extraction of features values to SVM.

REFERENCES

1. Vapnik VN. *IEEE Trans Neural Netw*, **10**, 988-999, 1999.
2. Hodges SJ, et al. *J Strength Cond Res*, **25**, 3107-3017, Nov 2011.
3. Soangra R, et al. *Ann Biomed Eng*, Dec 5, 2012.

Table 1: Three feature sets were used as inputs to SVM. 1) General features, 2) Selected features and 3) Complete concatenated waveform.

	General Features	Domain knowledge based Selected Features	Complete Concatenated Waveform
Data input for SVM	-Accelerometer and gyroscope data in all 3 directions of normalized representative gait cycle	-Accelerometer and gyroscope data in all 3 directions of normalized representative gait cycle - Resultant acceleration - Resultant Jerk	-Concatenated input of normalized representative gait cycle
	i) Mean ii) Standard deviation iii) Maximum iv) Minimum v) Mean Absolute Value $\bar{x} = \frac{1}{N}\sum_{k=1}^{N}\lvert x_k\rvert$	Resultant Acceleration features i) Skewness (temporal shift) ii) Energy iii) Dominant frequency iv) Maximum acceleration v) Minimum Acceleration Range of acceleration	--No Feature--
	i) Skewness ii) Kurtosis iii) Energy iv) Number of Slope sign changes v) Number of zero crossings	Resultant Jerk features i) Skewness (temporal shift) ii) Mean Jerk at heel contact iii) Absolute Maximum Jerk iv) Absolute Minimum Jerk	
	xi) Length of waveform xii) Dominant Frequency using low-pass filter and FFT	v) Range of Jerk Produced abs(max-min) vi) Jerk Cost $JC = \int_0^T \lvert\frac{d^3r}{dt^3}\rvert^2 dt$	

Table 2: Intra-subject ankle fatigue classification using IMU derived features. Accuracy, sensitivity, specificity and AUC (area under the Receiver operating curve) are tabulated for three kinds of feature selections methods and three kernels.

		Ankle Fatigue		
		Linear	Polynomial	RBF
General Features	Accuracy	97	92	96
	Sensitivity	97.78	93.33	95.56
	Specificity	95.56	91.11	95.56
	AUC	1	1	1
Domain knowledge based Selected Features	Accuracy	98	90	97
	Sensitivity	100	91.11	100
	Specificity	95.56	88.89	93.33
	AUC	1	0.96	0.96
Normalized complete concatenated waveform signals	Accuracy	99	83	98
	Sensitivity	100	86.67	100
	Specificity	97.78	80	95.56
	AUC	1	1	1

A COMPARISON BETWEEN ANGULAR MOMENTUM AND MARGIN OF STABILITY IN HEALTHY YOUNGER AND OLDER ADULTS

Arian Vistamehr and Richard R. Neptune

Mechanical Engineering Department, The University of Texas, Austin, TX, USA
email: arian.vistamehr@utexas.edu web: http://www.me.utexas.edu/~neptune

INTRODUCTION

Older adults are more susceptible to falling, which often leads to extensive musculoskeletal injuries and functional disabilities. In particular, lateral instability is a major concern in the elderly [1]. Previous work has shown that dynamic balance may be maintained passively in the sagittal plane. However, active control must be applied to stabilize the lateral motion [2]. To help diagnose and prevent balance disorders that may lead to falls, reliable measures are needed to quantify dynamic balance.

Whole-body angular momentum (*H*), a mechanics-based measure of body rotation, has been investigated in a range of balance studies including younger and older healthy adults [3] and amputee subjects [4]. The regulation of angular momentum is critical in maintaining dynamic balance and can be quantified by analyzing the rate of change of angular momentum (net external moment). Identifying the primary contributors to the external moment can provide insight into the underlying mechanisms for maintaining balance [4]. Another commonly used measure to quantify dynamic balance is the margin of stability (*MoS*), which is the minimum distance between the extrapolated center of mass (*XCOM*) and the base of support. This measure is based on foot placement and has been used to quantify balance in a number of patient populations (e.g., [5]).

However, no study has directly compared the two measures to see if they lead to similar conclusions. Thus, the purpose of this study was to analyze dynamic balance in healthy older and younger adults in the frontal plane (mediolateral motion) using peak-to-peak range of angular momentum and *MoS* and determine if the two measures of dynamic balance provide consistent results.

METHODS

Ten healthy young subjects (age= 27.3 ± 2.7) walked on an instrumented treadmill at 0.6 m/s and 1.2 m/s. From a previously collected dataset [6], we identified healthy older subjects who had a speed-matched self-selected walking speed. Seven subjects (age= 57.5 ± 9.4) walked at 0.6 m/s and nine subjects (age= 53.7 ± 8.5) walked at 1.2 m/s. In both data sets three 30-second trials were collected for each subject. Kinematic and ground reaction force (*GRF*) data were collected at 120Hz and 2000Hz, respectively. An inverse dynamics model was used to calculate the *COM* position and velocity for all the body segments. Whole-body angular momentum in the frontal plane was calculated as described in [4] and normalized with respect to subject mass, height and walking speed. *MoS* was calculated as described in [5].

The effect of age on changes in the peak-to-peak range of frontal plane angular momentum, range of *XCOM*, step width and *MoS* (all normalized by body height) was investigated at each walking speed using a student's t-test. In order to identify any correlation between *MoS* and the range of angular momentum, a Pearson correlation analysis was performed. Data from the younger and older adults were combined at each walking speed for the correlation analysis.

RESULTS AND DISCUSSION

The range of angular momentum increased significantly (p=0.005) with age at the lower walking speed of 0.6 m/s. However, at 1.2 m/s, there were no differences in the range of angular momentum between the older and younger adults (Figs. 1, 2). Also, the range of angular momentum decreased with increasing speed for both age groups, which was consistent with previous studies (e.g., [4]).

MoS (summed for left and right legs), peak-to-peak range of *XCOM*, and step widths are also shown for both age groups (Fig. 2). Significant differences between the age groups are identified with a "*". At the slower speed, the *XCOM* was not affected by age. Thus, a wider step in older adults (p=0.007) resulted in a higher *MoS* (p<0.001). However, there were no differences between the age groups during the fast walking speed.

Angular momentum was strongly correlated with *MoS* at both the slow (r =0.92, p<0.001, n=17) and fast (r =0.6, p=0.002, n=19) walking speeds (Fig. 3). The correlation between angular momentum and *MoS* indicate that a wider step may lead to greater lateral sway. It is commonly known that older adults increase their step width to maintain their balance. However, since the *XCOM* was not affected by age, the increased step width could have been a compensatory mechanism due to lack of muscle force generation (e.g., hip abductor torque capacity [1]), rather than foot placement corrections for maintaining dynamic balance. Future work is needed to investigate differences in external moments (i.e., moment arms and GRFs) between young and older adults to further understand the influence of increasing step width in older adults on dynamic balance.

The angular momentum and margin of stability measures were consistent in assessing dynamic balance in younger and older adults. Margin of stability is a relatively simple measure calculated using center of pressure, leg length, COM location and velocity data, and it can provide insight into foot placement relative to the COM location while accounting for the whole-body COM velocity. However, *MoS* does not provide insight into adaptations in the GRFs. In contrast, angular momentum is more complex measure (e.g., requires COM position, linear and angular velocity, as well as the mass and moment of inertia of all body segments) and provides a quantitative assessment of whole-body rotation. In addition, the rate of change of angular momentum (external moment) can provide insight into how adaptations in the GRFs and foot placement influence dynamic balance. Therefore, depending on the clinical question of interest, *MoS*, angular momentum, or a combination of both measures can be used to gain insight into dynamic balance.

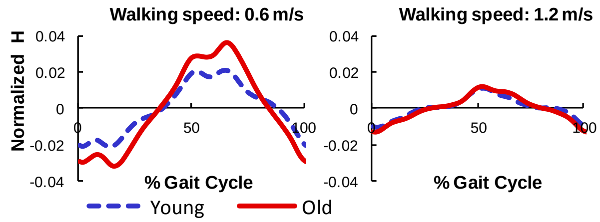

Figure 1: Frontal plane angular momentum (*H*).

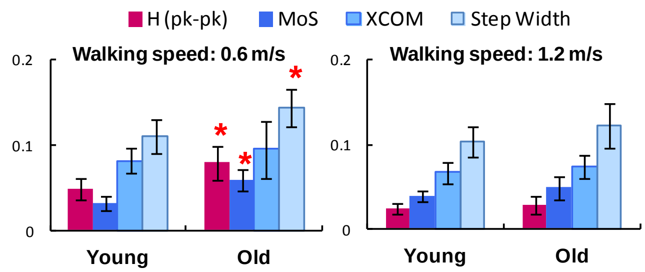

Figure 2: Range of angular momentum, *MoS*, range of *XCOM*, and step width, normalized with respect to the body height.

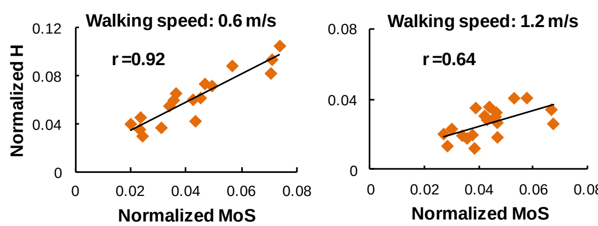

Figure 3: Correlations between *MoS* and range of angular momentum.

ACKNOWLEDGEMENTS

The authors would like to thank Dr. Steve Kautz for providing the experimental data. This work was supported by AHA SouthWest Affiliate pre-doctoral fellowship (12PRE12030414).

REFERENCES

1. Rogers, MW, et al. *Exerc Sport Sci Rev* **31**, 182-187, 2003.
2. Bauby, CE, et al. *J Biomech* **33**, 1433-1440, 2000.
3. Pijnappels, M, et al. *Gait & Posture,* **21** 388-394, 2005b.
4. Silverman, AK, et al. *J Biomech* **44**, 379-385, 2011.
5. Hof, AL, et al. *J Biomech* **25**, 250-258, 2007.
6. Bowden, MG, et al. *Arch Phys Med Rehabil* (in press).

EFFECTS OF VISUAL PERCEPTION OF SELF-MOTION ON GAIT IN PEOPLE WITH DIABETES

[1,2]Chun-Kai Huang, [2]Pariwat Thaisetthawatkul, [3]Vijay Shivaswamy and [1,2]Ka-Chun Siu

[1]Nebraska Biomechanics Core Facility, University of Nebraska at Omaha, Omaha, NE, USA
[2]Division of Physical Therapy Education, School of Allied Health Professions, [3]Department of Neurological Sciences, [4]Division of Diabetes, Endocrine & Metabolism, College of Medicine, University of Nebraska Medical Center, Omaha, NE, USA
email: chunkai.huang@unmc.edu web: http://nbcf.unomaha.edu/

INTRODUCTION

To maintain stability during locomotion, it relies on body-based and visual senses [1], such as perception of self-motion. People with more than 15 years of diabetes mellitus (DM) are at a high risk of suffering from diabetic neuropathy with abnormal sensation and sensory loss of their feet [2], which increases the incidence of fall injuries. Thus, the reliance on visual senses is crucial in DM population. The visual perception of self-motion has been previously shown to alter spatiotemporal gait characteristics in people with diabetes mellitus (DM) [3]. However, it is not clear if the visual perception exhibits the similar effect on gait alteration in people with and without DM.

Therefore, the aim of preliminary study was to investigate the differences of gait alteration between people with DM and their age-matched healthy control when self-motion was perceived during locomotion. We hypothesized that the perception of self-motion would alter gait patterns more prominently in DM group when compared those in age-matched group.

METHODS

Three chronic type 2 DM (mean year of diabetic diagnosis = 17 years; one female; mean age= 58.7 ± 6 years old) who have been diagnosed and pre-screened by both neurologist (P.T.) and endocrinologist (V.S.); two healthy age-matched adults (males; mean age= 58 years old) were recruited and walked on a treadmill (Bertec Corp. Columbus, OH).

Each subject walked five minutes at their self-selected pace for familiarization followed by three two-minute treadmill walking trials with and without virtual environment (VE). The VE was presented by three projectors in front of subjects that generated the visual flow of corridor matched with walking speed (Fig. 1). All subjects were given a seven-scale Presence Questionnaire to test their self-immersion to the VE at the end of the study.

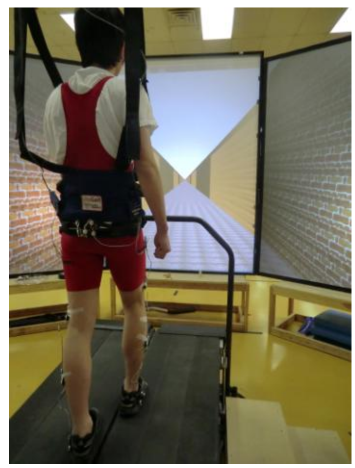

Figure 1: A subject walked on a treadmill with a safety harness while a virtual, speed-matched moving corridor was presenting ahead.

Three-dimensional spatiotemporal data were collected using NDI motion capture system at 100 Hz (Northern Digital Inc, Waterloo, Canada) and processed using custom-written MATLAB program (MathWorks, Inc., Natick, MA). Gait parameters (step length, step width, step time) were calculated. Step length was defined as the distance between two consecutive heel strikes of different legs; step width was the mediolateral distance between two heels at the moment of both feet contacted the treadmill belt; step time was the duration of two consecutive heel strikes of different legs. The average and variability (coefficient of variance, CV) of step length, step width and step time were calculated and reported.

Two-way ANOVA (VE vs. non-VE as within-subject factor and two subject groups as between-subject factor) with repeated measure was applied to compare all spatiotemporal gait parameters. Pair-wise comparison tests with Bonferroni adjustment were performed when significant effect was found. The significance level was set at 0.05.

RESULTS AND DISCUSSION

Age and body mass index did not show the significant difference between the two groups (p = 0.89 and p = 0.44 respectively). All participants had a strong self-immersion in the VE with Presence Questionnaire score 6.6 ± 0.55 (out of seven). A significant group effect was found in step length (p = 0.03; Fig. 2a), which DM group had shorter step length than control group. A significant interaction between group and VE exhibited in step width (p = 0.04). Individuals with DM decreased their step width more than those in control group when VE was presented ($p < 0.05$; Fig. 2b). No significant main effect was found on CV of gait parameters.

The finding of decreased step length in DM group is consistent with previous studies without VE that DM population adopt a new walking strategy in sagittal plane due to the fear of falling [4,5]. In addition, the DM group in this study altered their gait in frontal plane (decreased step width) when visual perception of self-motion was given by VE. It implies that, without normal sensory input, subjects with DM could rely on visual perception from VE to alter their gait patterns. More subjects are warranted to examine if the gait alternations found in the DM group is beneficial to their gait stability and fall reduction.

CONCLUSIONS

Overall, compared subjects with type 2 DM with their age-matched healthy control, this preliminary study provides further evidence that visual perception of self-motion plays a prominent role on gait adjustment/alteration in DM during treadmill walking. Virtual environment could be useful for DM to establish a walking strategy that is safe to prevent from future incidence of falls.

REFERENCES

1. Mohler B, et al. *Exp Brain Res* **181**, 221-228, 2007.
2. Simmons RW, et al. *Diabetes Res Clin* **36**, 153-160.
3. Huang CK, et al. *ENDO Society* **2013**.
4. Brach JS, et al. *Phys Ther* **88**, 1365-1374, 2008.
5. Lalli P, et al. *J Diabetes Complications* **2012**.

ACKNOWLEGEMENTS

This project was partly supported by the Nebraska Research Initiative and the UNMC SAHP Graduate Fellowship.

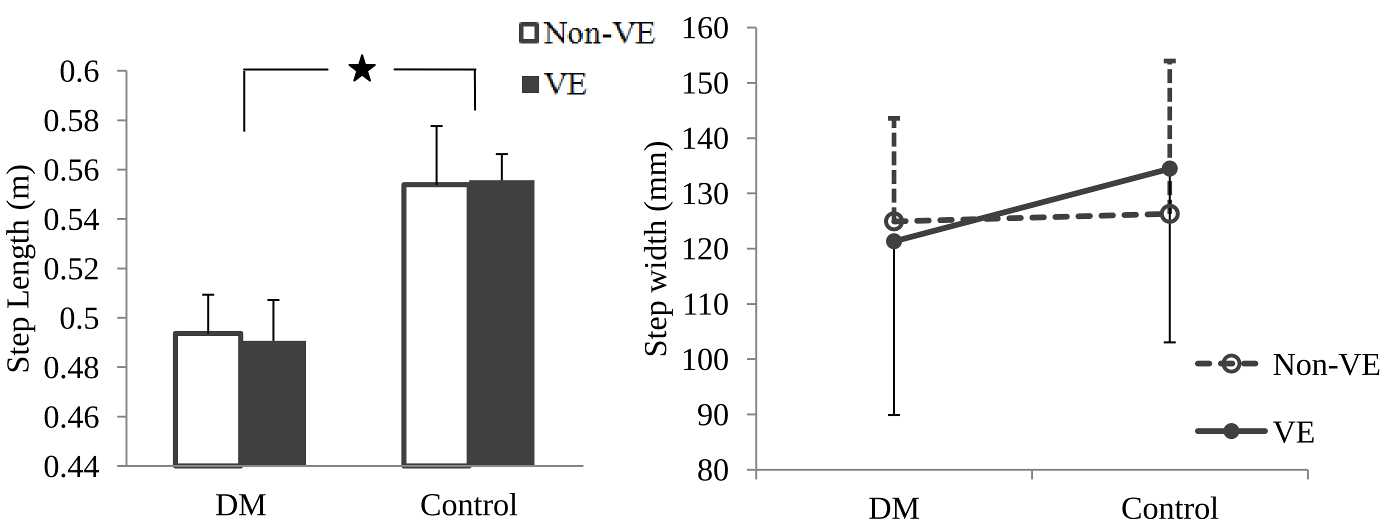

Figure 2: (a) The effect of DM condition on step length during treadmill walking; (b) The interaction of visual perception of self-motion and DM condition on step width during treadmill walking (VE: virtual environment; asterisk: $p < 0.05$).

OPTIMAL MONITOR LOCATION FOR POSTURE AND MOVEMENT DETECTION

Emma Fortune, Vipul Lugade and Kenton Kaufman

Mayo Clinic, Rochester, MN, USA
email: kaufman.kenton@mayo.edu, web: http://mayoresearch.mayo.edu/mayo/research/biomechanics

INTRODUCTION

Patient compliance is important when assessing physical activity, particularly using portable sensors at home when the patient applies their own activity monitors. Two main issues which can affect patient compliance in assessments are (a) requesting them to wear a large number of sensors [1] which can lead to complicated instructions and (b) sensor failure resulting in limited or no data and, therefore, no feedback for the patient. The aim of this study was to determine the validity of different monitor combinations for static posture and dynamic movement detection. We hypothesized that while the waist-thigh combination is the most accurate, single monitor use will also be sufficiently accurate.

METHODS

Accelerometer and video data were acquired from 12 healthy adults (3 M, 9 F; age (SD): 34.0 (9.7) yrs; BMI (SD): 24.7 (5.5) kg/m^2) using custom built activity monitors strapped bilaterally on the ankles, waist and thigh as they performed 5 minutes of static and dynamic activities involving standing, sitting, shuffling feet while standing and sitting, lying, walking and jogging. IRB approval and written informed consent were obtained prior to testing. Each activity monitor incorporated a tri-axial accelerometer (±16g, 100 Hz). Video data (60 Hz) were synchronized to accelerometer data by 3 jumps performed at data collection initiation. Four monitor combinations were investigated: 1) single waist, 2) single thigh, 3) single ankle, and 4) thigh and ankle monitors. These configurations were compared to the 'gold standard', waist and thigh monitors [2].

Different thresholds were used for the varying monitor configurations. For a single waist or ankle monitor, lying was determined when the vertical angle was between 50º-130º. For a single thigh monitor, standing was determined when the vertical angle was < 45º [3]. For the thigh-ankle combination, lying were identified when the ankle vertical angle was between 50º-130º and sitting and standing were distinguished when the thigh vertical angle was > or < 45º, respectively. Walking and jogging were detected when the acceleration signal magnitude area (SMA) exceeded thresholds. These thresholds were defined as .135g and .8g for detecting walking and jogging from the waist [2] and were scaled for the thigh and ankle as ratios of their mean SMAs to the waist SMA. Of the static epochs, a continuous Daubechy-4 Mother Wavelet transform was applied. Data within 0.1-2 Hz was classed as activity if it was > 1.5/s [2]. For the thigh-ankle combination, movement and jogging were detected using thigh accelerations. Transitions between postures were also identified. Video and accelerometer data were classified in 1 s windows. Sensitivities and positive predictive values (PPVs) were calculated for each monitor combination.

RESULTS AND DISCUSSION

All monitor combinations detected movement with substantial to excellent accuracy (both sensitivity & PPV > 60% to > 80% [4]) (Table 1) which were comparable to other studies [5]. All three postural orientations of standing, sitting and lying and transitions could only be identified with more than one monitor, which is consistent with previous studies [6, 7]. Transitions were detected with substantial accuracy using the waist-thigh combination and the single thigh monitor only. While single waist and ankle monitors could not distinguish between standing and sitting, the waist identified upright and lying postures with greater accuracy than the ankle. The waist-thigh combination detected all postures and movement more accurately than the thigh-ankle combination

(Table 2). The thigh monitor identified standing and walking/shuffling with the most accuracy for single monitor use, while the waist monitor produced the least accuracy due to missed shuffling steps. However, jogging was most accurately detected using a waist monitor. This is consistent with previous studies, showing that the waist location is optimal for detecting whole body movement, while the ankle or thigh are optimal for detecting limb movement [6]. Single waist monitor results were also more accurate than in other studies using different algorithms [8].

CONCLUSIONS

The waist and thigh combination produced the most accurate results overall. All monitor combinations detected jogging and walking/shuffling with sufficient accuracy. The results show that there is a trade-off between reducing the number of monitors per subject, choosing their locations and accuracy. The data suggests that researchers should carefully choose monitor numbers and their locations depending on the information required. While this study involves a simulated protocol conducted in a laboratory environment, the results suggest that the proposed analysis methods are suitable for movement detection using tri-axial accelerometers on the ankles, waist and thigh in a free living environment as long as data from at least one activity monitor is obtained. More detailed information on postures and transitions requires a thigh and waist (or similar trunk-based) monitor combination.

REFERENCES

1. Atallah L, et al. IEEE Trans Biomed Circuits Syst **5**, 320-329, 2011.
2. Lugade V, et al. ASB, Gainesville, FL, 2012.
3. Lyons G, et al. Med Eng Phys **27**, 497-504, 2005.
4. Landis J, et al. Biometrics **33**, 159-174, 1977.
5. Aminian K, et al. Med Biol Eng Comput **37**, 304-308, 1999.
6. Yang C, et al. Sensors **10**, 7772-7788, 2010.
7. Godfrey A, et al. Med Eng Phy **29** 930-934, 2007.
8. Dijkstra B, et al. Age Ageing **39**, 259-262, 2010.

ACKNOWLEDGEMENTS

Funding provided by DOD DM090896 and NIH T32 HD07447. Monitors provided by Mayo Clinic Special Purpose Processor Development Group.

Table 2: Accuracy for varying monitor locations.

Accuracy:	Best	Worst
Standing	thigh/waist-thigh	thigh-ankle
Sitting	waist-thigh	thigh-ankle
Lying	waist/waist-thigh	thigh-ankle
Walking/ Shuffling	thigh/waist-thigh	waist
Jogging	waist/waist-thigh	ankle
Transitions	waist-thigh	thigh-ankle

Table 1: Mean sensitivity (SD) and PPV (SD) for different monitor locations.
Bold indicates highest accuracy in each row, red indicates poor accuracy (≤ 60% [4]).

Sensitivity (%)	Waist & Thigh	Thigh & Ankle	Waist	Thigh	Ankle
Standing	**85 (7)**	74 (17)	79 (8)	76 (16)	55 (8)
Sitting	**94 (18)**	59 (8)	79 (8)	98 (1)	55 (8)
Lying	97 (2)	**99 (1)**	97 (2)	98 (1)	98 (2)
Walking/Shuffling	88 (7)	92 (7)	90 (7)	93 (6)	**95 (5)**
Jogging	**95 (7)**	92 (16)	**95 (7)**	92 (16)	83 (21)
Transitions	**87 (6)**	54 (12)	50 (14)	78 (9)	47 (10)
PPV (%)					
Standing	75 (16)	78 (11)	73 (11)	**84 (10)**	72 (8)
Sitting	**87 (4)**	86 (5)	73 (11)	83 (3)	72 (8)
Lying	**93 (12)**	65 (5)	**93 (12)**	83 (3)	69 (7)
Walking/Shuffling	**95 (3)**	90 (6)	78 (5)	91 (6)	77 (6)
Jogging	**99 (2)**	94 (12)	**99 (2)**	94 (12)	92 (15)
Transitions	70 (10)	75 (12)	82 (13)	72 (11)	**85 (11)**

FIXED CADENCE EFFECT ON SHOD & BAREFOOT GAIT KINEMATICS

Braden Romer, John Fox, Jay Patel, Jared Rehm, and Wendi Weimar

Auburn University, Auburn, AL, USA
email: bhr0002@auburn.edu, web: http://education.auburn.edu/kine/

INTRODUCTION

Barefoot and minimalist footwear has experienced incredible growth in recent years. While much of the recent success might be traced to an increased availability and marketing of minimalist footwear, advocates of this alternative footwear approach assert that the kinematic and kinetic changes associated with modern footwear is a contributing factor to lower extremity injuries.

Recent research has primarily focused on differences in running mechanics, with an increased stride length, decreased cadence, and increased impact transient associated with shod locomotion [1]. Remaining unanswered though is whether footwear changes are due to neural (e.g. reduced plantar feedback) or mechanical (e.g. increased inertia of the distal segment). Previous research has found an increased stride length when wearing athletic shoes as compared to flip-flops, which had been hypothesized as attributable to the increased mass of the athletic shoe [2]. However, more recent research has found that this relationship may not hold for all types of footwear as it has been reported that participants exhibited a longer stride length when wearing a lighter flip-flop as compared to a heavier version [3]. Therefore, the purpose of this study was to examine the effect of a fixed cadence on barefoot and shod gait kinematics.

METHODS

Twenty (10 female, 10 male) healthy participants volunteered for participation in the study. No participant had a lower-extremity injury within the year prior to participation in the study. Age of the participants was 23.7±2.4 years (m±SD) and body mass was 73.6±12.2kg. Participants walked approximately 11m on an instrumented walkway (GAITRite, CIR Systems, Inc., Havertown, PA, USA) and one full stride was captured for analysis. Markers were placed on the head of the fifth metatarsal, lateral malleolus, lateral femoral condyle, and greater trochanter. Kinematic data was averaged across a total of six trials per condition.

The three conditions included were: participants walking at a self-selected pace while barefoot (BFFW), shod while walking at a cadence matched to the barefoot cadence (SHBF), and barefoot while walking at a cadence matched to the barefoot cadence (BFBF). During the fixed cadence trials, participants were provided an audible metronome matching the desired cadence. Participants were dressed in identical polyester clothing and utilized commercially available non-running athletic shoes for all shod trials.

Separate Repeated Measures ANOVA's were completed with dependence on walking velocity, cadence, and sagittal plane lower-extremity joint angles (relative ankle, relative knee, absolute hip) at toe-off and foot strike. Post-hoc analyses were completed utilizing a least squares difference test to determine if significant differences (p<0.05) existed between conditions.

RESULTS AND DISCUSSION

No significant differences were found in joint angles at toe-off, however, significant main effects were found for velocity ($F_{(1.197,22.743)}$ = 5.335, p = 0.025, η^2 = 0.219), cadence ($F_{(2,38)}$ = 11.798.525, p < 0.001, η^2 = 0.383), knee angle at foot strike ($F_{(2,38)}$ = 3.525, p = 0.039, η^2 = 0.156), and ankle angle at foot strike ($F_{(2, 38)}$ = 4.178, p = 0.023, η^2 = 0.18). As indicated in Table 1, follow-up pairwise analyses indicated that participants walked significantly faster (p<0.001) during the fixed shod condition (SHBF) relative to the fixed barefoot condition (BFBF). Furthermore, though cadences were similar between all three conditions, BFBF was found to be significantly different (p=0.001) from the other conditions (Table 1).

Table 1: Spatiotemporal variables across the three conditions.

		Total (n = 20)
BFFW	[1] **Cadence** (steps*min^{-1})	116.8 (±7.5)
	Velocity (ms^{-1})	1.35 (±0.13)
SHBF	[1] **Cadence** (steps*min^{-1})	116.5 (±7.8)
	[2] **Velocity (** ms^{-1})	1.40 (±0.21)
BFBF	[1] **Cadence** (steps*min^{-1})	117.3 (±7.6)
	[2] **Velocity (** ms^{-1})	1.32 (±0.18)

[1] Significant differences in cadence were found between BFBF-SHBF (p<0.001).and BFBF-BFFW (p= 0.001).

[2] Significant differences in velocity were found between SHBF and BFBF (p < 0.001).

Figure 1 displays the relative joint angles for the knee and ankle at initial contact. Follow-up pairwise comparisons indicated that participants displayed significantly less plantarflexion at foot strike during BFBF than either BFFW (p=0.005) or SHBF (p=0.027). Likewise, participants exhibited greater knee flexion at foot strike during BFBF than either BFFW (p=0.033) or SHBF (p=0.027).

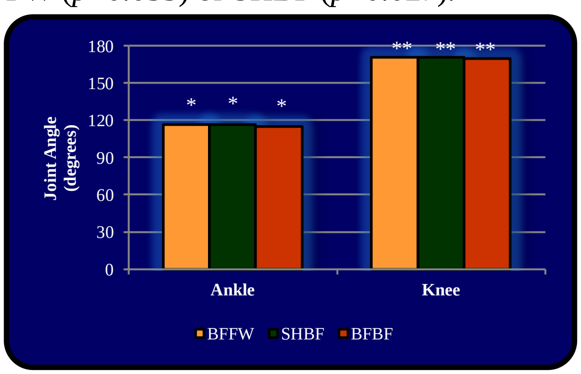

Figure 1: Joint kinematics at foot strike.

***** Sagittal Plane Ankle Angle for BFBF was significantly lower than either BFFW (p=0.005) or SHBF (p=0.027).

****** Sagittal Plane Ankle Angle for BFBF was significantly lower than either BFFW (p=0.033) or SHBF (p=0.027).

CONCLUSIONS

The results of the present study were unexpected, especially that footwear was not found to significantly alter joint kinematics. Conversely, participants displayed significantly greater dorsiflexion and knee flexion when walking barefoot at a fixed cadence (BFBF) which matched the naturally chosen cadence (BFFW). The results may have been confounded by the participant's inability to reproduce natural gait patterns when using a metronome as evidenced by the fluctuations in velocity and cadence. Furthermore, though significant differences were found between BFBF and the other two conditions (BFFW, SHBF), these differences were quite small. Specifically, participants displayed a tibiofemoral joint angle of approximately 171.2° during both BFFW and SHBF and 170.1° during the BFBF trials (Figure 1). Similarly, a talocrural joint angle of approximately 116.9° was found for both the BFFW and SHBF conditions and only 115.4° for the BFBF condition (Figure 1). Therefore, though the results were significant, the difference in joint kinematics and cadences are likely to be of little clinical or practical difference. Despite a slight difference in velocity between BFFW and SHBF, cadence and joint kinematics were not significantly different, lending support for a neural, rather than mechanical, interaction of footwear on gait mechanics. While previous research has indicated a significant footwear effect on pediatric walking, the lack of significant differences between barefoot and shod conditions in the present study was perplexing [4]. Future research should be directed towards two general areas. The use of a metronome appeared to significantly alter gait mechanics, therefore, future research should be directed towards developing a greater understanding of various approaches to adequately control cadence. Finally, only a single cadence and velocity condition was examined in the present study (barefoot, free walking); therefore, future research should examine the footwear effects on gait mechanics at a variety of velocities.

REFERENCES

1. Leiberman, DE, et al. *Nature*, **463**, 531 – 353, 2010.
2. Majundar, D, et al. *Indian J Physiol Pharmacol*, **50 (1)**, 33 – 40, 2006.
3. Shroyer, JF & Weimar, WH. *J Amer Podiatric Med Assn*, **100 (4)**, 252 – 257, 2010.
4. Wegener, C, et al. *J of Foot and Ankle Rsch*, **4(3)**, 1 – 13.

THE EFFECT OF LOAD ON SAGITTAL PLANE KINEMATICS DURING UNANTICIPATED CUTTING MANEUVERS

[1,2]Tyler N. Brown, [2]Meghan O'Donovan, [2]Leif Hasselquist, [2]Brian Corner, [2]Jeffrey M. Schiffman

[1]Oak Ridge Institute for Science and Education (ORISE), Belcamp, MD, USA
[2]U.S. Army Natick Soldier Research, Development and Engineering Center, Natick, MA,USA
email: tyler.n.brown4.ctr@mail.mil

INTRODUCTION

Load carriage has a detrimental effect on performance, which may be attributable to altered sagittal plane biomechanical profiles [1]. Previous biomechanics-based load carriage research has limited its assessment to straight line ambulation, i.e. treadmill walking [1]. It may be that changing the speed or direction of movement, i.e. dynamic maneuvers, during load carriage that result in greater adaptations of lower limb biomechanics than evident with straight line walking. Thus, greater performance decrements may also be associated with loaded dynamic cutting tasks. To date, however, the effect of load carriage during dynamic tasks is unknown. Reactive maneuvers, i.e. responding to an external, unplanned stimulus, may also produce substantial modifications of lower limb biomechanics that decrease performance [2]. With that in mind, the purpose of this study is to identify biomechanical parameters of anticipated and unanticipated cutting maneuvers during load carriage that determine performance of such tasks.

METHODS

Ten males (21.4 ± 3.6 years, 1.8 ± 0.1 m, and 74.8 ± 12.0 kg) had 3D hip and knee joint biomechanical data recorded during a series of single-leg cutting maneuvers. Each participant performed the cutting movements for two conditions: unloaded and loaded. During the unloaded condition (6 kg), participants wore a helmet and carried a mock weapon. For the loaded condition (20 kg), participants wore body armor with a fabric ammo panel attached on the anterior, in addition to carrying the weapon and donning the helmet. During each condition, participants performed five successful anticipated (AN) and unanticipated (UN) single-leg cutting maneuvers with their dominant limb. Each cut required the participants to run at 3.5 m/s ± 5% on a walkway, plant their dominant limb on a force platform (AMTI Optima HPS, Advanced Mechanical Technology Inc., Watertown, MA) embedded in the floor, and cut at 45° ± 15° to their non-dominant side. For the AN maneuver, each participant responded to a light stimulus delivered prior to initiation of the movement (~5 s). During the UN task, each participant responded to a light stimulus triggered during the approach phase of the run (~600 ms prior to force platform contact).

For each single-leg cut, hip and knee biomechanics were quantified based on the 3D coordinates of 36 reflective skin markers recorded with twelve high-speed (240 fps) optical cameras (Opus, Qualysis AB, Gothenburg, Sweden). A high-speed video recording of the subject standing in a stationary (neutral) position was taken following marker placement and used to define a kinematic model comprised of eight skeletal segments (bilateral foot, shank and thigh segments and the pelvis and trunk) with 24 degrees of freedom. The 3D marker trajectories recorded during each cutting trial were low-pass filtered with a fourth-order Butterworth filter at a cut-off frequency of 12. The filtered marker trajectories were subsequently processed by the Visual 3D (C-Motion, Rockville, MD) software to solve for the lower limb joint rotations, according to our previous work [3].

For analysis, initial contact (IC) and peak (PS) hip and knee sagittal plane rotations, and total stance time were assessed for the stance phase (0 – 100%) of each cutting maneuver. Subject-based means for both the AN and UN maneuvers were subsequently calculated for the dominant limb. The subject-based mean value for each dependent variable was then submitted to a repeated measures ANOVA to test the main effects of and possible interactions between the unloaded and loaded conditions, and movement type (AN and UN). Where statistically significant ($p < 0.05$) differences were observed, Bonferroni pairwise comparisons were used.

RESULTS AND DISCUSSION

Stance time did not significantly differ ($p = 0.590$) between the UN (0.29 ± 0.03 s) and AN (0.29 ± 0.03 s) single-leg cutting maneuvers, despite the fact participants adopted greater lower limb flexion during the reactive tasks. Specifically, significantly greater IC hip ($p = 0.042$) and knee ($p = 0.050$) flexion posture were evident during the UN as compared to the AN movements (Figure 1). Previous experimental evidence, however, suggests extended lower limb posture occurs during dynamic single-leg UN maneuvers [3]. The increased flexion posture currently associated with UN movements may be adopted to limit risky joint loads by placing the hamstrings at a mechanical advantage [4]. As such, the hamstrings may maximize their ability to stabilize the lower limb, and maintain the ability to perform the UN maneuvers.

Increased lower limb flexion was also evident during the unloaded condition (Figure 1). Specifically, significantly greater IC and PS hip ($p = 0.027$ and $p = 0.025$) and knee flexion ($p = 0.049$ and $p = 0.019$) were evident for the unloaded as compared to the loaded movements. During a cutting maneuver, the landing limb is required to rapidly decelerate and change of direction of the center of mass, while also controlling the inertias of the upper body [5]. Due to the added mass of the body armor and ammo panel for the loaded condition, the responsibilities of the landing limb musculature are substantially greater. As such, the extended lower limb posture may be necessary to avoid overloading the musculature and prevent collapse that may otherwise occur with greater flexion. The extended posture of the loaded condition may also be adopted to maintain performance during such tasks. The fact that stance time was not significantly different ($p = 0.145$) between the unloaded (0.28 ± 0.03 s) and loaded (0.29 ± 0.04 s) conditions supports this contention.

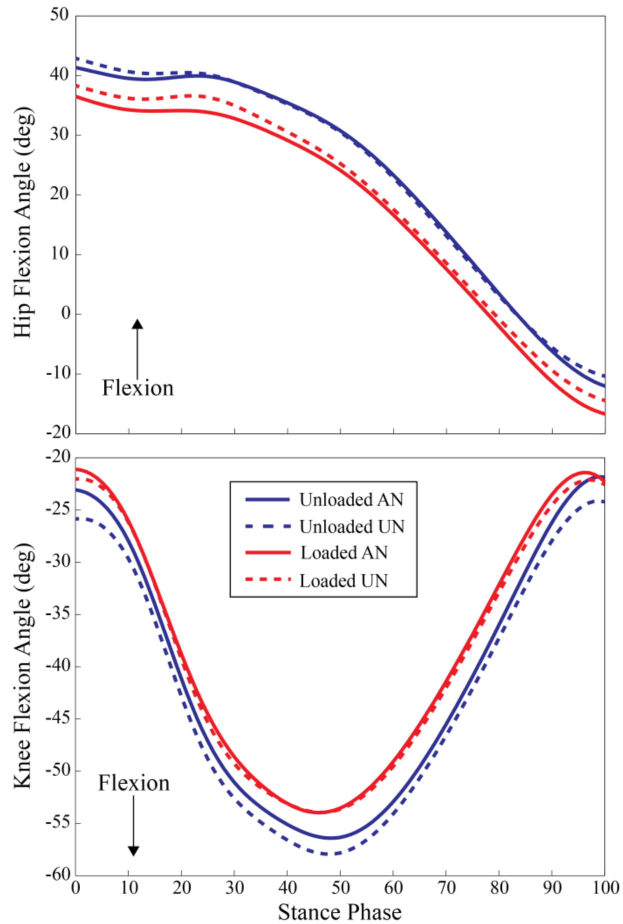

Figure 1: Hip and Knee flexion angles during the stance phase (0% - 100%) of both AN and UN cutting maneuvers for the unloaded and loaded conditions.

CONCLUSIONS

Sagittal plane adaptations of hip and knee posture during loaded and reactive cutting maneuvers may be adopted to maintain performance of each task. Further research to determine if these adaptations subsequently elevate injury risk of load carriage may be warranted.

REFERENCES

1. Patton JF, et al. *Eur J Appl Physiol*. **63**:89-93, 1991
2. Besier TF, et al. *MSSE*, **33**:1176-81, 2001
3. Brown TN, et al. *BJSM*. **43**:1049-1056, 2009
4. Decker MJ et al. *Clin Biomech*. **18**:662–9, 2003
5. McNitt-Gray et al. *Int. J. Sport Biomech*, **7**:201-4, 1991

ACKNOWLEDGEMENTS

The authors thank Ms. Marina Carboni and Mr. Albert Adams for their assistance with this study.

RELATIONSHIP BETWEEN FUNCTIONAL PERFORMANCE, COGNITION, GAIT AND BALANCE MEASURES IN OLDER ADULTS AFTER RESISTANCE TRAINING

Srikant Vallabhajosula, Francesco P. Worley, Robert L. Hensley, Stephen P. Bailey

Elon University, Elon, NC, USA
email: svallabhajosula@elon.edu, web: www.elon.edu/dpt

INTRODUCTION

Decline in functional performance, gait, balance and cognition are common among aging population. Such a decline could significantly affect their performance during activities of daily living Resistance training has been shown to be beneficial for older adults to improve their functional performance, gait and balance [1]. However, very few investigations have focused on the efficacy of resistance training to improve the cognitive function in geriatric population [2,3].

The purpose of the current study was two-fold. First, to determine the efficacy of a 4-week resistance training program on measures of functional performance, cognition, balance, and gait. Second, if after 4-weeks of resistance training, changes in functional performance measures like six minute walk, short physical performance battery, sit to stand time correlated with cognition (working memory and selective attention), instrumented gait and balance measures.

METHODS

Nine participants (7 females; mean age, 73.4 years; mean height, 1.63m; mean mass, 70.22kg) completed 4 weeks of resistance training. *Exercise intervention*: Each resistance training session lasted 30-45 min. consisting of the following exercises: squats, standing leg curl, knee extension, lateral hip raises, bicep curls, overhead press, upward row, heel raises. 2 sets of 8 repetitions were performed for each activity except heel raises, which was done by performing 1 set of 20 repetitions. The knee extensions and lateral hip raises were performed while wearing ankle weights (5-10 lbs). The bicep curls, overhead press and upward rows were performed using dumbbell weights (4-10 lbs). The following tests were conducted before and after the training period: 1) *Functional performance tests* included short physical performance battery, six minute walk test, sit-to-stand task and hand grip strength measurement using a hand-held dynamometer. 2a) For *Working Memory*, participants counted backwards by intervals of 7 from a randomly presented 3-digit number for 60s while sitting. The number of responses and wrong responses were analyzed. 2b) For *Selective Attention*, the Stroop test was used where the participants had to identify the color of the word instead of the actual word as quickly as possible. The reaction time and accuracy were analyzed. 3) *Instrumented gait testing* was done using a GaitRite system (CIR Systems Inc., Sparta, NJ). Participants performed five walking trials at their self-selected pace. An average of five trials was used for data analysis. Outcome variables included mean and coefficient of variation of walking speed, cadence, step time, step length, stride length, stance width, swing time, stance time, and double support time. 4) *Instrumented balance testing* was done using the Balance System SD (Biodex Medical Systems, Inc., Shirley, NY). Participants were tested under four conditions for 30s each with 10s rest between conditions: standing with eyes open/closed and on firm/foam surface. The maximum displacement of center of pressure in anterior-posterior and medio-lateral directions, sway area and sway index were analyzed. Statistical analyses for short physical performance battery, six minute walk test, hand grip strength, cognition, and gait was performed through a paired samples t-test. Balance data was analyzed using a 4(condition) x 2 (time) repeated measures ANOVA. A Pearson-product moment correlation coefficient was calculated between changes (from Pre- to Post-training) in the functional test measures with the cognition, gait and balance measures.

RESULTS AND DISCUSSION

After training, the coefficient of variation reduced significantly for cadence (by 45%; *P* = 0.025), step time (by 37%; *P* = 0.028) and stance time (by 45%; *P* = 0.019). The short physical performance battery score significantly increased by 17% after training (*P* = 0.044). Significant time main effect for sway area indicated a reduction by 28% after training (*P* = 0.012). The antero-posterior displacement during the eyes-closed and standing on foam surface condition also reduced by 15%. Significant strong correlation results are shown in Tables 1 and 2 below. Also, a significant moderate-to-strong negative correlation was found between change in hand-grip strength and change in coefficient of variation of step length (r = -0.668; *P* = 0.049). Similarly, a significant moderate-to-strong negative correlation was found between change in hand-grip strength and change in coefficient of variation of stance width (r = -0.697; *P* = 0.037).

CONCLUSIONS

Positive changes in functional performance measures were accompanied by positive changes in measures of gait variability and sway area after resistance training. Also, moderate-to-strong negative correlations between changes in temporal parameters of instrumented gait analysis and functional performance test measures (like a six-minute walk distance) might indicate that increased functional performance was achieved by altering the temporal aspects of gait. Results also showed that a change in a functional measure of balance (sit-to-stand time) was associated with a change in instrumented postural control parameters in challenging conditions (like standing on foam where the proprioceptive system is perturbed). Overall, results indicate that 4 weeks of resistance training improved the participants' neuromuscular function to maintain their balance based on the surrounding conditions (firm/foam surface). The resistance training also seemed to improve their functional performance and made their gait less variable. However, the training seemed to have lesser impact on cognition. A longer resistance training combined with a control group could highlight more advantages of resistance training for functional performance, cognition, gait, and balance in older adults.

REFERENCES

[1] Bird et al., *J Aging Phys Act*. 2009; Oct; 17(4):444-54

[2] Forte et al., *Clin. Interv. Aging*. 2013; 8: 19-27

[3] Chodzko-Zajko et al., Human Kinetics; 2009

Table 1: Pearson-product moment correlation coefficient between functional and instrumented measures of gait (* Significant difference, *P* < 0.05)

	Cadence	**Step time**	**Stance time**	**Swing time**	**Double support time**
6 minute walk distance	0.740* (*p=0.023*)	-0.776* (*p=0.014*)	-0.773* (*p=0.015*)	-0.742* (*p=0.022*)	-0.751* (*p=0.020*)

Table 2: Pearson-product moment correlation coefficient between functional gait and balance measures, and instrumented measures of balance (* Significant difference, *P* < 0.05)

	APD EC FIRM	**APD EO FOAM**	**MLD EC FOAM**	**SA EC FOAM**	**SI EO FOAM**
6 minute walk distance	-0.727* (*p=0.027*)	-0.191 (*p=0.622)*	0.773* (*p=0.015*)	0.758* (*p=0.018*)	-0.104 (*p=0.790*)
Sit-to-Stand time	0.651 (*p=0.057*)	0.753* (*p=0.019*)	-0.572 (*p=0.108*)	-0.733* (*p=0.025*)	0.755* (*p=0.019*)

APD – Antero-Posterior Distance; MLD – Medio-Lateral Distance; SA – Sway Area; SI – Sway Index; EO – Eyes Open; EC – Eyes Closed; FIRM – Firm surface; FOAM – Foam surface

GENERATING KINEMATICALLY CONSISTENT DATA FOR MUSCULOSKELETAL INVERSE DYNAMIC ANALYSES USING FINITE ELEMENT TOOLS

[1]Manoj Chinnakonda, [1]Prabhav Saraswat, [1]Jiang Yao, [1]Victor Oancea, [1]Juan Hurtado and [1]Subham Sett
[1]Dassault Systemes Simulia Corp., Providence, RI, USA
email: manoj.chinnakonda@3ds.com, web: www.3ds.com

INTRODUCTION

Motion capture data recorded using reflective markers can be noisy and be affected by skin artifacts or tracking errors [2]. These issues introduce the need to filter, correct and produce kinematically consistent motion data before using it to drive musculoskeletal inverse dynamics simulations. In this work, we show how Abaqus [1], a general purpose finite element tool, can be used effectively to produce kinematically consistent and averaged segment motions from motion capture inputs.

METHODS

A complete musculoskeletal analysis workflow comprising of musculoskeletal model set up, motion data processing, subject specific scaling, and muscle activation predictions using static optimization techniques has been recently implemented using Abaqus and Isight (a process automation and optimization tool) and activation results of right leg muscles have been validated against published EMG data [3]. This paper focuses on the motion data processing component of the workflow, while interested readers are advised to refer to [3] for more details on the complete workflow implementation.

The steps involved in motion data processing are as follows:

1. An Abaqus FE model is constructed with markers represented as nodes defined at their initial recorded coordinates. Shell elements are defined connecting 3-4 nodes designated per body segment and in turn each of these elements are coupled to reference nodes located at the segment center of masses through distributing coupling constraints [1]. During the finite element analysis, the motion of the marker points are completely prescribed through 3 translational degrees-of-freedom (DOF) coming from motion capture data. The shell elements along with the distributing coupling constraints help in computing an averaged motion (6 DOF) for each body segment at the coupling reference nodes based on translations available at each of the markers.

2. A subject specific musculoskeletal model comprising of rigid body segments connected by joints and spanned by muscles is developed in Abaqus/CAE (a GUI-based interactive pre-processing tool). The reference nodes of the rigid bodies located at the center of masses of the segments are each attached with CARTESIAN-CARDAN connectors (elements that model discrete point-point physical connections) with specified translational and rotational stiffnesses.

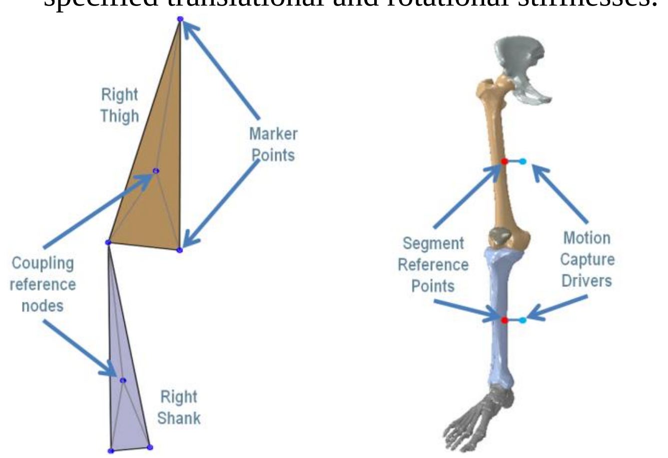

Figure 1: (Left) Abaqus model consisting of marker points, shell elements and distributing couplings for thigh and shank segments. (Right) Subject specific musculoskeletal model with CARTESIAN-CARDAN connectors attached to segment center of masses.

3. Motion recorded (6 DOF) at the reference nodes of distributing coupling constraints in step #1 are used to drive the end points of the CARTESIAN-CARDAN connectors. These connectors acting as stiff springs help alleviate any kinematic

inconsistency in the musculoskeletal model producing a filtered data for further inverse dynamics processing. The stiffness values of these connectors can be used as weight factors to control the segments for which the motion data should be closely followed. The steps involved in the motion data processing are shown in Fig.1

Prior to using real motion capture data, the accuracy of motion data processing set up was verified by using a set of artificial yet kinematically consistent and noise free marker motions as inputs and confirming that the same motion was reproduced after the data was processed.

RESULTS AND DISCUSSION

Reflective marker data of walking from 6 subjects (3 trials each) at self selected speeds (~ 1m/s) were used as inputs for validation of motion data processing component of the workflow for the right lower limb model. Marker motions before and after processing are compared and the resulting deviations are presented in Table 1. The values listed are average marker deviations, averaged over gait cycle, trials, marker locations (Pelvis, Knee, Ankle and Foot) and finally subjects.

Table 1: Average deviation in marker positions after data processing

Subject	Average deviation in marker positions (mm)			
	Pelvis	**Knee**	**Ankle**	**Foot**
1	9.78	5.14	3.03	3.33
2	6.30	4.18	3.10	4.48
3	6.78	5.15	2.64	3.05
4	7.91	4.74	2.68	1.85
5	7.63	3.60	3.31	4.96
6	6.80	3.55	2.92	2.41
Avg.	7.53	4.39	2.95	3.35

The marker deviations provide a measure of corrections needed to the marker motions in order to eliminate skin artifacts and kinematic inconsistency in the data. The maximum deviation happens at the Pelvis which is expected due to excess soft tissue causing the larger skin motions on pelvis markers. On a similar thought, corrections to Knee, Ankle and Foot are considerably smaller given that markers in these regions are less affected by skin motion.

Another measure of kinematic inconsistency is provided by the extensions recorded at the CARTESIAN-CARDAN connectors and results of one such subject/trial for the entire gait cycle is shown in Fig 2. The connector extensions are consistent with marker deviations reported earlier and show the maximum compromise in motion occurring at the Pelvis location.

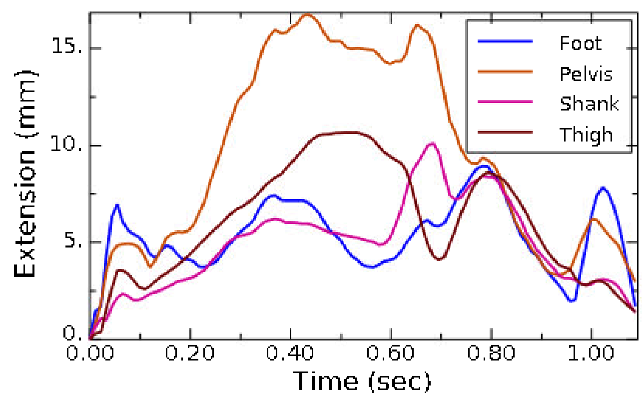

Figure 2: Extensions of CARTESIAN+CARDAN connectors during walking for one subject/trial.

Given that the dataset processed is for a slow walking activity, it is not expected for the skin motion or noise to affect the overall data quality and is corroborated by the fact that the marker deviations and the connector extensions measured are considerably small compared to the overall dimensions and displacements of the model.

REFERENCES

1. *Abaqus 6.12 Analysis User's Manual*, Dassault Systèmes Simulia Corp., 2012
2. Benoit D.L, et al. *Gait and Posture*. **24(2)**, 152-164, 2006.
3. Saraswat P, et al. *XXIV Congress of ISB,* Natal, Brazil, 2013.

ACKNOWLEDGEMENTS

We acknowledge Zygote for allowing use of their skeletal model.

EFFECT OF SHOE TREAD DEPTH ON FOOT SLIPPING KINEMATICS

[1]Devon Albert, [1]Aaron T. Ledgerwood, [1]April J. Chambers, [1]Mark S. Redfern and [2]Kurt Beschorner

[1]University of Pittsburgh, Pittsburgh, PA, USA
[2]University of Wisconsin-Milwaukee, Milwaukee, WI, USA
email: dla16@pitt.edu, web: http://www.engineering.pitt.edu/hmbl/

INTRODUCTION

Slips and falls account for over one million hospital emergency room visits each year [1]. Shoe tread, which has been shown to affect friction, may be an important parameter for predicting the likelihood of slips and slip severity [2]. A greater slip severity is characterized by increased peak slip velocity and slip distance, resulting in an increased risk of falling [3]. A gap in literature currently exists on whether shoe-tread is effective at reducing the severity of slips. In addition, most previous studies have focused exclusively on anterior-posterior slip path (slip distance), and the medial-lateral slip path has not received as much attention as a significant slipping parameter. The purpose of this study was to investigate the effect of tread type (treaded or non-treaded) on foot movements including slip path and peak slip velocity during slipping on a slippery glycerol surface. A secondary purpose was to quantify the amount of slipping in the medial-lateral direction. It was hypothesized that peak slip velocity and slip path will be greater for non-treaded shoe slips.

METHODS

Seventeen participants (10 female, mean ± standard deviation: age 23.5 ± 4.0 years, weight 70.0 ± 11.8 kg, height 1.71 ± 0.07 m) were asked to walk at a self-selected speed on an eight-meter vinyl walkway wearing either treaded or non-treaded shoes. Both shoe types were slip resistant footwear with a rubber sole. Treaded shoes had the tread intact (tread depth = 3 mm); non-treaded shoes had the tread completely removed by a belt-sander. The order in which participants wore each type of shoe was randomized.

A 90:10 glycerol:water solution was used to slip each participant on a 24” x 24” vinyl floor tile. At least five dry trials were collected before participants were unexpectedly slipped wearing the first type of shoes. After the first unexpected slip, at least fifteen dry trials with the second pair of shoes were collected to ensure participants returned to a normal gait [4]. Between each trial, participants were asked to listen to music and complete word searches to distract them from the possible application of a contaminant. Motion data were collected at 120 Hz using a 14 camera Vicon motion capture system. Subjects wore a safety harness throughout data collection to prevent injury.

Peak slip velocity (PSV) and slip path were calculated from the motion capture data of the slipping trials. PSV was calculated as the maximum resultant velocity of the heel between the beginning and end of the slip [3]. The beginning of the slip was defined as the first local minimum of the heel velocity after heel strike. Slip stop was defined as the first local minimum of the heel velocity after the slip. PSV was then normalized by gait velocity which was calculated from the sternum trajectory of the trial immediately preceding the slip. The anterior-posterior (AP) and medial-lateral (ML) directions, and resultant slip paths were defined as the total distance traveled by the heel in each respective direction between heel strike and slip stop. ANOVA tests were performed on AP, ML, and resultant slip paths and normalized peak slip velocity to assess the impact of tread conditions on slip parameters.

RESULTS AND DISCUSSION

Differences in slip paths in AP, ML, and resultant directions and PSV were found to be significant ($p<0.05$) between treaded (8 slips) and non-treaded

(14 slips) shoes (Table 1). The average PSV was 1.57 ± 0.80 m/s for non-treaded shoes and 0.063 ± 0.017 m/s for treaded shoes. The significantly higher PSV values for non-treaded shoes are indicative of more severe slips [3]. The average gait velocity was 1.29 ± 0.19 m/s for the non-treaded condition and 1.34 ± 0.24 m/s. Differences in gait velocity between treaded and non-treaded conditions were not significant. Furthermore, gait velocity was within the normal ranges for young adults [5].

Table 1: Calculated parameters' p-values between treaded and non-treaded conditions. Significant values ($p<0.05$) denoted by: *.

Parameter	p-value
Slip Path AP	0.0056*
Slip Path ML	0.0030*
Slip Path Resultant	0.0047*
Peak Slip Velocity	0.0015*
Gait Velocity	0.6283

Differences in slip path in the AP, ML, and resultant directions between treaded and non-treaded conditions were significant (Figure 1). Previous studies [6] report a slip distance greater than 10 cm indicates a severe slip; twelve of the fourteen slips for the non-treaded condition resulted in slip paths greater than 10 cm. None of the slip paths for the treaded condition were greater than 10 cm. The ratio between slip path in the ML and AP directions was 0.37 ± 0.17 for the non-treaded condition and 0.49 ± 0.27 for the treaded condition.

As hypothesized, the non-treaded condition resulted in severe slips (slip path AP > 10 cm) whereas the treaded condition did not result in severe slips. This confirms that shoe tread is effective at reducing slipping incidents. Although AP slip path (slip distance) has been used to benchmark slip severity [6], slip path in the ML direction may also be an indicator of slip severity. Medial-lateral foot slip may increase the risk of a fall and could lead to sideways falls that put the hip at risk. Slip parameters in all directions may need to be observed in order to fully understand the mechanics of a slip and how a slip manifests into a fall incident.

REFERENCES

1. NFSI. *Same Level Slip-and-Fall Statistics*. http://www.nfsi.org/the_costs.php.
2. Li KW, et al. *Applied Ergonomics* **37**, 743-748, 2006.
3. Moyer BE, et al. *Ergonomics* **49**, 329-343, 2006.
4. Timcho EA, et al. *Proceedings of ASB'09*, State College, PA, USA, 2009.
5. Kang HG, et al. *Gait & Posture* **27**, 572-577, 2008.
6. Cham R, et al. *Safety Science* **40**, 559-576, 2002.

ACKNOWLEDGEMENTS

We would like to thank our funding source: NIOSH R01 OH008986.

Table 2: Mean ± standard deviation of slip path in the AP, ML, and resultant directions for non-treaded and treaded conditions.

Condition	Slip Path AP (cm)	Slip Path ML (cm)	Slip Path Resultant (cm)
Non-Treaded	56.6 ± 38.3	17.3 ± 11.0	62.3 ± 40.6
Treaded	1.26 ± 1.17	0.50 ± 0.28	1.47 ± 1.20

ASSISTIVE FORCES AFFECT THE TEMPORAL STRUCTURE OF GAIT VARIABILITY

[1,2]Eric Cutler, [1,2]Shane R. Wurdeman, [3]Deborah L. Givens, [1,2]Nicholas Stergiou

[1]University of Nebraska at Omaha, Omaha, NE, USA
[2]University of Nebraska Medical Center, Omaha, NE, USA
[3]Creighton University, Omaha, NE, USA
email: ecutler@unomaha.edu, web: nbcf.unomaha.edu

INTRODUCTION

One out of three adults over the age of 65 years experiences a fall every year [1]. Recent estimates for direct medical costs from fall-related injury and death exceed $19 billion [2]. Previous studies have shown that elderly fallers exhibit an increased amount of gait variability (increased variance of stride parameters that describe the stride to stride fluctuations) and a loss of the complexity in the temporal structure of gait variability compared to their younger counterparts and healthy age-matched peers [3]. This loss of complexity is often demonstrated as a reduced predictability and increased attractor divergence between strides, resulting in gait variability that is closer to random white noise [4]. Thus, gait amongst elderly fallers is often described as noisy and unstructured. A method of restoring gait variability of elderly fallers to healthy levels and their characteristics could lead to a decrease in the incidence of falls.

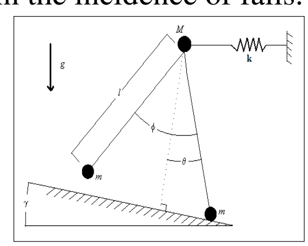

Figure 1: A passive dynamic walking model modified with an assistive force at the center of mass. Adopted from Kurz and Stergiou (2007).

Our preliminary research utilized a passive dynamic walking model (Figure 1). We demonstrated that implementing assistive actuators in the passive dynamic walker at the center of mass can provide a mechanism for altering the temporal structure of variability in gait [5]. The results of this study strongly indicated that the application of assistive forces is capable of shifting the model's gait into a more stable attractor [5]. Therefore, the purpose of this study was to transfer the model's results to human subjects and to determine if the effects of assistive forces are related to joint motion in young and elderly subjects.

METHODS

Six young subjects (age: 22±1.5 yrs, height: 1.7 m±0.4 m, mass: 70.3±5.4 kg) and three elderly subjects (age: 66±3.1 yrs, height: 1.5±0.3 m, mass: 73.1±4.0 kg) gave consent to participate in this study. Markers were placed at anatomical locations to track lower limb segment motion. All subjects performed 5 treadmill trials, each lasting 5 minutes in duration, at each subject's self-selected speed. Marker position data were recorded using a 12-camera 3-dimensional motion capture system (60 Hz; Motion Analysis Corp., Santa Rosa, CA, USA). Horizontal assistive forces in the anterior direction were applied at the waist via a custom device designed by the first author (Figure 2). The magnitude of assistive forces used spanned from 0 - 6% of each subject's bodyweight at 1.5% increments. The conditions were presented randomly and assistive forces were verified through an in-series strain gauge transducer (60 Hz; Omega Engineering, Stamford, CT, USA). Successive trials were separated by at least two minutes of rest in order to prevent subject fatigue.

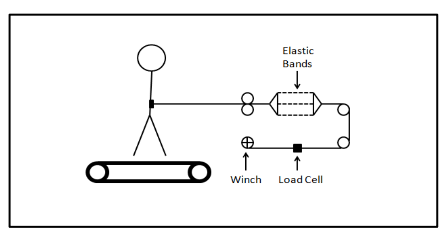

Figure 2: Assistive force device schematic. This custom design was utilized to apply

Marker position data for the left leg of each subject was transformed into three-dimensional joint angle flexion/extension time series and subsequently analyzed using the largest Lyapunov exponent (LyE) using custom MatLab code (MathWorks, Inc., Natick, MA) [6,7] LyE is a measure of the temporal structure of variability that quantifies the divergence within an attractor.

RESULTS AND DISCUSSION

The correlation coefficient between assistive force magnitude and LyE was positive for all parameters except for ankle dorsiflexion/plantarflexion in the young group (which was -0.29) (Table 1). Non-negative correlation coefficients ranged between 0.331 and 0.991 for the young group and between 0.892 and 0.976 for the old group. For the young group, the relationship between assistive force magnitude and LyE was small ($0.1<r<0.3$) for 1 joint angle, medium ($0.3<r<0.5$) for 2 joint angles, and very dependable ($r>0.5$) for 6 joint angles [8]. For the elderly group the relationship between assistive force magnitude and LyE was large ($r>0.5$) for all of the joint angles [8]. It would appear that there is a substantial relationship between assistive force magnitude and the temporal structure of gait variability. It also confirms the findings of our previous studies utilizing passive dynamic walkers [5].

Table 1: Correlation coefficient between assistive force magnitude and Lyapunov exponent.

		Young	Old
Ankle	Abd/Add	0.991432	0.914101
	Dorsi/Plant	-0.29038	0.952029
	Int/Ext	0.980812	0.903841
Knee	Abd/Add	0.383733	0.954935
	Flex/Ext	0.331375	0.975655
	Int/Ext	0.899618	0.957581
Hip	Abd/Add	0.955236	0.950848
	Flex/Ext	0.793099	0.892359
	Int/Ext	0.989937	0.892484

Additionally, the coefficients of determination for the old group showed that at least 79.6% of the variability in joint angle LyE can be attributed to the magnitude of the assistive forces, regardless of the specific joint or anatomic direction (Table 2).

Table 2: Coefficient of determination between assistive force magnitude and Lyapunov exponent

		Young	Old
Ankle	Abd/Add	0.9829	0.8356
	Dorsi/Plant	0.0843	0.9064
	Int/Ext	0.962	0.8169
Knee	Abd/Add	0.1473	0.9119
	Flex/Ext	0.1098	0.9519
	Int/Ext	0.8093	0.917
Hip	Abd/Add	0.9125	0.9041
	Flex/Ext	0.629	0.7963
	Int/Ext	0.98	0.7965

CONCLUSIONS

This study demonstrated that in young and elderly individuals there is a substantial relationship between anterior assistive force magnitude and the temporal structure of gait variability. The study provides support for the application of assistive forces as a method of altering the temporal structure of gait variability in the elderly.

REFERENCES

1. Hausdorff J, et al. *Arch Phys Med Rehabil* **82**, 1050-1056, 2001.
2. Stevens J. *Gerontologist*. **45**, 167-167, 2000.
3. Stergiou N, Decker LM. *Hum Mov Sci* **30**, 869-888, 2011.
4. Kurz MJ, et al. *Nonlin Dyn Psychol Life Sci* 14 151-164, 2010.
5. Kurz MJ and Stergiou N. *J Biomech Engr-Trans ASME* **129**, 216-222, 2007.
6. Vaughan C, et al. *Anonymous dynamics of human gait (2nd ed.)*, 1992.
7. Wolff R. *J Royal Stat Soc B-Meth*, **54**, 353-371, 1992.
8. Cohen, J. *Statistical power analysis for the behavioral sciences (2nd ed.)*, 1988.

ACKNOWLEDGEMENTS

This work was generously supported by the NASA Nebraska Space Grant, Creighton University and the University of Nebraska Medical Center.

THE EFFECTS OF PLANTAR FASCIITIS ON MULTI-SEGMENT FOOT RUNNING GAIT KINEMATICS

[1]Robin L. Bauer, [1]Carol K C Mitchell, [1]Mukta N. Joshi, [1]Stephen C. Cobb

[1]University of Wisconsin-Milwaukee, Milwaukee, WI, USA
email: rbauer1120@gmail.com

INTRODUCTION

Plantar fasciitis is a common lower extremity injury caused by mechanical overload that affects 10% of all runners. Despite its commonality, research results investigating the etiology of the condition and the most efficacious treatment have been equivocal [1]. A potential limitation of previous research assessing the mechanical changes associated with plantar fasciitis may be the modeling of the foot as a single segment. Previous studies on healthy adults have demonstrated the importance of using a multi-segment foot model during gait to identify midfoot and forefoot motion [2,3]. To date no study has investigated running kinematics in individuals with plantar fasciitis using a multi-segment foot model.

Clinical symptoms have historically been used for diagnosing plantar fasciitis. Recently, however, sonography has provided a more definitive measure for diagnosis [4,5]. In non-athletic populations, plantar fasciitis has been associated with a hypoechoic appearance and an adaptive thickening of the plantar fascia [4]. No studies have investigated the thickness of the plantar fascia in runners with plantar fasciitis.

The primary purpose of this study was to compare running kinematics between runners with plantar fasciitis and uninjured runners using a six-segment foot model. The secondary purpose was to investigate differences in plantar fascia thickness between the two groups.

METHODS

Fifteen runners (7 f, 8 m) with plantar fasciitis (age: 30 ± 8.74 yrs, height: 170.60 ± 8.25 cm; mass: 67.98 ± 8.20 kg) and 15 age, gender and mileage matched uninjured runners (age: 29.33 ± 6.53 yrs, height: 170.52 ± 7.78 cm, mass: 68.07 ± 9.99 kg) were recruited. Data collection consisted of a running gait analysis and ultrasound imaging.

A six foot segment model was used for this study [6]. Participants completed 10 running trials at 4.0 (±10%) m/s. 3D positions of the technical and anatomical marker clusters were collected at 200 Hz with a 10-camera Eagle system (Motion Analysis). A force plate (AMTI) sampling at 1000 Hz was used to identify initial contact and toe-off. A custom written Matlab program was used to filter the data, reconstruct the 3D position of each segment using the calibrated anatomical system technique with a single value decomposition optimization procedure, and compute joint angles between adjacent segments (Figure 1). Prior to completing the running trials, an anatomical calibration procedure was performed to identify anatomical landmarks and define local coordinate systems within each segment (Figure 1).

Stance phase was separated into 4 subphases, and MANOVAs ($\alpha \leq 0.05$) were performed to assess between-subject ROM differences for six functional articulations (rearfoot complex, calcaneocuboid, and calcaneonavicular complex, medial and lateral forefoot, and 1st metatarsophalangeal complex).

Ultrasound images were captured following a protocol similar to that reported by Rathleff [7]. The proximal attachment of each participant's plantar fascia was imaged using a 4.0 cm wide transducer head and 12 MHz transducer (Vivid-i, General Electric Healthcare) and a scan depth of 2.5 cm. Imaging of the plantar fascia consisted of real time scanning of longitudinal sonographic images. The thickness at the proximal insertion was measured on three successful images within 0.5 mm of each other. Independent t-tests ($\alpha \leq 0.05$) were conducted to investigate differences in plantar fascia thickness.

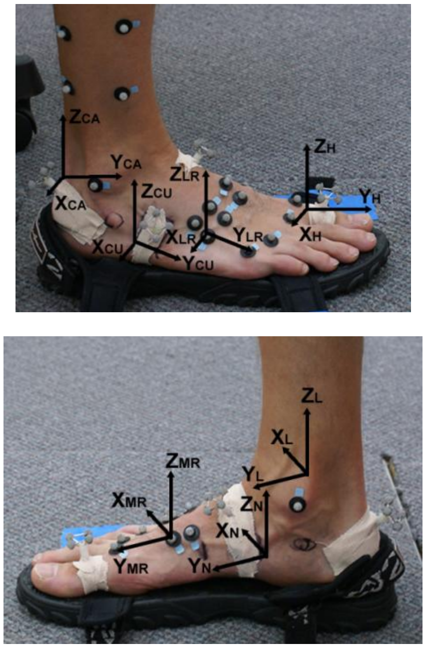

Figure 1: Technical and anatomical markers. **Top Figure:** calcaneus (X_{CA}, Y_{CA}, Z_{CA}), cuboid (X_{CU}, Y_{CU}, Z_{CU}), lateral rays (X_{LR}, Y_{LR}, Z_{LR}), and hallux (X_H, Y_H, Z_H) anatomical coordinate systems. **Bottom Figure**: Leg (X_L, Y_L, Z_L), navicular (X_N, Y_N, Z_N), and medial rays (X_{MR}, Y_{MR}, Z_{MR}) anatomical coordinate systems. All of the anatomical coordinate systems were defined using the appropriate anatomical landmarks.

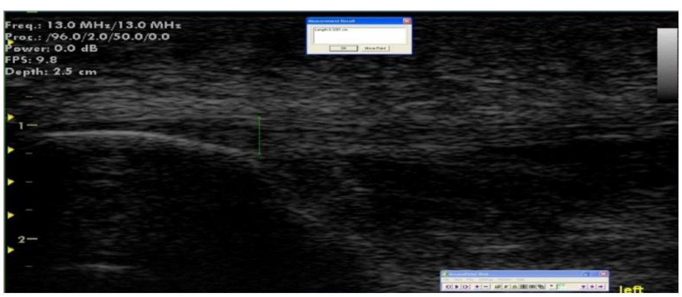

Figure 2: Representative ultrasound image of the left plantar fascia of an asymptomatic individual.

RESULTS AND DISCUSSION

Results revealed calcaneocuboid eversion ROM during early stance ($p = 0.003$) (Table 1), and plantar fascia thickness ($p = 0.007$) were significantly greater in the plantar fasciitis group. The increased eversion excursion of the calcaneocuboid in the plantar fasciitis group may suggest decreased lateral midfoot stability. Additionally, the increased thickness of the plantar fascia in the plantar fasciitis group (4.64 ± 1.07 mm) over the limb-matched control group (mean: 3.75 ± 0.54 mm) was consistent with previous findings [4,5].

The results of the study enhanced understanding of the effects of plantar fasciitis on running gait mechanics. Previous studies have only analyzed rearfoot kinematics. However, additional study on the influence of extrinsic and intrinsic foot musculature is warranted before conclusions regarding the effect of plantar fasciitis on running gait can be drawn.

REFERENCES

1. Cole C, et al. *Am Fam Phys*, **72**, 2237-42, 2005.
2. Arndt A, et al. *J Biomech*, **40**, 2672-8, 2007.
3. Cobb SC, et al. *Gait & Post*. **30**, 334-339, 2009.
4. Cardinal E, et al. *Radiology*, **201**, 257-9, 1996.
5. Karabay N, et al. *J Foot Ank Surg*, **46**, 442-6, 2007.
6. Cobb SC. *Proceedings of ASB '11*, Long Beach, CA, USA, 2011.
7. Rathleff MS, et al. *J Clin US*, **39**, 128-34, 2011.

ACKNOWLEDGEMENTS

This study was supported by the ASB Graduate Student Grant-In-Aid and the College of Health Sciences Research Grant.

Table 1: Mean (SD) sagittal, frontal, and transverse plane ROM for the calcaneocuboid joint during phase 1

		Plantar Fasciitis	**Control**	**p-value**
Sagittal Plane	Dorsiflexion	4.44 (3.74)	4.91 (2.73)	p = 0.701
Frontal Plane	Eversion	3.63 (2.73)	1.16 (1.14)	p = 0.003*
Transverse Plane	Adduction	3.63 (1.89)	3.28 (2.14)	p = 0.645

*Significantly different from control group ($p < 0.05$)

ASSOCIATIONS BETWEEN COGNITIVE PERFORMANCE AND GAIT VARIABILITY IN PARKINSON'S DISEASE

[1]Elizabeth Stegemöller, [1]Jonathan P. Wilson, [1]Audrey Hazamy, [1]Michael S. Okun, [1]Lori J.P. Altmann, and [1]Chris J. Hass

[1]University of Florida, Gainesville, FL, USA
email: estegemoller@hhp.ufl.edu

INTRODUCTION

Much research in Parkinson's disease (PD) has focused on motor symptoms of the disease. Yet, between 25 and 80% of persons with PD develop cognitive impairment [1, 2]. Cognitive impairments in PD manifest as deficits in speed of processing, working memory and executive function/attention abilities [3, 4]. Previous research has shown a relationship between executive function/attention and gait in persons with PD [5, 6], while the relationship between speed of processing and working memory with gait is lacking. Moreover, the relationship between executive function/attention and gait in PD has mainly been investigated during walking while completing a secondary cognitive task. There is little evidence examining the relationship between simple over ground walking and cognitive performance in persons with PD. In well-functioning older adults, executive function and memory are associated with gait/gait variability during simple over ground walking [5, 6]. Taken together, this would suggest that cognitive functions play an important role even in routine walking conditions without an additional cognitive load, potentially through overlapping neural systems or neural pathologies (as in PD). The purpose of this study was to examine the relationship between spatiotemporal gait parameters and variability, and cognitive performance across a broad range of cognitive domains (processing speed, working memory, and executive function/attention) during both over ground (single task) and dual task walking conditions in persons with PD.

METHODS

Thirty-five non-demented participants (65 ± 8) diagnosed with idiopathic PD completed the study. Testing was completed in the optimal "on" medication state. All participants gave written informed consent.

Participants completed a battery of 12 cognitive tests while seated in a quiet room. Scores from each test were obtained and were subsequently entered into a principal components analysis. This analysis yielded three distinct factors; 1) a processing speed factor, 2) a working memory factor, and 3) an executive function/attention impairment factor

Table 1. Cognitive Tests within Each Factor.

Processing Speed Factor
Star Task (sec)
Digit Symbol Substitution (sec)
Stroop Color Word (sec)
Stroop Index (sec)
0-Back (sec)
1-Back (sec)
Working Memory Factor
Operation Span (#)
Digit Span Forward (#)
Digit Span Backward (#)
Executive Function/Attention Impairment Factor
Stroop XXX (sec)
2-Back (accuracy)
Visual Working Memory (accuracy)
Digit Symbol Substitution (accuracy)

Participants also completed 10 trials of over ground walking along a 12-m walkway at their self-selected speed (single task) and 5 trials of walking while counting backwards from a three digit number by threes (dual task). Thirty-five retro-reflective markers placed over anatomical bony landmarks according to the Vicon's Plug-in-Gait marker system. Kinematic data were collected at 120Hz using a 10-camera Vicon Nexus motion capture system. Multiple toe-off and heel-strike events were identified and stride time, stride length, step width and walking speed were calculated. The coefficient of variation (CV) (CV = SD/mean * 100%) was calculated to determine within-subject variability of stride time, stride length, and step width.

A one-way repeated measures multivariate analysis of variance was completed to look for differences between single and dual task walking. Pearson correlation analyses were completed to compare the strength of the association between each cognitive factor and each gait variable for single task and dual task walking conditions.

RESULTS AND DISCUSSION

Results revealed significant differences between single and dual task walking for all variables ($p < 0.02$) except for stride length variability ($p = 0.06$).

Gait spatiotemporal measures and gait variability correlated significantly with only the processing speed factor and executive function/attention impairment factor. There were no significant correlations with the working memory factor.

Specifically, correlations revealed significant associations between the processing speed factor and stride length/variability, swing time/variability, and walking speed for both single and dual task conditions. This would indicate that slower cognitive processing speed times were associated with: 1) shorter stride length and increased stride length variability, 2) shorter swing time and increased swing time variability, and 3) slower walking speed.

For the executive function/attention impairment factor, step width/variability significantly correlated for both single and dual task conditions. Swing time/ variability significantly correlated with the executive function/attention factor during the single task condition only. This would indicate that less accurate executive function/attention scores were associated with 1) smaller step width and greater step width variability, and 2) longer swing times and less swing time variability.

These results would suggest that slower gait may be associated with slower cognitive performance. In addition, because changes in gait variability have been related to fall risk, executive function/attention impairments may be associated with poor postural control of gait in persons with PD. The associations with processing speed are strengthened during dual task, while the associations with executive function/attention impairment did not change. Thus, the slowing of overall processing speed may indicate a shared neural system underlying gait and cognitive performance that when challenged by increasing load affects both processes. The association between executive function/attention impairment and postural control of gait suggest the involvement of overlapping systems that are less affected by increasing cognitive load due to other available resources.

REFERENCES

1. Aarsland D et al. *Archiv Neurol* **60**, 387-92, 2003.
2. Cummings JL. *J Geriatr Psychiatry Neurol* **1**, 24-36, 1988.
3. Saint-Cyr JA et al. *Brain* **123**, 2091-108, 2000.
4. Taylor AE et al., *Brain* **109**, 845-83, 1986.
5. Plotnik M et al., *Exp Brain Res* **210**, 529-38, 2011.
6. Yogev G et al., *Eur J Neurosci* **22**, 1248-56, 2005.
7. Watson NL et al., *J Gerontol A Biol Sci Med Sci* **10**, 1093-100, 2010.
8. Beauchet O et al., *J Neuroeng Rehabil* **9**, Epub, 2012.

Table 2. Associations Between Cognitive Performance and Gait

	Processing Speed Factor		**Working Memory Factor**		**Executive Function/Attention Impairment Factor**	
	Single Task (r, p)	***Dual Task (r, p)***	***Single Task (r, p)***	***Dual Task (r, p)***	***Single Task (r, p)***	***Dual Task (r, p)***
Stride Time (ST)	0.14, 0.43	-0.15, 0.39	0.21, 0.23	-0.13, 0.94	-0.15, 0.39	-0.28, 0.11
ST Variability	0.25, 0.15	0.10, 0.57	0.24, 0.10	-0.13, 0.45	-0.08, 0.64	-0.10, 0.56
Stride Length (SL)	**-0.54, 0.001**	**-0.65, < 0.001**	0.13, 0.44	0.21, 0.23	-0.26, 0.13	-0.14, 0.43
SL Variability	**0.36, 0.03**	**0.70, < 0.001**	-0.10, 0.55	-0.31, 0.07	-0.09. 0.59	0.03. 0.87
Step Width (SW)	0.15, 0.40	0.16, 0.37	-0.01, 0.96	0.02, 0.92	**0.48, 0.004**	**0.49, 0.003**
SW Variability	0.26. 0.12	0.25. 0.14	-0.15, 0.38	-0.12, 0.47	**-0.58, < 0.001**	**-0.52, 0.001**
Swing Time (SwT)	**-0.46, 0.005**	**-0.69, < 0.001**	-0.14, 0.41	0.003, 0.99	**-0.42, 0.01**	-0.01, 0.96
SwT Variability	**0.42, 0.01**	**0.34, 0.04**	-0.24, 0.16	-0.16, 0.36	**0.37, 0.03**	-0.13, 0.47
Walking Speed	**-0.55, 0.001**	**-0.67, < 0.001**	-0.01, 0.95	0.09, 0.60	-0.15, 0.41	0.05, 0.76

VARIATIONS IN LEG STIFFNESS AND LOWER EXTREMITY RANGE OF MOTION VARIABILITY FROM STRIDE LENGTH PERTURBATIONS DURING GAIT

Andrew D. Nordin, Joshua P. Bailey, and Janet S. Dufek

University of Nevada, Las Vegas, Las Vegas, NV, USA
email: nordina@unlv.nevada.edu

INTRODUCTION

Human gait is a ubiquitous motor task, seemingly carried out with ease, but requiring considerable interactions within a complex locomotor system [1]. Investigations of human gait identify complex fluctuations in gait patterns despite unchanging environmental conditions, suggesting that variability within movement repetitions are not only inherent, but representative of function and adaptation [1,3,4]. Specifically, the healthy norm is considered to contain an optimal amount of variability, while excessively high or low variability is characteristic of system dysfunction [3].

The purpose of this examination was to explore the effect of stride length (SL) perturbations on leg stiffness and changes in lower extremity range of motion (ROM) variability during walking gait, relative to preferred walking (PW) and running (PR). Lower extremity ROM and ROM variability at the hip, knee, and ankle joints, in the sagittal plane were used in evaluating motor control of gait.

METHODS

Nine participants (5 male, 4 female; mean age 23.11±3.55 years, height 1.72±0.18m, mass 72.66±14.37kg) free from previous lower extremity injury were examined in this investigation. Informed consent was obtained prior to participation, as approved by the Research Ethics Board at the affiliated institution. Kinematic data were acquired using a 12-camera system (Vicon MX T40-S; 200Hz), and 35-point spatial model (Vicon Plug-in Gait Fullbody). Data filtering and interpolation included a low pass, 4th order (zero lag) Butterworth filter (cutoff frequency 15Hz) and cubic (3rd order spline).

Participants completed 5 trials in each stride condition for PW, PR, and subsequent SL manipulations computed as a percentage of leg length (LL; mean distance from anterior superior iliac spine to medial malleolus on each leg). SL perturbations used lengths of 60%, 80%, 100%, 120%, and 140% of LL. Participants were instructed to match their SL with cones spaced on the floor at corresponding distances. Kinematic analysis was carried out over 2 steps (1 stride) during each gait trial, assessing bilateral ROM at the hip, knee, and ankle from heel contact to toe-off for each limb.

Sagittal knee ROM was used to gauge leg stiffness during gait trials, where greater knee ROM has been shown to significantly reduce leg stiffness during locomotion [2]. Sagittal ROM and ROM variability, expressed via coefficient of variation (CV%), were evaluated at each joint. Knee ROM comparisons were made among stride conditions using one-way repeated measures ANOVA and Sidak *post-hoc* contrasts, via SPSS 20.0 (α=0.05). Lower extremity joint ROM variability comparisons involved 3x7 (joint x stride condition) mixed model ANOVA, with repeated measures on stride condition.

RESULTS AND DISCUSSION

Differences in sagittal knee ROM were detected among stride conditions ($F[3.840,322.547]=49.268$, $p<.001$). *Post-hoc* comparisons showed significant decreases in knee ROM during PR and among SLs at, and in excess of 100%LL, relative to PW, 60%LL, and 80%LL. This suggests increased SLs resulted in greater leg stiffness during walking, similar to that observed in running (Figure 1). As the majority of stride conditions showed significant differences ($p<.001$) in knee ROM, relative to each other condition, non-significant differences were highlighted in Figure 1, showing stride conditions of similar leg stiffness. All non-flagged differences were significant ($p<.005$).

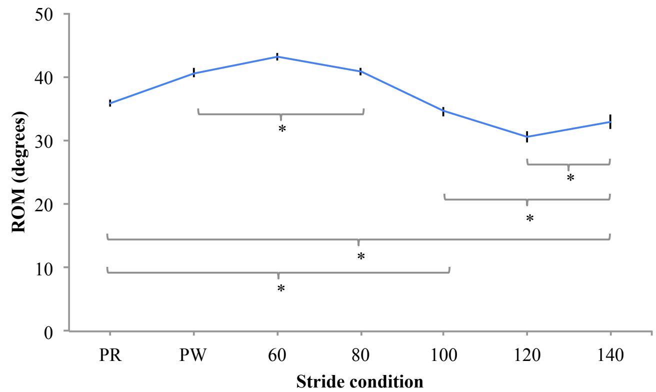

Figure 1: Stride condition vs. sagittal knee ROM (degrees; * is a non-significant difference; $p>.05$)

Differences in sagittal lower extremity ROM variability were detected among stride conditions ($F[3.510,178.986]=3.072$, $p=.023$). Greater ROM variability was observed at the 120% SL condition relative to the 80% SL condition (Figure 2). From the lack of significant differences among PW, 60%, 80%, and 100% SL conditions it is apparent that PW occurred within these SLs, while SLs exceeding 100%LL resulted in significant increases in lower extremity ROM variability, implicated in susceptibility to injury [3]. Running differed from the 80% SL condition (Figure 2), but did not reveal significant variability differences among remaining walking conditions, suggesting that running may present a separate, but stable gait pattern.

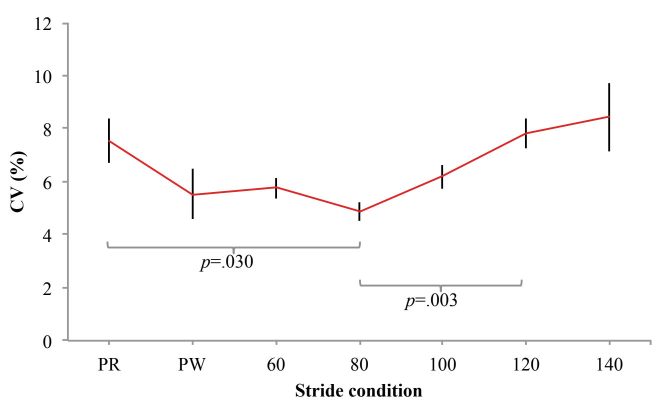

Figure 2: Stride condition vs. sagittal lower limb ROM variability (CV%)

Examining joint differences, ROM variability was significantly lower at the hip, relative to the ankle and knee joints (Figure 3). Greater variability reported among distal joints is in contrast to previous research on kinetic joint variability [5], suggesting that movement control may be altered during SL perturbations, or that kinematic and kinetic variables may respond differently.

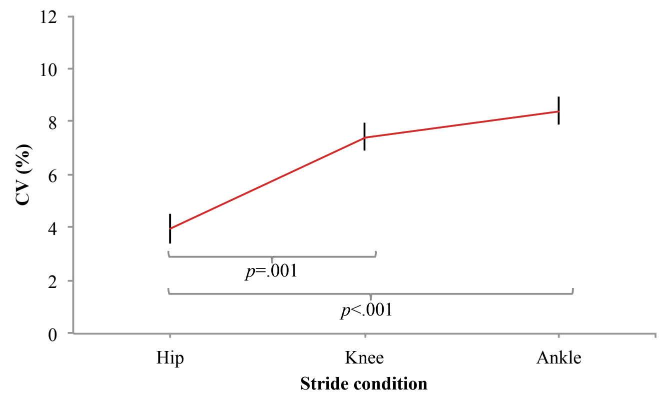

Figure 3: Lower extremity joint vs. sagittal ROM variability (CV%)

CONCLUSIONS

Overall, lesser knee ROM characterized greater leg stiffness at increased walking SLs and in running. This corresponded with stride conditions demonstrating greater lower extremity ROM variability, which may be representative of a loss of movement control, putting the system at greater risk of acute injury. Future research should further explore kinetic gait changes at altered stride lengths.

REFERENCES

1. Hausdorff JM, *Hum Mov Sci*. **26**, 555-589, 2007.
2. Lafortune MA, et al. *J Biomech* **29**, 1531-1537, 1996.
3. Stergiou N, Decker LM. *Hum Mov Sci*. **30**, 869-888, 2011.
4. Stergiou N, et al. *J Neuro PT* **30**, 120-129, 2006.
5. Winter DA. *Hum Mov Sci.* **3**, 51-76, 1984.

ACKNOWLEDGEMENTS

This poster was supported by grants from the National Center for Research Resources (5P20RR016464-11) and the National Institute of General Medical Sciences (8 P20 GM103440-1).

INDIVIDUALS WITH ANTERIOR CRUCIATE LIGAMENT RECONSTRUCTION DISPLAY ALTERED MECHANICS DURING SPLIT-BELT WALKING

Jaimie A. Roper, Ryan T. Roemmich, Chris J. Hass, Mark D. Tillman
University of Florida, Gainesville, FL, USA
email: jaimier@hhp.ufl.edu

INTRODUCTION

Individuals with anterior cruciate ligament (ACL) injury have an increased risk of developing osteoarthritis (OA). Even after ACL reconstruction (ACL-R), the rate of OA incidence remains between 62% and 80% [1]. Researchers have suggested that altered gait patterns coupled with repetitive abnormal cartilage loading after ACL injury may have implications for the development of OA [2]. When compared to a healthy population, individuals with ACL injury exhibit abnormal sagittal, frontal, and transverse plane kinematics, as well as sagittal and frontal kinetic patterns during the stance phase of walking [3]. Researchers have demonstrated that knee-joint moments and angles are not fully restored following ACL-R [3].

Interestingly, when compared to a healthy population, both the involved and uninvolved limb exhibit abnormal movement patterns [4]. These kinetic asymmetries at the knee and hip are evident after ACL injury and remain after ACL-R. This would suggest that bilateral changes that occur after unilateral ACL injury and surgery may be related to changes in the neurological control of the locomotor system.

To date, no study has investigated strategies aimed towards reducing abnormal, asymmetric kinetic and kinematic patterns during walking in individuals with ACL injuries. Therefore, interventions that may reduce the alterations and asymmetries in gait associated with ACL injury could produce improved walking patterns bilaterally. Split-belt treadmills (SBT) consist of two independently-controlled belts (one under each leg) and have been shown to acutely restore or improve symmetry in spatiotemporal parameters such as step length, double-limb support time, and spatial patterns of each limb in populations post-stroke [5]. However, utilizing the SBT to restore normal kinematic (spatial) and kinetic patterns in populations with ACL injury at the knee has not been investigated.

Examining movement strategies (SBT) that may improve alterations and asymmetries during walking that may reduce the incidence of OA after ACL injury is needed. The aim of this study was to compare knee-joint moments and angles in the sagittal and frontal planes during normal treadmill walking and SBT walking in individuals with ACL injury and healthy young adults [3,4].

METHODS

Four ACL-R participants (3 female, 1 male; Age: 21 ± 1 yr; Height: 1.65 ± 0.11 m; Mass: 60.2 ± 11.2 kg; Time following ACL-R: 15.5 ± 12.2 mo) and four healthy controls (3 female, 1 male; Age: 21 ± 1 yr; Height: 1.65 ± 0.10 m; Mass: 63.6 ± 8.77 kg) walked on an instrumented SBT (960 Hz; Bertec Corporation, Columbus, OH) during two conditions: slow and split. Participants initially selected his/her fastest comfortable walking speed, then walked for three minutes with both belts moving at 50% of the fast speed (slow). The participants then walked for eight minutes with the ACL-R involved/nondominant leg moving at the fast speed and the ACL-R uninvolved/dominant leg moving at the slow speed (split).

Kinematic and kinetic data were recorded during the last 30 seconds of the slow, fast, split, and re-split conditions. Sixteen passive reflective markers were attached to the lower body in accordance with the Vicon Plug-in-Gait lower body marker system. Kinematic data were collected using a 7-camera motion capture system (120 Hz; Vicon Nexus, Oxford, UK).

Averages for three-dimensional knee joint-angles were calculated during the braking and propulsive phases of gait. Force recordings, marker position data and the individuals' anthropometrics were used to calculate mean sagittal and frontal knee joint-moments during the propulsive and braking phases of gait via inverse dynamics.

Sagittal and frontal plane joint moments and GRFs were normalized to body mass (kg) and temporally to 100% of the gait cycle. Braking phase was defined as the period from heel-strike to the first 50% of single-limb stance period. Propulsive phase was defined as the period from second 50% of the single-limb stance to toe off [6].

Several 2x2 (group x condition) repeated measures MANOVAs with Bonferroni post-hocs for pairwise comparisons were used to analyze interactions of treadmill condition and group. Because this was a pilot study, a higher level of significance was used (α =0 .10).

RESULTS AND DISCUSSION

A significant group x condition interaction (p = 0.054) indicated the uninvolved knee (ACL-R) displayed different mean sagittal angle, sagittal moments and frontal moments in slow and split walking. We did not observe any further significant group x condition interactions.

Healthy controls showed no differences in knee angle, knee extensor/flexor moment, or knee abduction/adduction moment between slow and SBT walking. ACL-R individuals displayed larger uninvolved knee flexion angles (p = 0.001; Figure 1A) and smaller uninvolved knee flexor moments (p = 0.032; Figure 1B) during the propulsive phase in SBT walking compared to slow walking. ACL-R individuals also displayed larger uninvolved knee abduction moments (p = 0.023; Figure 1C) during the braking phase in SBT walking compared to slow walking (Figure 1).

We have demonstrated that the uninvolved knees of ACL-R individuals displays altered joint angles and moments during the braking and propulsive phase of gait when walking on the slow belt during the split condition. Changes in gait following ACL injury have been previously attributed to alterations in feedforward control to prevent anterior displacement of the tibia, and are present in both limbs. In addition to mechanical changes, these findings may provide further evidence of change in neurological control during walking after ACL-R. ACL-R may alter the mechanics of walking, particularly during a novel walking task (SBT). These alterations may lead to abnormal gait mechanics that could influence the individual's likelihood for developing OA.

The incidence of OA diagnosis in the uninvolved limb is unlikely as it typically develops in the involved limb. However, it is possible that compensatory alterations in the uninvolved knee

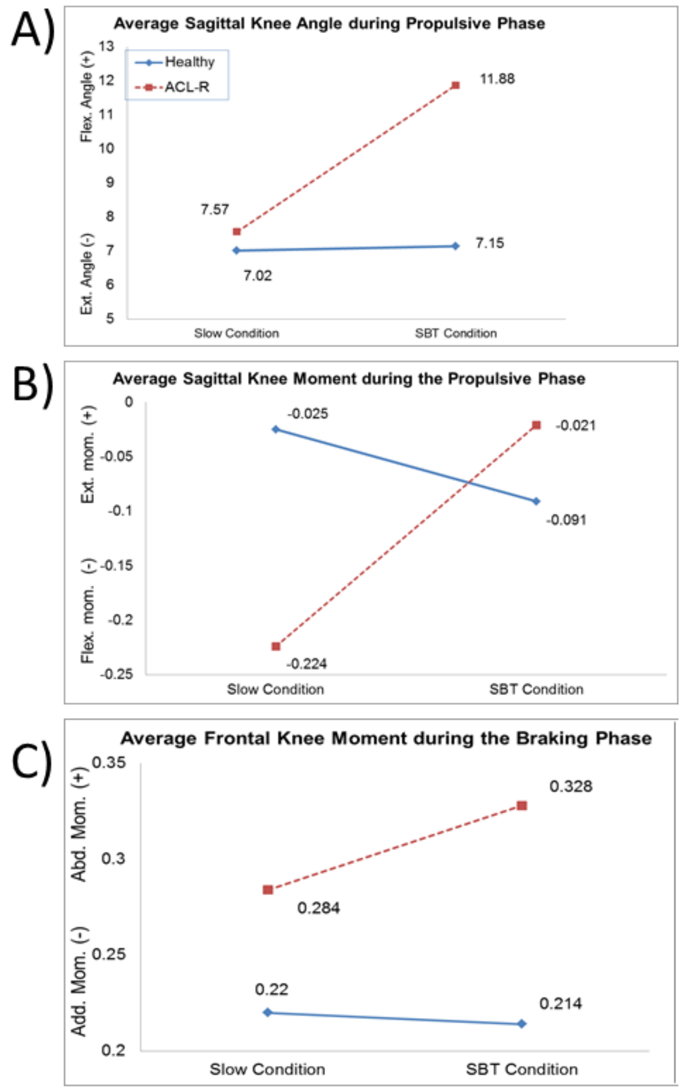

Figure 1. ACL-R individuals exhibit different mean values for (A) knee flexion angle (deg), (B) knee flexor moment (Nm/kg), and (C) knee abductor moment (Nm/kg).

may influence overall gait. Because the human body is a kinetic chain, joints of the uninvolved side may have an important role in compensation and adaptation in steady walking. Finally, this information could be useful for developing therapies aimed towards preventing OA in populations with ACL injuries.

REFERENCES

1. Oiestad et al. Am J Sports Med 2010.
2.Andriacchi et al. Ann Biomed Eng 2004.
3. Gao and Zheng. Clin Biomech 2010.
4. Ferber et al. Clin Biomech 2004.
5.Reisman et al. Neurorehabil Neural Repair 2009.
6. Turns et al. Arch Phys Med Rehabil 2007.

What predicts the first peak of the knee adduction moment? Implications for the treatment of knee osteoarthritis

[1]Anne Schmitz and [1]Brian Noehren

[1]University of Kentucky, Lexington, KY, USA
email: anne.schmitz@uky.edu

INTRODUCTION

Abnormal loading of the medial tibiofemoral compartment is an important factor in the development of osteoarthritis (OA) [1]. Gait modifications have been used as a non-surgical approach to reduce medial compartment loading in an attempt to slow disease progression. However, direct measurement of joint loading in intact joints is not possible to measure *in vivo*. Therefore, the knee adduction moment has been used as a clinical surrogate measure for loading of the medial compartment [2]. The first peak of the external knee adduction moment (EKAM) has been shown to predict the presence of medial compartment OA, the severity and rate of progression of the disease, and the presence of symptoms [3].

Gait modifications that alter the EKAM include decreased walking speed, increased stance width, toe out, medial thrust gait, trunk sway, high mobility shoes, variable stiffness shoes, wedge insoles, offloader braces, and canes [4]. These interventions aim to alter four fundamental variables that contribute to the EKAM: varus-valgus alignment of the tibia, magnitude of the ground reaction force (GRF), the location of the body's center of mass (COM), and the location of the center of pressure (COP). To date, no assessment has been done on the relative contributions of these variables to the EKAM. For clinicians to prescribe the most effective treatment, it is imperative to understand which of these variables contributes the most to the frontal plane knee moment. Therefore, the goal of this study was to determine which variable is the biggest determinant of the front plane knee moment: the location of the center of pressure, the location of the body's center of mass, the dynamic varus-valgus alignment of the knee, or the magnitude of the ground reaction force. Based on a recent review by Fregly on the effectiveness of various gait modification strategies [4], we expected varus-valgus alignment to explain the most variance, followed by COM location and superior-inferior GRF.

METHODS

Motion capture data was collected for 30 healthy subjects (average age 24, height 1.66 m, weight 59.6 kg) walking on a treadmill (average speed of 1.31 m/s). Retroreflective markers were placed on the subject using established procedure [5]. Three-dimensional marker trajectories were measured during walking by sampling at 200 Hz with a 15 camera motion analysis system (Motion Analysis Corp, Santa Rosa, USA) while simultaneously collecting force data at 1200 Hz using an instrumented Bertec treadmill (Bertec, Columbus, OH).

Visual 3D software (C-motion, Germantown, MD, USA) was used to filter the data, calculate a functional hip joint center [6], perform inverse kinematics, and perform inverse dynamics. Marker data was filtered at 8 Hz and force data filtered at 35 Hz using a fourth-order low-pass zero-lag Butterworth filter. Using previously described coordinate systems, joint angles and moments were then calculated using successive body fixed rotations using the order of flexion-extension, ab-adduction, followed by internal-external rotation [5].

Custom Matlab code (MathWorks Inc., Natick, MA) was used to extract the first peak external knee abduction moment calculated from inverse dynamics as well as kinematic variables at the same instant in time as the peak knee abduction moment: the adduction angle of the tibiofemoral joint; the location of the center of pressure relative to the foot origin, and the global position of the body's center of mass. Data was collected from 5 trials for each subject and then averaged. Knee abduction moment was normalized to body mass times height and ground reaction force by body weight squared. Using SPSS (SPSS Inc., Chicago, IL), Pearson's correlations coefficients were calculated and those variables significantly correlated with the peak knee abduction moment were input into a stepwise multiple linear regression model to determine the amount of variance in EKAM explained by the kinematic variables.

RESULTS AND DISCUSSION

Results of the correlation showed the first peak EKAM to be correlated with the superior-inferior location of the COP (r=-.450, p<0.05), the superior-inferior magnitude of the GRF (r=.676, p<0.01), and the knee adduction angle (r=.762, p<0.01). However, peak EKAM was not correlated with medial-lateral location of COP (r=-.094), medial-lateral location of the trunk COM (r=.220), superior-inferior location of the COM (r=-.025), or medial-lateral magnitude of the GRF (r=.275). It should be noted that our sample size of 30 subjects gives our test the power to accurately predict (β = 0.80) correlations of r ≥ .48.

A linear regression model was used to assess the ability of the superior-inferior location of COP, superior-inferior magnitude of the GRF, and knee adduction angle to predict the first peak EKAM (Table 1). The adduction angle explained 59% of the variance seen in peak EKAM (Figure 1), superior-inferior GRF explained 20% of the variance, and the superior-inferior location of COP explained 0%.

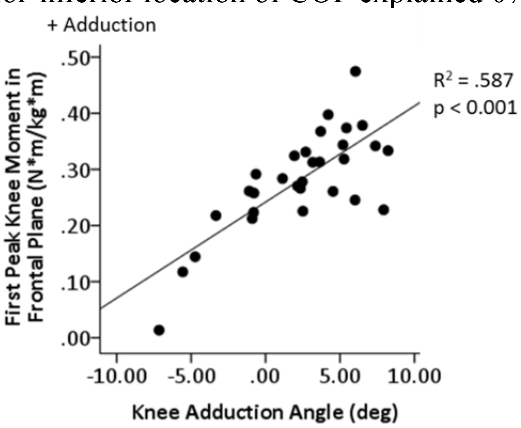

Figure 1: The adduction angle explained 59% of the variance seen in the first peak external knee adduction moment.

Our results agree with previous studies [4,7] that that ab-adduction alignment produces the greatest change in peak EKAM. Our results also suggest that the next effective treatment besides ab-adduction alignment is one that alters the superior-inferior GRF. These results suggest that interventions aimed at altering alignment through bracing or one that reduces superior-inferior GRF such as cane use maybe the most effective in reducing the first peak of the EKAM [4].

In contrast to previous research neither COM or COP were significant predictors of higher EKAM in the final model [7]. Trunk sway has been thought to alter the COP and line of action of the GRF [7]. As a secondary analysis we did find a significant correlation of the medial-lateral location of the COP with the medial-lateral location of the COM (r = -.420, p<0.05) and superior-inferior location of the COM (r = -.458, p<0.05). However, there was no correlation between COM and GRF magnitude in either direction. Our results suggest that the relationship between trunk sway and EKAM needs further investigation.

CONCLUSIONS

Knee adduction angle explains most of the variance in the first peak EKAM, thus suggesting interventions designed to change the angle might be the most effective treatment. Altered superior-inferior GRF magnitude explained the second most variance, suggesting another important variable in the modification of peak EKAM. These results provide insight into the critical variables which should be included in treatment strategies to reduce the EKAM.

REFERENCES

1.Andriacchi, T. P., et al. *Ann of BME* **32**, 447-57, 2004.
2.Zhao, D., et al. *J Orthop Res* **25**, 789-797, 2007.
3.Simic, M., et al. *Arth Care & Res* **63**, 405-426, 2011.
4.Fregly, B. J. *HSS Journal* 1-4, 2012.
5.Noehren, B., et al. *Gait & Posture* **36**, 596-599, 2012.
6.Schwartz, M. H., et al. *J Biomech* **38**, 107-16, 2005.
7.Hunt, M., et al. *Osteo and Cart* **16**, 591-599, 2008.

ACKNOWLEDGEMENTS

Collaborator Becca Williams, partially funded by NSF IIS 1231545

Table 1: Summary of stepwise multiple linear regression model

	R	R^2	Adjusted R^2	Change in R^2	p
Knee adduction angle	.762	.587	.566	-	<0.001
Knee adduction angle + superior-inferior GRF	.885	.783	.767	.203	<0.001

EFFECTS OF LOAD CARRIAGE AND FATIGUE ON GAIT COORDINATION AND VARIATION IN HEALTY MALES

[1]Cara Masterson, [1,3]Daniel Leib, [2]Henry Wang, and [1]Eric Dugan

[1]Boise State University, Boise, ID, USA
[2]Ball State University, Muncie, IN, USA
[3]University of Nebraska, Omaha, NE, USA

INTRODUCTION

Changing the environment or introducing perturbations to the system can lead to a change in segmental coordination. Variability in the coordination of a movement permits exploration of the task, allowing for development of stable coordinative states over time [1]. When significant constraints and/or large enough perturbations are introduced, a shift between these attractor regions allows for an individual to adapt to changes in the motor activity while achieving the same goal [2,3]. Adaptations to small perturbations are dealt with mainly by variation, maintaining the same coordination pattern but temporarily deviating from the theoretical optimal or normal pattern [4]. Too little or too much variability may have implications for injury risk [6]. The relationship between stability and variability allows for individuals to both achieve persistence at completing a task and to change the motor output as needed when perturbations are introduced.

The purpose of this study was to examine the effects of introducing load and fatigue on lower limb gait coordination and the variation of that coordination.
A better understanding of lower limb injury mechanisms may be derived from determining how coordination patterns change under loaded and/or fatigued conditions. Using mean absolute relative phase (MARP) as a measurement of coordination and deviation phase (DP) as a measure of variation within a coordinative strategy, the changes in inter- and intra-limb orientation were compared across conditions to determine if coordination or variation was altered due to the perturbations presented to the system. It was hypothesized that neither load nor fatigue would lead to significant changes in coordination.

METHODS

Twenty three male subjects were recruited from university student population convenience sampling. Following Army recruitment patterns, participants were 18-27 years of age and had a body mass index no greater than 28. Other exclusion criteria included current or previous military enlistment and current or previous musculoskeletal injury. Participants walked on the treadmill at a pace of 6km/h at a 0% incline under four different load/fatigue conditions. These conditions were:

1) unloaded-unfatigued (UU)
2) loaded-unfatigued (LU)
3) loaded-fatigued (LF) and
4) unloaded-fatigued (UL)

The loaded conditions refer to the participants carrying a 35 kg rucksack. The fatigued condition was induced by a fatiguing protocol completed between conditions 2 and 3. This protocol included loaded stepping, loaded heel raises, and maximal vertical jumping. This sequence of exercises was completed until the participants maximal vertical jump attempt fell to or below 80% of their original VJ_{max} height; at this point it was assumed that fatigue was reached [7]. This allowed for the fatigue protocol to be specific to each individual subject's capabilities.

Data were collected in 10 trials of 5 seconds each during the final minute of each walking stage. The angular positions and velocities of the foot, shank, and thigh of both limbs were calculated. Phase portraits were generated and phase plant trajectories were utilized to determine phase angles. Relative phase values were calculated for inter-limb and intra-limb coordination by determining the difference in phase values of relevant segments at each of 101 points in the gait cycle. The relative phase curves were averaged across all trials for each condition for all subjects [8].

In order to determine statistical differences, the curves were reduced to single numerical values of MARP and DP. The MARP is calculated by averaging the absolute values of the CRP curve for a given limb segment pair with a higher value indicating segments were more out of phase. The DP was calculated by averaging the standard deviation values of the CRP curve for a given limb segment pair with a higher value indicating more variable relationship between segments.

A repeated measures analysis of variance test ($\alpha = 0.05$) was utilized to test for differences in MARP and DP within participants across testing conditions.

RESULTS AND DISCUSSION

No significant changes in MARP were observed for any condition. Inter-limb DP at the ankle was significantly greater for LF than for UU and UF. Similar significance was seen at the knee with LF being greater than UU and UF. Only the shank-shank intra-limb pairing showed any significant variation differences, with UU being less than LF.

Participants tended to increase the variability in the chosen pattern instead of utilizing a new coordination pattern. The results suggest that with the combination of fatigue and load carriage, the variation in coordination is significantly higher than when not carrying the load no matter the state of fatigue.

The conditions utilized were designed to produce situations similar to military training exercises; a consistent gait velocity coupled with load bearing and fatigue. Results from this study revealed that some variability change did occur most often between the LF and UU testing conditions. It is important to note that coordination and variation values do not directly depend on each other. In other words, it is possible for MARP to change without a change in DP, and vice versa.

In this investigation, only sagittal plane angular position and velocities were assessed. It is important to note this because there may have been movement occurring in one of the other planes that was not represented with the data. An assessment of the frontal plane may have revealed greater hip abduction or excursion. This kind of movement may be viewed through the CRP assessment of the frontal plane, or possibly through more traditional gait parameters, such as steady step length and increased foot path length.

CONCLUSIONS

Coordination pattern did not change with the addition of load or fatigue relative to gait, but the variation in intra-limb coordination did increase. Future research should look further into the implications of variation changes with prolonged weight bearing gait tasks to fatigue.

REFERENCES

1. Glazier PS, et al. *Sportsscience 7*, 2003
2. Davids K, et al. *Sports Medicine* **33**, 245-260, 2003.
3. Scholtz JP, et al. *Experiemental Brain Research* **141**, 485-500, 2001
4. Hamill J, et al. *Clinical Biomechanics* **14**, 294-308, 1999.
5. Dingwell JB, et al. *Journal of Biomechanical Engineering* **123**, 27-32, 2001.
6. Hamill J, et al. *Movement System Variability*, Human Kinetics, 2006.
7. Weinhandl J, *Journal of Applied Biomechanics* **27**, 108-115, 2011.
8. Stergiou N, et al. *Gait and Posture* **13**, 210-220, 2001.

ACKNOWLEDGEMENTS

The authors would like to acknowledgement the Department of the Army grant #W81XWH-08-1-0587 as the primary funding source for this study.

BIOMECHANICAL VALUE OF TEMPERATURE IN ASSESSING PLANTAR LOADING

[1]Metin Yavuz, [1]Neha Delvadia, [1]Jayson Atves, [1]Jacqueline Goldfarb, [1]Joseph Stuto,
[1]Andrew Franklin, [1]Rebecca McGaha, [1]Jessica Rispoli, [1]Garneisha Torrence, [2]Nilin Rao
[1] Kent State University College of Podiatric Medicine, Independence, OH, USA
[2] Kent State University Department of Exercise Physiology, Kent, OH, USA
email: m.yavuz@gmail.com

INTRODUCTION

Many foot disorders have a biomechanical etiology. Ground reaction forces and related stresses that act under the foot are associated with complications such as diabetic ulceration, rheumatoid foot, hallux valgus and foot blistering. The normal component of the 3D plantar stresses, i.e., pressure, can be easily quantified by commercially available barefoot or in-shoe systems. However, few investigators have access to equipment capable of measuring 3D loading under the foot since measuring plantar shear stresses remains to be quite challenging.

Brand has suggested that temperature can be used to predict tri-axial loading under the foot [1]. Studies have also revealed that diabetic patients have increased plantar temperatures when compared to control subjects [2]. It is thought that diabetic feet experience elevated stresses that lead to inflammation within the foot, which can be observed as temperature increase on the plantar aspect of the foot. Unfortunately, this theory has not been validated before. The purpose of this study was to explore a site-wise association between peak plantar temperature and, peak pressure and shear stresses obtained from diabetic patients using a thermal camera and a custom-built pressure-shear plate. In addition, peak pressure and shear magnitudes were correlated against peak temperature in order to reveal a magnitude-wise association.

METHODS

The study was approved by the Institutional Review Board. Subjects gave informed consent before participation. Group DN consisted of 14 diabetic neuropathic patients (2 F, 64.8±6.8 years, 32.0±5.1 BMI). The second group (DC) comprised 14 diabetic patients (9 F, 52.4±12.9 years, 28.9±7.4 BMI) without neuropathy. Peripheral neuropathy was tested using a Biothesiometer and 5.07 Semmes-Weinstein monofilaments. Each subject waited ten minutes while barefoot in order to ensure the plantar temperatures reached steady-state conditions. After this period, resting plantar temperatures were recorded using an infrared thermal camera. Subjects then walked at self-selected speeds on the stress plate, which was installed on a 12-ft walkway and set flush. Data from three trials were averaged and used in statistical analysis. Data were collected implementing the two-step method. Subjects' feet were masked into five forefoot regions; hallux, lesser toes, first metatarsal head (MTH1), central forefoot (2^{nd} and 3^{rd} MTH) and lateral forefoot (4^{th} and 5^{th} MTH). Four major stress variables were identified in each subject; peak pressure (PP), peak shear (PS), peak pressure-time integral (PTI) and peak shear-time integral (STI). Peak values of the stress variables and peak temperature (PT) were found in five forefoot regions. Separately, locations of global peak values of all variables were determined for each person. Regional stress and temperature data were normalized. Each stress variable was correlated against temperature and Pearson Product Moment Correlation Coefficients (r) were calculated. Alpha was set at 0.05. Percentages of matches between the locations of peak stress and peak temperature values were found.

RESULTS AND DISCUSSION

All performed correlations were statistically significant ($p<.05$). However, except one, all r values were lower than 0.5. Table 1 displays the calculated r values and respective significance values. r values were relatively higher in group DC. Table 2 presents the site-wise correlation data between peak stress variables and peak temperature. Figure 1 displays the peak shear stress plantar temperature profiles of a representative DN subject.

Results indicated that despite statistically significant correlation coefficients, plantar temperature magnitudes are not good predictors of plantar loading. Plantar temperature values may vary depending not only on plantar loading, but also blood circulation, internal loading and the presence of kinetic friction at the foot-ground interface.

On the other hand, particularly in group DC, peak temperature values achieved a moderate success in identifying the location of peak stress values. This success was quite lower in group DN.

It is believed that the potential relationship between the magnitudes of stresses and temperature has a complicated, non-linear character. Appropriate modeling schemes can be implemented to explore such complicated potential relationships. The results of this study are thought to warrant further investigation on this topic.

REFERENCES

1. Brand PW. *Foot Ankle Int*, 24: 457-61, 2003.
2. Papanas N, et al. *Exp Clin Endocrinol Diabetes*, 117 (1): 44-7, 2009.

Table 1: Pearson Correlation Coefficients (p values) of stress and temperature correlations.

	Group DN	**Group DC**
PP - PT	0.414 (<.001)	0.479 (<.001)
PS - PT	0.405 (.001)	0.511 (<.001)
PTI - PT	0.429 (<.001)	0.480 (<.001)
STI - PT	0.448 (<.001)	0.476 (<.001)

Table 2: Site-wise correlation percentage values for peak stress and temperature.

	Group DN	**Group DC**
PP - PT	14% (2/14)	86% (12/14)
PS - PT	57% (8/14)	71% (10/14)
PTI - PT	14% (2/14)	71% (10/14)
STI - PT	57% (8/14)	50% (7/14)

ACKNOWLEDGEMENTS

This study was possible due to funds from the NIH grant 1R15DK082962.

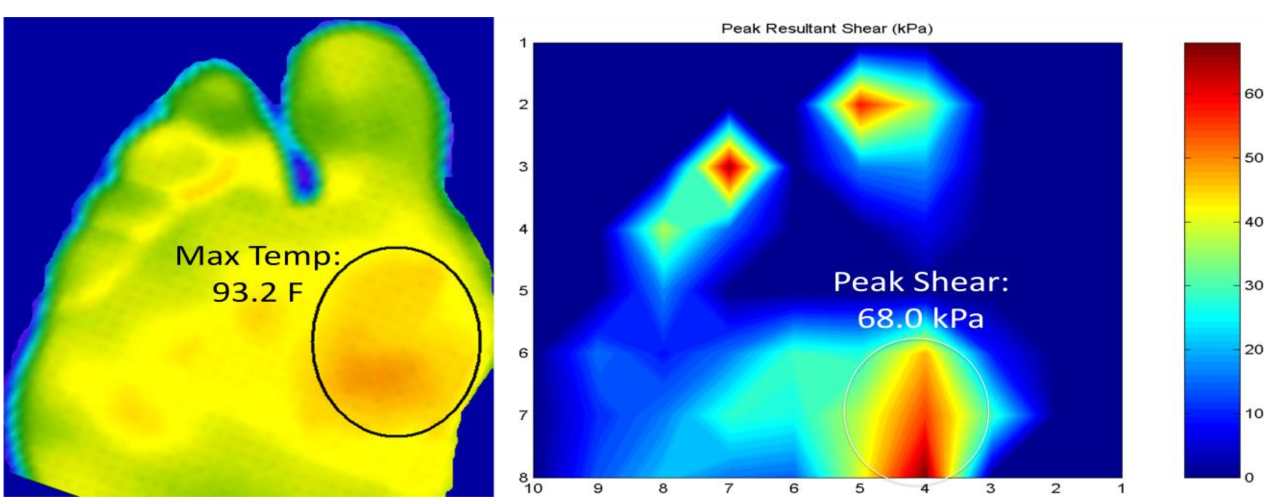

Figure 1: Resting plantar temperature (left) and peak plantar shear (right) profiles of a representative DN subject. Note the match between the sites of peak temperature and peak shear (MTH1)

ASSESSMENT OF BODY POSTURE USING INERTIAL MEASUREMENT UNITS: A VALIDATION STUDY

Gu Eon Kang and Melissa Gross

University of Michigan, Ann Arbor, MI, USA
email: guekang@umich.edu

INTRODUCTION

Depression is a widespread mental disorder among people of all ages that can be very severe with high suicide risk. Objective evaluation of psychomotor symptoms is important in diagnosing and managing depression. Emerging evidence suggests that body posture during walking changes with mood state and, conversely, that changes in body posture affect mood [1, 2]. Thus, monitoring body posture in real-time outside of the laboratory has potential in developing an adjunctive treatment for depression.

Inertial measurement units (IMUs) are a possible device type that could be used to measure postural angles while being worn on the body. Although angular data from IMUs have been validated for estimation of limb motions during gait and seated tasks [3-5], the feasibility and validity of using IMUs to measure body posture during walking has not yet been demonstrated. The purpose of this study was to assess the validity of IMUs to assess body posture during walking in healthy individuals.

METHODS

Ten healthy individuals (21.2 ± 4.3 years, 50% male) participated in the study after providing informed consent. Each participant wore three IMUs (Yost Engineering Inc., Portsmouth OH) on the forehead, right acromion and sternum. Sensor data were collected at 60 Hz. An optoelectronic motion analysis system was used as a reference system for validation. Four retroreflective markers were placed on each IMU and foot. Marker data were acquired with a motion analysis system with eight cameras (Motion Analysis Co., Santa Rosa CA) at 60 Hz and were filtered at 6 Hz using a Butterworth filter. Participants walked at normal speed while motion data were collected. Gait cycles were detected using coordinate data from the feet to detect heel strike. Postural angles were calculated using custom Matlab (MathWorks Inc., Natick MA) code for both measurement systems. Postural angles were then averaged over gait cycles from three trials for head extension, thorax extension and shoulder girdle elevation for each participant. Preliminary data are reported here for seven participants.

RESULTS AND DISCUSSION

Postural angles were highly correlated between measurement systems (Fig. 1). Pearson correlation coefficients were 0.88, 0.85 and 0.77 for head extension, thorax extension, and shoulder girdle elevation, respectively.

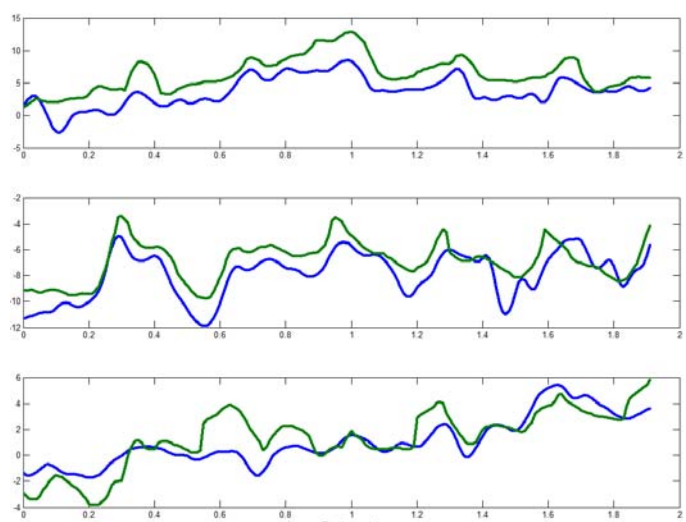

Figure 1: Postural angles (deg) for the reference system (blue) and IMUs (green) during 3 gait cycles (seconds) for one participant. Graphs are head extension (top), thorax extension (middle) and shoulder girdle elevation (bottom).

Values for the mean postural angles were similar between measurement systems (Table 1). Mean postural angles across participants were 0.9 ± 3.9

deg, -4.2 ± 3.6 deg, and 0.1 ± 1.3 deg from the reference system, and 1.2 ± 3.5 deg, -4.5 ± 2.2 deg, and 0.7 ± 1.0 deg from the IMUs, for head extension, thorax extension and shoulder elevation, respectively. The coefficients of determination (R^2) between mean postural angles were 0.537 (p=.67), 0.461 (p=.52) and 0.278 (p=.03) for head extension, thorax extension and shoulder girdle elevation, respectively (Fig. 2).

Differences in mean postural angles between the measurement systems were small, typically 2 deg or less. Mean differences in postural angles between measurement systems were -0.3 ± 2.7 deg, 0.4 ± 2.7 deg, and -0.6 ± 1.2 deg, for head extension, thorax extension and shoulder girdle elevation, respectively.

CONCLUSIONS

Strong correlations between postural angles measured with optoelectronic systems and IMUs suggest that IMUs can be used to assess changes in body posture during walking. Even though significant differences were observed in shoulder elevation angle, this may not be a limitation for clinical and scientific application, as the differences were very small. In conclusion, the proposed IMU system can be considered suitable to monitor body posture of patients with depression.

REFERENCES

1. Gross MM et al. *Hum Movement Sci* 31, 202 - 221, 2012.
2. Flack W. *Cognition Emotion* 20, 177 - 195, 2006.
3. Pérez R et al. *Sensors* 10, 10733 - 10751, 2010.
4. Cooper G et al. *J Biomech* 42, 2678 - 2685, 2009.
5. Cutti A et al. *Med Bio Eng Comput* 46, 169 - 178, 2008.

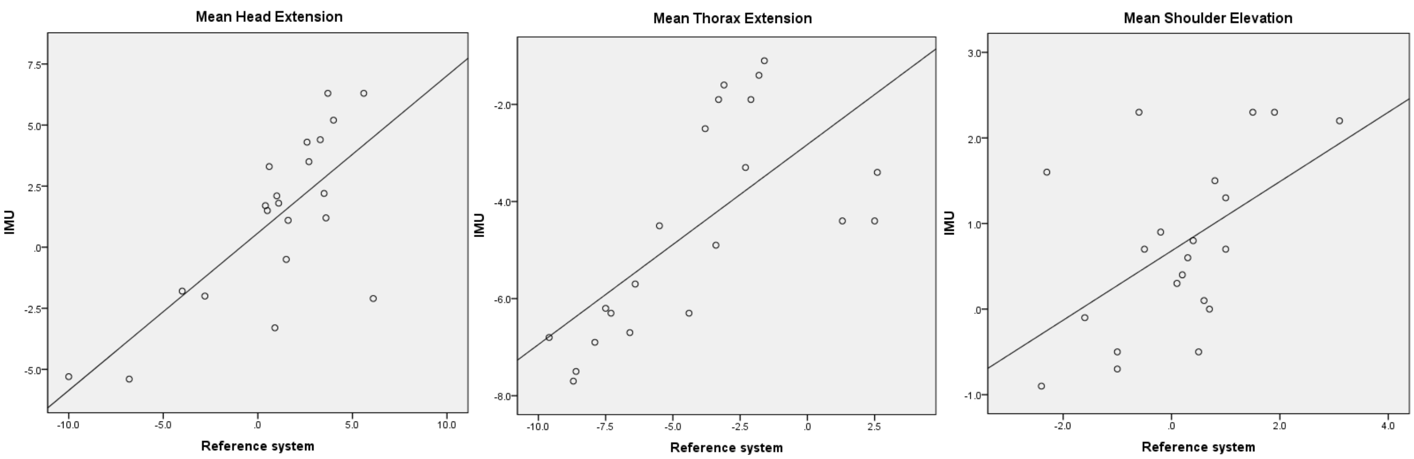

Figure 2: Correlation of mean postural angles (deg) between the reference system and IMUs. Correlation was strongest for mean head extension angles.

Table 1: Postural angles (deg) of each participant during gait trials for the reference system and IMUs.

Participant	Head Extension		Thorax Extension		Shoulder Girdle Elevation	
	Reference	IMU	Reference	IMU	Reference	IMU
1	2.1 ± 1.3	1.7 ± 0.6	-1.0 ± 3.2	-3.9 ± 0.9	0.2 ± 0.1	0.4 ± 0.2
2	-3.6 ± 8.5	-4.3 ± 1.9	-0.6 ± 4.3	-4.4 ± 0.1	-0.1 ± 0.7	1.0 ± 1.2
3	2.0 ± 1.4	0.9 ± 1.3	-7.5 ± 2.8	-6.9 ± 0.6	0.2 ± 0.4	0.4 ± 0.8
4	2.9 ± 3.8	3.8 ± 2.3	-6.8 ± 0.5	-6.2 ± 0.5	-1.8 ± 1.2	1.3 ± 1.2
5	-0.5 ± 2.0	-1.3 ± 2.5	-1.8 ± 0.3	-1.5 ± 0.4	0.8 ± 0.2	0.8 ± 0.7
6	3.2 ± 0.6	5.0 ± 1.1	-8.0 ± 0.7	-7.0 ± 0.7	2.0 ± 1.1	1.9 ± 0.6
7	0.2 ± 4.0	2.2 ± 3.6	-3.4 ± 0.4	-2.0 ± 0.5	-1.5 ± 0.8	-0.7 ± 0.2

Comparison of Functional Outcome Measures between Patients with Knee Disarticulation and Trans-Femoral Amputations Due to Trauma

Nancy A. Thesing, Trevor Kingsbury, Grant Myers, and Marilynn Wyatt

Naval Medical Center San Diego Gait Lab, San Diego, CA, USA
email: nancy.thesing@med.navy.mil

INTRODUCTION

With regards to gait in patients with amputation, previous studies have reported decreased velocity and cadence with increased energy consumption as the level of amputation moves more proximally [1,2]. Therefore, a knee disarticulation (KD) amputation should theoretically be favorable, because it preserves the femur as a long, stabilized lever for prosthetic control and end weight bearing and retains muscle strength by transecting the muscles at their distal tendinous insertion point [2]. However, functional data is lacking that proves a KD procedure is superior to a "long" trans-femoral (TF) amputation. This study aims to compare gait parameters and mechanical work in military patients with bilateral knee disarticulation/trans-tibial amputations to those with bilateral trans-femoral/trans-tibial amputations and to also correlate the residual femoral limb length to temporal-spatial, kinematic, kinetic, and mechanical work parameters.

METHODS

At Naval Medical Center San Diego (NMCSD), a retrospective review was conducted of active duty military males who had undergone a bilateral amputation, involving either a KD or a TF amputation on one side and a trans-tibial (TT) amputation on their other side due to trauma. Patients ranged in age from 23 to 41 years and had been walking unassisted for at least three months. They were matched for height (182.1 ± 0.02cm) and body mass index (BMI) (29.3 ± 4.0kg/m^2), resulting in groups of four KD/TTs and four TF/TTs. Patients wore their customized prostheses and walked at their self-selected paces as three-dimensional gait data were collected with a 12-camera Motion Analysis Corporation (MAC) system (Motion Analysis Corp., Santa Rosa, CA) and four, floor-embedded AMTI force plates (AMTI, Watertown, MA). Trials were processed with Cortex (MAC) and OrthoTrak (MAC) software. Variables examined included gait velocity, cadence, step width, step length, stride length, single limb support, total stance time on each side, vertical ground reaction forces at early stance (F1) and late stance (F3), and mechanical work. Visual3D (C-Motion inc., Germantown, MD) was used to calculate the total mechanical work as the sum of the potential, translational, and rotational energies of each body segment, integrated per stride length for both lower limbs and normalized per stride and body mass (Joules/kg*m). Independent T-Tests were used to identify significant differences between the groups with $\alpha = 0.05$. Femoral residual limb ratio was then linearly correlated with temporal-spatial, kinematic, kinetic, and mechanical work measures. Limb ratio was defined as the residual femoral length relative to the intact femoral length in percent [3]. The residual limbs were measured from the ASIS to the residual soft tissue of the femur or to the medial knee joint line.

RESULTS AND DISCUSSION

Table 1: Temporal-Spatial Parameters

Variable	KDA Grp	TFA Grp	P-Value
Velocity (m/sec)	1.22±0.17	1.22±0.10	0.964
Step Width (cm)	18.04±4.29	18.14±3.18	0.971
Cadence (steps/min)	103.18±5.44	106.55±6.07	0.440
Step Length (cm)	69.15±9.60 KD Side	69.48±2.41 TF Side	0.948
	72.35±6.89 TT Side	67.94±4.98 TT Side	0.339

(Table 1 continued)

Variable		KDA Grp	TFA Grp	P-Value
Stride Length (cm)		141.10±15.01 KD Side	137.66±6.44 TF Side	0.679
		141.67±14.59 TT Side	137.66±6.44 TT Side	0.633
Single Limb Support (% Gait Cycle)		34.33±1.00 KD Side	33.09±0.97 TF Side	0.126
		36.16±1.88 TT Side	35.23±0.38 TT Side	0.401
Total Stance (% Gait Cycle)		63.84±1.88 KD Side	64.76±0.38 TF Side	0.403
		65.67±1.00 TT Side	66.91±0.98 TT Side	0.126

Table 2: Mechanical Work (J/kg*m)

Group	KD or TF Side	TTA Side	Total Work Output
KDA	8.23±1.49	8.31±1.45	8.27±1.46
TFA	7.56±0.56	7.51±0.75	7.54±0.05
P-Value	0.451	0.366	0.396

No significant differences were found between groups for any of the temporal-spatial or work parameters (Tables 1 and 2). Furthermore, the groups loaded and unloaded their prosthetics with similar forces (Table 3). However, the analysis did show that the TFA group loaded their TT side significantly faster than the KD group. This quicker rate of loading could indicate that the patients with TF amputations do not fully trust their TF prosthetic and therefore want to get off of it quicker, resulting in an increased loading rate on their TT side. Additionally, femoral residual limb ratios did not linearly correlate with any of the temporal-spatial parameters: velocity (R^2=0.030), cadence (R^2=0.002), step width (R^2=0.002), single stance on KD/TF side (R^2=0.287), or KD/TF step length (R^2=0.001). Nor did it correlate with KD/TF peak hip power (R^2=0.423), KD/TF peak lateral trunk flexion (R^2=0.056), or KD/TF mechanical work (R^2=0.016). The shortest residual femur length was 58% of the length of the intact femur. Thus, the correlation findings suggest that as long as a residual femur is at least 58% of the length of the intact femur, gait and mechanical work parameters should not be significantly affected. This information could give surgeons more options when performing an amputation, especially on traumatic patients where significant soft tissue damage in the distal segment is a factor when determining the level of amputation. In the future it would be useful to determine if these findings hold true for patients with femurs shorter than 58% of the length of their intact femur.

REFERENCES

1. Waters RL, et al. *J Bone Joint Surg* **58A**, 42-6, 1976.
2. Smith DG. *InMotion* **14**(1), 2004.
3. Baum BS, et al. *Gait & Posture* **24S,** S265-S267, 2006.

Table 3: Force Parameters

	F1 (BW)		**F1 Rate of Change**		**F3 (BW)**	
	KD or TF Side	TTA Side	KD or TF Side	TTA Side	KD or TF Side	TTA Side
KDA Group	1.04±0.09	1.03±0.11	0.07±0.02	0.09±0.03	0.94±0.06	0.95±0.07
TFA Group	1.08±0.07	0.96±0.05	0.06±0.01	0.05±0.02	0.97±0.03	0.98±0.06
P-Value	0.571	0.151	0.485	0.047*	0.515	0.539

** Denotes Significance (α=0.05)*

Disclaimer: The views expressed are those of the authors and do not reflect the official policy or position of the Department of the Navy, Department of Defense, or the United States Government.

RELATIONSHIP BETWEEN MUSCLE FORCE AND SIZE OF HUMAN INTRINSIC FOOT MUSCLES

[1]Toshiyuki Kurihara, [1]Mituso Otsuka, [1]Nobuaki Tottori, [1]Takeshi Hashimoto, [1]Tadao Isaka, and [2]Junichiro Yamauchi

[1] Ritsumeikan University, Shiga, JAPAN
[2] Tokyo Metropolitan University, Tokyo, JAPAN
email: t-kuri-a@st.ritsumei.ac.jp

INTRODUCTION

Human foot is the only body parts that contact the ground during locomotion, hence the function of foot muscle is considered for an important. Human foot has many bones and muscles to construct a unique arch structure. Foot flexor muscles are aggregation of the muscles across metatarsal phalangeal and ankle joints and are divided into two muscle groups: the plantar intrinsic foot muscles (PIFM) and the extrinsic foot muscles. PIFM is the major foot muscle group due to that their origins and insertions of muscles are within a foot.

It has been reported that the toe flexor muscle strength is important determinants of balance or dynamic postural control [2]. Therefore, foot function should be evaluated with not only architecture of foot, but also force generating capacity of foot muscles. Understanding the architectural and neuromuscular function of foot could be a great hint for how human is evolutionally advanced to bipedal locomotion and then to provide practical information to prevent modern increases in the number of musculoskeletal disorders of a foot.

Evaluation of muscle force generating capacity along with muscle size is important way to quantify the physiological condition and muscle functions in human movements [8]; however, there is no information available how maximum force generating capacity of foot is related to the muscle size of PIFM. The purpose of this study was to investigate the relationship between force generating capacity and muscle size of PIFM.

METHODS

Twenty-eight young healthy sedentary volunteers (20.6 ± 2.0 yrs, body height 166.6 ± 8.0cm, body mass 59.8 ± 9.1 kg, means ± SD) were participated. They had no history of diagnosed neuromuscular disorder or lower limb injury, and no visible symptoms of hallux valgus and toe deformities. This study were approved by the Research Ethical Committee in Ritsumeikan University. Written informed consent was obtained from them.

The maximum voluntary isometric strength of the foot grip was measured by a custom designed dynamometer (T.K.K. 3361, Takei Scientific Instrument Co Ltd, Niigata, Japan). The subjects sat on a chair with 90 degrees of their hip, knee, and ankle joints. They were instructed to place their test foot on the dynamometer and placed another non-test foot on parallel side, and optimally grabbed the grip-handle bar of the dynamometer by toe and fingers of foot. Subjects first performed a few sub-maximum efforts to familiarize themselves with the measurements, and then exerted maximum voluntary isometric force as explosively as possible and tried to keep the force plateau for 3 seconds. Measurements of foot grip force (FGF) were repeated three times with at least one-minute rest period between bouts, and the largest value among the trials was chosen for the analysis. Both left and right feet were measured in randomized order.

The whole foot images were acquired by 1.5T MR system (Signa HDxt, GE Healthcare Co., USA). The serial T1-weighted MR images were acquired perpendicular to the plantar aspect of the foot using a fast spin-echo sequence (TE = 500 ms, TR = 16 ms, slice thickness = 4 mm, no gap, FOV = 120 × 120 mm). To measure the cross sectional area of plantar intrinsic foot muscles (CSA_{PIFM}), image at the metatarsophalangeal joint was selected due to that the anatomical cross-sectional area of the PIFM is the largest at this point [1]. Examining each images, wherever possible, non-contractile tissues such as bone, tendon, fat, connective tissue, nerve and blood vessels were excluded. All measurements and calculations were carried out by the same investigator using specially designed image analysis software (SliceOmatic 4.3, Tomovision Inc., Montreal, Canada).

RESULTS AND DISCUSSION

Significant correlations were found between FGF and CSA_{PIFM} in all feet ($n = 56$, $r = 0.748$, $p < 0.001$), and its correlations in male and female were $r = 0.682$ ($n = 28$, $p < 0.01$) and $r = 0.594$ ($n = 28$, $p < 0.01$), respectively (Figure 1). All the y-intercepts of the regression lines between FGF and CSA_{PIFM} were not significantly different from zero.

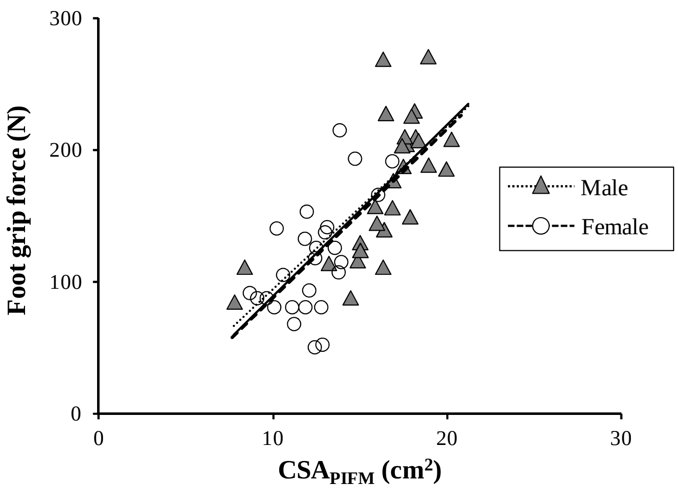

Figure 1: Relationships between cross sectional area of plantar intrinsic foot muscle (CSA_{PIFM}) and foot grip forces (FGF).

Gender differences were found in FGF (Male 173.1 ± 51.7 N, Female 119.8 ± 42.8 N) and CSA_{PIFM} (Male 16.4 ± 2.9 cm^2 , Female 12.3 ± 2.0 cm^2) All these values were significantly larger in male as compared to female. However, when FGF was normalized with CSA_{PIFM}, there was no significant difference between genders. The values of force per cross sectional area (FGF/CSA_{PIFM}) for male and female were 10.5 ± 2.4 N/cm^2 and 9.6 ± 2.8 N/cm^2, respectively.

It is well known that muscle force is related to the size of skeletal muscle. The muscle force generating capacity is generally determined with the maximum force normalized to cross sectional area, known as specific tension/force. The specific tension of human leg muscles was reported for ankle plantar flexor and dorsiflexor muscles [3,5,6] and quadriceps muscles [7]. Specific tension of plantar intrinsic foot muscles was first to show in this study. Our results of specific tension of PIFM were somewhat lower than its leg muscles shown in previous studies. This might be that, because measurement of FGF is a net force production of all conjunctive muscles, the force production of FGF is not able to isolate from the force production of only agonist intrinsic foot muscles. Also, the difficulty in determination of specific tension of PIFM was due to the fact that most of the major intrinsic foot muscles lay in oblique not directly the transverse or sagittal planes [4].

CONCLUSIONS

The relationships between FGF and CSA_{PIFM} were significantly correlated in young subjects. FGF was higher in male than in female subjects; however, the force generating capacity (FGF/CSA_{PIFM}) was not significantly different between male and female.

REFERENCES

1. Chang R, et al. *Clin Biomech* **27**, 500-505, 2012.
2. Endo M, et al. *J Gerontol Biol Sci Med Sci* **57**, 392-397, 2002.
3. Fukunaga T, et al. *J Applied Physiol* **80**, 158-165, 1996.
4. Kura H, et al. *Anat Rec* **249**, 143-151, 1997.
5. Maganaris CN, et al. *J Applied Physiol* **90**, 865-872, 2001.
6. Morse CI, et al. *J Applied Physiol* **99**, 1050-1055, 2005.
7. O'Brien TD, et al. *Exp Physiol* **95**, 202-210, 2010.
8. Yamauchi J, et al. *J Biomech* **40**, 1433-1442, 2007.

ACKNOWLEDGEMENTS

The authors especially acknowledge Dr. Sadayoshi Taguchi. This work was supported by JSPS KAKENHI Grant Numbers 23700688, 24700631, 22700652, 24300220, 70552321, and 70552321

DIRECTIONAL DIFFERENCES IN THE BIAXIAL MATERIAL PROPERTIES OF GOAT FASCIA LATA

[1]Carolyn M. Eng, [2]Francesco Q. Pancheri, [1]Daniel E. Lieberman, [1]Andrew A. Biewener, and [2]A. Luis Dorfmann

[1]Harvard University, Cambridge, MA, USA
[2]Tufts University, Medford, MA, USA
email: cmeng@fas.harvard.edu

INTRODUCTION

Despite the fact that fascia is ubiquitous in the body, little is known about its functional role during locomotion. Previous studies have shown that fascia may play a role in limb stability, muscle force transmission across segments, and storage and recovery of limb kinetic energy [1-5]. However, further investigation is critical in determining how fascia stiffness and hysteresis influence its potential to serve these functions during locomotion.

Because fascia has a sheet-like structure often attaching to muscles and bones at multiple sites, it is undoubtedly exposed to different states of biaxial strain and its functional potential cannot be captured with a simple uniaxial testing protocol. Thus, before we can further explore the mechanical role of fascia *in vivo*, its biaxial material response needs to be measured.

Planar biaxial tests with strain control were performed on goat fascia lata, which is a bi-layered structure composed of highly aligned collagen fibers. Tests were performed on longitudinally and transversely oriented samples to test the hypothesis that the fascia lata is stiffer and can store more strain energy in the longitudinal vs. transverse orientation. Furthermore, *in situ* experiments suggest that biaxial strains modulate longitudinal stiffness in aponeuroses, fascia-like structures found at muscle-tendon junctions [6]. Therefore, we also used these data to investigate the hypothesis that, like aponeuroses, fascia stiffness can be modulated by different biaxial strain conditions.

METHODS

Fascia lata (FL) samples were obtained from hindlimbs of five adult goats. Two samples were cut from each FL using a custom-made cruciform die, one oriented parallel with the longitudinal fibers while the other was oriented parallel to the transverse fibers. The longitudinal layer is parallel with the femur, while the transverse layer is 70-80° orthogonal to the longitudinal layer. Biaxial tests with strain control were performed using a previously described [7] custom-built Zwick/Roell planar biaxial testing system (Ulm, Germany). After preconditioning, samples were cycled to multiple strain levels of increasing magnitude while the perpendicular direction was held constant at 0% and 3% strain.

Engineering stress and strain were used to calculate initial stress, initial modulus, transition strain, elastic modulus, strain energy, and hysteresis. A multivariate linear mixed model was used to examine the effect of perpendicular strain (0% vs. 3%) and sample orientation (longitudinal vs. transverse) on tissue properties. All results were considered significant at a level of $p < 0.05$.

RESULTS AND DISCUSSION

Results show that FL stiffness and hysteresis are higher in the longitudinal vs. transverse direction and stiffness does not increase with perpendicular strain in either direction. While transition strain was not significantly different in the longitudinal vs. transverse orientation, initial stress, initial modulus, elastic modulus, strain energy, and hysteresis are significantly greater in the longitudinal vs. transverse orientation. These data confirm our hypothesis that the fascia lata is stiffer and has the potential to store more strain energy in the longitudinal vs. transverse orientation.

While tissue orientation has a large effect on the material properties of the fascia lata, an increase in perpendicular strain does not alter the shape of the stress-strain curve in either the longitudinal or transverse orientation. Contrary to our hypothesis, elastic modulus does not change with an increase in perpendicular strain (Fig. 1). Other parameters describing the shape of the stress-strain curve including initial modulus and transition strain also do not change when perpendicular strain is increased from 0% to 3%. Perpendicular strain also does not have a significant effect on hysteresis or strain energy. While the shape of the stress-strain curve does not change with perpendicular strain, initial stress increases as perpendicular strain is increased from 0% to 3% ($p < 0.05$).

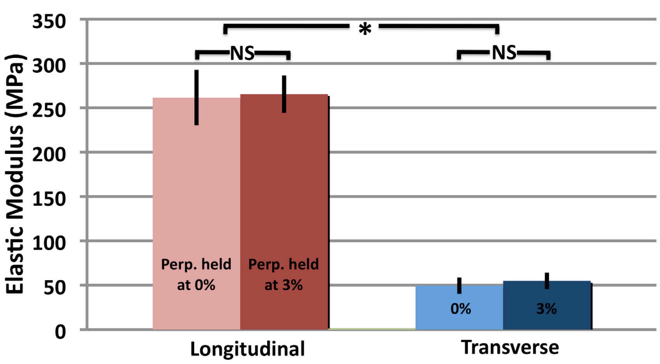

Figure 1: Elastic modulus was significantly greater in the longitudinal vs. transverse orientation ($p < 0.05$) but did not change with an increase in perpendicular strain ($p > 0.05$). Data are expressed as mean ± s.e.m.

CONCLUSIONS

Our results demonstrate that although the collagen layers in the goat fascia lata are not independent, they do not greatly influence one another's material properties. Differences in tissue properties in the longitudinal and transverse orientations are likely due to structural differences including layer thickness and collagen fibril size and density. Furthermore, differences in material properties between the longitudinal and transverse orientations suggest that differential loading in the longitudinal and transverse orientations during growth may lead to these structural changes, enhancing the ability of the longitudinal fascia lata to transmit force, store energy, or stabilize the limb.

REFERENCES

1. Bennett MB, et al. *J Zool* **217,** 469-475, 1989.
2. Eng CM, et al. *Proceedings of SICB 2012,* Charleston, SC, USA, 2012.
3. Evans P. *Ann Roy Coll Surg* **61**, 271-280, 1979.
4. Huijing PA, et al. *J Morphol* **256**, 306-321, 2003.
5. Stahl VA and Nicols TR. *Cells Tissues Organs* **193**, 325-335, 2011.
6. Azizi E and Roberts TJ. *J Physiol* **587**, 4309-4318, 2009.
7. Dorfmann A and Pancheri FQ. *Rubber Chem Technol* In press, 2013.

ENERGY DIFFERENCES BETWEEN A RIGID AND DEFORMABLE REPRESENTATION OF THE SHANK DURING DROP LANDINGS

Matthew T.G. Pain

Loughborough University, Loughborough, UK
email: m.t.g.pain@lboro.ac.uk, web: http://www.lboro.ac.uk/departments/ssehs/

INTRODUCTION

In the mechanical analysis of human movement body segments are frequently assumed to be rigid bodies. During impacts the shape of a body segment can change due to a mechanical wave propagating through soft tissue (Figure 1). Soft tissue deformation has been reported to account for up to 70% of the energy lost in some of these segments [1] during certain types of impact and occurs in conjunction with large changes in segment shape. More recently it has been shown that negative work produced by muscles during stair and ramp descent is not equal to the positive work produced when ascending, and it is suggested that this difference may be due to energy dissipation in soft tissue when foot collision occurs in the descending phase [2]. Zelik and Kuo [3] compared joint work to center of mass work and found differences that they associated with soft tissue motion not being included in the rigid body methods used with standard inverse dynamics. However, no measures of soft tissue energies of the lower limbs have been made or calculated directly from soft tissue motion. The aim of this study was to determine energy differences with deforming soft tissue of the shank during landings relative to a rigid body representation of the shank.

Figure 1: Stills from high speed video (1000 Hz) of a drop landing. Left is pre-impact, middle is post impact at minimum shank width, and right is post-impact at maximum shank width

METHODS

Six male subjects (age 23 $\pm$ 3 years, height 1.81 $\pm$ 0.08 m, body mass 81 $\pm$ 5 kg) who were free from lower extremity injury gave informed consent in accordance with the Loughborough University Ethical Advisory Committee procedures. Subjects performed a series of drop landings from four different heights (0.3, 0.5. 0.7 and 0.9 m) where the landing was heavily favoured onto one leg only. Two conditions were utilized: active markered leg landing on the force plate; and passive markered leg landing on the force plate. Active landings landed on the forefoot and controlled the impact. Passive landings landed as much onto the heel as comfortable and minimal effort was used in this leg to brake the landing. Each subject performed multiple landings and the landing with the most complete data set was used for further analysis.

A 10 camera Vicon motion analysis system (612 series, 1.3 megapixel cameras, Oxford, UK) operating at 700 Hz tracked 48 spherical markers (7.9 mm) placed on the shank in a 6×8 array. Incomplete marker trajectories were reconstructed using Vicon Nexus 1.4.116 and the pattern filling function. Reconstructed 3D marker locations were transformed in Matlab to give the rigid body least squares best fit [4]. For each trial, a stationary frame after landing was taken to represent the rigid frame configuration. Each frame, from just before impact to stationary, was rigid body transformed and the Euclidean distance between the i^{th} marker location in the rigid case and the free case was calculated per marker for all frames.

For simplicity it was assumed that each marker represented 1/48th of the mass of the shank of each subject. This allowed the RMS difference in marker positions, across all markers, to be used to represent the error in mass between the rigid body and the soft tissue body in each frame. The RMS difference time history power spectrum across all trials generally had 99.7% of the power under 75 Hz and almost no trials had a subsidiary peak in power >70 Hz. The RMS time history was low pass filtered at 75 Hz using a 2nd order zero lag Butterworth filter. This was then differentiated to get velocity and acceleration and these values, along with the segment mass, were used to determine the instantaneous absolute power values at each frame. Absolute power was then integrated over the period tissue oscillations associated with each impact were visible (generally around 200 ms) to give energy.

RESULTS AND DISCUSSION

Only a little over half of the trials were complete enough for full analysis due to marker drop out and reappearances introducing errors (up to 1000s of joules). During the impact phase the mean energy difference pooled across all subjects and good trials was 1.39 ± 1.09 J. There was no significant difference between energy values for either landing condition and no effect of height on energy values (paired t-test P>0.05), although the lack of significance at this could be due to the low number of complete trials. Across all trials the maximum RMS difference was 7.5 ± 2.9 mm, again no significant differences between conditions. Maximum positive and negative differences in marker locations between the rigid and free case gave changes in the medial-lateral diameter of the shanks of about twice the RMS value.

It should be noted that this method is not necessarily determining the total energy transferred through soft tissue motion, but rather it is evaluating what might be unaccounted for when using an optimal global reference frame rigid body fit to a single segment. If for instance all the soft tissue moves up in phase relative to the skeleton then the optimal rigid body could do a near perfect fit but at the incorrect height for a local skeletal based reference frame.

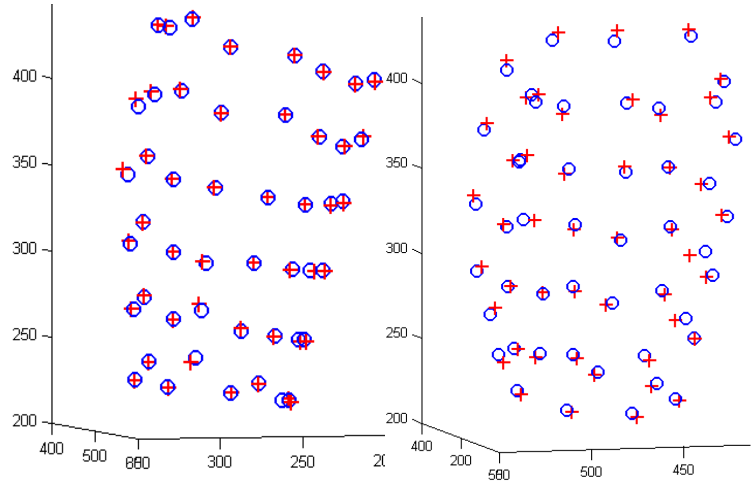

Figure 2: Rigid body marker positions, red crosses, and raw marker positions, blue circles, during late recovery, left, and mid impact, right, subject 1.

The results were quite sensitive to filtering. Filtering the RMS data at 20 Hz gave energy values of < 0.1 J. Filtering at 100 Hz gave energy values around twice those found here for the impact phase, but also started to produce energies of tenths of joules during the non-impact phases. Further processing of the current trials to deal with the marker drop out problems should result in more robust calculations. Preliminary analysis of one subject with 59 markers on the thigh gave an energy value of 3.7 J, which indicates that the values being determined here are comparable with those in the literature [1,2,3]. Direct measures of the energy difference between a rigid segment and wobbling segment can be determined. Further work to determine energy associated with soft tissue motion with respect to a local frame, and through wave effects, on these data will be performed in order to give a more complete understanding of this phenomenon.

REFERENCES

1. Pain MTG & Challis JH. *J App Biomech*, **18**, 231-242, 2002.
2. Devita P, et al. *J Exp Biol*, **210**, 3361-3373, 2007.
3. Zelick KE & Kuo AD. *J Exp Biol*, **213**, 4257-4264, 2010.
4. Challis JH. *J Biomech*. **28**, 733-737, 1995.

GAIT INITIATION VARIABILITY FOLLOWING A CONCUSSION

Thomas A. Buckley, Tiffen G. Tapia-Lovler, Hannah S. Brewer, and Barry A. Munkasy

Georgia Southern University, Statesboro, GA, USA.
email: TBuckley@Georgiasouthern.edu
web: http://www.georgiasouthern.edu/biomechanicslab

INTRODUCTION

Impaired postural control is a cardinal symptom of a concussion. Functional reserves and resource reallocation have been suggested to be compensatory mechanisms utilized by post-concussion individuals to successfully accomplish simple balance and posture tasks.[1] In moderate to severe traumatic brain injury, movement variability has been identified as an effective assessment tool which taxes the available neurological resources.[2] Gait initiation, literally the act of beginning to walk, has successfully identified impairments in postural control in a wide range of patient populations. Therefore, the purpose of this study was to evaluate variability during gait initiation in individuals who have suffered a sports-related concussion.

METHODS

The 17 participants (Female: 10, Age: 18.9 $\pm$ 0.9 years old, HT: 1.74 $\pm$ 0.10m, WT: 77.1 $\pm$ 14.4kg, MTBI history: 0.88 $\pm$ 1.17, 52.1%) were all NCAA Division I student-athletes. All participants underwent Gait Initiation (GI) assessment on two separate occasions: 1) during a baseline screening at the individuals' pre-participation physical examination (PRE), 2) within 24 hours of suffering a concussion (DAY 1). All participants completed 5 trials of self-selected pace cued GI on both testing days. Participants began each trial with one foot each on adjacent forceplates, initiated movement in response to a verbal cue, and proceeded down a 7m walkway with the initial step on a subsequent separate forceplate. (Figure 1)

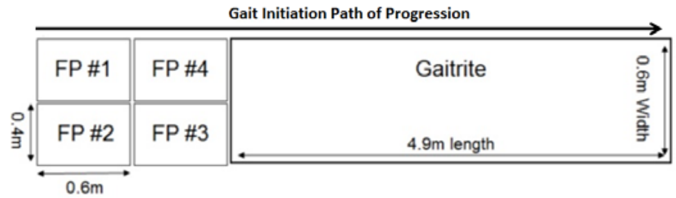

Figure 1. Lab Set-up. Participants begin the trials standing on forceplate 1 & 2 and walked from left to right with their initial step onto forceplate 3 or 4.

The kinetic data were sampled at 1,000 Hz from the 4 forceplates (AMTI, Watertown, MA, USA). The dependent variables quantified were both the mean and variability of the the center of pressure (COP) displacement during the anticipatory postural adjustment (APA) phases of GI in the posterior and lateral direction as well as the resulting initial step length and velocity which were calculated from kinetic data. Variability was calculated as the Coefficient of Variation (CV=SD/Mean * 100%). The dependent variables were compared between the two testing sessions with a paired samples t-test (alpha = .05) and Cohen's D effect sizes were calculated.

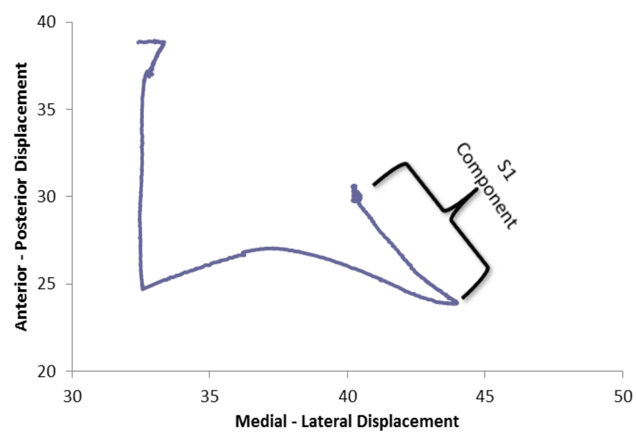

Figure 2. Exemplar COP excursion during GI.

RESULTS AND DISCUSSION

The participants' concussions in this study were graded retrospectively based on the Cantu revised evidence based guidelines and the majority (75%) were classified as grade II (symptoms lasting longer than 24 hours but less than 7 days). [3] The post-injury loss of consciousness rate was 11.8% and the post-traumatic amnesia rate was 41.2%.

There were between session differences in the APA COP displacement in both the posterior (t=8.43, P<0.001: *d*=2.14) and lateral (t=3.89, P=0.001; *d*=0.96) directions There was also a significant differences between test sessions for initial step length (t=2.28, P=0.0411, *d*=0.57), but no differences in step velocity (t=1.96, P=0.067).

	PRE	Day 1
S1 A/P*	6.1 ± 1.6cm	2.6 ± 0.9cm
S1 M/L*	6.3 ± 2.1cm	4.1 ± 1.6cm
Step Length*	0.65 ± 0.11m	0.59 ± 0.07m
Step Velocity	0.64 ± 0.17m/s	0.58 ± 0.11m/s

Table 1. Means and Standard Deviations. * indicates significant difference between sessions.

There were between session differences in the variability of the APA COP displacement in both the posterior (t=5.133, P<0.001, *d*=1.47) and lateral (t=3.125, P=0.007, *d*=1.05) directions. There were no differences between sessions for initial step length (t=0.077, P=0.94) or step velocity (t=0.89, P=0.38) variability.

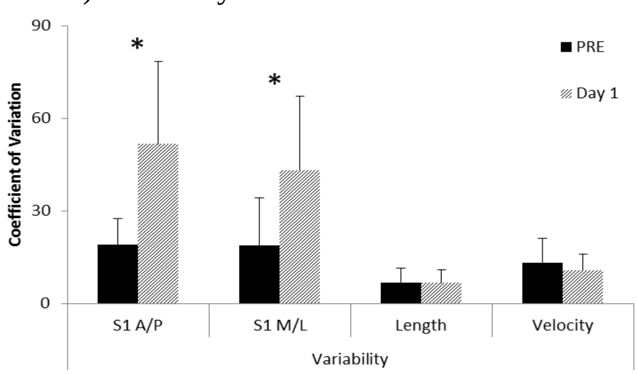

Figure 3. Gait Initiation Variability. * indicates significant difference between sessions.

The results of this study suggest that GI performance is impaired following a sports related concussion. Specifically, post-concussion individuals demonstrated reduced APA's and initial step length as well as increased variability in the COP displacements during the APA phase of GI.

Increased variability in performance is typically associated with instability in the postural control systems. [4] These instabilities are frequently associated with impaired central nervous system communication with the peripheral skeletal muscular system. Further, reduced attentional capacities have been associated with increased gait variability. In the post-concussion testing session, the individuals, had significant increases in COP displacement variability, during the APA phase, with large effect sizes evident between testing sessions (Cohen's D >0.8).

Increased gait variability is frequently associated with elevated fall risk; [4] however, this is an unlikely consequence in otherwise healthy young adults. More likely, this is evidence of impaired postural control and may be an intriguing approach to the study of concussion recovery as traditional gait metrics often normalize within a few days. [5]

REFERENCES

1. Chen JK, et al. Functional Abnormalities in Symptomatic Concussed Athletes: an fMRI study. *Neuroimage*. 2004; **22**:68–82.
2. McFadyen BJ, et al. Modality Specific, Multitask Locomotor Deficits Persist Despite Good Recovery After a Traumatic Brain Injury. *Arch Phys Med Rehabil*. 2009;**90**(9): 1596–1606.
3. Cantu RC. Posttraumatic Retrograde and Anterograde Amnesia: Pathophysiology and Implications in Grading and Safe Return to Play. *J Athl Train*. 2001;**36**(3) :244–248.
4. Hausdorff JM, et al. Increased gait unsteadiness in community-dwelling elderly fallers. *Arch Phys Med Rehabil*. 1997;**78**(3): 278–283.
5. Parker TM, et al. Gait Stability following Concussion. *Med Sci Sports Exerc*. 2006;38(6): 1032-1040.

ACKNOWLEDGEMENTS

Supported by: NINDS 1R15NS070744-01A and Georgia Southern University Faculty Development Committee.

DIFFERENCES IN PASSIVE CONTRIBUTIONS IN WALKING AMONG HEALTHY YOUNG AND OLDER ADULTS AND PERSONS WITH PAD

[1]Daniel Leib, [1]Shane Wurdeman, [1]Dylan Goodman [2,3]Iraklis Pipinos, [2,3]Jason Johanning and [1]Sara Myers

[1]University of Nebraska at Omaha, Omaha, NE, USA
[2] VA Nebraska-Western Iowa Health Care System, Omaha, NE, USA
[3]University of Nebraska Medical Center, Omaha, NE, USA
email: dleib@unomaha.edu, web: nbcf.unomaha.edu/

INTRODUCTION

Peripheral arterial disease (PAD) is a vascular disease in which the lower extremity blood vessels are occluded, resulting in pain during walking known as claudication. While most patients with PAD tend to walk more slowly than healthy controls, some are able to maintain similar speeds as controls despite decreased contributions from lower extremity joint powers [1]. It is currently thought that this decrease in joint power stems from changes to muscle physiology resulting from repeated cycles of ischemia and reperfusion [2]. The purpose of this study was to investigate potential differences in active and passive contributions to energy production during walking to understand the altered energetics that may explain the ability of certain patients with PAD to maintain a relatively high walking speed despite decreased joint powers. This was done by examining differences in external work and total joint work [3]. We hypothesized that to compensate for reduced muscle function, persons with PAD rely on greater levels of passive soft tissue work than speed matched younger and older healthy controls.

METHODS

Nine healthy young adults (age: 25.1 ± 5.7 years, height: 1.75 ± 0.11m, mass: 75.47 ± 22.96kg), nine healthy older adults (age: 66.5 ± 5.7 years, height: 1.73 ± 0.07m, mass: 78.94 ± 22.96kg), and nine persons with PAD (age 60.0 ± 9.1 years, height 1.73 ± 0.08m, mass 82.33 ± 17.56kg), were selected for analysis from an ongoing study related to PAD treatment outcomes. Subjects were selected for their matched preferred walking speeds (young: 1.33 ± 0.15m/s, older: 1.34 ± 0.11m/s, PAD: 1.27 ± .15m/s) to control for variations in joint kinetics that are a result of walking speed.

Five trials of overground walking data were collected using a 12- camera motion capture system (60 Hz; Motion Analysis, Santa Rosa, CA, USA) synchronized with a single force plate (600 Hz; Kistler Instruments, Winterhur, Switzerland). Data were collected prior to the onset of claudication for persons with PAD. Kinematic and kinetic data were calculated using the method of Nigg et al [4] utilizing Visual3D (C-Motion, Germantown, MD). Joint power data, sacral marker position data, and ground reaction force data for the right leg were exported for use in MATLAB 2012b (Mathworks, Natick, MA). External work was calculated as the dot product of the estimated center of mass velocity found by differentiating the sacral marker data [5] and ground reaction force data during stance for the right leg. Joint work was calculated as the time integral of joint power and then summed to find total joint work. An estimate of the contributions of passive and active work to walking was made by subtracting external work from total joint work [3]. Work data were separated into four phases of stance as outlined by Zelik and Kuo [3] and calculated as a dimensionless value for statistical analysis.

A 2-way ANOVA was first used to investigate the effects of subject group and phase of stance for the difference between joint and external work. An LSD post-hoc test was then performed to determine the sources of effects.

RESULTS AND DISCUSSION

A significant interaction was found between group and phase ($p<0.001$). Post-hoc analysis indicated that the young subject group was different from the

PAD group during collision, while young was different from both older adult groups during rebound.

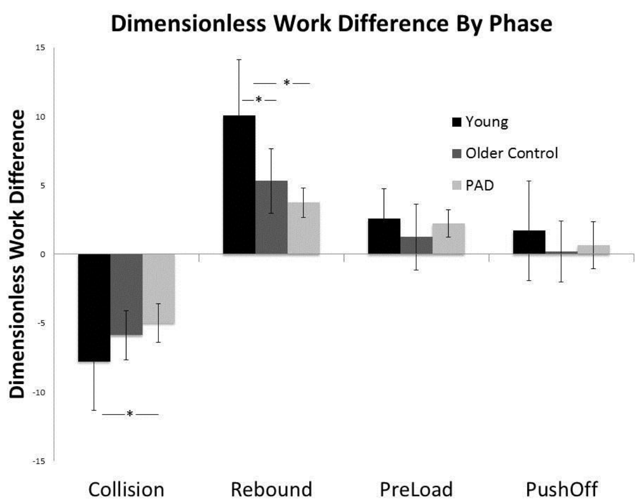

Figure 1: Plot of differences between dimensionless external work and joint work per phase for each subject group. Differences between subject groups at $p < 0.05$ are indicated by *. During collision, younger adults were different from PAD patients, while during rebound younger adults were different than both groups of older adults.

Although the estimate of active and passive contributions to work over the entirety of stance phase did not reach significance between groups (p=0.112), a difference between subject groups was found during the collision and rebound phase of stance. Young adults had a higher difference between external work and joint work than both older groups, indicating a greater amount of negative work accounted for in joint work calculations compared to external work. This indicates a larger relative contribution of passive elements, such as joint cartilage compression, bone deflection and energy return, and other passive factors to work during this phase of stance.

There are limitations to consider in this study. First, we make the assumption based on previous literature that differences in external work and joint work are the result of the ability of external work to be a more direct measure of total body work accounting for soft tissue and passive elements whereas joint work represents more directly active muscle work at each joint [3]. We also did not account for cadence (i.e. faster/slower joint rotational velocities without faster/slower walking speeds) as we chose to account for velocity, as matching subjects on both conditions would have reduced our sample size. It should also be noted that this method of estimating the difference between external work and joint work is not perfect, as energy due to motion relative to the center of mass are not captured in the analysis [3]. While these contributions are typically assumed to be insignificant and not included in gait kinetics calculations, it is possible that use of segmental motion above the hip may be a compensatory mechanism used by persons with PAD.

CONCLUSIONS

Older adults with PAD appear to not use larger amounts of passive soft-tissue work to achieve the same walking velocity as healthy older adults, as both groups of older adults use less passive work than young controls. This analysis suggests that increased reliance on passive soft-tissue work during gait is not the means by which persons with PAD who maintain a faster walking speed do so, despite reduced contributions from active joint contributions [1]. A possible alternative is reliance on upper body motion, perhaps through increased trunk lean or arm swing. An increase in cadence, which would allow for lower propulsive power per step, may also play a role. Future studies should investigate these possibilities as potential compensatory mechanisms in persons with PAD.

REFERENCES

1. Wurdeman SR, et al. *Gait and Posture*, **36**, 506-509, 2012.
2. Pipinos, II, et al. *Vasc Endovascular Surg*, **41**, 481-489, 2007.
3. Zelik KE and Kuo AD. *J Exp Biol*, **213**, 5257-4264, 2010.
4. Nigg BM, et al. *J Biomech*, **26**, 909-916, 1993.
5. Gard SA, et al. *Hum Mov Sci*, **22**, 597-610, 2004.

ACKNOWLEDGEMENTS

Funded by: NIH (1R01AG034995), VA RR&D (1I01RX000604) a NASA EPSCOR grant

GENDER DIFFERENCES IN RESPONSE TO LOAD CARRIAGE

Rebecca Krupenevich, Thomas Mahar, Jake Ridings, Rachel Tatarski, Patrick Rider, Zac Domire, Paul DeVita

East Carolina University, Greenville NC
Email: krupenevichr11@students.ecu.edu

INTRODUCTION

Female soldiers experience increased rates of injury compared to male soldiers. In particular, females have exhibited a high rate of overuse injuries at the knee [1]. Identifying the mechanisms that contribute to chronic knee pain could help to decrease injury rates among females in the military.

Many previous studies have determined the load amount to be carried as a relative load based on the participant's body weight [2]. This methodology may be masking gender differences in response to the load. In addition, relative loads are not applicable to the military population; load amounts carried in the military are absolute. They are based on the position or job being performed rather than body mass. A comparison of genders based on an absolute load, instead of loads relative to body weight, may help to explain the high rates of injury observed in female soldiers.

METHODS

A total of 13 healthy adults (8 males, 5 females) participated in this study after providing written informed consent. All subjects were members of the ECU Army ROTC. Subjects were asked to wear standard issue ROTC boots during testing and wore a MOLLE rucksack containing 24kg (U.S. Army fighting load) during loaded conditions. Subjects performed several walking trials at a standard speed of 1.5m/s up a ramp with 10 degree incline (Figure 1). Three load conditions (unloaded, mid-back, and low-back load placement) were tested. The low back load placement concentrated the load towards the bottom of the pack, and the mid back placement raised the load approximately 12cm from the low back position.

Kinematic data were captured using an eight camera Qualisys motion tracking system. AMTI force plates were used to capture force data. Data were analyzed using V3D and were combined in a musculoskeletal model to predict quadriceps forces and patellofemoral joint forces [3]. A 2x3 ANOVA was run to test for interactions between gender and load condition & for main effects for patellofemoral force, quadriceps force, maximum knee flexion angle, and knee extensor torque ($p<0.05$).

RESULTS AND DISCUSSION

There were no statistically significant interactions between gender and load condition for any of the variables we tested. A Tukey's HSD post-hoc test was run to determine significance on the main effects of load condition.

Males and females showed a significant increase in patellofemoral joint force (Fig 2) from unloaded to both low and mid load conditions ($p<0.05$). The gender effect was not significant ($p=0.09$). Similarly, there was a significant difference ($p<0.05$) between the unloaded condition & loaded conditions in quadriceps force (Fig 3) and knee extensor torque (Fig 5), but a non-significant gender effect, $p=0.21$ & $p=0.83$, respectively. Knee flexion angle (Fig 4) showed a significant load effect from the unloaded condition to the low load condition ($p<0.05$), but not to the mid load condition. There was also a significant difference in knee flexion angle between genders ($p<0.05$). Despite absence of interaction effect, females displayed a substantially larger percent increase in knee extensor torque, quadriceps force & patellofemoral joint force in response to loading compared to males (Table 1).

Figure 1: Click QR link or scan QR code to see incline walking videos

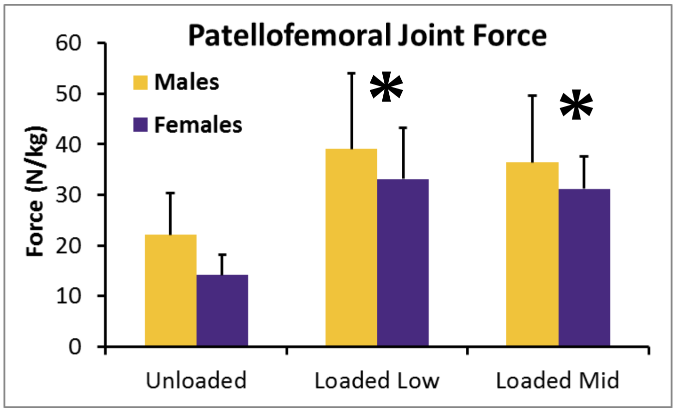

Figure 2: Patellofemoral joint force (*different from unloaded condition p<0.05)

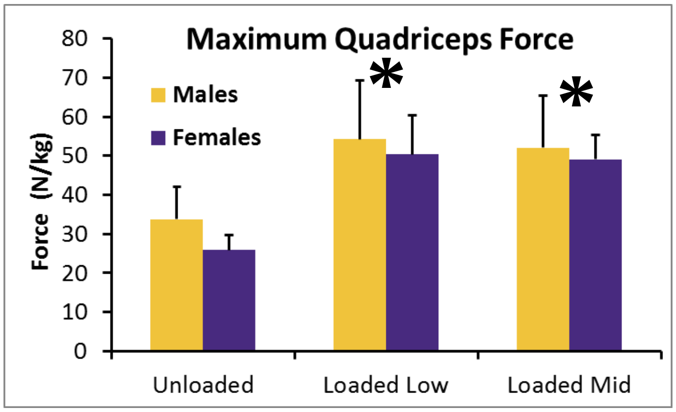

Figure 3: Maximum quadriceps force (*different from unloaded condition p<0.05)

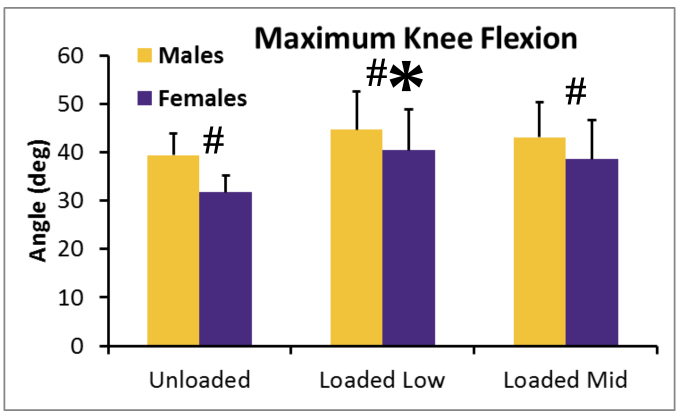

Figure 4: Maximum knee flexion (*different from unloaded condition p<0.05, #different between genders p<0.05)

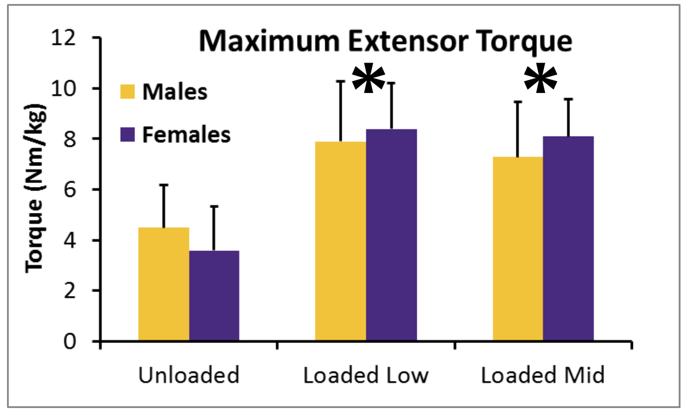

Figure 5: Maximum extensor torque (*different from unloaded condition p<0.05)

CONCLUSIONS

We think the approximately 2-fold increased response observed in knee kinetics in females compared to males in the loaded conditions may be a result of lower body mass and absolute strength in females. The load caused a 2-fold larger increase in knee flexion in females vs. males (~25% vs. 12%) leading to the 2-fold increase in knee torque, quadriceps force & patellofemoral force per unit mass. We propose the two-fold larger increase in patellofemoral force in females with load carriage may be one underlying mechanism for higher injury rates in female vs. male military personnel [4].

REFERENCES

1. Boling M, et al. *Scand. J Med. Sci. Sports* **20**, 725-730, 2010.
2. Quesada PM, et al. *Ergonomics* **43**, 293-309, 2000.
3. Messier SP, et al. *Osteoarthritis and Cartilage* **19**, 272-280, 2011.
4. Reynolds KL, et al. *US Army Research Institute of Environmental Medicine* **report no. 11-91**, 1990.

Table 1: Percent increase in kinetic variables

	Patellofemoral Joint Force		**Maximum Quadriceps Force**		**Maximum Knee Extensor Torque**	
	No load to low	No load to mid	No load to low	No load to mid	No load to low	No load to mid
M (n=8)	76%	64%	61%	54%	76%	62%
F (n=5)	134%	120%	95%	90%	134%	126%

PERSISTANCE OF ASYMMETRICAL LOWER-EXTREMITY JOINT WORK FOLLOWING ACL RECONSTRUCTION

[1,2] Benjamin D. Roewer, [1,2] Stephanie L. Di Stasi, PT, PhD [1,2,3,4] Timothy E. Hewett PhD

[1]OSU Sports Medicine, Ohio State University
[2]Sports Health and Performance Institute, Ohio State University Wexner Medical Center, Columbus, OH, USA
[3]Ohio State University, Depts. of Physiology and Cell Biology, Orthopaedic Surgery, Family Medicine, and Biomedical Engineering, Columbus, OH, USA
[4]Cincinnati Children's Hospital, Sports Medicine Biodynamics Center, Cincinnati, OH, USA
Email: ben.roewer@osumc.edu

INTRODUCTION

Anterior cruciate ligament (ACL) injuries are common among athletes who participate in running, cutting and jumping sports and often result in knee instability, reduced quadriceps strength and asymmetrical movement patterns. Athletes with an ACL-deficient knee typically achieve less peak knee flexion during normal walking and produce reduced peak internal knee extensor moments at the injured joint [1]. To compensate for reduced knee moments, poorer-functioning ACL-deficient athletes may increase the peak internal extensor moments in the hip [1].

After undergoing surgery to repair the injured ACL and restore stability to the knee, decreased knee moments may persist in the involved limb for two years or more despite participation in supervised, post-operative physical therapy [2]. Little is known about the contribution of each of the joints of the lower extremity to weight acceptance during gait and how asymmetrical knee moments and compensatory strategies are acutely affected by surgery. If changes in lower-extremity mechanics can be detected early after surgery and addressed in supervised physical therapy, then it may help spur the restoration of symmetrical movement patterns, and potentially reduce the risk for secondary ACL injury [3]. The purpose of this study was to quantify the relative contribution of the ankle, knee and hip to weight acceptance during gait after ACL injury and to test whether those contributions change early after surgery.

METHODS

Twelve subjects (age = 25.1 ± 11.6 years; height = 171.6 ± 10.7 cm; weight = 79.4 ± 13.9 kg) with a complete isolated rupture of their ACL provided informed consent to participate in the study. All subjects participated in two testing sessions (pre = prior to surgery; post = 6 weeks post-surgery) where they underwent a clinical examination and motion analysis.

All subjects participated in three-dimension (3D) motion analysis of level, overground walking. They were outfitted with 55 retroreflective markers using a modified Helen Hayes marker set and were instructed to walk at their self-selected speed along a ten-meter runway across two force platforms (1200 Hz, Bertec Corp., Worthington, OH). Trials were repeated until there were three acceptable trials in which subjects walked within +/- 5% of their self-selected walking speed and made isolated foot contact with one of the force platforms. 3D marker position data were collected at 240Hz using twelve passive, infrared cameras (Motion Analysis Corp, Santa Rosa, CA). Marker position and force platform data were filtered using a 4th order, bi-directional, lowpass, Butterworth filter with cutoffs of 6Hz and 40Hz, respectively. Sagittal-plane joint power of the ankle, knee, and hip, and peak knee flexion angles and moments were calculated during the first 25% of stance (i.e. weight acceptance) using Visual 3D (C-motion corp., Germantown, MD). Net negative work was computed using custom Matlab (Mathworks, Natick, MA) coding.

Peak knee angles and moments, and the proportion of negative joint work performed by each of the three lower-extremity joints were compared using an ANOVA with repeated measures (time x limb). Significance was defined as $p < 0.05$.

RESULTS AND DISCUSSION

There was an interaction in peak internal knee extensor moments ($p = 0.03$). Specifically, there was a significant asymmetry in peak internal knee extensor moments before surgery ($p < 0.01$), which increased after surgery due to a trend towards increasing peak internal knee moments in the uninjured limb ($p = 0.08$). There was not a significant time x limb interaction in peak knee flexion angles ($p = 0.90$).

Despite increasing asymmetry of peak internal knee extensor moments, there was no time x limb interaction in the proportion of negative joint work performed by the knees ($p = 0.32$; Figure 1); significantly more negative work was performed by the uninjured knee at both time points ($p < 0.001$).

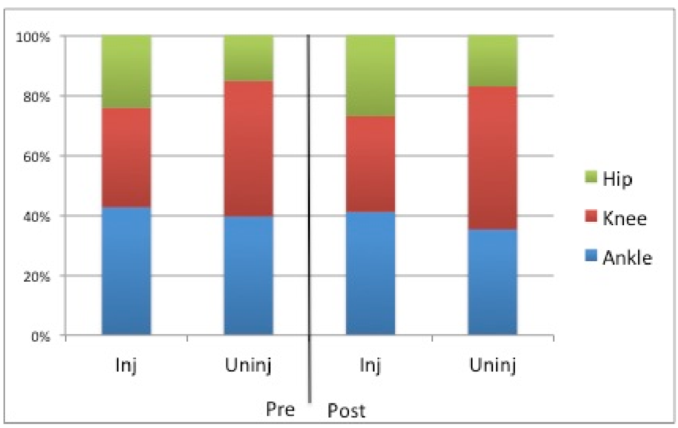

Figure 1: The relative amount of negative work produced by each joints during weight acceptance.

There were also no significant time x limb interactions in the relative proportion of negative joint work performed by the hips ($p = 0.90$) and ankles ($p = 0.89$). Significantly more negative work was performed by the hip on the uninjured limb at both time points ($p = 0.047$).

Despite detecting a significant increase in the peak internal knee extensor moment in the knee of the uninjured limb after surgery, there was no relative change in the proportion of net negative joint work performed by the knees during weight acceptance. We observed significant asymmetries in peak knee moments and the proportion of negative work performed by the joints, which may be of greater importance and may show that joint loading strategies prior to surgery may be immediately unaffected by the trauma of surgery.

These findings may also reasonably indicate that pre-operative gait mechanics may be significant predictors of post-operative gait mechanics. Future work will seek to fully characterize the effects of pre-operative interventions on post-operative outcomes to see if improvements in pre-operative gait mechanics and knee function lead to quicker recovery following surgery.

REFERENCES

1. Rudolph *Knee Surg. Sports Traumatol, Arthrosc* **9**, 62-71, 2001
2. Roewer, et al. *J Biomech* **44**, 1948-53, 2011.
3. Paterno, et al. *Am J Sports Med* **38**, 1968-78, 2010.

ACKNOWLEDGEMENTS

This study was funded by DJO Global (Vista, CA). We would like to thank Christopher Nagelli, Kari Stammen, Sam Wordeman, Dr. Chris Kaeding and the entire Sports Medicine Biodynamics staff, without whom this study would not be possible.

Table 1: Peak knee flexion angles and extensor moments during weight acceptance before and after surgery

	Peak Knee Flexion Angle (°)		Peak Internal Knee Extensor Moment (Nm/kg*m)	
	Pre	**Post**	**Pre**	**Post**
Injured	-38.7 ± 4.3	-37.9 ± 4.1	0.22 ± 0.8	0.21 ± 0.0
Uninjured	-38.7 ± 4.3	-38.1 ± 4.2	0.28 ± 0.9	0.33 ± 0.1

Contribution of Thigh and Tibial Motion to Knee Transverse Plane Motion in Runners with Anterior Knee Pain

[1]Pedro Rodrigues, [2]Brian Noehren, [3]Joseph Hamill

[1]New Balance Sports Research Lab, Lawrence, MA, USA
[2]University of Kentucky, Lexington, KY, USA
[3]University of Massachusetts, Amherst, MA, USA
email: pedro.rodrigues.a@gmail.com

INTRODUCTION

Anterior knee pain (AKP) is one of the most common overuse running injuries. While the exact etiology remains unknown, mechanical factors are recognized to play a critical role. Distal factors such as excessive calcaneal eversion have long been hypothesized to influence tibial internal rotation and in turn knee mechanics[1]. More recently, proximal factors such as abnormal hip adduction and internal rotation have also been found to be greater in those with PFP[2]. However, the relative contributions of proximal or distal segments on the kinematics of the knee have not been fully investigated in this population.

There have been a limited number of investigations of the transverse plane coordination in other populations. For example, Bellchamber et al.[3,] using an energy flow analysis, found that healthy runners presented with a proximal to distal energy flow. This finding suggests that the transverse plane motion of the knee was influenced relatively more by proximal factors. However, this pattern was found to vary across subjects and to change across different periods of stance. Furthermore, only healthy runners were evaluated in this study and it is feasible that the role of proximal and distal factors may change in those with injuries such as AKP.

The relative contribution of proximal and distal factors on knee motion can also be evaluated using correlations[4]. Using this approach, one could hypothesize that the segment (thigh or shank) that is most correlated with the motion of the knee is also the primary driver of its motion. Therefore, the purpose of this study was to evaluate the cross correlation between the transvers plane motion of the tibia and thigh relative to that of the knee.

METHODS

Nineteen healthy (10 male, 9 female, 34 ± 10 years, 1.7 ± 0.1m, 65 ± 12 kg) and seventeen runners with AKP (4 male, 13 female, 30 ± 7 years, 1.6 ± 0.1m, 60 ± 8 kg) completed the study. All subjects were running 12+ km per week for 6 months, utilized a heel-strike foot fall pattern and had no history of lower extremity surgeries.

Lower extremity segments were defined were defined using markers placed on the greater trochanters, medial/lateral knee, medial/lateral malleoli, sustentaculum tali, and peroneal tuberucle. Dynamic treadmill running trials were captured (Qualisys, Sweden, 200 Hz) using marker clusters attached to the lateral thigh, lower leg and directly to the calcaneus.

Kinematic data were analyzed in Visual 3D (C-Motion, USA). Marker trajectories were low pass filtered at 12 Hz. Joint and segment angles were calculated using Cardan X-Y-Z rotation sequence. Zero time lag cross correlations comparing the 1) transverse plane motion of the tibial segment and knee and 2) transverse plane motion of the thigh segment and knee were performed over five periods of stance. Subject specific correlation coefficients (R) were then evaluated using a two way ANOVA with health and segment as factors ($\alpha = 0.05$).

RESULTS AND DISCUSSION

Differences between runners with and without AKP were seen between 1% to 20% of stance (Table 1,

Figure 1). More specifically runners with AKP had higher correlation coefficients between tibia, thigh and knee rotation (Health R = 0.48 vs. AKP R = 0.74, p = 0.02). This finding indicates that the tibia and thigh were both moving in a pattern that resulted in knee internal rotation. The higher correlations in runners with AKP suggest they have less coordination variability between segments during weight acceptance, and could result in repetitive stress on the same tissues. These results add additional evidence of a lack of coordination variability in this population as was first shown by Hamill et al.[5].

The relative contribution of each segment to the transverse plane position of the knee also changed during stance (Table 1, Figure 1). Specifically, the thigh segment was found to have a greater contribution to knee position between 41% - 60% of stance (thigh R = 0.63 vs. tibia = 0.19, p < 0.01). This finding suggests that the reversal from a loading pattern to a propulsive pattern may be initiated proximally. In contrast, the tibia was found to have a greater influence on the transverse plane motion of the knee between 81 – 100% of stance (thigh R = 0.38 vs. tibia R = 0.76, p < 0.01). These finding supports those of Bellchamber et al.[3] who found the contribution of proximal and distal factors influencing the position of the knee may change over different periods of stance.

CONCLUSIONS

The transverse plane kinematics of the thigh, tibia and knee were more correlated in runners with AKP early in stance which may indicate a lack of coordination flexibility. Additionally, the relative contributions of the tibia and thigh segments to the knee's position appear to change across stance with contribution to knee rotation switching from the thigh at midstance to the shank towards terminal stance.

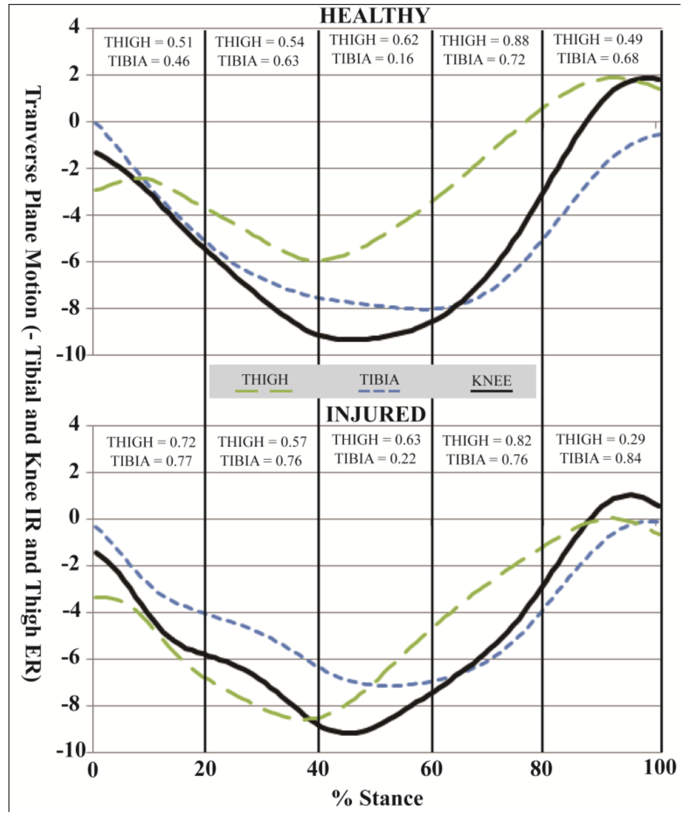

Figure 1. Transverse plane motion of the thigh, tibia and knee over stance. Cross-correlations with a zero time lag were performed over five periods of stance. Correlation coefficients (R) are reported for each time period.

REFERENCES

1. Tiberio D, JOSPT 9, 160-5, 1987.
2. Noehren B, Gait Posture 36, 596-9, 2012.
3. Bellchamber T, J Biomech 33,139-403, 2000.
4. Derrick T, Med Sci Sports Exerc 26, 919-28,1994.
5. Hamill J, Clin Biomech 14, 297-308,1999.

Table 1. An ANOVA was used to evaluate the correlation coefficients (R) over five periods of stance. P- values are presented below.

	% Stance				
	1-20	21-40	41-60	61-80	81-100
Group	**0.02**	0.36	0.79	0.93	0.86
Segment	0.98	0.13	**<0.01**	0.26	**<0.01**
Group * Segment	0.63	0.61	0.83	0.63	0.13

VISUAL FEEDBACK IMPROVES MOVEMENT SYMMETRY DURING SIT TO STAND

[1]Sumayah Abujaber, [2]Adam R Marmon, [2,3]Joseph Zeni Jr.

[1] Rehabilitation Sciences School, University Of Jordan, Amman, Jordan
[2]Biomechanics and Movement Science program, University of Delaware, Newark, DE, USA
3Department of Physical Therapy, University of Delaware, Newark, DE, USA
sumayah@udel.edu

INTRODUCTION

Patients with end stage of hip osteoarthritis (OA) demonstrate asymmetrical movement patterns during daily activities that increase the load on the non-affected limb [1]. Although total hip arthroplasty (THA) improves pain and function, altered kinetics and kinematics persist for a variety of motor tasks. During sit to stand (STS) task, patients after THA exhibited significantly more asymmetry compared to healthy individuals, with a shift toward the non-operated side [2]. Including symmetry training to the rehabilitation programs after THA may improve biomechanical outcomes. The purpose of this study is to examine whether providing real-time visual feedback of force under each limb can improve lower extremity biomechanics during a STS task in patients before and after THA. We hypothesized that patients would demonstrate improve kinetic and kinematic symmetry at the hip and knee when provided only with feedback of their ground reaction force under each limb.

METHODS

Ten patients participated in this study; five patients with end-stage hip OA (3 females, Age 66.8±5), and five patients 3 months after THA (5 females, Age 73.8 ± 6y). Patients performed STS task in two conditions (with and without visual feedback). Patients completed three trials of STS without visual feedback followed by three trials with visual feedback. Patients had two practice trials to become familiar with the task. All patients underwent 3D motion analysis of STS task using an 8 camera infrared motion system (Vicon) and 2 force-plates (Bertec). Joint angles and joint moments for each limb were calculated by inverse dynamic techniques. Feedback during STS was given through the use of a custom-written software program that runs on a laptop computer (Figure). The input to the feedback system is via two faceplates that transmits the relative medial/lateral weight distribution of the limbs. The visual display was on a monitor in front of patient, consists of two cylinders for each limb that fill or empty based on the percentage of weight that is distributed to each limb.

When visual feedback was provided, patients were asked to try putting equal weight under each limb, and to keep their trunk in the center with focusing on the feedback displayed on the monitor. The outcome measures use, during rising from chair, were the symmetry ratio of peak hip flexion moment (PHFM), hip sagittal angle (HSA), peak

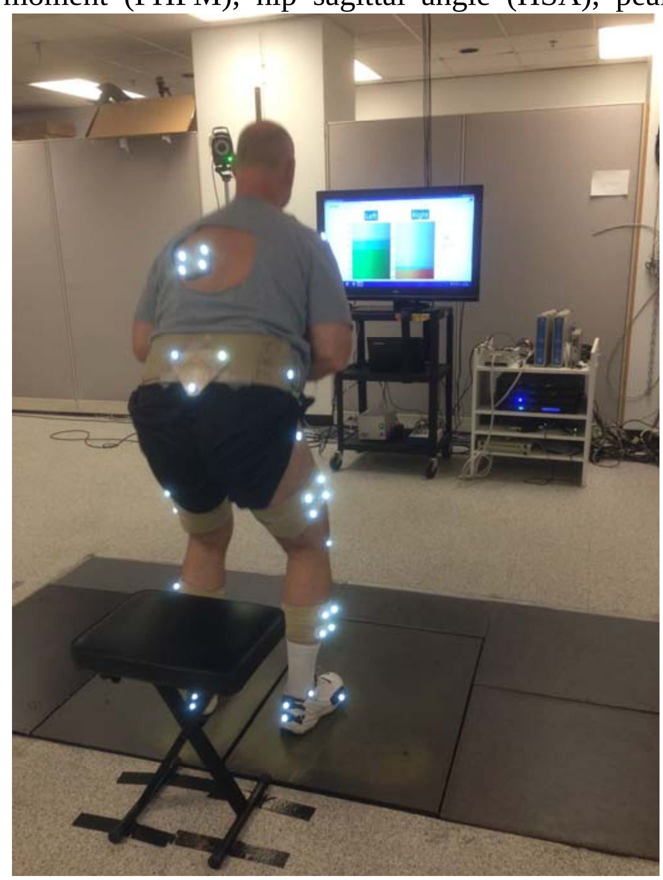

knee flexion moment (PKFM), and knee sagittal angle (KSA). Symmetry ratio of vertical ground reaction force (VGRF) calculated during sit to stand and while standing. Symmetry ratio was calculated by dividing the outcome value of operated side by that of the non-operated side. Descriptive statistics were calculated (mean and standard deviation) for all variables in the two conditions.

RESULTS AND DISCUSSION

There was an improvement in symmetry for all outcome variables when visual feedback was provided. Patients with end stage hip OA demonstrated more symmetrical movement patterns when receiving visual feedback, characterized by more inter-limb symmetry ratio for VGRF, PHSM and PKSM, and patients exhibited symmetrical KSA and HSA in both conditions (TABLE 1). Sagittal Hip and knee motion was very symmetrical during RFC in both conditions, the biomechanical symmetry for all other variables were improved in patients after THA (TABLE 2). These results indicate the effectiveness of real-time visual feedback on improving the symmetry of movement pattern during STS task. Visual feedback produced more symmetrical ratio of kinetics outcomes in patient before and after THA.

CONCLUSIONS

The improvements in biomechanical symmetry in the subjects who received visual feedback indicate that it may be effective for retraining kinetic and kinematic movement symmetry during a sit to stand task. Retention of these symmetrical movement patterns may reduce the risk of contralateral joint OA and reduce the risk for future joints replacement. Despite hip pain in patients with end-stage hip OA, these individuals were still able to improve movement symmetry during the retraining task. Because patients with THA also demonstrated improvement in joint symmetry, this feedback program may be effective at retraining movement patterns after surgery. Using only feedback of vertical ground reaction force, subjects were able to normalize kinetics and kinematics at the lower extremity joints. This technology can be implemented in the clinic using relatively inexpensive technology, such as a Wii Balance Board (Nintendo, Inc.) or bathroom scales.

REFERENCES

1. Miki H, et al. *Journal of biomechanics*, ***37***(4), 443–55, 2004
2. Talis V, et al. Clinical Biomechanics **23**(4), 424–33, 2008.

ACKNOWLEDGEMENTS

This study was supported by NIH grants (K12HD055931) and a scholarship from the University of Jordan.

Table 1: Symmetry ratios of biomechanical outcomes with and without visual feedback during RFC in patients with end-stage hip OA

	VGRF		HSA		PHFM		KSA		PKFM	
	NO VF	***VF***	***NO VF***	***VF***	***NO VF***	***VF***	***NO VF***	***VF***	***NO VF***	***VF***
Average	0.79	0.90	1.02	1.01	0.76	0.88	1.04	1.04	0.68	0.81
SD	0.13	0.19	0.12	0.10	0.11	0.09	0.14	0.13	0.16	0.23

Table 2: Symmetry ratios of biomechanical outcomes with and without visual feedback during RFC in patients 3 months after THA

	VGRF		HSA		PHFM		KSA		PKFM	
	NO VF	***VF***	***NO VF***	***VF***	***NO VF***	***VF***	***NO VF***	***VF***	***NO VF***	***VF***
Average	0.80	0.85	1.05	1.04	0.92	0.98	1.07	1.07	0.83	0.87
SD	0.15	0.14	0.07	0.09	0.24	0.29	0.12	0.13	0.23	0.30

STATIC AND DYNAMIC MEDIAL LONGITUDINAL ARCH ANGLE IN PATELLOFEMORAL PAIN SYNDROME INDIVIDUALS

[1] Sandra Aliberti, [1]Bruno Mezencio,[1]Alberto Carlos Amadio,[1]Julio Cerca Serrão ,[2]Joseph Hamill,[1]Luis Mochizuki
[1] Biomechanics Laboratory, Physical Education and Sport School, University of São Paulo - São Paulo
[2] Department of Kinesiology, University of Massachusetts – Amherst
email: aliberti@usp.br

INTRODUCTION

Patellofemoral Pain Syndrome (PFPS) is one of the most common musculoskeletal dysfunctions of the knee, affecting mainly physically active young women [1,2]. Rearfoot eversion has been related to PFPS as it may lead to a compensatory internal rotation of the tibia causing the patella to track laterally. Although there is limited evidence that foot orthoses provide greater short-term improvements in individuals with PFPS, kinematic studies that have investigated the relationship between PFPS and rearfoot eversion have produced controversial findings [3,4].

One limitation of these studies was that rearfoot motion could not be differentiated from forefoot motion. Modeling the foot as a rigid segment provides little information about foot roll over during locomotors tasks[5].The role of the longitudinal medial arch in PFPS during locomotor tasks is not clear. A multi-segmental foot model may improve information about foot arch mobility during dynamic tasks such as stair descent. Stair descent might be more challenging for PFPS individuals than walking due to the increase in pain that it often causes [6,7].

The aim of this study was to test the hypothesis that individuals with PFPS exhibit a greater static and dynamic medial longitudinal arch angle when compared to controls. The second hypothesis is that individuals with PFPS show a greater excursion of medial longitudinal arch, indicative of greater foot mobility.

METHODS

Stair descent data on two groups of 30 young adult females was collected: 1) 15 participants with PFPS for at least 2 months, who had knee pain in one of the following situations: resisted contraction of the quadriceps, squatting, prolonged sitting, descending or ascending stairs (23.5±6.8 yrs; 65.5±6.8 kg; 165 ± 6.8 cm); 2) 15 healthy controls (CG) similar in age, weight and height with PFPS group (26.1± 7.7 yrs; 61.7± 8 kg; 164± 6.7 cm).

A multi-segment foot model was used to track foot kinematics at 200Hz with a six camera motion analysis system during stair descent [7]. The stair was composed of 5 steps (19 cm in height, 28 cm in length). Each subject performed the stair descending task at 96 steps /min (the cadence was controlled by a metronome). The lower extremity was randomly chosen in the control group. In the PFPS group, the lower extremity chosen corresponded to the painful knee in participants with unilateral pain and to the most painful knee in participants with bilateral pain.A VAS was used to record knee pain intensity before and after stair descent task in PFPS [6].

Data analysis: A MATLAB program was written to calculate maximum value of the medial longitudinal arch angle (MLAA) during a static trial and maximum value of MLAA during the stance phase of the third step of the stair descent task among eight dynamic trials. MLAA is formed between the projections of the line segments of calcaneus posterior surface to the tuberosity of the navicular and the tuberosity of navicular to the head of the first metatarsal [7](see Figure1).
*Statistics:*Unpaired Student's t-test and Cohen's Effect Size were used to test for group differences. Paired t-test was used to compare VAS pain before and after stair descent in PFPS individuals (α= 5%).

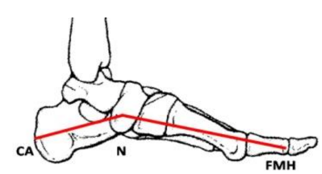

Figure1: Medial longitudinal arch angle (CA=calcaneus posterior surface, N=tuberosity of the navicular, FMH=first metatarsal head)[9].

RESULTS

The maximum value of the medial longitudinal arch angle (MLAA) during static trial was greater in the PFPS group (173^o±6.78) when compared to CG (164^o±11.18) (p=0.002) and the effect size of this difference was very strong (ES=1.0) (Figure 2a). The maximum value of the medial longitudinal arch angle (MLAA) was not different between groups (PFPS=176^o±2.22; CG=175^o±3.25 (p=0.463) and the effect size was weak (ES= 0.27)(Figure 2b).The maximum value of dynamic trial minus maximum value of static trial (DT – ST), MLAA excursion,was smaller in PFPS (3.5^o±7.42^o) than in CG (12^o±10.43) (p=0.042) with an effect size of this difference that was very strong (ES=0.95). Intensity of pain in PFPS individuals was greater after stair descent (2.5±2.48 cm) than it was before the task (0.7±1.25 cm) (p<0.000) with a very strong effect size(ES=1.0).

DISCUSSION

The hypothesis that individuals with PFPS would show a greater static MLAA when compared to controls was confirmed which may be indicative of a lower arch in the PFPS group. A low-arched foot has been associated with the development of knee injuries [8].

The hypothesis that individuals with PFPS would show a greater dynamic MLAA was not corroborated. Dynamic MLAA during stair descent showed very similar values as found for healthy adults during walking. This measure was also very consistent among trials for both CG and PFPS [7].

The difference between dynamic and static MLAA in PFPS was smaller, indicative of less excursion of MLAA when compared to controls. As the intensity of pain was greater after stair descent, the lower excursion of MLAA for PFPS may be associated with a protective pattern [6]. Consequently,the PFPS group may not have used their entire range of MLAA excursion during stair descent due to pain

This study investigated a planar angle of the foot that is clinically relevant for PFPS. A further analysis of 3D kinematic angles may enhance this discussion.

CONCLUSIONS

PFPS showed a lower static medial longitudinal arch and a lower excursion of medial longitudinal arch angle when compared to controls during stair descent.The dynamic longitudinal arch was not different between groups.

REFERENCES

1. Tauton JE et al. *Br J Sports Med*, **36**(2), 95 – 101, 2002.
2. Davis IR, Powers CM. *J Orthop Sports PhysTher*, **40**, 2010.
3. Barton CJ et al. *Gait and Posture* ,**30** , 405-416 , .2009.
4. Barton CJ et al. *Sports Med*, **40**, 377-95, 2010.
5. Powers C Et al. *Foot Ankle Int*.**23**, 634-640, 2002.
6.Aliberti S et al.*Phys Ther in Sport*, **11**, 30-34, 2010.
7. Leardini A et al.*Gait &Posture* . 2007; 25: 453–462
8.Williams DS et al. Clin Biomech, **16**, 341-47, 2001
9.Hamill J, Knutzen KM. *Biomechanical Basis of Human Movement*, Lippincott Williams & Williams, Inc., 2003.

ACKNOWLEDGEMENTS

This study was supported by CAPES Foundation (agency under the Ministry of Education of Brazil) (12466-12-3).

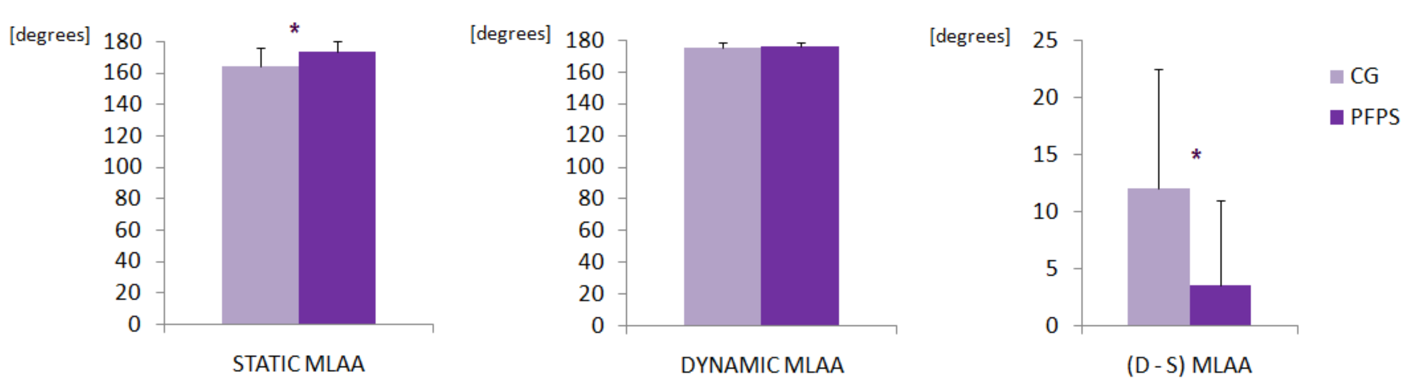

Figure 2: Mean and standard deviation of maximum value of static (a), dynamic (b) and the excursion (c) of the medial longitudinal arch angle (MLAA) between control group and patellofemoral pain syndrome group.*indicates a statistically significant difference.

ALTERED POWER GRIP FORCE DISTRIBUTION AND PHALANX FORCE TRAJECTORY FOR OLDER INDIVIDUALS

Lydia Lambert, Gregory P. Slota, Leah R. Enders, and Na Jin Seo

University of Wisconsin-Milwaukee, Milwaukee, WI, USA
email: lambertl@uwm.edu, web: https://pantherfile.uwm.edu/seon/www/

INTRODUCTION

Individuals 65 years or older accounted for 72.4% of the $185.5 billion increase in health care expenditures due to osteoarthritis from 1996 to 2005 [1]. Knowledge regarding a detailed power grip force profile for older individuals is sparse, even though altered power grip profiles (e.g., increased reliance on certain finger joints) could increase the rate of arthritis development [2] which is the leading cause of disability in the U.S. [3]. The purpose of this study was to determine the effect of aging on 1) normal force distribution patterns across phalanges and 2) phalanx force trajectory deviation during power grip. These power grip characteristics were investigated for their relevance in grip control [4,5] and the potential for development of arthritis [2] for the aging population [6].

METHODS

Thirteen young individuals (age = 25 ± 4 years) and nine older individuals (62 ± 9 years) participated as the younger and older groups, respectively. Subjects performed power grips at the maximum and 50% efforts on a custom-made grip dynamometer (Fig. 1), while proximal-distal shear force (tangential to grip surface) and normal force during power grip were recorded for each phalanx of individual fingers [5]. The entire surface of the grip dynamometer was varied for a rubber or paper surface.

Percent contribution of normal phalanx force was calculated as the percentage of each phalanx's normal force to the sum of all phalanges' normal forces of the hand. Phalanx force trajectory deviation was quantified as the angular deviation of the phalanx force from the direction normal to the cylinder surface (the arctangent of the ratio of the proximal-distal shear force to normal force).

Figure 1: A grip dynamometer recorded each phalanx's proximal-distal shear force (tangential to grip surface) and normal force during power grip.

Phalanx normal force contribution and phalanx trajectory deviation were compared for the two age groups (young vs. old), two effort levels, and two surfaces using ANOVA and Tukey post hoc analysis. Both the percent phalanx normal force contribution and the phalanx trajectory deviation data were non-normal and thus transformed using the 4th root and square root transformation, respectively, for ANOVA.

RESULTS AND DISCUSSION

Older individuals produced significantly greater normal force contribution with the distal phalanx and significantly less with the proximal phalanx compared to young individuals, independent of effort level and grip surface (Fig. 2, post hoc, p<.05). Percent normal force contribution was significantly dependent upon finger, phalanx, the interaction of age group and phalanx, and the interaction of effort and phalanx (ANOVA, p<.05).

Older individuals produced significantly greater phalanx force trajectory deviation with the proximal phalanx compared to young individuals, independent of effort level and grip surface (Fig.3, Tukey post hoc, p<.05). Phalanx force trajectory deviation was significantly dependent upon surface, effort, finger, phalanx, the interaction of age group and phalanx, the interaction of age group and finger, and the interaction of effort and phalanx (ANOVA, p<.05).

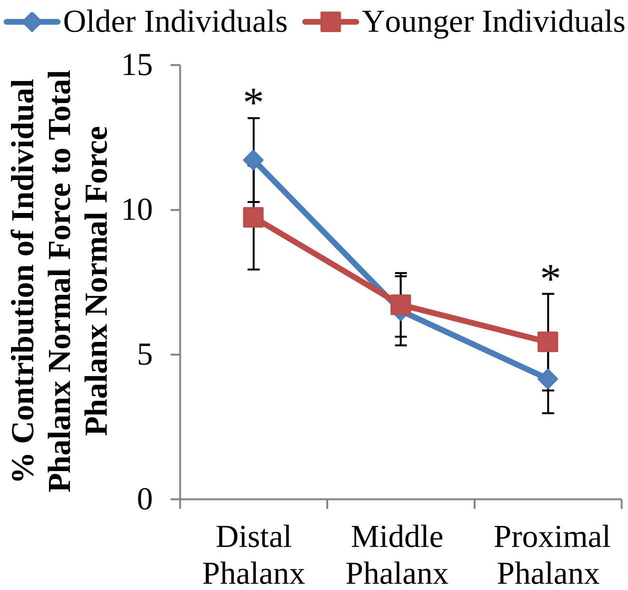

Figure 2: Mean ± SD phalanx normal force contribution significantly differed for older individuals' distal and proximal phalanges compared to younger individuals (finger, effort level, and grip surface pooled) (p<.05).

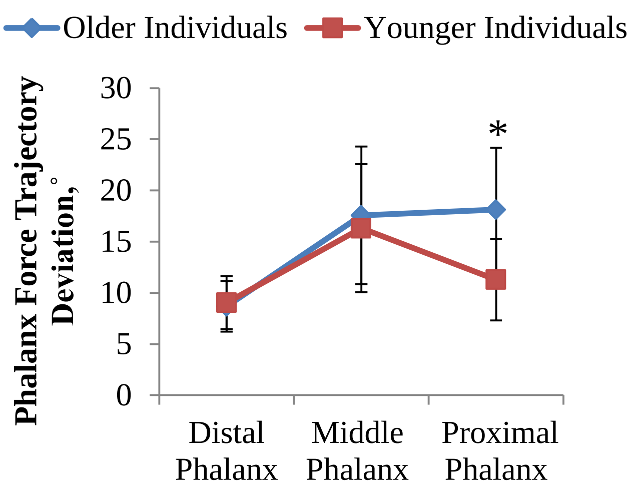

Figure 3: Mean ± SD phalanx force trajectory deviation was significantly greater for older individuals' proximal phalanx compared to younger individuals (finger, effort level, and grip surface pooled) (p<.05).

Older individuals displayed more uneven distribution of phalanx normal forces with increased force trajectory deviation of the proximal phalanx compared to younger individuals. Decreased proximal phalanx involvement and increased phalanx force trajectory deviation could be reflective of age-related weakening of the intrinsic muscles [7] that contribute to force generation at the proximal phalanx [8] and force direction control [7]. Therefore, the extrinsic finger flexor muscles that are less afflicted by age [7] and control more distal phalanges may be used to compensate for the weakened intrinsic muscles and contribute more to the overall power grip force. Consequently, increased distal phalanx involvement for force generation with aging may be associated with increased risk of developing arthritis in the distal interphalangeal joint [2,9].

CONCLUSIONS

Older individuals grip with a more uneven force distribution pattern with a higher force concentration at the distal phalanx and lower force concentration at the proximal phalanx compared to younger individuals. In addition, older individuals have greater grip force trajectory deviation at the proximal phalanx compared to younger individuals. This altered force distribution and trajectory deviation during power grip could be reflective of age-related weakening of intrinsic muscles. From a functional standpoint, high phalanx force trajectory deviation could lead to slippage/dropping of a grasped object from the hand [4]. In addition, increased reliance on the distal phalanx for force generation may be associated with prevalence of arthritis development in the distal interphalangeal joint in older individuals [2,9].

REFERENCES

1. Kotlarz H, et al. *Arthritis Rheum* **60**, 3546-3553, 2009.
2. Radin EL, et al. *Lancet* **297**, 377-379, 1971.
3. Center for Disease Control and Prevention, *MMWR*, **58**, 421-426, 2009.
4. Seo NJ, et al. *Exp Brain Res* **202**, 891-901, 2010.
5. Enders LR, Seo NJ. *J Biomech* **44**, 1447-1453, 2011.
6. Schoeni RF, Ofstedal MB. *Demography* **47**, 5-15, 2010.
7. Cole KJ. *Exp Brain Res* **175**, 285-291, 2006.
8. Long C., et al. *J. Bone Joint Surg.***52A**, 853-867, 1970.
9. Solovieva S, et al. *Rheumatology* **44**, 521-528, 2005.

FINGER ENSLAVING IN THE DOMINANT AND NON-DOMINANT HAND

[1]Luke A. Wilhelm, [2]Joel R. Martin, [1]Mark L. Latash, and [1]Vladimir M Zatsiorsky

[1]The Pennsylvania State University, University Park, PA, USA
[2] George Mason University, Manassas, VA
Email: law326@psu.edu

INTRODUCTION

Patterns of finger force production and finger coordination have been well documented. Force production patterns in multi-finger maximum voluntary contraction (MVC) tasks have been modeled with a neural network [1]. In particular, finger enslaving, the unintentional force production by non-task related fingers, has been consistently observed. Enslaving has been suggested as an indirect measure of dexterity, since lower enslaving would imply a greater ability to move the fingers independently. In addition, the dynamic-dominance theory states that the dominant (D) arm and hand are better suited for dynamic tasks, while the non-dominant (ND) arm and hand are better suited for stabilization tasks [2]. The purpose of this study was to compare enslaving values between the D and ND hands using the neural network approach. Previous work suggested that there are significant, though small, differences in enslaving between the hands [3]. Given the background of the dynamic-dominance theory, we hypothesized that the enslaving effects would be lower in the D hand.

METHODS

Twenty-two right-handed, young, healthy males were tested. Handedness was assessed by the Edinburgh Handedness Inventory, the Grooved Pegboard test, and the Jebsen-Taylor hand function test.

The MVC task was performed by 15 different finger combinations (I, M, R, L, IM, IR, IL, MR, ML, RL, IMR, IML, IRL, MRL, IMRL, where I designates the index finger, M – the middle finger, R – the ring finger, and L – the little finger). Subjects were instructed to produce maximal force with the fingers of a given combination and to pay no attention to the non-instructed fingers.

Neural network analysis resulted in the following equation:

$$[F] = \frac{1}{N}[w][X] + [v][X] \tag{1}$$

where [**F**] is a 4×1 matrix of individual finger forces, N is the number of fingers explicitly involved in the given task, [**w**] is a 4×4 finger connection weight matrix, [**X**] is a 4×1 matrix of neural command values ranging from zero (finger not explicitly involved) to one (finger maximally involved), and [**v**] is a 4×4 diagonal matrix of gain values. For the case when all four fingers are explicitly instructed to press, the equation can be reduced to:

$$[F] = [IFC][X] \tag{2}$$

where [**IFC**] is referred to as the interfinger connection matrix. The diagonal elements of the IFC represent the amount of force produced by the fingers due to direct commands, and the off-diagonal elements represent the amount of force produced due to enslaving effects. The elements of the IFC were normalized by the total four finger force. The sum of normalized, off-diagonal elements was taken to be the enslaving index for a given subject. Enslaving indices for each individual finger were calculated by summing the off-diagonal elements in the appropriate column of the IFC (first column for the index finger, second column for the middle finger, third column for the ring finger, and fourth column for the little finger).

RESULTS AND DISCUSSION

The results of a two-way ANOVA analysis (*hand* × *finger*) showed the index finger to have the lowest enslaving effects, while the ring finger showed the highest enslaving. This agrees with previous enslaving patterns found in the literature. However, no significant difference in enslaving indices was found between D and ND hands (Fig. 1).

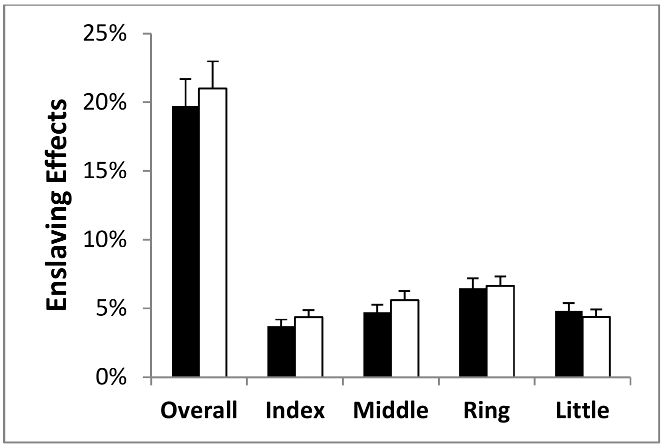

Figure 1: Percent of total force produced during the four finger task due to enslaving effects. Black bars are the D hand, and white bars are the ND hand.

The handedness scores from the Edinburgh Handedness Inventory, the Grooved Pegboard test, and the Jebsen-Taylor hand function test were compared with the enslaving indices with Pearson's *r*. All three tests showed greater hand function in the D hand. However, no significant correlations were found between any of the handedness tests and the enslaving indices.

Some previous work suggested that there are significant differences in enslaving effects between the D and ND hand. However, the reported differences were small, on the order of 2% [3]. In addition, these differences were only found in certain combinations of fingers, not all four fingers acting together. This, in combination with the current findings, suggests that any differences in enslaving effects between the hands are small.

Earlier studies have shown that although enslaving effects are a consequence of both peripheral mechanical coupling and central nervous system command coupling, neural factors play the largest role [4]. Furthermore, given appropriate practice and feedback, enslaving patterns have been shown to change, often in training sessions of no longer than one hour, suggesting that the neural mechanisms controlling enslaving are malleable [5]. Even though the D and ND hands are used differently in everyday tasks, the majority of tasks for both hands require multiple finger coordination as opposed to individual finger movement (e.g. grasping, object manipulation). We hypothesize that this prevalence of multi-finger tasks for both hands leads to similar patterns of enslaving in the D and ND hands.

CONCLUSIONS

Enslaving effects were not found to differ between D and ND hands when using the neural network method of analysis. We hypothesize that, although the D hand shows greater dexterity in functional tests, everyday use does not require extensive finger individuation. This creates similar patterns of enslaving between the D and ND hands.

REFERENCES

1. Zatsiorsky VM, et al. *Biol. Cybern* **79**, 139-150, 1998.
2. Sainburg R, *Exp Brain Res* **142**, 241-258, 2002.
3. Li S, *Human Move. Sci* **19**, 897-923, 2000
4. Latash ML, et al. *Brain Res* **924**, 198-208, 2002
5. Wu Y, et al. *J of Motor Behavior* **44**, 471-478, 2012

ACKNOWLEDGEMENTS

The study was in part supported by NIH grants NS-035032 and AR-048563.

NEUROMUSCULAR CONTROL OF SHOT DISTANCE USING THE DRIVER

Travis Peterson[1], P.S. Requejo[1,2,4], H. Flashner[3], Jill L. McNitt-Gray[1,2]

[1] Department of Biomedical Engineering, [2]Biological Sciences, [3]Aerospace and Mechanical Engineering
University of Southern California, Los Angeles, CA
[4]Rehabilitation Engineering, Rancho Los Amigos National Rehabilitation Center, Downey, CA
email: travispe@usc.com, web: http://dornsife.usc.edu/labs/biomech/

INTRODUCTION

Regulation of linear and angular momentum during the golf swing involves control of the total body center of mass trajectory (CM) in relation to the reaction forces generated during contact with the environment. During the golf swing, the resultant horizontal component of the reaction force (RFh) at each foot creates a moment about a vertical axis passing through the CM that accelerates rotation of the body toward the target. During competition, conditions often require that a player increase or decrease the shot distance when using the driver off the tee.

Previous research indicates scaling the resultant horizontal reaction force (RFh) of either the target and rear legs [2,3,4] can be an effective mechanism for controlling shot distance when using a shorter club (6-iron). A within-club analysis also revealed that regulation of shot distance was achieved in part by increasing the magnitude of the resultant horizontal reaction force without modification in the resultant horizontal reaction force-angle relationships within leg [2,3]. Within player consistency in RFh-angle relationships suggest that regulation RFh would involve selective activation of the same set of muscles activated during a player's preferred swing. In this study, we hypothesized that individual players would regulate shot distance by scaling RFh magnitude by selectively scaling muscle activation levels.

METHODS

Skilled golfers (n=6; handicap < 5, right handed) performed three swings using a driver (Taylor Made adidas golf) under normal swing, plus 10 yards (+10), and minus 10 yards (-10) conditions. Placement of the force plates allowed players to use their preferred address position to hit the golf ball toward the target. Subjects were on average 28.1 (12.4) years old, 1.77 (0.12) m in height, and 78.7 (18.7) kg in body mass. Reaction forces at the artificial turf-plate interface were quantified during each swing using dual force plates (Kistler, 1200 Hz) [5]. Kinematics of the body and club during the golf swing were captured at 110 Hz using reflective markers (MATT, Motion Reality, Inc.). Ball contact was synchronized at the time of club/ball contact using a microphone signal collected simultaneously with the reaction force-time data (t = 0s at ball contact). Activation of lower extremity muscles were monitored using electromyography using surface electrodes (1x1cm^2 Konigsberg, Pasadena, CA). Muscle activation (RMS filtered zero-lag fourth-order recursive Butterworth filter at 10-350 Hz, full wave rectified, and integrated in 20 ms bins) quantified and compared within player (normalized by manual muscle tests). The magnitude and direction of the peak resultant horizontal reaction forces were computed for each foot using reaction forces measured by each force plate during the swing. The interval of interest began at late backswing and ended at the time of ball contact.

RESULTS AND DISCUSSION

Comparison of lower extremity muscle activation patterns revealed that all players amplified muscle activation of target and rear leg muscles in the +10 yard condition compared to the -10 yard condition. This amplification in muscle activation corresponds with increases in RFh in both rear and target legs. During the downswing, posterior hip muscles (RGMax, RGMed, RBF & RSM/ST) of the rear leg were activated to generate anterior directed reaction forces at the feet (figure 2 for the exemplar subject). Anterior muscles (LRF) of the target leg were activated to generate posterior directed reaction

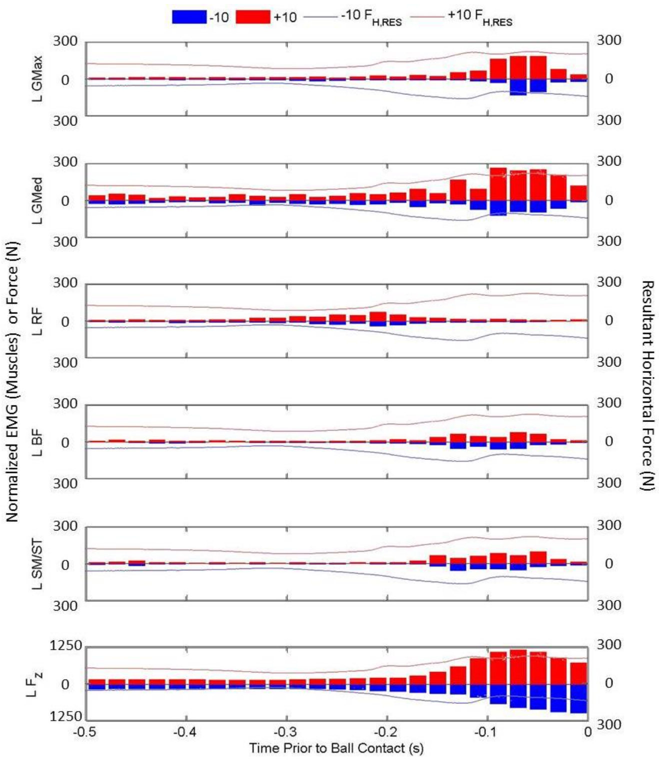

Figure 1: Target leg muscle activation and ground RFs of an exemplary subject for both the -10 (plotted negative) and +10 (plotted positive) yard conditions.

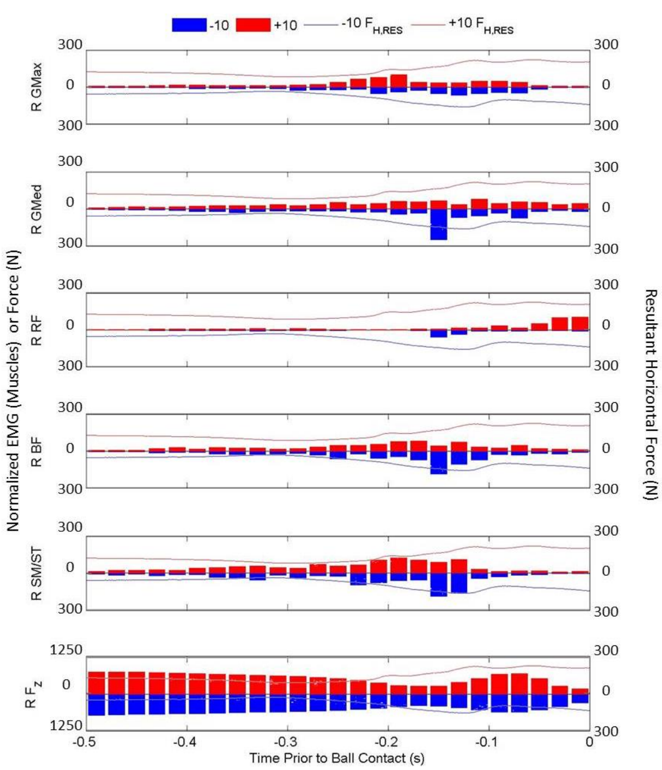

Figure 2: Rear leg muscle activation and ground RFs of an exemplary subject for both the -10 (plotted negative) and +10 (plotted positive) yard conditions.

forces as shown in figure 1 for the exemplar subject. These reaction forces created a force couple that acted to accelerate rotation of the body towards the target as shown in figure 3.

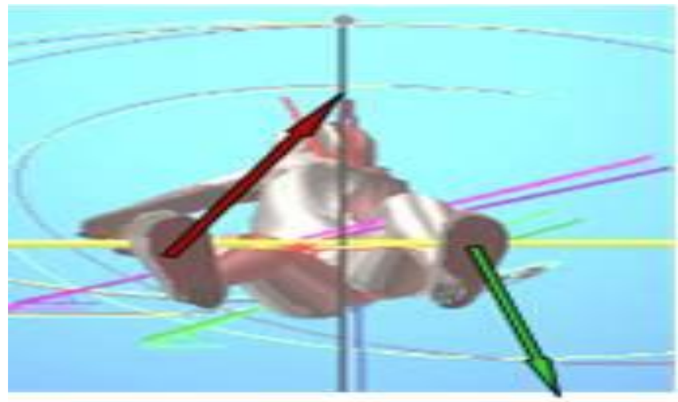

Figure 3: RFhs applied to the target and rear legs of the exemplary subject during the downswing create rotation to the target on the right. View from underneath, looking up.

CONCLUSIONS

Skilled players participating in this study maintained the same pattern of EMG activity, yet selectively scaled muscle activation to regulate reaction forces when modulating shot distance. This subtle, yet consistent regulation of muscle activation corresponding to increases in RFhs (associated with longer shot distances) is expected to provide multiple advantages from both a neuromuscular control and performance perspective.

REFERENCES

1. Mathiyakom W, et al. *J. Biomech*, **39**, 990-1000, 2006.
2. McNitt-Gray, JL et al. *Sports Biomech*, 2012.
3. Zaferiou, AZ et al. *ASB Proceedings*. 2011.
4. McNitt-Gray, JL et al. *ASB Proceedings* 2010.
5. Williams, K & Cavanagh, PR *MSSE* **15**(3), 247-255, 1983.

ACKNOWLEDGEMENTS

Partial funding for this research was provided by TaylorMade-adidas Golf.

A PILOT STUDY INVESTIGATING THE DIFFERENCE IN SENSE OF EFFORT BETWEEN CHRONIC STROKE SURVIVORS AND HEALTHY ADULTS

[1]Tarang K. Jain, [2]Clayton N. Wauneka, [1]Sara Ratzki, [1]Brenda Hozie, [1]Tommy VanTowle, [1]Bret Perry, [1]Grant Swanson, and [1,2]Wen Liu

Department of Physical Therapy and Rehabilitation Science, University of Kansas Medical Center, Kansas City, KS, USA
[2] Bioengineering Program, University of Kansas, Lawrence, KS, USA
Email: tjain@kumc.edu, web: http://www.ptrs.kumc.edu/research/neuromuscular-research-lab/index.html

INTRODUCTION

Past studies of muscle strengthening in healthy adults have reported that greater effort leads to higher gain and that the first significant change occurs in central nervous system as shown by increases in motor unit recruitment rate and firing rate [1]. Muscle weakness has been indicated in past studies as a primary factor for disability after stroke [2]. Intuitively one would expect significant outcome from strength training that uses the similar protocol developed in strength training of healthy adults. However, past studies using strength/resistance training in stroke rehabilitation have reported inconsistent results [3]. Various intensities of resistance have been tried in strength training of stroke survivors, but it is unclear whether there exits an optimal effort level for a specific sub-group of stroke survivors. Therefore, we set forth a study to investigate the effect of different effort levels on the elbow joint torque production and upper limb muscle activation using a sense of effort testing protocol in chronic stroke survivors and healthy adults.

METHODS

Five young healthy subjects (26.4±2.8 years) and thirteen chronic stroke survivors (64.2±6.3 years) > 3 months after stroke were enrolled. The subjects after stroke were classified into sub-categories based on severity of motor impairment (moderate n=4, mild n=9) using the Fugl-Meyer upper limb motor score. The testing of the torque production and upper limb muscle activation occurred in 2 sessions on two different days (Figure 1). During the first session, the maximum isometric voluntary elbow joint torque contraction (MVC) and maximal muscle activation (EMG) for biceps brachii, triceps, and auxiliary muscles (Anterior Deltoid, Middle Deltoid, Posterior Deltoid, Upper Trapezius, Pectoralis Major, and Lattisimus Dorsi) was established for flexion and extension motions on the unaffected side of the stroke survivors and the dominant side of the healthy subjects using the Biodex dynamometer. The subjects were then asked to contract elbow muscles in flexion and extension at different effort levels of MVC (30%, 50%, 70%, and 90%). During the second session, the affected side (stroke survivors) or non-dominant side (healthy subjects) was tested at different effort levels and the subjects were instructed to reproduce the effort levels.

The MVC and maximal muscle activation for biceps brachii, triceps, and auxiliary muscles in both flexion and extension were tested and recorded first. After that, the torque production and muscle activations at different effort levels were tested on both sides and the recorded data was normalized to MVC/maximal muscle activation to interpret the trends in both groups.

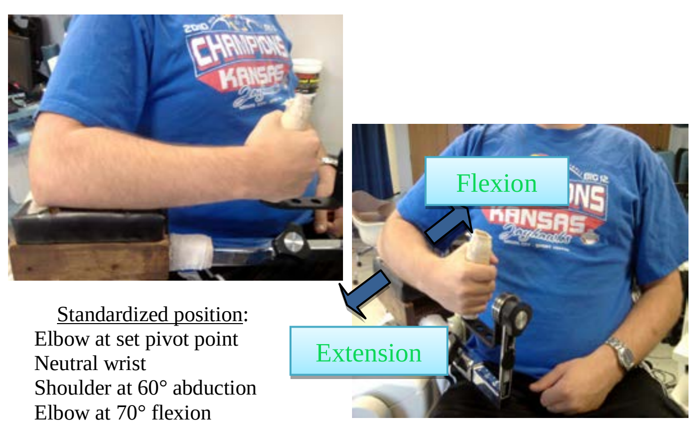

Figure 1: Experimental set-up using Biodex Dynamometer

RESULTS AND DISCUSSION

Healthy subjects demonstrated an expected pattern of linear increases in torque and agonist EMG activation with minimal co-activation of auxiliary and antagonistic muscle groups in isometric elbow flexion contraction (Figure 2). Stroke subjects with mild impairment demonstrated the similar pattern. Stroke subjects with moderate impairment differed from a linear progression in recorded torque and agonist EMG. There were no significant increases in activity levels of antagonist and auxiliary muscle groups as the effort level increased. Similar trends were observed for elbow extension.

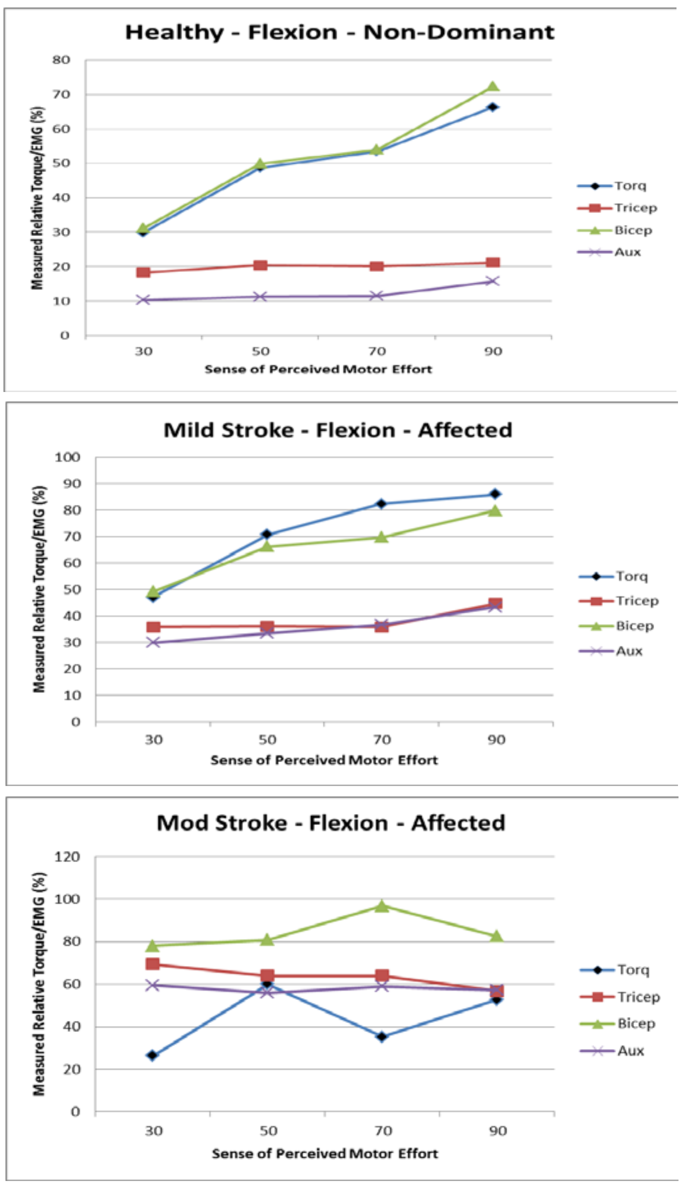

Figure 2: Trends in torque and muscle activation at different effort levels of elbow flexion for healthy and stroke patients.

The results of our study indicate that stroke survivors, depending on their levels of motor impairment, may/may not be able to scale their motor command according to a desired effort level. In this type of task, the stroke survivors with mild impairment showed similar behavior as healthy adults, while individuals with moderate impairment presented with abnormal behavior. This may be due to differences in the severity of disrupted motor neuron pathways after stroke.

We originally hypothesized that inability in accurately scaling force output in stroke survivors with moderate/severe impairment may come primarily from increased activity of either antagonist muscle or auxiliary muscles, as the literature indicated the increased co-contraction and abnormal muscle/movement synergy in stroke survivors in their attempt to compensate for their motor impairment. However, our data indicated no increase in activities of either antagonist or auxiliary muscle groups in company with the increase in effort level. The cause for the abnormal torque production scale in stroke survivors with moderate impairment in our data appeared to be a lack of accurate motor control on the agonistic muscle.

CONCLUSIONS

Our data indicate that the torque production and EMG activation in stroke subjects may differ from healthy subjects, depending on their impairment levels. Motor training with high resistance/high level of effort may benefit stroke survivors with mild impairment, but not necessary beneficial in individuals with moderate/severe impairment.

REFERENCES

1. Moritani T, deVries HA. *Am J Phys Med.* Jun; **58**(3): 115-30, 1979.
2. Wolf SL, et al. *Phys Ther.* Sep; **74**(9): 826-35, 1994.
3. Stein J, et al. *Am J Phys Med Rehabil.* Sep; **83**(9): 720-8, 2004.
4. Cirstea MC, et al. *Exp Brain Res* **151**: 289–300, 2003.

MUSCULAR CONTRIBUTIONS TO KNEE ACCELERATIONS DURING SINGLE-LEG JUMP LANDING IN AUSTRALIAN FOOTBALL PLAYERS

[1]Kristin D. Morgan, [2]Cyril J. Donnelly, and [1]Jeffrey A. Reinbolt

[1]University of Tennessee, Knoxville, TN, USA
[2]The University of Western Australia, Perth, Western Australia, AUS
email: kmorga12@utk.edu web: http://rrg.utk.edu

INTRODUCTION

Australia reports one of the highest rates of ACL injury in the world at 52/100,000 people annually [1, 2]. Approximately 60% of ACL injuries are non-contact injuries, the majority occur during single-leg jump landing (SLJL) [3, 4] when the knee is near full extension, experiences anterior tibial translation and under an external valgus load [5-7]. While previous studies have defined kinematic and kinetic characteristics of ACL injury, the muscular mechanisms behind ACL injury prevention are not well understood as indicated by the 50% increase in ACL injuries over the last decade [8]. ACL injury prevention programs are aimed at altering muscle force and activation patterns to circumvent the ACL injury mechanism; however, they are limited by their inability to assess individual muscle contributions to resist excessive knee loading during movement. This lack of understanding has limited the progress of the current ACL injury research.

Identifying how muscles contribute to movement during SLJL may help to mitigate injury risk. Muscles accelerate joints and determining how they accelerate the knee during landing may be the key to understanding ACL injury prevention. Induced acceleration analysis (IAA) determines the accelerations caused or "induced" by individual muscle forces acting on a model (e.g., contribution of muscle forces to knee accelerations). Hence, the contribution of each individual muscle to frontal, sagittal and transverse plane knee accelerations can be established and determine which muscles are responsible for resisting certain elevated knee accelerations and better understand the cause-effect relationship (i.e., muscle contributions to movement) between muscle forces and joint biomechanics specifically with regard to ACL injury risk.

METHODS

A subject-specific simulation was created in OpenSim of a male Australian football player conducting a SLJL task (Fig.1). Experimental kinematic, kinetic and sEMG data for six muscles (medial and lateral vasti, gastrocnemii and hamstrings) were recorded for each subject. A musculoskeletal model with 23 degrees-of-freedom (dof) and 92 muscle actuators was scaled to represent the size of the subject. The model included a 3 dof knee actuated by muscles and ideal torque actuators. Inverse kinematics and a residual reduction algorithm were used to generate the simulation of the weight-acceptance (WA) phase of SLJL that was dynamically consistent with experimental measured ground reaction forces (GRFs) (peak residual forces and moments < 4N and 8Nm, respectively). Computed muscle control estimated muscle excitations and subsequently muscle forces during landing. Then, IAA was conducted to compute individual muscle contributions during landing [9-11]. For muscles crossing the knee, their contribution to accelerating the knee in the frontal, sagittal, and transverse planes during the WA phase of SLJL were compared.

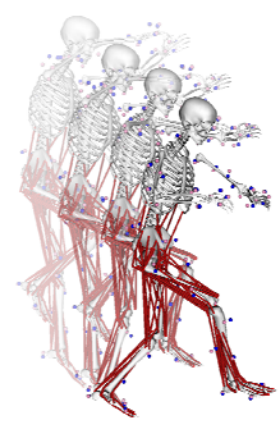

Figure 1: Simulation of SLJL task (model with 23 degrees of freedom and 92 muscle-tendon actuators).

RESULTS AND DISCUSSION

The muscular contributions to knee accelerations varied widely during the WA phase of SLJL (Fig. 2). In the frontal plane, the muscles that contributed to knee adduction based on peak and mean acceleration in descending order were the medial gastrocnemius, vastus medialis and medial hamstring muscles. The lateral gastrocnemius and hamstring muscles opposed adduction. In the sagittal plane, the muscles that accelerated the knee into extension in decreasing order were the vastus medialis, medial hamstring, lateral hamstring and vastus lateralis muscles. The gastrocnemii muscles resisted extension. In the transverse plane, the vastus medialis and medial hamstring muscles mainly contributed to internal knee rotation and the medial gastrocnemius muscle was the strongest contributor to external knee rotation.

The objective of this study was to understand how muscles contributed to accelerating the knee and mitigating injury risk. Thus muscles that opposed knee extension, abduction and also internal rotation could potentially reduce injury risk [6]. The results indicated that strong force production by the medial muscles served to counteract the early force production of the lateral gastrocnemius to adduct the knee and potentially mitigating ACL injury risk. Additionally, the gastrocnemii muscles flexed the knee to oppose the quadriceps muscles and increase knee flexion during landing also potentially reduce injury risk. However, the lateral gastrocnemii role in internally rotating and abducting the knee may mitigate its positive effect on flexing the knee.

This analysis was performed on one individual and future work will analyze additional subjects to determine if these trends are common across all individuals. Additionally, future analyses will investigate the contributions of muscles that do not cross the knee to knee accelerations in the frontal, sagittal and transverse planes.

ACKNOWLEDGEMENTS

We thank Caroline Finch, David Lloyd and Bruce Elliott for providing experimental data (NHMRC grant: 400937).

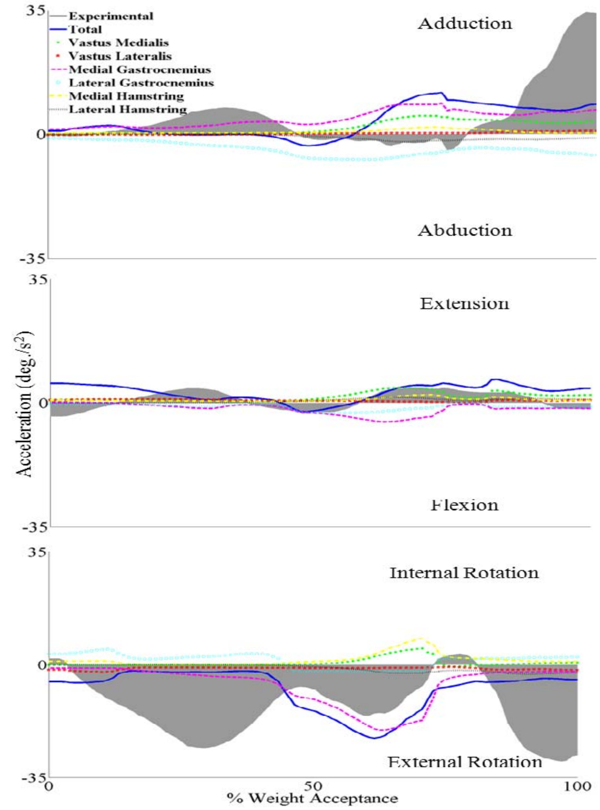

Figure 2: Muscle contributions to experimentally measured knee frontal, sagittal and transverse plane accelerations (shaded regions) for six muscles crossing the knee and the summation of the contributions of the six muscles (solid lines) during the WA phase of SLJL.

CONCLUSIONS

Based on these results, the medial gastrocnemius may be the best target for prevention programs to reduce ACL injury risk as it generated the strongest accelerations to oppose knee abduction and internal rotation. The lateral gastrocnemius was useful as a knee flexor and in this capacity could potentially resist the anterior translation of the tibia; however, its contributions to abducting the knee may diminish its role in lowering ACL injury risk.

REFERENCES

1. Janssen KW, et al. *Scand. J Med. & Sci in Sports* **22(**4), 495-501, 2012.
2. Moses B, et al.*Res in Sports Med*.**20** (3-4),157-70, 2012.
3. Ekegren CL, et al. *J Ortho Sports Phys Ther* **39**, 665-74, 2009.
4. Hewett TE, et al. *Am J Sports Med* **24**, 765-73, 1996.
5. Cochrane JL, et al., *J Sports and Med. in Sports* **10**, 96-104, 2007.
6. Koga H, et al. *Am J Sports Med* **38** (11), 2218-25, 2010.
7. Krosshau T, et al. *Am J Sports Med* **35** (3), 359-67, 2007.
8. Donnelly CJ, et al. *Res. in Sports Med* **20**, 239-62, 2012.
9. Liu MQ, et al., *J Biomech* **39**, 2623-30, 2006
10. Hamner SR, et al. *J Biomech* **43**, 2709-16, 2010.
11. Dorn TW, et al. *Comp Methods in Biomech and Biomed Eng.* **15** (6), 657-68, 2012.

ARM REACHING WITH VIBRATING MANIPULANDUM WITHIN A DYNAMIC ENVIRONMENT

[1]Clayton N. Wauneka, [2]Tarang K. Jain, and [2]Wen Liu

[1]University of Kansas, Lawrence, KS, USA
[2]University of Kansas Medical Center, Kansas City, KS, USA
email: claydn@ku.edu, web: http://www.ptrs.kumc.edu/research/neuromuscular-research-lab/index.html

INTRODUCTION

Feedback, such as vision and proprioception, are utilized to form internal models for human motor learning [1]. Internal models adapt to environments that vary dynamically due to velocity-dependent force fields. Vibration of muscles or tendons of the upper limb degrade proprioception and effect the development of an internal model by causing adaptation to be slower and more variable [2]. Vibration has been applied to upper limb muscles or tendons however, vibration has not been applied to the hand to show if decreased proprioception, due to vibration from the end effector, affects motor learning during reaching tasks.

METHODS

Sixteen subjects (age range – 25-38 years) with no neuromotor disorders enrolled in the study and were randomly assigned to two groups: the no vibration group (NVG) with only a velocity-dependent force field (n=8) or the vibration group (VG) with a velocity-dependent force field and end effector vibration (n=8).

Subjects were instructed to move a manipulandum (InMotion2, Interactive Motion Technologies) from a center point to a highlighted target (Figure 1). The subjects in both groups were exposed to the force field during reaching trials while the VG also experienced an additional end effector vibration with a 15 Hz frequency and 1.6±0.6 mm amplitude. The velocity-dependent force field was of the form

$$\begin{bmatrix} F_x \\ F_y \end{bmatrix} = B \begin{bmatrix} 0 & -1 \\ 1 & 0 \end{bmatrix} \begin{bmatrix} \dot{x} \\ \dot{y} \end{bmatrix}$$

where $\dot{x}$ and $\dot{y}$ represent the hand velocity on the horizontal plane, and B is a scalar gain of 15 Ns/m.

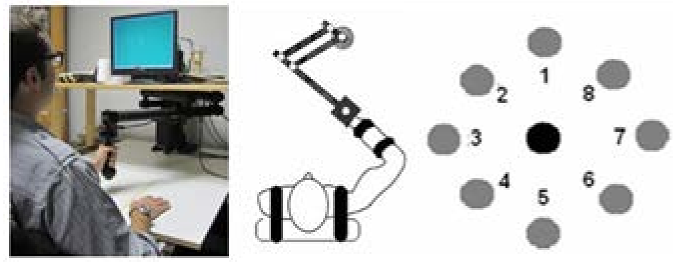

Figure 1: Experimental set-up: shoulder-elbow robot and monitor for limited visual feedback.

One cycle is a completion of reaching movements from the center to all 8 targets. A session had four phases: (1) *familiarization phase*, (2) *baseline phase* (4 cycles) with normal environment, (3) *testing phase* (25 cycles) with dynamic environment based on group assignment, (4) *washout phase* (15 cycles) with normal environment. Visual feedback of handle position was provided on a monitor for 500 ms after a visual cue signaled to begin reaching movement. During the 500 ms time, a velocity-dependent force field was applied and a vibratory motion to the handle depending on the group. Subjects were instructed to make a single, quick, uncontrolled movement toward the target.

Hand position in the horizontal plane was recorded. From the position recording several measures were calculated; normalized path length (nPL), mean absolute distance (MD), and initial angular error (iAE). nPL is defined as the actual path length divided by the theoretical path length and is a measure of efficiency. MD was obtained by the sum of mean absolute distance of each data point from the theoretical path, then divided by the total sample points. MD is a measure of accuracy. The instantaneous direction of hand movement was computed as the difference in angle of the actual path to the theoretical path for the first 150 msec after start and with velocity less than 0.2 m/sec. Recorded data were processed using a Matlab

(MathWorks, Inc.) program and paired t-tests were conducted to verify statistical significance (α=0.05) of change in measures from initial cycles and final cycles (test phase 2nd and 3rd cycles and final 2 cycles, respectively).

RESULTS AND DISCUSSION

The mean values of nPL decreased significantly ($p<0.05$) from initial cycles to final cycles in both groups. (Figure 2(a)). The changes in MD, though both mean values decreased, were not significant for either groups ($p=0.24$ and $p=0.08$, respectively) (Figure 2(b)). The mean value of iAE decreased in NVG group but not significant ($p=0.22$), and increased in VG, again not significant ($p=0.33$) (Figure 2(c)). The reason for the lack of statistical significance in changes in the measured MD could be partially due to a small sample size and low statistical power. A power analysis indicated relative small powers ranging from 14.1% to 25.6%

In nPL and iAE the mean values in initial cycles were significantly less ($p<0.05$) in the NVG group than VG group. The mean values in MD were less in the NVG group than VG group, but the difference was not statistically significant. These results might indicate that the vibration decreased reaching performance in initial cycles under a dynamic environment.

In addition to small sample size, another limitation of the study is the lack of estimation on the amount of contribution from vibration on the hand position measurement, which may have affected the outcome measures of the VG group.

CONCLUSIONS

Our results indicated that both groups in general adapted to the velocity-dependent force field. However, the adaptive behavior may depend on the specific measurement. With additional handle vibration, the adaptations in path length and movement error were in the same direction in both groups. For the initial angular error, the adaptation was negatively affected by the handle vibration. More research with large sample size is needed to further investigate such a complicated issue.

REFERENCES

1. Scmidt, R.A. and T.D. Lee, *Motor control and learning: A behavioral emphasis*, Human Kinetics Publishers, 2005.
2. Bock, O. and M. Thomas, *Human Movement Science*, 2011, **30**(3): 415-423.

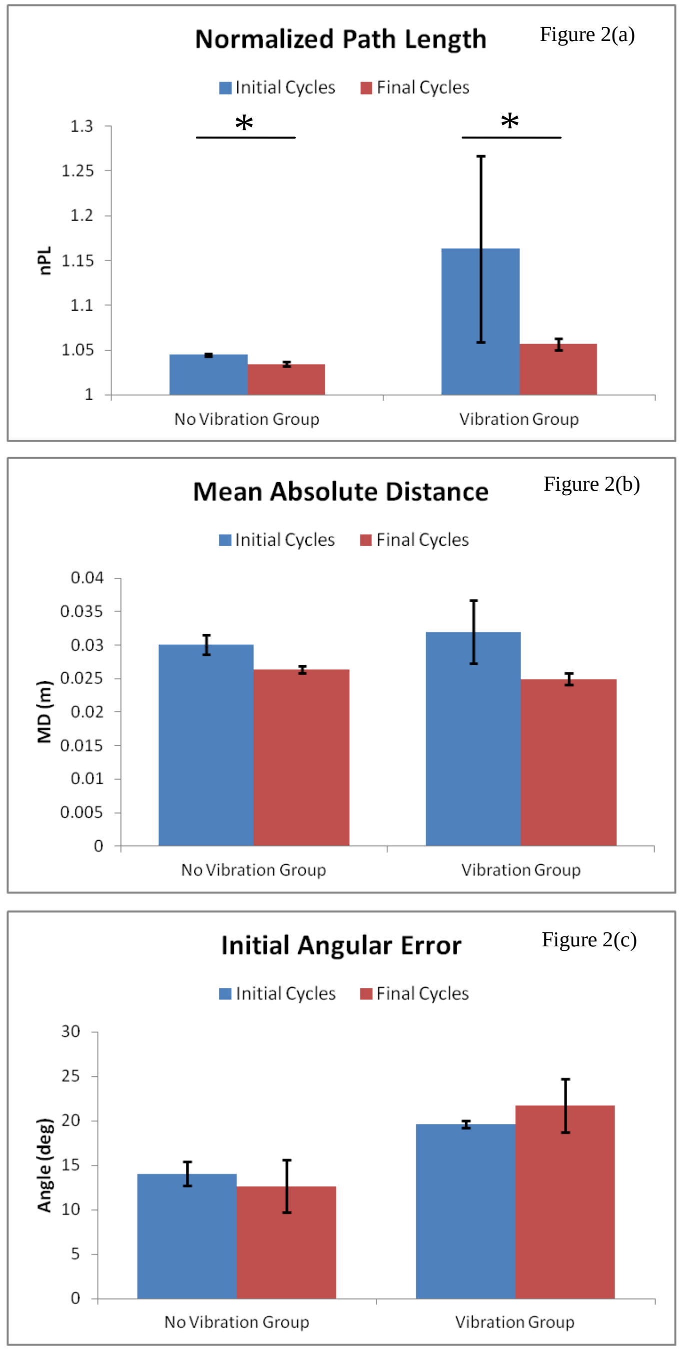

Figure 2: Comparison of initial trials to final trials of test phase for velocity-dependent force field with and without additional vibration at manipulandum. Figure 2(a) is of normalized path length. Figure 2(b) is of mean absolute distance. Figure 2(c) is of angular error.

DECREASED BONE MATERIAL STRENGTH IN SEVERE OSTEOGENESIS IMPERFECTA (OI)

[1,2]Carolyne Albert, [2]Peter Smith and [1,2]Gerald Harris

[1]Orthopaedic and Rehabilitation Engineering Center (OREC), Marquette University, Milwaukee, WI, USA
[2]Shriners Hospitals, Chicago, IL, USA
e-mail: carolyne.albert@marquette.edu

INTRODUCTION

Osteogenesis imperfecta (OI) is a disorder of bone fragility caused by genetic mutations that affect type I collagen. Severity varies widely, from mild to lethal in the perinatal period. The most severe form in children who survive the neonatal period, OI type III, can lead to several fractures over a lifetime.

Bone fragility in OI is believed to result from a combination of bone mass deficiencies and compromised material properties of the bone tissue. Little data, however, is available to describe bone material properties in individuals with OI. At the sub-microstructural scale, nanoindentation studies have found that the elastic modulus (E) of bone tissue is lower in children with severe OI (type III) than in normal controls [1], and that this property is slightly higher in mild vs. severe OI [2]. Bone material properties at the mesoscale, including strength and toughness, however, have not yet been characterized in individuals with OI.

The objectives of the current study were to measure the longitudinal and transverse flexural properties of cortical bone in individuals with severe OI and to compare these values with those of normal adults.

METHODS

Osteotomy specimens were collected from the tibial diaphyses of four adolescents (ages 13.5 ± SD 2.0, three males and one female) with OI type III (OI Group, N=4). These specimens were obtained during routine orthopaedic surgeries at Shriners Hospitals–Chicago, under an approved IRB protocol (Rush University Medical Center #10101309, Marquette University #HR-2167) and with informed consent from the donors. Control group specimens (N=4) were obtained from the mid-diaphyses of four cadaveric tibiae from adults (two males and two female donors, aged 50.5 ± SD 4.4) with no known musculoskeletal conditions.

The specimens were machined into rectangular beams using a low speed diamond saw. Each beam was machined such that its long axis was either longitudinal or transverse to the long tibial axis. A total of 1 to 6 beams per specimen were obtained in each the longitudinal and transverse directions. Beam depth and width were measured with a micrometer. Average depth and width were 628 μm (SD 49 μm) and 1018 μm (SD 43 μm). Beam lengths were 5-6 mm.

The beams were subjected to three-point flexural testing, using a validated method designed to characterize small bone specimens [3]. Yield strength (σ_y) was calculated using the 0.2% strain offset method. E was defined as the slope of the linear region of the flexural stress-strain curve, between 33% and 66% of σ_y. Flexural strength ($\sigma_{f,max}$) was determined as the maximum flexural stress. Toughness was estimated as the area under the stress-strain curve.

For each specimen, longitudinal properties were calculated as the average value over all available beams. The same was done for the transverse properties. Within-group (longitudinal vs. transverse orientation) and between-group (OI vs. control) comparisons were made using paired and unpaired t-tests, respectively.

RESULTS AND DISCUSSION

Representative flexural stress-strain curves for each group and each specimen orientation are shown in Fig. 1.

Within each group, all measured properties were significantly lower for transverse beams than longitudinal ones, p<0.04 (Table 1). In the control group, transverse properties were on average 60-96% lower than longitudinal ones. Similarly, in the

OI group, average transverse properties were 38-53% lower than those in the longitudinal direction.

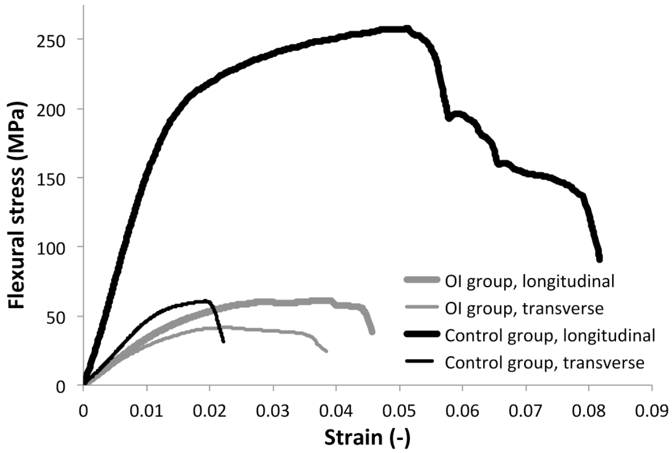

Figure 1: Flexural stress-strain curves for typical specimens in the OI (grey) and control (black) groups. Within each group, longitudinal and transverse specimens are shown as thick and thin lines, respectively.

It has been suggested, based upon nanoindentation data, that the properties of OI bone tissue may be less anisotropic than those of normal bone [4]. The current results, however, demonstrate that, similar to normal bone, OI bone exhibits anisotropic material behavior at the mesoscale.

Compared with the control group, longitudinal properties were significantly lower in the OI group, with average differences of 74-83% (Table 1). Transverse E, σ_y and $\sigma_{f,max}$ were also lower in the OI group by 46-65%. Toughness in the transverse direction, however, was not significantly different between the two groups.

In the control group, E and $\sigma_{f,max}$ were similar to longitudinal values published previously for normal adult cortical bone, e.g., 15 GPa and 220 MPa, respectively [5,6]. For the OI group, however, $\sigma_{f,max}$ was much lower than values reported for normal adolescent bone, i.e., 184-205 MPa [5].

Finally, although the two groups of donors in this study were not age-matched, similar $\sigma_{f,max}$ values have been reported between normal adolescent and adult bones [5]. Therefore, the large decrease in strength observed in the OI (vs. control) group may be attributed primarily to the genetic disorder rather than to age differences between the groups.

CONCLUSIONS

The results of this study provide insight into the mechanisms of bone fragility in OI. More specifically, the results support the assertion that compromised tissue properties play a part in the structural fragility of bones in individuals with OI.

REFERENCES

1. Weber M, et al. *Bone* **39**:616-22, 2006.
2. Albert C, et al. *Clin Biomech* **28**:110-6, 2013.
3. Albert C, et al. *J Eng Med* **227**:105-13, 2013.
4. Fan Z, et al. *J Biomed Mater Res* **79A**:71-7, 2006.
5. Sedlin E and C Hirsch. *Acta Orthop Scand* **37**:29-48, 1966.
6. Currey J and G Butler. *J Bone Joint Surg Am* **57**:810-4, 1975.

ACKNOWLEDGEMENTS

We thank Dr. Sergey Tarima for his assistance with the statistical analysis. This work was supported by NIDRR grant H133E100007 (U.S. ED), and CTSA grant UL1RR031973 (NIH). However, endorsement by the Federal Government should not be assumed. The study was also supported by a research fellowship from Shriners Hospitals.

Table 1: Longitudinal and transverse flexural cortical bone properties for each group. Means (SD).

Group	Orientation	E (GPa)	σ_y (MPa)	$\sigma_{f,max}$ (MPa)	Toughness (MJ/m^3)
OI	longitudinal	3.7 (1.6) *	53 (21) *	67 (25) *	3.0 (0.5) *
	transverse	2.3 (1.4) *†	30 (18) *†	37 (21) *†	1.4 (0.7) †
Control	longitudinal	16.2 (0.7)	205 (6)	261 (10)	17.2 (5.2)
	transverse	6.5 (1.2) †	64 (8) †	69 (7) †	1.3 (0.4) †

* $p \leq 0.05$ compared with control group (between group comparisons)

† $p \leq 0.05$ compared with longitudinal beams (within group comparisons).

DEVELOPMENT OF AGE AND GENDER-SPECIFIC THORAX FINITE ELEMENT MODELS

[1]Samantha L. Schoell, [1]Ashley A. Weaver, and [1]Joel D. Stitzel

[1]Virginia Tech-Wake Forest University Center for Injury Biomechanics, Winston-Salem, NC, USA
email: sschoell@wakehealth.edu, web: www.wakehealth.edu/cib

INTRODUCTION

In motor vehicle crashes (MVCs), thoracic injury ranks second only to head injury in terms of the number of fatalities and serious injuries, the body region most often injured, and the overall economic cost [1,2]. With a growing elderly population, there is a need to understand thoracic injury due to age and gender-specific variations. An image segmentation and registration algorithm was previously used to collect homologous rib and sternum landmark data and quantify age and gender-specific size and shape changes [3]. The purpose of this study was to morph an existing finite element (FE) model of the thorax using thin-plate spline interpolation to accurately depict thorax morphology for males and females of ages 0-100.

METHODS

The thin-plate spline is a smooth function that interpolates the connections between the nodes while minimizing the amount of change in landmark positions. An approach based on Stayton was modified for the purpose of morphing a reference FE mesh of the thorax to create age and gender-specific thoracic FE models [5]. In order to execute the thin-plate spline interpolation, homologous landmarks on the reference, target, and FE model are required**.** Homologous landmarks were previously collected and analyzed using the Generalized Procrustes Analysis to create functions describing the size and shape changes in the ribs and sternum for males and females of ages 0-100 [3]. These functions quantified the target geometry by defining the locations of homologous rib and sternum landmarks for every age and gender. A rigid transformation was performed to align the target geometry with the reference geometry in a meaningful way prior to FE morphing.

The thin-plate spline procedure as detailed by Bookstein involves the calculation of a bending energy matrix, L, and a partial warp score matrix, W, to determine the interpolation function and coefficients to map the reference landmark coordinates to the target landmark coordinates [4]. Subsequently, the calculated interpolation function and coefficients can be applied to other coordinates associated with the reference, i.e. the nodal coordinates of the FE model. Thin-plate spline regularization was employed to relax interpolation requirements so that resulting surface does not have to go exactly through all the control points. Regularization is controlled by the regularization parameter, λ, which was adjusted to achieve the highest element quality [6]. The element quality of the reference and morphed FE models was analyzed by comparing the Jacobian test, warpage test, and aspect ratio test results.

For the purposes of demonstration, the reference sternum and right ribs 1-12 were morphed to represent the anthropometry of a 25 year old male. The reference FE mesh of the ribs and the sternum was taken from the Global Human Body Models Consortium (GHBMC) full human body model [7]. The costal cartilage and intercostal muscles were included in the reference mesh. The sternum was simplified by removing the xiphoid process and removing the left half in order to preserve symmetry. The modified GHBMC atlas mesh used in this demonstration consisted of 52,886 nodes and 38,444 elements. The reference and target ribs and sternum consisted of 24,011 landmarks. The point clouds of the landmarks for the reference and target are shown in Fig. 1 (a) and (b), respectively.

RESULTS AND DISCUSSION

The results of the thin-plate spline interpolation are shown in Fig. 1. The regularization parameter, λ, was set to 0.5 to improve element quality. The results of the Jacobian test, warpage test, and aspect ratio test are shown in Table 1. The element quality of the morphed FE model was comparable to the reference FE model.

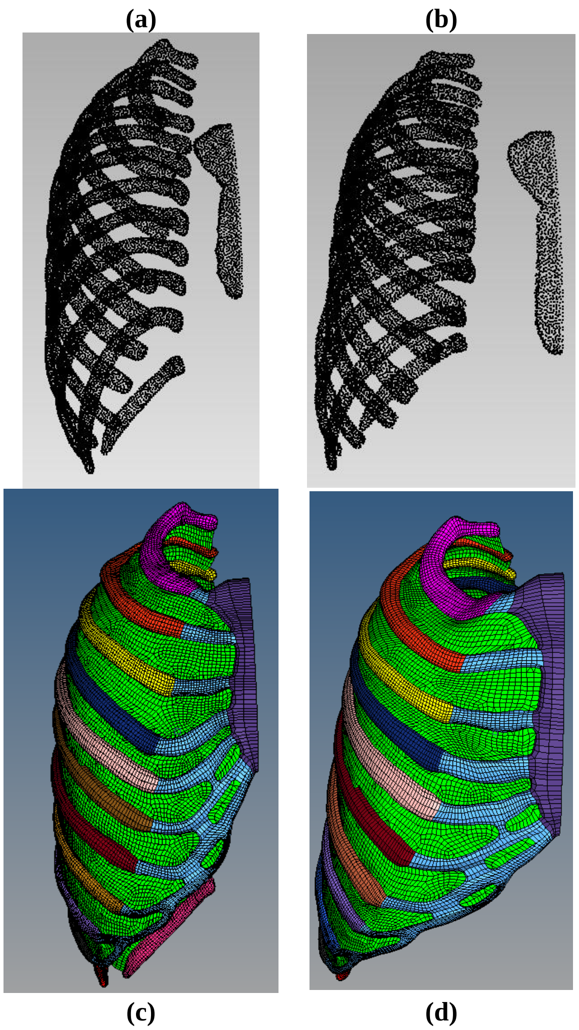

Figure 1: Comparison of point clouds of (a) reference landmarks (b) target landmarks (age 25 male) and FE models of (c) GHBMC reference and (d) morphed age 25 male.

CONCLUSIONS

A morphed age and gender-specific FE model of the thorax was developed using thin-plate spline interpolation. Thin-plate spline procedures generate smooth interpolation functions which transform an existing three dimensional mesh to a new geometry. The GHBMC thorax model was used as the reference mesh and the ribs, sternum, costal cartilage, and intercostal muscles were morphed accordingly based on the homologous landmark data for the ribs and sternum. The development of these age and gender-specific FE models of the thorax will lead to an improved understanding of the complex relationship between thoracic geometry, age, gender, and injury risk.

REFERENCES

1. Cavanaugh JM. *Accidental Injury: Biomechanics and Prevention*, New York, USA, 2002.
2. Ruan J, et al. *Stapp Car Crash* **47**, 299-321, 2003.
3. Weaver AA, et al. *Enhanced Safety of Vehicles Conference Proceedings*, 2011.
4. Bookstein, FL. *Morphometric Tools for Landmark Data: Geometry and Biology*, Cambridge, 1991.
5. Stayton, CT. *Evolution* **63**, 1348-1355, 2009.
6. Donato G, et al. *Computer Vision-ECCV*, 21-31, 2002.
7. Manual- Global Human Body Models Consortium (GHBMC) M50 Occupant Model, 2011.

ACKNOWLEDGEMENTS

Funding was provided by the National Highway Traffic Safety Administration.

Table 1: Morphing and element quality results.

	Jacobian	Aspect Ratio	Warpage
GHBMC Reference – 3D Elements	0.30 to 0.996	1.06 to 13.65	0.278 to 101.75
GHBMC Reference – 2D Elements	0.41 to 1.00	1.00 to 5.17	0.00 to 74.14
Male- Age 25 (λ=0.5) - 3D Elements	0.29 to 0.997	1.06 to 13.38	0.253 to 111.67
Male- Age 25 (λ=0.5) - 2D Elements	0.40 to 1.00	1.02 to 6.10	0.00 to 75.92

In Vitro Fixation Tests Utilizing an Adjustable Bone Plate

[1,2]Thomas M. Cervantes, [2,3]Alexander H. Slocum, Jr., [1]Rajiv Gupta, [1]Edward B. Seldin

[1]Massachusetts General Hospital, Boston, MA, USA
[2]Massachusetts Institute of Technology, Cambridge, MA, USA
[3]Marshall University School of Medicine, Huntington, WV, USA

INTRODUCTION

An adjustable bone plate intended for use in repairing mandibular fractures has previously been shown to be mechanically equivalent to existing bone plates [1]. Here, preliminary evaluation of the functional range of the plate, seen in Figure 1, is described in the form of an *in vitro* fracture repair test. Computed Tomography (CT) imaging is used to assess the functional range of the plate, as well as the gap between fracture segments before and after deformation.

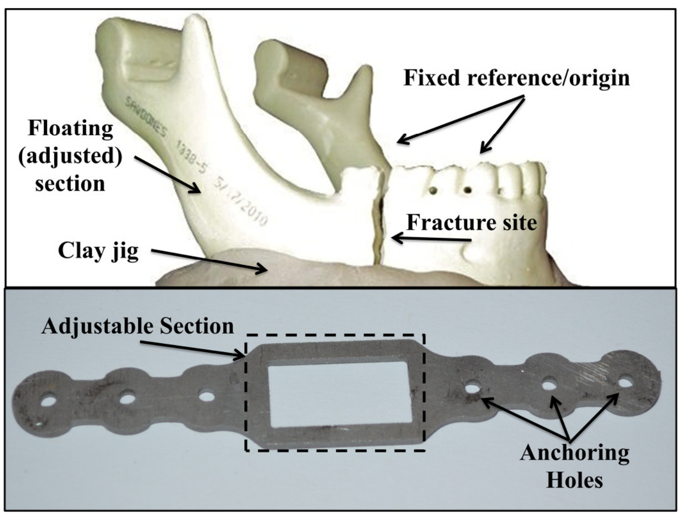

Figure 1: Clay jig for positioning fracture segments and applying the bone plate before deformation (top); stainless steel adjustable bone plate fabricated with waterjet technology (bottom).

Current practice in oral and maxillofacial surgery has developed to rely on Computed Tomography, especially when executing complex facial reconstructions to repair damage from trauma or congenital anomalies [2]. The current study seeks to demonstrate the use of CT in evaluating the deformation of an adjustable bone plate when it is used to repair a simulated mandibular fracture.

METHODS

Seven radiopaque markers are applied to different segments of a pre-fractured synthetic mandible, available from Sawbones® [3]. The markers allow for definition of an origin as well as the location of the segments in space with the CT scanner. Three are used for each segment to define a plane, and the origin is placed on the contralateral mid-ramus. Figure 2 shows an image of the mandible with a deformed bone plate attached, as well as the 7 markers and the respective planes they create.

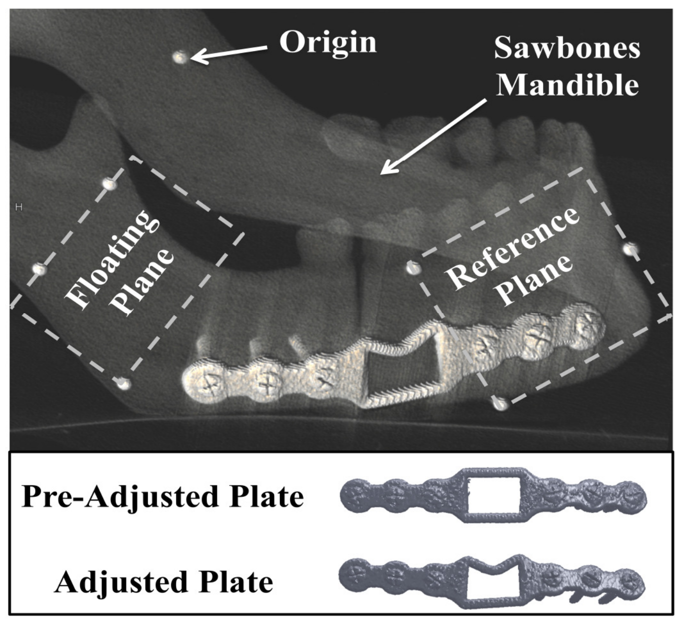

Figure 2: Volumetric CT scan showing the origin, reference plane, and floating plane (top); before and after scans of the adjustable bone plate (bottom).

An un-deformed adjustable plate was first applied to two segments of a synthetic mandible with a total fracture of the body between the first and second molar teeth on the right side. The two fracture segments were placed in a clay jig designed to enable repeatable relative positioning, and which simulated an angle encapsulating with the sagittal plane as well as a rotation about the A/P axis of the mandible. This positioning resulted in a gap between the superior sides of the fracture segments which was on the order of 2.5 mm. The inferior surfaces of the fracture halves remained in contact, resulting in an angular offset on the order of 6.5^{o}.

The plate was then contoured to the surface of the segments by EBS, holes were drilled, and trans-cortical screws placed in a manner similar to a typical ORIF procedure. The “repaired” mandible was then removed from the jig, and an initial volumetric image set was obtained using a Siemens SOMATOM Definition Flash CT scanner (Siemens, Munich, Germany). This was used to create a three dimensional (3D) reference configuration of the bone plate-mandible system prior to deformation.

Next, the “repaired” mandible was removed from the CT scanner, and deformations applied to the plate by EBS to reduce the apparent misalignment between the fracture segments, and bring the two sides into union. Subsequent re-imaging of the mandible demonstrated the proximity of the two segments to one another once the plate is deformed, as seen in Figure 2. The relative motion between the segments is then measured via a second volumetric CT image set.

Each data set was introduced as a DICOM file directory into Slicer 4 (3D Slicer, Boston, MA) to create an STL file of the bone plate and the markers. This was then imported into SolidWorks™ (Dassault Systems, Waltham, MA) for geometrical deformation analysis. First, the reference planes were compared to validate that their position did not change relative to the origin. The origins for the “normal” and “repaired” mandibles were constrained to be coincident, and the reference planes were constrained to be parallel. Translational movement of the reference plane before and after repair adjustment was established by measuring the distance between the centroid of the three fiducial markers that define the plane. Rotational movement was established by measuring the angle between vectors normal to the reference planes. The same procedure was applied to measure the translational and rotational changes of the floating planes.

RESULTS AND DISCUSSION

The results of this study are seen in Table 1, which shows the magnitudes of the translational and rotational adjustments of the reference plane and floating plane.

Table 1: Bone plate adjustment motions

Plane	Translational adjustment	Rotational adjustment
Reference	1.00 mm	0.74^{o}
Floating	6.94 mm	7.31^{o}

CONCLUSIONS

The results demonstrate that the adjustable bone plate has a respectable usable range; in this experiment it was able to reduce a malocclusion on the order of a few millimeters down to less than a millimeter. The methods presented herein will be used to conduct further tests on different deformation types; additional testing should also include static evaluation of the strength of the deformed plates after imaging. Currently, the deformations are similar to those evaluated in previous work by the authors [1].

REFERENCES

1. Cervantes, T. M., Slocum, Jr., A. H., Seldin, E. B., "Design and Experimental Evaluation of Adjustable Bone Plates for Mandibular Fracture Fixation", Journal of Biomechanics, January 2012, Vol. **45**:1, pp. 172-78.
2. Orentlicher, G., Goldsmith, D., Horowitz, A., “Applications of 3-Dimensional Virtual Computerized Tomography Technology in Oral and Maxillofacial Surgery: Current Therapy”, J Oral Maxillofac Surg, **68**:8 (2010) 1933-59.
3. Mandible with fracture, Part # 1338-5, Sawbones, Vashon, WA 98070. Online URL: www.sawbones.com/products/product.aspx?57.

ACKNOWLEDGEMENTS

The authors would like to acknowledge Irene Si Ming Wang for her assistance with organizing time on the scanner to conduct these experiments; and Ken Stone and the MIT Hobby Shop for providing waterjet access to cut the bone plates.

A NOVEL AUGMENTED REALITY SIMULATOR FOR TEACHING WIRE NAVIGATION SKILLS IN TREATING INTERTROCHANTERIC HIP FRACTURES

Brian Johns, Geb Thomas, Jenniefer Y Kho, Matthew D Karam, J Lawrence Marsh, and Donald D Anderson

The University of Iowa, Iowa City, IA, USA
email: Brian-Johns@uiowa.edu

INTRODUCTION

Standard surgical repair of an intertrochanteric fracture, the most common hip fracture, requires accurate placement of a wire across the fracture using static fluoroscopic images. Wire navigation is fundamental to a number of orthopedic procedures. Directing and advancing the wire in the correct plane relies on both visual-spatial and psychomotor dexterity skills [1]. Underdeveloped skills cause substandard wire positioning increasing fracture fixation failure rates [2].

Few practice methods exist for perfecting wire navigation skills outside the operating room. Completing the task in an artificial hip model, with radiopaque surrogate bone models and a C-arm fluoroscopy unit is the most common practice. Unfortunately, C-arm fluoroscopes are expensive, difficult to schedule, and expose trainees to potentially avoidable radiation. The few virtual orthopaedic simulators in existence use force-feedback devices in an attempt to simulate realistic drilling [3-5].

The augmented reality wire-navigation simulator (Fig. 1) combines real drills, wires, and surrogate bone models with virtually generated, radiation-free fluoroscopic images. Trainees navigate a wire from the lateral femoral cortex, through the femoral neck, in order to end within 5mm of the articular surface within the femoral head. The simulator exercises drilling dexterity, fluoroscopic interpretation, and visual-spatial wire navigation skills.

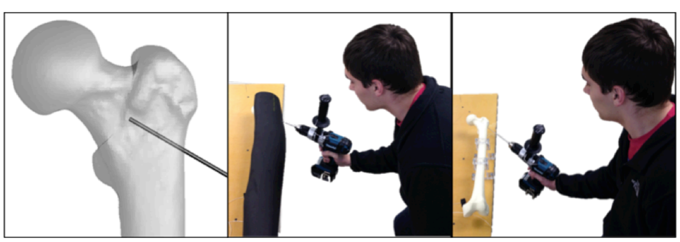

Figure 1: Trainees use virtual fluoroscopy (left) to complete wire navigation with (middle) and without (right) a visually obstructed view of the artificial femur.

METHODS

The simulator hardware consists of four major components: a personal computer, an artificial left femur (Sawbones Part No. 1129), a battery-powered portable electric drill, and two Ascension 3D Guidance trakSTAR 6-DOF electromagnetic tracking sensors. One sensor, attached to the bone, tracks the position and orientation of the femur. Simultaneously, the sensor connected to the drill tracks the advancement of the wire into the artificial femur.

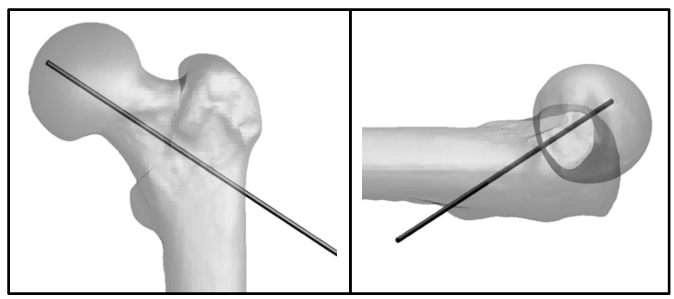

Figure 2: Sample views of virtual fluoroscopy showing AP (left) and lateral (right) views.

The computer generates virtual fluoroscopic images from two standard views used in this procedure: the anteroposterior (AP) and lateral view (Fig. 2). The software produces an AP or lateral view upon the trainee's request. Calibration techniques map the real-world environment to simulated fluoroscopy; ensuring actual movements of the wire correspond to the simulated images. The simulator saves and timestamps each image, while recording a continuous record of the wire positions throughout the exercise. Trainees review the accuracy of their entry and tip locations by rotating a 3D model of the wire and bone, augmented with an overlay of the optimal entry and ending positions (Fig. 3).

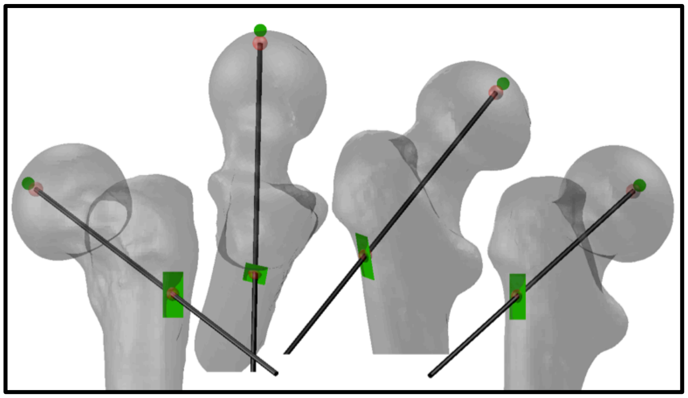

Figure 3: Geometric representation demonstrating the 3D model feedback to the trainees.

Six first-year orthopaedic residents, one third-year orthopaedic resident, and one expert surgeon completed three consecutive trials on the wire-navigation simulator. Before and after, the six first-year residents also completed a wire-guided training task with a C-arm and radiopaque surrogate bone models. Participants completed a survey pertaining to their individual experience.

The experiment tested three hypotheses:

1. Construct validity: The simulator can discriminate between levels of expertise.
2. Face validity: Subjects will report the simulator is realistic.
3. Trainees will report practicing on the simulator would improve their intraoperative skills.

RESULTS AND DISCUSSION

The team summed the standardized tip-apex distance (i.e. wire tip accuracy), number of fluoroscopic images, and accuracy of the entry point in the lateral cortex to create a composite final score. The entry location of one of the 24 trials was not in the lateral femoral cortex resulting in omission from the overall composite calculation.

The expert orthopaedic surgeon earned three out of the four top composite scores, exceeding the participant pool by an average of 1.00 standard deviations on each subcategory. Two out of the three trials for the third-year orthopaedic resident landed in the top five of all trials. The third trial ranked eighth out of the 23 trials. The worst resident trial averaged 1.06 standard deviations below the mean on each of the three scoring metrics. This preliminary data shows the simulator discriminates experienced surgeons from inexperienced residents, thus establishing grounds for construct validity.

The questionnaire contained three questions involving the realism of the simulator. Scores for realism ranged from one to five, with five being the most realistic. Questions concerned the realism of the virtual fluoroscopy, the realism of drilling of the artificial bone, and the overall simulator realism. Overall, subjects rated the simulator realistic (mean = 3.83), with the virtual fluoroscopy being slightly more realistic (mean = 4.17) than the drilling of artificial bone (mean = 3.67). Furthermore, 100% of participants agreed simulator practice would improve intraoperative skills for placing a wire in the femoral head during hip fracture surgery.

CONCLUSIONS

The composite scores of the experts and novices support the simulator has construct validity; though establishing the generality of this finding requires more participants. The experiment also supports the face validity of the simulator, with the same limitation on generality. These initial positive results forecast a worthy future and merits more trials to further the validation of the simulator.

REFERENCES

1. Atesok, K, et al. *J Am Acad Orthop Surg*. **20**, 410-422, 2012.
2. Herman A, et al. *Injury.* **43**, 856-863, 2011.
3. Tillander, B, et al. *Medical Teacher.* **26**, 189-191, 2004.
4. Tsai, M-D, et al. *Comput Biol Med.* **37**, 1709-1718, 2007.
5. Vankipuram, M, et al. *J Biomed Inform.* **43**, 661-669, 2010.

ACKNOWLEDGEMENTS

This project was funded (in part) by a National Board of Medical Examiners® (NBME®) Edward J. Stemmler, MD Medical Education Research Fund grant. Grants from the Orthopaedic Research and Education Foundation and from the Orthopaedic Trauma Association provided additional support.

Isokinetic Knee Torque in Early and Advanced Parkinson's disease: Relation to Physical Function

[1]Gurpreet Singh, [2]Kelly Lyons, [1]Wen Liu, [2]Rajesh Pahwa, and [1]Neena Sharma

[1]Department of Physical Therapy and Rehabilitation Sciences, University of Kansas Medical Center, KS, USA
[2]Department of Neurology, University of Kansas Medical Center, KS, USA
e-mail: gsingh2@kumc.edu, web: http://healthprofessions.kumc.edu/programs/physical_therapy/research/neuromuscular-research-lab/corr-lab.html

INTRODUCTION

Studies of isokinetic muscle testing have shown that muscle weakness is prominent in the more affected lower extremity and associated with difficulty in sit-stand transition in patients with Parkinson's disease (PD)[1,2]. Most past studies, however, are limited in assessing strength of knee extensors only, while ignoring the possible involvement of knee flexors in gait and balance problems. Furthermore, most of the studies used either less than 30°/sec or more than 90°/sec of isokinetic speed in testing their subjects. Considering that individuals with PD are generally older and walk with reduced speed due to gait and balance difficulties, a testing speed between 30°/sec and 60°/sec may best represent the lower limb speed in their daily activities. More importantly, past studies have not addressed the effect of the duration of PD disease that may alter muscle strength due to immobility or lack of activity over a relatively long time[2]. The objective of the present study was to assess changes in isokinetic knee strength in PD patients with various disease durations.

METHODS

Twenty people (15 males and five females; mean age 56.15± 6.7) diagnosed with PD were enrolled. Nine healthy adults (four males and five females; mean age 51.8±6.64) were also recruited to serve as controls. The participants with PD were divided into two groups, those with PD diagnosis less than 5 years and those with PD diagnosis for 5 years or longer. All PD patients were Hoehn & Yahr stage I-III, independently mobile with or without an assistive device. Physical function was assessed using the Timed Up and Go (TUG) test. All PD participants underwent isokinetic testing, while they were "ON" medication. The Cybex 3000 dynamometer (Figure 1) was used to assess isokinetic knee flexion and extension torque using speeds of 30°/sec and 60°/sec. The participants were instructed to move their leg between 0 and 90 degrees, three times as quickly as possible. The testing was conducted on both sides. All three trials were collected one after the other without any rest. A rest period of 5 seconds was given between the two different speeds. Two primary variables were analyzed: the peak value of muscle torque and time to peak torque. Analysis of Variance was used in data analysis, followed by post-hoc analysis if a significant difference was found.


Fig. 1: Cybex 6000 dynamometer

RESULTS AND DISCUSSION

We found significant differences in the flexion torque both at 30°/sec and 60°/sec velocities in more affected side ($p = 0.01$; $p = 0.01$) as well as in the less-affected sides ($p = 0.03$; $p = .02$) between the three groups (Fig 2). The post hoc analysis indicated that two PD groups were not significantly different in those measures.

Time to peak was significantly different among groups (Fig 3) for the more affected side in extension at 30°/sec ($p =0.022$) and the less affected side in extension at both 30°/sec ($p = 0.043$) and 60°/sec ($p = 0.03$). The post hoc analysis identified the significant differences between the two PD groups for more affected side time to extension at 30°/sec (MATE30), less affected side time to extension at 30 and 60°/sec (LATE30,LATE 60) ($p = 0.022$, $p = 0.043$, $p = 0.030$). The peak isokinetic torque was significantly negatively correlated with TUG for some of the outcome in PD groups described in the table. The strength of lower limbs is a major factor in mobility status. Previous studies have indicated muscle weakness in PD patients mostly in extensor muscles, tested under either at very low speed such as 5-30°/sec or high speed 90 - 180°/sec. Durmus[3] reported muscle weakness in hip flexors. Hip flexors are the major accelerators during swing phase of gait. The difficulty in individuals with PD with gait initiation might be related to hip flexor weakness. In our study, we found that three groups were significantly different in flexor strength at both 30°/sec and 60°/sec. This is in accordance with some previous studies which indicated muscle weakness in knee flexors of PD patients as compared to controls.

In our study, we find that isokinetic muscle strength in extension at 30°/sec and flexion at 60°/sec was significantly different between the more affected sides as compared to less affected side. Our results are comparable to the previous studies, indicating strength differences at higher velocities.

The time to reach the peak torque has been reported to be increased in PD as compared to controls. We find significant differences in the time to peak torque in extension at 30°/sec on more affected side and extension at both 30 and 60°/sec on the less affected side, when comparing our three groups. Additionally we found that time to reach the peak torque was significantly different between the more affected side and the less affected side, with the PD patients taken together from the two PD groups.

Several studies have looked at the relationships between knee extensor strength, postural stability, and functional task performance in elderly as well as disabled populations and suggest that decrease in muscular fitness associated with aging may lead to decreased postural stability and increased fall risk. We found that there was a significant negative correlation between the extension as well as flexion torque for the less affected side but not for the more affected side (Table 1).

CONCLUSIONS

Although muscle strength decreases in the lower extremities in PD, we did not find any differences in muscle strength in individuals with less than or more than five years of PD diagnosis. The evaluation of isokinetic muscle strength, time to peak torque and its relationship with functional activities have greater implications for treatment and designing rehabilitation programs for these individuals. However, it is suggested that more studies with emphasis on both types of strength testing that is isometric and isokinetic and various velocities and looking at the relationship of strength with function are needed to answer specific questions related to individual needs of these patients.

REFERENCES

1. Pedersen SW et al. *Scand J Rehabil Med.* Jun 1997.
2. Nogaki H et al. *Acta Neurol Scand.* Mar 1999;99(3)
3. Durmus B et al. *J Clin Neurosci.* Jul 2010;17

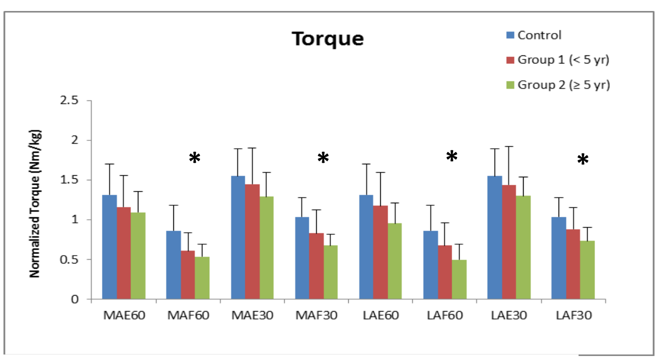

Fig. 2: Isokinetic Strength Test: Comparison of 3 groups

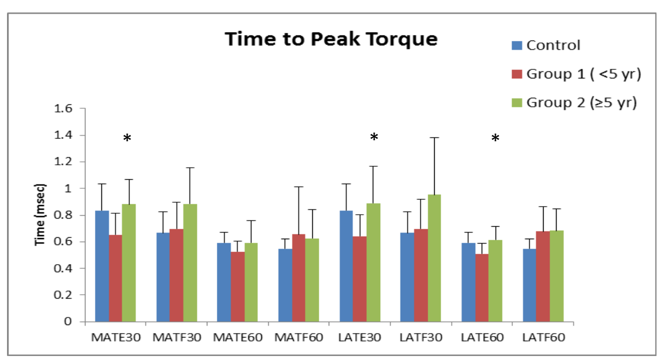

Fig. 3: Time to peak torque

	MAE30	MAF30	MAE60	MAF60	LAE30	LAF30	LAE60	LAF60
Group 1 (< 5 yr)	- 0.426	- 0.599	-0.541	- 0.713*	- 0.711*	- 0.822*	-0.784*	-0.827*
Group 2 (≥ 5 yr)	-0.482	- 0.485	- 0.565	- 0.644*	- 0.245	- 0.663*	- 0.588	- 0.826*
Control	-0.134	- 0. 154	- 0.169	- 0.153	- 0.134	- 0.154	- 0.169	- 0.153

Table 1: Correlations between peak knee torque and TUG

MAE30 & MAF30: More affected side extension and flexion at 30°/sec, MAE60 & MAF60: More affected side extension and flexion at 60°/sec
LAE30 & LAF30: Less affected side extension and flexion at 30°/sec, LAE60 & LAF60: Less affected side extension and flexion at 30°/sec

SUBJECT SPECIFIC MULTI-BODY MODLES OF THE HUMAN KNEE; DESIGN TECHNIQUES AND EXPERIMENTAL VERIFICATION

[1]Matthew G. deBock, [2]Rena F. Hale and [2]Roger V. Gonzalez

[1]LeTourneau University, Longview, Texas, USA
[2]University of Texas at El Paso, El Paso, Texas, USA
email: rvgonzalez@utep.edu, web: biomechanics.utep.edu

INTRODUCTION

Early onset joint degeneration and osteoarthritis (OA) have been associated with abnormal knee kinematics resulting from Anterior Cruciate Ligament (ACL) injuries [1]. While ACL reconstruction surgeries often restore knee function, they have not been shown to avert early onset of OA. A better understanding of joint kinematics and intersegmental forces in the knee might provide insight into improved reconstruction and injury prevention techniques of the ACL. Computational models able to accurately predict knee contact mechanics during movement will increase understanding of healthy and ACL deficient knee mechanics [2]. While finite element (FE) models have been created to this end, computational and development costs are excessive. Multi-body model simulations offer a shorter computational processing time than FE simulations [3]. Experimentally verified multi-body knee models are an important preliminary step in developing computationally efficient knee models for future use.

METHODS

Two subject specific multi-body models were developed in MSC Adams™ using knee geometries obtained from processed Magnetic Resonance Images (MRIs). Tibial, femoral, and patellar bones and cartilages, the medial, lateral, and cruciate ligaments, and the menisci were included in the model. Innovative techniques were applied to the design of the tibial cartilage, the ligaments, and the meniscus in order to better represent anatomical knee biomechanics.

Tibial cartilage was developed by dividing up the geometry into square sections which were then rigidly connected to each other [3]. Division of the cartilage allows for tibial plateau pressures to be observed following data processing (Fig. 1).

Medial and lateral meniscus geometries were horizontally split and radially sectioned (Fig. 1). Horizontally splitting the meniscus was a new technique which allowed for vertical compression of the meniscus. Connections between adjacent sections were defined using splines to replicate viscoelastic properties of the meniscus. Splines were created using Young's modulus values [4].

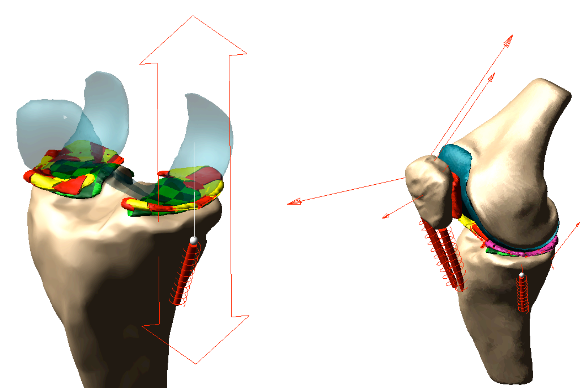

Horn insertions were approximated from MRI images and each was represented by two nonlinear springs [5].

Figure 1: Model shown with MCL wrapping emphasized (left) and with simulation forces (right).

Medial and lateral ligaments were innovatively modeled as a wrapping object attached by a stiff spring and a nonlinear force in Adams/View with a contact force defined between the object and the bone geometry (Fig. 1). Force was defined according to equations defined by Bloemker *et al* and was assumed to act equally throughout the length of the ligament [6]. Ligament length was defined as the total of the ligament sections. Cruciate ligaments without wrapping objects were modeled by the same equation.

Validation of the models against experimental data was performed using a six degree-of-freedom dynamic cadaver knee simulator [7]. Dynamic muscle forces were applied as described by Hale [7]. Hip and ankle positions were applied according to data acquired via VICON™, and a Tekscan™ force sensor placed on the tibial plateau acquired pressure data [7]. Muscle and position data from the fixture experiments were then applied to the corresponding subject specific multi-body model and used to run a simulation in Adams/View. Intersegmental force from the simulation was then compared to corresponding force from the *in-vitro* experiment.

RESULTS AND DISCUSSION

Preliminary trials showed ligaments modeled using bone wrapping methods produced stress-strain curves identical to simplified ligament models confirming the design methods used [2]. Force transmission through the meniscus in compression force simulations averaged approximately 30% and 20% of the total force on the medial and lateral tibial compartments respectively. Experimental studies on meniscus force transmission concluded forces should be approximately 50% and 70% for the medial and lateral compartments [8].

Discrepancies in meniscus forces may be attributed to several limitations, namely the age of the subject and quality of the MRI used to create the model. These two factors cause meniscus geometries to rest in abnormal anatomical positions resulting in decreased contact area and lower force transmission.

Simulation trials run at 55° flexion with muscle force input values obtained from squat data produced tibiofemoral intersegmental forces higher than those obtained experimentally (Fig. 2). Higher model forces are likely due to limitations in the experimental force collection sensors as discussed by Hale [7]. Both model and experimental data showed higher lateral tibial compartment forces compared to medial forces by approx. 50-100N.

Overall trends in experimental data matched the multi-body models, verifying that useful multi-body knee models may be produced using these methods.

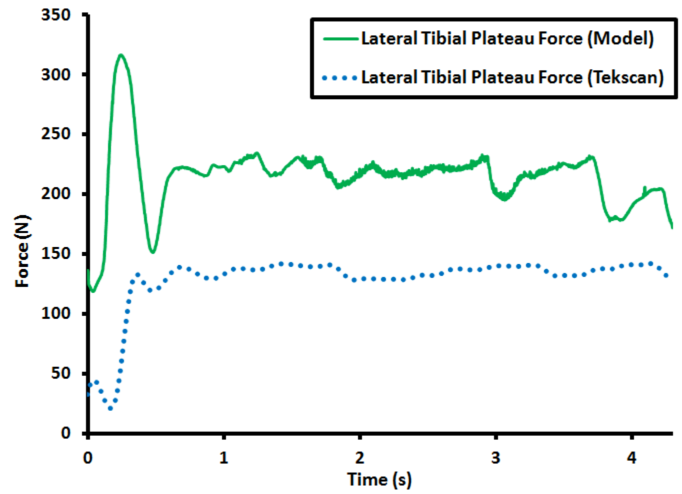

Figure 2: Tibial compartment force outputs during squat trial muscle inputs at 55° flexion.

CONCLUSIONS

Experimental and simulation outputs previously shown indicate the methods of multi-body modeling presented follow the trends of *in-vivo* intersegmental forces of the knee. This multi-body model creates a basis for the future development of computationally efficient, subject-specific knee models.

REFERENCES

1. Lohmander, L.S., et al. *Arthritis Rheum.* **50**, 3145-52, 2004.
2. Guess, T. M., et al. *The open biomedical engineering journal*. ***6*(816)**, 23–32, 2012.
3. Guess, T. M., et al. *Computer methods in biomechanics and biomedical engineering*, 37–41, 2011.
4. Fraser, C. A. et al. *University of Edinburgh School of Engineering and Electronics.* 2011.
5. Guess, T. M. et al. *Medical engineering & physics*, ***32*(5)**, 505–15, 2010.
6. Bloemker, K. H. et al. *The Open Biomedical Engineering Journal.* **6***,* 33–41, 2012.
7. Hale, R. F. Master's Thesis, 2012.
8. Seedhom, B. B., *Ann Rheum Dis.* **33**:111, 1974.

ACKNOWLEDGEMENTS

Special thanks to Alysa Nash & Stephen Wilson. This research was supported, in part, by NSF (BES 0966398) and NIH (R01AR046389-0851).

REPEATABLILITY OF A MODIFIED FINITE HELIAX AXIS METHOD: WITHIN AND BETWEEN SESSIONS

[1,2]Eveline S. Graf, [1]Darren J. Stefanyshyn

[1]Human Performance Laboratory, University of Calgary, Calgary, AB, Canada
[2]Spaulding National Running Center, Harvard Medical School, Cambridge, MA, USA
email: egraf@partners.org, web: http://www.kin.ucalgary.ca/hpl

INTRODUCTION

Torsion of the foot is defined as the relative rotation between the forefoot and rearfoot about an axis parallel to the longitudinal axis of the foot [1]. This movement has been studied during athletic movements and it was found that footwear limits maximal torsion. Therefore, torsion elements were introduced to sport shoes that allow torsion but restrict unwanted movement in the midfoot (e.g. bending) [1]. There is, however, no literature describing the appropriate position of torsion elements. In order to avoid that the shoe forces the foot into unnatural movements, it can be assumed that the shoe torsion axis location and orientation should be similar to the foot axis. Therefore, previous research has described a method to determine the foot torsion axis based on a modified finite helical axis (FHA) approach [2].

The FHA calculation is susceptible to error due to noise with small rotations. Both walking and running are movements with relatively small rotations in the midfoot; however, no work has been done on the repeatability of the finite helical axis location and orientation of the foot during these movements. Therefore, the purpose of this study was to quantify the repeatability of the helical axis parameters calculated with the modified FHA approach. The foot kinematics of walking, running, a lateral jab, and a shuffle cut were studied and the repeatability within- and between-sessions was determined.

METHODS

Part I: Twenty subjects (25.9±4.3 yrs, 1.7±0.8 m, 69.4±7.4 kg, 9 females) were recruited and signed informed consent. Each performed seven trials of walking (self-selected speed), running (3.7 m/s) and a lateral jab (maximal effort) with bare feet. Three retro-reflective markers were attached to each of the forefoot and the rearfoot. An additional two markers were placed on the head of the first and fifth metatarsal during the standing neutral trial (Figure 1). The marker trajectories were recorded using a Motion Analysis system with eight cameras (240 Hz). A Kistler force plate (2400 Hz) embedded in the floor was used to define stance.

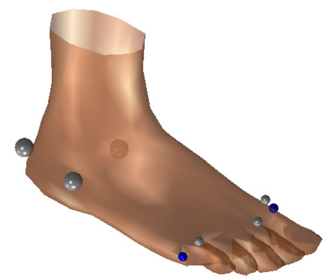

Figure 1: Marker setup with 3 rearfoot, 3 forefoot markers and 2 metatarsal head markers (neutral trial only)

Using Matlab, the orientation (alpha 1: angle in sagittal plane; alpha 2: angle from sagittal plane towards medio-lateral axis) and location of the finite helical axis of the midfoot was calculated using the modified FHA approach [2]. This method allows the calculation of the midfoot helical axis without the influence of metatarsophalangeal joint flexion. SPSS software was used to calculate the intra-class correlation coefficient (ICC, model (3,7)) in order to determine the within-session repeatability over the seven trials.

Part II: Nine male subjects (22.6±2.6 yrs, 1.9±0.8 m, 79.9±9.3 kg) participated in the part of the study assessing the between-session repeatability and visited the lab twice with at least one week in-between sessions. They performed seven repetitions of a lateral jab and a shuffle cut at maximal effort barefoot. The same data collection set-up as in part I was used. The ICC (model (3,2)) was calculated to determine the between session repeatability.

RESULTS AND DISCUSSION

Part I: The orientation variables of the FHA were repeatable between trials for all three movements (Table 1). However, the location variables were only repeatable for the lateral jab. Error or noise in the kinematic data has a larger effect on the FHA location calculation when only small rotations are occurring. The lateral jab is a movement with a maximal midfoot rotation of up to 30°. During walking or running, the midfoot rotation is much smaller (approximately 5°) and the noise due to skin movement and measurement artifacts led to a reduced repeatability of the FHA location calculation.

Part II: The ICC values indicated fair to good reproducibility of all FHA+ variables (Table 2). One variable that affects the overall repeatability is the marker placement on the foot. In the current study, the markers were placed on well defined regions on the foot by one examiner only. The results indicate that the marker positioning was done in a fairly repeatable manner.

The FHA location and orientation were expressed relative to the coordinate system that originated at the central heel marker. The orientation of this reference coordinate system was determined during a standing neutral trial. The repeatability of the FHA orientation (alpha 1 and 2) is dependent on the repeatability of the reference coordinate system orientation. The ICC values of alpha 1 and 2 indicate a good to excellent repeatability, which indicated a repeatable alignment of the foot. The repeatability of the FHA location was dependent on both the orientation of the reference CS as well as the origin location. Since the orientation of the reference CS has been determined as repeatable the reduced repeatability of the location variables results from differences in the origin location of the reference CS (central heel marker) between days. The central heel marker was placed on the center of the bare heel and not at a specific anatomical landmark. It can be assumed that when the reference CS origin would be chosen at an anatomical landmark (e.g. ankle joint center) the repeatability of the location of the FHA would be increased.

CONCLUSIONS

The modified FHA approach allowed the calculation of the helical axis during movements with large helical rotations with high repeatability within and between sessions. For movements with small rotation angles, however, the noise contained in the data led to a decreased repeatability of the location calculation. Therefore, for movements such as walking and running with small rotations between forefoot and rearfoot, the proposed method to calculate the foot torsion axis cannot be applied. For the lateral jab, which has large rotations in the midfoot area, the modified FHA approach was shown to be appropriate to determine the torsion axis.

REFERENCES

1. Segesser B, et al. *Sportverl Sportsch* **4**, 167-182, 1989.
2. Graf ES, et al. *Comput Math Methods Med*, 1-6, 2012.

Table 1: Intra-class correlation coefficients for helical axis location/orientation (within-session repeatability)

	Infero-superior location	Medio-lateral location	Alpha 1	Alpha 2
Lateral jab	0.984	0.988	0.982	0.984
Running	0.279	0.600	0.961	0.970
Walking	-0.391	-0.235	0.982	0.987

Table 2: Intra-class correlation coefficients for helical axis location/orientation (between-session repeatability)

	Infero-superior location	Medio-lateral location	Alpha 1	Alpha 2
Lateral jab	0.742	0.511	0.811	0.738
Shuffle cut	0.741	0.609	0.731	0.637

ANATOMICAL ASSOCIATIONS WITH KNEE KINEMATICS IN MATURING FEMALES

*[1]Shannon M. Pomeroy, [1]Grant C. Goulet and [1]Scott G. McLean
[1]School of Kinesiology, University of Michigan, Ann Arbor, MI, USA
Human Performance Innovation Laboratory
*Email: shanpom@umich.edu | Web: www.kines.umich.edu/lab/human-performance-innovation-laboratory

INTRODUCTION

Although the quantity and quality of anterior cruciate ligament (ACL) injury prevention programs has improved, ACL injury rates have not declined accordingly [1]. Non-modifiable knee morphologies are typically excluded from such prevention programs, despite the strong relationship between explicit knee joint anatomical indices and the risk for ACL injury [2]. However, the extent to which these associations vary throughout maturation, a sensitive growth period coupled with a large amount of osteogenic and neuromuscular adaptations, is currently unclear [1]. Thus, the purpose of this study was to examine the impact of key knee joint anatomical indices and single leg land-and-cut mechanics across three specific maturation states. Specifically, the associations between four anatomical indices and their ratios, and peak knee abduction, internal rotation, and anterior joint reaction force were explored.

METHODS

Thirty-eight active females without prior knee injury participated in the study. Subjects were stratified into *early*- (n=13; 9.5 ± 0.78 yrs), *middle*- (n=13; 12.9 ± 1.61 yrs), and *late*-pubertal (n=12; 14.1 ± 0.72 yrs) groups based on the presence of seven explicit anatomical indices [3]. Dominant limb knee scans and 3-D single leg knee biomechanics were obtained for each subject for within-group associations. Subject informed consent and University Institutional Review Board approval was obtained prior to study initiation.

Anatomical Indices

Knee joint anatomical data were recorded for each subject via a series of high-resolution multiplanar magnetic resonance images. From these data, medial tibial slope (MTS), lateral tibial slope (LTS) and their ratio (MTS:LTS), tibial plateau width (TPW), intercondylar distance (ICD) and their ratio (TPW:ICD) were quantified within Osirix 4.1 (Pixmeo). These indices were chosen for analysis based on their known links to ACL injury [2]. Measurements were made by a single experimenter on three separate occasions using our previously established techniques (Figure 1) [2]. Mean values for each indice were subsequently calculated for each subject and used in all statistical analyses.

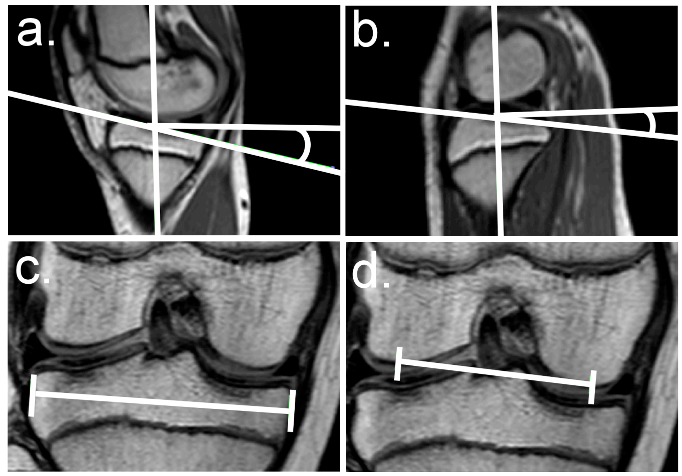

Figure 1. Medial tibial slope, lateral tibial slope, tibial plateau width, and intercondylar distance (a-d, respectively) were quantified and subsequently correlated with impact-induced knee mechanics.

Kinematic Analysis

Three-dimensional knee joint kinematic data were quantified for the dominant limb for a series of single leg land-and-cut maneuvers. Raw skin marker coordinate data were collected for 8 successful landing trials via standard motion capture techniques (Vicon Corp, CO) [2]. Data were imported into Visual 3D (C-Motion, MD) for computation of knee joint rotations. Peak stance phase (0-50%) knee abduction, internal rotations, and anterior joint force magnitudes were obtained and averaged for each subject across trials.

Mean subject-based data were submitted to linear stepwise (inclusion - $p<0.05$; exclusion - $p<0.15$) regression models to explore associations between the four discrete anatomical indices, their associated ratios, and impact-induced knee mechanics for each maturation state.

RESULTS AND DISCUSSION

Peak internal tibial rotation was found to be significantly correlated with TPW (r^2=0.335, *p*<0.028; Figure 2) and MTS:LTS (r^2 change=0.380, *p*<0.004) in early subjects (Table 1). Significant associations were not observed, however, between anatomical indices and both knee abduction angle and anterior joint reaction force in the same subjects. For the mid-maturation group, MTS (r^2=0.309, *p*<0.049), LTS (r^2 change=0.178, *p*<0.036), and TPW:ICD (r^2 change=0.454, *p*<0.024) were significantly correlated with peak knee abduction angle (Table 1). Only TPW:ICD, however, predicted peak stance internal tibial rotation (r^2=0.249, *p*<0.082; Table 1). Anterior joint reaction force was significantly correlated with TPW in middle maturation subjects (r^2=0.366, *p*<0.028; Table 1). Late-maturation subjects showed a significantly negative correlation between TPW:ICD and peak knee abduction angle (r^2=0.619, *p*<0.002; Table 1).

Table 1. Maturation-specific regression coefficients describing associations between knee anatomies and peak stance (0-50%) phase mechanics.

Peak Knee Abduction Angle			
Group	**Variable**	**β**	**t**
Middle	MTS	0.728	3.436
	LTS	0.605	2.683
	TPW:ICD	-0.425	-1.886
Late	TPW:ICD	0.787	4.030
Peak Knee Internal Rotation Angle			
Early	TPW	0.798	3.836
	MTS:LTS	0.411	2.343
Middle	TPW:ICD	0.499	1.911
Peak Knee Anterior Joint Reaction Force			
Middle	TPW	-0.605	-2.521

Outcomes demonstrated that high-risk kinematic variables linked to ACL injury are directly associated with explicit knee joint anatomies [2]. However, associations were largely group specific, varying across each of the three maturation states (Figure 2). Correlations between knee abduction angle and MTS, LTS, and TPW:ICD, for instance, existed in middle maturation subjects, while late subjects' peak abduction angles were predicted by TPW:ICD alone (Table 1).

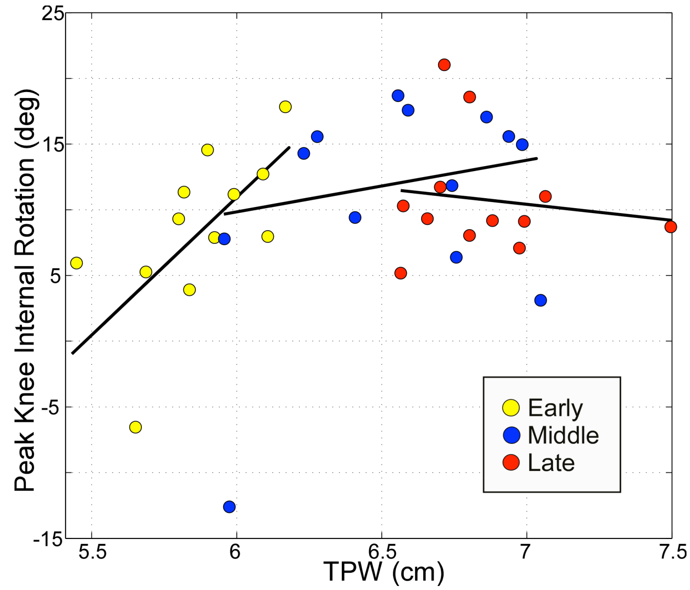

Figure 2: Variations in associations between TPW and peak stance (0-50%) phase knee internal rotation angle across three maturation states: early, middle, and late (r^2=0.629, r^2=0.384, r^2=-0.137, respectively).

These findings suggested that anatomical parameters governing debilitative mechanical loading patterns are sensitive to maturation state, similar to other adaptations, such as neuromuscular control [1]. Therefore, it is plausible that current risk screening and prevention methods for ACL injury would benefit from targeting such anatomical and high-risk mechanical associations at each stage of maturation by determining appropriate approach and timing of intervention. Such efforts are further validated as explicit anatomical indices evolve substantially throughout maturation [4]. Furthermore, understanding how such interactions are impacted by additional factors across maturation, such as habitual joint loading, will likely improve current prevention efforts. Thus, further detailed investigations of evolving knee joint morpho-mechanical profiles in maturing individuals are necessary.

REFERENCES

1. Griffin LY, et al., *J Am Acad Orthop Surg*. **8**:141-150, 2000.
2. McLean SG, et al., *Clin Biomech.* **25**:781-788, 2010.
3. O'Connor JE, et al., *Clin Anat.* In press. 2012.
4. Williams CJ, et al., *Orthop Res Soc.* 2013.

JUMPING PERFORMANCE MAY REFLECT LEVEL OF COMPETITION IN ORIENTEERING

[1] Kim Hébert-Losier

[1] Swedish Winter Sports Research Centre, Mid Sweden University, Östersund, Sweden
E-mail: kim.hebert-losier@miun.se

INTRODUCTION

In sports biomechanics, the legs are often modeled as springs that store and release elastic energy during ground contact using the stretch-shortening cycle. Since the ability of muscles to store and release energy is correlated to sports performance (e.g. better running economy) and the risk of musculoskeletal injury (e.g. low stiffness correlates to soft tissue injury), many scientists, clinicians and coaches are developing measures to quantify the efficiency of the stretch-shortening cycle.

This efficiency is often described in terms of *stiffness* or *pre-stretch augmentation* (*PSA*). Here, stiffness defines the ratio between the ground reaction force (GRF) and vertical displacement of the centre of mass during ground contact, whereas *PSA* defines the relative change in performance upon addition of an eccentric contraction prior to a concentric one. Both these indicators of the stretch-shortening cycle's efficiency can be computed using GRF data of jumping procedures in the absence of registrations of a vertical position coordinate.

Training for and competing in orienteering requires an individual to jump over obstacles, run up- or downhill and respond to rapid changes in terrain. Accordingly, together with strength and endurance, the ability of the leg to store and release elastic energy efficiently may be a key determinant of performance in this sport.

With this in mind, the present investigation was designed to characterize and compare the efficiency of the leg stretch-shortening cycle in elite and amateur male orienteer athletes. We hypothesized that the elite athletes would exhibit higher stiffness values and greater *PSA* than the amateur athletes.

METHODS

After providing written informed consent, a total of 16 male orienteer athletes (age: 29 ± 7 yr, height: 183 ± 5 cm, mass: 72 ± 7 kg) reported at a sports research facility for testing. Half the subjects were international or national level orienteer competitors, whereas the other half competed at an amateur level. All subjects were in good general health and none reported a current or recent (< 3 months) injury or medical condition that could limit their jumping abilities.

Prior to data collection, each subject watched a short instructional video that demonstrated the jumping tasks, performed a 5-min running warm-up on a self-driven treadmill (Woodway®, WI, USA) and practiced the jumping tasks under supervision and feedback from the investigator.

The experimental protocol contained 3 squat jumps, 3 counter movement jumps and one 15-s bilateral hopping task performed at a frequency of 2.2 Hz. Each jump was followed by 1-min of rest and replaced if not properly performed. During testing, the subject was barefoot and kept hands on hips. The subject was requested to land in a similar position than take-off (i.e. knees straight and ankle plantar-flexed). All trials were performed in the middle of a multi-axial force-plate (Kistler®, CH) that recorded GRF at 1000 Hz using the Kistler Measurement, Analysis and Reporting Software version 1.0.3 (MARS™ , S2P Ltd., SI).

The maximal vertical height calculated from the take off velocity of each squat jump (SJ_{max}) and each counter movement jump (CMJ_{max}) was extracted for each subject. These measures were used to calculate the *PSA* according to:

$$PSA = \frac{CMJ_{max} - SJ_{max}}{CMJ_{max}} \times 100\%$$

For stiffness, the GRF-curve from the 15-s hopping task was converted to vertical accelerations using the mass of the subject and gravitational acceleration (9.82 m·s^{-2}). The acceleration-curve was then doubly-integrated to yield velocity and position data based on central difference expressions with velocity values v evaluated halfway between stages for accelerations a and positions p with a time step $\Delta\tau = 0.001$ s.

The initial position integration constant was defined stating a zero vertical position of the centre of mass at the initial ground contact. The initial velocity integration constant was defined assuming a zero centre of mass position at take-off.

Leg stiffness (k) was computed as the ratio between the maximal vertical (upwards) GRF (f_{max}) and maximal vertical (downwards) displacement of the centre of mass (p_{max}) during ground contact, as:

$$k = \frac{f_{max}}{p_{max}}$$

After stiffness was calculated from each hop of the 15-sec trial, the values were sorted in an ascending order. The mean of the medial 22 stiffness values was extracted to provide a unique k value computed from a representative 10-sec of hopping data for each subject.

Descriptive statistics are reported as mean ± SD values. Student t-tests were used to compare the mean *PSA* and k values derived from the elite and amateur orienteer athletes, setting the statistical significance level at $p \leq 0.05$.

RESULTS

The results of all jumping procedures, summarized in **Figure 1**, revealed that although the amateurs jumped higher than the elite athletes during the squat jump (effect size 1, p=0.04), both groups attained similar heights in the counter movement jump (p=0.46). Accordingly, the elite group demonstrated greater *PSA* (effect size 1, p=0.05), but there was no difference in stiffness values measured from repeated hops (p=0.95).

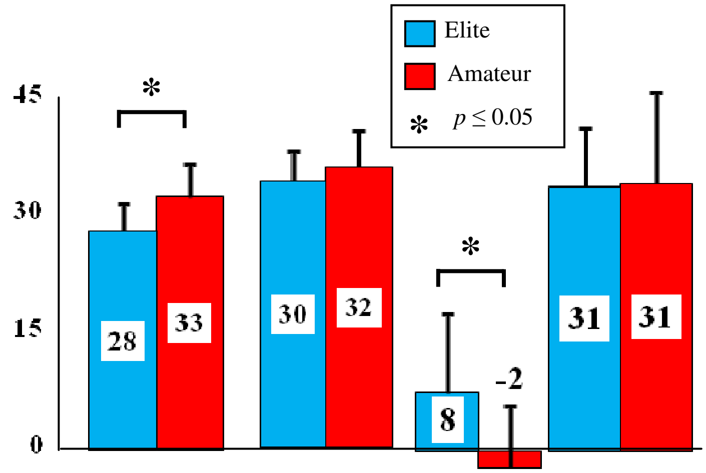

Figure 1. Mean ± SD (left to right) for maximal squat jump height (cm), maximal counter movement jump height (cm), pre-stretch augmentation (%) and leg stiffness (kN·m^{-1}).

DISCUSSIONS

Because endurance training negatively impacts power production [1], it is not surprising that the concentric power of our elite orienteer athletes was less than that of the amateurs. As anticipated, the elite group demonstrated greater *PSA*; suggesting more efficient use of the leg stretch-shortening cycle. However, this efficiency was not associated with more pronounced stiffness. This similarity in leg stiffness of the elite and amateur athletes probably reflects the fact that both employ running, a key determinant to leg stiffness, as a primary form of training. In fact, enhanced stiffness exerts a negative impact on *PSA* [2], which may be detrimental to leg responses to rapid alterations in running surface or terrain. Overall, our elite athletes demonstrated a distinct ability to utilize the *PSA*, highlighting the value of stretch-shortening exercises for the leg during training for orienteering.

REFERENCES

1. Abernethy PJ, et al. *Sports Med*, **10,** 365-89, 1990
2. Kubo K, et al. *Eur J Appl Physiol*, **96**, 305-14, 2006

ACKNOWLEDGEMENTS

The author thanks all the subjects for participating, Professor Anders Eriksson for his assistance in the technical computations and Professor Hans-Christer Holmberg for his mentorship.

KINEMATIC MARKERS OF PROLONGED PRONATION IN RUNNERS

[1,] James Becker, [1]Louis Osternig, [2]Stanley James, [3]Robert Wayner and [1]Li-Shan Chou

[1]Motion Analysis Laboratory, Department of Human Physiology, University of Oregon, Eugene OR, 97403
[2]Slocum Center for Orthopedics and Sports Medicine, Eugene OR 97401
[3]Cooperative Performance and Rehabilitation, Eugene, OR 97401
email: jamesb@uoregon.edu, web: http://biomechanics.uoregon.edu/MAL/

INTRODUCTION

Excessive amounts of velocities of foot pronation are commonly cited biomechanical factors for development of overuse injuries in runners [1]. However, while several studies suggest there is a relationship between the amount or velocity of pronation and injuries, an equal number of studies report no such relationship exists [1,2]. These inconclusive results suggest alternative theories on how abnormal pronation may be related to injury should be considered. Given the structural changes in the foot which occur during pronation, it may be that the duration the foot remains in a pronated position throughout stance, not necessarily the amount or velocity of pronation, is the more important variable for injury development [3].

However, before relationships between pronation duration and injury can be examined, biomechanical variables quantifying pronation duration, and specifically prolonged pronation, must be identified. Therefore, the purpose of this study was to identify biomechanical markers of clinically determined prolonged pronation. It was hypothesized that individuals who demonstrate prolonged pronation would not necessarily demonstrate excessive amounts or velocities of pronation but that they would demonstrate different kinematic patterns compared to non-prolonged pronators.

METHODS

Twenty competitive runners (sex: 14M, 6F, age: 22 ± 4.7 years, weekly mileage: 59.3 ± 16.2 miles) participated in this study. Subjects underwent a clinical exam measuring 10 variables documenting general lower limb alignment, flexibility, and mobility [3]. Subjects then participated in an observational gait analysis where they ran on a treadmill at speed approximating their easy training pace while their running gait was filmed with a high speed video camera sampling at 300 Hz (GC-PX10, JVC Corp.). Two clinicians independently reviewed the video and classified each subject as a non-prolonged (NPP) or prolonged (PP) pronator based on the relative alignment between the vertical axis of the shoe counter and the long axis of the tibia at the frame showing heel off.

Subjects then completed a 3D motion analysis where they ran continuous laps in the laboratory. Their whole body motion was recorded by a 10-camera motion capture system (Motion Analysis Corp.) sampling at 200 Hz. Ground reaction forces were recorded with three force plates (AMTI) sampling at 1000 Hz. For every subject, their foot strike pattern was characterized as rearfoot strike (RFS) or mid/forefoot strike (M/FFS). Filtered marker trajectories were used to calculate 17 variables describing orientations and movement of the leg segments.

Agreement between clinicians was evaluated with a kappa statistic. Discrepancies in classification were resolved by both clinicians viewing the video together. Differences between NPP and PP groups on clinical exam and kinematic variables were evaluated using a 2x2 (pronation group x foot strike pattern) analysis of variance. Arch height and running speed were entered as covariates. To examine odds of being in the PP group, variables with main effects of pronation group at $p < .2$ were entered into a binary forward logistic regression equation. The influence of each individual predictor variable was then assessed by sequentially evaluating the regression equation with variables entered at “low risk” and “high risk” values [4].

RESULTS AND DISCUSSION

The kappa statistic for agreement between the two clinicians was 0.73. After resolving discrepancies, 21 limbs were classified in the NPP group (12 RFS, 9 M/FFS) and 19 limbs were classified in the PP group (13 RFS, 6 M/FFS).

Neither the amount of pronation (NPP: 11.8 ± 4.1°, PP: 12.4 ± 4.7°, p = .544) nor the maximal velocity of pronation (NPP: 315.7 ± 120.4 °/s, PP: 370.8 ± 154.4 °/s, p = .224) were different between groups. From the 10 clinical exam measures and 17 kinematic variables, only 4 were significantly different between groups (Table 1).

Table 1. Variables which were significantly different between NPP and PP groups. All significant at $p < .01$.

Variable	NPP	PP
Period of pronation (%, Per_P)	67.5 (±15.2)	90.1 (±12.6)
Eversion at heel off (°, EHO)	-0.9 (±3.6)	-5.5 (±4.4)
Standing tibia varus angle relative to floor (°, SVA)	7.3 (±1.5)	9.2 (±1.7)
Static prone hip internal rotation ROM (°, $SHIR_{ROM}$)	35.9 (±12.1)	26.7 (±7.1)

Following an analysis for multi-colinearity, the following variables were entered into the logistic regression model: SVA, $SHIR_{ROM}$, hip internal rotation excursion during stance phase (HIR_{excur}), and static prone hip external rotation range of motion ($SHER_{ROM}$). The final model describing odds of being a prolonged pronator was: Odds = -9.39+1.63*HIR_{excur}+3.43*SVA+0.87*$SHIR_{ROM.}$

The final model was significant (χ^2 = 29.215, df = 3, $p < .001$), able to correctly classify 94.9% of the limbs, and explained 80% of the variance between NPP and PP groups (Nagelkerke R^2 = .80). Assuming the mean values for the NPP group represented a "low risk" condition and 1.5 standard deviations above or below these values represented "high risk" conditions [4], sequentially evaluating the regression equation resulted in the following combinations. With all variables entered at "low risk" values the odds of being in the PP group were 0.06. As HIR_{excur}, SVA, and $SHIR_{ROMeach}$ were each entered at "high risk" values, the odds of being in the PP group rose to 0.21, 1.29, and 7.2, respectively (Figure 1).

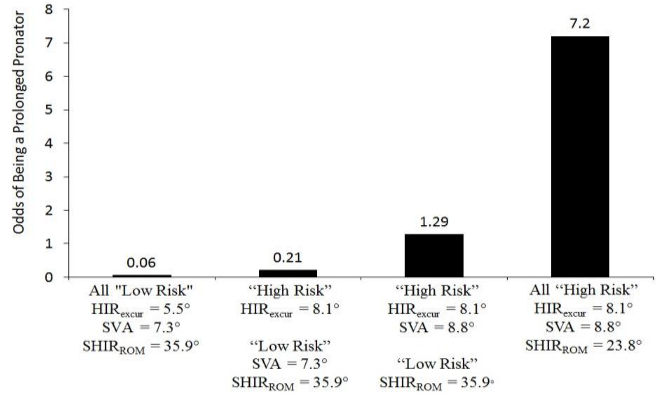

Figure 1. Illustrated results of the odds ratios resulting from sequentially evaluating the regression equation.

CONCLUSIONS

The results of this study suggest pronation duration should be considered as a unique variable in future studies on running injuries since individuals with prolonged pronation do not necessarily demonstrate excessive amounts or velocities of pronation. However, compared to non-prolonged pronators they demonstrate kinematic patterns which have prospectively been linked to the development of overuse running injuries [5]. While additional work is required to clarify the clinical implications of prolonged pronation, it currently appears that prolonged pronators can be identified using three simple biomechanical parameters, two of which are easy to measure in clinical settings

REFERENCES

1. Hreljac, A. et al. *Int SportMed J*. **7**:9-108, 2006
2. Ferber, R. *Athletic Training*. **1**: 242-246, 2009.
3. James, S. et al. *Am J Sports Med*. **6**:40-50, 1978.
4. Pohl, M. et al. *J Biomech*. **41**:1160-65, 2008.
5. Willems, T. et al. *Med Sci Sport Exer*. **39**:330-39, 2007.

ACKNOWLEDGEMENTS

This study was funded by the Eugene and Clarissa Evonuk Graduate Fellowship, the American Society of Biomechanics Dissertation Grant-in-Aid, and the International Society of Biomechanics Matching Dissertation Grant.

Quantification of the mechanical and neural components of finger enslaving by using the blind source separation (BSS) of EMG data

[1]Florent PACLET, [2]Marc LÉOUFFRE, [1]Stanislaw SOLNIK, [1]Luke WILHEM, [1]Mark LATASH and [1]Vladimir ZATSIORSKY

[1]Penn State University, University Park, PA, USA
[2]Grenoble University, Grenoble, FRANCE
email: fxp11@psu.edu

INTRODUCTION

Finger enslaving is the unintentional production of finger forces when only one finger is required to exert force. The quantification of the finger enslaving is done with two techniques: using one-finger force ramp production tasks [1] or a neural network (NN) method [2]. In both techniques, quantification of the total enslaving (TE) assumes the inclusion of the pure mechanical (such as tendon links or sticking) and the neural (linked command or muscle innervations) enslaving. The purpose of the study is to identify the mechanical enslaving (ME) and the neural enslaving (NE) components using a NN. We hypothesize that the unintended muscle activity (represented by EMG) reflects only the neural enslaving while both mechanical and neural enslaving are included in the unintended force production. Finger extension at P1 phalanx was selected as the experimental task. Only 3 muscles extend the P1 phalanx (i.e., EDC, EIP, and EDM). The EDC muscle has 4 compartments (one for each finger). Surface EMG of the EDC can be easily recorded because the muscle belly is close to the surface [3]. Thus, the physical separation of the EMG signal of each compartment of the EDC muscle is possible. The major issue is the recording of the surface EMG of the EIP and EDM. These muscles extend the Index and Little finger, respectively, and their bellies are close to each other. Recorded EMG represents the mixture of individual signals from these muscles. The blind source separation (BSS) has been demonstrated to successfully un-mix EMG signals from small and closely located muscles [4] and can be a good solution to solve this problem. The second objective of this study is to observe the effect of constraining a NN with a physiological variable such as EMG. We utilized [2] network and modified it by adding a layer (Fig. 1) and exploring its effects on the learning.

METHODS

Three subjects were tested in a finger extension task at P1. EMG bi-polar electrodes were placed over the four compartments of the EDC muscle, and two electrodes were placed over the EIP and EDM muscles. Subjects produced two sets of 15 combinations of MVC in extension at P1 with the four fingers. EMGs were bandpass [20 – 500 Hz] filtered and the BSS algorithm JADE [5], essentially the independent component analysis (ICA), was applied to separate signals from the EIP and EDM. Normal forces were used as the output to train both NNs. EMGs were used at the muscle layer level as a constraint to train the network (b). We computed the enslaving such that:

$$[TE] = [ME] \cdot [NE] \qquad (1)$$
$$[ME] = [TE] \cdot \{[NE]^T([NE][NE]^T)^{-1}\} \qquad (2)$$

$$\bar{\boldsymbol{e}} = [NE] \cdot \bar{\boldsymbol{c}} \qquad (3)$$
$$\bar{\boldsymbol{f}} = [ME] \cdot \bar{\boldsymbol{e}} \qquad (4)$$

where $\bar{\boldsymbol{c}}$ is the task requirement, $\bar{\boldsymbol{e}}$ the vector of EMGs and $\bar{\boldsymbol{f}}$ the vector of external forces

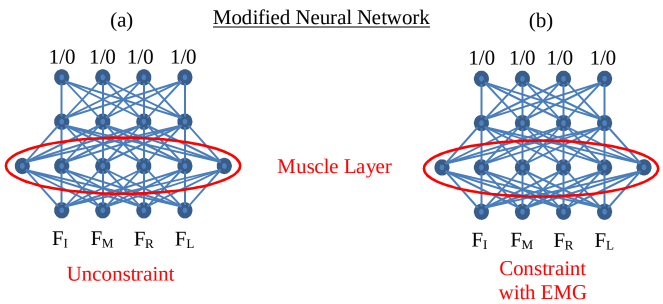

Figure 1: Modified NN without constraint (bottom left) and with EMG constraint (bottom right)

RESULTS AND DISCUSSION

Fig. 2 shows the result of the ICA algorithm on a representative subject. Signals from EIP and EDM muscles are well separated from the original mixed EMG signal.

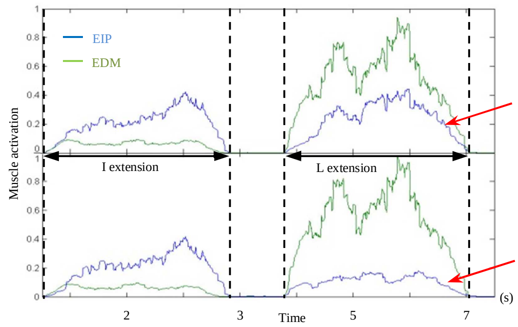

Figure 2: Integrated EMG mixture (on top) of the EIP (blue line) and EDM (green line) muscles during I extension (left) and L extension (right). The bottom shows the result of the ICA decomposition.

The normalized values (using weights normalization as in [2]) of the total enslaving given by the unconstrained NN across subjects were:

Table 1: Normalized values of TE from the unconstrained NN

	F_I	F_M	F_R	F_L
I	100.0	52,3	20,6	0.0
M	49.0	100.0	65.0	44.0
R	75.9	134.1	100.0	79.4
L	74.2	131.7	102.4	100.0

Normalized EMG values for each muscle were used at the muscle layer level as a constraint to train the network (2). Values of the enslaving were:

Table 2: Normalized values of TE from the constrained NN

	F_I	F_M	F_R	F_L
I	100.0	62.3	25.5	13.4
M	106.4	100.0	44.3	26.8
R	42.3	124.8	100.0	62.8
L	34.0	118.2	124.2	100.0

The EMG constraint changed the values in the enslaving matrix. Mean square error (MSE) was used to validate performance of the NNs. On average, constrained NN performed better compared to unconstrained NN (5.48 vs. 13.72, respectively).

From constrained NN we have extracted the *Neural enslaving* matrix from the total enslaving:

Table 3: Normalized values of the NE on the constrained NN

	EMG_I	EMG_M	EMG_R	EMG_L
I	100.0	102.8	82.5	60.2
M	68.7	100.0	71.7	42.0
R	62.5	97.1	100.0	87.2
L	46.7	26.7	69.4	100.0

Thus, we can deduce the *Mechanical enslaving* using Eq. (2):

Table 4: Normalized values of ME from the constrained NN

	F_I	F_M	F_R	F_L
EMG_I	100.0	3.1	-34.2	-10.0
EMG_M	-12.5	100.0	38.2	21.8
EMG_R	-79.7	54.9	100.0	22.5
EMG_L	-113.5	49.2	102.2	100.0

Surprisingly, some values are negative despite our initial assumption that assumes positive covariations between EMG and forces. This result cannot be true because muscles are only able to pull to generate forces, which would result in positive numbers. However, mechanical enslaving shows negative values because recorded forces include also the antagonist activity of the muscles spanning the MCP joint. Those muscles are also subject to the enslaving phenomenon with the neural and mechanical components.

CONCLUSIONS

Results have shown that it is possible to use the ICA for EMG blind separation. Using an extra layer to constrain a NN can help to find better solutions. Finally, identification of the involvement of the mechanical and the neural components of the enslaving is not clear and needs to be addressed in future studies. The extension of the fingers was also probably an unusual and difficult task and can be a limitation to this study.

REFERENCES

1. Latash ML, et al. *Exp. Brain Res.* **146(4)**, 419-432, 2002.
2. Zatsiorsky VM, et al. *Biol. Cybern.* **79**, 139-150, 1998.
3. Leijnse JNAL et al. *J Neurophysiol.* **100**, 64-75, 2008.
4. Farina D, et al. *IEEE transactions in Biomedical. Engineering* **51(9),** 1555-1567, 2004
5. Cardoso JF and Souloumiac A. *IEE Proceedings-F Radar and Signal Processing* **140(6),** 362-370,1993

ACKNOWLEDGEMENTS

This study is supported by NIH grants AR-048563, AG-018751, and NS-035032.

THE FUNCTIONAL ROLE OF THE MEDIAL GASTROCNEMIUS DURING CYCLING: A WORKLOOP APPROACH

Taylor Dick and James M. Wakeling

Simon Fraser University, Burnaby, BC, Canada
email: taylor_dick@sfu.ca

INTRODUCTION

Muscles have a variety of functions during locomotion and can act as motors, brakes, springs, and struts [1]. The specific role of the gastrocnemii during cycling is still controversial. Some suggest that their primary role is to act like struts and transfer power from limb segments to the crank during pedal downstroke [2,3]. Alternatively they may function like motors to propel the crank through the bottom of the pedal cycle [3]. It is possible that the function of the gastrocnemii change both during a pedal cycle, and also in response to the mechanical demands of activity.

Muscle function has previously been difficult to assess in humans because of the invasive techniques required, the estimates used in joint torque calculations, and inputs solely based on cadaveric data. The functional role of the gastrocnemius during cycling has not been evaluated using *in-vivo* measures of MTU length, belly length, and tendon forces under a wide range of cycling conditions. To date, work loops have been fairly restricted to animal studies because of limitations in quantifying muscle length and tendon force in humans, however with advances in 3D ultrasound this is now possible to achieve in humans. The aim of this experiment is to evaluate the functional role of the medial gastrocnemius (MG) during cycling using the work loop technique.

METHODS

Limb kinematics were recorded for 6 male subjects using an optical motion capture system (Certus Optotrak, NDI) pedaling over a range of 11 various combinations of crank torques and cadences on an indoor bike trainer (Indoor Trainer, SRM) equipped with pedal force sensors (Powerforce, Radlabor). A linear-array B-mode ultrasound probe (Echoblaster, Telemed) placed in custom-made fiberglass mount, with rigid-body clusters of LEDs was attached and secured over the distal muscle-tendon junction of the MG to track its 3D coordinates during cycling. Subject-specific Achilles tendon (AT) force-length curves were obtained from isometric tests in a custom made frame using 3D ultrasound and optical markers to estimate AT insertion (Fig.1). AT forces during cycling were calculated from the measured changes in tendon length (distance from AT insertion on calcaneous to MG muscle tendon junction in 3D space), using subject-specific AT force-length properties. Muscle tendon unit (MTU) length was calculated for each frame using the Grieves equations [4]. Belly lengths were calculated as the difference between MTU length and AT length. Seven complete revolutions of the pedal were combined and a Fourier series was used to fit the data. AT force versus muscle belly length was plotted to generate a workloop for each cycling condition (Fig. 3).

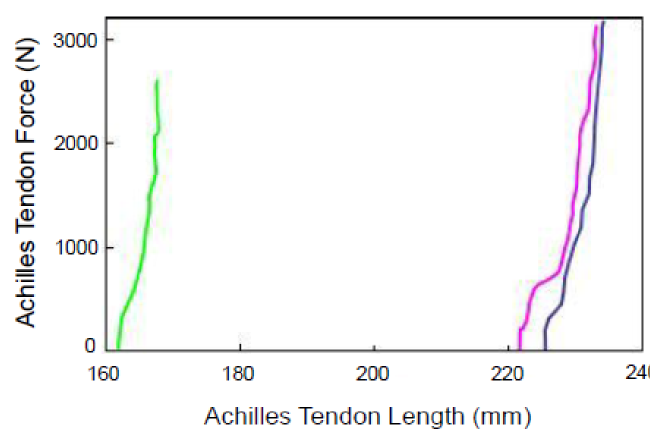

Figure 1: Subject-specific tendon force-length curves during ramped up isometric contraction, shown for 3 subjects

RESULTS AND DISCUSSION

MTU length, muscle belly length, and AT lengths were measured on a cycle by cycle basis over 7 revolutions. AT forces were calculated based on subject specific AT force length curves (Fig. 2).

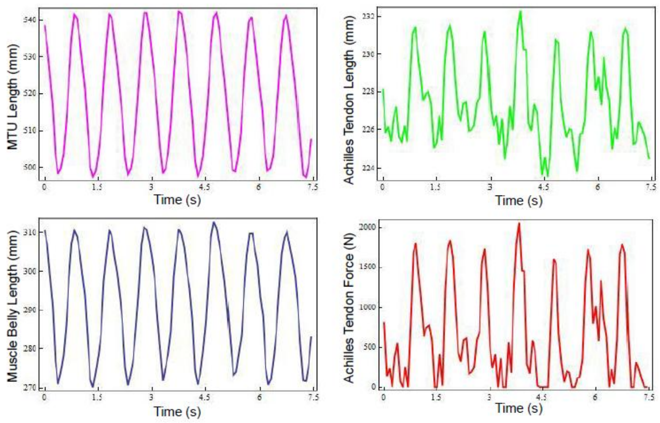

Figure 2: MTU length, muscle belly length, Achilles tendon length and Achilles tendon force over 7 cycles at 60 RPM and 4.5 N m crank torque.

Workloops for all 11 conditions showed a net positive work done by the MG muscle belly (Fig. 3). MG muscle belly produced the greatest work at 40 N m (highest crank torque) as dictated by the area within the loop. In all workloops, the muscle belly is at its shortest length at top dead centre (TDC), lengthens during pedal downstroke and then begins to shorten at between 165-175º of the pedal cycle. The workloops for all conditions show an increase in force both during the downstroke of the pedal cycle as well as in the last 135º of the pedal cycle. It is unknown whether the MG, a two-joint muscle, functions to transfer the power generated from the large upper leg muscles to the crank during downstroke [2,3] or whether they function as motors themselves. Our results indicate that the MG muscle belly transmits power during the down-stroke, and can also act as a motor: the second rise in force during the pedal revolution (at short belly lengths) is characteristic of all loops and likely contributes to knee flexion, pulling up on the crank arm and bringing the pedal back to TDC. It has also been suggested that activity in the gastrocnemii in the later phase of the pedal cycle may assist the contralateral limb during the propulsive phase [5].

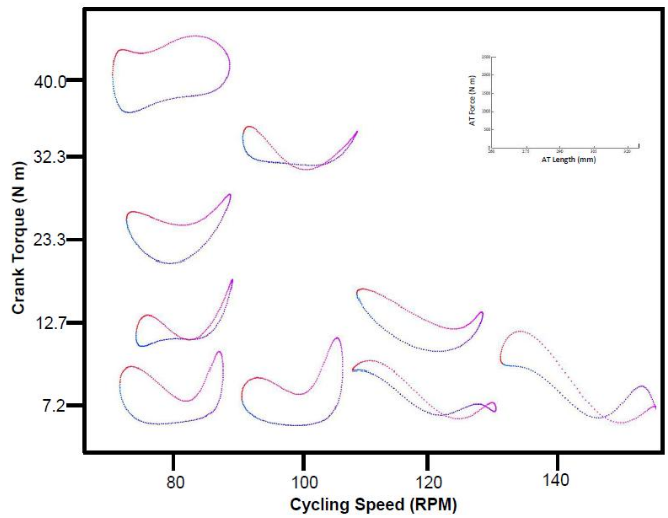

Figure 3: MG muscle belly workloops for 9 cycling conditions. Top dead centre (0º) shown in blue and this transitions to red during the cycle.

CONCLUSIONS

This is the first time that the functional role of the gastrocnemius during cycling has been determined using *in-vivo* measures of MTU length, belly length, and tendon forces. Previous studies relied on EMG to determine the role of the muscle during cycling and made conclusions based on excitation patterns. Paucity of information about muscle length has limited understanding of the function role of the muscle during specific movements. By combining *in-vivo* measures of AT force and muscle length, we can now assess the functional role of the MG during cycling. This study shows a dual role for the gastrocnemius at different phases of the pedal cycle, and that the muscle function changes in response to the mechanical demands of the movement.

REFERENCES

1. Dickinson et al. *Science* **288**, 100–106, 2000.
2. Neptune et al. *J Biomech* **33,** 155-164, 2000.
3. Neptune et al. *J Biomech* **30,** 1051-1058, 1997.
4. Grieves et al. *Int Ser Biomech* **2A**, 405-412, 1978.
5. Gregor and Conconi. *Road Cycling*. John Wiley & Sons, Ltd., 1996.

THE INFLUENCE OF COMPRESSIVE LOAD MAGNITUDE ON THE CENTRE OF ROTATION OF FUNCTIONAL SPINAL UNITS DURING IN VITRO BIOMECHANICS TESTING

Mamiko Noguchi, Chad E. Gooyers, and Jack P. Callaghan
Department of Kinesiology, University of Waterloo, Waterloo, ON, Canada
email: mnoguchi@uwaterloo.ca

INTRODUCTION

Center of rotation (CoR) is one measure commonly analyzed in *in vitro* spine biomechanics studies to assess normal and pathological (e.g. low back pain) behavior of the spine. CoR has been used to diagnose mechanical instabilities and to objectively evaluate arthroplasty techniques [1]. Therefore, it is important to identify mechanical factors that influence the location of the CoR to allow accurate interpretation of the results from *in vitro* research.

Spinal postures and passive tissue stiffness have been identified as factors influencing CoR location [1,2,3]. A number of studies have examined the instantaneous CoR in various postures [1,2]. In general, an instantaneous CoR is displaced anteriorly in flexion and posteriorly in extension. A recent study conducted in our laboratory demonstrated that increasing the magnitude of compressive load significantly increased the intact joint passive stiffness and decreased the range of the neutral zone [3]. Interestingly, only the extension limit, which defined one end of the neutral zone, was significantly different at each level of compressive load (10, 300, 900, and 1800 N), suggesting that facet joint contact may alter functional spinal unit (FSU) motion under different compressive loads. Although Panjabi et al. [4] also referred to this characteristic of the CoR as a function of the motion segment and the applied load, no study has examined how the magnitude of compressive load influences the location of the CoR.

The purpose of this study was to examine the effect of compressive load magnitude on the CoR during passive flexion-extension range of motion (ROM) tests. It was hypothesized that increasing the magnitude of compressive load would alter the trajectory of FSU motion, resulting in a significant change to the location of CoR.

METHODS

Eight porcine cervical FSUs (mean age=6 months), each consisting of two adjacent vertebrae and the intervening intervertebral disc, were excised. Rigid-bodies, each with four active infrared markers (Northern Digital Inc., Waterloo, ON), were rigidly fixed to anterior surface of the superior and inferior vertebra, and five virtual points (left and right frontal corners, facet joints and spinous process) were digitized using a four marker digitizing probe (Northern Digital Inc., Waterloo, ON). Each FSU received four repeats of a passive ROM test with varying magnitudes of compressive load (10, 300, 900, 1800 N) applied in a randomized order. Using a servomotor (AKM23D; Danaher Motion, Radford, VA, USA) connected in series with a torque cell (T120-106-1K, SensorData Technologies Inc., Sterling Heights, MI, USA), three complete flexion-extension cycles were applied at a rate of 0.5 degrees per second. Throughout each test, 3D marker positions were sampled at 100 Hz.

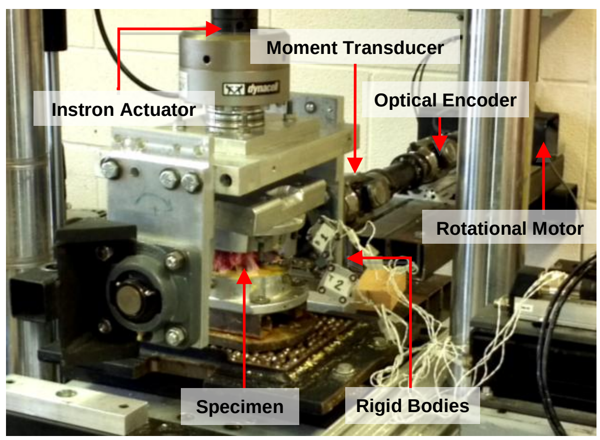

Figure 1: Experimental setup

The kinematic data of the superior vertebra were transformed into the inferior vertebral local coordinate system (origin defined as the midpoint between the digitized spinous process and vertebral body points). The trajectory of the rigid-body was fit to a sphere, using a least-squares algorithm implemented in MATLAB (Version 2012b, The

Mathworks Inc., Natick, MA, USA) and the CoR location, defined as the sphere center was computed. Anterior-posterior displacement of the sphere center was compared to the midpoint of inferior vertebrae local coordinate system across each loading condition using a one-way ANOVA with *post-hoc* pairwise comparisons of least square means (SAS Software, SAS Institute Inc., Cary, NC, USA). Measures of effect size were evaluated using Cohen's *d*.

RESULTS AND DISCUSSION

The CoR location at 10 N of applied compressive load, ($P<0.05$; d = 0.69-0.82), was located more posteriorly compared to the other loading conditions, while there were no significant changes among the higher compressive loads (d = 0.17-0.04) (Figure 2). The fit of the sphere to the kinematic data was excellent (SSE Range = 0.0001-0.0009) across all trials. On average, the CoR was displaced anteriorly by 12.10, 14.75 and13.98 mm when the magnitude of compressive load was increased from 10N to 300N, 900N, and 1800N, respectively.

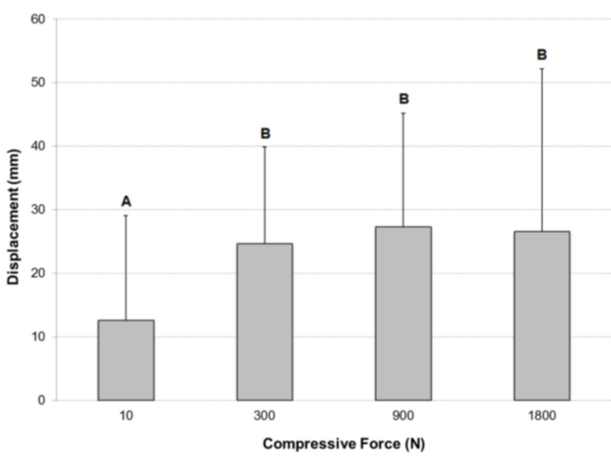

Figure 2: Anterior displacement of the CoR under different compressive loads

Findings from this work support our hypothesis that the CoR displaces anteriorly as the applied compressive load increases. A previous study conducted in our laboratory [3] demonstrated that the extension limit significantly decreased at each magnitude of compressive load whereas the flexion limit remained the same across all loading conditions (except 10 N), suggesting that the CoR may have been displaced anteriorly. The results of this study support our initial hypothesis; however, a significant difference was only revealed for the 10 N loading condition. In previous work [3], it was hypothesized that passive stiffness and neutral zone range changed linearly due to intradiscal pressure at different magnitudes of compressive load. However, the CoR location did not change linearly, which emphasizes that healthy facet joints play an important role in guiding vertebral joint motion of FSUs even at low magnitudes of compressive load (i.e. < 300 N). Therefore, a FSU's neutral zone range, particularly the extension limit, may be significantly impacted by intradiscal pressure, passive tissue stiffness and facet joint contact.

There are several limitations to this study. To date, kinematic data have only been collected on eight FSUs. Second, the test system used in the present work enabled the FSU to move with five degrees of freedom (joint lateral bending was constrained) and has shown (on average) increased angular displacement in flexion compared to other testing systems (e.g. follower-load apparatus) where the applied force is directed through the balance point of the FSU [5]. Although the instrumentation used in the present study allowed physiologically relevant loading, this artefact may have significantly altered the trajectory of FSU kinematics. Lastly, the current method did not calculate the geometric CoR of the vertebral joint. Hence, further investigation is necessary to track how adjacent vertebrae move with respect to each one another during dynamic flexion-extension tests.

CONCLUSIONS

The CoR of FSUs moved anteriorly under 300, 900, and 1800 N compressive loads, compared to a 10 N condition. This study demonstrated that variables frequently analyzed in *in vitro* spine biomechanics research, including the neutral zone range, passive stiffness, and CoR, are influenced by the magnitude of compressive load.

REFERENCES

1. Schmidt H, et al. *Clin Biomech*, **23**, 270-278, 2008.
2. Rosseau MA, et al. *Eur Spine J*, **15**, 299-307, 2006.
3. Noguchi M, et al. *J Biomech*, Submitted, 2013.
4. Panjabi M, et al. *J Biomech*, **9**, 185-192, 1976.
5. Cripton PA, et al. *J Biomech*, **33**, 1559-1568, 2000.

INFLUENCE OF LIGAMENTS ON ROTATION RESPONSE OF CERVICAL SPINE: FINITE ELEMENT STUDY

[1]Iman Zafarparandeh, [1,2]Deniz Erbulut, [1]Ismail Lazoglu, [2]Fahir Ozer

[1]Department of Mechanical Engineering, Koc University, Istanbul, Turkey
[2]Department of Neurosurgery, Koc University, Istanbul, Turkey
email: izafarparandeh@ku.edu.tr

INTRODUCTION

When a cervical motion segment exhibits abnormally large displacements in terms of either rotational or translational movements under physiologic load levels it is known as instability. The ligamentous tissues, articulating facets and disc nucleuses plays the main the role in the stability of the human cervical spine. Consequently, permanent damage to one of the stabilizing structures alters the role of others. Biomechanical models are helpful in understanding the influence of different tissues on spine stability. Among biomechanical models, finite element (FE) model is known as a versatile tool for analysis of the clinical biomechanics of the cervical spine [1].

The goal of this paper was to propose a three-dimensional FE model of full cervical spine and study the influence of ligaments on rotation response of the cervical spine in flexion loading. In comparison to symmetric models, to obtain more realistic results the asymmetry of cervical spine about mid-sagittal plane was considered. The model was validated against the published *in vitro* studies.

METHODS

The computed tomography (CT) scan data of a 35 year-old man was used to achieve the accurate three-dimensional geometry of each vertebra from C2 to C7. The asymmetric geometry of cervical spine about mid-sagittal plane was considered in modeling. Thus, the facet surface were not located in the same position on each side of the sagittal plane. The geometry of intervertebral discs were defined based on the average of their anterior and posterior thickness. Hexahedral mesh was generated on vertebrae and discs using the multi-block approach introduced by Kallemeyn et al. [2] , Fig.1. Truss elements were used to simulate different groups of ligaments including anterior longitudinal ligament (ALL), posterior longitudinal ligament (PLL), capsular ligament (CL), ligamentum flavum (LF) and interspinous ligament (ISL). The same number of truss elements were used on each side of the model. Facet joints were simulated using gap contact elements (GAPUNI) option of ABAQUS FEA software. The cartilaginous layer between the facet surfaces was simulated using "softened contact parameter", which exponentially adjust force transfer across the joint depending on size of the gap.

In each vertebra model, cancellous, cortical and posterior part were considered as deformable and isotropic material property was used. Six rings of elements were considered on the disc as the annulus fubrosus and were integrated with the nucleus part. The material property of annulus was simulated as the Neo-Hookean hyperelastic model. Incompressible fluid elements were used to simulate the material behavior of the nucleus. Rebar elements were embedded in each element of the annulus with the orientation of ±25º, in cervical region, to play the role of fibers. Hypoelastic model with no-compression option was used for simulation of fibers.

RESULTS and DISCUSSION

In the first step, the model was validated against *in vitro* studies [3,4] and a FE model [5] reported in the literature. Different loading types were chosen for validation, flexion/extension, lateral bend, axial rotation. The bottom surface C7 was fixed during the simulations. The loads were applied on a node located on top of the odontoid process of C2. In general, the simulation results were in experimental corridor of the published reports. In Fig. 2, the flexion/extension validation of the C4-C5 segment is presented. Then, the intact model was modified by omitting each group from the model and keeping others, to study the influence of ligaments on stability. Effect of ISL, LF and PLL were investigated in flexion. The load range included lower and higher loads to evaluate the effect of ligaments based on the amount of the load.

Fig. 3 compares the rotation response of the model after excluding each ligament group in flexion for two different amounts of load, 0.33 Nm and 2 Nm. In all segments there was a significant increase in the rotation response after omitting ISL, NoISL model, up to 75% and the maximum amount happened in C4-C5 segment for 2 Nm. The amount of increase for NoLF and NoPLL were up to 11% and 1% respectively and both happened for 2 Nm flexion loading. In higher load, 2 Nm, the difference between NoISL and other models rotation angle increased largely. In both load values, NoPLL model had a higher effect in C2-C3 segment. Excluding LF had a considerable effect on all loading cases in C2-C3 segment, but in other segments this effect was not obvious. Consequently, the ISL ligament preserved the normal motion while PLL or LF was excluded. However, when ISL was omitted other groups of ligaments did not preserve the stability. Thus, additional stabilization procedure such as posterior dynamic stabilization or fusion is unavoidable when is ISL injured.

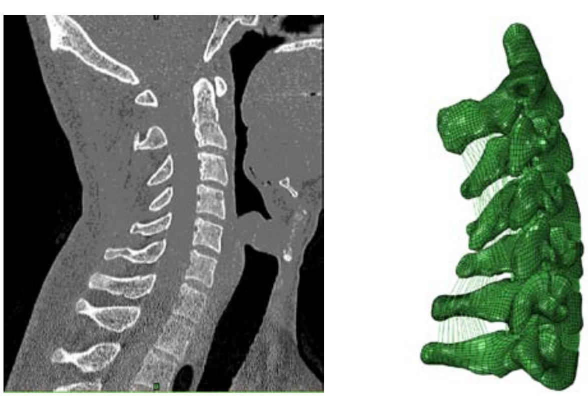

a) b)

Figure 1: a) CT data, b) FE model of cervical spine.

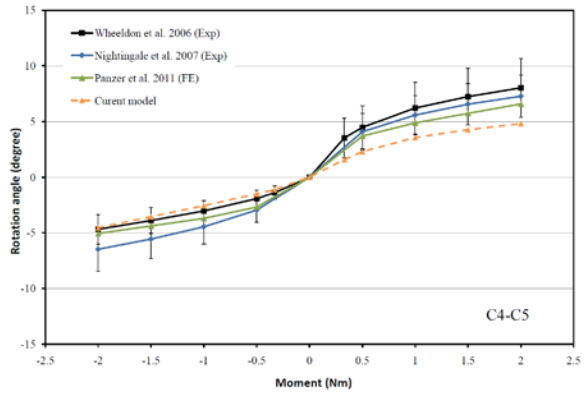

Figure 2: Comparison of the rotation response of C4-C5 segment with published in vitro studies and FE model in flexion/extension loading mode.

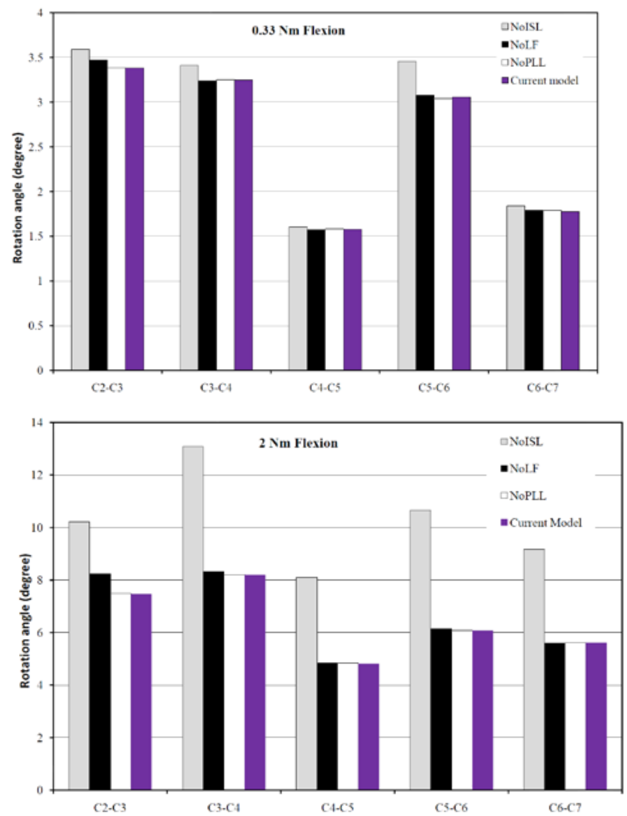

Figure 3: Comparison of rotation response of intact, NoISL, NoLF and NoPLL models.

REFERENCES

1. Teo EC, et al. *Med Eng Phys* **23**, 155-164, 2001.
2. Kallemeyn NA, et al. *Comput Meth Prog Bio* **95**, 227-235, 2009.
3. Wheeldon JA, et al. *J Biomech* **39**, 375-380, 2006.
4. Nightingale RW, et al. *J Biomech* **40**, 535-542, 2007.
5. Panzer MB, et al. *J Biomech* **42**, 480-490, 2009.

INCREASE IN BROADBAND EXCITATION IDENTIFIES VERTEBRAL ENDPLATE FRACTURES

[1]Matthew Coombs, [1]Kermit Davis, [1]Susan Kotowski, [2,3]Robert Parkinson, [2]Jack Callaghan

[1]University of Cincinnati, Cincinnati, OH, USA
[2]University of Waterloo, Waterloo, ON, Canada
[3]Giffin Koerth Forensics, Toronto, ON, Canada
email: daviskg@ucmail.uc.edu

INTRODUCTION

Low back disorders impact up to 80% of workers during their lifetime [1-3]. Common injury sites include the intervertebral discs and vertebral endplates. One hypothesized mechanism of injury is cumulative loading, which results in changes to the load bearing behavior of the intervertebral joint [4-7]. Traditionally, failure identification has occurred from observation of decreases in motion segment height, changes in force-deformation response, and following dissection. The purpose of this study was to determine whether changes in acceleration could identify vertebral endplate failures.

METHODS

Cervical functional spinal units (FSUs), four C3/C4 and two C5/C6 (n=6), were dissected from porcine spines, with all surrounding musculature removed. FSUs were potted in aluminum cups and instrumented with tri-axial accelerometers (Series 2 Accelerometers, NexGen Ergonomics, Quebec, Canada). Specimens were mounted to a servo-hydraulic materials test system (Instron 8872, Instron, Norwood, MA), oriented with the axis of compression (Fig. 1). Specimens were loaded cyclically with an initial magnitude of 4 kN, at a rate of 2 Hz. After every 20 cycles, a 1 kN impulse load was applied. After 200 impulses, or 4000 cycles, the cyclic load magnitude was increased by 1 kN. This pattern was repeated until audible fracture (Fig. 2). Loading was designed to mimic lifting, with impulse load magnitudes similar to heel strikes.

Specimen axial compression was measured from materials test system crosshead displacement, applied load was measured from the materials test system load cell, and specimen acceleration was measured from the affixed accelerometers. Fracture was hypothesized to have occurred when acceleration magnitude exceeded 1.5x the maximum magnitude of the first loading cycle. Fracture presence in the endplate was determined following dissection.

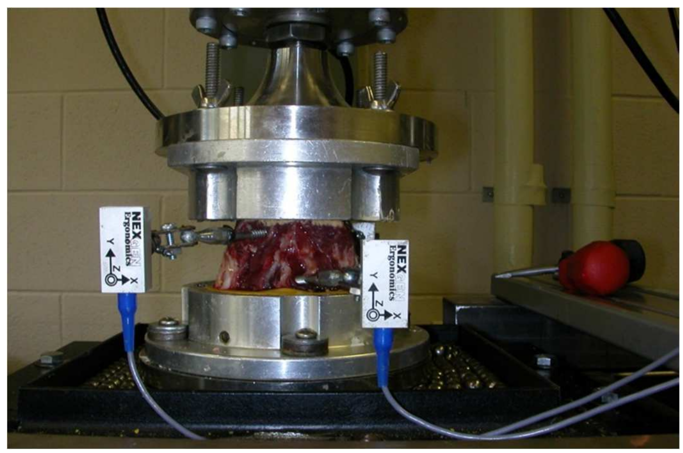

Figure 1: Functional spinal unit mounted in aluminum cups and connected to materials test system. Specimen is instrumented with tri-axial accelerometers, prepared for cyclic compression.

RESULTS AND DISCUSSION

Of the six specimens, three reached the fracture threshold criteria of a 1.5x increase in acceleration magnitude. Specimens meeting the fracture threshold criteria all demonstrated high broadband excitation in acceleration after predicted fracture occurrence (Fig. 3). All specimens determined as fractured by the threshold criteria possessed major fractures upon dissection (Fig. 4). Three specimens did not meet the threshold requirement in increased acceleration response. These specimens either had minor fractures of the endplate or damage to the underlying trabecular bone.

The change in acceleration response following fracture occurred before a significant change in displacement response, suggesting that broadband acceleration may be more sensitive than force-deformation. Initial small changes to broadband excitation correspond to hypothesized micro-fracture development before eventual specimen failure.

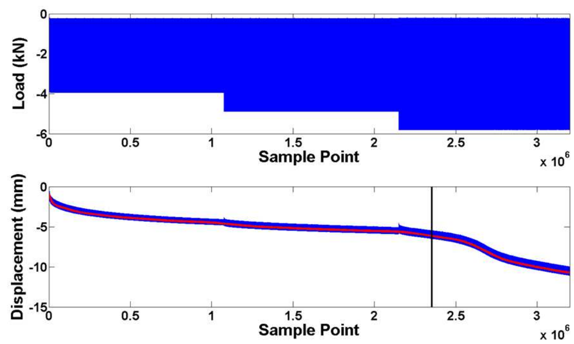

Figure 2: Compressive load applied to the cephalad vertebrae of cervical functional spinal units (top). Displacement response of representative specimen (bottom).

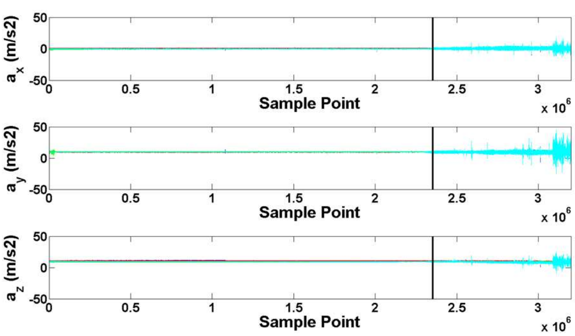

Figure 3: Acceleration response of a representative specimen during loading (same specimen as Fig. 2).

CONCLUSIONS

Clear differences were determined in acceleration response between intact and fractured FSUs. The presence of broadband excitation may be useful as a tool to determine the presence of some vertebral endplate fractures. Broadband acceleration response appears to be sensitive to the type and severity of endplate fracture. This may reflect a limitation with this method, specifically, the need for post-test fracture identification. This approach also has limited capability for identifying the exact cycle of fracture initiation.

In future work, correlation between initiation of increases in broadband excitation and changes in force-deformation response will be performed. This may allow for increased characterization of fracture behavior. Prediction of some types of fractures, including micro-fracture formation, may be possible by detection of increases in broadband excitation. Evaluation of changes in acceleration response following fracture may lead to insights in fracture development and propagation.

Figure 4: Functional spinal unit, meeting threshold criteria, with typical fracture (same specimen as Fig. 2). Specimens with major endplate fractures exhibited high levels of broadband excitation, following hypothesized fracture initiation.

REFERENCES

1. Biering-Sorensen F, et al. *Ugeskr Laeger* **145**, 2884-2888, 1983.
2. Cassidy JD, et al. *Spine* **23**,1860-1866, 1998.
3. Leboeuf-Yde C, et al. *Spine* **21**, 1518-1525, 1996.
4. Adams MA, et al. *Spine* **25**, 1625-1636, 2000.
5. Lotz JC, et al. *Spine* **23**, 2493-2450, 1998.
6. Lipson SJ, et al. *Arthritis Rheum* **24**, 12-21, 1981.
7. Osti OL, et al. *Spine* **15**, 762-767, 1990.

ACKNOWLEDGEMENTS

We gratefully acknowledge the ISB awards committee, and the University of Waterloo.

CANCELLOUS BONE FRACTURE VISUALIZATION METHOD

Nicole C. Corbiere, Orion L. Kafka, Kathleen A. Issen, and Laurel Kuxhaus

Clarkson University, Potsdam, NY, USA
email: lkuxhaus@clarkson.edu, web: http://people.clarkson.edu/~lkuxhaus/

INTRODUCTION

By 2020, half of Americans over the age of 50 will have either low bone density or osteoporosis [1]. Annually, 547,000 people suffer from vertebral fractures due to osteoporosis [1], yet the micro-mechanical origin of these fractures remains unclear. To identify the fracture initiation location and characterize the mode, visualization of the fracture surface is necessary. Complex fractures were created by mechanical compression [2] of cervine (deer) vertebral motion segments with physiologically realistic boundary conditions. Previous work used Micro-Computed Tomography (µCT) to view a 3D image of the motion segment before and after compression; however, the complex fractures were difficult to visualize. The method of crack visualization presented here originated in current research on porous materials, specifically metal foam specimens [3], and is applied to visualize fractures created in cancellous bone. The long-term research goal is to identify the individual trabeculae that fail first as a compression fracture forms. The immediate goal is to visualize the facture surface and use this visualization technique to infer how the fractures initiated and propagated.

METHODS

As part of a larger study, seventeen 3-vertebrae motion segments from three fresh-frozen white-tailed cervine specimens (two age 6 months, and one age 18 months) were compressed to form fractures. The segments were preconditioned [4] and compressed at a rate of 0.5 mm/min. The compressive load passed through the center of the intervertebral discs [5]. µCT scans (GE Phoenix Nanotom, General Electric, Wunstorf, Germany) were taken before and after loading. The work presented here discusses a representative fracture that was created in the L2 vertebra from an 18-month old specimen.

To visualize the fracture pattern, the post-compression µCT scan was reconstructed from the 2D projection images produced by the scanner. Once reconstructed, the 3D geometry was imported into the visualization software VGStudio MAX 2.2 (Volume Graphics GmbH, Heidelberg, Germany). This software allows easy manipulation of the scanned geometry and creation of pseudo-cutting planes to “fly though” the object, yet it is difficult to visualize only the fractured surface in 3D. Therefore, in VGStudio, virtual markers (points with x, y, and z coordinates) were manually placed along the fracture. Every 50 µCT slices (1.36 mm) along the frontal plane, another set of markers was placed along the fracture. Once the fracture had been mapped through the entire height of the vertebra, the same process was repeated in the median plane using the same increment as the frontal plane. After all markers had been placed, the points were exported to MATLAB (MathWorks, Natick, MA) to visualize the fracture surface.

RESULTS AND DISCUSSION

The force-displacement curve from a specimen used in this work is shown in Figure 1. There are two noticeable load drops. The first is approximately 5 kN, which is nearly 50% of the peak load of 10.69 kN. The specimen reloaded to approximately 7 kN and then experienced a second load drop of nearly 3 kN. Visual inspection of the µCT scan images revealed a mid-vertebral-body fracture in L2, the fracture was then digitized using the process described above. Figure 2 shows a comparison between the entire vertebral motion segment (L1-L3) from the µCT scan and the marked fracture surface from MATLAB.

The fracture surface resembles a wine glass consisting of a cup (concave to the cranial end) with a planar stem extending to the caudal end of L2. In the μCT images, the cup portion of the fracture is best seen in the dorsal and median planes. The fracture extends down the interior surface of the cortical shell and curves into a cup in the cancellous bone; however, one side of the cup is missing in the cortical and cancellous bone along the spinal cord canal. The approximate depth of the cup is 20 mm; the rim of the cup is just below the cranial endplate; the bottom of the cup, where the stem begins, is approximately in the middle of the vertebral body. In the μCT images of the isometric view and the frontal plane, the planar stem is seen as an open crack running along the median plane; the height of the planar crack is approximately 15 mm, running from the base of the cup and ending at the caudal endplate. By viewing the fracture surface, it is possible to infer where the fracture began and how it propagated. This fracture may have propagated caudally from the cup during the second load drop (Figure 1).

CONCLUSIONS

Marking and visualizing the fracture pattern and plotting the fracture surfaces separately allows clearer visualization of the fractured cancellous bone than the reconstructed μCT scan alone. This visualization method could be used for any medium that has an apparent fracture, and is especially valuable for porous materials such as cancellous bone.

Future work may automate the fracture surface identification. A limitation of this work is that the μCT scans were taken only before and after loading; future work will develop a loading fixture to hold the motion segment in place and permit iterative μCT scans at different loads. This will allow progressive images of the vertebral cancellous bone to visualize the fracture propagation during mechanical compression. Extensions of this work will include quantifying the geometric and material properties of trabeculae near the fracture zone, with the goal of predicting which trabeculae will fracture during subsequent loading.

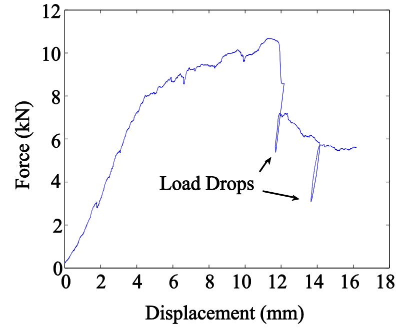

Figure 1: Force-displacement curve.

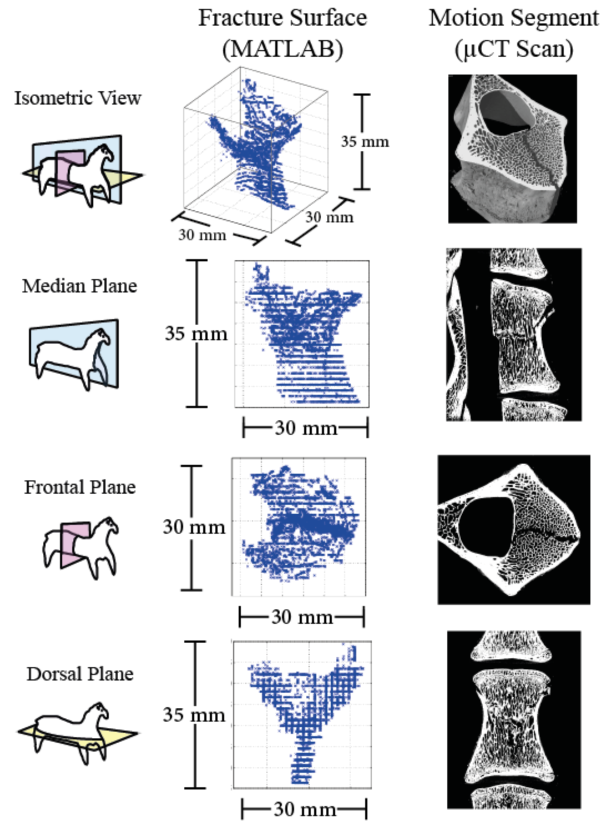

Figure 2: Visualization of fracture surface; isometric views (top) and planar projections shown.

REFERENCES

1. *National Osteoporosis Foundation*, Debunking the Myths, 2013. Fast Facts – Fractures, 2011.
2. Corbiere N et al. *ASB Annual Meeting*, 2012.
3. Ingraham M et al. *M S & E A*, **504**, 150-6, 2009.
4. Buckley J et al. *Spine Journal* **9**, 478-85, 2009.
5. Brown S et al. *J Biomech* **41**, 122-7, 2008.

ACKNOWLEDGEMENTS

We thank Cassie Christman, Dr. Mathew Ingraham and Dr. David Morrison for their contributions.

SHOULDER JOINT FORCE SENSITIVITY TO MUSCLE CHANGES FOLLOWING BRACHIAL PLEXUS BIRTH PALSY

[1,2]Dustin L. Crouch, [3]Johannes F. Plate, [3]Zhongyu Li and [1,2,3]Katherine R. Saul

[1] Virginia Tech-Wake Forest School of Biomedical Engineering and Sciences, Winston-Salem, NC, USA
[2]Department of Biomedical Engineering, Wake Forest School of Medicine, Winston-Salem, NC, USA
[3]Department of Orthopaedic Surgery, Wake Forest School of Medicine, Winston-Salem, NC, USA
e-mail: dcrouch@wakehealth.edu, web: http://www.sbes.vt.edu/kholzbau/MoBL/

INTRODUCTION

Nearly 1 in 3 children with brachial plexus birth palsy (BPBP) develop shoulder deformity secondary to muscle paralysis [1]. Researchers posit that muscles crossing the shoulder impart a posteriorly-directed force on the glenoid and high shoulder joint moments, leading to posterior humeral head subluxation, glenoid retroversion, and limited abduction and external rotation range of motion (ROM) at the glenohumeral (GH) joint. Muscles may produce these abnormal shoulder forces through two possible mechanisms: impaired longitudinal muscle growth [2] and strength imbalance between opposing muscles [3]. However, the extent to which these observed mechanisms are able to alter shoulder forces and produce deformity remains unknown. In this study, we performed a sensitivity analysis to determine which muscles and mechanisms are capable of producing shoulder forces consistent with the progression to deformity following BPBP.

METHODS

We used a well-tested upper limb musculoskeletal computer model [4] implemented for dynamic simulation [5] in OpenSim [6]. The model was simplified to include five degrees of freedom at the shoulder, elbow, and forearm. Thirty-two linear Hill-type muscle-tendon actuators represented muscles and muscle compartments crossing the shoulder and elbow.

In the model, we simulated impaired longitudinal muscle growth and strength imbalance, two possible mechanisms of deformity, to determine their potential to produce shoulder forces that are thought to contribute to deformity following BPBP. We simulated impaired longitudinal muscle growth by reducing the optimal fiber length of each muscle crossing the shoulder iteratively by up to 30%, in 5% increments. All muscles were inactive and could generate passive forces only. Active forces produced by non-paralyzed muscles that oppose paralyzed muscles are thought to lead to a strength imbalance condition [3]. Therefore, to simulate strength imbalance, each muscle crossing the shoulder was iteratively activated at 10% of its maximum activation level without changing other muscle properties; all other muscles were inactive and could generate passive forces only.

We evaluated the effect of each iteratively-applied muscle change on shouler forces. First, we calculated the change in GH bone-on-bone joint force from baseline due to the simulated deformity mechanisms. Muscle forces used to compute GH joint force were calculated with the arm fixed in a neutral posture: full adduction and neutral internal/external shoulder rotation. GH joint force changes were computed in the axial plane, since shoulder deformity occurs in this plane. Additionally, GH joint force changes were normalized to the resting GH joint force of the baseline model. We identified muscles that increased posteriorly-directed GH joint force and thus could contribute to bone deformity following BPBP.

Second, we determined whether deformity mechanisms reduced the ROM of the shoulder. Physiologically, at the limit of ROM, further joint rotation is resisted by opposing joint moments generated by soft tissues surrounding a joint. Therefore, we computed the net muscle-generated shoulder joint moments along three directions of movement: abduction in the frontal plane, external rotation in adduction (elbow flexed to 90°), and passive external rotation in 90° abduction (elbow flexed to 90°). The ROM limit was the joint angle at which muscle generated joint moments opposed a 34.3 N force applied at the wrist [7]. ROM limits were normalized to the baseline model ROM limits. We identified muscles capable of limiting shoulder abduction and external rotation ROM.

RESULTS AND DISCUSSION

At reduced optimal fiber length, the subscapularis, infraspinatus, and long head of biceps increased GH joint force in the posterior direction (Figure 1). These muscles are paralyzed in most cases of BPBP [8], and as a consequence may experience impaired growth. Furthermore, biceps and subscapularis have exhibited impaired longitudinal growth in a murine model of BPBP [2].

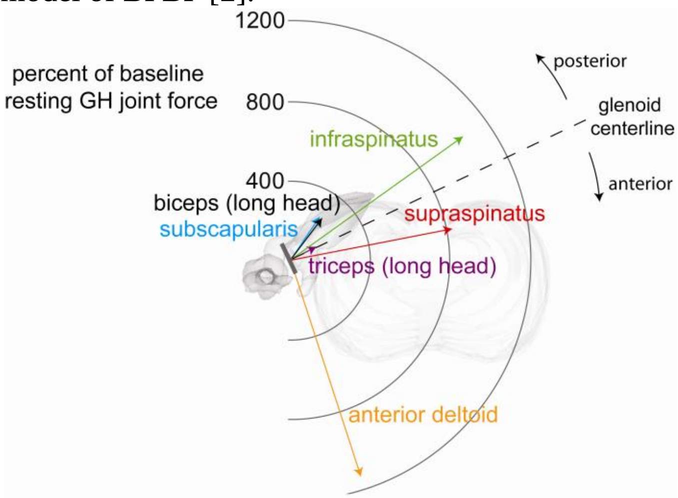

Figure 1: Superior view of the GH joint, superimposed with vectors representing normalized GH joint force changes generated passively by muscles at 30% reduced optimal fiber length.

At 10% muscle activation, the infraspinatus, subscapularis, teres major, teres minor, latissimus dorsi, posterior deltoid, and long head of biceps muscle increased GH joint force in the posterior direction. Of these muscles, only latissimus dorsi is not often paralyzed and, thus, could potentially contribute to bone deformity following BPBP.

At reduced optimal fiber length, the long head of triceps limited the abduction ROM, and the anterior deltoid and subscapularis muscles limited external rotation in adduction (Figure 2). Muscles at 10% activation did not limit shoulder ROM.

CONCLUSIONS

Impaired longitudinal growth of the subscapularis, infraspinatus, long head of biceps, long head of triceps, and anterior deltoid muscles could produce shoulder forces consistent with deformity following BPBP. These muscles may be potentially critical targets for treatments to prevent or alleviate shoulder deformity. The effect of strength imbalance on shoulder forces was limited, which supports findings that strength imbalance did not progress to shoulder deformity in a murine BPBP model [2]. Future studies should determine the extent to which the simulated deformity mechanisms occur clinically in patients with BPBP.

REFERENCES

1. Hoeksma AF, et al. *J Bone Joint Surg* **85A**, 316-322, 2003.
2. Nikolaou S, et al. *J Bone Joint Surg* **95A**, 461-470, 2011.
3. Waters PM, et al. *J Bone Joint Surg* **91A**, 2367-2375, 2009.
4. Holzbaur KRS, et al. *Ann Biomed Eng* **33**, 829-840.
5. Daly M. *WFU Graduate School*, Winston-Salem, NC, 2011.
6. Delp SL, et al. *IEEE Trans Biomed Eng* **54**, 1940-1950, 2007.
7. Osbahr DC, et al. *Am J Sports Med* **30**, 347-353, 2002.
8. Lagerkvist, et al. Dev Med Child Neurol **52**, 529-534, 2010.

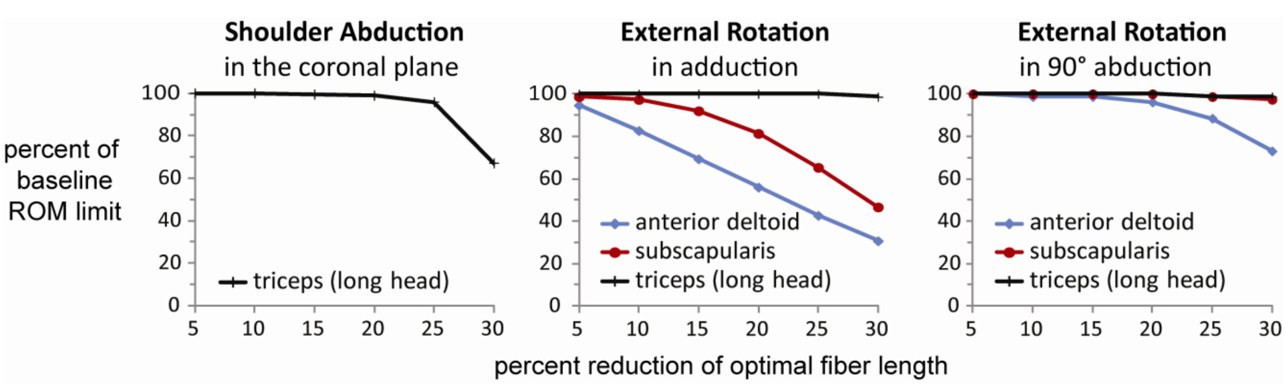

Figure 2: Effect of reduced optimal fiber length on passive shoulder ROM limits.

A FINITE ELEMENT MODELING APPROACH TO UNDERSTANDING CRITICAL MECHANICAL TRADE-OFFS IN REVERSE SHOULDER ARTHROPLASTY

Vijay Permeswaran, Jessica E. Goetz, Carolyn M. Hettrich, and Donald D. Anderson

The University of Iowa, Iowa City, IA, USA
email: vijay-permeswaran@uiowa.edu – web: http://poppy.obrl.uiowa.edu/

INTRODUCTION

Reverse shoulder arthroplasty (RSA) holds increasing attraction as a means to reliably restore pain-free function to patients with glenohumeral arthritis who are rotator cuff-deficient [1]. RSA utilizes a reverse ball-in-socket design, with the humeral component as the socket and the glenoid component the ball (glenosphere), to medialize and distalize the humeral center of rotation (Fig. 1).

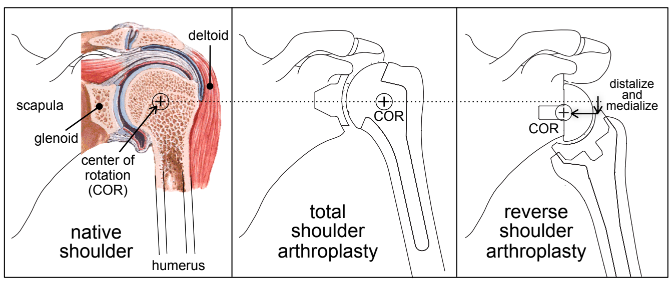

Figure 1. Comparison of the centers of rotation (COR) for the humerus (from left to right) in the native shoulder, in total shoulder arthroplasty, and in reverse shoulder arthroplasty.

In the wake of favorable post-op results, RSA has exhibited high early to mid-term complication rates. Scapular notching has been reported to occur after RSA in 31-97% of patients. Notching involves lateral bone loss in the scapula, attributed to contact between the humeral component and the scapula in terminal adduction. This recognition has led to modifications in implant design and surgical technique to reduce impingement risk. A common change has been to lateralize the center of rotation, either by placing bone graft behind the glenoid baseplate or by extending the glenosphere. Both of these modifications decrease the deltoid moment arm, and extending the glenosphere increases the risk of glenoid baseplate loosening or failure.

There is clear need for a better understanding of the mechanical trade-offs involved in RSA implant designs and implantation. A systematic finite element modeling approach to assess mechanical stresses in the implant and the neighboring bony tissues is here introduced.

METHODS

A finite element model of an Aequalis RSA design (Tornier, Montbonnot, France) was created. Two common implantation techniques were modeled: a 10° inferior tilt reamed into the glenoid surface and a **B**ony **I**ncreased **O**ffset (BIO) achieved using 10 mm of bone harvested from the humeral head [2]. The scapular geometry was segmented from CT scans of the Visible Female. The implant geometry was obtained from 3D laser scans of the actual implants, and surfaces were fit to the implant geometries using Geomagic Studio software (Geomagic USA, Morrisville, NC).

A finite element mesh was created (Fig. 2) from the generated surfaces using TrueGrid (v 2.3 XYZ Scientific Applications, Inc., Livermore, CA). The scapula, BIO bone wafer, humeral polyethylene cup, and cup liner were modeled as hexahedral three-dimensional elements while the glenosphere and humeral stem were modeled as rigid surfaces.

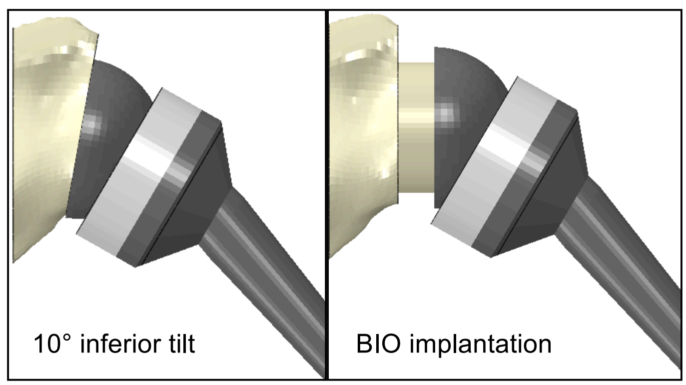

Figure 2. The finite elment model to the left shows a glenosphere implanted in a 10° inferior tilt, and to the right a bony increased offset (BIO) implantation.

The humeral component was initially placed in 30° of abduction. A force/moment combination representing the weight of the arm was applied to the end of the humeral stem. The humeral component was then allowed to freely adduct until contact with the scapula occurred. The adduction angle was then fixed for both models at the angle for which one of the two models first contacted the scapula. An internal-external rotation moment profile was then applied to the humeral implants while they were constrained to rotate about the center of the glenosphere, and contact stresses at the scapula-humeral cup interface were recorded. All jobs were run using Abaqus Explicit 6.11.1 (Dassault Systèmes, Vélizy-Villacoublay, France).

RESULTS AND DISCUSSION

Impingement between the humeral cup component and the inferior lateral scapular border was detected in both models (Fig. 3), but the contact stress was elevated and persisted across more angles in the 10° inferiorly tilted glenosphere compared to the BIO implantation. The point of contact stress was located in close proximity with the previously reported highest incidence of scapular notching.

These results suggest that a finite element modeling approach can provide insights into the nature of contact between the scapula and the humeral component in RSA. Prior developments with computational wear formulations [3] provide a means to study the progression from frank impingement motions to scapular notching. Additional work is needed to provide suitable kinematic/force-moment profiles reflective of activities of daily living in these cuff-deficient patients, specifically in poses where impingement is expected.

REFERENCES

1. Frankle M et al. J Bone Joint Surg Am. 87(8):1697-1705, 2005.
2. Boileau P et al. Clin Orthop Relat Res. 469(9):2558-2567, 2011.
3. Maxian TA et al. J Orthop Res. 14(4):668-675, 1996

ACKNOWLEDGEMENTS

This work was funded by faculty startup grant from the Department of Orthopaedics and Rehabilitation at the University of Iowa.

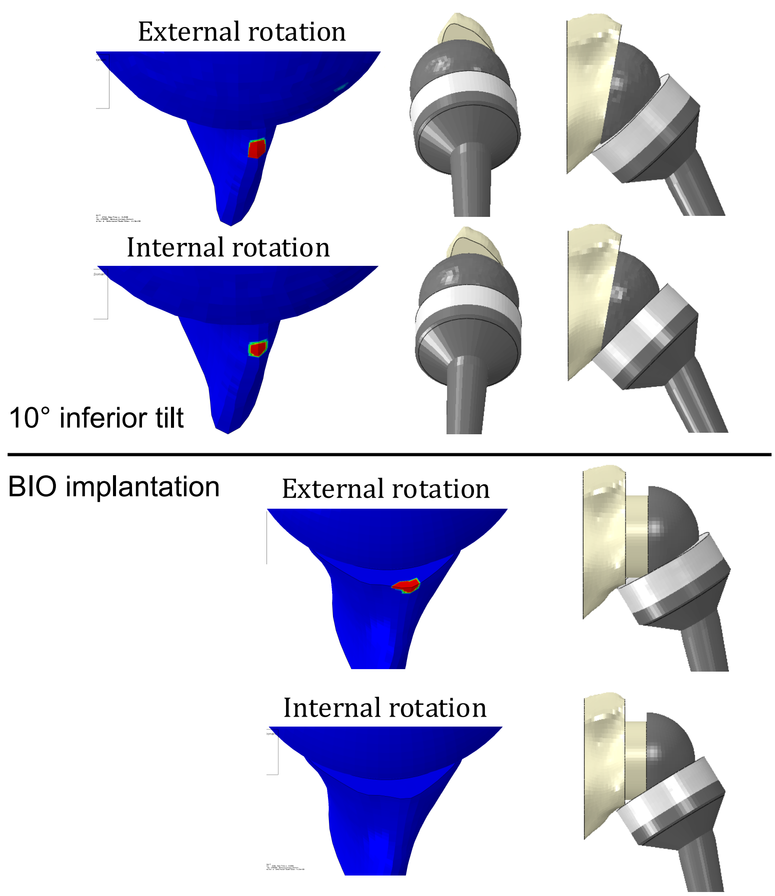

Figure 3. Contact stress at the interface between the glenosphere implanted in a 10° inferior tilt and the humeral cup was more elevated and persisted over a wider range of int/ext rotation compared to that of a bony increased offset (BIO) implantation.

THE ROLE OF PELVIC GIRDLE POSITION IN FORCE DEVELOPMENT AND ELECTROMYOGRAPHY OF THE LATISSIMUS DORSI

Jaynesh H. Patel, Adam E. Jagodinsky, Gretchen D. Oliver, and Wendi H. Weimar

Auburn University, Auburn, AL, USA
email: pateljh@auburn.edu, web: http://education.auburn.edu/kine/

INTRODUCTION

Multi-articulate muscles are subject to active insufficiency due to demands placed at the multiple joints that the muscle crosses. In many cases, when motion occurs at both joint simultaneously, the muscle cannot contribute to the muscle action at one joint due to the demands at the other joint. However, if the motion of the secondary joint were to improve the length of the muscle at the primary joint, then the contribution of the muscle at the primary joint would be enhanced. In overhead motions, such as throwing, the body seems to welcome this arrangement.

The latissimus dorsi (LD) is the broadest muscle of the back, originating at the iliac crest and inserting on the humerus [1]. It is generally accepted that the primary function of the LD is at the shoulder however, electromyographic studies confirm that it is active during trunk and pelvic girdle motions as well [2]. With this in mind it was hypothesized that changes in pelvic girdle position would affect the force production of the LD during internal rotation at the shoulder. Specifically, the purpose of this project was to investigate changes in electromyography (EMG) of the LD and isometric glenohumeral internal rotation force during six transverse pelvic girdle positions.

METHODS

All testing protocols were approved by the institution's IRB committee. Seventeen current resistance-training males volunteered to participate in the study. Following the securing of the informed consent, demographic data were collected (21.7 ± 1.04 yrs., 183 ± 6 cm., 83.5 ± 9.7 kg.). No participants had a previous upper-extremity injury within a year of participation in the study. The activity of the LD was recorded with a multichannel electromyography (EMG) amplifier/processor unit (MyoClinical, Noraxon USA INC; Scottsdale, AZ) using wet gelled bipolar Ag-AgCl disc surface electrode pairs (Blue Sensor SE, Ambu Inc. Denmark). Electrode placement sites were shaved, abraded, and cleaned according to standard electromyographic procedures. The electrode placement was similar to that used by Lehman et al. (2004), with the surface EMG electrodes placed over the muscle bell of the LD with 2 cm inter-electrode distance. Proper placement was verified by manual muscle testing. The raw EMG signal (μv) was amplified with an input impedance of 10 MΩ, the gain set at 1000x, and a common mode rejection ratio of >115 dB. Further data processing included band passed filtered (6^{th} order Butterworth, with cut off frequencies of 8 and 535 Hz), and full wave rectification.

A Biodex Isokinetic Dynamometer (Biodex System 4 Pro, Biodex Medical Systems, Inc.; Shirley, NY) was used in collection of torque data. Torque data was represented in foot * pounds^{-1}. Participants completed a maximal volitional isometric contraction (MVIC) of internal rotation in a neutral pelvic position with the right arm [90 degrees elbow flexion and shoulder abduction] on an isokinetic dynamometer for seven different conditions. Conditions were randomized: Neutral (N); 10 degrees contralateral transverse pelvic girdle rotation (10° CPR); 20 degrees contralateral transverse pelvic girdle rotation (20° CPR); 10 degrees ipsilateral transverse pelvic girdle rotation (10° IPR); 20 degrees ipsilateral transverse pelvic girdle (20° IPR) and full contralateral and ipsilateral transverse pelvic girdle rotation (Full CPR and Full IPR). Each participant completed three, two second contractions of maximal isometric internal rotation while EMG and peak torque data was recorded for each condition.

RESULTS AND DISCUSSION

Two, 1 x 7 (Condition) repeated measures ANOVA were completed for torque and EMG with follow-up pairwise comparisons where appropriate. Statistically significant main effects were noted for maximal torque values between the N condition and conditions 10° IPR and 20° IPR ($p < .05$)

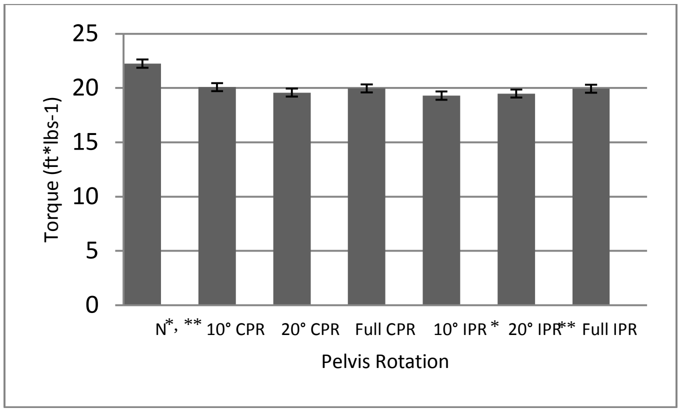

Figure 1: Isometric torque output of internal rotation at the glenohumeral joint. There were statistically main effects for maximal torque values between the neutral condition and conditions 10° IPR* and 20° IPR** ($p < .05$) [Figure 1].

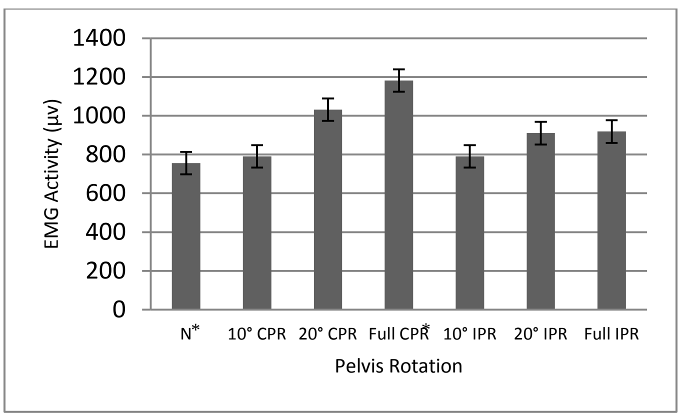

Figure 2: EMG activity of the LD during isometric internal rotation with different pelvis positions. There was a significant main effect between the N condition and Full CPR* ($p<.05$).

The purpose of this project was to determine if changing the static position of the pelvis in the transverse plane would alter the isometric torque production of the LD at the shoulder. It was anticipated that the altered pelvic girdle positions would yield a greater internal rotation torques than those noted for the neutral condition, however all statistical significance was noted for torques lower than at neutral.

It was anticipated that if a change were noted, it would be when the pelvis was in contralateral pelvic girdle rotation, a body position more aligned with a throwing motion. Though not significant this trend was noticed with three of the four largest torques noted during contralateral pelvic girdle rotation. This was also noted for the EMG.

CONCLUSIONS

The results of this study suggest that altering pelvic position does alter internal rotation force development, particularly with ipsilateral rotation, as is typically seen in overhand throwing motions. Further research is needed to determine how these combined motions affect the influence of the LD to specific joint motions.

This is a first step in a longer line of research that will investigate the relationship between pelvic girdle position and internal rotation torque production. Follow up studies will replicate this study during active transverse pelvic girdle rotation as well as with the inclusion of hip motion to evaluate the role of the lumbopelvic hip complex.

REFERENCES

1. Floyd, R.T. (2009). *Manual of Structural Kinesiology*. McGraw Hill, New York, New York.

2. Weimar, W. H., Patel, J. H., Sumner, A. M., Romer, B. H., Fox, J. & Rehm, J. (2012). The Role of the Latissimus Dorsi Muscle in Pelvic Girdle and Trunk Rotations. *Abstract presented at American Society of Biomechanics Conference, 2012.*

Evaluation of Midcarpal Capitate Contact Mechanics in Normal, Injured and Post-operative Wrist

[1] Modaresi S, [1] Kallem MS, [2] Lee P, [2] McIff TE, [2] Toby EB, [1,2] Fischer KJ

[1] University of Kansas, Lawrence, KS, USA
[2] University of Kansas Medical Center, Kansas City, KS, USA

INTRODUCTION

Carpal ligament injuries are among the frequently underreported and underdiagnosed injuries in the hand and wrist. Scapholunate (SL) dissociation is one of the most common forms of instability in carpal joints [1]. The SL joint plays a key mechanical role in stabilizing the overall carpus and in dampening excessive loads to the wrist in hyperextension and intercarpal supination [2]. Among carpal injuries, SL tears typically occur first with with loading in hyperextension and intercarpal supination. Diagnosis and reliable treatment of SL disassociation depends on factors such as the time after the injury, extent of the instability and arthritic changes in the wrist. When SL dissociation is left untreated, it leads to scapholunate advanced collapse (SLAC wrist) with osteoarthritis (OA) of the radiocarpal and capitolunate joints[3]. Investigating the in vivo joint kinematics and contact mechanics in normal, injured (with SL dissociation) and post-operative wrists will improve understanding of the injury, its implications for OA risk, and the effectiveness of the surgical repair. The goal of this study was to compare midcarpal joint mechanics of the capitate articulations with the scaphoid and lunate in normal (contralateral control) wrists, in wrists with scapholunate dissociation injury and in repaired wrists after healing. We hypothesized that injury will change mechanics and that post-operative mechanics will be similar to normal.

METHODS

Two human subjects with scapholunate ligament dissociation, who received direct SL surgical ligament repair, participated in this study. All research protocols were approved by the University of Kansas Medical Center’s Human Subject Committee. MRI images for the normal wrist, injured wrist and surgically repaired wrists were obtained using 3T MRI with a wrist coil. A constructive interface steady state (CISS) sequence was used for all images. We scanned each wrist twice- once while relaxed (0.15 mm pixels and 0.5 mm slice thickness) and during active controlled grasp (0.30 mm pixels and 1 mm slice thickness). To assure constant grip pressure during the grasp scan, visual feedback of grip pressure was provided. For evaluation of surgical efficacy, the injured wrists were imaged again at least 12 weeks after surgical reconstruction. High resolution images were used to construct model geometry. The capitate, scaphoid and lunate, along with their cartilage, were segmented from these images in Scan IP (Simpleware Ltd, Exeter, UK) and triangular faceted surface models were also created. Kinematics of the carpal bones from the unloaded to the functionally loaded state were obtained by image registration. Joint mechanics (contact areas, contact forces, average contact pressures and peak contact pressures) were calculated in Joint_Model software [4], assuming 1 mm uniform cartilage thickness and 4 MPa effective modulus.

RESULTS AND DISCUSSION

Quantitative magnitudes for contact parameters are shown in table 1. Contact force, contact area, and peak pressure in the scaphocapitate joint were higher in the injured and post-operative states compared to normal in both subjects. In the lunocapitate joint, contact force, contact area, peak pressure and average pressure are highest in the injured sate of the wrist for first subject, whereas in the post-operative wrist these contact parameters were similar to the normal wrist. For the second subject, contact force and contact area are highest in post-operative wrist, but peak pressure and average pressure are higher in injured wrist and follow the expected trend. For both subjects the scaphocapitate contact region spread distally in injured and post-operative wrists and peak pressure shifted volarly (Fig.1). There was no clear shift in lunocapitate contact between wrist states (Fig.2). This is consistent with observations of radiocarpal contact mechanics with injury, where changes in contact location are more pronounced for the scaphoid [5]. While no conclusion can be drawn from this preliminary data from two subjects, contact parameters for the injured wrists nearly all increased. Lunocapitate results generally support our second hypothesis that joint mechanics could return to normal after direct repair of the SL ligament. However, scaphocapitate results did not support this hypothesis increased force and contact area post-operatively compared to normal state. Scaphocapitate results after surgical repair remained similar to the injured joint mechanics in both subjects. This difference between scaphocapitate and lunocapitate results could be explained by some residual instability of the scaphoid. Even so, the direct repair may help prevent the development of lunocapitate arthritis. Contact forces and peak pressures are consistently higher in the scaphocapitate joint compared to lunocapitate, as expected from prior radiocarpal studies [5]. This helps establish the reliability of the results from these in vivo models.

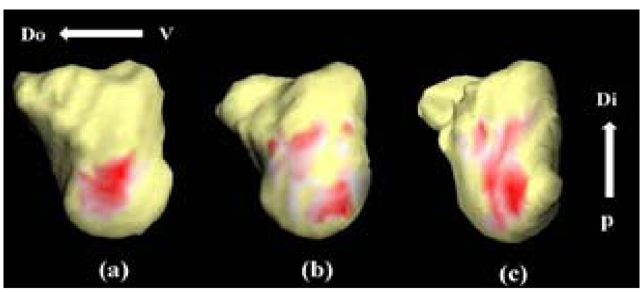

Figure 1: Contact pressure distribution on the capitate from scaphoid (Subject 1) for (a) normal, (b) injured, and (c) post-op wrist. Proximal=P, Distal =Di, Volar=V, and Dorsal=Do.

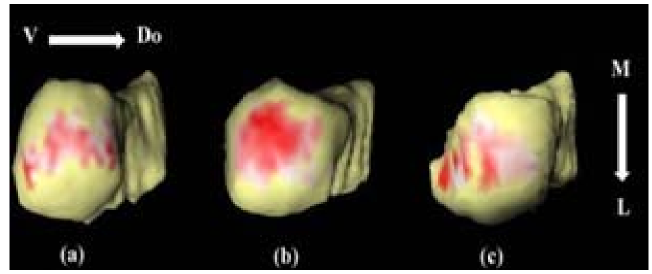

Figure2. Contact pressure distribution on the capitates from lunate(Subject 1) in (a) normal, (b) injured, and (c) post-op wrist. Medial=M, Lateral=L, Volar=V, and Dorsal=Do.

CONCLUSIONS

These in vivo data indicate that contact patterns greatly vary from the normal to injured wrist, which is consistent with development SLAC wrist and OA in the untreated injured wrist. Surgical repair appears to benefit midcarpal mechanics, but did not completely restore normal mechanics in these two subjects.

REFERENCES

1. Carg B, et al. *Orthop traumatol*, 2012.
2. Crisco JJ, et al. *Orthop Clin North Am 2001*, 32(2):219-231.
3. Igor Cizmar, et al. *past surg Hand surg*, 2010;44:245-251.
4. Kwak S, et al. *Comp Meth Biomech Biomed Eng. 2000*, 3(1):41-64. 5) Majima M, et al. J Hand Surg Am 2008. 33(2):182-188.
5. Johnson J, Doctoral Dissertation, University of Kansas Mechanical Engineering, 2012.

Table 1: Comparison of contact force (F), contact area (A), peak pressure (PP) and average pressure (AP) between Normal (N), Injured (I) and post-operative (P) wrist for the scaphoid and lunate articulations.

Subject	Condition	Scaphocapitate				Lunocapitate			
		F (N)	A (mm2)	PP (Mpa)	AP (Mpa)	F (N)	A (mm2)	PP (Mpa)	AP (Mpa)
S1	N	38.4	69	1.4	0.5	15.8	63	0.8	0.2
	I	54.6	125.8	1.5	0.4	28.3	81.7	1	0.3
	P	57	100	1.5	0.5	14	61	0.7	0.2
S2	N	40.6	62.8	1.3	0.6	14.6	30.1	1.3	0.4
	I	31.6	69.4	1.9	0.4	23.6	34.6	2.2	0.6
	P	41.4	81.4	2.1	0.5	28.6	80.6	1.1	0.3

KINEMATIC CALIBRATION OF A THIN-FILM PRESSURE GRID USING CIRCULAR DISK MARKERS

Erik W. Sinsel and Frank L. Buczek

National Institute for Occupational Safety and Health, Morgantown, WV, USA
email: Erik.Sinsel@cdc.hhs.gov

INTRODUCTION

Circular retroreflective disk markers have been used in video-based motion capture studies of handle gripping to kinematically calibrate a thin-film pressure grid wrapped around a cylindrical handle [1]. In that study, the pressure film was permanently adhered, and could not be removed and inspected for the purposes of measuring the accuracy of calibration marker placement.

Analogous to the kinematic calibration of human body segments, disk markers can be used to track and calibrate a pressure film grid Cartesian coordinate system. The *developable* property of a cylinder's surface allows it to be treated mathematically as a two-dimensional (2-D) plane [2], and allows the creation of a 2-D coordinate system on the surface of a cylinder, or on a closely wrapped film. Assessing anatomical landmark identification error (LIE) in the calibration of anatomical coordinate systems is critical for understanding the reliability of the resulting analyses [3]. Similarly, assessing LIE in the kinematic calibration of the pressure film is critical for understanding the reliability of resulting analyses.

We present a simple yet effective method empirically quantifying the accuracy and precision of the kinematic calibration of a thin-film pressure grid. We demonstrate the method in the case of applying calibration disk markers to a pressure film which has been adhered to a cylindrical handle.

METHODS

A thin-film pressure grid (Tekscan Inc., model 5101) was adhered to a cylindrical aluminum handle approximately 47 mm in diameter (Figure 1A). This setup was selected to closely replicate a combination in the previous study which used the same film model on a 50 mm handle [1].

The pressure film was taped to the cylinder in an attempt to align pressure cell rows with cylinder transverse planes. The pressure cell row closest to the thumb in a typical handle grip was designated as the "top", and the row farthest from the thumb as the "bottom". Circular disk markers approximately 5 mm in diameter were created from retroreflective tape. Ten calibration cells were selected, five each along the top and bottom rows, and were the same calibration locations used in the previous study.

Calibration markers were applied using the same method used previously. A desk-mounted magnifying glass with an articulating arm and circumferential light was used in applying the markers with a wide-tipped graphite tweezer. The cylinder rested on the desk during application, and was generally maintained in a position where its longitudinal axis was roughly aligned with the experimenter's sagittal plane with the bottom row being more proximal.

The pressure film was composed of two thin, transparent layers, each containing an array of parallel strips which were combined with the arrays orthogonal. When attached to the cylinder, the column strips were clearly visible (Figure 1A). The disk marker diameter was chosen so as to be roughly twice the length of a side of the square cell, which meant that adjacent column center lines could be used as a visual aid in locating the cell centroid along the underlying row. Pressure cell rows were identified by utilizing the intersections of small transparent gaps between adjacent rows and adjacent columns. When lit and viewed with the magnifying glass, these intersections provided visual cues for identifying the cell centroid along the column. The pressure film was removed and optically scanned in a consumer flatbed scanner at 600 dpi (Figure 1B). The bitmap image was imported into vector graphics software (Corel Draw X6) for analysis.

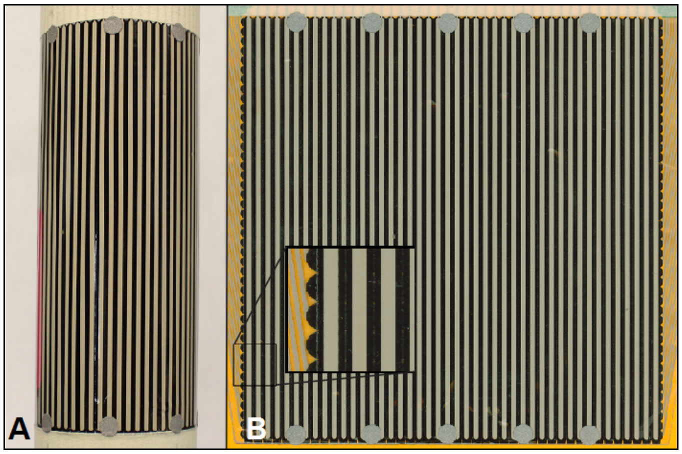

Figure 1: Calibration disk markers applied to a pressure film wrapped around a cylindrical handle; the optically scanned pressure film.

Visual landmarks were used to delineate rows and columns near calibration markers using graphical line objects. Calibration cell centroids in image coordinates were identified and recorded, and the line objects were removed from view. Circle objects 5 mm in diameter and with semi-transparent borders were manually fit to disk markers and their center image coordinates recorded. The empirical cell coordinates were used to create a least-squares pressure film orientation matrix and local origin position vector, which were used to perform coordinate transformations between the image and pressure film [4]. The origin was in the upper left corner with the row axis pointing down across rows, and the column axis pointing right across columns.

The LIE was calculated as the error vector **e** from cell to disk marker centroids, along pressure coordinate system axes. The kinematic calibration of the pressure grid coordinate system was assessed by calculating the root mean square error (RMSE) of disk marker centroids with their nominal cell landmark locations, given the manufacturer's specifications. Student's *t*-distribution was used to estimate the probability of an error vector magnitude of at least a quarter of the length of a side of the square cell. Three repetitions were conducted by the same experimenter.

RESULTS AND DISCUSSION

Landmark identification error was very low for all trials (Table 1). The greatest error was typically in the row component, where marker placement relied on the visibility of the intersections of gaps between rows and columns. The RMSE of the kinematic calibration was less than 0.5 mm for all cases. The probability of an error vector magnitude of at least one quarter of a cell side (0.64 mm) was less than 0.0002 for all trials.

REFERENCES

1. Sinsel EW, et al. *Proceedings of ASB'10*, Providence, RI, USA, 2010.
2. Salomon D. *Transformations and Projections in Computer Graphics*. Springer-Verlag, Ltd., 2006.
3. Della Croce U, et al. *Gait and Posture* **21**: 226-237, 2005.
4. Horn BKP, et al. *Journal of the Optical Society of America* **5**: 1127-1135, 1998.

DISCLAIMER

The findings and conclusions in this abstract have not been formally disseminated by the National Institute for Occupational Safety and Health and should not be construed to represent any agency determination or policy.

Table 1: LIE mean and standard deviation (SD) of pressure grid calibration markers (n=10), and coordinate system fit error for three trials. Vector components (e_r, e_c) are along row and column axes. The kinematic calibration RMSE is between transformed disk marker coordinates and their nominal landmarks. Student's *t*-distribution was used to calculate the probability of an error vector magnitude of at least ¼ of a square cell side.

	e_r (mm)	e_c (mm)	$\lvert e \rvert$ (mm)	RMSE (mm)	Pr($\lvert e \rvert \geq$ ¼ cell)
Trial 1	-0.02 (0.14)	0.00 (0.08)	0.14 (0.08)	0.39	< 0.0001
Trial 2	0.05 (0.13)	-0.04 (0.05)	0.12 (0.09)	0.41	< 0.0002
Trial 3	-0.02 (0.16)	-0.02 (0.03)	0.14 (0.08)	0.37	< 0.0001

Noncontact Photoacoustic and Laser-Ultrasound Imaging of Optical Absorbers and Acoustic Scatterers in Tissue Phantoms

Jami Johnson, Michelle Sabick and Kasper Van Wijk

Boise State University, ID, USA
email: jamijohnson1@u.boisestate.edu

INTRODUCTION

Photoacoustic (PA) imaging has gained increasing interest in the past decade since it has high optical contrast and the high-resolution and depth penetration capabilities of ultrasound [1]. Since the PA effect is absorption based, molecules can be mapped based on their optical properties. This is beneficial for imaging molecules in vascular structures with unique absorption spectra, such as hemoglobin. Unfortunately, structures without unique optical properties, such as vessel calcifications, are less readily detected with PA imaging.

The acoustic properties of calcified tissue *are* distinct compared to soft tissue due to differences in mechanical properties of the materials [2]. For source wavelengths beyond about 1000 nm, water absorbs the optical energy significantly at the body surface, causing an additional acoustic, or laser-ultrasound (LU), wave to be generated at the tissue surface. This LU wave propagates as in traditional ultrasound imaging and can provide information regarding acoustic impedance, which gives insight into the presence of constituents such as calcification.

In this abstract, we describe a new dual-modality imaging technique to exploit the unique characteristics of both LU and PA waves to distinguish both optical absorbers (such as blood) and acoustic scatterers (such as vascular calcification). This imaging technique has the potential to produce high-resolution images based on both optical and material properties of vascular structures. Our goal is to improve characterization of diseased vascular structures in a safe, noninvasive, noncontact manner.

METHODS

A solid tissue-mimicking phantom was constructed of Intralipid®, agar, and water, simulating the optical scattering and acoustic properties of human tissue. Two different blood vessel surrogates were embedded in the phantom at a fixed depth of 18 mm below the surface. A thin-walled polyester tube (12.7 µm wall thickness, 1.57 mm diameter) filled with infrared absorbing dye represented a healthy vessel filled with blood. A thicker-walled acrylic tube (467 µm wall thickness, 1.40 mm diameter) filled with the absorbing dye simulated a stiffer calcified artery filled with blood.

The experiments were performed in reflection configuration (Fig. 1). The imaging system consisted of an unfocused (8 mm diameter), 1064 nm Nd:YAG laser with a 15 ns pulse width and 11 Hz repetition rate as the excitation source. A scanning laser interferometer was the acoustic detector.

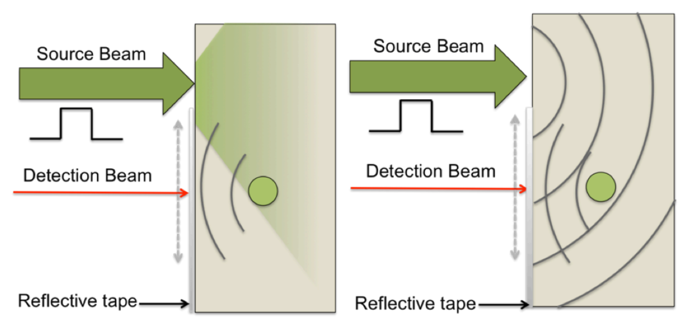

Figure 1: Experimental set-up, where source and receiver are incident on the same side of the tissue phantom. Left: the photoacoustic effect caused by absorption of optical energy by a tissue chromophore. Right: an LU wave generated at the surface and subsequently scattered by a structure with detectable acoustic contrast.

RESULTS AND DISCUSSION

After filtering irrelevant frequencies from the images, photoacoustic and laser-ultrasound waves were detected in both phantoms (Fig. 2 and Fig. 3). The PA wave arrives before the LU wave because the time for the optical energy to travel from the tissue surface to the tube is essentially instantaneous in comparison to the time it requires the acoustic wave to travel the same distance.

The thin tube had a larger inner diameter than the thick tube, allowing more light-absorbing dye to reside within the thin tube. The additional volume of absorbing agent within the thin tube resulted in a stronger PA wave in comparison to the thick tube, which contained less dye volume. Because PA imaging is absorption based, however, mechanical information about vascular structures, such as acoustic impedance and stiffness, are difficult to extract from a PA image.

The speed of sound through calcified tissue is significantly greater than through blood, resulting in higher acoustic contrast for calcified structures. Analogously, the acoustic contrast of acrylic is higher than the acoustically transparent polyester tube used in our experiment. This increase in contrast corresponded to increased amplitude of the scattered acoustic (LU) wave. In addition to analysis of acoustic contrast, parameters such as wall thickness and vessel stiffness can potentially be extracted from the LU wave.

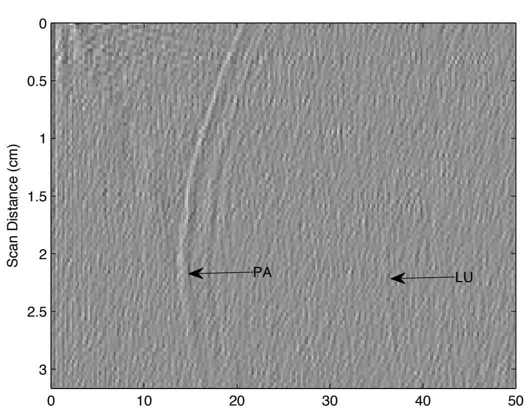

Figure 2: Results from scan with thin-walled tube filled with dye. Strong PA absorption and weak LU scattering is detected.

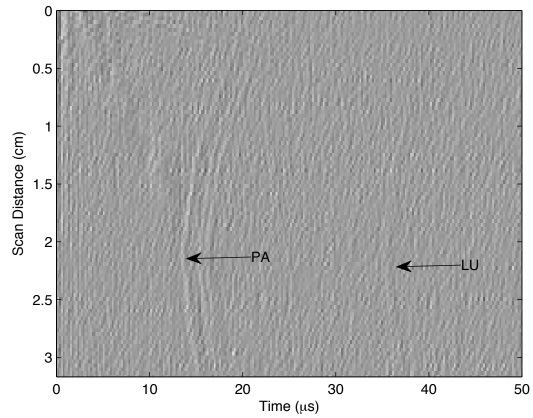

Figure 3: Thick-walled tube with dye. Reduced PA amplitude and increased LU contrast is observed when compared to the thin-walled trial, Figure 2.

CONCLUSIONS

The data show that both acoustic scatterers and optical absorbers of varying contrast can be detected with a dual PA-LU imaging modality. Noncontact, noninvasive methods were implemented to detect structures on the order of 1.5 mm. An increase in acoustic contrast is observed for the thick-walled tube, which is representative of a vessel with a stiff, thickened wall due to disease such as calcification. In traditional ultrasound imaging, calcifications smaller than 3 mm are unlikely to be detected [4]. Our detection of the thick-walled tube, with a thickness of less than 0.5 mm, shows promise toward a method of calcification detection with improved resolution. By detecting calcification in the beginning stages of the disease, or before intervention decisions are made, improved patient outcomes can be achieved.

In the future we hope to expand this technique to obtain high-resolution noninvasive vascular system maps indicating both vessel material properties and molecular makeup (both indicators of vascular health) without the use of ionizing radiation.

REFERENCES

1. Beard J. *Interface Focus* **1,** 602-631, 2011.
2. Allen TJ. *J Biomed Opt* **17**(6), 061209, 2012.
3. Rousseau G. *J Biomed Opt* **17**(6), 061217, 2012.
4. Taki.H. *J Med Ultrasonics* **39**, 127-135, 2012.

MODULATION OF TITIN ELASTICITY IN WORKING MUSCLE TO MINIMIZE ENERGY LOSS IN PASSIVE STRETCH-SHORTENING CYCLES

[1]Jens A. Herzog, [2]Tim R. Leonard, [2]Azim Jinha, and [2]Walter Herzog

[1]Mount Allison University, Sackville, NB, Canada
[2]University of Calgary, Calgary, AB, Canada
email: walter@kin.ucalgary.ca, web: http://www.ucalgary.ca/hpl/herzog

INTRODUCTION

Passive forces in skeletal muscles originate primarily from collagen fibrils in the connective tissues surrounding fibres, fascicles and muscles, and from titin, a giant molecular spring in sarcomeres (1). While the properties of collagen fibrils are well described, titin's properties are not well known, especially not within the structural framework of a sarcomere (2).

Titin is the third most abundant protein in a sarcomere and spans the half sarcomere from the M-band to the Z-line (Figure 1). Titin has spring-like properties in the I-band region. When a muscle is stretched, the randomly oriented Ig domains are aligned, followed by stretching of the PEVK segment, and the unfolding of Ig domains (3). Straightening of the Ig domains and stretching of the PEVK segment are thought to occur elastically, while *unfolding* of the Ig domains is thought to be highly viscoelastic (4).

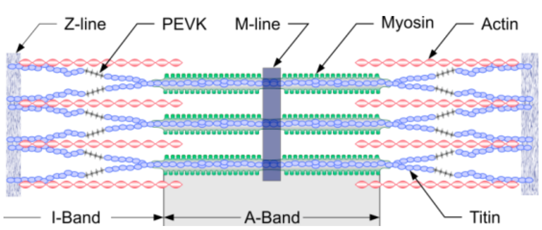

Figure 1: Schematic figure of a sarcomere with titin (in blue) extending from M-line to Z-line.

While the properties of isolated titin molecules have been identified in the past, titin's properties within the structural confines of the sarcomere are not well known. We hypothesized that titin is an essentially elastic spring as long as unfolding and refolding of Ig domains was prevented, and that the elastic domain of titin can be shifted to any sarcomere length by preventing un/refolding of Ig domains. Therefore, the purpose of this study was to identify the sarcomere length at which Ig domain unfolding occurs, and establish the unfolding and refolding kinetics of Ig domains of titin.

METHODS

Myofibrils (n=41) from rabbit psoas were used for all testing, as 95% of all passive force in myofibrils originates from titin (1), thus making it ideal for testing titin's properties (2). Myofibrils were harvested, isolated and prepared for testing as described previously (2). Myofibrils were attached at one end to a set of nano-levers for force measurements and at the other end to a glass needle to impose sub-nm length changes (Figure 2).

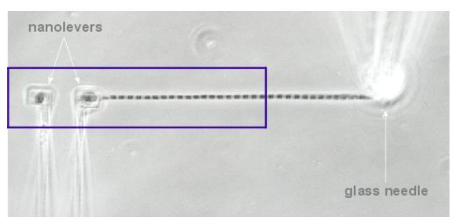

Figure 2: Micrograph of a myofibril attached to a glass needle and force levers for mechanical testing.

Eight myofibrils were used to assess the sarcomere length at which Ig domain unfolding occurred. This was done by stretching myofibrils from an initial average sarcomere length of 2.6µm to a length of up to 5.0µm and observing the characteristic inflection point associated with Ig domain unfolding (4).

Twenty-eight myofibrils were used to test the unfolding and refolding kinetics by stretching them from an initial sarcomere length of 2.6µm by 1-3 µm/sarcomere and returning them to the original length, and repeating these cycles three times. Following the three repeat cycles, myofibrils were rested at 2.6µm (n=20) or at 1.8µm (n=8) average sarcomere length for ten minutes before starting a new set of stretch-shortening cycles.

Finally, five myofibrils were stretched from a sarcomere length of 2.6µm by 2.0µm/sarcomere and were then subjected to ten stretch-shortening cycles of 1.0, 1.5, and 2.0µm/sarcomere magnitude.

RESULTS AND DISCUSSION

The inflection point of isolated myofibrils occurred first at an average sarcomere length of 3.5-3.7µm (Figure 3), suggesting that first Ig domain unfolding occurred at that length. This result agrees well with results on isolated titin molecules (4). Furthermore, Kellermayer et al. (4) observed Ig domain unfolding at ~25pN for a single titin molecule. When normalized to the size of our myofibrils (about 2700 titin molecules), the Ig domain unfolding would be expected to occur at approximately 68nN, which is exactly where we observed our inflection point (68±5nN, n=8), supporting the idea that we identified the start of unfolding of Ig domains.

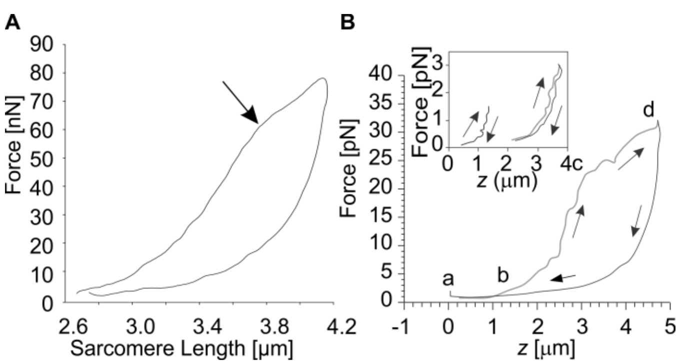

Figure 3: **A.** Inflection point (arrow) in a myofibril indicating first unfolding of Ig domains. **B**: inflection point (c) for an isolated titin molecule (4).

When resting myofibrils for ten minutes between sets at an average sarcomere length of 2.6µm, loading energy did not recover suggesting that refolding of Ig domains at this length is slow. In contrast, when resting myofibrils at 1.8µm, peak force and loading energy were fully recovered indicating that refolding kinetics at 1.8µm occurred more rapidly than at 2.6µm (Figure 4), despite the fact that there was no passive force at either length.

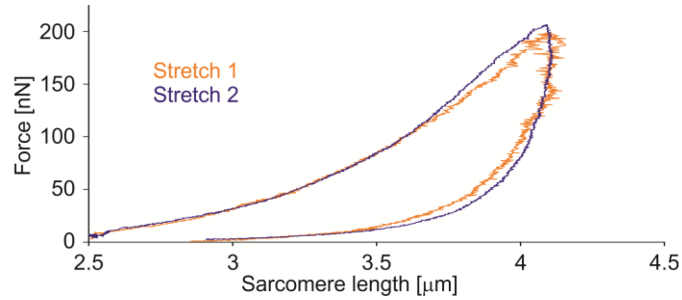

Figure 4: Full recovery (stretch 2) of peak force and loading energy for a myofibril rested for 10 minutes at a sarcomere length of 1.8µm.

Finally, when stretching titin to long lengths and preventing re-folding of Ig domains, myofibrils behaved virtually elastically with an average energy loss in a stretch-shortening cycle of 8% (Figure 5). This elastic behavior could be elicited at any lengths beyond 3.5µm, suggesting that passive muscle can work elastically at any length if titin Ig domain un/refolding is prevented.

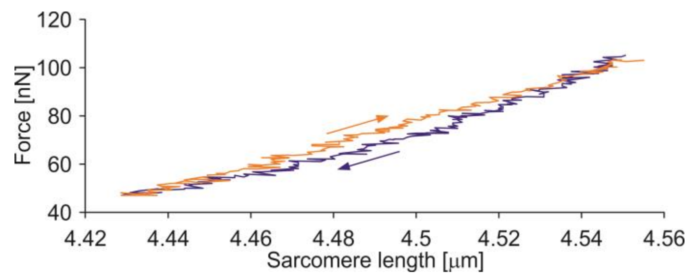

Figure 5: Virtually elastic behavior of a passive myofibril during a stretch-shortening cycle when Ig domain un/refolding was prevented.

CONCLUSION

Titin is a visco-elastic spring whose elastic region can be shifted to any sarcomere (muscle) length for minimal loss of energy in stretch-shortening cycles.

REFERENCES

1. Linke W, et al. *Biophys J* **67**: 672-682, 1994.
2. Herzog JA, et al. *J Biomech* **45**:1893-1899, 2012
3. Granzier H, et al. *Muscle Nerve* **36**:740-755, 2007
4. Kellermayer M, et al. *Science* **276**:1112-16, 1997

ACKNOWLEDGEMENTS

The Canada Research Chair Programme,
CIHR, and the Killam Foundation.

A PRACTICAL APPROACH TO DETERMINE APPROPRIATE CUTOFF FREQUENCIES FOR MOTION ANALYSIS DATA

[1,2]Evelyne Carbonneau, [3]Réjean Fontaine and [1,2]Cécile Smeesters

[1]Research Center on Aging, Sherbrooke QC, Canada
[2]Department of Mechanical Engineering, Université de Sherbrooke, Sherbrooke QC, Canada
[3]Department of Electrical and Computer Engineering, Université de Sherbrooke, Sherbrooke QC, Canada
e-mail: Cecile.Smeesters@USherbrooke.ca web: http://www.usherbrooke.ca/gmecanique

INTRODUCTION

To minimize the effect of noise on motion analysis data, filtering is often necessary. This requires the determination of an appropriate cutoff frequency, which will determine the amount of signal distortion and noise passed through the filter. Unfortunately, the literature on how to automatically select such a frequency for a data set is not very approachable for motion analysis researchers and does not provide sufficient details on how to implement such algorithms [1,2].

This study presents a practical approach to frequency analysis by: a) proposing an algorithm to determine appropriate cutoff frequencies using both power spectrum density (PSD) and residual analysis (RA), and b) evaluating the effect of these frequencies on a set of motion analysis results. The latter consisted of ground reaction force data from a study to determine the maximum forward, sideways and backward lean angles from which younger, middle-aged and older adults could be suddenly released and still recover balance [3].

METHODS

Our approach is summarized in 5 steps: 1) Make sure that the data is as clean as possible: eliminate noise if possible, choose sampling frequency, determine necessity of filtering. 2) Select the signals on which to perform the frequency analysis: select sample trials, identify useful signals. 3) Perform the frequency analysis using both PSD and RA with the Matlab code provided: select algorithm parameters, determine signals or factors to ignore, select cutoff frequencies. 4) Evaluate the effect of the selected cutoff frequencies: determine results to test, evaluate cutoff frequency impact, select definitive cutoff frequency. 5) Proceed with additional tests using the definitive cutoff frequency.

PSD: Thompson's multitaper method was used to estimate the PSD [1]. Only the PSD below f_{bin}, i.e. below the impact noise, was considered (Figure 1, top: dark gray area ignored). The power of the noise (PSD_0) was equal to the mean PSD between f_0 and f_{bin} (Figure 1, bottom: light gray area is noise). The PSD cutoff frequency (f_{cPSD}) was when the cumulative sum of the PSD reached 95% of the total power of the signal, i.e. the mean cumulative sum of the PSD between f_0 and f_{bin}.

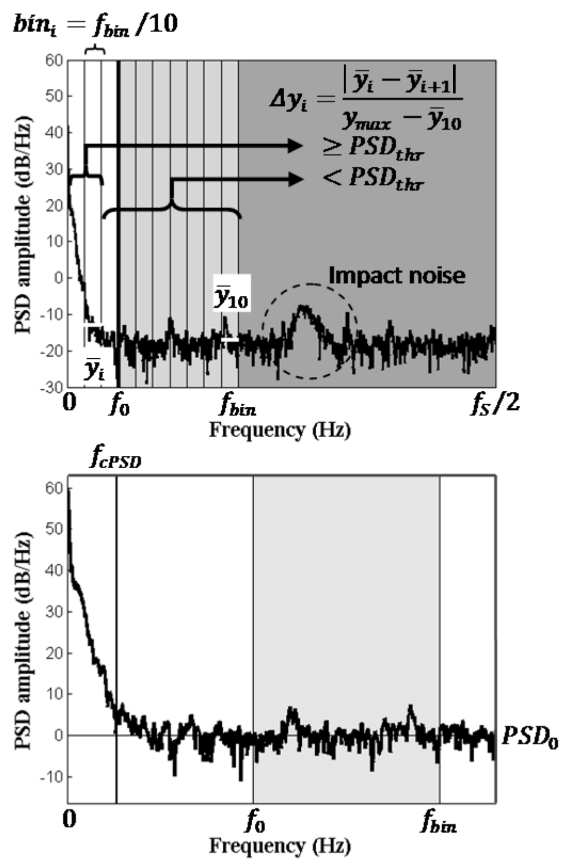

Figure 1: Cutoff frequency using PSD (f_{cPSD}).

RA: Winter's method was used to estimate the RA [2]. Only the residuals between the filtered and unfiltered signals below f_{bin}, i.e. below the impact noise, were considered (Figure 2, top: dark gray area ignored). The tangent line was the slope and intercept of the residuals between f_0 and f_1 (Figure 2, bottom: light gray area for tangent). Note that in the example shown f_1=f_{bin}, but this is not always the case. The RA cutoff frequency (f_{cRA}) was when the residual crossed the RMS of the noise, i.e. the intercept of the tangent line with the ordinate.

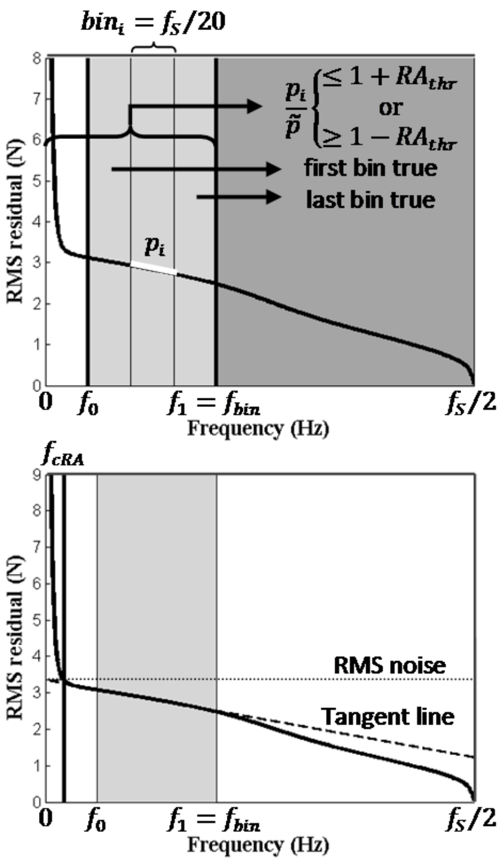

Figure 2: Cutoff frequency using RA (f_{cRA}).

RESULTS AND DISCUSSION

With f_{bin}=200Hz, PSD_{thr}=5% and RA_{thr}=20%, results showed that PSD (f_{cPSD}=76.6±36.3Hz, N=162) and RA (f_{cRA}=54.5±21.1Hz, N=162) gave different cutoff frequencies ($p<0.001$). More importantly, each method gave wide distributions of potential cutoff frequencies, emphasizing the fact that one cannot evaluate the effect of cutoff frequencies on a single signal, trial, factor or participant. Indeed, there is no "optimal" cutoff frequency because of the large variability of human movements, experimental setups and laboratory equipment, with their own signal to noise ratios.

Lean direction (forward, sideways or backward) and filter order (zero-phase-shift 4th or 8th order Butterworth filters) did not affect the performance measures (reaction time, weight transfer time and step time) of our motion analysis results [3]. However, age group (younger, middle-aged or older adults) did affect the performance measures as would be expected. The latter was thus entered as a covariate in the last analysis of variance, which showed that the two cutoff frequencies (55 and 75Hz) had only a negligible effect of 1ms on both reaction time (p=0.035) and step time ($p<0.001$), and no effect on weight transfer time (Table 1). In fact, time histories of the original and filtered signals were indistinguishable.

Table 1: Effect of cutoff frequencies on the performance measure results (mean±SD) [3].

Frequency(Hz)	N	Reaction time (ms)	Weight transfer time (ms)	Step time (ms)
55	36	75±2	162±10	198±5
75	36	76±2	162±10	199±5
Frequency difference		-1±1	0±1	-1±0
$p_{frequency}$		**0.035**	0.121	**<0.001**

CONCLUSIONS

Hopefully, this more user friendly, visual and intuitive approach will ease cutoff frequency selection and lead to a better comprehension of the importance of frequency analysis.

REFERENCES

1. Stergiou N. *Innovative Analyses of Human Movement*, Human Kinetics, 223-258, 2004.
2. Winter DA. *Biomechanis and motor control of human movement*, John Wiley & Sons, 13-58, 2005.
3. Carbonneau E and Smeesters C. 36th Annu Meet Am Soc Biomech, Gainesville FL, 2012.

ACKNOWLEDGEMENTS

Demers and Hamel for technical assistance and NSERC grant 298229-2009 for financial support.

Pilot Study of the Effect of an Acute Vestibular Therapy on Postural Stability of Children with Autism Spectrum Disorder and Typically Developing Children

[1]Senia Smoot, [1]Deborah Kinor and [1]Kimberly Edginton Bigelow

[1]University of Dayton, Dayton, OH, USA
email: senia.smoot@gmail.com web: http://academic.udayton.edu/~ewsl

INTRODUCTION

The prevalence of autism spectrum disorder (ASD) is growing in the United States, resulting in an increased need to expose children with ASD to effective therapeutic interventions [1,2]. Sensory integration (SI) therapy has been successful in improving social behaviors and sustained attention while reducing repetitive mannerisms and hypersensitivity [2]. It is difficult to accurately measure the effectiveness of SI therapy, however, due to the subjective nature of its results [2,3]. A literature search of the terms "SI therapy" "autism" and "evaluation" in Pubmed and Medline databases over the last 30 years yields no studies that quantitatively assess therapy data. One solution to this research gap is to quantitatively assess changes in sensory processing after therapy by measuring changes in physiological systems that require sensory interaction, such as postural control. Researchers have demonstrated that children with autism have atypical balance [4]. Therefore, as an improvement in sensory integration could result in a shift in postural stability, quantitative research could be conducted to determine the effectiveness of a SI program. As work in this field has been so limited to date, a preliminary, exploratory study was undertaken prior to initiating a full scale study. This research sought to determine whether SI therapies produce measurable, physiological trends, as well as identify any challenges that may arise in working with this special population. It was the objective of this pilot study to evaluate postural changes in children after a vestibular swing therapy. A further objective was to determine data trends, experimental feasibility, and data collection procedures for a larger, future study. It was hypothesized that subjects would demonstrate increased postural stability after undergoing a SI swing therapy protocol.

METHODS

Five children were tested for this study (8.6 ± 1.52 years old, 33.7 ± 9.7 kgs, 134.4 ± 12.5 cm). Three subjects were typically developing (TD) and two had been diagnosed with ASD. Subjects were required to be verbal, to have no medical conditions that would affect postural stability, and to have undergone no medication changes six weeks prior to testing. IRB consent was obtained from the University of Dayton prior to testing and the parents of all subjects gave written, informed consent. The test protocol to evaluate therapeutic effect was structured as a pre-test/post test. Subjects underwent static posturography testing on a Bertec Force Plate (BP 5050). Postural sway data was collected under four different sensory conditions: on a flat plate with eyes open/eyes closed, and on a foam pad with eyes open/eyes closed. For both the pre-test and the post-test two trials of every condition were taken, resulting in a total of 16 total trials for the entire session. Data was collected for a period of 20 seconds. As the subjects were younger children and two had ASD, additional measures were taken to increase the likelihood of a successful trial completion. These measures included a researcher quietly counting to 20 during each trial and using a photo of an animal as a visual fixation point. The photos were switched out for variety but the same image was used for each respective test condition – e.g. image A was always used for the eyes open/flat plate condition for each trial and for each subject.

The pre-test was conducted before the subject underwent a 10 minute SI therapy session on a vestibular swing. Following the therapy, the post-test was administered. The anterior-posterior (A/P) and medial-lateral (M/L) center of pressure (COP) data were used to calculate A/P sway range (APSR), medial-lateral sway range (MLSR), and mean velocity (MV). Due to small subject size, statistics could not be performed but trends and percent changes were examined.

RESULTS AND DISCUSSION

One of the purposes of this study was to test the feasibility of having children, including those with ASD, successfully complete the protocol. From this perspective, it appears that the strategies employed were helpful but problems with compliance still existed. Subjects with ASD had to repeat approximately 25% of the trials because they did not follow the testing instructions. Future studies might benefit from alternative means of data collection, such as shorter trials or seated posture.

As the vestibular swing seeks to stimulate vestibular function, there was particular interest in examining the effect of the swing on postural sway during the eyes closed, foam pad condition, as this condition is known to require vestibular reliance to maintain upright stance. After undergoing the swing therapy, 4 of the 5 subjects demonstrated an average A/P sway decrease of 3.95±2.4mm, as seen in Figure 1.

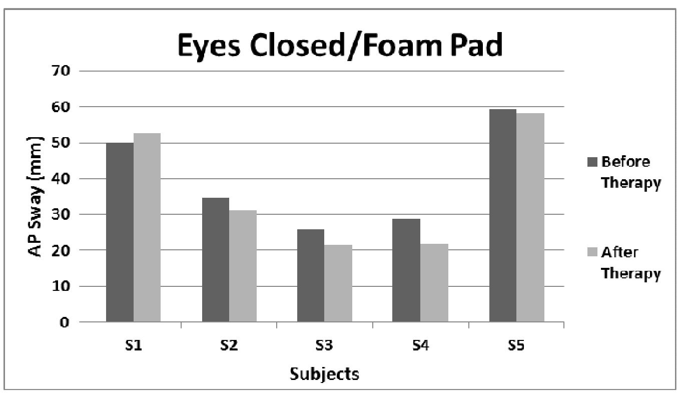

Figure 1: Average A/P sway range while standing on foam pad with eyes closed. Subects 4 and 5 were diagnosed with ASD.

Though minimal clinically important differences (MCID) have yet to be determined for postural sway, the data suggests that most subjects experienced improvements in balance, under this testing condition. Although these improvements are small in magnitude, they were noticeable after just ten minutes of a single therapy session. Future work should examine the effect of exposure to this therapy longitudinally.

Mean Velocity revealed perhaps the most interesting trends as subjects with ASD exhibited decreased MV (generally indicative of improved postural control), whereas the TD children exhibited increased mean velocity (generally indicative of poorer control). Future work should target this particular outcome to determine whether these findings exist in a larger data set, and seek to explain why these differences would exist. It is possible that the vestibular swing routine is only beneficial to those with sensory processing issues (i.e. children with ASD). On the other hand, despite the increases in MV, A/P and M/L sway ranges did not indicate poorer performance.

Although this study is limited by a small sample size, it is the first of its kind to indicate that SI therapy does produce measureable, albeit small, changes in postural control. If more information about SI therapy's physiological effect is procured, then it may be possible to start optimizing therapy sessions by identifying best evidence based practices. Furthermore, if the therapy is found to be beneficial, families may have grounds to seek reimbursement, increasing the number of children with ASD who could be exposed to this therapy.

CONCLUSIONS

It was found that SI therapy leads to small changes in postural stability in children with ASD. The clinical and practical significance of these findings is yet to be determined.

REFERENCES

1. Mash, Eric , Barkley Russell, editor. Treatment of childhood disorders. 2006.
2. Reynolds, S., et al. Journal of Neurodev Dis. 2010;2(3):120-32.
3. May-Benson, T. The Amer J of Occu Ther. 2010(64):403-14.
4. Molloy, C et al. Postural stability in children with ASD. J Autism Dev Disord. 2003;33(6):643-52.

ACKNOWLEDGEMENTS

This work has been supported by the NSF GRFP, researchers Abby Spohn and Martin Piszkiewicz, and Southpaw Enterprises and Therapy Connections for lending equipment.

QUANTIFICATION OF MUSCULOSKELETAL LOADING PROFILE OF THE THUMB DURING PIPETTING

[1*]John Z. Wu, [1]Erik W. Sinsel, [1]Justin F. Shroyer, [1]Daniel E. Welcome,
[2]Kristin D. Zhao, [2]Kai-Nan An, [1]Frank L. Buczek
[1] National Institute for Occupational Safety and Health, Morgantown, WV, USA. [2] Mayo Clinic, Rochester, MN, USA. *Email: jwu@cdc.gov

INTRODUCTION

Manual pipetting involves repetitive motion of the thumb for extracting and dispensing fluids, during which the muscles/tendons and articular joints of the thumb, hand and wrist are exposed to both highly repetitive motion and high loading. A survey-based study [1] showed that almost 90% of pipette users, who continuously used pipettes for more than an hour on a daily basis, reported hand and/or elbow disorders. One of the proposed mechanisms of the tenosynovitis is friction between the tendons and their synovial sheaths [2]. The friction is caused by the sliding of the tendon in its sheath and the contact force between the tendon and the sheath. Based on that injury mechanism, it is proposed to use tendon travel (i.e., displacement) as one of the measures to evaluate the biomechanical profile of selected occupational hand-intensive tasks [3]. The tendon displacement (or tendon excursion) has been utilized to quantitatively evaluate the biomechanical stress among different typing jobs [3]. In this study, we quantified tendon displacement to assess the cumulative loading exposure of the musculoskeletal system in the thumb during pipetting.

METHODS

The hand was modeled as a multi-body linkage system and includes four fingers (index, long, ring, and little finger), thumb, and a palm segment (Fig. 1B). Each of the fingers is comprised of a distal, an intermediate, and a proximal phalanx and a metacarpal. The thumb is comprised of a distal and a proximal phalanx, a metacarpal bone, and a trapezium. The metacarpals of the four fingers and the trapezium of the thumb were considered to be fixed to the palm segment. Although the model includes the entire hand, we have analyzed only the biomechanics of the thumb because it is the focus of the current study. The model includes only nine muscles that are attached to the thumb via tendons: flexor pollicis longus (FPL), extensor pollicis longus (EPL), extensor pollicis brevis (EPB), abductor pollicis longus (APL), flexor pollicis brevis (FPB), abductor pollicis brevis (APB), the transverse head of the adductor pollicis (ADPt), the

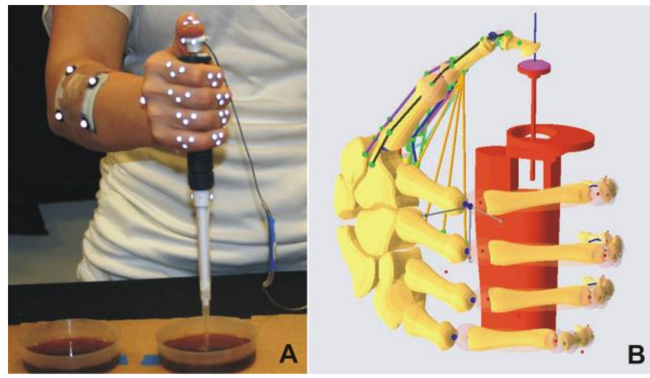

Figure 1. Experimental set-up and model. A: The subject operating the pipette during the testing. B: The AnyBody model of pipetting.

oblique head of the adductor pollicis (ADPo), and opponens pollicis (OPP). The model was developed using the commercial software package AnyBody (v4.0, AnyBody Technology, Aalborg, Denmark).

A typical thumb-activated pipette was used in the study (Fig. 1A). The pipette is actuated by a thumb-push button to extract and to dispense fluid, whereas there is a separate button to eject the disposable tip. Eight subjects (four male and four female; age 27.5(2.6) years; body mass 89.2(25.3) kg; height 170.1(8.6) cm) participated in the study following informed consent approved by the local human subjects committee. All subjects were right-handed laboratory technicians with a minimum of two years of experience using manual pipettes on a daily basis. The subjects first pressed the plunger to the first stop, extracted the sample fluid from the container by releasing the plunger, pointed the tip to a second container, and dispensed the fluid by depressing the plunger to the second stop (Fig. 1A). The subjects were instructed to repeat the same procedure for one minute in a test session.

Kinematics for the fingers, hand, and forearm were determined using methods previously described [4]. Retro-reflective markers (4 mm diameter hemispheres) were applied individually on the finger/thumb/hand segments using a thin self-adhesive tape (Fig. 1A). The measurement model consists of 12 finger segments (three segments for each of the four fingers), three thumb segments, a hand, and a forearm, with a total of 55 tracking markers being used to obtain pipetting kinematics. A 14-camera Vicon Nexus system (Oxford Metrics Ltd., Oxford England) provided marker trajectories at 100 Hz, with calibration residuals less than 0.5 mm for a control volume approximately 3 m (wide) x 3 m (long) x 2 m (high).

RESULTS

The accumulated tendon displacements during one hour were calculated by the sum of the tendon displacements in the time-histories, assuming that each subject's pipetting rate was maintained constant during a period of one hour (Figure 2 and Table 1). The accumulated tendon displacement in a work cycle is two times the magnitude of the maximal tendon displacement within the cycle. The average work period of pipetting of individual subjects is also listed in Table 1. The maximal accumulated displacement was found in the FPL and it reached approximately 29 m.

DISCUSSION AND CONCLUSIONS

We calculated the kinematics and tendon displacements during pipetting in the current study. Maximal tendon displacement during the pipetting was found in the FPL tendon. The average hourly accumulated tendon displacements in the FPL during pipetting was estimated to be 28.7 m (11.2-46.5 m), which was in a range of those observed in other occupational activities, such as typing and nail gun operations. Our results showed that the tendon displacement data contain relatively small standard deviations despite the high variances in the thumb kinematics (results not shown), suggesting that the accumulated tendon displacement may be used as a suitable parameter to evaluate the musculoskeletal loading profile.

REFERENCES

[1] David G, Buckle P. *Appl Ergon* 28 (4) (1997) 257–62.
[2] Moore A, Wells R, Ranney D. Ergonomics 34 (12) (1991) 1433–53.
[3] Sommerich CM, Marras WS, Parnianpour M, Clin Biomech (Bristol, Avon) 13 (4-5) (1998) 261–271.
[4] Buczek FL, Sinsel EW, Gloekler DS, Wimer BM, Warren CM, Wu JZ. *J Biomech* 44(9) (2011) 1805-9.

DISCLAIMER

The findings and conclusions in this report are those of the authors and do not necessarily represent the official position of the National Institute for Occupational Safety & Health. The mention of trade names, commercial products, or organizations does not imply endorsement by the US Government.

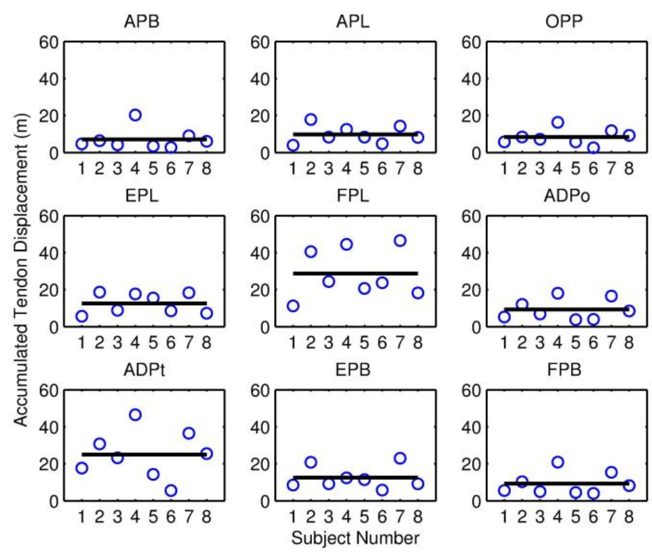

Figure 2. Accumulated tendon displacements during one hour for all eight subjects, assuming that subjects' pipetting rates were maintained constant during the pipetting.

Table 1. Average pipetting rate and accumulated tendon displacements during one hour for all eight subjects.

Tendon Displacement (m)	Subject Number 1	2	3	4	5	6	7	8	Mean	SD
APB	4.6	6.4	4.2	20.3	3.5	2.7	9.0	6.0	7.1	5.7
APL	3.9	17.8	8.3	12.5	8.3	4.8	14.3	8.1	9.8	4.8
OPP	5.7	8.4	7.2	16.3	5.7	2.6	11.8	9.3	8.4	4.2
EPL	5.6	18.7	8.9	17.7	15.5	8.5	18.3	7.2	12.5	5.5
FPL	11.2	40.6	24.3	44.5	20.7	23.7	46.5	18.2	28.7	13.3
ADPo	5.2	12.0	6.8	18.0	3.7	3.9	16.5	8.4	9.3	5.6
ADPt	17.6	30.8	23.2	46.5	14.3	5.6	36.5	25.5	25.0	13.0
EPB	8.5	20.8	9.2	12.4	11.4	5.8	23.0	9.2	12.5	6.1
FPB	5.5	10.3	5.0	20.9	4.4	4.0	15.4	8.2	9.2	6.1
Period (s)	4.8	2.1	4.1	2.4	3.5	4.6	2.4	4.6	3.6	1.1

COMPARISON OF THE KINEMATICS OF THE THRESHOLD OF BALANCE RECOVERY OF TWO POSTURAL PERTURBATIONS: LEAN RELEASE AND SURFACE TRANSLATION

[1,2]Victorien Thiaux, [3]Stephen N. Robinovitch and [1,2]Cécile Smeesters

[1]Research Center on Aging, Sherbrooke QC, Canada
[2]Department of Mechanical Engineering, Université de Sherbrooke, Sherbrooke QC, Canada
[3]Department of Biomedical Physiology and Kinesiology, Simon Fraser University, Burnaby BC, Canada
e-mail: Cecile.Smeesters@USherbrooke.ca web: http://www.usherbrooke.ca/gmecanique

INTRODUCTION

Balance recovery has been studied using a variety of postural perturbations such as lean releases, pulls, slips, surface translations and trips. Although the same step initiation, execution and geometry variables are often measured, to our knowledge only two studies have attempted to compare results from different postural perturbations.

Mansfield and Maki [1] compared medium pulls and surface translations while standing and walking in place in multiple directions and in both younger and older adults. Moglo and Smeesters [2] compared large forward lean releases, lean releases with pulls and pulls while walking in both younger and older adults. Moreover, the latter study was done at the threshold of balance recovery, since avoiding a fall was not always possible.

The purpose of this study was to continue these comparison efforts by comparing the kinematics of lean releases and surface translations at the threshold of balance recovery in younger adults.

METHODS

Six younger women (mean±SD=27.5±3.5yrs, range=22-30yrs) and 6 younger men (25.0±3.0yrs, 23-32yrs) participated in this study. We determined the maximum forward initial lean angle from which each participant could be suddenly released and still recover balance using a single step (Figure 1a). We also determined the maximum backward surface translation velocity from which each participant could be suddenly pulled and still recover balance using a single step (Figure 1b). Both postural perturbations resulted in forward losses of balance and their order was randomised by gender.

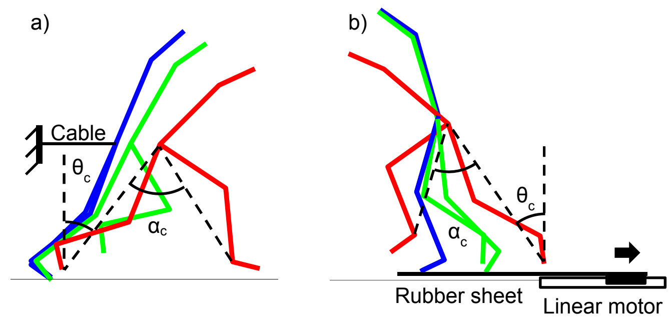

Figure 1: a) lean release and b) surface translation perturbations at onset of perturbation (blue), toe off (green) and heel strike (red).

For the lean release perturbation, participants were leaned forward from standing using a cable attached to a pelvic belt. The initial lean angle stared at ~10deg and was increased in ~5deg increments at each successful trial, until participants failed to recover balance twice at a given initial lean angle. For the surface translation perturbation, participants stood on a rubber sheet pulled backward by a linear motor. The translation velocity started at 1m/s and was increased in 0.25m/s increments at each successful trial, until participants failed to recover balance twice at a given translation velocity. Translation displacement and acceleration were kept constant at 700mm and 2.5m/s^2, respectively. For both postural perturbations, balance recovery was successful if participants used no more than one step (as instructed), did not touch the ground with their hands, and did not support their body weight in the safety harness (cable remained slack).

Using 2 force platforms and 1 load cell at 1000Hz, and 8 optoelectronic cameras with 16 passive markers at 100Hz, the following kinematic variables were obtained: maximum lean angle and maximum translation velocity, as well as reaction time, weight transfer time, step time, step velocity, step length and the ratio of stepping (α_c) over lean angle (θ_c) at heel strike (Figure 1) at the maximum perturbations.

For each perturbation, t-tests were used to confirm that the effect of gender on the maximum lean angle and the maximum translation velocity were not significant. Paired t-tests were then used to determine the effect of the two postural perturbations on each of the kinematic variables at the maximum perturbations.

RESULTS AND DISCUSSION

As expected, the maximum lean angle (p=0.772) and the maximum translation velocity (p=0.245) were not affected by gender.

At the maximum perturbations, the two postural perturbations did not have a significant effect on reaction time (p=0.057). However, the type of perturbation did affect weight transfer time (p=0.005), step time (p<0.001), step velocity (p=0.012), step length (p<0.001) and the ratio of stepping over lean angle at heel strike (p<0.001). Specifically, weight transfer times were longer while step times were shorter for surface translation. Step velocities were slower and step lengths were smaller for surface translation. Finally, the ratio of stepping over lean angle at heel strike was smaller for surface translation.

It is important to note that our results could have been affected by our experimental setup. For safety reasons, both lean releases and surface translations were conducted on top of a firm gymnasium mat (8ft or 2.4m long). For the lean release trials, participants started ~0.3m from one end of the mat and had nearly 2.1m of mat to recover balance by stepping. However, for the surface translation trials, participants started in the middle of the mat, were translated backward 0.7m and then had 1.9m of mat to recover balance by stepping. Some participants later reported being afraid of stepping off the mat given that the initial impression was of only 1.2m of mat available for stepping. Participants may thus have taken smaller step lengths in shorter step times, which lead to slower step velocities and smaller stepping over lean angle ratios.

CONCLUSIONS

From the onset of the perturbation to the onset of reaction, both perturbations are similar in their kinematics. However, the two perturbations do differ in their kinematics from the onset of reaction to heel strike, although these results could have been affected by our experimental setup and should be validated in future experiments.

REFERENCES

1. Mansfield A and Maki BE. *J Biomech* **42**, 1023-1031, 2009.
2. Moglo KE and Smeesters C. *30th Annu Meet Am Soc Biomech*, Blacksburg VA, 2006.

ACKNOWLEDGEMENTS

The personnel at the Injury Prevention and Mobility Laboratory for technical assistance as well as NSERC grant 298229-2009 and CIHR grants AMG-100487 & TIR-103945 for financial support.

Table 1: Effect of the postural perturbation on kinematic variables at the maximum perturbations (mean±SD).

Postural Perturbation	Gender	Maximum Lean Angle (deg) or Translation Velocity (m/s)	Reaction Time (ms)	Weight Transfer Time (ms)	Step Time (ms)	Step Velocity (m/s)	Step Length (mm)	Stepping angle (α_c) / Lean angle (θ_c)
Lean Release (LR)	YW	26.9±3.4deg	95±7	137±22	223±43	4.25±0.13	947±191	1.79±0.17
	YM	27.8±6.3deg	99±6	126±24	197±22	5.02±0.47	982±87	1.97±0.10
	Total	27.3±4.8deg	97±7	131±23	210±35	4.64±0.52	965±143	1.88±0.16
Surface Translation (ST)	YW	2.29±0.43m/s	97±9	157±28	171±14	4.14±0.27	711±95	1.41±0.20
	YM	2.54±0.25m/s	105±7	161±23	162±16	4.27±0.51	694±126	1.31±0.20
	Total	2.42±0.36m/s	101±8	159±24	166±15	4.21±0.39	702±107	1.36±0.20
$p_{\text{Perturbation}}$			0.057	**0.005**	**<0.001**	**0.012**	**<0.001**	**<0.001**
Perturbation difference	Mean			-28	43	0.43	262	0.52
	95% CI			-45/-10	23/63	0.11/0.75	180/345	0.35/0.70

YM: Younger Men (N=6), YW: Younger Women (N=6). Significant p-values (p≤0.05) are **bolded**.

BIOMECHANICAL RESPONSE TO LADDER SLIPPING EVENTS: EFFECTS OF HAND PLACEMENT ON RESPONSE AND RECOVERY

[1]Alyssa J. Paul, M.S., [1]Marissa Lovell, [1]Naira Campbell-Kyureghyan, Ph.D. and [1]Kurt Beschorner, Ph.D.

[1]University of Wisconsin Milwaukee, Milwaukee, WI, USA
email: paulaj@uwm.edu

INTRODUCTION

Falls are one of the most frequent work-related events causing fatal injury [1]. In 2011, the use of ladders resulted in 116 fatal injuries [2]. Additionally, non-fatal injuries involving ladders resulted in the most time away from work (a key measure of injury severity) at 14 days [2]. Studies have investigated the role of hand placement and grip strength during unperturbed ladder climbing [3, 4], as well as ladder design and orientation [5]. Few studies have considered ladder climbing as a whole body process or examined the body's response to a slip while climbing a ladder. This study characterizes the event sequencing of unexpected slips from a ladder and investigates muscle response to a slip. Furthermore, this study aims to identify differences in the response time to a ladder slip when using a rail grasping climbing strategy compared with a rung grasping strategy.

METHODS

IRB approval and informed consent were obtained from thirty-two subjects (10 females) aged 18 to 65. Inclusion criteria required regularly climbing a ladder. Exclusion criteria included: weight over 250 pounds, pregnancy and musculoskeletal, neurological or balance disorders. All subjects were fitted with shoes, athletic clothing and a harness. Forty-six reflective markers and 12 EMGs were placed on the subjects. Bilateral muscles included the vastus laterales, medial hamstrings, anterior deltoids, biceps, triceps, and forearm wrist flexors. A custom, vertically oriented ladder was equipped with a spinning fourth rung, which could be set in a position to freely spin or be secured. Marker position and EMG data were captured at 100 Hz and 1000 Hz respectively, via a Motion Analysis Corporation System (Santa Rosa, CA).

Subjects were randomly assigned to two different climbing strategies with their hands placed on the rung (RG) or rail (RL). A climbing trial consisted of one ascent and one descent of the ladder. For each climbing strategy, the subject performed 5 to 6 unperturbed trials, with the slip rung locked in place and then one trial with the slip rung allowed to freely spin to induce a slip or fall. In-between trials the subjects performed a fatigue walk outside of the lab so they were unaware of status of the spinning rung.

A belaying system (including: belayer, spotter, harness and impact mat) was used to ensure safety of all participants. Slips were defined as when the foot completely slipped off the slip rung during a perturbed trial. Slips and falls were analyzed with respect to their unperturbed baseline trials.

Events during climbing such as foot contact and foot off were identified by tracking the vertical position of markers attached to the foot during climbing. A second order, high pass Butterworth filter, with 10 Hz cutoff frequency, was applied to the electromyography (EMG) data. After filtering, root mean squared (RMS) signal smoothing was performed with a time constant of 30 ms. The resulting RMS signals for each trial were then normalized to maximum activity from baseline climbing. For each climbing strategy, the normalized RMS signals of the unperturbed trials were averaged together to provide mean and standard deviation baseline muscle activity. Muscle response onset was identified when the slip EMG activity exceeded 1 standard deviation of baseline climbing activity for a minimum of 50ms. An ANOVA was performed to determine the effect of hand placement on the onset of muscle activity after slip initiation.

RESULTS AND DISCUSSION

Of the 64 total perturbed trials, 16 resulted in slips, of which 5 became falls. Ten slips occurred on the rails and 6 slips on the rungs. Four of the 5 falls occurred with a rail hand placement. The average (standard deviation) time of events of a slip trial during ladder climbing were: 0 ms: the foot makes contact with the rung that is allowed to spin freely (the perturbed foot); 153 ms (64 ms): the foot contralateral to the slip steps off of the ladder rung; 218 ms (151 ms): perturbed foot slip is then initiated; 445 ms (196 ms): if there is a hand in motion it makes contact with the ladder; 602 ms (118 ms): the foot contralateral to the slip reestablishes contact with the ladder; 1428 ms (537 ms): the slip foot reestablishes itself on the ladder. Thus, ladder slips typically occur when one of the feet is in motion and all of the weight is being born on the slippery rung. The hands typically grasp the rungs during the initial part of the recovery period and then are followed by the leg contralateral to the slip reestablishing itself on the rung. The last event in the sequence is reestablishing the slip foot back on the rung. While the hands are first to respond to a ladder slip, the recovery process is a full body action, which occurs over a full second duration. Therefore, interventions aiming to improve recovery from ladder slips should consider both the upper and lower body contributions to recovery.

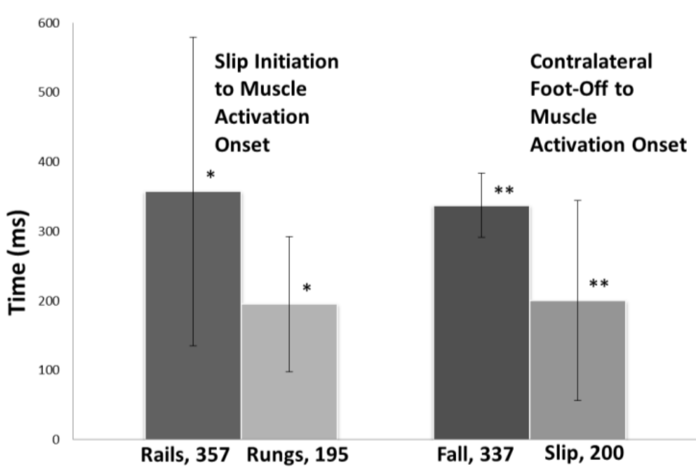

Figure 1: Average (standard deviation bars) time delay between slip initiation and muscle activation onset for rung versus rail hand placement and between contralateral foot-off and muscle activation onset for falls versus slips. (Statistically significant: * $p<0.001$, ** $p<0.01$)

The average delay of first muscle activation onset after slip initiation for all the slip trials ranged from 192 ms to 465 ms. A shorter delay occurred between slip initiation and first muscle activation onset for rung hand placement at 195 ms (97 ms) than rail hand placement at 357 ms (222 ms) ($p<0.001$), Figure 1. One possible explanation for this reduced response time is that participants may not have perceived the slip as quickly when holding rails because feeling a force tangential to the hands may be more difficult to detect than forces normal to the hand surface. For all of the slip trials the average delay between contralateral foot step off and the first muscle activation was 251 ms. Interestingly, slip trials where participants recovered had an onset of 200 ms (144 ms) while participants who fell had an onset time of 337 ms (46 ms) ($p<0.01$), Figure 1. Therefore, a slower onset time was associated with reduced ability to recover.

CONCLUSIONS

This study suggests that ladder slips typically initiate when one foot bears most of the body's weight. The recovery strategy is characterized by initially resetting the hands on the ladder and then resetting the feet back on the ladder. Holding on to the rails led to slower response times, which were associated with falling incidents. Therefore, grasping the ladder rungs during ladder climbing may be preferable for recovery from accidents.

REFERENCES

1. U.S Department of Labor- Bureau of Labor Statistics (BLS), *Census of Fatal Occupational Injuries*, 2010: Washington, D.C.
2. U.S Department of Labor- BLS, *Nonfatal Occupational Injuries and Illnesses Requiring Days Away from Work*, 2011: Washington, D.C.
3. Armstrong et al., 2009, *Proc Hum Fact Ergon Soc Annu Meet.* p. 935-39
4. Young et al., 2009, *Human Factors.* 51(5): p. 705-17
5. Bloswick and Chaffin, 1990, *Int J Ind Ergon,* 6(1): p. 17-27

ACKNOWLEDGEMENTS

This work was funded by University of Illinois-Chicago/NIOSH/CDC (5T42OH008672-08) and NIOSH R21 OH010038.

Effect of Compliant Flooring on Postural Stability in an Older Adult Population

Renee Beach, Kurt Jackson, PhD, Kimberly Edginton Bigelow, PhD

University of Dayton, Dayton, OH, USA
email: beachr1@udayton.edu

INTRODUCTION

Falls are prevalent in older adults, with one out of three adults age 65 and over falling each year [1]. Of those who fall, 20-30% will suffer moderate to severe injuries, leading to a decrease in quality of life, loss of mobility and an increased risk of death [2]. These issues are especially apparent in nursing homes, with nearly 40% of admissions stemming from falls and as many as 75% of residents falling annually [3,4]. Hip protectors have been proposed as a proven means of preventing fall-related injuries. However, a study that analyzed 24 hour compliance at residential care homes showed that of the 51% of residents who agreed to wear hip protectors, compliance at night was as low as 3% [5]. Since many individuals prefer not to wear hip protectors and yet falls continue to be a problem, it has been proposed that modifying flooring to be more compliant may be an alternative to reduce the risk of injuries from falls. Two commercially-made compliant floors have been identified as a passive intervention approach that may protect against multiple types of fall-related injuries by reducing femoral impact by up to 50% [6]. It has been proposed that the increased compliance in these floors minimally impacts balance, however, work in this area has been limited to date. The objective of this study was to analyze the effect of compliant flooring (SofTile and SmartCell) on quiet-standing and limits of stability in an older adult population.

METHODS

Ten healthy older adults participated in this study (4 female, 6 male; mean age 72.6 ± 7.6 years; mean height 169.9 ± 9.8 cm; mean weight 80.3 ± 15.9 kg). All subjects were free of diseases, disorders, or injuries that may have affected their ability to walk or stand without assistance. Subjects gave written informed consent and the University of Dayton IRB approved all procedures.

Each subject performed static balance tests while barefoot on a force plate (Bertec Corporation, Model BP 5050). The main factor of interest was the flooring condition: flat plate, SofTile, and SmartCell. Two trials of each the eyes open (EO) and eyes closed (EC) conditions, and the Limits of Stability (LOS) test, were collected on each floor in a random order, totaling 18 trials per subject. For the EO and EC conditions subjects were told to stand comfortably with their feet about hip width apart, looking straight ahead, arms at their side, without talking, and while remaining as still as they could. Anterior-posterior (A/P) and medial-lateral (M/L) center of pressure (COP) data was collected for thirty seconds at 1000 Hz for each trial. For the LOS condition the subjects were instructed to lean forward, backward, to the left, and to the right using an ankle strategy. Subjects stepped off of the plate after each floor sample and were given a 3-minute break. From the COP data the A/P Sway Range, M/L Sway Range and Mean Sway Velocity were calculated. A multivariate analysis of variance (MANOVA) was performed to determine the statistical significance ($p<0.05$) of the flooring conditions, as well as vision. A post hoc analysis to compare between floorings was also performed.

RESULTS AND DISCUSSION

Figure 1 shows the mean A/P and M/L sway ranges for quiet-standing on each of the flooring samples. Statistical analysis revealed that the factor 'flooring' significantly affected A/P Sway Range measures ($p=0.029$). No statistical differences existed for the other postural sway parameters. Though vision did, as expected, significantly affect postural sway, an interaction between vision and flooring was not found ($p>0.05$ for all). Table 1 provides the p-values for the statistical analysis.

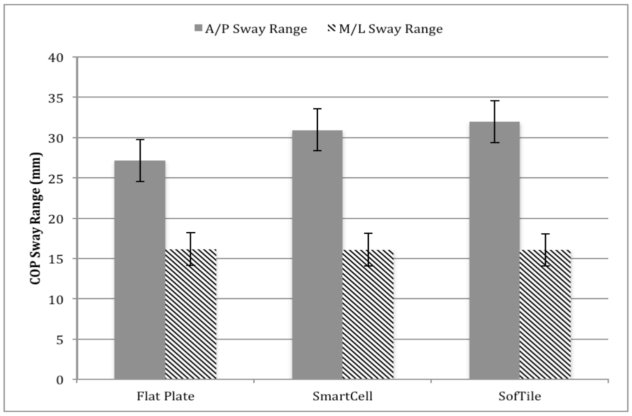

Figure 1: Mean A/P and M/L Sway Ranges for each floor condition, with error bars representing the 95% confidence intervals.

Table 1: P-values for flooring and vision, with statistically significant ($p<0.05$) denoted with *

COP Measure	Floor	Vision
A/P Sway Range	0.029*	0.000*
M/L Sway Range	0.997	0.096
Mean Velocity	0.211	0.000*

A post-hoc analysis revealed that for the A/P Sway Range results statistical differences were seen for the Flat Plate-SofTile (p=0.044) and Flat Plate-SmartCell (p=0.012) comparisons, but there was no statistical significance for the SmartCell-SofTile (p=0.582) comparison. A/P Sway Range was higher on the compliant surfaces, indicating increased instability/poorer performance.

These results suggest that compliant flooring may have an effect on the postural stability of an individual while standing. These findings are similar to those of Wright et al. who found small but significant differences in postural stability during quiet-standing across flooring samples in older women [6]. Increased sway can be an indicator of decreased postural instability and has previously been linked to increased likelihood of falling. More research now needs to be done to determine the implications of the significant, yet rather small (approximately 5 mm), differences observed in A/P Sway Range results.

This study also included the Limits of Stability task to examine how the flooring might impact movements requiring weight shifting. To date it appears that this is the first study to analyze LOS on compliant flooring. No statistically significant differences were found in sway ranges during the Limits of Stability task. With an observed power of 0.184 for A/P sway range and 0.124 for M/L sway range, more participants are needed to confirm this conclusion. Trends suggest individuals may achieve more range of motion (larger LOS) in the A/P direction on the flat plate, while the M/L sway range does not appear affected. It is possible that with a larger sample, these trends may become significant.

Future work is now underway to examine the effects of the compliant flooring on postural stability in older adults at higher risk of falling due to neurological impairment. This work will also examine how the flooring affects more functional movements such as while turning or retrieving an object from the floor.

CONCLUSIONS

It was found that compliant flooring may influence postural stability during quiet standing in the A/P direction. The clinical and practical significance of these findings as it relates to the dynamic balance and fall risk is yet to be determined.

REFERENCES

1. Hausdorff JM, et al. *Arch.Phys.Med.Rehabil.* 2001; **82**: 1050-1056
2. Alexander BH, Frederick P, Rivara and Wolf ME. *American Journal of Public Health* 1992; **82**: 1020-1023
3. American Geriatrics Society. *JAGS* 2001; 664-672
4. Centers for Disease Control and Prevention. 16 Sept 2011; 20 Jan 2012
5. Cryer C, Knox A, Martin D and Barlow J. *Injury Prevention* 2002; **8**: 202-206
6. Wright AD, Laing AC and Laing AC. *Accident Analysis and Prevention* 2011; **43**: 1480-1487

ACKNOWLEDGEMENTS

This work was supported by a National Science Foundation Graduate Research Fellowship to Renee Beach. The authors also wish to thank Haluk Ay.

DETERMINING VESTIBULAR CONTRIBUTIONS TO POSTURAL CONTROL DURING STANDING USING SUPRATHRESHOLD MECHANICAL STIMULATION

[1,2]Jung Hung Chien and [1]Mukul Mukherjee

[1]Nebraska Biomechanics Core Facility, University of Nebraska Omaha, Omaha, NE, USA
[2]College of Public Health, University of Nebraska Medical Center, Omaha, NE, USA
email: jchien@unomaha.edu web: http://nbcf.unomaha.edu/

INTRODUCTION

Successful postural control requires the integration of three major sensory systems: visual, somatosensory, and vestibular system [1]. A decline in postural control (e.g. increased center of pressure sway) is common in patients with vestibular disorders. The Sensory Organization Test (SOT; NeuroCom, Clackamas, OR, USA) has been widely used to investigate postural control during standing for patients with vestibular disorders. It categorizes patients with vestibular disorders into three groups: vestibular loss pattern, sensory selection pattern, and visually dependent pattern [2]. Patients identified having the vestibular loss pattern lose all sense of orientation and lose their balance in the SOT test conditions 5 and 6 in which orientation information from both proprioceptors and visual feedback are altered and the subject is forced to rely only on vestibular information. However, these patients can perform as well as normal subjects in conditions 1 through 4, in which sensory information from two sources is available to them. This type of patient is usually the patient with vestibular loss over a period of time. Such patients can use either visual or somatosensory information to compensate for the loss of the vestibular feedback for postural control [2]. In contrast to the patients with vestibular loss, patients who have uncompensated vestibular disorders may show increased sway in conditions where either the visual or the somatosensory system was perturbed or both the visual and the somatosensory systems were perturbed simultaneously [3]. These patients have difficulty orienting in conditions in which either or both the visual and the somatosensory systems are perturbed due to incomplete CNS adaptation to a vestibular lesion. This pattern of results is typical of patients with acute stages of vestibular lesions. Some patients who have distorted but not absent vestibular function such as acute hydrops which alters but does not eliminate vestibular input, show a visually dependent pattern of sensory organization [4]. These patients are sensitive to the visual sway-reference. Unfortunately, patients with vestibular disorders usually have vertigo, which might hinder the true response of the vestibular system to different environments. Besides, it is unknown whether the subjects sway more under unilateral or under bilateral vestibular stimulation when they stand under conflicting visual and somatosensory systems information. We attempted to answer this question by using suprathreshold mechanical vestibular stimulation (sMVS).

METHODS

Eight healthy young adults (24.7±5 years) were instructed to maintain their balance while standing on the Smart Balance Master (NeuroCom, Clackamas, OR, USA). The research module of the SOT was selected to investigate how participants maintained their balance under different conditions. Each trial lasted 90 seconds. There were total six sensory challenging conditions: 1) normal, 2) vision-blocked, 3) visual sway-reference, 4) surface sway-reference, 5) vision-blocked, surface sway-reference, and 6) visual and surface sway reference condition. In general, conditions 5 and 6 were used to indirectly detect the participant's ability to use inputs from the vestibular system to maintain balance. The suprathreshold mechanical vestibular stimulation (sMVS) contained two vibrating elements, called tactors (Engineering Acoustics, FL, USA.), were placed on the mastoid process on each side to perturb the vestibular feedback signals (Figure 1). The frequency and magnitude of the stimulation were communicated wirelessly to the tactor controller unit which transmitted these signals through cables to the tactors. The frequency of sMVS was set to 349 Hz and the magnitude was set to 17.5 db. A pulsed firing pattern was used where the duration of the firing period was 0.3 second and the duration of the resting period was 0.6 second. Three types of sMVS were given to the participants: bilateral, unilateral or none/control. A total of 18 trials were randomly arranged for each participant (3 sMVS types by 6 conditions). For unilateral stimulation, one side was randomly selected for each subject at the beginning of experiment and this side was consistent for all the unilateral trials. A performance index (PI) was calculated to determine the extent to which the body's sway in the Anterior-Posterior (AP) direction approached the limits of stability during the 90-second trials. The PI was calculated by numerically integrating the rectified COP signal in the AP direction (with the steady-state offset removed), and then scaling the result as a percentage of the maximum center of pressure signal in the AP direction. PIs near zero indicated a highly stable stance while stance was unstable when the PIs approached 100. A two-way mixed ANOVA was used to identify the effect of the sMVS type and sensory condition on the PI.

Figure 1. A) The tactors were secured by a cap and placed on the mastoid process on each side. B) The tactor controller unit: for communicating with the computer through bluetooth and transmit stimulus control signals to the tactors. C) A subject doing the SOT test on the NeuroCom with the tactors attached to the mastoid process.

RESULTS AND DISCUSSION

A significant main effect for the different sensory conditions was found (F=119.063, p<0.0001). A significantly main effect of the sMVS type was also found (F=5.709, p=0.01). A significant interaction of conditions and sMVS types was determined (F=2.881, p=0.003). Pairwise comparisons with Bonferroni correction indicated that the PI was significantly larger in condition 5 and condition 6 than any of the other four sensory conditions (Figure 2). This was true for all the sMVS types: non-sMVS, unilateral sMVS and bilateral sMVS. In addition, the PI was significantly larger when receiving unilateral sMVS than when receiving bilateral sMVS (p<0.0001) and when receiving no sMVS (p<0.0001) in condition 2 and condition 4 (Figure 2). In addition, the pairwise comparison showed that the PI was smaller when receiving no sMVS in comparison with when receiving bilateral sMVS (p=0.002) and when receiving unilateral sMVS (p=0.006) in the condition 6 (Figure 2).

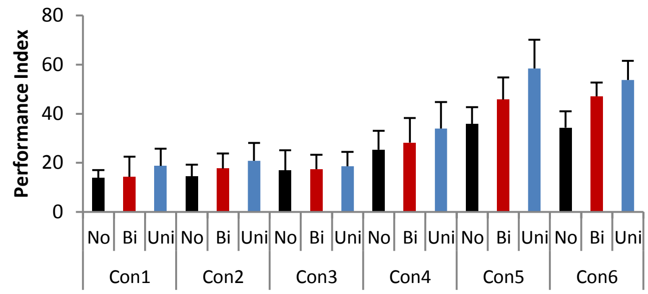

Figure 2. The performance index for the six SOT conditions under the two sMVS conditions.

Our study confirmed that using sMVS induced more body sway in the condition 5 and 6 than in the normal standing condition and sMVS caused healthy young subjects to behave like patients with vestibular loss. In addition, healthy young individuals swayed more under unilateral sMVS than under bilateral sMVS in conditions 5 and 6. This result is different from a previous study in which patients with bilateral vestibular loss swayed more than patients with unilateral vestibular loss in condition 5 [5]. Vestibular patients, because of long term sensory issues, may have learned how to use residual sensory systems for achieving better postural control. Therefore, unilateral loss had better results than bilateral. However, in an acute situation like in this study, postural control, which is primarily a bilateral coordination task, is affected more during unilateral stimulation in comparison to bilateral stimulation. Therefore, in the current study, postural control required less computational effort from the CNS for multisensory reweighting during bilateral vestibular stimulation than unilateral.

REFERENCES

1. Patla AE, et al., *J Exp Psychol Hum Percept Perform* **17**, 603-634, 1991.
2. Black FO, et al., *Progress in Brain Research* **76**, 263-275, 1988.
3. Zacharias G, et al., *Exp Brain Res* **41**, 159, 1981.
4. Black FO, et al., *Acta Otolaryngol*, **406**, 110, 1984.
5. Mbongo, et al., Audiology Neurotology **10**, 291, 2005.

ACKNOWLEDGEMENTS

This work was funded by the NASA EPSCoR grant (NNX11AM06A).

SINGLE-LEG STATIC STABILITY IN FIT, YOUNG ADULTS: LOWER EXTREMITY STRENGTH AND CORE STRENGTH AS PREDICTORS

Christopher Silvernale, Gary D. Heise, Emily Esselman, and Jeremy D. Smith

University of Northern Colorado, Greeley, CO, USA
email: gary.heise@unco.edu, web: http://www.unco.edu/nhs/ses/

INTRODUCTION

Postural stability, particularly static whole-body stability in older adults, has received considerable attention in the research literature. Whole-body stability in younger, athletic populations has received less attention, primarily because typical static, two-legged postural assessments do not sufficiently tax a younger person's overall stability.

Overall muscle strength, especially core and lower extremity muscle strength is thought to enhance stability and reduce the risk of injury [1]. Unfortunately, stability is used in a variety of applications with different definitions that depend on a person's perspective. For example, gerontologists may use stability to help predict the potential for independence, while sports medicine specialists may focus on an athlete's rehab from a lower extremity joint injury [2]. King et al. [3] showed a moderately strong relationship between postural stability of single-leg standing and the ratio of lower extremity strength and whole body moment of inertia in adolescents. In older adults, the relationship between lower extremity strength and postural stability is not very clear [4].

The purpose of this experiment was to identify whether lower extremity muscle strength and core strength was predictive of single-leg static stability among young, fit adults. It was hypothesized that stronger individuals would be more stable.

METHODS

Thirty-eight people volunteered for this study (18 men; 20 women). All participants were young, healthy, and active (age = 21.8 ± 2.4 yrs, mass = 73.3 ± 13.1 kg, body height = 172.9 cm ± 7.9 cm). At the beginning of a single test session, the experimental protocol was explained and a written informed consent was obtained. Demographic and anthropometric data were collected in addition to a self-assessment of fitness and some details about the frequency, duration, and intensity of weekly workouts.

Participants then performed a brief, 10-15 minute warm-up (e.g., walk, stretch, low-intensity exercise). Static, single-leg postural stability trials were collected on each leg and for two floor conditions (hard surface and soft surface). Ground reaction force (GRF) data were collected for 20 s at 100 Hz and the center of pressure (COP) coordinates were calculated for analysis. COP mean velocity, 95% confidence ellipse area, and 95% power frequency were calculated [5].

Lower extremity muscle strength was determined with an isokinetic dynamometer. Maximal, isometric efforts were measured for: knee flexion; knee extension; ankle plantarflexion; and ankle dorsiflexion. Four tests of core muscle endurance were also performed in a randomized order: 1) isometric trunk flexor posture; 2) isometric trunk extensor posture; 3) the "trunk side plank" exercise on the left side; 4) the "plank" exercise on the right side. Participants were required to hold these positions for as long as possible [6].

Stepwise multiple regression was used to evaluate the predictive power of strength measures for static stability. Lower extremity strength measures were normalized to body weight and core muscle endurance was expressed as a duration.

RESULTS AND DISCUSSION

Stepwise regression models for the dependent variable COP mean velocity were statistically significant for each foot-floor condition (see Table 1). Other dependent variables did not yield a significant regression model (95% confid. ellipse area and 95% power freq.). Back extensor muscle endurance was identified as the predictor variable for the left leg-hard surface condition, whereas normalized ankle dorsiflexor strength was identified for the other three conditions.

Table 1: Foot-floor conditions and stepwise regression results for the dependent variable COP mean velocity.

Condition	Predictor	r	adj r^2	*p*-value
Left-Hard	Core-Ext	-.33	.10	.034
Right-Hard	RtAnkleD	+.43	.19	.007
Left-Soft	LtAnkleD	+.35	.10	.033
Right-Soft	RtAnkleD	+.38	.12	.018

Core-Ext=back extensor endurance; Lt=left; Rt=right; AnkleD=normalized ankle dorsiflexor strength.

As shown in Figure 1, a lower COP mean velocity indicates better static stability and a longer endurance time for back extensor muscles is related to greater strength [6].

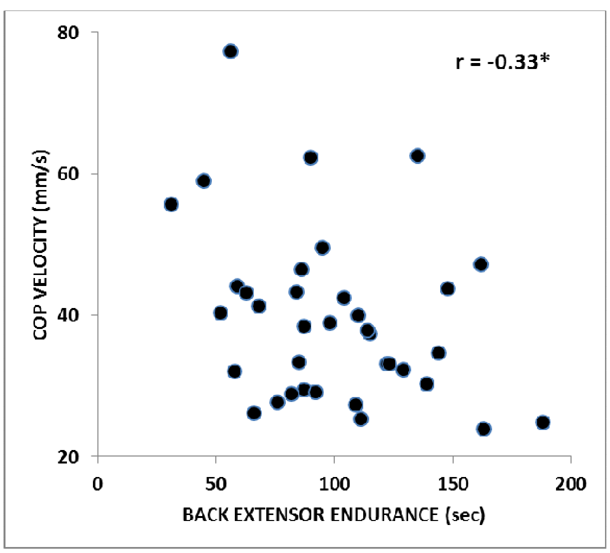

Figure 1: Scatterplot of back extensor muscle endurance and COP velocity for a left-footed, hard surface condition. **p*<.05

Therefore, the direction of the relationships between those variables in the first model shown in Table 1 was expected. (i.e., lower COP mean velocity associated with longer endurance times).

Upon closer examination, the three regression models that included ankle dorsiflexor strength as a significant predictor had an outlier that skewed the choice (See Figure 2). In addition, the positive correlation was opposite of our prediction.

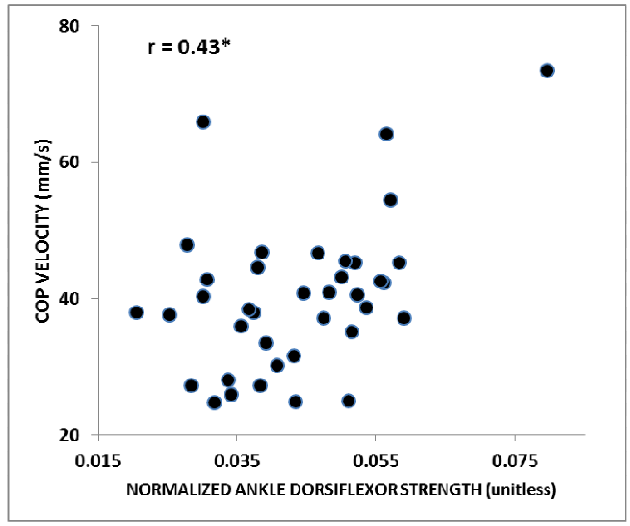

Figure 2: Scatterplot of normalized ankle dorsiflexor strength and COP velocity for a right-footed, hard surface condition. **p*<.05

Based on the results of the present experiment, the relationship between lower extremity strength and postural stability in a group of young, active people is unclear. This is similar to findings with older, less active adults [4]. The back extensor endurance time offers promise as a predictor of single-leg stability, but the amount of variability explained is modest.

REFERENCES

1. Leetun, DT et al. *Med Sci Sports Exerc*, **36**, 926-934, 2004.
2. Ross, S et al. *J Athl Training,* **40**, 298-304, 2005.
3. King, AC et al. *Gait & Posture*, **35**, 261-265, 2012.
4. Pizzagalli, L et al. *J Strength Cond Res*, **25**, 567-574, 2011
5. Prieto TE, et al. *IEEE Trans Biomed Eng* **43**, 956-966, 1996.
6. McGill, SM et al. *Arch Phys Med Rehab*, 80, 941-944, 1999.

WHOLE BODY POSTURE FOR RUNNING CHANGE OF DIRECTION TASKS

Kathryn L. Havens, Susan M. Sigward
Human Performance Laboratory
Division of Biokinesiology and Physical Therapy
University of Southern California, Los Angeles, CA, USA
email: khavens@usc.edu, web: www.usc.edu/go/mbrl

INTRODUCTION

Turning involves braking in the original direction of progression, and translation and rotation towards the new travel path, all without stopping ongoing locomotion [1]. Braking and translation are accomplished by appropriate separation of the body's center of mass (COM) and under-foot center of pressure (COP) for momentum manipulation. Braking is accomplished by separating the COM and COP in the anterior-posterior (AP) direction: the COM remains behind the foot to decelerate the body [2]. Translation of the body has been shown in walking turns to be accomplished through lateral foot placement [3], thus separating the COM and COP in the medial-lateral (ML) direction. While these have been characterized in walking turns, the postural strategies used to complete turns made at faster velocities have not yet been studied.

Running turns are commonly associated with lower extremity injuries, particularly anterior cruciate ligament (ACL) injury [4,5]. Cutting research has demonstrated differences in lower extremity mechanics when cuts are made to different angles [6], suggesting that task demand influences mechanics. Also, research has shown differences in mechanics based on anticipatory conditions. Cuts cued after the onset of movement resulted in mechanics considered to be more at risk, compared to those cued from the start [7]. This suggests that some anticipatory adjustments were made when adequate planning time was provided. However, more systematic research is needed both to understand the effect of task demand on mechanics and the role of anticipatory strategies.

The purpose of this study was to characterize the AP and ML COM-COP separation distances during two steps of a running and two cutting tasks (45˚ and 90˚ cuts).

METHODS

Twenty-five healthy soccer players (12 females) with no history of previous knee injury participated. Average age, height and weight were 22.4 ± 3.9 yrs, 1.74 ± 0.1 m and 70.9 ± 9.3 kg, respectively.

Subjects performed a straight running task, and two sidestep cutting tasks (to 45˚ and 90˚). For all tasks, subjects planted their non-dominant foot on the first force plate (approach step) and dominant foot on the second force plate (execution step). For the running task, subjects ran for 15 meters. For the cutting tasks, subjects ran 7.5 meters, planted their dominant foot on the force plate and changed direction away from the plant leg at a 45° or 90˚ and continued running for 7.5 meters. (Fig. 1). All tasks were performed as fast as possible.

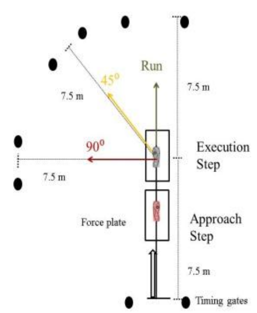

Figure 1: Experimental set-up for right dominant subject. Open arrow indicates original line of progression.

Three-dimensional kinematics were collected using a 10-camera motion capture system (Qualisys, Inc. Sweden), 250 Hz. Ground reaction forces (GRF) were quantified using AMTI force platforms (Newton, MA, USA), 1500 Hz. Whole body COM was calculated as the weighted sum of the COM of all 15 modeled segments (Visual3D™, C-Motion, Inc., Rockville, MD, USA). COP location, the application point of the resultant GRF vector, was determined from force plate recordings.

The distance between the COM and COP was calculated in the anterior-posterior (AP) and medial-lateral (ML) directions and then rotated to an anatomical reference system following the methods of Glaister [8]. Briefly, alignment of the anatomical reference system was calculated using the horizontal COM position, then the separation distances were aligned with this reference system using a rotation matrix. Peak separation distances were identified and normalized by height. Horizontal 2D COM velocity was calculated at initial contact. Data were averaged across four trials. Two-way repeated measures ANOVA (direction x step) were analyzed ($p \le 0.05$). Post-hoc analysis was done using t-tests ($p < 0.0056$).

RESULTS AND DISCUSSION

A main effect for direction ($F(2,48) = 348.555$, $p < 0.001$) revealed that greater body position for braking (greater AP COM-COP separation) was found during the cuts compared to straight running, with greater separation for the 90˚ cut than the 45˚ ($p < 0.001$) (Table 1). No main effect of step was found ($p = 0.168$). The greater body position for braking found in the cuts compared to straight running suggests that without adequate braking, successful completion of running turns may not be possible. Similar separation distance for both steps suggests that braking was accomplished over multiple steps.

Main effects for direction ($F(2,48) = 1171.104$, $P < 0.001$), and step ($F(1,24) = 466.845$, $p < 0.001$) and a direction x step interaction ($F2,48) = 208.052$, $p < 0.001$) were found for ML COM-COP separation (Table 1). When compared to the approach step, greater separation was found during the execution step of the cuts. During the execution step, greater separation was found in both cuts compared to the straight run ($p < 0.001$), and more for the 90˚ than the 45˚ cut ($p < 0.001$). For the approach step, greater ML COM-COP separation was found in the 45˚ cut than both the straight run ($p < 0.001$) and 90˚ cut ($p < 0.001$). This suggests that a greater proportion of the translation began before the 45˚ cut, even though the 90˚ cut required more translation. This was surprising, as the ML separation distance was expected to systematically increase with greater turn magnitude in both approach and execution steps.

CONCLUSIONS

Together, these data suggest that individuals modulated the distance between their COM and COP differently during tasks that involve varied angular demands, and that these were manipulated in advance of the execution step of the movement. More research is needed to understand how these postural strategies relate to joint kinematics and thus knee injuries.

REFERENCES

1. Hase K, et al. J Neurophysiol **81**, 2914-22, 1999.
2. Pai YC, et al. J Biomech **30**, 347-353, 1997.
3. Patla AE, et al. Exp Brain Res **129**, 629-34, 1999.
4. Boden BP, et al. Orthopadics **23**, 573-8, 2000.
5. Cochrane JL, et al. J Sci Med Sport **10**, 96-104, 2007.
6. Besier TF, et al. Med Sci Sports Exerc **33**,1168-75, 2001.
7. Besier TF, et al. Med Sci Sports Exerc **33**,1176-81, 2001.
8. Glaister BC, et al. J Biomech **40**, 3527-32, 2007.

Variable	Step	Run	45˚ cut	90˚ cut
Velocity (m/s)				
	Approach	6.21 ± 0.43	5.83 ± 0.45^{a}	4.72 ± 0.35^{a,b}
	Execution	6.55 ± 0.46	5.95 ± 0.48^{a}	3.84 ± 0.38^{a,b,c}
AP COM-COP (m/m)				
	Approach	-0.120 ± 0.025	-0.187 ± 0.036^{a}	-0.290 ± 0.027^{a,b}
	Execution	-0.135 ± 0.029	-0.189 ± 0.035^{a}	-0.294 ± 0.053^{a,b}
ML COM-COP (m/m)				
	Approach	-0.032 ± 0.018	0.162 ± 0.026^{a}	0.110 ± 0.038^{a,b}
	Execution	0.025 ± 0.023^{c}	0.257 ± 0.020^{a,c}	0.312 ± 0.024^{a,b,c}

Table 1: a denotes significant difference from straight run; b denotes significant difference from 45˚ cut; c denotes significant difference from approach step

THE EFFECT OF RECRUITMENT PROCESS ON POSTURAL SWAY: A PRELIMINARY COMPARISON ACROSS THREE CLINICAL STUDIES ON PATIENTS WITH LOW BACK PAIN

[1]Ting Xia, [1]Cynthia R. Long, [1]M. Ram Gudavalli, [2]Edward F. Owens Jr., [1]James W. DeVocht, [3]David G. Wilder, [4]William C. Meeker, and [1]Christine M. Goertz

[1]Palmer College of Chiropractic, Davenport, IA, USA
[2]TriMax Direct, 106 W. Water St., St. Paul, MN, USA
[3]Palmer College of Chiropractic – West Campus, San Jose, CA, USA
[4]University of Iowa, Iowa City, IA, USA
email: ting.xia@palmer.edu

INTRODUCTION

Low back pain (LBP) has long been recognized as a major health problem in modern societies. The severity of LBP is commonly evaluated using pain scales and disability questionnaires. It is well documented that LBP interferes with postural stability [1]. Typically, patients with LBP exhibit larger postural excursions and a faster swaying speed during quiet standing. However, the validity of the postural sway test as an objective evaluation tool for LBP severity has not been confirmed.

Previously, we have conducted three clinical trials on patients with LBP. In each study the mean postural sway characteristics, such as postural excursions in the anterior-posterior (AP) and medial-lateral (ML) directions, were examined. The postural sway test procedure was identical across the three studies. This allowed us to determine if the baseline postural sway characteristics were sensitive to study settings, such as inclusion and exclusion criteria, that significantly influence the study population. Specifically, we examined the results of those three clinical trials to see if the study sample demographic and clinical characteristics impacted postural sway.

METHODS

Study 1 (n = 192) [2]: Participants were eligible if they were 21-54 years old, presented with LBP of at least 4 weeks, scored 6 or above on the Roland Morris Disability Questionnaire (RMDQ), and met diagnostic classification of 1, 2, or 3 of the Quebec Task Force (QTF) Classification for Spinal Disorders.

Study 2 (n = 221) [3]: Participants were eligible if they were 21-65 years old, scored 4 or above in numerical rating scale (NRS) for pain in at least one screening point and ≥ 2 throughout the screening process, and met QTF classification of 1, 2, 3, or 7. While not a part of inclusion/exclusion criteria, all participants presented with LBP of at least 4 weeks.

Study 3 (n = 240) [4]: Participants were eligible for the study if they were at least 55 years old, presented with LBP of at least 4 weeks duration, and met QTF classification of 1, 2, or 3. There was no pain or RMDQ threshold required.

Mean excursions of center of pressure in the AP and ML directions were monitored using a force plate at 1000 Hz. Participants stood quietly first on a hard surface (hAP and hML), i.e. directly on the force plate, and then on a soft surface (sAP and sML), i.e. on a 10 cm thick latex foam pad, for 30 seconds, respectively. They were allowed to choose their comfortable stance while blindfolded and in stocking feet. The procedure was repeated twice. The average of the two trials was used for analysis.

The baseline postural sway was performed before participants received their first treatment. The major demographic factor under investigation was **age**. Sex, height, and weight were used to describe the samples. The major clinical factor was **RMDQ**. Visual analog scale (VAS-mm) for LBP pain was was used to describe the samples. Study 2 used NRS pain instead of VAS. For simplicity, VAS score was obtained by multiplying NRS by 10.

To enable comparisons between three studies, Study 2 participants were split into those of age 21-54 (2.a) and those of age 55-65 (2.b). The 2.a subgroup was further split into those with RMDQ < 6 (2.a.i) and those above (2.a.ii). For Study 3, the participants were split into those of age 55-65 (3.a) and those of age > 65 (3.b). The Study 3 participants were also split into those with RMDQ < 6 (3.c) and those above (3.d). As a preliminary investigation, only the descriptive statistics in mean ± standard deviation (SD) are presented. According to Study 1 (unpublished data), a minimum of 0.5-0.6 mm separation is necessary to satisfy a significant between-group difference. This criterion was used to interpret results on a qualitative basis.

RESULTS AND DISCUSSION

The mean postural excursions, as well as study and subgroup demographic and clinical characteristics, are summarized in Table 1. Two preliminary comparisons between study subgroups were performed. For those with RMDQ ≥ 6, Study 1 and Study 2-subgroup 2.a.ii shared similar RMDQ and age, as well as sex (% of male), height, weight and VAS. As shown in fig. 1, Study 1 exhibited higher excursions on the soft surface but not on the hard surface. Study 3-subgroup 3.d consisted of an older population than Study 1 and 2.a.ii. However, 3.d demonstrated higher excursions on the hard surface only compared to Study 1 but in all excursions compared to 2.a.ii. For those of age 55-65, Study 2-subgroup 2.b and Study 3-subgroup 3.a shared similar demographic and clinical characteristics. All mean excursions were higher in 3.a compared to 2.b.

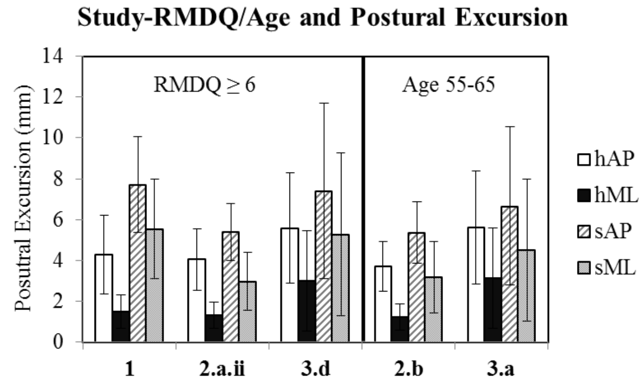

Figure 1. Mean±SD postural excursions across three studies grouped according to RMDQ and age.

CONCLUSIONS

These preliminary comparisons between study subgroups across three clinical trials demonstrate inconsistency in the postural sway testing results. The validity of this test as an objective evaluation tool for LBP severity needs further investigation.

REFERENCES

1. Ruhe A, et al. *Eur Spine J* **20**, 358–368, 2011.
2. Meeker WC, et al. *Clin Chiropractic* **14**, 145, 2011.
3. Wilder DG, et al. *Trials* **12**, 161, 2011.
4. Hondras MA, et al. *J Manipulative Physiol Ther* **32**, 330-343, 2009

Table 1: Summary of study and subgroup mean demographic, pain, disability, and postural excursions (mm).

Study	n	Male	M%	Age	Ht (cm)	Wt (Kg)	VAS	RMDQ	hAP	hML	sAP	sML
1	192	103	54	40.0	172.7	88.9	55.7	9.7	4.30	1.50	7.73	5.55
2	221	120	54	44.3	171.8	87.1	55.0	5.6	3.81	1.23	5.33	2.97
2.a	184	95	52	41.4	171.6	86.6	54.6	5.6	3.83	1.22	5.32	2.93
2.a.i	110	55	50	41.3	172.0	84.6	51.0	3.0	3.69	1.16	5.26	2.90
2.a.ii	74	40	54	41.7	171.1	89.5	60.0	9.6	4.05	1.31	5.41	2.96
2.b	37	25	68	58.7	172.5	89.7	57.0	5.6	3.71	1.24	5.37	3.18
3	240	135	56	63.1	171.1	86.2	42.3	6.4	5.84	3.45	6.78	4.79
3.a	167	93	56	59.4	171.0	86.7	41.6	6.5	5.61	3.13	6.67	4.51
3.b	73	42	58	71.3	171.4	85.1	43.9	6.1	6.37	4.19	7.06	5.43
3.c	118	76	64	63.1	172.3	86.2	33.5	2.8	6.10	3.92	6.18	4.30
3.d	122	59	63	63.1	170.0	86.2	50.9	9.8	5.58	3.00	7.40	5.27

CHARACTERIZING LUMBAR JOINT TORQUES DURING SITTING FOLLOWING MULTIDIRECTIONAL PERTURBATIONS: A CASE STUDY

[1,2]Albert H. Vette, [3,4]Takashi Yoshida, [3,4]Kei Masani, and [3,4]Milos R. Popovic

[1]University of Alberta, Edmonton, Alberta, Canada
[2]Glenrose Rehabilitation Hospital, Edmonton, Alberta, Canada
[3]University of Toronto, Toronto, Ontario, Canada
[4]Toronto Rehabilitation Institute, Toronto, Ontario, Canada
email: albert.vette@ualberta.ca, web: http://www.mece.engineering.ualberta.ca/

INTRODUCTION

Trunk instability during sitting is a major problem for individuals with spinal cord injury (SCI). It not only compromises their independence during activities of daily living, but can also lead to secondary health complications such as kyphosis or pressure sores. Consequently, it is not surprising that people with SCI prioritize the recovery of trunk stability over the recovery of walking function [1].

Recent developments in the field of neuro-rehabilitation suggest that neuroprostheses utilizing functional electrical stimulation (FES) have the potential to facilitate or restore trunk control during sitting. However, no study exists that provides a quantitative analysis of the lumbar joint torques in sitting following multidirectional perturbations. Along with a better understanding of intrinsic trunk stiffness, such analysis is essential for developing FES protocols that promote trunk stability following SCI. Accordingly, the objectives of this study were to: (1) use a three-dimensional (3D) dynamic model of the upper body [2] to estimate the lumbar joint torques during perturbed sitting; and (2) identify torque peaks and active stiffness at each joint as a function of perturbation direction.

METHODS

3D Dynamic Model: The 3D dynamic model (Fig. 1) consisted of five lumbar segments (L1 to L5), the thorax (TH), six cervical segments (C2 to C7), and the head (HD) [2]. The lowest lumbar and cervical joints (L5-PV and C7-TH) had three degrees of freedom each (DOF) and determined the 3D motion of the adjacent superior joints (see [2]). The model's 3D geometric and mass-inertia parameters were based on the *Visible Human Project* (see [2]) and could be scaled using anthropometrics and regression equations. The Newton-Euler inverse dynamics formulation was applied to predict lumbar joint torques during perturbed sitting using experimental motion data.

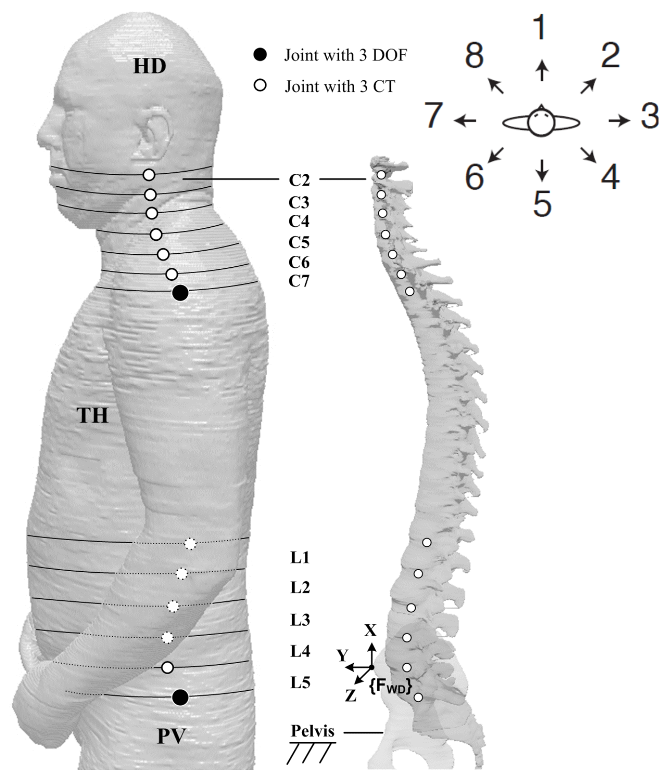

Figure 1: Schematic of the 3D dynamic model [2] and perturbation directions.

Data Acquisition: Kinematics from a healthy 34 year old male (height: 1.80 m; weight: 89 kg) were obtained during manual perturbations in eight horizontal directions (Fig. 1). Using an impulse force of approximately 180 N, five trials per direction were executed. Lumbar joint torques were calculated using the obtained 3D head and trunk angles and the inverse dynamics formulation.

<u>Data Analysis</u>: For each trial, maximum joint torques (τ_{max} [Nm]) and active joint stiffness (K_{active} [Nm/deg]) were quantified in dependence of perturbation direction. Torque peaks for any perturbation direction (0-360°) were estimated via a sinusoidal fit. The active joint stiffness required to ensure postural stability by counteracting the perturbation was predicted using linear regression analysis. For demonstration purposes, results are shown for the L5-PV joint only.

RESULTS AND DISCUSSION

Figure 2 shows the average perturbation force, anterior-posterior (AP) and medial-lateral (ML) trunk deflections, and L5-PV joint torques for a posterior-right perturbation (direction 4, 5 trials; see Fig. 1 for coordinate axes).

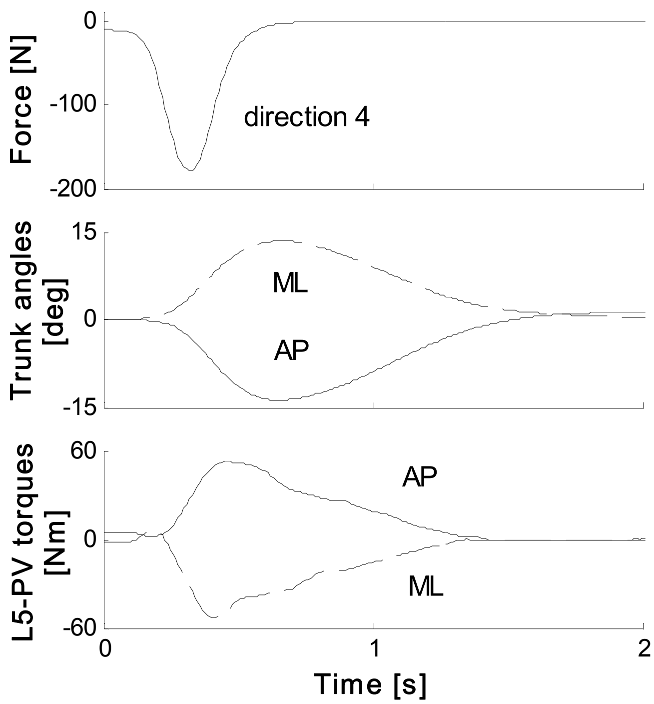

Figure 2: Perturbation and torque profiles (dir. 4).

Figure 3 depicts the maximum AP and ML trunk deflections (θ_{max} [deg] at L5-PV) and maximum AP and ML torques (τ_{max} [Nm] at L5-PV) in dependence of perturbation direction. A sinusoidal approximation adequately captured these dependencies, revealing an R^2 value of over 0.99.

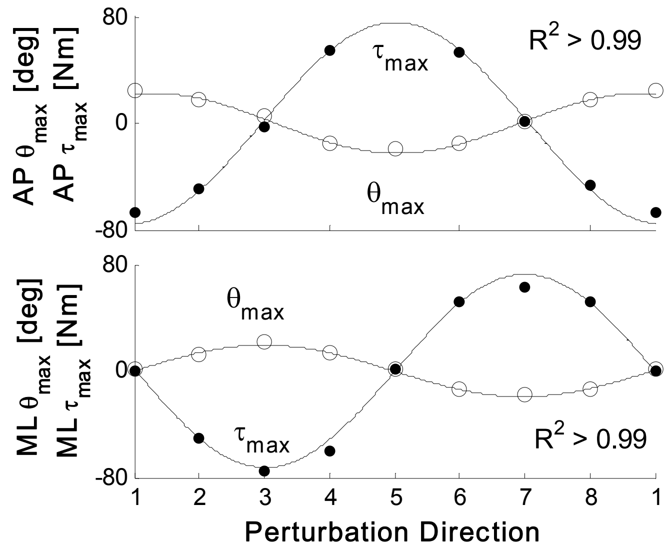

Figure 3: Maximum trunk angles and joint torques.

Table 1 lists active AP and ML joint stiffness (K_{active} [Nm/deg] at L5-PV) in dependence of perturbation direction. Due to the symmetry of the body, stiffness values were combined for directions 2 & 8 as well as directions 4 & 6. The results indicate that fairly consistent stiffness values are required for perturbation compensation, with ML stiffness being slightly larger than AP stiffness.

Table 1: Active joint stiffness for each direction.

	Perturbation Direction					
	1	**3**	**5**	**7**	**2&8**	**4&6**
$\mathbf{K_{AP}}$ $\mathbf{(R^2)}$	8.41 (0.93)	-	9.48 (0.97)	-	9.74 (0.90)	9.68 (0.88)
$\mathbf{K_{ML}}$ $\mathbf{(R^2)}$	-	12.10 (0.90)	-	11.14 (0.92)	11.12 (0.91)	14.24 (0.85)

The results of Fig. 3 suggest that trunk deflection can serve as feedback information for regulating FES-induced torques following SCI to restore upright posture post-perturbation. Moreover, the active stiffness values provide a benchmark for the *change* in torque that a potential neuroprosthesis needs to generate for trunk stabilization (Table 1). Future work will consolidate results from different lumbar joints in a representative sample of subjects.

REFERENCES

1. Anderson KD. *J Neurotrauma* **21**, 1371-83, 2004.
2. Vette AH, et al. *Med Eng Phys* **34**, 640-9, 2012.

LOADING ASYMMETRY DURING A STAND TO SIT TASK FOR PEOPLE WITH MULTIPLE SCLEROSIS

[1]Bradley Bowser, [2]Cathleen Brown, [2]Lesley White, and [2]Kathy Simpson

[1]South Dakota State University, Brookings, SD, USA
[2]University of Georgia, Athens, GA, USA
email: bradley.bowser@sdstate.edu

INTRODUCTION

Multiple sclerosis (MS) is a neurological disease characterized by lesions to the central nervous system. These lesions often cause sensory and motor dysfunction resulting in muscle weakness and poor balance for people with MS. During quiet standing people with MS display both mediolateral (ML) and anteroposterior (AP) postural instability. It has been suggested that ML stability during quiet standing for people with MS is largely influenced by asymmetries found in left and right limb loading [1]. When compared to controls, persons with MS have shown increased ML instability and loading asymmetries (LA) during a sit to stand movement [2]. In this study it appeared that the LA found in persons with MS may have been linked to leg extensor weakness.

Currently there is limited research examining balance and postural control during dynamic movements for people with MS. However, it is likely that ML instability and LA are not unique to the sit to stand movement and will also occur during the sitting down motion for people with MS. The purpose of this study was to compare ML stability and LA between MS and non-MS persons during a stand to sit movement. We hypothesize that persons with MS who have leg extensor weakness will display increased ML instability and LA during the stand to sit movement.

METHODS

Twenty-one ambulatory individuals diagnosed with relapsing-remitting MS were divided into two groups; persons with MS who displayed leg weakness (MS-LW; n = 10; 49±10yr; 1.67±0.07m; 82.2±15.5kg) and persons with MS who displayed comparable leg strength to controls (MS-CS; n = 11; 40±12 yr; 1.66±0.07m; 76.3±23.4kg). The control group consisted of 12 non-MS participants matched for age, height, and mass (CON; n=12; 43±12yr; 1.66±0.08m; 74.2±19.5kg).

Informed consent was obtained for all participants. Data was collected during 3 separate visits. The first 2 visits to obtain double baseline of the 1RM on leg press. The 3rd visit, 5 sit to stand to sit trials were performed. Participants began the movement in a standardized position with arms and hands folded across the chest, each foot on a separate force plate in a fixed position. For each trial the participant rose to a standing erect posture at a self-selected speed, stood motionless for 8-10s and then returned to a seated posture. Ground reaction forces (Bertec®: 1000Hz; LP filter 200Hz) were captured bilaterally.

ML stability was calculated as the standard deviation of the netCoP in the ML direction [3]. Absolute LA was calculated from the vertical ground reaction force from each force plate (Eq. 1) [1].

$$Absolute\ LA = \left(\frac{Fz_{high}}{Fz_{high}+Fz_{low}}\right) - \left(\frac{Fz_{low}}{Fz_{high}+Fz_{low}}\right) \qquad (1)$$

Absolute LA represents a percentage with 0% indicating no LA and 100% representing entire vertical load occurring on 1 limb. Relative LA was calculated similarly only replacing Fz_{high} and Fz_{low} with the vertical force from the dominant/stronger leg and the non-dominant/weaker leg sides respectively. ML stability and LA were calculated from initiation of the sitting down movement to seat contact. ANOVAs followed by post-hoc testing (α=0.05) were used to determine group differences for each of the variables of interest (Table 1).

RESULTS AND DISCUSSION

The self-reported expanded disability status score (EDSS) was 4.3±1.4 for MS-LW and 1.6±1.5 for MS-CS. The 1RM leg press values found in table 1 were used previously when postural stability measures for the standing up portion of the movement were presented [2]. 1RM leg press is presented here only to establish the difference that exists between groups and not as new information.

Our data suggests that LA is greater in the MS-LW group compared to the CON group (Table1). The absolute LA is an overall estimate of loading asymmetry that does not consider the specific limb that displays the greater loading. When examining the relative LA, it appears that persons with MS who have leg weakness, display greater vertical loading on their dominant/stronger limb when transitioning from a standing to sitting posture. It has been suggested that LA can be a reason for ML instability during dynamic movements. However, we were unable to find a significant group difference for ML stability (Table 1). A possible explanation could be the greater variability within each group during the stand to sit transition compared to the within group variability previously reported during the sit to stand movement.

Interestingly post-hoc comparisons revealed that group differences only occurred between the MS-LW and CON groups (Table 1). These findings would be consistent with the previous literature suggesting that LA is linked to leg extensor weakness. Although strength training has been reported to improve postural stability in persons with MS [4], there is limited research that examines the effects of symmetry training combined with strength training.

CONCLUSIONS

Persons with MS who have leg extensor weakness display greater absolute and relative loading asymmetries during the stand to sit transition than controls. MS training protocols that include symmetry training may be needed in order to maximize improvements to postural stability during dynamic tasks.

REFERENCES

1. Van Emmerik REA, et al. *Gait & Posture* **32**, 608-614, 2010.
2. Bowser BJ et al. *Proceedings of ACSM*, Indianapolis, IN, USA, 2013.
3. Winter DA. *Gait & Posture* **3**, 193-214, 1995
4. Huisinga JM, et al. *Motor Control* **16**, 50-63, 2012.

Table 1: Summary of p-values and effect sizes for all variables of interest

Variable	Group	Mean(SD)	ANOVA *P*-value (η_p^2)	Post-hoc Comparison (*p*-value; Cohen's *d*)
1RM Leg press (BW)	MS-LW	1.18(0.15)	0.0001(0.46)†	MS-LW < MS-CS (p = 0.003; d = 1.96)
(previously presented ACSM 2013)	MS-CS	1.91(0.50)		MS-LW < CON (p = 0.0001; d = 2.30)
	CON	2.13(0.56)		
Mediolateral Stability (M/L CoP displacement in mm)	MS-LW	11.2(4.60)	0.16(0.12)	NA
	MS-CS	10.0(5.97)		
	CON	7.50(2.57)		
Absolute Loading Asymmetry (%)	MS-LW	6.99(3.58)	0.01(0.27)*	MS-LW > CON (p = 0.01; d = 1.24)
(0% evenly loaded/100% complete loading on 1 limb)	MS-CS	5.82(2.44)		
	CON	2.96(2.89)		
Relative Loading Asymmetry (%) (+stronger limb/-weaker limb)	MS-LW	5.42(5.87)	0.01(0.26)*	MS-LW > CON (p = 0.01; d = 1.43)
	MS-CS	2.85(5.85)		
	CON	-1.69(3.85)		

*Significant difference with p < 0.05. †Significant difference with p < 0.001.

Dynamic Postural Stability Deficits Exist in Mechanically Lax Individuals but not those with Perceived Functional Ankle Instability

[1]Adam Rosen, [1]Jupil Ko, [1]Cathleen Brown Crowell

[1]University of Georgia, Athens, GA, USA
email: abr@uga.edu

INTRODUCTION

Lateral ankle sprains are among the most frequent athletic injuries. Lateral ankle sprains have been reported to recur at a rate in excess of 80%, and chronic ankle instability (CAI) is a frequent and serious pathologic consequence of sprains that develops in up to 50% of those with a history of ankle sprain [1]. These individuals often present with feelings of “giving way” and reports of sudden instability, which are characteristic of CAI. Contributing factors to CAI are debated, but contemporary theories include failure of the dynamic restraint mechanism resulting from proprioceptive deficiencies and/or excess mechanical ligamentous laxity [2]. The purpose of this study was to determine if differences exist in dynamic postural stability among healthy controls, copers, functionally unstable ankle individuals, and those with both functional instability and mechanical ankle laxity.

METHODS

A total of 93 individuals participated in this study. Participants were physically active and participated in at least 90 minutes of physical activity per week. Subjects were considered to have Functional Ankle Instability (FAI) with a history of mild to moderate ankle sprain at least 12 months before the study that required immobilization or non-weight bearing status for 3 days and the Cumberland Ankle Instability Tool (CAIT) score of ≤ 26, indicating poor function [3]. Subjects were included in the mechanical laxity group (MAI) using the same criteria as the FAI group plus mechanical laxity as indicated by an instrumented arthrometer (LigMaster Version 1.26, Sport Tech, Inc, Charlottesville, VA). MAI subjects' were considered mechanically lax with ≥29.4° of inversion based on previous literature [4]. Inclusion for ankle sprain copers included a history of ≤2 ankle injuries and a CAIT score of ≥ 28, indicating good function. Healthy controls had no history of ankle injury, and had CAIT scores of 29 or 30, indicating excellent function [3].

Participants completed the University's Institutional Review Board approved consent document prior to participation, and then completed ankle injury history and CAIT questionnaire documents. Participants were assessed for their maximal vertical jump height using a Vertec© jump trainer (Sports Imports, Columbus, OH), which was then set to 50% of that maximum as a target height. For the test trials, participants jumped off 2 legs at a distance of 70cm from a forceplate. Participants raised one arm to touch the target height, land on the test leg, and tried to "stick the landing," balancing for approximately 5 seconds after the landing [5]. Both limbs were tested in a randomized order.

Ground reaction force (GRF) data were transferred and reduced in MatLAB (version 7.0; the MathWorks, Natick, MA). Ground reaction forces were scaled to body weight. The first 3 seconds of data after initial ground contact (>10N) were analyzed. Stability index scores were calculated for anterior-posterior (APSI), medial-lateral (MLSI), vertical (VSI), and composite (DPSI), stability indices, according to previously established calculations [5]. Stability indices capture the ability to transition from a dynamic to a static state, which is important in sports and can be a possible mechanism of injury.

One-way ANOVA's ($\alpha<0.05$) were conducted on each of the stability index scores among the four groups. When significant differences among the groups were found, Tukey's post-hoc tests (α<0.05) were utilized to identify specifically where differences were seen.

RESULTS AND DISCUSSION

A summary of demographic data and dependent variable can be seen in Table 1. Significant differences were seen among the groups in the MLSI (*F*=3.438, *p*=.020) and DPSI (*F*=3.162, *p*=.029) variables. Specifically, for MLSI measures follow-up tests showed the MAI group had significantly higher (worse) scores than the coper group (*p*=.018). In DPSI composite (Figure 1), the MAI group had higher (worse) scores compared to both coper (*p*=.038) and FAI (*p*=.040) groups.

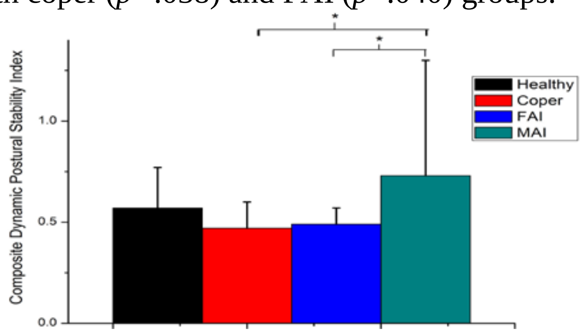

Figure 1: Composite Dynamic Postural Stability Index Among Each of the Four Groups (* Denotes Significant Tukey's Post-Hoc Test *p*<0.05)

The results demonstrate those who suffer from both mechanical and functional ankle instability have worse dynamic postural stability, compared to copers who have a history of ankle sprain but no complaints of instability. This seems particularly true in the medial-lateral GRF component. Cadaveric studies have demonstrated excess anterior tibial translation, internal rotation and supination when the anterior talofibular ligaments and calcaneal fibular ligaments are severed [6]. This alteration in range of motion may cause subsequent functional imbalances in those with mechanical ankle laxity. The results also indicate those who perceive they have deficiencies in functional tasks via self-reported questionnaires perform comparatively to both ankle sprain copers and healthy subjects. This finding is especially important, and may provide greater rationale for dichotomizing FAI and MAI groups in prospective investigations. It is interesting to note that the healthy controls were not significantly different compared to the MAI group, although they were trending in the same direction as the other results. We believe this may be attributed unequal sample sizes and insufficient power.

CONCLUSIONS

Mechanically lax subjects exhibit dynamic postural deficits compared to those with a previous history of ankle sprains. Future studies may warrant separation of mechanically lax subjects from the larger pool of CAI subjects.

REFERENCES

1. Yeung MS, et al. *Brit J Sport Med* **28,** 112-116, 1994.
2. Hertel J. *J Athl Training*, **7**, 364-375, 2003.
3. Hiller CE, et al. *Arch Phys Med Rehab*, **87,** 1235-1241, 2006.
4. Hirai D, et al. *Foot Ankle Int*, **30**, 1071-1077, 2009.
5. Wikstrom EA, et al. *J Athl Training*, **40,** 305-309, 2005.
6. Kovaleski JE, et al. *J Athl Training*, **37,** 467-474, 2002.

Table 1: Demographic data and dependent variables means ± standard deviation.

	Gender (M/F)	Age (yr)	Height (cm)	Mass (kg)	CAIT	Ankle Sprain History	APSI	**MLSI**	VSI	**DPSI**
Healthy	13/19	20.2±1.3	168.1±8.7	67.8±11.8	29.8±0.4	0.0±0.0	0.11±0.03	**0.41±0.24**	0.35±0.10	**0.57±0.20**
Coper	13/4	22.1±4.1	175.8±10.5	75.3±12.9	29.0±1.1	1.5±0.6	0.11±0.02	**0.24±0.20**	0.35±0.06	**0.47±0.13**
FAI	13/13	21.2±1.3	169.2±9.8	71.4±14.3	20.2±5.1	6.5±14.2	0.10±0.02	**0.32±0.14**	0.33±0.06	**0.49±0.08**
MAI	4/10	20.0±1.5	168.7±8.4	68.9±13.1	19.4±5.1	3.4±2.2	0.11±0.04	**0.57±0.62**	0.36±0.08	**0.73±0.57**

Note: Bold indicates significant difference among groups (α<0.05)

IMPACT OF OBESITY ON ANTROPOMETRIC PREDICTORS OF BODY FAT IN OLDER ADULTS

[1]Alicia Kolling, [1]Jenna Montgomery, [2]Jean L. McCrory, [1]Rakié Cham, [1]April J. Chambers

[1]University of Pittsburgh, Pittsburgh, PA, USA
[2]West Virginia University, Morgantown, WV, USA
email: alk93@pitt.edu, web: http://www.engineering.pitt.edu/hmbl/

INTRODUCTION

In recent years, obesity rates have continued to steadily increase. In 2009-2010, more than 35% of adults in the United States were obese, with obesity being more prevalent in adults over the age of 60 [1]. With obesity comes an increased risk of developing health conditions, such as type 2 diabetes and hypertension [1]. The prevalence of excessive body fat and the associated health risks have created a demand for simple and effective ways of measuring a person's obesity risk.

Various anthropometric measurements, such as circumference and ratios, are thought to be simple, inexpensive tools capable of diagnosing obesity. If accurate, these measurements would provide an easy way to monitor a patient's percent body fat and risk of obesity.

Previous studies have compared several anthropometric measurements to obesity and mortality risk in adolescents, adults, and older adults in various ethnic populations. Common measurements evaluated include body mass index (BMI), waist circumference, and waist-to-hip ratio.

A study of older adults, age ≥75 years, from the United Kingdom concluded that relative abdominal obesity and increased mortality risk were best measured using waist-to-hip ratio; additionally, waist circumference still predicted obesity and mortality risk better than BMI [2]. The Honolulu Heart Program, a study involving elderly Japanese-American men, showed consistent results that waist-to-hip ratio was positively correlated to mortality [3]. However, these studies determined mortality and obesity risk by evaluating measures such as BMI, smoking, heart rate and death rather than comparing to an accurately calculated percent body fat.

A dual-energy X-ray absorptiometry (DXA) scan is a method which can be used to accurately determine percent body fat. Though, DXA scans are expensive and time-consuming, making them inconvenient for use in a clinical setting.

Given the increased health risks associated with increased obesity, the correlation between percent body fat and waist circumference, hip circumference, and waist-to-hip ratio is important for understanding how health care providers can conveniently and effectively assess obesity in elderly adults. The goal of this research is to examine the impact of obesity on the relationship between waist and hip anthropometry and body fat percentages in older adults.

METHODS

Eighty-three adults (75.5 ± 5.0 years) were recruited as study participants. The adults were divided into four subgroups based on gender (41 male, 42 female) and obesity (42 non-obese BMI < 30, 41 obese BMI > 30). Each subject underwent a whole body DXA scan (Hologic QDR 1000/W, Bedford, MA) from which mass and percent body fat (%BF) were calculated on a total and per segment basis.

Hip and waist circumferences were measured by a trained technician using a cloth measuring tape. Waist-to-hip ratio was calculated.

Associations between each circumference and waist-to-hip ratio with %BF were explored using a correlation analysis. Statistical analysis was done to compare %BF to the measured circumferences for each of the four subgroups with an alpha value of 0.05.

RESULTS AND DISCUSSION

A positive correlation was found between waist circumference and %BF (Table 1).

Table 1. Correlation Values (r) between Percent Body Fat (%BF) and Anthropometric Measurements

	Female		Male	
	Non-obese	Obese	Non-obese	Obese
Waist Circumference	0.7227*	0.4983*	0.3917	0.7603*
Hip Circumference	0.8215*	0.8536*	0.5134*	0.7802*
Waist-to-Hip Ratio	0.2200	-0.2471	0.0552	0.2945

*denotes significant with p-value <0.05

This relationship was strongest for non-obese females and obese males; however, a lesser positive correlation was still observed for obese females and non-obese males (Figure 1). All conditions, except non-obese males, were significant.

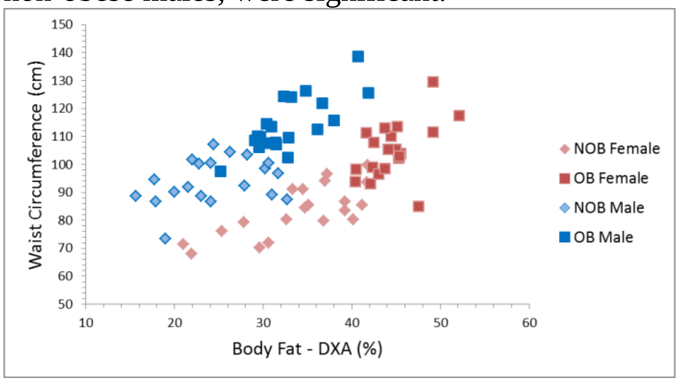

Figure 1: Waist circumference [cm] vs. body fat (%) for obese and non-obese males and females. As body fat increases, waist circumference increases.

Again, a positive relationship was found between hip circumference and %BF (Figure 2). This relationship was significant for both males and females, and independent of whether or not they were obese.

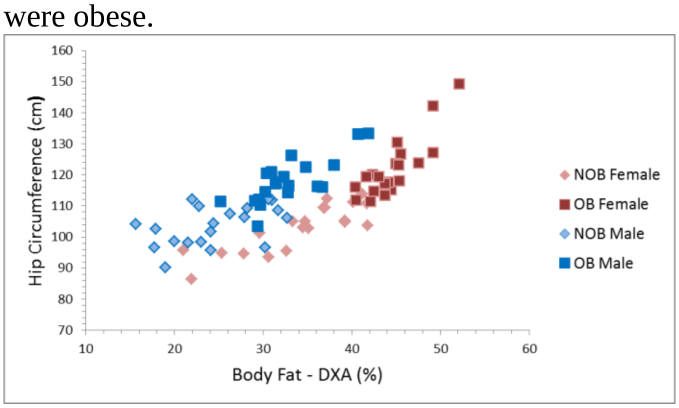

Figure 2: Hip circumference [cm] vs. body fat (%) for obese and non-obese males and females. As body fat increases, hip circumference increases.

No significant correlation was found between the waist-to-hip ratio and %BF (Figure 3).

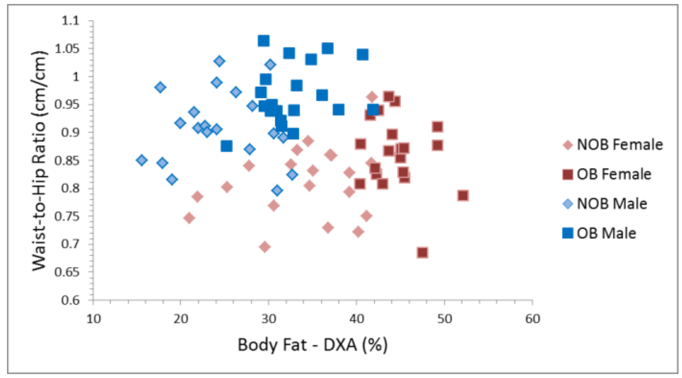

Figure 3: Waist-to-hip ratio vs. body fat (%) for obese and non-obese males and females. No significant correlation was observed.

The results shown do not support previous research suggesting that waist-to-hip ratio is a useful predictor of obesity in older adults. Of the three measurements examined, waist-to-hip ratio was least correlated to %BF. Waist and hip circumference were both positively correlated with %BF; however, hip circumference correlation values suggest it is a better measure in obese subjects, both male and female. For this reason, hip circumference has the potential to act as a better measure of %BF in elderly Americans.

Although more analysis is needed, initial findings suggest the waist-to-hip ratio should be avoided as an obesity determinant in older adults and, instead, waist or hip circumference should be used as an indicator until further methods are developed.

REFERENCES

1. Ogden CL, et al. *NCHS Data Brief* **82**, 2012.
2. Price GM, et al. *Am J Clin Nutr* **84**, 449-460, 2006.
3. Kalmijn S, et al. *Int J Obes Relat Metab Disord* **23**, 395-402, 1999.

ACKNOWLEDGEMENTS

Funding was provided by The Pittsburgh Claude D. Pepper Older Americans Independence Center & The University of Pittsburgh CTRC.

QUANTIFYING HEAD INJURY SEVERITY FOLLOWING PEDIATRIC PATIENT FALLS

[1]Janet S. Dufek, [2]Nancy A. Ryan-Wenger and [1]Kyle C. Mefferd

[1]University of Nevada, Las Vegas, Las Vegas, NV, USA
[2]Nationwide Children's Hospital, Columbus, OH, USA
email: janet.dufek@unlv.edu, web: kinesiology.unlv.edu/biomechanics

INTRODUCTION

It has been estimated that 30% of hospital falls result in serious injury to the patient [1]. The occurrence of pediatric patient falls in the hospital or medical clinic environment has been estimated to range from 1.2-10.8% of hospitalized children [2], with most children falling on their head [3]. Current procedures to characterize, minimize or eliminate fall occurrence are not uniform among health care facilities. Furthermore, fall treatment protocols following pediatric patient falls are non-standard and are even sometimes overlooked. A theoretical fall risk model has recently been introduced [4] and is the first to consider the triad of child human factors, environmental human factors and biomechanical factors as they relate to fall occurrence and injury potential. It was not the intent of this model to address the severity of falls when they do occur, which is of concern relative to administering appropriate follow-up care for the patient.

Presently, no criteria exist which associate the dynamics of a fall with injury severity for pediatric patients. The current study embraced the head injury criterion (HIC), a measure borrowed from the automotive industry, as a means of assessing potential bounds for injury severity, versus the Medical Error Prevention and Error scoring (MERP) value. The MERP rating scale, used in clinical settings, is a qualitative system with scores ranging from 1 (least severe) to 7 (most severe). Scores are assigned based upon the known facts of the fall and subjective reported recall. HIC values are dependent upon the system (person) and the mechanics of the fall scenario and are thus bound theoretically from zero to infinity. In most adult head impacts, HIC_{15} (collision Δ velocity modeled to be 15ms) values greater than 1000 suggest some level of head injury. Understanding the severity of the fall can potentially lead to policy change in healthcare delivery relative to follow-up care, reduce waste by eliminating unnecessary tests, and enhance the efficiency and effectiveness of healthcare delivery for children. Thus, the purpose of this study was to retrospectively calculate the head injury criteria (HIC) values for pediatric patient falls and correlate these values to documented injury severity (MERP) scores. This was done to assess the effectiveness of the current standard of fall injury severity (MERP score) relative to fall mechanics in an attempt to quantify fall severity. A second purpose was to examine the relationship between child ages and associated HIC_{15} values in an attempt to scale the values obtained from pediatrics to adult values.

METHODS

Adverse event report records for 33 young children (76.8 ± 2.2 cm, 10.4 ± 4.8 kg, 16.0 ± 10.1 m/o) who experienced falls while admitted to a pediatric hospital were examined. Pertinent information including age, height, mass, gender, fall description and qualitative injury severity score (MERP) were extracted from the records. Of the total number of cases, only 12 records had a MERP score recorded.

For each fall incident, an HIC value was computed. First, the child's center of gravity was modeled based upon age, gender, anthropometrics and fall scenario in order to accurately represent fall height. Several sources were used to estimate system center of gravity location including the anthropometric data base built into HumanCAD v1.2 (NexGen Ergonomics) software, AnthroKids Anthropometric Data Base (open access), and the Centers for Disease Control growth charts. Each fall was modeled for two positions, upright and lying, to simulate the child either climbing or rolling out of the hospital crib. Contact velocity and contact force were computed and an HIC_{15} (15 ms deceleration time independent of system deformation [3]) value computed using the following equation:

$$HIC = [(t_2 - t_1) \{1 / (t_2 - t_1 \int_{t1}^{t2} a(dt)\}^{2.5}]$$
$$HIC_{15} = a(t)^{2.5}$$

where a is acceleration (in units of gravity) and t is contact time (0.015 s).

Descriptive statistics were computed for contact velocity, force and HIC_{15} for the two modeled postures (n=33). The HIC_{15} value was correlated to the MERP score (n=12) to address the primary study purpose. In addition, the HIC_{15} value was correlated to age (n=33) to address the secondary study purpose.

RESULTS AND DISCUSSION

The demographic characteristics of the 33 cases evaluated reflected a very homogenous study sample. All falls occurred from a standard hospital crib (1.90m). The vertical COG location ranged from 1.92-2.47m (2.24±0.16m) and 1.57-2.01m (1.98±0.13m) for upright and lying postures, respectively. Descriptive modeled fall data are given in Table 1. The correlations between HIC_{15} and MERP were r=0.333 (upright) and r=0.045 (lying). The correlations between HIC_{15} and age were r=0.129 and r=-0.061 for upright and lying, respectively (Figure 1).

Table 1. Mean and standard deviation values for two modeled fall positions.

Model	Contact Velocity (m/s)	Contact Force (bodyweight)	HIC_{15}
Upright Posture			
Mean	6.63	4.59	204.79
sd	0.24	0.16	17.76
Lying Posture			
Mean	6.09	4.22	165.60
sd	0.22	0.15	14.15

Results suggest little to no relationship between HIC_{15} values and MERP scores assigned to each fall or age. The HIC_{15} values calculated for these pediatric falls were generally in the range of those reported for adults (135-519) which resulted in a headache or dizziness for the adults.

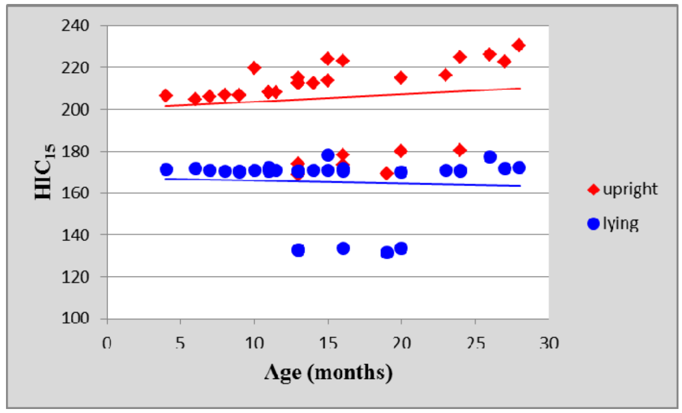

Figure 1. Correlation between HIC_{15} and age for two modeled fall positions.

CONCLUSIONS

This study explored the application of a unique approach to quantify the head injury severity of pediatric patient falls. The model is limited in that the fall was modeled as a rigid body. The homogenous nature of the falls (environment, child morphology) led to the inability to discriminate fall severity. A standard (adult) collision time (15ms) was used in this study. Modeling the falls with individualized parameters (skull deformation and/or floor surface) could provide additional insight into injury severity. Additionally, an alternative severity measure, such as the Abbreviated Injury Scale, may be a more appropriate correlate to HIC_{15} values.

REFERENCES

1. Stevens JA. In *Falls Free: Promoting A National Falls Prevention Action Plan,* National Council on Aging, 2004.
2. Child Health Corporation of America, 2009. Retrieved: http://chca.com/index_no_flash.html.
3. Cory CZ et al. *Forensic Sci Int,* **123,** 89-106, 2001.
4. Ryan-Wenger NA & Dufek JS. *J Spec Ped Nurs,* **18**, 4-12, 2013.

ACKNOWLEDGEMENTS

Partially supported by the President's Faculty Opportunity Award (#2221-272-76MH), University of Nevada, Las Vegas and the American Nurses Foundation (#2350-257-736T).

INDIVIDUAL MUSCLE CONTRIBUTIONS TO HANDCYCLING PROPULSION

Kotaro Sasaki

Boise State University, Boise, ID, USA
email: kosasaki@boisestate.edu

INTRODUCTION

Handcycling is gaining popularity as one of the few exercises available to manual wheelchair users. In theory, handcycling propulsion can be generated in any phases of crank rotation, because the hands are always in contact with handpedals to exert force. A previous study of handcycling has shown that propulsion arises during both pull and push phases [1]. (The pull phase is a phase during which the elbow is being flexed.) However, how individual upper-limb muscles generate or possibly impede propulsion is not well understood. Therefore, the purpose of this study was to identify individual muscle contributions to handcycling propulsion. Forward dynamics simulations emulating synchronous handcycling were used for the analysis.

METHODS

An upper-limb musculoskeletal model was generated based on a previous model [2] in OpenSim [3]. The model consisted of the thorax, clavicle, scapular, humerus, radius, ulna and hand segments. The inertial properties were obtained from literature [4]. Only the right upper limb was included in the model, assuming bilateral symmetry in synchronous handcycling. The model had five degrees of freedom at the sternoclavicular and acromioclavicular joints, and seven degrees of freedom at the glenohumeral, elbow and wrist joints. The joint coordinate system was based on the ISB recommendation [5]. The thorax segment was fixed in the global frame. Thirty Hill-type musculotendon actuators were included in the model.

Ten healthy male adults (age 25.5 ± 4.3 years old, height 178.0 ± 7.9 cm, body mass 78.1 ± 8.4 kg) without previous handcycling experience participated in the study after providing their informed consent to the protocol approved by Boise State University Institutional Review Board. After familiarizing themselves with a handcycle (*Top End Force, Invacare, Elyria, OH*) and warming-up, subjects performed stationary handcycling at a constant cadence of 60 rpm, with the power output of 90 watts controlled by a programmable bicycle trainer (*CompuTrainer, RacerMate, Inc., Seattle, WA*). Kinematics (100 Hz, *Vicon MX 460, Oxford, UK*), handpedal reaction forces and couples (2000 Hz, *MC1, Advanced Mechanical Technology, Inc., Watertown, MA*), and electromyography from ten upper-limb muscles (1000 Hz, *FreeEMG, BTS Bioengineering, Milano, Italy; Trigno, Delsys Inc, Boston, MA*) were collected for 15 seconds. These data were post-processed using zero-lag Butterworth digital filters.

Muscle-actuated forward dynamics simulations that emulate individual handcycling performance were generated using OpenSim [3]. A constraint force decomposition analysis [6] was used to obtain individual muscle contributions to handpedal forces. In the analysis, constraint forces (weld constraint) were used in the system equations of motion instead of applying experimental handpedal forces, and contributions to the constraint forces from all force components in the system (muscle forces, gravity, and velocity-related forces) were computed using an induced acceleration analysis [6]. Muscle contributions to the handpedal force were transformed into a local coordinate system that defines tangential direction to the circular path of the handpedal.

All data were time-normalized to crank angles (0-360^0), and averaged within and then across subjects. The pull and push phases were defined from 0^0 to 180^0, and from 180^0 to 360^0 of crank angles, respectively.

RESULTS AND DISCUSSION

The forward dynamics simulations well emulated handcycling performance with muscle excitation patterns matching EMG patterns (not shown here). Group-averaged root-mean-square errors in kinematics between the experimental data and simulations were less than 4 degrees in all joint angles. Reconstructed handpedal force (the sum of all force contributions obtained in the force decomposition analysis) closely matched experimental tangential handpedal force (Fig. 1), indicating that the decomposition analysis was successfully performed.

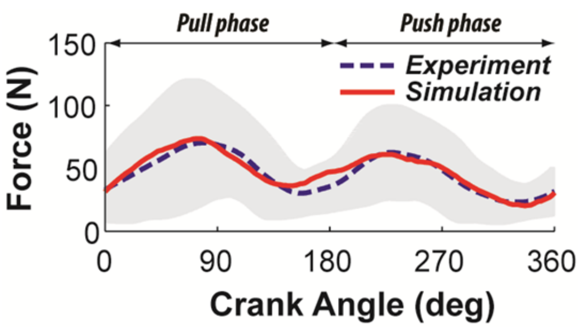

Figure 1: Group-averaged tangential handpedal force (propulsion) obtained in the experiments and simulations. The shaded area indicates one standard deviation from experimental average.

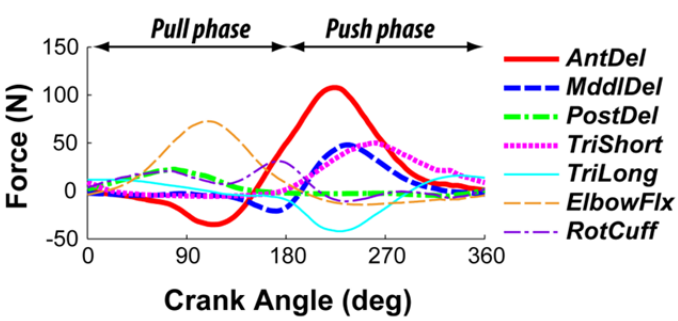

Figure 2: Individual muscle contributions to tangential handpedal force (propulsion). ***AntDel***: anterior deltoid, ***MddlDel***: middle deltoid, ***PostDel***: posterior deltoid, ***TriShort***: triceps short head, ***TriLong***: triceps long head, ***ElbowFlx***: biceps short head, brachialis and brachioradialis combined, ***RotCuff***: rotator cuff muscles.

Increased propulsion was observed during the pull and push phases (Fig. 1), which was consistent with previous study results [1]. In general, flexor muscles generated propulsion during the pull phase and extensor muscles did so during the push phase (Fig. 2). The primary contributors during the pull and push phases were the elbow flexors and the anterior deltoid, respectively. However, the anterior deltoid impeded propulsion during the pull phase. The triceps *short* head generated substantial propulsion during the push phase, but the triceps *long* head acted to impeded propulsion during early push phase. During the push-pull transition (around 360^0 or 0^0 crank angle), muscle contributions to propulsion were minimum.

The current study showed how individual muscles contribute to or impede synchronous handcycling propulsion among healthy adults. This information would be useful for individuals who aim to improve handcycling performance. Also, the information could serve as a basis for improving rehabilitation techniques such as functional electrical stimulation during handcycling or similar arm-crank exercises for individuals with impaired upper limb control. In addition, the force decomposition analysis can be applied to other upper-limb dynamic activities. Identifying muscle contributions to “endpoint forces” would provide valuable information in the research areas of rehabilitation, motor learning, and ergonomics.

REFERENCES

1. Arnet U, et al. *Med Eng Phys* **34**, 78-84, 2012.
2. Holzbauer, KR, et al. *Ann Biomed Eng* **33**, 829-840, 2005.
3. Delp SL, et al. *IEEE Trans Biomed Eng* **54**, 1940-1950, 2007.
4. Winter DA. *Biomechanics and Motor Control of Human Movement,* John Wiley & Sons, Inc., 1990.
5. Wu G, et al. *J Biomech* **38**, 981-992, 2005.
6. Hamner SR, et al. *J Biomech* **43**, 2709-2716, 2010.

ACKNOWLEDGEMENTS

This work was supported in part by NIH NCSRR travel grant by which technical support was obtained from the OpenSim team at Stanford University. The author is grateful to Jason Griswold for his help with data preparation.

EVALUATION OF NOVEL BIOFEEDBACK IN CHANGES OF ACVITATION OF THE TRAPEZIUS

[1]Brecca M. Gaffney, [2]Katrina S. Maluf, and [1]Bradley S. Davidson

[1]University of Denver, Human Dynamics Laboratory, Denver, CO, USA
[2]University of Colorado School of Medicine, Applied Neuromuscular Physiology Lab, Aurora, CO, USA
email: brecca.gaffney@du.edu

INTRODUCTION

Work-related chronic neck pain is a growing disorder in the United States that accounts for approximately 60% of all occupational disabling injuries [1]. Neck pain is linked to continuous and excessive activation in the upper trapezius (UT) muscle [2]. An effective treatment for chronic neck pain may be to reduce activation in the UT through an inferior shift in the muscle activity to the middle (MT) and lower trapezius (LT).

Because muscle architecture in the trapezius is complex and varied across the regions, the spatial information from high-density surface electromyography (HDsEMG) may provide a good signal on which to implement biofeedback for neck pain. Real-time EMG biofeedback using bipolar electrodes is used to assist a patient attempting to selectively activate and redistribute muscle activity [3]. Bipolar electrodes are typically used, which provide estimates of muscle activity only at the recording point. The real-time spatial distribution of the muscle activity (Fig. 1a) from HDsEMG may be particularly effective when using biofeedback to redistribute muscle activity from the UT to the MT and LT.

The objective of this investigation was to compare the redistribution of trapezius muscle activity using two different feedback interventions. We hypothesized that an HDsEMG interface would result in a more uniform and inferior distribution of trapezius muscle activity compared to traditional postural biofeedback.

METHODS

Twelve participants (5 males, 7 females) without a history of chronic neck or shoulder pain performed two, 15-minute typing tasks. Two types of feedback instruction were provided to the participants in a random order. The two types of feedback were (1) verbal feedback from the researcher prior to the typing task (NBF) and (2) verbal feedback from the researcher prior to the typing task plus visual feedback of HDsEMG signals during the typing task (BF). Verbal feedback consisted of a researcher coaching each participant how to sit at the computer with a “neutral posture.” The ideal neutral posture includes an upright trunk, tucked chin, and shoulder blades slightly depressed and adducted. Adopting this posture enacts an inferior shift in trapezius muscle activity [4]. Each participant practiced this posture for one minute with corrective manual and verbal feedback from the researcher before the typing tasks.

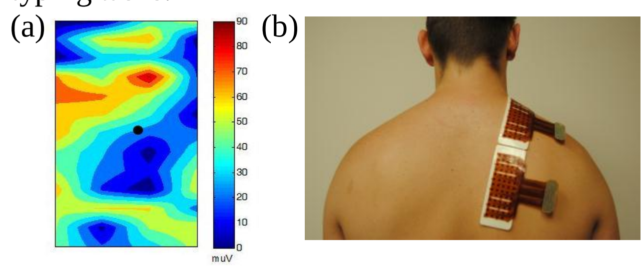

Figure 1: (a) Topographical map of ARV UT activity with Y_{COG} location (b) Electrode placement

Two HDsEMG electrode arrays (composed of 64 electrodes each) were placed over the UT, MT, and LT (Fig. 1b). The superior electrode array was placed 1 cm medial to the innervation zone with the 4th electrode row placed along the C7-acromion line [5]. HDsEMG signals were sampled during both typing tasks at 2,048 Hz. Fifty-one bipolar signals were extracted from each array.

The biofeedback intervention displayed a real-time onscreen indicator of trapezius muscle activity. Real-time EMG signals from both HDsEMG arrays were bandpass filtered (4th order Butterworth, 10-500 Hz) with a 1 second time constant. The signals were summed across all electrodes in each array, and the ratio of signal amplitude (superior/inferior) was calculated. An activity ratio (AR) was calculated that quantified how muscle activity was distributed between the superior and inferior fibers of the trapezius. An increase in AR indicated greater activation of the upper fibers relative to the lower fibers. Whenever the real-time AR exceeded the average AR recorded during the coached neutral posture for longer than one second, the participant received an onscreen visual alert to alter the distribution of their trapezius muscle activity through postural correction.

Average rectified values (ARV) of EMG signals were calculated over 0.5-s non-overlapping epochs. The distribution of trapezius muscle activity was represented by the *y*-component of the center of gravity (Y_{COG}) across both electrode arrays in the superior-inferior direction of trapezius muscle activity (Fig. 1). Homogeneity in trapezius muscle activation patterns of the UT was calculated using a measure of entropy:

$$entropy = -\sum_{i=1}^{51} p^2(i)\log_2(p^2(i))$$

where $p^2(i)$ is the square of the ARV value at electrode *i* normalized by the summation of activity in the squares of the 51 ARV values. Higher values correspond to a more heterogeneous distribution of muscle activity across the arrays [6]. The effect of biofeedback on trapezius muscle activity was examined by comparing dependent variables across typing tasks with a one-directional paired *t*-test. Level of significance was set at α=0.05.

RESULTS AND DISCUSSION

Three of the participants were unable to comply with the biofeedback instructions, shown by higher AR with the biofeedback interface than without (Table 1). Of the participants who were able to comply with the EMG biofeedback, the distribution of trapezius muscle activity shifted inferiorly and was spatially more homogeneous in activation patterns across the fibers of the UT muscle. However, these results were not statistically significant. AR was 10.16±33.31% lower with biofeedback. Y_{COG} was 11.38±11.37% lower (*P*=0.21) with biofeedback. Entropy was 5.95±1.89% lower (*P*=0.12) with biofeedback (Fig. 2). In addition, the participants who showed a larger inferior shift in Y_{COG} demonstrated more homogeneous spatial distribution patterns (lower entropy).

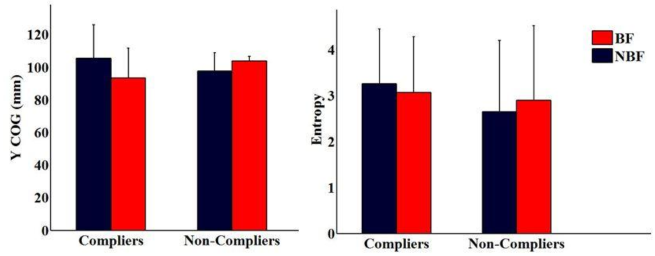

Figure 2: Mean±SD Y_{COG} and entropy between tasks.

The entropy of the ARV maps represents a measure of spatial heterogeneity of the UT. More uniform activation patterns in the UT reduces the risk for excessive activation in one area of the UT. The differences among participants in the distribution of muscle activity may indicate changes in motor unit recruitment patterns [6]. Throughout the duration of the typing task, the spatial reorganization of muscle activity may be a motor control mechanism to reduce muscle fatigue.

CONCLUSIONS

HDsEMG biofeedback successful changed the distribution of UT muscle activity for 75% (9 of 12) of the participants. The three participants unable to comply demonstrated more heterogeneous trapezius muscle activation patterns. These data indicate an inability to voluntarily redistribute muscle activity to the MT and LT in some individuals. These patients often do not respond to biofeedback-based interventions. Future work will investigate the effectiveness of HDsEMG biofeedback in patients with chronic neck pain.

REFERENCES

1. Piligan G. *Am J Ind Med*, **37**, 75-93, 2000
2. Voerman G. *Eur J Appl Physiol*, **102**, 1-9, 2007
3. Holterman A. *J Elect Kines*, **20**, 359-65, 2010
4. Wegner S. *Manual Ther*, **15**, 562-66, 2010
5. Farina D. *J Elect Kines*, **18**, 16-25, 2008
6. Samani A. *Eur J Appl Physiol*, **110**, 415-23, 2010

Table 1. Change in AR between typing tasks (* Non-Complier).

Subject	1	2	*3	4	5	6	7	8	*9	10	*11	12
ΔAR	-0.110	-0.054	0.014	-0.023	-0.108	-0.01	-0.320	-0.091	0.001	-0.094	0.053	-0.308

NORMATIVE 3D STRENGTH SURFACES IN HEALTHY SUBJECTS FOR THE HIP AND TRUNK JOINT COMPLEXES

[1]John M. Looft, [3]Allison A. Stockdale, [2]Keith G. Avin, [1]Laura A. Frey Law

[1]University of Iowa, Iowa City, IA, USA
[2]University of Pittsburgh, Pittsburgh, PA, USA
[3]Veterans Administration Hospital, Sacramento, CA
email: laura-freylaw@uiowa.edu

INTRODUCTION

As industrial advances continue in the United States, it is important to develop tools to protect workers from musculoskeletal disorders. Despite many advances in ergonomic workplace interventions, back pain remains one of the most common reasons for missed work days [1]. Further, healthcare costs associated with chronic and acute back pain have risen to between $84.1 to $624.8 billion dollars per year [2].

Digital human models (DHM) are currently being developed as one such tool to advance workplace assessments. These models are being used to predict kinetics and kinematics associated with performing various tasks. This process requires normative strength data to assess the relative task intensities. In particular, there is a lack of normative hip and trunk strength data available in the literature, considering both angle and velocity influences in multiple cardinal planes, i.e. flexion/extension, lateral flexion/extension, abduction/adduction, and rotation.

Thus, the purposes of this study were 1) to establish normative strength data for hip and trunk joint regions in healthy human subjects and 2) model 3D relationships of torque-angle-velocity strength for each torque direction in men and women.

METHODS

Subjects

51 subjects (24 F) participated in this study after providing written, informed consent, as approved by the University of Iowa institutional review board. All participants were reimbursed for their time.

Table 1: Mean (SD) subject demographic information by sex

	n	Height (cm)	Weight(kg)	Age (yr)
Men	27	182.3 (6.9)	79.1 (15.1)	23.9 (4.7)
Women	24	169.4 (8.3)	68.7 (14.4)	23.3 (4.1)

Subject age, height, weight, and % body fat were assessed during the initial visit (Table 1).

Experimental Procedures

Subjects performed both isometric and isokinetic maximum joint strength tests for the hip and trunk joints at two separate visits. The testing order was block randomized by joint plane of rotation to minimize the effects of testing order. A 2 min rest was provided between each angle/velocity test and a 5 min rest was provided between the isometric and isokinetic tests.

Strength Testing

Subjects first completed a 5 min warm-up on a stationary bike. Maximum voluntary torque was assessed for each joint at a variety of angles and velocities (Table 2) using a Biodex System 3 Isokinetic Dynamometer (Biodex Medical Systems, Shirley, New York). Normative strength data was collected for hip (flexion/extension and abduction/adduction) and trunk (flexion/extension, side bending, and rotation) complexes. To ensure proper testing, custom hip and trunk testing attachments were manufactured for the dynamometer and verbal encouragement was provided by the test administrator.

Table 2: Hip and trunk testing protocol

	Isometric Testing Angles (Deg)	Isokinetic Testing Velocities (Deg/s)
Trunk*	0, 10, 20, 30,40	30, 60, 90, 120
Hip	0, 15, 30, 45, 55	60, 90, 120, 180

*The maximum isometric trunk rotation angle was 30°

Isometric and Isokinetic Protocol

The maximum of three maximum voluntary contractions (MVICs) was used as the isometric angle-specific peak torque value (see Table 2). Isokinetic peak torques were assessed at multiple velocities (Table 2) at the joint angles assessed isometrically. Gravity corrections were used to account for the torque required to overcome the inertial limb weight. Total torque-velocity-angle triplets consisted of: 25 (trunk flexion/extension, side bending); 35 (trunk rotation); 20 (hip flexion/extension); and 15 (hip abd/adduction).

Data Processing

Labview 8.0 (National Instruments) was used to collect the raw torque, velocity, and position data at 1000Hz. Custom Matlab (Mathworks) programs were used for data processing, including filtering with a fourth-order Butterworth filter and extracting peak torque values. Isokinetic data was required to be within 15% of target velocity for inclusion. The mean, standard deviation (SD), and coefficient of variation (CV) were calculated for men and women. Eccentric strength was estimated as 120% of isometric MVCs for modeling 3D strength surfaces.

Strength Models

Torque-angle-velocity data triplets were curvefit using logistic equations (TableCurve 3D, SYSTAT) and 3D surfaces plotted using Sigmaplot (IBM). R^2 values were determined for each torque direction (4 trunk, 4 hip) and for males and females (16 total).

RESULTS AND DISCUSSION

Similar to previous 3D strength studies, the hip and trunk both demonstrated torque-angle and torque-velocity relationships with moderate interactions (see Fig 1 for one example). Men were consistently stronger than women for both joint complexes, particularly for trunk. The logistic equation surfaces fits were very reasonable for each joint and direction (see Table 3).

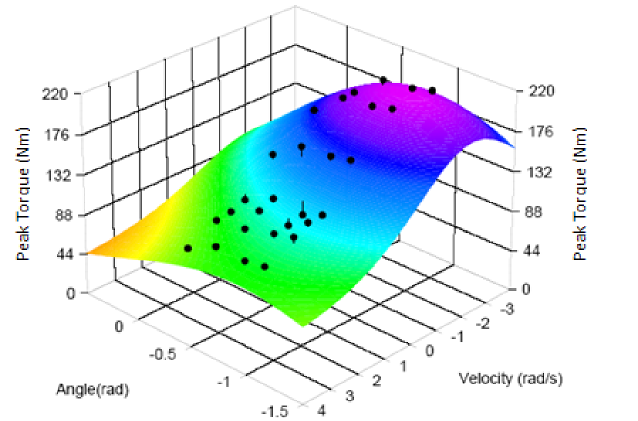

Figure 1: Example of the resulting 3D strength model for male hip extension.

CONCLUSIONS

This research effort has provided 3D strength surfaces for the hip and trunk joint complexes. With the addition of these surfaces and other joint strength models, DHMs will have more accurate models on which to base their kinetic predictions.

REFERENCES

1. Deyo, R.A., S.K. Mirza, and B.I. Martin, *Back pain prevalence and visit rates - Estimates from US national surveys, 2002.* Spine, 2006. **31**(23): p. 2724-2727.
2. Sadosky, A.B., et al., *Relationship Between Self-reported Low-back Pain Severity and Other Patient-reported Outcomes Results From an Observational Study*. Journal of Spinal Disorders & Techniques, 2013. **26**(1): p. 8-14.

ACKNOWLEDGMENTS

The authors were funded in part by National Institutes for Health, K01AR056134, United Council for Automotive Research (USCAR, Dearborn, MI), and the University of Iowa Heartland Center Graduate Student Fellowship

Table 3: Isometric peak torques (CV) and 3D surface fit results (R^2) for each joint, direction, and sex

Male		**PT (Nm)**	**CV**	**R^2**	**Female**		**PT (Nm)**	**CV**	**R^2**
Hip	*Flexion*	162.6	0.304	0.918	Hip	*Flexion*	121.6	0.340	0.944
	Extension	170.3	0.325	0.982		*Extension*	104.5	0.511	0.981
	Abduction	98.1	0.408	0.975		*Abduction*	81.6	0.470	0.940
	Adduction	107.1	0.610	0.986		*Adduction*	85.4	0.770	0.977
	Median		0.367	0.979		*Median*		0.491	0.961
Trunk	*Flexion*	188.7	0.350	0.984	Trunk	*Flexion*	108.2	0.430	0.974
	Extension	331.8	0.320	0.995		*Extension*	191.6	0.310	0.994
	Side Bending	152.2	.410	0.958		*Side Bending*	94.1	.470	0.979
	Rotation	72.2	.470	0.909		*Rotation*	45.5	.470	0.928
	Median		0.380	0.971		*Median*		0.450	0.977

COMPARISON OF SUPRASPINATUS AND INFRASPINATUS SURFACE AND FINE WIRE ELECTROMYOGRAPHY DURING ISOMETRIC HUMERAL ROTATION

[1]Rebecca L. Brookham, [1]Tyler R. Allen, [1]Alan C. Cudlip and [1]Clark R. Dickerson

[1]University of Waterloo, Waterloo, ON, CAN
email: clark.dickerson@uwaterloo.ca

INTRODUCTION

The rotator cuff (RC) rotates the humerus while maintaining stability of the glenohumeral joint. Electromyographic (EMG) monitoring of these muscles is crucial to understanding their function and dysfunction, but is complicated by the restricted access to these deep muscles. To record EMG from RC muscles, fine wire EMG is typically required to avoid cross-talk introduced by overlying, superficial muscles. Compared to surface EMG, fine wire EMG is more costly and invasive, requires specialized training and yields more localized muscle information. Using surface EMG to examine the RC is preferable if it sufficiently replicates fine wire signals. Synchronous surface and fine wire EMG have been compared for the lower limb [1, 2] and trunk musculature [3, 4], but only one recent study has made this comparison of maximal contractions of the RC [5]. The purpose of this study was to extend definition of the relationship between select surface and fine wire RC EMG to submaximal contractions.

METHODS

Surface and fine wire electrodes recorded EMG from the right supraspinatus and infraspinatus of 20 healthy adults (mean, range: age (years) 22, 18-32; stature (m) 1.69, 1.6-1.8; weight (kg) 66.6, 48.5-85.0). Participants performed 6s duration maximal voluntary force exertions of humeral internal rotation (IR) and external rotation (ER) which were used to normalize experimental exertion intensities. Muscle specific maximal voluntary contractions (MVCs) were performed to allow for EMG normalization. Participants performed 82 isometric IR or ER exertions in a combination of intensities (10%, 20%, 30%, 40%, 50%, 60%, 80% MVC) and postures (-45°, 0°, 45° of humeral rotation, and 0°, 45°, 90°, 135° of humeral abduction) with the elbow flexed to 90°. Raw EMG was high pass filtered (Fc 30Hz), linear enveloped (low pass filtered, Fc 2.5Hz) and normalized. Linear least squares best-fit regressions were used to compare the normalized EMG of surface and fine wire EMG recordings of supraspinatus and infraspinatus, respectively. Fine wire recordings were defined as the dependent variables, and surface recordings as the independent variables. Repeated measures ANOVA testing was then performed to assess the influence of intensity and humeral abduction and rotation angles on the relationships. Significant differences were identified using post-hoc (Tukey HSD) analysis.

RESULTS AND DISCUSSION

The regression equations for supraspinatus during ER and IR exertions are shown in Eq. 1 & 2, resp.:

$$EMG_{S,FW} = 1.6 + 0.76 \cdot EMG_{S,SF} \quad (r^2 = 0.76; p < 0.0001) \tag{1}$$

$$EMG_{S,FW} = -2.8 + 0.83 \cdot EMG_{S,SF} \quad (r^2 = 0.72; p < 0.0001) \tag{2}$$

The regression equations for infraspinatus during ER and IR exertions are shown in Eq. 3 & 4, resp.:

$$EMG_{I,FW} = 11.0 + 0.58 \cdot EMG_{I,SF} \quad (r^2 = 0.64; p < 0.0001) \tag{3}$$

$$EMG_{I,FW} = 1.8 + 0.20 \cdot EMG_{I,SF} \quad (r^2 = 0.62; p < 0.0001) \tag{4}$$

[where S=supraspinatus, I=infraspinatus, FW=fine wire, SF=surface. EMG is expressed as % MVC.] Regressions indicate that surface supraspinatus recordings overestimate respective fine wire recordings by 31.6%, plus 1.6% MVC offset across all ER trials, and this overestimation drops to 20.5%, minus 2.8% MVC offset across all IR trials. Surface infraspinatus recordings overestimate respective fine wire recordings by 72.4%, plus 11% MVC offset across ER exertions, and this overestimation spikes to 400%, plus 1.8% MVC offset across all IR exertions. Intercepts imply low levels of fine wire activation when surface records no activity, except for the infraspinatus during ER (11% MVC). Potential for cross-talk is high with surface infraspinatus recordings due to the overlying trapezius and interactions with the deltoid and latissimus dorsi. Cross-talk contamination may lower prediction capability, especially at activations lower than those which the models were built upon.

The relationships were influenced by humeral abduction ($p<0.0001$):

- for ER exertions (Fig. 1):

Supra activations at 135° were > than at 45°, 0° and Supra activations at 90°, 45° were > than at 0°.
Infra activations at 0° were > than at 45°, 90°, 135°.

- for IR exertions (Fig. 2):

Supra activations at 135°, 90° were > than 0°, 45°.
Infra activations at 0° were < than 45°, 90°, 135°.

The relationships were also influenced by intensity - as intensity increased, the bias in predicting fine wire from surface values also increased:

- for ER exertions:

1%↑ in intensity = 0.21%↑ fine wire Supra MVC% & 0.5%↑ fine wire Infra %MVC.

- for IR exertions:

1%↑ in intensity = 0.03%↑ fine wire Infra MVC%.

Humeral rotation did not influence predictions.

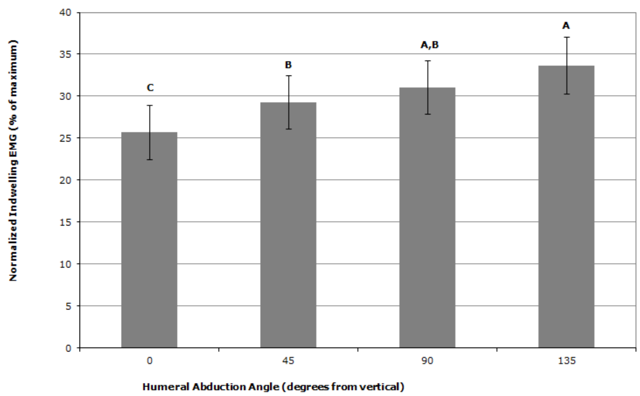

Figure 1: Supraspinatus activation during ER. [Different letters indicate significant differences.]

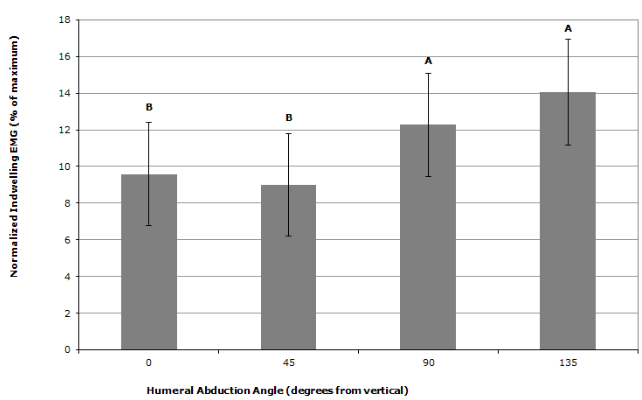

Figure 2: Supraspinatus activation during IR.

The relationships between surface and fine wire recordings were sensitive to arm posture and task intensity, which were attributable to changes in the muscle activity or recordable signal. RC muscle moment arms change with posture [6], and further, movement of the target muscle(s) beneath the skin and electrode may have altered signal content.

Submaximal exertions generated smaller overestimations and had more variance explained than those detailed in maximal exertions [5]. This may be because as relative intensity increases, the relationship to fine wire EMG signals becomes increasingly non-linear [7]. However, it is difficult to advocate universal surface electrode monitoring of the infraspinatus and researchers should use caution when examining exertions opposite to the primary action of the muscle investigated. Large overestimations of infraspinatus activation were seen during IR exertions.

CONCLUSIONS

Surface EMG can be used to reasonably multiplicatively estimate fine wire EMG of the supraspinatus and infraspinatus during submaximal humeral rotation exertions. These relationships are sensitive to changes in humeral abduction angles and task intensity. Caution should be taken when interpreting surface recordings as indicators of fine wire signals, especially for exertions where the muscle examined is not a primary mover.

ACKNOWLEDGMENTS

Support was received from the Natural Science and Engineering Research Council, Canada Foundation for Innovation and the University of Waterloo.

REFERENCES

1. Byrne C, et al. *J Electrom Kinesiol* **15**, 564-75, 2005.
2. Jacobsen WC et al. *J Electromyogr Kinesiol* **5,** 37-44, 1995.
3. Stokes IA et al. *Clin Biomech* **28**, 9-23, 2003.
4. McGill S et al. *J Biomech* **29**, 1503-7, 1996.
5. Waite DL et al. *J Electromyogr Kinesiol* **20**, 903-11, 2010.
6. Langenderfer JE et al. *J Orthop Res* **24,** 2006.
7. Onishi H et al. *J Electromyogr Kinesiol* 10, 59-67, 1999.

NEUROMAGNETIC ACTIVITY OF THE SENSORIMOTOR CORTICES DURING THE MOTOR PLANNING AND EXECUTION STAGES IN CHILDREN WITH CEREBRAL PALSY

[1]David J. Arpin, [2]Katherine M. Becker, [2]Elizabeth Heinrichs-Graham, [2]Tony W. Wilson & [1]Max J. Kurz

[1]Munroe-Meyer Institute, University of Nebraska Medical Center, Omaha, Nebraska
[2]College of Medicine, University of Nebraska Medical Center, Omaha, Nebraska
Email: mkurz@unmc.edu Web: http://www.unmc.edu/mmi/

INTRODUCTION

Cerebral palsy (CP) results from a perinatal brain injury that can impact the neuromuscular control of the lower extremities. A considerable amount of research efforts have been placed on cataloging and quantifying the motor impairments seen at the knee joint because it has been cited as a critical factor that limits the mobility of these children. These studies have shown that children with CP often present a wide variety of musculoskeletal impairments that may limit the knee's performance (e.g., co-contractions, spasticity, weakness, contractures). Based on these insights, the majority of treatment approaches have used a bottom-up treatment approach (e.g., surgery, strength training) in hopes of improving the knee joint's motor performance. However, systematic reviews indicate that there is little scientific support for these approaches, as the outcomes are often mixed and unpredictable [2].

Few investigators have suggested that the motor control problems seen in children with CP may be partially related to an abnormality in the ability of sensorimotor cortices to formulate a motor plan [1,3]. These studies have noted that children with CP have slower reaction times, and errors in muscular force production when performing motor tasks with the upper extremities. However, despite these novel behavioral insights, limited efforts have been made to evaluate if these results are due to aberrant activity of the sensorimotor cortices during the motor planning stage. Furthermore, no studies have evaluated if similar motor planning deficits exist while children with CP attempt to control the lower extremities; including the knee joint.

Magnetoencephalography (MEG) is the only brain imaging technique that can accurately separate the motor planning and execution stages of the sensorimotor cortices. Previous MEG studies have established that the beta-frequency (15-30 Hz) oscillatory activity in the sensorimotor cortices decreases before the movement onset, and represents the motor planning stage [4]. Moreover, it is well known that gamma-band (>50 Hz) oscillatory activity in the primary motor cortex is related to the execution of the motor command [4]. While the central role of beta and gamma neural oscillatory activity during movement is well appreciated, there has been no effort to use this knowledge to more precisely characterize the motor deficits seen in children with CP.

The purpose of this investigation was 1) to determine if motor planning deficits are present in children with CP while performing an isometric knee joint task, 2) to determine if beta event related desynchronization (ERD) and gamma event related synchronization (ERS) is altered in children with CP while moving the knee joint, and 3) to determine if there is a relationship between the beta ERD and gamma ERS and muscular control of the knee joint.

METHODS

Thirteen children with spastic diplegic or hemiplegic CP (Age = 11 $\pm$ 4 yrs.) and thirteen typically developing (TD) children (Age = 13.2 $\pm$ 3 yrs.) participated in this investigation. An isokinetic dynamometer (Biodex Inc., Shirley, NY) was used to measure the steady-state isometric torques generated by the knee joint extensors. The motor task involved matching and holding a target torque that was 20% of the child's maximum voluntary torque for 15 seconds. The target and the torque exerted by the child were displayed on a large monitor positioned ~1 meter away. The time to reach the target force was used as a surrogate assessment of the certainty of the motor plan. Additionally, the coefficient of variation (CV) was used to assess the steadiness of the motor output after the target value was achieved. A greater amount of variability was assumed to indicate more errors in execution and adjustment of the motor plan to remain at the target value.

A whole head 306-sensor MEG system (Elekta Neuromag, Helsinki, Finland) was used to assess the oscillatory activity of the sensorimotor cortices as children extended their knee when cued by an auditory stimulus. A linearly-constrained minimum variance vector beamformer algorithm was used to calculate 3D images that reflect the local power of neuronal current [4]. The single images generated were derived from the cross spectral densities of all combinations of MEG sensors averaged over the time-frequency ranges of interest. The beamforming analysis was performed for the beta-frequency spectrum (14-28 Hz) preceding movement onset, and the high-frequency gamma spectrum (>40 Hz) slightly preceding and during movement execution.

RESULTS AND DISCUSSION

The biomechanical results indicated that the children with CP took longer to reach the target (CP = 2.78 $\pm$ 0.20 sec; TD = 1.62 $\pm$ 0.13 sec; $p < 0.05$), and had greater errors in their ability to sustain the steady-state torque values (CP = 8.26 $\pm$ 2.30%; TD = 3.27 $\pm$ 0.48%; $p < 0.05$). These results imply that the children with CP take longer to formulate a motor plan, and have greater errors in adjusting and/or sustaining the motor output to match the desired motor output.

Exemplary results for a TD child and a child with CP are shown in Figure 1. The group MEG results indicated that children with CP had greater beta ERD responses (CP = -25.48 nAm; TD = -4.47 nAm; $p < 0.05$), and lower gamma ERS (CP = -16.93 nAm; TD = 6.82 nAm; $p < 0.05$) than the TD children. These results are the first to show that there is abnormal activity in sensorimotor cortices

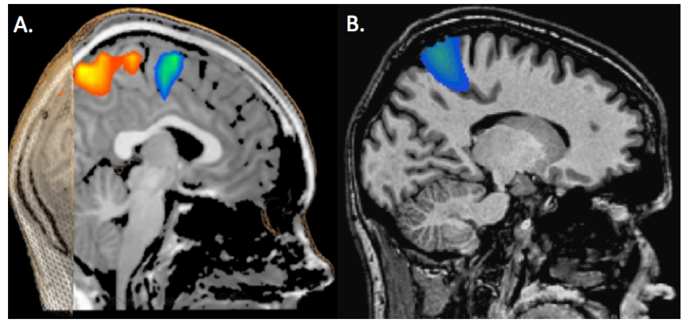

Figure 1. Motor activity for a representative TD child (A) and a child with CP (B). The gamma-frequency ERS that is associated with movement execution is shown in yellow (medial precentral gyrus) and the pre-movement beta-frequency ERD response appears in blue (supplementary motor area in TD and pre/postcentral gyri in CP). The darker blue indicates that the beta-frequency ERD was greater in the child with CP compared with the TD child.

during the motor planning stage, which may impact the later execution of the motor command by the primary motor cortices.

There was a moderate ($r = -0.48$; $p<0.05$) negative correlation between gamma ERS and the time taken to reach the target. Indicating that children who took longer to reach the target had a lower gamma ERS in the sensorimotor cortices. There also was a moderate ($r = -0.48$; $p<0.05$) negative correlation between the beta ERD and the CV. Indicating that greater errors in the knee joint's steady-state muscular performance were related to greater beta ERD during the motor planning stage.

Our results support the notion that children with CP have deficits in the formulation and execution of the motor command. We suspect that interventions focused on improving the ability of children with CP to formulate an adequate motor plan may result in an improved ability to control the knee joint.

REFERENCES

1. Duff SV & Gordon AM. *Dev Med Child Neurol* **45**, 746-757, 2003.
2. Mockford M & Caulton JM. *Ped Physical Ther* **20**, 318-333, 2008.
3. Valvano J & Newell KM. *Dev Med Child Neurol* **40**, 464-473, 1998.
4. Wilson TW, et al. *Brain Cogn* **73**(2), 75-84, 2010.

EFFECTS OF A NEWLY DESIGNED CERVICLE COLLAR ON NECK JOINT KINEMATICS

Jacob Gardner, Xuan Liu, Chen Wen, Songning Zhang

Biomechanics/Sports Medicine Lab, The University of Tennessee, Knoxville, TN, USA
email: jgardn25@utk.edu, web: http://web.utk.edu/~sals/resources/biomechanics_laboratory.html

INTRODUCTION

Cervical collars are often prescribed to patients who have sustained a cervical spine injury [1]. Spinal orthoses may be used to correct spinal deformities, immobilize intervertebral segments, provide regional stabilization, or protect the cervical region from damaging stresses during the healing process [2]. Adjustable cervical collars have recently emerged into the market to offer superior support and flexibility to fit a broader range of sizes for patients. A new cervical collar has been designed to provide more movement restrictions than currently available models as well as provide an increased distraction effect on the neck of the wearer. The objective of this research project was twofold: 1) to examine the restrictive effects of a newly designed adjustable cervical collar (Universal XTW, DeRoyal Industries, Inc.) on the 3D head-neck kinematics compared to two other similar cervical collars (Aspen Vista® and Miami J® Advanced), and 2) to compare the distraction effects of the three collars on the wearer.

METHODS

Nineteen healthy males and females (female: N=9, age 28.4 ± 6.8 yrs, height 1.66 ± 0.02 m, mass 62.5 ± 13.0 kg, BMI 22.6 ± 4.3 kg/m^2; male: N=10, age 27.1 ± 3.9 yrs, height 1.78 ± 0.08 m, mass 74.7 ± 13.9 kg, BMI 23.6 ± 3.3 kg/m^2) between the ages of 18 and 40 participated in the study. Subjects were free from injury at the time of the study and had no major past head, neck, or back injuries.

A 9-camera 3D motion analysis system (240 Hz, Vicon Motion Analysis Inc., UK) was used to collect kinematic data during testing. Reflective anatomical markers were placed on the subject's greater trochanters, acromion processes, and ear canals. A cluster of four markers on a rigid thermoplastic shell was placed on the trunk to track trunk motions. Four tracking markers placed on a head band were used to track head movements. Eight additional markers were placed on the cervical collars to track the movements during the dynamic testing.

The cervical collars were applied to the subject's in a supine position by the same researcher according to the manufacturers' instructions. Once the collar was applied, the head height was adjusted for each collar so that the subject's head remained in a neutral position while sitting.

For the dynamic testing, subjects sat in a customized testing chair equipped with two shoulder straps and a lap belt. The belts served to stabilize the trunk movements while allowing freedom of motion in the head and neck. The Subjects performed three movements: flexion/extension, lateral flexion, and axial rotation in 4 collar conditions: no collar and three collars. The movement speeds were controlled by the beat of a metronome set at 50 beats per minute.

3D kinematic data were processed and analyzed using Visual 3D software (C-Motion, Inc., Germantown, MD). Variables of interests were the range of motion (ROM) of flexion/extension, lateral flexion, and rotation movements. Additionally, the distance between the center of mass (COM) of the trunk and head were calculated to determine the distraction effects of each collar. A 2 x 4 (Gender x Collar) mixed design ANOVA was used to detect differences between genders and collars (SPSS 19.0, IBM, Chicago, IL.) Post hoc comparisons were performed using a paired samples t-test if a significant interaction was found. An alpha level of 0.05 was set a priori for all statistical procedures.

RESULTS AND DISCUSSION

The ANOVA revealed no significant gender main effect or gender by collar interaction. Thus, subsequent data were combined to focus on collar main effects. The results showed that no significant differences were found in head-trunk distraction values across the four collar conditions (Figure 1).

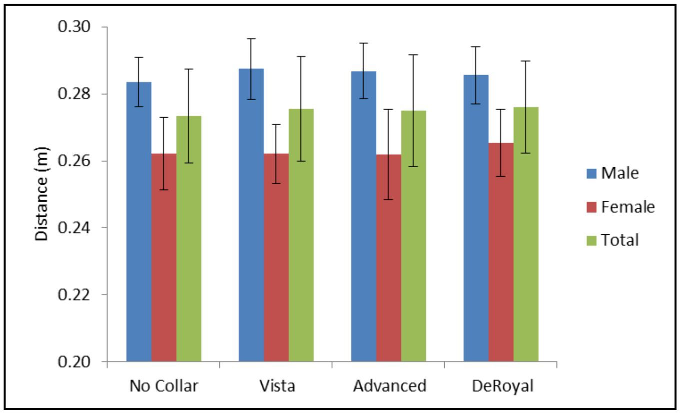

Figure 1: Mean head-trunk COM distraction values for males and females across the four collar conditions.

As expected, all collars significantly decreased the range of motion of all three movements compare to the no collar condition ($p < 0.001$, Table 1). Both the Advanced and the XTW showed significant reductions in the three movements compared to the Vista collar (except for the differences between Advanced and Vista in axial rotation ROM). Additionally, the XTW showed a significant reduction in axial rotation ROM compared to both the Vista and Advanced collars.

The results of this study suggest that the newly designed XTW collar provided a clear advantage in minimizing head movements when compared to the Vista collar. However, when compared to the Advanced collar, the differences were less significant, with the XTW collar restricting the axial movements more.

One of the missions of adjustable collars is to maintain and/or increase the head-trunk distance (distraction) during head/neck movements to provide a traction effect for the user. However, the results of this study showed that all adjustable collars tested in this study failed to increase the distraction. However, they were able to maintain the distraction.

CONCLUSIONS

The Universal XTW and Miami J® Advanced cervical collars provided greater restriction of head-neck movements in sagittal and frontal planes. However, the Universal XTW collar showed greater restriction on axial rotations of head-neck compared to Advanced and Vista collars.

REFERENCES

1. Richter D, et al. *J Trauma*, 50, 848-854, 2001.
2. White AA & Panjabi MM, *Clinical biomechanics of the spine.* J.B. Lippincott Co. 1990.

ACKNOWLEDGEMENTS

The funding for this study was provided in part by DeRoyal Industries.

Table 1: Total ROM of head/neck movements: mean ± SD.

Variable	**Brace Condition**				
	No Collar	**Vista**	**Advanced**	**XTW**	**P**
Flexion/Extension ROM	107.1±21.0	31.4±13.0 $	28.9±11.0 $#	27.0±8.7 $#	< 0.001
Lateral Flexion ROM	73.5±13.5	42.8±13.5 $	34.2±14.5 $#	31.4±11.2 $#	< 0.001
Axial Rotation ROM	132.0±22.9	35.4±18.6 $	35.6±20.3 $	27.3±15.4 $#@	< 0.001

Note: $: Significantly different from No Collar, #: Significantly different from Vista, @: Significantly different from Advanced.

THE EFFECTS OF A VARUS UNLOADER BRACE FOR LATERAL TIBIOFEMORAL OSTEOARTHRITIS AND VALGUS MALALIGNMENT AFTER ANTERIOR CRUICATE LIGAMENT RECONSTRUCTION: A PROOF OF CONCEPT

[1]Harvi Hart, [1]David Ackland, [1]Anthony Schache, [1]Marcus Pandy, [1]Natalie Collins and [1,2]Kay Crossley
[1]The University of Melbourne, Victoria, Australia
[2]University of Queensland, Queensland, Australia
Email: h.hart@student.unimelb.edu.au

INTRODUCTION

Anterior cruciate ligament reconstruction (ACLR) is a well recognized risk factor for knee osteoarthritis (OA) [1]. Lateral tibiofemoral joint OA (TFJOA) is observed in more than 50% of those with knee OA 10-15 years after ACLR [2]. Valgus bracing is frequently prescribed for medial TFJOA to reduce varus malalignment and external adduction moments, and to improve pain and function. However, valgus bracing may not be appropriate for those with lateral TFJOA after ACLR. Lateral TFJOA is associated with significantly greater knee abduction angles and smaller external knee adduction moments compared to those associated with medial TFJOA [3]. The varus unloader brace is one potential targeted intervention for individuals with lateral TFJOA after ACLR. It is designed to control sagittal and transverse plane rotations associated with ACLR and correct frontal plane malalignment. The purpose of this proof of concept study was to investigate the immediate effects of the varus unloader brace on knee-related symptoms (pain, confidence and stability), knee kinematics, and kinetics in a patient with lateral TFJOA and valgus malalignment after ACLR.

METHODS

A 48-year old man (height 1.83m, weight 78kg) was referred to a private physiotherapy clinic in Melbourne, Australia. He had undergone ACLR eight years previously on his left knee. Weight-bearing tasks such as walking, especially on uneven surfaces, were becoming increasingly difficult over time, and occasionally required a walking stick due to knee instability. The Knee Injury and Osteoarthritis Outcome Score [4] indicated severe limitations with function in sports and recreation, and reduced quality of life. Radiographs revealed evidence of OA in the lateral tibia of the left knee and valgus malalignment. The effects of the varus unloader brace were investigated on knee-related symptoms and biomechanics. The test conditions were: (i) no brace; (ii) brace with frontal-plane adjustment (varus re-alignment); and (iii) brace without frontal-plane adjustment (no varus re-alignment).

The immediate effects of the adjusted varus brace on symptoms were evaluated with the step down task [5], designed to replicate stair descent. On completion of the test performed with and without the varus brace, the patient rated his level of pain, difficulty of task, knee stability, and confidence on four separate 100mm visual analogue scales (VAS) where 100mm represents the worst possible symptoms (higher difficulty; greater instability; lower confidence; greater pain), and 0mm represents no symptoms.

Three-dimensional gait analysis was performed to assess the effects of the brace on knee biomechanics, according to a protocol described previously [6]. Reflective markers were attached at various locations on the trunk and the affected lower-limb of the subject. Markers on the thigh and leg of the affected lower-limb were positioned such that the brace could be easily fitted without altering any marker positions. Kinematic data were measured using a 9-camera video motion analysis system (Vicon, Oxford Metrics Ltd., Oxford), while ground reaction forces (GRF) were recorded simultaneously from three ground-embedded force platforms (Advanced Mechanical Technology Inc., Watertown, MA). Video and analog force-plate data were sampled at 120 Hz and 1,080 Hz, respectively. The patient walked at his self-selected speed under the three test conditions. Knee joint kinematics and external knee joint moments were calculated for the affected limb [7].

RESULTS

The patient reported reduced task difficulty (no brace 74mm; brace 33mm), lower knee instability (no brace 74mm; brace 28mm), increased confidence (no brace 75mm; brace 26mm) and no pain (no brace 3mm; brace 0mm) with the adjusted brace compared to not wearing the brace. The vertical and fore-aft GRFs were similar between the three test conditions (Table 1). At contralateral toe-off (CTO), an increase in the external knee flexion moment was noted with the adjusted brace (33%) and unadjusted brace (25%) when compared to the no brace condition (Table 1). In the frontal plane at CTO, a 24% reduction in the knee abduction angle was observed with the adjusted brace. A small decrease in the external knee adduction moment in both unadjusted and adjusted brace conditions was also observed (Table 1). At CTO the adjusted brace reduced the knee internal rotation angle by 56%, with only a 17% decrease in the knee internal rotation angle noted with the unadjusted brace (Table 1).

DISCUSSION

The varus brace produced immediate symptomatic improvements and changes in frontal and transverse plane knee kinematics and kinetics that were more pronounced for the adjusted than the unadjusted brace conditions. While these data represent bracing effects for a single patient only, they provide preliminary evidence for the potential efficacy of a brace that is specifically targeted for lateral TFJOA after ACLR. The adjusted brace reduced the knee abduction angle, which is important since valgus alignment is associated with greater risk of lateral TFJOA progression [8]. An intervention that increases the external knee adduction moment may heighten the risk of medial TFJOA progression; however, we observed a reduction in knee abduction angle and a slight decrease in the knee adduction moment. Given no change in GRF magnitude, the knee brace may have shifted the centre of pressure laterally, thus reducing the magnitude of the GRF moment arm about the knee joint center. In the transverse plane, the adjusted brace substantially reduced the knee internal rotation angle. This change may be significant, since previous studies have reported an increase in internal rotation following ACLR, which is thought to play, a role in initiation of knee OA following ACLR [9]. The ACL is essential in providing rotational knee stability. This study shows that an unloader knee brace may be able to mitigate abnormal knee joint behaviour in people with lateral TFJOA and valgus malalignment after ACLR.

REFERENCES

1. Lohmander LS, et al. *Am J Sports Med* **35**, 1756-69, 2007.
2. Ahn JH, et al. *Arthroscopy* **28**, 1114-23, 2012.
3. Butler RJ, et al. *Physical therapy* **91**, 1235-43, 2011.
4. Roos EM, et al. *JOSPT* **28**, 88-96, 1998.
5. Barton CJ, et al. *Br J Sports Med* **45**, 193-9, 2011.
6. Hunt MA, et al. *Arthrit Care Res* **63**, 293-297, 2011.
7. Schache AG, et al. *Gait Posture* **25**, 440-52, 2007.
8. Chaudhari AMW, et al. Med Sci Sports Exerc **40**, 215-222, 2008.
9. Sharma L, et al. *Ann Rheum Dis* **69**, 1940-5, 2010.

TABLE 1: Ground reaction forces, kinematics and kinetics data for three test conditions

		GRF (N/kg)		**Kinematics (degrees)**			**Kinetics (Nm/kg)**		
		Vertical	For-aft	Flexion	Abduction	IR	Flexion	Adduction	IR
No brace	CTO	1.10	-0.16	23.5	5.91	6.39	0.12	0.83	0.02
Unadjusted	CTO	1.09	-0.17	21.7	5.86	5.28	0.15	0.69	0.02
Adjusted	CTO	1.05	-0.16	23.7	4.49	2.81	0.16	0.73	0.02
No brace	PV	1.13	0.22	22.1	6.76	6.86	0.16	0.71	0.03
Unadjusted	PV	1.14	0.22	23.8	6.20	6.72	0.15	0.84	0.03
Adjusted	PV	1.14	0.22	24.3	5.19	3.38	0.18	0.77	0.03

GRF is ground reaction force; IR is internal rotation; CTO is contralateral toe-off; PV is peak value

THE RELATIONSHIPS OF FORCE GENERATION BETWEEN BIODENSITY TRAINING AND SIMILAR ATHLETIC TASKS

Boyi Dai, Erika M. Heinbaugh, Rebecca C. Moynes, Shawn S. Rockey, Derek T. Smith

University of Wyoming, Laramie, WY, USA
email: bdai@uwyo.edu, web: http://www.uwyo.edu/kandh/

INTRODUCTION

Osteoporosis is the loss of bone mineral density which increases the risk of bone fractures [1]. Mechanical loading with a high magnitude and a rapid application is effective in improving bone strength [2]. The high mechanical loading can be generated by impact force and muscle contractions [2]. High impact exercises such as hopping is effective in increasing bone mineral density [2]. However, high impact exercise might increase the risk of musculoskeletal injuries [3].

bioDensity training [4] is a recently developed tool to build bone mineral density and muscular strength. The training includes 4 exercises: chest press, core pull, leg press, and vertical lift. Individual's posture is adjusted to estimated optimal joint ranges to induce maximum muscle contractions. The loading is self-induced, so the training is considered as a safer way for osteogenic loading stimulation compared to high impact exercises. bioDensity training was designed to stimulate high mechanical loading through muscle contractions, but it was unknown how loading in bioDensity was different from loading in athletic tasks. In addition, because bioDensity training was limited to a small joint range of motion, it was unknown whether the strength developed in bioDensity could be transferred to athletic tasks involving a greater joint range of motions.

The purpose of the current study was to investigate the relationships of force generation between bioDensity training and similar athletic tasks. It was hypothesized that the maximum forces in bioDensity training would be greater than the maximum forces in similar athletic tasks. It was also hypothesized that the maximum forces in bioDensity training would be positively correlated with the maximum forces in similar athletic tasks.

METHODS

Twenty-five male and 39 female adults participated in this study (Age: 46.3 ± 14.8 years, Mass: 73.3 ± 14.8 kg, Height: 1.69 ± .09 m). Participants performed four maximal contraction exercises lasting 5 seconds each in a set of bioDensity training [4]. The four exercises were: 1) seated chest press, mainly involving chest, shoulder, and arm muscles; 2) seated core pull, mainly involving abdominal, hip flexor, and biceps muscles; 3) seated leg press, mainly involving hip extensor, knee extensor, and ankle plantar flexor muscles; and 4) standing vertical lift, mainly involving hip extensor, knee extensor, ankle plantar flexor, back, shoulder, and arm muscles. The chest press and core pull exercises mainly involved upper extremities and trunk. The leg press and the vertical lift mainly involved lower extremities and trunk. The maximum forces during these four exercises were recorded using bioDensity training device. Participants performed 3-4 sets of bioDensity training to obtain consistent results.

Participants performed 3 trials of a maximum push-up and 3 trials of a maximum countermovement jump with each limb on a force plate. The push-up was considered a task which mainly involved upper extremity and trunk. The countermovement jump was considered a task which mainly involved lower extremity and trunk. The maximum total vertical force during each jump and push-up was calculated and averaged across 3 trails.

The force data were normalized to body weight (BW). Wilcoxon Signed Ranks tests and Spearman correlation tests were performed for maximum forces between chest press and push-up, between core pull and push-up, between leg press and countermovement jump, and between vertical lift and countermovement jump. A type I error rate was set at 0.05 for statistical significance.

RESULTS AND DISCUSSION

Figure 1, 2. Maximum forces between chest press and push-up, and between core pull and push-up.

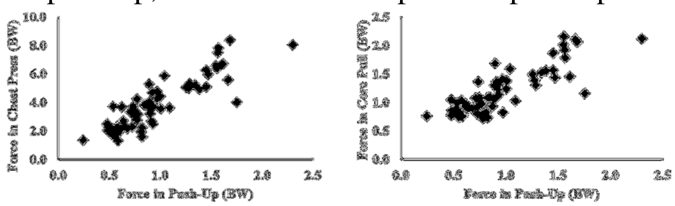

Figure 3, 4. Maximum forces between leg press and countermovement jump, and between vertical lift and countermovement jump.

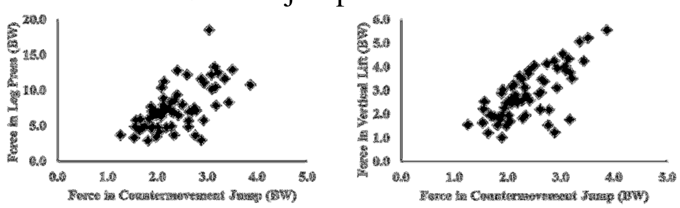

The maximum forces in chest press (3.8 ± 1.8 BW, $p < 0.001$) and core pull (1.2 ± 0.4 BW, $p < 0.001$) were greater than the maximum force in push-up (1.0 ± 0.4 BW). The maximum forces in leg press (7.5 ± 3.1 BW, $p < 0.001$) and vertical lift (2.8 ± 1.0 BW, $p < 0.001$) were greater than the maximum force in countermovement jump (2.4 ± 0.6 BW).

The maximum forces in chest press ($r = 0.85$, $p < 0.001$, Figure 1) and core pull ($r = 0.78$, $p < 0.001$, Figure 2) were correlated with the maximum force in push-up. The maximum forces in leg press ($r = 0.61$, $p < 0.001$, Figure 3) and vertical lift ($r = 0.66$, $p < 0.001$, Figure 4) were correlated with the maximum force in countermovement jump.

Our first hypothesis was supported that the maximum forces in bioDensity training would be greater than the maximum forces in similar athletic tasks. One goal of bioDensity training is to utilize muscle contractions instead of impact force to generate osteogenic loading stimulation. The bioDensity exercises are maximum limited-range contractions under estimated optimal joint ranges. The maximum forces developed in bioDensity training were greater than the maximum force during athletic tasks. The findings support that bioDensity can generate loading with high magnitude to improve bone strength. Future studies comparing internal bone forces between bioDensity training and athletic tasks can give us a better understanding of specific bone loading differences.

The second hypothesis was supported that the maximum forces in bioDensity training would be positively correlated with the maximum forces in similar athletic tasks. Another goal of bioDensity training is to develop muscular strength, but bioDensity training is limited to a small joint range. The forces generated at the estimated optimal joint ranges were correlated with the forces generated during athletic tasks with a great range of motions. The findings were consistent with previous studies that demonstrated strength gain could transfer from limited to full range of motion [5]. The results suggest that strength gain within bioDensity's limited range of motion is likely to be transferable to other larger joint ranges. Future intervention studies are needed to confirm this postulation.

CONCLUSIONS

The maximum forces in bioDensity training were greater than the maximum forces during similar athletic tasks. The maximum forces in bioDensity training were positively correlated with the maximum forces in similar athletic tasks. bioDensity training can generate loading with high magnitude to improve bone strength. Muscle strength gain during bioDensity training is likely to be transferable to other joint ranges of motion.

REFERENCES

1. Johnell O and Kanis JA. *Osteoporos Int* **17**, 1726-1733, 2006.
2. Bailey CA and Brooke-Wavell K. *Proc Nutr Soc* **67**, 9-18, 2008.
3. Heinonen A, et al. *Lancet* **16**, 1343-1347, 1996.
4. Jaquish J, et al. *Osteogenic Loading: A New Modality To Facilitate Bone Density Development* Jaquish Industrial Research, 2012.
5. Barak Y, et al. *Med Sci Sports Exerc* **36**, 1413-1420, 2004.

Effect of Glenohumeral Abduction on Supraspinatus Repair Tension

[1,2]Jacqueline R. Hawthorne, [1,2]Elise Carpenter, [1]Patrick H. Lam, [1]George A. C. Murrell

[1]Orthopaedic Research Institute, St George Hospital, Sydney, NSW, Australia
[2]The University of New South Wales, Sydney, NSW, Australia
email: patlam.ori@gmail.com, web: www.ori.org.au

INTRODUCTION

Rotator cuff tears are common, rotator cuff repair aim to re-attach the torn tendon back to the humeral head thus restoring shoulder function and reduce pain. However the re-tear rate post rotator cuff repair is reported to be 11 - 94%[1-3]. Some surgeons insist the use of slings and abduction pillows (small or large) post-operatively to unload or protect the repair while others do not.

Aims:

1) determine what position the shoulder is placed in when wearing a sling with large abduction pillow, a sling with small abduction pillow, sling with no pillow and

2) in a cadaver rotator cuff repair model, evaluate the tension on the supraspinatus tendon at each of these shoulder positions, with the ultimate aim to,

3) determine which type of sling places the repaired rotator cuff in the best position to heal without re-tearing.

METHODS

A pilot x-ray study was performed on three healthy subjects using a x-ray fluoroscopy InSight (Hologic, Inc. Bedford, MA, USA) in true anterior-posterior (AP) view, to determine what position the shoulder is placed in when wearing a sling only (Donjoy Ultrasling II (DJO, Normanhurst, NSW, Australia)), sling with small abduction pillow (Donjoy Ultrasling II (DJO)) and sling with large abduction pillow (ProCare Shoulder Abduction Kit (DJO)).

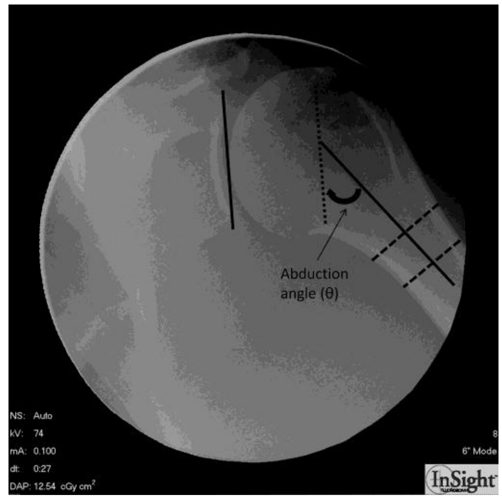

Figure 1: AP view of a shoulder X-Ray

These positions were reproduced in four human cadaveric shoulders using a custom made testing setup. The tension in the supraspinatus were evaluated both in the repaired tendon itself and the sutures used in the repair.

RESULTS AND DISCUSSION

The sling with no abduction pillow placed the glenohumeral joint (GH) in 4° ± 1° (mean angle ± SEM) of abduction and 29° ± 4° internal rotation, a sling with small abduction placed the GH joint in 13° ± 2° abduction and 20° ± 1° internal rotation and a sling with large abduction pillow placed the GH joint in 25° ± 3° abduction and 11° ± 0° internal rotation.

Placing the human cadaveric shoulders in the position of a sling with small abduction pillow caused a reduction in tension on the supraspinatus of 27% anteriorly ($p<0.05$) and 55% posteriorly ($p<0.006$) compared to placing the shoulder in the position of a sling with no abduction pillow.

Placing the shoulder in the position of a sling with large abduction pillow caused a further reduction in tension on the supraspinatus of 42% anteriorly ($p<0.0005$) and 56% posteriorly ($p<0.0001$) compared to the small abduction pillow.

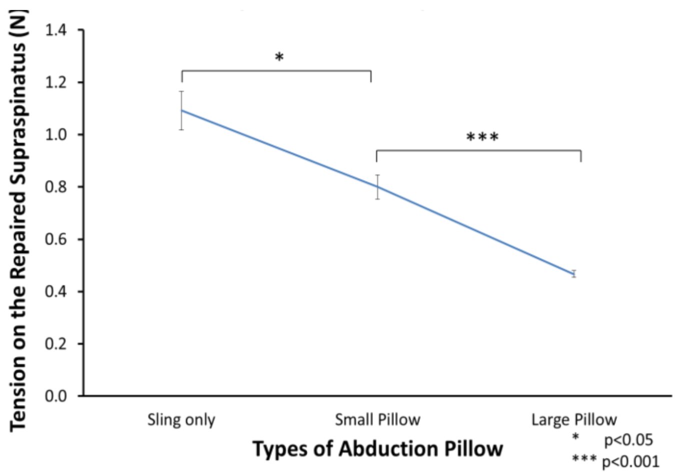

Figure 2: Effect of abduction pillow on repair tension (Anterior suture)

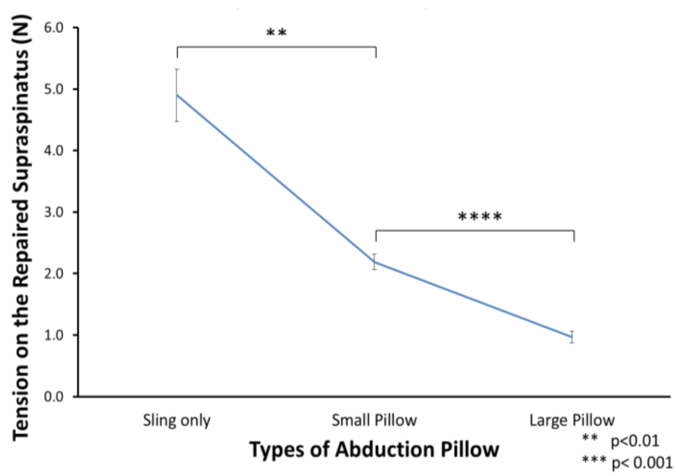

Figure 3: Effect of abduction pillow on repair tension (Posterior suture)

When the humerus was internally rotated from neutral to 30°, tension in the posterior suture was four times higher compared to tension in the anterior suture($P<0.0001$).

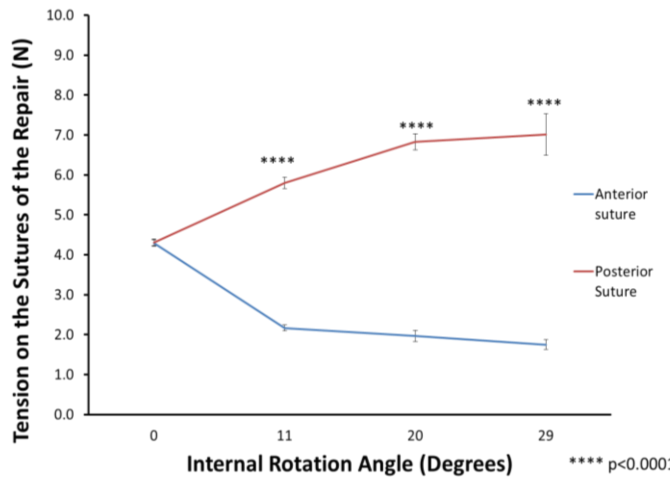

Figure 4: Effect of internal rotation on repair tension (at 0^o degree of abduction)

CONCLUSIONS

Angles of abduction clinically produced by commonly used slings and abduction pillows are lower than originally suggested in the literature. Abduction of the glenohumeral joint following rotator cuff repair at angles consistent with wearing small and large abduction pillows reduced tension on the supraspinatus by approximately 27% to 56%.

REFERENCES

1) Galatz, L.M., et al., *The outcome and repair integrity of completely arthroscopically repaired large and massive rotator cuff tears*. J Bone Joint Surg Am, 2004. 86-A(2): p. 219-24.

2) Lafosse, L., et al., *The outcome and structural integrity of arthroscopic rotator cuff repair with use of the double-row suture anchor technique*. J Bone Joint Surg Am, 2007. 89(7): p. 1533-41.

3) Harryman, D.T., 2nd, et al., *Repairs of the rotator cuff. Correlation of functional results with integrity of the cuff*. J Bone Joint Surg Am, 1991. 73(7): p. 982-9.

Data-driven Biomechanical Analysis of the Upper Trapezius Muscles and Neck Movement: A Pilot Study

[1]Qi Wei, [1]Naomi Lynn Gerber, [1]Zoran Duric, [1]Paul Otto, [1]Nalini Vishnoi, and [1]Siddhartha Sikdar

[1]George Mason University, Fairfax, VA, USA
email: qwei2@gmu.edu

INTRODUCTION

Chronic neck pain affects millions of Americans and is associated with significant healthcare expenditures, yet remains poorly understood. The long term goal of this project is to develop subject-specific biomechanical models informed by dynamic imaging and electromyographic (EMG) data to understand why specific regions of the neck muscles are vulnerable to local injury and to abnormal stretching during activities of daily living, and whether such injuries can cause biomechanical changes that perpetuate asymmetric loading of the neck muscles.

Our research group has been investigating the pathogenesis and pathophyiological mechanisms of myofascial trigger points (MTrPs) in the upper trapezius muscle. MTrPs appear as firm tender nodules on palpation and have been associated with myofascial pain syndrome [1]. In order to understand the mechanical causes and consequences of MTrPs, we design experiments to collect kinematic, muscle EMG, ultrasound imaging, and clinical data from controlled subjects and patients with neck pain who have symptomatic MTrPs. We develop subject-specific musculoskeletal models based on the acquired data which can predict muscle and joint forces during various movements. Through computational simulation and quantitative analysis, we can then investigate whether there is difference (1) in muscle activities, (2) muscle actions, and (3) joint loads between two groups of subjects and whether there is any correlation between these parameters and asymmetric cervical range of motion observed from neck pain patients. In the following, we present some preliminary results from a pilot study on collecting kinematic and EMG data which are used to guild biomechanical simulation and further analysis.

METHODS

Data Acquisition

The subject sat in a chair in an upright neutral position with shoulder relaxed and hands positioned on the laps. Two Optotrak® Certus ™ position sensors from which 3D real-time motion data was captured at 100Hz were positioned in front of the subject. Three Optotrak markers were placed on the shoulders and the chest to calibrate each subject's kinematics and to monitor potential shoulder motion. Smart marker rigid body consisting of three pre-calibrated markers was placed on the subject's forehead using a headband, which tracked 3DOF of the head. Two Delsys surface EMG sensors were affixed to the posterior surface of the neck at approximately C7 level. Each sensor made a 35° angle to the midline of the body to measure the activity of the upper trapezius muscle. EMG data was acquired at 1000Hz using the Delsys Myomonitor® IV EMG system, synchronized with the Optotrak motion capture system through an external trigger signal.

The subject was instructed to exert maximum voluntary efforts in attempted neck side bending and cervical rotation without moving the shoulders. The subject completed five repetitions of each target movement. Each repetition lasted for 10 seconds and a 5-second pause was taken between two repetitions.

Biomechanical Model

A computational musculoskeletal model of the neck [2] was used and slightly modified for dynamic simulation and analysis in OpenSim [3]. Wrapping surfaces were applied to realistically model the curved upper trapezius muscle paths during movement.

RESULTS AND DISCUSSION

Fig. 1 shows kinematic and EMG data of two representative trials, one side bending and one cervical rotation, both to the right hand side of the subject. The shoulder markers confirmed that there was little shoulder motion thus contraction of the upper traps muscles primarily contributed to cervical rotation. Three cervical rotation angles (flexion/extension, side bending, and cervical rotation) relative to the torso were computed and plotted, simplifying the neck joint as a 3DOF joint consistent with the biomechanical model [2]. Coupling between side bending and cervical rotation is known and was observed in our data. Bilateral upper trapezius muscle electrical activities were plotted on the second and third rows in each subfigure. During right side bending, the ipsilateral upper trapezius muscle was recruited while the contralateral upper trapezius muscle was inactive. During right cervical rotation, bilateral trapezius muscle coactivation was observed. The contralateral upper trapezius muscle had earlier onset and greater activation magnitude than the ipsilateral muscle, showing its recruitment as the agonist.

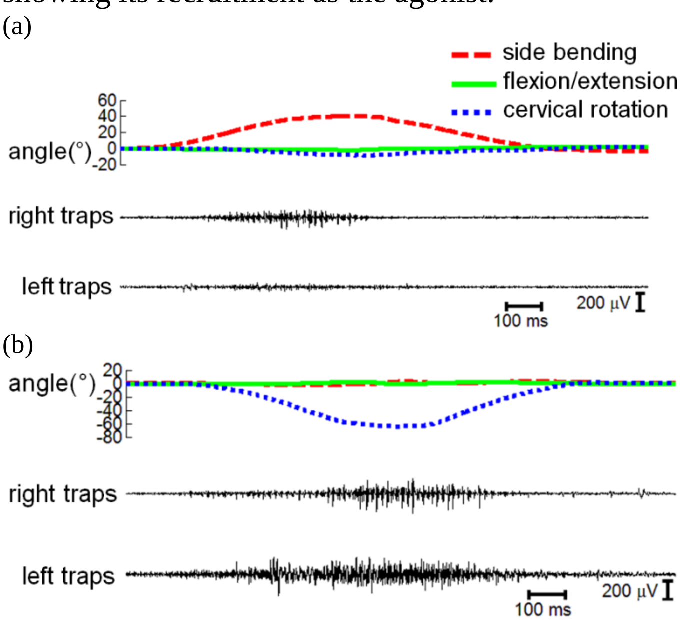

Figure 1. Head rotation angles and bilateral upper trapezius muscle EMG data during (a) right side bending and (b) right cervical rotation.

The captured kinematic data was loaded in the OpenSim neck model to analyze muscle deformation and actions through inverse dynamics simulation. Fig. 2 demonstrates simulation of the motions in Fig. 1. Musculotendon strains of the sternocleidomastoid muscle and the upper trapezius muscle, two major muscles involved in side bending and cervical rotation, were plotted over time. Snapshots of the simulated model were shown at the corresponding time frames. Combined with the measured EMG data in Fig. 1, eccentric and concentric contraction of the upper trapezius muscle during ipsilateral and contralateral movement can be further studied.

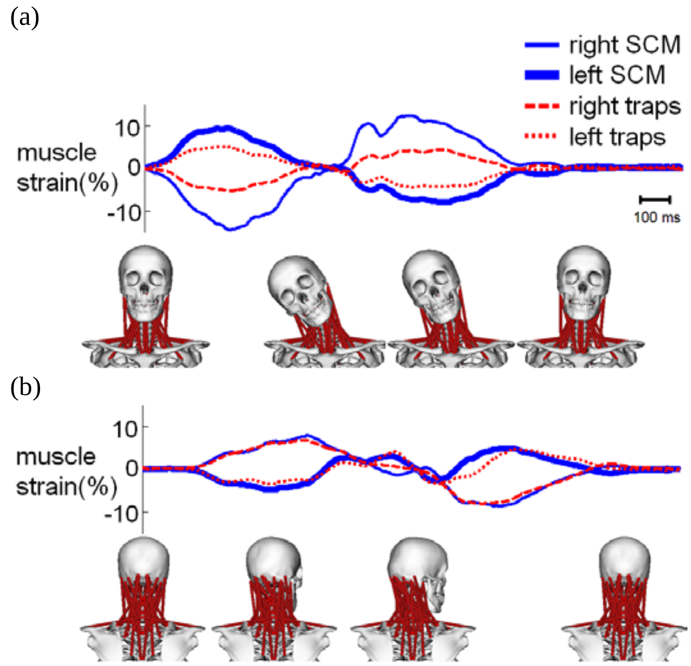

Figure 2. Simulated (a) right side bending and (b) right cervical rotation in OpenSim and predicted muscle strain. SCM - sternocleidomastoid muscle.

We demonstrate a data-driven neck biomechanics analysis framework through a pilot study. In future work, we plan to incorporate synchronized ultrasound imaging data acquired at various locations on the upper trapezius muscle. Longitudinal muscle strains will be estimated from these images. We will model upper trapezius muscle as connected compartments associated with realistic anatomical and physiological parameters. Image-based local muscle strains will be used to drive and evaluate the biomechanical model to investigate the mechanisms of MTrPs and the neck pain syndrome in the long term.

REFERENCES

1. Gerber NL, Sikdar S, Hammond J, and Shah J. *J. Spine Research Foundation* 6, 55-64, 2011.
2. Vasavada AN, Li S, and Delp SL. *Spine* 23(4), 412-422, 1998.
3. Delp SL, et al. *IEEE Trans Biomed Eng* 54, 1940-1950, 2007.

TIME-DEPENDENT CHANGES IN VELOCITY-DEPENDENT STIFFNESS OF THE ELBOW JOINT DURING STROKE RECOVERY

[1]Matthew Kindig, [1,2]Vennila Krishnan, and [1,2]Mehdi M. Mirbagheri

[1]Rehabilitation Institute of Chicago, Chicago, IL, USA
[2]Northwestern University, Evanston, IL, USA
email: mkindig@ric.org

INTRODUCTION

After stroke, one common neuromuscular abnormality is the development of hyperexcitability of the stretch reflex associated with spasticity. This arises due to a disruption in descending pathways from the brain to the limb, and it can impede or delay the successful recovery of motor function [1-4]. Spasticity is commonly characterized in terms of abnormal neuromuscular behavior of the affected muscles and joints [5]. Understanding the development of neuromuscular abnormalities associated with spasticity during recovery is extremely important for the development of successful therapeutic strategies for motor recovery.

When a joint (e.g. elbow) undergoes an angular perturbation, both stretch reflexes and the intrinsic neuromechanical properties of the muscles and other tissues contribute to the resistive torque; both of these mechanisms are velocity-dependent [6, 7]. Previously, we quantified the change in reflex and intrinsic characteristics in the hemiparetic elbow during a small-amplitude, quasi-stationary movement at various positions over the range of motion (ROM). However, it is also necessary to quantify the velocity-dependent nature of these mechanisms during a continuous movement that more closely approximates a functional movement of the upper extremity. To that end, Lee *et al.* quantified the velocity-sensitivity of the elbow joint during a constant-velocity stretching ramp, for hemiparetic subjects [8, 9]. However, as that study evaluated subjects only once at various times after injury (ranging from 8 weeks to 20 years), it does not provide insight into changes in this velocity-dependency over recovery time.

In this study, we extend our previous work and Lee's work by examining how the velocity-dependence of elbow stiffness changes over the course of six months of recovery after stroke.

METHODS

Subject Selection: 13 hemiparetic (7 left, 6 right) stroke survivors, recruited within four weeks of stroke, participated in this study. All subjects were drawn from the Rehabilitation Institute of Chicago in-patient pool and provided informed consent (approved by the Northwestern University IRB).

Experimental Procedure: Patients were seated, with their paretic forearm inserted into a customized fiberglass cast attached to an AC motor (Fig. 1). The motor applied controlled angular perturbations to the arm about the superior-inferior axis. A single-axis torque transducer measured the reaction torque around the elbow center of rotation.

Ramp waveforms were applied to the elbow at two constant velocities—10 deg/s (2 ramps) and 100 deg/s (5 ramps) —from the maximum flexion ROM to the maximum extension ROM. Ramps were applied while the subject was passive (no tonic contraction). This protocol was performed at a) time of recruitment (evaluation M0) b) one (M1) or two (M2) months thereafter, and c) six months (M6) after M0.

Analytical Procedure: For each test, the measured torque was inertially-compensated and then averaged across all ramp cycles to determine the mean position-torque curve. To quantify the velocity dependence of stiffness, the torque at both slow and fast speeds was determined from the mean

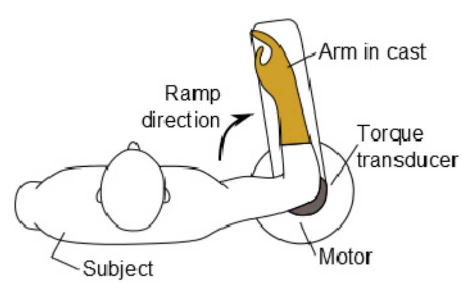

Figure 1: Illustration of experimental setup.

curve at the same elbow positions. These torques were plotted against each other, and the slope of the best-fit line was defined as the *dynamic gain* (γ). A dynamic gain of unity indicates no increase in torque due to increasing velocity.

RESULTS AND DISCUSSION

The elbow position *vs.* torque curve was nonlinear, with a larger stiffness (i.e., slope) towards the extremes of the ROM and a smaller slope closer to the neutral position, consistent with previous findings [3, 8, 10].

The dynamic gain was calculated for each evaluation time for all subjects. Subjects varied from having little velocity sensitivity ($\gamma \cong 1$) while others experienced a doubling of torque or greater over the velocity range ($\gamma > 2$); the average γ at M0 was 1.67 ± 0.50. Some subjects exhibited substantial increases or decreases in dynamic gain over recovery, while others presented little changes. To this end, subjects were classified based on the change $\Delta\gamma$ in dynamic gain between evaluations M0 and M6. Three distinct patterns of change over time were observed. The five subjects with $\Delta\gamma > +0.2$ were defined as the "substantial increase" class, while the four subjects with $\Delta\gamma < +0.2$ were defined as the "substantial decrease" class. (The four remaining subjects were considered to have "little change" (Fig. 2)). Notably, there was no apparent relationship between class membership and dynamic gain at M0: subjects with higher baseline velocity-dependencies did not tend to present more or less change in gain over time.

Previous studies [11, 12] have found that the reflex effect is negligible at the slow speed studied here (10 deg/s). Further, we have previously shown that the contributions due to the visco-elastic nature of the muscles are minimal over the velocity range considered here. Accordingly, the dynamic gain can be assumed to primarily quantify the increase in torque due to effects of hyperexcited reflexes. Thus, our results suggest that while some subjects present a significant decrease in stretch reflex responses over six months of recovery, others significantly increase or show no change during this time.

These results are consistent with our previous study using quasi-stationary perturbations [10], and supports our finding that the change with time in reflex behavior in the elbow varies substantially between stroke patients. The next step is to identify variables that can predict this change in dynamic gain over time, similar to our previous work [10, 13]. Overall, this work can help to provide a better understanding of the origin and nature and neuromuscular abnormalities associated with spasticity, and the role that they play in the development of motor impairment after stroke. This result is clinically significant, as appropriately-timed interventions that can reduce neuromuscular abnormalities associated with spasticity are vital for effective recovery of motor function after stroke.

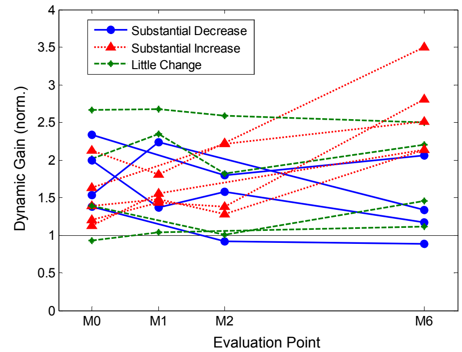

Figure 2: Dynamic gain at each evaluation point. Each line represents a unique subject.

ACKNOWLEDGEMENTS

Funding for this study was provided by National Institutes of Health, National Science Foundation, and the American Heart Association. We thank Krista Settle DPT and Cheng-Chi Tsao D-Sc. for their collaboration in data collection or analysis.

REFERENCES

1. Given, J., et al., *J Neurol Neurosurg Psychiatry*, **59**(3), 271-279, 1995.
2. Mirbagheri, M. M., et al., *Muscle Nerve*, **37**(3), 387-395, 2008.
3. Mirbagheri, M. M., et al., *J Neurophysiol*, **98**, 629-637, 2007.
4. Sinkjaer, T., et al., *Brain*, **117**, 355-363, 1994.
5. Mirbagheri, M. M., et al., *Ann Int Conf IEEE Eng Med Biol Soc*, 2002.
6. Lance, J. W., "Symposium synopsis," in *Spasticity: Disordered Motor Control*, Year Book Publishers, 1980.
7. Katz, R. T., et al., *Arch Phys Med Rehabil*, **70**, 144-155, 1989.
8. Lee, H.-M., et al., *Journal of Neurology, Neurosurgery & Psychiatry*, **72**(5), 621-629, 2002.
9. Ju, M.-S., et al., *Journal of Electromyography and Kinesiology*, **10**(1), 1-14, 2000.
10. Mirbagheri, M. M., et al., *Neurorehabilitation and Neural Repair*, **25**(5), 458-468, 2011.
11. Thilmann, A. F., et al., *Brain*, **114**, 233-244, 1991.
12. Powers, R. K., et al., *Ann Neurol*, **25**, 32-42, 1989.
13. Mirbagheri, M., et al., *IEEE Trans Neural Syst Rehabil Eng*, **20**(6), 762-770, 2012.

Thermal Conductivity of Prosthetic Elastomers, Fabrics, Liners, and Socket Materials

[2]Mena Klittich, [1]Brian Davis, [1]Christina Webber, [2]Ali Dhinojwala

[1]Department of Biomedical Engineering, University of Akron, Akron, OH, USA
[2]Department of Polymer Science, University of Akron, Akron, OH, USA
email: bdavis3@uakron.edu

INTRODUCTION

Thermal properties of materials are typically overlooked when designing a prosthetic because the focus is typically on designing a soft interface to reduce mechanical stresses[1]. As such, most liners and sockets end up acting as insulators around the residual limb, only allowing for a minimal amount of heat loss. Typical prosthetic liners consist of a layer of elastomer upon a fabric base. The residual limb comes in direct contact with the elastomer of the liner. Excess heat around the residual limb can cause sweating, discomfort and skin maceration that decreases the quality of life of the patient. These skin problems are common among amputees who use a prosthetic and include abrasions, blisters, dermatitis or bacterial infections [2].

Thermal conductivity of prosthetic liners and sockets is typically unknown or not reported. Recently Klute *et al.* experimentally determined the thermal conductivity of some prosthetic liners and sockets currently available [1]. Knowing these products' thermal conductivity values can aid in future development of improved prosthetics for amputees that are more comfortable and longer lasting. The purpose of this study was to determine the baseline thermal conductivity values of existing materials (elastomers, fabrics, liners, and socket materials) used in prosthetics.

METHODS

A heat flux meter apparatus (Fig. 1) was designed and built complying with ASTM standard C518-10 [3]. The configuration of the apparatus is such that the temperatures on each side of the specimen, as well as the flux on each side of the specimen are outputs after testing. It was concluded that under normal testing conditions, samples did not compress enough to bulge out over the edges of the heat flux transducers which could skew results. Since distributed pressure mimics the end use for the samples and did not significantly affect the sample shape, pressure was not restricted for most samples.

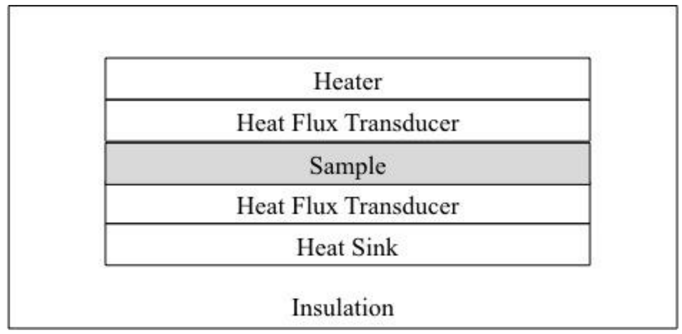

Figure 1: Diagram of the heat flux meter apparatus set up.

Testing was conducted with samples of elastomers (N=5), fabrics (N=9), liners (N=13), and socket materials (N=8) common in prosthetics. Each material was punched out to a 1" diameter circle with a uniform thickness across the sample. Clean samples were placed directly on the heat flux transducer, except in the case of socket materials where a thin layer of thermal grease was applied to both sides of the sample to ensure intimate contact between the sample and transducer. For liner samples, since the fabric side of the liner encounters cooler temperatures during use, it was placed on the cooler heat transducer. Each sample was tested until it reached a thermal steady state, defined by <0.1 °C temperature difference for each thermistor and <0.1 mV difference in each heat flux measurement over a 15 minute period. Thickness of the sample (L) was manually measured, then used to calculate the thermal conductivity of each sample, where Q is the flux and ΔT is the change in temperature.

$$\lambda = \frac{LQ}{\Delta T}$$

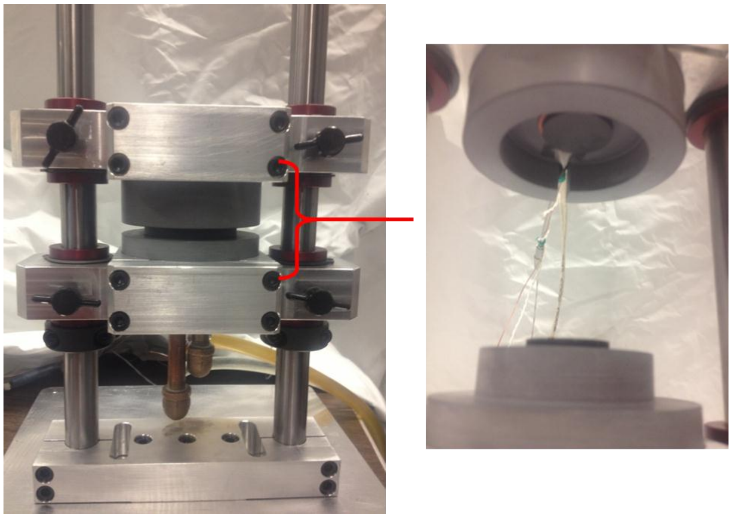

Figure 2. (Left) Heat flux meter, (right) close up of testing chamber (lower portion of chamber nests in upper part when closed)

RESULTS AND DISCUSSION

Overall, the materials used in current prosthetics had thermal conductivities substantially less than 1 W/m•K, indicating that they are poor heat conductors. The nine different fabric samples had the lowest conductivity values of all the materials tested (0.0483-0.0770 W/m•K). This was expected because of the air gaps present in the weave of the fabric. Using thermal grease in this situation to fill the air gaps would not have been appropriate because it would have saturated the fabric, making the measurement representative of only the conductivity of the thermal grease.

The thermal conductivity of five types of elastomers ranged from 0.1036-0.1521 W/m•K. The 13 different liners had similar thermal conductivity values (0.1020-0.1389 W/m•K). This similarity was anticipated because the liners are primarily comprised of an elastomer, with a thin fabric layer on one side. Overall, the fabric's thermal conductivity is quite low, but it is partially penetrated by the elastomer, reducing the air pockets. Because of this penetration, the liner's thermal conductivity was comparable to the elastomer's. Liners containing silicone had slightly higher thermal conductivities compared to liners comprised of thermoplastic elastomer (TPE).

Socket materials conducted heat better than the other prosthetic materials, with a range of conductivities for the eight different samples of 0.1153-0.1805 W/m•K. Although the socket materials had an improved thermal conductivity compared to the other tested materials, they are still considered an insulator because the conductivity values are less than 1 W/m•K.

CONCLUSIONS

Representative thermal conductivities of materials used in the production of prosthetic liners and sockets can be experimentally determined by using small samples of the materials loaded into a heat flux meter apparatus. These thermal conductivities can be used for future development of improved prosthetic liners and sockets for amputees.

REFERENCES

1. Klute GK, et al. *Prosthet Orthot Int* **31**, 292-299, 2007.
2. Koc E et al. *Int J of Derm* **47**, 463-466, 2008.
3. ASTM Standard C518-10, 2010, "Standard Test Method for Steady-State Thermal Transmission Properties by Means of the Heat Flow Meter Apparatus," ASTM International, West Conshohocken, PA, 2010, DOI: 10.1520/C0518-10, www.astm.org.

ACKNOWLEDGEMENTS

Funding through a contract issued through the Veterans Administration Innovation Initiative.

Integration of Musculoskeletal Analysis with Engineering Design for Virtual Prototyping of Exoskeletons

Priyanshu Agarwal, Pei-Hsin Kuo, Richard R. Neptune and Ashish D. Deshpande
The University of Texas at Austin, Austin, TX, USA
email: mail2priyanshu@utexas.edu, web: http://www.me.utexas.edu/~reneu/

INTRODUCTION

Human-worn exoskeletons have the ability to both augment the physical capacity of its wearer and assist in rehabilitation therapy. Design of these devices that physically interact with the human user is challenging because of user safety and comfort requirements in addition to typical robot performance measures (e.g. quick response, back-driveable etc.). Ultimately, models of the musculoskeletal and mechanical systems need to be combined so that the performance of the integrated human-exoskeleton system can be evaluated and optimized using computer simulations. We propose a novel framework for virtual prototyping of exoskeletons by merging musculoskeletal analysis with simulation-based engineering design. The framework provides a platform in which the design and control algorithm of exoskeletons can be iteratively optimized using three distinct types of performance measures—biomechanical, morphologi-cal, and controller. We present a case study that develops a virtual prototype of an index finger exoskeleton to illustrate the application of the framework using the OpenSim environment.

METHODS

Virtual Prototyping Framework

The framework provides a synergistic platform for developing and refining the engineering design and control algorithms for exoskeletons. With combined analysis of the musculoskeletal, mechanical and control systems, measures from the musculoskeletal model (e.g. muscle forces etc.) quantify the biomechanical performance, measures characterizing the physical design (e.g. stiffness etc.) of the exoskeleton (e.g. coupled system range of motion etc.) define morphological performance, and measures quantifying the performance of the exoskeleton controller (e.g. steady-state tracking error etc.) define controller performance.

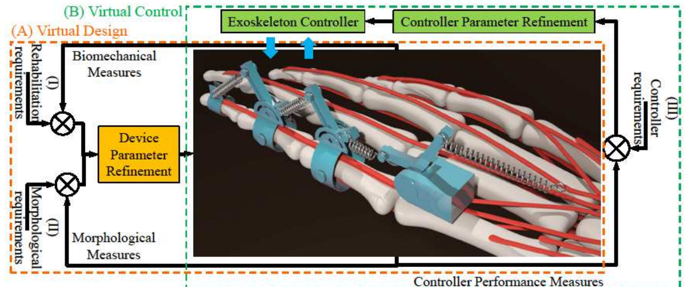

Figure 1: Framework for developing virtual prototypes of exoskeletons using biomechanical, morphological, and controller performance measures.

The virtual prototyping framework consists of the following steps (Fig. 1): (1) *Virtual Design*: develop an initial coupled exoskeleton-limb musculoskeletal model along with a controller. Identify the key biomechanical, morphological, and controller performance measures and a desired motion trajectory for the coupled model. Refine the coupled model using experimental data to improve its fidelity. Iteratively optimize the biomechanical or morphological performance measures or both while reproducing the desired motion trajectory. (2) *Virtual Control*: iteratively develop and refine control algorithms for the coupled system and optimize the controller performance measures while tracking the desired motion trajectory. (3) *Virtual Experimentation*: study specific "what-if" scenarios (e.g. specific muscle impairments in a patient) and modify design and control to improve performance. The presented framework can offer significant value not only for traditional hypothesis testing such as functional muscle group studies, but also for effective design, control, experimentation, and performance enhancement of exoskeletons with quantitative performance evaluation leading to shorter development life cycles.

Finger Exoskeleton Prototyping Case Study

We model and analyze an index finger exoskeleton system with the specific goal to identify the role of spring elements in achieving more comfortable interactions with the device and to accommodate

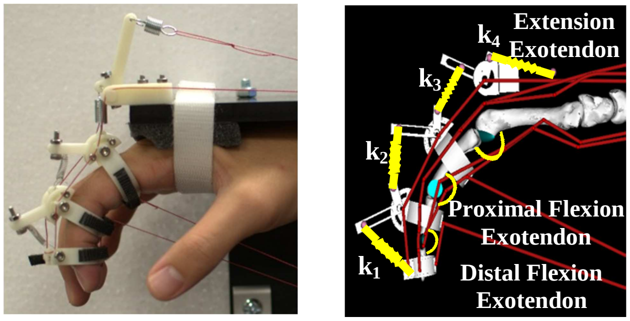

(a) (b)

Figure 2: Finger-exoskeleton coupled system. (a) Preliminary prototype of the device, and (b) combined musculoskeletal and mechanical system model used for the simulation. The model had 6 degrees of freedom consisting of index finger metacarpophalangeal (MCP) flexion, proximal interphalangeal (PIP) flexion, distal interphalangeal (DIP) flexion, and exoskeleton proximal, middle, distal link rotation.

misalignment between joint axes. A coupled finger-exoskeleton model was developed in OpenSim using the index-finger model [1] having wrapping surfaces and 4 Hill-type musculotendon actuators to closely resemble the preliminary prototype of the device (Fig. 2). Passive rotational stiffness was added at the three index finger joints to represent the passive torques due to ligaments and other structures. In addition, linear springs (k1-k4) coupling the various exoskeleton links were added to the model. We treated the three actuated tendons on the exoskeleton (exotendons) as the force generating elements and modeled them as musculotendon units. Their optimal fiber length was chosen such that the actuators can generate a wide range of forces over the exotendon excursions corresponding to the range of motion for the finger joints. To improve model fidelity, we also optimized (using an interior-point algorithm) the moment arm of each muscle individually by altering the muscle path based on experimental measurements [2].

Virtual design is carried out using Computed Muscle Control (CMC) analysis of the optimized model with sinusoidally varying finger joint angles as the desired flexion-extension motion trajectory in OpenSim. Also, a constraint was imposed on the maximum excitation of the index finger muscles to simulate a pathological finger. CMC analysis was carried out by changing the exoskeleton spring stiffness (k_1-k_4) to study its effect on muscle/exotendon forces, joint reaction forces, and joint angle tracking. A "what-if" study was performed to investigate how changing the upper limit on the excitation of the finger muscles (e.g., representing an improvement in a recovering finger) can be simulated to gain insight into the finger-exoskeleton interactions.

RESULTS AND DISCUSSION

Figure 3 presents the required actuator forces obtained using CMC for the tracking task. Finger muscle forces were generated due to their passive stretching. However, the majority of the forces were applied by the exotendons. Furthermore, increasing the stiffness of the exoskeleton resulted in better tracking of the joint angles, but with increased exotendon forces and joint reaction forces.

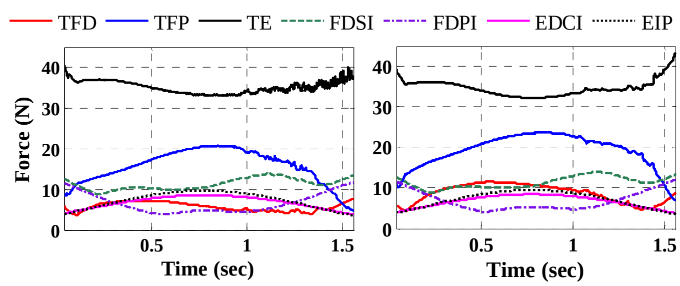

Figure 3: Actuator (muscle/exotendon) forces needed for position tracking as obtained from the CMC analysis with (a) lower stiffness, (b) higher stiffness.

CONCLUSIONS

We presented a framework for virtual prototyping of exoskeletons using musculoskeletal analysis and simulation-based design. Modeling and simulation of the coupled index finger and exoskeleton system led to the quantification of the exoskeleton performance in ways not possible with isolated mechanical models. The framework is generalizable to a wide range of exoskeleton systems designed for both augmentation and rehabilitation. In future work, we plan to apply this framework to optimize the design and controller of a wrist-hand exoskeleton.

REFERENCES

1. Holzbaur KR, et al. Ann Biomed Eng **33**, 829-840, 2005.
2. Fowler N, et al. *J Biomech* **34**(6), 791–797, 2001.

A BIOMECHANICAL MODEL FOR GLENOHUMERAL JOINT EVALUATION DURING PEDIATRIC MANUAL WHEELCHAIR MOBILITY

[1]Brooke A. Slavens, [1]Alyssa J. Paul, [2]Adam Graf, [2]Joseph Krzak and [2]Lawrence Vogel

[1]University of Wisconsin Milwaukee, Milwaukee, WI, USA
[2]Shriners Hospitals for Children - Chicago, Chicago, IL, USA
email: slavens@uwm.edu; paulaj@uwm.edu

INTRODUCTION

In 2010 there were 124,000 wheelchair users under the age of 21, and 67,000 under the age of 15 [1]. Manual wheelchair propulsion is highly repetitive and imposes considerable weight-bearing demands on the upper extremities (UEs) [2]. Upper limb pain and pathologies, reported in 50% of manual wheelchair users (MWU) with spinal cord injury (SCI) [3], have been associated with increased loads at extreme joint excursions [4]. Long-term improper propulsive techniques may predispose children to early-onset injury, particularly during development; however, few studies have attempted to evaluate joint dynamics during pediatric manual wheelchair use. We created, evaluated and applied a custom UE pediatric biomechanical model to quantify three-dimensional (3D) dynamics of pediatric MWUs to provide insight on UE joint demands.

METHODS

The UE inverse dynamics model computes 3D wrist, elbow and shoulder complex kinematics and kinetics and has been previously evaluated and reported [5].

The model includes a total of 11 rigid body segments, tracked by 27 markers, Figure 1, and follows ISB recommendations with the respective X, Y and Z – axes directed anteriorly, superiorly, and laterally [6]. The marker set used to describe the thorax followed a direct method of marker placement on thorax landmarks to reduce the influence of shoulder girdle movement on thoracic kinematic measurements. To avoid possible marker contact with the wheelchair during propulsion, a single marker tracked the olecranon. Bilateral scapula and clavicle segments were defined to provide a comprehensive description of the shoulder girdle, which comprises the glenohumeral (GH), acromioclavicular (AC) and sternoclavicular (SC) joints. Regression equations that employ the positions of five scapula markers were used to locate the GH joint center. For the TS and AI scapula markers, a tracking method based on rigid body theory was used to reduce the effects of skin motion artifact and possible marker-wheelchair interaction. [5]

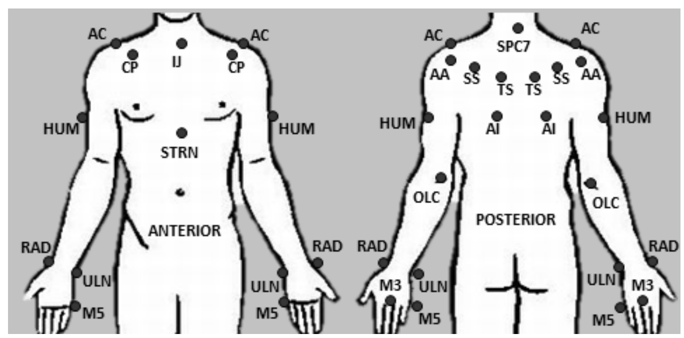

Figure 1: UE model marker set: IJ: suprasternal notch, STRN: xiphoid process, SPC7: spinal process C7, AC: acromioclavicular joint, AI: inferior angle, TS: trigonum spine, SS: scapular spine, AA: acromial angle, CP: coracoid process, HUM: humerus technical marker, OLC: olecranon, RAD: radial styloid, ULN: ulnar styloid, M3 and M5: third and fifth metacarpals. [5]

Three, 17 year-old MWU with SCI propelled their wheelchair along a 15-meter walkway at a self-selected speed and stroke pattern. Kinematic data was collected at 120 Hz using a 14 camera Vicon MX motion capture system. 3D force and moment data from the hand-handrim interface was simultaneously collected at 240 Hz using a SmartWheel (Out-Front, Mesa, AZ) on the subject's dominant side. Data was processed every 1% of the stroke cycle. 100% stroke cycle is defined by push and recovery phases, with 0% stroke cycle representing initial handrim contact. Ten total stroke cycles of each subject were analyzed using our custom pediatric inverse dynamics model. Mean joint angles, forces and moments, as well as peaks and ranges, during the wheelchair stroke cycle were computed.

RESULTS

Average GH joint kinematics for all subjects are characterized in Figure 2. Average dominant and non-dominant side peak extension was -18° and -13.7° respectively, and occurred at 97% and 98% of the stroke cycle, just prior to handrim contact. Average peak dominant and non-dominant GH joint flexion (38.6° and 43°, respectively) was achieved during the transition from push to recovery phase, which occurred on average at 49% stroke cycle. While peak internal rotation of 12.2° and 36° were largely different between the dominant and non-dominant sides, the peaks occurred at similar points in the stroke cycle: 38.7% and 43.3% for the dominant and non-dominant sides, respectively. The GH joint experienced average peak extension, adduction and external rotation at 48.7%, 36.3% and 98% stroke cycle respectively.

The largest average peak force of 7% body-weight (%BW) was superiorly directed and occurred at 11% stroke cycle. Notably though, not every subject experienced their personal peak force in the superior/inferior direction. The average peak anterior force was 2.9 %BW occurring at 18.7% stroke cycle and the average peak lateral force was 5.9 %BW at 18.3% stroke cycle.

DISCUSSION

The custom pediatric UE biomechanical model successfully quantified joint dynamics in adolescent MWUs with SCI. Differences between dominant and non-dominant sides are apparent, leading to a further need to investigate asymmetry in a larger population. Excessive joint motions combined with large joint forces and moments are concerning with regard to the development of pain and subsequent pathology in MWU. This work provides quantitative data to support training paradigms, alternative mobility patterns or assistive devices to reduce joint loading. Characterization of the wrist, elbow and glenohumeral joints is ongoing. Further research is underway to investigate wheelchair dynamics with a larger population to determine biomechanical factors during maturity and transition to adulthood to improve rehabilitative care.

CONCLUSIONS

Evaluation of UE joint dynamics during wheelchair mobility provides a comprehensive quantification of the biomechanical parameters associated with propulsion strategies and related upper limb pathologies. Future work involves correlations among joint dynamics, pain and functional outcomes, as well as to determine the underlying tissue level effects through musculoskeletal modeling. This research may ultimately guide improved treatment approaches for pediatric MWU and aid in injury prevention in wheelchair users.

REFERENCES

1. Brault, M.W. (2012) Curr Popul Rep, P70-P131.
2. Kulig, K. et al. (2001) Clin Biomech, 16: 744-51.
3. Boninger, M. L. et al. (2005) JRRD., 42:9-19.
4. Corfman, T.A. et al. (2003) J Spinal Cord Med, 26(2):135-140.
5. Paul, A. et al. (2012) IEEE EMBC, 4788-4791.
6. Wu, G. et al. (2005) J. Biomech, 38:981-992.

ACKNOWLEDGEMENTS

We would like to acknowledge the Department of Education NIDRR grant H133E100007.

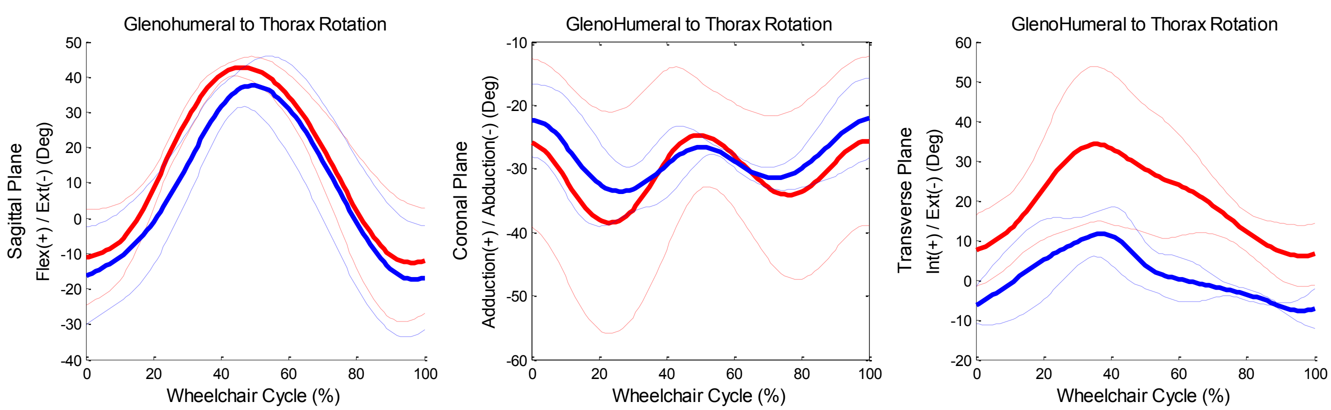

Figure 2: Mean **(bold)** and +/- 1 SD (dashed) glenohumeral (GH) joint kinematics with respect to the thorax segment: sagittal, coronal and transverse planes respectively (dominant side: blue, non-dominant side: red).

VARIABILITY OF UPPER EXTREMITY KINEMATICS AND SHOULDER PAIN DURING WHEELCHAIR PROPULSION: A VECTOR CODING ANALYSIS

[1]Iris M.-K. Hsu, [2]Yaejin Moon, [3]Chandrasekaran Jayaraman, [2]Ian M. Rice, [2]Jacob J. Sosnoff, [1]Elizabeth T. Hsiao-Wecksler

[1]Department of Mechanical Science and Engineering, [2]Department of Kinesiology and Community Health, [3]Department of Industrial and Enterprise Systems Engineering
University of Illinois at Urbana-Champaign, Urbana, IL, USA
email: mhsu7@illinois.edu

INTRODUCTION

Shoulder pain is common among manual wheelchair users with approximately 70% of them reported having shoulder pain [1]. Although variability of kinematics and kinetics of locomotion has been found to be indicative of motion dysfunction in gait literature, few studies have investigated the relationship between variability and dysfunction of upper extremities during wheelchair propulsion. One of the commonly used techniques to study variability is vector coding [3]. In this study, the peak angular deviation of the vector coding coupling angle ($VCAD_{peak}$) was used to study the variability as it represents the maximum amount of variability present in the system. The variability of upper extremity kinematics as a function of pain is assessed through $VCAD_{peak.}$ It was hypothesized that variability of the upper extremity coupling will be lower in people with severe shoulder pain.

METHODS

24 manual wheelchair users (11 female, 13 males, age = 24.3±10.1 years) with more than one year of experience were recruited for the study from the community. University IRB approval and informed consent were obtained. The average length of wheelchair usage was 15.0±8.5 years. Injury types included: spinal cord injury (N=11), spina bifida (N=8), amputation (N=2), spinal cyst (N=1), scaral agenesis (N=1), and arthogryposis (N=1).

Data collection and reduction

Wheelchair User Shoulder Pain Index (WUSPI) surveys were collected. WUSPI survey consists of 15 questions about the level of pain (no pain=0, severe pain=10) when performing various daily activities. The total WUSPI score, which ranges from 0 (no pain) to 150 (extreme pain) was calculated by adding the score of each item.

Each participant's wheelchair was bilaterally fitted with force and moment sensing wheels (SmartWheel, Three River Holdings LLC; Mesa, AZ) and placed on a stationary roller system. Real-time feedback of the propulsion speed was provided. The participants were asked to push at slow (0.7 m/s), fast (1.1 m/s) and a self-selected speed for three minutes in separate trials. Reflective markers were placed on anatomical landmarks and kinematic data were collected (Cortex 2.5, Motion Analysis Co.; Santa Rosa, CA). Both the kinematic and kinetic data were collected simultaneously at 100 Hz. SmartWheel data were used to define the start and end of a cycle. Each cycle was normalized to 100% propulsion cycle. The kinematic data were filtered with 2nd order Butterworth filter at 8Hz. Data from the fifth cycle onwards (i.e. steady-state behaviors) were analyzed.

Vector coding

Segment angles of the upper arm (θ_{AD}) and forearm (θ_{FA}) in the sagittal plan were calculated at each % cycle. An angle-angle plot of θ_{AD} vs. θ_{FA} was created and the vector coding coupling angle θ_{FA} was calculated [3]:

$$\theta_{VC,i} = \arctan \frac{\theta_{UA,i+1} - \theta_{UA,i}}{\theta_{FA,i+1} - \theta_{FA,i}}, i = 0 - 99\% \quad \text{— (1)}$$

Peak angular deviation of θ_{VA} ($VCAD_{peak}$) was used to analyze the variability of the upper extremity, where larger number indicates greater variability of the coupling between two segments.

Data analysis

Data were categorized into three groups based on the severity of pain: WUSPI=0 (N=6); WUSPI between 1 and 30 (N=15); and WUSPI greater than 30 (N=3). The stroke patterns of each participant were classified (See Table 1) [4]. A one-tailed one-way ANOVA was performed to test the statistical differences between groups (α=0.05). All statistical analyses were performed in SPSS Version 20.

Table 1: Distribution of stroke patterns and self-reported pain status.

Patterns	Semi-Circular (SC)	Double-Loop (DL)	Single-Loop (SL)	Arcing (ARC)
WUSPI = 0	5	1	0	0
0<WUSPI<30	7	2	2	4
WUSPI≥30	2	0	0	1
N =	**14**	**3**	**2**	**5**

RESULTS AND DISCUSSION

No statistical differences were found between groups of different severities of pain (Table 2).

Table 2: The $VCAD_{peak}$ at the three speeds.

	Average ± S.D. (deg)		
[Speed] (m/s)	Fast [1.18 ± 0.06]	Self-selected [0.97± 0.20]	Slow [0.76 ± 0.04]
WUSPI = 0	53.3 ± 18.7	56.9 ± 15.5	55.3 ± 12.8
0<WUSPI<30	54.4 ± 13.7	52.1 ± 11.3	55.8 ± 14.5
WUSPI ≥30	31.3 ± 17.1	43.9 ± 13.6	42.8 ± 20.3

As previous studies have suggested, kinematics and kinetics differences exist between different stroke patterns [4]. When $VCAD_{peak}$ values were broken into groups according to the stroke pattern (Fig. 1), decreasing $VCAD_{peak}$ was observed as the severity of pain increased in SC pattern. Therefore, a one-way ANOVA was performed on the group with SC stroke pattern. Due to the small sample size, we were not able to perform statistical analysis to compare the differences between different pain severities for other stroke patterns.

The analysis revealed statistical differences between groups of pain severity at fast speed (p=0.044). The LSD post hoc test showed that the group with WUSPI≥30 had significantly lower $VCAD_{peak}$ compared to the other two groups. However, there were no significant differences between WUSPI = 0 and 0<WUSPI<30. No group differences in $VCAD_{peak}$ were observed for the trials at self-selected and slow speeds.

These results indicate an association between increased shoulder pain and reduced peak variability in coupling between the forearm and upper arm motions when pushing at a more challenging pace. One possible reason is that the coupling between forearm and upper arm became stiffer as a response to underlying injury status.

Previous gait variability literature has shown differences in the amount of variability in spatiotemporal parameters at different percentages of comfortable speeds [5]. Our results are consistent with the literature.

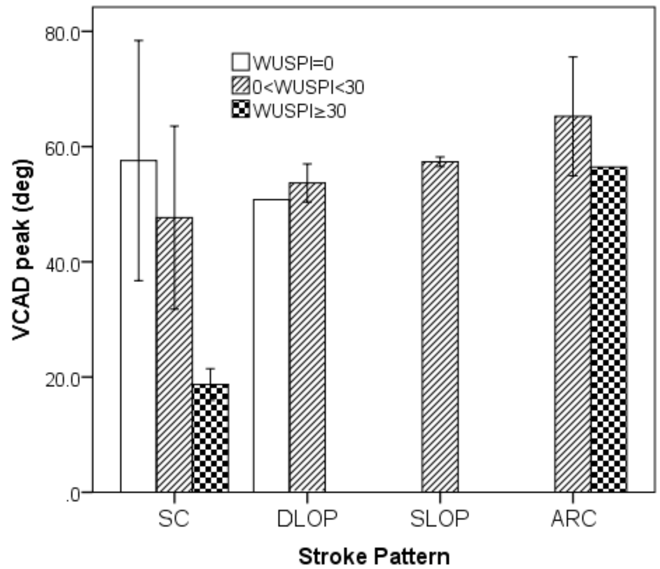

Figure 1: A plot of $VCAD_{peak}$ at fast speed categorized into different stroke patterns.

Limitations of this study were the small sample size of participants in the severe pain group and limited age range. Future studies shall incorporate wheelchair users with varying age and pain levels, and understand how stroke patterns affect variability.

REFERENCES

1. Gironda RJ, et al. *J Spinal Cord Med.* **27**(2):120-7, 2004
2. Srinivasan D, et al. *Clin Biomech.* **27**(10):979-93, 2012
3. Miller RH, et al. *J Biomech.* **43**(13):2554-60, 2010
4. Kwarciak AM, et al. *Disabil Rehabil Assist Technol.* **7**(6):459-63, 2012
5. Jordan K et al. *Gait Posture.* **26**(1):128-34, 2007

ACKNOWLEDGEMENTS

This project is funded by the Nation Institute of Health grant (#1R21HD066129-01A1). The authors extend their gratitude to the Illinois Simulator Laboratory.

ENHANCING FRICTION BETWEEN GLOVES AND PUSHRIMS FOR WHEELCHAIR RACING

[1]François Marcou, [1]Geneviève Masson, [1]François Martel, [1]Denis Rancourt, [1]Cécile Smeesters, [2]Félix Berrigan, [2]Jean Laroche and [1]Eve Langelier

[1]Department of Mechanical Engineering, Université de Sherbrooke, Sherbrooke QC, Canada
[2]Department of Kinanthropology, Université de Sherbrooke, Sherbrooke QC, Canada
e-mail: Eve.Langelier@USherbrooke.ca web: http://eureka.gme.usherbrooke.ca/perseus/

INTRODUCTION

Propulsion in wheelchair racing is achieved by friction between the pushrims, affixed on the wheels, and special gloves used to increase friction and protect the athlete's hands. Two types of gloves are typically used: 1) commercial soft gloves for beginners and sprinters with strong wrists, and 2) custom made hard gloves for longer races and athletes with weaker wrists. A recurring problem with hard gloves is slipping under rainy conditions or when the athletes exceed the friction limit at the glove-pushrim interface. Slipping can be disastrous as it leads to considerable time loss at crucial moments, such as at the start or while passing.

The friction force at the glove-pushrim interface is given by $F = \mu N$, where μ is the friction coefficient and N is the normal contact force. Based on this equation, we address two opportunities to avoid slipping and hence improve hard gloves: 1) increase the normal force by incorporating a wedge on the glove's contact surface, and 2) increase the friction coefficient by selecting new materials to cover the glove and/or pushrim.

METHODS

We developed a simple theoretical model to evaluate the impact of a wedge on the normal force (Fig. 1). We hypothesised that the glove and pushrim surfaces are in contact and do not deform. Assuming static equilibrium along the x axis, we obtain $N = A$ for flat glove surfaces ($\alpha = 90°$), and $N = N_1 + N_2 = \frac{A}{sin\alpha}$ for wedged glove surfaces ($0 < \alpha < 90°$). Therefore, $\mu_{Wedge} = \frac{\mu_{Flat}}{sin\alpha} > \mu_{Flat}$.

We also designed an apparatus to evaluate friction at the glove-pushrim interface (Fig. 2) as well as the effectiveness of a wedge on the glove surface. We glued material samples on two surfaces: 1) a glove mimicking surface that was either flat ($\alpha = 90°$) or wedged ($\alpha = 60$ and $45°$); and 2) a pushrim mimicking surface that consisted in a 15in diameter disk. A linear motor and a 6DOF load cell generated and measured a 100 or 200N normal contact force between the two surfaces. A rotary motor applied an increasing torque (49.5Nm/s) on the pushrim. Finally, an encoder measured the angular position of the disk, thus enabling the detection of the pushrim stall position (when the motor torque exceeds friction and the pushrim disk slips).

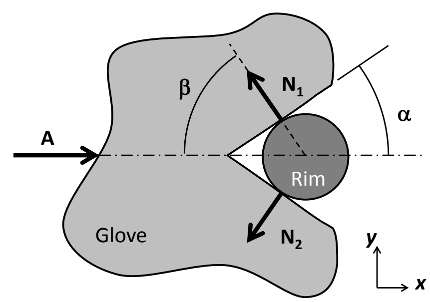

Figure 1: Wedge theoretical model. *A* was the force perpendicular to the pushrim applied by the athlete on the glove while N_1 and N_2 were the normal contact forces of the pushrim on the glove.

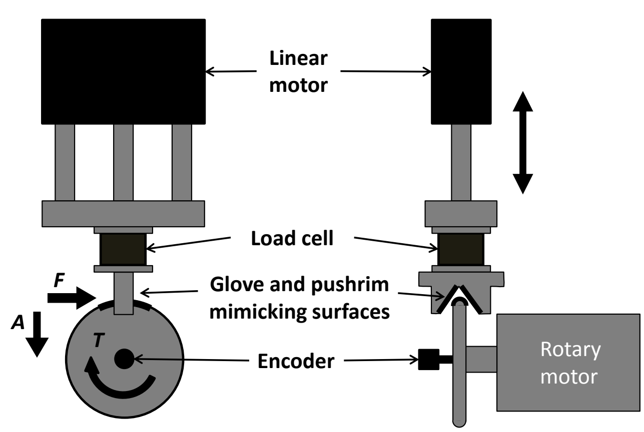

Figure 2: Apparatus to evaluate friction of different glove-pushrim material pairs.

We tested over 15 different materials for the glove mimicking surface, but only the actual rubber used by the athletes (natural rubber with additives) for the pushrim mimicking surface. This was requested by the athletes since this rubber is readily available. Finally, we conducted tests in dry and wet conditions to simulate field conditions.

RESULTS AND DISCUSSION

Adding a wedge to the hard glove surface improved friction (Table 1) for both dry and wet conditions. This may explain why athletes using soft gloves create a natural wedge between their thumb and index finger.

Table 1: Sample results for the wedge analysis (glove = suede, N = 200N, 5 repetitions) * = μ_{Flat} for theoretical model.

Glove surface	Condition	Experimental μ	Theoretical $\mu_{Wedge} = \frac{\mu_{Flat}}{sin\alpha}$
Flat (α = 90°)	Dry	0.87 ± 0.01	0.87*
	Wet	0.76 ± 0.03	0.76*
Wedged (α = 60°)	Dry	1.08 ± 0.03	1.00
	Wet	0.88 ± 0.01	0.88
Wedged (α = 45°)	Dry	1.35 ± 0.01	1.22
	Wet	1.11 ± 0.03	1.07

Our results also show that materials with asperities preserve a better friction coefficient in wet conditions than materials with smooth surfaces (Fig. 3). These observations are consistent with the theory of rubber friction and contact mechanics [1].

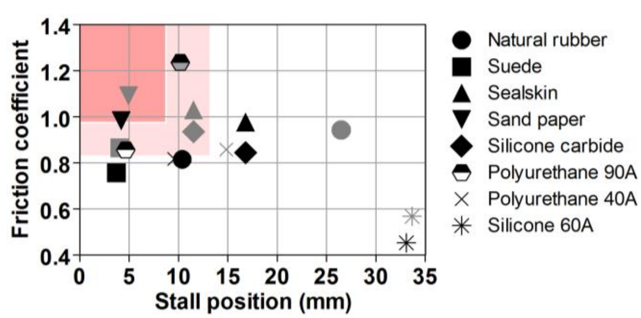

Figure 3: Sample results for the friction tests (flat glove surface, N = 200N, 5 repetitions). Gray symbols: dry conditions, black symbols: wet conditions. Pink areas: best results.

However, when designing a hard glove, other issues like durability must be considered. For example, sand paper gives excellent friction results but rapidly wears down under racing conditions, particularly for longer races. Moreover, the athlete's pushing technique must be examined before designing a wedged glove, to make sure there is no geometrical interference. To illustrate this point, we distributed pressure sensors over the glove's surface to evaluate the contact point trajectory during propulsion (Fig. 4). The pushrim draws a loop on the glove surface that should be considered to avoid geometric interference between the pushrim and the wedge on the glove's surface.

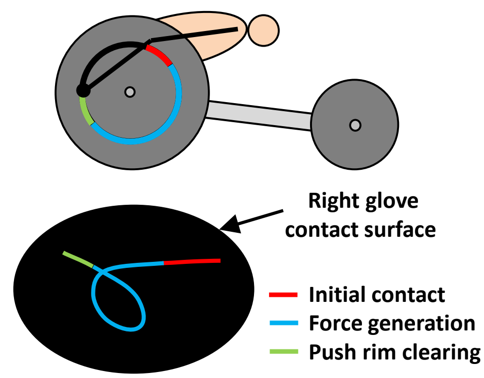

Figure 4: Contact point trajectory on the glove surface according to hand position on the pushrim.

CONCLUSIONS

We can improve hard glove performance under wet condition by choosing suede (wear resistant, high friction coefficients, low stall positions) as the glove surface material and/or by including a wedge. Based on motion analysis, this wedge can be narrower in the initial contact (red) and beginning of force generation (blue) phases, but must fade thereafter to allow for the inevitable contact loop and an easy pushrim clearance through wrist pronation.

REFERENCE

1. Persson BNJ. *J Chem Phys* **115**, 3840-3861, 2001.

ACKNOWLEDGEMENTS

This work was funded by the NSERC, Institut National du Sport du Québec and Athletics Canada. We would like to thank the Canadian Paralympics team for its kind participation to this project.

A NOVEL METHOD TO MODEL A CYCLIST IN SITU

[1]A Cole Meyers, [1]Moataz Eltoukhy, and [1]Joseph Signorile

[1]University of Miami, Coral Gables, FL, USA
email: a.meyers1@umiami.edu, web: www.education.miami.edu

INTRODUCTION

Until now, biomechanical modeling of cyclists has either stopped at the hip or assumed that the activity can be symmetrically modeled using 3 points of contact – feet, hips, and hands. Forces at the joints in a movement like walking are easily reconciled using force plate data; however, these analyses often reveal only joint forces without muscle forces or their points of application. Finding internal forces in the body using in-vivo experiments alone is difficult if not impossible. Additionally, it is difficult to determine muscle force/power output from multiple muscles simultaneously without affecting normal movement patterns. Computer modelling can provide useful biomechanical insights, allowing technicians and clinicians to examine each rider's strengths and weaknesses.

METHODS

In situ modeling requires measurement of forces at each of three contact points: the feet, hips, and hands. In the past, bicycle power meters were located in the rear wheel hub or bottom bracket, and provided a single value that represented the rider's power. Several companies (Garmin Ltd., Schaffhausen, CH; Look Cycle International, Nevers, Fr; Brim Brothers, Dublin, IE) have recently developed a system which inserts force transducers into the axle of a bicycle pedal (Fig. 1), allowing 3D reaction forces (RF) at the foot to be recorded during pedaling. Using these RF, forces and moments can be computed for the lower body.

Figure 1: Look Keo Power pedal

Because the hips are a critical contact point for a full-body diagram, computing forces above this point has not been possible. Innovative solutions from industry and academia have reduced this barrier.

For research, a tool capable of delivering 3D analysis is required; the biomech laboratory at UW Madison connected a JR3 30E15A4 load cell (JR3 Inc, Woodland, CA, USA) to a normal seatpost and saddle to gather RF data at the hips (Fig. 2).

Fig 2: UW Madison's bicycle saddle load cell

There are two approaches to approximate joint forces and moments for the upper extremity. In the first, the bicycle's front fork is rigidly attached to a force plate. An inverse dynamics model is solved using the RF at the feet and hips, and the upper extremities are assumed to be symmetrical. Model final forces calculated at the hands should equal the RF at the force plate. The second approach involves placing separate hand rests on individual force plates. This method, while more accurate, is not feasible if the researcher is seeking to model the cyclist on his or her own bicycle.

There is no practical way to measure the forces, stresses, and strains inside the human body during activity; however, musculoskeletal (MS) modeling allows estimation. It is a predictive computational approach consisting of representations of the bones, muscles and ligaments, driven in simulation by measurements of subjects' specific mechanics. MS inverse dynamics analysis offers a potential solution for predicting loading conditions over a wide range of body movements [1-4]. Because of redundancy in the MS system any motion can be achieved using an infinite number of muscle activation patterns. The muscle activation patterns of repeated movements are similar, indicating a logical criterion that dictates recruitment. This redundancy problem is solved by an optimization using AnyBody® modeling (Anybody Group, Aalborg, Denmark).

RESULTS AND DISCUSSION

Most cycling kinematic research has focused on the lower extremities. This is the case because analysis of joint forces and moments of the trunk, neck, and upper extremities depends on emerging technology. Force-actuated pedals are a relatively recent development (1981) [5,6], and until now have been the focus of research in the field. Because the nature of walking allows all external forces to be measured via force plates, analysis of forces in the back and upper extremities can be performed [7]. Many riders complain of back pain, from the neck to the sacrum [8-10]. Until now, these analyses were not available during cycling.

The mathematics of the problem is formulated below; the objective function implemented is a min/max criterion, which means that we are minimizing the fatigue of muscles in the system.

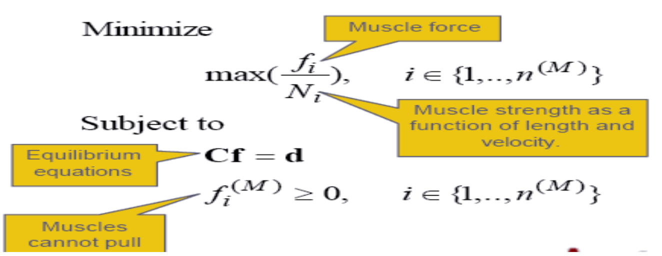

The model will start with the equations of equilibrium, determine the muscle forces based on the min/max criteria, and then decide which muscle forces are uniquely determined. These forces are removed from the model. The remaining system of muscles is solved again, and this cycle continues until no more muscles are left in the system.

Utilizing the proposed method, researchers can work with riders, trainers, and rehabilitation personnel to ascertain whether riders' back issues are the result of improper bicycle fitting or muscular inadequacies around the affected joints. Additionally, the use of such a system in conjunction with bicycle fitting systems like BGFit or RETÜL (Specialized Bicycle Components, Morgan Hill, CA, USA) should allow a more integrated picture of rider and bicycle, resulting in increased performance and decreased injury risk.

Figure 3: Full body musculoskeletal model

CONCLUSIONS

A method to create full body free-body diagrams of a cyclist while riding could be useful in increasing performance and reducing injury for cyclists.

REFERENCES

1. Eltoukhy M, et al. *XXIst Annual International Occupational Ergonomics and Safety Conference*, TX, USA, 2009.
2. Eltoukhy M, et al. *Int J Comp Vis Biomech* **3**, 99-106, 2010.
3. Eltoukhy M, et al. *Int J Comp Vis Biomech* **4**, 1-9, 2011.
4. Asfour S, et al. *Theoretical Biomechanics*, InTech, Austria, 2011.
5. Hull ML, et al. *J Biomech*, **14**, 843-856, 1981.
6. Hull ML, et al. (2) *J Biomech*, **14**, 857-872, 1981.
7. Callaghan JP, et al. *Clin Biomech* **14**, 203-216, 1999.
8. Clarsen B, et al. *Am J Sports Med* **38**, 2494-2501, 2010.
9. Collins K, et al. *Am J Sports Med* **17**, 675-680, 1989.
10. Weiss BD. *Am J Sports Med* **13**, 187-192, 1985.

ACKNOWLEDGEMENTS

The authors would like to thank Dr. Devin Berg for his help with completing this proof-of-concept.

MUSCULAR ACTIVATION OF LOWER LIMB MUSCLES DUE TO IN-FLIGHT POSTERIOR PERTURBATION DURING DROP LANDING

[1]Rumit Singh Kakar, [2]Scott W Arnett, [1]Yang-Chieh Fu, [1]Kathy J. Simpson
[1]University of Georgia, Athens, GA, USA
[2]The Western Kentucky University, KY, USA
email: rumit@uga.edu web: http://www.coe.uga.edu/kinesiology/research-service/biomechanics/

INTRODUCTION

In-flight perturbations applied by an opponent are commonly encountered when participating in team sports, such as basketball, football, soccer, and volleyball. Stable landings after such perturbations are needed to prevent ACL injuries [1]. However, the contributions of muscular responses to an in-flight perturbation are not understood. The purpose of the study was to determine how a posterior-directed linear perturbation influenced muscle activation strategies during drop landings and to understand anticipatory effects when expecting an in-flight perturbation. It was predicted that EMG of hip flexors, knee flexors and extensors and plantarflexors would increase pre- and post-touchdown when a perturbation was expected. We surmised that this increased activation would be a strategy to decrease the body's momentum and improve stability during landing.

METHODS

Healthy individuals, 5 males and 5 females (respectively, age: 20.8 ± .5 yrs, 20.8 ± 1.8 yrs; ht: 179.5 ± 6.2 cm, 165.4 ± 8.8 cm; mass: 77.2 ± 8.2 kg, 59.9 ± 10.6 kg) participating in competitive or recreational basketball, soccer, or volleyball provided informed consent. Ag/AgCl surface EMG electrodes were placed on 6 muscles of each lower limb: vastus lateralis (VL), vastus medialis oblique (VMO), rectus femoris (RF), long head of biceps femoris (BF), semitendinosus (ST), and medial gastrocnemius (GAS). EMG data were recorded using a Myopac® system (1200 Hz) and amplified (MPRD-101 Receiver/Decoder unit; CMRR 90 dB). Locations of 61 markers were collected using high-speed digital cameras (240 Hz). The perturbation cable was clipped to the posterior side of the participant (via a harness) at the medio-lateral and vertical location of the individual's center of mass (determined using the reaction board method [2]).

The participant hung from a suspended bar then dropped 55 cm onto 2 force plates in a normal landing pattern 5 times for each perturbation condition. The first condition was baseline (BASE); then no perturbation (NPER) and perturbation (PER) conditions were performed in a quasi-randomized order among participants. For PER, a posterior impulse (115% of mass) was applied via the cable attached to a perturbation device [3]. The raw EMG was band-pass filtered (10 – 100 Hz). Root mean square (RMS) EMG of each muscle group was calculated (window size = 33 ms; 4.78 Hz). RMS EMG was scaled to the peak value of the BASE RMS EMG. A muscle was considered active when values were $\geq$ 10% of BASE.

One-way ANOVA ($p < .05$) and Tukey's HSD (*posthoc*) for each muscle were used to compare the perturbation conditions for the EMG demonstrated during the flight phase and post-touchdown (from touchdown until maximum knee flexion).

RESULTS AND DISCUSSION

ST of both limbs ($p < .034$), and left limb BF ($p = .004$) significantly increased activation during PER compared to BASE during the flight phase. Right BF displayed the same tendency ($p = .078$). No other significant differences were detected (Tables 1-2). Lack of statistical significance of the majority of muscles among perturbation conditions may be due to inter-participant variability or activations truly were not different, based on the small magnitudes of differences among conditions.

Increased activation of hamstrings (BF and ST) may have served to decrease joint loading [4] and increase hip and knee stiffness to prevent joint collapse or loss of balance on landing. Increased hamstring activation may also have served to minimize anterior translation of the proximal tibia and distal proximal femur. Another possible explanation is that the posterior perturbation caused the lower trunk/ pelvis to be pulled posteriorly, resulting in hip/trunk flexion during the flight phase that, consequently, stimulated the hip extensors to increase their activation.

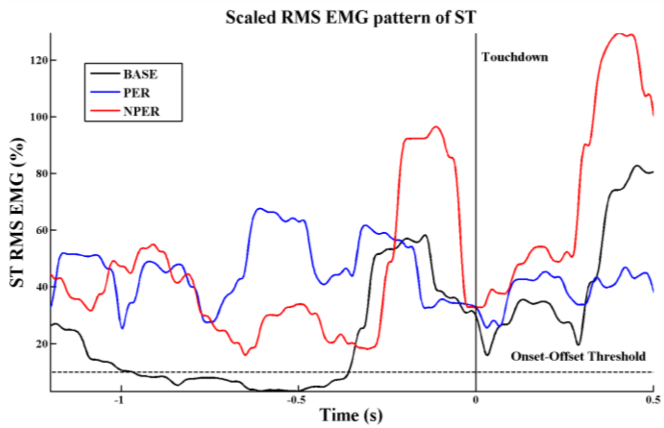

Figure 1: RMS EMG of semitendinosus of a representative participant for one trial of each perturbation condition.

Qualitatively, there were slight tendencies for increased activation of NPER compared to baseline. However, these were not statistically significant, suggesting that anticipating a perturbation did not have as much of an effect as an actual perturbation.

CONCLUSIONS

Increased hamstring activation before touchdown was the only muscle activation response to a posterior-directed in-flight perturbation. It appears that anticipatory effects likely do not account for the increased activation of the hamstrings. These results, along with knowledge of hip and knee mechanics, will further explain the knee joint biomechanics and strategies adopted to perform safe landings after this type of in-flight perturbation.

REFERENCES

1. Hewett, T. E. et al., Am J Sports Med 34(2): 299-311, 2006.
2. Hamill, J. et al., Biomech Basis of Human Movt. 430-431, 1995.
3. Arnett, S. W, Univ. of Georgia, [elec. source] 2007
4. Chappel, J.D. et al., Am J Sports Med. 35(2): 235-241, 2007.

Table 1: Scaled means ± SD of RMS EMG (% baseline EMG) of each muscle group for the flight phase.

	Right Limb			Omnibus	Left Limb			Omnibus
Muscle	BASE	PER	NPER	*p*	BASE	PER	NPER	*p*
RF	1.104 ± 0.522	1.095 ± 0.452	1.334 ± 0.638	.545	1.193 ± 0.506	1.236 ± 0.676	1.509 ± 0.931	.580
VMO	0.584 ± 0.347	0.668 ± 0.478	0.639 ± 0.576	.923	0.796 ± 0.541	0.957 ± 0.549	0.738 ± 0.477	.631
VL	0.816 ± 0.741	0.945 ± 1.085	0.968 ± 1.321	.944	0.773 ± 0.544	1.029 ± 1.065	0.941 ± 0.991	.426
BF	1.716 ± 0.941	3.462 ± 2.393	2.031 ± 1.627	.078	1.881 ± 1.082	5.097 ± 3.083	2.308 ± 1.681	.004*
ST	2.080 ± 1.043	5.100 ± 3.675	2.943 ± 2.067	.034*	2.175 ± 0.873	5.065 ± 2.819	2.655 ± 1.897	.008*
GAS	3.493 ± 1.669	3.977 ± 2.081	3.652 ± 1.771	.838	2.684 ± 1.253	2.954 ± 1.052	2.938 ± 1.089	.838

Table 2: Scaled means ± SD of RMS EMG (% baseline EMG) displayed post-touchdown.

	Right Limb			Omnibus	Left Limb			Omnibus
Muscle	BASE	PER	NPER	*p*	BASE	PER	NPER	*p*
RF	3.467 ± 0.742	3.582 ± 1.359	3.873 ± 1.144	.705	3.730 ± 1.193	3.821 ± 1.647	3.955 ± 1.625	.945
VMO	3.391 ± 0.933	3.528 ± 1.336	3.398 ± 1.010	.953	3.756 ± 0.905	4.531 ± 1.917	4.385 ± 1.790	.524
VL	3.429 ± 1.035	3.358 ± 1.215	3.623 ± 1.225	.871	3.523 ± 1.131	3.869 ± 1.891	4.035 ± 1.606	.762
BF	2.980 ± 1.307	2.870 ± 1.178	3.186 ± 1.285	.851	3.358 ± 1.041	4.516 ± 2.359	4.094 ± 1.582	.339
ST	2.910 ± 0.866	3.282 ± 1.554	3.913 ± 2.068	.471	2.462 ± 0.820	2.940 ± 1.384	3.456 ± 1.772	.291
GAS	2.191 ± 0.872	1.976 ± 0.892	2.501 ± 0.951	.438	1.645 ± 0.502	1.619 ± 0.421	1.960 ± 0.525	.233

A compact stereo-based motion capture solution for exercise monitoring

Mun Wai Lee, Sung Jung, Timothy Judkins, David Handelman, and Benjamin Bachrach

Intelligent Automation, Inc., 15400 Calhoun Drive, Suite 400
Rockville, MD 20855
email: mlee@i-a-i.com

INTRODUCTION

We propose a solution of a compact exercise monitoring system called ESPRIT: Exercise Sensing and Pose Recovery Inference Tool. This is a stereo camera system that monitors exercise activities, detects markers placed on the body, extracts image features, and recovers 3D kinematic body pose.

ESPRIT is being developed in support of NASA Exercise Countermeasure Program (ECP). Crew exercise is important during long-duration space flight for maintaining health and fitness, especially in preventing adverse health problems, such as losses in muscle strength and bone density. Monitoring of crew health and fitness is therefore important, and this includes performing motion capture and kinematic analysis to understand the effect of microgravity on exercise, and ensure that the exercise prescription (ExRx) is effective. Compared to standard multi-camera motion capture systems, ESPRIT is designed to be compact, relatively easy to set up and used in confined space.

To overcome the limitations of having only two cameras, ESPRIT uses strong prior knowledge and modeling of human body, pose, dynamics, and appearance. Preliminary result on ground-based laboratory has been promising and has demonstrated motion capture of several exercises, including walking, curling and dead lifting.

METHODS

The key innovations are: (1) a composite human body model that provides statistical priors on body shape, size, and appearance (see Fig. 1) (2) extraction of human silhouette and combining it with marker features to provide feature cues for pose estimation. (3) A robust and efficient marker detection algorithm with sub-pixel accuracy for depth estimation from stereo. (4) A statistical sampling-based method, Markov chain Monte Carlo (MCMC) [1], is used to compute a global optimization of the human pose trajectory, using multiple cues to help overcome temporary visual ambiguity due to partial occlusion. By using multiple feature cues and statistical inference techniques, it removes the need for multiple distributed cameras. With a stereo camera, the hardware footprint of the system is small, in terms of size, weight, power consumption, and setup time.

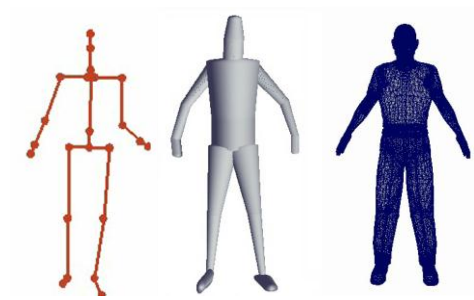

Figure 1: Composite human model with (i) skeleton, (ii) cylindrical, and (iii) mesh model.

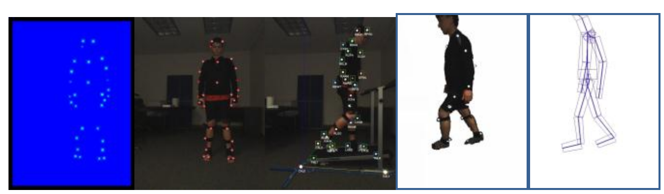

(a) (b) (c) (d) (e)

Figure 2: Feature extraction. (a) filter response, (b) marker detection, (c) marker labeling, (d) foreground, and (e) projected human model.

In this initial study, we developed an ESPRIT software prototype with a commercial stereo camera system (PointGrey Bumblebee). Key processing stages are: (a) foreground extraction, (b) markers detection and tracking, (c) stereo matching and 3D estimation, (d) markers labeling, and (e) pose estimation. Immediate result of these processing stages are shown in Fig. 2.

RESULTS AND DISCUSSION

Preliminary result in laboratory environment has been promising. We experimented with several exercises, including treadmill walking, curling and dead lifting. Screenshots of kinematic pose recovery are shown in Figure 3. For measuring relative locations of markers, at a range of 1-2 m, an average accuracy of 7.3 mm was achieved (Fig 4). This is based on the current hardware configuration of 12 cm stereo baseline, 640 pixel image width, and a workspace volume of approximately 2x2x1m.

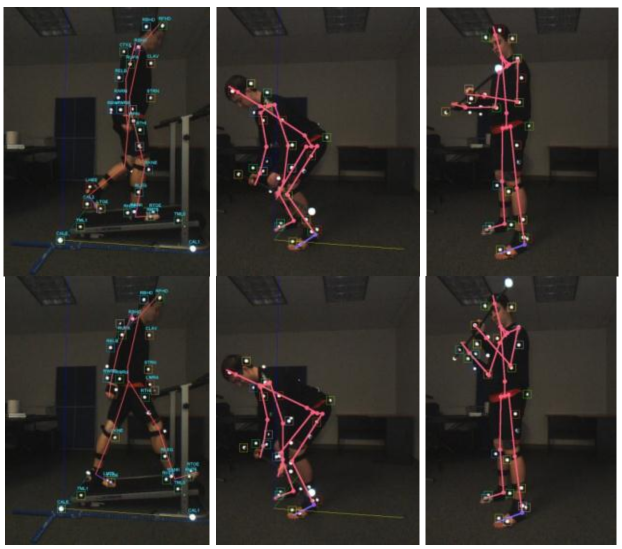

Figure 3: Result on stereo camera motion capture with exercise of treadmill, dead-lift, curl-lift.

Our ongoing work focuses on upgrading the hardware configuration and enhancing algorithms. Using a high-resolution (1024 pixel width) high-frame-rate stereo camera system, we project that the accuracy will be within 5mm or less (Fig 4), for an equivalent workspace volume. Marker clusters will be used to reduce set-up time and improve accuracy. A software simulation tool has been developed to help optimize the system design and to evaluate the algorithms. New algorithms are being developed to improve marker detection and localization, to overcome the issues of having only two cameras.

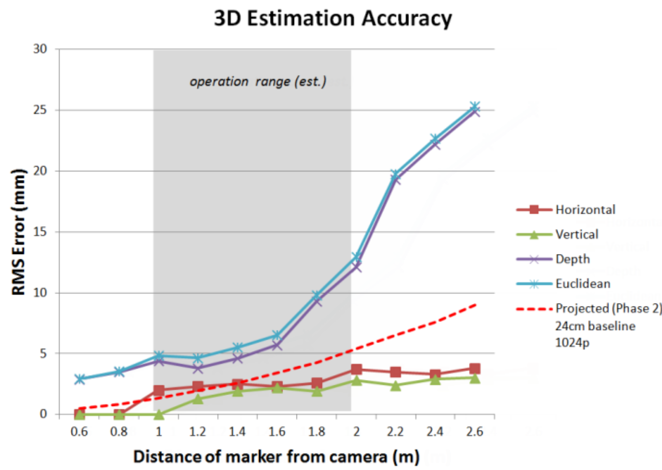

Figure 4: Achieved marker 3D distance accuracy as a function of distance.

CONCLUSIONS

The proposed solution is suitable for motion capture applications that require a compact portable system, short set up time with minimal cabling, and ease of use. It is suitable for targeted biomechanics studies that focus on certain body areas rather than full body kinematics. Initial experimental result shows that the solution is feasible and can achieve reasonable accuracy depending on hardware configuration and workspace volume.

REFERENCES

1. Lee M. and Nevatia R., (2009) *IEEE Trans. Pattern Analysis and Machine Intelligence*, vol. 31 no. 1, 27-38.

ACKNOWLEDGEMENTS

This work is supported by the NASA SBIR program under contracts #NNX11CG03P and #NNX12CA27C.

KINEMATIC COMPARISON OF SUCCESSFUL AND UNSUCCESSFUL LANDINGS DURING UNANTICIPATED MOVEMENT TASKS

[1]Kristof Kipp, [1]Christopher F. Geiser, [1]Claire M. Wood, [1]Carolyn M. Meinerz, and [2]Krista D. Watson

[1]Marquette University, Milwaukee, WI, USA
[2]Augustana College, Rock Island, IL, USA
email: kristof.kipp@marquette.edu, web: http://www.marquette.edu/exercise-science/

INTRODUCTION

An injury of the anterior cruciate ligament (ACL) is both a costly and detrimental event [1]. ACL injuries occur most often during cutting or landing tasks [1]. In addition, performing these tasks under unanticipated conditions elicits more high-risk biomechanics than when performed under preplanned conditions [2]. Research paradigms that use unanticipated cutting tasks to study landing biomechanics typically use only successful trials. It may, however, be prudent to analyze trials where the tasks are not executed successfully since lower extremity biomechanics may differ in a way that increases the risk of ACL injury.

METHODS

Twenty-eight female DI soccer players were recruited. Participants performed three randomly cued tasks: 1) single-leg land, 2) single-leg land and cut, and a single-leg land and forward run. Participants began each task by standing on a box, initiating a forward jump, and landing with their dominant limb on a force plate. Box height and forward jump distance were normalized to each participants' maximum vertical jump height and maximal single-leg stride distance, respectively. The random cue to perform each task was triggered from a switch mat placed on the take-off box.

For the purpose of this study, only data from the single-leg land task were analyzed. Data trials from this task were classified as either successful or unsuccessful landings, based on whether participants were able to stabilize their body over their dominant limb upon landing without touching the floor with the non-dominant limb. Further, data were only included for further analysis if a subject had more successful than unsuccessful landings.

A motion analysis system was used to collect position data from thigh and shank marker clusters [3]. Motion data were processed with Visual 3D to calculate 3-D knee joint angles [3]. Force plate data were used to determine foot contact during each landing. Knee flexion and abduction angle data were then interpolated to 100% of landing phase, which was defined as the time from the foot contact to maximum knee flexion.

Individual subject-based ensemble averages for each of the two knee rotations were created from between four to ten successful single-leg landings from each participant. Confidence intervals (95%) were then calculated around each participant's ensemble average knee data [4]. Data from successful and unsuccessful trials were compared across the entire interpolated landing phase with the use of the confidence intervals. The use of confidence intervals thus allows for statistical comparisons of point estimates to determine the difference between the 'average' of the successful trials and any given unsuccessful trial. Therefore, whenever unsuccessful trials were outside of the confidence interval, a significant difference in knee angle was present. The number of differences that were present between successful and unsuccessful trials throughout the landing phase were summed and then expressed as a percentage of the entire landing phase. This produced a variable that reflected the percentage difference between unsuccessful and successful landings.

RESULTS AND DISCUSSION

Eight participants matched our criteria for having more successful than unsuccessful landings. These participants had between four to ten successful landings and between one to three unsuccessful landings. The interpolated kinematic knee data of each participant differed between unsuccessful and successful landings (Table 1). On average, sagittal- and frontal-plane knee motions of unsuccessful trials differed by 66.8% and 41.2% from successful trials. Visual analysis of the kinematic landing data indicated that unsuccessful trials were characterized by less knee flexion and greater oscillations of knee motion in the frontal plane (Figure 1).

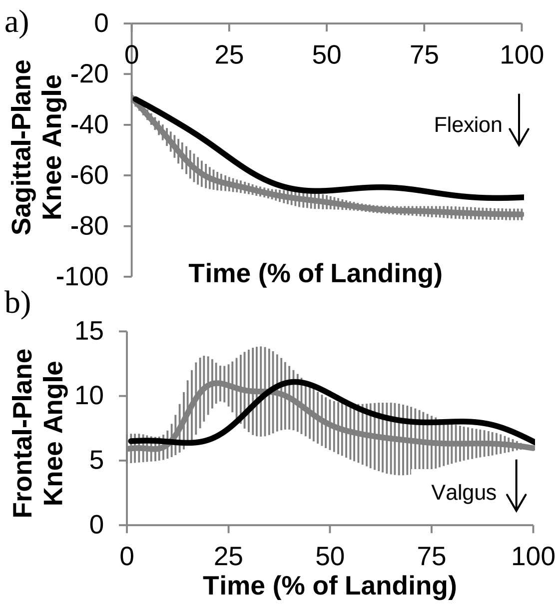

Figure 1: Sagittal (a) and frontal (b) plane knee angles (degrees) during the landing phases of successful and unsuccessful trials for participant 7. The grey line shows the ensemble average of all successful trials with the 95% confidence intervals in thin vertical bars. The black line shows one unsuccessful trial.

The analysis indicated that aspects of landing phase kinematics for unsuccessful trials differed significantly from successful trials. Differences were observed for both knee flexion and valgus/varus motions in all except for two participants. Most of the differences pointed to smaller knee flexion angles and greater frontal plane motion, both of which have been posited to manifest within the ACL injury mechanism [1, 5]. Given that performing landing tasks under unanticipated conditions is already associated with high-risk knee biomechanics, the smaller knee flexion and greater knee motion in the frontal plane during unsuccessful landings may lead to even greater high-risk landing scenarios.

CONCLUSIONS

The current findings suggest that unsuccessful landings are associated with greater high-risk knee motions and postures than successful landings when movements occur under unanticipated conditions or scenarios.

REFERENCES

1. Schultz SJ, et al. *J Athl Training* **45**, 499-508, 2010.
2. Besier TF, et al. *Med Sci Sports Exerc* **33**, 1176-1181, 2001.
3. Geiser CF, et al. *Med Sci Sports Exerc* **42**, 535-545, 2010.
4. Monaghan K, et al. *Clin Biomech* **21**, 168-174, 2006.
5. Hewett T, et al. *Am J Sports Med* **33**, 49-501, 2005.

Table 1: Percentage difference (%) in sagittal- and frontal-plane angles between unsuccessful and successful landings for each participant along with the group average.

	Participant								
Knee Angle	**1**	**2**	**3**	**4**	**5**	**6**	**7**	**8**	**Average**
Sagittal-Plane	67.3	0.0	81.2	97.0	5.0	100.0	96.0	88.1	66.8
Frontal-Plane	58.4	9.9	34.7	72.3	0.0	67.3	40.6	46.5	41.2

Note: The percentage difference indicates the percent of time during the landing phase that the unsuccessful trials were outside of the 95% confidence intervals of all successful trials.

DIFFERENCES IN THE MECHANICS BETWEEN THE DOMINANT AND NON-DOMINANT PLANT LIMB DURING INSTEP SOCCER KICKING

Cassidy M. Berlin and Eric L. Dugan

Boise State University, Boise, ID, USA
email: cassidyberlin@u.boisestate.edu, web: http://cobr.boisestate.edu/

INTRODUCTION

Soccer players are expected to be proficient at kicking with both limbs, however, most soccer players display a dominance of kicking ability causing asymmetry between the limbs [1]. This asymmetry in kicking mechanics may have injury implications. While there is some evidence that plant leg mechanics differ between the dominant (DL) and non-dominant (NDL) plant leg during kicking, there is little known about how these differences in mechanics relate to ACL injury risk [2].

Brophy and colleagues reported that female soccer players were more likely to injure their dominant support limb [3]. However, this study was a retrospective analysis of injury rates and did not provide insight about differences in lower extremity biomechanics. In contrast, Clagg and colleagues found that female soccer players exhibited greater knee extension, abduction, and external rotation joint moments in their non-dominant plant limb placing it at higher risk for ACL injury compared to the dominant plant limb [2]. These inconsistencies pose a question as to whether the dominant or non-dominant plant limb is more susceptible to ACL injury during instep soccer kicking of female soccer players.

The purpose of this study was to determine the differences in the mechanics between the dominant and non-dominant plant limb during instep soccer kicking of competitive female soccer athletes. It was hypothesized that the DL would exhibit greater posterior GRF impulse, net knee joint impulses in all three planes and lateral trunk lean.

METHODS

18 female participants were recruited for the study (age 20.7 +/- 2.4 years, height 65.3 +/- 2.2 inches, weight 135 +/- 17.9 lbs). All participants had one year of previous experience in competitive soccer. Competitive soccer was defined as soccer at the level of high school, club, collegiate or Olympic Development Program.

Following a warm-up and familiarization period, participants performed three instep kicks with each leg. The participants were aligned at a 60˚ angle from the direct approach of the ball and were allowed three preparation steps towards the soccer ball. This resulted in 3 kicks at a 60˚ approach angle from the right side of the ball and three kicks at a 60˚ approach angle from the left side of the ball. The participants were told to strike the ball as if they were trying to score a goal.

Three dimensional coordinate locations of a standard full-body marker set were recorded during the kicking trials with an 8 camera Vicon MX motion capture system (VICON, Denver, CO, USA). Labeled 3D trajectory and force plate data were imported into Visual 3D (C-Motion, Inc. Germantown, MD) for analysis of the kinematic and kinetic variables. The kinematic and kinetic data were filtered in Visual 3D using a Butterworth low pass filter at a cutoff frequency of 6 Hz for the kinematic data and 40 Hz for the kinetic data [4]. Custom processing protocols developed in Visual 3D were used to determine AP GRF impulse, knee joint impulse in all three planes, and lateral trunk lean. All variables were calculated between the times of initial plant foot contact (IC) to 50 ms after IC, as this may be a relevant time frame for the study of ACL injury risk [5].

In order to test for significant differences across the non-dominant and dominant limbs a Repeated Measures MANOVA was used with significance set at $p \leq 0.05$. A discriminate analysis was used as a post-hoc test to determine how the individual variables contributed to the difference between limbs.

RESULTS AND DISCUSSION

Descriptive statistics for the dependent variables are presented below.

Variable	DL Mean (SD)	NDL Mean (SD)
AP GRF Impulse (Nms)	-4.11 (3.73)	1.24 (4.40)
Net Sagittal Knee Moment Impulse (Nms)	0.00 (0.04)	-0.03 (0.01)
Net Frontal Knee Moment Impulse (Nms)	0.05 (0.02)	0.02 (0.02)
Net Transvers Knee Moment Impulse (Nms)	-0.02 (0.01)	-0.02 (0.01)
Trunk Lean (deg)	-2 (3)	-4 (3)

A significant multivariate main effect of limb was found (Wilks' $\lambda = 0.348$, $F(5,30) = 11.25$, $p = 0.000$). A discriminant analysis was performed to determine which variables were most responsible for the difference between limbs. This analysis revealed that the net frontal plane knee moment impulse, AP GRF impulse and knee sagittal plane knee moment impulse were the main contributors to the difference between conditions. The structure coefficients were 0.538, 0.493, and 0.424 respectively.

While there were significant differences between DL and NDL, these differences did not support our original hypotheses. We found that the dominant plant limb demonstrated greater values in the mechanics associated with increased ACL injury risk. These results were consistent with the study by Brophy et al. which concluded that female soccer players are statistically more likely to injury their dominant plant limb [3]. On the other hand, our results were contrary to the results of Clagg et al., who found greater "at risk" values in the non-dominant plant limb [3]. Results of the current study may have differed from those of Clagg et al. for several reasons including 1) kicking approach, 2) time frame of data analysis and 3) choice of variables.

While these results were inconsistent with those of Clagg et al. and our original hypotheses; these results are consistent with previous evidence suggesting that athletes may utilize a more protective strategy while performing a less familiar task. It has been found that females with more soccer experiences demonstrated larger knee moments than those exhibited by novice female soccer players [6]. It is possible that in the case of this study, the DL kicking strategy was analogous to the experienced player while the NDL kicking strategy was analogous to the novice player.

CONCLUSIONS

There is a difference between the dominant and non-dominant plant limb mechanics within competitive female soccer players. The differences we evident as the dominant plant limb produces greater net AP GRF impulse and knee joint moment impulse in the sagittal and frontal planes, exhibiting mechanics consistent with greater risk of ACL injury. As female soccer players gain experience in a task they may use more aggressive mechanics that place their dominant plant limb at a higher risk of ACL injury.

REFERENCES

1. Starosta, W. *Science and Football,* 346-355, 1988.
2. Clagg, S, Warnock, A, and Thomas, J. *Sports Biomechanics, 8(2)*: 141-153, 2009.
3. Brophy, R, et al. *Journal of Sports Medicine,* 44: 694-697, 2010.
4. Lin, F, et al. *Journal of Biomechanics,* 32: 395-400, 1999.
5. Park, K, et al. *American Journal of Sports Medicine,* 37: 1169-1177, 2009.
6. Sigward, S, and Powers, C. *Clinical Biomechanics,* 21: 740-747, 2006.

CHARACTERISTICS OF TIBIAL STRAINS DURING DIFFERENT TYPE OF PHYSICAL ACTIVITIES

Mohammad Kia, D. Clark Dickin, and Henry Wang
Biomechanics Laboratory, Ball State University

INTRODUCTION

There is evidence that an individual's past physical activity influences their risk of sustaining a tibial stress fracture. This evidence is based primarily on epidemiologic research on the rates of injury in different sub-populations [1]. The mechanisms that may explain these results have not been adequately examined. The goal of this study was to develop muscle driven forward dynamics simulations to investigate the influence of lower extremity exercises on tibial strains. The study hypothesized that high impact activities such as drop jump and cutting maneuvers produce different tibial strain profiles than those produced during walking. Experimentally measured kinematic data and ground reaction forces were used as inputs to the simulations while the tibial strain values were extracted.

METHODS

One healthy male subject (Age = 19 yr., height =1.80 m, and weight = 80 kg) performed the following four different type of exercises: drop-jump (JUM), cutting maneuver (CUT), running (RUN) and walking (WAK). A VICON motion capture system was used to record kinematics (240 Hz) and AMTI force plates were used to record ground reaction forces (2400 Hz). Computed tomography (CT) images of the subject were obtained in order to develop the right tibial bone geometry for a subject-specific lower extremity model. The 3D tibia was segmented in MIMICS 14.0 (Materialise, Leuven, Belgium).

MARC 2012 (MSC.Software, Santa Anna, CA) was used to develop a finite element (FE) model of the right tibia bone. Mechanical properties were assigned based on bone density. FE model was converted into a flexible tibia in MARC to incorporate the tibia geometry in LifeMod (LifeModeler Inc., San Clemente, CA). The subject's weight, height, gender, and age as well as the relative positions of the ankle, knee, and hip joints, determined from the motion capture, were used to scale the generic lower extremity models based on the GeBOD anthropometric database. The generic right tibia bone geometry was replaced with the developed flexible body of the subject specific tibia bone geometry. Tri-axis hinges combined with passive torsional spring-dampers were employed to model the hip joints. A hinge joint with a single degree of freedom was used for knee and ankle joints in the sagittal plane. A total of ninety muscles were added to the right/left legs. The measured kinematics, collected during lower extremity exercises, was used to drive the model with an inverse dynamics algorithm [2] while the muscle shortening/lengthening patterns were recorded. Next, kinematic constrains were removed, and muscles served as actuators to replicate the motions during forward dynamics (Fig.1).

A proportional–integral-derivative (PID) feedback controller was implemented to calculate each muscle force magnitude using the error signal between the current muscle length in the forward dynamics and the recorded muscle length during the inverse dynamics simulation. The force generated by individual muscle was limited by its force generating potential given by the following equation:

$$F_{max} = PCSA \times \sigma_{max} \quad (1)$$

Where F_{max} is the muscle's maximum force, $PCSA$ is the physiological cross sectional area and σ_{max} is the maximum tissue stress.

The maximum and minimum principle strain values (tension/compression) for all surface nodes of the tibial bone were computed in ADAMS (MSC. Software, Santa Ana, CA) during simulations. In order to compare the tibial strains during different activities in a consistent way, only maximum (*Max*) and average (*Mean*) strain values were reported for the nodes within mid-medial tibial shaft region [3].

RESULTS AND DISCUSSION

Although developing more computational models are in the process, the presented results are based on only one single subject specific model. Figure 2 illustrates tension (Fig.2a) and compression (Fig.2b) strains in color coded bars respectively during the stance phase of the cutting maneuver exercise. The average model predictions over the three trials of cutting maneuver are shown in figure 3 with a solid line and a shaded area corresponding to ±1 standard deviation. Table 1 summarizes the maximum and average values for the tibial strain on the mid-medial tibial shaft region over all four exercises during the stance phase.

Table 1: Tension (TEN) and Compression (COM) strain values during four different types of activities. COM strain values are rectified.

micro STRAIN		JUM	CUT	RUN	WAK
TEN	*Max*	1265	923	950	454
	Mean	390	580	338	206
COM	*Max*	437	1257	334	504
	Mean	179	572	162	212

This study produced a subject specific musculoskeletal model capable of concurrent simulation of muscle driven forward dynamics and calculated the tibial strain values. The current study shows that different types of physical activities exhibit different tibial strain profiles. High impact activities such as drop-jumping, cutting, and running elicit large tibial strain. Thus, participating in high impact activities may introduce mechanical stimulations to bone and lead to positive bone adaptations to resist unaccustomed loading environments. In summary, this modeling technique can provide useful insights of bone reactions to mechanical loadings during dynamic activities.

REFERENCES

[1] Milgorm, et al. Am J Sports Med, 2000

[2] Lifemodeler, I., 2010

[3] Milgorm, et al. J Biomech., 2003.

ACKNOWLEDGEMENTS

US ARMY, # W81XWH-08-1-0587

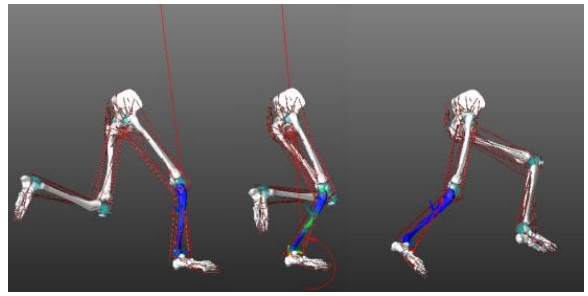

Figure 1: Lower extremity multi-body model of the subject with the flexible right tibial bone during the cutting maneuver.

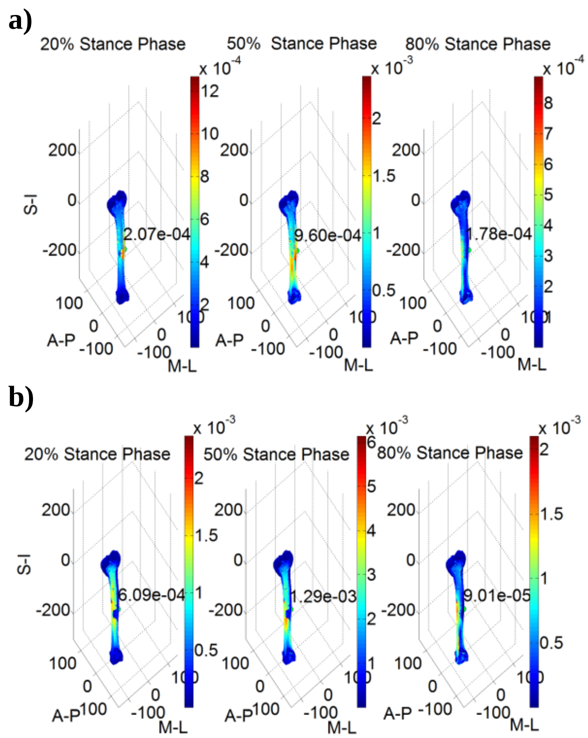

Figure 2: Computed strain at 20 %, 50% and 80% stance phase of the cutting maneuver.

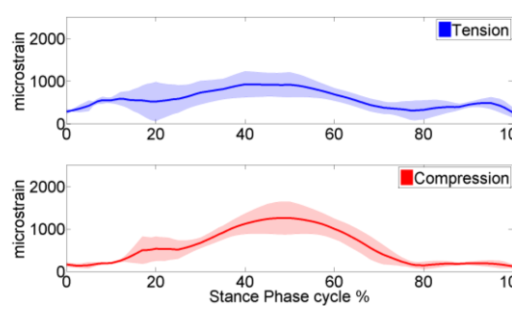

Figure 3: Model predicted strain on the mid-medial tibial shaft region.

KINEMATIC ANALYSIS OF SOCCER HEADING; COMPARISON OF TRAINING METHODS

[1]Shoko Suzuki, [2]Yasuo Nakamura and [1,3]Nozomu Inoue

[1]Graduate School of Life and Medical Sciences, Doshisha University, Kyoto, Japan
[2]Faculty of Health and Sports Science, Doshisha University, Kyoto, Japan
[3]Department of Orthopedic Surgery, Rush University Medical Center, Chicago, USA

email: ninoue@mail.doshisha.ac.jp

INTRODUCTION

Soccer is one of the most popular sports in the world. Heading is a technique of hitting a soccer ball using the head. There are several training methods to improve the heading technique. The most popular training method of the heading is heading the thrown ball. In this method, the ball is passed to the trainee directly; therefore, trajectory of the ball is similar to that seen in soccer games. However, reproducibility of the throwing is of concern. Another training method is that using a pendel to create motion of the ball [1,2]. This method employs simple equipment to hang the ball by rope. The ball moves like pendulum; therefore, its trajectory may not exactly duplicate the actual trajectory of the ball in the soccer game. However the pendel can create the ball trajectory with high reproducibility. The purpose of this study was to investigate differences of the heading motion between aforementioned two training methods.

METHODS

Thirteen university students were employed for this study (IRB approved). All subjects were skilled players with experiences of soccer of 12.9±2.9 years. Average age, height and weight of the players were 21.5±1.2 years old, 172.1±6.0 cm and 64.9±2.9 kg, respectively. A total of 55 spherical reflective markers were used (49 markers on subject's body, and 2 markers on a ball). 3D positions of each marker were recorded by a motion capture system (MAC 3D system, Motion Analysis). Three local coordinate systems were defined on the pelvis, thorax and head of the player's body to investigate kinematic parameters. Angular displacement of the head, thorax, and pelvis were calculated using coordinate transformation and Euler angles. Since a predominant heading motion is bending of the thorax, joint angles and angular velocity of forward and backward bending of the head and thorax were measured in this study. The period of heading motion was normalized by the period of the heading procedure. The start of the period (t=0[%]) was defined as the timing when subjects maximally bent the body backward. The end of the period (t=100[%]) was defined as an instance of ball impact. All subjects headed the soccer balls using two ball pass methods. First, the ball was passed to the subject by throwing with hands. The same passer threw the ball to the subject from a location 3 meters away from the subject. The subject was indicated to head the ball toward the passer. Next, the subject headed the ball using the pendel (Fig. 1). Ball height was adjusted according to the head position of each subject. The subject pushed the ball by him/her-self, moved back several steps, approached and headed the ball. The heading motion was recorded ten times in each method. The kinematic parameters in two methods were compared with a t-test. Significant level was set at $p<0.05$.

Figure 1: The experimental setup of the pendel

RESULTS

Significant difference was found in head backward tilt angles at both start (t=1) and end (t=100) of the heading period (Table 1). However, no significant difference was found in both thorax backward tilt angles (Table 1). In addition, no significant difference was found in each range of motion (Fig. 2).

Table 1: Angle of each segment

Segment	Normalized time	Angle (deg)	
		Throwing	Pendel
Head*	t=1	10.5±14.5	2.0±12.9
	t=100	7.1±19.5	-5.2±14.3
Thorax	t=1	17.2±9.8	15.4±7. 7
	t=100	4.0±10.4	5.0±6.8

Backward tilt(+)/Forward tilt(-), *:p<0.05

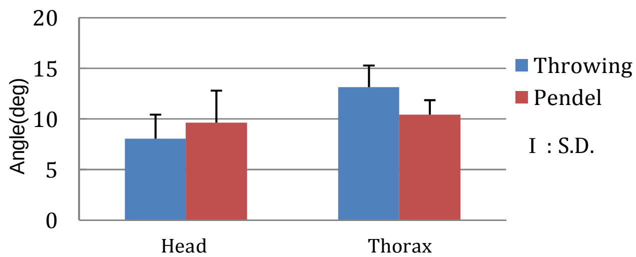

Figure 2: Range of motion

No significant difference was found in average angular motion and maximum angular velocity of head motion during the heading period (Figs. 3, 4). However, significant difference was found in average angular velocity and maximum angular velocity of thorax motion (Figs. 3, 4). No significant difference was found in height of ball impact (Table 2). However, significant difference was found in ball velocity just before impact (Table 2).

DISCUSSION

The present study showed more forwarded head position in the pendel method. This finding suggests that subject's visual axis was different in two methods. Training using the pendel may have made the players' view axis lower than that in the throwing training, which may caused lower angular velocity of the thorax in the pendel method.

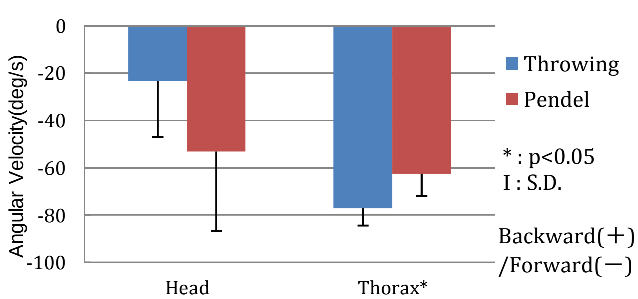

Figure 3: Average angular velocity

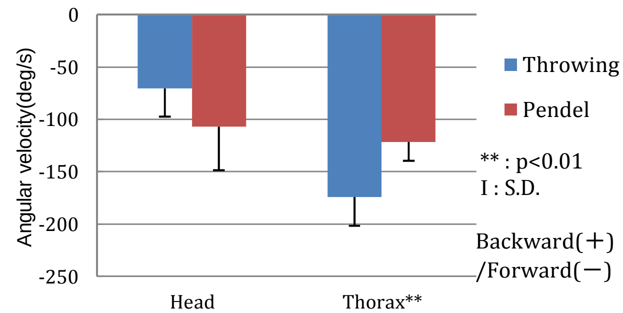

Figure 4: Maximum angular velocity

Table 2: Height and velocity of ball

	Throwing	Pendel
Height (mm)	1663±72.2	1647±57.9
Velocity (mm/s)*	4316±258.6	2029±397.6

*:p<0.05

If the ball velocity could be adjusted to the same velocity between pendel and throwing training methods, angular velocity of the thorax with the pendel may be same as that in the throwing method. However, there is an essential difference in the parabolic trajectory between the two methods (with a convex upward in the throwing method and a convex downward in the pendel method), and it may affects the motion tracking by the player. Therefore, the pendel may not be suitable for heading training. Nonetheless, the pendel method may be still suitable for beginners who afraid of the heading. It is natural for a human to be afraid of hitting a ball moving towards him/her with his/her head. Therefore, the first step of the heading is to overcome this fear. Due to lower velocity of the ball and no significant difference in the range of motion in the training using the pendel as compared with the throwing method, the pendel method is an effective training method for beginners. After the players have overcome the fear of heading, they may need to practice heading with the throwing ball.

REFERENCES

1. Nanba K, et al. *Bulletin of Faculty of Education, Shizuoka University Kyoka kyoiku series* **13**, 57-66, 1981.
2. Fukakura K. *Bulletin of the Faculty of Education, Fukushima University. Education-psychology* **34**, 119-126, 1982-12

GROUND REACTION FORCES AND IMPULSE DURING LANDING IS NOT CORRELATED WITH BALL SPEED IN HIGH SCHOOL BASEBALL PITCHERS

Masoumeh Soujoudi[1], Sakiko Oyama[1, 2], Joseph B. Myers [2]

[1]University of Texas at San Antonio, San Antonio, TX, USA
[2] University of North Carolina at Chapel Hill, Chapel Hill, NC, USA
Email: Sakiko.oyama@utsa.edu

INTRODUCTION

Baseball pitching is a whole-body movement that requires transfer of linear and angular momentum from the lower body to upper extremity, and then to the ball. Therefore, the kinematics and kinetics of lower extremity is considered important in production and transference of momentum to the ball. In fact, kinematic variables of the stride leg such as lower peak knee flexion angular velocity and greater knee extension velocity at ball release have been linked to increased ball speed. [1] It has also been described that the posterior and vertical ground reaction forces act to decelerate the lower body as the stride foot strikes the mound, which leads to transfer of momentum to the upper body to produce ball speed. [2]

Despite the perceived importance of lower extremity biomechanics on pitching performance, studies that investigated the ground reaction forces and impulse generated by the ground reaction forces in baseball pitching are limited [2, 3]. Therefore, the purpose of this study was to investigate whether the peak posterior and vertical ground reaction forces and impulses produced by the posterior and vertical ground reaction forces are correlated with ball speed in high school baseball pitchers. We hypothesize that ball speed is associated with ground reaction forces and impulses during landing.

MATERIAL AND METHODS

The data collection took place in a research laboratory. The pitches were performed from an indoor pitching mound into a backstop that was placed at a distance of 16.4m from the pitching rubber. The mound was instrumented with 2 force plates; one under the pitching “rubber” which was constructed from steel interfaced with the force plate and the other on the slope of the mound (**Figure 1**). The position of the force plate on the slope was adjusted based on the pitcher’s stride length. This force plate was used to capture the ground reaction forces during landing (900Hz). A seven-camera motions capture system was used to capture the kinematics (300Hz). A radar gun was used to capture ball speed.

A total of 55 high school baseball pitchers participated in this study (age: 15.5±1.2 years, height: 17.3±7.3m, mass: 73.3±10.6kg). The pitchers were fitted with reflective markers over tight-fitting clothing. After an adequate warm up, the pitchers pitched (fast-pitch) from wind-up until three strike pitches were captured.

Figure 1: Indoor pitching mound instrumented with force plates under the pitching rubber and on the slope

The filtered ground reaction forces were used to calculate the peak posterior and vertical ground reaction forces, and linear impulse produced by the posterior and vertical ground reaction forces before ball release. The impulse was calculated as the area under the force-time curve. The kinematic data were used to estimate the instant of ball release. The peak forces and impulses were normalized to subject’s body weight. Three-trial averages were used for statistical analyses.

Pearson product-moment correlation coefficients were used for data analysis. A priori-alpha was set to 0.05.

RESULTS AND DISCUSSION

The mean and standard deviation of the variables are presented in **Table 1**. An exemplary ground reaction force during landing is presented in **Figure 2**. The characteristics of the ground reaction force during landing were similar to what was reported in the study by MacWilliams et al [2].

Table 1: Mean and standard deviation (SD) of the variables examined in this study

	Mean	SD
Peak posterior ground reaction force (%BW)	-0.67	0.14
Peak vertical ground reaction force (%BW)	1.47	0.28
Posterior impulse (%BW)	-27.80	6.16
Vertical impulse (%BW)	64.68	10.88

BW: Body weight

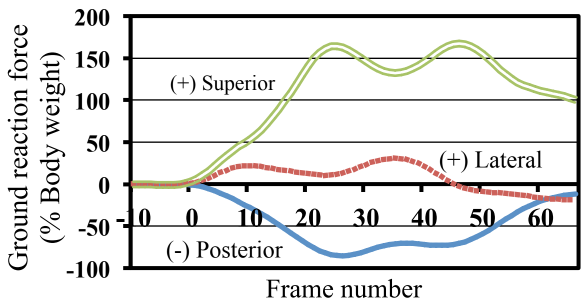

Figure 2: Exemplary ground reaction force during landing

Ball speed was not significantly correlated with any of the ground reaction force or impulse variables (**Table 2**).

Table 2. Correlation between ball speed and force variables examined in this study

	Posterior GRF	Vertical GRF	Posterior Impulse	Vertical Impulse
r	-.177	-.004	-.163	-.034
p	.200	.975	.240	.809

Our hypothesis that ball speed is associated with ground reaction forces and impulses during landing was rejected. This observation indicates that factors other than ground reaction force during landing have a larger influence on between-pitcher variance in ball speed.

MacWilliams et al [2] reported significant correlations between ball speed and peak posterior and vertical ground reaction forces within a single pitcher. This observation suggests that although the ground reaction forces during landing is not related to inter-pitcher variance in ball speed, it may be related to within-pitcher variance in ball speed. Therefore, we cannot dismiss the importance of the ground reaction forces during landing on pitching performance.

The relationship between ball speed and posterior and vertical impulses were examined in this study because the change in momentum is caused by the impulse, and not by the peak force. However, the relationships between ball speed and posterior/vertical impulses were non-significant, just like the relationships between ball speed and peak posterior/vertical forces.

Only the ground reaction forces and impulses during landing were analyzed in this study. Since the ground reaction forces acting on the stance leg produce pitcher's forward momentum, the relationships between ball speed and ground reaction forces and impulses during the stance phase (push off force) should be investigated in future studies. Additionally, examining the effects of lower extremity joint energetics on ball speed would help strength and conditioning specialists design effective exercise programs for baseball pitchers.

CONCLUSIONS

We observed that the posterior and vertical ground 1reaction forces or impulses produced by the posterior and vertical ground reaction forces during landing are not correlated with ball speed. Although ground reaction force during landing may be related to within-pitcher variance in ball speed, it does not seem to be related to inter-pitcher variance in ball speed.

REFERENCES

1. Matsuo T, et al. J Appl Biomech **17**, 1-13, 2001.
2. MacWilliams BA, et al. Am J Sports Med **26**, 66-71, 1998.
3. Guido JA, et al. J Strength Cond Res **26**, 1782-1785, 2012.

THE RELATIONSHIPS OF BAT QUICKNESS AND BAT VELOCITY WITH BATTING OUTCOMES FOR DIVISION I SOFTBALL PLAYERS

Travis Ficklin, Cassandra Reilly-Boccia, Robin Lund, Kara Beatty, and Javier Hervas
Biomechanics Laboratory, University of Northern Iowa, Cedar Falls, IA, USA
email: travis.ficklin@uni.edu

INTRODUCTION

The success of softball batters is often gauged statistically with measures such as batting average and slugging percentage. These are commonly used and provide information about game outcomes for hitters, but they are also dependent upon factors other than the physical characteristics of individual hitters. Bat quickness (BQ), the time it takes a the bat head to travel from a launch position at the onset of the swing to the point the bat makes contact with the ball [2], and bat velocity (BV), the linear velocity of the bat head at contact with the ball, are objective kinematic parameters that can be used to characterize a swing.

In professional baseball, BQ and BV have been found to be associated with "contact hitters" (batting average > .300) and "power hitters" (batting average < .300 with 35+ home runs) respectively [1]. However, no such relationships have been established for female softball players. The purpose of this study was to establish the relationships of BQ and BV to hitting outcomes for Division I collegiate softball players under game conditions.

METHODS

Video data were collected for all swings during a 15-game softball tournament in which six NCAA Division I teams played. For every pitch of the tournament, video cameras (JVC GC-PX1, Tokyo, JP) shooting at 300 Hz were used to capture any swing made. One camera was positioned on the first-base side of the field with its optical axis even with and parallel to the front edge of home plate. This camera was used to capture any swings made by right-handed hitters. The other, identical camera was positioned oppositely on the third-base side of the field, also with its optical axis parallel to the front edge of the plate. This second camera was used to capture any swings made by left-handed hitters. Though the cameras captured during all pitches, only data from trials in which a swing was made were kept. This resulted in a total of 1099 swings.

BQ was calculated by video analysis. The number of frames of video from the onset of the swing to contact, or, if the ball was missed, the frame in which the ball reached the same horizontal position as the bat tip, were counted. This number of frames was then multiplied by (1/300) s. The onset of the swing was determined to be the frame in which the bat tip made first movement on its trajectory to the hitting zone.

BV was calculated through digitization. The tip of the bat was digitized at contact, or, if there was no contact, in the frame in which the ball had reached the same horizontal position as the bat tip. The bat tip was also digitized five frames (1/60 s) prior to this instant. A reference distance was calculated between the back corner of home plate and the centroid of the front, inner corners of the batters' boxes. The distance covered by the bat tip in the 1/60 s immediately prior to contact or its equivalent frame was then converted to meters and divided by 1/60 s to yield BV.

All swings were rank ordered by BQ and BV. After rank ordering, each swing was placed in a quartile for each of the parameters (Q1-4_{BQ}, Q1-4_{BV}). Furthermore, two outcome variables were reported for each swing. For the first outcome variable, base hit (BH), a "hit" was recorded if the swing resulted in a single, double, triple or homerun. If it resulted in a miss, foul ball, or an out of any kind it was considered a "no hit." The second variable, total bases (TB) was determined by the number of bases achieved by each swing. If the swing resulted in a miss, foul ball or out of any kind a zero was recorded. Singles were recorded as a "1", doubles as a “2”, triples as a “3” and homeruns as a “4.” This variable was considered an indicator of “power hitting.” Due to the lack of normality, nonparametric statistical analyses were used. Two separate Kruskal-Wallis tests were conducted to determine if there were any differences between the quartiles for BQ and BV on either of the outcome variables (BH, TB). Mann-Whitney U tests were used as posthoc analyses when appropriate. Alpha was set at 0.05 for all tests.

RESULTS

Analysis of the quartiles indicated that there was no significant differences between Q1-4$_{BQ}$ for both BH (χ^2(3)=2.6, p=0.46) and TB (χ^2(3)=2.3, p=0.51). Differences were detected among Q1-4$_{BV}$ for both BH (χ^2(3)=10.4, p=0.02) and TB (χ^2(3)=9.9, p=0.02). The results of the posthoc analyses can be seen in Figures 1-2.

DISCUSSION

The results of the present study support the ability of BV to predict successful hitting outcomes, as a significantly greater number of BH and TB came from the quartiles with greater BV.

Surprisingly, BQ was not significantly related to hitting outcomes for the sample collected. Logically, better BQ would lead to more contact as less of the reaction time given to the batter would be needed for swinging and more could be used for judging the pitch.

The present data do support the previously found relationship between BV and power hitting as seen in the greater distribution of TB originating from the quartiles with best BV. Bigger BV at contact results in greater exit velocity for the ball, meaning more extra-base hits. Furthermore, better exit velocity should yield more BH as the ball becomes harder to field.

Because the present sample contains Division I players, it is probable that BQ for the population is sufficient for the level of play. This potentially leaves BV to be one source of differences in hitting success for the limited number of games in the tournament at which data was collected.

More data across more teams in more games need to be collected in order to further explain these relationships.

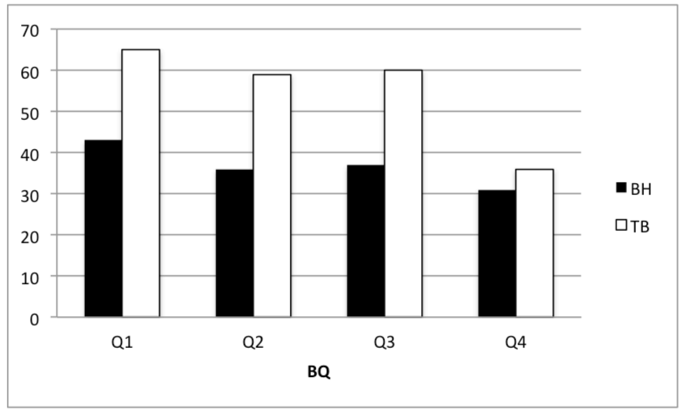

Figure 1: BH and TB by Q1-4$_{BQ}$.

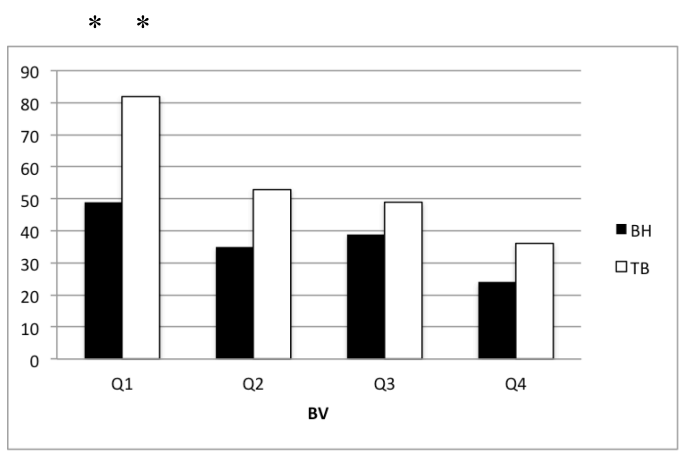

Figure 2: BH and TB by Q1-4$_{BV}$.
* sig. greater than Q3 and Q4.

REFERENCES

1. Stellar, T., et al. *The absolutes of hitting: Dynamic balance, kinetic links, axis of rotation, bat lag.* (Motion Picture) BioKinetics inc: Laguna Hills, Ca. (1993)
2. DeRenne, C., Stellar, T., & Blitzbau, A. *High tech hitting: Science vs. Tradition*. West Publishing. (1993)

RELATIONSHIP OF RATE OF TORQUE DEVELOPMENT AND CONTRACTILE IMPULSE DURING TIME CRITICAL PERIODS

[1]Samuel T. Johnson, [1]Marc F. Norcross, [2]Christine D. Pollard, and [1]Mark A. Hoffman

[1]Oregon State University, Corvallis, OR, USA
[2]Oregon State University-Cascades, Bend, OR, USA
email: sam.johnson@oregonstate.edu

INTRODUCTION

Rapid torque production is critical for joint stabilization during potentially injurious situations and during explosive athletic movements.[1] The most commonly used measure of rapid torque production is the rate of torque development (RTD), or the slope of the torque-time curve. Less commonly used is contractile impulse (CI), or the area under the torque-time curve. Regardless, both measures are typically calculated over the interval from torque onset to peak torque. However, the time it takes to reach peak torque is likely longer than the time available to stabilize a joint to prevent an injury (e.g., less than 50 ms) or complete an explosive movement (e.g., less than 250 ms). Due to this, there is increasing interest in measuring rapid torque production during time critical periods that are likely more closely associated with potentially injurious situations and/or explosive athletic movements.[2] Despite this interest, it is unknown how the choice of different length time intervals commonly used to evaluate RTD and CI might affect these measures. Therefore, we calculated RTD and CI over 0-50 ms and 0-250 ms and determined the relationships between the time intervals.

METHODS

Nineteen healthy, physically active volunteers (11 Males, 8 Females, Age: 20.84±1.61years, Height: 1.70±0.10m, Mass: 72.76±11.31kg) were tested after they provided informed consent.

Isometric plantarflexion torque-time curves of the dominant limb were measured using a Biodex System 3 Isokinetic Dynamometer (Shirley, NY) interfaced with a Biopac MP100 data acquisition system (Goleta, CA). Participants were seated recumbently with the dominant foot secured to the dynamometer footplate in 0° (neutral position) and the knee flexed to 60°.

Once positioned, participants were instructed to plantarflex against the footplate of the dynamometer as fast and as hard as possible in response to a light stimulus. Each contraction was held for approximately three to four seconds. A total of three trials with 60 seconds of rest between trials were collected.

Torque data were collected at 1000 Hz and upsampled to 2000 Hz. The data were low pass filtered at 10 Hz using a 4th order, zero-lag Butterworth filter. Torque onset was defined as the as the time when the torque exceeded 2.5% of the peak torque. RTD was calculated as the slope of the line of best fit for the torque-time curve from torque onset to 50 ms and onset to 250 ms. CI was calculated by integrating the area under the torque-time curve from torque onset to both of the two time windows. The average of each dependent variable across the three trials was used for statistical analysis.

Pearson correlation coefficients ($\alpha \leq 0.05$) assessed the relationships between RTD from 0-50 ms and 0-250 ms, and the relationships between CI from 0-50 ms and 0-250 ms.

RESULTS AND DISCUSSION

Both the RTD time intervals were significantly correlated to each other ($p<0.001$). Additionally, both of the CI time intervals were significantly correlated to each other ($p<0.001$). (Correlations are presented in Table 1 and raw data are presented in Table 2.)

While RTD and CI calculated using the different time intervals were significantly correlated, it is apparent that there is greater disagreement between RTD calculated over 0-50 ms and 0-250 ms than CI. An examination of the shared variance reveals a substantial reduction in shared variance in RTD (37% decrease) as the time interval increases (i.e., 0-50 ms vs. 0-250 ms). However, there is only 14.3% unexplained variance between CI calculated from 0-50 ms and 0-250 ms.

Table 1: Correlations and shared variance of RTD and CI between the selected time intervals.

	r	**r^2**
RTD 0-50 ms and 0-250 ms	0.794	0.630
CI 0-50 ms and 0-250 ms	0.926	0.857

The advantage of CI compared to RTD is that it takes into account the specific time history of the contraction.[3] This fact seems to help maintain the accuracy of the measure regardless of the time interval selected for analysis. RTD on the other hand, relies on an approximated line of best fit, and as such likely fails to account for subtleties in the torque-time curve.

CONCLUSIONS

When measuring rapid torque production it is important to consider time critical periods relevant to the task that is of interest. Based on these results, these time windows are differentially affected by the time interval chosen to quantify rapid torque production. In situations, where shorter time intervals are of interest, such as during potentially injurious situations, RTD or CI will both provide good estimates of rapid torque production. Whereas, when longer time intervals are of interest, such as during explosive athletic movements, CI appears to be a better choice.

REFERENCES

1. Aagaard P. *Exerc Sport Sci Rev*, ***31***, 61-67, 2003.
2. Andersen LL, et al. *Scand J Med Sci Sports* ***20***, e162-e169, 2010.
3. Aagaard P, et al. *J Appl Physiol*, ***93***, 1318-1326, 2002.

ACKNOWLEDGEMENTS

Funded through the OSU-Cascades Circle of Excellence Research Collaboration Award.

Table 2: Means ± Standard Deviation of RTD and CI over the different time intervals.

	Time Intervals	
	0-50 ms	**0-250 ms**
Rate of Torque Development (Nm/s)	233.44±147.34	191.44±108.94
Contractile Impulse (Nm·s)	0.34±0.20	7.27±3.95

Biomechanical variables during swing correlated with impact peak in running

[1]Anne Schmitz, [1]Michael Pohl, [1]Kaitlin Woods, and [1]Brian Noehren

[1]University of Kentucky, Lexington, KY, USA
email: anne.schmitz@uky.edu

INTRODUCTION

Up to 70% of runners develop an overuse injury within a 1 yr period [1]. While running injuries are multi-factorial in nature, abnormal biomechanics are considered an important contributing factor. In particular, a higher vertical impact peak of the ground reaction force in early stance has been associated with a history of overuse injuries such as tibial stress fractures and plantar fasciitis [2,3]. One potential way to reduce impact forces is to switch to making initial contact at midfoot or forefoot [4]. However, changing from a heel strike to forefoot strike pattern causes a greater demand at the foot and ankle due to greater ankle plantar flexion, thus shifting power absorption from the knee to the ankle [5]. This potential strategy may not be advisable for runners with less compliant tendons associated with aging, as well as individuals with injuries such as achilles tendonitis and plantar fasciitis. Therefore, other potential gait modifications are needed to reduce initial impact loading.

Given that the initial impact peak occurs early in stance, it is possible that its magnitude is dependent on running mechanics prior to initial contact with the ground [1]. Therefore, defining what biomechanical variables occurring prior to initial contact are associated with the impact peak may provide important information for the development of new gait modification strategies. To date, there have been few reports as to what factors play a role in high impact forces. For example, Lieberman et al. suggest decreases in the impact peak from running with a forefoot strike pattern may be due to increased ankle plantar flexion at landing, increased leg compliance, and a decreased effective body mass that impacts the ground (which is dependent on mass and velocity) [4]. Other investigators have reported that knee flexion angular velocity and hip extension power at the instant of peak impact were associated with the magnitude of the impact peak in rearfoot strikers [6]. However, both of the aforementioned studies focused solely on biomechanical variables measured during the stance phase. The swing phase of gait is where the body is positioning the leg for impact and could yield insight into other biomechanical variables that might be related to the impact peak. Therefore, the goal of our work was to determine which variables in swing phase were associated with the magnitude of the impact peak during running. The variables of interest were initial impact peak as well as superior-inferior segmental accelerations, velocity, and position at mid-aerial and terminal-swing. We expect impact peak to be most correlated with lower body segmental velocities [4,7,8].

METHODS

Instrumented motion capture data was collected for 32 healthy subjects (age 24 ± 3 yrs, height 1.66 ± 0.06 m, mass 60.1 ± 7.1 kg) running on a treadmill at a speed of 3.3 m/s. Using retroreflective markers, three-dimensional coordinate data were measured with a 15 camera motion analysis system (Motion Analysis Corp, Santa Rosa, USA) using a sampling rate of 200 Hz [9]. Force data was simultaneously collected at 1200 Hz using an instrumented Bertec treadmill (Bertec, Columbus, OH).

Visual 3D software (C-motion, Germantown, MD, USA) was used to filter the data, calculate a functional hip joint center, and calculate segmental kinematics. Raw marker coordinate data were filtered at 8 Hz and force data at 35 Hz using a fourth-order low-pass zero-lag Butterworth filter.

Custom Matlab code (MathWorks Inc., Natick, MA) was used to extract the impact peak of the vertical ground reaction force. It was also used to determine the position, velocity, and acceleration of the center of mass for the trunk, right thigh, right shank, and right foot at mid-aerial and terminal-swing of running. Terminal swing was defined as 10 ms prior to initial contact and mid-aerial the time halfway between left foot toe-off and right foot heel-strike.

Data were collected from 5 trials for each subject and then averaged. Using SPSS (SPSS Inc., Chicago, IL), Pearson's correlation coefficients were used to assess the relationship between the impact peak and variables of interest.

RESULTS AND DISCUSSION

The impact peak (average 1.6 ± 0.3BW) was significantly correlated with the superior-inferior velocity of the thigh ($r=-.370$, $p<0.05$) and shank ($r=-.556$, $p<0.01$) at mid-aerial, as well as with the foot acceleration at terminal swing ($r=.502$, $p<0.01$) and position at mid-aerial ($r=-.458$, $p<0.01$) (Figure 1). These results suggest the most effective way to decrease the impact peak would be to decrease the downward velocity of the shank.

A modeling study by Gerritsen found the impact peak to be largely influenced by the vertical velocity of the heel at touchdown [8]. While the foot velocity at terminal swing was not significantly correlated with the impact peak ($r=-.337$, $p=0.059$), the velocity of the shank at mid-aerial was largely correlated with the velocity of the foot at terminal swing ($r=.596$, $p<0.01$). This expands upon Gerritsen's study to identify factors that may be precursors to touchdown velocity.

The correlation of impact peak to trunk kinematics was not significant. Saunders proposed the theory that lower extremity kinematics are the main determinants of the motion of the COM during gait [7]. Our results suggest this may extend to running, in agreement with Zadpoor et al. [10] who used computer simulations to support the idea that the impact peak is due to the lower body extremities while the active peak during stance is the upper body's reaction to the impact.

The downward motion of the leg in terminal swing is largely controlled by gravity and the activity of the hamstrings [11]. Although not tested in running, Radin et al. has previously shown a larger downward velocity of the ankle, along with a lack of counterbalancing quadriceps force, at contact may be associated with larger heel strike transients in walking [11]. Our results suggest this may apply to running as well. One potential strategy that may be tested could be to train the individual to "tune" their quadriceps muscle prior to heel strike to better control initial impact peak and do what Radin refers to as "sliding" into stance rather than "digging" into the ground [11].

CONCLUSIONS

Investigating which biomechanical factors contribute to peak impact loads in running can help clinicians develop strategies to reduce joint loads during running that may cause overuse injuries. Our results suggest that an alternative to forefoot striking may be modifying lower extremity kinematics during swing in running. Future work will include more subjects to investigate the capability of the correlated variables to predict impact peak.

ACKNOWLEDGEMENTS

Partially funded by NSF IIS 1231545

REFERENCES

1.Hreljac, A. *Med Sci Sports Ex* **36**, 845-849, 2004.
2.Milner, C. E., et al. *Med Sci Sports Ex* **38**, 323-328, 2006.
3.Pohl, M. B., et al. *Clin J Sports Med* **19**, 372, 2009.
4.Lieberman, D. E., et al. *Nature* **463**, 531-535, 2010.
5.Williams III, D. B., et al. *Int J Sports Phys Ther* **7**, 525, 2012.
6.Noehren, B., et al. *Proc of ASB,* Gainesville, FL, 2012.
7.Saunders, J. B., et al. *J Bone Joint Surg Am* **35-A**, 543-58, 1953.
8.Gerritsen, K. G. M., et al. *J Biomech* **28**, 661-668, 1995.
9.Noehren, B., et al. *Gait & Posture* **36**, 596-599, 2012.
10.Zadpoor, A. A., et al. *J Biomech* **40**, 2012-2021, 2007.
11.Radin, E. L., et al. *J Orthop Res* **9**, 398-405, 1991.

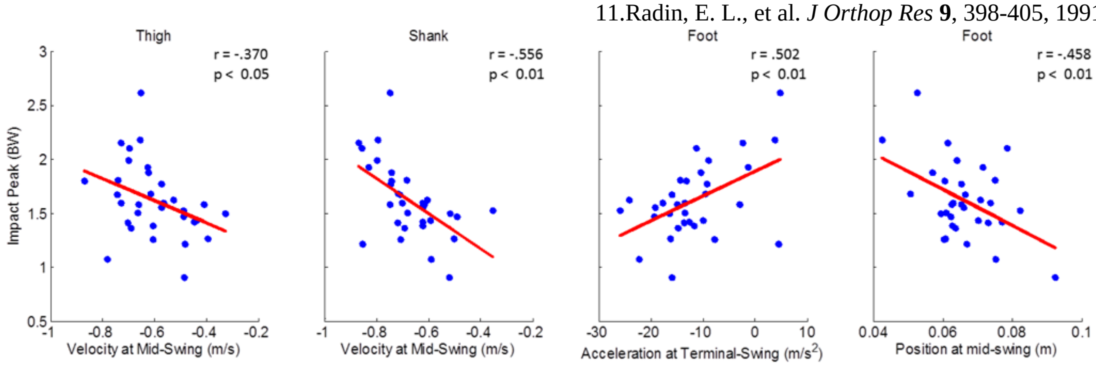

Figure 1: Significant correlations of lower extremity superior-inferior kinematics with impact peak. Positive values of position, velocity, and acceleration denote upward movement and position.

CAN INCREASED RUNNING CADENCE SIMULATE THE EFFECTS OF GOING BAREFOOT?

Jocelyn F. Hafer, Jennifer Bido, Leigh-Ann Plack, Jordan D. Metzl

Hospital for Special Surgery, New York, NY, USA
email: jocelynfhafer@gmail.com

INTRODUCTION

Running is a popular recreational sport and runners experience a high incidence of injury (1). Due to this incidence, injury prevention interventions have become a hot topic in running research. Currently barefoot running is a popular intervention, largely due to its portrayal as being safer and more natural in media (2). Scientific studies have found that barefoot or barefoot-style running can result in the reduction in mechanics typically associated with injury (3). These mechanics include increases in loading rate, impact forces (4), hip adduction angle (5, 6), and stride length. These kinematic and kinetic patterns have been associated with tibial stress fractures (4), iliotibial band syndrome (5), and patellofemoral pain syndrome (6). Barefoot running as an intervention aims to achieve changes such as decreased hip adduction during stance, decreased loading rate variables, increased knee flexion at initial contact, and decreased stride length.

While barefoot style running has been shown to achieve these changes in mechanics, barefoot running is not a viable option for all runners who wish to reap the injury prevention benefits of barefoot running. Some runners may be unable to run barefoot due to climate, available terrain, or inherent foot structure. Additionally, barefoot running may result in bony injuries in the foot (7). Running with an increased cadence has been shown to result in alterations to running mechanics that are similar to those seen with barefoot running (8). The purpose of this study was to determine if running with an increased cadence produces changes in running mechanics similar to barefoot running in a single group of runners.

METHODS

This study included 5 healthy runners. All were rearfoot strikers who had been injury free for at least 6 months prior to data collection. All runners did not wear orthotics and typically trained in neutral running shoes. No runners had experience training barefoot.

Kinematic and kinetic data were collected during overground running using a 12-camera motion capture system and 4 force plates. A full-body, six degree-of-freedom markerset was used to build the model for calculations. 3 running conditions were collected:

1. Normal: shod, preferred running cadence.
2. Cadence: shod, cadence 10% above preferred.
3. Barefoot: barefoot, cadence not controlled.

Before data were collected for conditions 2 and 3, runners were allowed to acclimate by running overground or on a treadmill. Runners were instructed to run “however you’re most comfortable” in each condition. Speed was monitored and controlled to match each runner’s preferred pace in each condition using a photogate system. Cadence was controlled using a metronome. Condition order was randomized.

The variables of interest in this study were vertical loading rate (VLR), impact force (IF), peak hip adduction angle during stance (PHAD), and heel strike distance (HSD), a measure used visually to identify overstriding. VLR was calculated as the slope of the vertical ground reaction profile between 20% and 80% of the curve before the first impact peak (or the first inflection point in cases where there was no definitive impact peak). IF was calculated as the value at the first impact peak (or the first inflection point) (Figure 1). HSD was calculated as the horizontal distance between the ankle and the runner's center of mass at initial contact. All variables were compared between conditions using repeated-measures ANOVA.

RESULTS

Participants included 5 runners (4 female) aged 34.2 ± 9.1 years, 1.6 ± 0.1 meters tall, 61.4 ± 2.8 kg. Average running velocity was 2.9 m/s.

VLR, and PHAD were significantly different between conditions (Table 1). VLR was decreased in cadence and barefoot conditions as compared to normal. PHAD was decreased in the cadence condition as compared to normal.

As expected, cadence was higher in the cadence than in the normal condition. Additionally, cadence was higher in the barefoot than in the normal condition. IF and HSD were not different between conditions.

Table 1: Kinematic and kinetic outcome variables. Post-hoc abbreviations indicate which conditions are different.

	Normal		Cadence		Barefoot		p-value	post-hoc
	Mean	SD	Mean	SD	Mean	SD		
cadence (steps/min)	85.7	6.23	93.78	6.23	90.9	4.82	**0.00**	NC, NB
VLR (BW/sec)	44.2	12.2	42.25	16.6	92.9	41	**0.01**	NB, CB
IF (BW)	1.57	0.35	1.27	0.69	1.29	0.37	0.28	
PHAD (°)	11.6	3.23	8.79	2.74	11.4	3.15	**0.01**	NC
HSD (cm)	0.21	0.04	0.20	0.04	0.21	0.04	0.16	

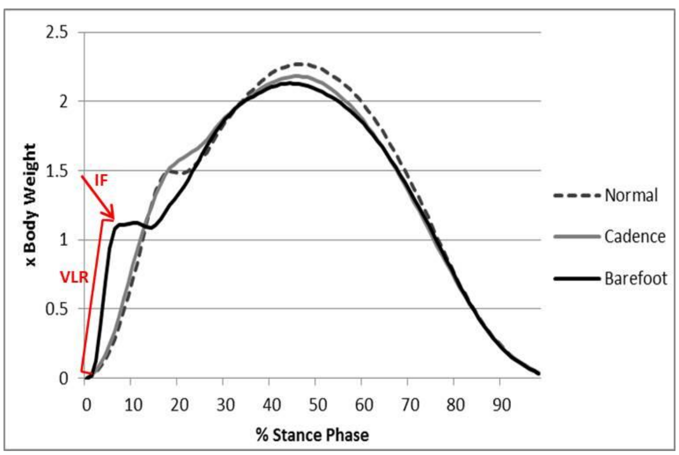

Figure 1: Vertical ground reaction force profile. Average of all subject data by condition. Example indicated for IF and VLR of barefoot condition.

DISCUSSION

The results of this study agree with those of earlier studies that looked at barefoot running or increased cadence individually. These results add to the current body of literature by demonstrating that a single group of runners demonstrates similar changes with the implementation of either of these two interventions (3, 8). The decreases in loading rate and hip adduction documented here suggest that runners with a history of injuries that are associated with increased loading rate (4) or hip adduction (5, 6) may benefit equally from increasing their cadence or running barefoot. This finding suggests that runners can achieve the benefits of barefoot running without changing their footwear. As removing shoe gear resulted in an increased cadence in this group of runners, it is possible that these changes are a result of increased cadence, not necessarily removing shoes.

While this study looked at an acute intervention, future studies should investigate what changes are seen in a long-term intervention. Additionally, in order to simulate real-world training conditions, runners in this study were not coached on correct running form. Future studies should investigate the effect of instruction or coaching on running form in these conditions.

REFERENCES

1. van Gent RN, et al. *Br J Sports Med* **41**, 469-480, 2007.
2. McDougall C. *Born to Run: a Hidden Tribe, Superathletes, and the Greatest Race the World Has Never Seen*. Alfred A. Knopf, 2009.
3. Squadrone R, et al. *J Sports Med Phys Fitness* **49**:1, 6-13, 2005.
4. Milner CE, et al. *Med Sci Sports Exerc* **38**, 323-328, 2006.
5. Noehren B, et al. *Clin Biomech* **22**(9), 951-956, 2007.
6. Willson JD, et al. *J Orthop Sports Phys Ther* **38**(10) 606-615, 2008.
7. Ridge ST, et al. *Med Sci Sports Exerc*
8. Heiderscheit BC, et al. *Med Sci Sports Exerc* **43**(2) 296-302, 2011.

THE EFFECTS OF FATIGUE ON VERTICAL LOADING DURING RUNNING

Danise L. Maas, ATC, Lars M. Mattison, EIT, Macie L. Michelson, Bradley Bowser, PhD

South Dakota State University, Brookings, SD, USA
Email: danise.maas@sdstate.edu

INTRODUCTION

It has been suggested that up to 70% of all runners sustain an overuse injury in a given year [1]. Research has indicated that both foot strike pattern and increased vertical loading during early stance may play a role in in these injuries.

Level of fatigue has been suggested to contribute to this high percentage of overuse injuries to runners. However, a recent meta-analysis indicates that vertical loading does not change following fatiguing protocols[2]. All of the studies examined in the meta-analysis used fatiguing protocols that involved running. However, there is no known research examining the use of a bicycle ergometer to induce fatigue. Fatiguing protocols using a bicycle ergometer may provide different results. This type of protocol may have implications for athletes who transition immediately from a cycling to a run such as triathletes.

When the legs are fatigued after riding a bicycle, cyclist often feel tightness and a certain degree of rigidity of their lower legs. It is likely that this sensation will carry over to running. As such, runners may run with a more leg stiffness. Increasing leg stiffness during running has been reported to increase vertical loading during early stance [3].

The purpose of this study is to examine the effects of a fatigue protocol using a bicycle ergometer on vertical impact peak (VIP), vertical instantaneous load rate (VILR), vertical average load rate (VALR), and leg stiffness (LS) during running. We hypothesize that there will be an increased VIP, VILR, VALR, and LS following the fatiguing protocol.

METHODS

This is an ongoing study where 8 Division I track and field athletes (age=21±3yr, height=1.81±0.12m, mass=67.0±10.3kg) have been studied to date. All participants were required to be injury free for two months prior to participation.

After obtaining informed consent, all participants were provided with Nike Air Pegasus footwear (Nike, Beaverton, OR). Reflective markers were then placed on their dominant leg side.

Participants were asked to run across a 30m runway imbedded with a force plate (Advanced Mechanical Technology Inc., Watertown, MA) at 3.7 m/s (± 5%). Qualisys Track Manager (Qualysis Medical AB, Gothenburg, Sweden) was used to capture motion (200Hz) and ground reaction force (1000Hz) data. Once 10 successful trials had been completed, the participant completed a variation of the Astrand-Rhyming cycle ergometer test. Participants started the test at 2 Kps and were asked to maintain a pace of 50-55 rpm. Every one minute the resistance of the bike increased by 0.5Kps. Fatigue was reached once participants were unable to maintain the required pace (50rpm) for 30 seconds. Immediately upon completion of the fatigue test, participants ran 10 more trials across the lab, of which the first three were analyzed.

All variables of interest were analyzed in a customized Labview (National Instruments, Austin, TX) program. VIP, VILR, VALR, and LS were compared pre and post-fatigue. Descriptive comparisons using percent difference and effect size (Cohen's *d*) were used to describe differences due to the small sample size.

RESULTS AND DISCUSSION

The data shows that participants had minimal differences between pre and post fatigue in their VIP and LS. The loading rate showed a meaningful drop of 9.55% for VILR and 11.8% for VALR. These loading rates also had the largest effect size indicating that they may be influenced by fatigue more than VIP and LS. A summary of the results are displayed in Table 1.

Table 1: Results from All Participants

	Pre Fatigue	Post Fatigue	% Diff	*d*
VIP	1.39(0.32)	1.37(0.10)	1.45%	0.08
VILR	72.9(22.8)	66.3(21.3)	9.55%	0.30
VALR	62.6(18.0)	55.6(19.4)	11.8%	0.37
LS	11.2(2.74)	10.7(2.56)	4.20%	0.17

Research has shown that foot strike patterns during running may influence loading variables [4]. We therefore decided to divide the runners into their strike pattern to determine if there were changes after fatigue that may be specific to the type of foot strike. The data was separated into midfoot strike runners (n=4) and heel strike runners (n=4). When examining the groups separately it appears that the midfoot strike runners had much greater loading than heel strike runners both before and after the fatiguing protocol. It appears that the midfoot strike runners also displayed greater reductions to in loading rates. A summary of this data is observed in Table 2.

Our hypothesis that an increase in leg stiffness would be observed was not supported by the data. The small drop in LS could be due to the fatigued runner having less control of the knee and a change in the knee flexion and extension during the running motion. The observed decrease in loading rates also may suggest that runners may have made changes to their joint kinematics. However, further investigation into the kinematic data is needed to provide greater insight into the small changes. The effects of being fatigued on a bicycle indicate that runners are reducing vertical loading and LS during early stance, but caution must be taken in the interpretation of these data due to the small sample size and the lack statistical comparisons.

CONCLUSIONS

A fatiguing protocol using a cycle ergometer appears to display small to no decrease in vertical loading during early stance. The small changes to VILR and VALR as a runner fatigues may indicate a reduction in injury risk from overuse running injuries. Responses to fatigue may depend on the foot strike pattern of the runner. However, larger sample sizes are needed in order to determine if this is the case.

REFERENCES

1. Van Gent, R.N. et al. *Br . Sports Med* 41, 469-480 2007.
2. Zadpoor, A. *J. Engineering in Medicine*. 226, 579-588, 2012.
3. Butler, RJ, et al., *Clin Biomech* 18, 511-517, 2003
4. Liberman, D.E. et al. *Nature* 463, 531-536, 2010

Table 2: A comparison of Midfoot and Heel Strike runners

	Midfoot Stike Runners (n=4)				**Heel Strike Runners (n=4)**			
	Pre Fatigue	Post Fatigue	% Diff	*d*	Pre Fatigue	Post Fatigue	% Diff	*d*
VIP	1.41(0.43)	1.37(0.33)	2.89%	0.01	1.37(0.23)	1.37(0.34)	0.00%	0.47
VILR	81.4(26.3)	71.9(25.7)	12.3%	0.33	64.5(16.7)	60.7(17.8)	6.18%	0.24
VALR	70.8(22.4)	61.8(26.4)	13.5%	0.39	54.4(8.64)	49.4(8.89)	9.59%	0.41
LS	13.2(1.29)	12.7(0.91)	4.03%	0.57	9.18(2.30)	8.77(2.12)	10.2%	0.20

LATERAL MOMENTUM GENERATION IN AN UNEXPECTED QUICK FIRST STEP

Christopher D. Ramos[1] and Jill L. McNitt-Gray[1,2]
[1]Department of Biomedical Engineering, [2]Biological Sciences, USC, Los Angeles, CA
email: rchristo@usc.edu

INTRODUCTION

A quick first step is advantageous in many sports. Defenders often need to read and react to an unexpected action of the opponent, and then quickly configure their body so that they can generate impulse in a desired direction. In the case of a quick first step, the mechanical objective is to quickly increase the horizontal velocity of the mass center (CM) so that their whole body quickly moves from an initial stationary position to the desired target (e.g. ideal body position to play a ball). Initiating a quick 'first step' out of the initial 'ready' position involves configuration of the extremities and trunk such that the center of pressure of the lead leg is behind the CM prior to push and initiation of joint extension [3,4,5,6].

In this study, we hypothesized that individuals who placed their lead foot under their CM would generate more impulse in a shorter amount of time compared to individuals who placed their lead leg more anterior to the CM. We tested this hypothesis by comparing the normalized impulse, force contact times, and peak to peak time between the lag and lead legs for both right and left directions.

METHODS

Collegiate-level female volleyball players (n=9) volunteered to participate in this study in accordance with the institutional review board. Participants initiated a quick first step to either the right or left in reaction to a launched ball. The ball was launched in an unexpected direction and participants were asked move in the direction of the ball as fast as possible. Sagittal and Coronal kinematics were recorded with a high speed camera (Casio, 300 Hz). Reaction forces were recorded using dual force plates (Kistler, 1200 Hz).

Shank and thigh angle relative to horizontal, stance width, and step length were calculated from coordinate data at first step with the lead leg. Duration of foot contact during impulse generation was determined for the lag and lead legs, as well as peak to peak (P2P) time between lag and lead leg force. Net horizontal impulse was then calculated for lag and lead legs by integrating force and normalized by mass to determine contribution of each leg. Participants' time to reach a cone 3.3 m away was recorded.

RESULTS AND DISCUSSION

Participants initiated lateral movement with one of three lead leg foot positions. During the first step, three participants (Group A) initiated contact with their lead leg foot under or posterior to the CM (ankle positioned posterior to hip, Fig 1A). Three participants (Group B) placed their lead foot in front of their CM, with the ankle posterior to the knee and anterior to the hip. Three other participants (Group C) placed their lead foot in front of their CM with the ankle anterior or under the knee.

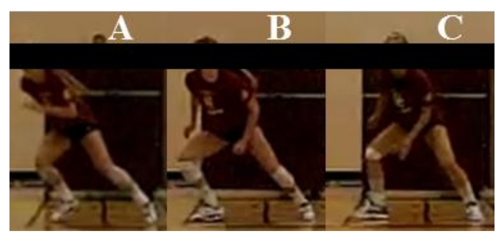

Figure 1. Example lead leg foot position at first step moving to the right for all three groups: exemplar participants with foot under CM (A), foot in front of CM and behind the knee (B), and foot in front of CM and under the knee (C).

Step length increased, shank angle increased and thigh angle decreased at initial contact as participants initiated contact with their feet more anterior to their CM (Table 1).

Duration between lag and lead leg peak push (P2P), lag foot contact time, and lead foot contact time increased when initiating foot contact more anterior to the CM. No significant change in horizontal velocity of the CM during foot contact (i.e. normalized impulse generation) was observed across groups (Fig 2, 3). This suggests that subjects who placed their foot closer under their CM were able to push faster to generate the same change in horizontal velocity of the CM.

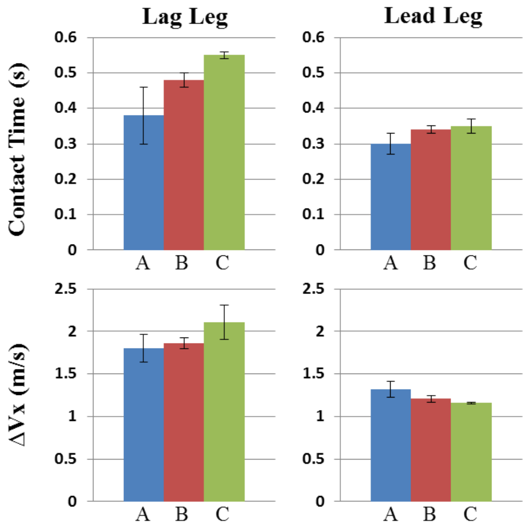

Figure 2. Mean lag and lead leg contact times and CM velocity changes for each group. Contact time increases from Group A (foot posterior to CM) to B to C (foot anterior to CM).

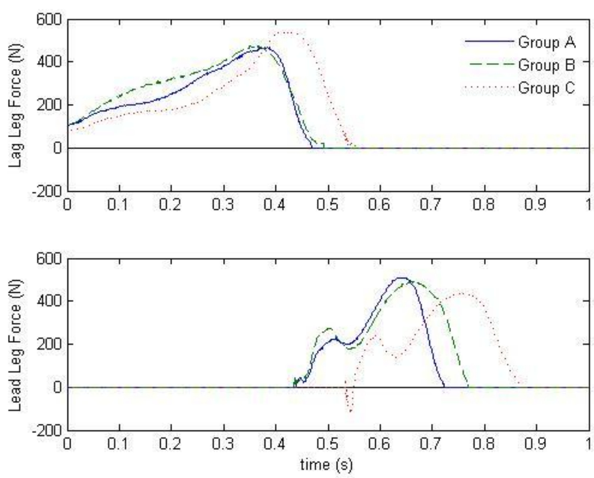

Figure 3. Representative lag and lead leg force-time curves synchronized at time of first reaction to ball launch for all 3 groups.

In addition, overall performance time (time from first reaction to a 3.3 m cone on either side of the player) decreased as participants initiated contact with their foot position more posterior to their CM (Table 1). These performance based results further support the idea that players initiating foot contact more underneath the body are able to initiate the push sooner and to generate comparable horizontal impulse in less time.

CONCLUSIONS

Results from this study indicate that individuals who placed their lead foot under their CM generate horizontal impulse in a shorter amount of time compared to individuals who placed their lead leg more anterior to the CM. Placing the foot underneath or posterior to CM puts the player in a position to initiate knee/hip joint extension sooner than when placing the foot anterior to the CM. Placing the foot more anterior to the CM introduces a delay in push (increase in P2P duration) because the player must wait for the CM to move anterior to the foot before initiating lead leg joint extension. Reducing the delay in push by initially placing the foot more posterior relative to the CM reduces movement time and improves performance at the whole body level.

REFERENCES

1.Mathiyakom W, et al. *J Appl Biomech* **23**, 149-161, 2007.
2.McNitt-Gray JL, et al. *J Biomech* **34**, 1471-1482, 2001.
3.Mathiyakom W, et al. *J Biomech* **39**, 990-1000, 2006.
4.Mathiyakom W, et al. *Exp Brain Res* **169**, 377-388 , 2006.

ACKNOWLEDGEMENTS

This work was supported by the USC Biomechanics Research Laboratory.

Table 1: Step length, shank and thigh angle, peak to peak time, and 3.3m time for A, B, and C to the Right

Group	Step Length (cm)	Shank Angle (deg)	Thigh Angle (deg)	P2P (s)	Time (s)
A	0 ± 2	44 ± 4	68 ± 4	0.26 ± 0.01	1.04 ± 0.04
B	8 ± 9	55 ± 8	45 ± 4	0.29 ± 0.01	1.09 ± 0.05
C	29 ± 13	63 ± 6	44 ± 6	0.44 ± 0.10	1.23 ± 0.10

GENERAL POSTER SESSION II – Thursday, 2:30-4:00
Grand Ballroom

ERGONOMICS			
2	Discrete Wavelet Transforms Can Detect Shoulder Muscle Fatigue During Light-duty Assembly Tasks **Xu X, Qin J, Lin JH**	5	Relative Rotations Of Pelvis And Ribcage In Seated And Standing Postures **Buschman J, Leitkam S, Bush TR**
8	Evaluation Of Grip Pressure And Hand-arm Vibration In Jack-hammering Task With And Without Lift Assist **Johnson B, Dix P, Campbell-Kyureghyan N**	11	The Effects Of Shoulder Abduction Angle And Wrist Angle On Upper Extremity Muscle Activity In Unilateral Right-handed Push/pull Tasks **Cudlip A, Allen T, Holmes M, Callaghan J, Dickerson C**
14	An Investigation Of Hand Force Distribution, Hand Posture And Surface Orientation **Figueroa R, Armstrong T**	17	Measurement And Analysis On The Posterior Intervertebral Gaps Based On X-ray Images Of Korean Lumbar System **Bae T, Park H, Yang J, Chun K, Ko C**
20	Trunk Inertial Estimates Of A Pregnant Female **Wicke J, Calleros A, DiMartino V**	23	Using A Stability Ball As A Task Chair: Spine Angles During Lateral Reaching **Karakolis T, Holmes M, Callaghan J**
26	The Influence Of Neck Posture And Canadian Forces Helicopter Helmet Configuration On Neck Muscular Demands **McKinnon C, Laing A, Dickerson C, Callaghan J**		

GAIT			
29	Stride Length At Controlled Walking Speeds Is Not Related To Redistribution Of Lower Extremity Joint Powers **Buddhadev H, Martin P**	32	The Relationship Between A Progressive Versus Single-stage Treadmill Test For Evaluation Of Claudication **Wurdeman S, Pipinos I, Johanning J, Myers S**
35	Does Slower Walking Speed In Older Adults Protect Against Distractions? **Kang HG, Thap D**	38	An Automated Iterative Method For Adjusting Virtual Model Markers In An Opensim Model **Mahboobin A**
41	Using Forward Simulations To Predict Saggital Kinematics During Fastfes **Ramsay J, Buchanan T, Higginson J**	44	Effects Of Electromyogram Signal Filtering On Muscle Activation Time **Soangra R, Lockhart T, Zhang J**
47	Comparison Of Methods To Determine Rotation Onset Of Upper Body Segments When Walking And Turning **Ambati VNP, Murray NG, Powell D, Reed-Jones R**	50	Body Orientation Affects The Distal Upper Extremity Impact Response Following Simulated Forward Falls **Burkhart T, Brydges E, Stefanczyk J, Andrews D**

53	Center Of Pressure Trajectory During Gait: A Comparison Of Four Foot Postures **Lugade V, Kaufman K**	56	The Effects Of Experimental Knee Pain On Co-contraction And Spatiotemporal Characteristics During A 30-min Run **Denning WM, Woodland S, Hunter I, Hopkins JT, Seeley M**
59	Association Between Peak Forefoot Plantar Shear Stresses And Physical Body Measures **Yavuz M, Delvadia N, Atves J, Goldfarb J, Stuto J, Rao N, Glaros A**	62	Analysis Of Foot Clearances In Firefighters During Ascent And Descent Of Stairs **Kesler R, Horn G, Hsiao-Wecksler E**
65	Sex Difference In Kinematic And Kinetic Patterns Of Treadmill Walking In Preadolescent Children **Wu J, Ajisafe T**	68	Do Increased Muscle Forces Lead To Increased Contributions To Support And Progression During Gait? **Schloemer S, Thompson J, Schmitt L, Best T, Siston R**
71	Assessing Gait Changes In Firefighters Due To Fatigue And Asymmetric Load Carriage **Sy J, Horn G, Kesler R, Petrucci M, Park K, Hsiao-Wecksler E**	74	Kinematic Analysis Of Foot Clearance During Stair Ambulation In Older Adult Unilateral Transfemoral Amputees **Luther A, Chambers A, Cham R**
77	New Adult Male Post Mortem Human Subject Segmental Weight, Centers Of Gravity, And Principal Moments Of Inertia **O'Donovan M, Hasselquist L, Albery C, Corner S, Corner B**	80	Prediction Of Load Accommodation Strategies During Walking From Lower Extremity Kinematic Variables **Atkins L, Dufek J, Bates B, James CR**
83	The Effect Of Trunk Flexion On Lower Limb Kinetics Of Able-bodied Gait **Major M, Kluger D, Fatone S, Gard S**	86	Gluteus Maximus And Soleus Compensate For Simulated Quadriceps Atrophy And Activation Failure Over A Range Of Walking Speeds **Thompson J, Chaudhari A, Schmitt L, Best T, Siston R**
89	The Influence Of Knee Bracing On Patellar Kinematics During Human Walking **Lee JY, Bailey S, Hardin E**	92	The Effect Of Split-belt Treadmill Speed Configurations On Interlimb Coordination And Gait Cycle Patterns **Hoover B, Roemmich R, Roper J, Hass C**
95	Sample Entropy Outperfoms Approximate Entropy With Small Data Sets **Yentes J, Hunt N, Schmid K, Kaipust J, McGrath D, Stergiou N**	98	Development Of A Geometric Model To Determine Inertial Parameters In Amputees **Siviy C, Luther A, Chambers A, Cham R**
101	Economization Of Stride Length In Level And Uphill Running **Hunter I, Robinson E**	104	Cardan Sequences On 1-mtp Joint Kinematics: Implications For Foot Bunion **Glasoe W, Pena F, Phadke V, Ludewig P**
107	Development And Evaluation Of A New Moving System Incorporated With Specific Function For Gait Rehabilitative Training Assistance **Lee B, Song L, Jung H, Jeon K, Jang K, Lim D**	110	Individual Limb Mechanical Analysis Of Gait Following Stroke **Mahon C, Farris D, Sawicki G, Lewek M**

113	Clinical Correlates And Effects Of Deep Brain Stimulation On Gait Variability In Essential Tremor **Roemmich R, Okun M, Zeilman P, McFarland N, Hass C**	116	Inter-joint Coordination For Individuals With Anterior Cruciate Ligament Reconstruction During Stair Ascent **Wang J, Hall M, Gillette J**
119	Persistent Deviations In Hip Dynamics During Gait In Women After Triple Innominate Osteotomy **Kolk S, Fluit R, Verdonschot N, Weerdesteyn V**	122	Femoral Neck Stresses During Stair Navigation **Deng C, Gillette J, Derrick T**
125	Evaluating Runners With And Without Anterior Knee Pain Using The Time To Contact The Ankle Joint Complex Range Of Motion Boundary **Rodrigues P, TenBroek T, van Emmerik R, Hamill J**	128	The Effect Of A New Microprocessor Controlled Prosthetic Knee On Obstacle Crossing In Patients With Unilateral Transfemoral Amputation **Aldridge Whitehead J, Wilken J**
131	Older Acl Non-copers Demonstrate Larger External Knee Adduction Moments One Year After ACLR **Wellsandt E, White K, Snyder-Mackler L**		

MOTOR CONTROL			
134	Controlling Redundancy In Wrist And Forarm Rotations **Peaden A, Dorman G, Charles S**	137	Short Term Learning And Sex Differences During Repeated Steadiness Tasks **Tracy B, Boesel E, Amin A**
140	The Role Of Variability In The Local Dynamic Stability Of Continuous Reach-and-point Movements **Heller D, Gregory R**	143	Torque Variability And EMG Activation Differs Between Adults With And Without Multiple Sclerosis At The Ankle **Davies BL, Arpin DJ, Kurz MJ**
146	Excitability Of The Middle Deltoid At Different Elevation Angles **Lin YL, Christie A, Karduna A**	149	Obesity-related Difference In Lower Extremity Strength Among Young Females: Preliminary Findings **Koushyar H, Matrangola S, Nussbaum M, Madigan M**

ORTHOPEDIC MECHANICS			
151	Treadmill Bone Loading During Spaceflight **Scott-Pandorf M, Buxton R, Ploutz-Snyder L, Peters B**	154	Relationships Between The Mechanical Quality Of Cortical Bone And FGF23 Levels In Mice Challenged By Fructose And Calcium Modified Diets **Williams E, Bajaj D, Douard V, Sabbagh Y, Ferraris R, Fritton JC**
157	Comparing Periosteal Morphology Between Cervine And Human Tibiae **Throop A, Landauer A, Clark A, Kuxhaus L**	160	Compression Force Substantially Increases The Tibiofemoral Joint Passive Stiffness And Moment In Sagittal And Frontal Planes **Marouane H, Shirazi-Adl A, Adouni M**

163	Secondary Kinematic Patterns Of Osteoarthritic Knees During Active Extension And Flexion **Freisinger G, Lewis J, Beal M, Pan X, Schmitt L, Siston R, Chaudhari A**	166	Estimation Of Individual Muscle Forces During Squatting And Lunging And Their Load Effect On The Tibial Plateau **Hale R, deBock M, Gonzalez R**
169	Leg Stiffness From Doubly Integrated Ground Reaction Forces Depend On The Integration Constant **Hébert-Losier K, Eriksson A**	172	Hip External Rotation Strength Impacts Lower Extremity Mechanics During Unanticipated Landing Activities In Collegiate Female Soccer Players. **Geiser C, Wood C, Meinerz C, Watson K, Kipp K**
175	Fatigue Effects On Intersegmental Accelerations During High-impact Landings: Piloting Performance Predictors **Davidson S, Cain S, Goulet G, Perkins N, McLean S**	178	Prolonged Pronation In Runners With Achilles Tendinopathy **Becker J, Osternig L, James S, Wayner R, Chou LS**
181	Changes In Passive Muscle Tension And Sarcomere Length Following Stroke **Tsai LC, Liu S, Wu YN, Liu C, Ren Y, Zhang LQ**	184	Association Between Iliotibial Band Syndrome Status And Running Biomechanics In Women **Foch E, Reinbolt J, Zhang S, Milner C**
187	Spine Motion During Activities Of Daily Living In Young Adults **Breloff S, Chou LS**	190	A Description Of Lumbar Intervertebral Configuration Using Principal Component-based Manifolds **Simons C, Cobb L, Davidson B**
193	A Refined Technique To Calculate Joint Motion Helical Axes From Six-dof Tracker Output **McLachlin S, Ferreira L, Dunning C**	196	Stress Distribution Formulation In A Linear Viscoelastic Bio-material **Peng Y, Zhou D**
199	Effects Of Distal Biceps Rupture On Supination Strength **Brown B, Schmidt C, Miller MC**	202	Age-related Changes To Shoulder Musculature In A Vervet Monkey Model **Santago A, Plate J, Smith T, Saul K**
205	Scaling And Architectural Similarity Of Common Models Of The Human Rotator Cuff **Mathewson M, Kwan A, Eng C, Lieber R, Ward S**	208	Three-dimensional Comparison Of Static And Dynamic Scapular Motion Tracking Techniques **MacLean K, Chopp J, Grewal TJ, Picco B, Dickerson C**

OTHER			
211	Experimental Design Influence On Detection Of Performance Differences **Bates B, James CR, Dufek J**	214	Analysis Of Hemodynamics In Abdominal Aortic Aneurysm (AAA) With Fenestrated Stent Graft **Kandail H, Hamady M, Xu XY**
217	Relationships Among Mechanical And Neuromuscular Control Variables In Healthy Individuals During Landing **Haddas R, Sawyer S, Sizer P, Brooks T, Chyu M, James CR**	220	A Flexible Orthopaedic Trauma Surgery Box Skills Trainer **Thomas G, Anderson D, Karam M, Johns B, Murillo SR, Marsh JL**

POSTURE & BALANCE			
222	Perception Of Complex Movement In Typically Developing Children And Children With Autism Spectrum Disorder **Haworth J, Kyvelidou A, Fisher W, Stergiou N**	225	Effect Of Forward Perturbation On The Trunk Neuromuscular Behavior **Shahvarpour A, Shirazi-Adl A, Larivière C, Mecheri H**
228	Postural Stability During Tandem Stance **Stevermer C, Gillette J**	231	An Attention Diverting Task Negatively Affects Recovery Step Kinematics And Fall Incidence **Hoops ML, Rosenblatt NJ, Grabiner MD**
234	Modeling The Lean Release And Surface Translation Perturbations With An Inverted Pendulum On A Cart **Thiaux V, Robinovitch SN, Smeesters C**	237	Single-leg Dynamic Stability In Fit, Young Adults: Lower Extremity Strength And Core Strength As Predictors **Heise G, Esselman E, Silvernale C, Smith J**
240	Differences In Center Of Pressure Regularity In Stable- And Unstable-surface Athletes **Powell D, Blaise Williams DS**	243	Measurement Of Human/bicycle Balancing Dynamics And Rider Skill **Cain S, Ashton-Miller J, Perkins N**
246	Effects Of Age And Obesity On Risk Of Slipping During Level Walking **Matrangola S, Rossi C, Nussbaum M, Madigan M**	249	The Test-retest Reliability Of Compensatory Stepping Thresholds Of Young Adults **Crenshaw J, Kaufman K**
252	Dynamic Lumbar Pursuit Task With Occupational Whole-body Vibration Exposure **Craig T, Wilson S**	255	Comparison Between Polynomial And Logistic Equations For Modeling Three Dimensional Strength Surfaces **Looft J, Frey-Law L**

REHABILITATION			
259	Optimization Of Porous Nitinol Geometry For Use In Bone Implants **Davis S, Elahinia M**	262	Investigation Of The Upper Cervical Spine Biomechanics Under Various Loading Type **Mesfar W, Moglo K**
265	Computerized Mallet Classification For Brachial Plexus Palsy **Ewert C, Crocher V, Seo NJ**	268	Rate Of Torque Development Deficits Following Total Knee Arthroplasty **Winters J, Christiansen C, Stevens-Lapsley J**
271	Muscle Architectural Changes Of The Post-stroke Tibialis Anterior **Wessel M, Ramsay J, Suydam S, Buchanan T, Higginson J**	274	Simple System For Isometric Muscle Strength Measurement And Biofeedback In An MRI Scanner **Wrigley T, Shanahan C**
277	Between Session Reliablity Of Quadricpes Percent Voluntary Activation And Force Measures In Healthy Participants **Grindstaff T, Katsavelis D, Morton S, Threlkeld AJ**	280	Similarities And Differences In Knee Mechanics Between Single Leg Squat And Single Leg Jump **Donohue M, Ellis S, Heinbaugh E, Zhu Q, Dai B**

283	Effects On Lumbar Loading Of Adding Upper Body Resistance To A Squat Exercise **Doran E, Pavol M**	286	Estimating Knee Adduction Moment In Real-time On An Elliptical Trainer **Kang SH, Lee SJ, Ren Y, Zhang LQ**
289	Stroke Induced Sensory Deficit Decreases Phalanx Force Control During Power Grip **Enders L, Seo NJ**	292	Somatosensory Cortex Activity In Response To Fingertip Stimulation Can Increase With Remote Subthreshold Vibrotactile Noise: An EEG Study **Hur P, Tseng YL, Seo NJ**
295	Comparison Of Load Reduction Abilities Of Camwalker And Corset-style Ankle Foot Orthoses **Wanamaker A, Davidson B, Christiansen C, Saint-Phard D**	298	In-bed Passive And Active Movement Rehabilitation Of Patients With Traumatic Brain Injury **Chen K, Liu L, Wang L, Ren Y, Gaebler D, Sisung C, Zhang LQ**
301	A Familiarization Protocol For Wheelchair Propulsion **Longworth J, Troy K**	304	A Principal Component Analysis Of Kinematic Variability During Wheelchair Propulsion **Jayaraman C, Rice IM, Moon Y, Hsu IMK, Hsiao Wecksler ET, Beck C, Sosnoff JJ**

SPORTS			
308	Proposal For A New Methodology For Tracking Arch Motion During Athletic Tasks **Hartigan EH, Zifchock R, Lawrence M, Tu C**	311	A Comparison Of Electromyography From Four Loading Configurations **Jagodinsky A, Fox J, Rehm J, Romer B, Patel J, Weimar W**
314	Gender Differences In Frontal Plane Lower Extremity Kinetic Variability During Landing **Nordin AD, Dufek JS**	317	Associations Between Clinical Dorsiflexion Flexibility And Landing Mechanics During A Drop Jump **Malloy P, Geiser C, Wood C, Meinerz C, Watson K, Kipp K**
320	Linear Prediction Of Kinematic And Kinetic Performance With Individual Anatomic Factors **Bates N, Myer G, Hewett T**	323	Effect Of Fatigue On High School Male And Female Pitchers **Gibbons M, Kraszewski A, Hafer J, Bido J, Graziano J, Levinson M, Backus S, Hillstrom H, Fealy S, Kontaxis A**
326	Peak Vertical Ground Reaction Forces Are Different During Stretch Vs. Wind-up Pitching In Collegiate Baseball Players **Rider P, Beaman B, McKinney T, DeVita P, Williams B**	329	The Effects Of Throwing Technique On Performance For Six Elite Javelin Throwers **Leigh S, Dapena J, Gross M, Li L, Myers J, Yu B**
332	A Comparison Of Two Different Sprint Start Techniques In Collegiate Linebackers **Lund R, Cusick J, Ficklin T**	335	Instantaneous Power Measurement In Wheelchair Racing **Pelland-Leblanc JP, Martel F, Langelier E, Smeesters C, Berrigan F, Laroche J, Rancourt D**
338	Dynamic Ankle Stiffness And Ankle Work In High- Compared To Low-arched Athletes During Barefoot Running **Powell D, Blaise Williams DS**	341	Can Cadence Manipulation Simulate The Joint Loading Benefits Of Barefoot Running? **Bido J, Hafer J, Plack LA, Metzl J**

344	A Triangulated Approach To Understanding Sports Surface Preferences **Tsui F, Forrester S**	

DISCRETE WAVELET TRANSFORMS CAN DETECT SHOULDER MUSCLE FATIGUE DURING LIGHT-DUTY ASSEMBLY TASKS

[1]Xu Xu, [2]Jin Qin and [1]Jia-Hua Lin

[1]Liberty Mutual Research Institute for Safety, Hopkinton MA, USA
[2]University of Massachusetts, Lowell MA, USA

email: xu.xu@libertymutual.com

INTRODUCTION

Shoulder musculoskeletal disorders are among the most prevalent work-related musculoskeletal disorders and constitute an important health problem. One of the occupations that are most affected is workers on assembly lines (Leclerc et al., 2004), as these jobs requires repetitive movement, which, as a risk factor, has been found positively associated with shoulder disorders. Repetitive movement is likely to result in muscle fatigue, and many hypothesize that shoulder muscle fatigue is a precursor of shoulder complaints (Takala, 2002). Short time Fourier transforms (STFT) is commonly used to analyze the changes in the frequency domain of surface electromyography (EMG) during muscle fatigue. Muscle fatigue can be demonstrated by a decreased median power frequency. However, STFT is only suitable for analyzing the signals with the same scale. During dynamic movement, the scale of EMG signals is changing so that using STFT to analyze EMG data could produce inaccurate results. Recently, discrete wavelet transform (DWT) has been adopted to analyze the EMG signals for dynamic conditions. The purpose of this study is to investigate whether DWT can be used for detecting shoulder muscle fatigue during light-duty assembly tasks.

METHODS

Twenty female participants (mean age = 43.5, S.D. 14.1) with no upper extremity musculoskeletal disorders participated in the study. A simulated workstation of a low intensity assembly task with repetitive motion was built in the laboratory. A wooden board with dowels was placed on the table. The dowels were coded in five different colors. Five bins containing the same color-coded washers were placed on the table as well (Figure 1). During the experiment, the participants were asks to pick a color-coded washer from a bin in turn and place it over a matching-color dowel using the pace of the metronome. The metronome was set to 2 seconds per beat, which was found to be long enough for completing an entire assembly cycle based on pilot tests. Each participant performed eight 10-minute trials, taking a one-minute break between trials.

Table 1: DWT decomposition of the surface EMG signal and the corresponding frequency

DWT decomposition	
CD1	256-512 Hz
CD2	128-256 Hz
CD3	64-128 Hz
CD4	32-64 Hz
CD5	16-32 Hz
CD6	8-16 Hz
CD7	4-8 Hz

Figure 1: Experiment setup

The surface EMG of the right upper trapezius and middle deltoid muscles were collected during the experiment at 1024 Hz (Ag-AgCl, Noraxon USA, Inc., Scottsdale, AZ). The EMG data of the 8th

minute of each session were extracted for performing DWT analysis with Bior1.3 being used as the orthogonal wavelet. Previous studies showed that the power of 5-30 Hz frequency band increases with the development of muscle fatigue. Therefore, the power of CD5 (16-32 Hz) and CD6 (8-16 Hz) (detail coefficients of level 5 and 6, see table 1) was calculated as an indicator of muscle fatigue.

RESULTS AND DISCUSSION

The results showed that from the beginning to the end of the assembly task, the power of CD5 and CD6 of the EMG signal of the upper trapezius and the infraspinatus gradually increased over the course (Figure 2). All the slopes of the regression lines are positive, which indicate a positive correlation between time and the power of the low frequency band of the EMG signals. Statistically, the slopes of the regression lines were significantly different than zero except for the CD6 of the infraspinatus. Such changes of power associated with the development of muscle fatigue in the lower frequency band are consistent with previous study on back muscles (Sparto, Parnianpour, Barria, & Jagadeesh, 2000).

The findings supported that discrete wavelet transform can be used to describe spectral changes of EMG signal induced by the development of the muscle fatigue during a light-duty assembly task.

CONCLUSIONS

This study used DWT to analyze the shoulder muscle EMG signals collected during a light-duty assembly tasks. The results indicate that DWT can effectively detect the spectral changes of EMG signal due to the development of muscle fatigue during dynamic movements.

REFERENCES

1. Leclerc, A., Chastang, J. F., Niedhammer, I., Landre, M. F., Roquelaure, Y., & Study Group on Repetitive, W. (2004). Incidence of shoulder pain in repetitive work. Occupational and Environmental Medicine, 61(1), 39-44.
2. Sparto, P. J., Parnianpour, M., Barria, E. A., & Jagadeesh, J. M. (2000). Wavelet and short-time Fourier transform analysis of electromyography for detection of back muscle fatigue. Ieee Transactions on Rehabilitation Engineering, 8(3), 433-436. doi: 10.1109/86.867887
3. Takala, E. P. (2002). Static muscular load, an increasing hazard in modern information technology. Scandinavian Journal of Work Environment & Health, 28(4), 211-213.

ACKNOWLEDGEMENTS

The authors are grateful to Raymond McGorry for many useful comments and suggestions, and Jacob Banks, Niall O'Brien, and Amanda Rivard for assistance in data collection.

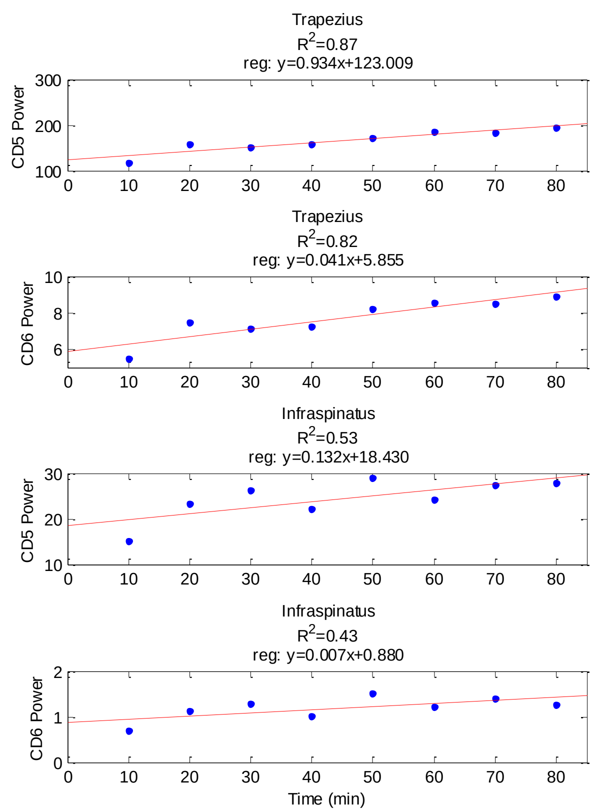

Figure 2: Linear regression between the time and the power of CD6 and CD7 obtained from Bior 1.3 discrete wavelet transform for the EMG signals of upper trapezius and infraspinatus.

RELATIVE ROTATIONS OF PELVIS AND RIBCAGE IN SEATED AND STANDING POSTURES

Jessica Buschman, Sam Leitkam, Tamara Reid Bush, PhD
Michigan State University Department of Mechanical Engineering
email: buschma5@msu.edu, leitkams@msu.edu, reidtama@msu.edu

INTRODUCTION

Digital human modeling is known for its ability to help improve the speed, value, and efficiency of creating products that involve human interaction. Digital human models are used in many sectors of industry from occupant positioning and seating design to assembly line movements of workers, but developing accurate human models is challenging. These challenges largely arise from the large variations in anatomy and movement [1]. For seating in particular, understanding how spinal articulation is achieved in the seated posture as compared to the standing posture has not been well defined. Spinal curvature is impacted by a large number of factors, but as Hubbard et. al. note there has not been ample research done on human spinal curvature regarding the relative rotations of the pelvis and ribcage [2]. The purpose of this research was to determine the relative influence of the ribcage and pelvis on spinal curvature in both seated and standing postures.

METHODS

The 19 subjects in this study were healthy individuals with no back pain. The subject pool consisted of eight males (average age 24.1 years, SD 2.2, range 22-27) and 11 females (average age 23.6 years, SD 1.4, range 22-26). In order to obtain spinal curvature data for seated and standing postures, a Qualisys motion capture system was used to track markers located on the subjects at key anatomical locations. Motion capture markers were placed over the seventh cervical vertebra (C7), the midway point between the two projections of the posterior superior iliac spine (MidPSIS), the sternum, the two anterior superior iliac spine (ASIS) projections and the lateral epicondyles of the femurs. Four postures were recorded: arched, erect, comfort, and slouched. These postures represented maximum kyphosis, comfortable or slight kyphosis, erect or slight lordosis, and maximum lordosis, all while maintaining a forward gaze. These postures were recorded in both the seated and standing positions.

From these data, three vectors were calculated to obtain the desired angles. The first vector started at the midpoint of the two virtually computed hip-joint centers (HJCs) and passed through the midpoint of the two ASIS markers. The second vector started at the sternum marker and passed through the C7 marker. Three angles were computed from these vectors. The first angle, α, was a measure from the ribcage vector to a vertical reference vector (Figure 1). The second angle, β, was from the pelvis vector to the reference vector. The third angle, also known as the openness angle or θ, measured the change between the ribcage and pelvis vectors. This angle change was previously linked to the amount of spinal curvature change [3].

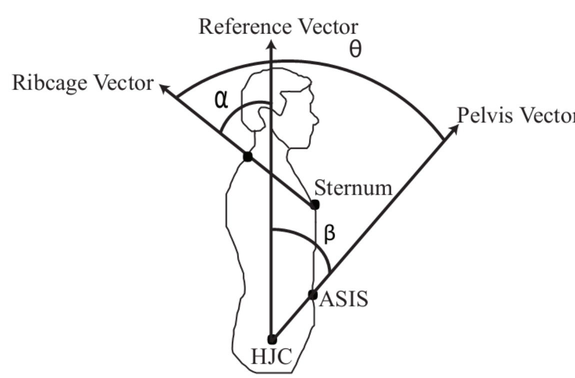

Figure 1: Vectors and angles used to identify the relative motion of the pelvis and ribcage: α is the angle between ribcage and a vertical reference vector, β is the angle between the pelvis and a vertical reference vector, and θ is the angle between pelvis and ribcage vectors

RESULTS AND DISCUSSION

To determine the relative influence of ribcage and pelvis on the openness angle, percentages of the motion of each were calculated for both sitting and standing spinal curvature. On average, the pelvis produced 27% of the total openness angle change while the ribcage produced 73% of the total openness angle change. This percent distribution was the same for both the seated and standing postures. Thus, regardless of standing and sitting, the ribcage rotates approximately 2.7 times more than the pelvis when moving between maximum lordosis and maximum kyphosis. Figures 2 and 3 show the relative ribcage and pelvis angles on an individual basis.

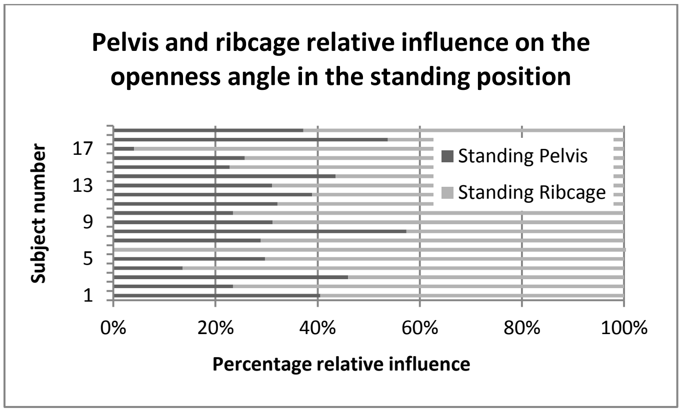

Figure 2: Stacked percentages comparing pelvis and ribcage relative influence on the openness angle in the standing position

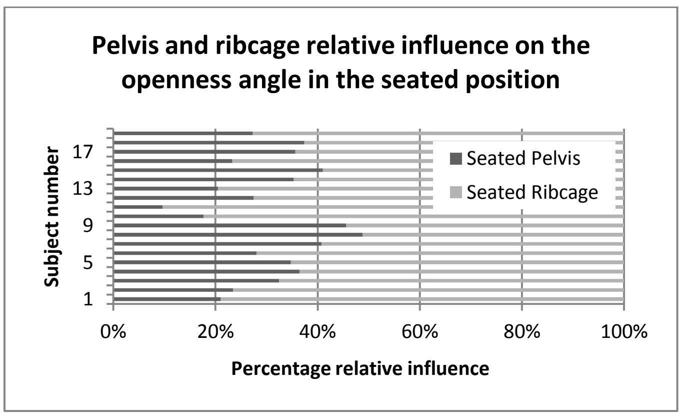

Figure 3: Stacked percentages comparing pelvis and ribcage relative influence on the openness angle in the seated position

The data collected in this study can also be compared on a macroscopic level in terms of the overall openness angle. Figure 4 compares the total openness angles of both seated and standing postures. The total openness angles of the two postures were similar, with the seated openness angle being slightly larger. In addition, the standard errors for the two measurements were 2.89 and 2.99 degrees for standing and seated, respectively.

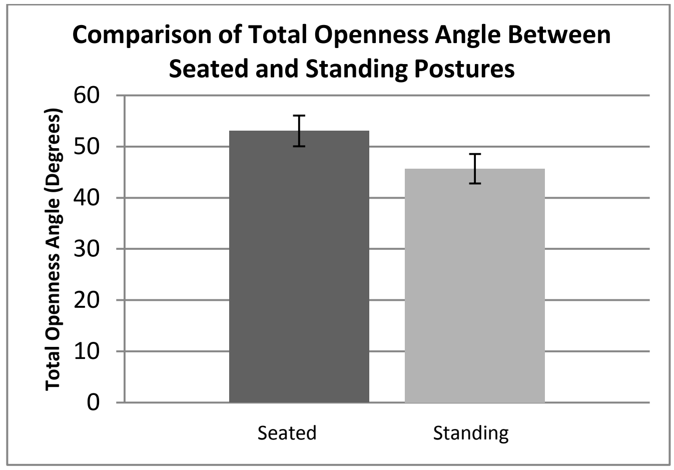

Figure 4: Comparison of the total openness angles between the seated and standing postures

Additionally, when these data were analyzed for differences in gender, no statistically significance differences were identified.

CONCLUSIONS

In summary, this research measured the relationship of pelvis and ribcage movement in the seated and standing positions. It was found that the relative influences between the pelvis and the ribcage on spinal curvature were 27% and 73%, respectively. However, the overall range of motion, as measured by the openness angle, was larger in the seated position than the standing position. These results can be used to support the development of digital human models that mimic the appropriate ratios of ribcage and pelvis motions, and total ranges of spinal articulation in seated and standing. These findings are useful regardless of anatomical diversity and gender; however future work to look at other populations such as the elderly and obese would also be beneficial.

REFERENCES

1. Chaffin (2001) Society of Automotive Engineers
2. Hubbard et. al. (1993) SAE Technical Paper Series
3. Leitkam et al. (2011) ASME

EVALUATION OF GRIP PRESSURE AND HAND-ARM VIBRATION IN JACK-HAMMERING TASK WITH AND WITHOUT LIFT ASSIST

Blake Johnson, BS, Patrick Dix, BS, and Naira Campbell-Kyureghyan, PhD

University of Wisconsin Milwaukee, Milwaukee, WI, USA
Email: john2742@uwm.edu

INTRODUCTION

There are many different tasks that expose construction workers to a variety of risks in their daily activities. One of the more common activities is the use of a jackhammer. Three of the various risk factors involved in using a jackhammer are overexertion, cumulative injury from repetitive lifting, and hand arm vibration (HAV). In the process of using a jackhammer, the operator must repeatedly lift the jackhammer onto the pavement. With the common weight of the jackhammer being 90lbs, this can lead to overexertion injuries.

Lift assist (LA) devices have been developed to be used as an add-on to an existing jackhammer. This device is designed to help lift the jackhammer from the pavement instead of manually lifting the jackhammer. LAs are intended to help reduce the overexertion and repetitive lifting risks associated with lifting the jackhammer. However, to date there have been no studies into whether and to what extent this device actually assists the operator in lifting the jackhammer. The goal of this study was to investigate if a LA device reduces the workload of the jack-hammering task and if the added weight will increase HAV. It is hypothesized that the LA device will reduce the amount of grip pressure needed to lift the jackhammer, and have no effect on HAV.

METHODS

Six healthy male subjects (ages 30-49 years) with between 7 and 20 years of experience as jackhammer operators were recruited to participate in the study. The average weight and height of the participants was 82kg and 167 cm. All subjects signed an inform consent that was approved by the IRB.

Each participant was asked to break up 6 inch thick reinforced concrete slabs, divided into 3ft x 3ft squares with a series of parallel diagonal lines across the sample area. The operators were told to follow the lines within each sample and to jackhammer in a way to mimic normal work day operation, no further instructions about operation were given. Subjects used a pneumatic jackhammer with and without LA.

Each trial was videotaped to record total task time and frequency of jackhammer lifting or LA operation. Any time spent on tasks that interfered with normal jackhammer operation was eliminated from total task time.

Grip pressure was measured using a Vista Medical FSA 24 sensor pressure glove placed on the operator's right hand, and collected at 5 Hz. A standard workman's glove was placed over the sensors. The amount of overall hand grip pressure was determined by summing all 24 sensors together at each time step.

The hand grip pressure data during lifting was analyzed using a custom MATLAB program. Grip pressure peaks were matched with video to assure that values during lifting were used. These values were normalized to the total weight of the device.

Hand grip pressure during operation was calculated by matching the data with video. The pressure during operation was averaged to obtain typical operating hand grip pressure. The pressure was also normalized to the total jackhammer weight.

Hand arm vibration (HAV) data was collected using a Biometrics W4X8 data collection system, and from a Nexgen S2-G10-MF accelerometer. Vibration data was processed using VATS software.

A paired t-test was conducted on the difference in hand grip pressure between a jackhammer with a LA from a jackhammer without a LA for both lifting and operating hand grip pressure. A paired t-test was also performed on HAV for operating a jackhammer with and without a LA. The confidence interval was set at 95%.

RESULTS AND DISCUSSION

The results showed that the LA helped to significantly reduce lifting grip pressure ($p < 0.05$). All but one of the subjects showed a decrease in lifting grip pressure (Figure 1) with an average of 30% (range 20-44%). One operator struggled with using the lift assist. The results suggest that the LA helps with the lifting portion that constitutes about 10% of the total jack hammering task. .

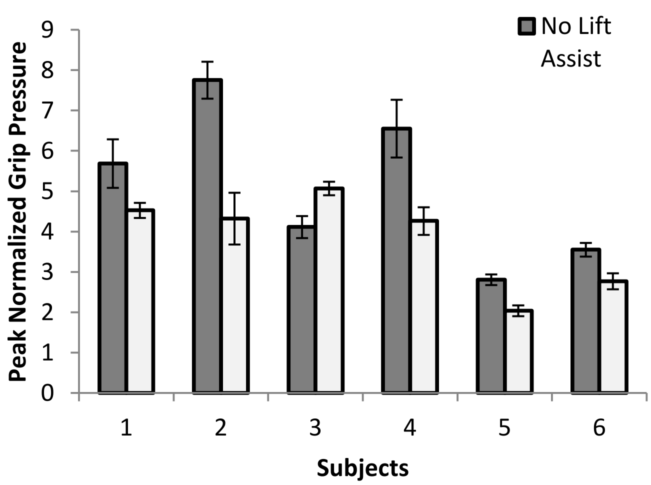

Figure 1: Peak grip pressure during lifting with and without a lift assist normalized jackhammer weight.

The National Institute for Occupational Safety and Health has suggested 51lbs as the maximum weight to be lifted in order to reduce overexertion and repetitive lifting injuries (1). The 90lb jackhammer is thus considered unsafe for lifting for all populations. The LA is intended to take the lifting portion out of jack-hammering and thus extend the ability to jackhammer to a more diverse group of people.

It has been established that hand arm vibration increases proportionally to the cube root of hand contact force (2) and that hand contact force is a function of grip and pushing forces (3). The LA added to the jackhammer did have a significant effect on contact force during operation ($p < 0.05$) with an average reduction of 12%. The decrease in grip pressure led to a HAV decrease of 11% on average, but the difference was not significant ($p=0.053$).

Four of the six operators had a decrease in total task time with the LA. The other two operators had trouble adjusting to the LA, and this could have caused the slower performance. This suggests the jack-hammering task can become faster by using the LA after experience is gained. A decrease in task time will reduce the overall workload of each individual jack-hammering task.

CONCLUSIONS

The LA did provide a reduction in grip pressure while lifting the jackhammer on the pavement and therefore helped with the lifting portion of the task. The LA also reduced grip pressure during operation. However, the reduction in grip pressure during operation did not lead to a significant decrease in HAV.

REFERENCES

1. Waters T, et. al. *Ergonomics*, **36**,7, 749-776, 1993.
2. Pyykkö I, et. al. *Scan. J. Work Environ and Health*, **2**, 87-95, 1976.
3. Welcome D, et. al. *J. of Ergonomics*, **34**, 507-518, 2004.

ACKNOWLEDGEMENTS

This study was supported by a grant from the Gas Technology Institute. The authors would also like to thank Alexa Hernandez Principe, John Bubaris and Nickolas Daniels for their assistance in data collection.

THE EFFECTS OF SHOULDER ABDUCTION ANGLE AND WRIST ANGLE ON UPPER EXTREMITY MUSCLE ACTIVITY IN UNILATERAL RIGHT-HANDED PUSH/PULL TASKS

[1]Alan C. Cudlip, [1]Tyler R. Allen, [1,2]Michael W. R. Holmes, [1]Jack P. Callaghan and [1]Clark R. Dickerson

[1]University of Waterloo, Waterloo, ON, Canada
[2]University of Ontario Institute of Technology, Oshawa, ON, Canada
email: cdickers@uwaterloo.ca

INTRODUCTION

High arm elevation and non-neutral wrist postures are independently associated with increased worker discomfort and muscle activity [1, 2]. Further, increased shoulder abduction angles increase activity of muscles surrounding the shoulder complex [3], which can accelerate muscular fatigue, especially in awkward postures [4]. However, potential interactions between these factors and their relative implications for strength and injury to the upper extremity remain unclear. This study intended to quantify upper extremity activity across a range of shoulder and wrist postures and describe how demands between these joints were modulated while performing pushes and pulls.

METHODS

20 participants (21.6 ± 1.5 yrs, 1.68 ± 0.12 m, 72.5 ± 16.5 kg) completed 72 seated right-handed isometric exertions in two force directions (push, pull) using combinations of shoulder angle (0, 45, 90, 120°), and wrist angle (flexion, neutral, extension). An absolute force of 30N was held for 7 seconds at each posture combination, with off-axis forces maintained below 5 N. All posture and force direction combinations were performed in a randomized order. Surface electromyography (EMG) was collected for 16 muscles (8 muscles surrounding the shoulder, 2 of the upper arm, and 6 of the forearm using a Noraxon Telemyo 2400 T G2), linear enveloped and normalized to muscle-specific maximal excitations (denoted as %MVE). Hand force was collected with an AMTI 6-DOF force transducer rigidly fixed to a MOTOMAN HP-50 robotic arm. Force was sampled synchronously with EMG at 1500 Hz using VICON Nexus 1.7.1 software. A 2-way repeated measures ANOVA (4 shoulder postures * 3 wrist postures) was completed to determine the effects of shoulder angle and wrist position on mean normalized muscle activity.

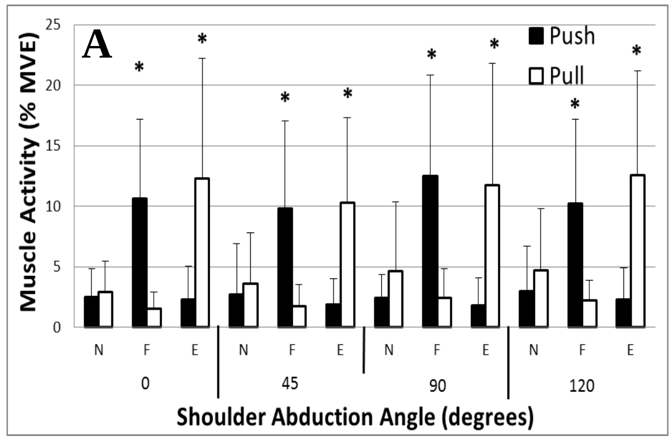

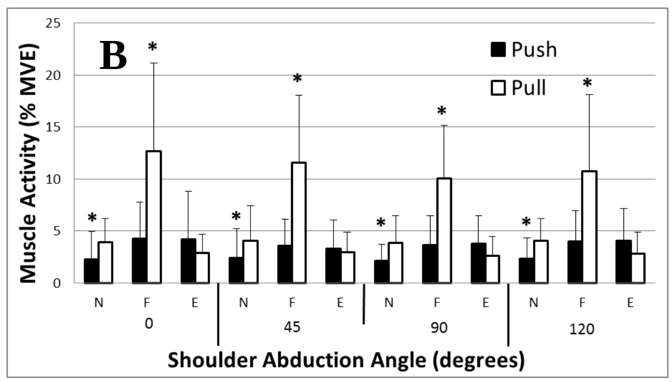

Figure 1. Normalized EMG of extensor carpi radialis (A) and flexor digitorum superficialis (B) during pushes and pulls across shoulder angles and wrist postures. Significant differences between wrist postures within directions are denoted by asterisks.

RESULTS AND DISCUSSION

Muscular activity changes were closely related to changes in local joint orientations and force direction, with the largest changes in activity outputs appearing in forearm musculature as wrist positions deviated from neutral postures. In push exertions, forearm extensor activity was greatest in flexed wrist postures, ranging from 11-20% MVE ($p<0.01$). During pulls, extensor activity was greatest in extended wrist postures, exceeding 25%

MVE in some cases (Figure 1A, p<0.01). Muscle activity for the forearm flexors was greatest in flexed wrist postures during pull exertions (Figure 1B, p<0.05). Increased shoulder abduction angle resulted in increased muscular activity of muscles surrounding the shoulder (Figure 2, p<0.01). Push exertions had variable effects on the anterior and posterior deltoid with increasing shoulder abduction angle, while middle deltoid increased with increasing abduction angle (p<0.0016).

Non-neutral wrist postures produced large increases in forearm activity for both force directions, with increases as much as 300% when compared to neutral positions in some instances. Activity levels for both forearm flexors and extensors exceeded recommended levels for intermittent forearm activity [5], even at low abduction angles. These activity levels were exacerbated as the wrist deviated from neutral in pull exertions for both forearm flexors and extensors, and for forearm extensors in pushing exertions (Figure 1). This suggests that the wrist may be prone to injury and strength limitations in these postures.

The large increases seen in shoulder musculature as abduction increased is likely due to moment arm changes and the increased difficulty to stabilize the glenohumeral joint during maintain body posture in these non-neutral positions [6]. Overall shoulder muscular activity increased by over 25 %MVE with increased shoulder abduction. Specific shoulder muscle activity levels varied markedly with force exertion direction. Exertions with increased humeral elevation relative to body position increase total muscle activity in both pushing and pulling exertions [7], and these elevated postures are a known risk factor in shoulder muscle fatigue, discomfort and shoulder pathology [8].

CONCLUSIONS

Overall joint demands switch with task conditions, with dependencies on local joint postures and force direction. Deviated wrist postures should be avoided as much as possible, as substantial changes in muscular activity occurred in these positions. Secondly, efforts should be focused to minimize shoulder abduction to decrease muscular activity and injury risk. There was limited evidence to suggest that shoulder posture influenced wrist activity levels or that wrist posture influenced shoulder muscle activity levels.

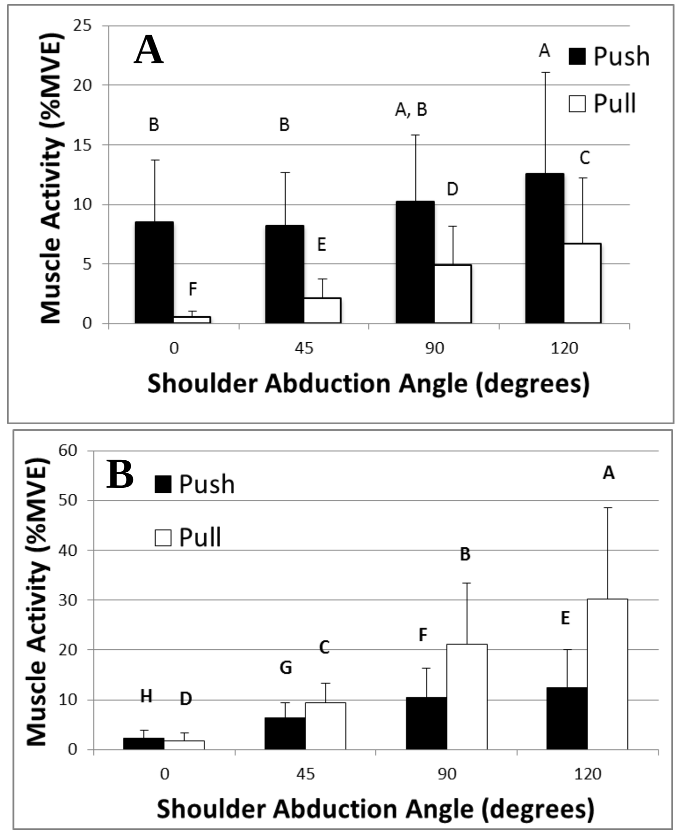

Figure 2. Normalized EMG of anterior deltoid (A) and middle deltoid (B) during pushes and pulls across shoulder angles and wrist postures for neutral wrist positions only. Other wrist postures are not shown as no effect was found. Significant differences within directions are denoted by different letters.

REFERENCES

1. Kim (2003). *HF & Ergonomics*, 13(2), 153-163.
2. Mogk & Keir (2003). *Ergo*, 46(9), 956-975.
3. Antony & Keir (2010). *J.Elec & Kin*, 20, 191-198.
4. Erdelyi et al (1988). *Int. Arc. Occ & Env Hlth*, 60, 119-124.
5. Byström & Fransson-Hall (1994). *HF*, 36(1) 158-171
6. Favre et al (2009). *J Shoulder Elbow Surg*, 18, 114-121
7. McDonald et al (2012). *App Ergo*, 43, 971-978.
8. Grieve & Dickerson (2008). *Occ Ergo*, 8, 53-88.

AN INVESTIGATION OF HAND FORCE DISTRIBUTION, HAND POSTURE AND SURFACE ORIENTATION

Rosemarie Figueroa[1], Thomas Armstrong PhD[1]

[1] Department of Industrial and Operations Engineering, University of Michigan, Ann Arbor, MI

INTRODUCTION

The hand is frequently exerted against surfaces to support the body and to hold work objects. These surfaces are often flat, such as a wall or a bench top. Failure to exert sufficient force can result in a fall or a loss of control of the work objects, property damage and injuries. Additionally repeated exertions can result in fatigue or activity related musculoskeletal disorders (MSDs) [1,2]. Data and models are needed that can be used to predict the strength capacity of the hand for various work objects and hand postures, and can be used to determine internal forces that contribute to muscle, tendon and nerve disorders [3]. Towards this end, this study aims to understand how maximum forces exerted with the hand against flat surfaces are influenced by posture and surface orientation. Additionally it examines how forces are distributed between the fingertips and the palm. The resulting force distributions can be used to determine joint moments for biomechanical analysis of tendon and muscle forces.

METHODS

Participants performed maximum exertions (100%MVC) perpendicular to an aluminum plate in 45˚, 0˚, 45˚ and 90˚ pitch at elbow height (Fig. 1), attached to a force transducer. Exertions were performed using 1) the whole hand (WH) (Fig. 2a) and 2) the fingertips (FT) (Fig. 2c).

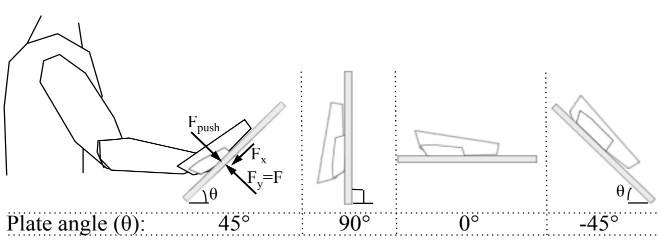

Figure 1: Maximum forces were exerted perpendicular to a surface oriented +45°, 90°, 0° and -45° with respect to horizontal. Frictional force is represented as Fx and normal force as Fy.

Six right-handed university students (3 males and 3 females) volunteered to participate in the study and gave written informed consent in accordance with IRB regulations. They were free of known movement disorders. The average stature was 181.7 ± 5.6 cm for males and 168.9 ± 3.0 cm for females. The average hand length was 19.7 ± 1.3 cm for males and 16.8 ± 0.3 cm for females. The average grip strength for the right hand was 457 ± 36 N for males and 299 ± 10 N for females as measured by a Jamar® grip dynamometer at position two (49 mm span). The average thumb-index finger pinch strength was 162 ± 13 N for males and 106 ± 13 N for females as measured by a B&L® pinch gauge.

The normal contact forces and force distribution were recorded using I-SCAN™ (Tekscan Inc., Boston, MA) at 60 Hz. LabVIEW (National Instruments, Inc., Austin, TX) at 5Hz program was written to show actual force exertion in the display for visual feedback. Data were averaged over 3s during maximum grip exertions. Statistical analyses were performed using MINITAB®.

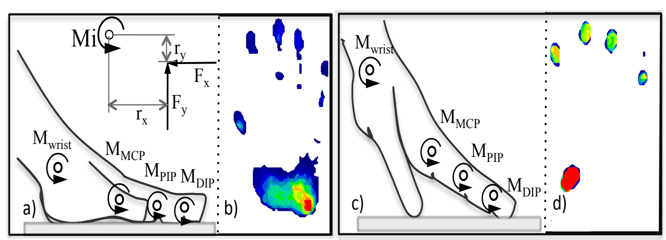

Figure 2: 0˚ pitch and 100%MVC exertions showing: posture- with (a) WH and (c) FT, and normal force distribution- with (b) WH and (d) FT (red represents highest pressure). Joint moments are represented as M_{DIP}, M_{PIP}, M_{MCP}, M_{wrist}.

Since participants exerted the force perpendicular to the surface, frictional force is negligible for moment calculation. Where,

$$Mi = r_y F_x + r_x F_y \approx r_x F sin\theta$$

$$F_x = \mu F_y$$

and Push Force = $\sqrt{\sum F_x^2 + \sum F_y^2} = \sum Fy$

RESULTS AND DISCUSSION

The higher percent of force distribution was located between the palm and thumb for WH cases and in the thumb for FT cases, and Figures 2b and 2d show this general pattern of pressure distribution. The force magnitude exerted by males was significantly larger ($p<0.05$) than females in 0˚ and 90˚ orientations for the WH cases, and in all the orientations for the FT cases (Table 1). Specifically in FT cases, there was a positive association between the plate angle and the %MVC (R^2 of .97 for females and .83 for males). Also, participants were able to get closer to the plate and use their body weight to create more force (as if they are performing a pushing task or supporting their body against a surface) leading to higher exertions at 90˚ pitch (Table 1).

Table 1: Average maximum exertions (Newton) per orientation for Females and Males, pushing with the whole hand (WH) and using just the fingertips (FT).

Orientation	Females		Males	
	WH	FT	WH	FT
-45˚	52.5 ±3.5	39.5 ±4.2	79.3 ±6.1	59.6 ±2.1
0˚	128.8 ±7.1	55.9 ±7.5	182.6 ±2.0	92.8 ±4.3
45˚	147.8 ±6.8	62.2 ±5.0	134.6 ±19.4	93.7 ±5.3
90˚	166.6 ±3.5	77.8 ±3.8	260.0 ±5.6	109.9 ±6.7

For both, females and males, Digit 1 (thumb) had a significantly higher force compared to the rest of the phalanges. On average, Digit 1 had 64.3% higher force for females (Fig. 3) and 52.5% for males (Fig. 4).

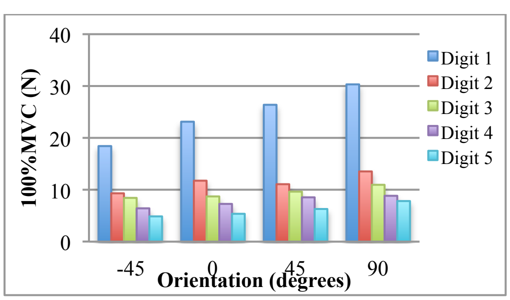

Figure 3: Female's force distribution per digit (FT-100%MVC) between orientations. Starting from Digit 1(thumb) to Digit 5 (pinky).

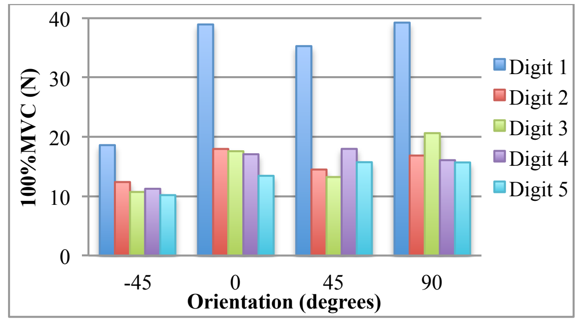

Figure 4: Male's force distribution per digit, (FT-100%MVC) between orientations. Starting from thumb (Digit 1) to pinky (Digit 5).

Phalange's joint moments were computed for 4 plate positions for participants 1-3. Results show that MCP has the highest load for all FT and WH cases. WH joint moments were lower than the FT cases, and this can be due to the fact that the palm had a high percent of the force distribution (Fig. 2b). For FT cases, joint moment values for 0˚ pitch were significantly higher ($P< 0.05$) in comparison to the rest of the plate orientations. Joint moment ratios were calculated for each joint and clustered by 'Digit 1' and 'Digit 2-5' (Table 2), since Digit 1 forces were significantly higher (Fig. 3 and 4).

Table 2: FT case at 100% MVC: Observed joint moment ratios for DIP, PIP and MCP joints of participants 1-3.

Orientation	**Digit 1** [DIP: MCP]	**Digits 2-5** [DIP: PIP: MCP]
-45º	[1: 2.83]	[1: 2.21: 2.26]
0º	[1: **4.32**]	[1: 2.33: **3.55**]
45º	[1: 3.59]	[1: 2.25: 2.58]
90º	[1: 2.63]	[1: 1.52: 2.10]

The joint moment calculations, finger force distributions and joint moment ratios can be used to compare strength capabilities from one position to another and for further biomechanical analyses.

REFERENCES

1. Marras, W. S., Cutlip, R. G., Burt, S. E., & Waters, T. R. *Applied ergonomics*, **40(1),** 15–22, 2009.
2. Garg, A., & Kapellusch, M. *Reviews of Human Factors and Ergonomics*, **7(1)**, 149–196, 2011.
3. Armstrong T. *Scand J WorkEnHith* **19(2)**, 73-84, 1993.

MEASUREMENT AND ANALYSIS ON THE POSTERIOR INTERVERTEBRAL GAPS BASED ON X-RAY IMAGES OF KOREAN LUMBAR SYSTEM

[1]Taesoo Bae, [1]Heesu Park, [2]Jaehyuk Yang, [3]Keyoung Chun and [3]Cheolwoong Ko

[1]Jungwon University, Goesan, Korea
[2]Korea University Guro Hospital, Seoul, Korea
[3]Korea Institute of Industrial Technology (KITECH), Cheonan, Korea
email: cheko@kitech.re.kr, web: http://www.kitech.ac.kr

INTRODUCTION

Recently, the world medical device market for spinal diseases is rapidly growing up above 20% per year. Especially in Korea, the number of surgery cases using spinal implants was increased by about 61% in 2004, compared to two years ago (New Tech-New Biz). Most of spinal implants in Korean market have been recently imported from the major foreign companies in Europe or USA. As the imported ones were developed primarily based on anthropometric data of Europeans or Americans, they were possibly not fit to the skeletal structure of Korean spine system.
Even though some Korean company had an experience to develop spinal implants considering the anatomical information of Korean spine system and there were several researches on intervertebral discs using 3D Korean spine models (Haiyun, 2010), the morphological measurement and analysis on Korean spinal structure are still rare. Referred to the previous studies on Korean lumbar spine, most of them were focused on abdominal and elector spinae muscles related to lower back pain (Hur et al., 2011). The objectives of this study were to measure the posterior intervertebral gap (PosIG) of Korean lumbar spine using radiography images as posture changes and to analyze the age-related effect of the PosIG between young and elderly Korean groups.

METHODS

This study newly fabricated a simplified chair device with 3-segmental rigid plates that can be adjusted to various angles (0°, 30°, 60° and 90°) (Figure 1) to obtain lumbar shape information (L1～L5) in each posture. The subjects included 10 males in their 20's (Height: 171.7±5.3cm, Weight: 71.3±9.9kg) and 10 elderly males in their 60's (Height: 163.6±5.6cm, Weight: 63.9±9.0kg), close to the Korean standard sizes (Sizekorea, 2004). Those who had been diagnosed with mental disorders, lumbar problems during the last 6 months or had a suspicious medical history were excluded from being subjects before X-ray examination. This study was approved by the Institutional Review Board (IRB NO. MD10024).
A total of 5 postures (Supine, Seatback-angle 30°, 60°, 90° and Standup) were defined, and the subjects maintained cross-arm-position (CAP) while the X-rays were being taken using digital X-ray equipment (DRS-8000, Listem Co., Korea) (Figure 1). To measure the gap of intervertebral cleft, the authors suggested three methods. The first is the shortest intervertebral distance using midline (method 1, $\overline{P1P2}+\overline{P1P2}$), the second is shortest distance using previously reported method (method 2, $\overline{P6P7}$), and the final one is the distance between intersection points of tangential lines to posterior shape of lumbar spine (method 3, $\overline{P5P7}$) (Figure 2). With the defined three methods, the authors analyzed the age-related effect to investigate the difference between the two groups. For each analysis, the paired student t-test was statistically performed.

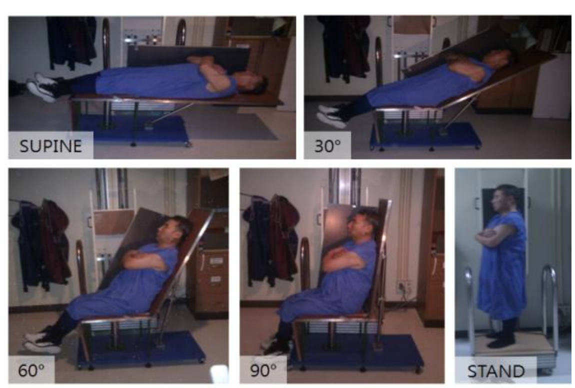

Figure. 1 Radiographical Assessment with customized Jig as posture changes from supine to standup

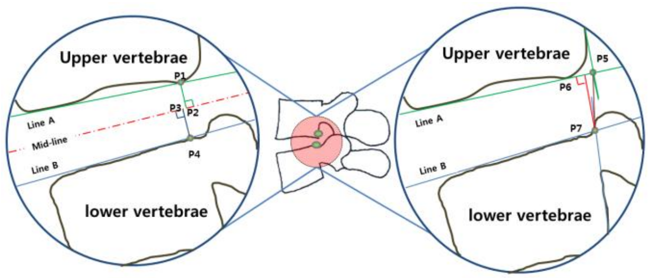

Figure. 2 Three different methods of measurement on posterior intervertebral gap

RESULTS AND DISCUSSION

The minimum value of intervertebral gap was found by method 1, while the maximum gap was obtained by method 3. According to the difference of the PosIG between the two groups, the results of method 2 averagely showed 0.01mm for 20s and 0.12mm for 60s greater than those of method 1, however, there was no statistical difference between the two groups. On the other hand, the results of method 3 were averagely 0.4mm for 20s and 0.63mm for 60s greater than method 1 and 2 (Figure 3). For the five postures, we analyzed the difference of the PosIG between 20s and 60s. At 0° (supine posture), the PosIGs for 20s were greater than those for 60s. At 30°, the PosIGs at L2-L3 and L5-S1 for 20s were greater than those for 60s. When the trunk posture was changed from 60° to 90°, the PosIGs from T12 to L3 for 20s were smaller than those of 60s. However, the PosIGs from L4 to S1 showed the greatest values. From these results, it was inferred that load distribution on lumbar spine in case of 60s during standup could be greater due to gradual decrease of the PosIG, compared to 20s (Figure 4).

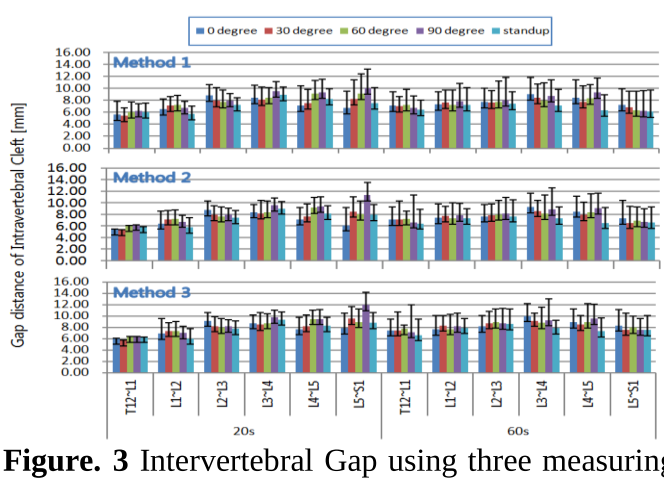

Figure. 3 Intervertebral Gap using three measuring methods for 20s and 60s

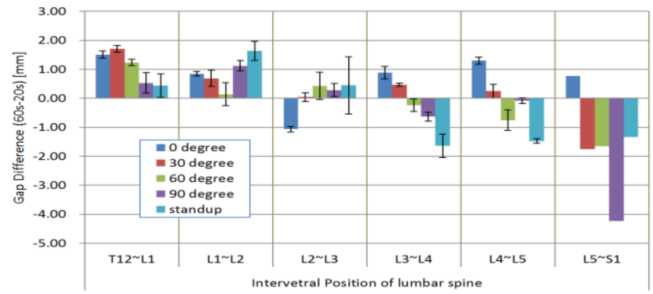

Figure. 4 Gap difference (60s-20s) of intervetral cleft at lumbar spine as postures change

Although the error of measurement was unavoidably existed, the tendency of load distribution on lumbar spine by method 1 and 2 was similar in all postures. As a future work, it is considered that it is necessary to discuss the precision of measurement for intervertebral gaps.

CONCLUSIONS

In this study, based on the X-ray images of Korean lumbar system, we measured the PosIG in five postures using the defined three methods for 20s and 60s and analyzed the age-differences between the two groups. In views of measurement methods, the shortest PosIGs using method 1 and 2 showed more meaningful results compared to the PosIG between intersection points from tangential lines (method 3). In addition, age-difference analysis depending on the trunk postures showed that the PosIGs at T12-L2 for 60s were greater than those for 20s in all postures, while the PosIGs at L5-S1 for 20s were greater in all postures except supine posture. Moreover, the PosIGs at L3-L5 for 60s in supine posture were greater, while the PosIGs toward standup posture were smaller, compared to those of 20s. These results would be useful to analyze risk of injury as fundamental data as well as to develop spinal implants.

REFERENCES

1. Haiyun Y, et al. *Spine*, **35(8)**, 2010.
2. Hur W, et al. *Korea J Pain*, **24(4)**, 2011.

ACKNOWLEDGEMENTS

This study was performed with assistance from the research fund of the Korea Institute of Industrial Technology (KITECH)

TRUNK INERTIAL ESTIMATES OF A PREGNANT FEMALE

Jason Wicke, Alex Calleros, Valerie DiMartino

William Paterson University, Wayne, NJ, USA
email: wickej@wpunj.edu

INTRODUCTION

Analysis of the forces and moments acting across the joints require several input parameters, including segment inertias (i.e. mass, center of mass location and moments of inertia). These inertias cannot be directly measured and therefore must be estimated using a body model. The accuracy of any body model is dependent on its ability to capture both the inter-individual differences and intra-individual variations in segment properties.

The more common body models used in biomechanic studies (e.g. Dempster, DeLeva, etc.) are primarily derived from the male population, though some female-specific models exist (e.g. Zatziorsky). Pregnant females are a unique population for which these traditional body models may not be appropriate, especially due to the necessary sensitivity required to capture the rapidly changing segments, primarily the trunk.

Models derived from the geometric method are most acute to capturing the rapid segment changes during pregnancy compared to models derived from other methods. The geometric-based Hatze model [1] is highly accurate but requires 133 anthropometric measures from the individual and complex algorithms not readily available. Jensen's model [2]only requires a front and side image of the individual, from which horizontal elliptical zones 2 cm in thickness are combined to estimate segment inertial parameters. Unfortunately, the use of elliptical zones creates cavities at the segment junctions (arm-trunk and trunk-leg) that result in relatively large underestimations of the segment inertial parameters.

The Wicke trunk model [3] has used sectioned ellipses to eliminate the cavity issue and also has included non-uniform density profiles separately for the trunk of college-aged males and females. However, whether this model is capable of accurately capturing the rapidly changing morphology of the pregnant trunk has yet to be determined. This pilot study examined the sensitivity of the volume function within the Wicke model to capture these changes.

METHODS

One pregnant female 39 years of age agreed to participate in this pilot study. Testing was conducted at 17, 23, 33 and 35 weeks of her pregnancy. During each testing session, a full body scan was taken, using a 3D scanner (TC^2®) that uses white light and infra-red technology resulting in approximately 1.5 million surface data points with an accuracy of within 1 mm. The participant wore a bikini to ensure accurate body surface capture. Immediately following the scan a front and side image of the participant was taken using traditional still digital cameras. Within each image, a horizontal and a vertical meter stick were captured to convert pixels to real units.

Cross sectional areas at specific heights along the trunk were calculated from the raw (object file) data of the full body scan using MatLab™. The side and front images of the participant were then digitized using the Slicer™ program. In short, this program calculates the anteroposterior and transverse dimensions at uniform intervals along the longitudinal axis of each segment. Using algorithms for geometric shapes, the volumes of each of these zones can be determined and combined with a density function to estimate the inertial parameters of each section. Where segments adjoin (e.g. hips at lower trunk & arms at upper trunk), sectioned ellipses were used to represent the cross-sectional area. At all other levels of the trunk, ellipses were adopted. The cross-sectional areas from the full body scan (criterion) were compared to the cross-sectional areas at the same longitudinal level from the Wicke model.

RESULTS AND DISCUSSION

An average of 24 upper trunk and 28 lower trunk cross sections were compared for each of the four weeks during the pregnancy (Table 1). The cross sectional area of the upper trunk slightly increased during the pregnancy, by approximately 100 cm^2. The Wicke model was accurate at estimating the upper trunk cross-sectional area with an average error within 5%. However, at each week tested, the model over-estimated the upper trunk region and can be mainly attributed to the cavity between the breasts that cannot be captured by an ellipse (Fig.1). The model may be more accurate at capturing the contour of the beasts if a separate shape was used, as does the Hatze model.

The lower trunk region showed much greater changes in the cross-sectional area as expected; increasing by approximately 250 cm^2. The model was more accurate at capturing this region compared to the upper trunk. At the 33rd week, the error was slightly greater than the other weeks. It is not certain why this happened, but could be simply due to the errors caused during the manual digitization process.

Overall, the volume function of the Wicke model appears to accurately capture the changes in the trunk region during pregnancy. However, the model needs to be tested on a greater sample to be more conclusive with the above statement. In addition, the overall error for the trunk inertial estimates during pregnancy has yet to be established. There are regions of over-estimation that counterbalance regions of under-estimation within the volume function. In addition, the density function will introduce further error, though the accuracy of geometric models are much more sensitive to the volume function compared to the density function [4].

The intra-individual changes that occur during pregnancy require adaptations in movement and the intersegmental moments concomitant to these inertial changes. In turn, proper adjustments to physical activities, equipment and other factors related to the pregnant female can be made to minimize the challenges that are faced during this period. The Wicke model shows potential for capturing

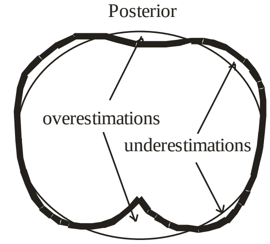

Figure 1: Cross-sectional area of breast region (dark line) being represented with an ellipse (light line).

REFERENCES

1. Hatze, H. *Theor. Issuse Ergonomics Sci*, **6**¸331-334, 2005.
2. Jensen, R. *J Biomech*, **11**, 349-358, 1978.
3. Wicke J, et al. *J Biomech*, **42**, 55-60, 2009.
4. Wicke J, et al. *J Appl Biomech*, **26**, 26-31, 2010.

Table 1: Mean ± SD of cross sectional areas (cm^2) and error (%) of the Wicke model for the upper and lower trunk.

	Upper Trunk			Lower Trunk		
Week	3D	Wicke	Error	3D	Wicke	Error
17	668.5 ± 134.6	637.8 ± 126.9	2.7 ± 5.1	757.9 ± 100.3	767.3 ± 105.6	-1.3 ± 2.5
23	772.6 ± 135.2	738.8 ± 131.0	4.3 ± 2.4	773.8 ± 108.2	770.41 ± 104.0	0.4 ± 2.7
33	784.1 ± 148.1	770.5 ± 136.2	1.6 ± 4.2	882.5 ± 120.6	849.07 ± 128.3	3.4 ± 4.0
35	752.0 ± 126.1	703.1 ± 130.8	3.7 ± 1.9	905.3 ± 152.3	899.9 ± 131.1	-0.5 ± 4.7

USING A STABILITY BALL AS A TASK CHAIR: SPINE ANGLES DURING LATERAL REACHING

[1]Thomas Karakolis, [2]Michael W.R. Holmes, and [1]Jack P. Callaghan

[1]Department of Kinesiology, University of Waterloo, Waterloo, ON, Canada
[2]Faculty of Health Sciences, University of Ontario Institute of Technology, Oshawa, ON, Canada
email: thomas.karakolis@uwaterloo.ca

INTRODUCTION

Despite evidence that using a stability ball, sometimes known as an Exercise ball or Swiss Ball, as a task chair does not result in increased core muscle activation while performing computer workstation tasks [1,2], numerous fitness suppliers continue to market stability balls as a positive alternative to conventional office chairs.

Typical office work can consist of prolonged tasks (i.e. typing, writing, reading, etc.), with periodic lateral reaching (i.e. for the phone, for a pen, for a binder, etc.). Both static postures and trunk lateral bend velocities have been identified as risk factors for low back disorders [3]. A stability ball can be considered a dynamic surface and may allow for lateral pelvic movement or perhaps even pelvic rotation during reaching. A consequence of this pelvic motion may be decreased trunk lateral bend. Therefore, the purpose of this study was to examine trunk lateral bend angles during reaching while sitting on a stability ball vs. a conventional task chair.

METHODS

Sixteen, right hand dominant, participants between the ages of 20 and 35 years, equally divided between males (n = 8; height = 1.81 ± 0.08 m; mass = 84.9 ± 14.3 kg; shoulder width = 0.40 ± 0.02 m) and females (n = 8; height = 1.64 ± 0.06 m; mass = 60.8 ± 10.3 kg; shoulder width = 0.33 ± 0.02 m), participated in this study.

Participants performed four reaching tasks using a target board placed on a desk, in two different seat conditions: an office chair with no armrests (control) and a stability ball. Seat conditions were presented in randomized order. Participants could self-select foot width, but were instructed to place their feet facing forward and in front of the ball/chair, as would be typical for office work. Once foot placement was selected, participants were asked not to move their feet throughout the approximately 5-minute long collection.

Chair and table height were adjusted such that elbow, hip, and knee angles were all 90 degrees at the beginning of each trial. Three different sized stability balls were available, and the most appropriate size was selected to ensure approximately enclosed hip and knee angles of 90 degree. The target board was placed on the table with the midline aligned with the participant’s midline. The target board was placed anteriorly to the participants at a distance of 20 cm from the thorax.

Each participant reached for four different lateral targets on the target board (80/110 cm from midline; left/right). Target distances were based on seated reach envelope guidelines by the Canadian Standards Association (CSA-Z412, 2000). The four reaches were presented in a randomized order. Participants were instructed to move only in the frontal plane, meaning they refrained from any voluntary flexion or axial rotation of the trunk. Lastly, participants were asked to start and end each reach trial in the same neutral posture, sitting on the chair/ball with their hands on the table.

Participants were instrumented with tri-axial accelerometers placed over the C7, L1, and S1 vertebrae. The accelerometers functioned as tilt sensors, with the relative angle between the C7 and L1 sensors in the frontal plane representing **thorax bend**, relative angle between L1 and S1 representing **lumbar bend**, and relative angle between C7 and S1 representing **trunk bend**. For each reach trial, maximum deviation from neutral for thorax, lumbar, and trunk bend were recorded as dependent measures. Two-way ANOVAs were performed for each dependant measure, with seating condition and target distance as within factors. Only reaches to the right (dominant side) were considered in this analysis.

RESULTS AND DISCUSSION

As would be expected, reaches to the target at 110 cm produced significantly greater average thorax, lumbar, and trunk lateral bend angles compared to the 80 cm target (Fig. 1; thorax p = 0.002; lumbar p = .012; trunk p = 0.000). The seating surface did not introduce any significant differences in the angles during the lateral reaches (Fig. 1; thorax p = 0.605; lumbar p = 0.772; trunk p = .830). Further, no interactions were found between seating condition and target distance (thorax p = 0.813; lumbar p = 0.811; trunk p = 0.993).

For the 80 cm reaches, trunk lateral bend was 7.9 ± 5.9 (SD) degrees while sitting on the stability ball and 8.5 ± 8.7 degrees while on the chair. Lumbar bend accounted for 52% (4.1 ± 5.3 degrees) of the total trunk bend on the ball versus 48% (4.0 ± 10.5 degrees) on the chair. A similar trend emerged in the 110 cm reach, where lumbar bend accounted for 49% of total trunk bend on the ball, and only 42% of trunk bend on the chair. Although not statistically tested, a trend was noticed such that a larger percent of total trunk lateral bend was accounted for in the lumbar spine on the ball. This trend does not support the initial hypothesis that the ball may allow for a more neutral spine during reaching.

Previously, it has been shown that there were no differences in muscle activation when using a stability ball while performing office work [2], counter to the idea of increased core muscle activation attributed to ball usage. Even in the absence of muscle activation increases, the potential for discomfort on the stability ball was significantly higher [2]. Recently, it has also been shown that the margin of safety in the base of support on a stability ball is lower [4]. These findings suggest that the potential to fall while working on a stability ball is greater than the potential to fall while working on a conventional office chair.

CONCLUSIONS

Although trunk lateral bend increased as reach distance increased, lateral bend angles did not differ between the stability ball and conventional task chair. There appears to be no added spine posture benefit for lateral workspace reach envelopes on a ball. Considering the increased stability/safety risk associated with the ball during lateral reaches our results do not support the use of a stability ball as a task chair for normal office work.

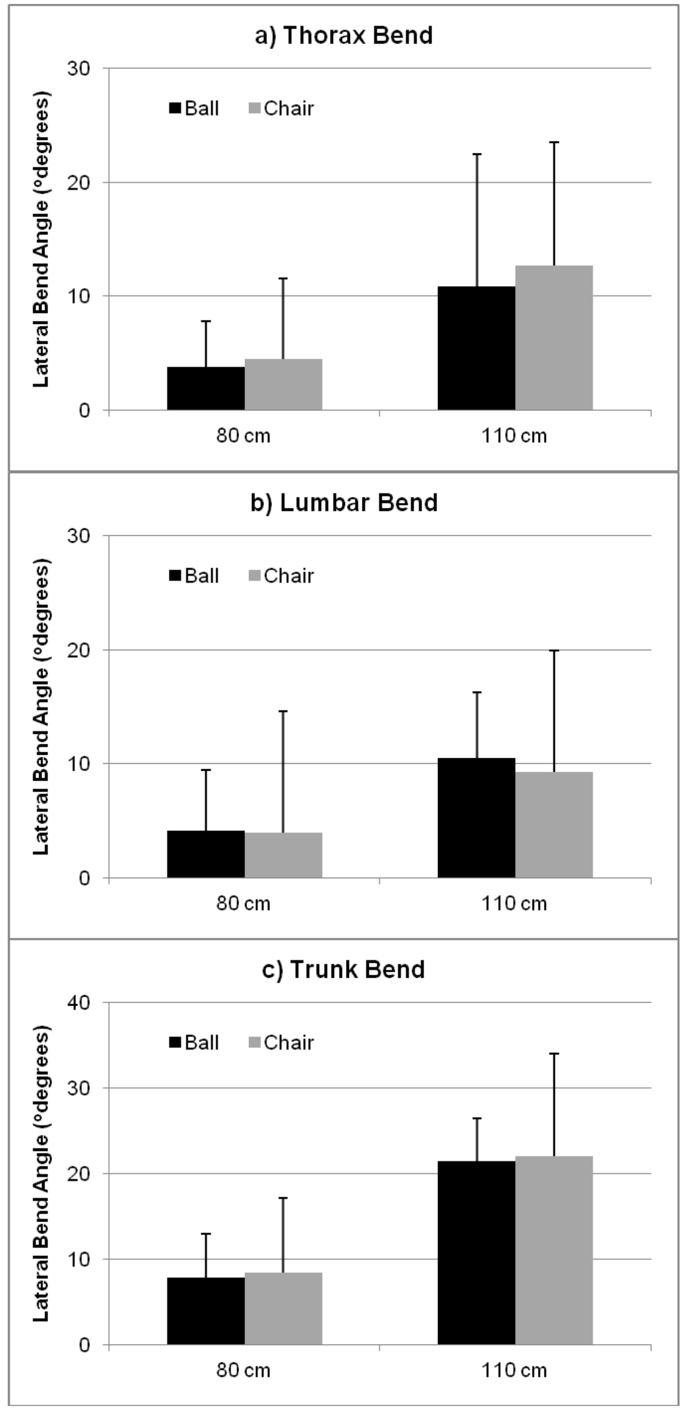

Figure 1: Maximum bend angles for (a) thorax, (b) lumbar, and (c) trunk during lateral reaches to targets 80 and 110 cm from midline.

REFERENCES

1. McGill SM et al. *Clin Biomech* **21**, 353-360
2. Gregory et al. *Hum Fac* **48**, 142-153
3. Marras WS et al. *J Biomech* **30**, 697-703.
4. Parmar R et al. *Ontario Kinesiology Association Conference*. Niagara Falls, ON, Canada, 2012

THE INFLUENCE OF NECK POSTURE AND CANADIAN FORCES HELICOPTER HELMET CONFIGURATION ON NECK MUSCULAR DEMANDS

Colin D. McKinnon[1], Andrew C.T. Laing[1], Clark R. Dickerson[1], Jack P. Callaghan[1]
[1]Department of Kinesiology, University of Waterloo, Waterloo, ON
Email: colin.mckinnon@uwaterloo.ca

INTRODUCTION

Neck pain and muscle fatigue are common among Canadian Forces (CF) pilots and flight engineers. Over 80% of CH146 Griffon helicopter pilots and flight engineers reported neck pain associated with in-flight task demands [1]. The constrained helicopter cockpit design requires awkward head and neck postures to scan terrain and to interact with the control display unit. From the perspective of helmets, attachment of a night-vision goggle (NVG) system increases the total helmet mass, creates a flexion neck moment, and alters the centre of mass location. This requires an increase in the activation of dorsal neck musculature, resulting in increased potential for muscle fatigue, and a corresponding increased risk of neck injury [2]. To balance the neck flexion moment created by the NVG and mitigate the elevated muscular demand, pilots use a counterweight (CW) attached to the posterior aspect of the helmet [1]. This study aimed to quantify neck muscle activity between no helmet, helmet, helmet with NVG and helmet with NVG and CW configurations in a range of head and neck postures.

METHODS

Eight male participants (21.3 ± 1.7 years; 177.9 ± 6.8 cm; 79.7 ±11.5 kg) were instrumented with passive optical motion tracking markers on the trunk, head and neck, and 10 pairs of surface EMG electrodes placed bilaterally over the erector spinae [ES], splenius capitis [SC], levator scapulae [LS], sternocleidomastoid [SCM], and upper trapezius [UT]. Participants sat with the legs and trunk restrained, and performed three maximum voluntary exertion (MVE) trials in each of seven neck postures (neutral, 45° flexion, 30° extension, 45° axial rotation, 20° lateral bend, 45° axial rotation + 45° flexion, and 45° axial rotation + 30° extension). Participants then performed three trials in each combination of six helmet configurations (no helmet, helmet only [hOnly], helmet with NVG in the up and down positions [hNVGup and hNVGdown], and helmet with NVG in the up and down positions with CW attached [hCWup and hCWdown]) and the seven neck postures for a total of 126 trials. For each trial, participants moved from a neutral posture to a marked target posture, held for 15 s, and returned to neutral. Target postures were confirmed in real-time as Euler rotation angles between the trunk and head segments. Trials for each helmet-posture combination were low-pass digitally filtered (single-pass, 2nd order Butterworth, 1.0 Hz cutoff), normalized to maximum activity across all MVE trials, ensemble averaged, and the peak muscle activity during the static hold plateau was extracted. Two-way repeated measures ANOVAs were used to assess the influence of posture and helmet configuration on the peak activity from each of the 10 recorded muscles.

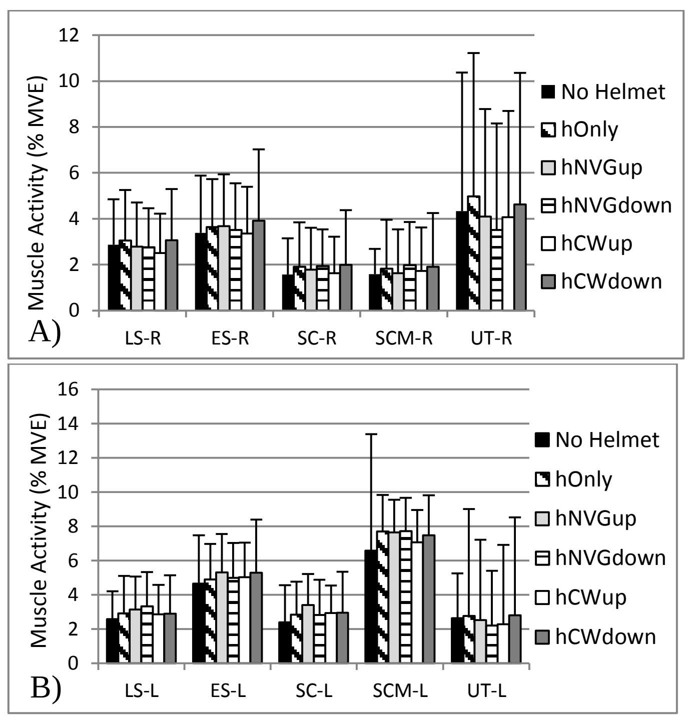

Figure 1: Mean muscle activity by helmet configuration for muscles on the A) right side and B) left side of the neck. Note: no significant differences were shown between helmet configurations.

RESULTS AND DISCUSSION

Muscle activation levels ranged from 1.8-7.4% MVE when collapsed across all conditions, and reached a maximum of 21.3% MVE for any single muscle in any condition. No significant posture-by-helmet effects were observed in the static hold phase of the task. Helmet configuration (main effect) did not influence any measured muscle activations (p = 0.270 to 0.850) (Figure 1). Significant main effects of posture existed for all recorded muscles (p < 0.0001 to p = 0.045). In general, muscle activity tended to be greatest in extension and combination movements for the lateral muscles (SC, LS, SCM), and greatest in flexion and flexion + rotation for ES (Table 1). In contrast, the activity of the right UT was significantly greater (p = 0.045) in the neutral posture (mean and standard deviation: 6.60 ± 8.5% MVE) compared to all other postures (3.0-4.6% MVE).

In general, muscle activity patterns corresponded to the primary action of each of the recorded muscles. Muscle activity tended to be highest in extension and combination postures and lowest in a neutral neck posture for the lateral neck muscles (LS, SC) and the SCM. With the head and helmet load forward (neck flexion), posterior muscle activity (ES) significantly increased.

No significant muscle activity differences were shown between the six helmet configurations evaluated. Considering the goal of the CW is to offset the forward shift in helmet centre of mass from the night-vision goggle system [3], intuitively one might expect decreases in muscle activitation when the CW is used. However, in agreement with previous findings [3], muscle activity was slightly higher with the CW than in the same configuration without the CW. This indicates that the addition of a CW may have no effect (or even a negative effect) on muscle activation, and that the weight of the head and neck has a greater influence on muscle activity than helmet weight in statically held positions. While this study analyzed static neck postures under controlled conditions, in reality helicopter pilots are exposed to high acceleration neck movements in addition to static postures. Inertial and kinetic analyses of helmet conditions are required to make conclusions about any related effects arising from increased helmet mass and distribution.

CONCLUSION

In summary, we observed distinct posture-based effects on muscle activity, but no effect of helmet configuration. Although the activation levels we observed were relatively low, it may be desirable to avoid neck extension coupled with rotation when designing vehicle instrumentation layouts. Though helmet configuration showed no effect on neck muscle activity in static postures, analysis of neck kinetics and of inertial effects during high accelerations is required to substantiate any conclusions about design of the NVG and CW system.

REFERENCES

1. Bridger *et al.* (2002). *Aviat Space Environ Med* **73**: 805-811.
2. Phillips *et al.* (1983). *Aviat Space Environ Med* **54**: 901-905.
3. Thuresson *et al.* (2003). *Aviat Space Environ Med* **74**: 527-532.

Table 1: Differences in muscle activity pooled across helmet configurations by posture compared to neutral.

	Muscle									
Posture	LS-R	LS-L	ES-R	ES-L	SC-R	SC-L	SCM-R	SCM-L	UT-R	UT-L
30° ext	>	>	--	--	>	>	>	--	--	--
45° flex	--	--	>	>	--	--	--	--	--	--
20° lat	--	--	--	--	--	--	--	--	--	--
45° rot	--	--	--	--	--	>	--	>	<	--
45° rot 45° flex	--	--	>	>	--	--	--	>	--	--
45° rot 30° ext	--	>	--	--	--	>	--	>	--	--

> and < indicate muscle activity significantly greater than or less than neutral (α = 0.05). Based on post-hoc pairwise comparisons.

STRIDE LENGTH AT CONTROLLED WALKING SPEEDS IS NOT RELATED TO REDISTRIBUTION OF LOWER EXTREMITY JOINT POWERS

Harsh Buddhadev and Philip E. Martin

Department of Kinesiology, Iowa State University, Ames, IA, USA
email: harshb@iastate.edu

INTRODUCTION

Compared to young adults, older adults display higher relative joint moment and power contributions at the ankle and lower contributions at the hip joint at any given speed of walking [1]. Two recent studies [2,3] demonstrated that systematically increasing stride length at a fixed walking speed leads to higher peak and average net joint moments and power at the ankle and lower values at the hip in young individuals. Allet and colleagues [3] suggested that differences between young and older adults in joint moment contributions may originate in stride length and cadence differences. However, in both studies [2,3] young participants walked under experimental constraints of stride length and cadence at one fixed walking speed. There is a need for further assessment of the potential relationship between stride length and the distribution of effort across the ankle, knee, and hip. Our purpose was to test the hypothesis that longer stride lengths are associated with higher relative power contributions at the ankle and lower contributions at the hip among a group of young, healthy adults.

METHODS

Thirteen healthy young adults (5 males, 8 females; 20.9 ± 2.8 yrs, 172.9 ± 8.8 cm, 63.7 ± 10.9 kg), who were free from conditions which can affect normal walking were recruited for the study. Reflective markers were placed on anatomical landmarks of the subject's trunk, pelvis and right lower extremity. Participants completed five successful walking trials for four randomly ordered speed conditions (1.1, 1.3, 1.5, or 1.7 $m \cdot s^{-1}$). Successful trials were ones in which the average speed through the measurement zone was within 3% of the target speed and there were no visible indications of adjusting the stride to impact a force platform. Three dimensional marker positions and ground reaction forces were sampled synchronously at 100 Hz and 500 Hz, respectively. A three-segment sagittal plane inverse dynamics model was used to estimate net joint forces and moments. Segment inertial properties for body segments were predicted using methods outlined by Vaughan [4]. Net joint average positive powers normalized to body mass were calculated over a full gait cycle for the ankle, knee, and hip as described previously [2]. Based on total average power (computed as a sum of all three average joint powers), relative powers at the three joints were computed as a percentage of the total. Correlations were computed between stride length normalized to leg length (SL/LL) and ankle, knee and hip relative joint powers for each speed condition. A one way ANOVA with repeated measures examined the effect of walking speed on ankle, knee and hip average and relative powers. Significant differences were considered at $p < .05$.

RESULTS

There were no statistically significant relationships between relative stride length and relative powers at ankle, knee and the hip joint for any speed condition (Table 1). Average powers for the ankle, knee and the hip significantly increased with walking speed (Figure 1). Walking speed did not significantly affect relative joint powers (Figure 2).

DISCUSSION

Correlations results indicated the absence of relationships between relative stride length and average positive powers at the three lower limb joints, which is inconsistent with a stride length and cadence-dependent effect on distribution of effort across the ankle, knee, and hip.

DeVita and Hortobagyi [1] speculated age related decline in strength of plantarflexor muscles is one

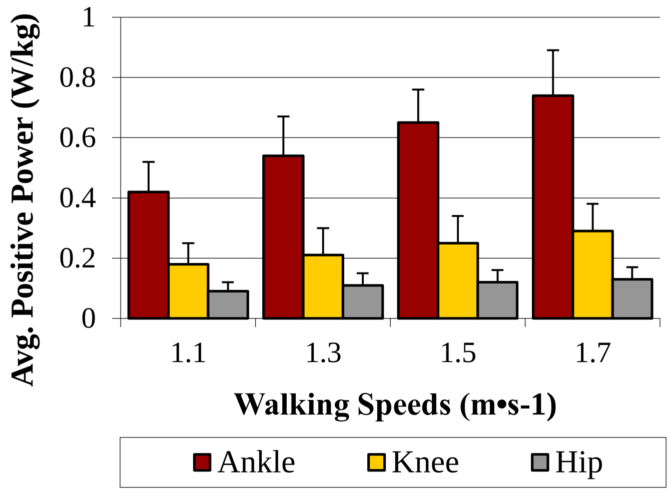

Figure 1: Average positive power (W/kg) for ankle, knee and hip joint for 1.1-1.7 $m \cdot s^{-1}$ walking speeds.

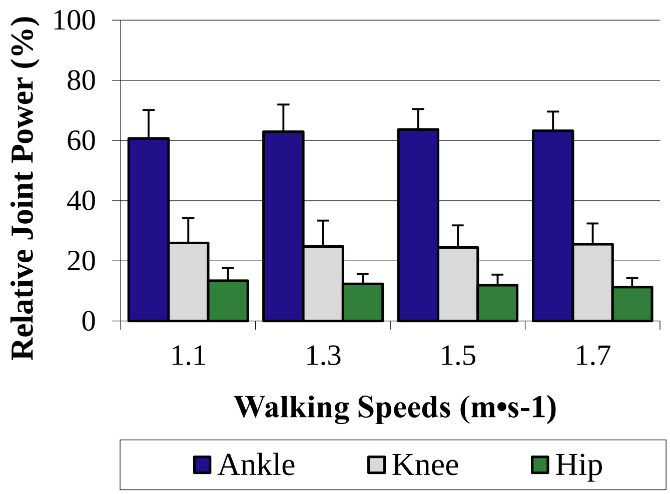

Figure 2: Relative joint power (%) for ankle, knee and hip joint for 1.1-1.7 $m \cdot s^{-1}$ walking speeds.

of the causes for redistribution of joint moments observed in the elderly. Since participants in our study were young healthy adults we may not expect such decline in strength. We speculate that redistribution as observed in previous studies may only occur at stride lengths relatively shorter or longer than self-selected stride lengths at controlled walking speeds. We, therefore, reject our hypothesis that at any given fixed walking speed, longer stride lengths are associated with higher relative power contributions at the ankle and lower contributions at the hip among a group of young, healthy adults.

CONCLUSIONS

Relative stride length at controlled walking speeds is not related to relative lower limb joint powers. Redistribution is more likely to occur at controlled walking speeds at stride lengths longer or shorter than self-selected.

REFERENCES

1. DeVita P et al. *J Applied Physiology* **88**, 1804-1811, 2000.
2. Umberger BR et al. *J Exp Biology* **210**, 3255-3265, 2007.
3. Allet L et al. *Gait & Posture* **34**, 300-306, 2011.
4. Vaughan CE et al. *Dynamics of Gait*, Kiboho Publishers, 1992.

Table 1: Correlations between relative stride length (SL/LL) and relative powers for ankle, knee, and hip joints for 1.1-1.7 $m \cdot s^{-1}$ walking speeds. *p* values are provided in parentheses.

	1.1 $m \cdot s^{-1}$	**1.3 $m \cdot s^{-1}$**	**1.5 $m \cdot s^{-1}$**	**1.7 $m \cdot s^{-1}$**
Relative SL (SL/LL)	1.44 ± 0.07	1.55 ± 0.06	1.68 ± 0.05	1.78 ± 0.05
Ankle (W/kg)	0.13 *(0.66)*	-0.29 *(0.34)*	0.14 *(0.65)*	0.04 *(0.89)*
Knee (W/kg)	0.04 *(0.89)*	0.29 *(0.34)*	-0.24 *(0.44)*	-0.11 *(0.72)*
Hip (W/kg)	-0.39 *(0.19)*	0.05 *(0.88)*	0.29 *(0.45)*	0.16 *(0.60)*

THE RELATIONSHIP BETWEEN A PROGRESSIVE VERSUS SINGLE-STAGE TREADMILL TEST FOR EVALUATION OF CLAUDICATION

[1]Shane R. Wurdeman, [2,3]Iraklis I. Pipinos, [2,3]Jason M. Johanning, and [1]Sara A. Myers

[1]University of Nebraska at Omaha, Omaha, NE, USA
[2]VA Nebraska-Western Iowa Health Care System, Omaha, NE, USA
[3]University of Nebraska Medical Center, Omaha, NE, USA
email: swurdeman@unomaha.edu, web: nbcf.unomaha.edu

INTRODUCTION

Peripheral arterial disease (PAD) is defined by atherosclerotic plaque buildup and subsequent blockages along the arterial walls of the extremities[1]. The narrowing of the arteries leads to reduced blood flow to the leg musculature upon exertion clinically resulting in complaints of leg pain. This pain, known as claudication, stops once muscular exertion ceases and metabolic demand returns to baseline[2]. Prior to 1991, the most common means to evaluate claudication was a single-stage treadmill walking test. The single-stage treadmill walking test consists of a fixed speed, fixed slope protocol. In 1991, Gardner et al.[1] reported results from a progressive treadmill walking test which consisted of a fixed speed with a progressively increasing slope protocol. The progressive test reduced testing time likely due to increased muscular demand. Due to the discrepant nature of the protocols, there has been no previous attempt to determine a relationship between these protocols. This has led to an inability to compare historical data to more recent data and allow for comparisons among different laboratories as the two protocols continue to be used. Therefore, the purpose of this study was to determine a relationship between the two protocols to allow for increased comparison of results among laboratories and studies. To allow for commonality, it was hypothesized that metabolic work demands of leg muscles are the primary cause of ischemic pain. Thus, a relationship in the mechanical work demands should similarly exist and thus allow for approximation of performance in one walking test based on the other.

METHODS

Thirty-one patients with PAD (age: 65.2±6.71 yrs; ht: 175.6±6.1 cm; mass: 87.5±15.6 kg) were screened and consented for participation. Subjects initially performed a progressive treadmill test followed by a rest period, and then several other biomechanical tests (e.g. overground walking trials and strength testing) as part of the larger study. Following these other tests, subjects rested before completing a single-stage treadmill test. The overall goal, and instructions given for each treadmill test, is to "walk until the pain in your leg forces you to stop". The time is then recorded as the maximum walk time. The single-stage test protocol is a fixed speed and slope at 1.5 mph (0.67 m/s) and 10% grade. The progressive test protocol is a fixed speed of 2.0 mph (0.89 m/s) and the slope starts at a 0% grade, but is then inclined 2% every 2 minutes[1]. Mechanical work for the treadmill tests was modeled as a point mass with work consisting of changes in translational kinetic and potential energy. Due to an overall upright posture during walking, contributions to work from rotational kinetic energy were assumed minimal and thus disregarded. A log transformation was then performed to remove nonlinearities. The calculation for mass-normalized work during the single-stage protocol was calculated as:

$$W = (V_x^2/2 + V_z^2/2 + V_z*g)*t \qquad (1)$$

where V_x and V_z are the forward and vertical velocity components, respectively, from treadmill speed and slope and t is time. This results in values of 0.667 m/s and 0.067 m/s for V_x and V_z, respectively. The calculation for mass-normalized work during the progressive protocol was similar with the exception that the values for V_x and V_z were adjusted every two minutes as the slope of the treadmill was increased. The relationship between performance in the single-stage and progressive protocols was evaluated through Pearson product-moment correlations with a significance level set at alpha equal to 0.05. We examined mechanical work since the primary cause of reduced walking performance seems to be associated with energy, however time measurements were also correlated.

RESULTS AND DISCUSSION

There was a large range in maximum walking times for the tests for the single-stage (avg: 308.19s ± 290.77, max: 1190s, min:50s) and the progressive protocols (avg: 429.61s ± 343.59; max: 1339s, min: 51s), allowing for a wide spectrum of performance to be included within the analysis. Significant relationships for time (r=0.630, p<0.001) and work (r=0.563, p=0.001) were found (Figure 1). But, this relationship was considerably stronger for work following the log transformation to remove nonlinearities (r=0.835, p<0.001).

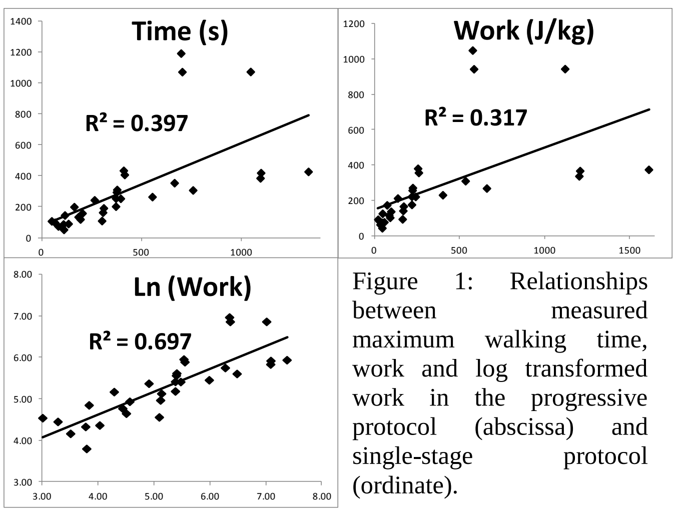

Figure 1: Relationships between measured maximum walking time, work and log transformed work in the progressive protocol (abscissa) and single-stage protocol (ordinate).

The relationship between maximum walking times for patients with PAD between the two protocols was not surprising. Unfortunately, visual inspection of the plots shows a less than desirable relationship for time when trying to make comparisons in walking times reported in the literature utilizing different walking protocols. Furthermore, time measurement does not account for varying slope and speed meaning that unless the studies being compared in the literature are utilizing the exact same single-stage and progressive protocols presented in this study, a regression equation would not be applicable.

Work, however, accounts for both slope and speed and thus makes it more desirable for comparing different studies presented in the literature. Visual inspection of work, however, revealed a similar problem with utilizing any regression equation. Specifically, the problems in the time domain are similarly seen but compressed with less spread, resulting in an even smaller coefficient of determination (R^2=0.317). But, when nonlinearities present were removed through a log transformation, the result was a marked relationship with a coefficient of determination that more than doubled (R^2=0.697). Thus, the following regression equation is proposed for comparing/translating maximum walking studies utilizing differing protocols:

$$SS = 0.5486*PP + 2.4257 \qquad (2)$$

Where SS is the natural log of the work calculated from a single-stage protocol utilizing eq. 1 above, and PP is the natural log of the work calculated from a progressive protocol similarly utilizing eq. 1 above but with varying velocity components according to the slope and speed.

CONCLUSIONS

Single point mass approximations of work during a treadmill walking task, following a log transformation, yields a valuable result of the individual's maximum walking performance. The log calculation of the work can then be compared to other individuals' performance in maximum walking tests regardless which protocol was used.

REFERENCES

1. Gardner AW, et al. *Med Sci Sports Exerc* **23**, 402-408, 1991.
2. McDermott MM, et al. *JAMA* **286**, 1599-1606, 2001.

ACKNOWLEDGEMENTS

This work was supported through an NIH-NIA grant (1R01AG034995), VA RR&D (1I01RX000604), UNMC Widaman Fellowship, and a NASA EPSCOR grant.

DOES SLOWER WALKING SPEED IN OLDER ADULTS PROTECT AGAINST DISTRACTIONS?

[1]Hyun Gu Kang and [2]Dan B. Thap

[1]California State Polytechnic University, Pomona, California
[2]Western University of Health Sciences, Pomona, California
email: hgkang@csupomona.edu www.csupomona.edu/~hgkang

INTRODUCTION

Slow gait in older adults predict dementia, disability, and falls[1]. Slow gait is associated with fear of falls and appear to be a behavioral adaptation[2]. Impairments in cognitive function, specifically executive function and attention, negatively affect gait in older adults, especially when cognitive distractions are present.[3] However, the mechanisms for these changes are not well understood. In particular, it is not clear which of these changes are due to a pathology and which are due to the adaptations around them.

The effect of cognitive impairments and dual tasking on gait has been studied in older adults, often based on self-paced protocols on a gait mat[1]. In these protocols, the specific effects of the pathology on gait are difficult to isolate since the walking individual also controls the speed at the same time as the other gait variables. As an alternative, we wanted to determine the changes in gait due to dual tasking in older adults while controlling for walking speed externally, to isolate the effects on gait separate from that of walking speed. In particular, we tested to see if slow walking in older adults minimizes the effect of dual taking on gait variability, by controlling for walking speed using a treadmill.

METHODS

Nine healthy older adults (mean age 72.2 ± 4.9) and 12 height- and weight-matched young adults (mean age 23.4 ± 1.9), with no orthopedic, neurological, or cognitive impairments, participated with informed consent. Each subject walked for 5 minutes on a L7 treadmill at each of three different speeds: 80%, 100%, and 120% of their preferred speed (PWS)[4]. Participants also performed serial subtractions as a dual task during walking by counting backwards out loud by 3 from 500. The order of presentation was randomized.

We used a treadmill to impose a walking speed on the subjects. Be imposing the walking speed externally, we controlled for behavioral adaptations that can occur when subjects perform the secondary cognitive task while attending to the pacing and velocity in the primary task.

VICON was used to measure the motion of the bilateral heel markers. Step length (SL) was calculated by taking the maximum anteroposterior distance between the heel markers during each step during each trial. Step length variability (SLV) was defined as the standard deviation of step length for each participant per trial. Step width (SW) from mediolateral distance between the heels at each step. Step width variability (SWV) was defined from the step width time series.

Gait parameters (SL, SLV, SW, SWV) from the two age groups, 3 walking speeds, and dual tasking conditions were compared using a full factorial ANOVA (SAS 9.3).

RESULTS AND DISCUSSION

Both groups exhibited PWS of 1.1 m/s ($p = 0.6$). Older adults exhibited longer average SL, SLV ($p=0.008$), SW ($p<0.001$) but not SWV ($p=0.6$). SL in older adults increased more with speed than in young adults. SLV was larger during slower speed in older adults.

SL lengthened with DT at fast speeds, and shortened at slow speeds. SLV, SW, SWV did not change with DT ($p<0.8$). Change in SL with dual tasking was more pronounced at faster speeds in older adults (p=0.056).

The increase in SL due to DT at fast speeds suggests that step time is becoming slower. Yet during slow walking, the adaptation appeared to be the opposite. This suggests that the externally imposed walking speed required a different stepping strategy due to dual tasking.

However, the change in the gait parameters due to dual tasking was not different between walking speeds, except at the fast walking speed. Therefore, slower walking did not reduce the impact of dual tasking on gait in these relatively healthy older adults, whose preferred walking speed was similar to that of young adults. However, they may be less likely to walk fast as their change in gait is exaggerated by dual tasking, eventually leading to slow gait. This phenomenon may occur in an older population with gait pathologies at slower speeds, and thus further work is needed.

CONCLUSIONS

Our objective was to test whether slower walking reduces the effect of dual tasking on gait. When we directly controlled for walking speed, walking speed did not influence the changes in gait parameters due to dual tasking except at the fast walking speed. Further work is necessary to confirm this in a population with existing gait disorders.

REFERENCES

1. Verghese J, et al. *J Am Geriatr Soc*, **54**, 255-61, 2006.
2. Maki BE. *J Am Geriatr Soc*, **45**, 313-20, 1997.
3. Yogev-Seligmann G, et al. *Mov Disord*, **23**, 329-42, 2008.
4. Dingwell JB and Marin LC. *J Biomech*, **39**, 444-52, 2006.

ACKNOWLEDGEMENTS

We thank Dominic Baiocco, William Hill, Mark Dela, Michelle Cotrupe, and Kaitlin Everhart for assistance with data collection.

Figure 1: Influence of Walking Speed and Dual Tasking on Step Length in Young and Older Adults

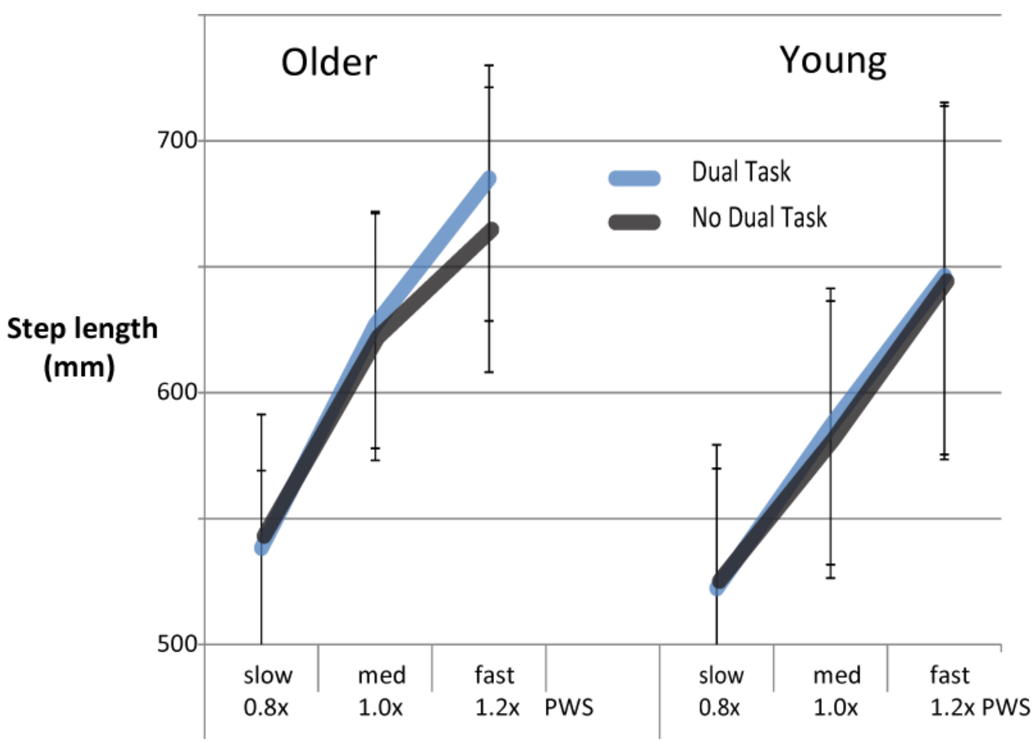

AN AUTOMATED ITERATIVE METHOD FOR ADJUSTING VIRTUAL MODEL MARKERS IN AN OPENSIM MODEL

Arash Mahboobin

University of Pittsburgh, Pittsburgh, PA, U.S.A.
Email: arm19@pitt.edu

INTRODUCTION

OpenSim [1], a widely used biomechanics software package, is a tool for developing and creating subject-specific multi-segment musculoskeletal models and dynamic simulations of movement. Subject-specific models are typically created by scaling a generic musculoskeletal model so that it matches the anthropometry of a particular individual. This is achieved by utilizing OpenSim's Scale Tool [2], where each body segment in the model is scaled based on relative distances between experimental and virtual marker locations, and mass properties (mass and moment of inertia) of each segment is scaled proportionally such that the total mass of the subject is reproduced. In addition to scaling the dimensions of the generic musculoskeletal model, the Scale Tool attempts to adjust the model's virtual markers by solving a weighted least-squares (WLS) problem to find a set of joint angles that minimize the position error between the model markers and the corresponding experimental markers. Both scaling and virtual model marker adjustment are important steps in the generation of dynamic simulations of movement.

Model marker adjustment through OpenSim's graphical user interface (GUI) is typically performed in an iterative manner by which the model can be viewed in a static pose, prior to adjusting model markers, providing the user with the ability to either manually alter the weighting factors on poorly tracked model markers that are included in the WLS problem, or change the x-, y-, and z-coordinates of virtual markers manually to have them match their corresponding experimental locations.

Given the importance of model scaling and marker adjustment, factors such as level of user experience, need for modeling large number of subjects, and use of extensive set of virtual model markers, to name a few, can potentially increase the length of time it takes to complete a Scale Tool process. In this paper an automated iterative approach for adjusting virtual model markers that yields small marker errors between the model and experimental markers is introduced.

METHODS

In the OpenSim's Scale Tool [2], model markers are adjusted by solving a weighted least-squares (WLS) problem, similar to the problem solved during inverse kinematics that finds a set of joint angles minimizing the position error between model and experimental markers. The weighting factors in the WLS problem determine how strongly the optimization should pay attention to adjusting virtual markers.

Finding a set of weighting factors through which the position errors between model and experimental markers are minimized could be both time consuming and challenging using the *manual iterative method*, especially if there are a large number of model markers involved. Here an *automated iterative method* is proposed that solves a series of WLS problems by highly weighting one marker at a time and using the newly scaled model and adjusted marker set obtained in step i as the starting point in step $i+1$ (Fig. 1).

Automated Iterative Marker Adjustment Algorithm
Model markers are iteratively adjusted by the following methodology (Fig. 1): During iteration i, a marker from the model marker set is selected and given a high weighting factor, leaving the rest of the model markers with a weighting factor of 1, therefore allowing the optimizer to pay more attention to the marker with the highest weight factor. A WLS problem is then solved to obtain a

newly scaled model with an adjusted model marker set. Iteration *i+1* then uses this scaled model and adjusted marker set as its starting point. The process is repeated until all model markers have been adjusted.

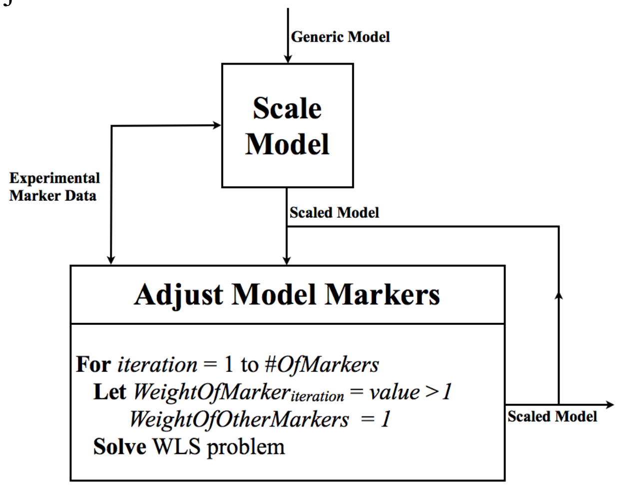

Figure 1. Flowchart representing automated iterative marker adjustment method.

Method Validation

The algorithm was tested on the example model (Gait2354) provided with the OpenSim package. Specifically, the generic musculoskeletal model was scaled and model markers were adjusted using (a) the manual iterative method, where the marker weighting factors suggested in the OpenSim example were used to adjust model markers, and (b) the iterative method described above. Matlab (The Math Works, Natick, MA) and OpenSim 3.0 were used to run the analysis.

RESULTS AND DISCUSSION

The overall RMS position error between the model and experimental markers for the manual and iterative methods were 3.4 cm and 0.02 cm, respectively. The maximum marker errors obtained were 6 cm and 0.04 cm for the manual and iterative methods, respectively. Maximum marker error for the manual method resulted from the left toe tip marker and for the iterative method from the left lateral toe marker.

There were noticeable differences between the side-to-side pelvis rotation, right hip flexion and adduction, right ankle and subtalar angles, and left hip rotation, knee, ankle, and subtalar angles, of which the left subtalar angle had the most significant improvement (-1.02° (iterative) versus 14.95° (manual)).

The total CPU time used by the Matlab process to scale and adjust 39 markers iteratively plus a final marker adjustment step, where all markers where assigned a weighting factor of 1, was 19.7 s.

Solutions of inverse kinematics and inverse dynamics problems are generally sensitive to the accuracy of scaling and model marker adjustment in OpenSim, therefore it is imperative to produce accurate subject-specific models to avoid these sensitivities as much as possible, especially when dealing with a large number of subjects and extensive number of virtual markers.

The manual iterative method is a good way of visualizing and adjusting model markers, producing results that are generally within a desired margin of error. However, the time it takes to adjust markers and therefore obtain reasonable joint angles could increase with factors such as user experience, number of subjects, and number of model markers. The automated iterative method can reduce this time and produce consistent model marker placement and joint angles during a static pose capture.

The results obtained here encourage use of this automated iterative method as an alternative way to adjusting model markers to match corresponding experimental locations as closely as possible. It is believed that the agreement obtained between the model and experimental markers is, to a large extent, due to the use of this iterative algorithm.

REFERENCES

1. Delp SL, et al. *IEEE T Bio-Med Eng* **54**, 1940-1950, 2007.
2. OpenSim Users Guide: *http://opensim.stanford.edu/support/*

ACKNOWLEDGEMENTS

Funding provided by the Pittsburgh Claude D. Pepper Older Americans Independence Center (P30AG024827).

USING FORWARD SIMULATIONS TO PREDICT SAGGITAL KINEMATICS DURING FASTFES

John W. Ramsay, Thomas S. Buchanan and Jill S. Higginson

University of Delaware, Newark, DE, USA
email: jramsay@udel.edu

INTRODUCTION

Stroke is a leading cause of long-term adult disability. Individuals who have suffered a stroke are often limited in performing functional tasks, especially walking. Therefore, regaining the functional ability to walk is a primary goal of post-stroke rehabilitation.

Fast treadmill training has emerged as a safe and effective way to improve walking performance in post-stroke individuals. Additionally, functional electrical stimulation (FES) provides active muscle contraction to muscles at specific times during gait and can also aid in motor learning [1]. FES is primarily used to correct paretic limb foot-drop during the swing phase of gait [2], yet deficits at other joints remain. A recent novel training intervention combining both fast walking speed and functional stimulation of multiple muscle groups (FastFES) has been proposed to address these other deficits [3].

The objective of this preliminary work was to investigate whether a forward dynamic simulation can replicate the experimental sagittal kinematics during FastFES. Using a simple foot-ground contact model, we hypothesized that the hip, knee, and ankle joint angles could be predicted during a simulated task within 5° of the experimental data during swing.

METHODS

One male post-stroke subject (age 59, right paretic) walked on a split belt treadmill (AMTI, Watertown, MA) at his fastest speed (0.6 m/s). Handrails were used and a harness (no bodyweight support provided) was attached for safety. Motion analysis was performed using an 8-camera motion analysis system (Vicon 5.2, Oxford, UK) at 100 Hz and synchronized with analog data at 2000 Hz. Two 20 second trials (NO STIM and STIM) were collected.

Electrical stimulation was delivered to paretic ankle dorsiflexor using surface electrodes. A Grass S8800 stimulator (Grass Instruments, MA), in combination with an SIU8 stimulus isolation unit was used to deliver electrical stimulation. A customized FES-system (CompactRIO, National Instruments, TX) using input from footswitch signals attached to both shoes was used to stimulate the ankle dorsiflexors during paretic swing phase.

Three dimensional kinematic and kinetic data were filtered in Visual 3D (C-Motion Inc., Bethesda, MD). Subject-specific anthropometric scaling parameters and motion data were exported by Visual3D and input into OpenSim 3.0 [4]. A musculoskeletal model with generic muscle parameters, 23 DOFs and 54 muscles was used for all computer simulations. To setup the forward simulations, a residual reduction algorithm was used to account for dynamic inconsistencies between the experimental kinematics and the ground reaction force data. Computed muscle control (CMC) [5] was then used to estimate muscle excitations and fiber lengths during the trial. The results from CMC were used as input to the forward dynamic simulations.

Forward dynamic simulations were performed on the paretic leg during swing. To allow the model to interact with the ground, foot-floor contact forces were modeled using contact spheres representing Hunt-Crossley contact forces [6] and were applied to the heel, first and fifth metatarsal. Additionally, the treadmill platform was given a prescribed speed of 0.6 m/s to match the experimental conditions. Simulations of the NO STIM condition were first used as a baseline to verify that the sagittal kinematics of the model matched the experimental data. Once the kinematics were verified, electrical stimulation was applied "virtually" by adjusting the dorsiflexor (tibialis anterior) muscle excitations during swing to simulate the experimental protocol. The predicted sagittal kinematics during "virtual" stimulation were compared to the kinematics observed experimentally. To limit instability in the system, simulations were performed for a 0.25 second time window occurring during mid-swing.

RESULTS AND DISCUSSION

Kinematic results for hip, knee and ankle joints under all conditions can be found in Figure 1. Sagittal kinematics during NO STIM swing were within 5° for all joint angles when compared between experimental and simulation. After STIM was applied to the simulation, the hip joint kinematics were within 5°, yet did not have the same profile as the experimentally observed data. Up to 50% mid-swing, both the knee and ankle joint angles tracked within the desired range, but diverged toward the end of the simulation.

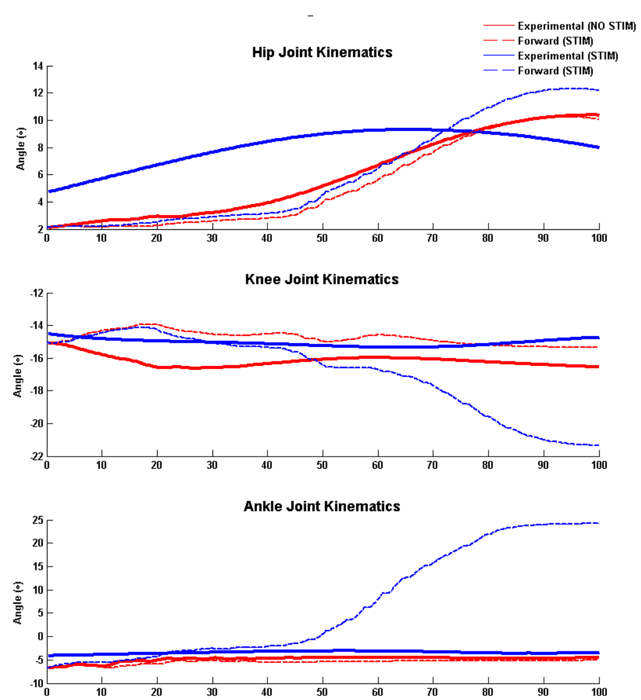

Figure 1. Sagittal kinematics for the knee, hip, and ankle joints during mid-swing. Experimental conditions are compared to forward dynamic simulation predictions during 1) NO STIM and 2) STIM.

The NO STIM kinematic results verified that, by using a few foot-ground contact forces, the forward dynamic simulation was able to match experimentally observed kinematics with prescribing ground reaction forces. The model was then used to predict the kinematics of a "virtual" electrical stimulation protocol. By stimulating the tibialis anterior muscle during swing to full activation, the model only predicted kinematics similar to the experimental data for the first 50% of mid-swing. It is possible that changing the states of the system (i.e. muscle excitation) for the entire duration of swing does not accurately represent the FES protocol, which applies individual electrical bursts separated by interpulse intervals.

More work is required to develop simulations that can overcome the limitations in this study. A simple foot-ground contact model may not be sufficient for post-stroke gait, and generic stiffness values for the forces were used. Additionally, to fully replicate the entire FastFES protocol, plantar flexor stimulation during terminal stance should be applied, resulting in a longer time frame of simulation.

CONCLUSIONS

We have shown that forward dynamic simulations have the capability of reproducing post-stroke experimental gait data within 5°. However, the simulations did not fully predict STIM conditions when electrical stimulation was applied virtually. This motivates the need to continue refining our model with more experimental data. By improving forward simulations with experimental data, novel therapeutic interventions may be eventually be investigated.

REFERENCES

1. Winchester P, et al. *Paraplegia* **32**, 680–686, 1994.
2. Burridge JH, et al., *Clin Rehabil* **11**, 201-210, 1997.
3. Kesar TM, et al., *Stroke* **40**, 3821-3827, 2009.
4. Delp SL, et al., *IEEE Trans on BME* **54**, 1940-1950, 2007.
5. Thelen, D., et al. *J Biomech* **36**, 321–328, 2003.
6. Hunt, KH, and Crossley, FRE. *ASME Journal of Applied Mechanics* 42, 440-445, 1975.

ACKNOWLEDGEMENTS

NIH P30-GM103333, ROI-AR040163, ROI-NS055383, UD Graduate Fellowship Awarded to JWR

Effects of Electromyogram Signal filtering on Muscle Activation Time

[1]Rahul Soangra, [1&2]Thurmon E Lockhart & [2]Jian Zhang

[1]School of Biomedical Engineering & Sciences, Virginia Tech-Wake Forest, VA, USA
[2]Industrial & Systems Engineering, Blacksburg, VA, USA
email: srahul@vt.edu, web: http://ise.locomotion.vt.edu

INTRODUCTION

Important information gained using dynamic electromyography is to accurately define the muscle action and phase timing within the gait cycle. Human gait relies on selective timing and intensity of appropriate muscle activations for stability, loading and progression over the supporting foot during stance, and further to advance the limb in swing phase. A traditional clinical practice is to low pass filter the integrated electromyogram (EMG) signals and to determine onset and cessation events using a predefined threshold. The accuracy of defining period of significant muscle activations by EMG varies with temporal shift involved in filtering of the signals. Low pass filtering with fixed order and cut-off frequency will introduce delay depending on the frequency of the signal. In order to precisely identify muscle activation and to determine onset and cessation times of the muscles, we explore onset and cessation epochs with denoised EMG signals using wavelets denoising, Empirical mode decomposition (EMD) and Ensemble empirical mode decomposition (EEMD) method, which are considered suitable tools for analyzing nonlinear and non-stationary signals such as EMG. Gastrocnemius muscle onset and cessation were determined in eight participants with two different walking conditions. Low pass filtering of integrated EMG (iEMG) signals resulted in premature onset (about 28% of stance duration) in younger when compared with iEMG signals. We also found significantly different onset time events ($p<0.02$ for normal speed walking, $p<0.01$ for fast speed walking) between those detected by low pass filtering and iEMG signals. Wavelet denoising accurately predicted onsets for normal walking. EEMD denoised signals could further detect preactivation onsets during fast walking condition.

METHODS

Eight young subjects (aged between 18-30 years old) of average height (176.25±6.08 cm) participated in the study. The Virginia Tech Institutional Review Board approved the study and the recruited participants had good health, with no cardiovascular, respiratory, neurological, and musculoskeletal abnormalities.

The subjects performed walking on 15 meter long walkway with two embedded forceplates (BERTEC #K80102, Type 45550-08, Bertec Corporation, OH, 43212, USA). A six-camera ProReflex system (Qualysis) was used to collect three-dimensional infra-red passive marker data of participants as they walked over the test floor surface. Kinematic data were sampled and recorded at 120 Hz. The sampling frequency of sampling frequency was set as 1200 Hz. An eight-channel EMG telemetry Myosystem 900 (Noraxon, USA), was used to record EMG signals of gastrocnemius muscle. Only those walking trials were used for analysis when subjects placed their left foot in the middle of forceplate. Kinematic events such as heel contact (HC) and toe off (TO) of both feet were determined by placing four markers at heel and toe (both right and left foot) and these events were verified by forceplates.

<u>Muscle Onset and cessation points were determined by the following algorithm </u>Raw EMG signals recorded during gait were band-pass filtered using a fourth order filter at 20-500Hz and full-wave rectified [1]. In this study, we have used classical threshold based approach for onset determination[2]. Baseline quiescent portion of EMG record was chosen of length 6msec data, starting from -50% of stance. Threshold was defined as shown below

$$Threshold = Baseline\ Mean + 3X\ Baseline\ STD$$

A threshold of three standard deviations above the baseline was used to identify muscle firing onset and cessation[2]. An algorithm was written with

3msec moving window and muscle onset was assumed to follow two conditions: (1) muscle activity was above the threshold for at least 0.1 sec and (2) If the muscle activity dropped below the threshold for more than 3% of stance duration (or 5% of gait cycle). The onset was updated to the new rise above the threshold and short duration EMG packet was discarded [3]. All muscle activity onset and cessation times are reported as percentage of stance duration. *Statistical Analysis:* Subject means used in statistical analyses were calculated as the mean of the two trials performed by each subject. A four factor analysis of variance (ANOVA) with a Tukey's posthoc was used to assess statistical differences between the four denoising methodologies (JMP , SAS USA). Alpha level was set at 0.05.

RESULTS AND DISCUSSION

Mean medial gastrocnemius muscle onset time events for low pass filtered (LPF) EMG signals of eight participants were found to be significantly different from those of iEMG for both normal ($p<0.02$) and fast walking ($p<0.01$) trials (Table 1). For most of the trials earlier onset were detected, when iEMG signals were filtered by low pass filter for normal speed walking trials (Table 1). We found that the duration of muscle activation was significantly different for both normal speed walking ($p=0.0049$) and fast speed walking ($p=0.0012$) for iEMG and low pass filtered (LPF) signals. Thus, traditional way of low pass filtering (LPF) was found to result in earlier onsets in normal walking whereas it was found to be advantageous in detecting preparatory pre-activations in fast walking.

In all fast walking trials, an earlier preparatory pre-activation was found, which was not detected by our threshold based algorithm for iEMG and wavelet denoised signals. This may be one of the reasons for finding significant difference among onsets for iEMG and LPF and that of Wavelet and LPF (Table 1). Thus EMD, EEMD and LPF signals posed advantageous as were able to detect preparatory pre-activations in fast speed walking trials (Figure 1 & 2).

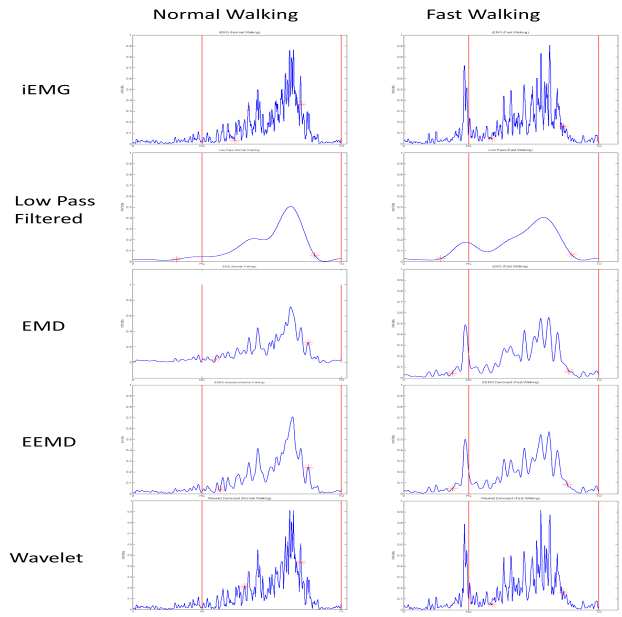

Figure 1: Onset and cessation for normal and fast walking with iEMG (as standard ground truth) and other denoised EMG signals for one participant.

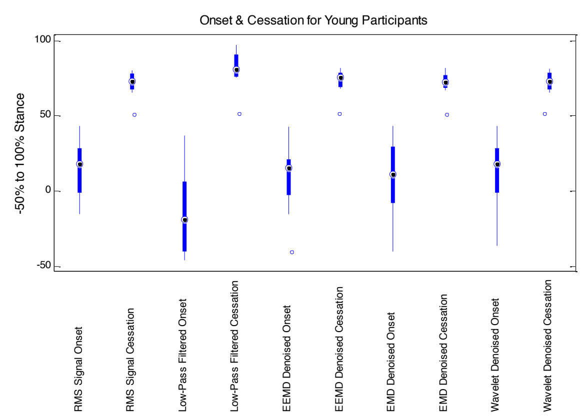

Figure 2: Onset and cessation points of medial gastrocnemius in eight participants

REFERENCES

[1] R. A. Chechile, "Human motion analysis: Current applications and future directions - Harris,GF, Smith,PA," *Journal of Mathematical Psychology,* vol. 41, pp. 126-126, Mar 1997.

[2] R. P. Difabio, "Reliability of Computerized Surface Electromyography for Determining the Onset of Muscle-Activity," *Physical Therapy,* vol. 67, pp. 43-48, Jan 1987.

[3] J. Perry, E. L. Bontrager, R. A. Bogey, J. K. Gronley, and L. A. Barnes, "The Rancho Emg Analyzer - a Computerized System for Gait Analysis," *Journal of Biomedical Engineering,* vol. 15, pp. 487-496, Nov 1993.

Table 1: Tukey's HSD comparison of onset point and time of muscle activation

		Onset Points [% of Stance]		**Muscle Activation Time [sec]**		**Onset Points [% of Stance]**		**Muscle Activation Time [sec]**	
		Fast Walking		Fast Walking		Normal Walking		Normal Walking	
		Difference	p-Value	Difference	p-Value	Difference	p-Value	Difference	p-Value
iEMG	LPF	43.55	0.001*	0.30	0.0012*	34.14	0.0118*	0.28	0.004*
Wavelet	LPF	35.88	0.005*	0.25	0.0091*	32.81	0.0171*	0.27	0.007*
iEMG	EEMD	28.91	0.039*	0.19	0.0923	12.84	0.7227	0.11	0.628
iEMG	EMD	22.73	0.162	0.16	0.2088	10.69	0.8358	0.08	0.825
Wavelet	EEMD	21.24	0.216	0.14	0.3298	11.51	0.7956	0.10	0.699
EMD	LPF	20.81	0.234	0.14	0.3040	23.44	0.1627	0.20	0.091
Wavelet	EMD	15.06	0.553	0.11	0.5646	9.36	0.8918	0.07	0.876
EEMD	LPF	14.63	0.581	0.11	0.5327	21.30	0.2432	0.17	0.188
iEMG	Wavelet	7.67	0.936	0.04	0.9640	1.32	0.9999	0.01	1.000
EMD	EEMD	6.17	0.970	0.02	0.9947	2.14	0.9996	0.02	0.997

COMPARISON OF METHODS TO DETERMINE ROTATION ONSET OF UPPER BODY SEGMENTS WHEN WALKING AND TURNING

[1]V.N. Pradeep Ambati, [1]Nicholas G Murray, [2]Douglas Powell and [1]Rebecca Reed-Jones

[1]The University of Texas at El Paso, El Paso, TX, USA
[2]Campbell University, Department of Physical Therapy, NC, USA
email: vambati@miners.utep.edu

INTRODUCTION

Studies investigating turning control while walking use segment rotation onset from three-dimensional kinematic data to determine segment coordination. Early studies of this behavior define rotation onset as the point where the movement trajectory deviates and continues beyond two (or sometimes three) standard deviations beyond the mean of a control (straight walking) ensemble average [1]. More recent studies have employed the first and third derivatives of displacement data to determine onset of body segment reorientation [2]. Currently it is unknown how these different methods alter the interpretation of segment coordination during turning. The purpose of this study was to compare data obtained using different methods of rotation onset criteria.

METHODS

Nine healthy young adults were recruited from the University of Texas at El Paso campus. Three-dimensional kinematic data were collected using an 8-camera motion capture system (120 Hz, Vicon, San Francisco, California). Participants performed straight path walking trials (control walking trials) and turning trials (both right and left). Displacement data were filtered with a recursive low-pass Butterworth filter with a cutoff frequency of 5 Hz. Straight trials were windowed and ensemble averaged together to create control trajectory movement profiles for the head, trunk, and pelvis during normal straight walking. Rotation onset was determined using two methods. The first method determined onset as the deviation of the displacement profile beyond two standard deviations of the ensemble control profiles. In the second method, displacement data was differentiated to the first derivative (velocity) and reanalyzed with respect to control velocity profiles.

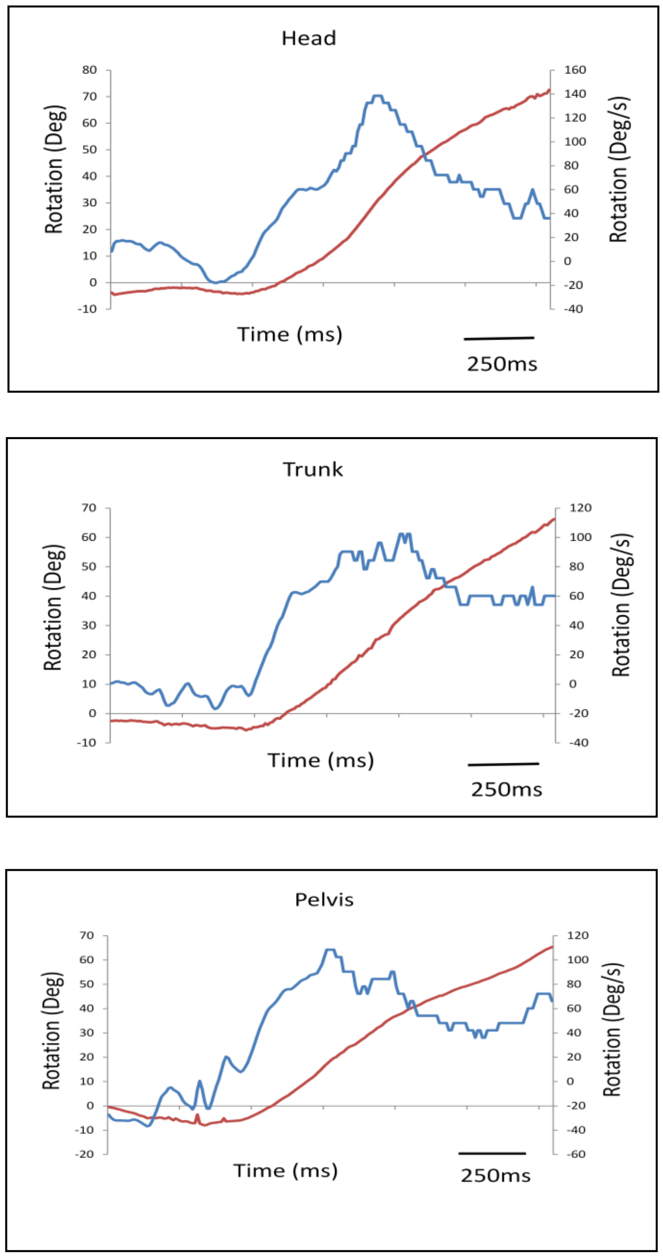

Figure 1: Representative velocity and displacement trajectories plotted together for head, trunk and pelvis segments.

Repeated measures ANOVA compared the onset timings of head, trunk and pelvis obtained using displacement data and velocity data.

RESULTS

There were no significant differences in head onset time obtained from displacement and velocity data. However, onset of trunk and pelvis rotations were significantly different (Table 1). The onset times for trunk and pelvis occurred significantly earlier in the data obtained from velocity compared to displacement analyses. When we plotted the velocity and position of the segments concurrently, it was clear that the velocity for the trunk and pelvis was deviating earlier than actual rotation (Fig 1 above).

DISCUSSION AND CONCLUSION

Though the onset time of head in displacement and velocity analysis were similar, significant differences were seen in trunk and pelvis onset (Table 1). We believe this difference in pelvis and trunk timing could be due to the ongoing movement of these segments during the normal gait cycle. The velocity of these segments begins to increase as the segment comes back to center to begin its rotation in the direction of the turn. Therefore, velocity trajectories for certain segments (trunk and pelvis) may not indicate a true point of rotation initiation. In addition, the use of velocity for onset analyses may limit comparisons to the greater body of literature that has used displacement analyses due to the significant differences observed in the current study between the two methods. Therefore use of displacement data seems to be a better choice for the analysis of turn onset time for body segments when turning while walking.

REFERENCES

[1] Hollands, M.A., Patla, A.E., & Vickers, J.N. (2002). "look where you're going!": gaze bheavior associated with maintaining and changing the direction of locomotion. *Experimental Brain Research*, (143), 221-230.

[2] Hollands, K. L., Vliet, P., Zietz, D., Wing, A., Wright, C., & Hollands, M. (2010). Stroke-related differences in axial body segment coordination during preplanned and reactive changes in walking direction. *Experimental Brain Research,* (202), 591-604. doi: DOI 10.1007/s00221-010-2162-1.

Table 1: The mean turn onset timings and standard deviations of different body segments obtained using displacement and velocity analyses.

	Head	**Trunk**	**Pelvis**
Displacement Data(ms)	668.4 ± 237.4	731.7 ± 253.1	605.7 ± 348.8
Velocity Data(ms)	659.8 ± 201.7	825.5 ± 208.8	751.1 ± 252.2
P value	0.856	0.048*	0.016*

BODY ORIENTATION AFFECTS THE DISTAL UPPER EXTREMITY IMPACT RESPONSE FOLLOWING SIMULATED FORWARD FALLS

[1]Timothy A. Burkhart, [2]Evan Brydges, [2]Jennifer Stefanczyk, [2]David M. Andrews

[1]Western University, London, Ontario, Canada
[2]University of Windsor, Windsor, Ontario, Canada
email: tburkhar@uwo.ca

INTRODUCTION

Injuries to the distal upper extremity frequently occur when people attempt to protect their head and torso with outstretched arms when they impact the ground after falling. The most common injury resulting from this scenario are distal radius fractures, which account for more than 50 % [1] of all fall-related injuries and cost more than $500B annually [2]. While considerable effort has been focused on preventing falls and fall-related injuries, their incidence has remained relatively constant over the last 20 years.

Previous work using a valid and reliable fall simulation method [3] presented the muscle activation patterns and kinematics of forward falls occurring from two fall heights and under three different fall conditions (straight-arm, bent-arm and self-selected). While this work provided valuable insight into the strategies individuals used to safely arrest a fall, only symmetric falls in a single body posture (trunk relative to the legs) were evaluated, which does not accurately reflect the various fall positions people adopt. Therefore, the purpose of this study was to determine the effect of asymmetric loading and body posture on the response of the upper extremity following simulated forward falls.

METHODS

The Propelled Upper Limb fall ARest Impact System (PULARIS) [3] was used to simulate forward fall conditions for 20 (9 male, 11 female) university aged participants. Participants were suspended from PULARIS in varying combinations of torso angles in the horizontal plane (sagittal plane: 0°; asymmetric: 30° and 45° relative to the sagittal plane), and torso to leg height (with respect to the ground) ratios (2:1 - legs below the hips, and 1:1 - legs even with the hips). Details of the fall protocol can be found in [3] but briefly, participants were suspended from PULARIS and raised so that the hands were 10cm above the force plates prior to release. The hands were aligned with the leading edge of the force plates (drop point) and then PULARIS was moved back (~2 m) to the start point. PULARIS was propelled forward from the start point and participants were released into free-fall at 1 m/s when they reached the drop point. Participants were instructed to arrest the fall with their left and right hands by landing onto one of two tri-axial force plates rigidly attached to the floor. Participants' hands impacted adjacent force plates in the 0° falls, and staggered plates in the 30° and 45° degree falls (Figure 1). A few no-fall trials were interspersed throughout the protocol to instill a sense of uncertainty common with actual falls.

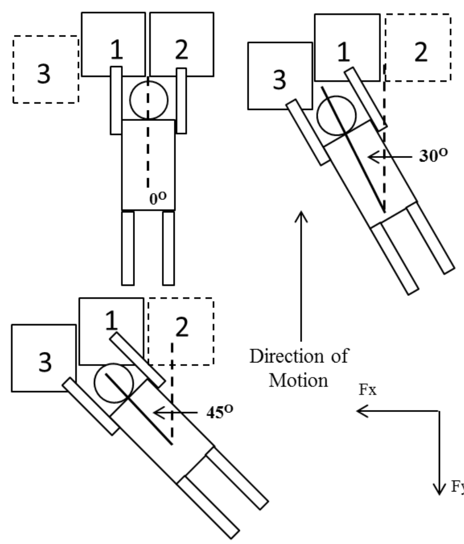

Figure 1: Top view of the experimental set-up showing the position of the force plates relative to the participant in the three fall directions. Note: Fz axis for the force plates is out of the page.

Participants were instrumented with a distal (radial styloid) and proximal (olecranon process) tri-axial accelerometer (right side only). The accelerometers measured the localized impact response in the axial (parallel with the long axis of the forearm), medio-lateral, and off-axis (perpendicular to the long axis of the forearm) directions. Peak forces and accelerations along all three axes were measured and a two-way (angle x direction) ANOVA was used to compare the means of the conditions tested.

RESULTS AND DISCUSSION

The overall mean (SD) resultant impact forces were 282.2 (88.5) and 246.1 (104.5) for the left and right hands, respectively, which agree well with previously reported symmetric fall data [3]. A significant fall direction main effect was found for the right Fx and the left Fx and Fz forces. The Fx forces during the asymmetric trials were almost eight (5.5 N vs. -39.6 N) and 14 (4.4 N vs. -53.5 N) times greater in magnitude compared to the symmetric falls, for the left and right hands, respectively (Figure 2). The left hand Fy and Fz forces decreased significantly by approximately 31 % and 20%, respectively from the symmetric to the asymmetric falls (Figure 2). Taken together, the impact force results suggest that the distal forearm is being loaded more medio-laterally during the asymmetric falls compared to the falls in the sagittal plane, where medio-lateral forces are negligible in relative terms. This shifting in the force vector during asymmetric falls may result in different injury mechanisms compared to symmetric falls.

The mean (SD) resultant distal and proximal accelerations were found to be 18.7 (4.3) g and 11.2 (4.6) g, respectively. A significant direction main effect was found for the proximal medio-lateral accelerations, such that the mean medio-lateral acceleration was a maximum of approximately 4 g less for the symmetric than the asymmetric falls. These acceleration findings further support the force data in that they reflect a similar change in the direction and magnitude of the joint loading.

In addition, a significant torso angle main effect was found for the proximal axial and off-axis peak accelerations. The proximal axial acceleration increased from a mean (SD) of -1.2 (3.9) g to 2.8 (3.4) g, while the off-axis acceleration decreased from -2.8 (4.1) g to -0.6 (4.5) g between the 1:1 and the 2:1 torso to leg height ratios. These results are consistent with the fact that falling with the legs positioned below the hips would reduce the percentage of body weight that is directed through the upper extremity at impact.

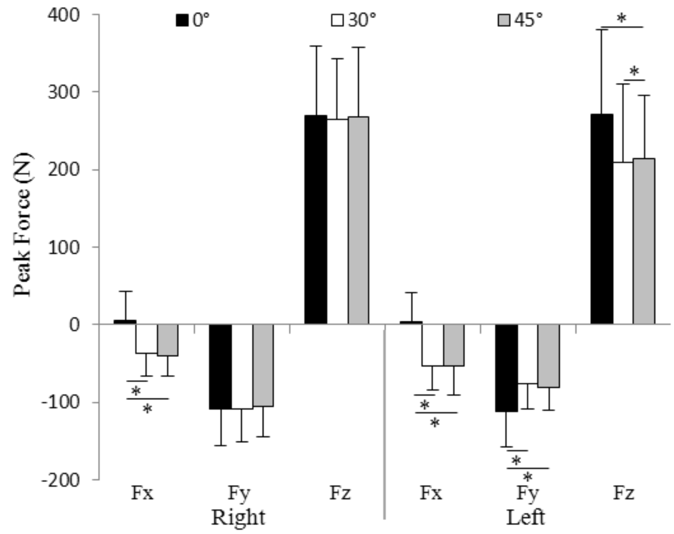

Figure 2: Comparison of the mean (SD) peak forces across the three fall directions for the left and right hands (*p<0.05).

CONCLUSIONS

A forward fall initiated impact can be affected by the way an individual falls. The force and acceleration results presented here suggest that falling asymmetrically can alter the magnitude and direction of the loading vector applied to the distal upper extremity, compared to falling in the sagittal plane. Specifically, falling asymmetrically may protect the distal upper extremity from injury by distributing the forces that cause a fracture inducing moment on the dorsal aspect of the radius, to occur in a more medio-lateral direction.

REFERENCES

1. Kim K-Y, et al. *Clin Biomech* **18**, 311-318, 2003
2. Burge R, et al. *J Bone Min Res* **22**, 465-475, 2007
3. Burkhart TA, et al. *JEK*, 2013 (in press)

ACKNOWLEDGEMENTS

Natural Sciences and Engineering Research Council of Canada and Don Clarke

CENTER OF PRESSURE TRAJECTORY DURING GAIT: A COMPARISON OF FOUR FOOT POSTURES

[1]Vipul A. Lugade and [1]Kenton R. Kaufman

[1]Mayo Clinic, Rochester, MN, USA
email: kaufman.kenton@mayo.edu

INTRODUCTION

The center of pressure (COP) movement has been identified as a measure of neuromuscular control during posture and gait. Defined as the centroid of all the external forces acting on the plantar surface of the foot, the COP has further been used to identify balance control, foot function, and treatment efficacy [1].

As patients with lower limb dysfunction often demonstrate modified gait patterns, it would be beneficial to characterize COP trajectories over a variety of possible foot strike conditions. Previous studies have demonstrated the effectiveness of orthoses in reducing the COP mediolateral movement among patients with forefoot valgus and forefoot varus [2], though no studies have demonstrated the expected COP trajectory across stance for a variety of foot postures during gait.

Knowledge of the proper COP trajectory can provide clinicians with proper diagnosis of foot pathology and treatment intervention. Therefore the purpose of this study was to investigate the COP movement when walking under normal and modified gait conditions.

METHODS

A total of 13 healthy young adults (8 females, age 25.1 ± 2.9 years), were asked to walk barefoot across an 8 meter walkway under four conditions: 1) plantigrade; 2) equinus; 3) inverted; and 4) everted walking. During equinus, inverted, and everted walking, subjects ambulated on their toes, lateral borders of their feet, and medial borders of their feet, respectively, in order to simulate walking with a pathology. All participants provided written informed consent prior to involvement in the study. The study protocol was approved by the Mayo Clinic Institutional Review Board.

Three-dimensional trajectories of 12 reflective markers bilaterally placed on the feet were collected using a 10-camera motion analysis system (Motion Analysis Inc., Santa Rosa, CA). Ground reaction forces and moments were collected from three force plates (AMTI Inc., Watertown, MA). Kinematic and kinetic data was collected at 120Hz and 720Hz, respectively. Foot anthropometrics including navicular height, foot length and foot width. The arch index was calculated during loaded conditions based on the ratio of navicular height and foot length [3].

The COP was computed for each limb throughout stance from the measured ground reaction forces and moments. The COP was converted into the foot coordinate system, with data normalized in the anterior-posterior and medial-lateral direction based on the foot length and foot width, respectively. Differences in the COM range of motion (ROM) across walking conditions was evaluated using a one-way ANOVA. A comparison of loaded foot arch index and the COP ROM was performed using a Pearson's correlation.

RESULTS AND DISCUSSION

A total of 26 feet were evaluated across all four walking conditions, with the COP traversing the forefoot, lateral boundary, and medial boundary of the foot during the three pathological gait conditions (Fig. 1). On average, the COP remained along the midline, the lateral portion, and the medial portion of the foot, during midstance for plantigrade, inverted and everted walking, respectively (Fig. 2). Towards end of stance, the COP progressed to the 1st metatarsal-phalangeal joint for all conditions.

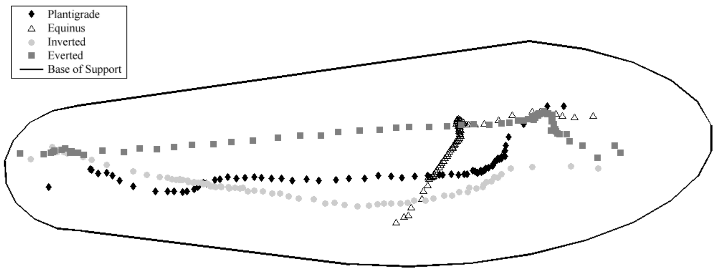

Figure 1: Representative trajectories of the COP for the right foot during plantigrade, equinus, inverted, and everted walking.

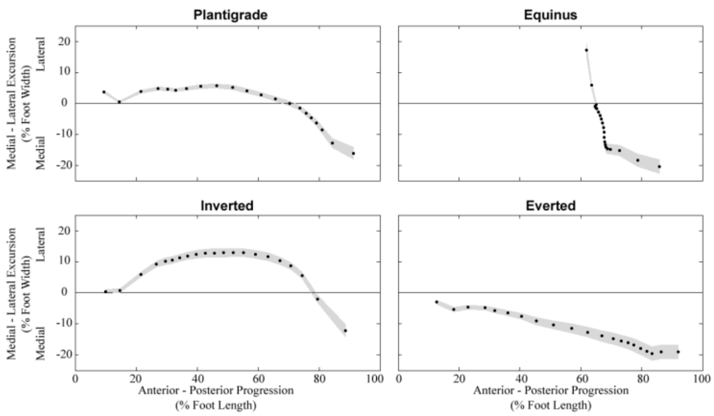

Figure 2: Excursion of the COP over the four walking conditions. Each point represents 5% of stance. Gray bands represent ± 1 SD.

Participants demonstrated a significant condition effect for both the anterior-posterior and medial lateral COP ROM (Fig 3; $P < 0.001$). The equinus walking condition demonstrated differences from all other conditions ($P < .001$), with the COP traversing across approximately 26% of the foot length and 41% of the foot width. The inverted walking condition also demonstrated a 10% greater COP ROM in the medial lateral direction than everted walking ($P = 0.036$).

The arch index was not correlated with the COP ROM for any measure except for the anterior posterior COP ROM during inverted walking ($R^2 = 0.31$; $P = 0.008$).

Results of the COP ROM are similar to those reported previously, in which the COP displacement corresponded to 83% of foot contact length and 18% of foot contact width [4]. During midstance, foot placement affected the COP by up to 10% in the medial lateral direction, revealing mechanisms for further complications. During pathological walking, balance ability and joint loading are affected, as the center of mass acceleration and lower extremity torques are altered by COP position. Investigation of the COP trajectory among patients is therefore crucial for proper intervention.

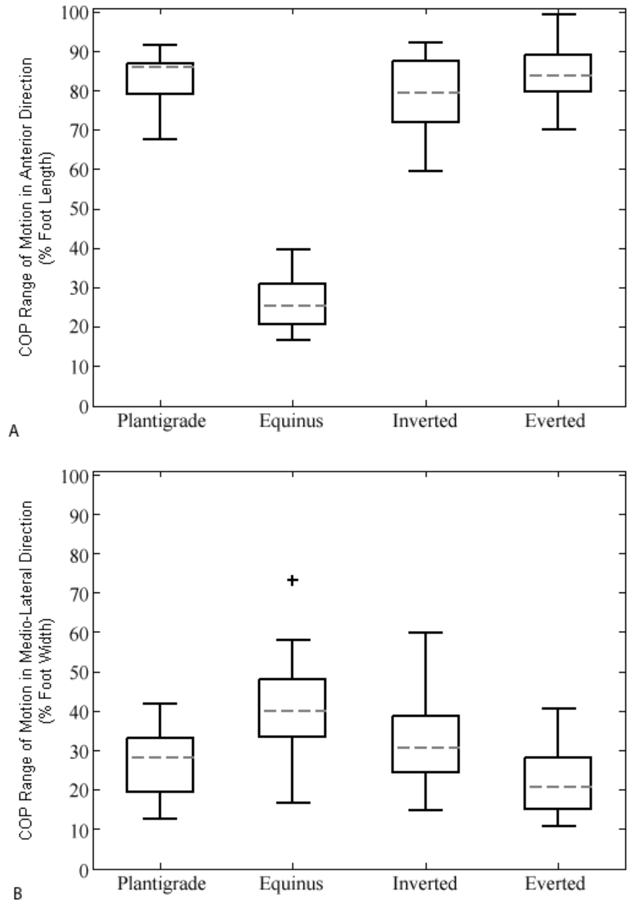

Figure 3: COP range of motion across four conditions. The central dashed line represents the median, the box edges are the 25th and 75th percentiles, and the whiskers extend to ± 2.7 SD. Outliers are labeled as +.

REFERENCES

1. Chesnin KJ, et al. *Gait Posture* **12,** 128-33, 2000.
2. McPoil TG, et al. *Phys Therapy* **69,** 149-54, 1989.
3. Kaufman KR, et al. *Am J Sports Med* **27,** 585-93, 1999.
4. Han TR, et al. *Gait Posture* **10,** 248-254, 1999.

ACKNOWLEDGEMENTS

Funding was provided by NIH T32 HD07447.

THE EFFECTS OF EXPERIMENTAL KNEE PAIN ON CO-CONTRACTION AND SPATIOTEMPORAL CHARACTERISTICS DURING A 30-MIN RUN

W. Matt Denning, Scott Woodland, Iain Hunter, J. Ty Hopkins, and Matthew K. Seeley
Brigham Young University, Provo, UT, USA
Email: mdenning@byu.edu

INTRODUCTION

Knee pathology will likely affect one in two Americans who reach the age of 85 and the related annual costs are approaching twenty billion dollars [1, 2]. Knee pathologies usually alter lower-extremity mechanics and eventually result in functional disability [3]. Researchers have demonstrated that knee pain can independently influence knee joint mechanics [4], however, studies investigating the effects of experimental knee pain on muscle activation during running are lacking. If knee pain, independent of other knee injury factors, alters muscle activation and lower-extremity mechanics during running, then knee pain could be a potential mechanism to predispose patients to chronic knee joint diseases. The purpose of this study was to determine if knee pain, independent of other knee pathology factors, influences muscle co-contraction and spatiotemporal characteristics.

METHODS

Twelve healthy subjects gave informed consent and participated in this study. Each subject completed three different conditions (pain, sham, and control) in a counterbalanced order. For each condition, subjects ran for 30 min at one of three speeds (3.0, 3.5, or 4.0 m/s). During the painful condition, subjects ran while receiving an 8-ml infusion of hypertonic saline (5.0% NaCl) into the infrapatellar fat pad, while the sham condition consisted of an 8-ml infusion of isotonic saline (0.9% NaCl) into the fat pad. The control condition consisted of subjects running with no infusion. Perceived pain levels were measured every three minutes using a 100-mm visual analog scale. Ten high speed cameras (VICON, Santa Monica, CA, USA) were used to collect 3D coordinate data (240 Hz) for bilateral heel and toe markers. Surface electrodes were use to measure bilateral ectromyography (EMG) for the: vastus medialis (VM), vastus lateralis (VL), medial hamstring (HM), lateral hamstring (HL), and medial gastrocnemius (GM). EMG data were processed using a root mean square algorithm (moving window = 50 ms). Each muscle was considered to be on when its amplitude was ≥ 20% of its maximum amplitude, calculated as the average of ten maximum stance-phase peaks during a 5 min warm-up trial prior to infusion.

Muscle co-contraction duration was determined to be the percentage of stance that at least one knee flexor and extensor was on. EMG and marker position data were recorded for 30 s at four different time points during the run (1, 10, 20, 30 min). Five gait cycles were identified during each 30 s trial and the average of the five gait cycles were averaged across the four different times, representing the entire 30 min run. EMG and marker position data were exported to MATLAB where co-contraction duration, stance time, swing time, stride rate, and stride length were calculated using custom algorithms. The independent variables for this study were condition (pain, sham, and control) and time (every 3 min from the start of the run for perceived pain). The dependent variables were muscle co-contraction duration, stance time, swing time, stride rate, stride length, and perceived pain. A mixed model repeated measures ANOVA was used to determine significance ($\alpha = 0.05$) for the dependent variables. A Tukey's post hoc comparison was used to evaluate significant between-condition differences and the nature of the interactions.

RESULTS AND DISCUSSION

A significant condition × time interaction existed for perceived pain ($p < 0.001$). Perceived pain remained significantly higher throughout the 30 min running trial during the painful condition only (Figure 1). Spatiotemporal characteristics for each condition can be found in Table 1. The painful condition resulted in lower stance times and decreased stride lengths when compared to the control ($p < 0.01$) and sham ($p < 0.05$) conditions. Additionally, stride rate increased during the painful condition when compared to the control ($p < 0.001$) and sham ($p = 0.01$) conditions. The three conditions did not result in any significant difference in co-contraction durations ($p = 0.13$; Figure 2).

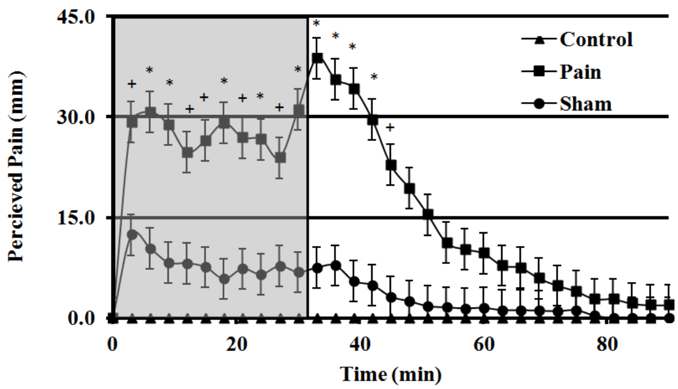

Figure 1: Means and standard errors for perceived pain. Gray area represents the 30 min run. * indicates significance from sham and control. + indicates significance from control only.

The spatiotemporal characteristics we observed during this study are similar to characteristics observed for individuals possessing knee pain due to knee pathologies [5]. This indicates that the experimental knee pain model in this study may be similar to knee pain related to actual knee pathologies. Additionally, it is important to note that this model was able to result in consistent experimental knee pain for 30 min, a relatively extended duration for experimental knee pain. While not measured in this study, the decreased stride length we observed could be due to decreased range of knee joint motion. With a shorter stride, stride rate would also be influenced in order for subjects to maintain the set running speed.

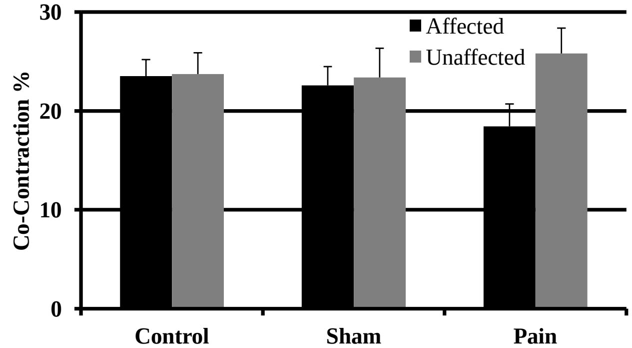

Figure 2: Co-contraction duration means and standard errors measured as a percent of stance phase for each of the three conditions.

CONCLUSIONS

Experimental knee pain during a 30 min running protocol did not affect muscle co-contraction duration. Spatiotemporal characteristics, however, were significantly affected by experimental knee pain; we observed decreased stance times, increased stride rates, and decreased stride lengths. These findings are consistent with idea that perceived pain is similar to pain found in knee joint pathologies. Additionally, the model was able to produce significant experimental knee pain for a relatively extended duration.

REFERENCES

1. Gottlob C, et al. *Clin Orthop Rel Res*, **367**, 272-282, 1999.
2. Murphy L, et al. *Arthritis Rheum*, **59**, 1207-1213, 2008.
3. Merle-Vincent F, et al. *Joint Bone Spine*, **74**, 612- 616, 2007.
4. Neogi T, et al. *Osteoarthr Cartilage*, **18**, 1250-1255, 2010.
5. Baliuman A, et al. *Osteoarthr Cartilage*, **10**, 573-579, 2010.

Table 1: Mean ± SD of spatiotemporal characteristics during each the three conditions. * indicates significance from the painful condition ($\alpha = 0.05$).

	Stance Time (sec)	Swing Time (sec)	Stride Rate (sec)	Stride Length (m)
Pain	0.29 ± 0.03	0.40 ± 0.04	1.45 ± 0.09	2.43 ± 0.32
Sham	0.30 ± 0.02*	0.40 ± 0.03	1.43 ± 0.08*	2.45 ± 0.31*
Control	0.31 ± 0.02*	0.40 ± 0.03	1.43 ± 0.09*	2.46 ± 0.32*

ASSOCIATION BETWEEN PEAK FOREFOOT PLANTAR SHEAR STRESSES AND PHYSICAL BODY MEASURES

[1]Metin Yavuz, [1]Neha Delvadia, [1]Jayson Atves, [1]Jacqueline Goldfarb, [1]Joseph Stuto, [2]Nilin Rao, [3]Alan Glaros
[1] Kent State University College of Podiatric Medicine, Independence, OH, USA
[2] Kent State University Department of Exercise Physiology, Kent, OH, USA
[3] Kansas City University of Medicine and Biosciences, Kansas City, MO, USA
email: m.yavuz@gmail.com

INTRODUCTION

Prelinimary studies have shown that plantar shear stresses are increased in diabetic patients with neuropathy. It is also known that diabetic patients tend to be overweight. Peak pressure has been long considered a risk factor for diabetic foot ulceration. Earlier studies on the relationship between body mass and/or weight and peak plantar pressures in diabetic patients revealed a realtively weak assocititation [1,2]. Cavanagh et al (1991) demonstrated a significant correlation between body mass and peak pressures in diabetic patients. Ahroni et al (1987) on the other hand, claimed that peak pressure values of heavier individuals may not necessarily be abnormally high. Another physical body attribute, body height, has been associated with step length [3]. It is also known that step length depends on anteroposterior ground reaction forces [4].

To our knowledge the literature does not contain any reports that discuss a potential correlation between peak plantar shear stress and body measures such as body mass or height. The purpose of this study was to explore these relationships using a custom-built pressure-shear plate.

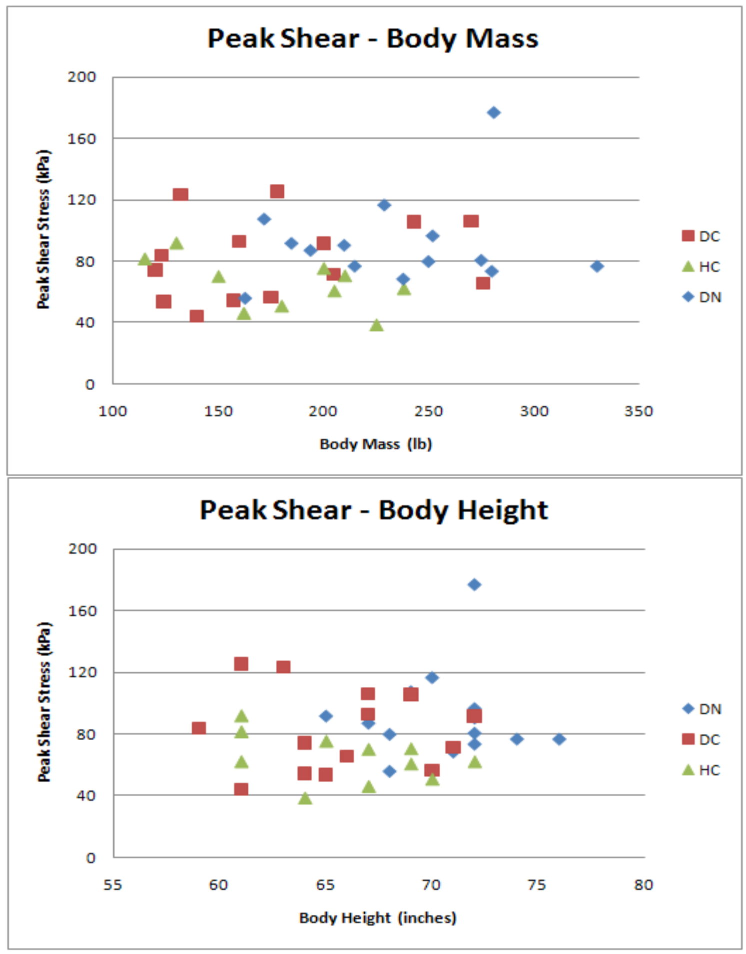

Figure 1: PS-Body Mass (top) and PS-Body Height (bottom) correlation graphs.

METHODS

The study was approved by the Institutional Review Board. Subjects gave informed consent before participation. Group DN consisted of 14 diabetic neuropathic patients (2 F, 64.8±6.8 years, 32.0±5.1 BMI). The second group (DC) comprised 14 diabetic patients (9 F, 52.4±12.9 years, 28.9±7.4 BMI) without neuropathy. The third group was the healthy control (HC) group, which included 11 individuals (7 F, 65.5±6.0 years, 27.8±5.9 BMI). Peripheral neuropathy was tested by a Biothesiometer and 5.07 Semmes-Weinstein monofilaments. Each subject walked multiple times at self-selected speeds on the stress plate, which was installed on a 12-ft walkway and set flush. Data from three trials were averaged and used in statistical analysis. Data were collected implementing the two-step method. Two shear stress variables were identified in each subject; peak shear (PS) and peak shear-time integral (STI). Two physical body measures of each subject group were correlated against the two stress parameters. These measures were body mass (pounds) and height (inches). Pearson Product Moment Correlation Coefficients (r) were calculated for each correlation. Multiple linear regression models were also generated for each group.

RESULTS AND DISCUSSION

No correlation was statistically significant. No absolute value of r was over 0.5. Neither body mass nor body height could account for any degree of variance in peak shear or peak shear-time integral values. Results indicated that plantar shear under the foot, regardless of a diabetic condition, do not depend on body mass or height. Table 1 displays the calculated r and respective p values. Figure 1 displays the correlation graphs for PS. Previous studies indicated that although there may be a statistically significant correlation between body mass and peak plantar pressures, this relationship is somewhat weak. The reason to the lack of a strong relationship might be variations in the structure of the foot. For example, in diabetic patients with peripheral neuropathy, compromised plantar fat may lead to bony prominent areas, where high pressure values can be seen. This may also be true for localization of plantar shear. Also, the proportional dimensions of the human body and foot may present great variation, which would also lead to substantial variations in the plantar surface area.

This study revealed that, PS and STI may vary regardless of body mass. These results also confirm an earlier report that showed that plantar shear stresses cannot be easily predicted based on plantar normal loads [5].

It was also found in this study that PS and STI may vary independent of body height. This might also indicate that PS and STI do not necessarily depend on gait speed; however this hypothesis needs to be further investigated.

It is thought that effective load bearing area, gait speed, muscle activity, frictional properties and moisture content of the skin, and other intrinsic factors might influence local shear stresses as well as body mass and height. Such a complicated relationship needs to be further investigated in a large sample study. The purpose of this study was to present preliminary data on the potential association of plantar shear stress and physical body measures.

REFERENCES

1. Cavanagh PR, et al. *Diabetes Care* **14** (8), 750-5, 1991.
2. Ahroni JH, et al. *Diabetes Care* **22** (6), 965-72, 1999.
3. Hof AL. *Gait & Posture* **4**, 222-3, 1996.
4. Martin PE, et al. *J Biomechanics* **25**, 1237-9, 1992.
5. Yavuz M, et al. *J Biomechanics* **40**, 3045-9, 2007.

ACKNOWLEDGEMENTS

This study was possible due to funds from the NIH grant 1R15DK082962.

Table 1: Pearson Correlation Coefficients (p values) of Group DN, DC and HC correlations.

	Group DN		Group DC		Group HC	
	Body Mass	**Body Height**	**Body Mass**	**Body Height**	**Body Mass**	**Body Height**
PS (kPa)	0.167 (.569)	0.039 (.896)	0.218 (.455)	-0.041 (.889)	-0.426 (.191)	-0.401 (.222)
STI (kPa.s)	0.187 (.522)	0.136 (.644)	0.289 (.316)	0.035 (.904)	0.439 (.177)	-0.038 (.911)

ANALYSIS OF FOOT CLEARANCES IN FIREFIGHTERS DURING ASCENT AND DESCENT OF STAIRS

[1,2]Richard M. Kesler, [1]Gavin P. Horn and [3]Elizabeth T. Hsiao-Wecksler

[1]University of Illinois, Fire Service Institute, Urbana-Champaign, IL, USA
[2]University of Illinois, Dept. of Bioengineering, Urbana-Champaign, IL, USA
[3]University of Illinois, Dept. of Mechanical Science and Engineering, Urbana-Champaign, IL, USA
email: rkesler2@illinois.edu, web: http://fsi.illinois.edu

INTRODUCTION

Slip, trip and fall (STF) injuries are the leading cause of moderate to severe injuries and the second leading cause of minor injuries to firefighters on the fireground [1].#Ascending and descending stairs is generally regarded as a common everyday activity, however the U.S. Consumer Product Safety Commission estimated that there were approximately one million stair related accidents in 1990. Results from a 2008 survey of 148 firefighters showed stairs as the fifth most prevalent cause of fireground injury [2]. Firefighters routinely traverse stairs in heavy firefighting personal protective equipment following significant amounts of work and fatigue, often while carrying heavy asymmetrical loads. The prevalence of STF injuries on the fireground, and the inherent risks associated with ascending and descending stairs indicate a need to examine stair ascent and descent in firefighters.

METHODS

Twenty-four firefighters (23 male, 1 female, age 28.6±7.9 years, height 1.8±0.1 m, weight 90.7±14.9 kg) participated in this study. All provided informed consent and IRB approval was obtained. All firefighters participated in three different fatiguing protocols, though only one, simulated firefighting in a burn building, is used in this analysis. Simulated firefighting was comprised of four activities done on a two-minute work-rest cycle: (1) a stair climb in which the subject climbed to the second step on a three-step, 1.2 m wide staircase, touched both feet to the second step, then stepped backward down to ground level, (2) a simulated hose advance, in which a section of hose was fixed to a modified weight pull machine, (3) a simulated secondary search, which included crawling around the perimeter of the room on hands and knees, and (4) a simulated overhaul task in which a pipe was attached to a modified weight pull machine that required pulling weight from overhead. For activities (2) and (4), 9.1 kg (20 lb) of weight were used to simulate the load of advancing a hose or pulling ceiling.#
#
Before and immediately after the fatiguing protocol, each subject went through a course consisting of six obstacles. The second obstacle was a 1.2 m wide, three step tall staircase where firefighters ascended one side and descended the opposite, always facing forward. Subjects then proceeded to the remaining four obstacles. Subjects passed through the full obstacle course twice and then twice through the first three obstacles carrying an 11.3 kg hose load on the right shoulder for a total of four trials before and four trials after the fatiguing protocol.#
#
Toe and heel clearances over the edges of the stairs were recorded using three-dimensional motion capture data sampled at 200 Hz (OQUS 100, Qualisys, Sweden). Reflective passive markers were placed on the boot in the vicinity of the heel, first metatarsal, fifth metatarsal and on the tip of the boot. A calibration trial was conducted to determine distance from the marker placement to the ground and to determine the angle of the foot during flat stance. The vertical offset was used to determine the bottom of the boot so true vertical clearance could be calculated. Vertical clearance of the toes (VCT) during ascent and vertical clearance of the heel (VCH) during descent were examined. VCT was calculated as the average vertical clearance of the "true" first and fifth metatarsals when each marker was vertically aligned with the stair edge. VCH was determined as the vertical clearance of the "true heel" and the stair edge when the two were vertically aligned. Considering subjects did not

always begin traversing the stairs using the same foot, 'leading' and 'trailing' limbs for landing and passing stairs were compared. The first foot on stair one was considered the leading limb and used to determine the Stair 1 Landing (S1L) clearance, with the first foot on stair two considered the trailing limb and used to determine the Stair 1 Passing (S1P) clearance (see Figure 1). For descent the same naming convention was used. The first foot on stair four was considered the lead descending limb, with the first foot to touch stair five considered the trailing descending limb. This naming convention was presented in [3].

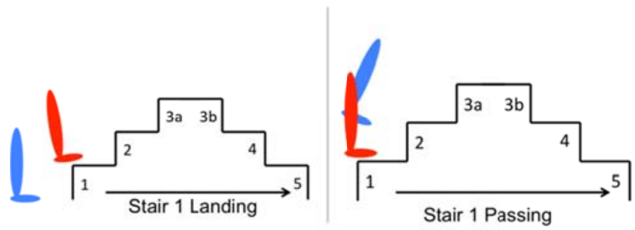

Figure 1: Illustration of stair edges and definition of landing and passing limbs during ascent. The left image shows landing clearance over stair one. The right image shows passing clearance over stair 1. Note that Stair 4 Landing (S4L) would indicate the clearance over edge 3b of the foot proceeding to land on stair 4.

RESULTS AND DISCUSSION

There was a significant *Time* main effect for stair clearances on five out of the 12 variables examined (SPSS 20, IBM, New York; Table 1). These included S1L ($p=0.005$), S3L ($p=0.003$), S4P ($p=0.039$), S5P ($p=0.002$) and FL ($p=0.048$). During ascent, clearances decreased across five of the six parameters examined, although only two were statistically significant (S1L and S3L). Clearances for S4L also decreased following fatigue. All other descent parameters (S4P, S5P, S5L, FL and FP) increased in clearance after fatigue, three of which were significant.

Previous studies have examined the negative effects of fatigue on postural control [4], stability [5,6] and gait [7]. Effects of fatigue also resulted in decreased sense of limb position [8]. The fatigue induced by simulated firefighting resulted in significant decreases in clearances while ascending and increases in clearances while descending stairs. The firefighters' lessened postural control and reduced sense of limb position may have carried them into the stairs during ascent and carried them away from the stair edges during descent.

CONCLUSIONS

The impact of fatigue on clearance over stair edges, especially the decrease seen during stair ascent could lead to increased risks of trips and falls while navigating stairs. An examination of the horizontal clearances could further the hypothesis that reduced postural control and sense of limb position due to fatigue carried the firefighter into the stair edges during ascent and away from the edges during descent. Further investigations into the effects of asymmetrical load carriage and different fatiguing conditions are still necessary.

REFERENCES

1. Karter MJ. *National Fire Protection Assoc*, 2012
2. Petrucci, MN, et al. *ASB Proceedings*, Gainesville, FL, 2012
3. Muhaidat J, et al. *Gait Posture* **33,** 504-506, 2011
4. Gribble PA, et al. *Arch Phys Med Rehabil* **85(4)**, 589-592, 2004
5. Dickin DC, et al. *Scand J Med Sci Sports* **18**, 765-772, 2008
6. Johnston RB, et al. *Med Sci Sports Exerc* **30(12)**, 1703-07, 1998
7. Park K, et al. *Safety Sci* **49**, 719-726, 2011
8. Allen TJ, et al. *Exp Brain Res* **170**, 30-38, 2006

ACKNOWLEDGEMENTS

The authors thank Matt Petrucci, David Li, Michael Angelini, Julian Sy, Lela DiMonte, and Dan Warner for their assistance. This project was funded by the Dept. of Homeland Security Fire Prevention & Safety Grant #EMW-2010-FP-01606.

Table 1: Stair Clearances (Mean±SE) over Stair Edges given in mm. Parameters indicated with a star (*) showed significant differences between pre- and post-fatiguing trials ($p<0.05$).

Ascent	S1 Landing	S1 Passing	S2 Passing	S2 Landing	S3 Landing	S3 Passing
Pre	43.9±4.3*	146.6±6.1	81.9±6.5	33.7±3.0	42.9±3.0*	47.9±6.4
Post	32.0±4.3*	141.2±5.4	77.3±7.1	30.2±3.2	35.8±3.6*	49.2±7.4
Descent	S4 Landing	S4 Passing	S5 Passing	S5 Landing	Floor Landing	Floor Passing
Pre	49.1±5.4	150.2±6.6*	136.5±3.2*	74.9±6.0	92.4±11.3	174.7±3.9*
Post	43.7±5.1	164.4±4.4*	151.0±4.2*	79.3±6.1	102.8±8.7	179.9±2.8*

SEX DIFFERENCE IN KINEMATIC AND KINETIC PATTERNS OF TREADMILL WALKING IN PREADOLESCENT CHILDREN

Jianhua Wu and Toyin Ajisafe
Georgia State University, Atlanta, GA, USA. Email: jwu11@gsu.edu

INTRODUCTION

Typically developing children are able to increase peak vertical ground reaction forces (GRF) while walking at a faster velocity [1]. It is not clear to what extent external ankle load (i.e., weights attached above the ankles) affects the kinematic and kinetic patterns of treadmill walking in typically developing children. External ankle load is a means of manipulating the inertial property of the lower extremities. This external load is found to facilitate the pendulum swing of the legs during locomotion [2] and enhance load sensory feedback during push off [3]. This study aimed to investigate the possible sex difference in the kinematic and kinetic patterns of treadmill walking in preadolescent children.

METHODS

Participants: Eight boys (mean age 9.1 years, height 1.32 m, and weight 29.1 kg) and five girls (mean age 8.9 years, height 1.29 m, and weight 24.9 kg) participated in this study.

Experimental design: There were two treadmill speed conditions: 75% (SS) and 100% (FS) of the participant's preferred overground walking speed. There were three external ankle load conditions: no load (A0), 2% load (A2), and 4% load (A4). A2 and A4 conditions were equal to 2% and 4% of the participant's body weight on each side, respectively.

Data collection:
A total of six conditions (2 speed by 3 ankle load) were tested. These conditions were randomized across the two groups. Two 60-second trials were collected for each condition. A Zebris instrumented treadmill was used to collect vertical GRF data.

Data analysis: Stride time was calculated from heel strike to heel strike of the same foot. The first peak force (F_{Z1}), the minimal force (F_{MIN}), and the second peak force (F_{Z2}) were determined for each gait cycle. Loading rate and unloading rate were calculated for the loading phase after heel strike and for the unloading phase before toe off, respectively, in a unit of BW/sec (Fig. 1). Total F_Z impulse was calculated for the area under the force curve, and it was the sum of vertical impact impulse (from heel strike to F_{MIN}) and vertical propulsive impulse (from F_{MIN} to toe off), in a unit of BW*sec.

Fig. 1

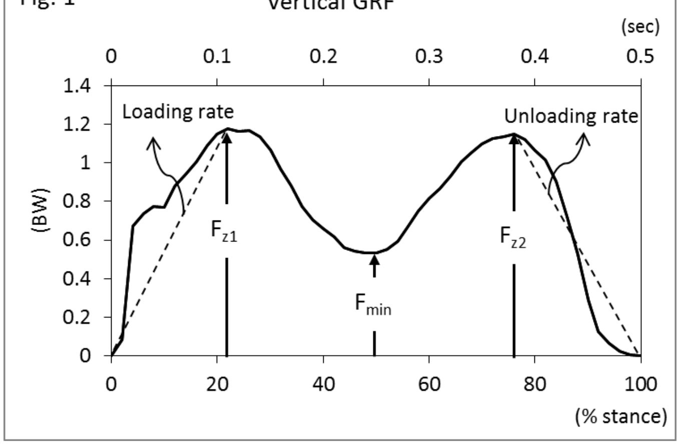

Statistical analysis: Three-way (2 group x 2 speed x 3 load) ANOVAs with repeated measures on the last two factors were conducted on each dependent variable. Statistical significance was set at $p<0.05$.

RESULTS AND DISCUSSION

Boys increased stride time with ankle load, while girls decreased it from A2 to A4. Both boys and girls decreased stride time with speed (Fig. 2).

Fig. 2

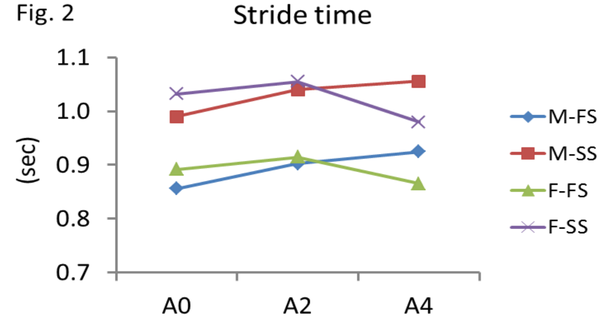

Boys increased F_{Z1} with ankle load, while girls decreased F_{Z1} from A2 to A4. Both boys and girls increased F_{Z1} with speed (Fig. 3).

Fig. 3

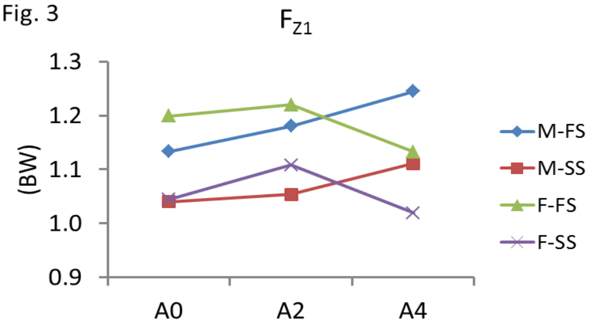

Boys increased F_{Z2} with ankle load, while girls decreased F_{Z2} from A2 to A4. Both boys and girls increased F_{Z2} with speed. There was a group by speed interaction on F_{Z2} (Fig. 4).

Fig. 4

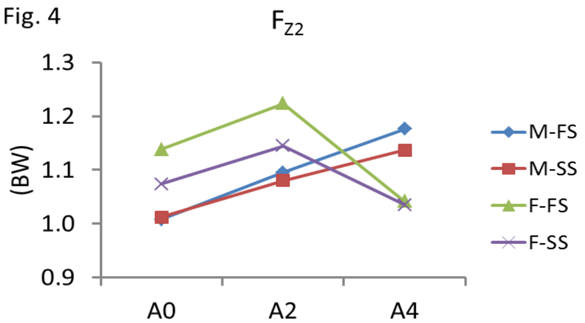

Boys increased the unloading rate with ankle load, while girls decreased the unloading rate from A2 to A4. Both boys and girls increased the unloading rate with speed (Fig. 5).

Fig. 5

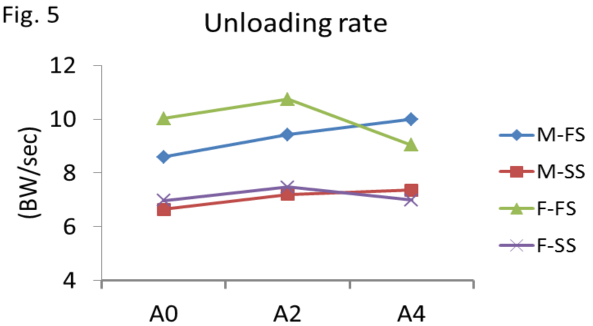

Neither a group nor a group by load interaction was found for total F_Z impulse (Fig. 6) and vertical propulsive impulse (Fig. 7). Both boys and girls increased the impulse variables with load and decreased the impulse variables with speed.

Both boys and girls increased stride time, F_{Z1}, F_{Z2}

Fig. 6

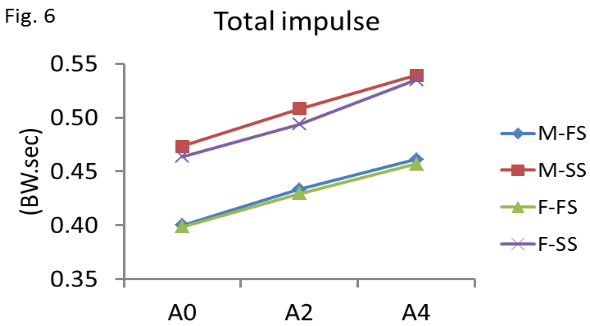

Fig. 7

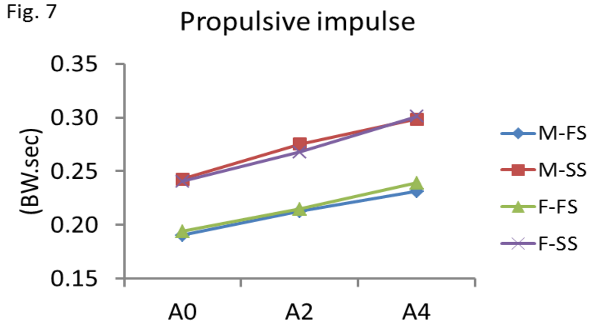

and unloading rate from no load (A0) to 2% load (A2) while walking on a treadmill. However, when the ankle load increased to 4% (A4), a sex difference was observed such that boys continued to increase stride time, F_{Z1}, F_{Z2} and unloading rate while girls decreased these variables. No difference was observed in the impulse variables between boys and girls. Future studies are warranted to investigate if this sex difference is due to different kinematic strategy or neuromuscular control.

CONCLUSIONS

A heavier ankle load may disrupt kinematic and kinetic patterns of treadmill walking in girls.

REFERENCES

1. Schwartz MH, et al. *J Biomech* **41**,1639-1650, 2008.
2. Browning RC, et al. *Med Sci Sports Exerc* **39**, 515-525, 2007.
3. Duysens J, et al. *Brain Res* **187**, 321-332, 1980.

ACKNOWLEDGEMENTS

This work was supported in part by the funding from the Jerome Lejeune Foundation.

DO INCREASED MUSCLE FORCES ALWAYS LEAD TO INCREASED CONTRIBUTIONS TO SUPPORT AND PROGRESSION DURING GAIT?

Sarah A. Schloemer, Julie A. Thompson, Laura C. Schmitt, Thomas M. Best, and Robert A. Siston

Ohio State University, Columbus, OH, USA
email: schloemer.7@osu.edu

INTRODUCTION

Muscle strength is essential to accomplish daily tasks of living such as walking and stair climbing. The forces produced by the muscles are used primarily for two main tasks during gait: vertical support and forward progression of the body mass center [1]. Many rehabilitation protocols target muscle strengthening to improve pathologic gait because muscle weakness has been associated with decreased function [2] and slower gait speeds [3]. However, targeted muscle strength gains alone do not always lead to improved function [4]. Therefore, there is a need to understand how changes in muscle strength due to disease or rehabilitation relate to the muscle's role in facilitating gait at various walking speeds. The purpose of this study was to determine the relationship between a given muscle's force and the contribution of that muscle to support and progression over a range of walking speeds.

METHODS

Six healthy subjects (2M/4F; 21.0 ± 2.3 years) provided IRB-approved written informed consent. Kinematic data were collected at 150 Hz using an 8-camera Vicon MX-F40 (Vicon, Oxford, UK) motion capture system and the Point-Cluster Technique [5] for each subject walking at a self-selected (SS) speed (1.31 ± 0.14 m/s), a fast speed (1.70 ± 0.25 m/s), and a slow speed (1.08 ± 0.14 m/s). Ground reaction force data were sampled at 600 Hz from six force places (Bertec Corp, Columbus, OH). Surface electromyography (Noraxon, Scottsdale, AZ) was sampled at 1500 Hz from bilateral lower extremity muscles. OpenSim 2.4 [6] was used to generate simulations of one gait cycle for each subject at each speed. The model was scaled to match the anthropometry of the individual subjects and experimental gait patterns were recreated by solving an inverse kinematics problem, using a weighted least-squares approach to minimize differences between experimental marker locations and the model's virtual marker locations. Muscle activations and forces in all lower extremity muscles were estimated using computed muscle control (CMC) [7] and were compared to the experimental EMG to ensure consistency between the simulated and experimental muscle activation patterns. An induced acceleration analysis (IAA) was used to determine individual muscle contributions to support and progression of the body mass center at each walking speed [8].

We then compared maximum muscle forces and maximum muscle contributions to support and progression for 16 major lower extremity muscles: gluteus maximus, gluteus medius, gluteus minimus, rectus femoris, vastus lateralis, vastus intermedius, vastus medialis, the long and short head of the biceps femoris, psoas major, meidal and lateral gastrocnemius, semimembranosus, semitendinosus, soleus and tibialis anterior. To determine how these measures change with speed, we then calculated the percent change in maximum muscle force and contributions to progression and support between slow and SS and SS and fast speeds.

RESULTS AND DISCUSSION

As speed increased from the slow to self-selected speed, increases in muscle force were generally accompanied by corresponding increases in muscle contributions to support and progression (Fig. 1). Of the 16 muscles, 15 (all but soleus) increased their force, 15 (all but gluteus minimus) increased their contributions to progression, and 12 increased their contributions to support.

In contrast, as speed increased further from the self-selected to fast speed, muscle forces generally continued to increase; however, changes in contributions to support and progression were not as consistent (Fig 1). Again, the same 15 muscles displayed an increase in force. However, only 8 muscles increased their contribution to progression and 11 increased their contribution to support. Percent changes in force and contributions to support and progression between speeds are shown in Table 1 from representative muscle groups.

It is believed that one of the main roles of muscles in the lower extremity is to propel and support the body. Our results suggest that although muscle force typically increases with walking speed, that an increase in force is not always accompanied by increased contributions to support and progression. The decreased contribution to center of mass acceleration observed in some muscles may suggest the muscle forces are used to accomplish a different task at higher speeds, such as increasing knee flexion acceleration prior to swing phase [9].

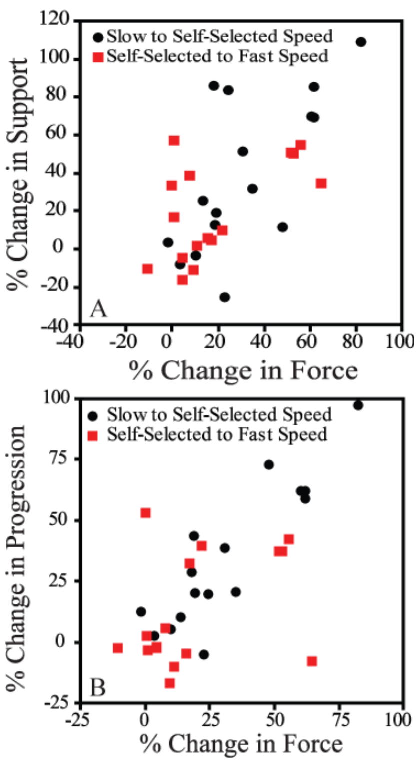

Figure 1: Effect of speed on relative changes in average muscle forces and contributions to support (A) and progression (B). Percent changes for each of the 16 muscles are represented by one marker.

CONCLUSIONS

Since increased muscle force may not directly translate to an increased capability to support and propel the body at higher gait speeds, increasing muscle strength alone may not be the sole means for achieving higher gait speeds. The ability of a muscle to accelerate the center of mass of the body involves a complex and interdependent interaction between muscle forces, moment arms, joint kinematics, and the ground reaction forces [8]. A more complete investigation of the interplay between joint kinematics, walking speed, and muscle forces may further explain how muscles are used to accelerate the lower extremity joints or support and propel the center of mass of the body. Such an understanding could establish a basis for the design of more comprehensive gait rehabilitation programs for individuals with pathologically weak muscles.

REFERENCES

1. Winter DA. *The Biomechanics and Motor Control of Human Gait: Normal, Elderly and Pathological*. University of Waterloo Press, 1991.
2. Wolfson L, et al. *J Gerontol A Biol Sci Med Sci* **50A**, 64-67, 1995.
3. Hurley MV, et al. *Ann Rheum Dis* **56,** 641-648, 1997.
4. Sullivan KJ, et al. *Phys Ther* **87**, 1580-1602, 2007.
5. Andriacchi TP, et al. *J BiomechEng* **120**, 743-749, 1998.
6. Delp SL, et al. *IEEE Trans Biomed Eng* **54**, 1940-1950, 2007.
7. Thelen DG, et al. *J Biomech* **36**, 321-328, 2003.
8. Zajac FE,et al. *Gait Posture* **16**, 215-232, 2002.
9. Fox MD and Delp SL. *J Biomech* **43**, 1450-1455, 2010

Table 1: Percent changes in force and contributions to support and progression from representative muscle groups between the slow and SS speeds and between the SS and fast speeds.

Muscle	Gluteus Maximus		Rectus Femoris		Vasti		Gastrocnemius		Hamstrings	
Speed	Slow to SS	SS to Fast	Slow to SS	SS to Fast	Slow to SS	SS to Fast	Slow to SS	SS to Fast	Slow to SS	SS to Fast
% Δ Force	61.8%	64.8%	19.4%	4.3%	67.0%	53.5%	9.0%	16.3%	13.4%	4.8%
% Δ Support	85.4%	34.5%	18.9%	-16.3%	79.5%	51.8%	-6.6%	6.9%	29.9%	22.6%
% Δ Progression	59.0%	-7.8%	20.2%	-2.2%	71.2%	38.7%	12.0%	24.2%	19.5%	4.1%

ASSESSING GAIT CHANGES IN FIREFIGHTERS DUE TO FATIGUE AND ASYMMETRIC LOAD CARRIAGE

[1]Julian F. Sy, [1,2]Gavin P. Horn, [1]Richard M. Kesler, [1]Matthew N. Petrucci, [3]Kiwon Park, and [1]Elizabeth T. Hsiao-Wecksler

[1]University of Illinois at Urbana-Champaign, Urbana, IL, USA
[2]Illinois Fire Service Institute, Champaign, IL, USA
[3]Trine University, Angola, IN, USA
email: ethw@illinois.edu, web: http://mechse.illinois.edu/research/hsiao-wecksler/

INTRODUCTION

One of the most common causes of firefighter injury on the fireground is slips, trips, and falls (STF). Every year, STF events account for over 8200, or over 21%, of all fireground injuries [1]. Previous studies have found correlations between gait characteristics and STF risk [2]. Thus, understanding the changes in gait characteristics after firefighting activities may aid developments in preventing STF-related injuries on the fireground.

Fatigue and load have been found to significantly impact gait characteristics [3-6]. Various fatiguing protocols have been used to assess the effects of fatigue on gait in firefighters [3,4] and it is therefore difficult to compare results from different studies in the current literature. One goal of this study was to compare the effects of different fatiguing protocols on gait to determine whether results from previous studies can be compared with one another.

Firefighters commonly carry asymmetric loads while traversing the fireground (e.g. air bottle, hose). Several studies have examined the effects of load on human gait [5,6], but no studies have been found that examine asymmetric loads on gait symmetry when subjects are fatigued. The second goal of this study was to investigate gait changes due to asymmetric load while fatigued, which may deepen the current understanding of risk factors in STF-related injuries.

METHODS

A total of 24 healthy male (n = 23) and female (n = 1) firefighters participated in this study (age 28.6 ± 7.9 years, height 182.1 ± 7.2 cm, weight 90.7 ± 13.9 kg). Each subject signed an informed consent and approval was obtained from the University of Illinois Institutional Review Board. Firefighters underwent three different fatiguing activities: (1) simulated firefighting activities in a live fire burn building (BBFF), (2) simulated firefighting activities in a temperature and humidity controlled environmental chamber (ECFF), and (3) treadmill walking in the environmental chamber (ECTM). Temperature in the live fire burn building varied from top to bottom due to the buoyant nature of the hot gasses generated by fire, but was kept at 82^{o} C at 1.2 m from the floor. Temperature and humidity throughout the environmental chamber was set at 49^{o} C and 30% humidity, respectively. The simulated firefighting activities consisted of 16 minutes of alternating work/rest cycles (with 2 minute intervals) and consisted of climbing stairs, overhead ceiling pulls, a room search, and advancing a hose. Treadmill walking consisted of 16 minutes of continuous walking at 4.5 km/h at 2.5% incline. The firefighters wore National Fire Protection Association (NFPA-1971) compliant structural firefighting personal protective equipment.

Gait performance was evaluated for each *fatiguing activity* at two separate *time* periods (pre/post-activity) under two different *load* conditions (with/without an 11.3 kg hose load over the right shoulder). Participants were instructed to look straight ahead and walk at fireground pace. Data were collected using a 29 foot long pressure sensitive gait mat (GAITRite Platinum, CIR Systems Inc., Havertown, PA). Six parameters were measured: step length (SL), stride length (STR_L), step width (SW), gait speed (GS), single leg support time (SLST), and double leg support time (DLST). SL, STR_L, and SW were normalized to each subject's corresponding leg length (greater trochanter to foot). SLST and DLST were measured as a percentage of gait cycle. Gait symmetry was quantified using the following symmetry index:

$$\text{SI} = \frac{P_L - P_R}{0.5(P_L + P_R)} 100\%$$

where P_L is the value of a measured gait parameter on the left side of the body and P_R is the value of the same parameter on the right side of the body.

Descriptive statistics were calculated for all measured gait parameters and a series of three-way repeated-measures analysis of variance tests were performed with *time*, *activity*, and *load* carriage as main effects. Statistical significance was set at $p < 0.05$. SPSS 20.0 (SPSS Inc., Chicago, IL, USA) was used for all analyses.

RESULTS AND DISCUSSION

Significant *time* main effects were found for SL (p = 0.038), STR_L (p = 0.032), SLST (p < 0.001), DLST (p < 0.001), and SW (p = 0.037), with shorter SL, STR_L, SLST, SW, and longer DLST after firefighting activity. Significant *load* main effects were found for SL (p < 0.001), GS (p = 0.001), STR_L (p < 0.001), SLST (p < 0.001), and DLST (p < 0.001). The addition of the hose load resulted in shorter SL, slower GS, shorter STR_L, longer DLST, and shorter SLST. A significant *activity* x *time* interaction was found for SL (p = 0.001), STR_L (p = 0.002), SLST (p = 0.002), DLST (p < 0.001), and SW (p < 0.001). Post-hoc analysis revealed significant differences post-activity for these parameters between BBFF and ECTM and between ECFF and ECTM, but no significant differences between BBFF and ECFF. Significant *time* x *load* interactions were also found for SL (p = 0.015), GS (p < 0.001), STR_L (p = 0.006), SLST (p = 0.042), and DLST (p < 0.001), with the differences between pre- and post-activity measures larger when carrying the hose load than without.

No significant main effects were found for symmetry index for STR_L, SLST, or DLST. A significant *load* main effect was found for SL symmetry (p = 0.003) with the right foot taking longer SL when carrying an asymmetric load. Additionally, a significant *load* x *time* interaction was found for SW symmetry with the right foot taking wider steps when carrying an asymmetric load, but only when fatigued (p = 0.001).

CONCLUSIONS

The effects of ECFF and BBFF conditions resulted in larger pre- to post-firefighting changes in various gait parameters when compared to the effects of ECTM. Additionally, no significant differences between the effects of ECFF and BBFF were found. These results suggest that studies employing fatiguing protocols using long term, low intensity treadmill walking may not be able to be directly compared with studies employing intermittent work/rest cycles similar to typical firefighting activities for evaluating changes in gait parameters.

Increased asymmetry in was found for SL and SW when firefighters were carrying the additional hose load. Larger SWs were found for the right foot when carrying a load while fatigued, which suggests that firefighters veer to the direction of the shoulder that is carrying the load. Additional load over the right shoulder might lead to hasty right heel strike in gait since the whole body center of mass is toward the right in the frontal plane. In order to compensate for this, subjects might use cautious strategies such as wider SW for reducing STF risk. In addition, this asymmetric load carriage requires additional hip moment which might result in fatigue of muscles related to hip joint.

REFERENCES

1. Qu X, et al. *Journal of Biomechanics* **44**, 1259-1263, 2011.
2. Hausdorff, et al. *Archives of Physical Medicine Rehabilitation* **82**, 1050-1067, 2001.
3. Park K, et al. *Safety Science* **49**, 719-726, 2011.
4. Kong PW, et al. *Gait and Posture* **31**, 284-288, 2010.
5. LaFiandra M, et al. *Journal of Biomechanics* **36**, 87-95, 2003.
6. Park K, et al. *Ergonomics* **53**, 882-891, 2010.

ACKNOWLEDGEMENTS

This project was funded by the Department of Homeland Security Fire Prevention & Safety Grant #EMW-2010-FP-01606. The authors thank David Li, Michael Angelini, Lela DiMonte, and Dan Warner for their assistance.

KINEMATIC ANALYSIS OF FOOT CLEARANCE DURING STAIR AMBULATION IN OLDER ADULT UNILATERAL TRANSFEMORAL AMPUTEES

Allison Luther, April Chambers, and Rakié Cham

Human Movement and Balance Laboratory, University of Pittsburgh, Pittsburgh, PA, USA
email: ajl77@pitt.edu, web: http://engineering.pitt.edu/hmbl/

INTRODUCTION

A growing prevalence of diabetes has led to an increase in the number of lower limb amputations occurring each year. Approximately 27% of the U.S. population over the age of 65 is affected by diabetes [1]. Vascular disease is the cause for 82% of all lower limb amputations, with over 25.8% of these occurring at a level above the knee [2]. The risk of falling during stair ambulation has been identified to be greater during stair descent for older, able-bodied adults [3], but the risk for older adults with unilateral transfemoral amputation has yet to be determined. Prior research with able-bodied individuals has evaluated foot clearance relative to the step edge during stair descent using a resultant distance method [4], and research with transtibial amputees has looked at horizontal and vertical distances [5]. However, there is no established methodology for examining minimum foot clearance during stair ascent and descent for transfemoral amputees. The objective of this study is to develop minimum foot clearance methodology for use in unilateral transfemoral amputee analysis. Furthermore, this method can aide in comparing the prosthetic and sound limbs, in order to understand foot placement strategies during stair ambulation.

METHODS

Three older adults (2 male/1 female, mean age 67 ± 3.46 yrs, weight 80.9 ± 14.93 kg, height 168.5 ± 9.58 cm) were included in the following analysis. Participants were asked to ascend and descend a series of three steps; three trials were collected for each condition. Vicon motion capture data was collected at 120 Hz. A custom foot marker set was used to reconstruct the bottom of the shoe sole along the forefoot (Fig. 1) and locate the inferior heel position. Stair ascent (SA) analysis took into consideration the forefoot markers for identifying the risk of tripping, while stair descent (SD) analysis focused on the inferior heel marker.

Figure 1: From left to right: toe tip, front forefoot, middle forefoot, break forefoot, and break (upper marker). Not pictured are the 3 corresponding forefoot markers placed along the medial sole. All 6 forefoot markers on each foot were recreated virtually using the static calibration data. The toe tip and break markers remained on the shoe during dynamic trials.

During ascent and descent three measures were used to evaluate minimum foot clearance over each step. A horizontal clearance was used to quantify the distance between the foot and the step edge when each marker was at the same vertical height as the step edge. Vertical clearance was the distance between the foot and the step edge when each marker was directly over the step edge. The resultant clearance took into consideration the overall smallest distance between each marker and the step edge at any time point during movement over the step.

RESULTS AND DISCUSSION

Table 1 provides SA clearance values for the sound and prosthetic limbs, along with the corresponding forefoot marker position that had the smallest clearance with respect to the step edge. Subjects 1 and 3 had a larger horizontal clearance with the prosthetic limb (PL) in comparison to the sound limb (SL); Figure 2 shows this progression for the prosthetic limb. Subject 2 utilized a sliding technique with the PL during ascent (Fig. 3), leading to a smaller horizontal clearance on the prosthetic side. Vertical and resultant clearances showed differences in where along the forefoot the minimum clearance occurred for each limb. Subject 1 had larger clearances with the PL. Subjects 2 and 3 had smaller vertical and resultant clearances with the PL. The toe tip, front forefoot and break forefoot positions had the smallest clearance with respect to step edge.

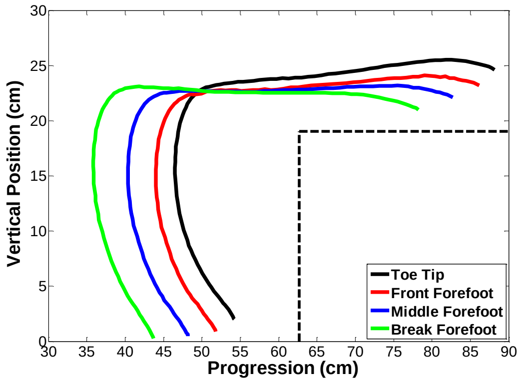

Figure 2: Typical prosthetic limb ascent motion.

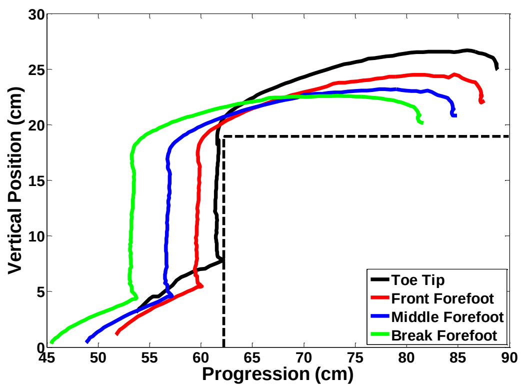

Figure 3: Sliding of the toe tip up the step riser.

During SD all subjects had an inferior heel horizontal clearance that was approximately twice as large with the PL in comparison to the SL. For all subjects, the PL vertical clearance was smaller by 1-2 cm than the SL. For the resultant clearance, Subjects 1 and 3 had less than a 1 cm difference between each limb, with the PL clearance greater than the SL. Subject 2 had a 1 cm smaller resultant clearance with the PL.

The marker set developed in this study was necessary because during SA, the commonly used toe tip marker cannot be the only defined location on the shoe for assessing clearance in unilateral transfemoral amputees. This methodology change allows minimum foot clearance to be evaluated regardless of gait style and shoe geometry. Spatial analysis of foot clearance is also possible, as different forefoot positions are identified as having the minimum foot clearance when passing over the step edge. The methods developed in this work are important for understanding the relation between minimum foot clearance and fall-risk during stair ambulation in older adults with unilateral transfemoral amputation. Additional subject analysis will provide strong evidence if the risk of falling is highest during ascent or descent, and where along the sole of the foot contact the step edge is likely to occur. Future work should also focus on how stair ambulation is affected by the use of different types of prosthetic knee joints.

REFERENCES

1. CDC. National diabetes fact sheet, 2011.
2. Dillingham, T.R., et al. *Southern Medical Journal*, **95**(8), 875-883, 2002.
3. Hamel, K.A., et al. *Gait & Posture*, **21,** 135-140, 2005.
4. Muhaidat, J., et al. *Gait & Posture*, **33**, 504-506, 2011.
5. Ramstrand, N., et al., *Prosthet Orthot Int*, **33**(4), 348-355, 2009.

ACKNOWLEDGEMENTS

Funding was provided by a grant from the American Orthotic and Prosthetic Association.

Table 1: Average minimum foot clearance (standard deviation) during stair ascent and the forefoot location.

Subject	Resultant Clearance (cm)		Horizontal Clearance (cm)		Vertical Clearance (cm)	
	Sound Limb	*Prosthetic Limb*	*Sound Limb*	*Prosthetic Limb*	*Sound Limb*	*Prosthetic Limb*
1	2.55 (0.89) Toe Tip	4.35 (1.42) Break Forefoot	-3.94 (1.87) Toe Tip	-11.30 (3.76) Toe Tip	4.39 (1.43) Toe Tip	4.41 (1.30) Break Forefoot
2	3.00 (0.62) Front Forefoot	0.71 (0.29) Toe Tip	-4.71 (1.30) Toe Tip	-0.75 (0.31) Toe Tip	3.63 (0.70) Front Forefoot	3.54 (2.03) Front Forefoot
3	5.93 (1.25) Toe Tip	4.25 (0.65) Front Forefoot	-9.10 (3.49) Toe Tip	-9.27 (4.37) Toe Tip	6.77 (1.34) Toe Tip	4.27 (0.69) Break Forefoot

NEW ADULT MALE POST MORTEM HUMAN SUBJECT SEGMENTAL WEIGHT, CENTERS OF GRAVITY, AND PRINCIPAL MOMENTS OF INERTIA

[1]Meghan O'Donovan, [1]Leif Hasselquist, [2]Chris Albery, [1]Samuel Corner, and [1]Brian Corner

[1]Natick Soldier Systems Center, Natick, MA, USA
[2]Infoscitex Corp, Wright Patterson Air Force Base, Dayton, OH, USA
email: meghan.p.odonovan.civ@mail.mil

INTRODUCTION

Accurate calculation and modeling of human kinetics requires knowledge of human segmental mass properties. Defined mass properties (mass, center of gravity, principal moments of inertia) of post mortem human subjects (PMHS) human body segments provide important information for dynamic calculations, human modeling and simulation, prosthetic and orthotic design, and for studies of human crashes, impacts, and falls. In addition, this data provides critical information for the validation of in-vivo findings on live human subjects. Limited data exists on directly measured human mass properties. In the last 60 years, only three studies have reported data of this kind [1,2,3]. Historical cadaveric data sets are limited by sample size, relevance to current populations of interest, and accuracy and validity of results due to the measuring methodologies of the time. The first purpose of this study was to correct calculation errors in the principal moments of inertia from previous data sets through the use of improved methods and modern, highly accurate measuring equipment. The second purpose was to develop a representative, population-based distribution of human body mass properties derived from a robust sample of PMHS. Results will lead to a new database that supersedes the current limited and dated information.

METHODS

Ten unembalmed male PMHS (age = 74.9 ± 12.22 years, weight = 79.4 ± 10.02 kg, stature = 1.75 ± .06 m, BMI = 25.84 ± 2.74 kg/m2) were selected based on stature and weight representative of a population distribution from the 1988 U.S. Army Anthropometry Survey (ANSUR) and the 2007 ANSUR II Pilot Survey. Additionally the PHMS were screened for bone mineral density and only those that met the criteria for healthy individuals (DEXA T-Score >1.00) were selected. Each PMHS was frozen and segmented into 15 segments: head, thorax (including neck), pelvis (including abdomen), and right and left upper arms, forearms, hands, thighs, lower legs, and feet (Figure 1). Methods of segmentation most closely followed that of Chandler et al. [2].

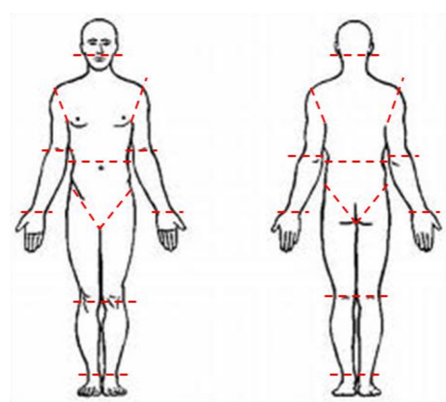

Figure 1: The approximate segmentation locations for each of the 15 measured segments.

The only exception included the segmentation of the trunk into pelvis and thorax. For the purposes of this study, a horizontal cut was made at the 10th rib mid spine, inferior to the diaphragm, which separated the thoracic cavity from the pelvis. For each segment, the mass, center of gravity (CG), and principal moments of inertia (MOI) were measured. Segment mass and CG were determined through the use of an electronic scale and moment table. The principal moments were measured using Space Electronics Moment of Inertia Instruments, Models XR – 50, and GB-3300AX (Space Electronics LLC, Berlin, CT), which operate on an inverted pendulum technique. For all segment weights, CGs, and

MOIs, the means and standard deviations for each were calculated.

RESULTS AND DISCUSSION

Table 1 gives the means and standard deviations for segment masses, centers of gravity, and principal moments of inertia. Data for segments that have both right and left components were averaged together. The current study attempts to reconcile the shortcomings of previous studies through the use of advanced measurement techniques and the correction of the principal moment of inertial errors. For example, Dempster [1] utilized basic suspension and balancing methods through the use of plumb lines and markings to determine values for segment centers of gravity. The study by Chandler et al. [2] did not attempt to provide a statistically valid sampling for establishing population estimates of segment MOIs and states that no attempt should be made to use the results reported as such. Zatsiorsky [4] reports that the Chandler et al. data set for the principal moments of inertia contained errors propagating from the inaccurate calculation of the inertial tensors for each segment. Advances in technology have resulted in the ability to obtain much higher fidelity data with less error.

CONCLUSIONS

Defining the mass properties of each segment of the human body is critical to the accurate calculation and modeling of human kinetics. This data may be used in lieu of limited and less accurate historical data sets.

REFERENCES

1. Dempster WT. *WADC TR-55-159*, 1955.
2. Chandler RF, et al. *TR-74-137*, 1975.
3. Clauser CE, et al. *TR-69-70*, 1969.
4. Zatsiorsky VM. *Kinetics of Human Motion*, Human Kinetics, 2002.

ACKNOWLEDGEMENTS

We would like to acknowledge Dr. John Bolte and Dr. Yun Seok Kang of the Injury Biomechanics Research Laboratory at Ohio State University for their contributions to this study.

Table 1: Average (± the standard deviation) centers of gravity (CG), principal moments of inertia (MOI), and mass of each PMHS segment.

	CG (cm)‡			MOI (kg·cm²)			Mass	
Segments	**X**	**Y**	**Z**	**X**	**Y**	**Z**	**(kg)**	**(%BW)**
Head	-0.07 ± 0.38	-0.08 ± 0.38	2.3 ± 0.51	173.89 ± 25.55	199.76 ± 16.02	171.56 ± 36.59	4.06 ± 0.3	5.34 ± 0.72
Thorax	0.55 ± 0.92	-0.81 ± 1.42	20.26 ± 1.36	6876.09 ± 1955.06	5398.3 ± 1578.73	3528.37 ± 1001.85	27.6 ± 4.84	35.66 ± 2.2
Pelvis	-0.69 ± 1.44	0.03 ± 0.86	-12.78 ± 1.68	2297.9 ± 799.43	1638.48 ± 832.64	1739.85 ± 448.21	15.81 ± 3.21	20.37 ± 2.15
Hand	6.89 ± 0.48	-0.08 ± 0.67	-0.3 ± 0.69	3.74 ± 1.05	10.03 ± 1.56	12.09 ± 2.00	0.5 ± 0.07	0.65 ± 0.05
Forearm	-0.2 ± 0.44	0.19 ± 0.31	-10.69 ± 0.71	61.66 ± 24.02	66.74 ± 18.68	16.51 ± 23.49	1.2 ± 0.26	1.55 ± 0.15
Upper Arm	-0.71 ± 1.12	0.19 ± 1.26	-13.65 ± 1.65	177.47 ± 43.7	180.87 ± 48.36	26.23 ± 9.47	2.15 ± 0.41	2.78 ± 0.29
Foot	5.97 ± 0.71	0.09 ± 0.61	-4.54 ± 0.87	8.88 ± 2.1	38.59 ± 7.86	37.66 ± 8.02	0.99 ± 0.14	1.29 ± 0.13
Lower Leg	-0.74 ± 0.59	0.27 ± 1.36	-15.75 ± 0.81	313.11 ± 73.97	315.74 ± 76.85	28.9 ± 12.29	2.55 ± 0.53	3.31 ± 0.48
Thigh	5.6 ± 9.58	-0.58 ± 2.5	-12.5 ± 8.64	1101.14 ± 352.64	1143.18 ± 365.27	185.46 ± 76.78	6.84 ± 1.41	8.84 ± 1.01

‡ **Segment Reference Origins:** Head - intersection of Y-axis (vector from right tragion to left tragion) and a normal passing through the right infraorbitale translated to sagittal. Thorax & Pelvis - at the 10th rib, midspine. Hand, Forearm, Upper Arm, Foot, Lower Leg, and Thigh – origin is at the proximal joint center with the z-axis vertical (for the hands and feet) or along the long bone (positive upwards), the y-axis positive left, and the x-axis parallel to ground (positive anterior direction).

Prediction of Load Accommodation Strategies During Walking from Lower Extremity Kinematic Variables

Lee T. Atkins[1], Janet S. Dufek[2], Barry T. Bates[3] and C. Roger James[1]

[1]Texas Tech University Health Science Center, Lubbock, TX, USA
[2]University of Nevada Las Vegas, Las Vegas, NV, USA
[3]University of Oregon, Eugene, OR, USA
email: lee.atkins@ttuhsc.edu

INTRODUCTION

Mechanical loading provides a stimulus for tissue remodeling [1]. Insufficient or excessive loading can be detrimental to tissue health [1]. Movement behaviors alter the magnitude of the ground reaction force and subsequently the force acting on a tissue [2,3,4]. Individuals may exhibit unique movement behaviors, or strategies. Load accommodation strategies may be elicited with the application of an external stressor during a dynamic activity, such as walking while carrying additional weight. Load accommodation strategies have been identified for running, landing and walking [5,6,7,8]. Strategies have been classified using a conceptual model based on observed vertical ground reaction force (vGRF) values in relation to the magnitude of an external stressor [9]. Based on Newtonian mechanics the magnitude of the vGRF should be predictable and increase at an equal rate to the applied external stressor. However, research has shown that while walking with extremity carried weights, subjects utilize an accommodation strategy with a rate of change in vGRF greater, lesser, or equal to the predicted vGRF [8]. Currently, it is unknown which lower extremity kinematic variables explain these strategies. The purpose of the study was to predict load accommodation strategies during walking using lower extremity kinematic variables.

METHODS

Twenty healthy subjects (10 male, 10 female) walked on a treadmill at 1.34 m/s while carrying 0, 44.5, and 89 N weights attached to the wrists while keeping hands clasped together (constrained) in front of their body. Vertical GRF data were obtained using an instrumented treadmill (Kistler Gaitway; 100 Hz). Lower extremity kinematics were obtained using a motion capture system (Vicon Motus; 120 Hz). Left side peak vGRF and sagittal plane kinematic excursions during loading response (initial contact to max vGRF) were extracted, averaged, and normalized to stride percentage across 10 footfalls for each load condition using a custom MATLAB algorithm. The load accommodation strategy was determined for each subject by calculating the rate of change (regression line slope) of the observed vGRF with respect to the known increases in system weight. Descriptive statistics were calculated for the strategy and kinematic variables. Kinematic variables from the three load conditions, including foot, leg and thigh segment, and ankle and knee joint excursions, were used to predict strategies using stepwise linear multiple regression (α_{entry} = 0.05, $\alpha_{removal}$ = 0.10) in SPSS. Stepwise regression also was used to predict the kinematic variables that explained the greatest variance in strategy from other kinematic variables. Excluded from these follow-up regression analyses were variables that were used to directly calculate the dependent variable. For example, leg and thigh segment excursions for all conditions were excluded from the prediction of knee joint excursion.

RESULTS AND DISCUSSION

Loaded walking elicited a mean load accommodation strategy greater than predicted by Newtonian mechanics (Figure 1). Individual subject strategies were variable. The kinematic variables initially entered into the stepwise regression model appeared minimally influenced by the load conditions (Table 1). Stepwise regression showed that two significant ($p<0.05$) predictor variables explained 56.4% of the strategy variance. The first predictor variable (x_1) was leg segment excursion in the 44.5 N load condition which was inversely

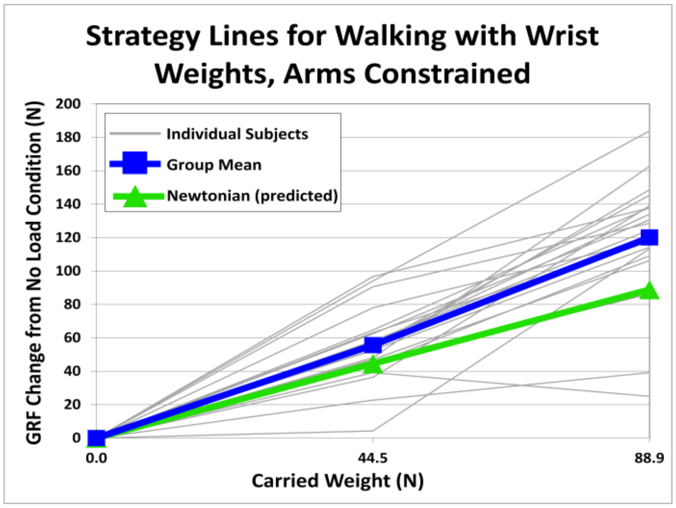

Figure 1. Group, individual, and predicted strategies.

related to strategy (y). The second predictor variable (x_2) was knee joint excursion in the 89 N load condition which was directly proportional to strategy (Table 2). The first follow-up stepwise regression showed that 36.4% of the variance in x_1 was explained by foot excursion in the 0 N condition (β=.554, p=0.005). Therefore, subjects who increased foot excursion with no load utilized increased leg segment excursion when carrying a 44.5 N load. The second follow-up stepwise regression showed that 93.7% of the variance in x_2 was explained by foot excursion in the 44.5 N condition (β=1.658, p<0.001) and ankle excursion in the 89 N condition (β=1.529, p<0.001). Thus, subjects who increased foot excursion with a 44.5 N load and ankle excursion with a 89 N load increased knee excursion when carrying a 89 N load.

CONCLUSIONS

Loaded walking with the wrists constrained elicited a group average super-Newtonian [9] load accommodation strategy partially explained by excursions of the knee, leg and foot. Individual subjects responded heterogeneously. Due to the implications of extreme load accommodation strategies, further research is needed to identify additional biomechanical variables related to these strategies.

Table 1. Kinematic Excursion Variables Entered into the Stepwise Linear Regression Model.

	Load Condition		
	0 N	**44.5 N**	**89 N**
Ankle Joint	-4.7(3.3)	-5.7(3.4)	-5.5(3.5)
Knee Joint	11.6(5.8)	11.7(5.1)	12.9(5.6)
Foot Segment	19.5(3.3)	18.7(3.5)	18.8(2.8)
Leg Segment	7.9(3.8)	6.9(3.2)	6.0(3.9)

Values are mean (standard deviation) degrees.

REFERENCES

1. Mueller MJ, et al. *Phys Ther* **82**, 383-403, 2002.
2. Peterman MM, et al. *J Biomech* **34**, 693-698, 2001.
3. Reilly SM, et al. *J Exp Biol* **208,** 993-1009, 2005.
4. Scott SH, et al. *Med Sci Sports Exerc* **22**, 357-369, 1990.
5. Bates, B. T., et al. *Proceedings of the 5th Biennial Conference of the CSB, University of Ottawa*, 40-41, 1988.
6. Caster BL, et al. *Med Sci Sports Exerc* **27**, 736-744, 1995.
7. Simpson KJ, et al. *Biomechanics XI-B*, Free University Press, Amsterdam, 701-704, 1988.
8. Atkins LT, et al. *Proceedings of the 36th Annual Meeting of the ASB*, Gainesville, FL, USA, 2012.
9. James CR, et al. *J Appl Biomech*, **19,** 106-118, 2003.

Table 2. Results of the Stepwise Linear Regression to Predict Strategy.

Model R	Model R^2	Variables Entered	β	β 95% CI	Bivariate Correlations		
					Pearson r	Semipartial ryx1.x2	Partial ry(x1.x2)
0.751	0.564	**Constant**	2.62	2.329, 4.066	-	-	-
		Leg Excursion 44.5 N *(p<0.001)*	-0.14	-.201, -.076	-0.561	-0.748	-0.744
		Knee Excursion 89.0 N *(p=0.006)*	0.057	.019, .096	-0.102	0.603	0.499

THE EFFECT OF TRUNK FLEXION ON LOWER LIMB KINETICS OF ABLE-BODIED GAIT

[1,2]Matthew J Major, [1]David Kluger, [1,2]Stefania Fatone, and [1,2]Steven A Gard

[1]Northwestern University Prosthetics-Orthotics Center,
Dept. of Physical Medicine and Rehabilitation, Feinberg School of Medicine, Chicago, IL, USA
[2]Jesse Brown VA Medical Center, Chicago, IL, USA
email: matthew-major@northwestern.edu, web: www.nupoc.northwestern.edu/

INTRODUCTION

Alterations in trunk flexion are associated with aging, spinal pathologies, and neuromuscular disorders [1]. For example, the pathology known as flatback causes a forward inclination of the trunk (referred to as positive sagittal spine balance) due to abnormal reductions in lumbar lordosis [2] and may induce crouch gait (i.e., excessive hip and knee flexion during stance) [3]. While these compensations may be necessary to maintain the body center-of-mass (COM) within the base of support [4] for upright balance, they place high demand on muscles and increase energy expenditure [5]. The unique joint configuration resulting from sustained trunk flexion and the increase in metabolic cost of crouch gait suggests changes in joint kinetics compared to normal posture.

Although the effect of varying levels of sustained trunk flexion on lower limb kinematics has been described [4], little is known of the effects on joint kinetics. Therefore, the purpose of this study was to investigate the effect of sustained trunk flexion on lower limb kinetics of able-bodied gait. We hypothesized that sustained trunk flexion and consequential adoption of crouch gait would increase hip extensor moments to support the trunk and reduce knee flexor moments resulting from sustained knee flexion. These results may serve as a model for developing insight into the joint kinetics and muscular demands of pathological populations that suffer from similar postural adaptations.

METHODS

Subjects without known musculoskeletal or neurological disorders were asked to walk at their self-selected normal walking speed under three trunk flexion conditions: 1) self-selected upright (UP), 2) 25 ± 7° trunk flexion (INT), and 3) 50 ± 7° trunk flexion (MAX). Participants were asked to bend from the hips to achieve their target trunk flexion as opposed to rounding at the lower or upper back. The Biofeedtrak feature in EVa RealTime software (Motion Analysis Corporation (MAC), Santa Rosa, CA) was used to provide auditory feedback to subjects while walking to assist them in maintaining the trunk flexion angle within the specified range during the INT and MAX conditions. The order of trunk flexion conditions was randomized to eliminate task order effects.

Retro-reflective markers were attached to subjects according to the Helen Hayes Marker Set [19], with an additional marker on the C7 spinous process. Sagittal plane trunk flexion was defined as the angle between the global vertical axis and a line connecting the sacral and C7 markers. Kinematic and kinetic data were collected with a digital motion capture system (MAC) at 120 Hz and six embedded forceplates (AMTI, Watertown, MA) at 960 Hz, respectively. Kinematic data were low-pass filtered with a 6 Hz cutoff frequency. Joint kinetics were estimated using inverse dynamics with OrthoTrak software (MAC). Joint work as an estimate of mechanical energy absorption or generation during stance was calculated by integrating joint power with respect to time. For each condition, data were averaged over at least three trials.

RESULTS AND DISCUSSION

Data were collected from 14 able-bodied subjects (7 male, 26±3 years, 174.2±9.9 cm, 72.3±12.1 kg). Trunk flexion resulted in noticeable changes in lower limb joint moments and powers (Figure 1). Increased trunk flexion systematically decreased the peak plantar flexor ankle moment, but systematically increased the plantar flexor moment at 25% of the gait cycle. Most noticeably, increasing trunk flexion systematically decreased the magnitude of the knee flexor moment in terminal stance and caused it to occur earlier in gait; at 46%, 42%, and 32% of the gait cycle for UP, INT and MAX conditions, respectively. This was expected, as sustained knee flexion would theoretically require less flexor moment for active flexion during mid stance. Furthermore, as the ground reaction force would remain posterior to the knee joint longer in stance as knee flexion increases, earlier extensor moments would be necessary to maintain this posture. Peak extensor moment at the hip increased systematically with trunk flexion and this was expected as subjects were requested to produce sustained trunk flexion at the hip.

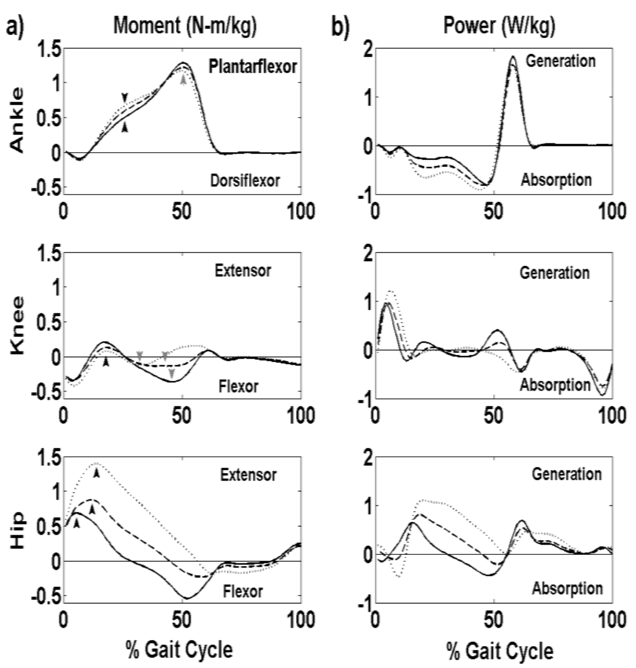

Figure 1: Joint moments (a) and powers (b). Solid=UP; dashed=INT; dotted=MAX. Arrows denote moments of interest.

As seen in Table 1, progressive trunk flexion produced a systematic increase in energy absorption at the ankle joint, as well as increased energy generation and decreased absorption at the hip joint. No consistent changes were observed at the knee, however, this joint acted to produce a net energy generation throughout stance for all conditions.

Table 1: Joint positive (energy generation) and negative (energy absorption) work.

Joint	**Mean ± SD (J/kg)**		
	UP	**INT**	**MAX**
Ankle	13.2 ± 2.9	11.2 ± 3.7	11.3 ± 5.3
	-19.2 ± 4.4	-24.4 ± 4.4	-28.0 ± 4.8
Knee	11.8 ± 3.6	9.6 ± 2.9	11.9 ± 4.1
	-5.4 ± 2.5	-4.7 ± 2.1	-7.4 ± 5.2
Hip	11.5 ± 3.7	20.4 ± 7.8	33.2 ± 9.1
	-9.2 ± 4.5	-3.6 ± 3.2	-3.6 ± 3.3

Importantly, whereas in normal posture (UP) hip moments transition into flexor toward the end of mid stance then gradually increase through terminal stance to aid in forward progression, sustained trunk flexion calls for increased and prolonged extensor moments to maintain this posture. Consequently, the mechanical energy generation demands on the hip increased systematically, suggesting a considerable increase in metabolic cost.

CONCLUSIONS

Walking with increasing trunk flexion places significant demand on the hip extensors to support the anteriorly displaced trunk COM and forces the knee joint to generate extensor moments earlier in stance. Importantly, the direct relationship between trunk flexion and energy absorption and generation at the ankle and hip joints, respectively, would suggest overall increased muscular demand during gait. These results support clinical observations that individuals with positive sagittal spine balance as a result of spinal pathology are susceptible to increased metabolic energy expenditure and premature muscular fatigue [6].

REFERENCES

1. Laroche M & Cintas P. *Joint Bone Spine* **77**, 593-596, 2010.
2. Potter BK, et al. *J Bone Joint Surg Am* **86-A**, 1793-1808, 2004.
3. Lin CJ, et al. *Gait Posture* **11**, 224-232, 2000.
4. Saha D, et al. *Gait Posture* **27**, 653-660, 2008.
5. Claus AP, et al. *Spine* **34**, E208-214, 2009.
6. Farcy JP & Schwab FJ. *Spine* **22,** 2452-2457, 1997.

GLUTEUS MAXIMUS AND SOLEUS COMPENSATE FOR SIMULATED QUADRICEPS ATROPHY AND ACTIVATION FAILURE OVER A RANGE OF WALKING SPEEDS

Julie A. Thompson, Ajit M.W. Chaudhari, Laura C. Schmitt, Thomas M. Best and Robert A. Siston

The Ohio State University, Columbus, OH, USA
email: thompson.1288@osu.edu

INTRODUCTION

Lower extremity muscles perform two main tasks during walking: generation or maintenance of forward progression and vertical support of the body mass center [1]. Not surprisingly, muscle weakness may impair someone's ability to maintain a normal gait. For example, quadriceps muscle weakness in some populations has been correlated with a decreased walking speed when compared to healthy individuals [2]. Quadriceps weakness may be a result of muscle atrophy and/or reduced voluntary muscle activation. Quadriceps strength deficits can be as high as 64% compared to the uninvolved side [3] and quadriceps activation deficits may approach 34% [4]. While quadriceps weakness has been correlated with a slower walking speed, the important cause-effect relationships between abnormal muscle function and reduced gait speed remain unknown.

The purpose of this study was to use muscle-driven simulations to estimate the muscle compensations needed to maintain normal kinematics over a range of walking speeds in response to quadriceps weakness (atrophy and activation failure).

METHODS

Six healthy subjects (2M/4F, Age: 21.0 ± 2.3 years) provided IRB-approved written informed consent. Each subject walked at a self-selected (1.31 ± 0.14 m/s), slow (1.08 ± 0.14 m/s), and fast (1.70 ± 0.25 m/s) speed while motion data were collected at 150 Hz using an 8-camera Vicon MX-F40 system and the Point-Cluster Technique [5]. Ground reaction forces were obtained from six force plates sampled at 600 Hz. Surface electromyography was simultaneously collected (1500 Hz) from the bilateral lower extremity muscles. We simulated one gait cycle for each subject and gait speed using OpenSim [6]. Computed muscle control [7] was used to calculate the muscle excitations and forces in all lower extremity muscles that produced a coordinated simulation of the subjects' gait. An induced acceleration analysis was then performed to determine the contributions of individual muscles to the forward progression and vertical support of the body mass center [8]. After completing the full-strength simulations, we weakened the quadriceps (rectus femoris and vasti) of one stance leg in three ways: 1) decreasing the quadriceps' peak isometric muscle force to 40% of normal (Atrophy Only), 2) constraining the peak activations of the quadriceps to 65% of the peak values that were calculated during the full-strength simulation (Activation Failure Only) and 3) a combination of simulated atrophy and activation failure (Atrophy + Activation Failure). We then forced the simulations to track normal gait kinematics, re-calculated muscle forces and contributions to progression and support in the weakened models, and identified changes in muscle forces and contributions to progression and support between the full-strength simulation and the simulations with quadriceps weakness.

RESULTS AND DISCUSSION

Of the major lower extremity muscle groups investigated, the gluteus maximus and soleus muscles displayed the greatest ability to compensate for simulated quadriceps weakness at all gait speeds by increasing force output and contributions to progression and support to maintain normal gait.

Muscle Forces

The gluteus maximus generated more force in early stance to compensate for quadriceps weakness, and increased its force output with increasing gait speed (Figure 1). Compensation by the gluteus maximus was greatest in response to the combination of simulated atrophy and activation failure of the quadriceps at all gait speeds. In contrast, we found that the soleus generated more force in late stance and decreased its force output with increasing gait speed. Compensation by the soleus was greatest in response to activation failure of the quadriceps, except for the slow gait speed, in which compensation was greatest in response to combined atrophy and activation failure (Table 1).

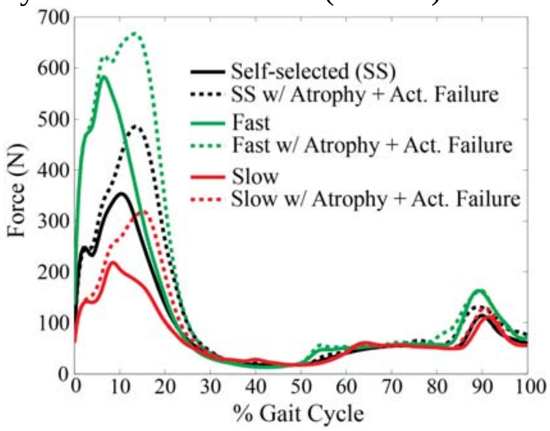

Figure 1: The effect of simulated quadriceps weakness on the force generated by the gluteus maximus over a range of gait speeds.

Contributions to progression and support

The gluteus maximus contributed more to slowing forward progression (braking) and providing vertical support in early stance to compensate for quadriceps weakness. Contributions to support increased with gait speed, but contributions to braking decreased when gait speed increased from self-selected to fast (Table 1). The soleus contributed more to progression and support in late stance to compensate for quadriceps weakness. Contributions to progression and support increased from a slow to a self-selected gait speed, but decreased from a self-selected to a fast gait speed.

Previous researchers have investigated muscle compensations due to weakness by simulating muscle atrophy only [9] or contributions to support and progression over a range of walking speeds [10]. To our knowledge, our study is the first use of muscle-driven simulations, albeit in healthy subjects, to investigate how lower extremity muscles could compensate for both quadriceps atrophy and activation failure to maintain normal gait kinematics over a range of walking speeds.

CONCLUSIONS

All simulations were able to track normal gait kinematics at all speeds, suggesting that it would be physiologically feasible for persons with quadriceps weakness to walk at a fast gait speed. Since persons with quadriceps weakness are known to walk slower than healthy individuals, our results indicate that other factors not simulated by our model (e.g. pain and perceptions of instability) likely contribute to reduced walking speeds in individuals with quadriceps weakness. Our findings lay the foundation for future work addressing factors that limit walking speed in pathological gait.

REFERENCES

1. Winter DA. *The Biomechanics and Motor Control of Human Gait: Normal, Elderly and Pathological*, University of Waterloo Press, 1991.
2. Hurley MV, et al. *Ann Rheum Dis* **56,** 641-8, 1997.
3. Mizner RL, et al. *Phys Ther* **83**, 359-65, 2003.
4. Hassan BS, et al. *Ann Rheum Dis* **60,** 612-8, 2001.
5. Andriacchi TP, et al. *J Biomech Eng* **120,** 743-9, 1998.
6. Delp SL, et al. *IEEE Trans Biomed Eng* **54,** 1940-50, 2007.
7. Thelen DG, et al. *J Biomech* **39,** 1107-15, 2006.
8. Hamner SR, et al. *J Biomech* **43**, 2709-16, 2010.
9. van der Krogt MM, et al. *Gait Posture* **36**, 113-9, 2012.
10. Liu MQ, et al. *J Biomech* **41**, 3243-52, 2008.

Table 1: Peak changes in muscle force and contributions to progression and support in response to activation failure alone (†) or combined atrophy and activation failure of the quadriceps (unmarked).

		Peak Force (N)			**Progression (m/s^2)**			**Support (m/s^2)**		
Muscle	**Speed**	**Change due to weakness**	**Change from self-selected (SS) speed**	**% Change from SS speed**	**Change due to weakness**	**Change from self-selected (SS) speed**	**% Change from SS speed**	**Change due to weakness**	**Change from self-selected (SS) speed**	**% Change from SS speed**
Gluteus Maximus	Slow	100.1	-167.6	-34.5	-0.080	0.078	-26.5	0.416	-0.813	-37.8
	SS	132.6	--	--	-0.077	--	--	0.442	--	--
	Fast	84.5	181.0	37.2	-0.071	0.023	-7.7	0.554	0.701	32.6
Soleus	Slow	115.5	-65.7	-3.4	0.060	-0.229	-13.1	0.527	-0.666	-7.8
	SS	211.8 †	--	--	0.104 †	--	--	0.952 †	--	--
	Fast	268.7 †	-127.7	-6.5	0.114 †	-0.031	-1.7	1.187 †	-0.550	-6.5

THE INFLUENCE OF KNEE BRACING ON PATELLAR KINEMATICS DURING HUMAN WALKING: A CASE STUDY

Joseph Y. Lee[1], Stephanie N. Bailey[2] and Elizabeth C. Hardin[1,2]

[1]Case Western Reserve University, Cleveland, OH, USA
[2]Louis Stokes Cleveland Department of Veteran Affairs Medical Center, Cleveland, OH, USA
email: jyl18@case.edu

INTRODUCTION

Knee braces can facilitate walking in those with pathological gait deficits, such as malalignment, pain, joint instability and lower extremity muscle weakness. These devices should influence the kinematics of the patella considering it is integral in knee function, increasing the quadriceps muscle leverage. In fact, studies have found that bracing changes the patella's trochlear position [1]. We present here a case study of a male patient prescribed a stance control knee-ankle-foot orthosis (KAFO, Sensor Walk Electronic KAFO, Ottobock, Minneapolis, US) for the left leg to facilitate walking. More recently, patellofemoral pain and instability in his right knee limited his walking for which he was prescribed a standard motion control knee brace (Townsend, Bakersfield, US). This prescription appeared to exacerbate the problems in this knee, the contralateral knee to the KAFO, during walking. We hypothesized that both braces were causing patellar maltracking. To investigate this hypothesis, gait analysis was performed

METHODS

Gait analysis was performed with a passive marker motion capture system (100 Hz, Vicon, Oxford, UK) and three force plates embedded in the ground (1000 Hz, AMTI, Watertown, MA). Reflective markers were placed on the left and right sides on the femur, the anterior superior iliac spines, the lateral epicondyles, the lateral malleoli, the tibia, the second metatarsal, the calcaneus, on the sacrum and on the anterior facet of the patella. The patient's anthropometric parameters were measured (height, weight, leg length, knee joint width and ankle joint width). Dara were collected under three experimental conditions: 1) unbraced walking, 2) walking with the KAFO on the left leg, and 3) walking with the KAFO on the left leg and the contralateral knee brace on the right leg.

The patient was required to walk at a fixed rate of 80 bpm to help maintain a walking speed of 0.65 m/s. These conditions were determined from preferred walking speed and cadence in the unbraced walking session. However, in session 2) and 3), the subject had difficulty maintaining the controlled speed with the KAFO; therefore, both preferred and controlled speed trials were collected. The patient walked for 10 m through the calibrated volume, repeating this for 5-10 times for each experimental condition. The marker data were processed (Plug-In Gait, Vicon, Oxford, UK) for 5-10 walking bouts and with custom software to determine the position of the patella in the global coordinate system.

RESULTS AND DISCUSSION

The unbraced motion of the patella showed the least mediolateral variability (Fig. 1a) whereas both braced conditions showed increased mediolateral variability (Fig. 1b and 1c). Patellar motion was also compared to the simultaneous knee flexion angle to determine the relationship between knee flexion during weight acceptance and mediolateral motion of the patella (Fig. 2), considering that the patella affects the quadriceps leverage. These results showed that both braced conditions produced more medial motion at foot strike and remained in longer in that position as the knee flexed with weight acceptance. Only the KAFO produced increased right knee flexion during weight acceptance whereas with the added right knee brace knee flexion was limited.

A limitation of this study is the assumption that mediolateral motion of the patella marker was related to patellar tracking. It is possible that internal-external rotation of the femur also contributed to this motion. There was greater internal rotation at the hip. In addition, these results show some hyperextension which was likely a result of marker placement. One experienced technician placed all the markers on the patient, and this error would have influenced each condition similarly.

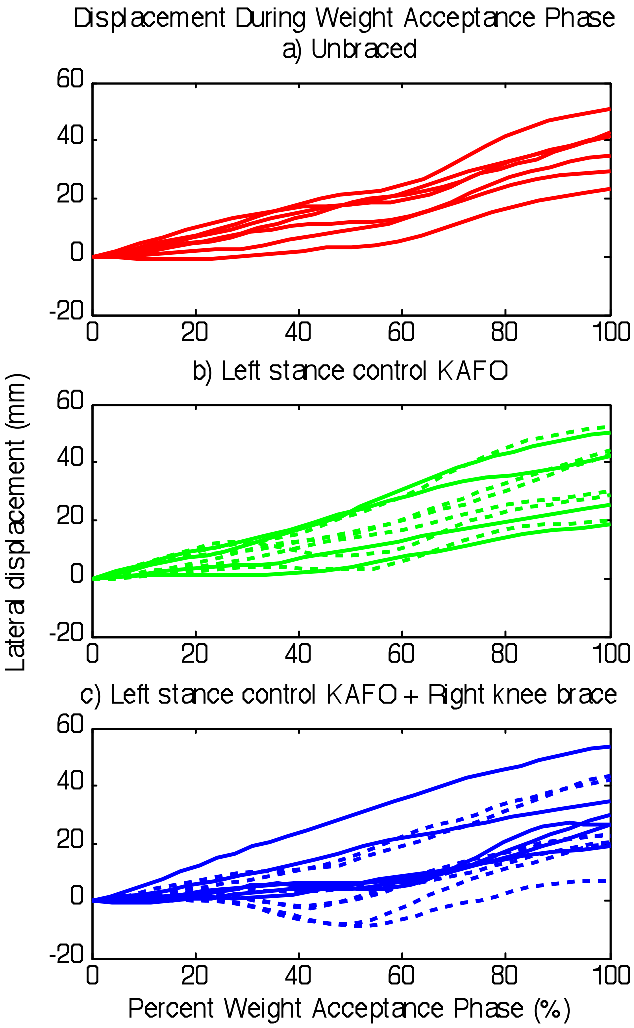

Figure 1: Mediolateral patella motion (+, lateral direction) of right patella during weight acceptance. Solid lines represent trials at 80 BPM speed and dotted lines represent preferred speed trials.

CONCLUSIONS

The patellar motion during the unbraced walking was consistently lateral whereas during both of the braced conditions there was initial medial motion likely from internal hip rotation. These findings show that the right knee patellar kinematics was influenced by the KAFO on the left knee, impairing knee joint function. Based on these findings, physical therapy was directed to minimize the use of knee bracing. Motion of the patella might be a simple clinical test which could be performed via video rather than a complex 3D analysis, but further validation would be required.

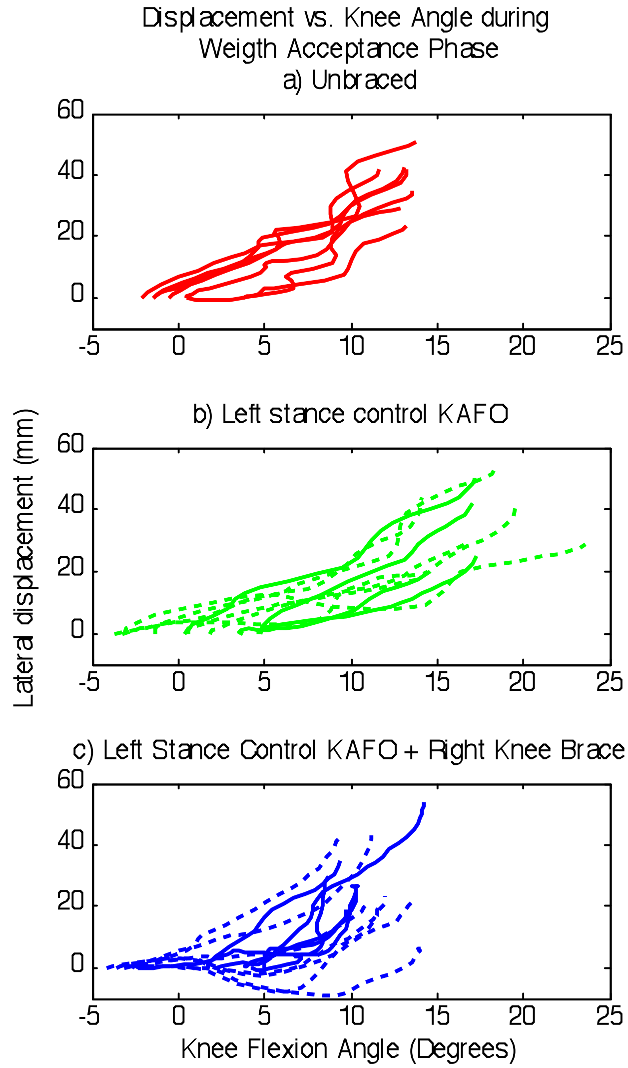

Figure 2: Mediolateral motion (+, lateral direction) of the right patella with respect to knee flexion angle during weight acceptance. Solid lines represent trials at 80 BPM speed and dotted lines represent preferred speed trials.

REFERENCES

1. Powers CM, et al. Med Sci Sports Exerc 31(12);1714-20.
2. Wilson NA, et al. *J Bone and Joint Surgery* 91**,** 558-66, 2009.

ACKNOWLEDGEMENTS

We acknowledge the assistance of Terese Hurin, CPO, at the Louis Stokes Cleveland Veteran's Affairs Medical Center.

THE EFFECT OF SPLIT-BELT TREADMILL SPEED CONFIGURATIONS ON INTERLIMB COORDINATION AND GAIT CYCLE PATTERNS

Brian Hoover, Ryan Roemmich, Jaimie Roper, and Chris Hass

University of Florida, Gainesville, FL, USA
email: bhoover@ufl.edu

INTRODUCTION

Synchronous arm and leg swing maintains dynamic stability during walking and is hypothesized to be controlled by limb-specific neural circuits [1]. However, the coordination between arm and leg swing appears to be dependent upon gait speed [2]. Advances in rehabilitation technology have led to the use of split-belt treadmills which allow the speed of the belt under each limb to be controlled independently. This independent control provides a unique means to perturb the walking pattern and to evaluate adaptation in arm and leg coordination. Because of the dynamic, everyday environments in which humans must ambulate, the ability to flexibly adapt gait patterns to maintain stability is crucial.

The purpose of this study was to investigate whether interlimb coordination changes during split-belt treadmill walking. Typical human gait consists of hip flexion paired with contralateral shoulder flexion. However, as gait speed is decreased, multiple arm swings per step are observed [2]. It is unknown what effect split-belt treadmill gait, which places different demands on each leg, has on coordination.

We utilized hip and shoulder angles to calculate two measures of interlimb coordination. To investigate the effect of the split-belt perturbation on gait, one discrete measure, the point estimate of relative phase (PRP, or the relationship between two segments based on the time required to reach a maximum or minimum value, which can range from 0° (in phase) to 180° (out of phase)), and one continuous measure in cross-covariance (COV, a measure ranging from -1 (out of phase) to 1 (in phase), with zero indicating no phasic relationship between the two signals (Fig. 1)), were used. Additionally, spatiotemporal gait parameters which have previously been described in the split-belt treadmill literature [3] were calculated.

METHODS

Seventeen participants (22±3 years, 10 female), in accordance with the Vicon Plug-In Gait model, were fitted with 35 retro-reflective markers and walked on a split-belt treadmill (Bertec Corporation, Columbus, OH). Kinematic data were collected using an 8 camera motion capture system (Vicon, Oxford, UK), sampling at a rate of 120 Hz. Self-selected Fast walking speed (FS) was determined when the participant identified the fastest speed which could be maintained for 10 minutes. Participants then walked at each Split and Tied condition for 90 seconds. During Split, the belt under the participant's non-dominant leg was set at FS, and the dominant-side belt moved at 90%, 70%, 50%, and 30% of FS. Both belts rotated at the same speed (90%, 70%, 50%, and 30% of FS) during the Tied Conditions. To allow for sufficient adaptation [3], only data from time 0:30-1:30 at each condition were analyzed. Outcome measures were calculated using a customized MATLAB (MathWorks, Natick, MA) script. A series of two-way and one-way ANOVAs, and Bonferroni post-hoc tests, were performed (GraphPad Prism, La Jolla, CA) using an α-level of 0.05.

RESULTS AND DISCUSSION

Statistical analysis revealed significant Condition (Split or Tied) X Speed (90%, 70%, 50%, or 30%) interactions among all contralateral limb COV and PRP measures. All gait measures resulted in significant Condition X Speed interactions except for the Fast leg Step Length. Within-measure results of all coordination and gait cycle measures can be found in Table 1.

Participants not only maintained coordination patterns throughout Split, but displayed improved coordination on all Split 30% measures when compared to Tied 30%. Consistent with previous literature, arm and leg swings became less coordinated as the Tied speeds decreased, particularly when treadmill was set at 30% of FS. These data support the hypothesis of multi-limb neural connections. Gait cycle measures mirrored past split-belt treadmill work. Longer stride lengths and shorter stance percentages were measured on the fast belt, and the slow belt elicited shorter stride lengths and greater stance percentages. These data indicate that the speed difference in belts should be taken into consideration when designing rehabilitation and research protocols.

REFERENCES

1. Kandel, E.R., et al. *Principles of neural science*. McGraw-Hill Professional, 2012.
2. Wagenaar, R.C. and R.E.A. van Emmerik, R. *J Biomech*, **33**, 853-861, 2000.
3. Dietz V, Zijlstra W, Duysens J. *Exp Brain Res* **101**, 513-520, 1994.

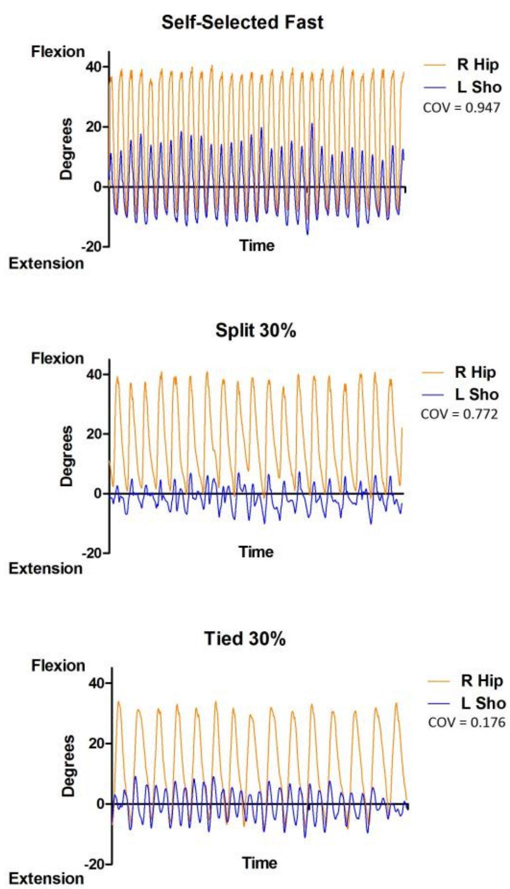

Figure 1: Flexion/extension and corresponding COV values of one participant's right (slow side) hip and left (fast side) shoulder during 3 speed configurations.

Table 1: Coordination and gait cycle results. † indicates a significant Condition X Speed interaction. Superscripts indicate within-measure significant differences of at least P<0.05.

Measure	Cond.	Speed			
		90%	70%	50%	30%
FastHip/ SlowSho COV†	Tied	0.88[a]	0.88[b]	0.84[c]	0.60[abc]*
	Split	0.90[u]	0.88	0.85	0.78[u]*
SlowHip/ FastSho COV†	Tied	0.89[a]	0.88[b]	0.83[c]	0.56[abc]*
	Split	0.89	0.88	0.88	0.84*
FastHip/ SlowSho PRP†	Tied	26.39[a]	25.48[b]	30.15[c]	59.04[abc]*
	Split	26.61	25.49	27.70	34.52*
SlowHip/ FastSho PRP†	Tied	27.02[a]	25.83[b]	29.14[c]	69.37[abc]*
	Split	28.98	28.03	28.44	35.49*
Fast Step Length (m)	Tied	0.61[abc]	0.55[ade]	0.48[bdf]	0.38[cef]
	Split	0.61[uv]	0.58[wx]	0.51[uwy]	0.43[vxy]
Slow Step Length (m) †	Tied	0.62[abc]	0.55[ade]^	0.47[bdf#]	0.37[cef]*
	Split	0.64[uv]	0.62[w]^	0.58[ux#]	0.50[vwx]*
Fast Stride Length (m) †	Tied	0.65[abc]	0.59[ade]^	0.53[bdf#]	0.45[cef]*
	Split	0.67	0.69^	0.69[#]	0.67*
Slow Stride Length (m) †	Tied	0.65[abc]	0.59[ade]	0.53[bdf#]	0.44[cef]*
	Split	0.63[uvw]	0.56[uxy]	0.47[vxz#]	0.33[wyz]*
Fast Stance (% gait cycle) †	Tied	62.13[abc]	64.13[ade]^	65.86[bdf#]	70.71[cef]*
	Split	60.40[uv]	58.06[wx]^	53.89[uwy#]	48.96[vxy]*
Slow Stance (% gait cycle) †	Tied	61.52[abc]	63.10[ade]^	64.78[bdf#]	69.58[cef]*
	Split	62.83[uvw]	65.86[uxy]^	69.51[vxz#]	74.60[wyz]*
Double Support (% gait cycle) †	Tied	23.64[abc]	27.23[ade]^	60.63[bdf#]	40.28[cef]*
	Split	23.22	23.92^	23.40[#]	23.56*

SAMPLE ENTROPY OUTPERFORMS APPROXIMATE ENTROPY WITH SMALL DATA SETS

[1]Jennifer M. Yentes, [2]Nathaniel Hunt, [3]Kendra K. Schmid, [1]Jeffrey P. Kaipust,
[4]Denise McGrath and [1]Nicholas Stergiou

[1]University of Nebraska at Omaha, Omaha, NE, USA
[2]University of California, Berkeley, CA, USA
[3]University of Nebraska Medical Center, Omaha, NE, USA
[4]University of Ulster, Belfast, Northern Ireland
email: jyentes@unomaha.edu, web: http://nbcf.unomaha.edu

INTRODUCTION

Originally formed out of the theories of thermodynamics, biologists have developed several algorithms that allow scientists to quantify entropy in biological time series. Two of the most popular algorithms are approximate entropy [ApEn; 1] and sample entropy [SampEn; 2]. Each algorithm takes three input parameters: (1) *m*, the length of the data segment that will be compared, (2) *r*, the similarity criterion, and (3) *N*, the length of the data. No clear consensus has been established to properly select the parameters, particularly for short data sets (N<500). In addition, it is vital that the parameters selected demonstrate relative consistency. That is that a small change in the parameter should not lead to a "flip" in the results; discrimination between groups should hold with small parameter changes. The aims of this research were to examine the effect of changing the three input parameter values on the calculation of ApEn and SampEn and describe the relative consistency of the algorithms in both short theoretical and experimental data sets (N<200).

METHODS

Theoretical data was generated in order to examine the effect of parameter choice in time series with known entropy values: (1) periodic, (2) chaotic and (3) white noise. Periodic and chaotic time series were generated using the logistic map and white noise was generated using the rand function in MatLab (Mathworks Inc., Natick, MA). Twenty chaotic and white noise time series were generated with initial conditions being chosen randomly. Only one periodic time series was generated using an initial condition equal to 3.4 for the logistic map.

Healthy young adults (n=26; 25.9$\pm$3.0 yrs) and healthy older adults (n=24; 70.9$\pm$4.1 yrs) were consented. After selecting a comfortable walking speed on a treadmill, subjects walked for three minutes while 3D marker trajectories were recorded (100Hz, NDI, Waterloo, Canada). Custom MatLab code generated three time series for each subject: step length, width and time. All time series were cut to *N* of 200.

ApEn(*m*,*r*,*N*) and SampEn(*m*,*r*,*N*) were calculated for each theoretical and experimental time series under all combinations of *m*=2, 3; *r*=0.05, 0.1, 0.15, 0.2, 0.25, 0.3 times the standard deviation of the entire time series; and *N*=100, 120, 140, 160, 180 and 200, for a total of 72 combinations. For ApEn and SampEn, a value of 0 indicates a perfectly repeatable time series. For perfect white noise, ApEn will result in a value of 2 and SampEn has no upper limit. A repeated-measures ANOVA (SAS, Cary, NC) was used to determine the effect of type (chaotic vs. white noise) and group (young vs. old) on ApEn and SampEn. The effect of changing *m, r,* and *N* was also investigated through significant 2-way or 3-way interactions.

RESULTS AND DISCUSSION

Theoretical Data: The periodic time series produced a value of 0 for all combinations of *m, r,* and *N*. A significant difference in ApEn ($p<0.0001$) and SampEn ($p<0.0001$) between the chaotic and white noise time series was found. The chaotic data set provided higher values of ApEn yet lower values of SampEn. The value of ApEn was different depending on the combination of *m, r,* and *N*

($p<0.0001$). However, SampEn was consistent across values of *N* but was different depending on values of *r* and *m* ($p<0.0001$).

Experimental Data: A significant difference in ApEn ($p=0.02$) and SampEn ($p=0.004$) between the step length time series for young and older adults was found. No difference in step width or step time was found between young and older adults for either ApEn or SampEn. For step length, width, and time, the value of ApEn was different depending on the combination of *m, r,* and *N* ($p<0.0001$) and SampEn tended to decrease as *r* increased although SampEn was consistent across values of *N* ($p<0.0001$).

Relative Consistency: With the white noise theoretical data at small *r* values, ApEn yielded lower ApEn values than the chaotic logistic map, which is known to be incorrect. ApEn demonstrated problems with relative consistency for all experimental data sets for $m=2$ and $r=0.25$ and 0.3. Older adults demonstrated a higher ApEn when $N=100$ but as *N* increased to 200, younger adults demonstrated a higher ApEn value. Relative consistency was challenged for small *r* values when calculating SampEn as well.

Based on our current findings, it appears that there is not a set combination of parameters that will work every time. ApEn values were influenced depending on input parameter combination regardless of whether theoretical or experimental data was analyzed. On the other hand, SampEn produced results for the experimental data sets that clearly demonstrated independence of data length regardless of the choice of *m* or *r*, consistent with previous findings [3].

For now, we recommend the *N* to be larger than 200 and as large as possible with respect to the practical constraints of the experiment. Another consider-ation to keep in mind when choosing *N* is whether or not the length of the time series being analyzed is sufficient to capture the dynamics of the system. It is possible that the dynamics and therefore, the related biological complexity of the movement pattern could not be captured in such short data sets thus affecting the results. On the other hand, for some gait or motor pathologies, collection of a trial of 200 data points may be difficult.

Our results also highlighted issues with relative consistency for both ApEn and SampEn. Relative consistency relates to the stability of the measure. When utilizing an entropy algorithm, the investigator should consider if it is providing a consistent value across different *r* values. Inconsistent values for ApEn and SampEn in the current results are problematic because the true relative direction of differences between young and older adults is unknown. When utilizing any nonlinear mathematical tool it is critically important that relative differences between groups are not an artifact of parameter choice. Slight changes in the input parameter choices should be investigated and their effect on the results should be reported. This will ensure that the relative difference, not necessarily the magnitude of difference but rather the direction of difference, between groups is stable.

CONCLUSIONS

It is essential to adopt a prudent approach to the various techniques available for the quantification of entropic properties of a signal. We suggest using $N>200$, an *m* of 2 and examine several *r* values before selecting your parameters. Based on our current findings, it appears that SampEn was less sensitive to changes in data length and demonstrated fewer problems with relative consistency.

REFERENCES

1. Pincus S. *Proc Natl Acad Sci USA* **88**, 2297-2301, 1991.
2. Richman JS and Moorman JR. *Am J Physiol Heart Circ Physiol* **278**, H2039-2049, 2000.
3. Molina-Pico AD, et al. *Artif Intell Med* **53**, 97-106, 2011.

ACKNOWLEDGEMENTS

Funding was provided by the NASA Nebraska Space Grant & EPSCoR, Patterson Fellowship through the University of Nebraska Medical Center and NIH/NIA (R01AG034995).

DEVELOPMENT OF A GEOMETRIC MODEL TO DETERMINE INERTIAL PARAMETERS IN AMPUTEES

Christopher Siviy, Allison Luther, April Chambers, and Rakié Cham

University of Pittsburgh, Pittsburgh, PA, USA
email: cjs142@pitt.edu, web: http://www.engineering.pitt.edu/hmbl/

INTRODUCTION

There are an estimated 623,000 lower-limb amputees in the United States [1]. Kinematic and kinetic gait analyses are widely used to analyze gait patterns of amputees and determine how safe prosthetic devices are. In this project, we focused on older adults with unilateral transfemoral amputations.

Kinetic gait analyses require knowledge of each body segment's inertial parameters, such as mass, Center of Mass (CoM), and mass moment of inertia. Directly measuring inertial parameters [2] requires time and disassembly of all prosthetic components, and typical regression models only work for healthy individuals. Geometric models have been used to provide estimates of segment parameters in both healthy individuals [3] and amputees [4]. Geometric models require only a series of anthropometric measurements, and therefore have the potential to be much less time-consuming and easier to implement than direct measurement. Additionally, a geometric model provides estimates of residual limb parameters, which is not possible via direct measurement. The goal of this research is to develop a simple geometric model to determine the inertial parameters of the prosthetic limb in a transfemoral amputee.

METHODS

This model was developed for one unilateral transfemoral amputee. Measurements were taken at the thigh (comprising the prosthetic socket, the residual limb, and any socket adapters), the shank (comprising the prosthetic knee, the pylon, and any associated pylon adapters) and the foot (comprising the prosthetic foot inside the shoe).

A certified prosthetist disassembled the prosthesis and direct measurements of mass and CoM were taken for all three segments on a laboratory force plate and balance board, respectively.

Figure 1 summarizes the measurements taken at the thigh socket. Diameters were taken in the Medial/Lateral (M/L) and Anterior/Posterior (A/P) direction every 3 cm. Straight distance from the first and last diameter locations to the proximal and distal edges of the socket were recorded along with the dimensions of any adapters and the socket's thickness.

For the shank, M/L, A/P, and overall length measurements of the knee were recorded at the proximal and distal edges of the prosthesis housing. The pylon's overall length and the dimensions of any adapters were recorded.

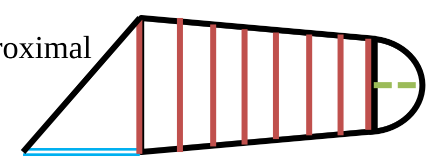

Figure 1: Socket measurements: Red solid lines are diameters taken every 3 cm. The blue double line is the straight distance from the most proximal diameter to the proximal edge of the socket. The green dashed line is the straight distance from the distal diameter measurement to the distal end of the socket.

The prosthetic foot remained in the shoe during all measurements. M/L and Superior/Inferior (S/I) measurements were recorded every 3 cm from the back of the shoe moving distally to the toe tip.

Five geometries were used in constructing the geometric model of the lower leg: (1) cylinder, (2) elliptical solid, (3) semi-ellipsoid of revolution, (4) rectangular prism, and (5) stadium solid. Mass, CoM, and mass moment of inertia were calculated for each geometry according to Kwon [5]. Tissue density was assumed to be 1.1 g cm^{-3} [6] and known densities were used for prosthetic components.

RESULTS AND DISCUSSION

The thigh is a series of elliptical solids capped by a semi-ellipsoid of revolution. The socket is a homogeneous shell whose major and minor radii are determined by the M/L and A/P diameters, and the residual limb is assumed to fill the inner volume. Adapters are modeled as rectangular prisms or cylinders. The shank contains three components. The prosthetic knee is an elliptical solid whose major and minor radii are determined by the A/P and M/L measurements. Knee mass is readily available in most manufacturers' specification sheets. The pylon was modeled as a hollow cylinder with standard dimensions of an inner diameter of 2.5 cm and an outer diameter of 3 cm. The foot consists of a series of stadium solids. The recorded foot mass is used to determine foot density.

Table 1. Selected comparisons between measured values and model estimates.

Parameter	Model Estimate	Measured Value
Shank CoM* [cm]	15.7	14.5
Foot CoM* [cm]	11.4	13.0
Socket Mass [kg]	1.65	1.31

* Distance from proximal end of segment

Table 1 provides selected comparisons between the directly measured values and model estimates of inertial parameters.
Due to the prosthetic knee's complexity the shank model assumes a homogeneous elliptical solid. The elliptical solid requires only four measurements and accurately predicts shank CoM within 1 cm. Likewise; the foot model predicts foot CoM within 2 cm.

The model overestimates socket mass. A socket is molded specifically to an amputee's residual limb, so socket thickness may vary over the length of the socket. Measuring socket thickness at multiple locations on the socket will likely increase the model's accuracy.

Further work will include a generalization of foot mass to eliminate the requirement to measure foot mass directly, and therefore eliminate the need to disassemble any part of the prosthesis. Additionally, application of the model to a larger pool of participants will further validate the model.

REFERENCES

1. Ziegler-Graham K, et al. *Arch Phys Med Rehabil* **89**(3), 422-429, 2008.
2. Selles RW, et al. *Arch Phys Med Rehabil* **84**(4), 569-567, 2003
3. Yeadon MR. *J Biomech* **23**(1), 67-74, 1990
4. Fowler EG, et al. *J Pediatr Orthop* **19**(6), 720-731, 1999
5. Kwon YH. http://kwon3d.com/. 1998
6. Mattes SJ, et al. *Arch Phys Med Rehabil* **81**(5), 561-568, 2000

ACKNOWLEDGEMENTS

Funding was provided by a grant from the American Orthotic and Prosthetic Association.

ECONOMIZATION OF STRIDE LENGTH IN LEVEL AND UPHILL RUNNING

Iain Hunter and Erin Robinson

Brigham Young University, Provo, UT, USA
email: iain_hunter@byu.edu web: http://biomechanics.byu.edu

INTRODUCTION

Selecting an optimal stride length in distance running makes a large difference in overall performance due to the large increases found in oxygen uptake when non-economical stride lengths are used (Cavanagh and Williams, 1982). Experienced runners naturally select stride rates and lengths that minimize oxygen uptake during distance running (Cavanagh and Williams, 1982; Hunter and Smith, 2007). These studies showed that runners have this ability to self-optimize stride length for economy on level ground when rested and fatigued.

When running uphill, the ratio of concentric to eccentric muscle activation is different than when running on level ground (Abe et al., 2011). Stride lengths are expected to be shorter during uphill endurance running since the speeds will be slower and the runner's foot will contact the ground a little earlier. This may lead to a difference in optimal stride length during uphill running. This study uses metabolic cost measures to determine whether experienced runners naturally select the most economical stride length when running uphill.

METHODS

Preferred and economical stride length was measured in 13 subjects during uphill and level treadmill running. An informed consent document was signed by each subject before she was allowed to begin. The study was approved by the Brigham Young University Institutional Review Board.

Each athlete ran three trials on three separate days: a familiarization trial for accommodation to treadmill running and practice matching a set cadence, and a level and uphill trial for a period of 20 minutes each. The trials were run at speeds of 3.83 m/s (7:00 min/mi) for level running and 2.68 m/s (10:00 min/mi) for a 6% uphill grade. These speeds were chosen through pilot testing which helped determine which uphill speed would have a similar oxygen uptake to level ground running. Preferred stride length was determined by manually timing 50 strides during the end of a five-minute warm up period. Oxygen uptake was measured throughout both of these trials while a computerized metronome helped subjects match their stride rate to plus and minus eight and 16 percent of their preferred stride rate for three minutes each. The final minute of oxygen uptake for each three-minute section was used in the final analysis. A best-fit second-degree polynomial was placed through oxygen uptake versus stride length. Solving for the minimum oxygen uptake value of this polynomial provided economical stride length. Repeated measures ANOVA with Sidak post-hoc tests were used to determine whether differences existed between preferred and economical stride lengths in uphill and level running.

RESULTS AND DISCUSSION

Preferred and economical stride lengths were no different during level ($p = 0.13$) or uphill running ($p = 0.98$). However, stride lengths were different between uphill and level running ($p < 0.01$). Mean stride lengths for each condition are found in Table 1. Average $\dot{V}O_2$ during the preferred stride length in the level trials was 44.05 ml/kg/min and the uphill trial was 44.66 ml/kg/min ($p = 0.64$).

Table 1: Stride lengths for the various conditions.

Level		Uphill	
Preferred	**Economical**	**Preferred**	**Economical**
2.59 ± .13	2.54 ± .10	1.88 ± .07	1.87 ± .06

Previous studies also observed no meaningful differences between preferred and economical strides during level running (Cavanagh and Williams, 1982; Hunter and Smith, 2007). Our main interest in this study was determining whether the same result would be found for uphill running. These experienced distance runners naturally selected the stride length that minimizes oxygen uptake while running uphill.

The mass-spring model of running explains why optimal stride length matches economical stride length (Hunter and Smith, 2007). While vertical or leg stiffness has not been reported during uphill running, the natural spring stiffness may explain why a preferred stride length is chosen in uphill running. We considered that the average applied force would be different during uphill running. However, runners appear to modify their technique in a way that the most economical stride length for running uphill is utilized. Future studies will investigate how vertical or leg stiffness changes with uphill and downhill running to better understand the connection between stiffness and economical stride lengths.

The steepness and shape of each curve varied from subject to subject (Figures 1 & 2. Some subjects were capable of using stride lengths substantially different than preferred without large increases in oxygen uptake during uphill and level running. Shorter strides than preferred were often less detrimental than longer strides within a given subject. A few runners had preferred stride lengths that were three to four percent away from the most economical. However, these were usually runners where only smaller increases in $\dot{V}O_2$ were observed due to non-optimization of stride length.

Some runners had a most economical stride length relatively far away from their preferred. However, these runners had very small increases in $\dot{V}O2$ as a result of this non-economization. It's seems that some runners have the ability to perform well using a relatively large range of stride lengths, while others must stay close to their naturally selected stride length when economy is their concern.

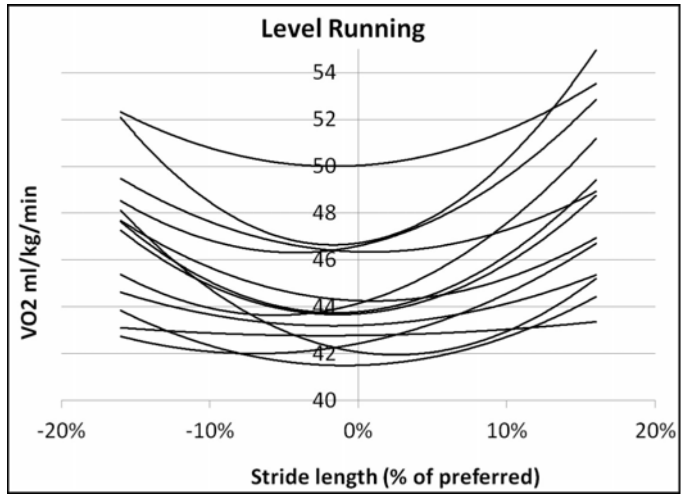

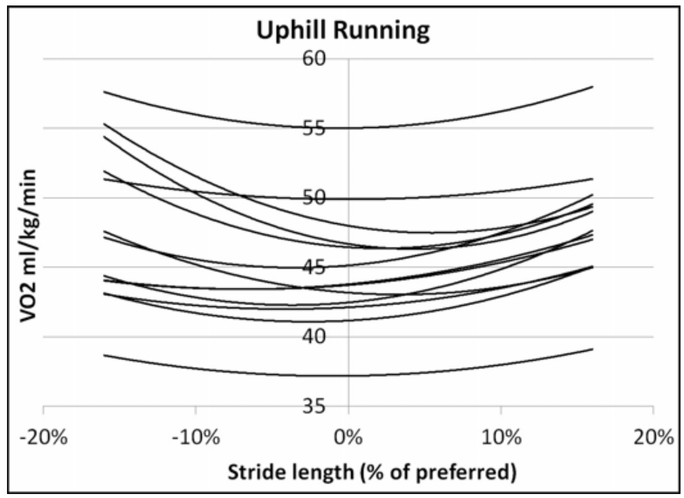

Figures 1 & 2: Prediction of economical stride length (ESL) based upon forcing strides ± 8 and 16% of preferred stride length (PSL).

CONCLUSIONS

Runners naturally select a stride length that optimizes running economy during level and uphill running. Small discrepancies between preferred and economical stride lengths existed, but only led to minor increases in $\dot{V}O_2$. Thus, distance runners should allow their bodies to naturally select stride length to minimize oxygen uptake. This will help them maintain their running pace using the least amount of energy.

REFERENCES

1. Cavanagh PR & Williams KR. *Sports Med* **22**, 30-35, 1982.
2. Hunter I & Smith GA. *Eur J App Physiol* **100**, 653-661, 2007.
3. Abe D et al. *J Physiol Anthro* **30**, 153-160, 2011.

CARDAN SEQUENCES ON 1-MTP JOINT KINEMATICS: IMPLICATIONS FOR FOOT BUNION

Ward M. Glasoe, Fernando Pena, Vandana Phadke, and Paula M. Ludewig

University of Minnesota, Minneapolis, MN USA
email: glaso008@umn.edu , web: http://www.med.umn.edu/physther/

INTRODUCTION

There is no standard for calculating first metatarso-phalangeal (1-MTP) joint kinematics. Sagittal motion is largest, thus it is typically calculated as the first rotation. But with bunion deformity, calculating the first rotation in the transverse plane may better represent rotations outside the sagittal plane. This study compared sagittal (*Z-Y'-X"*) vs. transverse (*Y-Z'-X"*) first rotation sequences to examine the influence of the different order of rotations in describing 1-MTP joint kinematics in controls, and in subjects with bunion.

METHODS

Twelve female control subjects, and 19 having bunion participated. Subjects were imaged while positioned in an open-upright .6 Tesla MR scanner, their foot posed on a system of wedges (Fig. 1) to simulate gait midstance (MS), heel off (HO) and terminal stance (TS).

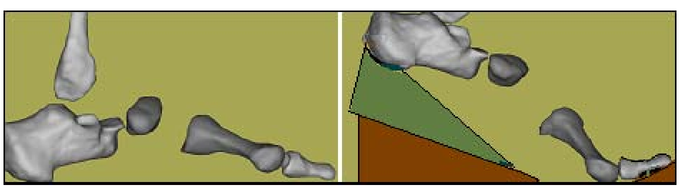

Figure 1: Sagittal view of the reconstructed bone models at midstance (MS) and terminal stance (TS).

The proximal phalanx of the hallux, the first metatarsal, and other tarsals were segmented and registered together in the MR coordinate system. Offset in 1-MTP joint posture was measured by the hallux valgus angle (Fig. 2), with 15° the threshold for classifying bunion.

Each tarsal was embedded with an inertial axis coordinate frame. Frames defining the hallux and first metatarsal aligned nearly coincident with MR reference. Coordinate frame axes were labeled positive Z-lateral, Y-up, and X anterior. Cardan angles were calculated using Mat Lab (Mathworks, Natick, USA). Descriptive results, and 1-MTP joint order of rotations were examined using a within factors (sequence; gait event) repeated measures ANOVA to analyze the mean differences in angles.

RESULTS AND DISCUSSION

Offset in 1-MTP joint posture was larger ($P < 0.05$) in the group with bunion (Table 1). Arch angle was not different between groups

Table 1: Mean ± SD group comparison results.

	Control	**Bunion**	***P*-value**
Demographics			
Age (yrs)	45 ± 17	50 ± 16	= 0.44
BMI (kg/m^2)	27 ± 6	26 ± 6	= 0.66
Foot Posture (°)			
Hallux Valgus Angle	8 ± 5	33 ± 15	< 0.01
Intermetatarsal Angle	11 ± 1	15 ± 3	< 0.01
Arch Angle	134 ± 7	134 ± 10	= 0.99

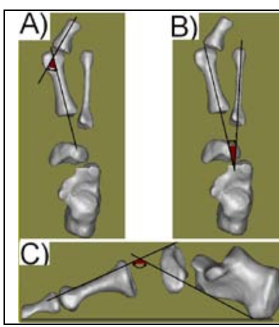

A) Hallux Angle: Lines bisect the hallux and 1-metatarsal.

B) Intermetatarsal Angle: Lines bisect the 1-2 metatarsals.

C) Arch Angle: Lines connect 1-metatarsal and calcaneus.

Figure 2: Planar measures of posture were made on the MS datasets. The foot shown had bunion.

The 2-way ANOVA results identified a significant interaction ($F \geq 25.1$; $P < 0.001$) between sequence and gait event. The *post-hoc* pairwise comparisons revealed the 1-MTP joint angle was different at TS for all statistical outputs (Fig. 3).

For sagittal 1-MTP joint angle rotation, both sequences captured an increasing pattern of dorsiflexion as should happen across a progression of late stance gait events. Dorsiflexion in the present study occurred in response to the foot being wedged forward to simulate gait (Fig. 1). In agreement with data reported in gait trials [1,2], dorsiflexion was the largest component rotation and this result showed the greatest consistency between Cardan sequences in both groups of subjects (Fig. 3).

For transverse 1-MTP joint angle rotation, only the use of the *Y-Z'-X"* Cardan sequence consistently found increasing abduction across the gait progression (Fig. 3). Abduction of the hallux is expected to occur when moving into late stance, especially in subjects having bunion deformity [1].

Frontal was the last rotation calculated. Differences in angles were largest at TS (Fig. 3), measuring 27° in controls and 40° in the bunion group. Note how different sequences output this rotation in opposite directions. Research interested in measuring hallux in/eversion are advised to explore other methods.

CONCLUSIONS

This study used a gait simulation imaging method to compare two different Cardan sequences on 1-MTP joint kinematics. Only the *Y-Z'-X"* sequence consistently found incremental increases in 1-MTP joint dorsiflexion, abduction, and eversion in females with and without bunion. Acknowledging that no data was offered to validate the measure of kinematics reported, continued research is needed to investigate whether the *Y-Z'-X"* sequence most accurately represents the direction and magnitude of 1-MTP joint motion during gait.

REFERENCES

1. Canseco K, et al. *Foot Ankle Int* **31**, 146-152, 2010
2. Deschamps K, et al. *Gait Posture* **32**, 102-106, 2010

ACKNOWLEDGMENTS

This work was funded by the Arthritis Foundation North Central Chapter

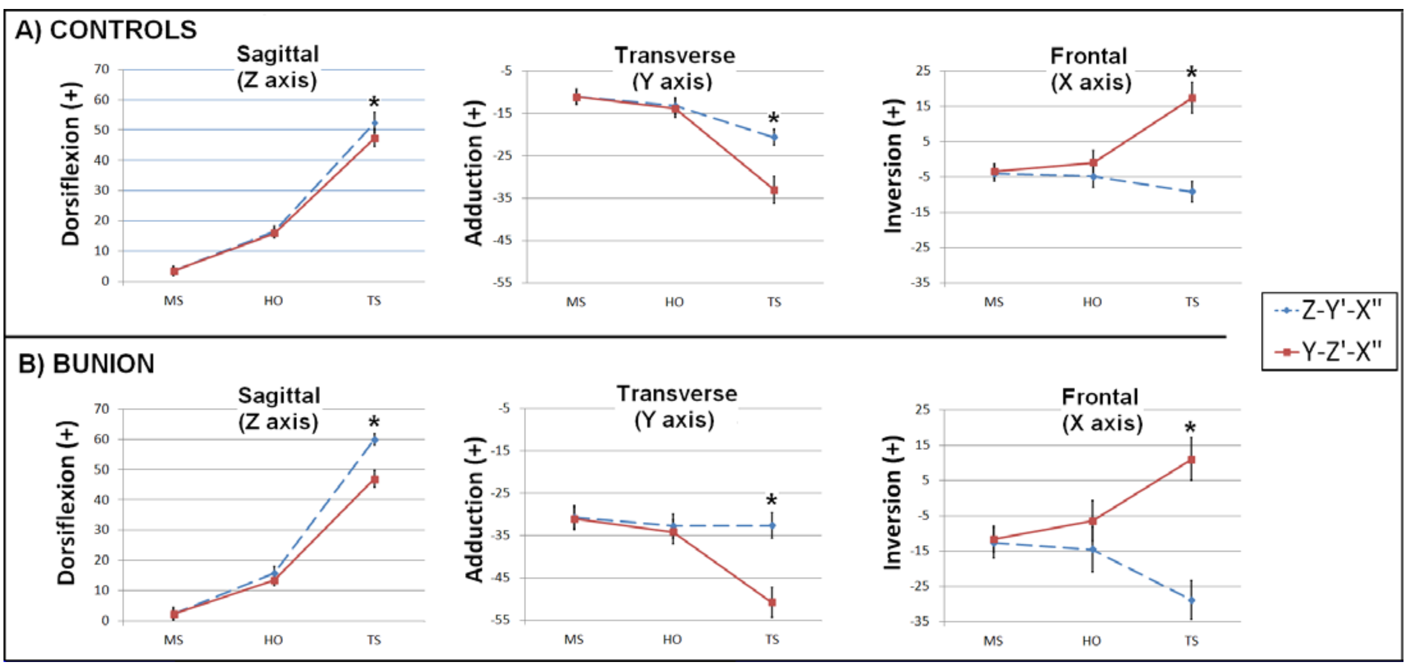

Figure 2: First metatarsophalangeal (1-MTP) joint angles with error bars (95% confidence intervals) plotted across conditions. Graph A) displays mean angles calculated for the control group (N = 12). Graph B) displays mean angles for the bunion group. Asterisks (*) indicates significant difference ($P < 0.05$) in pairwise comparison between sequence within conditions. Note scale change between graphs. Abbreviations: MS, midstance; HO, heel off; TS, terminal stance.

DEVELOPMENT AND EVALUATION OF A NEW MOVING SYSTEM INCORPORATED WITH SPECIFIC FUNCTION FOR GAIT REHABILITATIVE TRAINING ASSISTANCE

[1]Bumkee Lee, [1]Leeyong Song, [1]Hoyeon Jung, [2]Kyungjin Jeon, [3]Kyungbae Jang, [1]Dohyung Lim

[1]Dept. Mechanical Engineering, Sejong University, Seoul, Republic of Korea
[2]Smart Welfare Technology Research Group, KITECH, Cheonan, Republic of Korea
[3]Rehabilitation Research Institute, Korea National Rehabilitation Center, Seoul, Republic of Korea

Corresponding email: dli349@sejong.ac.kr

INTRODUCTION

According to CDC (U.S. Centers for Disease Control) statistics, 15.7 million adult Americans (7.1% of the total adult population) find it difficult or impossible to walk a quarter of a mile [1]. It has been widely recognized that a wheelchair is most useful substitution for their walking disability [2]. Most wheelchairs have, however, only a moving function generally, not the specific function designed for an assistance of a gait rehabilitative training [3]. The aims of this study are, therefore, to 1) develop a new moving system incorporated with the specific function above based on wheelchair platform and 2) evaluate its usefulness. The newly developed moving system is named S-MSGRTF (Sejong - Moving System with Gait Rehabilitative Training Function, Sejong University, Republic of Korea).

METHODS AND MATERIALS

Participants

Seven healthy subjects [males, between 22 and 25 years of age, 174±6cm (mean±s.d.) height, 71±12kg weight, 23±4kg/m^2 body mass index] were participated in this study. All subjects were free from musculoskeletal disorders and leg pain. The study protocol was approved by the Korean National Institute for Bioethics Policy Institutional Review Board, project number PIRB12-038-01. Consent was obtained from all subjects prior to participation in the study.

Data Acquisitions

Participants walked on a 30m ground walkway without/with wearing S-MSGRTF at a self-selected (natural gait) and a controlled (S-MSGRTF gait) speed, respectively. Three trials were then collected and their gait motion characteristics (kinematic and kinetic data) were recorded using a three-dimensional motion capture system with eight infrared cameras (VICON T-10s, Oxford, UK, 100Hz), two force-plates (AMTI OR6-7, Advanced Mechanical Technology Inc., Watertown, USA, 1000Hz) (Fig. 1). Here, a standard and a modified plug-in-gait models were used for the analysis of the gait motion characteristics.

S-MSGRTF Design and Development

S-MSGRTF was designed to embody both a moving and a gait rehabilitative training functions together capable of using during daily living activities of patients with walking disability (Fig. 1). The moving and gait rehabilitative training functions were then embodied based on a general wheelchair and lower extremity exoskeleton systems, respectively, and they were combined as one with the specifically designed mechanisms. For a gait rehabilitative training function, the part of the lower extremity exoskeleton of S-MSGRTF was consisted of the hip, knee and ankle joints and controlled by 12 artificial pneumatic muscles (Shadow Robot Com., London, UK) (Fig. 1). Artificial pneumatic muscles were then controlled based on the joint torques corresponding to the natural gait motion, particularly the flexion-extension motions of the hip, knee and ankle joints.

S-MSGRTF Evaluation

S-MSGRTF was evaluated to identify if it is well functioning properly for a moving and a gait rehabilitative training together, by comparing of the gait motion characteristics obtained from natural gait with them from S-MSGRTF gait. In addition, it was identified if a structural stability of S-MSGRTF is secured enough, through finite element analysis.

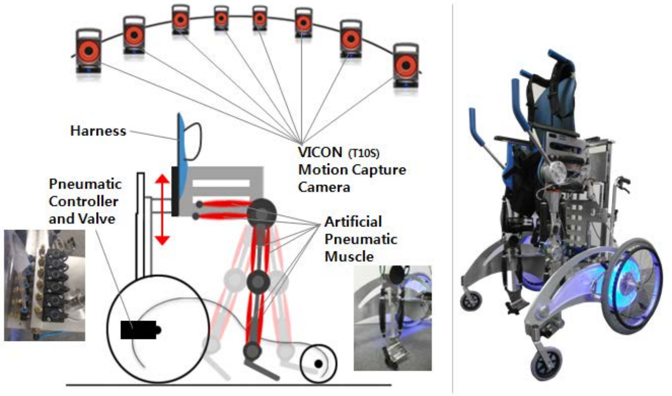

Figure 1: Schematic diagram for the gait motion analysis with S-MSGRTF and main components of S-MSGRTF

RESULTS AND DISCUSSIONS

Alteration patterns of the hip, knee and ankle joint angles for natural and S-MSGRTF gaits were shown in Fig. 2. A tendency of the alteration of the hip and knee joint angles during natural gait were similar to that during S-MSGRTF gaits, although a degree of deviation was initiated and bigger following 45% and 60% of gait cycles approximately in the hip and knee joint angles ($p>0.05$), respectively. Alteration pattern (tendency and magnitude) of the ankle joint angle during natural gait were, however, totally different to that during S-MSGRTF gaits ($p<0.05$). These findings indicate that S-MSGRTF may have potential to be applicable to a gait rehabilitative training assistant with wheelchair platform for movement, although it doesn't realize a natural gait completely, particularly in the ankle joint motion.

CONCLUSIONS

It is judged that a moving system (S-MSGRTF) developed newly in this study may be useful to the patient with walking disability because a gait rehabilitative training can be easily applied during their daily living activities. S-MSGRTF has, however, still many limitations. The limitations will be improved in our ongoing studies.

REFERENCES

1. Andrew McWilliams. Disabled and Elderly Assistive Technology in the U.S., BBC Research, Wellesley, MA, USA, 2008.
2. Kakimoto, A., et al. *Proceedings of the 19th Annual International Conference of the IEEE EMBS*, Chicago, IL, 1997.
3. Zeungnam Bien, et al. *Proceeding of the 2003 IEEE /ASME* AIM, Kobe, Japan, 2003.

ACKNOWLEDGEMENTS

This study was supported by a grant from the Korea Health-care Technology R&D Project, Ministry for Health, Welfare, & Family Affairs, Republic of Korea (A120126)

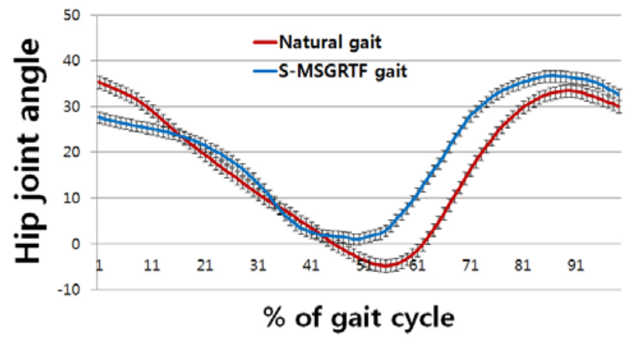

(A)

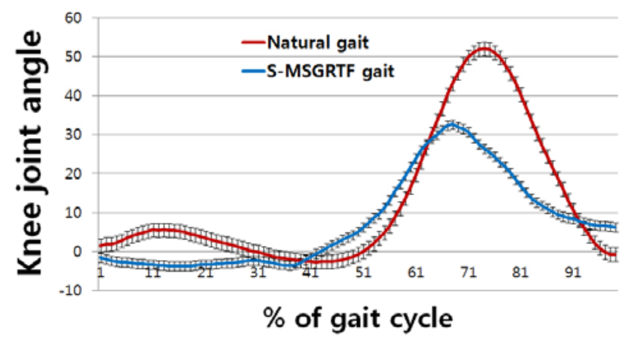

(B)

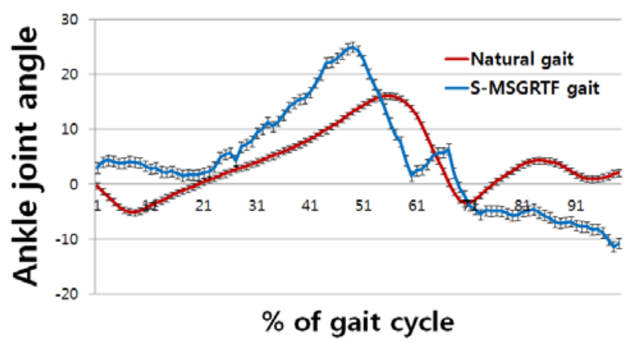

(C)

Figure 2: Alteration patterns of the (A) hip, (B) knee and (C) ankle joint angles at natural and S-MSGRTF gaits. Horizontal axis were presented in percentage of gait cycle.

INDIVIDUAL LIMB MECHANICAL ANALYSIS OF GAIT FOLLOWING STROKE

[1,2]Caitlin E. Mahon, [2]Dominic J. Farris, [1,2]Gregory S. Sawicki and [1]Michael D. Lewek

[1]University of North Carolina at Chapel Hill, Chapel Hill, NC, USA
[2]North Carolina State University, Raleigh, NC, USA
email: mahon.caitlin@gmail.com

INTRODUCTION

Total mechanical work and net metabolic cost of gait can be minimized when the timing and magnitude of the leading limb's negative mechanical work is equal to the trailing limb's positive mechanical work during double-support [1]. Following stroke, greater mechanical work requirements reduce metabolic efficiency [2]. We propose this is, in part, the result of inter-limb mechanical asymmetries.

We hypothesize that: (1) mechanical asymmetries between limbs will be greater in individuals with reduced gait functional ability. Based on analyses conducted on patient populations with similar impairments [3,4] we further hypothesize that: (2) gait following stroke will exhibit less positive power production from the paretic limb during the trailing double-support (DST) phase, greater negative power production from the non-paretic limb during the leading double-support (DSL) phase to redirect the COM, and greater positive power production from the non-paretic limb during the single-support (SS) phase to raise the COM (each in comparison to the contralateral limb).

METHODS

We recruited 26 individuals who presented with chronic (>6 months post-stroke) hemiparesis following unilateral, non-cerebellar brain lesion due to stroke. Individuals were stratified into "functional" groups based on self-selected overground speed: 13 high function (>0.8 m/s), 6 moderate function (0.5 m/s-0.8 m/s), and 7 low function (<0.5 m/s). The individual limbs method (ILM) [1] was used to calculate external mechanical power performed on the COM by the paretic and non-paretic limbs, during treadmill walking at a maintainable training speed.

Ground reaction forces, collected from a one-minute trial on a dual-belt treadmill, and vertical force from handrail support (when produced) were included in net force data prior to calculation of COM acceleration. Because the ILM assumes symmetric gait, and spatiotemporal asymmetries are often exhibited following stroke, the ILM was adjusted by: (1) assuming symmetry over strides, instead of steps, and (2) subtracting average COM acceleration over a trial from instantaneous COM acceleration prior to integration.

Five separate two-way (limb x functional group) ANCOVAs were performed (α=0.05) to examine differences in peak instantaneous mechanical power (P_{inst}) during (1) DST and (2) DSL and average mechanical power (P_{avg}) during (3) DST, (4) DSL and (5) SS, using treadmill speed as a covariate (all outcome variables were normalized to body mass). For the post-hoc analysis, adjusted means were computed and a Bonferroni adjustment was applied to account for multiple comparisons.

RESULTS AND DISCUSSION

Figure 1: The two-way ANCOVA analyzing peak P_{inst} during DST showed the paretic limb produced a significantly less positive P_{inst} peak than the non-paretic limb ($p<.0005$); no main effect for functional group ($p=.163$); and an interaction effect between limb and functional group ($p=.050$). Post-hoc analyses revealed the greatest difference between limbs (i.e., greatest asymmetry) existed for the moderate group and the least difference between limbs (i.e., least asymmetry) existed for the low group after applying the treadmill speed covariate (non-paretic/paretic adjusted means, (W/kg): high:

1.10/0.65; moderate: 1.10/0.45; low: 1.00/0.95). The two-way ANCOVA analyzing peak P_{inst} during DSL showed the non-paretic limb produced a significantly less negative P_{inst} peak than the paretic limb ($p=.047$); no main effect for functional group ($p=.288$); and no interaction effect between limb and functional group ($p=.944$).

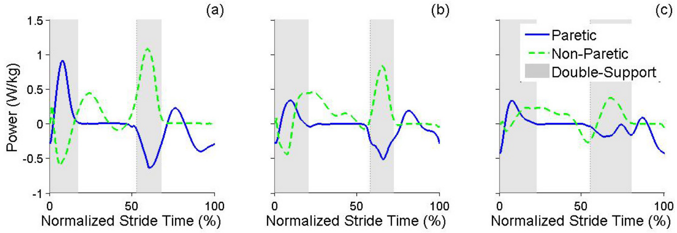

Figure 1: Normalized, mean P_{inst} for (a) high, (b) moderate and (c) low functional groups. Normalized Stride Time 0 indicates beginning of non-paretic limb DSL phase.

Figure 2: The two-way ANCOVA's analyzing P_{avg} produced during DST, DSL and SS, respectively, showed the paretic limb (compared to the non-paretic limb) produced significantly less positive P_{avg} during DST, and the non-paretic limb (compared to the paretic limb) produced significantly less negative P_{avg} during DSL and significantly greater positive P_{avg} during SS ($p<.0005$, $p<.0005$, $p<.0005$); no main effect for functional group ($p=.120$, $p=.452$, $p=.077$); and no interaction effect between limb and functional group ($p=.093$, $p=.453$, $p=.467$).

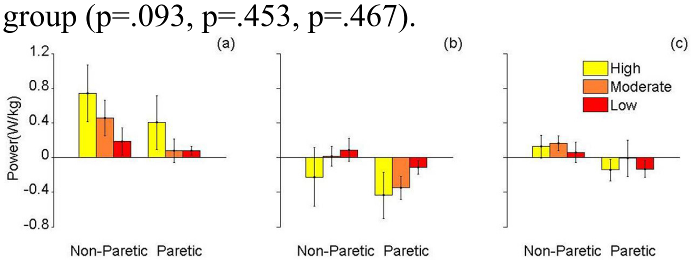

Figure 2: Total P_{avg} plotted over (a) DST, (b) DSL and (c) SS.

Although we observed significant mechanical asymmetries between limbs across all functional groups during each phase of the stride, we were surprised that these asymmetries were not significantly different *between* groups. The lone exception was peak P_{inst} during DST, for which asymmetry between limbs was larger in the moderate group compared to the low group. These results suggest that individuals with lower function do not exhibit less mechanical power production and absorption from solely the paretic limb, but from both limbs, compared to individuals with higher function.

Our second hypothesis was partially confirmed. We observed less positive peak P_{inst} and P_{avg} of the paretic limb (compared to the non-paretic limb) during DST. Although this may be due to the paretic ankle plantar-flexors producing less propulsive power than the non-paretic ankle plantar-flexors, further work is needed to confirm this.

We observed less negative peak P_{inst} and P_{avg} of the non-paretic limb (compared to the paretic limb) during DSL, contrary to our hypothesis. This may be due to step length asymmetry between limbs, which has been positively correlated with negative work production during heel-strike [5]. In our subjects, a greater mean paretic step length was exhibited across all functional groups.

There was greater positive P_{avg} for the non-paretic limb (compared to the paretic limb) during SS, as expected. Initiation of positive power production by the non-paretic limb immediately prior to SS was exhibited by the moderate and low groups (Figure 1) resulting in net positive P_{avg} values during DSL. Although this may be a compensation for less propulsive power produced by the trailing paretic limb or early initiation of power production to raise the COM, further work is needed to confirm this.

CONCLUSIONS

Robust differences in mechanical power produced between limbs exist, yet we observed little evidence of greater asymmetry in mechanical power production with reduced gait functional ability.

REFERENCES

1. Donelan JM, et al. *J Biomech* **35**, 117-124, 2002.
2. Stoquart G, et al. *Gait Posture* **36**, 409-413, 2012.
3. Houdijk H, et al. *Gait Posture* **30**, 35-40, 2009.
4. Doets HC, et al. *Hum Mov Sci* 2**8**, 786-797, 2009.
5. Donelan JM, et al. *J Exp Biol* **205**, 3717-3727, 2002.

CLINICAL CORRELATES AND EFFECTS OF DEEP BRAIN STIMULATION ON GAIT VARIABILITY IN ESSENTIAL TREMOR

[1,2]Ryan T. Roemmich, [1]Michael S. Okun, [1]Pamela R. Zeilman, [1]Nikolaus R. McFarland, and [1,2]Chris J. Hass

[1]Center for Movement Disorders and Neurorestoration, University of Florida, Gainesville, FL, USA
[2]Department of Applied Physiology and Kinesiology, University of Florida, Gainesville, FL, USA
Email: rroemmich@ufl.edu

INTRODUCTION

Essential tremor (ET) is one of the most prominent movement disorders in the adult population [1]. Persons with ET are typically characterized by an upper extremity action tremor which differs in origin and appearance from the resting tremor frequently observed in persons with Parkinson's disease. However, recent research has expanded beyond tremor and upper extremity dysfunction and begun to highlight gait deficits in persons with ET [2, 3]. Most frequently, studies with gait analysis have observed marked cerebellar-like dynamic instability in persons with ET.

Despite the frequently-noted dynamic instability during tandem gait, relatively little attention has been given to variability in normal gait in ET. This is surprising considering the well-established associations between variability in gait and dynamic instability. Data from our lab has suggested that gait variability is significantly higher in persons with ET as compared to their neurologically-healthy age-matched peers. However, the clinical correlates associated with gait variability in ET and treatment options for normalizing gait variability in this population remain unknown. As midline tremor severity has been shown to be related to various gait and balance deficits in ET, we postulate that midline tremor severity may also be associated with increased gait variability and that these symptoms may be responsive to surgical treatment.

Deep brain stimulation (DBS) has been established as a successful treatment option for reducing intention tremor in persons with ET. While this therapy has been shown to significantly reduce tremor, the impact of DBS on gait and dynamic stability is unclear. As unilateral thalamic stimulation has previously been shown to reduce midline tremor in persons with ET, we hypothesized that these reductions in midline tremor after DBS may also reduce gait variability in this population.

The purpose of this study was to investigate associations between itemized clinical scores on the Fahn-Tolosa-Marin Tremor Rating Scale (TRS) and gait variability measures in persons with ET in order to determine clinical correlates of gait variability in this population. We also aimed to investigate the effects of unilateral thalamic DBS on gait variability in persons with ET.

METHODS

Twenty-three persons with ET (66 ± 8 yrs, 175.4 ± 13.2 cm, 92.3 ± 23.6 kg) walked on a split-belt treadmill (Woodway USA, Waukesha, WI) for five minutes at a self-selected comfortable pace. Eight of these participants (69 ± 3 yrs, 177.0 ± 11.0 cm, 98.8 ± 20.0 kg) also underwent implantation of unilateral DBS on the ventral intermediate nucleus of the thalamus for tremor relief. Six months following surgery, the participants returned to the lab with the DBS on and walked for five more minutes on the split-belt treadmill at the same speeds tested previously. Participants also completed the TRS on each testing day.

Stride length was calculated as the anterior-posterior displacement of the ankle marker from heel-strike to ipsilateral toe-off. Stride time was calculated as the time from heel-strike to the next ipsilateral heel-strike. Step length was calculated as the anterior-posterior distance between the contralateral ankle markers at heel-strike. Step time was calculated as the time between heel-strike and the next contralateral heel-strike. Step width was calculated as the medial-lateral distance between the ankle markers at heel-strike. We defined variability in each of these measures by the coefficient of variation (CV), calculated by dividing the standard deviation by the mean across the entire five minute trial.

Two-tailed Spearman's correlations were performed to analyze associations between measures of gait variability and specific items of the TRS as well as between the pre-post change in gait variability measures and the pre-post change in specific items of the TRS in the participants who underwent DBS implantation. Related-samples Wilcoxon Signed Rank tests were performed to compare gait variability measures before and after DBS in the relevant participants. All levels of significance were set at α=.05.

RESULTS AND DISCUSSION

In the group of 23 persons with ET, stride length, stride time, and step length CVs were significantly associated with total TRS score as well as both resting and postural trunk tremor. Stride length and step length CVs were significantly associated with voice tremor.

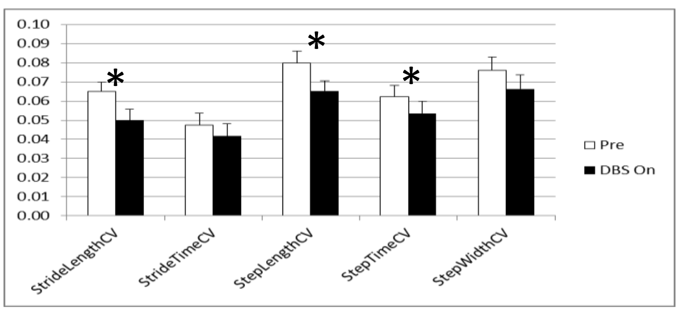

Figure 1. Unilateral thalamic DBS reduced stride length, step length, and step time CVs in persons with ET (* indicates p<.05).

After DBS, stride length, step length, and step time CVs were significantly reduced (Figure 1). The pre-post change in voice tremor was significantly associated with the pre-post change in step width CV. Pre-post changes in resting and postural trunk tremor were significantly associated with pre-post changes in stride time and step time CVs (Table 1).

CONCLUSIONS

Gait variability is significantly higher in persons with ET as compared to their neurologically-healthy peers. In this population, gait variability is associated with total TRS score and, more specifically, severity of midline tremors such as voice and trunk tremor. Gait variability is significantly reduced with DBS and reductions in the same midline tremors are associated with reductions in gait variability.

Deep brain stimulation appears to be an effective treatment to reduce gait variability in persons with ET through concurrent reduction of midline tremors. The effects of DBS on other gait characteristics remain controversial. Thus, further research is required to provide a more comprehensive understanding of the impact of DBS on locomotion in persons with ET.

REFERENCES

1. Louis ED, Ottman R, Hauser Wa. How common is the most common adult movement disorder? Estimates of the prevalence of essential tremor throughout the world. *Mov Disord* **13**(1), 5-10, Jan 1998.
2. Stolze H et al. The gait disorder of advanced essential tremor. *Brain* **124**, 2278-2286, 2001.
3. Louis ED, Rios ER, Rao AK. Tandem gait performance in essential tremor: clinical correlates and association with midline tremors. *Mov Disord* **25**(11), 1633-1638, August 2010.

Table 1. Spearman's correlation coefficients for associations between changes in TRS scores and gait variability measures after DBS.

		Change Stride Length CV	Change Stride Time CV	Change Step Length CV	Change Step Time CV	Change Step Width CV
Change TRS3 Voice	**Rho**	**.183**	**.639**	**.456**	**.456**	**.913***
	p	**.655**	**.088**	**.256**	**.256**	**.002**
Change TRS7 Trunk Rest	**Rho**	**.655**	**.764***	**.436**	**.764***	**.655**
	p	**.078**	**.027**	**.280**	**.027**	**.078**
Change TRS7 Trunk Post	**Rho**	**.630**	**.756***	**.378**	**.756***	**.630**
	p	**.094**	**.030**	**.356**	**.030**	**.094**

INTER-JOINT COORDINATION FOR INDIVIDUALS WITH ANTERIOR CRUCIATE LIGAMENT RECONSTRUCTION DURING STAIR ASCENT

[1]Junsig Wang, [2]Michelle Hall, and [1]Jason Gillette

[1]Iowa State University, Ames, IA, USA
[2]University of Melbourne, Victoria, Australia

INTRODUCTION

Anterior cruciate ligament (ACL) injuries are among the most common knee injuries for both athletes and non-athletes. After ACL reconstruction, long-term changes in knee and hip joint moment patterns have been observed during walking and stair negotiation [1]. Individuals likely alter their gait pattern after surgery to protect the reconstructed ACL in the presence of changes in knee joint structure and muscle weakness. Long-term gait adaptations are of concern, since almost 50% of these individuals display symptoms of knee osteoarthritis 10-20 years after the initial injury [2]. Describing inter-joint coordinative patterns post-ACL may provide insight into long-term gait compensations post-ACL reconstruction.

Stair negotiation is a prevalent task in daily life. Stair ascent creates a more demanding environment for the body and requires more dynamic control than normal walking [3]. The purpose of this study was to investigate inter-joint coordinative patterns for individuals with ACL reconstruction while ascending stairs. It was hypothesized that individuals post-ACL reconstruction would display significantly different inter-joint coordinative patterns than healthy matched controls.

METHODS

Ten individuals (6 female, 4 male) who experienced unilateral ACL reconstruction and ten healthy controls (6 female, 4 male) between 18-35 years old participated in this study. The ACL subjects were on average 5 years from ACL reconstruction surgery (range 1-11 years). A three-step staircase (step height 18.5 cm, tread depth 29.5 cm) was used for stair ascent. An eight-camera Vicon Nexus motion analysis system was use to collect three-dimensional kinematic data at a sampling rate of 160 Hz. Twenty-eight retro-reflective markers were placed on bony landmarks for a static standing trial. Eight markers were removed and then reconstructed during dynamic trials using transforms derived from the static trial. AMTI portable force platforms on steps one and two were used to detect the stance phase. Participants performed three trials of stair ascent with a left leg lead and a right leg lead at a self-selected speed.

Data were analyzed during the stance phase of the first and second steps. Hip flexion, knee flexion, and ankle dorsiflexion joint angles were calculated for each limb from kinematic data low-pass filtered at 6 Hz. Joint angular velocities were calculated from joint angles utilizing the central difference method. These data were then used to calculate phase angles from a phase plot, using the arctangent of angular velocity divided by angular displacement at each data point. Continuous relative phase (CRP) was calculated by subtracting the phase angles of the distal joint from the proximal joint. The CRP was evaluated for inter-joint coordination between the hip and knee joints and between the knee and ankle joints (Figure 1). A CRP value of 0° indicates completely in-phase joint coordination, while a CRP value of 180° indicates completely out-of-phase joint coordination.

Coordination patterns were quantified utilizing root-mean-square (CRP_{RMS}) and standard deviation (CRP_{SD}) of the ensemble CRP curves. Between group (post-ACL vs. control) differences for CRP_{RMS} and CRP_{SD} were compared using univariate ANOVA with a significance level of $p < 0.05$. The injured leg of ACL group (step one and step two) was compared to the right limb (step one) and left leg (step two) of the control group.

RESULTS

Hip-knee CRP_{RMS} was significantly lower ($p < 0.05$) for the post-ACL group as compared to the control group during step two of stair ascent (Table 1). There were no significant differences in hip-knee CRP_{RMS} for step one or for knee-ankle CRP_{RMS} for either step.

Hip-knee CRP_{SD} was significantly higher ($p < 0.05$) for the post-ACL group as compared to the control group during step two of stair ascent (Table 1). In addition, knee-ankle CRP_{SD} was also significantly higher ($p < 0.05$) for the post-ACL group during both steps. There was no significant difference in hip-knee CRP_{SD} for step one.

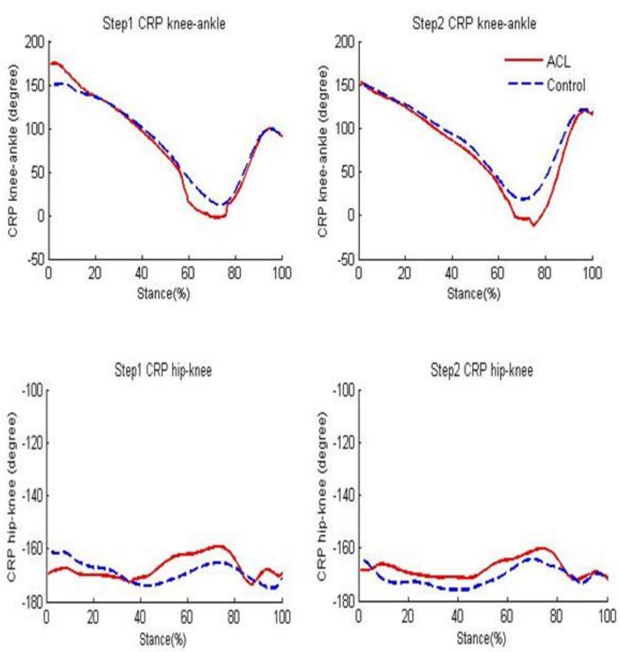

Figure 1. Mean knee-ankle and hip-knee CRP curves during for the post-ACL and control groups during stair ascent.

DISCUSSION AND CONCLUSIONS

The present study evaluated inter-joint coordination during stair ascent for individuals post-ACL reconstruction. The first finding was that hip-knee coordination for the post-ACL group exhibited more in-phase movement (lower CRP_{RMS}) and increased variability (higher CRP_{SD}) compared to the control group during the stair ascent second step. This is likely related to previous observations of decreased knee extension moments and increased hip extension moments for the post-ACL group during this step [1]. The second finding was that the post-ACL group exhibited increased knee-ankle variability during both steps of stair ascent. While decreased knee extension moments have been observed, no differences in ankle plantar flexion moments were found previously [1]. Referring to Figure 1, the greatest differences in knee-ankle CRP curves were seen between 60-80% of stance.

The findings from this study indicate that individuals post-ACL reconstruction display differences in inter-joint coordination when compared to controls. Of particular interest is the increased variability of knee-ankle coordination in the post-ACL group. The coupling of knee and ankle joint movement merits further investigation as a target for gait retraining and/or functional strengthening.

REFERENCES

1. Hall M, et al. *Gait Posture* **36**, 56-60, 2012.
2. Lohmander LS, et al. *Am J Sports Med* **35**, 1756-1769, 2007.
3. Hong Y, Xian J. *Gait Posture* **22**, 63-68, 2005.

Table 1: Mean CRP_{RMS} and CRP_{SD} for the post-ACL and control groups during stair ascent

	CRP_{RMS}				CRP_{SD}			
	Step1		Step2		Step1		Step2	
	Hip-knee	Knee-ankle	Hip-knee	Knee-ankle	Hip-knee	Knee-ankle	Hip-knee	Knee-ankle
Post-ACL	166.2±3.4	103.6±9.4	168.1±2.8*	95.5±10.9	7.7±1.3	56.9±8.9*	7.8±1.7*	55.1±4.8*
Control	168.7±3.2	99.1±6.2	171.2±1.3	101.1±14.8	7.1±1.7	46.4±6.2	6.3±1.5	46.1±7.9

*Indicates a significant difference in the post-ACL group as compared to the control at $p < 0.05$.

PERSISTENT DEVIATIONS IN HIP DYNAMICS DURING GAIT IN WOMEN AFTER TRIPLE INNOMINATE OSTEOTOMY

[1]Sjoerd Kolk, [2]René Fluit, [2,3]Nico Verdonschot, [1]Vivian Weerdesteyn

[1]Department of Rehabilitation, Nijmegen Centre for Evidence Based Practice, Nijmegen, The Netherlands
[2]Department of Biomechanical Engineering, University of Twente, Enschede, The Netherlands
[3]Orthopedic Research Laboratory, Nijmegen Centre for Evidence Based Practice, Nijmegen, The Netherlands

email: s.kolk@reval.umcn.nl, web: http://www.tlemsafe.eu/

INTRODUCTION

In adult patients with developmental dysplasia of the hip, a surgical procedure (Triple Innominate Osteotomy; TIO) of the pelvic bone can be performed to rotate the acetabulum in the frontal plane, which establishes better acetabular coverage. This procedure reduces pain and wear, and thereby greatly improves the quality of life of patients. Although all of these aspects show significant improvements in common clinical hip scores, very little is known about the effects of this procedure on a functional level, including gait [1]. This study therefore aimed to investigate the effects of TIO on the biomechanics of gait.

METHODS

Twelve women who had undergone a unilateral TIO and eight age and gender matched healthy controls participated in this study. The preliminary results presented in this abstract are based on a subset of five TIO patients (36±13 y, 68±6 kg, 1.70±0.05 m), and four healthy controls (31±10 y, 59±5 kg, 1.69±0.03 m). The TIO patients were operated between 3 and 12 years ago by the same experienced surgeon. They all followed the same post-operative rehabilitation programs involving physical therapy exercises. Besides their TIO, the patients were free of disease and other conditions that could alter their gait.

All participants walked barefoot at their own comfortable walking speed. A six-camera digital optical motion capture system (Vicon MX, Oxford, UK) was used to capture 35 retro-reflective markers placed on various landmarks of the participants. Two force platforms (AMTI, Watertown, MA, USA), embedded level in the laboratory floor measured ground reaction forces during the stance phase of the gait cycle.

A 21 degrees of freedom kinematic model consisting of trunk, pelvis, thigh, shank, talus and foot segments was built from the marker trajectories using the AnyBody Modeling System (version 5.3.1, AnyBody Technology A/S, Aalborg, Denmark). The model marker positions, segment lengths and knee joint axes were optimized using a parameter optimization algorithm [2]. Subsequently, inverse dynamic analysis was performed [3], yielding the outcome measures of interest (joint angles and joint moments).

Student t-tests were used for between group comparisons and paired samples t-tests for comparisons between operated and non-operated legs. The significance level was set at $p<0.05$.

RESULTS AND DISCUSSION

In the sagittal plane (Fig. 1), maximal hip extension angles in the TIO patients were 8° lower than in healthy controls, albeit not significantly (p=0.14). Maximal hip flexion moments (Fig. 2), were significantly lower in the TIO patients than in controls (p=0.04). There were no differences between the operated and non-operated legs.

In the frontal plane (Fig. 3), the hip adduction angle of the operated leg of the TIO patients was lower at midstance compared to healthy controls, but the differences did not reach significance (p=0.20) with the current sample size. It was also not significantly different compared to the non-operated leg (p=0.43).

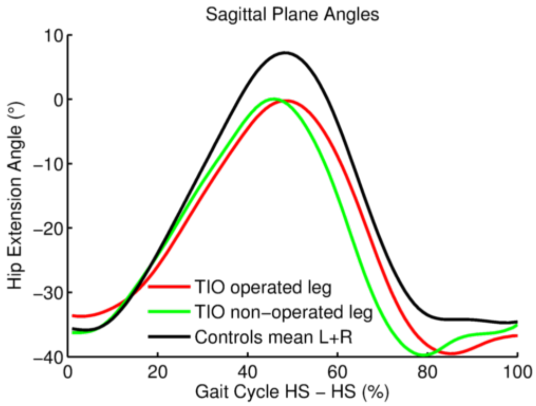

Figure 1: Hip kinematics in the sagittal plane.

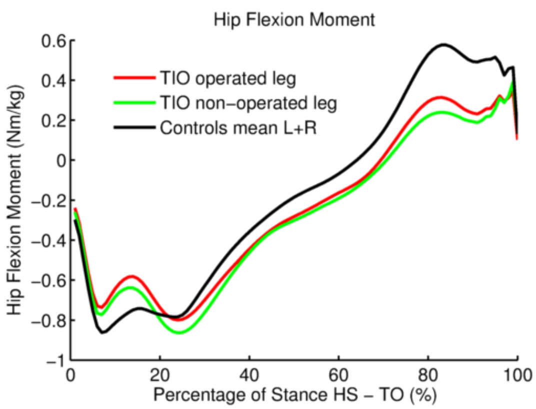

Figure 2: Sagittal plane hip moments, normalized to body weight.

The hip abduction moment at loading response was reduced in the TIO patients, both compared to the healthy controls and to the non-operated leg (Fig. 4). This difference did not reach significance between TIO patients and controls (p=0.08), but was significantly different between the operated and non-operated legs (p=0.03).

CONCLUSIONS

The preliminary results from the gait analyses revealed that the gait of TIO patients deviates from that of healthy controls in both the sagittal and frontal planes. The most striking differences were found in hip flexion moment in late stance, and in hip abduction moment at loading response. These findings might indicate muscle weakness in the hip flexors and abductors in TIO patients. It appears the TIO patients compensate for reduced abduction moment generating capacity in the operated leg by exerting a higher abduction moment with the contralateral leg, as the maximal hip abduction moment of the non-operated leg was higher than

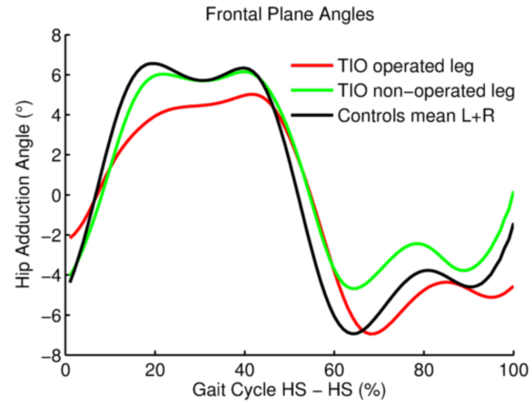

Figure 3: Hip kinematics in the frontal plane.

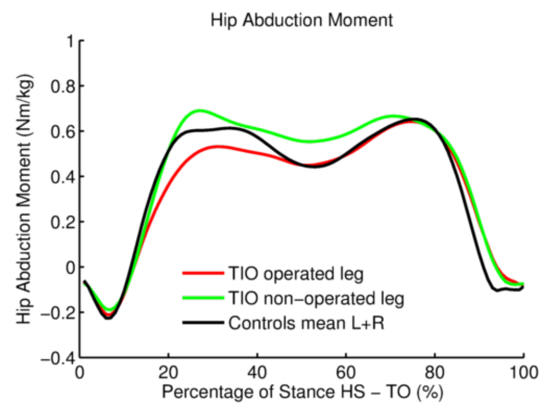

Figure 4: Frontal plane hip moments, normalized to body weight.

that of healthy controls. Although TIO generally improves the biomechanical geometry of the affected hip joint by increasing acetabular coverage [1], thus spreading joint forces across a larger surface, the osteotomy does not restore the hip to a normal functional level.

REFERENCES

1. van Hellemondt GG, et al. *J Bone Joint Surg [Br]* **87-B**, 911-915, 2005.
2. Andersen MS, et al. *Comput Method Biomec* **12(4)**, 371-84, 2009.
3. Damsgaard M, et al. *Simul Model Pract Th* **14**, 1100-1111, 2006.

ACKNOWLEDGEMENTS

This work is part of the TLEM*safe* project (http://www.tlemsafe.eu/), which is financially supported under the Seventh Framework Programme (FP7) of the European Commission.

FEMORAL NECK STRESSES DURING STAIR NAVIGATION.

[1]Chen Deng, [1]Jason C. Gillette, [1]Timothy R. Derrick

[1]Iowa State University, Ames, IA, USA
email: chend@iastate.edu , web: http:// www.kin.hs.iastate.edu/

INTRODUCTION

Fractures at the femoral neck play an important role in morbidity and mortality among older adults [1]. Understanding the loading environment is a crucial factor for reducing the incidence of fracture at this site [2,3]. The loading at the femoral neck can be measured or estimated using forces, moments, and stresses [3]. Based on previous studies, both sagittal and frontal hip moments are greater in stair ascent than descent [4], but it is unknown if stresses in the femoral neck have a similar pattern. In this study, the stresses at the superior and inferior sites of femoral neck during stair ascent and descent were estimated by applying a series of models. These femoral neck stresses were compared to the peak loading from sagittal and frontal plane internal hip moments.

METHODS

Five male and five female adult subjects (age: 59 ± 6.1 yrs; body mass: 68.90 ± 10.30 kg; height: 1.68 ± 0.05 m) with no lower limb injuries volunteered to participate. All subjects performed 5 successful trials of stair ascent and the same number trials of descent with a 3-stair staircase. Motion capture data (120 Hz, Vicon MX, Vicon, Centennial, CO, USA) and force data (1200 Hz, AMTI, Watertown, MA) were collected during each trial.

Raw force data and motion capture data were input into Matlab programs and low-pass filtered at 6 Hz. Inverse dynamics with rigid body assumptions was used to calculate 3-D joint moments and reaction forces at the hip, knee and ankle of the right leg. A musculoskeletal model was used to obtain maximal dynamic muscle forces, muscle moment arms and orientations for 43 lower limb muscles. Static optimization was used to select a set of muscle forces that minimized the sum of the squared muscle stresses and balanced the sagittal plane hip, knee and ankle moments and the frontal plane hip and ankle moments with the external moments for each frame of data. Muscle forces, joint reaction forces and joint moments were used to estimate the 3-D moments and forces at the midpoint of the femoral neck. These loads were then applied to a standardized elliptical model of the bone structure to estimate the stresses on the periphery of the inferior and superior portion of the ellipse model. The superior-inferior and anterior-posterior diameters of the model were 3.6 and 2.5 cm, which represented the diameters of the femoral neck; the superior-inferior and anterior-posterior thicknesses of the model were 0.6 and 0.3 cm, based on cortical bone thickness estimates of the femoral neck [5,6].

Differences in peak stresses and moments between stair ascent and descent were assessed by dependent t-test. All statistical tests were considered significant at $p < .05$. Statistical analyses were performed using IBM SPSS Statistics 19.

RESULTS

Table 1 shows the peak hip moments during stair ascent and descent. There was no statistical difference between peak abductor hip moments ($p = 0.705$), but the peak extensor hip moment was significantly greater during ascent compared to descent ($p = .001$).

Figure 1 and Table 1 show increased tension (positive values) at the superior site and increased compression (negative) at the inferior site of the femoral neck during stair descent. Stresses at both the superior and inferior sites displayed distinct peaks during the first half and second half of stance, so each peak was analyzed.

Significantly increased peak tensile stress was found in the 1st peak at the superior site during the descent condition (p = 0.005), but the 2nd peak showed no significant difference between stair ascent and descent (p = .098). Increased peak compressive stress at the inferior site during stair descent showed no significance in both peaks (P1: p =.105; P2: p = .071).

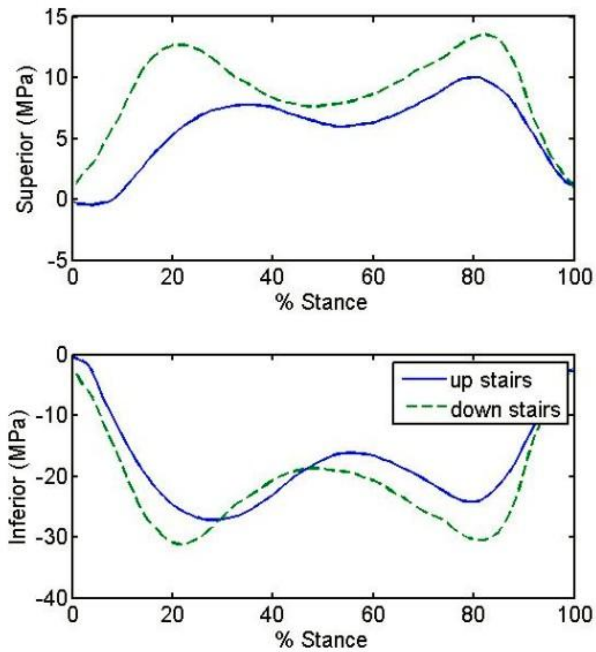

Figure 1. Ensemble average of stresses at the superior and inferior sites of the femoral neck, positive values indicated tension, negative indicated compression.

DISCUSSION

Peak tensile stress at the femoral neck increased in stair descent compared to ascent. On the other hand the peak hip extensor moment during stair navigation indicate greater loading during stair ascent. This agrees with a previous study comparing stair ascent and descent [4].

The 1st peak tensile stress during stair descent could be explained by increased deceleration of the body due to a higher contact velocity. In addition, the relatively extended position of the hip during decent places more of the vertical load on the inferior neck. During ascent the flexed position of the hip during this period places the vertical loads more toward the posterior surface of the neck.

In this study, conclusions concerning the loading of the proximal femur were contradictory depending on if loading was assessed via hip joint moments or from femoral neck stresses. Increased femoral neck stresses could help explanation why some older adults have reported more hip pain in stair descent than ascent. Researchers may benefit from a more comprehensive evaluation of the loading environment by estimating bone stresses as well as joint moments during stair ascent and descent.

REFERENCES

1. Graves, E. Vital Health Stat, 13(113), 1990.
2. Bergmann G, et al. J Biomech, 26, 969-990, 1993.
3. Bergmann G, et al. J Biomech 34, 859-871, 2001.
4. Novak A.C, et al. Gait & Posture, 33, 54-60, 2011.
5. Bell K.L, et al. J Bone Miner Res, 14(1), 111-119, 1999.
6. Alunni-Perret V, et al. J Forensic Sci, 48(3), 1-4, 2003.

Table 1. Means±SD of peak stresses at the superior and inferior sites of the femoral neck and peak hip moments during stair ascent and descent, P1 is the peak during the 1st half of stance, P2 is for the 2nd half.

	Superior Tensile Stress		Inferior Compressive Stress		Abductor Hip Moment	Extensor Hip Moment
Condition	P1 (MPa)	P2 (MPa)	P1 (MPa)	P2 (MPa)	(Nm)	(Nm)
stair ascent	8.4±3.4	10.8±3.9	28.3±6.5	25.5±6.0	63.2±11.3	52.1±17.4
stair descent	13.7±4.0	14.4±5.4	33.1±6.2	32.5±9.9	61.2±11.9	24.9±13.4

Evaluating Runners with and without Anterior Knee Pain Using the Time to Contact the Ankle Joint Complex Range of Motion Boundary

[1]Pedro Rodrigues, [1]Trampas TenBroek, [2]Richard van Emmerik and [2]Joseph Hamill

[1]New Balance Sports Research Lab, Lawrence, MA, USA
[2]University of Massachusetts, Amherst, MA, USA
email: pedro.rodrigues.a@gmail.com

INTRODUCTION

Excessive ankle joint complex (AJC) eversion is frequently reported as a risk factor in the development of overuse running injuries such as anterior knee pain (AKP)[1]. Orthotic studies have supported this link, providing evidence that when eversion is controlled, knee pain and function improve[2-3]. Conversely, prospective and retrospective biomechanical studies have not consistently shown a link between excessive eversion and AKP[4-5].

One potential reason for the discrepancy between biomechanical and orthotic studies could be in the definition of excessive eversion. Recent evidence has suggested that evaluating eversion in the context of a subject specific anatomical threshold, such as the joint's range of motion (ROM), may be more accurate at defining those with excessive eversion[6]. Using this technique, runners with AKP were found to come within 4.2º of their eversion ROM boundary while healthy runners maintained a buffer of 7.2º. In contrast, no differences in peak eversion were noted between groups. These findings suggest that excessive eversion should be evaluated in a subject specific and anatomically relevant context.

One limitation of this technique however is that it does not consider the velocity at which the joint is approaching its ROM boundary and therefore does not capture the time a runner's body has to react. In other words, two runners could have the same amount of time before reaching end range but accomplish this differently. One runner could have a large eversion buffer, but evert at a greater velocity. In contrast, a second runner could have a small eversion buffer but evert at a lessor velocity. Evaluating eversion in this neuromuscular context could provide greater insight into the association between calcaneal eversion and injury. Therefore the purpose of this study was to evaluate eversion using a neuromuscular threshold such as the time to contact (TtC) the AJC's ROM boundary in runners with and without AKP.

METHODS

Nineteen healthy (10 male, 9 female, 34 ± 10 years, 1.7 ± 0.1m, 65 ± 12 kg) and seventeen runners with AKP (4 male, 13 female, 30 ± 7 years, 1.6 ± 0.1m, 60 ± 8 kg) completed the study. All subjects were running 12+ km per week for 6 months, utilized a heel-strike foot fall pattern and had no history of lower extremity surgeries.

Lower extremity segments were defined from a single barefoot standing calibration with markers placed the greater trochanters, medial/lateral knee, medial/lateral malleoli, sustentaculum tali, and peroneal tuberucle. Dynamic movements were captured using marker clusters attached to the lateral thigh, lower leg and directly to the calcaneus. Passive eversion ROM (Figure 1) and dynamic running trials (2.9 m/s) were both captured (200 Hz) using an eight camera motion capture system (Qualisys, Sweden).

Kinematic data were analyzed in Visual 3D (C-Motion, USA). Marker trajectories were smoothed using a 12 Hz fourth order low pass Butterworth filter. Joint angles were calculated using Cardan angles with an X-Y-Z rotation sequence. The minimum angular distance from the eversion boundary during stance (eversion buffer) and the minimum TtC the eversion ROM boundary were averaged over 10 steps (Figure 1). Statistical differences were evaluated using a one way ANOVA and 95% confidence intervals.

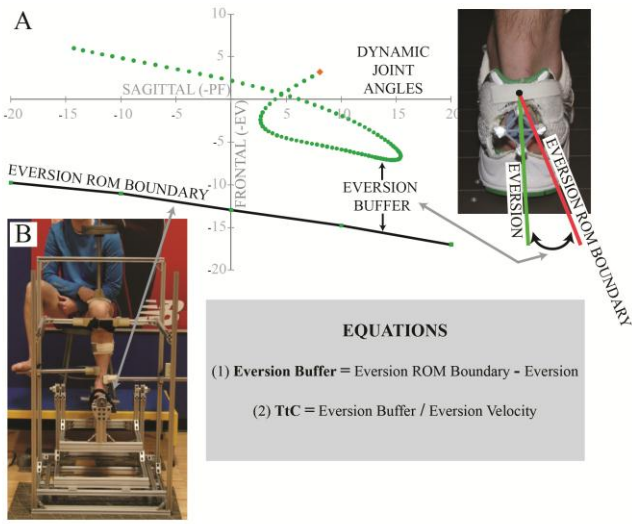

Figure 1. A runner's eversion buffer was determined by evaluating the frontal plane position of the AJC over stance relative to the joint's available ROM (A). The passive ROM of the AJC was measured using a custom built device, which passively everted the AJC using a 10 Nm torque (B). The eversion ROM boundary (A) was then defined by interpolating a virtual line between each measurement. The minimum angular distance between this boundary and the joint's angle during stance was deemed the eversion buffer (Equation 1). Additionally, the minimum time necessary to contact the eversion ROM boundary was recorded (TtC, Equation 2).

RESULTS AND DISCUSSION

Runners with AKP had significantly shorter TtC (35.63ms vs. 63.96ms, p = 0.03). This shorter TtC was in large part due to having a smaller eversion buffer (Table 1), however, velocity was found to have a substantial influence on the TtC of selected individuals.

A shorter TtC could increase a runner's risk of injury for several reasons. The reaction time of the AJC to quick inversion movements is, on average, between 54-70ms[7]. Injured runners in this study were found to have TtC's that were substantially shorter than these reported reaction times indicating that the surrounding musculature may not have sufficient time to react to unexpected perturbations. As a result, it is plausible that the joint could be forced to end range if perturbed, a position that places greater demands on the joint surfaces and surrounding soft tissue, which in turn would increase the risk of injury. Furthermore, functioning at end range could require that kinematic adjustments be made by surrounding joints, such as the knee and similarly increase its risk of injury.

CONCLUSIONS

These results provide evidence that a link between calcaneal eversion and AKP exists when using anatomical and neuromuscular based thresholds to define excessive pronation.

REFERENCES

1. Tiberio D, JOSPT **9**, 160-5, 1987
2. Mills K, et al. Br J Sports Med **46**, 247-52, 2012
3. Saxena A, et al. J Am Podiatr Med Assoc **93**, 264-71, 1993.
4. Hetroni I, et al. J Bone Joint Surg Br **88**, 905-08, 1988.
5. Kaufman KR, et al. Am J Sports Med **27**, 585-93, 1999.
6. Rodrigues P, et al. J Appl Biomechanics, "in press".
7. Waddington G, et al. Br J Sports Med **37**, 170-4, 2003.

Table 1. Comparison of time to contact and eversion buffer variables. Mean (SD)

	Healthy	AKP	Mean Difference	95% CI	p-value
Minimum TtC (ms)	**64.0 (46.9)**	**35.6 (22.8)**	**-28.3**	**-53.8 to -2.9**†	**0.03**
Buffer (°) @ min TtC	11.8 (6.3)	8.7 (5.2)	-3.2	-7.1 to 0.8	0.11
Velocity (°/sec) @ min TtC	-204.2 (75.9)	-208.9 (96.9)	-4.6	-63.2 to 54.0	0.87
Minimum Eversion Buffer (°)	**7.3 (4.3)**	**4.2 (3.6)**	**-3.1**	**-5.9 to -0.2**†	**0.03**

THE EFFECT OF A NEW MICRPROCESSOR CONTROLLED PROSTHETIC KNEE ON OBSTACLE CROSSING IN PATIENTS WITH UNILATERAL TRANSFEMORAL AMPUTATION

Jennifer M. Aldridge Whitehead[1] and Jason M. Wilken[1]

[1]Center for the Intrepid, Department of Orthopaedics and Rehabilitation, Brooke Army Medical Center, Ft. Sam Houston, TX

email: Jennifer.Aldridge@us.army.mil

INTRODUCTION

Obstacles are commonly encountered during walking and therefore it is important for individuals with lower limb amputation to be able to safely and effectively negotiate over obstacles. Safe negotiation of an obstacle requires sufficient clearance of the swing foot over the obstacle to avoid tripping. Individuals without amputation accomplish this by increasing lower extremity joint flexion, with the greatest importance placed on knee joint flexion, during the swing phase [1]. However, individuals with transfemoral (above the knee) amputation (TFA) are unable to actively control the knee joint during obstacle clearance. This results in persons with TFA commonly adopting a circumduction strategy to cross the obstacle [2].

Recently a new microprocessor controlled prosthetic knee (X2, Ottobock, Duderstadt, Germany) was developed with the goal of allowing persons with transfemoral amputation to cross obstacles without requiring circumduction. The X2 knee uses variable flexion/extension resistance to allow the user to flex the knee during the swing phase, contact the ground with a knee that has been preflexed to 4° and load the limb without the knee collapsing [3].

The purpose of this study was to compare the kinematics of obstacle crossing in persons with unilateral TFA while using the X2 and a conventional microprocessor controlled knee. It was hypothesized that persons with TFA would have increased prosthetic knee flexion during swing when the prosthetic limb was both leading and trailing while using the X2 device.

METHODS

7 male young adults with unilateral TFA (30.1 ± 5.8 years, 1.78 ± 0.08 m, and 87.2 ± 11.6 kg) participated in the study. Participants were assessed: 1) wearing their clinically prescribed prosthetic knee (CONV), and 2) wearing the X2. The two visits were separated by approximately 12 weeks and identical biomechanical testing was conducted during each visit.

Participants were instrumented with 57 reflective markers. A 26 camera optoelectronic motion capture system (120 Hz; Motion Analysis, Santa Rosa, CA) was used to track full-body movement. Marker data was filtered with a low pass Butterworth filter (6 Hz).

Participants were asked to cross a 10 cm x 135 cm x 10cm (height x width x depth) wooden obstacle that was placed in the middle of the walkway. Participants were allowed to cross the obstacle at a self-selected pace and were asked to lead with both their prosthetic and intact limbs. For each lead limb condition a minimum of three good trials were collected.

2x2 repeated measures ANOVA's were used to determine lead limb and device main effects (prosthetic lead and intact lead; CONV and X2) for both the leading and the trailing limbs. Estimated marginal means and a bonferroni correction were used to identify pairwise differences.

RESULTS AND DISCUSSION

Lead Limb (Fig. 1A): During obstacle clearance the intact limb knee was significantly more flexed than the prosthetic knee in both the X2 and CONV conditions ($p < 0.001$). Contrary to the hypothesis, peak prosthetic knee flexion during swing was not significantly different between devices ($p = 0.136$). While using the X2 device the knee was, however, more flexed than the CONV at initial contact after crossing the obstacle ($p = 0.006$). The approximately 4° increase was consistent with the design intentions of the device.

A

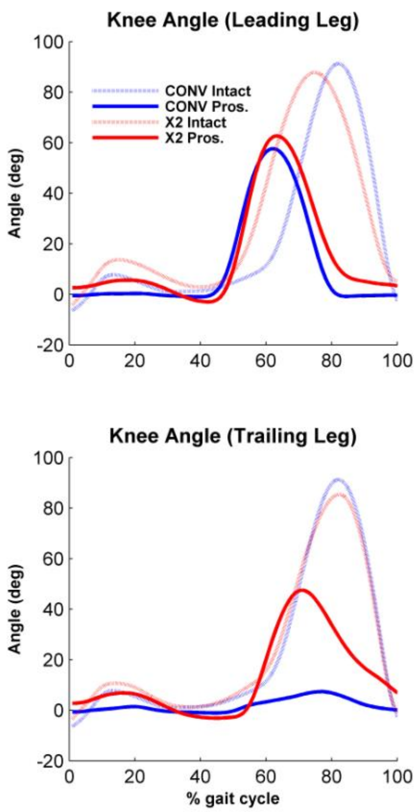

B

Figure 1: *Kinematics of the leading limb (A) and trailing limb (B) knee during obstacle clearance while using both CONV (blue) and X2 (red) knees for both the intact (dashed) and prosthetic limb (solid).*

Trail Limb (Fig. 1B): The intact limb knee was again significantly more flexed than the prosthetic knee in both the X2 and CONV conditions ($p < 0.001$). However, the X2 knee had approximately 40° greater peak knee flexion than the CONV device ($p = 0.023$; Table 1). Individuals primarily used a circumduction strategy with the CONV device and a knee and hip flexion strategy with the X2.

Additionally, the strategy difference resulted in significantly greater peak swing hip flexion while wearing the X2 compared to CONV ($p = 0.019$). As a result, the X2 peak trailing limb hip flexion values were not different between the prosthetic and intact limbs ($p = 0.472$).

Additionally, there was a trend (5 out of 7 participants) towards increased prosthetic knee flexion at initial contact after obstacle clearance when wearing the X2 compared to the CONV device. Increased prosthetic knee flexion at loading may suggest an increased user confidence that the device would support their body weight without collapsing.

CONCLUSIONS

A circumduction strategy is commonly used while crossing obstacles with a CONV device to ensure a fully extended knee at initial contact. While using the X2 participants were less likely to use a circumduction strategy, using greater hip and knee flexion when the device was the trailing limb. They also increased knee flexion at initial contact when leading with the X2 which may be indicative of greater confidence in the device.

Further study is underway to examine how increased knee and hip flexion while using the X2 affects toe clearance of the trailing prosthetic limb to aid in trip avoidance.

	CONV	X2
Lead Knee Flex - SW (deg)	59.9 (8.2)	64.2 (3.1)
Lead Knee Flex - IC (deg)	-0.3 (3.1)	3.6 (3.4)
Trail Knee Flex - SW (deg)	8.2 (5.1)	49.0 (37.2)
Trail Knee Flex - IC (deg)	0.2 (2.8)	8.0 (12.5)
Trail Hip Flex - SW (deg)	36.8 (5.1)	49.1 (11.5)

Table 1: *Mean (SD) peak kinematic values of interest for the prosthetic limb. (IC-Initial contact post obstacle clearance, SW – Swing)*

REFERENCES

1. Chou, L-S. and Draganich, L., J. Biomech., 1997. 30(4): p. 331- 337.
2. Vrieling, A., et al., Gait Posture, 2007. 26(4): p. 587-594.
3. Bellmann, M., et al., Arch. Phys. Med. Rehabil., 2012. 93: p. 541-549

ACKNOWLEDGEMENTS

Support provided by the U.S. Army Telemedicine & Advanced Technology Research Center and the Center for Rehabilitation Sciences Research (to JMW). Additionally, we would like to acknowledge Charles Scoville, Ashley Horta, Jordan Sturdy, and Derek Haight for their contributions.

Older ACL Non-Copers Demonstrate Larger External Knee Adduction Moments One Year after ACLR

Elizabeth Wellsandt[1], PT, DPT, Kathleen White[1], PT, DPT, Lynn Snyder-Mackler[1,2], PT, ScD, FAPTA
1-Biomechanics and Movement Science Program, University of Delaware, 2- Department of Physical Therapy, University of Delaware
email: ewellsan@udel.edu

INTRODUCTION

Over 250,000 anterior cruciate ligament (ACL) injuries occur annually in the US, with 125,000 reconstructions performed each year; however, long term knee joint health is a growing concern [1]. Knee osteoarthritis (OA) is traditionally associated with an aging population, however over 50% of athletes demonstrate radiographic changes 10 years after ACL reconstruction (ACLR) [2]. Increased medial tibiofemoral compartment loading is a potential mechanism for the progression of knee OA, and the external knee adduction moment has been used to quantify this increased loading [3]. Additional sagittal plane kinetic asymmetries are suspected factors in the progression of knee OA. These asymmetries are most characteristic of ACL non-copers, a sub-group of ACL-injured athletes who are the poorest functioning [4]. In the ACLR population, gait asymmetries, measured by the knee adduction moment and the knee flexion moment, have been reported between genders and compared to healthy controls, however the relationship to age has not yet been investigated [5,6]. Increased age has been shown to be a risk factor for articular cartilage damage at early follow-up following ACLR [7], and age may also be related to the risk for early OA as assessed by the knee adduction moment during gait. Therefore, the purpose of this study was to examine the relationship between age and the external knee adduction moment and knee flexion moment at peak knee flexion during gait in ACLR non-copers one year after surgery.

METHODS

Forty-two ACLR subjects (11 females, 29 males) who participated regularly (≥50 hrs/yr) in jumping, cutting, and pivoting activities were included in this study. Subjects were an average of 30.74 ± 10.70 yrs old at initial evaluation and underwent surgery an average of 12.7 wks (range 3-84, median 9.2) after initial evaluation. All subjects completed post-operative rehabilitation using criterion-based guidelines [8], and underwent 3D gait analysis using standard motion capture techniques an average 12.5 ± 0.76 months following ACLR. The external knee adduction moment and knee flexion moment at peak knee flexion during stance phase of gait for both limbs were the variables of interest. Paired t-tests were used to test for differences between limbs for the knee adduction and flexion moments. Linear regression was used to evaluate the relationship of age and walking speed with both the knee adduction moment and knee flexion moment for each limb. A priori significance level was set at the $p<.05$.

RESULTS AND DISCUSSION

There was no difference between limbs for the knee adduction moment ($p=0.549$, Inv: 0.22 Nm/kg*m (95% CI 0.19-0.25), Uninv: 0.23 Nm/kg*m (95% CI 0.20-0.26))(Figure 1). There was a significant difference between limbs for the knee flexion moment ($p<0.001$, Inv: 0.40 Nm/kg*m (95% CI 0.35-0.45), Uninv: 0.50 Nm/kg*m (95% CI 0.46-0.55))(Figure 1). A model including age and walking speed explained 18.5% of the variance for involved knee adduction moment ($R^2=0.185$, $p=0.018$), but did not significantly explain variance for the uninvolved limb ($R^2=0.035$, $p=0.500$). Age was the best predictor of knee adduction moment for the involved limb, ($\beta=0.431$, 95% CI 0.236-0.460, $p=0.005$)(Figure 2), while walking speed did not contribute significantly to the model ($\beta=0.003$, 95% CI 0.001-0.006, $p=0.986$). A model including age and walking speed explained 24.2% of the variance for knee flexion moment for involved limb ($R^2=0.242$, $p=0.005$) and 33.3% of the variance for the uninvolved limb ($R^2=0.333$, $p<0.001$). However, further examination shows that age did not contribute meaningfully to the model, with walking speed being the best predictor of knee flexion moment for both limbs (Inv: $\beta=0.458$, 95% CI 0.196-0.825, $p=0.002$; Uninv: $\beta=0.551$, 95% CI 0.278-0.790, $p<0.001$), while age was not a significant predictor in the model for either limb (Inv: $\beta=0.168$, 95% CI 0.002-0.007, $p=0.237$;

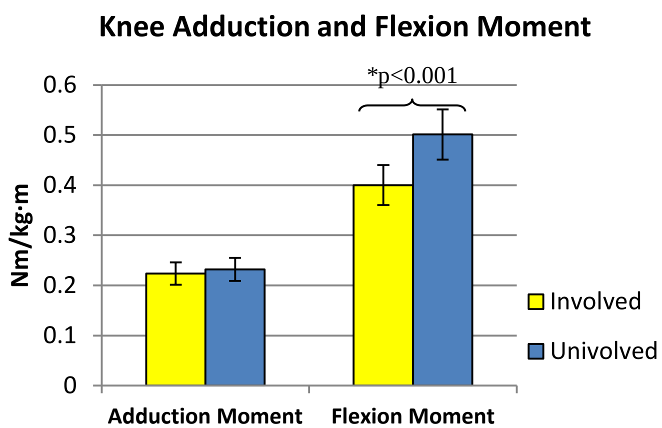

Figure 1: External knee adduction and flexion moments during peak knee flexion at stance phase during gait. Bars indicate 95% confidence intervals.

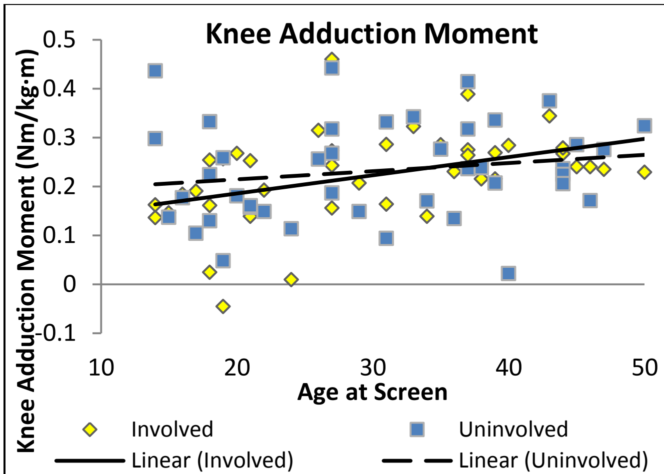

Figure 2: Age vs. knee adduction moment for involved and uninvolved limbs during peak knee flexion at stance phase of gait.

Uninv: β=0.158, 95% CI 0.001-0.006, p=0.233).

One year after ACLR, subjects continue to demonstrate significant limb-to-limb asymmetries in the sagittal plane. When looking at age with walking speed controlled, older individuals demonstrate a larger knee adduction moment for the involved limb. The external knee adduction moment is a useful estimate of the relative medial tibiofemoral joint loading. The larger adduction moment demonstrated in older subjects may be a mechanism that places these subjects at an increased risk for the development and progression of OA. Our findings relate to the risk factor of older age increasing the presence of osteoarthritic changes following ACLR [7].

The measured external knee adduction moment of both limbs in our cohort was smaller (0.22-0.23 Nm/kg*m) than healthy (0.30-0.40 Nm/kg*m) and ACLR patients (0.28-0.38 Nm/kg*m) reported by others [5,6]. Despite our smaller knee adduction moments, limb symmetry with regard to adduction moments of this cohort is consistent with ACLR patients of reported literature [6]. Lower peak knee adduction moments have been shown with slower gait speeds [9]. However, our results suggest gait speed may have a larger impact on sagittal plane than frontal plane kinetics.

While age was a significant predictor for involved limb knee adduction moment, it was not for knee flexion moment at either limb. Lower flexion moments of the involved limb in our subjects is consistent with previously reported values following ACLR [10]. Lower involved knee flexion moments may represent a compensatory strategy adopted by non-copers involving hamstring-quadriceps co-contraction and smaller knee flexion angles during stance as previously reported [11]. This stiffened knee gait pattern may provide a mechanism for increased joint loading and risk long-term knee joint health.

CONCLUSIONS

Larger external knee adduction moments for the involved limb during gait were present in older ACLR non-copers at one year following surgery. Further work is warranted to evaluate the risk factor of age and its relationship to the development and progression of OA following ACLR.

REFERENCES

1. Prodromos CC. *Arthroscopy* **23**, 1320-25, 2007.
2. Meuffels DA. *Br J Sports Med* **43**, 347-51, 2008.
3. Andriacchi TP. *Curr Opin Rheumatol* **18**, 2006.
4. Rudolph KS. *J Electromyogr Kinesiol* **8**, 1998.
5. Butler RJ. *Br J Sports Med* **43**, 366-70, 2009.
6. Webster KE. *Br J Sports Med* **46**, 355-59, 2011.
7. Asano MD. *Arthroscopy* **20**, 474-81, 2004.
8. Adams D. *J Orthop Sports Phys Ther* **42**, 2012.
9. Robbins SM. *Gait Posture* **30**, 543-46, 2009.
10. Hart JM. *Clin Biomech* **25**, 277-83, 2010.
11. Hurd WJ. *J Orthop* Res **25**, 1369-77. 2007.

CONTROLLING REDUNDANCY IN WRIST AND FORARM ROTATIONS

Allan Peaden[1], Garret R. Dorman[2], and Steven K. Charles[1,2]

[1]Department of Mechanical Engineering and [2]Neuroscience Center
Brigham Young University, Provo, UT
email: skcharles@byu.edu

INTRODUCTION

The wrist and forearm combined possess three degrees of freedom (DOF). In a simple pointing task, a virtual end effector could be positioned at any desired location by employing any two of these DOF. This implies that the neuromuscular system must solve an under-constrained problem when deciding how to position the combined wrist/forearm. The mechanism that determines how this motion is executed is currently unknown. Previous research suggests that the body may seek to optimize some cost function when making movements, such as minimizing torque change [1], maximizing accuracy [2], or maximizing stability [3]. In this light it has been proposed that the wrist joint may be utilizing some cost function to select a joint path for a pointing task in which wrist radial-ulnar deviation (RUD) and flexion-extension (FE) are considered the wrist's primary actuators, and forearm pronation-supination (PS) is considered to be unnecessary. More specifically, the purpose of this research is to test the following hypothesis:

- Involving the forearm (even when it is not required) allows the joints to traverse a shorter path than would be possible with the wrist joint alone
- The dynamics of the wrist are dominated by stiffness which is anisotropic creating paths that require less torque than others. Including forearm rotation allows the wrist to follow "paths of least stiffness."
- Admitting forearm rotation allows the nervous system to follow paths which minimize the total effort required to overcome the impedance of both the wrist and forearm.
- Forearm rotation is not part of a strategic plan to minimize the cost of moving; rather, it is the mechanical consequence (or kick-back) of moving the wrist joint.

METHODS

Ten young, healthy, right-handed subjects (five female and five male) participated in this study. Subjects were seated in a chair and required to point to different targets on a screen (2 DOF required) using their wrist and forearm (3 DOF available) (Figure 1). Subjects were free to move their forearm (PS) and wrist (FE and RUD), while elbow and shoulder motion were restricted. A cursor on a screen in front of the subject provided visual feedback and indicated the direction in which the subjects' hand was pointing (similar to the projection of a laser pointer on a screen).

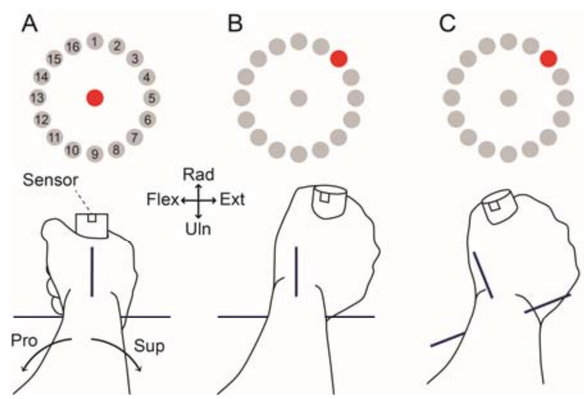

Figure 1: Subjects made 480 center-out movements to 16 targets in the periphery (15 visits to each). Each subject performed the task at both comfortable and fast speeds as well as to smaller and larger radii (15°and 22.5°).

The experiment took place in four sessions separated by 5 minute rest periods each. Sessions were separated by both speed and length of required displacement. The two speeds tested were "comfortable" and "fast." The two displacements required for movements were to targets displayed in a 15° or 22.5° radius. During each session trakSTAR motion sensors were attached both to a handle placed in the right hand and to the distal forearm from which forearm and wrist kinematics, from which PS, FE, and RUD were calculated. At the start of each session subjects' wrists were calibrated to a neutral position after which they made 480 step-tracking movements to 16 peripheral targets. No instruction was given regarding how to make the cursor move between targets, i.e. subjects were free to use only two or all three available DOFs.

After the data was collected, it was compared against predicted models of wrist behavior based on each of the four hypothesis. A 3DOF dynamic model of the wrist [4] was used to model behavior of the wrist using experimentally collected stiffness parameters [5].

RESULTS

Experimental data shows that forearm recruitment is indeed stereotyped across all subjects (Figure 2). Each hypothesis also predicts some amount of forearm recruitment (Figure 3). However, none of the proposed hypotheses match all features of the experimental observations.

DISCUSSION

None of the proposed hypothesis provide an accurate prediction of the amount of forearm recruitment that the body will employ for a two DOF pointing tasks. Hypothesis IV, which suggest that forearm recruitment is merely the result of a mechanical interaction between the joints (or “kick-back”) appears to follow the trend of the data most closely, though over-predicting its magnitude, while Hypothesis III predicts roughly the correct magnitude of forearm recruitment, with an incorrect shape of the trendline. Further research is needed, and possibly a more accurate model, to explain this phenomenon.

REFERENCES

[1] Scholz, JP, and G. Schoner. 1999. *Experimental Brain Research* 126 (3) (JUN): 289-306.
[2] Todorov, E., and MI Jordan. 2002. Nature Neuroscience 5 (11) (NOV): 1226-35
[3] Uno, Y., M. Kawato, and R. Suzuki. 1989. *Biological Cybernetics* 61 (2): 89-101.
[4] Peaden AW, and Charles SK. *In review.*
[5] Drake WB, and Charles SK. *In review.*

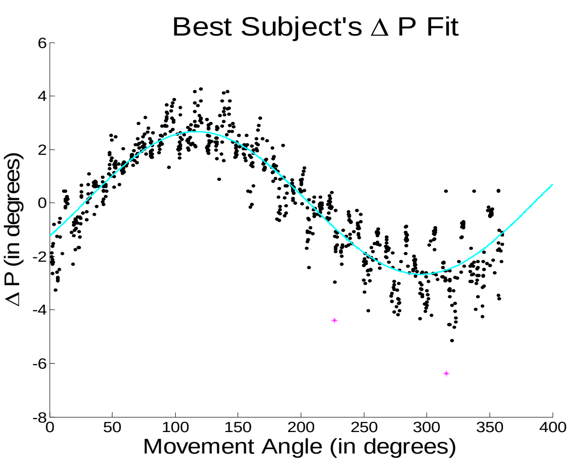

Figure 2: Collected data shows that (I) significant PS recruitment was used in redundant DOF movements (II) the degree of ΔP was predictable within subjects (III) the degree of ΔP was sinusoidal in nature.

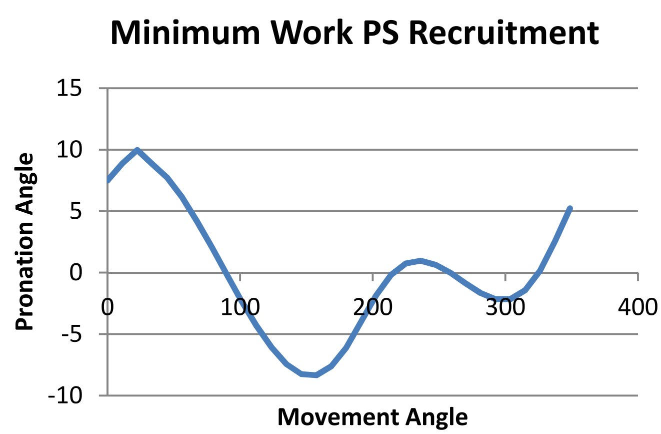

Figure 3: Predicted PS recruitment when seeking to minimize the amount of work done by the wrist/forearm to reach a target located at any arbitrary target located an equal distance from the origin, starting with pure radial deviation, and proceeding in a clockwise pattern.

SHORT TERM LEARNING AND SEX DIFFERENCES DURING REPEATED STEADINESS TASKS

Brian L. Tracy, Emma N. Boesel, Amin A. Amin

Neuromuscular Function Laboratory
Department of Health and Exercise Science
Colorado State University, Fort Collins, CO, USA
Email: brian.tracy@colostate.edu

INTRODUCTION

The ability of human subjects to control the variability of force about a target is a reflection of the integration of afferent input and the online correction of the ongoing motor command. This ability has been studied in aging, disease, and training [1]. In studies of muscle force variability, or steadiness, the experimental protocol often involves tasks during which the motor output of an isolated muscle group is maintained on a constant, submaximal target force [1]. In order to orient a subject to the task, minimize the contribution of immediate learning, and obtain a stable outcome measure, it is common to require at least one practice trial before two or more test trials. There is little definitive information to support the validity of that strategy during simple, submaximal force steadiness tasks. Furthermore, there is little information available on any potential differences in immediate learning effects between men and women. The purpose was to determine the extent of the immediate reduction in variability when young men and women perform repeated discrete trials of a constant-force (CF) steadiness task.

METHODS

Healthy young men (N=20, 23 ± 3yrs) and women (N=20, 22 ± 2yrs) underwent steadiness testing of the ankle dorsiflexors. The maximum voluntary contraction (MVC) force for dorsiflexion was first determined by performing 3-5 slow ramping trials until the maximal forces from two trials were within 5% of each other. The target force for the steadiness trials was set at 10% MVC. No practice trials were given. Subjects performed a sequence of ten 20s isometric constant-force trials with 40s rest between trials. Subjects had visual feedback of the exerted force and target force as bold horizontal lines on a large monitor and were instructed to match the target as steadily as possible for the whole trial. They rested completely during the 40s between trials. The first two seconds of the trials were discarded. The force fluctuations were quantified as the coefficient of variation of force (CV=SD force/mean force*100) for the first 3s, last 3s, and entire trial (15s). This allowed a within-trial and whole trial characterization of the normalized amplitude of the force fluctuations. Statistics: The CV of force was compared between the first 3s and last 3s for all trials, and across the ten consecutive trials using repeated-measures comparisons. The CV of force was also compared between the sexes (between subjects comparison).

RESULTS AND DISCUSSION

The linear trend across trials was significant, indicating a slight overall reduction in the CV across the ten trials (1.32% for trial 1 vs. 1.12% for trial 10, $P=0.008$, Fig. 1). Although trial 1 produced the highest average CV value, the reduction in CV from trial 1 to trials 2, 3, 4 or 5 was not significant (all $P>0.15$). The CV values for trials 6, 7, 9, and 10, however, were reduced compared with trial 1 ($P<0.05$). There were no differences in the across-trial effect between men and women ($P=0.5$, Fig. 2). Pooled across the ten trials, the CV of force was lower for women than men (1.03 vs. 1.36%, $P=0.049$, Fig. 2). Within trial effects: Pooled across all trials, the CV of force was lower in the last 3s of the trial compared with the first 3s of the trial (1.07 vs. 1.24%, $P<0.001$, Fig. 3). This within-trial effect was not different across trials ($P=0.86$) or between sexes ($P=0.12$).

The incremental reduction in the normalized amplitude of the fluctuations across a sequence of ten discrete trials performed over a 10 minute period suggests a small but relatively consistent effect of repeated performance of this simple task.

It appears that the amplitude of the force fluctuations are reduced, albeit slightly, even over the course of an 18s segment of a single trial. This effect does not diminish significantly over ten trials. Although the extent of the reduction in fluctuations is similar between young men and women both across and within trials, the normalized force variability overall is significantly less for women than men.

The results suggest that even for a simple, constant-force visuomotor task there is a quite rapid but subtle improvement in the ability to minimize the variability of force around a static submaximal target force, both within brief trials and across exposure to multiple trials performed in minutes. This is presumably the result of acute adjustments in brain function that rapidly minimize the difference between the force produced and the intended target force on a moment to moment basis [2].

Young women exhibited significantly better force control of the dorsiflexors than young men as evidenced by the lower CV values. This was consistent enough to be statistically significant. This is a new finding in the area of force steadiness. Although there is some information that suggests better force control for women than men [3], the small amount of literature cannot strongly suggest an unequivocal direction.

CONCLUSIONS

Young healthy adults exhibit subtle improvements in force steadiness during single trials and across multiple trials. These findings suggest the need for several practice trials in order to obtain a stable outcome measure in these subjects, and a careful selection of data segments within a trial to produce a representative outcome.

REFERENCES

1. Tracy, BL. *Advances in Neuromuscular Physiology of Motor Skills and Muscle Fatigue*, Research Signpost, 2009.
2. Floyer-Lea, A., et al *J Neurophysiol* **94**, 512-18, 2005.
3. Hudgens, GA, et al. *Human Factors* **30**, 51-60, 1988.

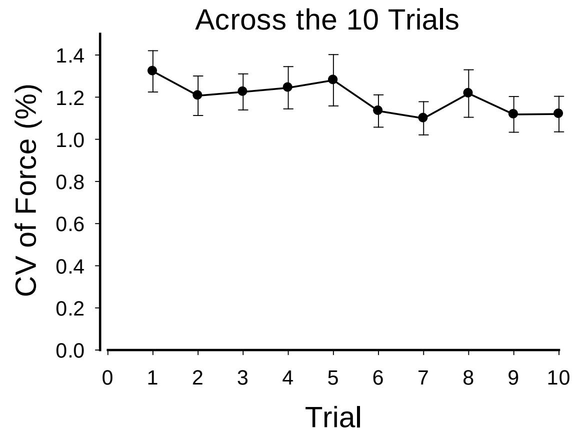

Figure 1. The linear trend for a reduction in the CV value across the 10 trials was significant (P=0.008).

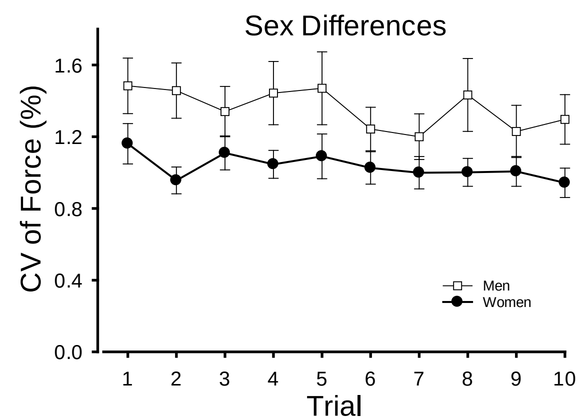

Figure 2. The CV values were lower for women than men (P=0.049).

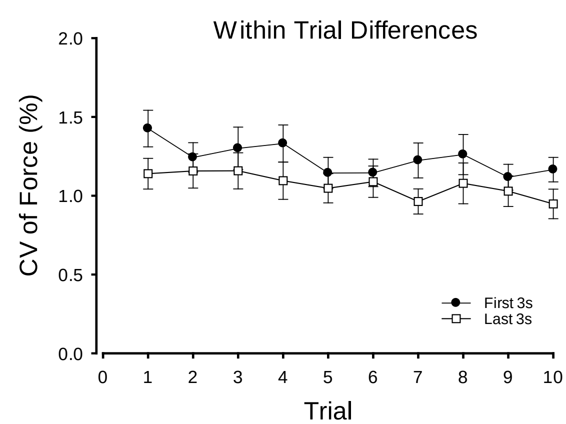

Figure 3. The CV values were lower on average for the last 3s of the trial compared with the first 3s of the trial (P<0.001).

THE ROLE OF VARIABILITY IN THE LOCAL DYNAMIC STABILITY OF CONTINUOUS REACH-AND-POINT MOVEMENTS

[1]David P. Heller, and [2]Robert W. Gregory

[1]Rockhurst University, Kansas City, MO, USA
[2]Southern Connecticut State University, New Haven, CT, USA
email: Dave.Heller@rockhurst.edu,
web: http://www.rockhurst.edu/academics/undergraduate/majors/exercise-and-sports-science/overview/

INTRODUCTION

Human voluntary movements are highly variable even when made by the same subject performing the same task. For example, the most reproducible feature of the trajectories of continuous, multi-joint reaching movements is the lack of reproducibility [1]. Despite, or perhaps because of, this variability, continuous multi-joint reaching movements exhibit remarkable stability in the face of minor perturbations.

It has been proposed that there is an optimal amount of movement variability associated with the most stable form of a movement [2]. Dingwell and Marin [3] demonstrated that during gait, subjects exhibit better stability at slower walking velocity while stride-to-stride variability revealed a U-shaped relationship with walking velocity indicating a non-linear relationship between variability and stability. In this study, the Lyapunov Exponent (LyE) was used as a measure of the local dynamic stability of a movement. The LyE is a quantification of the divergence of trajectories in a system's state space- a mathematical space that has both spatial and temporal aspects [2,3,4].

Variability in the timing of reaching movements has been shown to follow different principles than variability in space. It has been observed that increases in spatial variability are associated with increases in the velocity of reaching movements, whereas timing variability decreases [5]. Therefore, the relationship between variability and stability in reaching movements could differ depending if one is looking at timing or spatial variability. To our knowledge, no such correlation has ever been made. Thus, the purpose of this study was to examine the effect of velocity, displacement, and orientation, on the relationships between the spatial variability, timing variability, and local dynamic stability of reach-and-point movements.

METHODS

Twelve healthy, right-arm dominant individuals (6 males, 6 females) between 20-40 years of age performed reach-and-point movements while seated in front of a target grid oriented in the frontal plane. The center of the target grid was placed at 75% of maximum reach distance and aligned with the center of the shoulder joint for all individuals. The 3-cm diameter targets were positioned every 45° around a circle with radius 25 cm, including one target at the center. Subjects performed point-to-point reaching movements with their dominant arm over two displacements (25- and 50-cm) at two velocities (slow = 25 cm/s, fast = 50 cm/s) in the horizontal, vertical, or oblique directions. A motion capture system (Visualeyez VZ3000, PhoeniX Technologies) was used to record the three-dimensional position of the fingertip at a frequency of 100 Hz for 30 movement cycles. The 12 conditions (2 displacements × 2 velocities × 3 directions) were presented in random order.

Spatial variability ($\delta\mathbf{x}$) was quantified by the standard deviation of the length of the displacement vector between the terminal position values of each cycle. Timing variability (δt) was quantified by the standard deviation of the total time elapsed between the terminal position values of each cycle. Local dynamic stability was quantified using the LyE; all LyE values were calculated using Rosenstein et al.'s algorithm [4].

The effects of displacement, frequency, and direction on $\delta\mathbf{x}$, δt, and LyE values were tested for significance using a two-tailed *t*-test and the method of contrasts. Correlations between $\delta\mathbf{x}$ and LyE as well as between δt and LyE were obtained with Pearson correlations. The level of significance for both the *t*-values and the correlation coefficients was set at $p < 0.05$.

RESULTS AND DISCUSSION

The present study yielded several key findings. First, the effect of movement velocity on δ**x** values was significant ($p < 0.05$). Displacement variability was greater during the fast conditions (8.77 $\pm$ 1.17 mm) than the slow conditions (5.39 $\pm$ 1.11 mm) for both 25- and 50-cm movement displacements across all movement orientations (see Figure 1). This contrasts with the finding of path invariance with increased velocity during vertical reaching movements [6].

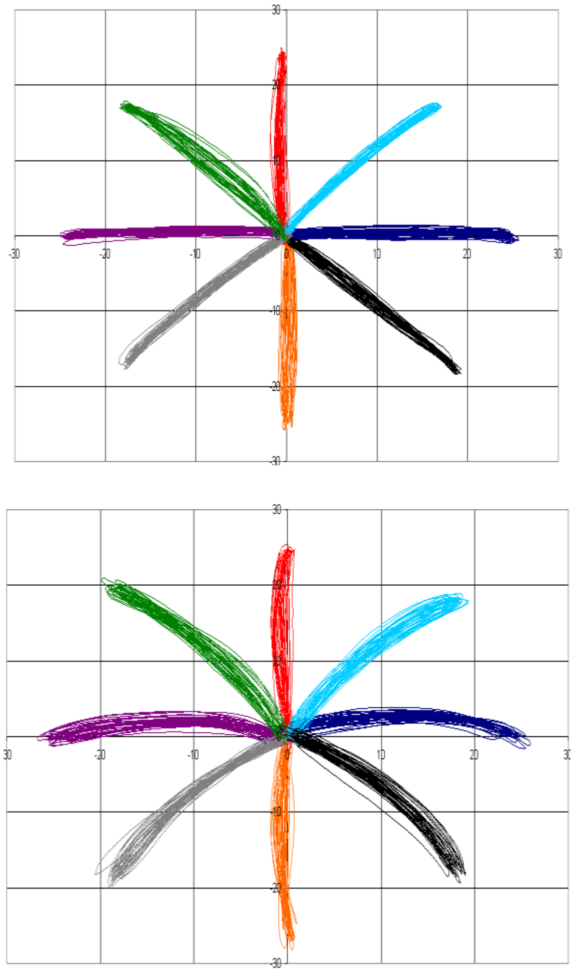

a)

b)

Figure 1: Representative fingertip trajectories during cyclic reach-and-point movements (subject RWG), axes are in cm. a) All 25-cm trials, slow velocity. b) All 25-cm trials, fast velocity.

Second, the effect of movement velocity on δt values was significant ($p < 0.05$). Temporal variability was greater during the slow velocity (63 $\pm$ 5 ms) conditions than the fast conditions (37 $\pm$ 8 ms) for both 25- and 50-cm movement displacements across all movement orientations. This finding agrees with data taken using a similar paradigm by Schmidt et al. [5].

Finally, a moderate but significant positive correlation was observed between δ**x** and LyE over all conditions (r = 0.320, $p < 0.05$), while δt and LyE showed a moderate but significant negative correlation (r = -0.377, $p < 0.05$). These inverse correlations highlight the complexity of spatiotemporal factors in the relationship between variability and stability.

CONCLUSIONS

Previously, spatial and temporal variability in reaching movements have been shown to follow different principles. The relationship between spatial variability and stability in gait has been shown to be non-linear. The present study indicates a positive correlation between spatial variability and stability, while indicating a negative relationship between timing variability and stability. The findings of this study suggest a complex spatiotemporal relationship between variability and stability in three-dimensional, multi-joint reaching movements. Future research will focus on the multidimensional aspect of spatial variability and its relationship to local dynamic stability as well as further exploring the possible non-linear relationship between variability and stability.

REFERENCES

1. Latash ML. *Neurophysiological Basis of Movement (2nd ed.)*, Human Kinetics, 2008.
2. Stergiou N, et al. *J Neurol Phys Ther* **30**, 120-129, 2006.
3. Dingwell JB, Marin LC. *J Biomech* **39**, 444-452, 2006.
4. Rosenstein MT, et al. *Physica D: Nonlinear Phenomena* **65**, 117-134, 1993.
5. Schmidt RA, et al. *Psychol Rev* **86**, 415-451, 1979.
6. Atkeson CG, Hollerbach, JM. *J Neurosci* **5**, 2318-2330, 1985.

ACKNOWLEDGEMENTS

The authors would like to thank students L. Beese, J. Keller, E. Kuster, R. Kleekamp, L. Tucker, and K. Walsh, as well as Dr. M. Clump, all of Rockhurst University, for help with data and statistical analysis, respectively.

TORQUE VARIABILITY AND EMG ACTIVATION DIFFERS BETWEEN ADULTS WITH AND WITHOUT MULTIPLE SCLEROSIS AT THE ANKLE

Brenda L. Davies, David J. Arpin, and Max J. Kurz

Munroe Meyer Institute, University of Nebraska Medical Center, Omaha, NE, USA
email: mkurz@unmc.edu web: http://www.unmc.edu/mmi/

INTRODUCTION

Multiple sclerosis (MS) is a demyelinating disease that occurs in young adults and often affects the control of the leg musculature. Many of these individuals with MS experience gait deficits and balance impairments that limit their activities of daily living. Previous research has shown that individuals with MS have significantly weaker muscles, and that the musculature fatigues at a faster rate than age matched controls. Yet, there has been limited research exploring how MS impacts the control of the ankle musculature. Control of the ankle joint is important for correcting the postural sway, clearing the foot during the swing phase of gait, and push-off at terminal stance.

Variability or error is present in all voluntary contractions and impacts the precision and control of the motor performance [1-3]. Several investigations have shown that aging results in greater variability in the steady-state isometric performance of the ankle joint, and that these variations may be a result of the inability to properly activate the motor unit pool that innervates the ankle musculature [1,2]. In spite of these novel findings, limited efforts have been made to extend these neurophysiological methods to understand how MS impacts the control of the ankle musculature. We suspect that the neurodegeneration associated with MS will result in an increased amount of variability in the motor control of the ankle joint. Identifying how the neurologic insult impacts the motor control of the ankle joint will provide a new framework for our future goals that are directed at assessing the efficacy of innovative therapeutic interventions that are aimed at promoting improved neuromuscular control in individuals with MS.

The purpose of this study was to quantify the steady-state isometric muscular control of the ankle plantar flexors in individuals with MS. We hypothesized that individuals with MS will have a higher coefficient of variation (CV) during a low level isometric contraction compared with healthy controls. Secondarily, we hypothesized that the surface EMG (sEMG) of the gastrocnemius in individuals with MS would exhibit altered harmonics when attempting to sustain the isometric contraction.

METHODS

Twenty-two adults (Age: 49.3 ± 8.34 years) with relapsing-remitting or secondary progressive MS participated in the study. The subjects had an average Kurtzke Extended Disability Status Score of 5.32 ± 1.02, which indicates that on average each subject could walk independently for at least 100 meters. Twenty normal, healthy adults served as a control group (Age: 45.1 ± 14.1 years).

Isometric control of the ankle plantar flexor muscles was measured using an isokinetic dynamometer (Biodex, Inc., Shirley, NY). Participants sat in the chair on the isokinetic dynamometer with the backrest angle at 90° with their knee fully extended and their ankle in a neutral position, with their foot strapped onto a metal footplate. The group with MS used their most affected leg for the testing while the control group used their dominant leg. Two isometric maximal voluntary contractions were completed, and the highest maximal voluntary torque (MVT) was used to calculate 20% of the MVT. A custom LabVIEW program was used to display the target and real-time torque generated by the ankle on a computer screen ~1 meter in front of the participants. Two submaximal steady state contractions at 20% MVT were held for 30 seconds each. The middle 15 seconds of each trial was utilized in order to ensure that a steady-state contraction had been reached. The coefficient of variation (CV) for each trial was calculated and the two trials were averaged. Concurrently, sEMG was collected from the gastrocnemius muscle. The sEMG was band pass filtered at a bandwidth of 20 – 350 Hz, and a fast Fourier transform was subsequently performed to determine the power spectral density. The power spectral density was normalized to the maximum value in the power spectrum, and was partitioned into seven 50 Hz bins. The amount of spectral content was calculated by integrating each bin.

RESULTS AND DISCUSSION

The MVT for the ankle plantarflexors was lower for the individuals with MS compared with the controls (MS: 41.6 $\pm$ 3.7 Nm; Control: 63.8 $\pm$ 5.9 Nm; p=0.0005). Additionally, the individuals with MS had a greater CV for the steady-state torque (Control: 1.97 ± 0.74%; MS: 3.96 ± 0.52%; p = 0.031). The CV results indicate that the individuals with MS had greater errors when attempting to match and sustain the target value. Previous results have shown that weaker muscles have more noise in their isometric force production [3]. Since the MVT for the individuals with MS were lower, we suspect that the higher variability may partially be a result of the inability to suppress the stochastic features that are present in the ankle joint's musculature performance.

There was a significant bin x group interaction (p = 0.005), and the post-hoc comparisons indicated that the participants with MS had less power between 101-150 Hz (p = 0.009) and 151-200 Hz (p = 0.03; Figure 1). This result suggests that the differences in the steadiness of the ankle torque between the respective groups may be related to the amount of power in these frequency bands. The reduction in power may be a result of the reduced firing rates of the motor units seen in individuals with MS [4]. Alternatively, it has been suggested that the amount of coherence between the oscillations in the sensorimotor cortices and the sEMG at 12-30 Hz can modulate the amount of power between 100-150 Hz [5]. Hence, it is also plausible that the reduced power may reflect an altered cortical drive to the muscle. We were not able to interrogate this speculation due to the bandwidth of the EMG system used in this investigation (Delsys Trigno; 20-350Hz). Therefore, the exact reason for the reduced amount of power in the 101-200 Hz remains unclear and deserves further investigation. Nevertheless, the difference at this frequency band provides evidence that the neural activation of the muscle was different for the individuals with MS.

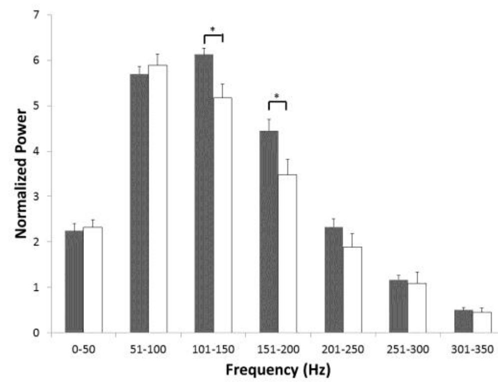

Figure 1: Amount of spectral power in each 50 Hz bin for the gastrocnemius muscle for the controls (black) and individuals with MS (white). *p<0.05.

REFERENCES

1. Kwon M, et al. *Hum Mov Sci* **31**, 1366-1378, 2012.
2. Kouzaki M & Shinohara M. *Muscle & Nerve* **42**, 78-87, 2010.
3. Hamilton AF, et al. *Exp Brain Res* **157**, 417-430, 2004.
4. Dorfman LJ, et al. *Electoenceph Clin Neurophys* **73**, 215-224, 1989.
5. Neto OP & Christou EA. *J Neurophys* **103**, 1093-1103, 2010.

EXCITABILITY OF THE MIDDLE DELTOID AT DIFFEFENT ELEVATION ANGLES

Yin-Liang Lin, Anita D. Christie and Andrew R. Karduna

University of Oregon, Eugene, OR, USA
email: yinliang@uoregon.edu, web: http:// physiology.uoregon.edu/

INTRODUCTION

The deltoid muscle is the primary mover of the shoulder joint. However, the moment arm of the deltoid changes during arm elevation. The moment arm is shorter at the initial range of elevation and gradually increases with arm elevation [1]. Compared to the initial range of elevation, electromyographic (EMG) studies show that the deltoid contributes more in the middle range of elevation [2], which indicates that the deltoid participates more when it is able to efficiently generate elevation torque. Therefore, central control of the deltoid may be different at different elevation angles.

Transcranial magnetic stimulation (TMS) can be used to assess the corticospinal excitability of muscles. The change of corticospinal excitability demonstrates the modulation of the corticospinal tract, which is from the primary motor cortex through the spinal cord to the muscle. The changes of the corticospinal control are associated with inter-joint torque reaction and different task execution [3]. The purpose of this study is to investigate the excitability of deltoid at different angles of elevation.

METHODS

Three healthy male subjects (20 – 24 years old) were tested. The corticospinal excitability of the middle deltoid was measured at 30° and 90° of arm elevation in the scapular plane. A MagStim 70mm double-coil stimulation coil (Magstim, Whitland, UK) was used to provide a single-pulse stimulation of the motor cortex. Surface EMG electrodes were taped on the middle deltoid to record the response to TMS stimulation. Maximum voluntary contractions (MVC) at 30° and 90° of arm elevation were collected before the TMS measures.

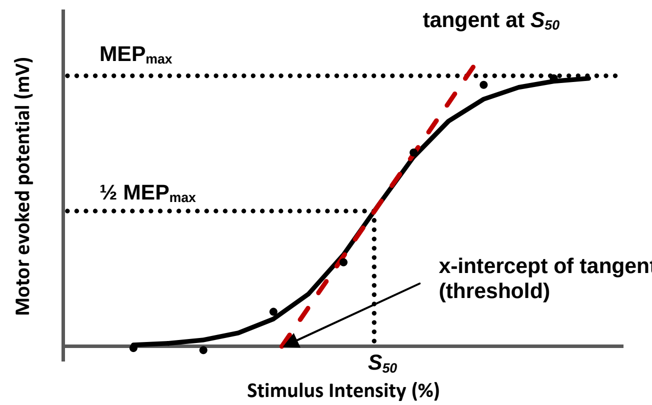

Figure 1: An example of a sigmoid fit to motor evoke potential (MEP) versus stimulus intensity plot. Three parameters (MEP_{max}, *m*, and x-intercept) are calculated from the curve.

The TMS stimulation was applied during 10% MVC of deltoid contraction. The coil was placed approximately 4 cm lateral of the bisection of the mid line and the biauricular line. It was moved around to find the optimal spot where the stimulus generated a maximum response from the middle deltoid. Stimulation intensity was then set at 10% below threshold and was increased in 5% increments until the response saturated. Five stimuli were delivered at each intensity of stimulation. The peak-to-peak amplitude of the motor evoked potential (MEP) was measured and averaged across the trials at each intensity. The curve of the relationship between stimulation intensity and the MEP amplitude was sigmoidal and was fit with the Boltzmann equation [4]:

$$\mathrm{MEP}_{(s)} = \frac{\mathrm{MEP}_{\max}}{1 + e^{m(S_{50}-s)}},$$

Where MEP(s) is the amplitude of motor evoked potential, MEP_{max} is the maximum MEP amplitude defined by the function; *m* is the slope parameter of the function; and S_{50} is the stimulus intensity at which the MEP is 50% of MEP_{max}. The peak slope of the function occurs at a stimulus intensity equal to S_{50} and is defined by the relationship: $\frac{m \text{ x } MEP_{max}}{4}$[4]. The threshold of activation is given by the x-intercept of the tangent to the curve at the point of S_{50}. MEP_{max}, m, and x-intercept were used to represent the corticospinal excitability of the middle deltoid (Fig. 1)

The value of the x-intercept threshold represents the stimulus intensity needed to activate the most excitable corticospinal motoneurons. The slope indicates the recruitment efficiency (gain) of the corticospinal tract. The MEP_{max} reflects the balance between excitatory and inhibitory components of the corticospinal tract [5].

RESULTS AND DISCUSSION

The MEP stimulus-response curves at 30° and 90° of arm elevation from one subject are shown in figure 2. Table 1 shows the mean and range of three parameters from all three subjects. Although there was variation between subjects, at 90° of elevation, the average of MEP_{max} was higher, the average slope was steeper, and the average threshold (x-intercept) was lower, compared to those at 30° of elevation.

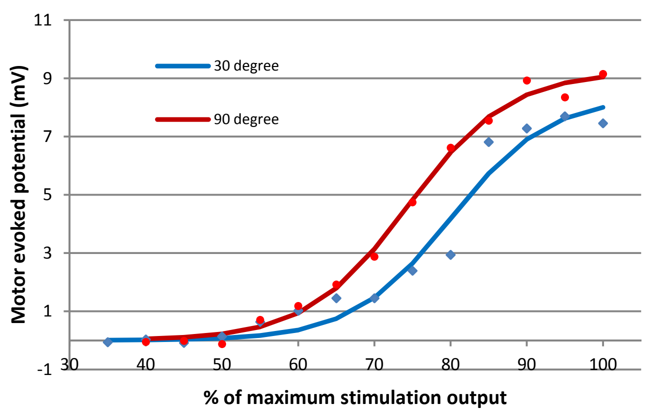

Figure 2. The curves of the motor evoked potential and stimulation intensity at 30° and 90° of arm elevation from one subject.

These results indicate that the stimulation needed to trigger the response of the corticospinal tract is lower, the recruitment efficiency (gain) of the corticospinal tract is higher, and the maximum response is higher at 90° of elevation, compared to those at 30° of elevation. Thus, the excitability of the middle deltoid increased at 90° of elevation, compared to at 30° of elevation.

CONCLUSIONS

The difference of the excitability at different elevation angles illustrates the differences in regulation of the corticospinal tract for the deltoid, which may be related to the changes in deltoid torque during arm elevation. In the future, we will also be testing the excitability of the rotator cuff muscles at different angles to investigate the difference in central control between the deltoid and rotator cuff muscles.

REFERENCES

1. Poppen NK and Walker PS. *Clin Orthop Relat Res* **135**, 165-170, 1978.
2. Alpert SW, et al. *J shoulder Elbow Surg* **9** 47-58, 2000
3. Gritsenko V, et al. *J Neurosci* **31**, 11968-79. 2011
4. Carroll TJ, et al. *J Neurosci Methods* **112**, 193-202, 2001.
5. Devanne H, et al. *Exp Brain Res* **114**, 329-338, 1997

ACKNOWLEDGEMENTS

The authors would like to thank Glenn Nutting and Jake Gacke for their assistance with protocol testing and data collection.

Table 1: The mean and range of the three parameters of deltoid excitability at 30° and 90° of arm elevation at the scapular plane

Arm elevation	MEP_{max} (mV)	Slope parameter	x-intercept (%)
30°	7.54 (5.63-8.63)	17.95 (15.63-21.28)	0.50 (0.38-0.67)
90°	8.27 (5.29-10.29)	18.94 (13.89-27.78)	0.48 (0.40-0.61)

OBESITY-RELATED DIFFERENCE IN LOWER EXTREMITY STRENGTH AMONG YOUNG FEMALES: PRELIMINARY FINDINGS

[1]Hoda Koushyar, [2]Sara Matrangola, [1]Maury A. Nussbaum, and [1]Michael L. Madigan

[1]Virginia Tech, Blacksburg, VA, USA
[2]High Point University, High Point, NC, USA
email: koushyar@vt.edu, web: http://www.biomechanics.esm.vt.edu/

INTRODUCTION

Individuals who are obese tend to be stronger than healthy-weight individuals in terms of absolute lower limb strength, but weaker in terms of relative strength when strength is normalized to body mass [1-3]. Previous studies on strength differences with obesity have focused on a specific joint or exertion type (e.g. knee extensors). A more comprehensive comparison of lower extremity strength between obese and healthy weight individuals that includes multiple joints and exertion types can provide more complete information on whether the effects of obesity might be joint- or exertion-dependent. Our current interest is in lower extremity capacity, and the purpose of this study was to investigate the effects of obesity on isometric and isokinetic strengths at ankle, knee, and hip among young females.

METHODS

Two groups of young females participated, including 10 healthy weight (HW, age: 21.7 ± 3.3 years, BMI: 22.5 ± 1.8 kg/m^2) and eight obese (OB, age: 21.75 ± 2.8 years, BMI: 34.1 ± 3.15 kg/m^2) individuals. Participants with a history of neurological, cardiac, or musculoskeletal disorders were excluded, and habitual activity levels were similar for both groups. The study was approved by the local IRB, and written consent was obtained from all participants.

Isometric and isokinetic (concentric and eccentric) maximum voluntary contractions (MVCs) were performed using the right lower extremity, with a Biodex System 3 dynamometer (Biodex Medical Systems, Inc., Shirley, NY), in plantar flexion (PF), dorsiflexion (DF), knee extension (KE), knee flexion (KF), hip extension (HE), and hip flexion (HF). Three isometric MVCs were performed at each of four different angles distributed evenly throughout the range of motion. Four concentric MVCs were performed at 150 deg/s for the knee, and at 120 deg/s for the ankle and hip. Four eccentric MVCs were performed at 75 deg/s for the knee, and 60 deg/s for the ankle and hip. Additional trials were completed to determine passive elastic/gravitational torques, which were subtracted from the isometric and isokinetic data during post-processing. For isometric MVCs, the peak torque over the four angles was determined. For isokinetic MVCs, the peak torque over the isokinetic region was determined. Mean values of absolute and normalized peak torques (to body mass) were compared between groups using Wilcoxon rank-sum tests. Statistical analyss was performed using JMP Pro 10 (SAS Institute, Inc., Cary, NC).

RESULTS AND DISCUSSION

Peak absolute torques tended to be higher in the OB group, but these differences were only statistically significant for concentric DF and eccentric HF MVCs (Figure 1). Peak normalized torque was lower in the OB group for 14 of the 18 testing conditions, with the exceptions being isometric PF, isometric HE, concentric HF, and eccentric PF MVCs (Figure 2).

The effect of obesity on normalized torque was apparent at all three joints, and in both flexion and extension directions, but was not uniform across all three types of contractions. Our results with respect to absolute and normalized concentric KE and KF peak torques were in general agreement with prior work (although prior work reported a significantly higher absolute torque among OB for KE) [1, 3]. Given that the effects of obesity may result, at least in part, from higher chronic physical exposure related to higher body mass, it was interesting to observe effects of obesity in muscle groups not as involved with body support (e.g., DF) as well as in muscle groups typically associated with body support (e.g., AP).

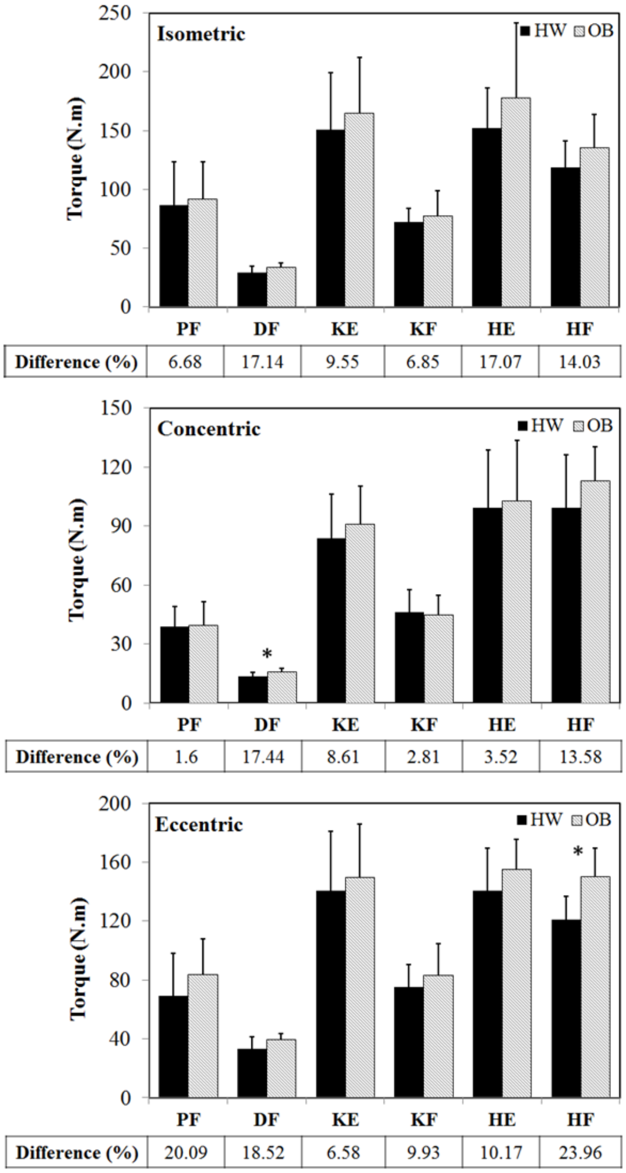

Figure 1: Peak isometric, concentric, and eccentric strength of lower extremity (mean ± s.d.). (0.01<p<0.05: *, p<0.01: **).

CONCLUSIONS

Minimal differences between OB and HW individuals were found in absolute strength, but OB exhibited less strength relative to body mass for most muscle groups and exertion types. Differences between joints, exertion directions, and exertion types may be related to a training effect associated with larger body mass, but this requires further study.

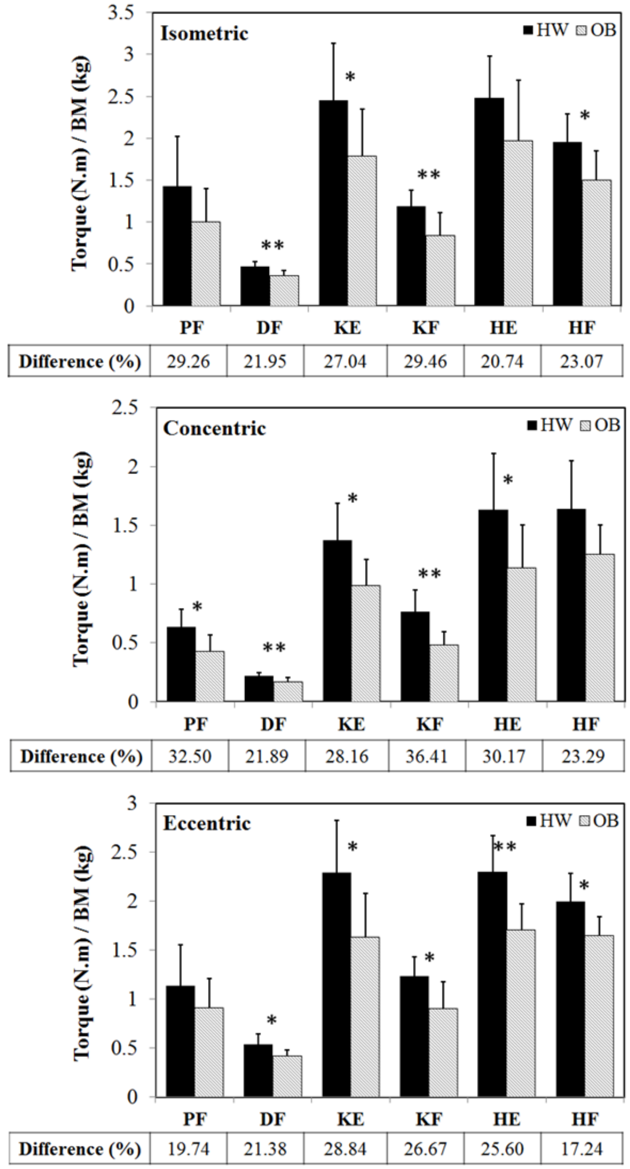

Figure 2: Peak isometric, concentric, and eccentric strength of lower extremity normalized to the body mass (mean ± s.d.). (0.01<p<0.05: *, p<0.01: **).

REFERENCES

1. Capodaglio P, et al. *BMC Musculoskeletal Disorder* **10**:47, 2009.
2. Maffiuletti NA, et al. *Eur J Appl Physiol* **101**, 55-59, 2007.
3. Hulens M, et al. *Int J Obes* **25**, 676-681, 2001.

ACKNOWLEDGEMENTS

This work was supported by grant R01OH009880.

TREADMILL BONE LOADING DURING SPACEFLIGHT

[1]Melissa Scott-Pandorf, [2]Roxanne Buxton, [3]Lori Ploutz-Snyder and [1]Brian Peters

[1]Wyle, Houston, TX, USA
[2]University of Houston, Houston, TX, USA
[3]Universities Space Research Association, Houston, TX USA
email: melissa.scott-pandorf@nasa.gov

INTRODUCTION

Exercise is the primary countermeasure for mitigating muscle and bone loss during spaceflight. The International Space Station (ISS) contains the most sophisticated exercise equipment to date, capable of providing loads and exercises similar to ground devices. Previous research has demonstrated that skeletal unloading in astronauts can result in a loss of bone mineral density (BMD) ranging from 0.4% to 2.7% per month [1]. The main concern with this significant loss is bone fracture. With limited medical resources available during a mission, a fracture could be detrimental and even life threatening. Limited information exists regarding the prescribed treadmill exercise programs and the gains/losses of bone. An understanding of the relationship between exercise loading forces and bone health outcomes is crucial in the implementation of efficient exercise countermeasures to mitigate deleterious changes in bone.

METHODS

A treadmill (T2) is onboard the ISS for aerobic exercise. The T2 is equipped with load cells capable of recording ground-reaction force (GRF) during crew exercise. GRF is measured directly underneath the T2 belt and the T2 system "floats" inside a vibration isolation system (VIS). Bungees are used to tether the crew to the treadmill as they run, in which, crew self-select a load near their max comfort. As the mission progresses crew often will increase this load by shortening the bungee length. T2 software requires the crew to take a static load measurement of the bungee setting before starting any exercise. Four T2 sessions per week are typically prescribed for crewmembers (CMs). CMs are instructed to run at the fastest pace possible for their prescribed interval times. Exercise GRF data is limited to the first 55 seconds of each stage in an exercise protocol as data storage and downlink bandwidth from ISS is limited. This T2 in-flight GRF data are new to ground personnel at NASA and we provide the data of one CM through an entire multi-month mission. These data include percentage of impact peaks (IP), peak vertical GRF (vGRF), impulse (Imp), and peak loading rate (LR) for representative prescribed exercise protocols as well as Total Mission T2 Bone Loading (TMBL) measures. The data have been normalized to "Earth body weights (BW)" to make comparisons with Earth running loads. The force loading through an entire workout and TMBL were projections from the 55-second samples that are provided. For the 55-second data sample, step time (ST) was determined as heel strike to heel strike. The number of steps per stage (# step/stage) was calculated as

Total stage run time / ST = # steps/stage

An average peak vGRF and average Imp were calculated for each stage sample and then multiplied by the # steps/stage. These values were summed for each stage in a single session workout for a total workout bone loading. Then all workouts were summed for TMBL. Preflight and postflight bone mineral density (DXA) is also reported.

RESULTS AND DISCUSSION

Across the entire mission, this CM made one notable change in bungee loading. In the first half of the mission he/she loaded to 79% ± 4% of their Earth body weight. In the last half that loading shifted to 88% ± 7%.

Table 1 shows 4 representative prescribed exercise sessions. IPs occurred 51% to 92% of the time and we suspect this may be attributed to type of prescribed protocol, the VIS on the T2 and the angle the runner approached T2 while using bungees. Changes in bungee load and running speed may generate more IPs. This CM had the greatest percentage of impact peaks per workout during the continuous 30-minute run. Notably the shortest intervals (30s/15s) had impact peaks for only half of all strides. For vGRF this CM experienced 1.3 to 1.5 BW per step across prescribed protocols. These values were not unlike the previous vertical force loading recorded on ISS using pressure insoles, which reported values of 1.2 to 1.7 BW [2]. The TMBL Imp for this CM was 21,208,886 (N·s) and TMBL for vGRF was 192,355 BW. For perspective, a slow/average running pace would result in peak vGRF of 2.5 BW force with each step while running on Earth [3]. We can conservatively estimate, based on total # steps, that if this CM were running on Earth instead of ISS they would have experienced 388,876 BW total. Therefore, we may say total loading is much less during running on ISS than Earth. The changes in DXA over the mission for this CM can be seen in Figure 1. Most regions had little to no decrement; however, the pelvis and calcaneus experienced 5% and 6% losses, respectively. Based on these results and IP reported in Table 1, it may benefit the calcaneus to prescribe exercise that will generate the most IP.

CONCLUSION

The forces applied during ISS exercise are considerably lower than Earth exercise; however, the relationship of these lower loads to bone loss is yet to be fully understood. Evaluating the loading forces per prescribed exercise may provide vital insight. The greatest loading force occurred in the 120/120 prescribed protocol; however, the 1800/0 had good IP and LR. The 30/15 protocol had the least loading force overall. T2 running is not the only exercise countermeasure for bone on ISS. The advanced resistive exercise device (ARED) provides resistive exercise training (for example, squat and deadlifts) up to 600-pound load and will soon provide GRF as well. These data will be catalogued for each crew and the bone density outcomes will be recorded. The use of bone saturation models is also being explored. It is the hope of the space health community to understand the bone loading/loss relationship better and use these data to inform our exercise prescriptions.

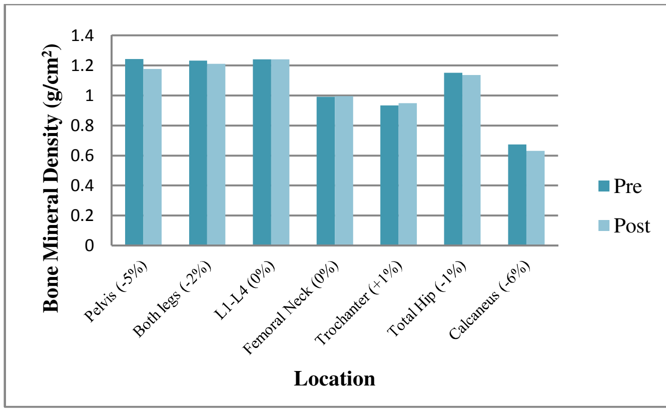

Figure 1. Pre/postflight DXA.

REFERENCES

1. Lang et al., *J Bone Min Res* **19**, 1006-1012, 2004.
2. Gopalakrishnan et al., Av Space Envir Med **81**, 2010.
3. Kluitenberg et al., *BMC Musc Dis,* 2012.

TABLE 1. Representative Prescribed T2 Exercise. Average and total force measures are reported. Percentage IP refers to the percentage of strides that had an impact peak while performing the prescribed protocol.

Prescribed Interval Protocol Warm-up + Run Time/Rest Time (s)	Speed (m/s)	IP (%)	vGRF (BW)	Total vGRF (BW)	LR (BW/s)	Imp (N·s)	Total Imp (N·s)
600 + 30 / 15 *8	2.32±1.31	50.5	1.39±0.04	3200	23.83±5.79	156.75±17.78	370,061
300 + 120 / 120 *6	3.24±1.50	87.4	1.45±0.10	7314	32.44±4.67	154.40±8.09	773,798
480 + 240 / 180 *4	3.20±1.24	81.6	1.41±0.09	7021	15.99±1.82	151.35±6.32	656,940
1800/0 *1	2.75±0.66	92.8	1.27±0.05	6093	26.84±2.04	152.02±4.49	737,606

*indicates # of intervals

RELATIONSHIPS BETWEEN THE MECHANICAL QUALITY OF CORTICAL BONE AND FGF23 LEVELS IN MICE CHALLENGED BY FRUCTOSE AND CALCIUM MODIFIED DIETS

[1,2]Edek Williams, [1]Devendra Bajaj, [1]Veronique Douard, [3]Yves Sabbagh, [1]Ronaldo Ferraris, [1,2]J. Chris Fritton

[1]New Jersey Medical School, Orthopaedics and Pharmacology/Physiology, Newark, NJ, USA
[2]Rutgers University, Biomedical Engineering, New Brunswick, NJ, USA
[3]Genzyme, A Sanofi Company, Cambridge, MA, USA
email: frittojc@umdnj.edu

INTRODUCTION

Serum levels of calcium, phosphate and 1,25(OH)$_2$ Vitamin D$_3$ (VitD3) have long been known to affect fracture risk. More recently, fibroblast growth factor 23 (FGF23), produced primarily by bone-forming osteoblasts and bone-resident osteocytes, has been demonstrated to be a potent cytokine that contributes to phosphate and VitD3 homeostasis [1].

Calcium (Ca^{2+}), the primary mineral component of bone, is tightly regulated. During periods of calcium need, a cascade of VitD3 driven processes maintain Ca^{2+} levels in serum. *In kidney*: Parathyroid hormone (PTH), released from the parathyroid gland, stimulates calcium reabsorption through activation of 25-Vitamin D3 to VitD3. *In intestine:* VitD3 increases calcium absorption through the upregulation of Ca^{2+} transporters [2]. *In bone*: VitD3 releases Ca^{2+} from bone by stimulating osteoblastic expression of RANKL, a ligand that promotes proliferation of bone-resorbing osteoclasts. VitD3 also acts in feedback by decreasing PTH expression in the Parathyroid gland and secondarily increases the expression of FGF23 by cells of the osteoblastic lineage [1,3].

Bone growth is affected by dietary intake of the elements of the cytokines: calcium, phosphate and VitD3. Importantly, the intake of these bone building agents has waned as consumption of foods with high fructose corn syrup has increased 10 fold over the past 30 years. However, few studies have investigated fructose effects on bone growth [5].

Here we have evaluated the effects of fructose on mouse bone during a period of increased calcium need (growth with dietary deficiency).

METHODS

Thirty-six, 3-week-old C57BL/6 mice (n=9/group) were fed a combination of normal- (0.5 %) /low-calcium (0.02%) and glucose/fructose (43%) diets for 5 wks. Animal care was IACUC approved. At 10d and 3d prior to sacrifice, all mice were administered calcein bone formation labels (20 mg/kg BW). At sacrifice, blood was sampled by cardiac puncture and serum was separated by centrifugation and stored at -80°C. Left humerii and femurs were excised and cleaned of soft tissue. Humerii were stored frozen prior to mechanical testing and femurs were fixed in formalin for staining and plastic embedding.

Frozen humerii were gradually thawed and tested in 3-point bending (Bose ElectroForce LM1 TestBench). Bones were pre-loaded at -0.4N and tested at a displacement rate of -0.05 mm/s until failure. Humerii remained hydrated prior to testing. Instantaneous force and displacement were captured at 200 Hz. Mechanical properties, including stiffness (E), ultimate load (P_u) and post-yield displacement (δ_{PY}) were quantified for individual load-deflection curves.

Femurs were dehydrated, bulk stained in basic fuchsin, embedded in poly-methyl-methacrylate, sectioned at the mid-shaft using a precision saw (Buehler 5000) and finely polished for confocal microscopy. The distal end was imaged with a high-resolution μCT scanner (Skyscan 1172) with calibration phantoms at ~8 μm resolution. Images were reconstructed and analyzed using packaged software. The trabecular region of interest (ROI) was a 1.7 mm length along the long-bone axis beginning 0.22 mm proximal to the growth plate. The cortical ROI was a 0.5 mm length, 2.2 mm proximal to the growth plate. Differences between groups were evaluated by one-way ANOVA ($p<0.05$). Post-hoc analysis was completed with Bonferroni corrections for multiple comparisons.

RESULTS AND DISCUSSION

µCT and microscopy demonstrated that calcium restriction leads to reduced trabecular mineral density (-39%, $p<0.01$) and decreased cortical area (-8%, n.s). 3-point bending demonstrated a decreased elastic stiffness (Fig 1b, -60%, $p<0.01$) and increased post-yield (plastic) deformation (+78%, $p<0.05$). The relationships between FGF23 and both BMD and stiffness (Fig 1a, c) suggests positive correlations. With high fructose diet this relationship was disrupted.

FGF23 is produced by osteocytes, terminally differentiated osteoblasts that are the most numerous cells of bone. Hypophosphatemic mineralization pathologies have been connected to the dysregulation of FGF23. One hypothesis is that the major effects are mediated by impaired intestinal calcium uptake through VitD3 dysregulation in kidney [4]. More work is required to determine if the dietary effects of fructose and calcium on FGF23 and bone growth may be more direct and regulated at the individual cell level or secondarily influenced by the number of osteocytes that become incorporated into bone matrix.

CONCLUSIONS

By challenging mice with a calcium-deficient diet we uncovered a surprising relationship between the serum level of FGF23, over a broad range, and bone's mechanical quality. Following up on this work may lead to better serum readouts for bone quality during growth that include FGF23. These are needed since other serum markers, such as systemic VitD3, have proven poor predictors of bone's structural and mechanical properties.

Fructose feeding disrupted the relationships between FGF23 and both BMD and stiffness, suggesting that fructose may impact mineralization of the bone matrix during growth.

REFERENCES

[1] Lu, *et al.*, *Curr Osteoporos Rep*, 9: 103-8, 2011.
[2] Williams, *et al.*, *ASBMR* Meeting, Minneapolis, MN, 2012.
[3] Barthel, *et al.*, *J Steroid Biochem Mol Biol*, 103: 381-8, 2007.
[4] Douard, *et al.*, *FASEB J*, 26:707-21, 2012.
[5] Tsanzi, *et al.*, *Bone*, 42: 960-8, 2008.

ACKNOWLEDGEMENTS

Luke Fritsky, Pat Buckendahl, and Joseph Geissler provided technical assistance. Funding was supported by NIH (AR063351) and NSF (1121049).

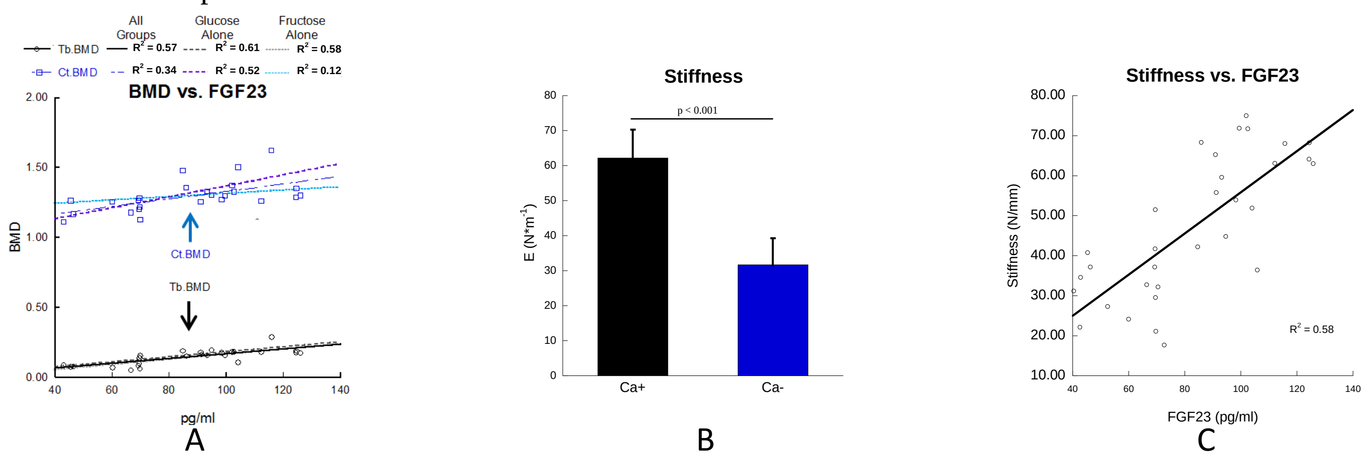

Figure 1: A) Relationship of Ct.BMD and Tb.BMD with serum FGF23. B) Calcium-deficient diet reduced the elastic stiffness as measured by 3-point bending of humerii. C) Relationship between serum FGF23 and humerus stiffness.

COMPARING PERIOSTEAL MORPHOLOGY BETWEEN CERVINE AND HUMAN TIBIAE

Alexander D.W. Throop[1], Alexander K. Landauer[1], Alexander Martin Clark Jr.[2], and Laurel Kuxhaus[1]

[1]Clarkson University, Potsdam, NY, USA
[2]Canton-Potsdam Hospital, Potsdam, NY, USA
email: lkuxhaus@clarkson.edu, web: http://people.clarkson.edu/~lkuxhaus/

INTRODUCTION

Novel fracture fixation devices, such as improved external fixators, fixation plates, or intramedullary nails, must be tested *in situ* before being used in patients [1]. Animal models are often more economical for preliminary testing; porcine and ovine tibiae morphology is similar to human tibiae [2, 3]. Furthermore, cervine vertebrae have been established as a suitable proxy for human vertebrae in mechanical testing [4]. Cervine (deer) tibiae are readily available in many regions and typically discarded after butchering. Yet there is no existing report of cervine tibiae dimensions. Therefore, the goal of this work is to compare periosteal dimensions of cervine tibiae to previously-reported human tibiae dimensions. If similar, cervine tibiae could be another cost-effective tibiae model for orthopaedic implant testing.

METHODS

This study used eight right tibiae from fresh-frozen cervine specimens (four males, *O. virginianus*, white tailed deer; approximate ages 1.5-3.5 years) that were obtained locally (Nolt's Custom Meat Cutting, Lowville, NY). All soft tissue was removed from each tibia. Following this preparation, external dimensions were measured three times by the authors of this work. All tibiae were kept hydrated with saline solution during the dissection and measurement.

Dimensions were measured on each tibia. Length (LN) was measured with a tape measure with accuracy of 1 mm (Kobalt 25-ft Metric and SAE tape measure, Lowe's, Mooresville, NC). The remaining measurements were made using calipers (6-inch dial caliper, General Tools, New York, NY) with an accuracy of 0.01 inches.

Eleven measurements were made in both the anterior-posterior (AP) and medial-lateral (ML) planes, as visually determined by the researchers. These measurements were: proximal epiphyseal (PE) and distal epiphyseal (DE) widths; proximal diaphyseal (PD) and distal diaphyseal (DD) widths at a distance of 20% of the overall length from each end; and mid-diaphyseal (MD) widths at 50% of its overall length. Figure 1 shows a cervine tibia with the location of each measurement.

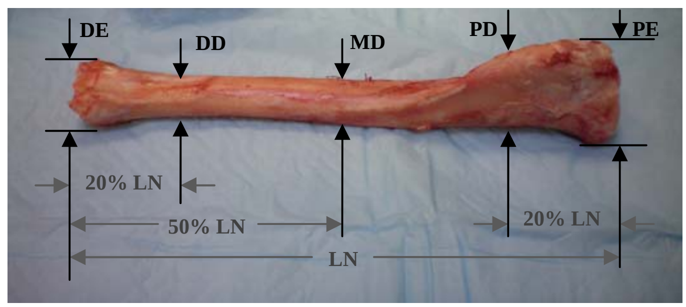

Figure 1: Cervine tibia measurement locations. Measurements (except LN) were made in the AP and ML planes.

RESULTS AND DISCUSSION

The mean measurement across researchers of each dimension was computed. These values were compared with previously-published measurements from cadaveric human tibiae [5]. The percent difference between each cervine and human dimension was calculated (Figure 2).

Several aspects of the cervine tibia are very similar to that of a human. Thirty-seven of the forty-eight diaphyseal measurements are within 20% of the median of the reported human values; in most cases, this difference was less than a few millimeters.

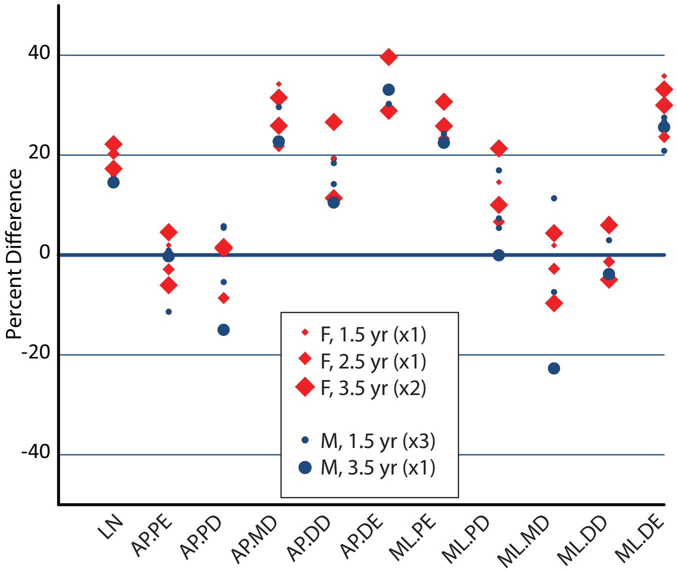

Figure 2: Percent difference of all eleven measured dimensions in deer compared to humans. A positive percent difference means that cervine measurement is smaller than the human measurement.

There is a marked difference between the epiphyseal dimensions; many differ by over 20% from the human dimensions. This variation could be attributed to the fact that the tibia in humans connects to the talus (ankle), yet in the deer, the tibia connects to the metatarsus (a distal leg segment.) This is consistent with the load-bearing roles of the human (biped) ankle compared to that of a quadruped. Given that the epiphysis is typically potted in a bonding material for testing fracture fixation devices, this dimensional difference should not notably influence the results when testing mid-shaft fixation devices.

Cervine tibia length (LN) is slightly shorter than that of human tibiae. This may be because four of the eight specimens measured were young, from a deer of approximately 18 months of age. It is notable that the tibia of greatest length was from the oldest male specimen (Table 1). The tibiae from older male cervine specimens may be the most appropriate model.

Limitations of this work include a limited sample size and the fact that only periosteal dimensions were measured. Comparison was made to previously-published human tibiae dimensions, which may not accurately capture anatomic variation. Additionally, the age estimation of the specimens is based on the expertise of the meat processor, and is therefore only approximate.

CONCLUSIONS AND FUTURE WORK

Based on the measurements collected here and compared with previously-reported human tibiae measurements, the cervine tibia can be a suitable proxy for the human tibia for evaluating new fracture fixation devices. This could impact biomechanical testing protocols, laboratory education in orthopaedic surgery, and the development of novel devices. Future work will include measuring more, older specimens; comparing the bone-mineral density between cervine and human tibia, and also making interior, endosteal measurements of the cervine tibiae to compare with human tibia measurements.

REFERENCES

1. ASTM International. Standard Specification and Test Methods for Intramedullary Fixation Devices: F1264-03
2. Lewis D, et al. *Arch Ortho Trauma Surgery* **129**, 817-22, 2009.
3. Klein P, et al. *J Ortho Research* **22**, 1072-78, 2004.
4. Kumar N, et al. *The Anatomical Record* **260**, 189-203, 2000.
5. Cristofolini L, et al. *J Biomech* **33**, 279-88, 2000.

ACKNOWLEDGEMENTS

We thank Nicole Corbiere and Sisi Zeng for helping with specimen preparation.

Table 1: Example of cervine tibia dimensions (in mm) compared to median human dimensions from [5].

Measured Dimensions	LN	AP.PE	AP.PD	AP.MD	AP.DD	AP.DE	ML.PE	ML.PD	ML.MD	ML.DD	ML.DE
Cervine (2.5, M)	312	57.7	45.7	21.6	20.1	28.4	61.6	33	26.7	24.4	38.9
Human	365	57.5	39.8	28	22.5	42.5	79.5	33	21.8	23.5	52.3

COMPRESSION FORCE SUBSTANTIALLY INCREASES THE TIBIOFEMORAL JOINT PASSIVE STIFFNESS AND MOMENT IN SAGITTAL AND FRONTAL PLANES

Hafedh Marouane, Aboulfazl Shirazi-Adl and Malek Adouni

Department of Mechanical Engineering,
École Polytechnique, Montréal, Québec, Canada
email: aboulfazl.shirazi@polymtl.ca

INTRODUCTION

In various activities of daily living, the human knee joint experiences large loads and motions. Recent *in vivo* measurements using instrumented knee implants have reported large compression forces on each tibiofemoral (TF) joint that could exceed 3 times total body-weight during level walking [1]. Experimental investigations of the knee joint, however, have commonly neglected the presence of such physiological compression forces due primarily to associated technical difficulties, joint instability and artifact loads. Similar to spinal intervertebral joints [2], such compression preloads likely substantially increase the passive stiffness and moment resistance of the knee joint in various directions. Nevertheless, musculoskeletal model studies of the knee joint routinely overlook the passive resistance of the joint when attempting to estimate muscle forces [3]. This assumption can markedly influence estimated muscle, contact and ligament forces. This study hence aimed to determine the effect of varying compression force (0-1800 N) on the passive response of the TF joint in both sagittal and frontal planes at different knee flexion angles (0-45^{o}). For this purpose, two validated finite element (FE) models of the tibiofemoral (TF) joint were employed [4]. To avoid artifact loads under compression forces, a novel approach was used in which compression was applied at the mechanical balance point (MBP) of the TF joint identified as a point where no rotations in sagittal and frontal planes are generated.

METHODS

Two validated FE models of the TF joint consisting of two bony structures (tibia and femur) and their compliant articular cartilage layers as well as menisci and four principal ligaments (ACL, PCL, LCL, MCL) are employed [4]. To simulate the transient response, the articular cartilage layers and menisci are simulated as a non-homogeneous nonlinear depth-dependent composite of collagen fibrils and an incompressible matrix. For comparison an equivalent but less refined model with isotropic depth-independent cartilage properties is also used. The TF joint response is studied at four flexion angles; 0 (full extension), 15, 30 and 45^{o} under compression preloads varying from nil to 1800 N (i.e., 3 times body weight of a female subject in our model constructed based on a female cadaver knee). Due to convergence problems, the response under 1800 N compression was obtained only with the less refined model.

To circumvent the artifact moments under compression, initially the MBP position (on the tibia) is determined as a point where a compression force does not generate any frontal and sagittal rotations in the unconstrained joint. This position alters, as expected, with the magnitude of applied compression force and the joint flexion angle. In the current simulations, the femur is fixed while the tibia remains unconstrained. With compression preloads applied at their respective MBP, the joint response is subsequently determined in the sagittal (flexion-extension) and frontal (varus-valgus) planes. The TF instantaneous (tangent) angular stiffness in these planes under various compression preloads is also determined by the perturbation method at the loaded configurations.

RESULTS AND DISCUSSION

Both nonhomogeneous and less-refined homogeneous models yielded similar results. The MBP location shifted medially with the compression force and posteriorly as the joint flexed from the full extension position. Flexion moments carried by the femur at its reference point (ie, mid-distance between epicondylar centers) increased significantly with the compression preload at all joint flexion angles (Fig. 1). The femoral valgus moments also increased with compression preload but were highest at the full extension. The instantaneous (tangent) angular rigidities in both sagittal (Fig. 2) and frontal planes also markedly increased with the compression preload and were highest at near full extension. The TF moment resistance at full extension substantially increased in both varus and valgus rotations as the compression preload increased (Fig. 3). Despite greater moments, forces in collateral ligaments decreased in varus/valgus rotations as the compression increased.

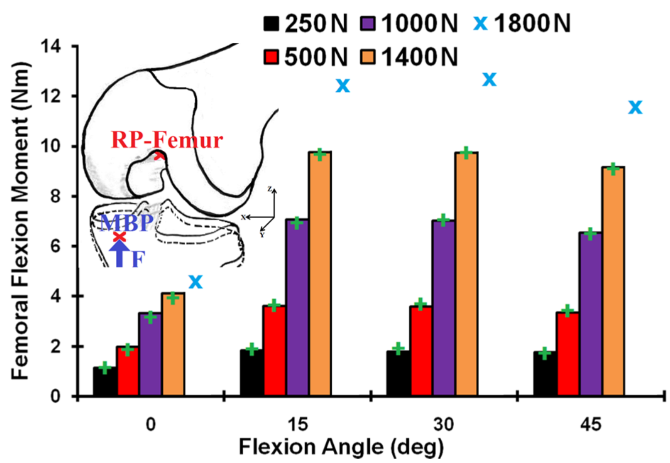

Figure 1: Knee flexion moment at various preloads. Results of less refined model are shown by + and x.

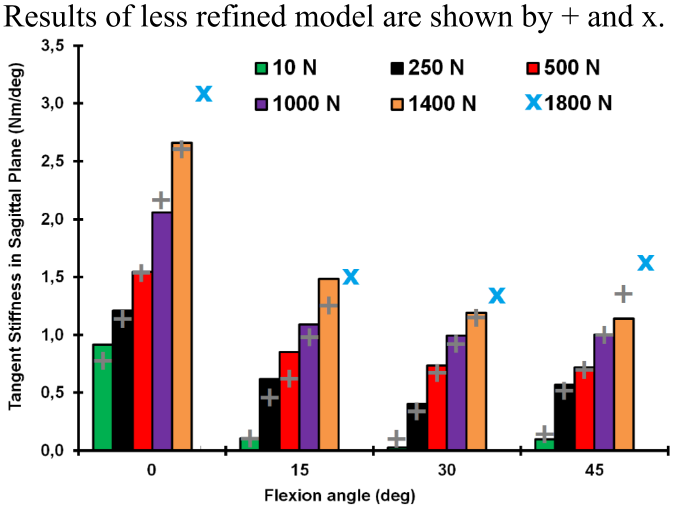

Figure 2: Tangent stiffness in the sagittal plane. Results of less refined model are shown by + and x.

Results under compression forces and moments acting alone or combined were in good agreement with those available in the literature. Determination of the joint MBPs allowed for the first time in the current study the proper application of physiological compression forces without any artifact moments. Under all joint flexion angles, the joint MBP shifted medially with compression thus increasing load transmission via the medial compartment. The compression preload substantially increased TF moment carrying capacity and instantaneous angular stiffness in both sagittal and frontal planes. Despite greater varus-valgus moment resistance, forces in collateral ligaments dropped as the compression force increased suggesting alterations in moment resistance from ligaments to contact forces and the protective role of compression force.

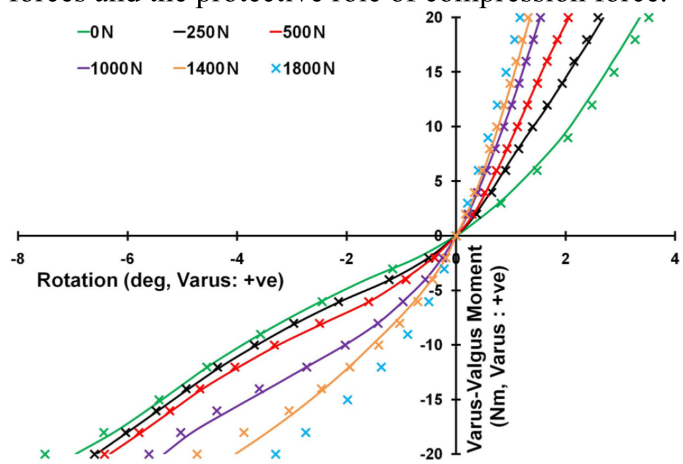

Figure 3: Varus-valgus moments at full extension. Results of less refined model are shown by x.

In conclusion, a novel TF joint MBP is identified at which location a compression force does not cause rotations in sagittal/frontal planes. The compression force substantially increases TF joint moment resistance and angular rigidities in frontal and sagittal planes. While the passive angular stiffness enhances the joint stability, the augmented passive moment resistance under compression preloads plays a role in supporting external moments and should as such be considered in the musculoskeletal models of the joint aiming for an accurate estimation of muscle forces and joint response.

REFERENCES

1. Kutzner et al, *J Biomech* 43:2164, 2010.
2. Shirazi-Adl, *J Biomech* 36 :267, 2006.
3. Kim et al, *J Orthop Res* 27 :1326, 2009.
4. Adouni et al, *J Biomech* 45:2149, 2012.

ACKNOWLEDGEMENTS

Work was supported by the NSERC-Canada and MUTAN-Tunisia.

SECONDARY KINEMATIC PATTERNS OF OSTEOARTHRITIC KNEES DURING ACTIVE EXTENSION AND FLEXION

Greg Freisinger, Jackie Lewis, Matthew Beal, Xueliang Pan, Laura Schmitt, Robert Siston, and Ajit Chaudhari

The Ohio State University, Columbus, OH, USA
email: chaudhari.2@osu.edu, web: http://sportsmedicine.osu.edu

INTRODUCTION

Motion of the healthy knee has been described by a coupled path of ab/adduction, int/external rotation and ant/posterior translation with flexion [1]. Kinematic patterns have been shown to differ between osteoarthritic and healthy knees [2], and it has been hypothesized that this may initiate or increase the rate of cartilage degeneration [3]. These kinematic differences have not been compared between unweighted open-chain knee extension and flexion, and it is unknown to what extent muscles activation influences the secondary knee kinematics. This study investigates seated knee extension and standing knee flexion in subjects with osteoarthritis and varus deformity. We hypothesize there will be differences in secondary knee kinematic patterns and lower extremity muscle activations between these two movements.

METHODS

Twelve subjects (4 males age=60.5±8.0 y, ht=1.77±0.03 m, wt=95.6±14.0 kg, standing varus alignment= 8.7±3.1°; 8 females age=60.5±4.7 y, ht=1.61±0.06 m, wt=87.1±9.1 kg, standing varus alignment=6.2±2.7°) awaiting unilateral total knee arthroplasty provided IRB approved informed consent to participate in this study. Each subject completed four repetitions of unilateral seated knee extension and unilateral standing knee flexion with their involved limb. A modified Point Cluster Technique [4] was used with ten motion capture cameras (MX-F40; Vicon), capturing at a frame rate of 150 Hz, to calculate the three degree of freedom angular motions and anterior-posterior (AP) translation between the tibia and femur. Surface electromyography was recorded at 1500Hz for the vastus medialis, vastus lateralis, rectus femoris, biceps femoris (long head), semitendinosus, medial gastrocnemius and lateral gastrocnemius using a wireless system (Telemyo DTS; Noraxon). Activation of each muscle was high-pass filtered, full wave rectified, smoothed and normalized to the maximum value recorded during standing bilateral calf raise, seated unilateral knee extension, and standing unilateral knee flexion. Normalized data were grouped to calculate overall average activations for the quadriceps (QUAD), hamstrings (HAM), gastrocnemii (GASTR).

The varus/valgus angle (VV), internal/external rotation (IER), AP translation, average muscle activation for the QUAD, HAM, and GASTR were discretized at 5 degree intervals of knee flexion during the concentric portion of the active extension and active flexion movements. These data were fit with a fourth order polynomial and the above variables of interest were evaluated at five knee flexion angles (15, 30, 45, 60, 75 degrees) for the extension and flexion curves.

A mixed model with two within-subjects factors (motion and flexion angle) and random subject effect was used for VV, IER, AP, QUAD, HAM, and GASTR. All two way interactions for fixed effects were included in the model. Holm's multi-comparison procedure was used to account for the tests of the difference between extension and flexion in the six variables of interest.

RESULTS AND DISCUSSION

For IER and AP translation, there was a significant difference between the single leg seated knee extension and standing knee flexion motions (Fig. 2, $P<0.001$). During seated knee extension, there was less internal rotation (mean difference ± SD: 4.2±3.2°) and less anterior translation of the femur (mean difference ± SD: 12.0±8.3 mm) compared to standing knee flexion. There was no significant difference in VV angle between the two activities (P=0.263). All variables were significantly different by flexion angle (P<0.001).

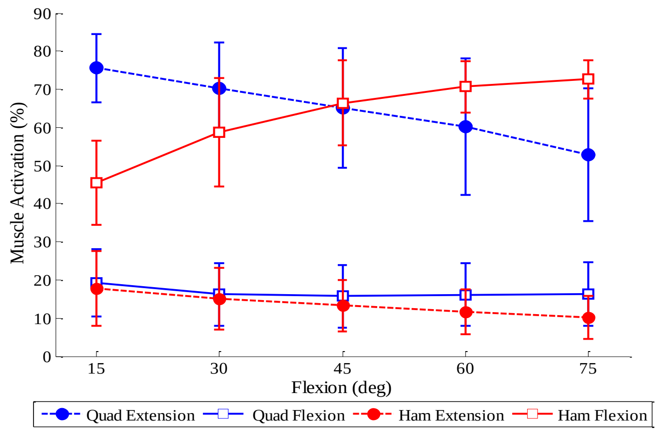

Figure 1: QUAD and HAM activation during extension and flexion.

QUAD, HAM and GASTR activity were also significantly different (Fig. 1, P<0.001) between motions. QUAD was more active in extension (mean difference ± SD: 48.1±15.4%), while HAM and GASTR were more active in flexion (mean difference ± SD: 49.2±9.1%, 13.3±7.6% respectively).

Gravity acts on the tibia differently in these two movements, which most likely causes the observed muscle activation changes. The larger QUAD and smaller HAM activation during seated extension, compared to standing flexion (Fig. 1), may account for the differences in AP translation of the femur. In extension the QUAD are pulling forward on the tibia and in flexion the HAM are pulling posteriorly on the tibia. The change in direction of muscle pull may account for the offset in AP curves seen with flexion (Fig. 2).

CONCLUSIONS

The secondary knee kinematic patterns showed significant differences even when comparing two unweighted, open-chain, single joint motions. These data show the interplay of changing muscle activations and secondary kinematics of the osteoarthritic knee. Future studies should consider the role of muscle activation in cartilage loading for patients with severe osteoarthritis.

REFERENCES

1. Dyrby CO, et al. *J. Orthop. Res.* **22**, 794-800, 2004.
2. Scarvell JM, et al. *J. Arthroplasty*. **22**, 383-393, 2007.
3. Chaudhari AM, et al. *Med Sci Sports Exerc*. **40**, 215-222, 2008.
4. Andriacchi TP et al. *J. Biomechanical Eng*. **120**, 743-749, 1998.

ACKNOWLEDGEMENTS

Funding for this study came from award number R01AR056700 from the National Institute of Arthritis and Musculoskeletal and Skin Diseases.

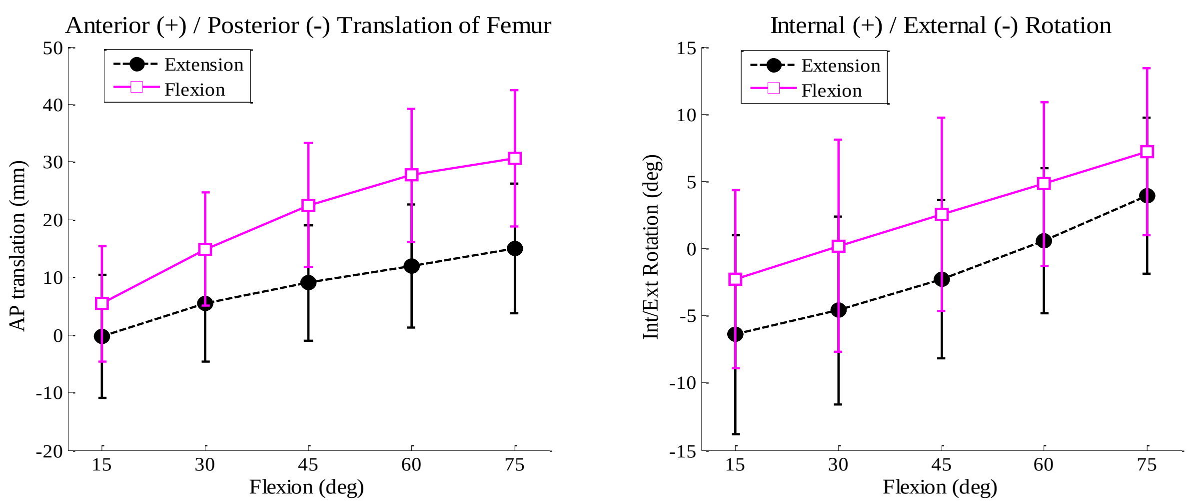

Figure 2: Mean and standard deviation for AP translation and IER for each motion by knee flexion angle.

ESTIMATION OF INDIVIDUAL MUSCLE FORCES DURING SQUATTING AND LUNGING AND THEIR LOAD EFFECT ON THE TIBIAL PLATEAU

[1]Rena Hale, [2]Matthew deBock, and [1]Roger Gonzalez

[1]University of Texas at El Paso, El Paso, TX, USA
[2]Letourneau University, Longview, TX, USA
email: rvgonzalez@utep.edu web:biomechanics.utep.edu

INTRODUCTION

Proper knee stability is essential in performing many isometric or slow knee movements, and even more critical during intense dynamic activities. Considerable interest has been given to knee stability clinically and with non-invasive research techniques such as computational modeling. The model validation process is often performed through *in-vitro* testing, but fixtures do not account for time varying muscle loads [1]. In quazistatic and dynamic tasks knee ligaments play a secondary role to muscles, which are the primary knee stabilizers [2]. We have developed a six degree-of-freedom (DOF) dynamic *in-vitro* knee simulator capable of simulating estimated time-varying muscle forces from multiple muscles. *In-vitro* simulations were conducted in conjunction with the development of a rigid body knee model. Tibiofemoral intersegmental forces due to time-varying muscle loads were measured during *in-vitro* experiments and estimated in computational simulations. Results were compared and quantified for model validation.

METHODS

Squat and lunge kinematics, ground reaction forces, and electromyography (EMG) data were collected from six healthy uninjured 18-21 year old males and females. Muscle activation was processed through an EMG-driven model, which predicted individual muscle force of eight muscles crossing the knee joint [3]. Flexor and extensor muscle forces were predicted during squatting and lunging maneuvers and compared between genders.

A cadaver knee was introduced into our six DOF knee simulator and instrumented with a Tekscan™ pressure sensor on the tibial plateau. During the dynamically loaded cadaver (DL-cadaver) experiments tibiofemoral inter-segmental force was measured at 20°/30°, 55°, and 80° knee flexion while estimated individual muscle forces from a squat and lunge (scaled to 25%) were loaded.

A multi-body dynamics (MD-Adams) knee model was developed from magnetic resonance images (MRI) of the cadaver specimen. Ligaments were modeled as spring and damper elements and force vectors replicated individual muscle forces. Muscle origin points were replicated origin points on the simulator and insertion points were based on the MRI. Hip and ankle points were simulated as rigid points. Joint position and the corresponding output muscle forces from the DL- cadaver experiment from both squatting and lunging trials were simulated on the MD-Adam's model. Tibiofemoral intersegmental forces were then compared between the DL-cadaver experiment and the model.

RESULTS AND DISCUSSION

Research suggests that vasti (vastus medialis and vastus lateralis) forces generate the highest muscle forces during walking [4] and during a sit-to-stand task [5]. Results of this study demonstrated estimated individual muscle forces with similar trends for both males and females during squatting and lunging motion, where vasti muscles generated the highest muscle force. High hamstring forces could be a result of high delay factors or noisy EMG readings. Standardized muscle and model parameters limit the accuracy of the predicted muscle forces.

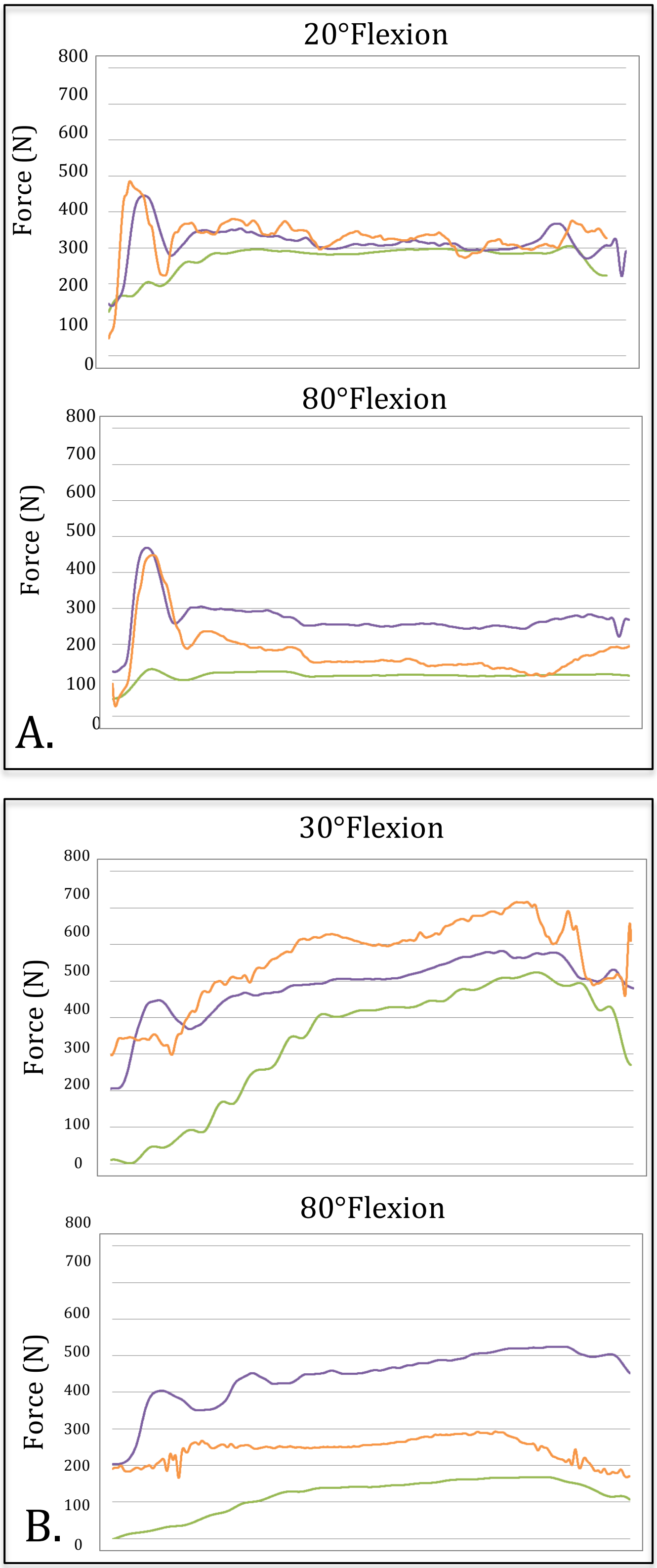

Figure 1 A.) Squatting B.) Lunging. Model verses DL-cadaver experiment under squatting muscle loads. X-axis is time of motion. Pressure senor (Green), Model (Orange), total muscle force (Purple).

DL-cadaver experiments under squatting muscle loads resulted in total applied muscle force of approximately 350 N (squatting), and 500 N (lunging). Forces generated from the simulator were low, but within the 400 N to 1000 N range [6]. Results from the MD-Adams model demonstrated comparable total intersegmental forces due to time-varying muscle force, in magnitude and trend, during both maneuvers (Fig 1).

Lunging simulations generated the most discrepancies at 30° flexion between fixture force loads and model output. However, at this joint angle, the computational model was inherently unstable and disregarded in assessment of validation. Passive force generated from model ligaments were seemingly high and affected the total contact force. Tibiofemoral contact forces due to dynamic muscle force application on the model displayed repeatability amongst squat and lunge data at simulated joint angles.

Future work for this study will include the DL-cadaver experiments simulating time-varying muscle loads during simultaneous joint motion and the further validation of our rigid body model.

CONCLUSIONS

This preliminary study illuminates the effect of estimated muscle forces on the tibial plateau, while developing a knee simulator capable of replicating multiple time-varying muscle loads. DL-cadaver experiments indicate that time-varying loads do affect the tibiofemoral load in a static flexion angle and can be demonstrated computationally and validated *in-vitro*.

REFERENCES

1. Wünschel, M., et al. *Knee surgery, sports traumatology, arthroscopy*. 2012.
2. Winby, R., et al. *Journal of biomech*, ***42***, 2294–300, 2009.
3. Buchann T. et al. *J Biomech* **20**, 367-95, 2004.
4.Sasaki and Neptune. *J Biomech*, **43**, 2780–4, 2010
5.Yoshioka et al. *J Biomech*, **45,** 699–705, 2012
6. Cottrell et al. *J Biomech*, **41**, 2324–2329, 2008.

ACKNOWLEDGEMENTS

This research was supported, in part, by NSF (BES 0966398) and NIH (R01AR046389-0851).

LEG STIFFNESS FROM DOUBLY INTEGRATED GROUD REACTION FORCES DEPEND ON THE INTEGRATION CONSTANT

[1]Kim Hébert-Losier and [1,2] Anders Eriksson

[1] Swedish Winter Sports Research Centre, Department of Health Sciences, Mid Sweden University, Sweden
[2] KTH Mechanics, Royal Institute of Technology, Sweden
E-mail: kim.hebert-losier@miun.se

INTRODUCTION

The efficiency of the stretch-shortening cycle is often expressed in terms of vertical or leg stiffness, defined as the ratio between the ground reaction force (GRF) and the vertical displacement of the centre of mass (CoM) or leg length deformation, respectively [2, 4]. Although vertical and leg stiffness is not synonymous *per se*, the two are equivalent when leg length shortening is estimated from a series of vertical hops [5].

Without registrations of a vertical position during hopping, it is common to compute leg stiffness from the GRF-curve using double integrations to define the vertical displacement of the CoM during ground contact [1]. An indeterminate integration constant must be selected to set the vertical velocity of the CoM at the initial ground contact, here denoted v_0. Although several options are possible to set this constant, those used in clinical sciences are not always verified against mechanical arguments.

Our aim was to contrast the results from leg stiffness measured from the double integration of the GRF-curve of repeated double-legged hops using four different assumptions to define the integration constant, v_0.

METHODS

After ethical approval, forty active men (age: 31 ± 9 yr, height: 182 ± 7 cm, mass: 77 ± 9 kg) provided written informed consent and were tested at a sports research facility. All subjects were in good general health at the time of data collection and none reported a current or recent (< 3 months) injury or medical condition that could limit ones' ability to hop repeatedly on two legs.

Prior to testing, each subject watched a short instructional video that demonstrated the double-legged hopping task. The subject then performed a 5-min cycling warm-up on an ergometer (Monark AB, Sweden) and practiced the task under the examiner's supervision. For data collection, each subject hopped for 15-s using both legs at 2.2 Hz, barefoot, knees straight and hands on hips. All trials were completed on a multi-axial force-plate (Kistler®, CH) that sampled GRF data at 1000 Hz using the Kistler MARS™ Software (S2P Ltd., SI).

Leg stiffness measures were obtained by converting the GRF-curve from each hopping trial to vertical accelerations using the subject's mass and the gravitational acceleration (9.82 $m\cdot s^{-2}$). The acceleration-curve was then doubly integrated to yield velocity and position data based on central difference expressions with velocity data v evaluated halfway between stages for accelerations, a, and positions, p, with a time step $\Delta\tau = 0.001$ s.

The initial position integration constant, p_0, was set stating a zero vertical CoM position at the initial ground contact (i.e. GRF becomes positive). The initial velocity integration constant, v_0, was set in four different ways, here denoted 'P', 'F', 'V' and 'T'. 'P' and 'F' considered data derived from one hop in isolation, whereas 'V' and 'T' considered an individual hop as part of a longer sequence. The assumptions were: 'P', zero CoM position at take-off; 'F', lowest CoM position at the same time as the peak GRF; 'V', landing velocity equal to take-off velocity, but of opposite sign; and 'T', based on an assumed ballistic motion between the preceding and the current ground contacts.

In all cases, stiffness was computed as the ratio between the maximal vertical (upwards) GRF (f_{max})

and the maximal vertical (downwards) CoM displacement ($p_{\max}$) during ground contact, as:

$$k = \frac{f_{\max}}{p_{\max}}$$

After stiffness was calculated from each hop of the 15-s trial, the values were sorted in an ascending order. The mean of the medial 22 stiffness values, representing 10-s of hopping data, was extracted to give a unique k value for each subject and for each choice of v_0.

Descriptive statistics are reported as mean ± SD values. A repeated measures ANOVA was used to determine whether the assumption used to define v_0 influenced the stiffness value, setting the statistical significance level at $P \leq 0.05$. Paired t-tests were used for comparing assumptions in post-hoc testing.

RESULTS

A summary of stiffness computations and between method comparisons is provided in **Fig. 1**. The choice of the integration constant v_0 had a significant impact on individual stiffness values computed, as well as on the mean stiffness obtained from the study cohort ($P < 0.0001$). Using the 'P', 'F', 'V' and 'T' assumptions provided mean values of 33.1 ± 6.7, 36.0 ± 7.9, 36.7 ± 7.5, and 37.2 ± 7.1 kN·m^{-1}, respectively. Post-hoc comparisons revealed that all assumptions provided significantly different results, except in the case of 'V' and 'T' (P = 0.3528)

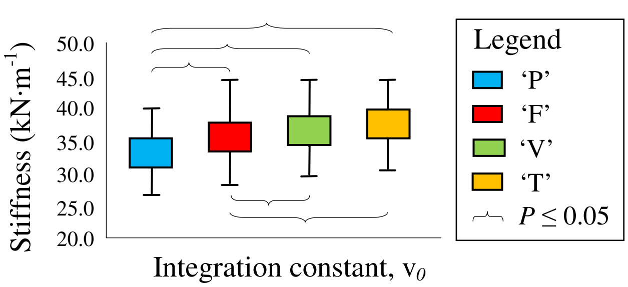

Fig 1. Mean ± SD of stiffness computed from the double integration of the ground reaction force data of 40 subjects performing a double-legged hopping task using four different methods to set the integration constant, v_0.

DISCUSSION

Our findings indicate that the choice of the integration constant for the landing velocity, v_0, can create as much as 10 % difference in the mean leg stiffness computed from doubly integrated GRF data of repeated double-legged hops. In its most simplistic definition, the spring-mass model assumes that during rhythmical hopping, velocities of the CoM at landing and take-off are symmetrical and displacements of the CoM during ground contact are sinusoidal. However, the assumptions of symmetric parameters for take-off and landing are not entirely valid in humanoid bounding gait [3]. Due to asymmetry of hops, all assumptions 'P', 'F', 'V' and 'T' are false to a certain extent, which directly impacts the stiffness values computed. Accordingly, the most reliable and valid computational method for determining the leg stiffness of an individual likely depends on the individualized level of hopping symmetry or asymmetry. Hence, we speculate that the most appropriate computational method to assess stiffness is subject- or group- dependent. In any case, stiffness values computed from double integrations of GRF registrations should always be accompanied by a detailed account of the evaluation method selected and, in particular, the assumption used to determine the velocity integration constant.

REFERENCES

1. Butler RJ, et al. *Clin Biomech* **18**, 511-7, 2003
2. Cavagna GA. *J Appl Physiol*, **39**:174-9, 1975
3. Cavagna GA. *Symmetry*, **2**, 1270-321, 2010
4. McMahon TA, et al. *J Biomech*, **23**, 65-78, 1990
5. Serpell BG, et al. *J Sports Sci,* **30**, 1347-63, 2012

ACKNOWLEDGEMENTS

The authors thank all the volunteers who took part in this study and Professor Hans-Christer Holmberg who supported this project and facilitated research collaboration

HIP EXTERNAL ROTATION STRENGTH IMPACTS LOWER EXTREMITY MECHANICS DURING UNANTICIPATED LANDING ACTIVITIES IN COLLEGIATE FEMALE SOCCER PLAYERS.

[1]Christopher F. Geiser, [1]Claire Wood, [1]Carolyn Meinerz, [2]Krista Watson, and [1]Kristof Kipp

[1]Marquette University, Milwaukee, WI, USA
[2]Augustana College, Rock Island, IL, USA
email: christopher.geiser@marquette.edu, web: http://www.marquette.edu/exercise-science/

INTRODUCTION

Lower extremity injuries have been linked to hip muscle weakness in both cross-sectional studies and theoretical papers [1,2] However, studies on the link between hip muscle strength measures and kinematic variables have been inconclusive or inconsistent [3] In studies examining hip strength and the effect on mechanical variables, participants were generally given preplanned tasks to perform, allowing them time to plan coordinated motions and responses to the tasks [4]. Performing these tasks under unanticipated conditions elicits more high-risk biomechanics than when performed under preplanned conditions [5,6]. The effects of the maximal strength of hip muscles may also be more apparent under unanticipated conditions than pre-planned conditions, as participants have to react in a shorter time frame without the ability to adjust body trajectory to the desired path, and where athletes generally adopt more of a co-contraction strategy in their controlling musculature [7].

METHODS

Twenty-three female D1 soccer players were recruited. Maximal isometric hip abduction and external rotation strength were measured with a standard protocol [4]. Participants then performed three randomly cued tasks: 1) single-leg land, 2) single-leg land and cut, and a single-leg land and forward run. Participants began each task by standing on a box, initiating a forward jump, and landing with their dominant limb on a force plate. Box height and forward jump distance were normalized to each participants' maximum vertical jump height and maximal single-leg stride distance, respectively. The random cue to perform each task was triggered from a switch mat placed on the take-off box.

A 14-camera Vicon motion analysis system was used to collect position data from thigh, shank, and heel marker clusters [4]. Hip, knee, ankle, and foot markers were positioned for a standing trial and used to define joint centers for each lower extremity joint. Motion data were processed with Visual 3D to calculate 3-D knee joint angles and moments [4]. Force plate data were used to determine initial foot contact during each landing.

Measured maximal isometric hip strength values were multiplied by segment length to calculate joint torque, and normalized to body mass. For the movement trials, hip and knee excursion, defined as initial contact angle minus the maximum angle during the landing phase, were calculated for each trial, averaged for each participant, and exported for analysis. Peak hip and knee moments in each plane were also identified during the same phase, averaged across trials, and exported for analysis. Moments reported are internal moments. Left lower extremity values were inverted in the frontal and transverse plane so the signs of all data are presented as right lower extremity data. No differences were found in the landing phase biomechanics between the three tasks, so data from all three tasks were pooled for statistical analysis

The effects of hip strength on landing mechanics were investigated with simple linear regressions. The level of statistical significance was set at $\alpha = 0.05$.

RESULTS

Hip abductor strength did not significantly correlate with any variables. Hip external rotation strength, however, correlated significantly with frontal-plane excursion of the hip into adduction (Figure 1; $R^2 = 0.24$; $p = 0.017$), peak hip external rotation moments in the transverse plane (Figure 2; $R^2 = 0.22$ $p = 0.021$), and with knee internal rotation moments in the transverse plane (Figure 2; $R^2 = 0.17$; $p = 0.048$).

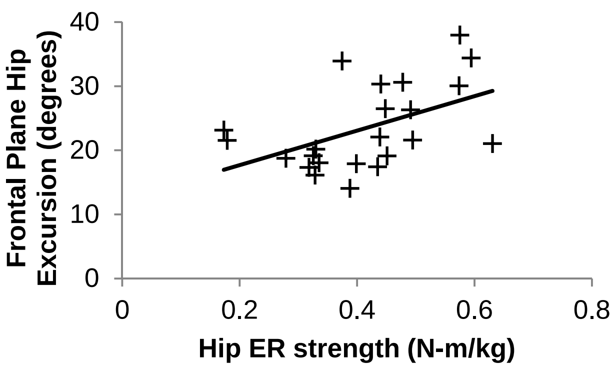

Figure 1: Hip Excursion in the frontal plane (degrees) plotted against measured Hip External Rotation static strength (N-m/kg).

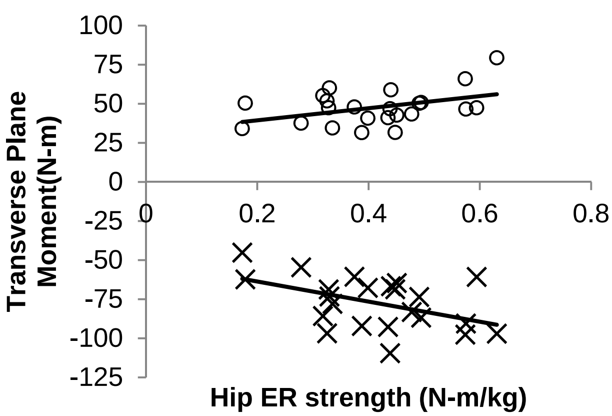

Figure 2: Hip (×) and Knee (○) transverse plane moments (N-m) plotted against measured Hip External Rotation static strength (N-m/kg).

DISCUSSION

Greater isometric hip external rotation strength correlated with a greater hip external rotation moment in women's D1 soccer players. In all participants, the femur was internally rotating after ground contact. The greater external rotator moment in those participants with greater hip strength suggests that those individuals controlled the femoral internal rotation with a stiffer landing strategy in that muscle group.

Further, participants with greater hip external rotator strength had a greater internal knee rotation moment. Oh et al [8] noted that an externally applied internal rotation moment contributed significantly to the loading of the ACL when combined with tibial abduction and axial loading. The participants in this study with greater hip external rotation strength had greater knee moments in the opposite direction, which would suggest that greater hip external rotation strength may ameliorate high-risk knee kinetics during unanticipated single leg landings, and therefore may have a protective effect at the knee.

CONCLUSIONS

The current findings suggest that hip external rotation strength affects the movement and loading of the lower extremity during the landing phase of unanticipated single leg activities. Individuals with greater static hip external rotator strength generated greater transverse plane moments at the hip during landing, possibly to counter deleterious externally applied internal rotation moments of the lower extremity while absorbing forces during impact.

REFERENCES

1. Leetun, et al. *Med Sci Sports Exerc* **36**, 926-934, 2004.
2. Chaudhari&Andriacchi, *J Biomech* **39**, 330-338, 2006.
3. DiMattia et al. *J Sport Rehab* **14**, 108-123, 2005
4. Geiser CF, et al. *Med Sci Sports Exerc* **42**, 535-545, 2010.
5. Sell TC, et al. *Am J Sports Med* **34**, 43-54, 2006.
6. Besier TF, et al. *Med Sci Sports Exerc* **33**, 1176-1181, 2001.
7. Besier TF, et al. *Med Sci Sports Exerc* **35**, 119-127, 2003.
8. Oh, YK, et al. *Am J Sports Med* **40**, 574-583, 2012.

FATIGUE EFFECTS ON INTERSEGMENTAL ACCELERATIONS DURING HIGH-IMPACT LANDINGS: PILOTING PERFORMANCE PREDICTORS

*[1]Steven P. Davidson, [2]Stephen M. Cain, [1]Grant C. Goulet, [2]Noel C. Perkins, [1]Scott G. Mclean
[1]School of Kinesiology and [2]Department of Mechanical Engineering
University of Michigan, Ann Arbor, MI, USA
Human Performance Innovation Laboratory
*E-mail: stevepd@umich.edu

INTRODUCTION

Intersegmental acceleration and velocity profiles help dictate body movement stability and resultant success. This will be particularly true for high-impact movement scenarios where kinematic transmissions across segments return high magnitudes. These large magnitudes increase the likelihood of “noisy” and potentially inaccurate precision movement responses. Degradation in precision will likely be exacerbated with the onset of fatigue, where sub-optimal muscle activation allows for greater mechanical transmission and adaptive/corrective responses up the kinetic chain. As an initial step in elucidating the contributions of intersegmental dynamics to performance, this study aimed to examine the effects of neuromuscular fatigue on segment specific angular velocity and acceleration profiles of a jump-landing task relevant to athletic activity.

METHODS

Subjects

Seven females (21.6 +/- 0.5 yrs.) were recruited to participate in this pilot study. Inertial measurement units (IMUs; Yost Engineering, Portsmouth, OH), containing tri-axial gyroscope and accelerometers, were secured to the dominant foot, shank and thigh, and the trunk (Figure 1). Prior to testing, sensors were time-synchronized via oscillating the dominant lower limb about the hip joint in the frontal plane.

Experimental Design

Subjects performed an initial series of jump-landing tasks to establish baseline pre-fatigue performance. Specifically, they executed six successful trails each of: 1) stationary double-leg front jump to dominant leg stabilization; 2) dominant leg cut-jumps (Figure 1); and 3) 0.6-m high box elevation jumps to dominant leg stabilization.

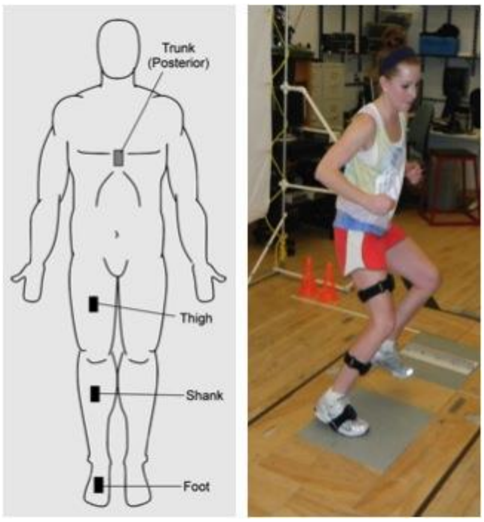

Figure 1. Location of IMU attachment (left), and example movement trial (right).

Subjects performed alternating jump-landing tasks and fatigue exercises until fatigue was reached. The fatigue protocol included three sets of specific exercises, with each set consisting of: 1) ten 0.6-m high box step–ups; 2) 10 double-leg squats; and 3) 20 stationary lunges (10 on each leg). Maximal fatigue was qualified as the inability to consistently perform fatigue exercises with proper athletic form. A single examiner determined when fatigue was achieved, and was denoted by any of the following: 1) inability to perform more than five full double-leg squats with knees flexed to 90-degrees; 2) inability to keep knee from touching the floor during five or more stationary lunges; and/or 3) inability to maintain constant frequency of step-up exercises. After maximal fatigue, subjects repeated the jump-landing tasks to assess post-fatigue performance.

Data Processing

Following testing, raw IMU data were processed within custom Matlab (Mathworks, Inc.) programs to extract segmental peak acceleration and angular velocity magnitudes during each baseline and post-fatigue jump-landing task. Average peak magnitudes were calculated for each jump-landing task from the six successful trials for each subject. After considering results, only data from elevation jump-landings was used in further analysis due to distinct impact peaks and the highest level of landing consistency across subjects. Paired two-tailed t-tests (SPSS Statistics 20) were conducted between baseline and post-fatigue kinematical measures.

RESULTS AND DISCUSSION

Peak resultant angular velocity occurred at initial ground contact and increased significantly post-fatigue for the thigh (25.3%; p=0.003) and trunk (65.8%; p=0.0004) segments compared to baseline. Foot angular velocity similarly peaked at initial contact, trending towards a post-fatigue increase (7.6%; p=0.057) (Figure 2). Peak resultant acceleration was significantly greater post-fatigue for the shank (13.2%; p=0.04) and trunk (35.9%; p=0.015) segments compared to baseline. Peak resultant acceleration again demonstrated an increasing trend post-fatigue for the foot segment (6.6%; p=0.057) (Figure 3).

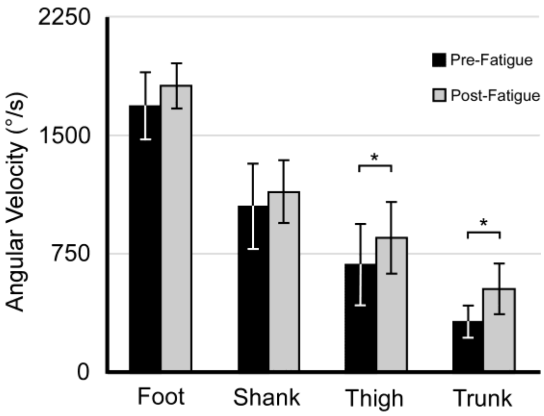

Figure 2. Effects of fatigue on peak resultant angular velocity magnitudes (*denotes p<0.05).

Fatigue increases the prevalence of lower limb overuse injuries such as stress fractures [1,3], due, in part, to the neuromuscular system's decreased ability to attenuate impact-induced accelerations [4]. Current outcomes support this tenet, with increased tibial accelerations being evident post fatigue for our dynamic landing task [2]. Increased kinematic transmission was also observed higher up the kinetic chain (thigh and trunk). Larger peak angular velocity and acceleration magnitudes evident in these segments in the presence of fatigue may directly impact their ability to stabilize and control movements requiring a high-degree of postural precision. This decreased dynamic stability may additional pre-empt additional joint injury scenarios, where passive joint structures must necessarily compensate for a compromised overarching neuromuscular strategy.

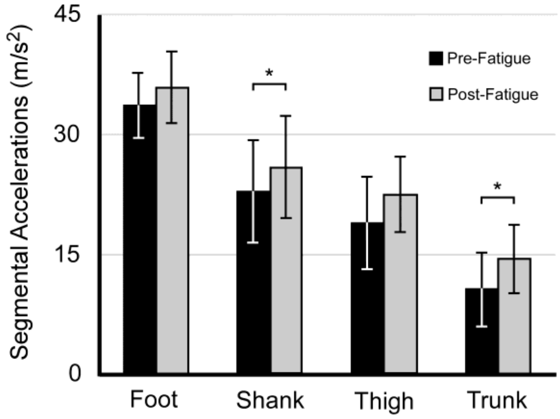

Figure 3. Effects of fatigue on peak resultant acceleration magnitudes (*denotes p<0.05).

The current pilot study, while providing important baseline information, is limited in its ability to identify key mechanical predictors of successful/degraded movement responses. Future efforts will expand on these initial efforts by additionally considering progressive fatigue contributions and assessments of explicit task accuracies with and without fatigue. Further, fatigue and movement tasks will continue to be refined to minimize confounding inter-subject neuromuscular control variations.

CONCLUSIONS

The influence of fatigue on performance is multi-factorial and detrimental to the overall ability to stabilize the body in an efficient manner. The data presented demonstrate increased acceleration and angular velocity transmission higher up the kinetic chain once fatigue sets in. The result of this increased transmission will likely be a decreased capacity to control movement precision, effectively reducing overall movement performance.

REFERENCES

1. Clansey A. et. al., *Med. Sci. Sports Exerc.* **44:** 1917-1923, 2012
2. Duquette A. et. al., *Hum.Movement Sci.* **29:** 567-577, 2010
3. Mizrahi J., et. al. , *Ann. Biomed. Eng.* **28:** 463-469, 2000
4. Mizrahi J., et. al. *Clin. Biomech.* **15:** 15-20, 2000

PROLONGED PRONATION IN RUNNERS WITH ACHILLES TENDINOPATHY

[1]James Becker, [1]Louis Osternig, [2]Stanley James, [3]Robert Wayner and [1]Li-Shan Chou

[1]Motion Analysis Laboratory, Department of Human Physiology, University of Oregon, Eugene OR, 97403
[2]Slocum Center for Orthopedics and Sports Medicine, Eugene OR 97401
[3]Cooperative Performance and Rehabilitation, Eugene, OR 97401
email: jamesb@uoregon.edu, web: http://biomechanics.uoregon.edu/MAL/

INTRODUCTION

Achilles tendinopathy (AT) is one of the most common overuse running injuries, a fact which has not changed in over thirty years of research [1,2]. Frequently cited biomechanical parameters for the development of AT include excessive amounts or velocities of foot pronation [3]. However, while several studies suggest there is a relationship between the amount or velocity of pronation and injuries, an equal number of authors report no such relationship exists [3]. Therefore, an alternative theory regarding the relationship between foot pronation and injury may be warranted

One such theory suggests it may be the duration the foot remains in a pronated position throughout stance, and not necessarily the amount or velocity of pronation, which is more important to consider for injury development [1]. While pronation is desirable early during stance, the foot should start supinating prior to push off, as supination will cause the axes of the transverse tarsal joints to diverge turning the foot into a rigid lever. Prolonging pronation past mid-stance would result in the foot being an inefficient lever during push-off, theoretically requiring greater muscular effort to stabilize the foot and generate sufficient propulsive impulse [1]. However, there are currently no reports in the literature which have examined the duration of pronation in runners with AT.

Therefore the purpose of this study was to compare the duration of pronation in runners currently symptomatic with AT with matched healthy control subjects. It was hypothesized that compared to healthy controls, runners with AT would demonstrate a longer duration of pronation but not excessive amounts or velocities of pronation.

METHODS

Thirteen runners currently symptomatic with AT and 13 healthy control subjects (CON) participated in this study (Table 1). The diagnosis of AT was made by one of the two clinicians participating in the study (SJ or RW). All CON subjects were healthy at the time of testing and had not history of AT. Subjects first underwent a clinical exam measuring 10 variables documenting general lower limb alignment, flexibility, and mobility [1].

Table 1. Subject characteristics. RFS = rearfoot strike. MFS = midfoot strike.

Variable	AT	Control
Sex	9M, 4F	9M 4 F
Weekly mileage	50.1 (± 15.1)	52.3 (± 14.7)
Foot strike pattern	7 RFS, 6 MFS	7 RFS, 6 MFS
Age	37.6 (± 15.9)	32.6 (± 12.4)

After the clinical exam subjects participated in a 3D motion analysis of their running gait. Their whole body motion was recorded by a 10-camera motion capture system (Motion Analysis Corp.) sampling at 200 Hz while they ran continuous laps around a short track in the laboratory. Ground reaction forces were recorded with three force plates (AMTI) sampling at 1000 Hz. Foot strike patterns were characterized as rearfoot strike (RFS) or mid/forefoot strike (M/FFS). Filtered marker trajectories were used to calculate 17 variables describing orientations and movement of the leg segments. Propulsive forces and impulses were calculated from the filtered anterior-posterior ground reaction force curves.

Differences between groups in descriptive characteristics (Table 1) were assessed using independent *t*-tests. Independent *t*-tests were also used to examine differences between AT and CON groups on clinical exam measures. Differences between groups in kinematic and kinetic variables were assessed using a 2X2 ANOVA (injury group x foot strike pattern). This allowed the inclusion of variance due to using different foot strike patterns. Running speed and arch height were included as covariates in the analysis. A binary logistic regression was used to examine the influence of the period of pronation (Per_P) on group assignment.

RESULTS AND DISCUSSION

No differences were observed for any of the descriptive characteristics between groups (Table 1). Compared to CON group, the AT group demonstrated higher standing tibia varus angle, reduced passive dorsiflexion range of motion, and a longer period of pronation (Figure 1).

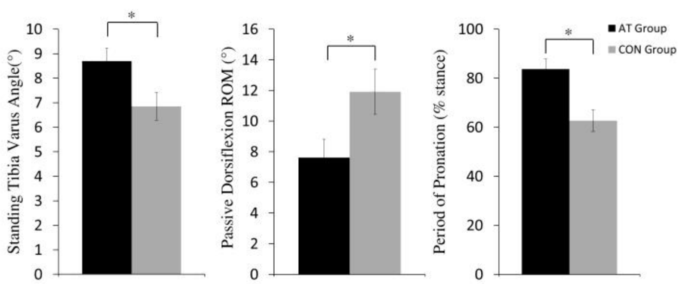

Figure 1. Standing tibia varus angle measured relative to vertical, passive dorsiflexion range of motion, and period of pronation. * indicates $p < .05$.

The time to heel off, peak propulsive force, and propulsive impulse were not different between groups (Figure 2). These results are in agreement with existing results in the literature [4,5] and suggest the overall mechanics of push off are similar between AT and CON subjects.

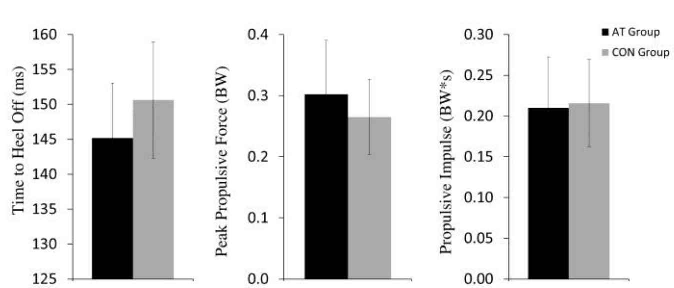

Figure 2. Time to heel off, peak propulsive force, and propulsive impulse for the AT and CON groups. None of these variables were different between groups.

Neither the amount of pronation (AT: 10.5° ± 3.5°; CON: 11.9° ± 2.5°; p = .383) nor the average velocity of pronation (AT: 239.7°/s ± 77.2°/s; CON: 196.8°/s ± 46.7°/s; p = .051) were different between groups.

The logistic regression model suggested each 1% stance increase in Per_P increased the odds of being in the AT group by 1.09 (p = .006). The overall model was significant (χ^2 = 12.36, df = 1, p < .001) and able to classify 80% of the subjects correctly.

CONCLUSIONS

Compared to healthy control subjects, individuals currently symptomatic with AT demonstrate longer periods of pronation. The lack of differences in propulsive forces or impulses between healthy runners and individuals with AT suggests the two groups apply force similarly during the push off. However, while their foot is still pronated, suggesting they are using a less efficient lever. Theoretically, this would result in less efficient force transmission. Therefore, to achieve similar acceleration of their center of mass, AT patients may need more force applied to the foot. Future work should investigate whether runners with AT are in fact producing greater muscular forces during push off. However, the results of this study suggest the duration of pronation is a variable to consider in future studies on AT, as no differences in either the amount or velocity of pronation were observed between injured and healthy subjects.

REFERENCES

1. James, S. et al. *Am J Sports Med.* **6**:40-50, 1978
2. Lopes, A. et al. *Sports Med*. **42**:891-905, 2012.
3. Munteanu, S. et al. *J Foot Ankle Res*. **4**:1-16, 2011.
4. Azevedo et al. *Br J Sports Med*. **43**:288-292, 2009.
5. McCrory et al., *Med Sci Sports Exer.* **31**:1374-1381, 19.

ACKNOWLEDGEMENTS

This study was funded by the Eugene and Clarissa Evonuk Graduate Fellowship, the American Society of Biomechanics Dissertation Grant-in-Aid, and the International Society of Biomechanics Matching Dissertation Grant.

CHANGES IN PASSIVE MUSCLE TENSION AND SARCOMERE LENGTH FOLLOWING STROKE

[1]Liang-Ching Tsai, [1]Shu Q. Liu, [2,3]Yi-Ning Wu, [3,4]Charley Liu, [3]Yupeng Ren, [1,3]Li-Qun Zhang

[1]Northwestern University, Chicago, IL, USA; [2]Brown University, Providence, RI, USA
[3]Rehabilitation Institute of Chicago, IL, USA; [4]University of Colorado, CO, USA
email: l-zhang@northwestern.edu, web: http://smpp.northwestern.edu/research/biodynamics

INTRODUCTION

Changes in muscle tension and sarcomere length play critical roles in regulating muscle cell function and adaptation [1]. Muscle adaptation may be associated with impairments following neurological disorders, such as cerebral palsy [2] and stroke [3]. However, there is a lack of understanding on how neurological disorders may affect muscle tension, how sarcomeres adapt to potential changes in mechanical loading, and the time course of muscle adaptation following neurological disorders. The objective of the study was to investigate *in vivo* changes in the passive tension and sarcomere length of the soleus muscle in a mouse model of ischemic stroke. This investigation provides insights into the mechanisms underlying pathological changes in the neuromuscular system post stroke.

METHODS

This study was approved by the Northwestern University Institutional Animal Care and Use Committee. To induce stroke, the right middle cerebral artery of C57L/6 mice was occluded permanently using suture ligation and bilateral common carotid arteries were ligated for one hour. Mice were tested at day 3 (D3), 10 (D10), and 20 (D20) after surgery (6 mice/group).

A force microscope (Fig. 1) capable of estimating *in vivo* muscle tension (through force and position sensors) and obtaining sarcomere images (using a CCD camera with an objective and tube lens) was used to evaluate the soleus muscle *in vivo*. Briefly, at a selected time point, mice were anesthetized and the tested hindlimb was secured at 0° knee flexion and 0° ankle dorsiflexion. The soleus muscle was exposed and held down at both ends near the muscle-tendon junction. The length, width, and thickness of the isolated soleus muscle were measured before testing. A 0.5mm prism (at the end of the metal tube) of the testing device was placed underneath the soleus muscle. The initial vertical position of the prism was aligned with the muscle so the muscle was not stretched during prism insertion. Starting from this defined initial position, stepwise lifting of the metal tube was performed until the isolated soleus muscle was stretched to 150% of its initial length (a total of 8-10 steps, about 0.3 mm/step). The lifting force, lifting distance, and sarcomere images (Fig. 2) were recorded *in vivo* at each lifting step. After testing, the isolated soleus muscle was removed and the mass of the muscle was measured. Both the impaired limb (left side) and the contralateral limb (right side) were tested.

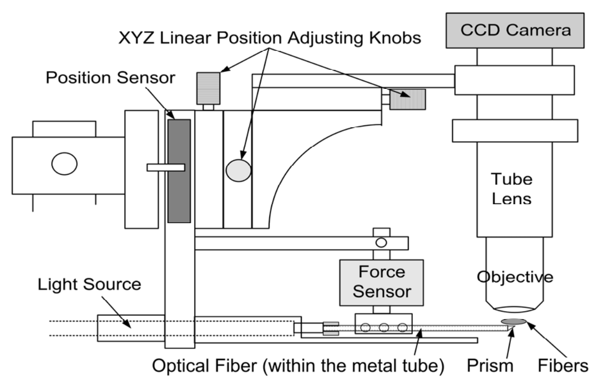

Figure 1: The force microscope used to obtain *in vivo* optic sarcomere images and estimate passive muscle tension simultaneously.

The sarcomere length of the soleus muscle at the initial position (0° knee flexion and 0° dorsiflexion) was measured from the optic images. The passive muscle tension at each lifting step was determined using the recorded lifting force and lifting distance based on force equilibrium equations (Fig. 3). Specifically, the passive muscle tension equals to the lifting force divided by $2\sin(\theta)$, where θ is the angle formed by the muscle and the horizontal line. Given the limitation of this equation on estimating muscle tension at the initial length (when $\theta = 0$, $1/\sin\theta = \infty$), an exponential curve was fitted to the other data points to estimate the muscle passive tension at the initial condition. The estimated passive tension was normalized to the cross sectional area to calculate passive muscle stress.

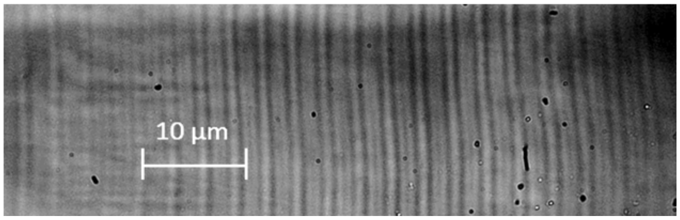

Figure 2: Image of sarcomeres obtained *in vivo* from the mouse soleus muscle.

Variables of interest included initial passive muscle stress, initial sarcomere length, and the density of the tested muscle (based on the mass and volume) for each of the 3 groups. For each variable of interest, the ratio of the impaired limb to the contralateral limb was calculated to minimize the potential influence due to variation across the mice.

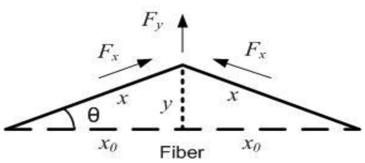

Figure 3: Free body diagram used to estimate the passive muscle tension (F_x) based on the lifting force (F_y) and lifting distance (y). The lifting angle (θ) can be calculated based on the lifting distance (y) and initial muscle length ($2x_0$).

RESULTS AND DISCUSSION

Following stroke, passive muscle stress and the density of the impaired hindlimb decreased in the D3 group, but increased in the D10 and D20 groups when compared to the contralateral hindlimb (Fig. 4). When compared to the contralateral limb, the sarcomere length of the impaired limb showed a trend of slight reduction in the initial flaccid phase (D3) and then increased slightly at D10 (Fig. 4).

Changes in the sarcomere length and mechanical properties of the skeletal muscle have been observed in cerebral palsy [2] but the time history of the *in vivo* fiber tension and sarcomere length following stroke have not been reported. Our findings indicate that, in mice, there were marked changes in the passive muscle stress post stroke, which may affect the subsequent sarcomere adaptation process. The observed changes in the passive muscle stress post stroke may not be explained by differences in the region of the passive length-tension curve where the muscles were tested as similar initial sarcomere lengths were observed between limbs. Instead, the changes in the passive stress may be associated with alterations in muscle composition (e.g., extracellular matrix, collagen accumulation) that may influence muscle density.

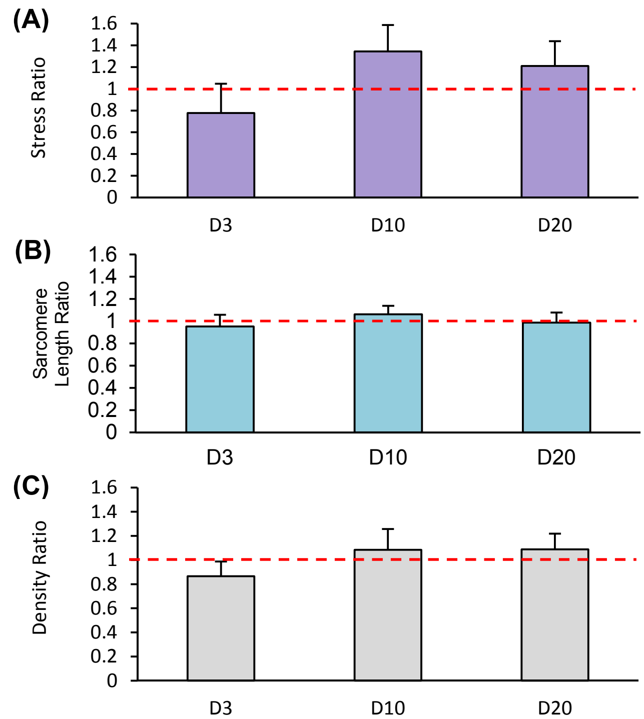

Figure 4: The ratio (impaired/contralateral) of the initial muscle stress (A), initial sarcomere length (B), and muscle density (C).

CONCLUSIONS

Changes in passive muscle fiber tension, sarcomere length, and time history following stroke were investigated *in vivo* using a mouse stroke model. Future studies with a larger sample, longer follow-up time, and histological testing for muscle content may provide a better understanding of the underlying mechanism(s) and process of muscular adaptation following ischemic stroke.

REFERENCES

1. Janmey PA & McCulloch CA. *Annu Rev Biomed Eng* **9**, 1-34, 2007.
2. Smith LR, et al. *J Physiol* **589**, 2625-2639, 2011.
3. Gao F & Zhang LQ. *J Appl Physiol* **105**, 1802-1808, 2008.

ASSOCIATION BETWEEN ILIOTIBIAL BAND SYNDROME STATUS AND RUNNING BIOMECHANICS IN WOMEN

Eric Foch, Jeffrey A. Reinbolt, Songning Zhang, and Clare E. Milner
University of Tennessee, Knoxville, TN, USA
email: efoch@utk.edu

INTRODUCTION

Iliotibial band syndrome (ITBS) is a common overuse running injury. Atypical secondary plane lower-extremity and trunk biomechanics during running are likely to play a role in the etiology of ITBS [1, 2]. Proximal factors such as a large hip adduction angle may increase the tensile strain in the iliotibial band during the stance phase of running [1]. A lack of ability to limit hip adduction may be due to hip abductor muscle weakness [1]. Furthermore, it has been postulated that runners with ITBS exhibit contralateral pelvic drop coupled with trunk lateral flexion away from the stance limb [2]. In this scenario, the whole body center of mass moves away from the stance limb. This would increase the moment arm between the knee joint and resultant ground reaction force. Consequently, a greater external knee adduction moment is produced potentially resulting in greater tensile strain in the iliotibial band [2]. In the transverse plane, the iliotibial band functions to limit knee internal rotation [3]. Excessive knee internal rotation may also increase the strain experienced by the iliotibial band [1]. The aforementioned joint and segment variables provide indirect information about the status of the iliotibial band during running. Musculoskeletal modeling and simulation can complement biomechanical analyses of lower-extremity joint motion to investigate how running pattern affects iliotibial band strain. Therefore, the purpose of this cross-sectional study was to determine if biomechanics during the stance phase of overground running, as well as isometric hip abduction strength differ among female runners with current ITBS, previous ITBS, and controls. It was hypothesized that biomechanics during running would differ among groups in peak: trunk contralateral flexion, contralateral pelvic drop, hip adduction, knee internal rotation, iliotibial band strain, and external knee adduction moment. Second, we hypothesized that hip abduction strength would be less in runners with current ITBS and previous ITBS compared to controls.

METHODS

As part of an ongoing investigation examining biomechanical factors associated with ITBS, 21 female runners between the ages of 18 and 45 were recruited. All procedures were approved by the Institutional Review Board prior to the commencement of the study. All women provided written informed consent prior to participating. Participants comprised three groups: current ITBS (n = 7 ; age: 25.9 ± 8.6 years; height: 1.63 ± 0.04 m; mass: 52.1 ± 3.3 kg; weekly mileage: 22.1 ± 16.9 mi·wk^{-1}), previous ITBS (n = 7 ; age: 25.0 ± 4.7 years; height: 1.67 ± 0.04 m; mass: 63.7 ± 10.4 kg; weekly mileage: 24.4 ± 12.8 mi·wk^{-1}), and controls (n = 7; age: 26.3 ± 7.5 years; height: 1.70 ± 0.04 m; mass: 58.6 ± 6.0 kg; weekly mileage: 28.1 ± 14.6 mi·wk^{-1}). Overground running data were collected using standard three-dimensional motion capture techniques. Passive reflective markers were placed bilaterally on the lower-extremity and trunk. Standard laboratory footwear was worn by participants. Marker trajectories were collected using a 9 camera motion capture system sampling at 120 Hz. Participants ran at a velocity of 3.5 m·s^{-1} ± 0.18 m·s^{-1} over a 17 m runway for 5 acceptable trials. A force plate sampling at 1200 Hz was used to determine the stance phase of the limb of interest. After completing the running trials, isometric hip abduction strength was measured using a hand-held dynamometer [4]. Right hip abductor strength was measured in the controls and previously or currently injured side measured in the ITBS groups. Hip abduction strength was normalized by participant body weight and height [3]. Kinematic data were processed using a joint coordinate systems method. Peak values of the joint and segment variables from five running trials were extracted from the first 60% of stance: trunk lateral flexion, contralateral pelvic drop, hip adduction, knee internal rotation, and external knee adduction moment. Musculoskeletal modeling of the iliotibial band and dynamic simulation of the running trials were performed in OpenSim [5] using a model developed previously [6]. Dependent variables from the running trials were averaged for each participant and group. Data were analyzed using descriptive statistics and one-way analysis of variance. *Post hoc* Fisher's least significant difference test was used to determine where any significant differences existed among dependent variables. Given the preliminary status of the study an alpha level of 0.10 was set for all statistical tests.

RESULTS AND DISCUSSION

Peak hip adduction during running was different among groups (Table 1; P = 0.044). Runners with previous ITBS exhibited deceased hip adduction compared to controls during overground running. Additionally, isometric hip abduction strength (P = 0.095) was different among groups. Hip abduction strength was less in runners with previous ITBS compared to controls. All other dependent variables were similar among groups.

No previous study has compared biomechanics during running and hip abduction strength among female runners with current ITBS, previous ITBS, and controls. Therefore, the purpose of this investigation was to determine if differences exist in secondary plane joint and segment biomechanics, iliotibial band strain, and hip abduction strength among the three groups. However, these preliminary findings do not support our hypotheses. Interestingly, runners with previous ITBS exhibited less hip abduction strength than controls. Hip abductor weakness has been suggested to be associated with increased hip adduction exhibited by runners with ITBS [1, 3]. However, our results indicate the opposite. Peak hip adduction angle was less in runners with previous ITBS compared to controls. Thus, hip abduction strength may not influence hip position during running.

CONCLUSIONS

Our preliminary data indicate that female runners with previous ITBS exhibit decreased peak hip adduction angle and hip abduction strength compared to controls. This suggests that large peak hip adduction angle may not be an etiological factor associated with ITBS.

REFERENCES

1. Noehren B, et al. *Clin Biomech* **22**, 951-956, 2007.
2. Powers C. *J Orthop Sports Phys Ther* **40**, 42-51, 2010.
3. Fredericson M, et al. *J Sci Med Sport* **10**, 169-175, 2000.
4. Ireland ML et al., *J Orthop Sports Phys Ther* **33**, 671-676, 2003.
5. Delp S et al., *IEEE Trans Biomed Eng* **54**, 1940-1950, 2007.
6. Foch E et al., *J Biomech* (in review).

Table 1: Peak biomechanical variables of interest during overground running, and hip strength among runners with current iliotibial band syndrome (ITBS), previous ITBS, and control groups (mean ± standard deviation)

	Current ITBS	Previous ITBS	Controls	*P*-value
Iliotibial Band Strain (%)	1.9 ± 1.2	2.2 ± 0.9	2.3 ± 0.9	0.719
Trunk Ipsilateral Flexion (º)	5.1 ± 1.6	3.8 ± 1.5	3.5 ± 1.8	0.160
Contralateral Pelvic Drop (º)	-6.6 ± 3.2	-3.9 ± 1.7	-5.8 ± 1.7	0.111
Hip Adduction Angle (º)	16.7 ± 2.9	13.8 ± 1.7	17.2 ± 2.8	0.021*
Knee Internal Rotation (º)	4.1 ± 6.5	4.2 ± 7.9	2.4 ± 3.7	0.832
Knee Adduction Moment ($Nm \cdot kg^{-1}$)	0.9 ± 0.2	1.0 ± 4.2	1.2 ± 0.7	0.588
Hip Abduction Strength (% BW*h)	19.7 ± 2.4	14.1 ± 5.6	22.7 ± 0.9	0.036*

* Indicates a significant difference between runners with previous iliotibial band syndrome and controls

SPINE MOTION DURING ACTIVITIES OF DAILY LIVING IN YOUNG ADULTS

[1,2]Scott P. Breloff and [1]Li-Shan Chou

[1]University of Oregon, Eugene, OR, USA
[2]University of Scranton, Scranton, PA, USA
email: scott.breloff@scranton.edu

INTRODUCTION

Various forms of back pain can affect up to 65% of the American population and is one of the top five reasons for missing work or visiting a health professional [1-3]. Despite this, there is no standard treatment method for this ailment [4].

During activities of daily living (ADLs), such as obstacle crossing, stair ascent and stair decent, different trunk or spine peak angles and range of motion (ROM) were reported [5]. However, the methods used to quantify the spine motion lacked the detail necessary to accurately describe the motion of the spine.

Limited biomechanical quantification methods of spine motion, frequency of back pain and the lack of treatment methods are the motivation for this study. Therefore, the purpose of this study was to examine differences in the kinematics of individual spinal segments of young adults when performing different activities of daily living, including level walking, obstacle crossing, stair ascending and stair descending. It was hypothesized that different activities of daily living will exhibit different kinematics at different spinal segments. Specifically, it was thought that normal level walking condition would have the least ranges of motion (ROM) and smallest peak angles when compared to deviations of level waking (obstacle crossing, stair ascent and stair descent).

METHODS

Fourteen healthy young adults (7 males/7 females; mean age: 27.9±5.9 years, mean height: 176.0±27.7 cm, mean mass: 67.8±17.2 kg) were recruited from the university community to participate in the study. All subjects read and signed informed consent approved by the Institutional Review Board.

A total of 65 (static) or 58 (dynamic) markers were placed on the subject. The maker set used in this study was modified from Pruess et al. [6] (Figure 1). Subjects then preformed four different ADL tasks (Figure 2). Kinematic data were captured using a 10-camera motion system at 60Hz (Motion Analysis Corporation, Santa Rosa, CA) and kinetic data were recorded using force platforms at 960Hz (Advanced Mechanical Technologies, Inc., Watertown, MA) in two configurations (Figure 2).

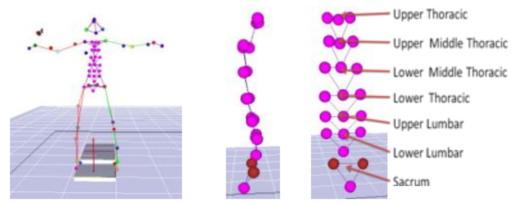

Figure 1: Anterior view of motion capture marker set with enhancements of the spine tracking markers. Sagittal view 2nd and posterior 3rd moving left to right.

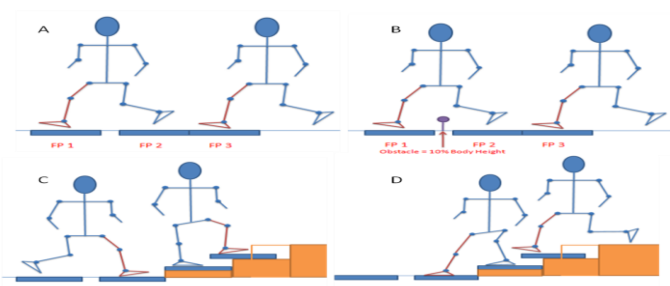

Figure 2. Definition of each task. (A) Level walking (W) – ipsilateral heel strikes, (B) Obstacle Crossing (OC) – Leading limb ipsilateral heel strikes, (C) Stair Ascent (SA) - ipsilateral heel strikes, (D) Stair Descent (SD) - ipsilateral heel strikes.

A MATLAB® (Mathworks, Natick, MA) program was used to calculate three-dimensional angles between each pair of adjoining spinal segments from heel strike (HS) to toe off (TO). Peak angles and ROM were calculated for each for the six angles as follows: Sacrum-to-Low Lumbar (SSL), Lower Lumbar-to-Upper (LLUL) Lumbar, Upper Lumbar-to-Lower Thorax (UPLT), Lower Thorax-to-Middle Lower Thorax (LTMLT), Middle Lower Thorax-to-Middle Upper Thorax (MLTMUT), and

Middle Upper Thorax-to-Upper Thorax (MUTUT). However, only the three most inferior adjacent spine segments (SLL, LLUL & UPLT) were examined in this study as most back pain presents in the low back [2]. A two-way within factor analysis of variance was used to detect the effects of ADL task and spinal level on the peak angles and ranges of motion.

RESULTS AND DISCUSSION

Main effects for the spine level were found for peak flexion angle (p=0.006) [Figure 3], sagittal ROM (p=0.001) [Figure 4a] and ipsilateral bending ROM (p=0.023). Furthermore, main effects on task were observed in the peak flexion angle (p=0.005) and sagittal ROM (p<0.001). Post-hoc pairwise comparisons on spine level marginal means found significant differences in the sagittal ROM (SSL > UPLT and LLUL > UPLT) [Figure 4b], frontal plane ROM (SSL > LLUL) and transverse plane ROM (SSL > UPLT and LLUL > UPLT).

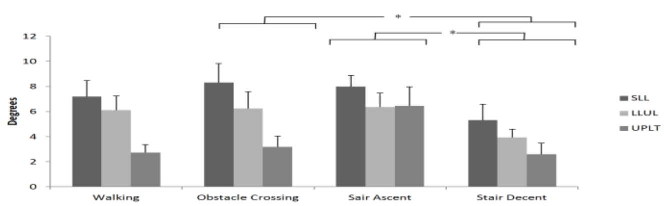

Figure 3: Significant differences between spinal levels with each condition for peak flexion angles in the sagittal plane. *indicates statistically significant change.

Significant interactions for the peak contralateral axial rotation angles (p=0.024) and ROM were detected (p=0.004). However, post-hoc pairwise comparisons of the marginal means (spine level and task) values and individual factor values were not significant.

Finally, specific significant differences were recorded in the UPLT frontal plane of motion where it was observed that the SA task had a greater ROM than the W task. Additionally, the SA task also had more ROM than the SD at the UPLT frontal spine level. In the transverse plane of motion, the SLL spine level presented with significantly larger OC ROM than the SD task.

The present study demonstrated promising results from the examination of detailed spine motion during ADL's. The results exhibited different kinematics (peak angle & ROM) during the ADL's.

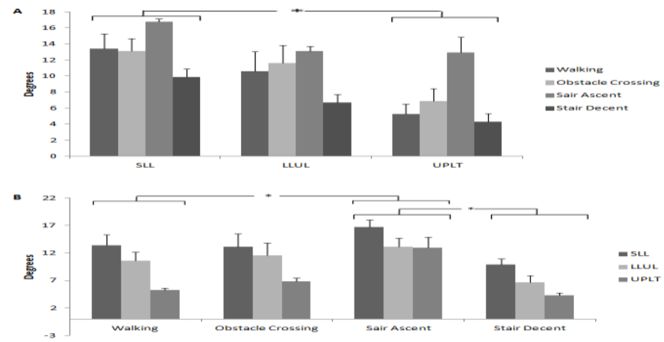

Figure 4: Range of motion in the sagittal plane of motion for various activities of daily living. A) is spine level ROM for each task of daily living. B) is the task specific ROM for all spine levels.

Changes in the sagittal plane might suggest momentum generation in a way to help complete the task or maintain balance depending on the task. Greater ranges of motion in the more distal segments (SLL) than the proximal (LLUL and ULUT) could provide evidence as to why most injuries occur in the low back as opposed to the middle or upper back.

CONCLUSIONS

Overall, this study was able to show how a segmental spine marker set could be an effective tool in determining different motion patterns from various spinal segments during multiple activity of daily living.

REFERENCES

1. Walker, B. F., *J Spinl Disord & Tech* **13**(3), 2000
2. NINDS, *Low Back Pain Fact Sheet*, 2011.
3. Taylor, V.M., et al., *Spine* **19**(11), 1994
4. Bigos, S.J., et al. *US Dept Health & Hum Serv.*, 1994
5. Chou, L.S., et al. *Gait & Posture* **13**(1): 17-26, 2001.
6. Preuss, RA. & Popovic MR. *J. of Electro and Kinesiology* **20**, 823-832, 2010

ACKNOWLEDGEMENTS

This work was funded in part thanks to the Eugene & Clarissa Evnouk Memorial Graduate Fellowship in Stress Physiology.

A DESCRIPTION OF LUMBAR INTERVERTEBRAL CONFIGURATION USING PRINCIPAL COMPONENT-BASED MANIFOLDS

[1]Craig J. Simons, [2]Loren Cobb, and [1]Bradley S. Davidson

[1]University of Denver, Denver, CO, USA
[2]University of Colorado Denver, Denver, CO, USA
email: craig.simons@du.edu

INTRODUCTION

Pathologic mechanisms that cause lumbar spine instability are poorly understood [1], which leads many researchers to answer their hypotheses using musculoskeletal models. Intervertebral kinematics are often modeled as a series of one or more hinge or spherical joints. Although convenient, this approach ignores the complex anatomic constraints provided by the surrounding passive tissues such as the discs, facets, and ligaments. However, these same anatomic complexities inhibit the ability to model their effects on kinematic constraints. An alternative approach to modeling lumbar kinematics is to develop phenomenological constraints for vertebral motion based on *in vivo* kinematic measurements. This approach assumes that intervertebral motion is relatively similar across populations, and can be scaled according to various anthropometric factors.

The objective of this investigation is to examine whether sagittal plane vertebral translation and rotation can be described using anthropometrically scaled ellipsoid manifolds parameterized with principal curves [2]. By accounting for anthropometry, a foundation is established to include subject-specific geometric constraints and apply this approach to individual musculoskeletal models.

METHODS

Magnetic resonance imaging (MRI) data were collected from 10 participants (6 men, 4 women, 30.9±6.5 years old) using a FONAR 0.6-Tesla Upright scanner. Scans were captured in six standing flexion and extension postures (full extension, partial extension, neutral standing, 1/3 flexion, 2/3 flexion, full flexion). Three-dimensional digitized reconstructions were created for each MR scan. Position and angular rotation of each vertebra relative to the sacrum was measured through vertebral body-fixed coordinate systems (Fig. 1).

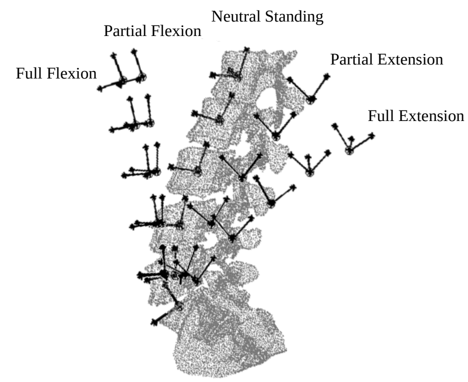

Figure 1: Reconstructed lumbar vertebrae with body-fixed coordinate systems in neutral standing. Body-fixed coordinate systems are shown for flexed and extended postures.

Vertebral position and angular rotation in the sagittal plane were modeled using an implicit function that consists of anthropometric data (height, weight, age) and measured coordinates (*y*, *z*) with linear and quadratic terms.

$$\sum_{i=1}^{m}\sum_{j=1}^{n} A_{ij}\, p_i q_j = 0 \tag{1}$$

where $p = \{1 \quad h \quad w \quad a\}$ and $q = \{y \quad z \quad y^2 \quad yz \quad z^2\}$. The coefficients, A_{ij}, were parameterized using principal component regression. Principal component regression minimizes the perpendicular distance between the implicit function and the y and z coordinates by obtaining the coefficient values from the eigenvectors of the covariance matrices. This procedure was applied to each lumbar vertebra, resulting in a family of ellipsoids that represent the available sagittal configuration of the lumbar vertebra.

RESULTS

The MR scans produced 60 sets of measurement data per vertebra (10 participants, 6 postures each). Measurements from all participants were grouped according to vertebra and principal curves were determined for describing sagittal plane vertebral position (Fig. 2). The curves include anthropometric effects for subject height, weight, and age. Goodness of fit was assessed with coefficients of determination, r^2, for each vertebra. Values ranged from 0.07 for L5 to 0.79 for L1, and were mostly moderately high.

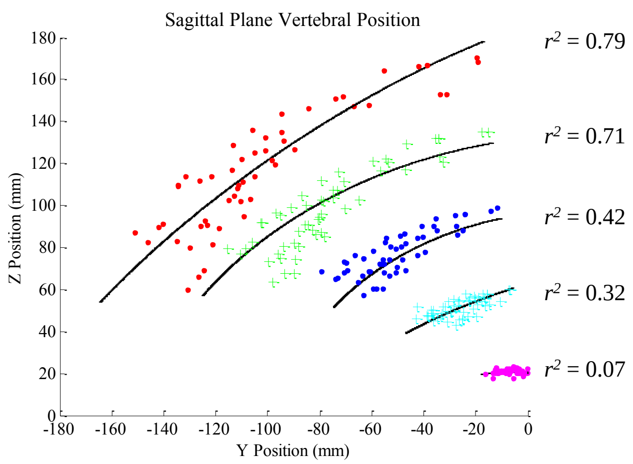

Figure 2: Scatter plot showing sagittal plane vertebral position for all 10 subjects and principal curves for L1 to L5. Measurements are referenced to the sacrum and full extension corresponds to most negative *y*-value.

DISCUSSION

Modeling these positions using geometric manifolds and parameterizing using principal curves provides a novel approach for evaluating intervertebral joint configuration. This approach assumes that lumbar vertebral joint trajectory can be modeled using a family of five ellipsoidal manifolds. This procedure uses physiologically-based constraints with minimal computational complexity and includes participant-specific anthropometry to determine parameterized vertebral position along five unique degrees of freedom for sagittal plane flexion and extension.

When unconstrained, the five lumbar spine vertebrae have 15 degrees of freedom in the sagittal plane, and musculoskeletal models apply constraints to reduce this to as few as a single degree of freedom [3]. Often these are mechanical constraints formulated on standard connections which do not account for the natural vertebral paths, and may not represent key stabilizing features of the lumbar spine such as lumbar lordosis.

By comparison, principal curves require minimal assumptions about the mechanism responsible for kinematics but can describe complex joint motion by incorporating ellipsoidal geometry and inferring a mechanistic outcome through the relationship between all available input data (comprised of subject specific vertebral measurements and anthropometry). Previous geometric model have used regression techniques that lack kinematics-based constraints and have required complex, sequential transformation and regression steps [4], increasing computational load and potential for error propagation. Principal curves provide a modular structure that can be expanded with nominal added complexity to evaluate any contributing factor of interest.

When the kinematic manifolds are created using a statistically representative data set, the model should be able to make accurate, subject-specific predictions. Because the model structure is not limited by simplifying assumptions, we expect that it will be capable of participant -specific predictions with low generalization error.

CONCLUSION

Principal component-based modeling offers unique advantages for predicting and interpreting performance of complex systems such as lumbar joint biomechanics because no assumptions are made regarding the governing mechanisms.

REFERENCES

1. Panjabi MM. *J Electromyogr Kines* **13**, 371-379, 2003
2. Hastie T and Stuetzle W. *J Am Stat Assoc* **84**, 502-516, 1989
3. Christophy M et al. *Biomech Model Mechanobiol* **11**, 19-34, 2012
4. Sicard C and Gagnon M. *Spine* **18**, 646-658, 1993

ACKNOWLEDGEMENTS

Thanks to MRI of America for providing access to the Fonar MR scanner. This work was supported in part by grant R00 AT004983-03 (to BSD) from NIH (NCAAM)

A REFINED TECHNIQUE TO CALCULATE JOINT MOTION HELICAL AXES FROM SIX-DOF TRACKER OUTPUT

[1]Stewart D. McLachlin, [1]Louis M. Ferreira, [1]Cynthia E. Dunning

[1]Western University, London, ON, CANADA
Email: cdunning@uwo.ca

INTRODUCTION

Tracking systems and associated kinematic algorithms are essential tools for understanding joint motion, as well as assessing the effects of pathologies and their related treatments on joint function and stability. One such technique, known as the finite helical axis (FHA) or screw displacement axis, defines the pose of an object in terms of a unique axis vector, coupled with a rotation about and a translation along the axis. With the majority of research in FHAs concerned with optimizing parameters from independent, non-rigid markers [1,2], few guidelines are available for calculating accurate FHAs using pre-packaged six degree-of-freedom (six-DOF) rigid body trackers. The goal of this study was twofold: (1) to present a simple technique to calculate FHA parameters from 6DOF pose information from a rigid body tracker using the screw matrix and (2) to investigate the concept of a "moving window" analysis method designed to maximize the number of accurate FHAs from a given data set.

METHODS

An Optotrak® Certus™ motion capture system was used to track the pose information of four Optotrak® Smart Markers (i.e., rigid body trackers). To determine the effectiveness of the trackers in calculating FHA parameters, a custom jig (CNC machined) that was capable of fixed planar rotations as small as 0.5° about a hinge joint was used. Two markers were connected to the moving portion of the jig, and two more to the fixed portion, at different distances from the true centre of rotation (Figure 1). The two moving trackers (trackers at the top of Figure 1) were positioned approximately 6cm and 10cm away from the hinge axis, respectively.

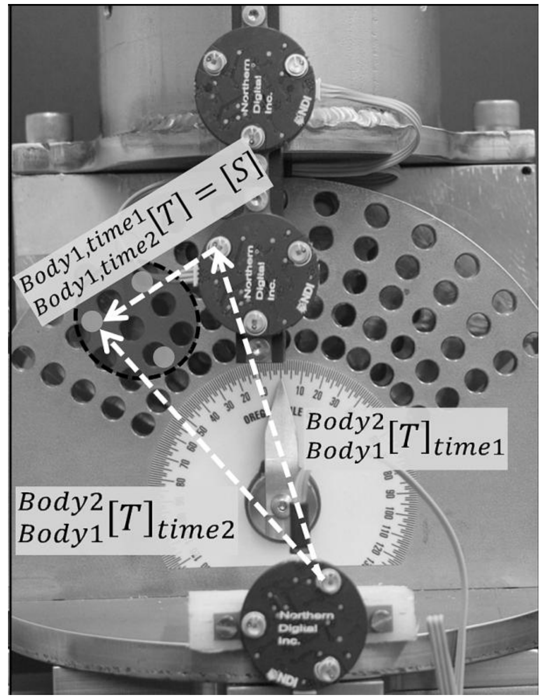

Figure 1: Four Smart Markers were used in this study (one fixed not shown). Transformation [T] matrices of a moving tracker "Body1" with respect to a reference "Body2" (either a fixed tracker or the camera) were determined by the Optotrak® software. The screw [S] matrix was then calculated for varying displacements (i.e., 1→2).

A data set was generated, comprised of six-DOF pose information captured in static 0.5° increments up to 25°. Screw matrices (which consider the moving tracker with respect to itself) were calculated directly from transformation (T) matrix output with respect to both the camera and fixed trackers. FHA output parameters calculated from the screw matrices using a common extraction technique included the rotation about the FHA, the direction cosines of the FHA, and the intercept of the plane normal to the hinge axis [3]. Data were initially evaluated as displacement from the neutral 0° position (*i.e.*, 0-0.5°, 0-1°, etc.). Subsequent evaluation explored the concept of a "moving window" analysis. With the understanding that FHA calculations are error-prone for small rotations, this technique defined a minimum rotation that needed to be achieved before the calculated FHA was considered acceptable. For example, with this data set, if the minimum rotation were set to 5°, the FHA between 0-5° would be the first accepted. The starting point would then be incremented to the next row of data, such that the next FHA generated in this case would be for 0.5-5.5°. The effect of window size was evaluated for minimum rotations of 0-10°, where a 0° window size would calculate FHAs between adjacent time points regardless of the rotation between them.

RESULTS AND DISCUSSION

Rotations calculated about the FHA were within 0.15° of the prescribed jig rotation. The most stable (*i.e.*, smallest standard deviation) FHA intercept was determined from the T matrices of the moving relative to the fixed trackers closest to the hinge axis. Moving window analysis improved the center of rotation and direction cosine precision (as evidenced by a decrease in the standard deviation of the measurement) with increasing minimum rotation size (Table 1). Smaller window sizes (<2°) had large intercept scatter, but as the window size was increased, the standard deviation of the intercept decreased to less than 1 mm for a minimum rotation of 2° or larger. There was a limited benefit to intercept scatter with window sizes greater than 5°, suggesting that a window size of 2-5° or higher would be appropriate for most biomechanical investigations.

For applications where the total range of motion is less than 2°, the current data suggests it would be challenging to recommend the FHA as a suitable technique, except for calculating an average FHA only. Furthermore, positioning trackers closer to the center of rotation, for both the moving and fixed trackers, improved the intercept stability, which agrees with previous investigations [1].

The topic of filtering was not included in this investigation, as the focus of this work was evaluating the FHA parameters generated from native tracker output. The hinge motion of the jig is also likely not representative of most biomechanics studies, yet for the preliminary evaluation of the moving window technique, it provided a reliable and stable axis of rotation.

CONCLUSIONS

This work presented a simple but effective starting point for researchers looking to readily calculate FHAs from rigid body trackers. Furthermore, the accuracy of the FHA parameters produced showed improvement with moving window analysis based on a minimum rotation of 2-5°.

REFERENCES

1.Metzger MF, *et al.*, *J Biomech* **43**, 2822-29, 2010.
2.Woltring H, *et al.*, *J Biomech* **18**, 379-89, 1985.
3.Spoor CS, *et al.*, *J Biomech* **13**, 391-393, 1980.

ACKNOWLEDGEMENTS

Funding assistance provided by the Natural Sciences and Engineering Research Council of Canada and the Joint Motion Program – A CIHR training program in Musculoskeletal Health Research & Leadership.

Table 1: Window Size Effect on Average *X-Y* Intercept and the Direction Cosines

Moving Window Size (°)	FHAs Created	Average *X* Intercept (mm)	Average *Y* Intercept (mm)	Average *X* Direction Cosine	Average *Y* Direction Cosine	Average *Z* Direction Cosine
0	50	20.2 ± 8.4	63.3 ± 7.9	0.019 ± 0.365	-0.005 ± 0.279	-0.895 ± 0.076
1	48	20.4 ± 1.6	65.0 ± 1.8	0.008 ± 0.130	0.000 ± 0.082	-0.987 ± 0.014
2	46	20.6 ± 0.9	65.5 ± 0.9	0.018 ± 0.088	-0.005 ± 0.052	-0.994 ± 0.006
3	44	20.4 ± 0.7	65.7 ± 0.5	0.029 ± 0.055	-0.005 ± 0.043	-0.997 ± 0.003
4	43	20.5 ± 0.5	65.8 ± 0.5	0.027 ± 0.045	-0.008 ± 0.034	-0.998 ± 0.002
5	40	20.5 ± 0.4	65.8 ± 0.4	0.028 ± 0.037	-0.005 ± 0.026	-0.999 ± 0.001

STRESS DISTRIBUTION FORMULATION IN A LINEAR VISCOELASTIC BIO-MATERIAL

Yun Peng and Debao Zhou

University of Minnesota, Duluth, MN, USA
Email: peng0234@d.umn.edu and dzhou@d.umn.edu

INTRODUCTION

In this paper, we present the formulation of the stress distribution within a viscoelastic material subjected to distributed pressure on the free surface. In the formulation, the stress tensor at any point in the material is obtained with two steps: in the first step, the elastic-viscoelastic correspondence principle is applied to obtain the stress solution for viscoelastic materials under a point load. In the second step, the obtained solutions from first step are integrated over the stress-applying area. Based on the formulation, the tress tensor at any point in the material is calculated numerically. This formulation can be used to simulate many practical contacting problems; one important example is the biomaterial cutting operations where a blade interacts with a biomaterial. In cutting, the effect of slicing angle on the stress distribution is an important factor to be included in the discussion. The slicing angle is determined by the magnitudes of tangential and normal components of the cutting force. Using the calculated principal stresses, it is possible to predict the location of damage using failure criterion such as Von-Mise criterion or Tresca's criterion. The results can serve as guidelines for several applications where the stress distribution and fracture prediction in viscoelastic materials are concerned.

METHODS

Contacting problems are frequently encountered in many situations. For example, in the design of a surgical simulator involving a scalpel, it is necessary to know the dynamic contacting force applied to the edge of the scalpel, in order to provide a vivid feeling of real surgeries. Such a force, once the stress distribution is known, can be calculated by integrating the stresses on the surface over the contacting area. In order to better understand a dynamic surgical process, it is also necessary to know the stress distribution in the material when the location of fracture initiation is a concern. To realize this, the blade-biomaterial contact problem is simplified as the model shown in Figure 1, where the tangential and normal force components are applied over a rectangular area on the surface of the half-plane. In Figure 1, the *o-xyz* is a frame fixed on the half-plane; $A(x, y, z)$ is a point in the material with coordinate x, y, z; $A'(x, y, 0)$ and $B(\zeta, \eta, 0)$ are two points on the surface; the distance from B to A' is r and from B to A is R; The normal and tangential components of the applied distribution force are p_n and p_t, respectively; and the angle between p_n and the resultant pressure is α, which is defined as slicing angle in this paper.

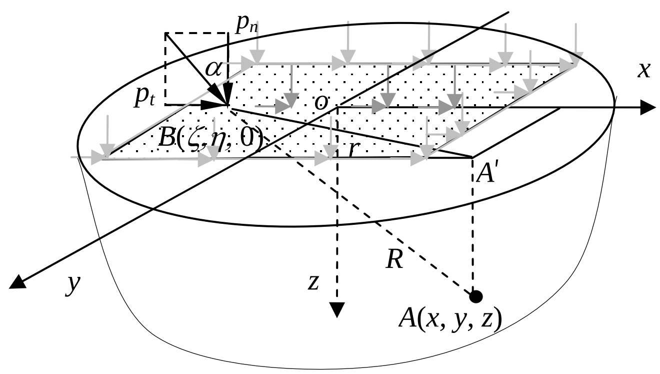

Figure 1: Simplified contacting model.

The material is approximated to be homogeneous and isotropic according to [1]. Under linear viscoelastic assumption, we directly derived the solutions for viscoelastic half-space subjected to point tangential and normal load by applying the elastic-viscoelastic correspondence principle. To obtain the solutions under uniform distributed pressure and tangential force, the surface integration is performed using the scheme in Figure1 over the rectangular region $S(-a<\xi<a, \ -b<\eta<b)$, which represents the contacting area. The results are given

in the form of stress tensor: $[\boldsymbol{\sigma}]_{3x3}=\{[\sigma_{xx}\ \sigma_{yx}\ \sigma_{zx}];\ [\sigma_{xy}\ \sigma_{yy}\ \sigma_{zy}];\ [\sigma_{xz}\ \sigma_{yz}\ \sigma_{zz}]\}$. The solutions to the stress distribution for any given point in the viscoelastic half-space subjected to uniform pressure are shown in the equation below. For simplicity, only the first component σ_{xx} in the stress tensor $[\boldsymbol{\sigma}]_{3x3}$ under normal pressure is presented. Noted is that there is another stress tensor $[\boldsymbol{\sigma}]_{3x3}$ under tangential pressure which is also not shown here due to page limit.

$$\sigma_{xx}=\frac{1}{2\pi}\left\{\left[\iint_S \frac{3(x-\xi)^2 z}{R^5}d\xi d\eta\right]P_n(t)\right.$$
$$\left.+\left[\iint_S\left(\frac{(x-\xi)^2-(y-\eta)^2}{Rr^2(R+z)}+\frac{(y-\eta)^2 z}{R^3r^2}\right)d\xi d\eta\right]\int_0^t p_n(\tau)V(t-\tau)d\tau\right\}$$

where $R=\sqrt{(x-\xi)^2+(y-\eta)^2+z^2}=\sqrt{r^2+z^2}$.

The applied distributed force is modeled using a cosine function. In the simulation in this paper, $p_n(t)=p_t(t)=a_1+a_2\cos\left[\pi(t-1)\right]$ with the unit of *kPa* and a_1=a_2=1. $V(t)$ describes the linear viscoelastic property and is derived from another two viscoelastic material properties: shear and bulk relaxations functions, which are modeled using exponential functions. In deriving its time-domain expression, the elastic-viscoelastic correspondence principle is applied, with Laplace and Inverse Laplace transform performed to its elastic counterpart: 1-2υ, where υ is the Poisson's ratio. Its time-domain form is $V(t)=m_1\delta(t)+n_1e^{-t/\tau}$ with m_1= 2, n_1=0.8, τ = 0.4s. $\delta(t)$ is the Dirac delta function.

RESULTS AND DISCUSSION

Based on these formulations and data, the stress for any given point inside the half-space can be both analytically and numerically calculated. Contour maps for each stress component can be plotted for any plane that we are interested, such as plane *xoz*, which is parallel to the direction of tangential forces, or plane *yoz*, which is perpendicular to the tangential forces. Knowing the stress tensor $[\boldsymbol{\sigma}]_{3x3}$, we are able to obtain the principal stress and predict the failure using criteria such as Von-Mise yield criterion, which requires the calculation of second deviatoric stress invariant, or Tresca's criterion, which requires the calculation of maximum shear stress. Previous research [2] has concluded that the maximum shear stress was the dominant reason in material failure, so we want to know the distribution of the maximum shear stress and to apply Tresca's criterion. The obtained the maximum shear stress distribution at peak external force with cutting angle equal to 45° is shown in Figure 2. Failure will happen at points where the Tresca stress exceeds the maximum shear strength according to Tresca's criterion.

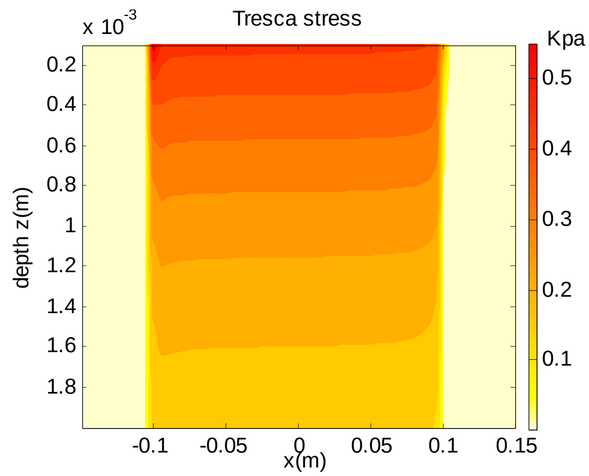

Figure 2: Plot of the Tresca stress in plane *xoz* at peak external force.

CONCLUSION

In this paper we derived the solution of viscoelastic half-space subjected to dynamic combined surface loading. The dynamic stress distribution can be used to design a surgical simulator with a scalpel involved. The solution we developed can help trainees view the stress map due to each movement during an operation. It is also feasible to predict the location of potential damage if the failure data is available.

REFERENCES

1. Umalea S., Decka C., Bourdeta N., Dhumaneb P., Solerb L., Marescauxb J. and Willingera R, *Journal of the Mechanical Behavior of Biomedical Materials* **17**, 22-33, 2013.
2. Zhou D. and McMurray G., *Modelling and Simulation in Engineering,* **2011,** 1-17.

Effects of Distal Biceps Rupture on Supination Strength

[1,3]Brown BT, [2]Schmidt CC, [1,3]Miller, Mark Carl

[1]University of Pittsburgh, Pittsburgh, PA, USA
[2]University of Pittsburgh Medical Center, Pittsburgh, PA, USA
[3]Allegheny General Hospital, Pittsburgh, PA, USA
email: brb102@pitt.edu

INTRODUCTION

Advocates for the non-operative treatment of distal biceps ruptures emphasize the limited functional loss.[1] Isometric supination strength loss of 26% - 40% has been reported in a neutral forearm position[1,2] and supination strength loss after biceps tendon reconstruction differs with forearm position.[7] Biomechanical studies have also demonstrated that the native biceps moment arm changes significantly with forearm position.[3-5] The purpose of this study was to quantify the effects of a complete distal biceps rupture. We hypothesized that supination strength loss would be significant, vary with forearm position, and be independent of arm dominance. Furthermore, strength loss would positively correlate with time from injury and negatively correlate with pain and disability.

METHODS

Individuals with complete avulsion of the distal biceps tendon were recruited to participate. Inclusion criteria consisted of individuals presenting in clinic seeking repair of the ruptured tendon and no other upper extremity injury. Subjects performed isometric supination strength testing using a custom-made torque-measuring device (Figure 1) and a previously published protocol.[6] Peak torque was recorded for each arm at three forearm positions; 60° of supination, (0°) neutral and 60° of pronation.

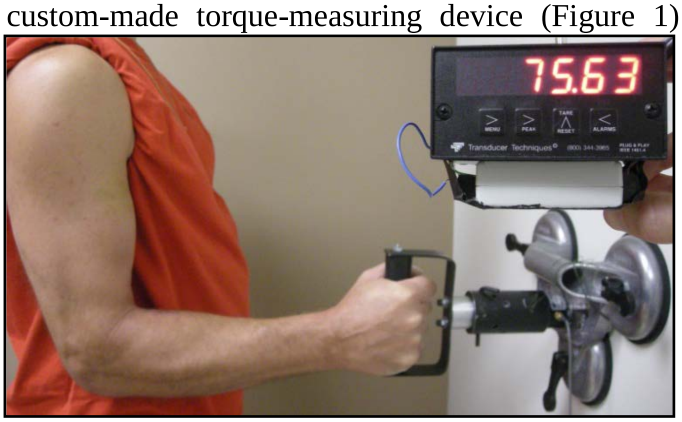

Figure 1: Isometric supination strength testing device. Industrial strength suction cups rigidly adhere the device to the wall and a torsional load cell records output of torque.

Supination strength loss was expressed as the ratio of the injured side to the contralateral side. Pain was assessed using a numeric visual analog pain scale (VAPS), ranging from 0-10 and functional outcomes were measured using the DASH questionnaire. Strength data were compared as a function of arm dominance, test angle, and biceps injury using a 3-way ANOVA, while relationships to strength were analyzed using linear regression (significance set at $p=0.05$). Outliers in the data were found by calculating the Mahalanobis distance, a metric gauging similarity in the dataset, accounting for Euclidean distance and correlations.[8]

RESULTS

Twenty three adult males with an average age of 49 ± 10 years suffered a complete distal biceps avulsion. There were 12 dominant and 11 non-dominant arm injuries. One individual was detected as an outlier, as his injury to evaluation was 10,951 days. The Mahalanobis distance for this data point was 4.58 where the threshold for the data set was 2.64. This data point was not used in the subsequent analyses, but will be discussed later as a relevant single case.

The average time of injury to evaluation was 25 days, ranging from 4 to 71 days. The supination strength loss was significant compared to the uninjured side (Figure 2): 59% in supination ($p<0.001$), 60% in neutral ($p<0.001$), and 52% in pronation ($p<0.001$). The strength values also showed the uninjured arm was significantly stronger in 60° of pronation and neutral compared to 60° of supination ($p<0.001$ and $p= 0.012$ respectively). The injured arm was also stronger in 60° of pronation compared to 60° of supination ($p= 0.043$).

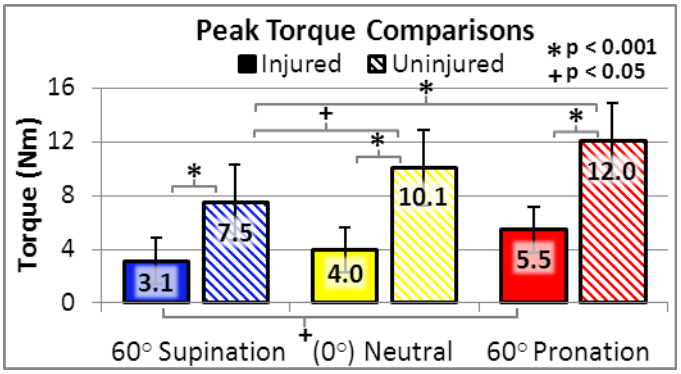

Figure 2: Supination torque values for all subjects; the data is divided into injured and uninjured arms regardless of arm dominance and highlights significant findings.

Analysis detected no differences in supination strength loss between the 3 forearm test positions ($p=0.094$) (Figure 3). Analysis revealed that arm dominance had no effect on strength loss ($p=0.76$). Strength loss, at any test angle, did not relate to the time from injury to evaluation ($p > 0.65$), VAPS score ($p > 0.06$), or DASH assessment ($p > 0.22$). The average VAPS score was 5 ± 2 and DASH score was 40 ± 21. Furthermore, time from injury did not correlate to the VAPS score ($p=0.10$) or to the DASH ($p=0.17$). The VAPS and DASH assessments positively correlated ($p=0.004$).

The outlying case with a lengthy time from injury to evaluation of 10,951 days (30 years), showed full recovery of strength in the pronated position (115%), partial recovery in neutral (72%), and less recovery in the supinated position (61%). (Figure 3)

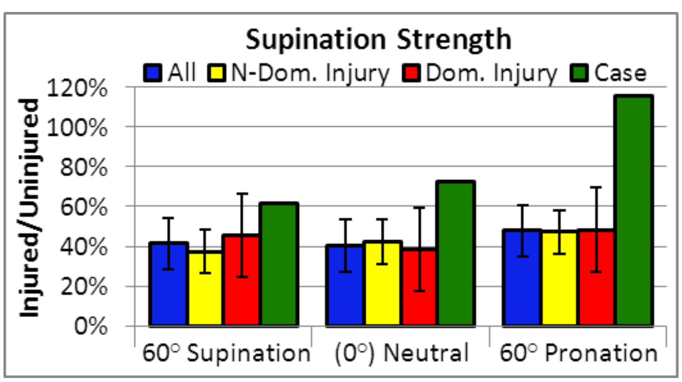

Figure 3: Injured limb is compared to the non-injured limb and expressed as percent loss. The data is further broken down to show strength loss involving non-dominant and dominant injuries. A single case of a distal biceps rupture 30 years from injury is also displayed.

DISCUSSION

The study shows that an individual loses 52% to 60% of their supination strength following distal biceps rupture. Pairing the literature on conservative treatment[1,2] with the current data involving no treatment demonstrates that significant deficits occur without surgical repair. Surgical intervention has been shown to restore biceps strength to 90% of normal.[6]

Supination strength loss was significant regardless of forearm position hinting at a dynamic interaction in the contribution of force between supinator muscles in the forearm. Forearm position showed variation in the amount of torque an individual could apply, even in the biceps deficient arm. This finding may be due to the co-contraction of the brachioradialis muscle, which acts as a supinator of the pronated forearm and then switches function to act as a pronator in the supinated forearm.

Reported disability and pain associated with the injury were not indicative of reduced strength, hinting that true weakness is independent of perception. Similarly, strength loss was not dependent on the time from injury to the evaluation. This suggests there is no immediate ability for the body to compensate for biceps rupture. The single case of an individual with a chronic biceps injury suggests that strength can be recovered at certain forearm positions. Long term data is needed to truly determine if supination strength, pain, and disability can improve without an attached distal biceps. We speculate that supination strength from pronation to neutral can improve as one strengthens the brachioradialis, but that strength deficits from neutral to supination will be difficult to overcome.

REFERENCES

1. Freeman C.R. *J Bone & Joint Surg.* 91, 2329-34, 2009
2. Morrey *J Bone & Joint Surg.*418-421, 1985
3. Bremer A.K. *Clin. Biomech.*21, 683-91, 2006
4. Murray W.M. *J Biomech.*28, 513-25, 1995
5. Schmidt CC *J Should. & Elbow Surg.*19, 1157-65, 2010
6. Schmidt CC *J Should. & Elbow Surg.*21, 1623-31, 2012
7. Hudak P.L. *Am. Ind. Med.*29, 602-8, 2002
8. Mahalanobis P.C. *J Nat. Inst. Sci. Ind.*1, 49-55, 1936

Age-related changes to shoulder musculature in a vervet monkey model

[1,2]Anthony C Santago II, [1]Johannes F Plate, [1]Thomas L. Smith, [1,2]Katherine Saul

[1]Wake Forest School of Medicine, Winston-Salem, NC
[2]Virginia Tech – Wake Forest School for Biomedical Engineering and Sciences, Winston-Salem, NC
email: asantag@wakehealth.edu website: http://www.sbes.vt.edu/kholzbau/MoBL

INTRODUCTION

Age-related changes to muscle tissue are well documented and include losses of mass and force as well as slowed shortening velocity [1]. In the upper limb, aging is also associated with reduced strength [2], rotator cuff tears, and arthritic changes. Characterizing the pathophysiology and progression of age-related changes to the upper extremity would help advance orthopaedic treatments to retain and improve function. An animal model of aging in the upper extremity would allow for longitudinal studies of musculoskeletal degradation that are difficult or expensive to perform in a human population. Additionally, animals are housed in a well-regulated environment, are more homogenous, and are easier to control than humans [3].

Non-human primates may be superior to other large animal models because their anatomical shoulder structure and functional use of the arm are more similar to those of humans [4]. Previous work in elderly vervet monkeys (*Chlorocebus pygerythrus*) demonstrated degenerative changes of the glenoid and more retroversion similar to changes observed in an older adult human population [5]. Additionally, the supraspinatus demonstrated decreased muscle fiber cross-sectional area which is consistent with aging humans. [5]. However, age-related changes in muscle architecture have not been studied in vervet monkeys. Therefore, the purpose of this pilot study was to quantify age-related changes to the rotator cuff and deltoid muscle architecture in a group of vervet monkeys.

METHODS

The right upper limb of two middle aged vervets, MA1 and MA2, (11.6 and 9.3 years; approximately 44 and 35 human years, respectively) and two older adult vervets, OA1 and OA2 (21.3 and 25.6 years; approximately 80 and 96 human years, respectively) were obtained from a previously-studied population of vervets [5]. Each limb was thawed, skinned, and fixed in 10% phosphate buffered formalin for 24 hours in a neutral shoulder and wrist posture with 90° of elbow flexion. The limb was then removed from formalin and placed in a 70% ethanol solution for a minimum of 24 hours to preserve the fixation and remove any excess formalin. The four rotator cuff muscles (supraspinatus, infraspinatus, subscapularis, teres minor) and the deltoid were dissected from the shoulder. Muscle belly length was measured using calipers from the most proximal end of the muscle fibers to the most distal end of the muscle fibers. Muscle volume was measured by placing the muscles in ethanol and measuring the displacement. Care was taken to remove all fascia and tendinous structures prior to volume and mass measurements. Infraspinatus, subscapularis, and deltoid were divided into subsections for mass, volume, and length measurements according to previous descriptions of muscle architecture [6]. For the muscles with multiple subsections, total volume was determined by adding the volume of the subsections, and average muscle belly length was calculated as the mean of the lengths of each subsection. A representative cross-sectional area of each muscle was determined by dividing volume by muscle belly length [7]. To determine muscle volume distribution, the volume fraction of the rotator cuff muscles and deltoid were calculated as a percentage of the total rotator cuff volume.

RESULTS AND DISCUSSION

The total mass of the rotator cuff muscles in the middle aged vervets, MA1 and MA2, was 42.24 and 32.10 grams, respectively; by comparison, the total rotator cuff mass of the older adult vervets, OA1 and OA2, was lower, at 30.89 and 26.92 grams, respectively. No evidence of rotator cuff tears was found during dissection for any of the vervet upper extremities, consistent with a previous study of the contralateral shoulders of these same animals [5].

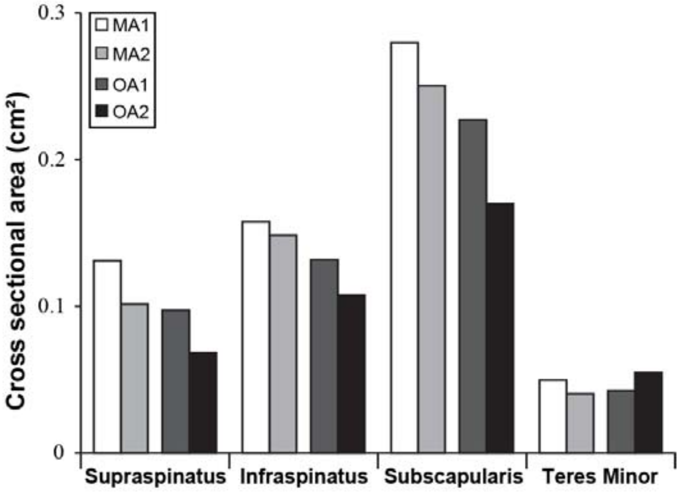

Figure 1: Cross-sectional area of rotator cuff muscles. The middle aged vervets had a larger cross-sectional area than the older adult vervets in the supraspinatus, infraspinatus and subscapularis.

With the exception of teres minor, the rotator cuff muscles of the older adult vervets had a smaller average cross-sectional area (Figure 1). Cross-sectional area is correlated with strength in human subjects and decreases with increasing age [10]. The observed reduced mass and cross-section in the older vervets warrants confirmation in a larger cohort of vervets.

Although our data set is small, our preliminary findings indicated similar muscle volume distributions in both middle-aged and old vervets (Figure 2). These findings are consistent with human data that demonstrated no difference in rotator cuff muscle volume distribution between young adult and older adult humans [2, 7]. However, the supraspinatus volume fraction is smaller in humans than in this vervet group. Additionally, the deltoid volume fraction is larger in humans than in this vervet group. The supraspinatus acts a dynamic stablizer in both humans and vervets [9], while the deltoid, an abductor, can contribute to superior translation of the humeral head and increase load on the supraspinatus [8]. Therefore, the relatively smaller deltoid and larger supraspinatus in these vervets may be associated with reduced loads on the supraspinatus muscle-tendon unit, which could explain the lack of rotator cuff tears seen in these vervets.

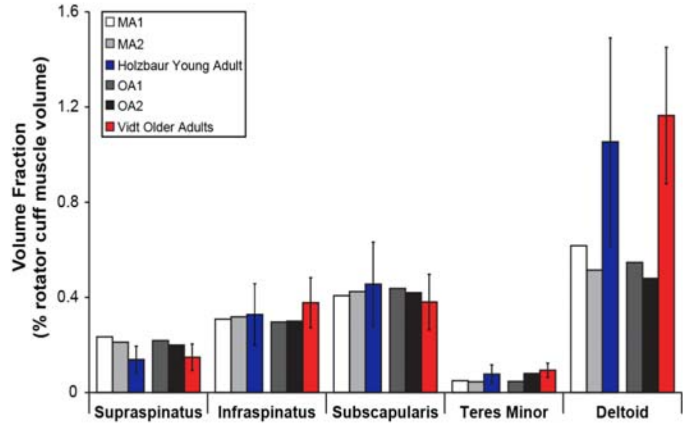

Figure 2: Volume fractions of the rotator cuff muscles and deltoid. Volume fractions of the supraspinatus and deltoid are smaller and larger, respectively, in humans than in the vervet subjects.

CONCLUSIONS

Our pilot data indicate that rotator cuff and deltoid muscles in vervet monkeys have reduced mass and cross-sectional area with increasing age. Additionally, our preliminary data did not provide evidence that the distribution of muscle mass in the rotator cuff and deltoid muscles change with age, which is consistent with aging in the human shoulder. However, the relative size differences between the supraspinatus and deltoid in humans and vervets may limit the vervet as a model to study rotator cuff tears. Future work will evaluate these and other structural parameters (such as optimal fiber length and PCSA) in a larger cohort of vervet monkeys, and will include analysis of the biceps, triceps, coracobrachialis, and teres major muscles.

REFERENCES

1. Choi S, et al. *J Gerontol A Biol Sci Med Sci*, **68**, 258-67, 2013.
2. Vidt M, et al. *J Biomech*, **45**, 334-41, 2012.
3. Lui PP, et al. *Scan J Med Sci Sports*, **21**, 3-17, 2011
4. Mannava S and Plate J, et al. *KSSTA*, doi:10.1007/s00167-012-2145-9.
5. Plate J, et al. *J Shoulder Elbow Surg*, doi: 10.1016/j.jse.2012.11.004.
6. Langenderfer J, et al. *Clin Biom*, **19**, 664-70, 2004.
7. Holzbaur K, et al. *J Biomech*, **40**, 742-49, 2007.
8. Potau J, et al. *Int J Primatol*, **30**, 697-708, 2009.
9. Larson S and Stern J, *Am J Phys Anthropol*, **79**, 369-77, 1989.
10. Hakkinen A and Hakkinen K. *Eur J Appl Physiol*, **62**, 410-14, 1991.

SCALING AND ARCHITECTURAL SIMILARITY OF COMMON MODELS OF THE HUMAN ROTATOR CUFF

[1]Margie Mathewson, [1]Alan Kwan, [2]Carolyn Eng, [1,3]Richard Lieber, and [1]Samuel Ward

[1]University of California, San Diego, San Diego, CA, USA
[2]Harvard University, Cambridge, MA, USA
[3]Department of Veterans Affairs Medical Center, San Diego, San Diego, CA, USA
email: srward@ucsd.edu, web: muscle@ucsd.edu

INTRODUCTION

Rotator cuff tears, especially in the supraspinatus muscle, are one of the most common causes of pain and disability in the upper extremity [1]. When attempting to model rotator cuff injury and repair, animal models are often used. However, questions remain regarding the relevance of the various animal models to humans due to differences in their basic anatomy, muscle architecture and functional use patterns [2]. Scaling of muscle architectural properties among different species is important for understanding how anatomy changes with animal size and locomotor style, but while general scaling information is available for some lower limb muscles, scaling data specific to the rotator cuff have not been published. Therefore, our aims were to: 1) compare the architecture of each of the four rotator cuff muscles among humans and ten species commonly used in rotator cuff research to determine the best animal model for the human rotator cuff, and 2) determine how rotator cuff muscle architecture scales with body size across species.

METHODS

Ten animals used in rotator cuff research were studied: mouse (n=3), rat (n=3), rabbit (n=3), dog (n=3), mini-pig (n=4), sheep (n=1), goat (n=1), cow (n=1), chimpanzee (n=1), and capuchin monkey (n=3), varying in size from less than 30 grams (mice) to nearly 600 kilograms (cow). Human data used for comparison were previously reported [1]. Shoulders were harvested and formalin fixed, and the supraspinatus (Sup), infraspinatus (I), teres minor (TM), and subscapularis (Sub) were removed. Muscle mass, muscle length (L_m), fiber length (L_f), pennation angle, and sarcomere length (L_s) were measured from fixed muscle, and moment arms (MA) were calculated from MRI images of shoulders prior to dissection. PCSA was calculated using the following equation:

$$PCSA = \frac{M \cdot \cos\theta}{\rho \cdot L_{fn}}$$

To compare architectural similarity between studied species and humans, the architectural difference index (ADI) was calculated using fiber length to muscle length ratio, fiber length to moment arm ratio, and PCSA percent [3]. A generalized least squares function, which accounted for phylogenetic similarity [4] (Fig. 1), was used in R [5] to calculate scaling relationships between $\log_{10}$ transformed body mass and muscle mass, fiber length, and PCSA.

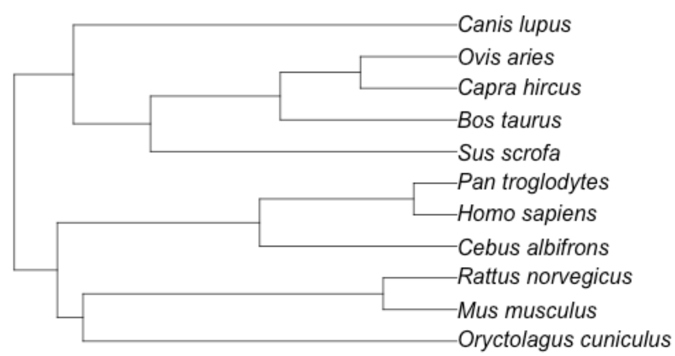

Figure 1: Phylogenetic tree for species of interest (*ovis aries* = sheep, *capra hircus* = goat, *bos taurus* = cow, *sus scrofa* = pig, *pan troglodytes* = chimp, *homo sapien* = human, *rattus norvegicus* = rat, *mus musculus* = mouse, *oryctolagus cuniculus* = rabbit; closely related canis lupus used in place of dog, and cebus albifrons used for capuchin monkey).

RESULTS AND DISCUSSION

As expected, there was variation among species for all architectural properties measured. To compare among species, normalized parameters were used. The percent of total rotator cuff PCSA contributed by each muscle was different among ungulates (sheep, goat, pig, cow), which were infraspinatus dominant, and other bipeds and quadrupeds, which were subscapularis dominant (Fig. 2).

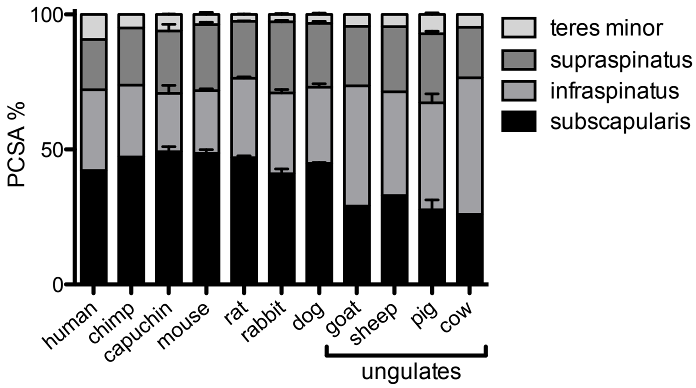

Figure 2: Percent contribution of each muscle to total rotator cuff PCSA.

When total ADI for all muscles was calculated, chimpanzees and capuchins were closest to humans, followed by small rodents (Fig. 3). Sheep showed the greatest calculated architectural difference from humans, with an ADI more than three times that of the chimpanzee.

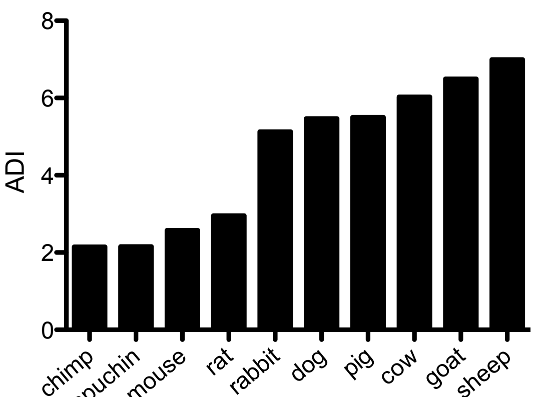

Figure 3: Combined ADI for all rotator cuff muscles. A perfect architectural match is an ADI of zero, so low values indicate greater similarity (human ADI=0).

Based on regression slopes and confidence intervals, geometric scaling was found for PCSA, muscle mass, and fiber length with respect to animal mass. Humans deviated from geometric scaling more than other species studied, but human exclusion or inclusion did not change the overall scaling relationships.

CONCLUSIONS

Animal models are crucial to further our understanding of human disease. Our results can be used to select the appropriate animal model for rotator cuff muscle studies. Geometric scaling was confirmed for all muscles and all parameters considered. These data demonstrate that, in terms of multiple measures of muscle design such as relative PCSA and mass, as well as L_f/L_m and L_f/MA ratios, primates and rodents are more relevant to humans compared to larger quadrupeds.

REFERENCES

1. Ward SR, et al. *CORR* **448**, 157-163, 2006.
2. Brand R. *CORR* **466**, 531-542, 2008.
3. Lieber RL, et al. *J Biomech* **25**, 557-560, 1992.
4. dos Reis M, et al. *Proc R Soc B: Bio Sci* **279**, 3491-3500, 2012.
5. R Core Team. *R: A Language and Environment for Statistical Computing*, 2012.

ACKNOWLEDGEMENTS

Thanks to H. Hoekstra, J. Chupasko, and M. Omura from the Harvard University Museum of Comparative Zoology for access to the chimpanzee shoulder, and to C.F. Ross at the University of Chicago for capuchin shoulders. This work was supported by NIH grant HD050837 and an NSF Graduate Student Research Fellowship.

Table 1: Phylogenetically adjusted regression exponents and coefficients of the scaling equation $y=aM^b$ for muscle mass, L_{fn} and PCSA relative to body mass. Values are mean ± SEM.

	Muscle Mass			PCSA			L_{fn}		
Muscle	**b**	**a**	**95% CI**	**b**	**a**	**95% CI**	**b**	**a**	**95% CI**
Supraspinatus	0.999±0.119	-2.665±0.498	0.730-1.268	0.635±0.125	-1.771±0.522	0.353-0.916	0.351±0.025	0.109±0.106	0.294-0.408
Infraspinatus	1.058±0.100	-2.880±0.418	0.832-1.284	0.713±0.104	-1.947±0.437	0.477-0.949	0.333±0.039	0.051±0.162	0.245-0.421
Teres Minor	1.049±0.089	-3.882±0.371	0.849-1.249	0.725±0.074	-2.842±0.310	0.557-0.892	0.317±0.052	-0.055±0.218	0.200-0.435
Subscapularis	0.953±0.109	-2.508±0.456	0.707-1.199	0.593±0.117	-1.377±0.492	0.328-0.859	0.355±0.040	-0.163±0.168	0.264-0.446

THREE-DIMENSIONAL COMPARISON OF STATIC AND DYNAMIC SCAPULAR MOTION TRACKING TECHNIQUES

Kathleen F. E. MacLean[1], Jaclyn N. Chopp[1], Tej-Jaskirat Grewal[1], Bryan R. Picco[1], Clark R. Dickerson[1]

[1]Department of Kinesiology, University of Waterloo, Waterloo, ON
email: k4maclea@uwaterloo.ca

INTRODUCTION

The shoulder is a complex joint comprised of many moving parts [1]. Accurately measuring shoulder rhythm is difficult, but imperative due to the shoulders susceptibility to numerous chronic and acute injuries. To identify pathological movement and risk for injury, clinicians typically assess shoulder motion dynamically through observation of humeral raising and lowering phases. However, static measures of shoulder rhythm are the preferred method of analysis and are often reported in shoulder rhythm descriptions [2]. Whether these two methods of scapular tracking identify the same shoulder rhythm is unknown. Clinicians and upper limb researchers would benefit from knowing whether dynamic measures of shoulder rhythm are useful and comparable indicators of static scapular positioning. The purpose of this paper was to determine how closely dynamic measures of scapular tracking represent static measures in a healthy population.

METHODS

Data for the present study were taken from two studies previously conducted at the University of Waterloo DIESEL lab using the same group of participants. Five shoulder angles were assessed for 24 participants ((13 M, 11 F; age 23+/- 2.47 years; weight 70+/-15.22 kg; height 174.25+/-10.66 cm) – scapulothoracic protraction/retraction, medial/lateral rotation and tilt, and sternoclavicular protraction/retraction and elevation/depression. Participants were monitored using dynamic and static tracking techniques during humeral elevation in three planes (frontal, scapular and sagittal). The static protocol instructed participants to elevate their arm to 0°, 45°, 90°, 120°, and 180° in each of the three planes. The dynamic protocol instructed participants to raise and lower their arm in the same three planes through 120° of elevation to the timing of a metronome. Elevation angles in the dynamic conditions were measured and recorded at 5° increments from 10° to 120°. Eight Vicon MX20+ cameras (Vicon Motion Systems, Oxford, UK) recorded the three-dimensional positions of reflective skin markers overlying upper extremity anatomical landmarks. Data reduction was performed in custom MATLAB 7.9.0 R2009b software. To compare between static and dynamic results, regression equation lines of best fit were generated for all static conditions for each participant. These equations were used to predict static measures that corresponded with each of the recorded dynamic elevation angles. Mean differences were determined between each of the tracking techniques – lowering-static, raising-static, and lowering-raising. ANOVAs were used to identify the influences of plane, elevation angle, and tracking technique (static, dynamic raising, dynamic lowering) on the between-technique differences.

RESULTS AND DISCUSSION

Mean differences existed across all techniques. These mean differences existed for all shoulder angles ($p<0.001$), except for elevation plane in scapulothoracic protraction/retraction ($p=0.955$).

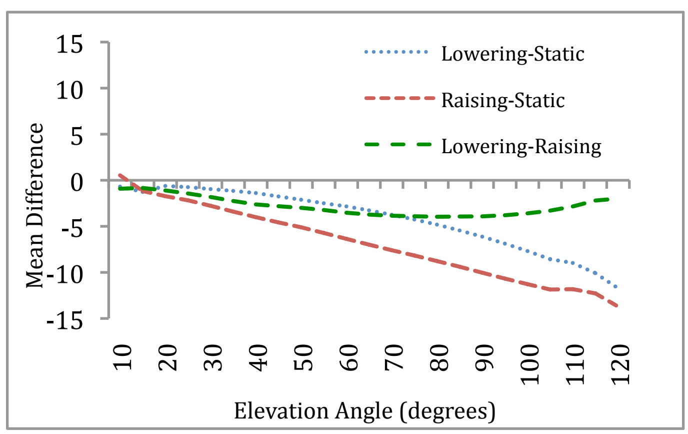

Figure 1: Mean differences between the three tracking techniques for the shoulder angle of Scapulothoracic Tilt.

Tracking techniques were influential ($p<0.001$), but the grouped mean differences fell below a relevant intra-individual variability benchmark of 5° [3], making them comparable to static measures. While mean differences remained small, the standard deviations were comparatively very large for all shoulder angles in the lowering-static and dynamic-static mean differences (Table 1). There was large variation in mean differences of the techniques across individuals.

Mean differences were most pronounced at higher humeral elevation angles, particularly in scapulothoracic tilt (Figure 1). It is hypothesized that the greater mean differences at higher elevation angles contributed to the large standard deviation noted in Table 1. Dynamic measures may under-estimate static measures, particularly at higher humeral elevations, such as above 90 degrees, as demonstrated by the negative mean differences in tracking methods (Figure 1 and Table 1). It has been demonstrated in previous research that dynamic scapular tracking techniques become increasing unreliable and harder to interpret at humeral elevation angles above 100° [4]. The lack of re-palpation in dynamic measures of shoulder angle could increase errors in this technique. This factor may be responsible for the differences found betweens static and dynamic measures at higher elevation angles. Both dynamic motion phases produced similar shoulder angles and thus had a small mean difference for all five shoulder angles (Table 1 Lowering-Raising), which was expected based on previous results.

Intra-individual differences were also large and may have contributed to the standard deviation in Table 1, but were mitigated by the group means. Previous work has demonstrated large intra-individual differences [5]. While perhaps not a concern for group analyses, intra-individual differences between static and dynamic measures have the potential to be quite large. This places further caution on the use and interpretation of dynamic measures in place of static measures, as the intra-individual differences are unpredictable and potentially large enough to skew data results and conclusions. However, both static and dynamic results are in agreement with previous research, demonstrating that both methods can represent a reliable representation of shoulder rhythm.

CONCLUSIONS

While population averages are similar, individual static and dynamic shoulder assessments may be different. Caution should be taken when dynamic shoulder assessments are performed on individuals, as the observed shoulder rhythm may not reflect that found in the more highly documented and thus preferred static shoulder rhythm assessment. Current dynamic approaches may require modification or repetition to identify pathological shoulder rhythm as robustly as the preferred static measures.

REFERENCES

1. Inman VT et al. (1944). *The Journal of Bone and Joint Surgery*. 26: 1-30.
2. Cutti, AG & Veeger HEJ (2009). *Medical and Biological Engineering and Computing*, 47, 463–466.
3. Tate AR et al. (2009). *Journal of Athletic Training*, 44(2), 165-73.
4. Van Andel C et al. (2009). *Gait & Posture*, 29, 123-28.
5. Grewal TJ & Dickerson CR (2013). *Journal of Biomechanics*, 46(3), 608-11.

Table 1: Mean differences and standard deviation (SD) in degrees, between the three levels of technique. Comparisons are made between dynamic lowering and static (Lowering-Static), dynamic raising and static (Raising-Static) and both phases of dynamic motion (Lowering-Raising).

Shoulder Angle	Lowering-Static (SD)	Raising-Static (SD)	Lowering-Raising (SD)
ST Protraction/Retraction	-4.98 (17.59)	-3.71 (17.42)	1.35 (3.38)
ST Med/Lateral Rotation	-1.02 (14.47)	0.37 (15.17)	1.49 (8.23)
ST Posterior/Anterior Tilt	-9.14 (15.05)	-10.62 (15.37)	-1.48 (3.65)
SC Protraction/Retraction	0.86 (10.44)	3.67 (10.32)	2.83 (2.54)
SC Elevation/Depression	-4.02 (7.41)	-3.48 (7.51)	0.55 (2.30)

EXPERIMENTAL DESIGN INFLUENCE ON DETECTION OF PERFORMANCE DIFFERENCES

[1]Barry T. Bates, [2]C. Roger James and [3]Janet S. Dufek

[1]Emeritus Professor, University of Oregon, Eugene OR, USA
[2]Texas Tech University Health Sciences Center, Lubbock, TX, USA
[3]University of Nevada, Las Vegas, Las Vegas, NV, USA
email: btbates@cox.net

INTRODUCTION

Numerous shoe manufacturers have been making marketing claims regarding the advantages of wearing what have been referred to as "toning shoes". The various shoe models each have uniquely shaped although similar rounded bottoms (rocker bottom outsoles) that manufacturers claim alter the user's normal walking gait resulting in benefits including toning muscles, improving posture and burning more calories. These assertions have generally been supported by in-house research/claims with additional anecdotal evidence, found online, from individuals who have worn the shoes and believe they have benefited in one or more of the claimed areas. As a result of public interest in the shoes and the manufacturers' stated claims, a number of researchers have chosen to investigate the functionality of the footwear relative to the stated claims [1, 5-8]. For the most part the claims have not been supported by independent research. Trends have been identified in lower extremity kinematics [7] with no significant group differences; however, a significant increase in ankle dorsiflexion in the rounded outsole shoe during the first half of support has been identified [5]. Others [6, 8] reported no differences in lower extremity muscle activity or metabolic cost. Andriacchi et al [1] identified several adaptation strategies in joint function for *individuals* walking in rounded outsole shoes. The use of unique strategies by individuals in response to perturbations presents a threat to external validity and can result in inability to identify group differences [2]. Thus, single subject methodology may be appropriate for this footwear assessment.

The primary rationale behind the single subject approach is that no two individuals are alike. The neuromuscular system is extremely pliable functionally allowing for numerous control options (performance strategies) based upon learning from past experiences. Performance strategies result in intersubject variability that cannot be controlled using traditional group statistical techniques. Another important performance characteristic of this functional complexity is variability. Intrasubject variability, inherent in all systems [4] can be managed by adding more subjects (group design) or trials (single subject design). Therefore, the purpose of this study was to demonstrate the effect of subject sample size and trial size on the statistical outcomes for single subject and group analyses.

METHODS

Volunteers (9 female, 3 male; 41.1±15.0 yrs; 1.74±0.08 m; 83.3±22.0 kg; BMI: 27.0±5.7) were solicited from the local community. All participants were free from lower extremity injury and able to walk on a treadmill unassisted at a speed between 1.12-1.58 m/s in 15 min increments (with rest). After granting institutionally approved written consent to participate, preferred treadmill walking speed was determined for each subject wearing his/her own footwear. Participants then walked on the treadmill at their preferred speed +10% in each of two shoe conditions: 1) traditional athletic shoe, and 2) a rocker bottom shoe, presented in a balanced randomized order. Subjects walked on the treadmill for 10 min. prior to data collection for each shoe condition. Fifty trials (strides) of data were collected in two blocks of 25 trials each using a high-speed video data collection system (120 Hz). Ten sagittal plane temporal and kinematic descriptive variables were identified for analysis for each of the right lower extremity joints. In addition, five stance variables were evaluated.

The two 25 trial data sets were combined to form a single sample of 50 trials. Data were analyzed for subject sample sizes of 5, 8, 10 and 12 subjects and trial sizes of 5, 10, 25 and 50. For trial sizes of 5, 10 and 25, three subsets of data were evaluated. The subsets consisted of the first, middle and last blocks of trials from the 50 trial sample for the respective trial size samples. This procedure, used to assure representation across the 50 trial sample for each subset, resulted in a total of 10 trial size samples for each subject: three each for 5, 10 and 25 trials and a single 50 trial sample. For subject sample sizes of 5, 8 and 10, three random samples were generated for each of the trial subsets (10 trial subsets * three subject sample sizes for a total of 30 samples). For the subject sample size of 12, only one sample was possible resulting in 10 additional samples. These 40 subject-trial data sets were evaluated using the Model Statistics single subject technique [3] and a traditional repeated measures ANOVA (shoe x subject) group analysis technique.

RESULTS AND DISCUSSION

The percentages of significant group and single subject comparisons collapsed across subjects and trials for all variables and selected subgroups of variables are given in Table 1. The final column (ratio) is the average ratio of the test statistic to the critical value for all comparisons.

Overall, 75% more significant differences were observed for the single subject analyses compared to group analyses (Table 1). In addition, group data show that sample size, independent of performance strategies, had a greater effect on observed significant differences than trial size. The single subject data illustrate the independence of results on sample size along with the importance of trial size on the number of observed significant differences.

CONCLUSIONS

The results identify the importance of study design on the ability to detect functional differences within- and between participants. Interpretation of footwear effects on performance may be highly influenced by individual morphology and experiences that can result in different performer strategies, which can be masked in traditional group designs.

REFERENCES

1. Andriacchi et al. *Unpublished laboratory report*, June 2008.
2. Bates, BT. *Med Sci Sports Exerc*, **28**, 631-638, 1996.
3. Bates, et al. *Med Sci Sports Exerc*, **24**, 1059-1068, 1992.
4. Newell & Corcos. *Variability and Motor Control*, 1993, Human Kinetics.
5. Nigg et al. *Clin Biomech*, **21**,82-88, 2006.
6. Porcari et al. *Unpublished laboratory report*, 2010.
7. Romkes et al. *Clin Boimech*, **21**, 75-81, 2006.
8. Santo et al. *J of Strength Cond Res*, **26**, 2426-2431, 2012.

Table 1: Proportion of Significant Group and Single Subject Comparisons Collapsed Across Number of Subjects and Trials by Selected Variable Category.

		Group Results								Single Subject Results							
Subj	Trials	Total	Kin	Temp	Stance	Ankle	Knee	Hip	ratio	Total	Kin	Temp	Stance	Ankle	Knee	Hip	ratio
5	50	0.247	0.263	0.263	0.147	0.423	0.230	0.137	1.009	0.630	0.810	0.561	0.512	0.818	0.632	0.499	0.693
8	50	0.374	0.414	0.337	0.273	0.583	0.397	0.193	1.444	0.644	0.823	0.583	0.528	0.838	0.654	0.498	0.733
10	50	0.453	0.559	0.315	0.260	0.757	0.460	0.240	1.686	0.645	0.829	0.574	0.523	0.842	0.647	0.506	0.731
12	50	0.500	0.619	0.322	0.320	0.790	0.530	0.270	2.081	0.627	0.801	0.571	0.410	0.844	0.648	0.498	0.728
12	5	0.350	0.408	0.311	0.180	0.593	0.350	0.193	1.385	0.471	0.548	0.412	0.253	0.727	0.484	0.310	0.430
12	10	0.385	0.452	0.307	0.240	0.620	0.397	0.210	1.474	0.650	0.727	0.570	0.469	0.844	0.663	0.533	0.712
12	25	0.379	0.438	0.315	0.247	0.620	0.393	0.190	1.441	0.744	0.786	0.681	0.686	0.907	0.742	0.614	0.957
12	50	0.380	0.433	0.267	0.360	0.580	0.370	0.200	1.596	0.798	0.810	0.749	0.835	0.936	0.798	0.642	0.946

ANALYSIS OF HEMODYNAMICS IN ABDOMINAL AORTIC ANEURYSM (AAA) WITH FENESTRATED STENT GRAFT

[1]Harkamaljot Kandail, [2]Mohamad Hamady and [1]Xiao Yun Xu

[1]Department of Chemical Engineering, Imperial College London, UK
[2]Department of Radiology, Imperial College Healthcare NHS Trust, London, UK
email: Hsk08@imperial.ac.uk, web: http://www3.imperial.ac.uk/chemicalengineering

INTRODUCTION

AAA is an abnormal and irreversible fusiform dilation of the terminal aorta, which can rupture if left untreated. The treatment options include highly invasive open surgical repair or minimally invasive Endovascular Aneurysm Repair (EVAR). Despite being minimally invasive, EVAR is not suitable for some patients due to unfavorable AAA morphology. Fenestrated Stent Graft (FSG) was designed to address these limitations. The aim of this study is twofold: (a) to investigate the hemodynamic effect of FSG on the renal arteries and (b) to evaluate the longitudinal drag force acting on the FSG. This is achieved by numerically computing the flow, pressure and stress fields in pre and post stented AAA. This quantitative analysis will help to predict the risk of future complications such as endoleaks and migration.

METHODS

Geometry

As shown in Fig. 1, patient specific 3D models of pre and post stented AAA were reconstructed from CT scans using Mimics.

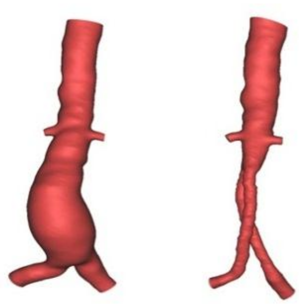

Figure 1: Pre and post stented AAA models reconstructed from CT scans.

Flow model and assumptions

The Navier-Stokes equations were used to describe the 3D, pulsatile blood flow in the lumen. Blood was assumed to be non-Newtonian, described by the Quemada model. The vessel wall and FSG were assumed to be rigid.

Boundary conditions

Physiologically realistic velocity and pressure waveforms were adopted and described using Fourier series [1]. Velocity profiles, derived from the Womersley solution [2] were imposed at the inlet, while volumetric flow rate and pressure waveforms were applied at the renal and iliac arteries respectively. No slip conditions were also specified at the wall. Numerical solutions were obtained using ANSYS CFX.

RESULTS AND DISCUSSION

In pre-stented AAA, there was a large recirculation zone in the sac as blood decelerated during transition from systole to diastole. However in post-stented AAA, more organized flow was observed over the whole cardiac cycle (Fig. 2). FSG had little effect on the blood flow patterns in the renal arteries. The longitudinal drag force acting on the FSG varied between 6.2 N and 9 N over one cardiac cycle (Fig. 3) and followed a very similar pattern to that of the cardiac pressure. FSG placement also significantly reduced the sac pressure.

Research is on-going to evaluate the hemodynamic effects and the drag force acting on the FSG for AAAs with different morphological features, e.g. angulated neck and/or angulated iliac bifurcations.

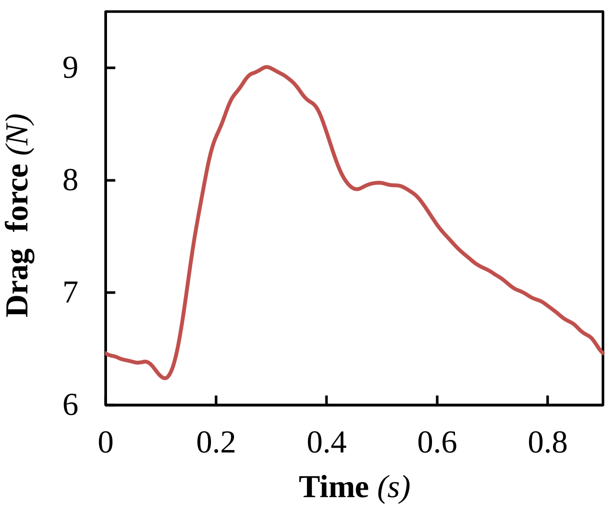

Figure 3: Longitudinal drag force acting on the FSG over one cardiac cycle.

Furthermore, fluid structure interaction simulations will also be carried out in order to gain a physical insight into the hemodynamics coupled with the structural mechanics of the aorta. This research will provide a full-fledged assessment tool for optimal FSG placement.

REFERENCES

1. Taylor CA, et al. *Ann Biomed Eng* **26**, 975 - 987, 1998.
2. Womersley JR. *J Physiol* **127**, 553 - 563, 1955.

ACKNOWLEDGEMENTS

This research is partially sponsored by Vascutek Ltd.

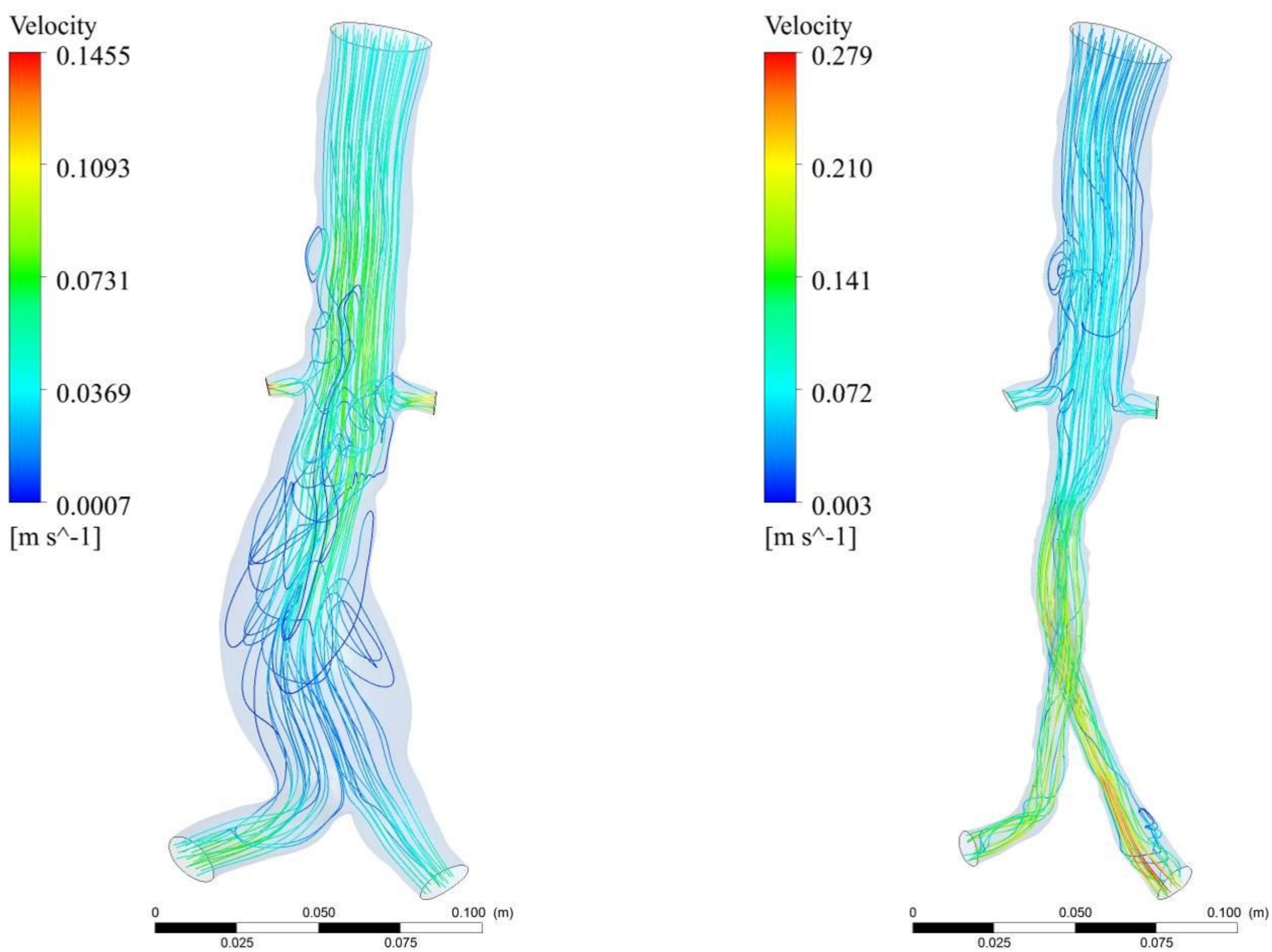

Figure 2: Velocity streamlines (at diastole) for comparison between pre-stented AAA and post-stented AAA.

Relationships among Mechanical and Neuromuscular Control Variables in Healthy Individuals during Landing

R. Haddas, S. Sawyer, P. Sizer, T. Brooks, M. Chyu, C.R. James

Texas Tech University Health Sciences Center, Lubbock, TX, USA
email: r.haddas@ttuhsc.edu

INTRODUCTION

Biomechanics investigators are often confronted with a dilemma when deciding which and how many variables to include when analyzing human motion. Advances in technology have allowed numerous measurements to be obtained simultaneously. Each measurement, such as knee angle time history, may in turn be reduced to provide numerous dependent variables. While the dependent variables should be determined by the research question, interacting factors include access to equipment and limited information about the interrelationships among variables. In addition to the obvious data management issues, a large number of dependent variables may lead to increases in statistical error. In some biomechanics settings, such as small research laboratories or clinical analysis settings, instruments may be limited to a set of cameras. In these settings, it would be ideal to take advantage of known interrelationships among variables. Strong interrelationships might permit the prediction of some kinetic variables from related kinematic variables. The purpose of this study was to explore the interrelationships among kinematic, kinetic and electromyographic (EMG) variables to (1) determine a parsimonious subset of dependent variables that explain the greatest amount of unique aspects of the data set variance during landing in healthy people, and (2) predict selected kinetic variable values from representative kinematic and EMG variables during landing.

METHODS

An intercorrelation design was used to determine a subset of kinematic, kinetic and EMG dependent variables that explained the greatest amount of unique variance during landing in healthy people in an exploratory fashion. A linear multiple regression design was used to determine a subset of kinematic and EMG dependent variables that predicted kinetic variables during landing in healthy subjects. Thirty-two subjects participated (age = 20.94 ± 2.27, height = 1.69 ± 9.62 m, mass = 71.18 ± 14.50 kg). Twenty-three reflective markers using locations and procedures adapted from Vaughan et al.[1] were incorporated in order to collect three-dimensional kinematics (VICON Nexus 1.7.1) of the lower extremity and lumbar spine at a sampling rate of 100 Hz. Raw 3D coordinate data were smoothed using a fourth order no-phase-shift Butterworth low pass digital filter with cutoff set to 6 Hz prior to exporting for further analysis. The ground reaction force (GRF) data were collected at 2000 Hz using two parallel force plates positioned side-by-side (AMTI). EMG data of the right side internal oblique (IO), external oblique (EO), multifidus (Mf) at the first lumbar (L5) spinal level, gluteus maximus (GM), semitendinosus (ST), vastus medialis (VM) and rectus femoris (RF) were measured at 2000 Hz using preamplified surface electrodes (Delsys, Inc).

Dependent variables included lumbar, hip, knee and ankle joint angles, and internal joint moments in 3D, sagittal plane lower extremity joint powers, and EMG onset times. Pearson product-moment correlations were used to calculate intercorrelations among 49 variables to explore and reduce the data set to a parsimonious set of variables that explained unique variance. Dependent variables strongly correlated with each other were evaluated for both logical and numerical redundancy. The criterion value for redundancy was initially set to r=0.707 or 50% explained variance [2]. The criterion value was progressively adjusted with additional iterations until five to eight dependent variables remained. After establishing a parsimonious set of variables, a separate analysis involving linear multiple regression was used to predict maximum vertical GRF, maximum knee moment in the sagittal plane, and maximum ankle moment in the sagittal plane from the larger set of 26 kinematic and EMG variables. Statistical analyses were conducted using SPSS, Version 21.0 (IBM, Inc, Chicago, IL).

RESULTS AND DISCUSSION

The original set of 49 variables was reduced to seven variables that effectively accounted for much of the unique variance within the data set. Evaluation of the intercorrelations among the 49 variables was used to reduce the data set to seven variables in a five step process. The final set of seven variables that explained unique variance were maximum knee angle in the sagittal plane, maximum pelvic angle in the frontal plane, pelvic angle in the sagittal plane at initial contact, lower lumbar angle in the sagittal plane angle at initial contact, maximum knee flexion moment in the sagittal plane, maximum vertical GRF, and ST onset.

Two techniques were employed to select the predictor independent variables for the regression analysis. First, the three kinematic or EMG independent variables that had the highest correlation with each dependent variable were manually identified and entered into a model to predict each selected kinetic variable. Second, a forward stepwise multiple regression model (p_{in} = 0.05; p_{out} = 0.10) was used to determine the best models for predicting the dependent variables from lower extremity kinematic and EMG predictor independent variables. The stepwise regression method was found to be more powerful and therefore became the focus of the remaining analysis.

The variables that were used to predict maximum vertical GRF were knee angle in the horizontal plane at initial contact, maximum knee angle in the sagittal plane, and hip angle in the sagittal plane at initial contact (R^2=0.42, p = 0.001, Eq. 1). The variables that were used to predict maximum knee moment in the sagittal plane were maximum pelvic angle in the sagittal plane, ankle angle in the horizontal plane at initial contact, and maximum ankle angle in the horizontal plane (R^2=0.503, p = 0.001, Eq. 2). No predictor variables successfully entered the stepwise model to predict maximum ankle moment in the sagittal plane (p > 0.05).

CONCLUSIONS

Seven biomechanical variables were found to explain unique aspects of the data set variance based on a systematic intercorrelational analysis. These variables should be considered as dependent variables in future drop vertical jump landing studies. In laboratory or clinical biomechanics settings which do not have access to a force platform, vertical GRF and maximum knee moment in the sagittal plane can be predicted moderately well from kinematic variables alone using multiple linear regression. Additionally, the findings of the current study indicate that future research should examine the effects of increasing maximum knee flexion, maximum ankle eversion angle, and ankle inversion angle at initial contact, and decreasing hip flexion angle at initial contact, and maximum pelvic anterior tilt angle to reduce GRF and maximum knee moments in the sagittal plane. Clinical and training interventions might target these key kinematic variables.

REFERENCES

1. Vaughan et al. *Dynamics of Human Gait (2nd ed.)*, Kiboho Publishers, 1999.
2. Tabachnick & Fidell. *Using multivariate statistics (2nd ed.)*, Harper Collins, 1989

Equation 1. Vertical GRF linear regression model

$$\widehat{VGRF} = 2967.74 - (23.39 \times KRIC) - (21.90 \times MKF) + (39.72 \times HFIC)$$

VGRF- Vertical ground reaction force (N), KRIC- Knee angle in the horizontal plane at initial contact (°), MKF - Maximum knee angle in the sagittal plane (°), HFIC - Hip sagittal plane angles at initial contact (°).

Equation 2. Knee sagittal plane moment linear regression model

$$\left(Knee\ sagittal\ \widehat{plane}\ moment\ = 36.48 + (19.54 \times MPF) + (3.20 \times ARIC) - (6.23 \times MAR)\right)$$

Knee sagittal plane moment (Nm), MPF - Maximum pelvic angle in the sagittal plane (°), ARIC - Ankle angle in the horizontal plane at initial contact (°), MAR - Maximum ankle angle in the horizontal plane (°).

A FLEXIBLE ORTHOPAEDIC TRAUMA SURGERY BOX SKILLS TRAINER

Geb W Thomas, Donald D Anderson, Matthew D Karam, Brian Johns,
Salvador Rojas Murillo, and J Lawrence Marsh

The University of Iowa, Iowa City, IA, USA
email: Geb-Thomas@uiowa.edu

INTRODUCTION

A 2010 review of virtual reality simulators for orthopaedic surgery[1] found only 23 articles exploring working simulators, and only three related to fracture management, compared with 246 citations for laparoscopic simulators. Many of the recent contributions to orthopaedic simulation technology have emphasized haptic feedback such as for bone drilling [2,3] and amputation surgery[4]. One of the most successful laparoscopic simulators is the Fundamental Laparoscopic Simulator[5], with which trainees manipulate rubber bands and rings and tie knots with laparoscopic tools while viewing their movements on a remote camera display.

This work introduces a skills acquisition approach similar to arthroscopically or fluoroscopically guided orthopaedic surgery by simulating single or two-plane assessments of three-dimensional tasks. In this simulator, two video camera images substitute for fluoroscopic images, and simple pins are analogous to the tip of guide wires used in surgery. The current skills trainer focuses on the task of quickly locating a precise position and orientation utilizing two orthogonal view planes. The simulator is relatively inexpensive and radiation free, improving its utility in training programs.

METHODS

The skills trainer consists of two video cameras mounted on an aluminum frame. The cameras view a roughly 4"x4"x4" workspace from orthogonal positions: one views the workspace from 1.5' above, the second camera points toward the participant from a position approximately 1.5' behind the workspace. A screen between the workspace and the participant obstructs the direct view of hand motions in the workspace. This requires the participant to rely on the camera views visible on a monitor placed conveniently nearby to navigate the 3D environment. Currently a proctor controls the simulation, although the task may be self-guided.

Three tasks were devised for the trainees. The horizontal peg-in-hole task consists of a 4"x4" acrylic pegboard with sixteen, 0.125" diameter drilled holes positioned in view of the top camera. The trainee is given one minute to place, in order, as many 1" long, 0.109" diameter steel pins into the holes as possible using camera guidance. The vertical peg-in-hole task is similar, except the pegboard is aligned specifically so the drilled surface is perpendicular to (and thus not directly visible in) both the top and side camera views. This forces the participants to rely on corresponding numbered indicators on the sides of the pegboard to correctly determine hole locations from perpendicular camera views. As in the first task, the participant inserts as many pins as possible in two minutes.

The final task, the angle task, uses a 3/8" diameter, 6" long shaft constrained to a spherical joint at one end. Unlike the previous two tasks, the participant must manipulate and match the shaft angle to a computer-generated line overlaid on the two orthogonal camera views. The objective is matching as many generated line positions with the shaft as

Figure 1. Box skills trainer. A resident trainee places a peg on the horizontal pegboard. The proctor updates video images, visible on a display located behind the keyboard.

possible within one minute.

Trainees are first acquainted with each task with live video. After familiarization, the camera mode is switched to only generate static views. The trainee must then verbally request either an “AP” to see a still image from the top camera, corresponding to a antero-posterior fluoro shot, or a “Lateral” to see a still image from the back camera. The static images remain visible until a new image is requested, which immediately replaces the old image. Scoring was standardized across all tasks. Each correct pin placement or shaft position received 100 points, but each requested image deducted 10 points from the total score. Subjects performed each task three times. Afterwards each trainee completed a survey.

Our hypotheses were:

1. Task performance improves with practice;
2. Trainees perceive that the task was helpful to improve their surgical skill.

Six post-graduate year one, male orthopaedic residents participated in the experiment. These trainees were also introduced to a more realistic surgical simulation involving the reduction and fixation of a tibial plafond fracture on the same day.

RESULTS AND DISCUSSION

The average scores for the horizontal peg-in-hole tasks were 511, 638 and 723 for the three respective trials. The average scores for the vertical tasks were 403, 503 and 572. For the angle task, averages were 800, 930 and 930. A general linear model of performance on the horizontal task as a function of order and participant with order as a covariate and participant as a random variable indicates a significant linear improvement with repetition: $F(1,11) = 8.21$, $p = 0.015$, with a model adjusted R-square of 24.9%. A similar model of vertical task performance also shows a significant linear improvement with repetition: $F(1,11) = 9.16$, $p = 0.012$, with a model adjusted R-square of 88.45%. A similar model did not lead to a significant linear improvement with repetition for the angle task.

The six questionnaire items generally yielded inconclusive findings. The respondents found that movements were moderately similar to a previously reported, more realistic tibial plafond fracture simulation[6] (four 3’s and two 4’s) on a 5-point scale with 5 being very similar. Responses to whether the dexterity requirements were similar were widely varying, ranging from 1 to 4 with a mean of 2.5 and standard deviation of 1.05. The participants moderately agreed that practice with the simulator would improve their performance on the more realistic simulator or real surgery (each 3 on a 5-point scale with standard deviations of 0.8 and 0.6, respectively). Five out of the six participants felt that scoring the simulator as a game enhanced their experience.

CONCLUSIONS

The results support the hypothesis that task performance improves with practice. The residents were moderately convinced that experience with the box trainer would improve performance with the more realistic tibial plafond facture simulator. Combining our positive results with the benefits of a low-cost, radiation free simulator demands further study. In addition, this low-fidelity simulator, once validated, may play an important role in basic orthopaedic trauma skill assessment (similar to the FLS trainer in General Surgery).

REFERENCES

1. Mabrey et al. Clin Orthop Relat Res. 468(10): 2586-2591, 2010.
2. Tsai et al. Comput Biol Med. 37(12):1709-1718, 2007.
3. Vankipuram et al. J Biomed Inform. 43(5):661-668, 2010.
4. Hsieh et al. Biomed. Eng.-App. Bas C 18(5):229-236, 2006.
5. Edelman et al. J. Surg. Res. 163:24–28, 2010.
6. Yehyawi et al. J Bone Joint Surg 2013.

ACKNOWLEDGEMENTS

This project was funded (in part) by a National Board of Medical Examiners® (NBME®) Edward J. Stemmler, MD Medical Education Research Fund grant and by a grant from the Orthopaedic Trauma Association. The efforts of Sebastian Surom in helping to construct the simulator are gratefully acknowledged.

PERCEPTION OF COMPLEX MOVEMENT IN TYPICALLY DEVELOPING CHILDREN AND CHILDREN WITH AUTISM SPECTRUM DISORDER

[1,2]Joshua Haworth, [2]Anastasia Kyvelidou, [1]Wayne Fisher, and [1,2]Nicholas Stergiou

[1]University of Nebraska Medical Center, Omaha, NE, USA
[2]University of Nebraska at Omaha, Omaha, NE, USA
email: jlhaworth@unomaha.edu, web: http://nbcf.unomaha.edu

INTRODUCTION

Typically developing children recognize biological motion in point-light displays. Interestingly, they specifically prefer to watch locomotion coherent with their own mode of locomotion; i.e. crawlers prefer to watch crawling whereas walkers prefer to watch walking [1]. This observation provides insight into how children recognize and replicate movements of others in their social environment.
The development of motor behavior relies, in part, on being able to incorporate the lessons learned from viewing others' attempts at similar motor performance. By watching others, we are able to vastly multiply our own experience and knowledge of successful movement strategies. For individuals with autism this is contingent, however, on whether or not the action of the model is perceptible; which unfortunately does not seem to be the case. Gepner and Feron [2] suggest that the phenotypic expressions of autism spectrum disorder are directly related to a neurophysiologic base stemming from temporo-spatial processing disorder. Disordered processing provokes confusion and discomfort in environments that contain rich sources of temporally relevant sensory information. Gepner and Feron present examples of an inability to perceive and produce overt responses, however even the observation of a more covert behavior such as another person's eye movements has been shown distracting to some with autism [3]. In light of a vast amount of work in biomechanics [4], we suggest that the specific aversion to the complex temporo-spatial aspects of others' movements is related directly to the perception of chaotic motion of the observed individual. Chaos is pervasive in human movement, and a deficit in recognizing this particular type of motion structure could be the basis for the lack of attention to biological motion, which is typical of children with autism.

Thus, the purpose of the current project was to assess gaze and postural behavior of young children, with and without autism in response to visual stimuli of different temporal complexity.

METHODS

Eight children (age matched, range from 3-6 years) participated; four have been diagnosed with autism (ASD), while four have not. Participants attended a single collection session during which synchronous measures of eye movement (Seeing Machines, faceLAB) and standing posture (Center of pressure; COP) was recorded via force plate; AMTI, OR6) were collected while viewing a point-light stimulus (Fig.1). The motion of the stimulus differed across three conditions, by scaling temporal complexity in terms of approximate entropy (ApEn); a sine wave (highly regular, ApEn=0.032), chaos (approximate to biological motion, ApEn=0.097), and brown noise (completely random, ApEn=0.136). Only mediolateral aspects were analyzed, to assess response to the horizontal motion of the stimulus.

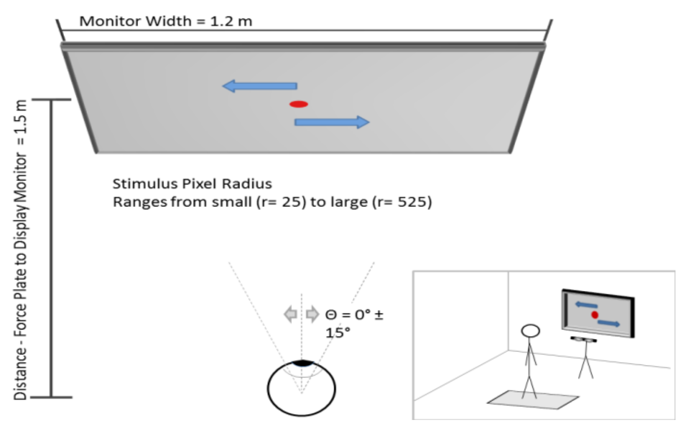

Figure 1: Diagram of experimental setup.

Trials lasted for three and a half minutes; with data recorded at 50 Hz. Post processing included identification of segments during which the child was speaking or making overt motions with their head or arms (none of the children moved their feet during the trial). The longest common segment was 3000 data points, or 60 seconds of continuous data. COP and gaze segments were further processed to produce the path length and the ApEn measure of variability using custom Matlab scripts (Mathworks Inc.). Data was filtered using a double pass Butterworth filter with a 20 Hz cutoff. Parameters for ApEn include m=2 and r=0.2*standard deviation. A 2x3 (Group x Stimulus) Mixed ANOVA was used for statistical comparisons.

RESULTS AND DISCUSSION

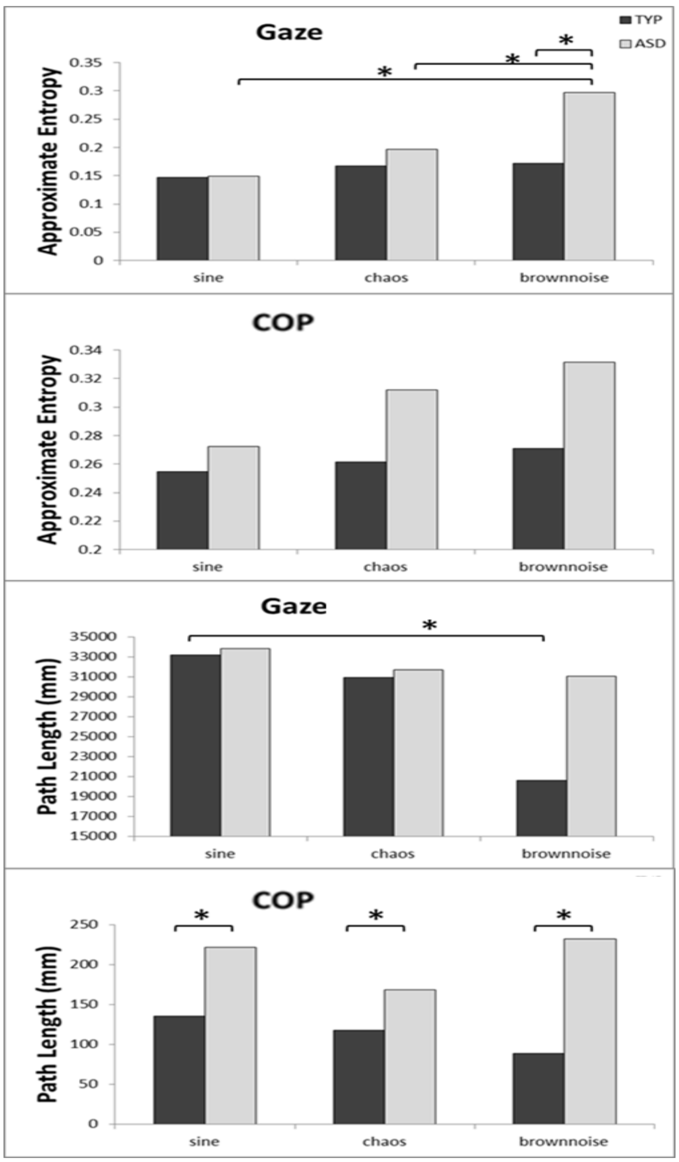

Figure 2: Approximate entropy (ApEn) and the total distance (Path) of Gaze and COP behaviors.
*near significant at $p<0.10$

Gaze and mediolateral postural sway were assessed for their responsiveness to the complexity of the horizontal motion of the presented stimulus (Fig. 2). Results suggest for Gaze ApEn, a main effect of Group ($p = 0.098$) and Stimulus ($p = 0.01$); as well as interaction ($p = 0.05$). No effects or interactions for COP ApEn. For Gaze Path, a main effect of Stimulus ($p = 0.091$) was suggested. COP Path showed a main effect of Group ($p = 0.017$), as well as an interaction ($p = 0.079$). While not directly supporting our proposed hypothesis, these results do highlight differing responsiveness to motion structure between children with and without ASD. A look at the Path of the gaze signal indicates that children without ASD did not follow the stimulus through its full distance in the brown noise condition. This finding exacerbates interest in how children attend to random motion.

It is of additional interest to note our results in Path of COP; showing that children with ASD move more than their non-ASD counterparts, regardless of the stimulus being shown.

CONCLUSIONS

The present data suggests that the gaze and postural sway of children with ASD differs from those without. These differences are noticeable in the complexity of temporal variations of each behavior, in response to a stimulus of specific complexity.

REFERENCES

1. Sanefuji, W, et al. *Inf Behav Dev* **31** 624-628, 2008.
2. Gepner, B, & Feron, F, *Neuro & Behav Reviews*, **33**, 1227-1242, 2009.
3. Grandin, T, *Thinking in Pictures and Other Reports from My Life with Autism*, Doubleday, 1995.
4. Stergiou, N, *Innovative Analysis of Human Movement*, Human Kinetics, 2004.

ACKNOWLEDGEMENTS

This work was supported by an American Society for Biomechanics Grant-in-Aid, a NASA Nebraska Space Grant Fellowship, the Nebraska Research Initiative, and a Dennis Weatherstone Pre-doctoral Fellowship from Autism Speaks (grant # 7070).

EFFECT OF FORWARD PERTURBATION ON THE TRUNK NEUROMUSCULAR BEHAVIOR

[1]Ali Shahvarpour, [1]Aboulfazl Shirazi-Adl, [2]Christian Larivière and [2]Hakim Mecheri

[1]École Polytechnique, Montréal, QC, Canada
[3] Institut de recherche Robert-Sauvé en santé et en sécurité du travail (IRSST), Montréal, QC, Canada
email: aboulfazl.shirazi@polymtl.ca

INTRODUCTION

In various occupational and recreational activities, the human trunk may experience sudden perturbations via additional loading or unloading. To avoid fall or loss of stability and control, the neuromuscular system reacts reflexively that tend to further overload the spine and increase the risk of injuries. The post-perturbation trunk response and associated risk of injury are influenced by the reflex response that in turn is likely modulated by the perturbation characteristics and the pre-existing initial conditions on posture and muscle activation. Investigation of the trunk response to sudden loading is hence promising to identify parameters that could diminish the risk of injury and overloading while augmenting the trunk stiffness and stability. Reflexive response following a perturbation is composed of stereotypical reflex patterns from low level neural centers in the central nervous system (CNS) [1]. The neuromuscular response is governed by perturbation characteristics. In this study, the trunk reflex response, including the latency period, peak amplitude, reflex rise time, EMG of select muscles and kinematics/kinetics is investigated. It is hypothesized that the perturbation magnitudes and initial conditions alter both reflex and voluntary response.

METHODS

In vivo measurement: Twelve young male subjects (weight 73.00±3.87 kg and height 177.42±3.12 cm) with no history of low-back pain participated. Subjects performed max voluntary contraction (MVC) in 6 directions. Superficial EMG signals of 12 muscles (6 bilateral pairs) were recorded; Longissimus (LG), Iliocostalis (IC), Multifidus (MF), Rectus abdominus (RA), External (EO) and Internal (IO) obliques. Subjects were semi-seated in the perturbation apparatus with the pelvis restrained and a harness placed at the T8 level [2]. The harness was connected to a load cell in front and to a potentiometer in the back in order to measure the load applied and the trunk displacement generated. A visual feedback system was used to monitor the initial trunk posture and abdominal pre-activation level. In presence of a steady initial pre-load, a sudden load was applied randomly within 5s interval. The perturbation force and displacement at the T8 level as well as EMG activity were measured for six testing conditions (Table 1). Five trials were performed for each condition with 30s of rest in between. In the condition 5, the T8 anterior displacement of 10 cm caused an initial trunk flexion rotation of about 20^{o}.

Table 1: Experimental conditions

Condition	Pre Load	Sudden Load	Initial Condition	Abdominal preactivation
1	5	50	Upright	-
2	5	100	Upright	-
3	50	50	Upright	-
4	50	100	Upright	-
5	5	50	10 cm T8 Translation	-
6	5	100	Upright	10%

Quantification of back muscles reflex: The onset of back muscles reflex was evaluated using two methods; (1) standard deviation (SD) [3] and (2) the approximated generalized likelihood-ratio (AGLR) [4]. The reflex latency was defined from the onset of trunk movement to the onset of muscle reflex [2]. In addition, the reflex amplitude (RatioPeak defined as the ratio of the first EMG peak over the initial EMG at the onset in a 250-ms window) was calculated. The normalized amplitude of the EMG peak (RawPeak) was also evaluated [2].

Statistical analyses: ANOVAs for repeated measures were used to analyze the effects of preload, sudden load, initial posture and preactivation of abdominal muscles on the trunk kinematics-kinetics and back muscle reflex response.

RESULTS AND DISCUSSION

The data of right and left muscles in all trials are pooled in light of preliminary statistical analyses demonstrating no side and trial effects. Latency period, using either SD or AGLR method, is found larger for the conditions 3-5 with greater preactivation in extensor muscles (Fig 1). The results of Tukey HSD post hoc analysis confirm the significant effect on latency in the condition 5 compared to others that may highlight the effects of initial strain and preactivation in extensor muscles.

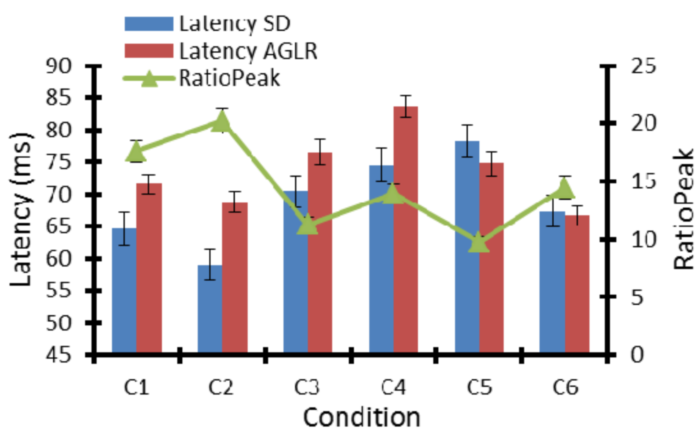

Figure 1: Mean of latencies and RatioPeak for various test conditions (Table 1).

Analysis of T8 displacement and force (Fig 2) reveals that, as expected, conditions 1,3 and 5 with smaller perturbation loads yield least trunk peak forces and displacements. Tukey`s test indicate significant differences between these three and remaining conditions ($p<0.0007$ for displacement and $p<0.0012$ for load). The RatioPeak of extensor muscles (Figs 1 and 3) is overall significantly larger in conditions 1 and 2 in contrast to conditions 3-6. This appears to suggest the role of initial pre-load in conditions 3 and 4 and preactivation in extensor muscles in conditions 5 and 6. Lower reflex activity (Figs 1 and 3) along with longer latency (Fig 1) in early post-perturbation period are hence likely related to larger preactivation levels present in these conditions 3-6. Results of this study therefore highlight the crucial role of the perturbation characteristics as well as preactivity in trunk muscles and initial posture on the trunk reflex and voluntary response under sudden loads.

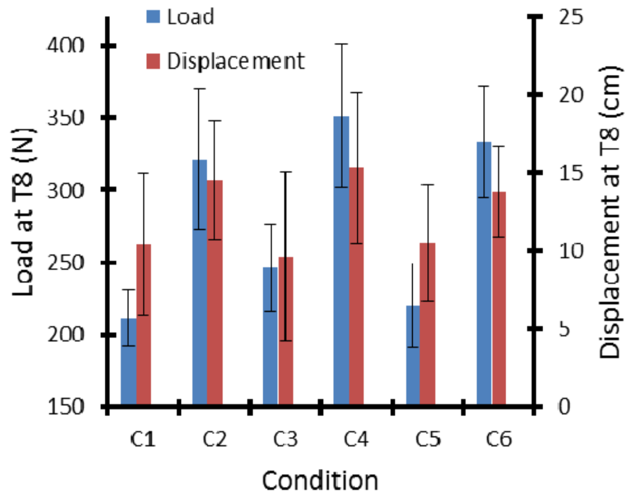

Figure 2: T8 peak displacement and load for various test conditions (Table 1).

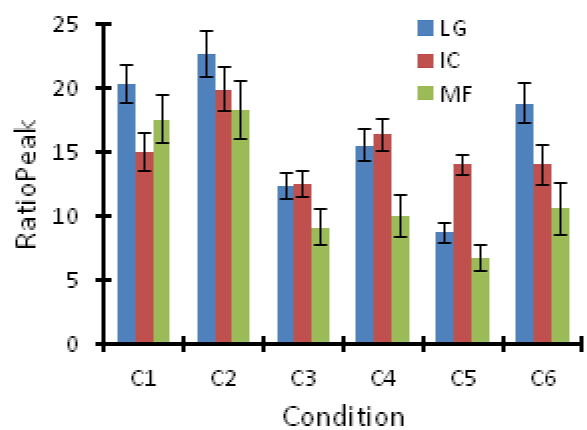

Figure 3: Ratio of peak (in post-perturbation 250 ms period) to initial EMGs for various extensor muscles and test conditions (Table 1).

REFERENCES

1. Scott SH, *Nature Neuroscience*, **5**, 534-546
2. Larivière et al, *Eur J Appl Physiol*, **109**, 577-590
3. Hodges/Bui, *Electro Clin Neuro*, **101**, 511-519
4. Staude, *IEEE Trans Biomed Eng*, **48**, 1292-2305

ACKNOWLEDGEMENT

This work has been supported by grants from the IRSST-Quebec and NSERC-Canada.

POSTURAL STABILITY DURING TANDEM STANCE

[1]Catherine A. Stevermer and [2]Jason C. Gillette
[1]Department of Physical Therapy, Des Moines University, Des Moines, Iowa
[2]Department of Kinesiology, Iowa State University, Ames, IA
e-mail: catherine.stevermer@dmu.edu

INTRODUCTION

Postural stability has been assessed by measuring center of pressure (COP) variables, and researchers interpret extremes in these values as indications of instability. As an alternative, researchers have used time-to-contact (TtC) measures of COP excursions as instability indicators during stance [1,2]. TtC estimates the time for the COP to reach the border of the support base as calculated from instantaneous COP trajectory. A lower TtC measure may indicate reduced postural stability and a potential risk for falls.

Various clinical balance assessments incorporate timed measures of static standing postures for determining stability. For balance screening, individuals often utilize timed assessment of single-limb stance to assess fall risk. In instances of pathology or pain, individuals may be unable to perform a single-limb standing task. Alternate tasks which challenge static balance include tandem stance where the base of support is reduced in the mediolateral direction [3] or a sharpened-Romberg test where vision is occluded.

The purpose was to evaluate stability measures in healthy young adults as a component of a larger project involving functional movement assessment. As previously proposed, we expected TtC measures to be lower for the more challenging tandem stance and eyes-closed conditions in comparison to normal stance and eyes-open conditions.

METHODS

Twenty-two young adults, 10 males and 12 females, (age 23 ± 2 yrs; height 1.7 ± 0.1 m; mass 78.5 ± 19.6 kg) participated in this project. Participants performed quiet standing for 30 seconds in three postures: tandem standing with the right foot placed anteriorly, tandem standing with the left foot placed anteriorly, and a self-selected comfortable stance with feet approximately hip width apart. Participants were instructed to stand on two adjacent force platforms (AMTI) during the trials, performing a trial in each posture with eyes open and eyes closed. If participants were unable to maintain the position for the full 30-second period, the trial was designated as a ‘failure’, but the attempt was not repeated. A total of 6 trials per participant were sampled at 160 Hz using Vicon Nexus software.

Analog data were filtered using a fourth-order, low-pass Butterworth filter using a cutoff frequency of 6 Hz. Center-of-pressure excursions, mean COP velocities, and maximum base of support percentages were calculated in the mediolateral (ML) and anteroposterior (AP) directions. Base of support (BOS) was based upon AP and ML origin determinations, such that the normal stance BOS was represented by anthropometrics of stance width and foot length. For the tandem stance condition, BOS was calculated using recorded foot width and foot length for each participant. TtC calculations were determined using COP velocities and accelerations. Failed trials were automatically detected using a 2.5% minimum weight-bearing (ground reaction force) requirement on each lower extremity and confirmed with experimental notation. All data processing was completed in Matlab.

Univariate ANOVA was conducted on stance and vision condition differences for weight-bearing asymmetry, BOS percentages, COP excursions and velocities, and TtC measures for successful trials. Using a Bonferroni correction ($p=0.05/9$), statistical significance was defined as $p<0.005$. Scheffe post-hoc comparisons indicated no statistical differences between the left and right tandem conditions ($p>0.51$), so the two conditions were combined. Using paired t-tests, tandem stance failures were compared with successful tandem trials with the opposite anterior foot position.

RESULTS AND DISCUSSION

With the exception of AP excursion with eyes open, all asymmetry, excursion, BOS percentage, and velocity parameters were significantly higher for the tandem stance as compared to the normal stance ($p<0.003$, Table 1). AP and ML TtC values were significantly lower for the tandem stance ($p<0.001$). For vision comparisons, AP/ML excursions, ML BOS, and AP/ML velocities were significantly higher for the tandem stance with eyes closed as compared to eyes open ($p<0.001$). AP and ML TtC values were significantly lower for the tandem stance with eyes closed ($p<0.001$).

The challenging tandem stance conditions and eyes closed conditions demonstrated higher COP velocity and lower TtC times than normal stance and eyes open conditions (Table 1). The 78% average reduction in TtC in tandem stance is consistent with tandem stance requiring more frequent ML COP shifts and using a smaller ML BOS which contributes to less time for balance adjustments. Without vision, participant performance on measured parameters was indicative of reduced postural stability.

Failures: A total of four 'failure' trials were captured involving three participants in tandem stance conditions. Significant differences between successful and failed trials were noted in the AP variables (Table 2). Weight-bearing symmetry reached 100% in all 4 cases, compared to an average asymmetry of 36.7±26.1% for successful tandem trials ($p<0.001$).

Differences between successful and unsuccessful standing trials in this young adult population appeared to occur in the AP direction as no differences were noted in ML parameters. These results suggest that healthy individuals prioritize ML control in the tandem stance posture and are less unaware of AP positioning until they are unable to compensate and must use a stepping strategy to recover balance.

Table 2: Comparison of Failure to Successful Trials (* = statistical significance at $p<0.02$)

Condition	AP Excursion (cm)	AP BOS (%)	AP Time-to-Contact (s)
Failure	13.8 ± 3.1*	69.9 ± 5.5*	0.18 ± 0.05*
Success	4.1 ± 1.7	36.3 ± 7.1	0.36 ± 0.03

CONCLUSIONS

The TtC measure appears to assess stability at increasing levels of difficulty in a healthy population. These findings support the recommended 30 second hold time for a tandem stance test [3], as it did appear to challenge balance in both eyes open and eyes closed conditions. Additional research may expand the use of the TtC measure with tandem stance in clinical populations in regards to fall risk assessment.

REFERENCES

1. Hertel J, et al. *J Appl Biomech*, **22**, 67-73, 2006.
2. Van Wegen EEH, et al., *Hum Mvmt Sci*, 21, 61-84, 2002.
3. Hile ES, et al., *Phys Ther*, **92**, 1316-1328, 2012.

Table 1: **Comparison of Stance and Vision Conditions.** (*) indicates statistically significant difference in parameter ($p<0.001$) between visual conditions during tandem stance.

Parameter of Interest	**Normal Stance**		**Tandem Stance**	
	Eyes Open	**Eyes Closed**	**Eyes Open**	**Eyes Closed**
Weight-bearing Asymmetry (%)	6.5 ± 5.0	6.2 ± 2.7	49.2 ± 17.6	56.3 ± 15.8
Anteroposterior (AP) Excursion (cm)	2.51 ± 1.97	2.37 ± 0.75	2.54 ± 0.83	4.47 ± 2.83*
Mediolateral (ML) Excursion (cm)	1.11 ± 1.66	0.83 ± 0.30	3.20 ± 0.67	4.97 ± 1.04*
AP Base of Support (%)	10.9 ± 8.1	10.1 ± 3.4	29.9 ± 10.6	31.9 ± 9.6
ML Base of Support (%)	6.7 ± 5.0	6.4 ± 4.1	36.6 ± 10.6	55.2 ± 13.7*
AP Velocity (cm/s)	0.64 ± 0.23	0.88 ± 0.37	1.45 ± 0.31	2.67 ± 0.90*
ML Velocity (cm/s)	0.43 ± 0.17	0.50 ± 0.18	1.84 ± 0.46	3.72 ± 1.05*
AP Time-to-Contact (s)	0.75 ± 0.18	0.65 ± 0.14	0.53 ± 0.08	0.37 ± 0.08*
ML Time-to-Contact (s)	1.09 ± 0.31	1.08 ± 0.25	0.25 ± 0.05	0.16 ± 0.04*

AN ATTENTION DIVERTING TASK NEGATIVELY AFFECTS RECOVERY STEP KINEMATICS AND FALL INCIDENCE

[1]Mackenzie L. Hoops, [1]Noah J. Rosenblatt, [1]Mark D. Grabiner

[1]University of Illinois-Chicago, Chicago, IL, USA
email: mhoops2@uic.edu, web: http://www.uic.edu/ahs/biomechanics/

INTRODUCTION

Mobility during daily life often occurs with concurrent cognitive or motor tasks. In light of this, dual-task paradigms are often used during fall risk assessment [1]. During postural control tasks, performance of a concurrent cognitive task distinguishes those with a history of falling from those without [2]. Indeed, performance of a concurrent cognitive task can influence recovery responses to small postural disturbances [3], especially during the later phases of the recovery response [4]. However, these studies have generally only used small postural disturbances after which subjects may not require a step to successfully recover their balance. How attention diverting tasks (ADT) influence the stepping kinematics required to successfully recover from a large postural disturbance, and subsequently, how it affects fall outcome has yet to be examined.

The purpose of this study was to examine how an ADT affects recovery step kinematics in response to a large, treadmill-delivered postural disturbance and, subsequently, how an ADT affects fall outcome of older women. We hypothesized that by diverting attention away from the recovery task, fall incidence would be greater than individuals who had their attention focused on recovering from a disturbance. Further, we hypothesized that recovery kinematics would be negatively altered by an ADT, evidenced by greater trunk flexion angle, greater trunk angular velocity, and a shorter initial recovery step length.

METHODS

Fifty-six middle aged and older women (64±7.1 yrs, 1.6±0.26 m, 76.4±17.0 kg) were included in this study. All subjects were part of a larger prospective study assessing the effectiveness of step training on fall incidence in the community. Subjects were free of musculoskeletal or neurological conditions that would limit functional mobility.

All subjects received a “standard” treadmill-induced postural disturbance. The treadmill disturbance was sufficient (zero to 0.89 m/s in 150 ms) to ensure that at least one step was required to avoid falling (Figure 1). The disturbance produced trunk flexion displacements and accelerations similar to those reported after an overground trip [5]. Seventeen subjects were randomly selected to perform an ADT during their initial postural disturbance. These subjects were instructed to count backwards by threes or sevens, from an arbitrary number greater than 100. After one minute of performing the ADT, the treadmill was manually triggered requiring the subject to perform a compensatory stepping response to avoid falling.

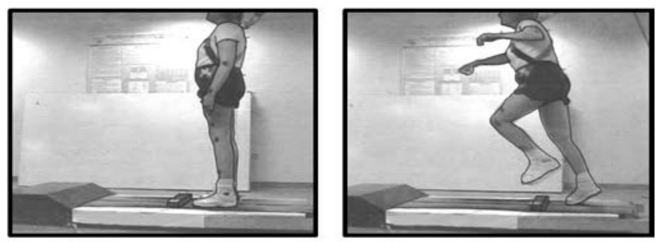

Figure 1: Subjects stood on a treadmill that suddenly accelerated posteriorly (left) causing forward rotation of the body and requiring several steps to recover balance (right). In all trials the subject is wearing a safety harness.

Fall outcome was documented for each subject. A successful recovery was considered a trial in which the subject was able to regain stability unambiguously without the assistance of the safety harness. Recovery step kinematics were captured using an eight camera motion capture system (120 Hz, Motion Analysis, Santa Rosa, CA) tracking movement of reflective markers placed on the extremities. Recovery variables of interest included those previously found to distinguish fallers from non-fallers [5]:

- Reaction time: time from when the treadmill starts to the instant the recovery foot leaves the treadmill
- Step length: distance between the centroids of the initial recovery foot to that of the stance foot as a percentage of body height (%BH)
- Trunk flexion angle at step initiation: angle of the trunk relative to orientation prior to disturbance at the instant the recovery foot leaves the treadmill
- Trunk flexion angle at recovery step completion: angle of the trunk relative to orientation prior to

disturbance at the instant the recovery step makes contact with the treadmill surface
- Trunk angular velocity at recovery step completion: derivative of trunk flexion angle at recovery step completion

Fall incidence was compared between the ADT and control group using a chi-squared test. The relative risk and 95% confidence interval of falling for the ADT group were calculated using a 2x2 contingency table. Separate 2x2 ANOVAs were used to examine the effects of fall outcome and task condition on recovery kinematics. Significance was set at the p=0.05 level.

RESULTS AND DISCUSSION

The proportion of fallers in the ADT group was significantly greater than the control group (RR=2.62; 95% CI=1.65-4.15; p=0.024). This is the first study to suggest that an ADT negatively affects the ability of older women to avoid falling following a postural disturbance that mimics a trip.

Recovery kinematics of the ADT and control groups are presented in table 1. The effect of task on reaction time and trunk flexion angle at recovery step initiation was not significant. These results support suggestions that step initiation is controlled by subcortical circuits that are unaffected by external distractions [4]. Later phases (i.e. those that control of the trunk kinematics during recovery step completion) are likely modified by the cortical circuits that may be affected by ADTs [6]. During these later phases, the cortex may need to select an "optimal" recovery response [4] to control the forward progressing COM and avoid a fall. The main effect of task on trunk angular velocity at recovery step completion and recovery step length was not significant suggesting that either these kinematics are not controlled by cortical circuits, or, the cortex has selected these kinematics as an "optimal" recovery strategy [4]. In contrast, the main effect of task on trunk flexion angle at recovery step completion was significant (p=0.005). These results suggest that following a large and unexpected loss of dynamic stability, when attention had been diverted to a different task, the "optimal" response may be focused on controlling the forward velocity of the trunk and establishing a sufficient step length rather than the orientation of the trunk at recovery step completion.

Table 1: Fall incidence and kinematic measures (mean±SD).

	ADT (n=17)	Control (n=39)
Fallers (n, %)	8 (47%)	7 (18%)
Age (yrs)	63 ± 5.7	64 ± 7.7
Height (m)	1.62 ± 0.06	1.63 ± 0.07
Weight (kg)	77 ± 16.6	76 ± 17.4
Reaction Time (s)	0.29 ± 0.05	0.30 ± 0.04
Step Length (%BH)	11.6 ± 4.4	14.5 ± 7.2
Trunk Flexion Angle at Step Completion (deg)	40.7 ± 10.1	30.5 ± 8.8
Trunk Flexion Angle at Step Initiation (deg)	16.4 ± 6.0	14.7 ± 6.0
Trunk Angular Velocity at Step Completion (deg/s)	2.3 ± 49.4	-12.5 ± 45.9

Supporting previous work from our laboratory [5,7], these results indicate that slower reaction time (p=0.014), shorter step length (p=0.028), greater trunk flexion angle at step initiation (p=0.012), and greater trunk flexion angular velocity at recovery step completion (p=0.001) were able to differentiate fallers from non-fallers.

One limitation to this study is that the ADT group only received instruction to perform the math task and was unaware that the treadmill would be triggered during their performance. The control group received instruction that if the treadmill moved, they should do whatever was required to regain their balance. Future work should include an ADT group that has received instruction that the treadmill may move in order to determine how instruction set and a cognitive task separately influence recovery kinematics and fall incidence.

CONCLUSIONS

The addition of an ADT significantly affected the ability to avoid falling following a large postural disturbance mimicking a trip. Control of the trunk during the latter, but not earlier, phase of the recovery step was negatively affected by the addition of an ADT. How step training with a concurrent distracting task could improve the efficacy of the training is yet to be determined.

REFERENCES

1. Woollacott M, Shumway-Cook A. *Gait Posture* 2002; 16:1-14
2. Shumway-Cook A, et al. *J Gerontol A Biol Sci Med Sci* 1997(52):M232-240
3. Brown LA, et al. *J Gerontol* 1999; 54A:M165-M171
4. Jacobs JV and Horak FB. *J Neural Transm* 2007(114):1339-1348
5. Owings TM, et al. *Clin Biomech* 2001(16);813-819
6. Norrie et al. *Exp Brain Res* 2002(146): 315-321
7. Pavol MJ et al. *J Gerontol* 2001(56A): M428-M437

MODELING THE LEAN RELEASE AND SURFACE TRANSLATION PERTURBATIONS WITH AN INVERTED PENDULUM ON A CART

[1,2]Victorien Thiaux, [3]Stephen N. Robinovitch and [1,2]Cécile Smeesters

[1]Research Center on Aging, Sherbrooke QC, Canada
[2]Department of Mechanical Engineering, Université de Sherbrooke, Sherbrooke QC, Canada
[3]Department of Biomedical Physiology and Kinesiology, Simon Fraser University, Burnaby BC, Canada
e-mail: Cecile.Smeesters@USherbrooke.ca web: http://www.usherbrooke.ca/gmecanique

INTRODUCTION

To our knowledge only two studies have attempted to compare results from different postural perturbations. Mansfield and Maki [1] compared medium pulls and surface translations while standing and walking in place in multiple directions and in both younger and older adults. Moglo and Smeesters [2] compared large forward lean releases, lean releases with pulls and pulls while walking in both younger and older adults. Moreover, the latter showed that the angular positions and velocities at reaction time of the threshold trials formed a disturbance threshold line separating falls from recoveries, regardless of the postural perturbation.

Unfortunately, balance recovery experiments are time consuming and can be dangerous, especially if large postural perturbations at the threshold of balance recovery, where avoiding a fall is not always possible, are used. It would thus be useful to be able to theoretically predict if a given postural perturbation will lead to an unavoidable fall or if balance recovery is possible.

The purpose of this study was to determine if an inverted pendulum on a cart model could simulate both lean releases and surface translations at the threshold of balance recovery from perturbation onset (PO) to reaction time (RT).

METHODS

Experimental procedure: We determined the maximum forward initial lean angle from which 12 younger men and women (mean±SD=26.2±3.4yrs, range=22-32yrs) could be suddenly released and still recover balance. We also determined the maximum backward surface translation velocity from which each participant could be suddenly pulled and still recover balance. The initial lean angle and translational velocity were increased in ~5deg and 0.25m/s increments, until participants failed to recover balance twice at a given initial lean angle or translation velocity (with constant displacement=700mm and acceleration=2.5m/s^2), respectively. Balance recovery was successful if participants used no more than one step, did not touch the ground with their hands, and did not support their body weight in the safety harness. For the maximum perturbations, the lean angles (θ) and translational displacements (x) were measured from PO to RT using 2 force platforms, 1 load cell and 8 optoelectronic cameras with 16 passive markers.

Inverted pendulum on a cart model: The maximum perturbations were modelled in Matlab using an inverted pendulum mounted on a horizontally moving cart (Figure 1). The inputs were the masses of the participant (m) and cart (M), height of the participant (h), gravity (g=9.81m/s^2), waist pull force (F_1=0), carpet pull force ($F_2=M\ddot{x}$ modelled as a step) and ankle torque (τ=0). The outputs were the angular (θ) and translational (x) positions, velocities and accelerations from PO to RT. The initial conditions were θ_o, $\dot{\vartheta}_o\approx0$, x=0 and $\dot{x}$=0 for lean release (M=∞), and $\theta_o=0$, $\dot{\vartheta}_o$=0, x=0 and $\dot{x}$=0 for surface translation.

Data analysis: The root mean square (RMS) error was calculated between the experimental and theoretical results for angular position and velocity from PO to RT (Figure 2, black lines). The error between the experimental and theoretical results for the angular position and velocity at RT was also calculated (Figure 2, dots). Finally, the experimental and theoretical disturbance threshold lines formed by the angular positions and velocities at RT for the maximum perturbations were compared (Figure 2, blue and green lines).

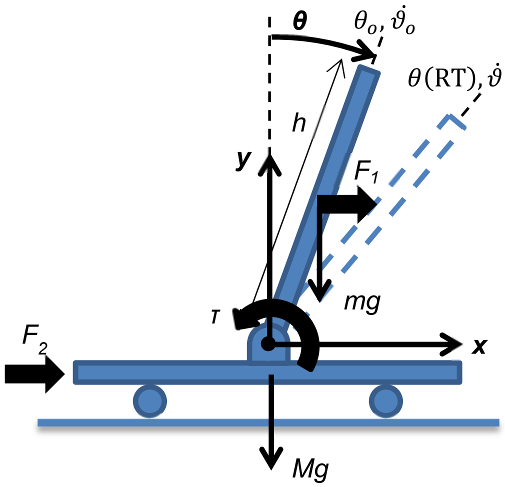

Figure 1: Inverted pendulum on a cart model.

RESULTS AND DISCUSSION

All RMS errors from PO to RT were significantly different from zero, but none exceeded 10% of the experimental disturbance threshold line intercepts (Table 1). Errors at RT were significantly different from zero only for angular position, and none exceeded 5% of the experimental disturbance threshold line intercepts. Finally, RMS errors for angular velocity were larger for surface translation than for lean release (p=0.005), while errors at RT for angular position were positive for lean release and negative for surface translation (p<0.001).

The experimental (y=-0.200x+36.1) and theoretical (y=0.172x+33.4) angular positions and velocities at RT for the maximum perturbations formed very similar disturbance threshold lines (Figure 2). Moreover, these disturbance threshold lines for lean releases and surface translations were very similar to the one obtained by Moglo and Smeesters [2] for lean releases, lean releases with pulls and pulls while walking.

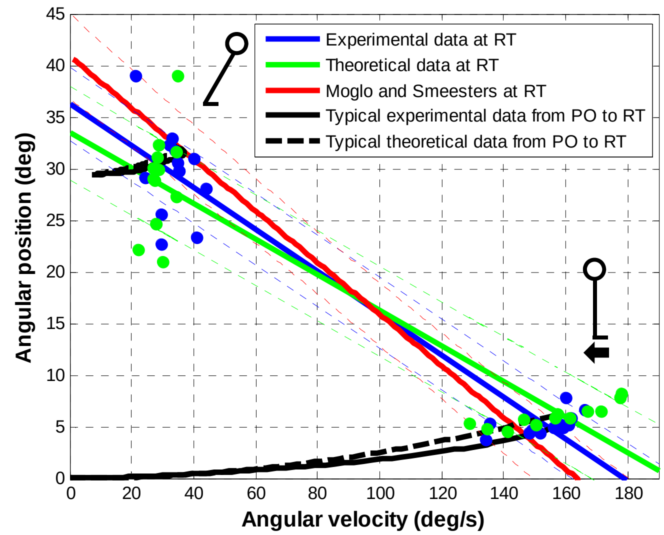

Figure 2 : Disturbance threshold lines (mean±SD).

CONCLUSIONS

The inverted pendulum on a cart model, having been validated, could be used to theoretically predict if a given lean release or surface translation perturbation will lead to an unavoidable fall or if balance recovery is possible, reducing the need for time consuming and dangerous experiments.

REFERENCES

1. Mansfield A and Maki BE. *J Biomech* **42**, 1023-1031, 2009.
2. Moglo KE and Smeesters C. *30th Annu Meet Am Soc Biomech*, Blacksburg VA, 2006.

ACKNOWLEDGEMENTS

The personnel at the Injury Prevention and Mobility Laboratory for technical assistance as well as NSERC grant 298229-2009 and CIHR grants AMG-100487 & TIR-103945 for financial support.

Table 1: Experimental versus theoretical errors (mean±SD) for angular position (θ) and velocity ($\dot{\vartheta}$).

	RMS error from PO to RT			Error at RT		
	Lean release	Surface Translation	p	Lean release	Surface Translation	p
θ (deg)	0.5±0.4 ***	0.6±0.3 ***	0.437	0.8±0.6 ***	-0.8±0.6 ***	**0.000**
θ / y intercept	1±1%	2±1%		2±2%	-2±2%	
$\dot{\vartheta}$ (deg/s)	8.7±5.7 ***	16.2±3.2 ***	**0.005**	4.0±7.2	-2.5±7.9	0.088
$\dot{\vartheta}$ / x intercept	5±3%	9±2%		2±4%	-1±4%	

PO: Perturbation Onset, RT: Reaction time. Significantly different from zero: * p≤0.05, ** p≤0.01, *** p≤0.001.

SINGLE-LEG DYNAMIC STABILITY IN FIT, YOUNG ADULTS: LOWER EXTREMITY STRENGTH AND CORE STRENGTH AS PREDICTORS

Gary D. Heise, Emily Esselman, Christopher Silvernale, and Jeremy D. Smith

University of Northern Colorado, Greeley, CO, USA
email: gary.heise@unco.edu, web: http://www.unco.edu/nhs/ses/

INTRODUCTION

Dynamic stability describes the process of transitioning from movement to a quiet, standing posture. Various measures, based on the diminishing fluctuations in ground reaction forces (GRF) and center-of-pressure (COP) trajectories, are often used to assess this transition [1]. Sports medicine clinicians have assessed dynamic stability in athletes with compromised joints (e.g., ACL injuries, ankle instability), but the influence of lower extremity strength has not been examined [2].

Overall muscle strength, especially core and lower extremity muscle strength, is thought to enhance stability and reduce the risk of joint injury [3]. Unfortunately, stability is used in a variety of applications with different definitions that depend on a person's perspective. For example, gerontologists may use stability to help predict the potential for independence, while sports medicine specialists may focus on an athlete's rehab from a lower extremity joint injury. Regardless of the perspective, improving muscle strength is thought to enhance stability of the entire body and lower extremity joints.

The purpose of this experiment was to identify whether lower extremity muscle strength and core strength was predictive of single-leg dynamic stability among young, fit adults. It was hypothesized that stronger individuals would be more stable.

METHODS

Thirty-eight people volunteered for this study (18 men; 20 women). All participants were young, healthy, and active (age = 21.8 ± 2.4 yrs, mass = 73.3 ± 13.1 kg, height = 172.9 ± 7.9 cm). At the beginning of a single test session, the experimental protocol was explained and a written informed consent was obtained. Demographic and anthropometric data were collected in addition to a self-assessment of fitness and some details about the frequency, duration, and intensity of weekly workouts.

Participants performed a brief, 10-15 minute warm-up (e.g., walk, stretch, low-intensity exercise). Four dynamic, single-leg postural stability trials were collected: two from a forward hop; two from a medially directed hop. Ground reaction force (GRF) data were collected for 20 s at 100 Hz. A stability index (SI), based on root-mean-square values, was computed for both the medial-lateral (ML) and anterior-posterior (AP) GRF components [1]. The SI was calculated over 3 seconds, beginning 0.5 s after impact to avoid inclusion of the impact GRF peak.

Lower extremity muscle strength was determined with an isokinetic dynamometer. Maximal, isometric efforts were measured for: knee flexion; knee extension; ankle plantarflexion; and ankle dorsiflexion. Four tests of core muscle endurance were also performed in a randomized order: 1) isometric trunk flexor posture; 2) isometric trunk extensor posture; 3) the "trunk side plank" exercise on the left side; 4) the "plank" exercise on the right side. Participants were required to hold these positions for as long as possible [4].

Stepwise multiple regression was used to evaluate the predictive power of strength measures for dynamic stability. Lower extremity strength measures were normalized to body weight and core muscle endurance was expressed as a duration.

RESULTS AND DISCUSSION

Six of the stepwise regression models were statistically significant with back extensor muscle endurance identified as the most frequent predictor variable. No secondary, predictor variables were identified after the primary one shown in Table 1. The regression model with the highest amount of explained variance is shown in Figure 1. The stability indices (SI) for the AP direction of the medial hops (right and left) produced no significant predictors (not shown in Table 1).

Table 1: Dependent variables (stability indices) and the significant predictor variable for each regression model.

Dep Var	Predictor	r	adj r^2	*p*-value
LF-SI-AP	Core-Ext	-.36	.11	.025
LF-SI-ML	Core-Ext	-.32	.08	.047
LM-SI-ML	LtKneeExt	-.34	.09	.034
RF-SI-AP	Core-Ext	-.38	.12	.019
RF-SI-ML	Core-Ext	-.47	.20	.003
RM-SI-ML	Core-Ext	-.35	.10	.029

L=left; R=right; F=forward; M=medial; SI-AP=stability index based on AP GRF; SI-ML=stability index based on ML GRF; Core-Ext=back extensor endurance; LtKneeExt=normalized knee extensor strength.

A lower SI indicates better dynamic stability and a longer endurance time for back extensor muscles is related to greater strength [4]. Therefore, the direction of the relationships between those variables in the five significant models shown in Table 1 was expected. (i.e., lower stability indices associated with longer endurance times).

Although one significant regression model included a lower extremity strength measure (for LM-SI-ML), it was surprising that no other leg strength measures were included. Our expectation was based on the findings of worse dynamic stability in subjects with functionally compromised ankle and knee joints [2]. Muscle strengthening is commonly prescribed to overcome such joint deficiencies, but our results did not show greater joint strength being associated with better dynamic stability. Overall core strength is frequently proposed as an important element of overall fitness and our results clearly show that back extensor muscle strength is the most important contributor to dynamic stability. These results are limited to young, active people and future work should focus on groups representing different ages and activity levels.

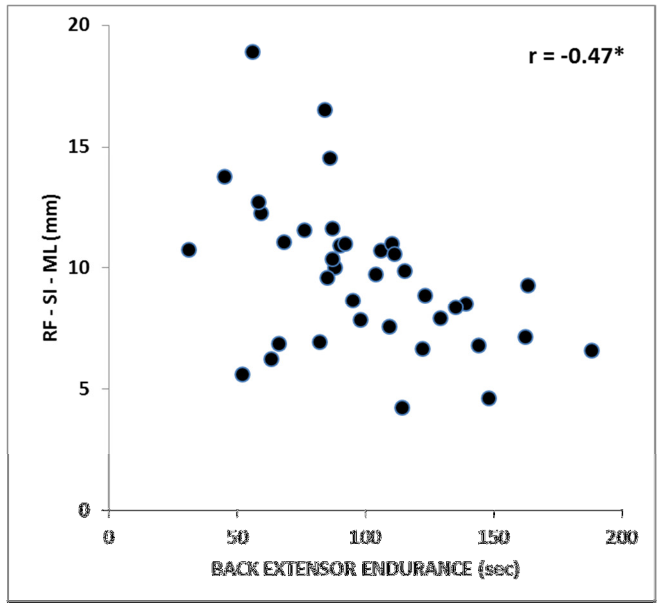

Figure 1: Scatterplot of extensor muscle endurance and the medial-lateral stability index (SI) for a right-footed, forward landing. *p<.05

CONCLUSIONS

After considering muscle strength at the knee and ankle, as well as musculature associated with the body's core, the endurance of back extensor muscles was the best predictor of dynamic stability. This conclusion was reached for multiple conditions (i.e., right and left leg; two different directions of movement-landings).

REFERENCES

1. Wikstrom, EA, et al. *J Sci Med Sport*, 11, 106-111, 2008.
2. Ross, S et al. *J Athl Training,* **40**, 298-304, 2005.
3. Leetun, DT et al. Med Sci Sports Exerc, 36, 926-934, 2004.
4. McGill, SM et al. *Arch Phys Med Rehab*, 80, 941-944, 1999.

DIFFERENCES IN CENTER OF PRESSURE REGULARITY IN STABLE- AND UNSTABLE-SURFACE ATHLETES

[1]Douglas Powell and [2]D.S. Blaise Williams

[1]Campbell University, Buies Creek, NC, USA
[2]Commonwealth Sports Medicine, Glen Allen, VA, USA
Email: dpowell@campbell.edu

INTRODUCTION

Biological signals contain inherent variability [1]. Exaggerated regularity (diminished variability) has been associated with advancing age, loss of function or pathology [1]. Previous research has investigated changes in the regularity of postural sway with advancing age, activity [2] and concurrent cognitive demands [3]. It has been demonstrated that active individuals exhibit better postural control compared to their inactive counterparts as measured by nonlinear measures of regularity [2]. However, no research has compared balance maintenance strategies in positive and negative feedback training paradigms. Therefore, the purpose of this study was to quantify differences in regularity of postural sway in individuals with positive and negative feedback training compared to sedentary individuals.

METHODS

Twenty-four healthy young adults volunteered to participate. Participants were free of musculoskeletal or neurological conditions that would affect postural steadiness. Participants were placed into one of three groups based on athletic experience. Unstable-surface athletes were characterized as individuals that regularly participated in sports associated with a negative feedback paradigm (i.e. surfing). A Smart Balance Master System 8.0 (NeuroCom International, Inc., Clackamas, OR, USA) was used to measure postural control. Force data were measured (100 Hz) using two force platforms (22.9 x 45.7 cm) within the Smart Balance Master System. Participants completed five successful 40-second trials during quiet standing.

Ground reaction forces were digitally filtered using a 50 Hz cut off frequency. Center of pressure was calculated from the given force platform data. ApEn was calculated as follows:

$$ApEn(m,r,N) = \ln\left[\frac{C_m(r)}{C_{m+1}(r)}\right]$$

where m was the length of compared runs (m = 2), r was the similar criterion (r = 0.20), N was the number of measurements in the time series (N = 4000) and C was the number of vectors defined by m based on the r criterion. Using Matlab software (Mathworks, Natick, MA) we calculated ApEn values for the ML and AP components of the CoP data, independently. A lag of 10 was used to counteract the effects of the excessively high sampling rate for nonlinear measures. Therefore, only every 10th point in the raw time series was used in the ApEn calculation, functionally reducing the sampling rate to 10 Hz.

Two univariate ANOVAs were used to determine the effect of group on ApEn values. In the presence of a significant main effect post-hoc t-tests were used to determine the source of the significant main effect. Significance was set at $p<0.05$.

RESULTS AND DISCUSSION

In the mediolateral direction (Figure 1), ApEn was significantly different between the non-athletes and stable-surface athletes ($p=0.006$) and between the stable- and unstable-surface athletes ($p=0.043$). No significant differences were observed between the non-athletes and unstable-surface athletes ($p=0.064$). In the anteroposterior direction (Figure 2), ApEn values were significantly lower in the unstable-surface athletes compared to the non-athletes ($p=0.041$) and stable-surface athletes ($p=0.043$). No differences were observed between the non-athletes and stable-surface athletes ($p=0.471$).

CONCLUSIONS

The findings of this study suggest that stable- and unstable-surface athletes exhibit unique postural control strategies. These observations likely relate surface paradigm in which the athletes train. Specifically, the unstable-surface athletes alter the position of the base of support with respect to the body's center of mass while the stable-surface athletes alter the position of their center of mass with respect to the base of support. The distal-to-proximal versus proximal-to-distal strategies may underlie the observed differences in regularity of postural sway.

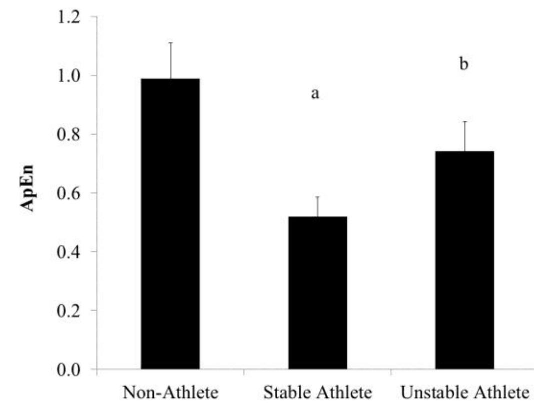

Figure 1. ApEn values for the ML CoP in non-athletes, stable-surface athletes and unstable-surface athletes. [a] – denotes significantly different than non-athletes, [b] – denotes significantly different than stable-surface athletes.

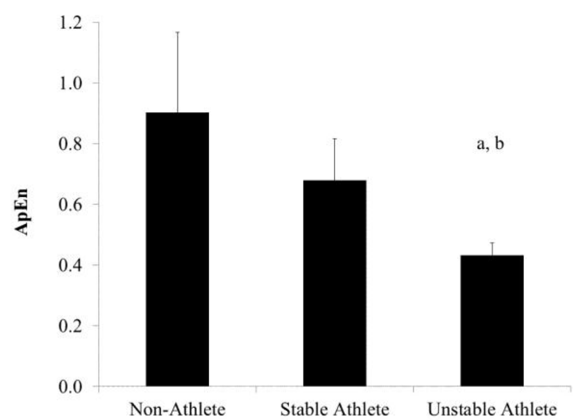

Figure 2. ApEn values in non-athletes, stable athletes and unstable athletes. [a] – denotes significantly different than non-athletes, [b] – denotes significantly different than stable-surface athletes.

REFERENCES

1. Pincus, SM et al., *J Clin Monit*. 7(4): 335-345, 1991.
2. Lamoth, CJ, et al., *Gait Posture.* 35(3): 489-493.
3. Cavanaugh, JT et al., *J Neuroeng & Rehabil.* 4:42, 2007.

MEASUREMENT OF HUMAN/BICYCLE BALANCING DYNAMICS AND RIDER SKILL

Stephen M. Cain, James A. Ashton-Miller and Noel C. Perkins

University of Michigan, Ann Arbor, MI, USA
email: smcain@umich.edu

INTRODUCTION

Experimental measurements of human/bicycle dynamics are needed to advance our understanding of how humans maintain balance of a bicycle and to identify metrics useful for quantifying rider skill. The objectives of this study were to use experimental data to quantify: 1) the relationship between center of pressure and center of mass movement of the bicycle/rider system, 2) the types of control used by riders, and 3) the differences between skilled and novice riders. We hypothesized that the lateral position of the center of mass is highly correlated to the lateral position of the center of pressure, steer rate is highly correlated to the roll rate of the bicycle, rider lean is highly correlated to bicycle roll, and skilled riders use significantly less steering effort and exhibit less variation than novice riders.

METHODS

We tested 14 subjects (4 females, 10 males; age = 26.4 ± 6.0 years, body mass = 71.1 ± 12.8 kg; mean ± standard deviation). The University of Michigan Institutional Review Board approved the study, and all subjects gave informed consent. We classified seven subjects as “cyclists” and seven subjects as “non-cyclists.” The cyclists all went on regular training rides, belonged to a cycling club or team, competed several times per year, and had experience using rollers for training. The non-cyclists knew how to ride a bicycle but did so only occasionally for recreation or transportation and did not identify themselves as skilled cyclists. Each subject rode a bicycle on training rollers in five experimental conditions distinguished by pedaling cadence (via a metronome) and bicycle speed (via gearing). The five conditions were executed in the following order: 1) cadence 80 rpm and speed 5.08 m/s, 2) cadence 80 rpm and speed 7.19 m/s, 3) cadence 80 rpm and speed 6.98 m/s, 4) cadence 80 rpm and speed 2.58 m/s, and 5) cadence 40 rpm and speed 1.29 m/s. Rollers, which constrain the bicycle in the fore/aft direction but allow free lateral movement, require the rider to maintain balance of the bicycle. The dynamics of a bicycle on rollers are similar to those of a bicycle overground [1].

We conducted experiments indoors utilizing an instrumented bicycle, a motion capture system, and training rollers mounted on a force plate. The bicycle [2] had embedded sensors that measure steer angle, steer torque, bicycle speed, and bicycle frame roll rate. In addition, we calculated the steering power from the steer torque and steer angular velocity. The motion capture system (Optotrak 3020, NDI) measured the positions of three markers attached to the bicycle frame, which we used to calculate the roll angle of the bicycle frame. The force plate (OR6-5-2000, AMTI) beneath the roller assembly measured the net force and moment that the rider/bicycle/rollers exerted on the ground. These reactions were later used to calculate the lateral position of the bicycle/rider center of pressure (y_{COP}) and center of mass (y_{COM}) [3] and the rider lean angle (Fig. 1A). Utilizing the measured and calculated quantities, we examined standard deviations of signals and cross-correlations between signals to quantify performance and control strategies. We used a mixed linear model to test for significant effects (α=0.05).

RESULTS AND DISCUSSION

For a perfectly balanced bicycle/rider traveling in a straight line, we would expect $y_{COM} = y_{COP}$. However during actual bicycle riding, similar to human standing, y_{COM} will deviate from y_{COP} in response to disturbances. Instead we expect that the center of mass will track the center of pressure, as illustrated by a representative trial in Fig. 1B. We quantify balance performance by calculating the cross-correlation (R^2) of y_{COM} to y_{COP}. For perfectly balanced riding, R^2 would be equal to one (1.0). However for actual bicycle riding, the value is less than one, as illustrated in Fig. 2.

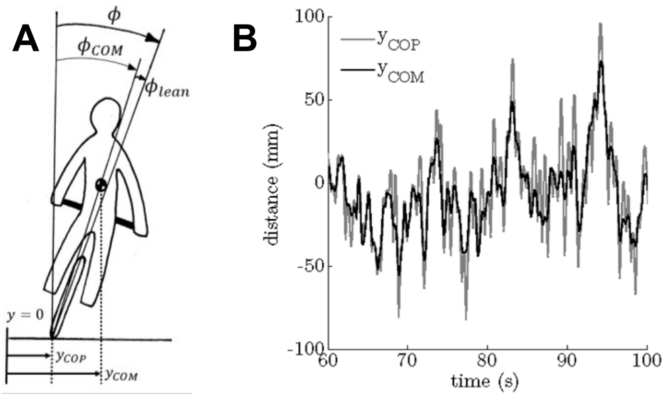

Figure 1. (**A**) Rear view of the bicycle/rider. The center of mass roll angle (ϕ_{COM}) minus the bicycle roll angle (ϕ) equals the rider lean angle (ϕ_{lean}). (**B**) The lateral COM location (y_{COM}) closely tracks the lateral COP location (y_{COP}) during riding.

As expected, the lateral positions of the center of mass and center of pressure are highly correlated during bicycle riding (R^2, Fig. 2). Our data do not indicate a significant effect of rider type (F=0.041, p=0.841), but do show significant effects for both speed (F=29.113, p<0.001) and the rider type/speed interaction (F=14.843, p<0.001). All riders demonstrated high R^2 values at low speeds; but as speeds increased, cyclists maintained higher R^2 values (i.e., better performance) than non-cyclists.

Having used cross-correlation to quantify balance performance, we also found that cross-correlation of steer rate to bicycle roll rate quantifies steer control (similar to [4]); and likewise the cross-correlation of rider lean angle to the bicycle roll angle quantifies rider lean control. At higher speeds, skilled riders (cyclists) achieved greater balance performance by employing more rider lean control (F=17.639, p<0.001) and less steer control (F=4.650, p=0.035) compared to novice riders (non-cyclists). In addition, skilled riders used less steer control effort as measured by average positive steering power (F=19.213, p<0.001) and standard deviation of steer angle (F=13.904, p<0.001) and less rider lean control effort as measured by the standard deviation of the rider lean angle (F=19.643, p<0.001).

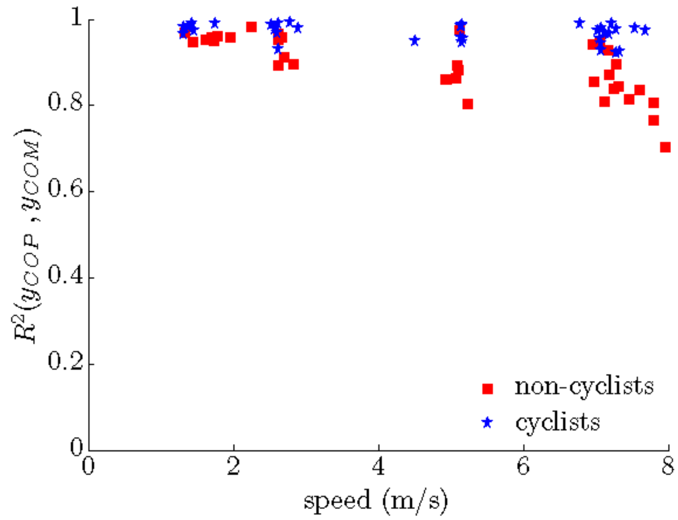

Figure 2. Cross-correlation of y_{COM} to y_{COP} versus speed.

CONCLUSIONS

The superior balance performance of skilled versus novice riders is revealed by highly correlated lateral positions of the center of pressure and center of mass (coefficients of determination of 0.97 versus 0.89, respectively). In achieving their superior balance performance, skilled riders employed more rider lean control, less steer control, and used less control effort than novice riders. The reduction in balance effort for skilled riders was not due to any reduced demands for balance. The metrics we introduce here can be used to quantify balance performance of the bicycle/rider system in many contexts including: 1) the analysis of bicycle designs, 2) the performance of assistive technologies, and 3) the assessment of bicycle training programs.

REFERENCES

1. Dressel A and JM Papadopoulos. *Eur J Phys* **33**, L21, 2012.
2. Cain SM and NC Perkins. *Vehicle Syst Dyn* **50**, 1341-1364, 2012.
3. Zatsiorsky VM and DL King. *J Biomech* **31**, 161-164, 1998.
4. Cain SM et al. *Proceedings of ASME DSCC 2012*, Fort Lauderdale, FL, USA, 2012.

EFFECTS OF AGE AND OBESITY ON RISK OF SLIPPING DURING LEVEL WALKING

[1]Sara L. Matrangola, [2]Christina M. Rossi, [2]Maury A. Nussbaum, and [2]Michael L. Madigan

[1]High Point University, High Point, NC, USA
[2]Virginia Tech, Blacksburg, VA, USA
email: sara.matrangola@gmail.com

INTRODUCTION

Obesity is a major health concern that afflicts more than one-third of all adults in the United States [1]. Older adults, aged 60 and over, are also more likely to be obese compared to younger adults [1]. One of the many negative consequences associated with obesity is an increased risk of falling and subsequent disability in older adults [2]. It is possible that this increased risk of falling may be due to an increased risk of slipping. To our knowledge, only one study has directly examined the effects of obesity on risk of slipping, and this study was limited to young adults and a small sample size (*n*=5 per group) [3]. Therefore, the effects of obesity on the risk of slipping, and the influence of age on this relationship, remains unclear. The goal of the current study was to investigate the effects of obesity, age, and their interaction on the risk of slipping during level walking. We hypothesized that obese adults would have an increased risk of slipping, and that age would exacerbate this difference.

METHODS

Seventy-eight participants completed this study including 21 healthy-weight (HW) young adults (age = 25.0±4.3 yrs, BMI = 22.3±2.2 kg/m^2), 20 obese (OB) young adults (age = 23.6±3.3 yrs, BMI = 33.6±3.3 kg/m^2), 23 HW older adults (age = 64.1±8.4 yrs, BMI = 24.2±1.8 kg/m^2), and 20 OB older adults (age = 63.5±9.5 yrs, BMI = 32.9±3.1 kg/m^2). All participants were required to pass a screening designed to exclude those with self-reported medical conditions, such as musculoskeletal, neurological, or balance disorders, that could impact the validity of the results, and all participants provided informed consent.

Participants walked at a self-selected speed along a 10m level walkway. During each of four trials, the positions of selected anatomical landmarks on the feet were sampled at 100 Hz using a Vicon MX motion analysis system with T10 cameras (Vicon Motion Systems Inc., Los Angeles, CA), and ground reaction forces were sampled at 1000 Hz using a force platform (Bertec Corporation, Columbus, OH). Risk of slipping was quantified using resultant heel velocity at heel contact, and the peak resultant required coefficient of friction (RCOF) during the weight acceptance portion of stance time, which was calculated as the ratio of total shear force to normal force during stance.

A three-way mixed-model analysis of covariance (ANCOVA) was used to investigate the effects of obesity (HW or OB), age (young or older adults), foot (dominant or nondominant), and obesity x age interaction on risk of slipping measures. Gait speed and step length were also included as covariates due to their effect on peak RCOF [4]. Effect sizes (ES) for significant main effects were calculated as the difference in the means divided by the standard deviation [5]. A two-way ANOVA was also used to investigate the effects of obesity, age, and their interaction on gait speed and step length. Statistical analyses were performed using JMP Pro 10 (SAS Institute, Inc., Cary, NC).

RESULTS AND DISCUSSION

At heel contact, older adults exhibited a 12.6% higher heel contact velocity compared to younger adults (p=0.013, ES=0.444). The non-dominant foot also exhibited a 2.2% higher heel contact velocity compared to the dominant foot (p=0.005, ES=0.078).

During weight acceptance in early stance, older adults exhibited a 2.5% lower peak resultant RCOF compared to young adults (p=0.031, ES=0.217), and OB adults exhibited a 2.8% higher peak resultant RCOF compared to HW adults (p=0.031, ES=0.203, Figure 1). The non-dominant foot also exhibited a 2.0% higher peak resultant RCOF compared to the dominant foot (p<0.001, ES=0.155).

During push-off in late stance, OB adults exhibited a 10.7% higher peak resultant RCOF (p<0.001, ES=0.790, Figure 1) compared to HW adults. The dominant foot also exhibited a 2.9% higher peak resultant RCOF compared to the non-dominant foot (p=0.006, ES=0.198).

Gait speed was 7.4% lower (p=0.008, ES=0.575) and step length was 4.2% shorter (p=0.019, ES=0.483) in obese adults (Table 1), but neither gait parameter differed with age.

Table 1. Gait Parameters (mean±s.d.)

	HW	OB
Gait Speed (m/s)^{ob}	1.34±0.17	1.24±0.15
Step Length (m)^{ob}	0.69±0.06	0.67±0.06

^{ob} denotes a significant obesity effect (p<0.05)

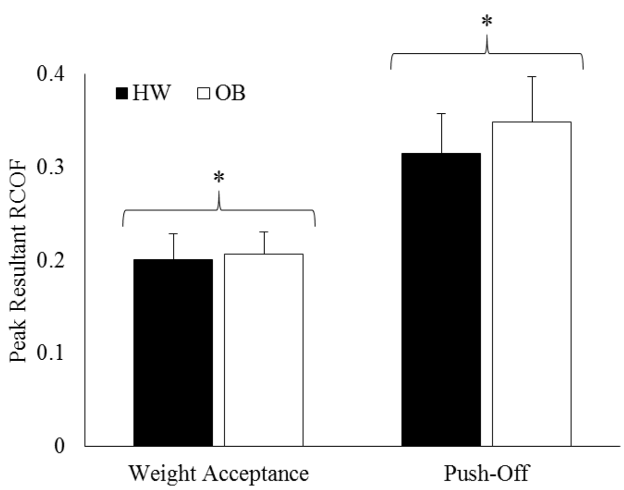

Figure 1. Least square means and standard errors for peak resultant RCOF.

Obesity was associated with an increased risk of slipping during the weight acceptance and push-off phases of stance. The small effect size during weight acceptance suggests that obese adults are only at a slightly greater risk of slipping during weight acceptance compared to their healthy-weight counterparts. The larger effect size observed during push-off suggests a larger risk of slipping during push-off. A prior study found no difference in resultant RCOF, gait speed, nor step length between young obese and healthy-weight adults [3].

We found no evidence that obesity increases the risk of slipping at heel contact. Additionally, we did not find evidence that age exacerbated the effects of obesity on risk of slipping.

Older adults exhibited a higher resultant heel velocity at heel contact and smaller resultant RCOF at weight acceptance compared to young adults. Effect sizes indicate that age moderately increases the risk of slipping at heel contact, but that age only minimally decreases the risk of slipping at weight acceptance. Similarly, previous research has shown older adults to have a significantly higher heel contact velocity, indicating a greater risk of slipping, though no significant differences were found in RCOF values between young and older adults [6]. Changes in gait associated with aging have been thought to produce a “safer” gait pattern, resulting in reduce RCOF values in older adults. However, in cases where the available coefficient of friction is below typical RCOF values for both young and older adults, the increased heel contact velocity could put older adults at a higher risk of slipping [6].

CONCLUSIONS

Obesity was associated with an increased risk of slipping during weight acceptance and push-off phases of stance, but age did not exacerbate these effects of obesity. Other effects of age were found that were similar to prior research.

REFERENCES

1. Ogden CL, et al. *NCHS Data Brief* **82**, 2012.
2. Himes CL, et al. *J Am Geriatr Soc* **60**,124-9,2012.
3. Wu X, et al. *J Biomech* **45**, 1042-7, 2012.
4. Anderson DE. *Proceedings of ASB ’09,* State College, PA, USA, 2009.
5. Portney LG and Watkins MP, *Foundations of Clinical Research*, Pearson Education, Inc., 2009.
6. Lockhart TE, et al. *Ergonomics* **46**,1136-60, 2003.

ACKNOWLEDGEMENTS

This work was supported by grant R01OH009880 and a NSF Graduate Research Fellowship (CMR).

THE TEST-RETEST RELIABILITY OF COMPENSATORY STEPPING THRESHOLDS OF YOUNG ADULTS

[1]Jeremy R. Crenshaw and [1]Kenton R. Kaufman

[1]Mayo Clinic, Rochester, MN, USA
email: kaufman.kenton@mayo.edu, web: http://mayoresearch.mayo.edu/mayo/research/biomechanics/

INTRODUCTION

Falls are the leading cause of accidental injury for older adults [1]. Identifying sensitive, reliable fall-risk assessments will improve the prescription of interventions. The ability to limit steps in response to a disturbance is reduced with old age, especially for those with a recent fall history [2-6]. This evidence suggests that compensatory stepping thresholds, or the minimum disturbance magnitudes that elicit single and multiple steps, may prospectively identify older-adult fallers. Clinically useful assessments, however, must be reliable. The purpose of this study was to initially evaluate the test-retest reliability of compensatory stepping thresholds by assessing young adults.

METHODS

Fifteen healthy, young adults (10 women / 5 men, age: 29 ± 7.5 years, height: 172.8 ± 8.8 cm, mass: 67.5 ± 13.8 kg) volunteered for this IRB-approved study. All participants provided written, informed consent prior to data collection.

Subjects visited the laboratory twice, with six to eight days between visits. At each visit, subjects were outfit with a harness attached to an overhead rail. As subjects stood on a microprocessor-controlled treadmill (ActiveStep®, Simbex, Lebanon, NH), 400 ms surface translations were delivered. The velocity profiles were triangle waveforms with peak velocities of 0.1-3.2 m/s, resulting in displacements of 2-64 cm.

Each visit consisted of three progressive series of disturbances to determine the following thresholds:

- *Anterior and Posterior Single-Stepping Thresholds*. Subjects were instructed to "try not to step" in response to anterior and posterior disturbances. Initial foot placement was at a comfortable width.
- *Anterior and Posterior Multiple-Stepping Thresholds*. Subjects were instructed to "try to take only one step" in response to anterior and posterior disturbances. Initial foot placement was at a comfortable width.
- *Lateral Single-Stepping Thresholds.* Subjects were instructed to "try not to step" in response to left and right disturbances. Feet were placed together, side-by-side. Thresholds were identified for the skill side (i.e. kicking limb) and stability side (i.e. non-kicking limb).

Within each progression, the direction (i.e. direction of the fall) and timing of disturbances were randomized. If a subject responded as instructed, the displacement was increased by one "level" for the next disturbance in that direction. Levels were incremented by 2 cm and 4 cm displacements for single- and multiple-stepping thresholds, respectively. The subject response was observed and recorded by a single investigator. Thresholds were defined as the disturbance displacement that elicited a failed response to four trials. Failed responses were due to stepping against instructions or support from the safety harness. The disturbance progression continued until thresholds in each direction were established.

The test-retest reliability of thresholds was assessed using intraclass correlations (ICC 2,1), Bland-Altman plots, and the true score 95% confidence interval [7,8].

RESULTS AND DISCUSSION

Stepping thresholds exhibited excellent agreement (ICC > 0.80, Figure 1). The anterior single-stepping threshold may have been less reliable (ICC = 0.65) because multiple available response strategies (ankle, knee, hip, mixed) increased inter-trial variability [9]. Repeatability was not analyzed for the anterior multiple-stepping threshold because nine subjects recovered from the largest disturbance in one step.

True single-stepping threshold confidence intervals were smaller than ±3.8 cm. A change of three levels would be considered real in all cases. The true posterior multiple-stepping threshold confidence interval was ±8.8 cm. A change of four levels would be considered real in all cases. For every decade of aging, the anterior single-stepping threshold decreases by about 1 cm, and the posterior multiple-stepping threshold decreases by about 5 cm [2,10]. Therefore, stepping thresholds are sensitive to the detrimental effects of aging that occur over 2-4 decades of life.

CONCLUSIONS

Compensatory stepping thresholds are reliable measures when assessing young adults. The ability of these measures to reliably and sensitively predict falls by older adults has yet to be determined.

REFERENCES

1. CDC WISQARS www.cdc.gov/injury/wisqars/index.html
2. Crenshaw JR, et al. *Proceedings of ASB,* Gainesville, FL, USA, 2012.
3. Mille M-L, et al., *J Neurophysiol* **90**, 666-674, 2003.
4. Pai YC, et al., *J Biomech* **31**, 1111-1118, 1998.
5. Rogers MW, et al. *J Gerontol* **56A**, M589-M594, 2001.
6. Hilliad MJ, et al. *Arch Phys Med Rehabil* **89**, 1708-1713, 2008.
7. Bland JM, et al., *Lancet* **327**, 307-310, 1986.
8. Weir JP, *J Strength Cond Res* **19**, 231-240, 2005.
9. Torres-Oviedo G, *J Neurophysiol* **98**, 2144-2156.
10. Crenshaw JR, *The Influence of Age on Compensatory Stepping Thresholds*, UIC, Chicago, 2011, hdl.handle.net/10027/9067.

ACKNOWLEDGEMENTS

Funding provided by NIH T32 HD0744

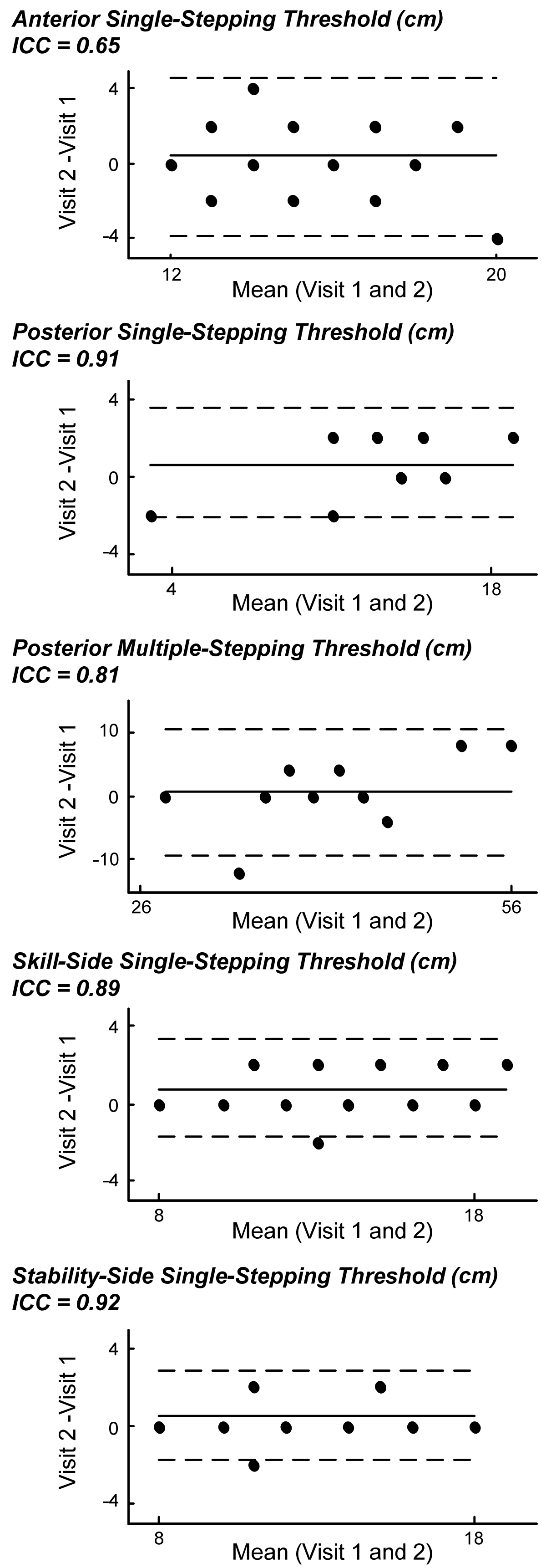

Figure 1: Bland-Altman plots of all thresholds.

DYNAMIC LUMBAR PURSUIT TASK WITH OCCUPATIONAL WHOLE-BODY VIBRATION EXPOSURE

Timothy D. Craig, and Sara E. Wilson

University of Kansas, Lawrence, KS, USA
email: sewilson@ku.edu,

INTRODUCTION

Whole body vibration has been identified as a significant risk factor in the etiology of low back pain and low back disorders [1-2]. Previous research has demonstrated changes in a variety of measures of lumbar neuromotor control with the exposure to vibration both during and after exposure [3-4]. These include increases in time to muscular response after sudden loading, increases in magnitude of motion after sudden loading, and increases in measures of proprioceptive errors [3-4]. The changes suggest that the neuromotor response is compromised by vibration exposure and that this compromise could lead to a greater risk for injury. However, the methods used to assess these changes have all been made in the laboratory and require a good deal of setup making them impractical for the industrial setting. As vibration exposures in the laboratory settings are more uniform and simplified relative to occupational exposures, there is a need to examine these effects in the occupational setting. The goal of this project was to develop a dynamic measure of lumbar neuromotor control that could be used easily in the workplace.

In a previous study, exposure to vibration was found to increase seated sway during exposure to vibration applied to the erector spinae musculature [5]. Since sway measures only require a force plate, such a measure could be used to test subjects in the workplace pre and post the workday. However, the previous study only looked at during vibration effects with a higher frequency exposure than typical in the workplace. Therefore, the goal of this study was to examine this measure post-exposure to a vibration at frequencies closer to the occupational setting.

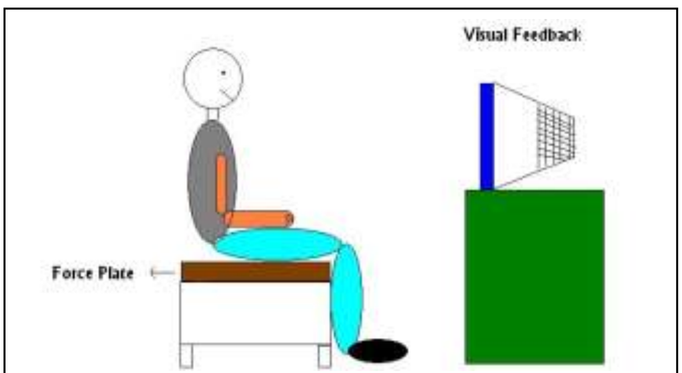

Figure 1: The experimental setup of the force plate and the visual feedback display on the computer screen

METHODS

Seven subjects (5 male, 2 female, weight 69 ± 11 kg, height 1.72 ± 0.05 m) participated in this study. Subjects with a history of low back pain and neuromuscular deficit were not allowed to participate. This study was approved by the human subjects committee, Univ. of Kansas-Lawrence. The subjects were tested under two conditions: before and immediately after whole body vibration exposure. For the testing, the subjects were instructed to sit on the force plate (Bertec, Columbus, OH) with hands on their lap and to let their feet and lower legs hang freely. An NI USB 6210 16-bit A/D board was connected to the force plate for the data acquisition and force plate data was collected at 100 Hz.

Three types of measures were assessed: 1. Quiet seated sway, 2. Tracking of a simple linear motion with center of pressure (COP), and 3. Tracking of a rotational motion with COP. For seated sway, the subjects were instructed to sit quietly on the force plate for 3 minutes with eyes closed. Subjects kept their hands on their laps and their feet were allowed to dangle freely.

For the tracking tasks, the COP was calculated and displayed on a computer screen (Fig. 1). Subjects were instructed to match their displayed center of pressure with a target that moved in 3 patterns: linear anterior-posterior (AP), linear medical lateral (ML), or circular . Each pattern was collected at a rate of 5s/cycle for 10 cycles.

Prior to the start of the experiment, the seated subjects were allowed to practice following the target until they were comfortable with the task. During the data collection, feedback was provided for the first 5 cycles of each pursuit task. During the last 5 cycles of each pursuit pattern the subjects were asked to continue following the pattern without feedback of their COP. This collection was performed before and after vibration exposure.

For the vibration exposure, the subjects were exposed to 20 minutes, seated, whole-body, random vibration (WBV) using a shaker table (Ling Electronics, Anaheim, CA). The random vibration profile was created to match the average vibration data collected from 3, 20-minute assessments of vibration exposure of a dump truck driver. Vibrations above 3 Hz (the lower frequency limit of the shaker table) were included in the creation of this profile. During the WBV period, subjects were also instructed to put their hands on their lap and to let their feet and lower legs hang freely.

RESULTS AND DISCUSSION

No significant differences were observed in mean sway speed during stable seated sway (p=1.0). There were no significant differences observed for the error in slope (p=0.214) or peak to peak (p=0.093) values for linear patterns. Errors were calculated by subtracting target position from actual COP. Nor were significant differences observed in the error of radius (p=0.165) or theta (p=0.543) for the circle pattern. However, examining the results of the circle task identified that iteration was significantly different (p=0.012) for the radius error and approaching significance (p=0.128) for the angle theta when examining repeatability.

CONCLUSIONS

Presently, the task created does not demonstrate a difference in the proprioceptive control of trunk posture resulting from WBV. A closer examination of the individual iterations identifies that the iterations progressively increase in differences for the circle pattern. This is believed to be a result of each successive iteration being further removed from the feedback condition. As the task is designed now, it is unable to provide useful information; however, it may be possible to adjust the task such that it would be sensitive to differences resulting from WBV. Based on the results of this study it would be recommended to remove the stable seated sway and increase the iterations of the pursuit patterns. This would allow for more iterations of the pattern and allow for alternating between feedback conditions. The observed trends may be strengthened with a larger sample size.

REFERENCES

1. Pope, M.H., Wilder, D.G., and Magnusson, M.L., A review of studies on seated whole body vibration and low back pain. 1999, Proc Inst Mech Eng [H], vol. 213, pp. 435-46.
2. Bernard, B.P., ed. Musculoskeletal disorders and work place factors. 1997, U.S. Department of Health and Human Services: Washington, D.C. 94-213.
3. Li, L., Lamis, F., and Wilson, S.E., Whole Body Vibration Alters Proprioception in the Trunk, International Journal of Industrial Ergonomics 38(9-10), pp. 792-800, 2008.
4. Arashanapalli, M., and Wilson, S.E. Paraspinal Muscle Vibration Alters Dynamic Stabilization in the Trunk, Journal of Biomechanical Engineering, 130(2), 2008.
5. Soltys, J.S., and Wilson, S.E., “Seated Postural Sway is Sensitive to Local Vibration”, Proceedings of the American Society of Biomechanics, Blacksburg, VA, 2006.

ACKNOWLEDGEMENTS

Research reported in this publication was supported by the National Institute of Arthritis and Musckuloskeletal and Skin Disease of the National Institutes of Health under Award Number 1R03AR061597-01. The content is solely the responsibility of the authors and does not necessarily represent the official views of the National Institutes of Health.

COMPARISON BETWEEN POLYNOMIAL AND LOGISTIC EQUATIONS FOR MODELING THREE DIMENSIONAL STRENGTH SURFACES

[1]John M. Looft, [1]Laura Frey Law

[1]University of Iowa, Iowa City, IA, USA
email: laura-freylaw@uiowa.edu

INTRODUCTION

Human strength capabilities have been studied for quite some time. Several strength relationships have been long recognized, such as torque-angle or length-tension relationships [1] and torque-velocity or force-velocity relationships [2]. These relationships have been used to characterize maximum joint torque using velocity or joint angle. Increasingly, three dimensional (3D) surfaces are being used as a function of both velocity and angle to represent human torque producing capability [3-8].

Modeling 3D force-length-velocity surfaces were first proposed at the single muscle level [9], as relatively uniformly saddle-shaped surfaces; particularly due to the “S-shaped” force-velocity relationship. Later this concept was expanded to joint complexes [3-8] to visually explain how these relationships affect maximum peak torque. While polynomial equations have been the most frequently used to model 3D strength surfaces [5-8]. We observed that polynomials can exhibit excessive curvature and non-physiological behaviors (i.e. torque crossing zero) when expanded outside of the originally measured data.

We hypothesized that logistic equations, often used to represent “S-shaped” relationships, may provide a better means to efficiently model 3D strength surfaces, while minimizing non-physiologic strength predictions near the end ranges of motion. Thus, the objective of this study was to compare polynomial and logistic equations when modeling normative 3D strength data, considering both quantitative (i.e., R^2 values) and qualitative (i.e. excessive curvature, torque crossing zero) assessments.

METHODS

We compared polynomial and logistic equation models based on existing 3D torque-angle-velocity data sets for the knee and elbow joints [4]. Up to 30 triplet data points, i.e., mean peak torque as a function of joint angle and movement velocity, were available for flexion and extension torque directions for both males and females for a total of 8, 3D strength surfaces. Eccentric peak torques were estimated as 120% of maximum torque based on a review of available literature (unpublished data)

The data were plotted and curve fit (TableCurve3D, Richmond, CA) using the Levenburg-Marquardt algorithm for fitting a third-order polynomial and a logistic equation. The polynomial equation had 10 parameters; the logistic equation had only 7. The parameters and R^2 values for each approach were recorded for each strength surface (8 total).

To assess each model’s strength predictions beyond the ranges of motion reported (15° – 100° and 15° – 110° for knee and elbow joints, respectively), the surfaces were plotted to a full normal joint range of motion (0° to 140°) [10]. Qualitatively the surfaces were examined to determine if the models predicted a non-physiological strength response (i.e. negative torque) or displayed excessive non-physiological curvature in the end ranges.

RESULTS AND DISCUSSION

The R^2 values and the minimum torque values for each of the 3D strength surfaces are provided in Table 1. Both sets of equations were able to fit the mean experimental data well; the median R^2 values were 0.983 and 0.971 for the polynomial and logistic equations, respectively. When extrapolating the models to the full range of motion, however, differences became apparent. All of the 8 polynomial strength surfaces (male and female, knee and elbow, flexion and extension) predicted non-physiological negative torque values (Table 1) as well as unlikely excessive curvature at the end ranges of motion (Figures 1A). Conversely, only 2 of the logistic equation surfaces (see Table 1) predicted negative torque values, with the minimum torque value magnitudes within 2 Nm of zero. One example of knee flexion strength surfaces are plotted in Figure 1.

A)

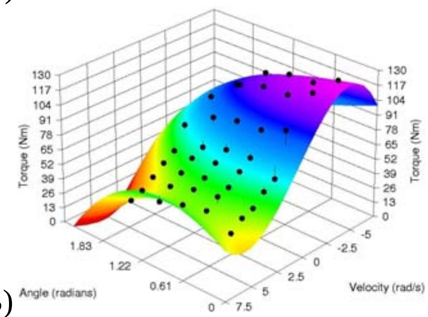

$R^2 = 0.979$

B)

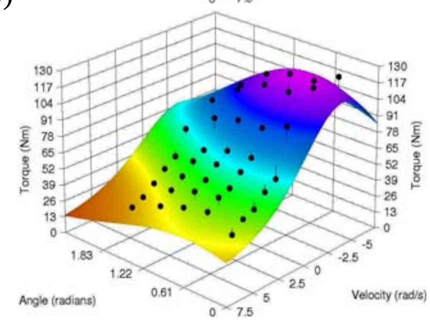

$R^2 = 0.970$

Figure 1: Knee flexion peak torque models for men are shown using A) a polynomial equation and B) a logistic equation.

CONCLUSIONS

This investigation found that while both polynomial and logistic equations fit torque-angel-velocity data for the knee and elbow joints equally well within the tested ROM, the logistic equations result in several qualitative advantages over the polynomial approach. The logistic equations demonstrated less extreme curvatures at the endpoints of motion and were better able to predict physiologically-consistent torque values through the full ROM (less negative torque values). The use of these logistic equations could provide DHMs more physiologically accurate strength predictions throughout the ROM, ultimately resulting in better assessments of task performance and safety.

REFERENCES

1. Gordon, A.M., A.F. Huxley, and F.J. Julian, *Variation in Isometric Tension with Sarcomere Length in Vertebrate Muscle Fibres*. Journal of Physiology-London, 1966. **184**(1): p. 170-+.
2. Hill, A.V., *The heat of shortening and the dynamic constants of muscle*. Proceedings of the Royal Society B-Biological Sciences, 1938. **126**(843): p. 136-195.
3. Anderson, D.E., M.L. Madigan, and M.A. Nussbaum, *Maximum voluntary joint torque as a function of joint angle and angular velocity: Model development and application to the lower limb*. Journal of Biomechanics, 2007. **40**(14): p. 3105-3113.
4. Frey-Law, L.A., et al., *Knee and Elbow 3D Strength Surfaces: Peak Torque–Angle–Velocity Relationships*. Journal of Applied Biomechanics, 2012. **28**(6): p. 726-737.
5. Khalaf, K.A. and M. Parnianpour, *A Normative Database of Isokinetic Upper-Extremity Joint Strengths: Towards The Evaluation of Dynamics Human Performance*. Biomedical Engineering Applications, Basis & Communications, 2001b. **13**: p. 79-92.
6. Khalaf, K.A., M. Parnianpour, and T. Karakostas, *Surface responses of maximum isokinetic ankle torque generation capability*. Journal of Applied Biomechanics, 2000. **16**(1): p. 52-59.
7. Khalaf, K.A., M. Parnianpour, and T. Karakostas, *Three Dimensional Surface Representation of Knee and Hip Joint Torque Capability*. Biomedical Engineering Applications, Basis & Communications, 2001. **13**: p. 79-92.
8. Khalaf, K.A., et al., *Modeling of functional trunk muscle performance: Interfacing ergonomics and spine rehabilitation in response to the ADA*. Journal of Rehabilitation Research and Development, 1997. **34**(4): p. 459-469.
9. Winters, J.M., *Hill-based muscle models: a systems engineering perspective*, in *Multiple Muscle Systems: Biomechanics and Movement Organization*, J.M. Winters and S.L.-Y. Woo, Editors. 1990, Springer: New York. p. 69-93.
10. Rothstein, J.M., S.H. Roy, and S.L. Wolf, eds. *The Rehabilitation Specialist's Handbook*. 2nd ed. 1998, Davis, F. A.: Philadelphia.

ACKNOWLEDGMENTS

The authors were funded in part by National Institutes for Health, K01AR056134, United Council for Automotive Research (USCAR, Dearborn, MI), and the University of Iowa Heartland Center Graduate Student Fellowship

Table 1: R^2 (minimum torque) values for the polynomial and logistic strength models

Male	**Flexion**	**Extension**	**Female**	**Flexion**	**Extension**
***Polynomial*†**			***Polynomial*†**		
Knee	0.979 (-15.9)	0.980 (-209.4)	**Knee**	0.986 (-26.6)	0.982 (-102.0)
Elbow	0.984 (-13.6)	0.988 (-7.1)	**Elbow**	0.973 (-3.1)	0.984 (-3.6)
***Logistic*‡**			***Logistic*‡**		
Knee	0.970 (14.1)	0.973 (19.1)	**Knee**	0.979 (19.5)	0.983 (14.0)
Elbow	0.971 (5.5)	0.968 (-1.7)	**Elbow**	0.952 (4.8)	0.955 (-0.5)

†$z = a + bx + cy + dx^2 + ey^2 + fxy + gx^3 + hy^3 + ixy^2 + jx^2y$

‡$z = 4ae^{(-((x-b)/c))} / ((1+e^{(-((x-b)/c))})^2) + 4de^{(-((y-e)/f))} / ((1+e^{(-((y-e)/f))})^2) + 16ge^{(-((x-b)/c)-((y-e)/f))} / ((1+e^{(-((x-b)/c))})^2 * (1+e^{(-((y-e)/f))})^2)$

OPTIMIZATION OF POROUS NITINOL GEOMETRY FOR USE IN BONE IMPLANTS

Sean Davis, Mohammed Elahinia, Ph.D

Department of Mechanical Engineering, University of Toledo
Contact: sean.davis2@rockets.utoledo.edu

INTRODUCTION

Nitinol shows promise for use in biomedical applications due to its high biocompatibility and super-elasticity. Recently Nitinol has drawn attention as a possible alternative to stainless steel and cobalt-chromium as a material for bone implants.[1] This is an appealing option as both Nitinol and bone exhibit a hysteretic stress-strain behavior (Fig. 1). More traditional metal implant materials are much stiffer than bone, which can lead to some regions of the bone being shielded from stress, possibly causing them to become osteoporotic. Although more similar to bone due to the hysteretic behavior, Nitinol is still much stiffer than any connective tissue. An option to decrease the stiffness of Nitinol is to use a porous material structure.[2] By varying the geometry, spacing, and volume of the pores in the structure, the implant can be tuned to various stiffness levels and hysteresis behaviors. This project aims to develop a system that makes use of Nitinol material models and shape optimization in order to design bone implants. The use of the shape optimization routine is unique in that it allows the mechanical properties of the implants to be customized precisely on a patient by patient basis.

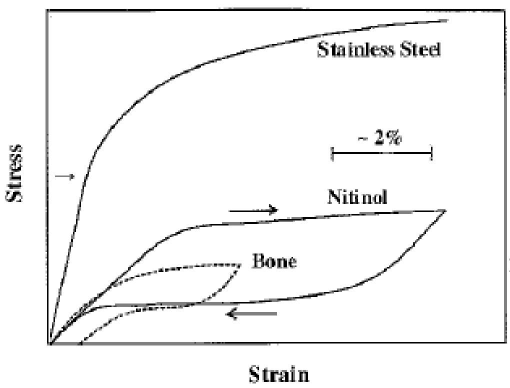

Figure 1: The stress strain relationships of bone and Nitinol.[3] Of special importance is the qualitatively similar hysteretic behavior of Nitinol and bone.

METHODS

To predict the behavior of porous Nitinol several simulations were performed using Abaqus FEA software. In order to account for the non-linear behavior of Nitinol the user-subroutine developed at Texas A&M was used.[4] By varying the relative densities of the Nitinol structure, relationships between porosity and compressive stress strain behavior were analyzed.

The geometries used during the initial simulations had a control placed on relative density, and relied on a random distribution of pore sizes and distribution. The results were then qualitatively compared to published stress-strain plots of porous Nitinol. The second set of simulations placed no control on relative density but instead strove to produce a porous structure with a target compressive behavior by varying the pore distribution, size and geometry. A simple shape optimization code was written to carry out this procedure.

RESULTS AND DISCUSSION

The preliminary results from the FEA simulations show promising qualitative similarities to published porous Nitinol compressive stress-strain behavior.[4,5] As the porosity of Nitinol structures increases we typically see a decrease in the initial slope of the stress strain behavior. This is reflected in the simulated behavior of porous Nitinol seen in Fig. 1. An additional quality that shows promise is the narrowing of the hysteresis between loading and unloading. The simulation also predicts this behavior seen in published stress-strain behavior. Moreover, the similarity between loading and unloading curves at strains greater than 8% is due to the material becoming denser as it is compressed. Once we begin actually producing porous structures a quantitative analysis will be carried out to further assess the model's predictions.

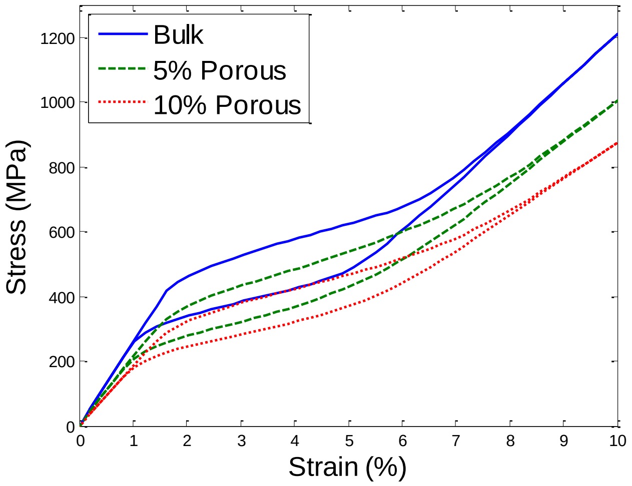

Figure 2: Stress-strain behavior of porous Nitinol collected during the first round of simulations

When a geometry corresponding to a desired compression behavior is determined, the Nitinol structure can be constructed using additive manufacturing techniques. Our lab recently purchased Phenix System's PXM which uses selective laser sintering to produce Nitinol parts from pre-alloyed Nitinol powders. With the PXM we will be able to verify that the geometries generated by the shape optimization routine do indeed match the prescribed compressive behavior.

In addition to the mechanical benefits obtained by creating a porous Nitinol material, there are also physiological implications. These include the potential negative consequences of increased surface area (and therefore possible increased risk for infection), and the positive benefits of bone ingrowth and implant stability. While important, these biological issues were beyond the scope of the current study.

CONCLUSIONS

The initial simulations show positive qualitative correlations to published experimental compressive behavior of porous Nitinol. A quantitative analysis of the accuracy of the model will be performed when samples of porous Nitinol are produced using the PXM. A promising initial result is that by varying the porosity of Nitinol structures the resulting stiffness and hysteresis can be varied.

REFERENCES

1. Bansiddhi A, et al. *Acta Biomaterialia* **4**, 773-782, 2008.
2. Bandyopadhyay A, et al. *Journal of Materials Science: Materials in Medicine* **20**, 29-34, 2009.
3. Silva T, et al. *Science and Technology of Materials* **17**, 34-37, 2005.
4. Aydoğmuş T, et al. *Journal of Alloys and Compounds* **478**, 705-710, 2009.
5. Bernard S, et al. *Journal of the Mechanical Behavior of Biomedical Materials* **13,** 62-68, 2012.

ACKNOWLEDGEMENTS

This work is funded by a grant "Nitinol Commercialization Accelerator" through Ohio's Third Frontier Program and by The University of Toledo.

INVESTIGATION OF THE UPPER CERVICAL SPINE BIOMECHANICS UNDER VARIOUS LOADING TYPE

[1,2] Wissal Mesfar and [1] Kodjo Moglo

[1] Royal Military College of Canada
[2] King Saud University
email: wissal.mesfar@rmc.ca, web: http://www.rmc.ca

INTRODUCTION

Understanding the biomechanical response of the cervical spine is of great interest in prevention from injuries, assessment and diagnosis. However, the complexity of the joint and its sensitivity let the experimental studies incapable to determine some specific parameters especially when it comes to estimate the stress and contact forces at the facets joint. Different movement can be done by the cervical joint complex and the biomechanical response can be different for each level to other. Due to the anatomy difference of the three levels of the upper cervical spine, the determination of the biomechanical response is more complex to be anticipated. That is why in this study we aim to quantify the contact force at different level of the upper cervical spine. We hypothesize that each level of the upper cervical spine reacts differently to a same applied loading.

METHODS

A previous 3D nonlinear head and neck (HN) complex finite element (FE) model is used for the simulation of this research. The model was developed and constructed based on adult CT scan and MRI images. The FE model consists of bony structures and their cartilage facet joints, the intervertebral discs (IVDs) and all the ligaments. Each ligament has been modeled by a number of uniaxial element except the transverse ligament which is modeled with shell element. All the ligaments were assigned a non-linear material properties [1]. However, linear and homogenous properties for the annulus and nucleus and the cartilage were considered. The bony structures were considered as rigid due to their greater stiffness to the adjacent soft tissue structures. For stable unconstrained boundary conditions, T1 is fixed while the cervical vertebrae are left free. In order to quantify the effect of the moment applied at different plane to the centre of mass of the head (CMH) on the upper cervical spine, a moment of 1.2 N.m was applied to simulate the left and right axial rotation, the left and right lateral bending, and the flexion and extension movement. The contact force at each level of the upper cervical spine was quantified in order to identify the most critical loading at each level. Only the results for the left facets joints were presented here since they can be concluded for the right facets joints.

RESULTS

The computed results indicate at 1.2 N.m moment loading applied to CMH that the highest contact force for the left C0-C1 facet joint is computed under the right axial rotation movement and the right lateral bending movement reaching 27 N and 18 N, respectively (Fig. 1). The CF under extension is nil until 0.6 N.m but it increases rapidly after 0.8 N.m to become higher than the CF computed in flexion at 1.2 N.m.

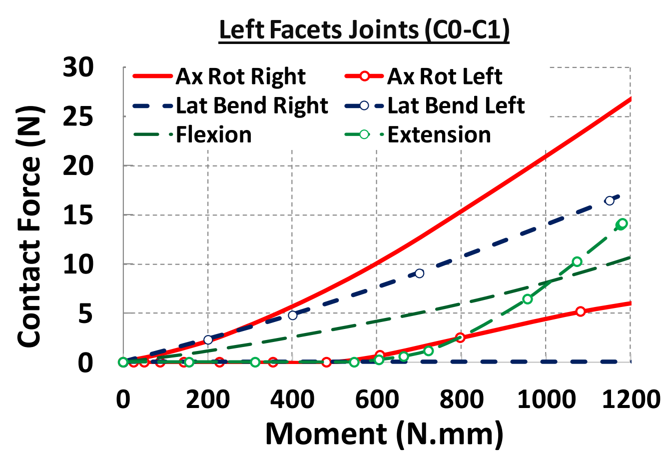

Figure 1: Contact force at C0-C1 left facet under 1.2N.m moment loading applied at the three major anatomical planes.

At the level C1-C2, the biomechanical effect is different than at C0-C1 and the highest CF was computed under the right lateral bending loading and the extension loading reaching 37 N and 33 N, respectively (Fig.2). The left and right axial rotation have a similar induced CF especially after 0.8 N.m. The CF under the right lateral bending loading continues to be nil as it is computed at left C0-C1.

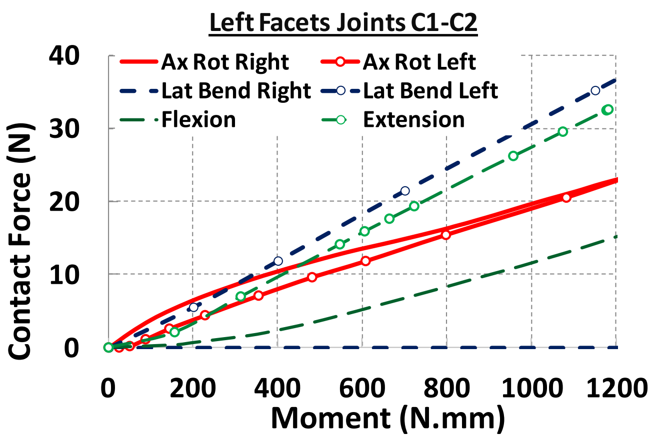

Figure 2: Contact force at C1-C2 left facet under 1.2N.m moment loading applied at the three major anatomical planes.

At C2-C3 left facet joint, the CF is maximum under 1.2N.m when the right axial rotation and extension were applied reaching 26N and 24N, respectively. For the same moment, the CF reaches 19N under the left lat bending movement (Fig.3).

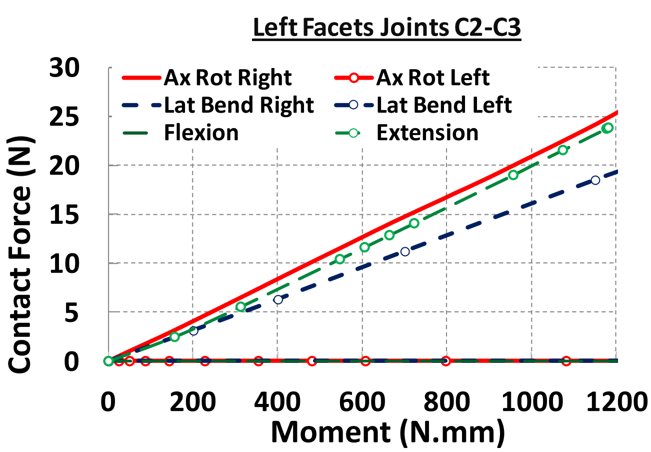

Figure 3: Contact force at C2-C3 left facet under 1.2N.m moment loading applied at the three major anatomical planes.

For all the other three considered movement, the CF at the left C2-C3 is nil.

DISCUSSION AND CONCLUSIONS

The biomechanical response of each level of the upper cervical spine depends of the applied loading. These results show clearly that each level of the upper cervical spine respond differently to a same type of loading. This can be explained by the difference of the anatomy of each level and of the interconnection mechanism between each level.

The right axial rotation movement is critical to the increase of the CF at the left C0-C1 and vise versa, i.e., the left axial rotation is the critical movement to the increase of the CF of the right C0-C1. This response is not conserved for the level left C1-C2, in which the left lateral bending becomes with the extension movement the most critical loading to the increase of the CF. Only one movement does not induce a CF for the two first levels, it is the right lateral bending. However at the left facets joint C2-C3, three movements do not induce any CF until 1.2N.m moment loading. These movements are the flexion, right lateral bending and the left axial rotation. The other loading induces at this level a CF that reaches a maximum of 26N at 1.2N.m applied in the right axial rotation moment. The presented results in this study were able to identify which is the critical movement for each of the three levels of the upper cervical spine. These results may be of great interest to the orthopedists to design rehabilitation adequate exercises following an injury in the upper cervical spine.

REFERENCES

1. Shim VPW, et al. *Exp. Mechanics*, **46**, 77–89, 2006.

ACKNOWLEDGEMENTS

The financial support from the Canadian Dept. of National Defence (DTAES 6) is gratefully acknowledged.

COMPUTERIZED MALLET CLASSIFICATION FOR BRACHIAL PLEXUS PALSY

Charlie Ewert, Vincent Crocher, and Na Jin Seo

University of Wisconsin-Milwaukee, Milwaukee, WI, USA
Email: crewert@uwm.edu, Web: https://pantherfile.uwm.edu/seon/www/

INTRODUCTION

The Mallet Classification assesses arm motion capability for patients with brachial plexus injuries using a series of five tasks [1]. For each task, the patient is given a score ranging from II to IV with IV being the best (Fig. 1). Doctors track the score to evaluate if a patient's arm motion improves after surgery or rehabilitation.

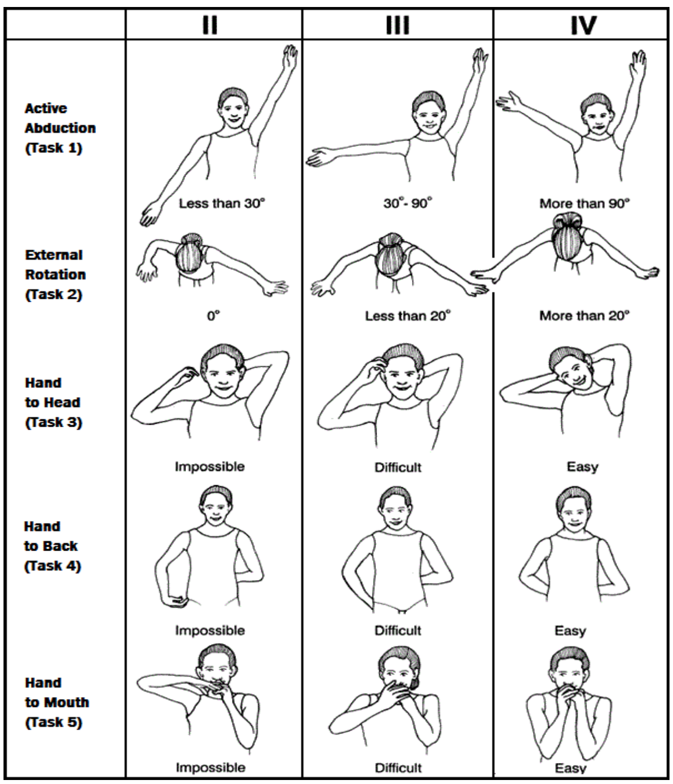

Figure 1: Illustration of the arm motions for each score for the five tasks of the Mallet Classification.

We developed a computerized Mallet Classification. This computerization provides a tool for patients' self-evaluation, thereby reducing therapists' workload. It can also improve the quality of clinicians' work by providing objective and detailed joint angle data compared to the crude II to IV score based on visual observation. In addition, the computerized clinical assessment can be useful for telemedicine, providing tele-evaluation to out-of-access patients.

METHODS

The computerized Mallet Classification is performed using our custom-developed computer program and a Kinect (Microsoft, Redmond, WA). The computer program prompts the patient to perform each task one by one, while obtaining the position data of the patient's body in three-dimensional space using the Kinect.

With the position data, the program calculates the shoulder abduction angle, shoulder external rotation angle, elbow flexion angle, as well as distances between body landmarks that relate to the task being conducted. The program makes a scoring decision based on the criteria detailed in Table 1, and displays the score for the patient upon completion of each task. The best score in the five second duration of the task is displayed.

In order to evaluate the accuracy of the computerized Mallet Classification, seven healthy young adults performed the tasks of the Mallet Classification while both the computer-based score and the conventional score from visual observation by the investigator were obtained for each task. Accuracy was computed as the percentage of match between the computerized and conventional scores.

RESULTS AND DISCUSSION

The computerized Mallet Classification ran well without computer errors and the need for additional instructions or assistance in person. The computerized Mallet Classification score matched with the conventional score 100% of the time for the first three tasks. However, the last two tasks were not perfect with Task 4 having the lowest accuracy (Table 2).

Table 1: Scoring criteria for the five tasks of the computerized Mallet Classification. Scores are based on the shoulder abduction angle (θ_{SA}), shoulder external rotation angle (θ_{SE}), elbow flexion angle (θ_{EF}), and distances between points including the hand (P_H), wrist (P_W), elbow (P_E), shoulder (P_S), opposite shoulder (P_{OS}), head (P_{HE}), and spine (P_{SP}, located approximately in the center of the spine).

Task	Criteria for score (II-IV)
1. Active Abduction	II: $\theta_{SA} < 30°$ III: $30° \leq \theta_{SA} < 90°$ IV: $90° \leq \theta_{SA}$
2. External Rotation	II: $\theta_{SE} \leq 0°$ or $d(P_E, P_{SP}) < d(P_E, P_W)$ III: $0° < \theta_{SE} < 20°$ IV: $20° \leq \theta_{SE}$
3. Hand to Head	II: $d(P_H, P_{HE}) \geq d(P_E, P_W)$ III: $d(P_H, P_{HE}) < d(P_E, P_W)$ IV: $d(P_{HE}, P_W) < d(P_E, P_W)$
4. Hand to Back	II: $\theta_{EF} \leq 80°$ or $d(P_H, P_{SP}) < d(P_S, P_{SP})$ III: $80° < \theta_{EF} \leq 120°$ IV: $120° < \theta_{EF}$
5. Hand to Mouth	II: $\theta_{SA} \geq 90°$ or $d(P_{HE}, P_H) < d(P_{OS}, P_S)$ III: $90° > \theta_{SA} \geq 60°$ IV: $60° > \theta_{SA}$

Table 2: Accuracy of test results

Task 1	Task 2	Task 3	Task 4	Task 5	Mean
100%	100%	100%	57%	93%	90%

This 10% overall inaccuracy is most likely due to two reasons. First, the worst accuracy for Task 4 may be related to the fact that, for this task only, subjects turned around and their backs were facing the Kinect so that their hand locations could be tracked. The Kinect appears to have difficulty tracking a person's arm movement when that person is backwards. It is possible that the movement detection algorithm for the Kinect software development kit may have been developed to track people who are directly facing the Kinect sensor.

Second, at times when two body points move into close proximity to one another, the Kinect showed difficulty distinguishing those two body points. This was the probable cause of inaccuracy for both Tasks 4 and 5.

Further improvements to the program are warranted given the results of our subject testing. The primary improvement areas are to increase the reliability of Task 4 by compensating for the subject having to be backwards as well as to improve the precision of the Kinect when two body points are near each other.

Needless to say, the future work includes evaluating the computerized Mallet Classification on patients and comparing the computerized scores to therapists' scores. Such studies would provide valuable information on critical areas of improvement such as the scoring algorithms, graphical user interface, and the overall program. In addition, given that the main patient populations for brachial plexus palsy are children, further evaluation is needed to examine if the computerized Mallet Classification works well with children with small body sizes as well as short attention spans.

CONCLUSIONS

The computerized Mallet Classification demonstrated the feasibility of our approach and yielded good accuracy for four of the five tasks. With further improvements to enhance the accuracy for Task 4, the computerized Mallet Classification has the following potential.

The computerized Mallet Classification enables a person to evaluate his or her own arm function without the need for other individuals such as a doctor and a therapist to take the measurements for him or her. The computerized test also has the capability to provide more detailed joint angle profiles than the simple clinical score, thereby providing guidance to clinicians regarding additional treatments or focus areas. Computerized clinical assessments also enable telemedicine and tele-evaluation.

REFERENCES

1. Piatt, J. H. *Pediatric Clinics of North America*, 51(2), 421-440, 2004.

RATE OF TORQUE DEVELOPMENT DEFICITS FOLLOWING TOTAL KNEE ARTHROPLASTY

[1]Joshua D. Winters, PhD, CSCS, [1]Cory L. Christiansen, PT, PhD, [1]Jennifer E. Stevens-Lapsley, PT, PhD

[1]Physical Therapy Program, Department of Physical Medicine and Rehabilitation, University of Colorado

email: joshua.winters@ucdenver.edu

INTRODUCTION

TKA is one of the most common elective surgical procedures performed in older adults with over 600,000 performed each year; costing approximately $9 billion/year.[1] Current rehabilitation efforts focused on improving strength training result in significant improvement, but are not sufficient to restore physical performance to that of healthy older adults.[2] While knee extensor strength is a key component, the speed of a muscle contraction, also has an important influence on physical function. Many aspects of physical function are dependent not only on strength, but also the speed with which force is developed (e.g. crossing a street or climbing stairs quickly). The importance of rapid torque generation in function and disability has prompted the development of exercise programs with a focus on improving the ability to rapidly generate torque in older adults.[3] However, following TKA, muscle strengthening is still commonly recommended without emphasis on the rate of torque development (RTD). Impaired knee extensor RTD is a modifiable risk factor and potential target of rehabilitation to improve functional outcomes following TKA.

Therefore, the purpose of this study was to assess changes in maximal knee extensor strength and RTD following TKA, compared to that of healthy older adults and determine if knee extensor RTD contributes to functional outcomes beyond that of knee extensor strength alone.

METHODS

Thirty-five patients following TKA and 23 healthy control subjects were retrospectively identified from two previous studies. All TKA subjects had a primary unilateral TKA secondary to knee osteoarthritis and participated in standardized rehabilitation programs following surgery. Patients were between the ages of 45 and 85 years of age. Exclusion criteria included uncontrolled hypertension, uncontrolled diabetes, body mass index > 40 kg/m^2, significant neurologic impairments, contralateral knee OA (as defined by pain greater than 4/10 with activity), or other unstable lower-extremity orthopedic conditions. Healthy control subjects had no history of hip or knee osteoarthritis or joint replacement and were of similar age as the TKA group subjects.

Knee extensor torque during maximal voluntary isometric contraction (MVIC) and rate of torque development (RTD) were assessed on the surgical limb preoperatively, 1 and 6-months following surgery using a HUMAC NORM (CSMi, Stoughton, Massachusetts) electromechanical dynamometer. Data were collected with a Biopac Data Acquisition System (BIOPAC Systems Inc, Goleta, California) and AcqKnowledge software, version 3.8.2 (BIOPAC Systems Inc). Subjects were asked to perform the knee extensor MVIC using both visual and verbal feedback up to 3 times. The trial with the steepest linear rise in force from rest was then used for data analysis. Peak RTD (RTD_{pk}) was calculated as the maximum value from the 1st derivative of the isometric knee extension torque data. RTD was also calculated as the change in force over the change in time from force onset to 25% MVIC (RTD_{25}) and 50% MVIC (RTD_{50}). The Timed-Up-and-Go (TUG) and stair climbing time (SCT) were used to measure physical function.

Independent samples t-tests were used to assess differences between the TKA and control groups in MVIC and RTD preoperatively, 1, and 6 months following TKA. Linear mixed models were used to analyze within subject differences for the repeated measures variables of MVIC and RTD for the TKA group. In the TKA group, hierarchical linear regressions were used to examine whether RTD provided a significant additional contribution to the explanation of the variability in TUG and SCT after accounting for the influence of MVIC. Pearson correlation coefficients were used to investigate the MVIC and RTD relationships with TUG and SCT at each time point in the TKA group.

RESULTS AND DISCUSSION

Independent samples t-tests revealed significant differences between the TKA and Control groups in both MVIC and RTD measures at all-time points (Figure 1).

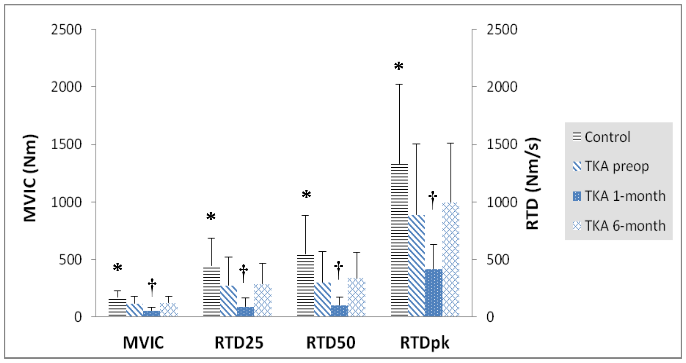

Figure 1: MVIC and RTD Measures at each Assessment Time Period.

* Significant differences between Controls and TKA patients (p<0.001)

† Significant differences for patients with TKA at 1-month post-surgery compared to preoperative and 6- months post-surgery (p<0.0001)

Linear mixed models showed a significant influence of time on quadriceps MVIC, RTD_{pk}, RTD_{25}, and RTD_{50} in the TKA group [(F=71.197, p<0.001; F=11.106 p<0.001; F=10.389 p<0.001; F=10.874 p<0.001, respectively)]. Bonferoni post-hoc tests revealed that both quadriceps MVIC and RTD significantly decreased 1-month following surgery (p<0.001) but at 6 months, were similar to preoperative levels (Figure 1).

Significant correlations were found between quadriceps MVIC, RTD and functional performance (TUG and SCT) at each of the 3 assessment time intervals (Table 1). The prediction of TUG and SCT scores 1-month post-surgery were significantly improved with the addition of RTD (RTD_{pk} or RTD_{50}) to the regression model after accounting for MVIC. Six months following surgery, RTD_{25} significantly improved the prediction of both TUG and SCT scores beyond that of strength alone.

CONCLUSIONS

Quadriceps performance following TKA is influenced by not only the maximal torque generating capacity of the muscle but also by the ability to *rapidly* generate torque. Significant deficits in quadriceps RTD exist following TKA and RTD significantly improves predicting function compared to MVIC alone for up to 6 months following surgery. These results suggest the importance of designing rehabilitative interventions that encompass all aspects of muscle function including RTD. Future studies are necessary to examine how interventions focused on knee extensor RTD following TKA may significantly improve current physical rehabilitation strategies.

REFERENCES

1. Cram, P., et al., *Total knee arthroplasty volume, utilization, and outcomes among Medicare beneficiaries, 1991-2010.* JAMA, 2012. **308**(12): p. 1227-36.
2. Bade, M.J., W.M. Kohrt, and J.E. Stevens-Lapsley, *Outcomes before and after total knee arthroplasty compared to healthy adults.* J Orthop Sports Phys Ther, 2010. **40**(9): p. 559-67.
3. Orr, R., et al., *Power training improves balance in healthy older adults.* J Gerontol A Biol Sci Med Sci, 2006. **61**(1): p. 78-85

Table 1: MVIC & RTD Correlations with Functional Performance.

Variable	Max Torque	RTD25	RTD50	RTDpk
Preoperative				
TUG	r=-0.516, p=0 .002	r=-0.440, p=0 .009	r=-0.443, p=0 .009	r=-0.460, p=0 .006
SCT	r=-0.490, p=0 .004	r=-0.397, p=0 .022	r=-0.408, p=0 .018	r=-0.439, p=0 .011
1-month post-surgery				
TUG	r=-0.591, p<0 .001	r=-0.416, p=0 .020	r=-0.616, p<0 .001	r=-0.652, p<0 .001
SCT	r=-0.652, p<0 .001	r=-0.488, p=0 .005	r=-0.651, p<0 .001	r=-0.638, p<0 .001
6-month post-surgery				
TUG	r=-0.536, p=0 .002	r=-0.588, p<0 .001	r=-0.526, p=0 .002	r=-0.528, p=0 .002
SCT	r=-0.502, p=0 .003	r=-0.573, p=0 .001	r=-0.539, p=0 .001	r=-0.518, p=0 .002

MUSCLE ARCHITECTURAL CHANGES OF THE POST-STROKE TIBIALIS ANTERIOR

Molly A. Wessel, John W. Ramsay, Stephen M. Suydam, Thomas S. Buchanan and Jill S. Higginson

University of Delaware, Newark, DE, USA
email: mwessel@udel.edu

INTRODUCTION

Stroke survivors often suffer from hemiparesis, or weakness and paralysis on one side of the body. In the lower leg, foot-drop commonly occurs in the paretic leg and manifests itself as a decrease in dorsiflexion range-of-motion. This change of range-of-motion may be due to increased muscle tone in the plantar flexor muscles, muscle weakness of the dorsiflexors, or some combination of both. A recent study investigated post-stroke ankle joint and muscle fascicle changes of the medial gastrocnemius and reported a decrease in muscle fascicle length, pennation angle, and range-of-motion [1]. Therefore, architectural changes such as these may contribute to post-stroke dorsiflexor weakness.

The objective of this study was to investigate the correlation between ankle joint motion and muscle fascicle length and pennation angle of the tibialis anterior (TA). Extended field-of-view (EFOV) was used to capture the entire muscle fascicle of the TA. We hypothesized that post-stroke fascicle length and pennation angles of the TA will be smaller compared to healthy controls.

METHODS

Multiple methods exist for determining fiber length. Point-to-point (Figure 1) and manual tracing methods (Figure 2) of analysis were performed to determine which method is better for curved muscle fascicles. Three individual raters performed three to five ultrasonic EFOV scans (10 MHz, 12mm linear probe) of a lamb soleus muscle for a total of fourteen ultrasonic images (LOGIQe, GE Healthcare). The primary researcher identified an individual fascicle on each image and performed both methods of measuring fascicle length. A paired t-test was performed to compare the fascicle lengths between point-to-point and tracing methods.

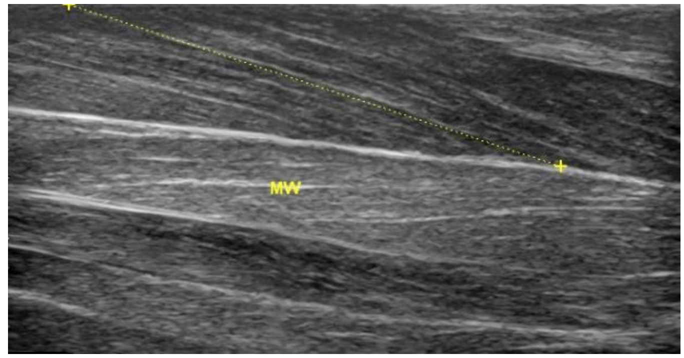

Figure 1: Point-to-point method of a muscle fascicle.

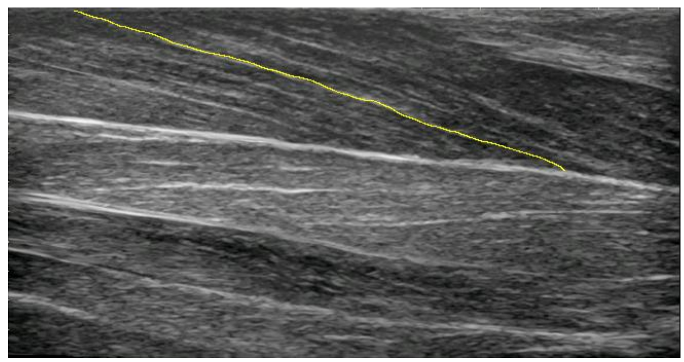

Figure 2: Trace method of a muscle fascicle performed in ImageJ (NIH.gov).

One stroke survivor (69 yrs old, 8 yrs post-stroke) and one healthy control (22 yrs old) were provided as preliminary data. Both subjects provided informed consent prior to testing. Longitudinal ultrasound images of the TA were collected using a B-mode scanner with a high-resolution linear array probe. Subjects were seated upright in an isometric dynamometer (Biodex, Shirley, NY) with their knee fully extended and ankle secured in neutral posture. Ankle range-of-motion was determined prior to testing. At least two ultrasonic images were taken of the muscle belly of the TA starting at 0º and incremented 10º in both plantar flexion and dorsiflexion until maximum range-of-motion was reached. All measurements were taken during a resting condition at each joint angle for both legs. Fascicle length and pennation angle were measured from each image using the point-to-point method and averaged for each joint angle. For the healthy subject, values from both legs were averaged together to obtain a single value. Linear regression lines were fitted to the data points for each limb.

RESULTS AND DISCUSSION

For this study there was no significance difference between the point-to-point and trace method of muscle fascicle length ($p>0.05$). Therefore, the point-to-point method was chosen due to simplicity and used for the remaining data collection.

Healthy TA fascicles were approximately 1 - 1.5 cm longer (y-intercept of 7.86 cm) than both non-paretic (y-intercept 6.94 cm) and paretic fascicles (y-intercept 6.27 cm) (Figure 3). The fascicle lengths for all 3 groups trended towards larger lengths at larger plantar flexor angles. Healthy and paretic fascicle lengths followed the same trend (slope 0.06). Non-paretic had a positive trend with a lower slope (0.04).

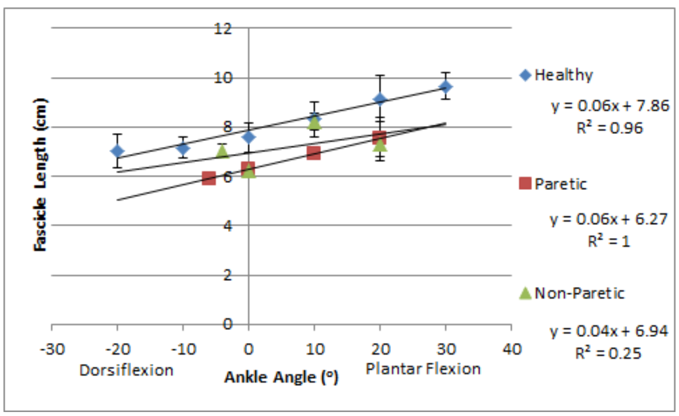

Figure 3: TA fascicle lengths across ankle angles in healthy, paretic, and non-paretic muscle.

Paretic TA pennation angles were 2.5 - 4° greater (y-intercept 14.07°) than both healthy (y-intercept 11.49°) and non-paretic angles (y-intercept 9.80°) (Figure 4). The pennation angles for all 3 groups trended towards smaller pennation angles at larger plantar flexion angles. Paretic and non-paretic pennation angles followed a similar trend (slope -0.12, -0.10, respectively), while healthy had a negative slope (-0.01) that was close to constant.

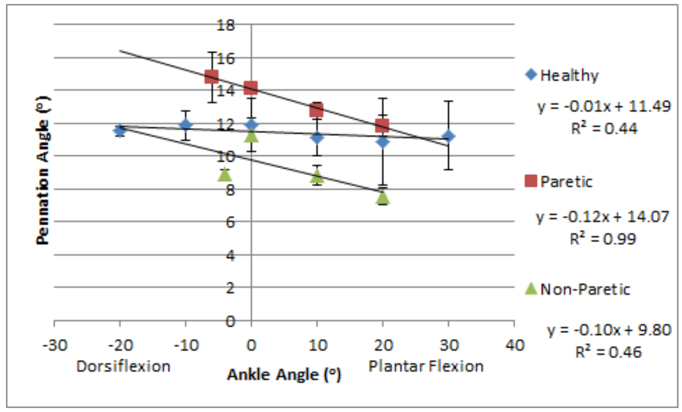

Figure 4: TA pennation angles versus ankle angles in healthy, paretic, and non-paretic muscle.

The point-to-point method to measure human fascicle lengths was chosen over the trace method because there was no significant difference between methods. However, we were unable to determine which method was more accurate. For highly curved muscle fascicles, it is possible that the trace method is more accurate.

In this study we found that fascicle lengths were smaller and pennation angles were greater in the paretic TA when compared to healthy values. Additionally, non-paretic fascicle lengths were slightly longer and pennation angles were smaller compared to paretic muscle. A previous study noted that TA volume was not significantly different between paretic and non-paretic sides [2]. Since we have observed architectural differences between these two sides, it is likely that paretic dorsiflexor strength is influenced by structural changes post-stroke. However, more subjects are needed to verify this claim. Overall, *in vivo* assessments of muscle structure may help provide a better understanding of the contributors to post-stroke foot drop.

REFERENCES

1. Gao F, et al. *Arch Phys Med Rehabil* **90**, 819-826, 2009.
2. Ramsay J, et al. *J Biomech* **44**(16), 2741-2746, 2011.

ACKNOWLEDGEMENTS

Funding provided by NIH P30-GM103333, ROI-AR040163, ROI-NS055383, UD Graduate Fellowship Awarded to JR

SIMPLE SYSTEM FOR ISOMETRIC MUSCLE STRENGTH MEASUREMENT AND BIOFEEDBACK IN AN MRI SCANNER

Tim V. Wrigley, Camille Shanahan

Centre for Health, Exercise and Sports Medicine (CHESM),
Department of Physiotherapy, University of Melbourne, Australia
email: timw@unimelb.edu.au, web: http://www.chesm.unimelb.edu.au

INTRODUCTION

A number of experimental protocols require that a research subject perform isometric contractions in an MRI scanner. These include imaging studies of joints under contractile loading [1], muscle metabolism studies [2], and functional MRI (fMRI) brain imaging studies of motor control tasks [3]. This requirement is difficult to meet, as space is limited, and the devices that are typically used for isometric force measurements in biomechanics contain ferromagnetic materials, which cannot be used in MRI.

This has led to the design of some complex, expensive devices, using special MRI-safe materials and novel methods of signal transmission specifically designed for use in MRI. However not all experiments need the sophistication of such devices. Here we describe a simple, inexpensive system for isometric strength measurement and biofeedback in MRI scanners, made from readily available materials which are safe for use in MRI, and which provides very good measurement capabilities consistent with many experimental requirements. The system is based on air pressure measurement, and was inspired by the use of sphygmomanometry pressure cuffs in some areas of clinical practice as a simple tool for muscle strength measurement, eg [4].

METHODS

For use in fMRI of knee osteoarthritis patients, where the lower limbs are outside the bore, an adjustable rig was designed for stabilizing the lower limb as the subject exerted an isometric knee extension contraction; it was constructed from aluminium, wood, and plastic (Figure 1). A cuff made from aluminium and webbing material with plastic buckles secured the subject's limb to the rig. A small sphygmomanometry pressure bag was placed between the cuff and the limb. Other rig configurations are conceivable using the same pressure measurement system, for example where a joint or muscle is imaged within the bore.

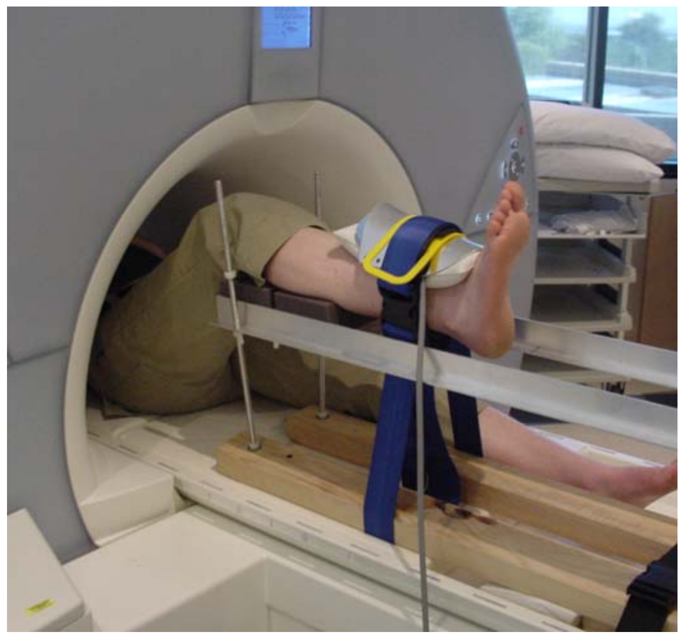

Figure 1: Rig configured for isometric knee extension. All materials (wood, aluminium, plastic, webbing) are MRI-safe. Limb cuff contains pressure bag for isometric force measurement.

The pressure bag was linked via air-tight plastic tubing to a pressure transducer unit housed outside the MRI room (Vernier Scientific GPS-BTA, Oregon USA). The relationship between pressure and force was derived by calibration with static weights, using a simulated leg assembly designed to mimic the way in which force is applied by the leg via the cuff.

The experimental paradigm for our fMRI experiments required the head to be in the scanner bore (Siemens Trio 3T, Germany) for brain imaging. Subjects were required to exert submaximal isometric muscle contractions in a sinusoidal pattern from 0% to 10% MVC. To achieve this, a digital frequency generator (Hewlett-Packard 33120A) was set to generate the stimulus sine wave, for the subjects to match with their muscle contractions, ie a force-matching paradigm. A trigger signal from the MRI scanner was used to start each sequence of this protocol, synchronized with image acquisition. Pressure and sine-wave voltage data were acquired, converted to force, and displayed in real-time by Matlab (Mathworks Inc, Mass., USA) using a DI-158 USB ADC (DATAQ, Ohio, USA). Subjects within the MRI scanner observed the biofeedback display showing the stimulus sine wave and their applied force via a PC screen projection and mirror system within the scanner.

RESULTS AND DISCUSSION

The calibration trials showed that a quadratic polynomial provided the best fit to estimate force from applied pressure up to forces of 500 Newtons (Figure 2). Pilot experiments outside the scanner also showed that this remote pressure measurement system had a similar transient response to a conventional S-beam type force transducer linked directly to the cuff.

Subjects for the fMRI experiments were readily able to apply variable knee extension forces via the rig, to match the stimulus sine wave (Figure 3). Head movement was minimal, an important requirement for fMRI. There was no MRI image distortion due to the rig.

CONCLUSIONS

While the MRI environment imposes considerable limitations on the space available for a research subject to perform muscle contractions, and restrictions on the type of measurement devices possible, simple but accurate systems such as that described here can be designed to work within these constraints.

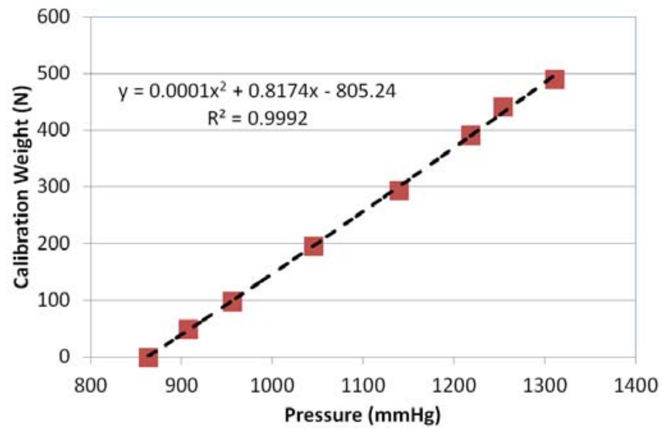

Figure 2: Calibration with fixed weights to derive empirical near-linear relationship between pressure and applied force.

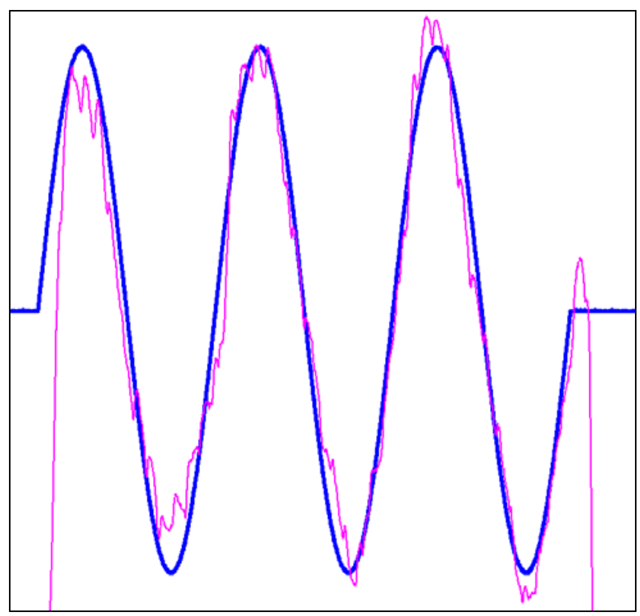

Figure 3: Example of use of the system for force matching paradigm in fMRI, showing the subject's applied isometric force derived from pressure measurement (purple), and the required sinusoidal force pattern (blue).

REFERENCES

1. Salsich GB, et al. *Clin Orthop Relat Res*. **417**, 277-84, 2003.
2. Layec G, et al. *Mag Res Mater in Phys, Biol & Med*. **21**, 227-35, 2008.
3. Newton JM, et al. *Neuroimage*, **43**, 136-46, 2008.
4. Bohannon RW, et al. *Arch Phys Med Rehabil*. **72**, 1991.

BETWEEN SESSION RELIABLITY OF QUADRICPES PERCENT VOLUNTARY ACTIVATION AND FORCE MEASURES IN HEALTHY PARTICIPANTS

Terry L. Grindstaff, Dimitrios Katsavelis, Sam K. Morton, and A. Joseph Threlkeld

Creighton University, Omaha, NE, USA
email: GrindstaffTL@creighton.edu web: rehablab.creighton.edu/

INTRODUCTION

Percutaneous electrical stimulation at maximal or supramaximal intensities is often used to estimate quadriceps voluntary activation, but may not be well-tolerated by some participants [1-2]. The use of a doublet pulse stimulus results in less discomfort and has quadriceps voluntary activation values that correlate well with the commonly used 10-pulse train of stimuli. No study has examined the between session reliability when using a doublet stimulus to determine quadriceps voluntary activation. Since measures of quadriceps voluntary activation are often used in research and clinical settings it is imperative to determine the reliability and minimal detectable change of these measures between sessions. Therefore, the purpose of this study was to determine the between session reliability and minimal detectable change for quadriceps voluntary activation and force output during maximal voluntary isometric contractions (MVIC).

METHODS

Eight healthy participants (6 male, 2 female; mean±SD, age= 25.5±3 years, height= 175.2±12.9 cm, mass= 75.2±15.4 kg) provided informed consent for study inclusion. Data were collected during two testing sessions, using identical procedures, at least 4 days apart.

Participants were seated on an isokinetic dynamometer (Biodex System 3; Biodex Medical Systems, Inc) with their hips flexed to 85°, knee flexed to 60°, and arms folded across their chest. The dominant limb was tested and defined as the limb which would be used to kick a ball. Two self-adhesive electrodes (8x14cm; Collins Sports Medicine) were placed over the proximal lateral aspect and the distal medial aspect of the quadriceps muscle.

Participants performed a standardized warm up consisting of submaximal and maximal muscle contractions coupled with submaximal electrical stimuli. A Digitimer Constant Current Stimulator (DS7AH; Digitimer Limited) with a Train/Delay Generator (DG2A; Digitimer Limited) was used to generate all electrical stimuli. A maximal electrical stimulus (2 pulses applied at 100Hz for 200ms duration, 450 mA) was applied to the quadriceps muscle in a relaxed state (resting twitch; RT). Participants then performed two MVICs coupled with a maximal electrical stimulus. Torque was displayed in real time and the examiner manually triggered the stimulus when the subject's MVIC torque reached and maintained a plateau.

Peak torques were extracted for each instance of stimulation (Figure 1). MVIC torque was calculated as the average torque produced over a 50 ms epoch prior to the delivery of the maximal electrical stimulus. Quadriceps percent voluntary activation was quantified using the interpolated twitch technique [3]. The average values between the two measures during each session were used for data analysis. Between session reliability was determined using an intraclass correlation coefficient ($ICC_{3,2}$) and associated confidence intervals (95% CI). Calculations were made for the standard error of measurement (SEM) and minimal detectable change (MDC).

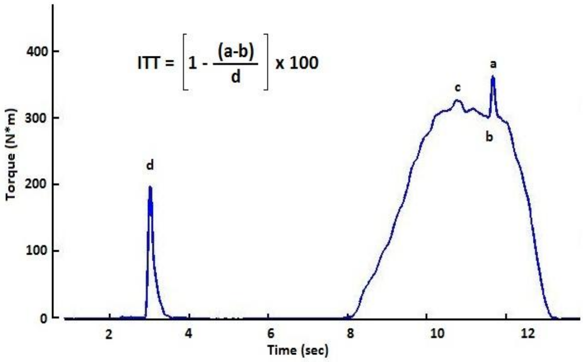

Figure 1. Schematic representation of the interpolated twitch technique utilized for the calculation of percent voluntary activation.

RESULTS AND DISCUSSION

The between session reliability was good for percent voluntary activation and MVIC measures (Table 1). The values are consistent with previously reported measures of between session reliability and slightly lower for minimal detectable change [4-5]. The results of this study indicate that if changes in percent voluntary activation that exceed 1.6% and MVIC torque values that exceed 8.9 N*m are beyond measurement error.

Results of this study should be interpreted with caution since only healthy participants, who were younger in age, were utilized. Estimates of quadriceps voluntary activation are often performed on individuals with knee joint injury. We did not estimate the clinical meaningfulness of these changes. Additionally, since estimates of quadriceps voluntary activation and force may also be obtained at other joint angles and using a variety of stimulation parameters these results may not be generalized to other methodological approaches.

CONCLUSIONS

Measures of quadriceps voluntary activation and force have good reliability between sessions in healthy participants. These results may be beneficial for researchers and clinicians who are responsible for measuring quadriceps function between sessions. The minimal detectable change provides a threshold which can be used to determine if measures obtained during subsequent testing sessions are beyond measurement error.

REFERENCES

1. Miller M, et al. *Scand J Med Sci Sports* **16**, 274-281, 2006.
2. Grindstaff TL, et al. *J Athl Train* **47**, 24-31, 2012.
3. Krishnan C & Williams GN. *Muscle Nerve* **41**, 868-874, 2010.
4. Kean CO, et al. *Arch Phys Med Rehabil* **91**, 1447-1451, 2010.
5. Morton J, et al. *Eur J Appl Physiol* **94,** 541-548, 2005.

ACKNOWLEDGEMENTS

This research was supported by the National Institute on Aging of the NIH (R15 AG040616). The content is solely the responsibility of the authors and does not necessarily represent the official views of the NIH.

Table 1. Descriptive Statistics (mean ± SD) and Reliability Estimates.

	Session 1	**Session 2**	**$ICC_{3,2}$ (95% CI)**	**SEM**	**MDC**
Percent Voluntary Activation (%)	85.8 ± 11.4	86.7 ± 13.0	0.97 (0.83, 0.99)	0.59	1.6
Peak Torque (N*m)	323.6 ±75.8	333.5 ± 75.5	0.96 (0.80, 0.99)	3.22	8.9

*SEM= Standard Error of Measure; MDC= Minimal Detectable Change

SIMILARITIES AND DIFFERENCES IN KNEE MECHANICS BETWEEN SINGLE LEG SQUAT AND SINGLE LEG JUMP

Michael R. Donohue, Samantha M. Ellis, Erika M. Heinbaugh, Qin Zhu, Boyi Dai

University of Wyoming, Laramie, WY, USA
Email: mdonohue@uwyo.edu

INTRODUCTION

Anterior cruciate ligament (ACL) injuries commonly occur during athletic tasks when individuals land with awkward postures which generate unbalanced forces to the knee joint [1]. Individuals demonstrated great knee valgus angle and small knee flexion when they injured their ACL [1, 2]. Great knee valgus angle and moment and small knee flexion angle were associated with great ACL loading [3].

Based on ACL injury characteristics and loading mechanisms, screening landing patterns during athletic tasks can identify individuals with high risk for ACL injuries [3]. Because of the similar motion between landing and squatting, squatting tasks have been used to identify ACL injury risks and included in rehabilitation following ACL injuries [4, 5, 6]. However, the exact mechanical similarities and differences between squatting and jump-landing are still unknown.

The purpose of this study was to investigate the similarities and differences in knee flexion angle, knee valgus angle and moment between a single leg squat (SLS) and a single leg jump (SLJ). It was hypothesized that maximum knee flexion angle, maximum knee valgus angle and moment in SLS would be positively correlated with those in SLJ. Maximum knee flexion angle would be greater in SLS and maximum knee valgus angle and moment would be greater in SLJ.

METHODS

Five male and four female recreational athletes without any major lower extremity injury participated in this study. (Age: 21.22 ± 2.19 years, Mass: 69.90 ± 15.73 kg, Height: 1.77 ± 0.10 m). Participants performed 3 trials of a SLS and a SLJ with a random order. The testing leg (left or right) was randomly selected. The SLS was performed with the non-testing leg bent at 90 degrees and behind the participant with their arms straight out and parallel to the ground. The participants were instructed to squat as low as possible while remaining under control and keeping their arms parallel to the ground. The SLJ was performed with participants starting on a 30 cm box positioned half their height away from a force plate. With both feet on the box, they were instructed to jump out to the force plate, land with only their testing leg on the force plate, and subsequently jump up as high as possible. Subjects’ motion was capture using a 6-camera opto-reflective system. The ground reaction force acting on the testing leg was recorded using a force plate. Knee joint angles were calculated as the Cardan angles from thigh reference frame to leg reference frame. An inverse dynamic approach was used to calculate external knee valgus moment. The maximum knee flexion angle (+), maximum knee valgus angle (+), and maximum knee valgus moment (+) were extracted as dependent variables for data analysis. Spearman correlation tests were performed for dependent variables between SLS and SLJ to test the similarities between them. Wilcoxon Signed Rank tests were performed for dependent variables between SLS and SLJ to test the differences between them. The significance level was set at 0.05.

RESULTS AND DISCUSSION

Maximum knee flexion angle ($r = 0.72$, $p = 0.03$, Figure 1), maximum knee valgus angle ($r = 0.93$, $p < 0.01$, Figure 2), and maximum knee valgus moment ($r = 0.75$, $p = 0.02$, Figure 3) in SLS were correlated with those in SLS. Maximum knee flexion angle in SLS (95.9 ± 10.0 deg) was greater than that in SLJ (74.7 ± 6.7 deg, $p < 0.01$) Maximum knee valgus angle in SLJ (4.8 ± 3.1 deg) was greater than that in SLS (0.5 ± 3.3 deg, $p < 0.01$). Maximum knee valgus moment in SLJ (54.2 ± 28.6 Nm) was greater than that in SLS (-7.0 ± 9.3 Nm, $p < 0.01$).

The first hypothesis was supported that maximum knee flexion angle, maximum knee valgus angle and moment in SLS were positively correlated with those in SLJ. The results supported utilizing SLS as a screening tool for biomechanical risk factors for ACL injuries. The results also suggested that squat training might modify jump-landing patterns. The findings are especially relevant for patients who have not been cleared to perform jump-landing task but would like to perform squat exercises to improve their jump-landing mechanics in the future.

The second hypothesis was supported that SLS had greater maximum knee flexion while SLJ had greater maximum knee valgus angle and moment. Although SLS and SLJ involved similar down and up motion, the most significant difference between them was the increased external forces and demand of jump-landing during SLJ. Because of a smaller loading, subjects were able lower their body more and achieve a greater knee flexion angle during SLS. Because of a greater loading, subjects increased non-sagittal knee motion and moment during SLJ.

Future injury prevention studies might focus on training individuals to increase their knee flexion angle and reduce their knee valgus angle and knee valgus moment during a SLS, as it is clear that this will affect their performance of a SLJ. A SLS would be more beneficial in a training environment as it is much more controllable and has less risk for an individual than does a SLJ, especially if the individuals are not cleared for athletic tasks or are at high risk for injury. Future intervention studies on training an individual's SLS are needed to confirm these statements. However, the inherent differences between SLS and SLJ suggested that squat training could not replace jump-landing training. Jump-landing training should be encouraged when individuals are cleared for athletic tasks and have good squat mechanics.

CONCLUSIONS

Maximum knee flexion angle, maximum knee valgus angle and moment in SLS were positively correlated with those in SLJ. SLS had greater maximum knee flexion while SLJ had greater maximum knee valgus angle and moment. SLS could be used as a screening and training tool especially for patients during early rehabilitation. However, SLS cannot completely substitute for SLJ.

REFERENCES

1. Boden BP, et al. *Orthopedics* **23**, 573-578, 2000.
2. Krosshaug T, et al. *Am J Sports Med* **35**, 359-367, 2007.
3. Dai B, et al. *Res Sports Med* **20**, 180-197, 2012.
4. Yamazaki J, et al. *Knee Surg Sports Traumatol Arthrosc* **18**, 56-63, 2010.
5. Beutler AI, et al. *J Athl Train* **37**, 13-18.
6. Butler RJ, et al. *Med Sci Sports Exerc* **44:5 Supplement**, 948, 2012.

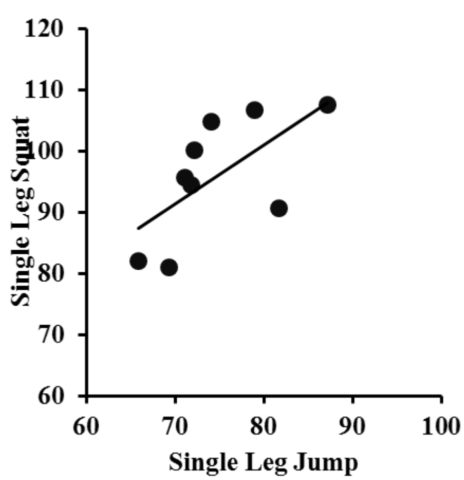

Figure 1. Maximum Flexion Angle (Deg)

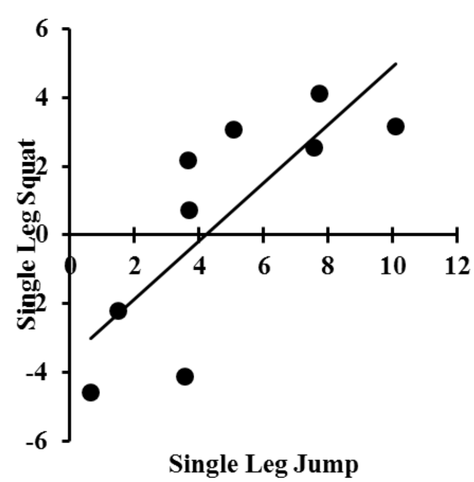

Figure 2. Maximum Valgus Angle (Deg)

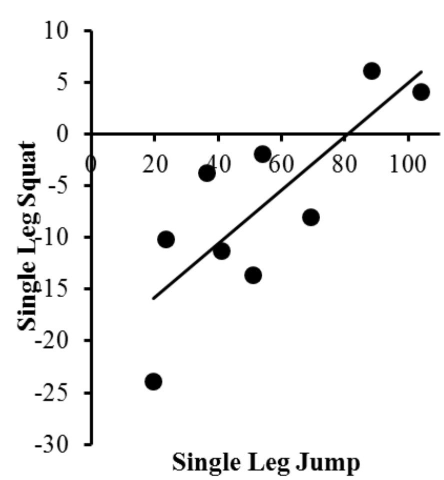

Figure 3. Maximum Valgus Moment (Nm)

EFFECTS ON LUMBAR LOADING OF ADDING UPPER BODY RESISTANCE TO A SQUAT EXERCISE

Elizabeth R. Doran and Michael J. Pavol

Oregon State University, Corvallis, OR, USA
email: mike.pavol@oregonstate.edu

INTRODUCTION

Osteoporotic fractures are a major concern for older women, with the spinal vertebrae being the most common fracture site [1]. One way to combat the vertebral bone loss that begins at menopause is resistance training, as the associated skeletal loading can stimulate bone formation if the loads are large enough. In particular, training against resistance applied to the upper body appears to be a key to eliciting osteogenic effects in the lumbar vertebrae [2]. Unknown, however, are the effects on lumbar loading of adding different types of upper body resistance to a squat exercise. Squat exercises have been included in fall and fracture prevention programs for the purpose of increasing lower body strength and femoral bone mass. Addition of upper body resistance to the squat could yield an exercise that also efficiently targets losses in lumbar bone mass. The objective of this study was thus to determine how adding static and dynamic upper body resistance, in the form of a weighted vest and a biceps curl, respectively, to a squat exercise would influence lumbar loading in middle-aged women.

METHODS

Twenty healthy, active women, aged 37-50 years (mean ± SD: 46 ± 4 yrs, 165 ± 6 cm, 62 ± 10 kg), participated in this study. After a task-specific warm-up, 34 reflective markers were attached to participants' upper and lower limbs, pelvis, thorax, and head. They then stood with each foot on a separate force plate (Bertec, Columbus, OH) and performed 4 sets of exercises in a counterbalanced order: a standing bilateral biceps curl with a 2.3 kg dumbbell in each hand, a bodyweight squat, a squat while wearing a 4.5 kg vest (Squat+Vest), and a squat while performing a bilateral biceps curl with the dumbbells (Squat+Curl). The squat and curl during the Squat+Curl were coordinated such that the elbows reached maximal extension at the lowest point of the squat. Participants were to squat as low as they safely could without exceeding 90° of knee flexion or touching the chair placed behind them. Participants performed 5 correct repetitions of each exercise, each in about 2 s with a brief pause in between. Kinematic data were collected at 60 Hz using a motion capture system (Vicon, Los Angeles, CA) and force plate data were collected at 360 Hz.

Motion capture and ground reaction force data were filtered at 5 Hz and 25 Hz, respectively, and were input, with participant-specific anthropometric data, into a rigid-body model of the lumbar spine and lower limbs within the AnyBody Modeling System (Aalborg, Denmark). The lumbar spine model from the AnyBody Managed Model Repository (v1.2) was adapted to the present application. This lumbar spine model included 7 rigid segments (pelvis, L1-L5 vertebrae, and thorax), 24 degrees of freedom, 154 muscles, and intervertebral disc stiffness [3]. Muscles were modeled as simple force generators whose strength was proportional to cross-sectional area. Each lower limb was modeled as 3 rigid segments (thigh, shank, and foot) with 3 degrees of freedom at each joint. The model was scaled to each participant. From the data input to the model, inverse dynamics and static optimization were used to solve for the muscle forces within the model and the compressive force and anterior-posterior (AP) shear force at each lumbar level over the trial. The cost function (J) minimized in the optimization was:

$$J = \max(\sigma_i) + 0.001\sum \sigma_i^2$$

where σ_i was the stress in muscle i.

The dependent variables selected for analysis were the peak magnitudes of the compressive and AP shear forces at L5/S1 and T12/L1, the levels at which the largest and smallest peak forces were observed. Apparent artifacts were removed before extracting the peaks. The first 3 correctly-performed trials with complete data were analyzed for each exercise, with peak forces averaged across like trials. Repeated-measures ANOVA identified differences in the dependent variables across the 4 exercises. Paired *t*-tests with a Bonferroni correction were used in the post hoc testing. Effects were considered significant at $p<.05$.

RESULTS AND DISCUSSION

Qualitatively, across exercises, peak compressive forces were greatest at L5/S1, whereas the largest anterior and posterior shear forces on the inferior vertebra were at T12/L1 and L5/S1, respectively. In all 3 squat exercises, the peak compressive and AP shear forces occurred near the lowest point of the squat (Figure 1). Peak loading during the curl occurred variously throughout the exercise. For all 4 exercises, peak loading tended to coincide with the peak muscle activity within the lumbar spine.

Differences between exercises existed in peak L5/S1 compressive force and peak T12/L1 AP shear force (both $p<.001$ in the respective ANOVA; Table 1). In both cases, the peak force was greater for the Squat+Vest than for the squat exercise and greater for the Squat+Curl than for the curl exercise. Peak forces for the Squat+Curl did not differ from those for either the squat or the Squat+Vest. Peak L5/S1 AP shear force and T12/L1 compressive force did not differ between exercises.

Lumbar loading during a squat exercise arises from the weight of the upper body, the forces used to accelerate it, and the muscle forces used to control its forward inclination. A weighted vest would act to increase all of these forces. To opposite effect, the torso is nearly stationary and erect during a curl.

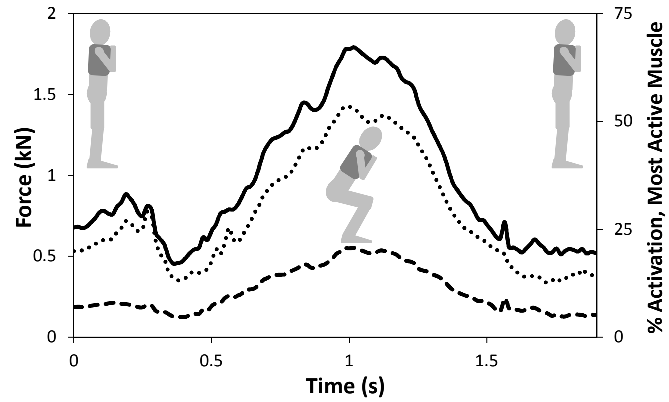

Figure 1: Predicted L5/S1 compressive force (—), anterior shear force on L1 at T12/L1 (– –), and activity of the most active muscle within the lumbar spine (····) for a typical repetition of the Squat+Vest.

Participants may also have kept the torso more erect during a Squat+Curl, moderating the effect of the dumbbells. These factors would explain the results.

CONCLUSIONS

Wearing a weighted vest acts to increase lumbar loading during a squat exercise, while performing a squat and curl together results in greater lumbar loading than performing a biceps curl alone. Adding upper body resistance to a squat exercise can thus increase lumbar loading relative to these exercises performed in isolation, with associated potential benefits to vertebral bone mass. Squat exercises with static upper body resistance, in particular, appear appropriate to consider in exercise programs for preventing osteoporosis of the lumbar spine.

REFERENCES

1. Burge R, et al. *J Bone Miner Res* **22**, 465-475, 2007.
2. Winters-Stone KM, et al. *Bone* **39**, 1203-1209, 2006.
3. de Zee M, et al. *J Biomech* **40**, 1219-1227, 2007.

Table 1: Mean ± SD peak loading on the inferior vertebra at two spinal levels as a function of exercise type.

Loading	Curl	Squat	Squat+Vest	Squat+Curl
T12/L1 compression (N)	1206 ± 402	1308 ± 389	1433 ± 426	1392 ± 365
T12/L1 anterior shear (N)	326 ± 132	610 ± 125	682 ± 134*	644 ± 113†
L5/S1 compression (N)	1285 ± 364	1835 ± 394	2002 ± 402*	1928 ± 370†
L5/S1 posterior shear (N)	206 ± 83	194 ± 90	199 ± 95	214 ± 82

* = $p<.01$ vs. Squat; † = $p<.001$ vs. Curl. Curl was not compared to Squat or Squat+Vest in post hoc testing.

ESTIMATING KNEE ADDUCTION MOMENT IN REAL-TIME ON AN ELLIPTICAL TRAINER

[1,2]Sang Hoon Kang, [2]Song Joo Lee, [1]Yupeng Ren, and [1,2]Li-Qun Zhang

[1]Rehabilitation Institute of Chicago, Chicago, IL, USA
[2]Northwestern University, Chicago, IL, USA
email: l-zhang@northwestern.edu, web: http:// smpp.northwestern.edu/research/biodynamics/

INTRODUCTION

External knee adduction moment (EKAM) is correlated with presence, severity, and progression of knee osteoarthritis (OA) [1], which affected more than 27 million Americans. *Reduction* of peak EKAM is thus often a major goal of knee OA rehabilitation [2]. Recently, real-time EKAM feedback, calculated from a 3-D inverse dynamics, was found to be helpful to reduce the peak EKAM on a treadmill in a motion analysis lab setting [3]. However, 3-D inverse dynamics calculation is difficult to implement, especially outside motion analysis laboratories, due to the usual requirement of complex and expensive motion capture systems potentially occupying large designated space and demanding cumbersome setup [3-5]. To address the issue, two EKAM prediction methods, a regression model [4] and an artificial neural network [5], were developed. However, the two methods may not be used for real-time EKAM estimation, because the former predicts only group un-normalized peak EKAM, and the latter needs percentage of stance phase [5]. Therefore, the *goal* of this research is to develop a practical and reliable *real-time* EKAM estimation method during stepping on an elliptical trainer (ET) by solving the 3-D inverse dynamics with kinematic data from a simple 6-DOF goniometer for the training and clinical evaluation of patients with knee OA.

METHODS

A healthy male (age: 19; height: 1.74m; body mass: 69Kg) participated in this study approved by the IRB of Northwestern University and gave informed consent.

An ET (Reebok Spacesaver RL; Fig. 1) was equipped with 6-axis F/T sensors (JR3, Woodland, CA) on both sides underneath the footplates.

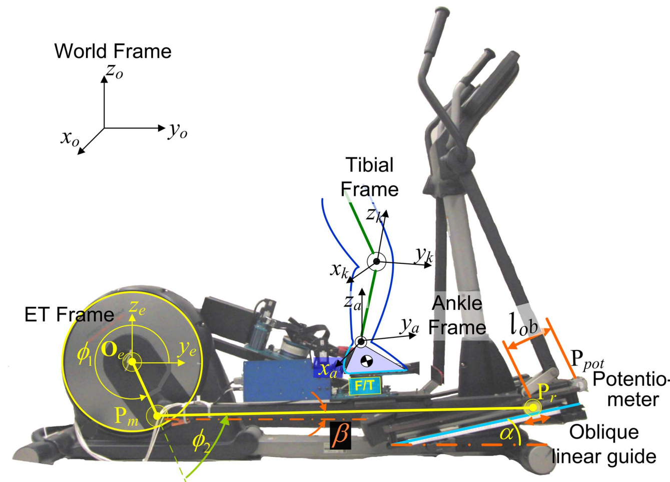

Figure 1: A modified elliptical trainer equipped with 6-axis F/T sensors (F/T below the footplate).

To measure ankle 3-D angle, one end of the goniometer was firmly strapped to the flat and bony anteromedial surface of the leg with neoprene bands to reduce its slip on subject's skin, and the other end was attached laterally to the footplate, which had no motion relative to the foot because of the foot straps. Before stepping, 3-D zero ankle angles were measured by the goniometer at the footplate's lowest position by aligning the 2nd metatarsal head, the midpoint between the lateral and medial malleoli and tibial tuberosity to be in the sagittal plane (y_a-z_a plane); and the center of the F/T sensor, lateral malleolus and lateral tibial condyle's superior margin to be in the frontal plane (z_a-x_a plane). Using the goniometer, the 3-D ankle angles were computed in real-time similar to [6]. Footplate angle, β, was determined by solving inverse kinematics of the ET's four-bar linkage structure, and foot Cartesian position from forward kinematics (Fig. 1). The subject's anthropometric data of foot and shank including lengths, masses, and inertia matrices were determined [7,8]. Considering that *non-zero pure moments* about x_a and y_a axes exerted to footplate's top surface may exist because foot was constrained to footplate, center of pressure (COP) may not be computed on the ET with the F/T sensor [7-9]. However, since the measured forces and torques were directly transmitted to the foot, a modified 3-D inverse dynamics, which does not require the COP, was developed to estimate EKAM with respect to the tibial anatomical frame (Fig. 1) [5]. The EKAM was obtained as the negative of the internal knee adduction moment calculated from the inverse dynamics. To account for regular stepping posture and possible ad/abducted knee postures of patients with knee OA and other injuries, the subject's EKAMs at three stepping conditions (regular, knee-adducted, and knee-abducted stepping) were estimated in real-time by using the proposed method, and corroborated with that from off-line estimation by using kinematic data from an optoelectric motion capture system (Optotrak 3020, Northern Digital, Waterloo, Canada) with 3 sets of markers (4 markers/set attached to a rigid shell) attached on thigh, shank, and foot in the same trials. The Optotrak data were sampled at 50 Hz and synchronized with all other signals collected at 100 Hz. The EKAM was computed at 100Hz using a custom real-time EKAM estimation program based on the modified 3-D inverse-dynamics. Elliptical cycle was defined as starting at the time the footplate reached the most anterior position and ending at the same position [10].

RESULTS AND DISCUSSION

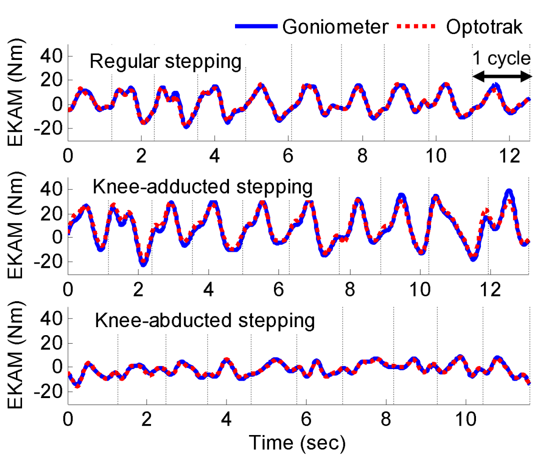

Figure 2: Estimated EKAM (10 cycles) during regular, knee-adducted, and knee-abducted stepping (top to bottom). EKAM estimated with the goniometer and Optotrak closely matched each other.

The estimated EKAM from the proposed real-time estimation method with 6-DOF goniometer closely matched that from the off-line method using Optotrak 3020 for all the three types of stepping (Fig. 2). Moreover, peak EKAM at each cycle was increased in knee-adducted stepping and decreased in knee-abducted stepping systematically compared to that of regular stepping. The goniometer is low-cost and its analog outputs can be conveniently connected to data acquisition systems.

CONCLUSIONS

The EKAM estimate from the practical *real-time* estimation method using the compact goniometer needs only a few minutes to set up, and the result well agreed with that from the off-line method using a motion capture system with much more involved setup. Combined with the ETs' advantages of lower impact during stepping, the real-time EKAM estimation method can be used for a subject-specific real-time biofeedback training of patients with knee injuries including knee OA so that the joint moment loading can be observed in real-time with different walking patterns, which can be used for clinical evaluation of walking pattern associated with excessive joint loading, and furthermore for guided rehabilitation training to reduce the excessive joint loading.

REFERENCES

1. Foroughi N, et al. *Knee* **16**, 303-309, 2009.
2. Reeves ND, et al. *Nat Rev Rheumatol* **7**, 113-122, 2011.
3. Wheeler JW, et al. *J Biomech Eng* **133**, 041007, 2011.
4. Hunt MA, et al. *Knee* **18**, 231-234, 2011.
5. Favre J, et al. *J Biomech* **45**, 692-698, 2012.
6. Shiavi R, et al. *J Biomech* **20**, 459-469, 1987.
7. Winter DA. *Biomechanics and Motor Control of Human Movement*, John Wiley & Sons, 2005.
8. Zatsiorsky V. *Kinetics of Human Motion*, Human Kinetics Publishers, 2002.
9. Cohen A, et al. *Bull Prosthet Res* **17**, 90-97, 1980.
10. Lu T-W, et al. *Med Sci Sports Exerc* **39**, 1651-1658, 2007.

STROKE INDUCED SENSORY DEFICIT DECREASES PHALANX FORCE CONTROL DURING POWER GRIP

Leah R. Enders and Na Jin Seo

University of Wisconsin-Milwaukee, Milwaukee, WI, USA
email: lrenders@uwm.edu, web: https://pantherfile.uwm.edu/seon/www/

INTRODUCTION

Many stroke survivors experience not only motor deficit but also somatosensory deficits, especially in the hand [1]. Knowledge regarding the role of this *sensory deficit* in stroke survivors' ineffective grip control is sparse. Not to mention little knowledge is available for grip control during *power grip*. New development of a power grip dynamometer in our laboratory allows investigation of grip force control and force direction during power grip [2]. The objective of this study was to determine the influence of stroke induced sensory deficit on (1) phalanx normal force control and (2) phalanx force trajectory deviation during lifting of an object in power grip. These two characteristics were investigated due to their functional implications for object slippage/dropping in impaired hands [3, 4].

METHODS

Thirteen chronic stroke survivors with tactile sensory deficit, 5 chronic stroke survivors with no tactile sensory deficit, and 12 age-matched neurologically-intact controls participated. Tactile sensory deficit was determined by the Semmes-Weinstein monofilament and Two-Point discrimination tests. Mean motor function and hand spasticity assessed by the upper extremity portion of the Fugl-Meyer Assessment (FM) and Modified Ashworth Scale (MAS), respectively, were similar for the two stroke survivor groups.

Subjects held the custom-made cylindrical grip dynamometer [2] vertically against gravity in power grip with the paretic (stroke survivors) or non-dominant (controls) hand, while each phalanx's normal force (normal to grip surface) and proximal-distal shear force (tangential to grip surface) were recorded for the thumb, index, and middle fingers. The phalanx force trajectory deviation was quantified as angular deviation of the phalanx force from the direction normal to the grip surface (the arctangent of the ratio of proximal-distal direction shear force to normal force). The grip dynamometer weighed 7N and was covered in a rubber surface.

The phalanx normal force magnitude and phalanx force trajectory deviation observed during the holding phase were compared among the three subject groups (stroke survivors with sensory deficit, stroke survivors without sensory deficit, and healthy controls) using ANOVA and Tukey post hoc analysis. Both sets of data were non-normal and thus transformed using a Box-Cox transformation.

RESULTS AND DISCUSSION

Stroke survivors with sensory deficit produced significantly less phalanx normal force during power grip compared to stroke survivors without sensory deficit and healthy controls (Figure 1, Tukey post hoc, $p<.05$). In other words, only stroke survivors *with* sensory deficit displayed reduced safety margin compared to control. Phalanx normal force was significantly dependent upon subject group, finger, and phalanx (ANOVA, $p<.05$).

Reduced safety margin [3] for stroke survivors with sensory deficit reflects an inability to detect micro-slips and greater likelihood for object dropping. The results also suggest that after stroke, those with sensory deficit behave differently than those without sensory deficit. Reduced safety margin for stroke survivors *with* sensory deficit and somewhat elevated safety margin for stroke survivors *without* sensory deficit may explain the previous research finding on no significant change in safety margin post stroke overall [5]. These differences in safety margins between the two stroke groups were not influenced by strength differences between the two groups, as additional analysis for maximum power grip force showed no significant strength capacity differences between the two stroke groups (p<.05).

Only stroke survivors with sensory deficit produced significantly greater phalanx force trajectory deviation compared to healthy controls (Figure 2, Tukey post hoc, p<.05). Phalanx force trajectory deviation was significantly dependent upon subject group, phalanx, and the interaction between group and finger (ANOVA, p<.05). Increased phalanx force trajectory deviation can increase chances of object slippage for those with sensory deficit due to force trajectories lying closer to the direction tangential to the object's surface [4].

CONCLUSIONS

Stroke induced sensory deficit, but not motor deficit, plays a role in reduced safety margin and increased phalanx force trajectory deviation during power grip, which can increase the likelihood of dropping or slippage of a grasped object. Tactile sensation is important for efficient grip control (i.e. appropriate safety margins [3] and phalanx force trajectory deviation [4]) to avoid object slippage. Hand motor rehabilitation may need to be preceded by somatosensory rehabilitation to maximize the recovery.

REFERENCES

1. Cary LM. *Crit Rev Phys Rehabil Med* **7**, 51-91, 1995.
2. Enders LR, Seo NJ, *J Biomech* **44**, 1447-1453, 2011.
3. Westling G, Johansson RS, *Exp Brain Res* **53**, 277-284, 1984.
4. Seo NJ et al. *Exp Brain Res* **202**, 891-901, 2010.
5. Blennerhassett JM, et al. *Arch. Phys. Med. Rehabil.* **87,** 418-429, 2006.

ACKNOWLEDGEMENTS

We thank funding from the ASB Graduate Student Grant-In-Aid Award, American Heart Association Midwest Affiliate, and Distinguished Fellowship from the National Institute of Disability and Rehabilitation Research.

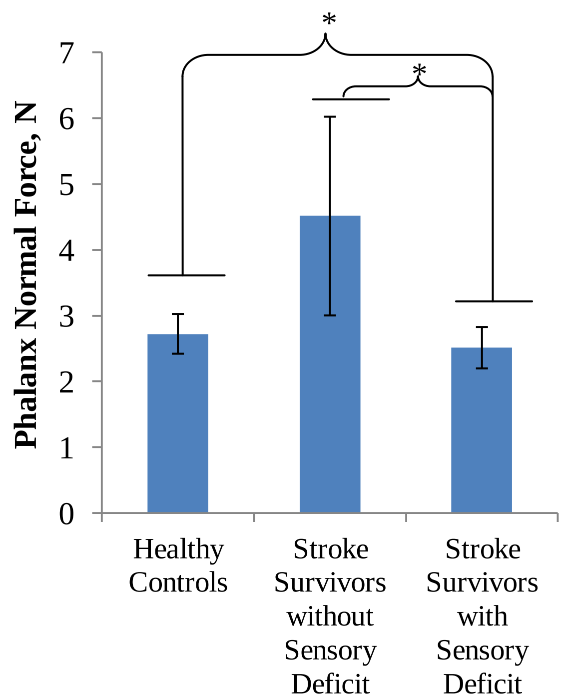

Figure 1: Mean ± SE phalanx normal force was significantly less for stroke survivors with sensory deficit compared to stroke survivors without sensory deficit and healthy controls (fingers and phalanges pooled) (p<.05).

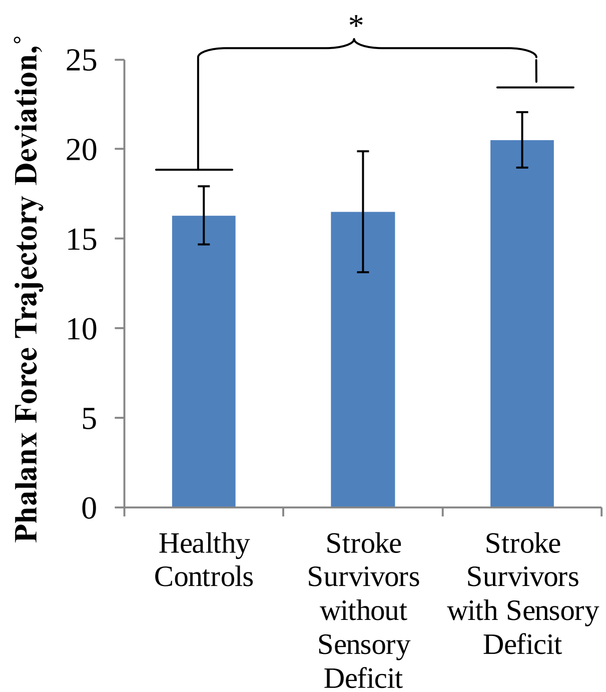

Figure 2: Mean ± SE phalanx force trajectory deviation was significantly greater for stroke survivors with sensory deficit compared to healthy controls (fingers and phalanges pooled) (p<.05).

SOMATOSENSORY CORTEX ACTIVITY IN RESPONSE TO FINGERTIP STIMULATION CAN INCREASE WITH REMOTE SUBTHRESHOLD VIBROTACTILE NOISE: AN EEG STUDY

Pilwon Hur, Ying-Ling Tseng, and Na Jin Seo

University of Wisconsin-Milwaukee, Milwaukee, WI, USA
E-mail: hur@uwm.edu, Web: pantherfile.uwm.edu/seon/www/

INTRODUCTION

Subthreshold vibrotactile noise at the wrist or dorsal hand can improve touch sensation of the fingertip in stroke survivors, as measured by the monofilament clinical test [1]. This finding extends the concept of stochastic resonance [2], by showing that noise applied remotely from the fingertip could influence sensation at the fingertip. Its mechanism, however, is unknown. The objective of this preliminary study was to investigate the effect of remote vibrotactile noise on the electroencephalography (EEG) activity in response to monofilament stimulation at the fingertip. We hypothesized that EEG activity increases with remotely applied subthreshold, but not suprathreshold, vibrotactile noise. Understanding of the mechanism behind sensory enhancement with remote subthreshold noise may help guide its clinical application to enhance patients' touch sensation.

METHODS

Monofilament touched one healthy young subject's index fingertip pad (Fig. 1a,b) while subthreshold (60% of the sensory threshold), suprathreshold (120% of the sensory threshold), or no vibrotactile noise was applied at the dorsal hand skin over the 2nd metacarpal bone (Fig. 1c). EEG activities were continuously recorded. A total of 150 monofilament touches were made for each of the three noise conditions, with the testing order randomized in multiple blocks. The interval between consecutive monofilament touches was random between 1 and 2 seconds. The location and parameters of the noise were chosen based on the previous study [1]. The vibrotactile noise was a white noise with frequencies between 0 to 500 Hz generated by C-3 Tactor (Engineering Acoustics Inc., Casselberry, FL, USA).

The 64 channel EEG data were collected at 1kHz in the international 10-20 system (Brain Products GmbH, Gilching, Germany) with a Synamps^2 amplifier system (Advanced Medical Equipment Ltd., Horsham, West Sussex, UK). To minimize auditory and visual artifacts, the subject wore ear plugs and headphone with white noise and was instructed to look at a fixation dot throughout the experiment, while the subject's hand, monofilament, and vibrotactile noise device were hidden behind a cardboard box (Fig. 1a).

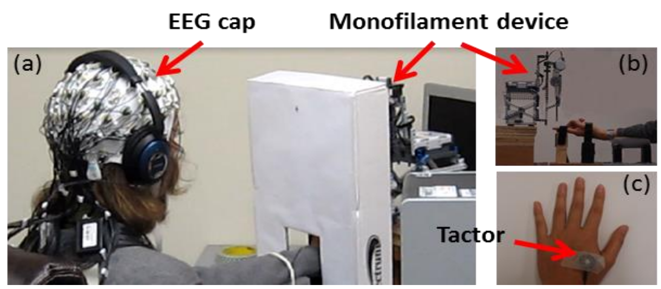

Figure 1: Experimental setup.

For initial analysis, the C4 electrode activity was examined for its location near the contralateral hand sensorimotor area (Fig 2). Event-related potentials (ERP) and power spectral densities (PSD) were analyzed, both in the time period between 350 ms before and 650 ms after the monofilament touch, using MATLAB (v8.0; The MathWorks, Natick, MA) and the EEGLAB toolbox [3]. The EEG data were initially filtered at 0.5-50 Hz to remove slow drifts and line noises. Independent component analysis was used to remove artifacts [4]. The 150 epochs were then averaged to have an ERP for each condition. Two-sample *t*-tests were used to compare the ERP peak to peak amplitudes and PSD at three different frequencies (5, 10, and 23 Hz) between the subthreshold and no noise conditions as well as between the suprathreshold and no noise conditions. The p-values were adjusted by the false discovery rate (FDR) correction.

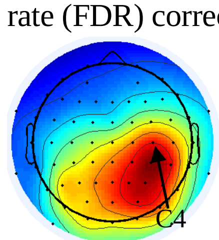

Figure 2: Independent component reflecting somatosensory cortex activity with the fingertip tactile stimulation shown in red.

RESULTS AND DISCUSSION

The peak to peak ERP in response to the monofilament stimulation of the fingertip significantly increased with the subthreshold vibrotactile noise (Fig. 3a) compared to the no noise condition (p<0.001). However, the suprathreshold noise did not significantly affect the peak to peak ERP compared to the no noise condition (Fig. 3b).

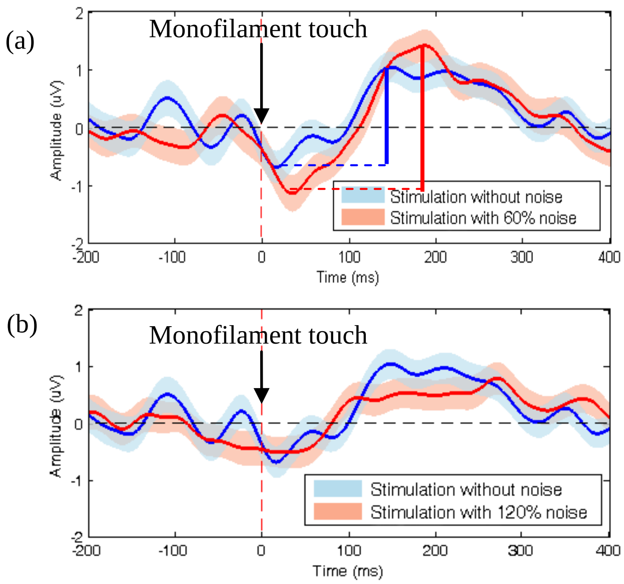

Figure 3: ERP when the dorsal hand received the subthreshold (a, 60% of the sensory threshold) and suprathreshold (b, 120%) vibrotactile noise compared to no noise

PSDs was also significantly affected by the subthreshold noise (Fig. 4a), but not the suprathreshold noise (Fig. 4b). With the subthreshold noise, upper β band activity (22-30 Hz) increased (p_{FDR}=0.01) and α band activity (around 10 Hz) decreased (p_{FDR}=0.05), compared to the no noise condition (Fig. 4a). Increased β band activity is known to be associated with strengthening of sensory feedback [5], and decreased α band activity is associated with increased sensorimotor information processing of related areas [6]. Subthreshold remote vibrotactile noise appears to facilitate reception of fingertip tactile sensation by increasing β band activity and decreasing α band activity at the hand area of the primary somatosensory cortex.

CONCLUSIONS

The subthreshold, but not suprathreshold, vibrotactile noise at the dorsum hand changed the brain activity

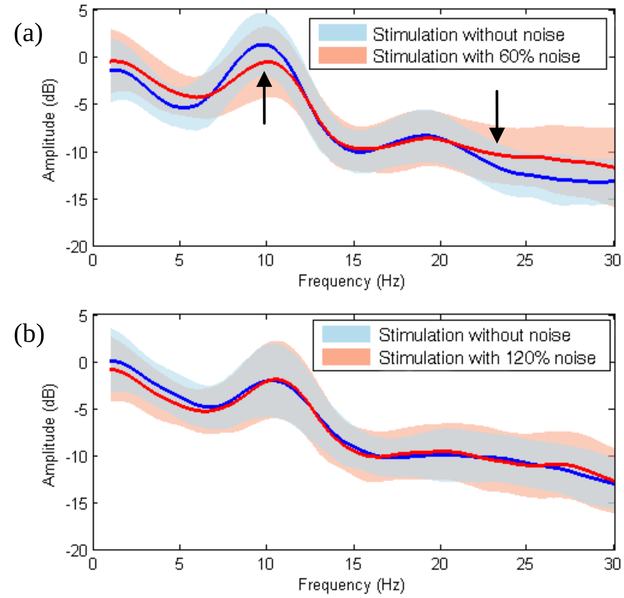

Figure 4: PSD when the dorsal hand received the subthreshold (a, 60% of the sensory threshold) and suprathreshold (b, 120%) vibrotactile noise compared to no noise

of the somatosensory cortex hand area in response to fingertip stimulation with increased event-related potentials and increased β and decreased α band activity, indicating strengthened sensation/sensory feedback and sensorimotor information processing. This study supports the role of remote subthreshold noise in enhancing touch sensation via cortical influence. Understanding of this mechanism may lead to a novel rehabilitation engineering technique for sensory enhancement in patients and older adults.

REFERENCE

1. Enders LR, Seo NJ, *The 42nd SfN*, New Orleans, LA, 2012.
2. Collins JJ, et al., *Physical Review E*, **56** 923-926, 1997.
3. Delorme A and Makeig S, *J Neurosci Methods*, **134** 9-21, 2004.
4. Mognon A, et al., *Pychophysiol*, **48**, 229-240, 2011
5. Baker SN, *Current Opinion in Neurobiol*, **17**, 649-655, 2007.
6. Pfurtscheller G, et al., *Int J Psychophysiol*, **24**, 39-46, 1996

ACKNOWLEDGEMENTS

We thank Mr. Ryan McKindles for advice on EEG data analysis and Dr. Brian Schmit for access to EEG equipment at Marquette University.

COMPARISON OF LOAD REDUCTION ABILITIES OF CAMWALKER AND CORSET-STYLE ANKLE FOOT ORTHOSES

[1]Andrea B. Wanamaker, [1,2]Bradley S. Davidson, [2]Cory L. Christiansen, and [2]Deborah Saint-Phard

[1]University of Denver, Human Dynamics Laboratory, Denver, CO, USA
[2]University of Colorado School of Medicine, Dept. of Physical Medicine and Rehabilitation, Aurora, CO, USA
Corresponding Author Email: bradley.davidson@du.edu

INTRODUCTION

Lower-extremity injuries, such as tibia and fibula stress fractures, require protection to heal and treatment sometimes can include complete unweighting on the injured limb [1, 2]. Complete unweighting can be achieved through crutches; however, crutches can cause discomfort and can be cumbersome with functional activity. In addition, some weight bearing promotes osteogenesis and may be beneficial for fracture management [1]. Ankle foot orthoses (AFOs) have become a common treatment method for lower-extremity fractures because they provide greater mobility than crutches [2, 3] and do not fully eliminate the weight bearing on the injured limb [4].

A common AFO used in fracture management is the camwalker (Fig. 1a). Despite this, there is no evidence that camwalker use reduces weight bearing on the injured limb. A possible alternative to the camwalker is the corset-style AFO (Fig. 1b). These custom devices were originally developed for use as a prosthesis. Although the corset-style paradigm based on circumferential pressure has been adapted for use as an AFO, it has not been fully evaluated in this context [5, 6]. The corset-style AFO may be more effective at reducing load transfer through the injured limb than the camwalker [5]. In addition, the corset-style AFO is low profile and may preserve natural gait kinematics better than the camwalker, which adds length and mass to the affected limb.

The objective of this investigation was to compare load reduction capacity during the stance phase of gait for the camwalker and corset-style AFOs. The difference between the ground reaction force applied to the shoe and the force applied to the foot is calculated as the percent unloading, and used to estimate the effectiveness of each AFO. We hypothesized that the use of the corset-style AFO would result in a larger percent unloading compared to the camwalker.

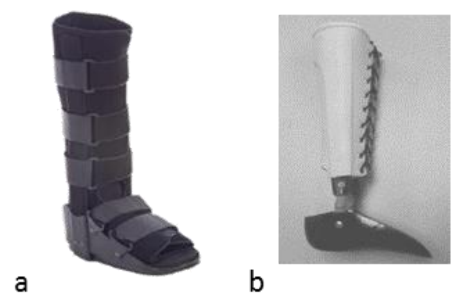

Figure 1: a) Camwalker AFO, b) Corset-style AFO.

METHODS

Eleven participants with no gait abnormalities were tested. Six used the camwalker (5 female, 1 male, 22.7±2.1 years, 173.0±11.5 cm, 166.2±37.7 lbs) and five used the corset-style AFO (4 female, 1 male, 38.4±8.9, 168.2±9.4 cm, 165.0±57.4 lbs). Two sets of insole pressure measurement devices (Tekscan, Boston, MA) were cut for each individual to be used during normal walking (tennis shoes) and braced walking (camwalker or corset-style AFO). Participants performed walking trials at an enforced speed of 1.5 m/s until three clean foot strikes on the force platforms were recorded for each limb during normal and braced conditions.

An Unloading Index (UI) was calculated across the stance phase to quantify the unloading across the entire stance phase and in three periods of stance (loading response, midstance, terminal stance). Mean UI was compiled from the three trials for each subject for their braced limb during the braced condition and for that same limb during normal walking. The difference between the braced and normal conditions were computed to obtain the relative UI difference. Data were compared across bracing mode (camwalker, corset-style AFO) using unpaired Student's *t*-test assuming unequal variances. Effect size was also calculated.

RESULTS

No significant differences were found between the bracing modalities; however, a trend was present in all periods of stance showing higher UI in the corset-style brace (Fig. 2). In the camwalker, the mean UI for the entire stance phase was 9.5±12.0% and in the corset-style was 33.7±35.0% (P=0.10). For the loading response, midstance, and terminal stance periods, mean UI for the camwalker and corset-style groups were 10.3±8.9% and 35.9±35.6% (P=0.10), 10.5±11.1% and 37.6±38.7% (P=0.09), and 8.8±10.6% and 28.7±30.3% (P=0.11), respectively.

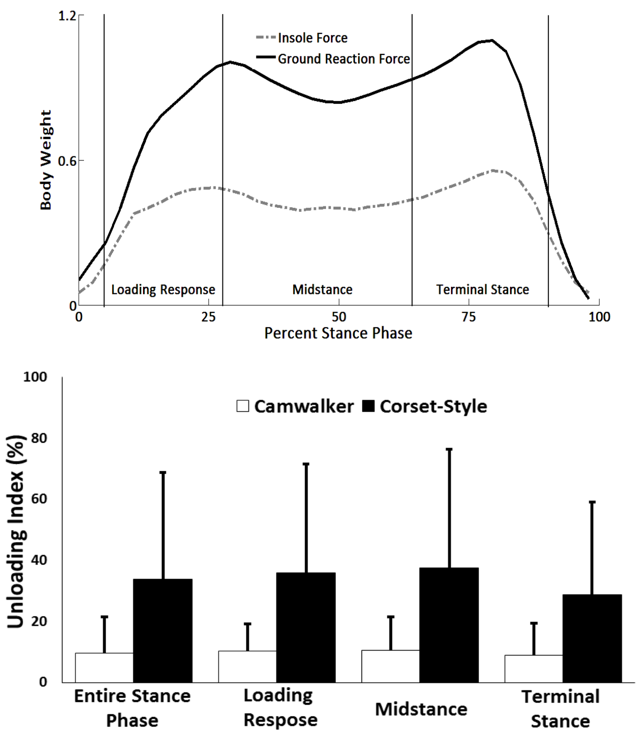

Figure 2: *Top*: Typical ground reaction force and insole force comparison for a corset-style AFO. *Bottom:* Ensemble group means (SD) for cam-walker and corset-style during each stance period.

For the entire stance phase, the effect size was 0.42. For the loading response, midstance, and terminal stance periods the effect sizes were 0.46, 0.43, and 0.40, respectively.

DISCUSSION and CONCLUSIONS

The results of this pilot examination indicate that the corset-style AFO may unload more than the camwalker during walking activity. None of the UI were significantly different between groups; however, all trended toward favoring the corset-style AFO in load reduction. Effect size results also trended toward a difference that could be clinically significant in lower extremity fracture management. Intersubject variability was high, possibly indicating that some subjects would benefit more than others from use of the corset-style brace. Further study is needed to determine what indicators best predict successful unloading with each brace.

The primary limitation in this investigation is that unloading of the lower extremity cannot be directly measured and the unloading index used is only a surrogate of the actual phenomenon. In addition, insole pressure devices, which measure forces normal to the sensor, are unable to account for shear components. However, in this investigation, this limitation results in a conservative estimation of load reduction.

In conclusion, the data indicate that using the corset-style AFO instead of the camwalker may be more beneficial to the patient if the goal is to decrease loading through the lower limb. Future investigations of these AFOs should include a clinical trial to further test this hypothesis.

REFERENCES

1. Sarmiento A, et al. *JBJS (Br)*, **71-B**, 602-609, 1989.
2. Sarmiento A. *JBJS* **52**(2), 295-311, 1970.
3. McCollough NC, et al. *JBJS* **60**(3), 314-319, 1978.
4. Sarmiento A, et al. *JBJS (Br)* **88-B**, 141-148, 2006.
5. Carlson JP, et al. *J Prosthetics and Orthotics* **4**(1), 41-44, 1991.
6. Sarmiento A, et al. *JBJS* **66**(9), 1328-1339, 1984.

In-Bed Passive and Active Movement Rehabilitation of Patients with Traumatic Brain Injury

[1,2]Kai Chen, [1,3]Lin Liu, [1]Liang Wang, [1,4]Yupeng Ren, [1,2]Deborah Gaebler, [1,2]Charles E. Sisung, [1,2]Li-Qun Zhang

[1]Rehabilitation Institute of Chicago, Chicago, IL, USA; [2]Northwestern University, Chicago, IL, USA; [3]XuanWu Hospital, Beijing, China; [4]Rehabtek LLC

email: l-zhang@northwestern.edu, web: http://smpp.northwestern.edu/research/biodynamics

INTRODUCTION

The applications of rehabilitation robotics have grown substantially during the past 10 years. Studies of lower limb robot-assisted therapy for children with moderate to severe cerebral palsy have shown significant gains compared with before and after 6 weeks training in balance, coordination, spasticity, strength and range of motion [1, 2]. While attempts to increase the application of robotic therapy in acute trauma brain injury (TBI) patients continue, our labs have recently extended our focus to rehabilitation of the children with lower-limb impairments in the hospital setup.

METHODS

Seven inpatients with traumatic brain injury (TBI) (5 girls, 2 boys, 12.8 ± 4.4 year old) recovering in hospital ward participated in this study. All had impaired lower-limb function with reduced or zero voluntary movement of the ankle and reduced selective motor control of the lower extremity.

A wearable rehabilitation robot with computer game interface was used to conduct guided motor relearning, passive stretching and active movement training and evaluate the outcome in terms of biomechanical and neuromuscular changes. The robotic device was equipped with a servomotor, a force sensor, and a digital controller. It was connected to a touchscreen computer for display and user interface (Figure 1). The interface allowed adjustment of the applied torque value, velocity, and difficulty levels of the exercise games, such as assistance or resistance level, according to each participant's ability.

The robot-aided therapy was conducted in the patient's ward 3~5 times a week (depend on patients' schedule and length of stay in hospital) for a total of about 18 sessions. The training in each session involved 10 minutes of passive stretching, 20 minutes of and assisted/resisted active movement, followed by 10 minutes of passive stretching.

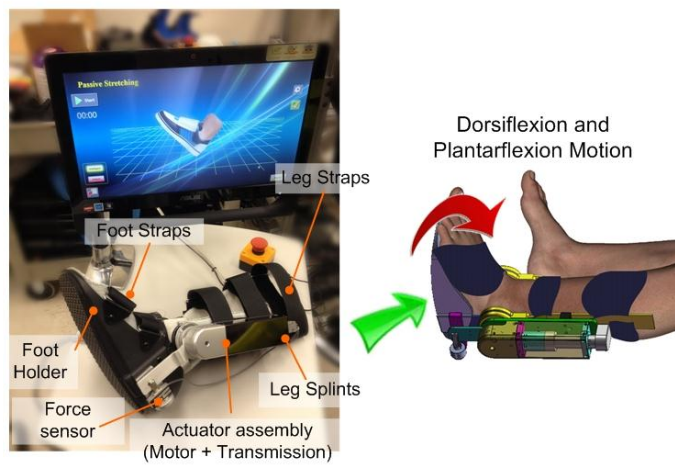

Figure 1: Diagram of the wearable robot for TBI inpatient rehabilitation.

Figure 2: Training setup. Participant lay supine on bed with the knee extended. The leg was supported by a pillowcase and foot was strapped onto the robotic boot with the ankle joint aligned with the robot rotation axis.

Children with TBI lay supine on bed with partially back and foot support by pillowcase. They wore the wearable robot on the ankle, the touchscreen computer placed in front of them with height and angle adjusted for proper view (Figure 2).

The same robot was used for training and evaluations. The participant's ankle was aligned with the rotation axis of the robot, and the joint ROM and torque limits were determined for passive stretching and controlled by an intelligent algorithm that allows strenuous and safe passive stretching [3]. Two types of active movement training were completed by the participants in which they voluntarily dorsiflexed and plantar flexed their ankle to play computer games. The choice of which type of active movement depended on the severity of disability of participants.

Clinical and biomechanical evaluations were done before and after the 18 sessions training period including the Modified Ashworth Scale (MAS) for spasticity, the Pediatric Balance Scales (PBS), and the Selective Control Assessment of the Lower Extremity (SCALE), passive range of motion (PROM), active range of motion (AROM), and muscle strength.

RESULTS AND DISCUSSION

All seven participants completed 18 sessions of training. Paired t-test showed improvements in biomechanical properties. The passive dorsiflexion was 19.14° ± 10.42° and 26.04° ± 5.75° (mean ± SD) before training and after training, respectively (P=0.0497), whereas the active dorsiflexion was 3.27° ± 7.96° prior to training and 12.68° ± 13.68° after training (*P=0.0255*); Averaged joint stiffness was reduced with training from 0.28 Nm/° before training to 0.21 N m/° after training. The dorsiflexor strength increased from 2.63 ± 2.09 Nm before training to 7.47 ± 4.04 Nm after training (*P = 0.0165*, Figure 3); the plantarflexion strength increased from 12.93 ± 9.51 Nm before training to 17.13 ± 11.42 Nm (P= 0.129). The MAS score at the ankle was 1.67 ± 0.74 before training and 0.67 ± 0.74 afterwards (P=0.070). The participants showed functional improvements in terms of SCALE, balance and locomotion with increasing scores, which were not significant due to missing measurements before training.

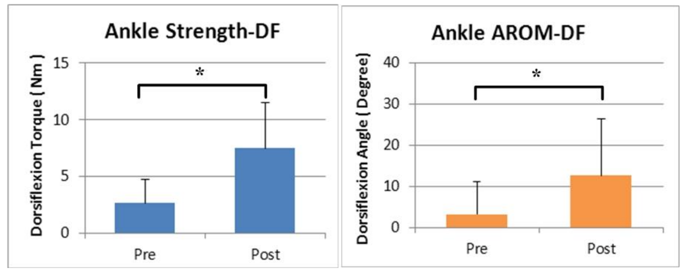

Figure 3: Biomechanical measures (AROM and strength of dorsiflexor).

CONCLUSIONS

Passive stretching combined with engaging active movement training was of benefit to children with TBI as seen in this pilot study. They demonstrated improvements in joint biomechanical properties, motor control performance, and functional capability in balance and mobility. The positive outcome of this study suggests that future studies include a larger sample of children with TBI in clinical settings to explore the impact of combined passive and active training on a single joint and adjacent joints. Further studies are needed to include control subjects and determine the optimal dose of therapy and examine translation of the observed gains to daily functional performance and participation in daily life.

REFERENCES

1. Wu YN, et al. *Neurorehabil Neural Repair*.**25,** 378-85, 2011.
2. Chung SG, et al. *Arch Phys Med Rehabil*. **85**, 1638-1646, 2004.
3. Zhang LQ, et al. *IEEE Trans Neural Syst Rehabil Eng*.**10,** 149-157, 2002.

A FAMILIARIZATION PROTOCOL FOR WHEELCHAIR PROPULSION

Jessica A. Longworth and Karen L. Troy

[1]University of Illinois at Chicago, Chicago, IL, USA
email: jlongw3@uic.edu, web: http://www.uic.edu/ahs/biomechanics

INTRODUCTION

The study of wheelchair propulsion biomechanics commonly employs the use of stationary rollers to simulate a smooth, over-ground propulsion environment and to allow for the collection of data during an extended period of propulsion using a limited amount of space. For most individuals, propelling on these rollers constitutes a novel task. It is imperative that distinctions be made between changes in a variable that occur as a result of the experimental treatment and those that are a result of acclimation to the experimental environment. For this reason, we propose the implementation of a familiarization protocol intended to account for this acclimatization period, and concurrently, improve the standardization with which this biomechanical data are collected.

The purpose of this study is to determine the number of propulsion cycles required for a subject to become familiarized to the task of wheelchair propulsion on stationary rollers, based on changes in kinematic variability.

METHODS

Twelve able-bodied, young adults (8 males, age 27 ± 5 yrs, height 1.8 ± 0.1 m, mass 77 ± 14 kg) volunteered to participate in this institutionally-approved study. All subjects provided written informed consent.

Subjects propelled a standard sport wheelchair (Quickie, Phoenix, AZ) on a set of stationary rollers (McLain, Lansing, MI). Subjects were instructed to propel at a self-selected speed which they might deem representative of everyday propulsion. When this speed was established (28 ± 14 sec), subjects were instructed to continue at that speed for an additional ten minutes. Instantaneous speed was recorded, and a speedometer was used to provide real-time visual feedback to the subject and investigator (6.8 ± 1.5 m/sec).

A three-dimensional motion capture system operating at 60 Hertz (Motion Analysis, Santa Rosa, CA) was used to collect kinematic data. Eighteen reflective markers were placed on the trunk and upper extremities to create a seven-segment rigid body model [1]. Segment angles of the right upper extremity were calculated relative to the global reference frame [2]. The data from each subject were divided into propulsion cycles that started and ended with maximal elbow extension (i.e. the end of the push phase, start of the recovery phase). For the purpose of this study, push time (i.e. duration of each propulsion cycle) was analyzed for each propulsion cycle.

Based on methods adapted from Owings and Grabiner, the running mean of push time was calculated for all of the recorded propulsion cycles [3]. Next, the final 10% of data points at the end of the running function were selected. The mean ±2 standard deviations (SDs) of push time was calculated for this subset of points. A 35-point sliding window progressed iteratively, one propulsion cycle at a time, through the running function until all 35 points fell within ±2 SDs of the mean of the 10% subset. The propulsion cycle number corresponding to the first point of the sliding window for which the 35 points fell within this range was considered the minimum number of propulsion cycles required to obtain a plateau in the variability for an individual subject. We considered this to represent familiarization (Figure 1).

These methods were also applied using the final 25% of the running mean, and ±1 SD and ±3 SDs to determine the most conservative estimate.

Table 1: Familiarization point based on the final 10% and 25% of all data points and ±1, 2, and 3 SDs. Data are presented as mean ± SD for propulsion cycle number and the corresponding time. (Results for the final 10% ±1 SD were not reported because five subjects did not reach familiarization under these parameters.)

	Final 10%		Final 25%	
	Cycle	Time	Cycle	Time
±1 SD	-	-	419 ± 97	7:36 ± 1:30
±2 SD	430 ± 111	7:54 ± 1:54	353 ± 114	6:24 ± 2:00
±3 SD	394 ± 123	7:18 ± 2:12	330 ± 107	5:24 ± 2:30

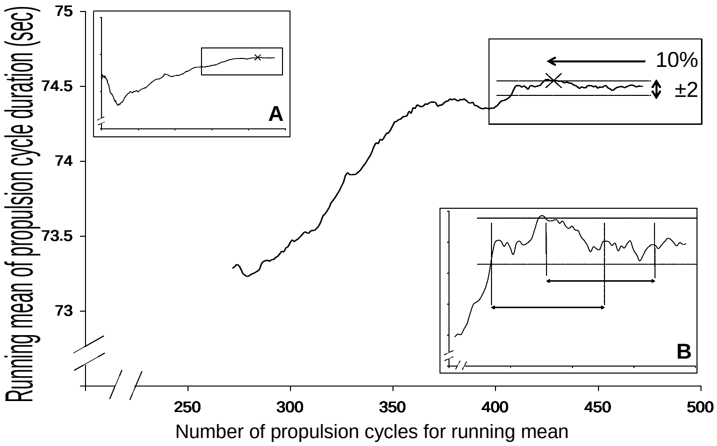

Figure 1: Representative running mean of propulsion cycle duration as a function of number of propulsion cycles, final 200 points. 'X' denotes familiarization. Final 10% and ±2 SDs are labeled. **Insert A:** Entire data series, 472 points. **Insert B:** Final 75 points with two example 35-point sliding windows labeled.

RESULTS AND DISCUSSION

During ten minutes of propulsion subjects performed an average of 542 ± 87 (range 434-666) propulsion cycles each. Using the final 10% of the total number of points of the running mean and a standard deviation of ±2 provided the most conservative estimate of the number of propulsion cycles required for familiarization and the time at which this occurred according our definition (Table 1). Based on these results, at least 430 ± 111 propulsion cycles (range 166-567) must be acquired before push time variability begins to plateau. This number of propulsion cycles occurs, on average, at 7:54 ± 1:54 during the ten minute trial. After this point the variability of the propulsion cycle duration is only minimally affected by additional propulsion cycles.

It is possible not all subjects will experience a stabilization of kinematics within 430 propulsion cycles, or during an 8-minute familiarization period. However, this value represents a relatively conservative estimate of familiarization. For example, if the final 10% of the data points were selected but a SD of ±3 was used, familiarization would occur among these subjects after 394 ± 123 cycles and after 7:18 ± 2:12. Similarly, if the final 25% of the data points were selected and a SD of ±2 was used, familiarization would occur among these subjects after 353 ± 114 and after 6:24 ± 2:00.

Able-bodied subjects were selected for this initial study instead of wheelchair users because they require familiarization to the stationary rollers as well as require familiarization to the propulsion task itself. This would be expected to lengthen the time to familiarization compared to manual wheelchair users, ensuring that the present estimate represents a familiarization time that applies to mean populations. A ten minute trial was selected as it was thought to be long enough to achieve familiarization but short enough to avoid the influence of fatigue on variability. Lastly, our estimate is based on one temporal kinematic index, push time, which is analogous to step length in gait. It is possible that spatial kinematics achieve temporal stabilization at a different time point than push time.

CONCLUSIONS

We have determined that propulsion cycle time in able-bodied subjects becomes stable after 430 ± 111 propulsion cycles on a set of stationary rollers. Therefore, we recommend allowing for approximately eight minutes of familiarization pushing prior to collecting biomechanical data. This may help minimize conflicting results due to methodological differences.

REFERENCES

1. Troy KL. *Disab & Rehab: Assist Tech* **6**(1), 22-28, 2011
2. Wu G, et al. *J Biomech* **38**, 981-992, 2005.
3. Owings TM & Grabiner MD. J Biomech 36, 1215-1218, 2003.

A PRINCIPAL COMPONENT ANALYSIS OF KINEMATIC VARIABILITY DURING WHEELCHAIR PROPULSION

Chandrasekaran Jayaraman, Ian M. Rice, Yaejin Moon, Iris M.-K. Hsu, Elizabeth T. Hsiao-Wecksler, Carolyn Beck, Jacob J. Sosnoff.

University of Illinois at Urbana-Champaign, Urbana, IL, USA
email: jayaram4@illinois.edu

INTRODUCTION

Manual wheelchair (MW) users are at high risk of developing shoulder pain. Consequently, mechanisms and factors that contribute to shoulder pain in manual wheelchair users have been a topic of scientific inquiry. Researchers to date have studied the association between various mean parameters of kinematic and kinetic propulsion mechanics and to shoulder pain. Examinations of wheelchair propulsion have divided the push cycle into two separate phases, the push phase when the hand is in contact with the wheel and the recovery phase when the hand is not in contact with the wheel. The majority of studies have focused on either the entire cycle or the push phase [1].

Although variability has been associated with musculoskeletal pain in various other motor tasks [2], there has been minimal investigation of this phenomena in wheelchair propulsion. Consequently, this project examined spatial variability of the recovery stroke as a function of shoulder pain during MW propulsion. Spatial variability analyzed using a principal component analysis (PCA) of the wrist trajectory was compared between groups with and without shoulder pain.

METHOD

Kinematic data of wheelchair propulsion from ten participants with spinal cord injury (five without shoulder pain and five with shoulder pain) were collected. All were experienced MW users with a Semi-circular pattern (SC) for their propulsion. All the subjects who participated in this study signed an institutionally approved informed consent form. The participant demographics and spinal injury diagnosis are listed in Table 1. Each participant's wheelchair was fitted bilaterally with force and moment sensing wheels (SmartWheel; Mesa, AZ, USA) and placed on a stationary roller with a tie-down system.

Table 1: Demographic details of participants. (SB-Spinal bifida, SA-Sacral agenesis, T-Thoracic ,C-cervical).

	Pain Group	**No Pain Group**
Injury	T8(n=1);T11(n=1); T6(n=1);SB(n=1);SA(n=1)	SB(n=2);T6-T9(n=2);C7(n=1).
Age (yrs)	28.8 (15.05)	23.3 (7.8)

Participants propelled for 3 trials at steady state speeds of 1.1 m/s (fast), 0.7 m/s (slow) and a self-selected speed for three minutes each. A 1 minute period was given between each trial. The sequence of speeds was randomized across participants. Real-time velocity feedback was provided to the participant. Kinematic data of wheelchair propulsion were collected using motion capture equipment (Cortex 2.5, Motion Analysis Co) at 100Hz.

Three-dimensional motion data from right arm segment markers, namely radial styloid (RS), ulnar styloid (US), were used for the variability analysis (Figure 1). The wrist centre motion coordinates were used to compute the PCA. Motion data were filtered using a 4^{th} order Butterworth filter (0 to 15 Hz). Cycles having any data points outside 3 standard deviations were excluded from the analysis. Each cycle in a trial was separated into propulsion and recovery phase based on handrim Mz (moment in z direction) values using a custom developed code in MATLAB. The recovery cycles in each trial were then time normalized to 1000 points (1 to 100%) using a shape preserving cubic spline interpolation. The mean recovery trajectory was computed for each trial. Principal components (PC's) were computed for the wrist motion coordinate data in directions orthogonal to mean recovery path at equally spaced (10%) intervals (from start of recovery 1% to end of recovery 100%) (Figure 1) [3]. The square root of the principal component (PC) values (standard deviation) at each spatial location was used as a measure of spatial variability.

A mixed model repeated measure ANOVA was used to determine if there were differences in spatial variability between groups. Speed was used as a within group factor and shoulder pain as the between group factor.

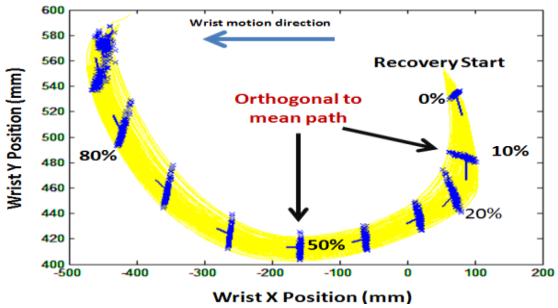

Figure 1: Sample wrist recovery trajectories (yellow) showing the spatial points (blue) orthogonal to mean recovery path at which PCA was computed (0% to 100% at every 10% interval).

RESULTS and DISCUSSION

Figure 1 shows a sample recovery trajectory from a participant with SC pattern. It was observed that the variance in the latter half of recovery phase (from 50% - 100% point) is higher than the variance in the first half (0% to 50%). During a typical SC recovery trajectory the wrist falls below the propulsion trajectory path and the hand switches the direction of motion. The shoulder joint has to abduct and also has to provide sufficient angular deceleration for the wrist to allow a smooth transition while switching. From the data trend, it was observed that the majority of this directional switch occurred around 10 to 20% of the recovery phase. At this point (10% in Figure 1), the shoulder has to couple a joint abduction with necessary angular deceleration. The region between 0% to 50% in Figure 1 shows higher variance in wrist path (around 10% to 20%) during this deceleration and directional transition phase.

Table 2 summarizes the results from the PCA. The standard deviations of the PC at the first 10% spatial location of recovery stroke between the two groups at three different test speeds are shown. Only at this point did variability significantly differ between groups regardless of speed (p=0.001). The wrist trajectory of the group with shoulder pain had a significantly larger amount of variability along the first PC direction compared to the group without shoulder pain. This observation is congruent with previous research examining shoulder pain and arm movement during ergonomic task [4]. Studies on repetitive reaching task in [5] demonstrate that subjects with shoulder pain exhibited higher relative variability in their kinematics than those without pain. We further note that most of the participants from the pain group in this study reported a pain score during shoulder abduction. So it is logical that the portion of the recovery phase related to maximal shoulder abduction is indicated. Due to the cross-sectional design of this investigation, it is not clear if shoulder pain causes increases in variability or vise versa.

Table 2: First principal component values between groups at 10% point along the recovery trajectory.

	√PC1(SD) (mm)			p value
	Fast	Self	Slow	
No pain	10.18 (3.2)*	11.83 (5.4)*	11.35 (2.62)*	*0.001
Pain	20.97 (2.92)	27.56 (8.02)	28.56 (13.2)	

CONCLUSIONS

There are two novel components of this project: 1) analysis of the recovery phase; and 2) examination of kinematic variability of wheelchair propulsion utilizing PCA. Wrist PC's were computed orthogonal to the mean wrist recovery path at every 10% spatial interval point along the mean recovery trajectory. The user group with shoulder pain had higher variability (at first 10% point of the recovery path) compared to the group without pain along the first PC direction. Further research is needed to determine if shoulder pain *results* from increased motor variability or rather if shoulder pain *leads* to more variability arm motion during wheelchair propulsion.

REFERENCES

1. Boninger, ML.,, et al. *Arch Phys Med Rehabil May;*83(5):718-23.,2002
2. Srinivasan D, Mathiassen SE. *Clin Biomech*. 27(10):979-93.,2012
3. Rajiv R., et al. *Neuroscience Letters*.469; 416–420.,2010
4. Madeleine, P., et al. *Exp.Brain.res*,185: 689-698,2008.
5. Lomond, K.V., et al. *Exp.Brain.res*,206: 271-282,2010.

ACKNOWLEDGEMENTS

This project is funded by the Nation Institute of Health grant (#1R21HD066129-01A1). The authors extend their gratitude to the Illinois Simulator Laboratory.

Authors: Hartigan EH, Zifchock R, Lawrence M, Tu C

Title: Proposal for a new methodology for tracking arch motion during athletic tasks

Background: Current methods to analyze foot motion require the placement of markers on the barefoot or through windows cut in the footwear. Placement of the markers in this manner reduces the external validity of a biomechanical study, since athletes typically use footwear in their activities of interest and movement is not similar between barefoot and shod conditions.[1] Furthermore, analysis of arch motion tends to mathematically force the rotation of the markers to occur along the long axis of the foot even though the anatomy of the arch is angled (e.g. arch height is higher at the mid-foot than the forefoot). A new marker set and model that describes motion of the foot's arch relative to the calcaneous around an axis created by the Feiss line (medial malleolus to 1st metatarsal head) would better replicate anatomy. Additionally, investigating the feasibility of analyzing foot control in athletes while they don normal footwear is warranted. If this new foot model for tracking motion around the Feiss line produces similar relative motion between markers on un-cut footwear (SHOD) and on the skin through cut footwear (WINDOW), then gross foot motion about the arch could be measured while wearing shoes. The purposes of this pilot study are two-fold: 1) to propose a new foot model to quantify mid-foot / forefoot relative to rearfoot motion around an anatomical axis; and 2) to compare relative excursions of arch motion between two shoe conditions (SHOD and WINDOW) during different athletic tasks.

Subjects: 15 healthy, uninjured recreational athletes 13M, 2F, aged 22.5 ± 3.1 years, with a mass of 74.3 ± 11.5 kg and a height of 1.72 ± 0.17 m participated in this study.

Methods: Three tasks (running, cutting, landing from a drop jump) were performed in sequence with the shoe conditions (SHOD and WINDOW) performed in random order. Retro-reflective markers were placed on the right leg only. Clusters of retro-reflective markers were placed on the lower leg and arch of the foot and single markers were placed on bony landmarks (medial malleolus, lateral malleolus,1st and 5th metatarsal heads, and calcaneus). The experimental model was a two segment foot model (heel and midfoot segments). The shoes were similar makes and models between conditions with only the right shoe cut for the WINDOW condition (e.g. heel and tongue of footwear). The experimental marker set consisted of superior, inferior and lateral heel markers on wands placed directly on the subject's skin via windows in the shoe to track the heel segment. A three marker cluster was also placed through a window cut in the tongue of the shoe to track the midfoot segment. The position of this 3 marker cluster was located by determining the mid-point on the Feiss line then moving laterally to the mid-point of the dorsum of the foot). This cluster was used to track motion of the arch of the foot. Laces were positioned to avoid contact with the arch cluster. The heel segment's superior point was defined as the ankle joint (equal distance between the malleoli markers) and the inferior point was defined as a point projected onto a plane created by the ankle joint, mid-point between the metatarsal heads and inferior heel marker that was the same height from the floor as the mid-metatarsal point. The mid foot segment was constructed along a line that ran from the medial malleolus marker to the first metatarsal head marker representing the anatomical Feiss line of the foot. The ankle joint was defined as the midpoint between the malleoli. Segments were all allowed six degrees of freedom. Motion was tracked during the stance phase of the 3 tasks with eight Oqus Series-3 cameras (Qualisys AB, Gothenburg, Sweden) set at 240 Hz. Trials were filtered with a low pass Butterworth filter with a cutoff of 10 for running, 15 for cutting, and 12 for drop jump landings. Arch excursions were calculated by subtracting the arch position at peak knee flexion from the arch position at initial contact. These excursions represent arch motion during the loading response of each task and mean excursions for the SHOD and WINDOW conditions were compared using paired t-tests (IBM, SPSS Statistics 19).

Results: Mean relative excursions were not statistically different between conditions during running, cutting, and drop jump landing tasks (Table 1).

Table 1. Arch excursions for the right foot: Window vs Shod

	Window	Standard Deviations	**Shod**	Standard Deviations	P value
Running	-0.730	2.279	0.055	0.803	0.164
Cutting	-4.142	4.574	-2.542	1.358	0.195
Jumping	-2.299	2.847	-1.535	1.339	0.320

Positive values indicate motion towards inversion whereas negative values indicate motion towards eversion.

Conclusion: Arch motion around the Feiss line appears to be no different when markers were placed on the footwear or when a window was cut to place the markers on the skin. These findings suggest that relative motion of the arch can be analyzed while a subject dons athletic footwear during the loading response of athletic tasks (e.g. run, cut, and drop jump landing). Each condition was measured using separate trials as both marker sets (WINDOW and SHOD) were unable to be tracked simultaneously on the foot. Therefore we cannot ascertain whether the arch motion was the same because trials were independent for each condition. We also appreciate the limitations of the model inability to accurately measuring specific bony motion within the shoe. Yet, these preliminary results suggest that gross neuromuscular control of the arch can be assessed while donning athletic footwear. This pilot work will allow effect size calculates for future studies to test if arch motion is different between limbs. The overall goal of this model is to determine whether movement of the arch while donning athletic footwear could be compared between limbs after anterior cruciate ligament (ACL) rupture and reconstruction (e.g arch motion of the healthy limb vs ACL reconstructed limb). Anecdotal evidence from the principle investigator's clinical expertise with athletes after ACL construction suggests that arch position may be different between the ACL reconstructed and healthy limb, yet methods are needed to quantify motion of the arch during athletic tasks.

References: **1.** Morio C, Lake MJ, Gueguen N, Rao G, Baly L. The influence of footwear on foot motion during walking and running. *J Biomech.* Sep 18 2009;42(13):2081-2088.

A COMPARISON OF ELECTROMYOGRAPHY FROM FOUR LOADING CONFIGURATIONS

Adam Jagodinsky, John Fox, Jared Rehm, Braden Romer, Jay Patel, and Wendi Weimar.

Auburn University, Auburn, AL, USA.
Email: aej0015@auburn.edu

INTRODUCTION

Countermovements are frequently used in athletic events for optimizing performance (1). Research has shown that the countermovement yields better performances compared to no countermovement (2). Given that canines lift their paws 4-8 cm before performing a countermovement in the canine sprint start (3), it should be considered that alternative loading configurations may improve performance. Therefore, the purpose of this project was to evaluate peak force and EMG amplitude during four loading configurations.

METHODS

Twenty male participants (83.7±8.8kg; 1.8±0.07m) were recruited. Electromyography of the pectoralis major and triceps brachii, and peak force were measured during plyometric pushups from the modified push-up position under 4 conditions. Condition 1 was performed from a pre-determined elbow flexed position. Condition 2, similar to a countermovement jump, involved beginning in the modified push-up position then lowering and pushing vertically. Condition 3 involved kneeling with arms positioned anteriorly. The participant fell forward into a countermovement, similar to a depth jump. The novel condition, condition 4, began from the modified push-up position. Each participant lifted his hands from the ground and fell into a countermovement.

RESULTS AND DISCUSSION

Peak force was found for each push-up. A 1 (Participant) x 4 (Condition) repeated measures ANOVA was used to analyze differences in peak force and EMG amplitude during the concentric phase. The peak force analysis indicated that significant differences exist between conditions (F = 43.329, $p < .001$) (Figure 1) with Condition 3 yielding the highest peak force. There was no significant difference between 1 and 2 (p = .791). However, peak force during 4 was greater than 1 and 2 ($p < .001$), but less than 3 ($p < .001$). EMG analysis revealed no significant differences of average peak amplitude for the pectoralis major (F = 1.197, p = .317) nor triceps brachii (F = .670, p = .531) across conditions (Figure 2).

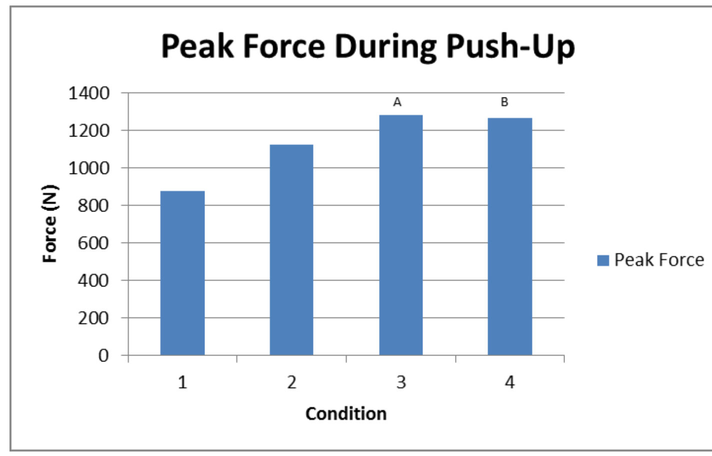

Figure 1: Peak force production during each push-up condition. (A: Significantly different than 1 &2; B: significantly different than 1, 2 & 3).

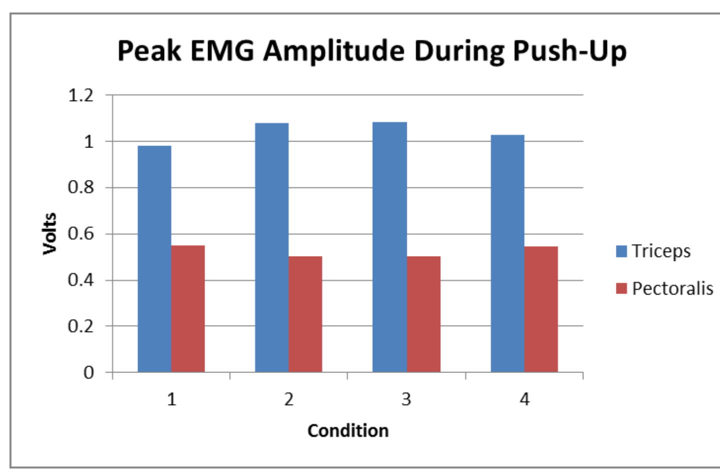

Figure 2: EMG activity of the pectoralis major and triceps brachii during each condition.

CONCLUSIONS

The peak force during the concentric phase was enhanced in condition 3 and 4; however muscle activity was not different across conditions. These findings suggest that higher force production from a countermovement is primarily dependent on the mechanical properties of the muscle rather than neuromuscular components. This research demonstrates improved performance with a novel loading pattern that may be useful in explosive athletic events since drop landings are impractical during most athletic events.

REFERENCES

1. Finni, T., Komi, P.V. & Lepola, V. *Eur J Appl Physiol, 83,* 416-426, 2000.
2. Arakawa, H., Nagano, A., Yoshioka, S. & Fukashiro, S. *J Electromyogr Kines, 20,* 340 – 347, 2010.
3. Angle, T.C. Gillette, R.L. & Weimar, W.H. *Australian Vet J*, *90,* 60-68, 2012.

GENDER DIFFERENCES IN FRONTAL PLANE LOWER EXTREMITY KINETIC VARIABILITY DURING LANDING

Andrew D. Nordin and Janet S. Dufek

University of Nevada, Las Vegas, Las Vegas, NV, USA
email: nordina@unlv.nevada.edu

INTRODUCTION

Investigations of human movement variability have been used as a means of exploring neuromotor functioning, where performance variability is thought to provide the system with flexibility and a mechanism for adaptation to movement repetition [1,2]. Operationally, variability has been considered to fall within optimal limits, while excessively high or low variability has been implicated in injury susceptibility [2]. Landing has been explored due to a high incidence of injury in athletic performance, as well as the ability to easily control task demands through increases in landing height [1].

The purpose of this investigation was to evaluate changes in lower extremity kinetic variability in the frontal plane, exploring gender comparisons during landing. Peak frontal plane joint moments were used to access variability across landing heights at the hip, knee, and ankle joints. Landing height was increased as a proportion of maximum vertical jump height (MVJH), which characterized lower extremity functioning across a range of task demands.

METHODS

Fourteen participants (7 male, 7 female; mean age 22.6±3.4 years; height 1.71±0.10m; mass 67.56±10.31kg) free from previous lower extremity injury were examined in this investigation. Informed consent was obtained prior to participation as approved by the Research Ethics Board at the affiliated institution.

Kinematic and kinetic data were simultaneously acquired using a 12-camera system (Vicon MX T40-S; 200Hz) and two synchronized force platforms (Kistler 9281CA, 9281B; 2000Hz). Data filtering and interpolation included a low pass, 4th order (zero lag) Butterworth filter and cubic (3rd order) spline. Ground contact was identified from force platform data (vertical ground reaction force >+20N). Landing phase was defined from ground contact to the point vertical center of mass (COM) velocity was zero (Figure 1).

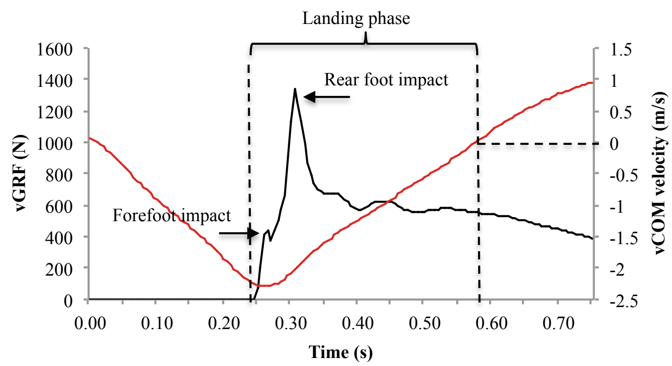

Figure 1: Vertical ground reaction force (GRF) and COM velocity vs. time, defining the landing phase

Participants completed a general warm up prior to testing. Five maximum vertical jump trials, measured using a Vertec, were averaged to determine maximum vertical jump height (MVJH). Five step-off bilateral landing trials were completed at four successive drop heights, calculated as a percentage of average MVJH (60%, 100%, 140%, 180%). Landing heights were ordered from lowest to highest to minimize risk of injury. Participants were instructed to land with both feet simultaneously, one foot on each force platform.

Variability was expressed using coefficient of variation (CV%). Comparisons were made using 2x3x4 (Gender x Joint x Height) mixed model ANOVAs, with repeated measures on height (α=0.05), for each dependent variable using SPSS 20.0 for Mac.

RESULTS AND DISCUSSION

Differences in frontal plane lower extremity peak moment variability were detected among landing heights, lower extremity joints, and between genders. A significant main effect for lower extremity joint (F[2,78]=7.771, p=.001, η^2=.166) showed lesser variability at the knee joint (16.9±3.4%) relative to the hip and ankle joints (25.0±4.5%, p=.001; 23.8±2.0%, p=.008; Figure 2). This suggests freezing at the knee joint during landing, which may have implications for injury susceptibility [1,2].

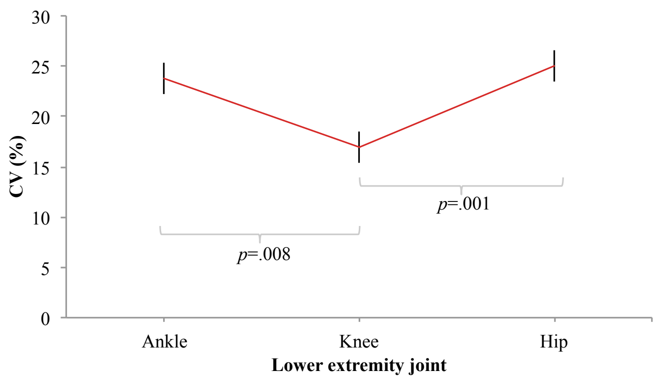

Figure 2: Lower extremity joint vs. peak frontal plane moment variability (CV%)

Females demonstrated greater overall lower extremity peak moment variability than males (23.8±%, 19.7±%, respectively) in the frontal plane (F[1,78]=6.126, p=.015, η^2=.073). Significant interaction was observed between landing height and gender (F[2.248,175.327]=7.159, p=.001, η^2=.084), suggesting that males and females differed in peak lower extremity joint moment variability across landing heights. As a result, simple main effects analyses were carried out.

Independent samples t-tests between genders identified lower extremity variability differences at the 60% MVJH landing height (t[53.786]=4.753, p<.001; Figure 3). From this, it appears that females responded differently to the landing task compared to males, where landing heights at, and in excess of 100% MVJH resulted in a significant decrease in peak lower extremity joint moment variability for females (F[2.125,82.880]=6.629, p=.002, η^2=.146; Figure 3). The lack of significant differences across landing heights for males (F[1.424,55.535]=3.210, p=.060, η^2=.076; Figure 3) suggests that male participants maintained a relatively constant level of lower extremity kinetic variability during landing, while females adopted a new landing strategy in excess of 100% MVJH. This may provide insight into gender differences in susceptibility to injury, particularly at increased landing heights [1]. These findings also suggest that females demonstrate greater lower extremity movement variability, working within operational limits that differ from males at lower task demands [2]. This may be a product of joint laxity relative to males, which may be associated with increased risk of lower extremity injury during landing [1,2].

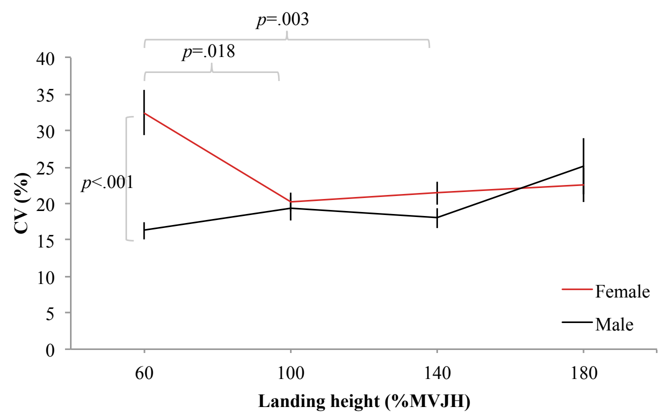

Figure 3: Landing height vs. lower extremity joint frontal plane moment variability (CV%) by gender

CONCLUSIONS

Overall, female participants demonstrated greater lower extremity kinetic joint variability during landing compared to males, but showed significant decreases when landing in excess of 100% MVJH. Future research should explore a wider range of task demands, seeking to better understand the relationship between movement variability and movement control, with attention to gender comparisons. Lesser kinetic variability at the knee may also shed light into the high rates of injury at this joint, providing avenues for future research.

REFERENCES

1. James, CR, et al. *Med & Sci Sports Ex.* **32**(11), 1833-1844. 2000.
2. Stergiou, N, Decker, LM. *Human Mov Sci.* **30**, 869-888. 2011.

ASSOCIATIONS BETWEEN CLINICAL DORSIFLEXION FLEXIBILITY AND LANDING MECHANICS DURING A DROP JUMP

[1]Philip Malloy, [1]Christopher F. Geiser, [1]Claire M. Wood, [1]Carolyn M. Meinerz, [2]Krista D. Watson and [1]Kristof Kipp

[1]Marquette University, Milwaukee, WI, USA
[2]Augustana College, Rock Island, IL, USA
email: philip.malloy@marquette.edu, web: http://www.marquette.edu/exercise-science/

INTRODUCTION

Anterior cruciate ligament (ACL) injuries are associated with altered neuromuscular control during landing tasks. Dynamic valgus, which is characterized by excessive frontal plane motion secondary to femoral adduction and tibial abduction, can place the knee in positions that have been associated with increased strain of the ACL [1,2,3].

While landing in an extended and abducted position at the knee results in deleterious loading associated with injury, the predictors of this dynamic valgus position have not been fully established[1,4]. Several other researchers have found that ankle flexibility is a predictor of such postures [5,6]. Individuals with less ankle dorsiflexion flexibility have demonstrated less knee flexion excursion and greater vertical and posterior ground reaction forces [5]. Greater knee excursion in the frontal plane has also been shown in individuals with less ankle dorsiflexion [6].

Ankle dorsiflexion flexibility is commonly measured during injury screenings of competitive athletes. The primary purpose of this study was to determine if ankle dorsiflexion flexibility is associated with knee abduction motion and moments during a drop landing task. The secondary purpose of this investigation is to determine if ankle dorsiflexion flexibility can predict energy attenuation during landing.

METHODS

Twenty two healthy DI female collegiate soccer players were recruited for a pre-season injury screening. Ankle dorsiflexion flexibility was measured using a goniometer, while subjects were in a long sitting position with the knee fully extended.

Subjects performed ten double leg drop vertical jumps off a box that was normalized to each individuals corresponding vertical jump height. Kinematic data from these jumps were recorded using a motion analysis system. Kinetic data were simultaneously collected using two force plates. Peak ankle flexion, knee flexion, knee abduction, knee abduction moment, total negative ankle and knee energies were calculated from these data during the landing phase, which was defined as the point of initial contact through peak knee flexion. Moments reported are external moments. Means and standard deviations of these variables were calculated and used for analysis.

Statistical analysis consisted of Pearson's correlations to determine the associations between the independent variable (ankle dorsiflexion flexibility) and each of the six dependent variables (peak ankle flexion, peak knee flexion, peak knee abduction, peak ankle energy, peak knee energy, and peak knee abduction moment). Statistical significance was set *a priori* at $\alpha = 0.05$.

RESULTS AND DISCUSSION

Significant correlations were found between ankle dorsiflexion flexibility and peak knee flexion (Figure 1: $r = -.385$, $p = 0.035$) and peak knee abduction (Figure 1: $r = .355$, $p = 0.048$). In addition, a significant correlation was found between ankle flexibility and peak knee abduction moment (Figure 2: $r = -.442$, $p = 0.017$).

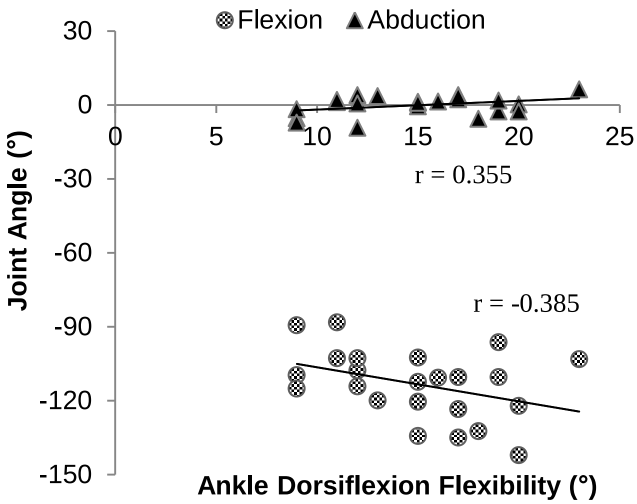

Figure 1: Peak knee flexion and abduction angles (degrees) as a function of ankle dorsiflexion flexibility (degrees).

These results suggest that less ankle dorsiflexion flexibility is associated with less knee flexion and greater knee abduction motion during landing. These findings are consistent with a previous report [5]. In addition to confirming previous findings, our study extends these findings and demonstrated that ankle dorsiflexion flexibility also predicted knee abduction moments. These results suggest that athletes with less ankle flexibility experience greater moments at a joint up the kinetic chain (i.e., the knee).

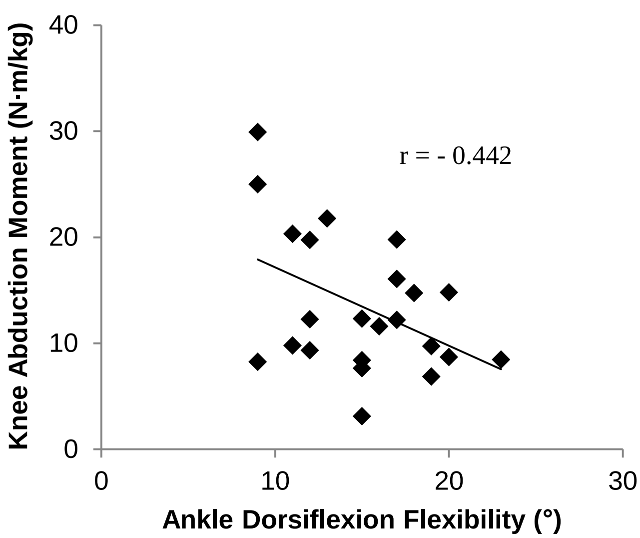

Figure 2: External knee abduction moment (N·m/kg) as a function of ankle dorsiflexion flexibility (degrees).

In investigating landing energetics we did not find any associations between ankle flexibility and the magnitude of either knee or ankle joint energies absorbed during landing. This may suggest that the greater moments at the knee are more due to factors such as landing posture and not distribution or dissipation of energy between segments of the lower extremity kinetic chain.

Less knee flexion, greater knee abduction, and greater knee abduction moments during landing have all been posited as risk factors for ACL injury through the dynamic valgus mechanism [1]. Our results suggest that less ankle dorsiflexion flexibility may precipitate anterior cruciate knee ligament loading by placing the knee in a more extended and abducted position during landing with simultaneous abduction moments. The combination of these factors may place athletes with less dorsiflexion flexibility at greater ACL injury risk during landing.

CONCLUSIONS

Female athletes with less ankle dorsiflexion flexibility demonstrated less peak knee flexion, greater peak knee abduction, and greater external knee abduction moments during landing from a drop jump. Ankle dorsiflexion range of motion may serve as a simple clinical measure to identify athletes at risk for ACL injury and opens the door for future interventions.

REFERENCES

1. Hewett TE, et al. *Am J Sports Med*. **33**, 492-501. 2005.
2. Markloff KL, et al. *J Orthop Res*. **13**, 930-935, 1995.
3. Withrow TJ, et al. *Clin Biomech*. **21**, 977-983, 2006
4. Griffin LY, et al. *Am J Sports Med. **34**,* 1512-1532, 2006.
5. Fong CM, et al. *J Athl Training* **46**, 5-10, 2011
6. Sigward SM et al. *J Orthop Sports Phys Ther*. **38**, 661-667, 2008.

LINEAR PREDICTION OF KINEMATIC AND KINETIC PERFORMANCE WITH INDIVIDUAL ANATOMIC FACTORS

Nathaniel A. Bates[1], Greg D. Myer[1,2], Timothy E. Hewett[1,2,3]

[1]University of Cincinnati, Cincinnati, OH, USA
[2]Cincinnati Children's Hospital Medical Center, Cincinnati, OH, USA
[3]OSU Sports Medicine Sports Health & Performance Institute, Ohio State University, Columbus, OH, USA
email: batesna@mail.uc.edu website: http://cincinnatichildrens.org/sportsmed

INTRODUCTION

Anterior cruciate ligament (ACL) ruptures are expensive, debilitating athletic injuries that lead to early onset osteoarthritis. [1] Kinematic and kinetic variables observed in tasks such as the drop vertical jump (DVJ) have been associated with increased ACL injury risk. [2] In order to prevent ACL rupture it is important to identify athletes that exhibit injury risk biomechanics, but the cost of motion capture systems needed for full biomechanical analysis is prohibitive to many institutions. As such complex nomograms have been developed to predict an athlete's injury risk biomechanics sans motion capture. [3] Early identification of injury risk mechanics may lead to injury prevention through the application of prophylactic interventions. [4] However, in some situations, such as the study of motion on cadaveric specimens, an investigator may lack some of the data points necessary to calculate a nomogram. The reproduction of *in vivo* motion on cadaveric specimens allows investigators to study injury mechanics in novel ways. Therefore, it is worthwhile to investigate how effective individual factors are at linearly modeling kinematic and kinetic performance. The purpose of this investigation was to establish whether individual anatomical factors can accurately predict kinematic and kinetic performance values during a DVJ task.

METHODS

239 female basketball players at the middle and high school level were evaluated through a series of biomechanical tests. Each subject was assessed for height with a stadiometer and weight with a calibrated physician's scale. Subjects were instrumented with 43 retroreflective markers and asked to perform three DVJ tasks from an initial height of 31 cm. 3D motion data was collected during each DVJ task with a 10-camera Motion Analysis Corp. system and dual AMTI force platforms. Kinematic and kinetic data were then calculated in Visual3d with a subject-specific biomechanical model. Isokinetic knee extension, knee flexion, and hip abduction strength were collected with a BIODEX dynamometer at a revolution speed of 300º /sec for the knee and 120º /sec for the hip. From this data four anatomical factors were selected to be evaluated against 12 kinematic and 12 kinetic measures for linear correlations. MATLAB was used to calculate the significance of each linear regression model and corresponding R-squared values. Statistical significance was determined at $\alpha < 0.05$.

RESULTS AND DISCUSSION

Most linear models exhibited poor R-squared values (Table 1). Anatomical factors expressed significant relationships ($P < 0.05$) with kinematic measures in 26 of 48 cases. However, R-squared values were universally poor ($R^2 < 0.18$). Similarly, though significant relationships ($P < 0.05$) were identified in 39 of 48 cases for kinetic measures, the maximum R-squared value was 0.69. Poor R-squared values indicate that, while significant, most of these models did not account for enough error to be clinically applicable predictors. The exceptions to this were height and mass relative to peak adduction moment (Figure 1) and flexion moment range. Unfortunately, these two measures have not been identified as indicators of ACL injury risk. Combination of factors, such as the height*mass, did not increase the number of measures for which models were significance or improve R-squared values relative to individual factors.

Table 1: Displays correlations between anatomical factors (columns) and performance measures (rows). Highlighted cells indicate a significant relationship was present and the corresponding R-squared value is indicated within that cell.

	Ht	Mass	H*M	Tib
Kinematics				
Flexion @ initial contact		0.03	0.02	
Abduction @ initial contact	0.06			0.05
Internal @ initial contact	0.04	0.04	0.05	0.05
Max flexion angle	0.12	0.17	0.18	0.02
Min flexion angle	0.06			0.05
Max abduction angle		0.04	0.03	
Max adduction angle	0.06	0.08	0.08	0.02
Max internal angle	0.09			0.08
Max external angle		0.04	0.04	
Flexion ROM				
Abduction ROM	0.06			0.06
Internal ROM				
Kinetics				
Flexion @ initial contact	0.02	0.07	0.06	
Abduction @ initial contact				
Internal @ initial contact				
Max Flexion Moment	0.12	0.32	0.31	0.04
Max Extension Moment	0.07	0.17	0.17	0.05
Max Abduction Moment	0.10	0.17	0.18	0.05
Max Adduction Moment	0.42	0.63	0.65	0.23
Max Internal Moment	0.09	0.07	0.08	0.06
Max External Moment	0.08	0.05	0.06	0.05
Flexion Moment Range	0.42	0.68	0.69	0.22
Abduction Moment Range	0.27	0.38	0.39	0.19
Internal Moment Range	0.25	0.27	0.30	0.14

Ht = subject height; **Mass** = subject mass; **H*M** = subject height multiplied by subject mass; **Tib** = subject tibia length

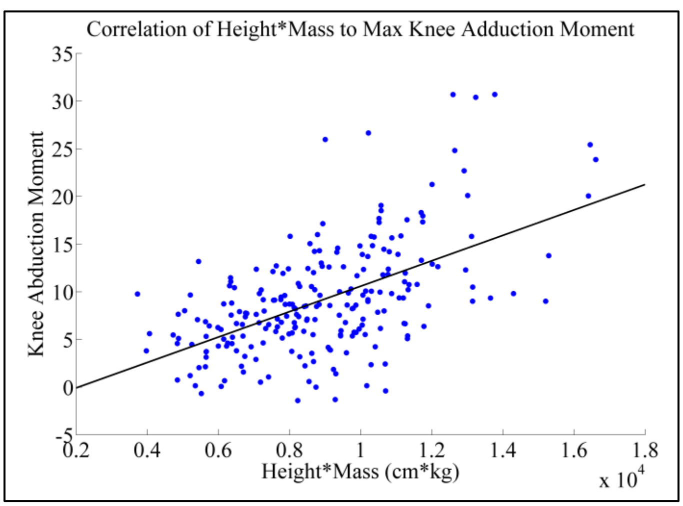

Figure 1: Graphic depiction of kinetic performance against anatomical factor (height*mass) data.

More complex models are necessary to correlate factors with most kinematic and kinetic measures. The nomogram developed by Myer et al. [3] predicts a single kinetic measure based on a multitude of anatomic, strength, and kinematic factors. Most of the current models are too oversimplified to accurately predict performance. As these linear prediction models do not accurately estimate kinematics, the adjustment of input kinematics relative to specimen size in cadaveric studies is not justified. Similar to clinical prediction, the poor R-squared values from linear models applied in this study account for too little kinematic variability to justify change. Therefore in studies that aim to recreate *in vivo* motion in cadaveric specimens, alteration of kinematic inputs relative to specimen size would be inappropriate.

Significant correlation between anatomic factors and kinetic measures were expected. Mechanics dictate that increased mass at a further distance will generate greater moments. However, even these factors mostly did not account for enough variation to be predictive beyond broad generalizations.

CONCLUSIONS

Linear models that correlate anatomical factors to kinematic and kinetic performance may not account for sufficient variance to accurately predict values. More robust, multi-factor nomograms are necessary to predict values and clinically significant variables such as relative ACL injury risk. [3]

REFERENCES

1. Delince P, et al. *Knee Surg., Sports Traumatology, Arthroscopy*. **20**, 48-61. 2009.
2. Hewett TE, et al. *Am. J. Sports Med.* **33**, 492-501. 2005.
3. Myer GD, et al. *Am. J. Sports Med.* **38**, 2025-2033. 2010.
4. Myer GD, et al. *J. Strength Cond. Res.* 20, 345-353. 2006.

ACKNOWLEDGEMENTS

Funding supported by NIH Grants R01-AR049735, R01-AR055563, and R01-AR056259.

EFFECT OF FATIGUE ON HIGH SCHOOL MALE AND FEMALE PITCHERS

[1]Mandi Gibbons, [1]Andrew Kraszewski, [1]Jocelyn Hafer, [1]Jennifer Bido,
[1]Jessica Graziano, [1]Michael Levinson, [1]Sherry Backus, [1]Howard Hillstrom, [1]Stephen Fealy, [1]Andreas Kontaxis

[1]Hospital for Special Surgery, New York, NY USA
email: mandigibbons@gmail.com, web: http://www.hss.edu/rehab-motion-analysis-lab.asp

INTRODUCTION

American baseball and softball are among the most popular sports for adolescents in the United States. Shoulder injuries are becoming increasingly prevalent in this population, with pitching volume being a significant risk factor. Pitchers may be vulnerable to shoulder injury due to fatigue-induced alterations in muscular strength and kinematics. There is limited published research describing the full 3D scapular and glenohumeral (GH) motion alterations and there are no data to show how fatigue can affect GH kinematics.

The objectives of this abstract are to investigate whether we can detect change in shoulder kinematics and strength in both male overhand and female underhand high school pitchers due to fatigue. This project received institutional IRB approval.

METHODS

A total of 24 pitchers (12 baseball, 12 softball) between the ages of 15 and 18 years, without history of shoulder pain or injury, were recruited to participate in this study.

Three-dimensional kinematics of upper extremity (head, thorax, scapula, humerus, forearm, hand) were recorded using a 12-camera optical motion system at 250 Hz. Markers were placed according to recommendations of Kontaxis et al [1]. Scapular kinematics were measured using a custom made cluster that follows the recommendations of Karduna et al [2].

Pitchers threw indoors from a pitching mound at regulation distance (male: 60.5 ft, female: 43 ft), and game-simulated volume (males: 90 pitches, females: 105 pitches). Pitchers threw only fastballs in sets of 15 with five-minute breaks between sets to allow for recovery. The last five pitches of the first set and the last five pitches of the last set were included in analysis (averages and standard deviations calculated for each set). Kinematics were calculated and compared between defined events (knee-up and follow through in males, initial drive and follow through in females).

Participants completed two abduction exercises moving between 60° and 120° of ROM, as indicated on a stationary guide, both before and after pitching. Scapulohumeral (SH) coupling was calculated from these trials.

Voluntary maximal isometric strength of the internal and external rotators was evaluated before and after pitching using a Biodex dynamometer (Biodex Medical Systems, Shirley, New York) in three positions (45° IR, 0° neutral, and 45° ER) with the arm abducted in 45 deg. A paired t-test (2-tail) was used to compare pre- and post-pitching strength.

RESULTS AND DISCUSSION

This is an ongoing investigation and for this abstract results from seven baseball and softball pitchers are reported. Significant increases in range of motion were seen in both softball and baseball pitchers (Figures 1A-B, Table 1). Significant decreases in strength as indicated by the isometric testing (Figures 2A-B) show that muscular fatigue is occurring in the baseball pitchers. There was no change in SH coupling.

As this is an ongoing investigation more analyses need to take place to specifically correlate these changes to fatigue. No changes were seen in SH coupling but male pitchers demonstrated a higher average value compared to the girls which was slightly decreased from pre to post testing.

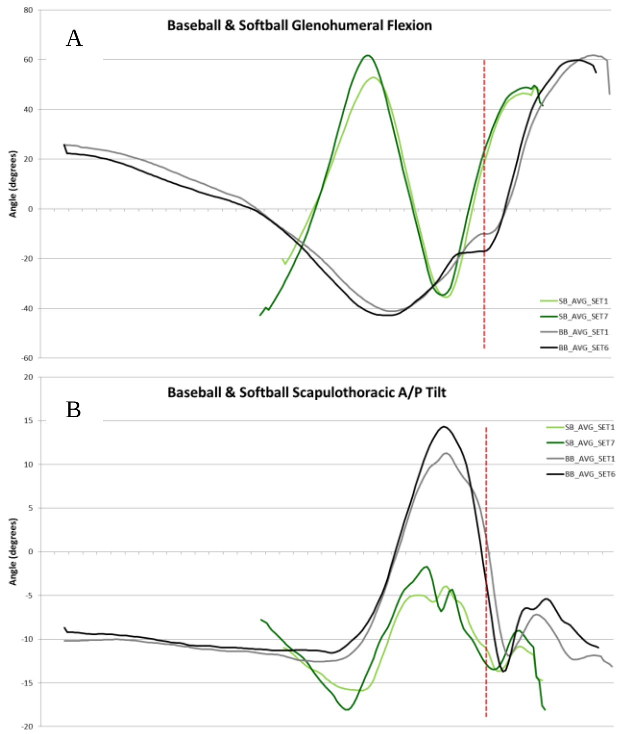

Figure 1A-B. Glenohumeral and scapulothoracic kinematics comparing first and last set of pitching (red dashed line = ball release; green = softball; black = baseball).

CONCLUSIONS

This study presents unique information regarding shoulder kinematics and strength in high school aged softball and baseball pitchers. Males did experience a decrease in muscular strength over a game-like bout of pitching, while females displayed more significant kinematic changes. Future analyses will include more subjects and clinical information in order to get a more comprehensive understanding of fatigue in these kinematic alterations.

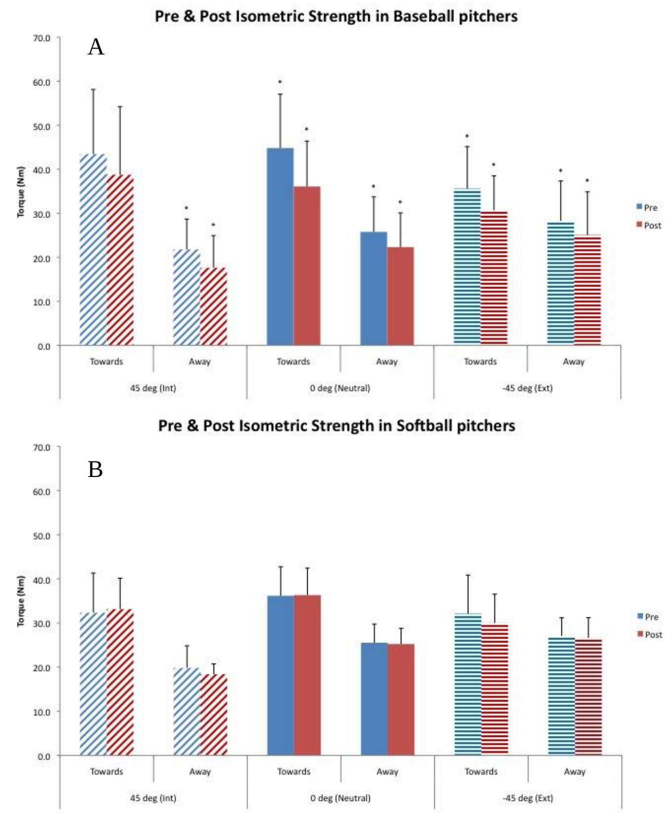

A

Figures 2A-B. Isometric strength in male and female pitchers (* indicates significant difference between pre and post; α = 0.05).

REFERENCES

1. Kontaxis A, et al. *Clin Biomech* 24, 246-253, 2009.
2. Karduna AR, et al. *ASME* **123**, 184-190, 2001.

ACKNOWLEDGEMENTS

Funded by the HSS Institute for Sports Medicine Research

Table 1: Comparison of shoulder joint ROM (mean ± SD) between the first and last set of pitching (* indicates significant difference between first and last set; α = 0.05)

Shoulder Joint Parameters	Baseball (n=7)		Softball (n=7)	
	Set 1	**Set 6**	**Set 1**	**Set 7**
GH Flexion ROM (°)	113.7 ± 11.8	115.9 ± 12.3	125.8 ± 13.1	129.4 ± 13.2*
GH Abduction (°)	84.5 ± 18.5	93.9 ± 33.5*	130.7 ± 12.3	141.4 ± 12.1
GH Rotation (°)	201.1 ± 39.5	210.6 ± 52.5	133.0 ±14.0	135.9 ± 22.1*
ST Tilt (°)	44.0 ± 12.7	42.56 ± 12.3	26.2 ± 3.0	28.5 ± 3.1
ST Protraction (°)	58.6 ± 8.1	57.7 ± 12.0	41.4 ± 6.0	43.4 ± 8.1*
ST Sup/Inf Rot (°)	27.4 ± 7.0	28.8 ± 7.2	49.7 ± 5.5	52.5 ± 5.8
Scapulohumeral Coupling	0.44	0.39	0.20	0.21

PEAK VERTICAL GROUND REACTION FORCES ARE DIFFERENT DURING STRETCH VS. WIND-UP PITCHING IN COLLEGIATE BASEBALL PLAYERS

[1]Patrick Rider, [2]Bret Beaman, [2]Taylor McKinney, [1]Paul DeVita and [3]Blaise Williams

[1]ECU Biomechanics Laboratory, Greenville, NC, USA
[2]ECU Human Movement Analysis Laboratory, Grenville, NC, USA
[3]Commonwealth Sports Medicine, Glen Allen, VA, USA
email: riderp@ecu.edu web: http://www.ecu.edu/cs-hhp/exss/biomechlab.cfm

INTRODUCTION

There are two mechanical patterns that baseball pitchers use to deliver the ball, commonly referred to as the stretch and the wind-up. Most biomechanical studies have investigated upper extremity kinematics and are typically focused on the wind-up pattern. Dun et al. is the only study to date that has examined differences between the stretch and wind-up. They found a small but significant difference in pitched ball velocity (0.2 m/s faster from the wind-up than from the stretch). Interestingly, in the upper extremity kinematic and kinetic variables investigated, the authors found no differences [1] between patterns. However, this study reported neither external ground reaction force data nor any lower extremity kinetics values.

Many studies have shown correlations between biomechanical variables and performance measures. However, few pitching studies have been conducted that have accounted for GRFs during the movement. A recent study investigated lower-extremity GRFs in baseball collegiate pitchers, and found strong correlations between GRF data and kinematic and kinetic variables [3]. However, this study failed to report any correlations of GRFs on performance measures.

The variance in ball velocity during pitching might be explained more so by differences in ground reaction forces than in upper body kinematics, since anecdotal evidence suggests that pitch velocity originates in the lower body. No studies have investigated the differences in GRFs between stretch and wind-up motions, therefore the purposes of this study were to compare the differences in ground reaction forces during stretch and wind-up pitching and to examine any relationships between ground reaction forces with pitched ball velocity in the two pitching patterns.

METHODS

Sixteen Division I collegiate pitchers were examined in this study (BM: 91.96 kg ± 8.36kg). All pitchers were on the active roster and had an approximate ¾ overhead delivery. Each participant provided university approved informed consent before testing. Each subject was fitted for standard bilateral full-body biomechanical motion capture and a familiarization period was allowed for the athlete to warm-up on the simulated mound. The mound consisted of two imbedded AMTI force plates; a small drive (rear) leg plate that was oriented parallel to the floor and a larger landing platform that was oriented at roughly a 10 degree angle to the floor, similar to the angle on a standard pitching mound. Data were collected with a 9 camera Qualisys motion capture system. Pitchers were instructed to throw four-seam fastballs at a target on a suspended net from their natural stretch/wind-up positions. Each pitcher threw 10 pitches from each starting position and starting position was randomized to minimize any fatigue effect between each trial. Ball velocity was recording using a radar gun.

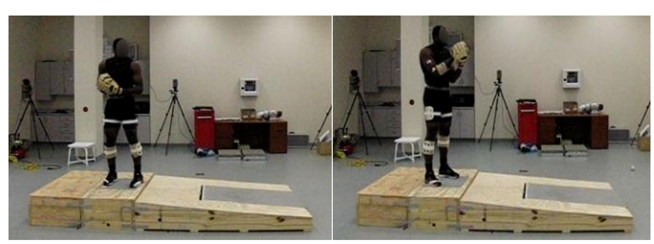

Figure 1: Data collection area with mound setup. Subject demonstrates typical starting positions for the stretch (left) and wind-up (right) pitching patterns.

Data were reduced and compared using Student's t-test to determine any significant (p<.05) differences between ball velocity and ground reaction forces between the two conditions. Regression analyses were conducted to determine if any significant relationships between variables existed.

RESULTS AND DISCUSSION

There was a small but statistically significant difference in pitched ball velocity between wind-up (36.81 mps ± 1.48) and stretch (36.48 mps ± 1.55). This difference is not practically significant as it is probably too small to have an impact on performance (less than 1 mph different). These values were slower than expected and could have been a result of the placement of the radar gun.

A significant difference in peak vertical GRF was observed between the groups (Wind-up: 1764.5 N ± 324.3 vs. Stretch: 1620.1 N ± 264.4) as shown in Figure 2. These data were similar to previously reported values [3, 4].

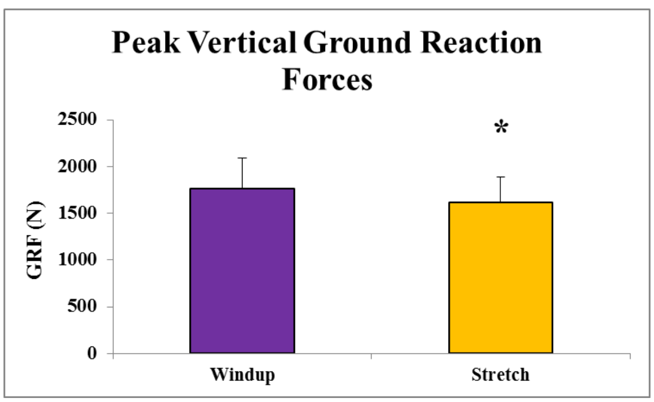

Figure 1: Mean (sd) peak vertical ground reaction forces of the landing leg during the wind-up and stretch conditions.

A moderate positive correlation (r=0.66) was found between mean ball velocity and mean landing vertical GRF. This was similar to many of the correlations among upper extremity kinematics and ball velocity found in other studies [2, 3].

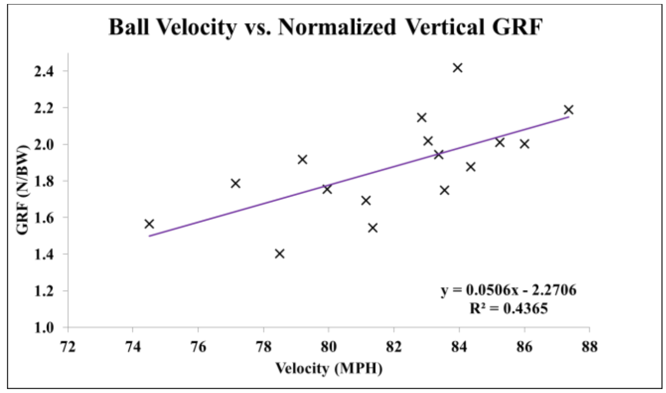

Figure 3: Relationship between mean ball velocity and mean landing vertical ground reaction force for both wind-up and stretch conditions.

CONCLUSIONS

Overall, peak ground reaction forces were greater in the landing leg during wind-up pitching vs. stretch pitching. Moderate correlations between ball velocity and vertical GRFs identify the importance of the interaction between the pitcher and the mound in generating high ball velocities. Further investigation into these external loads and their effects on other performance variables during baseball pitching is warranted.

REFERENCES

1. Dun, S., Kingsley, D., Fleisig, G. *American J of Sports Medicine*, **36(1)**, 137-41.

2. Toyoshima, S., et al. C. Morehouse(Eds.), University Park Press, pp. 169–174.

3. Guido, J., and Werner, S. *J of Strength and Conditioning Research*, **26(7)**, 1782-1785, 2012.

4. MacWilliams, B., et al. *American J of Sports Medicine*, **26(1),** 66-71.

ACKNOWLEDGEMENTS

The authors would like to acknowledge Greer Hoell and Matthew Salzano for their contributions during data collection and Meredith Hayek for her contribution to data reduction.

THE EFFECTS OF THROWING TECHNIQUE ON PERFORMANCE FOR SIX ELITE JAVELIN THROWERS

Steven Leigh[1] Jesus Dapena[2], Michael Gross[3], Li Li[4], Joseph Myers[3], and Bing Yu[3]

Montclair State University, Montclair, NJ, USA[1]
Indiana University, Bloomington, IN, USA[2]
The University of North Carolina at Chapel Hill, Chapel Hill, NC, USA[3]
Georgia Southern University, Statesboro, GA, USA[4]
email: leighst@mail.montclair.edu

INTRODUCTION

A javelin thrower makes complex, multi-joint movements to accelerate the javelin to great release speeds, while carefully controlling the direction of the release [1]. For maximum performance, a javelin thrower needs their technique to optimize the javelin release variables for maximum vacuum projectile motion and for beneficial aerodynamic effects. There are differences in technical training methods, strength, and anthropomorphics among javelin throwers. The optimal javelin throwing technique may be thrower-specific. The purpose of this study was to identify associations between technique variables and performance for six elite javelin throwers, and then to look for commonality.

METHODS

At least 10 trials each by three female and three male elite javelin throwers competing in meets from 2007 to 2010 were included in this study. All throws were recorded from behind and from the right side of the javelin runway with two HDV cameras operating at 60 frames/second. Twenty four body and javelin landmarks were digitized to obtain 2-D coordinate data from the video clips, and then time synchronized using multiple critical events. The Direct Linear Transformation procedure [2] was used to obtain real-life 3-D coordinate data.

Official distances were measured at each meet. Javelin release variables were calculated from the javelin's center of mass and javelin and global reference frames [1]. The aerodynamic distance was calculated from the official distance and the vacuum flight distance. Technique variables were reduced at right foot down, left foot down, and release. Shoulder and hip joint angles and trunk angles were calculated as Euler angles. Elbow, wrist, knee, and ankle joint angles were calculated between the longitudinal axes of their proximal and distal segments [3].

Associations between technique variables and the official distance, the release speed, and the aerodynamic distance were determined for each javelin thrower individually using a Pearson correlation analysis with a type I error rate of 0.05. Common associations between technique and performance among throwers were identified.

RESULTS AND DISCUSSION

There were significant correlations between technique variables and performance for every thrower individually. However, there were no technique variables that were significantly correlated with performance and were common to all six throwers. For all three female throwers, improved javelin throwing performance was associated with a lower javelin inclination at release, greater left hip flexion at release, greater right shoulder external rotation at left foot down, and greater right shoulder horizontal adduction at release. For all three male throwers, improved javelin throwing performance was associated with javelin oriented more to the right at left foot down.

Subject specific differences were found in the technique variables that were associated with performance. These differences do not mean that javelin throwing technique was different between subjects. The relative importance of technique varies depending on differences in technical training methods, anthropometrics, and specific strength and physical characteristics. In general, it is important for javelin throwers to use the approach run to transfer momentum into javelin release speed, to increase the gain in release speed through throwing arm motion during the delivery, and to control the release to minimize drag forces to gain aerodynamic distance.

The common results for the female javelin throwers suggest that all three mechanisms are necessary for performance. Left hip flexion may be the mechanism to transfer approach run momentum to javelin release speed. Externally rotating the right shoulder before the release and horizontally adducting the right shoulder at release may be the mechanism to increase release speed through throwing arm motion. Lowering the inclination angle of the javelin angle at release may be the mechanism to minimize contact surface area and drag forces to gain aerodynamic distance.

The common result for the male javelin throwers suggests that their ability to control the orientation of the javelin at release accounts for the most variation in throwing performance. Controlling the javelin at the release is important for minimizing drag forces and gaining aerodynamic distance. The lack of other common associations may be because they are proficient at converting runway momentum to release speed, and use a consistent throwing arm motion.

REFERENCES

1. Best RJ, Bartlett RM, and Morriss CJ. *J Sports Sci* **11(4)**, 315-28, 1993.
2. Abdel-Aziz YI, & Karara HM. *ASP Symposium on Close Range Photogrammetry*, Falls Church, VA, USA, 1971.
3. Liu H, Leigh S, & Yu B. *J Sports Sci* **28(13)**, 1459-67, 2010.

ACKNOWLEDGEMENTS

This project was financially supported by USATF, the International Society of Biomechanics, and the University of North Carolina Graduate School.

A COMPARISON OF TWO DIFFERENT SPRINT START TECHNIQUES IN COLLEGIATE LINEBACKERS

Robin Lund, Jason Cusick and Travis Ficklin
Biomechanics Laboratory, University of Northern Iowa, Cedar Falls, IA, USA
email: robin.lund@uni.edu

INTRODUCTION

Anecdotally, many linebacker coaches attempt to coach their players to eliminate the false step (rhythm step) during play. This motion has been deemed by many coaches as a wasted movement since the initial motion is backward [1]. The forward step is taught by numerous coaches to eliminate counterproductive movement, however it may be beneficial to step back before accelerating. By stepping back, the athlete utilizes the stretch-shortening cycle (SSC) which can lead to an increase in muscular force during push-off [2]. Stepping backward also allows the athlete to have a larger horizontal component of their ground reaction force (GRF). These benefits have been explored in previous work related to multiple activities [2,3,4], but not for the football linebacker position, where players are often coached to eliminate this rhythm step. The purpose of this study is to compare the rhythm step (RS) and the forward step (FS) on sprint start ability in collegiate linebackers.

METHODS

Fifteen collegiate football players who play the linebacker position executed three maximum effort sprints through 5 meters of both the RS and FS techniques in a randomized counterbalanced order following an auditory cue. Prior to this, three 5 meter sprint starts were also performed from track blocks (BS) to determine a best performance for comparison. For the RS and FS techniques, each subject started in the ready position they would use in game conditions.

Subjects were allowed to use their preferred leg to initiate each trial. High-Definition video of each trial was captured using a camera shooting at 60 Hz (JVC GC-PX1, Tokyo, JP). The camera was positioned such that its optical axis was perpendicular to a vertical plane bisecting the length of the running lane.

The forward-most point of the trunk was manually digitized for all frames of the run, starting at the subject's first movement after a visual signal that was made by the starter, simultaneously with the audio cue to start. This trunk position was converted to meters relative to the start line using calibration points visible in the video, and the time series location data were smoothed using a 4th-order zero-lag butterworth filter at 12 Hz. The times at which the forward-most point of the trunk crossed both the 2.5-m ($t_{2.5}$) and 5-m marks (t_5) were calculated by interpolation from time series horizontal position data.

This trunk point was chosen to be consistent with track and field timing rules and also represented meaningful forward progress by a linebacker trying to reach a location to execute a tackle. The time split between 2.5 m and 5 m was also recorded (t_{split}). The best trial for each technique was recorded in seconds (s).

Descriptive statistics (mean ± SD) were performed on all performance variables. A repeated measures MANOVA was used to compare the two techniques (RS, FS) as well as the block starts (BS) on $t_{2.5}$, t_5 and t_{split}. When appropriate, separate repeated measures ANOVA tests as well as paired samples t-tests were used as post hoc analyses. A Bonferroni correction was used to control for family wise error. Alpha was set at 0.05 for all tests.

RESULTS

Descriptive statistics can be found in Table 1. The repeated measures MANOVA indicated that there was a significant technique effect $(F(3,13)=32,$

p=0.001). Mauchley's test of sphericity was rejected for each of the three separate repeated measures ANOVA tests therefore a Greenhouse-Geisser penalty was assessed for these tests. A significant technique effect was observed for $t_{2.5}$ (F(1.4,21)=75.5, p=0.001) and t_5 (F(1.4,21.5)=67.4, p=0.001) but not for t_{split} (F(1.2, 18.6)=1.9, p=0.18). Paired samples t-tests indicated that BS was significantly faster than RS (p=0.001) and RS was faster than FS (p=0.001) for $t_{2.5}$. The same trend was observed for t_5. There were no differences between any of the techniques in t_{split} from 2.5 to 5 meters.

DISCUSSION

Horizontal forces are extremely important for acceleration/sprint starts. It is unsurprising that the BS resulted in the greatest horizontal forces because they maximize the forward horizontal component of GRF by allowing for normal forces with the blocks greater than those possible by friction with level ground.

Linebacker coaches may assume that the backward motion inherent to the RS is counterproductive. However, all subjects preformed better with the RS than the FS. First, using the RS allows the player to lower the center of mass (CM) and have more forward lean. This allows for more horizontal force, similar to using BS. Additionally, using the RS allows the player to utilize the SSC for generating initial force. Any benefit of SSC in the FS is likely to be less, if it exists at all, due to limited or eliminated range of stretching motion of the muscles.

The benefits of this technique are limited to the first few steps of the linebacker's motion (2.5 m) and are preserved through at least the 5-meter mark. All subjects were faster through 2.5 m in the RS condition, and through 5 m, but this benefit was realized in the first 2.5 m. After that, it seems that the player is moving similarly in any of the conditions.

Previous work [1,3,4] has shown also shown that the RS is superior for starting speed compared to FS. It is a naturally occurring motion that is often "coached out" of the athlete. The results of the present study suggest that in the case of the linebacker position it should not be. The players in the current study had previously been coached to perform only the FS, but were able to realize immediate benefit by abandoning it. Football coaches should be encouraged to revisit their methods for coaching this particular position.

Table 1. Descriptive statistics

	BS		RS		FS	
	Mean	SD	Mean	SD	Mean	SD
$t_{2.5}$ (s)	0.81**	0.05	0.95*	0.05	1.09	0.11
t_5 (s)	1.28**	0.06	1.43*	0.06	1.58	0.12
t_{split} (s)	0.47	0.02	0.46	0.02	0.47	0.03

** sig. faster than RS and FS

* sig. faster than FS

REFERENCES

1. Dewitt, J. (2010, June 20). *Linebacker play: Lead or get out of the way.* Retrieved from http://www.coacheslearningnetwork.com/index.php?PHPSESSID=b1a8b154df23db222da7182a12cd0120&nArticleID=119
2. Kraan, G. A., Veen, J. V., Snijders, C. J., & Storm, J. (2001). Starting from standing; why step backwards? *Journal of Biomechanics*, *34*, 211-215.
3. Frost, D. M., & Cronin, J. B. (2011). Stepping back to improve sprint performance: A kinetic analysis of the first step forwards. *Journal of Strength and Conditioning Research*, *25*(10), 2721-2728.
4. Frost, D. M., Cronin, J. B., & Levin, G. (2008). Stepping backward can improve sprint performance over short distances. *Journal of Strength and Conditioning Research*, *22*(3), 918-922.

INSTANTANEOUS POWER MEASUREMENT IN WHEELCHAIR RACING

[1]Jean-Philippe Pelland-Leblanc, [1]François Martel, [1]Ève Langelier, [1]Cécile Smeesters, [2]Félix Berrigan, [2]Jean Laroche and [1]Denis Rancourt

[1]Mechanical Engineering Department, Université de Sherbrooke, Sherbrooke QC, Canada
[2]Kinanthropology Department, Université de Sherbrooke, Sherbrooke QC, Canada
e-mail: Denis.Rancourt@usherbrooke.ca web: http://www.eureka.gme.usherbrooke.ca/perseus/

INTRODUCTION

In racing sports such as bicycle or wheelchair racing, power measurement is a key performance indicator that is less sensitive to variations in wind and road conditions. Though most commercial systems limit their feedback to an averaged power signal, instantaneous power gives more insights from a biomechanical point of view.

In the case of an athlete/wheelchair system, instantaneous power transfer to the system is defined as $P = vF$, with v, the instantaneous speed of the system center of mass (CoM) and F, the instantaneous force transmitted to the wheelchair in the direction of its movement. Since CoM motion is usually not measurable directly, the obvious alternative is to measure wheelchair motion. Measurement of external forces on the athlete/wheelchair system is, however, not a simple task. Instrumentation to directly measure pushing forces is often invasive. One potential alternative is to use Newton's second law with measurements of wheelchair acceleration. Hence, knowing the mass of the system, measurement of wheelchair motion alone may provide sufficient information to estimate instantaneous power transfer P.

The purpose of this study was to determine if, indeed, wheelchair motion data give valid estimates of instantaneous power P. Validation was achieved by comparing power transfer measured on the track versus on a validated laboratory ergometer [1].

METHODS

A national development team wheelchair athlete was asked to perform an all-out, standing start, 60m acceleration run both on the track and on a motorized ergometer mimicking resisting forces that occur while racing on a track.

When testing on the track, we instrumented the wheelchair using a BEI optical encoder mounted on a 12 inches circumference trailing wheel (Fig. 1), resulting in a resolution of 16400 pulses/m (i.e. per meter of chair motion). Signals were acquired using a NI Compact Rio and motion module system at a frequency of 1 kHz. Signals were sent from the wheelchair to a fixed station using a BEI SwiftComm real time wireless system.

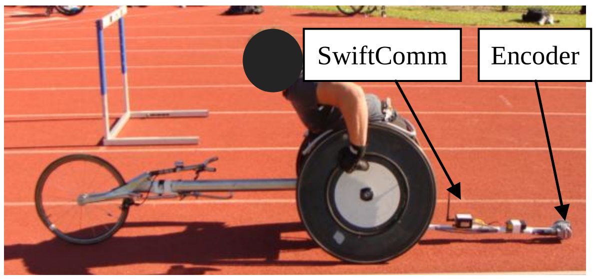

Figure 1: Encoder mounted on a trailing wheel.

When testing on the ergometer, we used a Sick DFS60A encoder mounted on a roller, resulting in a resolution of 309248 pulses/m. Data signals were acquired using the NI Compact Rio and motion module system at a frequency of 2 kHz. Signals were then down sampled to 1 kHz in Matlab.

Both signals (ergometer and track) were low pass filtered with a fourth order Butterworth filter with a cutoff frequency of 14 Hz, resulting in a filtered position signal (x). The instantaneous speed (v) and acceleration (a) were computed based on position data points with a centered derivative equation [2]:

$$v_i = \frac{x_{i+1} - x_{i-1}}{2\Delta t}, \qquad a_i = \frac{x_{i+1} - 2x_i + x_{i-1}}{\Delta t^2}$$

In order to compute the power produced by the athlete based on the measured data, forces opposing the movement were estimated. These opposing forces are composed of aerodynamic drag (F_A) and rolling resistance (F_R) and were approximated by the basic equations [3]:

$$F_A = \mu_R mg + k_f mgv^2, \qquad F_R = 0.5A\rho C_d v^2$$

The instantaneous power transfer could then be computed with: $P = v(ma + F_A + F_R)$.

RESULTS AND DISCUSSION

The small variations shown in table 1 demonstrate that the athlete had a similar performance in both testing conditions. However, when plotting the instantaneous power (Fig. 2), there is a significant discrepancy in peak power amplitude (factor of 2-3), which cannot be explained by the difference in time. Furthermore, a power peak is observed in between two pushes of track data, but not in the ergometer data. This could not be explained by a higher push frequency on the track as the number of push cycles to complete the runs is also similar.

Table 1: Time and number of pushes required to complete the runs.

Run	Time	Pushes count
60 m ergometer	11.24 s	28
60 m track	11.47 s	26

Based on other experimental data, the trailing wheel along with deformations of the wheelchair do not significantly contribute to those discrepancies. Spaepen [4] identified the second peak in the push cycle as the second fold of the positive mechanical work. From our point of view, this second peak is merely an artifact. Indeed, in track testing, we measure chair motion and not center of mass (CoM) motion of the athlete/wheelchair system. Chair motion is obviously not a good estimate of CoM motion since it is contaminated by the acceleration of the upper body segments. This bias on motion measurement leads to overestimated acceleration that explains the difference in power amplitude. This is not a problem on the ergometer since the wheelchair is constrained in the fore and aft direction.

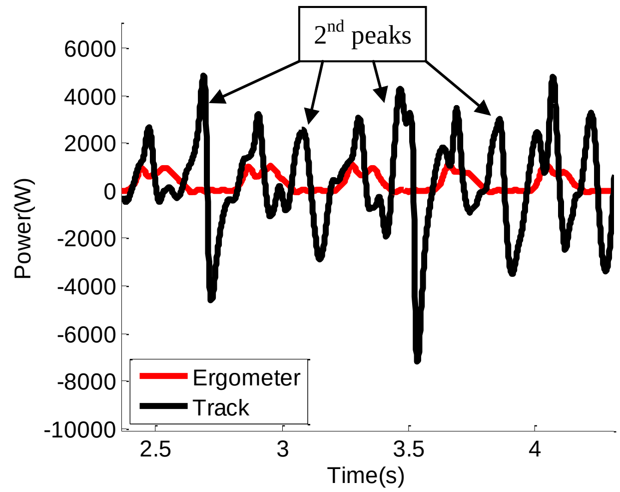

Figure 2: Instantaneous power on ergometer vs track, for five pushing cycles.

CONCLUSIONS

In sports requiring cyclic movements on a vehicle, measurement of vehicle motion to estimate center of mass motion may not be adequate to estimate instantaneous power transfer to the system. It is definitely the case for racing wheelchairs. Improvement to instantaneous power transfer estimates requires direct measurement of forces transmitted to the chair by the athlete.

REFERENCES

1. Lessard JL. Master's thesis, Université de Sherbrooke, 2013.
2. Winter DA. *Biomechanics and Motor Control of Human Movement*, John Wiley & Sons INC., 78, 2009.
3. Fuss FK. *Sports Engineering*, **12**, 41-53, 2009.
4. Vanlandewijck YC, et al. *Medicine and Science in Sports and Exercise, **26***, 1373-1381, 1994.

ACKNOWLEDGEMENTS

The athlete for his participation as a test subject and NSERC, the Institut National du Sport du Québec and Athletics Canada for financial support.

DYNAMIC ANKLE STIFFNESS AND ANKLE WORK IN HIGH- COMPARED TO LOW-ARCEHD ATHLETES DURING BAREFOOT RUNNING

[1]Douglas W. Powell & [2]D.S. Blaise Williams

[1]Campbell University, Buies Creek, NC, USA
[2]Commonwealth Sports Medicine, Glen Allen, VA, USA

INTRODUCTION

Individuals with mal-alignment or aberrant mechanics of the foot and ankle have been demonstrated to have a greater propensity of lower extremity injury [1]. Research has shown that low-arched individuals (LA) experience soft-tissue injuries to the medial aspect of the lower extremity while high-arched individuals (HA) experience bony injuries to the lateral aspect of the lower extremity [2]. It is suspected that a potential underlying mechanism for these unique injury patterns pertains to the role of the medial longitudinal arch in load attenuation. However, it has also been demonstrated that LA feet are significantly less stiff than normal and HA feet [3]. A foot that exhibits reduced stiffness may be a less effective lever for the transfer of muscle force to the ground during eccentric contraction associated with load attenuation and concentric contraction associated with propulsion.

Therefore, the purpose of this study was to examine the effect of foot type on dynamic ankle joint stiffness and ankle work in the braking versus propulsive phases of stance phase in running. It was hypothesized that low-arched individuals would exhibit significantly smaller dynamic ankle joint stiffness values and greater ankle joint work during the propulsive phase of running.

METHODS

Ten high- and 10 low-arched recreational athletes were recruited from a larger study. Arch height index [4] was used to classify participants as HA or LA (HA: AHI>0.377; LA: AHI<0.290). All participants performed five successful barefoot running trials at a self-selected pace while ground reaction forces (960 Hz, AMTI, Watertown, MA) and three-dimensional kinematics (480 Hz, 6-camera, Vicon, Oxford, UK) were recorded simultaneously. Data were filtered using a fourth order Butterworth filter with cutoff frequencies of 10 Hz and 50 Hz for kinematic and ground reaction force data, respectively. Visual 3D (C-Motion, Inc., Rockville, MD) was used to calculate ankle joint kinematics and kinetics.

Dynamic ankle joint stiffness was quantified as slope of the ankle joint angle-moment plot during the braking portion of the stance phase. Ankle joint work was calculated as the ankle moment integrated with respect to ankle position during the total stance phase as well as the braking phase and propulsive phases of stance. A Student's t-test was used to compare mean slopes between the high- and low-arched groups while a 2 x 3 group by phase repeated measures ANOVA was used to determine significant differences in ankle joint work variables.

RESULTS AND DISCUSSION

High-arched individuals exhibited significantly greater stiffness values compared to their low-arched counterparts (p= 0.021).

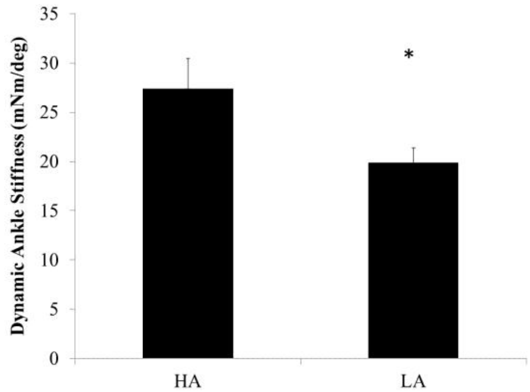

Figure 1. Dynamic ankle joint stiffness values in HA compared to LA athletes. * denotes significant difference between HA and LA athletes.

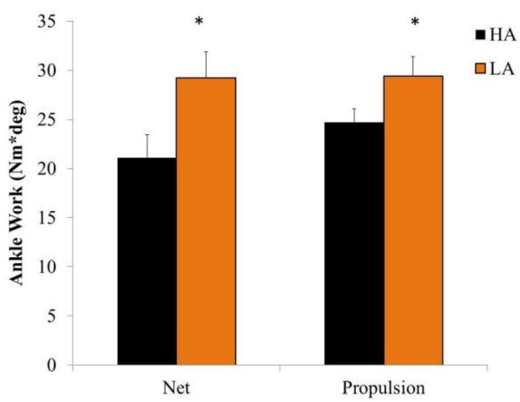

Figure 2. Ankle joint work during the total (net) and propulsive portions of the stance phase in HA (black) and LA athletes (orange). * denotes significant difference between HA and LA athletes.

These data demonstrate that differences in running kinetics exist in both the braking and propulsive phases of stance during running. The observed differences in dynamic ankle joint stiffness suggest that HA athletes attenuate load over a shorter period of time compared to their LA counterparts. Further, the ankle work data presented in this study demonstrate that HA athletes require reduced net and propulsive work at the ankle during a running task with similar mechanical demand. The increased muscular demand associated with the LA foot is a potential injury mechanism that should be further studied.

CONCLUSIONS

The findings of this study demonstrate differences in ankle joint mechanics during the load attenuation and propulsive portions of the stance phase of running. These differences may result in the unique injury patterns experienced by these two functionally different groups. Further research investigations may pertain to the efficacy of the foot as a mechanical lever during the stance phase of walking and running in these two groups.

REFERENCES

1. Kaufman, K.R. *Am J Sports Med* **27,** 585-593, 1999.
2. Williams, D.S. 3rd, et al. *Clin Biomech* **16**, 341-347, 2001.
3. Zifchock, R., et al., *Foot Ankle Int.* 27, 367-372, 2006.
4. Williams & McClay, *Phys Ther*. **80** (9), 864-871, 2000.

CAN CADENCE MANIPULATION SIMULATE THE JOINT LOADING BENEFITS OF BAREFOOT RUNNING?

Jennifer Bido, Jocelyn F. Hafer, Leigh-Ann Plack, Jordan D. Metzl

Hospital for Special Surgery, New York, NY, USA
email: jen.bido03@gmail.com

INTRODUCTION

Running remains a popular recreational activity despite the fact that the incidence of running injuries has been reported to be as high as 79.3% (1). Furthermore, the knee is the most common site of lower extremity injuries during running (1). This has recently led running related research to focus heavily on injury prevention. A popular mechanism for decreasing injury incidence is altering running mechanics, most notably by attempting to reduce joint loading through barefoot running and cadence manipulation.

Barefoot running has received strong media support and is experiencing increased popularity due to its portrayal as more natural and safer than running in regular running shoes (2). Studies have classified barefoot running as safer due to results showing decreases in kinetics and kinematics trends that have been previously tied to overuse injuries such as stress fractures (3), and patellofemoral pain (4). The variables that were decreased are: joint powers, impact forces, and decreased active knee flexion range of motion (5,6).

While barefoot running has many mechanical advantages, it may not be a realistic option for all. Recent studies have shown that even using minimalist running shoes, which seek to reduce the environmental constraints of barefoot running, can result in an increase in foot pathology (7). In light of this, cadence manipulation has been suggested as a viable alternative, as increasing running cadence has been shown to achieve similar kinetic and kinematic alterations to those seen in barefoot running (8). The objective of this study is to determine if similar changes in joint loading during the loading response (LR) of running occur when a single group of runners is in an increased cadence condition and a barefoot condition.

METHODS

Five healthy runners were included in this study. All trained at least 15 miles/week in neutral running shoes with no orthotics. All were rearfoot strikers with no experience running barefoot and no injury in 6 months prior to data collection.

Kinematic and kinetic data were collected during overground running using a 12-camera motion capture system and 4 force plates. A full-body, six degree-of-freedom markerset was used to build the model for calculations.

Three running conditions were collected:
1. Normal: shod, preferred running cadence.
2. Cadence: shod, cadence 10% above preferred.
3. Barefoot: barefoot, cadence not controlled.

All participants completed shod running trials in laboratory-provided neutral running shoes (New Balance). In order to acclimate to the assigned conditions before data were collected, runners were allowed to practice running overground or on a treadmill. Runners were instructed to run at a comfortable pace in each condition. Speed was monitored and controlled to match each runner's preferred pace in each condition. Cadence was controlled using a metronome. Condition order was randomized.

The variables of interest in this study were sagittal joint power and peak flexion angle (PFA) at the ankle, knee and hip during stance phase. Peak absorptive joint power and PFA during the LR were reported. LR was defined as the first 43% of stance phase. Repeated measures ANOVAs were calculated between conditions for each variable with significance set at $p \leq 0.05$. Post-hoc tests were run where ANOVA was significant.

RESULTS

Participants included 5 runners (4 female) aged 34.2 ± 9.1 years, 1.6 ± 0.1 meters tall, 61.4 ± 2.8 kg. Average running velocity was 2.9 m/s. Stance time was not significantly different between conditions.

Knee power and PFA were significantly different between conditions. Knee power was decreased in barefoot relative to normal, and knee PFA was decreased in cadence relative to normal (Table 1). Power and PFA were not different between conditions at both the ankle and hip.

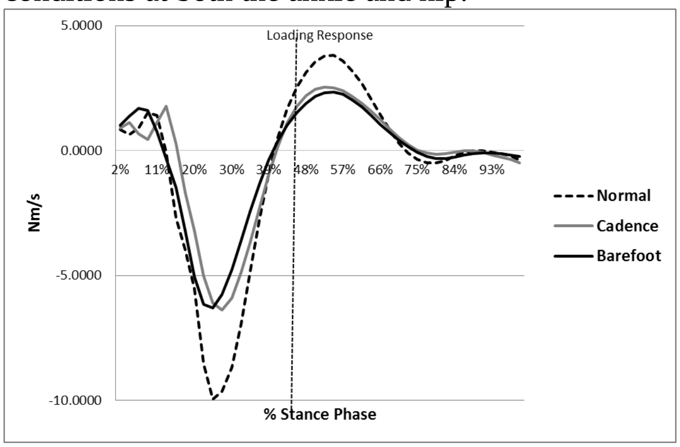

Figure 1: Knee power averages of all subject data across conditions. LR is indicated by a dashed line at 43% of stance phase.

DISCUSSION

The results of this study are in accordance with previous studies that have shown decreased joint powers, with greater sensitivity at the knee, in either cadence manipulation or barefoot running individually (5,7). This current study is novel because both conditions are studied in the same participants. As seen in Figure 1, there is a similar absolute decrease in knee power for both the cadence and barefoot conditions relative to normal, with barefoot being significantly different. For PFA, cadence is the condition that is significantly different from normal. The comparable results for barefoot and increased cadence conditions suggest that runners who seek injury prevention, specifically at the knee, may achieve similar benefits from either modification. Thus the removal of shoes or use of minimal running shoes may not be necessary to achieve the benefits of barefoot running.

As this is a pilot study of an acute intervention, future studies should seek to confirm the observations on a larger sample size as well as use an extended training period.

REFERENCES

1. Van Gent RN, et al. *BR J Sports Med* **41**, 469-480, 2007.
2. McDougall C. *Born to Run: a Hidden Tribe, Superathletes, and the Greatest Race the World Has Never Seen*. Alfred A. Knopf, 2009.
3. Milner CE, et al. *Med Sci Sports Exerc* **38**, 323-328, 2006.
4. Chumanov E, et al. *Gait and Posture* **36**, 231-235, 2012.
5. Williams DS 3rd, et al. *Int J Sports Phys Ther* **7**, 525-532, 2012
6. Squadrone R. *J Sports Med Phys Fitness* **49**, 6-13, 2009.
7. Ridge ST, et al. *Med Sci Sports Exerc*, 2013 Feb 22. [EPUB ahead of print] DOI: 10.1249/MSS.0b013e3182874769
8. Heiderscheit BC, et al. *Med Sci Sports Exerc* **43**, 296-302, 2011.

Table 1: Peak Flexion angle at each joint. Post-hoc abbreviations indicate which conditions are different. (* indicates post-hoc=0.08) Power is in Nm/s. PFA is in °.

	Normal		Cadence		Barefoot			
	Mean	SD	Mean	SD	Mean	SD	p-value	Post-hoc
Ankle Power	-6.16	1.33	-7.08	1.71	-6.47	1.45	0.32	
Knee Power	-10.42	2.73	-6.74	3.30	-6.67	2.75	**0.01**	NB, NC*
Hip Power	-2.45	1.75	-2.46	1.59	-2.32	0.87	0.94	
Ankle PFA	27.27	2.72	24.29	2.41	24.84	3.21	0.09	
Knee PFA	37.52	6.86	34.00	7.14	34.85	6.16	**0.01**	NC
Hip PFA	35.87	8.81	33.36	7.34	34.90	6.82	0.16	

A TRIANGULATED APPROACH TO UNDERSTANDING SPORTS SURFACE PREFERENCES

Felix Tsui and Steph Forrester
Sports Technology Institute, Loughborough University, LE11 3TU, UK
email: tsui.felix.4@gmail.com, web: http://sti.lboro.ac.uk

INTRODUCTION

In the design of sports surfaces, player preferences are seldom considered. This seems surprising as player perceptions on perceived injury risks or adverse playing conditions can ultimately affect overall performance. Instead, sports surfaces are typically designed to generate specific responses under mechanical and biomechanical testing. It is unclear, however, how these factors may meet the requirements of players from a preference perspective and, in turn, how this may relate to player comfort, safety and performance.

Mechanical testing is good at grading surfaces but poor at predicting player kinematics and ground reaction forces across different surfaces during running [1]. Moreover, biomechanical testing of player-surface interactions may provide insight into running mechanics but is likely influenced by player perception, particularly during competition [2]. Lastly, player perception may be a good way to determine which attributes constitute a "good" surface, but results from this method are difficult to put into practice. As such, triangulating the results from mechanical, biomechanical and perception testing may be necessary to fully optimize the play performance of a sports surface.

This study is a preliminary investigation into the relationship between three different techniques for assessing playing performance of a sports surface. The intention is to increase our understanding as to why certain surfaces are considered preferable.

METHODS

Fourteen healthy males (age 24±3 yrs, height 178±4 cm, body mass 74±8 kg) consented to participate in this study according to the protocol approved by the ethical advisory committee at Loughborough University. Each participant was asked to complete three successful runs along a ~20 m runway at 4.0 $m \cdot s^{-1}$ for three separate surfaces (*soft*, *medium* and *hard)*; *i.e.* where the right foot fully contacted the force platform and the velocity was within ± 5% of the target. Each surface had the same aesthetics and subjects were allowed to warm-up on each.

Ground reaction forces were measured at 1000 Hz during stance using two force platforms (Kistler 9281CA, Winterthur, SUI). Running kinematics were collected at 250 Hz by tracking opti-reflective markers using a 13-camera system (Vicon Motion Systems Ltd, Oxford, UK) system and processed in Visual3D (C-Motion, MD, USA). Running velocities were measured using SMARTSPEED timing lights (Fusion Sport Pty Ltd., Cardiff, UK) placed 4 m apart on either side of the force plates. Trials were compared using SPSS Statistics 20 (IBM, NY, USA) with $\alpha = 0.05$.

After each surface, participants were asked to fill out a questionnaire to assess their perception of the surface properties and their interaction with the surface. These two aspects were each described using five attributes scored using visual analogue scales. Subjects were also asked to rank the surfaces in order of preference. Mechanically, the hardness or stiffness of each surface was determined by the Advanced Artificial Athlete (AAA), a 2.25-kg Clegg Impact Hammer (CIH) and an Instron 9250 drop tester (Norwood, MA, USA).

RESULTS AND DISCUSSION

Overall, preferences were split between the *medium* and *hard* surfaces whilst the *soft* surface was ranked last by all subjects. Compared to perception data, this suggested that subjects based their preference on the uniformity and balance of the *medium* and *hard* surfaces, as these two attributes rated similarly but significantly different from the soft surface (Figures 1, 2). Perception data also suggested that there was a threshold in surface cushioning and hardness that could be tolerated in choosing a surface preference but that this range could be quite large. However, it was not immediately clear how their foot-strike patterns and usual play surface properties may have influenced these ratings.

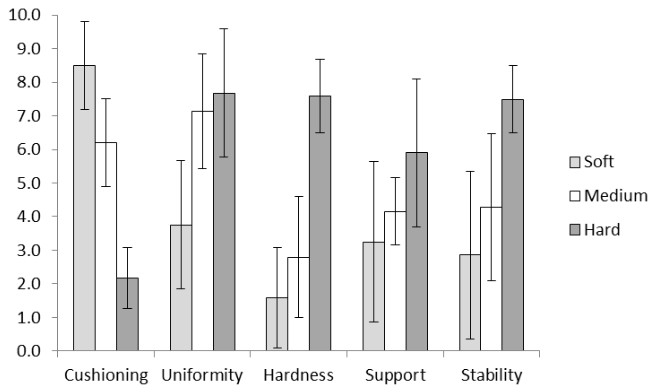

Figure 1. Perceptions on material performance.

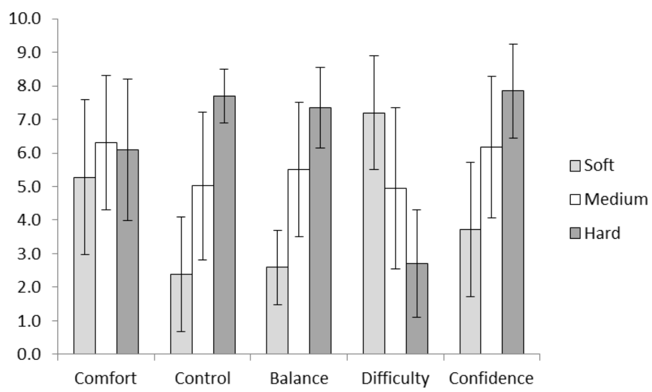

Figure 2. Perceptions on running performance.

Table 1. Mechanical performance of the surfaces.

Surface	Instron [kN·m^{-1}]	AAA [kN·m-1]	CIH [CIV]
Soft	44	50.3	31
Medium	70	67.3	40
Hard	180	151	63

Instron drop tests found that the surfaces covered a large range in surface stiffness (44-180 kN·m^{-1}). The AAA produced a similar range of stiffness but surface hardness, as measured by the CIH, seemed to be less sensitive (Table 1). This was likely due to the differing impact characteristics.

Comparing the preference for the *medium* and *hard* surfaces, the stance mechanics suggested that there may be an optimal or preferential running style (Table 2). On both preferred surfaces, leg stiffness and angle of attack were significantly different from the non-preferred surface. Both of these parameters may also help to explain the perceived increase in stability, control and balance of *medium* and *hard* surfaces along with the decrease in overall demand.

Given that hard sports surfaces have been linked to injuries, further work should investigate a wider range in surface hardness, including levels of greater hardness, in order to determine whether there exists an optimal hardness that subjects prefer. This may prove difficult as differences in surface deformation during stance will become very small possibly making it more difficult to perceive differences or to measure differences during stance. However, this can help add a level of sophistication to future sports surface design which accounts not only for its material properties but for its perceived performance.

REFERENCES

1. Dixon, S, et al. *Med & Sci in Sports Sci.*, **32**(11), 1919-1926, 2000.
2. Fleming, PR. *Proc. IMechE, Part P: J. Spo. Eng. and Tech.*, **225**(2), 43-64, 2011.

ACKNOWLEDGEMENTS

This research was supported by the EPSRC, UK (grant number EP/I020411/1).

Table 2: Stance mechanics (mean ± SD) for each surface.

Surface	$GRF_{z,PEAK}$ [N/kg]	Contact Time [ms]	Leg Stiffness [kN·m^{-1}]	Vertical Stiffness [kN·m^{-1}]	Angle of Attack [º]
Soft	3.06 ± 0.17[3]	231 ± 13[3]	53.4 ± 29.1[2,3]	34.0 ± 5.5	73.8 ± 1.6[2,3]
Medium	3.04 ± 0.16[3]	229 ± 16[3]	35.1 ± 8.9[1,3]	34.8 ± 5.2	75.7 ± 2.3[1]
Hard	2.99 ± 0.19[1,2]	223 ± 15[1,2]	31.0 ± 7.6[1,2]	36.5 ± 8.2	75.6 ± 2.0[1]

GENERAL POSTER SESSION III – Friday, 8:00-9:30
Grand Ballroom

ERGONOMICS			
3	Frequency Domain Features Of Semg During The Local Muscle Fatigue Of The Ankle With And Without Functional Instability **Zhang Q, Zhang L, Lu A, Wang G**	6	Measurements And Analysis On Muscle Activities In Female Subjects Depending On Drive-assisting Speeds Of A Shower Carrier **Ko C, Chun K, Bae, T**
9	Effects Of Prolonged Standing On Oxygen Saturation In The Soleus And Erector Spinae Muscles Of The Lower Back Using Near Infrared Spectroscopy **Haney J, Redfern M, Huppert T, Chambers A**	12	Muscle Activity In Simulated Overhead Drilling: The Influences Of Work Location, Force Direction, Hand Configuration And Body Posture **Maciukiewicz J, Cudlip A, Chopp J, Dickerson C**
15	Age-related Changes In Mechanical Properties Of Human Hand Digits **Park J, Pazin N, Friedman J, Zatsiorsky V, Latash M**	18	Kinematic Consistency-based Decision Rules For Discriminating Between Sincere And Feigned Trunk Motion Exertions **Almosnino S, McGillivary T, Stevenson J, Bruce O, Dvir Z**
21	The Effects Of Diurnal Changes In Behaviors Of Trunk Tissues On Trunk Mechanical Properties **Koch B, Agarwal A, Vazirian M, Bazrgari B**	24	Leg And Torso Muscle Response To Prolonged Kneeling **Lomo-Tettey D, Campbell-Kyureghyan N, Johnson B, Beschorner K**
27	Simulation To Improve Surgical Articular Fracture Reduction Skills **Ohrt G, Thomas G, Karam M, Yehyawi T, Westerlind B, Marsh JL, Anderson D**		

GAIT			
30	Circumventing Thigh Soft Tissue Artifact Via Shank Cluster-referencing Of Knee Joint Centers **Jongprasithporn M, Schulz B**	33	The Relationship Between The Stair Climbing Test, Knee Extension Strength, And Peak External Knee Flexion Moment In Patients Awaiting Total Knee Athroplasty **Lewis J, Freisinger G, Beal M, Schmitt L, Siston R, Chaudhari A**
36	Angular Momentum And Thorax-pelvis Coordination In Walking **Baird JL, Umberger BR, Hamill J, van Emmerik R**	39	Impact Of Total Menisectomy On Tibial Plateau Contact Forces, Femoral Cartilage Stress Level & Cruciate Ligament Forces In Passive Knee Flexion **El Sagheir S, Moglo K**
42	The Reliability Of Ultrasound In Obtaining Subject-specific Parameters **Leonardis J, Rider P, Black J, Kulas T, Domire Z**	45	Muscle Activation Changes In Responses To Orthotic Ankle Constraint During Walking **Hovorka C, Sung J, Eckert K, Gregor R, Chang YH**

48	Effects Of Age And Obesity On Risk Of Tripping During Level Walking **Rossi C, Matrangola S, Nussbaum M, Madigan M**	51	Step Length Perturbations Alter Variations In Center Of Mass Horizontal Velocity **Bailey J, Nordin A, Dufek J**
54	Execution Of Activites Of Daily Living In Persons With Parkinson's Disease. **Skinner J, Lee HK, Roemmich R, Amano S, Hass C**	57	Cadence Effets On Shod Gait Kinematics **Weimar W, Romer B, Fox J, Patel J, Rehm J**
60	Effects Of Prolonged Load Carriage Walking On Lower Extremity And Trunk Kinematics, Heart Rate, And Subjective Responses **Almosnino S, Kingston D, Bardana D, Stevenson J, Graham R**	63	Twelve Weeks Of Plantarflexor Strength Training Do Not Change Gait Biomechanics Of Healthy Old Adults Walking At A Safe Maximum Speed **Tatarski R, Beijersbergen C, Ridings J, Domire Z, Rider P, Hortobagyi T, DeVita P**
66	Kinetic Patterns Of Treadmill Walking In Preadolescents With And Without Down Syndrome **Wu J, Ajisafe T**	69	An Alternate Predictor Of Peak Medial Compartment Loading: The Product Of Peak Knee Extensor And Abductor Moments **Manal K, Gardinier E, Snyder-Mackler L, Buchanan T**
72	Young Adults Have Higher Arm Elevation Than Older Adults During Unexpected Slips **Merrill Z, Sandrian P, Chambers A**	75	Determining How Humans Regulate Variability During Walking **Bohnsack N, Cusumano J, Dingwell J**
78	The Mechanics Of Economical Walking: Insights From Chimpanzee And Human Bipedalism **Lee LF, O'Neill M, Demes B, Confer M, Thompson N, Larson S, Umberger B**	81	A Comparison Of Feedback Strategies In A Virtual Environment To Improve Gait Symmetry Of Service Members With Unilateral Transtibial Amputation **Nottingham E, Linberg A, Wolf E**
84	Mechanical Effectiveness Of A Combined Gait Modification Strategy To Reduce Knee Adduction Moment: Increasing Trunk Lean And Foot Progression Angle **Barrios J, Caldwell L**	87	Experimental Anterior Knee Pain Alters Electromyography During High-intensity Landing And Jumping **Seeley M, Pitt J, Park J, Cosgrave C, Chartrand S, Francom D, Hopkins T**
90	Transfemoral Amputation Alters Pelvis-trunk Coordination During Walking: Implications For Low Back Pain **Russell E, Aldridge Whitehead J, Wilken J**	93	A Comparison Of Torso Stability Between Bed Rest Subjects And Astronauts During Tandem Walk: Preliminary Findings **Miller C, Peters B, Kofman I, Brady R, Phillips T, Batson C, Mulavara A, Feiveson A, Reschke M, Bloomberg J**
96	Kinematic Variability And Accelerometers Demonstrate A Lack Of Agreement **Howe C, Hasenkamp R, Wurdeman S, Myers S, Arnold B**	99	Ankle Dynamics Of Walking At Varying Velocities And Inclines **Auyang A, Grabowski A**
102	Nonlinear Effects Of Body Weight On Ground Reaction Force Peaks **Shorten M**	105	Biplane Fluoroscopic Analysis Of The Hindfoot Using Model-based Tracking Techniques: A Static Phantom Study **Cross J, McHenry B, Harris G, Schmidt T**

108	Moments Of Inertia Of The Shank Change Markedly During Drop Landings **Pain M**	111	Does The Hallux Valgus Surgery Affect Spatiotemporal Parameters And Lower Extremity Kinematics During Gait? **Klugarova J, Janura M, Svoboda Z, Sos Z**
114	The Prevalence Of Gait Deviaitons In Individuals With Trans-tibial Amputation 4 Months After Independent Ambulation **Rodriguez K, Rabago C, Wilken J**	117	Does Quadriceps-strengthening Exercise Affect Quadriceps Force, Power, And Work During Stair Ascent In Adults With Knee Osteoarthritis? **Leonardis J, Rider P, Norbury J, Aaboe J, Christensen R, Bliddal H, Henriksen M, DeVita P**
120	Knee Angular Position And Muscle Activity During Modified Elliptical Exercise **Paquette M, Zucker-Levin A, DeVita P, Hoekstra J, Pearsall D**	123	Biomechanical Asymmetries During Gait In Individuals Before And Three Months After Unilateral Total Hip Arthroplasty **Pozzi F, Abujaber S, Zeni J**
126	Force Output Is More Variable In Patients With Peripheral Arterial Disease **Hasenkamp R, Wurdeman S, Johanning J, Pipinos I, Howe C, Myers S**	129	Sensitivity Of Vertical Ground Reaction Force Parameters In Normal And Amputee Running To Filter Design **Kiernan D, Koh K, Kwon HJ, Miller RH, Shim JK**
132	Do Biomechanical Loads Increase During Common Rehabilitation Exercises In Obese Individuals? **Singh B, Yack HJ, Janz K, Francis S**		

MOTOR CONTROL			
135	Why Are Wrist Rotations Less Smooth Than Reaching Movements? **Salmond L, Charles S**	138	The Relationship Between Visual Steadiness And Muscle Force Steadiness In Young And Old Adults **Krupenevich R, Reynolds K, Spangler L, Rider P, Murray N, DeVita P**
141	Muscle Recruitment And Angular Impulse Generation Strategies Used During Turn Tasks With Modified Hip External Rotation **Zaferiou A, McNitt-Gray JL**	144	Effects Of Volitional Spine Stabilization And Lower Extremity Fatigue On Landing Performance In A Recurrent Low Back Pain Population **Haddas R, Sizer P, Sawyer S, Brooks T, Chyu M, James CR**
147	Quadriceps Fatigue Affects Central Nervous System Activation **Morton S, Katsavelis D, Threlkeld AJ**		

ORTHOPEDIC MECHANICS			
152	Estimation Of Skull Cortical Thickness From Clinical Ct **Lillie E, Urban J, Weaver A, Stitzel J**	155	Finite Element Prediction Of Periosteal Strain At The Human Distal Radius During A Targeted Loading Task **Bhatia V, Edwards WB, Troy K**

158	The Vascular Structure Of Bone Is Compromised With Immobilization And Is Not Recovered With Anti-resorptive Treatment And Remobilization **Patel P, Bajaj D, Fritton C**	161	A Comprehensive Multiscale Characterization Of The Tibiofemoral Joint: Tissue Testing **Chokhandre S, Bennetts C, Colbrunn R, Bonner T, Erdemir A**
164	Evaluation Of New Total Knee Arthroplasty Considering Design Factors Capbling Of Reducing A Risk Of Tka Failures: Finite Element Analysis **Han P, Jang YW, Yoo OS, Kim JS, Lim D**	167	Influence Of Anticipation On Acl Loading When Ground Reaction Forces Are Perturbed During A Sidestep Cutting Maneuver **Weinhandl J, O'Connor K**
170	Relationships Between Lean Mass Asymmetry And Force Production Asymmetry In Jumping **Heinbaugh E, Moynes R, Rockey S**	173	Ankle Landing Strategy During A Vertical Stop-jump Maneuver Alters Knee Joint Resultant Forces **Akins JS, McGinn MA, Heebner NR, Sell TC, Lephart SM**
176	Single-joint Jump Height Correlates With Heel Length And Toe Length **van Werkhoven H, Piazza S**	179	Intrinsic Foot Muscle Deterioration And Metatarsophalangeal Joint Deformity In People With Diabetes And Neuropathy **Cheuy V, Hastings M, Commean P, Ward S, Mueller M**
182	The Passive Contributions Of The Vastus Medialis And Vastus Lateralis To Knee Extension And Hip Flexion **Lipps D, Baillargeon E, Sandercock T, Perreault E**	185	Prediction Of Failure Pattern In Spine Segments **Clouthier A, Hosseini H, Maquer G, Zysset P**
188	Prediction Of Trunk Neuromuscular Response Under Perturbations **Shahvarpour A, Shirazi-Adl A, Bazrgari B, Larivière C**	191	Quantification Of Reversal Of Lumbopelvic Rhythm During Active Forward Bending **Wattananon P, Sung W, Spinelli B, Biely S, Silfies S**
194	Repitative Freezing: Does It Change Nanoscale Material Properties Of Cancellous Bone? **Landauer A, Yuya P, Kuxhaus L**	197	Biomechanics Analysis Of Latissimus Dorsi Transfer In Reverse Shoulder Arthroplasty **Kontaxis A, Choi D, Gulotta L**
200	Changes In Windmill Pitch Mechanics Over Time **Konz S**	203	Kinematic Variables Associated With Acl Force During Unilateral Landings **Irmischer B, Hoch M, Ringleb S, Bawab S, Gaven S, Weinhandl J**
206	3D Surface Registration Of Partial Capitate Bones Using Spin Images **Breighner R, Holmes D, Leng S, An KN, McCollough C, Zhao K**	209	Time To Peak Force In Different Countermovement Configurations **Rehm J, Fox J, Patel J, Romer B, Jagodinsky A, Weimar W**

OTHER			
212	Angular Acceleration Of The Foot During Gait Using An IMU **Okita N, Sommer HJ**	215	Photoelastic And Finite Element Stress Analysis **Hassan JA, Abass SJ, Abud-Alhussian NA**

218	Toward Clinically Applicable Reconstruction Planning For Comminuted Articular Fractures **Kern A, Anderson D**		

POSTURE & BALANCE			
223	Inverse Dynamics Of Unstable Sitting: The Relationship Between Cop And Moment Control For Increasing Task Diffculty **Myers C, Shelburne K, Silfies S, Davidson B**	226	Model-Predicted Buckling Of The Adult Human Upper Extremity: Effects Of Peak Impulsive Force And Muscle States **Lee Y, Ashton-Miller J**
229	The Effect Of Occupational Footwear On Dynamic Balance **Chander H, Wade C, Dabbs N, Allen C, Cazas V, Lundahl J, Garner J**	232	Nonlinear Mathematics Detect Subtle Changes In Center Of Pressure **Rand T, Kyvelidou A, Myers S**
235	Postural Responses To Upper Limb Movements In Quiet Standing **Long B, Waxman J, Taylor J, Gosselin D, Rhea C**	238	The Temporal Structure Of Postural Control Variability During Standing Is Affected By Suprathreshold Mechanical Stimulation **Renz J, Chien JH, Mukherjee M**
241	Can We See Mathematical Chaos In Sensorimotor Coordination? **Haworth J, Kyvelidou A, Stergiou N**	244	The Effects Of Toning Shoes On The Postural Stability Of Women **Farley K, Niverson A, Rogge R**
247	Variability Of Postural Sway In Children With Autism Spectrum Disorders **Kyvelidou A, Haworth J, Stergiou N**	250	Effect Of Foot Wedge Positions On Lower Limb Muscle Activity During Standing **Samimi H, Anbarian M**
253	Involvement Of Central Nervous System In Functional Ankle Instability **Liu W, Jain T, Wauneka C**	256	Development Of Quantification Of Spatial Strain Distribution For Scoliotic Shape Using A Thin - Plate Spline Method **Kiriyama Y, Watanabe K, Matsumoto M, Toyama Y, Nagura T**
260	Multi Body Analsys Of Effect Of Injured Lateral Ligament **Kakigahara T, Matsuda M, Adachi K**	263	Finite Element Analysis Of Effects Of Gender-Dependent 3D Knee Geometry And Joint Laxity On ACL Impingement Against The Intercondylar Notch **Lee SJ, Zhang LQ**
266	Blood Flow Characterization In Multiple Anatomical Locations During Normal And Shear Loading **Drost J, Reid Bush T, Manorama A**	269	Individual Muscle Forces During A Sit To Stand Transfer **Caruthers E, Thompson J, Schmitt L, Best T, Chaudhari A, Siston R**
272	The Neuromagnetic Activity Of The Somatosensory Cortices And The Ankle Force Control Is Altered In Children With Cerebral Palsy **Kurz M, Arpin D, Heinrichs-Graham E, Becker K, Wilson T**	275	Within- And Between-Session Reliability For The Quantification Of The Thigh Muscles Co-activation Index During Isometric Contractions **Katsavelis D, Morton S, Threlkeld AJ**

278	The Effect Of Amputation Length And Interosseus Membrane Viability On Fibular Migration In Below Knee Amputations **Burkhart T, Asa B, Dunning C, Payne M, Wilson T**	281	The Effects Of Performance Demands On ACL Loading During A Stop-jump Task **Dai B, Garrett W, Gross M, Padua D, Queen R, Yu B**
284	Stretching With Vibration Improves Flexibility In Patients With Plantar Fasciitis **Russell E, Thompson B**	287	Towards Preventing Cancellous Bone Collapse: Cervine Model And Fracture Imaging **Corbiere N, Lewicki K, Issen K, Kuxhaus L**
290	Effect Of Sensory Manipulation On The Ability To Maintain Pinch Force **Tseng YL, Seo NJ**	293	Low-Cost Virtual Reality Game For Upper Limb Rehabilitation Using Kinect And P5 Glove **Arunkumar J, Hur P, Motawar B, Seo NJ**
296	Biomimetic Rocker Profile Restores Shank Progression During Walking With Orthotic Ankle Constraint **Oludare S, Hovorka C, Yan T, Chang YH, Kogler G**	299	An Exploration Of The Angular Orientation Of The Wrist During Arcing And Semicircular Wheelchair Propulsion **Zukowski L, Roper J, Otzel D, Hovis P, Tillman M**
302	Variability Of Peak Shoulder Force During Wheelchair Propulsion As A Function Of Shoulder Pain **Moon Y, Jayaraman C, Hsu IMK, Rice IM, Hsiao-Wecksler ET, Sosnoff JJ**	305	Racing Wheelchair Ergometer And Configurable Wheelchair Validations **Lessard JL, Pelland-Leblanc JP, Masson G, Rancourt D, Langelier E, Berrigan F, Laroche J, Smeesters C**

SPORTS			
309	Effects Of Impact Exposure And Thermal Annealing On Mechanical Properties Of An American Football Helmet Outer Shell Material **Krzeminski D, Fernando D, Lippa N, Rawlins J, Gould T, Piland S**	312	Evaluating Upsampling Methods For 3D Kinematic Data **Leigh S, Dapena J, Gross M, Myers J, Yu B**
315	The Influence Of Shoulder Rotation On Shoulder Kinetics In Catchers Throwing From The Knees **Plummer H, Oliver G**	318	Comparison Of Ankle Stabilization Techniques In Individuals With Functional Ankle Instability **McKelle Ulm H, Powell D**
321	Inter-Rater Reliability Of Two Commercial 3D Motion Capture Systems **McNally M, Roewer B, Hewett T**	324	Influence Of Pre-Release Range Of Motion On Overhead Back Throw Distance **Meyer B**
327	The Effect Of Fatigability In Lower Extremity Coordination Patterns In Softball Pitching **Forshaw B, Wu T, Postlmayr C, Laquale K**	330	Bat Quickness And Bat Velocity In Division I Softball Players **Reilly-Boccia C, Ficklin T, Lund R, Hervas J, Beatty K**
333	An Exploration Of Anxiety, Physiological Arousal, Stretching, And Performance **Rodden C, Mogus S, Hurst J, Mayhew J, Houser J, Bird M**	336	Variations In Step Width As Stride Length Shortens In Rearfoot And Mid/Forefoot Runners **Boyer E, Derrick T**

339	Biomechanically-Driven Mechanical Aging And Characterization Of Running Shoe Midsole Foam **Lippa N, Heskett M, Krzeminski D, Piland S, Rawlins J, Gould T**	342	Lower Extremity Muscle Activation During Barefoot, Minimalist And Shod Running **Standifird T, Mitchell U, Hunter I, Johnson W, Ridge S**
345	Running Mechanics During Stance For Surfaces Of Transient Stiffness **Tsui F, Forrester S**		

FREQUENCY DOMAIN FEATURES OF SEMG DURING THE LOCAL MUSCLE FATIGUE OF THE ANKLE WITH AND WITHOUT FUNCTIONAL INSTABILITY

[1,2]Qiuxia Zhang, [1]Lin Zhang, [1]Aming Lu and [1]Guodong Wang

[1]Soochow University, Suzhou, Jiangsu, China
[2]Biomechanics Laboratory, The Pennsylvania State University, USA
email: zhqiuxia@gmail.com

INTRODUCTION

Ankle joint sprains frequently occur during sporting activities. One of the commonest consequences of these sprains is subsequent functional ankle instability (FAI). Although much research has been conducted focusing on FAI, the analysis of movement patterns and muscle coordination in individuals with FAI during dynamic fatigue conditions is limited. The purpose of this study was to analyze the changing of frequency domain features of the surface electromyography (SEMG) data from four lower extremity muscles during maximal isokinetic concentric fatigue of the ankle musculature with and without functional instability.

METHODS

The ankles of 28 college-aged males were tested in this study. Fourteen of them had unilateral FAI (FAI Group: N=14, age: 20.8±1.1 yr; height: 180.0±4.6 cm; mass: 71.6±9.8 kg). To be characterized as FAI, the subjects satisfied the following criteria [1]: (1) experienced at least one significant lateral (inversion) ankle sprain of either the right or left ankle, but not both, in which the subject was unable to bear weight or was placed on crutches, within the last year, (2) no reported history of fracture to either ankle, (3) sustained at least one repeated injury or the experience of feelings of ankle instability or "giving way" in either the right or left ankle, but not both, (4) not undergoing any formal or informal rehabilitation of the unstable ankle, and (5) have no evidence of mechanical instability as assessed by a physician using an anterior drawer test. Subjects were pain free and full weight-bearing, without a limp, at the time of the study. While the other 14 subjects were matched-paired and served as controls (Control Group: N=14, age: 21.4±1.2 yr; height: 181.1±6.5 cm; mass: 71.3±7.1 kg). All procedures were approved by an institutional review board.

The unstable ankle of the FAI Group and the matched one of Control Group were tested. A CON-TREX Isokinetic Dynamometer and a Biovision System were used to synchronously collect: the peak torque, SEMG of the muscles and the angle of the joint. The range of motion was from 30° of plantar flexion to 10° dorsiflexion. Each subject performed three sub-maximal and three maximal trials at 105 °·s^{-1} for both warm-up and familiarization with the experimental set-up. After a period of rest the subjects performed consecutive maximal concentric trials at 60°·s^{-1}. Subjects were encouraged to continue their alternative maximal plantar flexion and dorsiflexion concentric muscle actions until three consecutive peak torques of both plantar flexion and dorsiflexion were less than 50% of the peak of the initial three concentric torques. The muscle peak torque of maximal concentric contraction and SEMG of Tibialis Anterior (TA), Soleus (SO), Medial Head of Gastrocnemius (GAM), Lateral Head of Gastrocnemius (GAL) were obtained.

The SEMG data were collected at a rate of 1000Hz, The mean power frequency (MPF), instantaneous median frequency (IMDF) based on wavelet analysis of the SEMG signal, using code written in MATLAB. The time was normalized to the total time to fatigue.

A mixed-model ANOVA was performed to compare the frequency domain features between the two groups using SPSS 18.0. The level of significance was set at α=0.05.

RESULTS AND DISCUSSION

During maximal isokinetic concentric fatigue of the ankle, there was significant difference between the two groups for the MPF and IMDF of the SEMG, not in TA and GAM (P>0.05), but in SO and GAL (P <0.05) （Figures 1 and 2）. For the control group，MPF and IMDF of the SEMG in the four muscles had the decreasing trend with increasing muscle fatigue (P<0.05). For the FAI group MPF and IMDF of the SEMG in SO and GAL, did not demonstrate this trend (P>0.05) （Figures 1 and 2).

Firstly, when the ankle is sprained, the sudden forces take the ankle beyond its normal range of motion, and cause lacerations of the soft tissue, such as joint capsule, ligaments and tendons around the ankle. In this case, the fast muscle fibers are more likely to be damaged than the slow twitch fibers. An increased proportion of slow twitch (ST) fibers would correspond to long sustained muscle force [2], More lactic acid is accumulated causing a decrease in pH which leads to the subtle change of the frequency of SEMG [3,4]. So in the muscle groups with a higher proportion of slow twitch fibers, the SO and GAL, the muscles in the FAI group are not likely to fatigue and therefore frequency domain features do not have the decreasing trend.

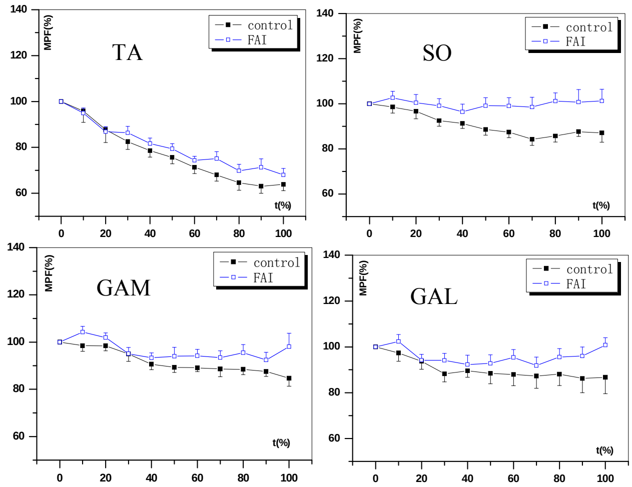

Figure 1: MPF changes of the SEMG during the local muscle fatigue of the ankle.

Secondly, the spectrum of SEMG shifts to the left, has a lower MPF, is an indicator of the fatigue of a muscle. Amann [5] considered that peripheral muscle fatigue may affect the central projection of thin fiber muscle afferents which provide inhibitory feedback to the CNS and thereby influence the magnitude of central motor drive during high-intensity whole-body endurance exercise. MPF and IMDF of SEMG in SO and GAL did not change with fatigue, which meant that the functional compensation deficiency after fatigue existed in the functional unstable ankle. This result would be due to both central and peripheral mechanisms.

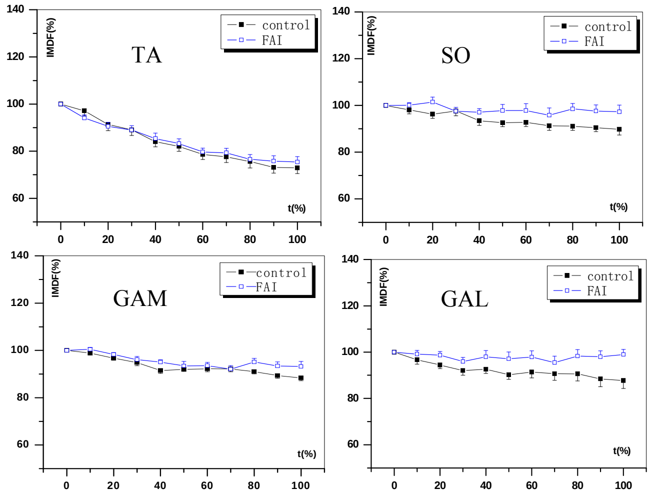

Figure 2: IMDF changes of the SEMG during the local muscle fatigue of the ankle.

CONCLUSIONS

During maximal isokinetic concentric fatigue of the ankle, frequency domain features are time-dependent for the muscles of a Control Group, and the TA and GAM of the FAI Group; but it is time-independent for SO and GAL of the FAI group. These results suggest that the central motor control strategy for the FAI Group was probably different from that for the Control Group; there was lack of ability for functional compensation in the functionally unstable ankle.

REFERENCES

1. Kaminski TW, et al. *J Athl Train*. **34**(3): 239-245, 1999
2. Sirca A, Susec-Michieli M. *J Neuro Sci*. **44**(2-3): 149-159, 1980
3. Tesch P. *Acta Physiol. Scand*. **104**(3): 373-374, 1978.
4. Tesch P, et al. *Acta Physiol Scand*. **103**(4): 413-420, 1978.
5. Amann M. *Med Sci Sports Exerc*. **43**(11): 2039-2045, 2011.

MEASUREMENTS AND ANALYSIS ON MUSCLE ACTIVITIES IN FEMALE SUBJECTS DEPENDING ON DRIVE-ASSISTING SPEEDS OF A SHOWER CARRIER

[1]Cheolwoong Ko, [1]Keyoung Chun, and [2]Taesoo Bae

[1]Korea Institute of Industrial Technology (KITECH), Cheonan, Korea
[2]Jungwon University, Goesan, Korea
email: cheko@kitech.re.kr web: http://www.kitech.re.kr

INTRODUCTION

From the viewpoint of quality of life (QoL), bathing/showering activities have the object of maintaining cleanliness, restricting diseases, and preventing secondary diseases, etc. Shower carrier is one of representative assisting equipment for care activities during showering the elderly in care facilities. In this study, for the development of a drive-assisting system to effectively move a shower carrier indoors, concept design was reviewed, and the muscle activities of test subjects were measured through the performance tests. Based on the test results, a drive-assisting system was proposed by which the muscle burden on caregivers could be reduced and the usage safety during moving a shower carrier could be secured.

METHODS

In this study, a new shower carrier prototype was developed considering usage conditions in elderly care institutions. The prototype was constituted with the bed frame (1,900 x 650mm) designed by considering the Korean elderly body information. A 3-step column type lifting module (maximum allowable load: 2,500N, lifting stroke: 500mm) with inbuilt dual linear actuators was also newly developed, and an integrated base frame (wheelbase: 1,250 x 580mm) whose static turn-over safety was secured through a turn-over analysis was fabricated (Figure 1).

Also, the suitable motor capacity and the drive-assisting wheel size were proposed. Based on the initial design criteria, the design parameters of the motor capacity (300kg·cm) and the drive-assisting wheel size (Ø210mm) were determined. An inbuilt hub motor was selected as a component of the driving unit, and the up-down link mechanism of the drive-assisting wheel was designed for the shower carrier prototype. A drive-assisting wheel prototype was prepared as an integrated type by molding the silicone ring on the hub motor (8FUN DX, ECOI). In addition, the drive-assisting wheel was fixed on the base frame with the left and right brackets for the performance tests (Figure 2).

For the performance tests for the drive-assisting system, six Korean females in their 40s (age: 43±4, height: 157±5cm, elbow height: 100.5±3.5cm, shoulder width: 38.3±2.3cm, and weight: 54.5±1.5kg) were selected as test subjects. For the measurement of the muscle activities from the subjects, 7 muscles in the upper body (TM/Trapezius Muscle, DM/Deltoid Muscle, BBM/Biceps Brachii Muscle, TBM/Triceps Brachii Muscle, ECRLM/Extensor Carpi Radialis Longus Muscle, FCUM/Flexor Carpi Ulnaris Muscle, and ESM/Erector Spinae Muscle) were selected. The muscle activities were measured using the EMG sensors (Electromyography, Delsys, Inc, USA) (Figure 3).

Fig. 1 Concept Design of Shower Carrier Prototype with Up-Down Link Mechanism of Drive-assisting Wheel

Fig. 2 Newly Developed Shower Carrier Prototype equipped with Drive-assisting System

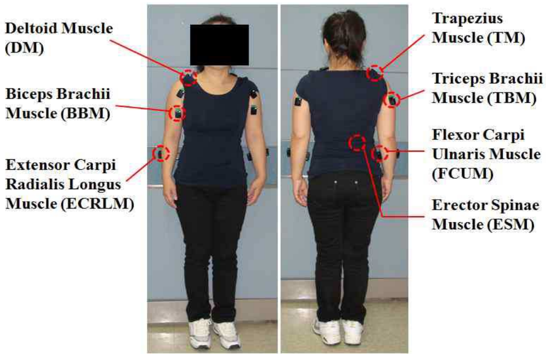

Fig. 3 EMG sensors attached to Female Subjects

Fig. 3 Performance Tests of Drive-assisting System on a Sloped Track

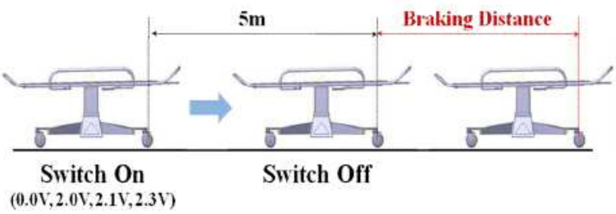

Fig. 4 Brake Distance Tests on a Flat Track

The performance tests were carried out on a sloped track of 10˚ (Standard of Korea Senior Products Association). In this study, the drive voltages of the drive-assisting wheel were set as 0.0V (0.00m/s), 2.0V (0.25m/s), 2.1V (0.5m/s), and 2.3V (0.75m.s), respectively. The gripping height of the shower carrier was set at the elbow height of the subject and a 60kg human dummy was loaded on the bed. The tests were repeated for 8 times per drive voltage, and the measured results from the 6 tests excluding the maximum/minimum values were analyzed.

To secure the safety caused by over-drive of a drive-assisting system, braking distances were also measured on a flat surface. First, the shower carrier was driven for 5 meters after switch-on of the drive-assisting wheel, and then the braking distance under each drive voltage was measured after switch-off of the drive-assisting wheel (Figure 4).

RESULTS AND DISCUSSION

The muscle activities in the TM, DM, UL (Upper Limb/UL=BBM+TBM+ECRLM+FCUM), and ESM, respectively. Here, change rates in the muscle activities in each muscle were investigated. First, in the TM, the change rates were observed as -21% by the drive voltage 2.0V compared to 0.0V, as -57% by 2.1V, and as -62% by 2.3V respectively ($p<0.05$), whereas -40% by 2.0V, -56% by 2.1V, and -69% by 2.3V compared to 0.0V were obtained respectively from the DM ($p<0.05$). Also, from the UL, the change rates of the muscle activities were observed as -17% by the drive voltage 2.0V compared to 0.0V, as -47% by 2.1V, and as -52% by 2.3V respectively ($p<0.05$), whereas the change rates from the ESM were found to be -20% by 2.0V, -34% by 2.1V, and -42% by 2.3V respectively compared to 0.0V ($p<0.05$). Meanwhile, the braking distances on the flat surface were found to be at 1.05m by the drive voltage 2.0V of the drive-assisting wheel, at 2.25m by 2.1V, and at 5.4m by 2.3V, respectively (Figure 5).

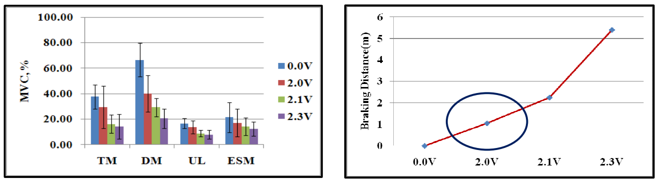

Fig. 5 Measurement Results of Muscle Activities and Brake Distance

CONCLUSIONS

In this study, a new shower carrier prototype with a drive-assisting system was developed by which reduction of the muscle burden on the caregivers during moving the shower carrier indoors could be expected. The performance test results indicated that, as the drive voltage of the drive-assisting wheel was increased, the muscle activities from the subjects became remarkably reduced. It was also found that the braking distance of 1.05m at the drive voltage 2.0V was suitable for the drive-assisting system of the shower carrier prototype developed in this study.

ACKNOWLEDGEMENTS

This study was carried out by research fund support from National R&D Program, Ministry of Health and Welfare, Korea (A101945) and KITECH.

EFFECTS OF PROLONGED STANDING ON OXYGEN SATURATION IN THE SOLEUS AND ERECTOR SPINAE MUSCLES OF THE LOWER BACK USING NEAR INFRARED SPECTROSCOPY

[1]Justin Haney, [1]Mark S. Redfern, [2]Theodore Huppert, [1]April J. Chambers

[1]Department of Bioengineering, University of Pittsburgh, Pittsburgh, PA, USA
[2]Department of Radiology, University of Pittsburgh, Pittsburgh, PA, USA
email: jmh141@pitt.edu, web: http://www.engineering.pitt.edu/hmbl

INTRODUCTION

Occupations, such as supermarket cashiers, health care employees, and assembly line workers, require workers to stand for prolonged periods of time. This has been associated with injury and health problems including lower extremity discomfort, low back pain, swelling of the lower limbs, and lower extremity venous blood restriction [1]. It is important to understand the reasons for the onset of fatigue and discomfort during prolonged standing in order to minimize these health problems. Psychophysical metrics, such as questionnaires that rate perceived levels of discomfort and fatigue can yield important insights, however are limited. Quantitative measures, such as electromyography (EMG), leg volume, underfoot center of pressure, and skin temperature, have also been used, but the findings are equivocal [1]. Therefore, new methods of exploring fatigue and discomfort due to long-term standing are needed.

Near infrared spectroscopy (NIRS) is a non-invasive technique that measures changes in absorption of near infrared light by oxyhemoglobin and deoxyhemoglobin to determine the change of oxygen saturation (SO_2) in a muscle over a period of time. A muscle experiences a decrease in SO_2 when it fatigues during a maximal voluntary contraction (MVC) followed by an increase in SO_2 immediately afterwards [2].

The goal of this pilot study was to compare perceived discomfort in selected regions of the lower extremity to changes in muscle SO_2 of the respective regions during prolonged standing on a hard surface. Based on previous findings, our hypothesis was that SO_2 will decrease in selected muscles of the lower extremity as participants experience lower extremity discomfort and fatigue during prolonged standing.

METHODS

Four healthy subjects (age: 23.2 ± 3.4 y; weight: 79.5 ± 19.0 kg) completed the testing protocol. Subjects were asked to stand still on a hard surface while keeping both feet on the ground for a duration of six hours with two minute sitting breaks after each hour. All subjects were given the same type of shoes and socks to wear throughout the testing session. A questionnaire was administered at the beginning of the session and every subsequent half hour of standing, which asked subjects to rate their perceived level of discomfort using a CR10 Borg scale. They rated their perceived level of discomfort in their upper and lower back, hips, upper legs, knees, lower legs, ankles, and feet ranging from 0 (no discomfort) – 10 (extreme discomfort) in a nonlinear fashion. Ratings of 11, "~", and "." were also an option to represent maximal discomfort [3].

NIRS was used to record SO_2 in the lateral portion of the soleus muscle and erector spinae muscle in the L3-L5 region of the lower back. The change in SO_2 (ΔSO_2) was calculated after each hour, defined as the average SO_2 of the final five minutes of the hour minus the average SO_2 during five minutes of initial baseline standing. Perceived discomfort ratings in the feet and lower back at the end of each hour were respectively compared to the ΔSO_2 in the soleus and erector spinae after each hour.

RESULTS AND DISCUSSION

The perceived level of discomfort for the feet and lower back were transformed to a linear Borg scale ranging from 6-23 with six corresponding to no discomfort at all [3]. Results of the ΔSO_2 in the soleus and perceived discomfort rating in the feet are plotted to show trends over each hour spent standing and across subjects (Fig. 1).

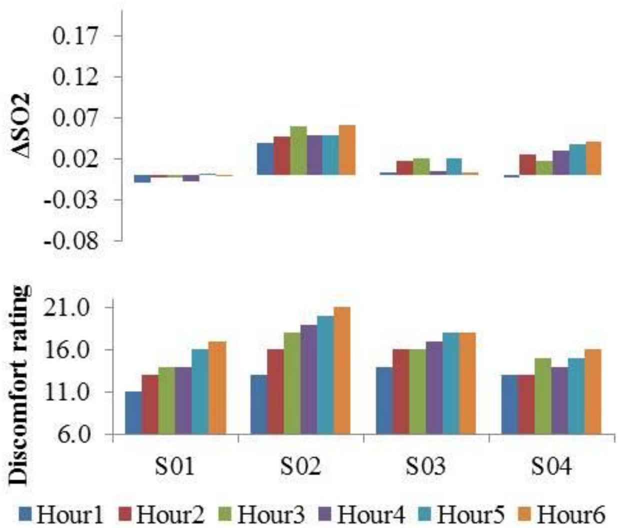

Figure 1: ΔSO_2 in the soleus and discomfort rating in the feet throughout entire six hours of standing and for all four subjects (S01-S04).

Results of the ΔSO_2 in the erector spinae muscle in the L3-L5 region and perceived discomfort rating in the lower back are plotted to show trends over each hour spent standing and across subjects (Fig. 2).

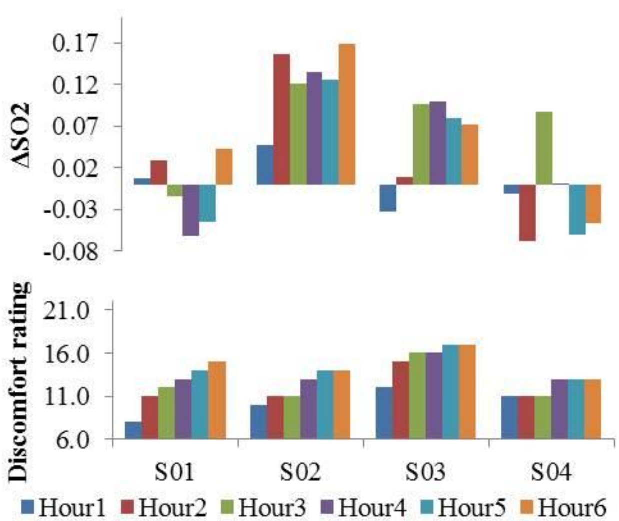

Figure 2: ΔSO_2 in the erector spinae and discomfort rating in the lower back throughout entire six hours of standing and for all four subjects.

As expected, the perceived discomfort level in the feet and lower back gradually increased over the six hours spent standing on the hard surface for all subjects. Unexpectedly, the ΔSO_2 in the soleus suggested increases over time spent standing for subjects S02, S03, and S04 while subject S01 experienced little or no change. The ΔSO_2 in the erector spinae muscle showed more variation over time and across subjects. Subjects S02 and S03 showed large increases after the first hour whereas subjects S01 and S04 showed varying trends of increases and decreases of ΔSO_2 across each hour.

The unexpected increase in SO_2 over time in the soleus and lower back erector spinae muscles could be due to the slow contractions experienced during long term standing. Previous research has related muscle fatigue during MVCs to decreased SO_2; however, during prolonged standing, the soleus and erector spinae muscles are never fully exerted. Instead, they undergo low intensity contractions that occur over a longer period of time. These contractions may cause a small influx of oxygenated hemoglobin to the muscles which increases SO_2.

REFERENCES

1. Redfern MS, Cham R, *AIHAJ*, **61**, 700-708, 2001.
2. Quaresima V. *Journal of Biomedical Optics*, **9**, 413-420, 2004.
3. Borg G. *Borg's Perceived Exertion and Pain Scales*, Human Kinetics, 1998.

ACKNOWLEDGEMENTS

Thank you to Dr. Patrick J. Sparto and the Medical Virtual Reality Center for the use of laboratory space and to Nancy Beluk and the Magnetic Resonance Research Center for help with equipment.

MUSCLE ACTIVITY IN SIMULATED OVERHEAD DRILLING: THE INFLUENCES OF WORK LOCATION, FORCE DIRECTION, HAND CONFIGURATION AND BODY POSTURE

Jacquelyn M. Maciukiewicz, Alan C. Cudlip, Jaclyn N. Chopp, Clark R. Dickerson

University of Waterloo, Waterloo, ON, Canada
email: cdickers@uwaterloo.ca

INTRODUCTION

Overhead work is associated with shoulder injury. Where overhead work is unavoidable, horizontal and vertical reach distance should be reduced [1]. Shoulder musculature, especially the rotator cuff, is highly susceptible to fatigue in these overhead postures [2]. This risk is exacerbated by strength deficits, with minimum outputs reported between 90°-120° of arm elevation [3]. Previous research has focused only on the dominant limb in drilling tasks, although the gross movement and stabilization efforts between limbs [4] makes inferences regarding bilateral tasks difficult. In addition, most strength data for the shoulder has focused on isolated joint exertions, and has not considered effects of the contralateral limb on these outputs [5]. The purpose of this study was to identify differences and quantify activity levels in unilateral and bilateral overhead drilling scenarios while manipulating overhead work locations and force application directions.

METHODS

8 right-handed male participants completed 24 overhead drilling exertions in two force directions (forward, upward) with two gross body postures (seated, standing) at three overhead work locations (15, 30, 45cm forward) in two configurations: 1) Bilateral: stabilization of a 1kg weight in the left hand at the work location while exerting force with the right hand, and 2) Unilateral: exerting force with only the right hand. Work heights were chosen to elicit 120° of humeral flexion in a 50th percentile male, ensuring at least 90° of flexion across the population. Right hand forces are 30N and held for 5 seconds. 6 muscles were monitored bilaterally (anterior (ADEL) and middle deltoid (MDEL), upper trapezius (UTRP), supraspinatus (SUPR), infraspinatus (INFR), thoracic erector spinae (THES) for 12 total sites) with surface electromyography (EMG) and normalized to muscle-specific maximal values.

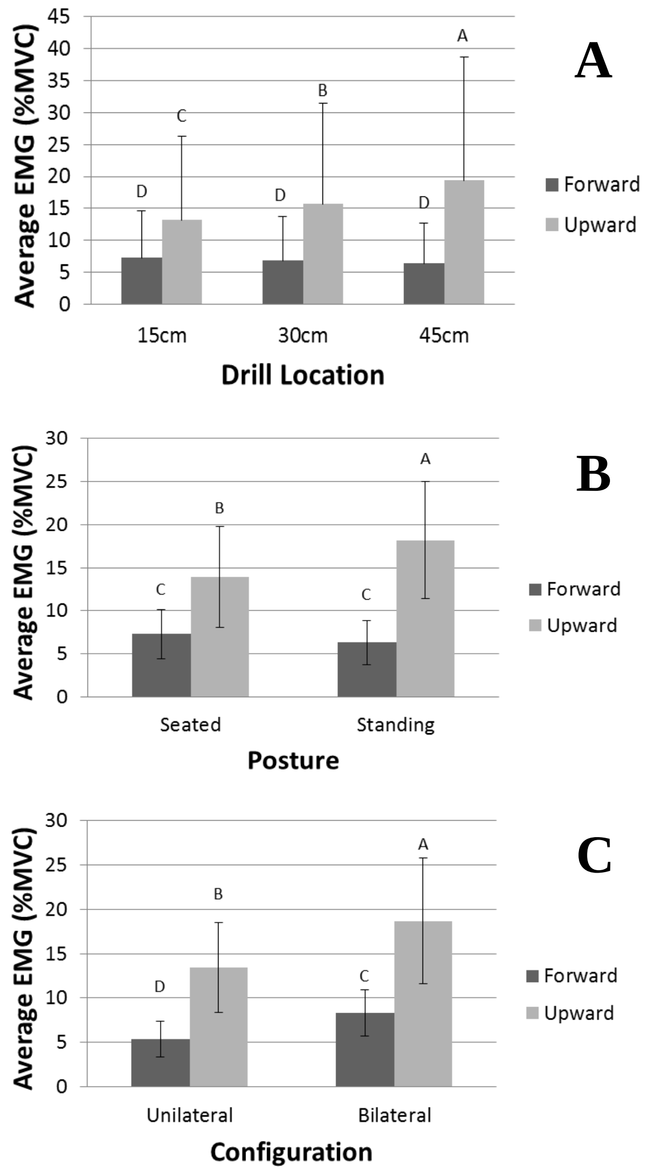

Figure 1. Normalized average muscular activity across all muscles showing interactions between force direction and drill location (A), posture (B) and configuration (C). Levels of significance are denoted by letters ($p<0.05$).

3-D right hand forces were recorded with a 6-DOF force transducer. A 4-way ANOVA (drilling location, configuration, force direction, and body posture) assessed influences on normalized individual and overall muscle activity (defined as an average over all muscles from both arms).

RESULTS AND DISCUSSION

Force direction, work location, posture and task configuration all had effects on muscular activity during these overhead drilling scenarios. Normalized EMG data from 8 participants shows upward exertions have increased overall muscular activity compared to forward exertions across postures (Figure 1B, $p<0.01$). Secondly, standing resulted in higher average activity than sitting ($p<0.01$). Finally, the most forward location generated more muscular activity than the other two locations in upward exertions, and changes in configuration (unilateral or bilateral) resulted in significant changes in muscle activity for most muscles ($p<0.05$). Force direction interacted with each other independent measure, but these other measures did not interact with each other ($p<0.01$).

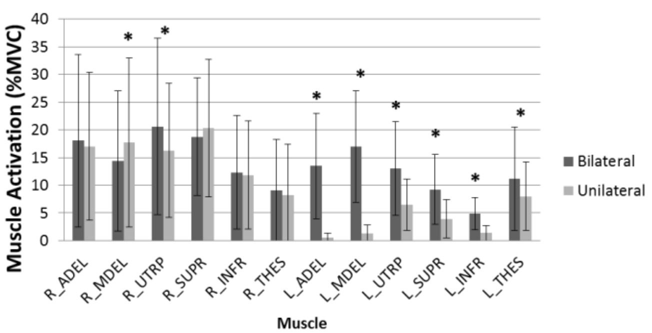

Figure 2. Normalized average individual muscle activity for unilateral & bilateral exertions. Asterisks indicate significant inter-configuration differences ($p<0.05$). R=right arm, L=left arm.

Direction of force application was the most significant factor identified. Exertions in a forward direction produced significantly lower average EMG outputs than upward exertions across work locations, body postures, and hand configurations (Figure 2). Forward exertions reportedly generate the lowest muscular demands in overhead postures [5], which is supported by the current results for both unilateral and bilateral drilling tasks (Figure 1C).

Work configuration profoundly influenced muscle activity. Bilateral configurations resulted in increased activity of middle deltoid and decreases in upper trapezius on the right side (Figure 2). These changes suggest redistribution of muscular effort in more symmetric positions. Bilateral exertions also caused higher average muscle activity in both force directions (Figure 1C), largely due to an increase in demand for the non-dominant (left) arm. Drill location and whole-body posture only affected upward force exertions, resulting in increased activity levels as locations moved further forward (Figure 1A), or in moving from a seated to a standing position (Figure 1B). Increased horizontal distances in overhead work are a reported risk factor for upper extremity disorders and injury [6]. The increased activity level in shoulder muscles found in this study for upward exertions supports this body of research, and overhead work should be positioned to minimize these reach distances.

CONCLUSIONS

Performing tasks that require the non-dominant arm modifies activity patterns on both sides of the body compared to a unilateral task. Generally, overall muscle demands increase. Much of the existing strength data for industrial tasks was collected on isolated joint exertions. These results are of potential utility to practicing ergonomists and work task designers in order to minimize injury fatigue risk when working in overhead positions, especially when interpreting potential exposures associated with performing bilateral tasks.

REFERENCES

1. Anton et al. (2001). *Ergonomics*, 44 (5), 489–501.
2. Herberts & Kadefors (1976). *Acta Orth. Scand.*, 47 (4), 381–387.
3. Garg et al. (2005). *Occ. Ergonomics*, 5, 131-140.
4. Wang & Sainburg (2007). *Experimental Brain Research*, 178: 241-258.
5. Harbo et al (2012). *Eur J App Phys*, 112, 267-275.
6. Chopp et al. (2009). *Ergonomics*, 1, 83-91.
7. Grieve & Dickerson (2008). *Occupational Ergonomics*, 8, 53-66.

Age-related changes in mechanical properties of human hand digits

[1]Jaebum Park, [1,2]Nemanja Pazin, [3]Jason Friedman, [1]Vladimir M. Zatsiorsky, and [1]Mark L. Latash
[1]Pennsylvania State University, University Park, PA, USA
[2]University of Belgrade, Belgrade, Serbia
[3]Tel Aviv University, Tel Aviv, Israel
email: jzp12@psu.edu

INTRODUCTION

Age-related physiological changes and functional deficits within the neuromotor system include reduction of muscle mass, impairment of tactile sensitivity, slowing down of muscle contractions, etc. In particular, healthy aging is known to be associated with higher grip forces and safety margins. The changes with advanced age in the manipulation strategies of hand/digit actions are partially due to the changes in mechanical properties of peripheral structures [1, 2]. In this study, we examined age-related differences in mechanical properties of the human hand digits by estimating the apparent stiffness [3, 5] and the friction coefficients between digit tips and contacting surfaces with the newly developed measurement devices.

METHODS

<u>Subject:</u> Twelve healthy elderly subjects and twelve healthy young subjects (age: 76.1 ± 5.6 for the elderly; 26.9 ± 4.9 years for the young; 6 females for each group) were recruited. All subjects were right-hand dominant. The elderly subjects were recruited from a local retirement community, and they passed a series of screening tests (e.g., cognition, depression, quantitative sensory tests, and general examination).

<u>*Equipment*</u>

Apparent stiffness estimation: Four hand digits (the thumb, and three fingers) grasped the handle, which was fixed to the table, and four miniature force sensors were used to measure the forces applied by the digits. The force sensors were connected to a rod, which was connected to an electromagnet. A compression spring was placed between the force sensor and the base. With this setup, when the electromagnet was turned on, the finger support was effectively rigid, when the electromagnet was off, the force sensor yielded under the corresponding digit resulting in a quick, low-amplitude motion. The electromagnets were controlled by the experimenter.

Friction coefficient estimation: A multi-axis force sensor was attached to the frame to measure normal and tangential forces, and a linear motor applied force that moved the sensor with respect to the digit [4]. The top of the sensor was covered with sand-paper (300-grit).

<u>*Experimental Procedure*</u>

Apparent stiffness estimation: There were fifteen experimental conditions: 5 digits (*Thumb, Index, Middle, Ring,* and *Little fingers*) × 3 force levels (15, 30, 45% of maximal voluntary contraction force, MVC). For each condition, the subjects were required to grasp the handle naturally and then to produce a steady-state level of force with a task-digit while keeping all non-task digits on the sensors for about 5 s. The normal force was displayed on the computer screen in %MVC of the task-digit. At a random time (uniformly distributed between 5 and 8 s), the electromagnet holding the task-digit was turned off, causing the task-digit to move into flexion. The displacement of the digit tip was approximately 5–10 mm. When the perturbation was applied, the task-digit force decreased immediately. The subjects were instructed to recover the dropped digit force to the original force level as quickly as possible. The sampling frequency was set at 500 Hz.

Friction coefficient estimation: There were fifteen experimental conditions: 5 digits (*Thumb, Index, Middle, Ring*, and *Little fingers*) × 3 normal force levels (15, 30, 45% of MVC). The subjects were instructed to exert a steady-state level of normal force by pressing with one of digits on the sensor while the sensor was moved horizontally. The subjects were instructed to keep the task-digit in the same position and configuration against sensor movement. The produced normal force was displayed on the computer screen. The subject performed three consecutive trials for each digit and condition.

Data analysis

Apparent stiffness estimation: We used a simple linear damped mass-spring model (one degree-of-freedom) for the hand digits [5]:

$$m\ddot{x}(t) + r\dot{x}(t) + kx(t) = f(t)$$

$x, \dot{x}, \ddot{x}$: digit tip position and its time derivatives; *f*: digit normal force; *m*: mass coefficient; *r*: damping coefficient; *k*: apparent stiffness coefficient. The apparent stiffness was estimated using the time window of 25 ms after the initiation of perturbation (0 ms) to avoid the influence of reflexes and voluntary reactions.

Friction coefficient estimation: the ratio between the tangential force during the sensor motion and the subject's normal force was computed as the dynamic coefficient of friction [3, 4].

RESULTS AND DISCUSSION

Apparent stiffness: In general, the elderly group showed larger values of *k* as compared to the young group (Young: 425. 9 ± 23.1 N/m; Elderly: 548.6 ± 23.1 N/m, mean ± standard error, $p < 0.01$). The stiffness increased with the magnitude of baseline force (15% < 30% < 45% of MVC) in both groups (Fig. 1). Also, both groups showed significant differences across digits (*thumb* > *index* > *middle* > *ring*, *little*) confirmed by post-hoc comparisons ($p < 0.05$).

Friction coefficient: Overall, the elderly group showed smaller friction coefficients as compared to the young group (Young: 0.81 ± 0.03; Elderly: 0.59 ± 0.03, mean ± standard error, $p < 0.001$). The friction coefficients decreased with the force level in the young group (15% > 30% > 45% of MVC) while there was no significant change between the force levels in the elderly group (Fig. 2). No significant differences were seen among digits.

CONCLUSIONS

1. Healthy aging is associated with higher apparent stiffness of the digits. Generally, the apparent stiffness increases with the magnitudes of digit-tip force.
2. Healthy aging is associated with smaller coefficients of dynamic friction between the skin and hand-held objects.

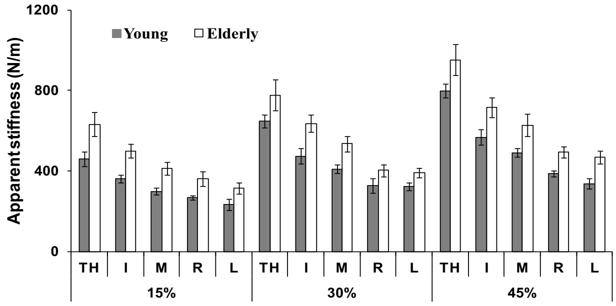

Figure 1. Apparent stiffness values of individual hand digits for three force levels (%MVC) for the young (gray bars) and elderly (white bars) groups. The average values across subjects are presented with standard error bars. TH, I, M, R, and L indicate thumb, index, middle, ring, and little fingers, respectively.

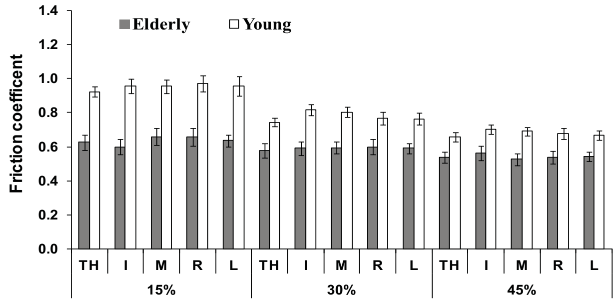

Figure 2. Coefficients of friction of individual hand digits in the three force conditions expressed in %MVC for the young (gray bars) and elderly (white bars) groups. The average values across subjects are presented with standard error bars.

REFERENCES

1. Escoffier C, et al. *J Invest Dermatol* **93**: 353-357, 1989
2. Cole KJ, et al. *J Neurosci* **19**: 3238-3247, 1999
3. Zatsiorsky, VM. *Kinetics of human motion. Champaign IL*: Human Kinetics, 2002.
4. Savescu AV, et al. *J Appl Biomech* **24**: 43-50, 2008
5. Hajian AZ, Howe RD. *J Biomech Eng* **119**: 109-114, 1997

KINEMATIC CONSISTENCY-BASED DECISION RULES FOR DISCRIMINATING BETWEEN SINCERE AND FEIGNED TRUNK MOTION EXERTIONS

[1]Sivan Almosnino, [2]Taya McGillivary, [1]Joan M. Stevenson, [1]Olivia Bruce, and [1,3]Zeevi Dvir

[1] Queen's University, Kingston, ON, Canada, [2]Univeristy of Waterloo, Waterloo, ON, Canada
[2]Tel Aviv University, Ramat Aviv, Israel
email: sivanalm@hotmail.com, web: http://www.skhs.queensu.ca/ergbio/

INTRODUCTION

Injuries to the lower back are common in work settings. During decision-making processes related to modification of rehabilitative procedures, as well as during establishment of impairment and possible disability rating resulting from such injuries, clinicians rely, in part, on scores attained from measurements of trunk range of motion (ROM) [2]. The validity of such scores, however, is based on the premise that during task performance, the patient was cooperative and performing to the best of their personal abilities. Due to several reasons, including the adversarial structure of the North American legal systems and the presence of various secondary gains, there is a documented suspicion among some health care professionals and compensation institutions that patients may have an incentive to exaggerate or feign pain or injuries [1]. In turn, this places patients in a compromised position since they are required, in effect, to prove the presence and extent of their claimed physical limitations. Thus, a necessity arises for ascertaining the type of effort performed during clinical evaluations of trunk ROM capabilities.

Previous investigations pertaining to this topic area have established kinematic measurement-based discriminatory models that rely on the notion that during sincere efforts, only minor variations exist in the performance of successive trunk movement exertions. On the other hand, during attempts to feign the presence of pain or injury; variations in performance across successive repetitions are greater, and are most apparent when examining higher derivatives of trunk angular position data [2,3].

In the current investigation, we aimed to exploit this phenomenon by using kinematic waveform similarity measures for development of a decision rule for differentiating between sincere and feigned trunk motion efforts.

METHODS

A convenience sample of 82 asymptomatic individuals (49 women, age range 19-50 years old) participated in the study. Written informed consent was obtained prior to testing, and the procedures were approved by Queen's University General Research Ethics Board. Three-dimensional trunk and pelvis kinematics were recorded using an electromagnetic tracking system sampling at 32 Hz (Polhemus Liberty, Colchester, VT). The experimental protocol consisted of two tasks: The first involved trunk flexion/extension movements, and the second was composed of trunk flexion, lateral bending and rotation to the participant's dominant side along a line situated at a 45° angle from standing posture. Each task was performed in two conditions: The first involved movement at a self-selected fast but comfortable speed through full ROM. In the second condition, the participants were asked to feign lower back injury or pain for secondary gain purposes, while simultaneously trying to convince the examiner that they are performing to the best of their ability. Two sets were performed in each condition, with each set composed of 6 continuous repetitions.

Trunk-pelvis angular joint positions were calculated and subsequently differentiated to obtain joint angular velocity data. The Euclidian norm of the joint angular positions was then calculated to obtain a single representative waveform for each trial. These data were subsequently segmented to individual repetitions and time normalized to 100% of the movement phase. For each task and condition, zero-phase, normalized, cross correlations and % root mean difference (%RMSD) scores were calculated between all trials. These were averaged to yield representative curve shape and relative magnitude difference scores for each set.

For classification purposes, two logistic regression models were constructed with an expanded input space to include quadratic terms for predicting efforts as being sincere or feigned in each of the tasks performed. A leave one-out cross validation routine was subsequently implemented to obtain unbiased estimates of the models' accuracies. The models' performance is reported in terms of the number of misclassifications per effort type and accompanying sensitivity and specificity percentages.

RESULTS AND DISCUSSION

In comparison to feigned attempts, sincere trials across both tasks were done in less time; were performed through a larger ROM, and achieved faster trunk angular velocities (Table 1).

The logistic regression-based decision boundary for the flexion/extension task performed in the sagittal plane is illustrated in Figure 1. In this a total of 140 of 164 efforts were classified correctly. Of the sincere efforts performed, 12 of 82 total sincere efforts were misclassified as being feigned, whilst 12 of 82 total feigned efforts were misclassified as being performed sincerely. The corresponding specificity and sensitivity values are both 85.4%.

For the task incorporating multidimensional trunk motion, the discriminatory model correctly classified 146 of 164 total efforts, with 11 of 82 sincere efforts misclassified as being feigned, and 7 of 82 feigned efforts classified as being performed sincerely. The specificity and sensitivity values are 86.6% and 91.5%, respectively.

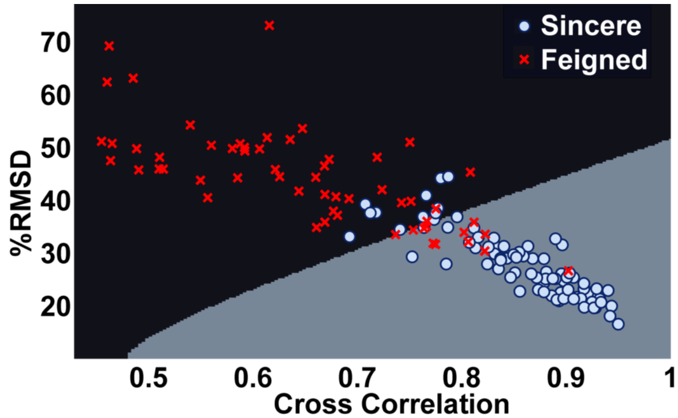

Figure 1: Logistic regression-based decision regions for classifying trunk motion flexion/extension efforts as being sincere or feigned. Axes are truncated for presentation purposes.

The performances of the decision rules obtained in this investigation are comparable to those reported previously [2,3]. However, the current investigation used less specialized equipment, and employs only 2 predictor variables (as opposed to 5) for discriminatory purposes. Since there are indications that those with low back disorders exhibit increased variability during trunk movement performance [3] the ability to generalize the proposed decision rules to those with low back disorders is unclear, and requires further research.

REFERENCES

1. Nova Scotia (Workers' Compensation Board) v. Martin [2003] 2 SCR 585.
2. Ferguson SA, et al. *Disabil Rehab* 2**5**, 236-241, 2003.
3. Marras WS, et al. *Spine* 2**5**, 587-595, 2000.

Table 1: Temporal-spatial characteristics of sincere and feigned effort attempts. Data presented as mean ± SD

	Sincere Trials		Feigned Trials	
Task	**Flexion/Extension**	**Multidimensional**	**Flexion/Extension**	**Multidimensional**
Task Time (s)	16.0 ± 3.8	15.5 ± 3.5	29.4 ± 13.8	28.3 ± 13.5
Maximal ROM (°)	81.0 ± 19.5	84.3 ± 17.0	66.4 ± 24.6	70.9 ± 21.2
Maximal Speed (°/sec)	158.4 ± 55.7	174.5 ± 72.4	94.6 ± 42.3	98.7± 44.6

THE EFFECTS OF DIURNAL CHANGES IN BEHAVIORS OF TRUNK TISSUES ON TRUNK MECHANICAL PROPERTIES

Brian Koch, Anuj Agarwal, Milad Vazirian, and Babak Bazrgari

University of Kentucky, KY, USA
email: babak.bazrgari@uky.edu, web: http://hmbl.engineering.uky.edu/

INTRODUCTION

Abnormal mechanics of the trunk has been suggested to play an important role in the development of low back pain (LBP) [1]. The trunk musculoskeletal system has both passive and active components contributing to its mechanical behavior. Daily alterations in behavior of tissues in the trunk musculoskeletal system are expected to affect trunk mechanics, though the extent of such diurnal effect is not yet clear. The objective of this study was to quantify changes in trunk mechanics following one day of low and high levels of physical activity and verify if changes in trunk mechanical behaviors fully recover after ~12 hours of rest period.

METHODS

Ten healthy males with no self-reported history of LBP participated after completing an informed consent procedure approved by the local IRB. Each participant completed three testing sessions involving both sudden perturbation and stress relaxation tests. Four of the participants (i.e., the high exposure group, age= 22 (3) years, stature= 185 (3) cm, weight=90 (9) kg) were members of the University's Ultimate Frisbee team and were tested before and after a daylong tournament. The other six participants (i.e., the low exposure group, age=26 (5) years, stature= 178 (4) cm, weight= 78 (9) kg) were University students and staff and were tested at the beginning and the end of their sedentary work day. All participants were also tested the following morning to evaluate recovery.

During each test session, participants stood in a rigid metal frame, were strapped in at the pelvis, and were attached to a servomotor (Kollmorgen, Radford, VA) via a rigid rod-harness assembly at the T8 level (Fig. 1). Initially, two replications of maximum voluntary pulling exertions (MVE) against the rigid rod were obtained using an in-line load cell (Interface SM2000, Scottsdale, AZ). Each participant then completed two perturbation tests while maintaining either 10% or 30% (±2%) of their MVE using real-time visual feedbacks of load cell readings. During each perturbation test once the required level of exertion achieved, horizontal position perturbations were generated by the servomotor and transmitted to the trunk via the rod-harness assembly. A one-minute sequence of trunk displacements (±5mm anterior-posterior) was induced with a pseudo-random set of delays between each perturbation. The driving force throughout the perturbations was measured using the in-line load cell and the resulting kinematics

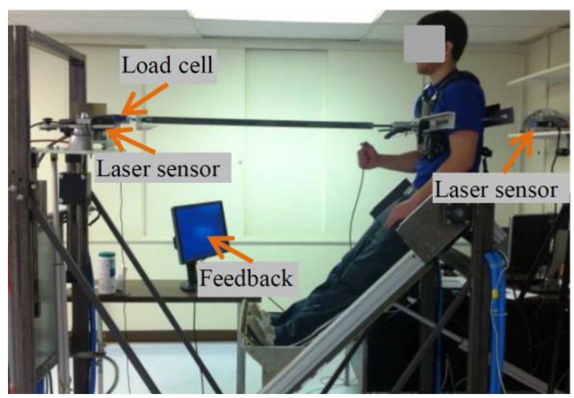

Figure 1: Experimental setup

were measured using two high-accuracy laser displacement sensors (Optex-FA, West Des Moines, IA), one targeting the participant's back at the T8 level and another targeting the load cell. Trunk intrinsic properties were obtained by relating measured trunk kinetics and kinematics during perturbation test and by using a system identification method that assumes the trunk as a single-degree-of-freedom system [2]. The stress-relaxation tests were performed in the same setup afterward. For this test, the participant's legs were raised to achieve a lower body rotation of 50 degree around the L5/S1 while keeping the trunk in a fixed upright posture using the rigid rod-harness assembly. Trunk response to such rotation (deformation) was measured by the in-line load cell.

The mean of maximum pulling force during the MVE trials, intrinsic stiffness and apparent mass from the perturbation tests along with initial passive resistance and relaxation after 4 minutes of exposure to 50 degree deformation from stress relaxation tests were used for subsequent statistical analyses. A repeated measure ANOVA was used to determine the effects of exposure level and time on these measures.

RESULTS AND DISCUSSION

Mean (SD) MVEs across all time points were similar ($F_{(1,8)}$=0.02; P=0.7) between the high and low exposure groups with respective values of 888 (265) N and 958 (302) N. There was, however, a significant ($F_{(2,7)}$=0.02; P=0.0005) time-by-group interaction (Fig. 2). MVEs in the high exposure group decreased ($t_{(6)}$=-3.07; P=0.026) by 22% after the exposure but then increased (recovered) ($t_{(6)}$= 3.67; P=0.016) by 14% during the rest period. MVEs were similar across all time points for the low exposure group. Intrinsic trunk stiffness while maintaining 30% of MVE was significantly different between ($F_{(1,8)}$=1.08; P=0.019) and within ($F_{(2,7)}$=1.75; P=0.029) subjects. Mean (SD) intrinsic stiffness with 30% effort across all time points were 16408 (2255) N/m and 13739 (2093) N/m for high and low exposure group respectively. Despite the recovery of MVEs following the rest period in the high exposure group, intrinsic trunk stiffness with 30% effort was 20% higher ($t_{(6)}$=2.25; P=0.042) than initial values (i.e., before exposure). Other measures of trunk intrinsic property with 10% and 30% efforts were not different between and within subjects. Initial passive resistance of the trunk was only different within subjects ($F_{(2,7)}$=1.63; P=0.034). Mean initial passive resistance increased 28% and 10% following exposure then decreased 28 % and 7% during the rest period in high and low exposure group respectively (Fig. 2). No difference was found in relaxation values after 4 minute.

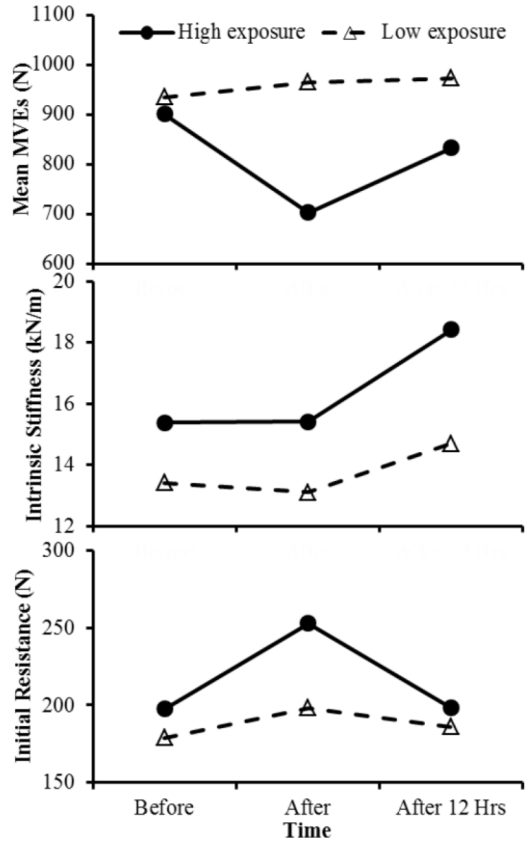

Figure 2: Alterations in MVEs, stiffness and initial resistance with time

CONCLUSIONS

Intrinsic trunk stiffness depends on the level of muscle activity and passive tissue resistance. Here, intrinsic trunk stiffness in the high exposure group increased following the recovery period. Such an increase in stiffness, despite recovery in MVE and passive resistance suggest an alteration (e.g., higher co-activation) in the activity pattern of trunk muscles during pulling efforts.

REFERENCES

1. Miller EM, et al. *J Biomech* ***46***; 801-6, 2013
2. Bazrgari B, et al. *Comp Meth. In Biomech & Biomed Eng* **15**, 1001-1009, 2012.
3. Gardner-Morse MG and Stokes IA. *J Biomech* **34**, 457-463, 2001.

ACKNOWLEDGEMENTS

This publication was supported by CDC-NIOSH grant number R21OH010195.

LEG AND TORSO MUSCLE RESPONSE TO PROLONGED KNEELING

Daniel Lomo-Tettey, MS, Naira Campbell-Kyureghyan, PhD, Blake Johnson, BS, Kurt Beschorner, PhD

University of Wisconsin-Milwaukee, WI, USA
Spine Biomechanics Laboratory of University of Wisconsin-Milwaukee, WI, USA
email: lomotet2@uwm.edu

INTRODUCTION

Many daily occupational tasks in construction, utilities, mining and other industries involve frequent and/or prolonged kneeling. Research suggests a link between lengthy kneeling and prevalence of chronic knee injuries such as knee joint inflammation, bursitis, osteoarthritis, and low back pain [1]. Prolonged kneeling and squatting have been identified as major work-related risk factors that predicted new-onset low back pain and knee osteoarthritis [2, 3]. A recent study reported that injuries to the knee, lower back, lumbar spine, and shoulder are among the most reported [4]. Consequently, medical treatment insurance claims for injury to the combined knee, lower back, and shoulder from eight mining companies in US from 1996 to 2008 are well over $9 million dollars [4].

Nevertheless, a gap in the literature exists regarding the biomechanical response to prolonged kneeling. As part of a larger study, this paper discusses leg and torso muscles response during prolonged kneeling on two legs at 90 degrees of knee flexion.

METHODS

Eight healthy subjects (age 20-50 years) volunteered to participate in the study (7 males, 1 female). The subjects were instructed to kneel on both knees at 90 degrees of knee flexion on a kneeling mat for up to 30 minutes. Subjects knelt with each knee on two identical force plates (AMTI, Watertown, MA) over which the kneeling mat was placed.

Electromyography (EMG) activity was recorded using 12 wireless surface electrodes (Delsys Inc, Boston, MA) placed on the muscle belly.

The EMG activity of the following twelve leg and torso muscles were recorded throughout the entire duration of the trial. The unilateral muscles recorded were: Rectus Femoris (RF), Vastus Lateralis (VL), Vastus Medialis (VM), Semitendinosus (SEM), Biceps Femoris (BF), Tibialis Anterior (TA), Medial Gastroc (MG), Lateral Gastroc (LG), bilateral Rectus Abdominis (RA), and bilateral Erector Spinae (ES).

The EMG data was recorded at 2000Hz and filtered using a 4th order Butterworth band-pass filter with corner frequencies set at 10Hz and 500Hz. Force plate data was collected at 1000Hz and filtered (Butterworth, pass through, amplifier gain 1000). The force plate data was part of a larger study and is not reported in this paper. The EMG root mean square (RMS) amplitudes were computed using a window size of 0.125s and an overlap window of 0.0625s. For each muscle, the EMG RMS values were normalized to the first one minute of initial kneeling (most subjects appeared to settle into the required kneeling posture by end of the first minute of kneeling). The normalization was performed by dividing all EMG RMS values by the RMS_0 value obtained at the one minute time point. Since the kneeling task did not involve force exertion, maximum voluntary contraction (MVC) data was not collected.

The effects of time on muscles response was determined using analysis of variance (ANOVA) tests with subjects blocked as random factors. Additionally, statistical significance of muscle activation between levels of kneeling time was determined using post hoc Tukey pair-wise comparisons at 95% confidence (Fig. 1 and Fig. 2). Statistical analyses were performed in Minitab (version 16).

RESULTS AND DISCUSSION

Greater muscle activations relative to the first minute's activity were observed for the hamstring (SEM and BF) and the torso (RA and ES) muscle groups. The lower leg muscles (MG, LG, and TA) and the quads (RF, VL, and VM) exhibited the least activation during kneeling. These findings are consistent with the fact that muscle groups are activated together.

For both knee flexors the RMS values first decreased and then increased as kneeling continued (Figure 1). Interestingly, SEM activity was found to be higher at 5 minutes (22%) and 30 minutes (21%) than at 15 minutes (p=0.013 and p=0.026 respectively).

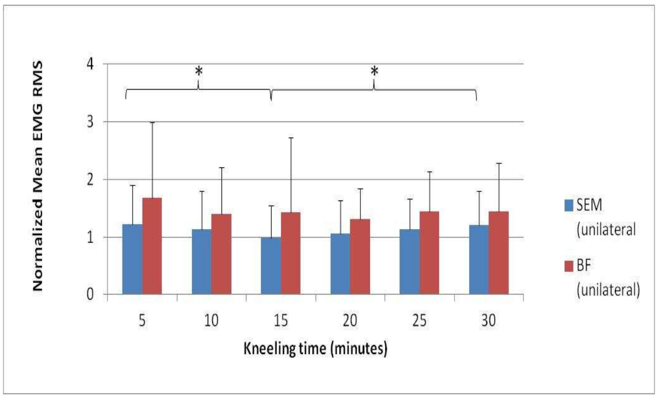

Figure 1: Unilateral knee flexors (SEM and BF) average RMS activity over time, normalized to the first minute of kneeling. *represents statistical significance.

While changes in RMS values for the BF exhibited similar trends over time, the difference was not found to be statistically significant. Similarly, RA activity was 90% higher at 5 minutes than 15 minutes (p=0.006) and 70% higher than at 30 minutes (p=0.046) (Figure 2). Statistically significant changes in muscle RMS were also observed for the ES. The data suggests that kneeling on two legs at 90 degrees of knee flexion over 10-15 minutes starts changing muscle activation patterns, primarily in knee and torso flexor muscle groups.

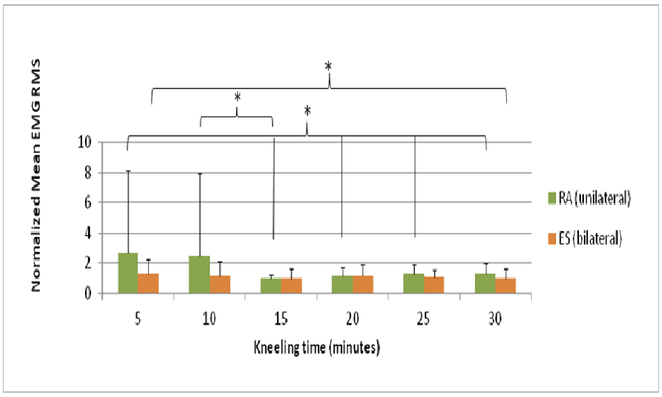

Figure 2: Bilateral torso flexors and extensors (RA and ES) average RMS activity over time, normalized to the first minute of kneeling. *represents statistical significance.

CONCLUSIONS

The main biomarkers, indicating activation pattern changes in response to kneeling on two legs at 90 degrees of knee flexion over 30 minutes were primarily the hamstrings and abdominal muscles. Stabilization of muscles in the lower leg as well as in the quadriceps was evident for the entire period of kneeling. Additional research is needed to determine the specific causes of these changes in activation patterns over time and how these changes might be related to tissue damage that causes kneeling-related disorders.

REFERENCES

1. Holmström, E. B., et al. (1992). *Spine* **17**, 672-677
2. Harkness, E. F., et al. (2003). *Rheumatology* **42**, 959-968.
3. Manninen, P., (2002). *Scandinavian journal of work, environment & health*, 25-32.
4. Gallagher, S., et al. (2009). *Journal of safety research* **40**, 233-237.

SIMULATION TO IMPROVE SURGICAL ARTICULAR FRACTURE REDUCTION SKILLS

Gary T. Ohrt, Geb W. Thomas, Matthew D. Karam, Tameem M. Yehyawi,
Brian O. Westerlind, J. Lawrence Marsh and Donald D. Anderson

The University of Iowa, Iowa City, IA, USA
email: don-anderson@uiowa.edu web: poppy.obrl.uiowa.edu

INTRODUCTION

Orthopaedic surgical skills acquisition during residency training is presently based on an apprenticeship model, with minimal practice outside of the operating room. This model does little to provide uniform training or assure technical competence. In a review of surgical errors, 63.5% of cases involved technical error and 29% included an error in judgment [1]. Both types of errors can be attributed to a lack of experience. Surgical simulation can help address shortcomings in training by ensuring residents the opportunity to (1) practice important procedures not otherwise encountered, (2) practice procedures until competency is achieved, and (3) prevent exposure of live patients to undue risk.

Surgical articular fracture reduction presents a challenging procedure involving a variety of skills needed in orthopaedic surgery. Partly for this reason, a laboratory simulation of the procedure was recently developed [2]. However, the complexity of the task makes it difficult for trainees to improve their skills working with this simulator. The goal of this study was to conduct preliminary assessments of the value of a flexible skills trainer and one-on-one coaching sessions to improve performance on the articular fracture reduction simulator.

METHODS

A simulation of the surgical reduction of a three-fragment tibial plafond fracture that has previously been described [2,3] was used to compare the performance of six first-year orthopaedic residents before (pre-test) and after (post-test) the use of a box skills trainer. A third (retention) test was performed two weeks later following a one-on-one coaching session. The simulator gives residents a 15 minute time window to reduce and fixate the fracture fragments using a standard set of surgical tools and stainless steel K-wires. The residents also use fluoroscopy to help determine the current position of the fragments. The fracture is housed in a surrogate soft tissue foot and ankle model (Sawbones Inc.). Among the changes recently introduced to the simulator, hand motion data were collected using a Polhemus G4 electromagnetic tracking system and the foot and ankle model (formerly homegrown) was produced by Sawbones Inc. and molded directly into the soft tissue model (Fig 1).

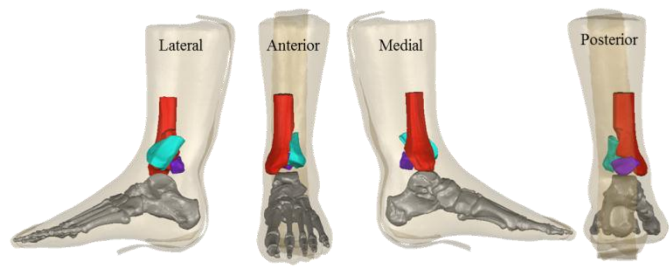

Figure 1: The foot and ankle fracture model used in the simulation is shown schematically in its soft tissue housing.

Data collected and analyzed following the simulation include the number of discrete hand motions and cumulative hand distance traveled, the number of fluoroscopy images (radiation exposure), and an objective structured scoring of performance (OSATS) done by an expert. Multiple angles of video were recorded, including a head-mounted camera (Go Pro Hero3) and multiple wide view angles.

The skills trainer consisted of two video cameras mounted on an aluminum frame. The cameras view a workspace from orthogonal positions: one from 1.5’ above, the second points toward the participant from a position approximately 1.5’ behind the workspace. A screen between the workspace and the participant obstructs the direct view of hand motions in the workspace. This requires the participant to rely on the camera views visible on a monitor placed conveniently nearby to navigate the 3D environment. Several tasks performed in the workspace (described in separate abstract) are used to exercise the trainees’ skills.

The video camera views obtained during the original fracture reduction simulation were edited together with the fluoroscopy images and were used in coaching the residents. The one-on-one coaching session consisted of a traumatologist viewing the videos with the resident in order to discuss surgical technique, proper use of tools (including fluoroscopy), and any other issue or questions that the resident may have had regarding the fracture reduction.

RESULTS AND DISCUSSION

The number of hand motions and distance traveled during the procedure became slightly less variable with each successive trial (Fig. 2), but the change was not significant (Table 1). The difference in the use of fluoroscopy was significant between the pre-test & retention test and the post-test and retention test (Fig. 3). Since the session with the traumatologist occurred immediately prior to the retention test, this would indicate that the one-on-one coaching session had a positive effect on use of fluoroscopy. Higher OSATS scores of performance on the post-test simulation compared to the pre-test suggests that time spent on the box skills trainer led to improved performance. Further performance improvements, as indicated by elevated OSATS scores, followed the one-on-one coaching. This also implies that coaching influenced performance.

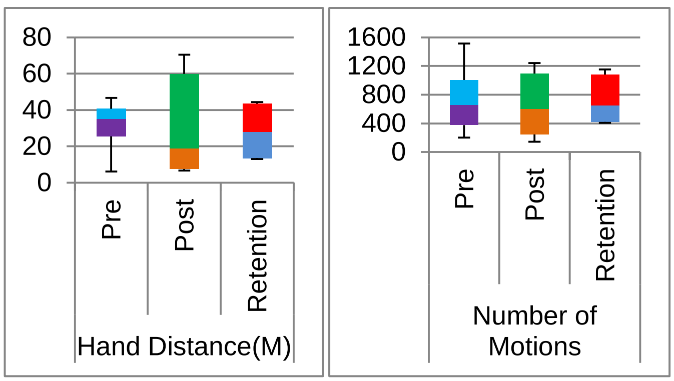

Figure 2: Left- box plot of distance in meters of hand travel during reduction **Right**-box plot of number of discrete hand motions during reduction.

Table 1: Student T-Test significance values for comparison between the three trials (significant results are highlighted.

	mAs	# of images	Distance (m)	# of motions	OSATS
Pre-Post	0.68	0.97	0.88	0.74	0.03
Pre-Ret	0.03	0.04	0.43	0.18	0.01
Post-Ret	0.01	0.01	0.64	0.86	0.14

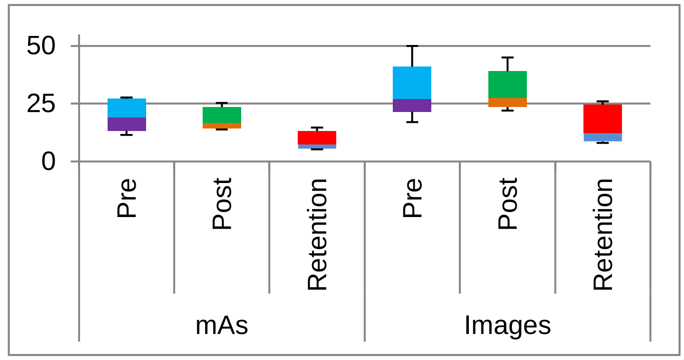

Figure 3: box plot of fluoroscopic data; on left radiation dose in mAs and on right number of images obtained.

CONCLUSIONS

Improvement shown by the residents both in their reduced use of fluoroscopy and improved OSATS scoring showed that the box skills trainer and the coaching provided by a senior traumatologist can be useful in resident education. We believe that this will lead to better trained surgeons; which will improve patient safety and patient outcomes.

REFERENCES

1. Fabri PJ, Zayas-Castro JL. *Surgery*. 2008. 177(1):28-32.
2. Karam MD, et al. *Iowa Orthop J*, 76-82, 2012.
3. Yehyawi TM, et al. *J Bone Joint Surg* [Am] (In Press) 2013.

ACKNOWLEDGEMENTS

This project was funded (in part) by a National Board of Medical Examiners® (NBME®) Edward J. Stemmler, MD Medical Education Research Fund grant and by a grant from the Orthopaedic Trauma Association. The assistance of Mr. Steven Long and Mr. Jon Myers in this work is gratefully acknowledged.

CIRCUMVENTING THIGH SOFT TISSUE ARTIFACT VIA SHANK CLUSTER-REFERENCING OF KNEE JOINT CENTERS

[1,2]Manutchanok Jongprasithporn and [1]Brian Schulz

[1]VA HSR&D/RR&D Center of Excellence in Maximizing Rehabilitation Outcomes,
James A. Haley VA Hospital, Tampa, Florida, USA
[2]Virginia Polytechnic Institute and State University, Blacksburg, Virginia, USA
email: mjongpra@vt.edu

INTRODUCTION

Passive motion analysis using skin markers is the most common method for kinematic analysis. Soft-tissue artifact (STA) is a primary source of error in dynamic task data such as gait, step up/down, and sit-to-stand/stand-to-sit and the greatest of these errors are found for the thigh [1]. During motor tasks, skin markers on the thigh showed larger displacement than using skin markers on the shank [2]. Thus, a marker set that circumvents thigh STA by locating both the knee and ankle joint centers relative to the shank cluster might improve kinematics [3]. Older and more impaired adults tend to have higher body mass index (BMI) and soft tissue than younger adults and might be more susceptible to thigh STA. To accurately quantify STA, invasive or radiographic methods are generally required, but an estimate of differences in STA error might be provided by changes in length of the thigh segment (i.e., distance between knee and hip joint centers), which based on the relatively small displacements of the hip and knee center should not substantially change in length. The purpose of this study is to investigate the effects of subject group and shank/thigh cluster-based references knee joint center on thigh length due to STA propagation. We hypothesize that 1) thigh length based on thigh cluster reference will exhibit greater lengthening, shortening, and range than thigh length based on shank cluster reference and 2) these effects will be greater in older and more impaired adults.

METHODS

Fourteen healthy young (age 26±5, BMI 23.67±3.26 kg/m^2), fourteen healthy older (age 73±7, BMI 27.00±2.15 kg/m^2) and eleven older adults who have fallen in the past 6 months (age 75±6, BMI 30.97±5.82 kg/m^2) participated in this study. Each participant traversed a 4.88m walkway 4 times at the preferred speed. Full-body motion data were recorded using passive markers. Kinematics calculated using previously described methods [3] based on shank and thigh cluster references. Thigh length during walking was calculated for right and left gait cycle events (heel contact to next heel contact of the same leg) using Visual3D. Three dependent variables (DVs) tested were 1) thigh lengthening (the difference between maximum and static thigh length) 2) thigh shortening (the difference between minimum and static thigh length) and 3) thigh range (the difference between maximum and minimum thigh length). A mixed design ANOVA, between-subjects (young x old x fall risk) and within-subject (shank x thigh cluster references) on DVs were performed to test the effects of subject group and cluster reference on thigh lengthening, shortening, and range. Post-hoc comparisons (Tukey's HSD) were performed to identify differences in the effects of different levels of the independent variables. Pearson correlation coefficient was performed to address relationships between DVs and BMI. JMP was used for all statistical analyses and effects were considered significant at $p<0.025$.

RESULTS AND DISCUSSION

Thigh lengthening ($p=0.0123$), shortening ($p<0.001$), and range ($p<0.001$) based on thigh cluster reference were all significantly larger than those based on shank cluster reference (Figure 1). These thigh length errors related to STA propagation could be influenced by locations of marker cluster references. There were significant differences in thigh lengthening ($p<0.001$), shortening (p=0.0007), and range (p=0.0106) between groups (Figure 1). Thigh lengthening in fall risk group was significantly greater than thigh lengthening in young and older. Fall risk group had the highest BMI among all groups. A higher BMI correlated with thigh lengthening based on thigh cluster reference (Figure 2, R^2=0.1805, p=0.0078). In contrast, there was no significant correlation between BMI and thigh lengthening based on shank cluster reference. There was an interaction between subject group and cluster reference on lengthening ($p<0.001$) where fall risk group with thigh cluster reference had greater lengthening than all other conditions.

CONCLUSIONS

Locating knee joint centers relative to thigh clusters results in greater thigh segment lengthening, shortening, and range than locating them relative to shank clusters. These effects increase in subjects with greater BMI or body fat. Shank cluster referencing of knee joint centers may reduce some effects of thigh STA when using skin markers.

REFERENCES

1.Peters A, et al. *Gait & Posture*, 31(1), 1-8

2.Stagni R, et al. *Clin Biomech*, 20(3), 320-9, 2005.

3.Schulz B, et al. *Clin Biomech*, 25, 687-92, 2010.

ACKNOWLEDGEMENTS

VA RR&D Career Development Award (E4941W). We thank Wendy Kimmel and Pradeep Ambati for assistance with data collection and Scott Barnett for statistical support. The contents of this manuscript are those of the authors alone and do not represent the views of the Department of Veterans Affairs or the United States Government.

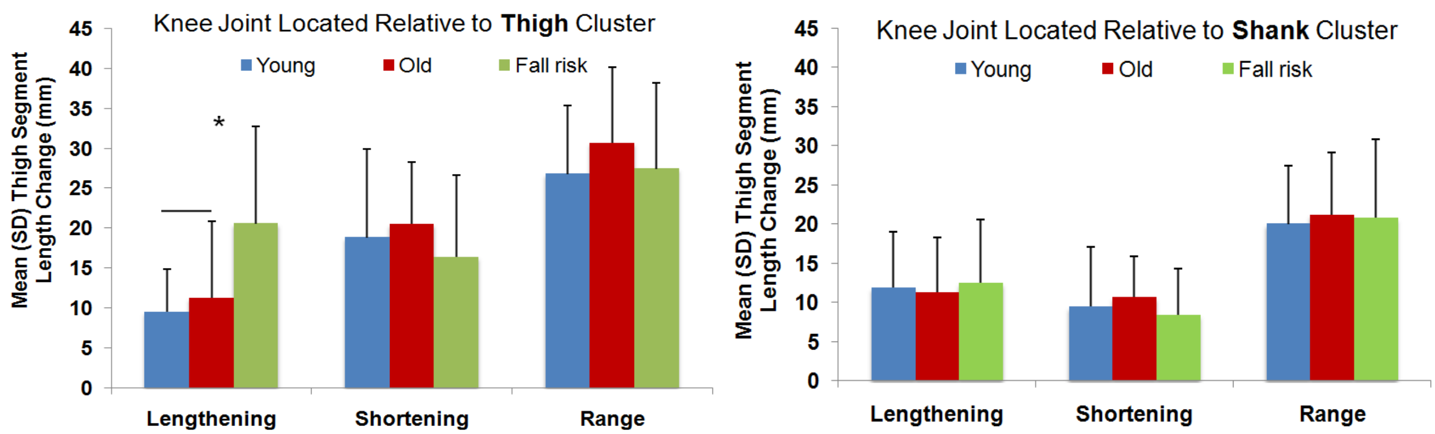

Figure 1: Thigh lengthening, shortening, and range by subject group for thigh cluster reference (left panel) and shank cluster reference (right panel) for knee joint center.

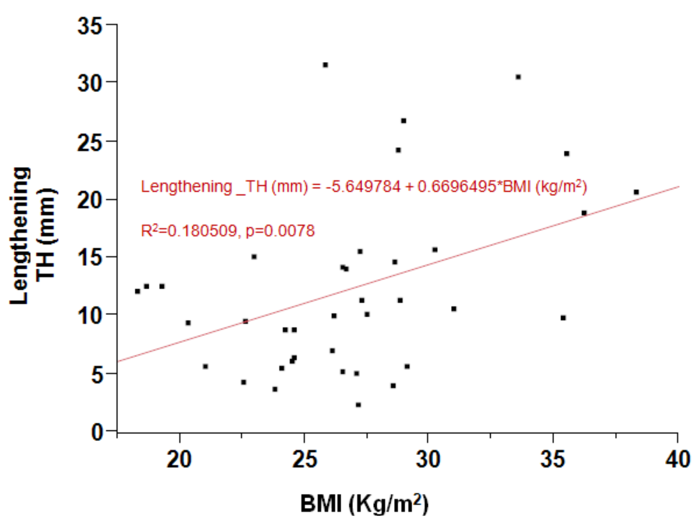

Figure 2: Correlation between body mass index (Kg/m^2) and thigh lengthening based on thigh cluster reference for knee joint center (R^2 =0.1805, p=0.0078).

THE RELATIONSHIP BETWEEN THE STAIR CLIMBING TEST, KNEE EXTENSION STRENGTH, AND PEAK EXTERNAL KNEE FLEXION MOMENT IN PATIENTS AWAITING TOTAL KNEE ATHROPLASTY

Jackie Lewis, Greg Freisinger, Matt Beal, Laura Schmitt, Robert Siston, and Ajit Chaudhari

The Ohio State University, Columbus, OH, USA
email: lewis.1127@osu.edu

INTRODUCTION

Stair climbing is one of the most challenging activities of daily living for an individual with severe osteoarthritis. Clinicians test leg strength and often use the stair climbing test (ascend and descend a flight of stairs as fast as possible) to track the progress of patients [1], with the presumption that patients with a faster stair climbing test (SCT) time have better knee function. Biomechanical studies of stair climbing often focus on the peak external knee flexion moment (pEKFM), which provides an estimate of the demand placed on the quadriceps to climb stairs [2-4]. Previous analyses of lower limb kinematics and kinetics during stair climbing have shown that osteoarthritic patients have lower pEKFMs when compared to healthy controls due to quadriceps avoidance mechanisms such a forward trunk lean [5]. Although the poor knee extension strength, slow SCT times and low pEKFMs have been linked to patients with severe osteoarthritis, to our knowledge no one has ever investigated the relationship between standard clinical tests and knee biomechanics. Therefore, the purpose of this study was to test the hypothesis that faster SCT time will be positively associated with greater knee extension strength and greater pEKFMs during stair ascent in individuals with knee osteoarthritis.

METHODS

Twelve subjects (4 males age=60.5±8.0y, ht=1.77±0.03m, wt=95.6±14.0kg; 8 females age=60.5±4.7y, ht=1.61±0.06m, wt=87.1±9.1kg) awaiting a total knee arthroplasty provided IRB to participate.

Each subject performed the clinical SCT (climb and descend a 12-step staircase as fast as possible (seconds), using a handrail if necessary), an isometric knee extension strength test at 60° of flexion (peak torque normalized by body mass)(System 3; Biodex, Inc.; Shirley, NY), and 8 stair ascent trials in our movement analysis laboratory.

Reflective markers were placed using a modified point cluster technique [6] on the femur and tibia segments to determine knee kinematics. 3D marker data were captured with 10 cameras at 150 Hz (Vicon MX-F40; OMG plc; Oxford, UK) and kinetic data from a three-step instrumented stair case (tread width: 10”, step height: 8”), custom designed with two steps attached to force plates (FP-4060; Bertec, Inc.; Columbus, OH) embedded in the floor, were collected at 1500 Hz.

Marker and force data were filtered with fourth order low-pass Butterworth filters at a cutoff frequency of 6 Hz and 12 Hz, respectively, to minimize skin artifact and artifacts due to resonance of the staircase structure. Inverse dynamics were calculated using custom Bodybuilder (Vicon; OMG plc; Oxford, UK) and Matlab scripts. pEKFM was normalized to a percentage of body weight times height..

The Spearman rank-order correlation coefficient was used to test the association between the pEKFM of the involved limb, the SCT time and knee extension strength of the involved limb.

RESULTS AND DISCUSSION

The average SCT times, peak external knee flexion moments during ascent of the involved limb and knee extension strength of the involved limb are shown in Table 1. The results supported the hypothesis in that individuals with a faster SCT time had greater knee extension strength (-0.81,

$p<0.05$). However, there was no association between pEKFM with SCT time or knee extension strength (Table 2), which did not support the hypothesis.

Table 1: Variable Average ± Standard Deviation

SCT (seconds)	pEKFM (% BWxHt)	Strength (Nm/kg)
24.69 ± 12.763	4.5 ± 1.1	1.03 ± 0.321

Table 2: Spearman Rank-Order Correlation Coefficients between the variables

	SCT time vs. pEKFM	SCT time vs. Strength	Strength vs. pEKFM
ρ	0.01	-0.81*	-0.07

* P < 0.05

The association between the SCT time and the knee extension strength suggests that more knee extension strength is needed to climb stairs faster. The lack of an association between pEKFM and extension strength suggests that in this population with end-stage osteoarthritis of the knee, pEKFM is not limited by quadriceps strength. However, this is consistent with our previous observation that pEKFM does not increase with increasing stair climbing speed [7], which is different from level ground walking [8].

We did not test uninjured individuals in this study, but compared to values in the literature, participants in this study had lower knee extension strength, lower pEKFM values and slower SCT times compared to healthy individuals, which is consistent with previous studies [2,5]. The lack of relationship between pEKFM and the other variables may be related to differences in task demands. These subjects may be employing a compensation strategy to reduce demand on the quadriceps during the short three-step climb in the laboratory, while they cannot avoid using the quadriceps during the isometric extension strength test or the timed SCT.Also, some patients used the handrail to climb and descend stairs, so they may be using more upper body strength to pull themselves up and lower themselves down the staircase.

There were several limitations to this study. The SCT time includes ascending as well as descending a full flight of stairs, and this was compared to the pEKFM during just ascent on a three-step staircase. Also, during the SCT, the patients are allowed to step one stair at a time, using only their uninvolved leg, while they are forced to go stair-over-stair when climbing the 3-step staircase in the motion capture volume. The lack of relationship may also be due to other biomechanical factors such as knee flexion angle, ground reaction force, or muscle activation patterns that were not analyzed in this analysis.

CONCLUSIONS

The results of this study suggest the necessity to reevaluate the relevance and meaning of estimating pEKFM in osteoarthritic patients during stair climbing, as it does not seem to change with stair climbing speed and was not correlated with knee extension strength. Further investigation of muscle activations, and other biomechanical variables such as knee flexion angle and ground reaction forces is necessary to make conclusive correlations between clinical tests and biomechanical measurements.

REFERENCES

1. Mizner RL, et al. *J of Orthopaedic and Sports Physical Therapy* **35.7**, 2005.
2. Andriacchi TP, et al. *J Bone Joint Surg Am* **62.5**, 1980.
3. Costigan PA, et al. *Gait and Posture* **16.1**, 2002.
4. Protopapadaki A, et al. *Clinical Biomechanics* **22.2**, 2007.
5. Asay JL, et al. *J of Orthopaedic Research* **27.3**, 2009.
6. Andriacchi TP, et al. *J of Biomechanical Engineering* **120.6**, 1998.
7. Lewis JM, et al. GCMAS 2013.
8. Andriacchi TP, et al. *Biomechanics of normal and pathological human articulating joints*, 1985.

ACKNOWLEDGEMENTS

Funding for this study came from award number R01AR056700 from the National Institute of Arthritis and Musculoskeletal and Skin Diseases.

Angular Momentum and Thorax-Pelvis Coordination in Walking

[1,2] Jennifer L. Baird, [2] Brian R. Umberger, [2] Joseph Hamill, [2] Richard van Emmerik

[1] St. Ambrose University, Davenport, IA, USA
[2] University of Massachusetts Amherst, Amherst, MA, USA
email: bairdjenniferl@sau.edu

INTRODUCTION

Transverse plane thorax-pelvis coordination becomes more out-of-phase as walking speed increases. It has been suggested that this coordination pattern is important for angular momentum control [1]. Since transverse plane angular momentum is primarily generated by the arms and legs, thorax-pelvis coordination should be related to arm swing. However, the relationship between arm swing and coordination, and the effects on angular momentum are unknown. Older adults demonstrate more in-phase thorax-pelvis coordination compared to young adults [2], which may be related to differences in angular momentum between young and old. The purpose of this study was to investigate the relationship between thorax-pelvis coordination and angular momentum of the arms in young and older adults.

METHODS

Ten young (23.3 years, SD 3.4 years) and ten older (69.6 years, SD 5.1 years) adults provided informed consent. Retroreflective markers were placed over the entire body to create a 13 segment full-body model. Subjects walked on a treadmill starting at 0.4 m/s, with speed increased every 60 s up to 1.8 m/s or the subject's fastest comfortable walking speed. Data were collected for 30 s at each speed. All young adults walked at all speeds, while 7 older adults walked at 1.6 m/s and 4 walked at 1.8 m/s.

Angular momentum was calculated for each individual segment and then summed for all segments according to:

$$H = \sum_{i}^{13}\left(I_i\omega_i + \left[m_i\dot{r}_i \times r_i\right]\right)$$

where H is the angular momentum, I_i is the inertia tensor, ω_i is the angular velocity, m_i is the segment mass, r_i is the position vector of the segment center of mass relative to the whole body center of mass, $\dot{r}_i$ is the time derivative of r_i and × is the cross product. To reduce variability due to differences in subject height and mass, angular momenta (kg•m^2/s) were scaled by subject mass (kg), center of mass height (m) and walking velocity (m/s), resulting in dimensionless values. The mean segmental contribution of the arms as a percentage of whole body angular momentum was calculated for each of 12 strides. Strides were determined from right heel strike to right heel strike, time normalized to the full gait cycle, and averaged over the strides. The range of upper, lower and whole body angular momentum was also calculated to get a more general idea of the distribution of angular momentum throughout the body.

Coordination was measured by continuous relative phase (CRP). CRP was calculated from normalized phase planes as the difference between the phase angles of the thorax and pelvis. CRP values range from 0° (in-phase) to 180° (anti-phase), where 180° was subtracted from all CRP angles between 180° and 360°. The mean CRP value of each stride was calculated. Reported values are the mean CRP of the twelve strides.

A two-way, mixed-model repeated measures ANOVA (2 age × 6 speed) was used to analyze angular momentum and CRP (SAS 9.2, Cary, NC, USA). Only speeds with data for all subjects were analyzed (up to 1.4 m/s), although the figures present data for all speeds. A covariance analysis was used to assess the relationship between thorax-pelvis CRP and the segmental contribution of the arms to angular momentum.

RESULTS AND DISCUSSION

The segmental contribution of the arms to whole-body angular momentum was greater in older adults compared to young at speeds of 0.6–1.0 m/s (interaction speed by age: $p<0.05$, Figure 1). Upper, lower and whole body angular momentum range all decreased with speed ($p<0.0001$ for all, Figure 2). The range of whole-body angular momentum was less in the older adults at speeds of 0.4-0.8 m/s (interaction speed by age: $p<0.01$, Figure 2).

Continuous relative phase became more out-of-phase with increasing speed for both groups ($p<0.0001$, Figure 1). The CRP was more out-of-phase for the young adults compared to the older adults at all speeds ($p<0.05$). Analysis of covariance revealed that there was no relationship between the continuous relative phase and mean segmental contribution of the arms to whole-body angular momentum ($p>0.05$).

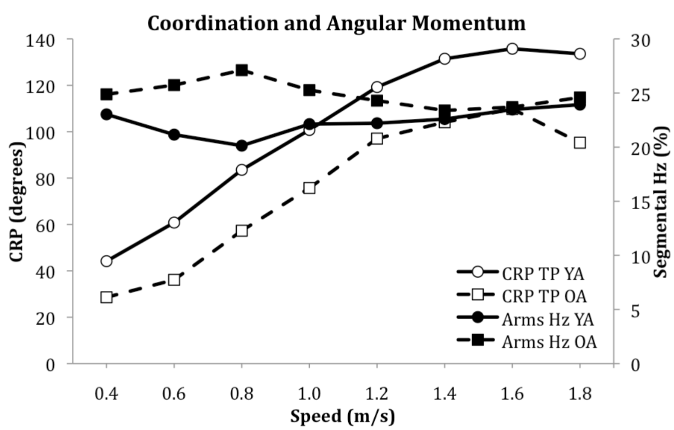

Figure 1: Relationship between continuous relative phase (CRP, primary axis) and segmental contribution of arms to whole body angular momentum (secondary axis) in young (YA) and older adults (OA). Hz = transverse plane angular momentum.

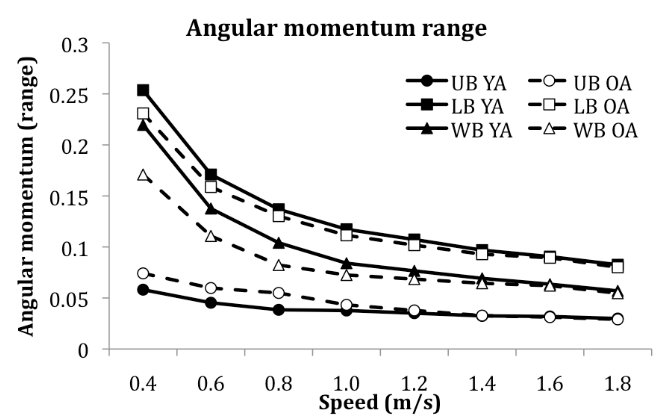

Figure 2: Angular momentum range for the upper body (UB), lower body (LB) and whole body (WB) in young (YA) and older (OA) adults across all walking speeds.

The segmental contribution of the arms to whole-body angular momentum was greater in the older adults than in the younger at slower walking speeds. Arm swing amplitudes would affect angular momentum. Although arm swing was an average of 4° greater in older adults at these slower speeds, this difference was not significant. Interlimb arm coordination may also affect angular momentum. At slower walking speeds, many people swing the two arms in-phase at twice the frequency of the legs [3]. This 2:1 pattern would decrease the angular momentum of the arms. Half of the young adults demonstrated a 2:1 arm to leg swing pattern, but only at the two slowest walking speeds. None of the older adults showed in-phase arm coordination. Finally, the greater segmental angular momentum of the arms in the older adults may be due to the smaller whole body angular momentum in light of no differences in upper body angular momentum.

The observed changes in CRP across speed and with age were expected based on previous research [2]. While CRP changed consistently across speeds, angular momentum of the arms did not. The results from the analysis of covariance support the lack of relationship between thorax-pelvis coordination and segmental arm angular momentum.

CONCLUSIONS

Differences in coordination between the young and older adults were accompanied by changes in angular momentum that depended upon speed, yet there was no clear relationship between coordination and angular momentum across all speeds. While arm and leg swing do result in a 'balance' or offsetting of upper and lower body angular momentum [4], it appears that this is not directly dependent upon thorax-pelvis coordination.

REFERENCES

1. Stokes VP et al. *J Biomech,* **22**, 43-50, 1989.
2. Van Emmerik REA et al. *Gait & Posture,* **22**, 233-239, 2005.
3. Wagenaar RC & van Emmerik REA. *J Biomech,* **33**, 853-861, 2000.
4. Herr H & Popovic M. *J Exp Biol,* **211**, 467-481, 2008.

IMPACT OF TOTAL MENISECTOMY ON TIBIAL PLATEAU CONTACT FORCES, FEMORAL CARTILAGE STRESS LEVEL & CRUCIATE LIGAMENT FORCES IN PASSIVE KNEE FLEXION

Sohaila El Sagheir and Kodjo Moglo

Department of Mechanical and Aerospace Engineering
Royal Military college of Canada, Kingston, Canada,
email: sohaila.el-sagheir@rmc.ca

INTRODUCTION

Cartilage degeneration in the knee joint is mainly caused by elevated stress level and high contact forces resulting from total meniscectomy procedures [1]. Statistics showed that among patients who had meniscectomy surgeries, 14.1% of men & 22.8% of women over 45 years show symptoms of Osteoarthritis (OA) which treatment costs around $185.5 billion in USA annually [2]. Previous studies lacked a full comparison between fully meniscectomized and intact knee joint during passive flexion. The objective of this study is to create a validated F.E. knee joint model that mimics biological behavior in order to predict results of complex scenarios and be used to provide full comparison of the above-mentioned cases. Parameters of interest are Von Mises (VM) stress, axial contact force, contact pressure and cruciate ligaments forces, In this study, the same passive knee joint model was analyzed under two scenario conditions:(1) Menisci Intact (control), (2) Total meniscectomy;(flexion 0-60 deg.) Only tibio-femoral joint was considered.

METHODS

A Finite Element knee joint model was constructed based on MRI scans of the right knee (Male:45 yr-70 kg) which were used to extract the 3D geometry of the knee joint model. The 3D geometry of the skeletal knee was built using Mimics and Abaqus software. Articular cartilages and menisci were considered to behave as linear elastic isotropic as reported in the literature [3]. Ligaments were modeled as springs which have an elastic nonlinear behaviour [4]. Since bone stiffness is much higher than soft tissues, bones are modeled as rigid bodies represented by a reference node and meshed with tetrahedral elements. Menisci and cartilages were meshed with 8 node hexahedron elements. Frictionless non-linear contact with finite sliding was assumed in all articulations. Boundary conditions were set to fix tibia & fibula in all D.O.F. Flexion was applied to the femoral reference node to flex in range (0-60) degrees.

RESULTS AND DISCUSSION

More load-bearing was noticed on the medial compartment in intact model which agrees with previous studies [5], while it shifted to lateral compartment in meniscectomy model. Results of axial contact forces on tibial plateau in intact case (Table 1) agreed with experimental validated results reported in previous study [6]. In case of meniscectomy, model predicted results showed a substantial increase of axial contact forces on the tibial plateau compared with the menisci intact case (Figure 1). Higher VM stress level values on femoral cartilage resulted in case of meniscectomy (Figure 2), results were within range of those reported in a previous experimental and numerical validated study [7] (Table 1). At 15 degrees of flexion, minor difference was noticed, however stress level started to ramp up at 30, 45 and 60 degrees flexion (Table 1) For cruciate ligaments forces, the model results of intact case were also validated with results reported in previous studies [4], in case of meniscectomy, much higher PCL forces were noticed compared to menisci intact case (Figure 3). Model predicted results of PCL forces in meniscectomy were (42N), (144N), (250N) and (424)N at 15, 30, 45 and 60 degree flexion respectively. ACL forces in case of meniscectomy were almost twice the value of the intact model between 0 and 15 degree flexion, then both values matched at higher flexion angles (almost zero force) which agrees with ACL curve pattern reported in previous studies [4] (Figure 4).

Table 1: Axial Contact Forces on tibial plateau and VM stress on femoral cartilage vs flexion in Menisci Intact and Meniscectomy

Flexion (Deg)	Axial Contact Force on Medial cartilage (N)			Axial Contact Force on Lateral cartilage (N)			VM stress on femoral cartilage (MPa)	
	Uncovered	Covered	Meniscectomy	Uncovered	Covered	Meniscectomy	Intact	Meniscectomy
30	313	100	915	190	95	1360	1.2	1.7
45	365	80	1040	140	60	1588	1.3	2.2
60	278	40	800	100	45	1618	1.68	2.2

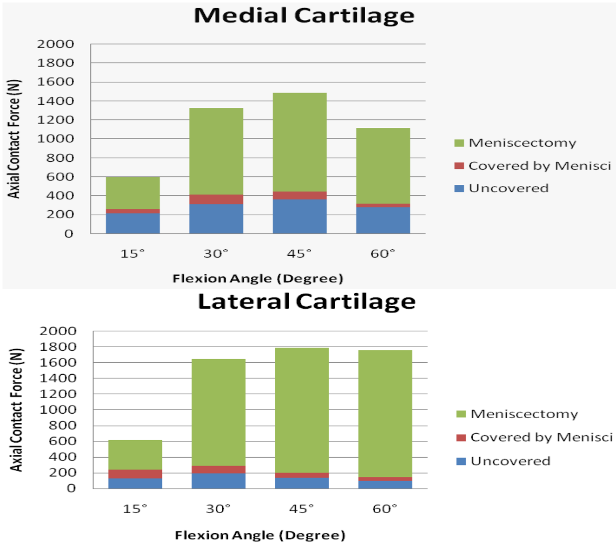

Figure 1: Axial contact forces on tibial plateau: Covered (via Menisci), uncovered (via cartilage) and complete Meniscectomy vs Flexion angles

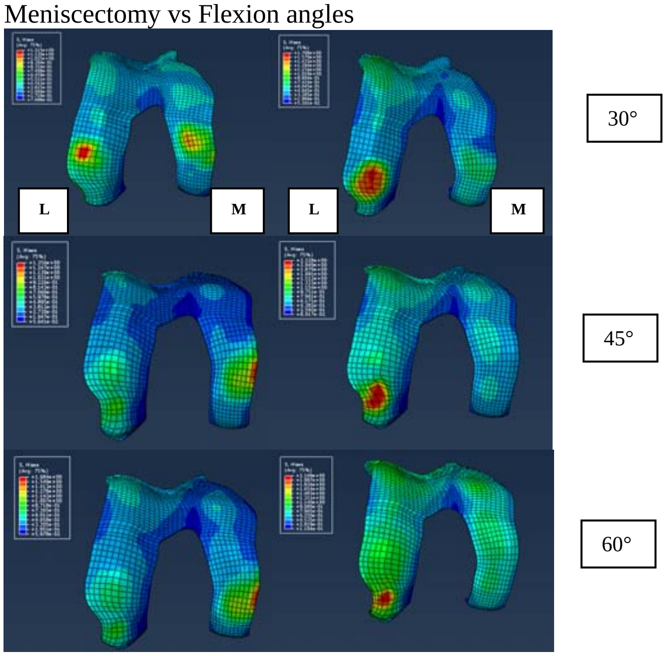

(a) Intact **(b) Meniscectomy**

Figure 2: VM stress on lateral (L), medial (M) femoral-compartments vs flexion (a) menisci intact. (b) meniscectomy.

Maximum contact pressure values on femoral cartilage were 3, 3.3 and 5.2 MPa (intact) versus 4.6, 6.4 and 7 MPa (meniscectomy) at 30, 45 and 60 degrees flexion respectively. Values of contact pressure were validated and agreed with experimental results of frozen cadaver knees under flexion testing as reported in study [8]

CONCLUSIONS

Total meniscectomy resulted in much higher cruciate ligaments forces, higher contact pressure, stress level on femoral cartilage and higher axial contact force on tibial cartilages in all analysis processed. The elevated values of contact force and VM stress on cartilages due to meniscectomy indicate higher cartilage degeneration risk, which promotes OA. Role of menisci in load bearing and shock absorption was highlighted when comparing covered, uncovered vs meniscectomy tibial cartilage axial contact force values (Figure1). It is interesting to notice that during flexion of meniscectomized model, more stress level was concentrated on the lateral compartment of femoral cartilage which shows a shift in loading than the intact model (concentrated on medial compartment), which recommends further investigation. Higher cruciate ligament forces indicate tear risk and instability of the joint. Total meniscectomy remains the most disrupting condition for the knee joint and is clinically recommended to be avoided as a fast treatment of meniscal injury.

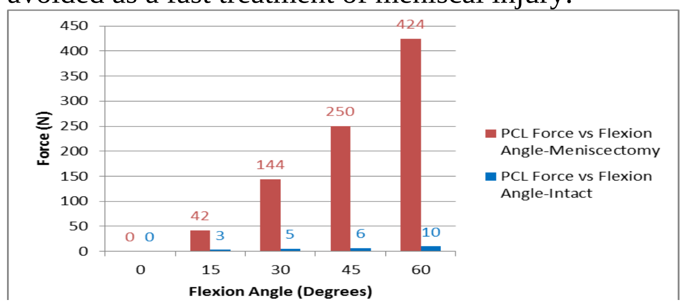

Figure 3: PCL forces vs flexion angle-Intact & Meniscectomy

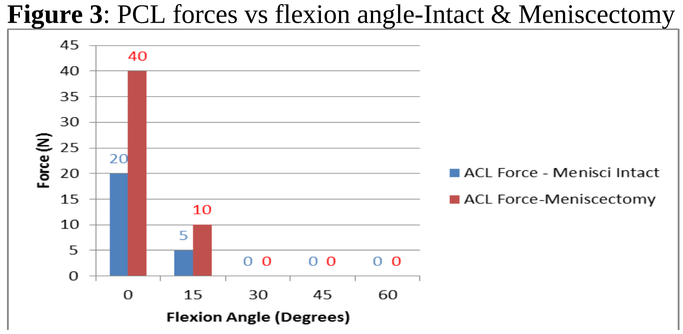

Figure 4:ACL forces vs flexion angle-Intact & Meniscectomy

REFERENCES

1. Clements KM, Burton-Wurster N, and Lust G, 2004. The spread of cell death from impact damaged cartilage: lack of evidence for the role of nitric oxide and caspases. OA Cartilage 12:577–585.
2. Chaoe et al. Managing OA: A multidisplinary approach. *The Journal of Musculoskeletal Medicine* Vol-27 No 10 (2010).
3. Pena B, et al. 3D FE. Analysis of the combined behaviour of ligaments & menisci in healthy human knee joint. *Journal of Biomechanics* 39, 1686-1701 (2006).
4. Mesfar W, et al. Biomechanics of the knee joint in flexion under various quadriceps forces. *The Knee* 12 424-434 (2005).
5. Shirazi A, et al. Biomechanical response of the passive knee joint under AP forces, *Clinical Biomechanics*, vol 13, 625-633 (1998).
6. W. Mesfar, A. Shirazi-Adl. Knee joint biomechanics in open kinetic chain flexion exercises *Clinical Biomechanics*, Volume 23, Issue 4, May 2008, Pages 477-482
7. Carpanen D. et al, The Effects of Partial Meniscectomy on Knee Joint Contact Stresses : A Finite Element Study. Angelia Ruskin University.
8. Robert Allaire et al, Biomechanical Consequences of a tear of the posterior root of medial meniscus, similar to total *The Journal of Bone & Joint Surgery*, Volume 90, Issue 9 (2008).

ACKNOWLEDGMENTS

This work is supported by Academic Research Program (ARP).

THE RELIABILITY OF ULTRASOUND IN OBTAINING SUBJECT-SPECIFIC PARAMETERS

Josh Leonardis, Patrick Rider, Jordan Black, Tony Kulas, & Zachary Domire

[1]Biomechanics Laboratory, Department of Kinesiology, East Carolina University, Greenville, NC
email: leonardisj10@students.ecu.edu, web: http://www.ecu.edu/cs-hhp/exss/biomechlab.cfm

INTRODUCTION

The accurate measurement of moment arms is critical for better understanding muscle function (1-4, 7-8). Moment arms help to describe musculotendon unit length changes, which allows for the estimation of muscle forces. Additionally, when combined with muscular forces, moment arms facilitate the generation of joint torques, making them essential to movement production.

Traditionally, moment arm measurements are obtained from cadavers where findings are often difficult to translate to the living human, or in vivo using expensive and commonly inaccessible imaging methods such as magnetic resonance imaging (3-4). Currently, portable diagnostic ultrasonography has been identified as an alternative imaging method, increasing the accessibility of subject-specific parameters and making the development of models more realistic and applicable (1, 3-6).

Ultrasound has been successfully used to obtain moment arm measurements of the tibialis anterior, gastrocnemius, soleus, and biceps brachii muscles, among others, with low variability between measurements and accuracy comparable to that of traditional methodology (1- 3-4). This technique, however, has not been tested using quadriceps musculature.

METHODS

Four healthy young adults (2 men and 2 women) volunteered for participation. Their (mean ± SD) height, weight, body mass index, and thigh length are detailed below (**Table 1**.).

Table 1: Participant characteristics

Subject	Height (m)	Weight (kg)	BMI (kg/m^2)	Thigh Length (cm)
1	1.70	75	25.9	46
2	1.63	52.3	19.8	44
3	1.65	56.8	20.8	45
4	1.80	86	26.6	47

Upon their arrival, and following a description of the procedure and associated risks, each participant gave their written consent.

Volunteers were then positioned sitting upright, with their right leg secured to a HUMAC NORM isokinetic dynamometer (CSMi, Stoughton, MA). The dynamometer head and seat position were adjusted individually for each subject and range of motion was set at anatomical zero and 105° of knee flexion. The dynamometer moved each participant's knee through a full range of motion twice, beginning and terminating in full extension. Using an Aixplorer ultrasonography unit (Supersonic Imagine, Aix-en-Provence, France), a video of the junction between the rectus femoris and patellar tendon was captured during the change in joint position.

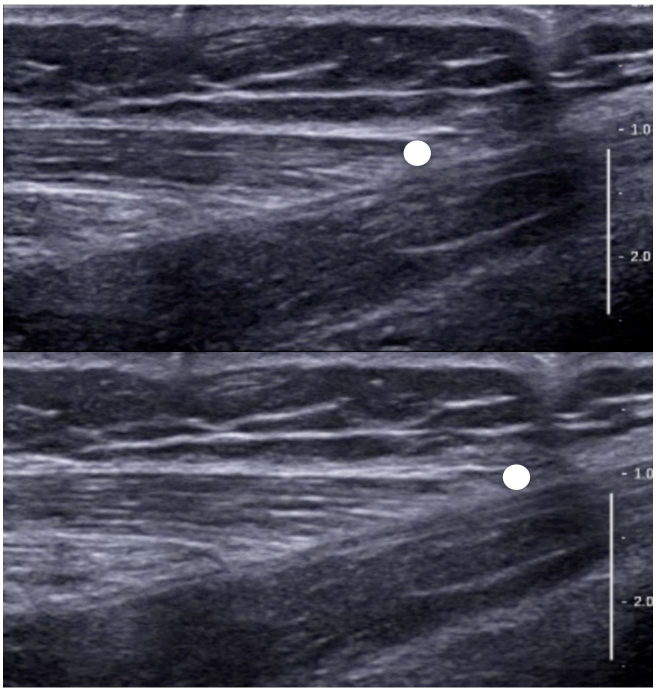

Figure 2: Example of tendon excursion methodology (Distal location marked with dots)

Moment arms (d_m) were determined using the tendon excursion method (**Fig. 2**). This technique fits a measured displacement of the tendon or muscle fiber (d_l) over the analogous angular displacement of the joint (d_θ), using:

$$(d_m) = (d_l) / (d_\theta)$$

By using the frame rate (20 Hz) that the ultrasound measurement was obtained at and the passive angular velocity (5°/s), we were able to track the distal end of the rectus femoris through a full range of motion measuring its displacement every 40 frames, or 10°.

RESULTS AND DISCUSSION

Our ultrasound-obtained rectus femoris moment arms were similar to values from the literature in pattern but were consistently shorter (**Fig 2**.). The longest moment arms were obtained at or near full knee extension while the shortest were measured at full flexion.

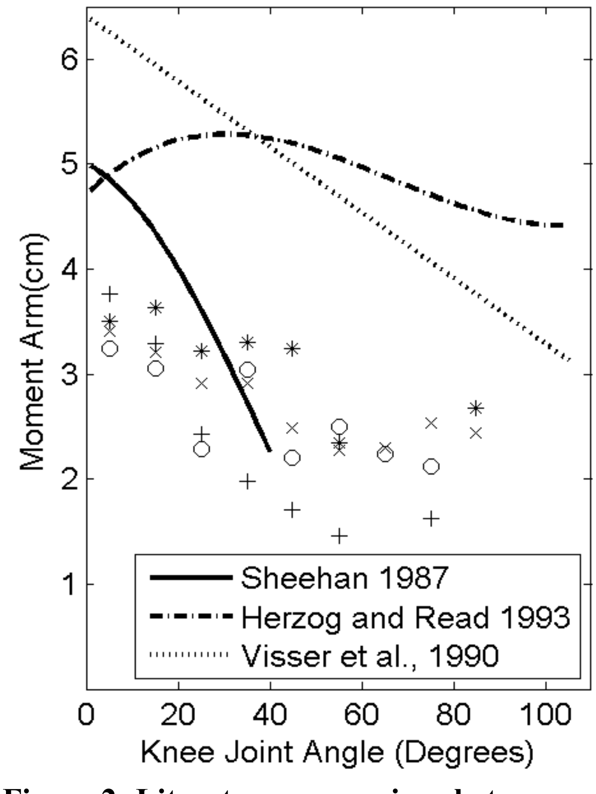

Figure 2: Literature comparison between patellar tendon (Sheehan) and rectus femoris (Herzog and Visser) moment arms.

No relationship existed between peak moment arm length and participant height or thigh length (**Fig. 3**).

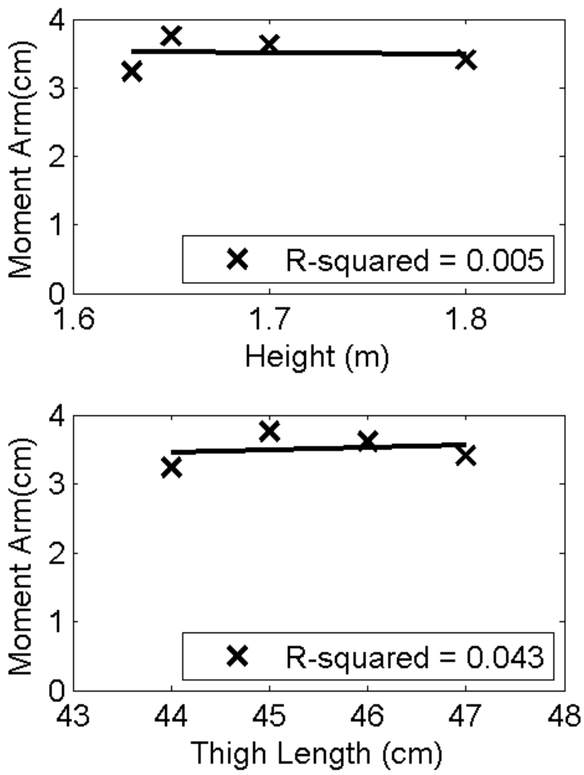

Figure 3: Subject heights and peak moment arms

CONCLUSIONS

The results of this study highlight the need for subject specific muscle moment arm determination, as in our subjects, there was no relationship between moment arm and either height or segment length. Ultrasound appears to be an appropriate imaging methodology for the acquisition of subject-specific quadriceps moment arms. However, future work is needed to determine if there is a systematic error that results in an under estimated moment arm length.

REFERENCE

1.Fath F, et al. *J Appl Phys* **109**, 1644-1654, 2010
2.Herzog W, et al. *J Anat* **182**, 213-230, 1993
3.Ito M, et al. *J Biomech* **33**, 215-218, 2000
4.Li L, et al. *Eng in Med & Bio*, 27th Meeting, 2005
5.Morse CI, et al. *J Appl Phys* **100**, 267-274, 2007
6.Reeves ND, et al. *J Appl Phys* **91**, 116-118, 2004
7.Sheehan FT, *J Biomech* **40**, 1968-1974, 2007
8.Visser JJ, et al. *Eur J Appl Phys* **61**, 453-460, 1990

MUSCLE ACTIVATION CHANGES IN RESPONSE TO ORTHOTIC ANKLE CONSTRAINT DURING WALKING

Christopher Hovorka, Jaemin Sung, Kathryne Eckert, Robert Gregor, Young-Hui Chang
School of Applied Physiology, Georgia Institute of Technology, Atlanta, GA, USA

email: chris.hovorka@ap.gatech.edu, web: http://www.ap.gatech.edu/Chang/Lab/CNL/home.html

INTRODUCTION

There is a dearth of information regarding the control of motion by lower limb orthoses and the elicited muscle activation changes in healthy and pathological populations. Long term constraint of lower limb motion (i.e., wearing a cast or motion constraining orthosis as fracture treatment) reveals muscle atrophy after several weeks [1]. Short term use of external power assist lower limb orthoses during walking suggests muscle activation decreases with continuous stepping to reduce feedback error [2]. Since the majority of prescribed lower limb orthoses constrain lower limb motion passively [3], we aim to better understand elicited muscle responses to conventional non-powered orthoses.

We hypothesized that using a unilateral ankle foot orthosis (AFO) that constrains right ankle motion will decrease muscle activation of right tibialis anterior and right soleus during the stance phase of gait when compared to walking with no constraint.

METHODS

Three healthy subjects (2 male, 1 female, mean age 20.93 ± 0.27 yr, mean weight 66.96 ± 5.44 kg) gave written informed consent and walked on an instrumented dual-belt treadmill at a comfortable speed (1.32 ± 0.08 m/s) in three conditions: use of footwear (control), use of right unilateral ankle foot orthosis-footwear combination (AFO-FC) with no ipsilateral ankle constraint (PFDF) and use of a right unilateral AFO-FC with maximal ipsilateral ankle constraint (PSDS). During the first visit, subjects were fit by a certified orthotist with custom designed footwear and a right ipsilateral AFO-FC and then briefly walked on the dual belt treadmill to identify comfortable walking speed. On the second visit, each subject walked at a comfortable speed for 15 minutes followed by 6 minutes seated rest between conditions. An initial control condition was followed by randomized order of AFO conditions. Kinematics, kinetics and EMG for 8 muscles were collected independently for each limb and synchronized as subjects walked on a custom dual-belt instrumented treadmill (1,080Hz, AMTI, Watertown, MA). Simultaneous kinematics data were captured using a 6-camera motion analysis system (120Hz, Vicon, Oxford, UK) and surface EMG (sEMG) data were collected using a wireless system (1,500Hz, Noraxon USA Inc. Scottsdale, AZ). Raw kinetics data were processed (filtered) and analyzed to determine stance and swing phases of the gait cycles. Each subject's lower limb was prepared for installation of adhesive bipolar surface electrodes in accordance with recognized procedures [4]. Raw sEMG data for the right and left tibialis anterior and soleus muscles were processed and are displayed in Figures 1-2. Muscle activation output was analyzed as the integrated area within the enveloped data that exceeded resting threshold (iEMG). To rule out muscle fatigue effects, a power spectrum analysis of the raw EMG data was performed using fast Fourier transformation and median frequency analysis [5].

RESULTS AND DISCUSSION

Fatigue analysis revealed no fatigue in tibialis anterior (TA) or soleus (SOL) muscles for the control, PFDF or PSDS conditions throughout the protocol. All conditions where the ankle was not constrained, i.e., control, PFDF, contralateral leg, showed similar TA and SOL muscle activation (Figures 3 and 4). In contrast, substantial reductions were observed in TA and SOL muscle activity immediately upon constraint of ankle motion (PSDS), which were sustained throughout the 15 minutes of walking.

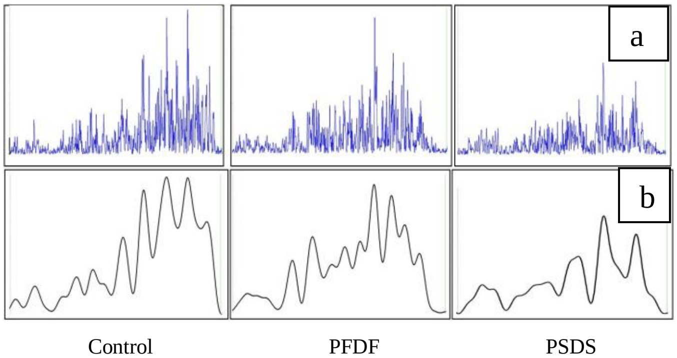

Figure 1: EMG data from a representative subject's right soleus muscle during stance phase of minute 9 to each condition (control, PFDF, and PSDS). Figure 1a shows the raw data after voltage offset adjustment and rectification, and Figure 1b shows the data after filtering.

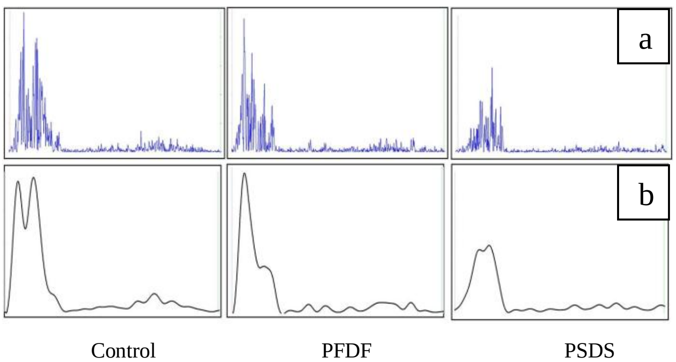

Figure 2: EMG data from a representative subject's tibialis anterior muscle during stance phase of minute 9 in each condition (control, PFDF, and PSDS). Figure 2a shows the raw data voltage offset adjustment and rectification, and Figure 2b shows the data after filtering.

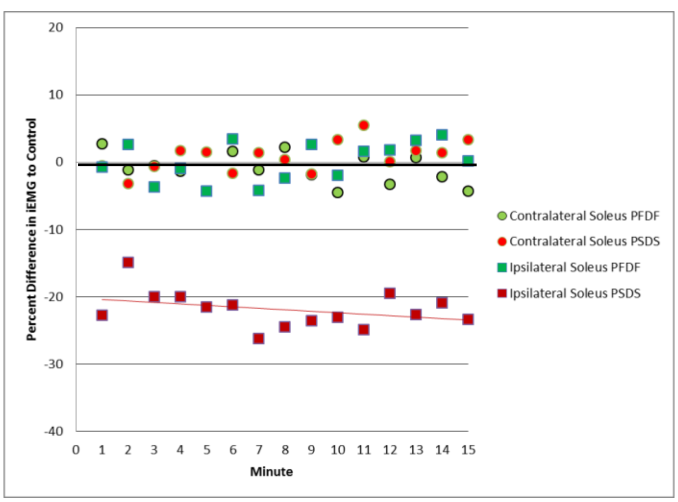

Figure 3: Soleus muscle activation (% difference) across all subjects' right and left legs in response to the conditions PFDF and PSDS. Contralateral soleus PFDF muscle output is -1.02 ± 1.34 %, contralateral soleus PSDS muscle output is 0.78 ± 1.25 %, ipsilateral soleus PFDF muscle output is -0.39 ± 1.97 %, and ipsilateral soleus PSDS muscle output is -22.11 ± 1.58 %.

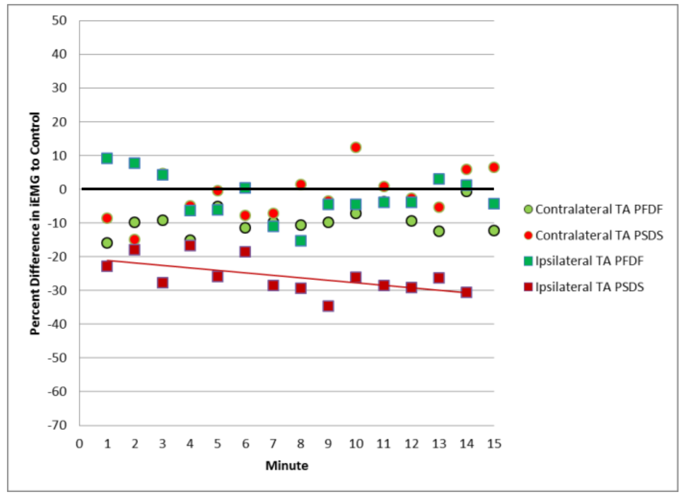

Figure 4: Tibialis anterior muscle activation (% difference) across all subjects' right and left legs in response to the conditions PFDF and PSDS. Contralateral TA PFDF muscle output is -10.14 ± 2.77 %, contralateral TA PSDS muscle output is -2.18 ± 4.19 %, ipsilateral TA PFDF muscle output is -2.18 ± 3.71 %, and ipsilateral TA PSDS muscle output is -25.50 ± 3.42 %.

CONCLUSIONS

Muscle activation (iEMG) of ipsilateral TA and ipsilateral SOL elicited a reduction in response to PSDS. The immediate decrease in muscle activity of these ankle muscles may be explained by a feedback control mechanism responding to a reduction of muscle length change with joint constraint. Increasing the sample size and additional investigation is planned to clarify the cause of muscle activation changes to orthotic constraint of ankle motion during walking.

REFERENCES

1. Appell HJ. *Sports Med* **10**, 42-58, 1990.
2. Reinkensmeyer DJ, et al. *IEEE EMBS*, 2009.
3. Gao F, Bedard B. *AAOP Annual Scientific Symposium*, 2013.
4. Stegeman DF, Hermens HJ. European recommendations for surface EMG (SENIAM), 1999.
5. Dingwell JB, et al. *IEEE Trans BME* **55**, 2666-2674, 2008.

ACKNOWLEDGEMENTS

This work was financially supported by the Center for Learning/Evidence Based Outcomes EBP-043011 and the Georgia Tech President's Undergraduate Research Award.

EFFECTS OF AGE AND OBESITY ON RISK OF TRIPPING DURING LEVEL WALKING

[1]Christina M. Rossi, [2]Sara L. Matrangola, [1]Maury Nussbaum, and [1]Michael L. Madigan

[1]Virginia Tech, Blacksburg VA, USA
[2]Highpoint University, Highpoint, NC, USA
email: rossic@vt.edu, web: http://www.biomechanics.esm.vt.edu/

INTRODUCTION:

Fall-related injuries are a major public health concern, and two major demographic trends in the United States threaten to exacerbate this problem: an increase in the older adult population and an increase in the prevalence of obesity. In 2009-2010, over one-third of adults were considered obese, and the likelihood of obesity increased with age [1]. Given these trends, it is important to understand how an individual's risk of tripping is affected by age and obesity.

The purpose of the study was to investigate the effects of age, obesity, and their interaction on the risk of tripping while walking over level ground. This risk was assessed by measuring minimum foot clearance (MFC) during the swing phase of normal gait.

METHODS

Four gender-balanced groups, comprised of 20 participants each, completed this study (Table 1). All participants were required to pass a screening designed to exclude participants with self-reported medical conditions, such as musculoskeletal, neurological, or balance disorders, that could impact the validity of the results.

Table 1: Participant demographics

Group	Age (y)	BMI (kg/m^2)
Young Healthy Weight	24±3.3	22.3± 2.2
Young Obese	23.1±3.0	33.4±3.3
Older Healthy Weight	62.4±8.2	24.2±1.8
Older Obese	64.1±9.8	32.7±3.0

Participants walked along a 10 m walkway at two speeds: a self-selected gait speed and a hurried speed of 1.9 m/s. Eight successful trials at each speed were completed, and each trial included the swing phase of both the dominant and non-dominant lower limbs. Thus, foot clearance from 16 swing phases for each participant was analyzed.

All participants wore the same brand of athletic shoes, to which were attached three reflective markers. A Vicon MX T10 motion analysis system (Vicon Motion Systems Inc., LA, CA) was used to sample marker positions at 100 Hz.

MFC was determined using a method adopted from Startzell et al [2]. A pointer with markers attached was used to define an average of 16 points on the sole of each shoe with respect to a shoe-fixed reference frame. MFC was defined as the lowest of all the points on the sole of the shoe during mid-swing. For each participant, the median MFC and MFC interquartile range (IQR) were determined. A lower median MFC and higher MFC IQR imply a greater risk of tripping [3]. A five-way, mixed-factor analysis of covariance was performed for median MFC and MFC IQR using JMP v7 (Cary, North Carolina, USA) with a significance level of $p<0.05$. Independent variables were age, obesity, gait speed, gender, and leg dominance; all two-way interactions were included, along with stature as a covariate

RESULTS AND DISCUSSION:

For median MFC, no two-way interactions were statistically significant. Median MFC was higher among older adults, higher at the hurried gait speed, higher for males, and higher for the non-dominant limb ($p<0.05$; Figure 1). Median MFC was also positively associated with stature ($p<0.05$).

MFC IQR was significantly affected by an age x speed interaction, in that IQR only increased with age at the hurried speed, and only increased with speed among older adults ($p<0.05$; Figure 2). In addition, MFC IQR increased for the non-dominant limb ($p<0.05$).

Participants who were obese exhibited a slower self-selected gait speed relative to the healthy weight participants ($p<0.05$).

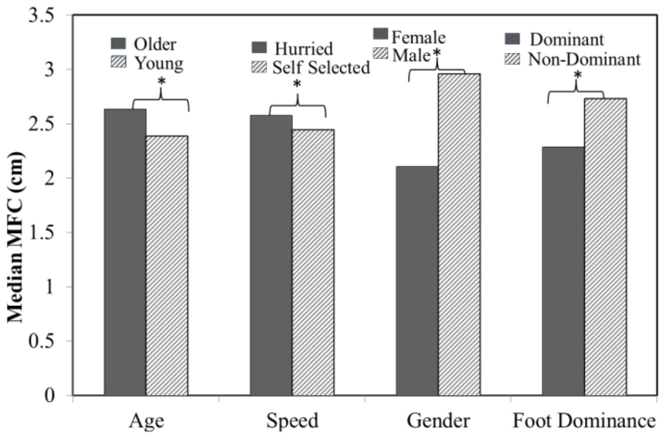

Figure 1: Median MFC values showing all significant main effects. * indicates $p<0.05$

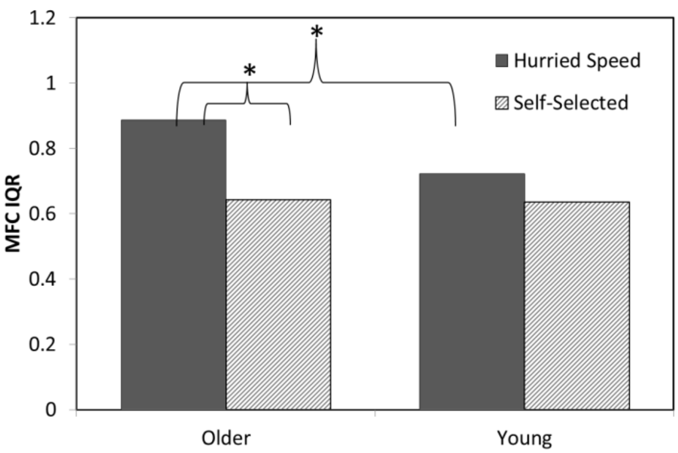

Figure 2: MFC IQR values showing significant age by speed interaction. * indicates $p<0.05$

The age by gait speed interaction effect on MFC IQR suggests that the older group, when walking at higher speeds, may have a higher risk of tripping due to greater variability in MFC. Conversely, the older adults showed a larger median MFC, and median MFC increased at the hurried gait speed, both of which suggest a decrease in risk of tripping. This increase in median MFC with age during overground walking has been previously reported [4] and could be a safety adaptation this group uses to compensate for sensory deficits that come with age. A potential cause for greater median MFC at higher gait speeds could be an adaptation used to offset greater MFC IQR at higher gait speeds.

Several studies have reported increased IQR with age during treadmill walking [5], however there was no significant main effect for age found here ($p=0.08$). It is possible that the effect of age on MFC IQR is reduced when walking overground as opposed to treadmill walking. Future work is needed to whether and under what conditions age influences MFC IQR.

There were no significant effects of obesity on median MFC or MFC IQR. Although obesity has been associated with alterations in temporal and angular components of gait (such as slower gait speed, smaller stride length, and larger stride width [6]) our results indicate that these alterations do not result in a greater risk of tripping.

CONCLUSIONS

Obesity was not found to substantially affect the risk of tripping, at least under the conditions examined here. Older adults at a hurried walking speed showed a greater risk of tripping, based on an increased MFC IQR. However, median MFC results indicated a decreased risk of tripping for older adults in addition to a decreased risk of tripping at hurried gait speeds. Potentially offsetting effects appear to be present when examining the risk of tripping among older adults, and these should be examined more closely in future work.

REFERENCES

1. Ogden C., et al *NCHS Data Brief.* ***82,*** *2012*
2. Startzell J.K, et al *Hum Mov Sci.* **18**,5 1999
3. Begg R, et al *Gait Post.* **25**,2 2007
4. Menant, et al *Gait Post*. **29**,3 2009
5. Barrett R.S et al, *Gait Post.* **32**,4 *2010*
6. Spyropoulos P, et al. *Arch Phys Med Rehabil* **72,** 1065-70, 1991

ACKNOWLEDGMENTS

This material is based upon work supported by the National Science Foundation Graduate Research Fellowship (to CMR), and 5R01OH009880.

STEP LENGTH PERTURBATIONS ALTER VARIATIONS IN CENTER OF MASS HORIZONTAL VELOCITY

Joshua P. Bailey, Andrew D. Nordin, and Janet S. Dufek

University of Nevada, Las Vegas, Las Vegas, NV, USA
email: bailey69@unlv.nevada.edu

INTRODUCTION

Speed of transport has previously been identified as an important factor in gait selection, with attention to transitions from walking to running [5]. Preferred gait speed has been attributed to optimization of mechanical efficiency and metabolic cost [2,4]. Previous investigations have explored steady-state gait speed, modeling the trajectory of the system center of mass (COM) as an inverted pendulum [2]. Speed adjustments are associated with alterations in step frequency and step length (SL), with the latter implicated in gait instability [1,5]. Specifically, longer SLs, exceeding preferred, have demonstrated greater vertical oscillation of the system COM, increasing the cost of transport [2]. From this, examining gait speed via system COM forward velocity ($COMv_x$) under contrasting stride conditions is considered valuable in gaining insight into selection of SL during locomotion.

The purpose of this research was to investigate the effects of SL perturbations on system COM forward velocity (v_x) during walking gait. Comparisons were made among step length perturbations and preferred stride walking (PW) and preferred stride running (PR) conditions.

METHODS

Eight participants (5 male, 3 female; age 23.5±3.6 yrs, height 1.72±0.18 m, mass 73.11±15.29 kg) free from previous lower extremity injury were included in this investigation. Informed consent was obtained prior to participation, as approved by the Research Ethics Board at the affiliated institution.

Kinematic data were acquired using a 12-camera system (Vicon MX T40-S; 200Hz), and 35-point spatial model (Vicon Plug-in Gait Fullbody). Data filtering and interpolation included a low pass, 4th order (zero lag) Butterworth filter (cutoff frequency 15Hz) and cubic 3rd order cubic spline.

PW, PR, and SL manipulations calculated as a percentage of leg length (LL; mean distance from anterior superior iliac spine to medial malleolus on each leg) were completed in a series of five trial blocks. SL perturbations used lengths of 60%, 80%, 100%, 120%, and 140% of LL. Participants were instructed to match their SL with cones spaced on the floor at corresponding distances. Gait speed and step frequency were not controlled in the current protocol. Kinematic analysis was carried out over two steps (one stride) during each gait trial.

Maximum and minimum system $COMv_x$ comparisons were made independently among stride conditions using one-way repeated measures ANOVA and Bonferroni *post-hoc* contrasts. Change in system $COMv_x$ ($\Delta COMv_x$; maximum v_x – minimum v_x) across the gait stride was also evaluated among stride conditions using one-way repeated measures ANOVA and Bonferroni *post-hoc* contrasts, via SPSS 20.0 (α=0.05). Degrees of freedom were adjusted using the Huynh-Feldt correction method where appropriate.

RESULTS AND DISCUSSION

Differences in maximum $COMv_x$ were detected among stride conditions (F[1.847,59.105]=339.458, p<.001, η^2=.914). *Post-hoc* comparisons showed significant increases (p<.001) in maximum $COMv_x$ at each successive SL from 60%LL to 140%LL (Figure 1). Due to the large number of significant differences among stride conditions, Figure 1 identifies non-significant differences (p>0.05), displaying stride conditions where $COMv_x$ values were similar. All non-flagged comparisons were significant ($p \leq .002$). From Figure 1, PW $COMv_x$ appeared to occur between SLs of 80%LL and 100%LL, but significantly differs from either of these two conditions ($p < .001$). PR predictably demonstrated significantly greater $COMv_x$ than PW and perturbed walking conditions ($p < .001$).

Similar to maximum $COMv_x$, differences in minimum $COMv_x$ were detected among stride conditions ($F[2.118,65.666]=130.951$, $p < .001$, $\eta^2=.809$). In contrast to maximum $COMv_x$, minimum $COMv_x$ did not differ between PW and SLs at, and in excess of 100%LL. Minimum $COMv_x$ appeared to plateau above the 60%LL stride condition, demonstrating a trend dissimilar to that observed for maximum $COMv_x$. As a result, $\Delta COMv_x$ across the gait stride was explored at each stride condition.

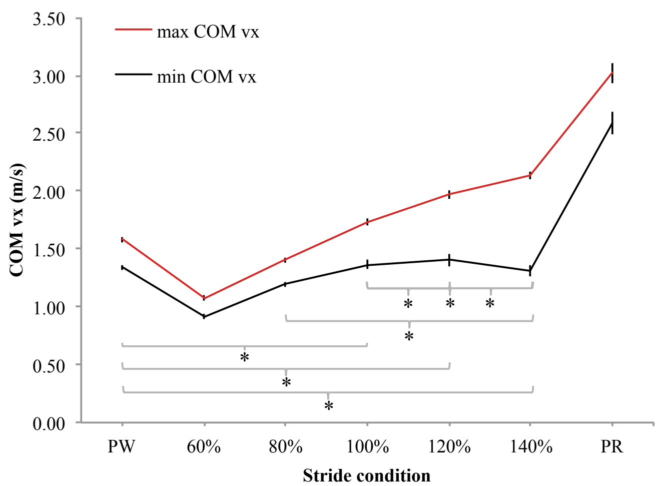

Figure 1: Step condition vs. horizontal COM velocity (* is a non-significant difference; $p > 0.05$)

Differences in $\Delta COMv_x$ were identified among stride conditions ($F[2.387,74.000]=40.364$, $p < .001$, $\eta^2=.566$). Pairwise comparisons detected significantly greater $\Delta COMv_x$ at 140%LL, and significantly lesser $\Delta COMv_x$ at 60%LL ($p \leq .005$; Figure 2). Greater $\Delta COMv_x$ was considered representative of larger fluctuations in gait speed as a result of braking during the gait stride [3]. Similar to Figure 1, Figure 2 depicts non-significant differences ($p > 0.05$), highlighting stride conditions of similar $\Delta COMv_x$. All non-flagged comparisons were significant ($p \leq .005$). Figure 2 suggests that $\Delta COMv_x$ was similar among PW, 80%LL, 100%LL, and PR, while 60%LL and 140%LL exhibited significant differences in $\Delta COMv_x$. From this, it appears as though increased SLs may become inefficient for locomotion, requiring large variations in forward velocity as a result of greater braking during gait.

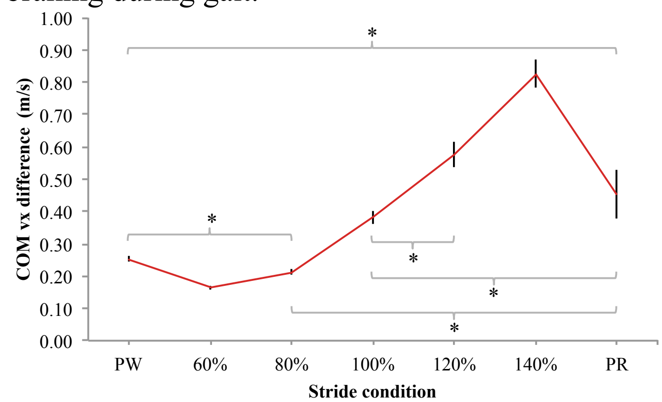

Figure 2: Step condition vs. horizontal COM velocity difference (max v_x – min v_x; * is a non-significant difference; $p > 0.05$)

CONCLUSIONS

The current research supports previous investigations relating preferred SL to metabolic and mechanical cost of transport [4]. Stride lengths greater than 100%LL demonstrate greater deviations in forward COM velocity, as a result of braking and subsequent loss of forward velocity. This outcome may provide insight into mechanisms responsible for transitions to running gait due to the increased energy expenditure needed to maintain steady-state speed during transport.

REFERENCES

1. Egerton T, et al. *Gait & Posture.* **34,** 178-182, 2011.
2. Gordon KE, et al. *Arch Phys Med Rehabil.* **90**, 136-144, 2009.
3. Peterson CL, et al. *Gait & Posture.* **33**, 562-567, 2011.
4. Usherwood JR, Bertram JEA. *Eur J Appl Physiol.* **90,** 647-650, 2003.
5. Zijlstra W, et al. *Gait & Posture.* **3,** 13-18, 1995.

ACKNOWLEDGEMENTS

This research was supported by grants from the National Center for Research Resources (5P20RR016464-11) and the National Institute of General Medical Sciences (8 P20 GM103440-1).

EXECUTION OF ACTIVITES OF DAILY LIVING IN PERSONS WITH PARKINSON'S DISEASE.

Jared W. Skinner, Hyo Keun Lee, Ryan Roemmich, Shinichi Amano and Chris J. Hass
University of Florida, Gainesville, FL, USA
Email: jskinner1@ufl.edu

INTRODUCTION

Parkinson's disease (PD) is a neurodegenerative disease that disrupts the functionality and quality of life in persons affected by the disease. Motor symptoms associated with PD include resting tremor, rigidity, bradykinesia, diminished postural stability and decreased muscular strength [3]. The combination of aging, degenerative effects of the disease, and reduced physical activity often manifest in reductions in stability, increased variability in force production and deficits in torque generation. These muscular deficits have been shown to be contributors to the bradykinesia frequently observed in this population. Muscular weakness and the subsequent movement difficulties associated with PD often manifest into increased inability to perform activities of daily living (ADL) and an increased risk for falls.

Healthy older adults (HOA) perform ADL at near maximal torque capabilities [1,2]. The increase in effort of torque production compared to young adults has been linked to the increase in age-related physiological differences. However, little is known about the role of muscular effort in the diminished capacity of persons with PD to perform ADLs. Indeed, whether or not persons with PD are limited in ADL performance by neuromuscular deficits, lack of motivation, or both remains unknown. Therefore, the purpose of this investigation was to determine the relative magnitude of lower extremity torque production with which persons with PD perform ADLs compared to HOA.

METHODS

Eight participants (65.25±8.89yr, 170.56±7.97cm, 77.37±10.4kg) with PD and 9 HOA (65.42±7.3yr, 170.4±10.4cm, 71.5±14.75kg) participated in this study. There were no significant differences in anthropometric data between groups. Patients with PD were tested while clinically "ON" approximately one hour after taking their medication. Participants performed a series of over ground walking and stair ascension tasks, two common ADLs. Participants first walked across an eight-meter long walkway containing three force plates (Bertec Corporation, Columbus, OH, USA) mounted flush to the laboratory floor. Subjects walked at a comfortable, self-selected pace while kinetic data were collected at 360Hz. Participants then ascended a single stair (6 inches high by 14 inches wide), that was positioned a top one of the force plates. Participants were instructed to initiate the movement by stepping onto the stair first with their dominant leg. A 10 camera Optical Capture System recorded kinematic data at 120 Hz (Vicon Nexus, Vicon, Oxford, UK). After an appropriate rest, participants were asked to perform a series of isokinetic muscular strength test bilaterally for hip flexion/extension, knee extension and ankle plantar flexion at speeds of 90°/sec and 120°/sec using the Kin-com dynamometer. The highest peak isokinetic moment at each joint for both velocities was recorded and used to normalize ADL joint moments. Total lower extremity peak moment during the ADL task was calculated by summing the peaks of the hip, knee and ankle moments produced during a given ADL trial. Percentage of hip, knee and ankle contribution was found by dividing the individual peak joint moment by the total peak moment. Statistical analysis was performed between groups (HOA vs PD), using an independent sample *t-test*. Level of Significance was set at $p < .05$.

RESULTS

The statistical analyses detected a significantly smaller max concentric ankle plantar flexion moment in persons with PD at both 90 and

120°/sec. However, there were no differences in peak moment for the knee or hip at the two speeds between the groups. The results also showed no difference in the proportion of their peak joint moment capabilities in PD and HOA when performing ADL's. However, the contribution of ankle was lower in PD during stair ascent when compared to HOA (22% vs. 32%, $p<.05$). There was no difference in the contribution of the knee in PD (42%) and HOA (39%). Lastly, the contribution of the hip was higher ($p<.05$) in PD (39%) when compared to HOA (26%). There were no differences in joint contribution of lower body moments in PD and HOA during over ground gait.

The current investigation indicated that lower extremity joint moment contribution were proportionally different between the PD and HOA groups. Individuals with PD have adapted a different strategy for stair negotiation. Our results demonstrate that persons with PD may compensate for diminished capabilities of the ankle plantar flexors by increasing the contribution of the hip to help in stair ascension. Our results may also indicate that persons with PD alter ADL strategies only during tasks which may challenge the musculoskeletal capabilities of the lower limbs to a greater extent, as we did not observe any differences during over ground gait.

Previous literature has shown that HOAs operate at a high proportion of their peak joint moment capabilities at the ankle, knee and hip while performing ADLs when compared to young adults[1]. However, the current investigation indicated that PD and HOA operate at similar proportions of their peak lower body joint moment capabilities. This however could be due to the severity level of the PD. Moderate to advanced stage PD has increased prevalence of motor dysfunction and impairments, which has been shown to affect the ability to produce joint torque [3]. Participants with PD in the current investigation had a mild level of severity, which could explain the similar magnitude of effort.

In summary, the investigation indicated persons with PD have a reduction in maximum ankle moment during plantar flexion. The reduction in the ankle moment is indicative of deficits in both strength and movement speed. Those with PD employ alternative strategies of muscle contribution to negotiate stairs, by enabling the hip flexors to contribute more to total moment production to stair ascension.

REFERENCES

1. Hortobágyi T, Mizelle C, Beam S, DeVita P. Old adults perform activities of daily living near their maximal capabilities. J Gerontol A Biol Sci Med Sci. 2003;58:M453–M460.
2. N.D. Reeves, M. Spanjaard, A.A. Mohagheghi, V. Baltzopoulos, C.N. Maganaris, Older adults employ alternative strategies to operate within their maximum capabilities when ascending stairs, Journal of Electromyography and Kinesiology, Volume 19, Issue 2, April 2009, Pages e57-e68, ISSN 1050-6411, 10.1016/j.jelekin.2007.09.009.
3. David, F.J., et al., Progressive resistance exercise and Parkinson's disease: a review of potential mechanisms. Parkinsons Dis. 2012: p. 124527.

Table 1: Percentage of Joint to Total Moment during Stair Accent and Gait (* indicates $p<.05$)

	PD Subjects n= 8	HOA Subjects n= 9	P-Value ($P<.05$)
Stair Accent (% of Total Moment)			
Ankle	22%	32%	.03*
Knee	39%	42%	.68
Hip	39%	26%	.03*
Gait (% of Total Moment)			
Ankle	44%	45%	.98
Knee	23%	26%	.52
Hip	33%	29%	.50

CADENCE EFFETS ON SHOD GAIT KINEMATICS

Wendi Weimar, Braden Romer, John Fox, Jay Patel, and Jared Rehm
Auburn University, Auburn, AL, USA
email: weimawh@auburn.edu, web: http://education.auburn.edu/kine/

INTRODUCTION

Recently, barefoot and minimalist footwear have been proposed as a more natural means of locomotion due to the kinematic and kinetic changes associated with shod gait [1]. While much of the research and discussion has focused on running, foot strike patterns, and the response of the intrinsic musculature of the foot, remaining unanswered whether changes in gait patterns are due to neural or mechanical.

Specific to walking, previous results found an increased stride length when wearing athletic shoes as compared to flip-flops, which the authors hypothesized was due to the increased mass of the athletic shoe [2]. However, more recent research found an increased stride length when participants wore a lighter flip-flop as compared to a heavier flip-flop, discounting the inertial component of footwear [3]. In addition, there is also support that increased tactile feedback can significantly alter walking kinematics [4].

Therefore, the purpose of this study was to investigate the effects of a fixed cadence on shod and barefoot walking mechanics.

METHODS

Twenty (10 female, 10 male) healthy participants volunteered for participation in the study. No participant had a lower-extremity injury within the year prior to participation in the study. Age of the participants was 23.7±2.4 years (m±SD) and body mass was 73.6±12.2kg. Participants walked approximately 11 m, and one full stride was captured for analysis. Markers were placed on the head of the fifth metatarsal, lateral malleolus, lateral femoral condyle and greater trochanter. Kinematic data was averaged across the six trials per condition.

The three conditions included: participants walking at a self-selected pace while wearing shoes (SHFW), shod while walking at a cadence matched to the shod cadence (SHSH), and barefoot while walking at a cadence matched to the shod cadence (BFSH). During the fixed cadence trials, participants were provided an audible metronome matching the desired cadence. Participants were dressed in identical polyester clothing and utilized commercially available non-running athletic shoes for all shod trials.

Separate Repeated Measures ANOVA's were completed with dependence on walking velocity, cadence, and sagittal plane lower-extremity joint angles (relative ankle, relative knee, absolute hip) at toe-off and foot strike. Post-hoc analyses were completed utilizing a least squares difference test to determine if significant differences ($p<0.05$) existed between conditions.

RESULTS AND DISCUSSION

No significant differences were found in knee or hip joint kinematics at toe-off or foot strike; however, significant main effects were found for the ankle at both foot strike ($F_{(2,34)} = 5.655$, $p = 0.008$, $\eta^2 = 0.250$) and toe-off ($F_{(2,34)} = 14.133$, $p < 0.001$, $\eta^2 = 0.454$). Significant main effects were also found for walking velocity $F_{(1.4,26.8)} = 33.761$, $p < 0.001$, $\eta^2 = 0.640$) and cadence $F_{(2,38)} = 11.265$, $p < 0.001$, $\eta^2 = 0.372$). As indicated in Table 1, follow-up pairwise analyses indicated that participants walked significantly faster ($p<0.001$) during both shod conditions (SHFW, SHSH) relative to the fixed barefoot condition (BFSH). During the fixed cadence conditions, cadence was found to be similar, though significantly ($p\leq0.001$) higher (0.6 steps*min^{-1} greater).

Table 1: Spatiotemporal variables across the three conditions.

		Total (n = 20)
SHFW	[1]**Cadence** (steps*min^{-1})	112.6
	[2]**Velocity** (ms^{-1})	1.39
SHSH	[1]**Cadence** (steps*min^{-1})	113.2
	[2]**Velocity** (ms^{-1})	1.39
BFSH	[1]**Cadence** (steps*min^{-1})	113.2
	[2]**Velocity** (ms^{-1})	1.26

[1] Significant differences in cadence were found between SHFW-SHSH and SHFW-BFSH ($p < 0.001$).

[2] Significant differences in velocity were found between SHFW-SHSH and SHSH-BFSH ($p \leq 0.001$).

Figure 1 displays the relative joint angles for the ankle at foot strike and toe-off. Follow-up pairwise comparisons indicated that participants displayed significantly (p=0.003) less plantarflexion at foot strike during BFSH than SHFW. Likewise, participants exhibited significantly less plantarflexion at toe-off during BFSH than either SHFW (p<0.001) or SHSH (p=0.002).

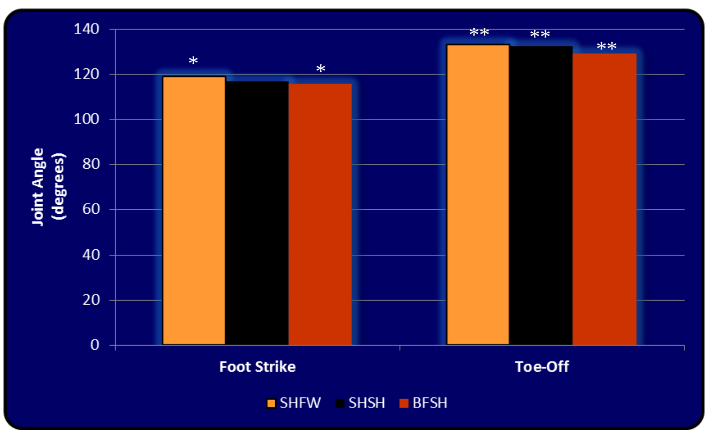

Figure 1: Relative Ankle Joint Kinematics at foot strike.

***** Sagittal Plane Ankle Angle for SHFW was significantly greater than BFSH (p=0.003).

****** Sagittal Plane Ankle Angle for BFSH was significantly lower than either SHFW (p<0.001) or SHSH (p=0.002).

CONCLUSIONS

Though a significant difference was found between the free-walking cadence and fixed cadence, the difference (0.6 steps*min^{-1}) is in all likelihood of little practical significance (Table 1). Furthermore, the lack of a significant difference between the fixed cadence conditions (SHSH, BFSH) suggests the efforts to control cadence were successful. Though stride length was not examined in the present study, walking velocity is the product of stride length and cadence. It would be expected that stride length was reduced during the BFSH condition due to the significant differences in velocity and lack of significance differences between cadences, lending support for a mechanical origin in gait alterations.

Conversely, while there was no significant difference between knee or hip joint kinematics at foot strike or toe-off, significant differences were found for the ankle (Figure 1). Specifically, participants exhibited less plantarflexion at foot strike when barefoot (BFSH = 115.6°) than during shod, free walking (SHFW = 118.9°). While this might be attributable to heel-height differentials commonly found in modern footwear, participants also displayed less plantarflexion during SHSH (116.8°), though this difference was non-significant. Therefore, it is more likely that this difference is due to the toe extension commonly seen in barefoot walking. This toe extension produces a dorsiflexion moment at the ankle and would contribute to this increased dorsiflexion position. Interestingly, participants displayed significantly lower plantarflexion (Figure 1) at toe-off during BFSH (129.2°) than SHFW (133°) or SHSH (132.4°). While heel-height could be responsible, the authors assert that this is more likely due to the significant differences in velocity (Table 1). It was anticipated that a fixed cadence would expand the understanding of kinematic differences between shod and barefoot gait. However, significant differences in velocity suggest that future research should focus on the influence of metronome directed cadences as well as footwear on gait kinematics.

REFERENCES

1. Leiberman, DE, et al. *Nature*, **463**, 531 – 353, 2010.
2. Majundar, D, et al. *Indian J Physiol Pharmacol*, **50 (1)**, 33 – 40, 2006.
3. Shroyer, JF & Weimar, WH. *J Amer Podiatric Med Assn*, **100 (4)**, 252 – 257, 2010.
4. Nurse, M, et al. *J of Electr & Kines*, **15**, 496-506

EFFECTS OF PROLONGED LOAD CARRIAGE WALKING ON LOWER EXTREMITY AND TRUNK KINEMATICS, HEART RATE, AND SUBJECTIVE RESPONSES

[1]Sivan Almosnino, [1]David Kingston, [1]Davide Bardana, [1]Joan Stevenson, and [1,2]Ryan Graham

[1]Queen's University, Kingston, ON, Canada
[2]Nippising University, North Bay, ON, Canada
email: sivanalm@hotmail.com, web: http://www.skhs.queensu.ca/ergbio/

INTRODUCTION

Load carriage walking utilizing a backpack is a common task performed in military settings [1,2]. This task is often performed over an extended period of time; a factor that may hamper performance and increase injury risk [1,2]. Load carriage walking tasks have been studied extensively with respect to biomechanical changes resulting from: participant characteristics; absolute or relative load magnitude; load location within the backpack and with respect to the bearer's center of mass; different types of backpacks; walking speed; walking surface (i.e. over ground vs. treadmill); and more [1]. However, the influences of these aforementioned factors have primarily been assessed utilizing data obtained from a small number of initial gait cycles. In addition, investigations that have of used experimental designs incorporating prolonged task duration offer conflicting results regarding alterations in biomechanical performance, particularly those related to joint kinematics [1,2].
As such, the primary aim of this investigation was to elucidate whether lower extremity joint and trunk kinematics are altered in response to prolonged load carriage treadmill walking. A secondary aim was to assess whether the task induces alterations in heart rate (HR), and self-reported exertion and body comfort.

METHODS

Seventeen healthy and physically active men participated in the study (mean ± SD age 25.9 ± 4.5 years; weight 80.6 ± 10.0 kg; height 177 ± 6 cm). Written informed consent was obtained from all participants prior to testing, and procedures approved by the University's General Research Ethics Board.

Three-dimensional kinematic data for the right lower extremity, pelvis, and trunk were obtained using a 9 camera Vicon 512 motion capture system (Vicon Motion Systems, Oxford, UK) sampling at 120 Hz (Figure 1). Participants were fitted with a 32.5 kg loaded military backpack (USMC MarPat ILBE rucksack, Arc'teryx Equipment Ltd., North Vancouver, BC, Canada), and donned the same type of military boots (Desert TFX® Rough-Out GTX®, Danner Boots Inc., Portland, OR, USA).

Figure 1: Experimental setup showing a participant performing the load carriage walking task with tracking-marker triads attached.

Testing was conducted in a climate-controlled laboratory. Participants performed 60 minutes of continuous treadmill walking at a speed of 1.53 m/s. Kinematic data were first recorded between minutes 7 and 10 from walk start, and during the last 3 minutes of the walk. At the end of each recording instance, participant HR, ratings of perceived exertion (RPE) and body region discomfort were recorded using standard techniques [2]. Following, mean sagittal plane lower extremity and trunk-pelvis joint angle waveforms were subjected to Principal Component Analysis (PCA) [3]. The number of PCs retained for analysis was determined using a 90% trace criteria. Differences in joint angular PC scores, as well as HR, RPE and discomfort scores were assessed using Bonferroni-corrected paired two-tailed t-tests (α=0.05) and accompanied by estimates of effect size (Pearson's r). PC interpretation was achieved via examination of loading vector and PC reconstruction plots [3].

RESULTS AND DISCUSSION

A total of 8 PCs were retained using the 90% trace criterion. Of these, only PC1 of the ankle joint exhibited statistically significant differences across the two measurement trials. Examination of the associated loading vector and PC reconstruction plot (Figure 2) suggests that at the end of the walking task, participants adopted a slightly more dorsiflexed foot throughout the gait cycle. However, the magnitude of this systematic difference is only 1-2 degrees at any given instant in the gait cycle. RPE scores were significantly greater at the end of the walk (11.1 ± 1.7) then at the start (10.2 ±1.9, $t(16) = -3.45$, $p<0.01$, $r = 0.65$). HR, expressed as a percentage of predicted maximum, did not differ between the final (63% ± 7%) and initial periods of the walk (63% ± 6%, $t(16) = 0.60$, $p = 0.55$, $r = 0.15$). Lastly, the only significant increases reported for body discomfort were for the neck/upper trapezius region (1.8 ± 1.1 vs. 3.9 ± 2.6, $p<0.001$, $r = 0.45$) and shoulders (1.4 ± 1.3 vs. 2.3 ± 1.6, $p<0.001$, $r = 0.29$).

The lack of meaningful changes in lower extremity and trunk kinematics in our investigation may be explained by the following factors: First, the relative HR values obtained suggest that the task performed was only of light aerobic intensity. As such, we postulate that fatigue, a factor that has been reported to alter biomechanical-related performance parameters during load carriage walking [1,2] was simply not induced by the experimental task. In this context, note that the choice of walking speed, duration, and load magnitude were consistent with current reported military training practices. However, in the current study, walking was performed in a controlled environment, with the load configuration dissimilar from that carried by soldiers during training and operations.

The second factor that may have contributed to the observed results relates to the equipment used in the investigation. The backpack, undershirt and footwear are state of the art, and in effect were designed to accommodate performance of tasks similar to the current one. Inferring from the relatively low discomfort experienced by the participants during trial performance in the current study, it may be that kinematic changes reported in previous studies were influenced, at least in part, by use of less accommodating equipment.

REFERENCES

1. Knapik JJ, et al. *Mil Med* **169**, 45-56, 2004.
2. Simpson KM, et al. *Ergonomics* **55**, 316-326, 2012.
3. O'Connor KM, et al. *Med Sci Sports Exerc* **41**, 867-878,2009.

Figure 2: Illustration of joint angle waveforms, 1st PC loading vectors and PC reconstruction plots

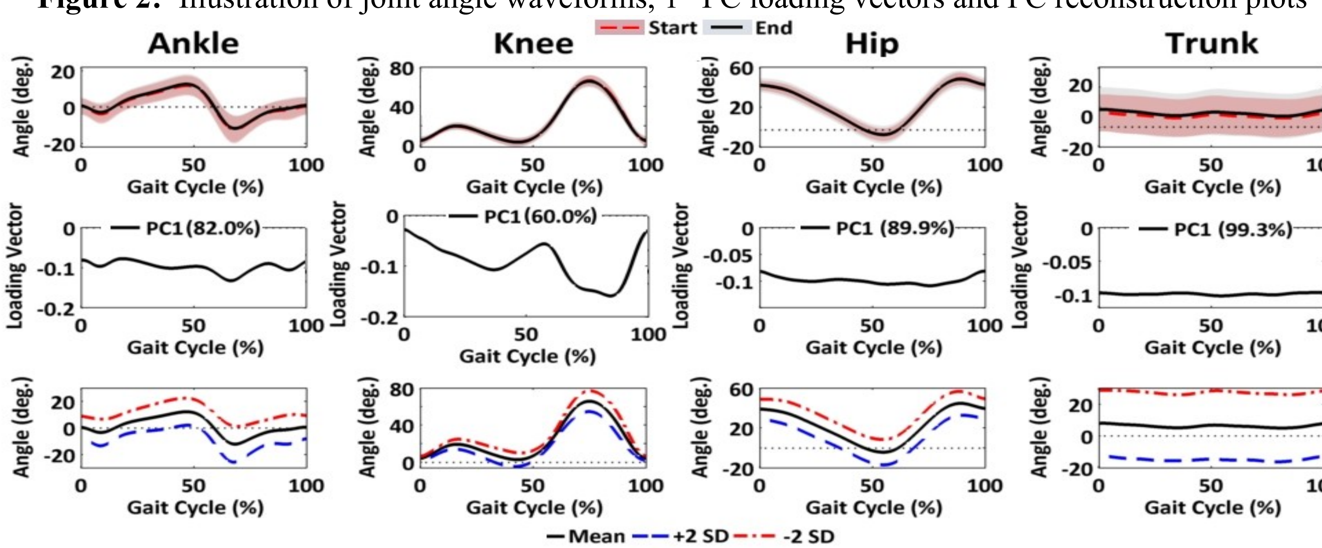

TWELVE WEEKS OF PLANTARFLEXOR STRENGTH TRAINING DO NOT CHANGE GAIT BIOMECHANICS OF HEALTHY OLD ADULTS WALKING AT A SAFE MAXIMUM SPEED

[1]Rachel Tatarski, [2]Chantal Beijersbergen, [1]Jake Ridings, [1]Zachary Domire, [1]Patrick Rider, [2]Tibor Hortobágyi, [1]Paul DeVita

[1]East Carolina University, Greenville, NC, USA
[2]University of Groningen, The Netherlands
email: tatarskir11@students.ecu.edu

INTRODUCTION

Locomotion is an important and inherent part of daily life and is integral in maintaining an independent lifestyle, especially in older adults whose functional capacity has declined. This decline is due to changes in many physiological characteristics, particularly a loss of muscle mass, strength and power [1] and it is manifested as a reduced walking velocity in old adults. Kinetically, old adults lose more torque and power at the ankle than at other joints [2,3]. This distal to proximal shift in muscle function could be due to plantarflexor weakness, so strengthening the plantarflexors may help reverse the negative physiological effects of aging and help preserve functional capacity in old adults. The purpose of this study was to determine the effect of a plantarflexor strength training program on gait biomechanics during level walking at a safe maximum speed in healthy old adults.

METHODS

Ten healthy adults, 65 to 85 years old have so far been recruited and randomly assigned to strengthening (n=6) or stretching (control, n=4) groups. Informed consent was obtained for all participants before testing or training. Pre- and post-test measurements of maximal plantarflexor strength were collected for each participant. This included obtaining a 1-repetition maximum (1RM) weight for the left limb ankle plantarflexors and then assessing the plantarflexor torque-velocity relationship using 20, 40, 60, 80, and 100% of the subject's 1RM. Force and motion data were captured with the subject on a supine leg press machine with a force plate mounted on the foot platform. Visual 3D was used to calculate ankle plantarflexor angular velocity and torque during the ankle press trials. Pre-and post-test gait kinematics and kinetics were collected while walking at a safe maximum speed using an 8-camera Qualisys motion tracking system, AMTI force plate and standard marker placements on the pelvis and left leg. Instructions were to, "walk as fast as you can without feeling like you are going to run or fall." Visual 3D was used to calculate ankle torque ankle power during the gait trials.

Between tests, both groups exercised three 3 per week for 12 weeks. During each exercise session, the strengthening group performed 2 sets of 10 repetitions of a bilateral ankle press for the gastrocnemius and two sets of 10 repetitions on a bilateral seated calf raise for the soleus muscles. Participants in the stretching group performed two 40-second repetitions for each of the static and dynamic gastrocnemius and soleus stretches. All subjects repeated the gait assessments, maximal plantarflexor strength testing and the ankle press trials at the end of the 12 week training period. Due the small sample sizes, t-tests were used to compare pre versus post-test values within each group to provide a preliminary analysis ($p<0.05$).

Figure 1: Scan the QR code to view simulation videos of torque-velocity strength testing, strengthening and stretching exercise protocols, and maximum speed walking test.

RESULTS AND DISCUSSION

The strengthening group significantly increased the average peak plantarflexor torque and peak velocity as seen in Figure 2 ($p<0.05$). The stretching group significantly increased average peak plantarflexor torque ($p<0.05$) but not peak velocity as seen in Figure 3.

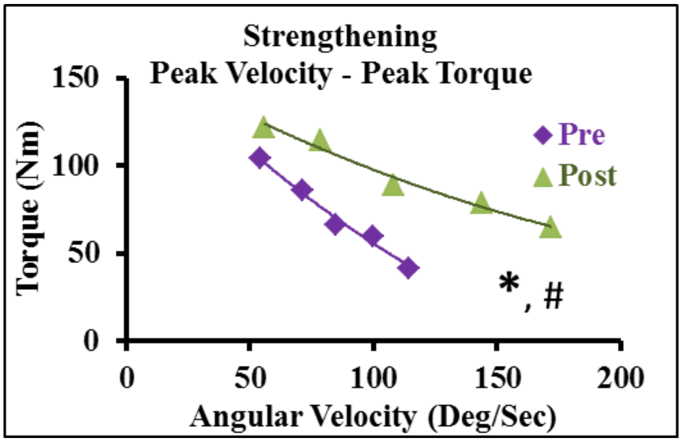

Figure 2: Pre and post torque-velocity relationships. * torque p<0.05; # velocity p<0.05

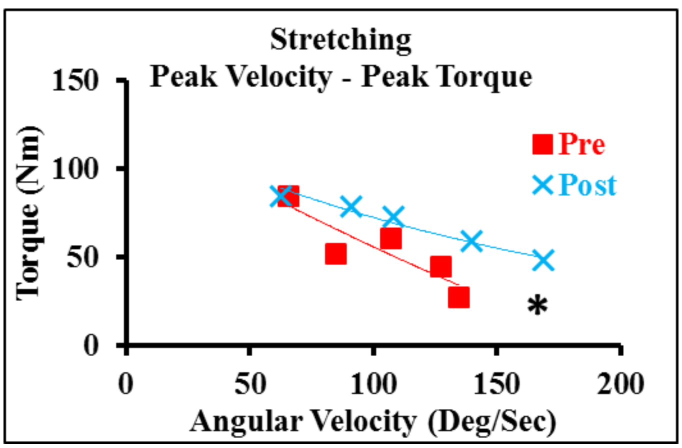

Figure 3: Pre and post torque-velocity relationships. * torque p<0.05

Despite this increase in peak torque, preliminary results showed no effect on the gait characteristics of old adults. As seen in Table 1, there were no changes in stride length, walking velocity, peak plantarflexor torque or peak plantarflexor power from the pre-test to post-test in either group while walking at a safe maximum speed.

CONCLUSIONS

Based on these preliminary results, a 12-week plantarflexor strength training program does not change the gait kinematics or kinetics of healthy old adults walking at a safe maximum speed. A possible explanation for the lack of gait changes could be due to the fact that our subjects were already healthy and mobile before the 12 weeks of exercise. At the pre-test, our subjects walked at 1.88m/s compared to the fastest speed of healthy old adults reported previously (1.66m/s) [4]. Perhaps our old adults do not have the capacity to further increase walking velocity. Additionally, it is possible that 12 weeks of strength training is not long enough to incorporate the increases in strength and joint torque capacity into gait adaptations.

REFERENCES

1. Metter EJ, et al. *J. Gerontol.Ser.A-Biol.Sci.Med.Sci* **52**, B267-B276, 1997.
2. DeVita P, et al. *J.Appl.Physiol* **88**, 1804-1811, 2000.
3. Graf A, et al. *Arch.Phys.Med.Rehabil* **86**, 2177-2183, 2005.
4. Ko S, et al. *Age and Ageing* **39**, 688-694, 2010.

Table 1: Gait kinematics and ankle kinetics of healthy old adults walking at a safe maximum speed.

	Strengthening		Stretching	
	Pre	Post	Pre	Post
Stride Length (m)	1.68 ± 0.29	1.66 ± 0.23	1.56 ± 0.20	1.57 ± 0.25
Velocity (m/s)	1.88 ± 0.30	1.81 ± 0.25	1.60 ± 0.18	1.57 ± 0.19
Torque (Nm/%BW*H)	9.0 ± 1.3	9.0 ± 0.7	9.5 ± 0.9	9.5 ± 0.8
Power (W/kg)	3.8 ± 1.4	3.9 ± 0.9	3.4 ± 0.9	3.6 ± 1.0

KINETIC PATTERNS OF TREADMILL WALKING IN PREADOLESCENTS WITH AND WITHOUT DOWN SYNDROME

Jianhua Wu and Toyin Ajisafe
Georgia State University, Atlanta, GA, USA. Email: jwu11@gsu.edu

INTRODUCTION

External ankle load is usually used to increase the moment of inertia of the legs and facilitate the pendulum swing of the legs during locomotion [1]. It is recognized that external ankle load can stimulate the activities of ankle plantar flexors and enhance load sensory feedback during push off [2]. A quick unloading has been found to trigger the stance-to-swing transition and initiate leg swing [3]. No study has been conducted to investigate how external ankle load affects the ground reaction force (GRF) and impulse variables in children with and without disabilities. This study aimed to investigate the effect of both treadmill speed and external ankle load on kinetic walking patterns in preadolescents with and without Down syndrome (DS).

METHODS

Participants: There were ten preadolescents with DS (8 M/2 F, mean age: 9.1 years, average height and weight: 1.25 m and 31.7 kg, respectively) and 10 children with typical development (TD) (8M/2F, mean age: 9.3 years, average height and weight: 1.34 m and 30.1 kg, respectively).

Experimental design: There were two treadmill speed conditions: 75% (SS) and 100% (FS) of the participant's preferred overground walking speed. Average SS and FS conditions were 0.76 m/s and 1.04 m/s, respectively, in the DS group, and 1.03 m/s and 1.37 m/s in the TD group. There were two external ankle load conditions: with (AL) and without (NL) bilateral external ankle load which was equal to 2% of the participant's body weight on each side. Average AL condition was 6.0 N in the DS group and 5.9 N in the TD group.

Data collection:
A total of four conditions (2 treadmill speed by 2 ankle load) were tested. Two 60-second trials were collected for each condition. The order of condition presentation was mostly randomized across the two groups. Because some participants in the DS group initially had difficulty executing treadmill walking under the FS condition, the SS condition was presented first to allow acclimation in these participants [4]. A Zebris FDM-T instrumented treadmill was used to collect vertical GRF data.

Data analysis: Customized Matlab programs were used to determine the first peak force (F_{Z1}), the minimal force (F_{MIN}), and the second peak force (F_{Z2}) for each gait cycle, in a unit of body weight (BW). To assess the rate of loading after heel strike and the rate of unloading before toe off, loading rate and unloading rate were calculated in these two regions, respectively, in a unit of BW/sec (Fig. 1).

Fig. 1

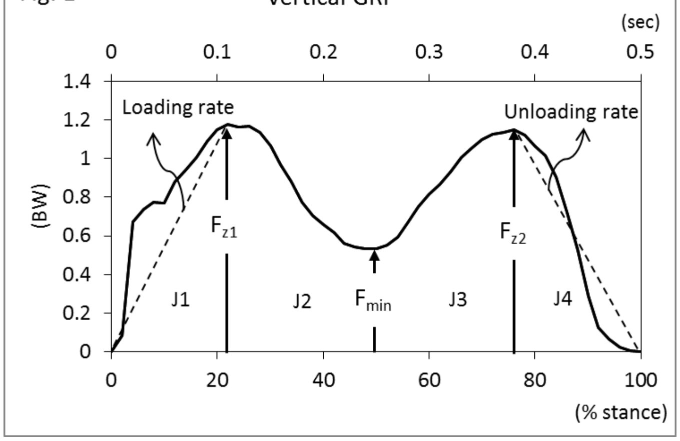

Impulse variables J1 to J4 were calculated in Fig. 1. Total F_Z impulse was the sum of J1 to J4. All the impulse variables had a unit of BW*sec.

Statistical analysis: A series of three-way (2 group x 2 speed x 2 ankle load) ANCOVA with repeated measures on the last two and with a covariate of speed were conducted on each dependent variable. Post hoc pair-wise comparisons with Bonferroni adjustments were conducted when appropriate. Statistical significance was set at $p<0.05$.

RESULTS AND DISCUSSION

There was a group by speed interaction on F_{Z2} (Fig. 2). The DS group decreased F_{Z2} from the SS to the FS condition while the TD group increased F_{Z2} accordingly. There was also a group by ankle load interaction on F_{Z2} (Fig. 2). The DS group increased F_{Z2} from the NL to the AL condition to a lesser extent than the TD group.

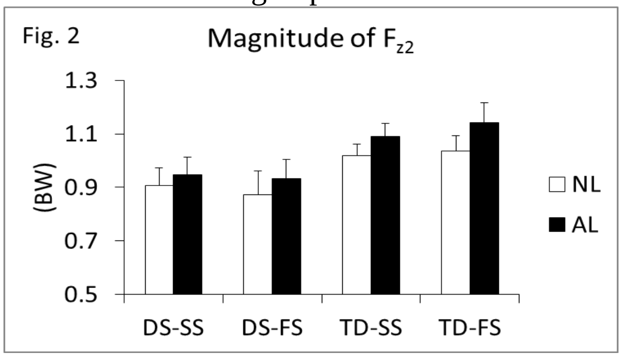

There was a group by speed interaction on the unloading rate (Fig. 3). The DS group increased the unloading rate from the SS to the FS condition to a lesser extent than the TD group.

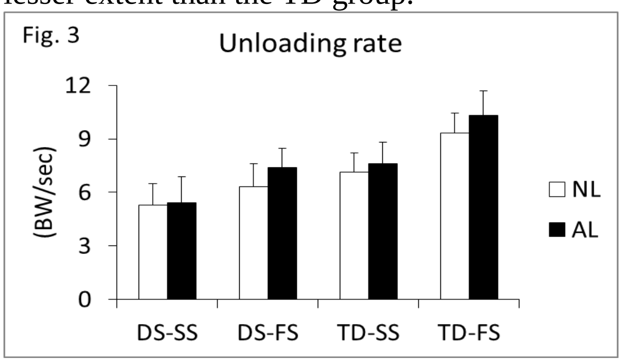

There was a group by ankle load interaction on J3 (Fig.4) and total F_Z impulse (Fig. 5). The DS group increased both J3 and total F_Z impulse from the NL to the AL condition to a lesser extent than the TD group.

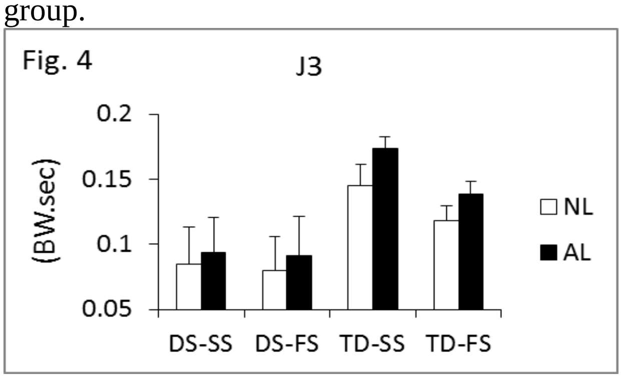

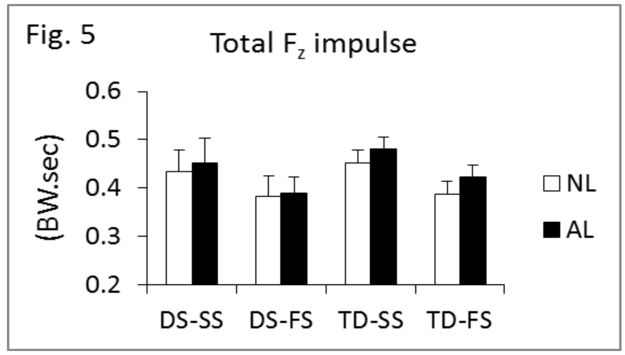

F_{Z2} was lower than body weight in the DS group but higher than body weight in the TD group (Fig. 2). The DS group may use hip flexors and extensors rather than ankle plantar flexors to accommodate the inadequate F_{Z2} during push off. When adapting to external ankle load, both groups increased the magnitude of F_{Z2}, suggesting that inclusion of external ankle load may be a promising approach to strengthening leg muscles and eliciting a more powerful push off in children with DS.

External ankle load may facilitate the DS group to increase vertical propulsive impulse and propel them upward during push off. However, the lower magnitude of impulses in the DS group suggests that even with external ankle load, the DS group still produced a less efficient push off.

CONCLUSIONS

External ankle load helps the DS group increase F_{Z2} and vertical propulsive impulse and may facilitate push off and the initiation of leg swing during treadmill walking.

REFERENCES

1. Browning RC, et al. *Med Sci Sports Exerc* **39**, 515-525, 2007.
2. Duysens J, et al. *Brain Res* **187**, 321-332, 1980.
3. Pearson KG, et al. *Exp Brain Res* **90**, 557-566, 1992.
4. Ulrich BD, et al. *Hum Move Sci* **23**, 133-146, 2004.

ACKNOWLEDGEMENTS

We would like to thank the funding support from the Jerome Lejeune Foundation.

AN ALTERNATE PREDICTOR OF PEAK MEDIAL COMPARTMENT LOADING: THE PRODUCT OF PEAK KNEE EXTENSOR AND ABDUCTOR MOMENTS

Kurt Manal, Emily Gardinier, Lynn Snyder-Mackler and Thomas Buchanan

University of Delaware, Newark, DE, USA
email: manal@udel.edu

INTRODUCTION

There is a high likelihood of developing knee osteoarthritis after ACL injury and altered joint loading has been implicated as a contributing factor (1). Joint loading cannot be measured directly and consequently surrogate measures, most commonly the knee abduction moment are used to infer medial loading. Therapies which reduce the abduction moment are assumed to reduce medial contact, however this may not be the case if there is a concomitant increase in the knee extensor moment (2,3). The knee extensor moment is directly related to quadriceps force, and muscle forces during gait are primary contributors to knee joint loading (4). The purpose of this study was to evaluate an alternate surrogate measure of medial loading; the product of peak extensor and knee abductor moments. Since the extensor moment is an indicator of quadriceps force and quadriceps force is associated with joint loading we hypothesized the product of extensor and abductor moments would yield a better estimate of medial contact force than the abduction moment alone.

METHODS

Ten healthy (5 male, 5 female) adults were evaluated approximately 6 months after ACL re-construction. All subjects had at least 90% side-to-side quadriceps strength. The average subject age was 34.1±7.9 years, height 1.75±0.08 meters and body mass 84.7±15.1 Kg. Visual3D was used to calculate stance phase kinematics and kinetics from marker and force platform data. Surface electromyography (EMG) was recorded from the major muscles crossing the knee and included the: biceps femoris long head (BFL), semimembranosus (SM), rectus femoris (RF), vastus medialis and lateralis (VM & VL), and the medial and lateral Gastrocnemii (MG & LG). EMG for the Vastus intermedius (VI) was equal to the average of the VM & VL, with Semitendinous (ST) and Biceps Femoris Short head (BFS) equal to the SM and BFL respectively. These data were input to an EMG-driven musculoskeletal model of the knee to predict individual muscle forces and medial compartment loading (5-6). Medial contact force predictions have been validated using publically available instrumented knee data as part of the third Grand Challenge to predict *in vivo* knee forces. The knee extension (Ext), abduction (Abd) and the product of the Abd and Ext moments (Abd*Ext) were used to predict peak medial loading. All data were time-normalized to 101 samples. Contact forces were reported as bodyweights (BWs) and joint moments were normalized to body BW*height. Three trials per subject were averaged in this manner.

RESULTS AND DISCUSSION

The abduction moment when used by itself was a good predictor (R^2 = 0.67) of medial contact force (Table 1). The prediction increased significantly when the product of abduction and extension moments was used to predict medial contact (R^2 = 0.87, p = 0.000) (Figure 3). The peak extension and abduction moments were not significantly correlated (R^2 = 0.04, p = 0.562) indicating the extensor moment provides unique information above and beyond the abduction moment when predicting medial contact force.

Table 1. R^2 between peak Abd, Ext and Abd*Ext moments with peak medial contact force (MC). These are highlighted in the first column. The Abd and Ext moments were not correlated (R^2 = 0.04).

	MC	**Abd**	**Ext**
Abd	0.67		
Ext	0.38	0.04	
Abd*Ext	0.87	0.68	0.52

The timing of the peak abduction and extensor moments was almost coincident (see Figure 1) and this corresponded with the timing of peak medial contact force (Figure 2).

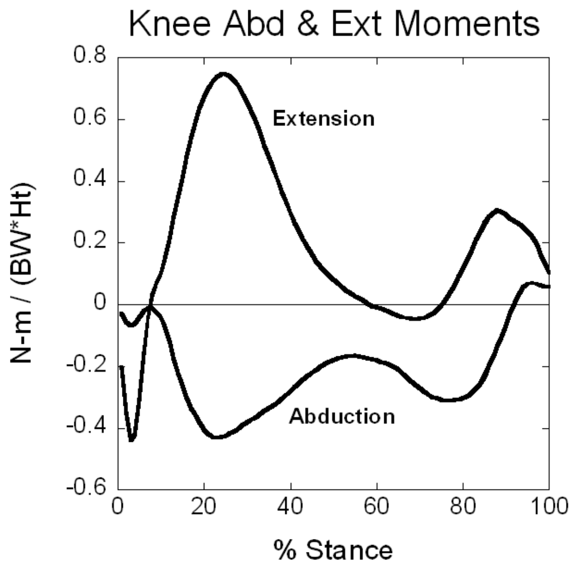

Figure 1. Ensemble averaged knee abduction and extension moments for 10 subjects. Standard deviations omitted for clarity.

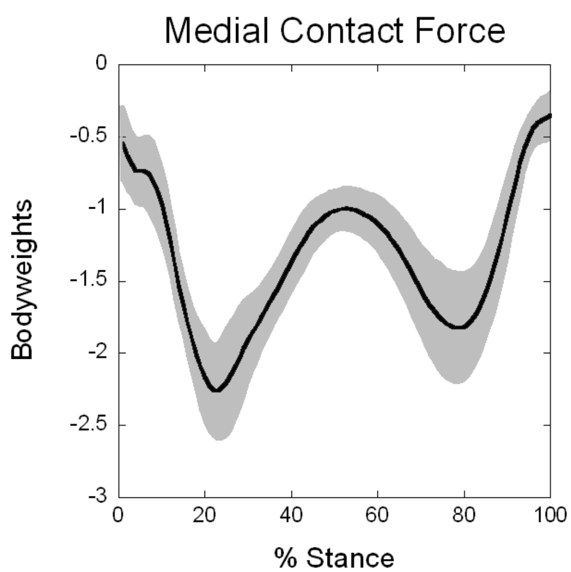

Figure 2. Ensemble averaged medial compartment contact force for 10 subjects (gray band = ± SD).

CONCLUSIONS

The product of peak knee extensor and abduction moments resulted in a better prediction of peak medial force compared to the abduction moment alone. This was because the peak abduction and extensor moments were not correlated. Using a surrogate measure of loading that is sensitive to quadriceps force may limit erroneous conclusions that can arise when inferring medial loading from the knee abduction moment alone [2,3]. This is especially relevant in studies investigating the effects of rehabilitation. The product of peak knee extensor and abduction moments is a simple measure that may have has clinical relevance.

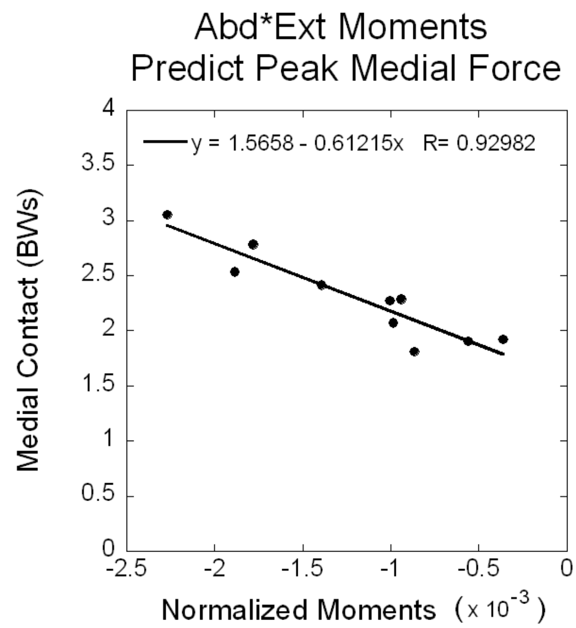

Figure 3. Linear regression between Abd*Ext moments and peak MC force. Joint moments were normalized by BW*height prior to multiplying and therefore the predictor is dimensionless.

REFERENCES

1. Fleming BC, et al. *Curr Opin Orthop*, 354–62, 2005.
2. Walter JP, et al. *J Orthop Res,* 1348-54, 2010.
3. Manal K, et al *J. Biomech. Eng*. 2013, PMID: 23445059
4. Sasaki K, et al. *J Biomech* 2780–4, 2010.
5. Buchanan TS, et al. *J. App Biomech*, 367–395, 2004.
6. Winby CR, et al. *J Biomech*, 2294-2300, 2009.

ACKNOWLEDGEMENTS

Supported by R01-AR048212, RO1-AR046386 & P30-GM103333

YOUNG ADULTS HAVE HIGHER ARM ELEVATION THAN OLDER ADULTS DURING UNEXPECTED SLIPS

[1]Zachary Merrill, [1]Peter Sandrian, [1]Rakié Cham, and [1]April J. Chambers

[1]University of Pittsburgh, Pittsburgh, PA, USA
email: zfm1@pitt.edu

INTRODUCTION

Slips and falls represent a serious problem faced by older adults, with the segment of the United States population over the age of 65 accounting for about three quarters of all fall related deaths [1], with these falls in the older age group accounting for $19 billion in annual medical costs [2]. Of these falls, about 5% require hospitalization or cause a fracture. The percentage leading to fracture or hospitalization increases with age, reaching approximately the rate of falls and injuries in the population over 75 years old. Between 30 and 50% of the total falls for the over 65 age group is due to accidental environment related falls, such as trips and slips [1].

While changes in gait mechanics and balance lead to an increased likelihood of falling in the elderly, arm activity as a response to gait perturbations has not been investigated to the same extent as the lower body, with very limited research describing the upper body responses in terms of kinetics, kinematics, and timing. The role of arms in gait is not fully understood, especially when dealing with gait perturbations. Several theories exist about upper body contributions during perturbations, including reaching for support, restoring the body's center of mass, and preparing for impact with the ground.

Differences in shoulder flexion angles and moments between young and elderly adults while slipping has already been documented, with younger adults having larger flexion angles and moments. Because test subjects have shown large and varying levels of abduction as well as flexion, the purpose of this abstract is to investigate how age affects the overall arm elevation angle and elevation angular velocity during unexpected slips.

METHODS

Twenty eight subjects (16 female, 12 male) in two age groups participated in this study; 16 were in the young adult (age 20-33) group, and 12 were in the older adult (age 55-67) group. Exclusion criteria included clinically significant histories or neurological, orthopedic, or cardiovascular issues interfering with normal gait and balance.

Before data collection, subjects practiced walking naturally with the motion tracking marker set and safety harness. The subjects were then exposed to two conditions: baseline dry walking, in which they walked at a natural, self-selected pace along a dry pathway, and unexpected slipping . To induce a slip, a slippery contaminant consisting of 75% glycerol and 25% water by volume was spread on the floor (unknown to the subject) where the subject stepped with his or her left foot. After slipping, each trial was classified as hazardous or nonhazardous, with a 1 m/s peak slip velocity cutoff [3].

The angular parameters calculated were derived from the left arm angle alpha, defined as the angle between the long axis of the humerus and the superior-inferior axis of the torso (Fig. 1). This angle was investigated because it takes into account

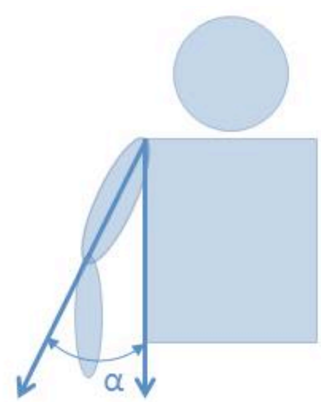

Figure 1: Definition of alpha angle. α is constrained between 0 and 180°, and is 0° in anatomical position, increasing as the arm is elevated.

both flexion/extension and adduction/abduction movements of the shoulder. After calculating and plotting the change in alpha over time, the slip reaction onset timing and angle were selected graphically based on the point where the angle after slip initiation began to deviate from the angle during baseline walking. Specific parameters investigated include maximum deviation in elevation angle during stance, maximum alpha angle after slip, and rate of alpha angle generation, alpha rate, after onset of the slip reaction. The maximum deviation during stance was defined as the difference between alpha at heel strike and maximum alpha during stance. This deviation was then used to find Δα, the difference in deviation between baseline and slipping trials. The rate of alpha angle generation, alpha rate, was defined as the average rate of change (degrees per second) of alpha between the onset of angle difference after slip initiation, and the peak value of alpha during the slip.

RESULTS AND DISCUSSION

Kinematic shoulder parameters related to the calculated α were analyzed with a linear regression model including age group (old or young) and slip hazardousness (hazardous or nonhazardous), as well as their interaction.

The analysis revealed significant effects of hazardousness and age on Δα (Figure 2), peak alpha angle while slipping, and alpha rate. As shown in Table 1, older adults had lower alpha angles when slipping, a smaller Δα, and a smaller average alpha rates when slipping. The interaction of age and hazardousness did not have a significant impact on any of the parameters, while age and hazardousness separately were a significant factor in all three parameters, and slip hazardousness was significant in peak alpha angle and alpha rate.

While both older and younger adults displayed similar upper extremity reactions to unexpected

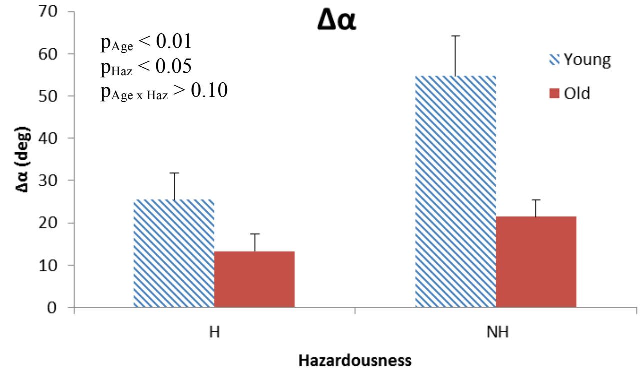

Figure 2: Comparison of Δα between age groups. Error bars represent standard error.

slips, the younger adults had significantly larger reactions in both hazardous and nonhazardous slips. Because younger adults had significantly higher Δα ($p=0.0223$), peak alpha angles ($p=0.0491$), and alpha rates ($p=0.0348$) in nonhazardous slips than in hazardous slips, they may have been able to correct their slipping motion with acute upper body reactions. By comparison, the older adult group had nearly identical alpha angles differences, peak alpha angles, and alpha rates in hazardous and nonhazardous slips.

CONCLUSION

Younger adults demonstrated several significant upper extremity slip reactions than older adults, including difference in maximum alpha angle deviation from normal walking, peak alpha angle, and alpha rate after reaction onset. While the exact purpose for these reactions is not entirely known, these upper body reactions appear to help younger adults to better maintain balance after an unexpected slip.

REFERENCES

1. Rubenstein LZ. *Age and Aging* **35-S2**, ii37-ii41, 2006.
2. Hanley A, et al. *Clinical Interventions in Aging* **6**, 19-25, 2011.
3. Moyer BE, et al. *Ergonomics* **4**, 329-343, 200

	Young Adults		Older Adults	
Hazardousness	**Hazardous**	**Nonhazardous**	**Hazardous**	**Nonhazardous**
Δα (deg)*^,+^	25.5	54.7	13.4	21.5
Peak Alpha Angle (deg)*^,+^	46.9	76.9	38.7	44.8
Alpha Rate (deg/s)*^,+^	32.3	64.7	22.6	27.2

Table 1: Mean values for Δα, peak α angle, and α rate during slipping. * indicates $p_{age} < 0.05$, and $^{+}$ indicates $p_{haz} < 0.05$. For all parameters, $p_{age\ x\ haz} > 0.10$.

DETERMINING HOW HUMANS REGULATE VARIABILITY DURING WALKING

Nicole K. Bohnsack[1], Joseph P. Cusumano[2], and Jonathan B. Dingwell[1]

[1] University of Texas, Austin, TX, USA, [2] Pennsylvania State University, University Park, PA, USA
E-mail: Nicole.Bohnsack@austin.utexas.edu
Web: http://www.edb.utexas.edu/faculty/dingwell/

INTRODUCTION

Walking is an essential task most people take for granted every day. However, human locomotion is a highly complex task that requires significant neural control. The neural systems that regulate walking continuously integrate multiple sensory inputs [1] and generate motor outputs to coordinate many muscles to achieve efficient, stable, and adaptable locomotion. This process is complicated both by the inherent redundancy of the system being controlled [2,3] and by inherent physiological noise [4].

This study sought to determine how effectively humans can alter how they regulate stride-to-stride fluctuations in their walking dynamics [5] when the *goals* of the walking task are directly manipulated.

METHODS

Walking on a treadmill at speed v only requires that you do not walk off the treadmill [5]. Of the *many* possible strategies that can achieve this goal, humans prefer to try to maintain ~constant speed (v) [5]. All combinations of stride length (L_n) and stride time (T_n) that satisfy $L_n/T_n = v$ define a "Goal Equivalent Manifold" [3, 5] for constant-speed walking (Fig. 1). "Goal equivalent" deviations tangent to the GEM (δ_T) do not affect v. Only "goal relevant" perpendicular deviations (δ_P) affect v.

7 healthy adults (age 18-35) walked on a motorized treadmill at the same constant speed for 2 trials of 6 min each under each of the following conditions:

- SPD: Normal walking at constant speed
- LEN: Walking at constant speed with stride length constrained (by targets on the treadmill)
- TIM: Walking at constant speed with stride time constrained (by a metronome)
- ALL: Walking at constant speed with both stride length *and* stride time constrained

3D movements of their feet were recorded (Vicon, Oxford Metrics, Oxford, UK) to compute stride length (L_n) and stride time (T_n) for each stride, n. Stride speeds were then computed as: $S_n = L_n/T_n$. Time series of δ_T and δ_P fluctuations relative to the originally hypothesized cons ant-speed GEM ([5]; Fig. 1) were extracted and analyzed.

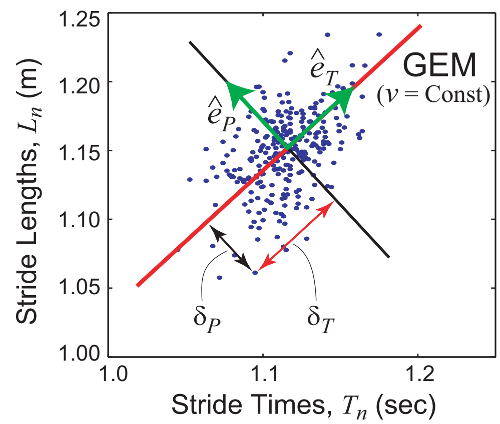

Figure 1: Stride lengths (L_n) vs. times (T_n) for a typical subject, showing the constant speed GEM ($L_n/T_n = v$) and scalar deviations δ_T and δ_P.

Means and standard deviations were computed for each variable. Detrended Fluctuation Analysis (DFA) [5] was used to compute an exponent, α, that quantifies the degree of statistical persistence or anti-persistence in each time series. Values of $\alpha > 0.5$ are "persistent", while $\alpha < 0.5$ indicate anti-persistence. Smaller values of α indicate more frequent/rapid corrections of stride-to-stride deviations and therefore also indicate greater control [5].

RESULTS AND DISCUSSION

Mean stride lengths (L_n), stride times (T_n), and stride speeds (S_n) remained nearly the same across all walking conditions (not shown). Interestingly, when we asked subjects to "constrain" their stride lengths and/or stride times to their mean preferred values, the *variability* in L_n, T_n, and S_n tended to increase rather than decrease (not shown).

For the SPD condition, fluctuations in L_n and T_n were both strongly persistent ($\alpha > 0.5$), consistent with previous findings [5]. For the LEN constrained task, α of L_n decreased significantly (i.e., tighter stride-to-stride control), but α of T_n did not (Fig. 2). Conversely, for the TIM constrained task, α of T_n decreased significantly, but α of L_n did not (Fig. 2). When stride length and time were both constrained (ALL), subjects corrected deviations in L_n much more so than deviations in T_n (Fig. 2).

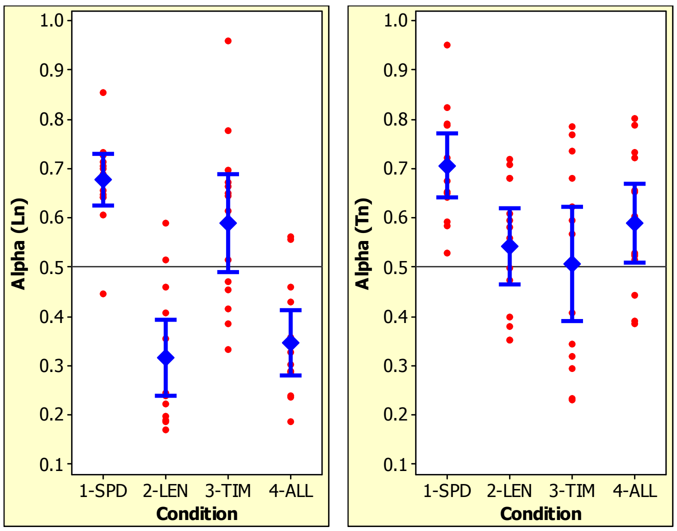

Figure 2: DFA α values for stride lengths (L_n) and stride times (T_n) for all 4 walking conditions. α(L_n) values decreased significantly ($p < 0.05$) for both LEN and ALL, relative to SPD. α(T_n) values decreased significantly ($p < 0.05$) only for TIM, relative to SPD.

For fluctuation analyses based on the constant-speed GEM (Fig. 1), subjects exhibited far greater variance along the GEM (δ_T) than perpendicular to the GEM (δ_P) (not shown), as expected [5]. However, this variance exhibited *no* changes across task conditions ($p > 0.40$; not shown). When subjects were asked to constrain their step lengths (LEN & ALL), they corrected δ_T deviations *along* the walking speed GEM significantly more rapidly than they did for the SPD trials (Fig. 3, Left). However, the same subjects corrected δ_P deviations to the *same* degree across *all* walking conditions (Fig. 3, Right).

CONCLUSIONS

Young healthy adults exploited different redundancy relationships in different ways when asked to control stride length and/or stride time in different contexts. In general, subjects made more rapid corrections of those stride-to-stride deviations that were most directly relevant to the different task goals imposed in each walking condition. This indicates that the central nervous system can adapt and achieve multiple goals simultaneously. Such flexibility could allow humans to accommodate a wide range of varying task demands as they walk. Demonstrating that we can directly *manipulate* these stride-to-stride control strategies suggests that this approach could be used to develop more effective rehabilitation interventions (e.g. [6,7]) that seek to minimize or eliminate only that variability which directly impacts task performance.

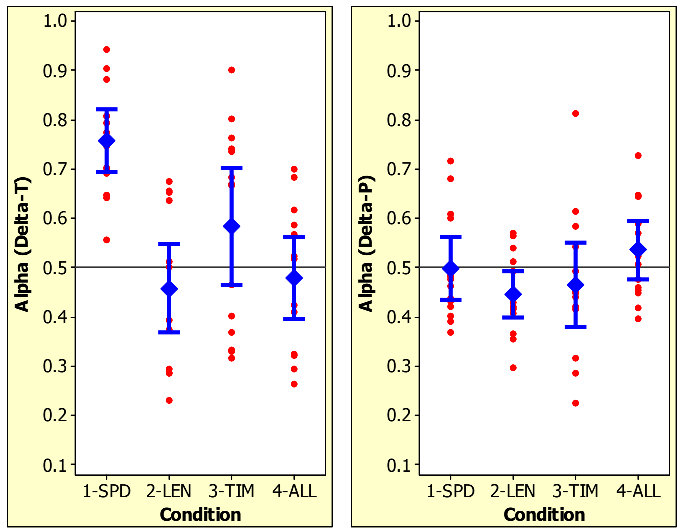

Figure 3: DFA α exponents for deviations tangent (δ_T) and perpendicular (δ_P) to the constant-speed GEM (Fig. 1) for all four walking conditions. α(δ_T) values were significantly reduced ($p < 0.05$) for both LEN and ALL, relative to SPD. However, α(δ_P) values did not vary across walking tasks ($p = 0.292$).

REFERENCES

1. Rossignol S et al. *Physiol. Rev.* **86**(1): 89-154, 2006.
2. Todorov E, *Nat. Neurosci.* **7**(9): 907-15, 2004.
3. Cusumano JP & Cesari P, *Biol. Cybern.* **94**(5): 367-379, 2006.
4. Faisal AA et al. *Nat. Rev. Neurosci.* **9**(4): 292-303, 2008.
5. Dingwell JB et al. *PLoS Comput. Biol.* **6**(7): e1000856, 2010.
6. Shah PK et al. *Eur. J. Neurosci.* **36**(1): 2054-62, 2012.
7. Lewek MD et al. *Phys. Ther.* **89**(8): 829-39, 2009.

ACKNOWLEDGEMENTS

Univ. of Texas Research Grant (to NKB & JBD)

THE MECHANICS OF ECONOMICAL WALKING: INSIGHTS FROM CHIMPANZEE AND HUMAN BIPEDALISM

[1]Leng-Feng Lee, [2]Matthew C. O'Neill, [2]Brigitte Demes, [1]Michelle Confer, [2]Nathan E. Thompson, [2]Susan G. Larson, and [1]Brian. R. Umberger

[1]University of Massachusetts Amherst, Amherst, MA, USA
[2]Stony Brook University School of Medicine, Stony Brook, NY, USA
email: umberger@kin.umass.edu, web: http://www.umass.edu/locomotion

INTRODUCTION

Human walking is remarkably economical, both in comparison to mammals as a group and especially compared to our closest living relative, the chimpanzee. Identifying factors that explain the differences in locomotor costs between humans and chimpanzees will help us understand the adaptive value of human musculoskeletal design.

It has been argued that the ~75% higher cost of walking in chimpanzees compared with humans can be understood in terms of differences in the volume of muscle that is activated to generate forces against the ground, and the duration of ground contact [3]. However, these analyses were based on joint moments from sagittal plane inverse dynamics analyses that were confined to the stance phase of walking. If substantial moments are generated outside of the sagittal plane, or during the swing phase, they may contribute to the differences in locomotor costs. Likewise, if joint powers are larger in chimpanzees, then a consideration of mechanical work may also be necessary to account for differences in the cost of walking between species.

To address these issues, we present initial results for three-dimensional (3-D) joint mechanics and mechanical energetics of the stance and swing phases of bipedal walking in chimpanzees and humans.

METHODS

Data were collected on three chimpanzees (age: 5.5 ± 0.3 yr, mass: 26.4 ± 1.7 kg, hip height: 0.34 ± 0.02 m) and twelve humans (age: 27.5 ± 4.7 yr, mass: 69.1 ± 12.0 kg, standing height: 1.70±0.07 m) during overground walking. Data for both species were collected in a laboratory setting. All experimental procedures were approved by the relevant ethics boards, and the human subjects provided informed consent.

The chimpanzees walked at self-selected speeds, averaging 1.1 ± 0.2 m/s, as they followed an animal trainer offering a juice reward. The human subjects all walked at a standardized speed of 1.2 m/s. Anatomical landmarks on the pelvis and hind/lower limbs were identified using non-toxic paint for the chimpanzees and reflective, spherical markers for the humans. Marker coordinates were recorded using high-speed motion capture systems, while ground reaction forces were simultaneously recorded using strain gauge-based force platforms. The kinematic and kinetic data were combined with estimates of body segment inertial properties to compute hip, knee and ankle joint moments using standard inverse dynamics equations. Joint powers were computed as the products of joint moments and joint angular velocities. To facilitate comparisons between species, joint moments and powers were scaled to body mass and limb length, yielding dimensionless moments and powers.

Chimpanzee data processing was performed in OpenSim using a chimpanzee musculoskeletal model [2] and human data processing was performed in Visual3D. We determined in a subset of human subjects that joint kinetics computed using OpenSim and Visual3D were nearly identical; thus, the use of different software packages for data processing did not affect our results or conclusions. The directions of positive joint moments are indicated in the vertical axis labels in Fig. 1. Positive joint powers indicated energy generation while negative joint powers indicated energy absorption.

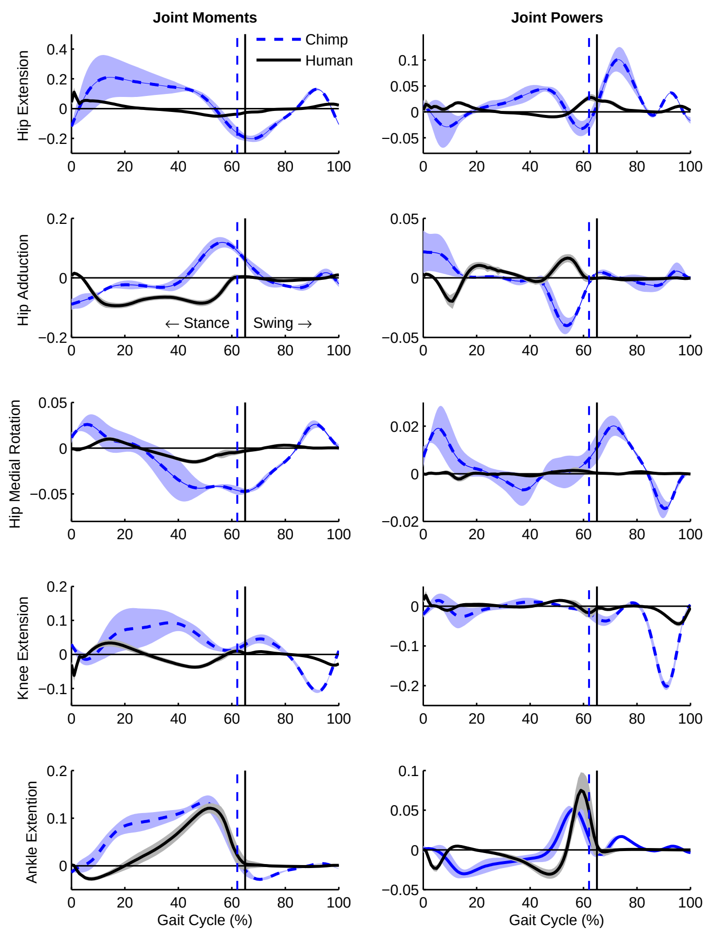

Figure 1: Dimensionless joint moments and joint powers for chimpanzee and human bipedal walking (shaded area is one standard deviation).

RESULTS AND DISCUSSION

Data for a representative chimpanzee subject are presented in Fig. 1 (mean of three trials) along with the group mean data for the human subjects (mean of five trials within a subject). Sagittal plane joint moments were positive (extensor) throughout the stance phase for chimpanzees, whereas they varied between extensor and flexor in humans. With the exception of the ankle joint, the peak moments and powers were larger in chimpanzees than in humans. There were considerable differences in the non-sagittal plane mechanics at the hip in both stance and swing phases. Hip rotation moments and powers were much larger in chimpanzees than in humans. Also, the substantial stance phase hip abduction moment seen in humans was reduced in chimpanzees, but was followed by a large adduction moment, which is related to the exaggerated frontal plane hip motion in chimpanzees [1].

Taken together, the 3-D hip joint moments and powers in the stance and swing phases of the chimpanzee stride tended to be relatively large compared with humans. For limb swing in particular, the hip extension and rotation moments and powers were of similar magnitude to the stance phase. This suggests a more actively controlled (i.e., less-pendular) leg swing motion in chimpanzees. Leg swing represents at least 25% of the net cost of walking [4]; thus, muscle actions during the swing phase may contribute to the higher metabolic cost of walking in chimpanzees relative to humans.

An important consideration in interpreting these results is that the walking speeds for the chimpanzees and humans were similar in absolute magnitude. In future work, we will also compare chimpanzees and humans walking at similar dimensionless speeds. Another issue to consider is the extent to which differences in metabolic cost can be related to joint-level expressions of force and power. To address that issue, the present data will form the basis for subsequent computer simulations that will provide more direct insight regarding differences in muscle function and energetic cost.

CONCLUSIONS

When walking bipedally, chimpanzees generate relatively large 3-D moments and powers in both the stance and swing phases. These differences help account for their higher cost of transport than humans.

REFERENCES

1. Lee L-F, et al. *Proceedings of ASB*, Gainsville, FL, USA, 2012.
2. O'Neill M, et al. *J Exp Biol*, in review.
3. Sockol M, et al. *PNAS* **104**, 12265-69, 2007.
4. Umberger B & Rubenson J. *ESSR* **39**, 59-67, 2011.

ACKNOWLEDGEMENTS

Thanks K. Lasek for animal care and training. Supported by NSF BCS-0935327 & BCS-0935321.

A COMPARISON OF FEEDBACK STRATEGIES IN A VIRTUAL ENVIRONMENT TO IMPROVE GAIT SYMMETRY OF SERVICE MEMBERS WITH UNILATERAL TRANSTIBIAL AMPUTATION

Elizabeth M. Nottingham, Alison A. Linberg and Erik J. Wolf
Walter Reed National Military Medical Center, Bethesda, MD, USA
E-mail: elizabeth.nottingham@med.navy.mil

INTRODUCTION

Traumatic lower extremity amputation alters gait mechanics. Deviations of gait symmetry within temporospatial, kinematic and kinetic parameters may lead to secondary injuries, including joint degeneration and pain, osteoarthritis, and low back pain [1-3]. Targeted rehabilitation strategies are necessary to ensure that service members (SM) with unilateral transtibial amputation receive appropriate and effective training to reduce such asymmetrical gait patterns. Visual feedback has been shown to reduce gait asymmetries in persons with unilateral transtibial amputation [4]. Recent clinical research indicates that patients with unilateral lower extremity amputations participating in computer assisted rehabilitation environment (CAREN; Motek Medical, Amsterdam, The Netherlands) training as an adjunct to standard of care physical therapy, display reductions in gait asymmetry and energy expenditure [5-6]. This study presents preliminary data comparing the ability of three types of feedback (direct, direct game, and indirect game) used in the CAREN to improve gait symmetry in SM with lower extremity amputation. CAREN intervention, including visual feedback in addition to standard of care physical therapy, could improve functional outcomes. Determining which specific type of feedback allows for the most immediate and lasting improvements should allow programmers and physical therapists to produce more efficient strategies for virtual reality based rehabilitation applications.

METHODS

A prospective three group pre-test/post-test design was used to compare three feedback methods using real-time display of vertical ground reaction force (vGRF) data. Direct (D) based feedback allows vGRF data to control the left to right movement of a simple object on the screen, providing direct feedback of the direction of any asymmetry. Direct game (DG) based feedback utilizes vGRF user data to control the left and right movement of a virtual airplane performing a task, directly indicating the direction of asymmetry. Indirect game (IG) based feedback uses vGRF data to control the speed of a racecar as it moves along a circular track, with increased symmetry resulting in a faster car speed. Staff advised each participant about how their biomechanics affected the visual feedback they were receiving; a physical therapist was able to provide verbal cuing to improve the subject's success with each task.

Three SM with traumatic unilateral transtibial amputation were block randomized into one of the three treatment groups. Participants wore their preferred prosthetic components without use of assistive devices and remained in the same components throughout the study.

Participants completed six 30 minute sessions in the CAREN over a three week period. Each session included 15 minutes of group-specific feedback training and 15 minutes of standard of care training which consisted of preselected non-walking based applications. Ground reaction forces were collected as participants walked on a treadmill (Bertec Inc., Columbus, OH). Feedback was displayed based on a symmetry index (SI) comparing peak vGRF during weight acceptance between prosthetic (p) and intact (i) limbs:

$$Symmetry\ Index = \frac{(i-p)}{(i+p)} * 100$$

Perfect symmetry is represented by an SI value equal to zero; negative values indicate an asymmetry toward the prosthetic side.

Gait assessments were conducted before and after CAREN training and involved walking overground at a forced velocity of 1.0 ms^{-1} as signaled by an auditory tone. Kinematic data were collected using a 27-camera motion capture system (Vicon, Oxford, UK), and five clean kinetic foot strikes were collected using six force platforms (AMTI, Inc., Watertown, MA) embedded in the walkway; an average of seven trials were required per session. Visual3D (C-Motion, Inc., Germantown, MD) was used to process and analyze the data. Symmetry index measures of average (across the five clean foot strikes) peak vGRF during weight acceptance, stance time, and step length were calculated. Normative gait data from six uninjured SMs were collected during a single session using identical collection methods.

RESULTS AND DISCUSSION

Age, height, and weight were comparable between the three participants and three controls. D and DG participants wore definitive carbon fiber sockets; the IG participant wore a temporary thermolyn socket. All used total surface bearing suction suspension sockets and energy storage and return prosthetic feet.

Symmetry in vGRF during weight acceptance improved for all participants following visual feedback training in the CAREN (Table 1). Step length and stance time symmetry index values changed minimally between sessions. Before and after training, step lengths and stance duration were longer in the prosthetic and intact sides, respectively. Based on this preliminary data set, the IG participant was more asymmetrical in vGRF at baseline than the other participants and showed the greatest improvement towards vGRF symmetry after training.

Table 1: Outcome measures for each SM by session*

Feedback Method	vGRF SI (%)	Step length SI (%)	Stance time SI (%)
Normative	1.1	0.4	0.7
Direct	**-2.8** **-2.7**	**1.2** **-0.8**	**4.1** **4.6**
Direct Game	**-5.5** **-2.2**	**-3.9** **-2.8**	**3.4** **3.2**
Indirect Game	**6.8** **-0.8**	**-1.5** **-5.3**	**2.6** **2.9**

* Pre training data are in black, post training data are in red

Improvement in outcomes measures were limited to the measure used in training, vGRF symmetry. This improvement occurred regardless of method of CAREN feedback. Improvements in vGRF symmetry were expected; the success of participants within each of their CAREN training applications was dependent on modifying this measure. All participants were able to learn a more symmetric vGRF gait pattern during feedback training, which was carried over to overground walking. Previous studies have seen greater effect with indirect feedback as more attention is directed to motor control features during training [7].

Consistent with previous literature on gait of individuals with unilateral transtibial amputation, participants took longer steps on their prosthetic side and spent more time in stance on their intact side [8]. These measures were not influenced by the feedback training.

CONCLUSIONS

The collection of additional data and further analyses will provide a better foundation for comparison between feedback methods. Metabolic data are being collected and may show improvements between sessions, similar to previous research [9]. A three-week post training follow up gait and metabolic data collection will reveal if these improvements in vGRF symmetry are maintained during the rehabilitation process without additional feedback training.

REFERENCES

1. Norvell DC et al. *Arch of Phys Med & Rehab* 2005; **86**(3): 487-93.
2. Burke MJ. *Annals of Rheumatic diseases* 1978; **37**(3): 252-4.
3. Lemaire ED. *Arch of Phys Med & Rehab* 1994; **75**(10):1094-9.
4. Dingwell JB et al. *Prost and Ortho International* 1996; 20(2):101-10.
5. Darter BJ. *Physical Therapy* 2011 Sep; **91**(9):1385-94.
6. Kruger SE. *Proceedings of IVRC* 2009; Haifa, Israel.
7. Davis BL. *Journal Prost & Ortho* 2004; **16**(2): 49-54
8. Nolan, L et al. *Gait and Posture* 2003; **17**(2): 142-51.
9. Magill RA. *Arch of Phys Med & Rehab* 1996; **77**(8): 811-5.

MECHANICAL EFFECTIVENESS OF A COMBINED GAIT MODIFICATION STRATEGY TO REDUCE KNEE ADDUCTION MOMENT: INCREASING TRUNK LEAN AND FOOT PROGRESSION ANGLE

[1]Joaquin A. Barrios and [1]Lydia K. Caldwell

[1]University of Dayton, Dayton, OH, USA
email: jbarrios1@udayton.edu

INTRODUCTION

The knee adduction moment (KAM) has received considerable attention in the biomechanical literature as proxy measure for medial knee joint load profile. In intervention studies, the KAM is often targeted as a variable for reduction. Recently, gait modification strategies have been explored. Two patterns have emerged as effective at reducing the early and late stance peaks of the KAM waveform, increased ipsilateral trunk lean (TL) and increased foot progression angle (FPA), respectively (Simic et al., 2012; Guo et al., 2007). Interestingly, no studies have combined these patterns in an effort to reduce KAM impulse throughout the stance phase (Maly et al., 2013). Therefore, the purpose of this study was to evaluate the mechanical effectiveness of three experimental patterns: increased ipsilateral TL, increased FPA, and a combination pattern (CP) of the two. We hypothesized the TL pattern would reduce the first peak of the KAM, the FPA pattern would reduce the second peak, and the CP would reduce the KAM impulse.

METHODS

Twenty healthy subjects were recruited for the study (Table 1). Potential subjects were excluded if they reported any history of lower extremity pathology. To prepare for data collection, subjects were fitted with a reflective marker set to the right lower extremity, pelvis and trunk. A static standing calibration and functional hip movement trial were then collected. Natural walking trials along a 23 m walkway were conducted at a self-selected speed, using sacral marker velocity along the line of progression. The experimental trials were then controlled at the established speed within 5%. For each experimental condition, subjects received verbal explanation of the pattern, followed by observing a demonstration from the investigator. Subjects then were allowed to practice the condition themselves for up to 5 minutes. For both the practice and actual trials, a mirror was positioned at the end of the walkway for feedback. The subjects were asked to perform the modifications to a self-determined “minimal” extent. The natural walking condition was collected first, the TL and FPA conditions were counterbalanced throughout the study as the 2nd and 3rd conditions to address possible order effects, and the CP was captured last.

Marker position data were captured using an 8-camera VICON (Oxford Metrics, Oxford, UK) Nexus motion analysis system (100 Hz), and kinetic data using a Bertec (Columbus, OH, USA) force platform (1500 Hz). Five successful trials were labeled in Nexus, exported in C3D format, and post-processed in Visual 3D (C-Motion, Bethesda, MD, USA). Stance-phase angles (XYZ Cardan sequence) and external moments (expressed in the distal coordinate system) were calculated. From the array data, custom Labview software (National Instruments, Austin, TX, USA) was used to derive and extract the discrete variables of interest. Specifically, we extracted first and second peak KAM, KAM impulse, peak TL angle and peak FPA. SPSS (v17.0, IBM, New York, USA) software was used to perform single-factor, repeated measures analyses of variance on the variables, with planned pairwise comparisons between the gait conditions. The pre-determined alpha level was set to 0.05.

RESULTS AND DISCUSSION

Table 1: Subject demographics

Gender	Age (y)	Height (m)	Weight (kg)	BMI (kg/m^2)
7M, 13F	20.6 (0.7)	1.7 (0.1)	67.7 (14.5)	23.4 (4.3)

In general, the purpose of this study was to evaluate the effects on the knee adduction moment of mirror-assisted, subjectively minimal increases in foot progression angle, increased ipsilateral trunk lean, or a combination the two. The rationale for utilizing a mirror was to provide a clinically relevant mode of feedback. The paradigm of employing small changes was based on our expectation that smaller changes in TL and FPA would still provide mechanical benefit at the knee while minimizing secondary effects such as increased metabolic and cognitive loads, altered mechanics at other joints, and a less natural appearance to gait.

The TL condition yielded some unexpected results. Foremost, first peak KAM did not significantly reduce, despite average increases in TL of approximately 6 degrees (Table 2). This amount of change has yielded significant KAM reductions in other studies (Simic et al., 2012). Further, we observed a reduction in second peak KAM, which has not been observed in the literature to our knowledge. This is likely to be related to the small but significant increase in FPA during the TL condition. In regards to KAM impulse, we observed a borderline reduction (p=0.06).

For the FPA condition, we observed an increase in angle of approximately 10 degrees. This was a larger change than expected, as we asked the subjects to perform changes to a minimal extent. As expected, second peak KAM was less, while trunk mechanics and first peak KAM were unaffected. Interestingly, this study is the first to observe a decrease in KAM impulse when utilizing an increased FPA gait pattern.

The combination of increased TL and FPA in this study was a novel gait modification strategy. As expected, increased angles of TL and FPA were observed, and were remarkably similar in change magnitude to the single pattern conditions. Surprisingly, we again observed no decrease in first peak KAM. However, the second peak did reduce. Importantly, and as hypothesized, we observed a reduction in KAM impulse. KAM impulse has recently been identified as an important loading variable in knee OA research, particularly with estimating cumulative knee loading over time (Maly et al., 2013).

CONCLUSIONS

In summary, we explored the mechanical effectiveness of combining increased TL and FPA during walking at reducing KAM parameters. We found that the CP led to reductions in KAM impulse and 2nd peak KAM, but did not reduce the first peak significantly. Future interventional research should consider the utility of this combined pattern at reducing knee loading.

REFERENCES

1. Simic M et al., (2012). *Arthritis Care Res* 64:1545-1553.
2. Guo M et al., (2007). *Gait Posture* 26:436-441.
3. Maly MR et al., (2013). *Gait Posture* 37:397-401.

Table 2: Means and standard deviations for the variables of interest for the four gait conditions. Italics indicate significant difference from natural walking at the 0.05 alpha level. TL = trunk lean, FPA = foot progression angle, CP = combined pattern, KAM = knee adduction moment

VARIABLE	**GAIT CONDITION**			
	Natural	**FPA**	**TL**	**CP**
Peak TL (°)	2.3 (1.3)	2.3 (1.6)	*8.6 (2.9)*	*8.5 (2.9)*
Peak FPA (°)	9.9 (5.9)	*19.4 (6.8)*	*11.6 (6.1)*	*19.8 (6.7)*
1st Peak KAM (Nm/(kg*m))	0.269 (0.063)	0.271 (0.065)	0.257 (0.063)	0.252 (0.068)
2nd Peak KAM (Nm/(kg*m))	0.174 (0.042)	*0.130 (0.050)*	*0.155 (0.051)*	*0.121 (0.056)*
KAM Impulse (Nm*s/(kg*m))	0.080 (0.021)	*0.071 (0.025)*	0.072 (0.032)	*0.066 (0.034)*

EXPERIMENTAL ANTERIOR KNEE PAIN ALTERS ELECTROMYOGRAPHY DURING HIGH-INTENSITY LANDING AND JUMPING

[1]Matthew K. Seeley, [1]Jordan D. Pitt, [2]Jihong Park, [1]Cory G. Cosgrave, [1]Sydney Chartrand, [1]Devin Francom and [1]J. Ty Hopkins

[1]Brigham Young University, Provo, UT, USA; [2]Marshall University, Huntington, WV, USA
email: matthewkseeley@gmail.com; web: biomech.byu.edu

INTRODUCTION

Anterior knee pain (AKP) is relatively common for physically active individuals and often results in altered movement neuromechanics [1-2]. Although AKP is a primary symptom of some common knee pathologies, the independent effects of AKP are unclear; i.e., it is unclear how AKP, independent from other knee pathology factors (e.g., patellofemoral joint inflammation or degradation), affects movement neuromechanics. The purpose of this study was to evaluate how movement intensity influences the independent effects of AKP on lower-extremity muscle activation during landing and jumping. We hypothesized that the independent influence of AKP on lower-extremity muscle activation would be greater during a more intense land and jump task, relative to a less intense land and jump task.

METHODS

Thirteen able-bodied subjects (mass = 70 ± 15 kg; height = 1.74 ± 0.11 m; age = 22 ± 2 years) gave informed consent and participated in two data collection sessions (control and pain). Sessions were separated by 48 hours. For each session, subjects performed three land and jump trials at two intensities (low and high), at three times (preinjection (T1), immediately postinjection (T2), and 20-min postinjection (T3)). The land and jump trials required subjects to jump forward over one obstacle, land on a force plate, and then jump forward over a second obstacle. Obstacle height was set to 50% and 80% of a maximal height that each subject could jump over for the low- and high-intensities, respectively. Bilateral surface electromyography (EMG) was recorded for the gastrocnemius (GA), vastus medialis (VM), biceps femoris (BF), gluteus medius (GMD), and gluteus maximus (GMX). EMG was measured from 200 ms before to 200 ms after the subjects contacted the force plate (1000 Hz; Delsys, Boston, MA, USA). This duration was time normalized to 100% for each trial; the first and second 50% were considered to be landing and jumping, respectively. For each session, EMG amplitudes were normalized to the average peak amplitude from the T1 trials.

For both sessions, subjects first performed the T1 trials at both intensities (low and high). Intensity order was counterbalanced. Next, for the pain session only, we injected 1-ml of hypertonic saline (5.0% NaCl) into the right infrapatellar fat pad to induce experimental AKP. Immediately after the injection, subjects performed the T2 trials. Twenty minutes after the completion of the T2 trials, subjects performed the T3 trials; these 20 minutes allowed for AKP resolution. Except for the injection, pain and control sessions were identical. We measured subject-perceived AKP for both sessions using a 10-cm visual analog scale.

We used functional linear models to evaluate the effect of session, intensity, time, and leg on EMG amplitude ($p < 0.01$). This statistical approach allowed us to evaluate effects of these independent variables on EMG amplitude throughout the entire land and jump task, rather than only at discrete time points.

RESULTS AND DISCUSSION

In addition to expected effects of intensity (EMG was often greater for high-intensity trials than for low-intensity trials), we observed three significant differences for EMG amplitude. For the high-intensity trials of the pain session only: (1) right GA

EMG was nearly 10% greater for T1 trials than for T2 trials at 20% of the land and jump task (Figure 1A); (2) right VM EMG was 10-20% greater for T3 trials than for T2 trials at 20%, 55%, and 75% of the land and jump task (Figure 1B); (3) for T2 trials only, left GMD EMG was 20% greater than right GMD EMG at 45% of the land and jump task (Figure 1C). Additionally, as was expected, subject-perceived pain levels were significantly increased during T2 trials of the pain session only. In summary: (1) AKP affected GA, VM, and GMD activation during the high-intensity, pain-session trials only. (2) Right GA activity decreased as a result of experimental AKP during the early part of landing. (3) Right VM activity, throughout the land and jump task, increased after AKP resolution. (4) GMD activity became bilaterally asymmetrical, as a result of AKP.

These results fit with results from a previous study regarding mechanical effects of independent AKP [3]. In this previous study, we observed that, during the stance phase of walking, plantarflexion angle and net torque, knee extension torque, and hip abduction torque decreased as a result of experimental AKP. We also observed that during the stance phase of running, plantarflexion and hip adduction angles decreased as a result of experimental AKP. Collectively, present and previous data indicate that AKP can independently alter lower-extremity neural patterns and corresponding mechanics. The cause(s) of these neural adaptations is unclear. It is unclear whether these alterations are voluntary or involuntary. More data are needed to understand causes and consequences (acute and chronic) of these neural adaptations. Also, interventions that effectively mitigate these neuromechanical alterations would likely benefit individuals suffering from AKP.

In conclusion, there are two primary findings from this study. First, during landing and jumping, AKP independently inhibited activation for the ipsilateral GA, VM, and GMD. Second, the magnitude of this independent effect was influenced by movement intensity; i.e., the effect was greater during high-intensity movement, relative to low-intensity movement.

REFERENCES

1. Fredericson M & Yoon K. *Am J Phys Med Rehabil,* **85**, 234-243, 2006.
2. Bazett-Jones DM et al. *Med Sci Sports Exerc*, Jan 30 [Epub ahead of print], 2013.
3. Seeley MK et al. *J Athl Train*, In Press.

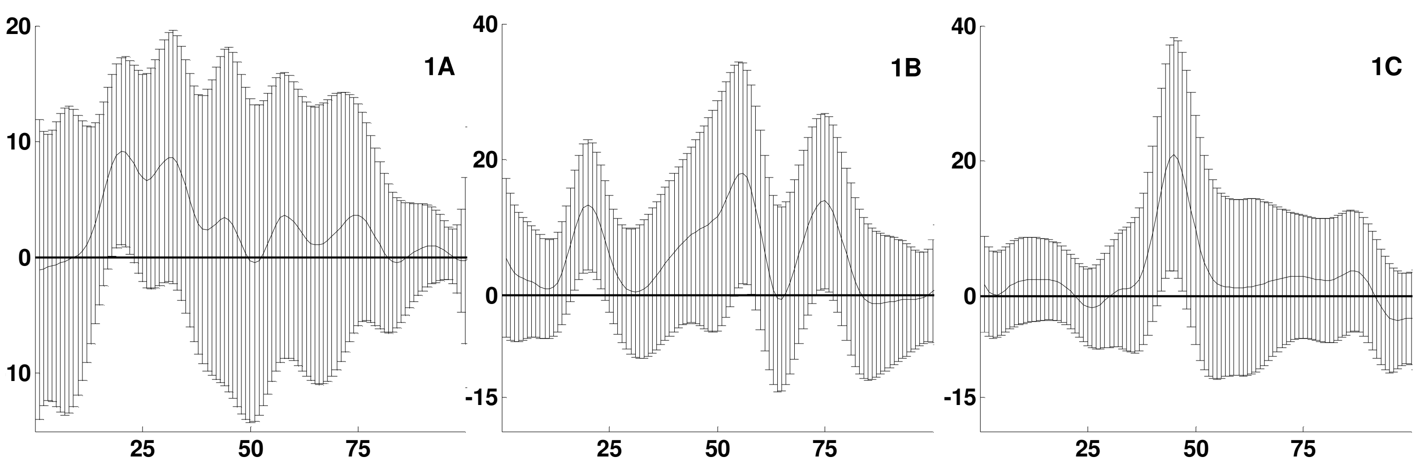

Figure 1. Mean differences and corresponding 99% confidence intervals for normalized EMG amplitude, plotted against normalized time during a high-intensity land and jump. Statistical differences are indicated when confidence intervals do not overlap zero lines. All differences occurred during the high-intensity T2 trials of the pain session.1A: right GA EMG was nearly 10% greater for T1 than for T2 at 20% of the land and jump. 1B: right VM EMG was 10-20% greater for T3 than for T2 at 20%, 60%, and 75% of the land and jump. 1C: left GMD EMG was 20% greater than right GMD EMG, during T2 only, at 45% of the land and jump.

TRANSFEMORAL AMPUTATION ALTERS PELVIS-TRUNK COORDINATION DURING WALKING: IMPLICATIONS FOR LOW BACK PAIN

Elizabeth M. Russell, Jennifer M. Aldridge Whitehead, Jason M. Wilken

Center for the Intrepid, Brooke Army Medical Center, Fort Sam Houston, TX, U.S.A.

E-mail: erussell.kin@gmail.com

INTRODUCTION

Low back pain (LBP) is common in individuals with transfemoral amputations (TFA) and their rates of pain are greater than in the general population [1]. The increased incidence of LBP is likely the result of altered gait mechanics from prosthetic use. Using continuous relative phase (CRP), Seay et al. [2] found that sufferers of LBP had greater synchronous, in-phase pelvis and trunk rotations in the frontal plane during walking than controls. Lamoth et al. [3] found that individuals with LBP never achieved the same degree of axial out-of-phase coordination as control subjects. LBP patients also have less ability to switch coordination patterns when exposed to perturbations, such as increases in walking speed [2,3,5].

The variability of CRP can also provide information on LBP. A movement with low variability is perceived as "safer" due to its predictability, but repetition may create an overuse situation [4]. Although the literature varies [2], Selles et al. [5] found lower pelvis-trunk coordination variability in patients with LBP relative to controls.

The purpose of this study was to determine if individuals with TFA, with and without LBP, demonstrate pelvis-trunk coordination consistent with populations with LBP. A secondary purpose was to determine if coordination modulates with walking speed.

METHODS

Seven TFA with LBP (TFA-LBP), nine TFA with no pain (TFA-NP), and twelve control subjects participated. TFA-NP indicated a response on a Prosthetics Evaluation Questionnaire of LBP frequency as "never" or "only once or twice" in the past 4 weeks. TFA-LBP indicated a LBP frequency ranging from "one time per week" to "all the time".

Overground gait was analyzed with three-dimensional motion capture (Motion Analysis, 120 Hz) as participants walked at slow, moderate and fast speeds corresponding to Froude numbers of 0.10, 0.16, and 0.23, respectively. Trunk and pelvis segment angles were calculated during eight strides initiated with the prosthetic limb in both TFA groups, and right limb in the control group. CRP and CRP variability were calculated as per Hamill et al. [4].

A repeated-measures ANOVA tested for significant main effects of group and speed. Paired t-tests and Tukeys post hoc tests identified pair-wise differences. Criterion for statistical significance was set at $p<0.05$.

RESULTS AND DISCUSSION

Group	Age (yrs)	Height (m)	Mass (kg)	Months ambulating
TFA-LBP	32.1* (5.2)	1.80 (0.06)	90.6* (10.9)	23 (21)
TFA-NP	28.4 (6.4)	1.79 (0.07)	82.4 (8.0)	43 (20)
Control	25.1 (3.1)	1.79 (0.06)	79.5 (10.0)	-

Table 1: Mean (standard deviation) subject characteristics. * indicates a significant difference from the control group. There were no significant differences between patient groups.

The TFA groups exhibited significantly different CRP values relative to the control group in the sagittal ($p<0.001$) and frontal ($p=0.001$) planes (Fig 1). Both TFA groups also responded in a manner similar to non-amputees with LBP [2].

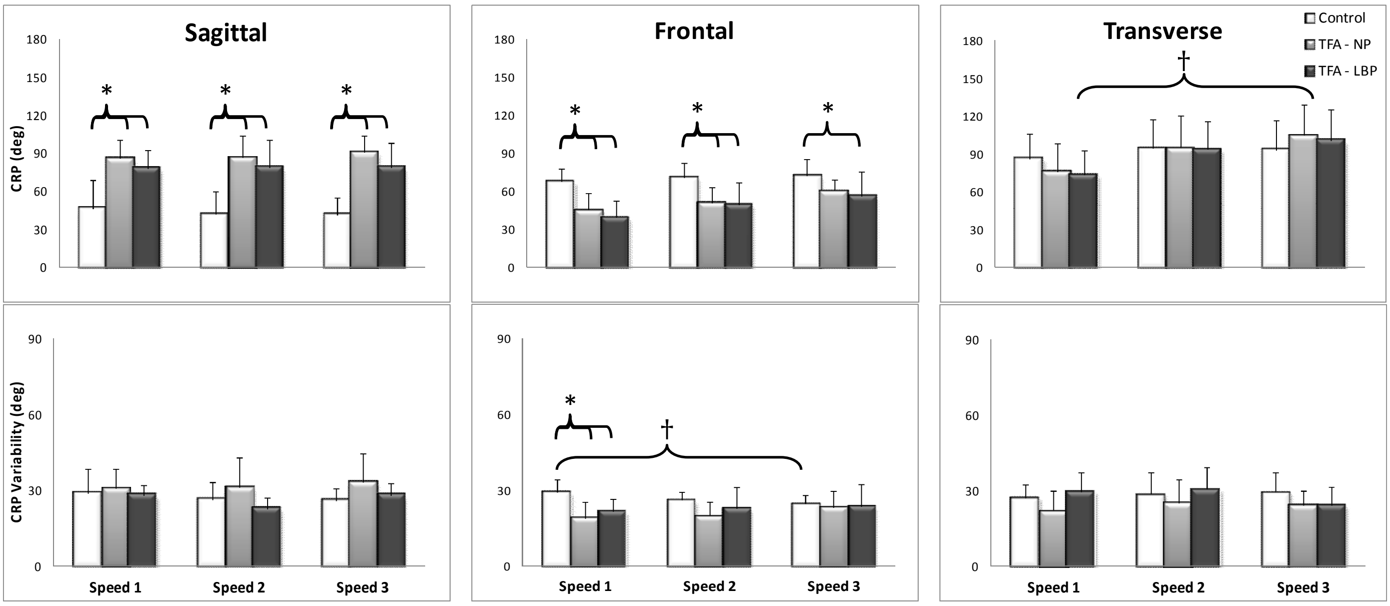

Figure 1: Mean CRP (top) and CRP variability (bottom) of trunk-pelvis coordination during walking with standard deviation bars. * indicates group differences and † indicates speed differences.

Although the greatest pelvis and trunk ranges of motion typically occur in the transverse plane during walking to control angular momentum, transverse CRP were not significantly different among groups.

Transverse CRP, in particular, was expected to increase with speed, but this was only found in the TFA groups ($p_{interaction} = 0.018$). Both TFA groups demonstrate an apparent phase transition between the lowest speeds. The speed differences may not have been sufficiently challenging to require adaptation by the control group but both TFA groups transitioned at lower levels of perturbation.

CRP variability was not significantly different among groups, with the exception of lower values in the TFA groups relative to the controls in the frontal plane at the slowest speed (p=0.014 and p=0.001 for TFA-NP and TFA-LBP, respectively, relative to controls).

SUMMARY/CONCLUSIONS

Individuals with TFA demonstrated some coordination patterns that were different from able-bodied individuals, but consistent with persons with LBP. The patient groups were able to control transverse plane rotations to the same extent as non-amputees, but may do so by neglecting optimal coordination in the sagittal and frontal planes. Interestingly, individuals with TFA with and without LBP were not significantly different.

Although a cause and effect relationship between CRP and future development of LBP has yet to be determined, the results of this study add to the literature attempting to characterize biomechanical parameters of LBP in high-risk populations.

REFERENCES

1. Ehde et al., (2000). *Arch Phys Med Rehabil*, **81**, 1039-44.
2. Seay et al., (2011). *Clin Biomech*, **26**, 572-8.
3. Lamoth et al., (2002). *Spine*, **27**, 92-9.
4. Hamill et al., (1999). *Clin Biomech*, **14**, 297-308.
5. Selles et al., (2001). *Clin Biomech*, **16**:175-81.

ACKNOWLEDGEMENTS

Funding for this study was provided by the U.S. Army Telemedicine & Advanced Technology Research Center and The Center for Rehabilitation Sciences Research.

A COMPARISON OF TORSO STABILITY BETWEEN BED REST SUBJECTS AND ASTRONAUTS DURING TANDEM WALK: PRELIMINARY FINDINGS

[1]Chris Miller, [1]Brian Peters, [1]Igor Kofman, [1]Rachel Brady, [1]Tiffany Phillips, [2]Crystal Batson, [3]Ajitkumar Mulavara, [4]Alan Feiveson, [4]Millard Reschke and [4]Jacob Bloomberg

[1]Wyle Science Technology & Engineering Group, Houston, TX, USA
[2]MEI Technologies Inc., Houston, TX, USA
[3]Universities Space Research Association, Houston, TX, USA
[4]NASA Lyndon B. Johnson Space Center, Houston, TX, USA
Email: chris.miller-1@nasa.gov

INTRODUCTION

During spaceflight, crewmembers experience a microgravity environment that results in a central reinterpretation of both vestibular and body axial-loading information by the sensorimotor system. Bed rest studies have been developed as a ground-based analog to spaceflight. Subjects lie at 6° head-down in strict bed rest to simulate the fluid shift and gravity-unloading of the microgravity environment. However, bed rest subjects still sense gravity in the vestibular organs. Therefore, bed rest isolates the axial-unloading component, thus allowing for the direct study of its effects.

The Tandem Walk (that is, walk on floor eyes closed) is a standard sensorimotor test of dynamic postural stability [1]. Normally, the performance metric is the number of steps the subject can complete without sidestepping. In this analysis, we used linear acceleration of the torso as the performance metric as it provides additional information about the subject's stability during the test. The purpose of this study was to compare torso stability during the Tandem Walk test between bed rest control subjects, short-duration (Space Shuttle) crewmembers, and long-duration International Space Station (ISS) crewmembers during their recovery from bed rest or spaceflight.

METHODS

All subjects provided written informed consent before participating in this study that was approved in advance by the NASA Lyndon B. Johnson Space Center Institutional Review Board.

This study is part of a larger protocol that uses a suite of physiologic tests and functional tasks to relate physiologic changes to changes in functional performance of mission-critical tasks immediately postflight or after bed rest. Subjects who have completed the study to date include: (a) 5 bed rest controls (4M/1F; 36.8 ± 7.9 yr; 66 ± 2.2 in.; 163.2 ± 17.9 lb), all of whom completed 70 days of 6-degrees head-down strict bed rest with no exercise countermeasure; (b) 6 short-duration crewmembers (4M/2F; 43.0 ± 5.6 yr; 70 ± 1.5 in.; 168.2 ± 17.6 lb) who completed Space Shuttle missions (13.2 ± 1.5 d), and (c) 7 long-duration crewmembers (6M/1F; 47.8 ± 2.3 yr; 70 ± 2.8 in.; 188.1 ± 32.8 lb) who completed missions aboard the ISS (152.6 ± 18.2 d). Data collection sessions occurred twice within a 2-month or 2-week time period before flight or bed rest, respectively (PRE), and four times after flight/bed rest: on the day of landing or end of bed rest (Post+0d), 1 day post (Post+1d), 6 days post (Post+6d) and a final session 10 days (bed rest) or 30 days (flight) post (Post+10/30). Due to logistical limitations, data could not be collected from long-duration crewmembers on landing day.

In the Tandem Walk test, the subject walked in a heel-to-toe fashion at a self-selected speed for 10 to 12 steps with their arms crossed on their chest and their eyes closed. A spotter walked next to the subject to ensure safety and to monitor the step count. Three Tandem Walk trials were performed per session.

Torso and head linear accelerations (relative to their respective local coordinate systems) were recorded using triaxial inertial measurement units (Xsens, North America Inc., Culver City, CA, USA) sampled at 50 Hz. During the analysis, the start and end of the trial were manually selected by inspection of the plot of the vertical acceleration of the head. Data were then rotated into the global coordinate system, and the gravitational acceleration was removed from the Z-component. The resultant linear acceleration of the torso was calculated at each time point of the trial. The root-mean-square (RMS) of the torso accelerations within a set window centered on the mid-point of the trial was then computed. A separate analysis revealed no significant difference between the two PRE sessions, so all PRE data were pooled. Finally, a preliminary mixed-model analysis of the differences in RMS values for each postflight/bed rest session relative to PRE (with three outliers removed) was used to compare group × session interactions; that is, changes from preflight/bed rest to postflight/bed rest values between groups.

RESULTS AND DISCUSSION

All groups exhibited increased torso instability (that is, higher RMS values) during Tandem Walk immediately postflight/bed rest (Figure 1). This suggests that axial-unloading alone – as is the case in bed rest – could result in decrements in Tandem Walk performance.

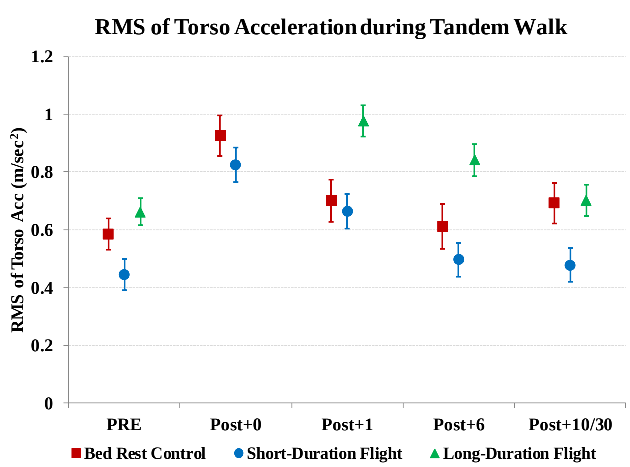

Figure 1: RMS estimated means (± SE) of the torso resultant acceleration across sessions and groups.

The preliminary mixed-model analysis showed confidence intervals for interaction effects that encompassed preponderantly positive values when comparing the long-duration crewmembers and the bed rest controls for the Post+1d and Post+6d sessions (Figure 2), and the short- and long-duration crewmembers for the Post+6d session. This seemed to indicate that, in long-duration crewmembers, the vestibular component further impaired torso stability postflight (that is, increased RMS), beyond that attributable to the axial-unloading component alone.

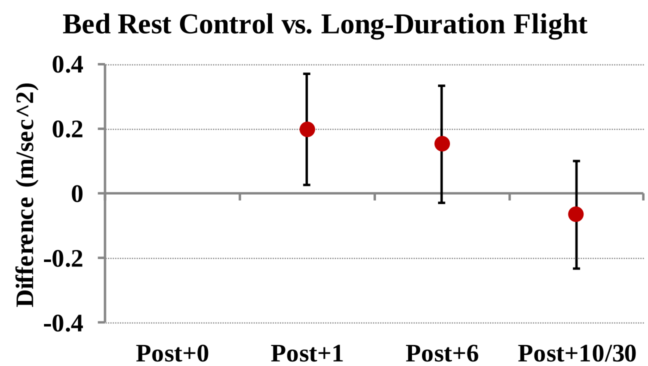

Figure 2: Mean estimate with 95% confidence intervals of the difference of the (post-PRE) session differences for the RMS of the torso acceleration between bed rest controls and long-duration fliers.

CONCLUSIONS

Body unloading alone, as in strict bed rest, resulted in decreased Tandem Walk performance (as measured by the RMS of torso acceleration) immediately post-bed rest. Central reinterpretation of vestibular information by the sensorimotor system during extended exposure to microgravity may further compromise torso stability during Tandem Walking postflight.

REFERENCES

1. Fregly, AR, et al. *Aerospace Medicine* **43**, 395-399, 1972.

ACKNOWLEDGEMENTS

This study is funded by the National Aeronautics and Space Administration.

KINEMATIC VARIABILITY AND ACCELEROMETERS DEMONSTRATE A LACK OF AGREEMENT

[1]Carlee Howe, [1]Ryan Hasenkamp, [1]Shane R. Wurdeman, [1]Sara A. Myers, [1]Bryan Arnold

[1]University of Nebraska at Omaha, Omaha, NE, USA
Email: samyers@unomaha.edu, web: nbcf.unomaha.edu

INTRODUCTION

Analysis of human gait variability can provide insight into the motor control of human movement. Gait variability can be quantified through both linear and nonlinear mathematical algorithms. Linear measures give insight into the amount of variability, or how far a time series deviates from the mean. Nonlinear measures give insight into the temporal structure of variability, or how a time series changes over time. Based upon nonlinear measurements, Optimal Variability Theory was developed stating that healthy gait has a specific temporal structure [1]. Deviations from this optimal variability have been associated with aging, disease, and delayed development [1, 2]. However, there are limitations to the current methods of assessing gait variability mainly because they utilize a laboratory setting usually using expensive 3-dimensional motion capture. Walking under laboratory conditions may not accurately reflect daily ambulation. Furthermore, the equipment and expertise to perform gait analysis may not be readily available to the clinicians who need to assess physical function. Inertial measurement sensors have been used for estimating the structure of variability during walking [3]. However, the use of such sensors and other accelerometers has not been validated. Accelerometers are less expensive and would thus be a more attractive clinical device. Therefore, the purpose of this study was to determine the agreement between the ambulatory activity obtained from an accelerometer and gait kinematic variability obtained through traditional gait analysis in the laboratory.

METHODS

Nineteen healthy young adults (age: 27 ± 4.9 years, weight: 69.8 ± 23.0 kg, height: 165.9 ± 38.0 cm) were recruited to participate in this study. Subjects walked on a treadmill while 3D marker trajectories (60 Hz; Motion Analysis Corp., Santa Rosa, CA) were recorded. Simultaneously, a tri-axial accelerometer (100 Hz; ActiGraph wGT3X+, Pensacola, FL) worn at the right hip recorded raw acceleration (milli-Gs). Subjects walked on the treadmill at self-selected speed (2.9 ± 0.4 mph) for ten minutes. The continuous joint angle time series was calculated at the right ankle, knee, and hip. Raw vertical acceleration was collected from the accelerometer. The largest Lyapunov exponent (LyE) was calculated for the joint angle time series at each joint and for the raw vertical acceleration using the Wolf's algorithm [4]. LyE is a nonlinear tool that evaluates the temporal structure of variability. For a continuous time series, it measures the divergence of the data set's trajectories in state space [4]. Bland Altman statistical methods were used to assess agreement and repeatability of measurements of LyE between gait kinematics and acceleration [5]. Bland Altman plots depicting the difference in the two measures against the mean of the two measures were used to graphically display the agreement and reliability. Agreement levels were set at ±2*standard deviation of the differences.

RESULTS AND DISCUSSION

Calculations of LyE are shown in Figure 2 (ankle: 0.93 ± 0.46, knee: 0.88 ± 0.25, hip: 0.78 ± 0.41 and acceleration: 2.62 ± 0.59). Results from the Bland-Altman statistic demonstrate how much the measurement from the accelerometer is likely to differ from the measurement of gait kinematics. The Bland-Altman plots in Figure 1 demonstrate a lack of agreement between gait kinematic variability at the ankle, knee, and hip and accelerometer measures with differences in LyE of up to 1.5 bits/s.

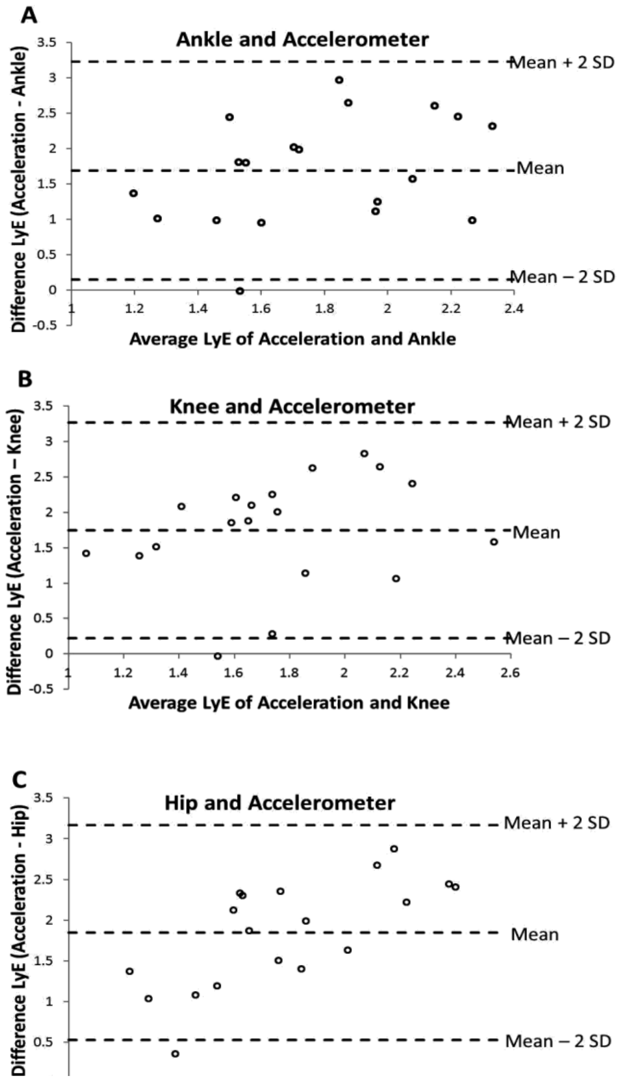

Figure 1. Bland-Altman plots depicting difference between LyE of acceleration and kinematics for A: the ankle B: the knee and C: the hip against the mean of the two measures.

The limits of agreement between LyE at the ankle and LyE of acceleration were 3.232 and 0.150. At the knee, the limits were 3.267 and 0.222. The limits of the hip were 3.167 and 0.529. These limits are large and should be considered beyond acceptable in a clinical setting.

The expanded measures from inertial sensors compared to accelerometers (i.e. angular measures) may improve agreement between the portable device and the gold standard motion capture system. However, importantly, the use of inertial sensors have also not been tested for agreement, but rather only shown to have a relationship. Such a means to verify inertial sensors can be questioned [5]. In addition, we have chosen to validate the accelerometer against joint angle measures due to

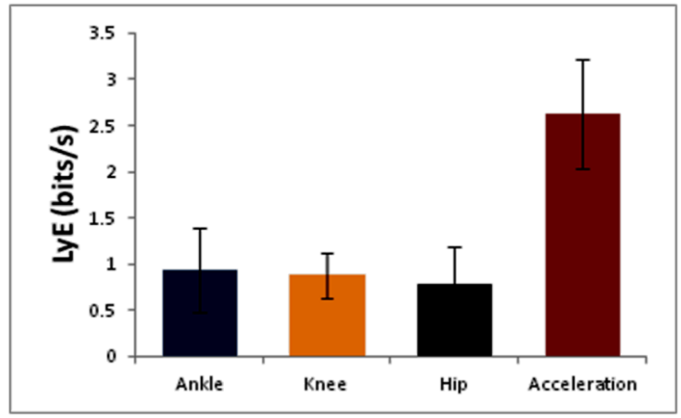

Figure 2. Lyapunov Exponent of the ankle, knee, hip, and acceleration.

the large amount of previous work showing the value of investigating joint angle measures compared to simple proximal trunk motions. The LyE is specific to the task, and thus any position sensor worn at the trunk may not be representative of task dynamics of the lower limbs.

CONCLUSION

There was a lack of agreement between the LyE of gait kinematic variability at the ankle, hip, and knee and accelerometer measures while walking on the treadmill. Further work is needed to investigate agreement between such portable movement devices (i.e. accelerometers, inertial sensors, etc.) and the structure of variability of the lower limbs. Validating such an instrument will allow for translation from the laboratory to the clinic.

REFERENCES

1. Stergiou N et al. *J Neurol Phys Ther*. 2006 Sep;**30**(3):120-9
2. Bruijn SM et al. *Ann Biomed Eng*. 2010 Aug;**38**(8):2588-93.
3. Myers S et al. *J Vasc Surg*. 2009 Apr;**49**(4):924-931.
4. Wolf A et al. *Physica D*. 1985 July;16(3):285-317
5. Bland J. Altman D. *The Lancet*. 1986 Feb;307-310

ACKNOWLEDGEMENTS

The work was supported by UNO UCRCA, NIH (1R01AG034995), VA RR&D (1I01RX000604).

GROUND REACTION FORCE AND LOWER EXTREMITY JOINT ANGLE ACCLIMATION DURING TREADMILL WALKING WITH AND WITHOUT LOAD

Angela C. Boynton
U.S. Army Research Laboratory, Aberdeen Proving Ground, MD, USA
email: angela.c.boynton.civ@mail.mil

INTRODUCTION

Treadmills provide a convenient means to collect multiple consecutive strides of gait data at precisely controlled speeds and grades. Numerous studies have evaluated differences in gait kinematics, muscle activity and energy expenditure between unloaded (i.e. without a backpack or other carried load) walking over ground and on a treadmill (TM), with the general conclusion that they are reasonably similar [1, 2]. However, there is some evidence that a period of acclimation to TM walking is needed to achieve these equivalent gait dynamics [3]. TMs are frequently used to collect biomechanics data during load carriage. Various changes in gait mechanics have been reported to occur in response to load carriage, suggesting that acclimation time may also be needed during loaded TM walking. To date, the time required for these changes in gait dynamics to stabilize remains unknown. Therefore, the purpose of this study was to quantify changes in ground reaction forces (GRFs) and sagittal plane knee and ankle angles over several minutes of treadmill walking with and without a carried load.

METHODS

Thus far, data has been collected for four males with recent military load carriage experience (mean age: 28.5 yrs, mean body mass: 77.3 kg). GRFs and lower extremity joint angles were evaluated over 7 minutes of walking at a self-selected pace on a force-sensing treadmill (AMTI, Watertown, MA), with and without load. Subjects wore a t-shirt, shorts and combat boots during both conditions. During the loaded condition they additionally carried a 33 kg rucksack. Peak vertical and anterioposterior GRFs, and sagittal plane knee and ankle angles were calculated from force plate and motion capture data collected at the 30-second mark during each minute of walking.

RESULTS AND DISCUSSION

Peak anterioposterior GRFs and stance phase ankle plantarflexion angle increased substantially over 7 minutes of walking with the rucksack load, and peak ankle dorsiflexion during stance increased over time for both conditions (Figure 1).

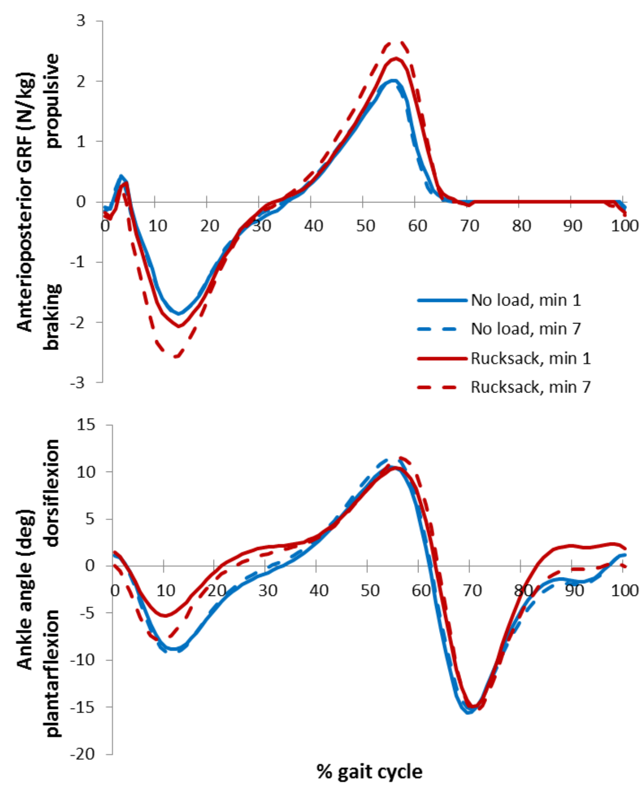

Figure 1: Anterioposterior GRF and sagittal ankle angle during walking with and without a rucksack.

During the rucksack condition, peak braking force increased from the first to third minute and then again between the final two minutes of walking, while propulsive force increased more progressively over the 7-minute period (Table 1). Stance phase plantarflexion during the loaded condition increased from minute 1 to 3 and again from minute 4 to 5, but was relatively unchanged during the remaining walking time. During both conditions, stance phase dorsiflexion increased by a similar amount over the entire walking period, stabilizing during minutes 4 and 5 and again during minutes 6 and 7. Peak vertical GRF, swing phase plantarflexion and knee flexion values were relatively unchanged over seven minutes of walking, regardless of load condition.

Matsas et al. [3] previously reported that 6 minutes of TM walking were required to achieve stable sagittal plane knee angles. However, the results of this study suggest that knee angles change very little during TM walking, even under load carriage. This finding is more consistent with those of other TM studies [1, 2].

Except for ankle dorsiflexion, peak values for the evaluated variables remained fairly stable over the entire unloaded walking period. In contrast, during load carriage, it appears that 5 to 6 minutes of walking are needed to achieve stable sagittal plane ankle angle and anterioposterior GRF and patterns.

As additional data are collected (11 more subjects planned), statistical significance of the changes observed during the loaded condition will be determined. Whether the resulting gait patterns are similar to those during over ground walking at the same speed will also be established. Further research is needed to ascertain the reasons for the observed changes and determine if additional changes occur over longer walking periods.

CONCLUSIONS

Preliminary results indicate that changes in anterioposterior ground reaction forces and sagittal plane ankle angles during treadmill walking differ between unloaded and loaded walking. It also appears that a treadmill acclimation period of at least 5 minutes is needed to achieve stable gait dynamics during load carriage.

REFERENCES

1. Alton F, et al. *Clin Biomech* **13**, 434-440, 1998.
2. Murray MP, et al. *J Appl Physiol* **59**, 87-91, 1985.
3. Matsas A, et al. *Gait & Posture* **11**, 46-53, 2000.

Table 1: Changes in ground reaction forces, knee and ankle angles over 7 minutes of treadmill walking. Bold italicized values indicate substantial change from prior minute.

% change from 1st minute		Minute of treadmill walking					
		2	3	4	5	6	7
Vertical GRF	**No load**	-1.31	-0.57	-1.41	-1.49	-0.94	-0.19
	Rucksack	0.92	-1.20	0.89	-1.22	-1.53	-2.23
Braking GRF	**No load**	1.63	-2.41	2.65	3.92	4.45	0.98
	Rucksack	***13.21***	***16.89***	20.17	18.78	17.93	***23.44***
Propulsive GRF	**No load**	-3.41	-2.95	-3.00	1.84	-0.64	-0.25
	Rucksack	1.18	***3.96***	3.92	***6.55***	6.20	***10.75***
Plantarflexion, stance	**No load**	0.55	7.72	2.33	1.02	-5.29	1.84
	Rucksack	***10.18***	***21.09***	19.20	***31.76***	27.62	30.87
Dorsiflexion, stance	**No load**	1.02	1.34	***4.26***	3.77	***9.01***	9.40
	Rucksack	1.62	***5.21***	6.65	6.12	***9.14***	8.27
Plantarflexion, swing	**No load**	-1.10	5.50	-3.25	0.04	0.07	1.11
	Rucksack	6.42	0.37	8.79	-2.69	-5.29	4.99
Knee flexion, stance	**No load**	1.01	1.38	1.79	2.27	1.97	1.41
	Rucksack	1.36	-0.11	-0.02	-0.12	0.82	-2.06
Knee flexion, swing	**No load**	-0.47	0.21	0.79	1.06	1.30	2.13
	Rucksack	0.95	1.79	2.55	2.23	3.39	1.99

NONLINEAR EFFECTS OF BODY WEIGHT ON GROUND REACTION FORCE PEAKS: IMPLICATIONS FOR NORMALIZATION

Martyn Shorten

BioMechanica LLC, Portland, OR, USA.
email: Martyn.Shorten@biomechanica.com

INTRODUCTION

Ground reaction force (GRF) measurements are commonly reported in bodyweight (BW) units. Division normalization of this type reduces the contribution of body size differences to the variance among subjects. Several researchers have noted that peak force measurements can remain significantly correlated with BW, even after normalization. Most recently, Wannop *et al*. [1] examined GRF components and inverse dynamic parameters in both walking and running and found multiple examples of statistically significant non-linear scaling with BW. In many cases, normalization using offsets and power curves more effectively removed correlations with BW than simple division.

The GRF scaling functions reported in [1] are empirical estimates and lack an underlying physical basis. This paper proposes that non-linear scaling of vertical GRF peaks with BW during running is a fundamental outcome of Newtonian dynamics.

THEORY

Force plate measurements implicitly assume a point-mass dynamic model. The notion that the vertical GRF component (*Fz*) scales with BW = *mg* is strictly only true under certain conditions - static loading (Eqn. 1) and constant acceleration (Eqn .2).

$$F_z - mg = 0; \quad \frac{F_z}{mg} = 1 \tag{1}$$

$$F_z - mg = ma; \quad \frac{F_z}{mg} = 1 + \frac{a}{g} \tag{2}$$

Also, for locomotion on a level surface, net impulse is constrained (Eqn. 3) so that over a sufficient time period (T) the *average* value of F_z, is proportional to BW. However, there is no requirement that instantaneous peaks scale with BW.

$$\int_0^T \left(F_z(t) - mg\right) = 0 \tag{3}$$

A mass-spring model of running [2] provides a simple example of non-linear scaling of peak loads with BW. A leg-spring with linear stiffness k has the characteristic equation $F_z - mg = k\,x$ and the (unscaled) equation of motion is

$$F_z(t) = mg\left(1 - Cos(\omega t)\right) + \sqrt{k\,m}\,v_0 Sin(\omega t) \tag{4}$$

where $\omega = \sqrt{k/m}$ is the natural frequency.

A leg-spring step with initial contact velocity v_0 at produces a peak vertical force of magnitude

$$F_{\max} = mg\left(1 + \sqrt{1 + \frac{k}{mg}\frac{v_0^2}{g}}\right) \tag{5}$$

While BW = *mg* is a factor in the peak force outcome, division normalization retains a residual effect since $F_{\max}/(mg)$ is also function of $f\,(mg)^{-½}$:

$$\frac{F_{\max}}{mg} = 1 + \sqrt{1 + \frac{k}{mg}\frac{v_0^2}{g}} \tag{6}$$

Also, during steady state running, the impulse criterion (Eqn. 2) constrains the relationship between $F_{\max}$ and contact time (Tc), introducing another nonlinear effect:

$$Tc = \frac{2}{\omega} Cos^{-1}\left(\frac{1}{1 - F_{\max}/mg}\right) \tag{7}$$

METHODS

The previously published data set included GRF records (1200 Hz) from 20 male subjects running multiple trials at 4.0 m s^{-1} ± 0.2 sd in moderately (57^{th} percentile) cushioned running shoes [3]. Results for the second vertical force peak (Fz_2) were examined for BW effects of the type reported by

Wannop *et al*. [1]. The same data were used to test the scaling effect proposed by Eqn. 6 using parameters calculated from net impulse and *Tc*.

RESULTS

After division normalization, a residual correlation between Fz_{max}/BW and BW was observed (Fig.1a). The trend was consistent with that reported by [1] but had low statistical significance (p<0.10). However, normalization preserved the important inverse relationship between Fz_{max}/BW and *Tc* predicted by Eqn 7 (Fig 2b).

Figure 1c shows evidence that the nonlinear scaling of Fz_{max} with BW resembles the effects of gravity acting on a simple mass-spring impact (Eqn. 6).

DISCUSSION

Normalizing biomechanical measures to account for dissimilar body sizes is a useful and widely employed analytical tool. However, scaling to BW is strictly only valid for static and steady state conditions. Under dynamic conditions residual effects of BW in the scaled force parameters are to be expected. A complete accounting of dynamic similarities requires force, dimension and time to be normalized. The common practice of scaling force alone may distort outcomes. Normalizing the time dimension to *Tc* (rather than the inter-step interval) adds complexity by destroying the impulse balance of Eqn. 3 and by masking the relationship between Fz_{max} and *Tc* (Eqn. 7, Fig 1b).

Both the theory and data presented here suggest a relationship between vertical GRF peaks and BW that includes both offset and a nonlinear (power law) effects. The offset and a portion of the nonlinearity are directly attributable to the effects of gravity. Gravity is not a component of horizontal forces (*Fxy*) but non-linear scaling of inertia effects persists ($Fxy/BW \propto (mg)^{-½}$) so scaling of *Fx*y to BW may not always be appropriate. Indeed, Wannop *et al*. [1] found that division scaling of medio-lateral force peaks could, in some cases, introduce a correlation with BW into the results.

This report is specifically limited to the vertical GRF component during running. However, since the observed scaling appears to be largely a consequence of gravity, the effect is probably more widely applicable. Also, the nonlinearities in *Fz* scaling must propagate to inverse dynamic parameters (e.g. joint moments) that depend on *Fz*.

CONCLUSION

The action of gravity has nonlinear effects on the relationship between dynamic vertical GRF peaks that are not removed by normalization to BW. Consistent with the empirical results of [1], the effects imply both offset and power law scaling.

REFERENCES

1. Wannop JW, et al. *J Applied Biomech* **28**, 665-676, 2012.
2. Blickhan R. *J Biomech* **22**,1217-1227, 1989.
3. Shorten MR. et al. *Footwear Science* **3**, 41-58, 2011.

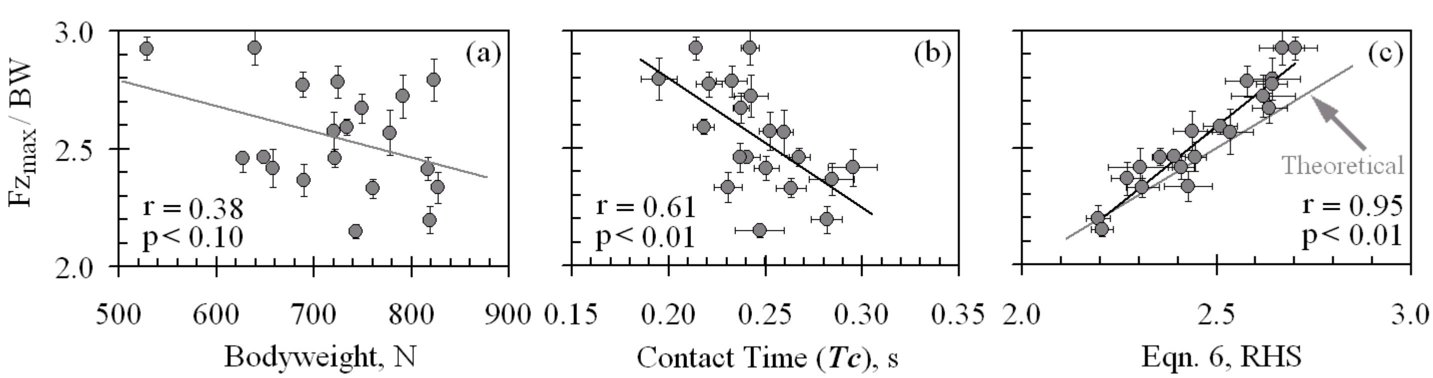

Figure 1: Normalized peak force (Fz_{max}) and (a) residual effect of bodyweight (b) contact time (c) Nonlinear scaling of the leg spring model (Eqn. 6). Errors bars show sd of subject trials.

BIPLANE FLUOROSCOPIC ANALYSIS OF THE HINDFOOT USING MODEL-BASED TRACKING TECHNIQUES: A STATIC PHANTOM STUDY

[1]Janelle A. Cross, [1]Ben McHenry, [1]Gerald F. Harris and [1]Taly Gilat Schmidt

[1]Marquette University, Milwaukee, WI, USA
email: janelle.cross@marquette.edu, web: http://www.tech4pod.org

INTRODUCTION

Dynamic assessment of skeletal kinematics is necessary for understanding normal joint function, in addition to effects of injury or disease [1, 2]. Conventional methods of motion analysis track skin-mounted optical markers with cameras to determine joint motion of the underlying bones. While these methods are simple, easy to implement and appropriate for various clinical and research related applications, they have been found to suffer from error due to movement (artifact) of the skin on which the markers are placed [3]. Due to the numerous bones and articulating surfaces within the foot and ankle, several rigid body assumptions are made to divide the foot into multiple segments for motion analysis. This method does not allow for obtaining inter-tarsal kinematics or kinetics of the hindfoot. A technique that locates the talus during gait analysis would allow for more advanced subtalar motion assessment and a more accurate estimate of hindfoot kinetics.

Fluoroscopy allows direct visualization of underlying bones by obtaining a sequence of x-ray images of a joint as it undergoes motion. This technology offers a valuable complement to conventional optical methods of motion analysis by providing a means of dynamic weight-bearing intra-articular motion measurements that are otherwise difficult to achieve. It has been used to track bone motion in animals, and in the human shoulder and knee [1, 2, 4]. Our group has previously reported hindfoot kinematics obtained from a single gantry in a population of adults, both shod and barefoot [5]. The ability of fluoroscopic analysis to have direct visualization of bony structures reduces the inaccuracies due to skin markers and enables analysis of the shod and orthotically braced foot [1].

Model-based fluoroscopy identifies bony position and orientation by comparing a three dimensional (3D) bone model to the acquired biplane fluoroscopic images. The 3D model is created from computed tomography (CT) or magnetic resonance (MR) images by identifying and segmenting the anatomy of interest. The accuracy of the model-based method was found to be within 0.8 mm of translation and 2.5° of rotation of the gold standard measurements performed with implanted bony markers [2]. The goal of this study was to develop a unique biplanar system that uses model-based tracking methods to perform *in vivo* analysis of the hindfoot.

METHODS

A biplane system was constructed centered along a 7 m raised walkway with an embedded 46.4 by 50.8 cm force plate (AMTI OR6-500 6-DOF, Watertown, MA). Two x-ray sources (OEC 9000, GE, Fairfield, CT), and two images intensifiers (15" diam., Dunlee, Aurora, IL) were mounted to the walkway with a 60 degree angle between the sources. High-speed cameras (N4, IDT, Pasadena, CA) were attached to each image intensifier. Cameras had 52mm lenses (Nikon, Melville, NY). The images were captured and digitized directly to a controller PC via Motion Studio 64 (Version 2.10.05, IDT, Pasadena, CA). The source-to-detector and source-to-object-center distances were 112 cm and 76 cm, respectively.

Open source software, X-Ray Reconstruction of Moving Morphology (XROMM, Brown University, Providence, RI) was used for image intensifier distortion correction. Two calibration frames of 1.20 mm thick perforated steel with 3.18 mm diameter holes spaced 4.76 mm apart in a staggered pattern were cut to fit the face of the image intensifiers (part no. 9255T641, McMaster-Carr, Robinson, NJ). The distortion correction algorithm in XROMM compares the spacing between the holes of the calibration frame in the fluoroscopic image with the true spacing and calculates a transformation matrix for correcting the images [4]. A foot/ankle phantom (XA241L, Phantom Lab Inc) was placed on the force plate in the middle of the irradiated area. Static images were collected with the x-ray sources set at 100 kV and 2.5 mA, with an estimated 10 µSv of radiation per trial.

RESULTS AND DISCUSSION

A unique biplane fluoroscopy system designed for hindfoot analysis was built, configured, tested and approved through the State and medical IRB for subject/patient testing. In order to quantify the cross-scatter contamination in the biplanar system, a study was performed [6]. Contamination was found to be relatively low when imaging distal extremities. Image intensifiers introduce distortion on the order of 10% that is corrected prior to motion analysis to minimize 3D tracking errors [1]. Images of the calibration frames were corrected for geometric distortion using the XROMM distortion correction algorithm to create a transformation matrix. This matrix was then applied to images of the static foot/ankle phantom. Figure 1A shows the raw distorted image of the phantom foot while figure 1B shows the foot after the application of the distortion correction algorithm. The undistorted image is smaller due to the edges of the image being reduced to their exact size. Further research is needed using dynamic phantom studies, along with continued patient pilot studies to further validate the biplanar system and model-based tracking software to implement full biplanar kinetic capability.

REFERENCES

1. Tashman S, et al. *J Biomech Eng* **125**, 238-245, 2003.
2. You BM, et al. *Medical Imaging, IEEE Transactions* **20**, 514-525, 2001.
3. Cappozzo A, et al. *Clin Biomech* **11**, 90-100, 1996.
4. Brainerd EL, et al. *J Exp Zool*, **313**, 262-279, 2010.
5. McHenry B, et al. *Proceeding of GCMAS*, Grand Rapids, MI, USA, 2012.
6. Cross JA, et al. *Proceeding of SPIE*, Lake Buena Vista, FL, USA, 2013.

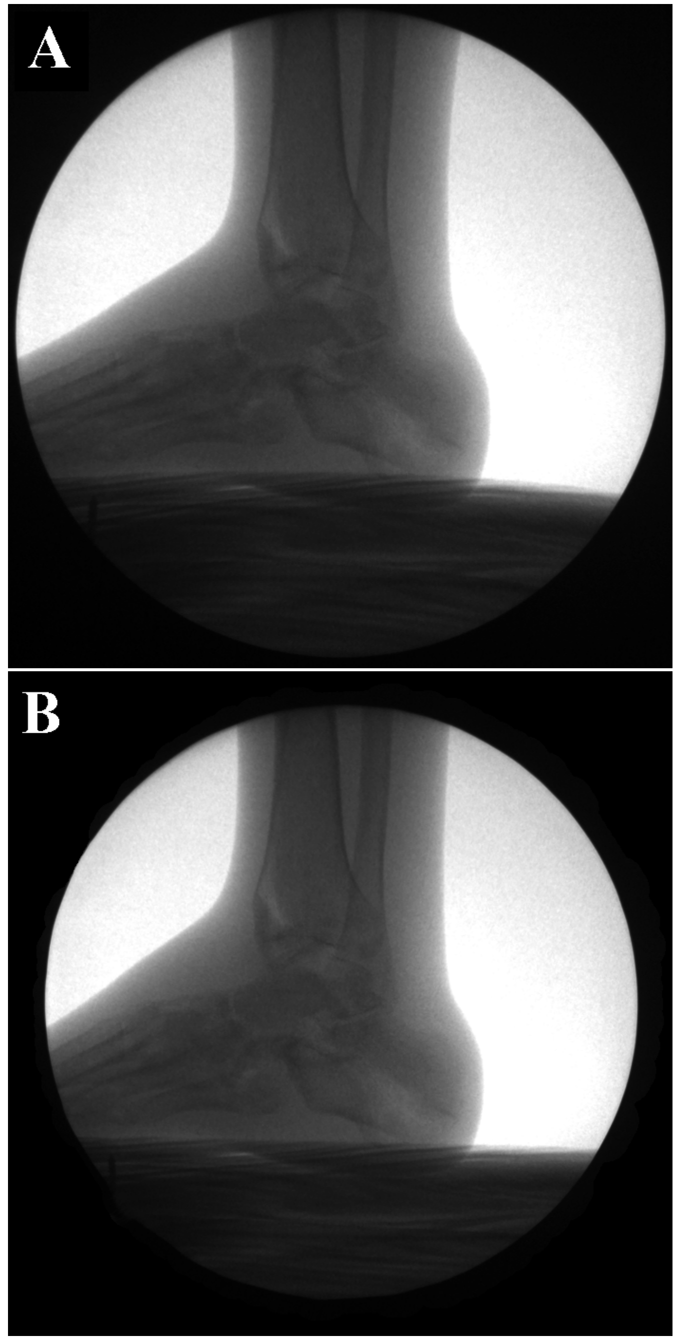

Figure 1: Correction of fluoroscopic distortion. A: Raw, distorted image of static phantom foot. B: After distortion correction algorithm applied.

ACKNOWLEDGEMENTS

Contents of this paper were developed under a grant from the Department of Education, NIDRR grant number H133E100007. However, contents do not necessarily represent the policy of the Department of Education, and you should not assume endorsement by the Federal Government.

MOMENTS OF INERTIA OF THE SHANK CHANGE MARKEDLY DURING DROP LANDINGS

Matthew T.G. Pain

Loughborough University, Loughborough, UK
email: m.t.g.pain@lboro.ac.uk, web: http://www.lboro.ac.uk/departments/ssehs/

INTRODUCTION

For the mechanical analysis of human movement body segments are frequently assumed to be rigid bodies, with the inertial parameters of these bodies required for detailed analyses fixed to a constant value. During impacts the shape of a body segment can change due to a mechanical wave propagating through soft tissue and had been represented by wobbling masses. Soft tissue deformation has been reported to account for up to 70% of the energy lost in some of these segments [1] during certain types of impact and occurs in conjunction with large changes in segment shape. We have previously reported that the inertial properties of the shank can change markedly solely due to active muscular contractions [2]. In [2] the volume of each segment varied on the same order as the repeatability but changes in maximum dimensions were around 10%. The moments of inertia increased by 5% about the longitudinal axis and decreased by 8% about the two transverse axes.

During impacts soft tissue motion is greater than during active muscular contractions but usually only lasts for tenths of a second, at most, and is difficult to measure. Previously we have shown [3] that by using arrays of small reflective markers and Vicon motion analysis system reasonable estimates of static segment volumes can be made at frame rates up to 1000 Hz (cylinder <3% error, forearm +2 to -8%). The worst case results were at the highest sample frequencies due to marker loss. For the forearm measures the worst values were obtained when the markers were placed on a thin nylon material rather than directly to the skin.

Some typical problems with measuring impacts with arrays of small markers are marker loss, marker confusion, and coverage of the complete area of interest, all of which previous methods [2] are sensitive to. The aim of this study was to use an array of markers on the shank to track soft tissue deformation during landing and rapidly approximate changes in inertial parameters with a more robust method. This makes use of the redundancy of multiple markers but at the expense of absolute accuracy in the inertial parameters by fitting an ellipsoid to the marker set. Thus the goal is to examine changes in inertial properties that can be related back to the static inertial parameters obtained by any preferred method

METHODS

Six male subjects (age 23 $\pm$ 3 years, height 1.81 $\pm$ 0.08 m, weight 81 $\pm$ 5 kg) who were free from lower extremity injury gave informed consent in accordance with the Loughborough University Ethical Advisory Committee procedures. Subjects performed a series of drop landings where landing was heavily favoured onto one leg only from four different heights (0.3, 0.5. 0.7 and 0.9 m). Two conditions were utilized active markered leg landing on the force plate and passive markered leg landing on the force plate. Active landings landed on the forefoot and controlled the impact. Passive landings landed as much onto the heel as comfortable and minimal effort was used in this leg to brake the landing. Each subject performed multiple landings and the landing with the most complete data set was taken forward for further analysis.

A 10 camera Vicon motion analysis system (612 series, 1.3 megapixel cameras, Oxford, UK) operating at 700 Hz tracked 48 spherical markers (7.9 mm) placed on the shank in a 6x8 array. Incomplete marker trajectories were reconstructed using Vicon Nexus 1.4.116 and the pattern filling function. Marker data were low pass filtered at 50 Hz with a 2nd order zero lag Butterworth filter.

Reconstructed marker locations were transformed in Matlab and for each frame an arbitrary ellipsoid was fitted (ellipsoid_fit, Y. Petrov, North Eastern, Boston USA). Inertial properties of the ellipsoids at each frame were calculated for each drop across subjects.

RESULTS AND DISCUSSION

Although the goal was not to reproduce accurate inertial parameters of the subjects the ellipsoid fits gave inertial parameters that were within the ranges seen in human subjects. For example Subject 1 had shank mass = 3.81 Kg, length 0.38 m, max width 0.14 m, and moments of inertia of 0.031, 0.032 and 0.007 N.m^2 indicating that the ellipsoid is providing a decent simulacrum of the whole shank. This should be advantageous when looking at changes with time and relating them to real changes in the human shank as there is a simpler level of mapping required.

An estimation of the change in width from stills of the shank from high speed video gave a total change in width of 15%. For a similar sized subject the ellipsoid fits had a change in width of ~10%. Changes in mass of the ellipsoid were 8% to 40% depending on the subject, condition and drop height. The larger values seemed to be mainly due to distinct short duration spikes and may be artifacts that need further consideration. This change in volume does not represent a change in the actual shank volume, which will remain constant, but is an indicator of the mass associated with that portion of the shank associated with the markers at any time which can change.

Changes in moment of inertia about the vertical axis were highly subject dependent, with changes of around 10% for some subjects and up to 30% for others, again condition and height dependent as well. Changes in the moments of inertia about the other two axes varied from 20% to 100% again depending on the subject, condition and drop height (Figure 1). Again the larger values seemed to be mainly due to distinct short duration spikes and may be artifacts that need further consideration. Further examining the results by subject and looking for

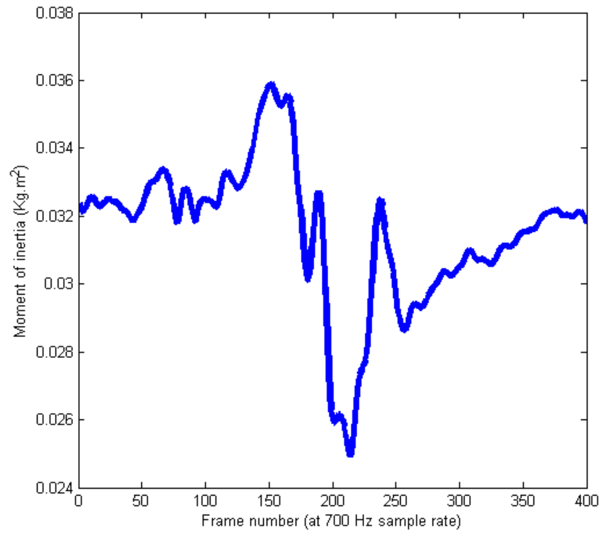

Figure 1: change in moment of inertia the ellipsoid about the medial-lateral axis.

systematic effects of drop height and condition on changes in inertial properties will aid in the understanding of the extent of soft tissue motion and when it will have a significant effect directly on joint moment calculations.

CONCLUSIONS

Using arrays of markers on the shank it is possible to track the deformation of the soft tissue under different impact conditions and produce a relatively realistic ellipsoid fit that can give some strong indication of the dynamic changes in segment inertia properties. It appears that the segment changes are considerable and should be considered during inverse dynamics analysis involving impacts.

REFERENCES

1. Pain, MTG & Challis, JH. *Journal of Applied Biomechanics*, **18** (3), 231, 42, 2002.
2. Pain, MTG & Challis, JH. *Journal of Applied Biomechanics* 17 (4), 326-334, 2001.
3. Perez Jimenez, I., and Pain, M.T.G. *4th North American Congress on Biomechanics,* Ann Arbor, USA, August 2008.

DOES THE HALLUX VALGUS SURGERY AFFECT SPATIOTEMPORAL PARAMETERS AND LOWER EXTREMITY KINEMATICS DURING GAIT?

[1]Jitka Klugarova, [1]Miroslav Janura, [1]Zdenek Svoboda and [2]Zdenek Sos

[1]Faculty of Physical Culture, Palacky University in Olomouc, Olomouc, Czech Republic
[2]Teaching Hospital Olomouc, Olomouc, Czech Republic
email: jitka.klugarova@upol.cz

INTRODUCTION

The hallux valgus (HV) deformity affects 23% of adults aged 18-65 years and 35.7% of elderly people aged over 65 years [1]. The patients usually complain of pain, difficulties during walking and problems with selection of the shoes. In severe stages of this deformity a surgery is required; however the difficulties during walking often persist after the surgery. A frequent postsurgical complication is a lateral deviation of the lesser toes [2]. There is luck of the evidence of the influence of HV surgery on spatiotemporal parameters and lower extremity and pelvic kinematics during walking. The aim of this study was to investigate if kinematic parameters of the gait cycle are affected after a HV surgery.

METHODS

Based on PICO format (P: patients with HV, over 40 years, I: first metatarsal osteotomy, C: control group, O: spatiotemporal parameters, lower extremity kinematics during gait) we formulated a clinical question: "Does the first metatarsal osteotomy affect spatiotemporal parameters and lower extremity kinematics during gait in patients with HV?

The experimental group consisted of 17 women with HV deformity (average age = 51.5±11.9 years, weight = 69.2±10.9 kg, height = 1.7±0.1 m) that underwent the first metatarsal osteotomy. We included only persons without an anamnesis of metabolic and neurological diseases and an ischemic disease of lower extremity. We also utilized a control group of 13 women (average age = 46.2±7.1 years, weight = 70.5±11.2 kg, height = 1.7±0.0 m) without HV. We used the optoelectronic system for the gait examination by Vicon MX (Vicon Motion System Ltd., Oxford, United Kingdom) with seven infrared cameras (200 Hz). Patients were instructed to walk at a self-selected pace. Five measured trials were evaluated. We focused on spatiotemporal parameters of the gait cycle and maximal and minimal peaks of the ankle, knee, hip and pelvic movement in sagittal, frontal and transversal plane during walking. These parameters were compared with those acquired from our control group.

After the Shapiro-Wilk normality test we decided to use a parametrical TWO-WAY ANOVA for repeated measurement and consequently Fisher´s LSD post hoc test (Statistica 10.0, Stat-Soft).

RESULTS AND DISCUSSION

Results showed that patients after HV surgery walked slower and with decreased cadence ($p<0.05$) as compared to their gait before surgery and to that of the control group. We also found that the operated leg exhibited longer step length and step time, as well as a shorter duration of single support and stance phase, compared to the non-operated leg ($p<0.05$) indicating the presence of asymmetry (Table 1). This image corresponds to the antalgic type of walking, in which the patient relieves the operated leg. The cause of the described asymmetry is probably the pain in the operated segment or substitute motion pattern used preoperatively, which HV surgery accentuates.

Furthermore, the operated leg exhibited greater dorsal flexion during mid-stance, as compared to the non-operated leg and the control group ($p<0.05$) (Fig. 1). Plantar flexion at the end of the stance phase was significantly reduced on operated leg ($p<0.01$) (Fig. 1).

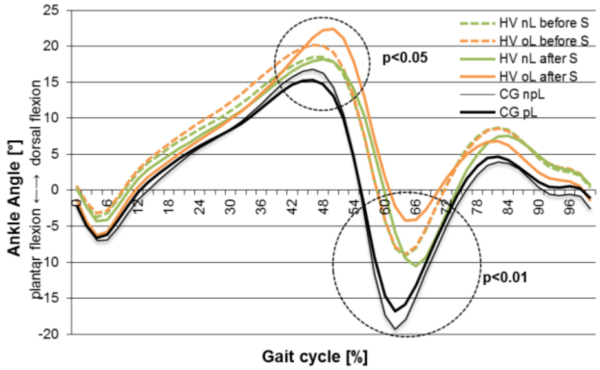

Legend: HV – HV group, nL – nonoperated leg, oL – operated leg, S – hallux valgus surgery, CG – control group, npL – non-preferred leg, pL – preferred leg, p – level of statistical significance.

Figure 1: Ankle kinematics in sagittal plane in the HV group and the control group.

Increased dorsal flexion during the midstance according Kirtley [3] compensates limited dorsal flexion of operated segment due to the pain. Consequently the toe-off at the end of stance phase could not be performed in the whole range.

Hallux valgus surgery did not significantly change angle parameters of pelvic movement (Fig. 2). Before HV surgery we found decreased pelvic elevation ($p<0.01$) at the beginning of the stance phase and greater pelvic depression ($p<0.01$) at the end of the stance phase on the side of operated leg.

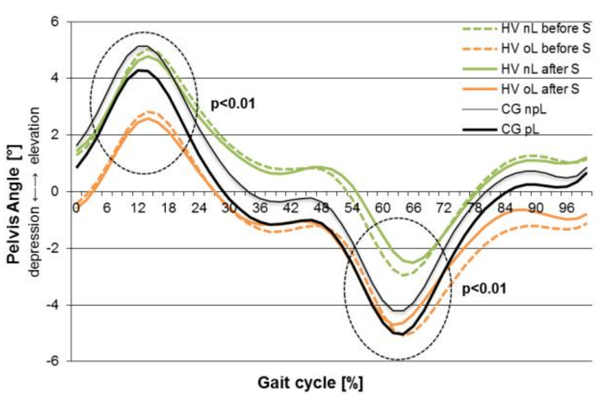

Legend: HV – HV group, nL – nonoperated leg, oL – operated leg, S – hallux valgus surgery, CG – control group, npL – non-preferred leg, pL – preferred leg, p – level of statistical significance.

Figure 2: Pelvic kinematics in frontal plane in the HV group and the control group.

This asymmetrical pelvic movement in the frontal plane persisted for four months after HV surgery. This follows that the pelvis was sloping during the whole gait cycle. The sloping pelvis is in most cases caused by asymmetric leg length, blocking or shift in sacroiliac joint, muscle imbalances between abductors and adductors in the hip [4].

CONCLUSIONS

HV surgery in the short term most markedly altered the preswing phase on the operated leg. After HV surgery is very important to recover the dorsal flexion of the hallux and re-educate heel-off and toe-off.

REFERENCES

1. Nix S, et al. Prevalence of hallux valgus in the general population: a systematic review and meta-analysis. *J Foot Ankle Res* **3**, 21, 2010.
2. Halebian JD & Gaines SS. Juvenile hallux valgus. *J Foot Surg* 22(4), 290-293, 1983.
3. Kirtley C. *Clinical gait analysis: theory and practice*, Churchill Livingstone, 2006:.
4. Lewit K. *Manipulative Therapy: Musculoskeletal Medicine*, Churchill Livingstone, 2009.

ACKNOWLEDGEMENTS

Our study was supported as a part of the grant 'Physical activity and inactivity of inhabitants of the Czech Republic in the context of behavioral changes', RP: 6198959221. Furthermore the study was supported by grant of the Palacky University Olomouc (FTK 2011 031).

Table 1: Description of spatiotemporal parameters of the gait in the HV group and the control group.

Group	HV group				Control group	
	nL		oL		pL	npL
	before S	after S	before S	after S		
Parameter	mean ± SD	mean ± SD	mean ± SD	mean ± SD	mean ± SD	mean ± SD
Cadence [step/min]	112.65 ± 9.2	*108.49 ± 9.5	111.76 ± 10.3	*108.53 ± 9.4	104.32 ± 22.1	104.29 ± 22.2
Walking speed [m/s]	1.15 ± 0.1	*”1.07 ± 0.1	ʿ1.14 ± 0.1	*ʿ1.07 ± 0.1	1.25 ± 0.2	1.25 ± 0.2
Step length [m]	ʿ0.61 ± 0.0	*ʿ0.56 ± 0.1	ʿ0.61 ± 0.1	#ʿ0.61 ± 0.0	0.65 ± 0.1	0.66 ± 0.1
Step time [s]	0.54 ± 0.0	0.54 ± 0.0	0.54 ± 0.0	*#ʿ0.57 ± 0.1	0.50 ± 0.1	0.50 ± 0.1
Single Support [%]	0.42 ± 0.0	*#0.45 ± 0.0	0.42 ± 0.0	#0.42 ± 0.0	0.44 ± 0.1	0.44 ± 0.0

Legend: S – surgery, nL – nonoperated leg, oL – operated leg, npL – non-preferred leg, pL – preferred leg, SD – standard deviation.

* Differences before and after hallux valgus surgery (ANOVA for repated measurement, LSD Fisher´s post hoc test): sygnificance at $p<0.05$.

Differences between operated and nonoperated leg (ANOVA for repated measurement, LSD Fisher´s post hoc test): sygnificance at $p<0.05$.

ʿ Differences between hallux valgus group and control group (ANOVA for repated measurement, LSD Fisher´s post hoc test): significance at $p<0.05$.

THE PREVALENCE OF GAIT DEVIAITONS IN INDIVIDUALS WITH TRANS-TIBIAL AMPUATION 4 MONTHS AFTER INDEPENDENT AMBULATION

Kelly M. Rodriguez, Christopher A. Rabago, Jason M. Wilken

Center for the Intrepid, Department of Orthopaedics and Rehabilitation, Brooke Army Medical Center, Ft. Sam Houston, TX
Email: Kelly.M.Rodriguez@us.army.mil

INTRODUCTION

Osteoarthritis, osteopenia, low back pain and other secondary musculoskeletal disorders are more prevalent in individuals with a history of prolonged lower extremity prosthetic use [1, 2]. These conditions are commonly attributed to deviations from able-bodied (AB) gait [1, 2]. A primary goal of rehabilitaiton after an amputation is to decrease gait deviations and restore normal gait patterns. However, the prevalence of deviations during early ambulation following transtibial amputation (TTA) has not been documented. The identification and correction of gait deviations during early ambulation may decrease the incidence of secondary musculoskeletal disorders in lower extremity prosthetic users.

Between group (i.e. able-bodied vs. injured) and inter-limb statistical comparisons are commonly used to identify gait deviations in individuals with TTA. Using these approaches, small between group differences are often discussed as having importance. A comparison of TTA gait measures to normative reference ranges may provide a supplementary approach for identifying deviations that are both statistically significant and prevalent amongst individuals within this population.

The purpose of this study was to characterize gait deviations in individuals with TTA within the first 4 months of ambulation using both prevalence and group mean approaches.

METHODS

Sixteen young adults with TTA and 40 AB individuals participated in this institutionally approved study. Individuals provided informed consent to participate in a biomechanical gait assessment walking at a predefined controlled velocity based on leg length [3].

A 26 camera optoelectronic motion capture system (120 Hz; Motion Analysis, Santa Rosa, CA) was used to track 13 body segments with a full-body, six degree-of-freedom marker set. Ground reaction force data was collected using eight AMTI force plates (AMTI Inc, Watertown, MA). Matlab (The Mathworks, Natick, MA) was used to compile peak kinematic and kinetic gait measures for the prosthetic and intact limbs. A normative reference range (mean ± 2SD) for each sagittal plane gait measure was calculated using the AB group data. Peak values outside normative reference ranges were defined as a gait deviation. The prevalence, or percent of patients with a deviation, was determined for each gait measure. Additionally, a one-way ANOVA (intact limb, prosthetic limb, AB limb) was used to identify differences in group means. Only comparisons between AB and the prosthetic and intact limbs are presented here.

RESULTS AND DISCUSSION

Gait deviation prevalence, means, and standard deviations for the TTA group are listed in Tables 1 and 2. All gait measures with greater than 30% prevalence of deviations were significantly different ($p<0.05$) between groups.

The highest prevalence of deviations in the intact limb occurred in the ankle and hip: 44% increased initial contact power absorption in the ankle, 31% increased hip stance extension, and 31% decreased hip swing flexion. These measures were not found to be significantly different in previous studies [5].

Table 1: Kinematic (°) deviation prevalence and direction of deviation in TTA group with mean (SD) of the group in the prosthetic and intact limbs.

Limb	Prosthetic		Intact	
Ankle	%	mean(SD)	%	mean(SD)
IC Plantflexion	↓ 19	-2.1(3.6)*	↓ 6	-3.3(2.7)
Dorsiflexion	↑ 6	16.3(2.9)	0	14(3.3)
Plantflexion	↓ 100	-4.7(2.7)*	↑ 13	-15.8(6.4)
Knee				
IC flexion	↑ 19	-1.0(6.2)*	↓ 6	-5.8(3.7)
ST flexion	↓ 25	7.8(7.7)	↓ 6	9.2(4.8)
ST extension	↓6, ↑13	2.5(6.7)	0	-1.3(3.2)
SW flexion	↓ 31	55.9(6.7)*	↓ 13	55.5(5.2)*
Hip				
ST flexion	↓6, ↑6	26.5(6.7)	↓ 19	21.5(6.0)*
ST extension	↑19	-13.1(6.4)	↑ 31	-15.0(6.5)*
SW flexion	↓13	27.9(6.0)	↓ 31	21.8(6.3)*

↑-increased peak in TTA group compared to AB group
↓- decreased peak in TTA group compared to AB group
*-means significantly different (p<.05) than AB group
IC-initial contact, ST-stance, SW-swing, TST-terminal stance, MST-mid stance, LR- loading response

In the prosthetic limb, the highest prevalence of deviations occurred in the ankle and knee: 100% with decreased plantarflexion, 50% with decreased ankle stance power generation, and 88% with decreased knee power generation at initial contact. These deviations are consistent with group mean measures reported to be significantly difference between TTA and AB populations [4, 5]. However, five prosthetic limb gait measures we found to be significantly different between groups had no individual subject values outside the normative reference ranges. This suggests ambulation in a minimally impaired range.

Although significant between groups differences were observed for nearly half of the measures, few deviations were present in a majority of individuals with TTA.

CONCLUSIONS

The current paper presents the use of prevalence as an additional means for identifying and characterizing deviations in individuals with TTA. Normative reference range comparisons provide a supplementary tool for the interpretation of statistically significant group mean comparisons.

Table 2: Prevalence of deviations in moments (Nm/kg) and powers (W/kg) and direction of deviation in TTA group with mean (SD) of the group in the prosthetic and intact limbs.

Limb	Prosthetic		Intact	
Ankle Moment	%	mean(SD)	%	mean(SD)
Dorsiflexion	↑ 13	-0.3(0.1)*	↑ 13	-0.3(0.1)
Plantflexion	↓ 6	1.3(0.2)*	0	1.4(0.1)
Ankle Power				
IC absorption	↑ 6	-0.3(0.1)	↑ 44	-0.4(0.2)*
ST absorption	↑ 13	-0.9(0.3)	↑ 13	-0.9(0.3)
TST generation	↓ 50	1.4(0.3)*	↑ 13	2.5(0.6)
Knee Moment				
IC flexion	↓ 6	-0.3(0.1)*	↑ 6	-0.5(0.1)*
ST extension	0	0.2(0.2)*	0	0.4(0.1)
MST flexion	↓ 13	-0.2(0.1)*	0	-0.4(0.1)
TST extension	↑ 6	0.2(0.1)	0	0.1(0.0)*
Knee Power				
IC generation	↓ 88	0.2(0.1)*	↑ 13	1.1(0.4)
LR absorption	0	-0.1(0.2)*	0	-0.5(0.3)
TST generation	0	0.2(0.1)*	0	0.5(0.2)
TST absorption	0	-0.8(0.2)	↓ 6	-0.5(0.2)*
Hip Moment				
IC extension	0	0.6(0.1)*	↑ 6	1.0(0.1)*
TST flexion	↑ 6	-0.8(0.2)	↓ 6	-0.6(0.1)*
SW extension	↑ 31	0.4(0.1)*	↑ 19	0.4(0.1)*
Hip Power				
ST generation	0	0.7(0.1)*	↑ 6	0.5(0.2)
ST absorption	↑ 13	-0.6(0.2)	↓ 6	-0.4(0.2)*
SW generation	↑ 6	0.9(0.2)	↓ 6	0.7(0.2)

↑-increased peak in TTA group compared to AB group
↓- decreased peak in TTA group compared to AB group
*-means significantly different (p<.05) than AB group
IC-initial contact, ST-stance, SW-swing, TST-terminal stance, MST-mid stance, LR- loading response

REFERENCES

1.Hungerford, D. JBJS, 1975. **57**
2.Kulkarni, J. Clin Rehab, 1998. **12**
3. Wilken, J. G&P, 2012. **2**
4. Gitter,A. AJPM&R, 1991. **70**
5. Bateni,H. JPO, 2002. **14**

DOES QUADRICEPS-STRENGTHENING EXERCISE AFFECT QUADRICEPS FORCE, POWER, AND WORK DURING STAIR ASCENT IN ADULTS WITH KNEE OSTEOARTHRITIS?

Josh Leonardis[1], Patrick Rider[1], John Norbury[2], Jens Aaboe[3], Robin Christensen[3], Henning Bliddal[3], Marius Henriksen[3], & Paul DeVita[1]

[1]Biomechanics Laboratory, Department of Kinesiology, East Carolina University, Greenville, NC
[2]Department of Physical Medicine and Rehabilitation, BSOM, East Carolina University, Greenville, NC
[3]Parker Institute, Copenhagen University Hospital, Frederiksberg, Denmark
email: leonardisj10@students.ecu.edu, web: http://www.ecu.edu/cs-hhp/exss/biomechlab.cfm

INTRODUCTION

Osteoarthritis (OA) is a chronic joint disease that accounts for more than half of all arthritis cases in the US by affecting ~27 million people (4). OA is characterized by joint space narrowing, exposure of subchondral bone, irregular bone growth, and joint pain and is most common in the knee (3, 4, 6). In addition to joint pain and degradation, knee OA causes the significant secondary problem of quadriceps weakness. The effects of knee joint pain and quadriceps muscle weakness are most evident during activities of daily living, such as ascending stairs, and can negatively affect quality of life.

Most treatment options for knee OA are limited to targeting the symptoms of the disease and a cure remains elusive. Many exercise interventions have reduced pain while quadriceps-strengthening exercise improves one's physical function in addition to the disease's symptoms (1, 5, 7). The mechanism behind improved symptoms, however, has yet to be identified. It is widely believed that by increasing quadriceps strength one improves quadriceps function during locomotion, thus reducing knee joint loads, pain, & disability. However, no empirical evidence has been found to support this theory. In fact, it has been found that with an exercise-induced increase in quadriceps strength, negligible changes occur to knee joint mechanics during locomotion, even with a cessation in pain (1-2). Therefore, we hypothesize that quadriceps-strengthening exercise will not affect quadriceps muscle biomechanics during locomotion in adults with knee osteoarthritis. The purpose of this pilot study was to determine the effects of a 12-week quadriceps strengthening protocol on maximum quadriceps muscle force, power, and work during stair ascent in adults suffering from knee OA.

METHODS

10 adults with physician-diagnosed tibiofemoral knee OA volunteered and were randomly placed into a *trained* or *untrained* group after providing written informed consent. Their characteristics were:

Table 1: Age, height, weight, and BMI.

	Trained	Untrained
Number	6	4
Age (yrs)	54.3 ± 5.8	57.4 ± 4.7
Height (m)	1.7 ± .04	1.7 ± .10
Mass (kg)	77.8 ± 8.9	76.0 ± 21.5
BMI (kg/m^2)	27.2 ± 3.2	26.9 ± 4.4

Participants had kinematic, ground reaction force, isokinetic strength, and WOMAC data collected before and after a 12-week interval. During this interval the trained group participated in a quadriceps-strengthening protocol 3 sessions per week, while the untrained group were not enrolled in any activity program. Training sessions consisted of 3 exercises performed for 3 sets of 10 repetitions with loads increasing from 65% to 80% of a previously determined 3RM. Quadriceps muscle force, power, and work were quantified using kinematic and kinetic data in combination with a biomechanical knee model (5, **Fig. 2**).

T-tests were used to determine significant pre- and post-test differences in strength and WOMAC data, while a 2-way repeated measures ANOVA was used to determine differences in quadriceps muscle force, power, and work between pre- and post-tests and treatment groups, all using $p<0.05$.

Figure 2. Biomechanical model

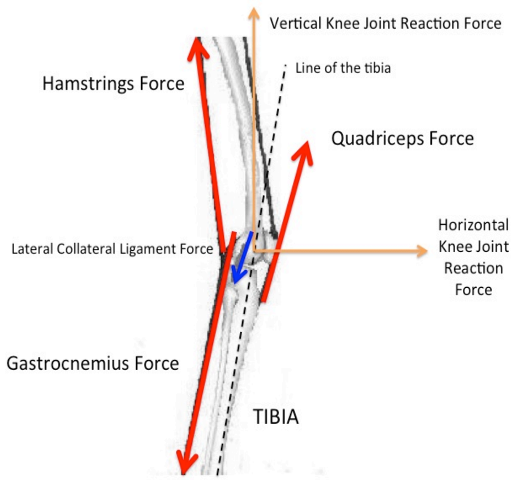

RESULTS AND DISCUSSION

Consistent with the literature, the training group exhibited significant increases in quadriceps strength as well as improvements in pain, function, and total WOMAC scores (all $p<0.05$). The control group showed no changes in strength or symptoms. Maximum quadriceps force and power (**Fig. 3**) were unchanged during ascent in both groups. These data are highlighted in **Table 2** for the strength-training group.

CONCLUSIONS

Despite improvements in strength, pain, and function, quadriceps-strengthening exercise did not change quadriceps force, power, or work during stair ascent. The findings of this pilot study suggest that the pain relief mechanism cannot be explained by improved quadriceps biomechanics.

Figure 3. Quadriceps force and power in stair ascent; solid & dotted: pre-test mean±sd; dashed: post-test mean

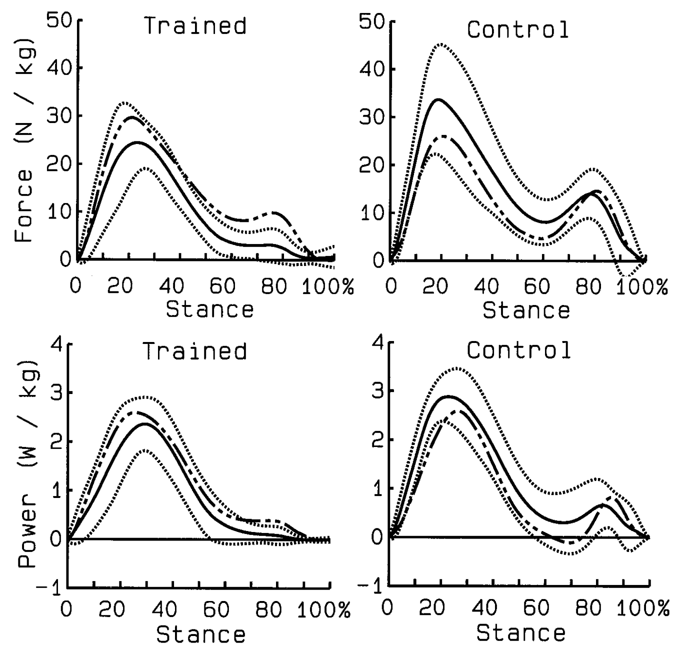

REFERENCES

1. Foroughi N, et al. *Cl Biomech* **26**, 167-174, 2011
2. Hurwitz DE, et al. *J Orth Res* **18**, 572-579, 2005
3. Lawrence RC, at al. *Arth & Rheum* **58 (1)**, 26-35, 2008
4. London NJ, et al. *Med Hyp* **76**, 887-892, 2011
5. Messier SP, et al. *Ost & Cart* **19**, 272-280, 2011
6. Vos T, et al. *Lancet* **380**, 2163-2196, 2010
7. Wang TJ, et al. *Cl Nursing* **20**, 2609-2622, 2010

Table 2: Pain, function, strength and quadriceps muscle biomechanics in strength training group.

	Pain	Function	Total	Strength	Force	Power	Work
Pre	3.5 ± 4.2	10.0 ± 12.2	20.9 ± 23.9	102 ± 41 Nm	28 ± 4.3 N	2.5 ± 0.5 W	0.7 ± 0.1 J
Post	1.5 ± 2.2*	1.0 ± 1.3*	8.6 ± 13.4*	133 ± 32 Nm*	31 ± 4.8 N	2.7 ± 0.4 W	0.8 ± 0.1 J

*Significant pre- post-test differences (p<.05)

KNEE ANGULAR POSITION AND MUSCLE ACTIVITY DURING MODIFIED ELLIPTICAL EXERCISE

[1]Max R. Paquette, [2]Audrey Zucker-Levin, [3]Paul DeVita, [1]Joseph Hoekstra and [4]David Pearsall

[1]University of Memphis, Health & Sport Sciences, Memphis, TN, USA
[2]University of Tennessee Health Science Center, Physical Therapy, Memphis, TN, USA
[3]East Carolina University, Kinesiology, Greenville, NC, USA
[4]McGill University, Kinesiology & Physical Education, Montréal, QC, Canada
Contact email: maxime.paquette@memphis.edu

INTRODUCTION

Medial compartment knee osteoarthritis (OA) is the most common type of knee OA. Peak knee adduction angle during gait strongly correlates with internal peak knee abduction moment, a surrogate measure of knee joint loading, in medial compartment knee OA patients [1]. Non-invasive interventions for medial compartment knee OA patients aim to reduce knee loads to help slow down disease progression and improve quality of life. Gait modifications including greater toe-out angle (TOA) and increased step width (SW) during level and stair walking have been found to reduce peak knee abduction moment in healthy and knee OA patients [2,3,4]. In addition, isolated hip abductor strengthening has been shown to reduce peak knee abduction moment in knee OA patients, by reducing pelvic drop and shifting the ground reaction force vector laterally (i.e., shortening the abduction moment lever arm) [5]. Obesity is the most important modifiable factor for knee OA development and progression and, weight loss has been shown to reduce compressive knee forces in knee OA patients during gait [6]. Further, a lateral motion elliptical device (i.e., skating simulation) would be expected to reduce peak knee adduction angle due to the lateral position of the foot relative to the hip joint during the load phase and, increase hip abductor involvement. This study compares exercise on a standard elliptical device using three different foot positions and on a lateral motion elliptical device to provide preliminary findings on knee angular position and muscle activity in healthy men. Greater TOA, wide SW and a lateral motion were expected to reduce the peak knee adduction angle and increase gluteus medius activity compared to straight foot position during elliptical exercise.

METHODS

9 healthy young men (22.6±1.7 yrs) volunteered for the study. A 9-camera motion analysis system (100 Hz, Qualisys, Sweden) and a wireless electromyography (EMG) system (2000 Hz, Delsys, USA) were used to obtain 3D lower extremity joint kinematics and muscle activity, respectively. The EMG surface electrodes were placed over the right vastus medialis (VM), biceps femoris (BF), gluteus maximus (GMax) and gluteus medius (GMed) according to existing guidelines [5]. The skin below each electrode placement site was shaved, lightly abraded and cleaned with an alcohol swab before application. Two maximal voluntary isometric contractions (MVIC) for each muscle were performed to obtain voluntary maximal muscle activity signals of each participant. The MVIC were performed using manual muscle testing by the researcher for all subjects. Uni-lateral retro-reflective markers were placed over bony landmarks of the pelvis and right lower extremity, and arrays of markers were attached to the thighs and shanks using elastic wrap. Participants performed a 30 second exercise bout at a stride rate of 50 strides per min on each of four elliptical device conditions: 1) lateral motion elliptical (Crossover, Technogym, USA) and on a standard elliptical trainer (EX-5, Matrix Fitness, USA) with 2) straight foot position, 3) increased TOA and, 4) increased SW. Exercise conditions were randomized and a 2-3 minute "familiarization" period was provided before the 30 second testing of each condition. The average of each variable in the middle six load-phases of the stride (i.e., most anterior to most posterior pedal position) during the 30 second bouts was analyzed. Visual3D (C-Motion, USA) was used to obtain the 3D lower extremity joint kinematic and EMG variables. The EMG signals were band-pass filtered

with cut-off frequencies of 20 and 400 Hz. The signals were full-wave rectified and smoothed using a root-mean-square (RMS) filter with a moving window of 150 ms. The EMG signals during exercise were normalized to the larger of the two MVIC RMS peak values for each muscle for each participant. The normalized EMG signals were then integrated (iEMG) during all six load-phases for each muscle. One-way repeated measure analyses of variance were used to compare all variables between elliptical conditions (α = 0.05).

RESULTS AND DISCUSSION

The peak frontal knee angle in early load-phase was greater in the TOA condition compared to the lateral (p=0.001), straight (p=0.001) and wide SW conditions (p<0.001) and; smaller during wide SW compared to the lateral condition (p=0.015). The peak frontal knee angle in late load-phase (i.e., abduction) was smaller in the TOA condition compared to the lateral (p=0.007), straight (p<0.001) and wide SW conditions (p<0.001). The smaller abduction angle in TOA may suggest greater late load-phase medial compartment knee loads in TOA compared to other conditions. The frontal plane knee range of motion (ROM) was significantly greater in the lateral condition compared to wide SW (p=0.019). The knee flexion-extension ROM during load-phase was greater in the lateral condition compared to all other conditions (p<0.001). This finding may suggest smaller localized peak knee forces during elliptical exercise in the lateral motion condition. However, the larger VM iEMG value in the lateral condition compared to the straight (p=0.001), TOA (p=0.004) and wide SW (p=0.001) conditions (Fig. 1) may indicate greater knee extensor force production during the lateral motion condition which could lead to larger peak compressive knee forces [6].

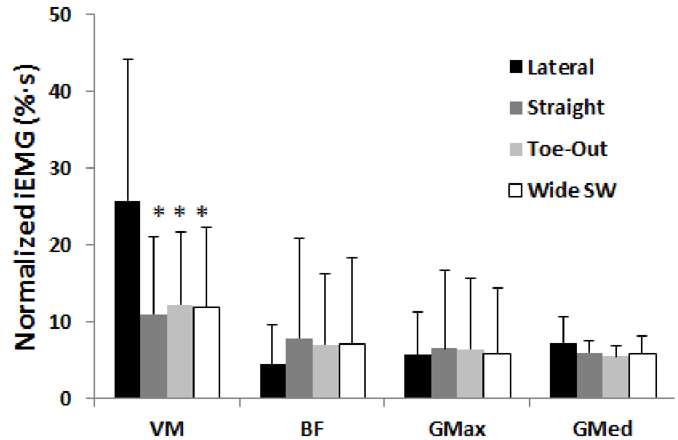

Figure 1: Mean (SD) normalized iEMG of VM, BF, GMax and GMed during the load-phase of elliptical exercise for all conditions. *: significantly different than the lateral condition (p<0.05).

CONCLUSIONS

Our findings refute the hypotheses that lateral motion, greater TOA and wide SW would reduce peak knee adduction angle and increase gluteus medius activation compared to straight foot elliptical exercise. The greater frontal and sagittal plane knee ROM may suggest that a lateral motion could help disperse forces within the knee to reduce peak compressive knee forces during elliptical exercise. However, increased VM activity may indicate greater muscle force contributions to yield larger peak compressive knee forces. Knee joint kinetic analyses using the current elliptical exercise methods are warranted to further study knee loads.

REFERENCES

1.Barrios, et al. J App Biom, 2012. **28**(5):551-9
2.Andrews, et al. J Orth Res, 1996. **14**(2): 289-95.
3.Paquette. Dissertation, 2012. U of Tennessee.
4.Guo, et al. Gait Posture, 2007. **26**(3): 436-41.
5.Thorp, et al. J Mus Neu Int, 2010. 10(2):166-173.
6.Messier et al. Osteo Cart, 2011. 19: 272-280.
7.Hermens, et al., 1999. Roessingh Res & Devel.

Table 1: Knee kinematic variables between elliptical exercise conditions (mean ± SD) and p-values.

	Elliptical Exercise				
Joint Angles (degrees)	**Lateral**	**Straight**	**Toe-Out**	**Wide SW**	**p**
Peak add-abduction in early load	0.02±3.85	-1.07±3.32	2.40±3.24 # & @	-2.02±3.24 #	**0.0001**
Peak add-abduction in late load	-6.86±6.32	-5.71±3.44	-1.65±2.60 # & @	-6.37±4.15	**0.003**
Add-abduction ROM	6.88±3.67 @	4.64±2.04	4.04±1.66	4.34±2.46	**0.018**
Flexion-extension ROM	50.13±4.92 &*@	23.63±4.64	21.90±7.19	22.92±5.73	**0.0001**

Note: Frontal peak knee and hip: abduction (-), adduction (+); Load: load-phase on elliptical device #: significantly different than Lateral; &: significantly different than Straight; *: significantly different than Toe-Out; @: significantly different than Wide SW (p < 0.05).

BIOMECHANICAL ASYMMETRIES DURING GAIT IN INDIVIDUALS BEFORE AND THREE MONTHS AFTER UNILATERAL TOTAL HIP ARTHROPLASTY

[1]Federico Pozzi, [1]Sumayah Abujaber, [1,2]Joseph Zeni Jr.

[1]Biomechanics and Movement Science program, University of Delaware, Newark, DE, USA
[2]Department of Physical Therapy, University of Delaware, Newark, DE, USA
fpozzi@udel.edu

INTRODUCTION

Patients with hip osteoarthritis (OA) demonstrate excessive lateral trunk lean toward the affected side during stance [1]. It is suggested that this strategy is adopted in the presence of hip pain and weakness to reduce the mechanical demand of the hip musculature and reduce hip compression force [2]. Although pain is largely resolved after total hip arthroplasty (THA) movement asymmetries persist. In particular, the surgical (SX) limb demonstrates lower external hip adduction moments during stance [3]. This alteration may be related to increased trunk lean toward the SX side, however most previous kinematic and kinetic analyses have not evaluated the effect of frontal plane trunk motion on more distal joints. Therefore, the aim of this study was to evaluate trunk, hip and knee kinematics and kinetics before and three months after unilateral THA. We hypothesized that following THA, movement asymmetries would persist in all planes.

METHODS

Six subjects scheduled for unilateral THA were recruited for this study. Subjects were excluded if the presented with any pathology (other than THA) that could affect movement patterns. Subjects were tested 2-4 weeks prior to THA and 3 months after THA. Gait analysis was performed using an eight camera motion capture system (VICON, London, England) and two force plates (Bertec Corp, Worthington, OH). Kinematic and kinetic data were sampled at 120Hz and 1080Hz, respectively. Retro-reflective markers were placed bilaterally on the acromion, iliac crest, greater trochanter, medial/lateral femoral condyle, medial/lateral ankle malleoli, heel (2), first and fifth metatarsal. Rigid thermo-plastic shells with four markers were secured bilaterally on the trunk, pelvis, thigh, and lower limb. Subjects walked naturally across the lab (~10m) and five walking trials were collected. Trials were discarded and performed again if subjects did not contact the force plate cleanly, targeted the force plates, and/or if speed exceeded ±5% of their pre-determined self-selected speed.

Visual3D software (C-Motion Inc., Germantown, MD) was used for the kinematic and inverse dynamic analysis. The model of the trunk segment (kinematic only) was created using the marker positioned on the acromion and iliac crests; the depth of the trunk was measured with a caliper and used to build the model. Lean angle was defined as a rotation of the trunk segment relative to the pelvis. Data were normalized according to 100% of the stance phase. Weight acceptance was defined as the first 30% of the stance phase; the interval between 50% and 90% of the stance phase was defined terminal stance. The following variables were calculated during weight acceptance: peak trunk lean angle; peak hip adduction angle; peak hip and knee adduction moment. Peak hip extension angle and peak extensor moment were calculated during terminal stance. Walking speed was calculated using two timing gates positioned 3m apart. All moments presented in this paper are external moments.

Data were compared between legs (SX vs. non-surgical [NSX]) and time (pre and 3-months after THA) using a 2x2 MANOVA with repeated measure on leg and time. Paired sample t-test was used to compare pre- and post-surgery walking speed.

RESULTS AND DISCUSSION

Despite subjects completed the walking trials 27% faster following the surgery, the statistical analysis showed only a statistical trend for gait speed (mean difference: 0.26m/s , $p=.06$).

Subjects with end stage hip OA had a 7° and 5° greater lean toward the SX side before and after THA, respectively (Fig. 1A). Despite this clinically meaningful difference, only a statistical trend for the main effect of legs was observed (p=.07, η^2=.51). A significant main effect of leg was found for hip angle in the frontal plane (p=.04, η^2=.60). Before and after surgery, subjects had greater hip adduction on the SX side compared to the NSX side during weight acceptance (pre and post main difference approximately 4°, Fig. 1D). This may be indicative of pelvic drop on the NSX side, which has been suggested to be a result of abductor weakness on the affected hip [2].

Knee adduction moment during weight acceptance in the SX side was approximately 33% lower compared to the NSX side before and after THA (main effect of leg, p=.04, η^2=.61), although no difference between limbs was seen for the hip adduction moment (Fig. 1E\F). The asymmetry in the frontal plane knee moment (decreased knee moment on the affected side) may be related to the excessive lateral trunk lean towards that side during stance [4].

Before THA, there were 8° difference in peak hip extension angles and 20% decrease in extension moments during terminal stance in the SX compared to the NSX hip (Fig. 1B\C). However, the significant leg*time interaction (peak extension angle, p=.03, η^2=.66; peak extensor moment, p=.01, η^2=.77) suggests that the sagittal plane hip asymmetries observed pre surgery were resolved after THA (3 months extension angle difference ~2°). Furthermore, the hip extensor moment in terminal stance was 20% higher in the SX compared to the NSX hip 3 months following surgery (main effect of time, p=.02, η^2=.77).

Sample size and absence of a control healthy group are considered limitations of this study. In addition, trunk and hip are not independent segments in our model.

CONCLUSIONS

Subjects with end stage hip OA present with abnormal gait mechanics. Although asymmetries in hip extension resolved following the THA, greater trunk lean and higher hip adduction angles may not resolve without targeted rehabilitation. Future work should determine if underlying weakness or range of motion deficits contribute to persistent movement asymmetries in the frontal plane. Failing to normalize excessive contralateral knee adduction moments may contribute to the high incidence of contralateral knee replacement and OA progression in the contralateral knee after THA.

REFERENCES

1. Reininga IHF, et al. *J Neurogen Rehabil* **9**:3, 2012.
2. Watelain E, et al. *Arch Phys Med Rehabil* **82**, 1705-1711, 2001.
3. Beaulieu ML, et al. *Gait Posture* **32**, 269-273, 2010.
4. Munderman A, et al. *J Biomech* **41**, 165-170, 2008.

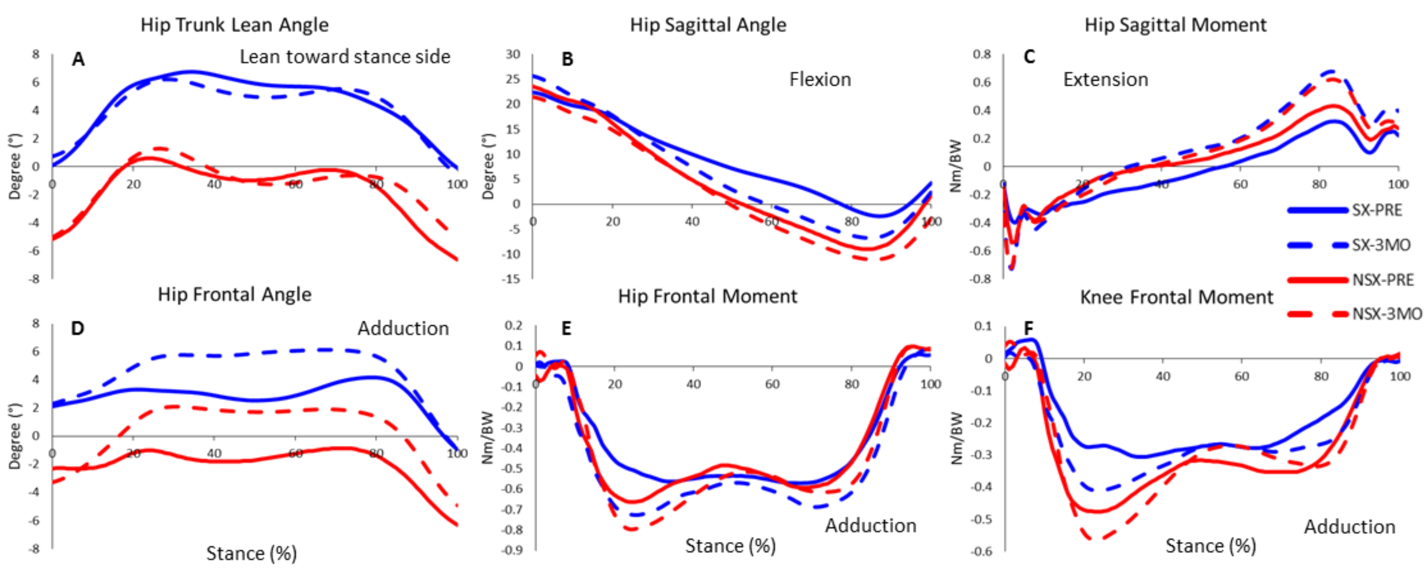

Figure 1. Kinematic and kinetic variables for the surgical (SX) and non-surgical (NSX) limbs. Data are presented according to 100% of the stance phase.

FORCE OUTPUT IS MORE VARIABLE IN PATIENTS WITH PERIPHERAL ARTERIAL DISEASE

[1]Ryan M. Hasenkamp, [1,3]Shane R. Wurdeman, [2,3]Jason M. Johanning, [2,3]Iraklis I. Pipinos, [1]Carlee Howe, and [1]Sara Myers

[1]University of Nebraska at Omaha, Omaha, NE, USA
[2] VA Nebraska-Western Iowa Health Care System, Omaha, NE, USA
[3]University of Nebraska Medical Center, Omaha, NE, USA
email: rhasenkamp@unomaha.edu, web: http://biomech.unomaha.edu/

INTRODUCTION

Peripheral arterial disease (PAD) is a major vascular disease affecting 8 to 12 million people in the United States. This disease is characterized by atherosclerosis in the lower extremity arteries and pain in the legs known as claudication. Patients with PAD have altered baseline gait as compared to healthy controls [1]. Walking is a complex interaction between nervous, muscular, and cardiovascular systems. In patients with PAD, the cardiovascular system is compromised due to lower extremity arterial blockages that reduce blood flow to the muscles in the legs. Previous studies have shown abnormal ankle moment and power in patients with PAD [2-6]. These altered parameters may be caused by insufficient ability of the plantarflexors to generate muscle force. Thus, the purpose of this study was to investigate muscular strength profiles in patients with PAD as compared to healthy age-matched controls.

Patients with PAD have poorer physical functioning than healthy controls, which coincides with reduced muscular strength and power at the ankle, knee, and hip [2-6]. Patients with PAD also have reduced cross-sectional area of muscle tissue, reduced nerve conduction velocity [6], and a decrease in type II (fast twitch) muscle fibers, which could lead to decreased muscular strength [7]. While much work has been done investigating muscular strength, there is little work that looks past peak maximal muscular strength. Walking however, is not a task requiring maximal effort. Therefore, this study investigated more comprehensive variables of muscular function including average, timing, and variability measures of force profiles. These measures were compared to healthy controls.

METHODS

Eight patients with PAD (age: 67.0 $\pm$ 7.0 yrs; height: 175.1 $\pm$ 9.0 cm; mass: 87.9 $\pm$ 13.6 kg) and eight age-matched controls (age: 66.9 $\pm$ 7.1 yrs; height: 176.0 $\pm$ 3.1 cm; mass: 86.7 $\pm$ 14.5 kg) performed isometric plantarflexion and dorsiflexion testing using a dynamometer (System 3.0; Biodex Medical Systems, Shirley, NY). Two maximal repetitions of isometric plantarflexion were performed for a duration of ten seconds for each repetition. Strength of patients with PAD was captured while they experienced claudication pain. To induce claudication, patients with PAD walked until the onset of claudication pain on a treadmill set at 0.67 m/s and 10% incline. Dependent variables during strength testing included peak torque, time to peak torque, average torque, and standard deviation of torque during the linear region. Average and standard deviation were calculated for the linear region of each trial as shown in Figure 2. Significant differences between patients with PAD and healthy controls for each variable were determined using independent t-tests ($\alpha = 0.05$).

RESULTS AND DISCUSSION

Significant differences between controls and PAD patients were discovered at peak torque (76.6 $\pm$ 17.4 ft*lbs and 56.9 $\pm$ 18.2 ft*lbs, $p = 0.04$), average torque during the linear region (72.5 $\pm$ 17.3 ft*lbs and 52.4 $\pm$ 18.9 ft*lbs, $p = 0.04$), and standard deviation of torque during the linear region (1.36 $\pm$ 0.5 ft*lbs and 2.6 $\pm$ 1.3 ft*lbs, $p = 0.02$, Figure 1). Patients with PAD were not able to generate as much maximum force during isometric plantarflexion as healthy controls. Furthermore, during the linear region, patients with PAD generated lower and more variable torque.

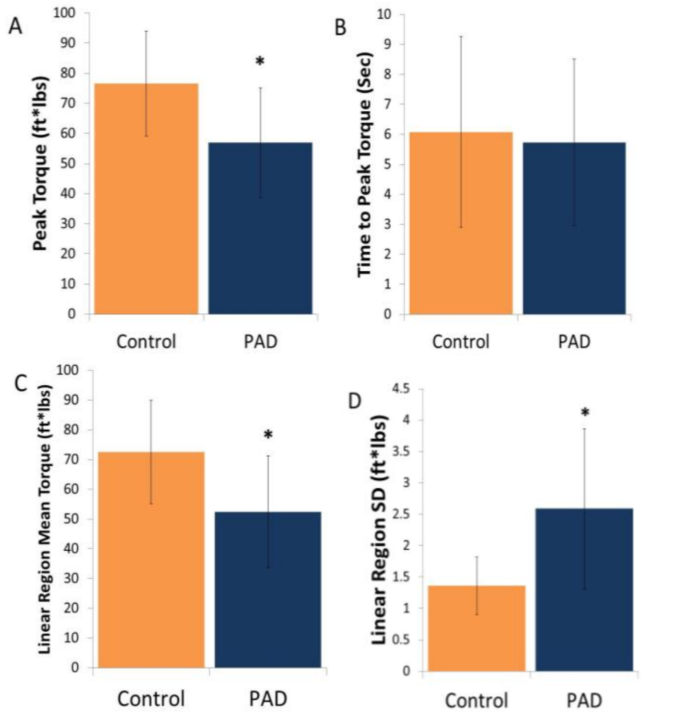

Figure 1: Differences between healthy controls and patients with PAD: A) Peak Torque, B) Time to Peak Torque C) Average Torque, and D) Standard Deviation of Torque.
* denotes significance from Controls p < 0.05.

There was no significant difference between controls and patients with PAD in time to peak torque (6.1 ± 3.2 s and 5.7 ± 2.8 s, p = 0.82).

The finding that healthy controls are able to generate more force than patients with PAD is consistent with the literature [2-6]. However the key finding from this study shows that patients with PAD demonstrate more variable force output during plantarflexion as shown by an increased standard deviation. This finding may explain why patients with PAD have altered ankle moment and power during walking [2-6].

CONCLUSIONS

The present study shows that patients with PAD cannot generate peak plantarflexor force similar to healthy controls. In addition their force output is significantly decreased and more variable than controls during the linear region. Overall, strength profiles are consistent with gait alterations seen in patients with PAD, specifically reduced ankle moment values and power generation compared with age-matched healthy controls.

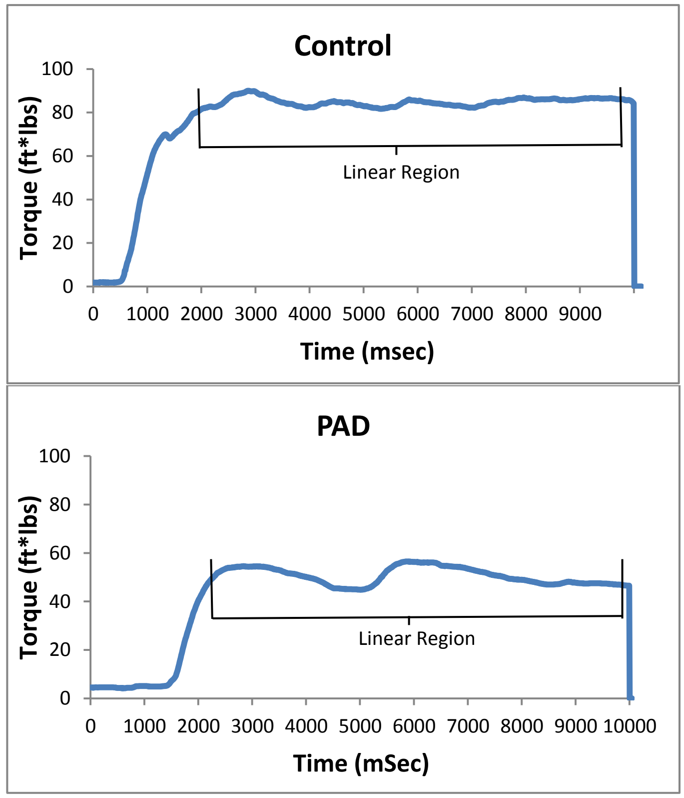

Figure 2: An example of the torque output curve during isometric plantarflexion for a healthy control subject (top) and a patient with PAD (bottom).

REFERENCES

1. Gardner AW, et al. *Vascular Medicine*, 6(1), 31-34, 2001.
2. McDermott MM, et al. *J American Medical Association*, 286(13), 1599-1606, 2001.
3. McDermott MM, et al. *J American Geriatrics Society*, 56(4), 724-729, 2008.
4. McDermott MM, et al. *J Vascular Surgery*, 39(3), 523-530, 2004.
5. Scott-Okafor HR, et al. *Angiology*, 52(1), 7-14, 2001.
6. McDermott MM, et al. *J American Geriatrics Society*, 52(3), 405-410, 2004.
7. Regensteiner JG, et al. *Circulation*, 87(2), 413-421, 1993.
8. Atkins LM, et al. *Angiology*, 55(4), 347-355, 2004.
9. Makris KI, et al. *Vascular*, 15(6), 336-343, 2007

Sensitivity of vertical ground reaction force parameters in normal and amputee running to filter design

Dovin Kiernan, Kyung Koh, Hyun Joon Kwon, Ross H. Miller, and Jae Kun Shim

University of Maryland, College Park, MD
email: rosshm@umd.edu; jkshim@umd.edu, web: http://www.sph.umd.edu/KNES

INTRODUCTION

Several studies have examined possible links between the characteristics of vertical ground reaction forces (GRF) in running and lower limb injuries [1-3]. Specifically, these studies have hypothesized that high *Magnitudes* and *Rates of loading* in the first, 'passive,' impact peak may cause lower limb stress fractures, medial tibial stress syndrome, plantar fasciitis, and/or pain in the hip, knee, low-back, or patellofemoral joint. With the increasing interest in these *impact peak variables* there is an emerging need to develop clear methodological guidelines for the processing and analysis of GRF data.

In motion capture and inverse dynamics several guidelines have been advocated to guide researchers' filtering techniques. For instance, Bisseling and Hof proposed that for movements with impact peaks, such as running, both kinematic marker data and GRF data should be filtered with a 20Hz low-pass cut-off [4]. In contrast, no clear guidelines exist regarding GRF filtering techniques for impact peak variables. Indeed, studies examining impact peak variables use a variety of methods. These methods range from no filter used/reported [1, 3] to a 4^{th} order Butterworth filter with a 50Hz low-pass cut-off [2]. Critically, the different processing methods used in these studies may: (1) lead to different, possibly erroneous, results and conclusions, and (2) make comparison of results across studies difficult.

The need for clear guidelines is further reinforced when examining different populations. In amputees the residual limb is composed of materials that have higher frequency components than the intact limb, or the limbs of controls [5]. Thus, using the same filtering techniques for amputees and controls may attenuate veridical GRF data and lead to erroneous results and conclusions.

The present study is designed to provide a preliminary analysis of the relationships between different filtering techniques and both the Magnitude and the Rate of loading in the impact peak of running.

METHODS

GRF data was collected from able-bodied controls (n=5) and unilateral trans-tibial amputees (n=5). Each participant ran around a 100m track at 2.5m/s, 3m/s, and 3.5m/s (±0.2m/s) at least five times for each speed. Ten 6 degree-of-freedom force platforms (Kistler, Amherst, NY) embedded in the track in series sampled GRF at 1000Hz. Three stance phases were randomly selected from the laps for each participant at each speed. For controls both legs were used for analysis; for amputees only the residual limb was used for analysis.

Raw vertical GRF data were filtered using a low-pass recursive Butterworth filter at three different orders (2^{nd}, 4^{th}, and 6^{th}) and at frequencies ranging from 1-100Hz in intervals of 1Hz. The Magnitude of the impact peak and the Rate of loading (slope of the vertical GRF from 20-80% of impact peak [3]) were identified and plotted against log(cut-off frequency) for each participant, order, and speed. A logarithmic line of best fit was calculated for each plot and the slope of that line (m, where $y = m*\ln(x) + b$) was used to characterize the relationship between cut-off frequency and each of the impact peak variables. These slopes were operationalized as the dependent variable. Slope data for Magnitude and Rate of loading were entered into two separate 2 (Group: Contol, Amputee) x 3 Speed (2.5m/s, 3m/s, 3.5m/s) x 3 (Order: 2^{nd}, 4^{th}, 6^{th}) mixed-measures ANOVAs.

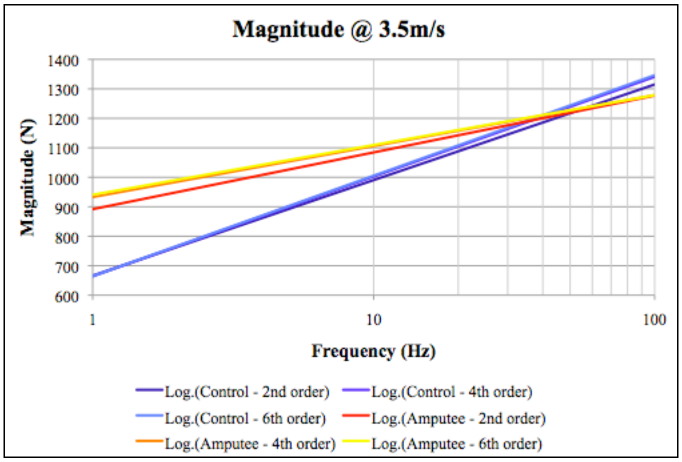

Figure 1: Logarithmic line of best fit for log(cut-off frequency) vs. mean Magnitude.

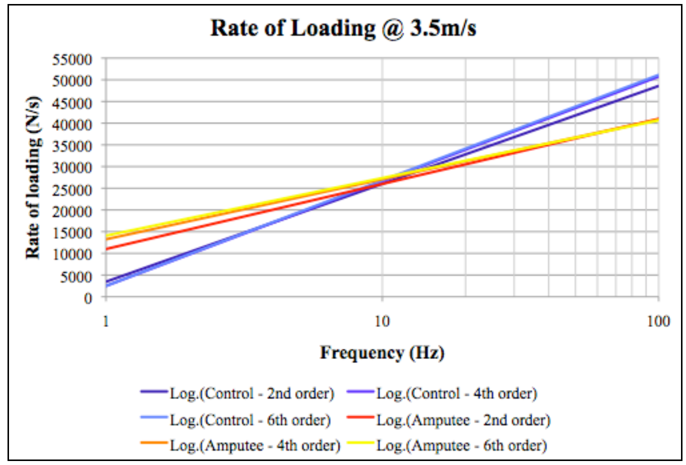

Figure 2: Logarithmic line of best fit for log(cut-off frequency) vs. mean Rate of loading.

RESULTS AND DISCUSSION

Analyses revealed a main effect of Order for both Magnitude ($F(2,16) = 4.007$, $p < 0.05$) and Rate of loading: $F(2,16) = 7.583$, $p < 0.01$). A main effect of Speed was also found for Magnitude ($F(2,16) = 32.667$, $p < 0.001$) and Rate of loading ($F(2,16) = 66.003$, $p < 0.001$). These findings indicate that different orders and running speeds produce different relationships between cut-off frequency and impact peak variables.

A Group by Order interaction was also found for both Magnitude: $F(2,16) = 4.783$, $p < 0.05$) and Rate of loading ($F(2,16) = 10.315$, $p = 0.001$). This finding indicates that the filter order used differentially affects the relationship between cut-off frequency and impact-peak variables in amputees as compared to controls.

Finally, the analyses revealed a three-way Group by Speed by Order interaction for both Magnitude ($F(4,32) = 5.615$, $p < 0.01$) and Rate of loading ($F(4,32) = 3.364$, $p < 0.05$). Figures 1 and 2 present a graphic representation of the findings discussed above.

CONCLUSIONS

The findings of this investigation demonstrate the sensitivity of vertical GRF parameters to filter method, and indicate that relationships between filter method and impact peak variables may be population- and running speed-specific. We suggest there is a need for methodological guidelines regarding filtering GRF data. Specifically, filter order and cut-off frequency need to be thoughtfully prescribed depending on the population and running speed used in a given study. Through the establishment of such methodological guidelines: (1) the findings of studies investigating impact peak variables will be more credible and, (2) more informed comparisons could be drawn between studies.

Further, the present findings suggest that filtering GRF at 20Hz, as advocated by Bisseling and Hof [4], may lead to a misrepresentation of the GRF profile and impact peak variables. Indeed, the slopes found in this study indicate that filtering at 20Hz may reduce both the Magnitude and Rate of loading. As GRF presumably has a high signal-noise ratio this reduction may constitute an attenuation of veridical frequency components.

REFERENCES

1. Davis et al. *Proceedings of ASB 2010,* Providence, Rhode Island, USA.
2. Pohl et al. *Journal of Biomechanics* **41(6)**, 1160-1165, 2008.
3. Milner et al. *Medicine and Science in Sports and Exercise* **38(2)**, 323-328, 2006.
4. Bisseling & Hof. *Journal of Biomechanics* **39(13)**, 2438-2444, 2006.
5. Wilson et al. *Prosthetics and Orthotics International* **33(3)**, 218-229, 2009.

DO BIOMECHANICAL LOADS INCREASE DURING COMMON REHABILITATION EXERCISES IN OBESE INDIVIDUALS?

[1]Bhupinder Singh, [2]Shelby L. Francis, [2]Kathleen F. Janz, and [1]H.John Yack
[1]Program in Physical Therapy & Rehabilitation Sciences
[2]Department of Health and Sport Studies
University of Iowa, IA, USA
Email: bhupindersingh@uiowa.edu

INTRODUCTION

Squat and lunge are classic exercises that have become an integral part of lower-extremity strengthening and postoperative rehabilitation programs [1]. Despite their widespread use across age and BMI spectrums, very few studies have looked at the biomechanics of these exercises. Of existing studies, most have focused on younger, normal weight, populations. The influence of obesity on the performance of squat and lunge has not been documented [2]. Despite the potential for biomechanical differences from normal weight subjects, there are no published data showing that clinicians make different recommendations when prescribing exercises for obese individuals. The purpose of this study was to analyze and compare the biomechanics of obese and normal weight individuals, as measured by hip and knee moments, while performing common physical therapy rehabilitation exercises. Taking the biomechanical stresses and strategies into consideration during common exercises may help to inform rehabilitation approaches used for obese individuals.

METHODS

Ten obese (BMI > 30 kg/m^2) female subjects age 37.4 ± 3.7 years, BMI 39.2 ± 3.7 kg/m^2 and ten normal weight (BMI<23 kg/m^2), female subjects, age matched 38.1 ±4.5 years, BMI 21.6 ±2.3 kg/m^2, volunteered for the study. Height, weight, waist circumference; hip circumference and tibial length were recorded. Infrared emitting markers were applied to the lower limbs, pelvis, and trunk segments. Anatomical landmarks were digitized, relative to segment local coordinate systems, to create a link-based model. Three-dimensional motion analysis system (Optotrak, NDI) and force plates (Kistler) were used to collect kinematic and kinetic data. Testing sessions included two trials: squatting down, feet shoulder width apart with right foot on force plate and held for 3 seconds at 3 different knee angles: 60, 70, and 80 degrees (full knee extension being 0 degree). Real time feedback was used to achieve the desired knee angle. Forward lunging, held for 3 seconds, with the right lead foot, on the force plate at, 3 different distances between feet- heel to toe: 1, 1.1, 1.2 times subject's tibial length.

DATA ANALYSIS

Visual 3D software (C-Motion) was used for processing. Mean values, over 3 s while holding the positions, were calculated for lower limb joint moments and support moments (summation of the lower limb extensor moments). The moments were normalized to body mass. A group (obese vs normal weight) by level of difficulty ANOVA was used to find differences in hip, knee and ankle moments across three levels of difficulty for the squat and lunge. Regression analysis was performed to find relationships between BMI or other anthropometric measures and extensor moments. SPSS 21.0 was used for analysis with p-value < 0.05.

RESULTS AND DISCUSSION

For the **squat**, hip and knee extensor moments in obese subjects were not different than normal weight subjects for all three levels of squat. However, ankle extensor moments were higher in obese subjects (Table 1). The support moment was higher in obese subjects, as compared to the normal weight subjects, for squat 70 (p = 0.03) and squat 80 (p= 0.01), but not different for squat 60 (p= 0.07).
Increased support moment across the three lower limb joints points to the possibility of an overall higher kinetic joint stress in obese subjects during squatting.

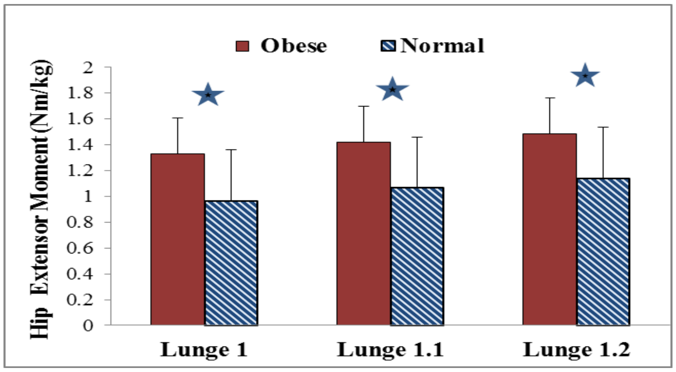

Figure 1: For the **lunge**, hip extensor moments were greater in obese than normal weight control subjects for level 1, 1.1 and 1.2 (p-values: 0.004, 0.003 and 0.007 respectively). Knee and ankle extensor moments were not different (Table1). Support moments showed an overall group effect between obese and normal weight subjects (p= 0.01).

Recent study looked at the effect of adding external load on the biomechanics of the lunge and showed an increase in hip extensor moments with little change in the knee contributions [3]. It could be argued that the external weight simulates the excess adipose tissue in obese subjects, causing a similar increase in hip moment.

Although there was no linear relationship, non-linear polynomial fit showed a moderate relationship between hip moments and BMI (Figure 2). Similar relationships were seen for squat 70 (r-square = 0.42) and squat 80 (r-square = 0.39). This points to the possibility of a ceiling effect in subjects with higher BMI's. A similar ceiling effect has been postulated for gait in obese females with BMI greater than 30 kg/m^2 [4].

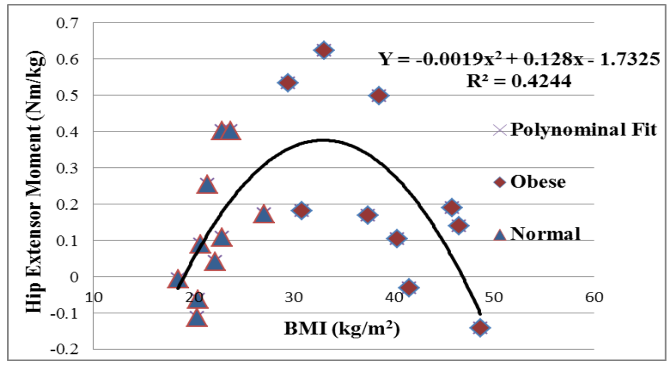

Figure 2: Non-Linear relationship between hip extensor moment for obese and normal weight subjects for squat 60.

CONCLUSIONS

The results suggest that obese individuals experience higher biomechanical stress than normal weight subjects while performing squat and lunge exercises. Non-linear associations were uncovered between anthropometric measures and kinetic measures, which makes the assessment of how best to approach exercise in this population even more challenging. Thus, while this study advocates for the need to consider obesity as a factor in exercise prescription, it acknowledges the apparent complexity that inhibits the understanding of issues that bias the kinetic measures.

REFERENCES

1. Flanagan SP, et al. *Med Sci Sports Exerc*. **35**, 635-43, 2003
2. Escamilla RF, et al. *Med Sci Sports Exerc*. **33**, 127-41, 2001.
3. Reimann BL, et al. *J Athl Train*. **47**,372-8, 2012.
4. Devita P, et al. *J Biomech*, **36**, 1355-1362, 2003.

Table 1: Mean (standard deviation) hip, knee, ankle extensor and support moment for different levels of squat and lunge exercises. The measures highlighted in grey color showed significant differences (p<0.05).

Moment(Nm/kg)		**Squat 60**	**Squat 70**	**Squat 80**	**Lunge 1**	**Lunge 1.1**	**Lunge 1.2**
Hip	Obese	0.22 (.24)	0.29 (.28)	0.37 (.30)	1.32 (.27)	1.41 (.28)	1.48 (.32)
	Normal	0.12 (.17)	0.17 (.18)	0.24 (.18)	0.96 (.39)	1.07 (.38)	1.14 (.39)
Knee	Obese	0.67 (.10)	0.73 (.12)	0.82 (.12)	0.53 (.15)	0.53 (.16)	0.50 (.22)
	Normal	0.59 (.22)	0.66 (.23)	0.75 (.26)	0.64 (.30)	0.56 (.29)	0.52 (.24)
Ankle	Obese	0.28 (.16)	0.31 (.19)	0.34 (.19)	0.42 (.20)	0.43 (.20)	0.47 (.21)
	Normal	0.19 (.10)	0.20 (.13)	0.20 (.11)	0.45 (.26)	0.42 (.25)	0.40 (.22)
Support	Obese	1.18 (.25)	1.33 (.32)	1.53 (.36)	2.33 (.36)	2.44 (.42)	2.52 (.47)
	Normal	0.92 (.27)	1.03 (.30)	1.18 (.34)	2.07 (.65)	2.05 (.64)	2.07 (.59)

WHY ARE WRIST ROTATIONS LESS SMOOTH THAN REACHING MOVEMENTS?

Layne H. Salmond[1] and Steven K. Charles[1,2]

[1]Department of Mechanical Engineering and [2]Neuroscience Center
Brigham Young University, Provo, UT, USA
email: lhsalmond@gmail.com and skcharles@byu.edu

INTRODUCTION

Early studies found that reaching movements are remarkably smooth, as demonstrated by the stereotypical bell-shaped velocity profile[1,2]. Models of movement which minimize jerk and maximize smoothness[3] provide a good approximation to many natural movements. Smoothness is an important measure to understand because the central nervous system's signals result in models that predict smooth trajectories. Even though the advantages of smoothness are not fully understood, abrupt changes have been found to require large driving signals, which carry more unwanted noise[4].

Later studies showed that the reaching movements of patients with certain disorders (such as stroke) are less smooth, and that movement smoothness improves with recovery[5].
Consequently, reaching movement smoothness may potentially diagnose and monitor recovery from disorders that affect reaching movements. This approach is especially appealing in rehabilitation robotics since the robot could monitor changes in movement smoothness during therapy[6].

In contrast, despite the development and implementation of robotic rehabilitation for the wrist[7], the smoothness of wrist rotations is unknown. Consequently, wrist rotation smoothness cannot currently be used to diagnose or monitor recovery from disorders affecting wrist rotations.

Recently, we characterized the smoothness of wrist rotations (Figure 1) in order to establish a foundation for future diagnosis and monitoring of disorders affecting wrist rotations. More specifically, we characterized the smoothness of wrist rotations under different speed and movement direction conditions. We found that:

1. Wrist rotations are significantly less smooth than reaching movements ($p<0.01$).
2. Slow wrist rotations are significantly less smooth than fast wrist rotations ($p<0.01$).
3. Wrist rotations in different directions exhibit significantly different smoothness ($p<0.05$).

While our study provides a baseline of normal smoothness in wrist rotations, and compares it to the well-known smoothness of reaching movements, it does not explain the cause of our findings. In our current work, we are uncovering the reasons why wrist rotations are less smooth than reaching movements, slow wrist rotations are less smooth than fast wrist rotations, and why movements in different directions exhibit significant differences in smoothness.

HYPOTHESES

We are currently testing the following hypotheses for each finding:

1. **Why are wrist rotations less smooth than reaching movements?**
   a. Mechanical: The low-pass filtering properties of the wrist do not suppress neuromuscular noise as well as those of the shoulder and elbow[8].
   b. Muscular: Distal muscles, which are known to have a higher coefficient of variation than proximal muscles[9], produce more noise during wrist rotations than shoulder and elbow muscles during reaching movements.
   c. Neural:
      i. Distal muscles have greater cortical control[10] than proximal muscles, which leads to longer feedback delays, more oscillations, and therefore less smoothness.
      ii. Proprioception at distal joints has less sensitivity than at proximal joints.
   d. Protocol-related: The speeds of wrist and reaching movements are not comparable.
2. **Why are slow movements less smooth than fast movements?**
   a. Slow movements require a lower action potential frequency, so the resulting train of

muscle twitches is less fused[11], decreasing movement smoothness.
   b. The signal-to-noise ratio is lower in slower movements.
3. **Why do wrist rotations in different directions exhibit significant differences in smoothness?**
   a. Differences in passive stiffness with direction[12,13] cause different smoothness.
   b. Muscles acting in different directions produce different amounts of noise.

METHODS

We are testing each hypothesis using the following methods:

1. **Why are wrist rotations less smooth than reaching movements?**
   a) Mechanical: Determination (using mathematical models for reaching and wrist movements) of the extent to which joint impedance (inertia, damping, stiffness) low-pass filters the effects of variation in muscle force.
   b) Muscular: Comparison of variation in muscle force (between wrist and reaching movements) given the known coefficients of variation (SD/mean) for proximal and distal muscles (combined with the models mentioned above).
   c) Neural:
      i) Investigation of differences in simulated smoothness when the models above are expanded to include differences in time delay.
      ii) Comparison of known proprioceptive thresholds between the wrist joint and the shoulder and elbow joints.
   d) Protocol-related: Comparison of smoothness by joint angular velocity instead of movement duration.
2. **Why are slow movements less smooth than fast movements?**
   a) Simulation of fast and slow movements using Hill-type model of excitation-contraction dynamics to simulate train of twitches and consequent variation in force output.
   b) Determination (using model mentioned above) of relationship between movement speed and signal-dependent noise.
3. **Why do wrist rotations in different directions exhibit significant differences in smoothness?**
   a) Comparison between pattern of variation in smoothness (with direction) and pattern of variation in wrist stiffness (which dominates wrist dynamics).
   b) Comparison of variation in force between wrist muscles acting in different directions.

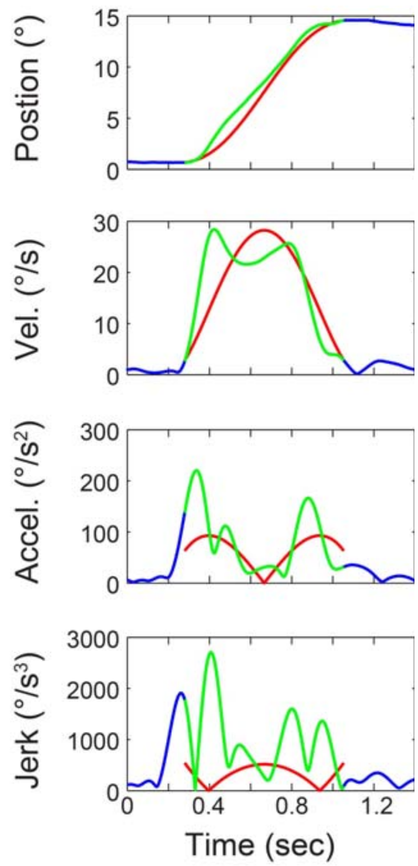

Figure 1: Actual movement (green) compared to maximally smooth movement (red)

REFERENCES

[1] Atkeson C and Hollerbach J (1985). J Neurosci, 5(9): 2318.
[2] Morasso P (1981). Exp Brain Res, 42(2): 223-227.
[3] Hogan N (1984). J Neurosci, 4(11): 2745.
[4] Harris C and Wolpert D (1998). Nature, 394(6695): 780-784.
[5] Rohrer B, et al (2002). J Neurosci, 22(18): 8297-8304.
[6] Hogan N, et al (2006). J Rehab Res & Dev, 43(5): 605.
[7] Krebs HI, et al (2007). IEEE TNSRE, 15(3): 327-335.
[8] Krylow A and Rymer W (1997). IEEE Trans Biomed Eng, 44(2): 165-176.
[9] de C Hamilton A, Jones K and Wolpert D (2004). Exp Brain Res, 157(4): 417-430.
[10] Lemon R, et al (2012). Brain, 135(7): 2290-2295.
[11] Faisal A, Selen L and Wolpert D (2008). Nature Rev Neurosci, 9(4): 292-303.
[12] Charles S and Hogan N (2012). J Neurophys, 107(4): 1230-1240.
[13] Charles S and Hogan N (2011). J Biomech, 44(4): 614-621.

THE RELATIONSHIP BETWEEN VISUAL STEADINESS AND MUSCLE FORCE STEADINESS IN YOUNG AND OLD ADULTS

Rebecca Krupenevich, Katie Reynolds, Luke Spangler, Patrick Rider, Nicholas Murray, Paul DeVita

East Carolina University, Greenville NC
Email: krupenevichr11@students.ecu.edu

INTRODUCTION

Old adults exhibit a decrease in both muscle force steadiness [1, 2] and visual capability [3] compared to young adults. Many studies investigating force steadiness have used a visual target as the stimulus for modulating muscle force [1, 2]. Since visual capability declines with age, and vision is used in most investigations of muscle force control with age, reduced muscle force control in older adults might be partially related to or explained by altered visual capacity. The purpose of this exploratory study was to compare the relationships between eye movement, as a component of visual steadiness, and quadriceps muscle force steadiness in young and old adults during isometric quadriceps contractions of constant and varying forces.

METHODS

19 healthy young adults (20.7±1.82yrs) and 18 healthy old adults (71.6±3.01yrs) participated in this study after providing written informed consent. Isometric quadriceps torque data were collected using an isokinetic dynamometer and used as a surrogate for muscle force. Horizontal and vertical eye movement data were collected using an eye-tracking system by recording motion of the pupil (Figure 1).

Visual feedback consisted of a cursor moving horizontally across the screen at a set speed and vertically in response to torque magnitude. The tasks consisted of three vision only tasks, two vision and torque tasks at a relative value of 40% MVC, and two vision and torque tasks at an absolute value of 54Nm. The vision only conditions consisted of a stationary cursor, the cursor moving across the middle of a blank screen, and the cursor moving across the middle of a screen on a straight white line. The torque conditions required the subject to bring the cursor up to a straight line in the middle of the screen and maintain the torque, or provide appropriate amounts of torque to increase and decrease the cursor on a parabola shaped target.

The middle 60% of each data set was plotted and a line of best fit was calculated. The horizontal and vertical vision and torque data were detrended before calculating measures of variance and central tendency**.** We used standard deviation to quantify steadiness for the vision and torque trials and Pearson Product Moment correlations to identify the relationships between steadiness in muscle torque and visual capacity.

Figure 1: Eye tracker device, click QR link or scan QR code to see video of tracking tasks

RESULTS AND DISCUSSION

Torque data from the straight-line vision and force conditions were used to quantify muscle torque steadiness (Figure 3). There were no significant differences between age groups for torque steadiness in the absolute condition ($p=0.19$) with young displaying an average torque variability of 0.76±0.25Nm and old displaying an average torque variability of 0.84±0.29Nm. Statistical significance was detected for the relative torque condition ($p<0.05$); these results were contrary to our expectations, with old adults showing less torque variability averaging 0.79±0.36Nm compared to young adults with an average of 1.16±0.44Nm.

Both groups displayed similar visual capacity, as measured by the three vision-only conditions. The static vision condition did not show a significant difference between the two groups for the horizontal (p=0.08) or vertical (p=0.28) visual components. The vision no-line and vision straight-line conditions did not show a significant difference between young and old adults for the vertical vision component, p=0.34 and p=0.47, respectively. A significant difference was observed in the horizontal component for the two conditions. Old adults showed decreased visual steadiness compared to young (p<0.05). Correlations performed between visual steadiness and muscle torque steadiness failed to show a statistically significant relationship for either condition in either age group using the following critical values for a two-tailed test at p<0.05: young adults (df=17) =0.456, old adults (df=16) =0.468 (Figure 2, Table 1).

Although decreased muscle force steadiness in old adults has been well documented [1, 2], our subjects failed to display this characteristic. The absence of a statistically significant difference in force steadiness is indicative of an extremely healthy, mobile, and capable old adult subject pool. The only differences between the two groups were age and maximal strength (young 209±68.44Nm, old 145±51.5Nm).

CONCLUSIONS

We were not able to identify any physiological relationship between muscle force steadiness and eye movement, as a component of visual steadiness.

It is possible that the relationship between force steadiness and visual feedback identified in previous research is due to decrements in visual processing capabilities and not due to a decline in visual steadiness. Regardless, present data support previous observations that reduced muscle force steadiness with age was in fact due to reduced neuromuscular capacity and not visual capacity.

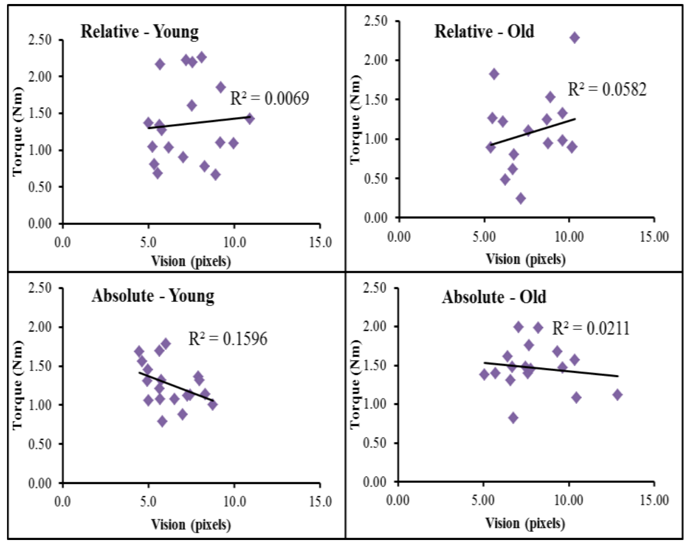

Figure 2: Correlations for absolute and relative parabola condition.

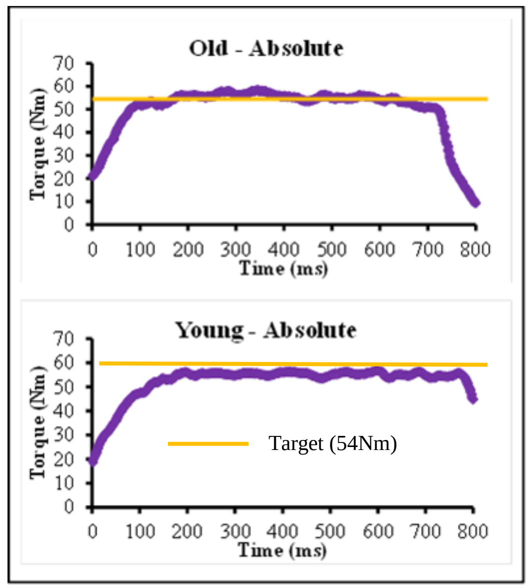

Figure 3: Representative torque data for one young and one old individual.

REFERENCES

1. Tracy BL, et al. *Med. Sci.Sports and Exerc.* **39**, 469-479, 2007.
2. Ofori E, et al. *Exp Brain Res* **203**, 299-306, 2010.
3. Moschner C, et al. *Journal of Gerontology: Medical Sciences* **49**, M235-M238, 1994.

Table 1: Correlation coefficients for relative and absolute conditions *r value <> 0, p<0.05

	Relative (40% MVC)		Absolute (54Nm)	
	Young	**Old**	**Young**	**Old**
Straight-Line	0.197	0.014	0.197	0.014
Parabola	0.083	0.241	0.083	0.241

MUSCLE RECRUITMENT AND ANGULAR IMPULSE GENERATION STRATEGIES USED DURING TURN TASKS WITH MODIFIED HIP EXTERNAL ROTATION

Antonia Zaferiou[1] and Jill L. McNitt-Gray[1,2]
Departments of [1]Biomedical Engineering and [2]Biological Sciences
University of Southern California, Los Angeles, CA, USA
email: zaferiou@usc.edu

INTRODUCTION

As we move through our environment in daily life, we encounter obstacles that require circumvention. Successful navigation requires us to turn effectively at speed and without losing our balance. Although this task may seem trivial for able-bodied individuals, performance of a turn requires satisfying multiple and often competing mechanical objectives, including generation of horizontal and angular impulse while maintaining balance. Failure to simultaneously satisfy these mechanical objectives can result in falls leading to injury or poor performance outcomes [1,2].

When tasks become more challenging, individuals selectively reallocate their physiological resources and in that process, reveal their preferred multijoint control priorities. When these regulatory mechanisms are identified within the control strategies of an elite performer, these findings can help identify feasible solutions for individuals with impaired mobility to accomplish simpler turning tasks. The piqué turn is similar to changing direction while walking, as it involves generation of linear and angular impulse occurs as support shifts from one leg to the other while the horizontal trajectory of the center of mass is maintained. Increasing the degree of rotation (from 360° to 720°) increases the rotation and balance control requirements of the task, revealing the dancer's preferred multijoint control priorities. Additionally, if the amount of hip external rotation is modified, muscle lengths at the hip change, thereby altering the force generation capacity of a muscle [3] and potentially changing muscle recruitment strategies.

The purpose of this study was to determine how skilled turners selectively activate lower extremity muscles to regulate reaction forces when (1) the degree of rotation increases and (2) the amount of hip external rotation at turn initiation is modified. We hypothesized that (1) muscle recruitment patterns during turns initiated using the same hip position would be consistent as the number of turns increases and (2) muscle activation levels would increase as the number of turns increased.

METHODS

Collegiate dancers with similar levels of dance experience and training (n=2) performed a series of piqué turns requiring varying degrees of rotation and hip external rotation. The amount of rotation required during each piqué was increased (360° (pk1 and npk1) and 720° (pk2 and npk2)) to systematically increase the rotation and balance control requirements between turn conditions. The piqué turn normally performed in ballet requires that the turn is performed with maximal hip external rotation (pk1 and pk2). These turns were compared to piqué turns performed with a neutral hip alignment (npk1 and npk2).

Turns were performed with each foot supported by a forceplate (Kistler, 1200Hz) while monitoring the activation of 9 muscles of the push leg using EMG surface electrodes (Konigsberg, 1200Hz). The EMG data were filtered using a 4th order zero-phase butterworth band-pass filter (10-400Hz) and quantified using root mean squared values in 20ms average bins. EMG data were normalized to the maximum binned values during isometric manual muscle tests [4]. Body segment kinematics were captured simultaneously in the frontal, sagittal, and transverse planes. A metronome was used as a timing constraint, just as dancers would normally adhere to a music based tempo requirement to control turn initiation and turn phase duration. The redirection of the horizontal reaction force (RFh), was compared across turn conditions during the push phase of a piqué. The average (+/- standard deviation) binned muscle recruitment data synchronized to push leg forceplate departure were compared across conditions to determine how the RFh were redirected.

RESULTS AND DISCUSSION

Consistent muscle recruitment was observed across hip muscle length conditions, however selective scaling corresponds to kinematic and kinetic contexts (Figure 1, blue vs. cyan). For example, activation of the gluteus maximus (GMa) and gluteus medius (GMe) of the push leg accompanied hip external rotation and hip extension and corresponded to antero-medially directed RFh. Both subjects used less biceps femoris (BF) recruitment (consistent with hip external rotation action of the BF) and less rectus femoris (RF) in npk1 than in pk1. This strategy is consistent with using RF to redirect RFh in the medial direction and translate the center of mass towards the turn stance leg when the lower extremity is externally rotated.

Selective modification of muscle recruitment strategies were found as the number of turns was increased (Figure 1, pk1 vs. pk2 and npk1 vs. npk2). There was an increase in hamstring activation consistent with redirecting the RFh in the antero-medial direction and generating hip external rotation required during the end of the push phase. Subject 1 modified RFh of push leg during pk2 and npk2 to create angular impulse earlier than in pk1 and npk1. This modification was due to earlier and higher levels of BF activation consistent with redirecting the RFh anteriorly (Figure 1). For subject 2, there was increased activation of the semimembranosus/ semitendinosus (SMST) from pk1 to pk2 with increased activation of BF from npk1 to npk2, consistent with the hip rotation actions of each muscle (Figure 1).

CONCLUSIONS

Selective modulation of lower extremity muscle activation was identified coincident with the subject- specific RFh reorientation. Recruitment patterns were similar but scaled across hip external rotation conditions and modified as number of turns increased. Subject-specific solutions were observed, even in this small sample, also emphasizing that there are multiple ways to satisfy the mechanical objectives in well-practiced goal-directed tasks such as piqué turns.

REFERENCES

1. Winter DA. *J Biomech*. **13(11)**:923-27, 1980
2. Mathiyakom W & McNitt-Gray JL J. *Rehabil Res Dev* **45(8):**1237-48, 2008
3. Loeb, Gerald E., and Claude Ghez. *Principles of Neural Science*. New York: McGraw Hill, 2000.
4. Kendall F.P. *Muscles: Testing and Function with Posture and Pain*, Baltimore, MD, USA 2005.

ACKNOWLEDGEMENTS

This work was supported by the USC Biomechanics Laboratory.

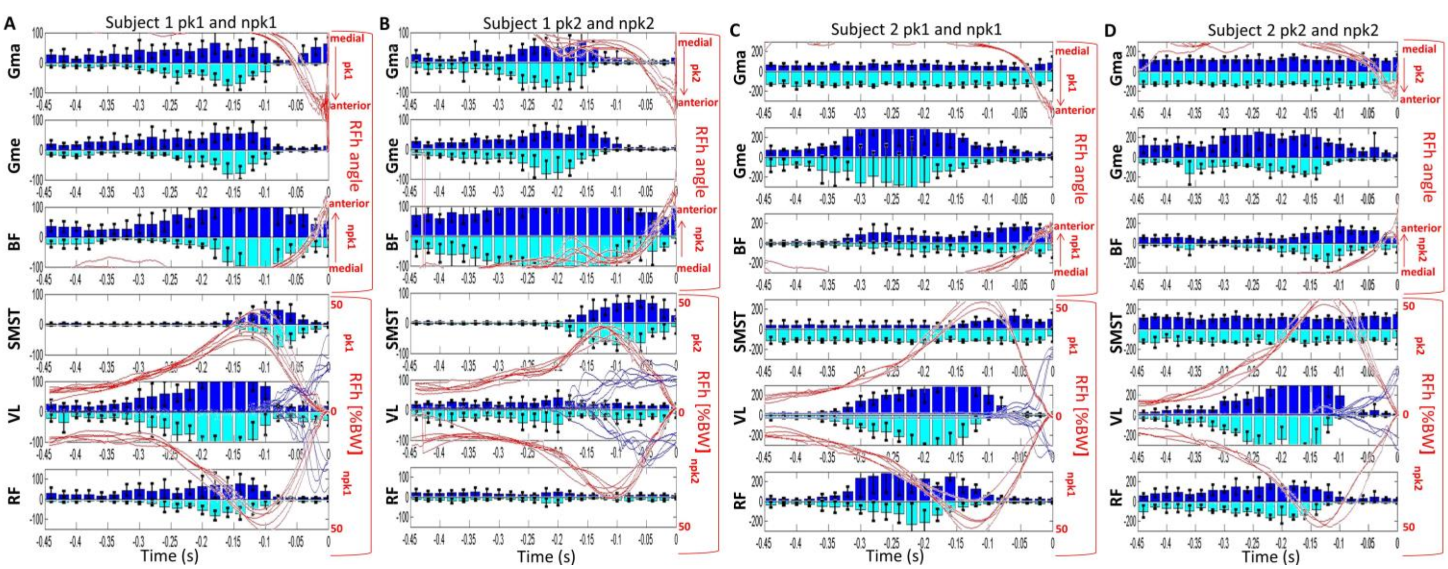

Figure 1: Subject 1 (A-B) and subject 2 (C-D) mean (+/- standard deviation) muscle recruitment for pk turns (blue) npk turns (cyan) with kinetic context overlay of RFh magnitude (red push leg, blue stance leg) and RFh angle trends from medial to anterior of push leg (top curves for pk turns, bottom curves for npk turns).

Effects of Volitional Spine Stabilization and Lower Extremity Fatigue on Landing Performance in a Recurrent Low Back Pain Population

R. Haddas, P. Sizer, S. Sawyer, T. Brooks, M. Chyu, C.R. James

Texas Tech University Health Sciences Center, Lubbock, TX, USA
email: r.haddas@ttuhsc.edu

INTRODUCTION

Lower extremity injuries and low back pain pervade everyday life. Along with injuries come the unavoidable physical, emotional, and economic costs, along with lost time and normal function [1]. Ankle sprains, anterior cruciate ligament (ACL) injuries, and hamstring muscle strains are the most common sports injuries [2]. Low back pain (LBP) can significantly influence an individual's quality of life and will affect between 60-80% of the population [3]. Additionally, LBP can alter functional ability and increase the risk of lower extremity injury [4]. A volitional preemptive abdominal contraction (VPAC) is commonly used to improve lumbar spine stabilization and reduce pelvic motion in individuals with spine dysfunction. The VPAC influences lower extremity motion control and potentially reduces the risk of injury [5]. Fatigue serves as a major risk for injury that alters muscle shock absorbing capacity and coordination of the locomotor system [6]. The effects of spine stabilization on people with recurrent low back pain are well documented [4]. The purpose of this study was to test the hypothesis that volitional spine stabilization strategies would modulate the effects of lower extremity fatigue on lower extremity and trunk mechanics, as well as neuromuscular control during landing in people with and without recurrent low back pain.

METHODS

Thirty-three healthy and 32 young adults with LBP participated. Three-dimensional kinematics (VICON Nexus) were collected from the lower extremity and lumbar spine at a sampling rate of 100 Hz. Ground reaction force (GRF) and electromyographic (EMG) data from the right side internal oblique (IO), external oblique (EO), and multifidus (Mf) at the first lumbar (L5) spinal level, as well as the right side gluteus maximus (GM), semitendinosus (ST), vastus medialis (VM) and rectus femoris (RF) were sampled at 2000 Hz. Subjects performed twelve DVJ trials: six with and without VPAC and six with and without VPAC in a fatigued state. Fatigue was induced using a submaximal squat protocol. A 2x2x2 mixed ANOVA was used to determine differences between groups and the VPAC and fatigue conditions for each dependent variable. Follow-up tests were conducted as necessary, with alpha correction at each step. Statistical analyses were conducted using SPSS.

RESULTS AND DISCUSSION

Semitendinosus onset exhibited a significant three-way interaction effect between subject groups, and the VPAC and fatigue conditions ($p=0.001$). No other variables exhibited a significant three-way interaction effect. Follow-up analyses were conducted to examine the significant three-way interaction effect for the ST onset variable and consisted of calculating six 2x2 ANOVAs with all combinations of group, VPAC and fatigue conditions. Semitendinosus onset exhibited significant two-way interaction effects for three of the six 2x2 follow-up ANOVAs. Semitendinosus onset exhibited a significant two-way interaction effect between the VPAC and fatigue conditions in the healthy group ($p=0.001$). In addition, semitendinosus onset exhibited a significant two-way interaction effect between group and VPAC condition during fatigue ($p=0.018$). Furthermore, semitendinosus onset exhibited a significant two-way interaction effect between group and fatigue condition during VPAC ($p=0.004$, Table 1).

Semitendinosus onset exhibited several significant simple main effects. Semitendinosus onset was significantly different between the VPAC conditions without (p=0.001) and with (p=0.001) fatigue in the healthy group. Semitendinosus onset occurred before contact with VPAC but after contact without VPAC in both fatigue conditions. Additionally, semitendinosus onset was significantly different between VPAC conditions in both the healthy (p=0.001) and LBP (p=0.001) groups with fatigue. Semitendinosus onset occurred before contact with VPAC but after contact without VPAC. Moreover, semitendinosus onset was significantly different between the fatigue conditions in the healthy (p=0.001) and LBP (p=0.001, Table 1) groups in the VPAC condition. Semitendinosus onset occurred before contact but earlier in both groups without fatigue compared to with fatigue. Several significant main effects were exhibited such as earlier onset with VPAC and later onset with fatigue in the LBP group; earlier onset with VACP and later onset in the LBP group without fatigue; and later onset with fatigue and in the LBP group without VPAC.

Maximum pelvic obliquity angle exhibited a significant two-way interaction effect between VPAC and fatigue conditions (p=0.045). No other significant two-way interactions were observed for this variable. Additionally, VPAC and fatigue decreased GRF and lumbar spine motion during landing, as indicated by several significant main effects (p = 0.001 to 0.002).

Based on our results, the VPAC appears to create a protective advantage for the knee and lumbar spine as suggested by the earlier ST activation in the VPAC conditions during the 0.30 m drop vertical jump landing, which could potentially translate into injury prevention if a perturbation is encountered during the landing task. In addition, these changes suggest that the neuromuscular system may be better prepared prior to initial ground contact for encountering the stresses imposed by the landing sequence. The VPAC can alter lower extremity neuromuscular control and improve pelvic and spine stabilization during a 0.30 m drop vertical jump in healthy individuals [5]. Moreover, our evidence suggests that lower extremity injury risk may increase when individuals are suffering from low back pain and while under the influence of fatigue, which is consistent with the literature [4,6].

CONCLUSIONS

Our results provide evidence that a VPAC strategy that is performed during a fatigued landing sequence decreases exposure to biomechanical factors that can contribute to lower extremity injury. This apparent protective response is present in both healthy and LBP individuals when landing from a 0.30 m height. Incorporating VPAC during dynamic stressful activities, with and without the presence of fatigue, appears to help improve sensorimotor control and facilitate positioning of the lower extremity, while protecting the lumbar spine. Clinicians can use this information when designing neuromuscular control training programs for people who have recurrent LBP to improve lower extremity control, spine stability, and potentially decrease injury risk.

REFERENCES

1. Whiting WC & Zernicke RF. *Biomechanics of mucsuloskeletal injury*. Human Kinetics, 2008.
2. Heiderscheit BC, et al. J Orthop Sports Phys Ther, **40**, 67-81, 2010.
3. Indahl A, et al. Spine **20**, 473-477, 1995.
4. Zazulak BT, et al. (2007). Am J Sports Med, **35**, 1123-1130, 2007.
5. Haddas R, et al. Abstr. 36th A. Mtng ASB, **97**, 2012.
6. James CR, et al. J Electromyography Kinesiol, **20**, 667-675, 2010.

Table 1. Semitendinosus Onset (seconds) for Healthy and LBP Groups in VPAC and Fatigue Conditions.

Healthy		**NFV** -.072						**NFNV** .009	**FV** -.006			**FNV** .034		
LBP					**NFV** -.039						**NFNV** .022	**FV** .317	**FNV** .040	
Group/Time	**-.080**	**-.070**	**-.060**	**-.050**	**-.040**	**-.030**	**-.020**	**-.010**	**.000**	**.010**	**.020**	**.030**	**.040**	**.050**

Time zero = Initial Contact. NFNV=No Fatigue and No VPAC, NFV=No Fatigue and VPAC, FNV= Fatigue and No VPAC, FV=Fatigue and VPAC

QUADRICEPS FATIGUE AFFECTS CENTRAL NERVOUS SYSTEM ACTIVATION

Sam K. Morton, Dimitrios Katsavelis, Terry L. Grindstaff and A. Joseph Threlkeld

Creighton University, Omaha, NE, USA
email: joethrelkeld@creighton.edu web: rehablab.creighton.edu/

INTRODUCTION

Fatigue has been shown to decrease voluntary activation of the quadriceps muscle [1,2] In these studies, fatigue was induced by requiring a set number of isokinetic contractions, usually 25-30. While repetitions remained the same, quantifiable fatigue states were not normalized between participants. Furthermore, these studies have not reported the characteristics of muscle activation during or after recovery from a fatigued state.

For the present study we used repetitive Maximum Voluntary Isometric Contractions (MVIC) to induce fatigue. Determination of fatigue was independent of the number of contractions a subject generated. We chose isometric contractions as they eliminated between-subject variations in the generation of smooth isokinetic contractions during fatigue development and isometric contractions were more consistent with our measurements of voluntary activation using the interpolated twitch technique (ITT).

METHODS

Eight healthy adult volunteers (6 male 2 female; (mean±SD, age= 25.5±3 years, height= 175.2±12.9 cm, mass= 75.2±15.4 kg) participated. After a 5 minute warm-up of treadmill walking, two self-adhesive percutaneous electrodes (8x14cm; Collins Sports Medicine) were placed on the skin of the dominant (preferred kicking) leg over the proximal vastus lateralis and the distal vastus medialis portions of quadriceps muscle.

Subjects were seated and secured in a Biodex System 3 isokinetic dynamometer (Biodex Medical Systems Inc., Shirley, NY) with the knee at 60 ^{o} of flexion and the hip at approximately 90 ^{o} of flexion [1].

A Digitimer Constant Current Stimulator (DS7AH; Digitimer Limited) with a Train/Delay Generator (DG2A; Digitimer Limited) was used to generate all electrical stimuli to the quadriceps (2 pulses applied at 100Hz for a 200msec duration, 450 mA). Prior to the fatiguing protocol, we measured the torque (Tpre) produced during two 5-second maximal voluntary isometric contractions (MVIC) of the quadriceps (yielding peak voluntary torque), two MVICs with superimposed electrical stimuli (yielding peak electrically augmented torque) and by an electrical stimulus to the muscle at rest (yielding peak electrically elicited torque).

After 2 minutes of rest, subjects undertook a fatigue protocol consisting of repetitive quadriceps MVICs (7 sec of contraction followed by 3 sec of rest). The 7-on, 3-off cycle was repeated until fatigue which was operationally defined as ≥35% decrement of a subject's peak torque output observed for three consecutive contraction relaxation cycles (≤65% of the highest pre-fatigue torque). Verbal encouragement and a real-time visual torque display were provided to the participant to elicit maximal effort during testing.

Immediately after the 35% voluntary torque decrement was obtained, the pre-fatigue torque and electrical stimulation protocol was duplicated (T0). Two minutes after fatigue, the torque and electrical assessments were repeated (T_2). If the participant was able to produce ≥80% of his or her highest pre-fatigue peak torque at T_2, testing was stopped. If they did not reach ≥80% of their initial peak torque, testing was repeated again at 5 minutes post-fatigue (T_5) or if needed at 10 minutes post-fatigue (T_{10}). The final testing session at which the participant recovered to ≥80% of initial peak torque (either T_2, T_5 or T_{10}) was termed Tlast .

Peak torques were extracted for each instance of stimulation (Figure 1). For purposes of determining percent voluntary activation, MVIC torque was calculated as the average torque produced over a 50 ms epoch prior to the delivery of the maximal electrical stimulus. Quadriceps percent voluntary activation was quantified using the interpolated twitch technique [1]. Statistical analysis was performed by using one-way ANOVA and post-hoc testing with $p<0.05$.

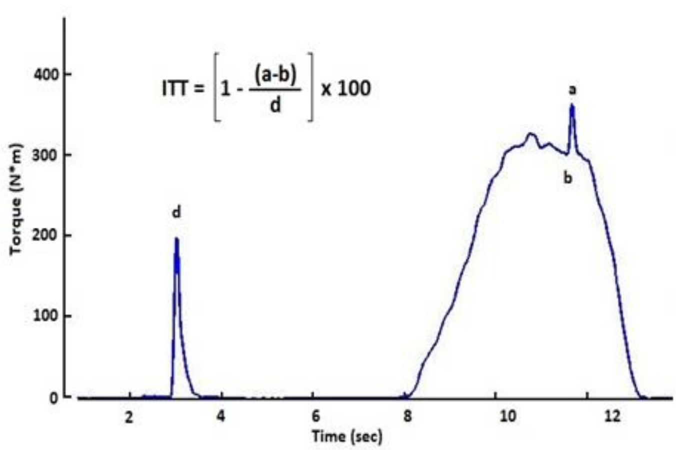

Figure 1. Schematic representation of the interpolated twitch technique utilized for the calculation of percent voluntary activation. Point d represents the peak torque produced by stimulating the muscle at rest. The larger curve to the right represents a voluntary contraction with a superimposed stimulus. Point b represents the average torque for the 50 msec preceding delivery of the electrical stimulation and point a represents the maximum torque produced by an active contraction with superimposed electrical stimulus.

RESULTS AND DISCUSSION

Significant differences were found in percent voluntary activation between stages ($p<.05$) (Figure 2). Post-hoc analysis showed significantly less percent activation at T0 in comparison to Tpre and Tlast. As depicted in Figure 2, percent voluntary activation at recovery (Tlast) was statistically the same as pre-fatigue activation (Tpre).

The majority of the subjects were able to recover within 2 minutes post-fatigue. Three subjects needed additional time to recover for one out of the two sessions.

CONCLUSIONS

Our results demonstrated that healthy participants experienced a significant suppression of the central component of quadriceps muscle activation immediately following a series of fatiguing isometric contractions. Muscle tension generated in a fatigued state was compromised by a lack of central activation [3]. Central activation was restored to Tpre levels when voluntary contractions could produce at least 85% of maximum torque (Tlast) thus the suppression of central activation was a short duration response.

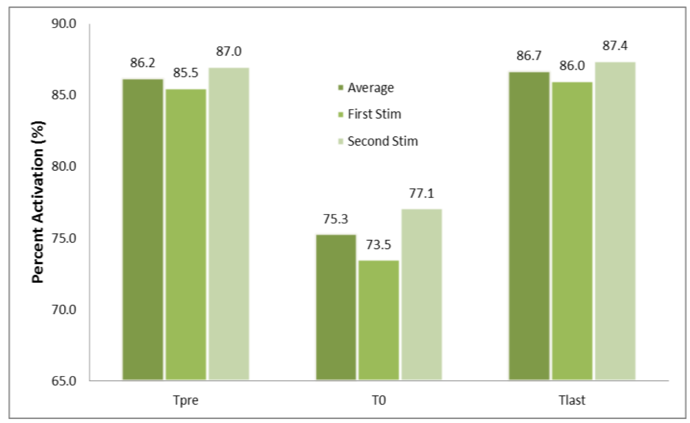

Figure 2. Percent activation with average, first and second stimulation separated.

REFERENCES

1. Krishnan C, Williams GN. Muscle Nerve **41**, 868-74, 2010.
2. Stevens-Lapsley J, et al. Neurorehabil Neural Repair **26**, 533-41, 2012.
3. Ranieri F, Neuromuscul Disor **3**, 157-61, 2012.

ACKNOWLEDGEMENTS

Research reported in this abstract was supported by the National Institute on Aging of the National Institutes of Health under grant number R15 AG040616. The content is solely the responsibility of the authors and does not necessarily represent the official views of the National Institutes of Health.

ESTIMATION OF SKULL CORTICAL THICKNESS FROM CLINICAL CT

[1,2]Elizabeth M. Lillie, [1,2]Jillian E. Urban, [1,2]Ashley A. Weaver, and [1,2]Joel D. Stitzel

[11]Wake Forest University School of Medicine, Medical Center Blvd, Winston-Salem, NC 27157
[2] Virginia Tech - Wake Forest University Center for Injury Biomechanics
email: elillie@wakehealth.edu, http://www.sbes.vt.edu

INTRODUCTION

In the United States traumatic brain injuries contributed to 30.5% of all injury related deaths from 2002 to 2006 [1]. The human cranial vault serves as the main mechanism of protection for the brain from these contact injuries. Despite the important role the skull plays in protecting the cranium, more needs to be known about its anatomy. Cortical thickness of bone is difficult to quantify due to the resolution limitation on clinical computed tomography (CT) scans. Thickness measurements of structures thinner than 3 mm are overestimated using the standard full width half max (FWHM) technique [2]. A better understanding of the physical properties of the skull would provide further insight into the mechanism of head injury. In this paper we present a technique that has been adapted from Treece et al to accurately interpret cranial vault cortical thickness from clinical CT scans [3]. With a large repository of clinical CT scans it would be advantageous to be able to evaluate thickness variations across the population by age and skull location.

METHODS

Two male cadavers (age 49 and 56) were used to evaluate the cortical thickness of the skull. Clinical CT scans of the head were collected at 0.625 mm isometric resolution for both specimens (GE 64-slice PET/CT Discovery VCT Scanner, Center for Biomolecular Imaging, Wake Forest University). The skulls were removed using a surgical saw at the base of the foramen magnum and cleaned by removing all skin and soft tissue.

One-quarter inch diameter sections of the skull were collected using neurosurgical equipment. These samples were then scanned using a GE CT-120 CT scanner (Biomedical Research Imaging Center, University of North Carolina at Chapel Hill) to evaluate the actual cortical thickness. The scans were collected at 25 micron resolution with isometric voxels and reconstructed at a 50 micron resolution. The FWHM technique was used to evaluate the actual cortical thickness from the microCT.

The software program Stradwin was used to estimate the cortical thickness of the skull from clinical CT scans [3]. The cortical density of the cadaver skull was measured and reported in Hounsfield Units and used to map cortical thickness estimates over a 3 dimensional (3D) surface of the bone [3, 4]. The location sampled for microCT was identified on the 3D reconstruction of the skull and the skull was then cropped to the appropriate size. Three dimensional volumes were calculated for both the microCT and the cropped clinical CT. The clinical CT was aligned to the microCT using both Geomagic Studio (Geomagic, Research Triangle Park, NC) and 3D Slicer (National Alliance for Medical Image Computing). The 3D volume from the clinical CT scan was converted to a point cloud and sub-selected to only contain points in contact with the surface of the microCT volume. The transforms created from the alignment were used to match the cortical thickness measurements from Stradwin between the clinical CT and the microCT. The thickness measurements corresponding with the surface label map of the clinical CT were then compared to the nearest thickness measurement from the microCT.

RESULTS AND DISCUSSION

A sample from the frontal bone of the 46 year old cadaver was selected for the validation of Stradwin for the skull. This sample contained the frontal suture which can be identified as a section of cortical bone from the outer to inner cortex as opposed to the two cortical tables separated by the diploe layer. The actual thickness measurements for the outer table of the frontal bone are shown in Figure 1A. The suture was determined to exceed 4 mm while much of the outer table fell between 1.5 to 2 mm. The thickness measurements calculated from the clinical CT scans are shown in Figure 1B. Qualitatively the thickness measurements between the microCT and the clinical CT were comparable (Figure 1C).

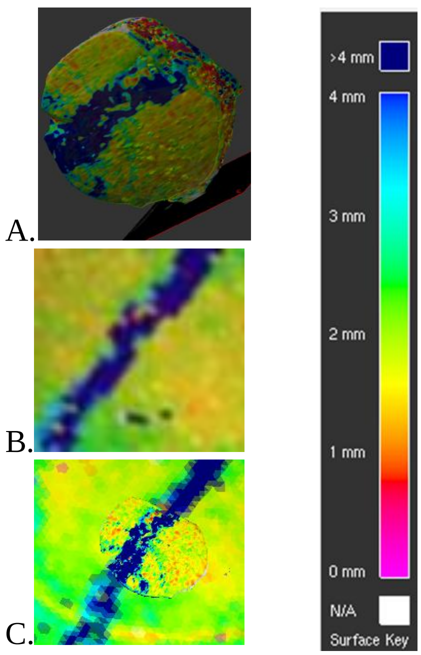

Figure 1: Thickness measurements from Stradwin represented as color maps over the 3D volume's outer surface for A) microCT, B) clinical CT, and C) microCT aligned with the clinical CT. The thickness scale is located on the right.

For a more quantitative analysis the thickness, calculations from the clinical CT that were associated with points on the surface label map were compared to the thickness of the nearest landmark on the microCT. In evaluating the difference in matched thickness calculations, 96% of all selected points fell within ±0.9 mm (Figure 2). The clinical CT thickness measurement overestimated actual thickness on average only 0.25 mm where the median actual thickness was 1.55 mm.

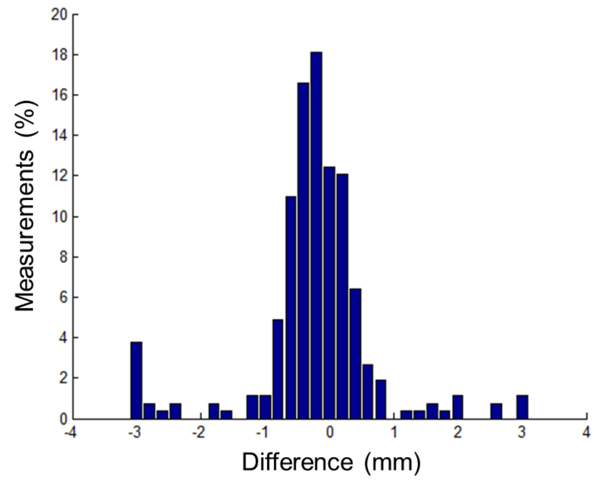

Figure 2: Distribution of difference in thickness measurements between the clinical CT and the thickness of the microCT.

CONCLUSIONS

With the exception of the suture within the sample, cortical thickness measurements on the skull were well below 3 mm and accurate thickness could not be calculated using FWHM on a clinical CT scan. The actual thickness of the skull has been shown to be more accurately determined from clinical CT scans using a cortical density based approach, facilitating the study of populations to assess skull table thickness by age and anatomical location.

REFERENCES

1. Faul M. *Centers for Disease Control and Prevention*, Atlanta, GA, 2010.
2. Newman DL. *Physics in Medicine and Biology* 43, 619-626, 1998.
3. Treece GM. *Med Image Anal* 14, 276-290, 2010.
4. Treece GM. *Med Image Anal* 16, 952-965, 2012.

ACKNOWLEDGEMENTS

The authors would like thank the National Highway Traffic Safety Administration for funding this research.

FINITE ELEMENT PREDICTION OF PERIOSTEAL STRAIN AT THE HUMAN DISTAL RADIUS DURING A TARGETED LOADING TASK

[1] Varun A. Bhatia, [2] W. Brent Edwards, [1,2] Karen L. Troy
[1]Bioengineering Department, University of Illinois at Chicago
[2]Department of Kinesiology and Nutrition, University of Illinois at Chicago
email: vbhati2@uic.edu, web: http://www.uic.edu/ahs/biomechanics

INTRODUCTION

Exercise based interventions have been used to maintain and improve bone strength in order to prevent fragility fractures in older populations [1]. Bone adapts to its mechanical environment (i.e., strain), and exercise interventions have been shown to increase bone mineral and mechanical properties in humans [2]. Although, empirical relationships between bone strain and bone adaptation have been well described using animal models, similar relationships for humans are limited and remain theoretical. In part, this is due to difficulties in adequately controlling and directly quantifying bone strain *in vivo*. The ability to accurately predict bone strain non-invasively under controlled experimental conditions, is an essential first step for deriving empirical relationships between bone strain and adaptation in humans. Knowledge of such relationships is a key prerequisite for the systematic development and evaluation of exercises to improve bone health and reduce the occurrence of fractures.

The objective of this study was to validate a subject-specific finite-element modeling technique to predict periosteal strains at the distal radius during a controlled mechanical loading task – leaning on to the palm of the hand (Fig 1a).

METHODS

Four female cadaveric forearms with hand intact (mean age 87 years) were obtained from anatomical gift. The distal most 12 cm of the forearms were imaged with a clinical CT scanner (BrightSpeed; GE Medical Systems, Milwaukee, WI, voxel size: 0.234mm X 0.234mm X 0.625mm). A calibration phantom (QRM, Moehrendorf, Germany) with calcium hydroxyapatite equivalent concentrations were used to establish a linear relationship between CT Hounsfield units (Hu) and calcium hydroxyapatite equivalent density (ρ_{ha}) in g/cm^3.

For each specimen, soft tissue proximal to the wrist was removed and osteotomy was performed 14 cm proximal to the distal dorsal tubercle of the radius; the proximal most 8 cm of the forearm was potted in polymethylmethacrylate. Six rectangular strain gage rosettes were adhered circumferentially to the periosteal surface of the distal radius, four on the dorsal side and two on the palmar side. The specimens were placed on a uniaxial material testing machine (MiniBionix 858, MTS Systems, Eden Prairie, MN) to mimic the mechanical task of leaning on to the palm of the hand (Fig 1b). The actuator was driven at 0.3 mm/sec until a load of 300 N was reached and analog data were collected at 100 Hz. Principal strains were calculated for each rosette at the instant of maximum load [3].

Segmented CT data were used to create surface geometries of the radius, lunate and scaphoid using the Mimics Innovation Suite (Materialise, Leuven, Belgium). Surface geometries were exported to 3-matic (Materialise, Leuven, Belgium), and finite element models were generated using quadratic tetrahedral elements. The scaphoid and lunate were given a nominal element size of 0.5 mm^3. Cartilage was modeled between the articular surface of the distal radius and carpal bones, and given a nominal element size of 0.25 mm^3. In accordance with a preliminarily mesh convergence analysis, the radius was given a nominal element size of 0.5 mm^3 (maximum 3.0 mm^3), corresponding to 35508 ± 3375 tetrahedral elements.

The scaphoid and lunate were defined as non-deformable rigid bodies. Cartilage was defined as a neo-Hookean hyperelastic material with a modulus of 10 MPa, and a Poisson's ratio of 0.45. The radius was assigned inhomogeneous linearly-isotropic material properties based on density. Four density-elasticity relationships were examined each with a Poisson's ratio of 0.4:

$E=10{,}500\rho_{ash}^{2.25}$ Eq (i) [4]
$E=2{,}500\rho_{app}^{3}$ Eq (ii) [5]
$E=6850\rho_{app}^{1.49}$ Eq (iii) [6]
$E=8920\rho_{app}^{1.83}$ Eq (iv) [6]

where E (MPa) is the elastic modulus, ρ_{app} (g/cm^3) is the apparent density equal to $\rho_{ha}/0.626$, and ρ_{ash} (g/cm^3) is the ash density equal to $\rho_{app}*0.6$.

Finite element models were solved using Abaqus 6.10 (Simulia, Providence, RI). Boundary conditions were created to match the experimental set-up (Fig 1c). The proximal part of the radius corresponding to the location of potting was fully constrained. The scaphoid and lunate were rotated to simulate 80° of wrist extension. Contact was modeled between the surfaces of the cartilage and scaphoid, and cartilage and lunate. A tied interface contact model was defined wherein the carpal bones were not allowed to slide once they were in contact and seated into the cartilage. A ramped force of 300 N was applied to the centroid of the scaphoid (180 N) and lunate (120 N) based on the assumption that 60% of the load transmitted through the wrist is borne by the scaphoid. The line of action of the resultant force vector was determined for each specimen using an unsymmetrical beam theory analysis based on proximal strain gage and CT information [7].

Finite element predicted principal strains at locations corresponding to strain gage site were calculated. Experimentally measured and model predicted principal strains (for each density-elastically relationship) were compared using Pearson's r, linear regression, and root mean square error (RMSE).

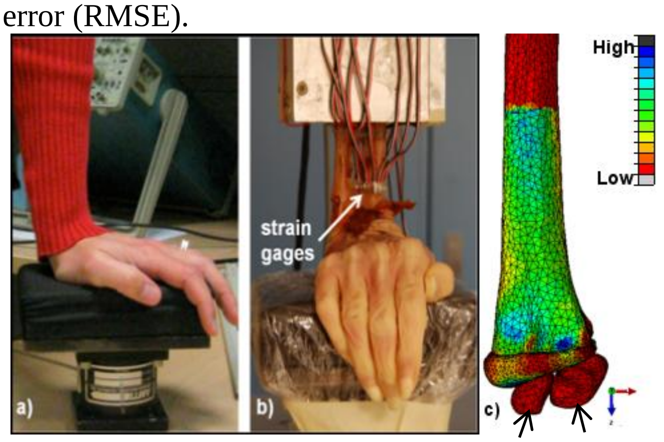

Figure 1: a) Targeted loading protocol, b) Experimental testing setup, c) Finite Element model showing minimum principal strains.

RESULTS AND DISCUSSION

The highest correlation and lowest RMSE between experimentally measured and finite element predicted strain was observed using Eq (iv). These models illustrated an r=0.928 and an RMSE of 424.3 ue (Table 1). One specimen illustrated substantial error (RMSE=713.8 με) relative to the other 3 specimens and upon further examination was found to be highly osteoarthritic. Using Eq (iv), exclusion of this specimen from our analysis resulted in a r=0.968, a slope of 0.984^{ns}, intercept of 51.1^{ns} (ns=not significantly different from 1 for slope and 0 for intercept), and a RMSE of 219.6 με (11.1% of maximum measured strain) (Fig 2).

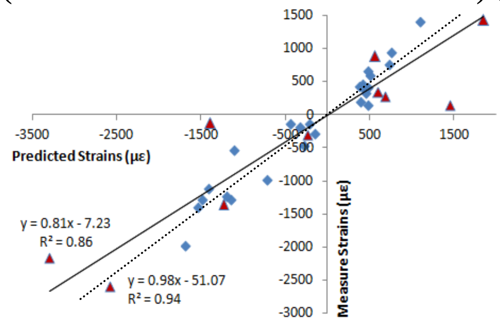

Figure 2: Plot of measured vs. predicted strains. Solid line: all specimens, dashed line: excluding specimen with OA.

This study is limited by the use of a small sample size, though many specimen-specific finite-element model validation studies have relied on sample sizes similar to ours. Additionally, the density-elasticity relationships examined herein were derived from anatomical locations other than the distal radius. However, we are unaware of a density-elasticity relationship specific to the distal radius.

CONCLUSIONS

We were able to validate a modeling method that can accurately (r=0.968, RMSE=11.1%) and non-invasively predict periosteal strains acting on the radius bone during a targeted loading task of leaning on to the palm of the hand. The validated model can be used to assess exercise-induced bone strain to better understand the mechanical factors contributing to bone adaptation in humans.

Table 1: Pearson's r, slope, intercept, root mean square error (RMSE), and RMSE as a percentage of the maximum absolute measured strain, for the four density-elasticity relationships. *[a] Significantly different, [ns] not significantly different from 1 (slope) or 0 (intercept)*

	Eq (i)	Eq (ii)	Eq (iii)	Eq (iv)
R	0.848	0.795	0.927	0.928
Slope	0.193^a	0.164^a	0.758^a	0.809^a
Intercept	-46.1^{ns}	-17.7^{ns}	1.2^{ns}	-7.2^{ns}
RMSE (ue)	3557.4	4117.2	472.3	424.3
RMSE (%)	136.8	158.4	18.2	16.3

REFERENCES

[1] Gomez-Cabello A, Sports Med. 2012, [2] Bailey CA, Bone 2010, [3] Bhatia VA, Proc. of the Orthop. Res. Soc 2012, [4] Carter DR, J Bone Joint Surg Am. 1977, [5] Keller TS, J Biomech 1994, [6] Morgan EF, J Biomech 2003 [7] Rybicki EF, J.Biomech 1977

THE VASCULAR STRUCTURE OF BONE IS COMPROMISED WITH IMMOBILIZATION AND IS NOT RECOVERED WITH ANTI-RESORPTIVE TREATMENT AND REMOBILIZATION

[1]Parth Patel, [1]Devendra Bajaj, [2]Paolo E. Palacio-Mancheno, [2]Mitchell B. Schaffler and [1]J. Christopher Fritton

[1]New Jersey Medical School, Department of Orthopaedics, Newark, NJ, USA
[2]City College of New York, CUNY, Department of Biomedical Engineering, New York, NY
email: frittojc@umdnj.edu

INTRODUCTION

Bisphosphonates are anti-resorptive drugs that suppress the bone loss of osteoporosis [1]. However, their use has been associated with atypical fracture of cortical bone in humans and lower cortical tissue toughness in animal models [2]. The bone loss associated with bed rest, spinal cord injury or space travel is more aggressive and we have been investigating the effects of bisphosphonates in these situations. Thus far we have demonstrated that cortical bone loss in an immobilized forelimb dog model is suppressed and allows for enhanced structural (endosteal and periosteal envelopes) recovery with remobilization [3,4]. However, mechanical fatigue life is adversely affected. In this study we have investigated the vascular structure of the intra-cortical envelope to gain a better understanding of how the largest pores of cortical bone may influence the mechanical properties of this tissue.

METHODS

Animal Model. In an IACUC-approved study adult female beagles were divided into 4 groups, plus age-matched control (n=6 /group, Figure 1a). The right forelimbs in the 4 groups were immobilized (IM) for 6 months (m) using thermoplastic splints (AquaPlast, Smith and Nephew) [5]. 2 groups were treated with daily doses of risedronate (RIS, 0.5 mg/kg/day) and 2 with sterile water vehicle (VEH). After 6 m IM, splints were removed in one RIS and one VEH-treated group, drug treatment was stopped, and dogs were allowed unrestricted weight-bearing and remobilization (RM) for 12 m. All groups (6m, 18m and age-matched control) were euthanized by pentobarbital overdose.

Cortical Beam Preparation. Beams (n=1/dog) with rectangular cross-sectional geometry (0.5x1.5x14 mm length) were sliced from the cortex of radii using a precision saw (Isomet 5000, Buehler). The osteon long axis was parallel to the long axis of each beam (Fig 1).

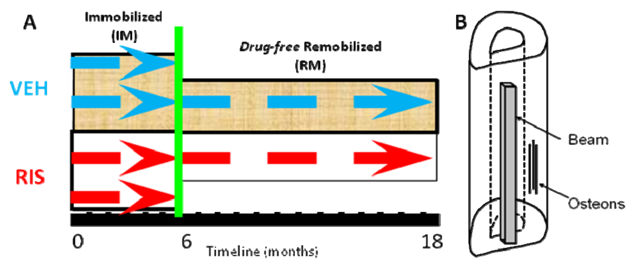

Figure 1. (A) Timeline for treatments (B) Beam in relative position with osteons in radius.

Micro-computed tomography. 3D micro-computed tomography (μCT) images of the beams were generated with a Skyscan 1172 system (Bruker, Belgium; 100kV; 100μA). The beams were immersed in PBS and individually scanned with a voxel resolution of 4.7μm. The measured porosity traits included total pore volume, degree of anisotropy and connectivity density (Conn).

Statistical Analysis. Results are shown as mean ± standard deviation (SD). Differences between groups were calculated by one way ANOVA with post-hoc Fisher's Least Significant Difference test for at $p<0.05$.

RESULTS AND DISCUSSION

With IM the total pore volume increased versus age-matched control and was not improved by either drug treatment or RM (Figure 2). The degree of anisotropy among all groups did not vary

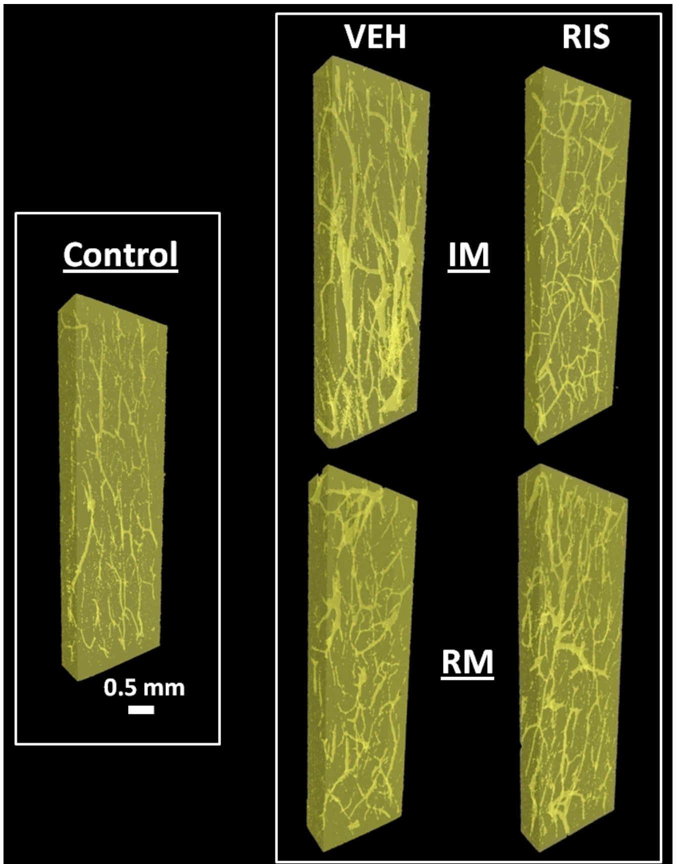

Figure 2. µCT images of the vascular pores of beams.

significantly (Fig. 2), remaining within 2% of control. Connectivity increased for all groups compared to control. The drug-treated remobilized (RM RIS) group was increased ($p < 0.05$) by 132% versus control (Fig. 3).

CONCLUSIONS

RIS is effective in slowing endosteal and periosteal bone loss. However, the intra-cortical envelope consisting mainly of the pores of the vascular supply appears not to be protected. In addition, very little recovery of this envelope occurs upon remobilization, regardless of whether previous drug treatment was attempted. This may partially explain some of our previous mechanical results for these beams, although not all, since drug treatment was beneficial to preventing the loss in toughness and fatigue life during immobilization. Regardless, a complete recovery of all the bone on all envelopes should be the goal of future work to optimize post-IM recovery, restore mechanical properties and prevent fractures after the extended disuse that occurs with bed rest, spinal cord injury and space flight.

REFERENCES

[1] Black et al. *The Lancet* **348**, 1535, 1996.
[2] FDA. *Meeting of Advisory Committee for Reproductive Health Drugs and Drug Safety*, 2011.
[3] Li et al. *NASA HRP Investigators' Workshop*, 11, 2007.
[4] Bajaj et al. *NASA HRP Investigators' Workshop*, 4092, 2012.
[5] Li et al. *JBMR* **20**, 117, 2005.

ACKNOWLEDGEMENTS

Drs. Richard Mann, Luis Cardoso, Chaoyang Li, Yilin Wang, Xiaobing Zhang and Mr. Edek Williams provided technical assistance. Supported by NIH/NIAMS (AR063351 & AR041210) and the NSBRI (PF02304, NASA contract NCC 9-58). Risedronate was provided by Procter & Gamble Pharmaceuticals.

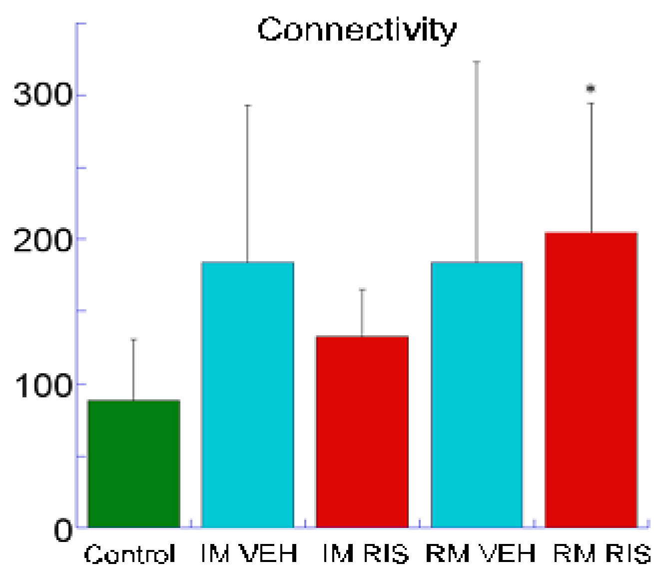

Figure 3. Comparison of connectivity. (* significance, $p < 0.05$, compared to control, in green)

A COMPREHENSIVE MULTISCALE CHARACTERIZATION OF THE TIBIOFEMORAL JOINT : TISSUE TESTING

Snehal Chokhandre[1,2], Craig Bennetts[1,2], Robb Colbrunn[3], Tara Bonner[3], Ahmet Erdemir[1,2]

[1]Computational Biomodeling (CoBi) Core
[2] Department of Biomedical Engineering
[3]BioRobotics and Mechanical Testing Core,
Lerner Research Institute, Cleveland Clinic, Cleveland, Ohio,44195, USA
email: chokhas@ccf.org, web: http://simtk.org/home/j2c

INTRODUCTION

The substructures of the tibifemoral joint significantly affect the mechanics of the joint. It is necessary to have a better understanding of the multiscale mechanics of the joint in order to develop treatment options and preventative measures for knee joint injuries and pathologies. With the growing focus on simulation studies of the knee joint for scientific and clinical purposes [1,2], data for model development and verification is becoming increasingly important. This is particularly important in instances where finite element (FE) analysis is used for clinical decision making.

Many studies employing FE analysis of the knee joint rely on literature for material properties and have limited validation, which may or may not be adequate to accurately represent the phenomena of interest. Expanding upon our previous study [3], where specimen-specific imaging and joint level mechanical testing data was acquired, this study aims to acquire specimen-specific tissue level mechanical response as well as cellular level information via histological analysis. This detailed dataset will provide complete multiscale information for development and confirmation of multi-resolution, finite element models to better understand the effects of macro (joint) level occurrences on micro (cell) level behavior.

METHODS

Mechanical testing was performed on a cadaver knee (34 year old female, normal BMI, no knee or foot injury, surgeries, osteoarthritis or inflammatory arthritis). The joint level testing was described previously [3] and is summarized here. The specimen was prepared such that only femur, tibia, femoral and tibial articular cartilage, anterior and posterior cruciate ligaments (ACL and PCL), medial and lateral collateral ligaments (MCL and LCL), and menisci were intact. Magnetic resonance (MR) images were acquired using a 4 Tesla scanner (Medspec, Bruker Biospin Corp., Billerica, MA) (Fig. 1). Mechanical testing of the joint was conducted on a six degrees of freedom (DoF) motion control robot (Rotopod R-2000, Parallel Robotic Systems Corp., Hampton, NH, USA) (Fig. 1). Laxity and combined loading tests were performed for flexion angles ranging from 0˚ to 90˚ in 30˚ increments.

Following joint testing, the substructures were dissected and tissue mechanical testing samples were prepared. Overall 12 samples were tested from femoral and tibial articular cartilage, cruciate and collateral ligaments and the menisci. Five mm diameter, full thickness cartilage and meniscus samples were tested under confined compression. Meniscus samples were also tested in uniaxial tension (dumbbell shaped, 5mm by 1mm test length). Ligament samples were tested under uniaxial tension (dumbbell shaped, 10mm by 2mm test length). All the tests were conducted on a uniaxial material testing system (MTS Systems Corporation, Eden Prairie, MN, USA). All the specimens were immersed in a saline bath and kept at 37 °C during testing. Stress relaxation tests were performed on all samples. Each cartilage and meniscus sample was tested at 5%, 10% and 15% strain at 20%/s strain rate for both confined compression and uniaxial tension. A preload of 0.05N was applied before the stress relaxation to obtain the initial test length of the cartilage and meniscus samples. In case of ligaments a preload of 0.1 N was applied followed by 10 preconditions cycles at ± 0.25 mm. A stress relaxation test was performed at 5% and 10% strain at 20%/s strain rate for all the ligament samples. Histology slides (H&E staining) were also prepared for all the tissue types.

RESULTS

The MR images and the joint testing data provided adequate specimen-specific anatomical information and mechanical response for joint level model development and evaluation (Fig. 1). The tissue testing data will be useful in specimen-specific tissue characterization, which in turn can be utilized to establish specimen-specific material properties in computational models (Fig. 2). Figure 3 shows the sample histology for femoral articular cartilage, ACL and medial meniscus.

DISCUSSION

The aim of this study was to obtain comprehensive multi-resolution mechanical testing and imaging data for the tibiofemoral joint, which can be used for the development of specimen-specific multiscale FE models of the joint. The study is first of its kind to obtain data at several spatial levels for a single specimen. Joint scale models can be developed based on specimen-specific anatomy. Specimen-specific material properties (cartilage, menisci, and ligaments) can be obtained from tissue mechanical testing. Experimental joint kinetics and kinematics can be used as an independent dataset for confirmation of model predictions. Histology data can be utilized to develop cell-scale models, again specific to the specimen. While this information provides significant value for simulation based-medicine, some limitations are apparent in its scope; only one specimen was tested, some tissue components (which may be of interest for other purposes) were removed prior to joint testing including the patella, and the total number of tissue testing samples were limited.

ACKNOWLEDGMENTS
The authors would like to thank Christopher Flask, PhD and Jack Jesberger for magnetic resonance imaging; Morgan Jones, MD, for specimen preparation and assessment; and Jason Halloran, PhD for help with joint level experimentation. This study was funded by R01EB009643, NIBIB, NIH.

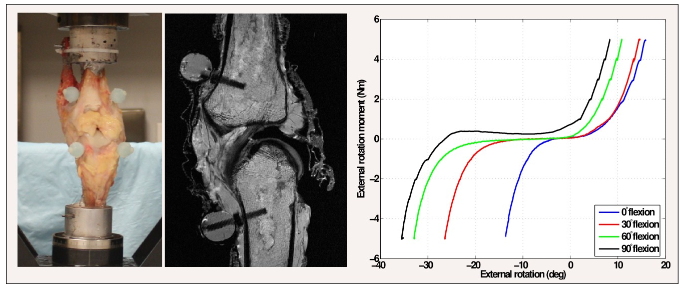

Figure 1: Testing at the joint scale provides *in vitro* joint geometry by magnetic resonance imaging and *in vitro* joint kinematics and kinetics by robotics testing.

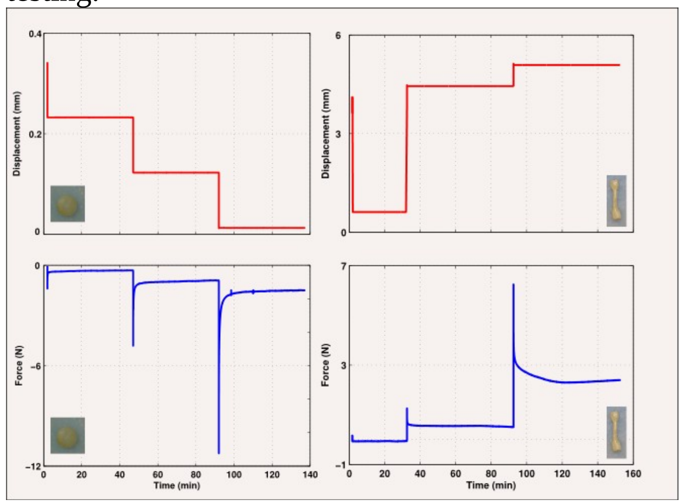

Figure 2: Time histories for applied deformations and resulting loads during lateral femoral cartilage confined compression test (left) and ACL uniaxial tensile test (right).

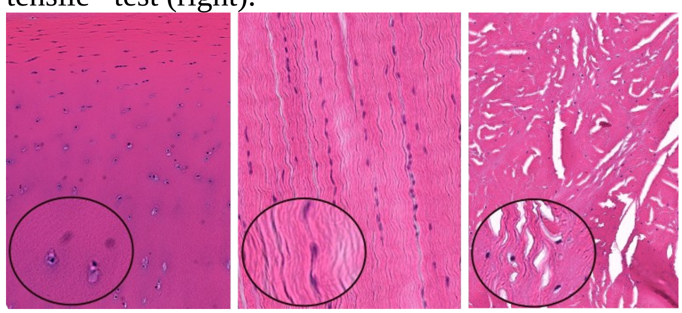

Figure 3: Histology sections of femoral articular cartilage, PCL and medial meniscus. Circular sections provide a magnified view.

REFERENCES

1. Peña E., et al., 2006, J Biomech, **39**(9), 1686-1701.
2. Shirazi R., et al., 2009, J Biomech, **42**(15), pp. 2458-2465.
3. Chokhandre S., et al., 2012, Proceedings of ASME 2012 SBC, Fajardo, Puerto Rico,USA.

EVALUATION OF NEW TOTAL KNEE ARTHROPLASTY CONSIDERING DESIGN FACTORS CAPBLING OF REDUCING A RISK OF TKA FAILURES: FINITE ELEMENT ANALYSIS

[1]Paul Han, [1]Young Woong Jang [2]Oui Sik Yoo [2]Jung Sung Kim [1]Dohyung Lim

[1]Dept. Mechanical Engineering, Sejong University, Seoul, Republic of Korea
[2]Central R&D Center, Cheonan, Chungnam, Republic of Korea
Corresponding e-mail: dli349@sejong.ac.kr

INTRODUCTION

Total knee arthroplasty (TKA) is frequently done and highly successful in the past decades [1]. It is therefore widely accepted that TKA an increasingly common procedure: more than 650,000 TKRs were done in the USA in 2008, more than 77,500 in the UK in 2009, and more than 100,000 in South Korea between 2002 and 2005 [2]. However, small percentage of TKA failures is still existed in a significant number of patients, when considering the large number of TKAs performed annually. Bone resorption, aseptic loosening, instability, wear are generally known as main reasons of TKA failures in mechanics. Recently a specific TKA (LOSPA, Corentec Co. LTD., Cheonan, Korea) adjusting design factors capable of reducing a risk of the failures above was developed. The aim is therefore to evaluate the TKA developed newly, through analyses of contact pressure patterns between the femoral and tibia TKA components, micromotion between the bone and TKA components, and stress/strain distribution within the tibia bone using a three-dimensional finite element (FE) analysis.

MATERIALS AND METHODS

LOSPA (Femur size #7: AP/ML 60/68mm, Spacer size #7: AP/ML 46/72mm, Baseplate size #7: AP/ML 46/72mm) was considered in this study. LOSPA was characterized by adjusting design factors of TKA component (anterior flange`s roundness, femoral condyle and tibial insert shape, etc.) for improvement of functions of deep flexion, wear resistance, joint stability, muscle force efficiency, ligament safety, etc.

A three-dimensional (3D) tibia FE model with TKA was generated based on sawbone (Tibia #3973, Sawbones Europe AB Co., Malmö, Sweden) and LOSPA. TKA was then aligned and inserted through a traditional TKR surgical guideline [3]. The total number of tetrahedral elements (C3H4) used for the FE model was 1,269,184 (Element size: 1.0). Here, material properties for the FE model were assigned referenced from literature with assumption of homogeneous, isotropic, and lineal elastic characteristics [4-5]. A compressive load of 2000N (about 3 times body weight) was applied to the FE model, sharing by the medial (60%) and lateral (40%) condyle, simulating a stance phase before toe-off. For the FE analysis, contact pressure patterns, micromotion and stress/strain distribution were evaluated for the prediction of the potential risks of wear, aseptic loosening and structural instability and resorption, respectively. Here, validation of FE model was performed through comparing of the results (contact pressure and strain) obtained from an actual mechanical test with those from the FE analysis.

RESULTS AND DISCUSSION

The developed FE model was validated with high accuracy, through comparing with contact pressure on the surface of the TKA spacer and strain on the cortical bone measured from the actual mechanical test.

Most of contact pressures were in the range of 0-30 MPa (Lateral and medial compartments: 99.0% and 96.3%, respectively) (Fig. 1). These findings are favorably comparable to the fact that contact pressures less than about 30 MPa are frequently occurred during walking, and may indicate that the potential risks of wear are low. Most of micromotions were in the range of 0-20 μm (82.5%) and not exceed a critical damage value (about 45 μm above), which is capable of inducing a negative effect on optimum bone in-growth (Fig. 2). These findings may indicate that the potential risks of aseptic loosening induced by micromotions are low. Stress/strain distributions within the cortical and cancellous bones were visualized in Fig. 3. In general, stress/strain distributions within the cortical (6.4 MPa / 424 μstrain) and cancellosus (1.4 MPa / 4,522 μstrain) bones were shown reasonably without the critical damage stress/strain (37.5 MPa / 2500 μstrain for cortical bone), which may reduce the capacity for bone remodeling, leading to bone degeneration. Also, peaked stresses (31.0 MPa and 2.64 MPa for cortical and cancellous bones, respectively) not exceed yield stresses (38.0 MPa and 5.0 MPa for cortical and cancellous bones, respectively) considering safety factor (N = 3.0). These findings may indicate that the potential risks of structural instability and bone resorption are low.

CONCLUSION

It is judged that newly developed TKA may be comparable at least with commercial TKAs in reduction of the potential risks of wear, aseptic loosening and structural instability and resorption. The current study had, however, a limitation in direct evaluation with commercial TKAs. It will be therefore considered in further studies.

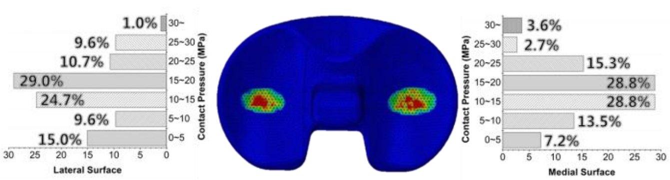

Figure 1: Percentage of contact area on surface of TKR spacer presenting with certain ranges of contact pressures

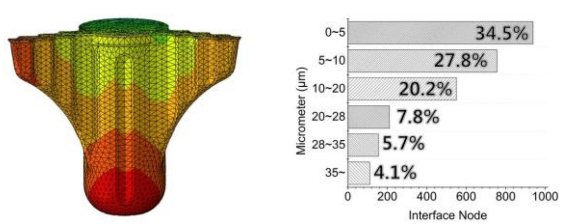

Figure 2: Percentage of bone and TKA component (keel part of base-plate) interface area presenting with certain ranges of micromotions

REFERENCES

1. E. Rubin, et al. *Bone and Joint: Pathology 2nd edition*, 1273-1347, 1994
2. A.J. Carr, et al. *Lancet* **379**, 1331-1340, 2012
3. M. Tew, et al. *J Bone Joint surg Br* **67**, 551-556, 1985.
4. M. Taylor, et al. *J Biomechanics* **31**, 303-310, 1998.
5. A.G. Au, et al. *Med Eng Phys* **27**, 123-134, 2005

ACKNOWLEDGEMENTS

This study was supported by a grant from the Korea Health-care Technology R&D Project, Ministry for Health, Welfare, & Family Affairs, Republic of Korea (A100023).

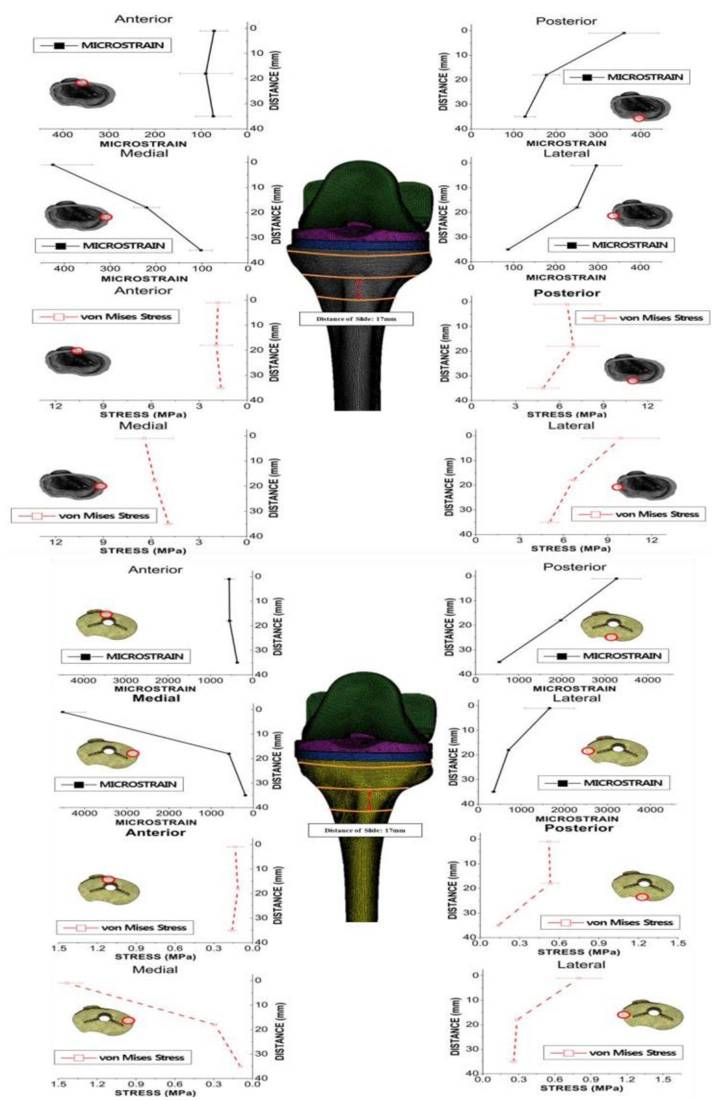

Figure 3: Stress/strain distribution within the a) cortical and b) cancellous bones (considered 48 regions of interests), from FE analysis

INFLUENCE OF ANTICIPATION ON ACL LOADING WHEN GROUND REACTION FORCES ARE PERTURBED DURING A SIDESTEP CUTTING MANEUVER

[1]Joshua T. Weinhandl & [2]Kristian M. O'Connor

[1]Old Dominion University, Norfolk, VA, USA
[2]University of Wisconsin-Milwaukee, Milwaukee, WI, USA
email: jweinhan@odu.edu

INTRODUCTION

Significant research efforts have been made in the last decade to determine modifiable risk factors of sustaining non-contact ACL injuries so prevention strategies can be developed [1]. Although previous studies have indicated that biomechanical factors such as frontal plane knee moments, quadriceps muscle activation, and proximal anterior tibia shear force may be risk factors for non-contact ACL injuries, a recent literature review failed to find convincing scientific evidence to support a cause-and-effect relationship between those proposed risk factors and non-contact ACL injuries [2].

Unanticipated cutting tasks offer a closer representation of movements that occur during game situations, and demonstrate increased risk to knee joint ligaments if there is limited time for appropriate postural adjustments [3]. However, these unanticipated cutting tasks are still an assessment of "safe" movement tasks. There is a need to more effectively bring together laboratory and field environments. Such an approach may provide crucial insights into the causal factors of non-contact ACL injury, facilitating the development of more effective and adaptable prevention methods.

Forward dynamics musculoskeletal modeling allows investigators to identify injury risk factors with cause-and-effect relationships [4]. For example, studies have shown that alterations in kinematic and muscle activation parameters at initial ground contact [4] and at peak posterior GRF [5] yield injury situations. The purpose of this study was therefore, to determine the influence of movement anticipation on ACL loading when presented with unexpected changes to the anteroposterior GRF during sidestep cutting. It was hypothesized that, as a result of GRF perturbations, peak ACL loading would increase more when the cutting direction was unanticipated compared to when the movement was anticipated.

METHODS

Twenty healthy recreationally active females (21 ± 1 years, 61.8 ± 6.4 kg, 1.66 ± 0.05 m) completed cutting tasks that consisted of four randomized conditions: anticipated (AC) and unanticipated (UC) cutting, a straight run, and a stop. Three-dimensional joint kinematics were collected using a ten-camera Motion Analysis Eagle system (200 Hz), and force plate data were collected with an AMTI force platform (1000 Hz).

Participant-specific musculoskeletal models were then generated in OpenSim [6] consisting of 21 degrees-of-freedom (*dof*). The left leg was actuated by joint torque actuators, while the right leg and back were actuated by 43 Hill-type muscle actuators. Maximum isometric force of each muscle in the model was scaled according to each participant's peak isokinetic strength. Pelvis position and orientation relative to the ground was defined with 6-*dof*. The head, arms, and torso were represented as a rigid segment connected with the pelvis by 3-*dof*. Each hip was modeled as a 3-*dof* ball-and-socket joint. The left knee was modeled as a 1-*dof* revolute joint, while the right knee was modeled as a 3-*dof* joint. Both ankles were modeled as 1-*dof* revolute joints. Computed muscle control (CMC) was then implemented to produce forward dynamic simulations for all AC and UC trials generally consistent with the experimentally measured kinematics [7].

Musculoskeletal model outputs were used in a three-dimensional knee model to estimate ACL force (F_{ACL}). Simulated perturbations of 120, 140 and 160% were applied to the anteroposterior ground reaction force GRF. For each perturbation model, muscle excitations, initial joint kinematics estimated by CMC, and perturbed GRFs served as inputs to a forward dynamics simulation and F_{ACL} was re-estimated. Changes in peak F_{ACL} due to movement GRF perturbations were assessed via a 4×2 repeated measures ANOVA. (perturbation magnitude (baseline, 120, 140 and 160%) × condition (AC, UC)). Significance was set *a priori* at $p<0.05$.

RESULTS AND DISCUSSION

Anteroposterior GRF perturbations did not result in significant magnitude×condition interactions in F_{ACL} or any planar component of F_{ACL} (Table 1). The main effect of perturbation magnitude revealed significant increases in F_{ACL} and the sagittal plane component as perturbation increased. The frontal plane component of F_{ACL} significantly decreased as perturbation magnitude increased. Similarly, the transverse plane component significantly decreased as perturbation magnitude increased to 140%. The main effect of cutting condition revealed F_{ACL} and the sagittal plane component were significantly greater during UC trials.

Table 1. Effects of cutting condition and perturbation magnitude on mean ± stdv peak ACL loading ($N \cdot kg^{-1}$).

	Anticipated	Unanticipated
Baseline	11.02 ± 4.65	12.40 ± 3.79
120%[a]	11.26 ± 4.60	12.65 ± 3.68
140%[ab]	11.43 ± 4.52	12.78 ± 3.58
160%[abc]	11.56 ± 4.42	12.83 ± 3.36

[a] significantly different from baseline
[b] significantly different from 120%
[c] significantly different from 140%

Previous studies have suggested F_{ACL} and potential for non-contact injuries are increased when performing cutting maneuvers in an unanticipated sporting situation [3]. In the frontal plane, increased knee adduction moments during initial weight acceptance of stance, when the movement is unanticipated, are thought to increase ACL loading [4]. However, this peak adduction moment occurs well before peak frontal plane ACL loading and has minimal influence on F_{ACL}. Rather, the increase in F_{ACL} observed in the current study was primarily due to changes in sagittal plane loading rather than frontal or transverse planes.

Perhaps more interestingly, anteroposterior GRF perturbations had similar effects regardless of cutting condition. Researchers have shown some level of pre-activation in the knee flexors and extensors during both anticipated and unanticipated sidestep cutting [3]. However, while there is a 70-90% increase in knee moments when the movement is unanticipated, there is only a 10-20% increase in activation of muscles surrounding knee [3]. This apparent mismatch between preprogrammed muscle activation patterns and external knee loads under unanticipated conditions appears to place larger loads on the ACL. This would suggest that initial joint configuration and appropriate pre-programmed muscle activation patterns are critical to increasing knee joint stiffness and effectively modulating ACL loading [4]. Thus, if given an initial joint configuration and a predetermined set of muscle excitations one could reasonably expect this difference in peak ACL loading would be magnified when GRFs unexpectedly change as a greater percentage of the energy would need to be absorbed through passive mechanisms.

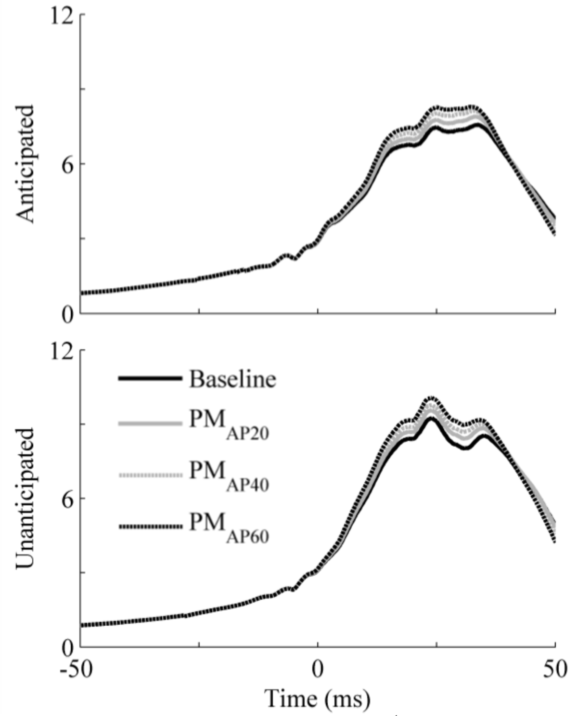

Figure 1. Mean ACL loading ($N \cdot kg^{-1}$) during anticipated (top panel) and unanticipated (bottom panel).

CONCLUSIONS

The results of this study indicate intervention studies aimed at preventing non-contact ACL injuries should include elements of reaction to unanticipated visual cues and unexpected perturbations. As the central nervous system has the ability to selectively alter postural adjustments based on information acquired from previous tasks, training to unanticipated visual cues, as well as unexpected perturbations, may provide an appropriate stimulus for the central nervous system to refine appropriate postural adjustments. Training programs might therefore focus on reducing reaction times to visual and mechanical stimuli. Whether these neuromuscular changes map over into performance of sporting tasks remains to be seen.

REFERENCES

1. Griffin et al. *AJSM*. **34**, 1512-32, 2006.
2. Yu & Garrett. *BJSM*. **41**, i47-51, 2007.
3. Besier et al. *MSSE*. **35**, 119-27, 2003.
4. McLean et al. *Clin Biomech*. **23**, 8926-36, 2008.
5. Lin et al. *J Biomech*. **42**, 418-23, 2009.
6. Delp et al. *IEEE TBE*, **54**, 1940-50, 2007.
7. Thelen et al. *J Biomech*, **36**, 321-8, 2003.

ACKNOWLEDGEMENTS

International Society of Biomechanics Dissertation Grant
University of Wisconsin-Milwaukee Dissertation Fellowship
UWM College of Health Sciences Student Research Grant

RELATIONSHIP BETWEEN LEAN MASS ASYMMETRIES AND FORCE PRODUCTION ASYMMETRIES DURING JUMPING

Erika M. Heinbaugh, Rebecca C. Moynes, Shawn Rockey, Derek T. Smith, Boyi Dai

University of Wyoming, Laramie, WY, USA
Email: eheinbaugh@uwyo.edu

INTRODUCTION

Bilateral force production asymmetries are associated with lower extremity musculoskeletal injuries [1,2]. The asymmetries may generate loading imbalance to the joints and increase injury risks [3]. It was suggested that force production asymmetries can be caused by a number of factors such as handedness, anthropometry, neurology, strength, previous injury, sport specific demands, and motor control stressors [4,5]. However, the underlying mechanism that causes force production asymmetry is still unknown.

From a neuromuscular control perspective, muscle force is determined by muscle activation level, muscle cross-sectional area, muscle stress, force-length relationship, and force-velocity relationship [4]. The bilateral muscle stress, force-length, and force-velocity relationships should be similar during a bilateral task. Therefore, muscle activation level and cross-sectional area are the two factors that may contribute to bilateral force production asymmetries. However, the relationships among muscle activation asymmetries, cross-sectional area asymmetries, and force production asymmetries are still unclear.

The purpose of this study was to investigate the relationships between force production asymmetries and lean mass asymmetries during a countermovement jump task. Lean mass asymmetry was used to approximate lower limb cross-sectional area asymmetries. It was hypothesized that force production asymmetries would be greater than lean mass asymmetries. It was also hypothesized that force production asymmetries would be positively and moderately correlated with lean mass asymmetries. Understanding the contribution of lean mass asymmetries to force production asymmetries could provide insight into developing training programs to normalize bilateral asymmetries as risk factors for injury.

METHODS

Ninety-five adults (Age: 45.15 ± 15.62 years, Mass: 74.45 ± 16.26 kg, Height: 1.68 ± .093 m) from the general population participated in the study. Each participant underwent a full-body Dual Energy X-ray Absorptiometry (DEXA) scan and performed three bilateral maximum countermovement jumps. Bilateral ground reaction forces (GRF) during jumps were collected using two force plates. Right and left leg lean mass were collected from the DEXA scan. Right and left average and maximum GRF were calculated from GRF data. Percent asymmetries were calculated for lean mass, max force and average force by subtracting the left side from the right side and dividing by the right side values. Positive values indicate the right leg produced more force and had more lean mass, while negative values indicate the left leg produced more force and had more lean mass. The dependent variables included lean mass asymmetry, lower extremity max GRF asymmetry, and average GRF asymmetry. One sample t-test was performed for max force, average force, and lean mass asymmetries to assess if these asymmetries were different from 0. Differences (Paired t-test) and correlations (Pearson Correlation) were used to assess and describe left and right side asymmetries. Asymmetry comparisons and correlations included: 1) lean mass to average GRF; and 2) lean mass to maximum GRF. A type I error rate was set at 0.05 for statistical significance.

RESULTS AND DISCUSSION

One sample t-test showed that max GRF (0.022 ± 0.081) and average GRF (0.027 ± 0.089) were significant from zero (p = 0.004 and p = 0.009) but the lean mass (-0.003 ± 0.034) was not (p = 0.404).

Percent asymmetries were significantly different for average GRF and lean mass (p=0.004) and max GRF and lean mass (p=0.013). There was no correlation between percent asymmetries for average GRF and lean mass (r = -0.116, p = 0.263) (Figure 1), however max GRF and lean mass showed a small but significant negative correlation (r = -0.290, p = 0.004) (Figure 2).

The first hypothesis, that the force asymmetries were greater than lean mass asymmetries, was supported. Participants demonstrate greater force on the right leg during jumps. However, the lean mass asymmetry was not significantly different from 0. The greater force on the right leg could be caused by leg preference during dynamic tasks even though the maximum force that can be generated by each leg might be similar. Right side dominant is observed only in force production but not lean mass.

The second hypothesis was not supported because of non-positive and weak correlations between force asymmetries and lean mass asymmetries. In general, the results show that the force asymmetries were not associated with or attributed to bilateral differences in lean mass distribution in participants who demonstrated force asymmetries during countermovement jumps. Indirectly, this evidence suggests that muscle activation asymmetries and not maximum force asymmetries may contribute to force production asymmetries.

Future injury prevention studies might focus on training neuromuscular control rather than lean mass distribution in normalizing force asymmetries in jumping tasks. Future studies with muscle activation measurements are needed to confirm this statement. In addition, the current study was limited to a general population, studying the mechanism of force asymmetries in athletic propulsion might be more relevant for injury prevention.

CONCLUSIONS

Right side dominant asymmetries were observed in force production during a counter-movement jump but not in lower extremity lean mass. Force asymmetries were not positively correlated with lean mass asymmetry. Muscle activation asymmetry rather than maximum force asymmetry may be a greater contributor to force production asymmetry.

REFERENCES

1. Hewett TE, et al. Am J Sports Med, 492-501, 2005.
2. Impellizzeri FM, et al. *Medicine & Science in Sport & Exercise*, 2044-2050, 2007.
3. Paterno MV, et al. AM J Sports Med, 1968-1978, 2010.
4. Newton RU, et al. *J of Strength & Conditioning Research* **20(4)**, 971-977, 2006.
5. Hodges SJ, et al. *J of Strength & Conditioning Research* **25(11)**, 3107-3117, 2011.
6. Escamilla RF, et al. *Medicine & Science in Sport & Exercise, 408-417, 2009*

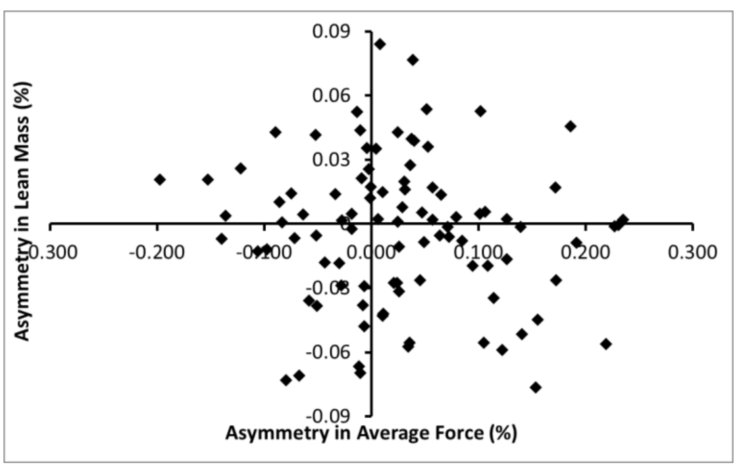

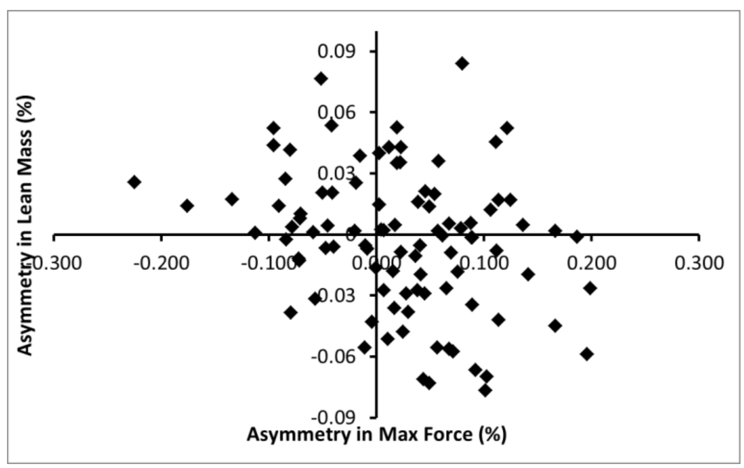

Figure 1. Percentage of Asymmetries in Average Force and Lean Mass

Figure 2. Percentage of Asymmetries in Max Force and Lean Mass

(Note: Negative values represent more force produced by left leg or more % lean mass in left leg)

ANKLE LANDING STRATEGY DURING A VERTICAL STOP-JUMP MANEUVER ALTERS KNEE JOINT RESULTANT FORCES

[1]Jonathan S. Akins, [2]Matthew A. McGinn, [1]Nicholas R. Heebner, [1]Timothy C. Sell, and [1]Scott M. Lephart

[1]University of Pittsburgh, Pittsburgh, PA, USA
[2]Carnegie Mellon University, Pittsburgh, PA, USA
email: jsa14@pitt.edu

INTRODUCTION

The majority of injuries among athletes are to the lower extremity with anterior cruciate ligament (ACL) injuries as one of the most common [1]. Despite prospective research, there has been no evidence of a reduction in ACL injury rates [1,2]. In an attempt to reduce the rate of ACL and other lower extremity injuries in sports, it is important to examine landing biomechanics. Previous studies have examined landing biomechanics during a stop-jump maneuver with a focus on reducing proximal tibia anterior shear force [3-5]. While ACL injuries are multi-planar, proximal tibia anterior shear force is likely the most direct loading mechanism [3]. Myers et al. demonstrated a reduction in proximal tibia anterior shear force following verbal instructions that included landing with increased knee flexion and toes first [5]. No studies were identified that specifically studied ankle joint position at landing. Landing in plantarflexion as compared to dorsiflexion allows the ankle to be an active component of the kinetic chain and may dampen the landing impact. The purpose of this study was to determine the effect of ankle landing strategy on vertical ground reaction forces (vGRFs), knee kinematics, and knee kinetics. We hypothesized that landing in plantarflexion would decrease vertical GRFs, decrease knee joint resultant forces and moments, and have no effect on knee kinematics.

METHODS

Three-dimensional lower extremity kinematics and kinetics were collected for 184 military personnel during a vertical stop-jump maneuver (Vicon Motion Systems, Centennial, CO, USA). Subjects stood at a distance of 40% of their height from the near edge of two force platforms (Bertec, Columbus, OH, USA), jumped with both legs to the force platforms, and landed with each foot on an individual platform. Immediately after landing, subjects performed a maximum vertical jump. Three successful trials were collected.

Lower extremity kinematics and kinetics were calculated using the Plug-In-Gait biomechanical model (Vicon Motion Systems, Centennial, CO, US). Vertical GRFs were used to identify initial contact of subjects with the force platforms. Initial contact was identified as the time when vGRFs exceeded 5% body weight. Knee kinematic data were calculated at initial contact and the peak values during the landing phase of the maneuver. Peak kinetic data were calculated during the landing phase of the maneuver and normalized by body weight. Means from three successful trials were used for data analysis.

Subjects were categorized based on ankle joint position in the sagittal plane at initial contact. An angle of 0° represented a neutral ankle position. Subjects landing in plantarflexion (≤0°) were placed in the plantarflexion group (age: 29.8 ± 7.1 years, height: 177.7 ± 6.2 cm, mass: 86.0 ± 8.8 kg). Subjects landing in dorsiflexion (>0°) were placed in the dorsiflexion group (age: 29.6 ± 5.9 years, height: 178.7 ± 5.9 cm, mass: 86.5 ± 8.5 kg).

Data were not normally distributed therefore a Mann-Whitney U test was used to identify significant differences between vGRFs, knee kinematics, and knee resultant forces and moments. All statistical analyses were performed using SPSS (Version 20, IBM, Armonk, NY, US). Alpha was set at .05 *a priori* for all analyses.

RESULTS AND DISCUSSION

No significant differences were identified between vGRFs or knee kinematics (Table 1). Landing in plantarflexion resulted in significantly less compressive tibia force (p=.033) and significantly greater anterior tibia shear force (p<.001) and lateral tibia shear force (p=.003). No significant differences were identified for knee resultant moments (p=.129-.288)

Landing in plantarflexion allows the ankle to be an active component of the kinetic chain which reduced compressive forces, but increased anterior and lateral shear forces. Increased compressive forces were expected when landing in dorsiflexion (heel first) because the GRFs directly load the tibia via the heel. Furthermore, a plantarflexed position allows the gastoc-soleus complex to absorb GRFs prior to contact. We hypothesized a reduction for anterior and lateral tibia shear forces, but found significant increases. Landing toes first shifts the GRF anteriorly with respect to the long axis of the tibia. This anterior shift creates a moment arm that the GRFs act upon. With similar vGRFs between groups, the moment arm likely increased the resultant forces/moments acting about the knee.

Knee resultant force and moment magnitudes from this study were similar to previous studies [3,4]. These studies identified biomechanical (hip and knee kinematics, GRFs) and neuromuscular (vastus lateralis activation) variables that are related to proximal tibia anterior shear force [3,4], but did not study ankle position during landing. These results identified that landing in dorsiflexion can reduce proximal tibia anterior shear force. Clinicians and coaches can use these results to assist in training of maneuvers similar to stop-jumps such as basketball rebounds, volleyball spikes, and related athletic maneuvers.

Future research should determine if ankle joint position at initial contact alters the distribution of ankle, knee, and hip joint kinetics, and the impact on maximal vertical jump height performance.

CONCLUSIONS

Landing in plantarflexion reduced compressive knee resultant forces, but increased proximal tibia anterior and lateral resultant forces.

REFERENCES

1. Hootman JM, et al. *J Athl Train* **42**, 311-319, 2007.
2. Siegel L, et al. *Clin J Sport Med* **22**, 349-355, 2012.
3. Sell TC, et al. *J Orthop Res* **25**, 1589-1597, 2007.
4. Yu B, et al., *Clin Biomech* **21**, 297-305, 2006.
5. Myers, et al., *J Biomech* **43**, 2657-2664, 2010.

Table 1: Vertical ground reaction forces, knee kinematics, and knee kinetics

	Plantarflexion Group (n=97)			Dorsiflexion Group (n=87)			p-value
Ankle Flexion at IC (°)*	-16.3	±	8.1	6.8	±	4.1	< 0.001
Knee Flexion at IC (°)	25.4	±	8.8	27.3	±	8.2	0.052
Knee Valgus at IC (°)	9.8	±	6.0	9.8	±	6.2	0.791
Peak Knee Flexion (°)	93.5	±	19.0	95.8	±	16.1	0.216
Peak Vertical Ground Reaction Forces (%BW)	202.6	±	55.2	192.1	±	59.9	0.063
Tibia Anterior Shear Force (BW)*	0.783	±	0.177	0.694	±	0.127	< 0.001
Tibia Lateral Shear Force (BW)*	0.368	±	0.152	0.309	±	0.136	0.003
Tibia Compression Force (BW)*	1.627	±	0.462	1.524	±	0.501	0.033
Knee Flexion Moment (BW)	193.4	±	46.2	180.3	±	35.7	0.129
Knee Varus Moment (BW)	30.2	±	14.7	36.2	±	23.4	0.288
Knee Internal Rotation Moment (BW)	4.16	±	4.16	3.31	±	3.37	0.147

* Significant difference (p < 0.05)

SINGLE-JOINT JUMP HEIGHT CORRELATES WITH HEEL LENGTH AND TOE LENGTH

Herman van Werkhoven, Stephen J. Piazza

The Pennsylvania State University, University Park, PA, USA
email: *piazza@psu.edu*

INTRODUCTION

Several recent studies have identified associations between foot and ankle structure and locomotor function. For example, the length of the heel has been found to correlate positively with energetic cost during running [1,2] and toe length has been found to correlate with toe flexor work during running [3]. Other studies have demonstrated that human sprinters have smaller Achilles tendon moment arms and longer toes than height-matched non-sprinters [4,5]. It is not clear, however, whether similar correlations between foot structure and performance exist for maximal height jumping.

Individuals with longer heels might be expected to have longer plantarflexor moment arms and thus better leverage for raising the body's center of mass. Musculoskeletal computer simulations have suggested, however, that large moment arms might reduce plantarflexor force due to force-velocity effects [4,6] and thus reduce moment and power during rapid plantarflexions.

The aim of this study was to test for correlations between performance in a single-joint maximal-height jumping task and either heel length or toe length. A single-joint jumping task was considered in order to allow for a focused investigation into the mechanisms of optimal performance. We hypothesized that jump height would correlate negatively with heel length, as each jump involves a rapid plantarflexion and shortening of the muscle fibers, but that jump height would correlate positively with toe length because longer toes would facilitate toe flexor work on the center on mass.

METHODS

Eight healthy male subjects performed five maximal height static jumps (without countermovement) using only the ankles (and not the knees or hips) for propulsion. Each subject wore braces to immobilize the knee joint and each was instructed not to rotate at the hips, bend the trunk, or move the arms or head. The arms were held stationary across the chest. Subjects wore platform shoes (JumpSoles, Metapro; Mountain View, CA) and a block was placed below the heel to prevent a countermovement.

Kinematics of the foot and shank were collected in order to calculate ankle angles. The peak rise of the centroid of four markers situated on the sacrum were used to measure jump height. Several foot, ankle and lower leg anthropometric values were recorded for each subject. These included: height; mass; lower leg length; maximum lower leg circumference; foot length; heel length (horizontal distance from lateral malleolus to back of the heel); and first toe length (distance from first metatarsal head to distal end of the hallux).

Correlation analyses were performed between all anthropometric variables and the jump height for each subject was averaged over five trials.

RESULTS AND DISCUSSION

Strong significant correlations were found between jump height and both heel length and toe length (Table 1, Figure 1, and Figure 2). No significant correlations were found between jump height and any of the other anthropometric variables.

Contrary to our hypothesis, a positive rather than a negative correlation was found between jump height and heel length (Figure 1). Our finding indicates that subjects with larger plantarflexor moment arms jump higher, suggesting that the increased leverage that follows from a longer plantarflexor moment arm outweighs the potential force reductions due to force-velocity effects. Previous studies have shown

Table 1: Correlations between anthropometric variables and average jump height (N=8, * p≤0.05)

measure	R^2	p-value
body mass	0.00	0.876
height	0.06	0.572
lower leg length	0.28	0.181
lower leg circumference	0.05	0.584
foot length	0.41	0.085
toe length	0.75	0.006*
heel length	0.71	0.009*

sprinters to possess smaller than normal plantarflexor moment arms, but it is possible that trained sprinters have undergone adaptations not found in our untrained subjects.

Previous modeling studies have suggested that a longer toe extends the duration of contact with the ground for sprinters, increasing the potential for forward propulsion [4,5]. This same mechanism could enhance maximal height jumping performance as a longer toe may keep the foot in contact with the ground longer and thus permit the muscles with more of an opportunity to propel the center of mass upwards.

The correlations we found are not simply a reflection of taller or heavier subjects jumping higher. Neither height nor body mass was correlated with jump height. A moderate correlation trending towards significance (R^2 = 0.41, p = 0.085) was found between foot length and jump height, although this dependency was not as strong as the relationships between heel length and jump height or toe length and jump height. Interestingly, foot length was strongly correlated with heel length (R^2 = 0.74, p = 0.006), but was not significantly correlated with toe length (R^2 = 0.16, p = 0.328).

We are currently working to develop a modified version of an existing computational simulation of the single-joint jumping task [7] to help explain the experimental findings of this study.

CONCLUSIONS

Maximal performance in a single-joint ankle jumping task was found to be significantly correlated with heel length and with toe length. For other motor tasks (e.g., sprinting and distance running) different combinations of heel and toe proportions seem to be favorable. Further investigation is needed to understand the mechanisms by which foot morphology potentially influences performance in different tasks and how differences in foot structure arise.

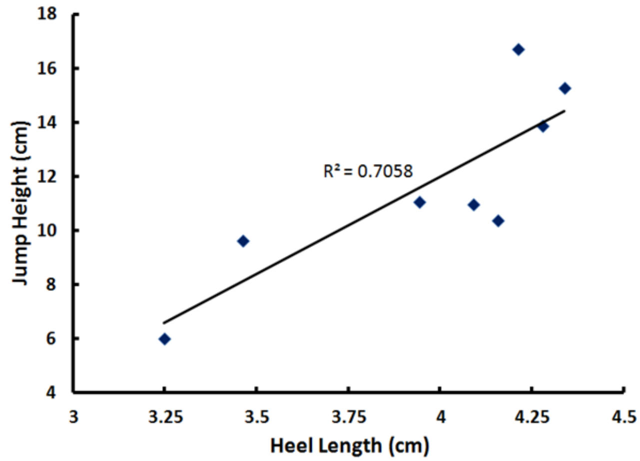

Figure 1: Correlation between average jump height and heel length (R^2 = 0.71, p = 0.009).

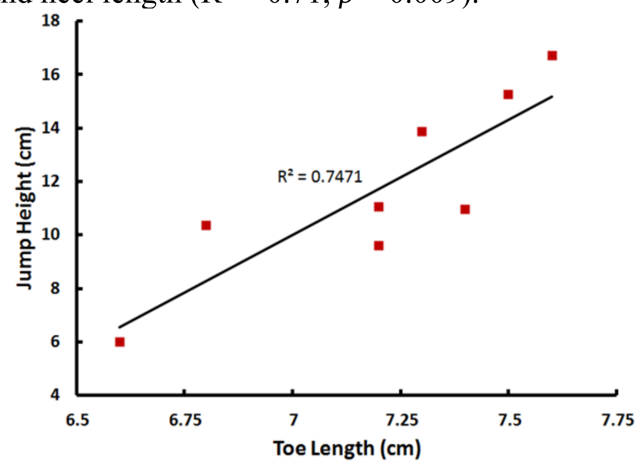

Figure 2: Correlation between average jump height and toe length (R^2 = 0.75, p = 0.006).

REFERENCES

1. Scholz MN, et al. *J Exp Biol* **211**, 3266-3271, 2008.
2. Raichlen DA, et al. *J Hum Evol* **60**, 299-308, 2011.
3. Rolian C, et al. *J Exp Biol* **212**, 713-721, 2009.
4. Baxter JR, et al. *P R Soc B* **279**, 2018-2024, 2012.
5. Lee SSM, et al. *J Exp Biol* **212**, 3700-3707, 2009.
6. Nagano A, et al. *J Biomech* **36**, 1675-1681, 2003.
7. van Werkhoven H, et al. *J Biomech*, in press.

INTRINSIC FOOT MUSCLE DETERIORATION AND METATARSOPHALANGEAL JOINT DEFORMITY IN PEOPLE WITH DIABETES AND NEUROPATHY

[1]Victor A. Cheuy, [1]Mary K. Hastings, [1]Paul K. Commean, [2]Samuel R. Ward, and [1]Michael J. Mueller

[1]Washington University in St. Louis, St. Louis, MO, USA
[2]University of California San Diego, San Diego, CA, USA
email: cheuyv@wusm.wustl.edu
web: https://pt.wustl.edu/research/FacultyResearch/Pages/AppliedBiomechanicsLaboratory.aspx

INTRODUCTION

Over 65,000 diabetes-related amputations occur annually, and over 80% are preceded by neuropathic plantar ulcers [1,2]. Previous studies have shown metatarsophalangeal joint (MPJ) hyperextension is associated with increased plantar pressures [3]. Clinical studies have shown that MPJ hyperextension deformities, such as hammer or claw toe, are associated with plantar ulcers [4,5]. The long-term objective of this research is to examine the contribution of intrinsic foot muscle (IFM) deterioration to the impairment cascade of MPJ hyperextension deformity, neuropathic plantar ulceration, and non-traumatic lower extremity amputation. Although IFM deterioration has been implicated as a contributing factor to neuropathic foot deformity [6], previous studies have been inconclusive [7,8].

The aims of this study were to compare IFM volume, IFM deterioration (ratio of adipose to lean muscle tissue volume), and physical performance in participants with diabetes mellitus and peripheral neuropathy (DMPN) to controls, and determine associations between IFM deterioration, physical performance, and second MPJ hyperextension.

METHODS

23 DMPN subjects (59 ± 10 years) and 12 age-matched controls (57 ± 14 years) were studied. The Foot and Ankle Ability Measure (FAAM) evaluated physical performance. Lateral radiographs were used to measure second MPJ angle (Figure 1A). A custom program developed in MatLab was used to measure IFM volume and deterioration from the hindfoot to midfoot (Figure 1B-D) [9]. To summarize, a histogram of all voxel intensities from the inputted MR slice is produced. A threshold between muscle and adipose intensities is automatically calculated using a multiple-Gaussian-function-fitting algorithm on an individual subject basis, unique to each MR image. An edge detection algorithm segments subcutaneous fat from the IFM. The remaining region of interest corresponding to the IFM is separated into lean muscle and adipose tissue volumes as determined by the threshold calculated earlier.

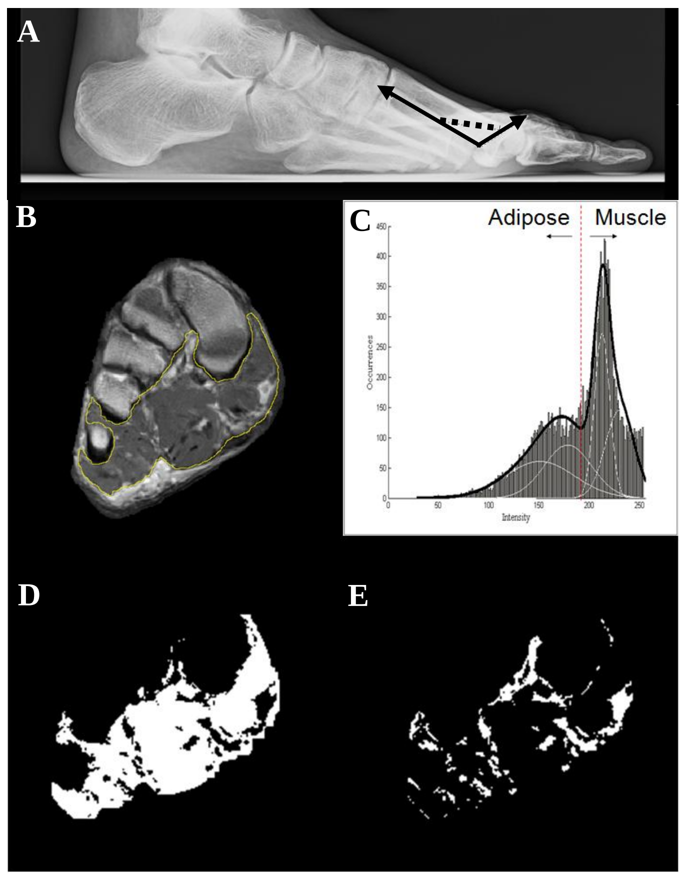

Figure 1: A) Lateral radiograph measure of the second metatarsophalangeal joint angle. B) Inputted MR image with the IFM group highlighted. C) Histogram of signal intensities with the multiple-Gaussian-function-fitting algorithm applied. D)

Lean muscle tissue and E) adipose tissue volumes calculated as determined by the threshold between tissue types.

RESULTS AND DISCUSSION

The DMPN group, compared to controls, had less lean muscle tissue (18.2 ± 11.0 vs. 31.6 ± 12.8 cm^3, P = 0.003) and more adipose tissue in the IFM (17.9 ± 10.5 vs. 9.3 ± 3.8 cm^3, P = 0.001) (Figure 2A). IFM deterioration (ratio of adipose to lean muscle volume) was higher in the DMPN group (1.6 ± 1.2 vs. 0.3 ± 0.2, P < 0.001), and FAAM scores were decreased (65.1 ± 24.4 vs. 98.3 ± 3.3 %, P < 0.001). The correlation between IFM deterioration and the second MPJ angle was r = -0.508 (P = 0.013) for all DMPN subjects (Figure 2B), but this correlation increased to r = -0.810 (P < 0.001) when only DMPN subjects with an IFM deterioration >1.0 were included (Figure 2C). There was no correlation between IFM deterioration and FAAM scores.

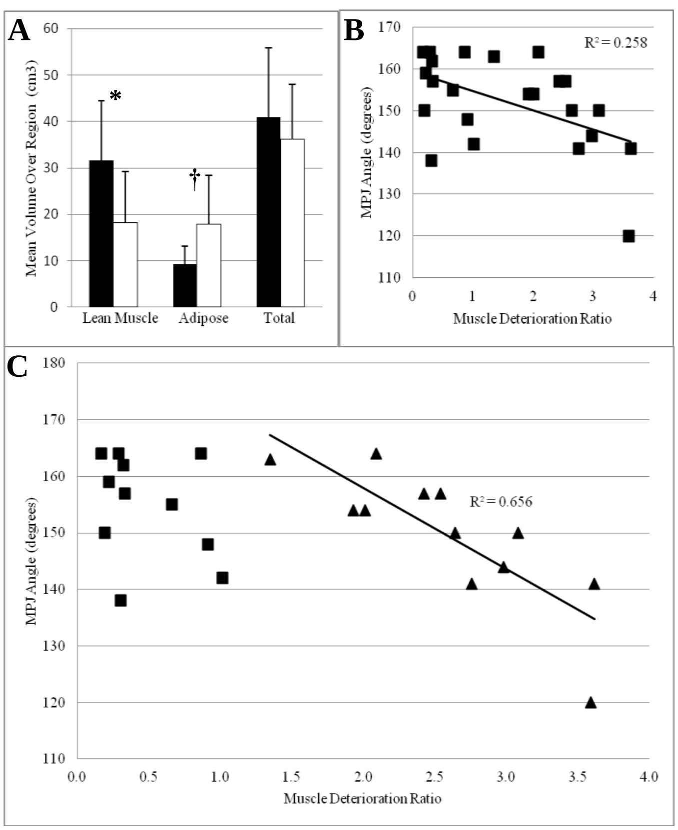

Figure 2: A) Mean volume of lean muscle, adipose tissue, and total IFM volume from the hindfoot to the midfoot (Black bars = control group, white bars = DMPN group. * P = 0.003, † P = 0.001 between groups). B) Scatter plot of MPJ angle vs. IFM deterioration ratio for all DMPN subjects. C) Scatter plot of the MPJ angle versus the muscle deterioration ratio for DMPN subjects with a ratio ≤ 1 (■) and with a ratio > 1 (▲).

This study shows DMPN subjects have almost 5 times as much IFM deterioration and lower physical performance than controls; and muscle deterioration is associated with second MPJ hyperextension angle, an important risk factor for skin breakdown and amputation.

CONCLUSIONS

The results of this study show that participants with diabetes and neuropathy have increased IFM deterioration, which was associated with MPJ angle hyperextension, especially with high values (>1.0) of IFM deterioration. Additional research is required to understand how IFM deterioration interacts with other impairments leading to forefoot deformity and skin breakdown. Intrinsic foot muscle deterioration may not be the primary causative factor of deformity, but it may be one in an interaction of multiple factors.

REFERENCES

1. CDC. *National diabetes fact sheet: national estimates and general information on diabetes and prediabetes in the United States, 2011*. Atlanta, GA, USA, 2011.
2. Pecoraro RE, et al. *Diabetes Care*, 1990; **13**, 513-21.
3. Mueller MJ, et al. *J Biomech* **36**, 1009-17, 2003.
4. Holewski JJ, et al. *J Rehabil Res Dev* **26**, 35-44, 1989.
5. Lavery LA, et al. *Arch Intern Med* **158**, 157-162, 1998.
6. Scheck M. *Clin Orthop* **123**, 63-69, 1977.
7. Bus SA, et al. *Diabetes Care* **25**, 1444-50, 2002.
8. Bus SA, et al. *Diabetes Care* **32**, 1063-67, 2009.
9. Cheuy VA, et al. *JMRI* **DOI 10.1002/ jmri.24069**, 2013.

THE PASSIVE CONTRIBUTIONS OF THE VASTUS MEDIALIS AND VASTUS LATERALIS TO KNEE EXTENSION AND HIP FLEXION

[1,2]David B. Lipps, [2]Emma Baillargeon, [2]Thomas G. Sandercock and [1,2]Eric J. Perreault

[1]Rehabilitation Institute of Chicago, Chicago, IL USA
[2]Northwestern University, Chicago, IL, USA
email: dlipps@ricres.org

INTRODUCTION

Muscles primarily transmit forces through tendon, but also transmit forces to neighboring muscles through myofascial connections. These adhesions strengthen following surgery as scar tissue, which produces greater myofascial force transmission and less tendon force transmission [1]. Musculoskeletal injuries may lead to greater intermuscular fibrosis [2], strengthening these myofascial connections. Since vastus medialis tendon elongation is reduced in patellofemoral pain [3], we seek to explore if patellofemoral forces are altered by the myofascia. First, we need to understand how healthy myofascial connections affect the vastus lateralis (VL) and vastus medialis (VM). The VL and VM articulate the knee, but are adjacent to hip flexor muscles (rectus femoris, tensor fasciae latae). The VL and VM will be isometric during passive hip flexion if the myofascial connections are irrelevant. Therefore, we investigated whether the healthy VL and VM will shorten during passive knee extension and remain isometric during passive hip flexion.

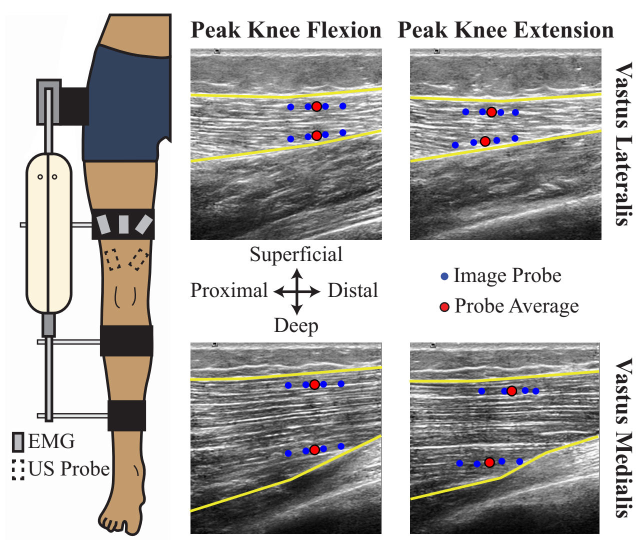

Figure 1: (left) Lokomat schematic. (right) Sample VL and VM ultrasound images with measurement probes tracked from peak knee flexion to peak knee extension.

METHODS

Three healthy adults (2 F, 1 M; 2 R, 1 L leg; mean age: 29 yrs, height: 175 cm, weight: 68 kg) had one leg moved within a Lokomat driven gait orthosis (Homoca, Inc.). The Lokomat was attached with three leg cuffs and a pad over the greater trochanter to prevent pelvic motion (Fig. 1). The Lokomat repeatedly moved the limb with a gait profile of 1 km/h. This profile was customized so the knee joint (10°–73° flexion) was passively moved with the hip fixed (0° flexion), or the hip joint (-16°–37° flexion) was passively moved with the knee fixed (8° flexion). The subjects were provided 50% body-weight support while standing on the contralateral limb. Muscle activity recorded with surface electromyography (EMG) of the VL, VM, rectus femoris (RF), biceps femoris (BF) and semitendinosus (ST) (Motion Lab Systems) was normalized to a maximum voluntary contraction and rectified. Data were sampled at 2 kHz.

A Siemens ACUSON Antares ultrasound system (B-mode, 13 MHz transducer, 38 mm width, 75 µm pixel resolution) was synchronized to the Lokomat and recorded motion of the VL and VM (40 Hz). The transducer was aligned to each muscle fiber orientation with a custom holder secured around the thigh to minimize movement. The transducer was distally located at ~20% femur length between the epicondyle and greater trochanter (Fig. 1). An automated Lucas-Kanade-Tomasi algorithm [4] tracked the spatial and temporal gradients between ultrasound images over one cycle of knee extension-flexion or hip flexion-extension. The displacement of two sets of four measurement probes (initially 30 mm apart) was tracked and averaged along the superficial and deep surface of the fascicle region (Fig. 1). Paired t-tests compared peak proximal displacement during hip flexion of the superficial and deep surfaces of the VL and VM to zero (i.e. isometric). Peak displacement of the VL and VM was analyzed with a 2x2 ANOVA (fixed: measurement surface (superficial/deep), joint moved (hip/knee); random: subject) with Tukey post-hoc tests (alpha: $p = 0.01$).

RESULTS AND DISCUSSION

Exemplar trials of VL during one cycle of passive knee and hip motion show tissue displacement was greater during knee extension than hip flexion, and greater deep than superficial (Fig. 2). The VL shortening during hip flexion is a novel finding since this muscle does not articulate the hip. Similar results were found for the VM (Fig. 3). EMG recordings confirm the muscles remained passive since all muscle activity was less than 1% MVC. The joint angles indicate only a single joint was moved during the experiment. During passive hip flexion, the proximal displacement of VL and VM indicates the muscles were not isometric, regardless if the measurement were superficial or deep (all 4 p-values < 0.001). There was a significant interaction between the measurement surface and the joint moved (VL & VM: $p < 0.001$). Post-hoc comparisons are provided in Fig. 3.

The present study shows that even in healthy subjects, the vasti muscles shorten during passive hip flexion, even though they do not articulate the hip. Similar results have been shown between the soleus and gastrocnemius [5]. It is known that myofascial connections can alter the relative motion of the quadriceps muscle following rectus femoris tendon transfer [6]. We posit that myofascial connections between the vasti and neighboring hip flexors contribute to these results. However, future work is needed to confirm this hypothesis and to determine if the length changes shown here result in significant intermuscular force transmission in both healthy and pathologic populations.

The study was limited by a small sample size and the lack of measurements of fascicle length, the distal rectus femoris (due to the thigh cuff), femoral internal rotation, and myofascial force transmission. The Lokomat also had a shorter knee cycle than hip cycle. Future work will address these concerns.

CONCLUSIONS

Displacement of the deep and superficial borders of the VL and VM indicates local shortening during passive hip flexion, even though these muscles do not articulate the hip. Future work will address if myofascial connections are responsible.

REFERENCES

1. Maas H, et al. *J Biomech* **45**, 289-96, 2012.
2. Williams, PE, et al. *J Anat*, **158**, 109-14, 1988.
3. Wilson N, et al. *J Appl Physiol* **107**, 422-8, 2009.
4. Darby J, et al. *J Appl Physiol* **112**, 313-27, 2012.
5. Bojsen-Moller J, et al. *J Appl Physiol* **109**, 1608-18, 2010.
6. Asakawa DS, et al. *J Biomech* **35**, 1029-37, 2002.

ACKNOWLEDGEMENTS

Dr. Yasin Dhaher, Dr. Wendy Murray, Tim Haswell, Andrew Tan, and Despina Kotsapouikis.

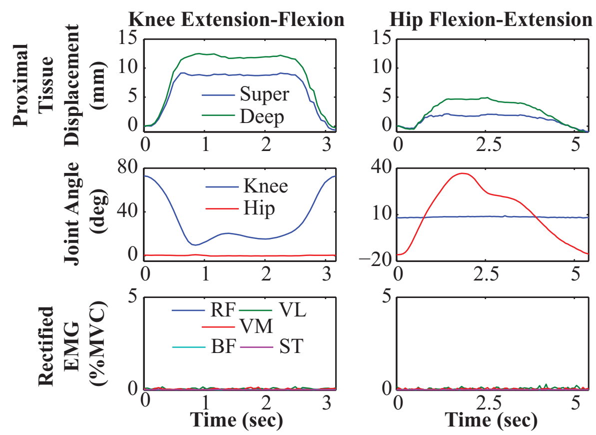

Figure 2: Exemplar trials of passive knee extension (left) and hip flexion (right) of the vastus lateralis.

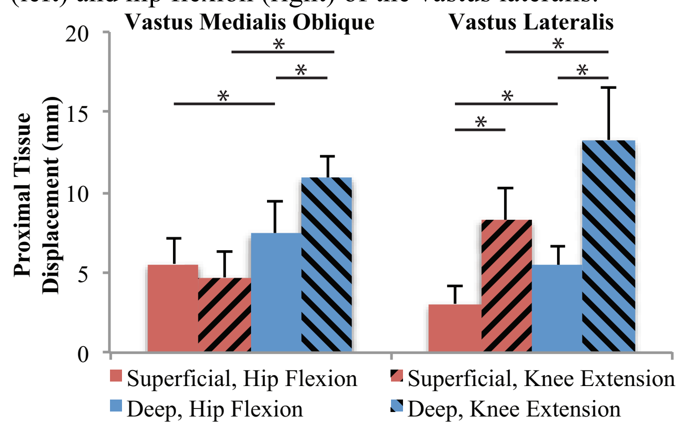

Figure 3: Peak muscle shortening of the superficial and deep borders of the vasti muscles during passive knee extension and hip flexion. * - significant post-hoc comparison ($p < 0.01$)

PREDICTION OF FAILURE PATTERN IN SPINE SEGMENTS

Allison L. Clouthier, Hadi S. Hosseini, Ghislain Maquer and Philippe K. Zysset

Institute for Surgical Technology and Biomechanics, University of Bern, Switzerland
email: philippe.zysset@istb.unibe.ch, web: http://www.istb.unibe.ch

INTRODUCTION

Vertebral compression fractures, which are associated with risk of further fracture, pain, loss of mobility, and mortality, are becoming increasingly common as our population ages [1]. While patient specific nonlinear finite element models have been shown to predict vertebral strength better than dual energy x-ray absorptiometry [2], the majority of models have been validated against experiments where the vertebral endplates are embedded in a stiff material or have been removed and do not replicate the boundary conditions imposed by the intervertebral discs. However, boundary conditions have a significant effect on predicted vertebral strength and damage patterns [3]. Models that have included the discs have used simplified bone models and were only subjected to small strains [5]. Therefore, the ability of a nonlinear model for vertebral bone to predict failure pattern was evaluated using both healthy and degenerated intervertebral disc conditions on two spine segments tested experimentally in large compression.

METHODS

Two spine segments including one vertebra surrounded by two intervertebral discs and two half-vertebra (T9-T11 and T11-L1) were cleaned of surrounding soft tissue and isolated from their posterior elements. The cranial and caudal half-vertebrae were embedded in PMMA and the specimens were fixed in a loading chamber filled with saline-solution. These were then mechanically tested in a stepwise fashion in which the segments were loaded, allowed to relax, and then imaged using high-resolution peripheral quantitative computed tomography (XtremeCT, Scanco Medical AG, Switzerland) for each loading step.

A finite element mesh was created for the spine segments using quadratic tetrahedral elements for the bone and linear hexahedral elements for the intervertebral discs. For bone elements, an implicit gradient enhanced over-nonlocal damage model including densification under large compression was implemented. Bone volume fraction and fabric orientation were obtained from the image of the initial configuration and used to assign material properties to each element [4]. The intervertebral discs were modelled as an isotropic hyper-elastic material. For the healthy case, the annulus fibrosus and nucleus pulposus were assigned separate material constants, with the nucleus being nearly incompressible, and moderate disc degeneration was simulated by assigning the entire disc the material properties of the healthy annulus fibrosus. Bone compaction in the vertebral bodies was visualized by showing the local change in volume, tr(**E**).

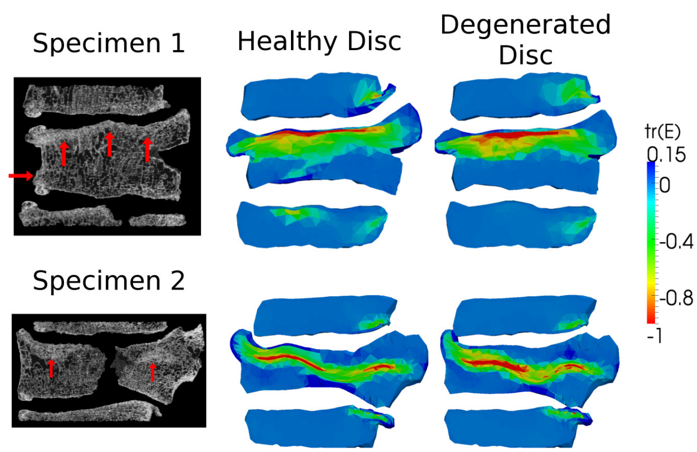

Figure 1: At the final loading step for each sample, the local change of volume, tr(**E**), is shown for models with healthy and degenerated discs. Experimentally obtained computed tomography images are shown for comparison.

RESULTS AND DISCUSSION

Specimen 1 sustained an anterior wedge fracture and the centre vertebra of the segment was deformed by an average of 30%. A large fracture occurred in Specimen 2, which was compressed 35%, separating the right-posterior section from the vertebral body.

A comparison between the local change of volume obtained from the simulations and visible bone compaction in the experimental images is shown in Figure 1 for the final loading step. The model was able to predict the failure pattern in both specimens. The main effect of disc condition was the amount of deformation in the endplates, which was reduced when the nucleus was made more compressible in the degenerated disc model.

The continuum model employed here is not able to simulate fractures; however, the model was able to predict fracture locations. Positive values of tr(**E**) indicate that elements have experienced tension, resulting in a volume increase. As observed in Figure 2, areas with positive values of tr(**E**) correspond quite well with fractures that occurred in the experiment.

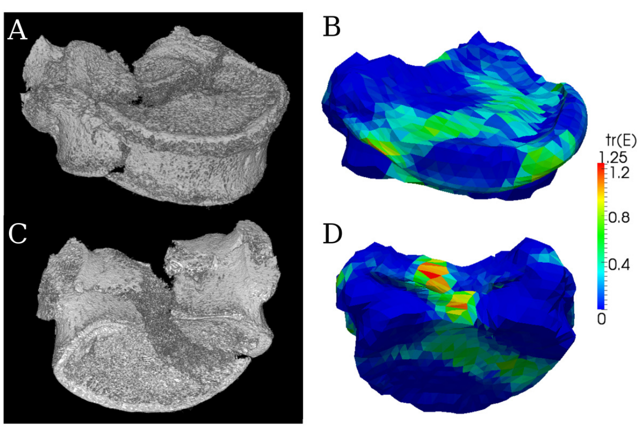

Figure 2: Positive values of tr(**E**) are shown corresponding to fracture locations for Specimen 2**.**

A limitation of the analysis presented here is the hyper-elastic model used for the intervertebral disc. While it is more sophisticated than previous models which have employed linear elasticity for small vertebral strains or have not included the disc, instead embedding the endplates in a stiff material, it is still a simplistic model for a complex, time-dependent, anisotropic, and heterogeneous material. As can be observed in Figure 1, more deformation occurs in the intervertebral discs experimentally than in either simulation. In the finite element model, problems of element distortion make such large deformations difficult to replicate. Hexahedral elements were used to mitigate this problem; however, experimental levels of compression were still not fully achieved. More sophisticated techniques for modelling the intervertebral discs may further improve the results of this model.

CONCLUSIONS

An implicit gradient enhanced over-nonlocal damage model for trabecular bone including densification was implemented for two spine segments with intervertebral discs experimentally tested in stepwise loading. The model was able to predict areas of bone localization as well as fracture locations in large compression.

REFERENCES

1. Vedantam R. *Am J Clin Med* **6(4)**, 14-18, 2009.
2. Dall'Ara E, et al. *Osteoporos Int* **23**, 563-572, 2012.
3. Maquer G, et al. *Compute Method Biomec* (in press), 2012.
4. Pahr DH and Zysset PK. *J Biomech* **42**, 455-462, 2009.
5. Eswaran SK, et al. *J Bone Miner Res* **212**, 307-314, 2006.

ACKNOWLEDGEMENTS

Funding for this project was provided by the European Community, Grant, 264 Agreement no. PITN-GA-2009-238690-SPINEFX.

PREDICTION OF TRUNK NEUROMUSCULAR RESPONSE UNDER PERTURBATIONS

[1]Ali Shahvarpour, [1]Aboulfazl Shirazi-Adl, [2]Babak Bazrgari and [3]Christian Larivière

[1]École Polytechnique, Montréal, QC, Canada
[2]Center for Biomedical Engineering, University of Kentucky, Lexington, KY, USA
[3]Institut de recherche Robert-Sauvé en santé et en sécurité du travail (IRSST), Montréal, QC, Canada
email: aboulfazl.shirazi@polymtl.ca

INTRODUCTION

Spinal stability is governed by passive ligamentous tissues, active musculature and neural feedback system [1]. Under a sudden perturbation, central nervous system (CNS) recruits muscles reflexively to provide sufficient trunk stability and control while avoiding the risk of fall and injury. The extent of this action, however, depends on and is modulated by not only the perturbation itself but the relative contributions of the other two subsystems as well. Alterations in trunk conditions and perturbation influence hence the risk of back disorders. An iterative kinematics-driven trunk finite element (FE) model has been developed to estimate muscle activity, spinal loads and trunk stability under static/transient loading conditions [2, 3]. The model has demonstrated that the trunk kinematics can be decoded to gain insight into the neuromuscular behavior and condition. In this work, the trunk neuromuscular response is investigated under various perturbation conditions. The required input kinematics-kinetics data are based on *in vivo* measurements on asymptomatic subjects under sudden forward perturbations.

METHODS

In vivo measurements: Twelve asymptomatic young male subjects (weight 73±4 Kg and height 177±3 cm) participated. Superficial EMG signals of 12 muscles were recorded. Subjects were semi-seated in the perturbation apparatus with the pelvis restrained [2]. A harness, placed at the T8 level, was connected to a load cell in front and a potentiometer on the back to measure trunk force and translation. A visual feedback system was employed to position subjects at specific trunk postures or abdominal pre-activity at the beginning of each test. The perturbation force and displacement at the T8 were measured for six randomly selected conditions (Table 1) with 5 trials with 30 sec rest in between.

Table 1: Experimental conditions

Condition	Preload (N)	Sudden Load N	Initial Posture	Abdominal Pre-activation
1	5	50	Upright	No
2	5	100	Upright	No
3	50	50	Upright	No
4	50	100	Upright	No
5	5	50	20° Flexion	No
6	5	100	Upright	10%

FE model studies: The trunk FE model was constructed with 7 rigid bodies representing the pelvis, lumbar vertebrae, T12 vertebra and thorax-neck-head as a single rigid body [2, 3]. Six shear-deformable beam elements with nonlinear load-displacement properties along with six linear and angular dampers interconnecting rigid bodies modeled the mechanical behavior of the passive ligamentous structures. The FE model was driven by prescribed segmental rotations (in the sagittal plane only due to the symmetry of the task) in a manner as to generate the temporal profile of the T8 translations recorded on subjects (Fig 1). The repartitioning of trunk rotations at T12-S1 levels was based on the literature [2, 3]. At each time instance and under prescribed segmental rotations (based on *in vivo* displacements), gravity loads along the spine (adjusted for each subject), measured perturbation force (Fig 1), passive resistance as well as damping/inertia forces, the FE model computed the net moments to be balanced by muscles at each vertebral level (T12 to L5). Once the muscle forces at different levels were calculated (i.e., by optimization at each level with minimum $\sum\sigma^3$), they were applied as additional external loads and analyses repeated till convergence. Iterative transient analyses were repeated to compute the response over the entire test period. The behavior of 4 individual subjects out of 12 (with trunk geometry close to that in the FE model) was analyzed.

RESULTS AND DISCUSSION

Under the suddenly applied load, subjects rotated forward with some delay and reached their peak trunk rotation around 0.5 sec at the maximum force and extended backward thereafter to their initial positions (Fig 1). The forward T8 translation increased under greater perturbations but significantly diminished when the initial steady pre-load increased from 5N to 50N. This tendency points to the effect of higher initial intrinsic stiffness in augmenting trunk stiffness and stability and hence improving the control of the neuromuscular system under sudden perturbations. After the onset of forward perturbations, sudden deviations in computed muscle activity from initial steady levels highlighted the latency periods found here in the range of 140 ms to 220 ms (Fig 2).

Large muscle forces were generated to counter the perturbation forces and net external moments that varied with the test conditions (Fig 3). The peak to low ratio in estimated net moments diminished in conditions 3 and 4 with higher initial pre-load (Fig 3). Large compression and shear forces were computed at the L5-S1 level (Fig 4). These forces increased under higher perturbations but decreased with greater initial preloads. Peak net moment and spinal loads occurred in the condition 5 with 20 deg initial flexion rotation indicating the crucial effect of posture on the trunk response.

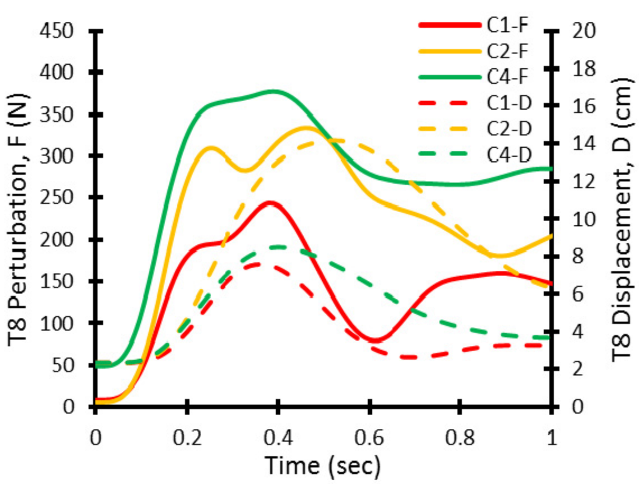

Figure 1: *In vivo* measured perturbation force and displacement at the T8 level for one subject.

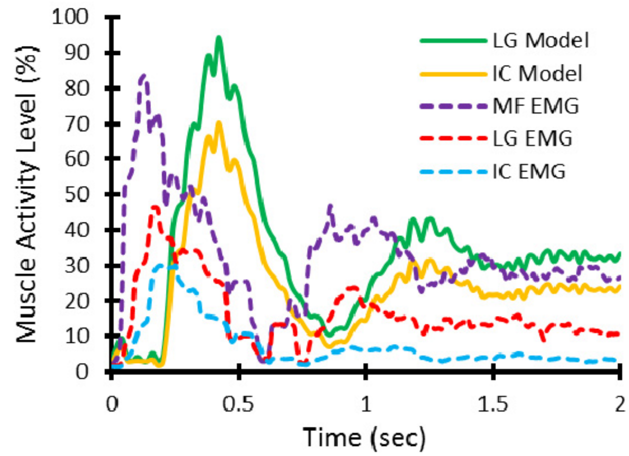

Figure 2: Muscle activity levels for condition 2.

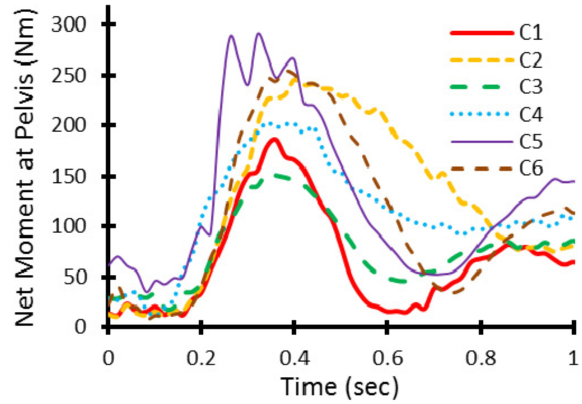

Figure 3: Net moment at the pelvis in a subject.

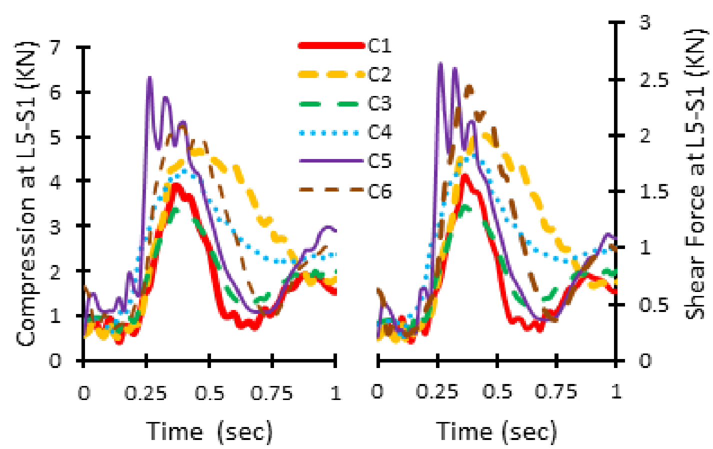

Figure 4: Compression/shear forces at the L5-S1.

REFERENCES

1. Panjabi MM, *J Spinal Disord*, **5**, 383-389, 1992
2. Bazrgari B et al, *J Biomech*, **42**, 1193-1200, 2009
3. Arjmand N et al, *J Biomech,* **39**, 510-521, 2006

ACKNOWLEDGEMENT

This work has been supported by grants from the IRSST-Quebec and NSERC-Canada.

QUANTIFICATION OF REVERSAL OF LUMBOPELVIC RHYTHM DURING ACTIVE FORWARD BENDING

PeemongkonWattananon,Won Sung, Bryan Spinelli, Scott A. Biely and Sheri P. Silfies

Drexel University, Rehabilitation Sciences Spine Research Lab, Philadelphia, PA, USA
email: pw86@drexel.edu web: http://www.drexel.edu/cnhp/rehab_sciences

INTRODUCTION

Reversal of lumbopelvic rhythm (LPR) is one type of aberrant movement pattern associated with low back pain (LBP) and used to identify patients who would benefit from core stabilization exercise[1].LPR is the movement interaction between the lumbar spine and pelvis observed during active forward bending (FWB). Clinical definitions of typical LPR and reversed LPR (rLPR) are provided in Table 1. Angle-angle plots have been used to graphically represent LPR (Fig. 1). Particular attention to the shape or trajectory of the angle-angle plots has been used to qualitatively assess the coordination between segments. It has been difficult to determine true differences between subjects or conditions (e.g., pre-, post-intervention) using qualitative analysis. Coupling angle plots address this problem by standardizing and quantifying the relationship between segments during movement[2]. The purpose of this study is to quantify typical LPR using coupling angle plots, and develop criteria that can accurately identify rLPR patterns during active FWB.

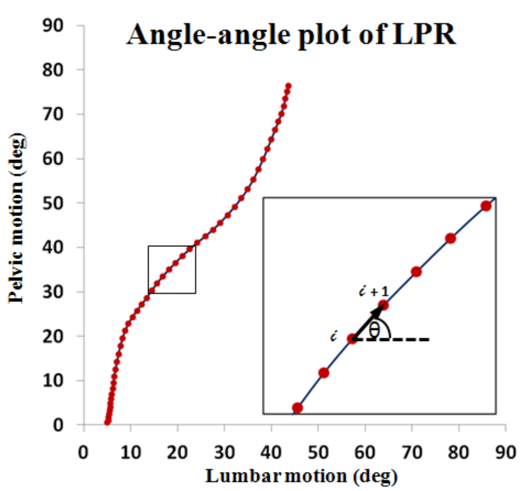

Figure 1: Example of angle-angle plot of LPR during forward bending with lumbar motion on the x-axis and pelvic motion on the y-axis. The coupling angle is represented by the angle (θ) of a vector (arrow) between two adjacent points relative to horizontal (dotted line).

METHODS

Simultaneous clinical observation and kinematic data were collected on 99 subjects during performance of 6 repetitions of active FWB. Clinicians were blinded to subject status of no LBP (n = 35), history of LBP (n = 32) and current LBP (n = 32). Individual kinematic patterns (n = 594) were stratified based on mutual agreement by two experienced physical therapists as typical movement pattern (n = 107) and rLPR (n = 57). Inter-rater reliability of clinical observation of rLPR was substantial (κ = .83; CI = .76-.91). Kinematic data from the femur, pelvis, lumbar and thoracic segments were recorded utilizing electromagnetic tracking system (Polhemus, Inc.).

All data analysis was performed using custom LabView programs (National Instrument, Corp.). Euler angles were derived from the position data and re-sampled to 100 data points across the task (forward bend = 50%; return to upright = 50%). Kinematic pattern consistency (CMC) ranged from .76-.98. Angle-angle plots were created and coupling angles were calculated by using the following equation:

$$Coupling\ angle\ (\theta) = atan\left[\frac{(Y_{i+1} - Y_i)}{(X_{i+1} - X_i)}\right]$$

Coupling angles from individuals rated as having typical movement patterns were used to derive the standard deviation for each data point. A typical coupling angle plot (percent of total motion vs. coupling angle) with a two standard deviation band (SDB) was created (Fig. 2).

The forward bend portion of each repetition was compared against the SDB. Individual plots were classified as rLPR if they exceeded the SDB. Kappa values were used to determine the agreement between clinical observation and kinematic classification of LPR and sensitivity/specificity calculated at each % of movement (potential cut point). A receiver operator characteristic curve (ROC) was used to determine the point that maximized agreement on classification. Sensitivity, specificity, and +/- likelihood ratio (LR) were calculated for this cut point.

RESULTS

The optimal cut point was 25% of total motion. Area under the ROC curve was .81. Diagnostic accuracy at this cut point is presented in Table 2.

DISCUSSION AND CONCLUSIONS

These finding indicate that rLPR can be accurately quantified using coupling angle with SDB. If coupling angles were outside the SDB at completion of 25% of total motion (half way through the forward bend phase of movement) it resulted in + LR of 8.45 (4.21-16.93) for identifying rLPR. This represents a moderate increase in the likelihood that the subject presented with a rLPR pattern during FWB. This method provides a first step toward identifying rLPR using kinematic data. The approach allows comparison of LPR between subjects or conditions (pre/post treatment) and provides a mechanism for quantifying timing or severity of rLPR impairment (when or how much the pattern deviates from typical). This information will provide both clinicians and researchers with a better understanding of the underlying movement coordination mechanism and impairment.

LIMITATIONS

Clinical observation of LPR was based only on two experienced physical therapists; which effects generalizability. The kinematic criteria for identification of rLPR were developed and validated on the same sample. The next step is to validate the criteria on an unrelated sample of subjects.

REFERENCES

1.Hicks G.E., et al. *Arch PhysMedRehabil*. 2005;**86**(9):1753-62.

2.Miller, R.H., et al. *Journal of Biomechanics*. 2010;**43**(13):2554-60.

ACKNOWLEDGEMENTS

This study was supported in part the by Orthopaedic Section, American Physical Therapy Association.

Table 1: Operational definition of clinical observation of typical and reversed LPR

Pattern	Definition
Typical	Observation of trunk forward bending in which lumbar spine and pelvis motion occur simultaneously with lumbar spine motion predominating in the first 1/3rd and pelvis motion predominating in the last 1/3rd.
Reversed	Observation of trunk forward bending in which pelvis motion is greater than lumbar spine motion during the first 1/3rd and/or lumbar motion greater than pelvis motion during the last 1/3rd.

Table 2: Kappa statistic and diagnostic accuracy of coupling angle plot using the 25% of total motion cut-off

%Agreement	Kappa(CI)	PABAK	*Sensitivity*	*Specificity*	+LR	-LR
82.32	**.59 (.43-.70)**	**.66 (.52-.75)**	**.63 (.49-.76)**	**.93 (.86-.97)**	**8.45 (4.21-16.93)**	**.40 (.28-.56)**

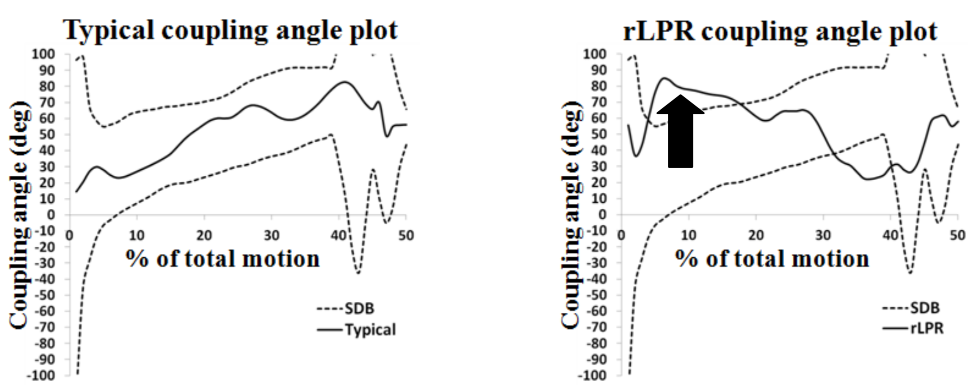

Figure 2: Example of LPR represented by coupling angle (solid line) with SDB (dotted line). Left plot represents typical LPR. Right plot represents reversal of LPR identified by coupling angle falling outside SDB before 25% of total motion (arrow).

REPITATIVE FREEZING: DOES IT CHANGE NANOSCALE MATERIAL PROPERTIES OF CANCELLOUS BONE?

Alexander K. Landauer, Philip A. Yuya and Laurel Kuxhaus

Clarkson University, Potsdam, NY, USA
email: lkuxhaus@clarkson.edu, web: http://people.clarkson.edu/~lkuxhaus/

INTRODUCTION

In vertebrates, the skeleton imparts physical form and bears load during daily activities. Cancellous bone, which comprises the interior of the vertebra, carries a portion of this load and its plate-and-rod structure may be damaged by repeated freeze-thaw cycling. While this is not a problem *in vivo*, it may affect laboratory work. Due to necessity, many research protocols use frozen tissue; specimens are often subjected to freeze-thaw cycling before use in experimental studies. Therefore, understanding of the effect of multiple freeze–thaw cycles on the mechanical properties of cancellous bone is critical to interpreting results.

Published studies of freeze-thaw cycling effects on biomaterials have focused on the macroscopic-level [1, 2], but the effects on individual trabeculae at the nanoscale remain unknown. The objective of this study is to use nanoindentation to quantify changes in nanoscale viscoelastic response characteristics (i.e. storage and loss moduli) of cancellous bone due to repeated freeze-thaw cycling.

METHODS

As part of a larger study, cervine (*O. virginianus*, white-tailed deer) vertebrae were obtained (Nolt's Custom Meat Cutting, Lowville, NY) from three male deer (ages approximately 1, 1.5 and 1.5 years). A single vertebra from the thoracic or lumber region of each spine was randomly chosen for each freeze-thaw cycle. The intact vertebrae were freeze-thaw cycled 0, 1, 4 and 5 times, from 21°C to -18°C. Cancellous bone cubes of approximately 1 cm^3 were excised from each vertebral body with an oscillating saw (Multi-Max 8300, Dremel, Waterloo, IA).

Following a procedure generalized in [3], specimen preparation began with ultrasonic cleaning in a mild soap bath. Then, specimens were dehydrated in ethyl alcohol with concentrations of 70%, 85% and 100% by volume for 2.5, 2.5 and 4.0 hours respectively and air-dried for 6.0 hours before fixation in a low-viscosity epoxy (EpoxySet, Allied High Tech Products, Inc., Rancho Dominguez, CA). To minimize the effects of surface roughness, specimens were polished on a mechanical polisher (EcoMet IV, Buehler, Lake Bluff, IL) using silicon-carbide paper (320, 400, 600, 800, and 1200 grit) and final polishing with 1 μm diamond and 0.05 μm alumina-silica slurries. Specimens were oriented such that the polished face was perpendicular to the primary *in vivo* loading axis of the vertebra.

To ensure surface roughness of the polished specimens would not interfere with measurements, the scanning probing microscopy function of the nanoindenter (TI950, Hysitron, Minneapolis, MN) was used to image 100 μm^2 areas on each polished surface. Given indentation specifications, a cutoff value for root mean squared roughness of 120 nm was used. Dynamic nanoindentation was performed with a calibrated Berkovich tip. Indentation parameters for the 90 to 200 Hz frequency sweep were: a static load of 6000 μN and load amplitude of 75 μN. Five regions of interest (ROI) on the exposed cancellous bone of each specimen were identified using the onboard optical microscope. At each ROI, a 4x4 pattern of indents was performed. The frequency response was analyzed as in [3, 4] to determine the stiffness, K_s, and damping, C_s.

These parameters were applied in the equations $E' = (K_s/2)\sqrt{\pi/A_c}$ and $E'' = (\omega C_s/2)\sqrt{\pi A_c}$ [4]. In these equations, the material elasticity is quantified by E', the storage modulus. The material damping is quantified with E'', the loss modulus. A_c

is the tip contact area and ω is the excitation frequency. The third reported parameter, the loss tangent, tan (δ), is quantified via the trigonometric tangent of the phase angle, δ, associated with damping between tip displacement and applied force. Known outliers (i.e. when the probe landed on epoxy) were discarded and a custom MATLAB (MathWorks Inc., Natick, MA) script was used to calculate mean and standard deviation for each property at each frequency.

RESULTS AND DISCUSSION

Figures 1-3 show the mean of 240 indentation measurements made across three specimens for each cycle at all frequencies; the standard deviation across all frequencies for each cycle is indicated in the legend. The results for storage modulus from cycles 1, 4, and 5 are within a standard deviation of Cycle 0, though the trend of these means is downward. This suggests that in later cycles the mean E' will decrease significantly from the fresh bone (i.e. Cycle 0) values. For loss modulus and loss tangent, a change in frequency response characteristics appears. For the initial cycles, material damping increased with indentation frequency. With additional cycles, E'' and tan (δ) are more constant across frequencies.

CONCLUSIONS

Nanoindentation was used to quantify micro-mechanical effects of freeze-thaw storage on cancellous bone. A trend of decreasing E' is apparent, which could be a result of the freeze-thaw cycling. Additionally, a change in slope between cycles 0 and 1, and 4 and 5, where E'' and tan (δ) are plotted against loading frequency is observed. This data suggests that viscoelastic properties were affected by initial freezing but not by subsequent cycles. The initial cycle may induce formation of micro-cracks or denaturation of the collagen. This suggests bone specimens that have been repeatedly freeze-thaw cycled can provide stable data in biomechanical testing. Future work includes testing additional cycles and statistical analysis. Results of this work may alter experimental methods that involve storage and testing trabecular bone and may address variability in previously published results.

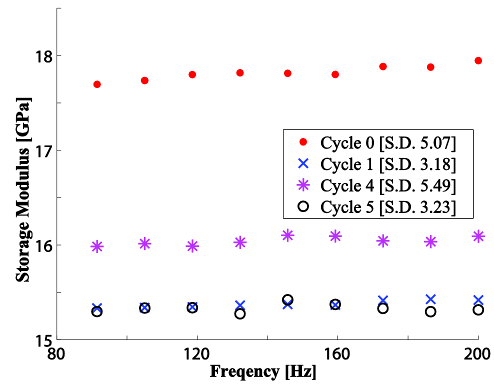

Figure 1: Mean storage modulus versus frequency.

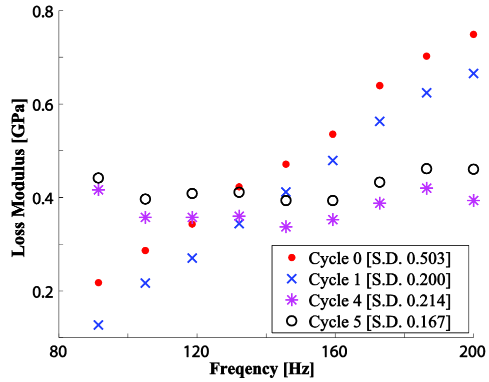

Figure 2: Mean loss modulus versus frequency.

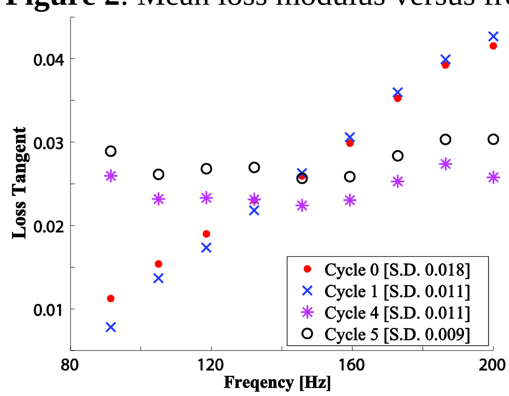

Figure 3: Mean loss tangent versus frequency.

REFERENCES

1. Moon D, et al. *J Biomech* **40**, 1153-57, 2006.
2. Borchers R, et al. *Biomaterials* **16,** 545-51, 1995.
3. Oyen M. *Handbook of Nanoindentation*, Pan Stanford Publishing Pte. Ltd., 2011.
4. Asif S, et al. *Rev Sci Instrum* **70,** 2408-13, 1999.
5. Polly B, et al. *Calcif Tissue Int* **90**, 286-93, 2012.

ACKNOWLEDGEMENTS

The authors thank Nimitt Patel, Joshua Gale, the Clarkson University Honors Program and the Coulter School of Engineering.

BIOMECHANICS ANALYSIS OF LATISSIMUS DORSI TRANSFER IN REVERSE SHOULDER ARTHROPLASTY

[1]Andreas Kontaxis, [1]Dan Choi, [1]Lawrence Gulotta

[1]Hospital for Special Surgery, New York, NY USA
email:KontaxisA@HSS.EDU, web: http://www.hss.edu/rehab-motion-analysis-lab.asp

INTRODUCTION

Reverse total shoulder arthoplasty (RTSA) is commonly used in patients with cuff tear arthropathy (CTA) to relief pain and to restore active humeral elevation ROM [1]. The reverse prosthetic designs medialise the humeral centre of rotation increasing the Deltoid moment arm and its performance [2]. However, clinical studies have shown that patients with RTSA usually show poor humeral internal/external ROM [1]. Especially in the case of atrophy or fatty infiltration of the posterosuperior part of the RC, involving both infraspinatus and teres minor (TM), the RTSA fails to restore active external rotation [3]. Latissimus dorsi (LD) tendon transfer has been proposed as a solution to restore active external rotation in patients with massive and irreparable rotator cuff (RC) tears [4].

There are only few studies investigating the biomechanics of LD transfer in RTSA and concentrate mostly on analyzing moment arm changes. The aim of the this investigation is to present an in depth biomechanical analysis of the LD transfer in RTSA, looking at moment arms (MA), muscle forces as well as joint contact loading in a variety of kinematic activities.

METHODS

An established shoulder biomechanical model, the Newcastle Shoulder Model (NSM) [5], was used to investigate the biomechanical properties of the LD transfer in RTSA. The model was adapted according to the techniques of Kontaxis et al., [2] that describes the geometry of a commercial reverse prosthesis (DELTA III®, DePuy). The model consists of six rigid bone segments (thorax, clavicle, scapula, humerus, radius and ulna), four joints and includes 31 muscles that are divided into a total of 90 lines of action that are modeled as elastic strings. The strings wrap around simple geometric shapes (e.g spheres and cylinders) that describe the bony geometry. The LD was modeled with 5 strings. The model can calculate muscle moment arms for a given motion and predict muscle and joint contact forces using inverse dynamic techniques.

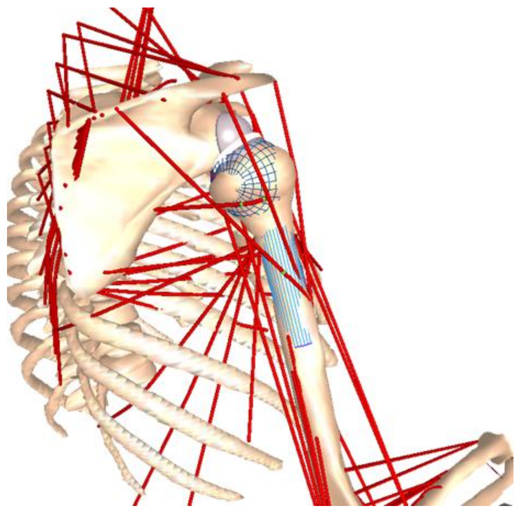

Figure 1: The NSM was adapted in order to simulate a RTSA with and without a LD transfer

Model set-up and kinematic inputs

Two different model set-ups were used: i) RTSA without LD transfer (anatomical attachment) ii) RTSA with LD transfer, where the attachment site of the LD were located at the posterolateral site of the humeral diaphysis, as it was described by Favre et al. [6]. During all simulations in both models, all the RC muscles (including the teres minor) were set inactive.

A set of kinematic tasks were used as an input to the model: i) Abduction 0-150 deg, ii) Forward Flexion 0-150 deg, iii) Int/External rotation in 90 deg of abduction, and iv) Simulation of an overhead Activity of Daily Living (ADL-Lift block to overhead shelf) as used by other upper extremity kinematic studies

Outcome variables
Muscle moment arms (MA), forces and glenoid joint loading were calculated for all tasks on both model set-ups. Rotational MA were evaluated for the external-internal task, while adduction MA was measured during abduction and forward flexion. The negative sign on the rotational angles and MA indicate external rotation and vice versa

RESULTS AND DISCUSSION

The MA results confirmed the ability of LD to externally rotate the arm after the tendon transfer. Comparing the MA values in the Int/Ext task, the model predicted a similar trend with the cadaveric study of Favre et al., even if the latter predicted much larger rotational MA for the LD (Fig 2). The adductive MA values were also increased for all the tasks (Abduction, Forward Flexion, ADL) but the differences were small (8.3% - 11.4%).

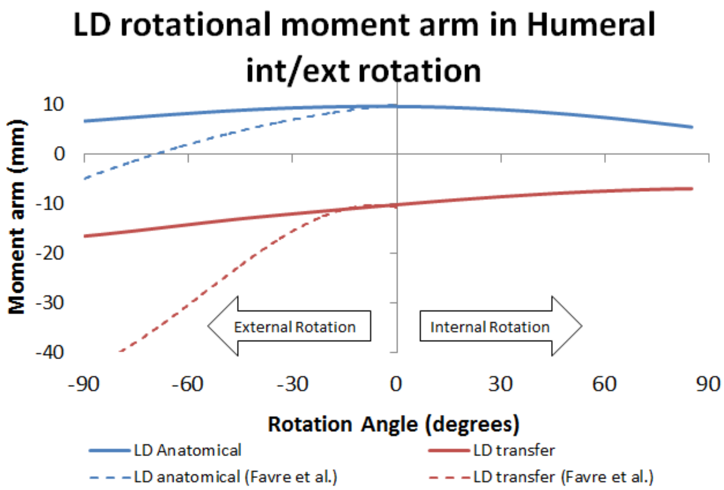

Figure 2: Rotational MA with LD in the anatomical and transfer attachment during Ext/Int task: Solid lines is for the current; dashed lines for the cadaveric study of Favre et al.

The change of MA had also an effect on the prediction of muscle and joint contact loads. The model predicted a much lower glenoid loading for the demanding task of ADL. The total load magnitude was reduced by 31%, while the biggest decrease was on the superior glenoid load (Fig. 3).

The high loading values on the model with the anatomical LD can be explained by the lack of the necessary muscles that generate external moment during the task. As a result the model has to activate excessively the posterior deltoid in order to achieve equilibrium and as a result increase the superior loading. The LD transfer model was able to generate the necessary external moment with a small activation of the LD, releasing the deltoid tensioning and thus the superior loading.

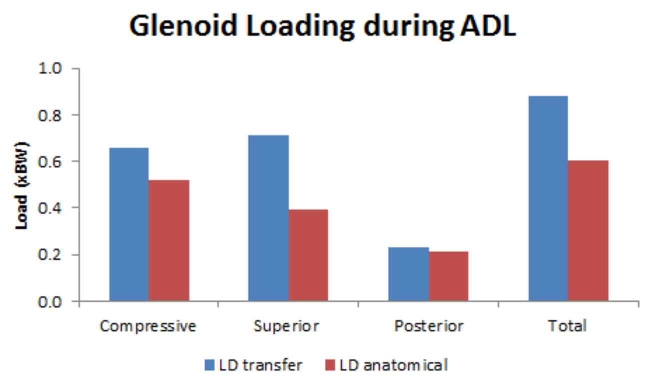

Figure 3: Glenoid loading during overhead ADL. The predicted loads were reduced on the model with the LD transfer

CONCLUSIONS

The results of the study indicate that LD transfer on RTSA can benefit the external rotation and loading of the glenoid when there is a full thickness RC tear with a weak (or lack) Teres minor. This is an ongoing investigation where multiple LD transfer attachment sites will be investigated together with a more comprehensive set of kinematic activities. The study aims to inform clinicians and orthopaedic manufacturers on how to optimize RTSA and improve functional outcomes in patients with CTA

REFERENCES

1. Boileau, P., et al., *J Shoulder Elbow Surg*, **15(5)**: p. 527-40, 2006.
2. Kontaxis, A. et al.,. *Clin Biomech (Bristol, Avon)*, **24(3)**: p. 254-60, 2009.
3. Sirveaux, F., et al., *J Bone Joint Surg Br*, **86(3)**: p. 388-95, 2004
4. Gerber,C.,*ClinOrthop Relat Res*,**232**:p.51-61,1988
5. Charlton, I.W. et al., *Proc Inst Mech Eng H*, **220(8)**: p. 801-12, 2006.
6. Favre, P., et al., *J Shoulder Elbow Surg*, **17(4)**: p. 650-8, 2008.

CHANGES IN WINDMILL PITCH MECHANICS OVER TIME

Suzanne M. Konz
Marshall University, Huntington WV

INTRODUCTION

Studies document softball injury rates and trends.(1, 2) A problem specifically identified with softball pitching injuries is a lack of limits on pitch count at any level.(3) The lack of pitch limitation results in softball rosters carrying a minimal number of pitchers and relying on those individuals to fulfill higher pitch counts in comparison to those pitchers on baseball rosters.(4) This could potentially translate to the softball pitcher pitching as many as 1500 to 2000 pitches in one weekend.(5) Suggestions have been made to regulate the frequency and volume of pitching to assist in managing injury in fast-pitch softball, but no current research addresses this issue specifically.(6)

A significant number of time-loss injuries to the upper extremity in elite windmill softball pitchers are documented.(7) The number of outings and pitches thrown in 1 week for a softball pitcher is typically in excess of those seen in baseball pitchers. Baseball team rosters list more pitchers than softball team rosters; developing into starters, middle relievers, or closers. Baseball teams provide rotations to give their pitching staff's recovery time. Softball teams are not afforded those options for their pitchers. As a result, windmill pitch athletes pitch multiple sessions on consecutive days or even multiple outings within a day. The forces have the possibility of creating overuse injury.

Previous studies have examined the one pitch thrown by the athlete or an average of the three highest velocity pitches out of ten thrown. No studies have investigated kinematic and kinetic changes over a session. The purpose of the study was to investigate changes in mechanics that occur through a game. From that, preventative programs can be established targeting the athlete training or player management.

METHODS

Fourteen female windmill pitchers competing in the 2009 Big XII Softball Championships in Oklahoma City, OK comprised the subject pool for this observational study. IRB waived consent due to the public domain nature of the data collection environment.

The researcher set a calibration tool around the pitching circle focusing on the pitching lane. Two digital video cameras (Canon DC 210, Canon USA Inc., Lake Success, NY) occupied positions behind home plate and above the third base dugout. RF sync units (Remote Video Synchronization Unit, Vicon – Colorado, Centennial, CO) attached to each camera provided an impulse to allow video syncing during analysis. All pitches thrown by the athletes during the game were filmed.

Five pitches for each subject were evaluated. The five pitches selected to be digitized were determined by the total pitch count for the individual athlete on the following basis: *p1*= the 10% mark, *p2* = the 35% mark, *p3* = the 60% mark, *p4* = the 85% mark, and *p5* = the 100% mark of total pitches thrown by the athlete. A 24-point model of the pitcher represents the softball-glove-pitcher system. 5 events occurring during the pitching motion were selected for comparison. The positions of the throwing arm at 3 o'clock, 6 o'clock, 9 o'clock, 12 o'clock and release were used. These were selected based upon previous research and coaching literature. Digitization began when the athlete was at set position and continued until 5 frames after the release of the ball. The raw video was converted to a computer-generated stick figure when the digitized film is processed. Athletes were separated into 2 groups based upon pitch count for analysis. Grouping was based upon a average pitch count of 41. Group 1 threw more than 41 pitches. Group 2 threw less than 41 pitches. Linear regressions determined the influence of the number of pitches thrown on each dependent variable. Dependent variables of importance were based upon previous literature. The independent variable was ball velocity at release.

RESULTS AND DISCUSSION

An analysis investigated the influence of stride factors on release velocity. The results of the regression indicated the predictors explained 55.2% of the variance (R^2=.305, $F(1,5)=7.26$, $p<.01$). Stride length ($p = .008$) was longer and stride angle ($p=.011$) was wider for athletes in Group1 when compared to athletes in Group 2. A second regression compared the relationship between hip and shoulder around the z-axis factors on release velocity. The results of the regression explained 52.6% of the variance (R^2=.277, $F(1,3)=7.28$, $p<.01$). Ball velocity at 12 o'clock (p.=.019) and shoulder angle in the z-plane ($p=.023$) were significant in their relationship to final release velocity. The third regression compared joint angles around the y-axis to the influence on release velocity. The results of the regression indicated the predictors explained 77.6% of the variance (R^2=.601, $F(1,25)=2.113$, $p<.021$). As this is an observational study, the researchers were trying to find focus aspects for future research. A final analysis was run focusing on the differences between the two groups at ball release related to previous significant factors. The focus was on stride leg and throwing arm and their influence on ball release velocity. The results of the regression indicated the predictors explained 72.4% of the variance (R^2=.524, $F(1,15)=3.303$, $p<.01$). Shoulder angle at of the throwing arm ($p=.005$), hip angle of the stride leg ($p=.037$), and ankle angle of the stride leg ($p=0.024$) were significant between the groups.

CONCLUSIONS

As pitch counts go above 41, windmill athletes lengthen and widen their strides in order to maintain velocity production. A longer and wider stride at release provides a lower release velocity due to a decrease in momentum. An interesting component related to stride is the impact of stride leg hip flex/ext angle and stride leg ankle PF/DF angle. The optimization of stride length juggles with the optimization of joint angles. A larger angle of the stride ankle and of the stride hip at the 12 o'clock position is a not an optimal contributor to high release velocities. A larger shoulder-shoulder angle around the z-axis at release is not good for optimal velocity. However, a greater shoulder flexion angle at the 12 o'clock position indicates a contribution to higher release velocity. The velocity of the ball at the 12 o'clock position impacts the overall release velocity.

Overall release velocity is not an indicator of decreased performance as athletes modify technique to non-optimal styles to maintain velocity. Protocols to address muscle strength of the upper extremity at 12 o'clock would be helpful. Limiting appearances or lower pitch counts help to preserve athlete health.

REFERENCES

1. Janda DH. The prevention of baseball and softball injuries. *Clinical orthopaedics and related research*. 2003;(409):20-8.
2. Loosli AR, Requa RK, Garrick JG, Hanley E. Injuries to pitchers in women's collegiate fast-pitch softball. *The American journal of sports medicine*. 1992;20(1):35-7.
3. Werner SL, Jones DG, Guido JA, Jr., Brunet ME. Kinematics and kinetics of elite windmill softball pitching. *The American journal of sports medicine*. 2006;34(4):597-603.
4. Werner SL, Fleisig GS, Dillman CJ, Andrews JR. Biomechanics of the elbow during baseball pitching. *The Journal of orthopaedic and sports physical therapy*. 1993;17(6):274-8.
5. Werner SL, Guido JA, McNeice RP, Richardson JL, Delude NA, Stewart GW. Biomechanics of youth windmill softball pitching. *The American journal of sports medicine*. 2005;33(4):552-60.
6. Doyle FM. Review of the windmill pitch: biomechanics and injuries. *Journal of chiropractic medicine*. 2004;3(2):53-62.
7. Flyger N, Button C, Rishiraj N. The science of softball: implications for performance and injury prevention. *Sports medicine*. 2006;36(9):797-816.

KINEMATIC VARIABLES ASSOCIATED WITH ACL FORCE DURING UNILATERAL LANDINGS

Bobbie Irmischer, Matthew Hoch, Stacie I. Ringleb, Sebastian Bawab, Stacey Gaven, Joshua T. Weinhandl

Old Dominion University, Norfolk, VA, USA
email: birmi001@odu.edu

INTRODUCTION

Anterior cruciate ligament (ACL) injuries occur between 80,000 to 250,000 times per year in the United States with 50% occurring in athletes between 15-25 years of age [1]. This problem is associated with large health care burdens and increased potential for loss of sports participation, which can lead to complications such as obesity, long-term disability, and increased risk of osteoarthritis [1]. For these reasons, understanding the etiology and pathomechanics of ACL injury has fueled many mechanistic [2] and interventional [3] studies.

Currently, many different techniques are used to evaluate risk factors and mechanisms for ACL injury. In vivo methodological approaches include observational (e.g., video analysis of injuries and athlete interviews), clinical (e.g., clinical imaging and physical exam), and laboratory (e.g., motion analysis) studies [4]. The development of musculoskeletal computer simulations in recent years has facilitated the exploration of ACL injury risk factors and mechanisms [5].

Despite vast attention devoted to exploring ACL injury mechanisms, a clear explanation or robust model that powerfully demonstrates the degree risk factors interact does not exist [4]. In fact, few studies demonstrate hypothesized risk factors actually increase an athlete's injury risk. The purpose of this study was to examine the relationship between lower extremity kinematics and ACL loading during unilateral landings. Identifying a combination of kinematic variables that explain a significant amount of explained variance in ACL loading may provide insights into ACL injury mechanisms and intervention strategies.

METHODS

Twenty-nine healthy, recreationally active participants aged 18 to 30 years (71.0 ± 19.1 kg, 1.71 ± 0.11m) volunteered to perform unilateral landings onto a force plate. Prior to data collection, participants were informed of study procedures and provided written informed consent in accordance with institutional guidelines. Single reflective markers were placed on specific anatomical landmarks [2] and a static standing calibration trial (neutral position) was collected. Participants were asked to complete five right side unilateral drop landings from 40 cm. Three dimensional marker coordinate data were collected at 200 Hz using an eight-camera Vicon motion analysis system. Synchronously, three-dimensional force data was collected at 1000Hz using a Bertec force plate.

Raw three-dimensional marker coordinate and GRF data were low-pass filtered using a fourth-order, zero lag, recursive Butterworth filter with cutoff frequencies of 12 Hz and 50 Hz, respectively. A kinematic model comprised of eight skeletal segments (trunk, pelvis, and bilateral thighs, shanks, and feet) was created from the standing calibration trial [2]. Three-dimensional ankle, knee, and hip angles were calculated using a joint coordinate system approach [6]. Twenty-one discrete kinematic variables commonly associated with ACL injury were identified. These variables were hip and knee flexion, adduction, and internal rotation angle, as well as, ankle plantar flexion and inversion at initial contact. Maximal values for hip and knee flexion, abduction, adduction, internal and external rotation, ankle dorsiflexion, inversion, and eversion were identified. Subject specific musculoskeletal models were created in OpenSim (SimTK, Stanford, CA) to estimate ACL force using measured kinematic and kinetic data [7].

Bivariate correlations were performed between ACL loading and individual kinematic variables. Significant correlations ($p<0.05$) were entered into a stepwise multiple-regression analysis conducted with ACL loading as the dependent variable. The initial model contained all predictor variables. After removing non-significant predictor variables, the overall percent of explained variance (R^2) for the regression analysis was identified along with predictive power of each variable. Significance was set *a priori* at p<0.05.

RESULTS AND DISCUSSION

Twenty-one initial predictors were reduced to four that significantly correlated with ACL force (Table 1); hip flexion at initial contact, maximum hip flexion, maximum knee adduction, and maximum knee abduction.

Table 1. Significant predictor variables

Predictor	Mean ± SD	*R*
Hip Flexion (IC)*	5.8 ± 11.1	-0.491
Hip Flexion (Max)	21.2 ± 15.5	-0.425
Knee Adduction (Max)*	3.8 ± 3.4	0.427
Knee Abduction (Max)	2.3 ± 3.3	0.483

* Indicates predictor variable included in final model

After stepwise regression analysis, the final model (Equation 1) included hip flexion at initial contact and maximum knee adduction.

$$(1)\quad F_{ACL} = 422.82 - (8.44)HFIC + (27.2)KAD$$

The final regression model accounted for 38% of the variance in ACL force during the drop landing (R=0.65, R^2=0.42, Adj R^2=0.38, p=0.001).

These results suggest landing with greater hip extension is a predictor of increased ACL loading. Due to the fast timing of peak ACL force during the deceleration phase of landing, lower extremity alignment at initial contact has been suggested as a predictor of peak ACL force [7]. Further, the relationship between landing in an extended position and increased GRF was previously identified [2]. Increased GRFs incurred landing with a more erect posture likely transfer up the kinetic chain, resulting in increased ACL loading.

The second predictor, peak knee adduction, was unexpected. Previous ACL research has focused primarily on knee abduction as a factor in ACL injury [1]. The findings of the current study suggest knee adduction may also be a critical factor. Visual analysis of the knee abd/adduction and ACL loading time series throughout the landing phase illustrates the relative timing of peaks in ACL loading corresponded with peaks in knee adduction (Fig. 1). On the other hand, the amount of knee abduction observed in the current study was minimal and therefore it is unclear how increases in knee abduction angle might influence ACL loading. Future studies may consider evaluating frontal plane knee range of motion during landings in addition to maximum abd/adduction values.

CONCLUSIONS

In the current study, lower extremity kinematic variables were used to formulate a model of ACL loading during a drop landing. A prediction equation of ACL force was generated using hip flexion at initial contact and maximum knee adduction, which explained 38% of ACL loading variance. While the addition of kinetic variables could potentially increase the explained variance in ACL loading, the two predictor variables currently included are easily measured clinically and in the field. Furthermore, hip flexion and knee adduction are easily modifiable components of landing mechanics.

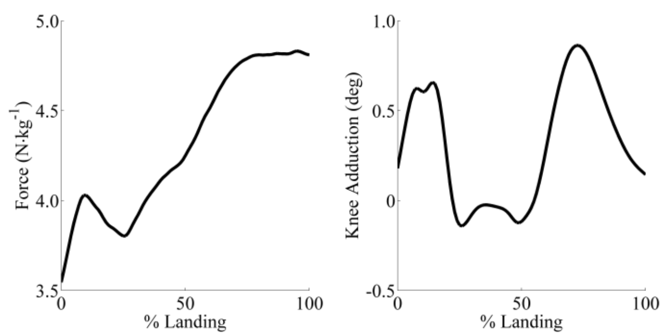

Figure 1. Mean knee adduction and estimated ACL force during landing.

REFERENCES

1.Hewett TE, et al. *Am J Sports Med*. **34**:299-311, 2006.
2.Weinhandl JT, et al. *J Appl Biomech*. **26**:444-53, 2010.
3.Pollard CD, et al. *Clin J Sport Med.* **16**:223-7, 2006.
4.Krosshaug T, et al. *Br J Sport Med*. **39**: 330-9, 2005.
5.Weinhandl JT, et al. *J Appl Biomech.* **27**:108-15, 2011.
6.Grood ES & Suntay WJ. *J Biomech Eng*, **105**:136-44, 1983.
7.Laughlin WA, et al. *J Biomech*, **44**:1845-51, 2011.

ACKNOWLEDGEMENTS

Multidisciplinary Seed Grant from the Office of Research at Old Dominion University, Norfolk, VA.

3D SURFACE REGISTRATION OF PARTIAL CAPITATE BONES USING SPIN IMAGES

[1]Ryan Breighner, [2]David R. Holmes III, [3]Shuai Leng, [1]Kai-Nan An, [3]Cynthia McCollough, and [1]Kristin Zhao

[1]Biomechanics Laboratory, Division of Orthopedic Research;
[2]Biomedical Imaging Resource; [3]Department of Radiology
Mayo Clinic, Rochester, MN
email: breighner.ryan@mayo.edu

INTRODUCTION

Registration refers to the process of aligning images or 3D image volumes. In order to extract as much information as possible from image-based motion capture, it is often necessary to register partial objects as they move into and out of the imaging field of view (FOV). In 4DCT of the wrist [1], this is of particular concern because of the present trade-off between longitudinal coverage and temporal resolution. Additionally, the large displacements inherent in image-based motion analysis make automated registration of objects impossible using pure optimization methods.

To simultaneously address the challenges of large displacements and partial object registration, this study utilized the spin-image algorithm: an object recognition and registration algorithm from the machine vision literature [2]. The large-displacement problem is directly overcome by the pose-independence of the algorithm, i.e. it generates registrations of similar accuracy regardless of the initial relative positions of the two surfaces to be aligned. However, because spin-image registration is correspondence based, the amount of available geometry in the two surfaces to be registered will affect the quality of the registrations. This study sought to determine the effect of available geometry on registration quality by applying the registration algorithm to successively smaller partial capitate surfaces.

METHODS

Under IRB approval and informed consent of the subject, an established 4DCT imaging technique [1] was used to acquire an 18-volume motion sequence of the wrist during a 2 second maximal flexion and extension cycle. A conventional static CT scan of the wrist was also obtained to capture surfaces and positions of the carpal bones in a neutral posture. The voxel dimensions for the scans were 0.234mm in-plane and 0.4mm in the longitudinal direction. Image volumes were subsequently converted to isotropic at the planar resolution.

From the motion sequence, a single volume in which the entirety of the capitate was visible was selected. The capitate bone was segmented from both the single 4DCT volume and the conventional CT using global thresholding followed by a graph-based connected-component method. The segmented bones were meshed using an adaptive deformation approach. Segmentation and meshing were done using Analyze 10.0 software (Mayo Clinic Biomedical Imaging Resource, Rochester, MN). Meshes were subsequently reduced to cortical hulls using the hidden-points-removal (HPR) algorithm, developed by Katz, et al. [3].

The resulting surface (mesh) from the conventional CT (‘model’) was then fit to the surface from the motion sequence (‘scene’) using the spin-image algorithm, establishing a ground-truth for subsequent partial- bone registration performance. The algorithm was then applied to the proximal 90% of the scene mesh. This was repeated in 10% increments until the algorithm ceased to align the surfaces.

The portion of points in the original (100%) scene that were within the mesh resolution of their nearest neighboring point in the registered model mesh was used as a general measure of fit quality. RMS error of mesh point location (comparing model meshes transformed by the 100% registration and the partial registrations) was calculated. Angular error was calculated by transforming an arbitrary unit vector by both the 100% and partial surface registration transformations, and determining the angle between the resulting vectors (as the inverse cosine of the dot product of the two unit vectors).

RESULTS AND DISCUSSION

Table 1 shows the relative accuracy of the registrations to the partial scene meshes. As shown, the effect of relative angular error resulting from partial geometry is relatively minimal. Additionally, looking at the results of the registration to the 60% capitate surface, it is apparent that information quantity alone is not the sole factor influencing registration accuracy when using the spin-image algorithm.

Table 1. Relative registration accuracy for partial mesh registrations

Proximal % Length	Angular error (°)	RMS error (mm)	% SRF
40	1.35	0.21	98.9
50	1.15	0.21	98.6
60	1.44	0.31	98.4
70	1.13	0.18	98.9
80	1.29	0.19	99.0
90	0.83	0.14	99.1
100	--	--	99.1

As the RMS errors are generally on the order of the image resolution from which the registered surfaces were created, it is likely that the bulk of the calculated RMS location error is attributable to disparities in mesh sampling between the model and scene meshes, rather than true errors in registration.

The algorithm ceased to accurately register model to scene when the partial geometry was reduced to the proximal 30%. This is likely because the amount of orientable geometry available for registration is insufficient. As shown in Figure 1, the proximal 30% of the capitate is nearly hemispherical, and thus minimally orientable.

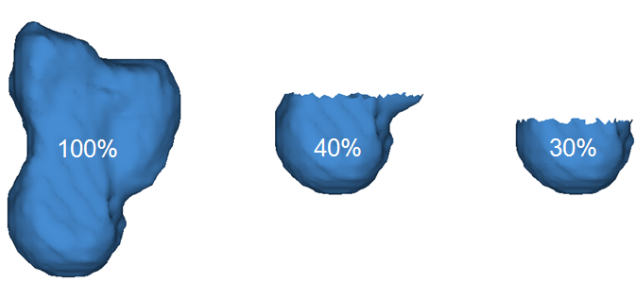

Figure 1. Sagittal views of complete, 40%, and 30% partial capitate surface meshes.

Note that the modest differences in mesh geometry between the 30% and 40% meshes are sufficient to allow for accurate registration fo the 40% partial scene. A sample registration is shown below in Figure 2 for the 60% partial scene (alignment view is scaled).

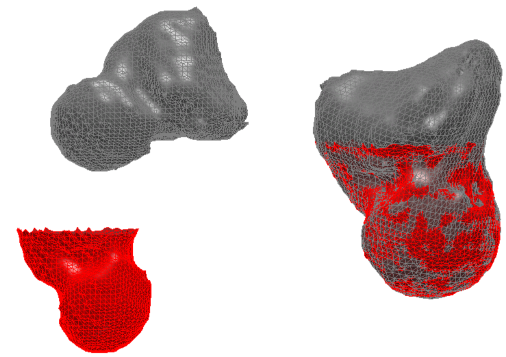

Figure 2. Alignment of model to 60% partial scene.

CONCLUSION

Evidenced by the RMS location errors (≤ 0.31 mm), low angular errors (≤ 1.44°), and high sub-resolution fit values (≥ 98.4%), the spin-image algorithm is well suited to the registration of partial capitate bones *when sufficient geometric information is present*. The amount of requisite information for accurate registration is dependent upon the direction in which the geometry of the imaged surfaces is limited and the uniqueness and orientablility of the available geometry. Had the elimination of geometry been from the proximal direction, less than 40% of the bone surface would likely still yield reasonable registrations.

REFERENCES

1. Leng S, Zhao K, Mingliang Q, An KN, Berger R, & McCollough CH. *Med. Phys. 38*(7), S50-S56 (2011).
2. Johnson AE & Herbert M. *Image and Vision Computing 16*, 635-651 (1998).
3. Katz S, Tal A, & Basri R. *Proc. SIGGRAPH 2007. ACM T. Graphic., 26*(3), 24-1–24-9 (2007).

ACKNOWLEDGEMENTS

This study was supported by award number R21AR057902 from the National Institute of Arthritis and Musculoskeletal and Skin Diseases and award number T32HD07447 from the National Institute of Child Health and Human Development.

TIME TO PEAK FORCE IN DIFFERENT COUNTERMOVEMENT CONFIGURATIONS

Jared Rehm, John Fox, Jay Patel, Braden Romer, Adam Jagodinsky and Wendi Weimar

Auburn University, Auburn, AL, USA
email: jmr0020@auburn.edu

INTRODUCTION

Sport activities often involve movements requiring high force and quick rate of force development. Countermovements are sometimes utilized to enhance performance [1,2]. Determining the optimal technique for a countermovement could have implications towards better sport performance. One technique that is being investigated as a result of canine research is a countermovement in which the participant removes his supporting limbs from the ground and falls into a countermovement [3]. This study seeks to find which of four types of countermovement in the upper extremity achieves peak force in the least amount of time.

METHODS

Twenty male participants (83.7±7.4kg; height, 1.8±0.07m) were recruited. The ground reaction force (GRF) was measured during plyometric pushups from the modified push-up position under 4 conditions: [A] was performed from a pre-determined elbow flexed position, [B] similar to a countermovement jump, involved beginning in the modified push-up position then lowering and pushing vertically, [C] standing on one's knees with arms positioned anteriorly participants fell forward into a countermovement, similar to a depth jump, and [D], beginning from the modified push-up position participants lifted their hands from the ground and fell into a countermovement. After each countermovement the participant would push maximally against a force plate embedded within the floor. The time from the initiation of movement to peak force produced during the push-up was collected.

RESULTS AND DISCUSSION

A one-way repeated measures ANOVA was utilized to find statistically significant differences in time to peak force during each condition. The mean times in seconds to peak force for each condition were found to be significantly different from each of the other times with $p<.01$ as shown in Figure-1 (A=.148s ±.055, B=.693s ±.191, C=.293s ±.058, D=.434s±.055).

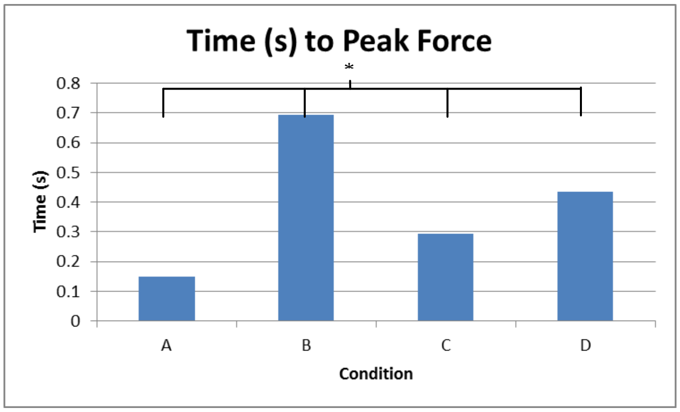

Figure 1: Time to peak force in seconds. All relationships signficant ($p<.01$).

[A] demonstrated the fastest time to peak force. This is not surprising because it lacked the countermovement and only involved the push up from the predetermined height. This agrees with previous research that countermovements take longer than no countermovement [4]. [C] yielded the fastest time with a countermovement. Further, study should investigate the mechanism for this occurrence. It could be due to the acceleration created by the falling into the countermovement without resistance from the arms to begin. The body could be reaching the time to produce the force for the desired movement faster because of the higher acceleration. [C] would not be applicable to many sport situations though so further investigation of [D] should be considered for specific sport actions that require countermovements. If the rate of force production is faster with [D], then it might be better to utilize a countermovement in which the limb is pulled away from the ground initially, instead of simply lowering the body.

CONCLUSIONS

Optimizing performance is a common athletic goal. Sometimes looking into the animal kingdom can give insight into potential ways for human performance optimization. The countermovement for [D] should be investigated further to see if there are directly applicable sport situations in which a bringing the limbs off the ground and falling into the countermovement offers an advantage over the more traditional countermovement.

REFERENCES

1. Arakawa, H., Nagano, A., Yoshioka, S. & Fukashiro, S. J Electromyogr Kines, **20**, 340 – 347, 2010.
2. Finni, T., Komi, P.V. & Lepola, V. *Eur J Appl Physiol*, **83**, 416-426, 2000.
3. Angle, T.C. (Unpublished doctoral dissertation). Auburn University, Auburn, AL, 2009.
4. Harman, Everrett A. et al. *Med Sci Sport Exer*, **20**(6), 825-833, 1990

ANGULAR ACCELERATION OF THE FOOT DURING GAIT USING AN IMU

Nori Okita and H. J. Sommer III

The Pennsylvania State University, University Park, PA, USA
Email: hjs1@psu.edu, web: http://mne.psu.edu/

INTRODUCTION

Recent advances in MEMS accelerometers have allowed cost effective and reliable angular acceleration measurement using two accelerometers mounted at fixed separation distance [1-3]. The angular acceleration measurements were successfully used to estimate foot orientation in pedestrian navigation [2], and to estimate angular velocity of an electric motor using a Kalman filter [3].

The purpose of the current paper was to compare two methods for measurement of angular acceleration of the foot (accelerometer versus gyroscope) using a wearable inertial measurement unit (IMU) that incorporates two MEMS multi-axis inertial sensors.

METHODS

An IMU with two 6-axis digital inertial sensors (MPU6050, Invensense, Sunnyvale, CA) was designed and fabricated (Fig 1). Each sensor contained a 3-axis gyroscope and a 3-axis accelerometer as well as signal conditioners and simultaneous 16-bit analog to digital converters in approximately 5mm x 5mm package.

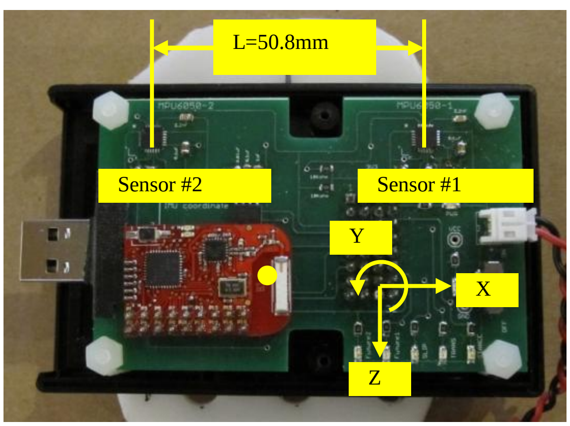

Figure 1: Top view of the IMU with two six-axis sensors separated by L=50.8 mm. IMU dimensions are approximately 60 x 95 x 20 mm.

The range of gyroscopes (gyro) and accelerometers were set at ±1,000º/s and ±16g, resulting in resolutions of 0.03º/s and 0.0005g. respectively. Signal bandwidth was set at approximately 180 Hz, with internal sampling at 1000 Hz. The digital data from each sensor was recorded into onboard memory at 200 Hz after receiving a wireless trigger to synchronize with force plate data collection (Kistler, Amherst, NY).

Three normal walking trials of one male subject were collected after approval from the Institutional Review Board of the university. The IMU was secured to the dorsal surface of the shoe with a shoe lace (Fig 2). The subject walked approximately 10 steps on the walkway at a comfortable pace of approximately 1 Hz stepping frequency.

Figure 2: IMU secured to the shoe with a shoe lace.

Data from the onboard memory was transferred to a PC to calculate angular acceleration about the medial-lateral axis by using Matlab (Natick, MA). Accelerometer- and gyro-based calculations were performed using two respective formulae:

$$\alpha_{accel,i} = \frac{a_{y1,i} - a_{y2,i}}{L} \qquad \alpha_{gyro,i} = \frac{d\omega_z}{dt} = \frac{\omega_{i+1} - \omega_{i-1}}{2\Delta t}$$

a_{y1} and a_{y2} were the vertical accelerations from sensor #1 and #2, respectively, L (50.8 mm) was the distance between the sensors, and ω_z was angular velocity about the medial-lateal axis measured by gyro. Three gyro-based angular accelerations were calculated for comparison purposes: sensor #1, sensor #2, and the average of the two. No data filtering other than DC offset removal was performed.

RESULTS AND DISCUSSION

Excellent agreement among four angular acceleration profiles was observed (Fig 3). Angular accelerations as large as ±1,500 rad/s^2 were measured during heel strike and toe off transients.

Root-mean-square (RMS) error values of all three gyro-based profiles with respect to the accelerometer-based profile resulted in approximately 50±3 rad/s^2. Maximum error ranged from 1,000 to 1,250 rad/s^2. Smoothing effects of averaging data from two gyros data were not apparent.

Noise amplification typically seen in numerical time derivatives of gyro signals was not observed due to accuracy of internal signal conditioning and analog-to-digital converters. The central difference formula provided higher-order truncation error, $\mathcal{O}(\Delta t^2)$, without phase shift. However, error between gyro- and accelerometer- based profiles still existed during heel contact and toe off transients (Fig 3).

Gyro-based finite-difference angular acceleration measurements provide several advantages over dual accelerometer-based measurements: fewer parts, smaller IMU size and sensor-to-sensor misalignment. However, current data suggests accelerometer-based angular acceleration measurements may be desired to capture high transients, such as heel contact and toe off, or during more dynamic activity.

CONCLUSIONS

Digital MEMS inertial sensors were used to measure the angular acceleration of a foot during normal walking. Gyro-based angular accelerations resulted in reasonable agreements with superior accelerometer-based measurements, except for the heel contact and toe off transients.

REFERENCES

1. Sommer H.J., IMU Tutorial, GCMAS, 2010
2. Stirling R. et. al, Proceedings of the European Navigation Conference GNSS, 2003.
3. Soo J. and Tomizuka M. Control Engineering Practice, **15**, 325-332, 2007.

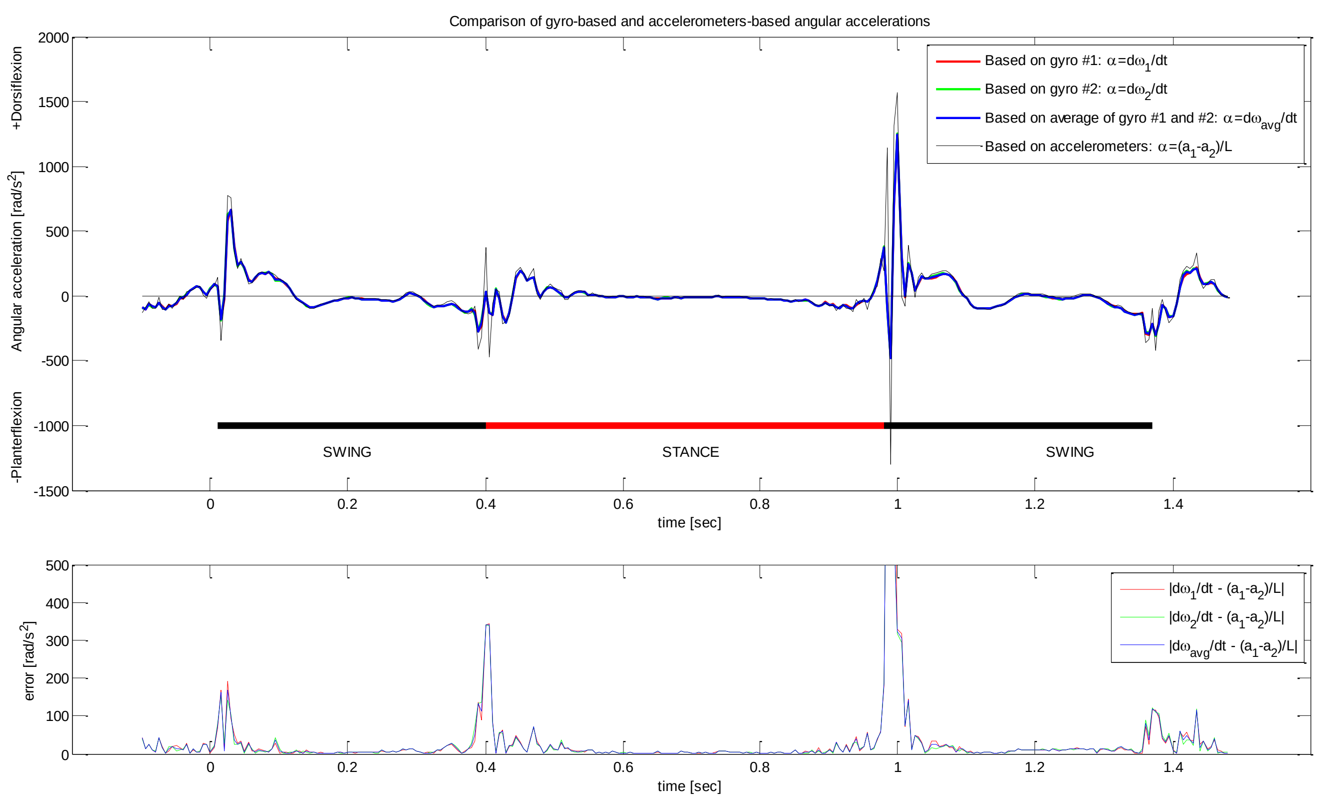

Figure 3: Representative angular accelerations during gait cycle from a single trial (top) and absolute value of error between gyro-based and accelerometer-based calculations (bottom). Larger angular accelerations and larger errors resulted during heel contact and toe off transients.

PHOTOELASTIC AND FINITE ELEMENT STRESS ANALYSIS OF HUMAN TEETH

Jamal A. Hassan, Sadiq J. Abass ,Noora A. Abud-Alhussian

Alnahrain University, Collage of Engineering, Medical Department

In this study, both the photoelastic, as well as the finite element methods, are used to study the stress distribution within various human teeth (mandibular first molar, mandibular central incisor and maxillary central incisor) under forces similar to those that occur during chewing. Two-dimensional models of teeth were created by the software AutoCAD using Wheeler's dental anatomy text book. The coordinates obtained from the Wheeler's data were fed into a computer numerical control (CNC) machine to fabricate the models from photoelastic sheets. Completed models were placed in a transmission polariscope and loaded with static forces (10N-100N) at 0° and 45° to the tooth axis. Stress can be quantified and localized by counting the number of fringes. The finite element models subdivided into small elements, resulting in a mesh where the mechanical properties of the material and applied loads to the component are taken into account. Materials were considered a homogeneous, isotropic, and linearly elastic. In both methods the Principle stresses were calculated at different regions, the crown, the cervical and the root. .It was found that when the teeth subject to the oblique load, the equivalent stress was concentrated on the coronal and middle thirds of the root. Under vertical load, the stresses were concentrated at the crown and cervical.

Keywords: Photoelasticity, Stress, Load, finite element

Toward Clinically Applicable Reconstruction Planning for Comminuted Articular Fractures

Andrew M. Kern and Donald D. Anderson

The University of Iowa, Iowa City, IA, USA
email: andrew-kern@uiowa.edu, web: http://poppy.obrl.uiowa.edu/

INTRODUCTION

Numerous clinical challenges arise in treating highly comminuted articular fractures. One germane to obtaining a precise reconstruction is a lack of knowledge of the pre-fracture anatomical origins of individual fragments [1]. A highly comminuted articular fracture is in many ways akin to a 3D puzzle. Knowledge of the puzzle solution gives a better understanding of the fracture, guides reconstruction and fixation planning, and potentially decreases the operative time.

A semi-automated system for obtaining such puzzle solutions from standard-of-care CT scans was previously developed using multiple software packages [1]. This system design was laborious and ultimately too unwieldy for clinical application. Furthermore, no means for conveying the solution to a clinician prior to surgery were made.

A more highly automated puzzle solving system is here presented, one allowing for computation of puzzle solutions within a 2 hour period, and requiring only ~35 minutes of user interaction. Puzzle solutions obtained using this new system are compared to ideal reconstructions, and the times required to obtain the solutions using the two systems are compared. The generality of the new methods are demonstrated by performing puzzle solutions on articular fractures of the distal tibia (ankle) and of the acetabulum (hip).

METHODS

The new puzzle solving software has been written in MATLAB 2012a (Mathworks, Natick, MA) in five discrete modules: Image Segmentation, Surface Partitioning, Surface Classification, Puzzle Solving, and Report Generation.

Image Segmentation

The accurate and rapid identification of many irregularly shaped bone fragments in CT images (segmentation) is a non-trivial task. The approach implemented first uses a marker-based watershed algorithm to roughly segment fragments, based on automatically selected seeds. This process tends to yield more "candidate" fragments than are actually present. A region-merging algorithm is then used to combine overly segmented candidate fragments. Finally, the user is allowed to manually delete, merge and split bone fragments interactively to produce the final surface models of each fragment.

Surface Partitioning

Following segmentation, it remains unclear which portions of the fragments belong to which anatomical surfaces. Surface partitioning aims to use 3D curvature information to divide a single fragment into discrete patches (Fig. 1). Based upon surface curvature weighting, a minimum spanning tree of the model is computed, identifying a globally optimal tree connecting all edges of high curvature. Cycles are created in the spanning tree by using a greedy algorithm to connect adjacent high-curvature leaves [2]. Following pruning, the surface patches contained within these cycles represent regions of anatomically similar geometry.

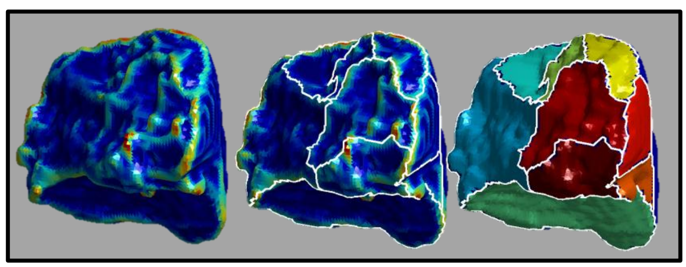

Figure 1. Surface partitioning begins with computation of surface curvature (left). Ridges of high curvature are found (center), and individual regions are isolated (right).

Surface Classification

The partitioned surface patches are identified as cortical, subchondral or inter-fragmentary using a supervised bagging-ensemble classification algorithm [3]. Vertex-specific surface curvatures, image intensities, and image gradients are sampled at different spatial scales and at varying depths to form a feature vector for use in classification. Each patch is then classified using these vertex-specific classifications, with majority rules enforcement across any given patch (Fig. 2).

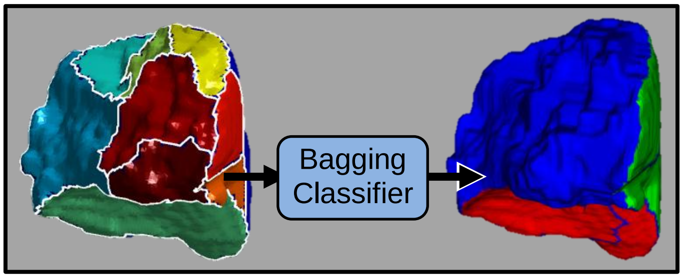

Figure 2. Surface partitions (left) are classified with ensemble bagging algorithm into three surface classes (right): Inter-fragmentary (blue), Subchondral (red), and Cortical (green).

Puzzle Solving

Fragment geometries and surface classifications are utilized to compute a final puzzle solution. Fragments are sorted by cortical surface area from largest to smallest and are progressively aligned to the surface of an intact contralateral template using an iterative closest point algorithm (ICP) [1]. The ICP matches cortical-to-cortical and subchondral-to-subchondral surfaces, while ignoring inter-fragmentary surfaces (Fig. 3).

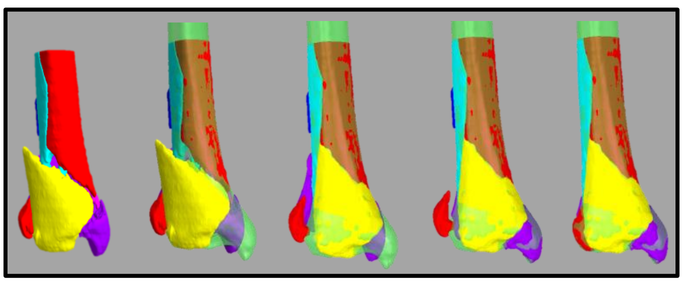

Figure 3. Fragments are aligned from smallest to largest using an Iterative Closest Point algorithm to register cortical and subchondral fragment surfaces to an intact template.

Report Generation

Following its computation the ideal fracture reconstruction needs to be conveyed to the clinician in an efficient and clear manner, which does not require the use of any esoteric software. A 3D-PDF file format was chosen as it is a common, cross-platform file that allows a user to visualize and manipulate the fractured bone and computer-reconstruction in real-time.

RESULTS AND DISCUSSION

Six comminuted ankle fractures and nine complex acetabular fractures were successfully reconstructed using the puzzle solving software (Fig. 4).

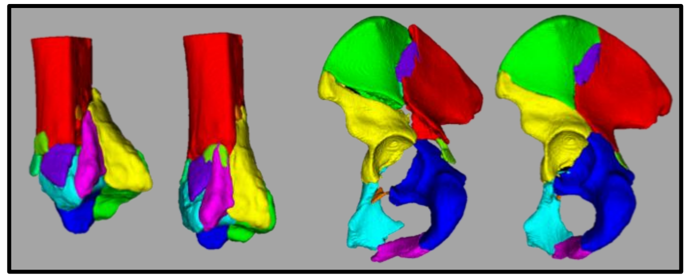

Figure 4. Representative reconstructions from tibial pilon (left) and acetabular (right) fractures.

Based on these results the approximate time from CT to final fracture reconstruction has been reduced from 12 hours to 2 hours while still obtaining an excellent fracture reconstruction. Additionally only ~35 minutes of interactive user time is required to perform these solutions, making it feasible for a technician to perform multiple puzzle solutions simultaneously (Fig. 5).

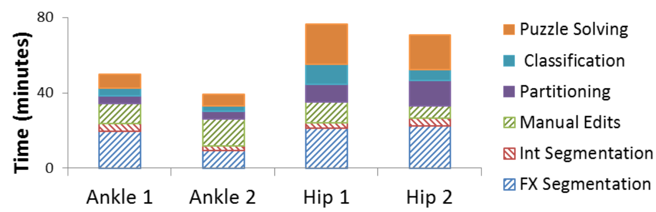

Figure 5. Reconstruction time for two representative ankle and hip fractures. Steps requiring active user input are textured.

These expedited methods pave the way for the evaluating the efficacy of computer-based fracture reconstructions in improving surgical outcomes. These inherently time-sensitive analyses can be performed and reported to clinicians within a reasonable timeframe. Future work involves trialing these methods on real fracture cases to refine the existing algorithms and improve report formatting and information, based upon clinician feedback.

REFERENCES

1. Thomas TP et al. *Comp. Methods. Biomech Biomed Eng*. 2011
2. Pauly M. et al. *Computer Graphics Forum.* 2003
3. Brieman, L. *Machine Learning.* 1996

ACKNOWLEDGEMENTS

This work was funded by Iowa Economic Development appropriations to the Grow Iowa Values Fund. Dr. Anderson is a co-owner of a company (FxRedux Solutions, LLC) founded to commercialize the puzzle solving technologies.

INVERSE DYNAMICS OF UNSTABLE SITTING: THE RELATIONSHIP BETWEEN COP AND MOMENT CONTROL FOR INCREASING TASK DIFFCULTY

[1]Casey A. Myers, [1]Kevin B. Shelburne, [2]Sheri P. Silfies, and [1]Bradley S. Davidson

[1]University of Denver, Human Dynamics Laboratory, Denver, CO, USA
[2]Drexel University, Rehabilitation Sciences Spine Research Lab, Philadelphia, PA, USA
email: casey.myers@du.edu

INTRODUCTION

Spinal instability is commonly associated with pathologic conditions such as multiple sclerosis and Parkinson's disease and is inherently linked to low back pain [1]. Although spinal instability remains poorly defined among both clinicians and researchers, an increasingly common paradigm used to quantify low back performance is to maintain a stable posture while sitting on an unstable platform (Fig. 1) [2]. Because this "unstable sitting" paradigm isolates torso kinematics, it provides a unique tool to investigate motor control in the lumbar spine musculature across a variety of conditions [3].

The majority of analyses for unstable sitting tasks mirror the traditional approach to standing balance, but it is not clear how these metrics relate to torso control strategies used to maintain stability. Center of pressure (COP) trajectory produced by contact of the hemisphere on a force plate allows calculation of summary statistics that are used to delineate cohorts as having better or worse "postural control". Although these metrics provide insight into the resulting motion that occurs during sitting tasks, the relations to kinematics or inverse dynamics has not been examined or reported.

The objectives of this study were to: 1) calculate the flexion/extension (F/E) moment at the lumbar spine during unstable sitting and determine its relationship to COP and rotational kinematics, and 2) quantify the effect of task difficulty on the F/E moment. We hypothesized that strong correlations would exist between COP position and kinematics. We also hypothesized that F/E moment would indicate strategy differences across tasks.

METHODS

Ten healthy participants (6 male, 4 female) sat on an unstable surface composed of a chair balanced on a hemisphere. Three ten-second trials were collected for each combination of the task to assess difficulty (large sphere (LS): 44cm diameter, small sphere (SS): 39cm diameter) and visual condition (eyes open (EO), eyes closed (EC)). Each participant was instructed to keep the chair as still as possible while maintaining an upright torso posture. The F/E moment was calculated for every time point using a sagittal plane inverse dynamics analysis (Fig. 1).

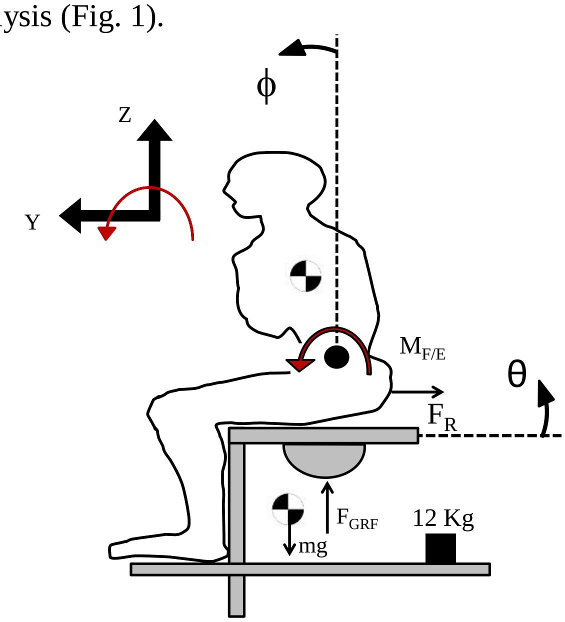

Figure 1: Diagram of unstable sitting illustrating the dependent variables of theta: angle of chair with respect to horizontal, COP: location of F_{grf} in the Y-direction, and F/E moment: $M_{F/E}$

Pearson product moment correlation was used to describe the relationship between F/E moment and chair rotation and F/E moment and COP. Differences across task combinations in theta, COP and F/E moment were compared with paired *t*-tests.

RESULTS AND DISCUSSION

Mean total theta and mean COP excursion significantly increased with increasing task difficulty. The easiest task was LS-EO and the hardest was SS-EC with theta for SS-EC 102.6% ±

12.2% greater than LS-EO (p<0.001) and SS-EC COP 96.7% ± 9.7 greater than LS-EO (p<0.001) (Table 1). Participants adopted a control strategy with an average extension moment that increased slightly with task difficulty. Two possible reasons exist for an extension moment preference. First, extensor muscle activity required to produce this moment may heighten their proprioception and allow for detection of small position changes. Second, a flexion moment applied in the wrong configuration at the wrong time may result in apprehension about falling forward. As expected, very strong correlations exist between theta and sagittal plane COP trajectory, which reflect kinematic constraints of rolling (Table 1).

A strong negative correlation existed between theta and F/E moment and a strong positive correlation existed between F/E moment and COP. The magnitude of these correlations were lower in the less difficult conditions than in the more difficult conditions (Fig. 2). During less difficult trials, it is

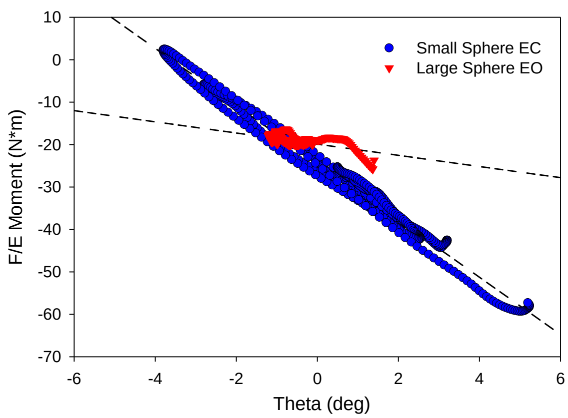

Figure 2: F/E moment vs. theta during a more difficult task with eyes closed compared to a less difficult sphere eyes open.

feasible that only intermittent corrective control would be needed [4], which would result in smaller F/E moment, low kinematic variability, and a lower moment-angle correlation than a more difficult task. During more difficult trials, a continuous control strategy was used that results in large F/E moment, large kinematic variability, and a strong F/E-angle relationship (Fig. 3). This strategy, which is likely more robust may enable rapid response to changes in angular position or perturbations.

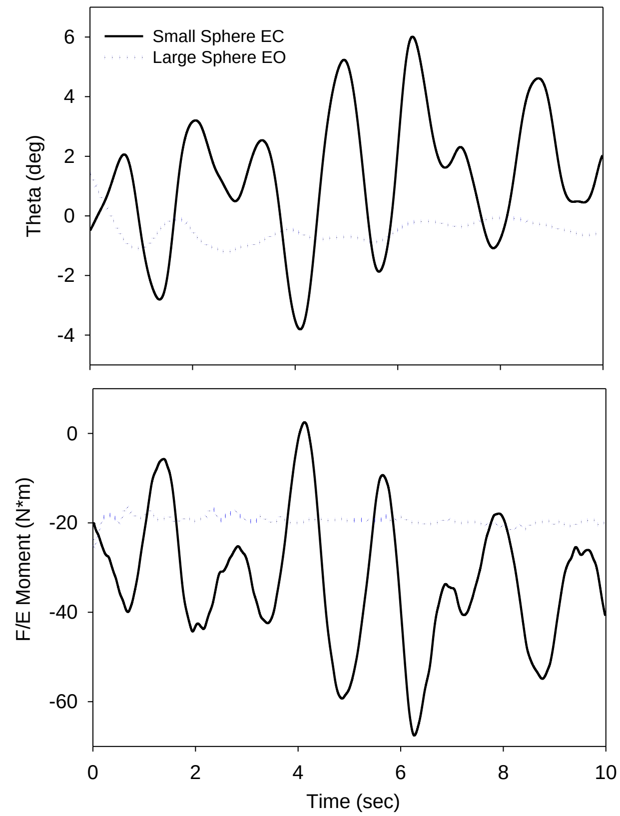

Figure 3: The more difficult task showed large changes in moment that correspond directly to changes in theta . The less difficult task showed smaller changes, with the F/E moment held relatively steady to maintain the chair position at theta = 0°.

CONCLUSION

This initial examination of inverse dynamics and kinematics during unstable paradigm revealed strong relationships between F/E moment and angular position and center of pressure. As we learn more about these metrics and how to interpret them, we anticipate using unstable sitting to gain insight into neuromuscular control strategies and low back stability across a range of task difficulty and pathology.

REFERENCES

1. Panjabi M. *J Spin Dis & Tech*, **4**(5) , 1992.
2. Cholewicki J. *J Biomech*, **33**, 1733-1737, 2000.
3. Van der Burg JCE. *Park & Rel Disord*, **12**, 492-498, 2006.
4. Bottaro A. *Hum Move Sci*, **24**(4), 588-615, 2005.

Table 1: mean (SD) values for dependent variables and correlations results for each of the four conditions.

	θ range (deg)	COP range (cm)	Avg F/E (N·m)	F/E Variability (N·m)	COP vs. θ (*r*)	F/E vs. θ (*r*)	F/E vs. COP (*r*)
Large Sphere EO	1.73 (0.65)	0.62 (0.28)	-30.34 (31.0)	2.0 (1.9)	0.98 (0.02)	-0.70 (0.27)	0.70 (0.27)
Large Sphere EC	3.96 (1.35)	1.47 (0.45)	-37.81 (21.4)	4.7 (3.8)	0.99 (0.01)	-0.88 (0.10)	0.88 (0.12)
Small Sphere EO	2.57 (0.63)	0.83 (0.20)	-34.81 (22.6)	3.0 (2.8)	0.98 (0.04)	-0.80 (0.19)	0.79 (0.18)
Small Sphere EC	5.37 (1.90)	1.80 (0.52)	-40.99 (16.5)	6.1 (2.9)	0.96 (0.07)	-0.87 (0.12)	0.87 (0.11)

MODEL-PREDICTED BUCKLING OF THE ADULT HUMAN UPPER EXTREMITY: EFFECTS OF PEAK IMPULSIVE FORCE AND MUSCLE STATES

[1]Yunju Lee and [1]James A. Ashton-Miller

[1]University of Michigan, Ann Arbor, MI, USA
email: yunjulee@umich.edu, web: http://me.engin.umich.edu/brl/

INTRODUCTION

When an arm is used to break a fall to the ground, the impact force on the hand can exceed several times body weight (BW) [1] on a hard surface or enough to cause wrist fracture. If the upper extremity were to buckle under that load then the risk of the head injury increases. However the factors that determine the arm buckling behavior remain poorly understood. We have previously reported pilot computer simulation results on the effects of age and gender on the magnitude of the impulsive load under which an arm could collapse [2], and measured the elastic and viscous resistance of the actively contracting elbow extensor muscles of young adults using an indirect approach [3]. Previous studies have focused only on the elbow and contribution of the elbow extensor muscles, so in this paper we explore (1) relationship between impulsive ground reaction peak force and arm joint (elbow and shoulder) deflexion angles and (2) the effect of the shoulder muscle properties and muscle stretch responses on the distal end impulsive load. To avoid a risk of wrist fracture or head injury, we used computer simulations to estimate upper extremity dynamics during the arrest of a forward fall.

METHODS

A 3-D, sagittally-symmetric, four-link (including hand, forearm, upper arm and clavicle), lumped parameter, musculoskeletal model of the adult upper extremity was developed using MD Adams™ 2010 engineering software. Segments were connected by two frictionless revolute joints representing wrist and elbow joints and by two frictionless spherical joints at shoulder and sternoclavicular joints. Segment anthropometric, mass, and inertial properties were taken from the literature [3].

The resistance of the precontracted elbow extensor muscles to forced flexion was modeled with a rotational spring and damper at the elbow whose linear coefficients we identified from impulsive measurements in 18 adults (9 females) [3]. We used these elbow data to identify muscular resistances (stiffness, K and viscosity, B) for the shoulder extensor (in sagittal plane) and adductor (in transverse plane) muscles based on measured 3-D kinematics during these experiments (Fig. 1).

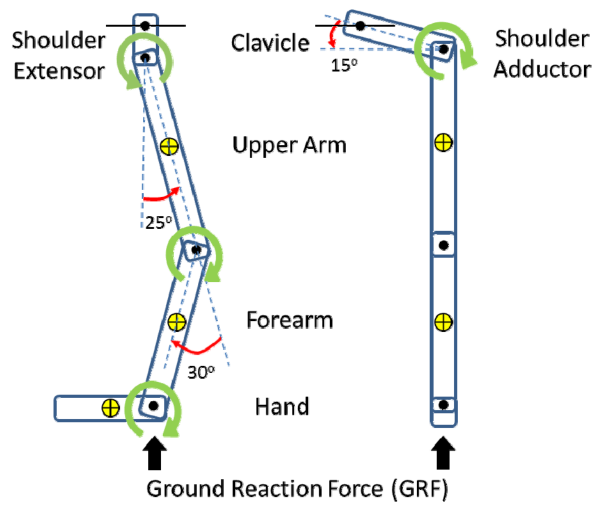

Figure 1: *In silico* model for simulating of the arrest of a sagittally-symmetric forward fall with the upper extremities (Left: sagittal plane, Right: axial plane). Black dots denote revolute joints at elbow and wrist joints and spherical joints at shoulder for extensor and adductor, and at the clavicle to ground.

Simulations were run with an initial pre-impact elbow flexion angle of 30° (where 0° denotes elbow extension) and shoulder extension angle of 25° (where 0° denotes the arm in the parasagittal plane (Fig. 1). Model simulations were run over the 200 msec post-impact at 1 msec increments. The sensitivity of arm load-deflexion behavior to changes in the peak load (F_1) of the impulsive ground reaction force on the hand with the usual muscle pre-contraction levels (70% of maximum voluntary contraction, MVC) were conducted from under 1*BW (785N) to 2.5 times BW in the peak force (F_1 = 500N – 2,000N). We also conducted a design of experiments (DOE) analysis for the effect of variations in shoulder extensor and adductor muscle pre-activation levels (K_{ext} = 1 – 8 Nm/deg for extensor stiffness and K_{add} = 1 – 6 Nm/deg for adductor stiffness) and elbow muscles (elbow stiffness, K_{elb} = 0.5 – 3 Nm/deg) on arm deflexion behavior. The effect of muscle viscosity, in units of Nm.s/deg, about a joint was assumed to have 1/10 the value of stiffness in Nm/deg [3].

The model extremity was considered to have *buckled* when the elbow angle, which was defined as the maximum angular deflexion under load from the initial elbow angle, reached 110°, or the vertical displacement of hand reached initial elbow height.

RESULTS AND DISCUSSION

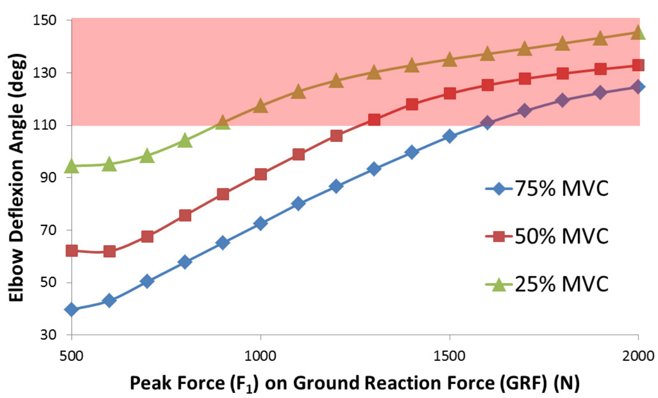

Figure 2: Predicted buckling behavior as a function of upper extremity distal peak load (F1) and elbow and shoulder muscle pre-contraction level (% MVC). The shaded region ($\Delta\Theta_{elbow} > 110^o$) denotes limb buckling.

The limb was predicted to buckle when the peak ground force exceeded 1,600 N for a 75% MVC elbow and shoulder muscle pre-contraction level, 1,300 N for 50% MVC, and 900N for 25% MVC, respectively (Fig. 2). The peak force (F_1) is known to be related to fall height and muscle pre-contraction levels [1]. We found earlier that the stiffness and viscosity acting about a planar elbow joint markedly affected its buckling behavior [3], and the same trend was found in this study. However, in this study, the shoulder adductor muscle properties significantly affected the shoulder adduction angle as well as the elbow deflexion angle, but neither the shoulder extensor muscle properties nor the shoulder adduction angle affected the final elbow angle (Table 1).

Table 1: Model sensitivity results shown as angle changes in percentage by varying muscle properties. The percentage to the left of the slash mark indicates the effect of a minimum modification in the parameter and the percentage to the right a maximum modification (see Methods).

Variable	Elbow Deflexion	Shoulder Extension	Shoulder Adduction
F_1	-72% / +82%	-48% / +21%	-6% / +11%
Elbow K & B	-80% / +43%	-10% / +40%	-15% / +2%
Shoulder Extensor K & B	-0% / +0%	-53% / +50%	-0%/ +0%
Shoulder Adductor K & B	-13% / +5%	-43% / +10%	-50% / +14%

The results suggest that the upper extremity buckling behavior was affected by both shoulder and elbow muscle pre-contraction level and the peak impulsive load acting on the limb.

CONCLUSIONS

These are estimates for the buckling load of an adult upper extremity during in a forward fall arrest show that limb buckling was sensitive to arm and shoulder muscle pre-contraction intensity. Because the shoulder adductor muscle state proved as important as the elbow extensor muscle state, it would wise to maintain good shoulder adductor strength, as well as triceps strength, if one is to prevent the head from striking the ground in a fall.

REFERENCES

1. DeGoede KM, et al. *J Biomech* **35**, 843-848, 2002.
2. Lee Y, et al. *Proceedings of NACOB'08,* Ann Arbor, MI, USA, 2008.
3. Lee Y, et al. *Ann Biomed Eng* **39**, 2542-2549, 2011.

ACKNOWLEDGEMENT

Funded by PHS Grant P30 AG0248

THE EFFECT OF OCCUPATIONAL FOOTWEAR ON DYNAMIC BALANCE

[1]Harish Chander, [2]Chip Wade, [1]Nicole C. Dabbs, [1]Charles R. Allen,
[1]Vanessa L. Cazas, [1]Jon Lundahl & [1]John C. Garner
[1]Applied Biomechanics Laboratory, University of Mississippi, University, MS
hchander@go.olemiss.edu
[2]TigErgonomics Laboratory, Auburn University, Auburn, AL

INTRODUCTION

Upright maintenance of balance, which requires the individual to keep the center of gravity within the base of support, is a fundamental part of daily activity under both static and dynamic conditions. Proper balance is crucial in occupational and industrial settings in order to prevent falls and fall related injuries. The Bureau of Labor Statistics reported 208,470 cases of work related falls in 2010 of which 646 were fatal [1]. The increased probability of falls has been related to a decreased balance performance and previous studies have shown decrements in balance as a result of different footwear [2]. Occupational footwear is often designed for safety and may fail to provide appropriate foot biomechanics which may impact balance characteristics. The purpose of the study is to examine the differences in dynamic balance in an acute period while wearing different types of commonly used occupational footwear.

METHODS AND PROCEDURES

Twenty five healthy male adults (aged 21.2±1.4 years; height of 179±9.4 cm; mass of 82.6±15.4 kg), with no history of orthopedic, musculoskeletal, cardiovascular, neurological and vestibular abnormalities participated in this study. The motor control test (MCT) on the Neurocom Eqitest was used to assess dynamic balance which uses the translational capabilities of the dual force platform to create two testing conditions with forward [medium (FWM)/ large (FWL)] and backward [medium (BWM)/ large (BWL)] translations. The testing procedure included an initial familiarization session where each participant was exposed to the MCT balance assessment and a second experimental testing session which was separated by at least 24 hours. The experimental testing session consisted of an initial barefoot (BF) balance measurement followed by randomized balance testing with three other occupational footwear conditions; work boot (WB) (mass 0.39±0.06 kg), tactical boot (TB) (mass 0.53±0.08 kg) and low top shoe (LT) (mass 0.89±0.05 kg) separated by a 10 minute rest/washout period. The subjects were seated during the 10 minute rest period to prevent any undue fatigue and any possible adaptation to the balance tests. Latencies, quantified as the time period (msec) between the onset of the translation and the initiation of the participant's active response were used as the balance dependent variable.

RESULTS

The latencies from the MCT were evaluated using a 1 x 4 [Testing Session x Footwear Condition (BF v. LT v. TB v. WB)] RMANOVA and independently for the backward and forward medium and large translations at an alpha level of 0.1 to identify any existing differences among the footwear conditions. Significant differences were found between the footwear conditions and post hoc pairwise comparisons revealed that BF condition had significantly lower latencies in the backward large (p=0.01) and forward medium (p=0.09) and large (p=0.04) translations compared to LT, TB and WB. No significant differences were found among the occupational footwear for any of the translations.

Fig.1: MCT Backward Translations

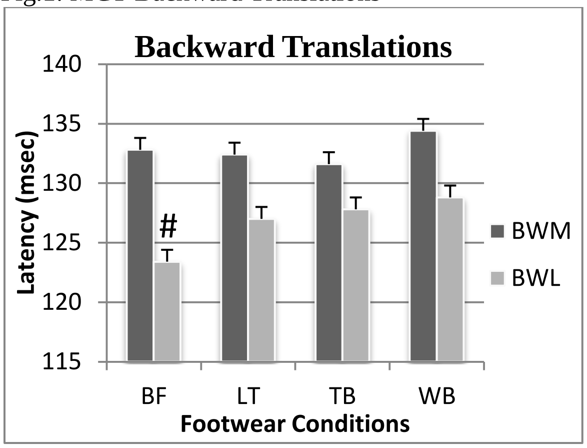

Fig.2: MCT Forward Translations

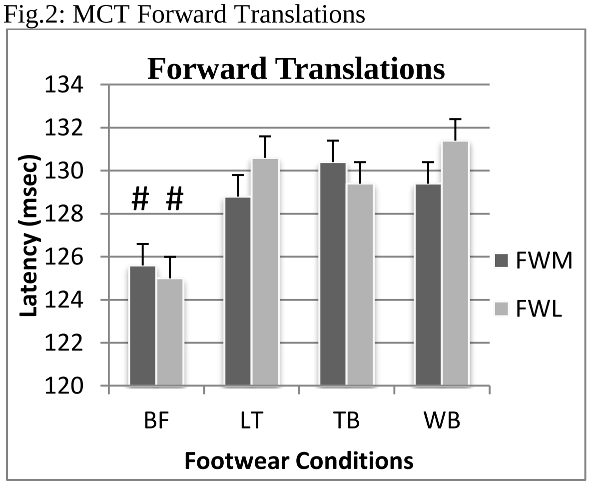

DISCUSSION

The MCT assesses the automatic motor control postural responses which are the first line of defense against unexpected external perturbations, that might lead to a fall [3]. The results indicate a significant difference in the MCT latencies between the barefoot and the three occupational footwear. These differences can be attributed to the increased somatosensory and proprioceptice feedback that are available in a barefoot condition unlike the shod conditions where the footwear acts as an interface between the ground and the foot, lowering the available somatosensory cues. A recent study showed significantly lower postural sway in the tactical and work boots compared to low top shoes in the eyes open and eyes closed sensory organization test, which was attributed to the above ankle elevated boot shaft that provided stability around the ankle [4]. However, in this study no significant differences were found between the three occupational footwear which suggessted that, although the elevated boot shafts of the tactical and work boots significantly reduced the center of pressure (COP) excursions, thereby decreasing the postural sway during quiet stance in the SOT, they did not influence the feedback control of postural adjustments to unexpected perturbations experienced during the MCT.

CONCLUSION:

The MCT latencies for the occupational footwear conditions although significantly higher than the barefoot conditions, were still under normal ranges for healthy adults. The findings from this study can be used as a series of recommendations for occupational footwear design. The midsole hardness of these footwear were not taken into consideration for this analysis. Future reasearch on the thickness-hardness of the midsole and its effects on the somatosensory system in maintaining dynamic balance is warranted. Additionally, dynamic balance assessment under occupational fatigue conditions may further help understand the efficiency of these occupational footwear.

REFERENCES

1. Bureau of Labor Statistics: 2012.
2. Menant, J. et al. Effects of shoe characteristics on dynamic stability when walking on even and uneven surfaces in young and older people. *Archives of Physical Medicine and Rehabilitation; 89:*1970-1976, 2008
3. Neurocom Equitest System operator's manual. Clackamas, OR: Neurocom Intl Inc.; 2002
4. Chander, H. Impacts on balance while walking in occupational footwear; 2012. (Master's Thesis) The University of Mississippi, University, MS.

NONLINEAR MATHEMATICS DETECT SUBTLE CHANGES IN CENTER OF PRESSURE

[1]Troy Rand, [1]Anastasia Kyvelidou, [1]Sara Myers

[1]University of Nebraska at Omaha, Omaha, NE, USA
email: troyrand@gmail.com, web: nbcf.unomaha.edu

INTRODUCTION

Falls are one of the most significant health concerns in an aging population and it is estimated that falls account for one third of the total cost of medical treatment for all injuries [1]. Because falling happens when the center of mass moves outside the base of support, studying postural control can give insights into the control mechanisms responsible for maintaining balance. Postural control is an intricate neuromuscular process with the goal of maintaining the body's center of mass over the base of support. Center of Pressure (COP) is a common measure used to assess postural control and represents the resultant forces acting on the ground and reflects the movement of the center of mass. There are three sensory systems responsible for maintaining balance: The visual system senses changes in body position through visual input, the somatosensory system senses changes in body position through mechanisms such as proprioception in the feet, limb position and muscle length, and the vestibular system senses changes in head position and movement. When measuring postural control there will be an inherent variability present since an individual cannot stand perfectly still. Previously it was thought that by reducing variability in standing posture a reduction in fall risk would occur. However it is now known that in a healthy biological system variability has a temporal structure that resembles mathematical chaos and has an ordered pattern [2]. Nonlinear methods have been used to explore the temporal structure of variability and have provided a stronger picture of the overall health of the neuromuscular system. It was hypothesized that nonlinear measures would be more sensitive to the changes in an aging population when compared to linear measures of postural control. These findings could help to determine changes in posture that could lead to a higher risk of falling earlier than the currently used clinical methods.

METHODS

Ten healthy young (age: 24.7 ±3.7 years; ht: 171.7 ±11.7 cm; mass: 70.6 ±15.5 kg) and seven healthy older adults (age: 67.7 ±5.4 years; ht: 175.1 ±8.1 cm; mass: 86.1 ±23.1 kg) were screened and consented for participation in this study. Two of the older adults were not able to maintain balance during the final two conditions so that data was excluded from analysis. Center of pressure was recorded for all participants using the Neurocom® Balance Manager™ System (Neurocom International Inc., Clackamas, OR; 100 hz). Each participant completed one trial in six separate conditions, each lasting 90-seconds. Subjects were instructed to stand with feet shoulder width apart and even weight distribution. The six conditions are the same as the Sensory Organization Test, which is a common clinical balance test designed to challenge the different sensory systems through the use of a movable visual surround and force platform. The conditions are 1) normal, 2) absent vision, 3) faulty vision, 4) faulty somatosensory, 5) faulty somatosensory and absent vision, and 6) faulty somatosensory and faulty vision. The COP signal was analyzed in the anteroposterior (AP) and mediolateral (ML) directions as well as the distance (D) from the previous point, which represents an integrated control of both the ML and AP directions (equation 1). The nonlinear dependent variables include detrended fluctuation analysis (DFA) and sample entropy to measure the temporal structure of the COP. DFA is a technique used to measure long-range correlations in non-stationary time series, and gives insight into the complexity of the temporal structure. Sample entropy quantifies the amount of regularity present in a time series and gives insight into the predictability of the temporal structure. The linear dependent variables include range to measure total displacement, sway path, which is a reflection of sway velocity, and the ellipse area containing 95% of the COP signal, which measures the total area the center of pressure covered throughout the trial. A two by six mixed ANOVA was used to compare between effects of age and condition. Significance was set at 0.05.

Equation 1: x = AP position; y = ML position

$$D_i = \sqrt{(x_{i+1} - x_i)^2 + (y_{i+1} - y_i)^2}$$

RESULTS AND DISCUSSION

Table 1: Main effects of age (Healthy young vs. Healthy older).

Measure	p-value
Range (AP)	0.032 *
Range (ML)	0.029 *
Sway Path	0.024 *
Ellipse Area	0.028 *
Sample Entropy (AP)	0.121
Sample Entropy (ML)	0.596
Sample Entropy (D)	0.329
DFA (AP)	0.027 *
DFA (ML)	0.599
DFA (D)	0.109

There were many significant differences due to the effect of condition, however it is beyond the scope of this abstract to discuss them all. Therefore, the analysis will be looking at group effect knowing that each group had all three sensory systems challenged. There was a significant group effect, with increases in all of the linear measures; however, the only significant difference in the temporal structure of variability was DFA in the AP direction (Table 1). This demonstrates that older adults are swaying more and with greater velocity, however the nonlinear measures are able to detect a more subtle change in neuromuscular control, as evidence by the condition effects. The significant difference in the DFA alpha values show a loss of complexity in the temporal structure, this was most notable in conditions five and six where vision and somatosensory systems were challenged (Figure 1, C). There was no significant difference in the sample entropy values, showing that the regularity of the temporal structure did not change. All of the healthy older participants in this study were physically active. Five of the seven older participants exercised three or more times per week and the other two exercised two times per week. The healthy older were also free of any known conditions that would affect postural control. Other research has recognized that it is hard to differentiate the effects of aging and the onset of disease [3].

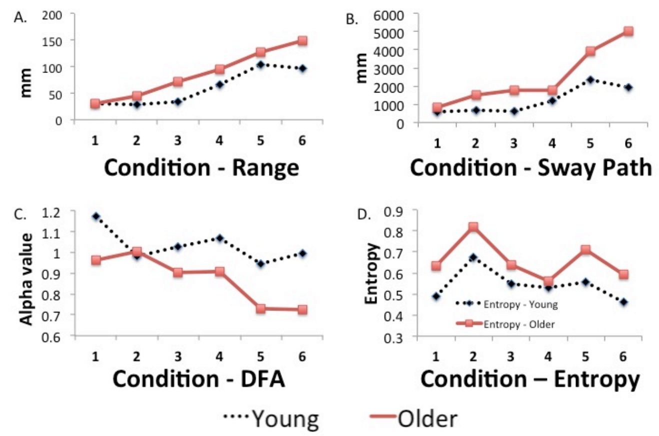

Figure 1: Healthy young vs. healthy older in the six experimental conditions. A) Range AP, B) Sway Path, C) DFA alpha value AP, D) Sample Entropy AP. Dotted line = Young, Solid line = Older.

CONCLUSIONS

Postural sway is a multifactorial component that has a strong neuromuscular basis. Typically aging is associated with decline of the neuromuscular system, however it appears that nonlinear measures provide a different view of neuromuscular control. More research needs to be done with a falling population to determine how the temporal structure of COP changes in relation to fall risk.

REFERENCES

1. Sjogren, H, et al. *Scand J Prim Health Care* **9**(3), 203-207, 1991.
2. Stergiou, N., et al. *J Neurol Phys Ther,* **30**(3), 120-129, 2006.
3. Vellas, B., et al. *Am J Clin Nutr*, **55**, 1225S-1230S, 1992.

ACKNOWLEDGEMENTS

This work was supported by the University Committee on Research and Creative Activity and Graduate Research and Creative Activity at the University of Nebraska at Omaha.

POSTURAL RESPONSES TO UPPER LIMB MOVEMENTS IN QUIET STANDING

[1]Benjamin L. Long, [2]Justin P. Waxman, [2,3]Jeffrey B. Taylor, [1]Dora J. Gosselin, & [2]Christopher K. Rhea

[1]Winston-Salem State University, Winston-Salem, NC, USA
[2]University of North Carolina at Greensboro, Greensboro, NC, USA
[3]High Point University, High Point, NC, USA
email: longbe@wssu.edu, web: http://www.biodynamicslab.org

INTRODUCTION

Internally generated perturbations from upper extremity movements alter the center of mass and require center of pressure (COP) adjustments to maintain upright stance. Besides affecting the amplitude of postural sway, the dynamics of the COP trajectory may also be affected by the perturbations, potentially reflecting less adaptable behavior [1]. Since postural stability is a function of the COP behavior within the base of support (BOS), a reduced BOS may affect the emergence of adaptive postural control behavior. Destabilizing upper extremity movements can be coupled with a reduced BOS, further challenging the postural control system. The purpose of this study was to identify the structure and magnitude of variability in the center of pressure in healthy college-age students during conditions of narrow base of support and bilateral arm movements of various speeds. It is hypothesized that internally generated perturbations of the center of mass via rhythmic, repetitive movements of the upper extremities will change the dynamics of postural control leading to a more regular COP time series.

METHODS

Three-dimensional kinematic and COP data were collected from 12 (6 female, 6 male) healthy college age subjects (24.4 ± 1.1 yrs; 169.9 ± 6.7 cm; 70.5 ± 15.4 kg) while standing on a force platform for 45 seconds under four randomized testing conditions: self-selected BOS with arms at side (SSBOS), narrow BOS (feet together) with arms at side (NBOS), narrow BOS with arm movements at 1Hz (NBSLOW), and narrow BOS with arm movements at 1.33Hz (NBFAST). During the arm movement conditions, subjects moved their arms vertically to shoulder height, in the scapular plane. A digital metronome was used as a reference for arm movement speed. In order to ensure that the system was not overly constrained, the metronome was turned off during testing. Two-minute rest periods were given between each condition in order to offset fatigue effects. Custom Matlab code (Mathworks, Newton, MA) was used to quantify measures of magnitude [Root Mean Square (RMS) and 95% Ellipse Area (COPEA)] and structure [Sample Entropy (SampEn)] from the COP time series. Separate one-way repeated measures ANOVAs were used to analyze the magnitude (RMS and COPEA) and structure (SampEn) of COP variability across all conditions (alpha = 0.05). Following a significant main effect, condition means were compared using pairwise comparisons with a Bonferroni correction.

RESULTS AND DISCUSSION

The purpose of this study was to examine the effect of both an altered BOS and repetitive arm movements on the magnitude and structure of COP variability. Switching from SSBOS to NBOS resulted in an increase in the magnitude (Figs 1, 2 & 3) of COP variability for both RMS and the COPEA. However, only RMS in the medial-lateral direction and COPEA were found to be statistically significant. The structure of variability (Figs 4 & 5) remained relatively unchanged between the SSBOS and NBOS conditions. As the task constraints increased with the addition of repetitive arm movements in a narrow base of support (conditions 3 & 4), participants were found to have a more irregular COP time series in both the medial-lateral and anterior-posterior directions, along with larger total COP movement (Figs 1-5). This irregularity and larger COP movement potentially reflects a system that is less adaptable and more unstable. Supporters of non-linear dynamics have advocated for the use of data obtained from young, healthy adults to be used as normative values for comparison with clinical populations, such as the elderly, injured, or those with neurological diseases [2,3]. The results of this study are a step towards establishing normative values for COP variability during conditions of an altered BOS and/or repetitive arm movements.

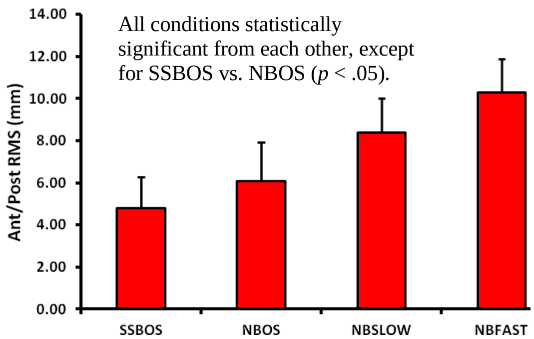

Figure 1: Root Mean Square (RMS) values for the anterior-posterior directions.

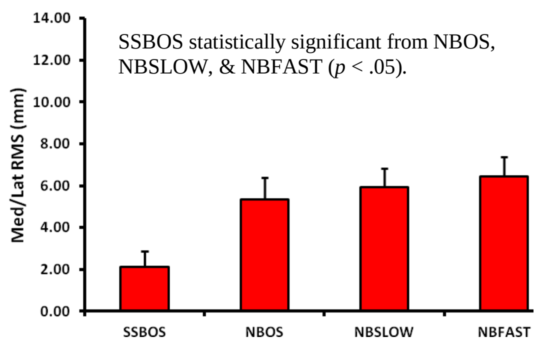

Figure 2: Root Mean Square (RMS) values for the medial-lateral directions.

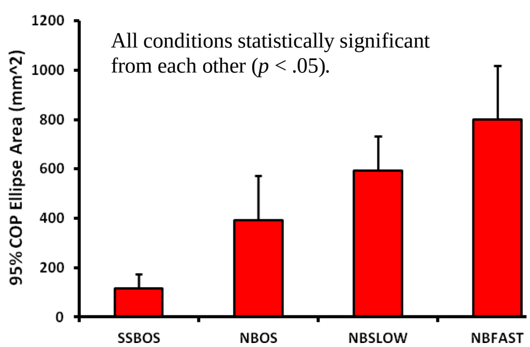

Figure 3: Center of Pressure (COP) 95% Ellipse Area.

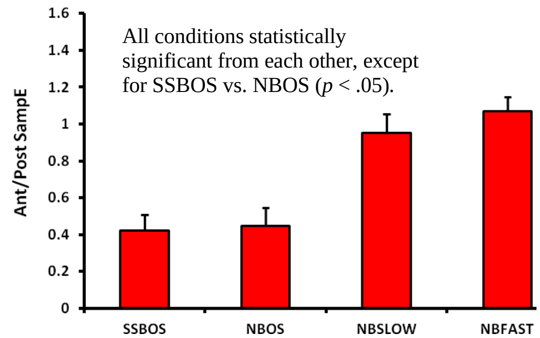

Figure 4: Sample Entropy values for the anterior-posterior direction.

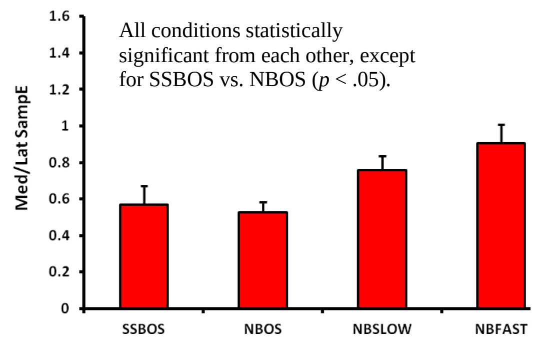

Figure 5: Sample Entropy values for the medial-lateral direction.

CONCLUSIONS

Rhythmic arm movements led to the emergence of less adaptive COP behavior, as evidenced by more variable and irregular trajectories. Interestingly, narrowing the BOS made relatively little difference in the variables of interest, possibly due to not manipulating the BOS enough. Future research should focus on postural responses to external perturbations when performing a concurrent upper limb task.

REFERENCES

1. Haddad, J.M., et al. *Experimental Brain Research*, **190**, 431-441, 2008.

2. Cavanaugh J.T., et al. *British Journal of Sports Medicine* **39**, 805-811, 2005.

3. Bodfish J.W., et al. *American Journal of Mental Retardation* **106**, 123-134, 2001.

THE TEMPORAL STRUCTURE OF POSTURAL CONTROL VARIABILITY DURING STANDING IS AFFECTED BY SUPRATHRESHOLD MECHANICAL STIMULATION

[1]Jessica Renz, [1,2]Jung Hung Chien, [1]Mukul Mukherjee, [1,2]Nick Stergiou

[1]Nebraska Biomechanics Core Facility, University of Nebraska at Omaha, Omaha, NE, USA
[2]College of Public Health, University of Nebraska Medical Center, Omaha, NE, USA
email: jchien@unomaha.edu web: http://nbcf.unomaha.edu/

INTRODUCTION

Variability is inherent in the maintenance of human posture and is reflective of the contribution of different sensory systems as postural sway. The structure of sway variability is often used to characterize subtle changes in the organization of the neuro-motor system during the maintenance of upright posture. Changes in the structure of postural sway variability under different task and sensory conditions are essential in understanding their role in the organization of human motor output. It has been shown that removing visual feedback during normal standing makes the Center of Pressure (COP) sway to become predictable [1]. Meyer et al., reported that plantar cutaneous desensitization through anesthesia revealed significant differences in postural sway variability in the short time-scale fluctuations [2]. This decrement in short time-scale fluctuation (more predictable behavior) occurred when the subjects were challenged during unipedal stance with eyes open or normal stance with eyes closed. This study suggested that the effects of cutaneous desensitization on postural sway variability were significant when sensory information from other sources were insufficient to overcome the loss of cutaneous sensation. Similarly, it was reported that the structure of postural sway variability became more predictable when cognitive loading was increased [3]. The aforementioned studies [1-3] have determined the effects of visual feedback, tactile feedback and cognitive processing on the temporal structure of postural sway variability during standing. However, the effect of the vestibular system on the structure of postural sway variability has not been explored. To address this issue, we used suprathreshold mechanical stimulation (sMVS). We hypothesized that the structure of postural sway variability would become predictable when sensory information from other sources became less reliable. Specifically, the structure of postural sway variability would become more predictable when the subject was forced to rely only on the vestibular system for postural control. This would be more evident with the vestibular system being perturbed with the sMVS.

METHODS

Eight healthy young adults (24.7±5 years) were instructed to maintain their balance while standing on the Smart Balance Master (NeuroCom, Clackamas, OR, USA). The research module of the SOT was selected to investigate how participants maintained their balance under different conditions. Each trial lasted 90 seconds. There were total six sensory challenging conditions: 1) normal, 2) vision-blocked, 3) visual sway-reference, 4) surface sway-reference, 5) vision-blocked, surface sway-reference, and 6) visual and surface sway reference condition. In general, conditions 5 and 6 were used to indirectly detect the participant's ability to use inputs from the vestibular system to maintain balance. The suprathreshold mechanical vestibular stimulation (sMVS) contained two vibrating elements, called tactors (Engineering Acoustics, FL, USA.), were placed on the mastoid process on each side to perturb the vestibular feedback signals (Figure 1). The frequency and magnitude of the stimulation were communicated wirelessly to the tactor controller unit which transmitted these signals through cables to the tactors. The frequency of sMVS was set to 349 Hz and the magnitude was set to 17.5 db. A pulsed firing pattern was used where the duration of the firing period was 0.3 second and the duration of the resting period was 0.6 second. Three types of sMVS were given to the participants: bilateral, unilateral or none/control. A total of 18 trials were randomly arranged for each participant (3 sMVS types by 6 conditions). For unilateral stimulation, one side was randomly selected for each subject at the beginning of experiment and this side was consistent for all the unilateral trials. We used Sample Entropy (SampEn) for describing the temporal structure of postural sway variability. The term SampEn has been defined as the negative natural logarithm for conditional properties that a series of data points, a certain distance apart *m*, would repeat itself at *m*+1. A time series with similar distances would result in a lower SampEn value and large differences would result in greater SampEn values with no upper limit. Thus, a perfectly repeatable time series elicits a SampEn value approaching to zero and a perfectly random time series would elicit a SampEn value converging toward infinity. A two-way mixed ANOVA measure was used to measure the effect of different sensory challenged conditions and the effect of sMVS on postural control during standing. Bonferroni correction was used for post hoc multiple comparisons.

Figure 1. A) The tactors were secured by a cap and placed on the mastoid process on each side. B) The tactor controller unit: for communicating with the computer through bluetooth and transmit stimulus control signals to the tactors. C) A subject doing the SOT test on the NeuroCom with the tactors attached to the mastoid process.

RESULTS

A significant main effect for the different sensory conditions was found ($F = 49.358$, $p < 0.0001$). A significant main effect of the sMVS type was also found ($F = 4.08$, $p = 0.032$) (Figure 2). No significant interaction between conditions and sMVS types was determined. The pairwise comparisons with Bonferroni correction indicated that the SampEn was significantly smaller in condition 5, and 6 than condition 1 to 4 in non-sMVS, unilateral sMVS and bilateral sMVS. In addition, SampEn was significantly smaller when receiving unilateral sMVS than when receiving bilateral sMVS and when receiving no sMVS (Figure 2).

DISCUSSIONS

Our study found that using sMVS caused the structure postural sway variability to be more predictable in condition 5 and 6. Our results supported the hypothesis that structure of postural sway variability became predictable if sensory information became less reliable [3]. In other words, normal standing provided high flexibility for postural control. In addition, the central nervous system might use conservative strategy to control posture (more regular movement) when receiving

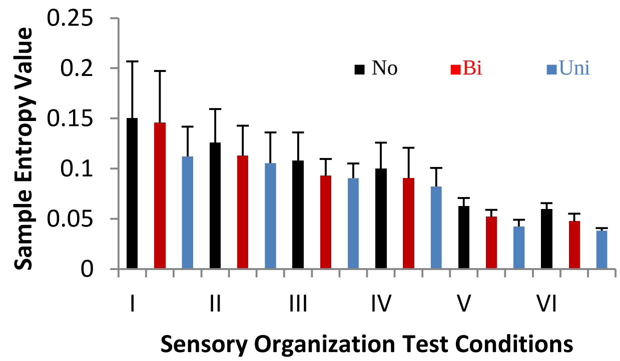

Figure 2. The Sample Entropy value for the six SOT conditions under the two sMVS conditions.

multiple sensory perturbations [4]. Our study also found that unilateral vestibular stimulation made postural sway to become more rigid than bilateral stimulation. This is probably because postural control is a bilateral coordination task requiring dynamic input from bilateral sources. If feedback is available from only one source, postural control requires more computational effort than if it is missing from bilateral sources.

REFERENCES

1. Riley MA, et al., *Gait Posture* **9**, 65-78, 1999.
2. Meyer PF, et al., *Exp Brain Research* **57**, 526-536, 2003.
3. Cavanaugh JT, et al., *J NeuroEngineering and Rehabilitation* **4**, 42, 2007.
4. Courtemanche R, et al., *Arch Phys Med Rehabil* **77,** 849-855.

ACKNOWLEDGEMENTS

This work was funded by NASA EPSCoR NNX11AM06A.

CAN WE SEE MATHEMATICAL CHAOS IN SENSORIMOTOR COORDINATION?

[1,2]Joshua Haworth, [2]Anastasia Kyvelidou, and [1,2]Nicholas Stergiou

[1]University of Nebraska Medical Center, Omaha, NE, USA
[2]University of Nebraska at Omaha, Omaha, NE, USA
email: jlhaworth@unomaha.edu, web: http://nbcf.unomaha.edu

INTRODUCTION

Work in biomechanics has revealed that the kinematics resultant from biological sources of motion can be characterized by nonlinear measures of the temporal structure of movement variability [1, 2]. The health of a biological system is related to an optimal state of this variability; characterized by the presence of mathematical chaos examined in movement over time. The suggestion that we may utilize chaos as a means to modulate our movement behaviors (possibly also to optimize our learning strategies) is quite a novel proposition. The assertion that optimum dynamics should include some factor of variance (from chaos) elegantly describes the way by which persons can interact with environments as complex as the world around us. However, it should be noted that not all environments are actually that complex. Often, either by natural order or imposed organization, we find ourselves operating under very routine circumstances. Other times, we may find our operations to be within an environment which truly has no organizational process to it, whatsoever. What is truly remarkable is our ability to organize our own behavior, which is almost ubiquitously robust against these environmental variances. In this experiment, we seek to test the human-environment coordination in the form of gaze and posture response to the motion structure of a presented visual stimulus. The stimulus is provided with rhythmic, chaotic, and random motion trajectories while gaze and postural responses are measured. We used cross recurrence quantification (cRQA) to address the coupling strength and quality between each of these systems. cRQA tests the relative likelihood of recurrence of behaviors across two time series [3]. cRQA output includes percent determinism and maxline representing probability and duration (respectively) of redundant behavior.

METHODS

Fourteen adults (4 male and 10 female, age 29.8 ± 10.5 years, height 1.638 ± 0.1 m, weight 67 ± 14.2 kg) attended a single data collection. Synchronous eye movement and standing posture recordings were taken while a moving point-light stimulus was displayed on a large monitor in front of the participant. FaceLab 4.5 (Seeing Machines, Acton, MA) eye-tracking equipment was used to track eye movements. An AMTI force platform (Advanced Mechanical Technology Inc., OR6-7, with MSA-6 amplifier) was used to record center of pressure (COP) data. Trials were managed through custom LabView software (National Instruments, Austin, TX), including software synchronization of the data from the eye-tracker and the force platform, as well as display of the visual stimulus. Data was collected at 50 Hz, the highest common frequency available amongst the equipment. The stimulus (see Fig. 1) was presented on a 55” 1920 x 1200 pixel LCD monitor, moving according to a predefined motion trajectory (sine, chaos, brown noise) updating position at 50 Hz. Trials lasted 5 minutes to ensure capture of adequate lengths of 15,000 data points. cRQA was used to test coupling between gaze and stimulus (Gaze), COP and stimulus (COP), and gaze and COP (SensMot, sensory-motor coordination).

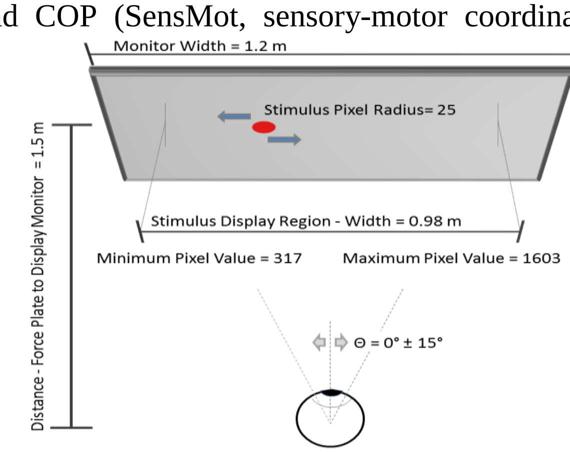

Figure 1: Diagram of experimental setup.

RESULTS AND DISCUSSION

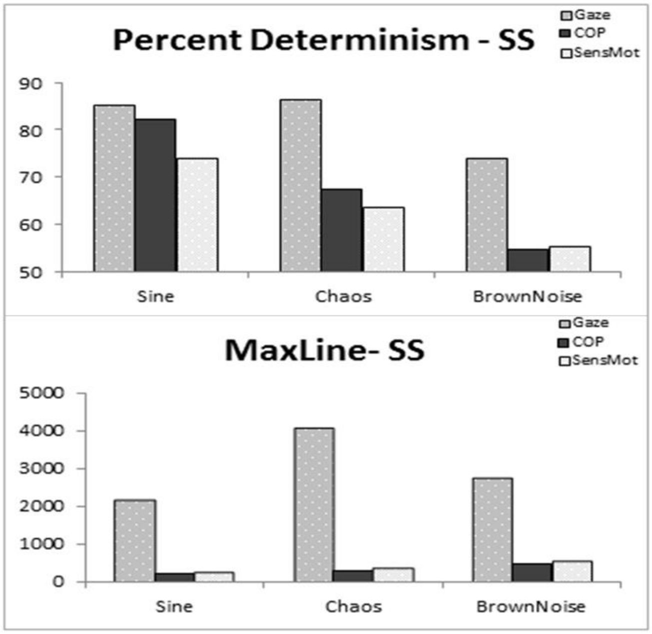

Figure 2: Results of cRQA, show coupling for Gaze and COP to stimulus motion separately, and related to one another (SensMot); across 3 stimulus types.

Percent Determinism shows that gaze has similar propensity to track Sine and Chaos. Gaze in response to Brown Noise has a significantly lower percent determinism, suggesting a lesser preference for coupling with this motion structure. However, an above 70% determinism shows we can coordinate with the random signal, yet in contrast with the other motion structures we tend to not couple as strongly. Our challenge here is to answer the question whether this reduced tendency is representative of a system limitation, or the demonstration of preference.

Maxline represents the longest duration (in data points) within which the two signals are sequentially recurrent. With regard to gaze behavior, we contend that this measure stands as a proxy for the attention span, or ability combined with interest, to maintain stimulus following. Our results indicate that the tendency for coupling is highest in the chaos condition, and similar for the sine and brown noise conditions. Interestingly, with regard to COP and SensMot (coordination between Gaze and COP), maxline increases across each of the three conditions, suggesting tighter couplings of posture (and separately between gaze and posture) in response to the least rhythmic (brown noise) stimulus motion.

These results suggest that our gaze behavior is proficient in response to a variety of motion structures, and is robust to motion variation of chaotic order. These results shed new light on the nature of how we attend to the motion of objects in our environments, and could go further than current theories in explaining the natural human interest in observing the movements of other persons [3]. This finding may also extend to help understand improvements in the way that we demonstrate skills in training or rehabilitation settings.

CONCLUSIONS

We have identified not only that persons are sensitive to the dynamics of a chaotic oscillator, but in some ways have a particular preference to certain aspects of their dynamics; i.e. chaos. Further work will focus on how this approach might allow us greater understanding of behavioral coordination in a dynamic world, rich with complex dynamics.

REFERENCES

1. Stergiou, N. *Innovative Analysis of Human Movement*, Human Kinetics, 2004.
2. Stergiou, N, et al. *J Neuro Phys Ther*, **30**, 120-129, 2006.
3. Shockley, K., et al. *Hum Perc Perf*, **29**, 326-332, 2003

ACKNOWLEDGEMENTS

This work was supported by an American Society for Biomechanics Grant-in-Aid, a NASA Nebraska Space Grant Fellowship,, the Nebraska Research Initiativeand a Dennis Weatherstone Pre-doctoral Fellowship from Autism Speaks (grant # 7070).

THE EFFECTS OF TONING SHOES ON THE POSTURAL STABILITY OF WOMEN

Kevin Farley, Audrey Niverson and Renee Rogge

Rose-Hulman Institute of Technology, Terre Haute, IN, USA
email: rogge@rose-hulman.edu, web: http://www.rose-hulman.edu/jrsi

INTRODUCTION

Postural stability is the ability to maintain an upright posture and to keep the center of pressure (COP) within the limits of the body's base of support. It is maintained through the dynamic integration of muscle activity and joint position. The foot, and therefore footwear, also plays a critical role in postural stability. The plantar surface of the foot contains cutaneous mechanoreceptors that detect tactile stimuli and relay this information to the central nervous system. Stimulation of cutaneous mechanoreceptors is believed to improve postural stability and proprioception (an awareness of where one's limbs are oriented in space). While traditional walking footwear is designed to provide stability and support to the foot, one of the hottest trends in the footwear industry has been "toning" shoes which have an intentionally unstable sole design. This unstable sole design forces the wearer's body to constantly work to find equilibrium or balance points. The manufacturers claim that this instability helps the wearer burn more calories, tone muscles, improve posture, and improve overall health. The goal of this study is to determine the effects of toning shoes on the postural stability of women.

METHODS

The study protocol was approved by the Institutional Review Board (#RHS-0160). Using a MatScan® Pressure System (TekScan, Boston, MA), dynamic balance data was collected for 55 women (18 – 65 yo, average = 34 ± 14 yo) wearing three types of footwear: toning shoes, tennis shoes and no shoes (barefoot). The order of footwear testing was randomized and the center of gravity was recorded for 30 seconds for repeated trials (with eyes open and eyes closed). In addition to medial-lateral (M-L) and anterior-posterior (A-P) displacement during quiet standing, the velocities of the sway was analyzed in the M-L and A-P directions. All statistical analyses were completed using student's t-tests and the two sample t-tests with a 95% significance level.

RESULTS AND DISCUSSION

The subjects demonstrated more balance and stability in the barefoot condition (i.e. A-P and M-L displacements were the smallest); therefore, the barefoot condition was the baseline of comparison for analyzing the other two footwear types. Subjects experienced a statistically significant increase ($p<0.05$) in A-P and M-L displacement when wearing toning shoes as compared to the barefoot data for eyes open and closed (Figure 1). The A-P and M-L displacement experienced while wearing tennis shoes fell between the toning shoe and barefoot data and no statistically significant differences were found.

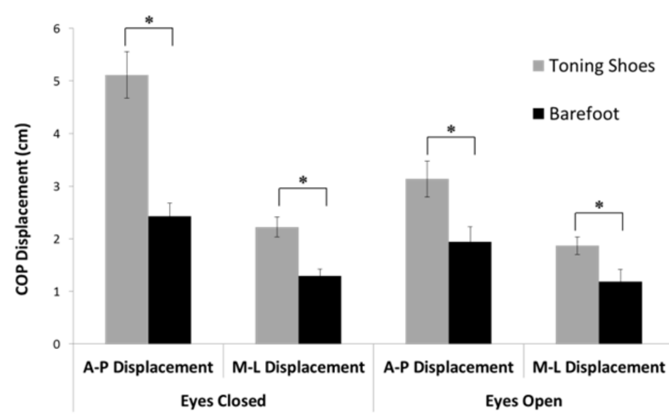

Figure 1: A-P and M-L displacements for eyes open and closed during quiet standing for barefoot and toning shoes. * indicates $p<0.05$.

There was a statistically significant increase ($p<0.05$) in the A-P velocity of the sway of the subjects for both eyes open and eyes closed (Figure 2). Note that there was a slight increase in M-L velocities, but the finding was not statistically significant.

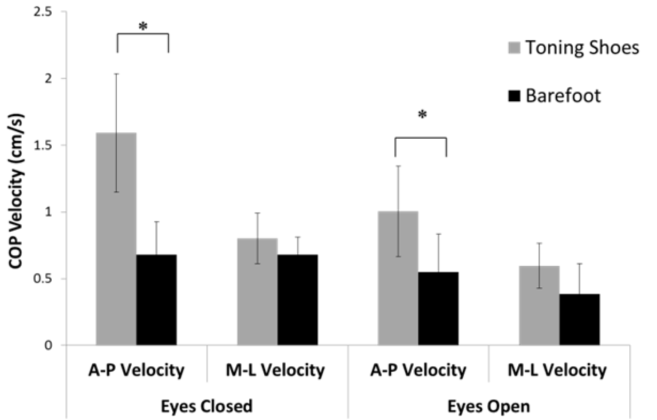

Figure 2: A-P and M-L sway velocities for eyes open and closed during quiet standing for barefoot and toning shoes. * indicates p<0.05.

Age also played a role in subject stability. Women over the age of 40 experienced increased A-P displacements and velocities when compared to women under the age of 40 (Figures 3 & 4).

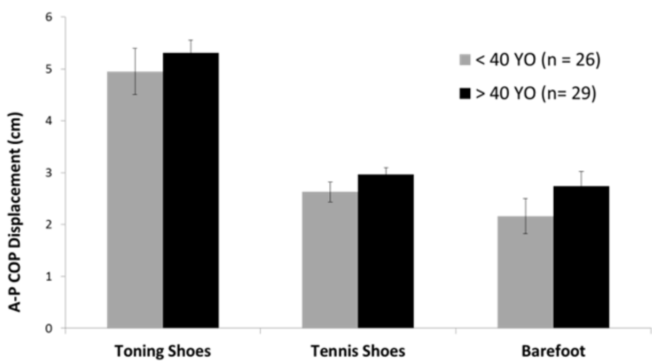

Figure 3: A-P COP for women younger and older than 40 for each type of footwear during quiet standing with eyes open.

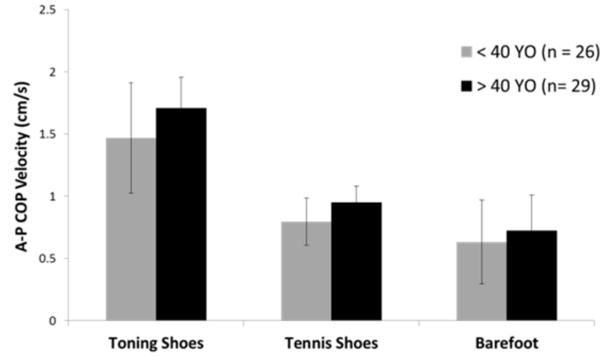

Figure 4: A-P COP velocity for women younger and older than 40 for each type of footwear during quiet standing with eyes open.

CONCLUSIONS

In this study stability was defined by measurements of the A-P and M-L displacements, as well as the velocity of the sway in each of these directions. This study provides evidence that toning shoes affect the balance of the women who wear them, regardless of age. However, researchers also observed that toning shoes might have a greater influence on the balance and stability of older women. The manufacturers of the toning shoes equate the decreased stability of customers as an opportunity for the customers to improve muscle tone as they work towards improving their balance. However, the increased instability of older women may be problematic as extreme instability may lead to falls and injuries in an older population. While the implications of the effects of footwear on static balance in this study are limited, an increased understanding of how different factors alter a subject's balance can be useful in further studies of footwear.

ACKNOWLEDGEMENTS

The authors gratefully acknowledge the support of the Rose-Hulman Independent Project/Research Opportunities Program and the Weaver Undergraduate Research Award for supporting this project.

VARIABILITY OF POSTURAL SWAY IN CHILDREN WITH AUTISM SPECTRUM DISORDERS

[1]Anastasia Kyvelidou, [2]Joshua Haworth, and [1]Nicholas Stergiou

[1]University of Nebraska at Omaha, Omaha, NE, USA
[2]University of Nebraska Medical Center, Omaha, NE, USA
email: akyvelidou@unomaha.edu, web: http://nbcf.unomaha.edu

INTRODUCTION

Children with Autism Spectrum Disorders (ASD) seem to exhibit more rigid and less adaptive behavior, including posture, under most conditions (Kohen-Raz, Volkmar, Cohen, 1992). It is plausible that children with ASD fixate on repetitive aspects of motion (i.e. watching wheels spin) and engage in repetitive motor responses (rocking). This perceptual and motor rigidity interferes with their attention to, and perception of the complex variability found in the motion of others and thus their ability to discriminate biological from non-biological motion. Gepner and Feron (2009) suggested that the phenotypic expressions of autism spectrum disorder are directly related to a neurophysiologic base stemming from temporo-spatial processing disorder (TSPD). Under this theoretical approach, it is entirely reasonable that posture (a continuous gross motor behavior which relies heavily on the online incorporation of sensory information) would suffer in persons with ASD. This has been shown to be the case by Molloy, Dietrich, and Bhattacharya (2003), who report drastic effects on posture under conditions of modified sensory input. Minshew, Goldstein, and Siegel (1997) have also shown that children with autism are less able to adapt to manipulations of somatosensory information, and continue throughout life to express developmentally delayed postural control.

The purpose of the current project was to assess the posture of young children, with and without ASD; particularly focusing on the associated variability.

METHODS

Center of pressure (COP) was recorded via force plate (AMTI, OR6) from a group of 10 children, age 4 to 6 years old. Four of these children have been diagnosed with ASD, while six have not. The children were provided a static point target on a television monitor, 1.5 m from where they stood (Figure. 1). The height of the monitor was adjusted so the target was positioned at the eye level of each child. Eye tracking equipment (Seeing Machines, faceLAB) was used to verify the maintenance of attention during collection. Trials lasted for three and a half minutes; with COP data was recorded at 50Hz. Post processing included identification of segments during which the child was speaking or making overt motions with their head or arms (none of the children moved their feet during the trial). The longest common segment across all children was 750 data points, or 15 sec of continuous COP.

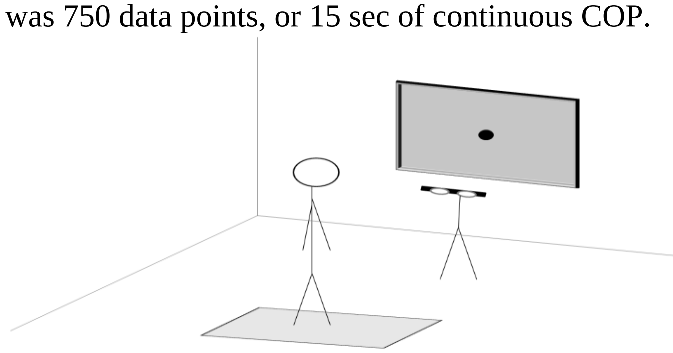

Figure 1: Diagram of the experimental setup.

These segments were further processed to generate the root mean square (RMS) and Lyapunov Exponent (LyE) measures of variability in both the anterior posterior (AP) and medial-lateral (ML) direction. Custom Matlab scripts (Mathworks Inc.) were used for post-processing. Data was filtered using a double pass Butterworth filter with a 20 Hz cutoff. RMS is the square root of the average of the squares of a time series and was used to describe the amount of variation within the data. LyE examines the rate of divergence of repeating trajectories and was used to describe the temporal aspect of variation. For statistical analysis, independent t-tests were performed to identify differences between typically developing children and children with ASD.

RESULTS AND DISCUSSION

RMS in the AP and the ML direction did not present any significant differences between children with typical development and children with ASD (Figure 2). However, the differences in the RMS in the ML direction were approaching significance (p=0.07), with children with ASD presenting lower RMS values than typically developing children.

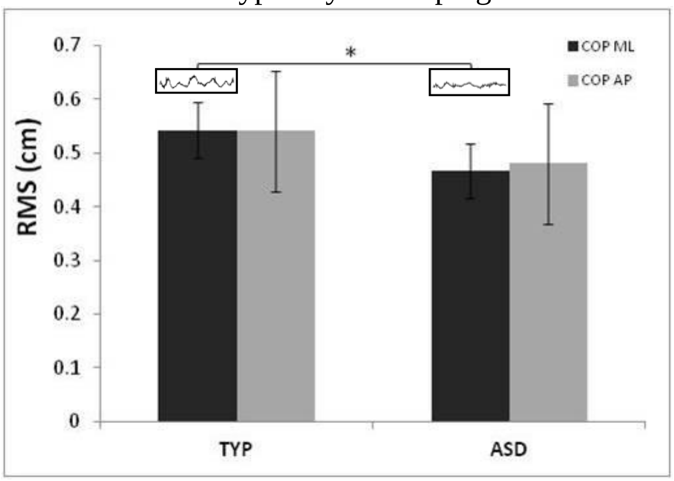

Figure 2: Root mean square (RMS) in the medial-lateral (ML) and anterior-posterior (AP) direction in typically developing children (TYP) and children with ASD. * indicates near significance, p = 0.07.

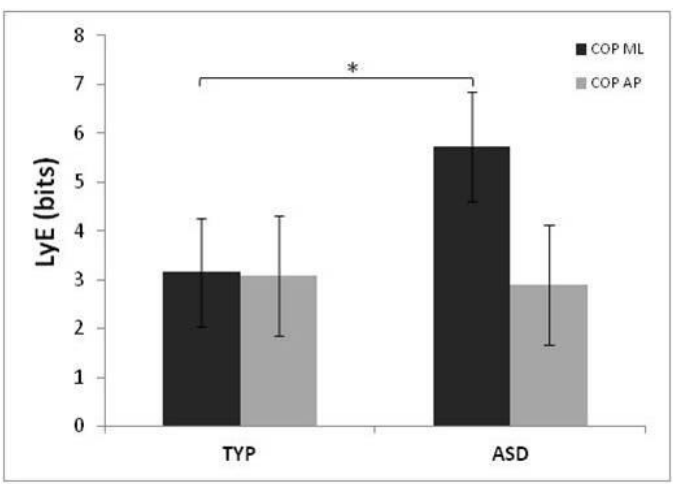

Figure 3: Lyapunov Exponent (LyE) in the medial-lateral (ML) and anterior-posterior (AP) direction in typically developing children (TYP) and children with ASD. * indicates significance, p = 0.01.

LyE in the AP direction did not present any significant differences between children with typical development and children with ASD (Figure 3). However, children with ASD presented statistically significant higher LyE values in the ML direction than typically developing children.

Overall, children with ASD appear to have reduced amount of COP variability, and redundant use of postural strategies in the ML direction. This is indicative of less cooperative behavior between the components of the underlying control system.

CONCLUSIONS

The present data suggest that the postural sway variability of children with ASD differs from typically developing children. These differences are noticeable in both the amount and temporal variations of COP sway during standing. It has been suggested that there is a developmental direct linkage between motor and social communication deficits in ASD highlighting the multi-interactive nature of the perception-action-cognition cycle, and thus the importance of motor deficits in children with ASD. These results have further implications for assessing motor development behavior in children with ASD and the development of future therapeutic protocols.

REFERENCES

1. Kohen-Raz R, et al. *J Autism Dev Disord.* **22**(3), 419-32, 1992.
2. Gepner B, et al. N*eurosc Biobehav R* **33**(8), 1227-42, 2009.
3. Molloy CA, et al. *J Autism Dev Disord* **33**(6), 643-52, 2003.
4. Minshew NJ, et al. *J Int Neuropsychol Soc*, **3**(4), 303-16, 1997.
5. Bhat AN, et al. *Physical Therapy*, **91**(7), 1116-29, 2011.

ACKNOWLEDGEMENTS

This work was supported by Autism Speaks and the Nebraska Research Initiative. We would also like to thank all the children and their families for participating in this study.

Effect of foot wedge positions on lower limb muscle activity during standing

Hamzeh Samimi[1*], Mehrdad Anbarian[2]

[1]Department of Physical Education, Bu-Ali Sina University, Hamedan, 12345, Iran
[2]Bu-Ali Sina University, Hamedan, Iran
*Hemin.samimi@yahoo.com

Abstract

Foot orthotics has been researched for their effect on postural stability in older persons. It is assumed that orthotic wedging could prevent abnormal compensatory motions in the proximal joints by aligning the subtalar joint and ankle and by improving the proprioception information of the foot. But, the effect of wedge positions on lower limb muscles activity in elderly are not well documented. Therefore, this study was aimed to determine the effects of two wedge positions on lower limb muscle activity during quiet bipedal standing balance with eyes open. Two wooden wedges with an inclination of 4.6 degrees were placed under lateral and medial sides of the 15 able-bodied elderly (age: 63 ± 7.8 years) feet. The surface electromyographic activity of selected lower limb muscles, namely biceps femoris (BF), semitendinous hamstring (SEM), vastus medialis (VM), vastus lateralis (VL). tibialis anterior (TA), peroneus langus (PL), medial gastrocnemius (MG) and soleus (SOL) were collected over 30 s period of time. Data were analyzed using paired t-test. Results indicated that muscle activity were greater in the barefoot condition rather than wedge positions. but this differences were not statistically significant. It may relate to postural strategy and responses employed by subjects against external sudden perturbation caused by wooden wedges. However, further researchs is needed to assess the effects of longer and discontinuous stimulations with foot wedge positions on postural control.

Keywords: Foot orthotics; Postural stability; Subtalar joint; Muscles activity

Involvement of central nervous system in functional ankle instability

[1,2]Wen Liu, [1]Tarang Jain, and [2]Clayton Wauneka

[1] Department of Physical Therapy and Rehabilitation Science, University of Kansas Medical Center, Kansas City, KS, USA

[2] Bioengineering Program, University of Kansas, Lawrence, KS, USA

Email: wliu@kumc.edu, web: http://www.ptrs.kumc.edu/research/neuromuscular-research-lab/index.html

INTRODUCTION

Patients after severe ankle sprains often develop chronic symptoms despite treatment. Functional ankle instability (FAI) is the term used to describe a condition with recurrent ankle sprains and/or ongoing episodes of ankle giving way. Past studies have suggested various etiological factors of FAI including joint laxity, proprioceptive deficiency, muscle weakness, and altered response time. However, findings on those FAI factors have been inconsistent [1-3]. Furthermore, none of those factors can explain how an ankle giving way occurs. An individual's reaction to an ankle giving way is usually dramatic as if there is tissue damage, when in fact no tissue damage occurs. We recently proposed a new FAI factor based on a well-known flexion reflex called "unloading reaction". An unloading reaction is characterized by a quick weight shift to the un-stimulated foot and body downward movement in flexion motions of the ankle, knee, and hip joints that generate upward inertial forces against vertical loads on the feet. It is possible that patients after severe ankle sprains may alter their triggering thresholds leading to a drastic reaction under a relatively mild ankle stretch. Such hyper-reactivity to an unloading reaction may cause ankle giving way episodes. In our previous studies, we have demonstrated that a static stretched ankle position led to significantly greater unloading reaction in health ankles, and ankles with FAI showed greater unloading reaction compared to the healthy ankles [4, 5]. However, the amount of unloading reaction observed in our previous studies was far less than a drastic reaction that usually occurs during ankle giving way. Here we report our pilot findings of dramatic unloading reactions in some FAI ankles tested under a dynamic stretch and nociceptive stimuli.

MATERIALS AND METHOD

We conducted our experiments on five subjects with FAI (1 male, 4 females; age: 41±3.16 years, height: 170.18±9.84 cm; weight: 84.09±17.62 kg). Participants were at least four weeks but not beyond one year after an unilateral ankle sprain (≥grade II), with ongoing ankle giving way incidence during functional activities, and active in exercise. The individuals were excluded if they had severe ankle pain and swelling, ankle surgery, gross limitation in ankle inversion (<15º), lower extremity injuries other than ankle sprain in past 12 weeks, current enrollment in formal rehabilitation program, any severe joint disease, or any previous experience of intolerance to electrical stimulation.

Two force plates were used to record ground reaction forces and two OPTOTRAK motion analysis units were used to record 3D motions at the ankle, knee, and hip joints of both limbs. Two surface electrodes (3x3 cm) were placed at the lateral aspect of the tested ankle, below and anterior to the lateral malleolus, to deliver nociceptive stimulation. A newly developed trapdoor had a tilt platform held at a level position by a remote-controlled deadbolt which, when released, allowed the platform to rotate 30° before hitting a mechanical stop (Figure 1). A potentiometer was used to record the rotation angle. During testing subjects stood with one foot on a level wooden box and the tested foot on the tilt platform centered over the pivot joint. The tested foot was secured to the tilt platform with rubber straps in order to avoid lifting of the foot during the experiment.

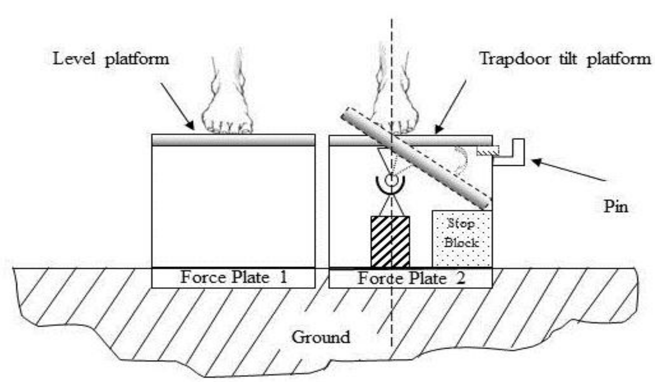

Figure 1: Illustration of the experimental setup.

Each subject was tested for unloading reaction on both ankles at two testing days separated by at least 3 days apart to minimize the potential habituation to nociceptive stimuli. During unloading reaction test, the subject wore a safety harness that was supported at the ceiling overhead. The safety harness was tightened up as subject approached 40º of knee flexion to allow certain amount of downward body motion during the test. The subject stood still with the tested foot on the trapdoor tilt platform and equal weight on both feet. The trapdoor was released without a warning. The subject went through the first five trials of the trapdoor drop test without nociceptive stimulation ("no stim"), followed by five trials of the combined trapdoor drop and nociceptive stimulation ("with stim"). The nociceptive stimuli were delivered to the tested ankle at a level of 20% above the tolerable pain threshold when the trapdoor rotated for about 20-25 degrees. Two key variables were examined: the vertical force variation (VFV) defined as the magnitude of decrease in the combined vertical ground reaction forces, and thee knee flexion variation (KFV) defined as the magnitude of averaged knee flexion angles of both knee joints. Pair-t test was used in statistical analysis.

RESULTS

Based on video tapes recorded during unloading reaction tests, three subjects were identified to have a drastic reaction when tested on their affected ankles using the combined dynamic stretch and nociceptive stimuli. They totally gave up their control of upright standing and left their bodies hanging onto the safety harness. The drastic reactions occurred only on the affected ankle with pain stimulation. The rest of two subjects did not show such reaction in any trial.

On average over five subjects, VFV of 329.2±347.4 N in the "with stim" trials of the affected ankle was the greatest compared to 74.6±34.3 N ("no stim" trials of the affected ankle), 68.5±35.4 N ("with stim" trials of the unaffected ankle), and 60.4±36.9 N ("no stim" trials of the unaffected ankle). The corresponding four mean values of KFV were 26.5±16.0º, 19.8±4.5º, 15.6±1.4º, and 13.5±1.4º, respectively. There were no statistically significant differences among all mean values.

DISCUSSION

In three out of five subjects, we observed a drastic reaction in that they totally gave up their control of upright standing when a combination of dynamic ankle stretching and nociceptive stimuli was applied on their affected ankles. This is the first time that an ankle giving way episode was duplicated in a laboratory without harming the subjects. There were several reasons that might be responsible for no significant differences among mean values of the measured VFV and KFV. The first is the small sample size. The second reason is due to limitations provided by the safety harness. The values of VFV and KFV in those drastic reaction trials would have been even greater if without safety harness. Finally, it is possible that the intensity of ankle stretching or nociceptive stimuli did not reach individual threshold for triggering a drastic reaction in those who did not show such reaction. An alternative explanation could be that some individuals with FAI might have no hyper-reactivity to unloading reaction. Nevertheless, the drastic reactions shown in three subjects along with large values of mean VFV and KFV in "with stim" trails indicated a unique reaction pattern in some FAI ankles.

Our new theory of mechanism of FAI may open doors for more research. Balance training is often used in treatment of FAI, however its clinical outcomes have not been shown to be associated with changes in examined potential underlying factors. Future studies may examine whether balance training can desensitize the hyper-reactive motor, thereby reducing the ankle "giving way" episodes.

REFERENCES

1. W. Liu, et al. *Clin Biomech (Bristol, Avon),* vol. 16, pp. 237-44, Mar 2001.
2. K. M. Refshauge, et al. *J Orthop Sports Phys Ther,* vol. 33, pp. 166-73; discussion 173-6, Apr 2003.
3. H. Tropp, *Int J Sports Med*, vol. 7, pp. 291-4, Oct 1986.
4. M. J. Santos and W. Liu, *Gait Posture,* vol. 26, pp. 106-12, Jun 2007.
5. M. J. Santos, et al. *Gait Posture,* vol. 27, pp. 589-94, May 2008.

DEVELOPMENT OF QUANTIFICATION OF SPATIAL STRAIN DISTRIBUTION FOR SCOLIOTIC SHAPE USING A THIN - PLATE SPLINE METHOD

Yoshimori Kiriyama, Kota Watanabe, Morio Matsumoto
Yoshiaki Toyama and Takeo Nagura

Keio University, Tokyo, JAPAN
kiriyama@mmm-keio.net

INTRODUCTION

Adolescent idiopathic scoliosis has not only malign configuration of vertebrae but also deformed vertebrae and rib cages. Thus the trunk including scoliotic deformity has a distribution of complicated spatial deformation three-dimensionally. This causes a difficulty to evaluate the symmetry of the spinal deformity quantitatively. The evaluation is, however, one of the most important in order to understand basic pathology of spinal disorder, and decide adequate plan of surgical treatment with spinal instruments. The objective of this study is to develop quantification method of spatial strain distribution of a scoliotic shape in order to evaluate the symmetry of the spinal deformity.

METHODS

Our method is divided into two procedures; symmetrization of a scoliotic spine, and evaluation of spatial strain distribution as shown in Fig.1.
In the symmetrization process, scoliotic spine was symmetrized using a thin plate spine method (TPS) [1]. TPS is the smooth and continuous method to deform shape corresponding the landmarks on a shape to target landmarks.

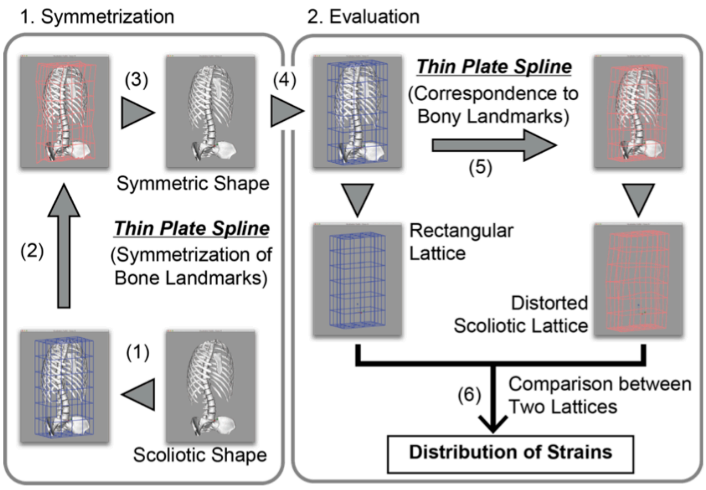

Figure 1: Outline of quantification of spatial strain distribution using a thin – plate spine

In this study, the spinal shape was wrapped with rectangular lattices of 4 by 4 by 6 (Fig.1 (1)). Depending on the node displacements, the scoliotic shape was deformed to symmetrize the scoliotic shape using TPS (Fig.1 (2) and (3)).
To symmetrize the scoliotic shape, multiple landmark points were extracted from the spinal shape. In this study, the points $\mathbf{P}_c$ that should be existed in a sagittal plane (104 points) and the pair of points $\mathbf{P}_r$ and $\mathbf{P}_l$ that should be existed in symmetric positions (466 points) were used. Here, x-axis is forward, y-axis is leftward and z-axis is superior directions. Using these points, adequate displacements of lattice nodes to minimize the following function.

$$\Omega = c_0 \sum P_{c,y}^2 + c_1 \sum P_{m,y}^2 + c_2 \sum \left(P_{s,x}^2 + P_{s,z}^2\right) + c_3 \int \left(\frac{1}{2}\mathbf{E} : \mathbf{E}\right) dV$$
$$\mathbf{P}_s = (\mathbf{I} - \mathbf{n}_y \otimes \mathbf{n}_y) \cdot (\mathbf{P}_l - \mathbf{P}_r) \quad , \qquad (1)$$

where $\mathbf{P}_m$ is a median point between $\mathbf{P}_r$ and $\mathbf{P}_l$, $\mathbf{n}_y$ is unit vector of y axis, $\mathbf{E}$ is a Green- Lagrange strain tensor, c_0, c_1 and c_3 were weight coefficients, and x, y, z mean each component. The first term evaluates the difference between $\mathbf{P}_c$ and a sagittal plane, the second and third terms evaluate symmetry of $\mathbf{P}_r$ and $\mathbf{P}_l$, and the forth term means internal strain energy of the lattice to restrict excessive deformation.
Obtained symmetric spinal shape was wrapped with new rectangular lattices again (Fig.1 (4)). The symmetric shape was restored to the original scoliotic shape. In the restoration, the new rectangular lattices were deformed using TPS corresponding landmark points on the symmetric shape to the scoliotic shape (Fig.1 (5)). As a result,

distorted lattices wrapping the original scoliotic shape was obtained.
Based on the new rectangular lattices, strain distribution of the distorted lattices was evaluated. Lattice by lattice, Green-Lagrange strain tensors were calculated (Fig.1 (6)).
In this study, CT image data of whole scoliotic spine that was obtained from a female adolescent idiopathic scoliosis was used. To reduce exposure of radiation, the images for preoperative evaluation were used. This study was approved by an institutional review board.

RESULTS

In the symmetric process, Cobb's angle was decreased from 35 degrees in the original shape

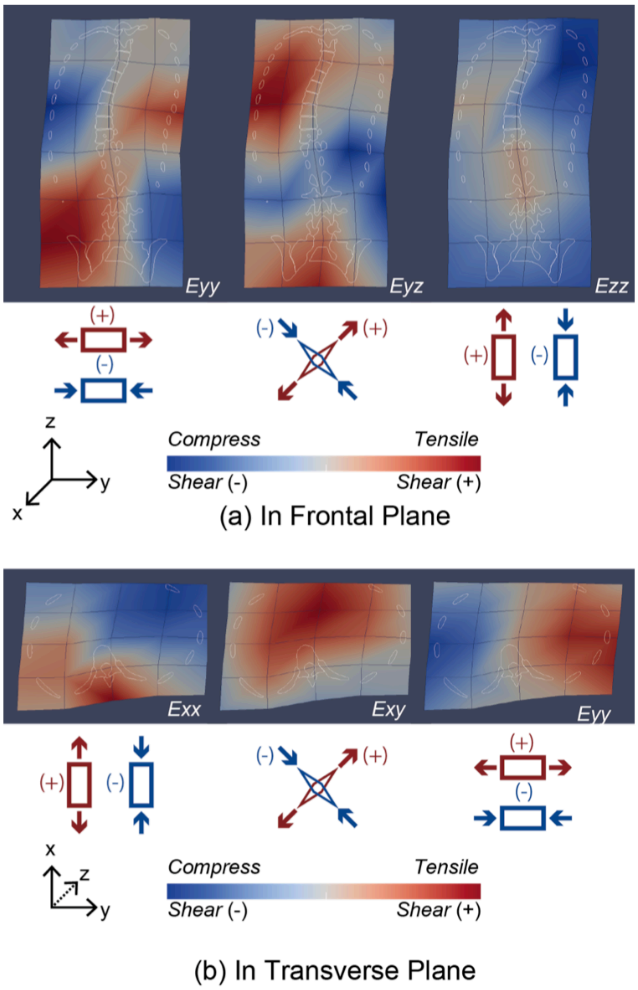

Figure 2: Stress distribution in frontal and transverse plane including the apical vertebra. (White line is a silhouette of the spine, the rib cages and the pelvis.)

decreased to 7 degrees in the symmetrized spinal shape. Based on a sagittal plane, $\mathbf{P}_c$ of Th7 had 7.7 mm maximally. Also, $\mathbf{P}_r$ and $\mathbf{P}_l$ of Th7 had the largest error in eq. 1, and the difference between $\mathbf{P}_r$ and the mirror position of $\mathbf{P}_l$ against x-z plane was 12.7 mm.
Fig. 2 shows the strain distribution in the frontal and transverse planes including the apical vertebra of the scoliotic spine respectively.

DISCUSSION

In this study, although the Th7 vertebra that showed the greatest inclination, had the largest calculational error, our method symmetrized the scoliotic shape mostly. Therefore, the calculated shape was used as a symmetric shape. As shown in Fig. 2, our method was possible to show that the various kinds of spatial strain consisting in compress, tensile and shear strains were distributed complicatedly in the scoliotic space. This qualification should be rationale of surgical treatment strategy with spinal instruments additional to Lenke's classification [2].
Our method is also possible to restore a sagittal plane that was distorted accompanying scoliotic deformity. This sagittal plane should be reference to evaluate the asymmetrical deformity.
One possible limitation was that we used only one kind of lattices. Additional limitation was that this method needed a lot of landmarks. To generalize our method, appropriate lattice partitions and the number of landmarks shape should be investigated with considering the curve patterns or severeness.
Thus, the quantification method was useful to elucidate the spatial strain distribution of spinal disorder.

REFERENCES

1. Bookstein FL, *Morphometric tools for landmark data Geometry and biology*, Cambridge University Press, 1991.
2. Lenke LG, et al. *J Bone Joint Surg Am* 83-A, 1169-1181, 2001.

ACKNOWLEDGEMENTS

A part of this study was supported by JSPS KAKENHI Grant Number 24659684.

MULTI BODY ANALYSIS OF EFFECT OF INJURED LATERAL LIGAMENT

[1]Takuya Kakigahara, [1]Mitsumasa Matsuda and [1]Kazuhiko Adachi

[1]Kobe University, Kobe, Hyogo, JAPAN
email: 101t317t@stu.kobe-u.ac.jp

INTRODUCTION

Foot and ankle joints are compound joints that are composed of 28 bones and a number of soft tissues, and support body weight. Therefore, injury of foot and ankle joints happens frequently, especially, lateral ligament sprain is most popular injury. There are some treatment methods for sprain, for example, setting ankle in plaster is used to immobilize the sprained joints and avoid resprain and extension of ligaments. Above all, taping is easy to use procedure for fixing joints and supporting ligaments. However, there is no conventional research that three dimensional model is used to simulate effect of injured ligaments and tape support.

The purpose of this study was to simulate the effect of injured lateral ligament, in which three ankle joints models that was normal, removed ATFL and removed ATFL + CFL with and without tape.

METHODS

Simulation model was composed of rigid bodies as bones and spring parts as rigid bodies and ligaments and cartilages in this study. The model was built using surface models of the 26 foot bones and the distal parts of the tibia and fibula, all obtained from CT scans (slice thickness is 1 millimeter) of the foot and ankle joints of a normal subject. Elastic contact conditions between the rigid bodies considered the influence of the cartilage reactions, and ligamentous structures were constructed using linear, tension-only spring elements. Elastic coefficient of the ligaments was set to 265 MPa [1] and elastic coefficient of the cartilage was set to 22.6 MPa [2]. The model is shown as Fig. 1.

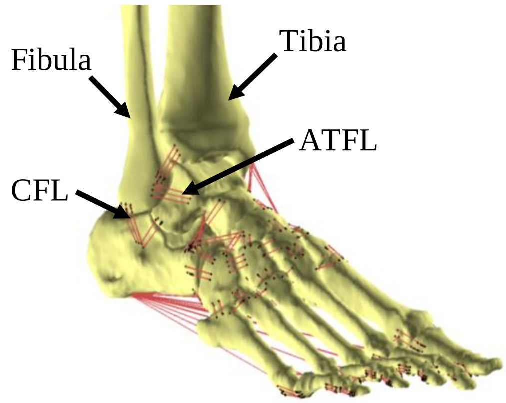

Figure 1: 3D multi body model of foot and ankle joints. Red lines indicate the ligament models that were consisted of a line or several lines.

Tape model was built on considerate position for thickness of subcutaneous tissue as flat surface model. Tape model was extensionless for holding on ankle joint and 38 millimeters wide. General taping procedure that was combined four types of taping, start up, horseshoe, heel lock and figure eight, was used for simulation.

Analysis condition was prepared with reference to [3] that reports dorsiflexion and internal rotation angles using 8 fresh frozen legs. Calcaneal bone and first and fifth metatarsal bones were defined as static, and axis of the tibia was set to perpendicular direction to the ground plane. The 3 kind of foot and ankle joints models that was normal, removed ATFL and removed ATFL + CFL with or without the tape model were used to simulated when internal rotation moment that was set to 1.96×10^3 Nmm was brought on axis of the tibia. In addition, inverted posture was modeled for the two different inversion angles: 5 and 10 degrees.

RESULTS AND DISCUSSION

Table 1 shows the internal rotation angles. Reference [3] shows that all in Normal, ATFL injury and ATFL + CFL injury model, the internal rotation angles without tape (5.7±2.0, 10.1±3.7, 13.6±5.2 degrees) and with tape (4.5±0.8, 7.0±1.6, 7.7 ± 2.4 degrees) in non-inverted posture. Analysis results are good agreement with the reported results, therefore these simulation models and results were considered appropriate. In removed ligaments condition, internal angles with tape were smaller than that without tape. This result suggests that the tape is also effective to put a brake on internal rotation in inverted posture.

In the non-inverted posture without tape, internal angle of removed ATFL + CFL model was larger than that of removed ATFL model. However, in the taping condition, there is no difference between that of removed ATFL + CFL model and that of removed ATFL model. This results show, ATFL is extended first followed by CFL when internal angle is increased. This is similar to development of lateral ligament sprain that usually ATFL is injured first followed by CFL. For this reason, we suggest that internal rotation is a cause of lateral ligament sprain.

Lateral ligament sprain often occur when inverted foot, however ATFL was not extended when tibia and fibula were shifted to inverted potion. This suggests that there is no direct damage to ATFL under inverted posture, on the other hand, inversion causes the excessive internal rotation that injures lateral ligament. In the normal condition without tape, comparison of internal rotation angle and tension of lateral ligament showed that the ATFL tension and internal angle of inverted posture were larger than that of non-inverted (Table 2). This result suggests that inverted posture increases the internal rotation angle and applied force to ATFL. On the other hand, ATFL tension of 10 degrees inverted is much the same that of 5 degrees, moreover, applied force to CFL occurred in 10 degrees inverted posture. These results consider that main braking ligament of internal rotation switches from ATFL to CFL when inversion angle is larger. Therefore, we suggest that low inversion angle causes the ATFL injury and the high angle causes the ATFL and CFL injury.

CONCLUSIONS

A novel computational model of the foot and ankle joints was developed to simulate the effect of taping and removed ATFL and/or CFL when the foot was internal rotated. The result shows that the taping is effective to put a brake on internal rotation in inverted posture, and inverted posture better rotated than non-inverted.

REFERENCES

1. Siegler S, et al. *Foot Ankle* **8**(8), 234-242, 1998.
2. Ide T, et al. *J Japanese Orthop* **12**, 125-131, 1990.
3. Hiroki O, et al. *Japanese Society of Clinical Sports Medicine* **18**(2), 290-296, 2010.

Table 1: Comparison of removed ligaments with or without tape for internal rotation angles

	Internal rotation angle (deg)					
Inverted angle (deg)	**0**		**5**		**10**	
Tape	**w/o***	**w***	**w/o**	**w**	**w/o**	**w**
Normal	4.93	4.87	6.56	6.31	7.05	6.54
Removed ATFL	9.46	6.38	7.61	6.92	7.38	6.82
Removed ATFL + CFL	12.1	6.38	14.6	6.70	15.6	6.70

* w/o: without tape, w: with tape.

Table 2: Internal rotation angles and tension of lateral ligament without tape

Target for comparison	Internal rotation angle (deg)	Tension of lateral ligament (N)		
		ATFL	**PTFL**	**CFL**
Non-invered	4.93	12.8	0	0
5 degrees inverted	6.56	19.3	0	0
10 degrees inverted	7.05	19.4	0	335

FINITE ELEMENT ANALYSIS OF EFFECTS OF GENDER-DEPENDENT 3D KNEE GEOMETRY AND JOINT LAXITY ON ACL IMPINGEMENT AGAINST THE INTERCONDYLAR NOTCH

[1, 2]Song Joo Lee and [1,2]Li-Qun Zhang

[1]Northwestern University, Evanston, IL, USA
[2]Rehabilitation Institute of Chicago, Chicago, IL, USA
email: l-zhang@northwestern.edu, web: smpp.northwestern.edu

INTRODUCTION

Females demonstrated 2-9 times higher ACL injury rate, narrow notch width and higher joint laxity in multi-planar directions [1,2]. One of potential ACL injury mechanisms is ACL impingement against the lateral wall of the femoral intercondylar notch [3], expressed as elongated and deformed ACL geometry [3] and contact area and contact pressure between the ACL and the intercondylar notch [4]. However, it has remained unclear about the contribution of gender-dependent joint laxity and 3D knee geometry on the susceptibility of ACL impingement against the femoral intercondylar notch. The goal of this study was to investigate the effects of gender-dependent joint laxity and 3D geometry of the knee on ACL impingement against the femoral intercondylar notch using a validated knee finite element model [4].

METHODS

Two knee FEMs (one female cadaver knee and one male knee from a live subject) including gender-dependent tibial external rotation laxity as kinematic boundary conditions were investigated. The finite element model was previously developed and validated using a cadaver specimen [4] with the following procedures. The three dimensional (3D) femur, tibia, and ACL images were segmented using commercial software, Mimics 14.01 image analysis software (Materialise N.V., Leuven, Belgium). Then, the reconstructed geometries of the femur, tibia, and ACL were meshed using HyperMesh™ (11.0, Altair Engineering, Inc, Michigan). The femur and tibia were meshed as rigid elements (R3D3). ACL was modeled as fiber-reinforced matrix models including hexahedral elements (C3D8RH) representing an isotropic hyper-elastic ground substance matrix and non-linear spring elements (SpringA) representing neo-Hookean materials to behave the ACL as transversely isotropic materials following the below constitutional equations (1) for the ground substance matrix , (2), and (3) for non-linear spring, similar to the previous study [4]. The connections between the ACL and femur, and the ACL and tibia were carefully meshed using HyperMorph function in HyperMesh™ to obtain anatomically realistic connections between ACL and femur, and between ACL and tibia.

$$\varphi_m = C_1(I_1 - 3) \tag{1}$$

$$\sigma = \begin{cases} 0 & \text{if } \lambda < 1 \\ C_2\left(e^{C_3(\lambda-1)} - 1\right) & \text{if } 1 \le \lambda < \lambda^* \\ C_4\lambda + C_5 & \text{if } \lambda^* \le \lambda \end{cases} \tag{2}$$

$$C_5 = C_2\left(e^{C_3(\lambda^*-1)} - 1\right) - C_4\lambda^* \tag{3}$$

where φ_m denotes the strain energy; I_1 the first invariant of the right Cauchy-Green strain; and C_1 a material constant. The spring elements are characterized by the nonlinear force-stretch relationship in Eqs (2) and (3) [4] and experimentally obtained ACL material properties. The fiber-reinforced FEM was analyzed using Abaqus (6.9, Dassault Systèmes). Knee flexion/ extension, abduction/adduction, and the internal /external rotation angle were defined in the joint coordinate system [5]. The femur and tibia represented as rigid bodies. Kinematic boundary conditions experimentally obtained from previous studies representing gender-dependent mean+1STD tibial external rotation laxity as 23.0° from 10 healthy males and as 31.7° from 10 healthy females [1] and a common knee abduction as 10.0° at a given knee flexion angle [4]. The notch width index (NWI) was compared between the female knee and the male knee and the femur geometries were normalized to the knee width.

RESULTS AND DISCUSSION

The NWI of the female knee was 0.25 and the male knee was 0.31. Overall, narrower 3D intercondylar notch shape in the normalized female knee was observed in comparison to the normalized male knee (Fig. 1).

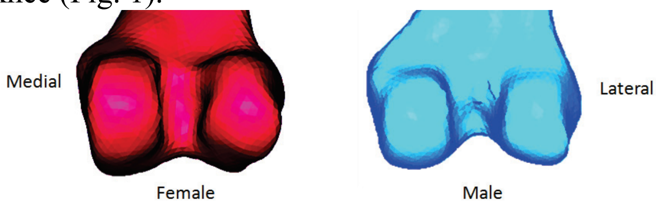

Figure 1. 3D intercondylar notch of the female knee and the male knee.

In the female knee model, ACL impingement against the intercondylar notch wall was seen during the kinematic sequence of knee abduction from 0° to 10.0° and tibial external rotation from 0° to 31.7°. Furthermore, higher tibial external rotation laxity led to higher maximum contact pressure and larger contact area (Fig. 2) as the ACL impinged against the intercondylar notch wall. Specifically, at the intermediate step corresponding to lower laxity of 21.1° tibial external rotation and 6.7° valgus, the maximum contact pressure was 3.55 MPa and the contact area was 4.11 mm^2, while at the higher laxity of 31.7° tibial external rotation and 10.0° valgus, the maximum contact pressure was 6.16 MPa and the contact area was 15.53 mm^2. Based on the known contact area and mean cell size of ACL as 90 μm, number of contacted ACL cells was estimated as $4.57*10^4$ at the lower laxity and $1.73*10^5$ at the higher laxity. The relationships between the laxity and contact area were not linear, which might be due to the non-linear biomechanical behaviors of the ACL.

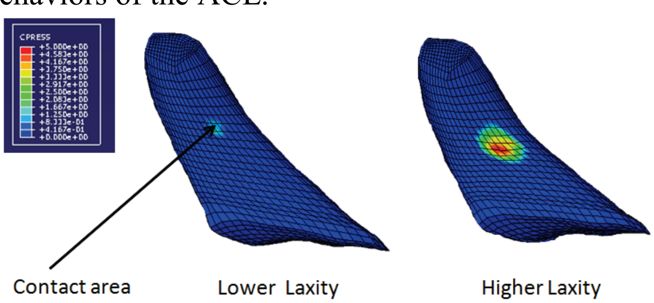

Figure 2. The contact area at the intermediate step (corresponding to lower female laxity of 21.1° tibial external rotation and 6.7° Abduction) and at the final step (corresponding to higher laxity of 31.7° tibial external rotation and 10.0° Abduction) in relation to the kinematic sequence of knee abduction from 0° to 10.0° and tibial ER from 0° to 31.7° in the female knee model.

In contrast, no impingement was observed in the male knee model in relation to the kinematic sequence of knee abduction from 0° to 10.0° and tibial external rotation from 0° to 23.0°. Furthermore, the minimum distance between the intercondylar notch wall and the ACL was 0.91 mm, occurring about the mid portion of ACL (at 67% of the ligament length from the origin at the femur).

CONCLUSIONS

In the female knee model, higher maximum contact pressure and larger contact area due to higher laxity and narrower notch were observed, while the male knee model did not show any impingement. The result may help us understand the causes for higher ACL injury rate in females. Stronger impingement with larger contact area between the ACL and the intercondylar notch wall indicated potential chronic sub-failure damage and cell death of ACL, such episodes may occur repeatedly, accumulate and lead to potential ACL rupture [4,6]. Although the models were generated from a female cadaver and a live male subject, the findings are justified because femur and tibia were rigid bodies with the ACL geometry obtained from "fresh-frozen" specimen. Further studies are needed over a larger sample to investigate clinical applications of the findings.

REFERENCES

1. Park HS, et al. *J Orthop Res* **26**, 937-44, 2008.
2. Shultz SJ, et al. *Am J Sports Med* **40**, 2836-44, 2012.
3. Fung DT, et al. *Clin. Orthop. Relat. Res.* **460**, 210-8, 2007.
4. Park HS, et al. *J Biomech* **43**, 2039-42, 2010.
5. Grood ES, et al. *J Biomech Eng* **105**, 136-44, 1983.
6. Fung DT, et al. *Anterior Cruciate Ligament (ACL): Causes of Injury, Adverse Effects and Treatment Options*, Nova, 2010.

Blood Flow Characterization in Multiple Anatomical Locations during Normal and Shear Loading

Joshua Drost, Abinand Manorama, Tamara Reid Bush

Department of Mechanical Engineering, Michigan State University
Email: drostjos@msu.edu, reidtama@msu.edu

INTRODUCTION

Decubitus ulcers, more commonly known as pressure ulcers or bed sores, are deep tissue wounds that extend from the skin to the muscle and bone and affect an estimated 3 million Americans. They are common among diabetics, individuals with spinal cord injury, the bedridden, and elderly [1].

Skin tissues require steady blood flow to stay healthy. Small changes in blood flow caused by external forces will stabilize in a healthy human. However, sustained occlusion or reduction of blood flow to the skin can lead to skin damage and tissue ischemia [2]. Populations with compromised vascular systems are particularly at risk for skin damage.

Previous studies have shown that external forces in the forearm cause a decrease in blood flow with the addition of normal forces (perpendicular to the skin) and a greater decrease with combined normal and shear (parallel to the skin) loading [3]. However, since only the forearm was evaluated in these prior studies, it was unclear if the blood flow in different regions of the body would have the same response to loading. Thus, the purpose of this work was to determine if the blood flow in different anatomical locations would react similarly to external forces.

METHODS

Twelve healthy participants with an average age of 22.08 years (2.75 SD) were tested. Blood flow was evaluated in four locations of each individual: heel, calf, sacrum, and forearm. For each test the subject laid prone on an examining table. The heel was tested on the center of the posterior surface of the right calcaneus. The calf was tested on the posterior of the right calf where the diameter was the greatest. The sacrum was tested at the midpoint between the subject's posterior superior iliac spines and intergluteal cleft (Figure 1). The forearm was tested three inches distal to the olecranon process superficial to the flexor compartment of the right pronated forearm. A Laser Doppler Perfusion Probe (Perimed, Stockholm, Sweden) was attached to each location to measure blood flow.

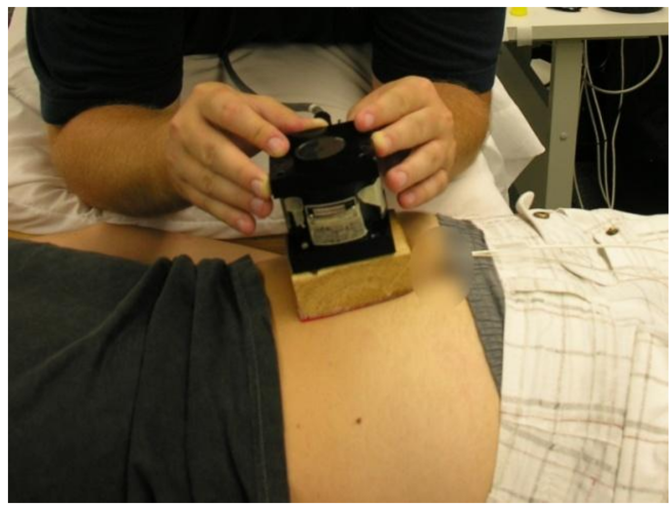

Figure 1. Experimental setup for the sacrum

Each location was tested under three conditions: baseline (no load), normal loading, and combined loading for one minute each. The baseline condition was always tested first. Both normal and shear loads were applied using a six axis load cell (Advanced Mechanical Technology, Inc., Watertown, MA, USA) and a custom wooden attachment designed to protect and apply loading around the probe. The loads were applied by the tester using a visual feedback system. During the normal loading condition, 20 N of normal force was applied. During the combined loading condition, 20 N of normal force and 10 N of shear force were applied. The shear loading was applied in a direction toward the center of the body relative to each location. The order of the normal condition and the combined condition was randomized for each subject. After loading, a resting period was provided and the next test did not begin until the blood perfusion stabilized. Following testing, a marking agent was applied to the skin at each location and a 20 N normal load was applied to determine the contact area of each test site.

RESULTS AND DISCUSSION

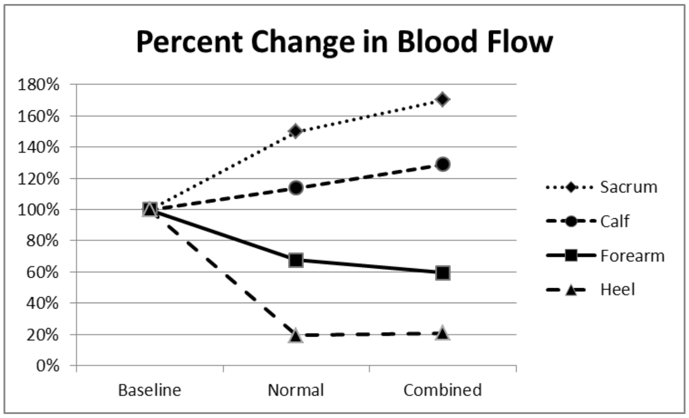

Figure 2. Average blood flow in each location tested for each of the loading conditions

The forearm results were similar to what had been previously reported: a decrease in blood flow with the application of a normal load and a further decrease with the addition of shear load [3]. A significant decrease in blood flow exists from both the baseline to normal and the baseline to combined loading conditions ($p<0.05$).

In the heel, there was a significant decrease in blood flow from the baseline to both the normal and combined loading conditions ($p<0.001$) as shown in Figure 2.

On average, the perfusion data from both the calf and sacrum increased with loading, but statistically analyzed, the data were not significant.

These differences in blood flow trends are likely related to pressure and contact area. This study kept the applied load constant for all anatomical locations; however, the contact area was not constant for all locations. The contact area for the sacrum and calf were similar, with the forearm and heel at approximately 75% and 15% of the sacral contact area. The smaller contact areas led to a higher pressure which is most likely the cause of the differences in response between body regions.

Another possible reason for the response differences between anatomical locations is the difference in the typical daily loading on the regions. In the seated position, or lying on a bed, the sacral region undergoes much larger loads than the forearm or the back of the heel. Therefore, rather than a constant load or pressure across all anatomical regions, the pressure should represent magnitudes seen on a daily basis.

CONCLUSIONS

This study looked at the changes of blood flow in different anatomical locations in response to external loading. Of the locations tested, the heel and the forearm presented a trend with a decrease in blood flow from no loading to normal loading, and a further decrease under both normal and shear loading. The calf and the sacrum did not display this trend. This is likely due to the differences in applied pressures and the differences in the typical daily loads of the applied regions.

To continue to better understand how pressure ulcers form in different regions of the body and how loading affects blood flow, a complete response profile of the loading, pressure and the different anatomical locations is necessary.

Future work will study the responses of location-specific loads or pressures that are representative of those applied to the regions in daily life. Studies could also be conducted on older, individuals to determine if the human body has a different response to loading as it ages and to assess differences in individuals with compromised vascular systems.

REFERENCES

1. Whitney J, et al. *Wound Repair Regeneration* **14**, 663–679. 2006.
2. Mak A, et al. *Annual Review of Biomedical Engineering* **12**, 29-53, 2010.
3. Manorama A, et al. *Clinical Biomechanics* **25**, 823–828. 2010.

INDIVIDUAL MUSCLE FORCES DURING A SIT TO STAND TRANSFER

Elena J. Caruthers, Julie A. Thompson, Laura C. Schmitt, Thomas M. Best, Ajit M.W. Chaudhari, and Robert A. Siston

The Ohio State University, Columbus, OH USA
e-mail: elena1caruthers@gmail.com

INTRODUCTION

Being able to rise and stand from a seated position is a basic, yet biomechanically demanding, activity of daily living [1]. However, due to weakened muscles or diseased joints, more than 2 million Americans over the age of 64 have difficulty accomplishing a sit-to-stand (STS) transfer independently, which can significantly limit mobility and independence [2, 3]. Several studies have determined joint torques and muscle activations associated with a STS transfer for various initial seating conditions by using traditional gait analysis techniques or rigid body models [2, 4, 5]. However, individual muscle forces in the STS transfer have yet to be fully explored. Understanding individual muscle function potentially informs rehabilitation strategies for patients with weakened muscles to improve performance with the STS transfer. As a first step toward that goal, the purpose of this study was to examine individual muscle forces in STS transfer in a young, healthy population.

METHODS

Seven healthy subjects (5 male and 2 female, Age: 22.7 ± 2.9 years) provided IRB-approved written consent. Subjects completed three trials of STS transfer, rising from a 55.2 cm position with their arms crossed over their chest while motion data was collected at 150 Hz using an 8-camera Vicon MX-F40 system and the Point-Cluster Technique (PCT) [6]. Ground reaction forces were obtained from two force plates sampled at 600 Hz, one placed under each of the subject's feet; no part of the chair touched the force plates. Bilateral surface EMG data was collected on the gluteus maximus, gluteus medius, rectus femoris, vastus lateralis, biceps femoris, tibialis anterior, medial gastrocnemius, and soleus using a 1500 Hz, 16-channel device.

Muscle-driven simulations of STS transfer were created for each subject's trial in OpenSim 2.4[7]. A generic lower limb musculoskeletal model was scaled to each subject's anthropometry. Inverse kinematics was implemented with a least-squares approach to reproduce the STS transfer motion in the scaled model with minimal difference between the experimental marker locations and the model's virtual marker locations. The joint forces and torques for each STS trial were determined through inverse dynamics and further resolved into individual muscle forces using static optimization (STO) [8].

The simulated muscle activations from STO were compared to the subject's experimental EMG after normalizing the EMG by peak activations in the simulation.

The data were sufficiently consistent between trials to use one trial per subject for analysis. We divided each STS trial into 3 phases: forward leaning (Phase 1), momentum transfer (Phase 2), and extension (Phase 3) [9]. The forward leaning phase begins when lumbar extension increases by .5 degrees from its initial value when the subject is at rest. The momentum transfer phase begins when hip flexion angle reaches its maximum value. The momentum transfer phase ends and the extension phase begins when the ankle reaches its maximum dorsiflexion value. The extension phase ends when the subject reaches their maximum hip extension value [9].

We investigated the gluteal muscles, quadriceps (vasti and rectus femoris), hamstrings, sartorius, gastrocnemius, soleus, and tibialis anterior, averaged the individual muscle forces across subjects and examined them across the three phases. After noticing that subjects had a tendency to lean sideways or have valgus knee positioning during the STS transfer, we further investigated the inter-limb differences in maximum muscle forces per phase.

RESULTS AND DISCUSSION

The quadriceps, hamstrings, soleus, and gastrocnemius generate a large amount of force during the STS transfer (Figure 1). In Phase 1, the quadriceps and hamstrings reach their peak values. In Phase 2, the forces in these muscles decrease while the force generated by the soleus increases. The soleus force continues to increase in Phase 3 as a standing position is attained. At the end of Phase 3, the gastrocnemius generates the greatest force of the muscles examined.

There were notable differences between the dominant and non-dominant leg average maximum muscle forces across subjects. Values are reported for muscles displaying a difference greater than 20% (Table 1). Some muscles, such as the soleus, also had negative percent differences between the dominant and non-dominant leg, implying that certain muscles generated a greater force in the non-dominant leg during the STS transfer.

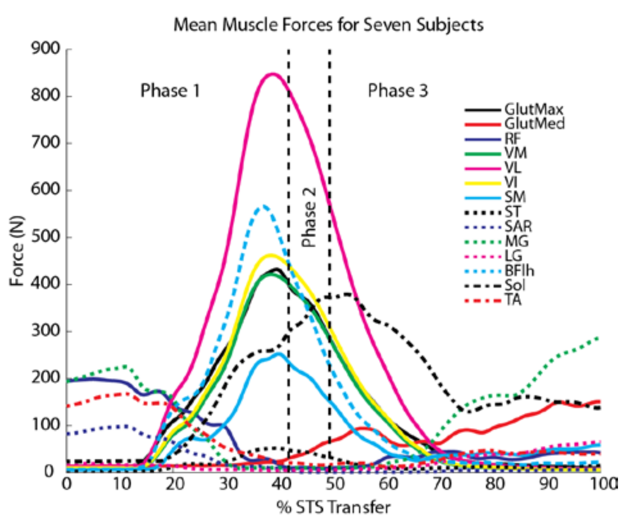

Figure 1: Selected muscle forces during STS transfer.

Our kinematic, kinetic, and EMG data compared favorably to those reported by other studies [4, 10], and we built upon those previous studies by estimating forces in individual muscles. It was expected that the quadriceps and hamstrings would play a large role in the STS transfer. However, the crossover between the forces in the quadriceps and hamstrings with the soleus in Phase 2 as well as the relatively large asymmetry between limbs in this healthy population were unexpected.

CONCLUSIONS

Understanding individual muscle forces as well as symmetry of muscle forces between legs during STS transfer in healthy subjects is the first step to analyzing muscle function and weakness in subjects with conditions such as osteoarthritis. These results set the stage for future work to investigate how unilateral and bilateral weakness affects a person's ability to perform the STS transfer and potentially inform rehabilitation strategies that could improve patients' functional performance with this task.

REFERENCES

1. Hughes MA, et al. *JRRD* **33**, 409-12, 1996.
2. Schultz AB, et al. *J Biomech* **25**, 1383-91, 1992.
3. Wretenberg P, et al. *Eur J Appl Physiol Occup Phys* **68,** 413-7, 1994.
4. Doorenbosch CA, et al. *J Biomech* **27**, 1299-307, 1994.
5. Scarborough DM, et al. *JRRD* **44**, 33-42, 2007.
6. Andriacchi TP, et al. *J Biomech Eng* **120**, 743-9, 1998.
7. Delp SL, et al. *IEEE Trans Biomed Eng* **54**, 1940-50, 2007.
8. Crowninshield RD. *J Biomech Eng* **100**, 88-92, 1978.
9. Schenkman M. *Phys Ther* **70**, 638-48, 1990.
10. Mak MYK, et al. *Clin Biomech* **18**, 197-206, 2003.

Table 1: Mean Percent Differences between Dominant and Non-Dominant Leg Maximum Muscle Forces

	GlutMax	**GlutMed**	**RF**	**SM**	**ST**	**SAR**	**LG**	**SOL**	**TA**
Phase 1	25.07	78.62	-13.50	38.19	35.93	-6.16	-11.70	-8.35	7.56
Phase 2	42.59	57.04	-17.08	89.94	72.01	-33.51	-46.72	-39.01	20.42
Phase 3	31.50	0.10	-64.02	54.40	39.17	-50.97	11.19	-27.21	50.49

THE NEUROMAGNETIC ACTIVITY OF THE SOMATOSENSORY CORTICES AND THE ANKLE FORCE CONTROL IS ALTERED IN CHILDREN WITH CEREBRAL PALSY

[1]Max J. Kurz, [1]David J. Arpin, [2]Elizabeth Heinrichs-Graham, [2]Katherine M. Becker & [2]Tony W. Wilson

[1]Munroe-Meyer Institute, University of Nebraska Medical Center, Omaha, Nebraska
[2]College of Medicine, University of Nebraska Medical Center, Omaha, Nebraska
Email: mkurz@unmc.edu Web: http://www.unmc.edu/mmi/

INTRODUCTION

It well recognized that children with cerebral palsy (CP) have somatosensory processing deficits that limit their proprioception, stereognosis, and tactile discrimination. Since CP involves damage to both the sensory and motor systems, it is unclear whether the noted sensory deficits contribute to the motor impairments seen in these children, or if they are more independent symptoms that share a common cause (i.e., perinatal brain damage). Results from diffusion tensor imaging (DTI) has provided some insight on this symptomatic relationship, by showing that the damaged thalamocortical tracts are related to the reduced muscular strength seen in children with CP [2]. Further understanding of how the somatosensory processing deficits interact with the motor impairments will be critical for improved understanding of the motor control problems seen in these children.

Magnetoencephalography (MEG) is a quantitative neurophysiological imaging technique that provides a direct measure of neuronal activity by measuring the minute magnetic fields that are generated by local electrical oscillations in activated neuronal populations. A considerable amount of research has used MEG to quantify the activation and organization of the primary and secondary somatosensory cortex through the use of evoked magnetic field paradigms [5]. Outcomes from these studies have confirmed that the somatosensory cortex is organized into well-defined "homunculus" like boundaries (*i.e.*, foot, arm, hand, leg, tongue, lips, *etc*.). In a recent exploratory investigation of four children with CP, we demonstrated that the responsiveness of the primary somatosensory cortices was diminished [4]. Furthermore, we have additionally shown, in a small cohort of children with CP, that the responsiveness of the primary somatosensory cortices is altered after gait training and that these neuromagnetic changes are accompanied by mobility improvements [3]. Together these results imply that the integrity of the somatosensory cortices is important for the motor control of the leg musculature.

Variability or error is present in all voluntary contractions and impacts the precision and control of the motor performance. Children with CP have greater variability in the lower extremity joints' performance when trying to hold an isometric force at a submaximal target [1]. We suspect that these greater errors may be partly due to deficiencies in the sensorimotor integration process for correcting the muscular force to match the prescribed target value [6]. Potentially, the breakdown in the error checking process may reside in the responsiveness of the primary somatosensory cortices to the external afferent feedback from the periphery.

The purpose of this investigation was 1) to evaluate the response of the somatosensory cortices of children with CP to an external stimulus, 2) to determine if the control of the ankle joint force is reduced in children with CP, and 3) to determine if there is a relationship between the activity of the somatosensory cortices and the amount of variability in the ankle joint's steady-state isometric force production.

METHODS

Eight children with spastic diplegia CP (Age = 11 $\pm$ 4 yrs.) and eight TD children (Age = 13.2 $\pm$ 3 yrs.)

participated in this investigation. An isokinetic dynamometer (Biodex Inc., Shirley, NY) was used to measure the steady-state isometric torques generated by the ankle joint plantarflexors. The motor task involved matching and holding a target torque that was 20% of the child's maximum voluntary torque for 15 seconds. The target and the torque exerted by the child were displayed on a large monitor positioned ~1 m away. The coefficient of variation (CV) was used to assess the amount of variability in the ankle joint's force production. A greater amount of variability was assumed to indicate greater errors in the adjustment of the motor plan to remain at the target value.

A whole-head 306-sensor MEG system (Elekta Neuromag, Helsinki, Finland) was used to assess the oscillatory activity of the somatosensory cortices as a small air bladder stimulated the bottom of the foot at the first metatarsal phalangeal joint. A linearly-constrained minimum variance vector beamformer algorithm was used to calculate 3D images that reflect the local power of neuronal current. The single images generated were derived from the cross spectral densities of all combinations of MEG sensors averaged over the 4-14 Hz frequency range from 25 to 275 milliseconds.

RESULTS AND DISCUSSION

The children with CP had a larger CV while attempting to sustain the steady-state torque values (CP = 18.8 $\pm$ 9%; TD = 2.5 $\pm$ 0.5%; $p = 0.01$), implying that they had greater errors in their ability adjust the force output to remain at the target value.

The beamformer imaging results showed that the children with CP had a lower amount of activity in the medial wall of the postcentral gyrus ($p < 0.05$, cluster-corrected). Further inspection of the data revealed that the somatosensory cortices of the children with CP desynchronized when the stimulus occurred, while the somatosensory cortices of the TD children had a synchronized response to the stimulus. These results indicate that the responsiveness of primary somatosensory cortices to the external afferent feedback was weaker and aberrant in the children with CP. In addition, there was a negative correlation between the CV and the amount of activity in the somatosensory cortices ($r = -0.60$; $p=0.008$), indicating that greater errors in matching the target force were related to less activity in the somatosensory cortices.

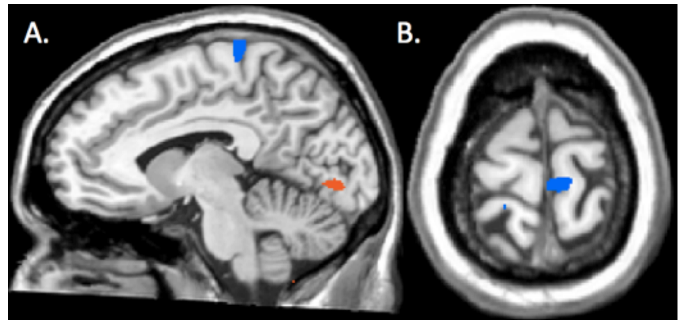

Figure 1. Beamformer images for the group differences shown in the sagittal (A) and transverse plane (B). The differences were located in the medial wall of the postcentral gyrus (shown in blue).

It is well established that the control of movement is based on an internal model that contains the desired muscular performance and the sensory information that should be returned as the motor plan is executed [6]. Comparisons between the actual afferent sensory information and the internal model's sensory predictions are used to detect errors in the motor performance. The reduced and aberrant response of the somatosensory cortices in the children with CP suggests that the neuronal groups that represent the foot may lack the ability to properly translate the external feedback for such comparisons. Based on this perspective, the increased amount of variability in the ankle's force production may be partly explained as a breakdown in the error correction networks.

REFERENCES

1. Arpin DJ, et al. *Res Dev Disabil* **34(4)**, 1134-1143, 2013.
2. Hoon AH, et al. *Dev Med Child Neurol* **51(9)**, 697-704, 2009.
3. Kurz MJ & Wilson TW. *Neurosci Let* **490(1)**, 1-5, 2011.
4. Kurz MJ, et al. *J Neurol Phys Ther* **36(4)**, 166-172, 2012.
5. Nakamura A, et al. NeuroImage **7**, 377-386, 1998.
6. Shadmehr R, et al. *Ann Rev Neurosci* **33**, 89-108, 2010.

WITHIN- AND BETWEEN-SESSION RELIABILITY FOR THE QUANTIFICATION OF THE THIGH MUSCLES CO-ACTIVATION INDEX DURING ISOMETRIC CONTRACTIONS

Dimitrios Katsavelis, Sam K. Morton, and A. Joseph Threlkeld
Creighton University, Omaha, NE, USA
email: joethrelkeld@creighton.edu web: rehablab.creighton.edu/

INTRODUCTION

Co-activation is the simultaneous activation of agonist and antagonist muscle groups around a joint, which contributes to joint stability and movement efficiency [1]. Co-activation becomes very important during ambulation and balance particularly around the knee. While certain levels of co-activation are normal in healthy populations, increased or reduced levels of co-activation may be associated with neuromuscular problems [2]. However, the wide range of methodological approaches for the quantification of co-activation makes comparison across studies and populations difficult. Most of the techniques that quantify co-activation index (CI) can be grouped within four categories, with normalization of each muscle with its respective maximum contraction to be considered the most advanced [2]. Nonetheless, there are still inconsistencies in smoothing techniques for the EMG signal. Root mean square (RMS) is the most commonly used smoothing approach [3] but the choice of RMS parameters may affect the reliability and meaning of results within and between sessions. Therefore, the purpose of the present study was to determine within- and between-session reliability of different methodological approaches for the quantification of the CI of the thigh extensor and flexor muscles of the knee during maximum voluntary isometric contractions (MVIC).

METHODS

Six healthy subjects with prior experience generating isokinetic contractions in a Biodex dynamometer (3 men and 3 women; 27.7±5yrs, 176.3±12cm; 81.8±14kg) completed two sessions of five knee MVICs. Surface electrode pairs were placed over the accessible segments of the quadriceps muscle of the dominant leg (vastus medialis, rectus femoris, and vastus lateralis) and the hamstring muscle groups (lateral hamstrings, medial hamstrings) according to the SENIAM guidelines. Subjects were secured to the Biodex chair with knee and hip joint angles of 60^o and 120^o, respectively. The dynamometer was aligned with the anatomic knee axis and the torque arm secured to the distal shank. Subjects performed one knee flexion MVIC followed by four extension MVICs with a minute of rest between each contraction. All subjects were retested to assess between–session reliability with at least 3 days between sessions.

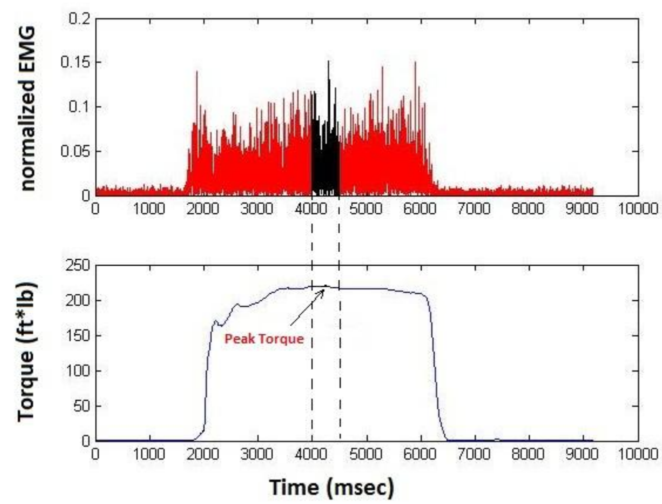

Figure 1: The Matlab algorithm calculated the RMS in a window of 500ms around the peak torque.

Torque and EMG signals were captured at 1kHz. Both peak torque (PT) and PT normalized to body weight (nPT) were extracted for analysis. The EMG signals were band-passed filtered (10 to 450Hz), corrected for zero offset, full-wave rectified, and normalized to MVIC. CIs were calculated based on the a) amplitude of the raw EMG signal, and b) root mean square (RMS) by calculating the quotient between the average EMG activity of the 2 antagonist and 3 agonist muscle groups. Five RMS methods were compared: smoothing the entire burst in windows of 20 and 50msec and smoothing a window of 20, 50, and 500msec around the PT (Figure 1). Intraclass correlation coefficient (ICC) analysis was used to assess the consistency of the different calculation approaches. Coefficients of variation (CV) were also calculated to determine within- and between-session variability.

RESULTS AND DISCUSSION

Torque (PT=406±139N*m; nPT=1.64±0.26) was highly reliable within- and between-sessions (ICC 0.982 and 0.958, respectively), which implied that subjects were able to reproduce their PT at both sessions and that any variation in CI values were not due to variations in torque output. CI values ranged from 13.4 to 16.1, with the calculations employing peak amplitude across the entire burst giving the highest values and methods using RMS around the PT producing the lowest values (Table 1).

Within-session

ICC analysis of the CI quantification approaches (Table 1) revealed that within-session coefficients were greater than 0.80, with most values greater than 0.90, while within-session CV values ranged from 8.6% to 21.6%. Within-session results indicated that quantification of CI was highly reliable for all approaches, with the 500ms-window yielding the most reliable and by far the least variable CI.

Between-session

ICC values for the between-session analysis ranged from 0.571 to 0.796, while CV values ranged from 24.9% to 30% (Table 1). The RMS approach in windows of 20 and 50ms throughout the entire burst as well as the RMS approach at a 500ms window around the PT produced higher ICC values and less variability than the other tested approaches. Between-session ICC values are consistently lower than within-session ICC values across all CI approaches. The opposite holds truth for CV values with between-session values to be consistently higher than within-session CV values.

CONCLUSIONS

The striking finding of the present study was the markedly lower reliability and the higher variability of the CI between-sessions in comparison to the within-session CI calculations. Small shifts in EMG electrode placement between sessions explain some of the differences. Also, the submaximal co-contraction of the hamstring muscles during knee extension could allow greater variability in the motor unit recruitment and firing frequency [4].

RMS at 500ms around the PT appeared to be a more reliable and less variable approach for the quantification of the CI. A possible explanation is that a 500ms window eliminated much of the motor unit size recruitment and firing rate variability that occurred across the entire contraction time or suppress potential artifacts that may occur using window sizes smaller than 500ms.

REFERENCES

1. Levine & Kabat. *Science* **116**, 115-8, 1952.
2. Busse ME, et al. *Phys Ther Rev* **10**, 247-53, 2005.
3. Hortobagyi T, et al. *Clin Biomech* **20**, 97-104, 2005.
4. Ounjian M, et al. *J Neurobiol* **22**,547-59, 1991.

ACKNOWLEDGEMENTS

Research reported in this abstract was supported by the National Institute on Aging of the National Institutes of Health under grant number R15 AG040616. The content is solely the responsibility of the authors and does not necessarily represent the official views of the National Institutes of Health.

Table 1: Within- and between-session reliability and variability for the different quantification methods of the co-activation index.

		Within-session		Between-session	
	CI (mean±SD)	CV (%)	ICC	CV (%)	ICC
Amplitude	16.1 (10.1)	14.2	0.859	28.9	0.672
RMS 20ms @PT	13.5 (8.0)	21.6	0.876	29.9	0.571
RMS 50ms @PT	13.5 (8.6)	19.9	0.902	30.0	0.646
RMS 500ms @PT	13.4 (8.8)	8.6	0.973	25.0	0.657
RMS 20ms	14.9 (9.9)	17.3	0.901	27.4	0.780
RMS 50ms	14.8 (10.3)	15.2	0.935	24.9	0.796

* CI = Coactivation Index, CV = Coefficient of Variation, and ICC = Intraclass Correlation Coefficient.

THE EFFECT OF AMPUTATION LENGTH AND INTEROSSEUS MEMBRANE VIABILITY ON FIBULAR MIGRATION IN BELOW KNEE AMPUTATIONS

[1]Timothy A. Burkhart, [1]Benjamin Asa, [1]Cynthia E. Dunning, [1]Michael Payne and [1]Timothy D. Wilson

[1]Western University, London, Ontario Canada
email: tburkhar@uwo.ca

INTRODUCTION

There are more than 180 000 new amputations involving the lower extremity every year [1]. It is predicted that the number of lower extremity amputations will double by the year 2050 [1] and of all lower extremity amputations, more than 50 % are trans-tibial (below the knee) [1].

One known complication of below knee amputations is a painful and debilitating condition involving migration of the fibula away from the tibia [3,4]. Although identified early in the medical literature [4], it has received little further attention despite clinical and ambulatory concerns. Among other hypothesized causes, it has been suggested that the loss of the distal tibial-fibular joint, a compromised interosseous membrane (IOM) [3,4] and unopposed action of the biceps femoris muscle contribute to this condition. With little empirical evidence to support these hypotheses, the purpose of the work described here was to determine the effect of amputation length and IOM viability on fibular migration in a cadaveric model.

METHODS

Below knee amputations were performed on twenty embalmed lower extremity (tibia and fibula) specimens. With the exception of the IOM, biceps femoris tendon and the tibio-fibular joint capsule all surrounding soft tissues were removed. Specimens were randomly assigned to one of four amputation groups defined by amputation length (long vs. short) and viability of the IOM (intact vs. sectioned) (Figure 1a). Long and short amputations were defined as the fibula being amputated to a length of 10 cm and 5 cm (measured from the tibial plateau), respectively. An incision was made along the length of the IOM to create a sectioned condition, while care was taken to ensure that no damage occurred to the IOM for the intact condition.

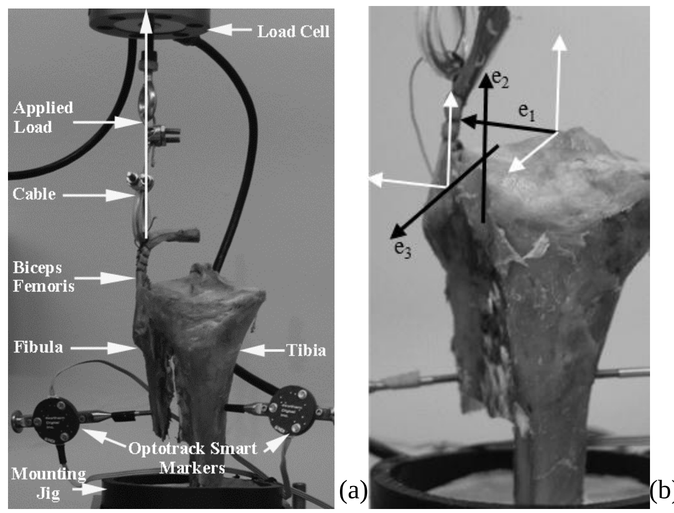

Figure 1: (a) Experimental set-up of a long amputation with a sectioned IOM and (b) the coordinate system used to define fibular motion (e1=tibia fixed axis; e3=fibula fixed axis; e2= floating axis).

The tibiae were cemented into 7 cm (10 cm diameter) sections of PVC that were mounted into a rigid testing jig within an Instron® materials testing machine (Figure 1a). The specimens wereϵ potted such that the biceps femoris tendon was vertical, simulating ~10^{o} knee flexion, an angle consistent with the position of the residual limb within a prosthesis. A suture sewn through the biceps femoris tendon was attached to an insulated cable, subsequently connected to the actuator of the Instron (Figure 1a).

Two Optotrack smart markers (Figure 1a) tracked the global motion of the fibula and tibia while a series of anatomical landmarks on each of the bones were digitized to develop fibular and tibial coordinate systems (Figure 1b). A floating axis coordinate system [5] was established to describe the motion of the fibula with respect to the tibia where the flexion/extension (e_1) and abduction/adduction (e_3) axes were fixed within the tibia and fibula, respectively (Figure 1b). A static calibration trial was collected to determine the initial position of the fibula with respect to the tibia.

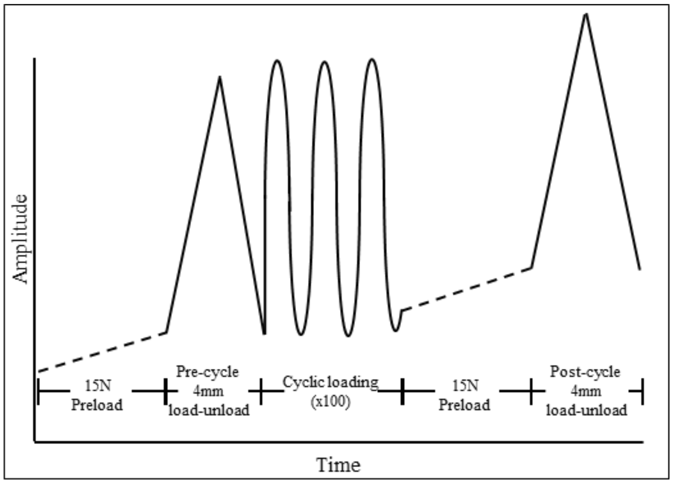

Figure 2: Example of the protocol used to load the biceps femoris tendon (dashed lines represent load control).

Following an initial 15 N preload (1 N/s), a 4mm (1 mm/s) loading-unloading phase was applied to the biceps femoris tendon (Figure 2). A position controlled cyclic waveform (sine wave; 0.5 Hz) with initial amplitude of 4 mm was then used to elicit continuous fibular motion for 100 cycles (Figure 2). Following the 100th cycle a preload and 4mm load-unload cycle were applied. This protocol continued with 2 mm increases in the sine wave amplitude until failure was observed (any occurrence that resulted in a sustained decrease of the load).

Outputs from the Instron® (force, moment) and Optotrack (joint kinematics) were calculated from the 14 mm displacement cycle across all specimens. Two-way ANOVAs (length x IOM condition) were used to assess the statistical significance associated with the four conditions.

RESULTS AND DISCUSSION

There were no statistically significant differences in the forces or moments applied to the specimens across all conditions. An overall mean (SD) moment of 2.0 (0.3) Nm resulted in 6.1 (2.7), 1.1 (4.7) and 2.8 (1.8) degrees of abduction, internal rotation and flexion of the fibula respectively (Figure 3). Although not significant, the long sectioned specimens abducted approximately 70 % more than the long intact specimens (8.2^{o} vs. 4.8^{o}) (Figure 3), and given the relatively thin layer of soft tissues overlying the fibula, would most likely result in residual limb deformation.

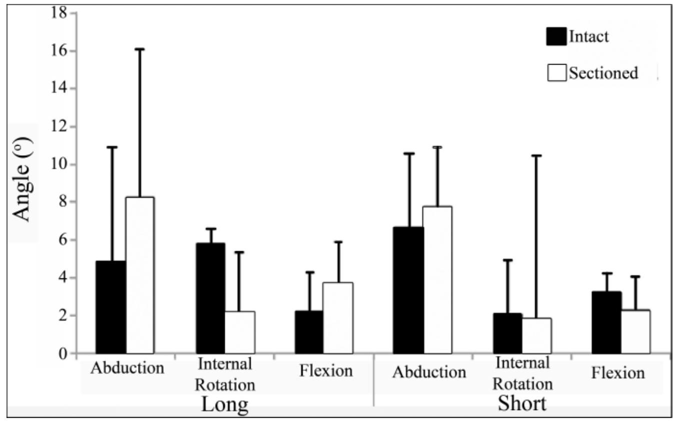

Figure 3: Effect of amputation length and IOM viability on tibio-fibular joint kinematics.

CONCLUSIONS

The results presented here suggest that the unopposed action of biceps femoris that results from a trans-tibial amputation is not significantly affected by the length of amputation or the viability of the IOM, However, this highlights the complex nature of these amputations and suggests that there may be additional abnormal loading applications interacting to produce fibular migration.

ACKNOWLEDGEMENTS

The Joint Motion Program- A CIHR Training Program in Musculoskeletal Health Research and Leadership. The ACB bequeathal program.

REFERENCES

1. Ziegler-Graham K, et al. *Arch Phys Med Rehab* **89**, 422-429, 2008.
2. Pinzur MS et al. *J Bone Joint Surg*, **89**, 1118-1127, 2007.
3. Loon HE. *Artificial Limbs*, **6**, 86-89, 1962.
4. Grood ES et al. *J Biomech Eng* **105,** 136-144, 1983.

THE EFFECTS OF PERFORMANCE DEMANDS ON ACL LOADING DURING A STOP-JUMP TASK

[1]Boyi Dai, [2]William E. Garrett, [3]Michael T. Gross, [3]Darin A. Padua, [2]Robin M. Queen, [3]Bing Yu

[1]University of Wyoming, Laramie, WY, USA
[2]Duke University, Durham, NC, USA
[3]The University of North Carolina at Chapel Hill, Chapel Hill, NC, USA
email: bdai@uwyo.edu, web: http://www.uwyo.edu/kandh/

INTRODUCTION

Anterior cruciate ligament (ACL) injuries usually occur during the early phase of landing tasks with a non-contact mechanism [1]. Jump landing tasks have been used to assess ACL injury risk factors [2,3].

In competitive situations, the same athletic task can be performed with different performance demands. For example, a basketball player might choose to jump as high as possible or to jump as faster as possible during a rebounding effort depending on the competitive situation. Previous investigators have screened athletes using maximum jump height as the performance demand [2,3]. However, it was unknown whether jump height was a sensitive performance demand when examining ACL loading. Screening and training athletes without knowing whether the task demands really represent an ACL injury scenario could establish inappropriate target variable for injury prevention.

The purpose of this study was to investigate the effects of both jump height and jump speed on ACL loading during a stop-jump task. It was hypothesized that ACL loading would increase when individuals performed a stop-jump task with a greater jump height and a faster jump speed.

METHODS

Eighteen male (Age: 23.1 ± 3.7 yrs; Height: 1.80 ± 0.05 m; Mass: 76.9 ± 8.8 kg) and eighteen female (Age: 21.6 ± 2.5 yrs; Height: 1.68 ± 0.07 m; Mass: 64.9 ± 6.0 kg) recreational athletes participated in the current study. The subjects performed a vertical stop-jump task with three different performance demands. The vertical stop-jump task consisted of a running approach, followed by a 1-footed take-off, followed by a 2-footed landing, and then a 2-footed take-off. During the first condition, subjects were instructed to jump as high as possible following the 2-footed take-off. During the second condition, subjects were instructed to jump off the ground as faster as possible following the 2-footed landing. During the third condition, subjects were asked to jump with 60% of maximum jump height following the 2-footed take-off. Three-dimensional kinematic and ground reaction force (GRF) data were collected. Lower extremity joint angles and joint resultant moments during the 2-footed landing were calculated for the dominant side. GRFs were normalized to each subject's body weight. Joint resultant moments were normalized to each subject's body weight multiplied by body height.

ACL loading variables included peak posterior GRF (PPGRF), timing of PPGRF, vertical GRF at PPGRF, and knee joint angles and moments at PPGRF. ACL loading variables among stop-jump conditions and between genders were tested using 3 x 2 mixed design ANOVAs. A Type I error rate was set at 0.05.

RESULTS AND DISCUSSION

PPGRF (Table 1) during the jumping fast condition was greater than the jumping for 60% of maximum height and the jumping for maximum height conditions. PPGRF during the jumping for maximum height condition was greater than the jumping for 60% of maximum height condition. Timing of PPGRF during the jumping fast condition was earlier than the jumping for 60% of maximum height and jumping for maximum height conditions.

Vertical GRF at PPGRF during the jumping fast condition was greater than the jumping for 60% of maximum height and jumping for maximum height conditions. Vertical GRF at PPGRF during the jumping for maximum height condition was greater than the jumping for 60% of maximum height condition. Knee flexion angle at PPGRF during the jumping for 60% of maximum height condition was less than the jumping fast and jumping for maximum height conditions. Knee external rotation angle at PPGRF during jumping for maximum height condition was less than the jumping for 60% of maximum height conditions. Knee extension moment at PPGRF during the jumping fast condition was greater than the jumping for 60% of maximum and jumping for maximum height conditions.

CONCLUSIONS

Increased external loading and decreased knee flexion were associated great ACL loading [1]. The results of this study supported the hypothesis that ACL loading would increase when individuals jumped with a faster speed because of the increased external loading and decreased knee flexion. However, the changes in ACL loading were inconclusive when individuals jumped for a higher jump height because of the increased external loading in conjunction with increased knee flexion.

Taylor et al. [4] proposed a hypothetical injury scenario during which injury could occur as a result of disruption in the timing of landing events. Additionally, the current study suggests that athletes could have an increased injury risk when landing with a shorter stance time following pre-landing or early landing perturbation.

Previous investigators generally have tested athletes with maximum jump height as the performance demand [2,3]. However, jump height might not be a sensitive performance demand when examining ACL loading. Testing athletes with a non-sensitive performance demand could result in misleading test results. Future injury risk studies might test subjects using other performance demands such as maximum jump speed in order to better represent ACL injury scenario. While a decrease in jump speed could result in decreased injury risk, jumping with a high speed might be unavoidable during competitive situations.

REFERENCES

1. Dai B, et al. *Res Sports Med* **20**, 180-197, 2012.
2. Yu B, et al. *Clin Biomech* **21**, 297-305, 2006.
3. Hewett TE, et al. *Am J Sports Med* **33**, 492-501, 2005.
4. Taylor KA, et al. *J Biomech* **44**, 365-371, 2011.

Table 1: Means (standard deviations) and *p* values of ANOVAs for ACL loading variables

	Jump Fast		Jump Max Height		Jump 60% Max Height		*P* Value		
Variables	Male	Female	Male	Female	Male	Female	Interaction	Condition	Gender
PPGRF (BW)	-0.93 (0.29)	-0.82 (0.25)	-0.64 (0.26)	-0.65 (0.26)	-0.57 (0.21)	-0.61 (0.18)	0.104	<0.001*	0.787
Time_PPGRF (ms)	29.30 (8.30)	25.84 (9.39)	30.60 (8.51)	31.27 (10.11)	32.80 (8.14)	29.35 (9.62)	0.120	0.004*	0.449
VGRF_PPGRF (BW)	2.23 (0.70)	1.82 (0.52)	1.63 (0.63)	1.52 (0.46)	1.44 (0.48)	1.37 (0.44)	0.078	<0.001*	0.225
KF_PPGRF (Deg)	35.95 (5.22)	27.12 (7.67)	38.51 (7.26)	31.70 (6.74)	31.81 (6.14)	27.38 (7.16)	0.049	<0.001*	0.002*
KIR_PPGRF (Deg)	-1.86 (5.14)	-0.04 (2.23)	-1.11 (5.01)	1.19 (3.52)	-1.35 (3.77)	-0.04 (2.72)	0.329	0.010*	0.152
KVA_PPGRF (Deg)	-1.31 (5.05)	-1.05 (6.05)	-1.00 (5.20)	0.12 (7.07)	-1.24 (4.53)	-0.12 (6.60)	0.588	0.299	0.658
KFM_PPGRF (BW*BH)	-0.11 (0.05)	-0.07 (0.03)	-0.06 (0.04)	-0.07 (0.03)	-0.06 (0.03)	-0.05 (0.03)	0.013	<0.001*	0.240
KIRM_PPGRF (BW*BH)	0.00 (0.05)	-0.01 (0.06)	-0.01 (0.03)	-0.01 (0.04)	-0.01 (0.02)	-0.01 (0.03)	0.653	0.241	0.749
KVAM_PPGRF (BW*BH)	0.00 (0.06)	-0.01 (0.03)	-0.01 (0.04)	-0.01 (0.02)	-0.01 (0.04)	-0.01 (0.03)	0.962	0.479	0.951

PPGRF: Peak posterior GRF; Time_PPGRF: Timing of PPGRF; VGRF_PPGRF: Vertical GRF at PPGRF; KF_PPGRF: Knee flexion angle at PPGRF; KIR_PPGRF: Knee internal rotation angle at PPGRF; KVA_PPGRF: Knee varus angle at PPGRF; KFM_PPGRF: Knee flexion moment at PPGRF; KIR_PPGRF: Knee internal rotation moment at PPGRF; KVA_ PPGRF: Knee varus moment at PPGRF. *: significant p values

STRETCHING WITH VIBRATION IMPROVES FLEXIBILITY IN PATIENTS WITH PLANTAR FASCIITIS

[1]Elizabeth M. Russell, PhD and [1,2]Benjamin Thompson, MD

[1]The Andrews Research and Education Institute, Gulf Breeze, FL, USA
[2]Milton Hospital Orthopaedic Department, Milton, MA, USA
email: elizabeth.russell@gmail.com

INTRODUCTION

Stretching the triceps surae complex is the most common conservative treatment for patients dealing with plantar fasciitis pain [1]. Lengthening the triceps surae increases the ankle dorsiflexion range of motion and numerous previous reports have supported stretching to relieve plantar fasciitis pain. However, sometimes static stretching of the muscle cannot provide adequate relief. It is possible that adding vibration to the stretching routines in plantar fasciitis patients may increase ankle dorsiflexion range of motion more than stretching alone in patients with plantar fasciitis. Stretching with locally-applied vibration induces acute increases in flexibility [2,3], which may be beneficial for this population.

The purpose of this study was to determine how stretching with vibration applied under the foot affected ankle dorsiflexion flexibility in patients with plantar fasciitis. It was hypothesized that stretching with vibration would improve flexibility more than static stretching alone.

METHODS

Fifty-three (N=53) male and female patients with current clinical diagnosis of plantar fasciitis were recruited for this study. All patients used conservative therapies to treat their plantar fasciitis pain, such as stretching, ice, and rolling the arch of the foot. Subjects were randomly assigned to either a control group (N=27, mean age: 45.3 ± 13.3 yrs, height: 1.77 ± 0.1 m, body mass index: 29.1 ± 7.5 kg/m^2) who experienced no vibration or an experimental group (N=26, mean age: 49.5 ± 10.8 yrs, height: 1.67 ± 0.09 m, body mass index: 27.4 ± 4.8 kg/m^2) who stretched with vibration.

Prior to data collection, all subjects lay prone on an exam table while ankle dorsiflexion range of motion was recorded at 90 and 180 degrees of knee flexion. Marks were placed on the center of the lateral malleolus, along the line of the fibula and on the head of the fifth metatarsal. The center of a goniometer and the goniometer arms were aligned with these respective marks. Care was taken by the investigator to ensure that the subject's foot did not rotate out of plane when taking these measurements.

A vibrating platform (PowerPlate Pro5, 30 Hz) was used to deliver the vibration under the foot to the experimental group. Subjects were instructed to extend the knee of the affected foot and keep the heel flat on the platform while lunging forward to stretch the triceps surae complex to the point of initial discomfort. The unaffected, or less affected, foot was placed on a platform of equal height. The distance between the feet was not controlled and subjects were able to adjust this distance to gain the greatest stretch. Range of motion measures were repeated after the stretching bout using the same marks previously described.

Student's unpaired t-tests were used to determine significant differences between the two groups in terms of the change in ankle dorsiflexion range of motion from baseline measures ($p<0.05$). Effect sizes (d) were also calculated.

RESULTS AND DISCUSSION

Stretching the triceps surae complex with vibration under the foot resulted in a greater percent increase in ankle dorsiflexion flexibility than stretching with no vibration at both 90 degrees ($p=0.024$, $d=0.914$) and at 180 degrees ($p=0.014$, $d=0.707$) (Figure 1). This resulted in an absolute change of 0.7 ± 3.4

degrees in the control group and 2.7 ± 3.3 degrees in the experimental group.

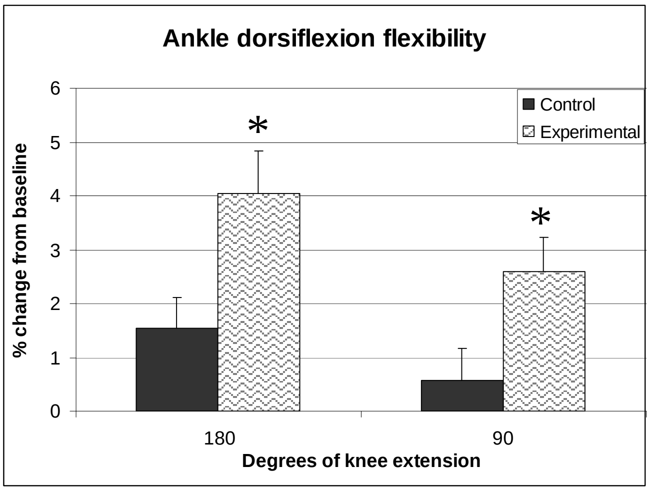

Figure 1: Mean percent change in ankle dorsiflexion flexibility during non-weight bearing and standard error bars.

There were no differences between groups for any of the subject characteristics of age, height, or body mass index.

In support of the hypothesis, stretching with vibration applied under the foot was a more effective way to increase flexibility in patients with plantar fasciitis than static stretching alone. Even though absolute and percent changes in range of motion were small, the moderate-to-high effect sizes indicate that these results may have a large degree of clinical relevance.

Therapy and conservative treatment for plantar fasciitis involves stretching, but previous research indicates that stretching alone may not be effective enough to adequately lengthen the triceps surae complex [4]. The use of vibration during stretching may augment flexibility. Feland et al. [5] reported that whole body vibration during stretching had long-term effects on flexibility retention in healthy populations. Therefore, it is possible that the positive effects of vibration during stretching may last longer than just the acute effect, however this has not been studied in a patient population with plantar fasciitis.

The positive effects of this therapy may result from three mechanisms: increased blood flow, increased pain threshold, or induced relaxation of the muscle. Vibration increases blood flow to the targeted area [6], which then increases temperature and has been linked to tissue extensibility [7]. The increase in flexibility may also be the result of decreased pain sensation from vibration [8] leading to the ability to stretch beyond initial discomfort. Lastly, vibration-induced flexibility may result from pre-synaptic inhibition of the Ia sensory fibers and the alpha motor neuron.

CONCLUSIONS

Patients with plantar fasciitis pain often need to stretch the triceps surae complex in the morning or throughout the day to relieve some of the tension on the plantar fascia during walking. Utilizing a form of vibration applied under the foot during their morning and daily stretching routines may enhance flexibility and improve mobility in this population. Future research will determine long-term successes of stretching with vibration on pain, function, and walking mechanics in patients with plantar fasciitis.

REFERENCES

1. Digiovanni et al., (2006) *J Bone Joint Surg Am*, **88**, 1775-81.
2. Issurin et al. (1994) *J Sports Sci*, **12**, 561-6.
3. Sands et al. (2006) *Med Sci Sports Exerc*, **38**, 720-5.
4. Grady and Saxena (1991) *J Foot Surg*, **30**, 465-9.
5. Feland et al. *Int J Sports Med*, **31**, 584-9.
6. Kerschan-Schindle et al., (2001) *Clin Physiol*, **21**, 377-82.
7. Lehmann et al. (1970) *Arch Phys Med Rehabil*, **51**, 481-7.
8. Staud et al. (2011) *Eur J Pain*, **15**, 836-42.

ACKNOWLEDGEMENTS

The authors gratefully acknowledge Drs. Erik Nilssen and Joshua Hackel for assistance with subject diagnosis and recruitment, and Athletes' Performance, Inc. for use of the PowerPlate.

TOWARDS PREVENTING CANCELLOUS BONE COLLAPSE: CERVINE MODEL AND FRACTURE IMAGING

Nicole C. Corbiere, Kathleen A. Lewicki, Kathleen A. Issen, and Laurel Kuxhaus

Clarkson University, Potsdam, NY, USA
email: lkuxhaus@clarkson.edu, web: http://people.clarkson.edu/~lkuxhaus/

INTRODUCTION

Fractures occur frequently in those with bone diseases, such as osteoporosis or osteopenia, which alter the structural and material properties of cancellous bone [1]. While fracture likelihood can be clinically estimated, the fracture initiation location cannot be predicted or prevented. Structural failure of a material is related to its geometry, the mechanical properties of the material, and the loading conditions. For example, vertebral compression fractures are common in patients with osteoporosis; burst fractures occur in those with osteopenia. Fracture likelihood may increase at certain postures. Thus, the long-term research goal is to predict fracture initiation location from cortical and cancellous bone geometry. Ultimately this information can be used to prevent vertebral fractures through prescribed exercise (mechanical loading) to strengthen trabeculae in those at risk.

To achieve these goals, fractures must be created mechanically in bones and the fractured trabecula regions must be identified both before and after fracture. This work uses cervine vertebrae, an appropriate model for mechanical testing [2,3]. This study demonstrates the feasibility of the mechanical testing and imaging methods, as a step towards clinical fracture prevention.

METHODS

A previously developed method for aligning the vertebrae during compression was used [3]. Three male cervine spines (white-tailed - thoracic and lumbar regions) were dissected; this resulted in 18 three-vertebra motion segments; one was used during load frame tuning, and is thus excluded from this analysis. Deer Spines A (DSA) and B (DSB) were approximately 6 months old and Deer Spine C (DSC) was approximately 18 months old. In preparation for mechanical loading, each three-vertebra motion segment was potted in Bondo™ (Auto Body Filler, 3M, St. Paul, MN) with half of the cranial and half of the caudal vertebrae submerged. The compressive load was transferred through the center of the intervertebral disc [6].

As described in [3], a Micro-Computed Tomography (μCT) scan (GE Phoenix Nanotom, General Electric, Wunstorf, Germany) was taken of the segment before and after compression (Figure 1). Each potted segment was placed in a loading fixture, gripped in a load frame (Instron 1331, Norwood, MA), and compressed at a rate of 0.5 mm/min until an abrupt load drop was observed. Two segments (DSB and DSC) were preconditioned (as in [7]) prior to compression. The data were analyzed from 0.0 mm to 8.0 mm of displacement; this range encompassed the mechanical response prior to any load drop in all segments.

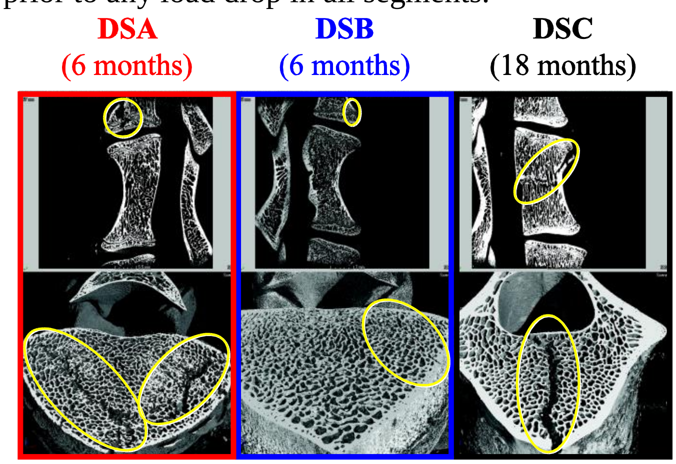

Figure 1: μCT scans showing a median plane view and 3D rendering; ovals indicate regions of fracture.

RESULTS AND DISCUSSION

Compression fractures were created in all 17 motion segments. Endplate fractures were common in the thoracic (7 of 11) and lumbar (3 of 6) vertebrae. Failure load increased from the cranial to the caudal segments, as expected, given the increasing cross-sectional area of vertebrae in the caudal direction. The two younger motion segments (DSA and DSB) fractured in the caudal endplate of the L1 vertebra, similar to a burst facture that would occur with trauma or osteogenesis imperfecta. DSC fractured in the vertebral body of L2, as shown in Figure 1, similar to osteoporotic vertebral fractures in humans. This apparent association between donor deer age and fracture type suggests that age of the specimen may influence fracture mode.

Figure 2 shows force versus displacement, both normalized at 8.0 mm of displacement. This normalization approximates a stress-strain curve for the motion segment.

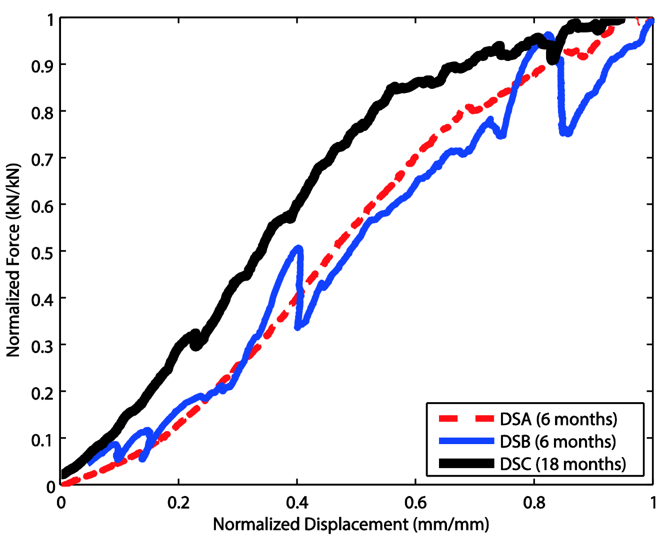

Figure 2: Normalized force-displacement for L1-L3 segments. The two noticeable peaks in DSB could indicate facet locking or other physical interference.

Since these normalized curves are not coincident, this suggests that, as expected, variations in vertebral geometry, such as cortical shell thickness and cancellous micro-structure, are important in deformation and failure processes. The convex-upward shape of these curves suggests that the deformation and failure progressed similarly for these motion segments, despite the different fracture types. The µCT scans, which show that each motion segment has formed fractures passing through both the cortical shell and cancellous structure of a single vertebra, confirm the similar processes. However, these similar loading conditions created different fracture types (as seen in Figure 1) in different specimens, so it is necessary to inspect the intact trabecular geometry in the regions which fractured.

CONCLUSIONS

This preliminary work suggests that the age of the donor animal may be an important factor in influencing fracture mode during mechanical loading. For example, to study osteoporotic compression fractures, older cervine specimens would be more appropriate, while younger specimens may be better models for osteogenesis imperfecta. Future work will test more specimens of a variety of ages, and in several different postures. The long-term goal is to quantify common parameters used to describe the trabecular geometry prone to failure. These trabeculae represent the weakest structural location; patient-specific exercise regimes could strengthen trabeculae via remodeling in these regions. Patient compliance should therefore decrease the incidence of vertebral fractures in those with bone diseases.

REFERENCES

1. *National Osteoporosis Foundation*, Fast Facts – Fractures, 2011.
2. Kumar N et al. *Anat. Rec.* **260**, 189-203, 2000.
3. Corbiere N et al. *ASB Annual Meeting*, 2012.
4. Rapillard L et al. *J Biomech* **39**, 2133-9, 2006.
5. Ebbesen E et al. *Bone* **25**, 713-24, 1999.
6. Brown S et al. *J Biomech* **41**, 122-7, 2008.
7. Buckley J et al. *Spine Journal* **9**, 478-85, 2009.

ACKNOWLEDGEMENTS

We thank Drs. Mathew Ingraham and David Morrison for load frame expertise, Cassie Christman and Lisa Ferrucci for potting help, and the machine shop at Clarkson University.

EFFECT OF SENSORY MANIPULATION ON THE ABILITY TO MAINTAIN PINCH FORCE

Ying-Ling Tseng, Na Jin Seo

University of Wisconsin-Milwaukee, Milwaukee, WI, USA
E-mail: tsengy@uwm.edu, Web: pantherfile.uwm.edu/seon/www/

INTRODUCTION

Sensory feedback from mechanoreceptors is essential for a person's ability to maintain force production during grip and object manipulation [1], especially in the absence of visual feedback [2]. While subthreshold stochastic vibrotactile stimulation has been shown to improve the fingertip's tactile sensation via the mechanism called stochastic resonance [3], its impact on motor control has not been much studied. Therefore, the objective of this study was to determine the effect of tactile sensory manipulation on persons' ability to maintain pinch force in the absence of visual feedback. Specifically, we examined the effect of vibrotactile stimulation to enhance tactile sensation as well as a bandage on the fingertip pad to decrease the tactile sensation while people maintain pinch force.

METHODS

Fifteen healthy subjects (19-36 years old, free of neuromuscular disorders) were instructed to maintain an isometric precision pinch grip at a target force level. Visual feedback for the target and actual pinch forces was given only for the first 8 seconds and then disappeared for the remaining 12 seconds of pinch grip. The pinch force error was determined as the absolute mean difference between the target pinch force and actual pinch force during the last 12 seconds of pinch without visual feedback, normalized by the target force (in % target force). Pinch force was measured using two load cells (Mini40, ATI Industrial Automation Inc., Apex, NC, USA).

The pinch force error was compared among three tactile sensory manipulation conditions and two target force levels. The three sensory manipulations were: bandaged thumb and index finger with DuoDERM CGF Extra Thin Dressings (ConvaTec Inc., Skillman, NJ, USA; Fig.1a); vibrotactile stimulation off condition simulating normal pinching; and vibrotactile stimulation on condition aiming for enhanced tactile sensation via stochastic resonance. The two target pinch forces were 5% and 20% maximum voluntary contraction (MVC) following a previous study [2].

The vibrotactile stimulation protocol including the stimulation locations and intensities followed our previous study that has shown effectiveness in enhancing tactile sensation [4]. Specifically, white noise with frequencies between 0 to 500 Hz was generated by EAI C-3 Tactor (Engineering Acoustics Inc., Casselberry, FL, USA; Fig. 1b-c). The vibrotactile stimulation was applied to one of five locations in the hand at a time: dorsum hand over the 1^{st} metacarpal bone, dorsum hand over the 2^{nd} metacarpal bone, thenar eminence, dorsal wrist, and volar wrist (Fig. 2). Vibrotactile stimulation intensities were at 60% and 80% of the sensory threshold. The sensory threshold was determined at each stimulation location for each subject.

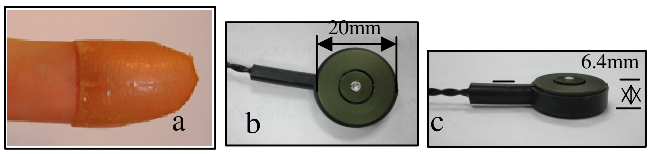

Figure 1: The sensory manipulations using the bandage (a) or vibrotactile stimulation (b, c).

Each condition was tested twice. Practice trials were given to ensure that subjects could reach and maintain the target force within +/- 1% MVC in the first 8 seconds. The non-dominant hand was used because the non-dominant hand typically reaches target force more slowly [4], maintains target force less accurately [5], and thus has more room to improve compared to the dominant hand.

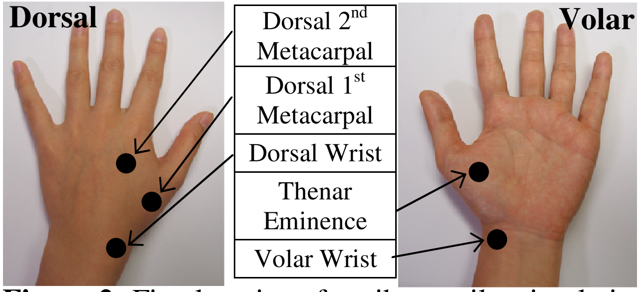

Figure 2: Five locations for vibrotactile stimulation.

Analysis of variance determined if the pinch force error was affected by sensory manipulation (bandaged finger, stimulation off/on), target force, stimulation intensity and location (nested under the stimulation on condition), and their interactions.

RESULTS AND DISCUSSION

The pinch force error changed with tactile sensory manipulation differently depending on the target force level ($p<.05$ for sensory manipulation × target force; Fig. 3). During pinch at 5% MVC, the bandaged finger resulted in 3.0% higher mean error compared to the normal pinching condition (stimulation off) (Fig. 3). The stimulation, on average, resulted in 0.5% lower error compared to the normal pinching condition. During pinch at 20% MVC, the error changed little with the tactile sensory manipulation and even slightly increased with stimulation.

The pinch force error was, on average, lower during pinch at 5% than 20% MVC ($p<.01$). Post-hoc analysis showed that the error was lower for the 5% than 20% MVC target force for the stimulation off and on conditions ($p<.01$), but not for the bandaged finger condition ($p>.05$). The locations and intensities of the vibrotactile stimulation did not significantly affect the pinch force error ($p>.05$).

The increased pinch force error with the bandages during pinch at 5% MVC may be due to the bandages blocking mechanoreceptors from receiving appropriate tactile information. At 20% MVC, the mechanoreceptors may have been overloaded and people may rely on sensorimotor memory [2] without tactile information. Vibrotactile stimulation marginally reduced error at 5% MVC, possibly because young healthy adults already have good tactile sensation even for the non-dominant hand. At 20% MVC, slight increase in the error with vibrotactile stimulation may represent the masking effect of the vibrotactile stimulation in perceiving strong signals [3].

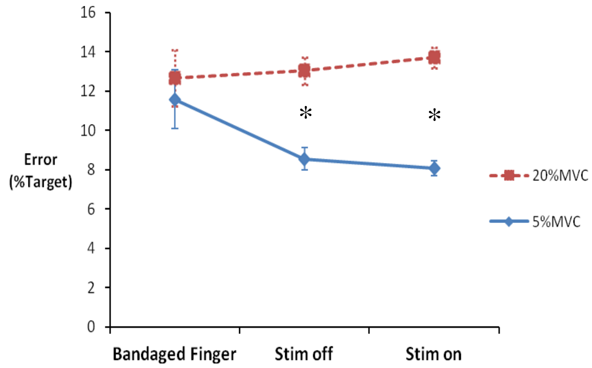

Figure 3: The pinch force error (mean ± standard error) normalized by the target force changed with tactile sensory manipulation (bandaged fingers, stimulation off, and on) differently depending on the target pinch force level.

CONCLUSIONS

Tactile sensation is crucial for maintaining a pinch force at the low force level, but not at the high force level. In precision tasks such as surgery, covering on the skin (e.g., bandage, glove) or existence of low-level vibration may influence mechano-receptors' sensing, tactile sensation, and thus the task performance at low force levels.

REFERENCES

1. Augurelle AS, et al. *J Neurophysiol* **89**, 665-671, 2003
2. De Serres SJ and Fang NZ. *Can J of Physiol and Pharmacol* **82**, 693-701, 2004
3. Collins JJ, et al. *Physical Review E* **56**(1), 923-926, 1997
4. Enders, LR, Seo, NJ. *The 42nd SfN*, New Orleans, LA, 2012.
5. Peters M. *Can J Psychol* **32**: 257–261, 1980
6. Henningsen H, et al. *Exp Brain Res* **105**: 304–311, 1995

ACKNOWLEDGMENT

We thank the Clinical and Translational Science Institute of Southeastern Wisconsin for funding.

LOW-COST VIRTUAL REALITY GAME FOR UPPER LIMB REHABILITATION USING KINECT AND P5 GLOVE

Jayashree Arunkumar, Pilwon Hur, Binal Motawar and Na Jin Seo

University of Wisconsin, Milwaukee, WI, USA
email: arunkum2@uwm.edu, web: pantherfile.uwm.edu/seon/www/

INTRODUCTION

After stroke, more than 50% of survivors report disability of upper extremity function even after conventional treatments [1]. Continuous intensive rehabilitation therapies in a virtual environment may enhance recovery [2]. However, access to virtual reality rehabilitation systems is currently not optimum due to high costs [3]. The need for low-cost virtual reality rehabilitation systems for use in clinics or at home is clear. The objective of this study was to develop a low-cost virtual reality game to engage patients in interactive kitchen activities for rehabilitation using low-cost commercially available motion tracking devices

METHODS

We have developed a virtual reality kitchen game for upper limb rehabilitation using two low-cost motion tracking devices, Kinect (Microsoft, Redmond, WA, USA) and P5 Glove (Essential Reality, LLC, New York, NY, USA) (Fig. 1). Kinect is used to detect the 3D position of the whole arm. The P5 Glove is used to capture the flexion/extension of individual digits and the 3D position and orientation of the hand.

The 3D virtual kitchen environment was developed using open-source software, Blender (Fig. 2). Users can interact with objects in the kitchen by moving their hand and arm whose motions are detected by the motion tracking devices and mimicked by the virtual hand and arm in the kitchen in real time (Fig. 3). A client program receives the joint position data from the motion tracking devices and transmits it to the server program (game engine in Blender) through a User Datagram Protocol connection. The server program then computes joint angles and maps them to the virtual arm. The virtual arm thus follows the user movement.

Compensatory movements such as reaching by moving the trunk [4] are programmed not to contribute to arm reaching to guide users toward normal reaching motion. To enhance the sense of reality, gravity is simulated in this kitchen such that objects fall to the floor if a user drops or pushes them.

Figure 1: Motion tracking devices used in the game (www.microsoftstore.com, vrealities.com)

Figure 2: 3D kitchen environment developed

Figure 3: Virtual arm reaching to grasp a glass

The game requires a user to perform a variety of functional tasks that involve grasping, moving and releasing of kitchen items, inspired by the clinical test, Fugl-Meyer Assessment. These tasks focus on individual and mass flexion/extension of the digits, grasping objects in different sizes and shapes, forearm pronation/supination, elbow extension, and shoulder abduction. For instance, the user is asked to move different items (plates, glasses, soda cans, soup cans) from the counter to an overhead shelf or from the overhead compartment to the cabinet under the counter to practice reaching and grasping motions.

In another task, the user has to pick up assorted utensils such as spoons, forks and knives one by one from the countertop and place them inside a drawer to practice precision grasps. The user is also asked to put toppings on a pizza or prepare salad using multiple ingredients to practice hand and arm coordination. The ingredients are in various shapes and sizes (e.g., pepperoni slices, salt shaker, dressing bottle, lettuce) to expose the user to various grip postures. In addition, the user is asked to flip an hour glass, dial a rotary phone, and wipe the table with a kitchen towel to practice other functional movements with the arm and hand.

To motivate the user, points are awarded per good performance by the user. If the user picks up a wrong item, places an item in an incorrect location, or performs with undesirable hand/arm postures, partial credits will be given. These points are stored to track and display to the user their own progress over repeated game plays.

RESULTS AND DISCUSSIONS

We have developed a virtual kitchen rehabilitation game containing a dynamic virtual arm. The virtual arm follows the user movement in real time well enough for playing the game. However, the need to improve accuracy and remove occasional jittering for the virtual arm movement exists for aesthetics and sense of reality, possibly by enhancing filtering and motion description algorithm for the data obtained from the low-cost devices. Additional future work includes user–specific calibration to accommodate patients with different functional capacities or ranges of motion and refinement of instructions for users.

This kitchen game with Kinect and P5 Glove demonstrates strong potential and feasibility for low-cost rehabilitation game systems for home or clinic use. The expected cost for this system is $310 for the hardware, as can be seen in Table 1. The game setup and content is designed to provide entertainment along with physical activity needed for rehabilitation.

CONCLUSIONS

We have developed a low-cost virtual game for patients to perform kitchen activities as a game with the virtual arm and hand. This kitchen game has the potential to complement occupational therapy and improve sensorimotor function of impaired hand and arms. Upon further technical and instructional improvements of the game, evaluation of the game for patients with hand/arm impairments will be performed to determine clinical efficacy and define future improvement needs.

REFERENCES

1. Peter RW, et al. *Stroke*, **28**, 507-512, 1997.
2. Henderson A, et al. *Topics in Stroke Rehabilitation*, **14**, 52-61, 2007.
3. Deutsch JE, et al. *Physical Therapy. J*, **88,** 1196-1207**,** 2008.
4. Cirstea MC, et al. *Brain*, **123**, 940-953, 2000.

Table 1: System cost analysis

System component	**The current system**	**Other options**
Arm motion detection system	Microsoft Kinect ~ $250	Optotrack ~$60,000
Finger motion detection	P5 Glove ~ $60	CyberGlove ~$10,000
Programming Toolkit	Blender (free software)	WorldToolKit ~$6,000

BIOMIMETIC ROCKER PROFILE RESTORES SHANK PROGRESSION DURING WALKING WITH ORTHOTIC ANKLE CONSTRAINT

[1]Simisola Oludare, [1]Christopher Hovorka, [1]Tiffany Yan, [1]Young-Hui Chang, [2]Géza Kogler
[1]Comparative Neuromechanics Laboratory, [2]Clinical Biomechanics Laboratory,
School of Applied Physiology, Georgia Institute of Technology, Atlanta, GA, USA

E-mail: chris.hovorka@ap.gatech.edu, Web: http://www.ap.gatech.edu/Chang/Lab/CNL/home.html

INTRODUCTION

Rocker profiles are commonly used in combination with lower limb orthoses as a motion control treatment for patients with neuromuscular deficits [**1**]. Although these designs are widely used, their motion control performance has not been clearly described [**1]**. We aim to describe the influence on shank progression by the rocker profile during walking. We hypothesized that walking with an orthosis that constrains ankle motion combined with footwear combination will elicit no difference in shank progression compared to walking with no constraint.

METHODS

The device used to constrain the ankle (talocrural) joint was a custom-made carbon fiber ankle foot orthosis footwear combination (AFO-FC) with a linear bearing locking/unlocking mechanism and a free fore-foot (Fig. 1a). The footwear portion of the AFO-FC was constructed with a series of foam materials: a low stiffness material in the heel and a high stiffness material in the mid section. For the data collection, subjects (n=3) walked on a dual belt treadmill at their comfortable walking speed for 15 minutes during a control condition which allowed free ankle plantarflexion and dorsiflexion (PFDF) and a constraint condition which stopped ankle plantarflexion and dorsiflexion (PSDS) with a 6 minute interval for rest between each condition. Movement data was collected onto the Vicon workstation via 6 high speed infrared cameras (sampling at 120 Hz) to capture coordinates of 16 passive reflective markers worn on each subject per a modified Helen Hayes protocol (in order to render a linked model of each subject's lower limb segments and joints); ground reaction force data was also collected via 2 AMTI force plates (sampling at 1080 Hz) beneath each treadmill belt. After the data was collected, it was processed and filtered in Vicon Plug-In gait and MATLAB, respectively. To quantify the shank progression during stance phase, we computed the whole and the within limb movement behaviors and the shank acceleration during the periods of stance. All data was analyzed for statistical analysis using a student's t-test.

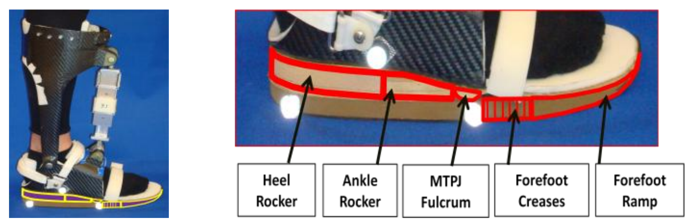

Figure 1. ***(Left)*** Custom right AFO footwear combination, ***(Right)*** Custom footwear system designed to restore lower limb roll over during constraint of shank motion by AFO. The reflective markers on the AFO-FC were used to calculate the periods of stance phase.

RESULTS

Right Ankle Constraint

During PSDS, plantarflexion and dorsiflexion constrained limb ankle motion were reduced by over 90% and 60%, respectively (Fig.2).

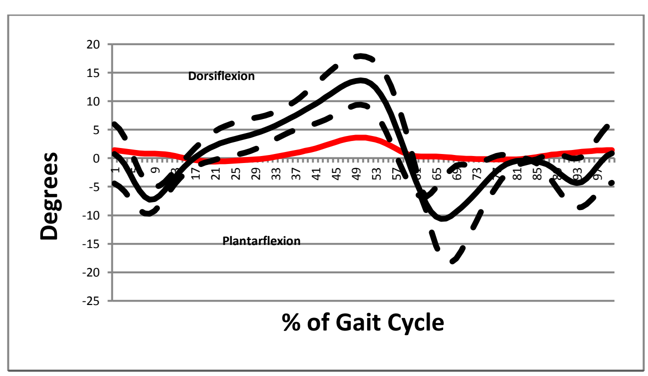

Figure 2. Mean sagittal plane angle during PFDF and PSDS for 3 subjects. The black dotted lines represent plus and minus one standard deviation from the control**.**

__Preservation of whole limb and within limb movement behaviors__

The whole limb movement behaviors analyzed were stance phase duration, step length and cadence; and the within limb movement behaviors analyzed were the ankle, knee and hip sagittal plane joint angles. There was no statistically significant difference ($p>0.05$) between PFDF and PSDS in whole limb and within limb movement behaviors for both constrained and unconstrained limbs (Table 1 and Fig. 3).

__Preservation of Shank Acceleration__

The shank acceleration was computed for the periods of stance phase. The periods of stance were calculated using the alignment of the foot over the course of the gait cycle as determined through three markers placed on the AFO-FC (Fig.1a). Although there was an increase in shank acceleration in loading response, mid and terminal stance due to ankle constraint, the differences were not statistically significant ($p>0.05$) (Table 2).

CONCLUSIONS AND DISCUSSION

Our findings support the rocker profile facilitated forward progression of the lower limb by maintaining shank acceleration in different periods of stance phase. These data suggest various components of the rocker profile serve as surrogate ankle-foot rockers to produce advancement of the lower limb during stance phase. To further clarify the performance of the rocker profile, additional analysis of the hip and knee torques on shank acceleration is needed**.**

REFERENCES

1. Hutchins S, et al. *The biomechanics and clinical efficacy of footwear adapted with rocker profiles – Evidence in the literature*. The Foot, 2009:19:165-170.

Table 1: Preservation of Whole limb movement behaviors

	Right		Left	
	PFDF	**PSDS**	**PFDF**	**PSDS**
Mean Stance Phase Duration (% of Gait Cycle)	60.42±0.21	59.30±0.64	63.10±0.34	62.80±0.16
Mean Step Length (meters)	0.91±0.01	0.89±0.01	0.95±0.11	0.94±0.01
Mean Cadence (steps/minute)	60.76±0.50	61.24±1.70	60.86±0.60	60.95±2.0

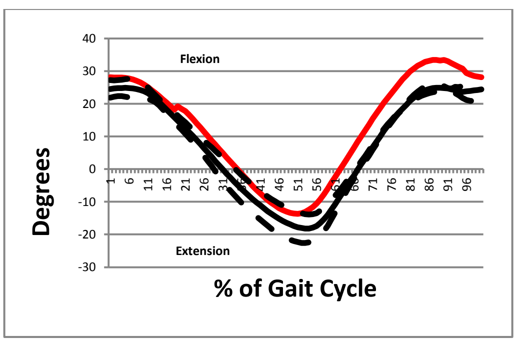

(a)

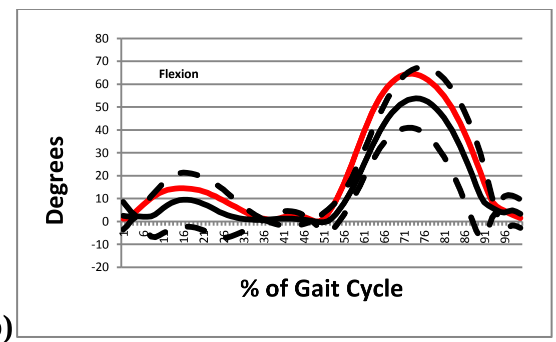

(b)

Figure 3: (a) The constrained (right) hip joint angle shows no significant difference between PFDF and PSDS **(b)** The constrained (right) knee joint angle shows no significant difference between PFDF and PSDS. The unconstrained (left) limb also shows similar results.

Table 2: The peak linear shank center of mass acceleration of the constrained is preserved in all periods of the stance phase.

	Right	
	PFDF	**PSDS**
Loading response shank acceleration (m/s^2)	4.50±1.93	5.08±1.32
Mid stance shank acceleration (m/s^2)	5.17±0.82	5.55±1.40
Terminal stance shank acceleration (m/s^2)	5.02±1.01	7.01±1.50

AN EXPLORATION OF THE ANGULAR ORIENTATION OF THE WRIST DURING ARCING AND SEMICIRCULAR WHEELCHAIR PROPULSION

[1]Lisa A. Zukowski, [1]Jaimie A. Roper, [1]Dana Otzel, [1]Patty Hovis, and [1]Mark. D. Tillman

[1]University of Florida, Gainesville, FL, USA
email: zukowski@ufl.edu

INTRODUCTION

Carpal tunnel syndrome (CTS) affects 49 to 63% of manual wheelchair users. This wrist pathology is a result of accumulated damage to the median nerve caused by compression within the carpal tunnel. Keir et al. [1] determined that wrist orientation beyond 48.6° of flexion, 32.7° of extension, 21.8° of radial deviation, or 14.5° of ulnar deviation leads to high carpal tunnel pressure levels (>30 mmHg) that are typical of median nerve damage. Wrist orientations beyond those cited above can lead to even higher pressures and faster development of chronic nerve damage. Wheelchair propulsion repetitively utilizes extreme angular orientations of the wrist, putting wheelchair users at a greater risk of developing CTS than the general population.

Semicircular and arcing propulsion are two commonly used wheelchair propulsion styles. Semicircular propulsion is characterized by long strokes, a larger range of motion, and the hand dropping below the pushrim in recovery, while arcing propulsion is characterized by short strokes, a smaller range of motion, and the hand following the pushrim in recovery. Previous research has indicated numerous advantages and disadvantages for each style but has not established the specific angular wrist orientations utilized. Determining whether one propulsion style utilizes more neutral wrist postures may enable wheelchair users to select a propulsion style that reduces trauma to the median nerve. The purpose of this project is to explore the different angular orientations of the wrist during arcing and semicircular propulsion.

METHODS

Six adults with paraplegia (three using arcing propulsion and three using semicircular propulsion, 36.2±14.3 yrs, 68.6±8.7 kg, 168.9±12.0 cm) participated in the study. All participants were medically and functionally stable and at least six months post injury.

Motion data were captured by 11 cameras as participants propelled across a length of 8 m. Each participant completed five trials at a self-selected pace using their preferred propulsion style in the same wheelchair.

Angular kinematics of the wrist were computed in the planes of flexion/extension and radial/ulnar deviation using Vicon Nexus software. A custom Matlab program was used for further processing. The pushes in each trial were combined to calculate an average push per participant. This average push was normalized to 100 time points for comparison by percentage of the total push. The maximum angular orientations of the wrist in flexion, extension, radial deviation, and ulnar deviation were compared between the propulsion styles using independent samples t-tests ($\alpha=0.10$). Because this is an exploratory study, a higher level of significance was used. Additional analyses were performed on the angular orientations that were outside of neutral as specified by Keir et al. [1]. The average wrist orientation and the percentage of time spent outside of neutral were compared between conditions using independent samples t-tests ($\alpha=0.10$). All statistical procedures were performed using SPSS 17.0.

RESULTS AND DISCUSSION

Arcing and semicircular propulsion utilize different angular wrist orientations. While most of the differences were not significant, many patterns were apparent (Table 1). Arcing propulsion utilizes more wrist flexion and less wrist extension during each

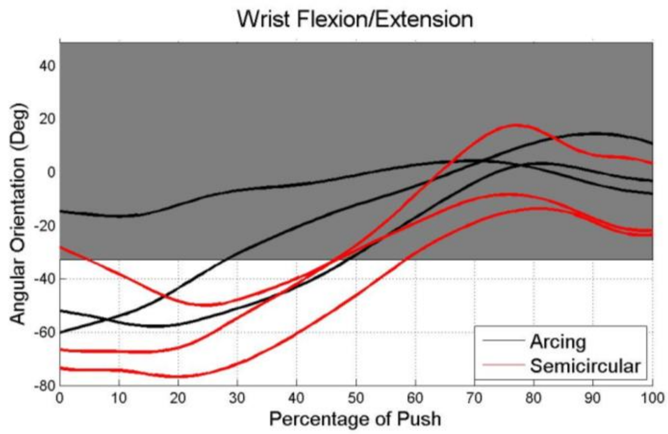

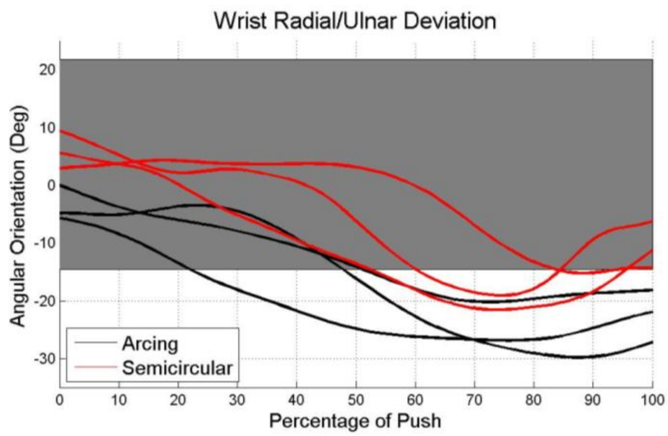

Figure 1: Wrist flexion/extension (negative values) and radial/ulnar deviation (negative values) during an average push in arcing versus semicircular propulsion. The gray box represents the limits of neutral angular orientation of the wrist.

push than semicircular propulsion (Figure 1). Further, semicircular propulsion positions the wrist 21.9° farther outside of neutral extension during 23.2% more of the push than arcing propulsion.

Some statistically significant differences and patterns for radial/ulnar deviation also became apparent (Table 1). Semicircular propulsion utilizes more radial deviation and less ulnar deviation during each push than arcing propulsion (Figure 1). Further, arcing propulsion positions the wrist 5.4° farther outside of neutral ulnar deviation during 32.6% more of the push than semicircular propulsion.

CONCLUSIONS

The more extreme ulnar deviation during arcing propulsion likely results in faster accumulation of median nerve damage. While not statistically significant, the extreme wrist extension during semicircular propulsion also possibly results in median nerve trauma. The continued self-selection of both propulsion styles may be explained by inter-individual differences in the effects of non-neutral extension and ulnar deviation.

REFERENCES

1. Keir PJ, et al. *Hum Factors* **49**, 88-99, 2007.

Table 1: Independent t-tests comparing wrist range of motion used with arcing versus semicircular propulsion.

	Arcing	Semicircular	Significance
Flexion			
Maximum (Deg)	7.58 ±6.15	-0.99 ± 16.7	p = 0.451
Extension			
Maximum (Deg)	-45.0 ± 24.7	-65.7 ± 13.3	p = 0.270
Percent of Time Outside of Neutral (%)	25.7 ± 24.5	48.9 ± 8.63	p = 0.198
Average Orientation Outside of Neutral (Deg)	-33.3 ± 28.8	-55.2 ± 11.0	p = 0.319
Radial Deviation			
Maximum (Deg)	-2.91 ± 2.83	6.53 ± 2.55	***p = 0.013**
Ulnar Deviation			
Maximum (Deg)	-25.8 ± 4.99	-18.8 ± 3.17	p = 0.109
Percent of Time Outside of Neutral (%)	59.7 ± 15.7	27.1 ± 15.6	***p = 0.063**
Average Orientation Outside of Neutral (Deg)	-22.7 ± 3.67	-17.3 ± 2.16	***p = 0.093**

Note. All values are mean ± standard deviation.

Variability of peak shoulder force during wheelchair propulsion as a function of shoulder pain

[1]Yaejin Moon, [2]C Jayaraman, [3]I.M. K. Hsu, [1]I.M. Rice, [3]E.T. Hsiao-Wecksler, [1]J.J. Sosnoff

[1]Department of Kinesiology and Community Health, [2]Department of Industrial and Enterprise Systems Engineering, [3]Department of Mechanical Science and Engineering, University of Illinois at Urbana-Champaign
email: ymoon9@illinois.edu

INTRODUCTION

Manual wheelchair users have a high prevalence of shoulder pain [1]. There is growing evidence that less variability in forces applied to biological tissue is related to the existence and development of chronic musculoskeletal pain [2].

Previous studies examining the effects of shoulder pain on wheelchair propulsion have focused on the average resultant force placed on the shoulder during wheelchair propulsion [3,4]. Consequently, very little information concerning the variability of forces applied to the shoulder is available.

The purpose of this investigation was to examine the variability of the resultant force acting on the shoulder during wheelchair propulsion as a function of shoulder pain in manual wheelchair users. It was predicted that manual wheelchair users with pain would demonstrate less variability of peak resultant force than those without pain.

METHODS

26 manual wheelchair users (14 females, 12 males, age=24.1±8.9years) participated in the investigation. Inclusion criteria included one year of manual wheelchair experience, and use of a manual wheelchair for 80% of their daily mobility. The participants' injury were diverse including spinal cord injury (n=11), spina bifida (n=9), cerebral palsy (n=2), and other (n=4). Participants were divided into groups based on self-report of shoulder pain. 12 subjects self-reported current shoulder pain, while 14 subjects reported no pain. For participants with pain, the shoulder with the most pain was analyzed. For participants without pain the dominant shoulder was analyzed (Right=20, Left=6).

Participants' wheelchairs were placed on a roller with a tie-down system. The participants were asked to propel at a fast speed of 1.1m/s, a self-selected speed (0.9±0.2m/s), and a slow speed of 0.7m/s for three minutes maintaining a constant speed. Kinetic data were collected with SMART wheels (Three Rivers Holdings, LLC, Mesa, AZ) that measures three-dimensional forces and torques applied to the push rim. Kinematic data were collected with motion capture system (Motion Analysis Co., Santa Rosa, CA) with eighteen markers at specific bony landmarks on the body. Both kinetic and kinematic data were collected at 100Hz and were digitally filtered with low pass Butterworth filter fourth order zero phase with 10Hz and 7 Hz cutoff frequency, respectively.

Inverse dynamics analysis was performed to calculate resultant forces applied to the shoulder during wheelchair propulsion using custom MATLAB code (The MathWorks, Natick, MA) based on previous study [3]. Peak values of resultant force during the push phase of each propulsion cycle were identified (Figure 1) and analyzed. Within individual variability was quantified as the coefficient of variation (CV=Standard deviation/Average) of cycle to cycle peak resultant forces.

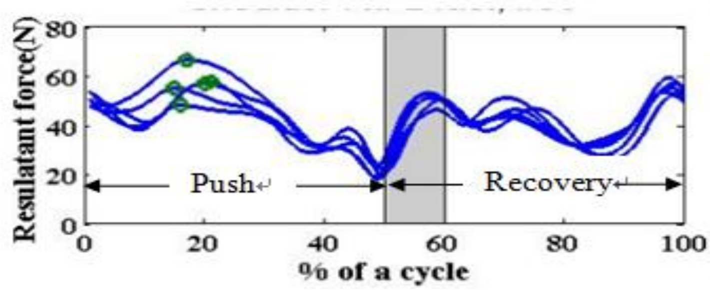

Figure 1: Sample of shoulder resultant force of five consecutive cycles indicating a peak with a dot.

All statistical analyses were performed using SPSS (V19.0, Chicago, IL). One-way analysis of covariance (ANCOVA) was used to compare peak shoulder force variability between pain and no pain group with body weight as a covariate in the analysis. Due to our directional hypothesis a one-tailed analysis was used with an alpha of 0.05.

RESULTS AND DISCUSSION

Analysis of group differences of demographics (e.g. age, gender composition, height, etc) revealed that body weight was significantly different. The pain group (75.4±12.6 kg) was heavier than the no pain group (59.4±26.5kg) (t-test, p=0.04). No other differences were noted.

Average Peak Resultant Force: Results from the study are presented in Table 1. The group with shoulder pain showed larger average peak force than the no pain group only in the fast propulsion condition. This result is consistent with previous reports and suggests that individuals with shoulder pain have a tendency to load larger forces on the shoulder during wheelchair propulsion [4].

Variability of Peak Resultant Force: The pain group had a significantly smaller CV of peak resultant force than the no pain group across all propulsion speeds. This is congruent with the proposition that decreased variability is associated with musculoskeletal pain or injury [2]. There are at least two potential reasons that the no pain group demonstrated greater variability than the pain group. First, it is possible that shoulder pain causes individuals to constrain their shoulder range of motion that results in decreased variability.

Secondly, it is possible that lower amounts of variability of peak shoulder force could be an underlying mechanism that leads to the development of shoulder pain by demanding relatively constant load on shoulder.

CONCLUSIONS

There was significantly less within individual variability of peak force in the push phase during wheelchair propulsion in wheelchair users with shoulder pain than those without shoulder pain. This observation is consistent with our hypothesis that variability of force applied on the shoulder is related to shoulder pain in wheelchair users. However, due to a cross sectional study design, the study cannot address whether decreased variability was a cause or a result of pain. Further work may investigate the relationship between pain and variability of shoulder forces with a longitudinal design or an experimental manipulation of pain [2]. In addition, uni-dimensional forces and moments should be studied to assess which direction of force and moment mainly influences variability of load on shoulder.

ACKNOWLEDGEMENTS

This project is funded in part by the Nation Institute of Health grant (#1R21HD066129-01A1). The authors extend their gratitude to Shawna Culp and Katie White for their assistance.

REFERENCES

1. Gutierrez, D. D. et al, *J Spin Cord Med, 30*(3), 251-255., 2007
2. Srinivasan, D., & Mathiassen, S. E. *Clin Biomech, 27(10), 979-993., 2012*
3. Collinger, J. L. et al, *Arch Phys Med Rehab, 89*(4), 667-676., 2008
4. Mercer, J. L., et al., *Clinic Biomech, 21*(8), 781-789. 20

Table 1: Comparison between groups with/without pain to peak shoulder forces as a function of speed.

		Pain		No pain		p-value
		AVG	STD	AVG	STD	
Fast speed (1.1 m/s)	Peak force Average (N)	48.79	13.82	35.74	9.82	*0.04
	Peak force Standard deviation (N)	5.38	2.10	5.07	1.65	0.14
	Peak force Coefficient variation	0.11	0.04	0.14	0.05	*0.01
Self selected speed (0.9±0.2 m/s)	Peak force Average (N)	47.26	12.62	35.84	11.06	0.06
	Peak force Standard deviation (N)	5.00	2.36	4.66	1.62	0.35
	Peak force Coefficient variation	0.11	0.04	0.13	0.04	*0.02
Slow speed (0.7 m/s)	Peak force Average (N)	45.15	12.53	34.84	10.78	0.10
	Peak force Standard deviation (N)	3.83	1.61	4.03	1.61	0.22
	Peak force Coefficient variation	0.09	0.02	0.12	0.04	*0.02

Note: AVG=Average, STD=Standard deviation

RACING WHEELCHAIR ERGOMETER AND CONFIGURABLE WHEELCHAIR VALIDATIONS

[1,2]Jean-Luc Lessard, [1,2]Jean-Philippe Pelland-Leblanc, [1,2]Geneviève Masson, [1,2]Denis Rancourt, [1,2]Eve Langelier, [1,3]Félix Berrigan, [1,3]Jean Laroche and [1,2]Cécile Smeesters

[1]Human Performance and Safety Research Group (PERSEUS), Sherbrooke QC, Canada
[2]Department of Mechanical Engineering, Université de Sherbrooke, Sherbrooke QC, Canada
[3]Department of Kinanthropology, Université de Sherbrooke, Sherbrooke QC, Canada
e-mail: Cecile.Smeesters@USherbrooke.ca web: http://www.usherbrooke.ca/gmecanique

INTRODUCTION

In wheelchair racing, athletes must be properly positioned in their wheelchair in order to perform. Although a few experimental studies have looked at the influence of an athlete's position on wheelchair propulsion [1], there is no consensus on the optimal position to improve performance. One of the reasons may be that it is not easy to realistically simulate track conditions such as aerodynamic drag, rolling friction, athlete-wheelchair inertia and center of mass position. Indeed, to adequately optimize an athlete's position, one must be confident that laboratory results will be transferable to the track.

Three types of ergometers are typically used to reproduce wheelchair propulsion in the laboratory (Table 1), but none have all the capabilities necessary to optimize an athlete's position. For this reason, the PERSEUS group chose to develop a hybrid type of ergometer consisting of a motorized roller ergometer with a configurable wheelchair simulator. It can be used with either the athlete's wheelchair or the configurable wheelchair. Moreover, it can reproduce track conditions including drag, friction and inertial force and to some extent the "wheelie effect" (front wheel lift).

Table 1: Ergometer capability to optimize position

Ergometer type		Simulate track	Use athlete's wheelchair	Change position
Treadmill [1]		+	+	–
Roller	Free roller [1]	–	+	–
	Brake unit [1,2]	±	+	–
	Motor unit [1]	+	+	–
Wheelchair simulator [1,3]		+	–	+

+ = possible, ± = not completely possible, – = not possible

The purpose of this study was to determine if the PERSEUS ergometer realistically simulates the track conditions and if the configurable wheelchair realistically simulates the athlete's wheelchair.

METHODS

A wheelchair athlete on the Canadian development team performed a series of 100m and 400m races: a) on the track or the ergometer using the athlete's wheelchair (track-ergometer validation), and b) on the ergometer using the athlete's wheelchair or the configurable wheelchair, which was set to exactly replicate the position on the athlete's wheelchair (athlete-configurable wheelchair validation).

Four variables were used to quantify the athlete's performance: the total race time, the maximum speed achieved, the total number of pushes and a distance constant (δ = distance travelled when 63% of the maximum speed is reached, Figure 1). For the track tests, a stopwatch (time), a 5Hz GPS (speed and distance) and a 30Hz video camera (pushes) were used. For the ergometer tests, a high resolution encoder and a motor-controller processing data at 2 kHz (time, speed, pushes and distance) were used.

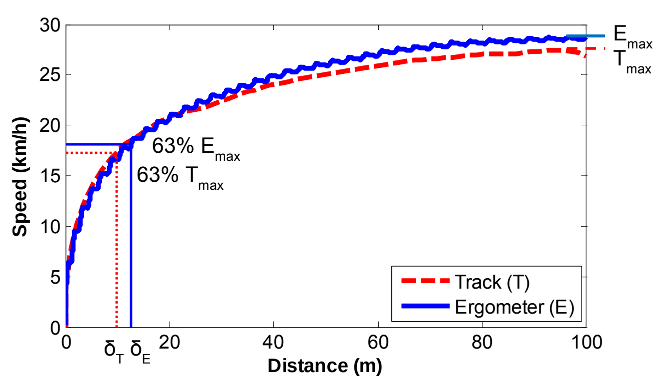

Figure 1: 100m race speed versus distance profile.

For the track-ergometer validation, the track session (am = morning) always preceded the ergometer session (pm = afternoon), so that the wind speeds could be measured during the track sessions and replicated on the ergometer. For the athlete-configurable wheelchair validation, a random order was used for the athlete's wheelchair (am/pm) and configurable wheelchair (pm/am) sessions. The am and pm sessions were separated by a minimum of 3h and included in order: 15min warm-up, wind measurement (track only), 100m race, 15min rest, 5min warm-up, wind measurement (track only), 400m race, cool down. Finally, the daily sessions were repeated over 3 days and 2 months separated the two validations.

Wilcoxon's non-parametric tests were used to determine the effect of track-ergometer or athlete-configurable wheelchair on all four variables.

RESULTS AND DISCUSSION

For the track-ergometer validation using the athlete's wheelchair (Table 2, left), there were no significant differences between the track and ergometer results for the 4 variables ($p \geq 0.109$). Therefore, using accurate simulation conditions, it is possible to use this ergometer to realistically simulate track conditions and transfer ergometer results to the track. Note that a greater sample size might show significant, but explainable, differences between the track and ergometer. Indeed, the ergometer does not simulate the 2 turns present in a 400m race, so a difference in race time and number of pushes was anticipated, since the athlete must use one arm to push and the other to execute the 3 steering changes on the track. Furthermore, the athlete had some difficulty remaining in his lane on the track due to his lack of experience.

For the athlete-configurable wheelchair validation on the ergometer (**Table 2**, right), there were no significant differences between the athlete's and configurable wheelchair results for the 4 variables ($p \geq 0.109$). Therefore, it is possible to use this configurable wheelchair to realistically simulate the athlete's wheelchair and transfer results from the configurable wheelchair to the athlete's wheelchair.

CONCLUSIONS

The racing wheelchair ergometer and configurable wheelchair developed in this project can thus be used to find an athlete's optimal position. A new wheelchair replicating this position could then be built for the athlete, which should improve performance on both the ergometer and the track.

REFERENCES

1. Vanlandewijck Y, et al. *Sports Med* **31**(5), 339-367, 2001.
2. Devillard X, et al. *Eur J Appl Physiol*, **85**(5), 479-485, 2001.
3. Niesing R, et al. *Med Biol Eng Comput*, **28**(4), 329–338, 1990.

ACKNOWLEDGEMENTS

The athletes of the Centre d'entraînement de haute performance de Sherbrooke for their participation as test subjects as well as NSERC, the Institut National du Sport du Québec and Athletics Canada for financial support.

Table 2: Racing wheelchair ergometer and configurable wheelchair validations (mean±SD).

	Track (T) versus Ergometer (E)					**Athlete's (A) versus Configurable (C) wheelchair**				
	Test	**100m**		**400m**		**Test**	**100m**		**400m**	
		Mean±SD	**p**	**Mean±SD**	**p**		**Mean±SD**	**p**	**Mean±SD**	**p**
Race time (s)	T&A	16.94±0.44	1.000	57.39±1.57	0.109	E&A	16.16±0.57	1.000	55.74±3.48	0.593
	E&A	16.90±0.35		55.04±1.36		E&C	16.19±0.74		56.00±2.76	
$Speed_{max}$ (km/h)	T&A	28.65±1.07	1.000	29.24±0.49	0.285	E&A	29.66±0.97	0.593	30.41±1.55	0.109
	E&A	28.55±0.68		29.57±0.64		E&C	29.99±1.67		30.02±1.38	
N_{push}	T&A	41.0±1.0	0.655	123.3±6.1	0.109	E&A	39.0±2.6	0.180	114.7±11.5	0.180
	E&A	40.7±2.3		118.0±7.2		E&C	38.0±3.5		117.7±11.2	
δ (m)	T&A	12.92±2.66	0.285	12.94±0.36	1.000	E&A	11.56±0.14	0.285	12.71±0.89	0.593
	E&A	11.76±0.44		13.24±1.77		E&C	12.46±1.10		12.82±0.69	

EFFECTS OF IMPACT EXPOSURE AND THERMAL ANNEALING ON MECHANICAL PROPERTIES OF AN AMERICAN FOOTBALL HELMET OUTER SHELL MATERIAL

David E. Krzeminski, Dilhan Fernando, Nadine M. Lippa, James W. Rawlins, Trenton E. Gould, Scott G. Piland

The University of Southern Mississippi, Hattiesburg, MS, USA
e-mail: david.krzeminski@eagles.usm.edu; web: www.usm.edu/shpm

INTRODUCTION

Degradative effects from a multitude of impact events and environmental conditions, along with periodic reconditioning exposure over the life-span of football helmets, are poorly understood. Changes to the outer shell materials may induce a systematic reduction in protective performance, potentially leading to a higher risk for head injury in athletes. Mechanical stress placed upon rubber toughened polycarbonate (PC) or polyethylene terephthalate (PET) will generate microscopic voids via particle cavitation which will macroscopically manifest to visibly whiten the material [1]. Pilot work has elucidated whitening in collegiate helmet outer shells after a single season [2]. Further, thermal annealing just above a material's glass transition temperature (T_g) is reported to rejuvenate its thermo-mechanical history [1].

Moreover, helmet outer shells are reused without a publicly available technical understanding between repetitive impact exposure inducing aesthetically unfavorable whitening and impact performance. The purpose of this study was to investigate the effects of impact exposure and thermal annealing on impact, bulk, and surface mechanical properties of an American football helmet outer shell material.

METHODS

Helmet-grade rubber-toughened PC/PET blend material (T_g = ~150°C) was injection molded into 4" x 6" x 1/8" plaques to match the thickness of an American football helmet outer shell. Four material conditions (non-impacted, non-impacted/annealed, impacted, and impacted/annealed) were investigated (Figure 1). Impact tests were performed upon a helmet surrogate plaque-foam system comprised of a plaque stacked atop 1" VN600 foam using an instrumented drop tower system (Dynatup 9250HV, Instron, Norwood, MA) [3]. The drop mass assembly of 5.04 kg contained a 44 kN load cell tup and a 2" diameter polyurethane dart (200H, Lixie Hammers, Central Falls, RI) with a measured Shore hardness (72 D) comparable to the helmet-grade plaque (81 D). Plaque-foam systems were impacted at 5.5 m/sec under ambient conditions against a 1" modular elastomer programmer (MEP) pad anvil [4, 5]. After an initial impact to quantify the performance of a non-impacted plaque (trial 1), an impact treatment of ten repetitive trials was performed (trials 2-11) followed by a final impact (trial 12) (Figure 1). Trials 1 and 12 were analyzed via a dependent t-test. Impact performance was measured with a 13th trial comparing impacted and impacted/annealed plaques, and results analyzed via an independent t-test. A total of 190 impacts were performed. Randomly selected plaques underwent a thermal annealing treatment at 175 °C for 5 minutes and then air cooled. Color change was quantified per CIELAB scale using a spectrophotometer (BYK Gardner, Columbia, MD) and analyzed via a one-way repeated measures ANOVA with 3 levels (pre-impact, pre-anneal, and post-anneal).

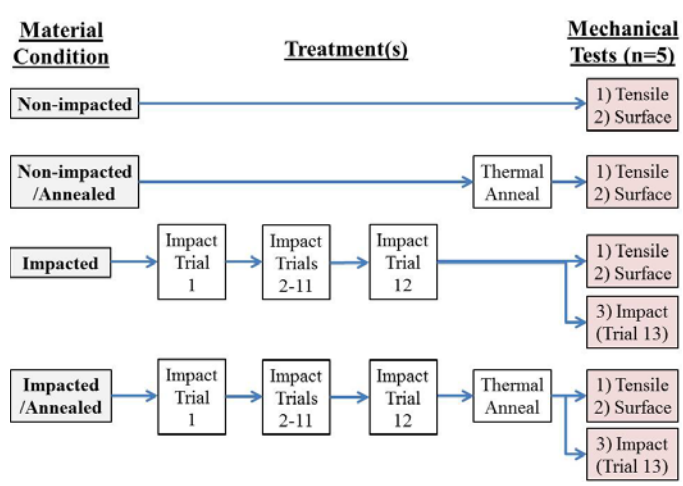

Figure 1: Experimental design showing treatments and mechanical tests across material conditions.

Tensile mechanical properties were measured (Insight 10, MTS, Eden Prairie, MN) at a strain rate of 25 mm/min and results analyzed via three separate one-way ANOVAs with 4 levels (material condition). Modified ASTM-D638 Type I tensile specimens (3.5" x 0.5" strips) were cut directly from plaques. Surface mechanical properties were quantified using load-controlled quasi-static nanoindentation (TI 900 Triboindenter, Hysitron, Minneapolis, MN) at pre-selected loads of 500, 1000, 1500, 2000, and 2500 μN, and analyzed with a 4 between (material condition) x 5 between (applied load) ANOVA. Post-hoc analyses were performed via Tukey HSD tests. For all statistical analyses, alpha level was set a priori at $\alpha = 0.05$.

RESULTS AND DISCUSSION

Each impact test induced visible whitening to the plaque. Furthermore, the change in characteristic curve shape between non-impacted and impacted plaques (Figure 2) along with a significant difference in mean peak force between trials 1 and 12 ($t=7.93$, $p<0.05$, $d=1.47$) indicated the impact treatment adequately induced a change in plaque impact performance. The visible disappearance of whitening along with a significant difference in mean L* ($F_{2,8}=563.38$, $p<0.05$) indicated the thermal annealing treatment adequately erased the impact-induced whitening.

The absence of significance in mean peak force along with no qualitative change in curve shape between impacted and impacted/annealed (Figure 2) suggested that the annealing treatment did not alter the impact energy management capabilities of a plaque with an impact history of 12 repetitive trials.

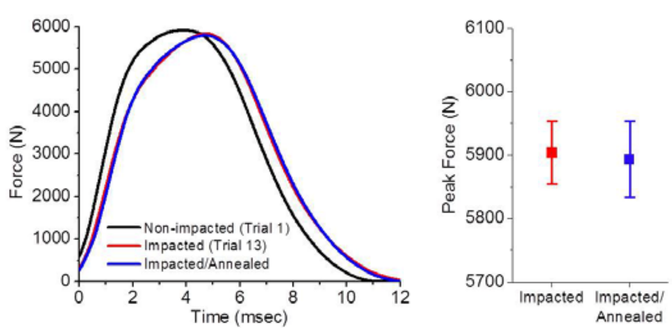

Figure 2: (left) Smoothed force-time curves for plaque-foam systems and (right) mean peak force for impacted and impacted/annealed plaques.

For surface, a difference in mean reduced modulus was observed ($F_{3,80}=4.35$, $p<0.05$, $f=0.39$) with annealed samples lower than non-annealed ($p<0.05$) (for a given impacted condition). Therefore, only annealing altered the surface mechanical properties up to a measured depth of ~1 μm.

Differences observed for yield stress ($F_{3,16}=6.93$, $p<0.05$, $f=1.32$) and ultimate tensile strength (UTS) ($F_{3,16}=21.21$, $p<0.05$, $f=2.30$) indicated both the impact and anneal treatments altered bulk tensile properties (Table 1). Impacted UTS was higher ($p<0.05$) than other conditions, indicating a change in strain hardening behavior during stress-strain testing. Further analysis revealed reductions in both Young's modulus (observed trend) and reduced modulus ($p<0.05$) when comparing annealed and non-annealed conditions, thus suggesting annealing softened the material. All impacted tensile specimens preferentially yielded at the whitened area. Whereas, impacted/annealed specimens did not preferentially yield at the whitened area that existed pre-anneal. As a result, annealing just above T_g aesthetically recovered the helmet-grade plaque, and potentially rejuvenated the thermo-mechanical history of the engineered material. Absence of surrogate-system differences in impact performance may be attributed to setup limitations, thus future work will employ a more accurate impact protocol. Our findings warrant exploring the effects of annealing outer shells as a potential way to mitigate the risk of head injury by providing greater helmet life-span consistency.

Table 1: Tensile properties of material conditions.

Material Condition	Tensile Mechanical Properties		
	Young's Modulus (MPa)	Yield Stress (MPa)	Ultimate Tensile Stress (MPa)
Non-impacted	955.5 ± 27.1	56.2 ± 0.3 ^{1}	44.0 ± 0.2 ^{1}
Non-impacted/Annealed	920.7 ± 26.7	55.0 ± 0.8 ^{1,2}	43.4 ± 1.9 ^{2,4}
Impacted	934.6 ± 21.6	55.3 ± 0.3	45.8 ± 0.2 ^{1,2,3}
Impacted/Annealed	910.9 ± 32.6	56.5 ± 0.8 ^{2}	44.7 ± 0.3 ^{3,4}

* Matching superscript number denotes post-hoc combination significance ($p<0.05$)

REFERENCES

1. Haward R and Young R. *Physics of Glassy Polymers*, 2nd Ed., Applied Science, Ltd., 1997
2. Krzeminski D. 2012 [unpublished data]
3. Krzeminski D, et al. *Sports Tech*, **4(1-2)**, 65, 2011
4. 001-11m11a, NOCSAE DOC (ND). 2011
5. ASTM F1446-11a. 2011. ASTM International

EVALUATING UPSAMPLING METHODS FOR 3-D KINEMATIC DATA

Steven Leigh[1] Jesus Dapena[2], Michael Gross[3], Li Li[4], Joseph Myers[3], and Bing Yu[3]

Montclair State University, Montclair, NJ, USA[1]
Indiana University, Bloomington, IN, USA[2]
The University of North Carolina at Chapel Hill, Chapel Hill, NC, USA[3]
Georgia Southern University, Statesboro, GA, USA[4]
email: leighst@mail.montclair.edu

INTRODUCTION

Prosumer high definition digital video (HDV) camcorders are commonly used to record sports activities to provide feedback to participants. These cameras may also used with the Direct Linear Transformation procedure to calculate real-life 3-D body landmark coordinates, for further quantitative analyses. HDV cameras record video images with a high resolution of 1920 x 1080 pixels, and are lightweight and portable. A significant disadvantage of these cameras is that they typically operate at a sampling frequency of 60 frames/second, which may be too low for analyzing high speed movements, such as throwing or kicking. Cameras with greater sampling frequencies tend to be considerably more expensive, or record images with significantly lower resolutions (640 x 480 pixels). Upsampling landmark coordinate data from HDV cameras would allow them to be used in a wider variety of settings with greater confidence in their accuracy, however, the errors associated with upsampling these data have not yet been determined. The purpose of this study, therefore, was to compare three-dimensional body landmark data calculated from video clips recorded at 60 frames/second and upsampled to 300 frames/second using linear interpolation and Shannon's sampling theorem with three-dimensional body landmark data calculated from video clips recorded at 300 frames/second natively.

METHODS

The trial with the longest official distance for the top ten female and male javelin throwers competing in the 2008 USATF Olympic Team Trials were included in this study. All throws were recorded from behind and from the right side of the javelin runway with two camcorders operating at 300 frames/second. Twenty-four body and javelin landmarks were manually digitized to obtain 2-D coordinate data at native 300 Hz from the video clips. These 2-D data were resampled at 60 Hz to produce a native 60 Hz data set. The native 60 Hz dataset was then upsampled to 300 Hz using a linear interpolation method. The native 60 Hz dataset was also upsampled to 300 Hz using Shannon's sampling theorem [1]. This resulted in three 2-D datasets with 300 Hz sampling frequencies: Set 1 native 300 Hz, Set 2 upsampled using linear interpolation, and Set 3 upsampled using Shannon's sampling theorem. Each of these three datasets were time synchronized using multiple critical events [2]. The Direct Linear Transformation procedure was used to obtain real-life 3-D coordinate data [3].

The 3-D coordinate data were compared between Set 1 and Set 2, and between Set 1 and Set 3 to evaluate errors due to the upsampling procedure. The mean absolute difference was calculated for the X (medial-lateral), Y (anterior-posterior), and Z (superior-inferior) coordinates of each body landmark between datasets. Set 2 and Set 3 were also compared to Set 1 using the coefficient of multiple correlation (CMC) to evaluate the similarity of the overall coordinate-time curves [4].

RESULTS AND DISCUSSION

The mean absolute difference between coordinate data upsampled to 300 Hz and data sampled natively at 300 Hz was less than 1% for distal landmarks and less than 4% for proximal landmarks. There was no difference between the errors found by comparing Set 1 to Set 2, or by comparing Set 1 to Set 3. The mean absolute difference was greatest for the right and left hip joint centers, where errors ranged from 0.05 meters along the medial-lateral axis to 0.02 meters along the superior-inferior axis. The mean absolute difference was smallest for the grip of the javelin, where errors were 0.01 meters along any axis.

The coefficient of multiple correlation was close to 1.000, indicating excellent reproducibility among coordinate-time curves for all landmarks. There was no difference between the CMCs found by comparing Set 1 to Set 2, or by comparing Set 1 to Set 3. The CMC was smallest for the right and left hip joints, and was 0.950. The CMC was greatest for the grip of the javelin, and was 0.999. The average CMC for all landmarks was 0.997.

The differences in the errors observed for the proximal landmarks compared with the distal landmarks are probably due to digitizing inconsistency when identifying the landmark. The digitizer was well trained with hundereds of hours of experience, however, digitizing was conducted with participants in a real-life situation, and proximal landmarks were difficult to identify. Conversely, distal landmarks were clear in every frame and were consistently identified.

Upsampling from 60 Hz to 300 Hz using linear interpolation or Shannon's sampling theorem introduces small errors and inconsistencies, and is a suitable method to be used with cheap, portable HDV cameras for high speed movements.

REFERENCES

1. Hamill J, Caldwell EC, & Derrick TR. *J Appl Biomech* **13(2)**, 226-38, 1997.
2. Yeadon MR, & King MA. *J Biomech* **32**, 983-6, 1999.
3. Abdel-Aziz YI, & Karara HM. *ASP Symposium on Close Range Photogrammetry*, Falls Church, VA, USA, 1971.
4. Yu B, *et al*. *J Orthop Res* **15**, 348-52, 1997.

ACKNOWLEDGEMENTS

This project was financially supported by USATF, the International Society of Biomechanics, and the University of North Carolina Graduate School.

THE INFLUENCE OF SHOULDER ROTATION ON SHOULDER KINETICS IN CATCHERS THROWING FROM THE KNEES

Hillary A. Plummer and Gretchen D. Oliver
Auburn University, Auburn, AL, USA. email: hplummer@auburn.edu

INTRODUCTION

A study examining shoulder injuries in high school baseball and softball athletes found that softball pitchers, first basemen, and catchers had an equal likelihood of sustaining shoulder injuries [6]. In addition, a study following 481 youth pitchers for 10 years determined that pitchers who also played catcher had two to three times higher risk of injury [3]. Injury statistics such as these have led to the evolution from focusing on throwing mechanics of pitchers to now examining catchers' mechanics when throwing to second base.

Catchers throwing to second base have a shorter stride length, open foot position, closed foot angle, and reduced pelvis-trunk separation at foot contact as well as excessive elbow flexion during arm cocking and less forward trunk tilt at ball release than pitchers' throwing long toss [4]. These differences led the authors to speculate that catchers may have an inefficient throwing motion. Another study examined the kinematic and kinetics of two different age groups of catchers throwing to second base from the stance [10]. This study revealed that pelvis-trunk separation was less than those reported by Fortenbaugh et al [4]. The group of younger catchers displayed greater upper extremity segmental velocity and pelvis rotation earlier in the throwing motion than those values displayed by the older catchers. It was therefore speculated that a rushed throwing motion may lead to dysfunction of the kinetic chain ultimately leading to greater upper extremity segmental velocities and kinetics due to the upper extremity compensating for lost energy.

Catchers not only have the option to throw from a squatted stance position when attempting to throw out a stealing base runner but may also throw from the knees. In many instances the method in which they chose to throw is determine by pitch location. The ideal pitch for a catcher to throw out a base runner is high and outside because this allows them to easily come out of the stance while avoiding the batter. However this ideal situation does not always occur and if the pitch is in the dirt the catcher must adapt and will often chose to throw from the knees. It is believed that throwing from the knees allows for the fastest release of the ball thus increasing the likelihood of throwing out the stealing base runner.

While it is currently unknown if throwing from the knees is truly beneficial it is important to examine the throwing mechanics from the knees. Throwing from the knees eliminates a majority of the kinetic chain (legs, hip, trunk) responsible for force production during dynamic activities such as throwing. The lower extremity has been reported to generate 54% of total force during a tennis serve emphasizing the importance of the proximal segments during dynamic movement [5]. The absence of the lower extremity may not only alter efficient kinetic chain sequencing but also may cause the glenohumeral joint to adapt and become a force producer to transfer forces to the ball. Thus the purpose of this study was to examine the influence of shoulder rotation on shoulder compressive forces in catchers throwing to second base from the knees.

METHODS

Twenty-two baseball and softball catchers (14.04 ± 4.05 years; 162.54 ± 18.91 cm; 62.21 ± 22.08 kg) participated. Participants were selected based on criteria that included coach recommendation, multiple years of catching experience, and freedom from injury within the past six months. Informed consent was obtained prior to testing.

The MotionMonitor^{TM} (Innovative Sports Training, Chicago, IL) synched with electromagnetic tracking system (Flock of Birds Ascension Technologies Inc., Burlington, VT) was used to collect data. Participants had a series of 10 electromagnetic sensors (Flock of Birds Ascension Technologies Inc., Burlington, VT) attached at the following locations: (1) the medial aspect of the torso at C7; (2) medial aspect of the pelvis at S1; (3-4) bilateral distal/posterior aspect of the upper arm; (5-6) bilateral distal/posterior aspect of the forearm; (7-8) bilateral distal/posterior aspect of lower leg; and (9-10) bilateral distal/posterior aspect upper leg [8-10]. The collection rate for these data describing the position and orientation of electromagnetic sensors was set at 144 Hz. Raw data were independently filtered along each global axis using a 4th order Butterworth filter with a cutoff frequency of 13.4 Hz. Raw data regarding sensor orientation and position were transformed to locally based coordinate systems for each of the respective body segments. Euler angle decomposition sequences were used to describe both the position and orientation. ISB standards and conventions were used to define trunk and shoulder movements. The catching surface was positioned so that the participant's knees would land on top of a 40 x 60 cm Bertec force plate (Bertec Corp, Columbus, Ohio) that was anchored into the floor. Force plate data were sampled at a frequency of 1000 Hz.

Following the attachment of the electromagnetic sensors and subsequent digitization, participants were given an unlimited time to warm-up in their gear (helmet, chest protector, and shin guards). Once the participants deemed themselves warm, testing began. In order to best simulate a game experience, the participant received a pitch from a pitcher and then threw the ball to a position player on second base. Data were collected for five accurate throws. An accurate throw to second base was one in which the position player did not have to move off the base when receiving the throw.

The throwing motion was broken down into the events of knee contact (KC), maximum shoulder external rotation (MER), ball release (BR), and maximum shoulder internal rotation (MIR) (Figure 1). Knee contact was defined as the point in the throwing motion where the participants' knees landed on the force plate as they dropped down to their knees to initiate the throw. Descriptive statistics and Pearson Product Moment Correlation Coefficients were calculated to identify relationships between humeral elevation and shoulder moment and compressive force. Type I error rate was set *a priori* at $p \leq 0.05$ and each event of throwing was analyzed independently.

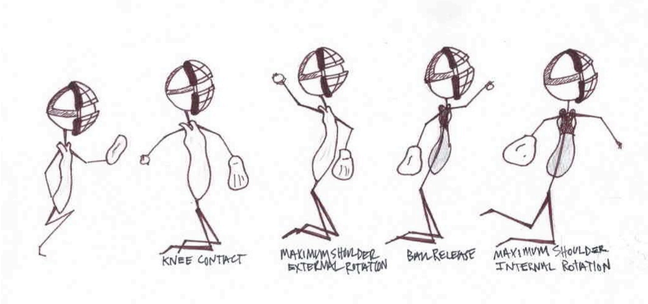

Figure 1: Events of the throwing motion from the knees.

RESULTS AND DISCUSSION

Shoulder kinematic and kinetic data are presented in Table 1. Maximum shoulder rotation was obtained at MER and averaged 100.4° of external rotation. Shoulder compressive force displayed the greatest value at BR reaching 803.2N. A significant relationship between shoulder rotation and shoulder compressive force was observed during MER ($r = -0.5$, $p = 0.01$) and BR ($r = 0.5$, $p = 0.02$).

Maximum shoulder rotation in younger catchers was reported to be 103.6° and older catchers reached 124.2°. The difference in shoulder rotation between younger and older catchers may reflect developmental differences due to age, osseous and soft tissue adaptations, or may be indicative of a rushed throwing motion. The amount of shoulder external rotation observed in catchers throwing from the knees is similar to the values reports in younger catchers throwing from the stance. The degree of shoulder external rotation has been reported to be proportional to the magnitude of stress imposed at the shoulder and elbow of pitchers, with the greatest stress occurring at MER [6,11]. In the current study, shoulder compressive force peaked at the point of BR whereas pitching and throwing from the stance produced the greatest kinetics at MIR [1-2,10]. Shoulder compressive force during the deceleration phase of pitching was reported to be 1090 N by Fleisig et al [1]. Additionally, production of maximum shoulder compressive force in pitchers resulted in minimal shear force anteriorly and inferiorly [1]. The difference in where maximum kinetics about the shoulder occurred between pitchers and catchers throwing from the stance compared to catchers throwing from the knees may be due to altered kinematics throughout the throw. The rotator cuff musculature acts to provide a compressive force necessary to resist shoulder distraction during throwing. The inability of the rotator cuff to adequately generate compressive force during throwing may lead to increased shoulder distraction ultimately placing not on the stabilizing musculature at risk for injury but also the glenoid labrum.

CONCLUSIONS

It is evident by the presented data that when catchers throw to second base from their knees, relationships exist between shoulder rotation and shoulder compressive force. Due to the excessive shoulder compressive force placed on the shoulder when throwing from the knees, this type of throw may need to be reduced or eliminated in catchers. Over time, large compressive force may lead to rotator cuff, glenoid labrum, or biceps tendon injury in catchers. Future research should examine both shoulder and elbow kinetics in catchers throwing from their knees to better understand potential injury risks.

REFERENCES

1. Fleisig GF, et al., *Am J Sports Med*. **23**(2):233-239, 1995.
2. Fleisig GF, et al., *J Biomech*. **32**:1371-1375, 1999.
3. Fleisig, GF, et al., *Am of Sports Med*. **39**:253-257, 2011.
4. Fortenbaugh D, et al., Proceedings of XXVIII International Society of Biomechanics in Sports Conference, Marquette, USA, 2010.
5. Kibler WB, *Clin Sport Med*. **14**:79-86, 1995.
6. Krajnik S, et al., *Pediatrics*. **125**:497-501, 2010.
7. Miyashita K, et al., *Am of Sports Med*. **38**:363-368, 2010.
8. Myers JB, et al., *Am of Sports Med*. **33**:263-271, 2005.
9. Oliver GD, et al., *J Strength Cond Res.* **24**:3015-3022, 2010.
10. Plummer HA, et al., *J Sports Sci:*2013.
11. Werner SL, et al., *Am of Sports Med*. **29**:354-358, 2001.

Table 1: Means and standard deviations at each event of the throw.

	KC	MER	BR	MIR
Shoulder Rotation (°)	-11.2±47.6	-100.4±49.2	-66.7±53.9	36.5±45.9
Shoulder Compressive Force (N)	15.2±53.2	326.8±488.4	-803.2±553.0	487.0±339.2

COMPARISON OF ANKLE STABILIZATION TECHNIQUES IN INDIVIDUALS WITH FUNCTIONAL ANKLE INSTABILITY

[1,2]H. McKelle Ulm and [1]Douglas W. Powell

Campbell University, Buies Creek, NC, USA
email: ulmh@campbell.edu, web: www.campbell.edu

INTRODUCTION

Lateral ankle sprains are a common occurrence in athletics with most sprains occurring in the Anterior Talofibular ligament (ATF) [1]. Disruption of the ATF not only results in a loss of mechanical stability, but also reduces proprioceptive feedback to the central nervous system. The loss of mechanical and dynamic stability often results in repeated sprains leading to functional ankle instability (FAI) [2].

Several interventions have been utilized to combat the deleterious effects of functional ankle instability on health and athletic performance including the use of ankle stabilizers [3]. Two common ankle stabilizers include ankle taping and ankle bracing. It has been demonstrated that ankle braces reduce the recurrence of ankle sprains; however, the mechanisms associated with efficacy of ankle bracing may increase the magnitude of forces transferred to higher joint structures including the knee.

Therefore, the purpose of this study was to quantify the effects of ankle bracing and taping on ankle and knee joint forces and moments during a landing task. It was hypothesized that ankle bracing and taping would be associated with reduced ankle joint forces and moments while concurrently increasing knee joint forces and moments.

METHODS

Fourteen recreational athletes (7 FAI, 7 Control) participated in this study. Participants were grouped based on self-reported scores on the Functional Ankle Instability Questionnaire (Hubbard & Kaminski, 2002). Questionnaire scores were confirmed via manual testing via anterior drawer and talar tilt tests, conducted by a single National Board Certified Athletic Trainer (HMU).

After assessment, participants performed a ten-minute warm up using a stationary cycle. Participants then performed three successful single-leg landing trials from a height of 0.60 meters in each of three conditions: Normal, Taped and Braced. Ground reaction forces (GRF, 960 Hz, AMTI, Watertown, MA, USA) and three-dimensional kinematics (120 Hz, 4-camera, Vicon, Oxford, UK) were recorded simultaneously.

Three-dimensional kinematics and GRFs were filtered using a 4th order Butterworth filter at 10 Hz and 50 Hz cutoff frequencies, respectively. Custom software (Matlab 2009, Mathworks, Natick, MA, USA) was used to calculate ankle and knee ranges of motion, and joint moments in the sagittal plane.

A 2 x 3 (group by condition) repeated measures analysis of variance with Tukey's post-hoc was used to determine significant effects of group and bracing condition for each measurement. Significance was set at $p < 0.05$.

RESULTS AND DISCUSSION

Table 1 presents peak vertical ground reaction forces, ankle and knee ranges of motion, and peak ankle and knee joint moments in each experimental condition.

The findings of this study demonstrate that ankle braces and ankle taping do not significantly alter peak vertical GRF ($p = 0.460$), sagittal plane ranges of motion (Ankle: $p = 0.863$; Knee: $p = 0.082$) or joint moments (Ankle: $p = 0.580$; Knee: $p = 0.877$) at the ankle and knee.

Further, no significant differences in peak vertical GRF ($p = 0.815$), sagittal plane ranges of motion (Ankle: $p = 0.784$; Knee: $p = 0.474$) or joint moments (Ankle: $p = 0.885$; Knee: $p = 0.850$) were observed between the healthy Controls and individuals with FAI.

These data demonstrate that sagittal plane mechanics are not different between individuals with FAI and healthy Controls. Due to the mechanism of injury, it is likely that differences in frontal or transverse plane mechanics may exists between these two functionally different groups.

These data further demonstrate that ankle stabilizers do not significantly alter lower extremity mechanics in the sagittal plane during a landing task. However, due to the design of ankle bracing, it is suspected that ankle bracing may result in altered frontal plane mechanics, potentially reducing forces associated with ankle sprains. Alternatively, ankle taping and bracing may provide additional sensory feedback to the central nervous system altering muscle activation strategies reducing the risk of ankle sprain.

The authors acknowledge there are limitations to the present study. Specifically, the small sample size reduces the generalizability and the statistical power. Further research should include investigation into other potential mechanisms of efficacy of ankle stabilizers including frontal and transverse plane mechanics and muscle activation patterns.

CONCLUSIONS

The findings of this study demonstrate that ankle stabilizers do not alter ankle and knee mechanics during a landing task. Further research is needed to expand the understanding of the mechanisms by which ankle stabilizers reduce ankle sprains.

REFERENCES

1. Fong, DT, et al. *Sports Med* **37**, 73-94, 2007.

2. Gribble, PA, et al. *Phys Ther Sport* **11**, 3-7, 2010.

3. Gross & Lu. *J Ortho Sports Phys Ther* **33**(10): 572-577, 2003.

Table 1: Peak vertical ground reaction forces, and ankle and knee ranges of motions and peak joint moments during the landing task in normal, braced and taped conditions. Presented mean (SD).

Group	Condition	pVGRF	Ankle ROM	Ankle Moment	Knee ROM	Knee Moment
Control	Normal	3.8 (0.3)	31.2 (7.6)	0.27 (0.15)	39.3 (7.7)	0.07 (0.13)
	Brace	3.7 (0.4)	30.1 (10.3)	0.18 (0.12)	38.4 (6.8)	0.06 (0.12)
	Tape	3.8 (0.4)	29.6 (5.7)	0.19 (0.12)	43.1 (5.9)	0.07 (0.10)
FAI	Normal	3.5 (0.6)	30.8 (12.5)	0.22 (0.18)	35.5 (11.8)	0.08 (0.10)
	Brace	3.8 (0.7)	29.8 (8.4)	0.22 (0.18)	33.7 (8.7)	0.09 (0.14)
	Tape	3.8 (0.6)	28.3 (8.3)	0.20 (0.17)	37.4 (9.7)	0.05 (0.12)

INTER-RATER RELIABILITY OF TWO COMMERCIAL 3D MOTION CAPTURE SYSTEMS

[1,2]Michael P. McNally, [1]Benjamin D. Roewer, [1,3,4]Timothy E. Hewett

[1],OSU Sports Medicine, Sports Health and Performance Institute, Ohio State University, Columbus, OH, USA
[2]Ohio State University, School of Health and Rehabilitation Sciences, Columbus, OH, USA
[3]Ohio State University, Depts. of Physiology and Cell Biology, Orthopaedic Surgery, Family Medicine, and Biomedical Engineering, Columbus, OH, USA
[4]Cincinnati Children's Hospital, Division of Sports Medicine, Cincinnati, OH, USA
email: michael.mcnally@osumc.edu

INTRODUCTION

Motion capture techniques are a commonly used in research settings to record and quantify human movement. They have been used in prospective research studies to identify biomechanical risk factors for athletic injuries such as anterior cruciate ligament (ACL) injuries. One study evaluated 205 females athletes and found that the peak knee abduction angle and knee range of motion were significant contributors to future ACL injury risk [2]. There were 9 ACL injuries in that cohort. In order to obtain the larger samples required for prospective studies, multi-center approaches to data collection may be necessary. However, data collected across several institutions may include more sources of error than data collected at a single site, thus making it difficult to confidently aggregate or compare data across sites.

One potential factor that may affect reliability of data is the use of different motion capture systems across sites. The use of a single system has shown excellent reliability within a testing session when testing a drop vertical jump [1]. Another study has shown excellent reliability for measurement of segmental foot kinematics across multiple institutions [3]. Common sources of kinematic variability include intra-subject, trial-to-trial variability and error in marker placement. To date, the reliability of data collected simultaneously has not been documented in order to characterize the variability introduced using different motion capture systems.

The purpose of this study was to assess the reliability of peak joint angles computed using data collected simultaneously on two different commercial, three-dimensional (3D) motion capture systems.

METHODS

Eighteen college football players were recruited to take part in laboratory research as part of a larger prospective coupled biomechanical-epidemiological study. Two motion capture systems (12camera, Raptor-4, Motion Analysis, Santa Monica, CA; and 10-camera, MX-40, Vicon, Oxford, UK) were set up in the same laboratory space to collect motion data simultaneously. Each camera system was independently aimed, focused, and calibrated according to manufacturer specifications to ensure that each camera had a 2D image error of less than 0.2 mm. A modified Helen Hayes marker set comprised of 55, 9 mm, retro-reflective markers was used with additional markers placed on the iliac crest, and bilaterally on the thighs, shanks, and feet. 3D marker position data was captured simultaneously with each system at 240 Hz while subjects performed three drop vertical jumps from a 31-cm box [2].

Marker position data were labeled and gaps less than 24 frames in length were filled using a cubic spline interpolation inherent within each system's motion capture software. Marker data from both systems were analyzed in Visual 3D (C-Motion Inc., Rockford, MD), to filter trajectories using a 4th order low-pass Butterworth filter with a 12 Hz cut-off frequency and compute Euler joint angles.

Following all collection, processing and quality control procedures, eight subjects were analyzed that contained complete matched knee data for both systems. Each leg from each of three drop jump trials was considered as an independent measurement that resulted in 48 data points for knee flexion and knee abduction angles at initial contact, peak knee flexion angle and peak knee abduction angle. Intra-class correlation coefficients (3,1) were used to test for absolute agreement in computed joint angles between systems. Excellent reliability was defined as ICC > 0.7.

RESULTS and DISCUSSION

The reliability of all peak sagittal plane joint angles in the ankle, knee and hip were rated as excellent. Of particular interest, knee flexion angles at initial contact, peak knee flexion and peak knee extension were all rated as excellent (ICC = 0.990, 0.999, and 0.731, respectively). The knee abduction angle at initial contact, peak knee abduction angle, and peak knee adduction angles were also rated as excellent (ICCs = 0.992, 0.844, 0.974, respectively). Bland-Altman plots are presented in Figure 1 to display the magnitude and variability of peak knee flexion and peak knee abduction angles measured using each system.

While data from two motion capture systems seems to be highly reliable, sources of variability appeared to be present that likely inhibited perfect agreement. One consideration is the greater variability of peak frontal plane angles. Peak frontal plane angles, while showing high reliability, also showed slight differences between systems (-1.17 and 0.45 degrees for valgus and varus angles). These differences could have significant implications for classification of individuals based on a specific cutoff point (i.e. determining high risk vs. low risk). In addition, small changes in joint angles may have a more pronounced effect on joint moments, which have been implicated as a significant variable when investigating ACL injury risk [2].

CONCLUSIONS

With high reliability and differences in angles of less than two degrees, which may not be clinically meaningful, the results of this study support the contention that data may be compared across multiple motion capture systems, provided standardized collection and processing procedures are administered. This has important implications for research, as it increases the possibility to obtain larger sample sizes across multiple sites, which is key to increasing generalizability and in obtaining sample sizes required for prospective studies to investigate injury risk.

REFERENCES

1. Ford KR, et. al. *Med Sci Sports Exerc* **39**, 2021-2028, 2007.
2. Hewett TE, et. al. *Am J Sports Med* **33**, 492-501, 2005.
3. Long JT, et. al. *Gait Posture* **31**, 32-36, 2010.

ACKNOWLEDGEMENTS

Special thanks to Stephanie Di Stasi and Sam Wordeman for assistance with data collection, Ajit Chaudhari and the OSU MAP lab for sharing lab space for data collections, and all members of the OSU Biodynamics laboratory, without which this study could not have been completed.

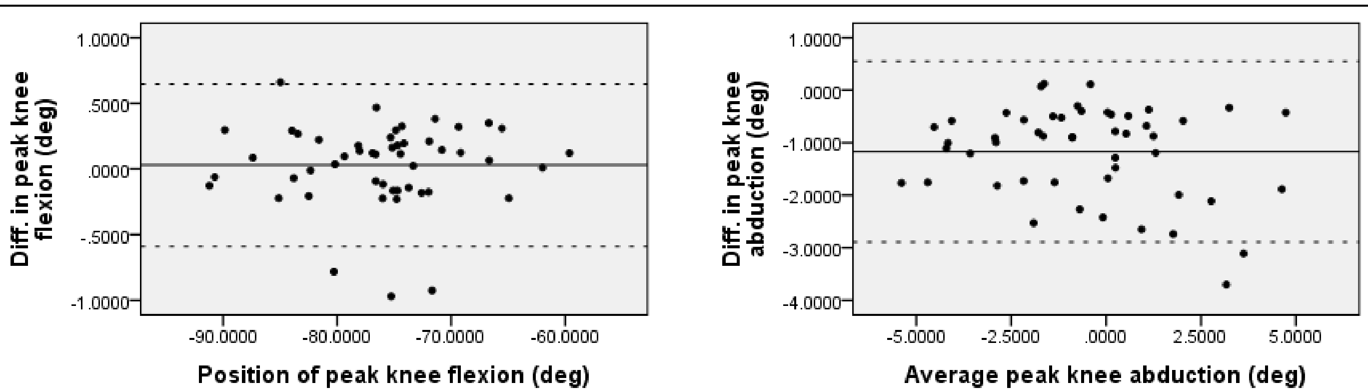

Figure 1. Bland-Altman plots for the difference between systems for peak knee flexion and peak knee abduction.

INFLUENCE OF PRE-RELEASE RANGE OF MOTION ON OVERHEAD BACK THROW DISTANCE

Ben Meyer
Shippensburg University, Shippensburg, PA, USA
email: bwmeyer@ship.edu

INTRODUCTION

Little is known about the mechanics of the overhead back throw (OHB). In the OHB throw, athletes use a countermovement technique to throw a weighted object (typically a medicine ball or shot). The countermovement consists of a descent phase and an ascent phase. (See Figure 1.) The distance traveled (ROM) by the shot during the descent phase is measured from the highest position of the shot to the lowest point in the range of motion. The ascent phase distance is measured from lowest point in the range of motion to the point of release. The sum of the descent and ascent distances is referred to as the total range of motion. Overall throw distance is measured from the starting line (the performer's feet must be behind the start line) to the closest mark made by the shot upon landing.

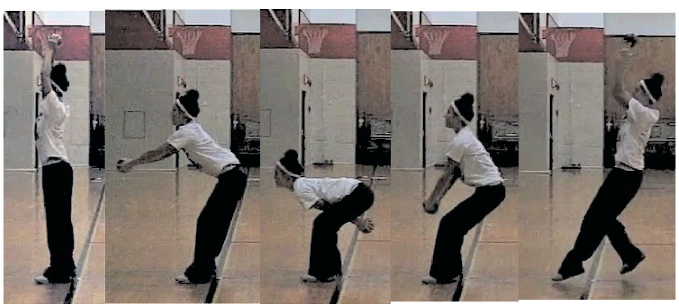

Figure 1. Overhead back throw technique.

The OHB is commonly performed by athletes in sports such as football and track & field during assessments of athletic power. The utility of the OHB as a measure of anaerobic power was investigated in Division I female basketball players, where it was found that OHB distance has a direct relationship to jumping ability, along with upper body strength and power [1].

The linear impulse-momentum relationship indicates that for an object of given mass, the greater the impulse exerted on the object, the greater the change in velocity of the object. Range of motion is often linked to time spent exerting force in throwing activities. It is therefore hypothesized that a moderate to strong relationship exists between the pre-release range of motion and the distance the object travels. The purpose of this study was to assess the relationship between pre-release range of motion and throw distances in the OHB technique.

METHODS

Eight male undergraduate students (height = 1.84 ± 0.05 m; mass = 82 ± 6 kg; age = 20 ± 1 yr) and twelve female undergraduate students (height = 1.64 ± 0.06 m; mass = 59 ± 7 kg; age = 20 ± 1 yr) participated in the study. Males used a 7.26 kg indoor shot and females used a 4 kg indoor shot to perform their throws.

Participants performed three trials, with the goal of achieving maximum distance. Each trial was recorded with a Casio Exilim EX-F1 camera at a sampling rate of 300 frames per second. For each participant, the best throw (based on largest measured distance) was used for further analysis. The center of the shot was digitized in every 15th frame of the video files using Logger Pro software to give data at 0.05 s intervals.

The pre-release range of motion values (descending, ascending, and total ROM) were computed using standard linear kinematics techniques.

RESULTS AND DISCUSSION

The results of this study are shown in Figures 2 & 3. Throw distances ranged from 4.0 m to 7.8 m for females, and from 7.3 m to 11.5 m for males. Figure 2 shows the relationship between throw distance and the total ROM. The relationship between total ROM and throw distance was very weak for females (R^2 = 0.0009), and moderate for males (R^2 = 0.42594). Figure 3 shows the relationship between throw distance and the ascending ROM. The relationship between ascending ROM and throw distance was again very weak for females (R^2 = 0.00015) and moderate for males (R^2 = 0.33569).

For females the slope of the trend line was flat between ROM (both ascending and total) and throw distance. However, for males the slope of the trend line was positive between total ROM and throw distance. Conversely, the slope of the trend line between ascending ROM and throw distance was negative for males.

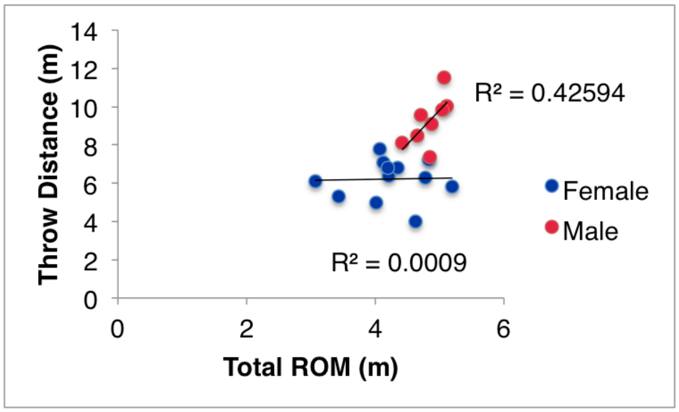

Figure 2: Relationship between throw distance and total ROM.

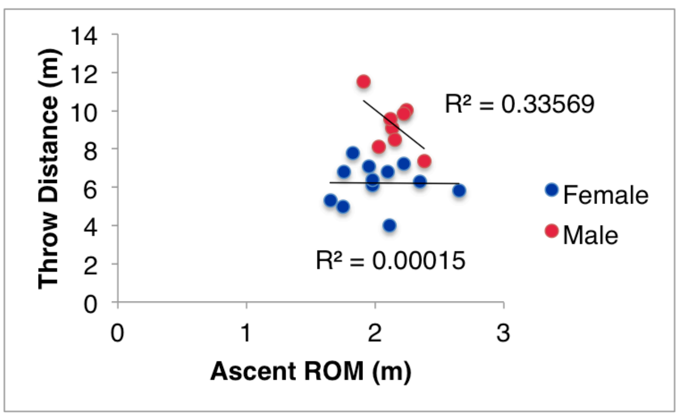

Figure 3: Relationship between throw distance and ascending ROM.

For the male participants in the study, using a larger pre-release total ROM led to larger throw distances. In contrast, the pre-release total ROM was not related to throw distance for the females in the investigation. In addition, the relationship between ascent ROM and throw distance did not match the expected outcome in either gender. This may be due to issues related to skill level and technique, as the participants in the study were not highly trained athletes and came from a wide variety of athletic participation backgrounds.

As a comparison, participants in a separate study threw a 3 kg medicine ball a distance of 12.8 m [2]. In contrast, our female subjects had an average throw distance of 6.2 m using a 4 kg shot, and our male participants threw an average of 9.3 m using a 7.26 kg shot. The distances thrown by participants in the present investigation are indicative of the heavier shots used and inexperience with the OHB technique.

CONCLUSIONS

In summary, athletes who wish to achieve large throw distances using the OHB technique should try to maximize the release velocity of the shot by the end of the pre-release ROM, as using a large ROM by itself does not guarantee a large throw distance. Athletes are also advised to use an appropriate release angle when performing the OHB throwing technique. Future research projects should address these kinematic factors, as well as kinetic factors such as lower extremity joint torques and transfer of momentum from the performer to the shot.

REFERENCES

1. Stauffer K, The comparison of the Max Jones Quadrathlon with the vertical jump and Wingate cycle tests as a method to assess anaerobic power in female Division I college basketball players, *Unpublished doctoral dissertation,* 2005.
2. Duncan MJ, et al. *Res in Sports Med,* **13**, 345-352, 2005.

ACKNOWLEDGEMENTS

The author would like to thank the participants for their assistance with this project.

THE EFFECT OF FATIGABILITY IN LOWER EXTREMITY COORDINATION PATTERNS IN SOFTBALL PITCHING

Bethany Forshaw, Tom Wu, Cara Postlmayr, and Kathleen Laquale
Bridgewater State University, Bridgewater MA, USA
Email: bforshaw07@gmail.com

INTRODUCTION

Softball is a fast growing sport, and the Amateur Softball Association (ASA) has reported that 1.3 million athletes have participated in 2008 [1]. There are two types of softball pitching, slingshot and windmill. Although one is no more accurate than the other, windmill pitching can generate a greater ball velocity because of a larger arm swing motion [2-4]. Previous research studies in other sports have indicated the importance of proper timing and sequencing of body joints to avoid injuries and increase skill performance [5-6]. Further, Frenandez, Yard, and Comstock (2005) reported that 52% of all reported sports injuries were lower extremity injuries [7]. Werner, Guido, McNeice, Richardson, Delude and Stewart (2005) indicated that windmill softball pitcher may throw between 1,200 to 1,500 pitches in a 3-day tournament [8]. The question of how fatigue would affect the pitching mechanic and performance remained to be addressed. Therefore, the purpose of this study was to examine the influence of fatigue on movement coordination patterns in windmill pitching in order to better understand the pitching mechanics and performance.

METHODS

Five female Division III college softball windmill pitchers between the ages of 18 to 23 participated in the study. Institutional ethics review board approved the study, and written informed consent was obtained prior to the study. These pitchers had no previous history of injury. The pitchers were instructed to bring their own gloves and catchers to simulate game scenario. Each pitcher was allowed to go through their normal warm-up routine for game simulation. After warm-up, six joint reflective markers were placed upon the right shoulder, hip, knee, ankle and toe joints. The five pitchers were then instructed to throw 70 fastball pitches. After every 10 pitches, the pitcher took a 2-minute break in order to simulate game activity. Only fastball pitches were chosen to prevent potential varying effects on the joint mechanics from other types of pitch. Pitching trials of #1-3 (beginning), #31-33 (middle) and #61-63 (end) were recorded, and these pitches were chosen so the researchers were able to analyze the development of fatigue over time. Joint angular velocities of the hip, knee, and ankle were analyzed with Ariel Performance Analysis System (APAS) software.

A standard two-dimensional kinematic analysis was conducted with a Casio Camera (Model: EX-FH25) operated at 120 Hz in conjunction with a 650W artificial light to assist in joint marker identification. A Butterworth filter function with a cutoff frequency of 18 Hz was applied to the data. The movement coordination pattern is defined as the timing and sequencing of joint movements, and a shared positive contribution (SPC) of proximal to distal joint and a reversed shared positive contribution (RSPC) of a distal to proximal joint techniques were used to assess movement coordination pattern [9-10]. A SPC or a RSPC of 0% indicates a sequential type of movement, and a SPC or a RSPC of 100% indicates a simultaneous type of movement. A one-way repeated measure ANOVA statistical analysis was conducted at α = 0.05 and followed by a t-test with Bonferroni adjustment if a significant difference was found. All statistical analyses were conducted with SPSS (v. 18) software.

RESULTS AND DISCUSSION

A one-way repeated measure ANOVA was conducted on the combined percentages of SPC and RSPC for the hip and knee joint angular velocities and for the knee and ankle joint angular velocities.

There was no statistical significant difference found in the combined percentages of SPC and RSPC for the hip and knee joint angular velocities (p = 0.174) and for the knee and ankle angular velocities (p = 0.174). The mean and standard deviation of the beginning (#1-3), middle (#31-33), and end (#61-63) pitches for the hip and knee and for the knee and ankle can be observed in Table 1.

From the results of this study, a large standard deviations of the mean for both combined percentages of SPC and RSPC for the hip and knee joints and for the knee and ankle joints were observed, which indicates a large variability in the lower body joint sequencing between participants. Further, this study showed that it did not make a difference if the participants displayed an SPC or an RSPC joint coordination pattern. Participants were able to use either SPC or RSPC to achieve the same task goal, windmill pitching. This finding implies that each participant has her own joint coordination sequencing in pitching, which demonstrated the same finding as a previous study conducted by Wu, et al (2012) on slo-pitch softball hitting [10].

Interestingly, as the pitchers thrown more pitches, there was however a trend of decreased in combined % SPC and % RSPC from the beginning to the middle and the end, particularly for the hip and knee joints. This finding suggests that pitchers demonstrated a more simultaneous type of coordination in the lower extremity in the beginning of a game, and as they become more fatigue, they tend to change to a more sequential type of coordination. Coaches may utilize this finding and use this as an indicator to assess the fatigability of their pitcher during the game.

CONCLUSIONS

The purpose of this study was to examine the effects of fatigability in the lower extremity movement coordination pattern in fast pitch softball pitchers. Fatigue may influence the timing and the sequencing of the lower body joints, which may increase the chances of injury. The findings of the study suggest the importance of strength training at the hip and knee joints. Future studies are warranted with a greater number of pitches, sample size, and different types of pitch.

REFERENCES

1. News Rx. *Health and Science*, 239, 2009.
2. Hofstetter JA. *Scholastic Coach* **49**(8), 59-60, 104-105, 1980.
3. Elliot B, et al. *Int J Sport Biomech*, **2,** 20-28, 1986
4. Barrentine SW, et al. *J Orthopedic Sports and physical Therapy* **28(**6), 405-415, 1998.
5. Hewett TE, et al. *Br J Sports Med* **39,** 347-350, 2005.
6. De Wit B, et al. *J Applied Biomech* **16,** 169-179, 2000.
7. Fernandez W, et al. *Acad Emerg Med* **14**(7), 641-645, 2007.
8. Werner SL, et al. *J Sports Medicine* **7,** 597-603, 2006.
9. Hudson JL. *Med Science of Sports Exercise* **18**(2), 242-251, 1986.
10. Wu T, et al. *XVIIth Biannual Conference for the CSB,* Vancouver, BC, Canada, 2012.

Table 1: Combined % SPC and % RSPC of coordination pattern in three pitching intervals

Coordination Pattern	Beginning	Middle	End
Hip and Knee	63.9 ± 75.4	12.0 ± 22.9	29.8 ± 47.3
Knee and Ankle	31.1 ± 33.3	14.9 ± 30.7	36.1 ± 25.3

BAT QUICKNESS AND BAT VELOCITY IN DIVISION I SOFTBALL PLAYERS

Cassandra Reilly-Boccia, Travis Ficklin, Robin Lund, Javier Hervas, and Kara Beatty
Biomechanics Laboratory, University of Northern Iowa, Cedar Falls, IA, USA
email: ccreibo@uni.edu

INTRODUCTION

Successful hitting in baseball and softball is dependent on many factors. Bat quickness (BQ) measured in seconds is defined as the time it takes the bat head to travel from its initial position at the launch phase to the point the bat makes contact with the ball [2]. Bat velocity (BV) is measured in meters/second and is the linear velocity of the bat head at contact with the ball. In baseball, BQ and BV and relationships between them have been previously reported for male athletes at the professional level [1]. However, no such parameters have been investigated or established for female softball players. The purpose of this study was to describe BQ and BV for Division I collegiate softball players in game conditions and investigate the relationships that exist between BQ and BV.

METHODS

Video data were collected for all swings during a 15-game softball tournament in which six NCAA Division I teams played. The Ratings Percentage Index (RPI) for the teams ranged from 1 to 271 for the sample. For every pitch of the tournament, video cameras (JVC GC-PX1, Tokyo, JP) shooting at 300 Hz were used to capture any swing made. One camera was positioned on the first-base side of the field with its optical axis even with and parallel to the front edge of home plate. This camera was used to capture any swings made by right-handed hitters. The other, identical camera was positioned oppositely on the third-base side of the field, also with its optical axis parallel to the front edge of the plate. This second camera was used to capture any swings made by left-handed hitters. Though the cameras captured during all pitches, only data from trials in which a swing was made were kept. This resulted in a total of 1099 swings.

BQ was calculated by video analysis. The number of frames of video from the onset of the swing to contact, or, if the ball was missed, the frame in which the ball reached the same horizontal position as the bat head, were counted. This number of frames was then multiplied by (1/300) s. The onset of the swing was determined to be the frame in which the bat head made its first movement on a continuous trajectory to the contact point.

BV was calculated through digitization. The head of the bat was digitized at contact, or, if there was no contact, in the frame in which the ball had reached the same horizontal position as the bat head. The bat head was also digitized five frames (1/60 s) prior to this instant. A reference distance was calculated between the back corner of home plate and the centroid of the front, inner corners of the batters' boxes. The distance covered by the bat head in the 1/60 s immediately prior to contact or its equivalent frame was then converted to meters and divided by 1/60 s to yield BV.

Means for BV and BQ were calculated for each player in the tournament. Additionally, correlation between BV and BQ was tested using Pearson's *r*.

RESULTS AND DISCUSSION

Mean BQ and BV for individual players were 0.208 (± 0.035) s and 28.71 (± 2.62) m/s respectively, compared to a reported 0.14 - 0.18 s and 29.06 - 35.76 m/s in major-league baseball hitters [1].

Mean BQ and BV for players were inversely correlated ($r = -0.40$, $p < .001$), meaning the shortest player swing times were associated with the greatest player bat velocities. When all swings are considered, BQ and BV is still inversely correlated ($r = -0.25$, $p < .001$).

Total reaction time given to hitters (the time between the release of the ball from the pitcher's hand to the instant at which contact needs to be made) is comparable between elite-level baseball and softball hitters. For example, a 95-mph fastball pitched from a 60 ft 6 in distance in baseball has comparable travel time to that of a 66 mph softball pitched from 43 ft in softball. It is therefore reasonable that BQ for the subjects in the present study was not dissimilar to that of elite baseball hitters in previous studies [1]. The differences probably stem from male and female strength differences, and it is unclear precisely how BV was measured in previous studies.

However, the existing differences are probably minimized by differences in equipment. For instance, major-league players must use wood bats, and college baseball players must use heavier bats. Both bats have bigger moments of inertia than those used by softball players.

The relationship between BQ and BV established previously for male professional baseball players indicated that a quicker bat resulted in a smaller velocity. This was thought to be true due to increased time of a swing leading to the greater accumulation of velocity. Thus, previous researchers have made a distinction between a "contact hitter" (a hitter with batting average > .299) and a "power hitter" (batting average < .300 and with 35 or more home runs) and shown that better BQ is associated with the former and better BV with the latter [1]. Superior athletes would then be able to have greater BV while still maintaining a low BQ.

This relationship did not materialize in the present study, either by individual player (see Figure 1), or by swing (see Figure 2). Instead, the greater BV were also associated also with better BQ (less time of swing). This is probably due to a vey wide range of player abilities, whereas previous research has been conducted with top-level, more homogenous sample. Additionally, in the present study, the best and worst hitters were probably disproportionately distributed as witnessed by the wide range in team RPI.

It is also probably the case that at the Division I level, most players are capable of executing a quick swing (i.e. - having good BQ). Therefore, meaningful ability differences are probably to be seen in BV. Future studies should address the relationships between these descriptive parameters and outcomes associated with hitting success.

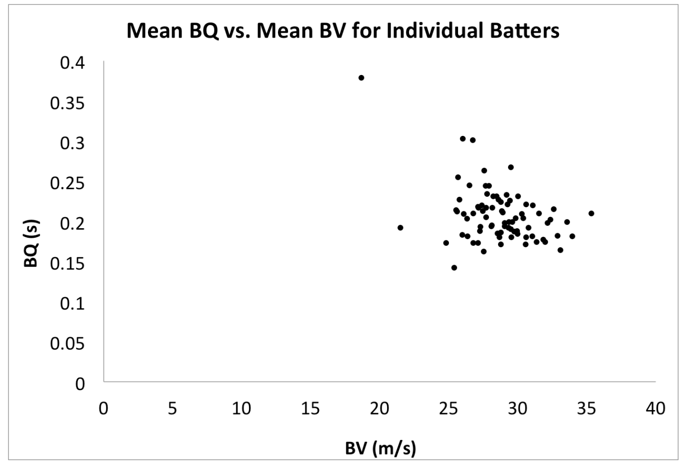

Figure 1: BQ vs. BV means for every player executing at least one swing in the tournament.

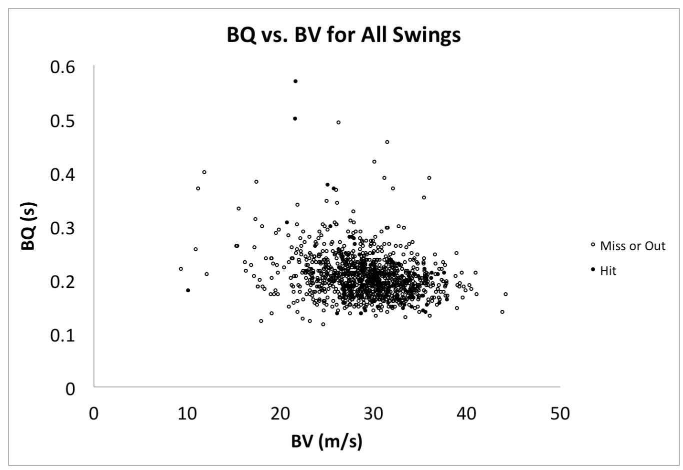

Figure 2: BQ vs. BV means for every swing executed during the tournament.

REFERENCES

1. Stellar, T., et al. *The absolutes of hitting: Dynamic balance, kinetic links, axis of rotation, bat lag.* (Motion Picture) BioKinetics inc: Laguna Hills, Ca. (1993)

2. DeRenne, C., Stellar, T., & Blitzbau, A. *High tech hitting: Science vs. Tradition*. West Publishing. (1993)

AN EXPLORATION OF ANXIETY, PHYSIOLOGICAL AROUSAL, STRETCHING, AND PERFORMANCE

[1]Cassandra Rodden, [1]Sarah Mogus, [1]Jennifer Hurst, [1]Jerry Mayhew, [2]Jeremy J Houser, and [1]Michael Bird

[1]Truman State University, Kirksville, MO, USA
[2]A.T. Still University, Kirksville, MO, USA
email: mbird@truman.edu, web: http://hes.truman.edu

INTRODUCTION

Previous examinations of the acute impact of stretching on performance were inconsistent. For example, when evaluating the stretch impact on a vertical jump, some researchers found a decrease in performance [1, 2], while others found no change in performance [3]. Subsequently, researchers found that the impact of stretching to be unreliable, and therefore not valid [4]. Yet something may explain the occasional small, negative impact of stretching on performance. In an effort to examine other factors that may have impacted performance, the objective of this study was to explore whether stretching would affect anxiety and physiological arousal levels.

METHODS

Subjects consisted of college-aged athletes (n=15, age =18-23 years). Two sessions were used to evaluate trait and state anxiety.

In the first session, subjects completed a modified form of the Competitive State Anxiety Inventory-2 (CSAI-2) to assess trait anxiety [5]. The questionnaire was modified slightly to ask the subjects how they generally feel before competition rather than how they felt right before a specific competition. Heart rate monitors were used to measure heart rate (HR), a physiological measure indicating arousal, but subjects were not able to see the values during either session. Subjects were randomly put in two groups of 3 or 4 after CSAI-2 assessment and HR was recorded. One group sat quietly for 7 minutes and one group stretched for 7 minutes. Four static stretches were performed, each held for 30 seconds: unilateral standing calf stretch, unilateral standing quadriceps stretch, unilateral seated hamstring stretch, and the unilateral gluteus stretch. After sitting for the designated time, HR was recorded. For the stretch group, HR was recorded 1 minute after the last stretch to prevent the movements related to stretching from affecting the values. Each group then switched activities and stretching or sitting was completed, followed by the recording of HR.

In the second session, the same subjects completed the CSAI-2 as an indication of state anxiety and the performance that would occur during that session. Heart rate monitors were again used to assess physiological arousal. Subjects again were not able to see the HR values during the session. Subjects were again split into two groups of 3 or 4. After an initial recording of HR, one group completed the same set of stretches they did in the first session, and the second group completed a set of dynamic warm-up exercises. The exercises were completed in 7 minutes and included jogging, high-knees, squats, and calf raises. After either stretching or dynamic warm-up, the subject's HR was recorded while completing the CSAI-2. HR recording was delayed to reflect a stable rate, not one of the immediate result of warm-up or stretching. After this they completed three vertical jumps at maximum effort. Groups then switched activities, with HR, CSAI-2, and vertical jumps completed in the same manner as described above.

Data was analyzed with a repeated measures ANOVA and an alpha level of 0.05.

RESULTS AND DISCUSSION

No significant changes were found concerning either anxiety measure in either session. Neither trait anxiety nor state anxiety changed before or after stretching. Even when utilizing trait anxiety levels as a covariate, difference in state anxiety were not found between treatments.

Heart rate, however, differed in several stages of each testing session. In the first session, HR was significantly lower than the initial value after stretching (8.3±2.6 bpm, $p<0.05$), and HR was significantly lower after stretching when compared to just sitting (3.5±1.4 bpm, $p<0.05$). It seems that stretching had a significant impact on arousal, as indicated by the lower HR. Further, the impact of stretching was significantly more than the impact of quiet sitting. Stretching potentially served to reduce the sympathetic nervous response, thus lowering HR.

In the second session, HR after warm-up and HR after stretching did not differ from initial values, but HR for the stretch group was significantly lower than HR in the dynamic warm-up group (5.2±1.6 bpm, $p<0.05$). HR not differing from the initial value was surprising for both treatments in this session.

Data were also examined for whether anxiety level (high or low) influenced HR, but no evidence was found to support anxiety levels and arousal levels within this group.

CONCLUSIONS

Within this limited sample, anxiety level does not seem to be affected by stretching. HR, an indication of arousal, seems to be influenced by stretching. According to the Inverted U-Hypothesis [6], the decreased HR may indicate a reduced arousal state that yielded poorer performance. For previous research the amount of change in performance may have depended on how much HR (and arousal) decreased in the performer during that session. In some cases, the reduction in physiological arousal may have reduced the performance in accordance with the inverted U-curve, in other cases the reduction in arousal may have had less impact on the performance, especially if the arousal level was beyond the ideal point in the U-curve for that performer. This may explain the variability in significant results and the lack of reliability of the stretching impact on performance. It seems that, with respect to performance, the order of events, and where stretching occurs, may matter with respect to arousal, but not other issues. If stretching changes arousal for the performer negatively, performance would decrease, if it changes arousal for the performer positively, performance would improve.

More research on arousal level, especially as it relates to stretching and subsequent performance, seems justified by this initial investigation.

REFERENCES

1. Bradley P, et al. *J Strength and Conditioning Res*, **26**, 223-226, 2007.
2. Hough, P, et al. *J Stretch and Conditioning Res*, **23**, 507-512, 2009.
3. Knudson, D, et al. *J Stretch and Conditioning Res*, **15**, 98-101, 2001.
4. Bird, M, et al. Proceedings of 28th ISBS, Marquette, MI, USA, 2010
5. Martens, R, et al. Competitive Anxiety in Sport, 1990.
6. Landers, D, & Arent, S, Handbook of Sport Psychology, 2nd ed., 2001.

VARIATIONS IN STEP WIDTH AS STRIDE LENGTH SHORTENS IN REARFOOT AND MID/FOREFOOT RUNNERS

[1]Elizabeth R. Boyer and [1]Timothy R. Derrick

[1]Iowa State University, Ames, IA, USA
email: ehageman@iastate.edu, web: http:// www.kin.hs.iastate.edu/

INTRODUCTION

Typical step width (SW) during running is approximately 3 cm and it has been noted that a narrower step causes greater ITB strain and strain rate [1] whereas a wider SW during gait may indicate medial-lateral (ML) instability and increase metabolic cost [2]. Because ML ground reaction forces (GRF) are greater in midfoot verus rearfoot (RF) running [3], it is possible SW may be larger in midfoot/forefoot (FF) striking. To our knowledge, no one has compared SW between RF and FF. Additionally, it has been suggested that shortening stride length (SL) 10% has positive implications for decreasing risk of tibial stress fractures and joint loading [4,5], but it is possible other spatial components of the stride, like SW, are altered by shortening SL. Therefore, our primary purpose was to compare SW between RF and FF striking. Our secondary purpose was to note if SW changed as SL was shortened 5% and 10%.

METHODS

Twenty-five recreational runners (19 RF and 6 FF) volunteered (mean±SD, age: 22±6 yrs; mass: 72.2±10.6 kg; height: 1.79±0.08 m). Participants visited the lab and reflective markers were placed on the lower extremities. Participants performed all conditions in their own shoes. First, they warmed up at a self-selected speed on the treadmill and then ran 5 minutes at 3.35 m/s with their habitual foot strike, during which preferred SL (PSL) was determined. Tape marks were placed on the floor corresponding to preferred step length. Participants performed 7 overground running trials at 3.35 m/s (±3%). Next participants ran on the treadmill for 3 minutes to the beat of a metronome indicating either a 5% or 10% shorter SL, followed by overground trials with the shortened SL. This was repeated for the other shortened SL condition. The 3 experimental conditions were repeated but with the opposite foot strike style (a new PSL was found).

Kinematic data were collected with an 8-camera Vicon system (200 Hz; filtered: 16 Hz). Kinetic data were collected by an AMTI force plate (1600 Hz, unfiltered). GRF were normalized to body weight (BW). SL and SW were calculated using the heel markers. A negative SW indicates crossing over. A 2×2 ANOVA (foot strike × SL) was performed in SPSS to compare SW, and polynomial contrasts were used to identify significant linear trends for SL.

RESULTS AND DISCUSSION

Actual overground SL reductions were 4.6% and 8.6% shorter than PSL. The foot strike × SL interaction was not significant ($p=0.133$). There was a main effect for foot strike ($p<0.001$), with SW being significantly wider in FF versus RF, (PSL: 3.3 v. 1.4 cm). There was also a main effect for SL ($p<0.001$), during which SW became narrower as SL decreased (linear trend $p<0.001$; Fig. 1). Perhaps as participants shortened their SL, their motor control system concomitantly reduced other spatial parameters, like ML step width. It has been suggested that a wider step is used to control ML balance [2], which may be less of a concern as SL shortens and stance time decreases.

This explanation, however, does not account for greater SW in FF even though PSL was significantly shorter compared to RF (2.42 v. 2.46 m; $p=0.043$). Therefore, foot strike style also seems to influence SW. In this sense, the increased medial GRF during the impact phase for FF (0.16 BW v. 0.04 BW for PSL; $p<0.001$) (Fig. 2) may dictate the increased SW. As seen in Fig. 2, immediately after contact in FF, there is a transient medial then lateral GRF peak, whereas the impact in RF is directed laterally and remains lateral throughout stance. Perhaps there is more ML instability during contact with a FF strike which the motor control system tries to manage by increasing SW. As suggested by Cavanagh [3], a wider SW during running will increase frontal plane moments to balance the increased ML GRF, which was apparent at the hip and ankle during FF (data not shown). These increased frontal plane muscle contractions presumably increase the economic cost of FF, although this is not supported for traditional running shoes [6].

Although both foot strike styles had a positive mean SW, the mean for RF was slightly lower than previously reported [1,7]. This may result from slightly different methods in calculating SW, or averages from [1] representing a combination of RF and midfoot strikers. However, it may also indicate our RF runners may have slightly increased ITB strains or strain rates because of using a narrower SW [1].

CONCLUSIONS

Step width during RF running was slightly narrower than FF, which may mean RF strikers that suffer from ITB may benefit from a wider SW [1]. Whether these different SW between foot strike styles are clinically meaningful and distinguishes between injury risk remains to be tested. Conversely, the wider SW in FF relative to RF may indicate elevated ML instability and partially account for the increased ML GRFs and frontal plane moments, although the mean SW is similar to those previously reported [1,7].

Regardless of foot strike style, SW slightly decreased as SL shortened. For runners who already have a crossover step or are at risk for ITB syndrome, shortening their stride is not recommended as it may also result in a narrower SW and possibly increase ITB strains. However, the benefits of a 10% shorter SL, such as reduced vertical loading rates and impact peak (data not shown), may outweigh the negatives of a narrower SW.

REFERENCES

1. Meardon SA et al. *Sports Biomech* **11**(4), 464-472, 2012.
2. Donelan et al. *J Biomech*, **37**, 827-835, 2004.
3. Cavanagh PR. *Foot & Ankle*, **7**, 197–217, 1987.
4. Edwards WB et al. *MSSE*, **41**(12), 2177-84, 2009.
5. Heiderscheit BC et al. *MSSE*, **43**(2), 296, 2011.
6. Perl DP et al., *MSSE*, ***44***(7), 1335-43, 2012.
7. Arellano CJ & Kram R. *J Biomech*, **44**, 1291-1295, 2011.

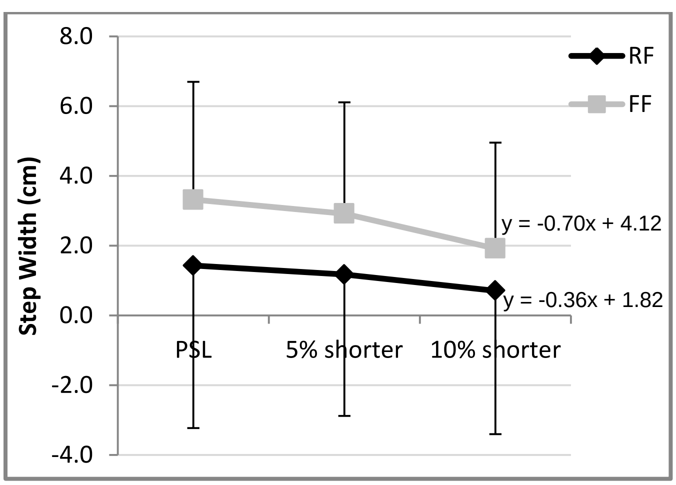

Figure 1. Step width for RF and FF striking and for the different stride length conditions. Linear equations for the different foot strikes are shown.

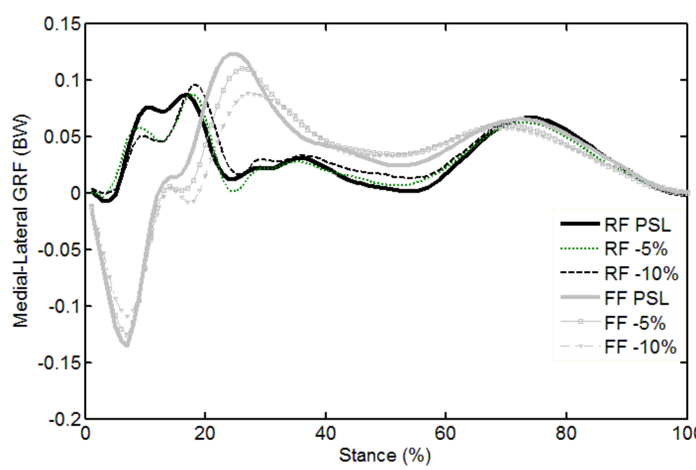

Figure 2. Ensemble medial-lateral GRF curves for the two foot strike styles (black = RF; gray=FF) and 3 SL conditions. Positive values are lateral.

BIOMECHANICALLY-DRIVEN MECHANICAL AGING AND CHARACTERIZATION OF RUNNING SHOE MIDSOLE FOAM

Nadine M. Lippa, Morgan D. Heskett, David E. Krzeminski, Scott G. Piland, James W. Rawlins, Trenton E. Gould

The University of Southern Mississippi, Hattiesburg, MS, USA
e-mail: nadine.lippa@eagles.usm.edu; web: www.usm.edu/shpm

INTRODUCTION

The goal of this study was to advance the knowledge of ethylene vinyl acetate (EVA) midsole foam performance to better elucidate the mechanisms of running overuse injury. Mechanical aging (MA) of footwear materials is successful when the cyclic forces incurred during human running are used to replicate material degradation. MA differs from the ASTM F1614 [1] footwear test, which primarily assesses short-term performance. Although ASTM tests are useful for laboratory comparisons, Verdejo [2] demonstrated F1614 to inaccurately represent running when implemented cyclically. Additionally, peer-reviewed literature is replete with biomechanically-inspired footwear testing that presents opportunities to improve input parameters and isolate the midsole contribution [2,3,4]. The three-fold purpose of this study was to: 1) develop a reasonable MA protocol to simulate 350 miles of heelstrike running; 2) determine whether the protocol effectively ages the foam; and 3) quantify the effect of simulated running on the extent of foam degradation via ASTM F1614.

METHODS

To inform a biomechanically-driven MA protocol, step length was estimated at 1 m [3,5], pilot testing estimated a single-leg frequency of 1.25 Hz [2,6,7], and human heelstrike running force plate data was employed (Fig. 1). The bimodal heelstrike was deconvoluted into its constituent frequencies of 24 Hz and 4 Hz for landing and pushoff, respectively, using a Fast Fourier transform and a 5 Hz low pass Butterworth filter. Due to the higher forces incurred, the pushoff event was the primary focus.

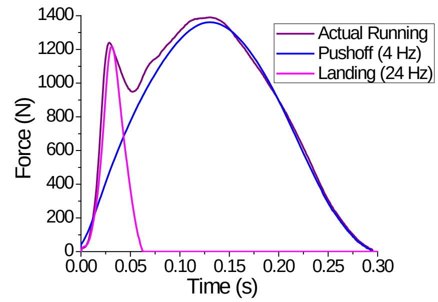

Figure 1: Bimodal heelstrike running waveform (forceplate data) and deconvoluted phases.

A Bose Electroforce 3300 mechanical testing unit (Eden Prairie, MN) performed MA. Platens of 100 mm diameter applied: 1) 250 ms of a 4 Hz sine wave from -3 N to -1390 N, and 2) 550 ms static hold at -3 N to secure the sample. To quantify degradation, ASTM F1614 was performed under ambient conditions using an instrumented drop tower (Dynatup 9250HV, Instron, Norwood, MA) with a dart diameter of 63.5 mm (versus standard recommendation of 45 mm) [8].

Sheets of EVA midsole foam matching properties of a running shoe (forefoot thickness 13 mm, Shore A 20-40, density 170-210 kg/m^3) were cut into 60mm diameter cylinders and divided into two groups: MA (n=3) and non-MA (n=3). For MA only, 1) net displacement (mm) and 2) energy absorbed (hysteresis area, J) were calculated for three cycles each at the beginning, middle, and end of aging. Both groups were impacted five times using ASTM F1614 to compare 3) impact peak force (N) and 4) duration (ms). For all statistical tests, alpha was set at α=.05 and results are presented as mean ± 95% CI.

RESULTS AND DISCUSSION

All statistical results are in Table 1. MA reduced mean foam thickness 2.3±.03 mm. Throughout MA, absorbed energy decreased, net displacement decreased, and hysteresis curve shape changed (Fig. 2), indicating the test's sufficient aging of the foam. ASTM F1614 peak force was greater for MA samples (Fig. 2). Duration was unexpectedly greater for non-MA, which may be explained by the trapezoidal curve shape for non-MA versus leptokurtic shape for MA foam. While the loading rate is higher, a trapezoidal curve limits peak force with less effect on duration. As previously reported [2,3], material change occurred most rapidly to foam during the first half of MA.

In addition to the MA protocol aging the foam, approximating 350 miles caused the foam to 1) lose 18% of its thickness, 2) lose 64% of its energy absorption, 3) lose 0.5 mm of net displacement, and 4) increase 45% in drop test peak force. If the MA test accurately mimics running, footwear performance may be significantly reduced before 350 miles. Thus, recommendations for replacement such as those by AAPSM [9] may require reevaluation. Future work will vary foam thickness to study the heelstrike event, compare results to literature, and further validate the MA procedure via biomechanically-aged foam.

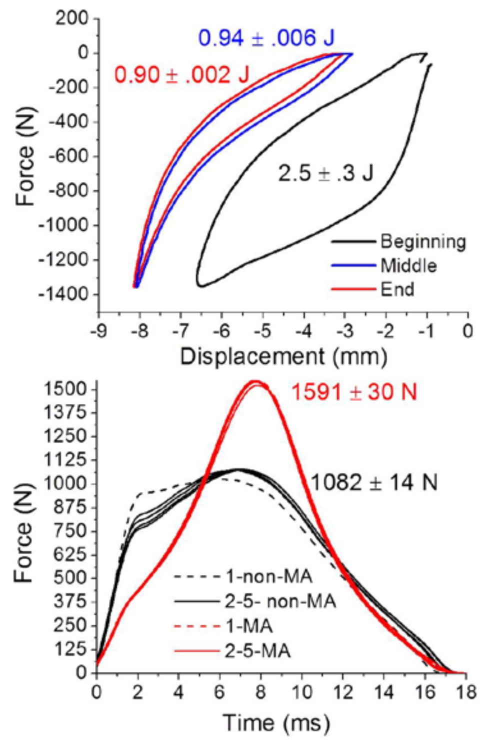

Figure 2: MA hysteresis with energy absorbed (top) and typical ASTM F1614 test with peak force (bottom).

Table 1: Summary of techniques, statistical tests, variables, and results ($p<.05$).

Technique	Statistical Test	Variables: IV-1	IV-2	DV	Between: df	F/t	p	f	Within: df	F/t	p	f	Interaction: df	F/t	p	f
Calipers	Dependent t-test	Point in Test	-	Thickness	-	-	-	-	2	173.5	<.001	3.46	-	-	-	-
Mechanical Aging (Bose)	3 x 3 RM ANOVA	Sample	Point in Test	Energy Absorbed	2,6	0.02	0.981	-	2,12	71.97	<.001	3.46	4, 12	0.016	0.999	-
				Net Displacement		795.44	<.001	15.78		952.84	<.001	12.87		153.7	<.001	7.19
				Peak Force		46.91	<.001	3.96		9.61	0.018	1.27		0.175	0.856	-
ASTM F1614 (Dynatup)	2 x 5 RM ANOVA	non-MA /MA	Drop Impacts	Peak Force	1,4	171.31	<.001	6.52	4,16	5.679	0.029	1.19	4,16	0.652	0.546	-
				Duration		0.259	0.637	-		5.053	0.008	1.12		11.29	<.001	1.67

ACKNOWLEDGEMENTS

The authors gratefully acknowledge Thomas Harris and Jessica Davison for their help with Bose testing. We also thank the Engineer Research and Development Center (ERDC W9132T-09-2-0019) for financial support and Der-tex Corporation for providing materials.

REFERENCES

1. ASTM F1614, Am Soc for Test Mat, 2009.
2. Verdejo. *Poly Testing* **23**(5), 2004.
3. Cook SD. *Am J Sports Med* **13**(4), 1985.
4. Brückner K. *Procedia Eng*. **2**(2), 2010.
5. Dillman CJ. *Exerc Sport Sci Rev* **3**(1), 1975.
6. Perl DP. *Med Sci Sport Ex* **44**(7), 2012.
7. Divert C. *Int J Sports Med*. **29**(6), 2008.
8. Krzeminski DE. *Sports Tech*. **4**(1), 2011.
9. AAPSM: www.aapsm.org. Accessed: 4/13/12.

LOWER EXTREMITY MUSCLE ACTIVATION DURING BAREFOOT, MINIMALIST AND SHOD RUNNING

[1]Tyler Standifird, [2]Ulrike Mitchell, [2]Iain Hunter, [2]Wayne Johnson and [2]Sarah Ridge

[1]University of Tennessee, Knoxville, TN, USA
[2]Brigham Young University, Provo, UT, USA
email: tstandif@utk.edu

INTRODUCTION

Research on running mechanics is a common area of biomechanical research. It is important to understand how varying running strategies may contribute to or decrease the risk of injury. At this time, barefoot and other minimalist running has gained popularity among many runners. Prior research has shown that barefoot running can be beneficial at reducing the amount of impact forces during running (1). Minimalist running shoes, like the Vibram FiveFingers (VF®), have been created to mimic barefoot running, though little is known about the specific mechanics used when wearing these types of running shoes.

EMG is a biomechanical tool that can compare muscle activations of different motor tasks. Lower extremity EMG has been measured and reported as a measure of muscle activation during a variety of activities including running. Although EMG has been compared previously for barefoot and shod conditions (2, 3), little research has looked at muscle activation during minimalist running.

One study which compared muscle activity during barefoot running and shod running reported increased tibialis anterior activation prior to foot strike during shod running (2), though this was the only muscle analyzed. Other research has looked at the tibialis anterior muscle along with the soleus, gastrocnemius and peroneus longus (3). This study reported no differences for pre-activation for the tibialis anterior or peroneus longus between shod and barefoot conditions, but did report pre activation levels to be greater for the plantar flexor muscles during barefoot running when compared with shod. The weight acceptance and push-off phases showed no differences between muscles.

The purpose of this project was to compare muscle activation during barefoot, shod and VF® running during three distinct time periods. It was hypothesized that the barefoot and VF® conditions would exhibit similar muscle activations and that both would be different than the shod condition.

METHODS

Ten injury free recreational runners with no barefoot/minimalist running experience were included in this study. Four wireless surface electrodes (Delsys Trigno, Boston, MA) were placed on the subjects' right leg at the following locations: tibialis anterior, soleus, gastrocnemius and peroneus longus. Prior to placement skin was prepped by shaving the area as well as cleansing with an alcohol wipe. Electrodes were placed according to the SENIAM recommendations (www.seniam.org). Prior to data collection electrodes were tested for proper location and cross talk. Once placement was deemed correct, the electrodes were secured using tape and wraps.

Following a warm-up of running the length of the Lab (15 m) a few times, subjects ran in VF®, barefoot and shoes (Nike Air Pegasus) in a randomized order at a speed of 3.84 m/s, controlled with timing lights. Subjects were required to meet this speed three times for each condition while making complete foot contact with the force platform. Visual 3d was used to analyze all EMG data. Data were filtered using a band-pass filter at 10-450 Hz, full-wave rectified and a moving RMS with a window size of 100 ms was applied. The max EMG value for each muscle was calculated as the overall max during all running trials. Each muscle's EMG signal during running trials was normalized to its max EMG value. Three different periods were identified during the gait cycle. The pre-activation period was calculated as the 50 ms prior to foot strike. The stance phase was split into two periods, by creating an event when the A/P ground reaction force moved from negative to positive. The first part of stance was labeled as impact phase and the last part was labeled as push-off phase. Normalized EMG signals were integrated for each time period and reported as I_{EMG}. ANOVA analysis was performed using mixed models and least square means were compared for the three conditions using Tukey adjustments.

RESULTS AND DISCUSSION

The tibialis anterior muscle showed differences between conditions during the pre-activation time period. The I_{EMG} value during the 50 ms prior to foot strike was the greatest during shod running and the smallest during barefoot running (the Vibram condition was not significantly different from either condition). The peroneus longus was found to be significantly less activated during push-off during the shod condition when compared with both the barefoot and Vibram condition. No other muscles had I_{EMG} values that were significantly different for any periods between conditions.

Our findings support the findings of some of the previous literature that have suggested that pre-activation of the tibialis anterior is greater in the shod condition when compared with barefoot running (2). Other studies have reported varying results, showing no difference in pre-activation levels of the tibialis anterior when comparing barefoot and shod running (3). With respect to pre-activation muscle activity in the gastrocnemius and soleus, our study found conflicting results to a previous study, as we found no differences in activation of these muscles (3). Additionally our findings on the differences in push-off activation of the peroneus longus muscles did not support previous literature (3). Differences between testing protocols may partially explain some of the discrepancies. The study reporting plantarflexor differences (3) instructed runners to run with a heel strike pattern. Our subjects were free to contact the ground in any manner.

CONCLUSIONS

We hypothesized that the EMG patterns during Vibram running would mimic those seen with barefoot running. We further suggested that both of these conditions would lead to different activation patterns when compared with shod running. The tibialis anterior during pre-activation differed between barefoot and shod conditions and the peroneus longus was less activated at push-off during shod when compared with the other two conditions. Muscle activation differences between shod and barefoot/minimalist running may be greater for runners with minimalist running experience. Our runners had no previous barefoot or minimalist running experience, an aspect similar to previous research (2,3). It may take time to alter running form including muscle activation patterns. In order to fully understand this effect it would be important to carry out similar studies on individuals with barefoot/minimalist running experience.

REFERENCES

1. Lieberman DE, et al. *Nature* **463**, 531-535, 2010
2. Tscharner V, et al. *J Biomech* **36**, 1169-1176, 2003
3. Divert C, et al. *Int J Sports Med* **26**, 593–598, 2005

Table 1: I_{EMG} values (%Max*s) for the tibialis anterior (TA), gastrocnemius (GAS), soleus (SOL) and peroneus longus (PL) Means (standard errors) *denotes significant difference from shod condition (p<.05)

Condition	Pre-Activation				Impact				Push-Off			
	TA	GAS	SOL	PL	TA	GAS	SOL	PL	TA	GAS	SOL	PL
Shod	.881 (.10)	.189 (.05)	.309 (.08)	.379 (.12)	1.51 (.18)	1.57 (.11)	2.43 (.67)	1.37 (.15)	.617 (.09)	1.27 (.14)	1.31 (.28)	.672 (.16)
Barefoot	.637 (.10)*	.262 (.05)	.265 (.08)	.337 (.12)	1.36 (.18)	1.51 (.11)	2.16 (.67)	1.35 (.15)	.636 (.09)	1.09 (.14)	1.45 (.28)	1.07 (.16)*
Vibram	.778 (.10)	.270 (.05)	.238 (.08)	.370 (.12)	1.27 (.18)	1.67 (.11)	1.95 (.67)	1.68 (.15)	.715 (.09)	1.24 (.14)	1.27 (.28)	.990 (.16)*

RUNNING MECHANICS DURING STANCE FOR SURFACES OF TRANSIENT STIFFNESS

Felix Tsui and Steph Forrester
Sports Technology Institute, Loughborough University, LE11 3TU, UK
email: tsui.felix.4@gmail.com, web: http://sti.lboro.ac.uk

INTRODUCTION

Governing bodies in major international sports (e.g. FIFA, IRB) provide guidelines for the properties of playing surfaces. However, these are based on performances under mechanical testing and it is unclear how athletes may be influenced by different surface properties. Changes in surface stiffness have been found to alter running mechanics during stance yet the path of the center of mass (CoM) has been found to remain unchanged [1].

The simplest model of human running represents the athlete as a point mass on a linear leg spring [2]. This approach has helped identify key control parameters such as the angle of attack (AOA), leg stiffness (k_{LEG}) and vertical stiffness (k_{VERT}). In response to increases in surface stiffness, leg stiffness was found to decrease by up to 68% [1]. Whilst these results were obtained on surfaces of constant stiffness, adaptations in leg stiffness to a step change in surface stiffness occurs within a single step [3]. However, it was argued that this control strategy may only apply to a single change in surface stiffness and not to transient changes.

This study compares running mechanics during stance for changes in surface stiffness under three conditions: constant stiffness, a single change in surface stiffness, and transient (step-by-step) changes. These results can provide insight into the strategies used by athletes for adapting to different surface playing conditions.

METHODS

Fourteen healthy males (age 21±3 yrs, height 178±4 cm, body mass 74±8 kg) provided consent to participate according to the protocol approved by the ethical advisory committee at Loughborough University. Each participant was required to complete three successful runs per surface condition on a ~20 m runway at 4.0 m·s^{-1}; *i.e.* where the right foot fully contacted the force plate and the velocity was within ± 5% of the target value.

A total of seven surface conditions were tested: three ***consistent*** (*soft*, *medium* and *hard)* to baseline overall performance; two ***single change*** (*hard* to *soft*, *soft* to *hard)*; and two ***transient change*** (random step-by-step profile of surface stiffness) trials. Each runway was formed using 12 foam sections each measuring 1.7 m long, 1.0 m wide and 0.7 m thick. The stiffness of *soft* (44 kN·m^{-1}), *medium* (70 kN·m^{-1}) and *hard* (180 kN·m^{-1}) surfaces were determined using force-deformation data obtained from mechanical drop tests with a similar effective mass to running impacts. There were no visual differences between the surface sections and participants had the opportunity to practice on each runway prior to data collection.

Ground reaction forces were measured at 1000 Hz using two force platforms (Kistler 9281CA, Winterthur, Switzerland). Running kinematics were collected at 250 Hz by tracking opti-reflective markers using a 13-camera sytem (Vicon Motion Systems Ltd, Oxford, UK) and processed using Visual3D (C-Motion, MD, USA). Running velocities were measured using SMARTSPEED timing lights (Fusion Sport Pty Ltd., Cardiff, UK) placed 4 m apart on either side of the force plate. Trials were compared using IBM SPSS Statistics 20 (NY, USA) with significance set at $\alpha = 0.05$.

RESULTS AND DISCUSSION

During ***consistent*** trials, k_{LEG} and k_{VERT} produced expected results (Table 1); i.e. k_{LEG} decreased significantly as surface stiffness increased whilst k_{VERT} was not statistically different across surfaces [1]. *Soft* and *medium* surfaces had similar peak ground reaction forces (GRF_{zPK}) suggesting similar CoM excursions; on the *soft* surface, the increased surface deformation was offset by a significantly shallower AOA. On the *hard* surface, AOA was similar to the *medium* surface, but with a significantly lower GRF_{zPK} suggesting a slightly lower CoM excursion.

During the ***single change*** in surface stiffness trials, a step transition from *hard→soft* generated similar GRF_{zPK} to all the ***consistent*** trials, but with a significantly lower k_{VERT} suggesting an increased CoM excursion. This can be attributed to the combination of a slightly steeper AOA and slightly lower k_{LEG}, a strategy closer to what was observed during ***consistent****-hard* trials. For the step transition of *soft→hard* trials, the AOA was similar to ***consistent****-soft* trials, but this was coupled with k_{LEG} similar to ***consistent****-hard* trials which acted to reduce CoM excursion and create a significantly greater k_{VERT}. To maintain similar ground contact times (CT), ground contact was used to generate greater horizontal impulse leading to longer steps off the force platform (Figure 1).

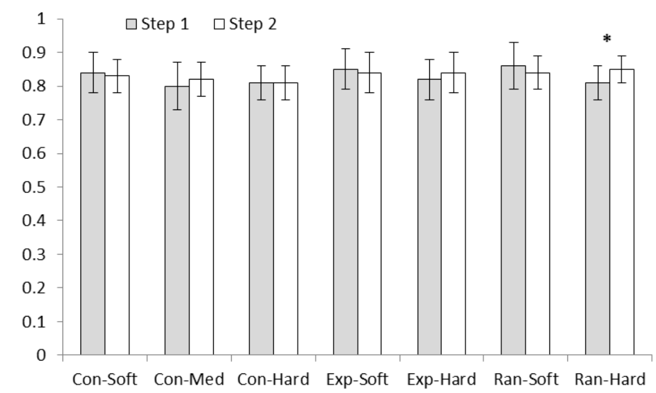

Figure 1. Normalized step-lengths (to body height) on-to (step 1) and off (step 2) the force platform. * denotes significance.

Stance mechanics for the ***transient change*** trials were statistically similar to those measured during the ***single change*** trials for the corresponding force platform surface stiffness. This suggested that during steady-state human running, the same strategy was adopted for changing stiffness surfaces regardless of whether it was a single change or a transient (step-by-step) change.

Future work can include multiple force platforms to capture the step immediately before and after the transition step and include lower limb joint mechanics to provide further understanding on how CoM excursions may be moderated.

CONCLUSIONS

For running on surfaces displaying changes in surface stiffness, stance mechanics appeared similar regardless of whether the change was a single abrupt transition or transient (step-by-step).

REFERENCES

1. Ferris, DP, et al. *Proc. Biol. Sci.*, **265**, 989-994, 1998.
2. Blickhan, R. *J. Biomech.*, **22**, 1217-1227, 1989.
3. Ferris DP, et al. *J. Biomech.*, **32**, 787-794, 1999.

ACKNOWLEDGEMENTS

This research was supported by the EPSRC, UK (grant number EP/I020411/1).

Table 1: Results for stance mechanics (mean±SD) for each surface condition.

Condition	$GRF_{z,PEAK}$ [N/kg]	CT [ms]	k_{LEG} [kN·m^{-1}]	k_{VERT} [kN·m^{-1}]	AOA [º]
Consistent					
Soft	3.06 ± 0.17[5-7]	231 ± 13[3,5,7]	42.3 ± 17.2[2,3,5,7]	34.0 ± 5.5[4,5,7]	73.8 ± 1.6[2,3]
Medium	3.04 ± 0.16[3,5-7]	229 ± 16[3]	35.4 ± 9.7[1,3,5-7]	34.8 ± 5.2[4-7]	75.7 ± 2.3[1,4-7]
Hard	2.99 ± 0.19[1,2,4-7]	223 ± 15[1,2]	27.0 ± 5.8[1,2,5-7]	36.5 ± 8.2[4-7]	75.6 ± 2.0[1,4-7]
Single Change					
Hard→ Soft	3.09 ± 0.18[3,5,7]	229 ± 12[3]	39.9 ± 14.4[2,3,5,7]	31.5 ± 4.8[1-3,5,7]	74.3 ± 2.3[2,3,7]
Soft→Hard	2.87 ± 0.19[1-4,6,7]	225 ± 15[1]	25.5 ± 5.4[1-4,6]	40.0 ± 10.2[1-4,6]	73.9 ± 2.0[2,3]
Transient Change					
Random→Soft	3.13 ± 0.17[2,3,5,7]	227 ± 14	40.2 ± 10.0[2,3,5,7]	32.1 ± 4.9[2,3,5,7]	74.4 ± 1.9[2,3,7]
Random→Hard	2.79 ± 0.21[1-6]	225 ± 17[1]	25.0 ± 6.3[1-4,6]	40.5 ± 8.4[1-4,6]	73.5 ± 2.1[2,3,4,6]